

Hugo A. Jakobsen

# Chemical Reactor Modeling

Multiphase Reactive Flows

 Springer

# Chemical Reactor Modeling

Hugo A. Jakobsen

# Chemical Reactor Modeling

Multiphase Reactive Flows

 Springer

Prof.Dr. Hugo A. Jakobsen  
Norwegian Univ. of Science & Technology  
Dept. of Chem. Engineering  
N-7491 Trondheim  
Norway  
hugo.jakobsen@chemeng.ntnu.no

ISBN: 978-3-540-25197-2

e-ISBN: 978-3-540-68622-4

Library of Congress Control Number: 2008924079

© 2008 Springer-Verlag Berlin Heidelberg

This work is subject to copyright. All rights are reserved, whether the whole or part of the material is concerned, specifically the rights of translation, reprinting, reuse of illustrations, recitation, broadcasting, reproduction on microfilm or in any other way, and storage in data banks. Duplication of this publication or parts thereof is permitted only under the provisions of the German Copyright Law of September 9, 1965, in its current version, and permission for use must always be obtained from Springer. Violations are liable to prosecution under the German Copyright Law.

The use of general descriptive names, registered names, trademarks, etc. in this publication does not imply, even in the absence of a specific statement, that such names are exempt from the relevant protective laws and regulations and therefore free for general use.

*Cover design:* eStudio Calamar, Girona, Spain

Printed on acid-free paper

9 8 7 6 5 4 3 2 1

springer.com

To Sara

---

## Preface

This book is based on lectures regularly taught in the fourth and fifth years graduate courses in transport phenomena and chemical reactor modeling, and in a post graduate course in modern reactor modeling at the Norwegian University of Science and Technology, Department of Chemical Engineering, Trondheim, Norway. The objective of the book is to present the fundamentals of the single-fluid and multi-fluid models for the analysis of single- and multiphase reactive flows in chemical reactors with a chemical reactor engineering rather than mathematical bias. Organized into 12 chapters, it combines theoretical aspects and practical applications and covers some of the recent research in several areas of chemical reactor engineering. This book contains a survey of the modern literature in the field of chemical reactor modeling.

I hope this book can serve as a guide for my future Ph.D. students, as well as other interested scientists, to get a thorough introduction to this field of research without spending too much of their invaluable time searching for and reading a large number of books and papers.

Comments on the contents of the book:

In chap 1 a survey of the elements of transport phenomena for single phase multicomponent mixtures is given. This theory serves as basis for the development of most chemical engineering models as well as the multiphase flow concepts to be presented in the following chapters. The first part of the chapter considers laminar single phase flows for multicomponent mixtures. In the second part of the chapter the governing equations are applied to turbulent flows.

Chapter 2 contains a summary of the basic concepts of kinetic theory of dilute and dense gases. This theory serves as basis for the development of the continuum scale conservation equations by averaging the governing equations determining the discrete molecular scale phenomena. This method is an alternative to, or rather both a verification and an extension of, the continuum approach described in chap 1. These kinetic theory concepts also determine the basis for a group of models used describing granular flows, further outlined in chap 4. A pedagogical advice basically for the students intending

to obtain their very first overview of the content of reactor modeling on the graduate level may concentrate on the continuum formulations first and, if strictly needed, go back to the chapters that are dealing with kinetic theory (i.e., chaps 2 and 4) after they feel confident with the continuum modeling concepts.

Chapter 3 contains a survey of a large number of books and journal papers dealing with the basic theory of multi-fluid flow modeling. Emphasis is placed on applying the multi-fluid model framework to describe reactive flows. This is perhaps the main contribution in this book, as there exist no textbook on reactive multiphase flow modeling intended for reactor engineers. In the more advanced textbooks the basic multicomponent multiphase theory is introduced in a rather mathematical context, thus there is a need for a less demanding presentation easily accessible for chemical reaction engineering students.

Chapter 4 contains a summary of the basic theory of granular flow. These concepts have been adopted describing particulate flows in fluidized bed reactors. The theory was primarily used for dense bed reactors, but modified closures of this type have been employed for more dilute flows as well. Compared to the continuum theory presented in the third chapter, the granular theory is considered more complex. The main purpose of introducing this theory, in the context of reactor modeling, is to improve the description of the particle (e.g., catalyst) transport and distribution in the reactor system.

In chap 5 an outline of the basic theory of the required closure laws and constitutive equations is provided. The first section presents the closures related to averaged products (i.e., the analogous to turbulence type of closures). The following sections describe models for the interfacial transport phenomena occurring in multiphase reactive systems. An overview of the important models for the different forces acting on a single particle, bubble or droplet is given. Model modifications due to swarm or cluster effects are discussed. The standard theories for interfacial heat and mass transfer are examined. In the last section the literature controversy originating from the fact that with the present level of knowledge, there is no general mathematical theory available to determine whether the 3D multi-fluid model is *well posed* as an initial-boundary value problem, is examined.

In chap 6 the derivation of the classical reactor models is examined starting out from the microscopic heat and species mass balances. In chemical reactor engineering the idealized models like the plug flow reactor (PFR) - and continuous stirred tank reactor (CSTR) models are well known from basic courses in chemical reaction engineering. For non-ideal flows the dispersion models (DMs) are frequently used. These standard models are deduced from the microscopic heat and species mass balances employing a cross-sectional area averaging procedure. Similar, but not identical, models can be obtained by simplifying the governing microscopic transport equations.

In chap 7 a brief summary of the agitation and fluid mixing technology is given. The main emphasis is placed on examining the modern strategies used

to model the momentum transfer from the impeller to the fluid. The methods are sketched and the basic equations are listed. A few model simulation examples are presented.

In chap 8 the basic bubble column constructions and the principles of operation of these reactors are described. The classical models for two- and three phase simple bubble column reactors are defined based on heat and species mass balances. The state of the art on fluid dynamic modeling of bubble column reactors is then summarized including a few simulations of reactive flows.

In chap 9 an outline of the basic theory of the population balance equation is provided. Three different modeling frameworks are defined, the macroscopic formulation, the microscopic continuum - and kinetic theory formulations. The macroscopic model is formulated directly on the macroscopic scales, enabling a suitable framework for practical engineering calculations. In this framework a simple and inaccurate numerical discretization scheme has become an integrated part of most closure laws. Since the numerical discretization schemes cannot be split from the physical closure laws in a trivial manner, the more popular closures for bubble coalescence and breakage rates are discussed in this chapter as well. The more rigorous microscopic formulations are presented and future reactor analysis should preferably be based on these concepts, enabling more accurate closure laws to be formulated and more optimized solution methods to be used. The status on population balance modeling of bubble coalescence and breakage phenomena is summarized.

Chapter 10 contains a literature survey of the basic fluidized bed reactor designs, principles of operation and modeling. The classical two- and three phase fluidized bed models for bubbling beds are defined based on heat and species mass balances. The fluid dynamic models are based on kinetic theory of granular flow. A reactive flow simulation of a particular sorption enhanced steam reforming process is assessed.

In chap 11 an overview of the basic designs, principles of operation, and modeling of fixed packed bed reactors is presented. The basic theory is applied to describe the performance of particular chemical processes operated in fixed packed bed reactors. That is, porous media reactive flow model simulations of particular packed bed sorption enhanced steam reforming processes are assessed.

In chap 12 a group of finite volume solution algorithms for solving the multi-fluid model equations is described. The basic single phase finite volume method solution strategies, spatial discretization schemes, and ODE solution methods in time are examined. The selected multiphase algorithms are extended versions of the single-phase SIMPLE-like algorithms. However, alternative algorithms can be found in the literature. Some of these methods are briefly outlined in this chapter. Moreover, several numerical methods for solving the population balance equation for dispersed flows are outlined. Finally, several solution methods for the resulting algebraic discretization equations are mentioned.

The book may be used as a reference book of the multi-fluid theory, or for teaching purposes at different educational levels. For example, at the graduate level, an introductory graduate course in single phase transport phenomena can be based on chap 1 (and parts of chap 2). Suitable numerical solution methods for the governing single phase equations can be found in chapter 12. An introduction to reactor modeling can be based on chaps 6-11. The material in chapters 2,3,4,5 and the multiphase parts of chap 12 may be better suited at the post graduate level. Taking these three courses in sequence, I hope the PhD students get the necessary knowledge to give future contributions in this field of science.

I have received a great deal of help from numerous persons, over the nearly twenty years association with this subject, in formulating and revising my views on both reactor modeling and chemical reactor engineering. I would like to acknowledge the inspiring discussions I have had with the colleagues at NTNU during my work on this book. I am particularly incepted to the present and former members of the staff at the Chemical Engineering Department at NTNU. In addition, I wish to thank the PhD students that have taken my graduate subjects and thus read the lecture notes carefully and supplied me with constructive criticisms (among other comments) and suggestions for further improvements on the text. It is fair to mention that my students, especially Dr ing Carlos A Dorao, MSc Håvard Lindborg, MSc Hans Kristian Rusten and MSc Cecilie Gotaas Johnsen, have contributed to this book in many ways. This includes technical contributions either in a direct or indirect way, and reading parts of the draft manuscript. I must also thank Associate Professor Maria Fernandino for her valuable suggestions and comments regarding chapter 2. Finally, my thoughts are due to my wife, Jana, who strongly believes quality is better than quantity. Her reviews and criticism of the contents surely improved the book.

Trondheim, November 2007

*Hugo A. Jakobsen*

---

# Nomenclature

## Latin Letters

$A$	Hamaker constant ( $J$ )
$A$	chemical component in general reaction
$A$	empirical model parameter ( $-$ )
$A$	macroscopic surface area defining the control volume ( $m^2$ )
$A$	model parameter ( $-$ )
$A$	shorthand notation for advective term
$a$	coefficient in the FVM discretization equation
$a$	non-linear function in PDE classification theory
$a$	stoichiometric coefficients in general reaction ( $-$ )
$A(t, \mathbf{r})$	generalized variable dependent on time and space
$A_0$	catchment area ( $m^2$ )
$A_0$	valve opening area ( $m^2$ )
$a_0$	parameter in prescribed velocity profile in laminar boundary layer theory ( $-$ )
$A_1$	surface of phase 1 in two phase system ( $m^2$ )
$a_1$	parameter in prescribed velocity profile in laminar boundary layer theory ( $-$ )
$A_2$	surface of phase 2 in two phase system ( $m^2$ )
$a_2$	parameter in prescribed velocity profile in laminar boundary layer theory ( $-$ )
$a_3$	parameter in prescribed velocity profile in laminar boundary layer theory ( $-$ )
$a_C(\tilde{\mathbf{x}}, \tilde{\mathbf{r}}; \mathbf{x}', \mathbf{r}', \mathbf{Y}, t)$	coalescence frequency or the fraction of particle pairs of states $(\tilde{\mathbf{x}}, \tilde{\mathbf{r}})$ and $(\mathbf{x}', \mathbf{r}')$ that coalesce per unit time ( $1/s$ )
$A_h$	heat exchange surface of reactor ( $m^2$ )
$A_I$	interface area ( $m^2$ )
$a_I$	interfacial area density denoting the interface area per unit volume ( $m^2/m^3$ )
$a_i$	coefficient in generic algebraic equation in TDMA outline
$a_i$	constants in MWR approximation of the solution

$A_P$	projected area, average projected area of particle area distribution on a plane normal to the flow ( $m^2$ )
$A_r$	chemical affinity of reaction $r$ ( $J/mol$ )
$A_S$	particle surface, average surface calculated from a particle surface distribution ( $m^2$ )
$a_{ij}$	coefficients in algebraic system matrix $\mathcal{A}$
$B$	baffle width ( $m$ )
$B$	chemical component in general reaction
$B$	coefficient consisting of inverted Maxwell-Stefan diffusivities ( $s/m^2$ )
$B$	displacement factor ( $-$ )
$B$	model parameter ( $-$ )
$B$	model parameter in logarithmic velocity profile ( $-$ )
$b$	constant of integration in laminar boundary layer theory ( $-$ )
$b$	constant term in the FVM discretization equation
$b$	impact parameter ( $m$ )
$b$	non-linear function in PDE classification theory
$b$	stoichiometric coefficients in general reaction ( $-$ )
$B(\mathbf{x}, \mathbf{r}, \mathbf{Y}, t)$	net birth term in population balance equation
$B_0$	permeability ( $m^2$ )
$b_B(\mathbf{x}, \mathbf{r}, \mathbf{Y}, t)$	particle breakup frequency ( $s^{-1}$ )
$b_i$	coefficient in generic algebraic equation in TDMA outline
$b_k$	total breakage rate of bubbles of group $k$ in multi-group model
$B_{B,i}$	birth rate due to breakup in bubble class $i$ ( $\frac{1}{s m^3}$ )
$B_{C_i}$	birth rate due to coalescence in bubble class $i$ ( $\frac{1}{s m^3}$ )
$B_{dd}(x)$	Kolmogorov second order velocity structure function ( $m^2/s^2$ )
$C$	chemical component in general reaction
$C$	clearance of turbulent impeller from the tank bottom ( $m$ )
$C$	constant in velocity structure function formula, $C = \frac{27}{55} \Gamma(\frac{1}{3}) C_k \approx 2.0$
$C$	( $-$ )
$C$	laminar impeller wall clearance ( $m$ )
$C$	model parameter ( $-$ )
$C$	shorthand notation notation for convective term
$C$	universal constant in the Kolmogorov two-third-law ( $-$ )
$c$	mole concentration of species ( $mol/m^3$ )
$c$	non-linear function in PDE classification theory
$c$	parameter in relation for the modulus of elasticity of the particulate phase ( $-$ )
$c$	speed of electromagnetic radiation propagation in a medium ( $m/s$ )
$c$	stoichiometric coefficients in general reaction ( $-$ )
$c^*$	mole concentration scale in turbulent boundary layer theory ( $-$ )
$c^+$	dimensionless mole concentration in turbulent boundary layer theory
$C$	( $-$ )
$C_L^M$	Magnus lift force coefficient ( $-$ )
$C_L^S$	Saffman lift force coefficient ( $-$ )
$C_L^T$	slanted wake transversal lift force coefficient ( $-$ )

$C_0$	model coefficient (-)
$C_\mu$	$k$ - $\varepsilon$ turbulence model parameter (-)
$C_\omega$	empirical model constant (-)
$C_b$	empirical parameter in two-phase $k$ - $\varepsilon$ turbulence model (-)
$C_c$	molar concentration of species $c$ in mixture ( $kmol/m^3$ )
$C_D$	$k$ - $\varepsilon$ turbulence model parameter (-)
$C_D$	drag coefficient (-)
$C_E$	empirical constant in LES model (-)
$C_f(f_{V_{i,j}})$	surface area increase coefficient (-)
$C_f$	friction factor (-)
$c_i$	coefficient in generic algebraic equation in TDMA outline
$C_K$	kinetic-energy velocity correction factor (-)
$C_k$	constant in the Kolmogorov five-third-law (-)
$C_L$	lift force (net) coefficient (-)
$C_M$	momentum velocity correction factor (-)
$C_P$	specific heat at constant pressure ( $J/kgK$ )
$C_p$	laminar impeller off bottom clearance ( $m$ )
$C_S$	Smagorinsky constant (-)
$C_S$	speed of sound ( $m/s$ )
$C_V$	specific heat at constant volume ( $J/kgK$ )
$C_V$	virtual - or added mass force coefficient (-)
$c_0$	speed of light in the medium. In a vacuum $c_0 = 2.998 \times 10^8$ ( $m/s$ )
$C_{\varepsilon 3}$	model parameter (-)
$C_{\varepsilon 1}$	$k$ - $\varepsilon$ turbulence model parameter (-)
$C_{\varepsilon 2}$	$k$ - $\varepsilon$ turbulence model parameter (-)
$C_{kl}$	rate of coalescence of bubbles of groups $g$ and $k$ in multi-group model
$C_{W1}$	empirical wall lift force coefficient (-)
$C_{W2}$	empirical wall lift force coefficient (-)
$C_{wb}$	bubble wall friction force coefficient (-)
$Ca$	Capillary number, $Ca = We/Re_P$ (-)
$CFL$	Courant number, used in the Courant-Friedrichs-Lewy necessary stability condition for hyperbolic equations
$D$	auxiliary factor in multiphase fractional step method implementation
$D$	bubble deformation factor (-)
$D$	chemical component in general reaction
$D$	diameter ( $m$ )
$D$	impeller diameter ( $m$ )
$D$	mass diffusion coefficient or diffusivity, binary or multicomponent systems ( $m^2/s$ )
$D$	model parameter (-)
$D$	shorthand notation notation for diffusive term
$d$	non-linear function in PDE classification theory
$d$	particle diameter ( $m$ )
$d$	stoichiometric coefficients in general reaction (-)
$d'$	diameter of daughter particle ( $m$ )

$d''$	diameter of the smallest daughter particle ( $m$ )
$D'_s$	effective mass based diffusion coefficient in the explicit expression for the Maxwell-Stefan flux ( $m^2/s$ )
$D'_{sm}$	effective diffusion coefficient of species $s$ in Wilke mass flux ( $m^2/s$ )
$D(\mathbf{x}, \mathbf{r}, \mathbf{Y}, t)$	net death term in population balance equation
$d(i)$	diameter of particle in class, group or phase $i$ ( $m$ )
$d\hat{S}$	entropy of mixture ( $J/K$ )
$D_{gp}^t$	gas-particle turbulent dispersion coefficient ( $m^2/s$ )
$d_A$	surface average diameter ( $m$ )
$d_a$	major axis of an ellipsoidal bubble ( $m$ )
$d_b$	minor axis of an ellipsoidal bubble ( $m$ )
$d_c$	critical bubble diameter ( $m$ )
$d_D$	drag diameter ( $m$ )
$d_e$	equivalent bubble diameter ( $m$ )
$D_h$	hydraulic diameter ( $m$ )
$d_H$	maximum horizontal dimension of a deformable particle ( $m$ )
$d_i$	coefficient in generic algebraic equation in TDMA outline
$d_i$	diameter of particle in interval $i$ ( $m$ )
$d_r$	reactor diameter ( $m$ )
$D_s$	effective diffusion coefficient for species $s$ in explicit Maxwell-Stefan flux expression ( $m^2/s$ )
$d_S$	Sauter mean diameter ( $m$ )
$D_s^e$	effective diffusivity of species $s$ in explicit expression for the dusty gas model flux ( $m^2/s$ )
$D_s^T$	multicomponent thermal diffusion coefficients ( $kg/ms$ )
$d_V$	maximum vertical dimension of a deformable particle ( $m$ )
$d_V$	volume average - or equivalent particle diameter ( $m$ )
$d_{12}$	distance between the centers of two hard spheres at collision ( $m$ )
$d_{\text{eff}}$	effective bubble diameter ( $m$ )
$d_{\text{max}}$	maximum stable fluid particle( $m$ )
$D_{B,i}$	death rate due to breakup in bubble class $i$ ( $\frac{1}{s m^3}$ )
$D_{C,i}$	death rate due to coalescence in bubble class $i$ ( $\frac{1}{s m^3}$ )
$d_{e,0}$	initial equivalent bubble diameter just above the distributor ( $m$ )
$d_{\text{max}}$	fixed maximum particle size ( $m$ )
$d_{\text{min}}$	fixed minimum particle size ( $m$ )
$D_{sm}$	Wilke effective diffusion coefficient for species $s$ ( $m^2/s$ )
$D_{sr}$	Fick's law binary diffusivity for the species $s$ and $r$ mixture ( $m^2/s$ )
$Da$	Damköhler number ( $-$ )
$da$	infinitesimal area on the sphere of influence denoting the face of the collision cylinder (in kinetic theory) ( $m^2$ )
$da$	infinitesimal surface element ( $m^2$ )
$Da_I$	Damköhler number, $Da_I = lr/u$ ( $-$ )
$dA_p$	differential area used to define the radiation intensity, $dA_p = da \cos \theta$ ( $m^2$ )

$DEN$	auxiliary parameter (denominator) in kinetic expression for steam reforming
$dl$	element of arc length ( $m$ )
$dl$	height of collision cylinder (in kinetic theory) ( $m$ )
$dm/dt$	mass change rate ( $kg/s$ )
$ds$	arc length ( $m$ )
$dt$	infinitesimal increment in time ( $s$ )
$dv$	infinitesimal volume element ( $m^3$ )
$dx$	infinitesimal increment in $x$ -coordinate direction ( $m$ )
$dy$	infinitesimal increment in $y$ -coordinate direction ( $m$ )
$dz$	infinitesimal increment in $z$ -coordinate direction ( $m$ )
$E$	empirical wall law model parameter ( $-$ )
$E$	energy of each photon ( $J$ )
$E$	generalized total energy of a given system in classical mechanics
$E$	heat flux emitted by a real surface ( $W/m^2$ )
$E$	total emissive power of thermal radiation ( $W/m^2$ )
$e$	non-linear function in PDE classification theory
$e$	thermal internal energy per unit mass of mixture ( $J/kg$ )
$e(\lambda)$	kinetic energy of eddy with size $\lambda$ ( $J$ )
$e(d_i, \lambda)$	turbulent kinetic energy of an individual eddy of size $\lambda$ breaking a bubble of size $d_i$ ( $J$ )
$E(k, t)$	three dimensional energy spectrum per unit mass ( $m^3/s^2$ )
$E(t)$	contact time distribution function in penetration theory ( $s^{-1}$ )
$E(t)$	normalized element age distribution function in surface renewal theory ( $s^{-1}$ )
$E_k^{\Gamma}$	interfacial energy transfer due to phase change ( $J/m^3s$ )
$E_k^E$	interfacial heat transfer ( $J/m^3s$ )
$E_k^W$	interfacial work by viscous and pressure forces ( $J/m^3s$ )
$E_{\lambda}(\lambda)$	spectral emissive power of thermal radiation ( $W/m^2 \mu m$ )
$E_{\text{eddies}}(\lambda)$	energy of discrete eddies of size $\lambda$ ( $\frac{J}{m^3[m]}$ )
$E_{\text{spectra}}(\lambda)$	energy of eddy wave function for eddies of size between $\lambda$ and $\lambda + d\lambda$ ( $\frac{J}{m^3[m]}$ )
$E_{\text{total}}$	total energy associated with the center of mass of a thermodynamic system ( $J$ )
$E_{\text{total}}$	total energy content within an arbitrary volume $V$ in the system ( $J$ )
$E_a$	activation energy of sorbent ( $J/kmol$ )
$E_b$	total thermal radiative power emitted by a blackbody ( $W/m^2$ )
$E_c(k)$	scalar spectrum in wave number space
$E_i$	internal energy associated with the center of mass of a thermodynamic system ( $J$ )
$E_k$	kinetic energy associated with the center of mass of a thermodynamic system ( $J$ )
$E_p$	potential energy associated with the center of mass of a thermodynamic system ( $J$ )

- $E_p$  scalar potential energy function or potential ( $J$ )  
 $E_p(\dot{q}, t)$  generalized potential energy of a given system in Lagrangian mechanics  
 $E_s(d)$  minimum energy required to deform a bubble of size  $d$  ( $J$ )  
 $e_s(d_i, d_j)$  increase of bubble surface energy required breaking the parent bubble  $d_i$  into a daughter bubble  $d_j$  and a second corresponding daughter bubble ( $J$ )  
 $E_T$  total kinetic energy of the macroscopic fluid motion ( $J$ )  
 $E_{\lambda, b}$  spectral thermal radiative power emitted by a blackbody ( $W/m^2 \mu m$ )  
 $E_{Total}$  total energy of two colliding particles ( $J$ )  
 $E_{k, fluid}$  kinetic energy (KE) of fluid surrounding a particle in virtual mass force analysis ( $J$ )  
 $EO$  Eötvös number ( $-$ )  
 $f(t, \mathbf{x})$  longitudinal autocorrelation function ( $-$ )  
 $F$  dimensionless drag coefficient ( $-$ )  
 $F$  mass flux component in FVM discretization  
 $F$  model parameter ( $-$ )  
 $F$  net flux of property  $\psi$  in elementary kinetic theory  
 $f$  continuous number density probability in least squares method outline  
 $f$  dimensionless constant in turbulent viscosity model ( $-$ )  
 $f$  friction factor ( $-$ )  
 $f$  non-linear function in PDE classification theory  
 $f$  surface force component ( $N$ )  
 $f$  wave frequency associated with Taylor hypothesis ( $radians/s$ )  
 $f(...)$  distribution function in Hamiltonian mechanics  
 $f(...)$  single distribution function in kinetic theory  
 $f(\mathbf{x})$  quadratic function in CG definition  
 $f(\zeta, \eta)$  function defining a curve on a given surface, expressed in the curvilinear coordinates  
 $f(m, \mathbf{r}, t)$  particle distribution function with particle mass as inner coordinate ( $\frac{1}{m^3[kg]}$ )  
 $f(t, \mathbf{r})$  general scalar, vector or tensor valued function  
 $F(x, y)$  explicit function defining a surface in 3D space, expressed in Cartesian coordinates  
 $f(x, y, z)$  implicit function defining a surface in 3D space, expressed in Cartesian coordinates  
 $f^{(1)}(\mathbf{r}, \mathbf{c}, \mathbf{r}_1, \mathbf{c}_1, t)$  single distribution function in kinetic theory,  $f \equiv f^{(1)}$   
 $f^{(1)}(\mathbf{x}, \mathbf{r}, t)$  single number distribution function denoting the number of particles per unit volume of the particle phase space at time  $t$  (general)  
 $f^{(1)}(d, \mathbf{r}, t)$  average single particle number density function using particle diameter as inner coordinate ( $\frac{1}{[m]m^3}$ )  
 $f^{(1)}(d, t)$  volume average particle number density probability with  $d$  as inner coordinate ( $\frac{1}{m^3[m]}$ )  
 $f^{(2)}(\mathbf{r}, \mathbf{c}, \mathbf{r}_1, \mathbf{c}_1, t)$  pair distribution function in kinetic theory  
 $f_1$  distribution function for molecule 1 in kinetic theory

$f_2$	distribution function for molecule 2 in kinetic theory
$f_\lambda$	number density of eddies of size between $\lambda$ and $\lambda + d\lambda$ ( $\frac{1}{m^3 s [m]}$ )
$f_b$	area (volume) fraction of bed gas taken by bubble phase gas ( $m^2$ )
$f_e$	area (volume) fraction of bed gas taken by emulsion phase gas ( $m^2$ )
$f_i^0$	fugacity of species $i$ in the mixture at the standard state ( $Pa$ )
$f_k$	auxiliary factor in PEA implementation
$F_s$	molar flow rate of species $s$ ( $mol/s$ )
$f_w$	bubble wake fraction ( $-$ )
$f_D$	Darcy friction factor ( $-$ )
$f_F$	Fanning friction factor ( $-$ )
$F_{in,\psi}$	total inflow of property $\psi$ into the calculation domain, used in convergence criterion
$f_{sr}$	proportionality or friction coefficient ( $kg/m^3 s$ )
$f_{V_{ij}}$	breakage volume fraction, $f_{V_{ij}} = d_j^3/d_i^3$ ( $-$ )
$ff$	fouling factor ( $Km^2/W$ )
$Fr$	Froude Number, $Fr = v^2/gL$ ( $-$ )
$g(t, \mathbf{x})$	transverse autocorrelation function ( $-$ )
$G$	auxiliary factor in multiphase fractional step method implementation
$G$	non-dimensional shear rate ( $-$ )
$G$	particle growth rate ( $m/s$ )
$G$	specific Gibbs free energy expressed in terms of mole ( $J/kg$ )
$G$	total irradiation of thermal radiation ( $W/m^2$ )
$g$	acceleration of gravity ( $m/s^2$ )
$g$	magnitude of the relative velocity vector ( $m/s$ )
$g$	non-linear function in PDE classification theory
$g$	source term in least squares method outline
$G_0$	modulus of elasticity of the particulate phase ( $kg/ms^2$ )
$G_\lambda(\lambda)$	spectral irradiation of thermal radiation ( $W/m^2 \mu m$ )
$g_I$	interface Gibbs free energy per unit mass ( $J/kg$ )
$g_k$	Gibbs free energy per unit mass ( $J/kg$ )
$g_{\alpha\beta}$	metric tensor
$Gr$	Grashof number, $Gr = l^3 \Delta\rho g / \rho\nu^2$ ( $-$ )
$H$	H-property function in the Boltzmann H-theorem
$H$	liquid height in standard turbulent stirred tank ( $m$ )
$H$	specific enthalpy, mixture enthalpy per unit mass expressed in terms of temperature, pressure and the mass fractions of the species in the mixture ( $J/kg$ )
$H$	stagnation enthalpy ( $J/kg$ )
$H$	wall distance in square duct ( $m$ )
$h$	Planck's constant = $6.6262 \times 10^{-34}$ ( $Js$ )
$h$	film thickness ( $m$ )
$h$	grid spacing ( $m$ )
$h$	grid spacing in multigrid method outline
$h$	head in head form of energy balance ( $m$ )

$h$	specific enthalpy, mixture enthalpy per unit mass expressed in terms of temperature, pressure and the mass fractions of the species in the mixture, a fluid dynamic quantity ( $J/kg$ )
$H(\mathbf{p}, \mathbf{q}, t)$	Hamiltonian function in Hamiltonian mechanics
$h(Re_P)$	dimensionless function in particle drag expression ( $-$ )
$h_k^T$	interfacial heat transfer due to phase change ( $J/m^3s$ )
$h_k^*$	specific enthalpy of ideal gas mixture ( $J/kg$ )
$h_k^{\text{cond, conv}}$	combined convective heat transfer coefficient accounting for conductive and convective heat transfer ( $W/m^2K$ )
$h_k^{\text{cond}}$	convective heat transfer coefficient accounting for conductive heat transfer ( $W/m^2K$ )
$h^{\text{excess}}$	specific mixture excess enthalpy ( $J/kg$ )
$h^{\text{excess}}$	specific residual enthalpy of mixture ( $J/kg$ )
$h^{\text{ideal mixture}}$	specific mixture enthalpy expressed in terms of enthalpies of pure real fluids ( $J/kg$ )
$h^{\text{rad}}$	heat transfer coefficient accounting for radiation transfer ( $W/m^2K$ )
$h_0$	initial film thickness ( $m$ )
$h_\alpha$	Lamé coefficients, metric coefficients, or scale factors
$h_C$	effective swept volume rate ( $m^3/s$ )
$h_c$	specific enthalpy associated with chemical species/component $c$ ( $J/kg$ )
$h_f$	final film thickness ( $m$ )
$H_I$	mean surface curvature ( $m^{-1}$ )
$h_I$	interface enthalpy per unit mass ( $J/kg$ )
$h_k$	enthalpy per unit mass ( $J/kg$ )
$h_v$	volumetric heat transfer coefficient ( $Jm^{-3}K^{-1}$ )
$h_{cd}$	interfacial heat transfer coefficient
$H_{GL}$	suspension height ( $m$ )
$h_{gp}$	gas to particle heat transfer coefficient ( $Jm^{-2}K^{-1}$ )
$I$	integral
$I$	turbulence intensity ( $-$ )
$I_e$	total intensity of emitted thermal radiation ( $W/m^2$ )
$I_i$	particle size interval ( $m$ )
$I_i$	total intensity of incident thermal radiation ( $W/m^2$ )
$I_R$	relative turbulence intensity ( $-$ )
$I_{\lambda,b}$	spectral radiation intensity of blackbody emission ( $W/m^2 \text{ sr } \mu m$ )
$I_{\lambda,e}(\lambda, \theta, \phi)$	spectral intensity of emitted thermal radiation ( $W/m^2 \text{ sr } \mu m$ )
$I_{\lambda,i}(\lambda, \theta, \phi)$	spectral intensity of incident thermal radiation ( $W/m^2 \text{ sr } \mu m$ )
$J(ff)$	approximate collision term in the Boltzmann equation as given by the Enskog expansion
$J$	Jacobian determinant
$J$	total radiosity of thermal radiation ( $W/m^2$ )
$J_{k,s}^T$	interfacial species mass transfer due to phase change ( $kg/m^3s$ )
$J_{k,s}^j$	interfacial species mass transfer due to ordinary diffusion ( $kg/m^3s$ )
$J_\lambda(\lambda)$	spectral radiosity of thermal radiation ( $W/m^2 \mu m$ )

$K$	equilibrium constant
$K$	generalized proportionality coefficient in the interfacial transfer flux relation
$K$	model parameter (—)
$K$	number of FEM elements that constitute a part of the domain
$K$	parameter in bubble size model for bubbling beds (—)
$K$	permeability constant in the Davidson-Harrison model characteristic of the particles and the fluidizing fluid ( $m^3s/kg$ )
$k$	Boltzmann constant ( $J/K$ )
$k$	constant in capture kinetics ( $1/s$ )
$k$	mean turbulent kinetic energy per unit mass ( $m^2/s^2$ )
$k$	parameter in cyclone pressure drop relation (—)
$k$	reaction rate constant
$k$	thermal conductivity ( $W/mK$ )
$k$	wave number ( $m^{-1}$ )
$K''$	model parameter (—)
$K'''$	model parameter (—)
$K(t - \tau)$	kernel function in history force expression (—)
$K_p^{coll}$	collisional diffusion coefficient ( $m^2/s$ )
$K_p^t$	particle turbulent (or kinetic) diffusion coefficient ( $m^2/s$ )
$k_0$	wave number for the integral scale of turbulence ( $m^{-1}$ )
$K_1$	empirical parameter in drag coefficient parameterization (—)
$K_2$	empirical parameter in drag coefficient parameterization (—)
$K_3$	empirical parameter in drag coefficient parameterization (—)
$k_{dilute}$	conductivity parameter for the dilute limit in granular theory ( $kg/ms$ )
$k_C$	cutoff wave number in LES ( $m^{-1}$ )
$k_d$	viscous Cutoff wave number in LES ( $m^{-1}$ )
$K_G$	overall gas-side mass transfer coefficient ( $m/s$ )
$K_g$	empirical parameter in breakage kernel closure (—)
$K_L$	overall liquid-side mass transfer coefficient ( $m/s$ )
$k_p$	mass transfer coefficient associated with a pressure driving force ( $m\ mole/Js$ )
$k_p$	turbulent kinetic energy analogue of the particulate phase ( $m^2/s^2$ )
$K_r$	overall rate coefficient ( $kg/m^3$ )
$k_{bc}$	bubble-cloud mass interchange coefficient ( $m^3/m^3s$ )
$k_{c,s}$	interfacial mass transfer coefficient ( $m/s$ )
$K_{eq}$	chemical reaction equilibrium constant
$k_{gp}$	gas-particle fluctuation covariance ( $m^2/s^2$ )
$k_{gp}$	gas-particle fluctuation kinetic energy (covariance) ( $m^2/s^2$ )
$k_{p,kin}$	kinetic thermal conductivities of the particle phase ( $W/mK$ )
$k_{p,m}$	molecular thermal conductivities of the particle phase ( $W/mK$ )
$k_{SGS,t}$	sub-grid scale kinetic energy per unit mass in LES ( $m^2/s$ )
$Kn$	Knudsen number (—)
$L$	height ( $m$ )
$L$	length of reactor ( $m$ )

$L$	length scale of turbulence, or integral length scale of turbulence ( $m$ )
$L$	length scale, characteristic length ( $m$ )
$l$	mixing length ( $m$ )
$l$	turbulence length scale ( $m$ )
$l$	upper horizontal boundary in laminar boundary momentum balance analysis ( $m$ )
$L(\dot{\mathbf{q}}, \mathbf{q}, t)$	Lagrangian function in Lagrangian mechanics
$L_c$	integral scale of scalar segregation ( $m$ )
$L_D$	height of solids in downcomer ( $m$ )
$l_e$	eddy size in the inertial subrange of the turbulence energy spectrum ( $m$ )
$l_I$	line formed by the intersection of $A_I(t)$ with $A(t)$ ( $m$ )
$l_j$	interfacial transport length for interface $j$ ( $m$ )
$l_S$	Smagorinsky lengthscale ( $m$ )
$l_W$	intersection of CV wall interface with the cross sectional plane ( $m$ )
$L_{\text{Total}}$	total angular momentum of two colliding particles ( $kg\ m^2/s$ )
$l_{k,s}$	film thickness on the phase $k$ side of the interface ( $m$ )
$L_{mf}$	height of the fixed bed at minimum fluidization conditions ( $m$ )
$l_{W,k}(t, z)$	closed curve of phase $k$ in the cross section plane ( $m$ )
$Le$	Lewis number, $Le = \alpha/D$ ( $-$ )
$M$	mass ( $kg$ )
$M$	total mass of mixture in CV ( $kg$ )
$M$	total mass of particulate system ( $kg$ )
$m$	empirical model parameter ( $-$ )
$m_1$	parameter in Davidson-Harrison two-phase model ( $-$ )
$m_2$	parameter in Davidson-Harrison two-phase model ( $-$ )
$M_c$	mass of species $c$ ( $kg$ )
$m_c$	mass of fluid enclosed in the volume of the particle in the pressure gradient force ( $kg$ )
$m_c$	total mass associated with the center of mass of a binary particle system ( $kg$ )
$m_g$	mass of particles in group $g$ ( $kg$ )
$M_I$	net interface property term
$m_i$	mass of one particle of type $i$ ( $kg$ )
$m_p$	mass of a single particle ( $kg$ )
$m_V$	virtual mass of a particle in virtual mass force analysis ( $kg$ )
$M_{in, mass}$	total inflow of mass into the calculation domain, used in convergence criterion
$M_{w_c}$	molecular weight of species $c$ ( $kg/kmol$ )
$Ma$	Mach Number, $Ma = v/C_S$ ( $-$ )
$Mo$	Morton number ( $-$ )
$MTKE$	mean turbulent kinetic energy per unit mass, coincides with the $k$ quantity ( $m^2/s^2$ )
$N$	impeller stirring rate ( $RPM$ )
$N$	number of experiments, or realizations

$N$	number of particles contained in a given system in classical mechanics
$N$	total number of species in a mixture
$n$	empirical model parameter (—)
$n$	number density (number of particles/ $m^3$ )
$n$	number of basis functions used in MWR solution approximation function
$n$	number of equations in matrix system, or number of unknowns in algebraic equation system
$n$	number of moles ( $mol$ )
$n_1$	parameter in capture kinetics (—)
$n_2$	parameter in capture kinetics (—)
$N_a$	Avogadro's number
$N_i$	number density of particles in the size interval $i$ ( $1/m^3$ )
$n_i$	number density of particles in size class $i$ ( $\frac{1}{m^3}$ )
$N_P$	particle number density (Number/ $m^3$ )
$N_p$	Newton number, $N_p = P/\rho N^3 D^5$ (—)
$N_Q$	pumping number (—)
$N_s$	moles of species $s$ ( $mol$ )
$Nu$	Nusselt number, $Nu = hl/k$ (—)
$O$	origo, an arbitrary reference point in space
$P$	impeller power consumption ( $W$ )
$P$	wave period associated with Taylor hypothesis ( $s$ )
$p$	function in MWR example
$p$	laminar impeller pitch ( $m$ )
$p$	pressure ( $Pa$ )
$p'_{k,I}$	temporal deviation between the instantaneous pressure and the interfacial mean pressure variable ( $Pa$ )
$p(\mu)$	probability density (—)
$p(\xi, \mathbf{r}, \mathbf{v}_\xi, \mathbf{c}, t)$	extended distribution function in kinetic theory
$P(\mathbf{r}, \mathbf{c}, t)$	normalized distribution function, or probability density function
$p(\mathbf{x}, \mathbf{r}, \mathbf{c}, t)$	advanced particle distribution function ( $\frac{1}{ \mathbf{x} (\mathbf{r})m}$ )
$p_C^B$	coalescence probability due to buoyancy processes (—)
$p_C^T$	coalescence probability due to turbulence processes (—)
$p_i^{(1)}(m, \mathbf{r}, \mathbf{c}, \omega_c, T, t)$	advance particle distribution function with multiple inner coordinates ( $\frac{1}{[kg,K](m/s)(\mathbf{r})m}$ )
$p_C^{LS}$	coalescence probability due to laminar shear (—)
$p_0$	constant in FEM example
$p_{kin}$	kinetic pressure in granular theory ( $N/m^2$ )
$P_b$	term in $k$ - $\epsilon$ turbulence model which represents the energy production rate per unit volume due to bubble motion ( $J/m^3s$ )
$p_B(d_i, \lambda_j)$	breakage probability function, determining the efficiency of the eddy-bubble collisions (—)
$p_B(d_i : d_j, \lambda)$	breakage probability function (—)
$p_C$	coalescence probability (—)

$p_e(d_i, \lambda)$	normalized distribution function used to describe the turbulent kinetic energy distribution of eddies of size $\lambda$ (-)
$P_i$	auxiliary coefficient in TDMA outline
$P_k$	term in $k$ - $\epsilon$ turbulence model which represents the energy production rate per unit volume due to fluid shear ( $J/m^3s$ )
$P_S$	pressure scale, or surface pressure ( $Pa$ )
$P_{C,kl}$	probability of coalescence of bubbles of groups $g$ and $k$ in multi-group model
$p_{p,crit}$	critical state frictional pressure for particle phase ( $Pa$ )
$p_{p,fric}$	frictional pressure for particle phase ( $Pa$ )
$Pe$	Péclet number, $Pe = v_{z,av}l/D = RePr$ (-)
$Pr$	Prandtl Number, $Pr = \mu C_P/k$ (-)
$Q$	heat ( $J$ )
$Q$	impeller pumping capacity ( $m^3/s$ )
$q$	mass of $CO_2$ adsorbed divided by mass adsorbent (-)
$q$	number of components/species in the mixture (-)
$q$	number of independent reactions
$q^{rad}$	total radiation heat transfer flux ( $W/m^2$ )
$q_\lambda(\lambda)$	spectral heat transfer flux ( $W/m^2\mu m$ )
$Q_b$	volumetric gas flow rate in bubble phase ( $m^3/s$ )
$Q_i$	auxiliary coefficient in TDMA outline
$Q_{ij}$	Eulerian correlation function which represents a normalized velocity correlation tensor (-)
$R$	impeller radius (-)
$R$	radius of pipe, tube or sphere ( $m$ )
$R$	radius of riser ( $m$ )
$R$	residual error
$R$	universal gas constant ( $J/mol K$ )
$r$	characteristic chemical reaction rate ( $s^{-1}$ )
$r$	model parameter (-)
$r$	radial coordinate in the Cylindrical and spherical coordinate systems ( $m$ )
$r$	smoothness monitor in TVD schemes
$r_0$	range of interaction defining a particle collision ( $m$ )
$R_b$	radius of bubble ( $m$ )
$r_b$	bubble radius ( $m$ )
$R_c$	radius of cloud ( $m$ )
$R_c$	rate of generation of species $c$ by chemical reaction per unit volume ( $kg/m^3s$ )
$r_c$	radius of core ( $m$ )
$R_d$	radius of the liquid disk between two coalescing bubbles ( $m$ )
$R_L(s)$	auto-covariance ( $m^2/s^2$ )
$R_n$	radius of curvature at the nose of the gas bubble ( $m$ )
$R_r$	reactor radius ( $m$ )

$r_r$	rate of generation for reaction $r$ defined independent of species, proportional to the extent of reaction ( $mol/m^3s$ )
$R_s$	dimensionless energy source due to mean force acting on particles in granular flow (-)
$r_s$	mass rate of production of species $s$ due to homogeneous chemical reaction ( $kg/m^3s$ )
$r_{AB}$	linear correlation coefficient (-)
$r_{ad}$	sorption rate ( $kmol/kg s$ )
$r_{ij}$	equivalent bubble radius ( $m$ )
$R_{ij}(t, \mathbf{x})$	two-point correlation tensor ( $m^2/s^2$ )
$R_{n_{k,s}}$	volumetric species mass transfer rate ( $kg/m^3s$ )
$R_{Q_k}$	volumetric heat transfer rate ( $W/m^3$ )
$R_{Q_{I,\lambda}}$	volumetric heat transfer rate due to condensation/vaporization ( $W/m^3$ )
$Re$	Reynolds Number, $Re = \rho v L / \mu$ (-)
$Re_\kappa$	shear Reynolds number (-)
$Re_\Omega$	rotation Reynolds number (-)
$S$	action integral in classical or Lagrangian mechanics
$S$	imaginary surface in phase space enclosing $\Omega$ , used in classical mechanics
$S$	specific entropy of mixture ( $J/kg K$ )
$s$	average surface renewal rate ( $s^{-1}$ )
$s$	model parameter (-)
$s$	specific entropy of mixture ( $J/kg K$ )
$s$	time variable used calculating the autocorrelation, $s = t' - t$ . Time difference between the two time instants at which the values of the time dependent velocity fluctuations are measured ( $s$ )
$S_\psi$	generalized source term
$s_A(\psi, g)$	scattering cross section expressed in terms of $\mathbf{k}$ ( $m^2$ )
$S_I$	perimeter ( $m$ )
$s_I$	interface entropy per unit mass ( $J/kg K$ )
$S_k$	momentum source term of phase $k$ ( $kg/m^2 s^2$ )
$s_k$	entropy per unit mass ( $J/kg K$ )
$S_W$	perimeter of the wall ( $m$ )
$S_{C,\psi}$	constant part of the linearized source term in FVM discretization
$S_{P,\psi}$	constant part of the linearized source term in FVM discretization
$Sc$	Schmidt Number, $Sc = \mu / \rho D$ (-)
$Sh$	Sherwood number, $Sh = k_c l / D$ (-)
$St$	Stanton number for heat, $St_h = h / (C_P \rho v_{z,av}) = \frac{Nu}{Re Pr}$ (-)
$St$	Stanton number for mass, $St_m = k_c / v_{z,av}$ (-)
$T$	diameter of standard turbulent stirred tank ( $m$ )
$T$	temperature ( $K$ )
$T$	time period over which time averaging is performed ( $s$ )
$t$	time coordinate ( $s$ )
$T(\dot{\mathbf{q}}, \mathbf{q})$	generalized kinetic energy in Lagrangian mechanics

$T^*$	temperature scale in turbulent boundary layer theory (-)
$T^+$	dimensionless temperature in turbulent boundary layer theory (-)
$T_{\text{Shaft}}$	shaft torque ( $W$ )
$t_b$	breakage time ( $s$ )
$t_b$	bubble breakage time ( $s$ )
$t_{\text{max}}$	time between the first contact and the time when the film area between two colliding bubbles reaches its maximum value ( $s$ )
$te$	contact time in surface renewal and penetration theories ( $s$ )
$U$	overall heat transfer coefficient ( $J/m^2sK$ )
$u_b$	average rise velocity of bubbles in a freely bubbling bed ( $m/s$ )
$u_b$	average rise velocity of bubbles in bubbling bed ( $m/s$ )
$u_e$	interstitial gas velocity in the emulsion phase ( $m/s$ )
$u_{bl,rise}$	rise velocity of a single bubble in a liquid ( $m/s$ )
$u_{br,0}$	ideal rise velocity of a single bubble in fluidized bed ( $m/s$ )
$U_{mf}$	superficial gas velocity at minimum fluidization conditions ( $m^3m^{-2}s^{-1}$ )
$V$	arbitrary macroscopic control volume fixed in space ( $m^3$ )
$V$	combined abstract volume $V = V_x + V_r$
$V$	speed of fluid flow; $V =  \mathbf{v} $ ( $m/s$ )
$V$	tank volume ( $m^3$ )
$V$	volume ( $m^3$ )
$V$	volume over which volume averaging is performed ( $m^3$ )
$v$	Kolmogorov micro velocity scale ( $m/s$ )
$v$	flow of gas through a bubble in bubbling bed
$v$	represents all admissible functions in the space $X(\Omega)$ of admissible functions in least squares method outline
$v$	speed of flow ( $m/s$ )
$v^+$	dimensionless velocity (-)
$v^S$	superficial velocity in tubular reactor ( $m/s$ )
$V_1$	volume region of phase 1 in two phase system ( $m^3$ )
$V_2$	volume region of phase 2 in two phase system ( $m^3$ )
$v_\infty$	terminal velocity ( $m/s$ )
$v_*$	friction velocity ( $m/s$ )
$v_{\text{breakage}}$	characteristic velocity of the bubble breakage process ( $m/s$ )
$v_{\text{rms}}$	root-mean-square of the fluctuating velocity components, rms-velocity ( $m/s$ )
$V_b$	bubble volume ( $m^3$ )
$V_b$	volume of bubble phase ( $m^3$ )
$V_c$	volume of cloud phase ( $m^3$ )
$V_i$	volume of a particle in class, group or phase $i$ ( $m^3$ )
$V_p$	volume of a single particle, or average of particle volume distribution ( $m^3$ )
$V_r$	volume in physical space
$V_r$	volume of gas in bubbling bed ( $m^3$ )
$v_t$	impeller tip speed ( $m/s$ )
$V_w$	bubble wake volume ( $m^3$ )

$V_x$	abstract volume in internal property space
$v_{\text{equa}}$	equatorial speed parameter used in experimental data analysis ( $m/s$ )
$v_{\text{slip}}$	fluid-particle velocity slip ( $m/s$ )
$V_{b,i}$	volume of bubble or particle in class $i$ ( $m^3$ )
$V_{bs}$	volume of solids in bubble phase ( $m^3$ )
$V_{cs}$	volume of solids in cloud phase ( $m^3$ )
$V_{es}$	volume of solids in emulsion phase ( $m^3$ )
$v_{z,\text{max}}$	maximum velocity at the center of a pipe ( $m/s$ )
$W$	impeller blade width ( $m$ )
$W$	weighting function in MWR discretization
$W_s$	solid feeding rate ( $kg/s$ )
$We$	Weber number, $We = \rho v^2 L / \sigma$ ( $-$ )
$x$	coordinate in Cartesian coordinate system ( $m$ )
$x$	fractional conversion of capture reaction ( $-$ )
$X(\Omega)$	space of admissible functions, used in least squares method outline
$x_i$	pivotal points in $I_i$
$X_k$	phase indicator function
$x_s$	mole fraction of species $s$ in gas or liquid mixture ( $-$ )
$X_{gkl}$	intergroup transfer matrix in multi-group method distributing the mass from groups $k$ and $l$ to group $g$ in the coalescence process
$X_{gk}$	matrix in multi-group method distributing the mass from the number of group $k$ bubbles broken to the number of group $g$ bubbles formed in the breakage process
$y$	coordinate in Cartesian coordinate system ( $m$ )
$y$	distance from wall ( $m$ )
$y^+$	distance from a wall measured in viscous lengths, or Reynolds number ( $-$ )
$y_0$	distance between the wall and the particle ( $m$ )
$Z$	reactor height ( $m$ )
$z$	coordinate in Cartesian coordinate system ( $m$ )
$z$	position above the distributor ( $m$ )
$Z_{s-r}$	collision frequency for one molecule of species type $s$ colliding with target molecules of type $r$ ( $s^{-1}$ )
$Z_{sr}$	collision density, the number of collisions between pairs of molecules $s$ and $r$ ( $m^{-3}s^{-1}$ )
$\langle \omega_k \rangle_{AI}^{\Gamma}$	interfacial mass flux weighted species mass fraction ( $-$ )
$\langle h_k \rangle_{AI}^{\Gamma}$	interfacial mass flux weighted heat transfer ( $J/kg$ )
$\langle H_s \rangle_{AI}$	surface average modified Henry's law constant for species $s$ in the mixture ( $-$ )
$\langle k_c \rangle_L$	length average mass transfer coefficient ( $m/s$ )
$\langle N_i \rangle_{te}$	average mass transfer rate in surface renewal and penetration theories ( $mol/m^2s$ )
$\langle v_{n,k}^{\text{rel}} \rangle_{AI}$	normal interface velocity due to phase change ( $m/s$ )
$\tilde{G}_s$	partial mass Gibbs free energy for species $s$ ( $J/kg$ )

$\check{H}_c$	partial specific enthalpy of species $c$ in the mixture ( $J/kg$ )
$\check{h}_c$	partial specific enthalpy of species $c$ in the mixture, a fluid dynamic quantity ( $J/kg$ )
$\dot{m}$	total mass flow rate ( $kg/s$ )
$\dot{m}_k$	interface mass transfer rate ( $kg/m^2s$ )
$\dot{m}_s$	mass flow rate of species $s$ ( $kg/s$ )
$\dot{Q}$	rate of heat added to the control volume $V$ ( $J/s$ )
$\dot{Q}_k^{\text{cond, conv}}$	combined convective heat transfer rate due to conduction and convection ( $W$ )
$\dot{Q}_k^{\text{cond}}$	convective heat transfer rate due to conduction ( $W$ )
$\dot{Q}^{\text{rad}}$	radiation heat transfer rate ( $W$ )
$\dot{Q}_\lambda$	spectral radiant heat transfer rate ( $W/\mu m$ )
$\dot{W}$	rate of work done on the control volume $V$ ( $J/s$ )
$\frac{dm}{dt}$	particle growth rate related to mass change by condensation, evaporation and dissolution ( $kg/s$ )
$\hat{G}$	Gibbs free energy expressed in terms of mole ( $J$ )
$\hat{D}_{sr}$	symmetric Fickian multicomponent diffusivity for the $s$ and $r$ pair of gases [17] [18] ( $m^2/s$ )
$\hat{C}_{sk}$	multicomponent inverse diffusivities ( $s/m^2$ )
$\hat{F}$	Helmholtz energy ( $J$ )
$\hat{f}_i$	fugacity of species $i$ in the mixture ( $Pa$ )
$\hat{G}$	Gibbs free energy ( $J$ )
$\hat{G}$	Gibbs free energy expressed in terms of mass ( $J$ )
$\hat{H}$	total mixture enthalpy (or enthalpy) expressed in terms of temperature, pressure and the masses of the various species in the mixture ( $J$ ); or enthalpy expressed in terms of temperature, pressure and the mole numbers of the various species in the mixture ( $J$ )
$\hat{h}$	total mixture enthalpy (or enthalpy) expressed in terms of temperature, pressure and the masses of the various species in the mixture, a fluid dynamic quantity ( $J$ ); or enthalpy expressed in terms of temperature, pressure and the mole numbers of the various species in the mixture, a fluid dynamic quantity ( $J$ )
$\hat{T}$	non-dimensional temperature ( $-$ )
$\hat{p}_{k,I}$	deviation between the local instantaneous pressure and the interfacial area averaged pressure ( $Pa$ )
$a_i$	activity of species $i$ in the mixture ( $-$ )
$f_j^{\text{pure}}$	fugacity of pure species $i$ ( $Pa$ )
$\tilde{D}_{sK}^e$	effective Knudsen diffusivity of species $s$ in porous medium ( $m^2/s$ )
$\tilde{D}_{sr}^e$	effective bulk diffusivity of binary pair $s-r$ in porous medium ( $m^2/s$ )
$\tilde{D}_{sk}$	Maxwell-Stefan diffusivities ( $m^2/s$ )
$\tilde{C}_{ij}$	residual stress tensor in LES ( $Pa$ )
$\tilde{L}_{ij}$	Leonard stress tensor in LES ( $Pa$ )
$\tilde{R}_{ij}$	residual stress tensor in LES ( $Pa$ )

$\tilde{S}_{ij}$	the large scale strain-rate tensor in LES ( $m^2/s$ )
$\mathcal{A}$	FEM characteristic matrix
$\mathcal{A}$	system matrix
$\mathcal{D}$	diagonal matrix containing interfacial coupling terms
$\mathcal{D}_{sr}$	generalized non-symmetric Fickian multicomponent diffusivity for the $s$ and $r$ pair of gases [16] [39] [3] ( $m^2/s$ )
$\mathcal{I}$	source term in generalized Boltzmann type of equation representing the effects of particle coalescence, breakage and collisions
$\mathcal{J}(\psi(\mathbf{c}))$	collision term in the Boltzmann equation
$\mathcal{D}_{sr}$	generalized non-symmetric multi-component Fickian mass diffusion coefficients ( $m^2/s$ )
$\mathcal{A}$	$\mathcal{A} : X \times X$ , a symmetric, continuous bilinear form, used in least squares method outline
$\mathcal{A}$	chemical reaction formula matrix ( $-$ )
$\mathcal{F}$	$\mathcal{F} : X$ , a continuous linear form, used in least squares method outline
$\mathcal{J}(f; g)$	norm equivalent functional in least squares method outline
$\mathcal{L}$	lower triangular matrix
$\mathcal{M}$	preconditioner in Krylov subspace methods outline
$\mathcal{P}$	process
$\mathcal{R}$	space domain
$\mathcal{U}$	upper triangular matrix
$\bar{e}(d_i, \lambda)$	mean turbulent kinetic energy of an eddy of size $\lambda$ breaking a bubble of size $d_i$ ( $J$ )
$\bar{G}_s$	partial molar Gibbs free energy for species $s$ ( $J/mol$ )
$\bar{p}$	mean pressure, defined as the mean value of the normal stresses across any three orthogonal planes ( $Pa$ )
$\bar{v}_\lambda$	average velocity of eddies of size $\lambda$ ( $m/s$ )
$\bar{v}_{\text{drops}}$	mean turbulent droplet velocity ( $m/s$ )
$\bar{v}_c$	continuous phase circulation velocity ( $m/s$ )
$\bar{v}_{r,d_i}$	average rise velocity of particle of size class $i$ ( $m/s$ )
$\bar{v}_{rel,t,ij}$	length of relative velocity between a pair of unlike bubbles ( $m/s$ )
$\bar{v}_{t,d}$	average speed of particles of size $d$ due to turbulence ( $m/s$ )
$\bar{v}_{t,i}$	mean turbulent bubble velocity ( $m/s$ )
$\frac{dv_c}{dr}$	average shear rate for the continuous phase ( $1/s$ )
$\bar{d}$	diameter of complementary daughter particle ( $m$ )
$\tilde{p}'_g$	fluctuation pressure component of the undisturbed flow ( $Pa$ )
$\underline{\underline{p}}_g$	local instantaneous pressure of the undisturbed flow ( $Pa$ )
$\underline{\underline{\mathcal{C}\mathcal{C}}}$	symmetrical, traceless and non-divergent tensor in Enskog expansion
$\mathbf{A}$	turbulence anisotropy tensor in extended $k-\epsilon$ model ( $-$ )
$\mathbf{B}$	tensor function in Enskog expansion
$\mathbf{e}$	unit tensor with components $e_{ij}$
$\mathbf{e}_I$	unit interface tensor
$\mathbf{P}$	pressure tensor ( $Pa$ )
$\mathbf{p}_{\text{coll}}$	collisional pressure tensor ( $Pa$ )

XXVIII Nomenclature

$\mathbf{p}_{\text{kin}}$	kinetic pressure tensor ( $Pa$ )
$\mathbf{T}$	total stress tensor ( $Pa$ ); $\mathbf{T} = p\mathbf{e} + \boldsymbol{\sigma}$
$\tilde{\mathbf{T}}_g$	total stress tensor of the undisturbed flow ( $Pa$ )
$g_{\alpha\beta}$	local metric tensor
$K_{\alpha\beta}$	curvature tensor ( $m^{-1}$ )
$\underline{G}$	specific molar Gibbs free energy expressed in terms of mole ( $J/kmol$ )
$\underline{H}$	specific molar enthalpy, mixture enthalpy per unit mole expressed in terms of temperature, pressure and the mole fractions of the species in the mixture ( $J/mol$ )
$\underline{h}$	specific molar enthalpy, mixture enthalpy per unit mole expressed in terms of temperature, pressure and the mole fractions of the species in the mixture, a fluid dynamic quantity ( $J/mol$ )
$\bar{\mathbf{F}}_l$	interfacial coupling term in two-phase $k-\epsilon$ turbulence model ( $N/m^3$ )
$\langle \mathbf{n}_{k,s} \rangle_{A_I}$	surface average combined species mass transfer flux ( $kg/m^2s$ )
$\langle \mathbf{v} \rangle_{N_i}$	number average velocity representative for particle size class $i$ ( $m/s$ )
$\mathbf{M}_k$	interfacial momentum transfer to phase $k$
$\mathbf{P}(\mathbf{p}, \mathbf{q}, t)$	a set of generalized momenta in Hamiltonian mechanics
$\mathbf{Q}(\mathbf{p}, \mathbf{q}, t)$	a set of generalized coordinates in Hamiltonian mechanics
$\dot{\mathbf{q}}$	generalized velocities in Lagrangian Mechanics
$\mathbf{C}$	vector function in Enskog expansion
$\mathbf{A}$	vector function in Enskog expansion
$\mathbf{a}$	acceleration of a single particle ( $m/s^2$ )
$\mathbf{a}_\xi$	generalized acceleration vector in property space
$\mathbf{B}$	general vector or tensor valued function
$\mathbf{b}$	constant vector in algebraic equation system
$\mathbf{b}$	element-abundance vector ( $mole$ )
$\mathbf{C}$	peculiar velocity ( $m/s$ )
$\mathbf{c}$	velocity of a single particle, or velocity of a collection of mono-atomic gas molecules ( $m/s$ )
$\mathbf{d}$	generalized diffusional driving force ( $m^{-1}$ )
$\mathbf{e}$	error vector in multigrid method outline
$\mathbf{e}$	unit vector with components $e_i$ in the $i$ ( $i = 1, 2, 3$ ) directions
$\mathbf{F}$	incident particle number flux or intensity ( $number/m^2s$ )
$\mathbf{F}$	net force acting on a single particle ( $N$ )
$\mathbf{f}$	FEM characteristic vector
$\mathbf{f}$	sum of forces acting on the mixture in the control volume ( $N$ )
$\mathbf{F}_{L,d}^W$	wall lift force acting on a collection of dispersed particles per unit mixture volume ( $N/m^3$ )
$\mathbf{F}_I$	surface force per unit area ( $N/m^2$ )
$\mathbf{F}_k$	generalized drag force per unit mixture volume ( $N/m^3$ )
$\mathbf{F}_L$	lift force acting on a collection of particles per unit mixture volume ( $N/m^3$ )
$\mathbf{F}_P$	net force acting on a collection of particles per unit mixture volume ( $N/m^3$ )

$\mathbf{f}_S$	total hydrodynamic surface force exerted by a fluid on a particle ( $N$ )
$\mathbf{F}_V$	virtual mass force acting on a collection of particles per unit mixture volume ( $N/m^3$ )
$\mathbf{f}_W$	net wall interaction force acting on a single particle ( $N$ )
$\mathbf{f}_{Buoy}$	buoyancy force on a single particle ( $N$ )
$\mathbf{f}_B$	Basset history force acting on a single particle ( $N$ )
$\mathbf{f}_D$	steady drag force acting on a single particle ( $N$ )
$\mathbf{f}_E$	body forces (except gravity) acting on a single particle ( $N$ )
$\mathbf{f}_G$	body force due to gravity acting on a single particle ( $N$ )
$\mathbf{f}_{hp}$	hydrostatic pressure force acting on a single particle ( $N$ )
$\mathbf{F}_{L,V}$	combined lift-virtual mass force acting on a collection of particles per unit mixture volume ( $N/m^3$ )
$\mathbf{f}_L$	lift force acting on a single particle ( $N$ )
$\mathbf{f}_{pg}$	pressure gradient force acting on a single particle ( $N$ )
$\mathbf{f}_p$	force due to external pressure gradient acting on a single particle ( $N$ )
$\mathbf{F}_{TD}$	turbulent dispersion force per unit volume ( $N/m^3$ )
$\mathbf{f}_V$	virtual- or added mass force acting on a single particle ( $N$ )
$\mathbf{G}$	velocity of the center of mass expressed in the laboratory frame ( $m/s$ )
$\mathbf{g}$	external force per unit mass, or gravity force per unit mass ( $m/s^2$ )
$\mathbf{g}$	relative particle velocity ( $m/s$ )
$\mathbf{g}_\alpha$	tangent basis vectors in orthogonal coordinate systems
$\mathbf{G}_c$	velocity of the center of mass expressed in the center of mass frame ( $m/s$ )
$\mathbf{H}$	angular momentum vector for a system ( $kgm^2/s$ )
$\mathbf{h}$	angular momentum vector for a particle ( $kgm^2/s$ )
$\mathbf{I}_k$	generalized interfacial transfer flux
$\mathbf{J}$	Jacobian
$\mathbf{J}$	local instantaneous diffusive flux of the generalized quantity $\psi$
$\mathbf{J}_s^*$	instantaneous diffusive molar flux of species $s$ in mixture ( $mol/m^2s$ )
$\mathbf{j}_m$	volumetric flux of the mixture ( $m^3/m^2s$ )
$\mathbf{J}_S$	molecular entropy flux ( $J/m^2sK$ )
$\mathbf{j}_s$	instantaneous diffusive mass flux of species $s$ in mixture ( $kg/m^2s$ )
$\mathbf{J}_{12}$	impulse of the force exerted by particle 1 on particle 2 ( $kgm/s$ )
$\mathbf{j}_c^g$	multi-component mass diffusion flux due to external force ( $kg/m^2s$ )
$\mathbf{j}_c^o$	ordinary multi-component mass diffusion flux ( $kg/m^2s$ )
$\mathbf{j}_c^p$	pressure gradient induced multi-component mass diffusion flux ( $kg/m^2s$ )
$\mathbf{j}_c^T$	temperature gradient induced multi-component mass diffusion flux ( $kg/m^2s$ )
$\mathbf{J}_{Vd}$	volumetric flux of the dispersed phase relative to the velocity of the volume centre of the mixture ( $m^3/m^2s$ )
$\mathbf{k}$	unit vector of the apse-line
$\mathbf{M}_k^F$	interfacial momentum transfer due to phase change ( $N/m^3$ )
$\mathbf{M}_k^T$	interfacial momentum transfer caused by stresses ( $N/m^3$ )

$\mathbf{m}_c$	instantaneous mass flux of molecules of species of type $c$ with respect to stationary coordinate axes ( $kg/m^2s$ )
$\mathbf{M}_I^\sigma$	net surface tension force term ( $N/m^2$ )
$\mathbf{M}_{k,l}$	interfacial momentum exchange between phases $k$ and $l$ ( $kg/m^2 s^2$ )
$\mathbf{M}_{sr}$	momentum transferred from species $r$ to $s$ per collision ( $kgm/s, collision$ )
$\mathbf{n}$	outwardly directed unit normal vector
$\mathbf{n}$	species-abundance vector ( <i>mole</i> )
$\mathbf{N}_I$	unit vector normal to $l_I(t)$ that is both tangent to and outwardly directed with respect to $A_I(t)$
$\mathbf{N}_s$	combined molar flux of species $s$ in gas or liquid mixture ( $mol/m^2s$ )
$\mathbf{n}_s$	combined mass flux of species $s$ in gas or liquid mixture ( $kg/m^2s$ )
$\mathbf{P}$	momentum associated with a macroscopic CV ( $kgm/s$ )
$\mathbf{p}$	generalized momenta in Hamiltonian mechanics
$\mathbf{p}_m$	search direction in $m$ -th iteration in Krylov subspace methods outline
$\mathbf{P}_{sr}$	diffusive force per unit volume exerted by species $r$ on species $s$ ( $N/m^3$ )
$\mathbf{q}$	generalized coordinates in Lagrangian and Hamiltonian mechanics
$\mathbf{q}$	heat flux vector ( $W/m^2$ )
$\mathbf{q}^{\text{rad}}$	total radiant energy flux arriving at a surface element ( $W/m^2$ )
$\mathbf{q}^c$	ordinary conductive heat flux, defined by Fourier's law ( $W/m^2$ )
$\mathbf{q}^d$	energy flux resulting from inter-diffusion of the chemical species ( $W/m^2$ )
$\mathbf{q}^r$	radiative heat flux ( $W/m^2$ )
$\mathbf{q}^x$	Dufour energy flux resulting from a temperature gradient induced by mass diffusion of chemical species ( $W/m^2$ )
$\mathbf{q}_I$	interface heat flux per unit length ( $J/m$ )
$\mathbf{q}_V$	volumetric radiant energy flux ( $W/m^3$ )
$\mathbf{q}_{\text{coll}}$	collisional granular heat flux ( $kg/s^3$ )
$\mathbf{q}_{\text{kin}}$	kinetic granular heat flux ( $kg/s^3$ )
$\mathbf{q}_{A_S}$	radiant surface energy flux ( $W/m^2$ )
$\mathbf{r}$	position vector, locating a point in space ( $m$ )
$\mathbf{r}$	residual vector
$\mathbf{r}_c$	definition of the center of mass point ( $m$ )
$\mathbf{r}_c$	position vector denoting the location of the center of mass ( $m$ )
$\mathbf{r}_i$	particle coordinates in Newtonian Mechanics ( $m$ )
$\mathbf{r}_p$	particle position vector, locating the center of mass ( $m$ )
$\mathbf{T}$	total torque applied to fluid mass in control volume ( $Nm$ )
$\mathbf{t}$	torque on a single sphere ( $Nm$ )
$\mathbf{t}$	unit tangent vector
$\mathbf{t}^{(k)}$	tangent surface vector
$\mathbf{T}_{Thrust}$	propulsive force developed by a jet-propeller motor ( $N$ )
$\mathbf{u}$	control volume surface velocity arising from the motion of the moving grid ( $m/s$ )
$\mathbf{u}$	generalized velocity in classical mechanics

$\mathbf{u}$	velocity of the control surface with respect to the coordinate reference frame (m/s)
$\mathbf{v}$	local instantaneous mixture velocity, mass average velocity (m/s)
$\mathbf{v}'_{d,s}$	modified mass diffusion velocity for species $s$ (m/s)
$\mathbf{v}^*_s$	species velocity of molecules of species $s$ generated by chemical reaction (m/s)
$\mathbf{v}_{\text{drift}}$	fluid particle drift velocity (m/s)
$\mathbf{v}_c$	instantaneous number mean velocity of molecules of species type $c$ with respect to stationary coordinate axes (m/s)
$\mathbf{v}_I$	interface velocity (m/s)
$\mathbf{v}_i$	mass average velocity of particle class $i$ (m/s)
$\mathbf{v}_i$	surface average velocity of particle class $i$ (m/s)
$\mathbf{v}_r$	external coordinate velocity (m/s)
$\mathbf{v}_x$	internal coordinate velocity
$\mathbf{v}_{\text{slip},d}$	slip velocity for dispersed phase $d$ (relative to the continuous phase $c$ ) (m/s)
$\mathbf{v}_\xi$	generalized velocity vector in property space
$\mathbf{v}_{c,d}$	instantaneous diffusion velocity for species $c$ , relative to the local motion of the mixture stream (m/s)
$\mathbf{v}_{i,d_i}$	size average velocity of particle class $i$ (m/s)
$\mathbf{v}_{i,n_i}$	number average velocity of particle class $i$ (m/s)
$\mathbf{v}_{i,V_i}$	volume average velocity of particle class $i$ (m/s)
$\mathbf{v}_{Mk}$	diffusion velocity of phase $k$ , the velocity of phase $k$ relative to the velocity of the mass center of the mixture (m/s)
$\mathbf{v}_{rel}$	relative velocity between particles or phases (m/s)
$\mathbf{v}_{rk}$	relative velocity between dispersed phase $k$ and continuous phase $c$ (m/s)
$\mathbf{v}_{Vk}$	drift velocity of phase $k$ , the velocity of phase $k$ relative to the velocity of the volume center of the mixture (m/s)
$\mathbf{w}$	velocity of the fluid at the control surface with respect to the control surface (m/s)
$\mathbf{x}$	internal property vector
$\mathbf{x}$	position vector defining the separation of two points in space ( $m$ )
$\mathbf{x}$	three coordinates in an arbitrary coordinate system fixed in space
$\mathbf{x}$	true solution of matrix system: $\mathcal{A}\mathbf{x} = \mathbf{b}$
$\mathbf{x}$	vector of unknowns in algebraic equation system
$\mathbf{x}^\nu$	intermediate solution of matrix system: $\mathcal{A}\mathbf{x}^\nu = \mathbf{b}$ after $\nu$ iterations
$\mathbf{x}^{\text{improved},\nu}$	corrected or improved solution in multigrid method outline
$\mathbf{x}_m$	approximate solution in $m$ -th iteration in Krylov subspace methods outline
$\mathbf{Y}$	vector representing the continuous phase variables
$d\mathbf{c}$	an infinitesimal element in a hypothetical velocity space containing the velocity $\mathbf{c}$
$d\mathbf{r}$	an infinitesimal spatial space containing the point $\mathbf{r}$

**Greek Letters**

$\alpha(T)$	total, hemispherical absorbtivity of a surface (-)
$\alpha_{sr}$	Onsager phenomenological coefficients ( $kg s/m^3$ )
$\alpha$	absorptivity, $\alpha = G_{\text{abs}}/G$ (-)
$\alpha$	isothermal compressibility ( $Pa^{-1}$ )
$\alpha$	ratio of CO <sub>2</sub> -acceptor to catalyst mass
$\alpha$	thermal diffusivity of conducting medium ( $m^2/s$ )
$\alpha^*$	parameter in relation for the modulus of elasticity of the particulate phase (-)
$\alpha_k$	instantaneous volume fraction of phase $k$ (-)
$\alpha_m$	auxiliary factor at iteration $m$ in Krylov subspace methods outline
$\alpha_P$	relaxation factor in FVM discretization
$\alpha_{\lambda,\theta}(\lambda, \theta, \phi, T)$	spectral, directional absorbtivity of a surface (-)
$\alpha_{\lambda}(\lambda, T)$	spectral, hemispherical absorbtivity of a surface (-)
$\beta$	bulk expansion coefficient ( $K^{-1}$ )
$\beta$	constant in time-splitting method
$\beta$	empirical parameter ( $\beta \approx 2.0$ ) in the Kuboi mean square droplet velocity relation (-)
$\beta$	interfacial friction coefficient
$\beta_k$	time fraction (-)
$\beta_m$	auxiliary factor at iteration $m$ in Krylov subspace methods outline
$\chi$	Enskog free volume correction function
$\chi$	energy ratio, $\chi = \frac{e(d_i, \lambda)}{\bar{e}(d_i, \lambda)}$ (-)
$\Delta \bar{h}_{lg,s}^{\text{vap}}$	latent heat of vaporization of pure species $s$ in the multicomponent mixture ( $J/mol$ )
$\Delta E$	translational energy change during an inelastic collision ( $kg m^2/s^2$ )
$\Delta h_{lg,mix}^{\text{vap}}$	latent heat of vaporization of the multicomponent mixture ( $J/kg$ )
$\Delta L$	bubbling bed expansion ( $m$ )
$\Delta p_C$	pressure drop through cyclone ( $Pa$ )
$\Delta p_D$	pressure drop across downcomer ( $Pa$ )
$\Delta p_f$	pressure drop due to friction ( $Pa$ )
$\Delta p_R$	pressure drop across riser ( $Pa$ )
$\Delta p_{CD}$	pressure drop through the solids flow control devices ( $Pa$ )
$\delta Q$	differential energy transfer to the thermodynamic system ( $J$ ). The $\delta$ symbol is used to indicate that the integration of $\delta Q$ which is not a state function is dependent on the path.
$\Delta t$	time increment ( $s$ )
$\Delta t_{\text{coal}}$	coalescence time interval ( $s$ )
$\Delta t_{\text{col}}$	collision time interval ( $s$ )
$\delta v$	turbulence velocity scale ( $m/s$ )
$\delta W$	differential work done on the thermodynamic system ( $J$ ). The $\delta$ symbol is used to indicate that the integration of $\delta W$ which is not a state function is dependent on the path.
$\Delta$	filter width in LES ( $m$ )

$\delta$	boundary layer thickness ( $m$ )
$\delta$	redundancy corrector in population balance
$\delta_c$	concentration boundary layer thickness ( $m$ )
$\delta_I(\mathbf{r} - \mathbf{r}')$	Dirac delta function which is zero everywhere except when $\mathbf{r} = \mathbf{r}'$ , infinite on interface, and integral unity
$\delta_v$	length scale characterizing the inner layer in turbulent boundary layers ( $m$ )
$\delta_{ij}$	Kronecker delta
$\delta_T$	thermal boundary layer thickness ( $m$ )
$\epsilon(T)$	hemispherical, total emissivity of a surface ( $-$ )
$\epsilon$	parameter in least squares method minimization statement
$\epsilon$	ratio of eddy size to the bubble size, $\epsilon = \lambda/d_i$ ( $-$ )
$\epsilon$	represent small threshold value in convergence criterion
$\epsilon$	surface roughness of pipe ( $m$ )
$\epsilon_I^\sigma$	net surface energy associated with surface tension ( $J/m^2s$ )
$\epsilon_{\lambda,\theta}(\lambda, \theta, \phi, T)$	spectral, directional emissivity of a surface ( $-$ )
$\epsilon_\lambda(\lambda, T)$	hemispherical, spectral emissivity of a surface ( $-$ )
$\epsilon_\theta(\theta, \phi, T)$	total, directional emissivity of a surface ( $-$ )
$\eta$	Kolmogorov micro length scale ( $m$ )
$\eta$	parameter called a surface coordinate or curvilinear coordinate of a point on a surface
$\Gamma$	boundary of the domain $\Omega$
$\Gamma$	mean flux of molecules in elementary kinetic theory (number/ $m^2s$ )
$\Gamma$	phase space symbol in classical mechanics
$\gamma$	energy dissipation rate term in the granular temperature equation ( $kg/ms^3$ )
$\gamma$	particle volume fraction ( $-$ )
$\Gamma(z)$	gamma function, a special function in advanced mathematics defined by means of an improper integral.
$\gamma_b$	volume fraction of solids in bubble phase with respect to the bubble volume ( $-$ )
$\gamma_c$	composition expansion coefficient associated with species $c$ ( $-$ )
$\gamma_c$	volume fraction of solids in cloud phase with respect to the bubble volume ( $-$ )
$\gamma_e$	volume fraction of solids in emulsion phase with respect to the bubble volume ( $-$ )
$\gamma_i$	activity coefficient for species $i$
$\Gamma_k$	average interface mass transfer rate from phase $k$ due to phase change ( $kg/m^3s$ )
$\gamma_k$	average occurrence of phase $k$ ( $-$ )
$\Gamma_L$	Lagrangian integral time scale ( $s$ )
$\Gamma_\psi$	general diffusion coefficient in FVM discretization
$\kappa$	curvature ( $m^{-1}$ )
$\kappa$	magnitude of fluid shear ( $1/s$ )
$\kappa$	von Kàrmàn constant ( $-$ )

### XXXIV Nomenclature

$\kappa$	wavenumber associated with Taylor hypothesis ( <i>radians/m</i> )
$\Lambda$	coefficient in the Zehner and Schlünder model for the convective heat transfer (–)
$\Lambda$	particle size ratio in bubble breakage kernel closure, $\Lambda = d_c/d$ (–)
$\lambda$	dimensionless constant in bubble size model (–)
$\lambda$	distance between two points in the flow where the second order velocity structure function is depends on $\lambda$ and $\varepsilon$ only ( <i>m</i> )
$\lambda$	eddy size ( <i>[m]</i> )
$\lambda$	length of electromagnetic radiation wave in a medium ( <i>m</i> )
$\lambda$	thermal conductivity of dilute gas ( <i>W/mK</i> )
$\lambda$	wavelength associated with Taylor hypothesis ( <i>m</i> )
$\lambda_d$	slip parameter for wall boundary condition in granular theory ( <i>m</i> )
$\Lambda_f(t)$	Eulerian longitudinal integral length scale ( <i>m</i> )
$\lambda_f(t)$	Eulerian longitudinal Taylor micro length scale, or longitudinal Taylor microscale ( <i>m</i> )
$\Lambda_g(t)$	Eulerian transverse integral length scale ( <i>m</i> )
$\lambda_g(t)$	Eulerian transverse Taylor micro length scale, or transverse Taylor microscale ( <i>m</i> )
$\langle \varepsilon_G \rangle_{\text{global}}$	effective global specific energy dissipation rate ( $m^2 s^{-3}$ )
$\mu$	mixture dynamic viscosity, or first viscosity coefficient ( <i>kg/ms</i> )
$\mu$	particular realization of the process $\mathcal{P}$
$\mu$	reduced mass ( <i>kg</i> )
$\mu$	specific realization involved in ensemble averaging
$\mu_{\text{dilute}}$	viscosity parameter for the dilute limit in granular theory ( <i>kg/ms</i> )
$\mu_B$	mixture bulk viscosity, dilatational or second viscosity coefficient ( <i>kg/ms</i> )
$\mu_c$	specific chemical potential of species <i>c</i> ( <i>J/kg</i> )
$\mu_j$	<i>j</i> -th moment of the population density function
$\mu_n$	<i>n</i> -th moment
$\mu_s$	partial mass Gibbs free energy for species <i>s</i> ( <i>J/kg</i> )
$\mu_t$	dynamic turbulent viscosity, or eddy viscosity ( <i>kg/ms</i> )
$\mu_{B,d}$	bulk viscosity parameter in granular theory ( <i>kg/ms</i> )
$\mu_{p,crit}$	critical state frictional viscosity for particle phase ( <i>kg/ms</i> )
$\mu_{p,fric}$	frictional viscosity for particle phase ( <i>kg/ms</i> )
$\nu$	frequency of electromagnetic radiation wave ( $s^{-1}$ )
$\nu$	mixture kinematic viscosity ( $m^2/s$ )
$\nu(\mathbf{x}', \mathbf{r}', \mathbf{Y}, t)$	average number of particles formed in the breakup processes (–)
$\nu_{gp}^t$	gas-particle turbulent viscosity ( $m^2/s$ )
$\nu_p^{coll}$	collisional viscosity of particule phase ( $m^2/s$ )
$\nu_p^t$	turbulent (or kinetic) viscosity of particule phase ( $m^2/s$ )
$\nu_{c,r}$	stoichiometric coefficient for element <i>c</i> in reaction <i>r</i> , negative for reactants, positive for products (–)
$\nu_{SGS,t}$	sub-grid kinematic viscosity in LES ( $m^2/s$ )

$\Omega(\psi)$	net source term denoting the loss of the property $\psi$ caused by inelastic collisions
$\Omega$	calculation domain in MWR and FEM examples
$\Omega$	imaginary arbitrary volume in phase space, used in classical mechanics
$\Omega$	rotational speed, $\Omega =  \mathbf{\Omega} $ ( $s^{-1}$ )
$\omega$	angle between the velocity $\mathbf{C}$ and the normal vector $\mathbf{n}$ in collision cylinder analysis
$\omega$	angular velocity ( $rad/s$ )
$\omega$	rotational speed of the shaft ( $rad/s$ )
$\omega$	species mixture mass fraction ( $-$ )
$\omega_B^T(d_i, \lambda)$	eddy-bubble collision probability density ( $\frac{1}{sm^3[m]}$ )
$\omega_{B,\lambda}^T(d_i, \lambda)$	eddy-bubble collision probability density, differential because it is eddy-bubble interaction specific ( $\frac{1}{sm^3[m]}$ )
$\omega_\alpha$	weight of the delta function centered at the characteristic particle size $d_\alpha$
$\Omega_{\text{Shaft}}$	shaft angular velocity ( $rad/s$ )
$\Omega_B$	macroscopic breakage rate ( $\frac{1}{sm^3}$ )
$\Omega_B(d_i)$	total breakage rate for particles of size $d_i$ ( $\frac{1}{sm^3}$ )
$\Omega_C$	macroscopic coalescence rate ( $s^{-1}m^{-3}$ )
$\omega_C$	bubble-bubble collision density ( $\frac{1}{m^3 s}$ )
$\omega_C^B$	buoyancy collision density ( $\frac{1}{sm^3}$ )
$\omega_C^T$	collision density caused by turbulent motion and expressed in the framework of a discrete numerical scheme ( $\frac{1}{sm^3}$ )
$\omega_C^{LS}$	collision density due to laminar shear ( $\frac{1}{sm^3}$ )
$\Omega_{\lambda,1}$	collision integral for thermal conductivity in kinetic theory ( $-$ )
$\Omega_{\mu,1}$	collision integral for viscosity in kinetic theory ( $-$ )
$\omega_{B(d_i, \lambda_j)}$	eddy-bubble collision rate ( $\frac{1}{sm^3}$ )
$\omega_C$	modified particle collision density ( $\frac{1}{m^3 s [m] [m]}$ )
$\Omega_{D,11}$	collision integral for self-diffusion in kinetic theory ( $-$ )
$\Omega_{D,12}$	collision integral for diffusion in kinetic theory ( $-$ )
$\omega_{ff}$	modified particle collision density ( $\frac{1}{m^3 s [m] [m]}$ )
$\omega_f$	single particle collision density ( $\frac{1}{s [m]}$ )
$\Phi(f)$	presumed PDF ( $-$ )
$\Phi_{\text{viscous}}$	viscous dissipation function ( $s^{-2}$ )
$\Phi$	perturbation function in Enskog expansion
$\Phi$	potential energy per unit mass ( $m^2/s^2$ )
$\phi$	blade attachment angle ( $^\circ$ ) or ( $rad$ )
$\phi$	coefficient in the Zehner and Schlünder model for the convective heat transfer ( $-$ )
$\phi$	local instantaneous source term of the generalized quantity $\psi$
$\phi$	polar coordinate
$\phi$	potential function in time-splitting method
$\phi$	unknown variable in TDMA outline
$\phi(r)$	limiter function in TVD schemes

$\Phi_{\text{eff}}$	effective global energy dissipation function ( $s^{-2}$ )
$\Phi_I(\frac{y}{\delta_v})$	non-dimensional function characteristic for the inner log-law or inertial sub-layer (-)
$\phi_i$	fugacity coefficient for species $i$
$\Phi_o(\frac{y}{\delta})$	non-dimensional function characteristic for the outer layer (-)
$\Phi_v(\frac{y}{\delta_v})$	non-dimensional function characteristic for the viscous sub-layer (-)
$\Phi_{\text{total}}$	entropy production rate ( $J/m^3 sK$ )
$\phi_{I,c}$	rate of production of the quantity $\psi_k$ per unit mass at each point on $A_I$
$\Pi_{\varepsilon_g}$	interaction term in $\varepsilon_g$ model equation for gas phase ( $kg/ms^4$ )
$\Pi_{gp}$	interaction term in $k_{gp}$ transport equation ( $kg/ms^3$ )
$\Pi_{kg}$	interaction term in $k_g$ model equation for gas phase ( $kg/ms^3$ )
$\psi$	generalized conserved quantity
$\psi$	microscopic molecular property of dilute gas (referred to a single molecule) in elementary kinetic theory
$\psi$	polar coordinate
$\psi(\mathbf{r}, \mathbf{c}, t)$	a generalized physical function that denotes a property of the molecules located at time $t$ near $\mathbf{r}$ with a velocity near $\mathbf{c}$
$\rho$	instantaneous field mass density ( $kg/m^3$ )
$\rho$	spectral reflectivity, $\rho = G_{\text{ref}}/G$ (-)
$\rho_L(s)$	autocorrelation coefficient (-)
$\rho_p$	mass density of particle ( $kg$ )
$\sigma_k$	$k$ - $\varepsilon$ turbulence model parameter (-)
$\sigma$	Stefan-Boltzmann constant, $= 5.67 \times 10^{-8}$ ( $W/m^2 K^4$ )
$\sigma'_{AT}$	alternative total (scattering) collision cross section ( $m^2$ )
$\sigma_1$	collision diameter used in kinetic theory ( $m$ )
$\sigma_A(\Omega)$	differential scattering cross section ( $m^2$ )
$\sigma_I$	surface tension ( $N/m$ )
$\sigma_s(d)$	surface restoring pressure of a bubble of size $d$ ( $Pa$ )
$\sigma_t(d)$	average deformation stress for bubbles of size $d$ ( $Pa$ )
$\sigma_\varepsilon$	$k$ - $\varepsilon$ turbulence model parameter (-)
$\sigma_{AT}$	total scattering cross section ( $m^2$ )
$\sigma_A$	standard deviation, the squared root of the variance (-)
$\sigma_A^2$	variance, a statistical measure of the dispersion of data about the mean (-)
$\tau$	Kolmogorov micro time scale ( $s$ )
$\tau$	average residence time of the elements in surface renewal theory ( $s$ )
$\tau$	time domain
$\tau$	time variable in history force expression ( $s$ )
$\tau$	tortuosity of porous medium (-)
$\tau$	transmissivity, $\tau = G_{\text{trans}}/G$ (-)
$\tau_p^c$	characteristic particle-particle collision time ( $s$ )
$\tau_g^t$	time scale of large turbulent eddies in gas phase ( $s$ )
$\tau_{gp}^t$	interaction time between particle motion and gas fluctuation or eddy life time seen by a particle ( $s$ )

$\tau_1$	collision time of molecules of type 1 (s)
$\tau_\omega$	time scale of scalar concentration fluctuations (s)
$\tau_b$	time constant associated with a bubble in $k$ - $\varepsilon$ turbulence model for bubbly flow [93] (s)
$\tau_e$	eddy turnover time scale (s)
$\tau_L$	Lagrangian micro time scale, or Lagrangian microscale (s)
$\tau_{gp}$	particle relaxation time (s)
$\sigma_{k,I}^*$	temporal deviation between the instantaneous stress and the interfacial mean stress variable (Pa)
$\theta_c$	mean circulation time in stirred tank (s)
$\theta_m$	mean mixing time in stirred tank (s)
$\theta$	granular temperature ( $m^2/s^2$ )
$\theta$	scattering angle
$\gamma$	rate of deformation or rate of strain ( $s^{-1}$ )
$\mathcal{T}$	function representing an expression in Boltzmann H-theorem relation
$\sigma_W$	wall shear stress (Pa)
$\varepsilon$	ensemble, consisting of a specific number of realizations $\mu$
$\varepsilon$	event space domain
$\varepsilon$	maximum energy of attraction between a pair of molecules in kinetic theory (J)
$\varepsilon$	perturbation parameter in Enskog expansion
$\varepsilon$	porosity of porous medium (-)
$\varepsilon$	turbulent energy dissipation rate per unit mass ( $m^2/s^3$ )
$\varepsilon_\omega$	scalar dissipation rate ( $s^{-1}$ )
$\varepsilon_b$	bed area occupied by bubble phase in bubbling bed (-)
$\varepsilon_{as}$	solids volumetric concentration in annulus (-)
$\varepsilon_{cs}$	solids volumetric concentration in core (-)
$\varepsilon_{gp}$	dissipation rate of the gas-particle fluctuation covariance ( $m^2/s^3$ )
$\varepsilon_{ijk}$	permutation symbol, or alternating unit tensor (-)
$\varepsilon_{mf}$	holdup of fluidized bed at minimum fluidization conditions (-)
$\varepsilon_{ov}$	gas holdup or overall void fraction (-)
$\varepsilon_{SGS}$	SGS dissipation rate per unit mass in LES ( $m^2/s^3$ )
$\varphi_i$	basis function used in MWR solution approximation function
$\lambda$	vector of Lagrange multipliers
$\Omega$	solid angle (steradians, sr)
$\psi_{\text{Collisional}}$	dense gas collisional transfer flux
$\psi_{\text{Kinetic}}$	dense gas kinetic transfer flux
$\psi_k$	spatial deviation of the point variable $\psi_k$ from the intrinsic volume average value $\langle \psi_k \rangle_{V_k}$
$\widehat{\sigma}_{k,I}$	deviation between the local instantaneous stress and the interfacial area averaged stress (Pa)
$\widehat{\psi}_k$	spatial deviation of the point variable $\psi_k$ from the mass-weighted volume average value $\langle \psi_k \rangle_V^{X_k \rho_k}$
$\widetilde{\psi}$	MWR solution approximation function

### XXXVIII Nomenclature

$\Xi$	function representing an expression in Boltzmann H-theorem relation
$\xi$	extent of reaction ( <i>mole</i> )
$\xi$	model parameter (-)
$\xi_{ij}$	ratio of the diameters of a pair of unlike bubbles $d_i/d_j$ (-)
$\zeta$	independent variable (-)
$\zeta$	parameter called a surface coordinate or curvilinear coordinate of a point on a surface
$b$	bubble phase
$d\chi$	differential plane angle
$d\xi_r$	extent of reaction for reaction $r$ ( <i>mole</i> )
$\langle \varepsilon_s \rangle_A$	cross sectional averaged solid volumetric concentration (-)
$\tilde{\sigma}_{ij}^n$	numerical stresses in LES ( <i>Pa</i> )
$\tilde{\sigma}_{ij}^R$	modeled residual stresses in LES ( <i>Pa</i> )
$\Omega$	angular momentum tensor ( <i>N/m</i> )
$\sigma$	viscous stress tensor ( $Pa = N/m^2$ )
$\sigma_{kin}$	deviatoric kinetic pressure tensor in granular theory ( $N/m^2$ )
$\sigma_{Mm}$	diffusion stress due to phase slip ( $N/m^2$ )
$\sigma_{Vm}$	drift stress due to the phase slip ( $N/m^2$ )
$\zeta_I \mathbf{e}_I$	fluxes of isotropic second order tensors
$(-\Delta \underline{H}_{r,A}^*)$	heat of reaction for reaction $r$ defined with species $A$ as basis ( <i>J/mol</i> )
$\Delta \underline{H}_c^*(T)$	molar enthalpy at temperature $T$ associated with species $c$ ( <i>J/mol</i> )
$\Delta \underline{H}_{f,c}^*$	standard molar heat of formation of species $c$ ( <i>J/mol</i> )
$\Psi(t)$	variable defined by a volume integral
$\kappa$	curvature vector ( $m^{-1}$ )
$\Omega$	angular velocity or rate of rotation; $\Omega = \frac{1}{2} \nabla \times \mathbf{v}$ ( $s^{-1}$ )
$\omega$	vorticity vector; $\omega = 2\Omega = \nabla \times \mathbf{v}$ ( $s^{-1}$ )
$\Phi(\psi)$	net flux denoting the transfer of the property $\psi$ during a set of particle collisions
$\Phi(\mathbf{r}, t)$	flux vector
$\psi_e$	FEM vector of nodal values of the solution
$\varphi_I$	flux of the quantity $\psi_I$ (per unit length of line) through $l_I(t)$
$\varsigma_I$	interface flux vector
$\xi$	material coordinates

#### Superscripts

'	prime, denotes a pseudo-mixture quantity associated with the dusty gas model
'	prime, denotes fluctuation quantity in conventional Reynolds (time) averaging
'	prime, denotes sub-grid-scale or residual quantity in LES
'	prime, primed quantities refer to the final property values after a binary molecular collision in kinetic theory.
'	property of one of the particles colliding or breaking in PBE modeling
'	small correction of a variable in FVM discretization

"	double prime, fluctuation component of an instantaneous quantity around it's mean weighted value. Used in the time- and ensemble averaging approaches.
*	fractional step index, or intermediate value
*	previous-iteration value of a variable, or provisional velocity value based on a guessed (or outer iteration) pressure, in FVM discretization
*	vector with properties after performing a rotation in space or reflection with respect to a given plane, or a combination
0	Maxwellian state property
0	constant property value
$\nu$	iteration counter index
new	fractional step iteration index indicating latest obtained value
$\sim$	property of a complementary particle in PBE modeling
*	asterisk denotes ideal gas state properties, or non-dimensional variables
<i>c</i>	cloud phase
<i>c</i>	ordinary
<i>cr</i>	critical quantity
<i>d</i>	diffusive
<i>dry</i>	dry conditions
<i>n</i>	old value at time $t$ in FVM discretization
$n + 1$	new value at time $t + \Delta t$ in FVM discretization
<i>r</i>	radiative
<i>s</i>	superficial
<i>V</i>	volume average quantity
<i>x</i>	mole fraction

**Subscripts**

0	inlet, or initial condition
$\psi$	representing a general quantity
BI	bubble induced quantity in $k$ - $\epsilon$ turbulence model for bubbly flow [92]
crit	critical or threshold value
eff	effective, sum of molecular and turbulent contributions
in	inlet condition
min	minimum value
SI	shear induced quantity in $k$ - $\epsilon$ turbulence model for bubbly flow [92]
surr	property of surroundings
sur	surface
sys	property of a simple subsystem
sys	property of surroundings
<i>A</i>	area
<i>a</i>	ambient property
<i>a</i>	annulus
<i>ad</i>	adiabatic conditions
<i>B</i>	breakage

XL Nomenclature

$B$	neighbor at the bottom (in the negative $z$ direction) in FVM discretization
$b$	grid cell volume face between $P$ and $B$ in FVM discretization
$b$	single bubble or bubble phase
$C$	coalescence
$c$	center of mass property
$c$	cloud phase
$c$	core
$c$	index to identify a species/component in a binary or multicomponent mixture
$cap$	capture particle property
$cat$	catalyst particle property
$E$	neighbor node on the east side (in the positive $x$ direction) in FVM discretization
$e$	element
$e$	emulsion phase
$e$	grid cell volume face between $P$ and $E$ in FVM discretization
$e_I$	interface average property in ensemble averaging procedure
$g$	group index
$I$	interface property
$i$	particle of type $i$ ( $kg$ )
$k$	phase
$L$	laboratory frame
$m$	mixture property
$mb$	minimum bubbling
$mf$	minimum fluidization
$N$	neighbor node on the north side (in the positive $y$ direction) in FVM discretization
$n$	grid cell volume face between $P$ and $N$ in FVM discretization
$n$	normal component of a vector
$nb$	general neighbor grid node in FVM discretization
$ov$	overall
$P$	central grid node under consideration in FVM discretization
$P$	index marking the first grid cell away from the wall
$p$	particle
$r$	relative
$S$	neighbor node on the south side (in the negative $y$ direction) in FVM discretization
$S$	surface
$s$	grid cell volume face between $P$ and $S$ in FVM discretization
$s$	solids phase or particle phase
$s$	species in a binary or multicomponent mixture
$T$	neighbor on the top (in the positive $z$ direction) in FVM discretization
$T$	time average quantity
$t$	grid cell volume face between $P$ and $T$ in FVM discretization

$t$	tube
$W$	neighbor on the west side (in the negative $x$ direction) in FVM discretization
$W$	wall
$w$	grid cell volume face between $P$ and $W$ in FVM discretization
$x$	$x$ -coordinate direction in Cartesian system ( $m$ )
$y$	$y$ -coordinate direction in Cartesian system ( $m$ )
$z$	$z$ -coordinate direction in Cartesian system ( $m$ )

**Operators**

$(\dots)$	component vector
$:$	multiplication sign, the scalar product (or double dot product) of two tensors
$[ \dots, \dots ]$	Poisson bracket operator in classical mechanics
$[ \dots ]$	square matrix
$\cdot$	multiplication sign, used for Scalar Product (or Dot Product) of two vectors, Divergence of a Vector Field, and other vector/tensor operations.
$\ddot{\psi}$	second order partial derivative of quantity $\psi$ with respect to time
$\delta$	denotes a variation about the motion of the system in Classical Mechanics
$\delta/\delta x$	generalized discretized spatial derivative
$\psi$	partial derivative of quantity $\psi$ with respect to time
$\frac{\partial ()}{\partial \mathbf{c}}$	gradient of $()$ with respect to $\mathbf{c}$
$\frac{\partial ()}{\partial \mathbf{r}}$	gradient of $()$ with respect to $\mathbf{r}$
$\frac{\partial ()}{\partial t}$	partial time derivative, denoting the partial derivative of the quantity $()$ with respect to $t$ , at constant $x, y, z, (()/s)$
$\frac{D ()}{Dt}$	substantial time derivative, material derivative, hydrodynamic derivative, derivative following the motion $(()/s)$
$\frac{d ()}{dt}$	total derivative operator
$\frac{D_c ()}{D_c t}$	hypothetical substantial time derivative operator in phase space
$\frac{d_c ()}{d_c t}$	hypothetical total time derivative operator in phase space
$\frac{d_I}{dt}$	material surface derivative ( $s^{-1}$ )
$\langle \dots \rangle$	general averaging operator
$\langle \dots \rangle_{A_I}^{\Gamma}$	mass flux weighted interfacial area average quantity
$\langle \dots \rangle^{X_k \rho_k}$	mass-weighted average
$\langle \dots \rangle_A$	area averaging operator
$\langle \dots \rangle_e$	ensemble averaging operator
$\langle \dots \rangle_M$	Maxwellian averaging operator
$\langle \dots \rangle_V$	volume averaging operator
$\langle \dots \rangle_{A_I}^{X_k}$	interface area averaged quantity
$\langle \psi_k \rangle_T^{X_k}$	$X_k$ -weighted average of $\psi_k$ over the entire time period $T$
$\langle \psi_k \rangle_V^{X_k}$	intrinsic volume averaging operator
$\langle \psi_k \rangle_{T_k}$	time average of $\psi_k$ over the accumulated time interval $T_k$

$\langle \psi_k \rangle_{V_k}$	intrinsic volume averaging operator
$\mathcal{L}$	linear first order differential operator in least squares method outline
$ \dots $	length of vector, magnitude of vector, or absolute value of scalar variable
$\nabla \cdot$	divergence operator
$\nabla$	gradient operator, vector differential operator, also known as <i>nabla</i> or <i>del</i> operator
$\nabla_I$	interface del or nabla operator
$\nabla_{\mathbf{c}}()$	gradient of () with respect to $\mathbf{c}$
$\nabla_{\mathbf{r}}()$	gradient of () with respect to $\mathbf{r}$
$\overline{\langle \dots \rangle}^f$	number weighted average quantity in external space
$\overline{\psi}$	overlines, time averaging operator
$\  \bullet \ _{Y(\Omega)}^2$	$L^2$ norm used in least squares method outline
$\partial$	partial derivative
$\Pi_i()$	product of all labeled variables in ()
$\times$	multiplication sign, vector product (or cross product) of two vectors
$\tilde{\phi}$	mesoscopic smoothly varying quantity in VOF
$\tilde{\psi}$	tilde, filtering operator
$covar(A, B)$	covariance between two variables, $A$ and $B$
$D$	linear differential operator in MWR example
$div()$	divergence of a vector
$G$	filtering function used in LES
$grad()$	gradient of a scalar

### Abbreviations

<i>ADI</i>	Alternating Direction Implicit
<i>ADM</i>	Axial Dispersion Model
<i>ASMM</i>	Algebraic Slip Mixture Model
<i>BBO</i>	Basset-Boussinesq-Osseen form of Newton's second law
<i>BC</i>	Bubble column
<i>BCG</i>	Bi-Conjugate Gradient
<i>BCGSTAB</i>	Bi-orthogonal Conjugate Gradient STABILized
<i>BFBC</i>	Bubbling Fluidized Bed Combustion
<i>CAFBC</i>	Circulating Atmospheric Fluidized Bed Combustor
<i>CARPT</i>	Computer Automated Radioactive Particle Tracer
<i>CBC</i>	Convection Boundedness Criterion
<i>CC – NUMA</i>	Cache Coherent Non-Uniform Memory Access-machines
<i>CDS</i>	Central Difference Scheme
<i>CFB</i>	Circulating Fluidized Bed
<i>CFBC</i>	Circulating Fluidized Bed Combustion
<i>CFBG</i>	Circulating Fluidized Bed Gasification
<i>CFD</i>	Computational Fluid Dynamics
<i>CFL</i>	Courant-Friedrichs-Lewy
<i>CG</i>	Conjugate Gradient
<i>CGS</i>	Conjugate Gradient Squared

- COSMIC* Conservative Operator Splitting for Multidimensions with Inherent Consistency
- CRE* Chemical Reaction (or Reactor) Engineering
- CSF* Continuous Surface Force
- CSS* Continuous Surface Stress
- CSTR* Continuous Stirred Tank Reactor model
- DCS* Deferred Correction Source
- DM* Dispersion Model
- DQMOM* Direct Quadrature Method of Moments
- EI* Embedded Interface
- EOS* Equation Of State
- FBC* Fluidized Bed Combustion
- FCC* Fluid Catalytic Cracking
- FCT* Flux Corrected Transport
- FDM* Finite Difference Method
- FEM* Finite Element Method
- FL* Flux Limiter
- FVM* Finite Volume Method
- GCV* Grid Cell Volume
- GLL* Gauss-Lobatto-Legendre collocation points
- GMRES* Generalized Minimal RESidual method
- IGCC* Integrated Gasification Combined Cycle
- ILU* Incomplete LU (ILU) -preconditioners in Krylov subspace methods outline
- IPSA* Implicit Interphase Slip Algorithm
- ISNAS* Interpolation Scheme which is Non-oscillatory for Advected Scalars
- LDA* Laser Doppler Anemometry
- LES* Large Eddy Simulation
- LS* Level Set
- LSM* Least Squares Method
- MAC* Maker And Cell
- MACHO* Multidimensional Advective Conservative Hybrid Operator
- MC* Monotonic Centered
- MinMod* MinMod function
- MPI* Message Passing Interface
- MUSCL* Monotone Upwind Scheme for Conservative Laws
- MUSIG* Multiple-Size-Group
- MWR* Method of Weighted Residuals
- NG* Number of Groups
- NIRVANA* Non-oscillatory, Integrally Restricted, Volume-Averaged Numerical Advection
- NUMA* Non-Uniform Memory Access-machines
- NV* Normalized Variable
- ODE* Ordinary Differential Equations
- PBE* Population Balance Equation

*PBR* Packed Bed Reactor  
*PDE* Partial Differential Equations  
*PDF* probability density function  
*PEA* Partial Elimination Algorithm  
*PFR* Plug Flow Reactor model  
*PISO* Pressure Implicit with Splitting of Operators  
*PLIC* Piecewise Linear Interface Construction  
*QMOM* Quadrature Method of Moments  
*QUICK* Quadratic Upwind Interpolation for Convective Kinematics  
*QUICKEST* QUICK with Estimated Streaming Terms  
*RNG* Re-Normalization-Group (RNG) theory  
*RTD* Residence Time Distribution  
*SEM* Spectral Element Method  
*SGS* Sub-Grid-Scale  
*SHARP* Simple High-Accuracy Resolution Program  
*SIMPLE* Semi-Implicit Method for Pressure-Linked Equations  
*SIMPLEC* SIMPLE Consistent  
*SIMPLER* SIMPLE Revised  
*SLIC* Simple Line Interface Calculation  
*SM* Spectral Method  
*SMART* Sharp and Monotone Algorithm for Realistic Transport  
*SOLA* SOLution Algorithm  
*SOLA – VOF* SOLution Algorithm for the Volume Of Fluid model  
*SOM* Second Order Moments  
*SOR* Successive Over-Relaxation  
*SUPERBEE* SUPERBEE function  
*TDMA* Tri-Diagonal Matrix Algorithm  
*TVD* Total Variation Diminishing  
*UDS* Upstream Differencing Scheme  
*ULTIMATE* Universal Limiter for Transient Interpolation Modeling of Advective Transport Equations  
*ULTRA* Universal Limiter for Tight Resolution and Accuracy  
*UTOPIA* Uniformly Third-Order Polynomial Interpolation Algorithm  
*VOF* Volume Of Fluid  
*CV* Control Volume

---

# Contents

---

## Part I Single Phase Flow

---

<b>1</b>	<b>Single Phase Flow</b> .....	<b>3</b>
1.1	Basic Principles of Fluid Mechanics .....	3
1.2	Equations of Change for Multi-Component Mixtures .....	8
1.2.1	Conservation of mass .....	15
1.2.2	Transport of species mass .....	19
1.2.3	Conservation of momentum .....	24
1.2.4	Conservation of total energy .....	35
1.2.5	Some useful simplifications of the governing equations .....	68
1.2.6	Gross Scale Average Forms of the Governing Equations .....	86
1.2.7	Dispersion Models .....	97
1.3	Application of the Governing Equations to Turbulent Flow .....	99
1.3.1	Origin and Characteristics of Turbulence .....	101
1.3.2	Statistical Turbulence Theory .....	104
1.3.3	Reynolds Equations and Statistics .....	117
1.3.4	Semi-Empirical Flow Analysis .....	121
1.3.5	Reynolds Averaged Models .....	129
1.3.6	Large Eddy Simulation (LES) .....	161
	<b>References</b> .....	<b>177</b>
<b>2</b>	<b>Elementary Kinetic Theory of Gases</b> .....	<b>187</b>
2.1	Introduction .....	187
2.2	Elementary Concepts in Classical Mechanics .....	193
2.2.1	Newtonian Mechanics .....	194
2.2.2	Lagrangian Mechanics .....	197
2.2.3	Hamiltonian Mechanics .....	201
2.3	Basic Concepts of Kinetic Theory .....	207

2.3.1	Molecular Models . . . . .	208
2.3.2	Phase Space, Distribution Function, Means and Moments . . . . .	210
2.3.3	Flux Vectors . . . . .	212
2.3.4	Ideal Gas Law . . . . .	217
2.4	The Boltzmann Equation . . . . .	218
2.4.1	The Boltzmann Equation in the Limit of no Collisions . . . . .	219
2.4.2	Binary Collisions . . . . .	223
2.4.3	Generalized Collision Term Formulation . . . . .	243
2.5	The Equation of Change in Terms of Mean Molecular Properties . . . . .	246
2.6	The Governing Equations of Fluid Dynamics . . . . .	249
2.7	The Boltzmann H-Theorem . . . . .	252
2.7.1	The H-Theorem Formulation . . . . .	252
2.7.2	The Maxwellian Velocity Distribution . . . . .	254
2.7.3	The H-Theorem and Entropy . . . . .	255
2.8	Solving the Boltzmann Equation . . . . .	256
2.8.1	Equilibrium Flow - The Euler Equations . . . . .	256
2.8.2	Gradient Perturbations - Navier Stokes Equations . . . . .	258
2.9	Multicomponent Mixtures . . . . .	262
2.10	Mean Free Path Concept . . . . .	309
2.11	Extending the Kinetic Theory to Denser Gases . . . . .	319
2.12	Governing Equations for Polydispersed Multiphase Systems . . . . .	324
<b>References . . . . .</b>		<b>327</b>

---

**Part II Multiphase Flow**

---

<b>3</b>	<b>Multiphase Flow . . . . .</b>	<b>335</b>
3.1	Introduction . . . . .	335
3.2	Modeling Concepts for Multiphase Flow . . . . .	339
3.2.1	Averaged Models . . . . .	340
3.2.2	High Resolution Methods . . . . .	344
3.3	Basic Principles and Derivation of Multi-Fluid Models . . . . .	365
3.3.1	Local Instantaneous Transport Equations . . . . .	370
3.3.2	The Purpose of Averaging Procedures . . . . .	393
3.4	Averaging Procedures . . . . .	394
3.4.1	The Volume Averaging Procedure . . . . .	397
3.4.2	The Time Averaging Procedure . . . . .	419
3.4.3	The Ensemble Averaging Procedure . . . . .	429
3.4.4	The Time After Volume Averaging Procedure . . . . .	441
3.4.5	The Mixture Models . . . . .	463

3.4.6	The Gross Scale Averaged Two-Phase Transport Equations.....	473
3.4.7	Heterogeneous Dispersion Models .....	484
3.5	Mathematical Model Formulation Aspects .....	485
<b>References</b> .....		489
<b>4</b>	<b>Flows of Granular Materials</b> .....	503
4.1	The Two-Fluid Granular Flow Model.....	508
4.1.1	Collisional Rate of Change .....	509
4.1.2	Dynamics of Inelastic Binary Collisions .....	514
4.1.3	Maxwell Transport Equation and Balance Laws..	516
4.1.4	Transport Equation in Terms of Peculiar Velocity	520
4.1.5	Initial- and Boundary Conditions for the Granular Phase Equations .....	530
4.2	Remarks on the Kinetic Theory of Granular Flows .....	531
4.2.1	Granular Flow Closure Limitations.....	534
<b>References</b> .....		537
<b>5</b>	<b>Constitutive Equations</b> .....	543
5.1	Modeling of Multiphase Covariance Terms .....	545
5.1.1	Turbulence Modeling Analogues .....	545
5.2	Interfacial Momentum Closure .....	553
5.2.1	Drag force on a single rigid sphere in laminar flow	559
5.2.2	Lift forces on a single rigid sphere in laminar flow	564
5.2.3	Lift and drag on rigid spheres in turbulent flows .	569
5.2.4	Drag force on bubbles .....	572
5.2.5	Lift force on bubbles .....	577
5.2.6	The Added mass or virtual mass force on a single rigid sphere in potential flow .....	581
5.2.7	Interfacial Momentum Transfer Due to Phase Change .....	587
5.3	Interfacial Heat and Mass Transfer Closures .....	588
5.3.1	Approximate Interfacial Jump Conditions .....	588
5.3.2	Fundamental Heat and Mass Transport Processes	597
5.3.3	Mass Transport Described by Fick's law .....	599
5.3.4	Heat Transfer Described by Fourier's Law .....	604
5.3.5	Heat and Mass Transfer Coefficient Concepts....	605
5.3.6	Heat Transfer by Radiation .....	635
<b>References</b> .....		647
<b>APPLICATIONS</b> .....		657

<b>6</b>	<b>Chemical Reaction Engineering</b> .....	659
6.1	Idealized Reactor Models .....	660
6.1.1	Plug Flow Reactor Models .....	660
6.1.2	Batch and Continuous Stirred Tank Reactors ....	663
6.2	Simplified Reactor Models .....	665
6.3	Chemical Reaction Equilibrium Calculations .....	666
6.3.1	Stoichiometric Formulation .....	670
6.3.2	Non-stoichiometric formulation .....	674
	<b>References</b> .....	677
<b>7</b>	<b>Agitation and Fluid Mixing Technology</b> .....	679
7.1	Tank Geometry and Impeller Design .....	679
7.2	Fluid Shear Rates, Impeller Pumping Capacity and Power Consumption .....	684
7.2.1	Fluid shear rates .....	685
7.2.2	Impeller Pumping Capacity .....	686
7.2.3	Impeller Power Consumption .....	687
7.2.4	Fundamental Analysis of Impeller Power Consumption .....	688
7.3	Turbulent Mixing .....	699
7.3.1	Studies on Turbulent Mixing .....	700
7.3.2	Flow Fields in Agitated Tanks .....	703
7.3.3	Circulation and mixing times in turbulent agitated tanks .....	705
7.3.4	Turbulent Reactive Flow in Stirred Tank .....	707
7.4	Heat Transfer in Stirred Tank Reactors .....	714
7.5	Scale-up of Single Phase Non-Reactive Turbulent Stirred Tanks .....	716
7.6	Mixing of Multi-Phase Systems .....	717
7.7	Governing Equations in Relative and Absolute Frames ....	723
7.7.1	Governing Eulerian Flow Equations in the Laboratory Frame .....	723
7.7.2	Coriolis and Centrifugal Forces .....	724
7.7.3	Governing Eulerian Equations in a Rotating Frame	727
7.8	Impeller Modeling Strategies .....	730
7.8.1	The Impeller Boundary Conditions (IBC) Method	730
7.8.2	The Snapshot (SS) Method .....	731
7.8.3	The inner-outer (IO) method and the multiple reference frame approach (MRF) .....	732
7.8.4	The Moving Deforming Mesh (MDM) Technique .	735
7.8.5	The Sliding Grid (SG) or Sliding Mesh (SM) Method .....	736
7.8.6	Model Validation .....	737

7.9	Assessment of Multiple Rotating Reference Frame Model Simulations .....	740
<b>References .....</b>		<b>751</b>
<b>8</b>	<b>Bubble Column Reactors .....</b>	<b>757</b>
8.1	Hydrodynamics of Simple Bubble Columns.....	757
8.1.1	Experimental Characterization of Cylindrical Bubble Column Flow .....	760
8.2	Types of Bubble Columns.....	764
8.3	Applications of Bubble Columns in Chemical Processes ...	766
8.4	Modeling of Bubble Column Reactors .....	767
8.4.1	Fluid Dynamic Modeling .....	770
8.4.2	Numerical Schemes and Algorithms .....	791
8.4.3	Chemical Reaction Engineering .....	793
8.4.4	Multifluid Modeling Framework .....	794
<b>References .....</b>		<b>797</b>
<b>9</b>	<b>The Population Balance Equation .....</b>	<b>807</b>
9.1	Three Alternative Population Balance Frameworks .....	812
9.1.1	The Continuum Mechanical Approach .....	812
9.1.2	The Microscopic Continuum Mechanical Population Balance Formulation .....	835
9.1.3	The Statistical Mechanical Microscopic Population Balance Formulation .....	853
<b>References .....</b>		<b>859</b>
<b>10</b>	<b>Fluidized Bed Reactors .....</b>	<b>867</b>
10.1	Solids Classification .....	868
10.2	Fluidization Regimes for Gas-Solid Suspension Flow .....	868
10.3	Reactor Design and Flow Characterization .....	872
10.3.1	Dense-Phase Fluidized Beds .....	873
10.3.2	Lean-Phase Fluidized Beds.....	875
10.3.3	Various Types of Fluidized Beds .....	880
10.3.4	Experimental Investigations .....	880
10.4	Fluidized Bed Combustors .....	883
10.5	Milestones in Fluidized Bed Reactor Technology .....	888
10.6	Advantages and disadvantages .....	892
10.7	Chemical Reactor Modeling .....	893
10.7.1	Conventional Models for Bubbling Bed Reactors ..	894
10.7.2	Turbulent Fluidized Beds .....	911
10.7.3	Circulating Fluidized Beds .....	911
10.7.4	Simulating Bubbling Bed Combustors Using Two-Fluid Models .....	915

10.7.5	Bubbling Bed Reactor Simulations Using Two-Fluid Models .....	928
<b>References</b> .....		945
<b>11 Packed Bed Reactors</b> .....		953
11.1	Processes Operated in Packed Bed Reactors (PBRs) .....	953
11.2	Packed Bed Reactor Design .....	954
11.3	Modeling and Simulation of Packed Bed Reactors .....	956
11.3.1	Fixed Bed Dispersion Models .....	957
11.3.2	Reactor Process Simulations .....	964
<b>References</b> .....		983
<b>12 Numerical Solution Methods</b> .....		985
12.1	Limitations of Numerical Methods .....	986
12.2	Building Blocks of a Numerical Solution Method .....	987
12.3	Properties of Discretization Schemes .....	989
12.4	Initial and Boundary Condition Requirements .....	991
12.5	Discretization Approaches .....	993
12.5.1	The Finite Difference Method .....	993
12.5.2	The Finite Volume Method .....	995
12.5.3	The Method of Weighted Residuals .....	995
12.5.4	The Finite Element Method .....	1002
12.6	Basic Finite Volume Algorithms Used in Computational Fluid Dynamics .....	1008
12.7	Elements of the Finite Volume Method for Flow Simulations .....	1012
12.7.1	Numerical Approximation of Surface and Volume Integrals .....	1014
12.7.2	Solving Unsteady Problems .....	1017
12.7.3	Approximation of the Diffusive Transport Terms .....	1022
12.7.4	Approximation of the Convective Transport Terms .....	1025
12.7.5	Brief Evaluation of Convection/Advection Schemes .....	1038
12.8	Implicit Upwind Discretization of the Scalar Transport Equation .....	1038
12.9	Solution of the Momentum Equation .....	1040
12.9.1	Discretization of the Momentum Equations .....	1040
12.9.2	Numerical Conservation Properties .....	1041
12.9.3	Choice of Variable Arrangement on the Grid .....	1043
12.9.4	Calculation of Pressure .....	1044
12.10	Fractional Step Methods .....	1056
12.11	Finite Volume Methods for Multi-fluid Models .....	1060
12.11.1	Special Challenges in Solving the Two-fluid Model Equations .....	1061

12.11.2	Explicit Fractional Step Algorithm for Solving the Two-Fluid Model Equations Applied to Bubble Column Flow . . . . .	1067
12.11.3	Implicit Fractional Step Method for Solving the Two-Fluid Granular Flow Model Equations Applied to Fluidized Bed Flow . . . . .	1070
12.11.4	Solution of Multi-fluid Models . . . . .	1076
12.12	Numerical Solution of the Population Balance Equation . .	1077
12.13	Solution of Linear Equation Systems . . . . .	1092
12.13.1	Point-Iterative Methods . . . . .	1092
12.13.2	The Tri-Diagonal Matrix Algorithm (TDMA) . . .	1093
12.13.3	Krylov Subspace Methods . . . . .	1095
12.13.4	Preconditioning . . . . .	1098
12.13.5	Multigrid Solvers . . . . .	1102
12.13.6	Parallelization and Performance Optimization . . .	1105

<b>References</b> . . . . .	1109
-----------------------------	------

**Part III APPENDIX**

<b>APPENDIX</b> . . . . .	1123
---------------------------	------

<b>A Mathematical Theorems</b> . . . . .	1125
A.1 Transport Theorem for a Single Phase Region . . . . .	1125
A.1.1 Leibnitz's Rule . . . . .	1125
A.1.2 Leibnitz Theorem . . . . .	1126
A.1.3 Reynolds Theorem . . . . .	1128
A.2 Gauss Theorem . . . . .	1130
A.3 Surface Theorems . . . . .	1131
A.3.1 Leibnitz Transport Theorem for a Surface . . . . .	1131
A.3.2 Gauss Theorem for a Surface . . . . .	1132

<b>References</b> . . . . .	1137
-----------------------------	------

<b>B Equation of Change for Temperature for a Multicomponent System</b> . . . . .	1139
B.1 The Problem Definition . . . . .	1139
B.2 Deriving the Equation of Change for Temperature . . . . .	1139

<b>References</b> . . . . .	1145
-----------------------------	------

<b>C Trondheim Bubble Column Model</b> . . . . .	1147
C.1 Model Formulation . . . . .	1147
C.2 Tensor Transformation Laws . . . . .	1157
C.2.1 Curvilinear Coordinate Systems . . . . .	1158

C.2.2	The Tensor Concept .....	1158
C.2.3	Coordinate Transformation Prerequisites.....	1160
C.2.4	Orthogonal Curvilinear Coordinate Systems and Differential Operators .....	1162
C.2.5	Differential Operators in Cylindrical Coordinates	1165
C.2.6	Differential Operators Required for the Two-fluid Model .....	1169
C.3	Two-Fluid Equations in Cylindrical Coordinates .....	1173
C.4	The 2D Axi-Symmetric Bubble Column Model .....	1176
C.4.1	Discretization of the Trondheim Bubble Column Model .....	1180
C.4.2	The Continuity Equation .....	1185
C.4.3	The Generalized equation .....	1187
C.4.4	The liquid phase radial momentum balance .....	1190
C.4.5	The Liquid phase axial momentum balance .....	1202
C.4.6	The gas phase radial momentum balance .....	1211
C.4.7	The gas phase axial momentum balance .....	1221
C.4.8	The Turbulent Kinetic Energy .....	1227
C.4.9	The Turbulent Kinetic Energy Dissipation Rate .	1230
C.4.10	The Volume fraction .....	1231
C.4.11	The Pressure-Velocity Correction Equations .....	1234
<b>References</b> .....		1237
<b>Index</b> .....		1239

**Single Phase Flow**

# Single Phase Flow

In this chapter the governing equations of change for single-phase reactive mixtures are presented.

An introduction to the basic continuum mechanics notation is given first ensuring that the fundamental principles are interpreted in an appropriate manner. Then, the derivation of the rigorous balance equations for multi-component fluid mixtures by use of the control volume approach is discussed. Alongside a standard set of approximate constitutive equations is listed. Thereafter several derived formulas, frequently also referred to by names like simplified-, macroscopic-, design-, or engineering models, are examined. In the latter context the primary aims are to explain how these formulas can be deduced from the fairly rigorous conservation equations, and to elucidate the inherent assumptions. The governing equations are applied to turbulent flows in the subsequent portion of sections in the chapter.

The theory of single phase materials is not only of principal importance analyzing single phase reactor systems, it also serves as basis for the description of multiphase flows.

## 1.1 Basic Principles of Fluid Mechanics

*Fluid mechanics* is the study of motions of gases and liquids. In the literature the subject is often divided into *compressible* and *incompressible* flows. However, the strict mathematical definitions of these two types of flows are not trivial. There is more to this than one may think, as will be discussed in sect. 1.2.5. Meanwhile, considering physical properties rather than strict mathematics, preliminary characterizations of these two classes of flows will provide important ideas why this subdivision of fluid mechanics is useful.

The majority of chemical engineers have stronger theoretical background in thermodynamics than fluid mechanics, so the vocabulary used in fluid mechanics literature may be a first barrier that one needs to pass. At this point, we thus intend to remove a possible source of confusion that is common among

chemical engineers. From a thermodynamic standpoint, gases and liquids have quite different characteristics. In thermodynamics liquids are often modeled as incompressible fluids. In this context, an incompressible fluid denotes a fluid having density that doesn't change significantly due to pressure variations (i.e.,  $\frac{1}{\rho} \frac{\partial \rho}{\partial p} |_{T, \omega_c} \approx 0$ ). Having this thermodynamic definition in mind, one may be surprised to learn about an incompressible flow of a compressible fluid in mechanics. However, *incompressible fluids* is a thermodynamical term, whereas *incompressible flow* is a fluid mechanical term. As will be discussed in sect. 1.2.5, the main criterion for incompressible flow is that the flow doesn't induce any significant fluid density changes. A criterion for such effects has been developed in fluid mechanics. That is, the so-called Mach number (i.e., that can be interpreted as a measure of the relative density changes due to flow effects) has to be low. Mathematical analyzes will be given at a later stage after the basic tools, the governing equations, have been presented.

Typical characteristics of compressible flows are given next. Under certain flow conditions density changes due to momentum (flow) effects must be considered in gas dynamics [168]. In practice, such compressible flows may be divided into the following categories:

- Flows where fluid dynamic wave propagation within the fluid are important.  
These phenomena may be important for a restricted number of chemical reactor systems, as for example certain industrial multi-phase systems operated in bubble column and fluidized bed reactors.
- Steady flow in which the fluid speed is of the same order of magnitude as the speed of sound.  
This situation hardly exist in chemical reactor systems. However, in an industrial chemical process plant there are many unit operations containing flows belonging to this category.
- Convection driven by body forces, e.g., gravity, acting on fluid subject to thermal expansion.  
These phenomena are very important in the geophysical sciences, but may be less important in the chemical industry.
- Large-scale convection of gases and liquids in the presence of body forces.  
A lot of work has been done on this subject in the geophysical sciences, but is not very important in the chemical industry.

Summarizing these results from fluid mechanics, a layman may erroneously conclude that the flows in chemical reactors are incompressible. Notice, however, that the analyzes referred were all performed on non-reactive flow systems. In chemical reactors, on the other hand, we may be dealing with flow situations where the densities of fluids vary both due to pressure and temperature changes, chemical reactions and non-ideal mixing. From a thermodynamic standpoint both compressible and incompressible fluids are considered in reactor modeling. This indicates that a general reactor technology modeling approach should be able to handle compressible flows.

The traditional modeling framework describing reactive flow systems is presented in the following. The basic conservation equations applied in most reactor model analyzes are developed from the concept that the fluid is a *continuum*. This means that a *fluid* is considered to be a matter which exhibits no finer structure [168]. This model makes it possible to treat fluid properties at a point in space and mathematically as continuous functions of space and time. From the continuum viewpoint, fluid mechanics and solid mechanics have much in common and the subject of both these sciences are traditionally called *continuum mechanics*.

The basic assumptions in fluid mechanics are thus that for lengths and time scales much larger than the characteristic molecular lengths and times, the continuum representation provides a quantitative correct description of the fluid dynamic behavior of the system. In general, the differential description is useful for processes where there is a wide separation of scales between the smallest macroscopic scales of interest and the microscopic scales associated with the internal structure of the fluid. The mean free path which is of the order of  $10^{-7}m$  for gases is commonly used as a suitable characteristic dimension (see sect 2.10). The continuum model in gas dynamics is thus expected to fail when the model resolution is no longer very much larger than the mean free path [168]. For liquids, a corresponding characteristic molecular dimension is not clearly defined but may be taken to be a distance equal to several intermolecular spacings which are of the order of  $10^{-10}m$ . These dimensions are so small that the continuum model is violated only in extreme cases. For single phase flow systems in reactor technology, we are usually not concerned with such extreme cases and the continuum approach is expected to provide useful information of the reactor performance.

Note, however, that in reactor technology we are very often dealing with dispersed and granular flows. Granular flow is referred to as flow of a powder in a vacuum [58]. Traditionally, the continuum approach have been adopted modeling these flows too. It might sometimes be useful to apply an alternative way of proceeding which is based on the results from elementary *kinetic theory of gases*, where such results enhance our physical insight of reactor performance. If this particulate view of matter is adopted we can, by use of a statistical procedure average over a large number of molecules or particles, derive a set of conservation equations which is analogue to the continuum equations. In fact, the results from these two alternative approaches are virtually identical. The latter method, which is more general in principle, is however much more complex theoretically and has been limited by theoretical difficulties to practically dilute gases. During the last decades several papers have been published, even on multiphase flow, presenting ideas on how to extend the kinetic theory closures to more general flow situations. These ideas are further discussed in later chaps. related to multiphase flows.

Keeping these basic assumptions in mind, the chemically reacting fluids can quantitatively be described in terms two categories of the governing equations [134]:

1. *Balance equations*, which summarize the experience of the last three centuries on the behavior of all forms of matter. The balance equations express that for any fluid, in any state of motion, the quantities being transported are balanced.

Experience have taught us that there are certain physical laws which must be valid irrespective of the type of fluid mixture being considered. These laws express *the balance principles* which impose constraints upon the coexisting field variables describing instantaneous motions of a chemically reacting fluid mixture. The term *conservation equations* usually refers to the equations expressing the classical laws of the separate conservation of total mixture mass, momentum and total energy. Based on the balance principle one can nevertheless formulate appropriate balance equations for other physical quantities which are not necessary conserved. Such equations are often called *transport equations* to imply that we are dealing with non-conservable quantities. However, the conservation equations can be formulated on a general form similar to the transport equations.

In many practical situations it is common to formulate *transport equations*, which are based purely on the balance principle and not on a physical law, to determine how the pertinent non-conservative quantities vary in time and space. Important examples:

- Transport of individual chemical species mass.  
Note that each chemical *element* is conserved. This means that ordinary chemical reactions involving the elements are merely changing partners, rather than being produced or destructed. Individual chemical species are however not really conserved since they can be generated or consumed in chemical reactions, but one can nevertheless write an appropriate balance equation or transport equation for each chemical species [134].
- Transport of the total entropy of the mixture, based on the second law of thermodynamics.
- Transport of the turbulent kinetic energy
- Transport of the turbulent dissipation rate
- Transport of the turbulent Reynolds stresses
- Transport of other covariances or turbulent moments
- Transport of probability density functions

Note that the conservation equations can be distinguished from the transport equations since they do not contain any production or destruction terms. Nevertheless, the conservation equations may contain terms on the RHS expressing a divergence of fluxes related to transport phenomena. The way in which these flux terms are divided into divergence of transport fluxes or source terms is rather involved, but procedures exist based on a number of requirements on the two types of terms which determine this separation uniquely.

The equations expressing these balance laws are, by themselves, insufficient to uniquely define the system, and statements on the material behavior are also required. Such statements are termed constitutive relations or constitutive laws.

2. *Constitutive equations*, which quantitatively describe the physical properties of the fluids. The most important constitutive equations used in this book are the Newton's viscosity law, the Fourier's law of heat conduction, and the Fick's law of mass diffusion. The equation of state and more empirical relations for the physical properties of the fluid mixture also belong to this group of equations.

To be able to formulate these continuum equations we need to apply certain mathematical theorems which are not expressing physical laws, but purely based on geometrical aspects of the fluid motion [104] [11] [13] [168] [134]. These relations are called *kinematic theorems*. The most important example of such a kinematic relation is the so-called *Leibnitz formula* for the derivative of an integral with variable limits. *Leibnitz theorem*, also known as the generalized transport theorem, represents a generalization of the fundamental Leibnitz formula. Note that in some physical sciences this transport theorem is called *the Reynolds transport theorem* to distinguish the generalized theorem from the original formula. A third variation is that a particular version of the generalized Leibnitz theorem is referred to as the Reynolds transport theorem ([182], sect. 3.4). To avoid any confusion, the various kinematic theorems applied are defined as we proceed deriving the governing equations.

Furthermore, for non-isothermal situations we need to be able to calculate the thermodynamics of fluid dynamics. However, thermodynamics deals with relatively permanent states, called equilibrium states, within uniform fields of matter [7] [145] [42] [54]. Any changes are assumed to be extremely slow. On the other hand, the fluid motions of interest in fluid mechanics are not necessarily slow. Nevertheless, it has been assumed that the classical thermodynamics can be directly applied to any flow system provided that an instantaneous *local* thermodynamic state is considered and that the rates of change are not too large [168]. A more common statement is that the thermodynamics require that the fluids are close to *local* equilibrium, but may not be in *global* equilibrium. However, all systems are supposed to be relaxing towards a state of *global* thermodynamic equilibrium.

The transport equations derived cannot be solved directly as they contain unknown terms which have to be expressed in terms of the known dependent variables, i.e., parameterized. A relation between observable effects and the internal constitution of matter are described by *constitutive equations or constitutive laws*. It is, however, hardly possible to formulate general expressions for these constitutive laws. The principles of constitutive equations given by Truesdell and Toupin [170] are considered to provide a rational means for obtaining descriptions of classes of materials, without inadvertently neglecting an important dependence. In reactor modeling practice only a limited

number of guiding principles (if any) which are considered to be the most fundamental and restrictive ones provided by continuum mechanics have been applied. According to Aris [3] and Malvern [104], the correct work on constitutive equations should consider the principles of consistency, coordinate invariance, isotropy, just setting, dimensional invariance, material indifference and equipresence. In addition, the set of model equations formulated should be well-posed as an initial value problem [130]. These mathematical principles are elaborated in chap 5 and sect 3.5 discussing multi-fluid models.

By use of the above mentioned framework and mathematical tools, and by reasonable assumptions based on analysis of *experimental data* we are hopefully able to formulate proper models providing reasonable predictions of the chemical reactor performance. In the following sects. the basic mathematical and conceptual tools determining the general reactor technology fundamentals are given and discussed.

## 1.2 Equations of Change for Multi-Component Mixtures

In this section the governing equations of change determining the behavior of multi-component mixtures are formulated on the general vector form. These fundamental balance equations can be transformed into any coordinate system by use of rigorous mathematical formulas [11] [13] [3] [17] ensuring that all the transport equations have the same physical meaning irrespective of the particular coordinate system used to locate points in space. The governing balance equations, as defined in the elementary orthogonal coordinate systems (e.g., Cartesian, cylindrical, spherical) commonly used in engineering practice, are tabulated in many textbooks (e.g., [11] [13]) to ease the work of the modelers. Nevertheless, it is still recommended to study this mathematical theory to be able to understand these transformations and, if necessary, transform the generalized equations into the body fitted non-orthogonal curvilinear coordinate system lately being very popular treating complex geometries in computational fluid dynamics (CFD). In general, however, the choice of coordinate system to describe any particular flow problem is determined largely by convenience.

There are also various ways that the physical laws (i.e., the laws of conservation of mass, linear - and angular momentum, and energy) can be applied describing the fluid behavior. It is usually distinguished between the *system approach* and the *control volume approach* (e.g., [70] [184] [134] [2][185] [114] [181]). In this context a *system* is defined as a collection of matter of fixed identity (i.e., a particular collection of atoms or molecules constituting a specified portion of the material), which may move and interact with its surroundings. A *control volume* (CV), on the other hand, is basically a volume in space (a geometric entity, independent of mass). Different types of CVs have been defined over the years, including some through which fluid may flow. In solid mechanics the system approach is generally used to describe the motion of

solid bodies because a given particle is easily identified. The control volume approach is normally used in fluid mechanics since the identification of a particular system becomes a tedious task.

An issue of fundamental importance is that the physical laws determining the fluid behavior are stated in terms of fluid systems, not control volumes. To formulate the governing laws in a control volume approach we must re-phrase the laws in an appropriate manner. In the integral formulation the Leibnitz- or Reynolds transport theorem provides the relationship between the time rate of change of an extensive property for a system and that for a control volume. For differential equations a similar interrelation between the system and control volume approaches is expressed through the substantial - or material derivative operator. Hence it follows that by use of these mathematical tools we may convert a system analysis to a control volume analysis.

One particular control volume definition might be confusing at first because it is interchangeable with a system as defined above (e.g., [134] [114] [104]). Such a control volume is called a *material* control volume (a geometric entity, dependent on mass) since it always retains the material originally present within its control surface (*CS*). The model framework for such an analysis of motion of material control volumes is termed *Lagrangian*. This is the familiar approach of particle and rigid body dynamics. An important alternative control volume retains stationary enabling a description of the material behavior at a fixed location. This framework is named *Eulerian*<sup>1</sup>. The relationship between the system and control volume approaches can be defined in terms of the material control volume representing a system. The Reynolds theorem, for example, defines the relationship between the material and Eulerian control volume descriptions.

To proceed formulating the governing equations, yet some important considerations concerning when or for what flow situations it is favorable to apply the alternative mathematical model frameworks are required. In general there is no single best choice of frame valid for all flow situations, rather several possibilities exist that can lead to the same useful predictions. Therefore, as expected perhaps, for most flow problems this decision is often based on convenience or level of detail sought. Nevertheless, in the context of reactor simulations a brief evaluation considering the complexity and use of the different control volumes might be given.

In continuum dynamics the balance principles and conservation laws can be applied to the fluid contained in a control volume of arbitrary size, shape and state of motion. Conceptually, the simplest control volume is perhaps the Lagrangian or material one that moves at every point on its surface with

<sup>1</sup> Note that according to Truesdell and Toupin [170] the material coordinates were introduced by Euler in 1762, although they are now widely referred to as the Lagrangian coordinates, while the spatial coordinates, often called Eulerian coordinates, were introduced by Jean le Rond d'Alembert (1717-1783) in 1752.

Elaborate discussions of these coordinates are given by Malvern [104] (sect 4.3) and Truesdell and Toupin [170] (pp. 326-327).

the local fluid velocity, see Fig 1.1(B). However, while the balance principles and conservation laws of fluid dynamics are readily stated for material control volumes, they are not so readily used in this form. This is because the use of Lagrangian material control volumes involve complex and computationally expensive mathematics as the Lagrangian control volume moving through space, may both change its volume and deform in shape. In this context, control volumes with *fixed* surfaces through which the fluid flows, offer the important advantage of involving simpler mathematics. Thus, most fluid dynamic reactor models are formulated using fixed (Eulerian) control volumes, see Fig 1.1(A). However, the most general type of control volumes is defined by surfaces that are neither fixed nor moving with the local fluid velocity, that is, the CV surfaces move with an arbitrary velocity. These generalized descriptions are commonly referred to as mixed Lagrangian-Eulerian-, generalized

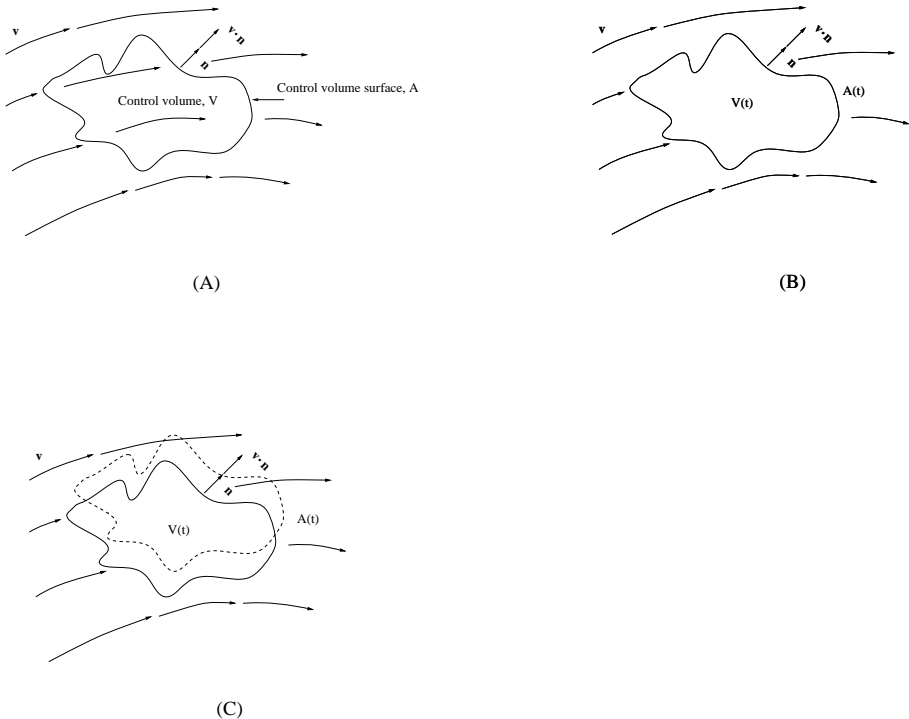


**Fig. 1.1.** (A) Finite Eulerian control volume *fixed* in space with the fluid moving through it. (B) Finite Lagrangian control volume *moving with the fluid* such that the same fluid particles are always in the same control volume (i.e., a material control volume). (C) Finite general Lagrangian control volume *moving with an arbitrarily velocity* not necessarily equal to the fluid velocity. The solid line indicate the control volume surface (CS) at time  $t$ , while the dashed line indicate the same CS at time  $t + dt$ .

Lagrangian- or arbitrary Lagrangian-Eulerian (ALE) methods [36] [37], and were first reported by Hirt et al. [68]. In this book this particular framework is termed *the general Lagrangian* approach, see Fig 1.1(C). This approach also involves quite complex mathematics and is thus hardly ever used in chemical reactor analysis.

It is remarked that in the standard literature on fluid dynamics and transport phenomena three different modeling frameworks, which are named in a physical notation rather than in mathematical terms, have been followed formulating the single phase balance equations [89]. These are: (1) The *infinitesimal particle* approach [89] [66] [144] [3] [2]. In this case a differential cubical fluid particle is considered as it moves through space relative to some fixed coordinate system. By applying the balance principle to this Lagrangian control volume the conservation equations for mass, momentum and energy are obtained. The value of a given property at a fixed position  $\mathbf{r}$  and time  $t$  coincides with the value appropriate to the particle which is at  $\mathbf{r}$  at time  $t$ . The substantial derivative operator establishes a connection between the Lagrangian and Eulerian frameworks. (2) The *infinitesimal control volume* approach [11] [13] [2]. In this method one considers a differential cubical volume element fixed in space, through which a fluid is flowing. By applying the balance principle to this Eulerian control volume the conservation equations for mass, momentum and energy are achieved. (3) The *finite control volume* approach [104] [12] [32] [168] [2]. In this approach a control volume of finite size is considered. This control volume can have any arbitrary shape and is either fixed in space or moves through space relative to some fixed coordinate system. By applying the balance principle to the finite control volume the conservation equations for mass, momentum and energy are written on the integral form. The Leibnitz theorem is used to define the time rate of change. The Gauss's theorem is used to relate the surface and volume integrals, resulting in an equation involving only volume integrals. It is then argued that the conditions must be satisfied for the integrand, since the integration is arbitrary.

Needless to say, the three approaches (1)-(3) give rise to identical results, the governing equations. However, it is not always clear which approach is being followed. There is also a subtle difference between the integral and differential forms of the governing flow equations [2]. The integral form of the equations allows for the presence of discontinuities inside the control volume (there is no inherent mathematical reason to assume otherwise). However, the differential form of the governing equations assumes the flow properties are differentiable, hence continuous. This consideration becomes of particular importance when calculating a flow with real discontinuities, such as shock waves and interfaces. In this book the *finite control volume* approach is applied for single phase flows because it coincides with the method adopted formulating the multi-fluid models (e.g., [182] [73] [39] [152] [148] [43]) in the subsequent chapters of this book.

To establish the integral form of the basic conservation laws for mass, momentum and energy, the fundamental approach is to start out from a system analysis and then transform the balance equations into a control volume analysis by use of the transport theorem. However, to achieve a more compact presentation of this theory it is customary to start out from a generic Eulerian form of the governing equations. That is, the material control volume analysis is disregarded.

The balance principle applied to an Eulerian CV is thus by definition expressed as a balance of accumulation, net inflow by convection and diffusion and volumetric production.

The Eulerian transport equations can be cast in the generalized form:

$$\left\{ \begin{array}{c} \text{Rate of } ( ) \\ \text{accumulation} \\ \text{in CV} \end{array} \right\} = \left\{ \begin{array}{c} \text{Net inflow} \\ \text{rate of } ( ) \\ \text{by convection} \\ \text{across} \\ \text{CV surface} \end{array} \right\} + \left\{ \begin{array}{c} \text{Net inflow} \\ \text{rate of } ( ) \\ \text{by diffusion} \\ \text{across} \\ \text{CV surface} \end{array} \right\} + \left\{ \begin{array}{c} \text{Net source} \\ \text{of } ( ) \\ \text{within CV} \end{array} \right\}$$

where  $( )$  applies to mass, momentum, energy, entropy, etc.

Therefore, as basis we formulate the generalized form of the local instantaneous transport equation for the mixture mass, component mass, momentum, energy and entropy in a fixed control volume (CV) on microscopic scales, as illustrated in Fig. 1.1.

This approach thus consider the conservation law of the quantity  $\psi$  within the fixed macroscopic volume  $V$  bounded by the fixed macroscopic surface area  $A$ .

$$\frac{\partial}{\partial t} \int_V (\rho\psi) dv = - \int_A (\rho\mathbf{v}\psi) \cdot \mathbf{n} da - \int_A \mathbf{J} \cdot \mathbf{n} da + \int_V \phi dv \quad (1.1)$$

The  $\mathbf{n}$  is the outward directed normal unit vector to the surface of the control volume,  $\mathbf{v}$  is the fluid velocity,  $\rho$  is the mixture density,  $\psi$  is the conserved quantity,  $\mathbf{J}$  is the diffusive flux and  $\phi$  is the source term.

The transient term in (1.1) can be manipulated as the order in which the partial time derivation and the integration is performed can be reversed. The convective and diffusive transport terms in (1.1) can be rewritten as a volume integral using Gauss' theorem (App. A).

Equation (1.1) can then be assembled in a single volume integral:

$$\int_V \left( \frac{\partial(\rho\psi)}{\partial t} + \nabla \cdot (\rho\mathbf{v}\psi) + \nabla \cdot \mathbf{J} - \phi \right) dv = 0 \quad (1.2)$$

Equation (1.2) must be satisfied for any macroscopic volume  $V$ , thus the expressions inside the volume integral must be equal to zero.

A generic local instantaneous equation for a general conserved quantity  $\psi$ , where  $\mathbf{J}$  represents the diffusive fluxes and  $\phi$  the sources of  $\psi$ , can be expressed as:

$$\frac{\partial(\rho\psi)}{\partial t} + \nabla \cdot (\rho\mathbf{v}\psi) + \nabla \cdot \mathbf{J} - \phi = 0 \quad (1.3)$$

The values for  $\psi$ ,  $\mathbf{J}$  and  $\phi$  for the different balances are listed in Table 1.1 (e.g., [11] [13] [32] [89]).

**Table 1.1.** The definitions of  $\psi$ ,  $\mathbf{J}$  and  $\phi$  for the different balance equations.

Balance Principle	$\psi$	$\mathbf{J}$	$\phi$
Total mass	1	0	0
Component mass	$\omega_c$	$\mathbf{j}_c$	$R_c$
Momentum	$\mathbf{v}$	$\mathbb{T}$	$\sum_{c=1}^N \rho_c \mathbf{g}_c$
Energy	$e + \frac{1}{2}v^2$	$\mathbb{T} \cdot \mathbf{v} + \mathbf{q}$	$\sum_{c=1}^N \rho_c (\mathbf{g}_c \cdot \mathbf{v}_c)$

where

$e$  is the internal energy of the multicomponent system,

$\mathbf{g}_c$  is the external forces per unit mass of component  $c$ ,

$\mathbf{j}_c$  is the molecular (diffusive) flux of component  $c$ ,

$N$  is the total number of species,

$\mathbf{q}$  is the multi-component energy flux vector,

$q$  is the number of independent reactions,

$R_c$  is the rate of generation of species  $c$  by chemical reaction.

$$R_c = \sum_{r=1}^q R_{r,c} \quad \text{where } R_{r,c} = R'_{r,c} M_{w_c} \left( \frac{kg}{m^3s} \right) \text{ and } R'_{r,c} \left( \frac{mol}{m^3s} \right),$$

$\mathbb{T}$  is the total stress tensor (i.e.,  $\mathbb{T} = p\mathbf{e} + \boldsymbol{\sigma}$ ),

$\omega_c$  is the mass fraction of component  $c$ ,

$\boldsymbol{\sigma}$  is the viscous stress tensor.

Note that the momentum and energy equations for mixtures and pure fluids differ in their last terms (e.g., [11] [12] [13] [169]), where  $\rho\mathbf{g}$  has been replaced by  $\sum_{c=1}^N \rho_c \mathbf{g}_c$  in the momentum equation and  $\rho(\mathbf{g} \cdot \mathbf{v})$  has been replaced by  $\sum_{c=1}^N \rho_c (\mathbf{g}_c \cdot \mathbf{v}_c)$  in the energy equation, respectively. In the mixture equations account are taken of the fact that each chemical species present may be acted on by a different external force per unit mass  $\mathbf{g}_c$ .

However, for the less experienced readers such a list of equations may not provide sufficient knowledge of the physical phenomena involved. Hence for that reason in the following sub-sections the governing equations are derived

again from scratch utilizing the advantages of the different descriptions to improve the elementary understanding of the physical phenomena and the basic modeling principles.

At this point a few mathematical prerequisites are required before the derivation of the equations of change can be discussed. First, the three kinds of time derivatives involved in this task are defined. Secondly, the transport theorem is introduced.

Let  $\psi = \psi(t, \mathbf{r})$  be a general scalar, vector or tensor function. By the *partial time derivative*,  $\partial\psi/\partial t$ , we mean the partial of  $\psi$  with respect to  $t$ , holding the independent space coordinate variables constant:  $\partial\psi/\partial t = \partial\psi/\partial t|_{\mathbf{r}}$ .

In Cartesian coordinates<sup>2</sup> the *total time derivative* of  $\psi$  is defined by:

$$\frac{d\psi}{dt} = \frac{\partial\psi}{\partial t}|_{x,y,z} + \frac{\partial\psi}{\partial x} \frac{dx}{dt}|_{y,z,t} + \frac{\partial\psi}{\partial y} \frac{dy}{dt}|_{x,z,t} + \frac{\partial\psi}{\partial z} \frac{dz}{dt}|_{x,y,t} \quad (1.4)$$

in which  $dx/dt$ ,  $dy/dt$  and  $dz/dt$  are the components of the arbitrary velocity of a given particle as seen by an observer in a framework not necessarily moving along with the fluid. The vector form is

$$\frac{D\psi}{Dt} = \frac{\partial\psi}{\partial t} + \mathbf{v}_S \cdot \nabla\psi \quad (1.5)$$

where  $\nabla$  is the gradient operator and  $\mathbf{v}_S$  denotes the arbitrary velocity.

In Cartesian coordinates the *substantial time derivative*,  $D/Dt$ , is given by

$$\frac{D\psi}{Dt} = \frac{\partial\psi}{\partial t} + v_x \frac{\partial\psi}{\partial x} + v_y \frac{\partial\psi}{\partial y} + v_z \frac{\partial\psi}{\partial z} \quad (1.6)$$

in which  $v_x$ ,  $v_y$  and  $v_z$  are the components of the velocity of a given particle as seen by an observer in a framework moving along with the fluid. The substantial time derivative is a special kind of total time derivative and is sometimes more logically called the total derivative following the motion. In (1.6) the last three terms on the right hand side are called the convective derivative, since they vanish if the velocity is zero or if  $\psi$  has no spatial change. The first term on the right hand side is called the local derivative. The vector form is given by

$$\frac{D\psi}{Dt} = \frac{\partial\psi}{\partial t} + \mathbf{v} \cdot \nabla\psi \quad (1.7)$$

where  $\nabla$  is the gradient operator.

To establish the relationship between the system and control volume representations we need to evaluate the rate of change of integrals of scalar and vector functions over a moving material volume occupied by fluid. Consider thus a material volume  $V(t)$  bounded by a smooth closed surface  $A(t)$  whose

<sup>2</sup> In the Cartesian coordinate system the independent space coordinates are  $x$ ,  $y$  and  $z$ .

points at time  $t$  move with the material velocity  $\mathbf{v} = \mathbf{v}(\mathbf{r}, t)$  where  $\mathbf{r} \in A$ . The material time derivative of the integral of a scalar function  $f(\mathbf{r}, t)$  over the time-varying material volume  $V(t)$  is given by the transport theorem.

$$\frac{D}{Dt} \int_{V(t)} f(\mathbf{r}, t) dv = \int_V \frac{\partial f(\mathbf{r}, t)}{\partial t} dv + \int_A f(\mathbf{r}, t) (\mathbf{v} \cdot \mathbf{n}) da \quad (1.8)$$

The volume integral on the RHS is defined over a control volume  $V$  fixed in space, which coincides with the moving material volume  $V(t)$  at the considered instant,  $t$ , in time. Similarly, the fixed control surface  $A$  coincides at time  $t$  with the closed surface  $A(t)$  bounding the material volume  $V(t)$ . In the surface integral,  $\mathbf{n}$  denotes the unit outward normal to the surface  $A(t)$  at time  $t$ , and  $\mathbf{v}$  is the material velocity of points of the boundary  $A(t)$ . The first term on the RHS of (1.8) is the partial time derivative of the volume integral. The boundary integral represents the flux of the scalar quantity  $f$  across the fixed boundary of the control volume  $V$ .

Noting that by use of the Gauss theorem (App A) yields:

$$\int_A f(\mathbf{r}, t) (\mathbf{v} \cdot \mathbf{n}) da = \int_V \nabla \cdot (f\mathbf{v}) dV \quad (1.9)$$

one obtains the familiar form of the transport theorem

$$\frac{D}{Dt} \int_{V(t)} f(\mathbf{r}, t) dv = \int_V \left[ \frac{\partial f(\mathbf{r}, t)}{\partial t} + \nabla \cdot (f\mathbf{v}) \right] dv \quad (1.10)$$

The transient term on the RHS might be manipulated as the order in which the partial time derivation and the integration is performed can be reversed.

Similar forms of the transport theorem hold for the material derivative of the volume integral for vector and tensor quantities.

### 1.2.1 Conservation of mass

The continuity equation for a mixture formulated in terms of the mass averaged mixture velocity has the same form as the continuity equation for single-component systems.

#### System analysis

The fundamental conservation of mass law for a multi-component system can be formulated employing the material Lagrangian framework (e.g., [11] [169] [89] [13]).

The mixture mass  $M$  in a macroscopic material control volume  $V(t)$ , is given by:

$$M = \int_{V(t)} \rho \, dv \quad (1.11)$$

The *mass conservation principle* can then be formulated for the system considering the material control volume  $V(t)$  which is moving in space and bounded by a closed material surface  $A(t)$ :

$$\frac{DM}{Dt} = \frac{D}{Dt} \int_{V(t)} \rho \, dv = 0 \quad (1.12)$$

The *transport theorem* (1.10) enables the time rate of change of the material volume integral (1.12) to be transformed into the Eulerian formulation. Hence,

$$\frac{D}{Dt} \int_{V(t)} \rho \, dv = \int_V \left[ \frac{\partial \rho}{\partial t} + \nabla \cdot (\rho \mathbf{v}) \right] \, dv = 0 \quad (1.13)$$

Equation (1.13) must be satisfied for any macroscopic volume  $V$ , thus the expressions inside the volume integral must be equal to zero. This result is termed the *equation of continuity* for a mixture, and is given by:

$$\frac{\partial \rho}{\partial t} + \nabla \cdot (\rho \mathbf{v}) = 0 \quad (1.14)$$

The fact that the control volume was fixed in space leads by definition to the specific differential form which is called the *conservative or flux form*.

### Finite Eulerian control volume analysis

The mixture mass  $M$  in a macroscopic Eulerian control volume  $V$ , at time  $t$  is given by:

$$M = \int_V \rho \, dv \quad (1.15)$$

In the Eulerian formulation the mass  $M$  can only be changed by convection across the CV surface considering non-nuclear-active materials. The conservation equation of mixture mass can thus be expressed like<sup>3</sup>:

$$\frac{\partial M}{\partial t} = \left[ \frac{\partial M}{\partial t} \right]_{\text{Convection}} \quad (1.16)$$

using a fractional time step notation for convenience.

The convective term is by definition given by:

$$\left[ \frac{\partial M}{\partial t} \right]_{\text{Convection}} = - \int_A (\rho \mathbf{v}) \cdot \mathbf{n} \, da \quad (1.17)$$

---

<sup>3</sup> The partial time derivation can be performed before the integration since the integration limits are fixed and no longer depend on the independent variable,  $t$ .

where  $\mathbf{n}$  is the outward directed normal unit vector to the surface of the fixed control volume.

The convective transport term in (1.17) can be transformed into a volume integral using Gauss' theorem (App A). The continuity equation (1.16), can then be expressed as:

$$\int_V \left[ \frac{\partial \rho}{\partial t} + \nabla \cdot (\rho \mathbf{v}) \right] dv = 0 \quad (1.18)$$

Equation (1.18) must be satisfied for any macroscopic volume  $V$ , thus the expressions inside the volume integral must be equal to zero. The resulting differential equation coincides with (1.14), as expected.

### Infinitesimal Eulerian control volume analysis

We end this subsection deriving the convective mass flux terms over an infinitesimal Eulerian control volume element, intending to provide improved understanding of the physics and mathematical concepts involved. Note that even though we consider convective mass fluxes only at this point, the mathematical flux concepts are general. That is, all convective and diffusive fluxes can be derived in a similar manner.

As we adopt a Cartesian coordinate system, the velocity and density are functions of  $(x, y, z)$  space and time  $t$ . In this  $(x, y, z)$  space we have placed an infinitesimally control volume of sides  $dx$ ,  $dy$  and  $dz$  fixed in space, with the fluid moving through it as illustrated in Fig. 1.2. Consider the left and right faces of the element which are perpendicular to the  $x$  axis. The area of these faces is  $dy dz$ . The mass flow through the left face is  $(\rho v_x) dy dz$ . Since the velocity and density are functions of spatial location, the value of the mass flux across the right face will be different from that across the left face. The difference in mass flux between the two faces is  $[\partial(\rho v_x)/\partial x] dx$ . Thus, the mass flow across the right face can be expressed as  $(\rho v_x + [\partial(\rho v_x)/\partial x] dx) dy dz$ . In a similar manner, the mass flow through both the bottom and top faces, which are perpendicular to the  $y$  axis, is  $(\rho v_y) dx dz$  and  $(\rho v_y + [\partial(\rho v_y)/\partial y] dy) dx dz$ , respectively. The mass flow through both the front and back faces, which are perpendicular to the  $z$  axis, is  $(\rho v_z) dx dy$  and  $(\rho v_z + [\partial(\rho v_z)/\partial z] dz) dx dy$ , respectively. Note that  $v_x$ ,  $v_y$ , and  $v_z$  are positive, by convention, in the positive  $x, y$ , and  $z$  directions, respectively. Hence, the arrows in Fig 1.2 show the contributions to the inflow and outflow of mass through the sides of the fixed element.

*Net inflow in x direction:*

$$(\rho v_x) dy dz - [\rho v_x + \frac{\partial(\rho v_x)}{\partial x} dx] dy dz = -\frac{\partial(\rho v_x)}{\partial x} dx dy dz \quad (1.19)$$

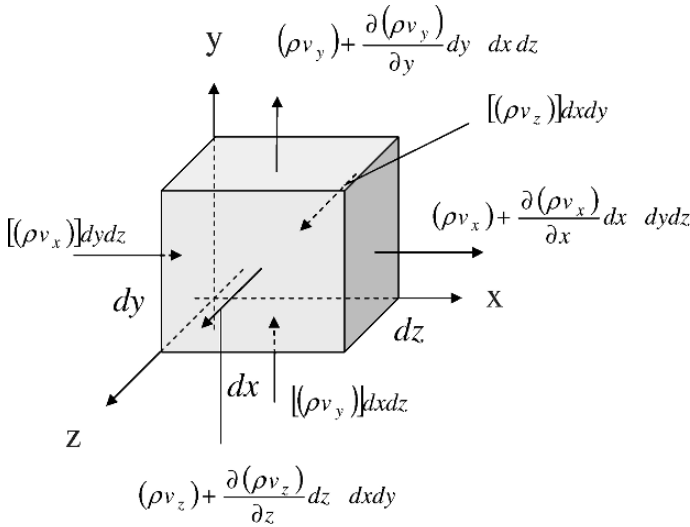


**Fig. 1.2.** A physical model of an infinitesimal Eulerian control volume fixed in space indicating the convective mass fluxes through the various faces of the volume element, used for derivation of the continuity equation.

*Net inflow in y direction:*

$$(\rho v_y) dx dz - \left[ \rho v_y + \frac{\partial(\rho v_y)}{\partial y} dy \right] dx dz = - \frac{\partial(\rho v_y)}{\partial y} dx dy dz \quad (1.20)$$

*Net inflow in z direction:*

$$(\rho v_z) dx dy - \left[ \rho v_z + \frac{\partial(\rho v_z)}{\partial z} dz \right] dx dy = - \frac{\partial(\rho v_z)}{\partial z} dx dy dz \quad (1.21)$$

Hence, the net mass flow into the element is given by

$$\text{Net mass inflow} = - \left[ \frac{\partial(\rho v_x)}{\partial x} + \frac{\partial(\rho v_y)}{\partial y} + \frac{\partial(\rho v_z)}{\partial z} \right] dx dy dz \quad (1.22)$$

The mixture mass of fluid in the infinitesimally small element is  $\rho (dx dy dz)$ , and the time rate of increase or accumulation of mass inside the element is given by

$$\text{Time rate of mass increase} = \frac{\partial \rho}{\partial t} dx dy dz \quad (1.23)$$

The physical principle that mass is conserved, when applied to the fixed element in Fig. 1.2, can be expressed in words as follows: *the net mass flow into the element must equal the time rate of increase or accumulation of mass inside the element.* This statement can mathematically be expressed as

$$\frac{\partial \rho}{\partial t} dx dy dz = -\left[\frac{\partial(\rho v_x)}{\partial x} + \frac{\partial(\rho v_y)}{\partial y} + \frac{\partial(\rho v_z)}{\partial z}\right] dx dy dz \quad (1.24)$$

or

$$\frac{\partial \rho}{\partial t} = -\left[\frac{\partial(\rho v_x)}{\partial x} + \frac{\partial(\rho v_y)}{\partial y} + \frac{\partial(\rho v_z)}{\partial z}\right] \quad (1.25)$$

In (1.25), the terms inside the brackets can be reformulated by use of vector and tensor notations. By comparing the terms inside the brackets with the mathematical definitions of the *nabla* or *del* operator, the vector product between this nabla operator and the mass flux vector we recognize that these terms can be written as  $\nabla \cdot (\rho \mathbf{v})$ .

The mass balance equation, (1.25), written in Cartesian coordinates can thus be rewritten in the general vector form as:

$$\frac{\partial \rho}{\partial t} = -\nabla \cdot (\rho \mathbf{v}) \quad (1.26)$$

We recall that the resulting equation is identical to the vector equation (1.14) formulated earlier based on a more direct mathematical approach.

### 1.2.2 Transport of species mass

The concentration of the various species in a multi-component mixture may be expressed in numerous ways. In this book the equations are formulated in terms of mass fluxes, thus mass concentrations are used. However, the equations could as well be formulated in terms of molar fluxes, and molar concentrations as usually applied in basic textbooks in Chemical Engineering (e.g., [11] [169] [13]). The mass concentration,  $\rho_c$ , is the mass of species  $c$  per unit of volume of solution. The species  $c$  mass density relates to the familiar molar concentration by the simple formula:  $C_c = \frac{\rho_c}{M_{w_c}}$ .  $M_{w_c}$  is the molecular weight of species  $c$ . The mass fraction,  $\omega_c = \frac{\rho_c}{\rho}$ , is the mass concentration of species  $c$  divided by the mixture mass density of the solution. The corresponding mole fraction,  $x_c = \frac{C_c}{C}$ , is the molar concentration of species  $c$  divided by the total molar concentration of the solution.

The individual chemical species in a mixture moves at different velocities. The  $\mathbf{v}_c$  denotes the velocity of the species  $c$  with respect to stationary coordinate axes. Thus, for a mixture of  $N$  species, the local mass-average velocity  $\mathbf{v}$  is defined as:

$$\mathbf{v} = \frac{\sum_{c=1}^N \rho_c \mathbf{v}_c}{\sum_{c=1}^N \rho_c} = \frac{\sum_{c=1}^N \rho_c \mathbf{v}_c}{\rho} = \sum_{c=1}^N \omega_c \mathbf{v}_c \quad (1.27)$$

where  $\rho = \sum_{c=1}^N \rho_c$  is the mixture density.

In flow systems, one is frequently interested in the velocity of a given species with respect to  $\mathbf{v}$  rather than with respect to stationary coordinates. This leads to the definition of the diffusion velocities:

$$\mathbf{v}_{c,d} = \mathbf{v}_c - \mathbf{v} \quad (1.28)$$

These diffusion velocities indicate the motion of component  $c$  relative to the local motion of the mixture stream.

The mass flux of species  $c$  is a vector quantity denoting the mass of species  $c$  that passes through a unit area per unit time. The mass flux relative to stationary coordinates is defined by:

$$\mathbf{m}_c = \rho_c \mathbf{v}_c \quad (1.29)$$

where  $\rho_c$  is the mass concentration or density of species  $c$ .

The *relative* mass flux is defined as:

$$\mathbf{j}_c = \rho_c (\mathbf{v}_c - \mathbf{v}) = \rho_c \mathbf{v}_{c,d} \quad (1.30)$$

The *convective* mass flux is thus defined by:

$$\rho_c \mathbf{v} = \mathbf{m}_c - \mathbf{j}_c \quad (1.31)$$

For binary mixtures the diffusive mass flux  $\mathbf{j}_c$  of species  $c$  is normally approximated by *Fick's first law*:

$$\mathbf{j}_c = -\rho D_c \nabla \omega_c \quad (1.32)$$

where the mass flux of species  $c$  is in the direction of decreasing concentration (which accounts for the minus sign). The quantity  $D_c$  is called the mass diffusion coefficient or diffusivity and has generally dimensions  $\frac{(\text{length})^2}{\text{time}}$ .

The rigorous kinetic theory, described in sect. 2.9, shows that the net species *relative* mass flux in a multi-component mixture will consist of three contributions associated with the mechanical driving forces and an additional contribution associated with the thermal driving force:

$$\mathbf{j}_c = \mathbf{j}_c^o + \mathbf{j}_c^p + \mathbf{j}_c^g + \mathbf{j}_c^T = \rho_c \mathbf{v}_{d,c} \quad (1.33)$$

as explained by Hirschfelder et al [67] and Bird et al. [11] [13].

The  $\mathbf{j}_c^o$  term denotes the *ordinary concentration diffusion* (i.e., multi-component mass diffusion). In general, the concentration diffusion contribution to the mass flux depends on the concentration gradients of all the substances present. However, in most reactor systems, containing a solvent and one or only a few solutes having relatively low concentrations, the binary form of Fick's law is considered a sufficient approximation of the diffusive fluxes. Nevertheless, for many reactive systems of interest there are situations where a multi-component closure (e.g., a Stefan-Maxwell equation formulated in terms

of mass average velocities) should be considered [166]. The *pressure diffusion* term  $\mathbf{j}_c^p$  accounts for the fact that there may be a net movement of the  $c$ 'th species in a mixture if there is a pressure gradient imposed on the system. The pressure diffusion effect is usually very small in chemical reactor systems as the local pressure gradients are much smaller than the concentration gradients. The pressure-diffusion proportionality coefficient is apparently much smaller than the mass diffusion coefficient. The *forced diffusion* term  $\mathbf{j}_c^g$  accounts for the fact that there may be a net movement of the  $c$ -th species in a mixture if there is an external force which is different for the individual species (e.g., electric field on an ionic system). This diffusion effect is seldom important in chemical reactor systems as only the gravity field is considered in most cases. The *thermal-diffusion* term  $\mathbf{j}_c^T$  describes the tendency for species to diffuse under the influence of a temperature gradient. The thermal-diffusion effect (or Soret effect) is usually neglected in chemical reactor systems because the thermal-diffusion coefficient is typically much smaller than the mass diffusion coefficient.

In reactor modeling only the ordinary concentration diffusion term  $\mathbf{j}_c^c$  is generally considered. The rigorous kinetic theory model derivation for multi-component mixtures is outlined in chap 2. Meanwhile, the Fick's law for binary systems is used.

## System analysis

For an individual species  $c$  in a multi-component mixture the *species mass balance principle* postulates that the time rate of change of the mass of a system of species  $c$  is equal to the rate at which the mass of  $c$  is produced by homogeneous chemical reactions.

The species  $c$  mass in a macroscopic material control volume  $V_c(t)$  is given by:

$$M_c = \int_{V_c(t)} \rho_c dv \quad (1.34)$$

Let  $V_c(t)$  denote the material volume occupied by species  $c$  (see Fig. 1.1B), and  $R_c$  denote the rate of production of species  $c$  per unit volume by homogeneous chemical reactions. The species mass balance can thus be expressed as:

$$\frac{DM_c}{Dt} = \frac{D}{Dt} \int_{V_c(t)} \rho_c dv = \int_{V_c(t)} R_c dv \quad (1.35)$$

To transform the system balance into an Eulerian control volume balance a particular form of the transport theorem applicable to single-phase systems of species  $c$  is required [149]. Let  $f$  be any scalar, vector or tensor field. The transport theorem for species  $c$  can be expressed as:

$$\frac{D}{Dt} \int_{V_c(t)} f(\mathbf{r}, t) dv = \int_{V_c} \left[ \frac{\partial f(\mathbf{r}, t)}{\partial t} + \nabla \cdot (f\mathbf{v}_c) \right] dv \quad (1.36)$$

The transport theorem (1.36) enables the time rate of change in the species mass balance (1.35) to be transformed into the Eulerian formulation. Hence,

$$\int_{V_c} \left[ \frac{\partial \rho_c}{\partial t} + \nabla \cdot (\rho_c \mathbf{v}_c) - R_c \right] dv = 0 \quad (1.37)$$

Equation (1.37) must be satisfied for any macroscopic volume  $V_c$ , thus at each point the differential mass balance for species  $c$  yields:

$$\frac{\partial \rho_c}{\partial t} + \nabla \cdot (\rho_c \mathbf{v}_c) = R_c \quad (1.38)$$

The species  $c$  total mass flux can be divided into the sum of convective and diffusive fluxes in accordance with (1.30). The result is:

$$\frac{\partial \rho_c}{\partial t} + \nabla \cdot (\rho_c \mathbf{v}) + \nabla \cdot \mathbf{j}_c = R_c \quad (1.39)$$

This equation is the Eulerian species  $c$  mass balance equation.

### Finite Eulerian control volume analysis

The species  $c$  mass in a fixed macroscopic volume  $V_c$ , is given by:

$$M_c = \int_{V_c} \rho_c dv \quad (1.40)$$

The Eulerian (see Fig. 1.1A) transport equation for the species  $c$  mass can be defined by:

$$\frac{\partial M_c}{\partial t} = \left[ \frac{\partial M_c}{\partial t} \right]_{\text{Convection}} + \left[ \frac{\partial M_c}{\partial t} \right]_{\text{Relative mass fluxes}} + \left[ \frac{\partial M_c}{\partial t} \right]_{\text{Reactions}} \quad (1.41)$$

The equation states that for non-nuclear-active mixtures the species  $c$  mass  $M_c$  can only be changed by convection and relative mass fluxes across the CV surface, and due to chemical reactions per unit volume.

The *convective term* can then be formulated as a surface integral, and converted to a volume integral by use of Gauss' theorem (App. A):

$$\left[ \frac{\partial M_c}{\partial t} \right]_{\text{Convection}} = - \int_{A_c} (\rho_c \mathbf{v}) \cdot \mathbf{n} da = - \int_{V_c} \nabla \cdot (\rho_c \mathbf{v}) dv \quad (1.42)$$

The *relative mass flux term* denotes the net rate of component  $c$  mass input per unit volume by concentration diffusion, pressure diffusion, forced

diffusion and thermal diffusion can then be formulated as a surface integral, and converted to a volume integral by use of Gauss' theorem (App. A):

$$\left[\frac{\partial M_c}{\partial t}\right]_{\text{Relative mass diffusion}} = - \int_{A_c} \mathbf{j}_c \cdot \mathbf{n} \, da = - \int_{V_c} \nabla \cdot \mathbf{j}_c \, dv \quad (1.43)$$

The reaction rate term, denoting the net rate of species  $c$  mass input per unit volume by chemical reactions is given by:

$$\left[\frac{\partial M_c}{\partial t}\right]_{\text{Reactions}} = \int_{V_c} R_c \, dv \quad (1.44)$$

The general form of the Eulerian transport equation for species  $c$  mass, can be formulated as:

$$\begin{aligned} \frac{\partial M_c}{\partial t} &= \left[\frac{\partial M_c}{\partial t}\right]_{\text{Convection}} + \left[\frac{\partial M_c}{\partial t}\right]_{\text{Relative mass fluxes}} + \left[\frac{\partial M_c}{\partial t}\right]_{\text{Reactions}} \\ &= - \int_{V_c} \nabla \cdot (\rho_c \mathbf{v}) \, dv - \int_{V_c} \nabla \cdot \mathbf{j}_c \, dv + \int_{V_c} R_c \, dv \end{aligned} \quad (1.45)$$

or with a little reformulation

$$\int_{V_c} \left[ \frac{\partial \rho_c}{\partial t} + \nabla \cdot (\rho_c \mathbf{v}) + \nabla \cdot \mathbf{j}_c - R_c \right] dv = 0 \quad (1.46)$$

Equation (1.46) must be satisfied for any macroscopic volume  $V_c$ , thus the expression inside the volume integral must be equal to zero. The resulting differential species mass balance coincides with (1.39).

Introducing the well known *Einstein summation notation* (e.g., described by [154]), the Cartesian form of the equation can be formulated

$$\frac{\partial \rho_c}{\partial t} + \frac{\partial (\rho_c v_i)}{\partial x_i} + \frac{\partial j_{c,i}}{\partial x_i} = R_c \quad (1.47)$$

where we have used the rigorous mathematical definitions of the Cartesian operators (e.g., [11]).

The divergence of a vector is defined as:

$$\text{div}(\mathbf{j}_c) = \nabla \cdot \mathbf{j}_c = \sum_{i=1}^3 \frac{\partial j_{c,i}}{\partial x_i} = \frac{\partial j_{c,i}}{\partial x_i} = \frac{\partial j_{c,x}}{\partial x} + \frac{\partial j_{c,y}}{\partial y} + \frac{\partial j_{c,z}}{\partial z} \quad (1.48)$$

Similarly, the gradient of a scalar is defined as:

$$\text{grad}(\rho) = \nabla \rho = \sum_{i=1}^3 \frac{\partial \rho}{\partial x_i} \mathbf{e}_i = \frac{\partial \rho}{\partial x_i} \mathbf{e}_i = \frac{\partial \rho}{\partial x} \mathbf{e}_x + \frac{\partial \rho}{\partial y} \mathbf{e}_y + \frac{\partial \rho}{\partial z} \mathbf{e}_z \quad (1.49)$$

From these definitions we see that  $grad()$  is a vector while  $div()$  is a scalar quantity.

The sum of the transport equations for all the  $N$  species in the mixture equals the *continuity* equation:

$$\frac{\partial \rho}{\partial t} + \nabla \cdot (\rho \mathbf{v}) = 0 \quad (1.50)$$

where by definition the sum of the relative or diffusive mass fluxes vanishes:

$$\sum_{c=1}^N \mathbf{j}_c = 0 \quad (1.51)$$

and, due to the mass conservation law, the sum of the reaction rate terms is by definition zero:

$$\sum_{c=1}^N R_c = 0 \quad (1.52)$$

Again, the fundamental principles are confirmed since (1.50) equals (1.14).

### 1.2.3 Conservation of momentum

The equation of motion is examined in this section.

#### System analysis

The momentum associated with a material control volume  $V(t)$  is defined by:

$$\mathbf{P} = \int_{V(t)} \rho \mathbf{v} dv \quad (1.53)$$

The basis for any derivation of the momentum equation is the relation commonly known as *Newton's second law of motion* which in the material Lagrangian form (see Fig. 1.1B) expresses a proportionality between the applied forces and the resulting acceleration of a fluid particle with momentum density,  $\mathbf{P}$ , (e.g., [89]):

$$\frac{D\mathbf{P}}{Dt} = \frac{D}{Dt} \int_{V(t)} (\rho \mathbf{v}) dv = \mathbf{f} \quad (1.54)$$

where  $\mathbf{f}$  is the net force acting on the fluid in the control volume.

Again, the system balance can be transformed into an Eulerian control volume balance by use of the transport theorem (1.10). Hence,

$$\frac{D}{Dt} \int_{V(t)} (\rho \mathbf{v}) dv = \int_{V(t)} \left[ \frac{\partial(\rho \mathbf{v})}{\partial t} + \nabla \cdot (\rho \mathbf{v} \mathbf{v}) \right] dv = \int_{V(t)} \mathbf{F} dv \quad (1.55)$$

where  $\mathbf{F}$  is the net force per unit volume acting on the fluid within the control volume. That is,

$$\mathbf{f} = \int_{V(t)} \mathbf{F} dv \quad (1.56)$$

Preliminarily, we keep the force undefined as our main purpose in this paragraph is to show the connection between the two formulations. The physical forces will be considered shortly.

The relation (1.55) must be satisfied for any macroscopic volume  $V(t)$ , so at each point the differential momentum balance yields:

$$\frac{\partial(\rho \mathbf{v})}{\partial t} + \nabla \cdot (\rho \mathbf{v} \mathbf{v}) = \mathbf{F} \quad (1.57)$$

This is the Eulerian control volume form of the momentum conservation equation.

### Finite Eulerian control volume analysis

The mixture momentum associated with an Eulerian control volume  $V$ , at time  $t$ , is given by:

$$\mathbf{P} = \int_V (\rho \mathbf{v}) dv \quad (1.58)$$

Hence, the Eulerian (see Fig. 1.1A) momentum balance equation is written considering a fixed control volume  $V$ :

$$\begin{aligned} \frac{\partial \mathbf{P}}{\partial t} &= \left[ \frac{\partial \mathbf{P}}{\partial t} \right]_{\text{Convection}} + \mathbf{f}_{\text{Forces}} \\ &= \left[ \frac{\partial \mathbf{P}}{\partial t} \right]_{\text{Convection}} + \mathbf{f}_{\text{Body Forces}} + \mathbf{f}_{\text{Surface Forces}} \end{aligned} \quad (1.59)$$

The equation states that the momentum density  $\rho \mathbf{v}$  can only be changed by convection across the CV surface and by the applied forces per unit volume on the fluid particle. The force term consists of two groups of forces. *The body forces* are due to external fields such as gravity or an applied electro-magnetic potential and act on the entire volume of the fluid element. *The surface forces* are applied by external stresses on the surfaces of the volume element.

*The convective term* can then be formulated as a surface integral (analogous to the mass flux formulation, Fig. 1.2), and converted to a volume integral by use of Gauss' theorem (App. A):

$$\left[ \frac{\partial \mathbf{P}}{\partial t} \right]_{\text{Convection}} = - \int_A (\rho \mathbf{v} \mathbf{v}) \cdot \mathbf{n} da = - \int_V \nabla \cdot (\rho \mathbf{v} \mathbf{v}) dv \quad (1.60)$$

The last term is somewhat complicated containing a *dyadic product*,  $\mathbf{v}\mathbf{v}$ . To be able to reformulate this expression into Cartesian coordinates we have to apply rigorous mathematical algorithms.

Using the algorithm given by Bird et al [11] [13], the component form is given by:

$$\begin{aligned}\nabla \cdot (\rho\mathbf{v}\mathbf{v}) &= \sum_{i=1}^3 \mathbf{e}_i \frac{\partial}{\partial x_i} \cdot \sum_{j=1}^3 \sum_{k=1}^3 \mathbf{e}_j \mathbf{e}_k (\rho v_j v_k) = \sum_{i=1}^3 \sum_{j=1}^3 \sum_{k=1}^3 (\mathbf{e}_i \cdot \mathbf{e}_j) \mathbf{e}_k \frac{\partial}{\partial x_i} (\rho v_j v_k) \\ &= \sum_{i=1}^3 \sum_{j=1}^3 \sum_{k=1}^3 \delta_{ij} \mathbf{e}_k \frac{\partial}{\partial x_i} (\rho v_j v_k) = \sum_{k=1}^3 \mathbf{e}_k \sum_{i=1}^3 \frac{\partial}{\partial x_i} (\rho v_i v_k)\end{aligned}\tag{1.61}$$

hence the  $k$ th component of  $\nabla \cdot (\rho\mathbf{v}\mathbf{v})$  is  $[\nabla \cdot (\rho\mathbf{v}\mathbf{v})]_k = \sum_{i=1}^3 \frac{\partial}{\partial x_i} (\rho v_i v_k)$  where  $\mathbf{e}_k$  is the unit vector in the  $k$  direction. The  $\delta_{ij}$  is the *Kronecker delta* defined as:

$$\delta_{ij} = \begin{cases} 1 & \text{if } i = j, \text{ and} \\ 0 & \text{if } i \neq j. \end{cases}\tag{1.62}$$

From the geometrical definition of the vector scalar- or dot product between the unit vectors, we can write:

$$(\mathbf{e}_i \cdot \mathbf{e}_j) = \delta_{ij}\tag{1.63}$$

*The body force terms* on unit volume basis are usually formulated in terms of the body forces per unit mass (e.g., [11] [169]):

$$\mathbf{f}_{\text{Body Forces}} = \left[ \frac{\partial \mathbf{P}}{\partial t} \right]_{\text{Body Forces}} = \int_V \sum_{c=1}^N \rho_c \mathbf{g}_c dv\tag{1.64}$$

where  $\mathbf{g}_c$  is the total sum of body forces per unit mass. In this term account is taken of the fact that each chemical species present may be acted on by different body forces per unit mass. Considering the gravitational body force only,  $\mathbf{g}_c$ , becomes the vector acceleration of gravity which is the same for all species.

*The surface force terms* per unit volume basis can be formulated as a surface integral in terms of the total stress tensor  $\mathbf{T}$ , and then converted to a volume integral by use of Gauss' theorem (App. A):

$$\mathbf{f}_{\text{Surface Forces}} = \left[ \frac{\partial \mathbf{P}}{\partial t} \right]_{\text{Surface Forces}} = - \int_A \mathbf{T} \cdot \mathbf{n} da = - \int_V \nabla \cdot \mathbf{T} dv\tag{1.65}$$

Stresses are the forces tending to produce deformation in a body, measured as a force per unit area.

The total stress tensor,  $\mathbf{T}$ , is thus interpreted physically as the surface forces per surface unit acting through the infinitesimal surface on the surrounding fluid with normal unit vector  $\mathbf{n}$  directed out of the CV. This means that the total stress tensor by definition acts on the surrounding fluid. The counteracting force on the fluid element (CV) is therefore expressed in terms of the total stress tensor by introducing a minus sign in (1.65).

The physical interpretation of tensors are not always obvious. We will therefore pay some attention to the definition of such a quantity in the hope of improving our understanding.

From basic mathematics (e.g., [3]) we recall that a Cartesian vector, as the velocity  $\mathbf{v}$ , in three dimensions is a quantity with three components,  $v_x$ ,  $v_y$  and  $v_z$  or

$$\mathbf{v} = \sum_{i=1}^3 v_i \mathbf{e}_i \quad (1.66)$$

The vector  $\mathbf{v}$  is regarded as an entity, just as the physical quantity it represents is an entity. Similarly, a second order Cartesian tensor, as the stress tensor, is defined as an entity having nine components:

$$\mathbf{T} = \sum_{i=1}^3 \mathbf{T}_i \mathbf{e}_i = \sum_{i=1}^3 \sum_{j=1}^3 T_{ij} \mathbf{e}_i \mathbf{e}_j \quad (1.67)$$

Note that scalars and vectors can be looked upon as tensors of zero and first order, respectively.

To proceed formulating the momentum equation we need a relation defining the total stress tensor in terms of the known dependent variables, a *constitutive relationship*. In contrast to solids, a fluid tends to deform when subjected to a shear stress. Proper constitutive laws have therefore traditionally been obtained by establishing *the stress-strain relationships* (e.g., [11] [12] [13] [89] [184] [104]), relating the total stress tensor  $\mathbf{T}$  to the rate of deformation (sometimes called rate of strain, i.e., giving the name of this relation) of a fluid element. However, the resistance to deformation is a property of the fluid. For some fluids, *Newtonian fluids*, the viscosity is independent both of time and the rate of deformation. For *non-Newtonian fluids*, on the other hand the viscosity may be a function of the prehistory of the flow (i.e., a function both of time and the rate of deformation).

The total stress tensor (i.e., force due to the stresses per surface unit, sometimes called ‘traction’) has commonly been divided into two components; *the hydrostatic pressure*,  $p\mathbf{e}$ , and *the viscous stress*,  $\boldsymbol{\sigma}$ , tensors ([11]):

$$\mathbf{T} = p\mathbf{e} + \boldsymbol{\sigma} \quad (1.68)$$

The first term on the right hand side denotes the pressure and is well known from thermodynamics. Pressure is a type of stress that can act on a fluid at rest. For an infinitesimally small fluid element, being in a state

of local equilibrium, pressure acts equally in all directions. Characteristics such as pressure that are the same in all directions are said to be *isotropic*. Note, however, that this assumption is rigorously only justified for systems consisting of spherical molecules or at very low densities. For other systems, the pressure tensor may contain an anti-symmetric part [32]. Pressure is a scalar quantity since it is not dependent on direction, and we need just one number to describe it at any point in space and time.

The second term on the right hand side denotes the viscous stresses, which exist when there are shearing motions in the fluid. The result of this stress is a deformation of the fluid. When one portion of a fluid moves, the intermolecular forces due to internal friction tend to drag adjacent fluid molecules in the same direction. The strength of these intermolecular forces depend on the nature of the fluid, and they determine the internal energy dissipation rate in the fluid relaxing the system towards a state of global thermodynamic equilibrium. Based on physical analysis, for example considering a conceptual cube, it has been found that these viscous forces can act in any of the three Cartesian directions on any of the three faces (as indicated in Fig. 1.3). This is one of the mathematical characteristics of a tensor, thus the viscous stress is a tensor with nine components. From a microscopic point of view one can say that the pressure tensor results from the short-range interactions between the molecules of the system, whereas the viscous term contain long-range interactions in the system [32].

A lot of confusion is related to the fact that several similar, but not equal, definitions of the total stress tensor have been observed in the literature. The different definitions deviate due to the introduction of pre factors of  $-1$  and/or  $\frac{1}{2}$ . In this book the definition of Bird et al. [11] [13] is used. There are three reasons why the adopted convention is preferred. Firstly, this convention is commonly used in chemical engineering. Secondly, in heat conduction described by Fourier's law it is customary to define the heat flux to be positive in the direction of decreasing temperature, when the heat is moving in the positive space directions. Similarly, in species mass diffusion described by Fick's law the mass flux is defined as positive in the direction of decreasing concentration, when the mass is moving in the positive space directions. Therefore in a shear flow it seems natural to define the total stress tensor so that it is positive in the direction of decreasing velocity. Thus, the laws for all three transport phenomena are formulated with the same sign convention. Thirdly, when the total stress tensor is divided into two parts, a pressure contribution and a viscous contribution, both parts have the same sign. In this way, the sign convention used here is in accordance with the sign convention normally applied in thermodynamics. That is, compression is positive in both terms.

This generalized form of the so-called *deformation law* have been used for most fluids, whereas the formulation of the  $\sigma$  term contains different expressions accounting for the various properties of the fluids. Since the Newtonian formulation is the simplest, and this law is satisfied by all gases and most common fluids [184] this formulation has been implemented into the majority

of the existing Computational Fluid Dynamic (CFD) program codes. When the momentum equation appears without a specific stress law (not even divided into pressure and viscous parts), it is known as *Cauchy's equation* (e.g., [3] [104], p. 214).

The constitutive equation for a Newtonian fluid in vector form is formulated by use of sophisticated tensor analysis (e.g., [11] [93] [184] [89] [2]). The following expression for the viscous stress tensor is applied:

$$\boldsymbol{\sigma} = -\mu[\nabla\mathbf{v} + (\nabla\mathbf{v})^T] + \left(\frac{2}{3}\mu - \mu_B\right)(\nabla \cdot \mathbf{v})\mathbf{e} \quad (1.69)$$

where  $\mu_B$  is known as the bulk viscosity, dilatational viscosity or second viscosity. The bulk viscosity is identically zero (shown by kinetic theory) for low density mono atomic gases and is probably not too important in dense gases and liquids (e.g., [11]). The bulk viscosity is usually negligible in combustion processes [89]. Therefore, the parameter is set to zero for most reactor models too. The quantity:

$$\boldsymbol{\gamma} = \nabla\mathbf{v} + (\nabla\mathbf{v})^T \quad (1.70)$$

is defined as *the rate of deformation (or rate of strain)*. Note, in some sciences it is common practice to define this variable deviating from this definition by a pre factor of  $\frac{1}{2}$ .

The component form of the dyadic product,  $\nabla\mathbf{v}$ , is given by:

$$\nabla\mathbf{v} = \sum_{i=1}^3 \sum_{j=1}^3 \frac{\partial}{\partial x_i} v_j \mathbf{e}_i \mathbf{e}_j \quad (1.71)$$

*The surface force term* is then given by:

$$\begin{aligned} \mathbf{f}_{\text{Surface Forces}} &= \left[ \frac{\partial \mathbf{P}}{\partial t} \right]_{\text{Surface Forces}} = - \int_{\mathcal{V}} \nabla \cdot \boldsymbol{\tau} \, dv \\ &= - \int_{\mathcal{V}} \nabla \cdot (p\mathbf{e}) \, dv - \int_{\mathcal{V}} \nabla \cdot \boldsymbol{\sigma} \, dv \\ &= - \int_{\mathcal{V}} \nabla p \, dv - \int_{\mathcal{V}} \nabla \cdot \boldsymbol{\sigma} \, dv \\ &= - \int_{\mathcal{V}} \nabla p \, dv + \int_{\mathcal{V}} \nabla \cdot (\mu[\nabla\mathbf{v} + (\nabla\mathbf{v})^T]) \, dv \\ &\quad + \int_{\mathcal{V}} \nabla \cdot \left[ (\mu_B - \frac{2}{3}\mu)(\nabla \cdot \mathbf{v}) \right] \, dv \end{aligned} \quad (1.72)$$

Applying the tensor algorithm given by [11] [13], the component form is given by

$$\begin{aligned}
\nabla \cdot \mathbb{T} &= \sum_{i=1}^3 \mathbf{e}_i \frac{\partial}{\partial x_i} \cdot \sum_{j=1}^3 \sum_{k=1}^3 \mathbf{e}_j \mathbf{e}_k T_{jk} = \sum_{i=1}^3 \sum_{j=1}^3 \sum_{k=1}^3 (\mathbf{e}_i \cdot \mathbf{e}_j) \mathbf{e}_k \frac{\partial}{\partial x_i} T_{jk} \\
&= \sum_{i=1}^3 \sum_{j=1}^3 \sum_{k=1}^3 \delta_{ij} \mathbf{e}_k \frac{\partial}{\partial x_i} T_{jk} = \sum_{k=1}^3 \mathbf{e}_k \sum_{i=1}^3 \frac{\partial}{\partial x_i} T_{ik}
\end{aligned} \tag{1.73}$$

hence the  $j$ th component of  $\nabla \cdot \mathbb{T}$  is  $[\nabla \cdot \mathbb{T}]_j = \sum_{i=1}^3 \frac{\partial T_{ij}}{\partial x_i}$ . Note that by convenience we simply changed the index denoting the direction of the stress from  $k$  to  $j$  in the mathematical operation above.

The total stress tensor written in Cartesian tensor notation is formulated:

$$T_{ij} = p\delta_{ij} - \mu \left( \frac{\partial v_i}{\partial x_j} + \frac{\partial v_j}{\partial x_i} \right) - \left( \mu_B - \frac{2}{3}\mu \right) \frac{\partial v_k}{\partial x_k} \delta_{ij} \tag{1.74}$$

where  $T_{ij}$  is the total stress acting in the positive  $j$ th direction on a face normal to the  $i$  axis.

The total stress tensor is a symmetric tensor (i.e.,  $T_{ij} = T_{ji}$ ), and in Cartesian coordinates it can thus be written:

$$T_{ij} = \begin{pmatrix} T_{xx} & T_{yx} & T_{zx} \\ T_{xy} & T_{yy} & T_{zy} \\ T_{xz} & T_{yz} & T_{zz} \end{pmatrix} = \begin{pmatrix} T_{xx} & T_{xy} & T_{xz} \\ T_{yx} & T_{yy} & T_{yz} \\ T_{zx} & T_{zy} & T_{zz} \end{pmatrix} \tag{1.75}$$

where the rows in the array correspond to the applied force (per surface unit) in each coordinate direction. The surface forces acting in the  $x$ -direction on the faces of the Cartesian fluid element, CV, are sketched Fig. 1.3.

As before, the convention used here is that  $T_{ij}$  denotes the total stress in the  $j$  direction exerted on a plane perpendicular to the  $i$  axis. Recall that the shear stresses are related to the time rate of change of the shearing deformation of the fluid element, whereas the normal stresses are related to the time rate of change of volume of the fluid element. As a result, both shear and normal stresses depend on velocity gradients in the flow. In most viscous flows, normal stresses are much smaller than shear stresses and usually neglected. The normal stresses may however become important when the normal velocity gradients are very large.

The surface forces which act directly on the surface of the fluid element are, as mentioned earlier, due to two sources only. The pressure distribution acting on the surface, imposed by the outside fluid surrounding the fluid element, and the viscous shear and normal stresses distribution acting on the surface imposed by outside fluid tugging or pushing on the surface by means of friction [2].

Before we proceed explaining the physical mechanism of the surface stresses, attention is put on the sign convention adopted regarding the direction of the stresses on the control volume surface. Contrary to the more common sign conventions applied for the surface stresses in standard literature on fluid mechanics (e.g., [184], pp. 65-72 [185], 225-230 [2], pp. 60-66), the

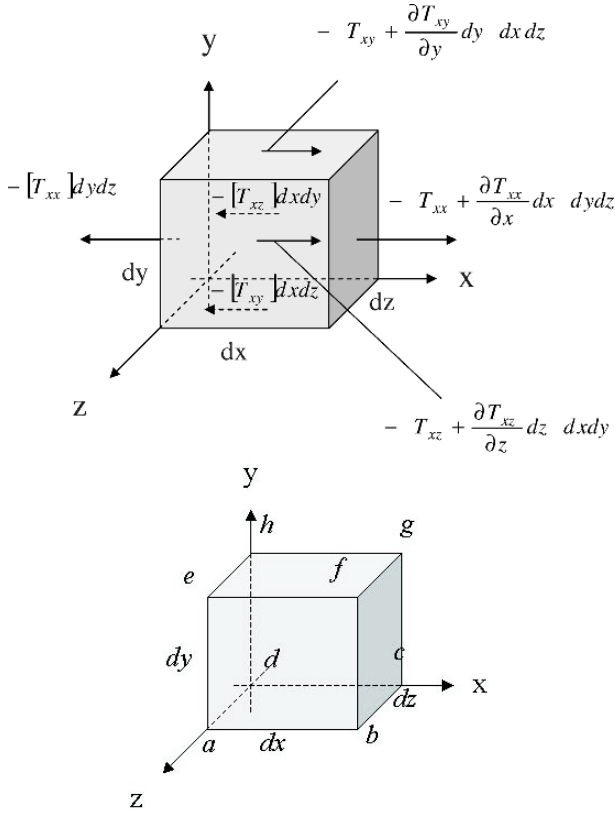


**Fig. 1.3.** A sketch of a Cartesian fixed control volume showing the surface forces acting on a moving fluid element. This Fig. is based on the illustrations of the surface forces given in the textbooks on fluid mechanics by [184], pp. 65-72 [185], 225-230 [2], pp. 60-66. However, contrary to the usual sign conventions applied in these books, the sign convention used in this book for the total stress tensor follows the approach given by Bird et al [11] [13]. Therefore, a pre factor of  $-1$  have been introduced for the forces in the Fig. Only the surface forces in the  $x$ -direction are shown.

sign convention used here for the total stress tensor follow the approach introduced by [11] [13]. Therefore, a pre factor of  $-1$  have been implemented for the total stress tensor acting on the fluid element, in contrast to the standard convention that positive stresses act on the fluid element surfaces.

By substitution of the given closures, the general form of the Eulerian conservation equation for the momentum density,  $\rho \mathbf{v}$ , can be formulated as:

$$\begin{aligned} \frac{\partial \mathbf{P}}{\partial t} &= \left[ \frac{\partial \mathbf{P}}{\partial t} \right]_{\text{Convection}} + \left[ \frac{\partial \mathbf{P}}{\partial t} \right]_{\text{Body Forces}} + \left[ \frac{\partial \mathbf{P}}{\partial t} \right]_{\text{Surface Forces}} \\ &= - \int_V \nabla \cdot (\rho \mathbf{v} \mathbf{v}) \, dv + \int_V \sum_{c=1}^N \rho_c \mathbf{g}_c \, dv - \int_V \nabla p \, dv - \int_V \nabla \cdot \boldsymbol{\sigma} \, dv \quad (1.76) \end{aligned}$$

or with a little rearranging

$$\int_V \left[ \frac{\partial(\rho\mathbf{v})}{\partial t} + \nabla \cdot (\rho\mathbf{v}\mathbf{v}) + \nabla p + \nabla \cdot \boldsymbol{\sigma} + \sum_{c=1}^N \rho_c \mathbf{g}_c \right] dv = 0 \quad (1.77)$$

Equation (1.77) must be satisfied for any macroscopic volume  $V$ , thus the expression inside the volume integral must be equal to zero. The result is known as the *momentum equation*:

$$\frac{\partial(\rho\mathbf{v})}{\partial t} = -\nabla \cdot (\rho\mathbf{v}\mathbf{v}) - \nabla p - \nabla \cdot \boldsymbol{\sigma} + \sum_{c=1}^N \rho_c \mathbf{g}_c \quad (1.78)$$

This relation coincides with (1.57) provided that the formulas for the forces are substituted into the latter one.

The physical meaning of the terms in the momentum equation (1.78) is inferred from the above modeling analysis. *The term on the LHS* denotes the rate of accumulation of momentum within the control volume per unit volume; *the first term on the RHS* denotes the net rate of momentum increase by convection per unit volume; *the second term on the RHS* denotes the pressure force acting on the control volume per unit volume; *the third term on the RHS* denotes the viscous force acting on the control volume per unit volume; and *the fourth term on the RHS* denotes the external body forces acting on the control volume per unit volume.

### **Infinitesimal Eulerian control volume stress analysis**

For somebody the physical meaning of the surface stresses might be intuitive and best explained formulating a stress balance over an infinitesimal Eulerian control volume.

Considering the surface forces in the  $x$ -direction exerted on the fluid element as sketched in Fig. 1.3, the physical mechanisms of the various stresses are described in the following.

At this point it may be informative to split the total stress tensor into two contributions, the viscous normal stresses and the pressure (note, only the net surface forces expressed in terms of the total stress tensor is indicated in the Fig. 1.3). The pressure is imposed by the outside fluid surrounding the fluid element, and is thus always defined positive acting on the fluid element. Considering the face *adhe*, which is perpendicular to the  $x$  axis, both the pressure and the viscous normal stresses act in the  $x$  - direction. The negative total stress tensor contains a negative pressure component that acts in the negative direction of the axis (to the left). The pressure negative force,  $-pdydz$ , acts in the direction out of the fluid element. Considering the face *bcbf* the negative total stress tensor contains a negative pressure component that acts in the positive direction of the axis (to the right). The negative

pressure force,  $-[p + (\partial p/\partial x)dx]dydz$ , acts in the direction out of the fluid element. The viscous stresses are defined in agreement with the convention that negative viscous stresses act in the direction of decreasing velocity ([2], pp. 60-66), and that an increase in all three components of velocity,  $v_x$ ,  $v_y$ , and  $v_z$ , occur in the positive directions of the axes. The direction of the viscous stresses acting on the *adhe* face can then be determined in the following way. When  $v_x$  increases in the positive  $x$ -direction,  $v_x$  is lower just in front of the face than on the face itself. This causes a retarding or dragging action on the fluid element, which acts in the negative  $x$ -direction (to the left). The negative total stress tensor contains a negative viscous stress component that acts in the negative  $x$ -direction,  $-\sigma_{xx}dydz$ . Considering the viscous stresses acting on the *bcgf* face,  $v_x$  still increases in the positive  $x$ -direction.  $v_x$  will now be higher just outside the face than on the face itself. This causes a tugging action (i.e., the fluid outside the CV moves outwards with a velocity higher than the CV surface velocity and the intermolecular forces due to internal friction in the fluid tend to drag adjacent fluid molecules out of the fluid element in the same direction) on the fluid element, which tries to pull the fluid element in the positive  $x$ -direction (to the right). The negative total stress tensor contains a negative viscous stress component that acts in the positive  $x$ -direction,  $-\left[\sigma_{xx} + (\partial\sigma_{xx}/\partial x)dx\right]dydz$ .

According to the conventions mentioned above,  $v_x$  increases in the positive  $y$  direction. Therefore, concentrating on face *efgh*,  $v_x$  is higher just above the face than on the face itself. This causes a tugging action on the fluid element, which tries to pull the fluid element in the positive  $x$ -direction (to the right). The negative total stress tensor contains a negative viscous stress component that acts in the positive  $x$ -direction. Face *efgh* is a distance  $dy$  above face *abcd*. The shear force in the  $x$ -direction on a face *efgh* is:  $-\left[\sigma_{yx} + (\partial\sigma_{yx}/\partial y)dy\right]dxdz$ . In turn, concentrating on face *abcd*,  $v_x$  is lower just beneath the face than on the face itself. This causes a retarding or dragging action on the fluid element, which acts in the negative  $x$ -direction (to the left). On the face *abcd* the only force in the  $x$ -direction is that due to tangential (or shear) stresses  $-\sigma_{yx}dxdz$ .

The directions of all the other stresses can be justified in a similar way.

With the above physical interpretation in mind, considering the front faces of a cubic CV, the surface force components due to the surface stresses are ([2] [184]):

$$\begin{aligned}
 f_{\text{Front Surface Force},x} &= -T_{xx}dydz - T_{yx}dxdz - T_{zx}dxdy \\
 f_{\text{Front Surface Force},y} &= -T_{xy}dydz - T_{yy}dxdz - T_{zy}dxdy \\
 f_{\text{Front Surface Force},z} &= -T_{xz}dydz - T_{yz}dxdz - T_{zz}dxdy
 \end{aligned}
 \tag{1.79}$$

For an element in equilibrium, these forces would be balanced by equal and opposite forces on the back faces of the element. If the element is accelerating, however, the front- and back- face stresses are different by differential amounts.

$$\begin{aligned}
& f_{\text{Back Surface Force},x+dx} \\
&= -[T_{xx} + \frac{\partial T_{xx}}{\partial x} dx] dy dz - [T_{yx} + \frac{\partial T_{yx}}{\partial y} dy] dx dz - [T_{zx} + \frac{\partial T_{zx}}{\partial z} dz] dx dy \\
& \\
& f_{\text{Back Surface Force},y+dy} \\
&= -[T_{xy} + \frac{\partial T_{xy}}{\partial x} dx] dy dz - [T_{yy} + \frac{\partial T_{yy}}{\partial y} dy] dx dz - [T_{zy} + \frac{\partial T_{zy}}{\partial z} dz] dx dy \\
& \\
& f_{\text{Back Surface Force},z+dz} \\
&= -[T_{xz} + \frac{\partial T_{xz}}{\partial x} dx] dy dz - [T_{yz} + \frac{\partial T_{yz}}{\partial y} dy] dx dz - [T_{zz} + \frac{\partial T_{zz}}{\partial z} dz] dx dy
\end{aligned} \tag{1.80}$$

A net surface force on the element can now be obtained using the relations derived for the forces acting on the front and back faces. That is, the leftward force on the left face is balanced by the rightward force on the right face, leaving only the net rightward force on the right face. Similar force balances can be formulated on the other four faces and for the other two axes directions, so that the net force on the control volume in each direction is due to three derivative terms:

$$\begin{aligned}
f_{\text{Surface Force},x} &= -f_{\text{Front Surface Force},x} + f_{\text{Back Surface Force},x+dx} \\
&= -\left(\frac{\partial T_{xx}}{\partial x} dx\right) dy dz - \left(\frac{\partial T_{yx}}{\partial y} dy\right) dx dz - \left(\frac{\partial T_{zx}}{\partial z} dz\right) dx dy
\end{aligned}$$

$$\begin{aligned}
f_{\text{Surface Force},y} &= -f_{\text{Front Surface Force},y} + f_{\text{Back Surface Force},y+dy} \\
&= -\left(\frac{\partial T_{xy}}{\partial x} dx\right) dy dz - \left(\frac{\partial T_{yy}}{\partial y} dy\right) dx dz - \left(\frac{\partial T_{zy}}{\partial z} dz\right) dx dy
\end{aligned}$$

$$\begin{aligned}
f_{\text{Surface Force},z} &= -f_{\text{Front Surface Force},z} + f_{\text{Back Surface Force},z+dz} \\
&= -\left(\frac{\partial T_{xz}}{\partial x} dx\right) dy dz - \left(\frac{\partial T_{yz}}{\partial y} dy\right) dx dz - \left(\frac{\partial T_{zz}}{\partial z} dz\right) dx dy
\end{aligned}$$

or, on a unit volume basis, dividing by  $dx dy dz$ , yields:

$$\begin{aligned}
F_{\text{Surface Force},x} &= -\frac{\partial T_{xx}}{\partial x} - \frac{\partial T_{yx}}{\partial y} - \frac{\partial T_{zx}}{\partial z} \\
F_{\text{Surface Force},y} &= -\frac{\partial T_{xy}}{\partial x} - \frac{\partial T_{yy}}{\partial y} - \frac{\partial T_{zy}}{\partial z} \\
F_{\text{Surface Force},z} &= -\frac{\partial T_{xz}}{\partial x} - \frac{\partial T_{yz}}{\partial y} - \frac{\partial T_{zz}}{\partial z}
\end{aligned} \tag{1.81}$$

which we note is equivalent to taking the divergence of the vector  $\mathbf{T}_k$ , the  $k$  component of the tensor  $\mathbf{T}$ .

Hence, the net surface force yields [11]:

$$\begin{aligned}
 \mathbf{F}_{\text{Surface Force},k} &= -\nabla \cdot \mathbf{T}_k = -\sum_{i=1}^3 \mathbf{e}_i \frac{\partial}{\partial x_i} \cdot \sum_{j=1}^3 T_{jk} \mathbf{e}_j = -\sum_{i=1}^3 \sum_{j=1}^3 (\mathbf{e}_i \cdot \mathbf{e}_j) \frac{\partial}{\partial x_i} T_{jk} \\
 &= -\sum_{i=1}^3 \sum_{j=1}^3 \delta_{ij} \frac{\partial T_{jk}}{\partial x_i} = -\sum_{i=1}^3 \frac{\partial T_{ik}}{\partial x_i} \quad (1.82)
 \end{aligned}$$

which is one of the total stress tensor components expressed in terms of the upper row of the total stress tensor. Note that  $\mathbf{T}_k$  denotes the tensor component  $k$  (i.e., a vector) which in Cartesian coordinates may be  $x$ ,  $y$  or  $z$ . To avoid any misunderstanding in formulating of the components of the vectors and tensors we have applied the index  $k$  denoting the direction of the stresses, instead of  $j$ .

The vector form of the momentum equation, adopted in (1.65), can now be obtained by comparing (1.82) and (1.73).

The components of the total stress tensor for Newtonian fluids in Cartesian coordinates  $(x, y, z)$  are defined as (e.g., [11] [13]):

$$T_{xx} = p + \sigma_{xx} = p - \mu \left[ 2 \frac{\partial v_x}{\partial x} - \frac{2}{3} (\nabla \cdot \mathbf{v}) \right] \quad (1.83)$$

$$T_{yy} = p + \sigma_{yy} = p - \mu \left[ 2 \frac{\partial v_y}{\partial y} - \frac{2}{3} (\nabla \cdot \mathbf{v}) \right] \quad (1.84)$$

$$T_{zz} = p + \sigma_{zz} = p - \mu \left[ 2 \frac{\partial v_z}{\partial z} - \frac{2}{3} (\nabla \cdot \mathbf{v}) \right] \quad (1.85)$$

$$T_{xy} = \sigma_{xy} = T_{yx} = \sigma_{yx} = -\mu \left[ \frac{\partial v_x}{\partial y} + \frac{\partial v_y}{\partial x} \right] \quad (1.86)$$

$$T_{yz} = \sigma_{yz} = T_{zy} = \sigma_{zy} = -\mu \left[ \frac{\partial v_y}{\partial z} + \frac{\partial v_z}{\partial y} \right] \quad (1.87)$$

$$T_{zx} = \sigma_{zx} = T_{xz} = \sigma_{xz} = -\mu \left[ \frac{\partial v_z}{\partial x} + \frac{\partial v_x}{\partial z} \right] \quad (1.88)$$

$$(\nabla \cdot \mathbf{v}) = \frac{\partial v_x}{\partial x} + \frac{\partial v_y}{\partial y} + \frac{\partial v_z}{\partial z} \quad (1.89)$$

### 1.2.4 Conservation of total energy

The balance principle, that is well known from the previous discussion, underlie any fundamental formulation of the total energy balance or conservation equation. Starting out from fluid dynamic theory the resulting partial differential equation contains unknown terms that need further consideration. We need a sound procedure for the formulation of closure laws.

Introductory it is noted that the constitutive relations we are assessing have traditionally been investigated by researchers in thermodynamics rather than fluid mechanics. This has the unfortunate consequence that the descriptions of these constitutive relations, as found in most textbooks on chemical reaction engineering, are vague as the conceptual vocabulary and nomenclature adopted in thermodynamics are not necessarily identical with the corresponding ones (i.e., if a true analogue exists at all) in fluid mechanics and visa versa. In addition, the fact that many of the thermodynamic relations adopted are developed under system restrictions very different from those under which chemical reaction engineering systems are operated investigating the rate of change of certain measurable physical quantities (e.g., species densities, temperature, pressure, mixture density, etc.), naturally makes a novice suspicious. The understanding is apparently improved as we grasp that thermodynamics is a very broad field of science that can be split into several disciplines.

However, at this point in our presentation it is obvious that we need a common language for the researchers working on the edge between the two fields of sciences (i.e., thermodynamics and fluid dynamics) to avoid any ambiguity. Therefore, to make sure that non-experts can follow the principal discussion in this paragraph, we define some basic thermodynamic concepts before we proceed describing the energy balance closures.

The word *thermodynamics*, which comes from Greek, means the power of heat [145]. The terms heat and energy are thus central to thermodynamics. Thermodynamics is a branch of science that deals with the properties of matter as related to change of temperature, where matter is anything that occupies space (including vacuum). The *state* of the system is defined by the set of values of all its primitive properties<sup>4</sup>. The succession of states through which a system passes during a change of state is called a *path*. Thermodynamics is based on a number of laws or postulates that enable the state of matter, which is affected by a vast quantity of properties, to be expressed in terms of a small number of properties. A property is defined as a quantity whose change in a process depends on the *end states* (i.e., equilibrium states) only, or alternatively, whose change in a cycle is always zero. The concept of equilibrium is fundamental to thermodynamics. *Classical thermodynamics* solely deals with states of *equilibrium*<sup>5</sup>, whereas in the context of chemical reaction engineering

---

<sup>4</sup> In thermodynamics one distinguishes between primitive properties and derived properties. A primitive property is a characteristic quantity of the system which can be determined by a test, i.e., a measurement ([145], p. 7). The outcome of the measurement is the value of the property.

<sup>5</sup> A thermodynamic system is in equilibrium when there is no change of intensive variables within the system. An equilibrium state is a state that cannot be changed without interactions with the environment. This definition includes that of mechanical equilibrium, but is a more general one. A state of thermodynamic equilibrium is a state of simultaneous chemical-, thermal-, and mechanical equilibrium. In other words, thermodynamic equilibrium is the state of the simultaneous vanishing of all fluxes ([32], p. 267). A thermodynamic system is thus

we are concerned with *non-equilibrium* situations in which momentum, heat and mass are being transferred (i.e., irreversible processes<sup>6</sup>).

Thermodynamics for non-equilibrium processes is referred to as *irreversible thermodynamics*. The scientific field of irreversible thermodynamics was established during the early 1900's<sup>7</sup>. There are three major reasons why irreversible thermodynamics is important for non-equilibrium systems. In the first place special attention is paid to the validity of the classical thermodynamic relations outside equilibrium (i.e., simple systems). In the second place the theory gives a description of the coupled transport processes (i.e., the Onsager reciprocal relations). In the third place the theory quantifies the entropy that is produced during transport. Irreversible thermodynamics can also be used to assess the second law efficiency of how valuable energy resources are exploited.

The thermodynamics of irreversible processes should be set up from the scratch as a continuum theory, treating the state parameters of the theory as field variables [32]. This is also the way in which classical fluid mechanic theory is formulated. Therefore, in the computational fluid dynamics literature, the transport phenomena and the extensions of the classical thermodynamic relations are both interpreted as closures of the fluid dynamic theory. The validity of the thermodynamic relations for fluid dynamic systems has been approached from the viewpoint of the kinetic theory of gases [13]. However, any firm distinction between irreversible thermodynamics and fluid mechanics

---

in equilibrium when the intensive (macroscopic) variables that specify the state of the system are uniform and do not change with time. This is a state at rest (static system) as the inertia terms vanish in the momentum equation at mechanical equilibrium. The mechanical equilibrium state is the condition in which the acceleration, the total derivative of the velocity vector, vanishes ([32], p. 43).

<sup>6</sup> In a reversible, cyclic process both the system and the surroundings are returned exactly to their original conditions [187]. A reversible process is thus a process during which the system is never away from equilibrium. In a reversible process there are no irreversible dissipation of energy to heat as no driving forces exists. It turns out that any reversible process is a hypothetical process, as one has failed to invent a perpetual motion machine.

On the other hand, an irreversible process is one in which, even when the system is cycled and thus returned to its original state, the surroundings is changed in a permanent way. Using a real process to do work requires that some of the energy is degraded. Velocity, temperature, and concentration gradients are always associated with losses of work, since energy is irreversibly transferred to internal energy through dissipation.

An irreversible process involves the natural movement of a system from a non-equilibrium state to an equilibrium state without intervention, thus it is a spontaneous process. Basically thermodynamics can tell us the direction in which a process will occur, but can say nothing about the speed (rate) of the process.

<sup>7</sup> Onsager might be counted as the founder of the field with his papers from in 1931 entitled *Reciprocal relations in irreversible processes*, *Phys. Rev.*, vol. 37, pp. 405-426; *Phys. Rev.*, vol. 38, pp. 2265-2279.

is difficult to define, as irreversible thermodynamics seems to overlap with transport phenomena and kinetics in many ways.

For the purpose of thermodynamic analysis one usually focus on a finite amount of matter (including vacuum), which is separated from its *surroundings*, and is called a *system* (e.g., [42] [54] [145]). In order to define a system one must specify its boundaries and describe the contents within the boundaries. Anything outside the boundary of the system is called the surroundings or the environment. A *closed* system is one in which *no* mass crosses the system boundaries. The amount of mass within the closed system is then constant, ignoring the effects of relativity and nuclear activity. An *open* system is one in which mass crosses the system boundaries. The system may gain or lose mass or simply have some mass passing through it. The selection of a suitable system for the application of the basic laws is quite flexible and is, in many cases, a complex problem. Any analysis utilizing a fundamental law must follow the designation of a specific system, and the difficulty of solution varies greatly depending on the choice made. It has been mentioned that the mobility of a fluid makes the identification of a particular system cumbersome. Thus, in fluid mechanics we normally transform the fundamental physical laws into a control volume formulation instead (i.e., in which the system may change from instant to instant), and in this way the analysis of fluid flow is greatly simplified. In particular, the non-material control-volume approaches circumvent the difficulty of system identification. Nevertheless, it might seem obvious that the fluid mechanical *control volume* has connexions to the thermodynamical *system* definitions. In general, it is convenient to imagine that an open system in thermodynamics coincides with an Eulerian control volume in fluid mechanics. In a similar manner a closed system coincides with a material Lagrangian control volume.

The concept in thermodynamics that describes what is happening to a system, is a *process*. When a change of states takes place in a system, the system is said to undergo a process. A process is completely specified by the end states, the path and the interactions that take place at the boundary.

Another important aspect of thermodynamics is the relationship between energy, heat and work. Energy describes a property that has a distinct value for each state, thus being a state function. Work and heat on the other hand are interactions and not properties. Hence, it is impossible to assign a value for work or heat to any state. Work and heat depend on the details of the process connecting to states. They can, therefore, be measured during a change of state only. The interactions called heat and work differ from one another. Work is an interaction which passes the test for equivalence of change in the level of a weight. Heat, on the other hand, does not. Heat is an interaction that may take place between two systems, each being in equilibrium but not in mutual equilibrium. The ability to have an interaction between systems in equilibrium is the main feature that distinguishes heat and work.

Thermodynamics also makes use of experimental facts. By experimental fact we mean an experiment that may be repeated many times, always

yielding the same result. Generalizations and extensions of experimental facts are known as laws or axioms. A law is formulated on the basis of all the experimental facts available without a single fact to contradict it. Of course, if we were to find even a single experimental fact that contradicts the law then we would have to modify the law or dispense with it altogether. Two such thermodynamic laws of especial importance, the first and second laws of thermodynamics, determine the main basis of modern thermodynamics. In the succeeding paragraphs we will thus convert the pertinent laws of thermodynamics from the system approach to the control volume approach (for further details, see e.g., [181], chap 6 and [114], chap 4).

To proceed supplementary knowledge of certain fundamental aspects of classical thermodynamics is required, revealing that the first law of thermodynamics leads to the law of conservation of total energy.

This field of thermodynamics was developed largely through the efforts of J. W. Gibbs during the late 1800's<sup>8</sup>. In two famous papers Gibbs was working with the mathematical transformations of energy and entropy in fluids. These transformations are subject to several constraints owing to the nature of state functions ([42], p. 173). In these studies one considers systems with no internal temperature gradients, rigid impermeable walls, and no external fields. These restrictions are said to comprise what is referred to as *simple* systems. For such simple systems the energy balance terms accounting for heat and work can be transformed from extensive properties (i.e., properties that depend on the size of the system) and expressed in terms of intensive properties (i.e., properties that do not depend on the size of the system) like density, temperature, and specific entropy. The set of thermodynamic variables used to specify the state of a fluid is referred to as state variables. As all engineering processes involve transition from one state (i.e., set of primitive property values) to another, one has to relate the state functions to each other mathematically to determine the changes in the state variables. It has been recognized that any transition calculation procedure is independent of path as long as it simply relates state properties.

The energy balance relates work, heat, and flow to the internal energy, kinetic energy, and potential energy of the closed system:

$$dE_{\text{total}} = d(E_i + E_k + E_p) = \delta Q + \delta W \quad (1.90)$$

where  $E_i$ ,  $E_k$  and  $E_p$  are the intensive internal, kinetic and potential energies of the center of mass of the system. It is seen that classical thermodynamics takes no account of the atomic structure of matter, but considers matter as a continuum. In (1.90) the symbol  $d$  indicates a differential element of a state

---

<sup>8</sup> Gibbs is counted as the founder of the field with his papers entitled 'On the equilibrium of heterogeneous substances', *Trans. Conn. Acad.*, vol. III, pp. 108-248, 1876; pp. 343-524, 1878.

function<sup>9</sup>, and the symbol  $\delta$  indicates a differential element of some quantity which is not a state function.

Eliminating all surface forces except those that cause expansion or contraction, because a simple system has no gradients or shaft work (i.e., the work of a turbine or a pump) and neglecting  $E_k$  and  $E_p$  changes by taking the system's center of mass as the frame of reference, the energy balance takes a specific simple form. The energy balance yields

$$dE_i = \delta Q + \delta W \quad (1.91)$$

This relation is recognized from introductory subjects on thermodynamics. Recall that in equilibrium thermodynamics a local formulation is generally not needed, since the intensive state variables are independent of the space coordinates. This fundamental formulation of the total energy balance is known as *the first law of thermodynamics* for a closed system, which expresses the fundamental physical principle that the total energy of the system,  $E_{\text{total}}$ , is conserved (a postulate).

Until this point we have limited our thermodynamic description to simple (closed) systems. We now extend our analysis considering an *open* system. In this case the material control volume framework might not be a convenient choice for the fluid dynamic model formulation because of the computational effort required to localize the control volume surface. The Eulerian control volume description is often a better choice for this purpose.

## System analysis

The total energy associated with a material control volume  $V(t)$  is defined by:

$$E_{\text{total}} = \int_{V(t)} \rho \left( e + \frac{1}{2} v^2 + \Phi \right) dv \quad (1.92)$$

where  $e$  is *the internal energy* per unit mass. From a microscopic point of view  $e$  represents the energy of thermal agitation as well as the energy due to the short-range molecular interactions.  $\Phi$  is *the potential energy* per unit mass, and  $\frac{1}{2}v^2$  is the *kinetic energy* per unit mass.

Note that in the derivation of the kinetic energy term we have used the scalar product of a vector with itself which is just the square of the magnitude of the vector

---

<sup>9</sup> From a thermodynamic point of view  $E_{\text{total}}$  is a state function, thus the integration of  $dE_{\text{total}}$  between two thermodynamic states gives a value which is independent of the thermodynamic path taken by the system between the two states. The situation is different when  $\delta Q$  and  $\delta W$  are integrated. The heat and work effects, which involve energy transfer, depend on the path taken between the two states, as a result of which the integrals of  $\delta Q$  and  $\delta W$  cannot be evaluated without knowledge of the path [54].

$$(\mathbf{v} \cdot \mathbf{v}) = |\mathbf{v}|^2 = v^2 \quad (1.93)$$

In the material *Lagrangian* framework the total energy balance also known as the first law of thermodynamics yields<sup>10</sup>:

$$\frac{DE_{\text{total}}}{Dt} = \dot{Q} + \dot{W} \quad (1.94)$$

where  $\dot{Q}$  and  $\dot{W}$  are energy transfer functions (i.e., not energy functions).

In the moving system, it is assumed that the heat transfer to the element,  $\delta\dot{Q}$ , is determined by the various forms of conduction and radiation across the CV surface.  $\delta\dot{W}$  denotes the work done on the fluid element due to surface forces. The potential energy term,  $\Phi$ , may be reformulated and treated as a term denoting the work done on the fluid element due to body forces. We will return to the derivation of the closure laws shortly.

Again, the system balance can be transformed into an Eulerian control volume balance by use of the transport theorem (1.10). In short, the result can be expressed as:

$$\begin{aligned} & \int_V \left[ \frac{\partial(\rho(e + \frac{1}{2}v^2 + \Phi))}{\partial t} \right. \\ & + \nabla \cdot (\rho\mathbf{v}(e + \frac{1}{2}v^2 + \Phi)) + \nabla \cdot \mathbf{q} + \nabla \cdot (p\mathbf{v}) + \nabla \cdot (\boldsymbol{\sigma} \cdot \mathbf{v}) \\ & \left. - \nabla \cdot \sum_{c=1}^N \rho_c \mathbf{v}_{c,d} \Phi_c \right] dv = 0 \end{aligned} \quad (1.95)$$

The energy balance must be satisfied for any macroscopic control volume  $V$ , so at each point the differential Eulerian energy balance can be written as:

$$\begin{aligned} & \frac{\partial(\rho(e + \frac{1}{2}v^2 + \Phi))}{\partial t} \\ & = -\nabla \cdot (\rho\mathbf{v}(e + \frac{1}{2}v^2 + \Phi)) - \nabla \cdot \mathbf{q} - \nabla \cdot (p\mathbf{v}) - \nabla \cdot (\boldsymbol{\sigma} \cdot \mathbf{v}) - \nabla \cdot \sum_{c=1}^N \rho_c \mathbf{v}_{c,d} \Phi_c \end{aligned} \quad (1.96)$$

This result is known as the *total energy equation*.

To solve the given energy equation the net energy flux  $\mathbf{q}$  has to be replaced by an appropriate multi-component heat flux closure. For single-component fluids the energy flux closure contains the familiar heat conduction- and the energy radiation fluxes. The rigorous kinetic theory of dilute gases shows that

<sup>10</sup> For a simple thermodynamic system the change in total energy,  $dE_{\text{total}}$ , is given by the differential of  $E_{\text{total}}$ , whereas for a fluid dynamic CV  $\frac{DE_{\text{total}}}{Dt}$  denotes the *substantial derivative* operator applied on the total energy variable.

for multi-component mixtures there are, in addition to the heat conduction- and thermal radiation fluxes, two additional contributions associated with the inter-diffusion of the different species in the mixture and a diffusion-thermo effect. For dilute multi-component gas mixtures Hirschfelder et al [67] and Bird et al [11] [13] proposed the following rigorous closure:

$$\mathbf{q} = \mathbf{q}^c + \mathbf{q}^d + \mathbf{q}^x + \mathbf{q}^r \quad (1.97)$$

It is well established in thermodynamics that heat flow is the result of temperature variations, i.e., a temperature gradient. This can be expressed as a proportionality between heat flux and temperature gradient, i.e., *Fourier's law*:

$$\mathbf{q}^c = -k\nabla T \quad (1.98)$$

where the  $\mathbf{q}^c$  is the *conductive heat flux* vector denoting the rate of heat flow per unit area. The flux of heat is in the direction of decreasing temperature (which accounts for the minus sign). The quantity  $k$  is a transport coefficient, i.e., the thermal conductivity, which in general has dimensions of heat per time per length per degree.

The energy flux contribution resulting from the *inter-diffusion* of the various species is denoted by  $\mathbf{q}^d$ . This energy flux is defined by:

$$\mathbf{q}^d = \sum_{c=1}^N \check{h}_c \rho_c \mathbf{v}_{c,d} = \sum_{c=1}^N \frac{\bar{h}_c}{M_{w_c}} \mathbf{j}_c \quad (1.99)$$

where  $\bar{h}_c$  is the partial molar enthalpy of species  $c$ .

A similar heat contribution is included implicitly within the  $e$  and  $h$  variables, thus occurring explicitly in the temperature equation.

However, the energy or heat flux contributions from these inter-diffusion processes are in general believed to be small and omitted in most applications (e.g., [148], p 816; [89], p 198; [11], p 566).

The *diffusion-thermal effect* or the *Dufour energy flux*  $\mathbf{q}^x$  describes the tendency of a temperature gradient under the influence of mass diffusion of chemical species. Onsager's reciprocal relations for the thermodynamics of irreversible processes imply that if temperature gives rise to diffusion velocities (the *thermal-diffusion effect* or *Soret effect*), concentration gradients must produce a heat flux. This reciprocal effect, known as the Dufour effect, provides an additional contribution to the heat flux [89].

For dilute gas mixtures we may employ the linearity postulate in irreversible thermodynamics to obtain the transport fluxes for heat and mass. The fundamental theory is examined in chap 2 and we simply refer to the expressions (2.456) and (2.457). Moreover, a particular form of the generalized Maxwell-Stefan equations, i.e., deduced from (2.298) in chap 2, is given by:

$$\mathbf{d}_r = \sum_{\substack{k=1 \\ k \neq r}}^q \frac{x_r x_k}{\bar{D}_{rk}} \left( \frac{D_k^T}{\rho_k} - \frac{D_r^T}{\rho_r} \right) \nabla \ln T + \sum_{\substack{k=1 \\ k \neq r}}^q \frac{x_r x_k}{\bar{D}_{rk}} \left( \frac{\mathbf{j}_k}{\rho_k} - \frac{\mathbf{j}_r}{\rho_r} \right), \quad r = 1, 2, 3, \dots, q \quad (1.100)$$

When the expression for  $\mathbf{d}_r$  in (1.100) is substituted into (2.456), we get:

$$\begin{aligned} \mathbf{q} - \sum_{r=1}^q \mathbf{j}_r \check{h}_r &= -\frac{1}{T} \alpha_{00} \nabla T - \sum_{r=1}^q \left( \frac{cRT D_r^T}{\rho_r} \right) \mathbf{d}_r \\ &= - \left[ \alpha_{00} + \sum_{r=1}^q \sum_{\substack{k=1 \\ k \neq r}}^q \left( \frac{cRT D_r^T}{\rho_r} \right) \frac{x_r x_k}{\tilde{D}_{rk}} \left( \frac{D_k^T}{\rho_k} - \frac{D_r^T}{\rho_r} \right) \right] \nabla \ln T \quad (1.101) \\ &\quad - \sum_{r=1}^q \sum_{\substack{k=1 \\ k \neq r}}^q \left( \frac{cRT D_r^T}{\rho_r} \right) \frac{x_r x_k}{\tilde{D}_{rk}} \left( \frac{\mathbf{j}_k}{\rho_k} - \frac{\mathbf{j}_r}{\rho_r} \right) \end{aligned}$$

It is already mentioned that the thermal conductivity of a mixture is defined to be the coefficient of proportionality between the heat flux and the temperature gradient when there are no mass fluxes in the system. Hence it follows that the quantity in brackets is the thermal conductivity  $k$  times the temperature  $T$ . The closure equation for the net heat flux thus yields:

$$\mathbf{q} = -k \nabla T + \sum_{r=1}^q \mathbf{j}_r \check{h}_r - \sum_{r=1}^q \sum_{\substack{k=1 \\ k \neq r}}^q \left( \frac{cRT D_r^T}{\rho_r} \right) \frac{x_r x_k}{\tilde{D}_{rk}} \left( \frac{\mathbf{j}_k}{\rho_k} - \frac{\mathbf{j}_r}{\rho_r} \right) \quad (1.102)$$

By comparison, we see that the Dufour term is given by:

$$\mathbf{q}^x = - \sum_{r=1}^q \sum_{\substack{k=1 \\ k \neq r}}^q \left( \frac{cRT D_r^T}{\rho_r} \right) \frac{x_r x_k}{\tilde{D}_{rk}} \left( \frac{\mathbf{j}_k}{\rho_k} - \frac{\mathbf{j}_r}{\rho_r} \right) \quad (1.103)$$

The Dufour term is usually small and can generally be neglected in reactor analysis.

The radiative heat-flux  $\mathbf{q}^r$  is generally treated separately from the other heat flux contributions because these physical phenomena are quite different in nature and involve unacquainted mathematics. Besides, the radiative contributions in the bulk of the fluid are limited because this flux is merely a surface phenomenon. Nevertheless, the radiative losses from solid surfaces are often significant in combustion and in particular chemical reactor processes. A brief introduction to the theory of thermal radiation is presented in sect 5.3.6.

In summary, the heat transport by conduction is generally important in reaction engineering applications. The thermal radiation flux is important in particular cases. The multi-component mixture specific contributions to the total energy flux are usually negligible.

## Finite Eulerian control volume analysis

The conventional *Eulerian* form of the conservation equation for total energy can be formulated<sup>11</sup>:

<sup>11</sup> Alternative presentations of the derivation of the first law of thermodynamics for open systems in the Eulerian CV framework on global scales are given by [47] [54] [42].

$$\frac{\partial E_{\text{total}}}{\partial t} = \left[ \frac{\partial E_{\text{total}}}{\partial t} \right]_{\text{Convection}} + \left[ \frac{\partial E_{\text{total}}}{\partial t} \right]_{\text{Heat}} + \left[ \frac{\partial E_{\text{total}}}{\partial t} \right]_{\text{Work}} \quad (1.104)$$

The *convective term*, denoting the net rate of total energy input per unit volume by convection can then be formulated as a surface integral, and converted to a volume integral by use of Gauss' theorem (App. A):

$$\left[ \frac{\partial E_{\text{total}}}{\partial t} \right]_{\text{Convection}} = - \int_A \left( \rho \left( e + \frac{1}{2} v^2 + \Phi \right) \mathbf{v} \right) \cdot \mathbf{n} \, da = - \int_V \nabla \cdot \left( \rho \left( e + \frac{1}{2} v^2 + \Phi \right) \mathbf{v} \right) \, dv \quad (1.105)$$

The *heat term*, denoting the net rate of total energy input per unit volume by conduction and radiation can then be formulated as a surface integral, and converted to a volume integral by use of Gauss' theorem (App. A):

$$\left[ \frac{\partial E_{\text{total}}}{\partial t} \right]_{\text{Heat}} = - \int_A (\mathbf{q} \cdot \mathbf{n}) \, da = - \int_V (\nabla \cdot \mathbf{q}) \, dv \quad (1.106)$$

The *work term*, for a multi-component mixture is commonly divided into two types, *mechanical work* and *potential work* (e.g., [32]):

$$\left[ \frac{\partial E_{\text{total}}}{\partial t} \right]_{\text{Work}} = \left[ \frac{\partial E_{\text{total}}}{\partial t} \right]_{\text{Mechanical Work}} + \left[ \frac{\partial E_{\text{total}}}{\partial t} \right]_{\text{Potential Work}} \quad (1.107)$$

The *mechanical work term*, denoting the net rate of work done on the fluid per unit volume by surface stress forces can be formulated as a surface integral, and converted to a volume integral by use of Gauss' theorem (App. A):

$$\begin{aligned} \left[ \frac{\partial E_{\text{total}}}{\partial t} \right]_{\text{Mechanical Work}} &= - \int_A [(\mathbf{T} \cdot \mathbf{v}) \cdot \mathbf{n}] \, da = - \int_V \nabla \cdot (\mathbf{T} \cdot \mathbf{v}) \, dv \\ &= - \int_V \nabla \cdot (p\mathbf{v}) \, dv - \int_V \nabla \cdot (\boldsymbol{\sigma} \cdot \mathbf{v}) \, dv \end{aligned} \quad (1.108)$$

The *potential work term*, denotes the rate at which work is done on each of the individual species  $c$  in the fluid per unit volume by *the individual species body forces*,  $\mathbf{g}_c$ , due to the diffusion of the various components in external fields such as an applied electro-magnetic potential. The term can be formulated as a surface integral, and as before converted to a volume integral by use of Gauss' theorem (App. A):

$$\left[ \frac{\partial E_{\text{total}}}{\partial t} \right]_{\text{Potential Work}} = - \int_A \left[ \left( \sum_{c=1}^N \rho_c \mathbf{v}_{c,d} \Phi_c \right) \cdot \mathbf{n} \right] \, da = - \int_V \nabla \cdot \left( \sum_{c=1}^N \rho_c \mathbf{v}_{c,d} \Phi_c \right) \, dv \quad (1.109)$$

Note that the expected contribution due to the gravity field vanishes because each species present is acted on by the same external force per unit mass,  $\mathbf{g}$ .

The general form of the Eulerian conservation equation for total energy,  $E_{\text{total}}$ , can then be formulated

$$\begin{aligned}
 \frac{\partial E_{\text{total}}}{\partial t} &= \left[ \frac{\partial E_{\text{total}}}{\partial t} \right]_{\text{Convection}} + \left[ \frac{\partial E_{\text{total}}}{\partial t} \right]_{\text{Heat}} + \left[ \frac{\partial E_{\text{total}}}{\partial t} \right]_{\text{Work}} \\
 &= - \int_V \nabla \cdot \left( \rho \left( e + \frac{1}{2} v^2 + \Phi \right) \mathbf{v} \right) dv - \int_V (\nabla \cdot \mathbf{q}) dv \\
 &\quad - \int_V \nabla \cdot (\rho \mathbf{v}) dv - \int_V \nabla \cdot (\boldsymbol{\sigma} \cdot \mathbf{v}) dv - \int_V \nabla \cdot \left( \sum_{c=1}^N \rho_c \mathbf{v}_{c,d} \Phi_c \right) dv
 \end{aligned} \tag{1.110}$$

or with a little rearranging (1.95) is obtained. Again, (1.95) must be satisfied for any macroscopic volume  $V$ , thus (1.96) is re-produced as expected.

The final form of this equation, often used in the literature, is obtained by introducing a transformation of the potential energy term,  $\Phi$ . In general, a force field is called *conservative* if it is the gradient of a scalar function.

Considering that the body forces  $\mathbf{g}_c$  are expressible in terms of the gradient of a scalar function (i.e.,  $\mathbf{g}_c = -\nabla \Phi_c$ ), then by use of the species continuity equation (1.39), we get:

$$\begin{aligned}
 &\frac{\partial(\rho\Phi)}{\partial t} + \nabla \cdot (\rho\mathbf{v}\Phi) + \nabla \cdot \sum_{c=1}^N \rho_c \mathbf{v}_{c,d} \Phi_c \\
 &= \frac{\partial}{\partial t} \left( \sum_{c=1}^N \rho_c \Phi_c \right) + \nabla \cdot \left( \sum_{c=1}^N \rho_c \mathbf{v}_c \Phi_c \right) \\
 &= \sum_{c=1}^N \rho_c \left[ \frac{\partial \Phi_c}{\partial t} + \mathbf{v}_c \cdot \nabla \Phi_c \right] + \sum_{c=1}^N \Phi_c \left[ \frac{\partial \rho_c}{\partial t} + \nabla \cdot (\rho_c \mathbf{v}_c) \right] \\
 &= \sum_{c=1}^N \rho_c \left[ \frac{\partial \Phi_c}{\partial t} - \mathbf{v}_c \cdot \mathbf{g}_c \right] + \sum_{c=1}^N \Phi_c \sum_{r=1}^q \nu_{c,r} R_r
 \end{aligned} \tag{1.111}$$

The last term vanishes if the potential energy is conserved in a chemical reaction (i.e.,  $\sum_{c=1}^N \Phi_c \nu_{c,r} = 0$ ;  $r = 1, 2, \dots, q$ ) [32]. This is the case if the property of the particles, which is responsible for the interaction with a field of force, is itself conserved. Examples for this case are the mass in a gravitational field and the charge in an electrical field.

For conservative forces, which can be derived from a potential  $\Phi$  being independent of time, the terms reduce to

$$\frac{\partial(\rho\Phi)}{\partial t} + \nabla \cdot (\rho\mathbf{v}\Phi) + \nabla \cdot \sum_{c=1}^N \rho_c \mathbf{v}_{c,d} \Phi_c = \sum_{c=1}^N \rho_c [-\mathbf{v}_c \cdot \mathbf{g}_c] = - \sum_{c=1}^N \rho_c (\mathbf{v}_c \cdot \mathbf{g}_c) \tag{1.112}$$

The term,  $-\sum_{c=1}^N \rho_c (\mathbf{v}_c \cdot \mathbf{g}_c)$ , reduces to the term applied for one component fluids,  $-\rho(\mathbf{v} \cdot \mathbf{g})$ , when  $\mathbf{g}_c$  is the same for all species. The interested reader is referred to de Groot and Mazur [32] for further discussion of these terms.

Adopting this simplified formulation (i.e., (1.112)), the total energy equation, (1.96), may be transformed to *the equation of internal- and kinetic [or mechanical] energy*

$$\frac{\partial(\rho(e + \frac{1}{2}v^2))}{\partial t} = -\nabla \cdot (\rho \mathbf{v}(e + \frac{1}{2}v^2)) - \nabla \cdot \mathbf{q} + \sum_{c=1}^N \rho_c (\mathbf{v}_c \cdot \mathbf{g}_c) - \nabla \cdot (p\mathbf{v}) - \nabla \cdot (\boldsymbol{\sigma} \cdot \mathbf{v}) \quad (1.113)$$

The physical meaning of the terms in this equation can be inferred from the above modeling analysis. *The term on the LHS* denotes the rate of accumulation of internal and kinetic energy within the control volume per unit volume; *the first term on the RHS* denotes the net rate of of internal and kinetic energy increase by convection per unit volume; *the second term on the RHS* denotes the net rate of heat addition due to heat conduction, interdiffusion effects, Dufour effects and radiation per unit volume; *the third term on the RHS* denotes the rate of work done on the fluid within the control volume by external body forces per unit volume; *the fourth term on the RHS* denotes the rate of work done on the fluid within the control volume by the pressure forces per unit volume; and *the fifth term on the RHS* denotes the rate of work done on the fluid within the control volume by the viscous forces per unit volume.

In convectational chemical reactor modeling the kinetic and potential energy terms are assumed to be negligible in comparison with the internal energy term (e.g., [47]). Therefore, only the thermal energy equation is applied in reactor models. Furthermore, the experimental studies on reaction kinetics provide empirical data and correlations which chemical engineers intend to utilize as far as possible. For numerical studies on chemical reactor performance, the heat generation due to chemical reactions should then be expressed by an explicit term in the energy equation. For real fluids this can be obtained by reformulating the equation in terms of temperature or a suitable enthalpy quantity. In the past the latter approach has seldom been used in reactor technology. Furthermore, there are two possible ways to formulate the thermal energy equation in terms of temperature. One approach is to relate the internal energy,  $e$ , to temperature by use of a constitutive relation from thermodynamics including the definition of *the specific heat capacity measured at constant volume*,  $C_V$ . In the second approach we reformulate the energy equation in terms of enthalpy,  $h$ , and thereafter relate the enthalpy to temperature by use of another constitutive relation from thermodynamics including the definition of *the specific heat capacity measured at constant pressure*,  $C_P$  (e.g., [7]). The second approach has conventionally been used in reactor technology. The heat of reaction can then be calculated from the standard heats of formation tabulated for many chemical compounds.

To proceed in our model derivation, the equation for internal energy,  $e$ , is obtained by subtracting the mechanical energy equation from the total energy equation. The first step in this mathematical exercise, is to formulate the equation for mechanical energy.

### Transport of kinetic energy

It is possible to derive the kinetic [mechanical] energy equation by forming the scalar product of the local velocity,  $\mathbf{v}$ , with the equation of motion (1.78). The result is

$$\mathbf{v} \cdot \frac{\partial(\rho\mathbf{v})}{\partial t} = -\mathbf{v} \cdot \nabla \cdot (\rho\mathbf{v}\mathbf{v}) - \mathbf{v} \cdot \nabla \cdot \mathbb{T} + \mathbf{v} \cdot \sum_{c=1}^N \rho_c \mathbf{g}_c \quad (1.114)$$

or reformulated by use of some vector and tensor algebra

$$\begin{aligned} \frac{\partial}{\partial t}(\rho\mathbf{v} \cdot \mathbf{v}) - \rho\mathbf{v} \cdot \frac{\partial\mathbf{v}}{\partial t} &= -\nabla \cdot [\rho\mathbf{v}(\mathbf{v} \cdot \mathbf{v})] + \rho\mathbf{v}\mathbf{v} : \nabla\mathbf{v} - \mathbf{v} \cdot \nabla \cdot \mathbb{T} + \mathbf{v} \cdot \sum_{c=1}^N \rho_c \mathbf{g}_c \\ &= -\nabla \cdot [\rho\mathbf{v}(\mathbf{v} \cdot \mathbf{v})] + \rho\mathbf{v} \cdot [(\mathbf{v} \cdot \nabla)\mathbf{v}] - \mathbf{v} \cdot \nabla \cdot \mathbb{T} \\ &\quad + \mathbf{v} \cdot \sum_{c=1}^N \rho_c \mathbf{g}_c \end{aligned} \quad (1.115)$$

where we have used following vector and tensor relations for the time derivative

$$\frac{\partial}{\partial t}(\rho\mathbf{v} \cdot \mathbf{v}) = \mathbf{v} \cdot \frac{\partial(\rho\mathbf{v})}{\partial t} + \rho\mathbf{v} \cdot \frac{\partial\mathbf{v}}{\partial t} \quad (1.116)$$

The vector and tensor differential operators that have been applied to the symmetrical dyad product  $\rho\mathbf{v}\mathbf{v}$  can be defined (e.g., [12], p. 574):

$$(\rho\mathbf{v}\mathbf{v} : \nabla\mathbf{v}) = \nabla \cdot [\rho\mathbf{v}\mathbf{v} \cdot \mathbf{v}] - \mathbf{v} \cdot [\nabla \cdot (\rho\mathbf{v}\mathbf{v})] \quad (1.117)$$

and the scalar product or double dot product of the two tensors occurring in this relation can be reformulated in accordance with ([12], p. 569):

$$(\mathbf{a}\mathbf{b} : \mathbf{c}\mathbf{d}) = (\mathbf{a} \cdot \mathbf{d})(\mathbf{c} \cdot \mathbf{b})$$

by setting  $\mathbf{a} = \rho\mathbf{v}$ ,  $\mathbf{b} = \mathbf{v}$ ,  $\mathbf{c} = \nabla$ ,  $\mathbf{d} = \mathbf{v}$  we obtain

$$\rho\mathbf{v}\mathbf{v} : \nabla\mathbf{v} = \rho\mathbf{v} \cdot [(\mathbf{v} \cdot \nabla)\mathbf{v}] \quad (1.118)$$

In the derivation we will also used the scalar product of a vector with itself which we recall is just the square of the magnitude of the vector

$$(\mathbf{v} \cdot \mathbf{v}) = |\mathbf{v}|^2 = v^2 \quad (1.119)$$

The scalar product of two vectors  $\mathbf{u}$  and  $\mathbf{w}$  is a scalar quantity defined by (e.g., [11] [12]):

$$(\mathbf{u} \cdot \mathbf{w}) = uw \cos \Phi_{u,w} \quad (1.120)$$

in which  $\Phi_{\mathbf{u},\mathbf{w}}$  is the angle between the vectors  $\mathbf{u}$  and  $\mathbf{w}$ . The scalar product is thus the magnitude of  $\mathbf{w}$  multiplied by the projection of  $\mathbf{u}$  on  $\mathbf{w}$ , or vice versa.

By inserting all these relations into (1.115), we can write

$$\frac{\partial}{\partial t}(\rho v^2) - \rho \mathbf{v} \cdot \left[ \frac{\partial \mathbf{v}}{\partial t} + (\mathbf{v} \cdot \nabla) \mathbf{v} \right] = -\nabla \cdot [\rho v^2 \mathbf{v}] - \mathbf{v} \cdot \nabla \cdot \mathbb{T} + \mathbf{v} \cdot \sum_{c=1}^N \rho_c \mathbf{g}_c \quad (1.121)$$

The equation of motion (1.78) will now, with a little reformulation of the terms, be reintroduced into the kinetic energy equation

$$\mathbf{v} \left[ \frac{\partial \rho}{\partial t} + \nabla \cdot (\rho \mathbf{v}) \right] + \rho \left[ \frac{\partial \mathbf{v}}{\partial t} + \mathbf{v} \cdot \nabla \mathbf{v} \right] = -\nabla \cdot \mathbb{T} + \sum_{c=1}^N \rho_c \mathbf{g}_c$$

after forming the scalar product of the local velocity with the latter equation which yields

$$\rho \mathbf{v} \cdot \left[ \frac{\partial \mathbf{v}}{\partial t} + \mathbf{v} \cdot \nabla \mathbf{v} \right] = -\mathbf{v} \cdot \nabla \cdot \mathbb{T} + \mathbf{v} \cdot \sum_{c=1}^N \rho_c \mathbf{g}_c - v^2 \left[ \frac{\partial \rho}{\partial t} + \nabla \cdot (\rho \mathbf{v}) \right] \quad (1.122)$$

the final form of the kinetic energy equation is obtained

$$\frac{\partial}{\partial t}(\rho v^2) = -\nabla \cdot [\rho v^2 \mathbf{v}] - 2\mathbf{v} \cdot \nabla \cdot \mathbb{T} + 2\mathbf{v} \cdot \sum_{c=1}^N \rho_c \mathbf{g}_c - v^2 \left[ \frac{\partial \rho}{\partial t} + \nabla \cdot (\rho \mathbf{v}) \right]$$

A minor modification is obtained multiplying the above equation by 1/2:

$$\frac{\partial}{\partial t}(\rho \frac{1}{2} v^2) = -\nabla \cdot (\rho \frac{1}{2} v^2 \mathbf{v}) - \mathbf{v} \cdot \nabla \cdot \mathbb{T} + \mathbf{v} \cdot \sum_{c=1}^N \rho_c \mathbf{g}_c - \frac{1}{2} v^2 \left[ \frac{\partial \rho}{\partial t} + \nabla \cdot (\rho \mathbf{v}) \right]$$

Moreover, by use of the continuity equation we obtain the form of the equation of change for kinetic energy which is usually given in the literature (e.g., [32]):

$$\frac{\partial}{\partial t}(\rho \frac{1}{2} v^2) = -\nabla \cdot (\rho \frac{1}{2} v^2 \mathbf{v}) - \mathbf{v} \cdot \nabla \cdot \mathbb{T} + \mathbf{v} \cdot \sum_{c=1}^N \rho_c \mathbf{g}_c \quad (1.123)$$

For convenience in subsequent discussions, we rewrite this equation in accordance with [11] splitting up the total stress tensor into two pressure and two viscous contributions.

$$\begin{aligned} \frac{\partial}{\partial t}(\rho \frac{1}{2} v^2) = & -\nabla \cdot (\rho \frac{1}{2} v^2 \mathbf{v}) - \nabla \cdot p\mathbf{v} + p(\nabla \cdot \mathbf{v}) \\ & - (\nabla \cdot [\boldsymbol{\sigma} \cdot \mathbf{v}]) + (\boldsymbol{\sigma} : \nabla \mathbf{v}) + \mathbf{v} \cdot \sum_{c=1}^N \rho_c \mathbf{g}_c \end{aligned} \quad (1.124)$$

At this point in the model derivation the physical meaning of some of these terms is not clear, but will be appreciated shortly after the internal energy equation has been investigated. Meanwhile, we proceed predicting the physical interpretations that are not obvious. *The term on the LHS* denotes the rate of accumulation of the kinetic energy within the control volume per unit volume; *the first term on the RHS* denotes the net rate of increase of kinetic energy by convection per unit volume; *the second term on the RHS* denotes the rate of work done by the pressure of the surroundings on the fluid within control volume; *the third term on the RHS* denotes the rate of reversible conversion of the kinetic energy to internal energy. As will be shown shortly, this term occurs with opposite sign in the equation for the internal energy; *the fourth term on the RHS* denotes the rate of work done by viscous forces on the fluid within the control volume; *the fifth term on the RHS* denotes the rate of irreversible conversion of kinetic energy to internal energy<sup>12</sup>.

As will be shown shortly, this term occurs with opposite sign in the internal energy equation; *the sixth term on the RHS* denotes the rate of work done by external body forces on the fluid within the control volume.

Because of the terms  $(\boldsymbol{\sigma} : \nabla \mathbf{v})$  and  $p(\nabla \cdot \mathbf{v})$ , the fluid may be heated (or cooled) internally. Hence, *an isothermal flow system* (i.e., for a system

---

<sup>12</sup> The *viscous dissipation* term  $(-\boldsymbol{\sigma} : \nabla \mathbf{v})$  is always positive for Newtonian fluids, because it can be written as a sum of quadratic terms [11]:

$$(-\boldsymbol{\sigma} : \nabla \mathbf{v}) = \mu \Phi_{\text{viscous}} = \frac{1}{2} \mu \sum_i \sum_j [(\frac{\partial v_i}{\partial x_j} + \frac{\partial v_j}{\partial x_i}) - \frac{2}{3} (\nabla \cdot \mathbf{v}) \delta_{ij}]^2 \quad (1.125)$$

in which  $i$  and  $j$  take on the values 1, 2, 3, the Cartesian coordinates  $x_i$  become  $x, y, z$  and the velocity components  $v_i$  become  $v_x, v_y, v_z$ .

The viscous dissipation function  $\Phi_{\text{viscous}}$ , i.e., which we have defined by  $\mu \Phi_{\text{viscous}} = (-\boldsymbol{\sigma} : \nabla \mathbf{v})$ , represents the rate at which the shear and deviatoric normal stresses do work on the fluid in the CV.  $\Phi_{\text{viscous}}$  may also be viewed as the rate at which the internal energy of the fluid is increased due to viscous dissipation. In accordance with irreversible thermodynamic theory this means that in all flow systems there is a degradation of mechanical to thermal energy since no real processes are reversible.

The  $(-\boldsymbol{\sigma} : \nabla \mathbf{v})$  term can cause considerable temperature rises in viscous high-speed flow systems. In chemical reactor systems, however, this term is usually very small and is generally neglected.

It is noted that an alternative definition of the dissipation function in which the viscosity parameter is included is quite common [184] [185] [181]. In this case the dissipation function coincides with the dissipation term.

operating in an adiabatic mode having no external heat fluxes through the boundaries,  $\int_{V, \text{Global}} \nabla \cdot \mathbf{q} dv = 0$ ) is a system in which the heat generated (or absorbed) through these terms does not cause appreciable temperature change.

### Transport of internal energy

Now we are in the position of being able to subtract the mechanical energy equation (1.124) from the total energy equation (1.113). The result is *the equation of internal [or thermal] energy*.

$$\frac{\partial(\rho e)}{\partial t} = -\nabla \cdot (\rho \mathbf{v} e) - \nabla \cdot \mathbf{q} - p(\nabla \cdot \mathbf{v}) - (\boldsymbol{\sigma} : \nabla \mathbf{v}) + \sum_{c=1}^N (\mathbf{j}_c \cdot \mathbf{g}_c) \quad (1.126)$$

The short-hand double dot product notation resembles (1.118) and is defined by:

$$\boldsymbol{\sigma} : \nabla \mathbf{v} = \nabla \cdot (\boldsymbol{\sigma} \cdot \mathbf{v}) - \mathbf{v} \cdot \nabla \cdot \boldsymbol{\sigma} \quad (1.127)$$

The physical meaning of the terms in the internal energy equation can be inferred from the modeling analysis above. *The term on the LHS* denotes the rate of accumulation of the internal energy within the control volume per unit volume; *the first term on the RHS* denotes the net rate of increase of internal energy by convection per unit volume; *the second term on the RHS* denotes rate of increase of internal energy by the heat flow (e.g., conduction, inter-diffusion effects, Dufour effects and radiation) per unit volume; *the third term on the RHS* denotes the *reversible* rate of increase of internal energy by compression per unit volume; *the fourth term on the RHS* denotes the *irreversible* rate of increase of internal energy by viscous dissipation per unit volume; *the fifth term on the RHS* denotes the rate of work done by the external body forces on the fluid mixture within the control volume. This term is due to species mass diffusion as the various chemical species present may be acted on by different external forces per unit mass  $\mathbf{g}_c$ . This term will thus vanish for one component systems and if the external force on all species is equal.

Comparing the mechanical energy equation (1.124) and thermal energy equation (1.126), we note that the terms  $(\boldsymbol{\sigma} : \nabla \mathbf{v})$  and  $p(\nabla \cdot \mathbf{v})$  occur in both equations. Since both terms have different signs in the two equations, they are apparently describing the inter-conversion of mechanical and thermal energy. The term  $p(\nabla \cdot \mathbf{v})$  is positive for those cases in which the fluid mixture is expanding, but negative in other situations where the fluid mixture is contracting. This term thus represents the *reversible* interchange processes. The term  $(\boldsymbol{\sigma} : \nabla \mathbf{v})$ , represents the *irreversible* degradation of mechanical energy to heat.

The absolute value of energy is not a convenient quantity for our calculations (i.e., in practice this quantity is not possible to determine for all systems

of interest), thus it is common in the study of thermodynamics to speak of energy changes relative to a appropriately chosen reference condition or a base state. Since we are focusing on the continuum scale changes in kinetic energy, potential energy, and energies of reaction, a convenient reference state chosen for determining the derived properties of any substance is *the standard state of formation* where the *elements* of the substance are in their most stable form at 25 °C and 1 bar. At this reference state the standard enthalpy of formation for the elements is conveniently taken as zero. The standard enthalpy of formation of a substance is defined as the enthalpy of that substance compared to the enthalpies of the elements from which it is formed.

In a general context (e.g., [72], p 15), the rate of change of internal energy for ideal mixtures within a control volume may consist of five components; a sensible or thermal component which accounts for the translational, rotational, and/or vibrational motion of the atoms/molecules comprising the matter; a latent component which relates to intermolecular forces influencing phase change between solid, liquid, and vapor states; a chemical component which accounts for energy stored in chemical bounds between atoms; and a nuclear component which accounts for binding forces in the nucleus. In this chap. we will not consider any phase change or nuclear processes, only the thermal - and chemical components are considered.

### The equation of internal energy in terms of enthalpy

For many engineering applications it is convenient to reformulate the equation of internal energy in terms of enthalpy or fluid temperature and heat capacity. To be able to transform the internal energy equation into a suitable form we need to apply some important thermodynamic relations which are discussed step by step in the following paragraphs.

The first step is to formulate the equation of internal energy in terms of enthalpy<sup>13</sup>. The enthalpy function is defined by (e.g., [89] [87]):

$$h = e + \frac{p}{\rho} \quad (1.128)$$

Introducing this relation into the thermal energy equation (1.126), we obtain *the enthalpy equation*

$$\frac{\partial(\rho h)}{\partial t} = -\nabla \cdot (\rho \mathbf{v} h) - \nabla \cdot \mathbf{q} + \frac{Dp}{Dt} - (\boldsymbol{\sigma} : \nabla \mathbf{v}) + \sum_{c=1}^N (\mathbf{j}_c \cdot \mathbf{g}_c) \quad (1.129)$$

---

<sup>13</sup> Enthalpy is a mathematical property defined for convenience in solving flow problems ([42], p. 48). Enthalpy is termed a convenience property because we have specifically defined it to be useful in problems where irreversible heat flow and pressure are manipulated ([42], p. 175).

The physical meaning of the terms in the enthalpy equation can be identified from the above modeling analysis. *The term on the LHS* denotes the rate of accumulation of enthalpy within the control volume per unit volume; *the first term on the RHS* denotes the net rate of increase of enthalpy by convection per unit volume; *the second term on the RHS*, that is already known from the foregoing discussion, denotes the rate of increase of enthalpy by the heat flow (e.g., conduction, inter-diffusion effects, Dufour effects and radiation) per unit volume; *the third term on the RHS* denotes the rate of work done by the pressure, which is induced by the surrounding fluid motion, acting on the mixture within the control volume per unit volume; the last two terms are already known from the foregoing discussion, nevertheless *the fourth term on the RHS* denotes the *irreversible* rate of increase of enthalpy by viscous dissipation per unit volume; *the fifth term on the RHS* denotes the rate of work done by external body forces acting on the mixture within control volume.

At this point we reiterate that the *specific enthalpy* of the mixture as defined in (1.128), also include *non-ideal mixing contributions* that should be calculated from a constitutive relation.

Two basic thermodynamic parameterizations may be formulated for the specific enthalpy. First, for real gases (i.e., for pure components or mixtures) and in principle also for liquids the specific enthalpy can be expressed in terms of enthalpies of ideal gases and residual functions (i.e.,  $h = h^* - h^{\text{residual}}$ , where the asterisk is used for ideal gas state, see e.g., [90], p. 115). The enthalpies for ideal gases are only functions of temperature and composition and can be found from the standard heats of formation or alternatively from standard heat capacities tabulated for many chemical compounds. The residual function can be found from a suitable equation of state (EOS). In reactor modeling we often assume that the gases are in an ideal gas state. For ideal gases the residual function is zero and the ideal gas law is valid. For liquids, on the other hand, the residual function becomes very large and often no suitable EOS is available. Most EOS formulations which are fitted to experimental data can in principle be applied for liquids too, but in many cases there are no experimental data available. Second, for real liquid mixtures the specific enthalpy can be expressed in terms of enthalpies of pure real fluids and excess enthalpies (i.e.,  $h = h^{\text{ideal mixture}} - h^{\text{excess}}$ , see e.g., [138], p. 400). The enthalpies for an ideal mixture is given by the mole number averaged pure component values (i.e., in some cases reformulated and given as the mass averaged component values). The excess enthalpy can be found from models for activity coefficients. The excess enthalpies (or heat of mixing) are negligible for many liquid systems. In reactor modeling we often assume that the liquid phases are ideal mixtures.

Further details on these relations are given in many textbooks on thermodynamics (e.g., [125]) and will not be repeated here. However, before we continue our derivation of the basic energy equation, the improved descriptions of the thermodynamic variables that can be embedded in single - and multiphase reactor models with limited costs are pointed out.

For low pressures (a few atmospheres and lower) we can apply the ideal gas model for gases and ideal mixture models for liquids. This formulation is very common in reactor technology. In some cases at higher pressures, the pressure effect on the gas phase is important. A suitable model for these systems is to use an EOS for the gas phase, and an ideal mixture model for liquids. However, in most situations at low pressures the liquid phase is more non-ideal than the gas phases. Then we will rather apply the ideal gas law for the gas phase, and excess properties for liquid mixtures. For polar mixtures at low to moderate pressures we may apply a suitable EOS for gas phases, and excess properties for liquid mixtures. All common models for excess properties are independent of pressure, and cannot be used at higher pressures. The pressure effect on the ideal (model part of the) mixture can be taken into account by the well known Poynting factor. At very high pressures we may apply proper EOS formulations for both gas and liquid mixtures, as the EOS formulations in principle are valid for all pressures. For non-volatile electrolytes, we have to apply a suitable EOS for gas phases and excess properties for liquid mixtures. For such liquid systems a separate term is often added in the basic model to account for the effects of ions. For very dilute solutions the Debye-Hückel law may hold. For many electrolyte systems we can apply the ideal gas law for the gas phase, as the accuracy reflected by the liquid phase models is low.

### Internal energy equation in terms of temperature

The enthalpy is an extensive thermodynamic property (i.e., a property that depends on the size or amount of the system). For an open system which can exchange mass with its surroundings we can write [87] [13]:

$$\hat{H}(T, p, M_1, M_2, M_3, \dots, M_N) = \sum_{c=1}^N M_c \left( \frac{\partial \hat{H}}{\partial M_c} \right)_{T,p,M'} = \sum_{c=1}^N M_c \check{H}_c \quad (1.130)$$

or

$$MH(T, p, \omega_1, \omega_2, \omega_3, \dots, \omega_{N-1}) = \sum_{c=1}^N M \omega_c \check{H}_c \quad (1.131)$$

in which the  $M_c$  are the masses of the various species,  $M$  is the total mass in the system given by the sum of the masses of all the species determining the system,  $M = \sum_{c=1}^N M_c$ , and the  $\omega_c = M_k/M$  are the corresponding mass fractions. Both  $\hat{H}$  and  $H$  are understood to be functions of  $T$ ,  $p$ , as well as composition. The subscript  $M'$  stands for  $M_1, M_2, \dots, M_{c-1}, M_{c+1}, \dots, M_N$ , and the subscript  $M$  stands for  $M_1, M_2, M_3, \dots, M_N$ .

The introduction of the mass fraction variable in (1.131) induces a constraint on the system:

$$\sum_{c=1}^N \omega_c = 1 \quad (1.132)$$

In this section we just keep this relation in mind and present a survey of the rather complicated mathematical derivation involved. A more rigorous model derivation is given in App. B.

The complete differential of  $\hat{H}(T, p, M_1, M_2, M_3, \dots, M_N)$  can then be expressed<sup>14</sup>:

$$d\hat{H} = \left(\frac{\partial \hat{H}}{\partial T}\right)_{p,M} dT + \left(\frac{\partial \hat{H}}{\partial p}\right)_{T,M} dp + \sum_{c=1}^N \check{H}_c dM_c \quad (1.133)$$

By use of the thermodynamic relations  $\hat{H} = MH$  and  $M_c = \omega_c M$ , we get:

$$HdM + MdH = M\left[\left(\frac{\partial H}{\partial T}\right)_{p,\omega} dT + \left(\frac{\partial H}{\partial p}\right)_{T,\omega} dp\right] + \sum_{c=1}^N [\check{H}_c \omega_c dM + \check{H}_c M d\omega_c] \quad (1.134)$$

and with the substitution of  $HdM = \sum_{c=1}^N \omega_c \check{H}_c dM$  from (1.131), the above relation can be rewritten as:

$$dH = \left(\frac{\partial H}{\partial T}\right)_{p,\omega} dT + \left(\frac{\partial H}{\partial p}\right)_{T,\omega} dp + \sum_{c=1}^N \check{H}_c d\omega_c \quad (1.135)$$

The first term on the right hand side of (1.135) can be recognized as the definition of *the specific heat at constant pressure*:

$$\left(\frac{\partial H}{\partial T}\right)_{p,\omega} = C_p \quad (1.136)$$

To formulate a proper relation for the second term we have to adopt another form of the Gibbs equation (i.e., an alternative form of (1.135)) and some of the Maxwell relations (e.g., [87]). Since  $H$  is a state variable, different pathways can be applied calculating the variation of this variable. Equivalent to expressing the state variable  $H$  in terms of  $T$ ,  $p$  and composition we can express  $H$  in terms of  $S$ ,  $p$  and composition:

$$dH = \left(\frac{\partial H}{\partial p}\right)_{S,\omega} dp + \left(\frac{\partial H}{\partial S}\right)_{p,\omega} dS + \sum_{c=1}^N \check{H}_c d\omega_c \quad (1.137)$$

By use of suitable Maxwell relations, this relation can be reformulated:

$$dH = \left(\frac{1}{\rho}\right) dp + TdS + \sum_{c=1}^N \check{H}_c d\omega_c \quad (1.138)$$

<sup>14</sup> Changes in one thermodynamic state variable can be related to changes in other state variables. The set of state functions that determines the simplest relationship between these functions is termed a *natural function*.

thus

$$\left(\frac{\partial H}{\partial p}\right)_{T,\omega} = \frac{1}{\rho} + T\left(\frac{\partial S}{\partial p}\right)_{T,\omega} \quad (1.139)$$

The second term on the right hand side of the equation is not easy to measure. By use of another of Maxwell's relations this term can be formulated in terms of density and temperature:

$$\left(\frac{\partial H}{\partial p}\right)_{T,\omega} = \frac{1}{\rho} - T\left(\frac{\partial(\frac{1}{\rho})}{\partial T}\right)_{p,\omega} \quad (1.140)$$

Introducing these relations into the first formulation (1.135) we obtain

$$dH = C_p dT + \left(\frac{1}{\rho} - T\left(\frac{\partial(\frac{1}{\rho})}{\partial T}\right)_{p,\omega}\right) dp + \sum_{c=1}^N \check{H}_c d\omega_c \quad (1.141)$$

In fluid dynamics the corresponding relation is conventionally written as a time rate of change, invoking the assumption of local instantaneous equilibrium. In particular the thermodynamic properties for a flowing fluid are assumed to be the same functions of temperature, pressure and composition as that for a fluid at equilibrium, as explained in chap 2. It follows that by use of the complete differential, the relation (1.141) can be transformed into the Lagrangian framework considering the enthalpy property on the form  $h[T(t, \mathbf{r}), p(t, \mathbf{r}), \omega_1(t, \mathbf{r}), \omega_2(t, \mathbf{r}), \omega_3(t, \mathbf{r}), \dots, \omega_N(t, \mathbf{r})]$ :

$$\frac{Dh}{Dt} = C_p \frac{DT}{Dt} + \left(\frac{1}{\rho} - T\left(\frac{\partial(\frac{1}{\rho})}{\partial T}\right)_{p,\omega}\right) \frac{Dp}{Dt} + \sum_{c=1}^N \check{h}_c \frac{D\omega_c}{Dt} \quad (1.142)$$

Substituting the equation of thermal energy (1.129) and the species mass transport equation (1.39) into the above equation yields the temperature equation<sup>15</sup>:

$$\begin{aligned} \rho C_p \frac{DT}{Dt} = & -\nabla \cdot \mathbf{q} - \frac{T}{\rho} \left(\frac{\partial \rho}{\partial T}\right)_{p,\omega} \frac{Dp}{Dt} - (\boldsymbol{\sigma} : \nabla \mathbf{v}) + \sum_{c=1}^N (\mathbf{j}_c \cdot \mathbf{g}_c) \\ & + \sum_{c=1}^N \check{h}_c \nabla \cdot \mathbf{j}_c + \sum_{c=1}^N (-\check{h}_c) R_c \end{aligned} \quad (1.143)$$

The last term in (1.143), denoting *the heat of reaction*, is seldom used in this form. The term denoting the rate of transformation can be given by:

<sup>15</sup> Recall that the relation,  $\sum_{c=1}^N \omega_c = 1$ , states that the weight fractions are linearly dependent. A rigorous model derivation, as given in App. B, may be needed to verify the given result.

There are two alternative paths available, either to formulate the complete differentiation of the enthalpy function in terms of  $N - 1$  species or in terms of  $N$  species and the constraint that  $\sum_{c=1}^N \omega_c = 1$  (e.g., [103], pp. 66-70).

$$R_c = \sum_{r=1}^q \nu_{c,r} M_{w_c} r_r \quad (1.144)$$

where  $r_r$  denotes the chemical reaction rate of reaction  $r$  per unit volume.

Considering the general homogeneous reaction:



and suppose that initially there are  $n_{A0}$  moles of  $A$ ,  $n_{B0}$  moles of  $B$ , etc. The rate of change of moles on one chemical species is related to that of any other by the stoichiometry of the reaction. Thus,

$$\frac{1}{a} \frac{dn_A}{dt} = \frac{1}{b} \frac{dn_B}{dt} = \frac{1}{c} \frac{dn_C}{dt} = \frac{1}{d} \frac{dn_D}{dt} \quad (1.145)$$

The reaction rate  $r_c$  is defined by:

$$r_c = \nu_C r = \frac{dn_C}{dt} \frac{1}{V}$$

where  $\nu_C$  is the stoichiometric coefficient of species  $c$ . If  $c$  refers to a reactant,  $\nu_C$  is negative, and for a product  $\nu_C$  is positive.

This relation shows that the rate divided by the stoichiometric coefficient is independent of the choice of reactant or product. The ratio between the reaction rate and the stoichiometric coefficient of anyone of the species can be expressed:

$$r = \frac{r_c}{\nu_C} = \frac{1}{\nu_C} \frac{dn_C}{dt} \frac{1}{V} = \frac{d\xi_r}{dt} \frac{1}{V} = \rho \frac{d\xi_r}{dt} \frac{1}{M} \quad (1.146)$$

where  $d\xi_r$  is the *extent of reaction* for reaction  $r$ .

The reaction rate quantity  $r$  is proportional with the extent of reaction and represents a useful way of maintaining consistency in reporting rate values, since  $r$  must be the same for all chemical species participating in the reaction (see [151], p. 38).

Introducing the  $r_r$  variable (i.e., characterizing the reaction rate of any reaction  $r$ ), the term in the temperature equation (1.143) denoting the heat of reaction can be reformulated:

$$-\sum_{c=1}^N \check{h}_c R_c = -\sum_{c=1}^N \check{h}_c \sum_{r=1}^q \nu_{c,r} M_{w_c} r_r = -\sum_{r=1}^q r_r \sum_{c=1}^N \check{h}_c M_{w_c} \nu_{c,r} = -\sum_{r=1}^q r_r \sum_{c=1}^N \bar{h}_c \nu_{c,r} \quad (1.147)$$

where  $M_{w_c} \cdot \check{h}_c$  is equal to the partial molar enthalpy of component  $c$ . That is, using the relation  $m_c = M_{w_c} \cdot n_c$ ,  $\check{h}_c = \left( \frac{\partial \hat{h}}{\partial m_c} \right)_{T,p,m'} = \frac{1}{M_{w_c}} \left( \frac{\partial \hat{h}}{\partial n_c} \right)_{T,p,n'} = \frac{1}{M_{w_c}} \bar{h}_c$  (see App. B).  $n_c$  is the number of moles of component  $c$  in the mixture, and  $\bar{h}_c$  is the partial molar enthalpy of component  $c$  in the mixture.

In Chemical Engineering it has become common practice to reformulate this term introducing the *the heat or reaction* quantity. The heat of reaction

is always given per mole of the species which is the basis of calculation (e.g., species  $c_{\text{ref}}$ ):

$$-\sum_{c=1}^N \bar{h}_c \nu_{c,r} = -\nu_{c_{\text{ref}},r} \sum_{c=1}^N \bar{h}_c \frac{\nu_{c,r}}{\nu_{c_{\text{ref}},r}} = \nu_{c_{\text{ref}},r} (-\Delta \bar{H}_{r,c_{\text{ref}}}) \quad (1.148)$$

thus

$$-\sum_{c=1}^N \check{h}_c R_c = -\sum_{r=1}^q r_r \sum_{c=1}^N \bar{h}_c \nu_{c,r} = \sum_{r=1}^q r_{r,c_{\text{ref}}} (-\Delta \bar{H}_{r,c_{\text{ref}}}) \quad (1.149)$$

The thermal energy equation in terms of temperature thus yields:

$$\begin{aligned} \rho C_p \frac{DT}{Dt} = & -\nabla \cdot \mathbf{q} - \frac{T}{\rho} \left( \frac{\partial \rho}{\partial T} \right)_{p,\omega} \frac{Dp}{Dt} \\ & - (\boldsymbol{\sigma} : \nabla \mathbf{v}) + \sum_{c=1}^N (\mathbf{j}_c \cdot \mathbf{g}_c) + \sum_{c=1}^N \bar{h}_c \nabla \cdot \left( \frac{\mathbf{J}_c}{M w_c} \right) + \sum_{r=1}^q r_{r,c_{\text{ref}}} (-\Delta \bar{H}_{r,c_{\text{ref}}}) \end{aligned} \quad (1.150)$$

Note that at this point the enthalpy equation is no longer formulated on conservative form.

It is important to identify the physical meaning of the terms in the temperature equation. *The term on the LHS* denotes the rate of gain of heat content per unit volume; *the first term on the RHS* denotes the rate of energy input by the heat flow (e.g., conduction and radiation) per unit volume; *the second term on the RHS* denotes the rate of work done by pressure of surroundings on the control volume per unit volume due to fluid motion; *the third term on the RHS* denotes the *irreversible* rate of internal energy increase per unit volume by viscous dissipation; *the fourth term on the RHS* denotes the rate of work done by body forces on the control volume; *the fifth term on the RHS* denotes an energy flux caused by inter-diffusion processes per unit volume<sup>16</sup>; *the sixth term on the RHS* denotes the thermal energy release by homogeneous chemical reactions per unit volume.

In the discussion above the specific enthalpies were expressed in the general form:

$$n\bar{h} = \sum_{c=1}^N n_c \bar{h}_c \quad (1.151)$$

where  $\bar{h}(T(t, \mathbf{r}), p(t, \mathbf{r}), y_1(t, \mathbf{r}), y_2(t, \mathbf{r}), y_3(t, \mathbf{r}), \dots, y_{N-1}(t, \mathbf{r}))$  is the *specific molar enthalpy* of the real mixture, and the *partial molar enthalpy* of component  $c$  in a real mixture is  $\bar{h}_c(T(t, \mathbf{r}), p(t, \mathbf{r}), y_1(t, \mathbf{r}), y_2(t, \mathbf{r}), y_3(t, \mathbf{r}), \dots,$

<sup>16</sup> This term can be reformulated by use of the vector differential operators for differentiation of products into the difference between two terms (e.g., [11], p. 567 [89], p. 198 [134], p. 225):  $\sum_{c=1}^N \check{h}_c \nabla \cdot \mathbf{j}_c = \sum_{c=1}^N \nabla \cdot (\check{h}_c \mathbf{j}_c) - \sum_{c=1}^N \mathbf{j}_c \cdot \nabla \check{h}_c$ . The first part of this term constitutes an additional component to  $\mathbf{q}$  in binary and multicomponent systems, as mentioned earlier.

$y_{N-1}(t, \mathbf{r})$ ). This formulation follows directly from the definition of the partial specific enthalpies. The partial specific enthalpies have to be derived from a differentiation of the specific enthalpies with respect to the mole number.

For an ideal mixture on the other hand, the calculations simplify considerably (e.g., [138], p. 397):

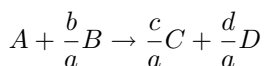
$$n\bar{h} = n\bar{h}^* = \sum_{c=1}^N n_c \bar{h}_c = \sum_{c=1}^N n_c \underline{h}_c^* \quad (1.152)$$

thus

$$\begin{aligned} \bar{h}_c &= \left( \frac{\partial \hat{h}}{\partial n_c} \right)_{T,p,n'} = \left( \frac{\partial (n\bar{h})}{\partial n_c} \right)_{T,p,n'} = \left( \frac{\partial (n\bar{h}^*)}{\partial n_c} \right)_{T,p,n'} = \left( \frac{\partial}{\partial n_c} \left( \sum_{c=1}^N n_c \underline{h}_c^* \right) \right)_{T,p,n'} \\ &= \underline{h}_c^* \end{aligned} \quad (1.153)$$

where  $\bar{h}_c(T(t, \mathbf{r}), p(t, \mathbf{r}), y_1(t, \mathbf{r}), y_2(t, \mathbf{r}), y_3(t, \mathbf{r}), \dots, y_{N-1}(t, \mathbf{r}))$  denotes the *partial molar enthalpy* quantity of component  $c$  in a mixture, whereas the  $\underline{h}_c^*(T(t, \mathbf{r}), p(t, \mathbf{r}))$ -quantity is *the molar enthalpy* of component  $c$  in an ideal mixture. We thus notice from the above derivation that for an ideal mixture yields  $\bar{h}_c(T(t, \mathbf{r}), p(t, \mathbf{r}), y_1(t, \mathbf{r}), y_2(t, \mathbf{r}), y_3(t, \mathbf{r}), \dots, y_{N-1}(t, \mathbf{r})) = \underline{h}_c^*(T(t, \mathbf{r}), p(t, \mathbf{r})) = \bar{h}_c(T(t, \mathbf{r}), p(t, \mathbf{r}))$ . Moreover, the subscript  $n'$  stands for  $n_1, \dots, n_{c-1}, n_{c+1}, \dots, n_N$ , and the subscript  $n$  stands for  $n_1, n_2, n_3, \dots, n_N$ .

To illustrate the manipulation needed to get the above equation into the form used in practice, following the approach given by [47] and [64], pp. 259 and 273), we shall use the generalized reaction with species  $A$  as basis:



The heat of reaction is defined as (e.g., species  $A$  is chosen as basis (joules per mole of  $A$  reacted)):

$$\Delta H_{r_A}^* = \frac{c}{a} \underline{h}_C^* + \frac{d}{a} \underline{h}_D^* - \frac{b}{a} \underline{h}_B^* - \underline{h}_A^* \quad (1.154)$$

and the relation to (1.143) is given by:

$$\sum_{c=1}^N (-\check{h}_c) R_c = r_A (-\Delta H_{r_A}^*) \quad (1.155)$$

For an ideal gas the enthalpy is independent of  $p$  at a given  $T$  (as can be verified by use of (1.140)). The heat of reaction at a particular temperature and pressure is thus expressed in terms of the enthalpy of formation at the reference temperature plus the change in enthalpy that results when the temperature is raised from the reference temperature to another temperature

$$\Delta \underline{H}_c^*(T) = \Delta \underline{H}_{f,c}^*(T_{\text{ref}}) + \int_{T_{\text{ref}}}^T \Delta \underline{C}_{p,c}^*(T) dT \quad (1.156)$$

where  $\Delta \underline{H}_{f,c}^*(T_{\text{ref}})$  is the *molar heat of formation* of species  $c$ .

As an aside, a possible alternative to the classical reactor modeling approach which consist in solving the temperature equation, is to use the enthalpy equation (1.129) in combination with the enthalpy-temperature relation (1.141). It is generally assumed that the enthalpy for a flowing fluid is the same function of temperature, pressure and composition as that for a fluid at equilibrium. Hence it follows that the two model formulations (1.141) and (1.142) are formally equivalent. As mentioned earlier, the transformation of the thermodynamic relation can be achieved using the total or complete differential for each independent operator at the time (i.e., illustrated using Cartesian coordinates):

$$\frac{\partial h}{\partial t} = \left(\frac{\partial h}{\partial T}\right)_{p,\omega} \frac{\partial T}{\partial t} + \left(\frac{\partial h}{\partial p}\right)_{T,\omega} \frac{\partial p}{\partial t} + \sum_{c=1}^{N-1} \left(\frac{\partial h}{\partial \omega_c}\right)_{p,T,\omega'} \frac{\partial \omega_c}{\partial t} \quad (1.157)$$

$$\frac{\partial h}{\partial x} = \left(\frac{\partial h}{\partial T}\right)_{p,\omega} \frac{\partial T}{\partial x} + \left(\frac{\partial h}{\partial p}\right)_{T,\omega} \frac{\partial p}{\partial x} + \sum_{c=1}^{N-1} \left(\frac{\partial h}{\partial \omega_c}\right)_{p,T,\omega'} \frac{\partial \omega_c}{\partial x} \quad (1.158)$$

$$\frac{\partial h}{\partial y} = \left(\frac{\partial h}{\partial T}\right)_{p,\omega} \frac{\partial T}{\partial y} + \left(\frac{\partial h}{\partial p}\right)_{T,\omega} \frac{\partial p}{\partial y} + \sum_{c=1}^{N-1} \left(\frac{\partial h}{\partial \omega_c}\right)_{p,T,\omega'} \frac{\partial \omega_c}{\partial y} \quad (1.159)$$

$$\frac{\partial h}{\partial z} = \left(\frac{\partial h}{\partial T}\right)_{p,\omega} \frac{\partial T}{\partial z} + \left(\frac{\partial h}{\partial p}\right)_{T,\omega} \frac{\partial p}{\partial z} + \sum_{c=1}^{N-1} \left(\frac{\partial h}{\partial \omega_c}\right)_{p,T,\omega'} \frac{\partial \omega_c}{\partial z} \quad (1.160)$$

or alternatively in vector form:

$$\begin{aligned} \frac{\partial h}{\partial t} + \mathbf{v} \cdot \nabla h &= \left(\frac{\partial h}{\partial T}\right)_{p,\omega} \frac{\partial T}{\partial t} + \left(\frac{\partial h}{\partial p}\right)_{T,\omega} \frac{\partial p}{\partial t} + \sum_{c=1}^{N-1} \left(\frac{\partial h}{\partial \omega_c}\right)_{p,T,\omega'} \frac{\partial \omega_c}{\partial t} \\ &+ \mathbf{v} \cdot \left[ \left(\frac{\partial h}{\partial T}\right)_{p,\omega} \nabla T \right] + \mathbf{v} \cdot \left[ \left(\frac{\partial h}{\partial p}\right)_{T,\omega} \nabla p \right] \\ &+ \mathbf{v} \cdot \left[ \sum_{c=1}^{N-1} \left(\frac{\partial h}{\partial \omega_c}\right)_{p,T,\omega'} \nabla \omega_c \right] \\ &= \left(\frac{\partial h}{\partial T}\right)_{p,\omega} \frac{\partial T}{\partial t} + \left(\frac{\partial h}{\partial p}\right)_{T,\omega} \frac{\partial p}{\partial t} + \sum_{c=1}^{N-1} \left(\frac{\partial h}{\partial \omega_c}\right)_{p,T,\omega'} \frac{\partial \omega_c}{\partial t} \\ &+ \left(\frac{\partial h}{\partial T}\right)_{p,\omega} \mathbf{v} \cdot \nabla T + \left(\frac{\partial h}{\partial p}\right)_{T,\omega} \mathbf{v} \cdot \nabla p + \sum_{c=1}^{N-1} \left(\frac{\partial h}{\partial \omega_c}\right)_{p,T,\omega'} \mathbf{v} \cdot \nabla \omega_c \end{aligned}$$

$$\begin{aligned}
&= \left(\frac{\partial h}{\partial T}\right)_{p,\omega} \frac{DT}{Dt} + \left(\frac{\partial h}{\partial p}\right)_{T,\omega} \frac{Dp}{Dt} + \sum_{c=1}^{N-1} \left(\frac{\partial h}{\partial \omega_c}\right)_{p,T,\omega'} \frac{D\omega_c}{Dt} \\
&= C_P \frac{DT}{Dt} + \left(\frac{1}{\rho} - T \left(\frac{\partial(\frac{1}{\rho})}{\partial T}\right)_{p,\omega}\right) \frac{Dp}{Dt} + \sum_{c=1}^{N-1} \left(\frac{\partial h}{\partial \omega_c}\right)_{p,T,\omega'} \frac{D\omega_c}{Dt}
\end{aligned} \tag{1.161}$$

The alternative procedure has the advantage of enabling the solution of an equation on the flux form, whereas the temperature equation is formulated on the advective form. Moreover, the enthalpy quantity is often representing a well behaved smooth function whereas the temperature variable might oscillate and represent steep gradients. However, the method has the drawback that in many cases the enthalpy variable has to be converted into temperature at a sufficient number of discretization points and for every time step in the solution process, since the boundary conditions used are normally expressed in terms of temperature. Besides, the transformation formulas for non-ideal reactive flow systems can be rather complex.

### Transport of entropy

From the formal macroscopic statement of *the second law of thermodynamics*, as developed from classical thermodynamics arguments, it is difficult to assign a physical significance to entropy. Ultimately, you must reassure yourself that entropy is defined mathematically, and like enthalpy, can be used to solve problems even though our physical connexion with the property is occasionally less than satisfying.

Historically, the concept of entropy as a state function was first introduced on macroscopic scales as a means of tracking transformations of heat into work in the context of heat engine design<sup>17</sup> [54]. On microscopic scales entropy has been interpreted as a measure of the molecular disorder of the system. Its value is related to the number of microscopic states available at a particular macroscopic state. From this point of view it is possible to appreciate the manner in which generation of disorder results in lost work (e.g., [42], chap. 3). The natural progression of real processes is from order to disorder, from lower entropy to higher entropy. Entropy is thus closely associated with probability. Nature spontaneously proceeds toward the states that have the highest probabilities of existing. We can conclude that the driving force for a spontaneous process is an increase in the entropy of the universe.

In irreversible thermodynamics entropy was introduced and discussed as a result of a need for quantification of the degree of irreversibility of a process. The theory thus explain the way in which the generation of disorder reflected by entropy change results in conversion of potentially useful work energy into practically useless thermal energy. In this discipline of thermodynamics the continuum balance equation for entropy plays a central role [32]. This equation expresses the fact that the entropy of a volume element changes with time for

<sup>17</sup> A heat engine is a device which converts heat into work.

two reasons. First it changes because entropy flows into the control volume, second because there is an entropy source due to irreversible phenomena inside the control volume. The entropy source is always a non-negative quantity, since entropy can only be created, never destroyed. For reversible transformation the entropy source vanishes.

To reduce the lost work in industrial process plants, the minimization of entropy production rates in process equipment is suggested as a strategy for future process design and optimization [81]. The method is based on the hypothesis that *the state of operation that has a minimum total entropy production is characterized by equipartition of the local entropy production*. In this context we need to quantify the entropy sources of the various irreversible unit operations that occur in the industrial system.

In fluid dynamics there is no specific use of the transport equation for entropy other than being a physical condition indicating whether a constitutive relation proposed has a sound physical basis or not (nevertheless, this may be a constraint of great importance in many situations). In this connexion we usually think of *the second law of thermodynamics* as providing an inequality, expressing the observation that irreversible phenomena lead to entropy production.

However, even though the application of the entropy equation in chemical reaction engineering is limited today, the understanding and physical interpretations of terms in the equation may be important in future process design and optimization<sup>18</sup>.

I view of the above evaluation, the formulation of the transport equation for entropy is outlined in the following paragraphs. If for no other reason, it is always advantageous to be a qualified debater governing the future direction of useful research.

By combining the total energy balance with simple thermodynamic relations between state variables, a transport equation that must be satisfied by the entropy density field  $\rho s$  is obtained.

At this point, the simplest way to formulate this equation is to reformulate the thermal energy equation written in terms of internal energy (i.e., (1.126)) or enthalpy (i.e., (1.129)) by use of the following thermodynamic relations (e.g., [7] [134] [32]):

---

<sup>18</sup> Kjelstrup and Bedeaux [81] speculate that the need in mechanical and chemical engineering for more accurate modeling tools to enable process equipment designs that waste less work will increase the use of irreversible thermodynamics in the near future. Better and more efficient use of energy resources is also a central future requirement. It may then no longer be sufficient to optimize the first law efficiency solely. The second law may have to be taken into account as well. Under future UN environmental protection conventions and protocols the process industry may be forced to report on their annual entropy production. As a political tool, economical benefits could also be given to those industries that limit or reduce their entropy production.

$$TdS = dE + pd\left(\frac{1}{\rho}\right) - \sum_{c=1}^N \mu_c d\omega_c \quad (1.162)$$

where  $S = S(E, \rho, \omega_c)$  or

$$TdS = dH - \left(\frac{1}{\rho}\right)dp - \sum_{c=1}^N \mu_c d\omega_c \quad (1.163)$$

where  $S = S(H, p, \omega_c)$ ,  $p$  is the equilibrium pressure, the functions  $\mu_c$  is the specific chemical potential of component  $c$ .

The specific chemical potentials refer to one unit of mass of the component concerned, and is defined by:

$$\mu_c = \left(\frac{\partial(\rho e)}{\partial M_c}\right)_{S,V,M'} \quad \text{for } (c = 1, 2, 3, \dots, N) \quad (1.164)$$

It is then assumed that, although the total system is not in equilibrium, there exists within small mass elements a state of local equilibrium, for which the local entropy is the same function of  $E$ ,  $\rho$  and  $\omega_c$  (or  $H$ ,  $p$  and  $\omega_c$ ) as in real equilibrium for a fluid parcel. In particular we assume that the above formulas remains valid written as a time rate of change for a mass element as described earlier.

The continuum mechanical analogues of the fundamental thermodynamic relations are written as:

$$T \frac{Ds}{Dt} = \frac{De}{Dt} + p \frac{D\left(\frac{1}{\rho}\right)}{Dt} - \sum_{c=1}^N \mu_c \frac{D\omega_c}{Dt} \quad (1.165)$$

or after introducing the enthalpy quantity (1.128):

$$T \frac{Ds}{Dt} = \frac{Dh}{Dt} - \frac{1}{\rho} \frac{Dp}{Dt} - \sum_{c=1}^N \mu_c \frac{D\omega_c}{Dt} \quad (1.166)$$

Note that the hypothesis of local equilibrium can only be justified by virtue of the validity of the conclusions derived from it.

Invoking these expressions and the transport equation for the species mass balance into the corresponding formulations of the thermal energy equation results in an explicit transport equation for the entropy density.

$$\begin{aligned} \rho \frac{Ds}{Dt} = & -\frac{1}{T} \nabla \cdot \mathbf{q} - \frac{1}{T} (\boldsymbol{\sigma} : \nabla \mathbf{v}) + \frac{1}{T} \sum_{c=1}^N (\mathbf{j}_c \cdot \mathbf{g}_c) + \frac{1}{T} \sum_{c=1}^N \mu_c \omega_c \left( \frac{\partial \rho}{\partial t} + \nabla \cdot (\rho \mathbf{v}) \right) \\ & + \frac{1}{T} \sum_{c=1}^N \mu_c \nabla \cdot \mathbf{j}_c - \frac{1}{T} \sum_{c=1}^N \mu_c R_c \end{aligned} \quad (1.167)$$

By use of the continuity equation the fourth term on the right hand side vanishes. The term is retained in the equation for convenience of the multi-phase analysis discussed in chap 3.3.

The last term in the equation above can be reformulated in terms of the chemical affinities as follows

$$-\frac{1}{T} \sum_{c=1}^N \mu_c R_c = -\frac{1}{T} \sum_{c=1}^N \mu_c \sum_{r=1}^q \nu_{c,r} r_r M_{w_c} = -\frac{1}{T} \sum_{r=1}^q r_r \sum_{c=1}^N \nu_{c,r} M_{w_c} \mu_c = \frac{1}{T} \sum_{r=1}^q r_r A_r \quad (1.168)$$

The chemical affinities of the reactions  $r$  ( $= 1, \dots, q$ ) are defined by

$$A_r = - \sum_{c=1}^N \nu_{c,r} M_{w_c} \mu_c, \quad (r = 1, \dots, q) \quad (1.169)$$

In irreversible thermodynamics the affinities act as the driving forces of the reactions [87].

We can then reformulate the entropy equation into the general form of a transport equation, which yields

$$\begin{aligned} \rho \frac{Ds}{Dt} = & -\nabla \cdot \left( \frac{\mathbf{q} - \sum_{c=1}^N \mu_c \mathbf{j}_c}{T} \right) - \frac{1}{T^2} (\mathbf{q} \cdot \nabla T) + \frac{1}{T} \sum_{c=1}^N \mu_c \omega_c \left( \frac{\partial \rho}{\partial t} + \nabla \cdot (\rho \mathbf{v}) \right) \\ & - \frac{1}{T} \sum_{c=1}^N \mathbf{j}_c \cdot \left( T \nabla \left( \frac{\mu_c}{T} \right) - \mathbf{g}_c \right) - \frac{1}{T} (\boldsymbol{\sigma} : \nabla \mathbf{v}) + \frac{1}{T} \sum_{r=1}^q A_r r_r \end{aligned} \quad (1.170)$$

The entropy flux,  $\mathbf{J}_s$ , and the entropy production,  $\Phi_{\text{total}}$ , are given by

$$\mathbf{J}_s = \frac{\mathbf{q} - \sum_{c=1}^N \mu_c \mathbf{j}_c}{T} \quad (1.171)$$

$$\begin{aligned} \Phi_{\text{total}} = & -\frac{1}{T^2} (\mathbf{q} \cdot \nabla T) + \frac{1}{T} \sum_{c=1}^N \mu_c \omega_c \left( \frac{\partial \rho}{\partial t} + \nabla \cdot (\rho \mathbf{v}) \right) - \frac{1}{T} \sum_{c=1}^N \mathbf{j}_c \cdot \left( T \nabla \left( \frac{\mu_c}{T} \right) - \mathbf{g}_c \right) \\ & - \frac{1}{T} (\boldsymbol{\sigma} : \nabla \mathbf{v}) + \frac{1}{T} \sum_{r=1}^q A_r r_r \end{aligned} \quad (1.172)$$

The entropy equation can now be used to express the Clausius' form of the second law of thermodynamics for open flow systems (e.g., [7] [145], p. 126). The inequality expresses that irreversible phenomena (diffusive momentum

transfer, energy transfer, mass transfer, and chemical reactions) lead to entropy production (i.e., energy dissipation)

$$\Phi_{\text{total}} \geq 0 \quad (1.173)$$

The way in which the separation of the terms of the right hand side of the entropy equation into the divergence of a flux and a source term has been achieved may at first sight seem to be to some extent arbitrary. The two groups of terms must, however, satisfy a number of requirements which determine this separation uniquely. First, one such requirement is that the entropy source term  $\Phi_{\text{total}}$  must be zero if the thermodynamic equilibrium conditions are satisfied within the system. Another requirement the source term must satisfy is that it should be invariant under a Galilean transformation (e.g., [147]), since the notations of reversible and irreversible behavior must be invariant under such a transformation. The terms included in the source term satisfy this requirement [32].

The physical meaning of the terms (or group of terms) in the entropy equation is not always obvious. However, *the term on the LHS* denotes the rate of accumulation of entropy within the control volume per unit volume. On the RHS the entropy flow terms included in  $\mathbf{J}_s$  show that for open systems the entropy flow consists of two parts: one is the reduced heat flow  $\frac{\mathbf{q}}{T}$ , the other is connected with the diffusion flows of matter  $\mathbf{j}_c$ ; Secondly, the entropy production terms included in  $\Phi_{\text{total}}$  demonstrates that the entropy production contains four different contributions. (*The third term on the RHS* vanishes by use of the continuity equation, but retained for the purpose of indicating possible contributions from the interfacial mass transfer in multiphase flows, discussed later). The first term in  $\Phi_{\text{total}}$  arises from heat fluxes as conduction and radiation, the third from diffusion, the fourth is connected to the gradients of the velocity field, giving rise to viscous flow, and the fifth is due to chemical reactions.

The structure of the expression for  $\Phi_{\text{total}}$  is that of a bilinear form: it consists of a sum of products of two factors. One of these factors in each term is a flow quantity (heat flux  $\mathbf{q}$ , mass diffusion flux  $\mathbf{j}_c$ , momentum flux expressed by the viscous stress tensor  $\boldsymbol{\sigma}$ , and chemical reaction rate  $r_r$ ). The other factor in each term is related to a gradient of an intensive state variable (gradients of temperature, chemical potential and velocity) and may contain the external force  $\mathbf{g}_c$  or a difference of thermodynamic state variables, viz. the chemical affinity  $A_r$ . These quantities which multiply the fluxes in the expression for the entropy production are called *thermodynamic forces* or *affinities*.

Even if the entropy equation formulated in this section is not independent of the other energy equations, the solution of this equation can provide some useful information.

- The second law of thermodynamics set important constraints on apparently possible physiochemical processes as for example minimum work to

separate a mixture, maximum possible efficiency of various unit operations often applied in chemical engineering and minimum electrical energy needed for production of various metals via electrolysis.

- This law may also provide a basis for process optimization analysis of engineering devices involving simultaneous transport phenomena and chemical reactions by use of *the principle of minimum entropy production*.
- The thermodynamic inequality may also guide the selection of *general constitutive laws* governing the diffusion of momentum, energy, and species mass in non-equilibrium chemical reacting mixtures.

### Remarks on the governing equations

- We have shown that all the balance laws for Eulerian CVs can be cast in the same standard form, applicable in any coordinate system. The coordinate system is chosen to proceed with the solution for the problem in question in a convenient way.
- Not all of the balance equations are independent of one another, thus the set of equation used to solve particular problems is not solely a matter of convenience. In chemical reactor modeling it is important to recall that all chemical species mass balance equations or all chemical element conservation equations are not independent of the total mass conservation equation. In a similar manner, the angular momentum and linear momentum constraints are not independent for flow of a simple fluid<sup>19</sup>.

On a microscopic scale perspective the angular momentum equation is an independent law [119]. In continuum mechanics the linear momentum equation may be used to derive the angular momentum equation and they are thus not independent. This statement is based on one condition. If the angular momentum of the microscopic particles is randomly oriented, then the vector sum for a large number of particles is zero. On the other hand, if we imagine that the microscopic particles have their axes of rotation aligned in a special direction, then the summation will give a net angular momentum on the continuum level. If this were the case, we would need to postulate a surface couple in addition to the surface force. Fortunately, in common fluids the microscopic angular momentum is randomly oriented and the couple does not exist. When this is true, we are able to show that the total stress tensor  $T_{ij}$  is symmetric. First we derive the angular momentum equation including a term for microscopic angular momentum. Then we shall show that the existence of a net microscopic angular momentum implies that the stress tensor is anti-symmetric. Conversely, if the net microscopic angular momentum vanishes, then the stress tensor is symmetric and the angular momentum equation is identical with the moment of the linear momentum equation.

<sup>19</sup> A *simple fluid* is defined as a fluid that can be described by a linear velocity law, a linear conduction law, and a state fixed by two thermodynamic variables [168].

For a system the angular momentum conservation law is stated as follows: *The rate of change of the angular momentum of a material volume  $V(t)$  is equal to the sum of the torques.* Let the vector  $r_j$  be the position of a point on the Lagrangian control volume surface with respect to a fixed origin. The relevant terms are formulated as follows [119] [134] [13]:

Angular momentum of material in element  $dv$  about origin:  $\mathbf{r} \times (\rho \mathbf{v}) dv$   
or  $\rho \epsilon_{ijk} r_j v_k dv$

Torque of body force about origin:  $\sum_{c=1}^N \mathbf{r} \times \rho_c \mathbf{g}_c dv$  or  $\sum_{c=1}^N \epsilon_{ijk} r_j \rho_c g_{k,c} dv$

Torque of surface force about origin:  $\mathbf{r} \times (\mathbf{T} \cdot \mathbf{n}) da$  or  $\epsilon_{ijk} r_j n_p T_{pk} da$

Net microscopic angular momentum:  $\mathbf{n} \cdot \boldsymbol{\Omega} da$  or  $n_k \Omega_{ki} da$

where the alternating unit tensor or *the permutation symbol*,  $\epsilon_{ijk} = (1/2)(i-j)(j-k)(k-i)$ , is defined as:

$$\epsilon_{ijk} = \begin{cases} +1 & \text{if } ijk = 123, 231, \text{ or } 312, \\ -1 & \text{if } ijk = 321, 132, \text{ or } 213, \text{ and} \\ 0 & \text{if any two indices are alike.} \end{cases} \quad (1.174)$$

Following Panton [119], in the last term an angular momentum tensor  $\Omega_{ki}$  is postulated, giving the transport of  $i$ -direction angular momentum across a  $k$ -direction plane by microscopic processes.

The angular momentum law then takes the following form:

$$\frac{D}{Dt} \int_V \rho \epsilon_{ijk} r_j v_k dv = \sum_{c=1}^N \int_V \epsilon_{ijk} r_j \rho_c g_{k,c} dv + \int_A [\epsilon_{ijk} r_j n_p T_{pk} + n_k \Omega_{ki}] da \quad (1.175)$$

The left side is converted using Leibnitz's and Gauss's theorems, while the last integral on the right-hand side is changed to a volume integral by Gauss's theorem. Since the region of integration is arbitrary, the integrands must be equal:

$$\begin{aligned} \epsilon_{ijk} \frac{\partial}{\partial t} (\rho r_j v_k) + \epsilon_{ijk} \frac{\partial}{\partial x_p} (v_p \rho r_j v_k) &= \epsilon_{ijk} \frac{\partial}{\partial x_p} (r_j T_{pk}) + \frac{\partial \Omega_{ki}}{\partial x_k} \\ &+ \sum_{c=1}^N \epsilon_{ijk} r_j \rho_c g_{k,c} \end{aligned} \quad (1.176)$$

The equation for the position vector  $r_i = x_i$  is independent of time, and its space derivative is  $\frac{\partial r_j}{\partial x_i} = \delta_{ij}$ . Using these facts, the equation above may be rearranged to:

$$\epsilon_{ijk} r_j \left[ \frac{\partial}{\partial t} (\rho v_k) + \frac{\partial}{\partial x_p} (\rho v_p v_k) - \sum_{c=1}^N \rho_c g_{k,c} - \frac{\partial T_{pk}}{\partial x_p} \right] = \epsilon_{ijk} T_{jk} + \frac{\partial \Omega_{ki}}{\partial x_k} \quad (1.177)$$

The term in brackets is the linear momentum equation and is equal to zero. The term  $\epsilon_{ijk} T_{jk}$  depends only on the anti-symmetric part of  $T_{jk}$ .

Thus, we have

$$-\epsilon_{ijk}T_{jk} = \frac{\partial\Omega_{ki}}{\partial x_k} \quad (1.178)$$

If we assume that the net microscopic flux of angular momentum,  $\Omega_{ki}$ , is zero, then  $\epsilon_{ijk}T_{jk}$  is zero and we have proved that  $T_{jk}$  is symmetric (see, e.g., [104], p 215; [11], p 114; [185], sect 4.4; [181], app C; [134], sect 2.2.2). Furthermore, a second consequence of this assumption is that the angular momentum equation is exactly equal to  $\mathbf{r} \times$  the linear momentum equation. In fluid mechanics the net microscopic flux of angular momentum is usually ignored, thus the the linear- and angular momentum equations are not independent (e.g., [149], sect 2.2.4 [13], sect 3.4; ). There is consensus in the literature that the stress tensor for fluids is symmetric except for a class of suspensions in which torques could be produced on each particle in the carrier fluid by an external field [88] [104]. This means, in practice, that for all chemical reactor systems of interest the stress tensor is symmetric. The motion of such fluids can be determined by an Eulerian vector angular-momentum balance equation on the form

$$\frac{\partial}{\partial t} \int_V \mathbf{r} \times (\rho \mathbf{v}) dv + \int_A \mathbf{r} \times \rho \mathbf{v} (\mathbf{v} \cdot \mathbf{n}) da = \int_A \mathbf{r} \times (\mathbf{T} \cdot \mathbf{n}) da + \sum_{c=1}^N \int_V \mathbf{r} \times (\rho_c \mathbf{g}_c) dv \quad (1.179)$$

which is particularly convenient for analyzing fluid flow in rotating turbo machinery like compressors, turbines, cyclones, etc.

The total energy equation expressing the physical law of conservation of total energy, can be reformulated into a set of energy transport equations expressing balance laws for the various forms of energy (i.e., kinetic, potential and internal energy). It has been shown in this paper that the entropy transport equation can be obtained from the energy balance equations, thus it is not independent of these equations.

Note also that compared to the momentum equation, the equation of change for kinetic energy and the equation for angular momentum do not introduce additional unknowns, nor do they include new information.

- It is common practice when applying CFD to chemical reactor modeling, to solve a set of independent transport equations consisting of; upto  $N - 1$  species transport equations; the mixture continuity equation; and the momentum equation and the internal (or thermal) energy equation formulated in terms of temperature.

For flow situations where the kinetic energy and/or the potential energy contributions become significant (e.g., high speed velocity flows within electrical fields), we may benefit from solving the transport equations for these variables as well.

### 1.2.5 Some useful simplifications of the governing equations

In chemical engineering we are usually not using the governing equations in their most fundamental forms, but apply suitable simplifications giving sufficient predictions of the different process units with minimum costs.

The ability to establish such quantitative links between measures of reactor performance and input and operating variables is essential in optimizing the operating conditions, in determining proper reactor scale-up and design, and in interpreting data in research and pilot-plant work.

#### Steady Flows

In many cases we consider steady flows. A *steady flow* is defined to be one for which, at any fixed point in the flow field, all the flow variables are independent of time. Thus, in all steady flow all partial derivatives with respect to time vanish.

#### Incompressible-, Compressible- and Variable Density Flows

The term *incompressible flow* is applied to any situation where changes in the density of a fluid particle are negligible [119]. A mathematical definition is

$$\frac{1}{\rho} \frac{D\rho}{Dt} = 0 \quad (1.180)$$

From the continuity equation we have

$$\frac{1}{\rho} \frac{D\rho}{Dt} = -\nabla \cdot \mathbf{v} \quad (1.181)$$

This shows that an alternative definition is that  $\nabla \cdot \mathbf{v} = 0$  (the rate of expansion is zero). An equivalent condition is to require that the fluid particles have constant volume, but not necessary constant shape. Furthermore, the different fluid particles do not need to have the same density. The only requirement is that the density of each individual fluid particle remain unchanged. The incompressible flow limit is approached when the density is constant along any streamline (i.e.,  $\frac{D\rho}{Dt} = -\rho(\nabla \cdot \mathbf{v}) \approx 0$ ). The resulting or derived constant volume condition, which occur in flow situations where density changes can be neglected, has sometimes erroneously been used defining incompressible flows in general. Such a procedure may lead to mathematical inconsistencies. The main criterion for incompressible flow (as defined in the non-reactive gas dynamics literature) is rather that the Mach number is low, and that no significant density changes occur due to changes in temperature.

In other cases the fluid velocity vector may be considered solenoidal<sup>20</sup> even though the mixture density is not constant.

Most chemical engineers relate the term *incompressible flow* to incompressible fluid systems. For non-reactive ideal liquid mixtures operated at nearly constant temperatures, the incompressible flow limit is obviously a reasonable approximation in practice.

However, for compressible systems, the gas dynamics analysis may not be that obvious although very important in the chemical process industry. To learn more about gas dynamics we are characterizing three seemingly very similar flow systems reflecting somewhat divergent behavior, starting out with a relatively simple incompressible non-reacting adiabatic gas flow in a vertical tube (i.e., representing an idealized design of chemical reactors), then we expand our analysis to a non-adiabatic system, and finally a reactive mixture is considered.

The first system constitutes a low Mach number internal gas flow with an adiabatic wall, i.e., an *incompressible flow* [119].

For such a one-component flow problem where the viscous dissipation is the only heat source, the density of the fluid is governed by the continuity equation and a thermodynamic equation of state (EOS). In the present case we write the EOS as

$$\frac{1}{\rho} \frac{D\rho}{Dt} = \alpha \frac{Dp}{Dt} - \beta \frac{DT}{Dt} \quad (1.182)$$

where the isothermal compressibility (e.g., [7] [138]) is:

$$\alpha(p, T) = \frac{1}{\rho} \left. \frac{\partial \rho}{\partial p} \right|_T \quad (1.183)$$

and the bulk expansion coefficient (e.g., [119] [138]) is:

$$\beta(p, T) = -\frac{1}{\rho} \left. \frac{\partial \rho}{\partial T} \right|_P \quad (1.184)$$

The functions  $\alpha$  and  $\beta$  are thermodynamic variables that characterize the fluid. Physically  $\alpha$  and  $\beta$  always take non-zero values. The right hand side of (1.182) is thus small only if the pressure and temperature changes are small enough. In turn, the magnitudes of these variables are governed by dynamic processes occurring in the flow field. The energy and momentum equations will play a major role in fixing the pressure and temperature. The advantage of writing the equation of state in the form (1.182) is that the flow field effects

---

<sup>20</sup> A vector field  $\mathbf{v}$  satisfying  $\nabla \cdot \mathbf{v} = 0$  is called *solenoidal*. A volume-preserving motion is called *isochoric*, i.e., a motion for which the density in the neighborhood of any particle remains constant as the particle moves. The flow of an incompressible fluid is necessarily isochoric, but there may also be isochoric flows of compressible fluids [104] (p. 212).

are isolated in  $Dp/Dt$  and  $DT/Dt$  while the thermodynamic character of the fluid is isolated in  $\alpha$  and  $\beta$ .

The governing equations determining the evolution of single-component fluid flow are:

Thermodynamics:

$$\frac{1}{\rho} \frac{D\rho}{Dt} = \alpha \frac{Dp}{Dt} - \beta \frac{DT}{Dt} \quad (1.185)$$

with  $\alpha = \alpha(p, T)$ ,  $\beta = \beta(p, T)$ ,  $C_P = C_P(p, T)$ ,  $\mu = \mu(p, T)$ ,  $k = k(p, T)$ .

Continuity:

$$\frac{1}{\rho} \frac{D\rho}{Dt} = -\nabla \cdot \mathbf{v} \quad (1.186)$$

Momentum:

$$\rho \frac{D\mathbf{v}}{Dt} = -\nabla p - \nabla \cdot \boldsymbol{\sigma} + \rho \mathbf{g} \quad (1.187)$$

Net viscous stress:

$$\nabla \cdot \boldsymbol{\sigma} = -\nabla \cdot \{ \mu [\nabla \mathbf{v} + (\nabla \mathbf{v})^T] \} + \nabla \cdot \{ (\frac{2}{3} \mu - \mu_B) (\nabla \cdot \mathbf{v}) \} \quad (1.188)$$

Energy:

$$\rho C_P \frac{DT}{Dt} = \nabla \cdot (k \nabla T) + \mu \Phi_{\text{viscous}} + \beta T \frac{Dp}{Dt} \quad (1.189)$$

The analysis rely on the boundary conditions specified. The boundary conditions at the inlet are  $v_i = (v_0, 0, 0)$ ,  $T = T_0$  and  $\rho = \rho_0$ . On the wall  $v_i = 0$  and  $n_i q_i = 0$ . That is, we have adopted the no-slip condition at the wall requiring that the velocity is zero. Since the wall is said to be adiabatic, no heat enters the flow through the walls. For the outlet several conditions are possible (e.g., zero gradients for fully developed flow, pressure boundary, free surface, etc.), for convenience we may overlook their importance in this analysis.

The fluid flow problem requires the solution of all these equations. The dependent variables are  $\rho$ ,  $p$ ,  $T$  and  $v_i$ . The governing equations are all coupled together. For instance, the momentum equation contains the density and pressure variables, and the viscosity parameter. These quantities depend on the local temperature. The temperature in turn is governed by the energy equation, which contains the velocity in the advective and dissipation terms. However, not all the terms in the equations have the same importance in determining the flow solution.

To determine which terms are large and which are small, we cast the equations into non-dimensional variables with scales that are governed by the dynamics of the flow. The appropriate scales for non-dimensionalizing the variables are usually found from the tube geometry (e.g., say, a characteristic length  $L$ ), the boundary conditions and from detailed analysis of the equations that govern the flow [119].

Most of the non-dimensional variables are then formed in a straightforward manner:

$$x_i^* = \frac{x_i}{L}, t^* = \frac{tv_0}{L}, v_i^* = \frac{v_i}{v_0}, \rho^* = \frac{\rho}{\rho_0}, \alpha^* = \frac{\alpha}{\alpha_0}, \beta^* = \frac{\beta}{\beta_0}, C_P^* = \frac{C_P}{C_{P0}}, \mu^* = \frac{\mu}{\mu_0}, k^* = \frac{k}{k_0} \text{ and } Fr = \frac{v_0^2}{|\mathbf{g}|L}.$$

Nevertheless, the temperature and pressure variables need further consideration.

The pressure scale is usually found indirectly by substituting all the other non-dimensional variable definitions into the momentum equation.

Accordingly, after substituting the dimensionless variables into the momentum equation, the non-dimensional pressure is defined as  $p^* = \frac{p-p_0}{\rho_0 v_0^2}$ . If  $p_S$  symbolizes the pressure scale, we write  $p^* = \frac{p-p_0}{p_S} = \frac{p-p_0}{\rho_0 v_0^2}$ . Thus, when the pressure changes in the flow are dominated by momentum effects,  $p^*$  is the proper non-dimensional pressure variable [119].

A further observation is that for incompressible flow, pressure plays the role of a force in the momentum equation. Since the pressure variable occurs only within a pressure gradient term in this equation, a reference level may be substituted without any effect. That is,  $\nabla(p - p_0) = \nabla p$ .

If we consider the thermal processes occurring in this problem, we expect that heat (thermal energy) is generated in the flow field by viscous dissipation. The heat will then be redistributed by conduction and carried to new places by advection. In this case a suitable temperature scale is given by  $T_{\text{scale}} = \mu_0 v_0^2 / k_0$ , [119]. This is an estimate of the temperature rise that one can expect because of viscous dissipation from a velocity gradient of order  $v_0/L$ . Thus, we define  $T^* = \frac{T-T_{\text{ref}}}{T_{\text{scale}}} = \frac{T-T_0}{\mu_0 v_0^2 / k_0} = \frac{T-T_0}{Pr v_0^2 / C_{P0}}$ . In the latter term, the Prandtl number ( $Pr = \mu_0 C_{P0} / k_0$ ) has been introduced.

After all the non-dimensional variables are substituted into the equations, several non-dimensional groups occur<sup>21</sup>:  $Re = \frac{\rho_0 L v_0}{\mu_0}$ ,  $Pr = \frac{\mu_0 C_{P0}}{k_0}$ ,  $\gamma_0 = \frac{C_{P0}}{C_{V0}}$ ,  $Fr = \frac{v_0^2}{|\mathbf{g}|L}$ ,  $Ma = \frac{v_0}{c_s}$ ,  $A = \alpha_0 \rho_0 C_{P0} T_0$  and  $B = \beta_0 T_0$ .

For any given flow problem these parameters have specific fixed values. If they are large or small, they magnify or diminish the effect of the terms in which they appear as coefficients. In non-dimensional variables the equations are written as:

Thermodynamics:

$$\frac{1}{\rho^*} \frac{D\rho^*}{Dt^*} = \gamma_0 Ma^2 \left[ \alpha^* \frac{Dp^*}{Dt^*} - \frac{Pr B \beta^*}{A} \frac{DT^*}{Dt^*} \right] \quad (1.190)$$

The thermodynamic functions  $\alpha^*$ ,  $\beta^*$ ,  $\mu^*$ ,  $k^*$  and  $C_P^*$  are still undetermined.

<sup>21</sup> In formulating these non-dimensional parameters we have used the expression for the speed of sound of an ideal gas (e.g., [119] [136], app. 4),  $C_S^2 = \frac{\gamma_0}{\rho_0 \alpha_0}$ . The details of the substitution are also simplified by noting that;  $Ma^2 = \frac{v_0^2}{C_S^2} = \frac{v_0^2 \rho_0 \alpha_0}{\gamma_0}$ , and that;  $\frac{v_0^2}{C_{P0} T_0} = \frac{Ma^2 \gamma_0}{A}$ .

Continuity:

$$\frac{1}{\rho^*} \frac{D\rho^*}{Dt^*} = -\nabla^* \cdot \mathbf{v}^* \quad (1.191)$$

Momentum:

$$\rho^* \frac{D\mathbf{v}^*}{Dt^*} = -\nabla^* p^* - \nabla^* \cdot \boldsymbol{\sigma}^* + \rho^* \frac{\mathbf{g}}{Fr|\mathbf{g}|} \quad (1.192)$$

Viscous stress:

$$\nabla^* \cdot \boldsymbol{\sigma}^* = -\frac{1}{Re} (\nabla^* \cdot \{\mu^* [\nabla^* \mathbf{v}^* + (\nabla^* \mathbf{v}^*)^T]\}) + \nabla^* \cdot \left\{ \left( \frac{2}{3} \mu^* - \mu_B^* \right) (\nabla^* \cdot \mathbf{v}^*) \right\} \quad (1.193)$$

Energy:

$$\begin{aligned} \rho^* C_P^* \frac{DT^*}{Dt^*} &= \frac{1}{Re} \frac{1}{Pr} (\nabla^* \cdot (k^* \nabla^* T^*)) + \mu^* \Phi_{\text{viscous}}^* \\ &+ \beta^* B \left( \frac{1}{Pr} + \frac{\gamma_0 Ma^2}{A} T^* \right) \frac{Dp^*}{Dt^*} \end{aligned} \quad (1.194)$$

$$\text{where } \mu^* \Phi_{\text{viscous}}^* = \frac{\mu}{\mu_0} \frac{\Phi_{\text{viscous}}}{v_0^2/L}.$$

Sample inlet boundary conditions are  $v_i^* = (1, 0, 0)$ ,  $T^* = 0$  and  $\rho^* = 1$ , and on the wall  $v_i^* = 0$  and  $n_i q_i^* = 0$ .

At this stage we can see that the incompressible flow limit results when the right side of the non-dimensionalized form of the thermodynamic relation (1.190) becomes small, that is, when  $Ma^2 \rightarrow 0$ . As a general rule of experience, if  $Ma < 1/3$ , then the incompressible flow assumption will give a fair result for external flows (e.g., [185], p. 221). When the non-dimensionalized term  $D\rho^*/Dt^* = 0$ , the density of a fluid particle is constant. From this result it follows that in the non-dimensionalized continuity equation the left side is zero, so that  $\nabla \cdot \mathbf{v}^* = 0$ . Terms containing  $\nabla \cdot \mathbf{v}^*$  in the viscous stress and dissipation relations become small, as does the term preceded by  $Ma^2$  in the energy equation.

For ideal gas dynamics it has been shown, by Taylor series expansions, that all the thermodynamic fluid property functions are constants in the limit of small Mach numbers [119] [185].

It is concluded that in this case the main criterion for incompressible flow is that the Mach number is low ( $Ma \rightarrow 0$ ), denoting that all the velocities are small compared to the speed of sound. That is, when the speed of sound  $C_S = \sqrt{\frac{\partial p}{\partial \rho}}|_S$  appears in the compressible flow analysis, its role is not to tell how fast waves travel, but to indicate how much density change accompanies a certain pressure change due to the flow (e.g., [119] [134]).

Using the pressure scale,  $\rho_0 v_0^2$ , a flow decelerated from  $v = v_0$  at one location in the flow to  $v = 0$  at another will undergo a pressure change  $\Delta p \propto \rho_0 v_0^2$  (neglecting viscosity). With these considerations the Mach number is interpreted as follows [119]

$$Ma^2 = \frac{v_0^2}{C_S^2} = v_0^2 \frac{\partial \rho}{\partial p} \Big|_S = \frac{\rho_0 v_0^2}{\rho_0} \frac{\partial \rho}{\partial p} \Big|_S \approx \Delta p \frac{1}{\rho_0} \frac{\Delta \rho}{\Delta p} = \frac{\Delta \rho}{\rho_0} \quad (1.195)$$

The parameter  $Ma^2$  is a measure of the size of density changes compared to fluid density. As  $Ma^2 \rightarrow 0$ , density changes become only a small fraction of the fluid density.

However, although  $Ma^2 \rightarrow 0$  is required for incompressible flow, it is not the only requirement. Some flows where  $Ma^2 \rightarrow 0$  are low speed compressible flows. However, in these cases density changes are usually caused by temperature and/or mixture composition changes. For the present one-component flow analysis such effects are not important as the wall boundary is considered adiabatic. There is then not enough heat generated by viscous dissipation to cause large temperature changes.

The governing equations for incompressible flow derived based on dimensional analysis yield [119]:

Thermodynamics:

$$\frac{D\rho^*}{Dt^*} = 0 \quad (1.196)$$

$$\alpha^* = \beta^* = \mu^* = k^* = C_P^* = \rho^* = 1$$

Continuity:

$$\nabla^* \cdot \mathbf{v}^* = 0 \quad (1.197)$$

Momentum:

$$\frac{D\mathbf{v}^*}{Dt^*} = -\frac{1}{\rho^*} \nabla^* p^* + \frac{1}{Re} \mu^* \nabla^{2*} \mathbf{v}^* + \frac{\mathbf{g}}{Fr|\mathbf{g}|} \quad (1.198)$$

Viscous stress:

$$\begin{aligned} \nabla^* \cdot \boldsymbol{\sigma}^* &= -\frac{1}{Re} (\nabla^* \cdot \{\mu^* [\nabla^* \mathbf{v}^* + (\nabla^* \mathbf{v}^*)^T]\}) \\ &\quad + \nabla^* \cdot \left\{ \left( \frac{2}{3} \mu^* - \mu_B^* \right) (\nabla^* \cdot \mathbf{v}^*) \right\} \\ &\approx \frac{1}{Re} \mu^* \nabla^{2*} \mathbf{v}^* \end{aligned} \quad (1.199)$$

Energy:

$$\frac{DT^*}{Dt^*} = \frac{1}{Re} \left( \frac{1}{Pr} \nabla^{2*} T^* + \mu^* \Phi_{\text{viscous}}^* \right) + \beta^* \frac{B}{Pr} \frac{Dp^*}{Dt^*} \quad (1.200)$$

The boundary conditions at the inlet are  $v_i^* = (1, 0, 0)$ ,  $T^* = 0$ ,  $p^* = 0$  and  $\rho^* = 1$ , and on the wall  $v_i^* = 0$  and  $n_i q_i^* = 0$ .

Inspection of these equations reveals quite a lot about incompressible flow.

First of all, the density and all the thermodynamic coefficients are constants. Secondly, when the density and the transport properties are constants, the continuity and momentum equations are decoupled from the energy equation. This result is important, as it means that we may solve for the three velocities and the pressure without regard for the energy equation or the temperature. Third, for incompressible flows the pressure is determined by the momentum equation. The pressure thus plays the role of a mechanical force and not a thermodynamic variable. Fourth, another important fact about incompressible flow is that only two parameters, the Reynolds number and the Froude number, occur in the equations. The Froude number,  $Fr$ , expresses the importance of buoyancy compared to the other terms in the equation. The Reynolds number indicates the size of the viscous force term relative to the other terms. It is mentioned that compressible flows are often high  $Re$  flows, thus they are often computed using the inviscid *Euler* (momentum) equations.

In the incompressible energy equation only derivatives of the temperature variable occur. This means that in incompressible flow, only changes in temperature with respect to some reference state are important. As with pressure, the level of the reference temperature does not affect the solution. The actual temperature in such a incompressible flow doesn't change noticeably.

The second system constitutes a low Mach number internal gas flow with non-adiabatic walls, i.e., a *compressible gas flow* [119].

In the foregoing discussion we have seen how the case  $Ma \rightarrow 0$  with an adiabatic wall is an example of incompressible flow. In other instances there is significant heat transfer through the wall. In this case we can isolate the flow situation by imagining that the wall is held at some fixed temperature  $T_W$  that is different from  $T_0$ . The non-dimensional scale for the temperature is redefined, so we need to redo the analysis of the resulting dimensionless equations. The problem now has a characteristic temperature scale,  $T_0 - T_W$ , which is a driving force for the conduction of heat from the wall into the fluid. Since we expect that all temperatures will lie between these two values, the proper non-dimensional temperature is:  $\hat{T} = \frac{T - T_0}{T_W - T_0}$ . The temperature variable,  $T^*$ , for the adiabatic wall problem is related to  $\hat{T}$  by the equation:  $T^* = \frac{T_W - T_0}{T_0} \frac{A}{\gamma_0 Pr Ma^2} \hat{T}$ . There is no change in the formulation for any of the other variables, thus we can substitute the new temperature variable into the governing equations and again let the Mach number approach zero.

The temperature variable does not appear in the continuity and momentum equations, so the previous dimensionless equations obtained in the adiabatic wall analysis remain unchanged. The equation of state is revised by substituting the new temperature variable. The EOS yields

$$\frac{1}{\rho^*} \frac{D\rho^*}{Dt^*} = \gamma_0 Ma^2 \alpha^* \frac{Dp^*}{Dt^*} - B\beta^* \left( \frac{T_W - T_0}{T_0} \right) \frac{D\hat{T}}{Dt^*} \quad (1.201)$$

When the new temperature variable is substituted into the energy equation, the equation changes to:

$$\begin{aligned} \rho^* C_P^* \frac{D\hat{T}}{Dt^*} = & \frac{1}{PrRe} \nabla^* \cdot (k^* \nabla^* \hat{T} + \frac{\gamma_0 Ma^2}{ARe} (\frac{T_0}{T_W - T_0}) \mu^* \Phi_{\text{viscous}}^*) \\ & + \frac{\beta^* B \gamma_0 Ma^2}{A} [\frac{T_0}{T_W - T_0} + \hat{T}] \frac{Dp^*}{Dt^*} \end{aligned} \quad (1.202)$$

Sample inlet boundary conditions are  $v_i^* = 0$  and  $\hat{T} = 1$  (or a known function).

The limit  $Ma^2 \rightarrow 0$  gives a low speed compressible flow where the thermodynamic state equation shows that the density changes occur only because of the large variations in temperature:

$$\frac{1}{\rho^*} \frac{D\rho^*}{Dt^*} = -B\beta^* (\frac{T_W - T_0}{T_0}) \frac{D\hat{T}}{Dt^*} \quad (1.203)$$

The energy equation for the flow shows that advection and conduction determine the temperature field:

$$\rho^* C_P^* \frac{D\hat{T}}{Dt^*} = \frac{1}{PrRe} \nabla^* \cdot (k^* \nabla^* \hat{T}) \quad (1.204)$$

The transport properties and the thermodynamic functions are not necessarily constants this time, but depend (weakly) on temperature. The flow is a low speed compressible flow as long as  $(T_0 - T_W)/T_0$  is finite. The continuity and momentum equations no longer simplify, but must be considered with their temperature dependence. The complete set of equations is coupled together through the transport properties and the density. These equations apply to flows where the wall supplies significant heating to the fluid, i.e., problems of natural convection.

The further special case of small temperature differences will turn out to be an incompressible flow. This flow is governed by the same equations as the adiabatic case except that the energy equation is a little different. The energy equation has only advection and conduction terms while in the adiabatic case the energy equation also includes a viscous dissipation and a pressure term.

The third system constitutes a low Mach number internal gas flow of a reactive mixture, i.e., a *variable density flow* [77].

In this book variable density flows are considered compressible in accordance with the view of [119], i.e., even though the density variations are not necessarily induced by pressure or compressibility effects, the terms *variable density flow* and 'compressible flow' are then equivalent phrases. This view may not agree with all the textbooks of classical gas dynamics.

In reactor modeling we are dealing with flow situations where the mixture density may vary both due to pressure and temperature changes, chemical reactions and non-ideal mixing. For these flow situations, we must consider

additional heat sources, changes in composition due to chemical reactions and fluid mixing, and thereafter redo the non-dimensional scales and reanalyze the resulting equations.

If we consider the physical processes occurring in this problem, we expect that heat is generated in the flow field by the heat of reaction and boundary temperatures at the wall and heating/cooling devices rather than viscous dissipation (as for the first case). In many systems pressure changes are dominated by chemistry rather than momentum effects, and density changes are caused by changes in composition rather than pressure and temperature changes. An extended thermodynamic state equation can be formulated assuming density to be a function of  $P$ ,  $T$  and  $\omega_c$  (e.g., [11] [13] [134] [115])

$$\frac{1}{\rho} \frac{D\rho}{Dt} = \alpha \frac{Dp}{Dt} - \beta \frac{DT}{Dt} + \sum_c \gamma_c \frac{D\omega_c}{Dt} \quad (1.205)$$

where  $\gamma_c = \frac{1}{\rho} \frac{\partial \rho}{\partial \omega_c} |_{P,T,\omega_{s \neq c}}$  defines the dependence of fluid density upon chemical composition, a composition expansion coefficient (e.g., [134], p. 320).

The state relation is not often used in this form in thermodynamics literature, but it is useful in flow analyzes. The chemistry and flow field effects are isolated in  $D\omega_c/Dt$ , determined by solving additional species transport equations. The thermodynamic character of the multi-component fluid is isolated in  $\gamma$  (and  $\alpha$  and  $\beta$ ). All the thermodynamic quantities are in principle functions of both temperature, pressure and composition.

An important question in reactive flow analysis is whether or not the density changes due to non-ideal mixing and reaction have significant effects on the flow. In many reactor systems both chemistry and flow scales are important. The formulation of proper non-dimensional scales is thus a difficult task. Therefore, in our subsequent analysis the pressure changes in the flow are supposedly dominated by momentum effects as in non-reactive systems.

Analyzing chemical reactor flows the starting point is a list of the fairly rigorous equations, as found in most textbooks (e.g., [11] [13] [89]), that should govern the reactor modeling problem.

Thermodynamics:

$$\frac{1}{\rho} \frac{D\rho}{Dt} = \alpha \frac{Dp}{Dt} - \beta \frac{DT}{Dt} + \sum_c \gamma_c \frac{D\omega_c}{Dt} \quad (1.206)$$

with  $\alpha = \alpha(p, T, \omega_c)$ ,  $\beta = \beta(p, T, \omega_c)$ ,  $C_P = C_P(p, T, \omega_c)$ ,  $\mu = \mu(p, T, \omega_c)$ ,  $k = k(p, T, \omega_c)$  and  $\gamma_c = \gamma(p, T, \omega_c)$ .

Continuity:

$$\frac{1}{\rho} \frac{D\rho}{Dt} = -\nabla \cdot \mathbf{v} \quad (1.207)$$

Momentum:

$$\rho \frac{D\mathbf{v}}{Dt} = -\nabla p - \nabla \cdot \boldsymbol{\sigma} + \sum_{c=1}^N \rho_c \mathbf{g}_c \quad (1.208)$$

Net viscous stress:

$$\nabla \cdot \boldsymbol{\sigma} = -\nabla \cdot \{\mu[\nabla \mathbf{v} + (\nabla \mathbf{v})^T]\} + \nabla \cdot \left\{ \left( \frac{2}{3}\mu - \mu_B \right) (\nabla \cdot \mathbf{v}) \right\} \quad (1.209)$$

Energy:

$$\begin{aligned} \sum_{c=1}^N \rho_c C_{p,\omega_c} \frac{DT}{Dt} = & -\nabla \cdot \mathbf{q} - \frac{T}{\rho_c} \left( \frac{\partial \rho_c}{\partial T} \right)_{p,\omega_c} \frac{Dp}{Dt} \\ & - (\boldsymbol{\sigma} : \nabla \mathbf{v}) + \sum_{c=1}^N (\mathbf{j}_c \cdot \mathbf{g}_c) + \sum_{c=1}^N h_c \nabla \cdot \mathbf{j}_c + \sum_{r=1}^q \left( \frac{R_{r,c}}{M_{w_c}} \right) (-\Delta H_{r,c}) \end{aligned} \quad (1.210)$$

Species mass:

$$\rho \frac{D\omega_c}{Dt} = \nabla \cdot (\rho D_c \nabla \omega_c) + R_c \quad (1.211)$$

with  $\rho_c = \rho \omega_c$ .

The reference boundary conditions at the inlet are  $v_i = (v_0, 0, 0)$ ,  $T = T_0$ ,  $\rho_c = \rho_{c,0}$  and  $\rho = \rho_0$ , and on the wall  $v_i = 0$  and either adiabatic  $n_i q_i = 0$  or non-adiabatic thus  $T = T_W$ .

Not all the terms in these equations have the same importance in determining the flow solution in chemical reactors. The only body force considered in most reactor models,  $\mathbf{g}_i$  (per unit mass), is gravitation which is the same for all chemical species,  $\mathbf{g}$ . The model equations for momentum and energy can then be simplified. In the momentum equation  $\sum_{c=1}^N \rho_c \mathbf{g}_c = \sum_{c=1}^N \rho_c \mathbf{g} = \rho \mathbf{g}$ . In the energy equation:  $\sum_{c=1}^N (\mathbf{j}_c \cdot \mathbf{g}_c) = \sum_{c=1}^N \mathbf{j}_c \cdot \mathbf{g} = 0$ . Furthermore, in most multicomponent flows, the energy or heat flux contributions from the interdiffusion processes are in general believed to be small and omitted in most applications,  $\sum_{c=1}^N h_c \nabla \cdot \mathbf{j}_c \approx 0$  (e.g., [148], p. 816; [89], p. 198; [11], p. 566).

To determine which of the remaining terms are large and which are small, we must again cast the equations into non-dimensional variables. For an ideal gas system many of the non-dimensional variables can still be formed in a straightforward manner using the boundary values. In this way we can, as in the preceding examples, define  $x_i^* = x_i/L$ ,  $t^* = tv_0/L$ ,  $v_i^* = v_i/v_0$ ,  $\rho^* = \rho/\rho_0$ ,  $\alpha^* = \alpha/\alpha_0$ ,  $\beta^* = \beta/\beta_0$ ,  $\gamma_c^* = \gamma_c/\gamma_{c,0}$ ,  $C_P^* = C_P/C_{P0}$ ,  $\mu^* = \mu/\mu_0$ ,  $k^* = k/k_0$ ,  $Fr = v_0^2/|\mathbf{g}|L$ ,  $D_c^* = D_c/D_{c,0}$  and  $R_c^* = R_c/R_{c,0}$ .

The temperature and pressure variables are more difficult to determine. If we assume that the pressure changes in the flow are dominated by momentum effects as in non-reactive systems, a proper non-dimensional pressure variable may be:  $p^* = \frac{p-p_0}{\rho_0 v_0^2}$ . Considering the physical and chemical processes occurring in this problem, one may expect that heat is generated in the flow field by chemical reactions or heating devices, rather than by viscous dissipation. The adiabatic temperature is an estimate of the maximum temperature ( $T_{\text{ad}} = T_0 + \frac{(-\Delta H_R)\omega_{c,0}}{C_{P0}}$ ) that can be obtained, due to the heat generated by reaction, in a reactor operating at adiabatic conditions (e.g., [52], p. 409). Using this

quantity the problem is supposed to have a characteristic scale  $T_{ad} - T_0$ , which is a driving force for conduction of heat from the reactive zones into the bulk fluid field. Thus, one may define:  $T^* = \frac{T - T_{ref}}{T_{scale}} = \frac{T - T_0}{T_{ad} - T_0}$ . At this point one may argue that for multiple reaction systems, we cannot estimate the exact adiabatic temperature without solving the problem. This may, however, not be important. In such cases one can use an estimate such as the maximum possible adiabatic temperature based on only one (e.g., the most exothermic one) reaction. Further discussion on this issue is given by [134] (p. 420) and [4] (pp. 278-282 and 302).

After suitable non-dimensional variables are substituted into the equations, the following non-dimensional groups occur:  $Re = \frac{\rho_0 L v_0}{\mu_0}$ ,  $Pr = \frac{\mu_0 C_{P0}}{k_0}$ ,  $\gamma_0 = \frac{C_{P0}}{C_{V0}}$ ,  $Fr = \frac{v_0^2}{|g|L}$ ,  $Ma = \frac{v_0}{C_S}$ ,  $A = \alpha_0 \rho_0 C_{P0} T_0$ ,  $B = \beta_0 T_0$ ,  $Da = \frac{t_{flow}}{t_{chem}} = \frac{(L/v_0)}{(\rho_0/R_{c,0})}$  (i.e., a Damköhler number (e.g., [18] [134], pp. 426-427)), and

$Q = \frac{(L/v_0)}{\rho_0 C_{P,0} (T_{ad} - T_0)} \sum_{r=1}^q \left( \frac{R_{r,c}}{M_{w,c}} \right) (-\Delta H r_{r,c})$  (i.e., a dimensionless heat of reaction term referred to as a Damköhler number (e.g., [18] [134], p. 421).

The final form of the mathematical problem statement in non-dimensional variables is as follows:

Thermodynamics:

$$\frac{1}{\rho^*} \frac{D\rho^*}{Dt^*} = \gamma_0 Ma^2 [\alpha^* \frac{Dp^*}{Dt^*}] - B\beta^* \left( \frac{T_{ad} - T_0}{T_0} \right) \frac{DT^*}{Dt^*} + \sum_c \gamma_c^* \gamma_{c,0} \frac{D\omega_c}{Dt^*} \quad (1.212)$$

Continuity:

$$\frac{1}{\rho^*} \frac{D\rho^*}{Dt^*} = -\nabla^* \cdot \mathbf{v}^* \quad (1.213)$$

Momentum:

$$\rho^* \frac{D\mathbf{v}^*}{Dt^*} = -\nabla^* p^* - \nabla^* \cdot \boldsymbol{\sigma}^* + \rho^* \frac{\mathbf{g}}{Fr|g|} \quad (1.214)$$

Viscous stress:

$$\nabla^* \cdot \boldsymbol{\sigma}^* = -\frac{1}{Re} (\nabla^* \cdot \{ \mu^* [\nabla^* \mathbf{v}^* + (\nabla^* \mathbf{v}^*)^T] \} + \nabla^* \{ (\frac{2}{3} \mu^* - \mu_B^*) (\nabla^* \cdot \mathbf{v}^*) \}) \quad (1.215)$$

Energy:

$$\begin{aligned} \rho^* C_P^* \frac{DT^*}{Dt^*} &= \frac{1}{Re} \frac{1}{Pr} \nabla^* \cdot (k^* \nabla^* T^*) + \frac{\gamma_0}{A} \frac{Ma^2}{Re} \left( \frac{T_0}{T_{ad} - T_0} \right) \mu^* \Phi_{viscous}^* \\ &+ \beta^* B \frac{\gamma_0 Ma^2}{A} \left( \frac{T_0}{T_{ad} - T_0} + T^* \right) \frac{Dp^*}{Dt^*} + Q \end{aligned} \quad (1.216)$$

where  $\mu^* \Phi_{viscous}^* = \frac{\mu}{\mu_0} \frac{\Phi_{viscous}}{v_0^2/L}$ .

Species mass:

$$\rho^* \frac{D\omega_c}{Dt^*} = \frac{1}{Re} \frac{1}{Sc} \nabla^* \cdot (\rho^* D_c^* \nabla^* \omega_c) + Da R_c^* \quad (1.217)$$

The governing equations for low Mach number flow derived based on the dimensional analysis can then be expressed as:

Thermodynamics:

$$\frac{1}{\rho^*} \frac{D\rho^*}{Dt^*} = -B\beta^* \left( \frac{T_{ad} - T_0}{T_0} \right) \frac{DT^*}{Dt^*} + \sum_c \gamma_c^* \gamma_{c,0} \frac{D\omega_c}{Dt^*} \quad (1.218)$$

Continuity:

$$\frac{1}{\rho^*} \frac{D\rho^*}{Dt^*} = -\nabla^* \cdot \mathbf{v}^* \quad (1.219)$$

Momentum:

$$\rho^* \frac{D\mathbf{v}^*}{Dt^*} = -\nabla^* p^* - \nabla^* \cdot \boldsymbol{\sigma}^* + \rho^* \frac{\mathbf{g}}{Fr|\mathbf{g}|} \quad (1.220)$$

Viscous stress:

$$\nabla^* \cdot \boldsymbol{\sigma}^* = -\frac{1}{Re} (\nabla^* \cdot \{\mu^* [\nabla^* \mathbf{v}^* + (\nabla^* \mathbf{v}^*)^T]\}) + \nabla^* \cdot \left\{ \left( \frac{2}{3} \mu^* - \mu_B^* \right) (\nabla^* \cdot \mathbf{v}^*) \right\} \quad (1.221)$$

Energy:

$$\rho^* C_P^* \frac{DT^*}{Dt^*} = \frac{1}{Re} \frac{1}{Pr} \nabla^* \cdot (k^* \nabla^* T^*) + Q \quad (1.222)$$

Species mass:

$$\rho^* \frac{D\omega_c}{Dt^*} = \frac{1}{Re} \frac{1}{Sc} \nabla^* \cdot (\rho^* D_c^* \nabla^* \omega_c) + Da R_c^* \quad (1.223)$$

A comparison of the two last mentioned sets of equations reveals the background for several classical reactor model simplifications. Most reactor systems are low velocity flows so that the terms with a pre factor containing the Mach number can be neglected. Then we see that the density is not significantly dependent on the pressure changes due to the flow, and the viscous dissipation and pressure terms in the temperature equation can be neglected. However, the density and thermodynamic coefficients are not constants, but may be functions of both temperature and mixture species composition. Therefore, the gas flows occurring in chemical reactors can in general be characterized as low velocity compressible flows.

Accordingly, a good starting point for the description of most chemical reactor systems is the following set of simplified conservation equations written in dimensionalized form:

Continuity:

$$\frac{1}{\rho} \frac{D\rho}{Dt} = -\nabla \cdot \mathbf{v} \quad (1.224)$$

Momentum:

$$\rho \frac{D\mathbf{v}}{Dt} = -\nabla p - \nabla \cdot \boldsymbol{\sigma} + \rho \mathbf{g} \quad (1.225)$$

Net viscous stress:

$$\nabla \cdot \boldsymbol{\sigma} = -\nabla \cdot \{ \mu [ \nabla \mathbf{v} + (\nabla \mathbf{v})^T ] \} + \nabla \{ (\frac{2}{3} \mu - \mu_B) (\nabla \cdot \mathbf{v}) \} \quad (1.226)$$

Energy:

$$\sum_{c=1}^N \rho_c C_{p,\omega_c} \frac{DT}{Dt} = -\nabla \cdot \mathbf{q} + \sum_{r=1}^q \left( \frac{R_{r,c}}{M_{w_c}} \right) (-\Delta H_{r,c}) \quad (1.227)$$

Species mass:

$$\rho \frac{D\omega_c}{Dt} = \nabla \cdot (\rho D_c \nabla \omega_c) + R_c \quad (1.228)$$

together with the corresponding thermodynamic constitutive relations:

Equation of state:

$$\frac{1}{\rho} \frac{D\rho}{Dt} \approx -\beta \frac{DT}{Dt} + \sum_c \gamma_c \frac{D\omega_c}{Dt} \quad (1.229)$$

with  $\alpha \approx \alpha(T, \omega_c)$ ,  $\beta \approx \beta(T, \omega_c)$ ,  $C_P \approx C_P(T, \omega_c)$ ,  $\mu \approx \mu(T, \omega_c)$ ,  $k \approx k(T, \omega_c)$  and  $\gamma_c \approx \gamma(T, \omega_c)$ .

## Bernoulli equation

For one component fluids the *Bernoulli equation* for inviscid<sup>22</sup> flow along a streamline can either be formulated by direct application of Newton's second law to a fluid particle moving along a streamline [114] [10] or derived projecting the generalized momentum equation (1.78) onto a streamline. Applying the latter approach, the Navier-Stokes equation for non-viscous fluids becomes:

$$\rho \frac{D\mathbf{v}}{Dt} = -\nabla p + \rho \mathbf{g} \quad (1.230)$$

Introducing vorticity<sup>23</sup> into the acceleration term, using the vector identity [184] [114]:

$$(\mathbf{v} \cdot \nabla) \mathbf{v} = \nabla \frac{v^2}{2} - \mathbf{v} \times \boldsymbol{\omega} \quad (1.231)$$

and let  $\mathbf{g} = -g\mathbf{e}_z$ . The result is

<sup>22</sup> In an inviscid flow the fluid is treated as non-viscous and non-conducting.

<sup>23</sup> The vorticity vector,  $\boldsymbol{\omega}$ , is a measure of rotational effects, being equal to twice the local rate of rotation (angular velocity) of a fluid particle (i.e.,  $\boldsymbol{\omega} = \text{curl}(\mathbf{v}) = \text{rot}(\mathbf{v}) = \nabla \times \mathbf{v} = 2\boldsymbol{\Omega}$ ) [168]. Many flows have negligible vorticity,  $\boldsymbol{\omega} \approx \text{curl}(\mathbf{v}) \approx 0$ , and are appropriately called *irrotational flows*.

$$\rho \frac{\partial \mathbf{v}}{\partial t} + \nabla(p + \frac{1}{2}\rho v^2 + \rho g z) = \rho \mathbf{v} \times \boldsymbol{\omega} \quad (1.232)$$

Again the LHS is the sum of the classical Euler terms of inviscid flow. We restrict our attention to steady flow, so the Euler equation in vector form becomes

$$\frac{\nabla p}{\rho} + \frac{1}{2}\nabla v^2 + g\nabla z = \mathbf{v} \times \boldsymbol{\omega} \quad (1.233)$$

We next take the dot product of each term with a differential length  $ds$  along a streamline. Hence,

$$\frac{\nabla p}{\rho} \cdot ds + \frac{1}{2}\nabla v^2 \cdot ds + g\nabla z \cdot ds = \mathbf{v} \times \boldsymbol{\omega} \cdot ds \quad (1.234)$$

Since  $ds$  has a direction along the streamline, the vectors  $ds$  and  $\mathbf{v}$  are parallel. However, the vector  $\mathbf{v} \times \boldsymbol{\omega}$  is perpendicular to  $\mathbf{v}$ , thus  $\mathbf{v} \times \boldsymbol{\omega} \cdot ds = 0$ .

Furthermore, as the dot product of the gradient of a scalar and a differential length gives the differential change in the scalar in the direction of the differential length, (1.234) becomes

$$\frac{dp}{\rho} + \frac{1}{2}d(v^2) + g dz = 0 \quad (1.235)$$

where the changes in  $p$ ,  $v$  and  $z$  are along the streamline. Integrating (1.235) gives

$$\int \frac{dp}{\rho} + \frac{v^2}{2} + g z = \text{Constant} \quad (1.236)$$

which indicates that the sum of the three terms on the LHS of the equation must retain a constant along a given streamline. The equation is also valid for both compressible and incompressible inviscid flows. However, for compressible fluids the variation in  $\rho$  with  $p$  must be specified before the first term in (1.236) is evaluated. Compressible flow is not of primary concern at this stage in the book, so we restrict the present analysis to incompressible flows. For further studies on compressible flows, the reader may consult the textbooks by [185] [114].

For inviscid, incompressible fluids (commonly called ideal fluids) (1.236) yields,

$$\frac{p}{\rho} + \frac{v^2}{2} + g z = \text{Constant} \quad (1.237)$$

It is often convenient to write (1.237) between two points (1) and (2) along a streamline and to express the equation in the head form by dividing each term by  $g$  so that

$$\frac{p_1}{\rho g} + \frac{v_1^2}{2g} + z_1 = \frac{p_2}{\rho g} + \frac{v_2^2}{2g} + z_2 \quad (1.238)$$

It is emphasized that the Bernoulli equation, derived from the Euler equation, is restricted to steady-, inviscid- and incompressible flow along a streamline.

For incompressible flows the same equation is valid even for viscous fluids if the flow is irrotational. This is shown next, starting out from the Navier-Stokes equation (1.78). If the fluid is incompressible, with constant  $\mu$  and  $\rho$ , the Navier-Stokes equation becomes

$$\rho \frac{D\mathbf{v}}{Dt} = -\nabla p + \mu \nabla^2 \mathbf{v} + \rho \mathbf{g} \quad (1.239)$$

Introducing vorticity into both the acceleration and the viscous terms, using the vector identity (1.231) for the acceleration and a similar one for the viscous term [184, 11]:

$$\nabla^2 \mathbf{v} = \nabla(\nabla \cdot \mathbf{v}) - \text{curl}(\boldsymbol{\omega}), \quad (1.240)$$

the result is:

$$\rho \frac{\partial \mathbf{v}}{\partial t} + \nabla(p + \frac{1}{2} \rho v^2 + \rho g z) = \rho \mathbf{v} \times \boldsymbol{\omega} - \mu \text{curl}(\boldsymbol{\omega}) \quad (1.241)$$

The LHS is the sum of the classical Euler terms of inviscid flow. The RHS vanishes if the vorticity is zero, regardless of the value of viscosity. Thus, if  $\boldsymbol{\omega} = 0$  which is the classic assumption of irrotational flow, the steady momentum equation reduces to the Bernoulli equation for steady incompressible flow:

$$\nabla(p + \frac{1}{2} \rho v^2 + \rho g z) = 0 \quad (1.242)$$

Under the given conditions, it is not necessary to integrate the equation along a streamline. Therefore, the Bernoulli equation can be written:

$$\frac{p_1}{\rho g} + \frac{v_1^2}{2g} + z_1 = \frac{p_2}{\rho g} + \frac{v_2^2}{2g} + z_2 \quad (1.243)$$

between any two points in the flow field. Equation (1.243) is seemingly exactly the same form as (1.238), but is not limited to application along a streamline.

It is emphasized that the Bernoulli equation (1.243), as derived from the Navier-Stokes equation, is still restricted to steady-, irrotational- and incompressible flow.

It may also be worthwhile noting that many more classical flow analysis are based on similar simplifications<sup>24</sup>.

<sup>24</sup> Inviscid, incompressible and irrotational flow fields are governed by Laplace's equation and are called *potential flows*, as the velocity in such flows can be expressed as the gradient of a scalar function called the velocity potential.

Another equation that resembles the Bernoulli equation very much is derived from the total energy balance [168]. For one component fluids the total energy equation (1.96) can be written:

$$\rho \frac{D}{Dt} \left( e + \frac{1}{2} v^2 + \Phi \right) = -\nabla \cdot \mathbf{q} - p \nabla \cdot \mathbf{v} - \mathbf{v} \cdot \nabla p - \nabla \cdot (\boldsymbol{\sigma} \cdot \mathbf{v}) \quad (1.244)$$

This equation can be reformulated by use of the continuity equation, to obtain the following relationship:

$$p \nabla \cdot \mathbf{v} = -\frac{p}{\rho} \frac{D\rho}{Dt} = \rho \frac{D}{Dt} \left( \frac{p}{\rho} \right) - \frac{Dp}{Dt} \quad (1.245)$$

which yields:

$$\rho \frac{D}{Dt} \left( e + \frac{p}{\rho} + \frac{1}{2} v^2 + gz \right) = -\nabla \cdot \mathbf{q} + \frac{\partial p}{\partial t} - \nabla \cdot (\boldsymbol{\sigma} \cdot \mathbf{v}) \quad (1.246)$$

where we have assumed that the only body force acting on the system is the gravity force.

In process engineering the energy equation (1.246) is often expressed in terms of enthalpy,  $h = e + \frac{p}{\rho}$ , hence<sup>25</sup>:

$$\rho \frac{D}{Dt} \left( h + \frac{1}{2} v^2 + gz \right) = -\nabla \cdot \mathbf{q} + \frac{\partial p}{\partial t} - \nabla \cdot (\boldsymbol{\sigma} \cdot \mathbf{v}) \quad (1.247)$$

Furthermore, if the flow is both steady and inviscid, the energy equation (1.247) reduces to:

---

A difficulty performing potential flow analysis is that these models do not satisfy the no-slip condition at a solid wall, which requires that both the normal and tangential velocity components vanish. This is because the assumption of irrotationality eliminates the second order velocity derivatives from the basic equation leaving only first order derivatives, so that only one velocity condition can be satisfied at a solid wall. In potential flow, then, we require only the normal velocity to vanish at a wall and put no restriction on the tangential velocity, which commonly slips at the wall. Apparently, at first sight potential solutions may not seem very useful in viscous analysis, but in fact at high Reynolds numbers a viscous flow past a solid body is primarily a potential flow everywhere except close to the body, where the velocity drops off sharply through a thin viscous boundary layer to satisfy the no slip condition. In many cases, the boundary layer is so thin that it does not really disturb the outer potential flow, which can be calculated by the methods of classical fluid dynamics. This approximation has been applied deriving expressions for many of the forces acting on solid and fluid particles (e.g., Magnus and Saffman lift forces) in dispersed flows.

<sup>25</sup> As the essential function of pumps, compressors, and turbines is to change the Bernoulli constant ( $h + \frac{1}{2} v^2 + \Phi$ ) of a flow, one conclusion from this equation is that such a device cannot operate without viscous forces and heat transfer in the absence of unsteadiness.

$$\rho \mathbf{v} \cdot \nabla (h + \frac{1}{2}v^2 + gz) = 0 \quad (1.248)$$

These inviscid flows are said to be *reversible adiabatic* or *isentropic*<sup>26</sup>.

For isentropic flow, the Gibb's equation (e.g., see (1.138) and set  $dS = 0$  and  $d\omega_c = 0$ , for  $c = 1, N$ ) gives  $dh = \frac{dp}{\rho}$ , and the energy equation (1.248) becomes:

$$\rho \mathbf{v} \cdot \nabla (\frac{p}{\rho} + \frac{v^2}{2} + gz) = 0 \quad (1.250)$$

That is, for incompressible flows the quantity  $(\frac{p}{\rho} + \frac{v^2}{2} + gz)$  has no variation in the direction of  $\mathbf{v}$  denoting a streamline. Therefore, under these conditions integration yields,

$$\frac{p_1}{\rho g} + \frac{v_1^2}{2g} + z_1 = \frac{p_2}{\rho g} + \frac{v_2^2}{2g} + z_2 \quad (1.251)$$

This relation is seemingly identical to the classical Bernoulli equation (1.238) along a given streamline. It is emphasized that the Bernoulli equation (1.251), as derived from the energy balance (1.96), is restricted to steady-, incompressible- and isentropic flows.

From the former discussion we conclude that proper use of the various forms of the Bernoulli equation requires close attention to the assumptions used in their derivation.

In addition, real process units are neither completely inviscid, irrotational or isentropic, thus several extended forms of the Bernoulli equation are used in practice constituting various forms of energy balances containing loss and/or work terms. Two extremely important variants of the original relation are outlined in the following paragraphs.

For steady incompressible flow with one inlet and one outlet, both assumed 1D, the integral form of (1.246) reduces to a simple relation between the flow at two cross section planes (1) and (2) as used in engineering calculations:

$$e_1 + \frac{p_1}{\rho} + \frac{v_1^2}{2} + gz_1 = e_2 + \frac{p_2}{\rho} + \frac{v_2^2}{2} + gz_2 - q + w_s + w_v \quad (1.252)$$

---

<sup>26</sup> The origin of this phrase is revealed analyzing the entropy equation. For isentropic flows the entropy equation (1.167) for one component fluids reduces to:

$$\frac{Ds}{Dt} = 0 \quad (1.249)$$

where both the heat conduction,  $\mathbf{q}$ , and the dissipation,  $\mu\Phi_{\text{viscous}}$ , are neglected.

It is seen that for isentropic flows the entropy of a given fluid particle is constant.

Further note that the terms *adiabatic* and *isentropic* are not synonymous. By definition, an *adiabatic* flow has  $\mathbf{q} = 0$  everywhere within the flow field. By virtue of the entropy equation (1.167), an *adiabatic* flow is *isentropic* only if the dissipation  $\mu\Phi_{\text{viscous}}$  is also zero.

where  $q$  denotes the heat transferred to the fluid per unit mass,  $w_s$  denotes the shaft work performed by pumps, turbines, etc and  $w_v$  denotes the viscous work.

If we again divide through by  $g$ , we express the equation in the head (length) form as:

$$\frac{e_1}{g} + \frac{p_1}{\rho g} + \frac{v_1^2}{2g} + z_1 = \frac{e_2}{g} + \frac{p_2}{\rho} + \frac{v_2^2}{2g} + z_2 - \frac{q}{g} + \frac{w_s}{g} + \frac{w_v}{g} \quad (1.253)$$

Applying the steady energy equation to low speed liquid flow in pipes with no shaft work and negligible viscous work, yields:

$$\frac{p_1}{\rho g} + \frac{v_1^2}{2g} + z_1 = \frac{p_2}{\rho g} + \frac{v_2^2}{2g} + z_2 + \frac{e_2 - e_1 - q}{g} \quad (1.254)$$

The last term on the RHS represents the loss of useful or available energy that occurs in an incompressible fluid because of friction [185, 114].

With the given restrictions this equation is identical to the 1D mechanical energy equation for the flow between the two points (1) and (2), as can be derived directly from (1.124) [11, 102]:

$$\frac{p_1}{\rho g} + \frac{v_1^2}{2g} + z_1 = \frac{p_2}{\rho g} + \frac{v_2^2}{2g} + z_2 + \frac{\Delta p_f}{\rho g} \quad (1.255)$$

where  $\Delta p_f$  denotes the pressure drop due to friction. Equation (1.255) is sometimes referred to as the extended Bernoulli equation for viscous flows.

Anyhow, (1.255) is not properly closed yet as the pressure drop variable is still undetermined. Therefore, before we can apply (1.255) we need to parameterize the losses in terms of known flow parameters in pipes, valves, fittings, and other internal flow devices. Assuming that the viscous stress tensor reduces to a single shear stress component per unit wall surface (e.g., [102] [185]),  $\Delta p_f$  per unit cross sectional area can be related directly to the friction drag force on the tube wall surface  $-\sigma_W \pi DL$ . That is, since the friction drag force in a horizontal tube with a constant rate of flow is given by  $\Delta p_f (\frac{\pi}{4}) D^2$ , the wall shear stress yields:

$$-\sigma_W = \frac{\Delta p_f \frac{\pi}{4} D^2}{\pi DL} = \frac{\Delta p_f D}{4L} = \mu \left( \frac{dv}{dy} \right)_W \quad (1.256)$$

or

$$\Delta p_f = -4 \frac{L}{D} \sigma_W \quad (1.257)$$

where the distance between the two points (1) and (2) is denoted by  $L$ , and the tube diameter is denoted by  $D$ .

Experience shows that the wall shear stress,  $-\sigma_W$ , is nearly proportional to the kinetic energy,  $\rho \frac{v^2}{2}$ . Hence, the pressure drop can be expressed

$$\Delta p_f \approx 4f\rho \frac{L}{D} \frac{v^2}{2} \quad (1.258)$$

where  $f = \frac{\sigma_w}{\rho \frac{v^2}{2}}$  is the Fanning friction factor which can be found from friction factor charts as a function of both the Reynolds number and the surface roughness of the tube. Such charts are given in most basic textbooks on transport processes [102] [185]. Equation (1.258) is valid for duct flows of any cross section (i.e., if the diameter  $D$  is replaced by the hydraulic diameter  $D_h$ ) and for laminar and turbulent flow. For other flow devices equivalent tube friction lengths can be determined experimentally [102].

### 1.2.6 Gross Scale Average Forms of the Governing Equations

The microscopic transport equations are often considered too complex for practical applications considering reactor optimization, scale-up and design. In engineering practice integral averages of the equations over one, two or three spatial directions are used reducing the model to that of an ideal reactor model type.

It is, for example, very common in reactors to have flow predominantly in one direction, say,  $z$  in a tubular reactor. The major gradients then occur in that direction. For many cases the cross-sectional average transport equations may thus be very useful.

A detailed derivation of the area-averaged single phase transport equations is presented in the this section.

### Area-Averaged Single Phase Transport Equations

The area averaging procedure that is examined in this section is based on the theory given by [14] [33] [34] [35]. The primary aim is to provide the necessary theorems to derive the cross-sectional averaged equations that coincide with the conventional 1D chemical reactor model from first principles. To formulate these theorems we chose to adopt the same concepts as are later used deriving the corresponding multiphase equations in sect 3.4.6. Following the approach of Delhaye and Achard we start out from an analysis of a small volume of a pipe with variable cross-section area and deduce the limiting forms of the Leibnitz' and Gauss' theorems for area considered valid in the limit  $\Delta z \rightarrow 0$ . For this reason it is emphasized that these theorems are actually derived for a volume but reduces to an area formulation introducing certain simplifying approximations.

Given a tube, axis  $Oz$  (unit vector  $\mathbf{e}_z$ ) in which a volume  $V$  is cut by a fixed cross section plane over area,  $A$ , as sketched in Fig. 1.4. The lateral dimensions of the control volume extend to the conduit walls. In this notation,  $\mathbf{n}$ , is the outward directed unit vector normal to the surface of the control volume.  $\mathbf{n}_l$  is the outward directed unit vector normal to the closed curve,  $l_W(t, z)$ ,

bounding the cross section plane.  $l_W(t, z)$  is the intersection of the control volume wall interface with the cross sectional plane.

The local instantaneous balance equation (1.3) is integrated over the cross section area  $A$  limited by the pipe wall boundary  $l_W(t, z)$ . The pipe cross section is not necessary uniform but it is assumed that there is no mass flow through the pipe wall. The basic averaging problem is defined by:

$$\int_{A(t,z)} \frac{\partial(\rho\psi)}{\partial t} da + \int_{A(t,z)} \nabla \cdot (\rho\mathbf{v}\psi) da + \int_{A(t,z)} \nabla \cdot \mathbf{J} da - \int_{A(t,z)} \sum_c \rho_c \phi_c da = 0 \tag{1.259}$$

To proceed we need to apply some particular forms of the Leibnitz rule and of the Gauss theorems.

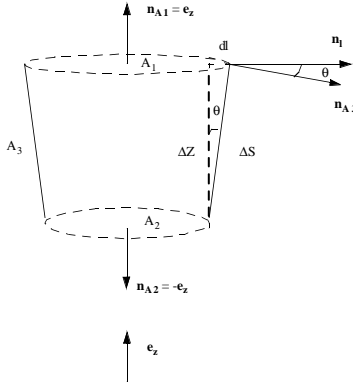


**Fig. 1.4.** Sketch of the control volume determining the basis for area-averaging of the single phase equations. For the mathematical derivation of the limiting form of the Leibnitz rule and of the Gauss theorem, note that  $\mathbf{n}_l \perp \mathbf{n}_{A_1}$  and  $\Delta z = \Delta s \cos \theta = \Delta s(\mathbf{n}_{A_3} \cdot \mathbf{n}_l)$

For small  $\Delta z$  the Leibnitz theorem can be expressed as (see Fig 1.4):

$$\begin{aligned} \frac{d}{dt} \int_{A(t,z)} f(t, \mathbf{r}) da \Delta z &= \int_{A(t,z)} \frac{\partial f(t, \mathbf{r})}{\partial t} da \Delta z + \int_{A_1(t,z+\Delta z)} f(t, \mathbf{r}) \mathbf{v}_{A_1} \cdot \mathbf{n}_{A_1} da \\ &\quad - \int_{A_2(t,z)} f(t, \mathbf{r}) \mathbf{v}_{A_2} \cdot \mathbf{n}_{A_2} da + \int_{l(t,z)} f(t, \mathbf{r}) \mathbf{v}_{A_3} \cdot \mathbf{n}_{A_3} \Delta s dl \\ &= \int_{A(t,z)} \frac{\partial f(t, \mathbf{r})}{\partial t} da \Delta z + \int_{l(t,z)} f(t, \mathbf{r}) \mathbf{v}_{A_3} \cdot \mathbf{n}_{A_3} \frac{\Delta z}{\mathbf{n}_{A_3} \cdot \mathbf{n}_l} dl \end{aligned} \tag{1.260}$$

where we have considered the control volume surfaces at  $z = z$  and at  $z = z + \Delta z$  to be stationary (i.e.,  $\mathbf{v}_{A_1} = \mathbf{v}_{A_2} = 0$ ). In certain physical situations the outer boundary face ( $A_3$ ) may not be stationary.

Dividing by  $\Delta z$ , the equation can be slightly reformulated:

$$\frac{d}{dt} \int_{A(t,z)} f(t, \mathbf{r}) da = \int_{A(t,z)} \frac{\partial f(t, \mathbf{r})}{\partial t} da + \int_{l(t,z)} f(t, \mathbf{r}) \mathbf{v}_{A_3} \cdot \mathbf{n}_{A_3} \frac{dl}{\mathbf{n}_{A_3} \cdot \mathbf{n}_l} \quad (1.261)$$

In the limit as  $\Delta z \rightarrow 0$ :

$$\frac{d}{dt} \int_{A(t,z)} f(t, \mathbf{r}) da = \int_{A(t,z)} \frac{\partial f(t, \mathbf{r})}{\partial t} da + \int_{l(t,z)} f(t, \mathbf{r}) \mathbf{v}_{A_3} \cdot \mathbf{n}_{A_3} \frac{dl}{\mathbf{n}_{A_3} \cdot \mathbf{n}_l} \quad (1.262)$$

In several papers the term on the left hand side in the above equation is reformulated using the partial derivative operator rather than the total derivative operator:

$$\frac{\partial}{\partial t} \int_{A(t,z)} f(t, \mathbf{r}) da = \int_{A(t,z)} \frac{\partial f(t, \mathbf{r})}{\partial t} da + \int_{l(t,z)} f(t, \mathbf{r}) \mathbf{v}_{A_3} \cdot \mathbf{n}_{A_3} \frac{dl}{\mathbf{n}_{A_3} \cdot \mathbf{n}_l} \quad (1.263)$$

The justification of this reformulation is apparently related to the physical interpretation of the mathematical operators used here. In this case the total derivative notation is adopted for an operator determining the time derivation at a fixed point in space, and not for a time derivative along a fluid particle trajectory (see [182], p. 79 [183], p. 51 [82], p. 13).

In a slightly generalized notation the limiting form of the Leibnitz theorem is given by:

$$\frac{\partial}{\partial t} \int_{A(t,z)} f(\mathbf{r}, t) da = \int_{A(t,z)} \frac{\partial f(\mathbf{r}, t)}{\partial t} da + \int_{l_W(t,z)} f(\mathbf{r}, t) \mathbf{v}_W \cdot \mathbf{n}_W \frac{dl}{\mathbf{n}_W \cdot \mathbf{n}_l} \quad (1.264)$$

where  $\mathbf{v}_W \cdot \mathbf{n}_W$  is the displacement velocity of a point on the boundary face,  $A_W$ .

For a control volume varying in the space dimensions only, this relation can be further simplified:

$$\frac{\partial}{\partial t} \int_{A(z)} f(\mathbf{r}, t) da = \int_{A(z)} \frac{\partial f(\mathbf{r}, t)}{\partial t} da \quad (1.265)$$

Similarly, for small  $\Delta z$  the Gauss theorem can be expressed as (see Fig. 1.4):

$$\begin{aligned}
 \int_{A(t,z)} \nabla \cdot \mathbf{B} da \Delta z &= \int_{A_1(t,z+\Delta z)} \mathbf{n}_{A_1} \cdot \mathbf{B} da + \int_{A_2(t,z)} \mathbf{n}_{A_2} \cdot \mathbf{B} da + \int_{l(t,z)} \mathbf{n}_{A_3} \cdot \mathbf{B} \Delta s dl \\
 &= \int_{A_1(t,z+\Delta z)} \mathbf{e}_z \cdot \mathbf{B} da - \int_{A_2(t,z)} \mathbf{e}_z \cdot \mathbf{B} da + \int_{l(t,z)} \mathbf{n}_{A_3} \cdot \mathbf{B} \frac{\Delta z dl}{\mathbf{n}_{A_3} \cdot \mathbf{n}_l}
 \end{aligned} \tag{1.266}$$

or

$$\int_{A(t,z)} \nabla \cdot \mathbf{B} da = \frac{1}{\Delta z} \left[ \int_{A_1(t,z+\Delta z)} \mathbf{e}_z \cdot \mathbf{B} da - \int_{A_2(t,z)} \mathbf{e}_z \cdot \mathbf{B} da \right] + \int_{l(t,z)} \mathbf{n}_{A_3} \cdot \mathbf{B} \frac{dl}{\mathbf{n}_{A_3} \cdot \mathbf{n}_l} \tag{1.267}$$

In the limit as  $\Delta z \rightarrow 0$

$$\int_{A(t,z)} \nabla \cdot \mathbf{B} da = \frac{\partial}{\partial z} \int_{A(t,z)} \mathbf{e}_z \cdot \mathbf{B} da + \int_{l(t,z)} \mathbf{n}_{A_3} \cdot \mathbf{B} \frac{dl}{\mathbf{n}_{A_3} \cdot \mathbf{n}_l} \tag{1.268}$$

In a slightly generalized notation the limiting form of the Gauss theorem (where we let  $\mathbf{B}$  be a vector or a tensor) is given by:

$$\int_{A(t,z)} \nabla \cdot \mathbf{B} da = \frac{\partial}{\partial z} \int_{A(t,z)} \mathbf{e}_z \cdot \mathbf{B} da + \int_{l_W(t,z)} \mathbf{n}_W \cdot \mathbf{B} \frac{dl}{\mathbf{n}_W \cdot \mathbf{n}_l} \tag{1.269}$$

In the case of  $\mathbf{B}$  being a vector, the component of the vector  $\mathbf{B}$  on  $Oz$  is given by  $\mathbf{e}_z \cdot \mathbf{B} = B_z$ .

If we take  $\mathbf{B} = \mathbf{e}_z$  we obtain:

$$\int_{A(t,z)} \nabla \cdot \mathbf{e}_z da = \frac{\partial}{\partial z} \int_{A(t,z)} \mathbf{e}_z \cdot \mathbf{e}_z da + \int_{l(t,z)} \mathbf{n} \cdot \mathbf{e}_z \frac{dl}{\mathbf{n} \cdot \mathbf{n}_l} \tag{1.270}$$

which gives the following definition:

$$\frac{\partial A(t,z)}{\partial z} = - \int_{l(t,z)} \mathbf{n} \cdot \mathbf{e}_z \frac{dl}{\mathbf{n} \cdot \mathbf{n}_l} \tag{1.271}$$

Introducing these relations into the cross section area averaged equation (1.259) yields:

$$\begin{aligned}
 \frac{\partial}{\partial t} \int_{A(t,z)} (\rho\psi) da + \frac{\partial}{\partial z} \int_{A(t,z)} (\rho v_z \psi) da + \frac{\partial}{\partial z} \int_{A(t,z)} (\mathbf{e}_z \cdot \mathbf{J}) - \sum_c \int_{A(t,z)} (\rho_c \phi_c) da \\
 = - \int_{l_W(t,z)} \mathbf{n} \cdot \mathbf{J} \frac{dl}{\mathbf{n} \cdot \mathbf{n}_l} + \int_{l_W(t,z)} \rho\psi \mathbf{n}_W \cdot (\mathbf{v}_W - \mathbf{v}) \frac{dl}{\mathbf{n}_W \cdot \mathbf{n}_l}
 \end{aligned} \tag{1.272}$$

where  $v_z$  is the  $z$ -component of the velocity vector,  $\mathbf{v}$ .

As we assume no mass flow through the pipe wall and adopt the no-slip condition, the wall convection in the last term equals zero as  $\mathbf{n}_W \cdot (\mathbf{v}_W - \mathbf{v}) = 0$  at the wall.

The area averaging operator is defined by:

$$\langle \psi \rangle_A = \frac{1}{A} \int_{A(t,z)} \psi da \quad (1.273)$$

If we apply (1.273) to the area averaged generic equation (1.272), the generic equation can be expressed as follows in terms of area averaged quantities:

$$\begin{aligned} & \frac{\partial(A\langle\rho\psi\rangle_A)}{\partial t} + \frac{\partial}{\partial z}(A\langle\rho v_z\psi\rangle_A) + \frac{\partial}{\partial z}(A\langle\mathbf{e}_z \cdot \mathbf{J}\rangle_A) - \sum_c A\langle\rho_c\phi_c\rangle_A \\ &= - \int_{l_W(t,z)} \mathbf{n} \cdot \mathbf{J} \frac{dl}{\mathbf{n} \cdot \mathbf{n}_l} \end{aligned} \quad (1.274)$$

For each balance law, the values of  $\psi$ ,  $\mathbf{J}$  and  $\phi$  defines the transported quantity, the diffusion flux and the source term, respectively.  $\mathbf{v}$  denotes the velocity vector,  $\mathbf{T}$  the total stress tensor,  $\mathbf{g}_c$  the net external body force per unit of mass,  $e$  the internal energy per unit of mass,  $\mathbf{q}$  the heat flux,  $s$  the entropy per unit mass,  $h$  the enthalpy per unit mass,  $\omega_s$  the mass fraction of species  $s$ , and  $T$  the temperature.

By means of these definitions, (1.274) gives the instantaneous area-averaged equations for the balance of total mass, momentum, total energy, and species mass.

*Continuity Equation:*

To achieve the mass balance the values of the generic quantities are defined as specified in Table 1.1:  $\psi = 1$ ,  $\mathbf{J} = 0$ , and  $\phi_c = 0$ .

$$\frac{\partial(A\langle\rho\rangle_A)}{\partial t} + \frac{\partial}{\partial z}(A\langle\rho v_z\rangle_A) = 0 \quad (1.275)$$

*Momentum Equation:*

To obtain the momentum balance the values of the generic quantities are defined as specified in Table 1.1:  $\psi = \mathbf{v}$ ,  $\mathbf{J} = \mathbf{T}$ , and  $\phi_c = \mathbf{g}_c$ .

$$\begin{aligned} & \frac{\partial(A\langle\rho\mathbf{v}\rangle_A)}{\partial t} + \frac{\partial}{\partial z}(A\langle\rho v_z\mathbf{v}\rangle_A) + \frac{\partial}{\partial z}(A\langle\mathbf{e}_z \cdot \mathbf{T}\rangle_A) \\ &= \sum_c A\langle\rho_c\mathbf{g}_c\rangle_A - \int_{l_W(t,z)} \mathbf{n} \cdot \mathbf{T} \frac{dl}{\mathbf{n} \cdot \mathbf{n}_l} \end{aligned} \quad (1.276)$$

If we split the total stress tensor  $\mathbf{T}$  into a pressure term  $pe$  and a viscous stress tensor  $\boldsymbol{\sigma}$  term, the vector equation can be expressed as:

$$\begin{aligned} & \frac{\partial(A\langle\rho\mathbf{v}\rangle_A)}{\partial t} + \frac{\partial}{\partial z}(A\langle\rho v_z\mathbf{v}\rangle_A) + \frac{\partial}{\partial z}(A\langle p\mathbf{e}_z\rangle_A) \\ & + \frac{\partial}{\partial z}(A\langle\mathbf{e}_z\cdot\boldsymbol{\sigma}\rangle_A) = \sum_c A\langle\rho_c\mathbf{g}_c\rangle_A - \int_{l_W(t,z)} \mathbf{n}\cdot\mathbb{T} \frac{dl}{\mathbf{n}\cdot\mathbf{n}_l} \end{aligned} \quad (1.277)$$

The momentum equation of interest in 1D engineering analysis is normally the linear momentum equation in the axial direction. It is therefore customary to project the terms in the equation along the tube axis. This operation is done by taking the scalar vector product of all the terms in (1.277) with the unit vector  $\mathbf{e}_z$ . The result is:

$$\begin{aligned} & \frac{\partial(A\langle\rho v_z\rangle_A)}{\partial t} + \frac{\partial}{\partial z}(A\langle\rho v_z v_z\rangle_A) + \frac{\partial}{\partial z}(A\langle p\rangle_A) \\ & + \frac{\partial}{\partial z}(A\langle(\mathbf{e}_z\cdot\boldsymbol{\sigma})\cdot\mathbf{e}_z\rangle_A) = \sum_c A\langle\rho_c g_{c,z}\rangle_A - \int_{l_W(t,z)} (\mathbf{n}\cdot\mathbb{T})\cdot\mathbf{e}_z \frac{dl}{\mathbf{n}\cdot\mathbf{n}_l} \end{aligned} \quad (1.278)$$

It is noted that if the velocity is not constant but varies across the cross sectional area, (1.273) can be used calculating the average of the product occurring in the momentum equation:

$$\langle v_z^2 \rangle_A = \frac{1}{A} \int_{A(t,z)} v_z^2 da \quad (1.279)$$

To assess the physical deviation between the average of products and the product of averages a momentum velocity correction factor can be defined by  $C_M = \langle v_z \rangle_A^2 / \langle v_z^2 \rangle_A$ . By use of the Hagen-Poiseuille law (1.353) and the power law velocity profile (1.354) it follows that at steady state  $C_M$  has a value of about 0.95 for turbulent flow and 0.75 for laminar flow [55]. In practice a value of 1 is used in turbulent flow so that  $\langle v_z^2 \rangle_A$  is simply replaced by the averaged bulk velocity  $\langle v_z \rangle_A^2$ . On the other hand, for laminar flows a correction factor is needed. For more precise calculations a simplified (not averaged!) 2D model is often considered for ideal axisymmetric pipe flows [52, 69].

Moreover, it is frequently assumed that the pressure  $p$  is almost constant along  $l_W$  and approximated by an average wall pressure  $\langle p \rangle_W$ . Therefore, by use of the definition (1.271), (1.278) can be written as:

$$\begin{aligned} & \frac{\partial(A\langle\rho v_z\rangle_A)}{\partial t} + \frac{\partial}{\partial z}(A\langle\rho v_z v_z\rangle_A) + A \frac{\partial\langle p \rangle_A}{\partial z} + \frac{\partial}{\partial z}(A\langle\boldsymbol{\sigma}_{zz}\rangle_A) \\ & = \sum_c A\langle\rho_c g_{c,z}\rangle_A - \int_{l_W(t,z)} (\mathbf{n}\cdot\boldsymbol{\sigma})\cdot\mathbf{e}_z \frac{dl}{\mathbf{n}\cdot\mathbf{n}_l} + (\langle p \rangle_W - \langle p \rangle_A) \frac{\partial A}{\partial z} \end{aligned} \quad (1.280)$$

A rough model closure can be achieved assuming that the averaged wall pressure  $\langle p \rangle_W$  is equal to the averaged pressure  $\langle p \rangle_A$ . The equation can then be slightly simplified:

$$\begin{aligned}
& \frac{\partial(A\langle\rho v_z\rangle_A)}{\partial t} + \frac{\partial}{\partial z}(A\langle\rho v_z v_z\rangle_A) + A\frac{\partial\langle p\rangle_A}{\partial z} + \frac{\partial}{\partial z}(A\langle\sigma_{zz}\rangle_A) \\
& = \sum_c A\langle\rho_c g_{c,z}\rangle_A - \int_{l_W(t,z)} (\mathbf{n} \cdot \boldsymbol{\sigma}) \cdot \mathbf{e}_z \frac{dl}{\mathbf{n} \cdot \mathbf{n}_l}
\end{aligned} \tag{1.281}$$

The last term on the RHS is the component of the averaged wall shear stress in the  $z$  direction. The wall shear stress term is often rewritten as:

$$- \int_{l_W(t,z)} (\mathbf{n} \cdot \boldsymbol{\sigma}) \cdot \mathbf{e}_z \frac{dl}{\mathbf{n} \cdot \mathbf{n}_l} = -\langle(\mathbf{n} \cdot \boldsymbol{\sigma}) \cdot \mathbf{e}_z\rangle_W S_I \tag{1.282}$$

where  $\langle(\mathbf{n} \cdot \boldsymbol{\sigma}) \cdot \mathbf{e}_z\rangle_W$  is the perimeter averaged wall stress, and  $S_I$  denotes the perimeter which is defined by  $S_I = \int_{l_W(t,z)} \frac{dl}{\mathbf{n} \cdot \mathbf{n}_l}$ . The averaged wall shear stress is approximated by the expression for steady flow given by

$$\begin{aligned}
-\langle(\mathbf{n} \cdot \boldsymbol{\sigma}) \cdot \mathbf{e}_z\rangle_{l_I} \frac{S_I}{A} & \approx -\frac{1}{2} f \langle\rho\rangle_A |v_z\rangle_A |v_z\rangle_A \frac{S_I}{4A} \\
& = -\frac{1}{2} f \langle\rho\rangle_A |v_z\rangle_A |v_z\rangle_A \frac{1}{D_h},
\end{aligned} \tag{1.283}$$

where  $D_h$  is the hydraulic diameter, and  $f$  is the Fanning friction factor [180] [6] [74] [9] [82]. For fully developed flows in circular pipes and tubes the friction factor has been determined experimentally and presented in a so-called Moody diagram which can be found in most introductory textbooks on engineering fluid flows. The commonly used semi-empirical friction factor relations for pipe flows are [114, 13]:

$$f = \begin{cases} \frac{16}{Re} & \text{for } Re < 2100, \\ \frac{0.0791}{Re^{1/4}} & \text{for } 2100 \leq Re < 10^5, \text{ and} \\ \frac{1}{(4.0 \log(Re\sqrt{f}) - 0.4)^2} & \text{for } 2300 < Re < 4 \times 10^6. \end{cases} \tag{1.284}$$

in which the Reynolds number is defined by:  $Re = \frac{\rho\langle v_z\rangle_A d_r}{\mu}$ .

### Energy Equation

To achieve the energy balance the values of the generic quantities are defined as specified in Table 1.1:  $\psi = (\frac{1}{2}v^2 + e)$ ,  $\mathbf{J} = (\mathbf{q} + \mathbb{T} \cdot \mathbf{v})$ ,  $\phi = \mathbf{g} \cdot \mathbf{v}$ .

$$\begin{aligned}
& \frac{\partial(A\langle\rho(\frac{1}{2}v^2 + e)\rangle_A)}{\partial t} + \frac{\partial}{\partial z}(A\langle\rho v_z(\frac{1}{2}v^2 + e)\rangle_A) \\
& + \frac{\partial}{\partial z}(A\langle(\mathbb{T} \cdot \mathbf{v}) \cdot \mathbf{e}_z\rangle_A) + \frac{\partial}{\partial z}(A\langle\mathbf{q} \cdot \mathbf{e}_z\rangle_A) \\
& = \sum_c A\langle\rho_c \mathbf{g}_c \cdot \mathbf{v}_c\rangle_A - \int_{l_W(t,z)} \mathbf{q} \cdot \mathbf{n} \frac{dl}{\mathbf{n} \cdot \mathbf{n}_l} - \int_{l_W(t,z)} (\mathbb{T} \cdot \mathbf{v}) \cdot \mathbf{n} \frac{dl}{\mathbf{n} \cdot \mathbf{n}_l}
\end{aligned} \tag{1.285}$$

Quite often  $\mathbf{v} \cdot \mathbf{v} = v^2 \approx v_z^2$  when the flow is dominant in the  $z$ -direction. This assumption is necessary in order to achieve a solvable set of equations considering that (1.280) is used calculating  $\langle v_z \rangle_A$ .

In engineering calculations of process units it is often convenient to introduce the enthalpy per unit of mass, i.e.,  $h = e + \frac{p}{\rho}$ , and rewrite the energy equation as:

$$\begin{aligned} & \frac{\partial(A\langle\rho(\frac{1}{2}v^2 + e)\rangle_A)}{\partial t} + \frac{\partial}{\partial z}(A\langle\rho v_z(\frac{1}{2}v^2 + h)\rangle_A) \\ & + \frac{\partial}{\partial z}(A\langle(\boldsymbol{\sigma} \cdot \mathbf{v}) \cdot \mathbf{e}_z\rangle_A) + \frac{\partial}{\partial z}(A\langle\mathbf{q} \cdot \mathbf{e}_z\rangle_A) \\ & = \sum_c A\langle\rho_c \mathbf{g}_c \cdot \mathbf{v}_c\rangle_A - \int_{l_W(t,z)} \mathbf{q} \cdot \mathbf{n} \frac{dl}{\mathbf{n} \cdot \mathbf{n}_l} \end{aligned} \quad (1.286)$$

It is noted that there is no work associated with the wall stresses since the velocity at the wall is zero (no-slip assumption) [25] [13].

### Species Mass Balance

For the species mass balance the values of the generic quantities are defined in accordance with Table 1.1:  $\psi = \omega_s$ ,  $\mathbf{J} = \mathbf{j}_s$ ,  $\phi = R_s/\rho_c$ .

$$\frac{\partial(A\langle\rho\omega_s\rangle_A)}{\partial t} + \frac{\partial}{\partial z}(A\langle\rho v_z\omega_s\rangle_A) + \frac{\partial}{\partial z}(A\langle\mathbf{e}_z \cdot \mathbf{j}_s\rangle_A) = A\langle R_s\rangle_A \quad (1.287)$$

## The Governing Instantaneous Area Averaged Equations

To obtain a solvable set of equations the averages of products have to be related to products of averages. One simple way of doing this operation is to approximate the averages of products by the products of averages<sup>27</sup>. A closed set of modeled instantaneous area averaged equations is listed below.

### Continuity Equation:

The instantaneous area averaged continuity equation deduced from (1.275) is expressed as:

$$\frac{\partial}{\partial t}(\langle\rho\rangle_A) + \frac{1}{A} \frac{\partial}{\partial z}(A\langle\rho\rangle_A\langle v_z\rangle_A) = 0 \quad (1.288)$$

### Momentum Equation:

The instantaneous area averaged momentum equation deduced from (1.280) is expressed as:

<sup>27</sup> There are also other more sophisticated methods available to relate the average of products to the products of average as discussed in chap 3.3. Nevertheless, the conventional model formulation used in chemical reaction engineering is normally derived in accordance with the procedure given in this section.

$$\begin{aligned}
& \frac{\partial}{\partial t} \left( \langle \rho \rangle_A \langle v_z \rangle_A \right) + \frac{1}{A} \frac{\partial}{\partial z} \left( A \langle \rho \rangle_A \langle v_z \rangle_A \langle v_z \rangle_A \right) \\
&= - \frac{\partial \langle p \rangle_A}{\partial z} - \frac{1}{A} \frac{\partial}{\partial z} \left( A \langle \sigma_{zz} \rangle_A \right) + \sum_c \langle \rho_c g_{c,z} \rangle_A \\
& \quad - \frac{1}{2} f \langle \rho \rangle_A | \langle v_z \rangle_A | \langle v_z \rangle_A \frac{S_I}{4A} + \frac{1}{A} (\langle p \rangle_W - \langle p \rangle_A) \frac{\partial A}{\partial z}
\end{aligned} \tag{1.289}$$

in which the last term is retained in case a more elaborated closure for the wall pressure is required.

### *Energy Equation*

The instantaneous area averaged energy equation deduced from (1.285) is expressed as:

$$\begin{aligned}
& \frac{\partial}{\partial t} \left( \langle \rho \rangle_A \left( \frac{1}{2} \langle v \rangle_A^2 + \langle e \rangle_A \right) \right) \\
& + \frac{1}{A} \frac{\partial}{\partial z} \left( A \langle \rho \rangle_A \langle v_z \rangle_A \left( \frac{1}{2} \langle v \rangle_A^2 + \langle e \rangle_A \right) \right) \\
& + \frac{1}{A} \frac{\partial}{\partial z} \left( A (\langle \mathbf{T} \rangle_A \cdot \langle \mathbf{v} \rangle_A) \cdot \mathbf{e}_z \right) + \frac{1}{A} \frac{\partial}{\partial z} \left( A \langle \mathbf{q} \cdot \mathbf{e}_z \rangle_A \right) \\
& = \sum_c \langle \rho_c \rangle_A \langle \mathbf{g}_c \rangle_A \cdot \langle \mathbf{v}_c \rangle_A - \langle \mathbf{n} \cdot \mathbf{q} \rangle_W \frac{S_I}{A}
\end{aligned} \tag{1.290}$$

To be able to apply the 1D equations one often has to estimate terms that cannot be calculated directly without further empirical information, or we might simply neglect the insignificant terms for each particular application. The work associated with the term  $(\langle \mathbf{T} \rangle_A \cdot \langle \mathbf{v} \rangle_A) \cdot \mathbf{e}_z$  can be split into two contributions. In chemical reactor analysis (and many other low Mach number flows in chemical engineering [13]) the viscous work  $(\langle \boldsymbol{\sigma} \rangle_A \cdot \langle \mathbf{v} \rangle_A) \cdot \mathbf{e}_z$  is normally neglectable relative to the pressure work  $\langle p \rangle_A \langle v_z \rangle_A$ .

The wall heat flux term can be approximated in terms of the convective heat transfer coefficient:

$$- \langle \mathbf{n} \cdot \mathbf{q} \rangle_W \frac{S_I}{A} = -h_W (\langle T \rangle_A - \langle T \rangle_W) \frac{S_I}{A} \tag{1.291}$$

Alternatively, the wall heat transfer flux can be expressed in terms of an overall heat transfer coefficient. For reactors with constant cross-sectional area  $A$  the geometric factor reduces to  $\frac{S_I}{A} = \frac{2\pi R_r}{\pi R_r^2} = \frac{2}{R_r} = \frac{4}{d_r}$ . It is understood that  $R_r$  and  $d_r$  are the radius and diameter of the reactor (tube).

Formulating the equation in terms of the enthalpy per unit of mass,  $h = e + \frac{p}{\rho}$ , we obtain:

$$\begin{aligned}
 & \frac{\partial}{\partial t} \left( \langle \rho \rangle_A \left( \frac{1}{2} \langle v \rangle_A^2 + \langle e \rangle_A \right) \right) \\
 & + \frac{1}{A} \frac{\partial}{\partial z} \left( A \langle \rho \rangle_A \langle v_z \rangle_A \left( \frac{1}{2} \langle v \rangle_A^2 + \langle h \rangle_A \right) \right) \\
 & + \frac{1}{A} \frac{\partial}{\partial z} \left( A (\langle \boldsymbol{\sigma} \rangle_A \cdot \langle \mathbf{v} \rangle_A) \cdot \mathbf{e}_z \right) + \frac{1}{A} \frac{\partial}{\partial z} \left( A \langle \mathbf{q} \cdot \mathbf{e}_z \rangle_A \right) \\
 & = \sum_c \langle \rho_c \mathbf{g}_c \cdot \mathbf{v}_c \rangle_A - \langle \mathbf{n} \cdot \mathbf{q} \rangle_W \frac{S_I}{A}
 \end{aligned} \tag{1.292}$$

### Mechanical Energy Equation

The engineering mechanical energy equation is derived by multiplying (1.289) with the averaged velocity  $\langle v_z \rangle_A$ . That is,

$$\begin{aligned}
 \langle v_z \rangle_A \left[ \frac{\partial}{\partial t} \left( \langle \rho \rangle_A \langle v_z \rangle_A \right) + \frac{1}{A} \frac{\partial}{\partial z} \left( A \langle \rho \rangle_A \langle v_z \rangle_A \langle v_z \rangle_A \right) \right] \\
 = - \frac{\partial \langle p \rangle_A}{\partial z} - \frac{1}{A} \frac{\partial}{\partial z} (A \langle \boldsymbol{\sigma}_{zz} \rangle_A) + \sum_c \langle \rho_c g_{c,z} \rangle_A \\
 - \frac{\langle \mathbf{n} \cdot \boldsymbol{\sigma}_z \rangle_W S_I}{A} + \frac{1}{A} (\langle p \rangle_W - \langle p \rangle_A) \frac{\partial A}{\partial z}
 \end{aligned} \tag{1.293}$$

After a little manipulation of the terms, we get:

$$\begin{aligned}
 & \frac{\partial}{\partial t} \left( \langle \rho \rangle_A \frac{1}{2} (\langle v_z \rangle_A)^2 \right) + \frac{1}{A} \frac{\partial}{\partial z} \left( A \langle \rho \rangle_A \langle v_z \rangle_A \frac{1}{2} (\langle v_z \rangle_A)^2 \right) \\
 & = - \langle v_z \rangle_A \frac{\partial \langle p \rangle_A}{\partial z} - \frac{\langle v_z \rangle_A}{A} \frac{\partial}{\partial z} (A \langle \boldsymbol{\sigma}_{zz} \rangle_A) \\
 & + \langle v_z \rangle_A \langle \rho \rangle_A \sum_c \langle \omega_c \rangle_A \langle g_{c,z} \rangle_A - \frac{1}{2} f \langle v_z \rangle_A \langle v_z \rangle_A^2 \frac{S_I}{4A} \\
 & + \frac{1}{A} (\langle p \rangle_W - \langle p \rangle_A) \langle v_z \rangle_A \frac{\partial A}{\partial z}
 \end{aligned} \tag{1.294}$$

A more rigorous formulation of the mechanical energy equation might be achieved by averaging the fundamental kinetic energy equation (1.124) over the cross-section area. If the velocity is not constant but varies across the cross sectional area we can use (1.273) to calculate the average of the products occurring in the corresponding 1D kinetic energy equation:

$$\langle v_z^3 \rangle_A = \frac{1}{A} \int_{A(t,z)} v_z^3 da \tag{1.295}$$

Again, to assess the physical deviation between the average of products and the product of averages a kinetic-energy velocity correction factor can be defined by  $C_K = \langle v_z^3 \rangle_A / \langle v_z \rangle_A^3$ . By use of the Hagen-Poiseuille law (1.353) and the power law velocity profile (1.354) it follows that at steady state  $C_K$  takes a value of about 0.95 for turbulent flow and 0.5 for laminar flow [55]. In practice a value of 1 is used in turbulent flow so  $\langle v_z^3 \rangle_A$  is simply replaced by the averaged bulk velocity  $\langle v_z \rangle_A^3$ .

*Internal Energy Equation*

The instantaneous area averaged internal energy equation can be derived by subtracting the mechanical energy equation (1.294) from the total energy equation (1.290). The result can be expressed as:

$$\begin{aligned}
& \frac{\partial}{\partial t} \left( \langle \rho \rangle_A \langle e \rangle_A \right) + \frac{1}{A} \frac{\partial}{\partial z} \left( A \langle \rho \rangle_A \langle v_z \rangle_A \langle e \rangle_A \right) \\
&= - \frac{\langle p \rangle_A}{A} \frac{\partial}{\partial z} (A \langle v_z \rangle_A) + \sum_c \langle \mathbf{j}_c \cdot \mathbf{g}_c \rangle_A \\
&\quad - \frac{1}{A} \frac{\partial}{\partial z} \left( A \langle \langle \boldsymbol{\sigma} \rangle_A \cdot \langle \mathbf{v} \rangle_A \cdot \mathbf{e}_z \right) + \frac{\langle v_z \rangle_A}{A} \frac{\partial}{\partial z} (A \langle \sigma_{zz} \rangle_A) \\
&\quad - \frac{1}{A} \frac{\partial}{\partial z} (A \langle \mathbf{q} \cdot \mathbf{e}_z \rangle_A) - \langle \mathbf{n} \cdot \mathbf{q} \rangle_W \frac{S_I}{A} + \frac{1}{2} f |\langle v_z \rangle_A| \langle v_z \rangle_A^2 \frac{S_I}{4A} \quad (1.296) \\
&\quad - \frac{1}{A} (\langle p \rangle_W - \langle p \rangle_A) \langle v_z \rangle_A \frac{\partial A}{\partial z} \\
&\approx - \frac{\langle p \rangle_A}{A} \frac{\partial}{\partial z} (A \langle v_z \rangle_A) + \sum_c \langle J_{c,z} \rangle_A \langle g_{c,z} \rangle_A \\
&\quad - \frac{1}{A} \frac{\partial}{\partial z} (A \langle q_z \rangle_A) - \langle \mathbf{n} \cdot \mathbf{q} \rangle_W \frac{S_I}{A} + \frac{1}{2} f |\langle v_z \rangle_A| \langle v_z \rangle_A^2 \frac{S_I}{4A} \\
&\quad - \frac{1}{A} (\langle p \rangle_W - \langle p \rangle_A) \langle v_z \rangle_A \frac{\partial A}{\partial z}
\end{aligned}$$

in which the bulk viscous dissipation terms are neglected. In addition, the work term given by the dot product between the species mass diffusion flux and the body forces other than gravity is approximated by the  $z$ -component of the actual term.

*Enthalpy Equation*

The instantaneous enthalpy balance can be derived from (1.296) by introducing the area averaged enthalpy per unit of mass:  $\langle h \rangle_A = \langle e \rangle_A + \frac{\langle p \rangle_A}{\langle \rho \rangle_A}$ . The result is [74]:

$$\begin{aligned}
& \frac{\partial}{\partial t} \left( \langle \rho \rangle_A \langle h \rangle_A \right) + \frac{1}{A} \frac{\partial}{\partial z} \left( A \langle \rho \rangle_A \langle v_z \rangle_A \langle h \rangle_A \right) \\
&\approx \frac{\partial \langle p \rangle_A}{\partial t} + \langle v_z \rangle_A \frac{\partial \langle p \rangle_A}{\partial z} + \sum_c \langle J_{c,z} \rangle_A \langle g_{c,z} \rangle_A \quad (1.297) \\
&\quad - \frac{1}{A} \frac{\partial}{\partial z} (A \langle q_z \rangle_A) - \langle \mathbf{n} \cdot \mathbf{q} \rangle_W \frac{S_I}{A} + \frac{1}{2} f |\langle v_z \rangle_A| \langle v_z \rangle_A^2 \frac{S_I}{4A} \\
&\quad - \frac{1}{A} (\langle p \rangle_W - \langle p \rangle_A) \langle v_z \rangle_A \frac{\partial A}{\partial z}
\end{aligned}$$

*Temperature Equation*

The instantaneous temperature equation can be derived from (1.297) by use of the complete differential (1.142). The area averaged form of the complete differential can be approximated as:

$$\begin{aligned}
 \frac{D\langle h \rangle_A}{Dt} &= \langle C_p \rangle_A \frac{D\langle T \rangle_A}{Dt} \\
 &+ \left( \frac{1}{\langle \rho \rangle_A} + \frac{\langle T \rangle_A}{\langle \rho \rangle_A^2} \left( \frac{\partial \langle \rho \rangle_A}{\partial \langle T \rangle_A} \right)_{p,\omega} \right) \frac{D\langle p \rangle_A}{Dt} \\
 &- \frac{1}{\langle \rho \rangle_A} \left[ \sum_{c=1}^N \langle \bar{h}_c \rangle_A \frac{\partial}{\partial z} \left( \frac{\langle J_{c,z} \rangle_A}{M_{w_c}} \right) + \right. \\
 &\quad \left. \sum_{r=1}^q \langle r_{r,c_{\text{ref}}} \rangle_A (-\Delta \langle \bar{H}_{r,c_{\text{ref}}} \rangle_A) \right]
 \end{aligned} \tag{1.298}$$

After reformulating the terms on the LHS of (1.297) by use of the area averaged continuity equation (1.288), we can eliminate the enthalpy quantity by use of the given relation (1.298). The area averaged enthalpy balance is then written as an equation for temperature:

$$\begin{aligned}
 &\langle \rho \rangle_A \langle C_p \rangle_A \left( \frac{\partial \langle T \rangle_A}{\partial t} + \langle v_z \rangle_A \frac{\partial \langle T \rangle_A}{\partial z} \right) \\
 &\approx - \frac{\langle T \rangle_A}{\langle \rho \rangle_A} \left( \frac{\partial \langle \rho \rangle_A}{\partial \langle T \rangle_A} \right)_{p,\omega} \frac{D\langle p \rangle_A}{Dt} + \sum_c \langle J_{c,z} \rangle_A \langle g_{c,z} \rangle_A \\
 &+ \sum_{c=1}^N \langle \bar{h}_c \rangle_A \frac{\partial}{\partial z} \left( \frac{\langle J_{c,z} \rangle_A}{M_{w_c}} \right) + \sum_{r=1}^q \langle r_{r,c_{\text{ref}}} \rangle_A (-\Delta \langle \bar{H}_{r,c_{\text{ref}}} \rangle_A) \\
 &- \frac{1}{A} \frac{\partial}{\partial z} (A \langle q_z \rangle_A) - \langle \mathbf{n} \cdot \mathbf{q} \rangle_W \frac{S_I}{A} + \frac{1}{2} f |\langle v_z \rangle_A| \langle v_z \rangle_A^2 \frac{S_I}{4A} \\
 &- \frac{1}{A} (\langle p \rangle_W - \langle p \rangle_A) \langle v_z \rangle_A \frac{\partial A}{\partial z}
 \end{aligned} \tag{1.299}$$

### Species Mass Balance

The instantaneous species mass balance is deduced from (1.287) replacing the average of products with the products of average:

$$\begin{aligned}
 &\frac{\partial (\langle \rho \rangle_A \langle \omega_s \rangle_A)}{\partial t} + \frac{1}{A} \frac{\partial}{\partial z} (A \langle \rho \rangle_A \langle v_z \rangle_A \langle \omega_s \rangle_A) \\
 &= - \frac{1}{A} \frac{\partial}{\partial z} (A \langle J_{s,z} \rangle_A) + \langle R_s \rangle_A
 \end{aligned} \tag{1.300}$$

### 1.2.7 Dispersion Models

In chemical reaction engineering single phase reactors are often modeled by a set of simplified 1D heat and species mass balances. In these cases the axial velocity profile can be prescribed or calculate from the continuity equation. The reactor pressure is frequently assumed constant or calculated from simple relations deduced from the area averaged momentum equation. For gases the density is normally calculated from the ideal gas law. Moreover, in situations where the velocity profile is neither flat nor ideal the effects of radial convective

mixing have been lumped into the dispersion coefficient. With these model simplifications the semi-empirical correlations for the dispersion coefficients will be system- and scale specific and far from general.

### Axial Dispersion models

The axial dispersion model is developed based on the 1D form of the governing equations given in sect 1.2.6. However, the instantaneous area averaged model equations are also Reynolds averaged to enable reactor simulations with practicable time resolutions. For the time after area averaged models, the instantaneous variables are decomposed and Reynolds averaged in the standard way. If we drop the averaging signs, the basic 1D species mass balance deduced from (1.300) is given by:

$$\frac{\partial}{\partial t}(\rho\omega_s) + \frac{\partial}{\partial z}(\rho v_z \omega_s) = \frac{\partial}{\partial z}(\rho D_{\text{eff}} \frac{\partial \omega_s}{\partial z}) + R_s \quad (1.301)$$

and the corresponding heat or temperature equation deduced from (1.299) yields:

$$\rho C_p \frac{\partial T}{\partial t} + \rho C_p v_z \frac{\partial T}{\partial z} = \frac{\partial}{\partial z}(k_{\text{eff}} \frac{\partial T}{\partial z}) + R_s(-\Delta H_{R_s}) + \frac{4U}{d_r}(T_{\text{sur}} - T) \quad (1.302)$$

where  $T_{\text{sur}}$  is the temperature of the surroundings and  $U$  is an overall heat transfer coefficient. In addition, the effective transport coefficients are included as a reminder that the temporal covariances resulting from the Reynolds averaging procedure are normally modeled adopting the gradient hypothesis and the Boussinesq turbulent viscosity concept.

The initial conditions used for dynamics reactor simulations depend upon the start-up procedure adopted in industry for each particular chemical process. A possible set of initial conditions corresponds to uniform variable fields given by the inlet values.

*The initial condition at  $t = 0$ :*

$$\begin{aligned} v_z &= v_{z,\text{in}} \\ \rho &= \rho_{\text{in}} \\ \omega_s &= \omega_{s,\text{in}} \\ T &= T_{\text{in}} \end{aligned} \quad (1.303)$$

The proper choice of boundary conditions has been extensively discussed in the literature. The conditions most frequently used those proposed by Danckwerts [26].

*The inlet boundary condition at  $z = 0$ :*

$$v_{z,\text{in}}\rho_{\text{in}}\omega_{s,\text{in}} = \rho v_z \omega_s - \rho D_{\text{eff}} \frac{d\omega_s}{dz}$$

$$\rho_{\text{in}} v_{z,\text{in}} c_p T_{\text{in}} = \rho v_z c_p T - k_{\text{eff}} \frac{dT}{dz} \quad (1.304)$$

The outlet boundary condition at  $z = L$ :

$$\frac{d\omega_s}{dz} = \frac{dT}{dz} = 0 \quad (1.305)$$

Baerns et al [4], Froment and Bischoff [52] and Scott Fogler [48] discuss numerous applications of this model in chemical reaction engineering.

### 1.3 Application of the Governing Equations to Turbulent Flow

Most flows occurring in nature and engineering applications are said to be turbulent. Still it is difficult to provide a complete definition of this phenomenon.

Hinze [66] presents the following definition: *Turbulent fluid motion is an irregular condition of flow in which the various quantities show a random variation with time and space coordinates, so that statistically distinct average values can be discerned.*

Tennekes and Lumley [167] find it more appropriate to list the characteristics of turbulent flow such as: *Irregularity (or randomness), diffusivity, large Reynolds numbers, three dimensional vorticity fluctuations and dissipation.* Turbulence is not a feature of fluids, but of fluid flows thus a continuum phenomenon.

In the modern theory of fluid dynamic systems *the term turbulence is accepted to mean a state of spatiotemporal chaos* (e.g., [155], chap 5). That is, the fluid exhibits chaos on all scales in both space and time. Chaos theory involves the behavior of non-linear dynamical systems and their response to initial and boundary conditions. Using such methods it can be shown that although the solution of the Navier-Stokes is apparently random for turbulent flows, its behavior presents some orderly structures. In addition, the numerical solution of the Navier-Stokes equations is sometimes strongly dependent on the initial conditions, thus even very small inaccuracies in the initial conditions may be fatal providing completely erroneous results<sup>28</sup>.

---

<sup>28</sup> The latter effect is often ‘nicely’ exemplified through poor weather forecasts. Naturally, the meteorologists are not able to define exact initial conditions based on their statistical analysis of the available weather observations. Consequently, poor forecasts are likely to be predicted for those regions or those times where the simulations are highly sensitive to the initial conditions. Fortunately, performing a large number of simulations of the same forecast, in which every single one of these simultaneous simulations is ran with small perturbations in the initial conditions, can provide information on the reliability of the forecast produced by use of an (ensemble) average model.

To quantitatively describe turbulent flows, we usually turn to the basic equations of fluid mechanics that describe the dynamics of the flow. This seems plausible because the average size of the turbulent structures is large in comparison with the mean free path of the molecules of the fluid. In principle, it is believed that single phase turbulent flows are exactly represented by these three dimensional time dependent transport equations (e.g., [112] [113] [66] [106] [121] [15], chap 10). Based on these equations three theoretical methodologies have been suggested in the literature enabling numerical analyzes of turbulent flows (for further details, see for example the textbook of [121]). Those are the direct numerical simulation (DNS), the large eddy simulation (LES), and the statistical approach. In DNS, the ‘un-averaged’ governing equations are solved to determine  $\mathbf{v}(\mathbf{r}, t)$  for one realization of the flow. Statistical analysis of the resulting numerical data could theoretically provide information such as turbulent fluctuations, the root-mean-square velocity, the frequency and wavenumber spectra, and their mutual interaction. However, although the existing numerical methods are capable of solving these equations, the numerical solutions are also limited due to constraints in computer time and storage since all length - and timescales in the flow have to be resolved. DNS is thus extremely computationally expensive and restricted to low Reynolds number flows as the computational cost increases rapidly with increasing Reynolds numbers. In addition, these equations contain time and space derivatives that require initial and boundary conditions for their solution. Although the governing equations may be applied directly to turbulent flows, rarely do we have sufficient initial and boundary condition information to resolve all turbulent scales down to the smallest eddy. Therefore, in practice, this approach is not very useful for chemical reactor analyzes. In LES, the governing equations are solved for a filtered velocity field which is representative of the larger scale turbulent motions. The equations solved usually include a model for the influence of the smaller scale motions which are not resolved. However, the LES approach still provides information on the dynamics and structure of turbulence on the larger scales. The filtering procedure is, of course, introduced to reduce the computational costs, compared to the DNS simulation approach. In practice, however, the method is still too computationally expensive for chemical reactor analyzes. Only a very limited number of preliminary reactor flow LES simulations have been performed in academia for research purposes so far, but the application of the LES concept (or LES hybrids) is expected to increase in the near future as the computer capacity continues to be improved. Therefore, the fundamental LES concepts are presented in the end of this chap. Consequently, in quantifying turbulent effects one necessarily has to resort to the statistical Reynolds averaging approach. The Reynolds averaged equations are solved to determine the mean velocity field,  $\bar{\mathbf{v}}(\mathbf{r}, t)$ . In the simplest versions of these approaches, the Reynolds stresses are obtained from a turbulent viscosity model. In reactor model simulations the turbulent viscosity is either obtained from an algebraic relation (such as the mixing length model) or from turbulence quantities such as  $k$

and  $\varepsilon$  for which modeled transport equations are solved. In a limited number of papers, the Reynolds stress model is used, for which modeled transport equations are solved for the Reynolds stresses, thus obviating the need for a turbulent viscosity.

The aim of this sect. is not to provide a comprehensive review of turbulence modeling, as can be found elsewhere (e.g., [66] [154] [106] [186] [139] [121] [15]). The intension is rather to outline the essential ingredients involved in single phase turbulence modeling, determining the basis theory for multiphase turbulent modeling in the context of engineering practice discussed in the subsequent chaps. in this book.

Although the main emphasis in this chap is put on the Reynolds averaging approach, some results obtained using more fundamental statistical approaches to turbulence are provided in an introductory paragraph. This highly theoretical work, together with experimental validation, has for example discovered the existence of a energy cascade mechanism, the characteristic length and time scales, the return to isotropy principle, etc. These are features of turbulence that could not be predicted by studying the conservation laws alone.

In the first three paragraphs of this chap some of the important characteristics of fluid turbulence are described. This includes the turbulence energy spectrum and Fourier analysis in wave space. Some basic statistics for describing turbulence are also presented. The fourth paragraph gives a semi-empirical analysis of turbulent boundary layer flows. In the fifth paragraph Reynolds averaged models are discussed. In the last paragraph large eddy simulation (LES) models are discussed.

### 1.3.1 Origin and Characteristics of Turbulence

In flows which are originally laminar, turbulence arises from instabilities at large Reynolds numbers. Turbulence cannot maintain itself but depends on its environment to obtain energy. A common source of energy for turbulent velocity fluctuations in single phase flow is shear in the mean flow. Other sources such as buoyancy is very important in the geophysical sciences. Thus, if turbulence arrives in an environment where there is no shear or other maintenance mechanism, it decays, the Reynolds number decreases and the flow tends to become laminar again. Mathematically, the details of transition from laminar to turbulent flow are rather poorly understood (e.g., [38]). Much of the theory of instabilities in laminar flows is linearized theory, valid for very small disturbances. It cannot deal with the large fluctuation levels in turbulent flow. On the other hand, almost all of the theory of turbulent flow is asymptotic theory, fairly accurate at very high Reynolds numbers but inaccurate and incomplete for Reynolds numbers at which the turbulence cannot maintain itself. Experiments have shown that the transition from laminar to turbulent flow is commonly initiated by a primary instability mechanism. The primary instability produces secondary motions, which may become unstable

themselves. A sequence of this nature generates intense localized disturbances, which arise at random positions at random times. These spots grow rapidly and merge with each other when they become large and numerous to form a field of developed turbulent flow. Many wake flows on the other hand become turbulent due to an instability that causes vortexes which subsequently become unstable. The latter mechanisms are very important in multi-phase flows.

Further discussions on the classical fluid dynamic stability theory can be found elsewhere (e.g., [112], chap 1; [38]; [139], chap 15).

Modern theories and concepts describing the initial dynamic evolution of fluid motions leading to the onset of turbulence, explaining experimental observations of instability phenomena, are typically rather theoretical and usually not considered by chemical reaction engineers. The interested reader is referred to texts on chaos theory and non-linear dynamics (e.g., [155], chap 5).

### Signature of Turbulence

Considering high resolution experimental data of velocity measured over a certain time period, as shown in Fig. 1.5, a number of features of turbulence stand out (e.g., [154], chap 2; [121]; [15], chap 1):

- The velocity varies in an irregular pattern, a characteristic signature of turbulence. This quasi-randomness is what makes turbulence different from other motions, like waves.
- The limited ability to find a statistically stable mean, or typical value, suggest that turbulence is not completely random (e.g., [112], chap 2).  
The interpretation that the fluctuations in the flow quantities are randomly distributed has been modified with the discovery of orderly structures, sometimes called *coherent structures*, within the flow. Coherent structures within fluid flows, and the modeling of these phenomena, are further discussed by [70] [71].
- There is a measurable and definable intensity to the turbulence that shows up as the small scale spread of velocity.  
Such a bounded characteristic of the velocity means that we can use statistics such as the variance or standard deviation to characterize the turbulence intensity.
- There appears to be a wide variety of time scales of velocity variations superimposed on top of each other.

For example, if we look closely at the high resolution experimental data we see that the time period between each little peak in the velocity profile has a certain characteristic small scale. The larger peaks seem to happen at another somewhat larger scale. There will also be other variations that indicate much larger time periods. If each of these time variations is associated with a different size turbulent eddy (i.e., the Taylor's hypothesis [164]), then we can conclude that we are seeing the signature of eddies

having different sizes. In other words, we are observing evidence of the spectrum of turbulence.

Perhaps an association to another physical phenomena which is more generally accepted, will help understanding this property of turbulence. The turbulence spectrum is analogous to the spectrum of colors that appears when you shine a light through a prism [164]. White light consists of many colors (i.e., many wavelengths or frequencies) superimposed on one another. The prism is a physical device that separates the colors. We could measure the intensity of each color to learn the magnitude of its contribution to the original light beam. We can performed a similar analysis on a turbulent signal using mathematical rather than physical devices to learn about the contribution of each different size eddy to the total turbulence kinetic energy. Therefore, although the physical interpretation of the experimental data may indicate a labyrinth of motions, turbulence may be idealized as consisting of a variety of different sized eddies. In this mathematical context, the eddies behave in a well-ordered manner when displayed in the form of a spectrum.

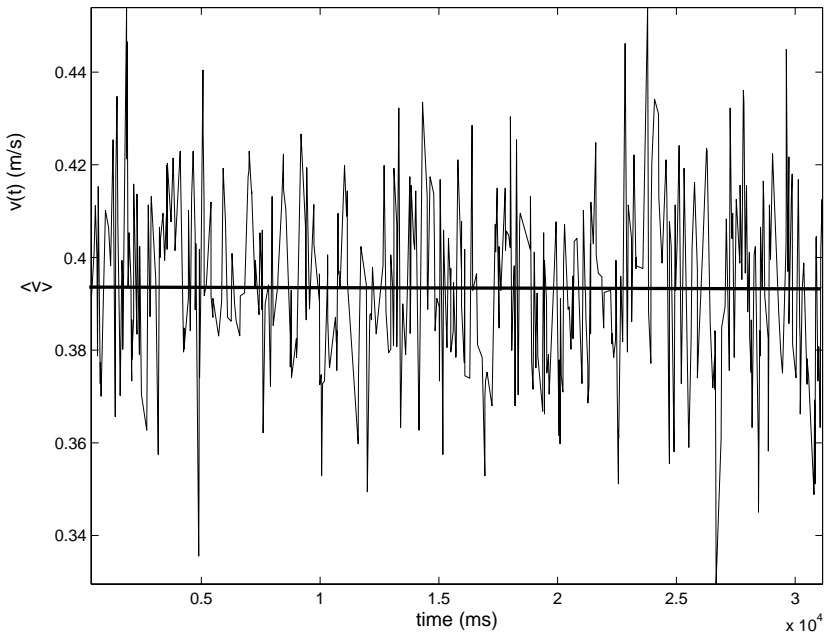


**Fig. 1.5.** A typical velocity signal recorded by a laser Doppler anemometer (LDA) in a liquid flow at NTNU.  $\langle v \rangle$  denotes the time average of the velocity over the time period displayed. The work was performed as a part of the strategic university program (SUP) entitled ‘CFD Applied to Reactor ProcEss Technology (CARPET)’.

### 1.3.2 Statistical Turbulence Theory

Introductory it is noted that the researchers developing the classical statistical turbulence theory were statisticians (statistical fluid mechanics), physicist and meteorologists rather than chemical engineers. This has the unfortunate consequence that the descriptions of this theory, as found in most textbooks on turbulence and statistical fluid mechanics, are not easily understood by chemical reaction engineers partly due to the unacquainted conceptual vocabulary and mathematical nomenclature adopted in these books. Another reason is language problems as much of the pertinent literature is not written in English, and so the references given in the english-language literature are often misleading as the original contents are neither precisely translated nor interpreted.

At this point in our presentation it is thus obvious that we need to define a common language for the researchers working on the edge between these fields of science (i.e., fluid dynamics, statistics, meteorology and chemical engineering) to avoid any ambiguity. However, the statistical turbulence theory is rather involved mathematically and difficult to explain in only a few words. Therefore, it is found more convenient to present a brief historical survey of the main milestones and scientific concepts developed during the last century. Emphasis is put on the physical interpretations of these concepts, avoiding future developments of ill posed reactor model closures. The fundamental theory is available elsewhere, for example in the books by [66] [8] [112] [113]. The classic papers on statistical turbulence theory have been collected in a publication by [51]. An early review of the statistical theory of turbulence was published by [40].

Turbulent motions are irregular and seemingly unpredictable. This is the most spectacular characteristic which distinguishes turbulent flows from laminar flows. The first scientific study of turbulence, performed by Reynolds [126], relates to this difference. Reynolds did study flows through pipes of constant diameter and by using the ‘method of color bands’ clearly established that there are two fundamentally different flow regimes, laminar and turbulent flows. Reynolds also determined the conditions under which transition took place. This is now described in terms of the *critical Reynolds number*. The *Reynolds number* used in modeling fluid flow is thus named after him.

Reynolds [127] provided the fundamental ideas about averaging and was the first to accomplish the formulation of the governing equations for turbulent flows in terms of mean and fluctuating flow quantities rather than instantaneous quantities. Reynolds stated the mathematical rules for forming mean values. That is, he suggested splitting a turbulent velocity field into its mean and fluctuating components, and wrote down the equations of motion for these two velocity quantities.

The decomposition of the instantaneous velocity variable into its mean and fluctuation is thus referred to as *Reynolds decomposition*. This procedure

is still the most common method of analyzing turbulent flows, and it is known as *Reynolds averaging*.

According to the ideas of Boussinesq [19] [20], the first turbulent closures was based on the gradient hypothesis and the coefficient of eddy viscosity.

The *eddy* concept was thus introduced. An eddy still eludes precise definition, but in one interpretation it is conceived to be a turbulent motion, localized within a region of a certain size, that is at least moderately coherent over this region. The region of a large eddy can also contain smaller eddies.

In an early study Taylor [157] put forth the mixing length ideas based on analogies with the discontinuous collisions between discrete entities that have been studied in the kinetic theory of gases (i.e., about ten years before Prandtl's similar ideas were published [123], but the idea has been traditionally attributed to Prandtl). However, logical difficulties arise considering the mixing length concept because there are no discrete fluid particles in the turbulent flow which retain their identity.

Later Taylor began to search for more suitable means for the the description of turbulence [165]. The statistical approach to the study of turbulence was initiated by a paper by Taylor [158]. In the work of Taylor [158] on turbulent transport the important role of the Lagrangian<sup>29</sup> correlation function (i.e., the one point time correlation) of the velocity field was first demonstrated. Taylor showed that the turbulent diffusion of particles starting from a point depends on the correlation between the velocity of a fluid particle at any instant and that of the same particle after a certain correlation time interval.

---

<sup>29</sup> The adjective 'Lagrangian' is used to indicate that the correlation relates to moving fluid particles (e.g., [167], p. 46 [113], p. 539). The adjective 'Eulerian' is used whenever correlations between two fixed points in a fixed frame of reference are considered.

Unfortunately, not all texts describing the turbulence correlation functions are using the same notation. Hinze ([66], p. 45) find it more logical to rename these functions using the opposite notation. That is, considering the correlation between the values of a velocity component in a given direction at a fixed point in the flow field at two different instants  $t'$  and  $t + t'$ , the resulting correlation was called Eulerian as the measurements were performed at one fixed point in space.

Subsequent textbooks considering statistical turbulence theory adopt either of the two notations possibly making some vagueness for the readers. The chemical engineering textbooks of Baldyga and Bourne [5] on turbulent mixing, and the interdisciplinary textbook of Biswas and Eswaran [15] on turbulent flow experiments and modeling both use the notation introduced by Hinze. However, the classical books (e.g., [167] [113]) and papers (e.g., Taylor's papers) on statistical turbulence theory use the other notation.

Therefore, to minimize the level of vagueness jumping from one notation to the other, in this book we adopt the original notation induced by Taylor as defined above.

For a statistically stationary process, the simplest multi-time statistic that can be considered is the *auto-covariance* (i.e., the one-point two-time correlation ):

$$R_L(s) = \overline{v'(t)v'(t+s)} \quad (1.306)$$

or, in normalized form, the *autocorrelation coefficient* (e.g., [167], sect. 6.4):

$$\rho_L(s) = \overline{v'(t)v'(t+s)}/\overline{v'^2(t)} \quad (1.307)$$

where  $v'(t) = v(t) - \overline{v(t)}$  is the fluctuation.

Because we are working with stationary variables, the autocorrelation gives no information on the origin of time, so that it can only depend on the time difference:  $s$ . The autocorrelation coefficient is the correlation coefficient between the process at time  $t$  and  $t + s$ .

The *Lagrangian integral time scale* of the process is defined by:

$$\Gamma_L = \int_0^{\infty} \rho_L(s) ds \quad (1.308)$$

The value of  $\Gamma_L$  is a rough measure of the longest interval over which  $v(t)$  is correlated with itself.

The microscale  $\tau_L$ , which is defined by the curvature of the autocorrelation coefficient at the origin (i.e., for  $s=0$ ):

$$\frac{d^2 \rho_L}{ds^2} \Big|_{s=0} = \frac{-2}{\tau_L^2} \quad (1.309)$$

Expanding  $\rho_L$  in a Taylor series about the origin, we can write, for small  $s$  ([158]; see also [167], sect 6.4; [66], sect 1-8),

$$\rho_L(s) = 1 + \frac{s^2}{2!} \left( \frac{\partial^2 \rho_L}{\partial s^2} \right) \Big|_{s=0} + \frac{s^4}{4!} \left( \frac{\partial^4 \rho_L}{\partial s^4} \right) \Big|_{s=0} + \dots = 1 - \frac{s^2}{\tau_L^2} + O(s^4) \quad (1.310)$$

in which  $\tau_L$  is the Lagrangian time scale which characterize the most rapid changes of  $v_1(t)$ .

Richardson ([129], page 66) introduced the idea of *the energy cascade*. Richardson's view of the energy cascade is that the turbulence can be considered to be composed of eddies of different sizes, and the energy is transferred from larger eddies to smaller eddies until it is drained out by viscous dissipation. Richardson's notation is that the large eddies are unstable and break up, transferring their energy to somewhat smaller eddies. However, Richardson did forward these general ideas only in qualitative form and did not make any deduction that could be formulated in precise mathematics.

In Taylor's analysis of turbulent flow the velocity field is considered random, in the sense that the variable does not have a unique value (i.e., the same value every time an experiment is repeated under the same set of conditions). Random functions of time in specific literature are also often called

random processes. However, this does not mean that turbulence is a random phenomena.

The idea that the correlation functions and other statistical moments of the fluid mechanical fields must be recognized as the fundamental characteristics of turbulence was first stated by Keller and Friedmann ([80]; see also [8], sect 2.2; [112], chap 2), who proposed a general method of obtaining the differential equations for the moments of arbitrary order for the description of turbulent flow. The determination of all such moments is equivalent to the determination of the corresponding probability distribution in the functional space. The total infinite Friedmann-Keller system of equations for all possible moments gives an analytical formulation of the problem of turbulence. However, analytical treatment of the problem is not feasible unless one confines attention to the very simplest kinds of averaged quantities (i.e., involving one- or two-point correlation functions). The desire to make practical calculations of complex flows has led to the development of approximate methods which make computer simulations of turbulent flows feasible. In one interpretation the hypothesis adopted in these theories permits the closure of a set of equations representing a lower order approximations to the infinite Friedmann-Keller system. A specific set of equations, the Reynolds equations, containing only single point first and second order moments of the fluid mechanical field is usually adopted. In statistical terms, the mean velocity and the Reynolds stresses are the first and second moments of the Eulerian probability distribution function (PDF) of velocity. Such a method doesn't provide much information about the structure (spectrum) of turbulence and the dynamics of interactions between the turbulent vortexes. The two-point correlations (or moments) contain more information about the structure of turbulence. Therefore, in the scientific literature it is implied that the methods employing the second-order two-point correlations (or even higher order functions) constitutes the fundamental, statistical approach to turbulence, while restricting the complexity to the use of the second-order one-point correlations only is considered an engineering approach. Nevertheless, the two-point structure function information is essential for improving the engineering models including second-order closures. In addition, the study of many physical phenomena in reactor systems requires information on the turbulence structure (e.g., phase and species mixing, coalescence and breakage of fluid particles).

A statistical theory of turbulence which is applicable to continuous movements and which satisfies the equations of motion was introduced by Taylor [159, 160, 161] and [162, 163], and further developed by von Kàrmàn [178, 179]. Most of the fundamental ideas and concepts of the statistical turbulence theory were presented in the series of papers published by Taylor in 1935. The two-point correlation function is a central mathematical tool in this theory. Considering the statistics of continuous random functions the complexity of the probability density functions needed in a generalized flow situations was found not tractable in practice. An idealized flow based on the assumption of

statistical homogeneity greatly simplified the analysis. Taylor [159, 160, 161] went further still and considered isotropic turbulence.

The velocity field is *statistically homogeneous* if all statistics are invariants under a shift in position. If the field is also statistically invariant under rotations and reflections of the coordinate system, then it is *statistically isotropic*. In chemical reaction engineering these mathematical definitions are usually somewhat relaxed, since turbulence is said to be *isotropic* if the individual velocity fluctuations are equal in all the three space dimensions. Otherwise it is said to be *an-isotropic*. Similarly, a flow field where turbulence levels do not change from one point to another is called *homogeneous*.

*Homogeneous isotropic turbulence* is a mathematical idealization of real turbulence, that was introduced by [159], allowing us to simplify the analysis of turbulence considerably, and thus gain insight into its behavior. Nevertheless, real turbulent flows do rarely approach homogeneity and isotropy. However, by using the homogeneous and isotropic turbulence concept the mathematical problem simplifies considerably and it is possible to obtain many specific mathematical results which explain several aspects of turbulent flows.

After Taylor's work was reported, von Kàrmàn [178] noticed that the mean values of the products of the velocities at two (or more points) were tensors. The realization of van Kàrmàn [178] that the correlation is a tensor simplified the analysis considerably because a known tensor in one coordinate system can be transformed into other coordinate systems simply by adopting the rules of such transformations for second order tensors. For the purposes of simplification, von Kàrmàn also introduced the assumption of *self-preservation* of the shape of the velocity product function during decay.

In the following we will consider some basic results of the statistics of such a homogeneous isotropic turbulent field. The consequences of homogeneity and isotropy for the correlation functions were worked out by von Kàrmàn and Howarth [179] and the full derivations are available in classical books like [66, 8, 112, 113].

The simplest statistic containing information on the spatial structure of the random field is the two-point, one time auto-covariance:

$$R_{ij}(t, \mathbf{x}) = \overline{v_i(\mathbf{r} + \mathbf{x}, t)v_j(\mathbf{r}, t)} \quad (1.311)$$

which is often referred to as the *two-point correlation*. For homogeneous turbulence in particular the correlation tensor  $R_{ij}(t, \mathbf{x})$  is a function of the vector  $\mathbf{x}$  defining the separation of the two points in space, but independent of  $\mathbf{r}$ . From this correlation tensor it is possible to define several integral length scales.

According to von Kàrmàn and Howarth [179], a consequence of isotropy is that  $R_{ij}$  can be expressed in terms of two scalar functions  $f(t, \mathbf{x})$  and  $g(t, \mathbf{x})$  identified as the longitudinal and transverse autocorrelation functions, respectively. There are two distinct longitudinal length scales,  $A_f$  and  $\lambda_f$ , that can be defined from  $f$ , and there are also two corresponding transverse

length scales  $\Lambda_g$  and  $\lambda_g$ , defined from  $g$ . The first of the Eulerian length scales obtained from  $f(t, \mathbf{x})$  is the longitudinal integral scale:

$$\Lambda_f(t) = \int_0^\infty f(t, \mathbf{x}) d\mathbf{x} \tag{1.312}$$

$\Lambda_f$  is a characteristic length of the larger eddies.

In isotropic turbulence, the transverse integral scale

$$\Lambda_g(t) = \int_0^\infty g(t, \mathbf{x}) d\mathbf{x} \tag{1.313}$$

is just half of  $\Lambda_f$ .

The second length scale obtained from  $f(t, \mathbf{x})$  is the longitudinal *Taylor microscale*,  $\lambda_f$ .

As  $f(t, \mathbf{x})$  and  $g(t, \mathbf{x})$  are even functions of  $\mathbf{x}$  because of isotropy (i.e.,  $f(t, \mathbf{x}) = f(-\mathbf{x}, t)$ , etc.), all the odd derivatives of  $f(t, \mathbf{x})$  and  $g(t, \mathbf{x})$  vanish as  $\mathbf{x} \rightarrow 0$ . Therefore, Taylor series expressions for  $f(t, \mathbf{x})$  and  $g(t, \mathbf{x})$ , around  $\mathbf{x} = 0$ , can be written as (e.g., [66], chap 1):

$$f(t, \mathbf{x}) = 1 + \frac{\mathbf{x}^2}{2!} \left( \frac{\partial^2 f}{\partial \mathbf{x}^2} \right) \Big|_{\mathbf{x}=0} + \frac{\mathbf{x}^4}{4!} \left( \frac{\partial^4 f}{\partial \mathbf{x}^4} \right) \Big|_{\mathbf{x}=0} + \dots = 1 - \frac{\mathbf{x}^2}{\lambda_f^2} + O(\mathbf{x}^2) \tag{1.314}$$

and

$$g(t, \mathbf{x}) = 1 + \frac{\mathbf{x}^2}{2!} \left( \frac{\partial^2 g}{\partial \mathbf{x}^2} \right) \Big|_{\mathbf{x}=0} + \frac{\mathbf{x}^4}{4!} \left( \frac{\partial^4 g}{\partial \mathbf{x}^4} \right) \Big|_{\mathbf{x}=0} + \dots = 1 - \frac{\mathbf{x}^2}{\lambda_g^2} + O(\mathbf{x}^2) \tag{1.315}$$

The Taylor microscale  $\lambda_f$  is now defined as a length scale which for a very small  $\mathbf{x}$  values gives:

$$f(t, \mathbf{x}) \approx 1 - \frac{\mathbf{x}^2}{\lambda_f^2} \tag{1.316}$$

where

$$\frac{1}{\lambda_f^2} = -\frac{1}{2} \left( \frac{\partial^2 f}{\partial \mathbf{x}^2} \right) \Big|_{\mathbf{x}=0} \tag{1.317}$$

and

$$g(t, \mathbf{x}) \approx 1 - \frac{\mathbf{x}^2}{\lambda_g^2} \tag{1.318}$$

where

$$\frac{1}{\lambda_g^2} = -\frac{1}{2} \left( \frac{\partial^2 g}{\partial \mathbf{x}^2} \right) \Big|_{\mathbf{x}=0} \tag{1.319}$$

It was shown by Taylor [159] that an analysis of the dissipation term occurring within the turbulent kinetic energy balance equation (derived later in this

chap) shows that in isotropic turbulence the energy dissipation rate is equal to:

$$\varepsilon = 15\nu \overline{\left(\frac{\partial v'_1}{\partial x_1}\right)^2} \quad (1.320)$$

Taylor re-formulated the expression for the length scale (see, e.g., [66], sect. 1-6) such that

$$\overline{\left(\frac{\partial v'_1}{\partial x_1}\right)^2} = \frac{2\overline{v'^2}}{\lambda_f^2} = \frac{2v_{\text{rms}}^2}{\lambda_f^2} \quad (1.321)$$

The turbulent velocity scale is often approximated by,  $v_{\text{rms}} = \sqrt{v'_i v'_i/3}$ , the root-mean-square of the fluctuating velocity components.

In isotropic turbulence, it was shown that  $\lambda_f \approx \sqrt{2}\lambda_g$ . It then follows that the energy dissipation rate is given by:

$$\varepsilon = 15\nu \frac{\overline{v'^2}}{\lambda_g^2} \quad (1.322)$$

The *dissipation rate* can be defined as:

$$\varepsilon = 15\nu \frac{v_{\text{rms}}^2}{\lambda_g^2} = 30\nu \frac{v_{\text{rms}}^2}{\lambda_f^2} \quad (1.323)$$

Taylor [159] stated that  $\lambda_g$  can be regarded as a measure of the diameter of the smallest eddies which are responsible for the dissipation of turbulent energy. Pope ([121], p. 199) stated that this statement is incorrect, because it incorrectly supposes that  $v_{\text{rms}}$  is the characteristic velocity of the dissipative eddies. The characteristic length scale of the smallest eddies are the Kolmogorov scale,  $\eta = (\frac{\nu^3}{\varepsilon})^{1/4}$  as will be further discussed shortly.

The Taylor microscale does not represent any distinct group of eddies, but the ratios  $\frac{v_{\text{rms}}}{\lambda_g}$  and  $\frac{v_{\text{rms}}}{\lambda_f}$  are fair estimates of the rate of strain characterizing viscous dissipation of energy (e.g., [5], p. 148).

Further details on this theory are given by Tennekes and Lumley ([167], sect. 3.2), Hinze ([66], chap 1) and Pope ([121], p. 198).

According to Taylor [159] [160] [161], the properties of the Lagrangian scales are similar to the Eulerian correlation scales. Although the statistical turbulence theory is derived in terms of the Eulerian correlation functions, accurate measurements of the Lagrangian scales and correlations are easier and direct. In contrast, the measurements of Eulerian correlations requires two probes simultaneously working at two different locations.

Taylor [164] thus suggested that turbulence might be considered “frozen” in a wind field as it advects past a sensor. A physical interpretation of this statement is that, if  $\bar{v} \gg v'$ , the fluctuations at a fixed point of the field may be imagined to be caused by the whole turbulent flow field passing that point as

a “frozen” field (i.e., the probe is assumed to be within a large almost homogeneous eddy during the time interval of sampling). The velocity fluctuations at that point will then be nearly identical to the instantaneous distribution of the velocity  $v'$  in a frame moving with the mean velocity (i.e., the probe follows the mean flow). Accordingly, as can be shown mathematically, the average wind speed could be used to translate Lagrangian turbulence measurements as a function of time to their corresponding Eulerian measurements in space.

In mathematical terms, the *frozen* turbulence approximation, known as Taylor’s hypothesis, refers to a simple mathematical relation between statistical temporal auto-covariances and spatial correlation functions approximately valid for quasi-steady homogeneous turbulent flow.

If we can assume that the homogeneous turbulent field has a constant mean velocity,  $\bar{v}_1$ , then we can express Taylor’s hypothesis of frozen turbulence as:

$$\frac{\partial}{\partial t} = \bar{v}_1 \frac{\partial}{\partial x_1} \quad (1.324)$$

The integral Lagrangian-Eulerian conversion relation yields:

$$A = \bar{v}_1 \Gamma_L \quad (1.325)$$

and the corresponding microscale relation is:

$$\lambda = \bar{v}_1 \tau_L \quad (1.326)$$

The mathematics involved is explained by several authors (e.g., [66], sect. 1-8; [121], p. 223; [15], p. 205; [154], p. 5).

Experimentalists often rely on this hypothesis interpreting experimental turbulence data. However, turbulence is not really “frozen”. The accuracy of this approximation depends both upon the properties of the flow and on the statistics being measured. Many experiments on complex turbulent flows have shown that Taylor’s hypothesis can fail.

Taylor [159] also formulated a relation estimating the energy dissipation rate in terms of the larger scales of turbulence. Taylor didn’t discuss the detailed derivation of this relation, but it may be derived in the following approximate manner ([167], p. 20). Assuming that the largest eddy sizes in turbulent flows do most of the transport of momentum and other quantities, these large eddies may be the relevant length scale in the analysis of the interaction of the turbulence with the mean flow. The amount of turbulent kinetic energy absorbed by the larger turbulent eddies per unit mass may then be proportional to the square of the characteristic turbulent velocity scale of the largest eddies,  $\overline{v'^2} = v_{\text{rms}}^2$ . The rate of energy transfer is assumed to be proportional to  $v/L$  (i.e., the reciprocal of the time scale of the large eddies), where  $L$  represents the size of the largest eddies. One may interpret the size of the large, energy containing eddies as the integral scale of turbulence<sup>30</sup>,

<sup>30</sup> The integral scales are those that correspond to the energy containing eddies, which also form the large (but not necessarily the largest) scales of the turbulent

$\Lambda$  (e.g., [15], sect. 2.2.5 [106] [167]), which can be measured by statistical methods. The rate of energy supply to the smaller scale eddies is thus of order  $v_{\text{rms}}^2 v_{\text{rms}}/\Lambda$ . It can be shown that the production of the kinetic energy of turbulence at the larger length scales ( $v_{\text{rms}}^3/L$ ) determines the rate of energy dissipation,  $\epsilon$ , at small length scales when the cascade of kinetic energy is in some kind of equilibrium. Hence, the energy is dissipated at a rate  $\epsilon$  and this equals the supply rate. In accordance with Taylor [159], we can thus write:

$$\epsilon \sim \frac{v_{\text{rms}}^3}{\Lambda} \quad (1.327)$$

This means that we can get an inviscid estimate for the dissipation rate from the large scale dynamics which do not involve viscosity. This implies that only a small fraction of the kinetic energy contained in the larger eddies is lost by direct viscous dissipation effects.

Taylor [159] further speculated that there may exist very small scale eddies which, though they play a very small part of diffusion, yet may be principal agents in the dissipation of energy.

Unfortunately, the simplified engineering method doesn't provide much information about the structure of turbulence and the dynamics of the interactions between the turbulent vortexes. The only structural information extracted from the second moments in relation to the structure of turbulence is the length scale,  $\Lambda$ , and the only information in relation to the dynamics of turbulence is the time constant representing the *eddy turnover time*<sup>31</sup>,  $\tau_e \approx \frac{\Lambda}{v_{\text{rms}}} \approx \frac{\Lambda}{(\Lambda\epsilon)^{1/3}} = \frac{\Lambda^{2/3}}{\epsilon^{1/3}}$ .

Further contributions to the subject were made by Taylor in 1938. Two important consequences of the non-linearity of the Navier-Stokes equations were identified: First, the skewness of the probability distribution of the difference between the velocities at two points, and the existence of an interaction or modulation between components of turbulence having different length scales. Secondly, the Fourier transform of the correlation between two velocities is an energy spectrum function in the sense that it describes the distribution of kinetic energy over the various Fourier wave-number components of the turbulence [164]. Taylor expressed in mathematical form the relation between the correlation function and the 1D spectrum function.

---

field (e.g., [66], chap 1). The integral length scales also roughly correspond to the distance over which the velocity fluctuations at one point are correlated with the velocity at another point, and the integral time-scales correspond to the time-intervals over which the velocity fluctuations at the same point are correlated.

<sup>31</sup>  $\tau_e$  can be interpreted as the time necessary to decrease significantly the size of the structure having initially size  $\Lambda$ . Another interpretation is that it is the time constant for the rate of kinetic energy dissipation when the cascade is in dynamic equilibrium (steady state), and a third interpretation could be that it is an estimate of a time necessary to transfer the kinetic energy from the scale  $\Lambda$  to the scale of dissipation.

The two-point one time correlation functions, in the form presented in the preceding discussion, are not suitable for analyzing motions at different scales and specifically they are not suitable for understanding relations between movements of fluid characterized by different length and time scales. That is why it is better to use the 3D Fourier transforms of two-point correlations and to decompose them into waves of different frequencies or wave numbers. Turbulence has by definition a 3D character so it is obvious that the spectrum has to be 3D as well, to characterize turbulence properly. The 1D spectrum of Taylor (see, e.g., [66]) oversimplifies the observed features of turbulence and may give misleading interpretations of the 3D field (see also, [113], p. 18). The differences and consequences of 1D and 3D spectrum analysis are discussed by Hinze ([66], sects. 1-12 and 3-4) and Pope ([121], sect. 6.5).

In the early investigations of the energy cascade by Richardson [129] and Taylor [159, 160, 161, 164], the transfer of energy to successively smaller scales was identified as a phenomenon of prime importance, but the precise mechanisms by which this transfer takes place was not identified or quantified. This was further accomplished by the work of Kolmogorov [83, 84].

The theory of Kolmogorov [83] was stated in the form of three hypotheses. The first hypothesis is apparently based on the homogeneous and isotropic concepts of Taylor [159] [160] [161]. Although the large eddies are in general anisotropic and affected by the boundaries of the flow, it was postulated by Kolmogorov [83], and later validated experimentally, that the smaller scales are less affected by the boundaries and thus demonstrate a certain degree of isotropy. In Kolmogorov's notation the orienting effect of the mean flow is weakened with each eddy breaking down, due to the chaotic nature of the energy transfer processes. The *theory of locally isotropic turbulence* thus constitutes an important addition to the assumptions on the energy cascade.

Approximately stated *Kolmogorov's hypothesis of local isotropy* yields ([83]; see also [121], p. 184): At sufficiently high Reynolds number, the small scale turbulent motions are statistically isotropic.

The second hypothesis concerns the very smallest dissipative eddies. Kolmogorov's [83] universal equilibrium theory of the isotropic small scale structure of turbulence is based on the assumption that when the Reynolds number is sufficiently high, a range of high wave numbers is produced in which turbulence is in both statistical- and dynamic equilibrium. The phrase 'statistical equilibrium' denotes the postulate that the rate of energy transfer from the large scales determines an almost constant rate of energy transfer through the successively smaller scales until the energy is dissipated at the very smallest scales. Hence, the net rate of energy transfer at all the scales within this range of wave numbers is given by the dissipation rate. The phrase 'dynamic equilibrium' denotes the postulate that the small eddies will evolve much more rapidly than the large eddies which contain most of the energy. That is, within a certain range of wave numbers, i.e., the *universal equilibrium range of wave numbers*, the timescales  $\tau_{e,l} \approx l/v_{\text{rms}}(l)$  are small compared with  $\tau_e \approx \Lambda/v_{\text{rms}}(\Lambda)$  so that the small eddies can adapt quickly to changes in

the large scale conditions. In this wavenumber range turbulence may be considered statistically quasi-steady. This statistically quasi-steady equilibrium state is said to be *universal* as turbulence in this wavenumber range is independent of the large scale conditions, thus any change in the length- and time scales of this part of turbulence can only be a result of the ‘local’ effect of the parameters  $\varepsilon$  and  $\nu$ .

Given these two parameters three unique length, velocity, and time scales can be formed from dimensional analysis, i.e., the Kolmogorov microscales:

$$\eta = \left(\frac{\nu^3}{\varepsilon}\right)^{1/4} \quad (1.328)$$

$$\tau = (\nu/\varepsilon)^{1/2} \quad (1.329)$$

$$v = (\nu\varepsilon)^{1/4} \quad (1.330)$$

Approximately stated *Kolmogorov’s first similarity hypothesis* yields ([83]; see also [121], p. 185): In every turbulent flow at sufficiently high Reynolds number, the statistics of the small scale motions have a universal form that is uniquely determined by  $\nu$  and  $\varepsilon$ .

The phrases ‘similarity hypothesis’ and ‘universal form’ refer to a mathematical consequence of the Kolmogorov hypothesis denoting that on the small scales all high-Reynolds-number turbulent velocity fields are statistically similar. That is, they are statistically identical when they are scaled by the Kolmogorov velocity scale ([121], p. 186).

The third hypothesis concerns the motions of scale  $l$  in the range  $L \approx \Lambda \gg l \gg \eta$  assumed to prevail in the universal equilibrium range. Kolmogorov postulated that the universal equilibrium range extends to scales much larger than  $\eta$ . If the energy is expected to be dissipated at the very smallest scales only, there must exist an *inertial subrange* of scales in which the viscosity will no longer play any role. That is, the statistical regime will be determined by a single parameter  $\varepsilon$ .

Approximately stated *Kolmogorov’s second similarity hypothesis* yields ([83]; see also [121], p. 186): In every turbulent flow at sufficiently high Reynolds numbers, the statistics of the motions of scale  $l$  in the range  $L \approx \Lambda \gg l \gg \eta$  have a universal form that is uniquely determined by  $\varepsilon$ , but independent of  $\nu$ .

Note that the Kolmogorov hypothesis, and deductions drawn from them, apparently have no direct connection to the Navier-Stokes equations.

Hinze ([66], sect 3-4) derived an analytical expression for the 3D spectrum  $E(k, t)$  as a function of wave number  $k$  and time  $t$ . This result shows that  $E(k = 0) \approx 0$ , then the spectrum function increases rapidly, reaches a maximum value, and decreases monotonously to zero as  $k$  increases.

Figure 1.6 shows an example of such a velocity spectrum determining a generalized spectral energy distribution for single phase flow. The ordinate

is a measure of the portion of turbulence energy that is associated with a particular size eddy. The abscissa gives the eddy size in terms of wave number ( $k$ ) which is proportional to the velocity fluctuation frequency ( $k \propto f/\bar{v}_1$ ). Small eddies have higher frequencies, thus larger wave numbers, than large eddies (using Taylor's hypothesis). According to Tennekes and Lumley ([167], p. 259), the eddy size  $l$  is roughly equal to  $2\pi/k$ . Peaks in the spectrum show which size eddies contribute the most to the turbulence kinetic energy. As seen from the Fig. 1.6, the smaller high frequency eddies are very weak. The large primary eddies, which are formed as the flow builds up, are known as macro eddies and cause large velocity fluctuations of low frequency. This eddy size is comparable to the characteristic dimensions of the flow system concerned.

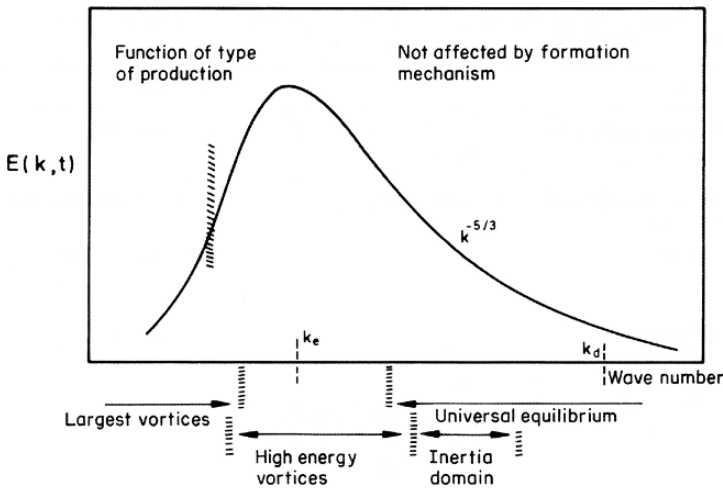


**Fig. 1.6.** Energy spectrum graph, taken from Hinze ([66], p. 229). The Fig is reproduced with permission of the McGraw-Hill Companies, copyright date January 07, 2005.

Large eddy motions can create shear regions, which can generate smaller eddies as a result of disruptions<sup>32</sup>.

Eddies with wave numbers in the region of ( $k_e$ ) (see Fig. 1.6) contain the largest part of the energy and contribute little to energy dissipation by internal friction. However, small eddies with wave numbers in the region of

<sup>32</sup> Tennekes and Lumley ([167], p. 258) presented a different mechanism. They imagined that the smaller eddies are exposed to the strain-rate field of the larger eddies. Because of the straining, the vorticity of the smaller eddies increases, with a consequent increase in their energy at the expense of the energy of the larger eddies.

( $k_d$ ) are produced from the non-ordered diffuse movement of the large high energy eddies. At the smallest size eddies, this cascade of energy is dissipated into heat by molecular viscosity. Hence, a turbulent flow situation is made up of macro eddies which act as an energy reservoir, these in turn producing micro eddies in which flux energy is dissipated by internal friction.

The hypotheses of Kolmogorov allow a number of additional deductions to be formulated on the statistical characteristics of the small-scale components of turbulence. The most important of them is the *two-third-law* deduced by Kolmogorov [84]. This law states that the mean square of the difference between the velocities at two points of a turbulent flow, being a distance  $\mathbf{x}$  apart<sup>33</sup>, equals  $C(\varepsilon\mathbf{x})^{2/3}$  when  $\mathbf{x}$  lies in the inertial subrange.  $C$  is a universal model constant. Another form of this assertion (apparently first put forward by Obukhov [116] [117]) is the *five-third law*. This law states that the spectral density of the kinetic energy of turbulence over the spectrum of wave numbers,  $k$ , has the form  $C_k\varepsilon^{2/3}k^{-5/3}$  in the inertial subrange.  $C_k$  is a new model constant (see e.g., [8], sect. 6.4).

From the experimentally determined energy spectrum we can obtain the mean turbulent energy per unit mass of fluid  $MTKE(t)$ , the turbulent energy dissipation rate per unit mass of fluid  $\epsilon(t)$ , and the integral length scale  $A_f(t)$ .

That is,  $MTKE(t)$  can be expressed in terms of the energy spectrum as (e.g., [15], p. 48):

$$MTKE(t) = \int_0^{\infty} E(k, t) dk = \frac{1}{2} \overline{v_i'v_i'} \quad (1.331)$$

Likewise, one can write  $\epsilon$  in terms of the energy spectrum as (e.g., [15], p. 51):

$$\epsilon(t) = 2\nu \int_0^{\infty} k^2 E(k, t) dk \quad (1.332)$$

and, for the integral length scale one may write (e.g., [15], p. 50; [106]; [121], p. 240):

$$A_f(t) = \frac{\frac{3\pi}{2} \int_0^{\infty} k^{-1} E(k, t) dk}{E(t)} \quad (1.333)$$

<sup>33</sup> Kolmogorov [83][84] introduce the concept of *structure functions* describing processes with stationary - or homogeneous increments.

By definition, the second order velocity structure function is the covariance of the difference in velocity between two points in space. A consequence of isotropy is that the structure function can be expressed in terms of a single scalar function. According to the similarity hypotheses of Kolmogorov, the scalar function can be expressed as:  $B_{dd}(x) = \delta v^2 \approx C(\varepsilon x)^{2/3}$ .  $\delta v$  is a derived velocity scale sometimes used in reactor analysis.

In parallel to the research on the turbulent velocity field, investigations were made concerning the local structure of the fields of passive scalars like chemical species concentrations and temperature. A thorough review of this theory is given by Baldyga and Bourne [5], so this vast theory will not be repeated in this book.

Instead, this paragraph is ended by a few comments on the validity of the basic hypotheses of Kolmogorov for chemical reactor flows. It is noted that the physical basis of the Kolmogorov similarity hypotheses was questioned by Landau and Lifshitz ([92], p. 126; i.e., note that the first Russian edition of the book was apparently printed as early as in 1944). Landau's remark was concerned with the effect of fluctuations in the energy dissipation rate on the small scale properties of turbulence. It was argued that these fluctuations must depend on the Reynolds number and other mean flow parameters, thus they cannot be strictly universal. A consequence of this correction is that the two-thirds and five-third laws may retain their form, but the coefficients in these relations are not universal constants as anticipated by Kolmogorov and Obukhov. It was speculated that these factors vary as functions of the probability distribution for  $\varepsilon$  (see also [113], p. 584). Obukhov [118] and Kolmogorov [86] obviously found these remarks valid, thus some refinements of the original hypotheses concerning the local structure of turbulence were discussed. However, these model limitations have apparently not yet attracted wide attention in the chemical engineering research community as many reactor model closures still rely on the preliminary ideas of Kolmogorov.

### 1.3.3 Reynolds Equations and Statistics

In engineering practice only very simple statistics of turbulence is used based on the average (mean), the fluctuation (standard deviation) and the second moment (fluxes) taken at one point in space (i.e., one point time correlation functions).

In the following we will thus present some basic statistical methods useful for determining turbulence quantities from experimental data, and show how these measurements of turbulence can be put into the statistical model framework. Usually, *this involves separating the turbulent from the non-turbulent parts of the flow, followed by averaging to provide the statistical descriptor*. We will survey some of the basic methods of statistics, including the mean, variance, standard deviation, covariance, and correlation (e.g., [66], chap 1; [154], chap 2; [156]).

By averaging our velocity measurements over a certain time period, we can eliminate or average out the positive and negative deviations of the turbulent velocities about the mean. Once we have the mean velocity,  $\bar{v}$ , for any time period, we can subtract it from the actual instantaneous velocity,  $v$ , to calculate the turbulent part,  $v'$ :

$$v' = v - \bar{v} \tag{1.334}$$

The velocity fluctuation represents the flow that varies with periods shorter than the averaging time period. Recall that turbulence is a 3D phenomena. Therefore, we expect that fluctuations in the  $x$ -direction might be accompanied by fluctuations in the  $y$ - and  $z$ - directions. Turbulence, by definition, is a type of motion. Yet motions frequently cause variations in the temperature and concentration fields as well, if there is some mean gradient of that variable across the turbulent domain. Hence, it is common practice to portion each of these variables into mean and turbulent parts in the same manner as for the velocity.

A *mean quantity* can be defined by time, space, and ensemble averages.

The *time average* applies at one specific point in space, and consists of a sum or integral over a time period  $T$ . For any variable,  $A(t, \mathbf{r})$ , that is a function of time,  $t$ , and space,  $\mathbf{r}$ :

$$\bar{A}(\mathbf{r}) = \frac{1}{N} \sum_{i=0}^{N-1} A(i, \mathbf{r}) \quad (1.335)$$

or

$$\bar{A}(\mathbf{r}) = \frac{1}{T} \int_{t=0}^T A(t, \mathbf{r}) dt \quad (1.336)$$

where  $t = i\Delta t$  for the discrete case.

The *spatial average*, which applies at some instant in time, is given by a sum or integral over the spatial domain. For example, the volume average is given by the sum or integral over the macroscopic volume  $V$ :

$$\langle A \rangle_V(t) = \frac{1}{N} \sum_{j=0}^{N-1} A(t, j) \quad (1.337)$$

or

$$\langle A \rangle_V(t) = \frac{1}{V} \int_{V=0}^V A(t, V) dv \quad (1.338)$$

where  $V = j\Delta V$  for the discrete case.

An *ensemble average* consists of the sum over  $N$  identical experiments:

$$\langle A \rangle_e(t, \mathbf{r}) = \frac{1}{N} \sum_{n=0}^{N-1} A_n(t, \mathbf{r}) \quad (1.339)$$

or

$$\langle A \rangle_e(t, \mathbf{r}) = \int_{\varepsilon} A(t, \mathbf{r}; \mu) p(\mu) d\mu \quad (1.340)$$

In the definitions above,  $\Delta t = T/N$  and  $\Delta V = V/N$ , where  $N$  is the number of data points.  $p(\mu)d\mu$  denotes the probability of observing  $\mu$  in the interval  $d\mu$ , where  $\mu$  is some realization and  $\varepsilon$  is all realizations of the ensemble.

In principle, for laboratory experiments the ensemble average is the most desirable because it allows us to reduce random experimental errors by repeating the basic experiment. However, we often have problems performing repeatable experiments in a operating process equipments and the physical interpretation of the experimental data is complicated.

Spatial averages are possible by deploying an array of sensors covering a line, area, or volume. If the turbulence is *homogeneous* (i.e., statistically the same at every point in space) then each of the sensors in the array will be measuring the same phenomenon, making a spatial average meaningful. Most practical flow situations are rarely homogeneous meaning that most spatial means are averaged over a variety of different phenomena. By proper choice of sensor array domain size as well as intra-array spacing, one can sometimes isolate scales of phenomena for study, while averaging out the other scales. Volume averaging is impossible using point measurements such as thermometers because of the difficulty of deploying these sensors at all locations within the grid volumes of finite extent. However, sensors that can scan volumes of the flow making proper volume averages of selected variables are available [156]. On the other hand, such measurements are difficult to perform due to enormous storage requirements. Area averaging is somewhat easier to perform within small area domains, but still proper measurements may be difficult to perform. Line averages are similarly performed by erecting sensors along one direction only.

Time averages are frequently used, and are computed from sensors mounted on a single fixed location site. The relative ease of making observations at a fixed point have made this technique the most popular one for practical applications.

For turbulence that is both homogeneous and stationary (statistically not changing over time), the time, space and ensemble averages should all be equal. This is called *the ergodic condition*, which is sometimes assumed to make the turbulence problem more tractable.

Using Reynolds decomposition the instantaneous quantities in the instantaneous equation are considered as sums of the mean (averaged) and fluctuating components. Substituting the instantaneous quantities with their decomposed sum and averaging, yields the averaged equations. The resulting time averaged equation will, in addition to proper means, contain unknown non-linear averaged terms which have to be modeled separately. These models are very often of semi-empirical nature and need to be validated.

Experimental measurements describing the detailed characteristics of the flow pattern including statistical data analysis is thus of vital importance. On the other hand, statistical descriptors such as the variance, covariance, standard deviation and turbulence intensity are of limited usefulness unless we can physically interpret them.

*The variance*,  $\sigma_A^2$ , is a statistical measure of the dispersion of data about the mean defined by:

$$\sigma_A^2 = \frac{1}{N} \sum_{i=0}^{N-1} (A_i - \bar{A})^2 \quad (1.341)$$

This is known as the biased variance. It is a good measure of the dispersion of a sample of a flow variable, but according to the statistical definition not the best measure of the dispersion of the whole population of possible observations. A better estimate of the variance (an unbiased variance) of the population, given a sample of data, is:

$$\sigma_A^2 = \frac{1}{N-1} \sum_{i=0}^{N-1} (A_i - \bar{A})^2 \quad (1.342)$$

When  $N$  is large  $1/N \approx 1/(N-1)$ , and as a result the biased definition is often used for convenience.

Recall that the turbulent part of the turbulent variable is given by  $a' = A - \bar{A}$ . Substituting this into the biased definition of variances and comparing the result with the definition of averages gives:

$$\sigma_A^2 = \frac{1}{N} \sum_{i=0}^{N-1} a_i'^2 = \overline{a'^2} \quad (1.343)$$

Thus, whenever we encounter the average of the square of a turbulent part of a variable, such as  $\overline{v_x'^2}$ ,  $\overline{v_y'^2}$ ,  $\overline{v_z'^2}$ , we can interpret these as variances.

The *standard deviation* is defined as the squared root of the variance:

$$\sigma_A = \overline{a'^2}^{1/2} \quad (1.344)$$

The standard deviation (or root-mean-square, rms, amplitude) always has the same dimensions as the original variable. It can be interpreted as a measure of the magnitude of the spread or dispersion of the original data from its mean. For this reason, it is used as a measure of the intensity of turbulence.

The turbulence intensity is expected to increase as the mean velocity  $\bar{v}_x$  increases, hence a dimensionless measure of the turbulence intensity,  $I$ , is often defined as:

$$I_x = \frac{\sigma_{v_x}}{\bar{v}_x} \quad (1.345)$$

$$I_y = \frac{\sigma_{v_y}}{\bar{v}_y} \quad (1.346)$$

$$I_z = \frac{\sigma_{v_z}}{\bar{v}_z} \quad (1.347)$$

In statistics, *the covariance* between two variables is defined as:

$$\text{covar}(A, B) = \frac{1}{N} \sum_{i=0}^{N-1} (A_i - \bar{A})(B_i - \bar{B}) \quad (1.348)$$

Using the Reynolds averaging methods, we can show that:

$$\text{covar}(A, B) = \frac{1}{N} \sum_{i=0}^{N-1} a'_i b'_i = \overline{a'b'} \quad (1.349)$$

Thus the non-linear turbulence products that were introduced by the averaging process applied to the governing equations have the same meaning as covariances.

The covariance indicates the degree of common relationship between the two variables,  $A$  and  $B$ . For example, let  $A$  represent air temperature,  $T$ , and let  $B$  be the vertical velocity,  $v_z$ . In the earth's atmosphere, we might expect the warmer than average air to rise (positive  $T'$  and positive  $v'_z$ ), and the cooler than average air to sink (negative  $T'$  and negative  $v'_z$ ). Thus, the product  $v'_z T'$  will be positive on the average, indicating that  $v_z$  and  $T$  vary together.

Sometimes, one is interested in a normalized covariance. Such a relationship is defined as *the linear correlation coefficient*,  $r_{AB}$ :

$$r_{AB} = \frac{\overline{a'b'}}{\sigma_A \sigma_B} \quad (1.350)$$

This variable ranges between  $-1$  and  $+1$  by definition. Two variables that are perfectly correlated (i.e., vary together) yield  $r = 1$ . Two variables that are perfectly negatively correlated (i.e., vary oppositely) yield  $r = -1$ . Variables with no net variation together yield  $r = 0$ .

The definition of kinetic energy per unit volume is  $\rho \frac{\mathbf{v}^2}{2}$ , whereas the kinetic energy per unit mass is just  $\frac{\mathbf{v}^2}{2}$ . It is common to partition the kinetic energy of the flow into a portion associated with the mean velocity,  $\frac{\bar{\mathbf{v}}^2}{2}$ , and a portion associated with the turbulence,  $\frac{\overline{\mathbf{v}'^2}}{2}$ . We can thus write the relations:

$$\text{Kinetic Energy of the Mean flow} = \frac{1}{2} (\bar{v}_x^2 + \bar{v}_y^2 + \bar{v}_z^2) \quad (1.351)$$

$$\text{Mean Turbulent Kinetic Energy} = k = \frac{1}{2} (\overline{v_x'^2} + \overline{v_y'^2} + \overline{v_z'^2}) \quad (1.352)$$

### 1.3.4 Semi-Empirical Flow Analysis

In industrial reaction engineering the simplest reactors are designed like tubes or pipes, and even the more complex reactor designs are often idealized as tubes to ease the modeling complexity. Therefore, before we proceed on the CFD related modeling issues the idealized or approximate engineering pipe velocity formulas are given as they are still very useful for simple hand calculations.

## Engineering Pipe Flow Design Formulas

From the introductory courses in fluid flow one recalls that the simple parabolic profile for laminar flow in a pipe, the *Hagen-Poiseuille law*, is derived by integration of a sufficiently simplified form of the generalized momentum equation (see e.g., [13], Example 3.6-1):

$$\frac{v_z(r)}{v_{z,\max}} = 1 - \left(\frac{r}{R}\right)^2 \quad (1.353)$$

where the maximum velocity at  $r = 0$  can be calculated from the cross-sectional averaged velocity,  $v_{z,\max} = 2\langle v_z \rangle_A$ .

Unfortunately, it is not possible to derive an analogue velocity profile for turbulent flow in an analytical manner based on the generalized momentum equations. However, a number of entirely empirical relations of similar simplicity exist for the velocity profile in turbulent pipe flow. One such relation often found in introductory textbooks on engineering fluid flow is the *power law velocity profile*:

$$\frac{\bar{v}_z(r)}{\bar{v}_{z,\max}} = \left(1 - \frac{r}{R}\right)^{1/7} \quad (1.354)$$

where  $\bar{v}_{z,\max}$  is the velocity at the centerline of the pipe (i.e., the centerline velocities are not the same in the two flow regimes).

The latter relation is often used as a reasonable approximation for turbulent pipe flows in engineering practice. That is, for fully developed turbulent flows this relation provides a reasonable approximation to the measured velocity profiles across most of the pipe radius. However, a brief examination of this relation shows that the power-law profile cannot be valid near the wall, since according to this equation the velocity gradient is infinite there. In addition, the simple relation cannot be precisely valid near the centerline because it does not give:  $\frac{d\bar{v}_z}{dr} = 0$  for  $r = 0$ .

The purpose of performing CFD model simulations is to obtain more accurate predictions of the flow fields, thus precise boundary conditions are needed. From the previous discussion it is rather obvious that for CFD reactor simulations the empirical turbulent velocity profile formula for simple pipes is not very useful providing accurate boundary conditions at reactor walls. In the following subsections we thus consider the Prandtl mixing-length model and a more advanced concept for analyzing simple wall shear flows, i.e., exemplified through a fully developed shear flow past a flat plate, where the mean velocity vector is assumed to be parallel to the wall. This simple flow is of practical importance and has played a prominent role in the historical development of the study of turbulent wall flows. The important step forward using this concept is that the boundary layer approach provides a local description of the flow structure in the vicinity of solid walls. That is, the model is apparently generic and valid on local scales for most turbulent solid wall flows.

### Prandtl's Mixing-Length Model

The mixing-length model of Prandtl [123] for flow near a solid boundary is based on an analogy between the chaotic motion of eddies and the random motion of molecules in dilute gases (kinetic theory).

In Cartesian coordinates the Reynolds shear stress  $\overline{\rho v'_x v'_y}$  represents a flux of  $x$ -momentum in the direction of  $y$ . Prandtl assumed that this momentum was transported by discrete lumps of fluid, which moved in the  $y$  direction over a distance  $l$  without interaction conserving the momentum and then mixed with the existing fluid at the new location. The mixing length,  $l$ , is supposed to be a variable analogous to the mean free path of kinetic theory in this process.

Prandtl's model derivation can then be briefly sketched, introducing the Boussinesq [19] [20] approximation for the turbulent viscosity. Starting out with the simple kinetic theory relation that the molecular viscosity equals the molecular velocity times the mean free path, an analogous relation can be formulated for the turbulent viscosity in terms of the turbulent mixing length and a suitable velocity scale,  $\nu_t \approx l v'_x$ .

The Prandtl velocity scale yields:

$$v'_x = l \left| \frac{d\bar{v}_x}{dy} \right| \quad (1.355)$$

Supported by experimental observations,  $v'_y$  is assumed to be of the same order of magnitude as  $v'_x$  in the constant stress layer near a solid boundary. Hence, we may define Prandtl's mixing length model as:

$$\overline{\rho v'_x v'_y} \approx -\mu_t \frac{d\bar{v}_x}{dy} \approx -\rho l^2 \left( \frac{d\bar{v}_x}{dy} \right)^2 \quad (1.356)$$

In the inner part of the boundary layer  $l$  is often estimated by  $l = \kappa y$  (e.g., [66]), where  $\kappa$  is known as the von Kàrmàn constant.

This relation has been used successfully for many boundary layer flows. However, it is today generally accepted that the physical equivalence between the turbulent mixing length and the molecular mean free path is completely erroneous. The turbulent eddies are not small compared to the width of the mean flow, and they interact continuously rather than collide instantaneously. This model limitation was already recognized by Taylor [157].

The mixing length model of Prandtl [123] is further discussed by McComb [106], sect. 1.5.2), Hinze ([66], sect. 5-2), Sideman and Pinczewski [146], Schlichting and Gersten ([139], sect 17.1.4) and Pope ([121], sect 7.1.7).

### Velocity Distribution in Turbulent Boundary Layers

Originally, the concept of *fluid boundary layer* was presented by Prandtl [122]. Prandtl's idea was that for flow next to a solid boundary a thin fluid layer (i.e.,

a boundary layer) develops in which friction is very important, but outside this layer the fluid behaves very much like a frictionless fluid.

To define a demarcation line between these two flow regions the thickness of the boundary layer,  $\delta$ , is arbitrarily taken as the distance away from the surface where the velocity reaches 99% of the free stream velocity (e.g., [106], p 12; [55], p 192; [114], p. 545).

To proceed giving a thorough description of the equations used for turbulent flows, we need some results from the semi-empirical turbulent boundary layer flow analysis.

For a generalized shear flow in the vicinity of a flat horizontal solid wall, the boundary layer flow can be described in Cartesian coordinates. The stress,  $-\overline{\sigma}_{xy,\text{eff}}$ , associated with direction  $y$  normal to the wall is apparently dominant, thus the stream-wise Reynolds averaged momentum equation yields:

$$\rho \frac{D\bar{v}_x}{Dt} \approx -\frac{\partial \bar{p}}{\partial x} - \frac{\overline{\sigma}_{xy,\text{eff}}}{\partial y} \quad (1.357)$$

where

$$\overline{\sigma}_{xy,\text{eff}} = -\mu \frac{\partial \bar{v}_x}{\partial y} + \rho \overline{v'_x v'_y} \quad (1.358)$$

Intuitively one could imagine that the boundary layer as a whole can be characterized in terms of the boundary layer thickness and related dimensionless groups. However, experimental data reveals that the laminar shear is dominant near the wall (i.e., in *the inner wall layer*), and turbulent shear dominates in *the outer wall layer*. There is also an intermediate region, called *the overlap wall region*, where both laminar and turbulent shear are important.

Consequently, Prandtl [123] postulated that, at high Reynolds numbers, close to the wall ( $y/\delta \ll 1$ ) there is an inner layer in which the mean velocity profile is determined by the viscous scales, independent of  $\delta$  and the free stream velocity,  $\bar{v}_x(y = \delta)$ .

Since ample experimental analyzes support the Prandtl hypothesis, it is evident that close to the wall the viscosity,  $\nu$ , and the wall shear stress,  $\sigma_W$ , are important parameters. From these quantities one can define viscous scales that are appropriate velocity scales and length scales in the near-wall region. Dimensional analysis confirmed by experiments indicates that the relevant velocity scale for the inner region is *the friction velocity*<sup>34</sup>, given by:

$$v_* = \sqrt{\frac{-\overline{\sigma}_W}{\rho}} \quad (1.359)$$

The corresponding length scale characterizing the inner layer, the viscous length scale, is defined as

<sup>34</sup> In most textbooks the friction velocity is defined as  $v_* = \sqrt{\frac{\overline{\sigma}_W}{\rho}}$ , where  $\overline{\sigma}_W \approx \overline{\sigma}_{xy} + \overline{\sigma}_{xy}^\dagger = \rho \nu \frac{d\bar{v}_x}{dy} - \rho \overline{v'_x v'_y}$ . However, due to the sign convention adopted in this book for the shear stresses, a negative sign has to be introduced in front of the wall stress variable.

$$\delta_v = \nu \sqrt{\frac{\rho}{-\bar{\sigma}_W}} = \frac{\nu}{v_*} \quad (1.360)$$

Two local Reynolds numbers can thus be formed based on the characteristic velocity and length scales for the boundary layer. One Reynolds number purely based on the viscous scales of the inner layer,  $v_*\delta_v/\nu$ , is identically unity, and the alternative dimensionless group called *the friction Reynolds number* is defined using scales reflecting both the inner and outer layers,  $\frac{v_*\delta}{\nu} = \frac{\delta}{\delta_v}$ .

The distance from the wall measured in viscous lengths, or wall units, can be denoted by:

$$y^+ = \frac{y}{\delta_v} = \frac{yv_*}{\nu} \quad (1.361)$$

Notice that  $y^+$  is very similar to the two local Reynolds numbers just defined for the boundary layer, thus the magnitude of this dimensionless length variable is sometimes interpreted as a kind of Reynolds number.

Subsequent experimental validation lead to additional partitioning of the inner constant stress layer according to the relative magnitude of the viscous and turbulent components of the total shear stress. The total shear stress takes the form:

$$\bar{\sigma}_{xy}^{\text{eff}} = \bar{\sigma}_{xy} + \bar{\sigma}_{xy}^t = -\rho\nu \frac{d\bar{v}_x}{dy} + \overline{\rho v'_x v'_y} \approx \bar{\sigma}_W \quad (1.362)$$

where the viscous part is given by Newton's law applied to the mean rate of strain and the turbulent contribution is just the corresponding component of the Reynolds stress tensor. At the wall, the boundary condition for the instantaneous velocity vector,  $\mathbf{v}(\mathbf{r}, t) = 0$ , dictates that all the Reynolds stresses vanish. Consequently, the wall shear stress is entirely due to the viscous contribution:

$$\bar{\sigma}_W = -\rho\nu \left[ \frac{d\bar{v}_x}{dy} \right]_{y=0} \quad (1.363)$$

The *viscous sub-layer* is defined as the region next to the wall where the first term on the RHS of (1.362) is dominant. For larger values of  $y$ , the second term on the RHS of (1.362) will become dominant, and this region is usually referred to as the the inertial - or *turbulent log-law sub-layer*. Evidently there will be an intermediate region where the two stresses will be of equal magnitude, and this transition sub-layer is called *the buffer layer*. This boundary layer theory is based on the assumption that the effective shear stress is constant throughout the inner layer.

### Viscous Sub-Layer Analysis

In the viscous sub-layer, the total shear stress is determined by the viscous shear contribution:

$$-\frac{\overline{\sigma}_{xy}^{\text{eff}}}{\rho} \approx -\frac{\overline{\sigma}_W}{\rho} = \nu \frac{d\bar{v}_x}{dy} \quad (1.364)$$

for  $y^+ < 5$ .

Since this relation is universal (e.g., [108]), it is convenient to introduce a non-dimensional function,  $\Phi_v(\frac{y}{\delta_v})$ , thus:

$$\frac{d\bar{v}_x}{dy} = \frac{v_*}{y} \frac{y v_*}{\nu} = \frac{v_*}{y} \Phi_v\left(\frac{y}{\delta_v}\right) \quad (1.365)$$

Integrating with respect to  $y$ , we get:

$$\bar{v}_x = \frac{u_*^2 y}{\nu} \quad (1.366)$$

or in the scaled variables  $y^+ = y/\delta_v$  and  $v^+(y^+) = \bar{v}_x/v_*$ , it yields:

$$v^+ = y^+ \quad (1.367)$$

where the constant of integration has been set equal to zero in order to satisfy the boundary condition,  $\bar{v}_x(y=0) = 0$ .

### Turbulent log-law Sub-Layer Analysis

At some further distance from the wall, in the turbulent log-law sub-layer, we may neglect the viscous term, and the total stress tensor reduces to:

$$\frac{\overline{\sigma}_{xy}^{\text{eff}}}{\rho} \approx \frac{\overline{\sigma}_W}{\rho} \approx \overline{v'_x v'_y} \quad (1.368)$$

By use of the Prandtl mixing-length model and the relation  $l \approx \kappa y$  [123], yields:

$$\frac{\overline{\sigma}_{xy}^{\text{eff}}}{\rho} \approx \frac{\overline{\sigma}_W}{\rho} \approx \overline{v'_x v'_y} \approx -l^2 \left(\frac{d\bar{v}_x}{dy}\right)^2 \approx -\kappa^2 y^2 \left(\frac{d\bar{v}_x}{dy}\right)^2 \quad (1.369)$$

and hence, by introducing the definition of the friction velocity we obtain:

$$u_*^2 \approx \kappa^2 y^2 \left(\frac{d\bar{v}_x}{dy}\right)^2 \quad (1.370)$$

The velocity gradient can thus be expressed in terms of a non-dimensional function analogous to the one defined for the viscous sub-layer (e.g., [108]),  $\Phi_I(\frac{y}{\delta_v})$ , hence:

$$\frac{d\bar{v}_x}{dy} = \frac{v_*}{y} \frac{1}{\kappa} = \frac{v_*}{y} \Phi_I\left(\frac{y}{\delta_v}\right) \quad (1.371)$$

or in the scaled variables:

$$\frac{dv^+}{dy^+} = \frac{1}{\kappa y^+} \quad (1.372)$$

Finally, integrating with respect to  $y^+$ , we obtain a logarithmic velocity profile:

$$v^+ = \frac{1}{\kappa} \ln y^+ + B \quad (1.373)$$

where  $B$  is a constant of integration. The two parameters in this relation are fitted to experimental velocity data obtained from pipe flow analyzes. However, the values of the constants,  $\kappa$ , and,  $B$ , vary slightly from one literature source to another probably reflecting the experimental accuracy of the analyzes. In most papers on reactor modeling the values  $\kappa = 0.40$  and  $B = 5.5$  are preferred.

A further limitation is that this logarithmic relation is only valid for smooth surfaces. That is, for flow situations where the height of any roughness element on the wall is less than the thickness of the viscous sub-layer. Contrary, if the roughness height is greater than the sub-layer thickness, the roughness height itself determines the inner region length scale. The latter approach is regularly applied in atmospheric weather forecast models (e.g., [22] [41] [75]).

For the inner region of the boundary layer, the mean velocity formulas for smooth surfaces can be generalized and expressed in a universal form:

$$v^+ = f(y^+) \quad (1.374)$$

which is known as *the law of the wall*, sketched in Fig. 1.7.

### Outer Layer Analysis

von Kàrmàn [177] deduced that in the outer layer the velocity gradient actually depends on the thickness of the boundary layer as a whole. Hence, based on dimensional arguments this implies that the velocity gradient can be expressed in terms of a non-dimensional function similar to those used for the viscous sub-layers [108]:

$$\frac{d\bar{v}_x}{dy} = \frac{v_*}{y} \Phi_o\left(\frac{y}{\delta}\right) \quad (1.375)$$

where the appropriate lengthscale has been introduced.

Integrating this equation between  $y$  and  $\delta$  yields the *velocity-defect law* for the outer layer. This, of course, requires that the non-universal non-dimensional function,  $\Phi_o$ , is known.

This function, at present being unknown, can be determined as we notice that the semi-empirical relations for the inner- and outer layers are different in form, but they must overlap smoothly in the intermediate layer. Mathematically, this implies that the dimensionless functions, i.e.,  $\Phi_I\left(\frac{y}{\delta_v}\right)$  and  $\Phi_o\left(\frac{y}{\delta}\right)$ , should approach the same asymptotic value in the overlap region (e.g., [108]; [121], p 275). The velocity gradient can thus be expressed in both sets of scales

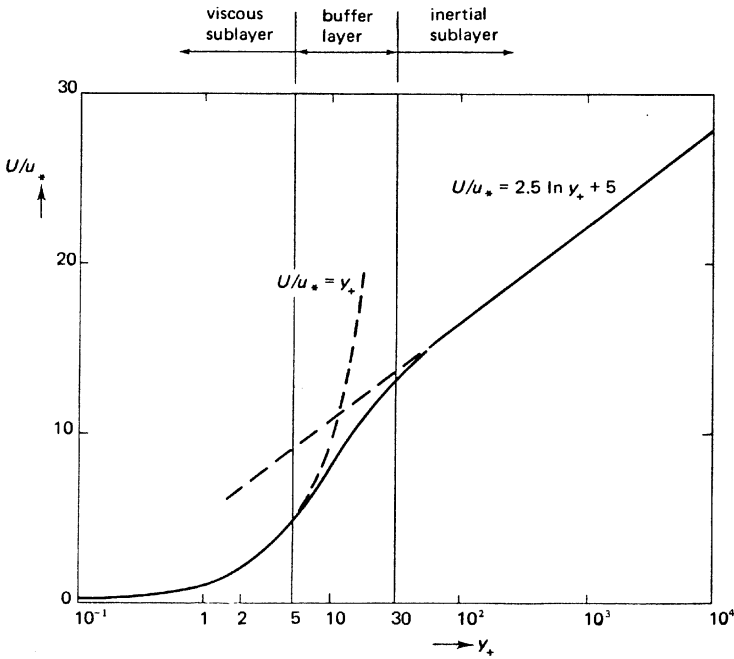


**Fig. 1.7.** The law of the wall, taken from Tennekes and Lumley ([167], p 160). In this figure the  $U$  and  $u_*$  variables correspond to the  $\bar{v}_x$  and  $v_*$  variables used in the present text. Reprinted with permission of the MIT Press as Publisher, 1/6/2005.

$$\frac{y}{v_*} \frac{d\bar{v}_x}{dy} = \Phi_I\left(\frac{y}{\delta_v}\right) = \Phi_o\left(\frac{y}{\delta}\right) = \frac{1}{\kappa} \approx 2.4 \quad (1.376)$$

This relation establishes the form of the velocity-defect law for small  $y/\delta$ , and indicates that the log-law can give reasonable predictions also for relatively large values of  $y^+$  provided that the overlap region has a significant width.

In summary, experimental data indicates that the turbulent boundary layer can be subdivided into an inner constant wall stress layer for the approximate range  $0 \leq y \leq 0.1\delta$ , and an outer non-constant stress layer bounded by  $0.1\delta < y \leq \delta$  [137] [121].

The inner layer is further classified as:

1. Viscous sub-layer:  $0 \leq y^+ \leq 5$
2. Transition sub-layer:  $5 < y^+ \leq 30$
3. Turbulent constant stress layer:  $30 < y^+ \leq 400$

The values used for  $\delta$  and  $y^+$  to classify the various layers may vary from one literature source to another. These discrepancies reflect the experimental accuracy obtained determining the boundaries between the various layers.

A common simplification adopted in many engineering CFD calculations is to neglect the influence of the deviating physics occurring in the buffer-layer. The inner part of the boundary layer is thus roughly subdivided into two more approximate sub-layers only, those are a viscous - and a turbulent sub-layer. The two sub-layers are separated at a certain distance from the wall  $y^+ = 11.63$  where the linear velocity profile in the viscous sub-layer meets the logarithmic velocity profile in the turbulent constant stress layer. For shorter distances from the wall ( $y^+ < 11.63$ ) the flow is assumed to be purely viscous and at larger distances from the wall ( $y^+ \geq 11.63$ ) the flow is purely turbulent.

The semi-empirical boundary layer analyzes of Prandtl [123] and von Kàrmàn [177] are further discussed by [108]; [106], sect 1.4.2; [66], sect 7-5; [139], sect 17; [121], sect 7.

### 1.3.5 Reynolds Averaged Models

Reynolds [127] postulated that the Navier-Stokes equations are still valid for turbulent flows, but recognized that these equations could not be applied directly due to the complexity and irregularity of the fluid dynamic variables. A true description of these flows at all points in time and space was not feasible, and probably not very useful at the time. Instead, Reynolds proposed to develop equations governing the mean quantities that were actually measurable.

To reformulate the governing equations in terms of mean flow quantities rather than instantaneous quantities, Reynolds postulated the fundamental ideas of averaging. In the averaging procedure devised by Reynolds [127] the instantaneous quantities are decomposed<sup>35</sup> into the sum of mean and fluctuating quantities.

The mean quantities were defined by time-averaging the instantaneous quantities over a sufficient time period ( $\Delta t$ ), i.e., being long enough to smooth out the turbulent fluctuations, separating the turbulent parts from the non-turbulent parts.

Introducing a generalized instantaneous quantity,  $\psi$ , the corresponding time average quantity is defined by:

<sup>35</sup> Note that the turbulent viscosity parameter has an empirical origin. In connection with a qualitative analysis of pressure drop measurements Boussinesq [19] introduced some apparent internal friction forces, which were assumed to be proportional to the strain rate ([20], p 8), to fit the data. To explain these observations Boussinesq proceeded to derive the same basic equations of motion as had others before him, but he specifically considered the molecular viscosity coefficient to be a function of the state of flow and not only on the system properties [135]. It follows that the turbulent viscosity concept (frequently referred to as the Boussinesq hypothesis in the CFD literature) represents an empirical first attempt to account for turbulence effects by increasing the viscosity coefficient in an empirical manner fitting experimental data. Moreover, at the time Boussinesq [19] [20] was apparently not aware of the Reynolds averaging procedure that was published 18 years after the first report by Boussinesq [19] on the apparent viscosity parameter.

$$\bar{\psi} = \frac{1}{\Delta t} \int_t^{t+\Delta t} \psi(t) dt \quad (1.377)$$

It has been shown that the averaging procedure is valid for statistically stationary variables only, thus the time average should be independent of the origin  $t$ . Apparently, the conventional Reynolds averaging procedure requires that the transients in the governing equations should be negligibly small (e.g., [66], p 6; [167], p. 28).

After the mean quantities have been obtained, the fluctuations can be obtained by subtracting the mean values from the corresponding instantaneous ones. The mean of a fluctuating quantity is zero by definition:

$$\bar{\psi'} = \frac{1}{\Delta t} \int_t^{t+\Delta t} (\psi(t) - \bar{\psi}) dt \equiv 0 \quad (1.378)$$

In the averaging procedure devised by Reynolds not only single quantities are considered, but also products of quantities constituting the governing equations.

Let  $A = \bar{A} + a'$  and  $B = \bar{B} + b'$  be two instantaneous variables, and let  $c$  represent a constant. Accordingly, the Reynolds [127] axioms or mathematical rules of averaging can be expressed as:

$$\begin{aligned} \bar{c} &= c \\ \overline{\bar{A}} &= \bar{A} \\ \overline{\bar{A}\bar{B}} &= \bar{A}\bar{B} \\ \overline{a'} &= 0 \\ \overline{\bar{A} + a'} &= \bar{\bar{A}} + \overline{a'} = \bar{A} \\ \overline{c\bar{A}} &= \bar{c}\overline{\bar{A}} + \overline{c a'} = c\bar{A} \\ \overline{b'} &= 0 \\ \overline{\bar{A}B} &= \overline{\bar{A}(\bar{B} + b')} = \bar{A}\bar{B} \\ \overline{A + B} &= \overline{\bar{A} + a' + \bar{B} + b'} = \bar{A} + \bar{B} \\ \frac{d\bar{A}}{dt} &= \frac{d\bar{A}}{dt} \\ \overline{\bar{A}B} &= \overline{(\bar{A} + a')(\bar{B} + b')} = \overline{\bar{A}\bar{B}} + \overline{\bar{A}b'} + \overline{\bar{B}a'} + \overline{a'b'} = \bar{A}\bar{B} + \overline{a'b'} \end{aligned} \quad (1.379)$$

Turbulence is a 3D phenomenon, thus it is expected that turbulence in one dimension might be accompanied by similar effects in the other two directions. In addition, as mentioned above, the turbulent motions frequently cause variations in the other quantities too. Hence, all the dependent variables defining the system can be partitioned into mean and turbulent parts.

Lately, a few alternative interpretations and extensions of the conventional Reynolds averaging procedure are given in the literature. A least two of these deviants deserve to be mentioned, as they are used frequently although not necessarily in reactor modeling.

The desire to make practical calculations of statistically non-stationary flows has led engineers to formulate semi-empirical extensions of the conventional method. In this case the instantaneous variables are said to be time averaged over a time interval which is large compared to the turbulent time scales, but still small compared to the time dependency of the mean component. Using this averaging procedure one should be aware of the problem of interpreting the simulated results, as the spectral split between the mean and turbulent contributions becomes rather vague and apparently related to both the time interval of averaging and the resolution of the numerical solution method.

An alternative interpretation of the Reynolds averaging procedure is regularly used in meteorology developing weather forecast models. The physical basis for this approach is neat and intuitive [154]. In boundary layer meteorology experimental analyzes show that a spectral energy gap is evident. This spectral gap provides a means to separate the turbulent from the non-turbulent scales of motion. By time-averaging the instantaneous quantities over a time period that corresponds to the spectral gap scales, the turbulent effects are eliminated from the mean. The turbulent part of the flow varies with periods shorter than the ones corresponding to the spectral gap scales, whereas the mean represents the part that varies with longer periods. These turbulence analyzes thus rely on the separation of scales enabling proper partitioning of the flow into the mean and turbulent parts. On physical reasons many of the operational numerical weather forecast models use grid resolutions or wavelength cutoffs that fall within the spectral gap. This means that larger scale motions can be explicitly resolved, whereas the smaller scale turbulent motions are modeled directly. That is, the effects of the sub-grid scale motions on the larger scales are parameterized by sub-grid scale statistical models. In one interpretation this averaging procedure is analogous to the filtering procedure used in the LES method as the averaging operator used is generic for time-, space- and ensemble averages. Unfortunately, for many practical flows one might not be able to obtain any vivid separation of scales, averaging the variables over a finite time period. Then the decomposition procedure may break down, and the simulated results may become inaccurate and difficult to interpret.

Stull ([154], sect. 2.4) and McComb ([106], app. B) discuss the statistical basis of the averaging procedures in further details.

However, while the convectional process of averaging the equations can be considered an exact procedure, the resulting averaged equations do not contain enough information about the turbulence to form a solvable set of equations. The statistical studies of the equations always lead to a situation in which there are more unknowns than equations. This is called *the closure*

problem of turbulence theory. One has to make ad hoc assumptions to make the number of equations equal to the number of unknowns.

The process of replacing the unknown averages or covariances, occurring in the governing equations after the equations have been averaged, with equations for variables which can be considered as dependent variables in the problem is called *turbulence modeling*. The resulting equations are termed a turbulence model. The turbulence model can be either an algebraic relation or a set of transport equations for some characteristic turbulent quantities. The various models are often classified according to the number of extra partial differential equations which are considered in addition to the Reynolds-averaged Navier-Stokes equations. That is, the zero-, one-, and two- equation models, as well as Reynolds Stress Models. All the average model formulations, except the Reynolds Stress Model, are based on the eddy viscosity hypothesis in what is often known as *the generalized Boussinesq hypothesis* [19, 20]:

$$\overline{v'_i v'_j} = \frac{2}{3} k \delta_{ij} - \nu_t \left( \frac{\partial \bar{v}_i}{\partial x_j} + \frac{\partial \bar{v}_j}{\partial x_i} \right) \quad (1.380)$$

where  $\delta_{ij}$  is the Kronecker delta and  $\nu_t$  is the eddy viscosity variable. The first term on the RHS is required as the sum of the normal stresses has to be consistent with the definition of  $k$ .

By formulating a proper turbulence model, the total number of equations involved equals the number of unknown variables, and a closed set of model equations is obtained. That is, adopting the eddy viscosity hypothesis we basically need to find proper expressions estimating the eddy viscosity variable. If the term containing the turbulent normal stresses is not neglected in equation (1.380), we need to determine the  $k$  variable too. The complexity of such model formulations may vary a lot, thus only a few of the most popular ones will be described below.

In multiphase reactor simulations the zero- and two equation models are very popular, only a few attempts have been made to implement Reynolds Stress Models, and LES models are still really rare.

## Zero-equation Models

Turbulence models containing the partial differential equations for the mean variable fields, and no differential equations for the turbulence are classified as *the zero-equation models*. All models belonging to this class is based on the eddy-viscosity concept. The eddy-viscosity is furthermore related to the mean flow field via an algebraic relation. Therefore, these models are also called algebraic models. Because of their simplicity, zero-equation models have received considerable interest over the years, and have been in common use for sophisticated engineering applications during the last decades.

The very simplest approximation of the turbulent effects on the mean flow can be achieved by assuming that the eddy-viscosity is proportional to the molecular viscosity:

$$\nu_t = f\nu \quad (1.381)$$

throughout the flow field. The dimensionless constant  $f$  is typically of the order 1000.

The mixing-length model of Prandtl [123] for flow near a solid boundary, i.e., that have been referred several times already, is perhaps the most popular zero-equation model.

## Reynolds Stress Models

Stull [154] presents an excellent review of the procedures for formulating transport equations for the turbulent fluxes and variances applied to boundary layer meteorology. Wilcox [186], Pope [121] and Biswas and Eswaran [15] provide alternative texts intended for the engineering community, the latter textbook also considers experimental aspects of the field.

Chou [23] was the first to derive and publish the generalized transport equation for the Reynolds stresses. The exact transport equation for the Reynolds stresses was established by use of the momentum equation, the continuity equation and a moderate amount of algebra.

Because the upcoming derivations are sometimes long and involved, it is *easy to lose sight of the forest for the trees*. The following summary gives the steps that will be taken in the subsequent subsections. to develop the governing equations in a form suitable for describing turbulent flows.

1. Apply the Reynolds decomposition procedure and expand the dependent variables within the instantaneous equations into mean and fluctuating parts.
2. Apply the time- or ensemble averaging procedure to get the equations for the mean variables describing turbulent flows.
3. Subtract the equations of step 2 from the corresponding ones of step 1 to get equations for the turbulent fluctuations.
4. Multiply the result of step 3 by other turbulent quantities and time- or ensemble average to yield the transport equations for turbulence statistics such as the Reynolds stresses and the turbulent kinetic energy.
5. Finally, formulate the transport equations for the other turbulent fluxes and variances (i.e., sometimes called turbulent correlations).

The conventional Reynolds averaging procedure is deduced from the governing equations for incompressible fluid systems. In Cartesian coordinates the corresponding instantaneous equation of continuity takes the following form (i.e., written in a compact form by use Einstein's summation notation):

$$\frac{\partial v_i(t, \mathbf{r})}{\partial x_i} = 0 \quad (1.382)$$

where  $v_i(t, \mathbf{r})$  is the fluid velocity at space position  $\mathbf{r}$  and time  $t$ .

For an incompressible fluid, the instantaneous equation expressing conservation of momentum is:

$$\frac{\partial v_i}{\partial t} + \frac{\partial v_j v_i}{\partial x_j} = -\frac{1}{\rho} \frac{\partial p}{\partial x_i} - \frac{1}{\rho} \frac{\partial \sigma_{ij}}{\partial x_j} \quad (1.383)$$

where  $\sigma_{ij}$  is the deviatoric stress tensor. For an incompressible Newtonian fluid,  $\sigma_{ij}$  is given by:

$$\sigma_{ij} = -\rho\nu \left( \frac{\partial v_i}{\partial x_j} + \frac{\partial v_j}{\partial x_i} \right) \quad (1.384)$$

where  $\nu$  is the kinematic viscosity of the fluid.

With the substitution of  $\sigma_{ij}$  from (1.384) and the use of (1.382), the resulting instantaneous equation of motion is known as the Navier-Stokes equation:

$$\frac{\partial v_i}{\partial t} + v_j \frac{\partial v_i}{\partial x_j} = -\frac{1}{\rho} \frac{\partial p}{\partial x_i} + \nu \frac{\partial^2 v_i}{\partial x_j \partial x_j} \quad (1.385)$$

By use of Reynolds averaging rules (1.379), the instantaneous continuity (1.382) can be averaged and we obtain:

$$\frac{\partial \bar{v}_i(\mathbf{r})}{\partial x_i} = 0 \quad (1.386)$$

Subtracting this result from (1.382) yields a similar equation for  $v'_i$ , thus the mean and fluctuating velocities separately satisfy the continuity equation. This is a trivial consequence of the linearity of (1.382).

In order to treat the equation of motion in the same way, we apply the Reynolds decomposition procedure on the instantaneous velocity and pressure variables in (1.385) and average term by term. It can be shown by use of Leibnitz' theorem that the operation of time averaging commutes with the operation of differentiating with respect to time when the limits of integration are constant [154, 106, 121, 15]).

The result is

$$\frac{\partial \bar{v}_i}{\partial t} + \bar{v}_j \frac{\partial \bar{v}_i}{\partial x_j} + \frac{\partial \overline{v'_i v'_j}}{\partial x_j} = -\frac{1}{\rho} \frac{\partial \bar{p}}{\partial x_i} + \nu \frac{\partial^2 \bar{v}_i}{\partial x_j \partial x_j} \quad (1.387)$$

Comparison with (1.385) shows that the equation for the mean velocity is just the Navier-Stokes equation written in terms of the mean variables, but with the addition of the term involving  $\overline{v'_i v'_j}$ . Thus, the equations of mean motion involve three independent unknowns  $\bar{v}_i$ ,  $\bar{p}$  and  $\overline{v'_i v'_j}$ . This is perhaps the best known version of the closure problem. Equation (1.387) is the Reynolds equation and the term  $\overline{v'_i v'_j}$  is the Reynolds stress. This term represents the transport of momentum due to turbulent fluctuations.

Equation (1.387) for the mean velocity is formally identical to the original Navier-Stokes equation, provided that we absorb the Reynolds stress into a more general stress tensor. An effective stress tensor is thus defined by

$$\overline{\sigma_{ij,\text{eff}}} = -\rho\nu\left(\frac{\partial\bar{v}_i}{\partial x_j} + \frac{\partial\bar{v}_j}{\partial x_i}\right) + \rho\overline{v'_i v'_j} \quad (1.388)$$

With a proper turbulence model the mean velocity is expected to be a fairly smooth function of time and position, and hence the problem of solving (1.387) should be very much simpler than the alternative direct numerical simulation task based on the primitive Navier-Stokes equation.

The simplest prescription for the Reynolds stress is apparently obtained from an algebraic turbulence model like the Prandtl [123] mixing-length model. The Prandtl model is, as explained in the foregoing analysis, based on the eddy viscosity concept and thus possesses the defects of this hypothesis. In addition, it lacks universality mainly because the prescription of the mixing length varies from one type of flow to another, and thus in complicated flows it may be impossible to specify any reliable parameterization for the mixing length.

The next category of turbulence closures, i.e., implying to be more accurate than the very simple algebraic models, is a hierarchy of turbulent models based on the transport equation for the fluctuating momentum field. These are the first-order closure models, i.e., those that require parameterizations for the second moments  $\overline{v'_i v'_k}$ , and the second-order closure models, i.e., those that require parameterizations for representing the third moments  $\overline{v'_i v'_j v'_k}$ . Since the Reynolds stress transport equation constitutes the basis for both the first- and second-order closure models, its derivation is presented next.

The equation of motion for the fluctuating velocity is obtained by subtracting (1.387) from (1.385):

$$\frac{\partial v'_i}{\partial t} + \bar{v}_j \frac{\partial v'_i}{\partial x_j} + v'_j \frac{\partial \bar{v}_i}{\partial x_j} + v'_j \frac{\partial v'_i}{\partial x_j} - \frac{\partial \overline{v'_i v'_j}}{\partial x_j} = -\frac{1}{\rho} \frac{\partial p'}{\partial x_i} + \nu \frac{\partial^2 v'_i}{\partial x_j \partial x_j} \quad (1.389)$$

In accordance with the equation for the fluctuating component  $v'_i$ , (1.389), a corresponding equation for the fluctuating component  $v'_k$  can be formulated simply by changing the index from  $i$  ( $x_i$ - momentum) to  $k$  ( $x_k$ - momentum) keeping all other indices and variables the same as before. The result is

$$\frac{\partial v'_k}{\partial t} + \bar{v}_j \frac{\partial v'_k}{\partial x_j} + v'_j \frac{\partial \bar{v}_k}{\partial x_j} + v'_j \frac{\partial v'_k}{\partial x_j} - \frac{\partial \overline{v'_k v'_j}}{\partial x_j} = -\frac{1}{\rho} \frac{\partial p'}{\partial x_k} + \nu \frac{\partial^2 v'_k}{\partial x_j \partial x_j} \quad (1.390)$$

Multiply (1.389) for the component  $i$  through with the fluctuating velocity  $v'_k$ , and time average yields

$$\overline{v'_k \frac{\partial v'_i}{\partial t}} + \overline{\bar{v}_j v'_k \frac{\partial v'_i}{\partial x_j}} + \overline{v'_k v'_j \frac{\partial \bar{v}_i}{\partial x_j}} + \overline{v'_k v'_j \frac{\partial v'_i}{\partial x_j}} = -\frac{1}{\rho} \overline{v'_k \frac{\partial p'}{\partial x_i}} + \overline{\nu v'_k \frac{\partial^2 v'_i}{\partial x_j \partial x_j}} \quad (1.391)$$

It is recognized that (1.391) doesn't completely constitute a transport equation for the second moments. However, combined with the corresponding transport equation, i.e., the one having the inverse  $i$  and  $k$  indexes, and

with some mathematical manipulation the exact transport equations for the Reynolds stresses are achieved.

For deriving the second equation, we multiply (1.390) for the component  $k$  through with the fluctuating velocity  $v'_i$ , and time average. The resulting equation can also be formulated by interchanging the  $i$  and  $k$  indices (i.e., replace each occurrence of  $i$  with  $k$ , and each occurrence of  $k$  with  $i$ ) in the above equation. The result is:

$$\overline{v'_i \frac{\partial v'_k}{\partial t}} + \overline{\bar{v}_j v'_i \frac{\partial v'_k}{\partial x_j}} + \overline{v'_i v'_j \frac{\partial \bar{v}_k}{\partial x_j}} + \overline{v'_i v'_j \frac{\partial v'_k}{\partial x_j}} = -\frac{1}{\rho} \overline{v'_i \frac{\partial p'}{\partial x_k}} + \overline{\nu v'_i \frac{\partial^2 v'_k}{\partial x_j \partial x_j}} \quad (1.392)$$

Summation of these two equations, and by use of the product rule of calculus to produce combinations like,  $\overline{v'_i \frac{\partial v'_k}{\partial t}} + \overline{v'_k \frac{\partial v'_i}{\partial t}} = \overline{\frac{\partial v'_i v'_k}{\partial t}}$ , yields

$$\begin{aligned} & \overline{\frac{\partial v'_i v'_k}{\partial t}} + \overline{\bar{v}_j \frac{\partial v'_i v'_k}{\partial x_j}} + \overline{v'_i v'_j \frac{\partial \bar{v}_k}{\partial x_j}} + \overline{v'_k v'_j \frac{\partial \bar{v}_i}{\partial x_j}} + \overline{v'_j \frac{\partial v'_i v'_k}{\partial x_j}} \\ & = -\frac{1}{\rho} \left( \overline{v'_i \frac{\partial p'}{\partial x_k}} + \overline{v'_k \frac{\partial p'}{\partial x_i}} \right) + \nu \left( \overline{v'_i \frac{\partial^2 v'_k}{\partial x_j \partial x_j}} + \overline{v'_k \frac{\partial^2 v'_i}{\partial x_j \partial x_j}} \right) \end{aligned} \quad (1.393)$$

The last term before the equal sign can be put into flux form by use of the continuity equation for the fluctuating components,

$$\frac{\partial}{\partial x_j} \overline{v'_i v'_j v'_k} = \overline{v'_j \frac{\partial v'_i v'_k}{\partial x_j}} + \overline{v'_i v'_k \frac{\partial v'_j}{\partial x_j}} = \overline{v'_i v'_j \frac{\partial v'_k}{\partial x_j}} + \overline{v'_j v'_k \frac{\partial v'_i}{\partial x_j}}$$

Each pressure term can be rewritten using the product rule of calculus, as illustrated in the following example:  $\overline{v'_k \frac{\partial p'}{\partial x_i}} = \overline{\frac{\partial p' v'_k}{\partial x_i}} - \overline{p' \frac{\partial v'_k}{\partial x_i}}$ .

The viscous terms can also be rearranged using the product rule in a similar manner. Consider a term of the form  $\overline{\frac{\partial^2 v'_i v'_k}{\partial x_j^2}}$ , using simple rules of calculus we can rewrite it as:

$$\begin{aligned} \overline{\frac{\partial^2 v'_i v'_k}{\partial x_j^2}} &= \overline{\frac{\partial}{\partial x_j} \left[ \frac{\partial v'_i v'_k}{\partial x_j} \right]} = \overline{\frac{\partial}{\partial x_j} \left[ v'_i \frac{\partial v'_k}{\partial x_j} + v'_k \frac{\partial v'_i}{\partial x_j} \right]} \\ &= \overline{\frac{\partial v'_i}{\partial x_j} \frac{\partial v'_k}{\partial x_j}} + \overline{v'_i \frac{\partial^2 v'_k}{\partial x_j^2}} + \overline{\frac{\partial v'_k}{\partial x_j} \frac{\partial v'_i}{\partial x_j}} + \overline{v'_k \frac{\partial^2 v'_i}{\partial x_j^2}} \\ &= 2 \overline{\frac{\partial v'_i}{\partial x_j} \frac{\partial v'_k}{\partial x_j}} + \overline{v'_i \frac{\partial^2 v'_k}{\partial x_j^2}} + \overline{v'_k \frac{\partial^2 v'_i}{\partial x_j^2}} \end{aligned}$$

If we multiply these terms by  $\nu$ , then the last two terms above will be identical to the last two terms in the transport equation. Thus, we can write the last two terms in the transport equation as

$$\overline{\nu v'_i \frac{\partial^2 v'_k}{\partial x_j^2}} + \overline{\nu v'_k \frac{\partial^2 v'_i}{\partial x_j^2}} = \nu \frac{\partial^2 \overline{v'_i v'_k}}{\partial x_j^2} - 2\nu \frac{\partial \overline{v'_i v'_j v'_k}}{\partial x_j \partial x_j}$$

The final form of the Reynolds stress transport equation (i.e., the transport equation for the turbulent momentum flux<sup>36</sup>) is:

$$\begin{aligned} \frac{\partial \overline{v'_i v'_k}}{\partial t} + \overline{v_j \frac{\partial v'_i v'_k}{\partial x_j}} &= -\overline{v'_i v'_j \frac{\partial \overline{v}_k}{\partial x_j}} - \overline{v'_k v'_j \frac{\partial \overline{v}_i}{\partial x_j}} - \frac{\partial \overline{v'_i v'_j v'_k}}{\partial x_j} \\ &\quad - \frac{1}{\rho} \left[ \frac{\partial \overline{p' v'_i}}{\partial x_k} + \frac{\partial \overline{p' v'_k}}{\partial x_i} - \overline{p' \left( \frac{\partial v'_i}{\partial x_k} + \frac{\partial v'_k}{\partial x_i} \right)} \right] \\ &\quad + \nu \frac{\partial^2 \overline{v'_i v'_k}}{\partial x_j^2} - 2\nu \frac{\partial \overline{v'_i v'_j v'_k}}{\partial x_j \partial x_j} \end{aligned} \quad (1.394)$$

The physical interpretation of the terms in the equation is not necessarily obvious. *The first term on the LHS* denotes the rate of accumulation of the kinematic turbulent momentum flux  $\overline{v'_i v'_k}$  within the control volume. *The second term on the LHS* denotes the advection of the kinematic turbulent momentum flux by the mean velocity. In other words, the left hand side of the equation constitutes the substantial time derivative of the Reynolds stress tensor  $\overline{v'_i v'_k}$ . *The first and second terms on the RHS* denote the production of the kinematic turbulent momentum flux by the mean velocity shears. *The third term on the RHS* denotes the transport of the kinematic momentum flux by turbulent motions (turbulent diffusion). This latter term is unknown and constitutes the well known moment closure problem in turbulence modeling. *The fourth and fifth terms on the RHS* denote the turbulent transport by the velocity-pressure-gradient correlation terms (pressure diffusion). *The sixth term on the RHS* denotes the redistribution by the return to isotropy term. In the engineering literature this term is called the pressure-strain correlation, but is nevertheless characterized by its redistributive nature (e.g., [131]). *The seventh term on the RHS* denotes the molecular diffusion of the turbulent momentum flux. *The eighth term on the RHS* denotes the viscous dissipation term. This term is often abbreviated by the symbol  $2\epsilon_{ik}$ .

For practical applications, second-order closure models are required for the third-order diffusion correlations, the pressure-strain correlation and the dissipation rate correlation as described by Launder and Spalding [94] and Wilcox ([186], sect. 6.3).

Launder and Spalding [94] argued that the pressure diffusion terms and the molecular diffusion of turbulent momentum fluxes are smaller than the rest of

<sup>36</sup> Momentum is by definition mass times velocity with units ( $\frac{kg\ m}{s}$ ). A momentum flux is thus a quantity with units ( $\frac{kg\ m}{s} \frac{1}{m^2\ s}$ ). These units are identical to ( $N/m^2$ ), which are the units for stress. For convenience, as we are usually measuring velocities and not fluxes, the fluxes are redefined in kinematic form by dividing by the mixture density. A kinematic momentum flux thus has units ( $\frac{m^2}{s^2}$ ).

the terms in the equation. These terms can thus be sufficiently approximated by a gradient type diffusion hypothesis. The third-order closure based on transport equations for the third moments are not considered worthwhile, as these correlations are considered small in engineering flows. The most common approach used in modeling the third moments is to adopt a gradient transport hypothesis for this term too. Because the turbulent energy dissipation occurs at the smallest scales, most modelers use the Kolmogorov [83] hypothesis of local isotropy to model the dissipation tensor ( $\varepsilon = \frac{2}{3}\rho\varepsilon\delta_{ik}$ ). A common feature of the full Reynolds stress models and the two-equation models is thus the limited accuracy reflected by the transport equation used for the turbulent length-scale (e.g., the  $\varepsilon$ -equation). Naturally, in conjunction with the Reynolds stress model second-order closures are used for the inherent terms in the length scale equation, whereas first-order closures are adopted in the corresponding two equation model equation. The pressure-strain correlation tensor, i.e., apparently being of the same order of magnitude as the production term [186], is also very difficult to parameterize further limiting the accuracy reflected by the Reynolds stress models. Considerable attention has been paid to this term by turbulence modelers, since there is no direct experimental information available for this correlation [186]. The recent LES and direct numerical simulations (DNS) have yet provided computer generated estimates for this term. Substantial improvements are also needed modeling near wall regions. Finally, in practice, each additional turbulence model equation increases both the computing time and the task of optimizing model parameters. It is easily seen that the Reynolds stress model basically includes 9 unknown terms for 3D simulations, since each term in equation (1.394) contains unrepeated  $i$  and  $k$  indices. Fortunately, the number of independent terms is reduced to 6 by symmetries. The computation of the nine terms in the Reynolds stress tensor thus requires that 7 additional transport equations are solved (i.e., including one transport equation for the turbulent energy dissipation rate). In addition, the Reynolds stress simulations are not as robust as the simpler two-equation model solution behavior.

Consequently, although the second-order closure models is considered a standard model in most commercial CFD codes, the Reynolds stress model is usually not considered worthwhile for complex reactor simulations. Actually, for dynamic simulations the interpretation problems, mentioned earlier in this paragraph, have shifted the attention towards the VLES simulations to be described shortly. In this book the second-order closure models are thus not considered in further details, the interested reader is referred to standard textbooks on turbulence modeling for CFD applications (e.g., [186] [121]).

## Two-Equation Models

Due to their robustness and reasonable accuracy, the first-order two-equation models, such as the  $k$ - $\varepsilon$  closure originally proposed by Harlow and Nakayama

[62] [63], have become very popular for reactor simulations. In this section the formal derivation of the  $k$ - $\varepsilon$  model equations are given and discussed.

A transport equation for *the turbulent kinetic energy*, or actually the momentum variance, can be derived by multiplying the equation for the fluctuating component  $v'_i$ , (1.389), by  $2v'_i$ , thereafter use the product rule of calculus to convert some of the terms in the provisional equation, and finally time average the resulting equation [154].

An alternative procedure is to simplify the transport equation for the kinematic momentum fluxes or Reynolds stresses. The contraction of the Reynolds stress transport equation (1.394) (that is, when the 3 equations for the 3 normal stresses, ( $i = k = 1, 2, 3$ ) are summed up) gives an exact transport equation for the turbulent kinetic energy (e.g., [167] [131] [106]).

Applying the latter procedure we set  $i = k$  in the Reynold stress equation (1.394), and we obtain the equation for the mean square of each component of the fluctuating velocity:

$$\begin{aligned} \frac{\overline{\partial v_i'^2}}{\partial t} + \bar{v}_j \frac{\partial \overline{v_i'^2}}{\partial x_j} = & -2\overline{v'_i v'_j} \frac{\partial \bar{v}_i}{\partial x_j} - \frac{\partial \overline{v'_j v_i'^2}}{\partial x_j} - \frac{2}{\rho} \left[ \frac{\partial \overline{p' v'_i}}{\partial x_i} - \overline{p' \left( \frac{\partial v'_i}{\partial x_i} \right)} \right] \\ & + \nu \frac{\partial^2 \overline{v_i'^2}}{\partial x_j^2} - 2\nu \overline{\left( \frac{\partial v'_i}{\partial x_j} \right)^2} \end{aligned} \quad (1.395)$$

The *first term on the LHS* denotes the rate of accumulation of the velocity variance  $\overline{v_i'^2}$  within the control volume. *The second term on the LHS* denotes the advection of the velocity variance by the mean velocity. *The first term on the RHS* denotes the production of velocity variance by the mean velocity shears. The momentum flux  $\overline{v'_i v'_j}$  is usually negative, thus it results in a positive contribution to variance when multiplied by a negative sign. *The second term on the RHS* denotes a turbulent transport term. It describes how variance  $\overline{v_i'^2}$  is moved around by the turbulent eddies  $v'_j$ . *The third term on the RHS* describes how variance is redistributed by pressure perturbations. This term is often associated with oscillations in the fluid (e.g., like buoyancy or gravity waves.) *The fourth term on the RHS* is called the pressure redistribution term. The factor in square brackets consists of the sum of three terms (i.e., here given in Cartesian coordinates):  $\frac{\partial v'_x}{\partial x}$ ,  $\frac{\partial v'_y}{\partial y}$ , and  $\frac{\partial v'_z}{\partial z}$ . These terms sum to zero because of the turbulence continuity equation. Hence, this term does not change the total variance (i.e., the sum of all three variance components). But it does tend to take energy out of the components having the most energy and put it into components with less energy. Thus, it makes the turbulence more isotropic, and is also known as *the return to isotropy term*. *The fifth term on the RHS* denotes molecular diffusion of the turbulent velocity variance. *The sixth term on the RHS* denotes the rate of viscous dissipation of velocity variance. It is noted that this formulation of the dissipation rate tensor term is not strictly correct [106]. The viscous energy dissipation rate for Newtonian fluids is generally defined by (1.125) in sect 1.2.4. For incompressible fluids it

can be slightly simplified and written as:

$$\epsilon = \frac{\nu}{2} \sum_i \sum_j \left( \frac{\partial v_i}{\partial x_j} + \frac{\partial v_j}{\partial x_i} \right)^2 \quad (1.396)$$

Consider the extension of this definition for the dissipation rate to the case of turbulence. We can introduce the mean dissipation rate by averaging both sides of (1.396), and introducing the decomposition of the velocity field into mean and fluctuating variables. The result is:

$$\bar{\epsilon} = \frac{\nu}{2} \sum_i \sum_j \overline{\left( \frac{\partial \bar{v}_i}{\partial x_j} + \frac{\partial \bar{v}_j}{\partial x_i} \right)^2} + \frac{\nu}{2} \sum_i \sum_j \overline{\left( \frac{\partial v'_i}{\partial x_j} + \frac{\partial v'_j}{\partial x_i} \right)^2} \quad (1.397)$$

For the particular case of homogeneous turbulence, we can set the mean velocity gradient to zero and consider only the dissipation of the kinetic energy of the fluctuating motions. That is, (1.397) becomes:

$$\bar{\epsilon} = \frac{\nu}{2} \sum_i \sum_j \overline{\left( \frac{\partial v'_i}{\partial x_j} + \frac{\partial v'_j}{\partial x_i} \right)^2} \approx \nu \sum_i \sum_j \overline{\left( \frac{\partial v'_i}{\partial x_j} \right)^2} \quad (1.398)$$

where it can be shown that the last step follows from the particular properties of homogeneous turbulence [159].

Therefore, the last term in the transport equation is not strictly the dissipation, unless the turbulence is homogeneous. However, it is usual to argue that the small scales responsible for the dissipation are homogeneous and hence this is probably quite a good approximation, except possibly near a solid surface.

It is obvious that this term is always positive, because it is a squared quantity. Therefore, when this term appears in the transport equation with the negative sign, it is always causing a decrease in the variance with time. In addition, it becomes larger in magnitude as the eddy size become smaller (i.e., using the hypothesis of Kolmogorov [83]). For these small eddies, the eddy motions are rapidly damped by viscous mechanisms and irreversibly converted into heat. This heating rate is so small, however, that it is often neglected in the energy conservation equation for turbulent flows.

By definition the turbulent kinetic energy per unit mass is one half of the variance  $\overline{v_i'^2}$ . Therefore, if we sum over  $i$ , then (1.395) gives us the balance equation for the turbulent kinetic energy,  $k$ , per unit fluid mass, which is defined by:

$$2k = \sum_i \overline{v_i'^2} \quad (1.399)$$

The only manipulation required is to divide all the terms in the equation by 2 and replace  $\frac{1}{2} \sum_i \overline{v_i'^2}$  on the left hand side by  $k$ . The turbulent kinetic energy equation then is given by [78, 95, 131]):

$$\frac{\partial k}{\partial t} + \bar{v}_j \frac{\partial k}{\partial x_j} = -\overline{v'_i v'_j} \frac{\partial \bar{v}_i}{\partial x_j} + \frac{\partial}{\partial x_j} \left( \frac{\overline{v_i'^2 v_j'}}{2} + \frac{1}{\rho} \overline{v'_j p'} \right) + \nu \frac{\partial^2 k}{\partial x_j^2} - \nu \left( \frac{\partial v'_i}{\partial x_j} \right)^2 \quad (1.400)$$

In (1.400), *the first term on the LHS* denotes the rate of accumulation of turbulent kinetic energy,  $k$ , within the control volume; *the second term on the LHS* denotes the advection of turbulent kinetic energy,  $k$ , by the mean velocity; *the first term on the RHS* denotes the production of turbulent kinetic energy by the mean velocity shear, and represents the rate at which kinetic energy is transferred from the mean flow to the turbulence; *the second and third terms on the RHS* denote turbulent transport of  $k$ . The triple velocity correlation is usually interpreted as the rate at which turbulent energy is transported through the fluid by turbulent fluctuations. The pressure-velocity correlation is interpreted as turbulent transport resulting from pressure and velocity fluctuations; *the fourth term on the RHS* denotes the molecular diffusion of turbulent energy,  $k$ ; *the fifth term on the RHS* represents the irreversible dissipation of turbulent kinetic energy to heat for homogeneous turbulence.

Closing the  $k$ - $\varepsilon$  model by turbulence modeling we relate the unknown Reynolds stress tensor and the turbulent transport terms to the fundamental mean flow variables, or the scaled variables in turbulent boundary layers, introducing additional approximations.

The second, third and fourth terms on the RHS of (1.400) (i.e., the triple moment, the pressure-velocity correlation, and the viscous diffusion term) are normally lumped together and modeled as diffusive transport processes being proportional to the gradient of the kinetic energy,  $k$ , (i.e., thus sometimes called the turbulent diffusion terms). That is, the triple moment is modeled as a turbulent diffusion process and approximated in accordance with the standard gradient hypothesis for scalar quantities. The pressure-velocity correlation is assumed to be small and approximated as a gradient-transport process too, apparently due to the lack of any better guess. The viscous diffusion term is negligible except near the wall (i.e., where the turbulence theory model is actually not valid since the flow is not fully turbulent).

The first-order closure models are all based on the Boussinesq hypothesis [19, 20] parameterizing the Reynolds stresses. Therefore, for fully developed turbulent bulk flow, i.e., flows far away from any solid boundaries, the turbulent kinetic energy production term is modeled based on the generalized eddy viscosity hypothesis<sup>37</sup>, defined by (1.380). The modeled  $k$ -equation<sup>38</sup> is

<sup>37</sup> Equation (1.380) is based on the assumption that all the normal stresses are equal thus representing an *isotropic* model for the Reynolds stresses.

<sup>38</sup> For the turbulent part of the inner boundary layer close to solid walls we usually adopt another closure for the Reynolds stresses and neglect the molecular diffusion term. The starting point for the boundary layer analysis, to be discussed shortly, is thus the  $k$ -equation in the following form:

$$\frac{\partial k}{\partial t} + \bar{v}_j \frac{\partial k}{\partial x_j} = -\overline{v'_i v'_j} \frac{\partial \bar{v}_i}{\partial x_j} + \frac{\partial}{\partial x_j} \left[ \left( \frac{\nu_t}{\sigma_k} \right) \frac{\partial k}{\partial x_j} \right] - \epsilon \quad (1.401)$$

written as:

$$\frac{\partial k}{\partial t} + \bar{v}_j \frac{\partial k}{\partial x_j} = \nu_t \left( \frac{\partial \bar{v}_i}{\partial x_j} + \frac{\partial \bar{v}_j}{\partial x_i} \right) \frac{\partial \bar{v}_i}{\partial x_j} + \frac{\partial}{\partial x_j} \left[ \left( \nu + \frac{\nu_t}{\sigma_k} \right) \frac{\partial k}{\partial x_j} \right] - \varepsilon \quad (1.402)$$

where  $\nu_t$  is the turbulent eddy kinematic viscosity and  $\sigma_k$  is an empirical constant.

The turbulent viscosity is modeled by analogy with kinetic gas theory (i.e.,  $\nu_t \propto v_{\text{rms}} L$ , and  $v_{\text{rms}} \approx k^{1/2}$ ), thus:

$$\nu_t = C'_\mu k^{1/2} L \quad (1.403)$$

where  $C'_\mu$  is an empirical parameter and  $L$  is an integral length scale. This is analogous to the relationship in kinetic theory between the viscosity, the particle energy, and the mean free path, and is often referred to as the *Kolmogorov-Prandtl relationship* (e.g., [85] [124]).

At first sight, though, this model seems to represent only marginal advance on the mixing length theory, if the length  $L$  still has to be fixed by simple empirical arguments. The turbulent energy dissipation rate,  $\varepsilon$ , is also unknown and needs to be parametrized.

To proceed it is apparently anticipated that the turbulence model will give more realistic predictions if the length scale,  $L$ , is calculated from a transport equation rather than from some local algebraic expression even though these models are not rigorously derived. In this way a second transport equation is introduced, from which the length scale can be derived. Models at this level are accordingly known as two equation models and there are many of them. In fact we do not formulate a transport equation for the length scale,  $L$ , itself, rather a transport equation for the product  $k^m L^n$  has been considered, where  $k$  is the kinetic energy of turbulence [94]. In order to obtain a dependent variable which really reflects the physics of the turbulence, several combinations of  $k$  and  $L$  have been considered over the years. Some of the combinations have an obvious physical interpretation. For example, the combination  $m = 1/2$  and  $n = -1$  represents a turbulent or eddy frequency, the combination  $m = 1$  and  $n = -2$  represents turbulent vorticity. The far most popular combination is  $m = 3/2$  and  $n = -1$ , by which the dependent variable is identified as the dissipation rate of turbulent energy. For this variable, in principle a rigorous equation can be derived from the transport equation for the fluctuating velocity, but in practice many empirical steps are needed to make it tractable (e.g., [15], chap 10.5). Instead, a simple semi-empirical procedure (i.e., apparently based on an analogy with the  $k$ -equation) is often used in engineering practice to draw up a transport equation for the dissipation rate,  $\varepsilon$ . An approximate transport equation can be expressed as:

$$\frac{\partial \varepsilon}{\partial t} + \bar{v}_j \frac{\partial \varepsilon}{\partial x_j} = -C_{\varepsilon 1} \frac{\varepsilon}{k} \bar{v}'_i \bar{v}'_j \frac{\partial \bar{v}_i}{\partial x_j} + \frac{\partial}{\partial x_j} \left[ \left( \frac{\nu_t}{\sigma_\varepsilon} \right) \frac{\partial \varepsilon}{\partial x_j} \right] - \frac{C_{\varepsilon 2} \varepsilon^2}{k} \quad (1.404)$$

where  $C_{\varepsilon 1}$  and  $C_{\varepsilon 2}$  are additional empirical constants.

This equation possesses production and dissipation terms that are similar to those in the kinetic energy transport equation, except that they are divided by the turbulence time scale of the energy containing eddies,  $\tau_t = \frac{k}{\epsilon}$ . As for the  $k$ -equation, the Reynolds stresses are parameterized based on the eddy viscosity hypothesis.

To close the  $k$ - $\epsilon$  model we need to eliminate the length scale variable,  $L$ , from the model relation (1.403). This has been achieved by relating the length scale to the dissipation rate and  $k$  through a semi-empirical relationship:

$$\epsilon = C_D \frac{k^{3/2}}{L} \quad (1.405)$$

that has been put up by Taylor [159] based on dimensional analysis (i.e.,  $\epsilon \propto \frac{v_{\text{rms}}^3}{L}$ , and one assumes  $v_{\text{rms}} \approx k^{1/2}$ ).  $C_D$  is an empirical parameter which in most instances is set to unity as it is very difficult to design experiments for direct validation of this parameter value.

By combining (1.403) and (1.405) we obtain a relation for the turbulent viscosity in terms of  $k$ , the obscure length scale variable  $\epsilon$ , and one empirical parameter:

$$\nu_t = \frac{C_\mu k^2}{\epsilon} \quad (1.406)$$

where  $C_\mu = C'_\mu C_D$ .

Examination of several two-equation models reveals that there is only very small differences between the various models of this type [106]. This may be expected since all proposals for formulating the 2nd equation are closely related, though they differ in the forms of diffusion and near wall terms employed [95]. However, as mentioned above, the  $k$ - $\epsilon$  model of Jones and Launder [78] has been predominant in the literature, and this model also determine the basis for most multi-phase turbulence models adopted in the more fundamental (CFD) reactor modeling approaches.

### Standard Model Parameter Values

The model parameter values have to be determined before the turbulence closure can be used in practice. The pioneering Imperial College group [59] [78] [61] [94] [96] [60] performed a few simple laboratory experiments and, combined with model analysis of these data, determined a set of parameter values which have later been referred to as the ‘standard’ parameter values. The specific flow situations investigated by the Imperial College group and the corresponding  $k$ - $\epsilon$  model simplifications used fixing this set of parameter values have been further discussed by Rodi [132] and Pope ([121], sect. 10). Basically, the parameter values are assumed to be universal and considered individually, as the problem specific  $k$ - $\epsilon$  model equations contain only one single unknown parameter for each flow situation studied. Accordingly, the

parameter values are fitted one by one to experimental data analyzing a few simple turbulent single phase flows only.

- In this manner, to determine the  $C_{\varepsilon 2}$  parameter, the  $k$ - $\epsilon$  model is applied to describe homogeneous decay of turbulence behind a grid. In this flow there are no velocity gradients so there are no diffusion terms and no production terms, only dissipation. The  $k$  and  $\epsilon$  equations (1.401) and (1.404) become:

$$\bar{v}_x \frac{dk}{dx} = -\epsilon \quad (1.407)$$

$$\bar{v}_x \frac{d\epsilon}{dx} = -C_{\varepsilon 2} \left( \frac{\epsilon^2}{k} \right) \quad (1.408)$$

$C_{\varepsilon 2}$  is then the only parameter appearing in the equations, and it can therefore be determined directly from the measured rate of decay of  $k$  behind a grid (e.g., [61]). The experimental data indicates that  $C_{\varepsilon 2} = 1.92$ .

- Correspondingly, the  $C_\mu$  parameter has been found analyzing simple turbulent shear flows where  $\frac{d\bar{v}_x}{dy}$  is the only non-zero mean velocity gradient. Applying the  $k$ -equation (1.401) to this flow situation we recognize that the dissipation and production terms are approximately equal. In statistical turbulence analysis (e.g., [66]), this property is said to be denoting an equilibrium shear flow. The simplified  $k$ -equation yields:

$$\overline{v'_x v'_y} \frac{d\bar{v}_x}{dy} \approx -\epsilon \quad (1.409)$$

By use of (1.406) the  $k$ -equation can be written as:

$$\overline{v'_x v'_y} \frac{d\bar{v}_x}{dy} \approx -C_\mu \frac{k^2}{\nu_t} \quad (1.410)$$

or, after minor reformulation, an expression for the unknown model parameter is given by:

$$C_\mu \approx \frac{\overline{v'_x v'_y}}{k^2} \left( -\nu_t \frac{d\bar{v}_x}{dy} \right) \quad (1.411)$$

The unknown Reynolds stress term can be calculated using the eddy viscosity hypothesis (1.380), or, alternatively, the term in the bracket on the RHS of this relation can be recognized as being approximately equal to the Reynolds stress:

$$\overline{v'_x v'_y} \approx -\nu_t \frac{d\bar{v}_x}{dy} \quad (1.412)$$

The  $C_\mu$  parameter can thus be determined experimentally based on the following model:

$$C_\mu \approx \frac{1}{k^2} [\nu_t \frac{d\bar{v}_x}{dy}]^2 \approx \left[ \frac{\overline{v'_x v'_y}}{k} \right]^2 \quad (1.413)$$

Measurements reported by Hanjalic and Launder [61] show that  $\left[ \frac{\overline{v'_x v'_y}}{k} \right] \approx 0.3$ , giving  $C_\mu \approx 0.09$ .

- $\sigma_k$  is set to unity in accordance with the standard Reynolds analogy for turbulent flows.
- Likewise,  $\sigma_\varepsilon$  is preliminarily set to unity in accordance with the standard Reynolds analogy for turbulent flows (i.e., later fixed at  $\sigma_\varepsilon = 1.3$  representing an optimization to experimental data for a number of 2D Couette flows. See next item.).
- The last parameter,  $C_{\varepsilon 1}$ , is determined investigating inhomogeneous high Reynolds number, fully developed channel flows (i.e., these flows are sometimes referred to as 2D Couette flows). Actually, the turbulence model is applied describing the flow in regions near walls, where the logarithmic velocity profile applies.

Starting out with fully developed channel flows the quantities of interest (i.e.,  $\bar{v}_x$ ,  $k$  and  $\varepsilon$ ) depend only on  $y$ , so the  $k$ - $\varepsilon$  model equations (1.401) and (1.404) reduce to:

$$0 = \frac{d}{dy} \left( \frac{\nu_t}{\sigma_k} \frac{dk}{dy} \right) - \frac{\bar{v}_x'}{v_x' v_y'} \frac{d\bar{v}_x}{dy} - \varepsilon \quad (1.414)$$

$$0 = \frac{d}{dy} \left( \frac{\nu_t}{\sigma_\varepsilon} \frac{d\varepsilon}{dy} \right) - C_{\varepsilon 1} \frac{\varepsilon}{k} \frac{\bar{v}_x'}{v_x' v_y'} \frac{d\bar{v}_x}{dy} - C_{\varepsilon 2} \frac{\varepsilon^2}{k} \quad (1.415)$$

This result shows that for the  $\varepsilon$ -equation (1.415), only the advective term is negligible. The transport equation for the dissipation rate cannot be further reduced, and we recognize that the diffusion term in the  $\varepsilon$ -equation may play an important role in near wall flows.

However, further simplifications can be achieved focusing on the log-law region. Considering the  $k$ -equation (1.414) experimental observations indicate that the production and dissipation terms balance (i.e., thus the dissipation and production terms are in local equilibrium), hence in the  $k$ -equation the diffusion term vanishes. This implies that  $k$  is approximately uniform.

Introducing the result that the dissipation- and production terms in the  $k$ -equation are in approximate local equilibrium, the  $\varepsilon$ -equation (1.415) yields:

$$\frac{d \left[ \left( \frac{\nu_t}{\sigma_\varepsilon} \right) \frac{d\varepsilon}{dy} \right]}{dy} + \frac{\varepsilon^2}{k} (C_{\varepsilon 1} - C_{\varepsilon 2}) \approx 0 \quad (1.416)$$

or

$$\frac{1}{\sigma_\varepsilon} \left( \frac{d\nu_t}{dy} \frac{d\varepsilon}{dy} + \nu_t \frac{d^2\varepsilon}{dy^2} \right) + \frac{\varepsilon^2}{k} (C_{\varepsilon 1} - C_{\varepsilon 2}) \approx 0 \quad (1.417)$$

This ordinary differential equation (ODE) indicates that there is a net source in the  $\varepsilon$ -equation that is balanced by the diffusion of  $\varepsilon$  away from the wall.

The last parameter in the  $\varepsilon$ -equation that still remains undetermined,  $C_{\varepsilon 1}$ , has been estimated recognizing that for the log-law region the given ODE reduces to a very simple algebraic relationship between the parameters in

the  $\varepsilon$ -equation. So, by fixing the values for the other model parameters just determined above,  $C_{\varepsilon 1}$  can be calculated directly from this relationship<sup>39</sup>. To reduce the  $\varepsilon$ -equation sufficiently deriving the afore mentioned algebraic relation between the model parameters only, all the physical variables have to be eliminated. This variable elimination is achieved by adopting a few hypotheses established in statistical turbulence theory and in the semi-empirical boundary layer flow analysis discussed in the foregoing sects., and by further analysis of the  $k$ - $\varepsilon$  model equations. In this manner, the  $\varepsilon$  and  $\nu_t$  variables can be expressed in terms of  $v_*$ ,  $y$  and the empirical model parameters only. After that,  $\frac{d\varepsilon}{dy}$ ,  $\frac{d^2\varepsilon}{dy^2}$  and  $\frac{d\nu_t}{dy}$  are easily deduced from the resulting expressions for  $\varepsilon$  and  $\nu_t$  since  $v_*$  is considered independent of  $y$ . Considering the  $\varepsilon$  variable first, the starting point is the semi-empirical relation (1.405) stating that  $\varepsilon$  can be estimated from  $L$  and  $k$ . Therefore, the unknown variables  $L$  and  $k$  are then expressed in terms of  $v_*$ ,  $y$  and the empirical model parameters, and thereafter eliminated from (1.405). So, the purpose of the forthcoming task is to derive an expression for the integral lengthscale,  $L$ , in terms of  $y$  and two empirical parameters only. Initially, the mathematical operations involved are outlined briefly in an easy to follow manner, thereafter the detailed model derivation is given. A relationship between the integral lengthscale,  $L$ , and eddy viscosity parameter,  $\nu_t$ , is found by introducing appropriate simplifications of the  $k$  equation (1.401), approximating the production term in accordance with the eddy viscosity hypothesis (1.380), and applying the Prandtl-Kolmogorov relation (1.403) to eliminate the turbulent kinetic energy variable from the equation. Thereafter, a relationship between the integral length scale,  $L$ , and the mixing length,  $l$ , is found by comparing the resulting expression for the viscosity parameter with the corresponding one deduced from the Prandtl mixing length model (1.356). Thus, in the inner part of the boundary layer  $L$  is determined by the mixing length and three model parameters. Finally, the mixing length is approximated in terms of  $y$  and an empirical parameter [174].

Accordingly, in mathematical terms, recognizing that the production and dissipation terms are approximately equal constituting an equilibrium flow, the  $k$ -equation is written as:

$$\frac{v'_x v'_y}{\partial y} \frac{\partial \bar{v}_x}{\partial y} \approx -\epsilon \approx -C_D \frac{k^{3/2}}{L} \quad (1.418)$$

where the turbulent energy dissipation rate has been substituted by (1.405).

<sup>39</sup> Alternatively, as the Reynolds analogy for turbulent flows is rather rough, it has also been speculated that by fixing  $C_{\varepsilon 1}$ ,  $\sigma_{\varepsilon 1}$  can be calculated directly from the given relationship instead. Of course, anyhow, it remains to find a plausible way of fixing one of the two parameters. Actually, the preliminary parameter values adjusted using the Reynolds analogy has later been optimized representing a best fit to a larger number of experimental data and flow situations.

On the LHS, the production term is modeled in accordance with the eddy viscosity hypothesis (1.380), hence

$$\nu_t \left( \frac{\partial \bar{v}_x}{\partial y} \right)^2 \approx C_D \frac{k^{3/2}}{L} \quad (1.419)$$

Next, the Prandtl-Kolmogorov relation (1.403) is used to eliminate  $k$  from the relation:

$$\nu_t \left( \frac{\partial \bar{v}_x}{\partial y} \right)^2 \approx C_D \frac{\left( \frac{\nu_t}{C'_\mu L} \right)^3}{L} = C_D \frac{\nu_t^3}{C'^3_\mu L^4} \quad (1.420)$$

After rearrangement, yields:

$$\nu_t \approx \left( \frac{C'_\mu}{C_D} \right)^{\frac{1}{2}} L^2 \left( \frac{\partial \bar{v}_x}{\partial y} \right) \quad (1.421)$$

By use of the eddy viscosity hypothesis (1.380) and the Prandtl mixing length model (1.356), a similar expression for the turbulent viscosity can be deduced, and given by

$$\nu_t \approx l^2 \left| \frac{d\bar{v}_x}{dy} \right| \quad (1.422)$$

Comparing the resulting relations (1.421) and (1.422), one may suggest that

$$L \approx l \left( \frac{C_D}{C'^3_\mu} \right)^{\frac{1}{4}} \approx \kappa y \left( \frac{C_D}{C'^3_\mu} \right)^{\frac{1}{4}} \quad (1.423)$$

This expression is used eliminating  $L$  from the relation for  $\varepsilon$  (1.405).

The purpose of the next task is thus to derive an expression for the turbulent energy,  $k$ , in terms of  $v_*$  and one empirical parameter only. Again, the mathematical operations involved are outlined briefly in an easy to understand manner, thereafter the detailed model derivation is given.

An expression for  $k$  in terms of the integral lengthscale,  $L$ , the mixing length,  $l$ , the average velocity gradient and one empirical parameter is derived using the Prandtl mixing length model (1.356), the eddy viscosity hypothesis (1.380), and the Prandtl-Kolmogorov relation (1.403). The integral length scale,  $L$ , is eliminated from the resulting expression using the relationship between the integral lengthscale,  $L$ , and the mixing length,  $l$  (1.423) just derived in the previous paragraph. Then, the velocity gradient near the wall is eliminated by use of the law of the wall (1.373).

Accordingly, in mathematical terms, the Prandtl mixing length model (1.356) is combined with the eddy viscosity hypothesis (1.380) to form an expression for the eddy viscosity parameter close to the wall. The result is given by:

$$\nu_t \approx l^2 \frac{d\bar{v}_x}{dy} \quad (1.424)$$

Eliminating the eddy viscosity parameter by use of the Prandtl-Kolmogorov relation (1.403) one obtains an expression for  $k$  near the wall:

$$C'_\mu k^{1/2} L \approx l^2 \frac{d\bar{v}_x}{dy} \quad (1.425)$$

or, after a little rearranging

$$k \approx \frac{l^2}{C'^{\frac{1}{2}}_\mu} \left( \frac{d\bar{v}_x}{dy} \right)^2 \quad (1.426)$$

The velocity gradient near a wall can be estimated from the logarithmic velocity profile (1.373):

$$\frac{d\bar{v}_x}{dy} \approx \frac{v_*}{\kappa y} \quad (1.427)$$

Eliminating the velocity gradient in (1.426) by use of (1.427), one can estimate  $k$  as:

$$k \approx \frac{l^2}{C'^{\frac{1}{2}}_\mu} \left( \frac{v_*}{\kappa y} \right)^2 \approx \frac{(\kappa y)^2}{C'^{\frac{1}{2}}_\mu} \left( \frac{v_*}{\kappa y} \right)^2 \approx \frac{v_*^2}{C'^{\frac{1}{2}}_\mu} \quad (1.428)$$

Inserting the resulting expressions for  $L$  (1.423) and  $k$  (1.428) into the relation for  $\varepsilon$  (1.405), yields:

$$\begin{aligned} \varepsilon &\approx C_D \frac{k^{3/2}}{L} \approx C_D \frac{k^{3/2}}{l \left( \frac{C_D}{C'_\mu} \right)^{\frac{1}{4}}} \approx (C_D C'_\mu)^{\frac{3}{4}} \frac{k^{3/2}}{\kappa y} \approx (C_D C'_\mu)^{\frac{3}{4}} \frac{\left( \frac{v_*^2}{\kappa y} \right)^{3/2}}{\kappa y} \\ &\approx \frac{v_*^3}{\kappa y} C_D^{3/4} \end{aligned} \quad (1.429)$$

From this expression two of the unknown derivatives in the ODE (1.417) can be deduced by simple rules of calculus:

$$\frac{d\varepsilon}{dy} \approx -C_D^{3/4} \frac{v_*^3}{\kappa y^2} \quad (1.430)$$

and

$$\frac{d^2\varepsilon}{dy^2} \approx 2C_D^{3/4} \frac{v_*^3}{\kappa y^3} \quad (1.431)$$

The last unknown variable in the ODE (1.417), the turbulent or eddy viscosity,  $\nu_t$ , is estimated from the Prandtl-Kolmogorov relation (1.403).

In this context the integral lengthscale,  $L$ , is eliminated by use of the Taylor [159] expression (1.405), where the  $k$  and  $\varepsilon$  variables therein have been substituted by use of (1.428) and (1.429), respectively. The result is:

$$\nu_t \approx C'_\mu k^{1/2} L \approx C_D C'_\mu \frac{k^2}{\varepsilon} \approx C_D C'_\mu \frac{\left( \frac{v_*^2}{\kappa y} \right)^2}{\frac{C_D^{3/4} v_*^3}{\kappa y}} \approx v_* \kappa y C_D^{1/4} \quad (1.432)$$

The derivative of the eddy viscosity parameter,  $\nu_t$ , with respect to  $y$  is expressed by

$$\frac{d\nu_t}{dy} \approx C_D^{1/4} v_* \kappa \quad (1.433)$$

To conclude, by insertion of (1.428) to (1.433) into the  $\epsilon$ -equation (1.417), the relationship between the model parameters yields

$$C_{\epsilon 1} - C_{\epsilon 2} \approx -\frac{\kappa^2}{C_\mu^{1/2} \sigma_\epsilon} \quad (1.434)$$

where  $\kappa$  is the von Kàrmàn constant and takes the value  $\kappa = 0.4$ .

This relationship (1.434) was, as a first approach, used to fix  $C_{\epsilon 1}$  when  $\sigma_\epsilon$  was fixed at unity in accordance with the well known Reynolds analogy. However, computer optimization fitting the parameters to experimental data gathered from several flow situations gives the values  $C_{\epsilon 1} = 1.44$  and  $\sigma_\epsilon = 1.3$ .

The two-equation turbulence closure with the prescribed parameters given above is called *the standard  $k$ - $\epsilon$  model*. With these parameters the model is able to predict several types of turbulent flow, in particular the flows used to determine the parameters.

Numerous papers have been published regarding the influence of the standard  $k$ - $\epsilon$  model parameters on the simulated results, both for single and multiphase flows, as outlined by Jakobsen [76]. Andersson [1] summarized the current experience applying the standard  $k$ - $\epsilon$  model to various single phase flow simulations. It was stated that the standard parameters by no means can be regarded as universal constants. Ad hoc correlations must often be made to the parameters in order to obtain good correspondence with experimental data. Experience has shown that even in certain fairly simple single phase flow situations some of the constants require other values. Furthermore, no direct method for establishing adequate parameters for a given flow situation has been proposed yet. These parameters are thus fixed only in the sense that they are not changed during a calculation. Of course this must also be an approximation, as flow condition may well vary considerably from one part of an apparatus to the other during a calculation.

Therefore, despite the great success of the  $k$ - $\epsilon$  model in engineering applications, caution is needed especially when high accuracy is required. Biswas and Eswaran [15], Pope [121], among others, list some of the major problems encountered in the application of the  $k$ - $\epsilon$  model.

In the context of reactor modeling, it is important to notice that this model rely on the Boussinesq eddy-viscosity concept which is based on the assumption that turbulence is isotropic. This means that the normal Reynolds stresses are considered equal and that the eddy viscosity is approximately isotropic. Therefore, the  $k$ - $\epsilon$  model cannot reproduce secondary flows which arise due to unequal normal Reynolds stresses. Unfortunately, the non-isotropic effects

are important in many chemical reactors like bubble columns, fluidized beds and stirred tanks. In addition, the standard  $k$ - $\varepsilon$  model also requires modifications when applied to swirling flows, thus making this closure usability rather limited for stirred tank simulations. Furthermore, the values of the empirical parameters need modifications when the model is applied to flows where the molecular viscosity plays an important role. Basically, the  $k$ - $\varepsilon$  model cannot be used near solid walls.

## Wall Functions

In this paragraph the wall function concept is outlined. The wall functions are empirical parameterizations of the mean flow variable profiles within the inner part of the wall boundary layers, bridging the fully developed turbulent log-law flow quantities with the wall through the viscous and buffer sub-layers where the two-equation turbulence model is strictly not valid. These empirical parameterizations thus allow the numerical flow simulation to be carried out with a finite resolution within the wall boundary layers, and one avoids accounting for viscous effects in the model equations. Therefore, in the numerical implementation of the  $k$ - $\varepsilon$  model one anticipates that the boundary layer flow is not fully resolved by the model resolution. The first grid point or node used at a wall boundary is thus placed within the fully turbulent log-law sub-layer, rather than on the wall itself [95]. In effect, the wall functions amount to a synthetic boundary condition for the  $k$ - $\varepsilon$  model. In addition, the limited boundary layer resolution required also provides savings on computer time and storage.

Both equilibrium and non-equilibrium wall boundary implementations are considered. For equilibrium flows the local production rate of turbulence equals the dissipation rate in the near wall grid node. The first set of wall function boundary conditions reported was apparently used for equilibrium flows by Gosman et al. [59]. Denoting the dependent variables in the first point near the wall by a subscript  $P$ , an approximate sketch of their approach is given next.

- The velocity components parallel to the wall are estimated from the logarithmic velocity profile relation (1.373). For example, using Cartesian coordinates, the x-component of the velocity vector is given as:

$$\bar{v}_{x,P} \approx \frac{v_*}{\kappa} \ln\left(E \frac{v_* y_P}{\nu}\right) = \frac{v_*}{\kappa} \ln(E y_P^+)$$
 (1.435)

where the parameter value (i.e., the constant of integration) is considered a function of surface roughness and shear stress variations (e.g., [59, 60, 154, 106]). In accordance with the practice of Gosman et al [59] and Gosman et al. [60], we suggest  $E = 9.793$  to be applied to chemical reactor models.

- Using a staggered grid arrangement the normal velocity component, say, the y-component, is set equal to zero at the wall (i.e., valid for impermeable walls only):

$$\bar{v}_{y,\text{wall}} = 0 \quad (1.436)$$

- The wall boundary condition for  $k_p$  is specified in accordance with (1.428):

$$k_P \approx \frac{v_*^2}{C_\mu'^{\frac{1}{2}}}$$

Accordingly, the wall boundary condition for the turbulent energy dissipation rate,  $\varepsilon$ , is given by (1.429):

$$\varepsilon_P \approx \frac{v_*^3}{\kappa y_P}$$

In the early FVM program codes, all the equilibrium variable values at the grid point, P, were simply calculated from the given parameterizations. However, in these steady state program codes the friction velocity is not known a priori but is an outcome of the iterative solution algorithm where the boundary values are coupled through the governing transport equations.

In addition, the logarithmic law is strictly valid for high-Reynolds number zero pressure gradient boundary layers only. Therefore, under practical flow conditions the physical basis is uncertain and the accuracy reflected by these relations becomes poor [186]. In consequence, the given wall function concept is not robust as severe numerical convergence- and stability problems often arise, thus more advanced implementations evolved. The wall functions and their implementations were subsequently extended to enable more robust boundary conditions providing solutions under almost any circumstances. One outcome of the subsequent model development is that in the modern FVM codes the transport equations for the velocity components being parallel to the wall and  $k$  are solved for the first grid node, P, within the calculation domain close to the wall boundary. For the velocity components being parallel to the wall there are no values stored at the solid surface in a staggered grid arrangement, so the wall friction force at the cell surface is replaced by an apparent source at the node point, P. The physical observation that the shear stress is approximately constant over the inner part of the boundary layer allows the modeler to relocate the point where the shear stress is actually calculated without further considerations. Since the physical value of  $k$  approaches zero at the wall, there is no  $k$ -flux contribution from the wall in the  $k$ -equation. Furthermore, at the node, P, close to the wall the turbulence production term reduces to a simple form expressed in terms of the wall shear stress. In this way the value of  $k$  at the wall node, P, is determined by the turbulence level in the mean flow and a modified turbulence generation term.

- For the velocity components parallel to the wall the calculation of the wall boundary conditions, i.e., the apparent bulk source term, for turbulent flows starts with the estimation of  $y_P^+$ , the dimensionless distance of the near wall node, P, to the solid surface. For turbulent flows where  $y_P^+ \leq 11.63$ , the value of the laminar wall shear stress is determined from:

$$-\overline{\sigma_W} = \mu \frac{\overline{v}_{x,P}}{y_P} \quad (1.437)$$

where  $\overline{v}_{x,P}$  is the velocity component parallel to the wall calculated at the first grid node inside the calculation domain. The resulting shear force,  $F_w$ , is defined by:

$$F_w = \overline{\sigma_W} A_{\text{Cell}} = -\mu \frac{\overline{v}_{x,P}}{y_P} A_{\text{Cell}} \quad (1.438)$$

where  $A_{\text{Cell}}$  is the wall area of the cell volume.

However, the friction force estimate calculated in this way is only valid in the laminar layer very close to the wall and rapidly becomes inaccurate as the node point enters the buffer layer. More important, nevertheless, the  $k-\varepsilon$  model is strictly not valid in the viscous sub-layer. In practice the first node is often incidentally placed within the laminar layer intending to make sure that the numerical grid resolution is sufficiently fine, with the unfortunate consequence that the simulated results are in poor agreement with the physical flow situation. Therefore, in such situations, it is recommended to choose a coarser grid resolution ensuring that the first grid node, P, is located in the log-law layer. For boundary layer flows for which the log-law relations are accurate, the overall solution is then insensitive to the choice of  $y_P$ . However, in other flows it is found that the solution is sensitive to the choice of  $y_P$  even within the log-law region. Unfortunately, it might not be possible to obtain numerically accurate, grid-independent solutions in these cases.

If  $y_P^+ > 11.63$ , node, P, is considered to be in the log-law region of the inner part of the turbulent boundary layer. In this region the law of the wall (1.373) (i.e., in the form  $v^+ = \frac{1}{\kappa} \ln(Ey^+)$ ) is used to calculate the shear stress variable.

Actually, several possibilities exist formulating the wall friction force. The natural boundary layer shear stress definition to use is the one deduced from the fundamental equilibrium boundary layer analysis. The wall shear stress is thus defined as  $-\overline{\sigma_W} = \rho v_* v_*$ .

Calculating the friction velocity from the log-law (1.373), yields:

$$-\overline{\sigma_W} = \rho \frac{\kappa^2 \overline{v}_{x,P}^2}{(\ln(Ey_P^+))^2} \quad (1.439)$$

In this approach the shear force,  $F_w$ , is defined by:

$$F_w = \overline{\sigma_W} A_{\text{Cell}} = -\rho \frac{\kappa^2 \overline{v}_{x,P}^2}{(\ln(Ey_P^+))^2} A_{\text{Cell}} \quad (1.440)$$

In other flow situations where the turbulent energy diffusion towards the wall is significant, appreciable departures from local equilibrium occur.

There are a variety of non-equilibrium boundary conditions suggested in the literature.

Launder and Spalding [95] recognized that the relation obtained for  $k$  in the log-law layer (1.428) permits us to redefine the friction velocity, when the  $k$  value is considered known from the previous iteration or time level. Hence, a non-equilibrium boundary layer shear stress approximation is given by  $-\overline{\sigma}_W = \rho v_* v_k$ .

Calculating the friction velocity from the log-law (1.373), and the non-equilibrium velocity scale from (1.428), yields:

$$-\overline{\sigma}_W \approx \rho C_\mu'^{1/4} k_P^{1/2} \frac{\kappa \bar{v}_{x,P}}{\ln(Ey_P^+)} \approx \rho C_\mu'^{1/4} k_P^{1/2} \frac{\bar{v}_{x,P}}{v^+} \quad (1.441)$$

In this approach the shear force,  $F_w$ , is given by:

$$F_w = \overline{\sigma}_W A_{\text{Cell}} = -\rho C_\mu'^{1/4} k_P^{1/2} \frac{\bar{v}_{x,P}}{v^+} A_{\text{Cell}} \quad (1.442)$$

For quite a few flow situations this relation provides results being in better agreement with experimental data, compared to the corresponding predictions obtained using the equilibrium formulation. Versteeg and Malalasekera [175] state that this approach represents the optimum near wall relationships from extensive computing trails.

To further minimize the numerical convergence- and stability problems related to the friction force calculations, yet another relation has been suggested based on the friction coefficient concept. In this approach the shear stress is defined by:

$$-\overline{\sigma}_W = \rho C_f |\bar{v}_P| (\bar{v}_{x,P} - \bar{v}_{x,w}) \quad (1.443)$$

where  $\bar{v}_{x,w}$  is a moving wall velocity set to zero for stationary walls.

The skin friction coefficient is calculated from the log-law relation in an implicit iteration loop

$$\frac{1}{\sqrt{C_f}} = \frac{1}{\kappa} \ln(E\sqrt{C_f} \frac{\bar{v}_{x,P} y_P}{\nu}) = \frac{1}{\kappa} \ln(E\sqrt{C_f} Re_y) \quad (1.444)$$

where  $-\overline{\sigma}_W = C_f \rho \bar{v}_{x,P}^2$  defines the friction factor.

Normally, simulating chemical reactor flows non-equilibrium wall boundary conditions are used. Basically, the solutions obtained based on the two non-equilibrium wall shear stress formulations given above do not diverge significantly, but the last one may have slightly better inherent numerical properties as the iteration process is sometimes converging a little faster.

- Assuming that  $\overline{v'_x v'_y} = \sigma_{xy,t} \approx \sigma_W$ , the  $k$ -equation (1.401) production term yields:

$$P_k \approx -\overline{x'_x v'_y} \frac{d\bar{v}_x}{dy} \approx -\sigma_W \frac{(\bar{v}_{x,P} - \bar{v}_{x,w})}{y_P} \approx \frac{-\sigma_W \bar{v}_{x,P}}{y_P} \quad (1.445)$$

The corresponding dissipation rate term is approximated using (1.405), the Prandtl-Kolmogorov relation (1.403), the eddy viscosity hypothesis (1.380), and the non-equilibrium boundary layer shear stress approximation (1.441):

$$\begin{aligned}\varepsilon_{k,P} &\approx C_D \frac{k_P^{3/2}}{L} \approx C_D C'_\mu \frac{k_P^2}{\nu_t} \approx C_D C'_\mu \frac{k_P^2}{\sigma_W} \rho \frac{d\bar{v}_x}{dy} \approx C_D C'_\mu \frac{k_P^2}{\sigma_W} \rho \frac{\bar{v}_{x,P}}{y_P} \\ &\approx C_D C'_\mu k_P^2 \frac{v^+}{\bar{v}_{x,P} (C_D C'_\mu)^{1/4} k^{1/2}} \frac{\bar{v}_{x,P}}{y_P} = (C_D C'_\mu)^{3/4} k_P^{3/2} \frac{v^+}{y_P}\end{aligned}\tag{1.446}$$

- The energy dissipation rate reaches its highest value at the wall. This makes it difficult to estimate the flux towards the wall from the transport equation, as it would require a very fine grid resolution. The energy dissipation,  $\epsilon_P$ , is therefore roughly estimated as a fixed value by the equilibrium relation (1.429):

$$\epsilon_P \approx C_D^{3/4} \frac{v_*^3}{\kappa y_P}$$

In the non-equilibrium approaches the dissipation rate is calculated as a function of the level of turbulent kinetic energy at the wall

$$\epsilon_P \approx (C_D C'_\mu)^{3/4} \frac{k_P^{3/2}}{\kappa y_P}$$

This approach works best within an iterative procedure, but can also be adopted in explicit discretization schemes calculating  $\varepsilon_P^{n+1}$  from  $k_P^n$  in the previous time level.

## Boundary Conditions

The solution of the governing reactor model equations are subjected to the boundary conditions specified. The number of boundary conditions required depends on the mathematical properties of the equations (e.g., elliptical, parabolic, hyperbolic, or mixed).

For single-phase turbulent reactor flows, the typical boundary conditions include impermeable solid walls, free surfaces, pressure boundaries, symmetry axis, inlet- and outlet conditions.

An impermeable solid wall is specified assuming that the no-slip velocity condition at the boundary is valid. In general, the scalar variable boundaries are specified by Neumann, Dirichlet- or mixed conditions.

A free surface is determined by fixing the normal component of the velocity at the surface to zero, and the partial derivative normal to the free surface of all other scalar quantities are set to zero.

An axis of symmetry is determined by fixing the radial component of the velocity to zero, whereas the partial derivative with respect to  $r$  of all the scalar variables is set to zero.

An inlet boundary is determined when the normal velocity component and the known scalar variables are specified. The turbulence quantities are generally estimated based on simple empirical relations.

An outlet boundary can be determined assuming that the flow is fully developed, thus the partial derivatives of all scalar variables are set to zero normal to the outlet surface plane.

A pressure boundary is determined by specifying the absolute pressure value.

Further details on the boundary condition implementations are given in chap 12 outlining the numerical algorithms, discretizations and solvers.

### Mean Kinetic Energy and Its Interaction with Turbulence

We learn quite a lot about the physics of turbulence by considering the ways in which energy is transported from one place to another, and transformed from one energy form to another. For the general case of a fluid occupying a global volume  $V$  bounded by a surface  $S$ , the total kinetic energy of macroscopic fluid motion  $E_T$  can be expressed in terms of the instantaneous velocity field  $v_i(t, \mathbf{r})$  as

$$2E_T = \sum_i \int_V \rho v_i^2 dv \quad (1.447)$$

An equation for  $E_T$  can be derived from the Navier-Stokes equation (1.124) in the form (i.e., noting that a few terms vanish when integrated)

$$\frac{dE_T}{dt} = \int_V \rho v_i g_i dv - \int_V \rho \epsilon dv \quad (1.448)$$

where, for simplicity, we have considered an incompressible flow of a one component mixture.  $g_i(t, \mathbf{r})$  is an externally applied force (per unit mass of fluid).  $\epsilon$  is the energy dissipation per unit time and per unit mass of fluid, given by

$$2\epsilon = \nu \sum_i \sum_j \left( \frac{\partial v_i}{\partial x_j} + \frac{\partial v_j}{\partial x_i} \right)^2 \quad (1.449)$$

Equation (1.448) tells us that the global rate of change of energy is equal to the rate at which the external forces do work on the fluid minus the rate at which viscous effects convert kinetic energy into heat. Note that the non-linear terms in the Navier-Stokes equation do no net work on the system. Mathematically, it can be shown that any term which appears as a divergence in the local energy equation vanishes when integrated over the system volume in order to obtain the global equation [106]. Furthermore, the viscous term can be divided into two parts, of which one is diffusive in character and vanishes when

integrated, and the other is dissipative and given by (1.449) for incompressible fluids.

In the turbulent case the total kinetic energy equation (1.447) is readily generalized to the form

$$2E_T = \sum_i \int_V \rho \bar{v}_i^2 dv + \sum_i \int_V \rho \overline{v_i'^2} dv \quad (1.450)$$

Normally, as discussed earlier, in reactor modeling we are interested in the energy associated with the velocity fluctuations  $v_i'$  only. The appropriate turbulent kinetic energy balance equation, the  $k$  equation, has therefore been derived via an equation for the Reynolds stress tensor.

The turbulent kinetic energy budget involves the production of turbulent kinetic energy by interaction of turbulence with the mean velocity. It was stated in the previous analysis that the production of  $k$  was accompanied by a corresponding loss of kinetic energy from the mean flow. No quantitative derivation was given at that point. To study this mechanism, a procedure analog to the derivation of the instantaneous kinetic energy equation can be applied to derive an equation for the mean kinetic energy of the flow.

We start with the transport equation for mean velocity in turbulent flow (1.387), multiply by  $\bar{v}_i$ , and use the chain rule to derive the following equation for mean kinetic energy per unit mass:

$$\frac{\partial(\frac{1}{2}\bar{v}_i^2)}{\partial t} + \bar{v}_j \frac{\partial(\frac{1}{2}\bar{v}_i^2)}{\partial x_j} + \bar{v}_i \frac{\partial \overline{v_i' v_j'}}{\partial x_j} = -\frac{\bar{v}_i}{\rho} \frac{\partial \bar{p}}{\partial x_i} + \nu \bar{v}_i \frac{\partial^2 \bar{v}_i}{\partial x_j \partial x_j} \quad (1.451)$$

The *first term on the LHS* represents the rate of accumulation of mean kinetic energy within the control volume. The *second term on the LHS* describes the advection of mean kinetic energy by the mean velocity. The *third term on the LHS* represents the interaction between the mean flow and turbulence. The *first term on the RHS* represents the production of *MKE* when pressure gradients accelerate the mean flow. The *second term on the RHS* represents the molecular dissipation of mean motions.

Using the product rule, the interaction term (i.e., the third term on the LHS) can be rewritten as

$$-\bar{v}_i \frac{\partial \overline{v_i' v_j'}}{\partial x_j} = \overline{v_i' v_j'} \frac{\partial \bar{v}_i}{\partial x_j} - \frac{\partial(\overline{v_i' v_j'} \bar{v}_i)}{\partial x_j} \quad (1.452)$$

This leaves

$$\frac{\partial(\frac{1}{2}\bar{v}_i^2)}{\partial t} + \bar{v}_j \frac{\partial(\frac{1}{2}\bar{v}_i^2)}{\partial x_j} = -\frac{\bar{v}_i}{\rho} \frac{\partial \bar{p}}{\partial x_i} + \nu \bar{v}_i \frac{\partial^2 \bar{v}_i}{\partial x_j \partial x_j} + \overline{v_i' v_j'} \frac{\partial \bar{v}_i}{\partial x_j} - \frac{\partial(\overline{v_i' v_j'} \bar{v}_i)}{\partial x_j} \quad (1.453)$$

If we compare the  $k$  equation (1.401) with the mean kinetic energy equation (1.453) we see that they both contain a term describing the interaction between the mean flow and turbulence. We are of course referring to the velocity

variance production term, which is the second last term in (1.453). The sign of this term differ in the two equations. Thus, the energy that is mechanically produced as turbulence is lost from the mean flow, and visa versa.

### Generalized Transport Equations for Specific Turbulent Fluxes and Variances of the scalar variables

Let  $\psi$  be a general instantaneous scalar variable representing quantities like energy, heat, temperature, species mass concentration, etc.. In Cartesian coordinates the general transport equation for  $\psi$  can be written as

$$\frac{\partial \rho \psi}{\partial t} + \frac{\partial}{\partial x_j} (\rho v_j \psi) = \frac{\partial}{\partial x_j} (\Gamma_\psi \frac{\partial \psi}{\partial x_j}) + S_\psi \quad (1.454)$$

where  $\Gamma_\psi$  is the molecular diffusion coefficient of quantity  $\psi$ , and  $S_\psi$  is the source term for the remaining processes not already in the equation, such as for example chemical reactions in the species transport equation. The physical interpretation of the terms in the general equation has been discussed earlier for the individual quantities of interest.

The general equation for the corresponding mean Reynolds averaged variables in a turbulent flow is derived in the following way. We start with the basic transport equation (1.454) and expand  $\psi$  into its mean and fluctuating parts (e.g., [153] [167] [66]):

$$\begin{aligned} \frac{\partial \rho \bar{\psi}}{\partial t} + \frac{\partial \rho \psi'}{\partial t} + \frac{\partial}{\partial x_j} (\rho \bar{v}_j \bar{\psi}) + \frac{\partial}{\partial x_j} (\rho v'_j \bar{\psi}) + \frac{\partial}{\partial x_j} (\rho \bar{v}_j \psi') + \frac{\partial}{\partial x_j} (\rho v'_j \psi') \\ = \frac{\partial}{\partial x_j} (\Gamma_\psi \frac{\partial \bar{\psi}}{\partial x_j}) + \frac{\partial}{\partial x_j} (\Gamma_\psi \frac{\partial \psi'}{\partial x_j}) + \bar{S}_\psi \end{aligned} \quad (1.455)$$

where we still assume that the fluid is incompressible (i.e.,  $\rho$  and  $\Gamma_\psi$  are constant). In addition, we have assumed that the remaining net source term,  $\bar{S}_\psi$ , is a mean forcing. Note that the latter assumption is not valid for many multicomponent reactive systems.

Next, we Reynolds average the instantaneous equation

$$\frac{\partial \rho \bar{\psi}}{\partial t} + \frac{\partial}{\partial x_j} (\rho \bar{v}_j \bar{\psi} + \overline{\rho v'_j \psi'}) = \frac{\partial}{\partial x_j} (\Gamma_\psi \frac{\partial \bar{\psi}}{\partial x_j}) + \bar{S}_\psi \quad (1.456)$$

The *first term on the LHS* denotes the rate of accumulation of the mean quantity  $\bar{\psi}$  within the control volume per unit volume. The *second term on the LHS* denotes the convection of the mean quantity  $\bar{\psi}$  by the mean velocity. The *third term on the LHS* represents the divergence of the turbulent  $\psi$  flux. The *first term on the RHS* represents the mean molecular diffusion of the  $\bar{\psi}$

quantity. *The second term on the RHS* denotes the mean net body source term for additional  $\psi$  processes<sup>40</sup>.

The general transport equation for the scalar quantity variance can be formulated, in analogy to the procedure applied for momentum, by subtracting (1.456) from (1.455) to obtain an equation for the turbulent fluctuations (e.g., [153] [167] [154]):

$$\begin{aligned} \frac{\partial \rho \psi'}{\partial t} + \frac{\partial}{\partial x_j} (\rho v'_j \bar{\psi}) + \frac{\partial}{\partial x_j} (\rho \bar{v}_j \psi') + \frac{\partial}{\partial x_j} (\rho v'_j \psi') - \frac{\partial}{\partial x_j} (\overline{\rho v'_j \psi'}) \\ = \frac{\partial}{\partial x_j} \left( \Gamma_\psi \frac{\partial \psi'}{\partial x_j} \right) \end{aligned} \quad (1.457)$$

Multiplying this equation by  $2\psi'$ , and using the product rule of calculus to covert terms like  $2\psi' \partial \psi' / \partial t$  into terms like  $\partial \psi'^2 / \partial t$ , yields:

$$\begin{aligned} \frac{\partial \rho \psi'^2}{\partial t} + 2\psi' \frac{\partial}{\partial x_j} (\rho v'_j \bar{\psi}) + \frac{\partial}{\partial x_j} (\rho \bar{v}_j \psi'^2) + \frac{\partial}{\partial x_j} (\rho v'_j \psi'^2) \\ = 2\psi' \frac{\partial}{\partial x_j} (\overline{\rho v'_j \psi'}) + 2\psi' \frac{\partial}{\partial x_j} \left( \Gamma_\psi \frac{\partial \psi'}{\partial x_j} \right) \end{aligned} \quad (1.458)$$

Next, we average, applying the Reynolds averaging rules, and rearrange the terms in the equation:

$$\frac{\partial \overline{\rho \psi'^2}}{\partial t} + \frac{\partial}{\partial x_j} (\rho \bar{v}_j \overline{\psi'^2}) = -2\overline{\psi' \frac{\partial}{\partial x_j} (\rho v'_j \bar{\psi})} - \frac{\partial}{\partial x_j} (\overline{\rho v'_j \psi'^2}) + 2\overline{\psi' \frac{\partial}{\partial x_j} \left( \Gamma_\psi \frac{\partial \psi'}{\partial x_j} \right)} \quad (1.459)$$

The first term on the right hand side is usually reformulated by use of the continuity equation for the fluctuations, and the last term is slightly rearranged assuming that  $\Gamma_\psi$  is a constant:

$$\frac{\partial \overline{\rho \psi'^2}}{\partial t} + \frac{\partial}{\partial x_j} (\rho \bar{v}_j \overline{\psi'^2}) = -2\overline{\rho \psi' v'_j \frac{\partial \bar{\psi}}{\partial x_j}} - \frac{\partial}{\partial x_j} (\overline{\rho v'_j \psi'^2}) + 2\overline{\Gamma_\psi \psi' \frac{\partial^2 \psi'}{\partial x_j^2}} \quad (1.460)$$

<sup>40</sup> Note that for multicomponent reactive systems the source term needs to be treated in a more sophisticated way if the time scale of the reaction rate is at the same order as the time scale of the turbulent fluctuations. For very rapid reactions, like in most combustion processes, the turbulent fluctuations will not influence the reaction rate directly but indirectly through the mixing properties of turbulence. Therefore, these reactions are often referred to as dispersion-controlled reactions. Further details are given by Jones [79], Baldyga and Bourne [5] and Fox [49]. For (very) slow reactions, like in many chemical processes, the turbulent transport processes perform relatively rapid mixing, thus allowing time for fresh reagent to mix with the local fluid. Therefore, calculating the average reaction rate the local reagent concentrations are assumed premixed and the turbulent species concentration variances appears to be small.

As was done for momentum, the last term in the equation is split into two parts, one determining the molecular diffusion of the  $\psi$  variance which is assumed to be small enough to be neglected. The remaining part is defined as twice the molecular dissipation term,  $\epsilon_\psi$ , by analogy with the kinetic energy term:

$$\epsilon_\psi \approx \Gamma_\psi \overline{\left(\frac{\partial \psi'}{\partial x_j}\right)^2} \quad (1.461)$$

Thus, the transport equation for the general scalar quantity  $\psi$  variance is

$$\frac{\partial \overline{\rho \psi'^2}}{\partial t} + \frac{\partial}{\partial x_j} (\overline{\rho \bar{v}_j \psi'^2}) = -2 \overline{\rho \psi' v'_j} \frac{\partial \bar{\psi}}{\partial x_j} - \frac{\partial}{\partial x_j} (\overline{\rho v'_j \psi'^2}) - 2\epsilon_\psi \quad (1.462)$$

*The first term on the LHS* represents the local rate of accumulation of the variance  $\overline{\psi'^2}$ . *The second term on the LHS* describes the convection of the quantity  $\psi$  variance by the mean velocity. *The first term on the RHS* denotes a production term, associated with the turbulent motions occurring within a mean  $\psi$  gradient. *The second term on the RHS* represents the turbulent transport of the  $\psi$  variance. *The third term on the RHS* denotes the molecular dissipation.

The general transport equation for the specific turbulent fluxes of scalar variables is derived in analogy to the corresponding momentum flux equations, i.e., the Reynolds stress equations. The derivation combines two equations for the fluctuations to produce a flux equation. For the first equation we start with the momentum fluctuation equation (1.389), multiply it by the scalar quantity perturbation  $\psi'$ , and Reynolds average:

$$\overline{\psi' \frac{\partial v'_i}{\partial t}} + \overline{\bar{v}_j \psi' \frac{\partial v'_i}{\partial x_j}} + \overline{\psi' v'_j \frac{\partial \bar{v}_i}{\partial x_j}} + \overline{\psi' v'_j \frac{\partial v'_i}{\partial x_j}} = -\frac{1}{\rho} \overline{\psi' \frac{\partial p'}{\partial x_i}} + \overline{\nu \psi' \frac{\partial^2 v'_i}{\partial x_j \partial x_j}} \quad (1.463)$$

Similarly for the second equation, we start with the equation for the fluctuating scalar variable (1.457) and multiply by  $v'_i$  and Reynolds average:

$$\overline{v'_i \frac{\partial \rho \psi'}{\partial t}} + \overline{v'_i \frac{\partial}{\partial x_j} (\rho v'_j \bar{\psi})} + \overline{v'_i \frac{\partial}{\partial x_j} (\rho \bar{v}_j \psi')} = -v'_i \frac{\partial}{\partial x_j} (\overline{\rho v'_j \psi'}) + v'_i \frac{\partial}{\partial x_j} (\Gamma_\psi \frac{\partial \psi'}{\partial x_j}) \quad (1.464)$$

we can reformulate some of the terms using the two forms of the continuity equation and the assumption that the fluid is incompressible

$$\overline{v'_i \frac{\partial \psi'}{\partial t}} + \overline{v'_i v'_j \frac{\partial \bar{\psi}}{\partial x_j}} + \overline{\bar{v}_j v'_i \frac{\partial \psi'}{\partial x_j}} + \overline{v'_i v'_j \frac{\partial \psi'}{\partial x_j}} = \frac{\Gamma_\psi}{\rho} \overline{v'_i \frac{\partial^2 \psi'}{\partial x_j^2}} \quad (1.465)$$

Next, add these two equations, put the turbulent flux divergence term into flux form using the continuity equations, and combine terms

$$\begin{aligned}
& \frac{\partial \overline{\psi'v'_i}}{\partial t} + \bar{v}_j \frac{\partial \overline{\psi'v'_i}}{\partial x_j} + \overline{\psi'v'_j} \frac{\partial \bar{v}_i}{\partial x_j} + \overline{v'_i v'_j} \frac{\partial \bar{\psi}}{\partial x_j} + \frac{\partial \overline{\psi'v'_i v'_j}}{\partial x_j} \\
& = -\frac{1}{\rho} \overline{\psi' \frac{\partial p'}{\partial x_i}} + \nu \overline{\psi' \frac{\partial^2 v'_i}{\partial x_j \partial x_j}} + \frac{\Gamma_\psi}{\rho} \overline{v'_i \frac{\partial^2 \psi'}{\partial x_j^2}}
\end{aligned} \tag{1.466}$$

Then, we split the pressure term into two parts, and assume  $\nu \approx \frac{\Gamma_\psi}{\rho}$  to combine the molecular diffusion terms:

$$\begin{aligned}
\frac{\partial \overline{\psi'v'_i}}{\partial t} + \bar{v}_j \frac{\partial \overline{\psi'v'_i}}{\partial x_j} & = -\overline{\psi'v'_j} \frac{\partial \bar{v}_i}{\partial x_j} - \overline{v'_i v'_j} \frac{\partial \bar{\psi}}{\partial x_j} - \frac{\partial \overline{\psi'v'_i v'_j}}{\partial x_j} \\
& - \frac{1}{\rho} \left[ \frac{\partial \overline{p' \psi'}}{\partial x_i} - \overline{p' \frac{\partial \psi'}{\partial x_i}} \right] + \nu \frac{\partial^2 \overline{\psi'v'_i}}{\partial x_j \partial x_j} - 2\nu \overline{\left( \frac{\partial v'_i}{\partial x_j} \right) \left( \frac{\partial \psi'}{\partial x_j} \right)}
\end{aligned} \tag{1.467}$$

The terms in this equation have physical interpretations analogous to those in the momentum flux equation (1.394), except for the additional term (i.e., the second term on the RHS), which is a production/loss term related to the mean scalar quantity gradient. Physically, this term suggests production of the scalar quantity flux when there is a momentum flux in a mean scalar quantity gradient. The turbulent momentum flux implies a turbulent movement of the fluid. If that movement occurs across a mean scalar quantity gradient, then the scalar quantity fluctuation would be expected.

Note that an additional term must be added if the source is assumed to fluctuate too.

Substituting  $2\epsilon_{u_i\psi}$  for the last term, and neglecting the pressure diffusion term and the molecular diffusion term leaves:

$$\frac{\partial \overline{\psi'v'_i}}{\partial t} + \bar{v}_j \frac{\partial \overline{\psi'v'_i}}{\partial x_j} = -\overline{\psi'v'_j} \frac{\partial \bar{v}_i}{\partial x_j} - \overline{v'_i v'_j} \frac{\partial \bar{\psi}}{\partial x_j} - \frac{\partial \overline{\psi'v'_i v'_j}}{\partial x_j} + \frac{1}{\rho} \overline{p' \frac{\partial \psi'}{\partial x_i}} - 2\epsilon_{u_i\psi} \tag{1.468}$$

where *the first and second terms on the LHS* are the rate of accumulation and advection terms, *the first and second terms on the RHS* relate to production/consumption, *the third term on the RHS* denotes turbulent transport, *the fourth term on the RHS* denotes redistribution, and *the fifth term on the RHS* denotes the molecular destruction or dissipation of the turbulent scalar quantity flux.

Turbulence closure models for the unknown terms in the flux- and variance equations for single phase reactor systems are discussed extensively by Baldyga and Bourne [5] and Fox [49] [50]. However, the application of these model closures should be treated with care as most of these parameterizations are expressed in terms of the turbulent eddy and other scalar dissipation rates (and dissipation energy spectra) which are about the weakest links in turbulence modeling. The predictive capabilities of the Reynolds averaged models

are thus very limited, and in most papers the use of these statistical concepts are restricted to the reproduction of known concentration and reaction rates. More elaborated statistical approaches have been proposed in which the governing equations are conditionally averaged invoking probability density functions and moments of the modeled quantities [121]. However, in this book no further consideration is given to the second order closure models.

For the purpose of reactor modeling, and in particular for multiphase systems, virtually only first order closures are adopted. Extensive use is made of the simple gradient transport hypothesis, even though it has long been realized that a gradient transport model requires (among other things) that the characteristic scale of the transporting mechanism must be small compared with the distance over which the mean gradient of the transported property changes appreciably [24]. In practice, this requirement is often violated and there exists experimental evidence that the gradient-diffusion models are not sufficiently accurate for variable density flows (e.g., [49]). Counter-gradient (or up-gradient) transport may even occur in certain occasions [100] [154]. In atmospheric simulations this phenomenon might be physically explained by large eddy transport of heat from hot to cold areas, regardless of the local gradient of the background environment.

Nevertheless, the second order closure models are avoided and usually not employed in industrial reactor flow simulations due to their complexity, negligible gain in accuracy and predictivity, and because of additional numerical convergence- and stability problems. Rather, the present trend in reactor modeling is to explore the capabilities of the large eddy simulation (LES) model.

### 1.3.6 Large Eddy Simulation (LES)

In this section the elementary concepts of the large eddy simulation (LES) technique are examined.

The LES approach has been thoroughly assessed by [150, 97, 27, 29, 30, 45, 46, 65, 110, 99, 176, 133, 109, 105, 128, 140, 141, 143, 53, 98, 137, 121]. These reports are recommended for complementary studies.

In some flows in boundary layer meteorology there appears to be a distinct lack of velocity variations at certain intervals of time periods or frequency intervals (e.g., [173]). The separation of scales is evident in the measured spectrum where the spectral gap appears as a wave number region containing very low energy separating the micro scale from the macro scale peaks. Motion to the left of the gap are said to be associated with *the mean flow*. Motions to the right constitute *turbulence*. Hence, *the spectral gap* provides a means to separate the turbulent from the non-turbulent influences on the flow (see also [137], p. 82). Most of the operational numerical weather prediction models use grid spacings or wavelength cutoffs that fall within the spectral gap.

This means that larger scale motions can be explicitly resolved and deterministically forecasted. The smaller scale motions, namely turbulence, are not explicitly resolved. Rather, the effects of those sub-grid scales on the larger scales are approximated by turbulence models. These smaller size motions are said to be parameterized by sub-grid scale stochastic (statistical) approximations or modes. The referred experimental data analyzes of the flow in the atmospheric boundary layer determine the basis for the large eddy simulation (LES) approach developed by meteorologists like Deardorff [27] [29] [30]. Large-Eddy Simulation (LES) is thus a relatively new approach to the calculation of turbulent flows.

The basic idea also stems from two additional experimental observations (see also the historical LES outline by Moin and Kim [110]). First, the large-scale structure of turbulent flows varies greatly from flow to flow and is consequently difficult, if not impossible, to model in a general way. Secondly, the small-scale turbulence structures are nearly isotropic, very universal in character, and hence much more amenable to general modeling. In LES, one actually calculates the large-scale motions in a time-dependent, three-dimensional computation, using for the large-scale field dynamical equations that incorporate relative simple models for small-scale turbulence. Only the part of the turbulence field with scales that are small relative to the overall dimensions of the flow field is modeled. This in contrast to phenomenological turbulence modeling, in which all the deviations from the mean velocity profile are modeled.

A typical LES calculation for wall-bounded turbulent flows imposes a great demand on computer speed and memory. At present, therefore, the use of LES for practical engineering applications is admittedly uneconomical. Thus, according to Reynolds [128], LES came to the attention of the engineering research community about a decade after it had been pioneered by scientists in weather forecast [101]. However, several considerations motivate the present development of the LES method in the engineering community. First, the information generated by simple flow calculations can be used as a research tool in studies of the structure and dynamics of turbulence. Secondly, the various correlations that can be obtained from the computed large-scale field may be used in developing phenomenological turbulence models for complex flows. Thirdly, the great bulk of routine engineering calculations of turbulent flows will always be made with the most economical representations of the turbulence that provide adequate predictions. For complex flows that are three dimensional, 3D calculations must be made with an appropriate approach. For these flows LES may actually prove to be faster and cheaper than the other turbulence models having the sophistication necessary to capture the complex effects [128]. The main reason for this is that the present methods based on the time (or ensemble) averaged Navier-Stokes equations require considerable experimental validation to be useful since it is difficult to develop a universal turbulence model representing all eddy sizes. Therefore, even with the experimental data available, the range of applicability of a particular model may be

limited. However, the cost of experimental research requires that model simulations should be carried out minimizing the number of experiments needed. Large eddy simulations is a compromise which attempts to fill the gap. The hypothesis is that by modeling just the small eddies, it may be possible to develop models which are sufficiently flow independent. According to Ferziger and Leslie [46], this is the premise of LES.

To provide an introductory mathematical description of the basic idea of Large Eddy Simulations, we consider the turbulent energy spectra. Suppose that we do not attempt to simulate all the wavenumber modes up to the viscous cutoff ( $> k_d$ ). Instead, we only simulate modes for which  $k \leq k_C$ , where the chosen cutoff wavenumber  $k_C$  satisfies the condition  $k_C \ll k_d$ . The situation we are envisaging in engineering practice is illustrated schematically in Fig. 1.8. Note that in engineering practice the cutoff wavenumber is often apparently arbitrarily chosen due to the missing energy gap in the energy spectrum, whereas in the geophysical sciences the choice of cutoff wavenumber  $k_C$  is not arbitrary but based on physical interpretations of experimental data (e.g., [154]).

However, the theoretical interpretation of LES is that we are simulating the Fourier-transformed Navier-Stokes equation with its wavenumber representation truncated to the interval  $0 \leq k \leq k_C$ . In accordance with the theory of

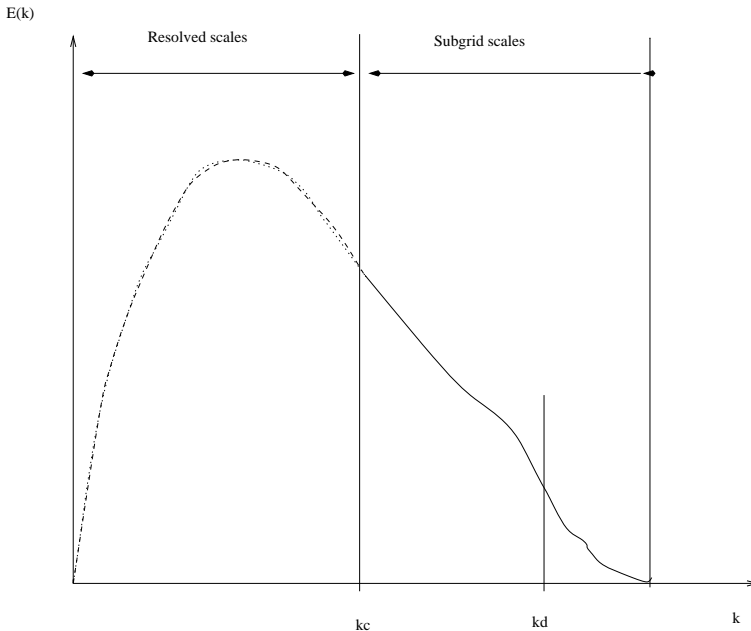


**Fig. 1.8.** The energy spectrum divided into resolved scales ( $k < k_C$ ) and subgrid scales ( $k > k_C$ ), for the purpose of large-eddy simulation.

Taylor [164] the non-linear convection term couples all wave numbers together thus the overall effect is a net transfer of energy from any one wavenumber to higher wave numbers<sup>41</sup> [106]. Hence, if we truncate at  $k = k_C$ , we are removing the mechanism by which energy is transferred from wave numbers below  $k_C$  to those above. In practice, such a simulation would fail because energy would be cascaded down to  $k = k_C$  and would pile up at the cutoff. To solve this problem we usually introduce an apparent viscosity, an analog to the eddy viscosity known from the foregoing discussion but with a different physical interpretation, to represent the effect of energy transfers to  $k > k_C$ . As can be seen from Fig. 1.8, the larger eddies ( $\lambda > \lambda_C$ , or  $k < k_C$  as  $\lambda = 2\pi/k$ ) carry most of the turbulent kinetic energy and most of the turbulent fluxes. Accordingly, in the ideal case, the smallest eddies carry only a small fraction of the turbulent kinetic energy and hardly any turbulent fluxes. Therefore, assuming that the energy flux to  $k > k_C$  is almost negligible, a rough model for it may still be sufficient providing accurate solutions for the larger eddies.

LES can also be performed in physical space, using the governing equations in a more familiar form. *The flow problems are then simulated using a 3D time-dependent numerical integration scheme which numerically resolves scales in between a lower limit of the order  $\Delta$  as given by the grid scale or any equivalent resolution limit of the numerical integration scheme, and an upper limit as given by the size of the computational domain.*

Basically, in further details, there are four conceptual steps in LES ([121], chap 13):

1. A *filtering* operation is defined to decompose the velocity,  $\mathbf{v}(\mathbf{r}, t)$ , into the sum of a filtered (or resolved) component,  $\tilde{\mathbf{v}}(\mathbf{r}, t)$ , and a residual (or sub-grid-scale, SGS) component,  $\mathbf{v}'(\mathbf{r}, t)$ :

$$v_i = \tilde{v}_i + v'_i \quad (1.469)$$

2. The equations for the evolution of the filtered velocity field are derived from the Navier-Stokes equations.
3. Closure is obtained by modeling the residual-stress tensor, most simply by an eddy-viscosity model.
4. The filtered model equations are solved numerically for  $\tilde{\mathbf{v}}(\mathbf{r}, t)$ , which provides a 3D and time dependent approximation to the large scale motions in one realization of the turbulent flow.

---

<sup>41</sup> If energy is feed into a certain band of scales, then turbulence has the tendency to distribute energy in a wave number space from the given mode to all other possible modes. In the absence of sources and sinks of energy, this process will continue to complete redistribution. However, in reality, geometry limits the lower end wave numbers and the viscosity damps out energy at high wave numbers. In order to balance the dissipation, more energy has to be transported from the large to small length scales. This is the reason for having a one-way transfer of energy from small to high wave numbers. Thus, the sub-grid scale model has to mimic the drainage of energy from the large scales.

There are, however, two viewpoints on the separation of the modeling issues (i.e., points 1-3 above) from the numerical solution (i.e., point 4 above).

- In one point of view, as expressed by Reynolds [128], the two issues are considered separately. The filtering and modeling are independent of the numerical method, and the closures are independent of the numerical grid used. Hence, the terms ‘filtered’ and ‘residual’ are more appropriate than the usual ‘resolved’ and ‘sub-grid’ phrases. In this case it is also expected that the numerical method provides accurate solutions to the filtered equations. In practice, however, the modeling and numerical issues are always connected.

In this approach the governing equations are usually transformed and solved numerically in wave number space by use of very accurate spectral methods.

The present LES concept has in most cases been used as a research tool to study isotropic and homogeneous turbulence within the more theoretical fields of science. Note that the residual-stress models for homogeneous turbulence are not adequate describing industrial non-isotropic inhomogeneous turbulent flows ([137] [121], chap 13).

- The alternative interpretation is that modeling and numerical issues should deliberately be combined. The governing equations are then solved in physical space often using a second order accurate finite difference or finite volume algorithm.

This LES concept is usually preferred in engineering practice. Note also that the residual-stress models used in physical space are usually different from those used in wave number space ([137] [121], chap 13).

In the numerical solution of the LES momentum equation, various numerical errors are incurred, the most important being the spatial truncation error. One way to express this error is through the modified equation, which is the PDE satisfied by the numerical solution. The modified equation corresponding to the LES momentum equation can be written:

$$\frac{\tilde{D}\tilde{v}_j}{\tilde{D}t} = \nu \frac{\partial^2 \tilde{v}_j}{\partial x_i \partial x_i} - \frac{\partial}{\partial x_j} (\tilde{\sigma}_{ij}^R - \tilde{\sigma}_{ij}^n) - \frac{1}{\rho} \frac{\partial \tilde{p}}{\partial x_j} \quad (1.470)$$

It is noted that the spatial-truncation error appears as an additional numerical stress,  $\tilde{\sigma}_{ij}^n$ , which depends on the grid spacing  $h$ . If the spatial discretization is  $p$ -th order accurate, then  $\tilde{\sigma}_{ij}^n$  is of order  $h^p$ .

There are also differing viewpoints on the role of the numerical stress in LES. The simplest view is that the LES equations should be solved accurately. That is, for a given filter width,  $\Delta$ , the grid spacing  $h$  should be chosen to be sufficiently small so that the numerical stress,  $\tilde{\sigma}_{ij}^n$ , is negligible compared with the modeled residual stress  $\tilde{\sigma}_{ij}^R$ . Kinetic energy is removed from the resolved motions by numerical dissipation at the rate  $\epsilon_{\text{num}} = -\tilde{\sigma}_{ij}^n \tilde{S}_{ij}$ .

The opposite viewpoint, advocated by Boris et al. [16], is that no explicit filtering should be performed and no explicit residual stress model should be used ( $\tilde{\sigma}_{ij}^R = 0$ ). Instead, an appropriate numerical method is used to attempt to solve the Navier-Stokes equation for  $\tilde{\mathbf{v}}(\mathbf{r}, t)$ . Because the grid is not fine enough to resolve the solution to the Navier-Stokes equation, significant numerical stresses  $\tilde{\sigma}_{ij}^n$  arise. Thus, filtering and residual-stress modeling are performed implicitly by the numerical method.

The numerical stress  $\tilde{\sigma}_{ij}^n$  depends on the type of numerical method used, and hence this choice is crucial. The ideal scheme is accurate for the well-resolved contributions to  $\tilde{\mathbf{v}}(\mathbf{r}, t)$ , while it attenuates poorly resolved shorter-wave length contributions.

Compared with explicit modeling of the residual stresses, this approach has advantages and disadvantages, advocates and detractors. The advantages are that for a given grid size as much as possible of the turbulent motion is represented explicitly by the LES velocity field  $\tilde{\mathbf{v}}(\mathbf{r}, t)$ , and that energy is removed from  $\tilde{\mathbf{v}}(\mathbf{r}, t)$  only where and when it is necessary to do so. A further advantage is that the time and effort required to develop and test a residual-stress model are eliminated. The primary disadvantage is that the modeling and the numerics are inseparably coupled. Another disadvantage is that there is no representation or estimation of the sub-grid scale motions that can be used for defiltering or in models for other sub-grid scale processes.

Leonard [97] was apparently the first to use the term *Large Eddy Simulation*. He also introduced the idea of filtering as a formal convolution operation on the velocity field and gave the first general formulation of the method. Since Leonard's approach forms the basis for application of LES to chemical reactor modeling, we discuss this approach in further details.

Leonard [97] defined a generalized filter as a convolution integral<sup>42</sup>:

$$\tilde{v}_i(\mathbf{r}, t) = \iiint G(\mathbf{r} - \boldsymbol{\xi}; \Delta) v_i(\boldsymbol{\xi}, t) d^3\xi \quad (1.471)$$

where  $G$  represents the filter function and the tilde denotes the large scale (or resolved) part of the velocity field. Over the years numerous filters have been proposed and used for performing the spatial scale separation (e.g., [137]).

The *filter function*,  $G$ , is normalized by requiring that:

<sup>42</sup> *Convolution*, the word comes from the folding together, one part upon another. In mathematics convolution can be considered as a generalized product of functions. In this context the purpose for introducing a convolution integral is to extend the integral over the whole flow field domain. Lower limit is  $-\infty$ , and upper limit is  $\infty$ . The filtering function  $G(\mathbf{r} - \boldsymbol{\xi}; \Delta)$  is a normalized weighting function with characteristic length  $\Delta$ . The argument  $\mathbf{r} - \boldsymbol{\xi}$  is a reminder for the limits of the original integral,  $\boldsymbol{\xi} \in (\mathbf{r} - \frac{1}{2}\Delta\mathbf{r}, \mathbf{r} + \frac{1}{2}\Delta\mathbf{r})$ . The symbol  $d\xi$  should still be thought of as simply an indication of what the independent variables are.

$$\iiint G(\mathbf{r} - \boldsymbol{\xi}; \Delta) d^3 \boldsymbol{\xi} = 1 \tag{1.472}$$

Three classical filters for large eddy simulation, as given by Leonard [97], are sketched in Fig. 1.9. In terms of the filter function (1.471), the volume-averaged box filter as defined in (1.486) is given by (e.g., [97] [186] [137]):

$$G(r_i - \xi_i; \Delta) = \begin{cases} 1/\Delta & \text{if } |r_i - \xi_i| \leq \Delta r_i/2, \\ 0 & \text{Otherwise} \end{cases} \tag{1.473}$$

and sketched in Fig. 1.9a. The physical box filter is not sharp in wave number space.

A Gaussian filter as sketched in Fig. 1.9b, is defined by:

$$G(r_i - \xi_i; \Delta) = \left(\frac{6}{\pi \Delta^2}\right)^{1/2} \exp\left(-6 \frac{|r_i - \xi_i|^2}{\Delta^2}\right) \tag{1.474}$$

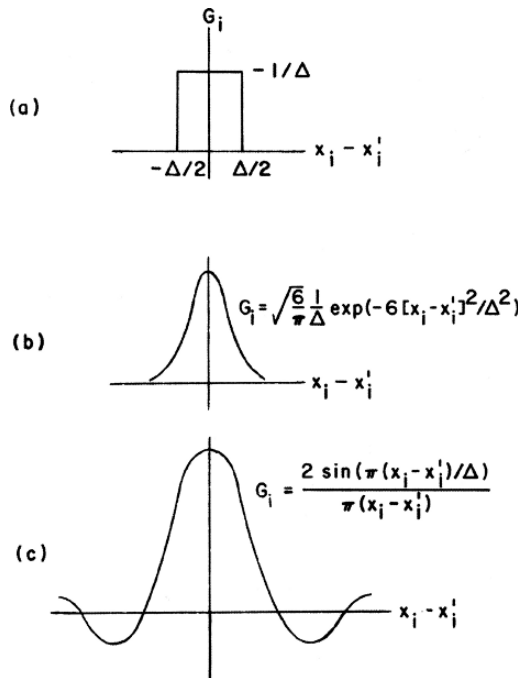


**Fig. 1.9.** Possible spatial filters defining large-scale quantities with  $G = G_1 G_2 G_3$ . The filter denoted by (a) is the volume-averaged box filter, the filter denoted by (b) is the Gaussian filter, and the filter denoted by (c) is the sharp cutoff filter. Note that the position vector,  $\mathbf{x}$ , used by Leonard corresponds to  $\mathbf{r}$  in this book. Reprinted from Leonard [97] with permission from Elsevier.

The Gaussian filter is fairly sharp both in physical space and in wave number space. This filter was for example used by Ferziger [45].

The Fourier transform of (1.471) is  $\widehat{\tilde{v}}_i(\mathbf{k}, t) = \widehat{G}(\mathbf{k})\widehat{v}_i(\mathbf{k}, t)$ , where  $\widehat{v}_i$  and  $\widehat{G}$  represent the Fourier transforms of  $v_i$  and  $G$ , respectively (e.g., [133, 186, 121, 137]).

A Fourier transform of the filter shown in Fig. 1.9c is a spectrally sharp cutoff filter, a kind of box filter in  $\mathbf{k}$ -space rather than  $\mathbf{r}$ -space. The spectrally sharp top-hat filter, i.e., the filter normally used in spectral simulations, is in physical space defined by (e.g., [97] [106]):

$$G(r_i - \xi_i; \Delta) = \frac{2 \sin(\pi(r_i - \xi_i)/\Delta)}{\pi(r_i - \xi_i)} \quad (1.475)$$

In physical space this filter is not sharp, as shown from the sketch in Fig. 1.9c.

The significance of the sharp spectral filter is apparent, it annihilates all Fourier modes of wave number  $|k|$  greater than the cutoff wave number,  $k_C = \pi/\Delta$ , whereas it has no effect on the lower wave number modes.

Illustrating the Reynolds averaging procedure in the previous sects. we started by formulating the average incompressible conservation equations for mass and momentum written in Cartesian coordinates, i.e., (1.382) and (1.383). Performing the corresponding derivation of the filtered LES equations we highlight the main similarities and differences between these two modeling approaches.

The filter operation defined by (1.471) is sometimes written in the contracted form (e.g., [106] [137]), intending to make the text more easy to follow:

$$\tilde{v}_i(\mathbf{r}, t) = G^* \{v_i\} \quad (1.476)$$

The continuity equation is a relatively simple starting point formulating the LES equations, neatly demonstrating the filtering procedure. Applying the mathematical operator  $G$ , defined according to (1.476), on (1.382) using a homogeneous filter (e.g., [140], p 380; [121], chap 13) yields<sup>43</sup>:

<sup>43</sup> This result can be proven by integration by parts with respect to  $\xi$ , provided only that  $v_i$  vanishes on the boundaries [106]:

$$\frac{\partial}{\partial x_i} \int G v_i d^3 \xi = \int \frac{\partial}{\partial x_i} (G v_i) d^3 \xi = \int G \frac{\partial v_i}{\partial x_i} d^3 \xi + \int \frac{\partial G}{\partial x_i} v_i d^3 \xi \quad (1.477)$$

or

$$\frac{\partial}{\partial x_i} (G^* \{v_i\}) = G^* \left\{ \frac{\partial v_i}{\partial x_i} \right\} + \int \frac{\partial G}{\partial x_i} v_i d^3 \xi \quad (1.478)$$

Note that

$$\int \frac{\partial G}{\partial x_i} v_i d^3 \xi = 0 \quad (1.479)$$

provided that  $v_i = 0$  at the boundaries.

Then,

$$G^* \left\{ \frac{\partial v_i}{\partial x_i} \right\} = \frac{\partial}{\partial x_i} (G^* \{v_i\}) = \frac{\partial \tilde{v}_i}{\partial x_i} \quad (1.480)$$

$$G^* \left\{ \frac{\partial v_i}{\partial x_i} \right\} = \frac{\partial}{\partial x_i} (G^* \{v_i\}) = \frac{\partial \tilde{v}_i}{\partial x_i} = 0 \quad (1.482)$$

It follows from (1.382), (1.476), and (1.482) that the resolved scales satisfy the continuity equation given by:

$$\frac{\partial \tilde{v}_i}{\partial x_i} = 0 \quad (1.483)$$

Considering the Navier-Stokes equation (1.383), the linear terms are straightly treated in a similar manner but, as in the Reynolds averaging procedure, the non-linear terms require further analysis. Applying the filter operator (1.476) on the non-linear terms in (1.383), yields

$$\frac{\partial \tilde{v}_i}{\partial t} + \frac{\partial \tilde{\sigma}_{ij}}{\partial x_j} = -\frac{1}{\rho} \frac{\partial \tilde{p}}{\partial x_i} + \nu \frac{\partial^2 \tilde{v}_i}{\partial x_j \partial x_j} \quad (1.484)$$

where the filtered non-linear term,  $\tilde{\sigma}_{ij}$ , is given by [97]:

$$\begin{aligned} \tilde{\sigma}_{ij} &= G^* \{v_i v_j\} = G^* \{\tilde{v}_i \tilde{v}_j + v'_i \tilde{v}_j + \tilde{v}_i v'_j + v'_i v'_j\} \\ &= \widetilde{v_i v_j} = \widetilde{\tilde{v}_i \tilde{v}_j} + \widetilde{v'_i \tilde{v}_j} + \widetilde{\tilde{v}_i v'_j} + \widetilde{v'_i v'_j} \\ &= \tilde{v}_i \tilde{v}_j + (\widetilde{\tilde{v}_i \tilde{v}_j} - \tilde{v}_i \tilde{v}_j) + (\widetilde{v'_i \tilde{v}_j} + \widetilde{\tilde{v}_i v'_j}) + \widetilde{v'_i v'_j} \\ &= \tilde{v}_i \tilde{v}_j + \tilde{L}_{ij} + \tilde{C}_{ij} + \tilde{R}_{ij} \\ &= \tilde{v}_i \tilde{v}_j + \tilde{\sigma}_{ij}^R \end{aligned} \quad (1.485)$$

where the instantaneous velocity field has been decomposed into resolved and sub-grid scales by use of (1.469).

The above equations describe the large-scale motion.  $\tilde{L}_{ij}$  represents the interactions among the large scales. The effect of small scales appears through the residual stress tensors (i.e.,  $\tilde{C}_{ij}$  and  $\tilde{R}_{ij}$ ). In particular,  $\tilde{C}_{ij}$  represents the interactions between the large and small scales, and  $\tilde{R}_{ij}$  reflects the interactions between subgrid scales. The tensors  $\tilde{L}_{ij}$ ,  $\tilde{C}_{ij}$  and  $\tilde{R}_{ij}$  are known as the *Leonard stress*, *cross-term stress* and the *residual Reynolds stress*, respectively.

---

thus the resolved scales satisfy the continuity equation.

Pope ([121], p. 562) shows that the operation of filtering and differentiating with respect to time commute. Pope also indicate that if we differentiate (1.471) with respect to  $x_j$  we will obtain the result

$$\frac{\partial \tilde{v}_i}{\partial x_i} = \frac{\partial \widetilde{v_i}}{\partial x_i} + \int v_i \frac{\partial G(\boldsymbol{\xi}, \mathbf{r})}{\partial x_i} d^3 \boldsymbol{\xi} \quad (1.481)$$

showing that the operations of filtering and differentiation with respect to position do not commute in general, but do so for homogeneous filters.

At first sight comparing the Reynolds decomposition and time averaging procedure with the corresponding steps in the filtering procedure there are certainly similarities, but also a few essential differences. Obviously, considering the Leonard stress terms, the filtering differs from the standard Reynolds averaging in one important respect,  $\tilde{\tilde{v}}_i \neq \tilde{v}_i$ . That is, a second averaging yields a different result from the first averaging ([53], chap 6). In a similar manner, considering the cross-term stress, we recognize that  $\tilde{v}'_i \neq 0$ . Comparing the resulting filtered equations of motion with the corresponding equations of mean motion obtained by Reynolds averaging the instantaneous equations, it is noted that the continuity equation (1.483) is formally identical with (1.386) for continuity, if we replace  $\tilde{v}_i$  by  $\bar{v}_i$ . There are also similarities between the Reynolds averaged and the Leonard filtered Navier-Stokes equations, as given by (1.387) and (1.484), respectively. The important differences lie in the presence of the cross-term stress term,  $\tilde{C}_{ij}$ , and the Leonard stress,  $\tilde{L}_{ij}$ , in (1.484). The Leonard stress term on the RHS of (1.485) is not a residual tensor, as it involves only the explicit scales and the filter function. The computation of the Leonard stresses may still cause practical difficulties as it requires a second application of the filter, but in principle there is no fundamental closure problem. However, even though there are formal similarities, an essential conceptual difference is that the Reynolds equations involve a mean field which is stationary, or slowly varying with time, and varies smoothly in space, while the large eddy simulations involve a field which may be extremely chaotic in space and time if the numerical grid spacing is small enough [98]. If the grid spacing is increased too much, however, the solution of the LES will, in some sense, converge towards the mean flow. In the other extreme limit, reducing the grid spacing sufficiently, a direct numerical simulation (DNS) is achieved.

In the following paragraphs only the engineering LES practice is considered, as this approach is relatively simple and based upon FD and FVM algorithms (i.e., note that almost all reactor models are discretized by the FVM).

The first engineering LES was Deardorff's [27] simulation of plane channel flow. Deardorff used Reynolds (spatial) averaging, applied to a unit cell of the finite difference mesh, to define the larger (or resolved) scales, and introduced the terminology *filtered variables*. Although only 6720 grid points were used, the comparison with literature laboratory experiments was sufficient favorable for the feasibility of the method to have been established.

The volume-average box filter used by Deardorff [27] is sketched in Fig. 1.9a. In Cartesian coordinates the filter is ([186] [137])<sup>44</sup>:

---

<sup>44</sup> Note that in these formulations a formal mathematical notation is used.  $\mathbf{r}$  is the position vector, while in the integrand we strictly need to use a vector which has components somewhere between the integration limits. The symbols  $d\xi$ ,  $d\eta$ , and  $d\zeta$  should be thought of as simply an indication of what the independent variables are.

$$\tilde{v}_i(\mathbf{r}, t) = \frac{1}{\Delta^3} \int_{x-\frac{1}{2}\Delta x}^{x+\frac{1}{2}\Delta x} \int_{y-\frac{1}{2}\Delta y}^{y+\frac{1}{2}\Delta y} \int_{z-\frac{1}{2}\Delta z}^{z+\frac{1}{2}\Delta z} v_i(\boldsymbol{\xi}, t) d\xi d\eta d\zeta \quad (1.486)$$

The quantity  $\tilde{v}_i$  denotes the *resolvable-scale filtered velocity*.

For finite difference and finite volume discretizations using the box filter, the *filter width*,  $\Delta$ , yields:

$$\Delta = h = (\Delta x \Delta y \Delta z)^{\frac{1}{3}} \quad (1.487)$$

To fully understand this concept of filtering, note that the values of flow properties at discrete points in a numerical simulation represent averaged values. To illustrate this explicitly, Rogallo and Moin [133] considered the central difference approximation for the first derivative of a continuous variable,  $v(x)$ , in a grid with points spaced a distance  $h$  apart. We can write this as follows (e.g., [133], p. 103 [186], p 323):

$$\frac{d\tilde{v}}{dx} \approx \frac{\tilde{v}(x+h) - \tilde{v}(x-h)}{2h} = \frac{d}{dx} \left[ \frac{1}{2h} \int_{x-h}^{x+h} v(\xi) d\xi \right] \quad (1.488)$$

This shows that the central-difference approximation can be thought of as an operator that filters out scales smaller than the mesh size. Furthermore, the approximation yields the derivative of an averaged value of  $\tilde{v}(x)$ .

In practice, the Leonard stress is often dominated by the numerical errors inherent in the finite difference (and finite volume) representation and is thus neglected or lumped into the deviatoric stress tensor (e.g., [97] [106] [186], p. 325). Consequently, as the box filter is applied to the Navier-Stokes equation, the residual stresses assume the form of sub-grid scale stresses:

$$\tilde{\boldsymbol{\sigma}}_{ij}^R = \widetilde{v_i v_j} - \tilde{v}_i \tilde{v}_j = (\widetilde{v_i v_j} - \tilde{v}_i \tilde{v}_j) + (\widetilde{v_i v_j'} + v_i' \tilde{v}_j) + \widetilde{v_i' v_j'} = \tilde{L}_{ij} + \tilde{C}_{ij} + \tilde{R}_{ij} \approx \tilde{C}_{ij} + \tilde{R}_{ij} \quad (1.489)$$

These stresses are similar to the classical Reynolds stresses that result from time or ensemble averaging of the advection fluxes, but differ in that they are consequences of a spatial averaging and go to zero if the filter width  $\Delta$  goes to zero.

For LES performed in physical space, the basic sub-grid stress model is the eddy-viscosity model proposed by Smagorinsky<sup>45</sup>. The Smagorinsky model is based on the gradient transport hypothesis and the sub-grid viscosity concept, just as the Reynolds stress models based on the Boussinesq eddy viscosity hypothesis, and expressed as:

$$\tilde{\boldsymbol{\sigma}}_{ij}^R = -2\nu_{SGS,t} \tilde{S}_{ij} + \frac{\delta_{ij}}{3} (\tilde{C}_{kk} + \tilde{R}_{kk}) \quad (1.490)$$

<sup>45</sup> The original idea of performing LES is due to Smagorinsky [150], who applied the technique to shear flows calculating the general circulation of the atmosphere on a finite difference grid and represented the drain of energy to turbulent scales smaller than the grid spacing  $h$  (i.e., the *sub-grid scales*) by a sub-grid model based on the effective viscosity hypothesis.

The model is based on the assumption of proportionality between the anisotropic part of the SGS-stress tensor,  $\tilde{\sigma}_{ij}^d = \tilde{\sigma}_{ij}^R - \frac{\delta_{ij}}{3}(\tilde{C}_{kk} + \tilde{R}_{kk})$ , and the large scale strain-rate tensor,  $\tilde{S}_{ij}$ . Hence,

$$\tilde{\sigma}_{ij}^d = -2\nu_{SGS,t}\tilde{S}_{ij} \quad (1.491)$$

where  $\tilde{\sigma}_{ij}^d$  denotes the deviator of  $\tilde{\sigma}_{ij}^R$ . This deviatoric tensor is necessary since the residual stress model being proportional to the large scale strain-rate tensor has a zero trace, thus we can only model a tensor that also has a zero trace.

Leonard [97] defined the complementary tensor,  $\frac{\delta_{ij}}{3}(\tilde{C}_{kk} + \tilde{R}_{kk})$ , and suggested that this term can be added to the filtered pressure,  $\tilde{p} + \frac{\delta_{ij}}{3}(\tilde{C}_{kk} + \tilde{R}_{kk})$ . In this way the complementary tensor requires no modeling. Analogous to the average turbulent kinetic energy quantity, one can also define a sub-grid scale kinetic energy variable,  $k_{SGS} = \frac{1}{2}(\tilde{C}_{ii} + \tilde{R}_{ii})$ . Hence, the anisotropic SGS tensor is given by  $\tilde{\sigma}_{ij}^d = \tilde{\sigma}_{ij}^R - \frac{2}{3}k_{SGS}\delta_{ij}$ .

Thereafter, the closure consists in determining the SGS eddy viscosity parameter. By analogy to the mixing length hypothesis, the Smagorinsky [150] model is defined as:

$$\nu_{SGS,t} = l_S^2 \tilde{S} \approx (C_S \Delta)^2 \tilde{S} \quad (1.492)$$

where  $\tilde{S} \approx (2\tilde{S}_{ij}\tilde{S}_{ij})^{1/2}$  is the characteristic filter rate of strain,  $\tilde{S}_{ij} = \frac{1}{2}(\frac{\partial v_i}{\partial x_j} + \frac{\partial v_j}{\partial x_i})$ ,  $C_S$  denotes the Smagorinsky constant,  $l_S$  denotes the Smagorinsky lengthscale (analogous to the mixing length), and the generalized filter width  $\Delta$  is a characteristic length scale of the resolved eddies (e.g., [150] [133] [106] [98] [186] [121], chap 13). Recall that in the present case,  $\Delta$  is proportional to the grid spacing,  $h$ .

If the grid scale  $h$  is close to the scale of the most energetic motions, such a simulation is called a *very large eddy simulation* (VLES) [128]. In LES, the filtered velocity field accounts for the bulk (say 80 %) of the turbulent kinetic energy everywhere in the flow field ([121], chap 13). In VLES the grid and filter are too large to resolve the energy-containing motions, and instead a substantial fraction of the energy resides in the residual motions. A VLES thus demands for more accurate sub-grid scale models than a LES in which the sub-grid scale fluxes and variances are small. Accurate modeling of the fluxes itself is necessary only where the sub-grid scales fluxes get large in comparison to the resolved fluxes. However, such a VLES may still be more accurate than a turbulence model which aims to describe all scales of motion together in one model [143].

Some workers reserve the term LES for the case where the filter scale  $\Delta$  corresponds to a wavenumber in the  $k^{-5/3}$  inertial range, and the term VLES when the residual field begins before the inertial range [128]. The reason for

this filter scale limit of subdivision between LES and VLES stems from the derivation of the Smagorinsky constant. Basically, the early LES models were constructed assuming that turbulence at the sub-grid scales corresponds to the Kolmogorov [83] inertial range of turbulence [101]. In particular, adopting the five-third law valid at these scales theoretical values for the Smagorinsky constant can be derived (e.g., [101] [137] [121]). For a coarser filter width, as those adopted in VLES, the assumption that the sub-grid scales corresponds to the inertial range of turbulence is significantly violated and the micro eddy movement is far from being isotropic and is not sufficiently independent of the macro eddy movement. Therefore, in VLES no analytical estimate of the Smagorinsky constant exists.

However, apparently the value of  $C_S$  is not universal in LES either. In practice,  $C_S$  is adjusted to optimize the model results. Deardorff [28] [29] quoted several values of  $C_S$  based on Lilly's estimates. The exact value chosen depends on various factors like the filter used, the numerical method used, resolution, and so forth, but they are generally of the order of  $C_S = 0.2$ . However, from comparison with experimental results, Deardorff concluded that the constant in the Smagorinsky effective viscosity model should be smaller than this, and a value of about  $C_S = 0.10$  was used. In addition, for the case of an anisotropic resolution (i.e., having different grid width  $\Delta x$ ,  $\Delta y$  and  $\Delta z$  in the different co-ordinate directions), the geometry of the resolution has to be accounted for.

Like all other models, LES requires the specification of proper boundary and initial conditions in order to fully determine the system and obtain a mathematically well-posed problem. However, this concept deviates from the more familiar average models in that the boundary conditions apparently represent the whole fluid domain beyond the computational domain. Therefore, to specify the solution completely, these conditions must apply to all of the space-time modes it comprises.

For 3D simulations of chemical reactors we generally need to specify inlet-, outlet - and wall boundary conditions. In such wall bounded flows the finest grid resolution is determined by the flow near walls where most of the turbulence energy production occurs. For industrial reactor simulations it is thus desirable to avoid the high cost of resolving the wall boundary layer by adopting the statistically average wall function approach based on the logarithmic law of the wall in line with the work of Deardorff [27], Schumann [140] and Moin and Kim [110]. The boundary conditions normally used in practical LES applications are neatly examined by Sagaut [137] and Pope [121]. It is noticed that the structure of the boundary layer flow has certain characteristics that require special treatment in LES [137]. That is, experimental and numerical investigations have revealed important dynamic processes within the boundary layer (e.g., anisotropic and intermittent bursting events, quasi-longitudinal and arch structures, etc.) that induce strong variations in the Reynolds stresses, and in the production and dissipation of the turbulent kinetic energy. Resolving these near wall dynamics directly is still not feasible,

and the existing sub-grid wall models are not sufficiently accurate. Another severe difficulty occurs at the reactor outlet boundary. Unfortunately, at such open boundaries the flow variables depend on the unknown flow outside the domain. However, this issue is not specific to LES, but constitutes a problem for most reactor simulations. The specification of accurate inlet conditions may also be a problem, since the flow upstream of the computational domain is usually not known in sufficient details (i.e., recall that we need to specify the space-time modes). In addition, the influence of the upstream conditions may persist for large distances downstream. Apparently, it is generally not clear how to specify suitable boundary conditions performing reactor LES analysis.

In an ideal single phase reactor flow situation a LES simulation could be initiated as a laminar flow, and by gradually increasing the inlet velocity the flow will evolve to a sufficiently high Reynolds number laminar flow. Then, by any physical disturbance the flow will sustain these instabilities and a flow regime transition from laminar to turbulent flow will take place. In a numerical simulation the necessary sustainable instabilities required for the flow regime transition to occur are caused by numerical instabilities normally emerging after a relatively long simulation time period. Of course, it is also possible that these numerical instabilities might grow or sustain as a pure numerical mode and do not represent physical turbulence so a proper validation procedure is necessary. To reduce the simulation time for the initial stage of the flow calculation obtaining fully turbulent flows, forced perturbations are commonly added to make the flow unstable and then evolving to become turbulent if the Reynolds number is sufficiently large. That is, it might not be necessary to add such perturbations deliberately as it is very difficult to specify consistent 3D fields for all the physical quantities involved to initialize the calculation. In practice, using inaccurate initial conditions, the flow develops neatly becoming fully turbulent but the higher order statistics might be physically realistic only after a certain adjustment period [133].

Applying LES the numerical resolution used is crucial achieving sufficiently accurate solutions. Schumann [143] stated that the size of the calculation domain should be large in comparison to the scale of the most energetic eddies. A reason for this requirement is that in LES the resolution requirements are determined directly by the range of scales contributing to the desired statistics and indirectly by the accuracy of the model [133]. The less accurate the model, the further the model scales must be separated from the scales of interest. This requirement may represent a problem in reactor simulations as the largest eddies are comparable to the reactor dimensions. Accordingly, if the size of the calculation domain adopted is too small we may neither get sufficient data for reliable statistics. Another numerical resolution requirement is that the scale  $h$  has to be much smaller than the scale of the large eddies. In VLES the grid scale  $h$  may be close to the most energetic motions but still smaller.

Validating LES, comparing the model predictions with experimental results, is also crucial. One must then ensure that the filtered experimental statistics are compared with the corresponding statistics of the filtered field.

Alternatively, one can compare the total field statistics from the simulation with the corresponding experimental data [128].

Progress in LES has taken place in various directions. Seeking more accurate models it might be natural to incorporate non-local effects through transport equations for the residual stresses and other quantities related to the residual motions. These LES model closures parallel the conventional turbulence modeling of Reynolds averaged closures. We have already stated that the Smagorinsky model is deduced from the mixing-length model. Moreover, transport equation models analogous to one-equation models, Reynolds stress models and PDF models have been proposed [121]. The most important difference between the two concepts is that in LES the filter width  $\Delta$  is taken as the characteristic lengthscale of the residual motions, so that no equation is needed for the turbulent length scale (analogous to the model equation for  $\varepsilon$ ). The most sophisticated SGS model used so far (i.e., counting the number of PDEs) was designed by Deardorff [30] for application to the atmospheric boundary layer. The model consists of 10 partial differential equations and bears a strong resemblance to a second-order closure model (a Reynolds Stress Model, RSM). In this particular model the dissipation rate is taken to be isotropic, hence the instantaneous dissipation rate  $\varepsilon_{SGS}$  of the residual or sub-grid scale kinetic energy ( $k_{SGS} = \frac{1}{2}\tilde{\sigma}_{ii}^R$ ) is related to  $k_{SGS}$  and the filter width by:

$$\varepsilon_{SGS} = \frac{C_E k_{SGS}^{3/2}}{\Delta} \quad (1.493)$$

where  $C_E = 0.7$ .

While the model apparently leads to improved predictions, its complexity has discouraged many researchers. Therefore, in a later study Deardorff [31] reverted to an isotropic eddy-viscosity model in order to decrease the computational costs. In the latter model version an additional equation was used to determine the residual kinetic energy, as the eddy viscosity  $\nu_{SGS}$  was expressed by:

$$\nu_{SGS} = C_\nu k_{SGS}^{1/2} \Delta \quad (1.494)$$

where  $C_\nu \approx 0.10$ .

Using the latter two relations we may also approximate the residual dissipation rate, e.g., in terms of the residual viscosity determined by other LES closures, in case this parameter is needed for reactor modeling purposes like in population balance kernels and in species mixing model parameterizations provided that the overall closure models remain consistent [21].

Germano et al. [56] and Germano [57] have devised a new concept that they describe as a *Dynamic SGS Model*. Their formulation is also based on the Smagorinsky eddy-viscosity approximation. However, rather than fixing the value of  $C_S$  a priori, they permit it to be computed as the LES proceeds. This is accomplished by using two filters.

A few rather preliminary attempts at performing LES describing turbulent reactive flows have also been reported (e.g., [142] [120]). For the study

of chemical processes within the atmospheric boundary layer zero-equation models are usually adopted for the mass fluxes. The variances are generally neglected. Moin et al [111] and Erlebacher et al. [44] pushed the frontiers of LES research into compressible flows. They derived a compressible flow SGS model and exercised it in computation of compressible isotropic turbulence. The main difference between incompressible and compressible flow formulations is that, instead of spatial filtering, it is customary to introduce mass weighted or Favre filtering,  $\tilde{f}^\rho = \tilde{\rho}f/\tilde{\rho}$ , in the latter case (e.g., [53]). The Favre-filtered SGS-stresses and the heat flux are then,  $\tilde{\tau}_{ij} = \tilde{\rho}(\tilde{v}_i\tilde{v}_j - \tilde{v}_i\tilde{v}_j)$  and  $\tilde{Q}_k = c_P\tilde{\rho}(\tilde{v}_k\tilde{T} - \tilde{v}_k\tilde{T})$ , where  $T$  is the temperature and  $c_P$  is the specific heat at constant pressure. The results presented are apparently in excellent agreement with DNS results. McComb [106] classified the various LES runs which have been carried out so far as, in effect, tests for sub-grid models. It was noted that variations from one simulation to another, in terms of choice of filter, filter width, grid resolution, and other numerical factors, can easily obscure differences between sub-grid models. Based on an evaluation of several investigations which have been performed specifically aiming at testing sub-grid models, the overall conclusion was that the Smagorinsky model predicts reasonable results and that the various modifications to it have little net effect on the actual LES. It was, however, indicated that when formulating the sub-grid models for LES, as for any constitutive equations, attention have to be drawn to the need to chose sub-grid models in such a way that the equation of motion for the large eddies is invariant under Galilean transformations. This simple requirement may lead to improved sub-grid models. Nevertheless, numerical aliasing errors can violate these invariance properties and lead to nonlinear numerical instabilities [133].

In conclusion, for chemical reactor simulations LES holds promise as a future design tool, especially as computers continue to increase in speed and memory. Basically, it turns out that the VLES approach performs well essentially due to the fine numerical grid resolution used thus an explicit SGS model is of minor importance. The approach is thus very appealing, as the tedious work fitting the turbulence closure to experimental data might be avoided. Apparently, the closure complexity represented by the Smagorinsky model seems sufficient for chemical reactor LES analyzes. Defining proper boundary conditions are presently more demanding.

---

## References

1. Andersson HI (1988) Introduction to Turbulence Modeling. Lecture Notes in Subject 76572 Turbulent Flow, Norwegian Institute of Technology, Trondheim
2. Anderson JD Jr (1995) Computational Fluid Dynamics: The Basics with Applications. McGraw-Hill, Inc., New York
3. Aris R (1962) Vectors, Tensors, and the Basic Equations of Fluid Mechanics. Dover, Inc., New York
4. Baerns M, Hofmann H, Renken A (1987) Chemische Reaktionstechnik. Georg Thieme Verlag Stuttgart, New York
5. Baldyga J, Bourne JR (1999) Turbulent Mixing and Chemical Reactions. John Wiley & Sons, Chichester
6. Banerjee S, Chan AMC (1980) Separated Flow Models-I: Analysis of the Averaged and Local Instantaneous Formulations. Int J Multiphase Flow 6:1-24
7. Barrow GM (1979) Physical Chemistry. Fourth Edition, McGraw-Hill International book Company, Auckland
8. Batchelor GK (1982) The Theory of Homogeneous Turbulence. Cambridge University Press, Cambridge
9. Bendiksen K, Malnes D, Moe R and Nuland S (1991) The dynamic two-fluid model OLGA: Theory and applications. SPE Production Engineers, pp. 171-180
10. Bird RB (1957) The equations of change and the macroscopic mass, momentum, and energy balances. Chem Eng Sci 6:123-181
11. Bird RB, Stewart WE, Lightfoot EN (1960) Transport phenomena. John Wiley & Sons, New York
12. Bird RB, Armstrong RC, Hassager O (1987) Dynamics of polymeric liquids. Volume 1, Fluid mechanics. John Wiley & Sons, New York
13. Bird RB, Stewart WE, Lightfoot EN (2002) Transport phenomena. Second Edition, John Wiley & Sons, New York
14. Birkhoff G (1964) Averaged Conservation Laws in Pipes. Journal of Mathematical Analysis and Applications 8:66-77
15. Biswas G, Eswaran V (2002) Turbulent Flows, Fundamentals, Experiments and Modeling. Alpha Science International Ltd., Pangbourne, England
16. Boris JP, Grinstein FF, Oran ES, Kolbe RL (1992) New insights into large eddy simulation. Fluid Dyn Res 10:199-228

17. Borisenko AI, Talapov IE (1979) *Vectors and Tensor Analysis*. Dover Publications Inc., New York
18. Boucher DF, Alves GE (1959) Dimensionless Numbers for Fluid Mechanics, Heat Transfer, Mass Transfer and Chemical Reaction. *Chemical Engineering Progress* 55(9):55-64
19. Boussinesq J (1877) Essai sur la théorie des eaux courants. Mèm près par div savants à l'Acad Sci, Paris 23(1):1-680
20. Boussinesq J (1897) Théorie de l'écoulement tourbillonnant et tumultueux des liquides dans les lits rectilignes à grande section I-II. Gauthier-Villars, Paris
21. Bove S (2005) *Computational Fluid Dynamics of Gas-Liquid Flows including Bubble Population Balances*. PhD Thesis, Aalborg University, Esbjerg
22. Businger JA, Wyngaard JC, Izumi Y, Bradley EF (1971) Flux profile relationships in the atmospheric surface layer. *J Atmos Sci* 28:181-189
23. Chou PY (1945) On Velocity Correlations and the solutions of the equations of turbulent fluctuation. *Quarterly of Applied Mathematics* 3:38-54
24. Corrsin S (1974) Limitations of Gradient Transport Models in Random Walks and in Turbulence. In: Landsberg HE, van Mieghem J (eds) *Advances in geophysics*, Academic Press, New York, 18A
25. Crowe CT, Sommerfeld M, Tsuji Y (1998) *Multiphase Flows with Droplets and Particles*. CRC Press, Boca Raton.
26. Danckwerts PV (1953) Continuous flow systems: Distribution of Residence Times. *Chem Eng Sci* 2(1):1-18
27. Deardorff JW (1970) A numerical study of three-dimensional turbulent channel flow at large Reynolds numbers. *J Fluid Mech Part 2* 41:453-480
28. Deardorff JW (1971) On the magnitude of the subgrid scale eddy coefficient. *J Comput Phys* 7(1):120-133
29. Deardorff JW (1972) Numerical Investigation of Neutral and Unstable Planetary Boundary Layers. *Journal of the Atmospheric Science* 29:91-115
30. Deardorff JW (1973) The Use of Subgrid Transport Equations in a Three-Dimensional Model of Atmospheric Turbulence. *Journal of Fluids Engineering (Transactions of the ASME)*, pp. 429-438
31. Deardorff JW (1980) Stratocumulus-capped mixed layers derived from a three-dimensional model. *Boundary-Layer Meteorol* 18:495-527
32. de Groot SR, Mazur P (1962) *Non-Equilibrium Thermodynamics*. North-Holland, Amsterdam
33. Delhaye JM, Achard JL (1977) On the averaging operators introduced in two-phase flow. In: Banerjee S, Weaver JR (eds) *Transient Two-phase Flow*. Proc. CSNI Specialists Meeting, Toronto, 3.-4. august
34. Delhaye JM (1977) Instantaneous space-averaged equations. In: Kakac S, Mayinger F *Two-Phase Flows and Heat Transfer*. Vol. 1, pp. 81-90, Hemisphere, Washington, DC
35. Delhaye JM, Achard JL (1978) On the use of averaging operators in two phase flow modeling: Thermal and Aspects of Nuclear Reactor Safty, 1: Light Water Reactors. ASME Winter Meeting
36. Donea J, Giuliani S, Halleux JP (1982) An Arbitrary Lagrangian-Eulerian Finite Element Method for Transient Dynamic Fluid-Structure Interactions. *Computer Methods in Applied Mechanics and Engineering* 33:689-723
37. Donea J, Huerta A, Ponthot JP, Rodríguez-Ferran A (2004) *Arbitrary Lagrangian-Eulerian Methods*. Encyclopedia of Computational Mechanics.

- Stein E, de Borst R, Hughes JR (eds), Volume 1: Fundamentals. John Wiley & Sons, Ltd (ISBN:0-470-84699-2)
38. Drazin PG, Reid WH (1981) *Hydrodynamic Stability*. Cambridge University Press, Cambridge
  39. Drew DA (1983) *Mathematical Modeling of Two-Phase Flow*. *Ann Rev Fluid Mech* 15:261-291
  40. Dryden HL (1943) A review of the statistical theory of turbulence. *Quart Appl Math* 1:7-42
  41. Dyer AJ (1974) A review of flux-profile relations. *Bound Layer Meteor* 1: 363-372
  42. Elliott JR, Lira CT (1999) *Introductory Chemical Engineering Thermodynamics*. Prentice Hall PTR, Upper Saddle River
  43. Enwald H, Peirano E, Almstedt AE (1996) Eulerian Two-Phase Flow Theory Applied to Fluidization. *Int J Multiphase Flow* 22:21-66, Suppl.
  44. Erlebacher G, Hussaini MY, Speziale CG, Zang TA (1992) Towards the Large-Eddy Simulation of Compressible Turbulent Flows. *J Fluid Mech* 238:155-185
  45. Ferziger JH (1977) Large Eddy Numerical Simulation of Turbulent Flows. *AIAA J* 15(9):1261-1267
  46. Ferziger JH, Leslie DC (1979) *Large Eddy Simulation: A Predictive Approach to Turbulent Flow Computation*. American Institute of Aeronautics and Astronautics, Inc., paper A79-45272
  47. Fogler H Scott (1992) *Elements of Chemical Reaction Engineering*. Second Edition, Prentice-Hall International, Inc., New Jersey
  48. Fogler H Scott (2006) *Elements of Chemical Reaction Engineering*. Fourth Edition, Prentice-Hall International, Inc., New Jersey
  49. Fox RO (1996) *Computational Methods for Turbulent Reacting Flows in the Chemical Process Industry*. *Revue De L'Institut Francais Du Petrole* 51(2): 215-243
  50. Fox RO (2003) *Computational Models for Turbulent Reacting Flows*. Cambridge University Press, Cambridge
  51. Friedlander SK, Topper L (1961) *Turbulence: Classic papers on statistical theory*. Friedlander SK, Topper L (eds), Interscience Publishers, Inc., New York
  52. Froment GF, Bischoff KB (1990) *Chemical Reactor Analysis and Design*. John Wiley and Sons, New York
  53. Galperin B, Orszag SA (1993) *Large Eddy Simulation of Complex Engineering and Geophysical Flows*. Cambridge University Press, Cambridge
  54. Gaskell DR (2003) *Introduction to the Thermodynamics of Materials*. Fourth Edition, Taylor & Francis, New York
  55. Geankoplis CJ (1993) *Transport Processes and Unit Operations*. Third edition, PTR Prentice Hall International Editions, Englewood Cliffs
  56. Germano M, Piomelli U, Moin P, Cabot WH (1991) A dynamic subgrid-scale eddy viscosity model. *Phys Fluids* A3:1760-1765
  57. Germano M (1992) Turbulence: The filtering approach. *J Fluid Mech* 238: 325-336
  58. Gidaspow D (1994) *Multiphase Flow and Fluidization-Continuum and Kinetic Theory Descriptions*. Academic Press, Harcourt Brace & Company, Publishers, Boston
  59. Gosman AD, Pun WM, Runchal AK, Spalding DB, Wolfshtein M (1969) *Heat and Mass Transfer in Recirculating Flows*. Academic Press, London and New York

60. Gosman AD, Launder BE, Reece GJ (1985) *Computer-Aided Engineering Heat Transfer and Fluid Flow*. John Wiley & Sons, New York
61. Hanjalic K, Launder BE (1972) A Reynolds Stress Model of Turbulence and its Application to Thin Shear Flows. *J Fluid Mech Part 4* 52:609-638
62. Harlow FH, Nakayama I (1967) Turbulence Transport Equations. *The Physics of Fluids* 10(11):2323-2332
63. Harlow FH, Nakayama I (1968) Transport of Turbulence Energy Decay Rate. Los Alamos National Laboratory Report, LA-3854
64. Hayes RE (2001) *Introduction to Chemical Reactor Analysis*. Gordon and Breach Science Publishers, Australia
65. Herring JR (1979) Subgrid Scale Modeling - An Introduction and Overview. *Turb Shear Flows* 1:347-352
66. Hinze JO (1975) *Turbulence*. Second Edition, McGraw-Hill, New York
67. Hirschfelder JO, Curtiss CF, Bird RB (1954) *Molecular Theory of Gases and Liquids*. John Wiley & Sons, Inc., New York
68. Hirt CW, Amsden AA, Cook JL (1974) An Arbitrary Lagrangian-Eulerian Computing Method for All Flow Speeds. *J Comput Phys* 14:227-253
69. Hoff KA, Poplsteinova J, Jakobsen HA, Falk-Pedersen O, Juliussen O, Svendsen HF (2003) Modeling of Membrane Reactor. *International Journal of Chemical Reactor Engineering* 1:1-12, Article A9, (<http://www.bepress.com/ijcre/vol1/articles.html>)
70. Hussain AKMF (1983) Coherent Structures - reality and myth. *Physics of Fluids* 26:2816-2850
71. Hussain AKMF (1986) Coherent Structures and Turbulence. *J Fluid Mech* 173:303-356
72. Incropera FP, DeWitt DP (2002) *Fundamentals of Heat and Mass Transfer*. Fifth Edition, John Wiley & Son, New York
73. Ishii M (1975) *Thermo-Fluid Dynamic Theory of Two-Phase Flow*. Eyrolles, Paris
74. Ishii M, Mishima K (1984) Two-Fluid Model and hydrodynamic Constitutive Equations. *Nuclear Engineering and Design* 82:107-126
75. Jakobsen HA, Berge E, Iversen T, Skaalin R (1995) Status of the development of the multi-layer Eulerian model. a) Model description. b) A new method for calculating mixing heights. c) Model results for sulphur transport in Europe for 1992 in the 50 km grid. EMEP/MSC-W Note No. 3/95. Research Report No. 21, The Norwegian Meteorological Institute (DNMI), Oslo, Norway
76. Jakobsen HA (2001) Phase Distribution Phenomena in Two-Phase Bubble Column Reactors. *Chem Eng Sci* 56(3):1049-1056
77. Jakobsen HA, Lindborg H, Handeland V (2002) A numerical study of the interactions between viscous flow, transport and kinetics in fixed bed reactors. *Computers and Chemical Engineering* 26:333-357
78. Jones WP, Launder BE (1972) The Prediction of Laminarization with a Two-Equation Model of Turbulence. *Int J Heat Mass Transfer* 15:301-314
79. Jones WP (1980) Models for Turbulent Flows with Variable Density and Combustion. In: Kollman W (ed) *Prediction Methods for Turbulent Flow*, Hemisphere Publishing Company
80. Keller LV, Friedman AA (1924) "Differentialgleichung für die turbulente Bewegung einer kompressiblen Flüssigkeit". *Proc 1st Intern Congr Appl Mech Delft*, pp. 395-405

81. Kjelstrup S, Bedeaux D (2001) Elements of irreversible thermodynamics for engineers. International Centre for Applied Thermodynamics, (ISBN: 975-97568-1-1), Istanbul
82. Kolev NI (2002) Multiphase Flow Dynamics 1, Fundamentals. Springer, Berlin
83. Kolmogorov AN (1941) The local structure of turbulence in incompressible viscous fluid for very large Reynolds numbers. Dokl Akad Nauk SSSR 30(4): 299-303 (in Russian)
84. Kolmogorov AN (1941) Energy dissipation in locally isotropic turbulence. Doklady AN SSSR 32(1):19-21
85. Kolmogorov AN (1942) The equation of turbulent motion in an incompressible fluid. Izvestia Acad Sci USSR Phys 6:56-58
86. Kolmogorov AN (1962) A refinement of previous hypotheses concerning the local structure of turbulence in a viscous incompressible fluid at high Reynolds number. J Fluid Mech 13(1):82-85
87. Kuiken GDC (1995a) Thermodynamics of Irreversible Processes. Applications to Diffusion and Rheology. John Wiley & Sons, Chichester
88. Kuiken GDC (1995) The Symmetry of the Stress Tensor. Ind Eng Chem Res 34:3568-3572
89. Kuo KK (1986) Principles of Combustion. John Wiley & Sons, New York
90. Kyle BG (1999) Chemical and Physical Process Thermodynamics. Third Edition, Prentice Hall PTR, New Jersey
91. Lahey RT Jr, Drew DA (1989) The Three-Dimensional Time-and Volume Averaged Conservation Equations of Two -Phase Flow. Advances in Nuclear Science and Technology 20:1-69
92. Landau LD, Lifschitz EM (1963) Fluid Mechanics. Pergamon Press, London
93. Langlois WE (1964) Slow Viscous Flow. Macmillan, New York
94. Launder BE, Spalding DB (1972) Mathematical Models of Turbulence. Academic Press, London
95. Launder BE, Spalding DB (1974) The Numerical Computation of Turbulent Flows. Computer Methods in Applied Mechanics and Engineering, No. 3, pp. 269-289
96. Launder BE, Sharma BI (1974) Application of the energy-dissipation model of turbulence to the calculation of flow near a spinning disc. Lett Heat Mass Transf 1:131-138
97. Leonard A (1974) Energy Cascade in Large-Eddy Simulations of Turbulent Fluid Flows. Adv Geophys 18A:237-248
98. Lesieur M (1993) Advance and State of the Art on Large-Eddy Simulations. 5th Int Symp on Refined Flow Modeling and Turbulence Measurements, Sep. 7-10, Paris
99. Leslie DC (1982) Simulation Methods for Turbulent Flows. In: Morton KW, Baines MJ (eds) Numerical Methods for Fluid Dynamics, Academic Press, London
100. Libby PA, Bray KNC (1981) Countergradient diffusion in pre-mixed flames. AIAA J 19:205-213
101. Lilly DK (1967) The representation of small-scale turbulence in numerical experiments. In: Proc IBM Scientific Computing Symposium on Environmental Sciences, IBM, White Plains, New York
102. Lydersen AL (1979) Fluid Flow and Heat Transfer. John Wiley & Sons, Chichester

103. Løvland J (2002) Applied Chemical Thermodynamics. Compendium in subject SIK 3035, Part II, Department of Chemical Engineering, The Norwegian University of Science and Technology
104. Malvern LE (1969) Introduction to the Mechanics of a Continuous Medium. Prentice-Hall, Inc., Englewood Cliffs
105. Mason PJ (1989) Large-Eddy Simulation of the Convective Atmospheric Boundary Layer. *J Atm Sci* 46(11):1492-1516
106. McComb WD (1990) The Physics of Fluid Turbulence. Clarendon Press, Oxford
107. Miller CA, Neogi P (1985) Interfacial Phenomena: Equilibrium and Dynamic Effects. Marcel Dekker, Inc., New York and Basel
108. Millikan CB (1938) A critical discussion of turbulent flows in channels and circular tubes. In: Den Hartog JP, Peters H (eds) Proc 5th Int Congr Applied Mechanics, New York, pp. 386-392, Wiley, New York
109. Moeng CH (1984) A Large-Eddy-Simulation Model for the Study of Planetary Boundary-Layer Turbulence. *J Atm Sci* 41(13):2052-2062
110. Moin P, Kim J (1982) Numerical investigation of turbulent channel flow. *J Fluid Mech* 118:341-377
111. Moin P, Squires K, Cabot W, Lee S (1991) A dynamic subgrid-scale model for compressible turbulence and scalar transport. *Phys Fluids* A3(11):2746-2757
112. Monin AS, Yaglom AM (1971) Statistical Fluid Mechanics: Mechanics of Turbulence. Volume 1. English edition updated, augmented and revised by the authors. Edited by John L. Lumley. The MIT Press, Cambridge
113. Monin AS, Yaglom AM (1975) Statistical Fluid Mechanics: Mechanics of Turbulence. Volume 2. English edition updated, augmented and revised by the authors. Edited by John L. Lumley. The MIT Press, Cambridge
114. Munson BR, Young DF, Okiishi TH (2002) Fundamentals of Fluid Mechanics. Fourth Edition, John Wiley & Sons, Inc., New York
115. Najm HN, Wychoff PS, Knio OM (1998) A semi-implicit numerical scheme for reacting flows I: Stiff chemistry. *J Comput Phys* 143:381-402
116. Obukhov AM (1949) Structure of the temperature field in a turbulent flow. *Izv Akad Nauk SSSR Ser Geogr i Geofiz* 13(1):58-69
117. Obukhov AM (1949) Pressure fluctuations in a turbulent flow. *Dokl Akad Nauk SSSR* 66(1):17-20
118. Obukhov AM (1962) Some specific features of atmospheric turbulence. *J Fluid Mech* 13(1):77-81
119. Panton RL (1996) Incompressible Flow. Second Edition, John Wiley & Sons, Inc., New York
120. Petersen AC, Beets C, van Hop H, Duynkerke PG, Siebesma AP (1999) Mass-Flux Characteristics of Reactive Scalars in the Convective Boundary Layer. *J Atm Science* 56:37-56
121. Pope S (2000) Turbulent Flows. Cambridge University Press, Cambridge
122. Prandtl L (1904) Über Flüssigkeitsbewegungen bei sehr kleiner Reibung. Verhandlg III Intern Math Kongr Heidelberg, pp. 484-491
123. Prandtl L (1925) Bericht über Untersuchungen zur ausgebildeten Turbulenz. *Z Angew Math Mech (ZAMM)* 5:136-139
124. Prandtl L (1945) Über ein neues Formelsystem für die ausgebildete Turbulenz. *Nachr Akad Wiss Göttingen Math-Phys* K1:6-19

125. Prausnitz JM, Lichtenthaler RN, de Azevedo EG (1999) *Molecular Thermodynamics of Fluid-Phase Equilibria*. Third Edition, Prentice Hall PTR, New Jersey
126. Reynolds O (1883) An experimental investigation of the circumstances which determine whether the motion of water shall be direct or sinuous, and the law of resistance in parallel channels. *Philos Trans Roy Soc London* A174:935-982
127. Reynolds O (1895) On the dynamical theory of incompressible viscous fluids and the determination of the criterion. *Philos Trans Roy Soc London* A186:123-164
128. Reynolds WC (1990) The Potential and Limitations of Direct and Large Eddy Simulations. In: Lumley JL (ed) *Turbulence at the crossroads*, Springer-Verlag, New York, pp. 313-343
129. Richardson LF (1922) *Weather Prediction by Numerical Process*. Cambridge University Press, Cambridge. An unabridged and unaltered republication of the work first published by Cambridge University Press, London in 1922 was later republished by 'Dover Publication, Inc.' in 1965.
130. Richtmyer RD, Morton KW (1957) *Difference Methods for Initial-Value Problems*. Second Edition, Interscience Publishers (John Wiley & Sons), New York
131. Rodi W (1981) *Turbulence Models and their Applications in Hydraulics*. IAHR/AIHR Monograph
132. Rodi W (1984) *Turbulence Models and Their Application in Hydraulics - A State of the Art Review*. Presented at the IAHR-Section on Fundamentals of Division II: Experimental and Mathematical Fluid Dynamics
133. Rogallo RS, Moin P (1984) Numerical Simulation of Turbulent Flows. *Ann Rev Fluid Mech* 16:99-137
134. Rosner DE (1986) *Transport Processes in Chemically Reacting Flow Systems*. Butterworths, Boston
135. Rouse H, Ince S (1957) *History of Hydraulics*. Iowa Institute of Hydraulic Research, State University of Iowa. Lithoprinted by Edwards Brothers Inc, Ann Arbor, Michigan, USA. Library of Congress Catalog Card Number 57-13474
136. Sabersky RH, Acosta AJ, Hauptmann EG, Gates EM (1999) *Fluid Flow: A First Course in Fluid Mechanics*. Fourth Edition, Prentice Hall, New Jersey
137. Sagaut P (1998) *Large Eddy Simulation for Incompressible Flows: An Introduction*. Springer, Berlin
138. Sandler SI (1999) *Chemical and Engineering Thermodynamics*. Third Edition, John Wiley & Sons, Inc., New York
139. Schlichting H, Gersten K (2000) *Boundary-Layer Theory*. Springer-Verlag, Berlin
140. Schumann U (1975) Subgrid Scale Model for Finite Difference Simulations of Turbulent Flows in Plane Channels and Annuli. *J Comput Phys* 18:376-404
141. Schumann U, Grötzbach G, Kleiser L (1980) Direct numerical simulation of turbulence. In: Kollmann W (ed) *Prediction Methods for Turbulent Flows*, Hemisphere, pp. 123-158
142. Schumann U (1989) Large-Eddy Simulation of the Turbulent Diffusion with Chemical Reactions in the Convective Boundary Layer. *Atmospheric Environment* 23(8):1713-1727
143. Schumann U (1992) Simulations and Parameterizations of Large Eddies in Convective Atmospheric Boundary Layers. In: *Proceedings of a workshop held at the European Centre for Medium-Range Weather Forecasts (ECMWF)*

- on Fine Scale Modelling and the Development of Parameterization Schemes, 16-18 September 1991, ECMWF.
144. Shames IH (1962) *Mechanics of fluids*. McGraw-Hill, New York
  145. Shavit A, Gutfinger C (1995) *Thermodynamics - From Concepts to Applications*. Prentice Hall, London
  146. Sideman S, Pinczewski W (1975) *Turbulent Heat and Mass Transfer at Interfaces: Transport Models and Mechanisms*. In: Gutfinger C (ed) *Topics in Transport Phenomena: bioprocesses, mathematical treatment, mechanisms*. Hemisphere, Washington
  147. Slattery JC (1972) *Momentum, Energy, and Mass Transfer in Continua*. Second Edition, McGraw-Hill Kogakusha, LTD, Tokyo
  148. Slattery JC (1990) *Interfacial Transport Phenomena*. Springer-Verlag, New York
  149. Slattery JC (1999) *Advanced Transport Phenomena*. Cambridge University Press, New York
  150. Smagorinsky J (1963) General Circulation Experiments with the Primitive Equations. *Monthly Weather Review* 91(3):99-164
  151. Smith JM (1981) *Chemical Engineering Kinetics*. Third Edition, McGraw-Hill International Book Company, Auckland
  152. Soo SL (1989) *Particles and Continuum: Multiphase Fluid Dynamics*. Hemisphere Publishing Corporation, New York
  153. Spalding DB (1971) Concentration fluctuations in a round turbulent free jet. *Chem Eng Sci* 26:95-107
  154. Stull RB (1988) *An Introduction to Boundary Layer Meteorology*. Kluwer Academic Publishers, Dordrecht
  155. Tabor M (1989) *Chaos and Integrability in Nonlinear Dynamics*. John Wiley & Sons, New York
  156. Tayebi D, Svendsen HF, Jakobsen HA, Grislingås A (2001) Measurement Techniques and Data Interpretations for Validating CFD Multiphase Reactor Models. *Chem Eng Comm* 186:57-159
  157. Taylor GI (1915) Eddy motion in the atmosphere. *Phil Trans Roy Soc A*215: 1-26
  158. Taylor GI (1921) Diffusion by continuous movements. *Proc London Math Soc, Serie 2*, 20:196-211
  159. Taylor GI (1935) Statistical Theory of Turbulence, I-III. *Proc Roy Soc London A*151(874):421-464
  160. Taylor GI (1935) Statistical Theory of Turbulence, IV. Diffusion in a turbulent air stream. *Proc Roy Soc London A*151(874):465-478
  161. Taylor GI (1935) Distribution of velocity and temperature between concentric rotating cylinders. *Proc Roy Soc London A*151(874):494-512
  162. Taylor GI (1936) Statistical Theory of Turbulence. V. Effect of turbulence on boundary layer. *Proc Roy Soc London A*156(888):307-317
  163. Taylor GI (1937) The Statistical Theory of Isotropic Turbulence. *Journal of the Aeronautical Sciences* 4(8):311-315
  164. Taylor GI (1938) The Spectrum of Turbulence. *Proc. Roy. Soc. London Series A* 164:476-490
  165. Taylor GI (1970) Some early ideas about turbulence. Boeing Symposium on Turbulence, *J Fluid Mech* 41:1-11
  166. Taylor R, Krishna R (1993) *Multicomponent Mass Transfer*. John Wiley & Sons, New York

167. Tennekes H, Lumley JL (1972) *A First Course in Turbulence*. The MIT Press, Cambridge
168. Thompson PA (1972) *Compressible-fluid dynamics*. McGraw-Hill, Inc. New York
169. Toong TY (1983) *Combustion Dynamics: The Dynamics of Chemically Reacting Fluids*. McGraw-Hill Book Company, New York
170. Truesdell C, Toupin R (1960) *The Classical Field Theories*. In: *Handbuch der Physik*, Vol. III, Pt. 1, Springer-Verlag, Berlin
171. Unverdi SO, Tryggvason G (1992) A Front-Tracking Method for Viscous, Incompressible, Multi-Fluid Flows. *J Comput Phys* 100:25-37.
172. Unverdi SO, Tryggvason G (1992) Computations of multi-fluid flows. *Physica D60*:70-83, North-Holland
173. van der Hoven I (1957) Power Spectrum of Horizontal Wind Speed in the Frequency Range From 0.0007 to 900 Cycles per Hour. *Journal of Meteorology* 14:160-164
174. van Driest ER (1956) On turbulent flow near a wall. *J Aero Sci* 23:1007
175. Versteeg HK, Malalasekera W (1995) *An introduction to computational fluid dynamics: The finite volume method*. Addison Wesley Longman Limited, Malaysia
176. Voke PR, Collins MW (1983) Large-Eddy Simulation: Retrospect and Prospect. *PhysicoChemical Hydrodynamics (PCH)* 4(2):119-161
177. von Kàrmàn T (1930) *Mechanische Ähnlichkeit und Turbulenz*. Proc Third Int Congr Applied Mechanics, Stokholm, pp. 85-105
178. von Kàrmàn T (1937) The fundamentals of the statistical theory of turbulence. *J Aeronaut Sci* 4(4):131-138
179. von Kàrmàn T, Howarth L (1938) On the statistical theory of isotropic turbulence. *Proc Roy Soc A164*(917):192-215
180. Wallis GB (1969) *One-dimensional Two-phase Flow*. McGraw-Hill Book Company, New York
181. Welty JR, Wicks CE, Wilson RE, Rorrer G (2001) *Fundamentals of Momentum, Heat, and Mass Transfer*. 4th Edition, John Wiley & Sons, Inc., New York
182. Whitaker S (1968) *Introduction to Fluid Mechanics*. Prentice-Hall, Inc., Englewood Cliffs
183. Whitaker S (1985) A Simple Geometrical Derivation of the Spatial Averaging Theorem. *Chemical Engineering Education*, pp. 18-21 and pp. 50-52
184. White FM (1974) *Viscous Fluid Flow*. McGraw-Hill, New York
185. White FM (1999) *Fluid Mechanics*. Fourth Edition, McGraw-Hill, Inc., New York
186. Wilcox DC (1993) *Turbulence modeling for CFD*. DCW Canada, California
187. Zumdahl SS (1992) *Chemical Principles*. D. C. Heath and Company, Lexington

## Elementary Kinetic Theory of Gases

In this chapter emphasis is placed on the mathematical derivation of the governing equations of fluid dynamics from first principles using the kinetic theory concepts. For dilute gases brief summaries of the Chapman-Enskog theory and the ultra simplified mean free path concept are provided, both shown to be useful methods deriving fundamental closures for the transport coefficients. The extended kinetic theory considering multi-component mixtures is sketched, and three different mass flux formulations are examined. An overview of the Enskog method extending the kinetic theory to denser gases is given, denoting a mathematical fundament for the theory of granular materials.

### 2.1 Introduction

The science of mechanics constitutes a vast number of sub-disciplines commonly considered beyond the scope of the standard chemical engineering education. However, when dealing with kinetic theory-, granular flow- and population balance modeling in chemical reactor engineering, basic knowledge of the principles of mechanics is required. Hence, a very brief but essential overview of the disciplines of mechanics and the necessary prescience on the historical development of kinetic theory are given before the more detailed and mathematical principles of kinetic theory are presented.

*Mechanics* is a branch of physics concerned with the motions of physical bodies and the interacting forces. The science of mechanics is commonly divided into two major disciplines of study called *classical mechanics* and *quantum mechanics*. Classical mechanics, which can be seen as the prime discipline of mechanics, describes the behavior of bodies with forces acting upon them. Quantum mechanics is a relatively modern field of science invented at about 1900. The term classical mechanics normally refers to the motion of relatively large objects, whereas the study of motion at the level of the atom or smaller is the domain of quantum mechanics. Classical mechanics

is commonly divided into *statics* and *dynamics*. Statics deals with bodies at rest, while dynamics deals with bodies in motion. The study of dynamics is sometimes further divided into *kinematics* and *kinetics*. Kinematics denotes the description of motion without regard to its cause, while in kinetics one intends to explain the change in motion as a result of forces. A third and very recent branch of dynamics is *non-linear dynamics and chaos*, which denotes the study of systems in which small changes in a variable may have large effects.

Frequently we also need to describe the behavior of large populations of interacting molecules in solids, gases and liquids, particulate systems, dense suspensions and dispersions. The science of classical mechanics may thus be grouped according to the state of matter being studied, into *solid mechanics* and *fluid mechanics*, both disciplines are often considered sub-disciplines of *continuum mechanics*<sup>1</sup> dealing with continuous matter. Hence, fluid mechanics or *fluid dynamics* denotes the study of the macroscopic physical properties and behavior of fluids. The continuity assumption, however, considers fluids to be continuous. That is, properties such as density, pressure, temperature, and velocity are taken to be well-defined at infinitely small points, and are assumed to vary continuously from one point to another. The discrete, molecular nature of a fluid is ignored. Hence, in many physical sciences this mathematical representation of the system is considered a simplifying engineering approach often useful in engineering practice, but of limited accuracy especially when the system considered doesn't allow sufficient inherent separation of scales. For those problems for which the continuity assumption does not give answers of desired accuracy we may (not always!) obtain better results using more fundamental concepts. *Statistical mechanics*<sup>2</sup> is the application of statistics, which includes mathematical tools for dealing with large populations, to the field of dynamics [33] [97] [83] [84]. Although the nature of each individual element of a system and the interactions between any pair of elements may both be well understood, the large number of elements and possible interactions present an infeasible problem to the investigators who seek to understand the behavior of the system. Statistical mechanics provides a mathematical framework upon which such an understanding may be built.

There have apparently been two parallel developments of the statistical mechanics theory, which are typified by the work of Boltzmann [6] and Gibbs [33]. The main difference between the two approaches lies in the choice of statistical unit [15]. In the method of Boltzmann the statistical unit is the molecule and the statistical ensemble is a large number of molecules constituting a system, thus the system properties are said to be calculated as

---

<sup>1</sup> Continuum mechanics is to a large degree based on the Leonhard Euler (1707-1783) axioms published in his book *Mechanica* in 1736-1737.

<sup>2</sup> The expression *statistical mechanics* was apparently first used in 1902 by Josiah Willard Gibbs in the title of his book *Elementary Principles in statistical Mechanics* [33].

average over a phase space trajectory resembling time average properties [38]. In the method of Gibbs the entire system is taken as a single statistical unit and the statistics are those of an ensemble of such systems, hence the system properties are calculated as averages over a large collection of imaginary systems each of which is an independent replica of the system of interest. The collection of independent systems supposedly spans the assembly of all possible micro-states consistent with the constraints with which the system is characterized macroscopically. The very first steps developing the theory dealing with irreversible processes was principally in accordance with the method of Boltzmann as outlined shortly. In the more modern research in statistical mechanics the method of Gibbs [33] has achieved considerable attention as it can be extended in a relatively simple and general way to the description of irreversible processes.

The discussion on the implications of choosing either of these methods usually goes along the following lines. If the positions and velocities of all the particles in a given system were known at any time, the behavior of the system could be determined by applying the laws of classical and quantum mechanics. This procedure is, of course, not feasible firstly because the actual positions and velocities of the individual particles are not known and secondly because the computational efforts needed calculating the macroscopic properties from the states of the individual particles are prohibitively great taking into consideration the large number of particles commonly present in the systems of interest. Instead, statistical methods are introduced with the object of predicting the most probable behavior of a large collection of particles without actually being concerned with the precise states of the individual particles. For this purpose the most probable particle states or a hypothetical ensemble of systems are considered calculating the macroscopic properties. Therefore, we may loosely say that the main reason for introducing the idea of an ensemble was to make it easier to accomplish averaging in statistical mechanics [51].

However, as the experimental characteristics are usually given as time average properties, the equivalence of the calculation and measurement data may be questionable. The ultimate question is whether the average over the ensemble of systems is the same as the average over an infinite time for a single system. Time averages and micro-canonical ensemble averages are commonly assumed to be identical by the *ergodic hypothesis*<sup>3</sup>.

Statistical mechanics is normally further divided into two branches, one dealing with equilibrium systems, the other with non-equilibrium systems. Equilibrium statistical mechanics is sometimes called *statistical thermodynamics* [70]. *Kinetic theory* of gases is a particular field of non-equilibrium statistical mechanics that focuses on dilute gases which are only slightly removed from equilibrium [28].

---

<sup>3</sup> In this context the *ergodic hypothesis* says that the time average and the average over a statistical ensemble are the same.

The main objective of performing kinetic theory analyzes is to explain physical phenomena that are measurable at the macroscopic level in a gas at- or near equilibrium in terms of the properties of the individual molecules and the intermolecular forces. For instance, one of the original aims of kinetic theory was to explain the experimental form of the ideal gas law from basic principles [65]. The kinetic theory of transport processes determines the transport coefficients (i.e., conductivity, diffusivity, and viscosity) and the mathematical form of the heat, mass and momentum fluxes. Nowadays the kinetic theory of gases originating in statistical mechanics is thus strongly linked with irreversible- or non-equilibrium thermodynamics which is a modern field in thermodynamics describing transport processes in systems that are not in global equilibrium.

In a series of impressive publications, Maxwell [65] [66] [67] [68] provided most of the fundamental concepts constituting the statistical theory recognizing that the molecular motion has a random character. When the molecular motion is random, the absolute molecular velocity cannot be described deterministically in accordance with a physical law so a probabilistic (stochastic) model is required.

Therefore, the conceptual ideas of kinetic theory rely on the assumption that the mean flow, transport and thermodynamic properties of a collection of gas molecules can be obtained from the knowledge of their masses, number density, and a probabilistic velocity distribution function. The gas is thus described in terms of the *distribution function*<sup>4</sup> which contains information of the spatial distributions of molecules, as well as about the molecular velocity distribution, in the system under consideration.

An important introductory result was the Maxwellian velocity distribution function heuristically derived for a gas at equilibrium. It is emphasized that a gas at thermodynamic equilibrium contains no macroscopic gradients, so that the fluid properties like velocity, temperature and density are uniform in space and time. When the gas is out of equilibrium non-uniform spatial distributions of the macroscopic quantities occur, thus additional phenomena arise as a result of the molecular motion. The random movement of molecules from one region to another tend to transport with them the macroscopic properties of the region from which they depart. Therefore, at their destination the molecules find themselves out of equilibrium with the properties of the region in which they arrive. At the continuous macroscopic level the net effect of these molecular transport processes is expressed through the non - equilibrium phenomena of viscosity, heat conduction and diffusion. Nowadays the phrase *transport processes* thus refers to the transport of mass, momentum and energy within a fluid smoothing out the macroscopic gradients in the physical variable fields enabling non-equilibrium systems to approach equilibrium states.

---

<sup>4</sup> The distribution function is sometimes given other names. Chapman [10] [11] and Chapman and Cowling [12], for example, introduced the name *velocity distribution function* which is also frequently used.

Analytical formulas quantifying the transport coefficients have been deduced in several ways, mostly based on the mean free path concept, the Maxwellian moment equations, and the Boltzmann equation. A preliminary theory of transport processes was suggested by Maxwell [65] in which the transport coefficients were determined on the basis of Clausius' empirical mean free path hypothesis<sup>5</sup>. In a subsequent study by Maxwell [66] the equation of transfer for non-equilibrium gases was derived, describing the total rate of change of any mean property of a gas consisting of molecules having certain predefined properties, neatly simplifying the analytical solution. The so-called *Maxwellian molecules* are point centers of force repelling each other with forces which are inversely proportional to the fifth power of their mutual distance. Almost needless to say, the resulting equations of change for the mean variables (or moments of the distribution function), also called *moment equations* or *equations of transfer*, play an important role in kinetic theory [100](p. 319 and p. 346). Based on these equations Maxwell deduced more accurate analytical relationships for the transport coefficients.

A few years later Boltzmann [6] presented the derivation of a more general integro-differential equation which describes the evolution of the distribution function in space and time. Two approximate methods<sup>6</sup> for solving the Boltzmann equation were given independently by Chapman [10] [11] and Enskog [24] [25], leading to the same novel relations for the transport coefficients. In this way the Boltzmann equation provides a more rigorous derivation of Maxwell's formulas quantifying the transport coefficients for a gas of Maxwellian molecules. Another important contribution was the H-theorem showing that the molecular collisions tend to increase entropy in an irreversible manner providing a firm theoretical justification of the second law of thermodynamics which was already accepted at that time<sup>7</sup>.

More or less as a spin-off result of the foregoing analysis determining the transport coefficients, a rigorous procedure deriving the governing equations of fluid dynamics from first principles was established. It is stressed that in classical fluid dynamics the continuum hypothesis is used so that the governing

---

<sup>5</sup> The mean free path is the average distance traveled by a molecule between successive collisions. The concept of mean free path was introduced by Clausius (1822-1888) in 1858 [8].

<sup>6</sup> Note that in 1949 Harold Grad (1923-1986) published an alternative method of solving the Boltzmann equation systematically by expanding the solution into a series of orthogonal polynomials. [36]

<sup>7</sup> The pioneering work in the direction of the second law of thermodynamics is considered to be performed in 1825 by Sadi Carnot investigating the Carnot cycle [51] [40]. Carnot's main theoretical contribution was that he realized that the production of work by a steam engine depends on a flow of heat from a higher temperature to a lower temperature. However, Clausius (1822-1888) was the first that clearly stated the basic ideas of the second law of thermodynamics in 1850 [13] and the mathematical relationship called the *inequality of Clausius* in 1854 [51]. The word *entropy* was coined by Clausius in 1854 [51].

equations of change are derived directly on the macroscopic scales applying the balance principle over a suitable control volume, as described in chap. 1. Thereafter, closure laws are required relating the internal stresses and diffusive transport fluxes of mass and energy (heat) to the gradients of the macroscopic quantities (e.g., Newton's law of viscosity, Fick's law of mass diffusion, and Fourier's law of conduction are commonly adopted). By using these constitutive relationships we also introduce several unknown parameters, the so-called transport coefficients of viscosity, mass diffusivities and thermal conductivity into the governing equations. Unfortunately, fluid dynamics does neither provide any guidelines on how to determine the mathematical form of the constitutive relations nor the values of transport coefficients.

Therefore, a unique application of kinetic theory emerges provided that an approximate solution of the Boltzmann equation is available. In this case particular moments of the distribution function can be obtained multiplying the Boltzmann equation by an invariant function (i.e., successively representing molecular mass, momentum and energy), and thereafter integrating the resulting equation over the whole velocity space. The moments of the distribution function (also called the probability-weighted average functions) represent macroscopic (ensemble) mean quantities like gas velocity, pressure, mass density, temperature and energy. In this way it is possible to derive rigorous equations of change for the evolution of the mean quantities starting out from the Boltzmann equation. The resulting transport equations are recognized as being analogue to the conservation equations of continuum mechanics. In addition, in contrast to the continuum mechanic formulation the ensemble averaged equations obtained from kinetic theory do not contain any unknown coefficients. That is, a particular set of closure laws is established. Alternatively, by comparing the kinetic theory results with the classical fluid dynamic equations, we may verify both the form of the constitutive laws and the values of the transport coefficients.

The kinetic theory of multi-component non-reactive mixtures was first described by Maxwell [65] [67] and Stefan [92] [93] and later thoroughly described by Hirschfelder et al. [39]. Hirschfelder et al. [39] also considers reactive systems. The latest contributions are reviewed by Curtiss and Bird [18] [19].

Basically, the Boltzmann equation is considered valid as long as the density of the gas is sufficiently low and the gas properties are sufficiently uniform in space. Although an exact solution is only achieved for a gas at equilibrium for which the Maxwell velocity distribution is supposed to be valid, one can still obtain approximate solutions for gases near equilibrium states. However, it is evident that the range of densities for which a formal mathematical theory of transport processes can be deduced from Boltzmann's equation is limited to *dilute* gases, since this relation is reflecting an asymptotic formulation valid in the limit of no collisional transfer fluxes and restricted to binary collisions only. Hence, this theory cannot without ad hoc modifications be applied to dense gases and liquids.

Enskog [26] made the first heuristic attempt to extend the kinetic theory of dilute mono-atomic gases to higher density gas systems. Enskog introduced corrections to the Boltzmann equation accounting for the finite size of the colliding molecules (a free volume correction), and that the centers of the two colliding particles are no longer at the same point. These model extensions resulted in a novel flux accounting for the mechanisms of instantaneous momentum and energy transfer over the distance separating the centers of the two colliding molecules. It is later stated that even at moderate densities the collisional transfer fluxes may become significant compared to the kinetic contribution, and they may dominate at slightly higher densities.

Nowadays the standard literature of kinetic theory of dilute gases usually refers to the books of Chapman and Cowling [12], Hirschfelder et al. [39], Huang [40], Reif [83], Present [77], Vincenti and Kruger [100], Ferziger and Kaper [28], Résibois and De Leener [85], Liboff [61], and Cercignani et al. [8]. Additional reviews on classical mechanics, for example the books of Goldstein [35], Arnold [2], McCall [69], Iro [43], and Panat [73], might also be needed deriving the elements of statistical mechanics, and in particular the dynamics of binary collisions. Moreover, the extensions of the elementary kinetic theory to liquid and polymeric liquid systems are examined by Hansen and McDonald [38] and Bird et al [4], respectively. The contents of the this chapter are to a large extent based on these reviews and the pioneering work summarized in this introductory section.

The present chapter is outlined in the following way. First, the elementary concepts of classical mechanics and kinetic theory are introduced. To illustrate the fundamental procedure deriving the governing equations of fluid dynamics from first principles, the Euler- and Navier-Stokes equations are derived for a dilute mono-atomic gas using the principal kinetic theory concepts. However, the mathematical details of the Enskog solution to the Boltzmann equation are outside the scope of this book because of its lengthy contents and complexity. Instead, the much simpler mean free path approach is used determining approximate values for the transport coefficients. In the following section the basic principles extending the mono-atomic equations to multi-component gas systems are outlined, since the multi-component transport equations are of fundamental importance for reactive system analysis. The subsequent section naturally contains an overview examining the multi-component mass diffusion concepts. Finally, Enskog's approach extending the kinetic theory to somewhat denser gases is outlined in the last section.

## 2.2 Elementary Concepts in Classical Mechanics

This section is devoted to a brief summary of the pertinent principles of dynamics and classical statistical mechanics. Hence, it establishes much of the notation used later presenting the kinetic theory concepts.

At the outset it is important to recognize that several mathematical frameworks for the description of dynamic systems are in common use. In this context classical mechanics can be divided into three disciplines denoted by *Newtonian mechanics*, *Lagrangian mechanics* and *Hamiltonian mechanics* reflecting three conceptually different mathematical apparatus of model formulation [35, 52, 2, 61, 38, 95, 60, 4].

### 2.2.1 Newtonian Mechanics

The initial stage in the development of classical mechanics is often referred to as Newtonian mechanics, and is characterized by the mathematical methods invented by Newton<sup>8</sup>, Galileo (the principle of relativity [2]), among others as summarized in further details by Arnold [2], Ferziger and Kaper [28] and Cercignani et al. [8]. The basic concepts of Newtonian mechanics include the use of point masses or particles, which is an object with negligible size with respect to the typical length scales of the system considered [43]. Point masses are thus mathematical points having mass but no structure. The motion of a point particle is characterized by a small number of parameters, i.e., the particle position, mass, and the forces applied to it. For an ensemble of particles the center of mass<sup>9</sup> of a composite object behaves like a point particle. The position of a point particle is defined with respect to an arbitrary point in space, which is called the origin,  $O$ . A point is represented by the position vector  $\mathbf{r}$  from  $O$  to the particle.

Newton's second law relates the mass and velocity of a particle to a vector quantity known as a force. This fundamental law is also referred to as the equation of motion:

---

<sup>8</sup> Although some of the physical ideas of classical mechanics is older than written history, the basic mathematical concepts are based on Isaac Newton's axioms published in his book *Philosophiae Naturalis Principia Mathematica* or *principia* that appeared in 1687. Translating from the original Latin, the three axioms or the laws of motion can be approximately stated [7] (p. 13) :

Law I: *Every body continues in its state of rest, or of uniform motion in a right line, unless it is compelled to change that state by forces impressed on it.*

Law II: *The change of motion is proportional to the motive force impressed; and is made in direction of the right line in which that force is impressed.*

Law III: *To every action there is always opposited an equal reaction: or, the mutual actions of two bodies upon each other are always equal, and directed to contrary parts.*

<sup>9</sup> A vector  $\mathbf{r}_c$  representing the average of the radii vectors of the particles, weighted in portion to their mass as:

$$\mathbf{r}_c = \frac{\sum m_i \mathbf{r}_i}{\sum m_i} = \frac{\sum m_i \mathbf{r}_i}{M} \quad (2.1)$$

defines a point known as the center of mass, or more loosely as the center of gravity. [73], p 11.

$$\frac{d(m\mathbf{c})}{dt} = \mathbf{F} \quad (2.2)$$

where the quantity  $m\mathbf{c}$  is called the momentum.

Given the initial coordinates and momenta of the particles, the particle position and velocity at any later time can in principle be obtained as the solution to Newton's equations of motion. Typically, the mass is constant in time, hence Newton's law can be written in the conventional form:

$$\mathbf{F} = m \frac{d\mathbf{c}}{dt} = m\mathbf{a} = m\dot{\mathbf{c}} = m\ddot{\mathbf{r}} \quad (2.3)$$

Newton used this equation as the basis of mechanics, hence it is sometimes called Newton's equation [2]. Note that Newton's 1. and 3. laws merely emerge as particular simplifications of the 2. law and are thus not explicitly stated.

A particular class of forces, known as conservative forces, can be expressed as the gradient of a scalar potential energy function (or potential) denoted by  $E_p$ :

$$m\ddot{\mathbf{r}} = \mathbf{F} = \nabla E_p(\mathbf{r}) \quad (2.4)$$

It is noticed that Newton's second law of motion forms a set of second order differential equations.

In order to formulate Newton's laws a suitable reference frame has to be chosen, as briefly sketched above. The inertial coordinate systems defined by the Galileo's principle of relativity are at rest or moving with a constant velocity [52]. In classical mechanics Newton's laws are valid in all inertial coordinate systems, since the rate of change of velocity equals the absolute acceleration of the system. Moreover, all coordinate systems in uniform rectilinear motion with respect to an inertial frame are themselves inertial. Strictly speaking Newton's laws are no longer valid if a system undergoes accelerations [37]. However, the Newtonian formulation can be extended for systems with arbitrary relative motion [73]. The modified relations are obtained by establishing the equations of motion in a fixed system and thereafter transforming them into the accelerated system. In the non-inertial frame of reference additional fictitious forces (e.g., Coriolis, centripetal and centrifugal forces) arise to account for the motion which is actually caused by the acceleration of the frame of reference.

Besides, to understand the basic principles of kinetic theory, granular flows and population balances we need to widen our knowledge of classical mechanics. Newton's mathematical formulation of the laws of motion is perhaps the most intuitive point of view considering familiar quantities like mass, force, acceleration, velocity and positions and as such preferred by chemical engineers. However, this framework is inconvenient for mathematical generalizations as required describing the motion of large populations of particles for which it is necessary to take into account the *constraints*<sup>10</sup> that limit the motion of the

<sup>10</sup> If the conditions of constraint can be expressed as equations connecting the coordinates of the particles and the time having the form:

system. In this book we restrict ourselves to holonomic constraints because most of the microscopic world has holonomic constraints.

Two types of difficulties in the solution of mechanical problems are introduced imposing constraints on the system. First, the coordinates of the  $N$  particles,  $\mathbf{r}_i, i = 1, \dots, N$ , are no longer all independent as they are connected by the equations of constraint, hence the set of  $N$  equations determining the motion of the individual particles are no longer independent. Second, interacting forces may be created by the constraints and are thus not known a priori as required in the Newtonian concepts [43]. Therefore, after Newton the field of classical mechanics became more general, mathematical and abstract. In the case of holonomic constraints, the first difficulty is solved by the introduction of *generalized coordinates*. The second difficulty is avoided by re-formulating the original theory of motion and forces in accordance with the Lagrangian and Hamiltonian theoretical formalisms. These two alternative formulations circumvent the concept of force, instead they are referring to other quantities such as energy, generalized coordinates, generalized velocities and generalized momenta for describing mechanical systems.

It is stressed that Lagrangian mechanics and Hamiltonian mechanics are equivalent to Newtonian mechanics, but these re-formulations are more convenient solving complex problems describing the behavior of a system of interacting particles. The main disadvantage of the Newtonian approach is that it is formally tied to the Cartesian coordinate system<sup>11</sup>. The Lagrangian and Hamiltonian formulations are independent of the coordinate system employed. That is, with the Lagrangian formalism one re-formulates the mechanical problem in terms of two scalar functions denoting the kinetic- and potential energy respectively, and this notation can greatly simplify the solution of many problems utilizing possible symmetries in the system in a better way. The Hamiltonian viewpoint is not particularly superior to the Lagrangian one for the direct solution of mechanical problems, but the Hamiltonian framework provides a better basis for theoretical generalizations in many areas of physics. In this context it is emphasized that the Hamiltonian formulation provides much of the language with which statistical mechanics and kinetic theory are constructed.

---


$$f(\mathbf{r}_1, \mathbf{r}_2, \mathbf{r}_1, \dots, t) = 0 \tag{2.5}$$

then the constraints are said to be *holonomic* [35, 73]. The constraints which cannot be expressed in the form of algebraic equations are non-holonomic constraints.

For the readers that are not familiar with the basics of Newtonian mechanics and the concepts of constraints, chap. I of [35] and chaps. 1-4 of [73] may serve as a understandable introduction to the subject.

<sup>11</sup> In principle, Newton regarded both space and time absolute entities, implying that they are the same for everyone [69]. No such frame does exist in nature, so in practice it is usually feasible to set up a coordinate system that comes as close to this idealization as may be required [73, 35, 70].

### 2.2.2 Lagrangian Mechanics

The Lagrange's equations can in general be expressed using either of two types of variational principles. These are called the differential and the integral principles. The latter group of methods is also referred to as the principles of minimum action, since in all these procedures the quantity to be varied has the dimension of an action (= energy  $\times$  time) [37] [2]. As an example we consider the Hamiltonian integral principle<sup>12</sup>, because it is the most general method and especially useful for holonomic systems with forces derivable from particular potentials. In the context of kinetic theory of dilute gases the application of the Lagrangian formulation may be convenient for the solution of scattering problems, i.e., the two-body mutual central force problem as viewed in the center of mass coordinate system [73] [35]. Nevertheless, the derivation of the Lagrangian equations merely serves as an intermediate step examining basic elements of the Hamiltonian formulation.

Considering a mechanical system consisting of a collection of particles which are interacting with each other in accordance with the equations of motion, the state of the system is completely described by the set of all the positions and velocities of the particles. In mechanics the minimum number of *independent parameters* necessary to uniquely determine the location and orientation of any system in physical space is called the number of *degrees of freedom*<sup>13</sup>. These quantities need not be the Cartesian coordinates of the particle, as was the case in Newton's work. Rather, the conditions of the problem may render some other more convenient choice of parameters. Any  $N$  independent parameters  $\mathbf{q} = \{q_1, q_2, \dots, q_N\}$  which completely define the position of a system with  $N$  degrees of freedom are called *generalized coordinates* of the system. The corresponding derivatives  $\dot{\mathbf{q}} = \{\dot{q}_1, \dot{q}_2, \dots, \dot{q}_N\}$  are called *generalized velocities*.

For a system placed in a conservative force field an alternative form of the equations of motion is obtained by introducing a Lagrangian function defined as the difference between the kinetic energy,  $T(\dot{\mathbf{q}}, \mathbf{q})$ , and the potential energy,  $E_p(\mathbf{q}, t)$ :

---

<sup>12</sup> An example of the alternative differential method is the principle of Jean Le Rond d'Alembert (1717-1783). Perspicuous descriptions of the d'Alembert principle and the derivation of the Lagrangian equations are, for example, given by Greiner [37] and Panat [73].

<sup>13</sup> The phrase *degrees of freedom* is not interpreted identically when it is used in the different branches of science. In physics and chemistry, each independent mode in which a particle or system may move or be oriented is one degree of freedom. In mechanical engineering, degrees of freedom describes flexibility of motion. In statistics, the degrees of freedom are the number of parameter values in probability distributions that are free to be varied. In statistical mechanics the number of degrees of freedom a given system has is equal to the minimum number of independent parameters necessary to uniquely determine the location and orientation of the system in physical space.

$$L(\dot{\mathbf{q}}, \mathbf{q}, t) = T(\dot{\mathbf{q}}, \mathbf{q}) - E_p(\mathbf{q}, t) = \frac{1}{2}m\dot{q}^2 - E_p(\mathbf{q}, t) \quad (2.6)$$

It is emphasized that Lagrangian mechanics is the description of a mechanical system in terms of generalized coordinates  $\mathbf{q}$  and generalized velocities  $\dot{\mathbf{q}}$ .

The final task in the Lagrangian procedure is to derive a differential equation for  $L(\mathbf{q}, \dot{\mathbf{q}}, t)$  by use of rather complex variational principles. Briefly stated, we are considering the effect of small excursions along the path of the system. The variation denotes a virtual displacement and the trajectory of an object is derived by finding the path which minimizes the action, a quantity which is the integral of the Lagrangian over time. Just a brief outline of the method is given in this book, because the main aim is to introduce elements of the notation to be used in kinetic theory analysis shortly. Further details on the technique are given elsewhere [52] [35] [61] [95].

The Hamiltonian variational principle states that the motion of the system between two fixed points, denoted by  $(q, t)_1$  and  $(q, t)_2$ , renders the action integral<sup>14</sup>

$$S = \int_{t_1}^{t_2} L(q, \dot{q}, t) dt \quad (2.7)$$

a minimum.

The necessary condition for  $S$  to have a minimum is that the variation of the integral is zero. Hence, the variational principle of least action is written in the form:

$$\delta S = \delta \int_{t_1}^{t_2} L(q, \dot{q}, t) dt = 0 \quad (2.8)$$

where  $\delta$  denotes a variation about the motion of the system.

Employing this concept to obtain a differential equation for  $L(q, \dot{q}, t)$ , which is defined by (2.6), the first variation of the action  $S$  is expressed by:

$$\delta S = \int_{t_1}^{t_2} L(q + \delta q, \dot{q} + \delta \dot{q}, t) dt - \int_{t_1}^{t_2} L(q, \dot{q}, t) dt = 0 \quad (2.9)$$

By expanding the first integral to first order, the variation can be expressed as:

$$\delta S = \int_{t_1}^{t_2} \left( \frac{\partial L}{\partial q} \delta q + \frac{\partial L}{\partial \dot{q}} \frac{d\delta q}{dt} \right) dt \quad (2.10)$$

Reformulating the second term of the integrand in accordance with:

$$\frac{d}{dt} \left( \frac{\partial L}{\partial \dot{q}} \delta q \right) = \frac{\partial L}{\partial \dot{q}} \frac{d\delta q}{dt} + \delta q \frac{d}{dt} \left( \frac{\partial L}{\partial \dot{q}} \right) \quad (2.11)$$

<sup>14</sup> For brevity we drop the vector font on the  $q$ 's and  $\dot{q}$ 's and assume a single degree of freedom.

implies that:

$$\delta S = \left. \frac{\partial L}{\partial \dot{q}} \delta q \right|_{t_1}^{t_2} + \int_{t_1}^{t_2} \left( \frac{\partial L}{\partial q} - \frac{d}{dt} \left( \frac{\partial L}{\partial \dot{q}} \right) \right) \delta q dt \quad (2.12)$$

Hence, the first term on the RHS vanishes, since the end points of the trajectory are held fixed in the variation. The second integral must vanish for any arbitrary, infinitesimal variation  $\delta q$ , hence the integrand is zero. The result is:

$$\frac{d}{dt} \frac{\partial L}{\partial \dot{q}} - \frac{\partial L}{\partial q} = 0 \quad (2.13)$$

The above derivation can be generalized to a system of  $N$  particles, noting that the variation must be effected for each variable independently. Hence, in terms of  $L$  the equations of motion are:

$$\frac{d}{dt} \frac{\partial L}{\partial \dot{q}_i} - \frac{\partial L}{\partial q_i} = 0 \quad i = 1, 2, 3, \dots, N \quad (2.14)$$

This set of equations are the famous Lagrangian equations<sup>15</sup>.

The second term on the LHS denotes the generalized forces defined by:

$$F_i = \frac{\partial L}{\partial q_i} \quad (2.15)$$

It can now be shown that the Lagrangian equations are equivalent to the more familiar Newton's second law of motion. If  $q_i = r_i$ , the generalized coordinates are simply the Cartesian coordinates. Introducing this definition of the generalized coordinates, and the corresponding Lagrangian function (2.6) into the Lagrangian equations of motion (2.14) we get:

$$\frac{d}{dt} (m\dot{q}) = \frac{\partial E_p}{\partial q} \quad (2.16)$$

or, since the gradient of the time independent potential energy field denotes a conservative force [43], the relation can be expressed in terms of a force:

$$m\ddot{q} = F(q, t) \quad (2.17)$$

The resulting relation is identical to the equation obtained in the Newtonian representation (2.3).

Given the Lagrangian for a system of interacting particles, a number of fundamental system properties can be deduced. Among these properties are the basic conservation<sup>16</sup> laws which can be deduced invoking the principle of

<sup>15</sup> The mathematical Lagrangian formalism in classical mechanics was first published in the book *Mécanique Analytique* by Joseph Louis Lagrange in 1788 [90].

<sup>16</sup> During the motion of a mechanical system, the generalized coordinates and generalized velocities which specify the state of the system vary with time. However, a set of functions of these quantities exist whose values remain constant during the motion of the system and depend only on the initial conditions. These functions are referred to as integrals of motion, and the quantities represented by these integrals are said to be conserved [52].

homogeneity of time and space for closed systems that do not interact with any external forces.

In this context examination of the total time derivative of the Lagrangian is informative. The relation can be expressed as:

$$\begin{aligned} \frac{d}{dt}L(\mathbf{q}, \dot{\mathbf{q}}, t) &= \sum_i \frac{\partial L}{\partial q_i} \dot{q}_i + \sum_i \frac{\partial L}{\partial \dot{q}_i} \ddot{q}_i + \frac{\partial L}{\partial t} \\ &= \sum_i \frac{d}{dt} \left( \dot{q}_i \frac{\partial L}{\partial \dot{q}_i} \right) + \frac{\partial L}{\partial t} \end{aligned} \quad (2.18)$$

or, by reorganizing the terms:

$$\sum_i \frac{d}{dt} \left( \dot{q}_i \frac{\partial L}{\partial \dot{q}_i} - L \right) = - \frac{\partial L}{\partial t} \quad (2.19)$$

Several classes of transformations between two frames or coordinate systems leave the Newtonian equation of motion invariant [43] [52]. The invariance of physical systems under translations of the coordinate system is often referred to as the *homogeneity of space*. The analogue invariance under rotations of the coordinate system is named the *isotropy of space*. Translations of the time origin also make the equation of motion remain invariant, this property is called the *homogeneity of time*. By virtue of the homogeneity of time, the Lagrangian of a closed system does not depend explicitly on time. Therefore, using (2.19) with  $L$  as defined by (2.6), it is verified that the energy of the system is conserved, as the quantity:

$$E = \sum_i \dot{q}_i \frac{\partial L}{\partial \dot{q}_i} - L = T + E_p \quad (2.20)$$

remains constant in time during the motion of the system.

In a similar manner the homogeneity in space leads to the law of conservation of linear momentum [52] [43]. In this case  $L$  does not depend explicitly on  $q_i$ , i.e., the coordinate  $q_i$  is said to be cyclic. It can then be seen exploring the Lagrange's equations (2.14) that the quantity  $\partial L / \partial \dot{q}_i$  is constant in time. By use of the Lagrangian definition (2.6), the relationship can be written in terms of more familiar quantities:

$$\frac{\partial L}{\partial \dot{q}_i} = m\dot{q}_i \quad (2.21)$$

It is stated that the momentum  $m\dot{q}_i$  is a constant of the motion, meaning that it is a conserved quantity. This result is, of course, only valid when all the interacting forces are conservative and there are no external forces acting on the system of particles.

Note also that the isotropy of space is the basis for the derivation of the law of conservation of angular momentum [52] [43].

### 2.2.3 Hamiltonian Mechanics

Hamiltonian mechanics<sup>17</sup> is based on the description of mechanical systems in terms of generalized coordinates  $q_i$  and generalized momenta  $p_i$ .

Starting out from Lagrangian mechanics in which the equations of motion are based on generalized coordinates  $q_i$  and the corresponding generalized velocities  $\dot{q}_i$ ,  $(q_i, \dot{q}_i)$ ,  $i = 1, 2, 3, \dots, N$ , the transformation of the problem to the Hamiltonian description can be performed adopting the Legendre's transformation technique. Hence, by replacing the generalized velocity variables  $\dot{q}_i$  with generalized momentum variables  $p_i$ , i.e., the latter quantities are also known as conjugate momenta, it is possible to further exploit the symmetry principles of mechanics. The concepts from Hamiltonian mechanics are pertinent to the phase space treatment of problems in dynamics. The Hamiltonian formulation thus provides the view in which the statistical mechanics and modern kinetic theory are constructed.

We define the Hamiltonian function by the Legendre transform of the Lagrangian function (2.6) [35] [37]:

$$H(\mathbf{p}, \mathbf{q}, t) = \sum_i \dot{q}_i p_i - L(\dot{\mathbf{q}}, \mathbf{q}, t) \quad (2.22)$$

in which  $p_i$  is given by:

$$p_i = \frac{\partial L}{\partial \dot{q}_i} \quad (2.23)$$

Given the Lagrange's equations of motion (2.14) and the Hamiltonian function (2.22), the next task is to derive the Hamiltonian equations of motion for the system. This can be achieved by taking the differential of  $H$  defined by (2.22). Each side of the differential of  $H$  produces a differential expressed as:

$$\begin{aligned} dH(\mathbf{q}, \mathbf{p}, t) &= \sum_i \frac{\partial H}{\partial \dot{q}_i} d\dot{q}_i + \sum_i \frac{\partial H}{\partial p_i} dp_i + \frac{\partial H}{\partial t} dt \\ &= \sum_i \left( p_i - \frac{\partial L}{\partial \dot{q}_i} \right) d\dot{q}_i + \sum_i \dot{q}_i dp_i - \sum_i \left( \frac{d}{dt} \frac{\partial L}{\partial \dot{q}_i} \right) dq_i - \frac{\partial L}{\partial t} dt \end{aligned} \quad (2.24)$$

Substituting the definition of the conjugate momenta (2.23) into (2.24) and matching coefficients,  $\sum_i \left( p_i - \frac{\partial L}{\partial \dot{q}_i} \right) d\dot{q}_i = 0$ , we obtain the equations of motion of Hamiltonian mechanics (i.e., also known as the canonical equations of Hamilton):

<sup>17</sup> Hamiltonian mechanics refers to a mathematical formalism in classical mechanics invented by the Irish mathematician William Rowan Hamilton (1805-1865) during the early 1830's arising from Lagrangian mechanics which was introduced about 50 years earlier by Joseph-Louis Lagrange (1736-1813). The Hamiltonian equations can however be formulated on the basis of a variational principle without recourse to Lagrangian mechanics [95] [2].

$$\dot{p}_i = -\frac{\partial H}{\partial q_i}, \quad (2.25)$$

$$\dot{q}_i = \frac{\partial H}{\partial p_i}, \quad (2.26)$$

An additional relationship of importance for explicitly time-dependent system functions, can be deduced by the same procedure and expressed as:

$$\frac{dL}{dt} = -\frac{\partial H}{\partial t} \quad (2.27)$$

The total time derivative of the Hamiltonian is achieved from (2.24)

$$\frac{dH}{dt} = \frac{\partial H}{\partial t} + \sum_i \frac{\partial H}{\partial q_i} \dot{q}_i + \sum_i \frac{\partial H}{\partial p_i} \dot{p}_i \quad (2.28)$$

Substitution of the Hamiltonian equations shows that the last two terms cancel, and so

$$\frac{dH}{dt} = \frac{\partial H}{\partial t} \quad (2.29)$$

In particular, if the Hamiltonian function does not depend explicitly on time, then

$$\frac{dH}{dt} = 0 \quad (2.30)$$

This means that  $H$  represents a conserved quantity. Eliminating the Lagrangian from (2.22) using (2.20) shows that the Hamiltonian function equals the total energy of the system,  $H = E$ .

It can now be shown that the Hamiltonian equations are equivalent to the more familiar Newton's second law of motion in Newtonian mechanics, adopting a transformation procedure similar to the one used assessing the Lagrangian equations. In this case we set  $p_i = r_i$  and substitute both the Hamiltonian function  $H$  (2.22) and subsequently the Lagrangian function  $L$  (2.6) into Hamilton's equations of motion. The preliminary results can be expressed as

$$\frac{\partial E_p}{\partial r_i} = -\dot{p}_i \quad (2.31)$$

and

$$\frac{1}{m_i} p_i = \dot{r}_i. \quad (2.32)$$

Then, we combine these two equations and introduce the force on particle  $i$ , defined in terms of the potential  $E_p$  by  $F_i = -(\partial E_p / \partial r_i)$ . The final result is thus given by  $\mathbf{F}_i = m_i \ddot{\mathbf{r}}_i$  in 3D which corresponds to Newton's second law of motion for particle  $i$  as expressed in the Newtonian formalism (2.3).

The Hamiltonian formalism has a number of important properties and implications. In the following paragraphs only a few of them are sketched in the context of a time-independent Hamiltonian function.

Most important, the concepts of Hamiltonian mechanics are fundamental to the phase space treatment of problems in dynamics. For a system with  $N$  degrees of freedom the set of  $2N$  canonically conjugate variables  $(\mathbf{p}, \mathbf{q})$  define a  $2N$ -dimensional *phase space* sometimes called the  $\Gamma$ -space<sup>18</sup> of the system [52] [61]. It is sometimes convenient to regard the phase space for a system as a whole as constructed out of the *configuration space* that corresponds to the set of coordinates chosen for the system taken together with the *momentum space* that corresponds to the set of momenta conjugate to those coordinates. Each point in phase space corresponds to a definite state of the system. When the system moves, the point representing it describes a curve called the phase path or *phase trajectory*. The motion of the phase point along its phase trajectory is determined by the canonical equations. Since the Hamiltonian equations are first order differential equations in time, the path of the representative point in phase space is determined by the initial point.

### Preservation of Phase Volume - Liouville Theorem

In the Hamiltonian formulation the Liouville equation can be seen as a continuity or advection equation for the probability distribution function. This theorem is fundamental to statistical mechanics and requires further attention.

Considering an *ensemble*<sup>19</sup> of initial conditions each representing a possible state of the system, we express the probability of a given ensemble or density distribution of system points in phase space  $\Gamma$  by a continuous function

$$f = f(\mathbf{p}, \mathbf{q}, t) \quad (2.33)$$

which is a normalized quantity with the following property

---

<sup>18</sup> For a collection of  $N$  identical particles the state of the system may be specified by giving the coordinates of each particle so that the system as a whole is represented by a cloud of  $N$  points in phase space. Alternatively, the state of the system as a whole constituting the gas phase can be completely specified by a single point in phase space. The phase for the system as a whole is called a  $\gamma$ -space or sometimes a  $\Gamma$ -space, and the phase space for any individual kind of particles (molecules) contained in the system is called a  $\mu$ -space for that particle [97] [28]. These notations may be linked to the theory of Gibbs [33] and Boltzmann [6], respectively.

<sup>19</sup> Willard Gibbs (1839-1903) introduced the idea of an ensemble of systems in his book entitled *Elementary Principles in Statistical Mechanics* published in 1902 [33]. An ensemble is a large number of of imaginary replicas of the system under consideration. Gibbs also introduced the ideas of canonical-, micro-canonical- and grand canonical ensembles which refer to ensembles having specific properties. [51]. For example, the micro-canonical ensemble is the assembly of all states with fixed total energy  $E$ , and fixed size. The canonical ensemble, another example, considers all states with fixed size, but the energy can fluctuate [9].

$$\int_{\text{all space}} f \prod_i dp_i dq_i = 1, \quad (2.34)$$

where  $\prod_i$  means product of all labeled variables and  $i$  runs from 1 to  $N$  degrees of freedom.

The distribution function  $f(\mathbf{q}, \mathbf{p}, t)$  is defined such that the product  $f(\mathbf{q}, \mathbf{p}, t) \prod_i dp_i dq_i = f(\mathbf{q}, \mathbf{p}, t) d\Omega$  represents the number of system points in the phase volume  $d\Omega$  about the point  $(\mathbf{q}, \mathbf{p})$  at the time  $t$ . The product of differentials  $d\Omega = \prod_i dp_i dq_i = dq_1 \dots dq_N dp_1 \dots dp_N$  may be regarded as an element of volume in phase space. It follows that the corresponding integral  $\int d\Omega$  taken over some region of phase space represents the volume of the particular region. This integral has the property of being invariant with respect to canonical transformations<sup>20</sup>. This means that the magnitude of a volume element in phase space is preserved under canonical transformations<sup>21</sup>. Therefore, at any given instant in time, the hypothetical ensemble points in the imaginary differential volume of  $\Gamma$ -space are consistently contained within a continuously closed surface. Thus, we let  $\Omega$  be an arbitrary volume element in  $\Gamma$ -space and  $S$  denotes its surface.

The rate of change of the number of phase points  $dN$ , within the infinitesimal phase space volume  $\prod_i dp_i dq_i$  is obtained from a balance equation expressing that the system points in an ensemble are neither created nor destroyed [60]. Hence, the rate of change of the number of system points in the volume  $\Omega$ ,  $\int_{\Omega} f d\Omega$  is equal to the net flux of points that pass through the closed surface that bound  $\Omega$ :

$$\frac{\partial}{\partial t}(f d\Omega) + \sum_i \left\{ \frac{\partial}{\partial p_i} (\dot{p}_i f d\Omega) + \frac{\partial}{\partial q_i} (\dot{q}_i f d\Omega) \right\} = 0 \quad (2.35)$$

We may divide by the volume to obtain the rate of change of density at a fixed position in phase space

$$\frac{\partial f}{\partial t} = - \sum_i \left\{ \frac{\partial}{\partial p_i} (\dot{p}_i f) + \frac{\partial}{\partial q_i} (\dot{q}_i f) \right\} = \sum_i \left\{ \dot{p}_i \frac{\partial f}{\partial p_i} + f \frac{\partial \dot{p}_i}{\partial p_i} + \dot{q}_i \frac{\partial f}{\partial q_i} + f \frac{\partial \dot{q}_i}{\partial q_i} \right\} \quad (2.36)$$

<sup>20</sup> The transformation from one pair of canonically conjugate coordinates  $\mathbf{q}$  and momenta  $\mathbf{p}$  to another set of coordinates  $\mathbf{Q} = \mathbf{Q}(\mathbf{p}, \mathbf{q}, t)$  and momenta  $\mathbf{P} = \mathbf{P}(\mathbf{p}, \mathbf{q}, t)$  is called a canonical transformation or point transformation. In this transformation it is required that the new coordinates  $(\mathbf{P}, \mathbf{Q})$  again satisfy the Hamiltonian equations with a new Hamiltonian  $H'(\mathbf{P}, \mathbf{Q}, t)$  [35] [43] [52].

<sup>21</sup> This theorem is known as the *Poincarè* theorem (1854-1912) [35] [43] [52], stating that:  $d\Omega = \prod_i dp_i dq_i = \prod_i dP_i dQ_i$ .

The invariance rests on the property of the Jacobian determinant of a canonical transformation:  $D = \det \left( \frac{\partial(\mathbf{Q}, \mathbf{P})}{\partial(\mathbf{q}, \mathbf{p})} \right) = 1$ . Consequently, the volume element is transformed as:  $\prod_i dp_i dq_i = \prod_i dP_i dQ_i = D \prod_i dp_i dq_i$ .

In particular, the evolution of a system in time also represents a canonical transformation which implies that the volume in phase space is conserved as it evolves in time. This is known as the *Liouville theorem* (1809-1882).

Since the Hamiltonian equations satisfy the *incompressibility* condition

$$\sum_i \left( \frac{\partial \dot{q}_i}{\partial q_i} + \frac{\partial \dot{p}_i}{\partial p_i} \right) = \sum_i \left( \frac{\partial^2 H}{\partial p_i \partial q_i} - \frac{\partial^2 H}{\partial q_i \partial p_i} \right) = 0 \quad (2.37)$$

a volume element in phase space is preserved under Hamiltonian flow. This relation is called the *Liouville's theorem* which is a fundamental property of Hamiltonian systems [60] [43].

This theorem further implies that the second and fourth terms in the summation on the RHS of (2.36) cancel to obtain

$$\frac{\partial f}{\partial t} + \sum_i \left( \dot{p}_i \frac{\partial f}{\partial p_i} + \dot{q}_i \frac{\partial f}{\partial q_i} \right) = 0 \quad (2.38)$$

This result is known as the *Liouville's equations* [61].

Notice that this equation is commonly written in the Poisson bracket form

$$\frac{\partial f}{\partial t} + [H, f] = 0 \quad (2.39)$$

where the Poisson bracket operator is defined by

$$[H, f] = \sum_{i=1}^N \left( \dot{q}_i \frac{\partial f}{\partial q_i} + \dot{p}_i \frac{\partial f}{\partial p_i} \right) = \sum_{i=1}^N \left( \frac{\partial H}{\partial p_i} \frac{\partial f}{\partial q_i} - \frac{\partial H}{\partial q_i} \frac{\partial f}{\partial p_i} \right) \quad (2.40)$$

The Poisson bracket is an operator in Hamiltonian mechanics which has convenient inherent properties considering the time evolution of dynamic variables [61] [73]. The most important property of the Poisson bracket is that it is invariant under any canonical transformation.

While this compact notation is convenient for the experienced user, to grasp the basic concepts a rough description may be preferable. Therefore, for the beginners that is not familiar with the concepts of statistical mechanics we reiterate the presentation of the abstract theory using an alternative notation equivalent to what is common in the fluid dynamic literature [40] [61]. The purpose is to provide introductory ideas about the practical implications of the Liouville equations describing the ensemble flow in  $\Gamma$ -space.

For this reason, we let  $\mathbf{u}$  denote a generalized velocity vector of the system points in the neighborhood of the element of surface  $dS$ :

$$\mathbf{u} = \{ \dot{q}_1, \dot{q}_2, \dots, \dot{q}_N; \dot{p}_1, \dot{p}_2, \dots, \dot{p}_N \} \quad (2.41)$$

In the particular case when the volume  $\Omega$  is thought to be fixed in phase space, the corresponding continuity equation can now be re-expressed as

$$\frac{\partial}{\partial t} \int_{\Omega} f d\Omega = - \oint_S \mathbf{u} \cdot f d\mathbf{S} = - \int_{\Omega} \nabla \cdot \mathbf{u} f d\Omega \quad (2.42)$$

where the net 'convective' flux out of the volume through the closed surface  $S$  is  $\oint \mathbf{u} \cdot f d\mathbf{S}$ .

Now, using a variant of Gauss theorem in  $\Gamma$ -space yields,

$$\int_{\Omega} \left[ \frac{\partial f}{\partial t} + \nabla \cdot (\mathbf{u}f) \right] d\Omega = 0 \quad (2.43)$$

Requiring that the integrand must be equal to zero for any volume, the resulting differential equation is given by

$$\frac{\partial f}{\partial t} + \nabla \cdot (\mathbf{u}f) = 0 \quad (2.44)$$

With (2.41) and (2.37), we find

$$\nabla \cdot \mathbf{u} = \sum_{i=1}^N \left( \frac{\partial \dot{q}_i}{\partial q_i} + \frac{\partial \dot{p}_i}{\partial p_i} \right) = \sum_{i=1}^N \left( \frac{\partial^2 H}{\partial q_i \partial q_i} - \frac{\partial^2 H}{\partial q_i \partial p_i} \right) = 0 \quad (2.45)$$

since the flow of system points is *incompressible*. Introducing the *solenoidal* vector field into the continuity equation returns the Liouville equation, which now appears as

$$\frac{\partial f}{\partial t} = -\mathbf{u} \cdot \nabla f - f \nabla \cdot \mathbf{u} = -\mathbf{u} \cdot \nabla f \quad (2.46)$$

In an engineering view the ensemble of system points moving through phase space behaves much like a fluid in a multidimensional space, and there are numerous similarities between our imagination of the ensemble and the well known notions of fluid dynamics [35]. Then, the substantial derivative in fluid dynamics corresponds to a derivative of the density as we follow the motion of a particular differential volume of the ensemble in time. The material derivative is thus similar to the Lagrangian picture in fluid dynamics in which individual particles are followed in time. The partial derivative is defined at fixed  $(q, p)$ . It can be interpreted as if we consider a particular fixed control volume in phase space and measure the time variation of the density as the ensemble of system points flows by us. The partial derivative at a fixed point in phase space thus resembles the Eulerian viewpoint in fluid dynamics.

## BBGKY-Hierarchy

In the more theoretical fields of science the conventional derivation of the Boltzmann equation for the one-particle distribution function, assumed to be valid for dilute gases, is considered far too heuristic and accordingly does not form an adequate formal basis for rigorous analysis. In this point of view a formal derivation starts out from a complete knowledge of the probability density formulated in terms of a  $N$ -particle density function<sup>22</sup>,  $f_N(\mathbf{q}, \mathbf{p}, t)$ , providing

<sup>22</sup>  $f_N$  denotes the  $N$ -body joint-probability density for the  $N$ -body system. This function gives the probability density of finding, at time  $t$ , particle 1 in the state  $(\mathbf{p}_1, \mathbf{q}_1)$ , particle 2 in the state  $(\mathbf{p}_2, \mathbf{q}_2)$ , ..., and particle  $N$  in the state  $(\mathbf{p}_N, \mathbf{q}_N)$ .

a general way of deducing the Boltzmann equation from the laws of dynamics via approximations of this rigorous equation. Deriving the Boltzmann equation in this manner may also provide novel guidelines for the extension of Boltzmann equation to higher densities.

The time evolution of this phase space probability density is governed by the Liouville equation expressed as

$$\frac{\partial f_N}{\partial t} = [H_N, f_N] \quad (2.47)$$

However, the description of the system governed by the complete phase space probability density is not feasible in practice for a large number of particles  $N$ . Therefore, one may rather consider the behavior of a subset of particles defining a reduced phase space distribution function. The unwanted information can be eliminated by integrating  $f_N$  over the coordinates and momenta of the remaining particles [38] [61] (i.e., resembling an averaging procedure). A particular system of integro-differential equations for such a reduced distribution function is known as the BBGKY-hierarchy (i.e., this abbreviation is written for N. N. Bogoliubov, M. Born, H. S. Greed, G. Kirkwood, and J. Yvon). Comprehensive discussions on this approach is given by Cercignani et al. [8] and Liboff [61]. Nevertheless, this approach is not very useful in practice since the BBGKY-hierarchy is not closed and an ad hoc problem contraction is required. It is noted that the first equation in this sequence is still most important as it governs the evolution of  $f_1(\mathbf{p}, \mathbf{q}, t)$  in time and space provided that an approximate closure for the pair density function  $f_{(2)}(\mathbf{p}', \mathbf{q}'; \mathbf{p}, \mathbf{q}, t)$  is available (i.e., this equation contains the lowest number of unknowns in the sequence), and it represents the generic form of all the kinetic equations. Much effort has been devoted to find approximate solutions to the BBGKY hierarchy on the basis of expressions that relate  $f_1(\mathbf{p}, \mathbf{q}, t)$  and  $f_{(2)}(\mathbf{p}', \mathbf{q}'; \mathbf{p}, \mathbf{q}, t)$ . The simplest approximation is to ignore the pair correlation altogether by writing:  $f_{(2)}(\mathbf{p}', \mathbf{q}'; \mathbf{p}, \mathbf{q}, t) = f_1(\mathbf{p}', \mathbf{q}', t)f_1(\mathbf{p}, \mathbf{q}, t)$ . This assumption implies that there is no statistical correlation between particles of states  $(\mathbf{p}', \mathbf{q}')$  and  $(\mathbf{p}, \mathbf{q})$  at any time  $t$ .

Various efforts along these lines have attempted to derive the Boltzmann equation from first principles. However, a number of assumptions come into play in all these derivations, which renders even the more formal analyzes somewhat ad hoc. Therefore, many practitioners do not consider the classical formalism worthwhile.

## 2.3 Basic Concepts of Kinetic Theory

In this section the statistical theorems or mathematical tools needed to understand the Boltzmann equation in itself, and the mathematical operations performed developing the macroscopic conservation equations starting out from the microscopic Boltzmann equation, are presented.

Introductory it is stressed that a heuristic theory, which resembles the work of Boltzmann [6] and the standard kinetic theory literature, is adopted in this section and the subsequent sections deriving the Boltzmann equation. Irrespective, the notation and concepts presented in sect. 2.2 are often referred, or even redefined in a less formal wrapping, thus the underlying elements of classical mechanics are prescience of outmost importance understanding the true principles of kinetic theory.

### 2.3.1 Molecular Models

For mono-atomic gases the spacing between the particles is considered large enough so that we can approximate the particles as points, or point centers of force. For this reason, in kinetic theory a gas molecule is characterized by its position  $\mathbf{r}$  and its velocity  $\mathbf{c}$ .

However, the intermolecular force laws play a central role in the model determining the molecular interaction terms (i.e., related to the collision term on the RHS of the Boltzmann equation). Classical kinetic theory proceeds on the assumption that this law has been separately established, either empirically or from quantum theory. The force of interaction between two molecules is related to the potential energy as expressed by

$$F(r) = -\frac{dE_P(r)}{dr} \quad (N) \quad (2.48)$$

where  $r$  is the distance between the two molecules.

For most purposes it is chosen to use the potential energy of interaction  $E_P(r)$  rather than the force of interaction  $F(r)$ . These two functions are related as:

$$E_P(r) = -\int_r^{\infty} F(r)dr \quad (J) \quad (2.49)$$

Several molecular models have been considered, each of them having certain advantages either in their physical interpretations or giving simple mathematical representations of the laws of interaction. The *billiard ball model* is one such exploratory molecular model which is frequently used because of its simplicity. In this model a molecule is viewed as a microscopic particle and approximated by a small featureless sphere, possessing a spherically-symmetric force field. For neutral particles this force field has a very short range, and the particles can be pictured as being almost rigid spheres, with an effective diameter equal to the range of the force field. Therefore, in an average sense each gas molecule is assumed to be a rigid, spherical, non-attracting, particle of diameter  $d$ , and mass  $m$ . These molecular characteristics resemble those of a billiard ball, thus this molecular representation is often referred to as the molecular 'billiard ball' model. As they have no structure, these particles have only energy of translation. The gas is further assumed to be sufficiently dilute for collisions involving more than two particles at a time to be ignored,

thus only binary collisions are considered. The collisions between these gas molecules are considered perfectly elastic<sup>23</sup>. It is also assumed that the gas obeys the ideal gas law.

The hard sphere potential is defined as:

$$E_P(r) = \begin{cases} \infty & \text{if } r \leq d \\ 0 & \text{if } r > d \end{cases} \quad (2.50)$$

This model is frequently used considering mono-atomic uncharged molecules. However, this model gives a very crude representation of the actual physics (e.g., repulsive forces and volume of sphere), since molecules in fact are complicated electronic structures, and can by no means resemble rigid spheres.

The *Maxwellian molecules* are useful in exploratory calculations in which a differentiable potential function is needed. For these molecules [66] the intermolecular force between pairs at a distance  $r$  apart is of the form  $Kr^{-5}$ , where  $K$  is a constant. Adopting this particular potential representation the solution of the equation of transfer reduces to a feasible problem, thereby Maxwell [66] obtained analytical expressions for the transport coefficients as mentioned earlier.

These two models represent the most important spherical symmetrical potential functions used in this book, but many others exist as well<sup>24</sup> [39] (pp. 31-35). In the two models adopted in this work the force is always repulsive and varies inversely as some power of the distance between the molecular centers. No redistribution of energy between the internal and the translational energy forms are allowed.

Depending on the molecular model chosen the interacting force may arise only upon contact, or act when the molecules are at any distance away from each other. Therefore, since many different molecular models and potentials are investigated, it is common practice in textbooks on kinetic theory to derive the expression for the collision term in a generalized or generic manner so that the framework is valid for any molecular model chosen.

---

<sup>23</sup> Considering a binary *elastic collision* two bodies collide and thereafter move apart again in such a way that both the overall momentum and the total kinetic energy of the center of mass of the two bodies are conserved ([96], p. 13) [43].

In a binary *in-elastic collision*, on the other hand, the two bodies collide and stick together. The overall momentum is normally conserved in these collisions too, but the overall kinetic energy of the center of mass of the two bodies is not conserved([96], p. 13).

During real collisions, the colliding molecules (particles) undergo both elastic and in-elastic deformations.

<sup>24</sup> The most frequently used model potentials are: Rigid sphere, point center of repulsion, Sutherland's model, Lennard-Jones potential, modified Buckingham potential, Kihara potential, Morse potential. Their advantages and disadvantages are thoroughly discussed elsewhere [39] [28].

### 2.3.2 Phase Space, Distribution Function, Means and Moments

A collection of mono-atomic gas molecules are characterized by their position  $\mathbf{r}$  in space and their velocity  $\mathbf{c}$  at time  $t$ . An infinitesimal spatial space containing the point  $\mathbf{r}$  is denoted by  $d\mathbf{r}$  (e.g., in Cartesian coordinates  $= dx dy dz$ ). In a similar manner, an infinitesimal element in a hypothetical velocity space containing the velocity  $\mathbf{c}$  is denoted by  $d\mathbf{c}$  (e.g., in Cartesian coordinates  $= dc_x dc_y dc_z$ ). The imaginary or hypothetical space containing both  $d\mathbf{r}$  and  $d\mathbf{c}$  constitutes the six-dimensional *phase space*<sup>25</sup>. Therefore, by a macroscopic point  $(\mathbf{r}, \mathbf{c}, t)$  in phase space is meant an infinitesimal volume,  $d\mathbf{r} d\mathbf{c}$ , centered at the point  $(\mathbf{r}, \mathbf{c}, t)$ , having an extension sufficient to contain a large number of molecules as required for a statistical description to be valid, but still small compared with the scale of the natural changes in the macroscopic quantities like pressure, gas velocity, temperature and density of mass.

A concept of principal importance in kinetic theory is the distribution function. The probabilistic *distribution function* containing the desired information about the spatial distribution of molecules and their velocity distribution is denoted by  $f(\mathbf{r}, \mathbf{c}, t)$ . This probability function is defined in such a way that  $f(\mathbf{c}, \mathbf{r}, t) d\mathbf{c} d\mathbf{r}$  denotes the probable number of molecules in the volume element  $d\mathbf{r}$  located at  $\mathbf{r}$ , whose velocities lie in the range  $d\mathbf{c}$  about  $\mathbf{c}$  at time  $t$ . We treat  $f$  as being a continuous and differentiable function of its arguments. When the distribution function is given, the macroscopic properties of the gas are determined using the concept of moments (or probability-weighted averages). We may now define a molecular *state vector*  $(\mathbf{r}, \mathbf{c})$  denoting the independent variables needed to specify the rate of change of the macroscopic properties.

The macroscopic property obtained by integrating  $f d\mathbf{c}$  over the whole velocity space is the *number density*,  $n(\mathbf{r}, t)$ , which denotes the number of particles per unit volume at the location  $\mathbf{r}$  at time  $t$ :

$$n(\mathbf{r}, t) = \int f(\mathbf{r}, \mathbf{c}, t) d\mathbf{c} \quad (2.51)$$

The mass *density* of the collection of gas molecules at  $\mathbf{r}$ , at time  $t$ , yields:

$$\rho(\mathbf{r}, t) = mn(\mathbf{r}, t) \quad (2.52)$$

<sup>25</sup> The classical phase space is formally defined in terms of generalized coordinates and momenta because it is in terms of these variables that Liouville's theorem holds. However, in Cartesian coordinates as used in the present section it is usually still true that  $p_i = mc_i$  under the particular system conditions specified considering the kinetic theory of dilute gases, hence phase space can therefore be defined in terms of the coordinate and velocity variables in this particular case. Nevertheless, in the general case, for example in the presence of a magnetic field, the relation between  $p_i$  and  $c_i$  is more complicated and the classical formulation is required [83].

Statistics means and moments are defined in terms of a suitable probability density function (PDF). Therefore, in the present context these statistical measures are expressed in terms of the normalized distribution function,  $P(\mathbf{r}, \mathbf{c}, t) = f(\mathbf{r}, \mathbf{c}, t)/n(\mathbf{r}, t)$ , having the important mathematical property of a PDF:

$$\int_{-\infty}^{\infty} P(\mathbf{r}, \mathbf{c}, t) d\mathbf{c} = \int_{-\infty}^{\infty} \frac{f(\mathbf{r}, \mathbf{c}, t)}{n} d\mathbf{c} = \frac{n}{n} = 1 \quad (2.53)$$

The mean (or expectation) of the random variable  $\mathbf{c}$  is defined by [75] [83] [84] [100]:

$$\mathbf{v}(\mathbf{r}, t) = \langle \mathbf{c}(\mathbf{r}, t) \rangle_M = \int_{-\infty}^{\infty} \mathbf{c} P(\mathbf{r}, \mathbf{c}, t) d\mathbf{c} \quad (2.54)$$

This measure is also referred to as the probability-weighted average of all possible values of  $\mathbf{c}$ .

More generally, let  $\psi(\mathbf{r}, \mathbf{c}, t)$  be a generalized physical function that denotes a property of the molecules located at time  $t$  near  $\mathbf{r}$  with a velocity near  $\mathbf{c}$ . Since  $\psi(\mathbf{r}, \mathbf{c}, t)$  is a function of  $\mathbf{c}$ , the mean of  $\psi$  is:

$$\langle \psi(\mathbf{r}, t) \rangle_M = \int_{-\infty}^{\infty} \psi(\mathbf{r}, \mathbf{c}, t) P(\mathbf{r}, \mathbf{c}, t) d\mathbf{c} = \frac{1}{n(\mathbf{r}, t)} \int_{-\infty}^{\infty} \psi(\mathbf{r}, \mathbf{c}, t) f(\mathbf{r}, \mathbf{c}, t) d\mathbf{c} \quad (2.55)$$

The  $n$ -th *moment about the origin* is defined to be:

$$\mu_n = \langle \mathbf{c}^n \rangle_M = \int_{-\infty}^{\infty} \mathbf{c}^n P(\mathbf{r}, \mathbf{c}, t) d\mathbf{c} \quad (2.56)$$

A first-order moment of  $\psi$  can thus be defined as:

$$\langle \psi(\mathbf{r}, t) \rangle_M = \int_{-\infty}^{\infty} \psi(\mathbf{r}, \mathbf{c}, t) P(\mathbf{r}, \mathbf{c}, t) d\mathbf{c} \quad (2.57)$$

It is noted that the moment (2.57) equals the mean (2.55).

It follows that the mean or macroscopic *fluid velocity* at the position  $\mathbf{r}$  and time  $t$ , yields:

$$\mathbf{v}(\mathbf{r}, t) = \frac{1}{n(\mathbf{r}, t)} \int \mathbf{c} f(\mathbf{r}, \mathbf{c}, t) d\mathbf{c} = \frac{1}{\rho(\mathbf{r}, t)} \int m \mathbf{c} f(\mathbf{r}, \mathbf{c}, t) d\mathbf{c} \quad (2.58)$$

The translational motion of a particular collection of molecules can either be specified by their velocity  $\mathbf{c}$  relative to a standard frame of reference, or by their velocity relative to a frame moving with a specified velocity. The molecular velocity defined in the frame of reference which moves with the local

fluid velocity  $\mathbf{v}$  is called the *peculiar velocity* of the collection of molecules, hence:

$$\mathbf{C} = \mathbf{c} - \mathbf{v} \quad (2.59)$$

It follows from the above definitions that the average peculiar velocity equals zero.

### 2.3.3 Flux Vectors

In a non-equilibrium gas system there are gradients in one or more of the macroscopic properties. In a mono-atomic gas the gradients of density, fluid velocity, and temperature induce molecular transport of mass, momentum, and kinetic energy through the gas. The mathematical theory of transport processes enables the quantification of these macroscopic fluxes in terms of the distribution function on the microscopic level. It appears that the mechanism of transport of each of these molecular properties is derived by the same mathematical procedure, hence they are collectively represented by the generalized property  $\psi$ .

In the gas we consider an infinitesimal element of surface area  $dA$  as sketched in Fig. 2.1. The orientation of the surface area is defined by a unit vector  $\mathbf{n}$  normal to the surface, and  $\omega$  is the angle between  $\mathbf{C}$  and  $\mathbf{n}$ . Imagine further that the element of surface area moves along with the fluid having the velocity  $\mathbf{v}(\mathbf{r}, t)$ . The collection of molecules will then move back and forth across this element area with their peculiar velocities  $\mathbf{C}$  about the mean velocity  $\mathbf{v}$ , in accordance with (2.59).

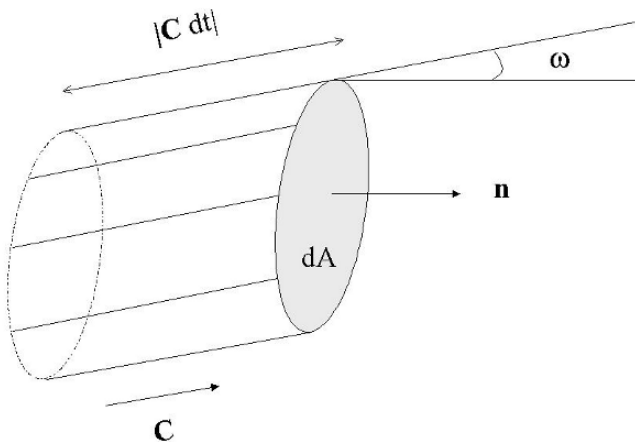


**Fig. 2.1.** A cylinder containing all molecules with peculiar velocity  $\mathbf{C}$  which cross the surface element  $dA$  during the time interval  $dt$ .

Ignoring any molecular collisions the number of molecules crossing the surface area  $dA$  during the infinitesimal time interval  $(t, t + dt)$  equals the number of molecules contained within an infinitesimal cylinder volume with cross-sectional area  $dA$  and length  $|\mathbf{C}|dt$  at time  $t$ . The volume of this cylinder,  $\mathbf{n} \cdot \mathbf{C} dt dA$ , contains  $f(\mathbf{r}, \mathbf{c}, t) d\mathbf{c} (\mathbf{n} \cdot \mathbf{C} dt dA)$  molecules.

Assuming that each molecule in an average sense carries with them the physical property  $\psi(\mathbf{r}, \mathbf{c}, t)$ , the amount of  $\psi$  transported by the molecules with velocities in the range  $d\mathbf{C}$  about  $\mathbf{C}$  across the area  $dA$  in the time  $dt$  is given by  $f(\mathbf{r}, \mathbf{c}, t) d\mathbf{c} (\mathbf{n} \cdot \mathbf{C} dt dA) \psi(\mathbf{r}, \mathbf{c}, t)$ . Accordingly, the flux of  $\psi$  denoting the amount which crosses  $dA$  per unit area per unit time is expressed as  $f\mathbf{n} \cdot \mathbf{C}\psi d\mathbf{c}$ .

The total flux of  $\psi$  across the elementary surface area  $dA$  is obtained by adding the contributions from molecules within all velocity ranges<sup>26</sup>:

$$\Phi_n(\mathbf{r}, t) = \int f\mathbf{n} \cdot \mathbf{C}\psi d\mathbf{c} \quad (2.60)$$

where  $\Phi_n(\mathbf{r}, t)$  denotes the  $\mathbf{n}$  component of the *flux vector*, thus  $\Phi_n(\mathbf{r}, t) = \mathbf{n} \cdot \Phi(\mathbf{r}, t) = n\langle C_n\psi(\mathbf{r}, t) \rangle_M$ .

The complete flux vector of the property  $\psi$  is give by:

$$\Phi(\mathbf{r}, t) = \int f\mathbf{C}\psi d\mathbf{c} \quad (2.61)$$

The physical interpretation of this vector is that the  $\mathbf{n}$ -component of the vector equals the flux of  $\psi$  across a surface normal to  $\mathbf{n}$ .

At this point it is appropriate to introduce the particular flux vectors associated with the transport of mass, momentum, and kinetic energy.

### Transport of Mass

In this case we set  $\psi = m$ :

$$\Phi(\mathbf{r}, t) = m \int f\mathbf{C}d\mathbf{c} = mn\langle \mathbf{C} \rangle_M = 0 \quad (2.62)$$

### Transport of Momentum

In this case we set  $\psi = mC_i$ , hence:

$$\Phi(\mathbf{r}, t) = m \int fC_i\mathbf{C}d\mathbf{c} = mn\langle C_i\mathbf{C} \rangle_M = \mathbf{p}_i \quad (2.63)$$

<sup>26</sup> The integration over  $\mathbf{c}$  is equivalent to integrating over  $\mathbf{C}$  since these two velocities differ by a constant (i.e., independent of  $\mathbf{c}$ ) only, and the integration is over the entire velocity space [39] (p. 457).

This flux vector denotes the transport of momentum relative to  $\mathbf{v}$  in the  $i$ -direction. In a 3D system the direction index  $i$  takes three different values, so there are a total of three flux vectors associated with momentum transfer. Together the three flux vectors constitute a symmetric second-order tensor with nine components. This tensor is usually referred to as the pressure tensor,  $\mathbf{P}$ . The pressure tensor is expressed by:

$$\mathbf{P} \equiv m \int f \mathbf{C} \mathbf{C} d\mathbf{c} \equiv \rho \langle \mathbf{C} \mathbf{C} \rangle_M = \rho \begin{pmatrix} \langle C_x^2 \rangle_M & \langle C_x C_y \rangle_M & \langle C_x C_z \rangle_M \\ \langle C_y C_x \rangle_M & \langle C_y^2 \rangle_M & \langle C_y C_z \rangle_M \\ \langle C_z C_x \rangle_M & \langle C_z C_y \rangle_M & \langle C_z^2 \rangle_M \end{pmatrix} \quad (2.64)$$

The diagonal elements  $\langle C_i^2 \rangle_M$  represent the *normal stresses*, in general denoting the sum of the static and the viscous forces per unit area acting on a surface at an instant in time. The non-diagonal elements, denoted by  $\langle C_i C_j \rangle_M$  for  $i \neq j$ , represent the *shear stresses* or the viscous shear forces per unit area.

We define the deviatoric - or viscous stresses as the negative thermal flux, determined by the difference between the thermodynamic pressure and the total pressure tensor, as follows:

$$\boldsymbol{\sigma}_{ij} \equiv [p\delta_{ij} - \rho \langle C_i C_j \rangle_M] \quad (2.65)$$

where the  $\delta_{ij}$  is the Kronecker delta.

The *mean pressure* (or *pressure*) is defined as the mean value of the normal stresses across any three orthogonal planes. The mean pressure,  $\bar{p}$ , is thus one third of the trace of the pressure tensor:

$$\bar{p} = \frac{1}{3} \rho \langle C^2 \rangle_M = \frac{1}{3} \mathbf{P} : \mathbf{e} \quad (2.66)$$

where the  $\mathbf{e}$  is the unit tensor.

The trace of the pressure tensor can be expressed in terms of the peculiar velocity:

$$\mathbf{P} : \mathbf{e} = P_{xx} + P_{yy} + P_{zz} = nm(\langle C_x^2 \rangle_M + \langle C_y^2 \rangle_M + \langle C_z^2 \rangle_M) = \rho \langle C^2 \rangle_M \quad (2.67)$$

In particular, when the system is at equilibrium (no macroscopic gradients), the viscous stresses vanish (i.e.,  $\boldsymbol{\sigma}_{ij} = 0$ ) and the total pressure tensor can be expressed in terms of the mean pressure or alternatively in terms of the *thermodynamic pressure*,  $p$ , as:

$$\mathbf{P} = \bar{p} \mathbf{e} = p \mathbf{e} \quad (2.68)$$

where  $P_{xx} = P_{yy} = P_{zz} = p$ . Since these conditions are satisfied in the static case only, such a pressure system is called *static*.

Strictly speaking the Maxwellian distribution function only applies to a gas in thermodynamic equilibrium which is a uniform steady state. The application of this function is thus basically restricted to a gas at rest. To force an

equilibrium gas system to flow, certain driving forces are necessary, hence all flowing systems must involve local gradients in the velocity and some other properties. Therefore, the Maxwellian distribution function is assumed valid also for certain classes of flows or in certain regions in a given flow in which the gradients are sufficiently small so that the gas can be considered in *local equilibrium* (see also sec. 2.7.2). Such a pressure system is often called *hydrostatic* as it is an apparent static state of flow [100] (p. 344). The equations of change derived from kinetic theory using the Maxwellian distribution function, assumed valid for the apparent *equilibrium flows*, correspond to the well known Euler equations in classical gas dynamics.

Hence, it follows that in general the net macroscopic surface stress is determined by two different molecular effects: One stress component associated with the pressure and a second one associated with the viscous stresses<sup>27</sup>. Again for a fluid at rest, the system is in an equilibrium static state containing no velocity or pressure gradients so the average pressure equals the static pressure everywhere in the system. The static pressure is thus always acting normal to any control volume surface area in the fluid independent of its orientation. For a compressible fluid at rest, the static pressure may be identified with the pressure of classical thermodynamics as derived from (2.64) using the Maxwellian distribution function (i.e., constituting the diagonal elements only). On the assumption that there is local thermodynamic equilibrium even when the fluid is in motion this concept of stress is retained at the macroscopic level. For an incompressible fluid the thermodynamic, or more correctly thermostatic, pressure cannot be defined except as the limit of pressure in a sequence of compressible fluids. In this case the pressure has to be taken as an independent dynamical variable [1] (sects. 5.13-5.24).

The macroscopic relationship between the total *molecular stress tensor*, which includes both the *hydrostatic*- or *thermodynamic pressure* and the *viscous stresses* is expressed as:

$$\mathbf{P} = p\mathbf{e} + \boldsymbol{\sigma} \quad (2.69)$$

or in matrix notation:

$$\mathbf{P} = \begin{pmatrix} p + \sigma_{xx} & \sigma_{xy} & \sigma_{xz} \\ \sigma_{yx} & p + \sigma_{yy} & \sigma_{yz} \\ \sigma_{zx} & \sigma_{zy} & p + \sigma_{zz} \end{pmatrix} \quad (2.70)$$

In practice the local pressure variable is assumed to be independent on the state of the fluid. If the gradients in the flow field of a mono-atomic gas are sufficiently large, viscous stresses and heat conduction phenomena emerge,

<sup>27</sup> The viscous stresses only come into play for systems containing significant velocity gradients within the fluid. Nevertheless, very large gradients are not required as the Navier-Stokes equations can be derived from the Chapman-Enskog perturbation theory. On the other hand, for the non-equilibrium boundary layer and shock wave systems, i.e., systems which deviates considerably from equilibrium, higher order expansions are apparently needed [28]. Actually, at least for shock waves the validity of the Maxwell-Boltzmann equation becomes questionable.

and the Maxwellian distribution function is no longer adequate. Therefore, when the fluid is in real motion, additional viscous normal stresses appear as denoted by  $\sigma_{ii}$ .

Adopting the Newton's viscosity law (1.69) derived from continuum mechanical principles [102] (sec. 2-4.2), the thermodynamic pressure deviates slightly from the mean pressure. It follows that the mean pressure is approximated as:

$$\bar{p} = \frac{1}{3}(P_{xx} + P_{yy} + P_{zz}) = p - (\mu_B + \frac{2}{3}\mu)\nabla \cdot \mathbf{v} \quad (2.71)$$

showing that the mean pressure in a deforming viscous fluid is not exactly equal to the thermodynamic property called pressure (i.e., apparently the constitutive relation is not consistent with the local equilibrium assumption).

This distinction is rarely important, as  $\nabla \cdot \mathbf{v}$  is normally very small in typical reactor flow problems, nevertheless adopting the rigorous form of the constitutive relation (1.69) the bulk viscosity  $\mu_B$  appears as an undetermined system parameter.

Stokes [94] solved this problem by introducing the novel assumption that  $\mu_B + \frac{2}{3}\mu = 0$ . Adopting this hypothesis we simply avoid the problem. Alternatively, when the incompressible flow limit  $\nabla \cdot \mathbf{v} = 0$  is applicable,  $\bar{p}$  equals  $p$ . Even for high speed compressible flows, i.e., for which  $\nabla \cdot \mathbf{v} \neq 0$ , we avoid the problem since the viscous normal stresses are normally negligible for such flows. Still a third assumption is often put forth, i.e., that the kinetic theory of gases proves that  $\mu_B + \frac{2}{3}\mu = 0$  for a mono-atomic gas<sup>28</sup> (e.g., Hirschfelder et al [39] p 521; Vincenti and Kruger [100] p 391; Ferziger and Kaper [28]). However, White [102] (p. 70) states that this is a specious argument since the kinetic theory actually assumes rather than proves this relationship to be valid. The discussion reported by Truesdell [99] also states that the theory is vague on this issue, as the different perturbation methods proposed in kinetic theory for solving the Maxwell-Boltzmann equation do not give consistent results even for mono-atomic gases. For polyatomic gases no formal theory exist determining this parameter value. It appears, apparently, that there exists no exact interpretation of Newton's viscosity law.

### Transport of Kinetic Energy

In this case we set  $\psi = \frac{1}{2}m\mathbf{C} \cdot \mathbf{C}$  and get:

$$\Phi(\mathbf{r}, t) = \int f \frac{1}{2}mC^2 \mathbf{C} d\mathbf{c} = \frac{1}{2}mn\langle C^2 \mathbf{C} \rangle_M = \mathbf{q}(\mathbf{r}, t) \quad (2.72)$$

<sup>28</sup> For example, the proof given by Vincenti and Kruger [100] (p. 391) is based on a comparison between the result obtained solving the Maxwell-Boltzmann equation using the Enskog expansion method and the corresponding expressions for the stress tensor derived in continuum gas dynamics. From this inter-comparison it is seen that for mono-atomic gases the kinetic theory result does not contain any terms corresponding to the bulk viscosity, thus it is concluded that this parameter equals zero.

By use of (2.59), the kinetic energy of the collection of particles may be expressed as:

$$\frac{1}{2}m\mathbf{c} \cdot \mathbf{c} = \frac{1}{2}m(\mathbf{C} + \mathbf{v}) \cdot (\mathbf{C} + \mathbf{v}) = \frac{1}{2}m(C^2 + 2\mathbf{v} \cdot \mathbf{C} + v^2) \quad (2.73)$$

The average of the second term on the RHS,  $\langle m\mathbf{v} \cdot \mathbf{C} \rangle_M$ , vanishes, whereas the average of the last term on the RHS,  $\langle \frac{1}{2}mv^2 \rangle_M$ , denotes the kinetic energy of the macroscopic fluid motion. The average of the first term on the RHS,  $\langle \frac{1}{2}mC^2 \rangle_M$ , is thus interpreted as the internal energy of the gas. It follows that the *internal energy per unit mass* of the gas,  $e(\mathbf{r}, t)$ , is defined as:

$$e(\mathbf{r}, t) = \frac{1}{n(\mathbf{r}, t)} \int \frac{1}{2}C^2 f(\mathbf{r}, \mathbf{c}, t) d\mathbf{c} = \frac{1}{\rho(\mathbf{r}, t)} \int \frac{1}{2}mC^2 f(\mathbf{r}, \mathbf{c}, t) d\mathbf{c} \quad (2.74)$$

The gas *temperature*,  $T$ , is defined in terms of  $e$  by the relation:

$$\rho e = \frac{3}{2}nkT \quad (2.75)$$

noting that for point particles equipartition of energy gives the relation<sup>29</sup>:  $mC^2 = 3kT$ .  $k$  is the universal Boltzmann constant,  $k = 1.380 \times 10^{-23}$  (J/K).

### 2.3.4 Ideal Gas Law

Strictly speaking an ideal gas is a system composed of particles, or quasi-particles, that do not interact with each other. In these simple systems the energy is due solely to translational motion.

---

<sup>29</sup> In classical statistical mechanics the principle of equipartition of energy states that the internal energy of a system composed of a large number of particles at thermal equilibrium will distribute itself evenly among each of the quadratic degrees of freedom allowed to the particle system [97] [35]. In particular, for any part of the internal molecular energy that can be expressed as the sum of square terms, each term contributes an average energy of  $\frac{1}{2}kT$  per molecule [100] [70]. The phrase *square term* refers to a term that is quadratic in some appropriate variable used to describe energy. It follows that for a dilute mono-atomic gas, the mean energy associated with the translational motion of the  $c$ -th molecule in each of the three space directions is  $\frac{1}{2}mC^2$ . The mean energy of the gas is obtained by adding the contributions from all the three directions:  $\frac{1}{2}mC^2 = \frac{1}{2}m(C_1^2 + C_2^2 + C_3^2) = \frac{3}{2}kT$ .

The equipartition principle was initially proposed by Maxwell [66] in 1867 who stated that the energy of a gas is equally divided between linear and rotational energy. The original theorem was later generalized by Boltzmann [6] in 1872 by showing that the internal energy is actually equally divided among all the independent components of motion in the system.

In kinetic theory, the temperature  $T$  of a gas at a uniform state at rest or in uniform translation is defined directly in terms of the peculiar speeds of the molecules, by the relation  $\frac{1}{2}m\langle C^2 \rangle_M = \frac{3}{2}kT$  obtained from (2.75) and (2.74). In accordance with (2.75) and (2.67) the static pressure  $p$  of a gas in equilibrium is given by  $p = \frac{1}{3}nm\langle C^2 \rangle_M = knT$ . Considering the mass  $M$  of gas contained in a volume  $V$ , the number of mono-atomic molecules  $N$  in the mass  $M$  is  $M/m$ , and the number density  $n$  is therefore  $N/V$ . The thermodynamic pressure is then given by  $pV = NkT$  [77] [12] [100] [28]. Alternatively one can write  $N = nN_a$ , where  $n$  is the number of moles of gas present and  $N_a$  is Avogadro's number. Then, the *ideal gas law*, yields

$$pV = nRT \quad (2.76)$$

where  $R = kN_a$  is the universal gas constant.

This formula may also valid for a gas not in equilibrium provided that the molecules possess only translatory energy.

## 2.4 The Boltzmann Equation

All the derivations of the Boltzmann equation are based on a number of assumptions and hypotheses, making the analyzes somewhat ad hoc irrespective of the formal mathematical rigor and complexity accomplished. So in this book a heuristic theory, which is physically revealing and equally ad hoc to the more fundamental derivations of the Boltzmann equation, is adopted. It is stressed that the notation used resembles that introduced by Boltzmann [6] and is not strictly in accordance with the formal mathematical methods of classical mechanics. However, some aspects of the formal formulations and vocabulary outlined in sect. 2.2 are incorporated although somewhat based on intuition and empirical reasoning rather than fundamental principles as discussed in sect. 2.3.

The Boltzmann equation can be derived using a procedure founded on the Liouville theorem<sup>30</sup>. In this case the balance principle is applied to a control volume following a trajectory in phase space, expressed as

$$\frac{d_c}{dct} \int \int f d\mathbf{r}d\mathbf{c} = \int \int \left( \frac{\partial f}{\partial t} \right)_{\text{Collision}} d\mathbf{r}d\mathbf{c} \quad (2.77)$$

denoting that the rate of change of  $f$  for a system of a number of particles moving with the phase space velocity vector  $(\frac{d\mathbf{r}}{dt}, \frac{d\mathbf{c}}{dt})$  equals the rate at which  $f$  is altered by collisions.

Applying numerous theorems, similar but not identical to those used in chap 1 deriving the governing equations in fluid dynamics, one arrives at the Boltzmann equation on the form

<sup>30</sup> The simplified interpretation of the Liouville theorem discussed in sect. 2.2 is used here deriving the translational terms, intending to make the formulation more easily available.

$$\frac{\partial f}{\partial t} + \mathbf{c} \cdot \frac{\partial f}{\partial \mathbf{r}} + \mathbf{F} \cdot \frac{\partial f}{\partial \mathbf{c}} = \left(\frac{\partial f}{\partial t}\right)_{\text{Collision}} \quad (2.78)$$

where  $\mathbf{c}$  and  $\mathbf{r}$  are considered independent coordinates. In addition, the force  $\mathbf{F}$  per unit mass is assumed to be independent of  $\mathbf{c}$  and replaces the instantaneous acceleration.

Symbolically the Boltzmann equation can be written as [40]:

$$\frac{D_{\mathbf{c}}f}{D_{\mathbf{c}}t} = \left(\frac{\partial f}{\partial t}\right)_{\text{Collision}} \quad (2.79)$$

where the LHS denotes the translational motion and the RHS represents the impact of collisions.

The model derivation given above using the Liouville theorem is in many ways equivalent to the Lagrangian balance formulation [83]. Of course, a consistent Eulerian balance formulation would give the same result, but includes some more manipulations of the terms in the number balance. However, the Eulerian formulation is of special interest as we have adopted this framework in the preceding discussion of the governing equations of classical fluid dynamics, chap 1.

For binary collisions the RHS of the Boltzmann equation (2.79) assumes the form<sup>31</sup>

$$\left(\frac{\partial f}{\partial t}\right)_{\text{Collision}} = \int_{\mathbf{c}_1} \int_{4\pi} (f' f'_1 - f f_1) g \sigma_A(\boldsymbol{\Omega}) d\Omega' d\mathbf{c}_1 \quad (2.80)$$

where the primes indicate the quantities after collision.

Presenting the basic theory involved we first discuss the translational part of the equation in the limit of no collisions, before the more complex collision term closure is outlined.

### 2.4.1 The Boltzmann Equation in the Limit of no Collisions

Preliminarily, deriving the terms on the LHS of the Boltzmann equation, we assume that the effects of collisions are negligible. The molecular motion is thus purely translational. We further assume that in an average sense each molecule of mass  $m$  is subjected to an external forces per unit mass,  $\mathbf{F}(\mathbf{r}, t)$ , which doesn't depend on the molecular velocity  $\mathbf{c}$ . This restriction excludes magnetic forces, while the gravity and electric fields which are more common in chemical and metallurgical reactors are retained.

### Ensemble of System Points Moving Along Their Trajectories in Phase Space

In this section we consider the translational terms in the context of a generalized advection equation [12, 77, 83, 40, 104, 39].

<sup>31</sup> Unprimed quantities will henceforth refer to initial values rather than values at arbitrary times, and primed quantities to final values after the collision.

The following shortening notation is thus introduced henceforth for the distribution function:  $f_1 \equiv f(\mathbf{c}_1, \dots)$ ,  $f' \equiv f(\mathbf{c}', \dots)$ ,  $f'_1 \equiv f(\mathbf{c}'_1, \dots)$ , etc.

The collection of molecules which at time  $t$  have positions and velocities in the range  $d\mathbf{r}d\mathbf{c}$  near  $\mathbf{r}$  and  $\mathbf{c}$  will, at an infinitesimal time  $dt$  later, have the positions and velocities in the range  $d\mathbf{r}'d\mathbf{c}'$  near  $\mathbf{r}'$  and  $\mathbf{c}'$  as a result of their motion under the influence of the force  $\mathbf{F}$ .

It follows that:

$$\mathbf{r}' = \mathbf{r} + \mathbf{c}dt \quad (2.81)$$

$$\mathbf{c}' = \mathbf{c} + \mathbf{F}dt \quad (2.82)$$

In mathematical terms the translational motion can be expressed as

$$f(\mathbf{r}', \mathbf{c}', t)d\mathbf{r}'d\mathbf{c}' = f(\mathbf{r}, \mathbf{c}, t)d\mathbf{r}d\mathbf{c} \quad (2.83)$$

The Lagrangian like control volume  $d\mathbf{r}d\mathbf{c}$  in the six dimensional phase space may become distorted in shape as a result of the motion. But, in accordance with the Liouville's theorem, discussed in sect. 2.2.3, the new volume is simply related to the old one by the relation:

$$d\mathbf{r}'d\mathbf{c}' = |\mathbf{J}|d\mathbf{r}d\mathbf{c} \quad (2.84)$$

where  $\mathbf{J}$  is the Jacobian of the transformation relations (2.81) and (2.82) from the old variables  $d\mathbf{r}d\mathbf{c}$  to the new variables  $d\mathbf{r}'d\mathbf{c}'$ . In this particular case where the force  $\mathbf{F}$  does not depend on the velocity  $\mathbf{c}$  of the molecules, we get  $\mathbf{J} = 1$  due to the Poincarè theorem. Hence,

$$f(\mathbf{r}', \mathbf{c}', t) = f(\mathbf{r}, \mathbf{c}, t) \quad (2.85)$$

or

$$f(\mathbf{r} + \mathbf{c}dt, \mathbf{c} + \mathbf{F}dt, t + dt) - f(\mathbf{r}, \mathbf{c}, t) = 0 \quad (2.86)$$

In terms of partial derivatives one obtains,

$$\left[ \left( \frac{\partial f}{\partial x}c_x + \frac{\partial f}{\partial y}c_y + \frac{\partial f}{\partial z}c_z \right) + \left( \frac{\partial f}{\partial c_x}F_x + \frac{\partial f}{\partial c_y}F_y + \frac{\partial f}{\partial c_z}F_z \right) + \frac{\partial f}{\partial t} \right] dt = 0 \quad (2.87)$$

or more compactly,

$$\frac{D_c f}{D_c t} \equiv \frac{\partial f}{\partial t} + \mathbf{c} \cdot \frac{\partial f}{\partial \mathbf{r}} + \mathbf{F} \cdot \frac{\partial f}{\partial \mathbf{c}} \quad (2.88)$$

where  $\frac{\partial f}{\partial \mathbf{r}} \equiv \nabla_{\mathbf{r}} f$  denotes the gradient of  $f$  with respect to  $\mathbf{r}$ , and  $\frac{\partial f}{\partial \mathbf{c}} \equiv \nabla_{\mathbf{c}} f$  denotes the gradient of  $f$  with respect to  $\mathbf{c}$ .

Therefore, in the limit of no molecular interactions, for which the collision term  $\left(\frac{\partial f}{\partial t}\right)_{\text{Collision}}$  vanishes, the Boltzmann equation yields

$$\frac{D_c f}{D_c t} = 0 \quad (2.89)$$

Equation (2.89) is a generalized advection equation stating that  $f$  remains unchanged if the observer moves along with the system points in phase space.

### Ensemble of System Points Moving Through a Fixed Volume in Phase Space

In this paragraph we consider the translational terms in the context of a generalized continuity equation [100, 83, 85].

Consider a fixed 6D control volume in phase space (i.e., an imaginary extension of the Eulerian control volume known from fluid dynamics, Fig. 1.2), containing a given range of molecular positions between  $\mathbf{r}$  and  $d\mathbf{r}$  and of velocities between  $\mathbf{c}$  and  $d\mathbf{c}$ . The number of molecules in this control volume  $d\mathbf{r}d\mathbf{c}$  of phase space changes as the positions and velocities of the molecules change. The net accumulation of molecules in this range in time  $dt$  is given by  $(\frac{\partial f}{\partial t})d\mathbf{r}d\mathbf{c}dt$ . The net change in the number of molecules within the control volume is determined by the number of molecules entering and leaving this range  $d\mathbf{r}d\mathbf{c}$  as a result of the random molecular motion.

In Cartesian coordinates the number of molecules entering the control volume,  $d\mathbf{r}d\mathbf{c}$ , in time  $dt$  through the face  $x = \text{constant}$  equals  $f(c_x dt)dydzdc_xdc_ydc_z$ . The corresponding number of molecules leaving through the face  $x + dx = \text{constant}$  is given by  $[fc_x + \frac{\partial}{\partial x}(fc_x)dx]dtdydzdc_xdc_ydc_z$  where both  $f$  and  $c_x$  are evaluated at  $x + dx$  and thereafter approximated using a first order Taylor expansion. Hence, the net number of molecules entering the control volume  $d\mathbf{r}d\mathbf{c}$  in time  $dt$  through the faces  $x$  and  $x + dx$  is:

$$\begin{aligned} f(c_x dt)dydzdc_xdc_ydc_z - [fc_x + \frac{\partial}{\partial x}(fc_x)dx]dtdydzdc_xdc_ydc_z \\ = -\frac{\partial}{\partial x}(fc_x)d\mathbf{r}d\mathbf{c}dt \end{aligned} \quad (2.90)$$

Net inflow in y- direction

$$\begin{aligned} f(c_y dt)dxzdc_xdc_ydc_z - [fc_y + \frac{\partial}{\partial y}(fc_y)dy]dtdxdzdc_xdc_ydc_z \\ = -\frac{\partial}{\partial y}(fc_y)d\mathbf{r}d\mathbf{c}dt \end{aligned} \quad (2.91)$$

Net inflow in z- direction

$$\begin{aligned} f(c_z dt)dxdydc_xdc_ydc_z - [fc_z + \frac{\partial}{\partial z}(fc_z)dz]dtdxdydc_xdc_ydc_z \\ = -\frac{\partial}{\partial z}(fc_z)d\mathbf{r}d\mathbf{c}dt \end{aligned} \quad (2.92)$$

Net inflow through the  $c_x$  face of the velocity space:

$$\begin{aligned} f(F_x dt)dxdydzdc_ydc_z - [fF_x + \frac{\partial}{\partial c_x}(fF_x)dc_x]dtdxdydzdc_ydc_z \\ = -\frac{\partial}{\partial c_x}(fF_x)d\mathbf{r}d\mathbf{c}dt \end{aligned} \quad (2.93)$$

Net inflow through the  $c_y$  face of the velocity space:

$$\begin{aligned} & f(F_y dt) dx dy dz dc_x dc_z - [f F_y + \frac{\partial}{\partial c_y}(f F_y) dc_y] dt dx dy dz dc_x dc_z \\ &= -\frac{\partial}{\partial c_y}(f F_y) d\mathbf{r} d\mathbf{c} dt \end{aligned} \quad (2.94)$$

Net inflow through the  $c_z$  face of the velocity space:

$$\begin{aligned} & f(F_z dt) dx dy dz dc_x dc_y - [f F_z + \frac{\partial}{\partial c_z}(f F_z) dc_z] dt dx dy dz dc_x dc_y \\ &= -\frac{\partial}{\partial c_z}(f F_z) d\mathbf{r} d\mathbf{c} dt \end{aligned} \quad (2.95)$$

Overall, the net inflow of molecules into the phase space  $d\mathbf{r} d\mathbf{c}$  is balanced by the transient term, hence:

$$\begin{aligned} \left(\frac{\partial f}{\partial t}\right) d\mathbf{r} d\mathbf{c} dt &= -\left[\frac{\partial}{\partial x}(f c_x) + \frac{\partial}{\partial y}(f c_y) + \frac{\partial}{\partial z}(f c_z)\right] d\mathbf{r} d\mathbf{c} dt \\ &\quad -\left[\frac{\partial}{\partial c_x}(f F_x) + \frac{\partial}{\partial c_y}(f F_y) + \frac{\partial}{\partial c_z}(f F_z)\right] d\mathbf{r} d\mathbf{c} dt \end{aligned} \quad (2.96)$$

Or, after dividing by  $d\mathbf{r} d\mathbf{c} dt$  and adopting Einsteins summation index notation:

$$\begin{aligned} \left(\frac{\partial f}{\partial t}\right) &= -\frac{\partial}{\partial x_i}(f c_i) - \frac{\partial}{\partial c_i}(f F_i) \\ &= -\left[c_i \frac{\partial f}{\partial x_i} + F_i \frac{\partial f}{\partial c_i}\right] - f\left[\frac{\partial c_i}{\partial x_i} + \frac{\partial F_i}{\partial c_i}\right] \end{aligned} \quad (2.97)$$

Further simplification can be achieved as we recall that the variables  $\mathbf{r}$  and  $\mathbf{c}$  are independent, hence:

$$\frac{\partial c_i}{\partial x_i} = 0 \quad (2.98)$$

In a similar manner,

$$\frac{\partial F_i}{\partial c_i} = 0 \quad (2.99)$$

since  $\mathbf{F}$  does not depend on  $\mathbf{c}$ .

Using the latter two relations the terms within the last bracket in (2.97) vanish, so the Boltzmann equation reduces to:

$$\frac{\partial f}{\partial t} = -\mathbf{c} \cdot \frac{\partial f}{\partial \mathbf{r}} - \mathbf{F} \cdot \frac{\partial f}{\partial \mathbf{c}} \quad (2.100)$$

This relation is known as the Liouville theorem as discussed in sect. 2.2.3.

Introducing a generalized form of the substantial derivative, measuring the rate of change as the observer moves along with the system points in

phase space, a compact form similar to (2.89) is achieved. Note also that it is common in the mechanics literature to assume that there always exists a sufficiently differentiable and single-valued function defining the position vector, even though it is unknown. In this interpretation the molecular positions and velocities changes in accordance with (2.81) and (2.82) [63] (sec. 4.3).

### 2.4.2 Binary Collisions

To determine the rate of change of  $f$  caused by molecular collisions we have to introduce a number of simplifying assumptions concerning the molecular motion and collisions. The most important assumptions are [83, 12, 28]:

- The gas density is assumed to be very low so that only binary collisions need to be taken into account. At higher densities, ternary and higher order interactions become significant.
- The interactions with the external boundaries of the system are ignored.
- We neglect all possible effects which can be exerted by the external force per unit mass,  $\mathbf{F}$ , on the magnitude of the collisional cross section.
- We assume *local equilibrium*. This means that the distribution function  $f(\mathbf{r}, \mathbf{c}, t)$  does not vary appreciably during a time interval of the order of the duration of a molecular collision, nor does it vary appreciably over a spatial distance of the order of the range of intermolecular forces.
- We assume *molecular chaos*. This means that in binary collisions both sets of molecules are randomly distributed so that the molecular velocity is uncorrelated with their position.

The time between two subsequent molecular collisions is also considered large enough so that one can neglect possible correlations between their initial velocities prior to the collision.

In other words, in approximate accordance with the original paper by Boltzmann [6], we assume that in a given volume element the expected number of collisions between molecules that belong to different velocity ranges can be computed statistically. This assumption is referred to as the Boltzmann *Stosszahlansatz*<sup>32</sup> (German for: Collision number assumption). A result of the Boltzmann *H-theorem* analysis is that the latter statistical assumption makes Boltzmann's equation irreversible in time (e.g., [28], sect. 4.2).

---

<sup>32</sup> This assumption is difficult to justify because it introduces statistical arguments into a problem that is in principle purely mechanical [85]. Criticism against the Boltzmann equation was raised in the past related to this problem. Nowadays it is apparently accepted that the molecular chaos assumption is needed only for the molecules that are going to collide. After the collision the scattered particles are of course strongly correlated, but this is considered irrelevant for the calculation since the colliding molecules come from different regions of space and have met in their past history other particles and are therefore entirely uncorrelated.

No exact expression for  $(\frac{\partial f}{\partial t})_{\text{Collision}}$  has been obtained since the nature of the interaction between the colliding molecules is not known in sufficient details. We resort to assume by hypothesis some laws of interaction which are validated comparing the overall results with experimental data.

Nevertheless, detailed experimental analysis of gases shows that, at distances large compared to the molecular dimensions, weak intermolecular forces exist, whereas at distances of the order of the molecular dimensions the molecules repel each other strongly. Moreover, collisions between complex molecules may in general also redistribute energy between the translational and internal energy forms.

To close the statistical Boltzmann equation determining the evolution of the distribution function, it is considered advantageous to derive constitutive relations for the collision term based on mechanistic analysis of simplified images or models of binary particle collisions. In this context simplifying assumptions about the nature of the forces between the two molecules during collisions must be made. Several molecular models have been considered, as already mentioned in sect. 2.3.1. Taking into account the molecular interactions we need a mathematical expression for the rate at which the distribution function  $f$  is being altered by collisions. In the Boltzmann equation, this phenomenon is represented by the net rate at which collisions increase or decrease the number of molecules entering the phase volume  $d\mathbf{r}d\mathbf{c}$ , hence:

$$\left(\frac{\partial f}{\partial t}\right)_{\text{Collision}} = \left(\frac{\partial f}{\partial t}\right)_{\text{Collision}}^+ - \left(\frac{\partial f}{\partial t}\right)_{\text{Collision}}^- \quad (2.101)$$

where the number of particles injected into  $d\mathbf{r}d\mathbf{c}$  due to collisions during the time  $dt$  is  $(\frac{\partial f}{\partial t})_{\text{Collision}}^+ d\mathbf{r}d\mathbf{c}dt$ , while those ejected is  $(\frac{\partial f}{\partial t})_{\text{Collision}}^- d\mathbf{r}d\mathbf{c}dt$ .

However, the equation cannot be applied in practice before constitutive relations for the unknown quantities  $(\frac{\partial f}{\partial t})_{\text{Collision}}^+$  and  $(\frac{\partial f}{\partial t})_{\text{Collision}}^-$  are formulated in terms of the distribution function  $f$  which is to be determined solving the Boltzmann equation.

To proceed we need to understand, and define in mathematical terms, the fundamental nature of binary collisions. In particular, it is desired to define the relationships between the initial and final velocities, the scattering cross sections, the symmetry properties of the collision, and the collision frequency.

## Dynamics of a Binary Collision

In this section we consider an elastic collision in free space between two spinless mono-atomic molecules<sup>33</sup> of masses  $m_1$  and  $m_2$ . In the laboratory frame the initial particle positions are denoted by  $\mathbf{r}_1$  and  $\mathbf{r}_2$ , and their initial velocities are indicated by  $\mathbf{c}_1$  and  $\mathbf{c}_2$ . The corresponding positions and velocities

<sup>33</sup> The theory may be useful even if the molecules are not mono-atomic, provided that their states of internal motion (e.g., rotation and vibration) are not affected by the collisions.

after the collision are  $\mathbf{r}'_1$ ,  $\mathbf{r}'_2$  and  $\mathbf{c}'_1$ ,  $\mathbf{c}'_2$ , respectively. In this frame the incident particle (i.e., sometimes called the projectile) ( $m_2$ ) moves in and the target ( $m_1$ ) is initially at rest. It is supposed that the particles interact through conservative forces only, so any external forces which act on the molecules are so small compared with the internal forces involved locally in the collision that their effect on the outcome of a collision can be neglected.

To express the dynamics of a binary collision in mathematical terms a more precise definition of a collision is needed. A collision occurs when two particles interact. The time taken for the interactions is assumed to be so small that we may consider them instantaneous compared to the time period between successive collisions. For this reason our interest lies on the particles' dynamics before and after the interaction takes place. It is essential to notice that the interacting particles do not necessarily touch physically for a collision to occur. We may then introduce a measure  $r_0$  that denotes the range of interaction. This parameter is thus defined so that, when the particles are sufficiently far away from each other ( $r > r_0$ ), the interaction vanishes. By definition, when the particles enter the interaction domain ( $r \leq r_0$ ), they experience a collision. The meaning of before and after collision is thus given in terms of the potential of interaction  $E_P(r)$  or the range of interaction  $r_0$ . Before interaction denotes the interval in which the particles are approaching one another and  $r > r_0$  or, equivalently,  $E_P(r) = 0$ . After collision denotes the interval in which the particles are receding from one another and, again,  $E_P(r) = 0$  and  $r > r_0$ .

*Before the particles are entering the interaction region,  $r > r_0$ , the two particles move freely with constant momenta towards each other. The total energy of the system equals the sum of the kinetic energies:*

$$E_{\text{Total}} = \frac{\mathbf{p}_1^2}{2m_1} + \frac{\mathbf{p}_2^2}{2m_2} \quad (2.102)$$

*After the particles are exiting the interaction region,  $r > r_0$ , they again move freely with constant momenta but now away from each other. The energy after interaction is:*

$$E'_{\text{Total}} = \frac{\mathbf{p}'_1{}^2}{2m_1} + \frac{\mathbf{p}'_2{}^2}{2m_2} = E_{\text{Total}} \quad (2.103)$$

*In the interaction region,  $r \leq r_0$ , the kinetic energy of the particles is generally converted partly into potential energy. The total energy of the two particles is still conserved:*

$$E'_{\text{Total}} = T + E_p = E_{\text{Total}} \quad (2.104)$$

For elastic collisions we examine this energy balance in further details considering hard sphere billiard ball like particles. In the laboratory frame the equations of motion for each of the interacting particles are:

$$m_1 \frac{d^2 \mathbf{r}_1}{dt^2} = \mathbf{F}_{12} \quad (2.105)$$

$$m_2 \frac{d^2 \mathbf{r}_2}{dt^2} = \mathbf{F}_{21} \quad (2.106)$$

where the force exerted on molecule 1 by molecule 2 is denoted by  $\mathbf{F}_{12}$ , and the force exerted on molecule 2 by molecule 1 is denoted by  $\mathbf{F}_{21}$ .

Provided that the interaction forces are conservative we may multiply (2.105) with the particle velocity  $\mathbf{c}_1 = \dot{\mathbf{r}}_1$  and (2.106) with the particle velocity  $\mathbf{c}_2 = \dot{\mathbf{r}}_2$ , and integrating in time. The result denotes the law of conservation of total energy [43]:

$$E_{\text{Total}} = \frac{1}{2} m_1 \mathbf{c}_1^2 + \frac{1}{2} m_2 \mathbf{c}_2^2 + E_p(|\mathbf{r}_1 - \mathbf{r}_2|) = \text{Constant} \quad (2.107)$$

It is now important to recollect that we regard the range  $r \leq r_0$  over which  $E_p$  is effective as being negligible small (i.e.,  $E_p(|\mathbf{r}_1 - \mathbf{r}_2|) \rightarrow 0$  for  $|\mathbf{r}_1 - \mathbf{r}_2| \geq r_0$ ), so our interest lies in what happens before and after the particles interact. Therefore, for elastic collisions the kinetic energy is conserved:

$$\frac{1}{2} m_1 c_1^2 + \frac{1}{2} m_2 c_2^2 = \frac{1}{2} m_1 c_1'^2 + \frac{1}{2} m_2 c_2'^2 = E_{\text{Total}} \quad (2.108)$$

Similarly, the sum of the cross products of (2.105) and (2.106) with  $\dot{\mathbf{r}}_1$  and  $\dot{\mathbf{r}}_2$ , respectively, leads to the law of conservation of total angular momentum:

$$L_{\text{Total}} = m_1 \mathbf{r}_1 \times \dot{\mathbf{r}}_1 + m_2 \mathbf{r}_2 \times \dot{\mathbf{r}}_2 = \text{Constant} \quad (2.109)$$

The relative position vectors in the laboratory frame are defined by:

$$\mathbf{r} = \mathbf{r}_2 - \mathbf{r}_1 \quad \text{and} \quad \mathbf{r}' = \mathbf{r}_2' - \mathbf{r}_1' \quad (2.110)$$

Accordingly, the relative displacements are:

$$r = |\mathbf{r}_2 - \mathbf{r}_1| \quad \text{and} \quad r' = |\mathbf{r}_2' - \mathbf{r}_1'| \quad (2.111)$$

The coordinate  $\mathbf{r}_c$  of the center of mass of two point particles is given by the weighted average of their coordinates  $\mathbf{r}_1$  and  $\mathbf{r}_2$ :

$$\mathbf{r}_c = \frac{m_1 \mathbf{r}_1 + m_2 \mathbf{r}_2}{m_1 + m_2} \quad (2.112)$$

where  $m_c = m_1 + m_2$  is the total mass.

The coordinates of the center of mass point  $\mathbf{r}_c$  lies on the straight line connecting the positions  $\mathbf{r}_1$  and  $\mathbf{r}_2$  of point masses  $m_1$  and  $m_2$ , respectively.

The velocity of the center of mass is given by:

$$\mathbf{G} = \frac{d\mathbf{r}_c}{dt} \quad (2.113)$$

It follows that the center of mass acceleration vanishes as:

$$m_c \frac{d\mathbf{G}}{dt} = m_c \frac{d^2 \mathbf{r}_c}{dt^2} = m_1 \frac{d^2 \mathbf{r}_1}{dt^2} + m_2 \frac{d^2 \mathbf{r}_2}{dt^2} = \mathbf{F}_{12} + \mathbf{F}_{21} = 0 \quad (2.114)$$

since the Newton 3. law of action and reaction states that  $\mathbf{F}_{12} = -\mathbf{F}_{21}$ . Note also that when the forces are given by the interaction potential  $E_p(r)$ , the local problem is spherically symmetric [43].

This result implies, when integrated in time, that the conservation of linear momentum yields:

$$m_c \mathbf{G} = m_1 \mathbf{c}_1 + m_2 \mathbf{c}_2 = m_1 \mathbf{c}'_1 + m_2 \mathbf{c}'_2 = \mathbf{P} = \text{Constant} \quad (2.115)$$

showing that the velocities are not independent. In fact (2.115) states that the total mass  $m_c$  of the two molecules moves uniformly throughout the collision. That is, the center of mass velocity  $\mathbf{G}$  remains unchanged since  $\mathbf{P}$  is conserved (constant) for elastic collisions.

Another quantity of interest is the relative velocity. Let  $\mathbf{g}_{21}$  and  $\mathbf{g}'_{21}$ , and  $\mathbf{g}_{12}$  and  $\mathbf{g}'_{12}$  denote respectively the initial and final velocity of the second molecule relative to the first, and of the first relative to the second, so that:

$$\mathbf{g}_{21} = \mathbf{c}_2 - \mathbf{c}_1 = -\mathbf{g}_{12} \quad \text{and} \quad \mathbf{g}'_{21} = \mathbf{c}'_2 - \mathbf{c}'_1 = -\mathbf{g}'_{12} \quad (2.116)$$

The magnitudes of  $\mathbf{g}_{21}$  and  $\mathbf{g}_{12}$  are equal and can be denoted by  $g$ , likewise for the final relative velocities. Thus:

$$g_{21} = g_{12} = g \quad \text{and} \quad g'_{21} = g'_{12} = g' \quad (2.117)$$

By means of (2.115) and (2.116) we can express  $\mathbf{c}_1$  and  $\mathbf{c}_2$ , and  $\mathbf{c}'_1$  and  $\mathbf{c}'_2$  in terms of  $\mathbf{G}$  and  $\mathbf{g}_{21}$ , as given by:

$$\begin{aligned} \mathbf{c}_1 &= \mathbf{G} - \frac{\mu}{m_1} \mathbf{g}_{21} \\ \mathbf{c}'_1 &= \mathbf{G} - \frac{\mu}{m_1} \mathbf{g}'_{21} \\ \mathbf{c}_2 &= \mathbf{G} + \frac{\mu}{m_2} \mathbf{g}_{21} \\ \mathbf{c}'_2 &= \mathbf{G} + \frac{\mu}{m_2} \mathbf{g}'_{21} \end{aligned} \quad (2.118)$$

where  $\mu = \frac{m_1 m_2}{m_1 + m_2}$  is the *reduced mass*.

The ratio between the kinetic energy (2.108) and momentum (2.115) is:

$$\frac{m_1(\mathbf{c}'_1{}^2 - \mathbf{c}_1{}^2)}{m_1(\mathbf{c}'_1 - \mathbf{c}_1)} = -\frac{m_2(\mathbf{c}'_2{}^2 - \mathbf{c}_2{}^2)}{m_2(\mathbf{c}_2 - \mathbf{c}'_2)} \quad (2.119)$$

and, after simple manipulations

$$\mathbf{c}'_1 + \mathbf{c}_1 = \mathbf{c}_2 + \mathbf{c}'_2 \quad \text{or equivalently} \quad \mathbf{g}'_{21} = -\mathbf{g}_{21} \quad (2.120)$$

Accordingly, by integration in time we also get:  $\mathbf{r}' = -\mathbf{r}$ .

From the momentum conservation relation (2.115) and (2.118), we obtain:

$$\mathbf{c}'_1 = \frac{2m_2\mathbf{c}_2 + (m_1 - m_2)\mathbf{c}_1}{m_c} = \frac{2m_2}{m_c}\mathbf{c}_2 \quad (2.121)$$

and

$$\mathbf{c}'_2 = \frac{2m_1\mathbf{c}_1 + (m_2 - m_1)\mathbf{c}_2}{m_c} = \frac{m_2 - m_1}{m_c}\mathbf{c}_2 \quad (2.122)$$

In the particular case of scattering from a stationary target,  $\mathbf{c}_1 = 0$ .

It is noticed that *in-elastic* collisions are characterized by the degree to which the relative speed is no longer conserved. For this reason the coefficient of restitution  $e$  in a collision is defined (i.e., with basis in (2.120)) as the ratio of the relative velocity after collision, divided by the relative velocity of approach [45] [69]:

$$\mathbf{c}'_2 - \mathbf{c}'_1 = -e(\mathbf{c}_2 - \mathbf{c}_1) \quad (2.123)$$

where  $e = 1$  denotes elastic collisions, whereas  $e = 0$  for totally inelastic collisions.

We now transform the model into a frame of reference that moves along with the center of mass in which  $\mathbf{r}_c = 0$  is taken as origin. In this coordinate system the center of mass motion is eliminated, and the origin point is at rest so  $\mathbf{P}_c = 0$ . The center of mass frame is 1D in the symmetric case.

By use of the relations given in (2.118), (2.108) becomes:

$$E_c = \frac{1}{2}m_c(G_c^2 + \frac{\mu}{m_c}g^2) = \frac{1}{2}m_c(G_c^2 + \frac{\mu}{m_c}g'^2) \quad (2.124)$$

The relative velocity changes from the value  $\mathbf{g}_{21}$  before the collision to the value  $\mathbf{g}'_{21}$  after the collision. Since the collision is assumed to be elastic so that the internal energies of the molecules remain unchanged, the total kinetic energy  $E_c$  remains unchanged in a collision.

By the definition of the center of mass frame, (2.115) yields:

$$\mathbf{P}_c = m_c\mathbf{G}_c = m_1\mathbf{c}_{1c} + m_2\mathbf{c}_{2c} = m_1\mathbf{c}'_{1c} + m_2\mathbf{c}'_{2c} = 0 \quad (2.125)$$

It then follows from (2.124) that  $E_c = \frac{\mu}{m_c}g^2 = \frac{\mu}{m_c}g'^2$  so that  $g = g'$ , as the center of mass velocity  $\mathbf{G}_c$  vanishes as a consequence of conservation of momentum (2.125). This result shows that the relative velocity is changed only in direction and not in magnitude by the collision. The dynamical effect of a collision is therefore known when the change in direction of  $\mathbf{g}_{21}$  is determined.

Further knowledge on the direction of  $\mathbf{g}_{21}$  is obtained by examining the simultaneous positions (or velocities) of the two particles in the center of mass framework. The position vectors  $\mathbf{r}_{1c}$ ,  $\mathbf{r}_{2c}$  and  $\mathbf{r}'_{1c}$ ,  $\mathbf{r}'_{2c}$  of the particles relative to the center of mass are defined by:

$$\mathbf{r}_{1c} = \mathbf{r}_1 - \mathbf{r}_c = -\frac{\mu}{m_1}\mathbf{r} \quad (2.126)$$

$$\mathbf{r}_{2c} = \mathbf{r}_2 - \mathbf{r}_c = \frac{\mu}{m_2} \mathbf{r} \quad (2.127)$$

$$\mathbf{r}'_{1c} = \mathbf{r}'_1 - \mathbf{r}'_c = -\frac{\mu}{m_1} \mathbf{r}' \quad (2.128)$$

$$\mathbf{r}'_{2c} = \mathbf{r}'_2 - \mathbf{r}'_c = \frac{\mu}{m_2} \mathbf{r}' \quad (2.129)$$

Eliminating the relative position vectors  $\mathbf{r}$  and  $\mathbf{r}'$  from these relations, yield:

$$m_1 \mathbf{r}_{1c} = -m_2 \mathbf{r}_{2c} \quad (2.130)$$

$$m_1 \mathbf{r}'_{1c} = -m_2 \mathbf{r}'_{2c} \quad (2.131)$$

This means that in the frame of reference which moves with the center of mass, the position vectors are at all times oppositely directed along a line, and their magnitudes have a fixed ratio.

It is further note that, by derivation of (2.126) to (2.129) with respect to time, we get:

$$\mathbf{c}_{1c} = \dot{\mathbf{r}}_{1c} = -\frac{\mu}{m_1} (\dot{\mathbf{r}}_2 - \dot{\mathbf{r}}_1) = -\frac{\mu}{m_1} \mathbf{c}_2 \quad (2.132)$$

$$\mathbf{c}_{2c} = \dot{\mathbf{r}}_{2c} = \frac{\mu}{m_2} (\dot{\mathbf{r}}_2 - \dot{\mathbf{r}}_1) = \frac{\mu}{m_2} \mathbf{c}_2 \quad (2.133)$$

$$\mathbf{c}'_{1c} = \dot{\mathbf{r}}'_{1c} = -\frac{\mu}{m_1} (\dot{\mathbf{r}}'_2 - \dot{\mathbf{r}}'_1) = \frac{\mu}{m_1} (\dot{\mathbf{r}}_2 - \dot{\mathbf{r}}_1) = \frac{\mu}{m_1} \mathbf{c}_2 \quad (2.134)$$

$$\mathbf{c}'_{2c} = \dot{\mathbf{r}}'_{2c} = \frac{\mu}{m_2} (\dot{\mathbf{r}}'_2 - \dot{\mathbf{r}}'_1) = -\frac{\mu}{m_2} (\dot{\mathbf{r}}_2 - \dot{\mathbf{r}}_1) = -\frac{\mu}{m_2} \mathbf{c}_2 \quad (2.135)$$

Since in the laboratory frame  $\mathbf{c}_1 = 0$ .

No further information about the collision can be obtained from the laws of conservation of momentum and energy. Instead, geometrical analysis of the interaction between molecules reveals that the direction of  $\mathbf{g}'_{21}$  depends not only on the initial velocities  $\mathbf{c}_1$  and  $\mathbf{c}_2$  (or in  $\mathbf{G}$  and  $\mathbf{g}_{21}$ ), but also on two independent geometrical variables.

Therefore, to determine the direction of  $\mathbf{g}'_{21}$  an investigation of the collision geometry is required. We naturally chose to work in a polar coordinate frame of reference where the trajectory is represented by the polar coordinates  $(r, \psi, \phi)$  with the polar axis lying along  $z$  being parallel to  $\mathbf{g}_{21}$ , as indicated in Fig. 2.2 and Fig. 2.3. The polar coordinates of a point molecule 2 give its position relative to a fixed reference point 0 and a given polar axis  $z$ . The radial coordinate  $r$  is the distance from 0 to the molecule 2.  $\theta$  is the angle between  $\mathbf{g}'_{21}$  and the  $z$  axis and  $\phi$  is the rotational angle of  $\mathbf{g}'_{21}$  about the  $z$  axis. Molecule 2 approaches  $O$  with velocity  $\mathbf{g}_{21}$  with a perpendicular distance  $b$  to the straight line between the source of the particle at  $r = -\infty$  and the scattering center  $O$ . The distance  $b$  is called the impact parameter. For elastic collisions in which  $|\mathbf{g}'_{21}| = |\mathbf{g}_{21}|$ , the final state is specified by the scattering angle  $\phi$  and the impact parameter  $b$ . Specifying  $\mathbf{G}$ ,  $\mathbf{g}_{21}$ , the angle  $\phi$ , and the impact parameter  $b$ , uniquely determines  $\mathbf{g}'_{21}$ .

At first sight, it may look like the two particle problem of describing the motion of a molecule 2 relative to molecule 1 is equivalent to the one particle problem of describing the motion of a single molecule 2 with reduced mass  $\mu$  acted on by the force  $\mathbf{F}_{21}$ . With respect to a fixed particle 1 the scattering process appears as shown in Fig. 2.2.

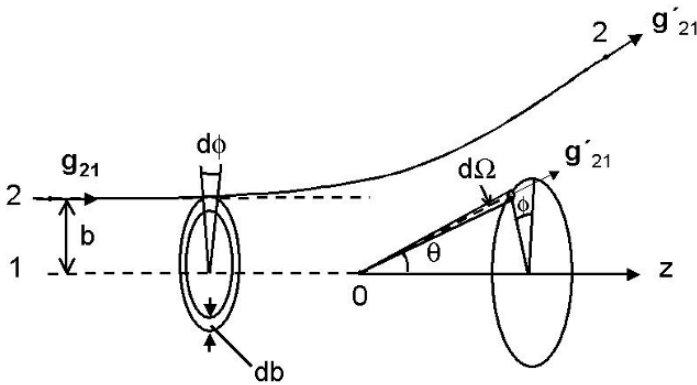


**Fig. 2.2.** Scattering of a molecule by a fixed center of force O. Molecule 1 is at rest with its center at the origin.

Using (2.118), the equation of motion for particle 2 (2.106) can be expressed as:

$$m_2 \frac{d^2 \mathbf{r}_2}{dt^2} = \mu \frac{d^2 \mathbf{r}}{dt^2} = \mathbf{F}_{21} \quad (2.136)$$

However, the problem cannot be solved that easily [35] [73]. The scattering angle  $\theta_L$  measured in the laboratory frame is the angle between the final and incident directions of the scattered particle, whereas the angle  $\theta$  calculated from the equivalent one-body problem is the angle between the final and initial directions of the relative vectors between the two particles. It is proven that the two angles are the same provided that the reference particle remains stationary throughout the scattering process (i.e., when the origin of the relative vector  $\mathbf{r}$  is fixed). On the contrary, in a real two-particle scattering event the reference particle recoils and is itself set in motion by the mutual force between the two particles, and it follows that the two angles are not the same. This means that for elastic binary particle collisions the scattering process is most conveniently described transforming the problem from the laboratory frame to a coordinate system moving with the center of mass of both particles [77] [35]. The angle between the initial and final directions of the relative vectors coincides with the scattering angle in this particular view. In this particular coordinate system it suffices to describe only one of the molecules in a binary collision as the second particle always moves oppositely.

Moreover, calculations are usually done in the *center of mass* frame, whereas the measurements are done in the *laboratory* frame [35]. Therefore, to calculate the kinematics of elastic collisions, it is often convenient to utilize both frames sequentially determining the scattering angles. That is, it is normally a better strategy to transform the problem to the center of mass frame, examine the kinetics of the collision and then transfer the result back to the laboratory frame, than to work directly in the laboratory frame. In particular, this procedure enables us to link the scattering angles in the laboratory frame  $\theta_L$  and the center of mass frame  $\theta$ .

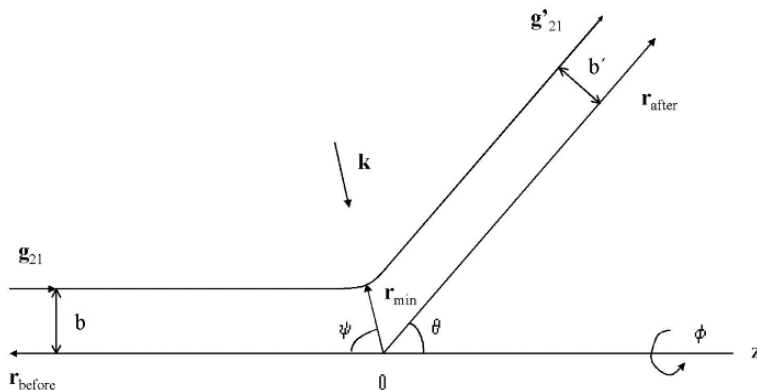


**Fig. 2.3.** Scattering in the frame of the relative vector  $\mathbf{r}$ . The scattering angle  $\theta$  is related to  $\psi$  through the relation  $\theta + 2\psi = \pi$ .

A simple geometrical analysis shows that after the scattering has taken place the velocity vectors  $\mathbf{c}'_2$  and  $\mathbf{c}'_{2c}$  make the angles  $\theta_L$  and  $\theta$ , respectively, with the vector  $\mathbf{G}$  lying along the initial direction of  $\mathbf{c}_1$  [35], Fig. 2.4. Using (2.118) which is expressed in the laboratory frame and (2.135) linking the two frames, we get:

$$\mathbf{c}'_2 = \mathbf{G} + \frac{\mu}{m_2} \mathbf{g}'_{21} = \mathbf{G} + \mathbf{c}'_{2c} = \frac{\mu}{m_1} \mathbf{c}_2 + \mathbf{c}'_{2c} \quad (2.137)$$

From Fig. 2.4 it can be seen that:

$$|\mathbf{c}'_2| \sin \theta_L = |\mathbf{c}'_{2c}| \sin \theta \quad (2.138)$$

since  $\mathbf{G}$  and  $\mathbf{c}_2$  are parallel vectors, and

$$|\mathbf{c}'_2| \cos \theta_L = |\mathbf{c}'_{2c}| \cos \theta + |\mathbf{G}| \quad (2.139)$$

by the scalar product of the two vectors  $\mathbf{c}'_2$  and  $\mathbf{G}$ , and noting that  $\mathbf{c}'_2 = \mathbf{G} + \mathbf{c}'_{2c}$  in accordance with (2.137).

The ratio of the latter two equations gives a relation between  $\theta_L$  and  $\theta$ :

$$\tan \theta_L = \frac{\sin \theta}{\cos \theta + \frac{|\mathbf{G}|}{|\mathbf{c}'_{2c}|}} = \frac{\sin \theta}{\cos \theta + \frac{\mu}{m_1} \frac{|\mathbf{c}_2|}{|\mathbf{c}'_{2c}|}} \quad (2.140)$$

By derivation of (2.129) we know that  $|\mathbf{c}'_{2c}| = \frac{\mu}{m_2} |\mathbf{g}_{21}| = \frac{\mu}{m_2} |\mathbf{c}_2|$ , so for elastic collisions we have [35] [37]

$$\tan \theta_L = \frac{\sin \theta}{\cos \theta + \frac{m_2}{m_1}} \quad (2.141)$$

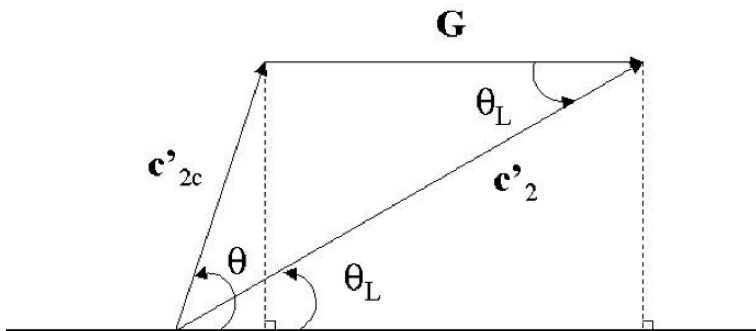


**Fig. 2.4.** The relations between the velocities in the center of mass and laboratory coordinates.

The use of this relationship is further elucidated calculating the scattering cross sections in sect. 2.4.2.

### Relative Velocity Variation

In this section we consider a scattering event, viewed in a frame where the origin of the relative vector  $\mathbf{r}$  is fixed (i.e., equivalent to the center of mass frame), as sketched in Fig. 2.3. The line joining the two molecules when at the points of closest approach,  $\mathbf{r}_{\min}$ , is called *the apse-line*. This apse-line passes through  $O$ , the intersection of the two asymptotes  $\mathbf{g}_{21}$  and  $\mathbf{g}'_{21}$ . The unit vector  $\mathbf{k}$  of the apse-line bisects the angle between  $-\mathbf{g}_{21}$  and  $\mathbf{g}'_{21}$ , as the orbit of the second molecule relative to the first is symmetrical about the apse-line. This symmetry is a consequence of the conservation of angular momentum  $L = \mu g b = \mu g' b'$  [61] [35].

The components of  $\mathbf{g}_{21}$  and  $\mathbf{g}'_{21}$  are equal in magnitude, but opposite in sign, hence  $\mathbf{g}_{21} \cdot \mathbf{k} = -\mathbf{g}'_{21} \cdot \mathbf{k}$ . It follows that  $\mathbf{g}_{21}$  and  $\mathbf{g}'_{21}$  differ by twice the component of  $\mathbf{g}_{21}$  in the direction of  $\mathbf{k}$ , thus:

$$\mathbf{g}_{21} - \mathbf{g}'_{21} = 2(\mathbf{g}_{21} \cdot \mathbf{k})\mathbf{k} = -2(\mathbf{g}'_{21} \cdot \mathbf{k})\mathbf{k} \quad (2.142)$$

The components of  $\mathbf{g}_{21}$  and  $\mathbf{g}'_{21}$  perpendicular to  $\mathbf{k}$  are equal:  $\mathbf{g} - \mathbf{k}(\mathbf{k} \cdot \mathbf{g}) = \mathbf{g}' - \mathbf{k}(\mathbf{k} \cdot \mathbf{g}')$ .

With the help of (2.118) we find that:

$$\mathbf{c}'_1 - \mathbf{c}_1 = \frac{\mu}{m_2}(\mathbf{g}_{21} - \mathbf{g}'_{21}) = 2\frac{\mu}{m_2}(\mathbf{g}_{21} \cdot \mathbf{k})\mathbf{k} = -2\frac{\mu}{m_2}(\mathbf{g}'_{21} \cdot \mathbf{k})\mathbf{k} \quad (2.143)$$

and

$$\mathbf{c}'_2 - \mathbf{c}_2 = \frac{\mu}{m_1}(\mathbf{g}_{21} - \mathbf{g}'_{21}) = 2\frac{\mu}{m_1}(\mathbf{g}_{21} \cdot \mathbf{k})\mathbf{k} = -2\frac{\mu}{m_1}(\mathbf{g}'_{21} \cdot \mathbf{k})\mathbf{k} \quad (2.144)$$

This result implies that when  $\mathbf{k}$ ,  $\mathbf{c}_1$  and  $\mathbf{c}_2$  are given, the velocities after the collision can be determined. That is, it is recognized from (2.80) that these relations are needed in order to calculate the part of the collision term concerning the inverse collision (i.e.,  $f'_1[\mathbf{c}'_1] = f'_1[\mathbf{c}_1 + 2\frac{\mu}{m_2}(\mathbf{g}_{21} \cdot \mathbf{k})\mathbf{k}]$  and  $f'_2[\mathbf{c}'_2] = f'_2[\mathbf{c}_2 - 2\frac{\mu}{m_1}(\mathbf{g}'_{21} \cdot \mathbf{k})\mathbf{k}]$ ).

### Concept of Solid Angle

The concept of solid angle, commonly used in kinetic theory, radiation and other scattering problem descriptions, is defined before the molecular scattering process is described in further details in the subsequent section.

Basically, the solid angle is the three dimensional analog of an ordinary angle. A differential plane angle  $d\chi$  is defined as the ratio of the element of arc length  $dl$  on the circle to the radius  $r$  of the circle, hence  $d\chi = dl/r$ . Analogous, the differential solid angle  $d\Omega$  subtended by an arbitrary differential surface  $dA$  is defined as the differential surface area  $d\Omega$  of a unit sphere covered by the arbitrary surface's projection onto the unit sphere [77] [42] [88]:

$$d\Omega = \frac{\mathbf{e}_r \cdot d\mathbf{A}}{|\mathbf{r}|^2} = \frac{\mathbf{e}_r \cdot \mathbf{n}dA}{r^2} \quad (2.145)$$

where  $\mathbf{e}_r = \frac{\mathbf{r}}{|\mathbf{r}|}$  denotes a unit vector in the direction of  $\mathbf{r}$ ,  $|\mathbf{r}|$  is the distance from the origin to the arbitrary differential area  $dA$ , and  $\mathbf{n}$  is the unit normal vector of the differential surface area  $dA$  as sketched in Fig. 2.5.

In kinetic theory we are using the solid angle to indicate the direction of the outgoing particles after the collision. In principle, we can calculate the solid angle from any given surface. We chose to use the particular surface that

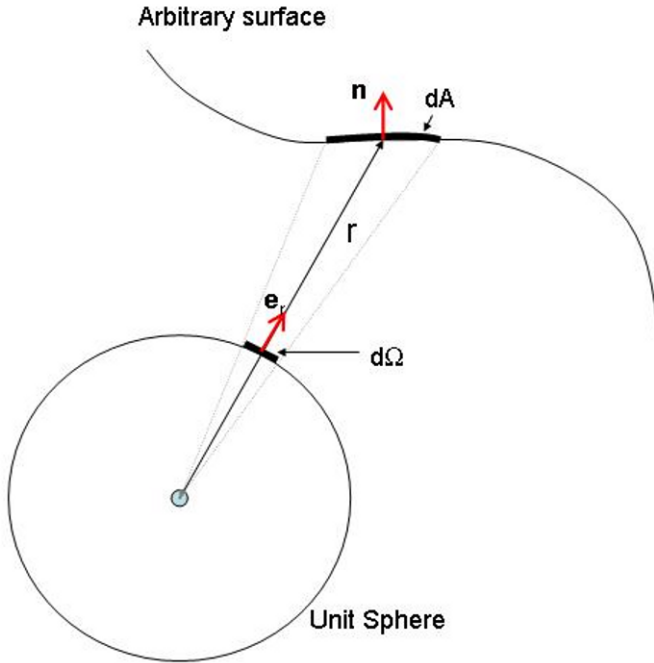


**Fig. 2.5.** An illustration of the differential solid angle,  $d\Omega = \sin\theta d\theta d\phi$ . The solid angle has the units of the steradian (sr) or  $\text{radian}^2$  ( $\text{rad}^2$ ).

coincides with the unit sphere making the mathematical complexity feasible. In this particular case we observe that  $\mathbf{n} = \mathbf{e}_r$  and  $|\mathbf{r}| = r = 1$ , and from (2.145) we get:  $d\Omega = dA$ . Hence, as illustrated in Fig. 2.6, in spherical coordinates the differential solid angle,  $d\Omega$ , subtended by a surface element on the sphere,  $dA$ , can be expressed as:

$$d\Omega = \frac{\mathbf{e}_r \cdot \mathbf{e}_r dA}{r^2} = dA = \sin\theta d\theta d\phi \quad (2.146)$$

## Scattering Cross Sections

In engineering practice we are often concerned with the scattering of a beam of identical particles incident with uniform velocity on the scattering center rather than with the deflection of a single particle. The different particles in the beam have different impact parameters and are therefore scattered through different angles. Hence, in these applications the complexity of the scattering processes involved cannot be described with the classical methods due to the prohibitive computational costs. Instead, the scattering of the particles

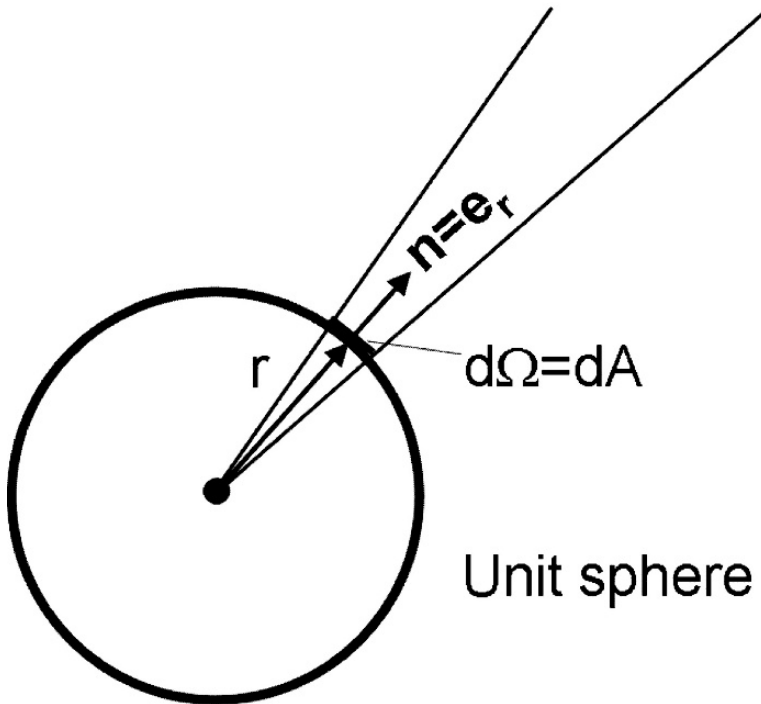


**Fig. 2.6.** A sketch of the solid angle in the special case when the arbitrary surface coincides with the unit sphere. In this particular case  $\mathbf{n} = \mathbf{e}_r$ ,  $|\mathbf{r}| = r = 1$ , hence from (2.145) it follows that  $d\Omega = dA$ .

in the incident beam are calculated in a statistical manner considering the distribution of the deflected particles to be proportional to the density of the incident beam. The corresponding proportionality factor is the *differential scattering cross section*.

Due to the symmetry properties of a binary collision, it is convenient to illustrate the basic ideas considering a one body scattering problem that is concerned with the scattering of particles by a fixed center of force.

We first state that as a particle approaches the center of force, its orbit will deviate from the incident straight line trajectory. After passing the center of force, the force acting on the particle will eventually diminish so that the orbit once again approaches a straight line (as sketched in Fig. 2.3). In general the final direction of motion is not the same as the incident direction, and the particle is said to be scattered.

To calculate the differential scattering cross section we need to define a particular system of reference for the differential solid angle. A suitable reference system can be defined in the following manner [12]. Let  $\mathbf{e}_g$  and  $\mathbf{e}_{g'}$  be unit vectors in the direction of  $\mathbf{g}_{21}$  and  $\mathbf{g}'_{21}$ , so that  $\mathbf{g}_{21} = g\mathbf{e}_g$  and  $\mathbf{g}'_{21} = g'\mathbf{e}_{g'}$ . The element of the surface  $d\Omega$  includes the point in a perpendicular plane

with unit normal  $\mathbf{\Omega} \equiv \mathbf{e}_g$ , whereas the element of the surface  $d\Omega'$  includes the point in a perpendicular plane with unit normal  $\mathbf{\Omega}' \equiv \mathbf{e}_{g'}$ .

The *differential scattering cross section* is defined in the following manner. Imagine a uniform beam of particles, i.e., all with the same mass, energy and initial velocity  $\mathbf{g}$ , incident upon a scattering center of force located at the origin  $O$ . Let the *incident flux* (or intensity),  $F = ng$ , be the number of molecules in the incident beam crossing a unit area normal to the beam in unit time ( $\frac{\text{number}}{s m^2}$ ).  $n$  is the number of particles per unit volume given by (2.51).

The number of particles scattered into the element of solid angle  $d\Omega'$  about  $\mathbf{\Omega}'$  is proportional to the incident flux  $F$  and the element of solid angle  $d\Omega'$ . The cross section for scattering in a given direction,  $\sigma_A(\mathbf{\Omega}'; g')$ , is thus defined so that,

$$F\sigma_A(\mathbf{\Omega}'; g)d\Omega' = \text{the number of molecules scattered into the solid angle element } d\Omega' \text{ about } \mathbf{\Omega}' \text{ per unit time (s),}$$

where  $d\Omega'$  is an element of solid angle around  $\mathbf{\Omega}'$ . The differential scattering cross section,  $\sigma_A(\mathbf{\Omega}'; g)$ , represents a statistical proportionality factor. Hence,  $\sigma_A(\mathbf{\Omega}'; g)d\Omega'$  denotes the surface in a plane perpendicular to the incident flow such that the molecules that cross this surface end up with a velocity  $\mathbf{g}'$  within the solid angle  $d\Omega'$ . The azimuthal angle  $\phi$ , which locates a section of the incident beam, is the same angle that appears in the spherical coordinate frame fixed with origin at the scatter.

Performing simple trigonometrical analysis of Fig. 2.2 it is seen that the number of deflected molecules considered equals the number of molecules that passed through the differential cylinder collision cross section area,  $bd\phi db$ , hence:

$$F\sigma_A(\mathbf{\Omega}'; g)d\Omega' = F\sigma_A(\theta; g)d\Omega' = Fb(\theta)db(\theta)d\phi \quad (2.147)$$

The relationship between  $\sigma_A(\mathbf{\Omega}', g)$  and the deflection angle  $\theta$  is established by trigonometry since with central forces there must be complete symmetry around the axis of the incident beam. It is then observed that all the particles with an impact parameter in the range  $(b, b + db)$  are deflected in the range  $(\theta, \theta + d\theta)$ , independently of  $\phi$ , hence  $\sigma_A(\mathbf{\Omega}', g) = \sigma_A(\theta, g)$  [85]. The detailed form of  $\sigma_A(\theta; g)$  depends on the intermolecular potential<sup>34</sup>.

Besides, the impact parameter  $b$  is generally considered a function of the energy and the corresponding scattering angle, thus (2.147) together with the solid angle relation in polar angles (2.146) constitute the classical formula for the differential scattering cross section,

$$\sigma_A(\theta, E(g)) = \frac{b(\theta, E(g))}{\sin \theta} \left| \frac{db(\theta, E(g))}{d\theta} \right| \quad (2.148)$$

<sup>34</sup> The differential cross section is a measurable quantity [40]. If the intermolecular potential is known,  $\sigma_A(\theta, g)$  can also be calculated using techniques from quantum mechanics. In this book we regard  $\sigma_A(\theta, g)$  as a specified property of the gas.

where  $E(g) = \frac{1}{2}\mu g^2$ , and  $\theta$  is the scattering angle. The absolute signs are required as  $b$  and  $\theta$  can vary in opposite directions, thus we avoid negative particle numbers.

In addition, as discussed earlier in sect. 2.4.2, the values of the differential scattering cross section  $\sigma_A$  depend on which of the two scattering angles  $\theta_L$  and  $\theta$  that is adopted. However, the number of particles scattered into a given element of solid angle must be the same whether we use  $\theta_L$  or  $\theta$ , so we may write:

$$2\pi F\sigma_A(\theta) \sin\theta |d\theta| = 2\pi F\sigma_A(\theta_L) \sin\theta_L |d\theta_L| \quad (2.149)$$

and

$$\sigma_A(\theta_L) = \sigma_A(\theta) \frac{\sin\theta}{\sin\theta_L} \left| \frac{d\theta}{d\theta_L} \right| \quad (2.150)$$

It is emphasized that both  $\sigma_A(\theta_L)$  and  $\sigma_A(\theta)$  are cross sections measured in the laboratory frame, only expressed in different coordinates. A formal expression for the scattering angle  $\theta$  as a function of  $b$  can be obtained from the orbit equation of the molecular model [35].

The *total scattering cross section* is another statistical quantity that can be derived from the differential cross section, defined as the integral of  $\sigma_A(\mathbf{\Omega}'; g)$  over all solid angle elements, hence:

$$\sigma_{A_T} = \int_{4\pi} \sigma_A(\mathbf{\Omega}', g) d\Omega' = \int_{2\pi} \int_{\pi} \sigma_A \sin\theta d\theta d\phi \quad (2.151)$$

In other words,  $\sigma_A(\mathbf{\Omega}'; g)$  denotes the proportionality factor for the number of particles scattered into a specific direction, whereas  $\sigma_{A_T}$  represents the proportionality factor for the total number of molecules scattered out of the incident beam.

For example, in the particular case when the molecules are rigid elastic spheres the apse-line becomes identical with the line of center at collision. In this case the distance  $d_{12}$  between the centers of the spheres at collision is connected with their diameters  $d_1, d_2$  by the relation [77]:

$$d_{12} = \frac{1}{2}(d_1 + d_2), \quad (2.152)$$

Note also that since  $\psi$  is the angle between the  $\mathbf{g}_{21}$  and  $\mathbf{k}$ , as sketched in fig. 2.7, it is shown that:  $\psi = \frac{1}{2}(\pi - \theta)$ .

Since the plane through  $\mathbf{k}$  and  $\mathbf{g}_{21}$  makes an angle  $\psi$  with a reference plane through  $\mathbf{g}_{21}$ ,  $\psi$  and  $\theta$  are polar coordinates specifying the direction of  $\mathbf{k}$  on the unit sphere. Thereby,

$$b = d_{12} \sin\psi = d_{12} \sin\left[\frac{1}{2}(\pi - \theta)\right] = d_{12} \cos\frac{\theta}{2} \quad (2.153)$$

The billiard ball model is unique in that  $\theta$  depends only on  $b$ , and not on  $g$ .

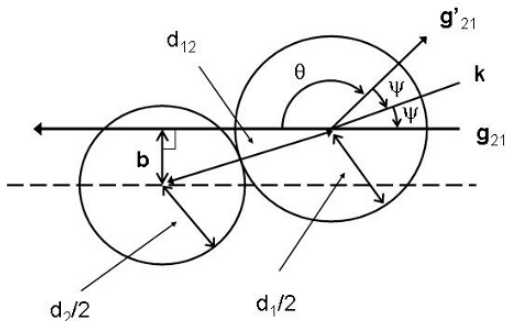


**Fig. 2.7.** A sketch defining the geometrical variables in scattering of rigid spheres.

It follows that,

$$b db = d_{12} \sin \psi \times d(d_{12} \sin \psi) = d_{12}^2 \sin \psi \cos \psi d\psi \quad (2.154)$$

Normally, we rather want to work with the angle  $\theta$  in place of the angle  $\psi$ :  $\theta = \pi - 2\psi$ . By use of standard formulas from trigonometry we may write:

$$\begin{aligned} \cos \theta &= \cos(\pi - 2\psi) = \cos(\pi) \cos(2\psi) - \sin(\pi) \sin(2\psi) \\ &= -1[\cos^2 \psi - \sin^2 \psi] - 0[2 \sin \psi \cos \psi] = \sin^2 \psi - \cos^2 \psi \\ &= 1 - \cos^2 \psi - \cos^2 \psi = 1 - 2 \cos^2 \psi \end{aligned} \quad (2.155)$$

so that

$$d \cos \theta = -4 \cos \psi d \cos \psi = -4 \cos \psi (-\sin \psi) d\psi = -4 \cos \psi \sin \psi d\psi \quad (2.156)$$

and

$$-\sin \theta d\theta = 4 \cos \psi \sin \psi d\psi \quad (2.157)$$

Therefore,

$$b db = d_{12}^2 \sin \psi \cos \psi d\psi = -\frac{d_{12}^2}{4} \sin \theta d\theta \quad (2.158)$$

or

$$b db d\phi = d_{12}^2 \sin \psi \cos \psi d\psi d\phi = -\frac{d_{12}^2}{4} \sin \theta d\theta d\phi = -\frac{d_{12}^2}{4} d\Omega' \quad (2.159)$$

where we let  $d\Omega'$  be the differential element of solid angle, which is the small area through which the unit vector  $\mathbf{e}_{g'}$  passes through. Hence,  $d\Omega' = \sin \theta d\theta d\phi$ .

The differential collision cross section is defined as a positive proportionality factor, but in our analysis we get:

$$\sigma_{A12} = \frac{b db}{\sin \theta d\theta} = -\frac{d_{12}^2}{4} \quad (2.160)$$

To avoid negative values we modify the relation slightly (e.g., [12], p. 60; [85], p. 81), in accordance with (2.148), hence:

$$\sigma_{A_{12}} = \left| \frac{b db}{\sin \theta d\theta} \right| = \frac{b}{\sin \theta} \left| \frac{db}{d\theta} \right| = \frac{d_{12}^2}{4} \quad (2.161)$$

From this relation we can deduce the important result,

$$b db d\phi = \sigma_{A_{12}} d\Omega' \quad (2.162)$$

and from (2.151) we obtain:

$$\sigma'_{A_{T_{12}}} = 2\pi \int_{-1}^1 \frac{d_{12}^2}{4} d \cos \theta = \pi d_{12}^2 \quad (2.163)$$

### Collision Symmetry Properties

The differential cross section has certain symmetry properties which are consequences of the electromagnetic nature of the molecular interactions. We briefly itemize two relevant symmetries:

- Invariance Under Time Reversal:

$$\sigma'_A(\mathbf{c}_1, \mathbf{c}_2 | \mathbf{c}'_1, \mathbf{c}'_2) = \sigma_A(-\mathbf{c}'_1, -\mathbf{c}'_2 | -\mathbf{c}_1, -\mathbf{c}_2) \quad (2.164)$$

The invariance of physical laws under time reversal<sup>35</sup> makes the cross sections for the original and *reverse* collisions equal [83] [97] [40]. This means that if we reverse the time each molecule will retrace its original trajectory, as sketched in Fig. 2.8.

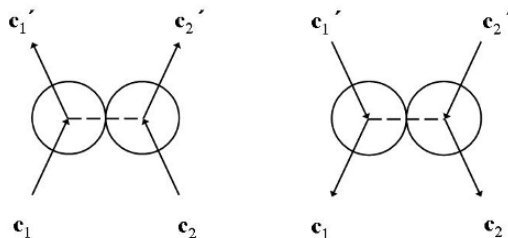


**Fig. 2.8.** A sketch illustrating an original collision (left) and an reverse collision (right). The scattering cross section are the same for both types of collision.

<sup>35</sup> From the definition of the Lagrangian function (2.6) it can be shown that the time coordinate is both homogeneous and isotropic meaning that its properties are the same in both directions [52]. For, if  $t$  is replaced by  $-t$ , the Lagrangian is unchanged, and therefore so are the equations of motion. In this sense all motions which obey the laws of classical mechanics are reversible.

- Invariance Under Rotation and Reflection:

$$\sigma'_A(\mathbf{c}_1, \mathbf{c}_2 | \mathbf{c}'_1, \mathbf{c}'_2) = \sigma_A(\mathbf{c}_1^*, \mathbf{c}_2^* | \mathbf{c}'_1, \mathbf{c}'_2) \quad (2.165)$$

where  $\mathbf{c}^*$  denotes the vector obtained from  $\mathbf{c}$  after performing a given rotation in space or a reflection with respect to a given plane, or a combination of both [83] [97] [40].

It is of particular interest to consider an *inverse* collision which is obtained from the original collision by interchanging the initial and final states, as sketched in Fig. 2.9:

$$\sigma_A(\mathbf{c}_1, \mathbf{c}_2 | \mathbf{c}'_1, \mathbf{c}'_2) = \sigma_A(\mathbf{c}'_1, \mathbf{c}'_2 | \mathbf{c}_1, \mathbf{c}_2) \quad (2.166)$$

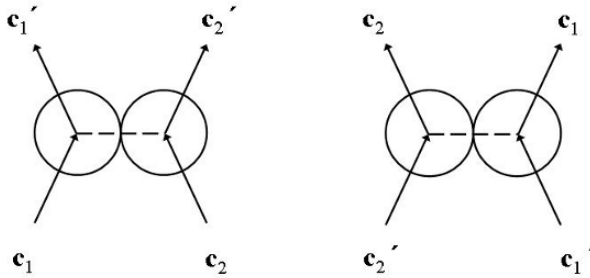


**Fig. 2.9.** A sketch illustrating an original collision (left) and an inverse collision (right). The scattering cross section are the same for both types of collision.

## Collision Frequency

To determine the rate of change of the distribution due to molecular collisions we also need to derive an expression for the expected number of collisions. From this measure the molecular *collision frequency* can be obtained as a spin-off result.

We first note that it is necessary to consider a small but finite range of velocity,  $d\mathbf{c}$ , rather than a specific value  $\mathbf{c}$ , as the probability is about zero that in  $d\mathbf{r}$  there is any molecule whose velocity is equal to any specified value  $\mathbf{c}$  out of the whole continuous range at a given instant.

In a similar manner, during a small time-interval  $dt$  the probable number of *collisions* in  $d\mathbf{r}$ , between molecules in the velocity ranges  $d\mathbf{c}_1$  and  $d\mathbf{c}_2$  is about zero if the geometrical collision variables  $b$  and  $\phi$  are assigned at specific values. Accordingly, we rather considered the finite ranges  $db$  and  $d\phi$  of  $b$  and  $\phi$ , respectively.

If we now consider the motion of molecules 2 relative to the center of molecules 1, as sketched in Fig. 2.2, a collision between the two molecules in which the impact parameter is in the range  $db$  about  $b$  and the azimuthal angle in the range  $d\phi$  about  $\phi$  can occur provided that the extension of the vector  $\mathbf{g}_{21}$  cut the plane through  $O$  perpendicular to the polar axis within the area bounded by circles of radii  $db$ ,  $b + db$  and center  $O$ , and by radii from  $O$  including an angle  $d\phi$ . It is customary to consider first only those collisions which involve particles of relative velocity  $\mathbf{g}_{21}$  and have impact parameters in  $db$  about  $b$ , and azimuths in  $d\phi$  about  $\phi$ . If such a collision is to occur in a time interval  $dt$ , then at the beginning of  $dt$  the center of molecule 2 must be within a cylinder having an area  $bd\phi db$  as base and generators equal to  $-\mathbf{g}_{21}dt$  (i.e., the length of the cylinder generators in the  $\mathbf{e}_g$  direction is given by the scalar product:  $(\mathbf{g}_{21} \cdot \mathbf{e}_g)dt = |\mathbf{g}_{21}||\mathbf{e}_g| \cos(0)dt = gdt$ ). The volume  $(gdt)(bd\phi db)$  is commonly referred to as *the collision cylinder*, as sketched in Figs. 2.10. The total number of molecules 2 in the collision cylinder which have their velocities in the range  $d\mathbf{c}_2$  about  $\mathbf{c}_2$  is equal to  $f_2(\mathbf{r}, \mathbf{c}_2, t)(gdt bd\phi db) d\mathbf{c}_2 dt$ .

Thereafter, one such collision cylinder is associated with each of the  $f_1(\mathbf{r}, \mathbf{c}_1, t)d\mathbf{c}_1 d\mathbf{r}$  molecules of type 1 within the specified velocity range  $d\mathbf{c}_1$  about  $\mathbf{c}_1$  in the volume element  $d\mathbf{r}$  about  $\mathbf{r}$ .

The expected number of collisions in  $d\mathbf{r}$  about  $\mathbf{r}$ , during a time interval  $dt$ , between molecules in the velocity range  $d\mathbf{c}_1$ ,  $d\mathbf{c}_2$  about  $\mathbf{c}_1$ ,  $\mathbf{c}_2$  with geometrical collision variables in the range  $db$ ,  $d\phi$  about  $b$ ,  $\phi$  is:

$$f_1 f_2 g b db d\phi d\mathbf{c}_1 d\mathbf{c}_2 d\mathbf{r} dt \quad (2.167)$$

On substituting  $\sigma_A(\Omega')d\Omega'$  for  $bd\phi db$ , we obtain the alternative expression:

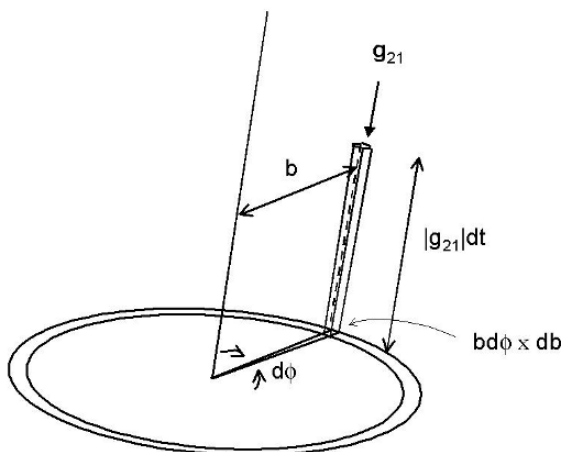


**Fig. 2.10.** Collision cylinder. Scattering in the  $\mathbf{c}_1$  molecular frame, where the  $\mathbf{c}_2$  molecules have velocity  $\mathbf{g}_{21}$ .

$$f_1 f_2 g \sigma_A(\boldsymbol{\Omega}') d\Omega' d\mathbf{c}_1 d\mathbf{c}_2 d\mathbf{r} dt \quad (2.168)$$

for the number of collisions.

For completeness it is stated that these relations rely on the molecular chaos assumption (i.e., valid for dilute gases only<sup>36</sup>), anticipating that the collisional pair distribution function can be expressed by:  $f^{(2)}(\mathbf{r}_1, \mathbf{c}_1, \mathbf{r}_2, \mathbf{c}_2, t) = f_1(\mathbf{r}_1, \mathbf{c}_1, t) f_2(\mathbf{r}_2, \mathbf{c}_2, t)$ . A more general expression for the number of collisions is then given by:

$$f^{(2)}(\mathbf{r}_1, \mathbf{c}_1, \mathbf{r}_2, \mathbf{c}_2, t) g \sigma_A(\boldsymbol{\Omega}') d\Omega' d\mathbf{c}_1 d\mathbf{c}_2 d\mathbf{r} dt \quad (2.169)$$

Adopting the molecular billiard ball model considering molecules that are smooth and symmetric rigid elastic spheres *not* surrounded by fields of force, the molecules affect each other motion only at contact.

Considering such binary collisions between billiard ball molecules of masses  $m_1$  and  $m_2$  in a gas mixture at rest in a uniform steady state, the number of collisions per unit volume and time is given by (2.168) after dividing by  $d\mathbf{r}$  and  $dt$ . Integrating the result over all values of  $\boldsymbol{\Omega}'$ ,  $\mathbf{c}_1$  and  $\mathbf{c}_2$ , we obtain the *collision density* representing the total number of collisions per unit volume and time between molecules of type  $m_1$  and molecules of type  $m_2$ :

$$\begin{aligned} Z_{12} &= \int_{\mathbf{c}_1} \int_{\mathbf{c}_1} \int_{4\pi} f_1 f_2 g \sigma_A(\boldsymbol{\Omega}') d\Omega' d\mathbf{c}_1 d\mathbf{c}_2 \\ &= \sigma_{A_{12}} \int_{-\infty}^{\infty} \int_{-\infty}^{\infty} \int_0^{2\pi} \int_0^{\pi} f_1 f_2 g \sin \theta d\theta d\phi d\mathbf{c}_1 d\mathbf{c}_2 \end{aligned} \quad (2.170)$$

where  $\sigma_{A_{12}}$  is the differential cross section for rigid spheres.

Adopting the absolute Maxwellian distribution function (anticipated at this point as it is discussed in sect 2.7.2), substituting  $f_1$  and  $f_2$  by the appropriate forms of the distribution function (2.224), i.e.,  $f_1 = n_1 (m_1/2\pi kT)^{3/2} \times \exp(-m_1 c_1^2/2kT)$  and  $f_2 = n_2 (m_2/2\pi kT)^{3/2} \times \exp(-m_2 c_2^2/2kT)$ , gives [12] (p 87):

$$Z_{12} = 2n_1 n_2 d_{12}^2 \left( \frac{2\pi kT m_c}{m_1 m_2} \right)^{1/2} = 2n_1 n_2 d_{12}^2 \left( \frac{2\pi kT}{\mu} \right)^{1/2} \quad (2.171)$$

This quantity is named the *bimolecular collision rate*. The  $\mu$  denotes the reduced mass and  $m_c = m_1 + m_2$  represents the total mass associated with the center of mass of a two particle system.

Note that the number of collisions between pairs of similar molecules  $m_1$  cannot be calculated by simply changing the suffix 2 to 1 in the given collision density relation for unlike molecules (2.171), because in this case one counts

<sup>36</sup> Let the mean free path between collisions be  $l$ , the Boltzmann equation is valid only when  $l \gg r_0$ . This constraint ensures rectilinear trajectories between collisions.

each collision between a pair of  $m_1$  molecules twice. The correct number of collisions between pairs of molecules  $m_1$  per unit volume and time is thus only half the value given by the formula for pairs of unlike molecules. Hence, for similar molecules the collision density is given by:

$$Z_{11} = 2n_1^2 d_1^2 \left( \frac{\pi k T}{m_1} \right)^{1/2} = \frac{1}{\sqrt{2}} \pi d_1^2 \langle c_1 \rangle_M n_1^2 \quad (2.172)$$

It is anticipated that the mean value of the speed of a gas which consists of molecules of type  $m_1$  in the Maxwellian state is given by  $\langle c_1 \rangle_M = \left( \frac{8kT}{\pi m_1} \right)^{1/2}$ . The derivation of this relationship is explained in (2.514) and (2.515).

The *collision frequency* denotes the average number of collisions undergone by each molecule of a certain type per unit time. The frequency of collisions between any one molecule of type  $m_1$  with other  $m_1$  molecules, is:

$$Z_{1-1} = \frac{2Z_{11}}{n_1} = 4n_1 d_1^2 \left( \frac{\pi k T}{m_1} \right)^{1/2} \quad (2.173)$$

since each collision affects two molecules at once. The type of target species considered calculating the frequency is indicated by the last index of  $Z_{1-1}$  that is separated by the hyphen [100].

The frequency of collisions between any one molecule of type  $m_1$  and a  $m_2$  molecule is given by:

$$Z_{1-2} = \frac{Z_{12}}{n_1} = 2n_2 d_{12}^2 \left( \frac{2\pi k T m_c}{m_1 m_2} \right)^{1/2} \quad (2.174)$$

The collision frequency for a molecule of type  $m_1$  colliding with all kinds of molecules in the mixture is:

$$Z_1 = \frac{Z_{11} + \sum_{j=2} Z_{1j}}{n_1} = Z_{1-1} + \sum_{j=2} Z_{1-j} \quad (2.175)$$

### 2.4.3 Generalized Collision Term Formulation

In this section we proceed deriving an explicit expression for the collision source term  $\left( \frac{\partial f}{\partial t} \right)_{\text{Collision}}$  in (2.78).

In the subsequent model derivation it is convenient to divide the velocity of all particles in the gas into two groups, the small range of velocities that fall into the interval  $d\mathbf{c}$  about  $\mathbf{c}$  and all other velocities denoted by  $\mathbf{c}_1$ .

The number of particles that are removed from the phase element  $d\mathbf{r}d\mathbf{c}$  in the time  $dt$  equals the total number of collisions that the  $\mathbf{c}$  particles have with the other  $\mathbf{c}_1$  particles in the time  $dt$ . The term  $\left( \frac{\partial f}{\partial t} \right)_{\text{Collision}}^+ d\mathbf{r}d\mathbf{c}dt$  considers all collisions between pairs of molecules that eject one of them out of the interval  $d\mathbf{c}$  about  $\mathbf{c}$ . By definition, the number of particles which is thrown out of the phase element is given by<sup>37</sup>:

<sup>37</sup> The notation used henceforth for the *pair distribution function* is defined by:  
 $f^{(2)}(\mathbf{r}, \mathbf{c}, \mathbf{r}_1, \mathbf{c}_1, t)$ .

$$\left(\frac{\partial f}{\partial t}\right)_{\text{Collision}}^- d\mathbf{r}d\mathbf{c}dt = \int_1 f^{(2)}(\mathbf{r}, \mathbf{c}, \mathbf{r}_1, \mathbf{c}_1, t) d\mathbf{r}_1 d\mathbf{c}_1 d\mathbf{r}d\mathbf{c} \quad (2.176)$$

Considering that the  $\mathbf{c}_1$  particles in  $d\mathbf{r}_1$  undergo a collision with the  $\mathbf{c}$  particles in  $d\mathbf{r}$  in the time  $dt$ , we need to determine  $d\mathbf{r}_1$  in terms of designable quantities. This can be achieved with the aid of the sketch showing a scattering event in the frame of the  $\mathbf{c}$  particles (equivalent to Fig. 2.10), revealing that all  $\mathbf{c}_1$  particles in the collision cylinder of height  $gdt$  and base area  $bd\phi db$  undergo a collision with the  $\mathbf{c}$  particles in the time  $dt$ . Hence, the volume of the collision cylinder is given by  $d\mathbf{r}_1 = gdt bd\phi db$ . It follows that the number of particles removed in  $dt$  is:

$$\begin{aligned} \left(\frac{\partial f}{\partial t}\right)_{\text{Collision}}^- d\mathbf{r}d\mathbf{c}dt &= \int_1 f^{(2)}(\mathbf{r}, \mathbf{c}, \mathbf{r}_1, \mathbf{c}_1, t) (gbd\phi db) d\mathbf{c}_1 d\mathbf{r}d\mathbf{c}dt \\ &= \int_1 f^{(2)}(\mathbf{r}, \mathbf{c}, \mathbf{r}_1, \mathbf{c}_1, t) g\sigma_A(\boldsymbol{\Omega}') d\Omega' d\mathbf{c}_1 d\mathbf{r}d\mathbf{c}dt \end{aligned} \quad (2.177)$$

Dividing by  $d\mathbf{c}d\mathbf{r}dt$ , we find that:

$$\left(\frac{\partial f}{\partial t}\right)_{\text{Collision}}^- = \int_1 f^{(2)}(\mathbf{r}, \mathbf{c}, \mathbf{r}_1, \mathbf{c}_1, t) g\sigma_A(\boldsymbol{\Omega}') d\Omega' d\mathbf{c}_1 \quad (2.178)$$

where we integrate over the solid angle,  $d\Omega'$ , and  $\mathbf{c}_1$  to sum up the rate of decrease for all the collisions occurring during  $dt$ . Note that we do not need to worry about any quantification of  $d\mathbf{c}d\mathbf{r}dt$  as these variables neatly disappear as we apply the usual theorem requiring that the argument of integration must vanish for any domain of  $d\mathbf{c}d\mathbf{r}dt$ .

The number of particles injected into  $d\mathbf{c}d\mathbf{r}$  due to collisions in the interval  $dt$ ,  $\left(\frac{\partial f}{\partial t}\right)_{\text{Collision}}^+ d\mathbf{r}d\mathbf{c}dt$ , considers all the binary collisions that can send one particle into the velocity interval  $d\mathbf{c}$  about  $\mathbf{c}$ .

This collision is recognized as being the inverse of the original collision, hence:

$$\begin{aligned} \left(\frac{\partial f}{\partial t}\right)_{\text{Collision}}^+ d\mathbf{r}d\mathbf{c}dt &= \int_1 f'^{(2)}(\mathbf{r}', \mathbf{c}', \mathbf{r}'_1, \mathbf{c}'_1, t) d\mathbf{r}'_1 d\mathbf{c}'_1 d\mathbf{r}d\mathbf{c}' \\ &= \int_1 f'^{(2)}(\mathbf{r}', \mathbf{c}', \mathbf{r}'_1, \mathbf{c}'_1, t) g\sigma_A(\boldsymbol{\Omega}) d\Omega d\mathbf{c}'_1 d\mathbf{r}d\mathbf{c}' dt \end{aligned} \quad (2.179)$$

where the primed variables refer to the inverse collision of the unprimed variables in (2.178).

We are considering a collision of the type (2.166) where  $\mathbf{c}$  is fixed at the center of mass (i.e., the origin of the relative vector is fixed).

To express (2.179) in terms of known variables the Liouville law for elastic collisions can be adopted, as several investigators (e.g., [28], sect. 3.1; [61],

---

The short notation henceforth introduced for the corresponding *single distribution function* is defined by:  $f(\mathbf{r}, \mathbf{c}, t) \equiv f^{(1)}(\mathbf{r}, \mathbf{c}, t)$ .

pp. 17-18; [12], pp. pp. 61-64; [40], p. 66; [83], p. 52) have shown that by symmetry (i.e.,  $\mathbf{G} = \mathbf{G}'$  and  $d\mathbf{g}_{21} = d\mathbf{g}'_{21}$ ) the Jacobian is unity<sup>38</sup>, hence  $d\Omega d\mathbf{c}'_1 d\mathbf{c}' = d\Omega' d\mathbf{c}_1 d\mathbf{c}$ . Note also that from the conservation of angular momentum the impact parameters  $b$  and  $b'$  before and after the collisions, respectively, are equal as  $L = \mu gb = \mu g'b'$ .

It follows that the number of particles added in  $dt$  is:

$$\left(\frac{\partial f}{\partial t}\right)_{\text{Collision}}^+ d\mathbf{r}d\mathbf{c}dt = \int_1 f'^{(2)}(\mathbf{r}', \mathbf{c}', \mathbf{r}'_1, \mathbf{c}'_1, t) g\sigma_A(\boldsymbol{\Omega}') d\Omega' d\mathbf{c}_1 d\mathbf{r}d\mathbf{c}dt \quad (2.180)$$

Dividing by  $d\mathbf{r}d\mathbf{c}dt$  we find that:

$$\left(\frac{\partial f}{\partial t}\right)_{\text{Collision}}^+ = \int_1 f'^{(2)}(\mathbf{r}', \mathbf{c}', \mathbf{r}'_1, \mathbf{c}'_1, t) g\sigma_A(\boldsymbol{\Omega}') d\Omega' d\mathbf{c}_1 \quad (2.181)$$

and again we integrate over the solid angle,  $d\Omega'$ , and  $\mathbf{c}_1$ , but this time to sum up the rate of increase for all the collisions occurring during  $dt$ .

Substituting these results into (2.101), yields the net collision rate:

$$\begin{aligned} \left(\frac{\partial f}{\partial t}\right)_{\text{Collision}} = & \int_1 f'^{(2)}(\mathbf{r}', \mathbf{c}', \mathbf{r}'_1, \mathbf{c}'_1, t) g\sigma_A(\boldsymbol{\Omega}') d\Omega' d\mathbf{c}_1 \\ & - \int_1 f^{(2)}(\mathbf{r}, \mathbf{c}, \mathbf{r}_1, \mathbf{c}_1, t) g\sigma_A(\boldsymbol{\Omega}') d\Omega' d\mathbf{c}_1 \end{aligned} \quad (2.182)$$

Finally, we impose the assumption of molecular chaos. That is, the pair distribution function can be expressed as [38] [61]:

$$f^{(2)}(\mathbf{r}, \mathbf{c}, \mathbf{r}_1, \mathbf{c}_1, t) = \frac{N-1}{N} f(\mathbf{r}, \mathbf{c}, t) f_1(\mathbf{r}_1, \mathbf{c}_1, t) \approx f(\mathbf{r}, \mathbf{c}, t) f_1(\mathbf{r}_1, \mathbf{c}_1, t) \quad (2.183)$$

and

$$f'^{(2)}(\mathbf{r}', \mathbf{c}', \mathbf{r}'_1, \mathbf{c}'_1, t) = \frac{N-1}{N} f'(\mathbf{r}', \mathbf{c}') f'_1(\mathbf{r}'_1, \mathbf{c}'_1, t) \approx f'(\mathbf{r}', \mathbf{c}', t) f'_1(\mathbf{r}'_1, \mathbf{c}'_1, t) \quad (2.184)$$

Substituting all these results into (2.78), gives the *Boltzmann* equation<sup>39</sup>:

$$\begin{aligned} \frac{\partial f}{\partial t} + \mathbf{c} \cdot \frac{\partial f}{\partial \mathbf{r}} + \mathbf{F} \cdot \frac{\partial f}{\partial \mathbf{c}} \\ = \int_1 [f'(\mathbf{r}, \mathbf{c}', t) f'_1(\mathbf{r}, \mathbf{c}'_1, t) - f(\mathbf{r}, \mathbf{c}, t) f_1(\mathbf{r}, \mathbf{c}_1, t)] g\sigma_A(\boldsymbol{\Omega}') d\Omega' d\mathbf{c}_1 \end{aligned} \quad (2.185)$$

For denser gases and rigid spheres the collision term is normally further reformulated in terms of  $\mathbf{k}$  [85] (pp. 83-85), as outlined in sect. 2.11.

<sup>38</sup> In Hamiltonian mechanics the Liouville's law for elastic collisions represents an alternative way of formulating Liouville's theorem stating that phase space volumes are conserved as it evolves in time [61] [43]. Since time-evolution is a canonical transformation, it follows that when the Jacobian is unity the differential cross sections of the original, reverse and inverse collisions are all equal. From this result we conclude that  $\sigma_A(\boldsymbol{\Omega}) = \sigma_A(\boldsymbol{\Omega}')$  [83] [28] [105].

<sup>39</sup> It is noted that this substitution is not strictly rigorous as a number of unspecified approximations are introduced as well [6].

## 2.5 The Equation of Change in Terms of Mean Molecular Properties

The emphasis in this section is to derive an equation of change for the average quantity  $\langle\psi\rangle_M$ . The mean value of the property function  $\psi(\mathbf{r}, \mathbf{c}, t)$  was defined by (2.55) in sec. 2.3.2. Notice that we are generally considering any property function  $\psi$  of a type of molecules that has position  $\mathbf{r}$  and velocity  $\mathbf{c}$  at time  $t$ .

The equation of change can be derived in two ways, either by analyzing the situation directly on the average scales<sup>40</sup>, or by starting out from the continuum microscopic Boltzmann equation (2.185) and thereafter apply a suitable averaging procedure to obtain the corresponding average - or moment equation.

In this section, an analysis based on the Boltzmann equation will be given. Before we proceed it is essential to recall that the translational terms on the LHS of the Boltzmann equation can be derived adopting two slightly different frameworks, i.e., considering either a fixed control volume (i.e., in which  $\mathbf{r}$  and  $\mathbf{c}$  are fixed and independent of time  $t$ ) or a control volume that is allowed to move following a trajectory in phase space (i.e., in which  $\mathbf{r}(t)$  and  $\mathbf{c}(t)$  are dependent of time  $t$ ) both, of course, in accordance with the Liouville theorem. The pertinent moment equations can be derived based on any of these two frameworks, but we adopt the fixed control volume approach since it is normally simplest mathematically and most commonly used. The alternative derivation based on the moving control volume framework is described by de Groot and Mazur [22] (pp. 167-170).

By virtue of the fixed control volume framework we first derive a generalized moment equation for  $\langle\psi\rangle_M$ . The average quantity  $\langle\psi\rangle_M$  is defined by (2.55). To find the equation that  $\langle\psi\rangle_M$  satisfies, we multiply on both sides of the Boltzmann equation (2.185) by  $\psi$  and integrate over all velocities  $\mathbf{c}$ . Thus, we get:

$$\int \frac{D_c f}{D_c t} \psi d\mathbf{c} = \int \left(\frac{\partial f}{\partial t}\right)_{\text{Collision}} \psi d\mathbf{c} \quad (2.186)$$

where

$$\int \frac{D_c f}{D_c t} \psi d\mathbf{c} \equiv \underbrace{\int \frac{\partial f}{\partial t} \psi d\mathbf{c}}_1 + \underbrace{\int \mathbf{c} \cdot \frac{\partial f}{\partial \mathbf{r}} \psi d\mathbf{c}}_2 + \underbrace{\int \mathbf{F} \cdot \frac{\partial f}{\partial \mathbf{c}} \psi d\mathbf{c}}_3 \quad (2.187)$$

Thereafter, we need to transform all the integrals in (2.187) into quantities which are direct averages, i.e., into integrals which involve  $f$  itself rather than its derivatives. For term 1 we obtain:

$$\int \frac{\partial f}{\partial t} \psi d\mathbf{c} = \int \left[ \frac{\partial}{\partial t} (f\psi) - f \frac{\partial \psi}{\partial t} \right] d\mathbf{c} = \frac{\partial}{\partial t} \int f\psi d\mathbf{c} - \int f \frac{\partial \psi}{\partial t} d\mathbf{c} \quad (2.188)$$

<sup>40</sup> The equation resulting from this approach is sometimes referred to as the *Enskog's equation of change* (e.g., [83], p. 527).

since the order of differentiation with respect to  $t$  and integration over  $\mathbf{c}$  can be interchanged when the integration limits of  $\mathbf{c}$  is not a function of  $t$  (i.e., applied to the first term on the RHS as the local time differentiation acts on the whole argument of the integral). Term 1 in (2.187) thus yields:

$$\int \frac{\partial f}{\partial t} \psi d\mathbf{c} = \frac{\partial}{\partial t} (n \langle \psi \rangle_M) - n \left\langle \frac{\partial \psi}{\partial t} \right\rangle_M \quad (2.189)$$

The integral term 2 in (2.187) can be rewritten in a similar manner, keeping in mind that  $\mathbf{r}$  and  $\mathbf{c}$  are *independent* dynamic variables.

It follows that term 2 is manipulated as:

$$\begin{aligned} \int \mathbf{c} \cdot \frac{\partial f}{\partial \mathbf{r}} \psi d\mathbf{c} &= \int \left[ \frac{\partial}{\partial \mathbf{r}} \cdot (f \mathbf{c} \psi) - f \mathbf{c} \cdot \frac{\partial \psi}{\partial \mathbf{r}} \right] d\mathbf{c} \\ &= \frac{\partial}{\partial \mathbf{r}} \cdot \int f \mathbf{c} \psi d\mathbf{c} - \int f \mathbf{c} \cdot \frac{\partial \psi}{\partial \mathbf{r}} d\mathbf{c} \\ &= \frac{\partial}{\partial \mathbf{r}} \cdot (n \langle \mathbf{c} \psi \rangle_M) - n \left\langle \mathbf{c} \cdot \frac{\partial \psi}{\partial \mathbf{r}} \right\rangle_M \end{aligned} \quad (2.190)$$

Finally, since we have assumed that the force,  $\mathbf{F}$ , is independent of the velocity  $\mathbf{c}$ , the integral term 3 in (2.187) can be expressed as:

$$\begin{aligned} \int \mathbf{F} \cdot \frac{\partial f}{\partial \mathbf{c}} \psi d\mathbf{c} &= \int \left[ \frac{\partial}{\partial \mathbf{c}} \cdot (\mathbf{F} f \psi) - \mathbf{F} \cdot f \frac{\partial \psi}{\partial \mathbf{c}} \right] d\mathbf{c} \\ &= [\mathbf{F} f \psi]_{\mathbf{c}} - \mathbf{F} \cdot \int f \frac{\partial \psi}{\partial \mathbf{c}} d\mathbf{c} \end{aligned} \quad (2.191)$$

The first term on the RHS vanishes, since for each direction (e.g., in Cartesian coordinates,  $i = 1, 2, 3$ ),  $f \rightarrow 0$  as  $|c_i| \rightarrow \infty$ , thus  $[F_i f \psi]_{c_i=-\infty}^{c_i=+\infty} \rightarrow 0$ . Hence, term 3 in (2.191) becomes:

$$\int \mathbf{F} \cdot \frac{\partial f}{\partial \mathbf{c}} \psi d\mathbf{c} = -\mathbf{F} \cdot n \left\langle \frac{\partial \psi}{\partial \mathbf{c}} \right\rangle_M \quad (2.192)$$

If we introduce the expressions from (2.189) through (2.191) into (2.187), we obtain the result:

$$\begin{aligned} \int \frac{D_c f}{D_c t} \psi d\mathbf{c} &= \frac{\partial}{\partial t} (n \langle \psi \rangle_M) + \frac{\partial}{\partial \mathbf{r}} \cdot (n \langle \mathbf{c} \psi \rangle_M) - \\ &\quad n \left[ \left\langle \frac{\partial \psi}{\partial t} \right\rangle_M + \left\langle \mathbf{c} \cdot \frac{\partial \psi}{\partial \mathbf{r}} \right\rangle_M + \mathbf{F} \cdot \left\langle \frac{\partial \psi}{\partial \mathbf{c}} \right\rangle_M \right] \\ &= \frac{\partial}{\partial t} (n \langle \psi \rangle_M) + \frac{\partial}{\partial \mathbf{r}} \cdot (n \langle \mathbf{c} \psi \rangle_M) - n \left\langle \frac{D_c \psi}{D_c t} \right\rangle_M \end{aligned} \quad (2.193)$$

in which we conveniently define:

$$\frac{D_c \psi}{D_c t} = \frac{\partial \psi}{\partial t} + \mathbf{c} \cdot \frac{\partial \psi}{\partial \mathbf{r}} + \mathbf{F} \cdot \frac{\partial \psi}{\partial \mathbf{c}} \quad (2.194)$$

At this point, we turn to the evaluation of the collision term given in (2.186). From (2.185) it is seen that the collision term takes the form:

$$\begin{aligned} \mathcal{J}(\psi(\mathbf{c})) &= \int \int \int \psi [f'(\mathbf{r}, \mathbf{c}', t) f'_1(\mathbf{r}, \mathbf{c}'_1, t) - f(\mathbf{r}, \mathbf{c}, t) f_1(\mathbf{r}, \mathbf{c}_1, t)] g \sigma_A(\boldsymbol{\Omega}') d\Omega' d\mathbf{c}_1 d\mathbf{c} \end{aligned} \quad (2.195)$$

Unfortunately, this relation is not particularly useful for a general  $\psi$  because of the very complex integrals. However, since mass ( $m$ ), momentum ( $m\mathbf{c}$ ), or kinetic energy ( $mc^2$ ) are conserved during a collision, it can be shown that<sup>41</sup>:

$$\begin{aligned} \mathcal{J}(\psi(\mathbf{c})) &= \int_1 \psi [f'(\mathbf{r}, \mathbf{c}', t) f'_1(\mathbf{r}, \mathbf{c}'_1, t) - f(\mathbf{r}, \mathbf{c}, t) f_1(\mathbf{r}, \mathbf{c}_1, t)] g \sigma_A(\boldsymbol{\Omega}') d\Omega' d\mathbf{c}_1 d\mathbf{c} = 0 \end{aligned} \quad (2.198)$$

This relation enable us to simplify the formulation of the general equation of change considerably. Fortunately, the fundamental fluid dynamic conservation equations of continuity, momentum, and energy are thus derived from the Boltzmann equation without actually determining the form of either the collision term or the distribution function  $f$ .

By substitution of the relations (2.193) and (2.195) into (2.186), we obtain the *Enskog's equation of change*:

---

<sup>41</sup> It is convenient to introduce the notion of *collisional invariants* (or *summational invariants*) (e.g., [39], p. 460; [61], p. 150). The validity of (2.198) is commonly justified by the following arguments:

Due to the symmetry properties of the collision term expression, interchanging variables gives the following equalities  $\mathcal{J}(\psi(\mathbf{c})) = \mathcal{J}(\psi_1(\mathbf{c}_1))$  for  $(\mathbf{c}, \mathbf{c}_1) \rightarrow (\mathbf{c}_1, \mathbf{c})$ ,  $\mathcal{J}(\psi'(\mathbf{c}')) = -\mathcal{J}(\psi(\mathbf{c}))$  for  $(\mathbf{c}, \mathbf{c}_1) \rightarrow (\mathbf{c}', \mathbf{c}'_1)$ , and  $\mathcal{J}(\psi'(\mathbf{c}')) = \mathcal{J}(\psi'_1(\mathbf{c}'_1))$  for  $(\mathbf{c}'_1, \mathbf{c}') \rightarrow (\mathbf{c}', \mathbf{c}'_1)$ . These symmetry properties can be combined to give the following relationship:  $4\mathcal{J}(\psi(\mathbf{c})) = \mathcal{J}(\psi(\mathbf{c})) + \mathcal{J}(\psi_1(\mathbf{c}_1)) - \mathcal{J}(\psi'(\mathbf{c}')) - \mathcal{J}(\psi'_1(\mathbf{c}'_1))$ .

The linearity of the  $\mathcal{J}$  operator allows us to rewrite the latter result as  $\mathcal{J}(\psi(\mathbf{c})) = \frac{1}{4}(\mathcal{J}(\psi(\mathbf{c})) + \mathcal{J}(\psi_1(\mathbf{c}_1)) - \mathcal{J}(\psi'(\mathbf{c}')) - \mathcal{J}(\psi'_1(\mathbf{c}'_1)))$ .

In conclusion, a function  $\psi(\mathbf{c})$  is a summation invariant if

$$\Delta\psi(\mathbf{c}) = \psi'(\mathbf{c}') + \psi'_1(\mathbf{c}'_1) - \psi(\mathbf{c}) - \psi_1(\mathbf{c}_1) = 0 \quad (2.196)$$

That is,  $\psi(\mathbf{c})$  is a property of a molecule that is preserved in a collision. Hence, for the conserved quantities mass, momentum and energy we can write:

$$\mathcal{J}(m) = \mathcal{J}(m\mathbf{c}) = \mathcal{J}(mc^2) = 0 \quad (2.197)$$

$$\frac{\partial}{\partial t}(n\langle\psi\rangle_M) = n\left\langle\frac{D_c\psi}{D_c t}\right\rangle_M - \frac{\partial}{\partial \mathbf{r}} \cdot (n\langle\mathbf{c}\psi\rangle_M) + \mathcal{J}(\psi) \quad (2.199)$$

where  $\mathcal{J}(\psi)$  denotes the rate of change of  $\psi$  per unit volume due to collisions.

## 2.6 The Governing Equations of Fluid Dynamics

In this paragraph the conservation equations of fluid dynamic are derived from the Boltzmann equation.

The equation of change, (2.199), becomes particularly simple if  $\psi$  refers to a quantity which is conserved in collisions between molecules so that  $\mathcal{J}(\Delta\psi = 0) = 0$ . Therefore, for conservative quantities (2.199) reduces to:

$$\frac{\partial}{\partial t}(n\langle\psi\rangle_M) + \frac{\partial}{\partial \mathbf{r}} \cdot (n\langle\mathbf{c}\psi\rangle_M) = n\left\langle\frac{D_c\psi}{D_c t}\right\rangle_M \quad (2.200)$$

By letting  $\psi$  in (2.200) be  $m$ ,  $m\mathbf{c}$ , and  $\frac{1}{2}mc^2$ , respectively, we obtain the three fundamental conservation equations that are all satisfied by the gas.

### Conservation of mass

We let  $\psi = m$ , hence (2.200) yields:

$$\frac{\partial}{\partial t}(nm) + \frac{\partial}{\partial \mathbf{r}} \cdot (nm\langle\mathbf{c}\rangle_M) = 0 \quad (2.201)$$

By averaging the peculiar velocity, defined by (2.59) in section 2.3.2, we get  $\langle\mathbf{c}\rangle_M = \mathbf{v}$  which is the mean velocity of the gas. Furthermore, the mass density of the gas, given by (2.52), is defined by  $\rho(\mathbf{r}, t) = mn(\mathbf{r}, t)$ . Equation (2.201) becomes:

$$\frac{\partial \rho}{\partial t} + \frac{\partial}{\partial \mathbf{r}} \cdot (\rho\mathbf{v}) = 0 \quad (2.202)$$

This is the *equation of continuity* of fluid dynamics.

### Conservation of momentum

We let  $\psi = m\mathbf{c}$ , hence (2.200) yields:

$$\frac{\partial}{\partial t}(nm\langle\mathbf{c}\rangle_M) + \frac{\partial}{\partial \mathbf{r}} \cdot (nm\langle\mathbf{c}\mathbf{c}\rangle_M) = nm\left\langle\frac{D_c\mathbf{c}}{D_c t}\right\rangle_M \quad (2.203)$$

By definition, (2.194), the last term in (2.203) can be rewritten as:

$$\frac{D_c\mathbf{c}}{D_c t} = \mathbf{F} \cdot \frac{\partial \mathbf{c}}{\partial \mathbf{c}} = \mathbf{F} \quad (2.204)$$

since  $\mathbf{c}$  is independent of  $\mathbf{r}$  and  $t$ .

By inserting (2.204), (2.203) becomes:

$$\frac{\partial}{\partial t}(\rho\mathbf{v}) + \frac{\partial}{\partial \mathbf{r}} \cdot (\rho\langle\mathbf{c}\mathbf{c}\rangle_M) = \rho\mathbf{F} \quad (2.205)$$

The second term on the LHS of (2.205) constitutes the sum of the pressure tensor (2.64) and the convective term. By use of (2.59), we set  $\mathbf{c} = \mathbf{v} + \mathbf{C}$ , and after some manipulation the dyad  $\langle\mathbf{c}\mathbf{c}\rangle_M$  can be expressed as:

$$\begin{aligned} \langle\mathbf{c}\mathbf{c}\rangle_M &= \langle(\mathbf{v} + \mathbf{C})(\mathbf{v} + \mathbf{C})\rangle_M = \langle\mathbf{v}\mathbf{v} + \mathbf{C}\mathbf{C} + \mathbf{v}\mathbf{C} + \mathbf{v}\mathbf{C}\rangle_M \\ &= \mathbf{v}\mathbf{v} + \langle\mathbf{C}\mathbf{C}\rangle_M \end{aligned} \quad (2.206)$$

since the average of the peculiar velocity is zero, i.e.,  $\langle\mathbf{v}\mathbf{C}\rangle_M = \mathbf{v}\langle\mathbf{C}\rangle_M = 0$ .

By use of the (2.206) and (2.64), (2.205) can be written as:

$$\frac{\partial}{\partial t}(\rho\mathbf{v}) + \frac{\partial}{\partial \mathbf{r}} \cdot (\rho\mathbf{v}\mathbf{v}) = -\frac{\partial}{\partial \mathbf{r}} \cdot \mathbf{P} + \rho\mathbf{F} \quad (2.207)$$

This relation corresponds to the *Cauchy equation of motion in fluid dynamics*.

### Conservation of energy

We let  $\psi = \frac{1}{2}mc^2$ , hence (2.200) yields:

$$\frac{\partial}{\partial t}\left(\frac{1}{2}nm\langle c^2\rangle_M\right) + \frac{1}{2}\frac{\partial}{\partial \mathbf{r}} \cdot (nm\langle\mathbf{c}\mathbf{c}^2\rangle_M) = \frac{1}{2}nm\left\langle\frac{D_c c^2}{D_c t}\right\rangle_M \quad (2.208)$$

By definition, (2.194), the last term in (2.208) is given by:

$$\frac{D_c(\mathbf{c} \cdot \mathbf{c})}{D_c t} = 2\mathbf{F} \cdot \left(\frac{\partial \mathbf{c}}{\partial \mathbf{c}} \cdot \mathbf{c}\right) = 2\mathbf{F} \cdot \mathbf{c} \quad (2.209)$$

since  $\mathbf{c}$  is independent of  $\mathbf{r}$  and  $t$ .

By inserting (2.209), (2.208) can be written as:

$$\frac{\partial}{\partial t}(\rho c^2) + \frac{1}{2}\frac{\partial}{\partial \mathbf{r}} \cdot (\rho\langle\mathbf{c}\mathbf{c}^2\rangle_M) = \rho\mathbf{F} \cdot \mathbf{v} \quad (2.210)$$

Equation (2.210) may be transformed, using the same methods as in the treatment of the equation of motion. The first term on the LHS of (2.210) can be manipulated by use of (2.59). We set  $\mathbf{c} = \mathbf{v} + \mathbf{C}$ , and after some manipulation the covariance  $\frac{1}{2}\langle c^2\rangle_M$  can be expressed as:

$$\frac{1}{2}\langle c^2\rangle_M = \frac{1}{2}\langle C^2\rangle_M + \frac{1}{2}\langle v^2\rangle_M = e + \frac{1}{2}v^2 \quad (2.211)$$

where  $e$  is defined in accordance with (2.74).

The second term on the LHS of (2.210) also needs some further manipulation. By use of (2.59), the covariance  $\frac{1}{2}\rho\langle\mathbf{c}\mathbf{c}^2\rangle_M$  can be expressed as:

$$\begin{aligned}\frac{1}{2}\rho\langle\mathbf{c}\mathbf{c}^2\rangle_M &= \frac{1}{2}\rho\langle\mathbf{c}(\mathbf{c}\cdot\mathbf{c})\rangle_M = \frac{1}{2}\rho\langle(\mathbf{C}+\mathbf{v})(C^2+2\mathbf{v}\cdot\mathbf{C}+v^2)\rangle_M \\ &= \frac{1}{2}\rho\left\{\langle\mathbf{C}C^2\rangle_M + \langle(2\mathbf{v}\cdot\mathbf{C})\mathbf{C}\rangle_M + \langle\mathbf{C}v^2\rangle_M + \langle\mathbf{v}C^2\rangle_M \right. \\ &\quad \left. + \langle\mathbf{v}(2\mathbf{v}\cdot\mathbf{C})\rangle_M + \langle\mathbf{v}v^2\rangle_M\right\} \quad (2.212) \\ &= \frac{1}{2}\rho\langle\mathbf{C}C^2\rangle_M + \rho\mathbf{v}\cdot\langle\mathbf{C}\mathbf{C}\rangle_M + \frac{1}{2}\rho\mathbf{v}\langle C^2\rangle_M + \frac{1}{2}\rho\mathbf{v}v^2 \\ &= \mathbf{q} + \mathbf{P}\cdot\mathbf{v} + \mathbf{v}e + \frac{1}{2}\rho\mathbf{v}v^2\end{aligned}$$

since the average of the peculiar velocity is zero, i.e.,  $\langle\mathbf{C}v^2\rangle_M = \mathbf{v}(2\mathbf{v}\cdot\langle\mathbf{C}\rangle_M) = 0$ . Furthermore, the last line on the RHS is obtained introducing the heat flux  $\mathbf{q}$  as defined by (2.72), the pressure tensor  $\mathbf{P}$  as defined by (2.64), and the internal energy variable  $e$  as defined by (2.74).

By use of (2.211) and (2.212), (2.210) can be expressed as:

$$\frac{\partial}{\partial t}(\rho[e + \frac{1}{2}v^2]) + \frac{\partial}{\partial \mathbf{r}}\cdot(\rho\mathbf{v}[e + \frac{1}{2}v^2]) = -\frac{\partial}{\partial \mathbf{r}}\cdot\mathbf{q} - \frac{\partial}{\partial \mathbf{r}}\cdot(\mathbf{P}\cdot\mathbf{v}) + \rho\mathbf{F}\cdot\mathbf{v} \quad (2.213)$$

This is the total energy equation, for which the potential energy term is expressed in terms of the external force  $\mathbf{F}$ . By use of the momentum equation we can derive a transport equation for the mean kinetic energy, and thereafter extract the mean kinetic energy part from the equation (i.e., the same procedure was used manipulating the continuum model counterpart in chap. 1, sect. 1.2.4). The result is:

$$\frac{\partial}{\partial t}(\rho e) + \frac{\partial}{\partial \mathbf{r}}\cdot(\rho\mathbf{v}e) = -\frac{\partial}{\partial \mathbf{r}}\cdot\mathbf{q} - \mathbf{P} : \frac{\partial}{\partial \mathbf{r}}\mathbf{v} \quad (2.214)$$

This may be even further restated in terms of temperature by using the continuity equation (2.202) and the definitions of  $e$ , (2.74), and  $T$ , (2.75):

$$\rho\frac{De}{Dt} = C_v\rho\frac{\partial T}{\partial t} + C_v\rho\mathbf{v}\cdot\frac{\partial T}{\partial \mathbf{r}} = -\frac{\partial}{\partial \mathbf{r}}\cdot\mathbf{q} - \mathbf{P} : \frac{\partial}{\partial \mathbf{r}}\mathbf{v} \quad (2.215)$$

where  $C_v = \frac{2m}{3k}$ , since the thermal energy consists of translational energy only for mono-atomic gases.

The conservation equations (2.202), (2.207) and (2.213) are rigorous (i.e., for mono-atomic gases) consequences of the Boltzmann equation (2.185). It is important to note that we have derived the governing conservation equations without knowing the exact form of the collision term, the only requirement is that we are considering summation invariant properties of mono-atomic gases. That is, we are considering properties that are conserved in molecular collisions.

Nevertheless, it is clear that, in order to obtain practically useful fluid dynamic equations from the general formulations derived above, one must find suitable closures determining explicit expressions for the unknown quantities, i.e., the pressure tensor  $\mathbf{P}$  and the heat flux  $\mathbf{q}$ , in terms of the known variables. Of course, (2.64) and (2.72) provide a prescription for calculating these quantities in terms of molecular quantities, but this requires finding the actual distribution function  $f$  which is a solution of the Boltzmann equation (2.185). It is noted that the pressure tensor is generally split into the pressure and the deviatoric or viscous stresses according to (2.69) shifting the problem to finding an expression for the viscous stresses instead. Anyhow, using the Chapman-Enskog series approximation of the distribution function, two well known forms of the fluid dynamic equations are obtained adopting the zero and first order perturbation approximations of the distribution function as will be outlined shortly.

Meanwhile the  $H$ -theorem is presented, as we need further knowledge on the distribution function and the embedded physics.

## 2.7 The Boltzmann H-Theorem

In this section the elementary definitions and results deduced from the  $H$ -theorem are given [6].

In summary, the statistical  $H$ -theorem of kinetic theory relates to the Maxwellian velocity distribution function and thermodynamics. Most important, the Boltzmann's  $H$ -theorem provides a mechanistic or probabilistic prove for the second law of thermodynamics. In this manner, the  $H$ -theorem also relates the thermodynamic entropy quantity to probability concepts. Further details can be found in the standard references [97] [39] [12] [100] [47] [28] [61] [85].

In practice, during the process of developing novel models for the collision term, the  $H$ -theorem merely serves as a requirement for the constitutive relations in order to fulfill the second law of thermodynamics (in a similar manner as for the continuum models).

### 2.7.1 The H-Theorem Formulation

We first derive the  $H$ -theorem in an approximate manner, starting out by introducing the differential  $H$ -property function defined by:

$$H = \int f \ln f d\mathbf{c}d\mathbf{r} \quad (2.216)$$

To determine how  $H$  changes in time we consider a uniform state in which the distribution function  $f$  is independent of position  $\mathbf{r}$  and no external forces

act upon the molecules. Thus (2.185) reduces to<sup>42</sup>:

$$\frac{df}{dt} = \frac{\partial f}{\partial t} = \int \int (f' f'_1 - f f_1) g \sigma_A(\boldsymbol{\Omega}') d\Omega' d\mathbf{c}_1 \quad (2.217)$$

Let the global quantity be defined by:

$$H = \int f \ln f d\mathbf{c} \quad (2.218)$$

$H$  is thus given by the integral over all velocities. Then,  $H$  is a number, independent of  $\mathbf{r}$ , but a function of  $t$ , depending only on the mode of distribution of the molecular velocities [12].

Multiplying the Boltzmann equation (2.185) by  $(1 + \ln f)$  and integrating over the phase space, yields:

$$\begin{aligned} \frac{dH}{dt} &= \frac{\partial H}{\partial t} = \int \frac{\partial}{\partial t} (f \ln f) d\mathbf{c} = \int (1 + \ln f) \frac{\partial f}{\partial t} d\mathbf{c} \\ &= \int \int \int (1 + \ln f) (f' f'_1 - f f_1) g \sigma_A(\boldsymbol{\Omega}') d\Omega' d\mathbf{c} d\mathbf{c}_1 \end{aligned} \quad (2.219)$$

Considering that  $(1 + \ln f)$  represents a summation invariant property, (2.219) can then be expressed as:

$$\frac{dH}{dt} = \frac{1}{4} \int \int \int \ln(f f_1 / f' f'_1) (f' f'_1 - f f_1) g \sigma_A(\boldsymbol{\Omega}') d\Omega' d\mathbf{c} d\mathbf{c}_1 \quad (2.220)$$

since  $4\psi(1 + \ln f) = \psi([1 + \ln f] + [1 + \ln f_1] - [1 + \ln f'] - [1 + \ln f'_1]) = \psi(\ln f + \ln f_1 - \ln f' - \ln f'_1) = \psi(\ln f f_1 - \ln f' f'_1) = \psi(\ln \frac{f f_1}{f' f'_1}) = -\psi(\ln \frac{f' f'_1}{f f_1})$ .

Setting  $\Xi = f f_1$  and  $\Upsilon = f' f'_1$ , (2.220) can be rewritten as:

$$\frac{\partial H}{\partial t} = \frac{1}{4} \int \int \int (\Upsilon - \Xi) \ln(\Xi/\Upsilon) g \sigma_A(\boldsymbol{\Omega}') d\Omega' d\mathbf{c} d\mathbf{c}_1 \quad (2.221)$$

with  $\Xi$  and  $\Upsilon$  positive, we examine the three cases  $\Xi = \Upsilon$ ,  $\Xi > \Upsilon$ , and  $\Xi < \Upsilon$ . For all three cases  $(\Upsilon - \Xi) \ln(\Xi/\Upsilon) \leq 0$ .

Moreover,  $g \sigma_A(\boldsymbol{\Omega}') d\Omega' d\mathbf{c} d\mathbf{c}_1$  is a positive measure, thus the integral on the right hand side of (2.220) is either negative or zero, so  $H$  can never increase. Hence, we can write:

$$\frac{\partial H}{\partial t} \leq 0 \quad (2.222)$$

This relation is known as Boltzmann's *H-theorem*.

This theorem states that, for any initial  $f$ ,  $H$  approaches a finite minimum limit, corresponding to a state of gas in which  $\partial H/\partial t = 0$  (steady state), and this can according to (2.220) occur, only if:

<sup>42</sup> We use the notation (index 1 or no index) to indicate the two sets of identical molecules having the same mass, but perhaps with different velocities.

$$\begin{aligned} f' f'_1 &= f f_1 \\ \ln f' + \ln f'_1 &= \ln f + \ln f_1 \end{aligned} \quad (2.223)$$

The  $H$ -theorem is thus equivalent to the second law of thermodynamics which states that the entropy cannot decrease. A formal relationship between the  $H$  quantity and the entropy  $S$  is discussed in sect. 2.7.3.

Equation (2.223) also relates  $H$  to the theory of *irreversible thermodynamics*, as it is a probabilistic confirmation of the irreversibility of physical processes.

### 2.7.2 The Maxwellian Velocity Distribution

To find the exact equilibrium distribution that is a solution to (2.223), it can be shown that the resulting equilibrium distribution is given by (see e.g., [77]; [61], p. 162; [12], p. 69):

$$f^0(\mathbf{c}) = n \left( \frac{m}{2\pi kT} \right)^{\frac{3}{2}} e^{-\frac{m\mathbf{c}^2}{2kT}} \quad (2.224)$$

where  $k$  is the Boltzmann constant. In the Maxwellian distribution the parameters  $n$ ,  $\mathbf{c}$  and  $T$  are constants in  $\mathbf{r}$  and  $t$ . This distribution formula is often referred to as the *absolute Maxwellian*.

For the imaginary equilibrium flows we assume that in the neighborhood of any point in the gas, the distribution function is locally Maxwellian, and  $\rho$ ,  $T$ , and  $\mathbf{v}$  vary slowly in space and time. It can be shown that the approximation  $f(\mathbf{r}, \mathbf{c}, t) \approx f^0(\mathbf{r}, \mathbf{c}, t)$  is also a solution to (2.223), when  $f^0(\mathbf{r}, \mathbf{c}, t)$  is defined by:

$$\begin{aligned} f^0(\mathbf{r}, \mathbf{c}, t) &= n(\mathbf{r}, t) \left( \frac{m}{2\pi kT(\mathbf{r}, t)} \right)^{\frac{3}{2}} e^{-\frac{m\mathbf{c}^2(\mathbf{r}, t)}{2kT(\mathbf{r}, t)}} \\ &= n(\mathbf{r}, t) \left( \frac{m}{2\pi kT(\mathbf{r}, t)} \right)^{\frac{3}{2}} e^{-\frac{m(\mathbf{c} - \mathbf{v}(\mathbf{r}, t))^2}{2kT(\mathbf{r}, t)}} \end{aligned} \quad (2.225)$$

It is important to note that this distribution function (2.225), defined so that it resembles (2.224) but with the constant values of  $n$ ,  $\mathbf{v}$  and  $T$  in (2.224) replaced by the corresponding functions of  $\mathbf{r}$  and  $t$ , remains a solution to (2.223). This distribution function, which is called the *local Maxwellian*, makes the kinetic theory much more general and practically relevant.

Both the absolute- and local Maxwellians are termed equilibrium distributions. This result relates to the local and instantaneous equilibrium assumption in continuum mechanics as discussed in chap. 1, showing that the assumption has a probabilistic fundament. It also follows directly from the local equilibrium assumption that the pressure tensor is related to the thermodynamic pressure, as mentioned in sect. 2.3.3.

### 2.7.3 The H-Theorem and Entropy

In this section a relationship between the equilibrium value of  $H$  and entropy,  $S$ , is derived [12] (p. 78).

Considering a gas at uniform steady state, (2.216) can be reformulated in terms of the absolute Maxwellian distribution (2.224), hence:

$$H = n \left\{ \ln n + \frac{3}{2} \ln \left( \frac{m}{2\pi kT} \right) - \frac{3}{2} \right\} \quad (2.226)$$

Integrating  $H$  over the gas volume ( $V = \frac{M}{\rho} = \frac{M}{mn}$ ), it follows that:

$$H_0 = \int_V H d\mathbf{r} = \frac{M}{m} \left[ \ln n + \frac{3}{2} \ln \left( \frac{m}{2\pi kT} \right) - \frac{3}{2} \right] \quad (2.227)$$

Assuming that the kinetic theory definition of temperature and the thermodynamic counterpart are consistent, the entropy variable may be considered a function of  $\rho$  and  $T$  as obtained combining the first and second law of thermodynamics [32]. The entropy of the gas is then given by [12] (p. 41):

$$\delta S = M \left( C_V \frac{\delta T}{T} + \frac{k}{m} \frac{\delta V}{V} \right) = \frac{Mk}{m} \left( \frac{3}{2} \frac{\delta T}{T} + \frac{\delta n}{n} \right) \quad (2.228)$$

After integration the relation can be written as:

$$S = \frac{Mk}{m} \ln \left( \frac{T^{3/2}}{n} \right) + \text{constant} = -kH_0 - \frac{3M}{2m} \left( \ln \left( \frac{2\pi k}{m} \right) + 1 \right) + \text{constant} \quad (2.229)$$

where  $\ln T$  has been eliminated using (2.227).

This relation connects  $H_0$  with the entropy when the gas is in a uniform steady state:

$$S = -kH_0 + \text{Constant}' \quad (2.230)$$

It is commonly argued that the constant reflects the arbitrariness of the zero point of entropy.

Due to the statistical relationship between  $H_0$  and  $S$  expressed through (2.230), the Boltzmann's  $H$ -theorem shows that for a gas that is not in a steady state  $H_0$  must decrease and the entropy  $S$  will increase accordingly. In accordance with (2.222) we can write:

$$\frac{dH_0}{dt} = -\frac{1}{k} \frac{dS}{dt} \leq 0 \quad (2.231)$$

or

$$\frac{dS}{dt} \geq 0 \quad (2.232)$$

The  $H$ -theorem is apparently a probability theory confirmation of the 2nd law of thermodynamics stating that the entropy cannot decrease in a physical process.

## 2.8 Solving the Boltzmann Equation

Various attempts have been made to obtain approximate solutions to the Boltzmann equation. Two of these methods were suggested independently by Chapman [10] [11] and by Enskog [24] giving identical results. In this book emphasis is placed on the Enskog method, rather than the Chapman one, as most modern work follows the Enskog approach since it is less intuitive and more systematic, although still very demanding mathematically.

The Enskog [24] expansion method for the solution of the Boltzmann equation provides a series approximation to the distribution function. In the zero order approximation the distribution function is locally Maxwellian giving rise to the Euler equations of change. The first order perturbation results in the Navier-Stokes equations, while the second order expansion gives the so-called Burnett equations. The higher order approximations provide corrections for the larger gradients in the physical properties like  $\rho$ ,  $T$  and  $\mathbf{v}$ .

The zero order approximation to  $f$  is valid when the system is at equilibrium and the gas properties contain no or very small macroscopic gradients. In particular, when the system is at equilibrium the heat fluxes and the viscous stresses vanish.

The Navier-Stokes equations are valid whenever the relative changes in  $\rho$ ,  $T$  and  $\mathbf{v}$  in the distance of the mean free path are small compared to unity. Inasmuch as the Enskog theory is rather long and involved, we will only provide a brief outline of the problem and the method of attack, and then rather discuss the important results.

When the second order approximations to the pressure tensor and the heat flux vector are inserted into the general conservation equation, one obtains the set of PDEs for the density, velocity and temperature which are called the Burnett equations. In principle, these equations are regarded as valid for non-equilibrium flows. However, the use of these equations never led to any noticeable success (e.g., [28], pp. 150-151); [39], p. 464), merely due to the severe problem of providing additional boundary conditions for the higher order derivatives of the gas properties. Thus the second order approximation will not be considered in further details in this book.

Further details of the Enskog method are given by Enskog [24] and in the standard references like Hirschfelder et al. [39], Ferziger and Kaper [28], Vincenti and Kruger [100], Chapman and Cowling [12] and Liboff [61].

### 2.8.1 Equilibrium Flow - The Euler Equations

Applying the local Maxwellian distribution function (2.225), explicit expressions can be obtained for the heat flux,  $\mathbf{q}$  and the pressure tensor  $\mathbf{P}$ .

Substituting  $f^0$  into the two flux formulas (2.64) and (2.72), give:

$$\mathbf{P} = m \int f^0 \mathbf{C} \mathbf{C} d\mathbf{c} = p\mathbf{e} \quad (2.233)$$

and

$$\mathbf{q} = \frac{1}{2}m \int f^0 \mathbf{C} C^2 d\mathbf{c} = 0 \quad (2.234)$$

In the zero order solution, there is no heat flow and the pressure tensor is diagonal. The diagonal elements in the pressure tensor denote the normal stresses that are identical to the thermodynamic pressure, as defined by (2.68).

These conclusions are not obvious at first sight, so a brief mathematical verification is provided. In Cartesian tensor notation, the pressure tensor (2.64) is given by:

$$P_{ij} = \rho \left( \frac{m}{2\pi kT} \right)^{3/2} \int C_i C_j \exp \left( -\frac{mC^2}{2kT} \right) dC = p\delta_{ij} \quad (2.235)$$

where  $dC = dc$ , since  $\mathbf{v}$  is not a function of  $\mathbf{c}$ .

Furthermore, as the integration is over the whole velocity space, it can be proved that any integral vanishes when the integrand is odd. Inspection of the pressure tensor shows that, since  $C_i$  and  $C_j$  themselves are odd functions of  $C_i$  and  $C_j$  respectively, whereas the exponential is an even function, the integrand as a whole is odd when  $i \neq j$  and even when  $i = j$ .

The derivation of the shear and normal stress terms is examined for two representative cases, for which we pick out the odd term ( $i = 1, j = 2$ ) and the even term ( $i = j = 1$ ). The two analytical integral solutions required are taken from the literature<sup>43</sup>.

For the particular odd term ( $i = 1, j = 2$ ) yields:

$$\begin{aligned} & \frac{P_{12}}{nm} \\ &= \left( \frac{m}{2\pi kT} \right)^{3/2} \int_{-\infty}^{\infty} C_1 \exp \left( -\frac{mC_1^2}{2kT} \right) dC_1 \int_{-\infty}^{\infty} C_2 \exp \left( -\frac{mC_2^2}{2kT} \right) dC_2 \int_{-\infty}^{\infty} \exp \left( -\frac{mC_3^2}{2kT} \right) dC_3 \\ &= \left( \frac{m}{2\pi kT} \right)^{3/2} \times 0 \times 0 \times 2 \left[ \frac{1}{2} \sqrt{\pi} \left( \frac{m}{2kT} \right)^{-1/2} \right] = 0, \end{aligned} \quad (2.236)$$

<sup>43</sup> In the following mathematical manipulation we are solving even integrals on the form:

$$\int_{-\infty}^{\infty} x^n \exp(-ax^2) dx = 2 \int_0^{\infty} x^n \exp(-ax^2) dx$$

Two even integral solutions are employed in this reformulation in which  $n = 0$  and  $n = 2$ , respectively, as listed below:

$$\int_0^{\infty} \exp(-ax^2) dx = \frac{\sqrt{\pi}}{2} a^{-1/2} \quad \text{and} \quad \int_0^{\infty} x^2 \exp(-ax^2) dx = \frac{\sqrt{\pi}}{4} a^{-3/2}$$

Further details can, for example, be found in [61] (pp. 526-527) and [12] (sect. 1.4).

and so on for the other shear stresses  $P_{13}$  and  $P_{23}$ . It is thus verified that for equilibrium flows all the viscous stresses vanish,  $\boldsymbol{\sigma} = 0$ .

For the particular even term ( $i = j = 1$ ) yields:

$$\begin{aligned} & \frac{P_{11}}{nm} \\ &= \left(\frac{m}{2\pi kT}\right)^{\frac{3}{2}} \int_{-\infty}^{\infty} C_1^2 \exp\left(-\frac{mC_1^2}{2kT}\right) dC_1 \int_{-\infty}^{\infty} \exp\left(-\frac{mC_2^2}{2kT}\right) dC_2 \int_{-\infty}^{\infty} \exp\left(-\frac{mC_3^2}{2kT}\right) dC_3 \\ &= \left(\frac{m}{2\pi kT}\right)^{3/2} \times 2 \left[\frac{\sqrt{\pi}}{4} \left(\frac{m}{2kT}\right)^{-3/2}\right] \times 2^2 \left[\frac{\sqrt{\pi}}{2} \left(\frac{m}{2kT}\right)^{-1/2}\right]^2 \\ &= p \left(\frac{1}{nkT}\right) \left(\frac{m}{2\pi kT}\right)^{3/2} (2\pi)^{3/2} \left(\frac{m}{kT}\right)^{-5/2} = \frac{p}{nm}, \end{aligned} \tag{2.237}$$

and so on for  $P_{22}$  and  $P_{33}$ . The total pressure tensor becomes,  $\mathbf{P} = pe$ .

The heat flux is treated in a similar manner. By substituting  $f^0$  from (2.225) into the definition of  $\mathbf{q}$  (2.72), it is seen that this expression constitutes an odd integral, hence  $\mathbf{q} = 0$  (e.g., [100], sect. 5).

Since we have just verified that both the viscous stresses and the heat conduction terms vanish for equilibrium flows, the constitutive stress tensor and heat flux relations required to close the governing equations are determined. That is, substituting (2.233) and (2.234) into the conservation equations (2.202), (2.207) and (2.213), we obtain the *Euler* equations for isentropic flow:

$$\frac{\partial \rho}{\partial t} + \nabla \cdot (\rho \mathbf{v}) = 0 \tag{2.238}$$

$$\frac{\partial}{\partial t} (\rho \mathbf{v}) + \nabla \cdot (\rho \mathbf{v} \mathbf{v}) = -\nabla p + \rho \mathbf{F} \tag{2.239}$$

$$\frac{\partial}{\partial t} \left(\rho \left[e + \frac{1}{2}v^2\right]\right) + \nabla \cdot \left(\rho \mathbf{v} \left[e + \frac{1}{2}v^2\right]\right) = -\nabla \cdot (p \mathbf{v}) + \rho \mathbf{F} \cdot \mathbf{v} \tag{2.240}$$

### 2.8.2 Gradient Perturbations - Navier Stokes Equations

Applying the Enskog perturbation method we intend to describe the properties of gases which are only slightly different from equilibrium. Only under these conditions will the flux vectors be about linear in the derivatives so that the formal definitions of the transport coefficients apply. In this limit the distribution function is still nearly Maxwellian, and the Boltzmann equation can be solved by a perturbation method. The resulting solutions are then used to obtain expressions for the heat and momentum fluxes and for the corresponding transport coefficients.

The first step in the Enskog expansion is to introduce a perturbation parameter  $\varepsilon$  into the Boltzmann equation to enforce a state of equilibrium flow as the gas is dominated by a large collision term:

$$\begin{aligned}\frac{D_c f}{D_c t} &= \frac{1}{\varepsilon} \int_1 [f'(\mathbf{r}, \mathbf{c}', t) f'_1(\mathbf{r}, \mathbf{c}'_1, t) - f(\mathbf{r}, \mathbf{c}, t) f_1(\mathbf{r}, \mathbf{c}_1, t)] g \sigma_A(\boldsymbol{\Omega}') d\Omega' d\mathbf{c}_1 \\ &= \frac{1}{\varepsilon} J(ff)\end{aligned}\tag{2.241}$$

where the perturbation parameter factor  $\varepsilon^{-1}$  measures the frequency of collisions. It is assumed that if  $\varepsilon \ll 1$ , the collisions are so frequent that the gas behaves like a continuum being in local equilibrium at every point.

Thereafter, the distribution function is expanded in a series in  $\varepsilon$ :

$$f = f^0 + \varepsilon f^1 + \varepsilon^2 f^2 + \dots\tag{2.242}$$

In a similar manner the time derivative is expanded as:

$$\frac{\partial}{\partial t} = \frac{\partial_0}{\partial t} + \varepsilon \frac{\partial_1}{\partial t} + \varepsilon^2 \frac{\partial_2}{\partial t} + \dots\tag{2.243}$$

stipulating that the time dependence of  $f$  is solely dependent on the fluid dynamic variables  $\rho$ ,  $T$ , and  $\mathbf{v}$ , and expressed in terms of an exact differential. The physical meaning of the expansion in time is that the lowest order terms vary most rapidly, whereas higher order terms are more slowly varying.

If these series expansions are introduced into the modified Boltzmann equation (2.241), and the coefficients of equal powers of  $\varepsilon$  equated, the distribution function can be uniquely determined to a specified order provided that  $f$  still satisfies the moment relations defining the physical properties like density, gas velocity and temperature.

Following this procedure, we get:

$$0 = J(f^0 f^0)\tag{2.244}$$

and

$$\frac{D_{c,0} f^0}{D_c t} = J(f^0 f^1)\tag{2.245}$$

The solution of (2.244) gives rise to the absolute Maxwellian,  $f^0$ , as discussed in sect 2.7.2.

Considering the first order approximation, (2.245) is supposedly solved for  $f^1$ . It is then required that the physical properties ( $\rho, \mathbf{v}, T$ ) are determined by the zero order approximation,  $f^0$ , whereas the higher order terms in the expansion contribute to  $\mathbf{q}$  and  $\boldsymbol{\sigma}$  only.

Next, in the first order perturbation solution  $f^1$  is written in terms of the perturbation function  $\Phi$ . Hence,

$$f \approx f^0 + f^1 \approx f^0 + \Phi f^0 = f^0(1 + \Phi)\tag{2.246}$$

where  $\varepsilon$  is set to unity.

After (2.245) has been solved for  $\Phi$  (i.e., instead of  $f^1$ ),  $f$  is known to second order  $f = f^0(1 + \Phi)$ . Note that when the perturbation function  $\Phi \neq 0$

but still  $\Phi \ll 1$ , the system is only slightly different from equilibrium as prerequisites.

After the first order approximation is introduced through (2.246), (2.245) is said to be an inhomogeneous linear integral equation for  $\Phi$ . The form of  $\Phi$  is then established without actually obtaining a complete solution. Instead, by functional analysis a partial solution is written in the form (e.g., Chapman and Cowling [12], sect. 7.3; Hirschfelder et al. [39], chap. 7, sect. 3):

$$\Phi = -\frac{1}{n} \left[ \sqrt{\frac{2kT}{m}} \mathbf{A} \cdot \frac{\partial}{\partial \mathbf{r}} (\ln T) + 2\mathbf{B} : \frac{\partial}{\partial \mathbf{r}} \mathbf{v} \right] \quad (2.247)$$

where  $\mathbf{A}$  is a vector function of  $\mathcal{C} = \sqrt{\frac{m}{2kT}} \mathbf{C}$ ,  $n$  and  $T$ , whereas  $\mathbf{B}$  is a tensor function of  $\mathcal{C}$ ,  $n$  and  $T$ .

To determine the form of these two functions (i.e.,  $\mathbf{A}$  and  $\mathbf{B}$ ) the solution for  $\Phi$  (2.247) is substituted into the linearized Boltzmann equation (2.245), and thereafter the coefficients of the different components of  $\nabla T$  and  $\nabla \mathbf{v}$  in the resulting relation are equated.

The only vectors that can be formed from these quantities are products of  $\mathcal{C}$  itself and scalar functions  $A(\mathcal{C}, n, T)$ , expressed as:

$$\mathbf{A} = A(\mathcal{C}, n, T) \mathcal{C} \quad (2.248)$$

$\mathbf{B}$  can be shown to be a symmetrical, traceless and non-divergent tensor [12, 28, 61]. The only second order symmetrical traceless tensors that can be formed from  $\mathcal{C}$ ,  $n$  and  $T$  are products of  $\overline{\mathcal{C}\mathcal{C}}$ <sup>44</sup> and scalar functions  $B(\mathcal{C}, n, T)$ . Hence, it follows that:

$$\mathbf{B} = \overline{\mathcal{C}\mathcal{C}} B(\mathcal{C}, n, T) \quad (2.249)$$

Finally, solutions to the integral flux equations like (2.64) and (2.72) are then obtained by expressing the scalar functions  $A(\mathcal{C}, n, T)$  and  $B(\mathcal{C}, n, T)$  in terms of certain polynomials<sup>45</sup> (i.e., Sonine polynomials).

However, without showing all the lengthy details of the method by which the two scalar functions are determined, we briefly sketch the problem definition in which the partial solution (2.247) is used to determine expressions for the viscous-stress tensor  $\boldsymbol{\sigma}$  and the heat flux vector  $\mathbf{q}$ .

Introducing the expressions for the first order approximation of the distribution function (2.246) and thereafter the partial solution for  $\Phi$  (2.247) into the pressure tensor definition, (2.64), we get [39]:

<sup>44</sup> This notation is used denoting a symmetrical, traceless and non-divergent tensor [12] [61] [28].

<sup>45</sup> The detailed mathematical analysis needed determining these integrals are omitted in this book as it is rather lengthy and involved, instead the reader being interested in these pure mathematics are referred to the formal mathematical procedures given in the standard references (e.g., Enskog [24]; Hirschfelder et al. [39]; Chapman and Cowling [12], p.126; Liboff [61], p. 187).

$$\begin{aligned}
\mathbf{P} &= m \int f \mathbf{C} \mathbf{C} d\mathbf{c} = m \int f^0 (1 + \Phi) \mathbf{C} \mathbf{C} d\mathbf{c} \\
&= m \underbrace{\int f^0 \mathbf{C} \mathbf{C} d\mathbf{c}}_1 + m \underbrace{\int f^0 \Phi \mathbf{C} \mathbf{C} d\mathbf{c}}_2 \quad (2.250)
\end{aligned}$$

where the parameter  $\varepsilon$  has been set equal to one.

From the previous section we recognize that term 1 on the RHS of (2.250) equals the pressure term,  $p\mathbf{e}$ , as for equilibrium systems. It can be shown by kinetic theory that term 2 on the RHS corresponds to the viscous stress tensor  $\boldsymbol{\sigma}$  as defined by the pressure tensor (2.69).

In order to determine the stress tensor term 2 in (2.250), the perturbation function  $\Phi$  in the integrand is substituted by the partial solution (2.247). Omitting integrals of odd functions of the components of  $\mathbf{C}$  or  $\mathbf{C}$ , only the term containing the  $\mathbf{B}$  remains. After some lengthy manipulations, the result is:

$$\boldsymbol{\sigma} = -\mu \left( \nabla \mathbf{v} + (\nabla \mathbf{v})^T - \frac{2}{3} (\nabla \cdot \mathbf{v}) \mathbf{e} \right) \quad (2.251)$$

Note that the viscosity parameter  $\mu$  has been introduced as a prefactor in front of the tensor functions by substitution of the kinetic theory transport coefficient expression after comparing the kinetic theory result with the definition of the viscous stress tensor  $\boldsymbol{\sigma}$ , (2.69). In other words, this model inter-comparison defines the viscosity parameter in accordance with the Enskog theory.

An analytical expression for the heat flux vector can be derived in a similar manner using the Enskog approach. That is, we introduce the first order approximation of the distribution function from (2.246) into the heat flux definition (2.72) and thereafter substitute the partial solution for  $\Phi$ , as defined by (2.247), into the resulting flux vector integrand as follows [39]:

$$\mathbf{q} = \frac{1}{2} m \int f^0 (1 + \Phi) C^2 \mathbf{C} d\mathbf{C} = -\lambda \nabla T \quad (2.252)$$

Hence, the conductivity  $\lambda$  in (2.252) is determined by model inter-comparison in accordance with the Enskog method<sup>46</sup>.

In conclusion, when these first order expressions for the pressure tensor and the heat flow vector are substituted into the general conservation equations (2.202), (2.207) and (2.213), we obtain the following set of partial differential equations:

$$\frac{1}{\rho} \frac{D\rho}{Dt} = -\nabla \cdot \mathbf{v} \quad (2.253)$$

$$\rho \frac{D\mathbf{v}}{Dt} = -\nabla p - \nabla \cdot \boldsymbol{\sigma} + \rho \mathbf{F} \quad (2.254)$$

<sup>46</sup> Overall, it is important to recognize that both the Newton viscosity law and Fourier's law of heat conduction are automatically generated from the approximate kinetic theory solution of Enskog.

$$\rho \frac{D}{Dt} \left( e + \frac{1}{2} v^2 \right) = -\nabla \cdot \mathbf{q} - \nabla \cdot (p\mathbf{v}) - \nabla \cdot (\boldsymbol{\sigma} \cdot \mathbf{v}) + \rho \mathbf{F} \cdot \mathbf{v} \quad (2.255)$$

where  $\boldsymbol{\sigma}$  and  $\mathbf{q}$  are given by (2.251) and (2.252), respectively.

The resulting set of conservation equations derived by kinetic theory corresponds to the Navier-Stokes equations of fluid dynamics.

## 2.9 Multicomponent Mixtures

In this section we briefly discuss some of the important issues that arise when the kinetic gas theory is extended to gas mixtures. For a more detailed study of kinetic theory of mixtures the reader is referred to Hirschfelder et al. [39], Williams [104] (app D) and Ferziger and Kaper [28].

It is first necessary to generalize the definitions of the important functions. If we denote the chemical species in a gas mixture by  $s$ , then  $n_s$ ,  $m_s$ ,  $f_s$ ,  $\mathbf{c}_s$ ,  $\mathbf{C}_s$ ,  $\mathbf{F}_s$ , etc. will in general be different for each species.

The starting point for the kinetic theory of low density, non-reacting mixtures of mono-atomic gases is the knowledge of the distribution function  $f_s(\mathbf{r}, \mathbf{c}_s, t)$ .  $f_s(\mathbf{r}, \mathbf{c}_s, t)$  is defined in such a way that the quantity  $f_s(\mathbf{r}, \mathbf{c}_s, t) d\mathbf{c}_s d\mathbf{r}$  represents the probable number of molecules of the  $s$ -th species which at the time  $t$  lie in a unit volume element  $d\mathbf{r}$  about the point  $\mathbf{r}$  and which have velocities within the range  $d\mathbf{c}_s$  about  $\mathbf{c}_s$ . It is emphasized that  $\mathbf{c}_s$  denotes the molecular velocity of a species  $s$  with respect to a coordinate system fixed in space.

The total number of molecules of species  $s$  per unit spatial volume yields:

$$n_s(\mathbf{r}, t) = \int f_s(\mathbf{r}, \mathbf{c}_s, t) d\mathbf{c}_s \quad (2.256)$$

For the mixture as a whole we have:

$$n(\mathbf{r}, t) = \sum_s \int f_s(\mathbf{r}, \mathbf{c}_s, t) d\mathbf{c}_s = \sum_s n_s \quad (2.257)$$

and

$$\rho(\mathbf{r}, t) = \sum_s m_s \int f_s(\mathbf{r}, \mathbf{c}_s, t) d\mathbf{c}_s = \sum_s m_s n_s = \sum_s \rho_s \quad (2.258)$$

The mean (number average) values of any function  $\psi_s(\mathbf{c}_s)$  over all the molecules of a particular species,  $s$ , yield:

$$\langle \psi \rangle_{M,s} = \frac{1}{n_s} \int \psi_s(\mathbf{c}_s) f_s(\mathbf{r}, \mathbf{c}_s, t) d\mathbf{c}_s \quad (2.259)$$

and the corresponding mean (number average) values of any function  $\psi_s(\mathbf{c}_s)$  over all the species in the mixture are:

$$\langle \psi \rangle_{M,n} = \frac{1}{n} \sum_s \int \psi(\mathbf{c}_s) f_s(\mathbf{r}, \mathbf{c}_s, t) d\mathbf{c}_s = \frac{1}{n} \sum_s n_s \langle \psi \rangle_{M,s} \quad (2.260)$$

The corresponding mixture mass average value of any function  $\psi_s(\mathbf{c}_s)$  is defined by:

$$\langle \psi \rangle_{M,m} = \frac{1}{\rho} \sum_s m_s \int \psi(\mathbf{c}_s) f_s(\mathbf{r}, \mathbf{c}_s, t) d\mathbf{c}_s = \frac{1}{\rho} \sum_s n_s m_s \langle \psi \rangle_{M,s} \quad (2.261)$$

In particular, the mass average velocity  $\mathbf{v}_m$  of the mixture is given by:

$$\mathbf{v}_m = \langle \mathbf{c}_s \rangle_{M,m} = \frac{1}{\rho} \sum_s \rho_s \langle \mathbf{c}_s \rangle_{M,s} \quad (2.262)$$

It is recognized that the mass average velocity for a mixture,  $\mathbf{v}_m$ , is not equal to the number or molar average velocity  $\langle \mathbf{c}_s \rangle_{M,n}$ .

The number average velocity for a particular species,  $s$ , is defined by:

$$\langle \mathbf{c}_s \rangle_{M,s} = \frac{1}{n_s} \int \mathbf{c}_s f_s(\mathbf{r}, \mathbf{c}_s, t) d\mathbf{c}_s = \frac{1}{n_s m_s} \int m_s \mathbf{c}_s f_s(\mathbf{r}, \mathbf{c}_s, t) d\mathbf{c}_s = \mathbf{v}_s(\mathbf{r}, t) \quad (2.263)$$

Note that for each species the molecular number and mass average velocities are equal, as all the molecules have the same mass.

The peculiar velocity of a molecule of species  $s$  is defined in terms of the mass average velocity:

$$\mathbf{C}_s(\mathbf{r}, \mathbf{c}_s, t) = \mathbf{c}_s - \mathbf{v}_m(\mathbf{r}, t) \quad (2.264)$$

The species  $s$  diffusion velocity denotes the average velocity of the particular type of species with respect to a reference frame moving with the mass average velocity of the gas mixture:

$$\mathbf{v}_{d,s} = \langle \mathbf{c}_s \rangle_{M,s} - \mathbf{v}_m = \mathbf{v}_s - \mathbf{v}_m \quad (2.265)$$

Thus, the diffusion velocity for a given species equals the average of the corresponding peculiar velocity and can be written in the form:

$$\mathbf{v}_{d,s} = \frac{1}{n_s} \int (\mathbf{c}_s - \mathbf{v}_m) f_s(\mathbf{r}, t) d\mathbf{c}_s \quad (2.266)$$

Hence, from the definitions of the diffusion and mass average velocities it follows that:

$$\sum_s n_s m_s \mathbf{v}_{d,s} = \sum_s m_s \int (\mathbf{c}_s - \mathbf{v}_m) f_s(\mathbf{r}, t) d\mathbf{c}_s = \sum_s m_s n_s (\langle \mathbf{c}_s \rangle_{M,s} - \mathbf{v}_m) = 0 \quad (2.267)$$

The kinetic theory temperature is defined in terms of the mean (number average) peculiar kinetic energy:

$$\begin{aligned} \frac{1}{2} \sum_s m_s \int (\mathbf{c}_s - \mathbf{v}_m)^2 f_s d\mathbf{c}_s &= \frac{1}{2} \sum_s m_s n_s \langle (\mathbf{c}_s - \mathbf{v}_m)^2 \rangle_M \\ &= \frac{1}{2} \sum_s m_s n_s \langle C_s^2 \rangle_M = \frac{3}{2} nkT \end{aligned} \quad (2.268)$$

The rigorous development of the kinetic theory of gases is based upon the Boltzmann equation for the velocity distribution function  $f_s$ . An extended Boltzmann equation, similar to (2.78), describes how  $f_s$  evolves in time and space,

$$\frac{\partial f_s}{\partial t} + \frac{\partial}{\partial \mathbf{r}} \cdot (\mathbf{c}_s f_s) + \frac{\partial}{\partial \mathbf{c}_s} \cdot (\mathbf{F}_s f_s) = \left( \frac{\partial f_s}{\partial t} \right)_{\text{Collision}} = \sum_r \mathcal{J}(f_s | f_r) \quad (2.269)$$

The external force per unit mass acting on a molecule of species  $s$  is denoted by  $\mathbf{F}_s$ , and  $\left( \frac{\partial f_s}{\partial t} \right)_{\text{Collision}} = \sum_r \mathcal{J}(f_s | f_r) = \int \int (f'_s f'_r - f_s f_r) g_{sr} \sigma_{A_{sr}} d\Omega_{sr} d\mathbf{c}_s$  denotes the molecular collision term accounting for the change in  $f_s$  due to molecular collisions.

The collective flux vector associated with the property  $\psi_s(\mathbf{c}_s)$  is given by:

$$\boldsymbol{\psi}_s = \int \psi_s f_s \mathbf{C}_s d\mathbf{c}_s = \int \psi_s f_s \mathbf{C}_s d\mathbf{C}_s \quad (2.270)$$

It is noted that, as for simple systems computing average quantities, integration over  $\mathbf{C}_s$  is equivalent to integration over  $\mathbf{c}_s$  since the two velocities differ by a constant, and the integration is over the entire range of velocities.

The specific species mass, heat and momentum fluxes can now be expressed by substituting the individual conservative properties for the function  $\psi_s$ .

The mass flux vector is obtained if  $\psi_s = m_s$ :

$$\mathbf{j}_s = m_s \int (\mathbf{c}_s - \mathbf{v}_m) f_s d\mathbf{c}_s = m_s \int \mathbf{C}_s f_s d\mathbf{C}_s = n_s m_s \langle \mathbf{C}_s \rangle_{M,s} = n_s m_s \mathbf{v}_{d,s}, \quad (2.271)$$

and, as shown earlier by (2.267), the sum of all the species mass flux vectors equals zero:

$$\sum_s \mathbf{j}_s = 0 \quad (2.272)$$

The three flux vectors associated with the species momentum transport in the  $x$ ,  $y$  and  $z$ -directions are obtained from (2.270) when  $\psi_s = m_s C_{s,x}$ ,  $\psi_s = m_s C_{s,y}$  and  $\psi_s = m_s C_{s,z}$ , respectively.

The nine components of these three vectors form a symmetric pressure tensor,  $\mathbf{P}_s$ , hence the mixture pressure yields:

$$\begin{aligned} \mathbf{P} &= \sum_s \mathbf{P}_s = \sum_s m_s \int (\mathbf{c}_s - \mathbf{v}_m)(\mathbf{c}_s - \mathbf{v}_m) f_s d\mathbf{c}_s = \sum_s m_s \int \mathbf{C}_s \mathbf{C}_s f_s d\mathbf{C}_s \\ &= \sum_s m_s n_s \langle \mathbf{C}_s \mathbf{C}_s \rangle_{M,s} = \rho \langle \mathbf{C}_s \mathbf{C}_s \rangle_{M,m} \end{aligned} \quad (2.273)$$

where the thermodynamic pressure is given by  $p = \frac{1}{3}tr(\mathbf{P}) = \frac{1}{3}\mathbf{P} : \mathbf{e} = \sum_s p_s = nkT$ , and the viscous stresses yield:  $\boldsymbol{\sigma} = \mathbf{P} - p\mathbf{e}$ .

The species  $s$  heat flux vector associated with the transport of kinetic energy is obtained if we let  $\psi_s = \frac{1}{2}m_s C_s^2$ , hence the mixture heat flux vector is determined by the sum over all the components:

$$\begin{aligned} \mathbf{q} &= \sum_s \mathbf{q}_s = \frac{1}{2} \sum_s m_s \int (\mathbf{c}_s - \mathbf{v}_m)^2 (\mathbf{c}_s - \mathbf{v}_m) f_s d\mathbf{c}_s = \frac{1}{2} \sum_s m_s \int C_s^2 \mathbf{C}_s f_s d\mathbf{C}_s \\ &= \frac{1}{2} \sum_s m_s n_s \langle C_s^2 \mathbf{C}_s \rangle_M \end{aligned} \quad (2.274)$$

Analytical expressions for the multicomponent flux vectors can be derived using the Enskog [24] perturbation method as sketched for one component mono-atomic gases in sect 2.8.

If the species  $s$  Boltzmann equation (2.269) is multiplied by the molecular property  $\psi_s(\mathbf{c}_s)$  and thereafter integrated over all molecular velocities, the general equation of change is achieved:

$$\frac{\partial}{\partial t} \int \psi_s f_s d\mathbf{c}_s + \frac{\partial}{\partial \mathbf{r}} \cdot \int \mathbf{c}_s \psi_s f_s d\mathbf{c}_s + \int \mathbf{F}_s \cdot \frac{\partial \psi_s}{\partial \mathbf{c}_s} f_s d\mathbf{c}_s = \int \psi_s \left( \frac{\partial f_s}{\partial t} \right)_{\text{Collision}} d\mathbf{c}_s \quad (2.275)$$

To derive the species equations of change we let  $\psi_s$  denote successively the mass  $m_s$ , the momentum  $m_s \mathbf{c}_s$ , and the energy  $\frac{1}{2}m_s(\mathbf{C}_s \cdot \mathbf{C}_s)$ . Thereafter, the corresponding mixture equations are obtained simply by adding all the specific species  $s$  equations. The governing equations are given by [39] (sect 7-2):

$$\frac{\partial \rho_s}{\partial t} + \nabla \cdot (\rho_s \mathbf{v}_m) + \nabla \cdot \mathbf{j}_s = 0, \quad (2.276)$$

$$\frac{\partial \rho}{\partial t} + \nabla \cdot (\rho \mathbf{v}_m) = 0, \quad (2.277)$$

$$\frac{\partial}{\partial t} (\rho \mathbf{v}_m) + \nabla \cdot (\rho \mathbf{v}_m \mathbf{v}_m) = -\nabla p - \nabla \cdot \boldsymbol{\sigma}_m + \sum_s \rho_s \mathbf{F}_s \quad (2.278)$$

$$\frac{\partial}{\partial t} \left( \rho \left[ e + \frac{1}{2} v_m^2 \right] \right) + \nabla \cdot \left( \rho \mathbf{v}_m \left[ e + \frac{1}{2} v_m^2 \right] \right) = -\nabla \cdot \mathbf{q} - \nabla \cdot (\mathbf{P} \cdot \mathbf{v}_m) + \rho \mathbf{F} \cdot \mathbf{v}_m \quad (2.279)$$

where the internal energy per unit volume is defined by  $\rho e = \frac{3}{2}nkT = \frac{1}{2} \sum_s m_s \int (\mathbf{c}_s - \mathbf{v}_m)^2 f_s d\mathbf{c}_s$ .

### Elementary Multicomponent Mass Diffusion

The Enskog series solution to the species  $s$  Boltzmann equation can be obtained in the same manner as sketched for the simple systems in sect. 2.8. Near equilibrium the perturbation function  $\Phi_s$  can be expressed as a linear function of the various gradients [39] (p. 469):

$$\Phi_s = -(\mathbf{A}_s \cdot \frac{\partial \ln T}{\partial \mathbf{r}}) - (\mathbf{B}_s : \frac{\partial}{\partial \mathbf{r}} \mathbf{v}_m) + n \sum_r \mathbf{C}_{s,r} \cdot \mathbf{d}_r \quad (2.280)$$

where the vector  $\mathbf{A}_s$ , the tensor  $\mathbf{B}_s$ , and the vectors  $\mathbf{C}_{s,r}$  are functions of  $\mathbf{c}_s$ ,  $\mathbf{r}$ , and  $t$ .

If this expression for  $\Phi_s$  is used in the integrals for the flux vectors, we obtain expressions for the mass diffusion vector, the pressure tensor, and the heat flux vector.

In particular, the integral for the diffusion flux can be expressed in terms of  $\Phi_s$ . Hence, for a  $q$  component gas mixture the multicomponent mass flux vector yields (Hirschfelder et al [39], p 478, p 516 and p 714; Curtiss and Bird [18, 19]):

$$\begin{aligned} \mathbf{j}_s &= n_s m_s \mathbf{v}_{d,s} = m_s \int \mathbf{C}_s f_s d\mathbf{C}_s \approx m_s \int \mathbf{C}_s f_s^0 \Phi_s d\mathbf{C}_s \\ &= m_s \int [ -(\mathbf{A}_s \cdot \frac{\partial \ln T}{\partial \mathbf{r}}) + n \sum_r \mathbf{C}_{s,r} \cdot \mathbf{d}_r ] \mathbf{C}_s f_s^0 d\mathbf{C}_s \\ &\approx p \sum_{r=1}^q \frac{\alpha_{sr}}{n_r m_s} \mathbf{d}_r - D_s^T \frac{\partial \ln T}{\partial \mathbf{r}} \\ &= \frac{n^2}{\rho} \sum_{r=1}^q m_s m_r \mathcal{D}_{sr} \mathbf{d}_r - D_s^T \frac{\partial \ln T}{\partial \mathbf{r}} \\ &= \rho_s \sum_{r=1}^q \hat{D}_{sr} \mathbf{d}_r - D_s^T \frac{\partial \ln T}{\partial \mathbf{r}} \end{aligned} \quad (2.281)$$

where the constants,  $\alpha_{sr}$ , correspond to the phenomenological coefficients of Onsager<sup>47</sup> which satisfy the reciprocal relations considering the processes of diffusion and thermal conduction. One of the phenomenological coefficient indexes refers to the temperature variable, whereas the other indexes refer to the components in the mixture.  $D_s^T$  denotes the multicomponent thermal diffusion coefficients<sup>48</sup>, having the property:

<sup>47</sup> The flux equations in irreversible thermodynamics describes the coupling among the fluxes of the various system properties. The linearity postulate states that the fluxes are linear functions of all the driving forces.

It is understood that these relations are derived adopting several relations from irreversible thermodynamics, e.g., the second law of thermodynamics, the Gibbs-Duhem relation, the linear law and the Onsager reciprocal relations [39, 22, 62, 18, 5].

<sup>48</sup> The latter serves as a reminder that the kinetic theory predicts the cross effects like the transport of mass resulting from a temperature gradient (thermal diffusion). It can also be shown that the theory predicts transport of energy resulting from a concentration gradient (the diffusion-thermo effects). These second-order effects are often referred to as the Soret - and Dufour effects. Unfortunately, no shortcuts are available as these terms do not appear when applying simple kinetic theory, only the more rigorous solution methods resolve these properties.

$$\sum_{s=1}^q D_s^T = 0. \quad (2.282)$$

For dilute mono-atomic gases the vector  $\mathbf{d}_s$  is defined by:

$$\mathbf{d}_s = \frac{\partial}{\partial \mathbf{r}} \left( \frac{n_s}{n} \right) + \left( \frac{n_s}{n} - \frac{n_s m_s}{\rho} \right) \frac{\partial \ln p}{\partial \mathbf{r}} - \frac{n_s m_s}{p \rho} \left[ \frac{\rho}{m_s} \mathbf{g}_s - \sum_{r=1}^q n_r \mathbf{g}_r \right] \quad (2.283)$$

constituting the so-called *generalized diffusional driving forces* due to concentration gradients, pressure gradients, and external force differences. From this result it follows that the diffusion flux, as defined in (2.281), contains terms proportional to the same driving forces which obey the property:

$$\sum_{s=1}^q \mathbf{d}_s = 0. \quad (2.284)$$

It is possible to justify several alternative definitions of the multicomponent diffusivities. Even the multicomponent mass flux vectors themselves are expressed in either of two mathematical forms or frameworks referred to as the generalized Fick- and Maxwell-Stefan equations.

The Fick first law of binary diffusion [29], expressing the mass flux as a function of the driving force, can be defined by:

$$\mathbf{j}_1 = -\rho D_{12} \nabla \omega_1 \quad (2.285)$$

and serves as basis for the generalized Fickian multicomponent formulations.

In the generalized Fickian equations (2.281) the given diffusivities,  $\mathcal{D}_{sr}$ , correspond to the diffusivity definition used by Curtiss and Hirschfelder [16], Hirschfelder et al. [39] (p. 715) and Bird et al. [3]:

$$\mathcal{D}_{sr} = -\frac{\rho p}{n^2 m_s m_r} \left( \frac{\alpha_{sr}}{n_r m_r} + \frac{1}{n_s m_s} \sum_{\substack{k=1 \\ k \neq s}}^q \alpha_{sk} \right) \quad (2.286)$$

These diffusivities are not symmetric,  $\mathcal{D}_{sr} \neq \mathcal{D}_{rs}$ .

However, the  $\mathcal{D}_{sr}$  coefficients relate to the alternative set of consistent multicomponent Fick diffusivities,  $\hat{D}_{sr}$ , by [18]:

$$\hat{D}_{sr} = -\mathcal{D}_{sr} \frac{\omega_s}{x_s x_r} + \sum_{\substack{k=1 \\ k \neq s}}^q \omega_k \mathcal{D}_{sk} \frac{\omega_s}{x_s x_k} = \frac{cRT \alpha_{sr}}{\rho_s \rho_r} \quad (2.287)$$

The multicomponent Fick diffusivities,  $\hat{D}_{sr}$ , are symmetric [17]:

$$\hat{D}_{sr} = \hat{D}_{rs} \quad s, r = 1, 2, 3, \dots, q \quad (2.288)$$

and obey the relation

$$\sum_{s=1}^q \omega_s \hat{D}_{sr} = 0 \quad r = 1, 2, 3, \dots, q \quad (2.289)$$

Hence, the corresponding multicomponent mass fluxes, i.e., the last line on the RHS of (2.281), denote a consistent set of generalized Fick equations derived from kinetic theory of dilute gases.

However, the multicomponent Fickian diffusivities,  $\hat{D}_{sr}$ , do not correspond to the approximately concentration independent binary diffusivities,  $D_{sr}$ , which are available from binary diffusion experiments or kinetic theory determined by the inter-molecular forces between  $s - r$  pair of gases. Instead, these multicomponent Fickian diffusion coefficients are strongly composition dependent.

Due to this difficulty it is preferable to transform the Fickian diffusion problem in which the mass-flux vector,  $\mathbf{j}_s$ , is expressed in terms of the driving force,  $\mathbf{d}_s$ , into the corresponding Maxwell-Stefan form where  $\mathbf{d}_s$  is given as a linear function of  $\mathbf{j}_s$ . The key idea behind this procedure is that one intends to rewrite the Fickian diffusion problem in terms of an alternative set of diffusivities (i.e., preferably the known binary diffusivities) which are less concentration dependent than the Fickian diffusivities.

This transformation can be done using the method suggested by Curtiss and Bird [18] [19] which is in accordance with the work of Merk [71]. To shorten the notation they temporarily define a modified diffusion velocity,  $\mathbf{v}'_{d,s}$ , by:

$$\rho_s \mathbf{v}'_{d,s} = \mathbf{j}_s + D_s^T \nabla \ln T \quad (2.290)$$

Thereafter, the diffusion velocity is expressed in terms of the driving forces using the last line on the RHS of (2.281). For species  $s$  and  $k$  the resulting relationships are given by:

$$\mathbf{v}'_{d,s} = \sum_{r=1}^q \hat{D}_{sr} \mathbf{d}_r \quad (2.291)$$

and

$$\mathbf{v}'_{d,k} = \sum_{r=1}^q \hat{D}_{kr} \mathbf{d}_r \quad (2.292)$$

Then each of the two relations is multiplied by the multicomponent inverse diffusivities,  $\hat{C}_{sk}$  (with  $k \neq s$  and dimensions time/length<sup>2</sup>), and when one equation is subtracted from the other, we get:

$$\hat{C}_{sk}(\mathbf{v}'_{d,k} - \mathbf{v}'_{d,s}) = - \sum_{r=1}^q \hat{C}_{sk}(\hat{D}_{kr} - \hat{D}_{sr}) \mathbf{d}_r \quad (2.293)$$

Next, the sum on  $k$  is performed:

$$\sum_{\substack{k=1 \\ k \neq s}}^q \hat{C}_{sk}(\mathbf{v}'_{d,k} - \mathbf{v}'_{d,s}) = - \sum_{r=1}^q \left[ \sum_{\substack{k=1 \\ k \neq s}}^q \hat{C}_{sk}(\hat{D}_{kr} - \hat{D}_{sr}) \right] \mathbf{d}_r, \quad s = 1, 2, 3, \dots, q \quad (2.294)$$

Curtiss and Bird [18] [19] and Slattery [89] (sect. 8.4.4) state that from kinetic theory of dilute gas mixtures it appears that the coefficients  $\hat{C}_{sk}$  are determined in such a way that the following relations are satisfied  $\sum_{\substack{k=1 \\ k \neq s}}^q \hat{C}_{sk}(\hat{D}_{kr} - \hat{D}_{sr}) = \delta_{sr} + \omega_s$ . Thus, by use of the property  $\sum_{s=1}^q \omega_s \hat{D}_{sr} = 0$ , the RHS of (2.294) reduces to  $+\mathbf{d}_s$ .

The modified diffusion velocity (2.290) can be related to the standard diffusion velocity (1.28), and expressed by:

$$\mathbf{v}'_{d,s} = \frac{\mathbf{j}_s}{\rho_s} + \frac{D_s^T}{\rho_s} \nabla \ln T = \mathbf{v}_{d,s} + \frac{D_s^T}{\rho_s} \nabla \ln T \quad (2.295)$$

Hence, the diffusion problem (2.294) can be expressed in terms of the actual diffusion velocities:

$$\sum_{\substack{k=1 \\ k \neq s}}^q \hat{C}_{sk}(\mathbf{v}_{d,k} - \mathbf{v}_{d,s}) = \mathbf{d}_s - \sum_{\substack{k=1 \\ k \neq s}}^q \hat{C}_{sk} \left( \frac{D_k^T}{\rho_k} - \frac{D_s^T}{\rho_s} \right) \nabla \ln T, \quad s = 1, 2, 3, \dots, q \quad (2.296)$$

These relations are called *the generalized Maxwell-Stefan equations* and are the inverted counterparts of the Fick diffusion equations (2.281). These two descriptions contain the same information and are interrelated as proven by Curtiss and Bird [18] [19] for dilute mono-atomic gas mixtures.

The Maxwell-Stefan diffusivities are now defined by:

$$\hat{C}_{sk} = \frac{x_s x_k}{\tilde{D}_{sk}} \quad (2.297)$$

Thereby, the generalized Maxwell-Stefan equations can be expressed in numerous ways:

$$\begin{aligned} \mathbf{d}_s - \sum_{\substack{k=1 \\ k \neq s}}^q \frac{x_s x_k}{\tilde{D}_{sk}} \left( \frac{D_k^T}{\rho_k} - \frac{D_s^T}{\rho_s} \right) \nabla \ln T &= \sum_{\substack{k=1 \\ k \neq s}}^q \frac{x_s x_k}{\tilde{D}_{sk}} (\mathbf{v}_{d,k} - \mathbf{v}_{d,s}), \quad s = 1, 2, 3, \dots, q \\ &= \sum_{\substack{k=1 \\ k \neq s}}^q \frac{x_s x_k}{\tilde{D}_{sk}} (\{\mathbf{v}_k - \mathbf{v}_m\} - \{\mathbf{v}_s - \mathbf{v}_m\}) = \sum_{\substack{k=1 \\ k \neq s}}^q \frac{x_s x_k}{\tilde{D}_{sk}} (\mathbf{v}_k - \mathbf{v}_s) \\ &= \sum_{\substack{k=1 \\ k \neq s}}^q \frac{x_s x_k}{\tilde{D}_{sk}} \left( \frac{\mathbf{n}_k}{\rho_k} - \frac{\mathbf{n}_s}{\rho_s} \right) = \sum_{\substack{k=1 \\ k \neq s}}^q \frac{x_s x_k}{\tilde{D}_{sk}} \left( \frac{\mathbf{j}_k}{\rho_k} - \frac{\mathbf{j}_s}{\rho_s} \right) \\ &= \sum_{\substack{k=1 \\ k \neq s}}^q \frac{1}{c \tilde{D}_{sk}} (x_s \mathbf{N}_k - x_k \mathbf{N}_s) = \sum_{\substack{k=1 \\ k \neq s}}^q \frac{1}{c \tilde{D}_{sk}} (x_s \mathbf{J}_k^* - x_k \mathbf{J}_s^*) \end{aligned} \quad (2.298)$$

where the combined molar flux with respect to stationary axes is given by:

$$\mathbf{N}_s = c_s \mathbf{v}_s = c x_s \mathbf{v}_s = c_s \mathbf{v}_m^* + \mathbf{J}_s^*, \quad (2.299)$$

and the corresponding combined mass flux is defined by:

$$\mathbf{n}_s = \rho_s \mathbf{v}_s = \rho \omega_s \mathbf{v}_s = \rho_s \mathbf{v}_m + \mathbf{j}_s \quad (2.300)$$

In general, this equation ought to be written in terms of the difference of molecular velocities  $\mathbf{v}_k - \mathbf{v}_s$ , so that the relation can be expressed in terms of any desired mass or molar fluxes.

A more rigorous derivation of these relations were given by Curtiss and Hirschfelder [16] extending the Enskog theory to multicomponent systems. From the Curtiss and Hirschfelder theory of dilute mono-atomic gas mixtures the Maxwell-Stefan diffusivities are in a first approximation equal to the binary diffusivities,  $\tilde{D}_{sr} \approx D_{sr}$ . On the other hand, Curtiss and Bird [18] [19] did show that for dense gases and liquids the Maxwell-Stefan equations are still valid, but the strongly concentration dependent diffusivities appearing therein are not the binary diffusivities but merely empirical parameters.

Considering pure diffusion problems (i.e., no convection) or Engineering multicomponent systems with predefined molar velocities (i.e., not involving the momentum equations), the molar flux description is often used. Accordingly, in ordinary diffusion problems the Fickian flux formulation can be replaced by a set of  $q - 1$  independent equations. For simplicity we generally adopt a set of assumptions considered very good approximations for dilute gas systems, i.e., the thermal diffusion is negligible, the body force per unit mass is the same on each species, and either the pressure is constant or the molecular weights of all the species are about the same. Hence, the driving force (2.283) reduces to:

$$\mathbf{d}_s \approx \nabla x_s \quad (2.301)$$

The resulting set of equations, i.e., using the last line on the RHS of (2.298), is given by:

$$\nabla x_s = - \sum_{r=1}^q \frac{x_s x_r}{\tilde{D}_{sr}} (\mathbf{v}_s - \mathbf{v}_r) = - \sum_{r=1}^q \frac{1}{c \tilde{D}_{sr}} (x_r \mathbf{N}_s - x_s \mathbf{N}_r), \quad s = 1, 2, 3, \dots, q \quad (2.302)$$

This relation is referred to as the Maxwell-Stefan model equations, since Maxwell [65] [67] was the first to derive diffusion equations in a form analogous to (2.302) for dilute binary gas mixtures using kinetic theory arguments (i.e., Maxwell's seminal idea was that concentration gradients result from the friction between the molecules of different species, hence the proportionality coefficients,  $\hat{C}_{sk}$ , were interpreted as inverse friction or drag coefficients), and Stefan [92] [93] extended the approach to ternary dilute gas systems. It is emphasized that the original model equations were valid for ordinary diffusion only and did not include thermal, pressure, and forced diffusion.

It is seen from (2.302), or maybe easier from the Fickian formulation (2.281), that when the driving force (2.283) is approximated by the mole fraction gradients, there is an important difference between binary diffusion and multicomponent diffusion fluxes (e.g., Toor [98]; Taylor and Krishna [96]). In binary systems the movement of species  $s$  is always proportional to the negative of the concentration gradient of species  $s$ . In multicomponent diffusion, however, we may also experience *reverse diffusion* in which a species moves against its own concentration gradient, *osmotic diffusion* in which a species diffuses even though its concentration gradient is zero, and *diffusion barrier* when a species does not diffuse even though its concentration gradient is nonzero.

It is sometimes convenient to cast the governing set of equations into a  $q - 1$  dimensional matrix form. Starting out from the diffusive molar fluxes, as given by the last term on the RHS of (2.298), yield:

$$\mathbf{d}_s = - \sum_{r=1}^q \frac{x_r \mathbf{J}_s^* - x_s \mathbf{J}_r^*}{c \tilde{D}_{sr}} \quad (2.303)$$

However, only  $q - 1$  of the diffusion fluxes are independent, hence:

$$\mathbf{J}_q^* = - \sum_{r=1}^{q-1} \mathbf{J}_r^* \quad (2.304)$$

Using the latter relation, (2.303) may be rewritten as:

$$\begin{aligned} \mathbf{d}_s &= - \sum_{r=1}^q \frac{x_r \mathbf{J}_s^* - x_s \mathbf{J}_r^*}{c \tilde{D}_{sr}} = - \sum_{r=1}^{q-1} \frac{x_r \mathbf{J}_s^* - x_s \mathbf{J}_r^*}{c \tilde{D}_{sr}} - \left( \frac{x_q \mathbf{J}_s^* - x_s \mathbf{J}_q^*}{c \tilde{D}_{sq}} \right) \\ &= - \sum_{r=1}^{q-1} \frac{x_r \mathbf{J}_s^* - x_s \mathbf{J}_r^*}{c \tilde{D}_{sr}} - \left( \frac{x_q \mathbf{J}_s^* - x_s \left( - \sum_{r=1}^{q-1} \mathbf{J}_r^* \right)}{c \tilde{D}_{sq}} \right) \\ &= - \sum_{r=1}^{q-1} \left( - \frac{x_s \mathbf{J}_r^*}{c \tilde{D}_{sr}} + \frac{x_s \mathbf{J}_r^*}{c \tilde{D}_{sq}} \right) - \sum_{r=1}^{q-1} \frac{x_r \mathbf{J}_s^*}{c \tilde{D}_{sr}} - \frac{x_q \mathbf{J}_s^*}{c \tilde{D}_{sq}} \\ &= - \sum_{r=1}^{q-1} \left( - \frac{x_s \mathbf{J}_r^*}{c \tilde{D}_{sr}} + \frac{x_s \mathbf{J}_r^*}{c \tilde{D}_{sq}} \right) - \sum_{r=1}^q \frac{x_r \mathbf{J}_s^*}{c \tilde{D}_{sr}} \\ &= - \sum_{\substack{r=1 \\ r \neq s}}^{q-1} \left( - \frac{x_s}{c \tilde{D}_{sr}} + \frac{x_s}{c \tilde{D}_{sq}} \right) \mathbf{J}_r^* - \sum_{\substack{k=1 \\ k \neq s}}^q \frac{x_k}{c \tilde{D}_{sk}} \mathbf{J}_s^* - \frac{x_s}{c \tilde{D}_{sq}} \mathbf{J}_s^* \\ &= \frac{1}{c} \left\{ - \sum_{\substack{r=1 \\ r \neq s}}^{q-1} B_{sr} \mathbf{J}_r^* - B_{ss} \mathbf{J}_s^* \right\} \end{aligned} \quad (2.305)$$

where the coefficients  $B_{ss}$  and  $B_{sr}$  are defined by:

$$B_{sr} = -x_s \left( \frac{1}{\tilde{D}_{sr}} - \frac{1}{\tilde{D}_{sq}} \right) \quad (2.306)$$

and

$$B_{ss} = \frac{x_s}{\tilde{D}_{sq}} + \sum_{\substack{k=1 \\ k \neq s}}^q \frac{x_k}{\tilde{D}_{sk}} \quad (2.307)$$

Let  $(\mathbf{d})$  and  $(\mathbf{J}^*)$  denote, respectively, the vectors of independent driving forces  $\mathbf{d}_1, \mathbf{d}_2, \mathbf{d}_3, \dots, \mathbf{d}_{q-1}$  and independent diffusion fluxes  $\mathbf{J}_1^*, \mathbf{J}_2^*, \mathbf{J}_3^*, \dots, \mathbf{J}_{q-1}^*$ , hence we may write the  $q - 1$  equations in  $q - 1$  dimensional matrix form as:

$$c(\mathbf{d}) = -[B](\mathbf{J}^*) \quad (2.308)$$

where  $[B]$  is a square matrix of order  $q - 1$ .

Then, to find an explicit expression for  $(\mathbf{J}^*)$  we pre-multiply by the inverse of  $[B]$ :

$$c[B]^{-1}(\mathbf{d}) = -[B]^{-1}[B](\mathbf{J}^*) = -(\mathbf{J}^*) \quad (2.309)$$

or, more conveniently:

$$(\mathbf{J}^*) = -c[B]^{-1}(\mathbf{d}) \quad (2.310)$$

Multicomponent mass transport problems can be approximated by linearization replacing the variable properties in the governing equations (i.e.,  $[B]$ ) with constant reference values (i.e.,  $[B]_{x_{\text{ref}}}$ ) [96]. This approach provides significant computational savings in many cases, but this model linearization should be treated with caution as it gives accurate predictions only when the property variations are not too large.

In particular cases it is desired to work with an explicit expression for the mole flux of a single species type  $s$ ,  $\mathbf{J}_s^*$ , avoiding the matrix form given above. Such an explicit model can be derived manipulating the original Maxwell-Stefan model (2.303), with the approximate driving force (2.301), assuming that the mass fluxes for all the other species are known:

$$\begin{aligned} \mathbf{J}_s^* &= \frac{-c\nabla x_s + \sum_{\substack{r=1 \\ r \neq s}}^q \frac{\mathbf{J}_r^* x_s}{\tilde{D}_{sr}}}{\sum_{\substack{r=1 \\ r \neq s}}^q \frac{x_r}{\tilde{D}_{sr}}} \\ &= D_s \left( -c\nabla x_s + \sum_{\substack{r=1 \\ r \neq s}}^q \left( \frac{\mathbf{J}_r^* x_s}{\tilde{D}_{sr}} \right) \right) \end{aligned} \quad (2.311)$$

where  $D_s$  is given by:

$$D_s = \left( \sum_{\substack{r=1 \\ r \neq s}}^q \frac{x_r}{\tilde{D}_{sr}} \right)^{-1} \quad (2.312)$$

Wilke [103] proposed a simpler model for calculating the effective diffusion coefficients for diffusion of a species  $s$  into a multicomponent mixture of stagnant gases. For dilute gases the Maxwell-Stefan diffusion equation is reduced to a multicomponent diffusion flux model on the binary Fick's law form in which the binary diffusivity is substituted by an effective multicomponent diffusivity. The Wilke model derivation is examined in the sequel.

The combined molar flux of species  $s$  in a binary mixture is defined in accordance with (2.299), using Fick's law:

$$\mathbf{N}_s = c_s \mathbf{v}_m^* + \mathbf{J}_s^* = x_s c \mathbf{v}_m^* - c D_{sr} \nabla x_s = x_s (\mathbf{N}_s + \mathbf{N}_r) - c D_{sr} \nabla x_s \quad (2.313)$$

in which  $c \mathbf{v}_m^* = \mathbf{N}_s + \mathbf{N}_r$  for binary mixtures.

Wilke [103], among others, postulated that an analogous equation for the combined molar flux of species  $s$  in a multicomponent mixture can be written as [3](p 571):

$$\mathbf{N}_s = x_s \sum_{r=1}^q \mathbf{N}_r - c D_{sm} \nabla x_s \quad (2.314)$$

where  $D_{sm}$  represents the effective diffusion coefficient of component  $s$  with respect to the composition of the multicomponent gas mixture.

To express the effective diffusion coefficient in terms of the known binary diffusivities Wilke invoked the Maxwell-Stefan equation. From the last line on the RHS of (2.298) a particular form of the Maxwell-Stefan equation is given:

$$\nabla x_s = \sum_{\substack{r=1 \\ r \neq s}}^q \frac{1}{c \tilde{D}_{sr}} (x_s \mathbf{N}_r - x_r \mathbf{N}_s) \quad (2.315)$$

For dilute systems all gases except the species  $s$  molecules are being stagnant, hence all the fluxes denoted by  $\mathbf{N}_r$ , for  $r \neq s$ , are zero. Thus, the Wilke relation (2.314) reduces to:

$$\mathbf{N}_s = - \frac{c D_{sm}}{1 - x_s} \nabla x_s, \quad (2.316)$$

and the Maxwell-Stefan equation (2.315) yields:

$$\nabla x_s = - \sum_{\substack{r=1 \\ r \neq s}}^q \frac{1}{c \tilde{D}_{sr}} x_r \mathbf{N}_s \quad (2.317)$$

Then, by solving (2.316) for  $\nabla x_s$  and equating the result to the simplified driving force (2.301) in the Maxwell-Stefan equations (2.315), we get [23] [3] (p 571):

$$\frac{1}{D_{sm}} = \frac{1}{(1-x_s)} \sum_{\substack{r=1 \\ r \neq s}}^q \frac{x_r}{\tilde{D}_{sr}} \quad (2.318)$$

The diffusion of species  $s$  in a multicomponent mixture can then be written in the form of Fick's law of binary diffusion, using the effective diffusion coefficient  $D_{sm}$  instead of the binary diffusivity. The Wilke equation is defined by:

$$\mathbf{J}_s^* = -cD_{sm}\nabla x_s \quad (2.319)$$

However, the Wilke equation does not in general satisfy the constraint that the species mole fractions must sum to 1 [14].

A similar model often used by reaction engineers is derived for the limiting case in which all the convective fluxes can be neglected. Consider a dilute component  $s$  that diffuses into a homogeneous mixture, then  $\mathbf{J}_r^* \approx 0$  for  $r \neq s$ . To describe this molecular transport the Maxwell-Stefan equations given by the last line in (2.298) are adopted. With the given restrictions, the model reduces to:

$$\nabla x_s = \sum_{\substack{r=1 \\ r \neq s}}^q \frac{1}{c\tilde{D}_{sr}} (x_s \mathbf{J}_r^* - x_r \mathbf{J}_s^*) \approx - \sum_{\substack{r=1 \\ r \neq s}}^q \frac{1}{c\tilde{D}_{sr}} x_r \mathbf{J}_s^* \quad (2.320)$$

By solving the effective multicomponent diffusion flux as postulated by Wilke (2.319) for  $\nabla x_s$  and equating the result to the simplified driving force (2.301) in the Maxwell-Stefan equations (2.320), we get:

$$\frac{1}{D_{sm}} = \sum_{\substack{r=1 \\ r \neq s}}^q \frac{x_r}{\tilde{D}_{sr}} \quad (2.321)$$

This simple relation provides fair approximations of the molecular fluxes for several ternary systems in which  $s$  is a trace component [82] (p 597).

To describe the combined bulk and Knudsen diffusion fluxes the *dusty gas model* can be used [44] [64] [48] [49]. The dusty gas model basically represents an extension of the Maxwell-Stefan bulk diffusion model where a description of the Knudsen diffusion mechanisms is included. In order to include the Knudsen molecule - wall collision mechanism in the Maxwell-Stefan model originally derived considering bulk gas molecule-molecule collisions only, the wall (medium) molecules are treated as an additional pseudo component in the gas mixture. The pore wall medium is approximated as consisting of giant molecules, called *dust*, which are uniformly distributed in space and held stationary by an external clamping force. This implies that both the diffusive flux and the concentration gradient with respect to the dust particles vanish.

For the  $q + 1$ -component pseudo-mixture we may modify the formulation of the Maxwell-Stefan equation given in the last line of (2.298) and the generalized diffusional driving force expression (2.283). The dusty gas model, for  $s = 1, 2, \dots, q + 1$ , yields:

$$\begin{aligned}
 -\sum_{r=1}^q \frac{\mathbf{N}'_s x'_r - \mathbf{N}'_r x'_s}{c' \tilde{D}'_{sr}} - \frac{\mathbf{N}'_s x'_{q+1} - \mathbf{N}'_{q+1} x'_s}{c' \tilde{D}'_{s,q+1}} = \nabla x'_s + \frac{(x'_s - \omega'_s) \nabla p'}{p'} \\
 - \frac{c'_s \mathbf{g}'_s - \omega'_s \sum_{r=1}^{q+1} c'_r \mathbf{g}'_r}{p'}
 \end{aligned} \tag{2.322}$$

However, only  $q$  of these equations are independent. It is thus required to solve  $(q - 1)$  equations for the bulk species and 1 for the pseudo-component denoting the pore wall medium.

The quantities marked with a prime refer to the pseudo-mixture, that is the gas mixture with the dust molecules. This distinction will be maintained by writing  $p'$ ,  $c'$ ,  $x'_s$ ,  $\tilde{D}'_{sr}$  and  $\omega'_s$  for the quantities referred to the pseudo-mixture and  $p$ ,  $c$ ,  $x_s$ ,  $\tilde{D}_{sr}$  and  $\omega_s$  for the same quantities referred to the actual ideal gas. Note also that for the species concentrations  $c_s$ , partial pressures  $p_s$  and the molar flux vectors there are no distinction between the two quantities.

To ensure that the dust molecules are motionless,  $N'_{q+1} = 0$ , a net external force is used to prevent them from moving in response to any gas pressure gradients [49]:

$$\nabla p = c_{q+1} \mathbf{g}_{q+1} \tag{2.323}$$

Moreover, it is assumed that there are no external forces acting on the actual species,  $\mathbf{g}_s = 0$  for  $s = 1, \dots, q$ . The form of the  $q$  independent equations is thus given by:

$$-\sum_{r=1}^q \frac{\mathbf{N}'_s x'_r - \mathbf{N}'_r x'_s}{c' \tilde{D}'_{sr}} - \frac{\mathbf{N}'_s x'_{q+1}}{c' \tilde{D}'_{s,q+1}} = \nabla x'_s + \frac{(x'_s - \omega'_s) \nabla p'}{p'} + \frac{\omega'_s c_{q+1} \mathbf{g}_{q+1}}{p'} \tag{2.324}$$

To obtain a form of the dusty gas model that can be used in practice the primed variables associated with the pseudo-mixture have to be transformed to the unprimed variables associated with the gas.

The two first terms on the RHS can be formulated as:

$$\begin{aligned}
 \nabla x'_s + \frac{x'_s}{p'} \nabla p' &= \nabla \left( \frac{p'_s}{p'} \right) + \frac{x'_s}{p'} \nabla p' = p'_s \nabla \left( \frac{1}{p'} \right) + \frac{1}{p'} \nabla p'_s + \frac{x'_s}{p'} \nabla p' \\
 &= -\frac{p'_s}{p'^2} \nabla p' + \frac{1}{p'} \nabla p'_s + \frac{x'_s}{p'} \nabla p' \\
 &= -\frac{x'_s}{p'} \nabla p' + \frac{1}{p'} \nabla p'_s + \frac{x'_s}{p'} \nabla p' = \frac{1}{p'} \nabla p'_s
 \end{aligned} \tag{2.325}$$

From the equation of state for an ideal gas we observe:

$$p' = c' RT = (c + c_{q+1}) RT = p + c_{q+1} RT \tag{2.326}$$

Hence, applying the nabla operator yields:

$$\nabla p' = \nabla p + c_{q+1} R \nabla T \tag{2.327}$$

Inserting this result into (2.323), gives:

$$c_{q+1}\mathbf{g}_{q+1} = \nabla p' - c_{q+1}R\nabla T \quad (2.328)$$

By use of the ideal gas law, (2.325) can be rewritten as:

$$\frac{1}{p'}\nabla p'_s = \frac{1}{c'RT}\nabla(c'_sRT) = \frac{c'_s\nabla(\ln T)}{c'} + \frac{\nabla c'_s}{c'} \quad (2.329)$$

Then, employing these formulas, (2.324) can be rewritten as:

$$\begin{aligned} -\sum_{r=1}^q \frac{N'_s x'_r - N'_r x'_s}{c' \tilde{D}'_{sr}} - \frac{N'_s x'_{q+1}}{c' \tilde{D}'_{s,q+1}} &= \nabla x'_s + \frac{x'_s \nabla p'}{p'} - \frac{\omega'_s \nabla p'}{p'} + \frac{\omega'_s c_{q+1} \mathbf{g}_{q+1}}{p'} \\ &= \frac{1}{p'} \nabla p'_s - \frac{\omega'_s \nabla p'}{p'} + \frac{\omega'_s (\nabla p' - c_{q+1} R \nabla T)}{p'} \\ &= \frac{c'_s \nabla(\ln T)}{c'} + \frac{\nabla c'_s}{c'} + \frac{\omega'_s c_{q+1} R \nabla T}{p'} \end{aligned} \quad (2.330)$$

To complete the transformation of the dusty gas model containing primed quantities into the unprimed variables associated with the actual gas, one must employ the following definitions:

$$x'_s = \frac{c'_s}{c'} \quad (2.331)$$

$$c'_s = c_s \quad (2.332)$$

$$\tilde{D}_{sr}^e = \frac{c' \tilde{D}'_{sr}}{c} \quad (2.333)$$

$$\tilde{D}_{sK}^e = \frac{\tilde{D}'_{s,q+1}}{x'_{q+1}} \quad (2.334)$$

$$x_s = \frac{c_s}{c} \quad (2.335)$$

$$\mathbf{N}'_s = \mathbf{N}_s \quad (2.336)$$

Multiplying the first term on the LHS of (2.330) by  $c'/c'$ , we obtain:

$$-\sum_{r=1}^q \frac{N'_s x'_r c' - N'_r x'_s c'}{c'^2 \tilde{D}'_{sr}} = -\sum_{r=1}^q \frac{N_s c_r - N_r c_s}{c'^2 \tilde{D}'_{sr}} = -\sum_{r=1}^q \frac{N_s x_r - N_r x_s}{c' \tilde{D}'_{sr}} \quad (2.337)$$

The mass fraction of species  $s$  can be expressed as:

$$\omega'_s = \frac{m_s}{m_{total}} = \frac{\frac{m_s}{V}}{\frac{m_{total}}{V}} = \frac{\rho_s}{\rho_{total}} = \frac{\rho_s}{\sum_{r=1}^q \rho_r + \rho_{q+1}} = \frac{c_s M_{w_s}}{\sum_{r=1}^q (c_r M_{w_r}) + c_{q+1} M_{w_{q+1}}} \quad (2.338)$$

When  $M_{w_{q+1}} \rightarrow \infty$ ,  $\omega'_s \rightarrow 0$ , so the last term on the RHS of (2.330) vanishes. Hence, (2.330) becomes:

$$-\sum_{r=1}^q \frac{\mathbf{N}_s x_r - \mathbf{N}_r x_s}{\tilde{D}_{sr}^e} - \frac{\mathbf{N}'_s x'_{q+1}}{\tilde{D}'_{s,q+1}} \approx c_s \nabla(\ln T) + \nabla c_s \quad (2.339)$$

By employing the relations;  $\tilde{D}_{sK}^e = \frac{\tilde{D}'_{s,q+1}}{x'_{q+1}}$  and  $\mathbf{N}'_s = \mathbf{N}_s$ , we get:

$$-\sum_{r=1}^q \frac{\mathbf{N}_s x_r - \mathbf{N}_r x_s}{\tilde{D}_{sr}^e} - \frac{\mathbf{N}_s}{\tilde{D}_{sK}^e} = c_s \nabla(\ln T) + \nabla c_s \quad (2.340)$$

Moreover, by use of the ideal gas law;  $c_s = \frac{p_s}{RT}$ , the RHS can be manipulated like:

$$\begin{aligned} -\sum_{r=1}^q \frac{\mathbf{N}_s x_r - \mathbf{N}_r x_s}{\tilde{D}_{sr}^e} - \frac{\mathbf{N}_s}{\tilde{D}_{sK}^e} &= \frac{p_s}{RT} \nabla(\ln T) + \nabla \frac{p_s}{RT} \\ &= \frac{p_s}{RT^2} \nabla T + \nabla \frac{p_s}{RT} \\ &= \frac{p_s}{RT^2} \nabla T + \frac{p_s}{R} \nabla \left( \frac{1}{T} \right) + \frac{1}{RT} \nabla p_s \quad (2.341) \\ &= \frac{p_s}{RT^2} \nabla T - \frac{p_s}{RT^2} \nabla T + \frac{1}{RT} \nabla p_s \\ &= \frac{1}{RT} \nabla p_s = \frac{c}{p} \nabla p_s = c \nabla x_s \end{aligned}$$

Note that the final expression on the RHS is valid for ideal gases at constant pressure only.

By splitting the combined molar flux (2.299), we obtain:

$$\sum_{r=1}^q \frac{(\mathbf{J}_s^* + c_s \mathbf{v}_m^*) x_r - (\mathbf{J}_r^* + c_r \mathbf{v}_m^*) x_s}{\tilde{D}_{sr}^e} + \frac{\mathbf{J}_s^* + c_s \mathbf{v}_m^*}{\tilde{D}_{sK}^e} \approx -c \nabla x_s \quad (2.342)$$

By simple manipulation, the commonly used mole form of the dusty gas model is achieved:

$$\sum_{r=1}^q \frac{\mathbf{J}_s^* x_r - \mathbf{J}_r^* x_s}{\tilde{D}_{sr}^e} + \frac{\mathbf{J}_s^* + c_s \mathbf{v}_m^*}{\tilde{D}_{sK}^e} \approx -c \nabla x_s \quad (2.343)$$

It is sometimes advantageous to use an explicit expression, similar to (2.311), for the diffusive flux. To achieve such an expression, we must reformulate the model by first re-arranging the terms in the following way:

$$\mathbf{J}_s^* \sum_{r=1}^q \frac{x_r}{\tilde{D}_{sr}^e} - \sum_{r=1}^q \frac{\mathbf{J}_r^* x_s}{\tilde{D}_{sr}^e} + \frac{\mathbf{J}_s^*}{\tilde{D}_{sK}^e} + \frac{c_s \mathbf{v}_m^*}{\tilde{D}_{sK}^e} \approx -c \nabla x_s \quad (2.344)$$

Observing that the terms occurring for  $r = s$  in the two sums cancel out, we get:

$$\mathbf{J}_s^* \left( \sum_{\substack{k=1 \\ k \neq s}}^q \frac{x_k}{\tilde{D}_{sk}^e} + \frac{1}{\tilde{D}_{sK}^e} \right) - \sum_{\substack{r=1 \\ r \neq s}}^q \frac{\mathbf{J}_r^* x_s}{\tilde{D}_{sr}^e} + \frac{c_s \mathbf{v}_m^*}{\tilde{D}_{sK}^e} \approx -c \nabla x_s \quad (2.345)$$

or, explicitly:

$$\mathbf{J}_s^* \approx D_s^e \left( \sum_{\substack{r=1 \\ r \neq s}}^q \frac{\mathbf{J}_r^* x_s}{\tilde{D}_{sr}^e} - \frac{c_s \mathbf{v}_m^*}{\tilde{D}_{sK}^e} - c \nabla x_s \right) \quad (2.346)$$

where

$$D_s^e \approx \left( \sum_{\substack{k=1 \\ k \neq s}}^q \frac{x_k}{\tilde{D}_{sk}^e} + \frac{1}{\tilde{D}_{sK}^e} \right)^{-1} \quad (2.347)$$

In some cases the convective term on the LHS of (2.343) can be neglected since  $\mathbf{J}_s^* \gg c_s \mathbf{v}_m^*$ . For these particular problems the dusty gas model (2.343) reduces to:

$$\sum_{\substack{r=1 \\ r \neq s}}^q \frac{\mathbf{J}_s^* x_r - \mathbf{J}_r^* x_s}{\tilde{D}_{sr}^e} + \frac{\mathbf{J}_s^*}{\tilde{D}_{sK}^e} \approx -c \nabla x_s \quad (2.348)$$

This relation can be written in the matrix form:

$$\mathbf{J}_s^* \left( \sum_{\substack{k=1 \\ k \neq s}}^q \frac{x_k}{\tilde{D}_{sk}^e} + \frac{1}{\tilde{D}_{sK}^e} \right) - \sum_{\substack{r=1 \\ r \neq s}}^q \frac{\mathbf{J}_r^* x_s}{\tilde{D}_{sr}^e} \approx -c \nabla x_s \quad (2.349)$$

or more compactly:

$$\mathbf{J}_s^* B_{ss} + \sum_{\substack{r=1 \\ r \neq s}}^q \mathbf{J}_r^* B_{sr} \approx -c \nabla x_s \quad (2.350)$$

with the coefficients:

$$B_{ss} = \left( \sum_{\substack{k=1 \\ k \neq s}}^q \frac{x_k}{\tilde{D}_{sk}^e} + \frac{1}{\tilde{D}_{sK}^e} \right) \quad (2.351)$$

$$B_{sr} = -\frac{x_s}{\tilde{D}_{sr}^e} \quad (2.352)$$

In vector notation we get:

$$[B](\mathbf{J}^*) = -c(\nabla \mathbf{x}) \quad (2.353)$$

or, after multiplying both sides by  $[B]^{-1}$ , we obtain:

$$(\mathbf{J}^*) = -c[B]^{-1}(\nabla\mathbf{x}) \quad (2.354)$$

It is emphasized that in this description the gas molecule-dust interactions are accounted for by a set of effective Knudsen diffusion coefficients. Therefore, the dusty gas model contains two types of effective binary diffusion coefficients, the effective binary pair diffusivities in the porous medium and the effective Knudsen diffusivities. The effective diffusivities are related to the corresponding molecular diffusivities by:

$$\tilde{D}_{sr}^e = \tilde{D}_{sr} \frac{\varepsilon}{\tau} \quad (2.355)$$

and

$$\tilde{D}_{sK}^e = \tilde{D}_{sK} \frac{\varepsilon}{\tau} \quad (2.356)$$

where the porosity-to-tortuosity factor ( $\frac{\varepsilon}{\tau}$ ) characterizes the porous matrix and is best determined by experiment. Epstein [27] provides physical interpretations of the  $\varepsilon$  and  $\tau$  parameters. For dilute gases, both the molecular bulk and Knudsen diffusivities can be derived from kinetic theory.

### Consistent Diffusive Mass Flux Closures for the Governing Reactive Flow Equations

The conventional modeling practice considers the mass average mixture velocity as a primitive variable instead of the number or molar averaged mixture velocity. The mass averaged velocity is the natural and most convenient basis for the laws of conservation of mixture mass, momentum and energy. It is noticed that the total number of moles of the molecules in a mixture is not necessarily conserved in reactive systems, whereas the elements and the mixture mass are preserved quantities. Separate equations of motion and energy for each species  $s$  can be derived by continuum arguments [5]. However, for mixtures containing a large number of different species the resulting sets of separate species mole, momentum and energy equations are neither feasible nor needed for solving transport problems. Besides, the species momentum and energy fluxes are not measurable quantities. Therefore, for the calculation of multicomponent problems containing convective transport phenomena the mass average velocity based description of the diffusion has an essential advantage. If this description is chosen, then all the conservation equations contain only mass average velocities, while in the molar description of the diffusion the equations of motion and energy contain mass average velocities whereas the species mass balance equations contain number or mole average velocities. The two velocities are equal only when all the components of the system have the same molar mass, hence the mass average velocity based diffusion flux formulation is recommended for reactor simulations.

The rigorous derivation of the Maxwell-Stefan equations by use of the kinetic theory of dilute gases has already been explained in connection with

(2.290) to (2.298). Nevertheless, although not very useful in practical application, it might be informative from a physical point of view to start out from the complete macroscopic species momentum balance when examining the consistent derivation of the Maxwell-Stefan equations in terms of the mass diffusion fluxes. However, it is noted that the following macroscopic derivation is not as rigorous as the alternative kinetic theory approach.

The linear momentum principle for species  $s$  states that the rate of change of momentum is balanced by the forces acting on the system and the rate of production of momentum of species  $s$  [101] [78]:

$$\begin{aligned} \frac{D}{Dt} \int_{V_s(t)} \rho_s \mathbf{v}_s dv &= \int_{V_s(t)} \rho_s \mathbf{g}_s dv + \int_{A_s(t)} \mathbf{n} \cdot \mathbf{T}_s da + \int_{V_s(t)} \sum_{r=1}^q \mathbf{P}_{sr} dv \\ &+ \int_{V_s(t)} r_s \mathbf{v}_s^* dv \end{aligned} \quad (2.357)$$

where  $\rho_s \mathbf{g}_s$  represents the body force acting on species  $s$ . The term  $\mathbf{n} \cdot \mathbf{T}_s$  represents the species stress vector. The term  $\mathbf{P}_{sr}$  denotes the force per unit volume exerted by species  $r$  on species  $s$ , and the sum in the balance equation represents the force exerted on species  $s$  by all the other species. The last term  $r_s \mathbf{v}_s^*$  designates the source of species momentum<sup>49</sup>. Note that the velocity of the molecules of species  $s$  generated by chemical reaction,  $\mathbf{v}_s^*$ , need not be equal to the species  $s$  velocity  $\mathbf{v}_s$ .

To convert the system balance description into an Eulerian control volume formulation the transport theorem is employed (i.e., expressed in terms of the species  $s$  velocity,  $\mathbf{v}_s$ ):

$$\frac{D}{Dt} \int_{V_s(t)} f dv = \int_{V_s} \frac{\partial f}{\partial t} dv + \int_{A_s} f \mathbf{v}_s \cdot \mathbf{n} da \quad (2.358)$$

in which  $f$  represents any scalar, vector or tensor valued function.

To convert the area integrals into volume integrals the Gauss theorem is used (App A) in the standard manner.

The transformed momentum balance yields:

$$\int_{V_s} \left( \frac{\partial(\rho_s \mathbf{v}_s)}{\partial t} + \nabla \cdot (\rho_s \mathbf{v}_s \mathbf{v}_s) - \rho_s \mathbf{g}_s - \nabla \cdot \mathbf{T}_s - \sum_{r=1}^q \mathbf{P}_{sr} - r_s \mathbf{v}_s^* \right) dv = 0 \quad (2.359)$$

From chap 1 it is known that this balance has to be valid for any volume, hence the integral argument must be equal to zero:

$$\frac{\partial(\rho_s \mathbf{v}_s)}{\partial t} + \nabla \cdot (\rho_s \mathbf{v}_s \mathbf{v}_s) - \rho_s \mathbf{g}_s - \nabla \cdot \mathbf{T}_s - \sum_{r=1}^q \mathbf{P}_{sr} - r_s \mathbf{v}_s^* = 0 \quad (2.360)$$

<sup>49</sup> The fundamental derivation of the species balance equation for systems with homogeneous chemical reactions, starting out from from a Boltzmann type of equation, is briefly discussed in the following subsection.

This balance equation can also be derived from kinetic theory [101]. In the Maxwellian average Boltzmann equation for the species  $s$  type of molecules, the collision operator does not vanish because the momentum  $m_s \mathbf{c}_s$  is not an invariant quantity. Rigorous determination of the collision operator in this balance equation is hardly possible, thus an appropriate model closure for the diffusive force  $\mathbf{P}_{sr}$  is required. Maxwell [65] proposed a model for the diffusive force based on the principles of kinetic theory of dilute gases. The dilute gas kinetic theory result of Maxwell [65] is generally assumed to be an acceptable form for dense gases and liquids as well, although for these mixtures the binary diffusion coefficient is a concentration dependent, experimentally determined empirical parameter.

The elementary modeling of the *diffusion force* is outlined in the sequel. For dilute multicomponent mixtures only elastic binary collisions are considered and out of these merely the unlike-molecule collisions result in a net transfer of momentum from one species to another. The overall momentum is conserved since all the collisions are assumed to be elastic (see sect 2.4.2), hence the net force acting on species  $s$  from  $r$  per unit volume,  $\mathbf{P}_{sr}$  equals the momentum transferred from  $r$  to  $s$  per unit time and unit volume [77] (sect 4-2). The diffusion force yields:

$$\mathbf{P}_{sr} = \mathbf{M}_{sr} Z_{sr} \quad (2.361)$$

where  $\mathbf{M}_{sr}$  represents the momentum flux transferred per collision, and  $Z_{sr}$  denotes the number of collisions between species  $s$  and  $r$  molecules per unit time and unit volume (the collision density).

Several closures have been proposed to calculate the collision density for molecules in gas mixtures [77] (pp 52-55). To derive these expressions for the collision density one generally perform an analysis of the particle-particle interactions in an imaginary container [77] [91] [51], called the conceptual collision cylinder in kinetic theory, as outlined in sect 2.4.2. A fundamental assumption in this concept is that the rate of molecular collisions in a gas depends upon the size, number density, and average speed of the molecules. Following Maxwell [65] each type of molecules are considered hard spheres, resembling billiard balls, having diameter  $d_s$ , mass  $m_s$  and number density  $n_s$ . These hard spheres exert no forces on each other except when they collide. Moreover, the collisions are perfectly elastic and obey the classical conservation laws of momentum and energy. In addition, the particles are uniformly distributed through the gas. Different approximations of the hitherto unknown average molecular speeds  $\langle c_s \rangle_M$  and  $\langle c_r \rangle_M$  can then be made. Suppose that a molecule of type  $s$  moves with an average speed of  $\langle |\mathbf{c}_s| \rangle_M = \langle c_s \rangle_M$  in an imaginary container that contains both  $s$  and  $r$  molecules. Preliminary, in line with the early models, we may assume that the molecules of  $r$  are stationary (this restriction will be removed shortly). Since we are using the billiard ball molecular model, a collision occurs each time the distance between the center of a molecule  $s$  and a molecule  $r$  becomes equal to  $d_{sr} = (d_s + d_r)/2$  in accordance with (2.152). This means that if we construct an imaginary sphere

of radius  $d_{sr}$  around the center of molecule  $s$ , a collision occur every time another molecule  $r$  is located within this sphere as the molecule  $s$  enclosed within the imaginary sphere travels with its average speed sweeping out a cylindrical volume  $\sigma_{A_T} \langle c_s \rangle_M = \pi d_{sr}^2 \langle c_s \rangle_M$  per unit time. If  $n_r$  is the total number of  $r$  molecules per unit mixture volume, the number of centers of  $r$  molecules in the volume swept out is  $\sigma_{A_T} \langle c_s \rangle_M n_r$ . This number equals the number of collisions experienced by the one molecule of  $s$  in unit time, hence the collision frequency can be expressed by:

$$Z_{s-r} = \sigma_{A_T} \langle c_s \rangle_M n_r \quad (2.362)$$

adopting the same notation as used in the last part of sect 2.4.2. A reasonable approximation of the molecular speed may be calculated from the Maxwellian distribution function following the kinetic theory presented in sect 2.4.2.

Moreover, if there is a total of  $n_s$  molecules of  $s$  per unit volume in addition to the  $r$  molecules, the collision density  $Z_{sr}$  denoting the total number of  $s-r$  collisions per unit volume per unit time is:

$$Z_{sr} = Z_{s-r} n_s = \sigma_{A_T} \langle c_s \rangle_M n_r n_s \quad (2.363)$$

If only the  $s$  type of molecules are present, the collision density  $Z_{ss}$  represents the collisions of  $s$  molecules with one another. The expression for this density resembles that for  $Z_{sr}$  but a pre-factor 1/2 has to be introduced to avoid counting each collision twice:

$$Z_{ss} = \frac{1}{2} \sigma_{A_T} \langle c_s \rangle_M n_s n_s \quad (2.364)$$

which coincides with (2.172) when the speed is calculated from the Maxwellian velocity distribution function.

In the collision density formulas presented so far the target molecules  $r$  within the collision cylinder are assumed stagnant, hence only the averaged speed  $\langle c_s \rangle_M$  of the  $s$  molecules is considered. A better estimate of the collision density might be obtained allowing the target molecules to move within the collision cylinder, thus the average relative speeds  $\langle |\mathbf{c}_{rel, sr}| \rangle_M$  and  $\langle |\mathbf{c}_{rel, ss}| \rangle_M$  of the molecules should be used instead of the average speed of the individual species.

Furthermore, dealing with a mixture containing two types of molecules  $s$  and  $r$  of different masses, the  $\langle c_s \rangle_M$  and  $\langle c_r \rangle_M$  values are different. A fairly accurate model is achieved considering that the average relative speed is given by  $\langle |\mathbf{c}_{rel, sr}| \rangle_M = (\langle c_s \rangle_M^2 + \langle c_r \rangle_M^2)^{1/2}$ . This average speed relation is derived using the Maxwellian distribution function as shown by Present [77] (p 79, p 53, p 30). A rigorous collision density model can then be expressed as:

$$Z_{sr} = \sigma_{A_T} \langle |\mathbf{c}_{rel, sr}| \rangle_M x_r x_s n^2 = \sigma_{A_T} \sqrt{\langle c_s \rangle_M^2 + \langle c_r \rangle_M^2} x_r x_s n^2 \quad (2.365)$$

If the gas contains only type  $s$  molecules, the average relative speed of two molecules becomes  $\langle |\mathbf{c}_{rel, ss}| \rangle_M = (\langle c_s \rangle_M^2 + \langle c_s \rangle_M^2)^{1/2} = \sqrt{2} \langle c_s \rangle_M$ . Hence, the expression for  $Z_{ss}$  has to be modified replacing  $\langle c_s \rangle_M$  by  $\sqrt{2} \langle c_s \rangle_M$ , giving:

$$Z_{ss} = \frac{1}{\sqrt{2}} \sigma_{AT} \langle c_s \rangle_M n_s n_s \quad (2.366)$$

The corresponding expression for the number of collisions of one molecule of  $s$  per unit time, when only  $s$  molecules are present, becomes:

$$Z_s = \sqrt{2} \sigma_{AT} \langle c_s \rangle_M n_s \quad (2.367)$$

It is noted that the collision cross-sectional area, also referred to as the total scattering cross section (2.163), can be approximated in different ways too. In one approach the target particles are approximated as point-like particles. Thus, the cross section of the target particles are not considered in calculating the effective cross-sectional area, so  $\sigma_{AT} \approx \pi d_s^2/4$ . To achieve an improved estimate of the effective cross-sectional area the size of the target particles should be taken into account as well, thus  $\sigma_{AT} = \pi d_{sr}^2$ .

The net *momentum flux* transferred from molecules of type  $s$  to molecules of type  $r$  can be approximated by the difference between the average momentum of molecule  $s$  before and after the collision:

$$\mathbf{M}_{sr} = m_s (\mathbf{v}_s - \mathbf{v}'_s) \quad (2.368)$$

In the literature the net momentum flux transferred from molecules of type  $s$  to molecules of type  $r$  has either been expressed in terms of the average diffusion velocity for the different species in the mixture [77] or the average species velocity is used [96]. Both approaches lead to the same relation for the diffusion force and thus the Maxwell-Stefan multicomponent diffusion equations. In this book we derive an approximate formula for the diffusion force in terms of the average velocities of the species in the mixture. The diffusive fluxes are introduced at a later stage by use of the combined flux definitions.

Nevertheless, the given momentum flux formula (2.368) is not useful before the unknown average velocity after the collisions  $\mathbf{v}'_s$  has been determined. For elastic molecular collisions this velocity can be calculated, in an averaged sense, from the classical momentum conservation law and the definition of the center of mass velocity as elucidated in the following.

The velocity of the center of mass referred to a fixed point in space can be obtained from the expression given for position vector of the center of mass (2.112):

$$\mathbf{G} = \frac{m_s \mathbf{v}_s + m_r \mathbf{v}_r}{m_s + m_r} \quad (2.369)$$

If all possible particle-particle approaches are considered, the ensemble average velocities after the collision will be equal to  $\mathbf{G} = \mathbf{G}' = \text{Constant}$ , because all directions of reflection or rebound are assumed to occur with equal likelihood in kinetic theory of dilute gases [77]. By ensemble averaging, we may write:

$$\mathbf{v}'_s = \mathbf{v}'_r = \mathbf{G}' = \mathbf{G} \quad (2.370)$$

One recalls from (1.339) that the ensemble averaged of a species  $k$  velocity  $\langle \mathbf{c}'_k \rangle_e$  is defined by:

$$\mathbf{v}'_k = \langle \mathbf{c}'_k \rangle_e = \frac{1}{N} \sum_{i=1}^N \mathbf{c}'_{k,i} \quad (2.371)$$

where  $N$  is the number of events (collisions) observed.

An ensemble averaged momentum balance considering  $N$  binary collisions between  $s$  and  $r$  molecules is obtained by averaging (2.115). The result is:

$$m_s \mathbf{v}_s + m_r \mathbf{v}_r = m_s \mathbf{v}'_s + m_r \mathbf{v}'_r \quad (2.372)$$

Inserting (2.370) into (2.372) gives:

$$m_s \mathbf{v}_s + m_r \mathbf{v}_r = m_s \mathbf{v}'_s + m_r \mathbf{v}'_r = m_s \mathbf{G}' + m_r \mathbf{G}' = (m_s + m_r) \mathbf{G}' \quad (2.373)$$

Solving for  $\mathbf{v}'_s = \mathbf{G}'$  the relation becomes:

$$\mathbf{v}'_s = \mathbf{G}' = \frac{m_s \mathbf{v}_s + m_r \mathbf{v}_r}{m_s + m_r} = \text{Constant} \quad (2.374)$$

By assuming that an ensemble average velocity equals a Maxwellian average velocity, we might introduce (2.374) into (2.368). In this way we get:

$$\mathbf{M}_{sr} = m_s \left( \mathbf{v}_s - \frac{m_s \mathbf{v}_s + m_r \mathbf{v}_r}{m_s + m_r} \right) \quad (2.375)$$

If we multiply the first term on the RHS by  $\frac{m_s + m_r}{m_s + m_r}$ , we get:

$$\begin{aligned} \mathbf{M}_{sr} &= m_s \left( \mathbf{v}_s \left( \frac{m_s + m_r}{m_s + m_r} \right) - \frac{m_s \mathbf{v}_s + m_r \mathbf{v}_r}{m_s + m_r} \right) \\ &= m_s \left( \frac{m_s \mathbf{v}_s + m_r \mathbf{v}_s - m_s \mathbf{v}_s - m_r \mathbf{v}_r}{m_s + m_r} \right) \\ &= m_s \left( \frac{m_r \mathbf{v}_s - m_r \mathbf{v}_r}{m_s + m_r} \right) \\ &= \frac{m_s m_r (\mathbf{v}_s - \mathbf{v}_r)}{m_s + m_r} \end{aligned} \quad (2.376)$$

By inserting (2.365) and (2.376) into (2.361), we achieve:

$$\mathbf{P}_{sr} = \mathbf{M}_{sr} Z_{sr} = x_r x_s (\mathbf{v}_s - \mathbf{v}_r) \frac{m_s m_r \pi n^2 d_{sr}^2 \sqrt{\langle c_s \rangle_M^2 + \langle c_r \rangle_M^2}}{m_s + m_r} \quad (2.377)$$

If we insert a proportionality (drag or friction) coefficient that does not depend on the mole fractions and the velocities  $\mathbf{v}_s$  and  $\mathbf{v}_r$ , we obtain:

$$\mathbf{P}_{sr} = x_r x_s (\mathbf{v}_s - \mathbf{v}_r) f_{sr} \quad (2.378)$$

The binary friction coefficient has been related to the binary diffusivity by the following relation [65] [96]:

$$f_{sr} = \frac{p}{\tilde{D}_{sr}} \quad (2.379)$$

The diffusion force can thus be expressed as<sup>50</sup>:

$$\mathbf{P}_{sr} = \frac{px_r x_s (\mathbf{v}_s - \mathbf{v}_r)}{\tilde{D}_{sr}} \quad (2.380)$$

By inserting (2.380) into (2.360), the species momentum equation yields:

$$\begin{aligned} \frac{\partial(\rho_s \mathbf{v}_s)}{\partial t} + \nabla \cdot (\rho_s \mathbf{v}_s \mathbf{v}_s) &= \rho_s \mathbf{g}_s + \nabla \cdot \mathbf{T}_s + \sum_{r=1}^q \mathbf{P}_{sr} + r_s \mathbf{v}_s^* \\ &= \rho_s \mathbf{g}_s - \nabla p_s + \nabla \cdot \boldsymbol{\sigma}_s + p \sum_{r=1}^q \frac{x_r x_s (\mathbf{v}_r - \mathbf{v}_s)}{\tilde{D}_{sr}} + r_s \mathbf{v}_s^* \end{aligned} \quad (2.381)$$

where the species stress tensor has been decomposed in the standard manner:

$$\mathbf{T}_s = -p_s \mathbf{e} + \boldsymbol{\sigma}_s \quad (2.382)$$

where  $\boldsymbol{\sigma}_s$  is the species  $s$  viscous stress tensor.

The balance (2.381) can be simplified to obtain the Maxwell-Stefan equation, due to the following assumption:

$$\frac{\partial(\rho_s \mathbf{v}_s)}{\partial t} + \nabla \cdot (\rho_s \mathbf{v}_s \mathbf{v}_s) - \rho_s \mathbf{g}_s - \nabla \cdot \boldsymbol{\sigma}_s - r_s \mathbf{v}_s^* \ll p \sum_{r=1}^q \frac{x_r x_s (\mathbf{v}_r - \mathbf{v}_s)}{\tilde{D}_{sr}} - \nabla p_s \quad (2.383)$$

It has been shown that this inequality is valid for a wide variety of conditions [101]. That is, (2.381) can be reduced to:

$$p \sum_{r=1}^q \frac{x_r x_s (\mathbf{v}_r - \mathbf{v}_s)}{\tilde{D}_{sr}} \approx \nabla p_s = p \nabla x_s + x_s \nabla p \quad (2.384)$$

If we assume that the last term on the RHS is small,

$$\sum_{r=1}^q \frac{x_r x_s (\mathbf{v}_r - \mathbf{v}_s)}{\tilde{D}_{sr}} - \nabla x_s \gg \frac{x_s}{p} \nabla p, \quad (2.385)$$

the Maxwell-Stefan equation (2.298) is reproduced for the particular cases in which the driving force can be approximated by the mole fraction gradient, the gravity force is the only body force acting on the system and the thermal diffusion is neglectable. Therefore, in one instructive view, it is stated that the

<sup>50</sup> This model was first obtained by Maxwell [65] for binary systems. Present [77] (sect 8-3) outlines a more accurate treatment by the moment transfer method which is not restricted to the billiard-ball molecular representation.

Maxwell-Stefan equations represent a particular simplification of the species momentum equation.

The corresponding combined mass flux form of the Maxwell-Stefan relation can be expressed like:

$$\mathbf{d}_s = - \sum_{r=1}^q \frac{x_s x_r (\mathbf{v}_s - \mathbf{v}_r)}{\tilde{D}_{sr}} = - \sum_{r=1}^q \frac{x_s x_r \left( \frac{\mathbf{n}_s}{\omega_s} - \frac{\mathbf{n}_r}{\omega_r} \right)}{\rho \tilde{D}_{sr}} \quad (2.386)$$

The combined flux variable in the Maxwell-Stefan equation given above is then eliminated using the definition (2.300), thus:

$$\mathbf{d}_s = - \sum_{r=1}^q \frac{x_s x_r \left( \frac{\mathbf{j}_s + \rho \omega_s \mathbf{v}_m}{\omega_s} - \frac{\mathbf{j}_r + \rho \omega_r \mathbf{v}_m}{\omega_r} \right)}{\rho \tilde{D}_{sr}} = - \sum_{r=1}^q \frac{x_s x_r \left( \frac{\mathbf{j}_s}{\omega_s} - \frac{\mathbf{j}_r}{\omega_r} \right)}{\rho \tilde{D}_{sr}} \quad (2.387)$$

Moreover, for computational purposes, it is convenient to convert the mole fractions into mass fractions:

$$\begin{aligned} \mathbf{d}_s &= - \sum_{r=1}^q \frac{x_s x_r \frac{\mathbf{j}_s}{\omega_s} - x_s x_r \frac{\mathbf{j}_r}{\omega_r}}{\rho \tilde{D}_{sr}} \\ &= - \sum_{r=1}^q \frac{\left( \frac{\omega_s M_w}{M_{w_s}} \right) \left( \frac{\omega_r M_w}{M_{w_r}} \right) \frac{\mathbf{j}_s}{\omega_s} - \left( \frac{\omega_s M_w}{M_{w_s}} \right) \left( \frac{\omega_r M_w}{M_{w_r}} \right) \frac{\mathbf{j}_r}{\omega_r}}{\rho \tilde{D}_{sr}} \\ &= - \frac{M_w^2}{\rho M_{w_s}} \sum_{r=1}^q \frac{\omega_r \mathbf{j}_s - \omega_s \mathbf{j}_r}{M_{w_r} \tilde{D}_{sr}} \end{aligned} \quad (2.388)$$

However, only  $q - 1$  of the diffusion fluxes are independent, hence:

$$\mathbf{j}_q = - \sum_{r=1}^{q-1} \mathbf{j}_r \quad (2.389)$$

Eliminating the diffusive flux  $\mathbf{j}_q$  from (2.388), by use of (2.389), yields:

$$\begin{aligned} \mathbf{d}_s \frac{\rho M_{w_s}}{M_w^2} &= - \sum_{r=1}^{q-1} \frac{\omega_r \mathbf{j}_s - \omega_s \mathbf{j}_r}{M_{w_r} \tilde{D}_{sr}} - \left( \frac{\omega_q \mathbf{j}_s - \omega_s \mathbf{j}_q}{M_{w_q} \tilde{D}_{sq}} \right) \\ &= - \sum_{r=1}^{q-1} \frac{\omega_r \mathbf{j}_s - \omega_s \mathbf{j}_r}{M_{w_r} \tilde{D}_{sr}} - \left( \frac{\omega_q \mathbf{j}_s - \omega_s \left( - \sum_{r=1}^{q-1} \mathbf{j}_r \right)}{M_{w_q} \tilde{D}_{sq}} \right) \\ &= - \sum_{r=1}^{q-1} \left( - \frac{\omega_s \mathbf{j}_r}{M_{w_r} \tilde{D}_{sr}} + \frac{\omega_s \mathbf{j}_r}{M_{w_q} \tilde{D}_{sq}} \right) - \sum_{r=1}^{q-1} \left( \frac{\omega_r \mathbf{j}_s}{M_{w_r} \tilde{D}_{sr}} \right) - \left( \frac{\omega_q \mathbf{j}_s}{M_{w_q} \tilde{D}_{sq}} \right) \\ &= - \sum_{r=1}^{q-1} \left( - \frac{\omega_s \mathbf{j}_r}{M_{w_r} \tilde{D}_{sr}} + \frac{\omega_s \mathbf{j}_r}{M_{w_q} \tilde{D}_{sq}} \right) - \sum_{r=1}^q \left( \frac{\omega_r \mathbf{j}_s}{M_{w_r} \tilde{D}_{sr}} \right) \end{aligned}$$

$$\begin{aligned}
&= - \sum_{\substack{r=1 \\ r \neq s}}^{q-1} \left( -\frac{\omega_s \mathbf{j}_r}{M_{w_r} \tilde{D}_{sr}} + \frac{\omega_s \mathbf{j}_r}{M_{w_q} \tilde{D}_{sq}} \right) - \left( -\frac{\omega_s \mathbf{j}_s}{M_{w_s} \tilde{D}_{ss}} + \frac{\omega_s \mathbf{j}_s}{M_{w_q} \tilde{D}_{sq}} \right) \\
&\quad - \sum_{\substack{r=1 \\ r \neq s}}^q \left( \frac{\omega_r \mathbf{j}_s}{M_{w_r} \tilde{D}_{sr}} \right) - \left( \frac{\omega_s \mathbf{j}_s}{M_{w_s} \tilde{D}_{ss}} \right) \\
&= - \sum_{\substack{r=1 \\ r \neq s}}^{q-1} \left( -\frac{\omega_s}{M_{w_r} \tilde{D}_{sr}} + \frac{\omega_s}{M_{w_q} \tilde{D}_{sq}} \right) \mathbf{j}_r - \left( \frac{\omega_s}{M_{w_q} \tilde{D}_{sq}} + \sum_{\substack{k=1 \\ k \neq s}}^q \left( \frac{\omega_k}{M_{w_k} \tilde{D}_{sk}} \right) \right) \mathbf{j}_s
\end{aligned} \tag{2.390}$$

A more compact notation is achieved introducing two coefficient matrices:

$$\mathbf{d}_s = -\frac{M_w^2}{\rho M_{w_s}} \left( \sum_{\substack{r=1 \\ r \neq s}}^{q-1} B'_{sr} \mathbf{j}_r + B'_{ss} \mathbf{j}_s \right) \tag{2.391}$$

where the coefficient matrices  $B_{sr}$  and  $B_{ss}$  are defined by:

$$B'_{sr} = -\omega_s \left( \frac{1}{M_{w_r} \tilde{D}_{sr}} - \frac{1}{M_{w_q} \tilde{D}_{sq}} \right) \tag{2.392}$$

and

$$B'_{ss} = \frac{\omega_s}{M_{w_q} \tilde{D}_{sq}} + \sum_{\substack{k=1 \\ k \neq s}}^q \frac{\omega_k}{M_{w_k} \tilde{D}_{sk}} \tag{2.393}$$

The diffusion flux can then be written in a vector form:

$$(\mathbf{j}) = -\frac{\rho(\mathbf{M}_w)}{M_w^2} [B']^{-1} (\mathbf{d}) \tag{2.394}$$

For the particular cases in which the expression for the driving force reduces to the mole fraction gradient, we can derive an explicit expression for  $\mathbf{j}_s$  assuming that all the other fluxes  $\mathbf{j}_r$  are known. Besides, when the mass based formulation is used, it is convenient to rewrite the driving force in terms of the corresponding mass fraction gradient:

$$\mathbf{d}_s \approx \nabla x_s = \nabla \left( \frac{\omega_s M_w}{M_{w_s}} \right) = \frac{1}{M_{w_s}} \nabla (\omega_s M_w) = \frac{1}{M_{w_s}} (\omega_s \nabla M_w + M_w \nabla \omega_s) \tag{2.395}$$

By inserting (2.395) into (2.388), gives:

$$\frac{1}{M_{w_s}} (\omega_s \nabla M_w + M_w \nabla \omega_s) = -\frac{M_w^2}{\rho M_{w_s}} \sum_{r=1}^q \frac{\omega_r \mathbf{j}_s - \omega_s \mathbf{j}_r}{M_{w_r} \tilde{D}_{sr}} \tag{2.396}$$

If we multiply the expression by  $M_{w_s}/M_w$ , we can re-arrange the relation like:

$$\omega_s \nabla \ln(M_w) + \nabla \omega_s = \frac{M_w}{\rho} \sum_{r=1}^q \frac{\omega_s \mathbf{j}_r - \omega_r \mathbf{j}_s}{M_{w_r} \tilde{D}_{sr}} \quad (2.397)$$

The RHS of the relation can also be manipulated slightly, as the terms for  $r = s$  cancel out. The result is given by:

$$\omega_s \nabla \ln(M_w) + \nabla \omega_s = \frac{M_w}{\rho} \left( \sum_{\substack{r=1 \\ r \neq s}}^q \frac{\omega_s \mathbf{j}_r}{M_{w_r} \tilde{D}_{sr}} - \mathbf{j}_s \sum_{\substack{r=1 \\ r \neq s}}^q \frac{\omega_r}{M_{w_r} \tilde{D}_{sr}} \right) \quad (2.398)$$

An explicit relation for the diffusive flux of species  $s$ ,  $\mathbf{j}_s$ , can be obtained with minor manipulation:

$$\mathbf{j}_s = D'_s \left( -\rho \omega_s \nabla \ln(M_w) - \rho \nabla \omega_s + M_w \omega_s \sum_{\substack{r=1 \\ r \neq s}}^q \frac{\mathbf{j}_r}{M_{w_r} \tilde{D}_{sr}} \right) \quad (2.399)$$

where the effective mass based diffusion coefficient is defined by:

$$D'_s = \left( M_w \sum_{\substack{r=1 \\ r \neq s}}^q \frac{\omega_r}{M_{w_r} \tilde{D}_{sr}} \right)^{-1} \quad (2.400)$$

The relation (2.399) can be used to solve the set of Maxwell-Stefan equations iteratively.

Kleijn [46] used this Maxwell-Stefan formulation simulating chemical vapor deposition reactors. One advantage of this explicit formula is that the multicomponent flux is relatively easy to implement as user defined functions in commercial flow codes. However, the conventional matrix form probably enables the design of more efficient solution strategies.

An alternative to the complete Maxwell-Stefan model is the Wilke approximate formulation [103]. In this model the diffusion of species  $s$  in a multicomponent mixture is written in the form of Fick's law with an effective diffusion coefficient  $D'_{sm}$  instead of the conventional binary molecular diffusion coefficient. Following the ideas of Wilke [103] we postulate that an equation for the combined mass flux of species  $s$  in a multicomponent mixture can be written as:

$$\mathbf{n}_s = \omega_s \sum_{r=1}^q \mathbf{n}_r - \rho D'_{sm} \nabla \omega_s \quad (2.401)$$

where  $D'_{sm}$  represents the effective diffusion coefficient of component  $s$  with respect to the mass based composition of the multicomponent gas mixture.

From the second last line on the RHS of (2.298) a particular form of the Maxwell-Stefan equation is given:

$$\nabla x_s = \sum_{\substack{r=1 \\ r \neq s}}^q \frac{x_s x_r (\mathbf{n}_r - \frac{\mathbf{n}_s}{\omega_s})}{\rho \tilde{D}_{sr}} \quad (2.402)$$

For dilute systems all gases except the species  $s$  molecules are being stagnant, hence all the fluxes denoted by  $\mathbf{n}_r$ , for  $r \neq s$ , are zero. Hence, the Wilke relation (2.401) reduces to:

$$\mathbf{n}_s = -\frac{\rho D'_{sm}}{1 - \omega_s} \nabla \omega_s, \quad (2.403)$$

and the Maxwell-Stefan equation (2.402) reduces to:

$$\nabla x_s \approx -\sum_{\substack{r=1 \\ r \neq s}}^q \frac{x_s x_r \frac{\mathbf{n}_s}{\omega_s}}{\rho \tilde{D}_{sr}} \quad (2.404)$$

Noting that the driving force can be expressed in terms of mass fractions instead of mole fractions in according to (2.395), and by transforming the mole fractions on the RHS into mass fractions, the relation above can be written as:

$$\omega_s \nabla M_w + M_w \nabla \omega_s \approx -\frac{M_w^2 \mathbf{n}_s}{\rho} \sum_{\substack{r=1 \\ r \neq s}}^q \frac{\omega_r}{M_{w_r} \tilde{D}_{sr}} \quad (2.405)$$

With minor manipulation the previous relation can be written as:

$$\nabla \omega_s \approx -\frac{M_w \mathbf{n}_s}{\rho} \sum_{\substack{r=1 \\ r \neq s}}^q \frac{\omega_r}{M_{w_r} \tilde{D}_{sr}} - \omega_s \frac{\nabla M_w}{M_w} \quad (2.406)$$

For dilute mixtures consisting of species having about the same molecular weight the last term on the RHS of (2.406) might be neglected:

$$\nabla \omega_s \approx -\frac{M_w \mathbf{n}_s}{\rho} \sum_{\substack{r=1 \\ r \neq s}}^q \frac{\omega_r}{M_{w_r} \tilde{D}_{sr}} \quad (2.407)$$

By solving (2.403) for  $\nabla \omega_s$  and equating the result to the same gradient as derived from the simplified Maxwell-Stefan equations (2.407), we obtain an expression for the effective mass based diffusivity:

$$\frac{1}{D'_{sm}} \approx \frac{M_w}{1 - \omega_s} \sum_{\substack{r=1 \\ r \neq s}}^q \frac{\omega_r}{M_{w_r} \tilde{D}_{sr}} \quad (2.408)$$

This effective diffusivity expression is consistent with the multicomponent diffusive flux written on the Fick's law form:

$$\mathbf{j}_s = -\rho D'_{sm} \nabla \omega_s, \quad (2.409)$$

which might be applied when the given restrictions are fulfilled.

In reactive flow analysis the Fick's law for binary systems (2.285) is frequently used as an extremely simple attempt to approximate the multicomponent molecular mass fluxes. This method is based on the hypothesis that the pseudo-binary mass flux approximations are fairly accurate for solute gas species in the particular cases when one of the species in the gas is in excess and acts as a solvent. However, this approach is generally not recommendable for chemical reactor analysis because reactive mixtures are normally not sufficiently dilute. Nevertheless, many industrial reactor systems can be characterized as convection dominated reactive flows thus the Fickian diffusion model predictions might still look acceptable at first, but this interpretation is usually false because in reality the diffusive fluxes are then neglectable compared to the convective fluxes.

To describe the combined bulk and Knudsen diffusion fluxes the *dusty gas model* can be used. It is postulated that on a mass basis the dusty gas model can be written in analogy to (2.330) in the following way:

$$-\sum_{r=1}^q \frac{\frac{\mathbf{n}'_s x'_r x'_s}{\omega'_s} - \frac{\mathbf{n}'_r x'_s x'_r}{\omega'_r}}{\rho' \tilde{D}'_{sr}}} - \frac{\frac{\mathbf{n}'_s x'_s x'_{q+1}}{\omega'_s}}{\rho' \tilde{D}'_{s,q+1}} = \frac{c'_s \nabla(\ln T)}{c'} + \frac{\nabla c'_s}{c'} \quad (2.410)$$

when  $M_{w_{q+1}} \rightarrow \infty$ ,  $\omega'_s \rightarrow 0$  in accordance with (2.338).

To close the mass form of the dusty gas model, using a similar transformation procedure as employed for the mole based formulation, three novel definitions are required:

$$\mathbf{n}'_s = \mathbf{n}_s \quad (2.411)$$

$$\mathbf{j}'_s = \mathbf{j}_s \quad (2.412)$$

$$\rho'_s = \rho_s \quad (2.413)$$

We multiply the first term on the LHS by  $c'^2/c'^2$  and the second term on the LHS by  $c'/c'$ :

$$-\sum_{r=1}^q \frac{\frac{\mathbf{n}_s}{\omega'_s} (x'_r c') (x'_s c') - \frac{\mathbf{n}_r}{\omega'_r} (x'_s c') (x'_r c')}{(c')^2 \rho' \tilde{D}'_{sr}} - \frac{\frac{\mathbf{n}_s}{\omega'_s} (x'_s c') x'_{q+1}}{c' \rho' \tilde{D}'_{s,q+1}} = \frac{c'_s \nabla(\ln T)}{c'} + \frac{\nabla c'_s}{c'} \quad (2.414)$$

Thereby, all the primed terms of the pseudo-mixture can then be transformed into the actual un-primed variables:

$$-\sum_{r=1}^q \frac{\frac{\mathbf{n}_s}{\rho_s} c_r c_s - \frac{\mathbf{n}_r}{\rho_r} c_s c_r}{c D^e_{sr}} - \frac{\frac{\mathbf{n}_s}{\rho_s} c_s}{D^e_{sK}} = c_s \nabla(\ln T) + \nabla c_s \quad (2.415)$$

Thereafter, the terms containing the actual unprimed mixture variables can be re-written by use of (2.300) and the ideal gas law:

$$\sum_{r=1}^q \frac{x_r x_s \mathbf{j}_s - x_s x_r \mathbf{j}_r}{D_{sr}^e} + \frac{x_s \mathbf{j}_s + \mathbf{v}_m c_s M_w}{D_{sK}^e} = -\rho \nabla x_s \quad (2.416)$$

This form of the mass based dusty gas model equation, which corresponds with the mole based formulation (2.342), is restricted to constant pressure systems.

To enable effective computations it is convenient to rewrite the mole fractions into mass fractions, hence the dusty gas model takes the form:

$$\frac{M_w^2}{M_{w_s}} \sum_{\substack{r=1 \\ r \neq s}}^q \frac{\omega_r \mathbf{j}_s - \omega_s \mathbf{j}_r}{M_{w_r} D_{sr}^e} + \frac{M_w \mathbf{j}_s + \mathbf{v}_m \rho_s M_w}{M_{w_s} D_{sK}^e} = -\frac{\rho}{M_{w_s}} (\omega_s \nabla M_w + M_w \nabla \omega_s) \quad (2.417)$$

From this expression an explicit expression for  $\mathbf{j}_s$  can be obtained:

$$\mathbf{j}_s = D_s^e \left( M_w^2 \sum_{\substack{r=1 \\ r \neq s}}^q \frac{\omega_s \mathbf{j}_r}{M_{w_r} D_{sr}^e} - \frac{\mathbf{v}_m \rho_s M_w}{D_{sK}^e} - \rho (\omega_s \nabla M_w + M_w \nabla \omega_s) \right) \quad (2.418)$$

where

$$D_s^e = \left( M_w^2 \sum_{\substack{r=1 \\ r \neq s}}^q \frac{\omega_r}{M_{w_r} D_{sr}^e} + \frac{M_w}{D_{sK}^e} \right)^{-1} \quad (2.419)$$

In the particular cases in which the convective term can be neglected,  $\mathbf{j}_s \gg \rho \mathbf{v}_m \omega_s$ , the dusty gas model (2.417) reduces to:

$$M_w^2 \sum_{\substack{r=1 \\ r \neq s}}^q \frac{\omega_r \mathbf{j}_s - \omega_s \mathbf{j}_r}{M_{w_r} D_{sr}^e} + \frac{M_w \mathbf{j}_s}{D_{sK}^e} = -\rho (\omega_s \nabla M_w + M_w \nabla \omega_s) \quad (2.420)$$

The model can be written in a matrix form:

$$\mathbf{j}_s \left( M_w^2 \sum_{\substack{k=1 \\ k \neq s}}^q \frac{\omega_k}{M_{w_k} D_{sk}^e} + \frac{M_w}{D_{sK}^e} \right) - M_w^2 \sum_{\substack{r=1 \\ r \neq s}}^q \frac{\omega_s \mathbf{j}_r}{M_{w_r} D_{sr}^e} = -\rho (\omega_s \nabla M_w + M_w \nabla \omega_s) \quad (2.421)$$

A more compact notation is obtained introducing two coefficient matrices:

$$\mathbf{j}_s B_{ss} + \sum_{\substack{r=1 \\ r \neq s}}^q \mathbf{j}_r B_{sr} = -\rho (\omega_s \nabla M_w + M_w \nabla \omega_s) \quad (2.422)$$

The coefficient matrices are defined by:

$$B_{ss} = M_w^2 \sum_{\substack{k=1 \\ r \neq s}}^q \frac{\omega_k}{M_{w_k} D_{sk}^e} + \frac{M_w}{D_{sK}^e} \quad (2.423)$$

and

$$B_{sr} = -M_w^2 \frac{\omega_s}{M_{w_r} D_{sr}^e} \quad (2.424)$$

Using vector notation the dusty gas model for the mass fluxes yields:

$$(\mathbf{j}) = -\rho[B'']^{-1} \left( (\boldsymbol{\omega}) \nabla M_w + M_w \nabla(\boldsymbol{\omega}) \right) \quad (2.425)$$

From (2.341) a less restricted driving force can be derived avoiding the constant pressure assumption. The extended driving force can be expressed by:

$$\mathbf{d}_s \approx c \frac{\nabla p_s}{p} \approx \frac{\nabla(p x_s)}{RT} = \frac{1}{M_{w_s} RT} (p(\omega_s \nabla M_w + M_w \nabla \omega_s) + M_w \omega_s \nabla p) \quad (2.426)$$

In this case the dusty gas diffusive mass flux can be written as:

$$(\mathbf{j}) = -\rho[B'']^{-1} \frac{1}{RT} \left( p(\boldsymbol{\omega}) \nabla M_w + M_w \nabla(\boldsymbol{\omega}) + M_w (\boldsymbol{\omega}) \nabla p \right) \quad (2.427)$$

The design of a complete set of *governing equations* for the description of reactive flows requires that the combined fluxes are treated in a convenient way. In principle, several combined flux definitions are available. However, since the mass fluxes with respect to the mass average velocity are preferred when the equation of motion is included in the problem formulation, we apply the species mass balance equations to a  $q$ -component gas system with  $q - 1$  independent mass fractions  $\omega_s$  and an equal number of independent diffusion fluxes  $\mathbf{j}_s$ . However, any of the formulations derived for the multicomponent mass diffusion flux can be substituted into the species mass balance (1.39), hence a closure selection optimization is required considering the specified restrictions for each constitutive model and the computational efforts needed to solve the resulting set of model equations for the particular problem in question.

Let  $(\boldsymbol{\omega})$  and  $(\mathbf{j})$  denote, respectively, the column arrays of independent mass fractions  $\omega_1, \omega_2, \omega_3, \dots, \omega_{q-1}$  and independent diffusion fluxes  $\mathbf{j}_1, \mathbf{j}_2, \mathbf{j}_3, \dots, \mathbf{j}_{q-1}$ . For multicomponent mixtures with no homogeneous chemical reactions the governing species mass balance can be written on the vector form:

$$\frac{\partial(\rho(\boldsymbol{\omega}))}{\partial t} + \nabla \cdot (\rho \mathbf{v}_m(\boldsymbol{\omega})) = -\nabla \cdot (\mathbf{j}) \quad (2.428)$$

For multicomponent systems the diffusive flux term may be written in accordance with the Maxwell-Stefan equations (2.394) with the driving force

expressed in terms of mass fractions (2.395). With this rigorous diffusion flux closure, the species mass balance becomes:

$$\rho \frac{D(\omega)}{Dt} = \nabla \cdot \left( \rho [B']^{-1} \left( (\omega) \nabla M_w + M_w \nabla (\omega) \right) \right) \quad (2.429)$$

where  $[B']$  is a squared matrix of order  $q - 1$ .

The mass diffusion flux may alternatively be calculated in accordance with the approximate Wilke equation (2.409). In this case the species mass balance reduces to:

$$\rho \frac{D(\omega)}{Dt} = \nabla \cdot \left( \rho [\text{diag}(\mathbf{D}'_m)] \nabla (\omega) \right) \quad (2.430)$$

where  $[\text{diag}(\mathbf{D}'_m)]$  is a diagonal squared matrix of order  $q - 1$  and the vector  $(\mathbf{D}'_m)$  denotes a column array with dimension  $(q - 1)$ .

To described the combined bulk and Knudsen diffusion fluxes in porous media the dusty gas model (2.427) can be used. The corresponding transport equation is given by:

$$\varepsilon \rho \frac{D(\omega)}{Dt} = \nabla \cdot \left( \rho [B'']^{-1} \frac{1}{RT} \left( p(\omega) \nabla M_w + M_w \nabla (\omega) + M_w (\omega) \nabla p \right) \right) \quad (2.431)$$

where the matrix  $[B'']$  has dimensions  $(q - 1) \times (q - 1)$ . It is noted that numerous approximations have been made deriving this equation, for this reason any application in reactor simulations should be carefully validated.

In order to develop a more rigorous expression for the *driving forces in mass transfer*, use is normally made of physical laws and postulates taken from irreversible thermodynamics. For multicomponent systems it is advantageous to relate the diffusion fluxes to the activity rather than number - or mass fractions, since the activity formulation is valid for ideal as well as non-ideal systems. Notwithstanding, the binary diffusivities,  $D_{sr}$ , and the Maxwell-Stefan diffusivities,  $\tilde{D}_{sr}$ , are almost identical for ideal gas mixtures solely. For non-ideal gas mixtures and liquids the multi-component diffusivities are empirical parameters only. However, the generalized driving force formulation is claimed to be more useful in describing the inter-diffusion in dense gases and liquids (e.g., Curtiss and Bird [18, 19]; Taylor and Krishna [96]).

To avoid vagueness the notation used in the forthcoming mathematical manipulations of the thermodynamic variables are specified. The extensive thermodynamic functions (e.g., internal energy, Gibbs free energy, Helmholtz energy, enthalpy, entropy, and volume) can be expressed in two ways, either in terms of mass or mole. Using the Gibbs free energy as an example, i.e., it is postulated that this thermodynamic property is a function of pressure, temperature and composition, hence we can write:

$$\hat{G} = \hat{G}(T, P, M_1, M_2, M_3, \dots, M_q) \quad (2.432)$$

in terms of mass, and

$$\hat{G} = \hat{G}(T, P, n_1, n_2, n_3, \dots, n_q) \quad (2.433)$$

in terms of mole.

In irreversible thermodynamics it is more convenient to use intensive or specific variables instead. Again we have two possible ways of defining the specific functions, either using molar specific variables which are given per mole or specific variables which are given per unit mass. Hence,

$$G = \frac{\hat{G}}{M} = G(T, P, \omega_1, \omega_2, \omega_3, \dots, \omega_{q-1}) \quad (2.434)$$

and

$$\underline{G} = \frac{\hat{G}}{n} = \underline{G}(T, P, x_1, x_2, x_3, \dots, x_{q-1}) \quad (2.435)$$

In thermodynamics partial variables are also used intensively. Accordingly, two sets of partial variables can be defined. The *partial mass variable* yields:

$$\mu_s = \check{G}_s = \left( \frac{\partial \hat{G}}{\partial M_s} \right)_{T, p, M_{k \neq s}} \quad (2.436)$$

This quantity is related to the corresponding intensive variables in the following way [89] (sec. 8.4):

$$\left( \frac{\partial \hat{G}}{\partial M_s} \right)_{T, p, M_{k \neq s}} - \left( \frac{\partial \hat{G}}{\partial M_q} \right)_{T, p, M_{k \neq q}} = \left( \frac{\partial G}{\partial \omega_s} \right)_{T, p, \omega_{k \neq s, q}} \quad (2.437)$$

The corresponding *partial molar variable* is written as:

$$\bar{G}_s = \left( \frac{\partial \hat{G}}{\partial n_s} \right)_{T, p, n_{k \neq s}} \quad (2.438)$$

which is related to the corresponding intensive variables:

$$\left( \frac{\partial \hat{G}}{\partial n_s} \right)_{T, p, n_{k \neq s}} - \left( \frac{\partial \hat{G}}{\partial n_q} \right)_{T, p, n_{k \neq q}} = \left( \frac{\partial G}{\partial x_s} \right)_{T, p, x_{k \neq s, q}} \quad (2.439)$$

The partial mass and the partial molar variables are simply related by:

$$\bar{G}_s = M_{w_s} \mu_s \quad (2.440)$$

Finally, we relate the intensive variables to the partial variables in the following manner:

$$\hat{G}(T, P, \omega_1, \omega_2, \omega_3, \dots, \omega_{q-1}) = \sum_{s=1}^q \left( \frac{\partial \hat{G}}{\partial M_s} \right)_{T, p, M_{k \neq s}} \omega_s \quad (2.441)$$

and

$$\underline{G}(T, P, x_1, x_2, x_3, \dots, x_{q-1}) = \sum_{s=1}^q \left( \frac{\partial \overset{\circ}{G}}{\partial n_s} \right)_{T, p, n_{k \neq s}} x_s \quad (2.442)$$

The Gibbs-Duhem equation is derived from the Euler and Gibbs equations (e.g., Prausnitz et al. [76], app. D; Slattery [89], p. 443). The two forms of the Gibbs-Duhem equation are:

$$MSdT - Vdp + \sum_{s=1}^q M\omega_s d\mu_s = 0 \quad (2.443)$$

using specific variables, and

$$n\overset{\circ}{S}dT - Vdp + \sum_{s=1}^q nx_s d\bar{G}_s = 0 \quad (2.444)$$

in terms of specific molar variables.

The starting point for the rigorous derivation of the diffusive fluxes in terms of the activity is the entropy equation as given by (1.170), wherein the entropy flux vector is defined by (1.171) and the rate of entropy production per unit volume is written (1.172) as discussed in sec. 1.2.4.

To eliminate  $S$  from the Gibbs-Duhem relation formulated in terms of specific quantities (2.443) we need the definitions of  $MH$ :

$$MH = ME + pV = \sum_{s=1}^q M\omega_s \check{H}_s \quad (2.445)$$

and  $MG$ :

$$MG = MH - TMS = \sum_{s=1}^q M\omega_s \mu_s \quad (2.446)$$

From these two relations we find:

$$MS = \frac{MH - MG}{T} = \frac{ME + pV - \sum_{s=1}^q M\omega_s \mu_s}{T} \quad (2.447)$$

Hence, by substitution of the given expressions for  $MS$  (2.447) into the mass form of the Gibbs-Duhem equation (2.443) yields:

$$\left( \frac{MH - MG}{T} \right) dT - Vdp + \sum_{s=1}^q M\omega_s d\mu_s = 0 \quad (2.448)$$

After division by the volume and the temperature, this equation can be put in a form useful to manipulate the entropy production term. Thus, by use of (2.445) and (2.447), we get:

$$\sum_{s=1}^q \rho_s d\mu_s - \frac{1}{T} \sum_{s=1}^q \rho_s \mu_s dT - \frac{1}{T} dp + \frac{1}{T^2} \sum_{s=1}^q \rho_s \check{H}_s dT = 0 \quad (2.449)$$

or

$$\sum_{s=1}^q \rho_s d\left(\frac{\mu_s}{T}\right) - \frac{1}{T} dp + \frac{1}{T^2} \sum_{s=1}^q \rho_s \check{H}_s dT = 0 \quad (2.450)$$

Assuming that this relation is valid at the state of local equilibrium, the differentiation can be exchanged by the  $\nabla$ -operator (Curtiss and Bird [18] [19]):

$$\sum_{s=1}^q \rho_s \nabla\left(\frac{\mu_s}{T}\right) - \frac{1}{T} \nabla p + \frac{1}{T^2} \sum_{s=1}^q \rho_s \check{h}_s \nabla T = 0 \quad (2.451)$$

With the aim of expressing the rate of entropy production  $\Phi_{\text{total}}$  due to mass diffusion in terms of a convenient driving force,  $\frac{cRT}{\rho_s} \mathbf{d}_s$ , we add some extra terms in the third term on the RHS of (1.172) in such a way that the entropy production term remains unaltered utilizing the property that  $\sum_s \mathbf{j}_s = 0$ . The form of the terms that are added is guided by the terms in the Gibbs-Duhem equation (2.451).

The modified entropy production rate (1.172) is commonly written as [18] [19]:

$$\begin{aligned} \Phi_{\text{total}} = & -\frac{1}{T^2} (\mathbf{q} \cdot \nabla T) - \frac{1}{T} (\boldsymbol{\sigma} : \nabla \mathbf{v}) - \frac{1}{T} \sum_{r=1}^q A_r r_r - \\ & \sum_{s=1}^q \left( \frac{\mathbf{j}_s}{\rho_s} \cdot \left[ \rho_s \nabla\left(\frac{\mu_s}{T}\right) - \frac{\rho_s}{\rho T} \nabla p + \frac{\rho_s \check{h}_s}{T^2} \nabla T - \frac{\rho_s \check{h}_s}{T^2} \nabla T - \frac{\rho_s \mathbf{g}_s}{T} + \frac{\rho_s}{\rho T} \sum_{r=1}^q \rho_r \mathbf{g}_r \right] \right) \end{aligned} \quad (2.452)$$

The entropy production term has been written as a sum of products of fluxes and forces. However, there are only  $q - 1$  independent mass fluxes  $\mathbf{j}_s$ , and the Gibbs-Duhem equation (2.451) tells us that there are only  $q - 1$  independent forces as well [5].

Furthermore, it is noted that the first three terms in the brackets on the RHS of (2.452) are similar to the terms in the Gibbs-Duhem relation (2.451). However, two of these three terms do not contribute to the sum. The pressure term vanishes because  $\sum_s \mathbf{j}_s = 0$ . The two enthalpy terms obviously cancel because they are identical with opposite signs. Moreover, the last term in the brackets on the RHS of (2.452), involving the sum of external forces, is zero as  $\sum_s \mathbf{j}_s = 0$ . One of the two remaining terms, i.e., the one containing the enthalpy, we combine with the  $\mathbf{q}$  term. Hence, the modified entropy flux vector (1.171) and production terms (1.172) become:

$$\mathbf{J}_s = \frac{1}{T} \left( \mathbf{q} - \sum_{r=1}^q \mathbf{j}_r \check{h}_r \right) + \sum_{r=1}^q \check{s}_r \mathbf{j}_r \quad (2.453)$$

and

$$T\Phi_{\text{total}} = -\frac{1}{T} \left[ \mathbf{q} - \sum_{r=1}^q \mathbf{j}_r \check{h}_r \right] \cdot \nabla T - \sum_{r=1}^q \mathbf{j}_r \cdot \frac{cRT}{\rho_r} \mathbf{d}_r - \boldsymbol{\sigma} : \nabla \mathbf{v} - \sum_{r=1}^q A_r r_r \quad (2.454)$$

where

$$\frac{cRT}{\rho_s} \mathbf{d}_s = T \nabla \left( \frac{\mu_s}{T} \right) + \frac{\check{h}_s}{T} \nabla T - \frac{1}{\rho} \nabla p - \mathbf{g}_s + \frac{1}{\rho} \sum_{r=1}^q \rho_r \mathbf{g}_r \quad (2.455)$$

Due to the linearity postulate in irreversible thermodynamics, each vector flux must depend linearly on all the vector forces in the system. We may thus rewrite the fluxes as [18] [19]:

$$\mathbf{q} - \sum_{r=1}^q \mathbf{j}_r \check{h}_r = -\frac{1}{T} \alpha_{00} \nabla T - \sum_{r=1}^q \left( \frac{cRT \alpha_{0r}}{\rho_r} \right) \mathbf{d}_r \quad (2.456)$$

$$\mathbf{j}_s = -\alpha_{s0} \nabla T - \rho_s \sum_{r=1}^q \left( \frac{cRT \alpha_{sr}}{\rho_r} \right) \mathbf{d}_r \quad (2.457)$$

in which the  $\alpha_{sr}$  are the phenomenological coefficients being symmetric according to the Onsager reciprocal relations. Henceforth, the thermal diffusion coefficients are denoted by  $D_s^T = \alpha_{s0} = \alpha_{0s}$  and the Fickian diffusivities are given by  $\hat{D}_{sr} = \frac{cRT \alpha_{sr}}{\rho_s \rho_r}$  as foreseen in the preceding paragraphs.

It is sometimes convenient to reformulate the generalized diffusional driving forces  $\mathbf{d}_s$  either in terms of mass or molar functions, using the partial mass Gibbs free energy definition,  $\check{G}_s = \check{h}_s - T \check{s}_s$ , and the chain rule of partial differentiation assuming that the chemical potential (i.e.,  $\mu_s = \check{G}_s$ ) is a function of temperature, pressure and concentration (Slattery [89], sect. 8.4).  $\mathbf{d}_s$  can then be expressed in several useful forms as listed below. Expressing the thermodynamic functions on a mass basis we may write:

$$\begin{aligned} \mathbf{d}_s &= \frac{\rho_s}{cRT} \left( \check{s}_s \nabla T + \nabla \mu_s - \frac{1}{\rho} \nabla p - \mathbf{g}_s + \frac{1}{\rho} \sum_{r=1}^q \rho_r \mathbf{g}_r \right) \\ &= \frac{\rho_s}{cRT} \left[ \sum_{\substack{r=1 \\ r \neq s}}^q \left( \frac{\partial \mu_s}{\partial \omega_r} \right)_{T,p,\omega_{k \neq s,q}} \nabla \omega_r + \left( \check{V}_s - \frac{1}{\rho} \right) \nabla p - \mathbf{g}_s + \frac{1}{\rho} \sum_{r=1}^q \rho_r \mathbf{g}_r \right] \\ &= \frac{\rho_s}{cRT} \left[ \nabla_{T,p} \mu_s + \left( \check{V}_s - \frac{1}{\rho} \right) \nabla p - \mathbf{g}_s + \frac{1}{\rho} \sum_{r=1}^q \rho_r \mathbf{g}_r \right] \end{aligned} \quad (2.458)$$

These relations may also be reformulated on a mole basis:

$$\begin{aligned}
\mathbf{d}_s &= \frac{c_s M_{w_s}}{cRT} \left( \frac{\bar{S}_s}{M_{w_s}} \nabla T + \nabla \left( \frac{\bar{G}_s}{M_{w_s}} \right) - \frac{1}{\rho} \nabla p - \mathbf{g}_s + \frac{1}{\rho} \sum_{r=1}^q \rho_r \mathbf{g}_r \right) \\
&= \frac{x_s}{RT} \left[ \sum_{\substack{r=1 \\ r \neq s}}^q \left( \frac{\partial \bar{G}_s}{\partial x_r} \right)_{T,p,x_{k \neq s,q}} \nabla x_r + \bar{V}_s \nabla p \right] + \\
&\quad \frac{x_s M_{w_s}}{RT} \left( -\frac{1}{\rho} \nabla p - \mathbf{g}_s + \frac{1}{\rho} \sum_{r=1}^q \rho_r \mathbf{g}_r \right) \\
&= \frac{x_s}{RT} \nabla_{T,p} \bar{G}_s + \frac{x_s M_{w_s}}{RT} \left[ \left( \check{V}_s - \frac{1}{\rho} \right) \nabla p - \mathbf{g}_s + \frac{1}{\rho} \sum_{r=1}^q \rho_r \mathbf{g}_r \right]
\end{aligned} \tag{2.459}$$

The transformations of the thermodynamic quantities like the partial mass Gibbs free energy might need further explanation. By use of the chain rule of partial differentiation the chemical potential on a mass basis is expanded considering that the chemical potential,  $\mu_s$ , is a function of  $T$ ,  $p$  and  $\omega_s$ :

$$d\mu_s = \left( \frac{\partial \mu_s}{\partial T} \right)_{p,\omega} dT + \left( \frac{\partial \mu_s}{\partial p} \right)_{T,\omega} dp + \sum_{\substack{r=1 \\ r \neq s}}^q \left( \frac{\partial \mu_s}{\partial \omega_r} \right)_{T,p,\omega_{k \neq s,r}} d\omega_r \tag{2.460}$$

where the partial derivatives with respect to  $T$  and  $p$  are eliminated by the thermodynamic relations,

$$\left( \frac{\partial \mu_s}{\partial T} \right)_{p,x} = -\check{S}_s \tag{2.461}$$

and

$$\left( \frac{\partial \mu_s}{\partial p} \right)_{T,\omega} = \check{V}_s \tag{2.462}$$

where  $\check{V}_s$  is the partial mass volume.

Alternatively, expressing the chemical potential on a molar basis we get:

$$d\bar{G}_s = \left( \frac{\partial \bar{G}_s}{\partial T} \right)_{p,x} dT + \left( \frac{\partial \bar{G}_s}{\partial p} \right)_{T,x} dp + \sum_{\substack{r=1 \\ r \neq s}}^q \left( \frac{\partial \bar{G}_s}{\partial x_r} \right)_{T,p,x_{k \neq s,r}} dx_r \tag{2.463}$$

where the partial derivatives with respect to  $T$  and  $p$  are substituted by the thermodynamic relations,

$$\left( \frac{\partial \bar{G}_s}{\partial T} \right)_{p,x} = -\bar{S}_s \tag{2.464}$$

and

$$\left( \frac{\partial \bar{G}_s}{\partial p} \right)_{T,x} = \bar{V}_s \tag{2.465}$$

where  $\bar{V}_s$  is the partial molar volume.

Assuming that these relations are valid for a system at local equilibrium, the differential 'd' may be substituted by the  $\nabla$ -operator. Hence, from (2.460) and (2.463) we may define the following short notations:

$$\nabla_{T,p}\mu_s = \sum_{\substack{r=1 \\ r \neq s}}^q \left( \frac{\partial \mu_s}{\partial \omega_r} \right)_{T,p,\omega_{k \neq s,r}} d\omega_r \quad (2.466)$$

and

$$\nabla_{T,p}\bar{G}_s = \sum_{\substack{r=1 \\ r \neq s}}^q \left( \frac{\partial \bar{G}_s}{\partial x_r} \right)_{T,p,x_{k \neq s,r}} dx_r \quad (2.467)$$

in which we are keeping the temperature  $T$  and pressure  $p$  constant.

For the description of inter-diffusion in dense gases and liquids the expression for  $\mathbf{d}_s$  is further modified introducing a fugacity (i.e., a corrected pressure) or an activity (i.e., a corrected mole fraction) function [76]. The activity  $a_s(T, \omega_1, \omega_2, \omega_3, \omega_{q-1})$  for species  $s$  is defined by:

$$\mu_s = \mu_s^0 + RT \ln \frac{\hat{f}_s}{f_s^0} = \mu_s^0 + RT \ln a_s \quad (2.468)$$

where the auxiliary fugacity and activity functions are related by  $a_s = \frac{\hat{f}_s}{f_s^0} \cdot \mu_s^0$  denotes the chemical potential at some reference state. While either  $\mu_s^0$  or  $f_s^0$  is arbitrary, both may not be chosen independently, since when one is chosen the other is fixed.

For liquids it is convenient to chose a particular reference state, *a standard state*, that can be defined by the Gibbs free energy of 1 mole of pure  $s$  at the mixture temperature,  $T$ , and a specified pressure, say 1 bar. Hence, in this case  $\mu_s^0$  is a function of temperature only,  $\mu_s^0 = \mu_s^0(T, p = 1\text{bar}, \omega \rightarrow 1)$ . Alternatively,  $\mu_s^0$  may be chosen as the chemical potential for pure species  $s$  at the system temperature and pressure in which  $\mu_s^0 = \mu_s^0(T, p)$ . That is, numerous reference states are possible, which one to be chosen matters little provided that the model formulation is consistent. Henceforth, we are using the given standard state as defined above.

For dense gases it often more convenient to use the fugacity,  $\hat{f}_s$ , defined by<sup>51</sup>:

$$\mu_s = \mu_s^* + RT \ln \frac{\hat{f}_s}{f_s^*} \quad (2.469)$$

where  $\mu_s^*$  denotes a reference state being an ideal gas state at the system temperature and a standard pressure state (e.g.,  $p^* = 1$  bar). However, in either case using fugacities or activities the model derivation is very similar so we proceed considering the activity formulation only.

Introducing the activity variable, the first term on the RHS of (2.455) is rewritten by use of the chain rule of partial differentiation considering that the chemical potential is a function of temperature, pressure and composition. The

<sup>51</sup> Chemical potentials are not the easiest of quantities to deal with, especially considering the use of consistent reference states for all the species that may be involved in multiphase multicomponent systems.

mass and mole based relations are given by (2.460) and (2.467), respectively. It follows that the first term on the RHS of the mass based expression (2.455) can be written as:

$$\begin{aligned}\rho_s T \nabla \left( \frac{\mu_s}{T} \right) &= \rho_s T \nabla \left( \frac{\mu_s^0}{T} \right) + \rho_s R T \nabla \ln a_s = \rho_s \nabla \mu_s^0 - \rho_s \mu_s^0 \nabla \ln T + \rho_s R T \nabla \ln a_s \\ &= -\rho_s \check{s}_s^0 \nabla T - \rho_s \mu_s^0 \nabla \ln T + \rho_s R T \nabla \ln a_s \\ &= -\rho_s (T \check{s}_s^0 + \mu_s^0) \nabla \ln T + \rho_s R T \nabla \ln a_s\end{aligned}\quad (2.470)$$

In the derivation given on the last page the relation:

$$\nabla \mu_s^0 = \left( \frac{d\mu_s^0}{dT} \right) \nabla T = -\check{s}_s^0 \nabla T \quad (2.471)$$

has been used since  $\mu_s^0(T)$  is a function of temperature only.

Substitution of (2.470) into (2.455) gives:

$$\frac{cRT}{\rho_s} \mathbf{d}_s = RT \nabla \ln a_s + (\check{h}_s - \check{h}_s^0) \nabla \ln T - \frac{1}{\rho} \nabla p - \mathbf{g}_s + \frac{1}{\rho} \sum_{r=1}^q \rho_r \mathbf{g}_r \quad (2.472)$$

Then, by use of the chain rule of partial differentiation on  $\mu_s$  we get (2.460), and thereafter eliminating the partial derivatives therein by (2.461) and (2.462), introducing the activity through (2.468), and eliminating the standard state potential by (2.471) as well as the Gibbs free energy definition:

$$\mu_s = \check{h}_s - T \check{s}_s \quad (2.473)$$

We may thus write:

$$RT \nabla \ln a_s = RT \sum_{\substack{r=1 \\ r \neq s}}^q \left( \frac{\partial \ln a_s}{\partial \omega_r} \right)_{T,p,\omega_{k \neq s,r}} \nabla \omega_r + \check{V}_s \nabla p - (\check{h}_s - \check{h}_s^0) \nabla \ln T \quad (2.474)$$

where  $\check{V}_s$  denotes the partial mass volume which can be related to the volume fraction of species  $s$  by:  $\phi_s = \rho_s \check{V}_s = c_s \bar{V}_s$ .

Inserting (2.474) into (2.472), gives:

$$\frac{cRT}{\rho_s} \mathbf{d}_s = RT \sum_{\substack{r=1 \\ r \neq s}}^q \left( \frac{\partial \ln a_s}{\partial \omega_r} \right)_{T,p,\omega_{k \neq s,r}} \nabla \omega_r + (\check{V}_s - \frac{1}{\rho}) \nabla p - \mathbf{g}_s + \frac{1}{\rho} \sum_{r=1}^q \rho_r \mathbf{g}_r \quad (2.475)$$

A problem related to the use of thermodynamic quantities on a mass basis instead of molar basis is that all the existing thermodynamic models naturally are expressed in terms of molar quantities. For example, in the case of concentrated non-ideal liquid mixtures the thermodynamic quantities can be

calculated from the existing models of the excess Gibbs energy  $G^E$  which are normally expressed in terms of specific molar functions. There are numerous models for  $G^E$  available, e.g., NRTL, UNIQUAC and UNIFAC, all providing thermodynamic properties on the molar basis [76].

We may easily rewrite the important quantities in (2.472) to molar basis as the partial mass and partial molar variables of species  $s$  are simply related by the molecular weight. We start by changing the thermodynamic quantities within the two first terms on the RHS of (2.455) using molar concentrations defined by  $\rho_s = M_{w_s} c_s$ .

Then, we redefine the activity for species  $s$  by:

$$\bar{G}_s = \bar{G}_s^0 + RT \ln a_s^m \quad (2.476)$$

where  $a_s^m = a_s^m(T, x_1, x_2, x_3, \dots, x_{q-1})$ .

Again, by use of the chain rule of partial differentiation and consistent formulas from thermodynamics, we get:

$$c_s RT \nabla \ln a_s^m = c_s RT \sum_{\substack{r=1 \\ r \neq s}}^q \left( \frac{\partial \ln a_s^m}{\partial x_r} \right)_{T,p,x_{k \neq s,r}} \nabla x_r + c_s \bar{V}_s \nabla p - (\bar{h}_s - \bar{h}_s^0) \nabla \ln T \quad (2.477)$$

Hence, on the molar form the driving force (2.472) becomes:

$$\begin{aligned} cRT \mathbf{d}_s &= c_s RT \sum_{\substack{r=1 \\ r \neq s}}^q \left( \frac{\partial \ln a_s^m}{\partial x_r} \right)_{T,p,x_{k \neq s,r}} \nabla x_r + (c_s \bar{V}_s - \omega_s) \nabla p \\ &\quad - \rho_s \mathbf{g}_s + \omega_s \sum_{r=1}^q \rho_r \mathbf{g}_r \end{aligned} \quad (2.478)$$

The ratio of activity and mole fraction defines the activity coefficient,  $a_s^m = x_s \gamma_s$  [76]. For an ideal solution the activity is equal to the mole fraction since the activity coefficient equals unity.

That is, we may expand the first term on the RHS in a convenient manner, excluding  $x_q$  (i.e., for a solvent containing several solutes it might be convenient to label the solvent as species  $q$ ):

$$\begin{aligned} x_s \sum_{r=1}^{q-1} \left( \frac{\partial \ln a_s^m}{\partial x_r} \right)_{T,p,x} \nabla x_r &= x_s \sum_{r=1}^{q-1} \left( \frac{\partial \ln(\gamma_s^m x_s)}{\partial x_r} \right)_{T,p,x} \nabla x_r \\ &= x_s \sum_{r=1}^{q-1} \left( \frac{1}{\gamma_s^m x_s} \frac{\partial \gamma_s^m x_s}{\partial x_r} \right)_{T,p,x} \nabla x_r \\ &= x_s \sum_{r=1}^{q-1} \left( \frac{\partial \ln x_s}{\partial x_r} + \frac{\partial \ln \gamma_s^m}{\partial x_r} \right)_{T,p,x} \nabla x_r \\ &= \sum_{r=1}^{q-1} \left( \delta_{sr} + x_s \frac{\partial \ln \gamma_s^m}{\partial x_r} \right)_{T,p,x} \nabla x_r \end{aligned} \quad (2.479)$$

For ideal solutions  $\gamma_s^m = 1$ , hence the  $q - 1$  independent driving forces yield:

$$\mathbf{d}_s = \nabla x_s + \frac{1}{cRT} (c_s \bar{V}_s - \omega_s) \nabla p - \frac{\rho_s}{cRT} \mathbf{g}_s + \frac{\omega_s}{cRT} \sum_{r=1}^q \rho_r \mathbf{g}_r \quad (2.480)$$

### *Applications in Chemical Reactor Engineering*

The applicability of the multicomponent mass diffusion models to chemical reactor engineering is assessed in the following section. Emphasis is placed on the first principles in the derivation of the governing flux equations, the physical interpretations of the terms in the resulting models, the consistency with Fick's first law for binary systems, the relationships between the molar and mass based fluxes, and the consistent use of these multicomponent models describing non-ideal gas and liquid systems.

The *rigorous Fickian multicomponent mass diffusion flux* formulation is derived from kinetic theory of dilute gases adopting the Enskog solution of the Boltzmann equation (e.g., [17] [18] [19] [89] [5]). This mass flux is defined by the relation given in the last line of (2.281) :

$$\mathbf{j}_s = -D_s^T \nabla \ln T - \rho_s \sum_{r=1}^q \hat{D}_{sr} \mathbf{d}_r \quad s = 1, 2, 3, \dots, q$$

where the driving force can be expressed in any of the given forms, e.g., (2.458) and (2.459), either on molar or mass basis.

For binary systems the Fickian mass flux vector reduces to:

$$\begin{aligned} \mathbf{j}_1 &= -D_1^T \nabla \ln T - \rho_1 (\hat{D}_{11} \mathbf{d}_1 + \hat{D}_{12} \mathbf{d}_2) \\ &= -D_1^T \nabla \ln T + \rho \hat{D}_{12} \mathbf{d}_1 = -D_1^T \nabla \ln T + \rho \left\{ -\tilde{D}_{12} \frac{\omega_1 \omega_2}{x_1 x_2} \right\} \mathbf{d}_1 \\ &= -D_1^T \nabla \ln T - \frac{c^2}{\rho} M_{w_1} M_{w_2} \tilde{D}_{12} \mathbf{d}_1 \end{aligned} \quad (2.481)$$

where we have used the additional requirements that  $\mathbf{j}_1 + \mathbf{j}_2 = 0$ ,  $\mathbf{d}_1 + \mathbf{d}_2 = 0$ ,  $\omega_1 \hat{D}_{11} + \omega_2 \hat{D}_{21} = 0$ , and  $\hat{D}_{12} = \hat{D}_{21}$  in accordance with (2.272), (2.284), (2.289) and (2.288), respectively. For dilute gases the multicomponent Fickian diffusivities are also related to the binary Maxwell-Stefan diffusivities as shown by Curtiss and Bird [18] [19], i.e.,  $\hat{D}_{11} = -\frac{\omega_2 \omega_2}{x_1 x_2} \tilde{D}_{12}$  and  $\hat{D}_{12} = -\frac{\omega_1 \omega_2}{x_1 x_2} \tilde{D}_{12}$ . It is further noticed that for gases at low density the Maxwell-Stefan diffusivities are approximately equal to the Fick first law binary diffusivities, i.e.  $\tilde{D}_{12} \approx D_{12}$ . In addition, for binary systems the mass fractions are related to the corresponding mole fractions by:

$$\omega_1 = \frac{M_{w_1}}{M_w} x_1 \quad \text{and} \quad \omega_2 = \frac{M_{w_2}}{M_w} x_2. \quad (2.482)$$

For flowing systems it may seem natural to express the driving force in terms of mass fractions using (2.458), thus:

$$\begin{aligned} \mathbf{d}_1 &= \frac{\rho_1}{cRT} \left[ \left( \frac{\partial \mu_1}{\partial \omega_2} \right)_{T,p} \nabla \omega_2 + \left( \check{V} - \frac{1}{\rho} \right) \nabla p - \omega_2 (\mathbf{g}_1 - \mathbf{g}_2) \right] \\ &= \frac{\rho}{c} \left( \frac{\partial \ln a_1}{\partial \ln \omega_1} \right)_{T,p} \nabla \omega_1 + \frac{\rho_1}{cRT} \left[ \left( \check{V} - \frac{1}{\rho} \right) \nabla p - \omega_2 (\mathbf{g}_1 - \mathbf{g}_2) \right] \end{aligned} \quad (2.483)$$

where we have introduced an activity on a mass basis. However, this activity is an unused variable and there exists no model for it yet. In addition, a principal disadvantage of working in terms of  $a_1$  is that for ideal solutions  $(\frac{\partial \ln a_1}{\partial \ln \omega_1})_{T,p} \neq 1$  in general.

Instead, the driving force is usually rewritten on a molar basis using (2.458), (2.459) and (2.476). Hence, we obtain:

$$\begin{aligned} \mathbf{d}_1 &= \frac{\rho_1}{cRT} \left[ \left( \frac{\partial \mu_1}{\partial \omega_2} \right)_{T,p} \nabla \omega_2 + \left( \check{V} - \frac{1}{\rho} \right) \nabla p - \omega_2 (\mathbf{g}_1 - \mathbf{g}_2) \right] \\ &= \left( \frac{\partial \ln a_1^m}{\partial \ln x_1} \right)_{T,p} \nabla x_1 + \frac{Mr_1 x_1}{RT} \left[ \left( \check{V} - \frac{1}{\rho} \right) \nabla p - \omega_2 (\mathbf{g}_1 - \mathbf{g}_2) \right] \end{aligned} \quad (2.484)$$

The principal advantage of working in terms of  $a_1^m$  is of course that for ideal solutions  $(\frac{\partial \ln a_1^m}{\partial \ln x_1})_{T,p} = 1$ .

It may be informative to express the overall mass flux as the sum of four terms<sup>52</sup> [39] [3] [89] [5]:

$$\mathbf{j}_1 = \mathbf{j}_1^o + \mathbf{j}_1^p + \mathbf{j}_1^g + \mathbf{j}_1^T \quad (2.485)$$

The *ordinary diffusion flux*, which is normally significant in reactor analysis, is expressed as:

$$\mathbf{j}_1^o = -\frac{c^2}{\rho} M_{w_1} M_{w_2} \tilde{D}_{12} \left( \frac{\partial \ln a_1^m}{\partial \ln x_1} \right)_{T,p} \nabla x_1 \quad (2.486)$$

For ideal solutions this relation naturally reduces to Fick's first law:

$$\mathbf{j}_{1,id} = -\frac{c^2}{\rho} M_{w_1} M_{w_2} \tilde{D}_{12} \nabla x_1 \quad (2.487)$$

For non-ideal mixtures, the Fick first law binary diffusivity,  $D_{12}$ , can thus be expressed in terms of the Maxwell-Stefan diffusivity,  $\tilde{D}_{12}$ , by:

$$D_{12} = \tilde{D}_{12} \left( \frac{\partial \ln a_1^m}{\partial \ln x_1} \right)_{T,p} \quad (2.488)$$

The latter relationship may not be entirely obvious at present but clarified shortly as it is further discussed in connection with (2.498).

However, strictly speaking, the fundamental kinetic theory concept is valid for dilute gases solely because the mass flux diffusivities are known for ideal gas mixtures only,  $\tilde{D}_{12} \approx D_{12}$ .

<sup>52</sup> See also sect 1.2.2 concerning the importance of the various contributions to the overall mass diffusion flux in chemical reactor analysis.

The *pressure diffusion* is given by:

$$\mathbf{j}_1^p = \frac{M_{w_1} x_1}{RT} \left( \check{V} - \frac{1}{\rho} \right) \nabla p \quad (2.489)$$

and is significant in systems where there are very large pressure gradients [62]. However, the operating pressure gradients in chemical reactors are usually not large enough so this term is not significant in reactor models.

The *forced diffusion* is expressed as:

$$\mathbf{j}_1^g = -\frac{M_{w_1} x_1 \omega_2}{RT} (\mathbf{g}_1 - \mathbf{g}_2) \quad (2.490)$$

which may be of importance describing aqueous electrolytes [62]. If gravity is the only external force, as in most chemical reactors, then  $\mathbf{g}_1 = \mathbf{g}_2 = \mathbf{g}$  and  $\mathbf{j}_1^{(g)}$  vanishes.

The *thermal diffusion* term is written as:

$$\mathbf{j}_1^T = -D_1^T \nabla \ln T \quad (2.491)$$

This term is usually not important in reactor modeling, since sufficiently large temperature gradients are not common in chemical process plants.

The *multicomponent generalization of Fick's first law of binary diffusion* is the second mass flux formulation on the Fickian form considered in this book. The generalized Fick's first law is defined by<sup>53</sup> [72] [22] [62] [20] [96]:

$$\mathbf{j}_s = -\rho \sum_{r=1}^{q-1} \check{D}_{sr} \nabla \omega_r \quad s = 1, 2, 3, \dots, q-1 \quad (2.492)$$

and restricted to multicomponent systems, i.e.,  $q > 2$ . The diffusivities,  $\check{D}_{sr}$ , defined by this relation may take negative values and are not, in general, symmetric ( $\check{D}_{sr} \neq \check{D}_{rs}$ ). The vector form of this mass flux is given by (2.493):

$$(\mathbf{j}) = -\rho [\text{diag}(\check{\mathbf{D}})] \nabla(\boldsymbol{\omega}) \quad (2.493)$$

A multicomponent Fickian diffusion flux on this form was first suggested in irreversible thermodynamics and has no origin in kinetic theory of dilute gases. Hence, basically, these multicomponent flux equations represent a purely empirical generalization of Fick's first law and define a set of empirical multicomponent diffusion coefficients.

That is, as described by de Groot and Mazur [22] (chap. XI), Taylor and Krishna [96] and Cussler [20], it can be shown using the linearity postulate and the Onsager relations from irreversible thermodynamics that not all of

<sup>53</sup> In the chemical engineering literature the generalized or multicomponent form of Fick's first law of binary diffusion is normally written on a molar basis.

these diffusion coefficients are independent but are subject to certain constraints. However, these theoretical constraints are not very useful in practice, since they require detailed thermodynamic information that is rarely available. Anyhow, the thermodynamic theory does not provide any values for (quantification of) the multicomponent diffusion coefficients,  $\tilde{D}_{sr}$ , so in practice all of them have to be determined from experiments. Hence, these coefficients cannot be interpreted simply, and there is therefore no fundamental theory predicting any formal relationships between the multicomponent - and the Fick first law binary diffusivities even for dilute gases in this particular diffusion model formulation.

The *generalized multicomponent Maxwell-Stefan equation* (2.298) represents the third multicomponent mass diffusion formulation considered in this book. The rigorous form of Maxwell-Stefan equation can be expressed as:

$$\sum_{\substack{k=1 \\ k \neq s}}^q \frac{x_s x_k}{\tilde{D}_{sk}} \left( \frac{\mathbf{j}_k}{\rho_k} - \frac{\mathbf{j}_s}{\rho_s} \right) = \mathbf{d}_s - \sum_{\substack{k=1 \\ k \neq s}}^q \frac{x_s x_k}{\tilde{D}_{sk}} \left( \frac{D_k^T}{\rho_k} - \frac{D_s^T}{\rho_s} \right) \nabla \ln T, \quad s = 1, 2, 3, \dots, q$$

where the Maxwell-Stefan diffusivities  $\tilde{D}_{sk}$  are less concentration dependent than  $\hat{D}_{sk}$  and  $\bar{D}_{sk}$  for dilute gases.

For binary systems the generalized Maxwell-Stefan relation reduces to:

$$\frac{x_1 x_2}{\tilde{D}_{12}} \left( \frac{\mathbf{j}_2}{\rho_2} - \frac{\mathbf{j}_1}{\rho_1} \right) = \mathbf{d}_1 - \frac{x_1 x_2}{\tilde{D}_{12}} \left( \frac{D_2^T}{\rho_2} - \frac{D_1^T}{\rho_1} \right) \nabla \ln T \quad (2.494)$$

With the additional constraints that  $\mathbf{j}_1 + \mathbf{j}_2 = 0$  and  $D_1^T + D_2^T = 0$ , and by expressing the mass fraction in terms of mole fractions (2.482), we can rewrite (2.494) as:

$$\mathbf{j}_1 = -D_1^T \nabla \ln T - \frac{c^2}{\rho} M_{w_1} M_{w_2} \tilde{D}_{12} \mathbf{d}_1 \quad (2.495)$$

where

$$\begin{aligned} \mathbf{d}_1 &= \frac{x_1}{RT} \left[ \left( \frac{\partial \bar{G}_1}{\partial x_2} \right)_{T,p} \nabla x_2 + \bar{V}_1 \nabla p \right] \\ &\quad + \frac{x_1 M_{w_1}}{RT} \left( -\frac{1}{\rho} \nabla p - \mathbf{g}_1 + \frac{1}{\rho} (\rho_1 \mathbf{g}_1 + \rho_2 \mathbf{g}_2) \right) \\ &= \left( \frac{\partial \ln a_1^m}{\partial \ln x_1} \right)_{T,p} \nabla x_1 + \frac{x_1 M_{w_1}}{RT} \left( \tilde{V}_1 - \frac{1}{\rho} \right) \nabla p - \frac{x_1 M_{w_1} \omega_2}{RT} (\mathbf{g}_1 - \mathbf{g}_2) \end{aligned} \quad (2.496)$$

If we drop the pressure-, thermal-, and forced-diffusion terms, the binary diffusivities can be expressed as:

$$\mathbf{j}_1 = -\frac{c^2}{\rho} M_{w_1} M_{w_2} \tilde{D}_{12} \mathbf{d}_1 = \frac{c^2}{\rho} M_{w_1} M_{w_2} \left\{ \tilde{D}_{12} \left( \frac{\partial \ln a_1^m}{\partial \ln x_1} \right)_{T,p} \right\} \nabla x_1 \quad (2.497)$$

The driving force can also be expressed in terms of the mass fraction gradient using (2.482):

$$\begin{aligned} \mathbf{j}_1 &= -\frac{c^2}{\rho} M_{w_1} M_{w_2} \tilde{D}_{12} \left( \frac{\partial \ln a_1^m}{\partial \ln x_1} \right)_{T,P} \left\{ \left( \frac{\rho}{c} \right)^2 \frac{1}{Mr_1 Mr_2} \nabla \omega_1 \right\} \\ &= -\rho \left\{ \tilde{D}_{12} \left( \frac{\partial \ln a_1^m}{\partial \ln x_1} \right)_{T,P} \right\} \nabla \omega_1 = -\rho D_{12} \nabla \omega_1 \end{aligned} \quad (2.498)$$

This result confirms that (2.488) is valid, and for dilute gases, i.e., ideal gas systems,  $D_{12}$  and  $\tilde{D}_{12}$  are about equal. Similarly, it is easily shown that the Fick's first law diffusivity is the same whether this law is formulated on a mass or molar basis.

For non-ideal systems, on the other hand, one may use either  $D_{12}$  or  $\tilde{D}_{12}$  and the corresponding equations above (i.e., using the first or second term in the second line on the RHS of (2.498)). In one interpretation the Fick's first law diffusivity,  $D_{12}$ , incorporates several aspects, the significance of an inverse drag ( $\tilde{D}_{12}$ ), and the thermodynamic non-ideality. In this view the physical interpretation of the Fickian diffusivity is less transparent than the Maxwell-Stefan diffusivity. Hence, provided that the Maxwell-Stefan diffusivities are still predicable for non-ideal systems, a passable procedure is to calculate the non-ideality corrections from a suitable thermodynamic model. This type of simulations were performed extensively by Taylor and Krishna [96]. In a later paper, Krishna and Wesselingh [49] stated that in this procedure the Maxwell-Stefan diffusivities are calculated indirectly from the measured Fick diffusivities and thermodynamic data (i.e., fitted thermodynamic models), showing a 'weak' composition dependence. In this engineering approach it is not clear whether the total composition dependency is artificially accounted for by the thermodynamic part of the model solely, or if both parts of the model are actually validated independently.

From a more scientific point of view, the Maxwell-Stefan diffusivities for multicomponent dense gases and liquids deviate from the Fick first law binary coefficients derived from kinetic theory and are thus merely empirical parameters [18]. Hence, for non-ideal systems one needs to fit either  $D_{12}$  or  $\tilde{D}_{12}$  to the experimental data in accordance with the corresponding equations above (i.e., using the first or second term on the RHS of (2.498)). It is then, generally, more convenient to measure  $D_{12}$  directly since this procedure requires no additional activity data. Because the Maxwell-Stefan diffusivities are the binary values found from binary experiments or calculated from the Enskog theory for the case of dilute gases only, the various forms of the multicomponent diffusion flux formulations are all of limited utility in describing multicomponent diffusion for non-ideal systems as they all contain a large number of empirical parameters that have to be determined. The non-ideal corrections in terms of the activity are apparently not very useful even for binary systems as the Maxwell-Stefan diffusivities are not the binary ones except for dilute gases where the solution becomes ideal.

A qualified question is then whether or not the multicomponent models are really worthwhile in reactor simulations, considering the accuracy reflected by the flow, kinetics and equilibrium model parts involved. For the present multiphase flow simulations, the accuracy reflected by the flow part of the model is still limited so an extended binary approach like the Wilke model suffice in many practical cases. This is most likely the case for most single phase simulations as well. However, for diffusion dominated problems multicomponent diffusion of concentrated ideal gases, i.e., for the cases where we cannot confidently designate one of the species as a solvent, the accuracy of the diffusive fluxes may be significantly improved using the Maxwell-Stefan approach compared to the approximate binary Fickian fluxes. The Wilke model might still be an option and is frequently used for catalyst pellet analysis.

To describe the mass diffusion processes within the pores in catalyst pellets we usually distinguish three fundamentally different types of mass diffusion mechanisms [64, 49, 48]:

- *Bulk diffusion* that are significant for large pore sizes and high system pressures in which gas molecule-molecule collisions dominate over gas molecule-wall collisions.
- *Knudsen diffusion* becomes predominant when the mean-free path of the molecular species is much larger than the pore diameter and hence molecule-wall collisions become important.
- *Surface diffusion* of adsorbed molecular species along the pore wall surface. This mechanism of transport becomes dominant for micro-pores and for strongly adsorbed species.

The bulk diffusion processes within the pores of catalyst particles are usually described by the Wilke model formulation. The extended Wilke equation for diffusion in porous media reads:

$$\mathbf{J}_s^* = -cD_s^e \nabla x_s \quad (2.499)$$

where  $D_s^e = D_{sm}^e = (\varepsilon/\tau)D_{sm}$  for bulk diffusion. The  $D_{sm}$  is calculated from the Wilke equation (2.319).

If Knudsen diffusion is important, the combined effective diffusivity may be estimated as [23]:

$$\frac{1}{D_s^e} = \frac{1}{D_{sK}^e} + \frac{1}{D_{sm}^e} \quad (2.500)$$

On the other hand, the more rigorous Maxwell-Stefan equations and the dusty gas model are seldom used in industrial reaction engineering applications. Nevertheless, the dusty gas model [64] represents a modern attempt to provide a more realistic description of the combined bulk and Knudsen diffusion mechanisms based on the multicomponent Maxwell-Stefan model formulation. Similar extensions of the Maxwell-Stefan model have also been suggested for the surface diffusion of adsorbed molecular pseudo-species, as well as the combined bulk, Knudsen and surface diffusion apparently with limited success [48] [49].

However, if convective transport of heat and species mass in porous catalyst pellets have to be taken into account simulating catalytic reactor processes, either the Maxwell-Stefan mass flux equations (2.394) or dusty gas model for the mass fluxes (2.427) have to be used with a variable pressure driving force expressed in terms of mass fractions (2.426). The reason for this demand is that any viscous flow in the catalyst pores is driven by a pressure gradient induced by the potential non-uniform spatial species composition and temperature evolution created by the chemical reactions. The pressure gradient in porous media is usually related to the consistent viscous gas velocity through a correlation inspired by the Darcy's law [21] (see e.g., [5] [49] [89], p 197):

$$\mathbf{v}_m = -\frac{B_0}{\mu} \nabla p \quad (2.501)$$

Generally, the permeability  $B_0$  ( $m^2$ ) has to be determined experimentally. However, for simple structures the permeability coefficient  $B_0$  can be determined analytically. Considering a cylindrical pore, for example, the permeability can be calculated from the Poiseuille flow relationship  $B_0 = d_0^2/32$  [49].

Solving this flow model for the velocity the pressure is calculated from the ideal gas law. The temperature therein is obtained from the heat balance and the mixture density is estimated from the sum of the species densities. It is noted that if an inconsistent diffusive flux closure like the Wilke equation is adopted (i.e., the sum of the diffusive mass fluxes is not necessarily equal to zero) instead, the sum of the species mass balances does not exactly coincide with the mixture continuity equation.

A few investigations on the practical applications of the dusty gas model are reported in the literature. In a representative study of the interacting phenomena of diffusion and chemical reaction in porous catalyst pellets for the steam reforming and methanation reactions under industrial conditions [23], the dusty gas model was used as basis for the evaluation of the limitations in the applicability of the simplified model (2.499). The models used in the study were derived considering a set of simplifying assumptions: (1) The reaction mixture was treated as an ideal gas. (2) The system was operated at steady state. (3) The external heat and mass transfer resistances were neglected. (4) The viscous flow was negligible and the pellet was under isobaric conditions. (5) Both Knudsen and ordinary diffusion fluxes were considered. (6) The pellet was assumed to be isothermal. (7) The pellet slab is symmetric about the center. Under industrial operating conditions it was shown that at low steam to methane ratios the diffusion fluxes calculated using the simplified Fickian formulation (2.499) were in excellent agreement with the dusty gas model results. At higher steam to methane ratios the simplified model predictions did deviate a little yet significantly from the dusty gas model results, indicating that it might be worthwhile to solve the full dusty gas model in this case. However, the use of the more complex dusty gas model in reaction

engineering is generally not considered an essential issue in the investigations reported in the literature. That is, in view of the uncertainties reflected by the other terms (e.g., reaction kinetics, interfacial fluxes and convection) in a typical reactor model these deviations are normally negligible. Therefore, it is generally anticipated that the simplified model (2.499) is sufficient for most practical reactor simulations.

## Polyatomic Reactive Systems

For polyatomic reactive systems the mixture continuity, momentum and energy equations seemingly remain unchanged compared to the corresponding conservation equations for multicomponent non-reacting mono-atomic gases, as  $m_s$ ,  $m_s \mathbf{C}_s$ , and  $e_s^{\text{total}} = \frac{1}{2} m_s C_s^2 + e_s^{\text{int}}$  are summation invariants. Note that  $e_s^{\text{total}}$  denotes the total energy which equals the sum of the translational and internal energy forms. However, for polyatomic reactive systems the species mass balance deviates from the corresponding one for non-reactive systems in that it includes a reaction rate term resulting from collisions of molecules of type  $s$  with all types of molecules [39]. This means that when deriving this particular transport equation from basic principles, the collision term on the RHS of the Boltzmann equation (2.275) must be modified to account for the effects of chemical reactions. Correspondingly, transforming the mixture energy balance in terms of temperature the resulting temperature equation is slightly different from that of mono-atomic gases in that it contains a heat of reaction term. In addition, as expected, the Enskog perturbation solution of the mixture Boltzmann equation (2.269) is a little more involved than the corresponding one for simple systems containing one type of species only. Fortunately, the expressions for the fluxes in terms of the distribution function are basically unaffected by the reaction taking place in the gas mixture.

## 2.10 Mean Free Path Concept

In this section the determination of the transport properties, i.e., using the empirical method suggested by Maxwell [65], on the basis of Clausius' mean free path concept is outlined.

That is, instead of determining the transport properties from the rather theoretical Enskog solution of the Boltzmann equation, for practical applications we may often resort to the much simpler but still fairly accurate mean free path approach (e.g., [12], section 5.1; [87], chap. 20; [34], section 9.6). Actually, the form of the relations resulting from the mean free path concept are about the same as those obtained from the much more complex theories, and even the values of the prefactors are considered sufficiently accurate for many reactor modeling applications.

## Transport Properties

The overall aim in this analysis is to determine a rough estimate of the transfer fluxes in dilute one-component gases using the elementary mean free path concept in kinetic theory. In this approach it is assumed that the only means for transport of information in the fluid is via molecular collisions. Due to the physical similarity of the flux phenomena of mass, momentum and energy, a common mathematical formalism is outlined (e.g., [104] app E; [61] sect 3.4.2; [77] sect 3-4; [39] sect 2).

Considering a dilute gas containing  $n$  molecules per unit volume inducing a macroscopic transfer flux of property  $\psi$ . The symbol  $\psi$  denotes any property of a single molecule that can be changed by collisions, and  $\langle\psi\rangle_M$  represents the average value of  $\psi$  for the gas. The molecules are assumed to move in a geometrical configuration in which  $\frac{\partial\langle\psi\rangle_M}{\partial x} = \frac{\partial\langle\psi\rangle_M}{\partial y} = 0$ , so that the molecular motion transport the property  $\langle\psi\rangle_M$  in the  $z$ -direction only. For illustrative purposes we consider a gas confined between two infinite parallel planes denoted by  $z = z_0$  and  $z = z_2$ . Imagine a net flux of the properties in the positive  $z$ -direction through a plane at an arbitrary location  $z = z_1$  between the two planes located at  $z = z_0$  and  $z = z_2$ . Let  $F_\psi$  denote the net molecular flux of the property  $\psi$  in the  $z$ -direction.

At each collision it is assumed to be an equalizing transfer of properties between the two molecules, so in consequence  $F_{z_1}$  is determined by the relative location of the last collision experienced by a molecule before it crosses the plane at  $z = z_1$ . This particular distance is thus expected to be related to the mean free path,  $l$ . It is supposed throughout that the mean free path is small compared to the dimensions of the vessel containing the gas.

It may be expected that on the average molecules crossing the plane  $z = z_1$  from the  $z_1 - l$  side will transfer the property  $\psi_{z_1-l}$  and those crossing from the  $z_1 + l$  side will transfer the property  $\psi_{z_1+l}$ . Hence,  $F_{z_1} = \Gamma\langle\psi\rangle_M|_{z_1-l} - \Gamma\langle\psi\rangle_M|_{z_1+l}$ , where  $\Gamma_{z_1-l}$  denotes the number of molecules per unit area per second crossing the plane  $z = z_1$  from the  $z_1 - l$  side and  $\Gamma_{z_1+l}$  denotes the number of molecules per unit area per second crossing the plane  $z = z_1$  from the  $z_1 + l$  side.

This means that  $\Gamma_{z_1-l} = \Gamma_{z_1+l} = \Gamma_{z_1}$ , where  $\Gamma_{z_1} = \frac{1}{6}\langle|\mathbf{C}|\rangle_M n$ . The factor  $\frac{1}{6}$  accounts for the fact that only one-sixth of the molecules on plane  $\Gamma_{z_1-l}$  move in the  $(+z)$ -direction<sup>54</sup>. Hence:

$$F_{z_1} = \frac{1}{6}\langle|\mathbf{C}|\rangle_M n (\langle\psi\rangle_M|_{z_1-l} - \langle\psi\rangle_M|_{z_1+l}) \quad (2.502)$$

<sup>54</sup> Consider isotropic molecular motion in a Cartesian coordinate system. If there are  $n$  molecules per unit volume, about one-third of them have velocities along the  $x$ -direction. Half of these, i.e.,  $\frac{1}{6}n$  per unit volume, move in the  $(+x)$ -direction and the other half of them move in the  $(-x)$ -direction. Accordingly, one-sixth of the  $N$  molecules move in the  $(+y)$ -direction, another one-sixth of them move in the  $(-y)$ -direction, another one-sixth of them in the  $(+z)$ -direction, and finally the last one-sixth of them will move in the  $(-z)$ -direction.

The properties  $\langle\psi\rangle_M|_{z_1-l}$  and  $\langle\psi\rangle_M|_{z_1+l}$  in (2.502) may then be expanded in a Taylor series about  $z = z_1$ , since the mean free path is small compared to the distance over which  $\langle\psi\rangle_M$  changes appreciably. Neglecting terms of order higher than one the result is<sup>55</sup>:

$$F_{\psi,z_1} = \frac{1}{6}\langle|\mathbf{C}|\rangle_M n (\langle\psi\rangle_M|_{z-l} - \langle\psi\rangle_M|_{z+l}) = \frac{2l\langle|\mathbf{C}|\rangle_M n}{6} \times \left( \frac{\langle\psi\rangle_M|_{z-l} - \langle\psi\rangle_M|_{z+l}}{2l} \right) \approx -\frac{l\langle|\mathbf{C}|\rangle_M n}{3} \frac{d\langle\psi\rangle_M}{dz} \quad (2.503)$$

assuming that the gradient of the property  $\langle\psi\rangle_M$  is constant over distances of the order  $l$ .

To determine the species mass diffusion a concentration gradient is induced by assuming that the species number concentration is different at each of the planes  $z_0, z_1, z_2$ . To estimate the viscosity we create a gradient in the  $z$ -momentum by assuming that the molecules at the plane  $z_0$  are moving in the negative  $z$ -direction, at the plane  $z_1$  the molecules are stationary, and those at plane  $z_2$  are moving in the positive  $z$ -direction. To induce a thermal conduction flux the three planes are taken to be at different temperatures.

Then, the specific fluxes are achieved letting the symbol  $F_\psi$  successively represent the  $y$ -component of the flux of momentum through a plane with normal in the  $z$ -direction, the flux of energy through the same plane, and the mass flux of species  $c$  through the same plane, respectively. The symbol  $\langle\psi\rangle$  represents correspondingly the  $y$ -direction momentum per molecule of mass  $m$ ,  $mv_y$ , the energy per particle ( $me$ ), and the mass per molecule of species  $c$ ,  $m_c$ .

Comparing the fluid dynamic closures with the corresponding kinetic theory results we see that:

$$F_{mv_y} = -\frac{1}{3}\langle|\mathbf{C}|\rangle_M l n m \frac{dv_y}{dz} = P_{yz} = -\mu \frac{dv_y}{dz} \quad (2.504)$$

$$F_{me} = -\frac{1}{3}\langle|\mathbf{C}|\rangle_M l n m \frac{de}{dT}|_V \frac{dT}{dz} = q_z = -\lambda \frac{dT}{dz} \quad (2.505)$$

$$F_{m\omega_c} = -\frac{1}{3}\langle|\mathbf{C}|\rangle_M l n m \frac{d\omega_c}{dz} = j_z = -\rho D \frac{d\omega_c}{dz} \quad (2.506)$$

The molecular fluxes can be extended to systems containing gradients in the other two space dimensions as well, denoting a complete three dimensional flux formulation.

Note that in determining the viscosity parameter we consider a spatially uniform fluid in a state of shear such that  $\mathbf{v} = v_y(z)\mathbf{e}_y$ . In the heat conduction case we imagine that a gas is heated at constant volume so that all the energy supplied is increasing the energy of the molecules, thus  $n[d(me)/dT] = \rho C_v$ , where  $C_v = \frac{3k}{2m}$  is the specific heat per unit mass at constant volume. The mass diffusion flux is determined considering a binary mixture in which both

<sup>55</sup> The subscript  $z_1$  is omitted since the choice of the position  $z = z_1$  was arbitrary.

the total pressure and temperature are uniform. The form of the species mass flux used above deviates from the standard literature on elementary kinetic theory in that the mass fraction is used in instead of the species number density. A brief discussion of the two formulations is given by [87] (p 495).

The standard self-diffusion flux can be derived in a similar way. The flux of particles in the positive  $z$ -direction that crosses the  $z_1$  plane is equal to the number of molecules that reach the same plane from  $z_1 - l$ , minus those that reach it from  $z_1 + l$ . The result is [61]:

$$\begin{aligned} \Gamma_{z_1} &= \Gamma|_{z_1-l} - \Gamma|_{z_1+l} = \frac{1}{6} \langle |\mathbf{C}| \rangle_M (\langle n \rangle_M|_{z-l} - \langle n \rangle_M|_{z+l}) \\ &= \frac{2l \langle |\mathbf{C}| \rangle_M}{6} \left( \frac{\langle n \rangle_M|_{z-l} - \langle n \rangle_M|_{z+l}}{2l} \right) \\ &\approx - \frac{l \langle |\mathbf{C}| \rangle_M}{3} \frac{d \langle n \rangle_M}{dz} = -D \frac{d \langle n \rangle_M}{dz} \end{aligned} \quad (2.507)$$

Comparing the two last terms, we may conclude:  $D = \frac{1}{3} l \langle |\mathbf{C}| \rangle_M$ .

The molecular flux models are still not closed as the mean free path  $l$  and the molecular speed quantities  $\langle |\mathbf{C}| \rangle_M$  are not determined yet. A frequently used closure is examined in the next paragraph.

## Mean Free Path

In this section approximate mathematical models determining the molecular mean free path are derived.

It is anticipated that for dilute gases the mean free path is a significant parameter that governs the mechanism of transfer, defined as the mean distance traveled by a molecule between two successive collisions [87]. The basic physical interpretation of the transfer phenomenon is thus that a molecule traveling a free path of a certain distance is in effect transferring momentum, energy and mass over that distance.

To derive a simple expression for the mean free path we preliminarily examine the molecular motion from the point of view of an elementary kinetic theory of dilute gases adopting the billiard ball molecular model. Consider a pure gas composed of a collection of rigid, non-attracting spherical molecules of diameter  $d_1$ , mass  $m_1$ , and number density  $n_1$  colliding at random. A molecule is singled out as it travels in straight paths from one collision to the next, anticipating that the molecular speed and direction of motion change with each collision. It is then further imagined that at a given instant all the molecules but the one in question are frozen in position, whereas this particular molecule moves with an average speed  $\langle |\mathbf{c}_1| \rangle_M$ . At the instant of a collision, the center to center distance of the two molecules is  $d_1$  (see Fig. 2.7). The total collision cross section or target area,  $\sigma_{AT}$ , of the moving molecule is then given by  $\sigma_{AT} = \pi d_1^2$ . In time  $t$  the moving molecule sweeps out a cylindrical volume of length  $\langle |\mathbf{c}_1| \rangle_M t$  and cross section  $\sigma_{AT}$  (see Fig 2.10).

Any molecule whose center is in this cylinder will be struck by the moving molecule. The number of collisions in time  $t$  is given by  $\sigma_{A_T} n_1 \langle |\mathbf{c}_1| \rangle_M t$ , where  $n$  is the number of molecules present in a unit volume, assumed to be uniformly distributed in space. A crude estimate of the mean free path,  $l_1$ , is then given by the ratio of the distance traveled in time  $t$  over the number of collisions in this time [100]:

$$l_1 = \frac{\langle |\mathbf{c}_1| \rangle_M t}{\sigma_{A_T} n_1 \langle |\mathbf{c}_1| \rangle_M t} = \frac{1}{\sigma_{A_T} n_1} \quad (2.508)$$

The corresponding collision frequency is defined as the average number of collisions per unit time experienced by any one molecule of type 1:

$$Z_{1-1} = \sigma_{A_T} n_1 \langle |\mathbf{c}_1| \rangle_M = \frac{\langle |\mathbf{c}_1| \rangle_M}{l_1} \quad (2.509)$$

The mean time between successive collisions of molecules of type 1, called the *collision time*  $\tau_1$ , is approximated by:

$$\tau_1 = \frac{1}{Z_{1-1}} = \frac{l_1}{\langle |\mathbf{c}_1| \rangle_M} \quad (2.510)$$

Several extensions of the crude model sketched above have been derived over the years, for example considering the situation that all the molecules in the cylindrical volume move with the same average speed. A third model providing results being in better agreement with the Enskog relations is obtained assuming that all the molecules possess a Maxwellian speed distribution.

The Maxwellian representation of the collision frequency of one molecule of type  $m_1$  with similar molecules (2.173) is commonly rewritten using the ideal gas law:

$$Z_{1-1} = \frac{2Z_{11}}{n_1} = 4n_1 d_1^2 \sqrt{\frac{\pi kT}{m_1}} = 4 \frac{p_1}{kT} d_1^2 \sqrt{\frac{\pi kT}{m_1}} = 4p_1 d_1^2 \sqrt{\frac{\pi}{m_1 kT}} \quad (2.511)$$

The mean free path,  $l_1$ , traveled by a molecule of type  $m_1$  between successive collisions in a given time  $t$  is found by dividing the total distance traveled by all molecules of type  $m_1$  in this time by the total number of the collisions between them:

$$l_1 = \frac{n_1 \langle |\mathbf{c}_1| \rangle_M t}{\frac{n_1 t}{\tau_1}} = \langle |\mathbf{c}_1| \rangle_M \tau_1 = \frac{\langle |\mathbf{c}_1| \rangle_M}{Z_{1-1}} \quad (2.512)$$

From this formula it is seen that to calculate  $l_1$  we need to determine the mean molecular speed  $\langle |\mathbf{c}_1| \rangle_M$ . For real systems the average molecular speed is difficult to determine. Assuming that the system is sufficiently close to equilibrium the velocity distribution may be taken to be Maxwellian. For molecules in the absolute Maxwellian state the peculiar velocity equals the microscopic molecular velocity, i.e.,  $\mathbf{C}_1 = \mathbf{c}_1$ , because the macroscopic velocity

is zero  $\mathbf{v}_1 = 0$ , hence it follows that the speed of the microscopic molecular velocity equals the thermal speed:  $\langle C_1 \rangle_M = \langle |\mathbf{C}_1| \rangle_M = \langle c_1 \rangle_M = \langle |\mathbf{c}_1| \rangle_M$ .

The mean value of a generalized function of the molecular velocity for a gas in the absolute Maxwellian state is defined by:

$$n\langle \psi \rangle_M = \int_{-\infty}^{\infty} \psi f d\mathbf{c} = n \left( \frac{m}{2\pi kT} \right)^{3/2} \int_{-\infty}^{\infty} \psi \exp\left(-\frac{mC^2}{2kT}\right) d\mathbf{c} \quad (2.513)$$

The present form of the integral is not really defined in a consistent manner as the integrand contains the peculiar speed  $C$ , which is defined by  $C = |\mathbf{C}|$ , whereas the integration is over the velocity space  $d\mathbf{c}$ . Transforming from Cartesian coordinates  $(C_x, C_y, C_z)$  to spherical polar coordinates  $(C, \theta, \phi)$ , we get with spherical symmetry:  $d\mathbf{c} = d\mathbf{C} = C^2 \sin\theta d\theta d\phi dC$  (e.g., [105], p. 34; [12], p. 70; [34], p. 242).

The mean value of the thermal speed  $C (= |\mathbf{C}|)$  can then be derived as follows<sup>56</sup>:

$$\begin{aligned} \langle C \rangle_M &= \left( \frac{m}{2\pi kT} \right)^{3/2} \int_{-\infty}^{\infty} C \exp\left(-\frac{mC^2}{2kT}\right) d\mathbf{C} \\ &= \left( \frac{m}{2\pi kT} \right)^{3/2} \int_0^{\infty} C^3 \exp\left(-\frac{mC^2}{2kT}\right) \int_0^{2\pi} \int_0^{\pi} \sin\theta d\theta d\phi dC \\ &= 4\pi \left( \frac{m}{2\pi kT} \right)^{3/2} \int_0^{\infty} C^3 \exp\left(-\frac{mC^2}{2kT}\right) dC \\ &= 4\pi \left( \frac{m}{2\pi kT} \right)^{3/2} \times \frac{1}{2} \left( \frac{m}{2kT} \right)^{-2} = \left( \frac{8kT}{\pi m} \right)^{1/2} \end{aligned} \quad (2.514)$$

Thus, for a molecule of type 1 the mean value of the peculiar speed  $\langle C_1 \rangle_M$  for a gas in the Maxwellian state yields:

$$\langle C_1 \rangle_M = \langle c_1 \rangle_M = \sqrt{\frac{8kT}{\pi m_1}} = 2\sqrt{\frac{2kT}{\pi m_1}} \quad (2.515)$$

<sup>56</sup> In these manipulations we have used a mathematical formula solving odd integrals on the form:

$$\int_0^{\infty} x^n \exp(-ax^2) dx$$

The solution for  $n = 3$  is (e.g., [61] (pp. 526-527), [12], sect. 1.4):

$$\int_0^{\infty} \exp(-ax^2) dx = \frac{1}{2} a^{-2}$$

The mean free path can then be determined from (2.512) and (2.511):

$$\begin{aligned}
 l_1 = \langle |\mathbf{c}_1| \rangle_M \tau_1 &= \frac{\langle |\mathbf{c}_1| \rangle_M}{Z_{1-1}} = \left( 2\sqrt{\frac{2kT}{\pi m_1}} \right) \left( \frac{1}{4n_1 d_1^2 \sqrt{\frac{\pi kT}{m_1}}} \right) \\
 &= \frac{1}{\sqrt{2} n_1 d_1^2 \pi} = \frac{kT}{\sqrt{2} p_1 d_1^2 \pi}
 \end{aligned} \tag{2.516}$$

### Transport Coefficients

In this section we derive theoretical expressions for the transport coefficients (i.e., viscosity, thermal conductivity, and diffusivity) for dilute gases.

Using the elementary mean free path theory (2.508), the viscosity, thermal conductivity<sup>57</sup> and self-diffusion coefficients in (2.504) and (2.506) are estimated to be (e.g., [77]; [28], sect. 6.7 and chap. 7; [100], chap. 5; [74], chap. 3):

$$\mu_1 = \frac{1}{2} \rho_1 l_1 \langle C_1 \rangle_M = \frac{1}{\pi d_1^2} \sqrt{\frac{m_1 kT}{\pi}} \tag{2.517}$$

$$\lambda_1 = \frac{1}{2} \rho_1 l_1 \langle C_1 \rangle_M C_{v,1} = \mu_1 C_{v,1} \tag{2.518}$$

$$D_{11} = \frac{1}{2} l_1 \langle C_1 \rangle_M = \mu_1 / \rho_1 \tag{2.519}$$

In a one-component gas it is conceptually still possible to label a certain subset of particles with 1 and the complement, 2. The resulting motion of the conceptually labeled subgroup of particles is called *self-diffusion*. Diffusion in a two-component system is called *mutual diffusion*.

The following set of parameter values may be more common because they are obtained adopting a refined proportionality coefficient in the flux expressions and the more accurate mean free path relation (2.516). The parameter values are<sup>58</sup> [77] (sect 3-5) [74] (chap 3) [5] (sects 1-4, 9-3 and 17-3):

$$\mu_1 = \frac{1}{3} \rho_1 l_1 \langle C_1 \rangle_M = \frac{2}{3\pi d_1^2} \sqrt{\frac{m_1 kT}{\pi}} \tag{2.520}$$

$$\lambda_1 = \frac{1}{3} \rho_1 l_1 \langle C_1 \rangle_M C_{v_1} = \mu_1 C_{v-1} = \frac{1}{\pi d_1^2} \sqrt{\frac{k^3 T}{\pi m_1}} \tag{2.521}$$

<sup>57</sup> In this section we denote the thermal conductivity by the symbol  $\lambda$  to distinguish this parameter from the Boltzmann constant.

<sup>58</sup> Maxwell [65] was able to obtain these fairly accurate expressions for the transport coefficients which describe their primary dependence of upon temperature, pressure, mass and size of the molecules in the gas based on rather crude arguments. Historically, the mean free path theory given by Maxwell [65] predates the more accurate theory based on the Boltzmann equation by about half a century.

The self diffusivity which is valid for two species of identical mass and size yields:

$$D_{11} = \frac{1}{3} l_1 \langle C_1 \rangle_M = \mu_1 / \rho_1 = \frac{2}{3} \left( \frac{kT}{\pi^3 m_1} \right)^{1/2} \frac{1}{n d_1^2} = \frac{2}{3} \left( \frac{k^3}{\pi^3 m_1} \right)^{1/2} \left( \frac{T^{3/2}}{p_1 d_1^2} \right) \quad (2.522)$$

For species of differing mass and size, the mean free paths, velocities, and collision frequencies will be different. The derivation of the binary diffusivity is more complicated but may be expressed as [28] [74] [5] (sect 17-3):

$$D_{12} = \frac{2}{3} \left( \frac{k}{\pi} \right)^{3/2} \left( \frac{1}{2m_1} + \frac{1}{2m_2} \right)^{1/2} \left( \frac{T^{3/2}}{p \left( \frac{d_1 + d_2}{2} \right)^2} \right) \quad (2.523)$$

A similar result was obtained by Present [77] (p 149) for the rigid-sphere molecular model:

$$D_{12} = \frac{1}{3} l_1 \langle C_1 \rangle_M = \frac{3}{8} \left( \frac{\pi kT}{2\mu} \right)^{1/2} \frac{1}{n \pi d_{12}^2} \quad (2.524)$$

The pressure dependence expressed by these relations is fairly accurate for pressures up to about 10 – 20 atmospheres. At higher pressures, multi-body collisions become important and the pressure dependence is greater. Experimental evidence also show that a temperature dependence of  $T^{3/2}$  is too weak leading to the search for more accurate relations as derived by use of the Enskog approach.

Alternative estimates of the transport coefficients can be obtained from the rigorous Chapman-Enskog expansion method of mono-atomic gases at low densities (e.g., [24] [25] [12] [61] (p 202) [28]). The transport coefficients deduced from the Chapman-Enskog kinetic theory with the rigid elastic spheres interaction model yield (e.g., [39] sect 8.2; [61], p 202):

$$\mu_1 = \frac{5}{16 d_1^2} \sqrt{\frac{m_1 kT}{\pi}}, \quad (2.525)$$

$$\lambda_1 = \frac{5}{2} \mu_1 C_{v_1} = \frac{75}{64 d_1^2} \sqrt{\frac{k^3 T}{m_1 \pi}} \quad (2.526)$$

$$D_{11} = \frac{3}{8 n_1 d_1^2} \sqrt{\frac{kT}{m_1 \pi}} \quad (2.527)$$

The binary diffusivity can also be determined in a similar manner considering a binary mixture of dilute gases:

$$D_{12} = \frac{3}{16 n_1 d_{12}^2} \sqrt{\frac{2kT}{\pi \mu}} \quad (2.528)$$

The Chapman-Enskog kinetic theory actually gives general expressions for the transport properties in terms of the intermolecular potential energy which is

related to the intermolecular force as expressed by (2.48) and (2.49). The molecular interaction is most frequently described by the empirical Lennard-Jones 12 – 6 potential.

The transport coefficients like viscosity, thermal conductivity and self-diffusivity for a pure mono-atomic gas and the diffusivity for binary mixtures obtained from the rigorous Chapman-Enskog kinetic theory with the Lennard-Jones interaction model yield (e.g., [39], sect 8.2; [5], sects 1-4, 9-3 and 17-3):

$$\mu_1 = \frac{5}{16} \frac{\sqrt{\pi m_1 kT}}{\pi \sigma_1^2 \Omega_{\mu,1}} \quad (2.529)$$

$$\lambda_1 = \frac{25}{32} \frac{\sqrt{\pi m_1 kT}}{\pi \sigma_1^2 \Omega_{\lambda,1}} C_{v_1} \quad (2.530)$$

$$D_{11} = 3.2027 \times 10^{-5} \sqrt{\frac{T}{M_{w_1}}} \frac{1}{c \sigma_1^2 \Omega_{D,11}} \quad (2.531)$$

$$D_{12} = 0.0018583 \sqrt{T^3 \left( \frac{1}{M_{w_1}} + \frac{1}{M_{w_2}} \right)} \frac{1}{p \sigma_{12}^2 \Omega_{D,12}} \quad (2.532)$$

in which  $\sigma_1$  is a characteristic diameter of the molecules of type 1, often called the collision diameter, and may be defined differently for each molecular model. In the Lennard-Jones potential  $\sigma_1$  has the significance of being the distance from the center of mass of the two molecules to the point at which the potential changes from repulsive to attractive [28]. To calculate  $\sigma_{12}$  an analog of the rigid sphere model is generally adopted:  $\sigma_{12} = (\sigma_1 + \sigma_2)/2$ . This approach has little theoretical justification and is not accurately verified by experimental data. The collision integrals<sup>59</sup>  $\Omega_{\mu,1}$ ,  $\Omega_{\lambda,1}$ ,  $\Omega_{D,11}$ , and  $\Omega_{D,12}$  account for the details of the paths that the molecules take during a binary collision and are usually of order unity. In one view these integrals are interpreted as describing the deviation from the rigid sphere behavior. The  $\varepsilon$  quantity in the Lennard-Jones potential is a characteristic energy denoting the maximum energy of attraction between a pair of molecules. For binary mixtures  $\varepsilon_{12}$  is usually approximated by a geometric average of the contributions from the two species  $\varepsilon_{12} \approx \sqrt{\varepsilon_1 \varepsilon_2}$ .

By use of these formulas accurate calculations of the transport coefficients can thus be performed provided that the Lennard-Jones potential parameters like  $\varepsilon_1$  and  $\sigma_1$  are known. Extensive lists of these parameters are given for many substances by Hirschfelder et al [39] and Bird et al [5], among others.

<sup>59</sup> Chapman and Cowling [12] have shown that in kinetic theory the transport coefficients can be expressed in terms of the Sonine polynomial expansion coefficients which are complicated combinations of the bracket integrals. In the given solutions these integrals are written as linear combinations of a set of these *collision integrals*. See also Hirschfelder et al [39], sect 7-4.

### Dilute gas hypothesis

The phrase *dilute gas* indicates that the physical volume  $n[\frac{3}{4}\pi d^3]$  occupied by the gas particles (molecules) is small compared to the volume  $V$  available to the gas. Mathematically this condition can be expressed as:

$$n \left[ \frac{4}{3} \pi d^3 \right] \ll V, \quad (2.533)$$

or

$$\frac{n \left[ \frac{4}{3} \pi d^3 \right]}{V} \ll 1, \quad (2.534)$$

where  $n$  denotes the number of particles and  $d$  is the radius of the particle.

A real gas can thus be considered dilute provided that the mean free path  $l$  is much larger than the particle size, i.e.,  $l \gg d$ .

Assuming that the molecules are rigid elastic spheres a typical value for the mean free path for a gas, say oxygen, can be calculated from (2.516). Consider a typical room temperature at 300 (K) and a pressure of 101325 (Pa). The collision diameter of molecular oxygen can be set to  $3.57 \times 10^{-10}$  (m) in accordance with the data given by [51], example 1.4. We can then calculate the mean free path  $l$  for oxygen:

$$\begin{aligned} l &= \frac{RT}{\sqrt{2}\pi d^2 N_a p} \\ &= \frac{8.314(JK^{-1}mol^{-1}) \times 300(K)}{\sqrt{2}\pi [3.57 \times 10^{-10}(m)]^2 \times 6.022 \times 10^{23}(mol^{-1}) \times 101325(Pa)} \\ &= 7.22 \times 10^{-8}(m) \end{aligned} \quad (2.535)$$

Since the molecular diameters for the different gases are of the same order, the mean free path in any gas at the given temperature and pressure is of the order  $10^{-5}(cm)$ . In this case it follows that the mean free path is about hundred times the diameter of the molecule, thus the gas is dilute. However, it is noted that at higher gas pressure, say 10132500 (Pa), the mean free path is reduced and comparable with the dimensions of a molecule. In this case the assumption of molecular chaos may not be valid so the gas cannot be considered dilute [12].

### Continuum hypothesis

A dilute gas mixture is assumed to behave as a continuum when the mean free path of the molecules is much smaller than the characteristic dimensions of the problem geometry. A relevant dimensionless group of variables, the Knudsen number  $Kn$ , is defined as [47, 30, 31]:

$$Kn = \frac{l}{L}, \quad (2.536)$$

where  $l$  is the mean free path of the molecules and  $L$  a characteristic dimension of the apparatus region in which the relevant physical phenomena take place (e.g., the thickness of boundary layers in which large gradients appear, the diameter of catalyst pores, the reactor diameter, etc).

In general the *continuum hypothesis* is considered valid for  $Kn < 0.01$ .

By use of the typical numerical value for the mean free path given above for a gas at temperature  $300K$  and pressure  $101325Pa$ , this condition indicates that the continuum assumption is valid provided that the characteristic dimension of the apparatus is  $L > 0.001cm$ . Nevertheless, it is noted that at low gas pressures, say  $10Pa$ , the mean free path is increased and might be comparable with the characteristic dimensions of the apparatus. In particular, for low pressures and small characteristic dimensions we might enter a flow regime where the continuum assumption cannot be justified.

## 2.11 Extending the Kinetic Theory to Denser Gases

The preceding sections in this chapter deal with the kinetic theory of dilute gases summarizing the statistical modeling concepts, deriving the governing conservation equations and fairly accurate relations determining the transport coefficients from first principles.

The starting point for the kinetic theory of dilute mono-atomic gases is the Boltzmann equation determining the evolution of the distribution function in time and space. The formulation of the collision term is restricted to gases that are sufficiently dilute so that only binary collisions need to be taken into account. It is also required that the molecular dimensions are small in comparison with the mean distance between the molecules, hence the transfer of molecular properties is solely regarded as a consequence of the free motion of molecules between collisions.

Obviously, these restrictions are not met in dense gases, so the dilute gas results are not acceptable for higher-density systems (e.g., Ferziger and Kaper [28], p. 356). After recognizing these model restrictions, Enskog [26] made a first attempt to extend the kinetic theory of dilute mono-atomic gases to slightly higher densities.

Basically, Enskog's kinetic theory extension consists in the introduction of corrections that account for the fact that for dense gases the molecular diameter is no longer small compared with the average intermolecular distance.

The fundamental postulate is that as a dilute gas is compressed two novel effects become important because the molecules have finite volumes. First, it is expected that during a molecular collision momentum and energy are transferred over a distance equal to the separation of the molecules. In the particular case of rigid spherical molecules this collisional transfer of momentum and energy takes place instantaneously and results in a transfer over the distance between their centers. Second, the collision frequency may be altered. One possible mechanism is that the collision frequency is increased

because the particle diameter is not negligible small compared with the average distance between the molecules. However, the collision frequency may also decrease because the molecules are close enough to shield one another from oncoming molecules. Nevertheless, the probability of multiple simultaneous collisions is considered negligible.

### Enskog's Equation

For dilute mono-atomic gases we have shown that the evolution of the distribution function is given by the Boltzmann equation as expressed by (2.185). Hence, considering dense gases it might be natural to start out from this result. Enskog [26] derived a modified Boltzmann equation for the evolution of the distribution function supposedly valid for denser gases. No changes was made to the LHS of the equation, whereas an extended form of the collision term was introduced due to the finite size of the molecules.

More precisely, Enskog considered a mono-atomic gas composed of rigid spherical molecules of diameter  $d$ . The restriction to rigid spheres was made because multi-body collisions need not be considered, as for this special molecular model there are essentially no three-body and higher order collisions. The major aim was to take into account the mechanisms of instantaneous momentum and energy transfer over the distance separating the centers of the two colliding molecules,  $d_{12} = d$ . Another important goal was to extend the collision frequency formula correcting for the finite size of the molecules.

Considering the impact of collisions for dilute mono-atomic gases we have shown in the foregoing paragraphs that we need to know the numbers of pairs of molecules both lying in the element  $d\mathbf{r}$  which are going to collide in the time interval  $dt$  and elementary knowledge from scattering theory. Hence, during a time interval  $dt$  the expected number of collisions in the volume element  $d\mathbf{r}$  about  $\mathbf{r}$  between molecules in the velocity ranges  $d\mathbf{c}$  about  $\mathbf{c}$  and  $d\mathbf{c}_1$  about  $\mathbf{c}_1$ , with the infinitesimal solid angle in the range  $d\Omega'$  about  $\Omega'$ , is given by the collision term on the RHS of (2.185).

For dense gases Enskog started out from the given result for dilute gases, examined the basic collision term formulation and thereafter introduced certain extensions to the collision term. The pertinent modifications certainly need further considerations and are thus briefly outlined next.

In the analysis of a binary collision between molecules with velocities  $\mathbf{c}_1$  and  $\mathbf{c}_2$  the direction of the line of centers at collision can be specified by the unit vector  $\mathbf{k}$  along the apse-line (i.e. in the particular case of rigid spherical molecules, the apse-line corresponds to the line joining the centers of the two molecules at the instant of contact), Fig. 2.7. This unit vector is precisely characterized by the polar angles  $(\psi, \phi)$ .

Therefore, instead of describing the deflection<sup>60</sup> with the angles  $(\theta, \phi)$ , it is more convenient to use the angles  $(\psi, \phi)$  since in these variables the

<sup>60</sup> The deflection angle  $\theta$  is defined as the angle between the final and initial velocities:  $\theta = \pi - 2\psi$ . It appears that the phrase scattering is used for the case

final velocity  $\mathbf{g}'_{21}$  is more simply related to the initial velocity  $\mathbf{g}_{21}$  (i.e., by symmetry the projections of  $\mathbf{g}_{21}$  and  $\mathbf{g}'_{21}$  on  $\mathbf{k}$  are equal and of opposite sign:  $\mathbf{k} \cdot \mathbf{g}_{21} = -\mathbf{k} \cdot \mathbf{g}'_{21}$ , as discussed in sect. 2.4.2). In particular, in sect. 2.4.3 we found that when the collision term in (2.185) is expressed in terms of the impact parameter (i.e.,  $b db d\phi$ ),  $\mathbf{c}'$  and  $\mathbf{c}'_1$  should be given as functions of  $\mathbf{c}$ ,  $\mathbf{c}_1$ ,  $b$  and  $\phi$ . Alternatively, when the collision term is rewritten in terms of  $\sigma_A(\theta, g) d\Omega'$  the velocities  $\mathbf{c}'$  and  $\mathbf{c}'_1$  must be given as functions of  $\mathbf{c}$ ,  $\mathbf{c}_1$  for given  $\Omega'$ , through the law of collision. We can then, for example, use (2.142), (2.143) and (2.144) expressed in the particular reference frame chosen (i.e., laboratory system). However, a third and more common approach is to use the unit vector  $\mathbf{k}$  to describe the scattering. That is, we express the scattering cross section in terms of the variable  $\mathbf{k}$  rather than  $\theta$ . Therefore, when the scattering cross section is expressed in terms of the unit vector  $\mathbf{k}$ , (2.142), (2.143) and (2.144) can be used directly to compute  $\mathbf{c}'$  and  $\mathbf{c}'_1$  as these relations are independent of the laboratory frame. The latter formulation plays a fundamental role in the applications of kinetic theory to denser gases, hence it is worthwhile to display its derivation in further details.

The scattering cross section is expressed in terms of the variable  $\mathbf{k}$ , simply by defining a function  $s_A(\psi, g)$  by [85] [77]:

$$s_A(\psi, g) \sin \psi d\psi d\phi = \sigma_A(\theta, g) \sin \theta d\theta d\phi \quad (2.537)$$

in such a way that the number of particles deflected into the corresponding differential surface element of a sphere of unit radius per unit time (2.147) becomes:

$$F \sigma_A(\theta, g) \sin \theta d\theta d\phi = F s_A(\psi, g) \sin \psi d\psi d\phi \quad (2.538)$$

By trigonometric manipulations using (2.157), we obtain

$$s_A(\psi, g) = \sigma_A(\theta, g) \frac{\sin \theta d\theta d\phi}{\sin \psi d\psi d\phi} = 4\sigma_A(|\pi - 2\psi|; g) \cos \psi \quad (2.539)$$

where we have required that  $s_A$  is a positive factor by using a positive angle:  $\theta = |\pi - 2\psi|$ .

It appears that the variable  $\mathbf{k}$  will be convenient shortly calculating the collision term because it allows us to write down the number of scattered particles in a form independent of the particular system of coordinates used in the previous calculations (i.e., the laboratory frame). Trigonometrical considerations imply that:

$$\cos \psi = \mathbf{k} \cdot \mathbf{e}_{g'} = \mathbf{k} \cdot \frac{\mathbf{g}'_{21}}{|\mathbf{g}'_{21}|} \quad (2.540)$$

or,

$$\psi = \arccos(\cos \psi) = \arccos\left(\frac{\mathbf{k} \cdot \mathbf{g}'_{21}}{g}\right) \quad (2.541)$$

---

of Maxwellian billiard ball particles, whereas the phrase deflection is used in the more general case considering a center of force.

and we introduce a novel quantity

$$dk = \sin \psi d\psi d\phi \quad (2.542)$$

denoting a differential area of a sphere of unit radius. Hence,  $\psi$  and  $\phi$  represent the polar angles around  $\mathbf{k}$ .

It follows that the number of particles scattered into the differential area element per unit time, given by (2.538), can be rewritten using (2.542), (2.541) and (2.540). The result is

$$\begin{aligned} F\sigma_A(\theta, g) \sin \theta d\theta d\phi &= F s_A(\psi, g) \sin \psi d\psi d\phi = F s_A(\psi, g) dk \\ &= F s_A(\arccos(\frac{\mathbf{k} \cdot \mathbf{g}'_{21}}{g}), g) dk \\ &= F s_A(\arccos(\mathbf{k} \cdot \mathbf{e}_{g'}), |\mathbf{g}'_{21}|) dk = F s_A(\mathbf{k}, \mathbf{g}'_{21}) dk \end{aligned} \quad (2.543)$$

which is independent of the laboratory reference frame, as it is expressed in a system of coordinates moving with the center of mass.

For hard spheres (2.543) takes a particularly simple form, using (2.539), (2.540) and (2.161), we get:

$$\begin{aligned} s_A(\mathbf{k}, \mathbf{g}'_{21}) &= s_A(\arccos(\frac{\mathbf{k} \cdot \mathbf{g}'_{21}}{g}), g) = 4\sigma_A(\psi, g) \mathbf{k} \cdot \mathbf{e}_{g'} = 4(\frac{d_{12}^2}{4}) \mathbf{k} \cdot \mathbf{e}_{g'} \\ &= d_{12}^2 \mathbf{k} \cdot \mathbf{e}_{g'} \end{aligned} \quad (2.544)$$

Making an inversion of the trajectory with respect to the origin  $O$  and reversing the velocities, the unit vector along the apse line changes sign, whereas the deflection angle  $\theta$  does not change in these transformations [85]. Hence, in accordance with the Liouville law for elastic collisions, the cross sections of the two processes are the same and consistently  $s(\mathbf{k}', \mathbf{g}_{21}) = s(\mathbf{k}, \mathbf{g}_{21}) = s(-\mathbf{k}, \mathbf{g}_{21})$ .

Reformulating (2.543), using (2.540) and (2.544), we get:

$$|\mathbf{g}_{21}| F\sigma_A(\theta, g) d\Omega' = |\mathbf{g}_{21}| F s_A(\mathbf{k}, \mathbf{g}'_{21}) dk = F d_{12}^2 \mathbf{k} \cdot \mathbf{g}_{21} dk \quad (2.545)$$

or, simply

$$g\sigma_A(\theta, g) d\Omega' = d_{12}^2 \mathbf{k} \cdot \mathbf{g}_{21} dk = d_{12}^2 g dk \cos \psi \quad (2.546)$$

The frequency of collision in (2.168) can now be rewritten as:

$$f(\mathbf{r}, \mathbf{c}, t) f_1(\mathbf{r}_1, \mathbf{c}_1, t) d_{12}^2 \mathbf{g} \cdot \mathbf{k} dk d\mathbf{c}_1 d\mathbf{c} d\mathbf{r} \quad (2.547)$$

where it is assumed that the molecules having a velocity in the range  $\mathbf{c}_1, \mathbf{c}_1 + d\mathbf{c}_1$  may collide with the target molecule within the collision cylinder and form a homogeneous incident beam with flux  $dF = g f_1(\mathbf{r}, \mathbf{c}_1, t) d\mathbf{c}_1$ . Moreover, we have dropped the subscript in the relative velocity because from this point on we are interested only in the velocity before ( $\mathbf{c}, \mathbf{c}_1$  and  $\mathbf{g}$ ) and after ( $\mathbf{c}', \mathbf{c}'_1$  and

$\mathbf{g}'$ ) the collision and never in the intermediate velocities during the scattering process.

Two modifications are made to this expression in order to describe the frequency of collisions in a dense gas of rigid spheres. First, the frequency of collisions is changed by a factor  $\chi$ :

$$\chi f(\mathbf{r}, \mathbf{c}, t) f_1(\mathbf{r}_1, \mathbf{c}_1, t) d_{12}^2 \mathbf{g} \cdot \mathbf{k} dk d\mathbf{c}_1 d\mathbf{c} d\mathbf{r} \quad (2.548)$$

where  $\chi$  is a free volume correction function that is unity for dilute gases, and increases with increasing gas density towards infinity as the gas density approaches the state of closest packing where no motion is possible. The correction function  $\chi$  is related to the virial expansion of the equation of state and fitted to experimental data [39].

Second, due to the finite size of the colliding molecules the centers of the two molecules are not at the same point. If, at the instant of collision, the center of the first molecule is at  $\mathbf{r}$ , the center of the second one is at  $\mathbf{r} - d_{12}\mathbf{k}$ , so that  $f(\mathbf{r}_1, \mathbf{c}_1, t)$  is replaced by  $f(\mathbf{r} - d_{12}\mathbf{k}, \mathbf{c}_1, t)$ . The correction function is determined at the point of contact between the two particles, hence:

$$\chi(\mathbf{r} - \frac{1}{2}d_{12}\mathbf{k}) f(\mathbf{r}, \mathbf{c}, t) f_1(\mathbf{r}_1, \mathbf{c}_1, t) d_{12}^2 \mathbf{g} \cdot \mathbf{k} dk d\mathbf{c}_1 d\mathbf{c} d\mathbf{r} \quad (2.549)$$

As for dilute gases, corresponding to any direct collision specified by the variables  $\mathbf{c}, \mathbf{c}_1, \mathbf{k}$  there is an analogous inverse collision in which  $\mathbf{c}, \mathbf{c}_1$  are the velocities of the molecules after the collision, while  $-\mathbf{k}$  is the direction of the apse-line. In such a collision the center of the second molecule is at  $\mathbf{r} + d_{12}\mathbf{k}$ , while the point of contact is at  $\mathbf{r} + \frac{1}{2}d_{12}\mathbf{k}$ . Hence, the extended Boltzmann equation describing the evolution of the the distribution function for a dense gas of rigid spherical molecules is analogous to (2.185):

$$\begin{aligned} \frac{D_c f}{D_c t} = & \int \int [\chi(\mathbf{r}_1 + \frac{1}{2}d_{12}\mathbf{k}) f'(\mathbf{r}_1, \mathbf{c}_1, t) f'_1(\mathbf{r}_1 + d_{12}\mathbf{k}, \mathbf{c}_2, t) \\ & - \chi(\mathbf{r}_1 - \frac{1}{2}d_{12}\mathbf{k}) f(\mathbf{r}_1, \mathbf{c}_1, t) f_1(\mathbf{r}_1 - d_{12}\mathbf{k}, \mathbf{c}_2, t)] d_{12}^2 (\mathbf{g} \cdot \mathbf{k}) dk d\mathbf{c}_1 \end{aligned} \quad (2.550)$$

This extended Boltzmann equation is called the *Enskog equation*.

Applying the Enskog approximate solution method, consistent flux vectors are derived for dense gases accounting for the finite size of the molecules. Because of the inherent corrections there are two contributions to the dense gas fluxes, one flux associated with the collisional transfer which is important in dense gases only, and another flux due to the motion of molecules between collisions as for dilute gases. The total flux of the property  $\psi$  is determined by the sum of these two contributions:

$$\psi = \psi_{\text{Collisional}} + \psi_{\text{Kinetic}} \quad (2.551)$$

In particular, for mono-atomic dense gases both the pressure tensor,  $\mathbf{P}$ , and the heat flow vector  $\mathbf{q}$ , contain two flux contributions [12] [28] [39].

Although the Enskog theory is formally valid for rigid spheres only, fairly accurate results have been obtained for real gases as well provided that the effective collision diameter is appropriately adjusted.

Enskog's dense gas theory for rigid spheres is also used as basis developing granular flow models. The modifications suggested extending the dense gas kinetic theory to particulate flows are discussed in chap 4.

## 2.12 Governing Equations for Polydispersed Multiphase Systems

To describe polydispersed multiphase systems the Boltzmann equation can be extended by including the dependency of the internal property coordinates such as the particle size and shape in the definition of the distribution function. In this way a statistical balance formulation can be obtained by means of a distribution function on the form:  $p(\boldsymbol{\xi}, \mathbf{r}, \mathbf{v}_\xi, \mathbf{c}, t)d\xi d\mathbf{r} d\mathbf{v}_\xi d\mathbf{c}$ , defined as the probable number of particles with internal properties in the range  $d\xi$  about  $\boldsymbol{\xi}$ , with a velocity range in property space  $d\mathbf{v}_\xi$  about  $\mathbf{v}_\xi$ , located in the spatial range  $d\mathbf{r}$  about the position  $\mathbf{r}$ , with a velocity range  $d\mathbf{c}$  about  $\mathbf{c}$ , at time  $t$ . The particular Boltzman type of equation is given by:

$$\frac{\partial p}{\partial t} + \nabla_{\mathbf{r}} \cdot (\mathbf{c}p) + \nabla_{\mathbf{c}} \cdot (\mathbf{F}p) + \nabla_{\boldsymbol{\xi}} \cdot (\mathbf{v}_\xi p) + \nabla_{\mathbf{v}_\xi} \cdot (\mathbf{a}_\xi p) = \mathcal{I} \quad (2.552)$$

where the first term on the LHS denotes the time variation of the distribution function  $p$ . The second term on the LHS represents the change in the number density distribution because of fluid particle convection into and out of the range  $d\mathbf{r}$ . The third term on the LHS represents the change in the number density distribution because of acceleration of the fluid particle into and out of the range  $d\mathbf{c}$  in the standard manner. However, in this case the net force  $\mathbf{F}$  acting to accelerate or decelerate the fluid particle includes the body and drag forces (per unit mass). The fourth term on the LHS represents the change in the number density distribution because of transport processes in the property space for example due to fluid particle growth into and out of the range  $d\xi$ . The fifth term on the LHS represents the change in the number density distribution because of accelerations in the property space for example due to acceleration of the fluid particle interface into and out of the range  $d\mathbf{v}_\xi$ . The term on the RHS represents the rate of change in the number density distribution due to particle coalescence, breakage and collisions.

Following the same procedure as outlined in sects 2.5 and 2.6 deriving the governing single phase conservation equations from the original Boltzmann equation, the extended Boltzmann equation can be multiplied by a generalized property function whereupon the resulting equation is integrated over the whole velocity space to give a generic transport equation for the conserved multiphase quantities [86]. In particular, considering that the property function is unity a transport equation for the number distribution function

$f(\boldsymbol{\xi}, \mathbf{r}, t)$  is obtained [53]. This transport equation is generally referred to as the *population balance equation*.

Hulburt and Katz [41] applied this approach to derive a transport equation for the number distribution function describing particulate systems considering growth, nucleation and agglomeration processes. Reyes Jr [86] and Lafi and Reyes [50] derived an extended set of mass, momentum and energy equations to describe polydispersed bubbly flows using a fluid particle continuity equation analogous to the Boltzmann's transport equation. In a similar manner Laurent et al [59] derived the governing conservation equations for polydispersed dense sprays of evaporating liquid droplets. Lathouwers and Bellan [54, 55, 56, 57, 58] proposed a similar model for polydispersed gas-solid multicomponent reactive processes in fluidized beds.

The main challenge in formulating these equations is related to the definition of the collision operator. So far this approach has been restricted to the formulation of the population balance equation. That is, in most cases a general transport equation which is complemented with postulated source term formulations for the particle behavior is used. Randolph [80] and Randolph and Larson [81] used this approach deriving a microscopic population balance equation for the purpose of describing the behavior of particulate systems. Ramkrishna [79] provides further details on this approach considering also fluid particle systems.

The population balance modeling framework is further discussed in chap 9.

---

## References

1. Aris R (1962) *Vectors, Tensors, and the Basic Equations of Fluid Mechanics*. Dover, Inc., New York
2. Arnold VI (1989) *Mathematical Methods of Classical Mechanics*. Second Edition, Springer-Verlag, New York
3. Bird RB, Stewart WE, Lightfoot EN (1960) *Transport phenomena*. John Wiley & Sons, New York
4. Bird RB, Curtiss CF, Armstrong RC, Hassager O (1987) *Dynamics of polymeric liquids*. Volume 2, Kinetic Theory. John Wiley & Sons, New York
5. Bird RB, Stewart WE, Lightfoot EN (2002) *Transport phenomena*. Second Edition, John Wiley & Sons, New York
6. Boltzmann L Weitere Studien über das Wärmegleichgewicht unter Gasmolekülen. *Sitzungsberichte Kaiserl Akad der Wissenschaften*, 66(2):275-370
7. Cajori F (1947) *Sir Isaac Newton's Mathematical Principles of Natural Philosophy and his System of the World*. Translated into English by Andrew Motte in 1729. The Translations revised, and supported with an historical and explanatory appendix, by Florian Cajori. University of California Press, Berkeley, California
8. Cercignani C, Illner R, Pulvirenti M (1994) *The Mathematical Theory of Dilute Gases*. Springer-Verlag, New York
9. Chandler D (1987) *Introduction to Modern Statistical Mechanics*. Oxford University Press, New York
10. Chapman S (1916) On the Law of Distribution of Molecular Velocities, and on the Theory of Viscosity and Thermal Conduction, in a Non-Uniform Simple Monoatomic Gas. *Phil Trans Roy Soc London* 216A:279-348
11. Chapman S (1918) On the Kinetic Theory of a Gas. Part II: A Composite Monoatomic Gas: Diffusion, Viscosity, and Thermal Conduction *Phil Trans Roy Soc London* 217A:115-197
12. Chapman S, Cowling TG (1970) *The Mathematical Theory of Non-Uniform Gases*. Third edition, Cambridge Mathematical Library, Cambridge
13. Clausius R (1850) Ueber die bewegende Kraft der Wärme und die Gesetze, welche sich daraus für die Wärmelehre selbst ableiten lassen. *Ostwald's klassiker der exakten wissenschaften*, Wilhelm Engelmann in Leipzig
14. Coffee TP, Heimerl JM (1981) Transport Algorithms for Premixed, Laminar Steady-State Flames. *Combustion and Flame* 43:273-289

15. Cox RT (1950) The Statistical Method of Gibbs in Irreversible Change. *Reviews of Modern Physics* 22 (3):238-248
16. Curtiss CF, Hirschfelder JO (1949) Transport Properties of Multicomponent Gas Mixtures. *J Chem Phys* 17(6):550-555
17. Curtiss CF (1968) Symmetric Gaseous Diffusion Coefficients. 49(7):2917-2919
18. Curtiss CF, Bird RB (1999) Multicomponent Diffusion. *Ind Eng Chem Res* 38:2515-2522
19. Curtiss CF, Bird RB (2001) Additions and Corrections. *Ind Eng Chem Res* 40:1791
20. Cussler EL (1997) *Diffusion: Mass Transfer in Fluid Systems*. Second Edition, Cambridge University Press, Cambridge
21. Darcy HP (1856) *Les Fontaines Publiques de la Ville de Dijon*. Paris:Dalmont
22. de Groot SR, Mazur P (1962) *Non-Equilibrium Thermodynamics*. North-Holland, Amsterdam
23. Elnashaie SSEH, Abashar MEE (1993) Steam reforming and methanation effectiveness factors using the dusty gas model under industrial conditions. *Chem Eng Proc* 32:177-189
24. Enskog D (1917) *Kinetische Theorie der Vorgänge in Mässig Verdünnten Gases*. Inaugural Dissertation, Uppsala
25. Enskog D (1922) Die numerische Berechnung der Vorgänge in mässig verdünnten Gases. *Ark Mat Astron Fys* 16(16):1-60
26. Enskog D (1922) *Kinetische Theorie der Wärmeleitung, Reibung und Selbstdiffusion in gewissen verdichteten Gasen und Flüssigkeiten*. *Kungl Svenska Vet-Ak Handl* 63(4):1-44
27. Epstein N (1989) On the tortuosity and the turtuosity factor in flow and diffusion through porous media. *Chem Eng Sci* 44:777-779
28. Ferziger JH, Kaper HG (1972) *Mathematical Theory of Transport Processes in Gases*. North-Holland Publishing Company, Amsterdam
29. Fick A (1855) Ueber Diffusion. *Ann der Physik* 94:59-86
30. Gad-el-Hak M (1999) The Fluid Mechanics of Microdevices - the Freeman Scholar Lecture. *Journal of Fluids Engineering-Transactions of the ASME* 121:5-33
31. Gad-el-Hak M (2006) Gas and Liquid Transport at the Microscale. *Heat Transfer Engineering* 27 (4):13-29
32. Gaskell DR (2003) *Introduction to the Thermodynamics of Materials*. Fourth Edition, Taylor & Francis, New York
33. Gibbs JW (1902) *Elementary Principles in Statistical Mechanics: Developed with especial reference to the rational fundation of thermodynamics*. Charles Scribner's Sons, New York
34. Gidaspow D (1994) *Multiphase Flow and Fluidization-Continuum and Kinetic Theory Descriptions*. Academic Press, Harcourt Brace & Company, Publishers, Boston
35. Goldstein H (1980) *Classical Mechanics*. Second Edition, Addison-Wesely Publishing Company, Reading Massachusetts
36. Grad H (1949) On the kinetic theory of rarified gases. *Comm Pure Appl Math* 2:331-407
37. Greiner W (2003) *Classical Mechanics: Systems of Particles and Hamiltonian Dynamics*. Springer, New York
38. Hansen JP, McDonald IR (1990) *Theory of Simple Liquids*. Second Edition, Academic Press, London

39. Hirschfelder JO, Curtiss CF, Bird RB (1954) *Molecular Theory of Gases and Liquids*. John Wiley & Sons, Inc., New York
40. Huang K (1963) *Statistical Mechanics*. John Wiley & Sons, Inc., New York
41. Hulburt HM, Katz S (1964) Some Problems in Particle Technology: A statistical mechanical formulation. *Chem Eng Sci* 19:555-574
42. Incropera FP, DeWitt DP (2002) *Fundamentals of Heat and Mass Transfer*. Fifth Edition, *John Wiley & Son*, New York
43. Iro H (2002) *A Modern Approach to Classical Mechanics*. World Scientific, New Jersey
44. Jackson R (1977) *Transport in Porous Catalysts*. Elsevier, Amsterdam, the Netherlands
45. Jenkins JT, Savage SB (1983) A Theory for Rapid Flow of Identical, Smooth, Nearly Elastic Spherical Particles. *J Fluid Mech* 130:187-202
46. Kleijn C (1991) *Transport Phenomena in Chemical Vapor Deposition Reactors*. PhD thesis, the Technische Universiteit Delft, the Netherlands
47. Kogan MN (1969) *Rarefied Gas Dynamics*. Trilling L ed translated from Russian, Plenum Press, New York
48. Krishna R (1993) Problems and Pitfalls in the use of the Fick Formulation for Interparticle Diffusion. *Chem Eng Sci* 48(5):845-861
49. Krishna R, Wesselingh JA (1997) The Maxwell-Stefan Approach to Mass Transfer. *Chem Eng Sci* 52(6):861-911
50. Lafi AY, Reyes Jr JN (1994) General Particle Transport Equation. Report OSU-NE-9409, Department of Nuclear Engineering, Oregon State University, Oregon
51. Laidler KJ, Meiser JH (1995) *Physical Chemistry*. Second Edition. Houghton Mifflin Company, Boston
52. Landau LD, Lifschitz EM (1976) *Mechanics*. Third Edition, Pergamon Press, Oxford
53. Lasheras JC, Eastwood C, Martínez-Bazán, Montañés JL (2002) A review of statistical models for the break-up of an immiscible fluid immersed into a fully developed turbulent flow. *Int J of Multiphase Flow* 28:247-278
54. Lathouwers D, Bellan J (2000) Modelling and simulation of bubbling fluidized beds containing particle mixtures. *Proc of the Comb Inst* 28:2297-2304
55. Lathouwers D, Bellan J (2001) Modelling of biomass pyrolysis for hydrogen production: The fluidized bed reactor. *Proc of the 2001 DOE Hydrogen Program Review*. NREL/CP-570-30535
56. Lathouwers D, Bellan J (2001) Modelling of dense gas-solid reactive mixtures applied to biomass pyrolysis in a fluidized bed. *Int Journal of Multiphase Flow* 27:2155-2187
57. Lathouwers D, Bellan J (2001) Yield optimization and scaling of fluidized beds for tar production from biomass. *Energy & Fuels* 15:1247-1262
58. Lathouwers D, Bellan J (2001) Modelling of dense gas-solid reactive mixtures applied to biomass pyrolysis in a fluidized bed. *Proc of the 2001 US DOE Hydrogen Program Review*. NREL/CP-570-28890
59. Laurent F, Massot M, Villedieu P (2004) Eulerian Multi-fluid modeling for the numerical simulation of coalescence in polydisperse dense liquid sprays. *J Comp Phys* 194:505-543
60. Lichtenberg AJ, Lieberman MA (1992) *Regular and Chaotic Dynamics*. Second Edition, Springer-Verlag, New York

61. Liboff RL (1998) Kinetic Theory: Classical, Quantum, and Relativistic Descriptions. Second Edition, John Wiley & Sons, Inc., New York
62. Lightfoot EN (1974) Transport Phenomena and Living Systems. John Wiley & Sons, Inc., New York
63. Malvern LE (1969) Introduction to the Mechanics of a Continuous Medium. Prentice-Hall, Inc., Englewood Cliffs
64. Mason EA, Malinauskas AP (1983) Gas Transport in Porous Media: The Dusty-Gas Model. Chemical Engineering Monographs. Volume 17, Elsevier, Amsterdam
65. Maxwell JC (1860) Illustrations of the Dynamical Theory of gases. - Part I. On the Motions and Collisions of Perfectly Elastic Spheres. Phil Mag 19:19-32
66. Maxwell JC (1867) On the Dynamical Theory of gases. Phil Trans Roy Soc London 157:49-88
67. Maxwell JC (1868) Illustrations of the Dynamical Theory of gases. Phil Mag 20:33-36
68. Maxwell JC (1890) The scientific papers of James Clerk Maxwell. Ed. Niven WD Cambridge University Press, vol. I & II, Cambridge
69. McCall MW (2001) Classical Mechanics: A Modern Introduction. John Wiley & Sons LTD, Chichester
70. McQuarrie DA (1973) Statistical Thermodynamics. Harper & Row, New York
71. Merk S (1959) The Macroscopic Equations for Simultaneous Heat and Mass Transfer in Isotropic, Continuous and Closed Systems. Appl Sci Res A8:73-99
72. Onsager L (1945) Theories and Problems of Liquid Diffusion. Ann N Y Acad Sci 46:241-265
73. Panat PV (2005) Classical Mechanics. Alpha Science International Ltd, Harrow
74. Plawsky JL (2001) Transport Phenomena Fundamentals. Marcel Dekker, Inc., New York
75. Pope S (2000) Turbulent Flows. Cambridge University Press, Cambridge
76. Prausnitz JM, Lichtenthaler RN, de Azevedo EG (1999) Molecular Thermodynamics of Fluid-Phase Equilibria. Third Edition, Prentice Hall PTR, New Jersey
77. Present RD (1958) Kinetic Theory of Gases. McGraw-Hill Book Company, Inc, New York
78. Quintard M, Bletzacker L, Chenu S, Whitaker S (2006) Nonlinear, multicomponent, mass transport in porous media. Chem Eng Sci 61:2643-2669
79. Ramkrishna D (2000) Population Balances. Academic Press, San Diego
80. Randolph A (1964) A population balance for countable entities. Canadian J Chem Eng 42:280-281
81. Randolph A, Larsson MA (1988) Theory of Particulate Processes: Analysis and Techniques of Continuous Crystallization. Academic Press, Harcourt Brace Jovanovich, Publishers, San Diego
82. Reid RC, Prausnitz JM, Poling BE (1987) The Properties of Gases & Liquids. Fourth Edition, McGraw-Hill Book Company, New York
83. Reif F (1965) Fundamentals of statistical and thermal physics. McGraw-Hill Book Company, New York
84. Reif F (1967) Statistical physics. McGraw-Hill Book Company, New York
85. Résibois P, De Leener M (1977) Classical Kinetic Theory of Fluids. John Wiley & Sons, New York

86. Reyes Jr JN (1989) Statistically Derived Conservation Equations for Fluid Particle Flows. Nuclear Thermal Hydraulics 5th Winter meeting, Proc ANS Winter Meeting.
87. Rohsenow WM, Choi H (1961) Heat, Mass, and Momentum Transfer. Prentice-Hall, Inc., Englewood Cliffs, New Jersey
88. Siegel R, Howell JR (2002) Thermal Radiation Heat Transfer. Fourth Edition, Taylor & Francis, New York
89. Slattery JC (1999) Advanced Transport Phenomena. Cambridge University Press, New York
90. Smits AJ (2000) A Physical Introduction to Fluid Mechanics. John Wiley & Sons, Inc., New York
91. Smoluchowski M (1918) Versuch einer mathematischen Theorie der Koagulationskinetik kolloider Lösungen. Zeitschrift für Physikalische Chemie, Leipzig, Band XCII pp 129-168
92. Stefan J (1871) Über das Gleichgewicht und die Bewegung, insbesondere die Diffusion von Gasgemengen. Sitzungsberichte Akad Wiss Wien 63:63-124
93. Stefan J (1872) Über die dynamische Theorie der Diffusion der Gase. Sitzungsberichte Akad Wiss Wien 65(2):323-363
94. Stokes GG (1845) On the Theories of the Internal Friction of Fluids in Motion, and of the Equilibrium and Motion of Elastic Solids. Trans Camb Phil Soc 8:287-305
95. Tabor M (1989) Chaos and Integrability in Nonlinear Dynamics. John Wiley & Sons, New York
96. Taylor R, Krishna R (1993) Multicomponent Mass Transfer. John Wiley & Sons, New York
97. Tolman RC (1938) The Principles of Statistical Mechanics. Oxford University Press, First Edition, London
98. Toor HL (1957) Diffusion in Three-component Gas Mixtures. AIChE J 3(2):198-207
99. Truesdell C (1954) The Present Status of the Controversy Regarding the Bulk Viscosity of Fluids. Proc R Soc London 226A(1164):59-69
100. Vincenti WG, Kruger CH Jr. (1967) Introduction to Physical Gas Dynamics. Second Printing, John Wiley and Sons, Inc., New York
101. Whitaker S (1987) Mass Transport and Reaction in Catalyst Pellets. Transport in Porous Media 2:269-299
102. White FM (1974) Viscous Fluid Flow. McGraw-Hill, New York
103. Wilke CR (1950) Diffusional Properties of Multicomponent Gases. Chem Eng Prog 46:95-104
104. Williams FA (1985) Combustion Theory: The Fundamental Theory of Chemically Reacting Flow Systems. Second Edition, The Benjamin/Cummings Publishing Company, Inc., California
105. Woods LC (1993) An Introduction to the Kinetic Theory of Gases and Magnetoplasmas. Oxford University Press, Oxford

**Multiphase Flow**

## Multiphase Flow

In this chapter the pertinent multiphase modeling concepts established in fluid mechanics are examined. The modeling framework constituting the basis for the next generation of chemical reactor models is presented. The average multi-fluid model represents a trade-off between accuracy and computational efforts. This concept is a direct multi-dimensional extension of the conventional reactor models with the addition of the momentum equations. The multi-fluid model is actually the only approach that can be used analyzing chemical reactive systems on industrial scales considering both inherent physics and feasible computational efforts. The remaining sections of the chapter are devoted to the derivation of the two-fluid and multi-fluid models, and to the description of the averaging procedures commonly used in multi-phase flow analysis.

### 3.1 Introduction

It is primarily a knowledge of chemical kinetics and reactor design that distinguishes the chemical engineers from other engineers. This multi-disciplinary profession emerged as a branch of engineering that is concerned with the design, construction and operation of chemical process plants in which the chemical reactor is a central unit. Both catalytic and non-catalytic chemical processes are operated in these chemical reactor units, as described in basic reaction engineering courses [78]. However, the major motivation for performing multi-phase flow analysis in chemical reaction engineering is highly linked to the discovery of catalysts.

A catalyst is, as is well known by chemical engineers, a substance that affects the rate of a reaction but emerges from the process unchanged. The major application of catalysis are in petroleum refining and in chemical production, and this is thus a very important field of research in an oil and gas producing country like Norway. The development and use of catalysts has been a major part of the constant search for new ways of increasing product

yield and selectivity from chemical reactions. Catalysis is usually referred to as the occurrence, study, and use of catalysts and catalytic processes. In this context *yield* refers to the amount of a specific product formed in a given process per mole of entering reactant, while *selectivity* is related to the number of moles of desired product formed per mole of undesired product formed. Both homogeneous and heterogeneous catalytic systems are used. Homogeneous catalysis concerns processes in which a catalyst is in solution with at least one of the reactants. A heterogeneous catalytic process involves more than one phase, usually the catalyst is a solid and the reactants and products are in liquid or gaseous form.

The discovery of solid catalyst and their application to chemical processes led to a breakthrough of the chemical industry [61]. Catalytic processing, involving multiphase systems, is utilized in the production of most industrial chemicals. The chemical or biochemical catalysts employed have a determining influence on the plant size, complexity, product distribution, by-products, economy and emission to the environment. The success of catalytic processing of multiphase systems has resulted from a synergetic approach to the problem by industrial chemistry and chemical engineering researchers. Traditionally, the focus of the industrial chemistry scientists has been on the catalyst, its preparation, active form, activity, active centers, kinetics and poisons that might damage it. Chemical engineers were mainly concerned with how to provide chemicals in sufficient amounts, enable mixing of the reactants on the molecular scales bringing the species effectively in contact with the chosen catalyst, and how to separate the products (and the catalyst particles) from the effluent process mixture (suspension). The engineers also concerned themselves with design and scale-up issues, as to how to produce the selectivity and rates reached in the laboratory on the industrial process scale.

Chemical reaction engineering (CRE) emerged gradually as a powerful methodology that quantifies the interplay between transport phenomena and kinetics on a variety of scales. A fundamental task for chemical reaction engineers is the formulation of a reactor model for which the basis are the species mass transport equations and the heat balance. The fluid velocity is normally considered a model parameter, or approximated by idealized flow formulas. These models have been used successfully determining various quantitative measures of reactor performance such as production rate, conversion and selectivity. The ability to establish such quantitative links between measures of reactor performance and input and operating variables is essential in optimizing the operating conditions in manufacturing, for proper reactor selection in design and scale-up, and in correct interpretation of data in research and pilot plant work.

However, the conventional reactor model formulations are normally strictly not precise on the microscopic scales (yet usually sufficient in engineering practice) as the fundamental or 'rigorous' version of the governing transport equations were considered too complex to be conveniently solved for practical applications. There are generally two ways to obtain simplified models,

i.e., either by direct simplification of the fundamental equations neglecting insignificant terms that have no practical interest or by averaging/integrating the governing equations over suitable scales in time - and space. The averaging procedure is more common in practice, as the direct simplifications are only applicable for a few idealized flows.

The choice of averaging scales in space (e.g., whole reactor, reactor section or differential volume) to which the averaging procedure is applied determines the level of sophistication of the reactor model on macroscopic scales. As it is very common in chemical reactors to have flow predominantly in one direction, i.e., normally in the axial direction as in tubular reactors, a cross-sectional averaged model may be used when only the spacial gradients in the principal flow direction have to be considered. The resulting equations are conventionally referred to as the non-ideal *axial dispersion model* (ADM). In the presence of packing or multiple fluid phases, a distinction is made between the true local fluid velocity, sometimes called the interstitial velocity ( $m/s$ ), and the velocity considered over the whole cross section, as if there were only one phase and no packing, called the superficial velocity ( $m^3$  fluid/ $m^2$  cross section  $s$ ). If the convective transport is completely dominant over any diffusive transport, the idealized *Plug Flow Reactor* (PFR) model is achieved. Otherwise, when the dispersion terms are very large, we can average out all space gradients in the species mass densities and the enthalpy quantity leading to the ideal *Continuous Stirred Tank Reactor* (CSTR) model.

The conventional models are often sufficient for determining proper descriptions of the kinetics and the molecular transport processes, which then enables us to properly quantify the species overall or effective generation rates. Hence, the idealized reactor models are still preferred for the conventional chemical reactor analysis. They are also frequently utilized in chemical process simulations, optimization and control. However, it is obvious that all terms in a reactor model should be described at the same level of accuracy. It is certainly not optimal to have a detailed description of one term in the model if the others can only be very crudely described. Therefore, the improvement in accuracy obtained by the more detailed description of the kinetics at the molecular scale in turn required a more detailed description of the flow fields. The search for more fundamental reactor models solving all the pertinent balance equations simultaneously (e.g., the continuity equation, species mass balances, heat balance and momentum equations) in a predictive manner is gradually emerging, defining a strategic goal in chemical reaction engineering. Sufficient modeling progress achieving such predictive capabilities is not imminent. It appears that the fundamental multi-phase reactor models still have limited inherent capabilities to fully replace the empirically based analysis in use today.

Nevertheless, in the last two or three decades an increasing trend in applying fundamental modeling approaches to elucidate details of the reactor flow performance has been seen in the literature and recognized as useful by the industry. It is emphasized that almost only cold flow analysis of the

reactor flow fields have been performed hitherto concluding that even the flow patterns in industrial reactors are almost prohibitively complex, hence the fundamental modeling is a challenging task. So, in chemical reactor engineering the multi-fluid flow models are merely related to modern academic research investigating details of cold flow patterns, physicochemical hydrodynamics and to a very limited extent improving the basic understanding of the complex interactions between flow phenomena, thermodynamics, molecular and turbulent transport processes, and chemical reaction kinetics.

## Chemical Reactor Flow Structure Characteristics

Detailed descriptions of the chemical reactor flow patterns are given in chaps 8, 10, 7 and 11. Meanwhile, a preliminary overview of the pertinent reactor flow characteristics is given to determine which modeling concepts are available describing the behavior of the relevant flows.

Typical multiphase flow regimes identified in general gas-liquid and gas-solid flows in vertical and horizontal tubes are illustrated in Fig 3.1.

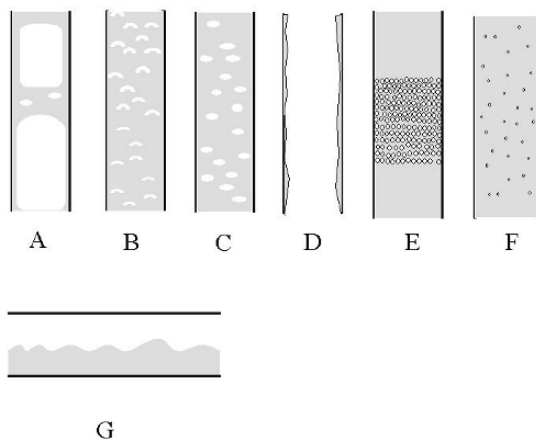


**Fig. 3.1.** Multiphase flow regimes. A: Slug flow. B: Bubbly flow. C: Droplet Flow. D: Annular flow. E: Packed and porous fixed bed. F: Particulate flow. G: Stratified free surface flow.

Examples of typical reactor flows are listed belows:

- Single phase fluid flows (single phase reactors, i.e., laminar and turbulent flows).
- Flow through porous beds of solids (fixed bed reactors, i.e., continua of gas; three phase fixed beds, i.e., continua of gas through a porous fixed solid and trickling liquids on the solid surface).

- Granular flows (fluidized bed reactors, i.e., discrete particles in a continuous gas phase).
- Bubbly flows (two phase bubble columns, stirred tank reactors, waste water treatment, i.e., bubbles in liquid).
- Slurries (i.e., discrete particles in liquid).
- Complex multiphase flows (e.g., slurry bubble columns and stirred tank reactors i.e., bubbly flows in slurries; three phase fluidized beds, i.e., liquid droplets and particles in continuous gas) where many phases interact simultaneously.

In addition to the complex flow structure encountered in these reactor systems, typically one has to deal with component and energy transport within the individual phases and momentum, heat and mass transfer both between the various phases and to the external reactor walls. The interactions with chemical reaction kinetics are difficult both with respect to physical modeling and numerical solution approximations due to the very wide range of time and length scales involved.

## 3.2 Modeling Concepts for Multiphase Flow

The development of computational methods for multiphase flows was pioneered by Harlow and Welch [96], Hirt [106], Amsden and Harlow [6], Harlow and Amsden [97], Nichols and Hirt [155], Hirt and Nichols [108], and Hirt and Nichols [107] at the Los Alamos science laboratory in New Mexico. These methods were based on finite difference discretizations of the continuity and Navier-Stokes equations using velocity and pressure as the primitive variables. The early work on incompressible flows showed the need to use staggered grids and upwind differencing at high Reynolds numbers to obtain stable and physical solutions. The idea of solving the pressure from the continuity equation was accepted. In Europe the interest in computational fluid mechanics was initiated by the publication of a book by another pioneering group at Imperial College in London UK introducing the basic principles of the finite volume method and the wall function concept making primitive turbulence simulations feasible [86]. The work of Spalding on multiphase modeling and solution methods [207] [208] [209] [210] [211] at Imperial College is perhaps better known as he produced the very first commercial CFD program code (PHOENICS) for solving multiphase flow problems. An excellent review on models and numerical methods for multiphase flow has been presented by Stewart and Wendroff [212]. Similar reviews with emphasis on dilute gas-particle flows models have been published by Crowe [36], Crowe et al. [37] and Crowe et al. [38].

For multiphase systems a rough distinction can be made between systems with *separated flows* and those with *dispersed flows*, as sketched in Fig 3.1 (i.e., regime G versus regimes B, C and F). This classification is not only important

from a physical point of view, but also from a computational perspective since for each class different computational approaches are required.

In view of the multi-phase reactor flow structure characteristics summarized in sect 3.1, it is obvious that dispersed flow systems are dominating. For these flows roughly three different computational strategies can be distinguished based on the scales resolved by the model formulation:

1. The *Eulerian-Lagrangian models* for very dilute flows where small discrete particles are considered in the control volume formulating the governing microscopic model equations. For slightly denser flows different types of Eulerian and Lagrangian averaging procedures are applied deducing the more practical macroscopic model equations.
2. The *Eulerian-Eulerian multifluid models* for dense flows where a relatively large number of particles are considered determining a continuous phase in the control volume formulating the governing microscopic model equations. Different types of Eulerian averaging procedures are applied deducing the corresponding macroscopic model equations.
3. The *High resolution methods* for multiphase flows containing any number of particles where the model equations are formulated considering very small control- and averaging volumes. That is, the relative size of fluid particles with respect to the averaging volumes is large enough so the particles (not the interfaces!) can in principle be resolved [11, 245, 222, 223].

The modeling frameworks used are Eulerian, Lagrangian, or a combination of these concepts.

In the sequel the averaged *Eulerian- Lagrangian*, averaged *Eulerian-Eulerian*, and *High Resolution* methods are outlined.

### 3.2.1 Averaged Models

In this section the governing equations determining the averaged Eulerian-Lagrangian and the Eulerian - Eulerian modeling concepts are discussed.

#### Averaged Eulerian-Lagrangian Multi-Phase Models

For dispersed multiphase flows a Lagrangian description of the dispersed phase are advantageous in many practical situations. In this concept the individual particles are treated as rigid spheres (i.e., neglecting particle deformation and internal flows) being so small that they can be considered as point centers of mass in space. The translational motion<sup>1</sup> of the particle is governed by the Lagrangian form of Newton's second law [103, 148, 120, 38]:

<sup>1</sup> For non-spherical rigid particles the particle rotation may become important. This requires that an angular momentum equation for each particle has to be solved [38].

$$\frac{d}{dt}(m_p \mathbf{v}_p) = \mathbf{f}_{hp} + \mathbf{f}_p + \mathbf{f}_E + \mathbf{f}_G + \mathbf{f}_D + \mathbf{f}_V + \mathbf{f}_L + \mathbf{f}_B \quad (3.1)$$

where  $m_p = \rho_p V_p$  is the mass of the particle. Treating the dispersed phase as rigid spheres  $\rho_p$ ,  $V_p$  and  $m_p$  are constants in time. The forces listed on the RHS of (3.1) denote surface and body forces acting on the particle as considered in sect 5.2.  $\mathbf{f}_{hp}$  denotes the force due to the hydrostatic pressure,  $\mathbf{f}_p$  designates the force due to any external pressure gradients,  $\mathbf{f}_G$  denotes the body force due to gravity,  $\mathbf{f}_E$  denotes any body force created by external fields apart from gravity,  $\mathbf{f}_D$  is the steady drag force,  $\mathbf{f}_V$  is the virtual mass force,  $\mathbf{f}_L$  is the transversal lift force, and  $\mathbf{f}_B$  is the Basset history force.

The particle trajectory is calculated from the definition of the translational velocity of the center of mass of the particle:

$$\frac{d\mathbf{r}_p(t)}{dt} = \mathbf{v}_p(t, \mathbf{r}_p(t)) \quad (3.2)$$

A group of Euler-Lagrangian concepts are classified with respect to the complexity involved describing the interfacial coupling between the phases [66]. In a *one way coupled* system the particle volume loading is assumed to be small enough so that any effects that the presence of the dispersed phase may have on the continuous phase can be neglected. Thus, the local velocity of the continuous phase has a direct impact on the particle while the reverse is not true. For slightly denser systems the effects of the particles on the carrier fluid cannot be ignored and *two way coupling* is required. For dense systems *four way coupling* is necessary to take into account the additional particle-particle collision effects and any fluid turbulence modification caused by the particles.

When one way coupling is used, the Eulerian velocity field is computed independent of the particle tracking by a standard single-phase simulation. Thereafter, the trajectories of the individual particles are computed independently from one another. In contrast, a two way coupled Euler-Lagrangian simulation must solve the fully time dependent dispersed and continuous phase equations in an iterative manner. In a four way coupled system there are mutual (binary) interactions between the individual particles as well as a two way coupling between the dispersed and continuous phases, making the dynamic equations of all the phases strongly coupled so the iterative process becomes even more difficult to handle both regarding computational time and stability.

The complexity of the interfacial coupling depends mainly on the value of the dispersed phase volume fraction and the number of particles. That is, for a given value of the dispersed phase volume fraction the number of particles depends on the current particle size distribution. In practice, as a general rule of thumb, for very dilute flows (say  $\alpha_p < 10^{-6}$ ) containing very small particles a simple one-way coupling between the dispersed and continuous phases is assumed sufficient, while two way coupling is considered a reasonable approach for moderately dense dispersions (say  $\alpha_p \leq 10^{-3}$ ). For denser systems four-way coupling is recommended [38] [203]. However, the computational speed and storage capabilities of the present computers are limited so in

many practical simulations the number of particles are prohibitively large and the computational loads have to be reduced considering statistical methods. It is thus distinguished between direct Euler-Lagrangian models which are tracking all the particles simultaneously, and statistical model formulations computing an ensemble of representative particle trajectories only. For flows involving a relative small number of tiny particles (typically less than  $10^3$  particles) it is normally feasible to solve a set of Lagrangian equations for every element. However, if the number of tiny particles is large (typically more than  $10^4$  particles), a statistical approach is more practical. In such a description the total population is represented by a finite number of computational parcels, each of which represents a group of particles having the same properties. In this case caution is required as the Euler-Lagrange method is not fully consistent whenever the cloud of particles tracked constitutes a volume larger than the fluid parcel considered averaging the governing equations. Moreover, the number of computational parcels (samples) must be large enough so that the properties of the whole population are well represented.

For simulations involving two- and four way coupling the continuous phase is described by slightly modified single phase momentum equations formulated in the Eulerian framework [148, 152, 125, 130, 49, 50]. That is, the Eulerian momentum equations contain an additional interaction term denoting the sum of the individual interactions by each particle. These interaction terms are deduced based on Newton's 3. law (i.e., the individual drag forces experienced by the particles act with equal magnitude but in the opposite direction on the continuous phase, *actio=reactio*). It is noted the drag terms require the interpolation of the continuum phase velocity from the Eulerian grid to the local particle position.

The main advantage of the Eulerian-Lagrangian approach (i.e., compared to the alternative Euler-Euler model described in the next subsection) is its flexibility with respect to the incorporation of the microscopic transport phenomena. Particle dynamics can in principle be described in detail, a particle size distribution can easily be incorporated, direct particle-particle interactions can be accounted for as well as the hydrodynamic interaction between neighboring particles.

The major disadvantage of the Eulerian-Lagrangian approach is its relatively high computational load (i.e., again compared to the Eulerian-Eulerian approach). The flows in multiphase chemical reactors, for example, are usually very dense so it is not feasible to keep track of the high number of dispersed particles, thus only the statistical approach can be used [120]. Note also that all the averaged multiphase model formulations require appropriate closure laws for the interfacial transport of momentum. The correct form of these closure laws is still being debated. Rigorous derivations of the constitutive relations and model coefficients exist at best solely for idealized flow situations, whereas semi-empirical parameterizations and parameter fitting are used in practical applications in which the flow characteristics deviate largely from the idealized cases.

### Averaged Eulerian-Eulerian Multi-fluid Models

The averaged Eulerian-Eulerian multi-fluid model denotes the averaged mass and momentum conservation equations as formulated in an Eulerian frame of reference for both the dispersed and continuous phases describing the time-dependent motion. For multiphase isothermal systems involving laminar flow, the averaged conservation equations for mass and momentum are given by:

$$\frac{\partial}{\partial t}(\alpha_k \rho_k) + \nabla \cdot (\alpha_k \rho_k \mathbf{v}_k) = \Gamma_k \quad (3.3)$$

and

$$\begin{aligned} \frac{\partial}{\partial t}(\alpha_k \rho_k \mathbf{v}_k) + \nabla \cdot (\alpha_k \rho_k \mathbf{v}_k \mathbf{v}_k) = & -\alpha_k \nabla p - \nabla \cdot (\alpha_k \boldsymbol{\sigma}_k) \\ & + \mathbf{M}_{k,l} + \Gamma_k \mathbf{v}_I + S_k + \alpha_k \rho_k \mathbf{g}_k \end{aligned} \quad (3.4)$$

where  $\rho_k$ ,  $\mathbf{v}_k$ ,  $\alpha_k$  and  $\boldsymbol{\sigma}_k$  represent, respectively, the density, velocity, volume fraction and viscous stress tensor of the  $k$ -th phase,  $p$  the pressure,  $\Gamma_k$  a source term describing mass exchange between phase  $k$  and the other phases,  $\mathbf{M}_{k,l}$  the interface momentum exchange term between phase  $k$  and phase  $l$ , and  $S_k$  a momentum source term of phase  $k$  due to external forces other than gravity.

An advantage of the multi-fluid model is that in principle it can be used to compute any multiphase flow regime, provided that an adequate closure relation for the interfacial coupling terms are provided. Besides, when this model is applied to describe dense dispersed flows, the Euler-Euler approach is normally less computationally demanding than the alternative Euler-Lagrangian model simulations described in the previous sub-section. Nevertheless, at the same time, a severe disadvantage of a multi-fluid model is the need for empirical closure laws for the interfacial transport processes. The formulation of the Eulerian interfacial closure laws for both dilute and dense suspensions are based on simple average of the Lagrangian single particle relationships for idealized flows, thus the accuracy reflected by the Eulerian interfacial coupling terms is generally even poorer than for the corresponding Lagrangian models. Although promising results have been obtained in recent years, there are still no general agreement on the correct mathematical form of the net interfacial forces acting on the dispersed phase particles, nor on the net hydrodynamic and fluid-particle turbulence interactions. Prudence must also be shown to limit numerical diffusion in the Eulerian model fields, for instance, by applying at least second order schemes both in time and space instead of the first order schemes commonly applied in the commercial program codes [30, 79, 140, 201, 202, 123].

Notwithstanding, as the flow in most operating chemical reactors is dense, the Euler-Euler type of models has been found to represent a trade-off between accuracy and computational efforts for practical applications [120].

### 3.2.2 High Resolution Methods

The purpose of this section is to give an overview of the pertinent high resolution methods often referred in the literature on multiphase reactor modeling. These are: The Marker and Cell (MAC) method [96], the Simplified MAC method [6], the volume of fluid (VOF) method [108], the level set (LS) front capturing method [214, 20, 186], and finally the front tracking method<sup>2</sup> [227, 221].

Using the volume averaged Eulerian-Eulerian and Eulerian-Lagrangian multi-phase models the spatial resolution considered deriving the constitutive relations is generally coarse compared to the size of the particles. However, small-scale structures in the fluid and most likely also within the dispersed fluid particles may under specific conditions govern important phenomena encountered in multiphase reactors. In this context the physicochemical phenomena affecting the fluid particle coalescence and breakage rates are highlighted. In this area much fundamental work remains to be done.

In view of the discussion in sect 3.2.1, numerical methods that are designed to resolve the interfacial configurations in time and space are attractive elucidating the impacts of the microscopic phenomena on the macroscopic quantities. Such high resolution models are often divided into various classes due to their mathematical characteristics. One class of these methods can be recognized by the use of a single set of transport equations for the whole flow field [183, 224], *the whole field formulation*. Another useful formulation of the balance equations decomposes the problem into any number of bulk phase domains where the usual single phase transport equations holds, and the interfaces across which the physical quantities are required to have specific jumps. This alternative formulation is thus sometimes called *the jump-condition form*. In the latter approach each phase is treated separately. From another mathematical point of view the various methods for interface simulation can be divided into two classes, depending on whether a fixed or a moving grid is used in the bulk of the phases as well as to locate the interface and determining its orientation. In *fixed-grid* methods, there is a predefined grid that does not move with the interface. In this case the interface is making a 2D plane cut across the fixed 3D grid. In *moving-grid* methods, the interface is a boundary between two elements or sub-domains of the bulk grid. The interface then identifies, at some order of approximation, with element boundaries [183]. Lately, the complexity of the methods has increased tremendously, so a more compound characterization is frequently used to distinguish the different techniques. Hence, three important methods are named in accordance with the concepts used to identify the position and orientation of the interface, the grids adopted, as well as the frameworks employed formulating the governing

<sup>2</sup> It is noticed that after some re-evaluation Tryggvason and co-workers [228, 222] classified their front tracking method [227] as an embedded interface method, since it is best described as a hybrid between a front tracking and a front capturing method.

equations. In the early *particle methods* the flow fields of the bulk phases are solved on a fixed grid, and the position of the interface is identified using passive marker particles which are following the bulk flow. In the modern *front capturing* methods, the interface or front separating the bulk phases appears directly on a fixed grid as a region with steep gradients in the primary variables [228]. The *front tracking* methods are usually constructed by explicitly tracking the interface by use of a moving grid, a front, determining a material boundary between the fluid phases which are thus treated separately on a fixed grid [224] [228].

Following these classifications, the MAC, SMAC, VOF and LS techniques are all front capturing methods. The MAC and SMAC techniques are also referred to as particle methods. In the VOF and LS methods a similar marker function is used to identify the phases and reconstruct the interface, hence they are sometimes called *volume tracking* methods [111] [227]. The embedded interface (EI) method can be characterized as a hybrid between a front capturing and a front tracking technique [222] [224]. In this type of methods a stationary or fixed regular grid is used for the fluid flow, but the interface is tracked by a separate grid of lower dimension. This grid is usually called the front. However, unlike front tracking methods where each phase is treated separately, the embedded interface method follows most front capturing methods and treats all phases by a single set of governing equations for the whole flow field.

### The Marker and Cell Method (MAC)

The original MAC method of Harlow and Welch [96] was the first marker method developed aiming at numerical simulations of time-dependent *incompressible* flows with a free surface [111]. The MAC model constitutes the continuity and Navier-Stokes equations for the continuous fluid, and the Lagrangian equations of motion for the marker particles. As part of this method Harlow and Welch proposed a novel staggered grid arrangement of the dependent variables (i.e., separate grid cells were used for  $v_x$ ,  $v_y$  and  $p$  in 2D), which is essential for treating the pressure-velocity coupling in the Navier-Stokes equations and is still frequently used in fluid flow codes. On this grid the continuity and Navier-Stokes equations were discretized using a second order finite difference scheme in space, applying simple averaging for points where the variables are not defined in the grid. As in all incompressible flow codes, the continuity equation was treated implicitly. The velocity tendencies were approximated using a first order explicit scheme. Hence, all the terms in the Navier-Stokes equations are approximated using the velocity values at time level  $t_n$ .

In the first phase of the MAC algorithm the pressure at time level  $t_{n+1}$  is calculated, solving a Poisson equation in which the source term is a function of the velocity values at time level  $t_n$  only. Thereafter, the full Navier-Stokes equations are used to find the time level  $t_{n+1}$  velocities. It is emphasized that

the Poisson equation is derived by combining the implicit incompressibility condition with the momentum equations, thus the resulting momentum equations satisfy the continuity automatically. The pressure field obtained from this procedure is the true pressure instead of a pseudo pressure as used in later methods such as SIMPLE [160] and the typical fractional step projection algorithms [33]. In the second phase of the MAC method marker particles are scattered initially to identify the spatial region occupied by a single fluid with a free surface (facing vacuum) and to track the movement of the free surface during the simulation. The particles are transported in a Lagrangian manner along with the materials. Surfaces are then defined as lying at the boundary between regions with and without marker particles, hence the location and shape of the free surface can be found. However, the free surface stresses and the effects of the surface tension were ignored.

The simplified MAC method, the SMAC technique of Amsden and Harlow [6], denotes a three-stage fractional time step advancement procedure that resembles the technique suggested by Chorin [33]. In the SMAC procedure tentative estimates of the  $t_{n+1}$  time level velocity field is determined first using an explicit algorithm approximating the momentum equations, ensuring that the vorticity is correct but the continuity may not be satisfied. Then, a corrected pressure is calculated from the continuity in-balance in such a way as to preserve the vorticity but bringing the divergence to zero. Finally, an updated velocity is calculated from the new pressure estimate. The advantages of SMAC, compared to the original MAC method, are related to simpler program implementations, higher convergence rates, and more convenient boundary treatment. In the second phase of the algorithm the free surface treatment is still the same as for the original MAC method.

It appears that a method that defines fluid regions rather than interfaces offers the advantage of logical simplicity for situations involving interacting multiple free boundaries. While the marker particle method provides this simplicity, it suffers from a significant computer memory and storage demand. It also requires considerable computational efforts to move all the particle points to the new locations. Besides, no successful extensions of the MAC method which enable proper reconstruction of sharp interfaces seemed feasible. It was thus natural to seek an alternative interface capturing method which requires less computer resources but still provides sufficient accuracy. No real breakthrough in this respect was achieved till the use of marker particles was abandoned and a marker function advected by the flow was used instead [108].

### **The Volume of Fluid (VOF) Method**

In this sub-section the basis elements of the volume of fluid method are described. In general the VOF model is composed of a set of continuity and momentum equations, as well as a transport equation for the evolution of a

phase indicator function which is used to determine the location and orientation of the interface. We distinguish between the jump condition - and the whole field formulations of the method, in which both forms are based on a macroscopic view defining the interface as a 2D surface. The jump condition form is especially convenient for free-surface flow simulations, whereas the whole field formulation is commonly used for interfacial flow calculations in which the internal flow of all the phases are of interest.

A common feature for all the different formulations of the VOF model is that the location and orientation of the interface are defined through a volume fraction function. The evolution of this volume fraction function in time and space is determined by a scalar advection equation defined by:

$$\frac{D\alpha_1}{Dt} = \frac{\partial\alpha_1}{\partial t} + (\mathbf{v}_m \cdot \nabla)\alpha_1 = 0 \quad (3.5)$$

The propagation procedure contains the calculation of the volume fraction,  $\alpha_1$ , that represents the fractional volume of the cell occupied by fluid 1. A unit value of  $\alpha_1$  corresponds to a cell full of fluid 1, while a zero value indicates that the cell contains no fluid 1. Cells with  $\alpha_1$  values between zero and one must then contain an interface.

The VOF models thus require a proper numerical advection scheme to approximate the transport of the scalar function in an accurate manner avoiding numerical diffusion. Most VOF algorithms solve the problem of updating the volume fraction field,  $\alpha_1$ , given the fixed grid and the velocity field,  $\mathbf{v}_m$ , using a second order explicit discretization scheme in time and a higher (second) order discretization scheme on the flux form in space. In many program codes the fractional step or operator split method, which updates the volume fraction by advecting the interface along one spatial direction at the time, has been used [179, 180, 226, 92, 183, 123]. Thus, in 3D three consecutive reconstruction and convection steps are required per time step. In unsplit methods there is only one reconstruction step and the volume fluxes across the cell faces are computed simultaneously.

In the *jump-condition formulation* the physical problem is generally decomposed into  $k$  bulk phase domains where the continuity and momentum equations for isothermal incompressible flows holds, and at the interface between these domains boundary conditions are specified using the interface jump conditions. That is, across the interface some quantities are required to be continuous, while others are required to have specific jumps. The discontinuous (singular) momentum jump condition can be derived by use of the surface divergence theorem<sup>3</sup> (see e.g., [63] p 51; [26]). A rigorous derivation of the jump balances for the multi-fluid model is given in sect 3.3.

<sup>3</sup> The work of Brenner [26] also contains a micro-mechanical derivation of the differential equation of interface statics that clearly distinguish between micro-scale and macro-scale viewpoints. From thermodynamic analysis it is concluded that the surface tension manifests itself in the normal direction as a force that drives surfaces towards a minimum energy state characterized by a configuration of minimum surface area.

The governing equations for the jump condition form of the VOF method are thus defined by [164]:

$$\nabla \cdot \mathbf{v}_k = 0 \quad (3.6)$$

$$\frac{\partial \mathbf{v}_k}{\partial t} + \mathbf{v}_k \cdot \nabla \mathbf{v}_k = -\frac{1}{\rho_k} \nabla p_k + \nu_k \nabla^2 \mathbf{v}_k \quad (3.7)$$

The interface boundary conditions, i.e., the momentum jump conditions, are expressed as (i.e., no surface tension gradients are considered):

$$\sum_{k=1}^2 \mathbb{T}_k \cdot \mathbf{n}_k = 2\sigma_I H_I \mathbf{n}_I \quad (3.8)$$

This condition may be split into a normal stress condition:

$$\sum_{k=1}^2 \mathbf{n}_I \cdot \mathbb{T}_k \cdot \mathbf{n}_k = \mathbf{n}_I \cdot 2\sigma_I H_I \mathbf{n}_I \quad (3.9)$$

or

$$\sum_{k=1}^2 [(\mathbf{n}_I \cdot \mathbf{n}_k) p_k + \mathbf{n}_I \cdot \boldsymbol{\sigma}_k \cdot \mathbf{n}_k] = 2\sigma_I H_I \quad (3.10)$$

and a tangential stress condition:

$$\sum_{k=1}^2 [\mathbf{t}_k^{(k)} \cdot \boldsymbol{\sigma}_k \cdot \mathbf{n}_k]_I = 0 \quad (3.11)$$

where the vectors  $\mathbf{t}^{(k)}$  may be any set of  $d - 1$  independent tangent vectors to the interface  $A_I$ , and  $d$  is the dimension of space [132, 245, 183].

Performing macro-scale experiments it has been observed that the normal surface tension force induces higher normal stresses in the fluid on the concave side of the interface than on the other fluid on the convex side of the interface. In a micro-scale view we may say that this interfacial tension force is exerted by the interfacial material lying on the convex side of the surface upon the material lying on the concave side. The normal component of the surface force is thus frequently (not always!) defined positive into the mean curvature of the surface, in line with the physical observations. The direction of the normal component of the interface force given by (3.9) is determined by two factors, the interface normal unit vector  $\mathbf{n}_I$  which we have defined positive into the curvature<sup>4</sup>, and the mean curvature variable which we have chosen to define as an absolute value. That is, the variable used here determining the mean curvature of the surface ( $H_I = (\kappa_1 + \kappa_2)/2$ ) is consistent with the definition

<sup>4</sup> If we define  $\mathbf{n}_I$  positive out of the curvature instead, the curvature itself must be defined in a consistent manner with sign defining its orientation. Note that several variations of sign conventions may be chosen. The choice of conventions is to a large extent a matter of convenience.

given by Slattery [199] (p 1116) and by most classical textbooks on differential geometry.  $\kappa_1$  and  $\kappa_2$  denote the absolute values of the principal curvatures of the surface. The principal curvatures are the maximum and minimum values of the normal curvature. Another mode of expressing the principal curvatures  $\kappa_1$  and  $\kappa_2$  is in terms of the principal radii of curvature  $R_1$  and  $R_2$ :  $\kappa_1 = 1/R_1$  and  $\kappa_2 = 1/R_2$ . Finally, the mean curvature of a surface may also be expressed in terms of the variation of the unit surface normal  $\mathbf{n}_I$  with position in the surface. Thus, the mean surface curvature may be given by:  $H_I = -\frac{1}{2}\nabla \cdot \mathbf{n}_I$ .

*Free-surface flow* is a limiting case of flow with interfaces, in which the treatment of one of the phases is simplified. For instance, for some cases of gas-liquid flow, we may consider the pressure  $p_{\text{gas}}$  in the gas to depend only on time and not on space and the viscous stresses in the gas to be negligible. For such flows the jump condition formulation must be used, since the bulk momentum equation breaks down. The jump conditions become boundary conditions on the border of the liquid domain [245, 183]:

$$p_l + \mathbf{n}_l^{lg} \cdot \boldsymbol{\sigma}_l \cdot \mathbf{n}_l^{lg} = p_{\text{gas}} + 2\sigma_I H_I \quad (3.12)$$

and

$$\mathbf{t}_l^{lg,(k)} \cdot \boldsymbol{\sigma}_l \cdot \mathbf{n}_l^{lg} = 0 \quad (3.13)$$

The original VOF model designed for free surface flow simulations constitutes the mass and momentum conservation equations for incompressible fluids in the jump condition form [155, 108].

The pioneering SOLA-VOF method [108] evolved from the MAC/SMAC techniques [96, 6], thus the velocity and pressure fields are obtained in accordance with the SMAC method with only minor modifications. That is, in the SOLA codes the condition of a zero velocity divergence is still treated as an equation for the pressure but now, merely to save memory, the pressure-velocity coupling is solved iteratively adjusting the pressure and velocity simultaneously. The original SOLA-VOF method considers the motion of a fluid zone in vacuum. Therefore, no shear forces were present at the fluid surface. The effect of velocity gradients on the surface pressure was neglected, hence at the free surface a fixed boundary value was specified for the pressure,  $p_s(t)$ . Later on, the surface tension effects have been included with only minor additional efforts. The boundary pressure values were then determined from the surface tension force,  $p = p_s - 2H_I\sigma_I$ , where  $H_I$  is the mean curvature of the interface.

The SOLA-VOF method time integration consists of three basic steps:

- A tentative estimate of the velocity field in the new time-step is achieved by an explicit step, using the previous time level values for all advective, pressure and diffusive terms.
- Iterate on the pressure-velocity changes until the continuity is satisfied.
- The new fluid distribution is determined updating the volume fraction function.

The SOLA-VOF method has been used simulating bubble motion in liquid [12]. An important part of this simulation is the tracking of the free surface and determining boundary conditions on it. The simplified jump condition form of the VOF method was applicable because for large differences in liquid and gas densities and large Reynolds numbers the motion of the gas inside the bubble becomes unimportant and the pressure distribution in it can be assumed uniform constituting a free surface flow.

The alternative VOF models designed to describe stratified and dispersed flows with internal motions in all the phases are based on the *whole domain formulation*. The basis for this approach is a set of equations valid for the whole calculation domain, in which the governing mass and momentum balances are expressed as [132, 214, 32, 183, 164, 92, 222, 227]:

$$\nabla \cdot \mathbf{v}_m = 0 \quad (3.14)$$

$$\frac{\partial}{\partial t}(\rho \mathbf{v}_m) + \nabla \cdot (\rho \mathbf{v}_m \mathbf{v}_m) = -\nabla p_m - \nabla \cdot \boldsymbol{\sigma}_m + \rho \mathbf{g} + 2\sigma_I H_I^{12} \mathbf{n}_I \delta_I(\mathbf{r} - \mathbf{r}') \quad (3.15)$$

where  $\sigma_I$  is the surface tension,  $H_I$  the local mean curvature, and  $\mathbf{n}_I$  the normal to the interface pointing into phase 1.  $\delta_I(\mathbf{r} - \mathbf{r}')$  is a Dirac delta function that is zero everywhere except at the interface, where  $\mathbf{r} = \mathbf{r}'$ . The effect of the discontinuous (singular) surface tension force is to act as an additional forcing term in the direction normal to the fluid interface.

The density and viscosity occurring in these equations are defined as:

$$\rho_m = \alpha_1 \rho_1 + (1 - \alpha_1) \rho_2 \quad (3.16)$$

and

$$\mu_m = \alpha_1 \mu_1 + (1 - \alpha_1) \mu_2 \quad (3.17)$$

The model can be classified as a homogeneous mixture model which is formulated directly on the averaging scales (i.e., the control volume coincides with the averaging volume). It is further assumed that the relative velocity in the interface grid cells is zero ( $\mathbf{v}_r = 0$ ), and that all the scales of turbulence are resolved (i.e., in this respect this homogeneous model formulation resembles a direct numerical simulation).

The derivation of the given whole field formulation, introducing the Dirac delta function ( $\delta_I$ ) into the surface tension force relation to maintain the discontinuous (singular) nature of this term, is to a certain extent based on physical intuition rather than first principles (i.e., in mathematical terms this approach is strictly not characterized as a continuum formulation on the differential form). Chandrasekhar [31] (pp 430-433) derived a similar model formulation and argued that to some extent the whole field momentum equation can be obtained by a formal mathematical procedure. However, the fact that the equation involves  $\delta_I$ -functions means that to interpret the equation correctly at a point of discontinuity, we must integrate the equation, across the interface, over an infinitesimal volume element including the discontinuity.

In addition, we need to specify which quantities are continuous and which bounded at an interface between two fluids. Similar whole field formulations have been used and further discussed by Lafaurie et al. [132], Sussman et al. [214], Chang et al. [32], Popinet and Zaleski [164], Gueyffier et al. [92] and Tryggvason [222] [183].

Several numerical techniques have been proposed to approximate the singular interface terms occurring in the VOF model formulations. A convenient way to categorize these techniques is due to the physical images of the interface used as basis designing the numerical method.

It is so that interfacial physics are conventionally described adopting either a superficial 2D macroscopic - or a somewhat more physical 3D microscopic representation of the interface. Since an interface is generally observed and characterized on a macroscopic scale that is large relative to the thickness of the interfacial zone, an interface is often conveniently idealized as a 2D, discontinuous (singular) surface possessing a macroscopically defined location, configuration and orientation between a pair of contiguous, 3D, immiscible bulk fluid phases. The alternative representation of the interface is more fundamental denoting a microscopic, 3D interface structure, accounting for the diffuse transition region existing between the two fully developed bulk fluid phases on either side. These two models are mutually consistent describing the interface behavior on the macroscopic scales, but the microscopic view possibly affords a more rational means for deriving interfacial constitutive laws when the microscopic physics are known allowing for the deduction of macroscale models by proper averaging. Such approaches may also be valuable explaining the underlying mechanisms determining the 2D interfacial properties which are normally parameterized directly on the macroscopic scales.

The first generation methods that were proposed involved interface reconstruction and approximation of the singular interfacial term from the 2D interface properties. These models thus rely on a proper numerical procedure to locate the interface within the mesh based on the volume fraction field. The local curvature may then be calculated in each surface grid cell.

The first VOF methods were naturally developed for 2D problems. Such an interface is considered to be a continuous, piecewise smooth line and the problem of its reconstruction is that of finding an approximation to the section of the interface in each cell, by knowing only the volume fraction,  $\alpha_1$ , in that cell and in the neighboring ones. The simplest types of VOF-methods are the Simple Line Interface Calculation (SLIC) as used in the SOLA-VOF algorithm [108]. Typically, the reconstructed interface is made up of a sequence of segments aligned with the grid. The more accurate techniques attempt to fit the interface through piecewise linear segments. These techniques are known as the Piecewise Linear Interface Construction (PLIC) methods [8] [179]. The key part of the reconstruction step is the determination of the location of the segment. This is equivalent to the determination of the unit normal vector,  $\mathbf{n}_I$ , to the segment. This kind of VOF methods can be generalized to three dimensions with little conceptual difficulty [245, 183].

The second fairly modern group of methods introduces (of numerical reasons) a 3D continuous surface force (CSF) or a 3D continuum surface stress (CSS) acting locally within the whole transition region constituting a meso-scale interface. Notice that since we are primarily interested in the interfacial forces, the latter group of techniques were used approximating the surface effects without actually reconstructing the interface.

The pioneering work, determining the basis for all the techniques in this group, was performed by Brackbill et al. [25] developing the *the continuum surface force method (CSF)* for modeling the surface tension effects on fluid motion. In the CSF model the interface discontinuity (singular) term has been smoothed to avoid numerical instabilities, and the surface tension force becomes replaced by a continuous formulation. In other words, the discontinuous (singular) surface tension force determined from a macro-scale point of view, is reformulated considering a more diffuse transition region (inspired by microscopic physics and the micro-scale point of view) that is not necessarily aligned with the grid. Brackbill et al. [25] replaced the discontinuous characteristic function by a smooth variation of fluid volume fraction  $\tilde{\alpha}_1$  between 0 and 1 over a distance of order  $h$ , where  $h$  is a length comparable to the resolution afforded by a computational mesh with spacing  $\Delta V = h^3$ . This replaces the jump condition boundary-value problem at the interface by an approximate continuous model and mimics the problem specification in a numerical calculation, where one specifies the values of  $\alpha_1$  at grid points and interpolates between. The interface where the fluid changes from fluid 1 to fluid 2 discontinuously is replaced by a continuous transition, and the surface tension force acts everywhere within the transition region. The CSF method thus eliminates the need for interface construction, simplifies the calculation of the surface tension effects, enables accurate modeling of two- and three-dimensional fluid flows driven by surface forces, and imposes no modeling restrictions on the number, complexity, or dynamic evolution of fluid interfaces having surface tension. A restriction related to this numerical approximation is of course that we are introducing a smoothed representation (i.e., in itself relying on the assumption that the interface is limited to an explicitly defined finite thickness) of the physical phenomena which are occurring at very small scales. In addition, the Eulerian discretization schemes applied approximating (3.5) are diffusive and smear out the  $\alpha_k$  profile and thus the interface. Therefore, the main difficulty in using these methods is to maintain a sharp interface between the different phases.

It might be worth mentioning that, as this numerical discretization technique replaces the conventional 2D interface specification with a 3D description, the interface reformulation makes it convenient to introduce an alternative notation for the interface characteristics as well expressing the curvature with sign defining its orientation. The reformulated surface force is then defined positive acting on one of the fluid fields, in accordance with the choice of unit normal sign convention. A common practice is to define the unit normal vector positive pointing out of phase 1. A constraint therefore is to make sure

that consistent sign conventions are adopted for the normal unit vector and the orientation of the surface curvature (as the unit normal vector pointing out of phase 1 may at some instants be oriented into the curvature and at other instants out of the curvature, since the surface orientation may change with time).

On the meso-scopic scale the smoothly varying volume fraction  $\tilde{\alpha}_1$  is constructed as follows:

$$\tilde{\alpha}_1(\mathbf{r}) = \frac{1}{\Delta V} \int_{\Delta V} \alpha_1(\mathbf{r}') \delta_I(\mathbf{r} - \mathbf{r}') dv' \quad (3.18)$$

where  $\delta_I(\mathbf{r} - \mathbf{r}')$  is a smooth integration kernel (i.e., an interpolation function like the B-spline [25]). We let  $\delta_I(\mathbf{r} - \mathbf{r}') \rightarrow \delta_I$  as the grid spacing  $h \rightarrow 0$ .

Further,  $\tilde{\alpha}_1$ , is differentiable because  $\delta_I$  is, hence:

$$\nabla \tilde{\alpha}_1(\mathbf{r}) = \frac{1}{\Delta V} \int_{\Delta V} \alpha_1(\mathbf{r}') \nabla \delta_I(\mathbf{r} - \mathbf{r}') dv' \quad (3.19)$$

Using Gauss' theorem and noting that  $\alpha_1$  is constant within each fluid, Brackbill et al [25] converted the volume integral into an integral over the interface  $\delta A_I$ :

$$\nabla \tilde{\alpha}_1(\mathbf{r}) = \frac{[\alpha_1]}{\Delta V} \int_{\delta A_I} \mathbf{n}_1 \delta_I(\mathbf{r} - \mathbf{r}'; \epsilon) da' = \frac{1}{\Delta V} \int_{\delta A_I} \mathbf{n}_1 \delta_I(\mathbf{r} - \mathbf{r}'; \epsilon) da' \quad (3.20)$$

where  $[\alpha_1]$  is the jump in the volume fraction variable, i.e.,  $[\alpha_1] = 1$ .

This relation can be used calculating a weighted mean of the surface normal. This approximation of the normal converges to the true normal of the interface as the smoothing kernel becomes more concentrated on the interface. Several alternative high-order kernels have been discussed by Aleinov and Puckett [5].

The volume averaged force formulation then yields:

$$\begin{aligned} \mathbf{F}_{I,1} &= \frac{1}{\Delta V} \int_{\Delta V} 2\mathbf{n}_1 \sigma_I \delta_I H_I dv' \approx \frac{2}{\Delta V} \int_{\Delta V} \sigma_I \nabla \tilde{\alpha}_1 H_I dv' \approx \frac{2}{\Delta V} \sigma_I \nabla \tilde{\alpha}_1 H_I \int_{\Delta V} dv' \\ &\approx 2\sigma_I \nabla \tilde{\alpha}_1 H_I \end{aligned} \quad (3.21)$$

Brackbill et al [25] also found it very difficult to use the classical expressions calculating the mean curvature of any 3D surface in a numerical model, since they require an algorithm determining the principal curvatures being the maximum and minimum values of the normal curvature (see e.g., [63], pp 44-47). To improve on this limitation of the VOF model, Brackbill et al [25] suggested an alternative and computationally much simpler expression

for the mean curvature,  $H_I$ , which could be used determining the net surface force per unit area,  $\mathbf{F}_{I,1}$ , on any element of the surface  $A_I$ .

The mean curvature is expressed in terms of the unit normal pointing into phase 1:

$$H_I = -\frac{1}{2}\nabla_I \cdot \mathbf{n}_1 \quad (3.22)$$

The unit normal vector is determined from the spatial distribution of the volume fraction of the phase 1 field:

$$\mathbf{n}_1 = -\frac{\nabla\tilde{\alpha}_1}{|\nabla\tilde{\alpha}_1|} \quad (3.23)$$

The normal component of the volume force, that is non-zero only within the phase transition regions, can then be expressed in terms of the volume fraction gradient [25]:

$$\mathbf{F}_{I,1} \approx 2[-\nabla\tilde{\alpha}_1]\sigma_I\left(-\frac{1}{2}\right)\nabla \cdot \left[-\frac{\nabla\tilde{\alpha}_1}{|\nabla\tilde{\alpha}_1|}\right] \approx -\nabla\tilde{\alpha}_1\sigma_I\nabla \cdot \left[\frac{\nabla\tilde{\alpha}_1}{|\nabla\tilde{\alpha}_1|}\right] \quad (3.24)$$

where Chang et al. [32] stated that the color function is defined so that the normal vector points in the outward direction<sup>5</sup>.

The momentum equations in the whole field formulation can also be rewritten in a momentum conserving form [132] [183] [92], defining a 3D capillary pressure tensor

$$\mathbf{T}'_I = -\sigma_I(\mathbf{e} - \mathbf{n}_I\mathbf{n}_I)\delta_I \quad (3.25)$$

where  $\mathbf{e}$  is the unit tensor  $\delta_{ij}$ . To enable a physical interpretation of this tensor, the particular normal vector used in this relation is required to give meaning outside the surface  $A_I$ . Using this quantity the capillary force can be represented as the divergence of  $\mathbf{T}'_I$ ,

$$\nabla \cdot \mathbf{T}'_I = \sigma_I\nabla \cdot \{(\mathbf{e} - \mathbf{n}_I\mathbf{n}_I)\delta_I\} = \sigma_I H_I \mathbf{n}_I \delta_I \quad (3.26)$$

The momentum equation (3.15) can then be cast in a conservative form

$$\frac{\partial}{\partial t}(\rho\mathbf{v}) = -\nabla p - \nabla \cdot (\rho\mathbf{v}\mathbf{v} + \boldsymbol{\sigma} + \mathbf{T}'_I) + \rho\mathbf{g} \quad (3.27)$$

For this reason the surface tension force can be interpreted as a correction to the momentum stress tensor, i.e., it represents a continuum surface stress (CSS) tensor.

<sup>5</sup> In the case of two immiscible fluids, a characteristic phase indicator function,  $X_I$ , may be defined that is equal to 1 in one of the phases and 0 in the other phase. Then  $X_I$  and  $\mathbf{n}_I$  are related by  $\mathbf{n}_I\delta_I = \nabla X_I$  analogue to the relations used in standard volume averaging procedures [54] [164]. An averaged representation of this relation may be given as  $\frac{1}{\Delta V} \int_{\delta A_I} \mathbf{n}_I \delta_I da' = -\nabla\tilde{\alpha}_1$

This model formulation constitutes a volume conserving (i.e., exact only when  $\rho_1 = \rho_2$ ) variant of the VOF algorithm. The model is considered relatively simple to implement in a program code, computationally efficient and easy to parallelize. Both the 2D and 3D CSS simulations performed well without using the smoothed function (3.18) calculating the normal vector and the curvature, indicating that the CSS method may be more stable than the original CSF technique. The volume conservative algorithm can thus use the volume fraction itself which varies sharply over one or two grid cells across the interface. If (3.18) is used instead, the CSS methods amounts to a variant of the basic CSF method.

The CSF and CSS based versions of the VOF method have been used to calculate improved estimates of the single particle drag and lift coefficients and for simulating breakage and coalescence of dispersed flows containing a few fluid particles [49, 218, 50, 141, 18].

A third variant of the VOF method calculates the interface tension force by the CSS method and perform an independent PLIC reconstruction of the interface to improve the design of the advection schemes. In this way the tailored advection discretization schemes prevent numerical smoothing of the interface [149].

In reactor technology the VOF methods have become very popular for such simulations because they are reasonable accurate, relative simple to implement and much faster than the more accurate level set and front tracking methods (discussed shortly). However, it is noted that none of the VOF approaches are useful in predicting the rebound outcome of colliding fluid particles because the surface tension force or stress approximation fails to predict the complex physics involved in these cases. That is, when two interfaces from two different particles are placed in the same grid cell, the particles might automatically merge or coalesce as a numerical mode due to the low order local approximation of the interface normal in combination with an insufficient interface resolution. Hence, this approach cannot be used in coalescence - rebound outcome studies determining a physical coalescence criterion. However, by use of an in-house code<sup>6</sup> based on the CSS-PLIC approach Gotaas et al [88] simulated binary droplet collisions under conditions that gave permanent coalescence, and coalescence followed by reflexive or stretching separation. It was concluded that the VOF predictions were in excellent agreement with experimental data in most cases. A typical collision map for the air/water system is given in Fig 3.2. Nevertheless, for head-on collisions the simulated outcomes for operating conditions on the border between the coalescence and reflexive separation regimes did not always coincide with experimental observations, as a coalescence outcome prevailed somewhat into the experimental reflexive separation regime. It was revealed that in these odd cases the in-house code is not

---

<sup>6</sup> These droplet-droplet collisions are simulationed by use of an in-house VOF code called FS3D developed at University of Stuttgart and Institut für Thermodynamik der Luft-und Raumfahrt, ITLR

able to conserve the thin liquid film which is present when the droplets are at their maximum deformation. Instead the film ruptures and this in turn results in a unphysical loss of kinetic energy so that the final separation observed in the experimental analysis doesn't occur. It is mentioned that this film rupture problem did not occur simulating the coalescence outcome conditions. Gotaas et al [88] did use a model resolution of  $1 \mu\text{m}$  which represents the present computer capacities at the University in Trondheim. The VOF code might thus become inaccurate due to insufficient numerical resolution or, more severely, because the macroscopic VOF model breaks down when such a film or interface becomes very thin as the basic model concept is based on the continuum hypothesis. In such flow situations the liquid film might reach scales much less than the scales on which short range molecular forces act to attract or repel interface molecules. These mechanisms are normally considered significant on scales of the order of  $10\text{-}40 \text{ nm}$  and are thus generally not taken into account by the VOF model. However, the given threshold is very uncertain as the molecular forces are largely affected by the fluid properties and the presence of surfactants [93, 183, 158]. In this area much fundamental work remains to be done.

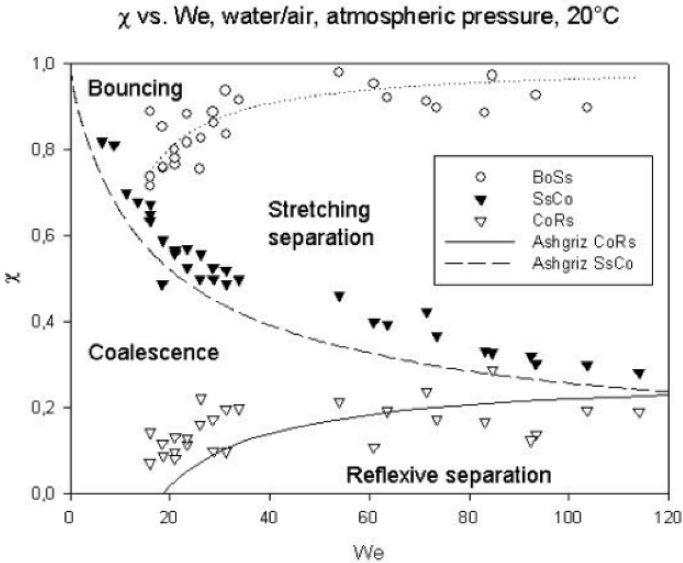


**Fig. 3.2.** Typical droplet-droplet collision outcome map with four regimes [88]; Bouncing (Bo), Coalescence (Co), Stretching Separation (Ss), and Reflexive Separation (Rs).  $\chi$  denotes the impact factor, and  $We$  is the Weber number.

The VOF technique thus works best analyzing flow situations where the macroscopic interface motion may be nearly independent on the microscopic

interface physics. For example, many analyzes on stratified or free-surface flows may be performed successfully by such a model.

It is also noted that the VOF model concept is not primarily intended for multicomponent reactive flow analyzes, so no interfacial heat- and mass transfer fluxes or any variations in the surface tension are usually considered.

### The Level Set (LS) Method

In the previous sub-section we did learn that the VOF algorithms locate the interface by tracking a marker function,  $\alpha_k$ , which corresponds to the local volume fraction of the phase  $k$ . At an interface,  $\alpha_k$  goes between 0 and 1, hence identifies its location. As  $\alpha_k$  is discontinuous at an interface, a practical computation method smears out the  $\alpha_k$  profile and thus the location of the interface. This numerical problem, leading to a thickening of the interface, led researchers to propose an extension of the VOF technique. These extended VOF algorithms, introducing a modified interface tracking function, are called level set (LS) methods. The level set algorithms are defined with a fixed interface thickness. These LS models can therefore be implemented and solved using the same numerical difference techniques for the advection terms as those used for the VOF technique, without allowing the interface to smear out in space.

The design of the LS methods may be sketched as follows. To determine the exact location of the interface, we utilize some inherent properties of a mathematical function characterized as a distance function. In this context a distance function,  $d$ , denotes the signed normal distance to the interface. This type of functions satisfies:

$$|\nabla d| = 1 \quad \text{for } \mathbf{r} \in \Omega \quad \text{with } d = 0 \quad \text{for } \mathbf{r} \in \Gamma \quad (3.28)$$

and  $\nabla d$  determines a unit normal vector at the interface,  $\Gamma$ .

If such a function did exist, the surface tension force could be represented by [214] [186] (p.151):

$$\mathbf{F}_I = 2\mathbf{n}\sigma_I\delta(d)H_I \quad (3.29)$$

In this formulation the surface tension term is considered to be a force concentrated on the interface,  $\Gamma$ .

In practice, a mathematical function that behave like a distance function over the whole calculation domain as the interface evolves in space is very difficult to define. Therefore, as a compromise, we may utilize the so-called zero level set of a smooth function,  $\varphi$ , that behaves like a distance function locally in the vicinity of the interface. The novel idea of the level set methodology is thus to introduce a higher dimensional smooth function  $\varphi(\mathbf{r}, t = 0)$  defined as:

$$\varphi(\mathbf{r}, t = 0) = \pm d \quad (3.30)$$

where  $\mathbf{r}$  is a point in space and  $d$  is still the shortest distance from  $\mathbf{r}$  to the initial interface. The sign of  $\varphi(\mathbf{r}, t = 0)$  indicates whether  $\mathbf{r}$  is inside or

outside the regions closed by the initial interface (i.e., for two-phase flow the positive sign denotes one of the phases, whereas the negative sign denotes the transition interface zone).

As pointed out by Sussman et al [214] and Chang et al. [32], the surface tension force can be cast into the level set formulation:

$$\mathbf{F}_I = 2\mathbf{n}\sigma_I\delta(d)H_I = 2\nabla\varphi\sigma_I\delta(\varphi)H_I(\varphi) \tag{3.31}$$

This relation is true only for the ideal case where  $\varphi$  remains a distance function, as:  $\mathbf{n} = (\frac{\nabla\varphi}{|\nabla\varphi|})_{\varphi=0}$ ,  $H_I = \nabla \cdot (\frac{\nabla\varphi}{|\nabla\varphi|})_{\varphi=0}$ , and  $|\nabla\varphi|_{\varphi=0} = 1$ .

The derivation of this relation can apparently be found in Chang et al [32], in which it was also shown (using rather complex mathematics) that this formulation admits solutions that are consistent with the boundary condition applied in the jump-condition formulation.

In a similar manner as for the VOF technique, the evolution of the interface is determined solving a transport equation for the level set function. That is, instead of solving equation (3.5), the following equation is solved [179]:

$$\frac{D\varphi}{Dt} = \frac{\partial\varphi}{\partial t} + (\mathbf{v} \cdot \nabla)\varphi = 0 \tag{3.32}$$

The level set equation (3.32) describes the evolution of the distance function as the interface moves along its normal vector field with normal speed  $F = \mathbf{n} \cdot \mathbf{v}$ . By use of the relation determining the normal vector pointing into the positive phase,  $\mathbf{n} = \frac{\nabla\varphi}{|\nabla\varphi|}$ , we may rewrite the equation as:

$$\frac{D\varphi}{Dt} = \frac{\partial\varphi}{\partial t} + (\mathbf{v} \cdot \nabla)\varphi = \frac{\partial\varphi}{\partial t} + \mathbf{v} \cdot \frac{\nabla\varphi}{|\nabla\varphi|} |\nabla\varphi| = \frac{\partial\varphi}{\partial t} + \mathbf{v} \cdot \mathbf{n} |\nabla\varphi| = \frac{\partial\varphi}{\partial t} + F |\nabla\varphi| = 0 \tag{3.33}$$

Both forms of the transport equation have been used describing the evolution of the interface. The choice of formulation seems to be a matter of convenience.

Since the density and viscosity are constant in each fluid, they take two different values depending on the sign of  $\varphi$ , we may write:

$$\rho(\varphi) = \rho_2 + (\rho_1 - \rho_2)H(\varphi) \tag{3.34}$$

and

$$\mu(\varphi) = \mu_2 + (\mu_1 - \mu_2)H(\varphi) \tag{3.35}$$

where  $H(\varphi)$  is the Heaviside function given by ([215], p. 273):

$$H(\varphi) = \begin{cases} 0 & \text{if } \varphi < 0 \\ \frac{1}{2} & \text{if } \varphi = 0 \\ 1 & \text{if } \varphi > 0. \end{cases} \tag{3.36}$$

In practice, however, a smoothed level set function is defined so that  $|\nabla\varphi| = 1$  when  $|\varphi| \leq \epsilon$  due to the finite resolution applied in numerical simulations smearing the front out on several grid cells.

To alleviate further numerical problems due to sharp changes in some of the physical variables across the front and also because of the numerical difficulties presented by the Dirac delta function in the surface tension term, the interface is defined having a fixed thickness that is proportional to the spatial mesh. This allows us to smooth the functions across the interface and replace the Dirac delta function with a smoothed delta function  $\delta_\epsilon$ . In other words, we maintain a fixed thickness of the interface within the LS approach.

The approximated delta function is defined as (e.g., [214]):

$$\delta_\epsilon(\varphi) = \begin{cases} \frac{1}{2}(1 + \cos(\pi\varphi/\epsilon))/\epsilon & \text{if } |\varphi| < \epsilon, \\ 0 & \text{Otherwise.} \end{cases} \quad (3.37)$$

where  $\epsilon$  denotes the prescribed *thickness* of the interface (e.g., [214] used  $\epsilon = \frac{3}{2}\Delta x$ ).

The Heaviside function is also replaced with a smoothed Heaviside function  $H_\epsilon(\varphi)$  defined as ([215], p. 274):

$$H_\epsilon(\varphi) = \begin{cases} 0 & \text{if } \varphi < -\epsilon \\ \frac{1}{2}[1 + \frac{\varphi}{\epsilon} + \frac{1}{\pi}\sin(\frac{\pi\varphi}{\epsilon})] & \text{if } \varphi \leq \epsilon \\ 1 & \text{if } \varphi > \epsilon. \end{cases} \quad (3.38)$$

The smoothed delta function is then given by  $\delta_\epsilon = \frac{dH_\epsilon}{d\varphi}$ , whereas the thickness of the interface can be approximated by  $2\epsilon/|\nabla\varphi|$ .

The smoothed density and viscosity are now given as:

$$\rho_\epsilon(\varphi) = \rho_2 + (\rho_1 - \rho_2)H_\epsilon(\varphi) \quad (3.39)$$

and

$$\mu_\epsilon(\varphi) = \mu_2 + (\mu_1 - \mu_2)H_\epsilon(\varphi), \quad (3.40)$$

respectively.

The surface tension force is represented by [32] [214] [215]:

$$\mathbf{F}_I = 2\mathbf{n}\sigma_I\delta(d)H_I \approx 2\nabla\varphi\sigma_I\delta_\epsilon(\varphi)H_I(\varphi) \quad (3.41)$$

We can derive this force relation from the CSF model of Brackbill et al. [25] if we let the smoothed color function,  $\nabla\tilde{\alpha}_l$ , be given as a smoothed Heaviside function  $H_\epsilon$ . This implies that<sup>7</sup>:  $\nabla\tilde{\alpha}_l = \delta_\epsilon(\varphi)\nabla\varphi$ .

The mean curvature,  $H_I$ , of the zero level set is then found from:

$$H_I(\varphi) = -\frac{1}{2}\nabla \cdot \mathbf{n}(\varphi) = -\frac{1}{2}\nabla \cdot \left( \frac{\nabla\varphi}{|\nabla\varphi|} \right) \quad (3.42)$$

where the last term is given by appropriate finite difference approximations (e.g., [214]; [186], p 58).

<sup>7</sup> The reformulation is based on the relationship:  $\nabla H_\epsilon(\varphi) = \frac{\partial H_\epsilon}{\partial x} + \frac{\partial H_\epsilon}{\partial y} + \frac{\partial H_\epsilon}{\partial z} = \frac{\partial H_\epsilon}{\partial \varphi} \left( \frac{\partial \varphi}{\partial x} + \frac{\partial \varphi}{\partial y} + \frac{\partial \varphi}{\partial z} \right) = \frac{\partial H_\epsilon}{\partial \varphi} \nabla\varphi$

So, it is clear that we can choose  $\varphi(\mathbf{r}, t = 0)$  to be a distance function. However, under the evolution of  $\varphi(\mathbf{r}, t)$ , solving (3.32) or (3.33), it will not necessarily remain a distance function (i.e.,  $|\nabla\varphi| \neq 1$ ). A procedure is needed to reinitialize the level set function at each time step to retain its distance function properties without changing its level set. Sussman and Smereka ([215], p 275) suggested that this can be achieved by solving the following PDE:

$$\frac{\partial d}{\partial t'} = \text{sign}(\varphi)(1 - |\nabla d|) \quad (3.43)$$

with initial conditions  $d(\mathbf{r}, 0) = \varphi(\mathbf{r})$ , where

$$\text{sign}(\varphi) = \begin{cases} -1 & \text{if } \varphi < 0 \\ 0 & \text{if } \varphi = 0 \\ 1 & \text{if } \varphi > 0 \end{cases} \quad (3.44)$$

and  $t'$  is an artificial time.

The steady state solution of this PDE are distance functions. Furthermore, when  $\text{sign}(0) = 0$ ,  $d(\mathbf{r}, t')$  has the same zero level set as  $\varphi$ . Therefore, Sussman and Smereka [215] solved this PDE to steady state and then replaced  $\varphi(\mathbf{r})$  by  $d(\mathbf{r}, t'_{\text{steady}})$ .

They also found that  $\varphi$  only needs to be a distance function close to the front. Therefore, it is not necessary to solve the PDE to steady state over the whole domain. We may then locate the interface as the local areas within the calculation domain where  $|d| \leq \epsilon$ , and we iterate on  $d$  until  $|\nabla d| = 1$  near the interface. The front will then have a uniform thickness, as this solution corresponds to  $|\nabla\varphi| = 1$  when  $|\varphi| \leq \epsilon$ .

Compared to the VOF method, the level set methods offer interface identification through the use of a distance function which is continuous everywhere in the field. The solution of the field equation for this function then identify the interface location, the zero level sets. Furthermore, this level set function reflects advantageous numerical properties being a smooth function. In other words, the main difference between the VOF and the level set methods is related to the properties of the improved marker function formulation. Advantages of the level-set method are that, unlike the VOF method, the interface is represented as a continuous surface. Furthermore, there is no need for the complex interface reconstruction algorithms. The improved function formulation also reduces the main disadvantage of the VOF method, that is, it does not smear out the location of the interface. However, according to Rider et al. [179], level set methods although conceptually appealing suffer from a number of detriments. First among these is the lack of volume (mass) conservation. Computational cost is also an issue. For these reasons the LS method has not (yet) become as popular as the VOF method, analyzing dispersed flows in chemical reactors. However, the LS method has been used to describe the detailed flow around individual fluid particles and thus may contribute to improve our understanding of these phenomena.

Pan and Suga [159], for example, performed 3D dynamic simulations of binary droplets collisions for cases of different Weber numbers and impact parameters. The systems used are water drops in air and tetradecane drops in nitrogen at atmospheric conditions. The bulk fluids are considered incompressible. The simulations cover the four major regimes of binary collision: bouncing, coalescence, reflexive separation, and stretching separation. The method predicted the outcomes of both head on and off-center collisions in all the regimes for both systems in excellent agreement with the available experimental data. However, contrary to the work of Gotaas et al [88] in which a VOF method was used to investigate the capacity of accurately predicting the flow regime transition lines as sketched in Fig 3.2, Pan and Suga focused on operating conditions in the bulk of the different flow regimes. Nevertheless, from the results presented in their papers it can be seen that both the VOF and LS methods have problems to conserve the thin liquid films created when the drops collide and a reflexive separation outcome is expected at the transition areas between the coalescence and reflexive separation regimes. On the other hand, it is emphasized that the LS model captures the bouncing collision outcome even though the model in principle can predict automatic coalescence in cases when the gas film becomes extremely thin before rupture due to the computational model limitations which are similar to those of the VOF method. No physical coalescence criterion is prescribed in any of these models. At first sight, it may thus seem like the inherent interface force discretization and the *continuous* level set function reinitialization procedure give slightly more accurate predictions of the collision outcome than the VOF method. However, at lower Weber numbers than that of the bouncing collision, the LS model fails to predict the expected coalescence regime seen in the experimental data. The simulated results might thus suggest that the mechanism of bouncing collision is governed by macroscopic dynamics, whereas the collision regime of coalescence after minor deformation may be related to microscopic phenomena. Typical errors in mass conservation were reported to be less than 5% by volume.

The LS models are apparently more accurate than the computationally cheaper VOF methods, but the LS models still suffer from not having the possibility to prescribe a physical coalescence criterion instead of relying on the numerical mode outcome of the discretization approximations.

In reactor engineering the level-set method is generally too computationally demanding for direct applications to industrial scale units. The level set method can be applied for about the same cases as the VOF method and works best analyzing flows where the macroscopic interface motion is independent of the microscopic phenomena. These concepts are not primarily intended for multi-component reactive flows, so no interfacial heat- and mass transfer fluxes or any variations in the surface tension are normally considered.

### The Embedded Interface (EI) Method

In this sub-section the *embedded interface method* (frequently referred to as a front tracking method) developed for direct numerical simulations of viscous multi-fluid flows is outlined and discussed. The unsteady model is based on the whole field formulation in which a sharp interface separates immiscible fluids, thus the different phases are treated as one fluid with variable material properties. Therefore, equations (3.14) and (3.15) account for both the differences in the material properties of the different phases as well as surface tension effects at the phase boundary. The bulk fluids are incompressible. The numerical surface tension force approximation used is consistent with the VOF and LS techniques [222] [32], hence the major novelty of the embedded interface method is in the way the density and viscosity fields are updated when the fluids and the interface evolve in time and space.

Tryggvason and co-workers [227, 228, 127, 128, 170, 224, 71, 72, 225] solve the Navier-Stokes equations using a projection method very similar to the MAC method [96]. The interface is tracked explicitly by connected marker points. In the solution procedure a fixed structured grid is used for the transport equations, and a moving grid of lower dimension marks the boundary between the bulk phases. This moving grid is called the *front*.

The properties of each fluid particle remain constant, thus a set of advection equations can be set up expressing these constraints:

$$\frac{D\rho}{Dt} = 0 \quad (3.45)$$

$$\frac{D\mu}{Dt} = 0 \quad (3.46)$$

These relations are referred to as the EOSs for the material properties [228, 158, 95, 224].

However, an essential feature of the EI method is that the fluid properties are not advected solving the above EOSs directly. Instead, the interface between the different fluids is moved. This is achieved by explicit tracking points on the interface between the two fluids in a Lagrangian manner [227]:

$$\frac{d\mathbf{r}_I}{dt} = \mathbf{v}_I \quad (3.47)$$

After the discrete points on the interface are moved with the flow, the continuous interface is reconstructed by connecting these points by appropriate linear or triangular elements (i.e., a finite element technique). It is noticed that explicit front tracking is generally more complex than the advection of a marker function as in the VOF and LS methods, nevertheless this technique is also considered more accurate [224].

Seeing that the momentum equations are solved on a fixed grid but the surface tension is found on the front, it is necessary to convert the interface quantity that exists at the front to a grid value. It follows that at each

time step information must be passed between the moving Lagrangian interface and the stationary Eulerian grid by interpolation since the Lagrangian interface points do not necessarily coincide with the Eulerian grid points. This is done by a method known as the immersed boundary technique [228] [127]. With this technique, the interface is approximated by a smooth distribution function that is used to distribute the interface terms over grid points nearest to the interface. In a similar manner, this function is used to interpolate the variables from the stationary grid to the interface. In particular, an indicator function,  $I(\mathbf{r})$ , that is 1 inside the fluid particle and 0 in the continuous fluid, is constructed from the known position of the interface. In fact, the jump in the indicator function across the interface is distributed to the fixed grid points nearest to the interface using the distribution function. The immersed boundary technique then generates a grid-gradient field  $\nabla I(\mathbf{r}) = \int_{\text{Font}} \delta_I(\mathbf{r} - \mathbf{r}_{\text{Font}}) \mathbf{n}_{\text{Font}} dA_{\text{Font}}$  which is zero except in a thin zone near the interface. This transition zone has a finite thickness which is fixed during the simulation. The indicator function (i.e., a Heaviside function) is then obtained by solving a Poisson equation [71]:

$$\nabla^2 I = \nabla \cdot \nabla I = \nabla \cdot \int_{\text{Font}} \delta_I(\mathbf{r} - \mathbf{r}_{\text{Font}}) \mathbf{n}_{\text{Font}} dA_{\text{Font}} \quad (3.48)$$

To relate the gradient to the  $\delta_I$  function marking the interface, it is found convenient to express the indicator function in terms of an integral over the product of 1D  $\delta_I$  functions [224].

Since the property variables are discontinuous across the interface, one may expect either excessive numerical diffusion or problems with oscillations around the jump if no special treatment is used at the front. To avoid these problems local smoothing of the variables across the discontinuous interface is introduced. This is accomplished by use of the smoothed indicator function calculating the fluid properties at each point on the fixed grid by:

$$\mu(\mathbf{r}) = \mu_c + (\mu_d - \mu_c) \mathbf{I}(\mathbf{r}) \quad (3.49)$$

$$\rho(\mathbf{r}) = \rho_c + (\rho_d - \rho_c) \mathbf{I}(\mathbf{r}) \quad (3.50)$$

Notice that these relations imply that the material properties in each phase have a smooth incompressible extension into the other phase.

The net effects of the immersed boundary technique are that in the interface transition zone the fluid properties change smoothly from the value on one side of the interface to the value on the other side. The artificial interface thickness is fixed as a function of the mesh size applied to provide stability and smoothness, and it does not change during the calculations. Therefore no numerical diffusion is present. The finite thickness also serves to position the interface more accurately on the grid. The surface tension force (normal contribution only) is then calculated estimating the mean curvature based on geometric information obtained from the restructured interface.

Describing collisions between fluid particles using the EI model, the fluid film drainage and particle deformation processes will be described in detail. However, after the fluid within the film between the particles has drained until there are only the thickness of the two interfaces left (i.e., one interface grid for each particle), the particles move together being influenced by the interfaces, until the particles eventually rebound. Coalescence of the two particles is only allowed if an empirical closure, i.e., a *coalescence model*, is used together with a numerical procedure for merging the two moving grids. To accommodate topology changes in the model, the interface is artificially reconnected when two points come closer than a specified small distance. The threshold is chosen rather arbitrarily since there exist no reliable model for the critical interface thickness. So far Tryggvason and coworkers have either used a given drainage time or a specified thickness of the film as criteria for coalescence. It occurs that an advantage of front tracking is that it is possible to control the distance at which interfaces merge and study the effect of varying coalescence criteria, unlike front capturing methods where there is no active control over topological changes.

In the EI method the interface is explicitly tracked by connected marker points, so such changes in topology are accounted for by changing the connectivity of the points in an appropriate way. Tryggvason and coworkers state that this numerical operation is very time consuming and represents the greatest disadvantage of front-tracking methods. However, in methods like VOF and LS which identify the phase boundary by a marker function, topology changes take place automatically whenever two interfaces, or different parts of the same interface, come closer than about one grid cell spacing. Coalescence is apparently related to the drainage of the fluid between the coalescing interfaces in a complex manner, and a method that is simply connecting parts of the interface that are close certainly give an incorrect solution because these films supposedly rupture as a result of short-range molecular forces. Therefore, to calculate the draining of these films prior to rupture a prohibitive fine grid resolution is required. However, performing EI model simulations using feasible grid resolutions Tryggvason and co-workers have confirmed that the flow in the film between two colliding droplets is commonly so simple that the drainage process can be accomplished by analytical lubrication models [93, 199].

The embedded interface method has not been applied describing industrial scale chemical reactor operation. However, the EI method has been applied examining numerous multi-fluid phenomena relevant to reactor analysis. Unverdi and Tryggvason [228, 228] and Tryggvason et al [221] investigated the interactions of two 2D and 3D bubbles. The impact of variations in viscosity and the effects of surface tension were illustrated. They further stated that the model can be used to inspect the validity of the classical model simplifications (e.g., inviscidness, Stokes flow, two-dimensionality or axisymmetry) and to confirm the applicability of these idealizations for specific problems. The motion of a few 2D bubbles at low Reynolds numbers was simulated by

Esmaeeli and Tryggvason [70], indicating that in such bubbly flows there is an inverse energy cascade. Esmaeeli et al. [69] and Ervin and Tryggvason [68] computed the rise of a single bubble in a vertical shear flow and showed that the lift force changes sign when the bubble deforms. Nobari et al [158] and Han and Tryggvason [95] simulated binary collisions of axisymmetric drops, predicting the breakage after initial coalescence in reasonable agreement with experimental data. Juric and Tryggvason [127] developed a front tracking or EI method for the solidification of pure materials and used it to examine the growth of dendrites. The EI model has been extended and used to elucidate the motion of a premixed flame by Qian et al. [170]. The EI method has also been extended to simulate boiling flows [128, 71, 72, 225].

The variety of applications clearly demonstrate that the EI method has the potential of resolving many problem aspects in reactor technology. However, it is noted that the EI concept is not primarily intended for multicomponent reactive flow analyzes, but still interfacial heat- and mass transfer fluxes and variations in the surface tension have been considered [224]. Nevertheless, in most cases the bulk phases are considered incompressible.

No direct model intercomparisons between the EI, VOF and LS methods have been performed, so it is difficult to evaluate which method are preferable regarding computational costs and accuracy for different applications. However, it seems that the VOF method is faster but suffers from lower accuracy. The LS methods are usually more accurate than VOF methods, but suffers from higher computational costs and problems regarding mass conservation. The EI method is quite accurate, but is probably the most time consuming one comparing these methods. However, although the LS model predictions can be very good for fluid particle collision simulations, the EI method has the advantage of controlling the coalescence process explicitly provided that a proper coalescence criterion is available. Notwithstanding, the VOF technique is still generally preferred in engineering research and industrial practice, whereas the LS and EI methods are regarded as academic research tools.

### 3.3 Basic Principles and Derivation of Multi-Fluid Models

In the following chapters on multiphase modeling we first present the underlying principles used developing the microscopic two-fluid model. Then we introduce the averaging theorems and learned about the detailed mathematical manipulations required formulating the macroscopic multi-fluid transport equations. The concepts of averaging are employed to overcome the scale disparity dealing with the complex flow regimes occurring in multiphase chemical reactors.

An introductory summary of the basic ideas underlying the conventional single phase modeling concepts is given to emphasize the inherent limitations reflected by the different continuum model formulations [173]. It is generally

accepted that solids, liquids, and gases are composed of distinct molecules or atoms. Therefore, in single phase flow there is numerous modeling approaches available that can be taken depending upon the application in question. These include the atomistic simulation of the behavior at the molecular level, kinetic theory, local instantaneous continuum modeling and averaged macro-scale modeling. It is further noticed that the evolution of these modeling approaches starts with a particle formulation at the atomic level. Then, by Maxwellian averaging over systems of particles, a local instant continuum model in the form of partial differential equations (PDEs) can be derived from kinetic theory, as shown in chap. 2. In the context of kinetic theory it is essential to point out the conceptual ideas that each macroscopic point in the continuum description represents a mean value for a large number of discrete molecules (although the exact number is not explicitly specified). In the particular cases in which very fine scales are considered as basis for the PDE model formulation (e.g., for micro channel analysis), the basic continuum assumption might become questionable as each macroscopic point only represent a limited number of molecules so no reliable weighted mean values can be determined as the representativity of the distribution function is questionable. The macro-scale model is obtained by still another averaging of the local instantaneous continuum model. These modeling approaches applied to single phase fluid dynamics yield the Boltzmann equation, the Navier-Stokes equations, and the Reynolds averaged Navier-Stokes equations, respectively.

In most engineering models materials are conveniently treated as continuous media instead of individual molecules or atoms. This is because engineers are mostly concerned about the averaged features of material, represented by primitive variables like density, velocity, pressure, temperature, and mass fractions, which vary continuously in space and time. The only approach that is numerically tractable even for the single phase case, considering the current state of computer capability, is the averaged macro-scale model. In kinetic theory the macroscopic transport equations that correspond to the local instantaneous conservation laws are derived in terms of moments of invariant quantities by use of the Boltzmann equation. It is noted that the local instantaneous equations deduced from kinetic theory are inherently closed, so no additional constitutive relations are required. In continuum mechanics, on the other hand, the governing equations are formulated directly on macroscopic scales adopting the continuum hypothesis. In this approach closure laws are required, as the inherent characteristics of the molecular or atomic movement are ignored in this framework. In fluid mechanics the Newton's law of viscosity, the Fourier's law of conduction, and the Fick's law of diffusion constitute the closure laws for momentum, energy, and mass, respectively. Nevertheless, introducing the constitutive relations in the continuum mechanical approach, the resulting local instantaneous equations deduced from the two concepts coincide. It is thus apparent that the given PDEs in both formulations are not exact, they are merely very useful approximations. However, the partial differential descriptions typically break down at very short length

and time scales in the sense that the underlying model assumptions are violated so no physical solution can be ensured. The length and time scales below which continuum descriptions become inaccurate are on the order of the characteristic lengths and times associated with the micro-structure of the medium. Only for lengths and times much larger than characteristic molecular lengths and times do the Navier-Stokes equations provide a quantitatively correct description of fluid dynamic behavior. In single phase flow the importance of rarefaction effects are frequently assessed by the magnitude of the *Knudsen number* which is defined as the ratio of the mean free path of the molecules to the particle diameter  $Kn = \lambda/d_p$ . If the Knudsen number is large, say  $Kn \gg 10^{-3}$ , the flow can not be regarded as a continuum [38]. Moreover, in kinetic theory a similar Knudsen number is defined in terms of some characteristic macroscopic dimension and measures the relative importance of collisions and particle streaming, and this dimensionless group must be small if the Chapman-Enskog expansion is to be valid [77].

In general, the differential description is useful for processes where there is a wide separation of scales between the smallest macroscopic scales of interest and the microscopic scales associated with the internal structure of the fluid. If the micro-scales were always of molecular magnitude then questions of scale separation would seldom arise. But, in many of the models employed for engineering purposes, the characteristic scales of the internal structure being described are themselves macroscopic in nature. In such situations the desired separation between the calculated and modeled scales is much less clear cut, and one must be careful not to attribute quantitative significance to any predicted solution features with scales comparable to the internal micro-scale. When a continuum description is pushed to far, i.e. applied on scales too small, one can only hope that such inaccuracies are not catastrophic in nature.

The local instant behavior of Newtonian multiphase flow is considered accurately described by the continuum equations with the addition of interfaces across which appropriate jump conditions hold. Nevertheless, just as for single phase flows, the application of the local instantaneous equations to large-scale engineering problems is numerically intractable. Therefore, to obtain macro-scale solutions we must resort to further averaging and seek solutions for the average values of the system dependent variables. In essence there are three approaches to averaging the continuous phase equations, these are time, volume and ensemble averaging. Considering time and volume averaging a central point is that the length and time scales associated with the detailed flow structures are not always widely separated from the macroscopic length and time scales on which one would like to predict the average behavior. Therefore, the continuum description rely on proper separation of scales. However, proper separation of scales rarely occurs in multiphase flows, as the scales of the internal structures over which we desire to average may be comparable to the macroscopic scales over which the desired averaged quantities vary. This is precisely the sort of situation in which a simple partial differential description may be expected to break down as the field variables are not

sufficiently smooth to be considered continuous functions [173] [112]. Thus, in these particular flow regimes, it is somewhat doubtful whether the PDEs for the averaged flow variables can accurately predict the rate of change on the length and time scales of interest. The second averaging operation also introduces the need for additional closure models, and the details of the averaging methods have been the subjects of debate. It is important to note that the characteristic lengths and times over which these averages are performed clearly define lower limits for the scales over which the equations accurately represent differential variations. Nevertheless, the resulting PDEs can still be accurately solved to ensure reliable predictions of the physics inherently accounted for by the closed set of model equations, since the numerical approximations and the physical closure models are not coupled. Of course, the resulting numerical solution doesn't reflect any small scale physics which was not taken into account formulating the closure laws.

Considering multiphase LES simulations, on the other hand, the situation is very different as the numerical representation and the physical model can be directly coupled. To perform a LES simulation a differential model is formulated, discretized and implemented in a program code. In this particular case careful considerations are required as the length and time scales of the eventual discretization may not be compatible with those in which the interfacial model closures were based. Besides, in many situations of single phase simulations having wide spread of scales the discretization errors reflected by the finite difference and finite volume methods can be separately analyzed and dealt with by conventional techniques such as convergence and truncation-error analysis based on the Taylor series expansions. That is, from a mathematical point of view, the PDEs resulting from the volume averaging or filtering procedures are based on the continuous function assumption, and thus they can in principle be solved with finer and finer numerical resolution in time and space intending to improve the accuracy of the numerical representation of the proposed PDEs. On the other hand, from a physical point of view, if the numerical resolution becomes finer than the cut off filtering scales (in time and space) determining the basis for the interfacial closure formulation, severe physical interpretation problems occur (strictly not defined). Proper model validation can then only be performed on scales larger than the filtered scales. In multiphase flow one is thus hardly ever in a position to keep on refining the resolution until the solution no longer changes (i.e., basically because no adaptive interfacial closures are available), and one must seek other means of obtaining the most accurate results possible under the circumstances. In any case, there is clearly no point in examining the behavior of the system in the limit of infinitely fine resolution when the interfacial closures do not apply on scales less than those considered in their parameterization.

Therefore, ensemble averaging is frequently used intending to avoid the shortcomings of time and volume averaging, as ensemble averaging is not limited by any volume or time constraints [38] [59] (i.e., still limited by the continuum hypothesis adopted formulating the underlying single phase equa-

tions). Ensemble averaging is based on the probability of the flow field being in a particular configuration at a given time. That is, theoretically an ensemble denotes an infinite set of replicas of the same system that are identical in all respects apart from being in different microscopic multiphase system states at a particular instant in time. Nevertheless, in a more practical view a useful conceptualization of the ensemble average assumes that the flow is deterministic, but the randomness arises through uncertainty in the initial conditions itself, the physical transport coefficients or the empirical model parameters and the chaotic behavior of the evolving flow [58] [59]. Let a realization of the flow denote a possible motion that could have happened. An ensemble average is then taken over many different flow realizations that have the same initial and boundary conditions. In the limit that the number of realizations is going to infinity, the ensemble average approaches the ensemble mean which may be a function of both time and space. In numerical weather prediction a similar ensemble average is computed by averaging over many different forecasts for the same domain and time period, but starting from slightly different initial conditions or using different numerical models or parameterizations. In this sense an ensemble average is a generalization of the simple principle of adding the values of the variables for each realization, and dividing by the number of observations. It is further emphasized that ensemble averaging does not require that any representative volume contains a large number of particles in any given realization [58]. Besides, the interfacial coupling terms can in principle be considered representative for an ensemble of identical multiphase system states, thus they do not restrict the ensemble average in terms of a representative volume in their fundamental form. Nevertheless, the interface closures adopted in all continuum model formulations are conveniently derived per unit volume based on simple volume averaging considering one single particle in a relatively large volume of the continuous phase so that the particle can be considered a point mass. The interfacial constitutive relations may also be parameterized in terms of the relevant time scales for the problem in question. Therefore, these characteristic length and time scales obviously define limitations for the scales over which the closed ensemble average equations accurately represent differential variations. In effect all the closed macro-scale model formulations reflect similar restrictions for their applications.

In a conceptual interpretation the time and volume averages are representative measures for one realization only, so these averages rely on an implicit assumption that the statistics are the same for any one realization [58]. In a theoretical sense the ensemble average is thus considered fundamental, and time and space averages can only be used to approximate the ensemble average in special situations. That is, the ergodic hypothesis states that for statistically stationary and homogeneous flows the ensemble, time and volume averages are identical, otherwise the ergodic hypothesis is to be considered a rough approximation [105]. On the other hand, the experimental data used for model validation is normally obtained in a time or volume averaged framework [216]. Moreover, the accuracy limitations in performing experiments and

the implicit assumptions related to the time and volume averaging techniques make the link between purely theoretical model considerations and practical applications difficult. In most applications it is thus referred to the ergodic hypothesis assuming that experimental data determined using any averaging procedure can be used validating any model formulation. However, such a model validation procedure is only approximate (at best) and indicates the accuracy that can be achieved using any of these modeling concepts.

Based on the considerations presented above, it was found necessary to carry out a critical evaluation of the various model formulations available aiming to achieve a proper description of the multiphase flow regimes occurring in chemical reactors.

### 3.3.1 Local Instantaneous Transport Equations

In this section we apply the *control volume approach* to derive the governing equations for two-phase flows in the Eulerian framework. The mathematical formulation of the local instantaneous equations starts with the integral balance principle written for a fixed control volume (CV), through which the fluid flows, containing two continuous phases separated by an interface across which the physical properties are discontinuous and may jump. The integral equations are then transformed by means of the Leibniz rule and the Gauss theorems to obtain a sum of two volume integrals and a surface integral. The volume integrals lead to the local instantaneous PDEs valid in each of the continuous phases whereas the surface integral denotes the local instantaneous jump conditions valid on the interface only. Literature cited [185, 9, 13, 42, 112, 43, 47, 41, 26, 197, 48, 24, 198, 197, 118, 199, 63, 25, 146, 147, 67, 40, 82].

By definition a phase interface is the region in space separating two immiscible phases in which the system properties differ from those of the contiguous phases. When a physical phase interface is investigated on a sufficiently fine length scale, the transition zone is characterized as a highly inhomogeneous 3D region over which rapid changes and steep normal gradients in the continuum mechanical fields and material properties occur [82]. Several modeling approaches have been proposed describing the interfacial transport processes, yet the results are not in complete agreement. Basically, the physical nature of such a phase interface allows two different views to be taken formulating continuum models for the interface region. Hence the interface region is either regarded as a *microscopic* 3D diffuse transition region or a *macroscopic* 2D dividing surface as observed over an experimental length scale that is large relative to the thickness of the physical interfacial transition zone.

From an academic viewpoint one might assume that on microscopic scales the system properties are continuous functions across the interface region as well as throughout the bulk phases, the phase interface might be regarded as a *3D region with finite thickness*. Applying the general balance principle to a material CV containing two phases, in a similar manner as we did for a

continuous 3D media in chap 1, the governing balance equations can be cast in the generic form:

$$\frac{D}{Dt} \int_{V(t)} (\rho\psi) dv = - \int_{A(t)} \mathbf{J} \cdot \mathbf{n} da + \int_{V(t)} \sum_c \rho_c \phi_c dv \quad (3.51)$$

where  $\mathbf{n}$  is the outward directed normal unit vector to the surface of the control volume  $A$ ,  $D/Dt$  is the substantial time derivative,  $\mathbf{v}$  is the velocity,  $\rho$  is the density,  $\psi$  is the conserved quantity,  $\mathbf{J}$  is the diffusive flux and  $\phi_c$  is the source term. The given system balance can be transformed into an Eulerian control volume balance formulation by use of an extended form of the generalized transport theorem, which takes the discontinuous interface into consideration, in a similar manner as described in chap 1 for single phase flow. When the specific field variables indicated in Table 1.1 are substituted, the familiar local instantaneous balance equations are obtained governing the transport of mixture mass, species mass, mixture momentum, mixture energy, temperature and entropy etc. for the continuous media.

Although it is appealing from a scientific point of view to regard the interface as a 3D region of finite thickness, the computational difficulties involved considering the implicit numerical grid resolution requirements make the application of this concept infeasible.

From a practical viewpoint instrumentation size limitations enable only indirect observations of the interfacial properties through their influence upon the surrounding bulk phases. Therefore, in engineering applications an interface has traditionally been viewed as a *singular 2D dividing surface* separating two immiscible homogeneous bulk phases<sup>8</sup>. In this concept the cumulative effects of the interface upon the adjoining phases are taken into account by the assignment to the dividing surface of any excess properties not accounted for by the homogeneous bulk phases [1]. Adopting these ideas describing two-phase flows it is essential to note that the conventional single phase differential balance equations can be applied to each bulk phase up to the interface, but not across it. Therefore, in the presence of a discontinuous interface the governing equations must be supplemented by appropriate boundary conditions or *jump conditions* at the interface. This is accomplished by writing separate conservation and constitutive equations for each of the two bulk fluids and the dividing surface.

Furthermore, adopting the macro scale viewpoint several alternative modeling approaches are proposed in the literature for deriving the jump conditions. Moreover, coinciding results are achieved from independent thermodynamical and mechanical derivations, since the surface tension is equivalently defined from energy and force considerations [150]. The relevant concepts can be briefly summarized as follows. In a series of papers a general balance principle in which the interface is represented by a 2D dividing surface of no thickness

---

<sup>8</sup> The 2D dividing surface model was originally proposed by Gibbs [83] (p 219).

was formulated for a generic quantity associated with a two-phase material body [185, 194, 42, 41, 197, 48, 199, 200]. A second group of interface model formulations applied a very similar balance principle in which the interface was represented by a 3D region over an infinitesimal CV of negligible thickness which was fixed to and spans the interface [135]. Ishii [112] derived an alternative interfacial balance equation based on a CV analysis, introducing surface mean properties which were averaged over a thin layer in the neighborhood of the interface. A third group of methods is proposed deriving the macro-scale interfacial conservation and constitutive equations from knowledge of the underlying micro-scale equations and thermodynamic principles [151, 150, 26, 63, 146, 147, 82]. Matched asymptotic expansion techniques are used for systematically reconciling the macro- and micro scale views.

In this book the generic balance equations for discontinuous 3D media are formulated adopting the generic surface excess concept [83, 1, 63]. The physical interface view adopted admits the use of two disparate length scales, so the physical variables are decomposed into the sum of a bulk phase quantity and an interface quantity. The bulk quantities represent the macro scale view that we are not resolving distances of the order of the thickness of the interfacial region. In the micro scale viewpoint, on the other hand, a more physical field density becomes apparent which is fully continuous throughout  $dV$ . It is only in the vicinity of the fluid interface that differences between the interface and bulk properties emerge, and these differences are attributable to large normal gradients in  $\psi$  existing within the interfacial transition zone. Thus, as a means of reconciling the usual discontinuous macro-scale view of fluid interfaces with the more physical continuous micro-scale view, the residual difference is assigned to the macroscopic surface  $A_I$  as representing the total surface excess amount of the property  $\psi$  in  $A_I$ . Therefore, the generic area field density  $\psi_I$  is connected to the excess amount of the property per unit area at the points of the 2D interfacial continuum.

Consider a joint material control volume (CV) containing two phases with phase index  $k(= 1, 2)$  and an interface with area  $A_I(t)$  moving with the velocity  $\mathbf{v}_I$ , as illustrated in Fig. 3.3. The macroscopic volume occupied by the CV is denoted by  $V = V_1(t) + V_2(t)$ , and  $A = A_1(t) + A_2(t)$  is the closed macroscopic surface of the CV. Hence it follows that for each phase  $k$  separately, an arbitrary non-material control volume  $V_k(t)$  bounded by a closed surface having partly an external CV surface  $A_k(t)$  and partly an interface surface  $A_I(t)$  is employed.  $l_I(t)$  is the line formed by the intersection of  $A_I(t)$  with  $A(t)$ . It is emphasized that the interface is not a material surface because mass transfer may occur between the volumes  $V_1(t)$  and  $V_2(t)$  through  $A_I(t)$ .

With the use of the excess property relations, the first term on the LHS of (3.51) is written as:

$$\frac{D}{Dt} \int_{V(t)} (\rho\psi) dv = \frac{d}{dt} \int_{V_1(t)+V_2(t)} (\rho\psi) dv + \frac{d_I}{dt} \int_{A_I(t)} (\rho_I\psi_I) da \quad (3.52)$$

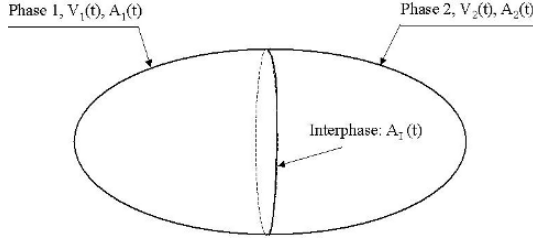


**Fig. 3.3.** A material control volume containing two phases with a moving non-material interface.

in which the quantities  $\psi$ ,  $\rho$  and  $\mathbf{v}$  are assumed to be continuously differentiable in the regions  $V_1(t)$  and  $V_2(t)$ , and the surface quantities  $\psi_I$ ,  $\rho_I$  and  $\mathbf{v}_I$  are assumed to be continuously differentiable on the surface  $A_I(t)$ . Since in general the dividing surface  $A_I(t)$  is non-material, the regions  $V_1(t)$  and  $V_2(t)$  are not material.

The molecular (diffusive) fluxes of the property  $\psi$  through the boundaries of the macroscopically discontinuous CV depicted by  $V$  are rewritten in a similar manner, in which we are led to define the surface excess lineal flux of  $\psi$  through  $A_I$  [63]:

$$-\int_{A(t)} \mathbf{J} \cdot \mathbf{n} da = -\int_{A_1(t)+A_2(t)} \mathbf{J} \cdot \mathbf{n} da - \int_{l_I(t)} \boldsymbol{\varphi}_I \cdot \mathbf{N}_I dl \quad (3.53)$$

The volume source relation adopts the form:

$$\int_{V(t)} \sum_c \rho_c \phi_c dv = \int_{V_1(t)+V_2(t)} \sum_c \rho_c \phi_c dv + \int_{A_I(t)} \sum_c \rho_{I,c} \phi_{I,c} da \quad (3.54)$$

By substituting these macro-scale excess property relations (3.52)- (3.54) into the generic microscopic transport equation (3.51), the macroscopic balance principle, as applied to the overall material CV for an arbitrary property  $\psi$  (per unit mass) associated with a two-phase system, is by definition expressed as a balance of the rate of change of the property within the two volumes  $V_k(t)$  ( $k = 1, 2$ ) and the interface  $A_I(t)$ , net inflow fluxes by diffusion through  $A_k(t)$ , production within the bulk volumes  $dV_k$  and the interface surface  $A_I(t)$ , and net inflow fluxes through the interface  $A_I$  (per unit length of line). The resulting generic macroscopic balance equation is expressed on the form<sup>9</sup>:

<sup>9</sup> The notation used in the generic equation is strictly only valid for scalar properties. In the particular case when a vector property is considered the tensor order of the corresponding variables is understood to be adjusted accordingly. Hence, the quantities  $\psi_k$ ,  $\phi_k$  and  $\phi_I$  may be vectors or scalars, while  $\mathbf{J}_k$  and  $\boldsymbol{\varphi}_I$  may be vectors, or second order tensors.

$$\begin{aligned}
\sum_{k=1}^2 \left( \frac{d}{dt} \int_{V_k(t)} (\rho_k \psi_k) dv \right) + \frac{d_I}{dt} \int_{A_I(t)} \rho_I \psi_I da = - \sum_{k=1}^2 \int_{A_k(t)} \mathbf{J}_k \cdot \mathbf{n}_k da \\
+ \sum_{k=1}^2 \int_{V_k(t)} \sum_c \rho_{k,c} \phi_{k,c} dv + \int_{A_I(t)} \sum_c \rho_{I,c} \phi_{I,c} da - \oint_{l_I(t)} \boldsymbol{\varphi}_I \cdot \mathbf{N}_I dl
\end{aligned} \tag{3.55}$$

in which  $t$  is the time coordinate,  $A(t)$  is the closed surface bounding the whole body,  $l_I(t)$  is the line formed by the intersection of  $A_I(t)$  with  $A(t)$ ,  $\rho_k \psi_k$  is the density of the property per unit volume within the bulk phase  $k$ ,  $\frac{d_I}{dt}$  is the surface material derivative following a multi-component surface particle moving with the mass-averaged surface velocity  $\mathbf{v}_I$ ,  $\rho_I \psi_I$  is the density of the quantity per unit area on  $A_I(t)$ ,  $\rho_I$  is the mass density per unit area on  $A_I(t)$ ,  $\mathbf{J}_k$  is the diffusive flux of the quantity  $\psi_k$  (per unit area) through  $A_k(t)$ ,  $\mathbf{n}_k$  is the unit vector normal and outward directed with respect to the closed surfaces constituted by  $A_k(t)$ ,  $\phi_{k,c}$  is the rate of production of the quantity  $\psi_k$  per unit mass at each point within the bulk phases,  $\phi_{I,c}$  is the rate of production of the quantity  $\psi_k$  per unit mass at each point on  $A_I$ , and  $\boldsymbol{\varphi}_I$  is the flux of the quantity  $\psi_I$  (per unit length of line) through  $l_I(t)$ ,  $\mathbf{N}_I$  is the unit vector normal to  $l_I(t)$  that is both tangent to and outwardly directed with respect to  $A_I(t)$ .

For the purpose of describing interfacial transport phenomena it is convenient to describe the 2D surface geometry using a 3D reference system with origin located outside the surface in the CV in which the surface is embedded (e.g., [63], chap. 3; [217], sect. 11.4; [62], pp. 486-492). This framework is named *extrinsic* and connects the 2D surface and the ambient 3D bulk phases. The *intrinsic* perspective of an observer located internally within the surface is then used as a component part providing a simpler description of the interface in terms of a 2D representation which is independent of the 3D space in which the interface is embedded. Due to the mathematical complexity involved, the notation of the 2D differential geometry is examined briefly. A more comprehensive introduction can be found in, for instance, references [63, 217, 25, 129, 1, 62, 94, 199, 241, 232, 29].

Let us consider surfaces in a Cartesian frame, whence these results can be generalized to any set of three coordinates  $\mathbf{x}$  in an arbitrary coordinate system fixed in space. A surface in 3D space can generally be defined in several different ways. Explicitly,  $z = F(x, y)$ , implicitly,  $f(x, y, z) = 0$  or parametrically by defining a set of parametric equations of the form  $x = x(\zeta, \eta)$ ,  $y = y(\zeta, \eta)$ ,  $z = z(\zeta, \eta)$  which contain two independent parameters  $\zeta, \eta$  called surface coordinates or curvilinear coordinates of a point on the surface. In this coordinate system a curve on the surface is defined by a relation  $f(\zeta, \eta) = 0$  between the curvilinear coordinates. By eliminating the parameters  $\zeta, \eta$  one can derive

the implicit form of the surface and by solving for  $z$  one obtains the explicit form of the surface. Moreover, using the parametric form of the surface we can define the position vector to a point on the surface which is then represented in terms of the parameters  $\zeta, \eta$  as  $\mathbf{r}_I = \mathbf{r}(x(\zeta, \eta), y(\zeta, \eta), z(\zeta, \eta))$ . The curves  $\mathbf{r}(\zeta, c_2)$  and  $\mathbf{r}(c_1, \eta)$  with  $c_1, c_2$  constants define two surface curves called coordinate curves, which intersect at the surface coordinates  $(c_1, c_2)$ . The family of curves with equally spaced constant values define a surface coordinate grid system. The vectors  $\mathbf{a}_\zeta = \frac{\partial \mathbf{r}}{\partial \zeta}$  and  $\mathbf{a}_\eta = \frac{\partial \mathbf{r}}{\partial \eta}$  evaluated at the surface coordinates  $(c_1, c_2)$  on the surface, are tangent vectors to the coordinate curves through the point and basis vectors for any vector lying in the surface. The position vector is then expressed in the form  $\mathbf{r}_I = x(\zeta, \eta)\mathbf{e}_x + y(\zeta, \eta)\mathbf{e}_y + z(\zeta, \eta)\mathbf{e}_z$ . From the basis vectors we may construct a unit normal vector to the surface at the point  $P$  by calculating the cross product of the tangent vectors  $\mathbf{n}_I(\zeta, \eta) = \mathbf{a}_\zeta \times \mathbf{a}_\eta / |\mathbf{a}_\zeta \times \mathbf{a}_\eta|$ , denoting a right handed system of coordinates. In this frame a vector  $\mathbf{c}$  associated with points in the surface can be expressed by  $\mathbf{c} = c^\alpha \mathbf{a}_\alpha + c_n \mathbf{n}_I = c_\alpha \mathbf{a}^\alpha + c_n \mathbf{n}_I$ , where  $c^\alpha (\alpha = 1, 2)$  are the contra-variant components of  $\mathbf{c}$  and  $c_\alpha (\alpha = 1, 2)$  are the covariant components of  $\mathbf{c}$ . For orthogonal coordinate systems, a set of unit vectors  $\mathbf{i}_\alpha = \mathbf{a}_\alpha / |\mathbf{a}_\alpha|$  can be defined. Hence, at each point  $P$  on  $A_I$  one can define a set of orthonormal basis vectors  $(\mathbf{i}_1, \mathbf{i}_2, \mathbf{n}_I)$ , where  $\mathbf{i}_1$  and  $\mathbf{i}_2$  are lying in the tangent plane and  $\mathbf{n}_I$  is the unit normal to  $A_I$ . In this frame the vector  $\mathbf{c}$  associated with points in the surface can be expressed by  $\mathbf{c} = \hat{c}_\alpha \mathbf{i}_\alpha + c_n \mathbf{n}_I$ .

Let the position  $(\zeta, \eta)$  of a moving particle in the surface be represented by the position vector  $\mathbf{r}_I = \mathbf{r}_I(\zeta, \eta, t) = x(\zeta, \eta, t)\mathbf{e}_x + y(\zeta, \eta, t)\mathbf{e}_y + z(\zeta, \eta, t)\mathbf{e}_z$ . The velocity of the surface point  $(\zeta, \eta)$  is then defined by:

$$\mathbf{v}_I = \left( \frac{\partial \mathbf{r}_I}{\partial t} \right)_{\zeta, \eta} \quad (3.56)$$

A rigorous model formulation must consider all the relevant interfacial transport phenomena. By constructing a moving coordinate system at each point on the interface one can describe the geometry in terms of a *curvature* which is a measure of how the tangent vector to the coordinate curves in the surface are changing along the curves. To compute the curvature we parameterize a curve in the surface in yet another way in terms of the arc length parameter  $s$ , thus  $\mathbf{r}_I = \mathbf{r}_I(s)$  where  $\zeta = \zeta(s)$  and  $\eta = \eta(s)$ . Thereafter we design a moving frame of orthogonal unit vectors traveling along a curve in space consisting of three vectors, the unit tangent vector, the unit normal vector and a bi-normal vector which is perpendicular to both the tangent and normal vectors<sup>10</sup>. From these prerequisites the method for determining the curvature proceeds with the construction of a unit normal  $\mathbf{n}_I$  at a general point  $P$  on the surface, and the design of a plane which contains the unit surface normal vector  $\mathbf{n}_I$ . Let  $\mathbf{r}_{I,1} = \mathbf{r}_{I,1}(s_1)$  denote the position vector defining a curve 1 which is the intersection of the selected plane with the surface, where  $s_1$  is the arc length

<sup>10</sup> This frame is named the *Frenet frame* after Jean-Frédéric Frenet (1816-1900).

along the curve measured from the point  $P$ . The curve's unit tangent vector evaluated at the point  $P$  is then given by:

$$\mathbf{t}_1 = \frac{d\mathbf{r}_{I,1}}{ds_1} = \frac{d\mathbf{r}_{I,1}/dt}{ds_1/dt} = \frac{d\mathbf{r}_{I,1}/dt}{|d\mathbf{r}_{I,1}/dt|} \tag{3.57}$$

Differentiating  $\mathbf{t}_1 \cdot \mathbf{t}_1 = 1$ , with respect to arc length  $s_1$  we find  $\mathbf{t}_1 \cdot d\mathbf{t}_1/ds_1 = 0$  which implies that the vector  $d\mathbf{t}_1/ds_1$  is perpendicular to the tangent vector  $\mathbf{t}_1$ . Therefore, if we divide  $d\mathbf{t}_1/ds_1$  by the length  $|d\mathbf{t}_1/ds_1|$ , we obtain a unit vector which is orthogonal to  $\mathbf{t}_1$ .

Hence, the principal unit normal vector to the space curve  $\mathbf{n}_{s_1}$  is defined by:

$$\mathbf{n}_{s_1} = \pm \frac{1}{|d\mathbf{t}_1/ds_1|} \frac{d\mathbf{t}_1}{ds_1} \tag{3.58}$$

in which we normally choose the sign of  $\mathbf{n}_{s_1}$  so that  $\mathbf{n}_{s_1}$  points in the direction in which the curve is bending [62]. In other words, the unit normal vector  $\mathbf{n}_{s_1}$  is positive pointing into the concave side of the curve.

The bi-normal unit vector of a space curve  $\mathbf{b}_1 = \mathbf{t}_1 \times \mathbf{n}_I$  is perpendicular to both the surface tangent vector  $\mathbf{t}_1$  and the surface normal vector  $\mathbf{n}_I$ , such that the vectors  $(\mathbf{t}_1, \mathbf{n}_I, \mathbf{b}_1)$  form a right handed system. It is noted that the vector  $\mathbf{n}_{s_1}$  lies in the plane which contains the vectors  $\mathbf{n}_I$  and  $\mathbf{b}_1$ , yet the direction of the two normal vectors in this plane generally differ by an angle  $\theta$ .

For curve 2 a consistent orthogonal Frenet frame is defined by  $(\mathbf{t}_2, \mathbf{n}_I, \mathbf{b}_2)$ . Therefore, for each of the two Frenet frames the curvature vectors  $\boldsymbol{\kappa}_1 = \frac{d\mathbf{t}_1}{ds_1}$  and  $\boldsymbol{\kappa}_2 = \frac{d\mathbf{t}_2}{ds_2}$  denote the rate at which the unit tangent vectors to the two curves turn with respect to the arc length  $s_1$  and  $s_2$ , respectively, along these curves. Since  $\mathbf{t}_1$  and  $\mathbf{t}_2$  are unit vectors, the length remain constant and only the direction changes as the particles move along the curves. The curvature vectors can be written in the component form as

$$\boldsymbol{\kappa}_1 = \frac{d\mathbf{t}_1}{ds_1} = \kappa_1 \mathbf{n}_{s_1} = \kappa_{n_1} \mathbf{n}_I + \kappa_{g_1} \mathbf{b}_{s_1} = \boldsymbol{\kappa}_{n_1} + \boldsymbol{\kappa}_{g_1} \tag{3.59}$$

$$\boldsymbol{\kappa}_2 = \frac{d\mathbf{t}_2}{ds_2} = \kappa_2 \mathbf{n}_{s_2} = \kappa_{n_2} \mathbf{n}_I + \kappa_{g_2} \mathbf{b}_{s_2} = \boldsymbol{\kappa}_{n_2} + \boldsymbol{\kappa}_{g_2} \tag{3.60}$$

where  $\kappa_n$  is called the normal curvature and  $\kappa_g$  is called the geodesic curvature. The curvatures along  $s_1$  and  $s_2$  are conventionally defined by

$$\kappa_1 = \left| \frac{d\mathbf{t}_1}{ds_1} \right| \quad \text{and} \quad \kappa_2 = \left| \frac{d\mathbf{t}_2}{ds_2} \right| \tag{3.61}$$

for curve 1 and 2, respectively.

To determine how much a curve is curving near a point on the surface the normal curvature components suffice, since the geodesic curvature rather concerns a property of curves in a metric space which reflects the deviance of

the curve from following the shortest arc length distance along each infinitesimal segment of its length. So far the two perpendicular planes containing the unit normal were arbitrarily selected. If we vary the plane containing the unit surface normal  $\mathbf{n}_I$  at  $P$  we get different curves of intersection with the surface, in which each curve has a curvature associated with it. By examining all such planes we can identify the maximum and minimum normal curvatures associated with the surface point  $P$ . The values of these normal curvatures are called the principal curvatures  $\kappa_{n_1}$  and  $\kappa_{n_2}$ . We omit details here, making only loose statements about the results of differential geometry of surfaces.

The local geometry of a surface is generally characterized by two surface tensors, the metric tensor and curvature tensor. Letting  $(\zeta, \eta) = (\zeta^1, \zeta^2)$ , the tangent vectors to each of the coordinate curves at a point  $P$  can be represented as the basis vectors  $\mathbf{a}_\alpha = \frac{\partial \mathbf{r}_I}{\partial \zeta^\alpha}$  ( $\alpha = 1, 2$ ) where the partial derivatives are to be evaluated where the coordinate curves on the curves intersect. It follows that an element of arc length with respect to the surface coordinates is represented by:

$$ds^2 = d\mathbf{r}_I \cdot d\mathbf{r}_I = \frac{\partial \mathbf{r}_I}{\partial \zeta^\alpha} \cdot \frac{\partial \mathbf{r}_I}{\partial \zeta^\beta} d\zeta^\alpha d\zeta^\beta = g_{\alpha\beta} d\zeta^\alpha d\zeta^\beta \quad (3.62)$$

where the components of the local metric tensor is defined by  $g_{\alpha\beta} = \mathbf{a}_\alpha \cdot \mathbf{a}_\beta$  ( $\alpha, \beta = 1, 2$ ) in terms of the basis vectors. It has an inverse  $g^{\alpha\beta}$  which satisfies by definition  $\mathbf{a}_\alpha \cdot \mathbf{a}^\beta = g^{\alpha\beta} g_{\alpha\beta} = \delta_\alpha^\beta$  ( $\alpha, \beta = 1, 2$ ), where  $\delta_\alpha^\beta$  is the Kronecker delta and the repeated Greek superscript-subscript indices imply summation following the Einstein summation convention. The metric tensor and its inverse are used to raise and lower Greek indices as in the following example:  $\mathbf{a}^\alpha = g^{\alpha\beta} \mathbf{a}_\beta$  and  $\mathbf{a}_\alpha = g_{\alpha\beta} \mathbf{a}^\beta$  ( $\alpha, \beta = 1, 2$ ). It is noted that the quadratic form of (3.62) is called *the first fundamental form of the surface*. Many important local properties of a surface can be expressed only in terms of this fundamental form. The study of these properties is called the *intrinsic geometry* of the surface.

The normal curvature which is determined from the dot product relation  $\kappa_n = \mathbf{n}_I \cdot \boldsymbol{\kappa} = \mathbf{n}_I \cdot \frac{d\mathbf{t}}{ds}$ . From the orthogonality condition  $\mathbf{n}_I \cdot \mathbf{t} = 0$  we obtain by differentiation with respect to the arc length  $s$  the relation  $\mathbf{n}_I \cdot \frac{d\mathbf{t}}{ds} + \mathbf{t} \cdot \frac{d\mathbf{n}_I}{ds}$ , so the normal curvature can be rewritten as  $\kappa_n = -\mathbf{t} \cdot \frac{d\mathbf{n}_I}{ds} = -\frac{d\mathbf{r}_I}{ds} \cdot \frac{d\mathbf{n}_I}{ds}$ . We can then define the quadratic form

$$\kappa_n ds^2 = -d\mathbf{r}_I \cdot d\mathbf{n}_I = K_{\alpha\beta} d\zeta^\alpha d\zeta^\beta \quad (3.63)$$

where the components of the curvature tensor (dyadic)  $K_{\alpha\beta}$  is defined via the second derivative of the surface shape function,  $K_{\alpha\beta} = \mathbf{n}_I \cdot \frac{\partial}{\partial \zeta^\alpha} \frac{\partial \mathbf{r}_I}{\partial \zeta^\beta}$ . The curvature tensor for the surface is defined by the relation  $\mathbf{K} = -\nabla_I n_I$ , and the signed mean curvature  $H_I = -\frac{1}{2} g^{\alpha\beta} K_{\alpha\beta} = -\frac{1}{2} \nabla_I \cdot n_I$  of the surface is positive<sup>11</sup> when the mean curvature is concave in the direction of  $\mathbf{n}_I$ . The surface

<sup>11</sup> Note that other sign conventions exist as well.

gradient operator is defined as  $\nabla_I = \mathbf{e}_I \cdot \nabla = \mathbf{a}^\alpha \frac{\partial}{\partial \zeta^\alpha}$ . The quadratic form of (3.63) is called *the second fundamental form of the surface*. The investigation of the properties of the surface expressible in terms of the second fundamental form are called extrinsic geometry of the surface.

Adopting an alternative interpretation of the second fundamental form of the surface the normal and mean curvatures can be computed from a procedure for determining the radii of curvature instead. In general, a curved surface is uniquely characterized by two radii of curvature. Again, to compute the curvature at a given point  $P$  of an arbitrary surface embedded in 3D space, one erects a normal to the surface at the point in question and then passes a plane through the surface and containing the normal. The line of intersection will in general be curved, so the local curvature at differential dimensions is approximated as the arc of a circle that is tangent to the curve at the given surface point. Thus, the first *radius of curvature* coincides with the radius of the imaginary circle. The second radius of curvature is obtained by passing a second plane through the surface, also containing the normal, but perpendicular to the first plane. The mean curvature,  $H_I$ , is then defined as the geometric mean value of the two radii of curvature,

$$H_I = \frac{1}{2} \left( \frac{1}{R_1} + \frac{1}{R_2} \right) \quad (3.64)$$

It is emphasized that the radii of curvature  $R_1$  and  $R_2$  obtained in this way are not necessarily the principal radii of curvature, but the geometric mean value of the reciprocals of the radii of curvature equals the mean curvature as this sum is independent of how the first plane is orientated [1]. On the other hand, if we rotate the first plane through a full circle, the first radius of curvature will go through a maximum, and its value at this maximum is called the *principal radius of curvature*. The second principal radius of curvature is then that in the second plane, yet kept fixed and perpendicular to the first. From the preceding discussion we conclude that the principle curvatures correspond to the reciprocals of the principal radii of curvature  $\kappa_1 = 1/R_1$  and  $\kappa_2 = 1/R_2$ .

From a mathematical point of view this geometrical surface representation forms a rigorous basis for calculating the interfacial transport processes. The geometrical surface model can, for example, be adopted describing the macro-scale experimental observations that the normal surface tension force induces higher normal stresses in the fluid on the concave side of the interface than in the other fluid on the convex side of the interface. Nevertheless, in practice it is difficult to use these mathematical expressions for estimating the curvature of a surface in a numerical model, since it requires an algorithm for finding and choosing two convenient curves  $s_1$  and  $s_2$ , and calculating the mean curvature from these two curvatures. Instead, the mean curvature is expressed in terms of the unit normal that are determined based on so-called level curves as discussed in sect. 3.2.2 presenting the VOF- and LS methods. A geometrical interpretation of the directional derivative shows that the gradient to a level curve at a given point on the surface determines a normal vector to the level

surface. The normal vector is directed in the direction in which the level function increases most rapidly (corresponding to the direction of steepest ascent on a surface). The position of a point on a moving and deforming dividing surface may be described by the single scalar equation (e.g., [199], p 24; [217], sect 12.7):

$$f(\mathbf{r}, t) = 0 \quad (3.65)$$

upon differentiating this function with respect to time following a particular point on the surface  $(\zeta, \eta)$ , we find:

$$\frac{\partial f}{\partial t} + \mathbf{v}_I \cdot \nabla f = 0 \quad (3.66)$$

Since the interface is considered a level surface, the unit normal vector  $\mathbf{n}_I$  to  $A_I$  is defined by:

$$\mathbf{n}_I = \pm \frac{\nabla f}{|\nabla f|} \quad (3.67)$$

where the sign (+) is conventionally used for the normal directed outwards and (-) is used for  $\mathbf{n}_I$  directed inwards [246]. Nevertheless,  $\mathbf{n}_I$  can point in the same direction as  $\mathbf{n}_k$  or in the opposite direction depending on the choice of level function (i.e., the level function is usually set to be the volume fraction of either the continuous or dispersed phase). The unit normal of the dispersed phase, for example, is pointing outside the particle when it is defined from the spatial distribution of the volume fraction fields as follows:

$$\mathbf{n}_d = -\frac{\nabla \alpha_d}{|\nabla \alpha_d|} = \frac{\nabla \alpha_c}{|\nabla \alpha_c|} \quad (3.68)$$

The speed of displacement of the surface is defined as the scalar product of  $\mathbf{v}_I$  by  $\mathbf{n}_I$ . We then deduce, by use of (3.66) and (3.67):

$$\mathbf{v}_I \cdot \mathbf{n}_I = \mathbf{v}_I \cdot \frac{\nabla f}{|\nabla f|} = -\frac{\frac{\partial f}{\partial t}}{|\nabla f|} \quad (3.69)$$

The next task in our model derivation is to transform the system description (3.55) into an *Eulerian control volume formulation* by use of an extended form of the generalized transport theorem (see App A). For phase  $k$  the generalized Leibnitz theorem is written:

$$\begin{aligned} \frac{d}{dt} \int_{V_k(t)} (\rho_k \psi_k) dv &= \int_{V_k(t)} \frac{\partial(\rho_k \psi_k)}{\partial t} dv + \int_{A_k(t)} \rho_k \psi_k \mathbf{v}_k \cdot \mathbf{n}_k da \\ &+ \int_{A_I(t)} \rho_k \psi_k \mathbf{v}_I \cdot \mathbf{n}_k da \end{aligned} \quad (3.70)$$

Likewise, the second term on the LHS of (3.55) is transformed using the Leibnitz theorem for the area  $A_I$  (see app A). The surface theorem yields:

$$\frac{d_I}{dt} \int_{A_I(t)} (\rho_I \psi_I) da = \int_{A_I} \left( \frac{d_I(\rho_I \psi_I)}{dt} + \rho_I \psi_I \nabla_I \cdot \mathbf{v}_I \right) da \quad (3.71)$$

in which  $d_I/dt$  is the material derivative in the surface denoting the time derivative of a surface quantity following the motion of a surface particle (e.g., [199], p 14; [58], p 90; [63], sect 3.4). A material interface does not exchange mass at any point  $\mathbf{r}_I$  with the surrounding bulk phases, but moves and deforms with the mass averaged motion of the neighboring fluid phases [63], Sect 3.4. In particular, the normal component of the velocity vector at some point  $\mathbf{r}_I$  of a material fluid interface, is identical to the actual normal surface velocity at that point. However, it is possible to allow for net solute or solvent molecular exchange to occur by molecular diffusion without violating the condition of no net mass exchange. Therefore, we often restrict the model derivation considering a material interface, with the interpretation that there are no convective transport across the interface, but we do not rule out the possibility of diffusive transport across the interface. This is possible because the molecular mass diffusion flux is measured relative to the mass averaged velocity, hence there is not net mass transport when there is no convective flux. That is, for a material surface, the velocity of a point lying permanently on the interface is the same as the mass-averaged velocity of the two 3D fluid continua lying on either sides of the interface. For a non-material interface the interface velocity will generally differ from the velocities of the two 3D fluid continua lying on either sides of the interface. However, the kinematical treatment of the interface as being a material surface may in many cases be a sufficiently accurate approximation for reactive systems. Nevertheless, to present a general description, we proceed assuming that the interface is non-material.

The convective and diffusive transport terms in (3.55) are rewritten as the sum of a volume and an interface surface integral using Gauss' theorem (see app A). For each bulk phase we get:

$$\int_{V_k(t)} \nabla \cdot \mathbf{J}_k dv = \int_{A_k(t)} \mathbf{J}_k \cdot \mathbf{n}_k da + \int_{A_I(t)} \mathbf{J}_k \cdot \mathbf{n}_k da \quad (3.72)$$

and

$$\int_{V_k(t)} \nabla \cdot (\rho_k \mathbf{v}_k \psi_k) dv = \int_{A_k(t)} (\rho_k \mathbf{v}_k \psi_k) \cdot \mathbf{n}_k da + \int_{A_I(t)} (\rho_k \mathbf{v}_k \psi_k) \cdot \mathbf{n}_k da \quad (3.73)$$

We can now combine the generalized transport theorem (3.70) and the Gauss' theorem (3.73) to obtain:

$$\begin{aligned}
 \frac{d}{dt} \int_{V_k(t)} (\rho_k \psi_k) dv &= \int_{V_k(t)} \left[ \frac{\partial(\rho_k \psi_k)}{\partial t} + \nabla \cdot (\rho_k \mathbf{v}_k \psi_k) \right] dv \\
 &+ \int_{A_I(t)} \rho_k \psi_k (\mathbf{v}_I - \mathbf{v}_k) \cdot \mathbf{n}_k da
 \end{aligned} \tag{3.74}$$

We may refer to (3.74) as the transport theorem for a region where the closing control volume surface partly consists of a non-material phase interface.

Finally, the interfacial flux terms in (3.55) are transformed from a line integral into an interface surface integral using the surface divergence theorem (app. A). In the momentum equation the interfacial stress term involving surface tension appears as a line integral  $\int_{l_I(t)} \mathbf{N}_I \cdot \mathbb{T}_I dl$  over the curve  $l_I(t)$  which is the intersection of the fixed  $CV$  and  $A_I(t)$ .  $\mathbb{T}_I$  is the surface stress tensor and  $\mathbf{N}_I$  is the unit normal vector located in the tangent plane and directed outward the area  $A_I$  (Fig. 3.4). The surface fluid is normally assumed to be inviscid and thus isotropic, so this force reduces to  $\int_{l_I(t)} \mathbf{N}_I \sigma_I dl$ , where  $\sigma_I$  is the surface tension (a scalar). The Gauss theorem for a surface enable the transformation of a line integral into a surface integral, hence the surface tension term is conventionally written as:

$$\int_{l_I(t)} \mathbf{N}_I \sigma_I dl = \int_{A_I(t)} [\nabla_I \sigma_I - (\nabla_I \cdot \mathbf{n}_I) \sigma_I \mathbf{n}_I] da = \int_{A_I(t)} [\nabla_I \sigma_I + 2H_I \sigma_I \mathbf{n}_I] da \tag{3.75}$$

where  $\nabla_I$  is the surface del operator. The surface divergence  $-(\nabla_I \cdot \mathbf{n}_I)$  is equal to twice the mean curvature,

$$-\nabla_I \cdot \mathbf{n}_I = 2H_I \tag{3.76}$$

The first term on the RHS of (3.75) is a force acting tangential to the interface toward regions of higher surface tension. The second term on the RHS of (3.75) is a force acting normal to the interface, proportional to the curvature  $H_I$ . The normal force tends to smooth regions of high curvature, whereas the tangential force tends to force fluid along the interface towards regions of higher surface tension.

Surface tension arises due to short range intermolecular forces. The most important ones are van der Waals forces, London dispersion forces, hydrogen and metallic bondings [1]. The contributions from the individual forces are assumed independent, and the effective surface tension are calculated as the linear sum of the individual force contributions. The different molecular attraction forces at the two sides of the interfaces induce a resulting attraction force at the interface. Imagine that the molecules at an interface between two fluids exist in a state different from that of the molecules in the interior of the fluid. The phase  $k$  molecules are (on the average) surrounded by phase  $k$  molecules on only one side within the interface, whereas the interior

molecules are completely surrounded. Consequently, the configurational energy of the surface molecules differs from that of the interior molecules and the surface exists in a state of tension [234]. From a micro-scale point of view we may then say that the interfacial tension force is exerted by the interfacial material lying on the convex side of the surface upon the material lying on the concave side.

Two somewhat different definitions of the surface tension exist in the literature [1]. First, as discussed above, the surface tension can be viewed as a force per unit length intending to reduce the area of the interface. We can thus define it in accordance with the following interface force:

$$\int_{A_I(t)} \mathbf{F}_I da = - \oint_{l_I(t)} \mathbf{N}_I \sigma_I dl \quad (3.77)$$

where  $\sigma_I$  has units  $N/m$ . This interpretation is usually adopted for experimental determination of the surface tension.

Second, in thermodynamics it is more common to define surface tension in terms of work or the amount of energy needed to increase the surface with one unit area (i.e., the energy needed to bring a certain amount of molecules from the bulk to the surface). In this context the surface tension has a character of a surface free energy per unit area. The latter definition is in fact equivalent to the unit force per unit length (i.e.  $Nm/m^2 \equiv N/m$ ). The energy interpretation is by many researchers in thermodynamics considered the more fundamental one, and thus this interpretation is usually adopted for theoretical derivations. The surface tension is then defined as [1] [166]:

$$\sigma_I = \left( \frac{d\hat{G}}{dA} \right)_{T,P,\mathbf{n}} = \left( \frac{d\hat{F}}{dA} \right)_{T,V,\mathbf{n}} \quad (3.78)$$

where  $dA$  determines the increase in surface area,  $d\hat{G}$  denotes the change of surface Gibbs free energy, and  $d\hat{F}$  denotes the change of surface Helmholtz energy. In this case  $\sigma_I$  has units  $Nm/m^2$ .

Further details on the force balance at an arbitrary curved fluid interface is given in app A.

In the total energy and heat equations a similar line integral term appears  $\int_{l_I(t)} \mathbf{q}_I \cdot \mathbf{N}_I dl$  accounting for the heat flux entering the CV through  $l_I$ . Using another form of the Gauss theorem for a surface (app. A) transforming the line integral into a surface integral, the surface heat flux term is conventionally written as:

$$\int_{l_I(t)} \mathbf{q}_I \cdot \mathbf{N}_I dl = \int_{A_I(t)} \nabla_I \cdot \mathbf{q}_I da \quad (3.79)$$

For convenience, the generic interface flux  $\varphi_I$  of arbitrary tensorial order in (3.55) is split into two groups of contributions in accordance with their tensorial order (i.e., considering the mentioned surface tension and interfacial

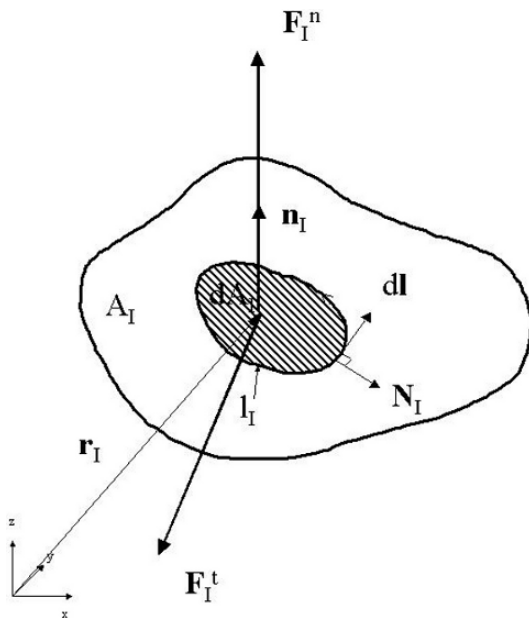


Fig. 3.4. Diagram for Gauss surface theorem.

heat fluxes only). The first group represents flux vectors  $\varsigma_I$ , whereas the second group denotes fluxes of isotropic second order tensors  $\zeta_I e_I$ .

The resulting surface terms are then written applying the different forms of the surface divergence theorem [63]:

$$\begin{aligned}
 - \oint_{l_I(t)} \varphi_I \cdot \mathbf{N}_I dl &= - \oint_{l_I(t)} \left( \varsigma_I \cdot \mathbf{N}_I + (\zeta_I e_I) \cdot \mathbf{N}_I \right) dl \\
 &= - \int_{A_I(t)} \nabla_I \cdot \varsigma_I da - \int_{A_I(t)} \nabla_I \cdot (\zeta_I e_I) da \\
 &= - \int_{A_I(t)} \nabla_I \cdot \varsigma_I da - \int_{A_I(t)} \left[ \nabla_I \zeta_I - (\nabla_I \cdot \mathbf{n}_I) \zeta_I \mathbf{n}_I \right] da
 \end{aligned} \tag{3.80}$$

where  $\nabla_I \cdot e_I = 2H_I \mathbf{n}_I$ .  $e_I$  denotes the *dyadic surface idemfactor* defined by  $e_I = \mathbf{e} - \mathbf{n}_I \mathbf{n}_I$ , in which the dyadic  $\mathbf{e}$  is the 3D spatial idemfactor [63]. It is further noted that the  $\varsigma_I$  vector is tangent to the surface  $A_I$ .

Using these theorems and excess definitions, (3.55) takes the form:

$$\begin{aligned}
 & \sum_{k=1}^2 \int_{V_k(t)} \left( \frac{\partial(\rho_k \psi_k)}{\partial t} + \nabla \cdot (\rho_k \mathbf{v}_k \psi_k) + \nabla \cdot \mathbf{J}_k - \sum_c \rho_{k,c} \phi_{k,c} \right) dv = \\
 & - \int_{A_I(t)} \left( \frac{d_I(\rho_I \psi_I)}{dt} + \rho_I \psi_I \nabla_I \cdot \mathbf{v}_I - \sum_c \rho_{I,c} \phi_{I,c} \right. \\
 & \quad - \sum_{k=1}^2 (\rho_k (\mathbf{v}_k - \mathbf{v}_I) \psi_k + \mathbf{J}_k) \cdot \mathbf{n}_k \\
 & \quad \left. + \nabla_I \cdot \zeta_I - \nabla_I \zeta_I + (\nabla_I \cdot \mathbf{n}_I) \zeta_I \mathbf{n}_I \right) da
 \end{aligned} \tag{3.81}$$

It is seen that the governing system equation (3.51) is transformed into a generic Eulerian control volume formulation (3.81) consisting of a volume integral determining the microscopic transport equations for the bulk phases and a surface integral determining the jump balance at the interface.

The balance (3.81) must be satisfied for any  $V_k(t)$  and  $A_I(t)$ , thus the arguments in the volume and surface integrals must all independently be equal to zero. The local instantaneous two-phase balance equations for a quantity  $\psi$  in the  $k$ th phase where  $\mathbf{J}_k$  and  $\phi_k$  are the fluxes and sources of  $\psi_k$  can then be expressed as:

$$\frac{\partial(\rho_k \psi_k)}{\partial t} + \nabla \cdot (\rho_k \mathbf{v}_k \psi_k) + \nabla \cdot \mathbf{J}_k - \sum_c \rho_{k,c} \phi_{k,c} = 0 \tag{3.82}$$

The balance principle applied to mass, momentum and energy for an interface is expressed by the jump condition:

$$\begin{aligned}
 & \sum_{k=1}^2 \left( \rho_k (\mathbf{v}_k - \mathbf{v}_I) \psi_k + \mathbf{J}_k \right) \cdot \mathbf{n}_k = \\
 & \frac{d_I(\rho_I \psi_I)}{dt} + \rho_I \psi_I \nabla_I \cdot \mathbf{v}_I - \sum_c \rho_{I,c} \phi_{I,c} + \nabla_I \cdot \zeta_I - \nabla_I \zeta_I + (\nabla_I \cdot \mathbf{n}_I) \zeta_I \mathbf{n}_I
 \end{aligned} \tag{3.83}$$

### Continuity

The mass balance is then found by substituting  $\psi = 1$ ,  $\mathbf{J}_k = 0$  and  $\phi_{k,c} = 0$  into (3.82):

$$\frac{\partial \rho_k}{\partial t} + \nabla \cdot (\rho_k \mathbf{v}_k) = 0 \tag{3.84}$$

This equation expresses the constraint of conservation of mass at every point within phase  $k$ .

Introducing the values for the interface parameters  $\zeta_I = 0$ ,  $\phi_{I,c} = 0$  and  $\zeta_I = 0$  into (3.83), the jump mass balance for the dividing surface becomes (e.g., [199], p. 87; [42], p. 400; [205], p. 44):

$$\sum_{k=1}^2 \rho_k (\mathbf{v}_k - \mathbf{v}_I) \cdot \mathbf{n}_k = \frac{d_I \rho_I}{dt} + \rho_I \nabla_I \cdot \mathbf{v}_I \quad (3.85)$$

In practical applications one normally neglects the terms describing the interfacial effects, thus the jump mass balance may be written as

$$\sum_{k=1}^2 \rho_k (\mathbf{v}_k - \mathbf{v}_I) \cdot \mathbf{n}_k = \sum_{k=1}^2 \dot{m}_k = 0 \quad (3.86)$$

### Species Mass Balance

The species mass balance is established by substituting  $\psi = \omega_s$ ,  $\mathbf{J}_k = \mathbf{j}_{k,s}$  and  $\phi_{k,c} = R_{k,s}/\rho_{k,c}$  into the (3.82):

$$\frac{\partial \rho_{k,s}}{\partial t} + \nabla \cdot (\rho_{k,s} \mathbf{v}_k) = -\nabla \cdot \mathbf{j}_{k,s} + R_{k,s} \quad (3.87)$$

Introducing the values for the interface parameters  $\zeta_I = 0$ ,  $\phi_{I,c} = -R_{I,s}/\rho_{I,c}$  and  $\zeta_I = 0$  into (3.83), the jump mass balance equation for the dividing surface becomes (e.g., [199], pp. 679-708):

$$\sum_{k=1}^2 \left( \rho_{k,s} (\mathbf{v}_k - \mathbf{v}_I) + \mathbf{j}_{k,s} \right) \cdot \mathbf{n}_k = \frac{d_I \rho_{I,s}}{dt} + \rho_{I,s} \nabla_I \cdot \mathbf{v}_I + R_{I,s} \quad (3.88)$$

where  $R_{k,s}$  is the rate at which species  $s$  is produced by homogeneous chemical reactions per unit volume, and  $R_{I,s}$  is the rate at which species  $s$  is produced by heterogeneous chemical reactions per unit area.

In practical applications one normally neglects the terms describing the interfacial transport phenomena, thus the jump component mass balance may be written as:

$$\sum_{k=1}^2 \left( \rho_{k,s} (\mathbf{v}_k - \mathbf{v}_I) + \mathbf{j}_{k,c} \right) \cdot \mathbf{n}_k = R_{I,s} \quad (3.89)$$

In line with single phase flows, the diffusive flux,  $\mathbf{j}_{k,s}$ , is commonly parameterized adopting Fick's law for binary systems,  $\mathbf{j}_{k,s} = -\rho_k D_s \nabla \omega_{k,s}$ .

### Momentum Balance

The momentum balance is found by substituting  $\psi = \mathbf{v}$ ,  $\mathbf{J}_k = \mathbf{T}_k$  and  $\phi_{k,c} = \mathbf{g}_{k,c}$  into the generalized transport equation (3.82):

$$\frac{\partial}{\partial t}(\rho_k \mathbf{v}_k) + \nabla \cdot (\rho_k \mathbf{v}_k \mathbf{v}_k) = -\nabla \cdot \mathbb{T}_k + \sum_c \rho_{k,c} \mathbf{g}_{k,c} \tag{3.90}$$

This is Cauchy’s first law for a multicomponent mixture (e.g., [199], p 710).

Introducing the values for the interfacial parameters  $\boldsymbol{\sigma}_I = 0$ ,  $\boldsymbol{\phi}_{I,c} = \mathbf{g}_{I,c}$  and  $\zeta_I = \sigma_I$  into (3.83), the jump momentum balance for the dividing surface becomes<sup>12</sup>(e.g., [199], p 710; [42], p 400; [205], p 44):

$$\begin{aligned} \sum_{k=1}^2 \left( \rho_k \mathbf{v}_k (\mathbf{v}_k - \mathbf{v}_I) + \mathbb{T}_k \right) \cdot \mathbf{n}_k = \\ \frac{d_I(\rho_I \mathbf{v}_I)}{dt} + \rho_I \mathbf{v}_I \nabla_I \cdot \mathbf{v}_I - \sum_c \rho_{I,c} \mathbf{g}_{I,c} - \nabla_I \sigma_I + (\nabla_I \cdot \mathbf{n}_I) \sigma_I \mathbf{n}_I \end{aligned} \tag{3.91}$$

where  $(\nabla_I \cdot \mathbf{n}_I) \sigma_I \mathbf{n}_I$  and  $\nabla_I \sigma_I$  denote the normal and tangential components of the surface force [25], respectively.

In practical applications considering fluid particles one normally neglects all the interface terms in (3.91), except the interfacial tension terms. Hence, the jump momentum balance is given by:

$$\sum_{k=1}^2 \left( \rho_k \mathbf{v}_k (\mathbf{v}_k - \mathbf{v}_I) + \mathbb{T}_k \right) \cdot \mathbf{n}_k = -\nabla_I \sigma_I + (\nabla_I \cdot \mathbf{n}_I) \sigma_I \mathbf{n}_I \tag{3.92}$$

Each of the two tangential unit vectors  $\mathbf{t}_i$  ( $i = 1, 2$ ) is perpendicular to  $\mathbf{n}_I$  and to the other vector,  $\mathbf{t}_1 \cdot \mathbf{t}_2 = 0$ . Therefore, the tangential components of the jump condition (3.92) can be expressed as:

$$\sum_{k=1}^2 \left( \mathbb{T}_k \cdot \mathbf{n}_k \right) \cdot \mathbf{t}_i = -\nabla_I \sigma_I \cdot \mathbf{t}_i \quad \text{for } i = 1, 2 \tag{3.93}$$

From this equality it follows that when the surface tension is constant, the tangential stress is continuous over the interface. In fluid mechanics it is thus frequently assumed that the tangential components of velocity are continuous across a phase interface [199]. With this simplification,  $v_{I,t} = v_{k,t}$ , the jump momentum balance yields:

$$\begin{aligned} \sum_{k=1}^2 \left( \rho_k (\mathbf{v}_k \cdot \mathbf{n}_k - \mathbf{v}_I \cdot \mathbf{n}_k)^2 \mathbf{n}_k + \mathbb{T}_k \cdot \mathbf{n}_k \right) = \\ \frac{d_I(\rho_I \mathbf{v}_I)}{dt} + \rho_I \mathbf{v}_I \nabla_I \cdot \mathbf{v}_I - \sum_c \rho_{I,c} \mathbf{g}_{I,c} - \nabla_I \sigma_I + (\nabla_I \cdot \mathbf{n}_I) \sigma_I \mathbf{n}_I \end{aligned} \tag{3.94}$$

in which we have used a particular identity for a spatial vector field in a surface given on the next page.

<sup>12</sup> The surface tension parameter (a scalar) has the same role as the pressure term in the three dimensional case (e.g., [42], p 398; [199], p 163).

The mentioned identity for a spatial vector field in a surface is defined by:

$$\mathbf{v} = (\mathbf{v} \cdot \mathbf{n}_I) \mathbf{n}_I + (\mathbf{e} - \mathbf{n}_I \mathbf{n}_I) \cdot \mathbf{v} = (\mathbf{v} \cdot \mathbf{n}_I) \mathbf{n}_I + \mathbf{e}_I \cdot \mathbf{v} = v_n \mathbf{n}_I + v_t \hat{\mathbf{t}} \quad (3.95)$$

where  $\mathbf{e}_I$  is the dyadic surface idem-factor which can be regarded as a tangential projector [246]. The tangential vector  $\hat{\mathbf{t}}$  can be written as linear combinations of the two basis vector fields associated with an orthogonal surface coordinate system  $\hat{\mathbf{t}} = \hat{t}_i \mathbf{t}_i$  [199].

The surface tension force is usually significant when one of the materials is a liquid and the other is either a gas, solid or a liquid. A computational methodology to determine the surface tension for solids in liquids are outlined by [60] [242]. In gas-solid particle flows the surface tension terms are commonly ignored, since these forces are usually very small compared to the viscous terms within the particle phase [57].

### Energy Balance Equation

The energy balance is found by substituting  $\psi = (e_k + \frac{1}{2}v_k^2)$ ,  $\mathbf{J}_k = \mathbf{T}_k \cdot \mathbf{v}_k + \mathbf{q}_k$  and  $\phi_{k,c} = \mathbf{v}_{k,c} \cdot \mathbf{g}_{k,c}$  into (3.82) (e.g., [199], pp. 715-723):

$$\frac{\partial \rho_k (e_k + \frac{1}{2}v_k^2)}{\partial t} + \nabla \cdot (\rho_k (e_k + \frac{1}{2}v_k^2) \mathbf{v}_k) = -\nabla \cdot \mathbf{T}_k \cdot \mathbf{v}_k + \sum_c \rho_{k,c} \mathbf{v}_{k,c} \cdot \mathbf{g}_{c,k} - \nabla \cdot \mathbf{q}_k \quad (3.96)$$

Introducing the values for the interfacial parameters  $\boldsymbol{\varsigma}_I = \mathbf{q}_I - \sigma_I \mathbf{v}_I$  and  $\zeta_I = 0$  into (3.83), the jump energy balance equation for the dividing surface becomes (e.g., [42], pp 400-401):

$$\begin{aligned} \sum_{k=1}^2 \left( \rho_k (e_k + \frac{1}{2}v_k^2) (\mathbf{v}_k - \mathbf{v}_I) + \mathbf{v}_k \cdot \mathbf{T}_k + \mathbf{q}_k \right) \cdot \mathbf{n}_k &= \frac{d_I \rho_I (e_I + \frac{1}{2}v_I^2)}{dt} + \\ \rho_I (e_I + \frac{1}{2}v_I^2) \nabla_I \cdot \mathbf{v}_I - \sum_c \rho_{I,c} \mathbf{v}_{I,c} \cdot \mathbf{g}_{c,I} + \nabla_I \cdot \mathbf{q}_I - \nabla_I \cdot (\sigma_I \mathbf{v}_I) & \end{aligned} \quad (3.97)$$

### Internal Energy Balance

The differential transport equations for mechanical energy, internal energy, and temperature in the bulk phases are derived as described for the single phase equations in chap. 1. The derivation of the corresponding jump balances, on the other hand, may need some further comments. To derive the jump internal energy balance we start with the jump total energy balance and subtract the jump kinetic (mechanical) energy balance, in a similar way as we did for the derivation of the transport equations for the bulk phases.

The jump kinetic energy balance is derived by taking the scalar product of the jump momentum balance (3.91) with  $\mathbf{v}_I$  (e.g., [199], p 720; [42], p 401):

$$\sum_{k=1}^2 \left( \rho_k \mathbf{v}_I \cdot \mathbf{v}_k (\mathbf{v}_k - \mathbf{v}_I) + \mathbf{v}_I \cdot \mathbb{T}_k \right) \cdot \mathbf{n}_k = \frac{d_I}{dt} \left( \frac{1}{2} \rho_I v_I^2 \right) + \rho_I v_I^2 \nabla_I \cdot \mathbf{v}_I - \sum_c \rho_{I,c} \mathbf{v}_I \cdot \mathbf{g}_{c,I} - \mathbf{v}_I \cdot \nabla_I \sigma_I + (\nabla_I \cdot \mathbf{n}_I) \sigma_I \mathbf{v}_I \cdot \mathbf{n}_I \tag{3.98}$$

Subtracting the jump kinetic energy balance (3.98) from the jump total energy balance (3.97), yields:

$$\begin{aligned} \sum_{k=1}^2 \left( \rho_k \left( e_k + \frac{1}{2} v_k^2 - \mathbf{v}_k \cdot \mathbf{v}_I \right) (\mathbf{v}_k - \mathbf{v}_I) + (\mathbf{v}_k - \mathbf{v}_I) \cdot \mathbb{T}_k + \mathbf{q}_k \right) \cdot \mathbf{n}_k = \\ \frac{d_I(\rho_I e_I)}{dt} + \rho_I \left( e_I - \frac{1}{2} v_I^2 \right) \nabla_I \cdot \mathbf{v}_I + \nabla_I \cdot \mathbf{q}_I - \sum_c \rho_{I,c} \mathbf{j}_{I,c} \cdot \mathbf{g}_{c,I} \\ + \mathbf{v}_I \cdot \nabla_I \sigma_I - (\nabla_I \cdot \mathbf{n}_I) \sigma_I \mathbf{v}_I \cdot \mathbf{n}_I - \nabla_I \cdot (\sigma_I \mathbf{v}_I) = \\ \frac{d_I(\rho_I e_I)}{dt} + \rho_I \left( e_I - \frac{1}{2} v_I^2 \right) \nabla_I \cdot \mathbf{v}_I + \nabla_I \cdot \mathbf{q}_I - \sum_c \rho_{I,c} \mathbf{j}_{I,c} \cdot \mathbf{g}_{c,I} \\ - (\nabla_I \cdot \mathbf{n}_I) \sigma_I \mathbf{v}_I \cdot \mathbf{n}_I - \sigma_I \nabla_I \cdot \mathbf{v}_I \end{aligned} \tag{3.99}$$

Since our concern is primarily with interface energy transfer rather than with the energy associated with the dividing surface, we normally neglect all interfacial effects and write the jump internal energy balance (3.99) as:

$$\sum_{k=1}^2 \left( \rho_k \left( e_k + \frac{1}{2} v_k^2 - \mathbf{v}_k \cdot \mathbf{v}_I \right) (\mathbf{v}_k - \mathbf{v}_I) + (\mathbf{v}_k - \mathbf{v}_I) \cdot \mathbb{T}_k + \mathbf{q}_k \right) \cdot \mathbf{n}_k = 0 \tag{3.100}$$

There is no experimental evidence to suggest that the interfacial effects neglected in the jump energy balance significantly affect interface energy transfer ([199] p 721). On the other hand, the interfacial effects in the jump momentum balance may affect the velocity distribution within the immediate neighborhood of the interface and in this way indirectly influence the interface energy transfer. Nevertheless, even if the interfacial energy has no practical effect upon interface energy transfer, it is not zero, since interfacial tension is a derivative of  $e_I$  (see [199], sect 5.8.6). In engineering practice we normally neglect the effect of mass transfer upon the interchange of kinetic energy, and the work done at the phase interface with respect to its effect upon the interchange of internal energy at the interface. Adopting these simplifying assumptions the jump internal energy balance further reduces to (e.g., [205], p 45):

$$\sum_{k=1}^2 \left( \rho_k e_k (\mathbf{v}_k - \mathbf{v}_I) + \mathbf{q}_k \right) \cdot \mathbf{n}_k = 0 \tag{3.101}$$

*Jump Enthalpy Balance*

Let the enthalpy be defined by  $h_k = e_k + p_k/\rho_k$ , the deviatoric stress tensor by  $\mathbf{T}_k = p_k \mathbf{e} + \boldsymbol{\sigma}_k$ , and the surface enthalpy  $h_I = e_I - \sigma_I/\rho_I$ , hence the jump internal energy balance (3.99) can be cast into the following form (e.g., [42]; [205] p 45):

$$\begin{aligned} & \sum_{k=1}^2 \left( \rho_k (h_k + \frac{1}{2} v_k^2 - \mathbf{v}_k \cdot \mathbf{v}_I) (\mathbf{v}_k - \mathbf{v}_I) + (\mathbf{v}_k - \mathbf{v}_I) \cdot \boldsymbol{\sigma}_k + \mathbf{q}_k \right) \cdot \mathbf{n}_k = \\ & \frac{d_I(\rho_I h_I)}{dt} + \rho_I (h_I - \frac{1}{2} v_I^2) \nabla_I \cdot \mathbf{v}_I + \frac{d_I \sigma_I}{dt} + \nabla_I \cdot \mathbf{q}_I - \sum_c \rho_{I,c} \mathbf{j}_{I,c} \cdot \mathbf{g}_{c,I} \\ & - (\nabla_I \cdot \mathbf{n}_I) \sigma_I \mathbf{v}_I \cdot \mathbf{n}_I \end{aligned} \quad (3.102)$$

where we have used the fact that  $(\mathbf{v}_k - \mathbf{v}_I) \cdot p_k \mathbf{e}_k \cdot \mathbf{n}_k = (\mathbf{v}_k - \mathbf{v}_I) \cdot \mathbf{n}_k p_k$ .

At catalytic surfaces chemical reaction engineers often prefer to use a heat jump formulation which contains an explicit term for the heat generation due to the heterogeneous chemical reactions. The reformulation of the surface enthalpy term in the above enthalpy jump condition follows the same principles as explained in sect 1.2.4 deriving the single phase temperature equations from the enthalpy equation.

By use of the species mass jump condition (3.88) or its simplified form (3.89), the surface version of the complete differential (1.142) can be expressed as:

$$\begin{aligned} \frac{d_I h_I}{dt} &= C_{p,I} \frac{d_I T_I}{dt} + \left( \frac{1}{\rho_I} + \frac{T_I}{\rho_I^2} \left( \frac{\partial \rho_I}{\partial T_I} \right)_{p,\omega} \right) \frac{d_I p_I}{dt} \\ &- \frac{1}{\rho_I} \left[ \sum_{c=1}^N \bar{h}_{I,c} \nabla_I \cdot \left( \frac{\mathbf{J}_{I,c}}{M_{w_c}} \right) + \sum_{r=1}^q r_{r,c_{\text{ref}},I} (-\Delta \bar{H}_{r,c_{\text{ref}},I}) \right] \end{aligned} \quad (3.103)$$

This result is then used to rewrite the surface enthalpy substantial derivative term in (3.102), and so the required form of the jump enthalpy balance is obtained. However, in practical applications of the jump condition for catalytic surfaces, one generally neglects the terms describing the interfacial transport phenomena and retains only the heat of reaction term. Therefore, the approximate jump heat balance is written as:

$$\sum_{k=1}^2 \left( \rho_k h_k (\mathbf{v}_k - \mathbf{v}_I) + \mathbf{q}_k \right) \cdot \mathbf{n}_k \approx \sum_{r=1}^q r_{r,c_{\text{ref}},I} (-\Delta \bar{H}_{r,c_{\text{ref}},I}) \quad (3.104)$$

This jump enthalpy condition determines the basis for the derivation of the conventional temperature equation used in heterogeneous catalysis (3.204).

#### *Jump Entropy Balance*

In order to transform the enthalpy balance into a jump entropy balance, we introduce the Gibbs free enthalpies defined by ([42], p. 402):

$$g_k = h_k - T_k s_k \tag{3.105}$$

$$g_I = h_I - T_I s_I \tag{3.106}$$

The Gibbs equation, written for the interface, has the following form:

$$\frac{d_I h_I}{dt} = T_I \frac{d_I s_I}{dt} - \frac{1}{\rho_I} \frac{d_I \sigma_I}{dt} \tag{3.107}$$

Using these definitions, the jump enthalpy balance becomes:

$$\begin{aligned} \sum_{k=1}^2 \left( \rho_k (g_k + T_k s_k + \frac{1}{2} v_k^2 - \mathbf{v}_k \cdot \mathbf{v}_I) (\mathbf{v}_k - \mathbf{v}_I) + (\mathbf{v}_k - \mathbf{v}_I) \cdot \boldsymbol{\sigma}_k + \mathbf{q}_k \right) \cdot \mathbf{n}_k = \\ \frac{d_I \rho_I g_I}{dt} + \frac{d_I \rho_I T_I s_I}{dt} + \rho_I (g_I + T_I s_I - \frac{1}{2} v_I^2) \nabla_I \cdot \mathbf{v}_I + \frac{d_I \sigma_I}{dt} + \nabla_I \cdot \mathbf{q}_I \\ - \sum_c \rho_{I,c} \mathbf{j}_{I,c} \cdot \mathbf{g}_{c,I} - (\nabla_I \cdot \mathbf{n}_I) \sigma_I \mathbf{v}_I \cdot \mathbf{n}_I \end{aligned} \tag{3.108}$$

### Summarizing the Governing Equations and Jump Balances

The generic instantaneous transport equation for a balanced quantity  $\psi$  in the  $k$ th phase is expressed by (3.82), in which  $\mathbf{J}_k$  and  $\phi_k$  are the fluxes and source of  $\psi_k$ . It is noted that the bulk phase equation is identical to the single phase equation (1.3) presented in chap. 1.

Ignoring the interface transport terms, the local instantaneous jump balances for a quantity  $\psi$  can be expressed in a generic form as:

$$\begin{aligned} \sum_{k=1}^2 \left( \rho_k (\mathbf{v}_k - \mathbf{v}_I) \psi_k + \mathbf{J}_k \right) \cdot \mathbf{n}_k \approx - \sum_c \rho_{I,c} \phi_{I,c} + \nabla_I \cdot \boldsymbol{\varsigma}_I \\ - \nabla_I \zeta_I + (\nabla_I \cdot \mathbf{n}_I) \zeta_I \mathbf{n}_I \\ \approx - M_I \end{aligned} \tag{3.109}$$

where  $M_I$  denotes the relevant terms associated with  $\psi$  at the dividing surface.

The values for  $\psi$ ,  $\mathbf{J}$ ,  $\phi$  and  $M_I$  are given in Table 3.1:

**Table 3.1.** The definitions of  $\psi$ ,  $\mathbf{J}$  and  $M_I$

Conservation Principle	$\psi$	$\mathbf{J}$	$\phi$	$M_I$
Total mass	1	0	0	0
Component mass	$\omega_s$	$\mathbf{J}_s$	$R_s$	$R_{I,s}$
Momentum	$\mathbf{v}$	$\boldsymbol{\Gamma}$	$\mathbf{g}_c$	$-M_I^\sigma$
Energy	$e + \frac{1}{2} v^2$	$\boldsymbol{\Gamma} \cdot \mathbf{v} + \mathbf{q}$	$(\mathbf{g}_c \cdot \mathbf{v}_c)$	$-(\epsilon_I^\sigma + \nabla_I \cdot \mathbf{q}_I)$

where

- $\omega_s$  is the mass fraction of component  $s$ ;
- $\mathbf{J}_s$  is the molecular (diffusive) flux of component  $s$ ;
- $R_s$  is the rate of production of species  $s$  by homogeneous reactions;
- $R_{I,s}$  is the rate of production of species  $s$  by heterogeneous reactions;
- $\mathbf{T}$  is the total stress tensor ( $= p\mathbf{e} + \boldsymbol{\sigma}$ );
- $\mathbf{g}_c$  is the external forces per unit mass of component  $c$ ;
- $M_I$  is a net surface property term:
  - $\mathbf{M}_I^\sigma = -\nabla_I \sigma_I + (\nabla_I \cdot \mathbf{n}_I) \sigma_I \mathbf{n}_I$  is the surface tension force;
  - $\epsilon_I^\sigma = -\nabla_I \cdot (\sigma_I \mathbf{v}_I)$  is the surface energy associated with surface tension;
- $e$  is the internal energy of the multicomponent system;
- $\mathbf{q}$  is the multicomponent energy flux vector;
- $\boldsymbol{\sigma}$  is the viscous stress tensor;
- $\sigma_I$  is the surface tension;
- $\nabla_I$  is the surface del or nabla operator.

### The Microscopic Transport Equations for a Finite Number of Dispersed Phases - the Multi-Fluid Model

The generic microscopic transport equation for a generalized quantity  $\psi$  can be formulated considering a material control volume  $V(t)$  containing  $N$  continuous phases separated by several interfaces across which the physical properties are discontinuous and may jump, as sketched in Fig. 3.5. This formulation represents a direct extension of the two-fluid modeling procedure described in the preceding section. Among the most rigorous model formulations proposed hitherto are those by Slattery [194, 197, 199] and Deemer and Slattery [41].

The generic balance equation for the variable  $\psi$  in  $V(t)$  is written as:

$$\begin{aligned}
 & \sum_{k=1}^N \left( \frac{d}{dt} \int_{V_k(t)} \rho_k \psi_k dv \right) + \frac{1}{2} \sum_{k=1}^N \sum_{j=1}^N (1 - \delta_{jk}) \frac{d_{I,jk}}{dt} \int_{A_{I,jk}(t)} \rho_{I,jk} \psi_{I,jk} da = \\
 & - \sum_{k=1}^N \int_{A_k(t)} \mathbf{J}_k \cdot \mathbf{n}_k da \\
 & + \sum_{k=1}^N \int_{V_k(t)} \sum_c \rho_{k,c} \phi_{k,c} dv + \frac{1}{2} \sum_{k=1}^N \sum_{j=1}^N (1 - \delta_{jk}) \int_{A_{I,jk}(t)} \sum_c \rho_{I,jk,c} \phi_{I,jk,c} da \\
 & - \frac{1}{2} \sum_{k=1}^N \sum_{j=1}^N (1 - \delta_{jk}) \oint_{l_{I,jk}(t)} \varphi_{I,jk} \cdot \mathbf{N}_{I,jk} dl
 \end{aligned} \tag{3.110}$$

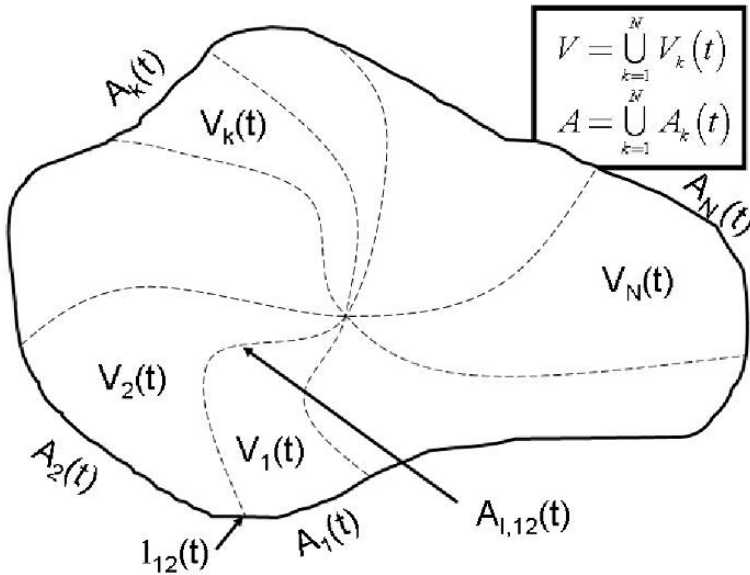


**Fig. 3.5.** A material control volume  $V(t)$  containing  $N$  phases with moving interfaces. The closed surface bounding the CV is  $A(t)$ , and the dividing surfaces enclosed by  $A(t)$  are  $A_{I,jk}(t)$ . The lines formed by the intersection of  $A_{I,jk}(t)$  with  $A(t)$  are  $l_{jk}(t)$ . Any anomalous physical phenomena occurring in the union of all common lines formed by the intersection of the dividing surfaces are ignored [199].

where  $A_{I,jk}(t)$  denotes the interface between the  $j^{\text{th}}$  and  $k^{\text{th}}$  phases. Defining the location of the surface  $A_{I,jk}(t)$  as  $\mathbf{r}_{I,jk} = \mathbf{r}_{I,jk}(x(\zeta, \eta, t), y(\zeta, \eta, t), z(\zeta, \eta, t))$  the velocity of the surface point  $(\zeta, \eta)$  is defined by  $\mathbf{v}_{I,jk} = (\partial \mathbf{r}_{I,jk} / \partial t)_{\zeta, \eta}$ .

The two first terms on the LHS of (3.110) can be transformed into a volume and a surface integral using the Leibnitz's theorem:

$$\begin{aligned} \frac{d}{dt} \int_{V_k(t)} \rho_k \psi_k dv &= \int_{V_k(t)} \frac{\partial}{\partial t} (\rho_k \psi_k) dv + \int_{A_k(t)} (\rho_k \mathbf{v}_k \psi_k) \cdot \mathbf{n}_k da \\ &+ \sum_{j=1}^N (1 - \delta_{jk}) \int_{A_{I,kj}(t)} \rho_k \psi_k \mathbf{v}_{I,kj} \cdot \mathbf{n}_{kj} da \end{aligned} \tag{3.111}$$

The convective and diffusive terms can be written as a sum of a volume and a surface integral using the Gauss' theorem:

$$\begin{aligned} \int_{V_k(t)} \nabla \cdot (\rho_k \psi_k \mathbf{v}_k) dv &= \\ \int_{A_k(t)} \rho_k \psi_k \mathbf{v}_k \cdot \mathbf{n}_k da &+ \sum_{j=1}^N (1 - \delta_{jk}) \int_{A_{I,kj}(t)} \rho_k \psi_k \mathbf{v}_k \cdot \mathbf{n}_{kj} da \end{aligned} \tag{3.112}$$

and

$$\int_{V_k(t)} \nabla \cdot \mathbf{J}_k \, dv = \int_{A_k(t)} \mathbf{J}_k \cdot \mathbf{n}_k \, da + \sum_{j=1}^N (1 - \delta_{jk}) \int_{A_{I,kj}(t)} \mathbf{J}_k \cdot \mathbf{n}_{kj} \, da \quad (3.113)$$

Accordingly, (3.110) can be rewritten as:

$$\begin{aligned} \sum_{k=1}^N \int_{V_k(t)} \left( \frac{\partial(\rho_k \psi_k)}{\partial t} + \nabla \cdot (\rho_k \mathbf{v}_k \psi_k) + \nabla \cdot \mathbf{J}_k - \sum_c \rho_{k,c} \phi_{k,c} \right) dv = \\ - \sum_{k=1}^N \sum_{j=1}^N (1 - \delta_{ij}) \int_{A_{I,kj}(t)} \left( \frac{1}{2} \frac{d_{I,kj}}{dt} (\rho_{I,kj} \psi_{I,kj}) + \frac{1}{2} \rho_{I,kj} \psi_{I,kj} \nabla_{I,kj} \cdot \mathbf{v}_{I,kj} \right. \\ \left. - \frac{1}{2} \sum_c \rho_{I,kj,c} \phi_{I,kj,c} - (\rho_k (\mathbf{v}_k - \mathbf{v}_{I,kj}) \psi_k + \mathbf{J}_k) \cdot \mathbf{n}_k \right. \\ \left. + \frac{1}{2} \nabla_{I,kj} \cdot \varsigma_{I,kj} - \frac{1}{2} \nabla_{I,kj} \zeta_{I,kj} + \frac{1}{2} (\nabla_{I,kj} \cdot \mathbf{n}_{I,kj}) \zeta_{I,kj} \mathbf{n}_{I,kj} \right) da \end{aligned} \quad (3.114)$$

The balance (3.114) must be satisfied for any  $V_k(t)$  and  $A_{I,kj}(t)$ , thus the arguments in the volume and surface integrals must all independently be equal to zero. The local instantaneous multi-fluid balance equations for a quantity  $\psi$  in the  $k$ th phase where  $\mathbf{J}_k$  and  $\phi_k$  are the fluxes and sources of  $\psi_k$  can then be expressed as:

$$\frac{\partial(\rho_k \psi_k)}{\partial t} + \nabla \cdot (\rho_k \mathbf{v}_k \psi_k) + \nabla \cdot \mathbf{J}_k - \sum_c \rho_{k,c} \phi_{k,c} = 0 \quad (3.115)$$

The generic jump condition is expressed as:

$$\begin{aligned} \dot{\mathbf{m}}_{I,kj} \psi_k + \dot{\mathbf{m}}_{I,jk} \psi_j + \mathbf{J}_k \cdot \mathbf{n}_{kj} + \mathbf{J}_j \cdot \mathbf{n}_{jk} = \\ \frac{d_{I,kj} (\rho_{I,kj} \psi_{I,kj})}{dt} + \rho_{I,kj} \psi_{I,kj} \nabla_{I,kj} \cdot \mathbf{v}_{I,kj} - \sum_c \rho_{I,kj,c} \phi_{I,kj,c} \\ + \nabla_{I,kj} \cdot \varsigma_{I,kj} - \nabla_{I,kj} \zeta_{I,kj} + (\nabla_{I,kj} \cdot \mathbf{n}_{I,kj}) \zeta_{I,kj} \mathbf{n}_{I,kj} \end{aligned} \quad (3.116)$$

where  $\dot{\mathbf{m}}_{I,kj} = \rho_k (\mathbf{v}_k - \mathbf{v}_{I,kj}) \cdot \mathbf{n}_{I,kj}$  is the mass transfer per unit area of the interface and unit time from the  $k^{\text{th}}$  phase to the  $j^{\text{th}}$  phase through the interface.

The particular local instantaneous equations are specifically defined when the values for  $\psi$ ,  $\mathbf{J}$ ,  $\phi$  and  $M_I$  are given in accordance with Table 3.1 for multi-fluid systems.

### 3.3.2 The Purpose of Averaging Procedures

From the preceding discussion in this chapter, one can conclude that the pertinent modeling approaches to be applied in practice must involve some kind of

average representation of the flow structure in the reactors. Starting out from the local instantaneous equations proper averaging is needed on the macroscopic scales to avoid solving the multiphase flow problem as a deterministic multi-boundary problem with the interface relations of mass, momentum, and energy as boundary conditions (e.g., [205, 112, 67, 58]). The purpose of averaging is thus to allow a coarser mesh and a longer time step to be used in the numerical simulation. Unfortunately, as a consequence of the averaging of the instantaneous jump conditions valid across the interface between the phases, new expressions that lack formal description are introduced. Closure models for such terms thus become necessary. These models are often formulated by recourse to approximate local flow field analysis and sometimes by recourse to empiricism. Usually, it is here that the approach loses some of the precision that is inherent in the derivation of the rigorous differential equations. In fact all the averaging methods have the important drawback that the resulting macroscopic equations have lost most of the topological information about the flow structure. For example, after averaging the governing equations for gas-liquid flows operating in the bubbly flow, stratified flow or slug flow regimes the resulting set of macroscopic equations are apparently identical. This means that all these flows are represented by the same set of governing equations, so for each particular flow regime the physical structure properties have to be re-introduced through the constitutive equations. Nevertheless, this framework is still the most rigorous concept that can be put to practice for performance optimization, scale-up and design of industrial scale reactors.

### 3.4 Averaging Procedures

This section deals with the formulation of proper transport equations representing some kind of averaged continuum mechanical description of the flow system. There are two main strategies that have been used deriving the existing macroscopic models, denoted the averaging and mixture approaches, respectively. The *Averaging approach* consist in the postulation of the local instantaneous conservation equations prior to the application of an averaging procedure deriving macroscopic Eulerian multi-fluid models. In the *mixture approach* the mixture properties are postulated directly at the macroscopic scales, and a set of macroscopic balance equations is formulated based on the conventional conservation laws and the mixture properties. So, in this particular modeling concept the control volume and the averaging volume coincide.

The averaging approach might be considered fundamental and preferred compared to the mixture approach, because averaging provides certain advantages as the resulting macroscopic variables are explicitly related to the local variables. Nevertheless, averaging cannot circumvent the need to postulate constitutive equations, but it can give insight into the types of terms expected to be important in the constitutive relations. The major difference between the averaging and mixture approaches thus lies in the level at which

we introduce the necessary postulates and empiricism. Moreover, embedded in the practice of using either average or mixture equations is the assumptions that, for the investigation of multiphase flows in reactor systems, the local microscopic details of the flow are not needed (eluding a multi-scale approach). However, even though it is the macroscopic characteristics that are of interest, the effect of the microscopic details on the macroscopic characteristics can be very important for particular multiphase systems.

Depending on the mathematical formulation used to describe the multiphase problem in question, the different averaging procedures can be classified into three groups, the Eulerian averaging, the Lagrangian averaging and the Boltzmann statistical averaging [112]. In this section emphasis is placed on the Eulerian integral averaging operators since the main purpose is to smooth out instant and local variations of the local instantaneous variable fields. Besides, these averages are conventionally used in continuum mechanics and experimental analyzes.

The philosophy taken in this book is that any understanding that can be gained from averaging is worthwhile, thus a general introduction to this topic is given before all the mathematical details are presented. Many mathematically different Eulerian averaging procedures for deriving the macroscopic equations and jump conditions for multiphase flows have been proposed in the literature. These are the *volume averaging*-, the *time averaging*- and the *ensemble averaging* techniques, as well as combinations of the basic single averaging operators. Besides, some researches also introduce mass- or phase averaged variables. The first step in a general averaging procedure is to form the average of the local instantaneous transport equations and the corresponding jump conditions. The resulting averaged equations cannot be solved directly, as they contain averages of products of the dependent variables. The second step in an averaging procedure is thus to obtain a solvable set of equations by relating the averages of products to expressions containing products of averaged variables. This has commonly been done either by employing concepts similar to conventional single phase Reynolds decomposition [177] or methods similar to single phase Favre decomposition before averaging [75, 76]. Note that the Reynolds and Favre decomposition and averaging rules are normally used in the field of single phase turbulence modeling in order to separate the fluctuating components of the variables from the averaged variables (separation of scales), whereas when applied to multiphase flow models the main purpose of these procedures is rather to separate the averages of product into products of average. Moreover, these procedures give rise to extra terms in the transport equations, containing covariances of the fluctuating components, analogous to the Reynolds stress terms obtained in the case of single phase turbulence modeling. A general procedure for formulating a multi-fluid model is sketched in Fig. 3.6. Finally, for completeness it ought to be mentioned that a lot of work has been focused on formulating multi-fluid models for dispersed phases based on kinetic theories [176, 175, 133], and on the kinetic theories of granular materials as outlined in chap 4. It is noted that the fundamental

basis for such model formulations is related to dispersed particle statistics (Maxwellian averaging) rather than continuum mechanics.

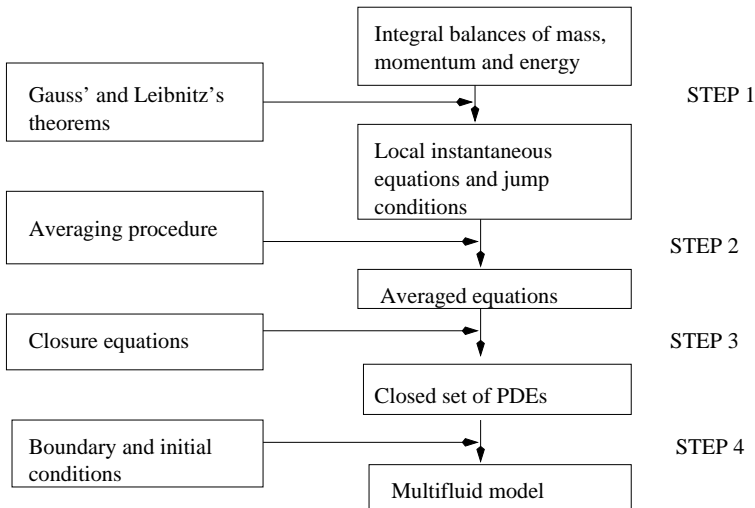


**Fig. 3.6.** General procedure for formulating a multi-fluid model.

From a mathematical point of view there are still no complete agreement on the properties of the different averaging operators and their suitability for deriving the macroscopic equations.

In continuum mechanics a proper averaging procedure should lead to flow variables that are continuous [10]. Considering the pure time and space averages which were the first methods to appear around 1950 [54], some doubts or difficulties related to the continuity of the flow variables were pointed out by [43, 47, 10, 48, 205]. To deal with these matters the basic averages were thus refined by weighting, by multiple application, and by various choices of averaging scales.

On the other hand, experimental techniques have been developed over the years exclusively to determine time- and volume average measures of the flow keeping the expenses as low as possible. Therefore, in the past the time averaging, volume averaging and time- or ensemble averaging after volume averaging solely have been used in the engineering sciences deriving multiphase models. In particular the time- after volume averaging operator was frequently used. In this method the purpose of the time averaging after volume averaging is to express averages of products in terms of products of averages and to account for the high frequency fluctuations retained by the instantaneous volume averages (separation of scales) [205]. A convenient consequence of this approach is that the conventional single phase Reynolds and Favre decomposition and time averaging concepts are considered appropriate, thus the established single

phase turbulence models are often adopted closing the resulting model equations. However, detailed inspections of the flows in laboratory scale, pilot scale and industrial scale chemical reactors under typical operating conditions reveal that the validity conditions of the time- and volume averaging operators are frequently violated thus an ensemble average operator might be preferable. Therefore, in the last few years the mass-weighted ensemble averaging procedure has gained considerable interest.

In the subsequent sections the averaging procedures most frequently used in multiphase reactor modeling are examined. Hence it follows that the basic principles of averaging are presented with emphasis on disperse two phase systems.

### 3.4.1 The Volume Averaging Procedure

In this section we assess the volume averaging technique. The literature cited considering different forms of *spatial averaging* (i.e., area or volume) are [43, 44, 243, 156, 10, 24, 192, 52, 54, 21, 2, 135, 205, 206, 157, 193, 14, 81, 89, 90, 91, 7, 194, 195, 196, 197, 198, 199, 200, 233, 234, 235, 237, 238, 239, 110, 17, 163, 165, 230, 153, 154, 181, 37, 38, 171, 98, 99, 100, 101, 102, 168, 129] which might be recommended for complementary studies.

The condition under which the volume averaging operators can be applied handling the scale disparity in a suitable manner<sup>13</sup> can be expressed as [235, 156, 89, 205, 206]:

$$\left\{ \begin{array}{l} \text{Characteristic} \\ \text{dimension of} \\ \text{phases, } d_p \end{array} \right\} \ll \left\{ \begin{array}{l} \text{Characteristic} \\ \text{dimension of} \\ \text{averaging volume, } l \end{array} \right\} \ll \left\{ \begin{array}{l} \text{Characteristic} \\ \text{dimension of} \\ \text{physical system, } L \end{array} \right\}$$

This means that we require that the averaging volume is sufficiently large so that the microscopic variations in  $\psi_k$  are essentially smoothed out and the averaged functions  $\langle \psi_k \rangle_V$  are continuous, and that the average of the average equals the average,  $\langle \langle \psi_k \rangle_V \rangle_V = \langle \psi_k \rangle_V$ . That is, when the averaging volume is very small the average quantities of the mixture fluctuates because portions of the phases included in the averaging volume are location-dependent. This fluctuation diminishes as the size of the volume increases, and within a certain characteristic size of  $V$  the average quantities become independent of  $V$ . However, the characteristic size of  $V$  should not be too large, otherwise it becomes dependent upon the global variations of the quantities and the dimensions of the system.

<sup>13</sup> It is noted that the requirement of proper separation of scales represents the main drawback of the volume averaging method. The constitutive equations used generally depend strongly on this assumption which is hardly ever fulfilled performing simulations of laboratory, pilot and industrial scale reactor units.

The *volume averaging operator* which can be applied to any scalar, vector or tensor valued property function  $\psi_k$  associated with phase  $k$ , is defined by<sup>14</sup>:

$$\langle \psi_k \rangle_V = \frac{1}{V} \int_V X_k \psi_k dv = \frac{1}{V} \int_{V_k(t)} \psi_k dv \quad (3.117)$$

where  $X_k$  is the phase indicator function which equals 1 in phase  $k$  and zero elsewhere. The mathematical properties of the generalized function  $X_k$  ensure that the ordinary mathematical operations of vector calculus can be performed on the local variables. In particular, as the fluid properties is discontinuous across the 2D interface between the two bulk phases, the phase indicator function is used as a weighting function in forming averages of the local variables to ensure that the differentiation of the discontinuous variables within the integrals are performed in a valid manner [58] [7]. Besides, it is claimed that the introduction of the weighted averages leads to considerable mathematical simplification deriving the averaged equations [54] [171]. However, the trade-off for the simple derivation is that all the manipulations involve generalized functions<sup>15</sup>. Hence it is emphasized that the conventional space averaging operator was defined avoiding the explicit use of the phase indicator function [43, 47, 24, 54, 205, 206, 239]. On the other hand, under certain conditions the  $X_k$ -weighted volume average coincides with the conventional single volume average operator [171].

The *intrinsic* volume average is defined as:

$$\langle \psi_k \rangle_{V_k} = \langle \psi_k \rangle_V^{X_k} = \frac{\frac{1}{V} \int_V X_k \psi_k dv}{\frac{1}{V} \int_V X_k dv} = \frac{1}{V_k(t)} \int_{V_k(t)} \psi_k dv \quad (3.118)$$

where the intrinsic volume average has been expressed as the  $X_k$ -weighted volume average. In other words, the  $X_k$ -weighted volume average as defined by (3.118) is assumed to coincide with  $\langle \psi_k \rangle_{V_k}$  which represents the averaged value of  $\psi$  in the phase  $k$  over the volume  $V_k(t)$ .

By comparing the averaging operators (3.117) and (3.118), we can see that:

$$\langle \psi_k \rangle_V = \frac{V_k}{V} \langle \psi \rangle_{V_k} = \alpha_k \langle \psi \rangle_{V_k} \quad (3.119)$$

in which the instantaneous *volume fraction*  $\alpha_k$  of phase  $k$  is given by:

<sup>14</sup> It is emphasized that  $\langle \psi_k \rangle_V$  is the average of the quantity  $\psi$  in phase  $k$  over the entire averaging volume  $V$ . This averaging operator is sometimes called the *extensive* or *superficial* volume average of  $\psi$  for phase  $k$ .

<sup>15</sup> Mathematicians may say that this approach leads to more elegant mathematics, since the phase indicator function might be imagined as a sensor which enables local instantaneous phase identification. However, this somewhat mathematical formulation may also impede physical understanding for an inexperienced reaction engineer having a more practical background.

$$\alpha_k = \frac{V_k}{V} \quad (3.120)$$

To derive a local volume average of the generic differential balance equation for phase  $k$  (3.82) is integrated over the phase  $k$  averaging volume  $V_k$ , and thereafter multiplied with the reciprocal averaging volume  $V$ . The resulting volume averaged equation is given by:

$$\frac{1}{V} \int_{V_k} \frac{\partial(\rho_k \psi_k)}{\partial t} dv + \frac{1}{V} \int_{V_k} \nabla \cdot (\rho_k \mathbf{v}_k \psi_k + \mathbf{J}_k) dv - \frac{1}{V} \int_{V_k} \sum_c \rho_{k,c} \phi_{k,c} dv = 0 \quad (3.121)$$

or, using a more compact notation:

$$\left\langle \frac{\partial(\rho_k \psi_k)}{\partial t} \right\rangle_V + \langle \nabla \cdot (\rho_k \mathbf{v}_k \psi_k + \mathbf{J}_k) \rangle_V - \left\langle \sum_c \rho_{k,c} \phi_{k,c} \right\rangle_V = 0 \quad (3.122)$$

The first, second and third terms in (3.122) have to be reformulated using the conventional volume averaging theorems<sup>16</sup>. The first theorem one makes use of relates the spatial average of a time derivative to the time derivative of a spatial average, and is called the *Leibnitz rule* for volume averaging:

$$\frac{1}{V} \int_{V_k} \frac{\partial \psi_k}{\partial t} dv = \frac{\partial}{\partial t} \left[ \frac{1}{V} \int_{V_k} \psi_k dv \right] - \frac{1}{V} \int_{A_I} \psi_k \mathbf{v}_I \cdot \mathbf{n}_k da \quad (3.123)$$

or, using the compact notation:

$$\left\langle \frac{\partial \psi_k}{\partial t} \right\rangle_V = \frac{\partial}{\partial t} \langle \psi_k \rangle_V - \frac{1}{V} \int_{A_I} \psi_k \mathbf{v}_I \cdot \mathbf{n}_k da \quad (3.124)$$

In this theorem  $A_I$  is the area of the interface between phase  $k$  and the other phase,  $\mathbf{n}_k$  is the outward unit normal of the infinitesimal element of area  $a$  of phase  $k$ , and  $\mathbf{v}_I$  is the velocity of the local interface. The theorem, which was originally derived by [236], represents a special form of the Leibnitz rule which is necessary for the particular case when the time derivative is discontinuous and reflects a Dirac delta function like character [90, 239, 58].

For the particular case when  $\psi_k = 1$  it is recognized that (3.117), (3.118) and (3.124) can be manipulated and expressed as

$$\langle 1 \rangle_V = \frac{1}{V} \int_V X_k dv = \frac{1}{V} \int_{V_k} dv = \alpha_k \quad (3.125)$$

and

$$0 = \frac{\partial \alpha_k}{\partial t} - \frac{1}{V} \int_{A_I} \mathbf{v}_I \cdot \mathbf{n}_k da \quad (3.126)$$

<sup>16</sup> The volume averaging theorems have been derived rigorously by several researchers [194, 199, 200, 38, 233, 235, 236, 237, 239, 110, 89, 90, 91].

in accordance with the work of [98, 99, 205, 239], among others.

The second theorem we utilize relates the average of a spatial derivative to the spatial derivative of the average, and is called the *Gauss rule* for volume averaging:

$$\frac{1}{V} \int_{V_k} (\nabla \psi_k) dv = \nabla \left[ \frac{1}{V} \int_{V_k} \psi_k dv \right] + \frac{1}{V} \int_{A_I} \psi_k \mathbf{n}_k da \quad (3.127)$$

or

$$\langle \nabla \psi_k \rangle = \nabla \langle \psi_k \rangle + \frac{1}{V} \int_{A_I} \psi_k \mathbf{n}_k da \quad (3.128)$$

This spatial averaging theorem was independently derived by Anderson and Jackson [7], Slattery [194] and Whitaker [233] applying three different methods [110]. In the method of Slattery [194] the theorem is elegantly deduced from the three dimensional Leibnitz's theorem<sup>17</sup> using advanced mathematics and a compact notation for the geometry [196] [38]. On the other hand, the use of weighted averages emerged from the work of Anderson and Jackson [7].

A special case of (3.128) is the theorem for the volume average of a divergence:

$$\langle \nabla \cdot \boldsymbol{\psi}_k \rangle_V = \nabla \cdot \langle \boldsymbol{\psi}_k \rangle_V + \frac{1}{V} \int_{A_I} \boldsymbol{\psi}_k \cdot \mathbf{n}_k da \quad (3.129)$$

where  $\boldsymbol{\psi}_k$  is interpreted as a vector or a second order tensor field [200]. The theorems (3.128) and (3.129) represent special forms of the Gauss rule which are necessary in the particular case when the spatial derivatives are discontinuous and reflect a Dirac delta function like character [58].

For the particular case when  $\psi_k = 1$  it is recognized that (3.128) reduces to:

$$0 = \nabla \alpha_k + \frac{1}{V} \int_{A_I} \mathbf{n}_k da \quad (3.130)$$

This is an important relationship frequently utilized manipulating the averaged terms [205] [239].

This completes the list of the mathematical tools required to reformulate the volume averaged equation (3.121) into a more practically useful form.

Applying the Leibnitz's rule (3.123) to the first term in (3.121) yields:

$$\frac{1}{V} \int_{V_k} \frac{\partial(\rho_k \psi_k)}{\partial t} dv = \frac{\partial}{\partial t} \left[ \frac{1}{V} \int_{V_k} \rho_k \psi_k dv \right] - \frac{1}{V} \int_{A_I} \rho_k \psi_k \mathbf{v}_I \cdot \mathbf{n}_k da \quad (3.131)$$

or, in the compact notation:

$$\left\langle \frac{\partial(\rho_k \psi_k)}{\partial t} \right\rangle_V = \frac{\partial}{\partial t} \langle \rho_k \psi_k \rangle_V - \frac{1}{V} \int_{A_I} \rho_k \psi_k \mathbf{v}_I \cdot \mathbf{n}_k da \quad (3.132)$$

<sup>17</sup> The three dimensional Leibnitz theorem is also referred to as the *general transport theorem*.

Applying the Gauss' rule (3.129) to the second and the third terms gives:

$$\frac{1}{V} \int_{V_k} \nabla \cdot (\rho_k \mathbf{v}_k \psi_k) dv = \nabla \cdot \left[ \frac{1}{V} \int_{V_k} (\rho_k \mathbf{v}_k \psi_k) dv \right] + \frac{1}{V} \int_{A_I} (\rho_k \mathbf{v}_k \psi_k) \cdot \mathbf{n}_k da \quad (3.133)$$

for the convective terms. In the compact notation we write

$$\langle \nabla \cdot (\rho_k \mathbf{v}_k \psi_k) \rangle_V = \nabla \cdot \langle \rho_k \mathbf{v}_k \psi_k \rangle_V + \frac{1}{V} \int_{A_I} (\rho_k \mathbf{v}_k \psi_k) \cdot \mathbf{n}_k da \quad (3.134)$$

Likewise, the diffusive terms are written:

$$\frac{1}{V} \int_{V_k} \nabla \cdot \mathbf{J}_k dv = \nabla \cdot \left[ \frac{1}{V} \int_{V_k} \mathbf{J}_k dv \right] + \frac{1}{V} \int_{A_I} \mathbf{J}_k \cdot \mathbf{n}_k da \quad (3.135)$$

and, in the compact notation:

$$\langle \nabla \cdot \mathbf{J}_k \rangle_V = \nabla \cdot \langle \mathbf{J}_k \rangle_V + \frac{1}{V} \int_{A_I} \mathbf{J}_k \cdot \mathbf{n}_k da \quad (3.136)$$

The fourth term is given directly by use of the volume average operator:

$$\frac{1}{V} \int_{V_k} \sum_c \rho_{k,c} \phi_{k,c} dv = \langle \sum_c \rho_{k,c} \phi_{k,c} \rangle_V \quad (3.137)$$

Substituting the novel relations (3.132), (3.134), (3.136) and (3.137) into the generic equation (3.122), the volume averaged equation becomes:

$$\begin{aligned} \frac{\partial \langle \rho_k \psi_k \rangle_V}{\partial t} + \nabla \cdot \langle \rho_k \mathbf{v}_k \psi_k \rangle_V + \nabla \cdot \langle \mathbf{J}_k \rangle_V = \\ - \frac{1}{V} \int_{A_I} (\psi_k \rho_k (\mathbf{v}_I - \mathbf{v}_k) + \mathbf{J}_k) \cdot \mathbf{n}_k da + \langle \sum_c \rho_{k,c} \phi_{k,c} \rangle_V \end{aligned} \quad (3.138)$$

Introducing the phase  $k$  volume fraction (3.120) and the intrinsic volume average operator (3.118), we get:

$$\begin{aligned} \frac{\partial (\alpha_k \langle \rho_k \psi_k \rangle_{V_k})}{\partial t} + \nabla \cdot (\alpha_k \langle \rho_k \mathbf{v}_k \psi_k \rangle_{V_k}) + \nabla \cdot (\alpha_k \langle \mathbf{J}_k \rangle_{V_k}) = \\ - \frac{1}{V} \int_{A_I} (\dot{m}_k \psi_k + \mathbf{J}_k \cdot \mathbf{n}_k) da + \alpha_k \langle \sum_c \rho_c \phi_c \rangle_{V_k} \end{aligned} \quad (3.139)$$

where  $\dot{m}_k$  is the interface mass transfer rate defined by:

$$\dot{m}_k = \rho_k (\mathbf{v}_k - \mathbf{v}_I) \cdot \mathbf{n}_k \quad (3.140)$$

The local jump conditions are averaged in a similar manner. Integrating the local jump condition (3.109) over the interfacial area  $A_I$  and then multiplying the result with the reciprocal averaging volume  $V$ , the averaged jump condition becomes:

$$\frac{1}{V} \int_{A_I} \left( \sum_k [\dot{m}_k \psi_k + \mathbf{J}_k \cdot \mathbf{n}_k] + M_I \right) da = 0 \quad (3.141)$$

The averaged equations governing each phase and the corresponding jump conditions are then achieved defining the specific values of the generic variables in (3.139) and (3.141) in accordance with Table 3.1.

The governing instantaneous volume averaged equations are examined next with focus on the principal approximations normally applied to the interfacial integral terms.

*Mass:*

The volume averaged continuity equation appears by substituting  $\psi_k = 1$ ,  $\mathbf{J}_k = 0$  and  $\phi_{c,k} = 0$  into (3.139):

$$\frac{\partial(\alpha_k \langle \rho_k \rangle_{V_k})}{\partial t} + \nabla \cdot (\alpha_k \langle \rho_k \mathbf{v}_k \rangle_{V_k}) = -\frac{1}{V} \int_{A_I} \dot{m}_k da \quad (3.142)$$

Introducing the values for the interface properties  $M_I = 0$  into (3.141), yields:

$$\sum_k \Gamma_{V_k} = 0 \quad (3.143)$$

where the interfacial mass transfer terms due to phase change is defined by:

$$\Gamma_{V_k} = \frac{1}{V} \int_{A_I} \rho_k (\mathbf{v}_I - \mathbf{v}_k) \cdot \mathbf{n}_k da = -\frac{1}{V} \int_{A_I} \dot{m}_k da = a_I \langle \dot{m}_k \rangle_{A_I} \quad (3.144)$$

in which  $\langle \dot{m}_k \rangle_{A_I} = -\int_{A_I} \dot{m}_k da / A_I$  denotes the interfacial area averaged mass transfer rate [112]. The interfacial area density is defined by:

$$a_I = A_I / V \quad (3.145)$$

*Momentum:*

The volume averaged momentum equation appears by substituting  $\psi_k = \mathbf{v}_k$ ,  $\mathbf{J}_k = \mathbf{T}_k$  and  $\phi_{c,k} = \mathbf{g}_{c,k}$  into (3.139):

$$\begin{aligned} \frac{\partial(\alpha_k \langle \rho_k \mathbf{v}_k \rangle_{V_k})}{\partial t} + \nabla \cdot (\alpha_k \langle \rho_k \mathbf{v}_k \mathbf{v}_k \rangle_{V_k}) + \nabla \cdot (\alpha_k \langle \mathbf{T}_k \rangle_{V_k}) = \\ -\frac{1}{V} \int_{A_I} (\dot{m}_k \mathbf{v}_k + \mathbf{T}_k \cdot \mathbf{n}_k) da + \alpha_k \langle \sum_c \rho_c \mathbf{g}_c \rangle_{V_k} \end{aligned} \quad (3.146)$$

Introducing the values for the interface properties  $\mathbf{M}_I = 2\sigma_I H_I \mathbf{n}_I + \nabla_I \sigma_I$  into (3.141), yields:

$$\sum_k (\mathbf{M}_k^I + \mathbf{M}_k^T) = \frac{1}{V} \int_{A_I} \mathbf{M}_I da \quad (3.147)$$

The interfacial momentum transfer due to phase change is defined by:

$$\mathbf{M}_k^I = \frac{1}{V} \int_{A_I} \rho_k \mathbf{v}_k (\mathbf{v}_I - \mathbf{v}_k) \cdot \mathbf{n}_k da = -\frac{1}{V} \int_{A_I} \dot{m}_k \mathbf{v}_k da = \Gamma_{Vk} \langle \mathbf{v}_k \rangle_{A_I}^{\Gamma_{Vk}} \quad (3.148)$$

in which the mass transfer weighted interfacial area averaged velocity  $\langle \mathbf{v}_k \rangle_{A_I}^{\Gamma_{Vk}}$  is defined in analogy to the mass-weighted averaged variables known from turbulence theory [112] (p. 133).

The interfacial momentum stresses yield:

$$\mathbf{M}_k^T = -\frac{1}{V} \int_{A_I} \mathbf{T}_k \cdot \mathbf{n}_k da = -\frac{1}{V} \int_{A_I} (p_k \mathbf{e} + \boldsymbol{\sigma}_k) \cdot \mathbf{n}_k da \quad (3.149)$$

where the total stress tensor of both phases has been modeled using the Newtonian strain-stress formulation.

It has become customary to rewrite the interfacial momentum transfer term  $\mathbf{M}_k^T$  in terms of the interfacially averaged pressure  $\langle p_k \rangle_{A_I}$  and shear stresses  $\langle \boldsymbol{\sigma}_k \rangle_{A_I}$  of phase  $k$  to separate the mean field effects from local effects [233, 194, 112, 54, 56, 153, 154, 193]. In the volume averaging approach the interfacial area averaged pressure is defined by:

$$\langle p_k \rangle_{A_I} = \frac{1}{A_I} \int_{A_I} p_k da \quad (3.150)$$

and the interfacial area averaged viscous stress term is defined by:

$$\langle \boldsymbol{\sigma}_k \rangle_{A_I} = \frac{1}{A_I} \int_{A_I} \boldsymbol{\sigma}_k da \quad (3.151)$$

The deviation between the local instantaneous pressure and the interfacial area averaged pressure is defined as:

$$\widehat{p}_{k,I} = p_k - \langle p_k \rangle_{A_I} \quad (3.152)$$

and similarly, the interfacial stress deviation yields:

$$\widehat{\boldsymbol{\sigma}}_{k,I} = \boldsymbol{\sigma}_k - \langle \boldsymbol{\sigma}_k \rangle_{A_I} \quad (3.153)$$

Using these definitions of the interfacial quantities, the stress terms in (3.146) can be expressed as:

$$\begin{aligned}
& -\nabla \cdot (\alpha_k \langle \mathbf{T}_k \rangle_{V_k}) - \frac{1}{V} \int_{A_I} (p_k \mathbf{e} + \boldsymbol{\sigma}_k) \cdot \mathbf{n}_k da \\
& = - \left[ \nabla (\alpha_k \langle p_k \rangle_{V_k}) + \nabla \cdot (\alpha_k \langle \boldsymbol{\sigma}_k \rangle_{V_k}) \right] \\
& - \left[ \langle p_k \rangle_{A_I} \mathbf{e} \cdot \frac{1}{V} \int_{A_I} \mathbf{n}_k da + \langle \boldsymbol{\sigma}_k \rangle_{A_I} \cdot \frac{1}{V} \int_{A_I} \mathbf{n}_k da \right. \\
& \quad \left. + \frac{1}{V} \int_{A_I} (\widehat{p}_{k,I} \mathbf{e} + \widehat{\boldsymbol{\sigma}}_{k,I}) \cdot \mathbf{n}_k da \right] \tag{3.154}
\end{aligned}$$

Besides, by making use of (3.130), introducing the interfacial momentum transfer term  $\mathbf{M}_k^T$  given by (3.149), and defining the generalized drag term by:

$$\mathbf{F}_k = \frac{1}{V} \int_{A_I} (\widehat{p}_{k,I} \mathbf{e} + \widehat{\boldsymbol{\sigma}}_{k,I}) \cdot \mathbf{n}_k da \tag{3.155}$$

we can further manipulate the stress terms in (3.154) in the following manner:

$$\begin{aligned}
& -\nabla \cdot (\alpha_k \langle \mathbf{T}_k \rangle_{V_k}) + \mathbf{M}_k^T \\
& = - \left[ \nabla (\alpha_k \langle p_k \rangle_{V_k}) + \nabla \cdot (\alpha_k \langle \boldsymbol{\sigma}_k \rangle_{V_k}) \right] \\
& - \left[ -\langle p_k \rangle_{A_I} \nabla \alpha_k - \langle \boldsymbol{\sigma}_k \rangle_{A_I} \cdot \nabla \alpha_k - \mathbf{F}_k \right] \tag{3.156} \\
& = -\alpha_k \nabla \langle p_k \rangle_{V_k} + (\langle p_k \rangle_{A_I} - \langle p_k \rangle_{V_k}) \nabla \alpha_k \\
& - \nabla \cdot (\alpha_k \langle \boldsymbol{\sigma}_k \rangle_{V_k}) + \langle \boldsymbol{\sigma}_k \rangle_{A_I} \cdot \nabla \alpha_k + \mathbf{F}_k \\
& \approx -\alpha_k \nabla \langle p_k \rangle_{V_k} - \nabla \cdot (\alpha_k \langle \boldsymbol{\sigma}_k \rangle_{V_k}) + \mathbf{F}_k = -\alpha_k \nabla \langle p_k \rangle_{V_k} + \mathbf{M}_k^d
\end{aligned}$$

where

$$\mathbf{M}_k^d = \langle p_k \rangle_{A_I} \nabla \alpha_k + \langle \boldsymbol{\sigma}_k \rangle_{A_I} \cdot \nabla \alpha_k + \mathbf{F}_k \tag{3.157}$$

The terms  $(\langle p_k \rangle_{A_I} - \langle p_k \rangle_{V_k}) \nabla \alpha_k + \langle \boldsymbol{\sigma}_k \rangle_{A_I} \cdot \nabla \alpha_k$  are referred to as the interfacial pressure difference effect (or the concentration gradient effect) and the combined interfacial shear and volume fraction gradient effect [67] [115], respectively. The interfacial pressure difference effect is normally assumed to be insignificant for the two-fluid model [54, 4, 125, 119]. That is, for two-phase flows one generally assumes that  $\langle p_k \rangle_{A_I} = \langle p_k \rangle_{V_k} = \langle p_l \rangle_{A_I} = \langle p_l \rangle_{V_l}$  for phases  $k$  and  $l$ , respectively. Moreover, for separated flows the combined interfacial shear and volume fraction gradient effect normally dominates over the generalized drag  $\mathbf{F}_k$ , whereas this combined effect is generally ignored for dispersed flows [115].

The generalized drag force per unit mixture volume which is acting on the dispersed phases of mean diameter  $d$  is commonly formulated as [112, 113, 114, 115, 168, 4, 54, 57, 58, 154, 119, 120]:

$$\begin{aligned}\mathbf{F}_d &= -\frac{1}{V} \int_{A_I} (\widehat{p}_{d,I} \mathbf{e} + \widehat{\boldsymbol{\sigma}}_{d,I}) \cdot \mathbf{n}_d da = N_d (\mathbf{f}_D + \mathbf{f}_V + \mathbf{f}_B + \mathbf{f}_L) \\ &= \frac{6\alpha_d}{\pi d^3} (\mathbf{f}_D + \mathbf{f}_V + \mathbf{f}_B + \mathbf{f}_L)\end{aligned}\quad (3.158)$$

where the  $\mathbf{f}$ -terms in the bracket denote the forces acting on a single sphere in a dilute mixture (assuming no particle-particle interactions) which are normally including the steady drag, virtual mass, Basset history and the lift forces. The  $N_d$  denotes the number of particles per unit volume and is defined by  $N_d = \frac{6\alpha_d}{\pi d^3}$ . The generalized drag force hypothesis is assumed valid for dilute flows provided that that the different forces are independent. Further details on the modeling of the interfacial coupling terms are discussed in the sect 5.2.

For wall bounded flows the wall interaction forces have a similar origin as the interfacial momentum transfer terms [129]. These terms are assessed in further details in sect 3.4.6.

For the surface tension forces we can utilize (3.130) and the mean value theorem for integrals, hence the term on the RHS of (3.147) can be expressed as [112] [129]:

$$\begin{aligned}\frac{1}{V} \int_{A_I} \mathbf{M}_I da &= \frac{1}{V} \int_{A_I} (2\sigma_I H_I \mathbf{n}_I + \nabla_I \sigma_I) da \\ &\approx 2\langle \sigma_I H_I \rangle_{A_I} \frac{1}{V} \int_{A_I} \mathbf{n}_I da + \frac{1}{V} \int_{A_I} \nabla_I \sigma_I da \\ &\approx 2\langle \sigma_I \rangle_{A_I} \langle H_I \rangle_{A_I} \nabla \alpha_2 + a_I \langle \nabla_I \sigma_I \rangle_{A_I}\end{aligned}\quad (3.159)$$

where  $\langle H_I \rangle_{A_I}$  is the interfacial area averaged curvature [112] [54] [129]. In this relation we adopt the sign convention defined by  $\mathbf{n}_I = \mathbf{n}_1$ . The mean curvature is still defined in accordance with (3.76).

For dispersed flows containing very small fluid particles the interfacial tension effects have occasionally been considered significant [129]. In this case, the average momentum jump condition (3.147) becomes [112] [54] [129]:

$$\begin{aligned}& \Gamma_{V_k} \langle \mathbf{v}_k \rangle_{A_I}^{\Gamma_{V_k}} + \langle p_k \rangle_{A_I} \nabla \alpha_k + \langle \boldsymbol{\sigma}_k \rangle_{A_I} \cdot \nabla \alpha_k + \mathbf{F}_k \\ & + \Gamma_{V_l} \langle \mathbf{v}_l \rangle_{A_I}^{\Gamma_{V_l}} + \langle p_l \rangle_{A_I} \nabla \alpha_l + \langle \boldsymbol{\sigma}_l \rangle_{A_I} \cdot \nabla \alpha_l + \mathbf{F}_l \\ & = 2\sigma_I \langle H_I \rangle_{A_I} \nabla \alpha_l + a_I \langle \nabla_I \sigma_I \rangle_{A_I}\end{aligned}\quad (3.160)$$

Nevertheless, it is common to neglect the variations in surface tension at the interfaces, and the interfacial pressures are generally related by the Young-Laplace equation [244] [138] [54]:

$$\langle p_k \rangle_{A_I} - \langle p_l \rangle_{A_I} \approx -2\sigma_I \langle H_I \rangle_{A_I} = -\sigma_I \left( \frac{1}{R_1} + \frac{1}{R_1} \right) \quad (3.161)$$

in which the curvature radii is defined in accordance with (3.64). In this case the averaged momentum jump condition can be expressed by:

$$\Gamma_{V_k} (\langle \mathbf{v}_k \rangle_{A_I}^{\Gamma_{V_k}} - \langle \mathbf{v}_l \rangle_{A_I}^{\Gamma_{V_l}}) + (\langle \boldsymbol{\sigma}_k \rangle_{A_I} - \langle \boldsymbol{\sigma}_l \rangle_{A_I}) \cdot \nabla \alpha_k + \mathbf{F}_k + \mathbf{F}_l \approx 0 \quad (3.162)$$

Provided that the interfacial area averaged velocities are parameterized in a consistent manner (i.e.,  $\Gamma_{V_k} (\langle \mathbf{v}_k \rangle_{A_I}^{\Gamma_{V_k}} - \langle \mathbf{v}_l \rangle_{A_I}^{\Gamma_{V_l}}) = 0$ ), this condition shows that the introduction of the surface tension force is in accordance with Newton's 3. law.

In practice, however, it is difficult to parameterize the interfacial area averaged velocity so in the momentum equation it's often set equal to the bulk velocity and in the momentum jump condition the mass transfer terms are simply neglected enabling a closure relation for the interfacial drag terms which are in agreement with Newton's 3. law. Hence,

$$(\langle \boldsymbol{\sigma}_k \rangle_{A_I} - \langle \boldsymbol{\sigma}_l \rangle_{A_I}) \cdot \nabla \alpha_k + \mathbf{F}_k + \mathbf{F}_l \approx 0 \quad (3.163)$$

For dispersed systems the interfacial tension terms are generally more important in the high resolution models simulating details of the local flow close to each individual interface.

*Energy:*

The volume averaged energy equation appears by substituting  $\psi_k = e_k + \frac{1}{2}v_k^2$ ,  $\mathbf{J}_k = \mathbf{T}_k \cdot \mathbf{v}_k + \mathbf{q}_k$  and  $\phi_{c,k} = \mathbf{v}_k \cdot \mathbf{g}_{c,k}$  into (3.139):

$$\begin{aligned} & \frac{\partial}{\partial t} \left( \alpha_k \langle \rho_k (e_k + \frac{1}{2}v_k^2) \rangle_{V_k} \right) + \nabla \cdot \left( \alpha_k \langle \rho_k \mathbf{v}_k (e_k + \frac{1}{2}v_k^2) \rangle_{V_k} \right) \\ & + \nabla \cdot \left( \alpha_k \langle \mathbf{T}_k \cdot \mathbf{v}_k \rangle_{V_k} \right) + \nabla \cdot \left( \alpha_k \langle \mathbf{q}_k \rangle_{V_k} \right) \\ & = -\frac{1}{V} \int_{A_I} \left( \dot{m}_k (e_k + \frac{1}{2}v_k^2) + (\mathbf{T}_k \cdot \mathbf{v}_k + \mathbf{q}_k) \cdot \mathbf{n}_k \right) da \\ & + \alpha_k \left\langle \sum_c \rho_{k,c} \mathbf{v}_{k,c} \cdot \mathbf{g}_{k,c} \right\rangle_{V_k} \end{aligned} \quad (3.164)$$

Introducing the values for the interface properties

$M_I = \nabla_I \cdot \mathbf{q}_I - \nabla_I \cdot (\sigma_I \mathbf{v}_I)$  into (3.141), yield:

$$\sum_k (E_k^E + E_k^W + E_k^\Gamma) = -\frac{1}{V} \int_{A_I} M_I da \quad (3.165)$$

where the interfacial energy transfer due to phase change is defined by:

$$\begin{aligned}
E_k^{\Gamma} &= \frac{1}{V} \int_{A_I} \rho_k (e_k + \frac{1}{2} v_k^2) (\mathbf{v}_I - \mathbf{v}_k) \cdot \mathbf{n}_k da = -\frac{1}{V} \int_{A_I} \dot{m}_k (e_k + \frac{1}{2} v_k^2) da \\
&= \Gamma_{V_k} \langle (e_k + \frac{1}{2} v_k^2) \rangle_{A_I}^{\Gamma_{V_k}}
\end{aligned} \tag{3.166}$$

in which  $\langle (e_k + \frac{1}{2} v_k^2) \rangle_{A_I}^{\Gamma_{V_k}}$  denotes the mass transfer weighted interfacial (internal and mechanical) energy [112] (p. 137).

The interfacial heat transfer is given by:

$$E_k^E = -\frac{1}{V} \int_{A_I} \mathbf{q}_k \cdot \mathbf{n}_k da = a_I \langle \mathbf{q}_k \cdot \mathbf{n}_k \rangle_{A_I}, \tag{3.167}$$

in which  $\langle \mathbf{q}_k \cdot \mathbf{n}_k \rangle_{A_I}$  denotes the interfacial area averaged heat transfer flux.

The interfacial work by viscous and pressure forces yields:

$$E_k^W = -\frac{1}{V} \int_{A_I} (\mathbf{T}_k \cdot \mathbf{v}_k) \cdot \mathbf{n}_k da \tag{3.168}$$

and the surface energy sources are expressed as the product of the interfacial area concentration and the averaged interfacial fluxes:

$$\begin{aligned}
\frac{1}{V} \int_{A_I} M_I da &= -\frac{1}{V} \int_{A_I} (-\nabla_I \cdot (\sigma_I \mathbf{v}_I) + \nabla_I \cdot \mathbf{q}_I) da \\
&= \langle \nabla_I \cdot (\sigma_I \mathbf{v}_I) \rangle_{A_I} a_I - \langle \nabla_I \cdot \mathbf{q}_I \rangle_{A_I} a_I
\end{aligned} \tag{3.169}$$

where  $-\langle \nabla_I \cdot \mathbf{q}_I \rangle_{A_I}$  and  $\langle \nabla_I \cdot (\sigma_I \mathbf{v}_I) \rangle_{A_I}$  are the interfacial area averaged interfacial energy fluxes.

*Internal Energy:*

It is not convenient to use (3.139) averaging the internal energy balance, as some of the terms do not fit within the generalized framework. Instead the averaged form of the internal energy equation is obtained by averaging (1.126). The resulting volume averaged internal energy equation is given by [192] [205]:

$$\begin{aligned}
&\frac{\partial}{\partial t} (\alpha_k \langle \rho_k e_k \rangle_{V_k}) + \nabla \cdot (\alpha_k \langle \rho_k \mathbf{v}_k e_k \rangle_{V_k}) = \\
&\quad - \alpha_k \langle \mathbf{T}_k : \nabla \mathbf{v}_k \rangle_{V_k} - \nabla \cdot (\alpha_k \langle \mathbf{q}_k \rangle_{V_k}) \\
&\quad - \frac{1}{V} \int_{A_I} (\dot{m}_k e_k + \mathbf{q}_k \cdot \mathbf{n}_k) da + \alpha_k \langle \sum_c \mathbf{j}_{k,c} \cdot \mathbf{g}_{k,c} \rangle_{V_k} \\
&= -\alpha_k \langle \sigma_k : \nabla \mathbf{v}_k \rangle_{V_k} - \alpha_k \langle p_k \nabla \cdot \mathbf{v}_k \rangle_{V_k} - \nabla \cdot (\alpha_k \langle \mathbf{q}_k \rangle_{V_k}) \\
&\quad - \frac{1}{V} \int_{A_I} (\dot{m}_k e_k + \mathbf{q}_k \cdot \mathbf{n}_k) da + \alpha_k \langle \sum_c \mathbf{j}_{k,c} \cdot \mathbf{g}_{k,c} \rangle_{V_k}
\end{aligned} \tag{3.170}$$

Alternatively, the internal energy balance can be deduced from the averaged counterparts of the kinetic energy equation (1.124) and the total energy equation (1.113).

The averaged form of the internal energy jump balance (3.101) can be written as

$$\sum_k (E_k^E + e_k^\Gamma) \approx 0 \quad (3.171)$$

and from (3.166) it is seen that  $e_k^\Gamma = \Gamma_{V_k} \langle e_k \rangle_{A_I}^{\Gamma_{V_k}}$ .

*Enthalpy:*

It is not convenient use (3.139) averaging the enthalpy equation as some of the terms do not fit within the generalized framework. Instead the averaged form of the enthalpy equation can be obtained by averaging (1.129) directly or from (3.170) and the enthalpy definition (1.128).

The volume averaged enthalpy equation is given by [192] [205]:

$$\begin{aligned} & \frac{\partial}{\partial t} (\alpha_k \langle \rho_k h_k \rangle_{V_k}) + \nabla \cdot (\alpha_k \langle \rho_k \mathbf{v}_k h_k \rangle_{V_k}) = \\ & \frac{\partial (\alpha_k \langle p_k \rangle_{V_k})}{\partial t} + \nabla \cdot (\alpha_k \langle \mathbf{v}_k p_k \rangle_{V_k}) \\ & - \alpha_k \langle \boldsymbol{\sigma}_k : \nabla \mathbf{v}_k \rangle_{V_k} - \alpha_k \langle p_k \nabla \cdot \mathbf{v}_k \rangle_{V_k} - \nabla \cdot (\alpha_k \langle \mathbf{q}_k \rangle_{V_k}) \\ & - \frac{1}{V} \int_{A_I} \left( \dot{m}_k \left( h_k - \frac{p_k}{\rho_k} \right) + \mathbf{q}_k \cdot \mathbf{n}_k \right) da + \alpha_k \langle \sum_c \mathbf{j}_{k,c} \cdot \mathbf{g}_{k,c} \rangle_{V_k} \end{aligned} \quad (3.172)$$

The averaged form of the simplified enthalpy jump balance (3.102) can be written as

$$\sum_k (E_k^E + h_k^\Gamma) \approx 0 \quad (3.173)$$

in which we have neglected the interfacial tension and heat flux effects. Besides, the additional interfacial jump condition term which occurs within the averaging process

$$\frac{1}{V} \int_{A_I} p_k (\mathbf{v}_I - \mathbf{v}_k) \cdot \mathbf{n}_k da \approx 0 \quad (3.174)$$

since the effect of wave propagation is assumed to be negligible [199] [192]. The interfacial heat transfer due to phase change is expressed as

$$h_k^\Gamma = \Gamma_{V_k} \langle h_k \rangle_{A_I}^{\Gamma_{V_k}} \quad (3.175)$$

*Temperature:*

The averaging of the temperature equation for multiphase reactive systems is not straight forward and numerous forms of the averaged equation can be found in the literature.

It is obviously not convenient to use (3.139) averaging the temperature equation, as the terms in the equation do not fit within the generalized framework. Instead the averaged form of the temperature equation might be deduced by averaging (1.150).

The volume averaged temperature equation is then given by:

$$\begin{aligned}
& \alpha_k \langle \rho_k C_{p,k} \frac{\partial T_k}{\partial t} \rangle_{V_k} + \alpha_k \langle \rho_k C_{p,k} \mathbf{v}_k \cdot \nabla T_k \rangle_{V_k} = \\
& - \nabla \cdot (\alpha_k \langle \mathbf{q}_k \rangle_{V_k}) - \alpha_k \langle \frac{T}{\rho} (\frac{\partial \rho}{\partial T})_{p,\omega} \frac{Dp}{Dt} \rangle_{V_k} \\
& - \nabla \cdot (\alpha_k \langle \boldsymbol{\sigma}_k : \nabla \mathbf{v}_k \rangle_{V_k}) + \alpha_k \langle \sum_c \mathbf{J}_{k,c} \cdot \mathbf{g}_{k,c} \rangle_{V_k} \\
& + \alpha_k \langle \sum_{c=1}^N \bar{h}_c \nabla \cdot (\frac{\mathbf{j}_c}{M_{w_c}}) \rangle_{V_k} + \alpha_k \langle \sum_{r=1}^q r_{r,c_{\text{ref}}} (-\Delta \bar{H}_{r,c_{\text{ref}}}) \rangle_{V_k} \\
& - \frac{1}{V} \int_{A_I} \mathbf{q}_k \cdot \mathbf{n}_k da
\end{aligned} \tag{3.176}$$

To achieve the solvable temperature equation frequently used in reactor analysis it is necessary to assume that  $C_{p,k}$  is constant within the averaging volume. In this particular case the continuity equation can be used manipulating the terms on the LHS of (3.176). In addition, in this approach the interfacial heat transfer term due to phase change has to be included by postulation.

Alternatively, a similar result is obtained from (3.172) by use of the complete differential (1.142). This method seems more appropriate as the derivation of the interfacial terms for example is in accordance with the standard averaging theorems, hence this method might be more rigorous. The alternative form of the averaged temperature is given in (3.204). However, the choice of model approximations should of course always be determined by comparison with physical observations.

*Chemical species:*

The volume averaged species mass balance appears by substituting  $\psi_k = \omega_{k,s}$ ,  $\mathbf{J}_k = \mathbf{j}_{k,s}$  and  $\phi_{c,k} = -R_{k,s}/\rho_{k,c}$  into (3.139):

$$\begin{aligned}
& \frac{\partial (\alpha_k \langle \rho_{k,s} \rangle_{V_k})}{\partial t} + \nabla \cdot (\alpha_k \langle \rho_{k,s} \mathbf{v}_k \rangle_{V_k}) + \nabla \cdot (\alpha_k \langle \mathbf{j}_{k,s} \rangle_{V_k}) = \\
& - \frac{1}{V} \int_{A_I} (\dot{m}_k \omega_{k,s} + \mathbf{j}_{k,s} \cdot \mathbf{n}_k) da + \alpha_k \langle R_{k,s} \rangle_{V_k}
\end{aligned} \tag{3.177}$$

Introducing the values for the interface properties  $M_I = R_{I,s}$  into (3.141), yields:

$$\sum_k (\mathbf{J}_{k,s}^I + \mathbf{J}_{k,s}^j) = \frac{1}{V} \int_{A_I} R_{I,s} da \tag{3.178}$$

The interfacial species mass transfer due to phase change is defined by:

$$\begin{aligned}\mathbf{J}_{k,s}^\Gamma &= \frac{1}{V} \int_{A_I} \rho_k \omega_{k,s} (\mathbf{v}_I - \mathbf{v}_k) \cdot \mathbf{n}_k da = -\frac{1}{V} \int_{A_I} \dot{m}_k \omega_{k,s} da \\ &= \Gamma_{V_k} \langle \omega_{k,s} \rangle_{A_I}^{\Gamma_{V_k}}\end{aligned}\quad (3.179)$$

in which the  $\langle \omega_{k,s} \rangle_{A_I}^{\Gamma_{V_k}}$  denotes the mass transfer weighted interfacial species  $s$  mass fraction [112] (p. 133).

The other interfacial mass transfer fluxes are given by:

$$\mathbf{J}_{k,s}^j = -\frac{1}{V} \int_{A_I} \mathbf{j}_{k,s} \cdot \mathbf{n}_k da = a_I \langle \mathbf{j}_{k,s} \cdot \mathbf{n}_k \rangle_{A_I} \quad (3.180)$$

in which  $\langle \mathbf{j}_{k,s} \cdot \mathbf{n}_k \rangle_{A_I}$  denotes the interfacial area averaged mass transfer flux.

The interfacial production term due to heterogeneous reactions is normally rewritten as:

$$\frac{1}{V} \int_{A_I} M_I da = \frac{1}{V} \int_{A_I} R_{I,s} da = \langle R_{I,s} \rangle_{A_I} a_I = \rho_{\text{Bulk}} \langle R_{I,s} \rangle^m \quad (3.181)$$

in which the interfacial reaction rate per unit interface area is commonly substituted by the more practical reaction rate per unit mass  $\langle R_{I,s} \rangle^m = \langle R_{I,s} \rangle_{A_I} a_I / \rho_{\text{Bulk}} (kg/kg, cat \times s)$  in which  $\rho_{\text{Bulk}}$  denotes the bulk density of the catalyst ( $kg, cat/m_r^3$ ).

In order to carry out computations with the volume averaged equations on the form (3.138) or (3.139), we need to relate the average of products to products of averages and derive constitutive equations for the interfacial coupling terms.

The first problem is generally solved by introducing mass- and phase weighted volume averaged variables and the concept of *spatial decomposition* of these variables [98, 81].

The mass-weighted volume average of the quantity  $\psi_k$  is defined by:

$$\langle \psi_k \rangle_V^{X_k \rho_k} = \frac{\frac{1}{V} \int \rho_k \psi_k X_k dv}{\frac{1}{V} \int \rho_k X_k dv} = \frac{\langle \rho_k \psi_k \rangle_V}{\langle \rho_k \rangle_V} = \frac{\langle \rho_k \psi_k \rangle_{V_k}}{\langle \rho_k \rangle_{V_k}}, \quad (3.182)$$

in which the intrinsic volume average coincides with the  $X_k$ -weighted average as defined by (3.118).

We can now adopt the concept of *spatial decomposition* of the mass-weighted variables to relate the average of products to products of average.

Let  $\hat{\psi}_k$  represent the spatial deviation of the point variable  $\psi_k$  from the mass-weighted volume average value  $\langle \psi_k \rangle_V^{X_k \rho_k}$ , as defined by:

$$\widehat{\psi}_k = \psi_k - \langle \psi_k \rangle_V^{X_k \rho_k} \quad (3.183)$$

where  $\psi_k$  represents the local variable at a point in space  $\mathbf{r}$ . The concept of spatial decomposition of the volume averaged variables was initially proposed by Whitaker [233] [235] [236] for applications in multiphase flow models in analogy to the conventional temporal decomposition of the instantaneous variables used in the study of turbulent transport phenomena [75] [131]. The spatial decomposition concept was later slightly modified by Gray and co-workers [89] [98] [99] [91] to eliminate an inherent inconsistency for modeling dispersion as a diffusive mechanism.

Introducing (3.183) into (3.182) we obtain the important result:

$$\begin{aligned} \langle \rho_k \rangle_V \langle \psi_k \rangle_V^{X_k \rho_k} &= \langle \rho_k \psi_k \rangle_V \\ &= \langle \rho_k (\langle \psi_k \rangle_V^{X_k \rho_k} + \widehat{\psi}_k) \rangle_V \\ &= \langle \rho_k \rangle_V \langle \psi_k \rangle_V^{X_k \rho_k} + \langle \rho_k \widehat{\psi}_k \rangle_V \\ &= \langle \rho_k \rangle_V \langle \psi_k \rangle_V^{X_k \rho_k}, \end{aligned} \quad (3.184)$$

in which we have shown that  $\langle \rho_k \widehat{\psi}_k \rangle_V = \alpha_k \langle \rho_k \widehat{\psi}_k \rangle_{V_k} = \langle \widehat{\psi}_k \rangle_V^{X_k \rho_k} = 0$  because  $\langle \psi_k \rangle_V^{X_k \rho_k}$  is constant within  $V$ .

Moreover, utilizing (3.184) the convective term in the averaged equation (3.139) can be rewritten as:

$$\begin{aligned} \langle \rho_k \mathbf{v}_k \psi_k \rangle_{V_k} &= \langle \rho_k \mathbf{v}_k \psi_k \rangle_V^{X_k} \\ &= \langle \rho_k (\langle \mathbf{v}_k \rangle_V^{X_k \rho_k} + \widehat{\mathbf{v}}_k) (\langle \psi_k \rangle_V^{X_k \rho_k} + \widehat{\psi}_k) \rangle_{V_k} \\ &= \langle \rho_k \rangle_{V_k} \langle \mathbf{v}_k \rangle_V^{X_k \rho_k} \langle \psi_k \rangle_V^{X_k \rho_k} + \langle \rho_k \widehat{\psi}_k \widehat{\mathbf{v}}_k \rangle_{V_k} \end{aligned} \quad (3.185)$$

Introducing the mass-weighted variables (3.182) and manipulating the convective terms by use of the concept of spatial decomposition (3.183), the averaged equation (3.139) can be written as:

$$\begin{aligned} \frac{\partial (\alpha_k \langle \rho_k \rangle_{V_k} \langle \psi_k \rangle_V^{X_k \rho_k})}{\partial t} &+ \nabla \cdot (\alpha_k \langle \rho_k \rangle_{V_k} \langle \mathbf{v}_k \rangle_V^{X_k \rho_k} \langle \psi_k \rangle_V^{X_k \rho_k}) \\ &+ \nabla \cdot (\alpha_k \langle \mathbf{J}_k \rangle_{V_k}) = -\frac{1}{V} \int_{A_I} (\dot{m}_k \psi_k + \mathbf{J}_k) \cdot \mathbf{n}_k da + \alpha_k \sum_c \langle \rho_{k,c} \phi_c \rangle_{V_k} \\ &- \nabla \cdot (\alpha_k \langle \rho_k \widehat{\mathbf{v}}_k \widehat{\psi}_k \rangle_{V_k}) \end{aligned} \quad (3.186)$$

It is easily seen that the principal closure problem is maintained since three undetermined terms appear in the volume averaged equations (3.186). The first term,  $-\nabla \cdot (\alpha_k \langle \rho_k \widehat{\mathbf{v}}_k \widehat{\psi}_k \rangle_{V_k})$ , is called the microscopic deviation term. In principle these terms correspond to the single phase SGS turbulence fluxes and might be modeled adopting a single phase turbulence model. In LES

these covariance terms are normally modeled as sub-grid scale turbulence fluxes adopting the Smagorinsky model. On the other hand, in connection with the double averaging operators (i.e., adopting the time or ensemble after volume averaging procedures) these terms are normally neglected [243, 10]. The second term,  $-\frac{1}{V} \int_{A_I} \mathbf{J}_k \cdot \mathbf{n}_k da$ , accounts for the effects of interfacial stress, heat and species mass transfer, whereas the third term,  $\frac{1}{V} \int_{A_I} \dot{m}_k \psi_k da$ , accounts for the interfacial transfer due to phase change.

To illustrate the remaining covariance modeling task required closing the model, the fairly rigorous instantaneous volume averaged equations expressed in terms of mass-weighted quantities are listed below.

*Mass:*

The modified volume averaged continuity equation deduced from (3.142) can be written as:

$$\frac{\partial}{\partial t} \left( \alpha_k \langle \rho_k \rangle_{V_k} \right) + \nabla \cdot \left( \alpha_k \langle \rho_k \rangle_{V_k} \langle \mathbf{v}_k \rangle_V^{X_k \rho_k} \right) = \Gamma_{V_k} \quad (3.187)$$

The interfacial mass transfer flux  $\Gamma_{V_k}$  needs to be approximated providing parameterizations for the unknown quantities in (3.144).

*Momentum:*

The modified volume averaged momentum equation deduced from (3.146) can be written as:

$$\begin{aligned} & \frac{\partial}{\partial t} \left( \alpha_k \langle \rho_k \rangle_{V_k} \langle \mathbf{v}_k \rangle_V^{X_k \rho_k} \right) + \nabla \cdot \left( \alpha_k \langle \rho_k \rangle_{V_k} \langle \mathbf{v}_k \rangle_V^{X_k \rho_k} \langle \mathbf{v}_k \rangle_V^{X_k \rho_k} \right) \\ &= -\nabla \cdot \left( \alpha_k \langle \langle \mathbf{T}_k \rangle_{V_k} + \langle \mathbf{T}_k \rangle_{V_k}^{Re} \right) + \mathbf{M}_k^T \\ & \quad + \Gamma_{V_k} \langle \mathbf{v}_k \rangle_{A_I}^{\Gamma_{V_k}} + \alpha_k \left\langle \sum_c \rho_{k,c} \mathbf{g}_c \right\rangle_{V_k} \\ & \approx -\alpha_k \nabla \langle p_k \rangle_{V_k} - \nabla \cdot \left( \alpha_k \langle \langle \boldsymbol{\sigma}_k \rangle_{V_k} + \langle \mathbf{T}_k \rangle_{V_k}^{Re} \right) + \mathbf{F}_k \\ & \quad + \Gamma_{V_k} \langle \mathbf{v}_k \rangle_{A_I}^{\Gamma_{V_k}} + \alpha_k \left\langle \sum_c \rho_{k,c} \mathbf{g}_c \right\rangle_{V_k} \end{aligned} \quad (3.188)$$

in which  $\langle \mathbf{T}_k \rangle_{V_k}^{Re} = \langle \rho_k \widehat{\mathbf{v}}_k \widehat{\mathbf{v}}_k \rangle_{V_k}$ . In addition, closure relations are needed for the interfacial terms (3.148), (3.158) and (3.159).

*Energy:*

The modified volume averaged energy equation deduced from (3.164) can be written as:

$$\begin{aligned} & \frac{\partial}{\partial t} \left( \alpha_k \langle \rho_k \rangle_{V_k} \langle e_k \rangle_V^{X_k \rho_k} + \frac{1}{2} \langle \langle v_k \rangle_V^{X_k \rho_k} \rangle^2 + \frac{1}{2} \langle \widehat{\mathbf{v}}_k \cdot \widehat{\mathbf{v}}_k \rangle_V^{X_k \rho_k} \right) \\ & + \nabla \cdot \left( \alpha_k \langle \langle \rho_k \rangle_{V_k} \langle \mathbf{v}_k \rangle_V^{X_k \rho_k} \langle e_k \rangle_V^{X_k \rho_k} + \langle \rho_k \widehat{\mathbf{v}}_k \widehat{e}_k \rangle_{V_k} \right) \end{aligned}$$

$$\begin{aligned}
& + \frac{1}{2} \nabla \cdot \left( \alpha_k \langle \rho_k \rangle_{V_k} \langle \mathbf{v}_k \rangle_V^{X_k \rho_k} (\langle v_k \rangle_V^{X_k \rho_k})^2 + \langle \widehat{\mathbf{v}}_k \cdot \widehat{\mathbf{v}}_k \rangle_V^{X_k \rho_k} \right) \\
& + \nabla \cdot \left( \langle \mathbf{v}_k \rangle_V^{X_k \rho_k} \cdot (\alpha_k \langle \rho_k \widehat{\mathbf{v}}_k \widehat{\mathbf{v}}_k \rangle_{V_k}) \right) \\
& + \frac{1}{2} \nabla \cdot \left( \alpha_k \langle \rho_k \rangle_{V_k} \langle \widehat{\mathbf{v}}_k (\widehat{\mathbf{v}}_k \cdot \widehat{\mathbf{v}}_k) \rangle_V^{X_k \rho_k} \right) + \nabla \cdot \left( \alpha_k \langle \mathbf{q}_k \rangle_{V_k} \right) \\
& + \nabla \cdot \left( \alpha_k (\langle \mathbf{T}_k \rangle_{V_k} \cdot \langle \mathbf{v}_k \rangle_V^{X_k \rho_k} + \langle \mathbf{T}_k \cdot \widehat{\mathbf{v}}_k \rangle_{V_k}) \right) \\
& = \Gamma_{V_k} \left( \langle e_k \rangle_{A_I}^{\Gamma_{V_k}} + \frac{1}{2} (\langle \mathbf{v}_k \rangle_{A_I}^{\Gamma_{V_k}})^2 \right) + E_k^W + E_k^E \\
& \quad + \alpha_k \left\langle \sum_c \rho_{k,c} \mathbf{v}_{k,c} \cdot \mathbf{g}_{k,c} \right\rangle_{V_k}
\end{aligned} \tag{3.189}$$

The interfacial work by viscous and pressure forces (3.168) can be rearranged decomposing the velocity as:

$$\begin{aligned}
E_k^W &= - \frac{1}{V} \int_{A_I} (\mathbf{T}_k \cdot \mathbf{v}_k) \cdot \mathbf{n}_k da \\
&= - \frac{1}{V} \int_{A_I} (\mathbf{T}_k \cdot (\langle \mathbf{v}_k \rangle_V^{X_k \rho_k} + \widehat{\mathbf{v}}_k)) \cdot \mathbf{n}_k da \\
&= \mathbf{M}_k^T \cdot \langle \mathbf{v}_k \rangle_V^{X_k \rho_k} + E_k^{\widehat{W}}
\end{aligned} \tag{3.190}$$

where  $E_k^{\widehat{W}}$  is called the interfacial extra work [56].

Besides, constitutive equations are required for the unknown quantities in (3.166), (3.167) and (3.169).

#### *Mechanical Energy:*

The volume averaged kinetic energy equation can be derived by talking the scalar product of the averaged velocity with the momentum equation (3.188). Without introducing the normal simplifications assumed valid for dispersed flows, the result is:

$$\begin{aligned}
& \frac{\partial}{\partial t} \left( \alpha_k \langle \rho_k \rangle_{V_k} \frac{1}{2} (\langle v_k \rangle_V^{X_k \rho_k})^2 \right) \\
& + \nabla \cdot \left( \alpha_k \langle \rho_k \rangle_{V_k} \langle \mathbf{v}_k \rangle_V^{X_k \rho_k} \frac{1}{2} (\langle v_k \rangle_V^{X_k \rho_k})^2 \right) \\
& = - \langle \mathbf{v}_k \rangle_V^{X_k \rho_k} \cdot \nabla \cdot \left( \alpha_k (\langle \mathbf{T}_k \rangle_{V_k} + \langle \mathbf{T}_k \rangle_{V_k}^{Re}) \right) + \langle \mathbf{v}_k \rangle_V^{X_k \rho_k} \cdot \mathbf{M}_k^T \\
& \quad + \Gamma_{V_k} \langle \mathbf{v}_k \rangle_{A_I}^{\Gamma_{V_k}} \cdot \langle \mathbf{v}_k \rangle_V^{X_k \rho_k} + \alpha_k \left\langle \sum_c \rho_{k,c} \mathbf{g}_c \right\rangle_{V_k} \cdot \langle \mathbf{v}_k \rangle_V^{X_k \rho_k}
\end{aligned} \tag{3.191}$$

A simplified formulation of the volume averaged mechanical energy equation supposedly valid for dispersed flows only can be expressed as:

$$\begin{aligned}
& \frac{\partial}{\partial t} \left( \alpha_k \langle \rho_k \rangle_{V_k} \frac{1}{2} (\langle v_k \rangle_V^{X_k \rho_k})^2 \right) \\
& + \nabla \cdot \left( \alpha_k \langle \rho_k \rangle_{V_k} \langle \mathbf{v}_k \rangle_V^{X_k \rho_k} \frac{1}{2} (\langle v_k \rangle_V^{X_k \rho_k})^2 \right) \\
& = -\alpha_k \langle \mathbf{v}_k \rangle_V^{X_k \rho_k} \cdot \nabla \langle \rho_k \rangle_{V_k} \\
& \quad - \langle \mathbf{v}_k \rangle_V^{X_k \rho_k} \cdot \nabla \cdot \left( \alpha_k (\langle \boldsymbol{\sigma}_k \rangle_{V_k} + \langle T_k \rangle_{V_k}^{Re}) \right) + \langle \mathbf{v}_k \rangle_V^{X_k \rho_k} \cdot \mathbf{F}_k \\
& \quad + \Gamma_{V_k} \langle \mathbf{v}_k \rangle_{A_I}^{\Gamma_{V_k}} \cdot \langle \mathbf{v}_k \rangle_V^{X_k \rho_k} + \alpha_k \left\langle \sum_c \rho_{k,c} \mathbf{g}_c \right\rangle_{V_k} \cdot \langle \mathbf{v}_k \rangle_V^{X_k \rho_k}
\end{aligned} \tag{3.192}$$

In which the identity:

$$\begin{aligned}
& \langle \mathbf{v}_k \rangle_V^{X_k \rho_k} \cdot \left( \frac{\partial}{\partial t} (\alpha_k \langle \rho_k \rangle_{V_k} \langle \mathbf{v}_k \rangle_V^{X_k \rho_k}) + \nabla \cdot (\alpha_k \langle \rho_k \rangle_{V_k} \langle \mathbf{v}_k \rangle_V^{X_k \rho_k}) \right) \\
& = \frac{\partial}{\partial t} \left( \alpha_k \langle \rho_k \rangle_{V_k} \frac{1}{2} (\langle v_k \rangle_V^{X_k \rho_k})^2 \right) \\
& \quad + \nabla \cdot \left( \alpha_k \langle \rho_k \rangle_{V_k} \langle \mathbf{v}_k \rangle_V^{X_k \rho_k} \frac{1}{2} (\langle v_k \rangle_V^{X_k \rho_k})^2 \right)
\end{aligned} \tag{3.193}$$

has been used [112, 56].

An apparent internal energy equation can be derived by subtracting (3.192) from (3.183). The result is:

$$\begin{aligned}
& \frac{\partial}{\partial t} \left( \alpha_k \langle \rho_k \rangle_{V_k} (\langle e_k \rangle_V^{X_k \rho_k} + \frac{1}{2} \langle \widehat{\mathbf{v}}_k \cdot \widehat{\mathbf{v}}_k \rangle_V^{X_k \rho_k}) \right) \\
& + \nabla \cdot \left( \alpha_k (\langle \rho_k \rangle_{V_k} \langle \mathbf{v}_k \rangle_V^{X_k \rho_k} \langle e_k \rangle_V^{X_k \rho_k} + \langle \rho_k \widehat{\mathbf{v}}_k \widehat{e}_k \rangle_{V_k}) \right) \\
& + \frac{1}{2} \nabla \cdot \left( \alpha_k \langle \rho_k \rangle_{V_k} \langle \mathbf{v}_k \rangle_V^{X_k \rho_k} \langle \widehat{\mathbf{v}}_k \cdot \widehat{\mathbf{v}}_k \rangle_V^{X_k \rho_k} \right) \\
& + \frac{1}{2} \nabla \cdot \left( \alpha_k \langle \rho_k \rangle_{V_k} \langle \widehat{\mathbf{v}}_k (\widehat{\mathbf{v}}_k \cdot \widehat{\mathbf{v}}_k) \rangle_V^{X_k \rho_k} \right) + \nabla \cdot \left( \alpha_k \langle \mathbf{q}_k \rangle_{V_k} \right) \\
& + \alpha_k \left( \langle \boldsymbol{\sigma}_k \rangle_{V_k} + \langle T_k \rangle_{V_k}^{Re} \right) : \nabla \langle \mathbf{v}_k \rangle_V^{X_k \rho_k} + \nabla \cdot \left( \alpha_k \langle T_k \cdot \widehat{\mathbf{v}}_k \rangle_{V_k} \right) \\
& + \alpha_k \langle p_k \rangle_{V_k} \nabla \cdot \langle \mathbf{v}_k \rangle_V^{X_k \rho_k} = \Gamma_{V_k} \left( \langle e_k \rangle_{A_I}^{\Gamma_{V_k}} + \frac{1}{2} (\langle \mathbf{v}_k \rangle_{A_I}^{\Gamma_{V_k}})^2 \right) \\
& - \langle \mathbf{v}_k \rangle_{A_I}^{\Gamma_{V_k}} \cdot \langle \mathbf{v}_k \rangle_V^{X_k \rho_k} \Big) + E_k^{\widehat{W}} + E_k^E \\
& + \alpha_k \left( \left\langle \sum_c \rho_{k,c} \mathbf{v}_{k,c} \cdot \mathbf{g}_{k,c} \right\rangle_{V_k} - \left\langle \sum_c \rho_{k,c} \mathbf{g}_c \right\rangle_{V_k} \cdot \langle \mathbf{v}_k \rangle_V^{X_k \rho_k} \right)
\end{aligned} \tag{3.194}$$

For the particular systems where gravity is the only external force considered, the corresponding energy source terms vanish.

*Internal Energy:*

The modified volume averaged internal energy equation can be deduced from (3.170) introducing a spatial decomposition of the velocity variable. The result is:

$$\begin{aligned}
& \frac{\partial}{\partial t} \left( \alpha_k \langle \rho_k \rangle_{V_k} \langle e_k \rangle_V^{X_k \rho_k} \right) + \nabla \cdot \left( \alpha_k \langle \rho_k \rangle_{V_k} \langle \mathbf{v}_k \rangle_V^{X_k \rho_k} \langle e_k \rangle_V^{X_k \rho_k} \right) \\
&= -\alpha_k \langle \boldsymbol{\sigma}_k \rangle_{V_k} : \nabla \langle \mathbf{v}_k \rangle_V^{X_k \rho_k} - \alpha_k \langle p_k \rangle_{V_k} \nabla \cdot \langle \mathbf{v}_k \rangle_V^{X_k \rho_k} \\
&\quad - \alpha_k \langle \boldsymbol{\sigma}_k : \nabla \widehat{\mathbf{v}}_k \rangle_{V_k} - \alpha_k \langle p_k \nabla \cdot \widehat{\mathbf{v}}_k \rangle_{V_k} - \nabla \cdot (\alpha_k \langle \mathbf{q}_k \rangle_{V_k}) \\
&\quad + \Gamma_k \langle e_k \rangle_{A_I}^{\Gamma V_k} + E_k^E - \nabla \cdot (\alpha_k \langle \rho_k \widehat{\mathbf{v}}_k \widehat{\mathbf{e}}_k \rangle_{V_k}) + \alpha_k \left\langle \sum_c \mathbf{j}_{k,c} \cdot \mathbf{g}_{k,c} \right\rangle_{V_k}
\end{aligned} \tag{3.195}$$

The averaged form of the internal energy jump balance (3.101) can be written as

$$\sum_k (E_k^E + e_k^\Gamma) \approx 0 \tag{3.196}$$

From (3.165) we observe that  $e_k^\Gamma = \Gamma_{V_k} \langle e_k \rangle_{A_I}^{\Gamma V_k}$ .

Subtracting the equation for the averaged internal energy (3.195) from the apparent internal energy equation (3.194) gives an equation for the spatial covariance expressing an average deviating kinetic energy:

$$\begin{aligned}
& \frac{\partial}{\partial t} \left( \alpha_k \langle \rho_k \rangle_{V_k} \left( \frac{1}{2} \langle \widehat{\mathbf{v}}_k \cdot \widehat{\mathbf{v}}_k \rangle_V^{X_k \rho_k} \right) \right) \\
&+ \nabla \cdot \left( \alpha_k \langle \rho_k \rangle_{V_k} \langle \mathbf{v}_k \rangle_V^{X_k \rho_k} \left( \frac{1}{2} \langle \widehat{\mathbf{v}}_k \cdot \widehat{\mathbf{v}}_k \rangle_V^{X_k \rho_k} \right) \right) \\
&+ \nabla \cdot \left( \alpha_k \langle \rho_k \rangle_{V_k} \left( \frac{1}{2} \langle \widehat{\mathbf{v}}_k (\widehat{\mathbf{v}}_k \cdot \widehat{\mathbf{v}}_k) \rangle_V^{X_k \rho_k} \right) \right) \\
&+ \alpha_k \langle \mathbb{T}_k \rangle_{V_k}^{Re} : \nabla \langle \mathbf{v}_k \rangle_V^{X_k \rho_k} + \nabla \cdot \left( \alpha_k \langle \mathbb{T}_k \cdot \widehat{\mathbf{v}}_k \rangle_{V_k} \right) \\
&= \Gamma_{V_k} \left( \frac{1}{2} \langle (\langle \mathbf{v}_k \rangle_{A_I}^{\Gamma V_k})^2 \rangle - \langle \mathbf{v}_k \rangle_{A_I}^{\Gamma V_k} \cdot \langle \mathbf{v}_k \rangle_V^{X_k \rho_k} \right) \\
&+ \alpha_k \left( \left\langle \sum_c \rho_{k,c} \mathbf{v}_{k,c} \cdot \mathbf{g}_{k,c} \right\rangle_{V_k} - \left\langle \sum_c \rho_{k,c} \mathbf{g}_{k,c} \right\rangle_{V_k} \cdot \langle \mathbf{v}_k \rangle_V^{X_k \rho_k} \right) \\
&- \alpha_k \left\langle \sum_c \mathbf{j}_{k,c} \cdot \mathbf{g}_{k,c} \right\rangle_{V_k} + E_k^{\widehat{W}}
\end{aligned} \tag{3.197}$$

*Enthalpy:*

The modified volume averaged enthalpy equation can be deduced from (3.172) or alternatively from (3.195) and the relations between the averaged internal energy and the enthalpy:

$$\langle e_k \rangle_V^{X_k \rho_k} = \langle h_k \rangle_V^{X_k \rho_k} - \langle p_k \rangle_{V_k} / \langle \rho_k \rangle_{V_k} \tag{3.198}$$

$$\langle e_k \rangle_{A_I}^{\Gamma_{V_k}} = \langle h_k \rangle_{A_I}^{\Gamma_{V_k}} - \langle p_k \rangle_{A_I}^{\Gamma_{V_k}} / \langle \rho_k \rangle_{A_I}^{\Gamma_{V_k}} \quad (3.199)$$

The result is:

$$\begin{aligned} & \frac{\partial}{\partial t} (\alpha_k \langle \rho_k \rangle_{V_k} \langle h_k \rangle_V^{X_k \rho_k}) \\ & + \nabla \cdot \left( \alpha_k \langle \rho_k \rangle_{V_k} \langle \mathbf{v}_k \rangle_V^{X_k \rho_k} \langle h_k \rangle_V^{X_k \rho_k} \right) = \\ & \frac{\partial (\alpha_k \langle p_k \rangle_{V_k})}{\partial t} + \nabla \cdot (\alpha_k \langle \mathbf{v}_k \rangle_V^{X_k \rho_k} \langle p_k \rangle_{V_k}) + \nabla \cdot (\alpha_k \langle \widehat{\mathbf{v}}_k p_k \rangle_{V_k}) \\ & - \alpha_k \langle \boldsymbol{\sigma}_k \rangle_{V_k} : \nabla \langle \mathbf{v}_k \rangle_V^{X_k \rho_k} - \alpha_k \langle p_k \rangle_{V_k} \nabla \cdot \langle \mathbf{v}_k \rangle_V^{X_k \rho_k} \\ & - \alpha_k \langle \boldsymbol{\sigma}_k : \nabla \widehat{\mathbf{v}}_k \rangle_{V_k} - \alpha_k \langle p_k \nabla \cdot \widehat{\mathbf{v}}_k \rangle_{V_k} - \nabla \cdot (\alpha_k \langle \mathbf{q}_k \rangle_{V_k}) \\ & - \nabla \cdot (\alpha_k \langle \rho_k \widehat{\mathbf{v}}_k \widehat{h}_k \rangle_{V_k}) + \alpha_k \left\langle \sum_c \mathbf{j}_{k,c} \cdot \mathbf{g}_{k,c} \right\rangle_{V_k} \\ & + \Gamma_{V_k} \langle h_k \rangle_{A_I}^{\Gamma_{V_k}} + E_k^E \end{aligned} \quad (3.200)$$

The averaged form of the enthalpy jump balance (3.101) can be written as:

$$\sum_k (E_k^E + h_k^\Gamma) \approx 0 \quad (3.201)$$

in which  $h_k^\Gamma = \Gamma_{V_k} \langle h_k \rangle_{A_I}^{\Gamma_{V_k}}$ .

*Temperature:*

The averaged temperature equation can be derived from the averaged enthalpy equation (3.200) by use of the complete differential (1.142). In this case the averaged enthalpy equation is first reformulated by use of the averaged continuity equation (3.187). The intermediate result is:

$$\begin{aligned} & \alpha_k \langle \rho_k \rangle_{V_k} \left( \frac{\partial \langle h_k \rangle_V^{X_k \rho_k}}{\partial t} + \langle \mathbf{v}_k \rangle_V^{X_k \rho_k} \cdot \nabla \langle h_k \rangle_V^{X_k \rho_k} \right) = \\ & \frac{\partial (\alpha_k \langle p_k \rangle_{V_k})}{\partial t} + \langle \mathbf{v}_k \rangle_V^{X_k \rho_k} \cdot \nabla (\alpha_k \langle p_k \rangle_{V_k}) + \nabla \cdot (\alpha_k \langle \widehat{\mathbf{v}}_k p_k \rangle_{V_k}) \\ & - \alpha_k \langle p_k \nabla \cdot \widehat{\mathbf{v}}_k \rangle_{V_k} - \alpha_k \langle \boldsymbol{\sigma}_k \rangle_{V_k} : \nabla \langle \mathbf{v}_k \rangle_V^{X_k \rho_k} - \alpha_k \langle \boldsymbol{\sigma}_k : \nabla \widehat{\mathbf{v}}_k \rangle_{V_k} \\ & - \nabla \cdot (\alpha_k \langle \rho_k \widehat{\mathbf{v}}_k \widehat{h}_k \rangle_{V_k}) + \alpha_k \left\langle \sum_c \mathbf{j}_{k,c} \cdot \mathbf{g}_{k,c} \right\rangle_{V_k} - \nabla \cdot (\alpha_k \langle \mathbf{q}_k \rangle_{V_k}) \\ & + \Gamma_{V_k} \langle h_k \rangle_{A_I}^{\Gamma_{V_k}} + E_k^E - \Gamma_{V_k} \langle h_k \rangle_V^{X_k \rho_k} \end{aligned} \quad (3.202)$$

The volume averaged form of the complete differential (1.142) can be approximated as:

$$\begin{aligned}
\frac{D\langle h_k \rangle_V^{X_k \rho_k}}{Dt} &= \langle C_{p,k} \rangle_{V_k} \frac{D\langle T_k \rangle_{V_k}}{Dt} \\
&+ \left( \frac{1}{\langle \rho_k \rangle_{V_k}} + \frac{\langle T_k \rangle_{V_k}}{\langle \rho_k \rangle_{V_k}^2} \left( \frac{\partial \langle \rho_k \rangle_{V_k}}{\partial \langle T_k \rangle_{V_k}} \right)_{p,\omega} \right) \frac{D\langle p_k \rangle_{V_k}}{Dt} \\
&- \frac{1}{\langle \rho_k \rangle_{V_k}} \left[ \left\langle \sum_{c=1}^N \bar{h}_c \nabla \cdot \left( \frac{\mathbf{j}_c}{M_{w_c}} \right) \right\rangle_{V_k} + \left\langle \sum_{r=1}^q r_{r,c_{\text{ref}}} (-\Delta \bar{H}_{r,c_{\text{ref}}}) \right\rangle_{V_k} \right]
\end{aligned} \tag{3.203}$$

in which the average of products are assumed equal to the product of averages.

By substitution the temperature equation yields:

$$\begin{aligned}
\alpha_k \langle \rho_k \rangle_{V_k} \langle C_{p,k} \rangle_{V_k} \left( \frac{\partial \langle T_k \rangle_{V_k}}{\partial t} + \langle \mathbf{v}_k \rangle_V^{X_k \rho_k} \cdot \nabla \langle T_k \rangle_{V_k} \right) &= \\
- \alpha_k \frac{\langle T \rangle_{V_k}}{\langle \rho \rangle_{V_k}} \left( \frac{\partial \langle \rho \rangle_{V_k}}{\partial \langle T \rangle_{V_k}} \right)_{p,\omega} \frac{D\langle p_k \rangle_{V_k}}{Dt} + \langle p_k \rangle_{V_k} \frac{D\alpha_k}{Dt} & \\
- \nabla \cdot (\alpha_k \langle \boldsymbol{\sigma}_k \rangle_{V_k} : \nabla \langle \mathbf{v}_k \rangle_V^{X_k \rho_k} + \alpha_k \langle \boldsymbol{\sigma}_k : \nabla \widehat{\mathbf{v}}_k \rangle_{V_k}) & \\
+ \alpha_k \left( \left\langle \sum_{c=1}^N \bar{h}_c \nabla \cdot \left( \frac{\mathbf{j}_c}{M_{w_c}} \right) \right\rangle_{V_k} + \left\langle \sum_{r=1}^q r_{r,c_{\text{ref}}} (-\Delta \bar{H}_{r,c_{\text{ref}}}) \right\rangle_{V_k} \right) & \\
- \nabla \cdot (\alpha_k \langle \mathbf{q}_k \rangle_{V_k}) + \Gamma_{V_k} \langle \langle h_k \rangle_{A_I}^{V_k} - \langle h_k \rangle_V^{X_k \rho_k} \rangle + E_k^E & \\
+ \alpha_k \left\langle \sum_c \mathbf{j}_{k,c} \cdot \mathbf{g}_{k,c} \right\rangle_{V_k} &
\end{aligned} \tag{3.204}$$

The interfacial heat transfer flux involves the interfacial heat which can be related to the heat of vaporization or condensation and the heat flux of the phase on the  $k$  side of the interface [112].

For incompressible and porous media flows we may follow the approaches of [239, 200] wherein the variations of the factor  $\rho_k C_{p,k}$  within the averaging volume are neglected to enable application of the Leibnitz' and Gauss' averaging rules on the temperature and apparent flux terms. For this particular case the modified volume averaged enthalpy equation in terms of temperature can be deduced from (3.176) as follows:

$$\begin{aligned}
\rho_k C_{p,k} \left( \frac{\partial (\alpha_k \langle T_k \rangle_{V_k})}{\partial t} + \langle \mathbf{v}_k \rangle_{V_k} \cdot \nabla (\alpha_k \langle T_k \rangle_{V_k}) \right) &= \\
- \nabla \cdot (\alpha_k \langle \mathbf{q}_k \rangle_{V_k}) - \nabla \cdot (\alpha_k \langle \boldsymbol{\sigma}_k \rangle_{V_k} : \nabla \langle \mathbf{v}_k \rangle_{V_k}) & \\
+ \alpha_k \left\langle \sum_{c=1}^N \bar{h}_c \nabla \cdot \left( \frac{\mathbf{j}_c}{M_{w_c}} \right) \right\rangle_{V_k} + \alpha_k \left\langle \sum_{r=1}^q r_{r,c_{\text{ref}}} (-\Delta \bar{H}_{r,c_{\text{ref}}}) \right\rangle_{V_k} & \\
+ \Gamma_{V_k} \langle C_{p,k} T_k \rangle_{A_I}^{V_k} + E_k^E + \alpha_k \left\langle \sum_c \mathbf{j}_{k,c} \cdot \mathbf{g}_{k,c} \right\rangle_{V_k} & \\
- \nabla \cdot (\rho_k C_{p,k} \langle \widehat{\mathbf{v}}_k \widehat{T}_k \rangle_{V_k}) &
\end{aligned} \tag{3.205}$$

in which the terms on the LHS are manipulated by use of the continuity equation. Moreover, the average of products resulting from the convective term is reformulated using spatial decomposition of the temperature and velocity variables.

The procedure can be summarized in three steps:

$$\begin{aligned}
& \left\langle \frac{\partial T_k}{\partial t} \right\rangle_V + \langle \mathbf{v}_k \cdot \nabla T_k \rangle_V \\
& \approx \frac{\partial}{\partial t} (\alpha_k \langle T_k \rangle_{V_k}) + \nabla \cdot (\alpha_k \langle \mathbf{v}_k T_k \rangle_{V_k}) - \frac{\Gamma_{V_k}}{\rho_k C_{p,k}} \langle C_{p,k} T_k \rangle_{A_I}^{\Gamma_{V_k}} \\
& = \frac{\partial}{\partial t} (\alpha_k \langle T_k \rangle_{V_k}) + \langle \mathbf{v}_k \rangle_{V_k} \cdot \nabla (\alpha_k \langle T_k \rangle_{V_k}) + \nabla \cdot (\langle \widehat{\mathbf{v}}_k \widehat{T}_k \rangle_{V_k}) \\
& \quad - \frac{\Gamma_{V_k}}{\rho_k C_{p,k}} \langle C_{p,k} T_k \rangle_{A_I}^{\Gamma_{V_k}}
\end{aligned} \tag{3.206}$$

*Chemical species:*

The modified volume averaged species mass balance deduced from (3.177) can be expressed as:

$$\begin{aligned}
& \frac{\partial}{\partial t} \left( \alpha_k \langle \rho_k \rangle_{V_k} \langle \omega_{k,s} \rangle_V^{\alpha_k \rho_k} \right) \\
& + \nabla \cdot \left( \alpha_k \langle \langle \rho_k \rangle_{V_k} \langle \mathbf{v}_k \rangle_V^{\alpha_k \rho_k} \langle \omega_{k,s} \rangle_V^{\alpha_k \rho_k} + \langle \rho_k \widehat{\mathbf{v}}_k \widehat{\omega}_k \rangle_{V_k} \right) \\
& + \nabla \cdot \left( \alpha_k \langle \mathbf{j}_{k,s} \rangle_{V_k} \right) = \Gamma_{V_k} \langle \omega_{k,s} \rangle_{A_I}^{\Gamma_{V_k}} - \mathbf{J}_{k,s}^j + \alpha_k \langle R_{k,s} \rangle_{V_k}
\end{aligned} \tag{3.207}$$

in which constitutive equations are needed for the unknown quantities in (3.179), (3.180) and (3.181).

For *incompressible* flows the fluid properties (e.g.,  $\rho_k$ ,  $\mu_k$ ) are constants so the covariances between the fluctuating components of  $\rho_k$  and  $\psi_k$ , i.e.,  $\langle \widehat{\rho}_k \widehat{\psi}_k \rangle_{V_k}$ , vanish. The density variable is thus conveniently denoted by  $\rho_k$  and simply moved outside the averaging bracket. Therefore, for constant density flows the mass-weighted variables coincide with the phase-weighted or intrinsic variables, thus the Favre like mass-weighted variable procedure used above can be replaced by a simpler method resembling the conventional Reynolds averaging procedure used in turbulence analysis [153, 154, 193].

Since the spatially averaged model for incompressible systems is used occasionally in chemical engineering practice, we will briefly outline the Reynolds like spatial decomposition and averaging procedure for completeness. In this case the  $\widehat{\psi}_k$  represents the spatial deviation of the point variable  $\psi_k$  from the intrinsic volume average value  $\langle \psi_k \rangle_{V_k}$ , and is defined by:

$$\widehat{\psi}_k = \psi_k - \langle \psi_k \rangle_{V_k} \tag{3.208}$$

where  $\psi_k$  represents the local variable at a point in space  $\mathbf{r}$ .

The average of the spatial deviation  $\widehat{\psi}_k$  is computed applying the intrinsic average operator (3.118) on (3.208). The obvious result is:

$$\langle \widehat{\psi}_k \rangle_{V_k} = \langle \psi_k \rangle_{V_k} - \langle \langle \psi_k \rangle_{V_k} \rangle_{V_k} = \langle \psi_k \rangle_{V_k} - \langle \psi_k \rangle_{V_k} = 0 \quad (3.209)$$

It follows that the average of the product of the two local variables  $\psi_k$  and  $\phi_k$  can be written as the product of the averaged variables plus a covariance term, as follows:

$$\langle \psi_k \phi_k \rangle_{V_k} = \langle \psi_k \rangle_{V_k} \langle \phi_k \rangle_{V_k} + \langle \widehat{\psi}_k \widehat{\phi}_k \rangle_{V_k} \quad (3.210)$$

Having related the average of products to the products of averages, the averaged equation (3.139) becomes:

$$\begin{aligned} \frac{\partial(\alpha_k \rho_k \langle \psi_k \rangle_{V_k})}{\partial t} + \nabla \cdot (\alpha_k \rho_k \langle \mathbf{v}_k \rangle_{V_k} \langle \psi_k \rangle_{V_k}) + \nabla \cdot (\alpha_k \langle \mathbf{J}_k \rangle_{V_k}) = \\ - \frac{1}{V} \int_{A_I} (\dot{m}_k \psi_k + \mathbf{J}_k) \cdot \mathbf{n}_k da - \nabla \cdot (\alpha_k \rho_k \langle \widehat{\mathbf{v}}_k \widehat{\psi}_k \rangle_{V_k}) + \alpha_k \sum_c \rho_{k,c} \langle \phi_c \rangle_{V_k} \end{aligned} \quad (3.211)$$

The averaging approach for incompressible flows has been applied describing solidification processes in metallurgy [153, 81, 14, 193]. For example, for the modeling of materials solidification Shyy et al [193] did derive a set of macroscopic transport equations intended to be valid in solid, liquid, and mushy zones. In particular, since the volume averaged covariance terms can be interpreted as sub-grid stresses they adopted the LES concept developing a microscopic deviation model and constitutive equations based on the Smagorinsky eddy viscosity coefficient hypothesis. The suggested models have their limitations as the constitutive relations are not generally valid, thus experimental data is always required to fit the unknown model parameters and for model validation.

The conventional constitutive equations are discussed in chap 5.

### 3.4.2 The Time Averaging Procedure

In this section we assess the single time averaging technique. Pure *time averaging* has been examined by [229, 112, 45, 43, 47, 53, 48, 24, 54, 116, 157]. These investigations are recommended for complementary studies.

The conditions under which the time averaging procedure can be applied for multiphase flows coincide with those for which time averaging can be used for single phase turbulence flows<sup>18</sup>, and can be expressed as [112, 43, 47]:

<sup>18</sup> It is noted that the requirement of proper separation of scales represents the main drawback of the time averaging method. The constitutive equations used generally depend strongly on this assumption which is hardly ever fulfilled performing simulations of turbulent reactive flows.

$$\left\{ \begin{array}{l} \text{Characteristic} \\ \text{time scale of} \\ \text{the turbulent} \\ \text{fluctuations in} \\ \text{the flow, } \tau_t \end{array} \right\} \ll \left\{ \begin{array}{l} \text{Characteristic} \\ \text{time period of} \\ \text{averaging, } T \end{array} \right\} \ll \left\{ \begin{array}{l} \text{Characteristic} \\ \text{time scale of} \\ \text{the overall} \\ \text{variations in} \\ \text{the flow, } \tau_L \end{array} \right\}$$

In this averaging procedure we imagine that at any point  $\mathbf{r}$  in a two-phase flow, phase  $k$  passes intermittently so a function  $\psi_k$  associated with phase  $k$  will be a piecewise continuous function. However, the interfaces are not stationary so they do not occupy a fixed location for finite time intervals. For this reason the average macroscopic variables are expected to be continuous functions (but this hypothesis has been questioned as it can be shown that the first order time derivative might be discontinuous which is not physical, hence an amended double time averaging operator was later proposed as a way of dealing with this problem [43, 47]). Since  $T$  is the overall time period over which the time averaging is performed, phase  $k$  is observed within a subset of residence time intervals so that  $T = \sum_k T_k$  for all the phases in the system. In this context the time averaged equations are established treating the interfaces as discontinuous jumps with no thickness [43, 47], in contrast to the interface model used by Ishii [112].

In the conventional averaging procedure a phase indicator function  $X_k$  is defined by:

$$X_k(\mathbf{r}, t) = \begin{cases} 1 & \text{if location } \mathbf{r} \text{ pertains to phase } k, \\ 0 & \text{otherwise.} \end{cases} \quad (3.212)$$

The mathematical properties of  $X_k$  ensure that the ordinary mathematical operations of vector calculus can be performed on the local instantaneous variables which are discontinuous [112, 58].

The local instantaneous equations can be time averaged over a defined time interval  $[t - T/2; t + T/2]$ . The *single time averaging operator* which can be applied to any scalar, vector or tensor valued property function  $\psi_k$  associated with phase  $k$ , is defined by:

$$\langle \psi_k \rangle_T = \frac{1}{T} \int_{t-T/2}^{t+T/2} X_k \psi_k dt' = \frac{1}{T} \int_{t_k - T_k/2}^{t_k + T_k/2} \psi_k dt' \quad (3.213)$$

It is emphasized that  $\langle \psi_k \rangle_T$  is by definition the time average of the quantity  $\psi_k$  over the entire time averaging period  $T$ .

The corresponding time average of  $\psi_k$  over the time interval  $T_k$ , which coincides with the  $X_k$ -weighted average of  $\psi_k$  over the entire time period  $T$ , is defined by:

$$\langle \psi_k \rangle_{T_k} = \langle \psi_k \rangle_T^{X_k} = \frac{\frac{1}{T} \int_{t-T/2}^{t+T/2} X_k \psi_k dt'}{\frac{1}{T} \int_{t-T/2}^{t+T/2} X_k dt'} = \frac{1}{T_k} \int_{t_k-T_k/2}^{t_k+T_k/2} \psi_k dt' \quad (3.214)$$

By comparing the averaging operators (3.213) and (3.214), the following relationship is achieved:

$$\langle \psi_k \rangle_T = \frac{T_k}{T} \langle \psi_k \rangle_{T_k} = \beta_k \langle \psi_k \rangle_{T_k} \quad (3.215)$$

in which the *time fraction*  $\beta_k$  of phase  $k$  is defined by:

$$\beta_k = \frac{T_k}{T} \quad (3.216)$$

To derive a time average of the generic differential balance equation for phase  $k$  (3.82) is multiplied with  $X_k$ , integrated over the entire averaging time interval  $T$ , and thereafter multiplied with the fixed reciprocal overall time averaging period  $T$ . The resulting time averaged equation is given by:

$$\frac{1}{T} \int_{t-T/2}^{t+T/2} \left( X_k \frac{\partial(\rho_k \psi_k)}{\partial t} + X_k \nabla \cdot (\rho_k \mathbf{v}_k \psi_k + \mathbf{J}_k) - X_k \sum_c \rho_{k,c} \phi_{k,c} \right) dt' = 0 \quad (3.217)$$

or, using a more compact notation:

$$\left\langle \frac{\partial(\rho_k \psi_k)}{\partial t} \right\rangle_T + \langle \nabla \cdot (\rho_k \mathbf{v}_k \psi_k + \mathbf{J}_k) \rangle_T - \left\langle \sum_c \rho_{k,c} \phi_{k,c} \right\rangle_T = 0 \quad (3.218)$$

The first, second and third terms in (3.218) have to be reformulated using the conventional time averaging theorems<sup>19</sup>. The first theorem one makes use of relates the average of a time derivative to the time derivative of an average quantity, and is called the *Leibnitz's rule* for time averaging:

$$\frac{1}{T} \int_{t-T/2}^{t+T/2} X_k \frac{\partial \psi_k}{\partial t} dt' = \frac{\partial}{\partial t} \left[ \frac{1}{T} \int_{t-T/2}^{t+T/2} X_k \psi_k dt' \right] - \frac{1}{T} \sum_{t_I^k \in (t-\frac{T}{2}; t+\frac{T}{2})} \frac{\mathbf{v}_I \cdot \mathbf{n}_I}{|\mathbf{v}_I \cdot \mathbf{n}_I|} \psi_k(t_I^k) \quad (3.219)$$

or, expressed in the compact notation

$$\begin{aligned} \left\langle \frac{\partial \psi_k}{\partial t} \right\rangle_T &= \frac{\partial}{\partial t} \langle \psi_k \rangle_T - \frac{1}{T} \sum_{t_I^k \in (t-\frac{T}{2}; t+\frac{T}{2})} \frac{1}{|\mathbf{v}_I \cdot \mathbf{n}_I|} \psi_k(t_I^k) \mathbf{v}_I \cdot \mathbf{n}_I \\ &= \frac{\partial}{\partial t} (\beta_k \langle \psi_k \rangle_{T_k}) - \frac{1}{T} \sum_{t_I^k \in (t-\frac{T}{2}; t+\frac{T}{2})} \frac{1}{|\mathbf{v}_I \cdot \mathbf{n}_I|} \psi_k(t_I^k) \mathbf{v}_I \cdot \mathbf{n}_I \end{aligned} \quad (3.220)$$

<sup>19</sup> The time averaging theorems have been derived by [112] [47].

where  $\mathbf{n}_k$  is the outward unit normal of the element of area  $A_k$  of phase  $k$ , and  $\mathbf{v}_I$  is the velocity of the local interface.  $\psi_k(t_I^k)$  denotes the value of  $\psi$  on the phase  $k$  side of the interface. It is also noted that  $\mathbf{v}_I \cdot \mathbf{n}_I$  is positive when the interface is approaching the point under consideration and negative when the interface is leaving it [112, 47].

For the particular case when  $\psi_k = 1$  it is recognized that (3.213), (3.214) and (3.220) can be manipulated and expressed as:

$$\langle 1 \rangle_T = \frac{1}{T} \int_{t-T/2}^{t+T/2} X_k dt' = \frac{T_k}{T} = \beta_k \tag{3.221}$$

and

$$0 = \frac{\partial \beta_k}{\partial t} - \sum_{t_I^k \in (t-T/2; t+T/2)} \frac{\mathbf{v}_I \cdot \mathbf{n}_I}{|\mathbf{v}_I \cdot \mathbf{n}_I|} \tag{3.222}$$

in accordance with the work of [112, 43, 47, 24].

The second theorem we utilize relates the average of a spatial derivative to the spatial derivative of the average, and is termed the *Gauss rule* for time averaging:

$$\frac{1}{T} \int_{t-T/2}^{t+T/2} (X_k \nabla \psi_k) dt' = \nabla \left[ \frac{1}{T} \int_{t-T/2}^{t+T/2} X_k \psi_k dt' \right] + \frac{1}{T} \sum_{t_I^k \in (t-\frac{T}{2}; t+\frac{T}{2})} \frac{1}{|\mathbf{v}_I \cdot \mathbf{n}_I|} \mathbf{n}_I \psi_k(t_I^k) \tag{3.223}$$

In the compact notation, we get:

$$\begin{aligned} \langle \nabla \psi_k \rangle_T &= \nabla \langle \psi_k \rangle_T + \frac{1}{T} \sum_{t_I^k \in (t-\frac{T}{2}; t+\frac{T}{2})} \frac{1}{|\mathbf{v}_I \cdot \mathbf{n}_I|} \mathbf{n}_I \psi_k(t_I^k) \\ &= \nabla (\beta_k \langle \psi_k \rangle_{T_k}) + \frac{1}{T} \sum_{t_I^k \in (t-\frac{T}{2}; t+\frac{T}{2})} \frac{1}{|\mathbf{v}_I \cdot \mathbf{n}_I|} \mathbf{n}_I \psi_k(t_I^k) \end{aligned} \tag{3.224}$$

A special case of (3.224) is the theorem for the time average of a divergence:

$$\begin{aligned} \langle \nabla \cdot \boldsymbol{\psi}_k \rangle_T &= \nabla \cdot \langle \boldsymbol{\psi}_k \rangle_T + \frac{1}{T} \sum_{t_I^k \in (t-\frac{T}{2}; t+\frac{T}{2})} \frac{1}{|\mathbf{v}_I \cdot \mathbf{n}_I|} \mathbf{n}_I \cdot \boldsymbol{\psi}_k(t_I^k) \\ &= \nabla \cdot (\beta_k \langle \boldsymbol{\psi}_k \rangle_{T_k}) + \frac{1}{T} \sum_{t_I^k \in (t-\frac{T}{2}; t+\frac{T}{2})} \frac{1}{|\mathbf{v}_I \cdot \mathbf{n}_I|} \mathbf{n}_I \cdot \boldsymbol{\psi}_k(t_I^k) \end{aligned} \tag{3.225}$$

where  $\boldsymbol{\psi}_k$  is interpreted as a vector or a second order tensor field.

For the particular case when  $\psi_k = 1$  it is recognized that (3.224) reduces to:

$$0 = \nabla \beta_k + \frac{1}{T} \sum_{t_I^k \in (t-\frac{T}{2}; t+\frac{T}{2})} \frac{1}{|\mathbf{v}_I \cdot \mathbf{n}_I|} \mathbf{n}_I \tag{3.226}$$

which is an important relationship frequently utilized manipulating the averaged terms [47]. The same relationship is obtained from (3.225) if  $\psi_k$  is replaced with the unit tensor  $\psi_k = \mathbf{e}$ .

By taking into account the particular forms of the Leibnitz's and Gauss' theorems valid for time averaging (3.220), (3.224) and (3.225), the averaged generic equation (3.218) becomes:

$$\begin{aligned} & \frac{\partial(\beta_k \langle \rho_k \psi_k \rangle_{T_k})}{\partial t} + \nabla \cdot (\beta_k \langle \rho_k \mathbf{v}_k \psi_k \rangle_{T_k}) + \nabla \cdot (\beta_k \langle \mathbf{J}_k \rangle_{T_k}) = \\ & - \frac{1}{T} \sum_{t_I^k \in (t - \frac{T}{2}; t + \frac{T}{2})} \frac{1}{|\mathbf{v}_I \cdot \mathbf{n}_I|} (\dot{m}_k \psi_k + \mathbf{J}_k \cdot \mathbf{n}_k) + \beta_k \langle \sum_c \rho_c \phi_c \rangle_{T_k} \end{aligned} \quad (3.227)$$

where  $\dot{m}_k$  is the interface mass transfer rate as defined by (3.140).

The interfacial transfer terms occurring on the RHS of (3.227) can be rewritten as [112]:

$$- \frac{1}{T} \sum_{t_I^k \in (t - \frac{T}{2}; t + \frac{T}{2})} \frac{1}{|\mathbf{v}_I \cdot \mathbf{n}_I|} (\dot{m}_k \psi_k + \mathbf{J}_k \cdot \mathbf{n}_k) = - \sum_j l_j^{-1} (\dot{m}_k \psi_k + \mathbf{J}_k \cdot \mathbf{n}_k)_j \quad (3.228)$$

where  $j$  denotes the  $j$ -th interface passing through  $\mathbf{r}$  during the time interval  $T$  and where  $l_j = T |\mathbf{v}_I \cdot \mathbf{n}_I|_j$  is the interfacial transport length for interface  $j$ .

The local jump conditions are time averaged in a similar manner. To derive the averaged form of the generic condition we multiply (3.109) with  $\frac{1}{|\mathbf{v}_I \cdot \mathbf{n}_I|}$ , take the sum over all the interface occurrences obtained within the entire averaging time interval  $t_I^k \in [t - T/2; t + T/2]$ , and thereafter multiply the resulting relation with the fixed reciprocal averaging time period  $T$ . The averaged jump condition becomes:

$$\begin{aligned} & - \frac{1}{T} \sum_{t_I^k \in (t - \frac{T}{2}; t + \frac{T}{2})} \frac{1}{|\mathbf{v}_I \cdot \mathbf{n}_I|} \left( \sum_k [\dot{m}_k \psi_k + \mathbf{J}_k \cdot \mathbf{n}_k] + M_I \right) = \\ & - \sum_j l_j^{-1} \left( \sum_k [\dot{m}_k \psi_k + \mathbf{J}_k \cdot \mathbf{n}_k] + M_I \right)_j = 0 \end{aligned} \quad (3.229)$$

The averaged equations governing each phase and the corresponding jump conditions are then achieved defining the specific values of the generic variables in (3.227) and (3.229) in accordance with Table 3.1.

*Mass:*

The time averaged continuity equation appears by substituting  $\psi_k = 1$ ,  $\mathbf{J}_k = 0$  and  $\phi_{c,k} = 0$  into (3.227):

$$\frac{\partial(\beta_k \langle \rho_k \rangle_{T_k})}{\partial t} + \nabla \cdot (\beta_k \langle \rho_k \mathbf{v}_k \rangle_{T_k}) = - \sum_j l_j^{-1} \dot{m}_{kj} = \Gamma_{Tk} \quad (3.230)$$

Introducing the values for the interface properties  $M_I = 0$  into (3.229), yields:

$$\sum_k \Gamma_{Tk} = 0 \quad (3.231)$$

where the interfacial mass transfer terms due to phase change is defined by

$$\Gamma_{Tk} = - \sum_j l_j^{-1} \dot{m}_{kj} = a_{T_I} \langle \dot{m}_k \rangle_{T_I} \quad (3.232)$$

in which  $\langle \dot{m}_k \rangle_{T_I} = - \sum_j \frac{\dot{m}_{kj}}{l_j} / a_{T_I}$  denotes the interfacial area averaged mass transfer rate [112]. The interfacial area density is defined in accordance with (3.233). The surface area concentration per volume is given by [112]:

$$a_{T_I} = \sum_j l_j^{-1} \quad (3.233)$$

*Momentum:*

The time averaged momentum equation appears by substituting  $\boldsymbol{\psi}_k = \mathbf{v}_k$ ,  $\mathbf{J}_k = \mathbf{T}_k$  and  $\boldsymbol{\phi}_{c,k} = \mathbf{g}_{c,k}$  into (3.227):

$$\begin{aligned} \frac{\partial(\beta_k \langle \rho_k \mathbf{v}_k \rangle_{T_k})}{\partial t} + \nabla \cdot (\beta_k \langle \rho_k \mathbf{v}_k \mathbf{v}_k \rangle_{T_k}) + \nabla \cdot (\beta_k \langle \mathbf{T}_k \rangle_{T_k}) = \\ - \sum_j l_j^{-1} (\dot{m}_k \mathbf{v}_k + \mathbf{T}_k \cdot \mathbf{n}_k)_j + \beta_k \langle \sum_c \rho_c \mathbf{g}_c \rangle_{T_k} \end{aligned} \quad (3.234)$$

Introducing the values for the interface properties  $\mathbf{M}_I = 2\sigma_I H_I \mathbf{n}_I + \nabla_I \sigma_I$  into (3.229), yields:

$$\sum_k (\mathbf{M}_{Tk}^\Gamma + \mathbf{M}_{Tk}^T) = \sum_j l_j^{-1} \mathbf{M}_{Ij} \quad (3.235)$$

where the interfacial momentum transfer due to phase change is defined by:

$$\mathbf{M}_k^\Gamma = - \sum_j l_j^{-1} \dot{m}_{kj} \mathbf{v}_{kj} = \Gamma_{Tk} \langle \mathbf{v}_k \rangle_{T_I}^{\Gamma_{Tk}} \quad (3.236)$$

in which the mass transfer weighted interfacial area averaged velocity  $\langle \mathbf{v}_k \rangle_{T_I}^{\Gamma_{Tk}}$  is defined in analogy to the mass-weighted averaged variables known from turbulence theory [112] (p. 133).

The interfacial momentum stresses yield:

$$\mathbf{M}_k^T = - \sum_j l_j^{-1} \mathbf{T}_{kj} \cdot \mathbf{n}_{kj} = - \sum_j l_j^{-1} (p_k \mathbf{e} + \boldsymbol{\sigma}_k)_j \cdot \mathbf{n}_{kj} \quad (3.237)$$

where the total stress tensor of both phases has been modeled using the Newtonian strain-stress formulation.

In a similar manner as for the volume averaging method in sect 3.4.1, the stress terms are normally rewritten introducing interfacial mean quantities weighted by the interfacial mass transfer rate (i.e., in the volume averaging method the interfacial area averaged stresses are not weighted by the mass transfer rate). The interfacial mean pressure weighted by the interfacial mass transfer rate per unit surface area becomes:

$$\langle p_k \rangle_{T_I} = \frac{\sum_j \frac{p_{kj} \dot{m}_{kj}}{l_j}}{\sum_j \frac{\dot{m}_{kj}}{l_j}} \quad (3.238)$$

Naturally, the interfacial mean viscous stress weighted by the mass transfer rate per unit surface area is then defined by:

$$\langle \boldsymbol{\sigma}_k \rangle_{T_I} = \frac{\sum_j \frac{\boldsymbol{\sigma}_{kj} \dot{m}_{kj}}{l_j}}{\sum_j \frac{\dot{m}_{kj}}{l_j}} \quad (3.239)$$

The corresponding fluctuating interfacial quantities are defined by:

$$p'_{k,I} = p_k - \langle p_k \rangle_{T_I} \quad (3.240)$$

$$\boldsymbol{\sigma}'_{k,I} = \boldsymbol{\sigma}_k - \langle \boldsymbol{\sigma}_k \rangle_{T_I} \quad (3.241)$$

Proceeding in the same way as explained presenting the volume averaging procedure, we obtain the following result

$$\mathbf{M}_k^T = \langle p_k \rangle_{T_I} \nabla \beta_k + \langle \boldsymbol{\sigma}_k \rangle_{T_I} \cdot \nabla \beta_k + \mathbf{F}_k \quad (3.242)$$

The interfacial pressure difference effect and the combined interfacial shear and time fraction gradient effect are treated in the same manner as suggested discussing the analogous terms in (3.156). The modified definition of the generalized drag force follows naturally from an analogy to (3.158). Utilizing (3.226) and the mean value theorem for integrals, the term on the RHS of (3.235) can be expressed as

$$\begin{aligned} \sum_j l_j^{-1} \mathbf{M}_{Ij} &= \sum_j l_j^{-1} (2\sigma_I H_I \mathbf{n}_I + \nabla_I \sigma_I)_j \\ &\approx 2\langle \sigma_I H_I \rangle_{T_I} \sum_j \frac{\mathbf{n}_{I,kj}}{T |\mathbf{v}_{I,kj} \cdot \mathbf{n}_{kj}|} + \sum_j l_j^{-1} \nabla_{Ij} \sigma_I \\ &\approx 2\langle \sigma_I \rangle_{T_I} \langle H_I \rangle_{T_I} \nabla \beta_2 + a_{T_I} \langle \nabla_I \sigma_I \rangle_{T_I} \end{aligned} \quad (3.243)$$

where  $\langle H_I \rangle_{T_I}$  is the interfacial area averaged curvature [112]. The mean curvature is defined in accordance with (3.76). In this equation the sign convention is given by the definition  $\mathbf{n}_I = \mathbf{n}_1$ .

*Energy:*

The time averaged energy equation appears by substituting  $\psi_k = e_k + \frac{1}{2} v_k^2$ ,  $\mathbf{J}_k = \mathbf{T}_k \cdot \mathbf{v}_k + \mathbf{q}_k$  and  $\phi_{c,k} = \mathbf{v}_k \cdot \mathbf{g}_{c,k}$  into (3.227):

$$\begin{aligned}
& \frac{\partial}{\partial t} \left( \beta_k \langle \rho_k (e_k + \frac{1}{2} v_k^2) \rangle_{T_k} \right) + \nabla \cdot \left( \beta_k \langle \rho_k \mathbf{v}_k (e_k + \frac{1}{2} v_k^2) \rangle_{T_k} \right) \\
& + \nabla \cdot \left( \beta_k \langle \mathbf{T}_k \cdot \mathbf{v}_k \rangle_{T_k} \right) + \nabla \cdot \left( \beta_k \langle \mathbf{q}_k \rangle_{T_k} \right) \\
& = - \sum_j l_j^{-1} \left( \dot{m}_k (e_k + \frac{1}{2} v_k^2) + (\mathbf{T}_k \cdot \mathbf{v}_k + \mathbf{q}_k) \cdot \mathbf{n}_k \right)_j \\
& \quad + \beta_k \left\langle \sum_c \rho_{k,c} \mathbf{v}_{k,c} \cdot \mathbf{g}_{k,c} \right\rangle_{T_k}
\end{aligned} \tag{3.244}$$

Introducing the values for the interface properties

$M_I = \nabla_I \cdot \mathbf{q}_I - \nabla_I \cdot (\sigma_I \mathbf{v}_I)$  into (3.229), yields:

$$\sum_k (E_k^E + E_k^W + E_k^G) = \sum_j l_j^{-1} M_{I,j} \tag{3.245}$$

The interfacial energy transfer due to phase change is defined by:

$$\begin{aligned}
E_k^G &= \sum_j l_j^{-1} \rho_{kj} (e_k + \frac{1}{2} v_k^2)_j (\mathbf{v}_I - \mathbf{v}_k)_j \cdot \mathbf{n}_{kj} = - \sum_j l_j^{-1} \dot{m}_{kj} (e_k + \frac{1}{2} v_k^2)_j \\
&= \Gamma_{T_k} \langle (e_k + \frac{1}{2} v_k^2) \rangle_{T_I}^{\Gamma_{T_k}}
\end{aligned} \tag{3.246}$$

in which  $\langle (e_k + \frac{1}{2} v_k^2) \rangle_{T_I}^{\Gamma_{T_k}}$  denotes the mass transfer weighted interfacial (internal and mechanical) energy [112] (p. 137).

The interfacial heat transfer is given by:

$$E_k^E = - \sum_j l_j^{-1} \mathbf{q}_{kj} \cdot \mathbf{n}_{kj} = a_{T_I} \langle \mathbf{q}_k \cdot \mathbf{n}_k \rangle_{T_I}, \tag{3.247}$$

in which  $\langle \mathbf{q}_k \cdot \mathbf{n}_k \rangle_{T_I}$  denotes the interfacial area averaged heat transfer flux.

The interfacial work by viscous and pressure forces yield:

$$E_k^W = - \sum_j l_j^{-1} (\mathbf{T}_k \cdot \mathbf{v}_k)_j \cdot \mathbf{n}_{kj} \tag{3.248}$$

The surface energy sources are expressed as the product of the interfacial area concentration and the averaged interfacial fluxes:

$$\begin{aligned}
\sum_j l_j^{-1} M_{I,j} &= - \sum_j l_j^{-1} (-\nabla_I \cdot (\sigma_I \mathbf{v}_I) + \nabla_I \cdot \mathbf{q}_I)_j \\
&= \langle \nabla_I \cdot (\sigma_I \mathbf{v}_I) \rangle_{T_I} a_{T_I} - \langle \nabla_I \cdot \mathbf{q}_I \rangle_{T_I} a_{T_I}
\end{aligned} \tag{3.249}$$

where  $-\langle \nabla_I \cdot \mathbf{q}_I \rangle_{T_I}$  and  $\langle \nabla_I \cdot (\sigma_I \mathbf{v}_I) \rangle_{T_I}$  are the interfacial accumulated residence time averaged interfacial energy fluxes.

*Chemical species:*

The time averaged species mass balance appears by substituting  $\psi_k = \omega_{k,s}$ ,  $\mathbf{J}_k = \mathbf{j}_{k,s}$  and  $\phi_{c,k} = R_{k,s}/\rho_{k,c}$  into (3.227):

$$\begin{aligned} \frac{\partial(\beta_k \langle \rho_{k,s} \rangle_{T_k})}{\partial t} + \nabla \cdot (\beta_k \langle \rho_{k,s} \mathbf{v}_k \rangle_{T_k}) + \nabla \cdot (\beta_k \langle \mathbf{j}_{k,s} \rangle_{T_k}) = \\ - \sum_j l_j^{-1} (\dot{m}_k \omega_{k,s} + \mathbf{j}_{k,s} \cdot \mathbf{n}_{kj})_j + \beta_k \langle R_{k,s} \rangle_{T_k} \end{aligned} \quad (3.250)$$

Introducing the values for the interface properties  $M_I = R_{I,s}$  into (3.229), yields:

$$\sum_k (\mathbf{J}_{k,s}^I + \mathbf{J}_{k,s}^j) = \sum_j l_j^{-1} M_{Ij} \quad (3.251)$$

where the interfacial species mass transfer due to phase change is defined by:

$$\mathbf{J}_{k,s}^I = \sum_j l_j^{-1} \rho_{kj} \omega_{kj,s} (\mathbf{v}_I - \mathbf{v}_k)_j \cdot \mathbf{n}_{kj} = - \sum_j l_j^{-1} \dot{m}_{kj} \omega_{kj,s} = \Gamma_{T_I} \langle \omega_{k,s} \rangle_{T_I}, \quad (3.252)$$

in which the  $\langle \omega_{k,s} \rangle_{T_I}$  denotes the mass transfer weighted interfacial species  $s$  mass fraction [112] (p. 133).

The other interfacial mass transfer fluxes are given by:

$$\mathbf{J}_k^j = - \sum_j l_j^{-1} \mathbf{j}_{kj} \cdot \mathbf{n}_{kj} = a_{T_I} \langle \mathbf{j}_k \cdot \mathbf{n}_k \rangle_{T_I} \quad (3.253)$$

in which  $\langle \mathbf{J}_k \cdot \mathbf{n}_k \rangle_{T_I}$  denotes the interfacial area averaged mass transfer flux.

The interfacial production term due to heterogeneous reactions is normally rewritten as:

$$\sum_j l_j^{-1} M_{Ij} = \sum_j l_j^{-1} R_{Ij,s} = \langle R_{I,s} \rangle_{T_I} a_I = \rho_{\text{Bulk}} \langle R_{I,s} \rangle_{T_I}^m \quad (3.254)$$

in which the interfacial reaction rate per unit interface area is commonly substituted by the more practical reaction rate per unit mass  $\langle R_{I,s} \rangle_{T_I}^m = \langle R_{I,s} \rangle_{T_I} a_I / \rho_{\text{Bulk}}$  ( $kg/kg, cat \times s$ ) in which  $\rho_{\text{Bulk}}$  denotes the bulk density of the catalyst ( $kg, cat/m_r^3$ ).

In order to carry out computations with the time averaged equations on the form (3.227), we need to relate the average of products to products of averages and derive constitutive equations for the interfacial coupling terms.

Proceeding in a similar manner as suggested deriving the volume averaged equations, the first problem is generally solved introducing mass- and phase weighted time averaged variables and the concept of *temporal decomposition* that is analogous to the temporal decomposition conventionally used in the study of turbulent transport phenomena [89] [112].

The mass-weighted time average of the quantity  $\psi_k$  is defined by:

$$\langle \psi_k \rangle_T^{X_k \rho_k} = \frac{\frac{1}{T} \int_{t-T/2}^{t+T/2} (X_k \rho_k \psi_k) dt'}{\frac{1}{T} \int_{t-T/2}^{t+T/2} (X_k \rho_k) dt'} = \frac{\langle \rho_k \psi_k \rangle_T}{\langle \rho_k \rangle_T} = \frac{\langle \rho_k \psi_k \rangle_{T_k}}{\langle \rho_k \rangle_{T_k}} \quad (3.255)$$

In analogy to the conventional Favre decomposition and time averaging procedure we let  $\psi_k''$  denote the temporal fluctuation of the instantaneous variable  $\psi_k$  about the mass-weighted time average value  $\langle \psi_k \rangle_T^{X_k \rho_k}$ , as defined by:

$$\psi_k'' = \psi_k - \langle \psi_k \rangle_T^{X_k \rho_k} \quad (3.256)$$

Introducing (3.256) into (3.255) we obtain an important relationship:

$$\begin{aligned} \langle \rho_k \rangle_T \langle \psi_k \rangle_T^{X_k \rho_k} &= \langle \rho_k \psi_k \rangle_T \\ &= \langle \rho_k (\langle \psi_k \rangle_T^{X_k \rho_k} + \psi_k'') \rangle_T \\ &= \langle \rho_k \langle \psi_k \rangle_k^{X_k \rho_k} \rangle_T + \langle \rho_k \psi_k'' \rangle_T \\ &= \langle \rho_k \rangle_T \langle \psi_k \rangle_T^{X_k \rho_k} \end{aligned} \quad (3.257)$$

in which we have shown that  $\langle \rho_k \psi_k'' \rangle_T = \beta_k \langle \rho_k \psi_k'' \rangle_{T_k} = \langle \psi_k'' \rangle_T^{X_k \rho_k} = 0$  because  $\langle \psi_k \rangle_T^{X_k \rho_k}$  is constant within  $T$ .

Using (3.257) the convective term in the averaged equation (3.227) can be written as:

$$\begin{aligned} \langle \rho_k \mathbf{v}_k \psi_k \rangle_{T_k} &= \langle \rho_k \mathbf{v}_k \psi_k \rangle_T^{X_k} \\ &= \langle \rho_k (\langle \mathbf{v}_k \rangle_k^{X_k \rho_k} + \mathbf{v}_k'') (\langle \psi_k \rangle_k^{X_k \rho_k} + \psi_k'') \rangle_T^{X_k} \\ &= \langle \rho_k \rangle_T \langle \mathbf{v}_k \rangle_T^{X_k \rho_k} \langle \psi_k \rangle_T^{X_k \rho_k} + \langle \rho_k \mathbf{v}_k'' \psi_k'' \rangle_T \end{aligned} \quad (3.258)$$

Introducing the mass weighted variables (3.256) and manipulating the convective terms by use of the concept of temporal decomposition (3.255), the averaged equation (3.227) becomes:

$$\begin{aligned} \frac{\partial (\beta_k \langle \rho_k \rangle_{T_k} \langle \psi_k \rangle_T^{X_k \rho_k})}{\partial t} + \nabla \cdot (\beta_k \langle \rho_k \rangle_{T_k} \langle \mathbf{v}_k \rangle_T^{X_k \rho_k} \langle \psi_k \rangle_T^{X_k \rho_k}) \\ + \nabla \cdot (\beta_k \langle \mathbf{J}_k \rangle_{T_k}) = - \sum_j l_j^{-1} (\dot{m}_k \psi_k + \mathbf{J}_k)_j \cdot \mathbf{n}_{kj} + \beta_k \sum_c \langle \rho_{k,c} \phi_c \rangle_{T_k} \\ - \nabla \cdot (\beta_k \langle \rho_k \mathbf{v}_k'' \psi_k'' \rangle_{T_k}) \end{aligned} \quad (3.259)$$

As in the volume averaged equations discussed in sect 3.4.1, three undetermined terms can be identified in the time averaged equations (3.259). The first term,  $-\nabla \cdot (\beta_k \langle \rho_k \mathbf{v}_k'' \psi_k'' \rangle_{T_k})$  denotes the covariance or correlation terms. The second term,  $-\sum_j l_j^{-1} \mathbf{J}_{kj} \cdot \mathbf{n}_{kj}$ , accounts for the effects of interfacial stress,

heat and species mass transfer, whereas the third term,  $-\sum_j l^{-1} \dot{m}_{kj} \psi_{kj}$ , account for the interfacial transfer due to phase change.

To save space the governing time averaged equations for each of the primary variables are *not* listed here as their mathematical form coincides with the volume averaged model formulation given in sect 3.4.1. Nevertheless, it is important to note that the physical interpretations of the mean quantities and the temporal covariance terms differ from their spatial counterparts. Furthermore, the conventional constitutive equations for the unknown terms are discussed in chap 5, and the same modeling closures are normally adopted for any model formulation even though their physical interpretation differ.

### 3.4.3 The Ensemble Averaging Procedure

In this section we examine the ensemble averaging method in the framework of the generic single averaging procedure proposed by Drew [54] and further elaborated in [55, 137, 56, 58]. The paper by Enwald et al [67] summarizes this approach nicely in the setting of fluidized bed reactor simulations.

Other statistical averaging methods exist as well, some of them have been assessed by [27, 104, 28, 3, 126, 247, 248, 249, 169, 142]. These reports might be recommended for complementary studies.

As distinct from the time and volume averaging procedures, the application of the ensemble averaging operator is not restricted by any space- and time scales. The ensemble averaging is thus considered the fundamental method [58, 59].

Generally, an ensemble average is defined in terms of an infinite number of realizations of the flow, consisting of variations of position, configuration, and velocities of the discrete units and the fluid between them. This means that we imagine that one can measure a local instantaneous quantity for each of an infinity of experiments which are alike except for presumably unimportant details of their behavior, and obtain the averaged values by averaging the quantity over the ensemble. For this reason the ensemble average can be interpreted as a measure related to the repeatability of experiments. On the other hand, for chaotic multiphase systems an exact experiment or realization is hardly repeatable since physical characteristics like the detailed boundary and initial conditions cannot be controlled with sufficient accuracy [56]. An inaccurate repetition of the experiment will thus rather lead to another member of the ensemble. Besides, it goes without saying that in physical analysis an infinite number of experiments cannot be realized, so the measured data is not averaged over an infinity of realizations. The best that one can do is to compute ensemble averages over a sufficiently large but finite number of realizations to ensure that the average measures become stable and do not fluctuate significantly. For such systems a correct detailed prediction cannot be made either because the physical characteristics like the boundary and initial conditions cannot be specified [59].

Consider a local instantaneous scalar, vector or tensor valued function defined by  $\psi \equiv \psi(\mathbf{r}, t)$ , and let  $\langle \psi \rangle_\varepsilon(\mathbf{r}, t)$  denote the corresponding averaged field. The ensemble averaging operator can be defined in terms of a continuous probability density function [54, 58, 137]. For this purpose a few mathematical prerequisites are needed. Let  $\mathcal{R}$  denote an appropriate space domain,  $\tau$  a time domain and  $\varepsilon$  an event space of a process  $\mathcal{P}$ . In this method a statistical process refers to the set of possible flows that could occur using appropriate initial and boundary conditions<sup>20</sup>. In this notation a generic local instantaneous variable  $\psi$ , defined in  $\mathcal{P}$ , is written as  $\psi \equiv \psi(\mathbf{r}, t; \mu)$ . It follows that  $\mathbf{r} \in \mathcal{R}$  is the position vector,  $t \in \tau$  is the time and  $\mu \in \varepsilon$  is a particular realization of the process  $\mathcal{P}$ . A realization of the flow designates a possible motion that could have happened.

In order to avoid mathematical difficulties when applying the averaging operators to the generic equation we introduce the phase indicator function  $X_k(\mathbf{r}, t; \mu)$  in any realization. This Heaviside function picks the phase  $k$  while ignoring the other phases and the interface. The characteristic function is defined by:

$$X_k(\mathbf{r}, t; \mu) = \begin{cases} 1 & \text{if phase } k \text{ is present at location } \mathbf{r} \text{ in the realization } \mu, \\ 0 & \text{otherwise.} \end{cases} \quad (3.260)$$

The  $X_k$  is considered a generalized function which is especially useful in connection with differentiation of discontinuous functions within an integral.

The ensemble average of  $\psi$  is then defined by:

$$\langle \psi_k \rangle_\varepsilon = \int_\varepsilon \psi_k(\mathbf{r}, t; \mu) p(\mu) d\mu = \int_\varepsilon \psi_k(\mathbf{r}, t; \mu) dm(\mu) \quad (3.261)$$

where  $p(\mu)d\mu = dm(\mu)$  is the probability density for observing a realization  $\mu$  in the interval  $d\mu$  on the set of all possible events  $\varepsilon$ . In this method one refers to  $\varepsilon$  as the ensemble.

From the definition of a probability density function we note:

$$\int_\varepsilon p(\mu) d\mu = 1 \quad (3.262)$$

---

<sup>20</sup> For some turbulent flows, the boundary conditions and initial conditions cannot be controlled sufficiently to allow repeatable experiments. In this case, although turbulent flows are not really deterministic, a useful conceptualization of the ensemble average assumes that the flow is deterministic but that randomness may arise through the uncertainty in the initial and boundary conditions [58].

Another possible conceptualization of the ensemble average imagines that the process is affected by small random forces through the motion. Particulate flows can then be described by distributions of positions, velocities and sizes adopting the basic principles of kinetic theory [85, 247, 248, 169, 249]. This alternative ensemble averaging approach is examined in relation to granular flows in chap 4.

Before the averaging operator can be applied to the generic transport equation we need to take into account that multiphase mixtures are characterized by the presence of discontinuities in the fields. It is generally assumed that the fields of interest are smooth within each separate phase  $k$ , but that they can change discontinuously across the interfaces dividing the phases. Thereby the property functions are well behaved within each of the continuous phases, but in order to average the exact local instantaneous equation taking the discontinuous interfaces into account we need extended expressions for  $\langle \partial\psi_k/\partial t \rangle_e$  and  $\langle \nabla\psi_k \rangle_e$ . That is, for a well behaved function  $\psi_k$  connected to the bulk phases conventional axioms similar to (1.379) can still be applied, while to deal with the discontinuous fields related to the interfaces we introduce the phase indicator function so that  $\langle X_k\partial\psi_k/\partial t \rangle_e$  and  $\langle X_k\nabla\psi_k \rangle_e$  are considered generalized functions which can be manipulated in terms of test functions as outlined by [54] [55] [58]. Compared to the previous averaging procedures (e.g., [43] [47]), the use of generalized functions eliminates certain difficulties encountered when applying the averaging operators to discontinuous fields<sup>21</sup>. The trade-off for the simple derivation of the averaged equations and jump conditions is that all the mathematical manipulations involve generalized functions [54].

The particular forms of the Leibnitz's and Gauss' rules used for ensemble averaging are given by:

$$\begin{aligned} \langle X_k \frac{\partial\psi_k}{\partial t} \rangle_e &= \langle \frac{\partial X_k \psi_k}{\partial t} \rangle_e - \langle \psi_k \frac{\partial X_k}{\partial t} \rangle_e \\ &= \frac{\partial \langle X_k \psi_k \rangle_e}{\partial t} - \langle \psi_k \frac{\partial X_k}{\partial t} \rangle_e \end{aligned} \quad (3.263)$$

and

$$\begin{aligned} \langle X_k \nabla\psi_k \rangle_e &= \langle \nabla X_k \psi_k \rangle_e - \langle \psi_k \nabla X_k \rangle_e \\ &= \nabla \langle X_k \psi_k \rangle_e - \langle \psi_k \nabla X_k \rangle_e \end{aligned} \quad (3.264)$$

The last term on the RHS in both of these equations are related to the surface average of  $\psi_k$  over the interface and evaluated on the phase  $k$  side of the face [58]. The other terms on the RHS in both equations are related to the bulk phase average of  $\psi_k$  and are treated applying the conventional averaging axioms on the form (1.379).

The ensemble average of the phase indicator function is equivalent to the average occurrence of phase  $k$ :

<sup>21</sup> It is noted that the original Reynolds axioms are not applicable to discontinuous functions as normally occur across the interfaces in multiphase flow. As a remedy, Drew [54] extended these functions making them continuous by use of the generalized function concept connecting the functions of the continuous phases on each side of the interface across the interface. Hence the discontinuous functions are modified to be continuous but locally very steep functions across the interface. Formally the averaging axioms can then be extended to include the interfaces, giving rise to the modified formulations of the axioms.

$$\gamma_k = \langle X_k \rangle_e \quad (3.265)$$

where

$$\sum_{k=1}^2 \gamma_k = 1 \quad (3.266)$$

It is noted that both the time fraction  $\beta_k$  and the average occurrence or number fraction  $\gamma_k$  are often treated as equivalent to the local volume fraction  $\alpha_k$  of phase  $k$ . However, this assumption is strictly correct for stationary and homogeneous flows only.

This equivalence of averages is not obvious so some kind of justification might be needed. Drew [54] pointed out that mathematically the local averaging operators for the volume, time and ensemble averages are formally similar. Besides, both the time and volume averages can be viewed as approximations to the ensemble average provided that the ergodic hypothesis holds on the local scale. Under these restrictions, with the ensemble averaging notation as basis, all the single averaging operators can be written in a generic manner.

In this notation the time average of  $\psi_k$  is defined by taking one realization  $\mu^*$ , integrating over the time interval from  $t-T/2$  to  $t+T/2$ , and normalizing:

$$\langle \psi_k(\mathbf{r}, t; \mu^*) \rangle_T = \frac{1}{T} \int_{t-T/2}^{t+T/2} \psi_k(\mathbf{r}, \tau; \mu^*) d\tau \quad (3.267)$$

which has the practical advantage that we need not sample the ensemble repeatedly but rather perform a large number of samples in time within one realization.

In a similar manner the volume average can be seen as an ensemble average in which  $\psi_k$  is integrated over a sub-ensemble represented by  $\mu_\eta$  for  $\eta \in V$ . The volume average is then defined by:

$$\langle \psi_k \rangle_V = \frac{1}{V} \int_V \psi_k(\mathbf{r}, t; \mu_\eta^*) dv = \frac{1}{V} \int_V \psi_k(\mathbf{r} + \boldsymbol{\eta}, t; \mu^*) dv_\eta \quad (3.268)$$

It is emphasized that these time and volume averaging operators are appropriate only for statistically steady and homogeneous flows in which the ergodic hypothesis holds.

The averaged balance equations are obtained by multiplying the exact local instantaneous equations (3.82) and (3.109) by  $X_k$  and then applying the single generic averaging operator.  $X_k$  is a generalized function satisfying the topological equation on the form [54] [56]:

$$\frac{D_I X_k}{Dt} = \frac{\partial X_k}{\partial t} + \mathbf{v}_I \cdot \nabla X_k = 0 \quad (3.269)$$

This relation is imagined as the material derivative of  $X_k$  following the interface [56]. For a point in space that is located on the interface  $X_k$  takes

the value  $X_k = 0$ , otherwise  $X_k = 1$ . In either case the partial derivatives are both zero, so all the terms in (3.269) are zero. On the other hand, considering a point located on the surface that move with the interface velocity, Drew [54] [56] [58] imagines that the function  $X_k$  is expressing a constant jump determined by the generalized functions. Thus its material derivative is zero.

Using the  $X_k$  function we can average the generic transport equation. Preliminarily, we put up the resulting equation in the compact notation:

$$\begin{aligned} \langle X_k \frac{\partial(\rho_k \psi_k)}{\partial t} \rangle_e + \langle X_k \nabla \cdot (\rho_k \mathbf{v}_k \psi_k) \rangle_e + \langle X_k \nabla \cdot \mathbf{J}_k \rangle_e \\ = \langle X_k \sum_c \rho_{k,c} \phi_{k,c} \rangle_e \end{aligned} \quad (3.270)$$

The first, second and third terms in (3.270) have to be reformulated using the extended forms of the conventional averaging theorems.

The extended form of the Leibnitz's rule can be derived by use of the phase indicator function (3.260), the topological equation (3.269), the Reynolds averaging rules (1.379) and the chain rule [54]:

$$\begin{aligned} \langle X_k \frac{\partial \psi_k}{\partial t} \rangle_e &= \langle \frac{\partial(X_k \psi_k)}{\partial t} - \psi_k \frac{\partial X_k}{\partial t} \rangle_e \\ &= \langle \frac{\partial(X_k \psi_k)}{\partial t} + (\psi_k \mathbf{v}_I) \cdot \nabla X_k \rangle_e \\ &= \langle \frac{\partial(X_k \psi_k)}{\partial t} \rangle_e + \langle (\psi_k \mathbf{v}_I) \cdot \nabla X_k \rangle_e \\ &= \frac{\partial \langle X_k \psi_k \rangle_e}{\partial t} + \langle (\psi_k \mathbf{v}_I) \cdot \nabla X_k \rangle_e \end{aligned} \quad (3.271)$$

In a similar manner the extended form of Gauss' rule can be derived by use of the phase indicator function (3.260), the topological equation (3.269), the Reynolds averaging rules (1.379) and the chain rule [54]:

$$\begin{aligned} \langle X_k \nabla \psi_k \rangle_e &= \langle \nabla(X_k \psi_k) - \psi_k \nabla X_k \rangle_e \\ &= \langle \nabla(X_k \psi_k) \rangle_e - \langle \psi_k \nabla X_k \rangle_e \\ &= \nabla \langle X_k \psi_k \rangle_e - \langle \psi_k \nabla X_k \rangle_e \end{aligned} \quad (3.272)$$

Applying the generic form of Leibnitz's theorem (3.271) to the first term in (3.270), we get:

$$\langle X_k \frac{\partial(\rho_k \psi_k)}{\partial t} \rangle_e = \frac{\partial \langle X_k \rho_k \psi_k \rangle_e}{\partial t} + \langle (\rho_k \psi_k \mathbf{v}_I) \cdot \nabla X_k \rangle_e \quad (3.273)$$

Similarly, by applying the generic form of Gauss' rule (3.272) to the second and the third terms in (3.270) we obtain the following results:

$$\langle X_k \nabla \cdot (\rho_k \mathbf{v}_k \psi_k) \rangle_e = \nabla \cdot \langle X_k \rho_k \mathbf{v}_k \psi_k \rangle_e - \langle (\rho_k \mathbf{v}_k \psi_k) \cdot \nabla X_k \rangle_e \quad (3.274)$$

and

$$\langle X_k \nabla \cdot \mathbf{J}_k \rangle_e = \nabla \cdot \langle X_k \mathbf{J}_k \rangle_e - \langle \mathbf{J}_k \cdot \nabla X_k \rangle_e \quad (3.275)$$

Introducing these modified formulations (3.273), (3.274) and (3.275), the averaged generic equation (3.270) can be written as:

$$\begin{aligned} & \frac{\partial \langle X_k \rho_k \psi_k \rangle_e}{\partial t} + \nabla \cdot \langle X_k \rho_k \mathbf{v}_k \psi_k \rangle_e + \nabla \cdot \langle X_k \mathbf{J}_k \rangle_e - \langle X_k \sum_c \rho_{k,c} \phi_{k,c} \rangle_e \\ &= \langle (\rho_k \mathbf{v}_k \psi_k) \cdot \nabla X_k \rangle_e + \langle \mathbf{J}_k \cdot \nabla X_k \rangle_e - \langle \rho_k \psi_k \mathbf{v}_I \cdot \nabla X_k \rangle_e \\ &= \langle [\rho_k \psi_k (\mathbf{v}_k - \mathbf{v}_I) + \mathbf{J}_k] \cdot \nabla X_k \rangle_e \end{aligned} \quad (3.276)$$

The RHS of (3.276) denotes the interfacial transport terms.

The averaged equations of the form (3.276) cannot be solved directly, as they contain averages of products of the dependent variables. To obtain a solvable set of equations, we need to relate the average of products to products of average variables. For this purpose the phase- and mass weighted quantities are introduced.

The weighted mean quantities are defined in agreement with the standard single phase Favre averaging procedure [112, 48, 67]. That is, we define:

*Phase-weighted averaging:*

$$\langle \psi_k \rangle_e^{X_k} = \frac{\langle X_k \psi_k \rangle_e}{\langle X_k \rangle_e} = \frac{\langle X_k \psi_k \rangle_e}{\langle \gamma_k \rangle_e} \quad (3.277)$$

*Mass-weighted averaging:*

$$\langle \psi_k \rangle_e^{X_k \rho_k} = \frac{\langle X_k \rho_k \psi_k \rangle_e}{\langle X_k \rho_k \rangle_e} \quad (3.278)$$

The generalized instantaneous quantity  $\psi_k$  is decomposed into a weighted mean component and a fluctuation component in analogy to the Favre averaging procedure for compressible flows [75, 131]:

$$\psi_k = \langle \psi_k \rangle_e^{X_k \rho_k} + \psi_k'' \quad (3.279)$$

where  $\psi_k''$  is the superimposed fluctuation component of the instantaneous quantity  $\psi_k$  around its mean weighted component  $\langle \psi_k \rangle_e^{X_k \rho_k}$ . The average of a mass weighted fluctuating quantity like  $\langle \psi_k'' \rangle_e^{X_k \rho_k}$  is equal to zero by definition,  $\langle \psi_k'' \rangle_e^{X_k \rho_k} = 0$ . This result can be verified decomposing  $\psi_k$  on the RHS of the weighted variable definition (3.278) using (3.279):

$$\begin{aligned} \langle X_k \rho_k \rangle_e \langle \psi_k \rangle_e^{X_k \rho_k} &= \langle X_k \rho_k \psi_k \rangle_e \\ &= \langle X_k \rho_k (\langle \psi_k \rangle_e^{X_k \rho_k} + \psi_k'') \rangle_e \\ &= \langle X_k \rho_k \langle \psi_k \rangle_e^{X_k \rho_k} \rangle_e + \langle X_k \rho_k \psi_k'' \rangle_e \end{aligned} \quad (3.280)$$

Comparing this result with the definition of the weighted component of  $\psi_k$  given by (3.278), it follows that  $\langle X_k \rho_k \psi_k'' \rangle_e = 0$ . From the latter relation we can deduce, the important result:

$$\begin{aligned} \langle X_k \rho_k \psi_k'' \rangle_e &= \langle X_k \rho_k \rangle_e \langle \psi_k'' \rangle_e^{X_k \rho_k} = \langle X_k \rangle_e \langle \rho_k \rangle_e^{X_k} \langle \psi_k'' \rangle_e^{X_k \rho_k} \\ &= \gamma_k \langle \rho_k \rangle_e^{X_k} \langle \psi_k'' \rangle_e^{X_k \rho_k} \\ &= 0 \end{aligned} \quad (3.281)$$

By definition the phase indicator function  $X_k$  cannot be decomposed into a mean component and a fluctuation component, thus the only way this relation can be fulfilled is by defining  $\langle \psi_k'' \rangle_e^{X_k \rho_k} = 0$ .

If we adopt (3.281), all the terms in the generic equation (3.276) can be reformulated and expressed in terms of weighted quantities and a large number of unknown covariances. The different terms in the equation are rewritten as:

*The transient term:*

$$\begin{aligned} \langle X_k \rho_k \psi_k \rangle_e &= \langle X_k \rho_k \rangle_e \langle \psi_k \rangle_e^{X_k \rho_k} \\ &= \langle X_k \rangle_e \langle \rho_k \rangle_e^{X_k} \langle \psi_k \rangle_e^{X_k \rho_k} \\ &= \gamma_k \langle \rho_k \rangle_e^{X_k} \langle \psi_k \rangle_e^{X_k \rho_k} \end{aligned} \quad (3.282)$$

*The convective term:*

$$\begin{aligned} \langle X_k \rho_k \mathbf{v}_k \psi_k \rangle_e &= \langle X_k \rho_k (\langle \mathbf{v}_k \rangle_e^{X_k \rho_k} + \mathbf{v}''_k) (\langle \psi_k \rangle_e^{X_k \rho_k} + \psi_k'') \rangle_e \\ &= \langle X_k \rho_k (\langle \mathbf{v}_k \rangle_e^{X_k \rho_k} \langle \psi_k \rangle_e^{X_k \rho_k} + \langle \mathbf{v}_k \rangle_e^{X_k \rho_k} \psi_k'' \\ &\quad + \mathbf{v}''_k \langle \psi_k \rangle_e^{X_k \rho_k} + \mathbf{v}''_k \psi_k'') \rangle_e \\ &= \langle X_k \rho_k \rangle_e \langle \mathbf{v}_k \rangle_e^{X_k \rho_k} \langle \psi_k \rangle_e^{X_k \rho_k} \\ &\quad + \langle X_k \rho_k \psi_k'' \rangle_e \langle \mathbf{v}_k \rangle_e^{X_k \rho_k} \\ &\quad + \langle X_k \rho_k \mathbf{v}''_k \rangle_e \langle \psi_k \rangle_e^{X_k \rho_k} + \langle X_k \rho_k \mathbf{v}''_k \psi_k'' \rangle_e \\ &= \langle X_k \rangle_e \langle \rho_k \rangle_e^{X_k} \langle \mathbf{v}_k \rangle_e^{X_k \rho_k} \langle \psi_k \rangle_e^{X_k \rho_k} \\ &\quad + \langle X_k \rangle_e \langle \rho_k \mathbf{v}''_k \psi_k'' \rangle_e^{X_k} \\ &= \gamma_k \langle \rho_k \rangle_e^{X_k} \langle \mathbf{v}_k \rangle_e^{X_k \rho_k} \langle \psi_k \rangle_e^{X_k \rho_k} + \gamma_k \langle \rho_k \mathbf{v}''_k \psi_k'' \rangle_e^{X_k} \end{aligned} \quad (3.283)$$

The covariances of phase  $k$  are normally defined by the phasic average of the product of the fluctuating arbitrary variable and the velocity components:

$$\mathbf{J}_k^{Re, X_k} = \frac{\langle X_k \rho_k \mathbf{v}''_k \psi_k'' \rangle_e}{\langle X_k \rangle_e} = \frac{\langle X_k \rho_k \mathbf{v}''_k \psi_k'' \rangle_e}{\gamma_k} \quad (3.284)$$

*The diffusive term:*

$$\langle X_k \mathbf{J}_k \rangle_e = \langle X_k \rangle_e \langle \mathbf{J}_k \rangle_e^{X_k} = \gamma_k \langle \mathbf{J}_k \rangle_e^{X_k} \quad (3.285)$$

The volume production term:

$$\begin{aligned}
 \langle X_k \sum_c \rho_{k,c} \phi_{k,c} \rangle_e &= \sum_c \langle X_k \rho_{k,c} \rangle_e \langle \phi_{k,c} \rangle_e^{X_k \rho_k} \\
 &= \langle X_k \rangle_e \sum_c \langle \rho_{k,c} \rangle_e^{X_k} \langle \phi_{k,c} \rangle_e^{X_k \rho_k} \\
 &= \gamma_k \sum_c \langle \rho_{k,c} \rangle_e^{X_k} \langle \phi_{k,c} \rangle_e^{X_k \rho_k}
 \end{aligned} \tag{3.286}$$

Introducing the reformulated forms of the terms examined above, the exact macroscopic transport equation (3.276) (i.e., without including any constitutive equations for the unknown terms) can be expressed as:

$$\begin{aligned}
 &\frac{\partial (\gamma_k \langle \rho_k \rangle_e^{X_k} \langle \psi_k \rangle_e^{X_k \rho_k})}{\partial t} + \nabla \cdot (\gamma_k \langle \rho_k \rangle_e^{X_k} \langle \mathbf{v}_k \rangle_e^{X_k \rho_k} \langle \psi_k \rangle_e^{X_k \rho_k}) \\
 &+ \nabla \cdot (\gamma_k (\mathbf{J}_k^{X_k} + \mathbf{J}_k^{Re, X_k})) - \gamma_k \sum_c \langle \rho_{k,c} \rangle_e^{X_k} \langle \phi_{k,c} \rangle_e^{X_k \rho_k} \\
 &= \langle [\rho_k \psi_k (\mathbf{v}_k - \mathbf{v}_I) + \mathbf{J}_k] \cdot \nabla X_k \rangle_e = \langle (\dot{m}_k \psi_k + \mathbf{J}_k \cdot \mathbf{n}_k) \frac{\partial X_k}{\partial n} \rangle_e
 \end{aligned} \tag{3.287}$$

The gradient of the phase indicator function, being a generalized scalar function [54], can be expressed as<sup>22</sup>:

$$\nabla X_k = \left( \frac{\partial X_k}{\partial n} \right) \mathbf{n}_k = -\delta(\mathbf{r} - \mathbf{r}_I) \mathbf{n}_k \tag{3.288}$$

in which  $\delta(\mathbf{r} - \mathbf{r}_I)$  denotes the Dirac's delta function for the interface and  $\mathbf{n}_k$  is the unit normal to the interface between the phases in the direction out of phase  $k$ . Thus, the Dirac delta function or the gradient in the phase indicator function serves to pick out the mass and molecular fluxes at the interface. The Dirac delta function has the property:

$$\int_{-\infty}^{+\infty} f(\xi) \delta(\xi - a) d\xi = f(a) \tag{3.289}$$

Averaging the product of the absolute value of the gradient and the fluxes gives as the result the average contributory effect of mass and molecular fluxes at the interfaces over the whole domain of integration [67]. Drew [54] defined the averaged interfacial area per unit volume by:

<sup>22</sup> It is noted that two different sign conventions are in common use considering the definitions of the interfacial terms. We follow the sign convention by [54, 67], but a different set of consistent definitions are proposed in the latest reports [136, 55, 56, 57, 58]. The reason for switching the sign convention becomes clear shortly, as all the interfacial fluxes in our derivation apparently have opposite sign compared to the conventional formulations presented in this chapter.

$$a_{eI} = \left\langle \frac{\partial X}{\partial n} \right\rangle_e \quad (3.290)$$

The averaged jump conditions are derived by multiplying the exact jump condition (3.109) by  $\frac{\partial X_k}{\partial n}$  (for a specific value of  $k$  [56, 67]) and averaging, recognizing that  $\mathbf{n}_1 = -\mathbf{n}_2$  and  $\frac{\partial X_1}{\partial n} = \frac{\partial X_2}{\partial n}$ :

$$\sum_k \left\langle (\dot{m}_k \psi_k + \mathbf{J}_k \cdot \mathbf{n}_k) \frac{\partial X_k}{\partial n} \right\rangle_e = - \left\langle M_I \frac{\partial X_l}{\partial n} \right\rangle_e \quad (3.291)$$

or

$$\sum_k \left\langle [\rho_k (\mathbf{v}_k - \mathbf{v}_I) \psi_k + \mathbf{J}_k] \cdot \nabla X_k \right\rangle_e = - \left\langle M_I \frac{\partial X_l}{\partial n} \right\rangle_e \quad (3.292)$$

in which it is understood that on the RHS no summation should be made (henceforth we drop the index  $l$  inferring that we have chosen either  $l = 1$  or  $l = 2$ ) and the factor  $\frac{\partial X_l}{\partial n} = \mathbf{n}_l \cdot \nabla X_l$  is to be expressed in accordance with the prevailing sign convention for the interface terms (3.288).

The averaged equations governing each phase and the corresponding jump conditions are then achieved defining the specific values of the generic variables in (3.287) and (3.291) in accordance with Table 3.1:

*Mass:*

The volume averaged continuity equation appears by substituting  $\psi_k = 1$ ,  $\mathbf{J}_k = 0$  and  $\phi_{c,k} = 0$  into (3.287):

$$\frac{\partial (\gamma_k \langle \rho_k \rangle_e^{X_k})}{\partial t} + \nabla \cdot (\gamma_k \langle \rho_k \rangle_e^{X_k} \langle \mathbf{v}_k \rangle_e^{X_k \rho_k}) = \langle \dot{m}_k \frac{\partial X_k}{\partial n} \rangle_e = \Gamma_k \quad (3.293)$$

Introducing the values for the interface properties  $M_I = 0$  into (3.291), yields:

$$\sum_k \Gamma_k = 0 \quad (3.294)$$

where the interfacial mass transfer terms due to phase change is defined by:

$$\Gamma_k = \left\langle \dot{m}_k \frac{\partial X_k}{\partial n} \right\rangle_e = a_{eI} \langle \dot{m}_k \rangle_{eI} \quad (3.295)$$

in which  $\langle \dot{m}_k \rangle_{eI} = \langle \dot{m}_k \frac{\partial X_k}{\partial n_k} \rangle_e / a_{eI}$  denotes the interfacial area averaged mass transfer rate [58]. The interfacial area density is defined in accordance with (3.290).

*Momentum:*

The averaged momentum equation appears by substituting  $\psi_k = \mathbf{v}_k$ ,  $\mathbf{J}_k = \mathbf{T}_k$  and  $\phi_{c,k} = \mathbf{g}_{c,k}$  into (3.287):

$$\begin{aligned} & \frac{\partial (\gamma_k \langle \rho_k \rangle_e^{X_k} \langle \mathbf{v}_k \rangle_e^{X_k \rho_k})}{\partial t} + \nabla \cdot (\gamma_k \langle \rho_k \rangle_e^{X_k} \langle \mathbf{v}_k \rangle_e^{X_k \rho_k} \langle \mathbf{v}_k \rangle_e^{X_k \rho_k}) \\ & + \nabla \cdot (\gamma_k (\langle \mathbf{T}_k \rangle_e^{X_k} + \langle \mathbf{T}_k \rangle_e^{Re, X_k})) = \left\langle (\dot{m}_k \mathbf{v}_k + \mathbf{T}_k \cdot \mathbf{n}_k) \frac{\partial X_k}{\partial n} \right\rangle_e + \\ & \gamma_k \langle \rho_k \rangle_e^{X_k} \sum_c \langle \omega_{k,c} \rangle_e^{X_k \rho_k} \langle \mathbf{g}_{k,c} \rangle_e^{X_k \rho_k} \end{aligned} \quad (3.296)$$

Introducing the values for the interface properties  $\mathbf{M}_I = 2\sigma_I H_I \mathbf{n}_I + \nabla_I \sigma_I$  into (3.291), yields:

$$\sum_k (\mathbf{M}_k^\Gamma + \mathbf{M}_k^T) = -\langle \mathbf{M}_I \frac{\partial X}{\partial n} \rangle_e \quad (3.297)$$

where the interfacial momentum transfer due to phase change is defined by:

$$\mathbf{M}_k^\Gamma = \langle \dot{m}_k \mathbf{v}_k \frac{\partial X_k}{\partial n} \rangle_e = \Gamma_k \langle \mathbf{v}_k \rangle_{e_I}^{\Gamma_k} \quad (3.298)$$

in which the mass transfer weighted interfacial area averaged velocity  $\langle \mathbf{v}_k \rangle_{e_I}^{\Gamma_k}$  is defined in analogy to the mass-weighted averaged variables known from turbulence theory [112] (p. 133).

The interfacial momentum stresses yield:

$$\mathbf{M}_k^T = \langle \mathbf{T}_k \cdot \mathbf{n}_k \frac{\partial X_k}{\partial n} \rangle_e = \langle (p_k \mathbf{e} + \boldsymbol{\sigma}_k) \cdot \mathbf{n}_k \frac{\partial X_k}{\partial n} \rangle_e \quad (3.299)$$

where the total stress tensor of both phases has been modeled using the Newtonian strain-stress formulation.

In a similar manner as for the single averaging methods in sects 3.4.1, 3.4.2 and 3.4.3, the stress terms are normally rewritten introducing an interfacial averaged pressure  $\langle p_k \rangle_{e_I}$  and an interfacial averaged viscous stress  $\langle \boldsymbol{\sigma}_k \rangle_{e_I}$ . In this method the interfacial pressure is normally defined by:

$$\langle p_k \rangle_{e_I} = \frac{\langle p_k \frac{\partial X_k}{\partial n} \rangle_e}{\langle \frac{\partial X_k}{\partial n} \rangle_e} = \frac{\langle p_k \frac{\partial X}{\partial n_I} \rangle_e}{a_{e_I}} \quad (3.300)$$

Naturally, the interfacial viscous stress is defined by:

$$\langle \boldsymbol{\sigma}_k \rangle_{e_I} = \frac{\langle \boldsymbol{\sigma}_k \frac{\partial X_k}{\partial n} \rangle_e}{\langle \frac{\partial X_k}{\partial n} \rangle_e} = \frac{\langle \boldsymbol{\sigma}_k \frac{\partial X_k}{\partial n} \rangle_e}{a_{e_I}} \quad (3.301)$$

The corresponding fluctuating interfacial quantities are defined by:

$$p''_{k,I} = p_k - \langle p_k \rangle_{e_I} \quad (3.302)$$

$$\boldsymbol{\sigma}''_{k,I} = \boldsymbol{\sigma}_k - \langle \boldsymbol{\sigma}_k \rangle_{e_I} \quad (3.303)$$

Proceeding in the same way as explained presenting the volume averaging procedure, we obtain the following result:

$$\begin{aligned} \mathbf{M}_k^T &= \langle \mathbf{T}_k \cdot \nabla X_k \rangle_e = \langle p_k \nabla X_k \rangle_e + \langle \boldsymbol{\sigma}_k \cdot \nabla X_k \rangle_e \\ &= \langle p_k \rangle_{e_I} \langle \nabla X_k \rangle_e + \langle \boldsymbol{\sigma}_k \rangle_{e_I} \cdot \langle \nabla X_k \rangle_e + \langle \mathbf{T}''_k \cdot \nabla X_k \rangle_e \\ &= \langle p_k \rangle_{e_I} \nabla \gamma_k + \langle \boldsymbol{\sigma}_k \rangle_{e_I} \cdot \nabla \gamma_k + \mathbf{F}_k \end{aligned} \quad (3.304)$$

The interfacial pressure difference effect and the combined interfacial shear and time fraction gradient effect are treated in the same manner as suggested discussing the analogous terms in (3.156). The modified definition of the generalized drag force follows naturally from an analogy to (3.158). Utilizing (3.288), (3.272) with  $\psi_k = 1$  and the mean value theorem for integrals, the term on the RHS of (3.297) can be defined by the index  $l = 1$  and expressed as:

$$\begin{aligned} -\langle \mathbf{M}_I \frac{\partial X}{\partial n} \rangle_e &= -\langle (2\sigma_I H_I \mathbf{n}_1 + \nabla_I \sigma_I) \frac{\partial X_1}{\partial n_1} \rangle_e \\ &\approx -2\langle \sigma_I H_I \rangle_{e_I} \langle \mathbf{n}_1 \frac{\partial X_1}{\partial n_1} \rangle_e - \langle \nabla_I \sigma_I \frac{\partial X_1}{\partial n_1} \rangle_e \\ &\approx -2\langle \sigma_I \rangle_{e_I} \langle H_I \rangle_{e_I} \nabla \gamma_2 - a_I \langle \nabla_I \sigma_I \rangle_{e_I} \end{aligned} \quad (3.305)$$

where  $\langle H_I \rangle_{e_I}$  is the interfacial area averaged curvature [112]. The mean curvature is defined by (3.76). Again, we have used the sign convention that occurs by  $\mathbf{n}_I = \mathbf{n}_1$ .

*Energy:*

The averaged energy equation appears by substituting  $\psi_k = e_k + \frac{1}{2}v_k^2$ ,  $\mathbf{J}_k = \mathbf{T}_k \cdot \mathbf{v}_k + \mathbf{q}_k$  and  $\phi_{c,k} = \mathbf{v}_k \cdot \mathbf{g}_{c,k}$  into (3.287):

$$\begin{aligned} &\frac{\partial}{\partial t} \left( \gamma_k \langle \rho_k \rangle_e^{X_k} (\langle e_k \rangle_e^{X_k \rho_k} + \frac{1}{2} (\langle v_k \rangle_e^{X_k \rho_k})^2 + \frac{1}{2} \langle \mathbf{v}_k'' \cdot \mathbf{v}_k'' \rangle_e^{X_k \rho_k}) \right) \\ &+ \nabla \cdot \left( \gamma_k (\langle \rho_k \rangle_e^{X_k} \langle \mathbf{v}_k \rangle_e^{X_k \rho_k} \langle e_k \rangle_e^{X_k \rho_k} + \langle \rho_k \mathbf{v}_k'' e_k'' \rangle_e^{X_k}) \right) \\ &+ \frac{1}{2} \nabla \cdot \left( \gamma_k \langle \rho_k \rangle_e^{X_k} \langle \mathbf{v}_k \rangle_e^{X_k \rho_k} ((\langle v_k \rangle_e^{X_k \rho_k})^2 + \langle \mathbf{v}_k'' \cdot \mathbf{v}_k'' \rangle_e^{X_k \rho_k}) \right) \\ &+ \nabla \cdot \left( \langle \mathbf{v}_k \rangle_e^{X_k \rho_k} \cdot (\gamma_k \langle \rho_k \mathbf{v}_k'' \mathbf{v}_k'' \rangle_e^{X_k}) \right) \\ &+ \frac{1}{2} \nabla \cdot \left( \gamma_k \langle \rho_k \rangle_e^{X_k} \langle \mathbf{v}_k'' (\mathbf{v}_k'' \cdot \mathbf{v}_k'') \rangle_e^{X_k \rho_k} \right) + \nabla \cdot \left( \gamma_k \langle \mathbf{q}_k \rangle_e^{X_k} \right) \\ &+ \nabla \cdot \left( \gamma_k (\langle \mathbf{T}_k \rangle_e^{X_k} \cdot \langle \mathbf{v}_k \rangle_e^{X_k \rho_k} + \langle \mathbf{T}_k \cdot \mathbf{v}_k'' \rangle_e^{X_k}) \right) \\ &= \Gamma_k \left( \langle e_k \rangle_{e_I}^{\Gamma_k} + \frac{1}{2} (\langle v_k \rangle_{e_I}^{\Gamma_k})^2 \right) + E_k^W + E_k^E \\ &+ \gamma_k \left\langle \sum_c \rho_{k,c} \mathbf{v}_{k,c} \cdot \mathbf{g}_{k,c} \right\rangle_e^{X_k} \end{aligned} \quad (3.306)$$

Introducing the values for the interface properties

$M_I = \nabla_I \cdot \mathbf{q}_I - \nabla_I \cdot (\sigma_I \mathbf{v}_I)$  into (3.291), yields:

$$\sum_k (E_k^E + E_k^W + E_k^E) = -\langle M_I \frac{\partial X}{\partial n} \rangle_e \quad (3.307)$$

where the interfacial energy transfer due to phase change is defined by:

$$\begin{aligned} E_k^\Gamma &= - \left\langle \frac{\partial X_k}{\partial n} \rho_k \left( e_k + \frac{1}{2} v_k^2 \right) (\mathbf{v}_I - \mathbf{v}_k) \cdot \mathbf{n}_k \right\rangle_e \\ &= \left\langle \frac{\partial X_k}{\partial n} \dot{m}_k \left( e_k + \frac{1}{2} v_k^2 \right) \right\rangle_e = \Gamma_k \langle (e_k + \frac{1}{2} v_k^2) \rangle_{e_I}^{\Gamma_k}, \end{aligned} \quad (3.308)$$

in which  $\langle (e_k + \frac{1}{2} v_k^2) \rangle_{e_I}^{\Gamma_k}$  denotes the mass transfer weighted interfacial (internal and mechanical) energy [112] (p. 137).

The interfacial heat transfer is given by:

$$E_k^E = \langle \mathbf{q}_k \cdot \mathbf{n}_k \frac{\partial X_k}{\partial n} \rangle_e = a_{e_I} \langle \mathbf{q}_k \cdot \mathbf{n}_k \rangle_{e_I}, \quad (3.309)$$

in which  $\langle \mathbf{q}_k \cdot \mathbf{n}_k \rangle_{e_I}$  denotes the interfacial area averaged heat transfer flux.

The interfacial work by viscous and pressure forces yields:

$$E_k^W = \langle (\mathbf{T}_k \cdot \mathbf{v}_k) \cdot \mathbf{n}_k \frac{\partial X_k}{\partial n} \rangle_e \quad (3.310)$$

and the surface energy sources are expressed as the product of the interfacial area concentration and the averaged interfacial fluxes:

$$\begin{aligned} - \langle M_I \frac{\partial X}{\partial n} \rangle_e &= \langle (-\nabla_I \cdot (\sigma_I \mathbf{v}_I) + \nabla_I \cdot \mathbf{q}_I) \frac{\partial X_I}{\partial n_I} \rangle_e \\ &= - \langle \nabla_I \cdot (\sigma_I \mathbf{v}_I) \rangle_{e_I} a_{e_I} + \langle \nabla_I \cdot \mathbf{q}_I \rangle_{e_I} a_{e_I} \end{aligned} \quad (3.311)$$

where  $\langle \nabla_I \cdot \mathbf{q}_I \rangle_{e_I}$  and  $-\langle \nabla_I \cdot (\sigma_I \mathbf{v}_I) \rangle_{e_I}$  are the interfacial averaged interfacial energy fluxes.

*Chemical Species:*

The averaged species mass balance appears by substituting  $\psi_k = \omega_{k,s}$ ,  $\mathbf{J}_k = \mathbf{j}_{k,s}$  and  $\phi_{c,k} = R_{k,s}/\rho_{k,c}$  into (3.287):

$$\begin{aligned} &\frac{\partial (\gamma_k \langle \rho_k \rangle_e^{X_k} \langle \omega_{k,s} \rangle_e^{X_k \rho_k})}{\partial t} \\ &+ \nabla \cdot (\gamma_k \langle \rho_k \rangle_e^{X_k} \langle \omega_{k,s} \rangle_e^{X_k \rho_k} \langle \mathbf{v}_k \rangle_e^{X_k \rho_k}) + \nabla \cdot (\gamma_k \langle \mathbf{j}_{k,s} \rangle_e^{X_k}) = \\ &\langle (\dot{m}_k \omega_{k,s} + \mathbf{j}_{k,s} \cdot \mathbf{n}_k) \frac{\partial X_k}{\partial n} \rangle_e + \gamma_k \langle R_{k,s} \rangle_e^{X_k} \end{aligned} \quad (3.312)$$

Introducing the values for the interface properties  $M_I = R_{I,s}$  into (3.291), yields:

$$\sum_k (\mathbf{J}_{k,s}^\Gamma + \mathbf{J}_{k,s}^j) = - \langle M_I \frac{\partial X}{\partial n} \rangle_e \quad (3.313)$$

where the interfacial species mass transfer due to phase change is defined by:

$$\begin{aligned} \mathbf{J}_{k,s}^I &= - \langle \rho_k \omega_{k,s} (\mathbf{v}_I - \mathbf{v}_k) \cdot \mathbf{n}_k \frac{\partial X_k}{\partial n} \rangle_e = \langle \dot{m}_k \omega_{k,s} \frac{\partial X_k}{\partial n} \rangle_e \\ &= \Gamma_k \langle \omega_{k,s} \rangle_{e_I}^{\Gamma_k}, \end{aligned} \quad (3.314)$$

in which the  $\langle \omega_{k,s} \rangle_{e_I}^{\Gamma_k}$ , denotes the mass transfer weighted interfacial species  $s$  mass fraction [112] (p. 133).

The other interfacial mass transfer fluxes are given by:

$$\mathbf{J}_{k,s}^j = \langle \mathbf{j}_{k,s} \cdot \mathbf{n}_k \frac{\partial X_k}{\partial n} \rangle_e = a_{e_I} \langle \mathbf{j}_{k,s} \cdot \mathbf{n}_k \rangle_{e_I} \quad (3.315)$$

in which  $\langle \mathbf{j}_{k,s} \cdot \mathbf{n}_k \rangle_{e_I}$  denotes the interfacial area averaged mass transfer flux.

The interfacial production term due to heterogeneous reactions is normally rewritten as:

$$- \langle R_{I,s} \frac{\partial X}{\partial n} \rangle_e = \langle R_{I,s} \rangle_{e_I} a_{e_I} = \rho_{\text{Bulk}} \langle R_{I,s} \rangle_{e_I}^m \quad (3.316)$$

in which the interfacial reaction rate per unit interface area is commonly substituted by the more practical reaction rate per unit mass  $\langle R_{I,s} \rangle_{e_I}^m = \langle R_{I,s} \rangle_{e_I} a_{e_I} / \rho_{\text{Bulk}}$  ( $kg/kg, cat \times s$ ) in which  $\rho_{\text{Bulk}}$  denotes the bulk density of the catalyst ( $kg, cat/m_r^3$ ).

As expected, three groups of undetermined terms appear in the averaged equations (3.287). The first term,  $\nabla \cdot (\gamma_k \langle \rho_k \mathbf{v}'' \psi'' \rangle_e^{X_k})$  denotes the covariance or correlation terms. The second term,  $\langle \mathbf{J}_k \cdot \mathbf{n}_k \frac{\partial X_k}{\partial n} \rangle_e$ , accounts for the effects of interfacial stress, heat and species mass transfer, whereas the third term,  $\langle \dot{m}_k \psi_k \frac{\partial X_k}{\partial n} \rangle_e$ , account for the interfacial transfer due to phase change. The conventional constitutive equations are discussed in chap 5.

### 3.4.4 The Time After Volume Averaging Procedure

In this section we examine the *multiple averaging* operators with emphasis on the time after volume averaging technique. The literature cited concerning the multiple averaging operators like the space followed by time or ensemble averaging are [229, 243, 46, 43, 47, 24, 10, 174, 189, 190, 191, 192, 64, 135, 205, 206, 74]. These reports might be considered for complementary studies.

The time after volume averaging procedure can be applied under a unified set of conditions denoting the sum of the two sub-sets of requirements formulated in sects 3.4.1 and 3.4.2 for the pure volume and time averaging procedures to handle the scale disparity in a proper manner.

It has been shown that the time-volume and volume-time averaging operators are mathematically commutative [43, 47]. Nevertheless, Sha and Slattery [189] argued that in experimental analysis the instrumentation often records space average followed by a time average data. For this reason it might be convenient to formulate a consistent model formulation for the theoretical

analysis. Later, Soo and co-workers [190, 191, 205, 206] on the other hand state that the order of performing volume averaging and time averaging cannot be arbitrarily chosen due to the different physical interpretations of the different averages. Hence, volume averaging was preferred for constructing a continuum for each phase while time averaging was performed after volume averaging to account for the high-frequency fluctuations.

To close the rigorous time after volume averaged equations several modeling strategies have emerged over the years relating the average of products to products of averages. We may roughly divide these methods into two groups, one class of concepts dealing with separated flows and a second group of approaches considering dispersed flows.

In this context it is worth mentioning that when formulating the early stratified flow models the time after area averaging method was preferred describing one-dimensional two-phase pipe flows [231, 43, 47, 24, 16] and thermo-fluid dynamics in boiling water nuclear reactors [229, 10, 243, 190, 191]. Moreover, a three-dimensional generalization of the area averaging method intended for stratified flows was derived by [135]. It is pointed out that no decomposition of the field variables was performed in any of the early time and spatially averaged stratified flow models [229, 243, 10, 51]. Instead, correlation or distribution coefficients are introduced and defined as the ratio between the average of the product of macroscopic variables and the product of the averaged macroscopic field variables

$$C_k = \frac{\overline{\alpha_k \langle \rho_k \rangle_{V_k}^{\alpha_k} \langle \psi_k \mathbf{v}_k \rangle_V^{\alpha_k \rho_k}}}{\overline{\alpha_k} \langle \rho_k \rangle_{V_k}^{\alpha_k} \langle \psi_k \rangle_V^{\alpha_k \rho_k} \langle \mathbf{v}_k \rangle_V^{\alpha_k \rho_k}} \quad (3.317)$$

In this theory the covariance coefficients are affected by the size of the averaging scales in time and space [51]. However, in engineering practice these coefficients are commonly set to unity because very little data on the distribution coefficients are available [229, 243, 10].

In this work the application of the time after volume averaging method to dispersed flows is of particular interest. In this specific application the variables are usually decomposed both in time and space. However, the spatial covariances are generally neglected merely due to a general lack of understanding of the physical processes considered by these terms. It is generally assumed that for dispersed mixtures the effect of non-locality and thus the spatial covariances can be neglected [51, 205, 206]. The temporal decomposition of the spatially averaged variables gives rise to terms of mean and fluctuating quantities where the temporal covariances are interpreted as the turbulent contributions. Therefore, in this double averaging procedure the first part of the model formulation coincides with the standard volume averaging method as outlined in sect 3.4.1. The time averaging theorems used are similar to the conventional Reynolds or Favre averaging procedures, and deviate from the time averaging operator described in sect 3.4.2 in that the operator is

applied to the continuous variable fields achieved after the smoothing volume averaging.

Let the time averaging operator, when applied to any volume averaged scalar, vector, or tensor valued function  $\langle \psi_k \rangle_V$  associated with phase  $k$ , be defined by:

$$\overline{\langle \psi_k \rangle_V} = \frac{1}{T} \int_{t-T/2}^{t+T/2} \langle \psi_k \rangle_V dt \quad (3.318)$$

where  $\langle \psi_k \rangle_V$  is continuous and has no jump discontinuities. That is,  $\langle \psi_k \rangle_V$  has no jump discontinuities in space because this function is already spatially smoothed.

In accordance with the conventional Reynolds axioms (1.379), the Leibnitz's rule is given by:

$$\overline{\frac{\partial \langle \psi_k \rangle_V}{\partial t}} = \frac{\partial \overline{\langle \psi_k \rangle_V}}{\partial t} \quad (3.319)$$

Likewise, the Gauss' rule for a scalar field yields:

$$\overline{\nabla \langle \psi_k \rangle_V} = \nabla \overline{\langle \psi_k \rangle_V} \quad (3.320)$$

and the particular form of Gauss' rule used for vectors and tensors is written:

$$\overline{\nabla \cdot \langle \psi_k \rangle_V} = \nabla \cdot \overline{\langle \psi_k \rangle_V} \quad (3.321)$$

An instantaneous volume-averaged quantity can be decomposed into two parts, the mean and the fluctuation<sup>23</sup>:

$$\langle \psi_k \rangle_V = \overline{\langle \psi_k \rangle_V} + \langle \psi_k \rangle'_V \quad (3.323)$$

where  $\langle \psi_k \rangle'_V$  denotes the superimposed fluctuation component of the instantaneous variable  $\langle \psi_k \rangle_V$  around it's mean component  $\overline{\langle \psi_k \rangle_V}$ .

Defining a Favre averaging procedure the generalized instantaneous quantity,  $\psi_k$  is *decomposed* into a weighted mean component and a fluctuation component [75] [131]:

$$\langle \psi_k \rangle_V = \overline{\langle \psi_k \rangle_V^{\alpha_k \rho_k}} + \langle \psi_k \rangle''_V \quad (3.324)$$

where  $\langle \psi_k \rangle''_V$  denotes the deviation between the instantaneous variable  $\langle \psi_k \rangle_V$  around it's mean weighted component  $\overline{\langle \psi_k \rangle_V^{\alpha_k \rho_k}}$ .

<sup>23</sup> For comparison we note that if we reverse the order in which we apply the averaging operators to the generalized quantity  $\psi$ , the deviation  $\widehat{\psi}_k$  between the un-smoothed local time averaged  $\widehat{\psi}_k$  and the time- and volume averaged property value  $\overline{\langle \psi_k \rangle_V}$  is defined by:

$$\widehat{\psi}_k = \overline{\psi}_k - \langle \overline{\psi}_k \rangle_V \quad (3.322)$$

Alternatively, for the mass-weighted variables we can define:

$$\langle \psi_k \rangle_V^{\alpha_k \rho_k} = \overline{\langle \psi_k \rangle_V^{\alpha_k \rho_k}} + \langle \psi_k \rangle_V''^{\alpha_k \rho_k} \quad (3.325)$$

where  $\langle \psi_k \rangle_V''^{\alpha_k \rho_k} = \langle \rho_k \rangle_V \langle \psi_k \rangle_V''$  is the superimposed mass-weighted fluctuation component of the instantaneous mass-weighted quantity  $\langle \psi_k \rangle_V^{\alpha_k \rho_k}$  around its mean component  $\overline{\langle \psi_k \rangle_V^{\alpha_k \rho_k}}$ . The mass-weighted average is given by:

$$\overline{\langle \psi_k \rangle_V''^{\alpha_k \rho_k}} = \overline{\langle \rho_k \rangle_V \langle \psi_k \rangle_V''} = 0 \quad (3.326)$$

By definition the time average of the fluctuating components in (3.323) and (3.325) equals zero, whereas the time average of the fluctuating component in (3.324) is not:

$$\overline{\langle \psi_k \rangle_V''} \neq \overline{\langle \psi_k \rangle_V'} = \overline{\langle \psi_k \rangle_V''^{\alpha_k \rho_k}} = 0 \quad (3.327)$$

Furthermore, we have

$$\begin{aligned} \overline{\langle \psi_k \rangle_V} &= \frac{1}{T} \int_{t-T/2}^{t+T/2} \left[ \frac{1}{V} \int_V (\overline{\psi_k} + \psi_k') dv \right] dt = \frac{1}{V} \int_V \left[ \frac{1}{T} \int_{t-T/2}^{t+T/2} (\overline{\psi_k} + \psi_k') dt \right] dv \\ &= \overline{\langle \psi_k \rangle_V} \end{aligned} \quad (3.328)$$

which shows that the time average of an instantaneous volume averaged quantity equals the volume average of a time averaged quantity.

Again, it is emphasized that the particular forms of the Leibnitz's and Gauss' rules which are valid for time averaging of discontinuous functions as used in sect 3.4.2 are not applicable for the time after volume averaging process considered in this sub-section, since the discontinuities related to the interface are smoothed out after volume averaging has been performed [205]. It follows that the conventional single phase Favre and Reynolds temporal decomposition and time averaging concepts are valid and can be applied without modifications [177, 75, 131]. Besides, we find it is worth mentioning that in connection with the single averaging operators like the volume averaging procedure described in sect 3.4.1, the main purpose of the Reynolds and Favre decomposition and averaging rules is to separate the averages of product into products of average. On the other hand, applying a time averaging operator to the instantaneous volume averaged variables the main purpose is to separate the high frequency fluctuating components from the time-averaged variables in analogy to single phase turbulence modeling.

Taking (3.138) and (3.141) as starting point for the time averaging, we can write:

$$\begin{aligned} \frac{\partial \overline{\langle \rho_k \psi_k \rangle_V}}{\partial t} + \nabla \cdot \overline{\langle \rho_k \mathbf{v}_k \psi_k \rangle_V} + \nabla \cdot \overline{\langle \mathbf{J}_k \rangle_V} = \\ - \frac{1}{V} \int_{A_I} \overline{(\dot{m}_k \psi_k)} da + \frac{1}{V} \int_{A_I} \overline{(\mathbf{J}_k \cdot \mathbf{n}_k)} da + \overline{\langle \sum_c \rho_{k,c} \phi_{k,c} \rangle_V} \end{aligned} \quad (3.329)$$

and

$$\overline{\frac{1}{V} \int_{A_I} \left( \sum_k [\dot{m}_k \psi_k + \mathbf{J}_k \cdot \mathbf{n}_k] + M_I \right) da} = 0 \tag{3.330}$$

So far in the derivation of the averaged equations the basic concepts used are considered fairly rigorous, but in order to put (3.329) and (3.330) into directly usable forms several modeling approaches have emerged proposing quite different manipulations and approximations of the undetermined terms.

The rigorous form of the averaged equations for the particular quantities governing phase  $k$  and the corresponding jump conditions can be achieved defining the specific values of the generic variables in (3.329) and (3.330) in accordance with Table 3.1.

*Mass:*

The time after volume averaged continuity equation appears by substituting  $\psi_k = 1$ ,  $\mathbf{J}_k = 0$  and  $\phi_{c,k} = 0$  into (3.329). The result is:

$$\frac{\partial(\overline{\langle \rho_k \rangle_V})}{\partial t} + \nabla \cdot (\overline{\langle \rho_k \mathbf{v}_k \rangle_V}) = -\overline{\frac{1}{V} \int_{A_I} \dot{m}_k da} \tag{3.331}$$

Introducing the values for the interface properties  $M_I = 0$  into (3.330), we get:

$$\sum_k \overline{\Gamma_{V_k}} = 0 \tag{3.332}$$

where the interfacial mass transfer terms due to phase change is defined by:

$$\overline{\Gamma_{V_k}} = -\overline{\frac{1}{V} \int_{A_I} \dot{m}_k da} = \overline{a_I \langle \dot{m}_k \rangle_{A_I}} \approx \overline{a_I} \overline{\langle \dot{m}_k \rangle_{A_I}} \tag{3.333}$$

in which the turbulent contributions are commonly lumped into the empirical model parameters or simply neglected.

*Momentum:*

The time after volume averaged momentum equation appears by substituting  $\psi_k = \mathbf{v}_k$ ,  $\mathbf{J}_k = \mathbf{T}_k$  and  $\phi_{c,k} = \mathbf{g}_{c,k}$  into (3.329). The result is:

$$\begin{aligned} \frac{\partial(\overline{\langle \rho_k \mathbf{v}_k \rangle_V})}{\partial t} + \nabla \cdot (\overline{\langle \rho_k \mathbf{v}_k \mathbf{v}_k \rangle_V}) + \nabla \cdot (\overline{\langle \mathbf{T}_k \rangle_V}) = \\ -\overline{\frac{1}{V} \int_{A_I} (\dot{m}_k \mathbf{v}_k + \mathbf{T}_k \cdot \mathbf{n}_k) da} + \overline{\langle \sum_c \rho_c \mathbf{g}_c \rangle_V} \end{aligned} \tag{3.334}$$

Introducing the values for the interface properties  $\mathbf{M}_I = 2\sigma_I H_I \mathbf{n}_I + \nabla_I \sigma_I$  into (3.330), yields:

$$\sum_k \overline{(\mathbf{M}_k^T + \overline{\mathbf{M}_k^T})} = -\frac{1}{V} \int_{A_I} \overline{\mathbf{M}_I} da \quad (3.335)$$

where the interfacial momentum transfer due to phase change is defined by time averaging (3.148):

$$\overline{\mathbf{M}_k^T} = -\frac{1}{V} \int_{A_I} \overline{\dot{m}_k \mathbf{v}_k} da = \overline{\Gamma_{V_k} \langle \mathbf{v}_k \rangle_{A_I}^{\Gamma_{V_k}}} \approx \overline{\Gamma_{V_k} \langle \mathbf{v}_k \rangle_{A_I}^{\Gamma_{V_k}}} \quad (3.336)$$

in which the turbulent contributions are usually lumped into the empirical model parameters or simply neglected.

The interfacial momentum stresses (3.149) yield:

$$\overline{\mathbf{M}_k^T} = -\frac{1}{V} \int_{A_I} \overline{\mathbf{T}_k \cdot \mathbf{n}_k} da = -\frac{1}{V} \int_{A_I} \overline{(p_k \mathbf{e} + \boldsymbol{\sigma}_k) \cdot \mathbf{n}_k} da \quad (3.337)$$

in which the turbulent contributions are taken into account through the empirical drag coefficients. Sha et al. [191] also indicate that several additional covariance momentum transfer terms may occur due to high frequency fluctuations. For example, there may be interfacial stresses akin to Reynolds stresses, interfacial momentum transfer associated with the high frequency fluctuating mass generation which may not vanish locally, and interfacial momentum transfer due to eddy mass diffusion. However, experimentally its hard to distinguish between the different contributions, and the contributions of the high frequency correlation terms on the net interfacial momentum transfer flux are usually assumed to be of the same order of magnitude as the uncertainty reflected by the empirical drag coefficients.

By time averaging the term on the RHS of (3.147) can be expressed as

$$\begin{aligned} \frac{1}{V} \int_{A_I} \overline{\mathbf{M}_I} da &\approx 2 \overline{\langle \sigma_I \rangle_{A_I} \langle H_I \rangle_{A_I} \nabla \alpha_2} + \overline{a_I \langle \nabla_I \sigma_I \rangle_{A_I}} \\ &\approx 2 \overline{\langle \sigma_I \rangle_{A_I} \langle H_I \rangle_{A_I} \nabla \alpha_2} + \overline{a_I \langle \nabla_I \sigma_I \rangle_{A_I}} \end{aligned} \quad (3.338)$$

In these terms the turbulent contributions are usually neglected due to limited knowledge of the turbulent interfacial processes.

*Energy:*

The time after volume averaged energy equation appears by substituting  $\psi_k = e_k + \frac{1}{2} v_k^2$ ,  $\mathbf{J}_k = \mathbf{T}_k \cdot \mathbf{v}_k + \mathbf{q}_k$  and  $\phi_{c,k} = \mathbf{v}_k \cdot \mathbf{g}_{c,k}$  into (3.329). The averaged energy equation takes the form:

$$\begin{aligned} \frac{\partial}{\partial t} \left( \overline{\langle \rho_k (e_k + \frac{1}{2} v_k^2) \rangle_V} \right) &+ \nabla \cdot \left( \overline{\langle \rho_k \mathbf{v}_k (e_k + \frac{1}{2} v_k^2) \rangle_V} \right) \\ &+ \nabla \cdot \overline{\langle \mathbf{T}_k \cdot \mathbf{v}_k \rangle_V} + \nabla \cdot \left( \overline{\langle \mathbf{q}_k \rangle_V} \right) \end{aligned}$$

$$\begin{aligned}
 &= -\frac{1}{\bar{V}} \overline{\int_{A_I} \left( \dot{m}_k \left( e_k + \frac{1}{2} v_k^2 \right) + (\mathbf{T}_k \cdot \mathbf{v}_k + \mathbf{q}_k) \cdot \mathbf{n}_k \right) da} \\
 &\quad + \overline{\left\langle \sum_c \rho_{k,c} \mathbf{v}_{k,c} \cdot \mathbf{g}_{k,c} \right\rangle V}
 \end{aligned} \tag{3.339}$$

Introducing the values for the interface properties  $M_I = \nabla_I \cdot \mathbf{q}_I - \nabla_I \cdot (\sigma_I \mathbf{v}_I)$  into (3.330), yields:

$$\sum_k (\overline{E_k^E} + \overline{E_k^W} + \overline{E_k^F}) = \frac{1}{\bar{V}} \overline{\int_{A_I} M_I da} \tag{3.340}$$

where the time after volume averaged interfacial energy transfer due to phase change is defined by:

$$\begin{aligned}
 \overline{E_k^F} &= -\frac{1}{\bar{V}} \overline{\int_{A_I} \dot{m}_k \left( e_k + \frac{1}{2} v_k^2 \right) da} = \overline{\Gamma_{V_k} \langle (e_k + \frac{1}{2} v_k^2) \rangle_{A_I}^{\Gamma_{V_k}}} \\
 &\approx \overline{\Gamma_{V_k} \langle (e_k + \frac{1}{2} v_k^2) \rangle_{A_I}^{\Gamma_{V_k}}}
 \end{aligned} \tag{3.341}$$

in which the turbulent contribution is commonly lumped into the empirical model parameters.

The time after volume averaged interfacial heat transfer is given by:

$$\overline{E_k^E} = -\frac{1}{\bar{V}} \overline{\int_{A_I} \mathbf{q}_k \cdot \mathbf{n}_k da} = \overline{a_I \langle \mathbf{q}_k \cdot \mathbf{n}_k \rangle_{A_I}} \approx \overline{a_I \langle \mathbf{q}_k \cdot \mathbf{n}_k \rangle_{A_I}} \tag{3.342}$$

in which the turbulent contributions are usually lumped into the empirical model parameters. Nevertheless, in a few approaches the effective flux is split into a laminar and a turbulent contribution. It can be shown that the concepts of the averaging indicates that there may be contributions to the interfacial energy flux due to the high frequency fluctuations [190]. The interfacial work by viscous and pressure forces yields:

$$\overline{E_k^W} = -\frac{1}{\bar{V}} \overline{\int_{A_I} (\mathbf{T}_k \cdot \mathbf{v}_k) \cdot \mathbf{n}_k da} \tag{3.343}$$

and the surface energy sources are expressed as the product of the interfacial area concentration and the averaged interfacial fluxes:

$$\begin{aligned}
 \frac{1}{\bar{V}} \overline{\int_{A_I} M_I da} &= -\frac{1}{\bar{V}} \overline{\int_{A_I} (-\nabla_I \cdot (\sigma_I \mathbf{v}_I) + \nabla_I \cdot \mathbf{q}_I) da} \\
 &= \overline{\langle \nabla_I \cdot (\sigma_I \mathbf{v}_I) \rangle_{A_I} a_I} - \overline{\langle \nabla_I \cdot \mathbf{q}_I \rangle_{A_I} a_I}
 \end{aligned} \tag{3.344}$$

The turbulent contributions are usually neglected due to limited understanding of the phenomena involved.

*Chemical species:*

The time after volume averaged species mass balance appears by substituting  $\psi_k = \omega_{k,s}$ ,  $\mathbf{J}_k = \mathbf{j}_{k,s}$  and  $\phi_{c,k} = R_{k,s}/\rho_{k,c}$  into (3.329). The averaged species mass balance becomes:

$$\frac{\partial(\overline{\langle \rho_{k,s} \rangle_V})}{\partial t} + \nabla \cdot (\overline{\langle \rho_{k,s} \mathbf{v}_k \rangle_V}) + \nabla \cdot (\overline{\langle \mathbf{j}_{k,s} \rangle_V}) = -\frac{1}{V} \int_{A_I} (\dot{m}_k \omega_{k,s} + \mathbf{j}_{k,s} \cdot \mathbf{n}_k) da + \overline{\langle R_{k,s} \rangle_V} \quad (3.345)$$

Introducing the values for the interface properties  $M_I = R_{I,s}$  into (3.330), yields:

$$\sum_k (\overline{\langle \mathbf{J}_{k,s}^I \rangle} + \overline{\langle \mathbf{J}_{k,s}^j \rangle}) = \frac{1}{V} \int_{A_I} M_I da \quad (3.346)$$

The interfacial species mass transfer due to phase change is defined by:

$$\overline{\langle \mathbf{J}_{k,s}^I \rangle} = -\frac{1}{V} \int_{A_I} \dot{m}_k \omega_{k,s} da = \overline{\langle \Gamma_{V_k} \langle \omega_{k,s} \rangle_{A_I}^{\Gamma_{V_k}} \rangle} \approx \overline{\langle \Gamma_{V_k} \langle \omega_{k,s} \rangle_{A_I}^{\Gamma_{V_k}} \rangle} \quad (3.347)$$

In the interfacial coupling terms the turbulent contributions are commonly taken into account through the empirical model parameters.

The other interfacial mass transfer fluxes are given by:

$$\overline{\langle \mathbf{J}_k^j \rangle} = -\frac{1}{V} \int_{A_I} \mathbf{j}_k \cdot \mathbf{n}_k da = \overline{\langle a_I \langle \mathbf{j}_k \cdot \mathbf{n}_k \rangle_{A_I} \rangle} \approx \overline{\langle a_I \langle \mathbf{j}_k \cdot \mathbf{n}_k \rangle_{A_I} \rangle} \quad (3.348)$$

The turbulent contributions are usually taken into account through the empirical model parameters or simply neglected due to the lack of understanding of these processes.

The interfacial production term due to heterogeneous reactions is normally rewritten as

$$\frac{1}{V} \int_{A_I} M_I da = \frac{1}{V} \int_{A_I} R_{I,s} da = \overline{\langle R_{I,s} \rangle_{A_I} a_I} \approx \overline{\langle \rho_{\text{Bulk}} \langle R_{I,s} \rangle^m \rangle} \quad (3.349)$$

The turbulent contributions to the interfacial terms are normally normally neglected since our knowledge concerning these phenomena are limited.

In order to carry out computations with the time after volume averaged transport equations on the form (3.329) and (3.330), we need to relate the average of products to products of averages and derive constitutive equations for the interfacial coupling terms.

## The Favre Decomposition Method

One way to solve the first problem is to introduce mass- and phase weighted volume averaged variables and the concepts of spatial and temporal decomposition of the volume averaged variables. The mass-weighted volume average of the quantity  $\psi_k$  is defined by (3.182) and the phase-weighted volume average is defined by (3.118). However, for dispersed flows all the spatial covariances are neglected in this averaging method [205, 206, 74]. The turbulence effects are thereafter considered by temporal decomposition of the weighted quantities followed by time averaging in a way resembling the analysis of variable density single phase flows [75, 131]. In particular, mass-weighted averaging akin to Favre averaging in compressible flows is employed in accordance with the work of [87, 117, 139]. This approach has the merit of reducing the number of covariance terms emerging after the averaging operation as compared to conventional Reynolds averaging. The phase velocities and the scalar variables representing the balanced quantities are normally mass-weighted before they are temporally decomposed into phase mean and fluctuating components, while the remaining scalar variables are decomposed into phase mean and fluctuating components without any prior mass-weighting.

From (3.184) the volume averaged mass flux of phase  $k$  in (3.138) is reformulated using a spatial decomposition (3.183) of the velocity variable. Thus, we can write:

$$\langle \rho_k \mathbf{v}_k \rangle_V = \langle \rho_k (\langle \mathbf{v}_k \rangle_V^{\alpha_k \rho_k} + \widehat{\widehat{\mathbf{v}}}_k) \rangle_V = \langle \rho_k \rangle_V \langle \mathbf{v}_k \rangle_V^{\alpha_k \rho_k} \quad (3.350)$$

In the subsequent temporal decomposition of the scalar variables is as a main rule performed in accordance with (3.323), while the velocity is decomposed using the approach for mass-weighted variables (3.325). After time averaging the mass flux (3.350) of phase  $k$ , we obtain:

$$\begin{aligned} \overline{\langle \rho_k \mathbf{v}_k \rangle_V} &= \overline{\langle \rho_k \rangle_V (\langle \mathbf{v}_k \rangle_V^{\alpha_k \rho_k} + \langle \mathbf{v}_k \rangle_V^{\prime\prime, \alpha_k \rho_k})} \\ &= \overline{\langle \rho_k \rangle_V} \overline{\langle \mathbf{v}_k \rangle_V^{\alpha_k \rho_k}} + \overline{\langle \rho_k \rangle_V} \overline{\langle \mathbf{v}_k \rangle_V^{\prime\prime}} \\ &= \overline{\langle \rho_k \rangle_V} \overline{\langle \mathbf{v}_k \rangle_V^{\alpha_k \rho_k}} \end{aligned} \quad (3.351)$$

Besides, the term  $\overline{\langle \rho_k \rangle_V} = \overline{\alpha_k \langle \rho_k \rangle_{V_k}}$  is treated as one field variable for compressible flows, whereas for incompressible flows the mass-weighted average variable reduces to a phase-weighted average.

In accordance with (3.185) the convective term in the generic volume averaged equation (3.138) is manipulated introducing mass-weighted variables (3.182) and the concept of spatial decomposition (3.183). Hence, the volume averaged convection term is given by:

$$\begin{aligned} \langle \rho_k \mathbf{v}_k \psi_k \rangle_V &= \langle \rho_k \rangle_V \langle \mathbf{v}_k \rangle_V^{\alpha_k \rho_k} \langle \psi_k \rangle_V^{\alpha_k \rho_k} + \langle \rho_k \widehat{\widehat{\psi}}_k \widehat{\widehat{\mathbf{v}}}_k \rangle_V \\ &\approx \langle \rho_k \rangle_V \langle \mathbf{v}_k \rangle_V^{\alpha_k \rho_k} \langle \psi_k \rangle_V^{\alpha_k \rho_k} \end{aligned} \quad (3.352)$$

in which the volume average of products is approximated by the product of averages. That is, the covariance of the spatial deviation variables are normally neglected.

With a temporal decomposition of the volume averaged variables (3.323) and (3.325), we get:

$$\begin{aligned}
 \overline{\langle \rho_k \mathbf{v}_k \psi_k \rangle_V} &\approx \overline{\langle \rho_k \rangle_V \langle \mathbf{v}_k \rangle_V^{\alpha_k \rho_k} \langle \psi_k \rangle_V^{\alpha_k \rho_k}} \\
 &= \overline{\langle \rho_k \rangle_V (\langle \mathbf{v}_k \rangle_V^{\alpha_k \rho_k} + \langle \mathbf{v}_k \rangle_V'') (\langle \psi_k \rangle_V^{\alpha_k \rho_k} + \langle \psi_k \rangle_V'')} \\
 &= \overline{\langle \rho_k \rangle_V \langle \mathbf{v}_k \rangle_V^{\alpha_k \rho_k} \langle \psi_k \rangle_V^{\alpha_k \rho_k}} + \overline{\langle \rho_k \rangle_V \langle \psi_k \rangle_V'' \langle \mathbf{v}_k \rangle_V^{\alpha_k \rho_k}} \\
 &\quad + \overline{\langle \rho_k \rangle_V \langle \mathbf{v}_k \rangle_V'' \langle \psi_k \rangle_V^{\alpha_k \rho_k}} + \overline{\langle \rho_k \rangle_V \langle \mathbf{v}_k \rangle_V'' \langle \psi_k \rangle_V''} \\
 &= \overline{\langle \rho_k \rangle_V \langle \mathbf{v}_k \rangle_V^{\alpha_k \rho_k} \langle \psi_k \rangle_V^{\alpha_k \rho_k}} + \overline{\langle \rho_k \rangle_V \langle \mathbf{v}_k \rangle_V'' \langle \psi_k \rangle_V''}
 \end{aligned} \tag{3.353}$$

Using (3.351) and (3.353) the averaged equations governing phase  $k$  can be modeled as:

*Mass:*

The reformulated time after volume averaged continuity equation appears by substituting (3.351) into (3.331). The result is:

$$\frac{\partial (\overline{\langle \rho_k \rangle_V})}{\partial t} + \nabla \cdot (\overline{\langle \rho_k \rangle_V \langle \mathbf{v}_k \rangle_V^{\alpha_k \rho_k}}) = \overline{\Gamma_k} \tag{3.354}$$

in which the source term  $\overline{\Gamma_k}$  may be a complex function of low and high frequency contributions. However, in most reactor simulations only the low-frequency contributions are taken into account.

*Momentum:*

The reformulated time after volume averaged momentum equation appears by substituting (3.182) and (3.353) into (3.334). The result is:

$$\begin{aligned}
 &\frac{\partial}{\partial t} \left( \overline{\langle \rho_k \rangle_V \langle \mathbf{v}_k \rangle_V^{\alpha_k \rho_k}} \right) + \nabla \cdot \left( \overline{\langle \rho_k \rangle_V \langle \mathbf{v}_k \rangle_V^{\alpha_k \rho_k} \langle \mathbf{v}_k \rangle_V^{\alpha_k \rho_k}} \right) \\
 &= -\nabla \cdot \left( \overline{\langle \alpha_k \rangle_V \langle p_k \rangle_{V_k}} \right) - \nabla \cdot \left( \overline{\langle \alpha_k \rangle_V \langle \boldsymbol{\sigma}_k \rangle_V^{\alpha_k} + \langle \boldsymbol{\sigma}_k \rangle_V^{Re \alpha_k}} \right) \\
 &\quad - \frac{1}{V} \int_{A_I} (\dot{m}_k \mathbf{v}_k + \mathbf{T}_k \cdot \mathbf{n}_k) da + \overline{\langle \rho_k \rangle_V} \sum_c \overline{\langle \omega_{k,c} \rangle_V^{\alpha_k \rho_k}} \mathbf{g}_{k,c}
 \end{aligned} \tag{3.355}$$

where the time after volume averaged momentum flux is given in accordance with (3.353) as:

$$\overline{\langle \rho_k \mathbf{v}_k \mathbf{v}_k \rangle_V} = \overline{\langle \rho_k \rangle_V \langle \mathbf{v}_k \rangle_V^{\alpha_k \rho_k} \langle \mathbf{v}_k \rangle_V^{\alpha_k \rho_k}} + \overline{\langle \rho_k \rangle_V \langle \mathbf{v}_k \rangle_V'' \langle \mathbf{v}_k \rangle_V''} \tag{3.356}$$

The second term on the RHS of (3.356) represents the Reynolds stress of phase  $k$ , defined by:

$$\overline{\langle \boldsymbol{\sigma}_k \rangle_V^{Re}} = \overline{\langle \rho_k \rangle_V \langle \mathbf{v}_k \rangle_V'' \langle \mathbf{v}_k \rangle_V''} \quad (3.357)$$

or we may introduce a phase weighted Reynolds stress in analogy to the quantities used in the multiphase single averaging operators [139]. The phase-weighted Reynolds stress term can be defined by:

$$\overline{\langle \boldsymbol{\sigma}_k \rangle_V^{Re \alpha_k}} = \frac{\overline{\langle \boldsymbol{\sigma}_k \rangle_V^{Re}}}{\overline{\alpha_k}} = \frac{\overline{\langle \rho_k \rangle_V \langle \mathbf{v}_k \rangle_V'' \langle \mathbf{v}_k \rangle_V''}}{\overline{\alpha_k}} \quad (3.358)$$

which needs to be modeled by a suitable turbulence model for phase  $k$ . A consistent phase-weighted definition of the time after volume averaged viscous stress term yields:

$$\overline{\langle \boldsymbol{\sigma}_k \rangle_V^{\alpha_k}} = \frac{\overline{\langle \boldsymbol{\sigma}_k \rangle_V}}{\overline{\alpha_k}} \quad (3.359)$$

The pressure term is normally rewritten using the conventional Reynolds decomposition concept, thus:

$$\begin{aligned} \nabla \cdot \overline{\langle p_k \mathbf{e} \rangle_V} &= \nabla \overline{\langle p_k \rangle_V} = \nabla \left( \overline{\langle p_k \rangle_{V_k}} + \overline{\alpha'_k \langle p_k \rangle'_{V_k}} \right) \\ &\approx \nabla (\overline{\alpha_k \langle p_k \rangle_{V_k}}) \end{aligned} \quad (3.360)$$

The temporal covariance term is normally neglected due to the lack of knowledge on the physical processes taking place (i.e.  $\overline{\alpha'_k \langle p_k \rangle'_{V_k}} \approx 0$ ). Preliminary analysis based on a hypothesis that these terms are of diffusive nature has been performed by [119].

The source term is derived in the following way:

$$\sum_c \overline{\langle \rho_k \rangle_V} \mathbf{g}_{k,c} = \sum_c \overline{\langle \rho_k \omega_{k,c} \rangle_V} \mathbf{g}_{k,c} = \overline{\langle \rho_k \rangle_V} \sum_c \overline{\langle \omega_{k,c} \rangle_V^{\alpha_k \rho_k}} \mathbf{g}_{k,c} \quad (3.361)$$

in which the particular scalar  $\omega_{k,c}$  denoting the balanced species mass fraction is represented by a mass-weighted quantity.

*Energy:*

The reformulated time after volume averaged energy equation appears by substituting (3.182) and (3.353) into (3.339). The energy equation takes the form

$$\begin{aligned} &\frac{\partial}{\partial t} (\overline{\langle \rho_k \rangle_V} \overline{\langle E_k \rangle_V^{\alpha_k \rho_k}}) + \nabla \cdot (\overline{\langle \rho_k \rangle_V} \overline{\langle \mathbf{v} \rangle_V^{\alpha_k \rho_k}} \overline{\langle E_k \rangle_V^{\alpha_k \rho_k}}) \\ &= -\nabla \cdot (\overline{\langle p_k \rangle_V} \overline{\langle \mathbf{v}_k \rangle_V^{\alpha_k \rho_k}}) - \nabla \cdot (\overline{\langle \mathbf{q}_k \rangle_V}) \\ &\quad - \nabla \cdot (\overline{\langle \mathbf{v}_k \rangle_V^{\alpha_k \rho_k}} \cdot (\overline{\langle \boldsymbol{\sigma}_k \rangle_V} + \overline{\langle \boldsymbol{\sigma} \rangle_V^{Re}})) \\ &\quad + \nabla \cdot (\overline{\langle \rho_k \rangle_V} D_{k,t}^{e_k} \overline{\langle e_k \rangle_V^{\alpha_k \rho_k}}) \\ &\quad - \frac{1}{V} \int_{A_I} \left( \dot{m}_k (e_k + \frac{1}{2} v_k^2) + (\mathbf{T}_k \cdot \mathbf{v}_k + \mathbf{q}_k) \cdot \mathbf{n}_k \right) da \\ &\quad + \overline{\langle \rho_k \rangle_V} \sum_c (\overline{\langle \omega_{k,c} \rangle_V^{\alpha_k \rho_k}} \overline{\langle \mathbf{v}_k \rangle_V^{\alpha_k \rho_k}} - D_{k,t}^{\omega_{k,s}} \nabla \overline{\langle \omega_{k,c} \rangle_V^{\alpha_k \rho_k}}) \cdot \mathbf{g}_{k,c} \end{aligned} \quad (3.362)$$

where  $\overline{\langle E_k \rangle_V^{\alpha_k \rho_k}} = \overline{\langle e_k \rangle_V^{\alpha_k \rho_k}} + \frac{1}{2} \overline{\langle \mathbf{v}_k \rangle_V^{\alpha_k \rho_k} \cdot \langle \mathbf{v}_k \rangle_V^{\alpha_k \rho_k}}$

The transient terms in (3.339) are reformulated in the following way:

$$\begin{aligned} \overline{\langle \rho_k (e_k + \frac{1}{2} v_k^2) \rangle_V} &= \overline{\langle \rho_k e_k \rangle_V} + \frac{1}{2} \overline{\langle \rho_k v_k^2 \rangle_V} \\ &= \overline{\langle \rho_k e_k \rangle_V} + \frac{1}{2} \overline{\langle \rho_k (\mathbf{v}_k \cdot \mathbf{v}_k) \rangle_V} \end{aligned} \quad (3.363)$$

in which we adopt (3.182) for the *internal energy*-density covariance:

$$\overline{\langle \rho_k e_k \rangle_V} = \overline{\langle \rho_k \rangle_V} \overline{\langle e_k \rangle_V^{\alpha_k \rho_k}} \quad (3.364)$$

where the particular scalar  $e_k$  denoting the internal energy is represented by a mass-weighted quantity.

The *kinetic energy term* in (3.339) is more cumbersome to deal with. The volume average kinetic energy term yields:

$$\begin{aligned} \langle \rho_k (\mathbf{v}_k \cdot \mathbf{v}_k) \rangle_V &= \langle \rho_k ((\langle \mathbf{v}_k \rangle_V^{\alpha_k \rho_k} + \widehat{\mathbf{v}}_k) \cdot (\langle \mathbf{v}_k \rangle_V^{\alpha_k \rho_k} + \widehat{\mathbf{v}}_k)) \rangle_V \\ &= \langle \rho_k (\langle \mathbf{v}_k \rangle_V^{\alpha_k \rho_k} \cdot \langle \mathbf{v}_k \rangle_V^{\alpha_k \rho_k} + 2 \langle \mathbf{v}_k \rangle_V^{\alpha_k \rho_k} \cdot \widehat{\mathbf{v}}_k + \widehat{\mathbf{v}}_k \cdot \widehat{\mathbf{v}}_k) \rangle_V \\ &= \langle \rho_k \rangle_V (\langle \mathbf{v}_k \rangle_V^{\alpha_k \rho_k} \cdot \langle \mathbf{v}_k \rangle_V^{\alpha_k \rho_k}) + \langle \rho_k (\widehat{\mathbf{v}}_k \cdot \widehat{\mathbf{v}}_k) \rangle_V \\ &\approx \langle \rho_k \rangle_V (\langle \mathbf{v}_k \rangle_V^{\alpha_k \rho_k} \cdot \langle \mathbf{v}_k \rangle_V^{\alpha_k \rho_k}) \end{aligned} \quad (3.365)$$

After time averaging the volume averaged kinetic energy term, we get:

$$\begin{aligned} \overline{\langle \rho_k (\mathbf{v}_k \cdot \mathbf{v}_k) \rangle_V} &\approx \overline{\langle \rho_k \rangle_V (\langle \mathbf{v}_k \rangle_V^{\alpha_k \rho_k} \cdot \langle \mathbf{v}_k \rangle_V^{\alpha_k \rho_k})} \\ &= \overline{\langle \rho_k \rangle_V ((\langle \mathbf{v}_k \rangle_V^{\alpha_k \rho_k} + \langle \mathbf{v}_k \rangle_V'') \cdot (\langle \mathbf{v}_k \rangle_V^{\alpha_k \rho_k} + \langle \mathbf{v}_k \rangle_V''))} \\ &= \overline{\langle \rho_k \rangle_V (\langle \mathbf{v}_k \rangle_V^{\alpha_k \rho_k} \cdot \langle \mathbf{v}_k \rangle_V^{\alpha_k \rho_k})} + \overline{\langle \rho_k \rangle_V (\langle \mathbf{v}_k \rangle_V'' \cdot \langle \mathbf{v}_k \rangle_V'')} \\ &\approx \overline{\langle \rho_k \rangle_V (\langle \mathbf{v}_k \rangle_V^{\alpha_k \rho_k} \cdot \langle \mathbf{v}_k \rangle_V^{\alpha_k \rho_k})} \end{aligned} \quad (3.366)$$

The *convective energy flux* in (3.339) is also split into two separate contributions:

$$\begin{aligned} \overline{\langle \rho_k \mathbf{v}_k (e_k + \frac{1}{2} v_k^2) \rangle_V} &= \overline{\langle \rho_k \mathbf{v}_k e_k \rangle_V} + \frac{1}{2} \overline{\langle \rho_k \mathbf{v}_k v_k^2 \rangle_V} \\ &= \overline{\langle \rho_k \mathbf{v} e_k \rangle_V} + \frac{1}{2} \overline{\langle \rho_k \mathbf{v} (\mathbf{v}_k \cdot \mathbf{v}_k) \rangle_V} \end{aligned} \quad (3.367)$$

The time after volume averaged internal energy flux, i.e., the first term on the RHS of (3.367), is reformulated in accordance with (3.353) and given by:

$$\overline{\langle \rho_k \mathbf{v}_k e_k \rangle_V} = \overline{\langle \rho_k \rangle_V} \overline{\langle \mathbf{v}_k \rangle_V^{\alpha_k \rho_k}} \overline{\langle e_k \rangle_V^{\alpha_k \rho_k}} + \overline{\langle \rho_k \rangle_V} \overline{\langle \mathbf{v}_k \rangle_V''} \overline{\langle e_k \rangle_V''} \quad (3.368)$$

The second term on the RHS of (3.368) represents the thermal transport due to the fluctuations in velocity and internal energy. This term can be

modeled in accordance with the gradient hypothesis and the Boussinesq transport coefficient concept. That is, we approximate the covariance by:

$$\overline{\langle \rho_k \rangle_V \langle \mathbf{v}_k \rangle_V'' \langle e_k \rangle_V''} = -\overline{\langle \rho_k \rangle_V D_{k,t}^{e_k} \nabla \langle e_k \rangle_V^{\alpha_k \rho_k}} \quad (3.369)$$

and  $D_{k,t}^{e_k}$  is the eddy thermal diffusivity.

The volume averaged *kinetic energy flux* in (3.367) is given by:

$$\begin{aligned} & \overline{\langle \rho_k \mathbf{v}_k (\mathbf{v}_k \cdot \mathbf{v}_k) \rangle_V} \\ &= \overline{\langle \rho_k (\langle \mathbf{v}_k \rangle_V^{\alpha_k \rho_k} + \widehat{\mathbf{v}}_k) (\langle \mathbf{v}_k \rangle_V^{\alpha_k \rho_k} + \widehat{\mathbf{v}}_k) \cdot (\langle \mathbf{v}_k \rangle_V^{\alpha_k \rho_k} + \widehat{\mathbf{v}}_k) \rangle_V} \\ &= \overline{\langle \rho_k \rangle_V \langle \mathbf{v}_k \rangle_V^{\alpha_k \rho_k} (\langle \mathbf{v}_k \rangle_V^{\alpha_k \rho_k} \cdot \langle \mathbf{v}_k \rangle_V^{\alpha_k \rho_k})} + \\ & \quad \overline{\langle \rho_k \rangle_V \langle \mathbf{v}_k \rangle_V^{\alpha_k \rho_k} (2 \langle \mathbf{v}_k \rangle_V^{\alpha_k \rho_k} \cdot \widehat{\mathbf{v}}_k + \widehat{\mathbf{v}}_k \cdot \widehat{\mathbf{v}}_k)} + \\ & \quad \overline{\langle \rho_k \widehat{\mathbf{v}}_k (\langle \mathbf{v}_k \rangle_V^{\alpha_k \rho_k} \cdot \langle \mathbf{v}_k \rangle_V^{\alpha_k \rho_k} + 2 \langle \mathbf{v}_k \rangle_V^{\alpha_k \rho_k} \cdot \widehat{\mathbf{v}}_k + \widehat{\mathbf{v}}_k \cdot \widehat{\mathbf{v}}_k) \rangle_V} \\ &= \overline{\langle \rho_k \rangle_V \langle \mathbf{v}_k \rangle_V^{\alpha_k \rho_k} (\langle \mathbf{v}_k \rangle_V^{\alpha_k \rho_k} \cdot \langle \mathbf{v}_k \rangle_V^{\alpha_k \rho_k} + \langle \widehat{\mathbf{v}}_k \cdot \widehat{\mathbf{v}}_k \rangle_V)} + \\ & \quad 2 \overline{\langle \mathbf{v}_k \rangle_V^{\alpha_k \rho_k} \cdot \langle \rho_k \widehat{\mathbf{v}}_k \widehat{\mathbf{v}}_k \rangle_V} + \overline{\langle \rho_k \widehat{\mathbf{v}}_k (\widehat{\mathbf{v}}_k \cdot \widehat{\mathbf{v}}_k) \rangle_V} \approx \\ & \quad \overline{\langle \rho_k \rangle_V \langle \mathbf{v}_k \rangle_V^{\alpha_k \rho_k} (\langle \mathbf{v}_k \rangle_V^{\alpha_k \rho_k} \cdot \langle \mathbf{v}_k \rangle_V^{\alpha_k \rho_k})} \end{aligned} \quad (3.370)$$

After introducing a temporal decomposition of the mass-weighted velocity variable and time averaging the volume averaged term in (3.370), we get:

$$\begin{aligned} \overline{\langle \rho_k \mathbf{v}_k (\mathbf{v}_k \cdot \mathbf{v}_k) \rangle_V} &\approx \overline{\langle \rho_k \rangle_V \langle \mathbf{v}_k \rangle_V^{\alpha_k \rho_k} (\langle \mathbf{v}_k \rangle_V^{\alpha_k \rho_k} \cdot \langle \mathbf{v}_k \rangle_V^{\alpha_k \rho_k})} \\ &= \overline{\langle \rho_k \rangle_V \langle \mathbf{v}_k \rangle_V^{\alpha_k \rho_k} (\langle \mathbf{v}_k \rangle_V^{\alpha_k \rho_k} \cdot \langle \mathbf{v}_k \rangle_V^{\alpha_k \rho_k})} \\ & \quad + \overline{\langle \mathbf{v}_k \rangle_V^{\alpha_k \rho_k} \langle \rho_k \rangle_V (\langle \mathbf{v}_k \rangle_V'' \cdot \langle \mathbf{v}_k \rangle_V'')} \\ & \quad + 2 \overline{\langle \mathbf{v}_k \rangle_V^{\alpha_k \rho_k} \cdot \langle \rho_k \rangle_V \langle \mathbf{v}_k \rangle_V'' \langle \mathbf{v}_k \rangle_V''} \\ & \quad + \overline{\langle \rho_k \rangle_V \langle \mathbf{v}_k \rangle_V'' (\langle \mathbf{v}_k \rangle_V'' \cdot \langle \mathbf{v}_k \rangle_V'')} \\ &\approx \overline{\langle \rho_k \rangle_V \langle \mathbf{v}_k \rangle_V^{\alpha_k \rho_k} (\langle \mathbf{v}_k \rangle_V^{\alpha_k \rho_k} \cdot \langle \mathbf{v}_k \rangle_V^{\alpha_k \rho_k})} \\ & \quad + 2 \overline{\langle \mathbf{v}_k \rangle_V^{\alpha_k \rho_k} \cdot \langle \rho_k \rangle_V \langle \mathbf{v}_k \rangle_V'' \langle \mathbf{v}_k \rangle_V''} \end{aligned} \quad (3.371)$$

in which the second term on the RHS of (3.371) represents the energy transport due to the fluctuations in velocity. This term can be expressed in terms of the Reynolds stresses as:

$$\overline{\langle \mathbf{v}_k \rangle_V^{\alpha_k \rho_k} \cdot \langle \rho_k \rangle_V \langle \mathbf{v}_k \rangle_V'' \langle \mathbf{v}_k \rangle_V''} = \overline{\langle \mathbf{v}_k \rangle_V^{\alpha_k \rho_k}} \cdot \overline{\langle \boldsymbol{\sigma}_k \rangle_V^{Re}} \quad (3.372)$$

In addition, the volume averaged expansion work in (3.339) is estimated by:

$$\begin{aligned} \nabla \cdot (\langle p_k \mathbf{e} \cdot \mathbf{v}_k \rangle_V) &= \nabla \cdot (\langle p_k \mathbf{v}_k \rangle_V) \\ &= \nabla \cdot (\langle \langle p_k \rangle_V + \widehat{p}_k \rangle_V (\langle \mathbf{v}_k \rangle_V^{\alpha_k \rho_k} + \widehat{\mathbf{v}}_k))_V \\ &= \nabla \cdot (\langle p_k \rangle_V \langle \mathbf{v}_k \rangle_V^{\alpha_k \rho_k} + \langle p_k \rangle_V \langle \widehat{\mathbf{v}}_k \rangle_V \\ & \quad + \langle \widehat{p}_k \rangle_V \langle \mathbf{v}_k \rangle_V^{\alpha_k \rho_k} + \langle \widehat{p}_k \widehat{\mathbf{v}}_k \rangle_V) \\ &\approx \nabla \cdot (\langle p_k \rangle_V \langle \mathbf{v}_k \rangle_V^{\alpha_k \rho_k}) \end{aligned} \quad (3.373)$$

After time averaging the volume averaged expansion work term, the result is:

$$\begin{aligned}
\nabla \cdot \overline{\langle p_k \mathbf{e} \cdot \mathbf{v}_k \rangle_V} &= \nabla \cdot \overline{\langle p_k \mathbf{v}_k \rangle_V} \\
&\approx \nabla \cdot \overline{\langle p_k \rangle_V \langle \mathbf{v}_k \rangle_V^{\alpha_k \rho_k}} \\
&= \nabla \cdot \left( \overline{\langle p_k \rangle_V} + \overline{\langle p_k \rangle'_V} \right) \left( \overline{\langle \mathbf{v}_k \rangle_V^{\alpha_k \rho_k}} + \overline{\langle \mathbf{v}_k \rangle''_V} \right) \\
&= \nabla \cdot \left( \overline{\langle p_k \rangle_V} \overline{\langle \mathbf{v}_k \rangle_V^{\alpha_k \rho_k}} + \overline{\langle p_k \rangle_V} \overline{\langle \mathbf{v}_k \rangle''_V} \right. \\
&\quad \left. + \overline{\langle p_k \rangle'_V} \overline{\langle \mathbf{v}_k \rangle''_V} \right) \\
&\approx \nabla \cdot \left( \overline{\langle p_k \rangle_V} \overline{\langle \mathbf{v}_k \rangle_V^{\alpha_k \rho_k}} \right)
\end{aligned} \tag{3.374}$$

The work performed by the viscous forces in (3.339) is treated in a similar manner. The volume averaged term is approximated as:

$$\begin{aligned}
\nabla \cdot (\langle \boldsymbol{\sigma}_k \cdot \mathbf{v}_k \rangle_V) &= \nabla \cdot \left( \langle (\boldsymbol{\sigma}_k)_V + \widehat{\boldsymbol{\sigma}}_k \rangle \cdot \left( \langle \mathbf{v}_k \rangle_V^{\alpha_k \rho_k} + \widehat{\widehat{\mathbf{v}}}_k \right) \right)_V \\
&= \nabla \cdot \left( \langle (\boldsymbol{\sigma}_k)_V \rangle \cdot \langle \mathbf{v}_k \rangle_V^{\alpha_k \rho_k} + \langle (\boldsymbol{\sigma}_k)_V \rangle \cdot \widehat{\widehat{\mathbf{v}}}_k \right)_V \\
&\quad + \langle \widehat{\boldsymbol{\sigma}}_k \rangle_V \cdot \langle \mathbf{v}_k \rangle_V^{\alpha_k \rho_k} + \langle \widehat{\boldsymbol{\sigma}}_k \rangle \cdot \widehat{\widehat{\mathbf{v}}}_k \rangle_V \\
&\approx \nabla \cdot \left( \langle (\boldsymbol{\sigma}_k)_V \rangle \cdot \langle \mathbf{v}_k \rangle_V^{\alpha_k \rho_k} \right)
\end{aligned} \tag{3.375}$$

and, by time averaging the result is:

$$\begin{aligned}
\nabla \cdot \overline{\langle \boldsymbol{\sigma}_k \cdot \mathbf{v}_k \rangle_V} &\approx \nabla \cdot \overline{\langle (\boldsymbol{\sigma}_k)_V \rangle \cdot \langle \mathbf{v}_k \rangle_V^{\alpha_k \rho_k}} \\
&= \nabla \cdot \left( \overline{\langle (\boldsymbol{\sigma}_k)_V \rangle} + \overline{\langle (\boldsymbol{\sigma}_k)'_V \rangle} \right) \cdot \left( \overline{\langle \mathbf{v}_k \rangle_V^{\alpha_k \rho_k}} + \overline{\langle \mathbf{v}_k \rangle''_V} \right) \\
&= \nabla \cdot \left( \overline{\langle (\boldsymbol{\sigma}_k)_V \rangle} \cdot \overline{\langle \mathbf{v}_k \rangle_V^{\alpha_k \rho_k}} + \overline{\langle (\boldsymbol{\sigma}_k)_V \rangle} \cdot \overline{\langle \mathbf{v}_k \rangle''_V} \right. \\
&\quad \left. + \overline{\langle (\boldsymbol{\sigma}_k)'_V \rangle} \cdot \overline{\langle \mathbf{v}_k \rangle''_V} \right) \\
&\approx \nabla \cdot \left( \overline{\langle (\boldsymbol{\sigma}_k)_V \rangle} \cdot \overline{\langle \mathbf{v}_k \rangle_V^{\alpha_k \rho_k}} \right)
\end{aligned} \tag{3.376}$$

The variables in the body force (3.339) are spatially decomposed and volume averaged, the result can be expressed as:

$$\begin{aligned}
\left\langle \sum_c \rho_{k,c} \mathbf{v}_{k,c} \cdot \mathbf{g}_{k,c} \right\rangle_V &= \sum_c \langle \rho_k \omega_{k,c} \mathbf{v}_{k,c} \rangle_V \cdot \mathbf{g}_{k,c} \\
&= \sum_c \left( \langle (\rho_k)_V \rangle \langle \omega_{k,c} \rangle_V^{\alpha_k \rho_k} \langle \mathbf{v}_{k,c} \rangle_V^{\alpha_k \rho_k} + \langle \rho_k \widehat{\omega}_{k,c} \widehat{\widehat{\mathbf{v}}}_{k,c} \rangle_V \right) \cdot \mathbf{g}_{k,c} \\
&\approx \langle (\rho_k)_V \rangle \sum_c \left( \langle \omega_{k,c} \rangle_V^{\alpha_k \rho_k} \langle \mathbf{v}_{k,c} \rangle_V^{\alpha_k \rho_k} \right) \cdot \mathbf{g}_{k,c}
\end{aligned} \tag{3.377}$$

and by subsequent time averaging, yields:

$$\begin{aligned}
\overline{\left\langle \sum_c \rho_{k,c} \mathbf{v}_{k,c} \cdot \mathbf{g}_{k,c} \right\rangle_V} &= \sum_c \overline{\langle \rho_k \omega_{k,c} \mathbf{v}_{k,c} \rangle_V} \cdot \mathbf{g}_{k,c} \\
&\approx \sum_c \overline{\langle (\rho_k)_V \rangle \langle \omega_{k,c} \rangle_V^{\alpha_k \rho_k} \langle \mathbf{v}_{k,c} \rangle_V^{\alpha_k \rho_k}} \cdot \mathbf{g}_{k,c}
\end{aligned}$$

$$\begin{aligned}
&= \sum_c \left( \overline{\langle \rho_k \rangle_V} \overline{\langle \omega_{k,c} \rangle_V^{\alpha_k \rho_k}} \overline{\langle \mathbf{v}_{k,c} \rangle_V^{\alpha_k \rho_k}} \right) \cdot \mathbf{g}_{k,c} \\
&\quad + \sum_c \left( \overline{\langle \rho_k \rangle_V} \overline{\langle \omega_{k,c} \rangle_V''} \overline{\langle \mathbf{v}_{k,c} \rangle_V''} \right) \cdot \mathbf{g}_{k,c} \\
&\approx \overline{\langle \rho_k \rangle_V} \sum_c \left( \overline{\langle \omega_{k,c} \rangle_V^{\alpha_k \rho_k}} \overline{\langle \mathbf{v}_{k,c} \rangle_V^{\alpha_k \rho_k}} - D_{k,t} \nabla \overline{\langle \omega_{k,c} \rangle_V^{\alpha_k \rho_k}} \right) \cdot \mathbf{g}_{k,c}
\end{aligned} \tag{3.378}$$

in which the second term on the RHS represents the species mass transport due to the fluctuations in velocity and species mass fractions. This term is modeled as:

$$\overline{\langle \rho_k \rangle_V} \overline{\langle \mathbf{v}_k \rangle_V''} \overline{\langle \omega_{k,s} \rangle_V''} \approx -\overline{\langle \rho_k \rangle_V} D_{k,t}^{\omega_{k,s}} \nabla \overline{\langle \omega_k \rangle_V^{\alpha_k \rho_k}} \tag{3.379}$$

and  $D_{k,t}^{\omega_{k,s}}$  is the eddy mass diffusivity.

*Chemical species:*

The reformulated time after volume averaged species mass balance appears by substituting (3.182) and (3.353) into (3.345). The averaged species mass balance becomes:

$$\begin{aligned}
&\frac{\partial}{\partial t} \left( \overline{\langle \rho_k \rangle_V} \overline{\langle \omega_{k,s} \rangle_V^{\alpha_k \rho_k}} \right) + \nabla \cdot \left( \overline{\langle \rho_k \rangle_V} \overline{\langle \mathbf{v}_k \rangle_V^{\alpha_k \rho_k}} \overline{\langle \omega_{k,s} \rangle_V^{\alpha_k \rho_k}} \right) \\
&= -\nabla \cdot \left( \overline{\langle \mathbf{j}_{k,s} \rangle_V} \right) + \nabla \cdot \left( \overline{\langle \rho_k \rangle_V} D_{k,t}^{\omega_{k,s}} \nabla \overline{\langle \omega_k \rangle_V^{\alpha_k \rho_k}} \right) \\
&\quad - \frac{1}{V} \int_{A_I} \left( \dot{m}_k \omega_{k,s} + \mathbf{j}_{k,s} \cdot \mathbf{n}_k \right) da + \overline{\langle R_{k,s} \rangle_V}
\end{aligned} \tag{3.380}$$

The transient term in (3.345) is modeled as:

$$\begin{aligned}
\overline{\langle \rho_{k,s} \rangle_V} &= \overline{\langle \rho_k \omega_{k,s} \rangle_V} = \overline{\langle \rho_k \rangle_V} \overline{\langle \omega_{k,s} \rangle_V^{\alpha_k \rho_k}} \\
&= \overline{\langle \rho_k \rangle_V} \left( \overline{\langle \omega_{k,s} \rangle_V^{\alpha_k \rho_k}} + \overline{\langle \omega_{k,s} \rangle_V''} \right) \\
&= \overline{\langle \rho_k \rangle_V} \overline{\langle \omega_{k,s} \rangle_V^{\alpha_k \rho_k}} + \overline{\langle \rho_k \rangle_V} \overline{\langle \omega_{k,s} \rangle_V''} \\
&= \overline{\langle \rho_k \rangle_V} \overline{\langle \omega_{k,s} \rangle_V^{\alpha_k \rho_k}}
\end{aligned} \tag{3.381}$$

The time after volume averaged convective mass flux of species  $s$  in (3.345) is approximated in accordance with (3.353) and given by:

$$\begin{aligned}
\overline{\langle \rho_k \mathbf{v}_k \omega_{k,s} \rangle_V} &= \overline{\langle \rho_k \rangle_V} \overline{\langle \mathbf{v}_k \rangle_V^{\alpha_k \rho_k}} \overline{\langle \omega_{k,s} \rangle_V^{\alpha_k \rho_k}} \\
&\quad + \overline{\langle \rho_k \rangle_V} \overline{\langle \mathbf{v}_k \rangle_V''} \overline{\langle \omega_{k,s} \rangle_V''} \\
&\approx \overline{\langle \rho_k \rangle_V} \left( \overline{\langle \mathbf{v}_k \rangle_V^{\alpha_k \rho_k}} \overline{\langle \omega_{k,s} \rangle_V^{\alpha_k \rho_k}} - D_{k,t}^{\omega_{k,s}} \nabla \overline{\langle \omega_k \rangle_V^{\alpha_k \rho_k}} \right)
\end{aligned} \tag{3.382}$$

We end this subsection by summarizing the governing equations valid for *incompressible flows*, since this model formulation is often used in engineering research. For incompressible flows the fluid properties (e.g.,  $\rho_k$ ,  $\mu_k$ ) are constants so the density variable is conveniently denoted by  $\rho_k$  and simply moved outside the averaging over-lined bracket.

For these particular flows the mass-weighted and the phase-weighted averaged quantities are equal, thus:

$$\overline{\langle \psi_k \rangle_V^{\rho_k \alpha_k}} = \frac{\rho_k \overline{\langle \psi_k \rangle_V}}{\rho_k \overline{\alpha_k}} = \overline{\langle \psi_k \rangle_V^{\alpha_k}} = \frac{\overline{\alpha_k \langle \psi_k \rangle_V}}{\overline{\alpha_k}} \quad (3.383)$$

The relationship between the conventional Reynolds time average in (3.323) and the weighted Favre time average variables in (3.324) follows directly from their definitions [131]:

$$\langle \psi_k \rangle_V = \overline{\langle \psi_k \rangle_V} + \langle \psi_k \rangle'_V = \overline{\langle \psi_k \rangle_V^{\alpha_k \rho_k}} + \langle \psi_k \rangle''_V \quad (3.384)$$

in which we recall that  $\overline{\langle \psi_k \rangle'_V} \neq \overline{\langle \psi_k \rangle''_V^{\alpha_k \rho_k}} = 0$ .

Decomposing the phase-weighted quantity in (3.383) using the Favre procedure, we get:

$$\begin{aligned} \overline{\alpha_k \langle \psi_k \rangle_V^{\alpha_k}} &= \overline{\alpha_k \langle \psi_k \rangle_V} = \overline{\alpha_k (\langle \psi_k \rangle_V^{\alpha_k} + \langle \psi_k \rangle''_V)} \\ &= \overline{\alpha_k \langle \psi_k \rangle_V^{\alpha_k}} + \overline{\alpha_k \langle \psi_k \rangle''_V} \\ &= \overline{\alpha_k \langle \psi_k \rangle_V^{\alpha_k}} \end{aligned} \quad (3.385)$$

Comparing (3.385) with the definition of the weighted component of  $\psi_k$  given by (3.383), it follows that:

$$\overline{\alpha_k \langle \psi_k \rangle''_V} = 0 \quad (3.386)$$

An important consequence of (3.386) is that:

$$\overline{\alpha_k \langle \psi_k \rangle''_V} = \overline{(\overline{\alpha_k} + \alpha'_k) \langle \psi_k \rangle''_V} = \overline{\alpha_k \langle \psi_k \rangle''_V} + \overline{\alpha'_k \langle \psi_k \rangle''_V} = 0 \quad (3.387)$$

or after rearranging the resulting relation:

$$\overline{\langle \psi_k \rangle''_V} = -\frac{\overline{\alpha'_k \langle \psi_k \rangle''_V}}{\overline{\alpha_k}} \neq 0 \quad (3.388)$$

meaning that the time average of the fluctuation component related to the phase weighted averaged variables is not zero by definition.

Besides, multiplying both sides of the expression (3.384) by  $\alpha_k$  and thereafter time averaging the resulting equation, we get a relation between the Favre and Reynolds averaged variables:

$$\overline{\alpha_k \langle \psi_k \rangle_V} = \overline{\alpha_k \langle \psi_k \rangle_V} + \overline{\alpha'_k \langle \psi_k \rangle'_V} = \overline{\alpha_k \langle \psi_k \rangle_V^{\alpha_k \rho_k}} + \overline{\alpha_k \langle \psi_k \rangle''_V} \quad (3.389)$$

Then, since  $\overline{\alpha_k \langle \psi_k \rangle''_V} = 0$  by (3.386), we observe that:

$$\overline{\langle \psi_k \rangle_V^{\alpha_k \rho_k}} - \overline{\langle \psi_k \rangle_V} = \frac{\overline{\alpha'_k \langle \psi_k \rangle'_V}}{\overline{\alpha_k}} \quad (3.390)$$

Furthermore, taking the time average of (3.324), we get:

$$\overline{\langle \psi_k \rangle_V} = \overline{\langle \psi_k \rangle_V^{\alpha_k \rho_k}} + \overline{\langle \psi_k \rangle_V''} \quad (3.391)$$

and it follows that:

$$\overline{\langle \psi_k \rangle_V^{\alpha_k \rho_k}} - \overline{\langle \psi_k \rangle_V} = -\overline{\langle \psi_k \rangle_V''} = \frac{\overline{\alpha_k' \langle \psi_k \rangle_V''}}{\overline{\alpha_k}} = \frac{\overline{\alpha_k' \langle \psi_k \rangle_V'}}{\overline{\alpha_k}} \quad (3.392)$$

From this result it is seen that  $\overline{\langle \psi_k \rangle_V''}$  equals the difference between the two average values of the variable  $\psi_k$ , and can be expressed in terms of either forms of the volume fraction covariances.

The governing equations for incompressible flows can thus be expressed by:

*Mass:*

The incompressible form of the time after volume averaged continuity equation (3.354) becomes:

$$\frac{\partial(\overline{\alpha_k} \rho_k)}{\partial t} + \nabla \cdot (\overline{\alpha_k} \rho_k \overline{\langle \mathbf{v}_k \rangle_V^{\alpha_k}}) = \overline{\Gamma_k} \quad (3.393)$$

*Momentum:*

The incompressible form of the time after volume averaged momentum equation (3.355) is given by:

$$\begin{aligned} & \frac{\partial}{\partial t} (\overline{\alpha_k} \rho_k \overline{\langle \mathbf{v}_k \rangle_V^{\alpha_k}}) + \nabla \cdot (\overline{\alpha_k} \rho_k \overline{\langle \mathbf{v}_k \rangle_V^{\alpha_k}} \overline{\langle \mathbf{v}_k \rangle_V^{\alpha_k}}) \\ & = -\nabla \cdot (\overline{\alpha_k} \overline{\langle p_k \rangle_{V_k}}) - \nabla \cdot \left( \overline{\alpha_k} (\overline{\langle \boldsymbol{\sigma}_k \rangle_V^{\alpha_k}} + \overline{\langle \boldsymbol{\sigma}_k \rangle_V^{Re \alpha_k}}) \right) \\ & \quad - \overline{\frac{1}{V} \int_{A_I} (\dot{m}_k \mathbf{v}_k + \mathbf{T}_k \cdot \mathbf{n}_k) da} + \overline{\alpha_k} \rho_k \sum_c \overline{\langle \omega_k \rangle_V^{\alpha_k}} \mathbf{g}_{k,c} \end{aligned} \quad (3.394)$$

*Energy:*

The incompressible form of the time after volume averaged energy equation (3.362) can be expressed as:

$$\begin{aligned} & \frac{\partial}{\partial t} (\overline{\alpha_k} \rho_k \overline{\langle E_k \rangle_V^{\alpha_k}}) + \nabla \cdot (\overline{\alpha_k} \rho_k \overline{\langle \mathbf{v} \rangle_V^{\alpha_k}} \overline{\langle E_k \rangle_V^{\alpha_k}}) \\ & = -\nabla \cdot (\overline{\langle p_k \rangle_V} \overline{\langle \mathbf{v}_k \rangle_V^{\alpha_k}}) - \nabla \cdot (\overline{\alpha_k} \overline{\langle \mathbf{q}_k \rangle_{V_k}}) \\ & \quad - \nabla \cdot (\overline{\langle \mathbf{v}_k \rangle_V^{\alpha_k}} \cdot (\overline{\langle \boldsymbol{\sigma}_k \rangle_V} + \overline{\langle \boldsymbol{\sigma} \rangle_V^{Re}})) \\ & \quad + \nabla \cdot (\overline{\alpha_k} \rho_k D_{k,t}^{e_k} \nabla \overline{\langle e_k \rangle_V^{\alpha_k}}) \\ & \quad - \overline{\frac{1}{V} \int_{A_I} \left( \dot{m}_k (e_k + \frac{1}{2} v_k^2) + (\mathbf{T}_k \cdot \mathbf{v}_k + \mathbf{q}_k) \cdot \mathbf{n}_k \right) da} \\ & \quad + \overline{\alpha_k} \rho_k \sum_c (\overline{\langle \omega_{k,c} \rangle_V^{\alpha_k}} \overline{\langle \mathbf{v}_{k,c} \rangle_V^{\alpha_k}} - D_{k,t}^{\omega_{k,c}} \nabla \overline{\langle \omega_{k,c} \rangle_V^{\alpha_k}}) \cdot \mathbf{g}_{k,c} \end{aligned} \quad (3.395)$$

*Chemical Species:*

The incompressible form of the time after volume averaged species mass balance equation (3.380) can be expressed as:

$$\begin{aligned} & \frac{\partial}{\partial t} (\overline{\alpha_k \rho_k \langle \omega_{k,s} \rangle_V^{\alpha_k}}) + \nabla \cdot (\overline{\alpha_k \rho_k \langle \mathbf{v}_k \rangle_V^{\alpha_k} \langle \omega_{k,s} \rangle_V^{\alpha_k}}) \\ &= -\nabla \cdot (\overline{\langle \mathbf{j}_{k,s} \rangle_V}) + \nabla \cdot (\overline{\rho_k D_{k,t}^{\omega_{k,s}} \nabla \langle \omega_{k,s} \rangle_V^{\alpha_k}}) \\ & \quad - \frac{1}{V} \int_{A_I} (\dot{m}_k \omega_{k,s} + \mathbf{j}_{k,s} \cdot \mathbf{n}_k) da + \overline{\langle R_{k,s} \rangle_V} \end{aligned} \quad (3.396)$$

### The Conventional Reynolds Decomposition Method

The alternative Reynolds averaged equations are derived without introducing any weighted-average variables. Instead we adopt the conventional Reynolds averaging method [64, 205, 125, 119]. In the past, almost all the practical problems of multiphase flow and reactor modeling were dealt with using these equations. By applying the Reynolds averaging rules (1.379) to the volume averaged equations (3.138), the terms in the averaged generic equation (3.329) can be expressed as follows:

*The transient term:*

$$\begin{aligned} \overline{\alpha_k \langle \rho_k \rangle_{V_k} \langle \psi_k \rangle_V} &= \overline{\alpha'_k \langle \rho_k \rangle'_{V_k} \langle \psi_k \rangle'_V} + \overline{\overline{\alpha_k} \langle \rho_k \rangle'_{V_k} \langle \psi_k \rangle'_V} \\ & \quad + \overline{\alpha'_k \langle \psi_k \rangle'_V \langle \rho_k \rangle_{V_k}} + \overline{\alpha'_k \langle \rho_k \rangle'_{V_k} \langle \psi_k \rangle_V} \\ & \quad + \overline{\overline{\alpha_k} \langle \rho_k \rangle_{V_k} \langle \psi_k \rangle_V} \end{aligned} \quad (3.397)$$

*The convective term:*

$$\begin{aligned} \overline{\alpha_k \langle \rho_k \rangle_{V_k} \langle \mathbf{v}_k \rangle_V \langle \psi_k \rangle_V} &= \\ & \overline{\alpha'_k \langle \rho_k \rangle'_{V_k} \langle \mathbf{v}_k \rangle'_V \langle \psi_k \rangle'_V} + \overline{\overline{\alpha_k} \langle \rho_k \rangle'_{V_k} \langle \mathbf{v}_k \rangle'_V \langle \psi_k \rangle'_V} + \\ & \overline{\langle \rho_k \rangle_{V_k} \alpha'_k \langle \mathbf{v}_k \rangle'_V \langle \psi_k \rangle'_V} + \overline{\overline{\alpha_k} \langle \rho_k \rangle_{V_k} \langle \mathbf{v}_k \rangle'_V \langle \psi_k \rangle'_V} + \\ & \overline{\alpha'_k \langle \rho_k \rangle'_{V_k} \langle \psi_k \rangle'_V \langle \mathbf{v}_k \rangle_V} + \overline{\langle \rho_k \rangle_{V_k} \langle \mathbf{v}_k \rangle_V \alpha'_k \langle \psi_k \rangle'_V} + \\ & \overline{\overline{\alpha_k} \langle \mathbf{v}_k \rangle_V \langle \rho_k \rangle'_{V_k} \langle \psi_k \rangle'_V} + \overline{\alpha'_k \langle \rho_k \rangle'_{V_k} \langle \mathbf{v}_k \rangle'_V \langle \psi_k \rangle_V} + \\ & \overline{\overline{\alpha_k} \langle \rho_k \rangle'_{V_k} \langle \mathbf{v}_k \rangle'_V \langle \psi_k \rangle_V} + \overline{\langle \rho_k \rangle_{V_k} \alpha'_k \langle \mathbf{v}_k \rangle'_V \langle \psi_k \rangle_V} + \\ & \overline{\alpha'_k \langle \rho_k \rangle'_{V_k} \langle \mathbf{v}_k \rangle_V \langle \psi_k \rangle_V} + \overline{\overline{\alpha_k} \langle \rho_k \rangle_{V_k} \langle \mathbf{v}_k \rangle_V \langle \psi_k \rangle_V} \end{aligned} \quad (3.398)$$

*The diffusive term:*

$$\overline{\alpha_k \langle \mathbf{J}_k \rangle_{V_k}} = \overline{\alpha'_k \langle \mathbf{J}_k \rangle'_{V_k}} + \overline{\overline{\alpha_k} \langle \mathbf{J}_k \rangle_{V_k}} \quad (3.399)$$

The volume production term:

$$\begin{aligned}
& \overline{\alpha_k \langle \rho_k \rangle_{V_k} \sum_c \langle \omega_{k,c} \rangle_V \langle \phi_{k,c} \rangle_V} = \\
& \sum_c \left( \overline{\alpha_k \langle \rho_k \rangle_{V_k} \langle \omega_{k,c} \rangle_V \langle \phi_{k,c} \rangle_V} + \overline{\alpha_k \langle \rho_k \rangle_{V_k} \langle \omega_{k,c} \rangle'_V \langle \phi_{k,c} \rangle'_V} + \right. \\
& \quad \overline{\alpha_k \langle \omega_{k,c} \rangle_V \langle \rho_k \rangle'_V \langle \phi_{k,c} \rangle'_V} + \overline{\alpha_k \langle \phi_{k,c} \rangle_V \langle \rho_k \rangle'_V \langle \omega_{k,c} \rangle'_V} + \\
& \quad \overline{\alpha_k \langle \phi_{k,c} \rangle_V \langle \rho_k \rangle'_V \langle \omega_{k,c} \rangle'_V} + \overline{\alpha_k \langle \rho_k \rangle'_V \langle \omega_{k,c} \rangle'_V \langle \phi_{k,c} \rangle'_V} + \\
& \quad \overline{\langle \rho_k \rangle_{V_k} \langle \omega_{k,c} \rangle_V \alpha'_k \langle \phi_{k,c} \rangle'_V} + \overline{\langle \rho_k \rangle_{V_k} \langle \phi_{k,c} \rangle_V \alpha'_k \langle \omega_{k,c} \rangle'_V} + \\
& \quad \overline{\langle \rho_k \rangle_{V_k} \alpha'_k \langle \omega_{k,c} \rangle'_V \langle \phi_{k,c} \rangle'_V} + \overline{\langle \omega_{k,c} \rangle_V \langle \phi_{k,c} \rangle_V \alpha'_k \langle \rho_k \rangle'_V} + \\
& \quad \overline{\langle \omega_{k,c} \rangle_V \alpha'_k \langle \rho_k \rangle'_V \langle \phi_{k,c} \rangle'_V} + \overline{\langle \phi_{k,c} \rangle_V \alpha'_k \langle \rho_{k,c} \rangle'_V \langle \omega_{k,c} \rangle'_V} + \\
& \quad \left. \overline{\alpha'_k \langle \rho_{k,c} \rangle'_V \langle \omega_{k,c} \rangle'_V \langle \phi_{k,c} \rangle'_V} \right) \tag{3.400}
\end{aligned}$$

Substituting the given expressions (3.397) to (3.400) for the terms in the governing equation, (3.329) is expressed as:

$$\begin{aligned}
& \frac{\partial}{\partial t} (\overline{\alpha_k \langle \rho_k \rangle_{V_k} \langle \psi_k \rangle_V}) + \nabla \cdot (\overline{\alpha_k \langle \rho_k \rangle_{V_k} \langle \mathbf{v}_k \rangle_V \langle \psi_k \rangle_V}) \\
& = -\nabla \cdot \left( \overline{\alpha_k \langle \mathbf{J}_k \rangle_{V_k}} + \overline{\alpha'_k \langle \mathbf{J}_k \rangle'_V} \right) \\
& + \sum_c \overline{\alpha_k \langle \rho_k \rangle_{V_k} \langle \omega_{k,c} \rangle_V \langle \phi_{k,c} \rangle_V} \\
& - \frac{1}{V} \int_{A_I} (\overline{\dot{m}_k \psi_k}) da - \frac{1}{V} \int_{A_I} (\overline{\mathbf{J}_k \cdot \mathbf{n}_k}) da \\
& - \left[ \frac{\partial}{\partial t} \left( \overline{\alpha'_k \langle \rho_k \rangle'_V \langle \psi_k \rangle'_V} + \overline{\alpha_k \langle \rho_k \rangle'_V \langle \psi_k \rangle'_V} \right. \right. \\
& \quad \left. \left. + \overline{\alpha'_k \langle \psi_k \rangle'_V \langle \rho_k \rangle_{V_k}} + \overline{\alpha'_k \langle \rho_k \rangle'_V \langle \psi_k \rangle_V} \right) \right] \\
& - \left[ \nabla \cdot \left( \overline{\alpha'_k \langle \rho_k \rangle'_V \langle \mathbf{v}_k \rangle'_V \langle \psi_k \rangle'_V} + \overline{\alpha_k \langle \rho_k \rangle'_V \langle \mathbf{v}_k \rangle'_V \langle \psi_k \rangle'_V} \right. \right. \\
& \quad + \overline{\langle \rho_k \rangle_{V_k} \alpha'_k \langle \mathbf{v}_k \rangle'_V \langle \psi_k \rangle'_V} + \overline{\alpha_k \langle \rho_k \rangle_{V_k} \langle \mathbf{v}_k \rangle'_V \langle \psi_k \rangle'_V} \\
& \quad + \overline{\alpha'_k \langle \rho_k \rangle'_V \langle \psi_k \rangle'_V \langle \mathbf{v}_k \rangle_V} + \overline{\langle \rho_k \rangle_{V_k} \langle \mathbf{v}_k \rangle_V \alpha'_k \langle \psi_k \rangle'_V} \\
& \quad + \overline{\alpha_k \langle \mathbf{v}_k \rangle_V \langle \rho_k \rangle'_V \langle \psi_k \rangle'_V} + \overline{\alpha'_k \langle \rho_k \rangle'_V \langle \mathbf{v}_k \rangle'_V \langle \psi_k \rangle_V} \\
& \quad + \overline{\alpha_k \langle \rho_k \rangle'_V \langle \mathbf{v}_k \rangle'_V \langle \psi_k \rangle_V} + \overline{\langle \rho_k \rangle_{V_k} \alpha'_k \langle \mathbf{v}_k \rangle'_V \langle \psi_k \rangle_V} \\
& \quad \left. \left. + \overline{\alpha'_k \langle \rho_k \rangle'_V \langle \mathbf{v}_k \rangle_V \langle \psi_k \rangle_V} \right) \right] \tag{3.401}
\end{aligned}$$

$$\begin{aligned}
 & + \sum_c \left( \overline{\overline{\alpha_k \langle \rho_k \rangle_{V_k} \langle \omega_{k,c} \rangle'_V \langle \phi_{k,c} \rangle'_V}} + \right. \\
 & \quad \overline{\overline{\alpha_k \langle \omega_{k,c} \rangle_V \langle \rho_k \rangle'_{V_k} \langle \phi_{k,c} \rangle'_V}} + \overline{\overline{\alpha_k \langle \phi_{k,c} \rangle_V \langle \rho_k \rangle'_{V_k} \langle \omega_{k,c} \rangle'_V}} + \\
 & \quad \overline{\overline{\alpha_k \langle \phi_{k,c} \rangle_V \langle \rho_k \rangle'_{V_k} \langle \omega_{k,c} \rangle'_V}} + \overline{\overline{\alpha_k \langle \rho_k \rangle'_{V_k} \langle \omega_{k,c} \rangle'_V \langle \phi_{k,c} \rangle'_V}} + \\
 & \quad \overline{\overline{\langle \rho_k \rangle_{V_k} \langle \omega_{k,c} \rangle_V \alpha'_k \langle \phi_{k,c} \rangle'_V}} + \overline{\overline{\langle \rho_k \rangle_{V_k} \langle \phi_{k,c} \rangle_V \alpha'_k \langle \omega_{k,c} \rangle'_V}} + \\
 & \quad \overline{\overline{\langle \rho_k \rangle_{V_k} \alpha'_k \langle \omega_{k,c} \rangle'_{V_k} \langle \phi_{k,c} \rangle'_V}} + \overline{\overline{\langle \omega_{k,c} \rangle_V \langle \phi_{k,c} \rangle_V \alpha'_k \langle \rho_k \rangle'_{V_k}}}} + \\
 & \quad \overline{\overline{\langle \omega_{k,c} \rangle_V \alpha'_k \langle \rho_k \rangle'_{V_k} \langle \phi_{k,c} \rangle'_V}} + \overline{\overline{\langle \phi_{k,c} \rangle_V \alpha'_k \langle \rho_{k,c} \rangle'_{V_k} \langle \omega_{k,c} \rangle'_V}} + \\
 & \quad \left. \overline{\overline{\alpha'_k \langle \rho_{k,c} \rangle'_{V_k} \langle \omega_{k,c} \rangle'_V \langle \phi_k \rangle'_V}} \right)
 \end{aligned}$$

An obvious drawback related to the application of this particular averaging procedure is the extensive need for constitutive relations to achieve a solvable set of equations. The number of covariances are substantially reduced for the cases in which the density fluctuations can be neglected. Nevertheless, the conventional Reynolds averaging procedure gives rise to several covariance terms which lack physical interpretation and are thus generally ignored in spite of limited physical justification.

The incompressible flow form of the volume and time averaged equations which can be derived adopting the conventional Reynolds averaging procedure are more practical. Moreover, the covariance terms of order higher than two are normally neglected in accordance with the conventional single phase turbulence modeling procedure assuming that their relative magnitude is small compared to the lower order covariances. Considering the transient term of the generic transport equation all covariances are usually neglected based on the hypothesis that these terms are smaller than the product of averaged quantities.

The transient term (3.397) is normally approximated by:

$$\overline{\overline{\alpha_k \rho_k \langle \psi_k \rangle_V}} \approx \overline{\overline{\alpha_k}} \overline{\overline{\rho_k}} \overline{\overline{\langle \psi_k \rangle_V}} \tag{3.402}$$

The convection term (3.398) can be expressed as:

$$\begin{aligned}
 & \overline{\overline{\alpha_k \langle \rho_k \rangle_{V_k} \langle \mathbf{v}_k \rangle_V \langle \psi_k \rangle_V}} \approx \\
 & \overline{\overline{\alpha_k}} \overline{\overline{\rho_k}} \overline{\overline{\langle \mathbf{v}_k \rangle'_V \langle \psi_k \rangle'_V}} + \overline{\overline{\rho_k}} \overline{\overline{\langle \mathbf{v}_k \rangle_V}} \overline{\overline{\alpha'_k \langle \psi_k \rangle'_V}} \\
 & + \overline{\overline{\rho_k}} \overline{\overline{\alpha'_k \langle \mathbf{v}_k \rangle'_V \langle \psi_k \rangle_V}} + \overline{\overline{\alpha_k}} \overline{\overline{\rho_k}} \overline{\overline{\langle \mathbf{v}_k \rangle_V \langle \psi_k \rangle_V}}
 \end{aligned} \tag{3.403}$$

The diffusion term (3.399) is normally approximated by:

$$\overline{\overline{\langle \mathbf{J}_k \rangle_{V_k}}} \approx \overline{\overline{\alpha_k}} \overline{\overline{\langle \mathbf{J}_k \rangle_{V_k}}} \tag{3.404}$$

The volume production term (3.400) is approximated by:

$$\overline{\overline{\alpha_k \langle \rho_k \rangle_{V_k} \sum_c \langle \omega_{k,c} \rangle_V \langle \phi_{k,c} \rangle_V}} \approx \overline{\overline{\alpha_k}} \overline{\overline{\rho_k}} \sum_c \overline{\overline{\langle \omega_{k,c} \rangle_V \langle \phi_{k,c} \rangle_V}} \tag{3.405}$$

The model equations for incompressible flows which are frequently used in engineering research are thus written as:

$$\begin{aligned}
 & \frac{\partial}{\partial t} (\overline{\alpha_k \rho_k \langle \psi_k \rangle_V}) + \nabla \cdot (\overline{\alpha_k \rho_k \langle \mathbf{v}_k \rangle_V \langle \psi_k \rangle_V}) \\
 &= -\nabla \cdot \left( \overline{\alpha_k \langle \mathbf{J}_k \rangle_{V_k}} \right) + \overline{\alpha_k \rho_k} \sum_c \overline{\langle \omega_{k,c} \rangle_V \langle \phi_{k,c} \rangle_V} - \frac{1}{V} \int_{A_I} (\dot{m}_k \psi_k) da \\
 & - \frac{1}{V} \int_{A_I} (\mathbf{J}_k \cdot \mathbf{n}_k) da - \left[ \nabla \cdot \left( \overline{\alpha_k \rho_k \langle \mathbf{v}_k \rangle'_V \langle \psi_k \rangle'_V} \right. \right. \\
 & \left. \left. + \rho_k \overline{\langle \mathbf{v}_k \rangle_V \alpha'_k \langle \psi_k \rangle'_V} + \rho_k \overline{\alpha'_k \langle \mathbf{v}_k \rangle'_V \langle \psi_k \rangle_V} \right) \right]
 \end{aligned} \tag{3.406}$$

It is easily seen that the incompressible model formulation contains less covariance terms than the model equations for compressible flows (3.401). For this reason the compressible formulation is seldom used, instead the formulation valid for incompressible flows is often used for weakly compressible systems as well.

For convenience, we normally remove the  $\langle \dots \rangle_V$  volume averaging signs from the equations. By introducing the consistent sets of values for the generalized variables we get, as before, the transport equations for the specific balanced quantities.

*Mass:*

$$\frac{\partial(\overline{\alpha_k \rho_k})}{\partial t} + \nabla \cdot (\overline{\alpha_k \rho_k \overline{\mathbf{v}_k}}) = \nabla \cdot (\rho_k D_{k,t}^{\alpha_k} \nabla \overline{\alpha_k}) + \overline{\Gamma_k} \tag{3.407}$$

where the covariance is modeled by use of the gradient hypothesis and the Boussinesq turbulent transport coefficient concept:

$$\rho_k \overline{\alpha'_k \mathbf{v}'_k} \approx -\rho_k D_{k,t}^{\alpha_k} \nabla \overline{\alpha_k} \tag{3.408}$$

*Momentum:*

$$\begin{aligned}
 & \frac{\partial(\overline{\alpha_k \rho_k \overline{\mathbf{v}_k}})}{\partial t} + \nabla \cdot (\overline{\alpha_k \rho_k \overline{\mathbf{v}_k} \overline{\mathbf{v}_k}}) \\
 &= -\nabla \cdot (\overline{\alpha_k \overline{p}_k}) - \nabla \cdot (\overline{\alpha_k \overline{\boldsymbol{\sigma}}_k}) + \overline{\alpha_k \rho_k \mathbf{g}} - \nabla \cdot (\overline{\alpha_k \rho_k \overline{\mathbf{v}'_k \mathbf{v}'_k}}) \\
 & + 2\nabla \cdot (\rho_k \overline{\mathbf{v}_k} D_{k,t}^{\alpha_k} \nabla \overline{\alpha_k}) + \overline{\mathbf{M}_k^\Gamma} + \overline{\mathbf{M}_k^T} \\
 &= -\nabla \cdot (\overline{\alpha_k \overline{p}_k}) - \nabla \cdot (\overline{\alpha_k (\boldsymbol{\sigma}_k + \boldsymbol{\sigma}_k^{Re})}) + \overline{\alpha_k \rho_k \mathbf{g}} + 2\nabla \cdot (\rho_k \overline{\mathbf{v}_k} D_{k,t}^{\alpha_k} \nabla \overline{\alpha_k}) \\
 & + \overline{\mathbf{M}_k^T} + \overline{\mathbf{M}_k^\Gamma}
 \end{aligned} \tag{3.409}$$

in which the Reynolds stresses are defined by

$$\boldsymbol{\sigma}_k^{Re} = \rho_k \overline{\mathbf{v}'_k \mathbf{v}'_k} \tag{3.410}$$

Moreover, gravity is often the only body force considered in reactor analysis, and the covariance term is frequently approximated in accordance with (3.408).

*Energy:*

$$\begin{aligned}
 & \frac{\partial(\overline{\alpha_k \rho_k \overline{E_k}})}{\partial t} + \nabla \cdot (\overline{\alpha_k \rho_k \mathbf{v}_k \overline{E_k}}) \\
 &= -\nabla \cdot (\overline{\alpha_k \overline{p_k} \mathbf{v}_k}) - \nabla \cdot (\overline{\alpha_k \overline{\boldsymbol{\sigma}}_k \cdot \mathbf{v}_k}) + \nabla \cdot (\overline{\alpha_k \overline{\mathbf{q}}_k}) + \overline{\alpha_k \rho_k \mathbf{v}_k} \cdot \mathbf{g} \\
 &+ \nabla \cdot \left( \overline{\alpha_k \rho_k \mathbf{v}_k} \cdot \overline{\mathbf{v}'_k \mathbf{v}'_k} + \rho_k \overline{\mathbf{v}_k \mathbf{v}_k} \cdot \overline{\alpha'_k \mathbf{v}'_k} \right) + \nabla \cdot (\overline{\alpha_k \rho_k \mathbf{v}'_k e'_k}) \\
 &+ \nabla \cdot (\overline{e_k \rho_k \alpha'_k \mathbf{v}'_k}) \\
 &= -\nabla \cdot (\overline{\alpha_k \overline{p_k} \mathbf{v}_k}) - \nabla \cdot \left( \overline{\alpha_k (\overline{\boldsymbol{\sigma}}_k + \overline{\boldsymbol{\sigma}}_k^{\text{Re}})} \cdot \mathbf{v}_k \right) + \nabla \cdot (\overline{\alpha_k \overline{\mathbf{q}}_k}) + \overline{\alpha_k \rho_k \mathbf{v}_k} \cdot \mathbf{g} \\
 &+ \nabla \cdot (\rho_k \overline{\mathbf{v}_k \mathbf{v}_k} \cdot (D_{k,t}^{\alpha_k} \nabla \overline{\alpha_k})) + \nabla \cdot (\overline{\alpha_k \rho_k D_{k,t}^{e_k} \nabla e_k}) \\
 &+ \nabla \cdot (\overline{e_k \rho_k D_{k,t}^{\alpha_k} \nabla \alpha_k})
 \end{aligned} \tag{3.411}$$

where the additional covariance is modeled as the earlier one by use of the gradient hypothesis and the Boussinesq turbulent transport coefficient concept:

$$\rho_k \overline{\alpha_k \mathbf{v}'_k e'_k} \approx -\rho_k \overline{\alpha_k} D_{k,t}^{e_k} \nabla \overline{e_k} \tag{3.412}$$

*Chemical Species:*

$$\begin{aligned}
 & \frac{\partial}{\partial t} (\overline{\alpha_k \rho_k \overline{\alpha_k} \overline{\omega_{k,s}}}) + \nabla \cdot (\overline{\alpha_k \rho_k \overline{\alpha_k} \mathbf{v}_k \overline{\omega_{k,s}}}) = -\nabla \cdot (\overline{\alpha_k \overline{\mathbf{j}}_{k,s}}) \\
 &+ \nabla \cdot (\overline{\alpha_k \rho_k} D_{k,t}^{\omega_{k,s}} \nabla \overline{\omega_{k,s}}) - \frac{1}{V} \int_{A_I} (\dot{m}_k \omega_{k,s} + \mathbf{j}_{k,s} \cdot \mathbf{n}_k) da + \overline{\langle R_{k,s} \rangle_V}
 \end{aligned} \tag{3.413}$$

where the velocity-mass fraction covariance is modeled by use of the gradient hypothesis and the Boussinesq turbulent transport coefficient concept:

$$\rho_k \overline{\alpha_k \mathbf{v}'_k \omega'_{k,s}} \approx -\rho_k \overline{\alpha_k} D_{k,t}^{\omega_{k,s}} \nabla \overline{\omega_{k,s}} \tag{3.414}$$

In one view the time after volume averaging averaging operator gives rise to a set of model equations which is closed introducing numerous simplifying assumptions reducing the accuracy of the simulated results. However, in another viewpoint it is argued that for model validation it is more convenient to use this double averaging method in comparison with the models derived adopting the single averaging operators, since the measured data is in better consistency with the simulated results obtained applying this particular model.

More important perhaps, because of the fluctuating volume fraction variable the mathematical form of the resulting time after volume averaged equations differ slightly from those derived using the single averaging operators discussed in sects 3.4.1, 3.4.2 and 3.4.1. Not only are the physical interpretations of the various terms different, there are also additional and mathematically deviating terms occurring in this model formulations. It is observed that this fact has induced some confusion in the literature, as inconsistent constitutive equations are sometimes erroneously exchanged between the single- and multiple averaged equations. For this reason caution is needed ensuring that only consistent constitutive equations are used to approximate the unknown covariance terms occurring in the more advanced reactor models.

### 3.4.5 The Mixture Models

The basic mixture model concept considers the whole multiphase mixture as a single macroscopic continuum. In the literature the mixture model equations are derived applying various approaches which we conveniently divide into two groups. Basically, the mixture models are either derived applying the balance principle over a macroscopic Eulerian CV or by taking the sum of the averaged equations for the individual phases [15]. The first group of models is known from the work of Wallis [231], Sha and Soo [187] and Bennon and Incropera [17], whereas the second group of formulations emerged from the work of Zuber and Findlay [250], Soo [204] and Ishii [112].

Bedford and Drumheller [15] reviewed the basic principles of the continuum theories that have been developed to model mixtures of immiscible constituents, such as bubbly flows, fluid-particle mixtures, fluid saturated porous media, and composite materials. In the classical continuum theory of mixtures the pseudo-fluid is given effective macroscopic properties which have to be postulated. Balance equations are written for the pseudo-homogeneous mixture mass, momentum and energy in terms of the postulated mixture properties. These three macroscopic mixture conservation equations may be supplemented by postulated phasic balance equations. In these extended versions of the classical theories the mixture properties are given as a volume fraction weighted sum of the phasic properties. To close this model separate continuity equations of the dispersed phases are postulated and incorporated in the formulation to account for the phase distribution phenomena. In particular using the mixture equations together with the continuity equations of the dispersed phases computationally efficient descriptions of the multiphase flow are achieved, since we are considerably reducing the number of transport equations to be solved compared to the full multi-fluid model. It is generally accepted that the extended mixture model concept is appropriate to describe mixture flows in which the dynamics of the phases are closely coupled [112]. In the second group of mixture models the phasic equations are adopted from one of the existing macroscopic multi-fluid model formulations which can be derived from the local instantaneous equations applying different averaging

procedures. The mixture model equations are then achieved by taking the sum of the averaged equations for all the individual phases in the system. In the ideal case both approaches provide the same macroscopic equations.

To determine the dispersed phase velocities as occurring in the phasic continuity equations in both formulations, the momentum equation of the dispersed phases are usually approximated by algebraic equations. Depending on the concept used to relate the phase  $k$  velocity to the mixture velocity the extended mixture model formulations are referred to as the algebraic slip-, diffusion- or drift flux models.

These mixture models have been applied to investigate chemical engineering problems by [17, 163, 202, 182, 145, 165, 230, 85, 193, 19], among others.

### The Classical Homogeneous Mixture Model

In this section the classical continuum theory of mixtures is reviewed [15]. In this concept the multiphase mixture is treated as a single homogeneous continuum. Thereby the balance principle can be applied to derive conservation laws for the macroscopic pseudo-fluid in analogy to the single phase formulation examined in chap 1. Approximate constitutive equations are postulated for the expected macroscopic behavior of the phases.

Consider any quantity  $\psi_m$  associated with a mixture of phases. For an arbitrary material macroscopic control volume<sup>24</sup>  $V_m(t)$  bounded by the surface area  $A_m(t)$ , a generalized integral balance can be postulated stating that the time rate of change is equal to the molecular transport flux plus the volumetric production [187]:

$$\frac{D}{Dt} \int_{V_m(t)} \rho_m \psi_m dv = - \int_{A_m(t)} \mathbf{J}_m \cdot \mathbf{n} da + \int_{V_m(t)} \rho_m \phi_m dv \quad (3.415)$$

In this notation,  $\mathbf{n}$  is the outward directed normal unit vector to the external mixture surface  $A_m(t)$  closing the mixture volume  $V_m(t)$ ,  $D/Dt$  is the substantial time derivative,  $\mathbf{v}_m$  is the velocity associated with the mixture,  $\rho_m$  is the mixture density,  $\psi_m$  is any mixture quantity,  $\mathbf{J}_m$  is the mixture diffusive flux and  $\phi_m$  is the source term. Virtually no mixture theory includes any interfacial properties, so we chose not to include the interface mechanisms in the basic model formulation [115].

It follows from the continuum assumption that the integrands in (3.415) are continuous and differentiable functions, so the integral theorems of Leibnitz and Gauss (see app. A) can be applied transforming the system description into an Eulerian control volume formulation. The governing mixture

<sup>24</sup> To relate the classical mixture theory to the more familiar volume averaging method we may assume that the mixture CV, which is larger than a phase element but smaller than the characteristic domain dimension, coincides with the averaging volume used in the volume averaging approach.

equations are thus derived in the same manner as outlined for single phase flow in chap 1. The resulting equation is written:

$$\int_{V_m} \left( \frac{\partial(\rho_m \psi_m)}{\partial t} + \nabla \cdot (\rho_m \mathbf{v}_m \psi_m) + \nabla \cdot \mathbf{J}_m - \rho_m \phi_m \right) dv = 0 \quad (3.416)$$

Since (3.416) must be satisfied for any  $V_m$ , the macroscopic equation can be transformed into its differential form:

$$\frac{\partial(\rho_m \psi_m)}{\partial t} + \nabla \cdot (\rho_m \mathbf{v}_m \psi_m) + \nabla \cdot \mathbf{J}_m - \rho_m \phi_m = 0 \quad (3.417)$$

in which the properties and the constitutive equations required for the mixture mass, momentum, energy, and species transport equations have to be postulated. To deduce the different mixture balance equations the variables in (3.417) are defined in analogy with the single phase variables in Table 3.1. The resulting set of partial differential equations is sometimes called the *macroscopic continuum mixture equations* [193].

The basic mixture model equation (3.417) contains several undetermined quantities which have to be determined. These variables are conventionally postulated as the sum of the volume fraction weighted property values of the phases in the mixture.

The mixture density  $\rho_m$  yields:

$$\rho_m = \sum_k \alpha_k \rho_k \quad (3.418)$$

The mixture viscosity  $\mu_m$ :

$$\mu_m = \sum_k \alpha_k \mu_k \quad (3.419)$$

The mixture diffusive flux  $\mathbf{J}_m$ :

$$\mathbf{J}_m = \sum_k \alpha_k \mathbf{J}_k \quad (3.420)$$

The mixture mass averaged velocity  $\mathbf{v}_m$ :

$$\mathbf{v}_m = \frac{\sum_k \alpha_k \rho_k \mathbf{v}_k}{\sum_k \alpha_k \rho_k} = \frac{\sum_k \alpha_k \rho_k \mathbf{v}_k}{\rho_m} \quad (3.421)$$

The generic mass averaged quantity  $\psi_m$ :

$$\psi_m = \frac{\sum_k \alpha_k \rho_k \psi_k}{\sum_k \alpha_k \rho_k} = \frac{\sum_k \alpha_k \rho_k \psi_k}{\rho_m} \quad (3.422)$$

where the actual phase  $k$  volume fraction  $\alpha_k = V_k/V_m$  have been introduced relating the superficial variables and the actual phase variables.

To preserve the system volume the volume fractions  $\alpha_k$  are subject to the natural constraint:

$$\sum_k \alpha_k = 1 \quad (3.423)$$

Since the mixture properties are given as the sum of the volume fraction weighted property values of the different phases in the mixture, the dispersed phase volume fractions were originally calculated from the postulated dispersed phase continuity equations. In the past these macroscopic equations were expressed based on hypothesis and physical intuition rather than basic principles. The modern versions of the classical mixture theories are thus derived starting out from the averaged equations for the individual phases to ensure that the governing equations are correctly formulated.

The main disadvantage reflected by the classical mixture model is that no direct connection is made with the microscopic phenomena. In consequence essential features of the multi-phase systems are easily overlooked, and sometimes unnecessary assumptions are imposed on the macroscopic quantities [102]. For this reason the classical mixture model is seldom used for reactor analysis involving fluid flow calculations, since it is very difficult to postulate reliable parameterizations for the mixture properties and the constitutive equations. However, the mixture model concept determines the basis for the pseudo-homogeneous reactor models which are well known from conventional reactor modeling [80]. In these reactor simulations simplified descriptions of the flow or even predefined velocity profiles are used, nevertheless these empirical models are computationally efficient and thus very useful analyzing the interactions between the reaction kinetics and the different transport processes occurring in such reactive systems. It is emphasized that for many chemical processes idealized flow profiles prevail or the chemical kinetics and the molecular diffusion processes are the rate determining steps so the details of the flow are not essential determining the chemical conversion and heat transport in the reactor [122].

In problems in which the dispersed phase momentum equations can be approximated and reduced to an algebraic relation the mixture model is simpler to solve than the corresponding multi-fluid model, however this model reduction requires several approximate constitutive assumptions so important characteristics of the flow can be lost. Nevertheless the simplicity of this form of the mixture model makes it very useful in many engineering applications. This approximate mixture model formulation is generally expected to provide reasonable predictions for dilute and uniform multiphase flows which are not influenced by any wall effects. In these cases the dispersed phase elements do not significantly affect the momentum and density of the mixture. Such a situation may occur when the dispersed phase elements are very small. There are several concepts available for the purpose of relating the dispersed phase velocity to the mixture velocity, and thereby reducing the dispersed

phase momentum equation to a much simpler relation. The algebraic relations frequently mentioned in the multiphase flow literature are outlined in the following sub-sections.

### The Algebraic-Slip Mixture Model

In this section we derive the algebraic-slip mixture model equations for cold flow studies starting out from the multi-fluid model equations derived applying the time- after volume averaging operator without mass-weighting [204, 205]. The momentum equations for the dispersed phases are determined in terms of the relative (slip) velocity.

Under isothermal cold flow conditions only the continuity and momentum equations are required as defined by (3.417) choosing appropriate values for the generalized functions analogous to those in Table 3.1. The governing mixture equations are then expressed as:

$$\frac{\partial \rho_m}{\partial t} + \nabla \cdot (\rho_m \mathbf{v}_m) = 0 \quad (3.424)$$

and

$$\frac{\partial (\rho_m \mathbf{v}_m)}{\partial t} + \nabla \cdot (\rho_m \mathbf{v}_m \mathbf{v}_m) = -\nabla p_m - \nabla \cdot (\boldsymbol{\sigma}_m + \boldsymbol{\sigma}_{m,t}) + \rho_m \mathbf{g} \quad (3.425)$$

where  $\mathbf{v}_m$  is the mixture velocity vector which represents the velocity of the mixture mass center,  $\mathbf{g}$  is the acceleration due to gravity,  $p_m$  is the mixture pressure,  $\boldsymbol{\sigma}_m$  is the mixture viscous stress tensor, and  $\boldsymbol{\sigma}_{m,t}$  is the turbulent mixture stress tensor.

For Newtonian fluids the effective stress tensor (i.e., the sum of the viscous and turbulent stresses) is given by:

$$\boldsymbol{\sigma}_{m,\text{eff}} = \boldsymbol{\sigma}_m + \boldsymbol{\sigma}_{m,t} = -\mu_{\text{eff}}(\nabla \mathbf{v}_m + (\nabla \mathbf{v}_m)^T) - \frac{2}{3}\mathbf{e}(\nabla \cdot \mathbf{v}_m) \quad (3.426)$$

In order to approximate the effective viscosity  $\mu_{\text{eff}} = \mu_{m,t} + \mu_m$  for the mixture flows, separate models are needed for the turbulent viscosity  $\mu_{m,t}$  and the mixture viscosity  $\mu_m$ . The standard k- $\epsilon$  model originally developed for single-phase flows has been used to compute the turbulent viscosity  $\mu_{m,t}$  in the majority of publications on numerical simulations of two-phase flows. Nevertheless, it is still an open question whether the approximate turbulence models which were originally developed for single-phase flow are appropriate for two-phase flow simulations [122].

The volume fractions of the dispersed phases can be calculated from the time-after volume averaged phase  $k = d$  continuity equations, as examined in sect 3.4.4. A common form of the modeled continuity equations yields:

$$\frac{\partial (\alpha_d \rho_d)}{\partial t} + \nabla \cdot (\alpha_d \rho_d \mathbf{v}_d) = \nabla \cdot (\rho_d D_{\alpha,t}^{\alpha_d} \nabla \alpha_d) \quad (3.427)$$

in which the diffusive terms accounts for dispersive effects of the dispersed phase due to random fluctuations of the fluid-particle motions. This term stems from the modeled volume fraction-velocity covariance in the continuity equation [205, 119]. For turbulent flows the turbulent diffusivity  $D_{\alpha,t}^{\alpha d}$  is normally determined by the turbulent viscosity as the turbulent Schmidt number is about 1.

In (3.427) the dispersed phase velocity  $\mathbf{v}_d$  occurs as an undetermined variable. The phasic velocities are related to the mixture velocity through the mixture velocity definition (3.421). The dispersed phase velocity is computed from the continuous phase velocity  $\mathbf{v}_c$  and a relative (slip) velocity  $\mathbf{v}_{rk}$ , in accordance with the definitions:

$$\mathbf{v}_{rk} = \mathbf{v}_k - \mathbf{v}_c \quad (3.428)$$

For the relative (slip) velocity  $\mathbf{v}_{rd}$  numerous empirical correlations are available in the literature [34]. Hence it follows that each component of the dispersed phase momentum equation is reduced to an algebraic-slip relation (3.428). This is the reason why this mixture model formulation is referred to as the *algebraic-slip mixture model*.

In particular applications alternative relations for the slip velocity (3.428) can be derived introducing suitable simplifying assumptions about the dispersed phase momentum equations comparing the relative importance of the pressure gradient, the drag force, the added mass force, the Basset force, the Magnus force and the Saffman lift force [125, 119, 58]. For gas-liquid flows it is frequently assumed that the last four effects are negligible [201, 19].

The relation for the slip velocity is then written as:

$$\mathbf{v}_{\text{slip},d} = -\frac{\nabla p}{C_{D,d}} \quad (3.429)$$

where  $C_{D,d}$  is a drag force coefficient for which a large number of correlations can be found in literature. It is noted that each of these expressions is only valid under specific operating conditions. The  $C_{D,d}$  depends primarily on the particle Reynolds number  $Re_p$ . In the past the bubble size dependency was considered negligible for air bubbles in water in the mean diameter size range 1 – 10 mm. Hence,

$$C_D = 50 \frac{g}{cm^3 s} \quad (3.430)$$

was used in this bubble size range, leading to a mean bubble slip velocity of about 20 cm/s, which is in approximate agreement with experimental velocity data of air bubbles in tap water [34, 184].

For dispersed gas-liquid flows it is further assumed that  $p_m = p_c = p$ . The density of the continuous liquid phase is commonly assumed constant  $\rho_l \approx \text{constant}$ , while the density of the gas phases is either given in accordance with the ideal gas law  $\rho_g = \frac{pM_w}{RT}$  or assumed constant. The viscosities of both phases are commonly given constant values.

The bubble wake effects are occasionally considered important describing the transversal movement of the bubbles [73, 218]. In these cases it is imagined that small bubbles are accelerated in the wake of larger ones and others are pushed aside. Hence, there is a considerable particle path dispersion on the bubble size scale which appears as a random motion on the macro scale level considered in the model. The impacts of these random spatially dispersive effect are often assumed embedded in the diffusion-like term occurring in the the continuity equation for the gas phase (3.427). The corresponding diffusion coefficient has been related to the turbulent eddy viscosity of the liquid phase [120]. This approach assumes an isotropic dispersion. However, since real bubbles rise relative to the liquid predominantly in the vertical direction, the dispersion will probably not be an isotropic effect [121]. A more general representation might be expressed in terms of a dispersion tensor. However, at present there are neither sufficient knowledge available to model the tensor elements nor enough experimental data to validate such models.

This gas-liquid modeling approach has been used performing dynamic simulations of two-phase bubble column reactor flows operating at low gas holdups [201, 202, 19]. A major limitation revealed in these simulations is that there is some difficulties in conserving mass for the dispersed phases, so this concept is not recommended for the purpose of simulating chemically reactive flows.

### The Diffusion Mixture Model

In this section we derive the diffusion mixture model equations starting from the time averaged multi-fluid model expressed in terms of phase- and mass weighted variables [112]. The relative movement of the individual phases is given in terms of diffusion velocities.

The continuity and momentum equations for each phase  $k$  are given by:

$$\frac{\partial}{\partial t}(\alpha_k \langle \rho_k \rangle^{X_k}) + \nabla \cdot (\alpha_k \langle \rho_k \rangle^{X_k} \langle \mathbf{v}_k \rangle^{X_k \rho_k}) = \Gamma_k \quad (3.431)$$

and

$$\begin{aligned} \frac{\partial}{\partial t}(\alpha_k \langle \rho_k \rangle^{X_k} \langle \mathbf{v}_k \rangle^{X_k \rho_k}) + \nabla \cdot (\alpha_k \langle \rho_k \rangle^{X_k} \langle \mathbf{v}_k \rangle^{X_k \rho_k} \langle \mathbf{v}_k \rangle^{X_k \rho_k}) = \\ - \alpha_k \nabla \langle p_k \rangle^{X_k} - \nabla \cdot (\alpha_k [\langle \boldsymbol{\sigma}_k \rangle^{X_k} + \langle \boldsymbol{\sigma}_{t,k}^{Re} \rangle^{X_k}]) \\ + \alpha_k \langle \rho_k \rangle^{X_k} \langle \mathbf{g} \rangle^{X_k \rho_k} + \mathbf{F}_k \end{aligned} \quad (3.432)$$

where the turbulent stress tensor is given by:

$$\langle \boldsymbol{\sigma}_{t,k}^{Re} \rangle^{X_k} = \langle \rho_k \mathbf{v}''_k \mathbf{v}''_k \rangle^{X_k} \quad (3.433)$$

and the corresponding time averaged jump conditions yields:

$$\sum_k \Gamma_k = 0 \quad (3.434)$$

$$\sum_k \mathbf{F}_k = \mathbf{F}_I \quad (3.435)$$

where we have neglected the effect of interfacial mass transfer upon the interfacial momentum transfer.

Based on the Favre-averaged continuity equations (3.431), the mixture continuity equation is obtained by taking the sum over all phases:

$$\frac{\partial}{\partial t} \sum_k \langle \alpha_k \langle \rho_k \rangle^{X_k} \rangle + \nabla \cdot \sum_k \alpha_k \langle \rho_k \rangle^{X_k} \langle \mathbf{v}_k \rangle^{X_k \rho_k} = \sum_k \Gamma_k \quad (3.436)$$

At the interface the total mass is balanced in accordance with the jump mass condition (3.434), thus the RHS of (3.436) must vanish. Hence, by use of the Favre averaged form of (3.418) and (3.421) we obtain the continuity equation for the mixture (3.424).

The mixture momentum equation can be deduced in a similar way from the sum of the momentum balances of the individual phases:

$$\begin{aligned} & \frac{\partial}{\partial t} \sum_k \alpha_k \langle \rho_k \rangle^{X_k} \langle \mathbf{v}_k \rangle^{X_k \rho_k} + \nabla \cdot \sum_k \alpha_k \langle \rho_k \rangle^{X_k} \langle \mathbf{v}_k \rangle^{X_k \rho_k} \langle \mathbf{v}_k \rangle^{X_k \rho_k} \\ &= - \sum_k \alpha_k \nabla \langle p_k \rangle^{X_k} - \nabla \cdot \left( \sum_k \alpha_k [\langle \boldsymbol{\sigma}_k \rangle^{X_k} + \langle \boldsymbol{\sigma}_{t,k}^{Re} \rangle^{X_k}] \right) \\ &+ \sum_k \alpha_k \langle \rho_k \rangle^{X_k} \langle \mathbf{g} \rangle^{X_k \rho_k} + \sum_k \mathbf{F}_k \end{aligned} \quad (3.437)$$

Ishii [112] introduced the *diffusion velocity*  $\mathbf{v}_{Mk}$  of phase  $k$  defined as the velocity of phase  $k$  relative to the velocity of the mass center of the mixture:

$$\mathbf{v}_{Mk} = \langle \mathbf{v}_k \rangle^{X_k \rho_k} - \mathbf{v}_m \quad (3.438)$$

Using the given definition of the diffusion velocity (3.438), the Favre form of the mixture density (3.418) and the Favre form of the mixture velocity (3.421), the second term in the mixture momentum balance (3.437) can be reformulated:

$$\begin{aligned} & \nabla \cdot \sum_k \alpha_k \langle \rho_k \rangle^{X_k} \langle \mathbf{v}_k \rangle^{X_k \rho_k} \langle \mathbf{v}_k \rangle^{X_k \rho_k} = \\ & \nabla \cdot (\rho_m \mathbf{v}_m \mathbf{v}_m) + \nabla \cdot \sum_k (\alpha_k \langle \rho_k \rangle^{X_k} \mathbf{v}_{Mk} \mathbf{v}_{Mk}) \end{aligned} \quad (3.439)$$

Introducing the mixture- and diffusion velocity variables (3.421) and (3.438), the momentum equation (3.437) takes the form:

$$\frac{\partial}{\partial t} (\rho_m \mathbf{v}_m) + \nabla \cdot (\rho_m \mathbf{v}_m \mathbf{v}_m) = -\nabla p_m - \nabla \cdot (\boldsymbol{\sigma}_m + \boldsymbol{\sigma}_{m,t}^{Re} + \boldsymbol{\sigma}_{Mm}) + \rho_m \mathbf{g} + \mathbf{F}_I \quad (3.440)$$

The last term on the right hand side of the mixture momentum equation (3.440) accounts for the influence of the surface tension force  $\mathbf{F}_I$  on the mixture in accordance with (3.435).

The three stress tensors are defined as:

$$\boldsymbol{\sigma}_m = \sum_k \alpha_k \langle \boldsymbol{\sigma}_k \rangle^{X_k} \quad (3.441)$$

$$\boldsymbol{\sigma}_{m,t}^{Re} = \sum_k \alpha_k \langle \rho_k \mathbf{v}''_k \mathbf{v}''_k \rangle^{X_k} \quad (3.442)$$

$$\boldsymbol{\sigma}_{Mm} = \sum_k \alpha_k \langle \rho_k \rangle^{X_k} \mathbf{v}_{Mk} \mathbf{v}_{Mk} \quad (3.443)$$

and represent the average viscous stress, turbulent stress and diffusion stress due to the phase slip, respectively.

In (3.440) the pressure of the mixture is defined by the relation:

$$\nabla p_m = \sum_k \alpha_k \nabla \langle p_k \rangle^{X_k} \quad (3.444)$$

In practice, the phase pressures are often assumed to be equal, i.e.,  $\langle p_k \rangle^{X_k} = p_m = p$ .

If we now return to consider an individual phase, we may use the definition of the diffusion velocity (3.438) to eliminate the phase velocity in the continuity equation for phase  $k$ :

$$\frac{\partial}{\partial t} (\alpha_k \langle \rho_k \rangle^{X_k}) + \nabla \cdot (\alpha_k \langle \rho_k \rangle^{X_k} \mathbf{v}_m) = \Gamma_k - \nabla \cdot (\alpha_k \langle p_k \rangle^{X_k} \mathbf{v}_{Mk}) \quad (3.445)$$

In practice, the diffusion velocity has to be determined through the relative velocity (3.428). Hence, it follows that:

$$\begin{aligned} \mathbf{v}_{Md} &= \langle \mathbf{v}_d \rangle^{X_d \rho_d} - \mathbf{v}_m \\ &= [\mathbf{v}_{rd} + \langle \mathbf{v}_c \rangle^{X_c \rho_c}] - \left[ \frac{1}{\rho_m} \sum_{k=1}^n \alpha_k \langle \rho_k \rangle^{X_k} \langle \mathbf{v}_k \rangle^{X_k \rho_k} \right] \\ &= [\mathbf{v}_{rd} + \langle \mathbf{v}_c \rangle^{X_c \rho_c}] - \left[ \frac{1}{\rho_m} \sum_{k=1}^n \alpha_k \langle \rho_k \rangle^{X_k} (\mathbf{v}_{rk} + \langle \mathbf{v}_c \rangle^{X_c \rho_c}) \right] \\ &= [\mathbf{v}_{rd} + \langle \mathbf{v}_c \rangle^{X_c \rho_c}] \\ &\quad - \left[ \frac{1}{\rho_m} \sum_{d=1}^{n-1} \alpha_d \langle \rho_d \rangle^{X_d} \mathbf{v}_{rd} + \frac{1}{\rho_m} \sum_{k=1}^n \alpha_k \langle \rho_k \rangle^{X_k} \langle \mathbf{v}_c \rangle^{X_c \rho_c} \right] \\ &= \mathbf{v}_{rd} - \frac{1}{\rho_m} \sum_{d=1}^{n-1} \alpha_d \langle \rho_d \rangle^{X_d} \mathbf{v}_{rd} \end{aligned} \quad (3.446)$$

When the diffusion velocity is eliminated, the main difference between the particular diffusion- and algebraic-slip mixture models presented in this

section is that the algebraic-slip model is derived using a double time- after volume averaging operator [205], while the diffusion model is derived applying a single time averaging operator combined with the introduction of phase- and mass weighted variables [112].

The given diffusion model formulation has been used simulating the gas-liquid dynamics in cylindrical bubble column reactors [182].

### The Drift-Flux Mixture Model

In this section we derive the drift-flux mixture model starting out from the time averaged multi-fluid model expressed in terms of phase- and mass weighted variables [112]. The relative moment of the phases is given in terms of drift velocities. This approach can be applied for systems where the phase densities are constants and the interface mass transfer can be neglected.

The drift velocity  $\mathbf{v}_{V_k}$  of phase  $k$  is defined as the velocity of phase  $k$  relative to the velocity of the volume center of the mixture [112, 85]:

$$\mathbf{v}_{V_k} = \langle \mathbf{v}_k \rangle^{X_k \rho_k} - \sum_k \alpha_k \langle \mathbf{v}_k \rangle^{X_k \rho_k} = \langle \mathbf{v}_k \rangle^{X_k \rho_k} - \mathbf{j}_m \quad (3.447)$$

where  $\mathbf{j}_m = \sum_k \alpha_k \langle \mathbf{v}_k \rangle^{X_k \rho_k}$  is the volumetric flux of the mixture representing the velocity of the volume center of the mixture.

We may then write:

$$\sum_k \alpha_k \mathbf{v}_{V_k} = \sum_k \alpha_k \langle \mathbf{v}_k \rangle^{X_k \rho_k} - \sum_k \alpha_k \mathbf{j}_m = \mathbf{j}_m - \mathbf{j}_m = 0 \quad (3.448)$$

The flux of the dispersed phase relative to the velocity of the volume centre of the mixture is given by [85]:

$$\mathbf{J}_{Vd} = \alpha_d (\langle \mathbf{v}_d \rangle^{X_d \rho_d} - \mathbf{j}_m) = \alpha_d \mathbf{v}_{Vd} \quad (3.449)$$

Introducing the mixture- and drift velocity variables (3.421) and (3.447), the momentum equation (3.437) takes the form:

$$\frac{\partial}{\partial t} (\rho_m \mathbf{v}_m) + \nabla \cdot (\rho_m \mathbf{v}_m \mathbf{v}_m) = -\nabla p_m - \nabla \cdot (\boldsymbol{\sigma}_m + \boldsymbol{\sigma}_{m,t}^{Re} + \boldsymbol{\sigma}_{Vm}) + \rho_m \mathbf{g} + \mathbf{F}_I \quad (3.450)$$

The three stress tensors are defined as:

$$\boldsymbol{\sigma}_m = \sum_k \alpha_k \langle \boldsymbol{\sigma}_k \rangle^{X_k} \quad (3.451)$$

$$\boldsymbol{\sigma}_{m,t}^{Re} = \sum_k \alpha_k \langle \rho_k \mathbf{v}''_k \mathbf{v}''_k \rangle^{X_k} \quad (3.452)$$

$$\boldsymbol{\sigma}_{Vm} = \sum_k \alpha_k \langle \rho_k \rangle^{X_k} \mathbf{v}_{V_k} \mathbf{v}_{V_k} \quad (3.453)$$

and represent the average viscous stress, turbulent stress and drift stress due to the phase slip, respectively.

For systems with constant densities and no phase change, the Favre averaged continuity equation (3.431) reduces to:

$$\frac{\partial \alpha_k}{\partial t} + \nabla \cdot (\alpha_k \langle \mathbf{v}_k \rangle^{X_k \rho_k}) = 0 \quad (3.454)$$

By use of the drift velocity (3.447), the continuity equation can be rewritten as:

$$\frac{\partial \alpha_k}{\partial t} + \nabla \cdot (\alpha_k \mathbf{j}_m) + \nabla \cdot (\alpha_k \mathbf{v}_{V_k}) = 0 \quad (3.455)$$

After some manipulations we get:

$$\frac{\partial \alpha_k}{\partial t} + \mathbf{j}_m \cdot \nabla \alpha_k = -\nabla \cdot (\alpha_k \mathbf{v}_{V_k}) \quad (3.456)$$

where the relation  $\nabla \cdot \mathbf{j}_m = 0$  is derived taking the sum of the individual continuity equations for all the phases in the system.

In practice, the drift velocity (3.447) is determined from the slip velocity (3.429) as follows:

$$\begin{aligned} \mathbf{v}_{V,k} &= \langle \mathbf{v}_k \rangle^{X_k \rho_k} - \sum_k \alpha_k \langle \mathbf{v}_k \rangle^{X_k \rho_k} \\ &= [\langle \mathbf{v}_c \rangle^{X_c \rho_c} + \mathbf{v}_{rk}] - \left[ \sum_k \alpha_k (\langle \mathbf{v}_c \rangle^{X_c \rho_c} + \mathbf{v}_{rk}) \right] = \mathbf{v}_{rk} - \sum_k \alpha_k \mathbf{v}_{rk} \end{aligned} \quad (3.457)$$

This form of the mixture model is called the *drift flux* model. In particular cases the flow calculations is significantly simplified when the problem is described in terms of drift velocities, as for example when  $\alpha_d$  is constant or time dependent only. However, in reactor technology this model formulation is restricted to multiphase cold flow studies as the drift-flux model cannot be adopted simulating reactive systems in which the densities are not constants and interfacial mass transfer is required.

The drift-flux model equations have been assessed in multiphase flow analysis by several authors [112, 85, 145, 231].

### 3.4.6 The Gross Scale Averaged Two-Phase Transport Equations

The area averaging theory described in this section is based on the papers by [229, 243, 44, 46, 47, 22, 10, 24, 115, 135, 16]. The main object in this section is to provide the necessary theorems to derive the cross-sectional averaged equations that coincide with the conventional 1D multiphase chemical reactor model from first principles. To formulate these theorems we chose to adopt the same concepts as were used deriving the corresponding single phase equations

in sect 1.2.6. Following the approach of Delhaye and Achard [47] we proceed performing an analysis of a small volume of a pipe with variable cross-section area containing a two phase mixture and deduce the limiting forms of the Leibnitz' and Gauss' theorems for area considered valid in the limit  $\Delta z \rightarrow 0$ . For this reason it is emphasized that these theorems are actually derived for a volume but reduces to an area formulation introducing certain simplifying approximations.

Given a tube with axis  $Oz$  (unit vector  $e_z$ ) in which a volume  $V_k$  is limited by a boundary,  $A_I$  and cut by a cross section plane over area,  $A_k$ , as sketched in Fig 3.7. The lateral dimensions of the control volume extend to the conduit walls. In this notation,  $\mathbf{n}_k$  is the outward directed unit vector normal to the interface of phase  $k$ .  $l_I(t, z)$  is the intersection of interface,  $A_I$ , with the cross sectional plane.  $\mathbf{n}_{l,k}$  is the outward directed unit vector normal to the closed curve of phase  $k$ ,  $l_{W,k}(t, z)$ , in the cross section plane.

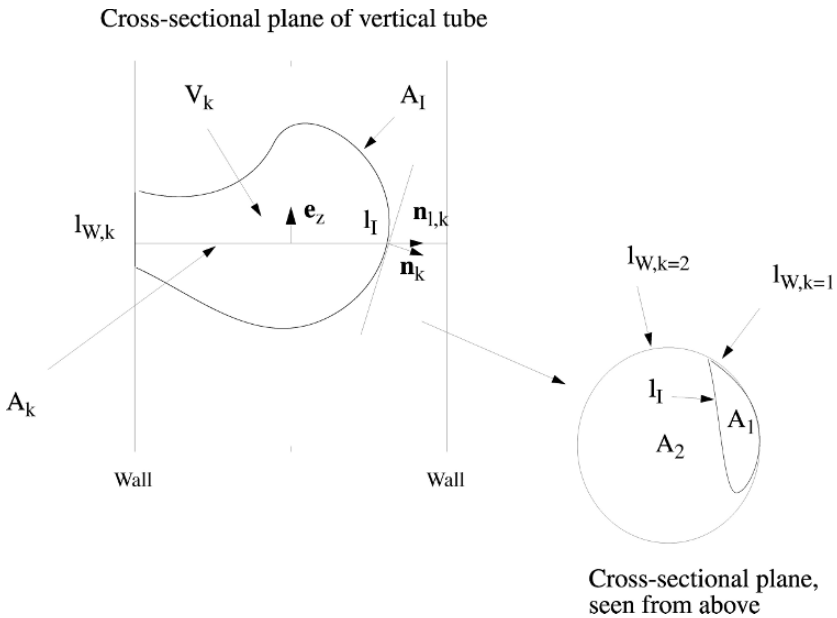


**Fig. 3.7.** Sketch of the control volume determining the basis for area-averaging of the two phase equations.

The purpose of this derivation is to average the local, instantaneous balance equation over the variable cross-section area of a pipe occupied by the two phases, as sketched in Fig 3.7.

The local, instantaneous balance equation (1.3) is integrated over the cross section area,  $A_k(t, z)$ , limited by the boundaries,  $l_I(t, z)$ , with the other phase

and with the pipe wall boundary,  $l_{W,k}(t, z)$ :

$$\int_{A_k(t,z)} \frac{\partial(\rho_k \psi_k)}{\partial t} da + \int_{A_k(t,z)} \nabla \cdot (\rho_k \mathbf{v}_k \psi_k) da = - \int_{A_k(t,z)} \nabla \cdot \mathbf{J}_k da + \int_{A_k(t,z)} \sum_c \rho_{c,k} \phi_{c,k} da \quad (3.458)$$

To proceed the limiting forms of the Leibnitz and the Gauss theorems<sup>25</sup>, appropriate for two phase flow, are applied. These theorems are considered direct extensions of the single phase theorems examined in sect 1.2.6 so no further derivation is given here. In most reactor model formulations the pipe walls are supposed to be fixed and impermeable. In the limit  $z \rightarrow 0$ , the limiting form of the Leibnitz theorem for volume reduces to the following relation for area [43, 47]:

$$\begin{aligned} \frac{\partial}{\partial t} \int_{A_k(t,z)} f(\mathbf{r}, t) da &= \int_{A_k(t,z)} \frac{\partial f(\mathbf{r}, t)}{\partial t} da + \int_{l_I(t,z)} f(\mathbf{r}, t) \mathbf{v}_I \cdot \mathbf{n}_k \frac{dl}{\mathbf{n}_k \cdot \mathbf{n}_{l,k}} \\ &+ \int_{l_{W,k}(t,z)} f(\mathbf{r}, t) \mathbf{v}_W \cdot \mathbf{n}_k \frac{dl}{\mathbf{n}_k \cdot \mathbf{n}_{l,W}} \end{aligned} \quad (3.459)$$

where  $\mathbf{v}_I \cdot \mathbf{n}_k$  is the displacement velocity of a point on the interface,  $A_I$ , and  $\mathbf{v}_W \cdot \mathbf{n}_k$  is the displacement velocity of a point on the wall boundary face,  $A_W$ .

For the particular case when the phase  $k$  control volume is varying both in time and space at the interface, but in space only at the wall boundary face, this relation is simplified as  $\mathbf{v}_W \cdot \mathbf{n}_W = 0$ :

$$\frac{\partial}{\partial t} \int_{A_k(t,z)} f(\mathbf{r}, t) da = \int_{A_k(t,z)} \frac{\partial f(\mathbf{r}, t)}{\partial t} da + \int_{l_I(t,z)} f(\mathbf{r}, t) \mathbf{v}_I \cdot \mathbf{n}_k \frac{dl}{\mathbf{n}_k \cdot \mathbf{n}_{l,k}} \quad (3.460)$$

In the limit  $z \rightarrow 0$ , the limiting form of the Gauss theorem for volume reduces to the following relation for area (where we let  $\mathbf{B}$  be a vector or a tensor):

$$\int_{A_k(t,z)} \nabla \cdot \mathbf{B} da = \frac{\partial}{\partial z} \int_{A_k(t,z)} \mathbf{e}_z \cdot \mathbf{B} da + \int_{l_I(t,z)} \mathbf{n}_k \cdot \mathbf{B} \frac{dl}{\mathbf{n}_k \cdot \mathbf{n}_{l,k}} + \int_{l_{W,k}(t,z)} \mathbf{n}_k \cdot \mathbf{B} \frac{dl}{\mathbf{n}_k \cdot \mathbf{n}_{l,W}} \quad (3.461)$$

In the case of  $\mathbf{B}$  being a vector, the component of the vector  $\mathbf{B}$  on  $Oz$  is given by  $\mathbf{e}_z \cdot \mathbf{B} = B_z$ .

<sup>25</sup> Area averaging can be considered to be a limiting case of local volume averaging [43, 47, 189]. Thus the phrase *limiting form* refers to the modified forms of the averaging theorems which are applicable to the governing 3D equations to derive a set of equations valid for 1D problems.

If we take  $\mathbf{B} = \mathbf{e}_z$  we obtain:

$$\begin{aligned} \int_{A_k(t,z)} \nabla \cdot \mathbf{e}_z da &= \frac{\partial}{\partial z} \int_{A_k(t,z)} \mathbf{e}_z \cdot \mathbf{e}_z da + \int_{l_I(t,z)} \mathbf{n}_k \cdot \mathbf{e}_z \frac{dl}{\mathbf{n}_k \cdot \mathbf{n}_{l,k}} \\ &+ \int_{l_{W,k}(t,z)} \mathbf{n}_k \cdot \mathbf{e}_z \frac{dl}{\mathbf{n}_k \cdot \mathbf{n}_{l,W}} \end{aligned} \quad (3.462)$$

With minor rearrangement this gives the following important result:

$$\frac{\partial A_k(t,z)}{\partial z} = - \int_{l_I(t,z)} \mathbf{n}_k \cdot \mathbf{e}_z \frac{dl}{\mathbf{n}_k \cdot \mathbf{n}_{l,k}} - \int_{l_{W,k}(t,z)} \mathbf{n}_k \cdot \mathbf{e}_z \frac{dl}{\mathbf{n}_k \cdot \mathbf{n}_{l,W}} \quad (3.463)$$

Introducing these relations into the cross section area averaged equation, gives:

$$\begin{aligned} \frac{\partial}{\partial t} \int_{A_k(t,z)} (\rho_k \psi_k) da &+ \frac{\partial}{\partial z} \int_{A_k(t,z)} (\rho_k v_{z,k} \psi_k) da + \frac{\partial}{\partial z} \int_{A_k(t,z)} (\mathbf{e}_z \cdot \mathbf{J}_k) da = \\ &- \int_{l_{W,k}(t,z)} \mathbf{n}_k \cdot \mathbf{J}_k \frac{dl}{\mathbf{n}_k \cdot \mathbf{n}_{l,W}} - \int_{l_{W,k}(t,z)} \mathbf{n}_k \cdot (\rho_k \mathbf{v}_k \psi_k) \frac{dl}{\mathbf{n}_k \cdot \mathbf{n}_{l,W}} \\ &- \int_{l_I(t,z)} \mathbf{n}_k \cdot \mathbf{J}_k \frac{dl}{\mathbf{n}_k \cdot \mathbf{n}_{l,k}} - \int_{l_I(t,z)} \mathbf{n}_k \cdot (\rho_k \mathbf{v}_k \psi_k) \frac{dl}{\mathbf{n}_k \cdot \mathbf{n}_{l,k}} \\ &+ \int_{l_I(t,z)} \rho_k \psi_k (\mathbf{v}_I \cdot \mathbf{n}_k) \frac{dl}{\mathbf{n}_k \cdot \mathbf{n}_{l,k}} + \int_{A_k(t,z)} \sum_c (\rho_{c,k} \phi_{c,k}) da \end{aligned} \quad (3.464)$$

where  $v_{z,k}$  is the  $z$ -component of the velocity vector,  $\mathbf{v}_k$ .

As we assume no mass flow through the pipe wall, the wall convection term is equal to zero as  $\mathbf{n}_k \cdot \mathbf{v}_k = 0$  at the wall. The equation reduces to:

$$\begin{aligned} \frac{\partial}{\partial t} \int_{A_k(t,z)} (\rho_k \psi_k) da &+ \frac{\partial}{\partial z} \int_{A_k(t,z)} (\rho_k v_{z,k} \psi_k) da + \frac{\partial}{\partial z} \int_{A_k(t,z)} (\mathbf{e}_z \cdot \mathbf{J}_k) da = \\ &- \int_{l_{W,k}(t,z)} \mathbf{n}_k \cdot \mathbf{J}_k \frac{dl}{\mathbf{n}_k \cdot \mathbf{n}_{l,W}} - \int_{l_I(t,z)} \mathbf{n}_k \cdot (\rho_k \mathbf{v}_k \psi_k + \mathbf{J}_k) \frac{dl}{\mathbf{n}_k \cdot \mathbf{n}_{l,k}} \\ &+ \int_{l_I(t,z)} \rho_k \psi_k (\mathbf{v}_I \cdot \mathbf{n}_k) \frac{dl}{\mathbf{n}_k \cdot \mathbf{n}_{l,k}} + \int_{A_k(t,z)} \sum_c (\rho_{c,k} \phi_{c,k}) da \end{aligned} \quad (3.465)$$

or

$$\begin{aligned}
 & \frac{\partial}{\partial t} \int_{A_k(t,z)} (\rho_k \psi_k) da + \frac{\partial}{\partial z} \int_{A_k(t,z)} (\rho_k v_{z,k} \psi_k) da + \frac{\partial}{\partial z} \int_{A_k(t,z)} (\mathbf{e}_z \cdot \mathbf{J}_k) da = \\
 & - \int_{l_{W,k}(t,z)} \mathbf{n}_k \cdot \mathbf{J}_k \frac{dl}{\mathbf{n}_k \cdot \mathbf{n}_{l,W}} - \int_{l_I(t,z)} (m_k \psi_k + \mathbf{n}_k \cdot \mathbf{J}_k) \frac{dl}{\mathbf{n}_k \cdot \mathbf{n}_{l,k}} \\
 & + \int_{A_k(t,z)} \sum_c (\rho_{c,k} \phi_{c,k}) da
 \end{aligned} \tag{3.466}$$

where  $m_k$  is the interfacial mass transfer rate given by (3.140).

Introducing area averaged quantities by use of the area averaging operator defined by:

$$\langle \psi_k \rangle_{A_k} = \frac{1}{A_k} \int_{A_k(t,z)} \psi da, \tag{3.467}$$

The balance equation can be written as:

$$\begin{aligned}
 & \frac{\partial (A_k \langle \rho_k \psi_k \rangle_{A_k})}{\partial t} + \frac{\partial}{\partial z} (A_k \langle \rho_k v_{z,k} \psi_k \rangle_{A_k}) + \frac{\partial}{\partial z} (A_k \langle \mathbf{e}_z \cdot \mathbf{J}_k \rangle_{A_k}) = \\
 & - \int_{l_{W,k}(t,z)} \mathbf{n}_k \cdot \mathbf{J}_k \frac{dl}{\mathbf{n}_k \cdot \mathbf{n}_{l,W}} - \int_{l_I(t,z)} (m_k \psi_k + \mathbf{n}_k \cdot \mathbf{J}_k) \frac{dl}{\mathbf{n}_k \cdot \mathbf{n}_{l,k}} \\
 & + \sum_c A_k \langle \rho_{c,k} \phi_{c,k} \rangle_{A_k}
 \end{aligned} \tag{3.468}$$

The cross-section averaged equations governing phase  $k$  are obtained defining the specific values of the generalized variables in (3.468) in accordance with Table 3.1 gives the instantaneous area-averaged equations for the balance of mass, momentum, total energy, species mass and entropy.

#### *The Balance of Mass:*

In this case we define  $\psi_k = 1$ ,  $\mathbf{J}_k = 0$ , and  $\phi_{c,k} = 0$ , hence:

$$\frac{\partial (A_k \langle \rho_k \rangle_{A_k})}{\partial t} + \frac{\partial}{\partial z} (A_k \langle \rho_k v_{z,k} \rangle_{A_k}) = - \int_{l_I(t,z)} m_k \frac{dl}{\mathbf{n}_k \cdot \mathbf{n}_{l,k}} = \Gamma_{A_k} A \tag{3.469}$$

where  $\Gamma_{A_k}$  is the area averaged interfacial mass transfer rate defined by:

$$\Gamma_{A_k} = - \frac{1}{A} \int_{l_I(t,z)} m_k \frac{dl}{\mathbf{n}_k \cdot \mathbf{n}_{l,k}} \tag{3.470}$$

*The Balance of Momentum:*

In this case we define  $\psi_k = \mathbf{v}_k$ ,  $\mathbf{J}_k = \mathbb{T}_k$ , and  $\phi_{c,k} = \mathbf{g}_{c,k}$ , thus:

$$\begin{aligned} & \frac{\partial(A_k \langle \rho_k \mathbf{v}_k \rangle_{A_k})}{\partial t} + \frac{\partial}{\partial z}(A_k \langle \rho_k v_{z,k} \mathbf{v}_k \rangle_{A_k}) + \frac{\partial}{\partial z}(A_k \langle \mathbf{e}_z \cdot \mathbb{T}_k \rangle_{A_k}) \\ &= - \int_{l_{W,k}(t,z)} \mathbf{n}_k \cdot \mathbb{T}_k \frac{dl}{\mathbf{n}_k \cdot \mathbf{n}_{l,W}} - \int_{l_I(t,z)} (m_k \mathbf{v}_k + \mathbf{n}_k \cdot \mathbb{T}_k) \frac{dl}{\mathbf{n}_k \cdot \mathbf{n}_{l,k}} \\ & \quad + \sum_c A_k \langle \rho_{c,k} \mathbf{g}_{c,k} \rangle_{A_k} \end{aligned} \quad (3.471)$$

and after the total stress tensor,  $\mathbb{T}_k$ , is split into a pressure term,  $p_k \mathbf{e}$ , and a viscous stress tensor,  $\boldsymbol{\sigma}_k$ , we get:

$$\begin{aligned} & \frac{\partial(A_k \langle \rho_k \mathbf{v}_k \rangle_{A_k})}{\partial t} + \frac{\partial}{\partial z}(A_k \langle \rho_k v_{z,k} \mathbf{v}_k \rangle_{A_k}) + \frac{\partial}{\partial z}(A_k \langle p_k \mathbf{e}_z \rangle_{A_k}) = \\ & - \frac{\partial}{\partial z}(A_k \langle \mathbf{e}_z \cdot \boldsymbol{\sigma}_k \rangle_{A_k}) + \sum_c A_k \langle \rho_{c,k} \mathbf{g}_{c,k} \rangle_{A_k} \\ & - \int_{l_{W,k}(t,z)} \mathbf{n}_k \cdot \mathbb{T}_k \frac{dl}{\mathbf{n}_k \cdot \mathbf{n}_{l,W}} - \int_{l_I(t,z)} (m_k \mathbf{v}_k + \mathbf{n}_k \cdot \mathbb{T}_k) \frac{dl}{\mathbf{n}_k \cdot \mathbf{n}_{l,k}} \end{aligned} \quad (3.472)$$

If we project the terms in (3.472) along the tube axis, we obtain:

$$\begin{aligned} & \frac{\partial(A_k \langle \rho_k v_{z,k} \rangle_{A_k})}{\partial t} + \frac{\partial}{\partial z}(A_k \langle \rho_k v_{z,k} v_{z,k} \rangle_{A_k}) + \frac{\partial}{\partial z}(A_k \langle p_k \rangle_{A_k}) = \\ & - \frac{\partial}{\partial z}(A_k \langle (\mathbf{e}_z \cdot \boldsymbol{\sigma}_k) \cdot \mathbf{e}_z \rangle_{A_k}) + \sum_c A_k \langle \rho_{c,k} g_{c,z,k} \rangle_{A_k} \\ & - \int_{l_{W,k}(t,z)} (\mathbf{n}_k \cdot \mathbb{T}_k) \cdot \mathbf{e}_z \frac{dl}{\mathbf{n}_k \cdot \mathbf{n}_{l,W}} - \int_{l_I(t,z)} (m_k \mathbf{v}_k + \mathbf{n}_k \cdot \mathbb{T}_k) \cdot \mathbf{e}_z \frac{dl}{\mathbf{n}_k \cdot \mathbf{n}_{l,k}} \end{aligned} \quad (3.473)$$

If we assume that the pressure,  $p_k$ , is constant along  $l_I$  and  $l_W$ , and equal to the averaged pressure,  $\langle p_k \rangle_{A_k}$  over  $A_k$ . Then, by using the definition (3.463), (3.473) can be written as:

$$\begin{aligned} & \frac{\partial(A_k \langle \rho_k v_{z,k} \rangle_{A_k})}{\partial t} + \frac{\partial}{\partial z}(A_k \langle \rho_k v_{z,k} v_{z,k} \rangle_{A_k}) + \frac{\partial}{\partial z}(A_k \langle p_k \rangle_{A_k}) \approx \\ & - \frac{\partial}{\partial z}(A_k \langle (\mathbf{e}_z \cdot \boldsymbol{\sigma}_k) \cdot \mathbf{e}_z \rangle_{A_k}) + \sum_c A_k \langle \rho_{c,k} g_{c,z,k} \rangle_{A_k} \\ & - \int_{l_{W,k}(t,z)} (\mathbf{n}_k \cdot \boldsymbol{\sigma}_k) \cdot \mathbf{e}_z \frac{dl}{\mathbf{n}_k \cdot \mathbf{n}_{l,W}} - \int_{l_I(t,z)} (m_k \mathbf{v}_k + \mathbf{n}_k \cdot \boldsymbol{\sigma}_k) \cdot \mathbf{e}_z \frac{dl}{\mathbf{n}_k \cdot \mathbf{n}_{l,k}} \\ & + \langle p_k \rangle_{A_k} \frac{\partial A_k}{\partial z} \end{aligned} \quad (3.474)$$

or

$$\begin{aligned}
& \frac{\partial(A_k \langle \rho_k v_{z,k} \rangle_{A_k})}{\partial t} + \frac{\partial}{\partial z} (A_k \langle \rho_k v_{z,k} v_{z,k} \rangle_{A_k}) + A_k \frac{\partial \langle p_k \rangle_{A_k}}{\partial z} \approx \\
& - \frac{\partial}{\partial z} (A_k \langle (\mathbf{e}_z \cdot \boldsymbol{\sigma}_k) \cdot \mathbf{e}_z \rangle_{A_k}) + \sum_c A_k \langle \rho_{c,k} g_{c,z,k} \rangle_{A_k} \\
& - \int_{l_{W,k}(t,z)} (\mathbf{n}_k \cdot \boldsymbol{\sigma}_k) \cdot \mathbf{e}_z \frac{dl}{\mathbf{n}_k \cdot \mathbf{n}_{l,W}} - \int_{l_I(t,z)} (m_k \mathbf{v}_k + \mathbf{n}_k \cdot \boldsymbol{\sigma}_k) \cdot \mathbf{e}_z \frac{dl}{\mathbf{n}_k \cdot \mathbf{n}_{l,k}}
\end{aligned} \tag{3.475}$$

where the interfacial momentum transfer due to phase change is defined by:

$$M_{k,z}^\Gamma = -\frac{1}{A} \int_{l_I(t,z)} m_k \mathbf{v}_k \cdot \mathbf{e}_z \frac{dl}{\mathbf{n}_k \cdot \mathbf{n}_{l,k}} = \Gamma_{Ak} \langle v_z \rangle_{l_I}^{\Gamma_{Ak}} \tag{3.476}$$

For dispersed flows the interfacial momentum viscous stresses acting on the dispersed phase can be approximated by:

$$M_{z,d}^\sigma = -\frac{1}{A} \int_{l_I(t,z)} (\mathbf{n}_d \cdot \boldsymbol{\sigma}_d) \cdot \mathbf{e}_z \frac{dl}{\mathbf{n}_d \cdot \mathbf{n}_{l,d}} \approx -\frac{3}{4} \rho_c \frac{C_D}{d_S} \alpha_d |\langle v_{z,r} \rangle_A| \langle v_{z,r} \rangle_A \tag{3.477}$$

where  $d_S$  is the Sauter mean diameter and  $v_{z,r} = (v_{z,d} - v_{z,c})$  denotes the relative velocity. That is, the averaged drag force is related to the averaged local relative velocity  $\langle v_{z,r} \rangle_A$  and not to the difference between the area averaged velocities of the individual phases [115].

The wall momentum viscous stresses, i.e., the friction drag, yields:

$$\begin{aligned}
M_{k,z}^{Drag} &= -\frac{1}{A} \int_{l_{W,k}(t,z)} (\mathbf{n}_k \cdot \boldsymbol{\sigma}_k) \cdot \mathbf{e}_z \frac{dl}{\mathbf{n}_k \cdot \mathbf{n}_{l,W}} \\
&\approx -f_{D,W} \frac{1}{2} \rho_k |\langle v_{z,k} \rangle_A| \langle v_{z,k} \rangle_A \frac{S_W}{4A}
\end{aligned} \tag{3.478}$$

where  $S_W$  is the perimeter of the wall.

By the principles of material indifference Slattery [196] (pp 228-230) elucidated the functional relationship between the variables in the empirical friction or drag force parameterizations<sup>26</sup>. It is noted that the dimensionless wall drag or friction factors of Darcy ( $f_D$ ) and Fanning ( $f_F$ ) are related in the following manner (e.g., [124, 240]):

<sup>26</sup> Whitaker [234] (chap 8) explains the convention normally used to distinguish between these two types of parameters. The friction factors for dispersed bodies immersed in a flowing fluid is traditionally referred to as dimensionless drag coefficients, whereas the drag force for flow inside closed conduits is generally expressed in terms of a dimensionless friction factor.

$$f_F = \frac{|\boldsymbol{\sigma}_w|}{\frac{1}{2}\rho\bar{v}_z^2} = \frac{f_D}{4} \quad (3.479)$$

The friction factor for laminar flow in pipes ( $Re < 2300$ ) is given by  $f_D = 4f_L = \frac{64}{Re}$ . For turbulent flow in rough pipes the friction factors depends on both the Reynolds number and the surface roughness of the tube. Colebrook [35] devised an implicit relation for the Darcy friction factor which reproduce the well known Moody diagram quite well.

$$\frac{1}{\sqrt{f_D}} \approx 1.74 - 2.0 \log\left(2\frac{\epsilon}{D} + \frac{18.7}{Re\sqrt{f_D}}\right) \quad (3.480)$$

Similar parameterizations exist for flows past a flat plate, jets and wakes [240].

*The Balance of Total Energy:*

In this case we define  $\psi_k = (\frac{1}{2}v_{z,k}^2 + e_k)$ ,  $\mathbf{J}_k = (\mathbf{q}_k + \mathbb{T}_k \cdot \mathbf{v}_k)$ ,  $\phi_{c,k} = \mathbf{g}_{c,k} \cdot \mathbf{v}_{c,k}$ , so it follows that:

$$\begin{aligned} & \frac{\partial(A_k \langle \rho_k (\frac{1}{2}v_{z,k}^2 + e_k) \rangle_{A_k})}{\partial t} + \frac{\partial}{\partial z}(A_k \langle \rho_k v_{z,k} (\frac{1}{2}v_{z,k}^2 + e_k) \rangle_{A_k}) = \\ & - \frac{\partial}{\partial z}(A_k \langle (\mathbb{T}_k \cdot \mathbf{v}_k) \cdot \mathbf{e}_z \rangle_{A_k}) - \frac{\partial}{\partial z}(A_k \langle \mathbf{q}_k \cdot \mathbf{e}_z \rangle_{A_k}) \\ & + \sum_c A_k \langle \rho_{c,k} \mathbf{g}_{c,k} \cdot \mathbf{v}_{c,k} \rangle_{A_k} - \int_{l_{W,k}(t,z)} \mathbf{q}_k \cdot \mathbf{n}_k \frac{dl}{\mathbf{n}_k \cdot \mathbf{n}_{l,W}} \\ & - \int_{l_I(t,z)} (m_k (\frac{1}{2}v_{z,k}^2 + e_k) + \mathbf{n}_k \cdot (\mathbb{T}_k \cdot \mathbf{v}_k) + \mathbf{q}_k \cdot \mathbf{n}_k) \frac{dl}{\mathbf{n}_k \cdot \mathbf{n}_{l,k}} \end{aligned} \quad (3.481)$$

or by introducing the enthalpy per unit of mass,  $h_k = e_k + \frac{p_k}{\rho_k}$ , we obtain:

$$\begin{aligned} & \frac{\partial(A_k \langle \rho_k (\frac{1}{2}v_{z,k}^2 + e_k) \rangle_{A_k})}{\partial t} + \frac{\partial}{\partial z}(A_k \langle \rho_k v_{z,k} (\frac{1}{2}v_{z,k}^2 + h_k) \rangle_{A_k}) = \\ & - \frac{\partial}{\partial z}(A_k \langle (\boldsymbol{\sigma}_k \cdot \mathbf{v}_k) \cdot \mathbf{e}_z \rangle_{A_k}) - \frac{\partial}{\partial z}(A_k \langle \mathbf{q}_k \cdot \mathbf{e}_z \rangle_{A_k}) \\ & + \sum_c A_k \langle \rho_{c,k} \mathbf{g}_{c,k} \cdot \mathbf{v}_{c,k} \rangle_{A_k} - \int_{l_{W,k}(t,z)} \mathbf{q}_k \cdot \mathbf{n}_k \frac{dl}{\mathbf{n}_k \cdot \mathbf{n}_{l,W}} \\ & - \int_{l_I(t,z)} (m_k (\frac{1}{2}v_{z,k}^2 + e_k) + \mathbf{n}_k \cdot (\mathbb{T}_k \cdot \mathbf{v}_k) + \mathbf{q}_k \cdot \mathbf{n}_k) \frac{dl}{\mathbf{n}_k \cdot \mathbf{n}_{l,k}} \end{aligned} \quad (3.482)$$

where the interfacial energy transfer due to phase change is defined by:

$$E_{k,z}^\Gamma = -\frac{1}{A} \int_{l_I(t,z)} m_k (\frac{1}{2}v_z^2 + e)_k \frac{dl}{\mathbf{n}_k \cdot \mathbf{n}_{l,k}} = \Gamma_{Ak} \langle (\frac{1}{2}v_z^2 + e)_k \rangle_{l_I}^{\Gamma_{Ak}} \quad (3.483)$$

The interfacial energy source yields:

$$E_{k,I}^E = -\frac{1}{A} \int_{l_I(t,z)} (\mathbf{n}_k \cdot \mathbf{q}_k) \frac{dl}{\mathbf{n}_k \cdot \mathbf{n}_{l,k}} = a_I \langle \mathbf{n}_k \cdot \mathbf{q}_k \rangle_{l_I} \quad (3.484)$$

The interfacial work by viscous and pressure forces yield:

$$E_{k,I}^W = -\frac{1}{A} \int_{l_I(t,z)} \mathbf{n}_k \cdot (\mathbb{T}_k \cdot \mathbf{v}_k) \frac{dl}{\mathbf{n}_k \cdot \mathbf{n}_{l,k}} \quad (3.485)$$

The external wall heat transfer is expressed as:

$$E_{k,Wall}^E = -\frac{1}{A} \int_{l_{W,k}(t,z)} (\mathbf{n}_k \cdot \mathbf{q}_k) \frac{dl}{\mathbf{n}_k \cdot \mathbf{n}_{l,W}} = \langle \mathbf{n}_k \cdot \mathbf{q}_k \rangle_W \frac{S_W}{A} \quad (3.486)$$

*The Entropy equation:*

In this case we define:

$$\begin{aligned} \psi_k &= s_k, \\ \mathbf{J}_k &= \frac{\mathbf{q}_k - \sum_c \mu_{c,k} \mathbf{j}_{c,k}}{T_k}, \text{ and} \\ \frac{\phi_k}{\rho_k} &= -\frac{1}{T_k \rho_k} \left[ \frac{1}{T_k} (\mathbf{q}_k \cdot \nabla T_k) + \sum_c \mathbf{j}_{c,k} \cdot (T_k \nabla \left( \frac{\mu_{c,k}}{T_k} \right) - \mathbf{F}_{c,k}) + \boldsymbol{\sigma}_k : \nabla \mathbf{v}_k \right. \\ &\quad \left. + \sum_r A_{r,k} r_{r,k} \right] \end{aligned} \quad (3.487)$$

Hence it follows that:

$$\begin{aligned} &\frac{\partial (A_k \langle \rho_k s_k \rangle_{A_k})}{\partial t} + \frac{\partial}{\partial z} (A_k \langle \rho_k v_{z,k} s_k \rangle_{A_k}) \\ &+ \frac{\partial}{\partial z} (A_k \langle \left( \frac{\mathbf{q}_k - \sum_c \mu_{c,k} \mathbf{j}_{c,k}}{T_k} \right) \cdot \mathbf{e}_z \rangle_{A_k}) \\ &+ \int_{l_{W,k}(t,z)} \left( \frac{\mathbf{q}_k - \sum_c \mu_{c,k} \mathbf{j}_{c,k}}{T_k} \right) \cdot \mathbf{n}_k \frac{dl}{\mathbf{n}_k \cdot \mathbf{n}_{l,W}} \\ &+ \int_{l_I(t,z)} \left( m_k s_k + \left( \frac{\mathbf{q}_k - \sum_c \mu_{c,k} \mathbf{j}_{c,k}}{T_k} \right) \cdot \mathbf{n}_k \right) \frac{dl}{\mathbf{n}_k \cdot \mathbf{n}_{l,k}} - \frac{1}{T_k} \left[ \frac{1}{T_k} (\mathbf{q}_k \cdot \nabla T_k) \right. \\ &\left. + \sum_c \mathbf{j}_{c,k} \cdot (T_k \nabla \left( \frac{\mu_{c,k}}{T_k} \right) - \mathbf{g}_{c,k}) + \boldsymbol{\sigma}_k : \nabla \mathbf{v}_k + \sum_r A_{r,k} r_{r,k} \right] = 0 \end{aligned} \quad (3.488)$$

The final form of the entropy equation is consistent with the formulation given for one component fluids by [136].

*The Species Mass Balance:*

In this case we define  $\psi_k = \omega_{k,s}$ ,  $\mathbf{J}_k = \mathbf{j}_{k,s}$ , and  $\phi_{c,k} = R_{k,s}/\rho_{k,c}$ , and we get:

$$\begin{aligned} & \frac{\partial(A_k \langle \rho_k \omega_{k,s} \rangle_{A_k})}{\partial t} + \frac{\partial}{\partial z}(A_k \langle \rho_k \omega_{k,s} v_{z,k} \rangle_{A_k}) = \\ & - \frac{\partial}{\partial z}(A_k \langle \mathbf{e}_z \cdot \mathbf{j}_{k,s} \rangle_{A_k}) - \int_{l_{W,k}(t,z)} \mathbf{n}_k \cdot \mathbf{j}_{k,s} \frac{dl}{\mathbf{n}_k \cdot \mathbf{n}_{l,W}} \\ & - \int_{l_I(t,z)} (m_k \omega_{k,s} + \mathbf{n}_k \cdot \mathbf{j}_{k,s}) \frac{dl}{\mathbf{n}_k \cdot \mathbf{n}_{l,k}} + A_k \langle R_{s,k} \rangle_{A_k} \end{aligned} \quad (3.489)$$

The interfacial species mass transfer due to phase change is defined by:

$$J_{k,s}^\Gamma = -\frac{1}{A} \int_{l_I(t,z)} m_k \omega_{k,s} \frac{dl}{\mathbf{n}_k \cdot \mathbf{n}_{l,k}} \approx \Gamma_{A_k} \langle \omega_{k,s} \rangle_{l_I}^{\Gamma_{A_k}} \quad (3.490)$$

The other interfacial mass transfer fluxes are given by:

$$J_{k,s}^j = -\frac{1}{A} \int_{l_I(t,z)} \mathbf{n}_k \cdot \mathbf{j}_{k,s} \frac{dl}{\mathbf{n}_k \cdot \mathbf{n}_{l,k}} \approx a_I \langle \mathbf{n}_k \cdot \mathbf{j}_{k,s} \rangle_{l_I} \quad (3.491)$$

in which  $\langle \mathbf{n}_k \cdot \mathbf{j}_{k,s} \rangle_{l_I}$  denotes the averaged interfacial mass transfer flux. The area averaged wall mass transfer flux of species  $s$  is given by:

$$J^{\text{Wall}} = -\frac{1}{A} \int_{l_{W,k}(t,z)} \mathbf{n}_k \cdot \mathbf{j}_{k,s} \frac{dl}{\mathbf{n}_k \cdot \mathbf{n}_{l,W}} \quad (3.492)$$

but normally vanishes as we consider impermeable walls only.

In the present state of knowledge numerous hypothesis are generally admitted to achieve a solvable set of equations [229, 243, 46, 10]. The fairly rigorous set of equations are thus simplified neglecting both the time - and spatial covariance terms, so the average of products are approximated by the products of average. In addition, it is assumed that the EOS valid for local quantities apply to averaged quantities. Besides, as often adopted in chemical reactor analysis, in vertical flows the pressure is considered constant over the cross-section. Moreover, as the reactor flows are assumed to be symmetrical with respect to a straight line, the vectorial momentum equation reduces to its projection on the symmetry axis. It is further noted that the area phase fraction,  $\alpha_k$ , is defined by:

$$\alpha_k = \frac{A_k}{A} \quad (3.493)$$

which can be introduced into the equations eliminating the phase cross sectional area,  $A_k$ , variable [135].

On the basis of these hypotheses, the set of modeled equations used in chemical engineering practice are obtained as follows, as we drop the cross-sectional averaging sign  $\langle \dots \rangle_{A_k}$  for convenience, expressing the necessary balances:

*The Balance of Mass:*

The fairly rigorous equation (3.469) is modeled as:

$$\frac{\partial(\alpha_k \rho_k)}{\partial t} + \frac{1}{A} \frac{\partial}{\partial z} (\alpha_k \rho_k v_{z,k} A) = \Gamma_{A_k} \quad (3.494)$$

*The Balance of Momentum:*

The fairly rigorous equation (3.475) is modeled as:

$$\begin{aligned} & \frac{\partial(\alpha_k \rho_k v_{z,k})}{\partial t} + \frac{1}{A} \frac{\partial}{\partial z} (\alpha_k \rho_k v_{z,k} v_{z,k} A) + \alpha_k \frac{\partial p_k}{\partial z} \approx \\ & - \frac{1}{A} \frac{\partial}{\partial z} (\alpha_k (\mathbf{e}_z \cdot \boldsymbol{\sigma}_k) \cdot \mathbf{e}_z) A + \sum_c \alpha_k \rho_{c,k} g_{c,z,k} + \Gamma_{A_k} \langle v_z \rangle_{l_I}^{\Gamma_{A_k}} + M_{z,k}^\sigma \\ & - f_{D,W} \frac{1}{2} \rho_k |v_{z,k}| v_{z,k} \frac{S_W}{4A} \end{aligned} \quad (3.495)$$

*The Balance of Total Energy:*

The modeled form of the energy equation (3.496) can be expressed as:

$$\begin{aligned} & \frac{\partial(\alpha_k \rho_k (\frac{1}{2} v_{z,k}^2 + e_k))}{\partial t} + \frac{1}{A} \frac{\partial}{\partial z} (\alpha_k \rho_k v_{z,k} (\frac{1}{2} v_{z,k}^2 + e_k) A) = \\ & - \frac{1}{A} \frac{\partial}{\partial z} (\alpha_k \langle (\mathbf{T}_k \cdot \mathbf{v}_k) \cdot \mathbf{e}_z \rangle_{A_k} A) - \frac{1}{A} \frac{\partial}{\partial z} (\alpha_k \langle \mathbf{q}_k \cdot \mathbf{e}_z \rangle_{A_k} A) \\ & + \sum_c \alpha_k \rho_{c,k} \mathbf{g}_{c,k} \cdot \mathbf{v}_{c,k} + \langle \mathbf{n}_k \cdot \mathbf{q}_k \rangle_W \frac{S_W}{A} \\ & + \Gamma_{A_k} \langle (\frac{1}{2} v_z^2 + e)_k \rangle_{l_I}^{\Gamma_{A_k}} + E_{k,I}^W + a_I \langle \mathbf{n}_k \cdot \mathbf{q}_k \rangle_{l_I} \end{aligned} \quad (3.496)$$

*The Species Mass Balance:*

The modeled form of the species mass balance (3.489) can be expressed as:

$$\begin{aligned} & \frac{\partial(\alpha_k \rho_k \omega_{k,s})}{\partial t} + \frac{1}{A} \frac{\partial}{\partial z} (\alpha_k \rho_k \omega_{k,s} v_{z,k} A) = \\ & - \frac{1}{A} \frac{\partial}{\partial z} (\alpha_k j_{z,k,s} A) + \Gamma_{A_k} \langle \omega_{k,s} \rangle_{l_I}^{\Gamma_{A_k}} + a_I \langle \mathbf{n}_k \cdot \mathbf{j}_{k,s} \rangle_{l_I} + \alpha_k R_{s,k} \end{aligned} \quad (3.497)$$

The governing 1D two phase flow equations assessed in this section are very often used in industry, academia and in engineering research. For example, these 1D area-averaged equations (with slightly different constitutive equations) determine the basis for the commercial dynamic two-fluid model

simulator named *OLGA* developed at the Institute for Energy Technology (IFE) at Kjeller in Norway [16] for the oil and gas processing industry. The model is intended for dynamic simulations of two-phase oil and gas flows in pipelines. It has been used analyzing terrain slugging, pipeline startup and shut-in, production rates, and pigging. These simulations have been performed for pipelines of several kilometers length with time spans ranging from hours to weeks.

### 3.4.7 Heterogeneous Dispersion Models

In chemical reaction engineering the two phase or heterogeneous versions of the dispersion models discussed in sect 1.2.6 are frequently used simulating multiphase reactor like fixed bed, fluidized bed and slurry bubble column reactors. However, this model is most successfully applied to fixed bed reactors as the flow profile in these reactors is being fairly flat. For such reactors the effective dispersion coefficient typically considers both molecular - and turbulent diffusion, and the gross scale dispersion caused by the packing of catalyst particles. Besides, in reactor simulations the cross section averaged enthalpy and temperature equations are required for non-isothermal systems. These two balance equations can with minor struggle be deduced from the total energy equation following the same steps as examined for single phase flows in sect 1.2.6. In a heterogeneous model the effective thermal conductivity contains various contributions, such as conduction in the solid and in the fluid, and radiation in gas-filled voids between solid surfaces.

### Heterogeneous Axial Dispersion models

The axial dispersion model equations for the continuous phase is developed based on the 1D form of the governing equations given in sect 3.4.6. However, the instantaneous area averaged model equations are also Reynolds averaged to enable reactor simulations with practicable time resolutions. For the time after area averaged models, the instantaneous variables are decomposed and Reynolds averaged in the standard way. If we drop the averaging signs, the basic 1D species mass balance deduced from (3.497) is given by:

$$\frac{\partial}{\partial t}(\alpha_k \rho_k \omega_{k,s}) + \frac{\partial}{\partial z}(\alpha_k \rho_k v_{z,k} \omega_{k,s}) = \frac{\partial}{\partial z}(\alpha_k \rho_k D_{z,k,\text{eff}} \frac{\partial \omega_{k,s}}{\partial z}) + \Gamma_{Ak} \langle \omega_{k,s} \rangle_{I_I}^{\Gamma_{Ak}} \quad (3.498)$$

in which it is customary to define the superficial velocity by  $v_{z,k}^S = \alpha_k v_{z,k}$ . The interfacial mass transfer term  $\Gamma_{Ak} \langle \omega_{k,s} \rangle_{I_I}^{\Gamma_{Ak}}$  has to be parameterized for the chemical process in question, normally a simple film model suffices.

The corresponding heat or temperature equation can be derived following a similar procedure as adopted formulating the single phase equation (1.299). The result is:

$$\alpha_k \rho_k C_{p,k} \left( \frac{\partial T_k}{\partial t} + v_{z,k} \frac{\partial T_k}{\partial z} \right) = \frac{\partial}{\partial z} (\alpha_k k_{z,k,\text{eff}} \frac{\partial T_k}{\partial z}) + \Gamma_{Ak} \langle h_k \rangle_{LI}^{\Gamma_{Ak}} + \frac{4U}{d_r} (T_{\text{sur}} - T) \quad (3.499)$$

where the interfacial heat transfer rate has to be parameterized for the chemical process in question, normally a simple film model suffice. The effective transport coefficients are included as a reminder that the temporal covariances resulting from the Reynolds averaging procedure are normally modeled adopting the gradient hypothesis and the Boussinesq turbulent viscosity concept.

There are several ways of describing the solid phase processes. One way of treating the solid phase is to consider the packed bed as a porous media and simply adopt a similar set of model equations for the solid phase, as put up for the fluid, noting that the solid phase is often fixed so there is no convection. A more common modeling approach in chemical reaction engineering is to investigate the intra-particle processes formulating a diffusion model for a single representative particle.

The alternative pseudo-homogeneous model is a kind of mixture model (see sect 3.4.5) which is achieved by taking the sum of the individual equations for the two phases.

The initial conditions used for dynamics reactor simulations depend upon the start-up procedure adopted in industry for each particular chemical process. A possible set of initial conditions corresponds to uniform variable fields given by the inlet values as outlined in sect 1.2.6. The standard Danckwerts [39] boundary conditions are normally applied.

### 3.5 Mathematical Model Formulation Aspects

The well-posedness of the two-fluid model has been a source of controversy reflected by the large number of papers on this issue that can be found in the literature. This issue is linked with analysis of the characteristics, stability and wavelength phenomena in multi-phase flow equation systems. The controversy originates primarily from the fact that with the present level of knowledge, there is no general way to determine whether the 3D multi-fluid model is well posed as an initial-boundary value problem. The mathematical theory of well posedness for systems of partial differential equations describing dispersed chemical reacting flows needs to be examined.

Introductory work has however been made to analyze the mathematical properties of the equations. In their pioneer work Gidaspow [84] and Lyckowski et al [144] consider the 1D, incompressible, in-viscid two-fluid flow equations with no added mass or lift effects given by:

$$\frac{\partial \alpha_k}{\partial t} + \frac{\partial (\alpha_k \langle v_k \rangle_{V_k})}{\partial x} = 0 \quad (3.500)$$

$$\alpha_k \rho_k \left( \frac{\partial \langle v_k \rangle_{V_k}}{\partial t} + \langle v_k \rangle_{V_k} \frac{\partial \langle v_k \rangle_{V_k}}{\partial x} \right) = -\alpha_k \frac{\partial \langle p_k \rangle_{V_k}}{\partial x} + F_{x,k} \quad (3.501)$$

where  $F_{x,g} = -F_{x,l} = K_l(v_g - v_l)$ , and  $K_l$  is assumed to be constant.

If the characteristics of the system of equations are found to be complex, the initial-value problem is said to be ill-posed [178]. A physical interpretation of this mathematical statement can be found by analyzing the flow instabilities predicted by this set of model equations. The instabilities predicted by a *well-posed model system* has some realistic physical meaning, while the instability always present in an *ill-posed system* is a mathematical mode having no physical origin indicating that the model is not treating small-scale phenomena correctly.

Traditionally, this so-called ill-posed nature of the model makes it desirable to seek physical modifications of the simple model to find a well-posed mode. Several attempts have thus been made to improve the mathematical properties of the equations by re-examining some of the basic assumptions made in the derivation of the model equations. *The idea is that by introducing more physical and exact formulations into the description, the final set of equations will be well posed.*

Ramshaw and Trapp [172] incorporated surface tension effects, which had traditionally been ignored. Travis et al [220] considered viscous stresses, Lahay et al [134] considered the added mass force, Prosperetti and Wijngaarden [167] considered compressibility effects. Trapp [219] considered Reynolds stresses, while Stuhmiller [213], Bourè [22], Pauchon and Banerjee [161, 162], Sha and Soo [188], Prosperetti and Jones [168] and Holm and Kupersmidt [109] have put their main focus on the adoption and interpretation of the interfacial pressure forces (see sects 3.4.1 and 3.4.6). The simplest choice for the interfacial pressure distribution  $\langle p_k \rangle_{A_I}$  is to assume that it is equal to the fluid bulk pressure. This implies that  $\langle p_g \rangle_{V_g} = \langle p_l \rangle_{V_l} = \langle p_g \rangle_{A_I} = \langle p_l \rangle_{A_I}$  for a two-phase system and as a result the current engineering practice is obtained (e.g., [168, 125, 119]). However, this approach leads to an equation set involving a single pressure, which has real characteristics only when the two fluid velocities are equal [219].

Considering low-pressure bubbly flows a slightly more general assumption is that the interfacial pressure in the gas phase is related to the average pressure of the gas phase by:

$$\langle p_g \rangle_{A_I} - \langle p_g \rangle_{V_g} \approx 0 \quad (3.502)$$

since the averaged pressure within the spheres will be very close to the average interfacial pressure [213, 161, 136, 143].

In contrast, the difference between the interfacial averaged pressure and the mean pressure in the liquid phase is, for a non-pulsating bubble, given by [213]:

$$\langle p_l \rangle_{A_I} - \langle p_l \rangle_{V_l} = \xi \rho_I (\langle \mathbf{v}_g \rangle_g - \langle \mathbf{v}_l \rangle_{V_l}) \quad (3.503)$$

It was shown that this approach gives real characteristics only if  $\langle p_l \rangle_{A_I}$  is lower than  $\langle p_l \rangle_{V_l}$ . A value of  $\xi = -\frac{1}{4}$  is used by several researchers [136] [161].

However, Drew [54] also discusses this approach and argues that this formulation is questionable, as it may not be consistent with the interfacial drag parameterizations used.

Sha and Soo [188] dealt with essentially the same problem from a more physical angle. Their discussion focuses on what form the  $\nabla(\alpha_k \langle p_k \rangle_{V_k})$  term in the momentum equation should take. They gave an overview of the terms  $\nabla(\alpha_k \langle p_k \rangle_{V_k}) = \alpha_k \nabla \langle p_k \rangle_{V_k} + \langle p_k \rangle_{V_k} \nabla \alpha_k$  and divided the literature approaches into three groups. These includes those who favor (1) dropping  $\langle p_k \rangle_{V_k} \nabla \alpha_k$  for the reason of being canceled out by the interfacial source term in the momentum equation when the bulk mean pressure is assumed equal to the interfacial mean pressure. Those who favor (2) retaining a part of it as a stabilizing force. Sha and Soo [188] argued that the physical effect of the  $\langle p_k \rangle_{V_k} \nabla \alpha_k$  term is to spread the dispersed phase which has an initial concentration gradient. They proposed to replace the term by:

$$\alpha_k \nabla \langle p_k \rangle_{V_k} + (1 - B) \langle p_k \rangle_{V_k} \nabla \alpha_k \quad (3.504)$$

where  $B$ ,  $0 \leq B \leq 1$ , is a displacement factor which is a function of the flow configuration. The last group, those who favor (3) retaining  $\langle p_k \rangle_{V_k} \nabla \alpha_k$  for the reason of an extension of the continuum mechanics, as a compressive force to fulfill the laws of thermodynamics.

In an attempt to close the non-constructive controversy, Bourè [23] claims that both forms of the pressure terms are acceptable. The occurrence of complex roots in the momentum equations is not related to the correct use of the pressure terms, but is primarily a problem of mathematical form of the constitutive terms.

In reaction engineering the 2D and 3D multi-fluid model equations used are obviously solvable although with certain struggle, hence to some extent affected by the mathematical model properties reflected by the simplified model equations examined in the above mentioned work. Besides, in some cases numerical problems occur due to the inadequate mathematical properties reflected by the constitutive equations used in particular in the limit as  $\alpha_k \rightarrow 0$  or  $\alpha_k \rightarrow 1$ . Another source of problem encountered in dense reactor flows is the highly recirculating flow patterns located at the outlets making consistent formulations of the necessary boundary conditions difficult, especially for reactive variable density flows. Further analysis of the mathematical properties of the model equations are still considered useful, in the sense that this can assist in developing novel closure laws having more appropriate properties and to ensure that the need for ad hoc tricks to obtain somewhat ill-conditioned solutions can be avoided.

---

## References

1. Adamson AW (1967) *Physical Chemistry of Surfaces*. Second Edition, Interscience Publishers (John Wiley & Sons), New York
2. Ahmadi G (1987) On the mechanics of incompressible multiphase suspensions. *Adv Water Res* 10:32-43
3. Ahmadi G, Ma D (1990) A thermodynamical formulation for dispersed multiphase turbulent flows-I Basic theory. *Int J Multiphase Flow* 16:323-340
4. Albråten PJ (1982) *The Dynamics of Two-Phase Flow*. PhD thesis, Chalmers University of Technology, Göteborg, Sweden
5. Aleinov I, Puckett EG (1995) Computing Surface Tension with High-Order Kernels. In: Oshima, K., (ed) *Proceedings of the 6th International Symposium on Computational Fluid Dynamics*, pp. 13-18, Lake Tahoe, CA, USA.
6. Amsden AA, Harlow FH (1970) A Simplified MAC Technique for Incompressible Fluid Flow Calculations. *J Comput Phys* 6:322-325
7. Andersson TB, Jackson R (1967) A Fluid Mechanical Description of Fluidized Beds: Equations of Motion. *Ind Engng Chem Fundam* 6(4):527-539
8. Ashgriz N, Poo JY (1991) FLAIR: Flux Line-Segment Model for Advection and Interface Reconstruction. *J Comput Phys* 93:449-468.
9. Aris R (1962) *Vectors, Tensors, and the Basic Equations of Fluid Mechanics*. Dover, Inc., New York
10. Banerjee S, Chan AMC (1980) Separated Flow Models-I: Analysis of the Averaged and Local Instantaneous Formulations. *Int J Multiphase Flow* 6:1-24
11. Banerjee S (1999) Multifield Formulations. In: *Modelling and Computation of Multiphase Flows*, Short Course, Zurich, Switzerland, March 8-12, 14B:1-49.
12. Barkhudarov MR, Chin SB (1994) Stability of a numerical algorithm for gas bubble modelling. *Int. J Numer Meth Fluids* 19:415-437
13. Batchelor GK (1970) *An Introduction to Fluid Dynamics*. Cambridge University Press, Cambridge
14. Beckermann C, Viskanta R (1993) Mathematical modeling of transport phenomena during alloy solidification. *Appl Mech Rev* 46(1):1-27
15. Bedford A, Drumheller DS (1983) Theories of Immiscible and Structured Mixtures. *Int J Engng Sci* 21(8):863-960
16. Bendiksen K, Malnes D, Moe R and Nuland S (1991) The dynamic two-fluid model OLGA: Theory and applications. *SPE Production Engineers*, pp. 171-180

17. Bennon WD, Incropera FP (1987) A continuum model for momentum, heat and species transport in binary solid-liquid phase change systems-II. Application to solidification in a regular cavity. *Int J Heat Transfer* 30(10): 2171-2187
18. Bertola F (2003) Modelling of Bubble Columns by Computational Dynamics. PhD thesis, Politecnico Di Torino, Torino
19. Bertola F, Grundseth J, Hagesaether L, Dorao C, Luo H, Hjarbo KW, Svendsen HF, Vanni M, Baldi G, Jakobsen HA (2005) Numerical Analysis and Experimental Validation of Bubble Size Distribution in Two-Phase Bubble Column Reactors. *Multiphase Science & Technology*, 17(1-2):123-145
20. Beux F, Banerjee S (1996) Numerical Simulation of Three-Dimensional Two-Phase Flows by Means of a Level Set Method. *ECCOMAS 96 Proceedings*, John Wiley.
21. Biesheuvel A, Wijngaarden L van (1984) Two-phase flow equations for a dilute dispersion of gas bubbles in liquid. *J Fluid Mech* 168:301-318
22. Bourè JA (1978) Constitutive Equations for Two-Phase Flows. In: *Two-phase flows and heat transfer with application to nuclear reactor design problems*, chap 9, von Karman Inst. Book, Hemisphere, New York
23. Bourè JA (1979) On the form of the pressure terms in the momentum and energy equations of the two-phase flow models. *Int J Multiphase Flow* 5: 159-164
24. Bourè JA, Delhay JM (1982) General Equations and Two-Phase Flow Modeling. In: Hetsroni G (ed) *Handbook of Multiphase Systems*, Section 1.2, pp. (1-36) - (1-95), McGraw-Hill, New York
25. Brackbill JU, Kothe DB, Zemach C (1992) A Continuum Method for Modeling Surface Tension. *J Comput Phys* 100:335-354.
26. Brenner H (1979) A Micromechanical Derivation of the Differential Equation of Interfacial Statics. *Journal of Colloid and Interface Science* 68 (3):422-439
27. Buyevich YA (1971) Statistical hydrodynamics of disperse systems. Part 1. Physical background and general equations. *J Fluid Mech* 49(3):489-507
28. Buyevich YA, Shchelchkova IN (1978) Flow of Dense Suspensions. *Prog Aerospace Sci* 18:121-150
29. Carmo MP do (1976) *Differential Geometry of Curves and Surfaces*. Prentice-Hall, Inc, Englewood Cliffs
30. Celik I (1993) Numerical Uncertainty in Fluid Flow Calculations: Needs for Future Research. *ASME J Fluids Engineering* 115:194-195.
31. Chandrasekhar S (1981) *Hydrodynamic and hydromagnetic stability*. Dover Publications, New York.
32. Chang YC, Hou TY, Merriman B, Osher S (1996) A Level Set Formulation of Eulerian Interface Capturing Methods for Incompressible Fluid Flows. *J Comput Phys* 124:449-464.
33. Chorin AJ (1968) Numerical solution of the Navier-Stokes equations. *Math Comput* 22:745-762.
34. Clift R, Grace JR, Weber ME (1978) *Bubble, Drops, and Particles*. Academic Press, New York
35. Colebrook CF (1939) Turbulent Flow in Pipes, with particular reference to the Transition Region between Smooth and Rough Pipe Laws. *J Inst Civ Eng* 12(4):133-156
36. Crowe CT (1982) Review: numerical models for dilute gas-particle flows. *J Fluids Engng* 104:297-303

37. Crowe CT, Truitt TR, Chung JN (1996) Numerical Models for Two-Phase Turbulent Flows. *Annu Rev Fluid Mech* 28:11-43.
38. Crowe CT, Sommerfeld M, Tsuji Y (1998) *Multiphase Flows with Droplets and Particles*. CRC Press, Boca Raton.
39. Danckwerts PV (1953) Continuous flow systems: Distribution of Residence Times. *Chem Eng Sci* 2(1):1-18
40. Danov KD, Gurkov TD, Dimitrova T, Ivanov IB, Smith D (1997) Hydrodynamic Theory for Spontaneously Growing Dimple in Emulsion Films with Surfactant Mass Transfer. *Journal of Colloid and Interface Science* 188:313-324
41. Deemer AR, Slattery JC (1978) Balance Equations and Structural Models for Phase Interfaces. *Int J Multiphase Flow* 4:171-192
42. Delhaye JM (1974) Jump Conditions and Entropy Sources in Two-Phase Systems: Local Instant Formulation. *Int J Multiphase Flow* 1:395-409
43. Delhaye JM, Achard JL (1977) On the averaging operators introduced in two-phase flow. In: Banerjee S, Weaver JR (eds) *Transient Two-phase Flow*. Proc. CSNI Specialists Meeting, Toronto, 3.-4. august
44. Delhaye JM (1977) Instantaneous space-averaged equations. In: Kakac S, Mayinger F *Two-Phase Flows and Heat Transfer*. Vol. 1, pp. 81-90, Hemisphere, Washington, DC
45. Delhaye JM (1977) Local time-averaged equations. In: Kakac S, Mayinger F *Two-Phase Flows and Heat Transfer*. Vol. 1, pp. 91-100, Hemisphere, Washington, DC
46. Delhaye JM (1977) Space/time and Time/space-averaged equations. In: Kakac S, Mayinger F *Two-Phase Flows and Heat Transfer*. Vol. 1, pp. 101-114, Hemisphere, Washington, DC
47. Delhaye JM, Achard JL (1978) On the use of averaging operators in two phase flow modeling: Thermal and Aspects of Nuclear Reactor Safty, 1: Light Water Reactors. ASME Winter Meeting
48. Delhaye JM (1981) Basic Equations for Two-Phase Flow Modeling. In: Bergles AE, Collier JG, Delhaye JM, Hewitt GF, Mayinger F (eds) *Two-Phase Flow and Heat Transfer in the Power and Process Industries*. Hemisphere Publishing, Washington
49. Delnoij E, Kuipers JAM, van Swaaij WPM (1997) Computational fluid dynamics applied to gas-liquid contactors. *Chem Eng Sci* 52 (21/22):3623-3638.
50. Delnoij E (1999) *Fluid Dynamics of Gas-Liquid Bubble Columns*. PhD thesis, University of Twente, The Netherlands, Twente.
51. Dobran F (1983) On the formulation of conservation, balance and constitutive equations for multiphase flows. In: Vezirogly TN (ed) *Proc 3rd Multiphase Flow and Heat Transfer Symposium*.
52. Drew DA (1971) Averaged Field Equations for Two-Phase Media. *Stud Appl Math* 50(2):133-166
53. Drew DA, Lahey RT Jr (1979) Application of general constitutive principles to the derivation of multidimensional two-phase flow equations. *Int J Multiphase Flow*. 5:243-264
54. Drew DA (1983) Mathematical Modeling of Two-Phase Flow. *Ann Rev Fluid Mech* 15:261-291
55. Drew DA (1992) Analytical Modeling of Multiphase Flows: Modern Developments and Advances. In: Lahey RT jr (ed) *Boiling Heat Transfer*, pp. 31-83, Elsevier Science Publishers BV, Amsterdam

56. Drew DA, Lahey RT Jr (1993) Analytical Modeling of Multiphase Flow. In: Roco MC (ed) Particulate Two-Phase Flow, Chapt. 16, pp. 509-566, Butterworth-Heinemann, Boston
57. Drew DA, Wallis GB (1994) Fundamentals of Two-Phase Flow Modeling. Multiphase Science and Technology 8:1-67
58. Drew DA, Passman SL (1999) Theory of Multicomponent Fluids. Springer, New York
59. Drew DA (2005) Probability and repeatability: One particle diffusion. Nuclear Engineering and Design 235:1117-1128
60. Duckworth OW, Cygan RT, Martin ST (2004) Linear Free Energy Relationships between Dissolution Rates and Molecular Modeling Energies of Rhombohedral Carbonates. Langmuir 20:2938-2946
61. Duducovič MP (1999) Trends in Catalytic Reaction Engineering. Catal Today 48 (1-4):5-15
62. Edwards CH Jr, Penny DE (1982) Calculus and Analytic Geometry. Prentice-Hall Inc, Englewood Cliffs, New Jersey
63. Edwards DA, Brenner H, Wasan DT (1991) Interfacial Transport Processes and Rheology. Butterworth-Heinemann, Boston
64. Elghobashi SE, Abou-Arab TW (1983) A two-equation turbulence model for two-phase flows. Phys Fluids 26(4):931-938.
65. Elghobashi SE, Truesdell GC (1993) On the two-way interaction between homogeneous turbulence and dispersed solid particles. I: Turbulence modification. Phys Fluids A5 (7):1790-1801
66. Elghobashi SE (1994) On predicting particle laden turbulent flows. Appl Sci Res 52:309-329.
67. Enwald H, Peirano E, Almstedt AE (1996) Eulerian Two-Phase Flow Theory Applied to Fluidization. Int J Multiphase Flow 22:21-66, Suppl.
68. Ervin EA, Tryggvason G (1997) The rise of bubbles in a vertical shear flow. ASME J Fluid Engineering 119:443-449
69. Esmaeeli A, Ervin E, Tryggvason G (1994) Numerical simulations of rising bubbles. In: Blake JR, Boulton-Stone JM, Thomas NH (eds) Bubble Dynamics and Interfacial Phenomena. Kluwer Academic Publishers, Dordrecht
70. Esmaeeli A, Tryggvason G (1996) An Inverse Energy Cascade in Two-Dimensional Low Reynolds Number Bubbly Flows. J Fluid Mech 314:315-330
71. Esmaeeli A, Tryggvason G (2004) Computations of film boiling. Part I: numerical method. Int J Heat Mass Transfer 47:5451-5461
72. Esmaeeli A, Tryggvason G (2004) A front tracking method for computations of boiling in complex geometries. Int J Multiphase Flow 30:1037-1050
73. Fan F-S, Tsuchiya K (1990) Bubble Wake Dynamics in Liquids and Solid-Liquid Suspensions. Butterworth-Heinemann, Boston
74. Fan F-S, Zhu C (1998) Principles of Gas-Solid Flows. Cambridge University Press, Cambridge
75. Favre A (1965) Equations des gaz turbulents compressibles. J Mécanique 4(3):361-390
76. Favre A (1969) Statistical Equations of Turbulent Gases. Problems of Hydrodynamics and Continuum Mechanics. SIAM, pp. 231-266, Philadelphia (PA)
77. Ferziger JH, Kaper HG (1972) Mathematical Theory of Transport Processes in Gases. North-Holland Publishing Company, Amsterdam
78. Fogler Scott H (2006) Elements of Chemical Reaction Engineering. Fourth Edition, Prentice-Hall International, Inc, New Jersey

79. Freitas J (1993) Editorial. Transactions of the ASME, Journal of Fluids Engineering. New York: American Society of Mechanical Engineers 115:339-340.
80. Froment GF, Bischoff KB (1990) Chemical Reactor Analysis and Design. John Wiley and Sons, New York
81. Ganesan S, Poirier DR (1990) Conservation of Mass and Momentum for the Flow of Interdendritic Liquid during Solidification. Metallurgical Transactions B 21B:173-181
82. Ganesan V, Brenner H (2000) A diffuse interface model of two-phase flow in porous media. Proc R Soc Lond A 456:731-803
83. Gibbs JW (1928) The Collected Works of J. Willard Gibbs. Longmans, Green & Co, New York
84. Gidaspow D (1974) Introduction to Modeling of Two-Phase Flow. Round Table Discussion (RT-1-2). Proc 5th Int Heat Transfer Conf Vol VII, p. 163.
85. Gidaspow D (1994) Multiphase Flow and Fluidization-Continuum and Kinetic Theory Descriptions. Academic Press, Harcourt Brace & Company, Publishers, Boston
86. Gosman AD, Pun WM, Runchal AK, Spalding DB, Wolfshtein M (1969) Heat and Mass Transfer in Recirculating Flows. Academic Press, London and New York
87. Gosman AD, Lekakou C, Polits S, Issa RI, Looney MK (1992) Multidimensional Modeling of Turbulent Two-Phase Flows in Stirred Vessels. AIChE J 38(12):1946-1956
88. Gotaas C, Havelka P, Roth N, Hase M, Weigand B, Jakobsen HA, Svendsen HF (2004) Influence of viscosity on droplet-droplet collision behaviour: Experimental and numerical results. CHISA 2004, Prague, Czech Republic, August 22-26.
89. Gray WG (1975) A Derivation of the Equations for Multi-Phase Transport. Chem Eng Sci 30:229-233
90. Gray WG, Lee PCY (1977) On the Theorems for Local Volume Averaging of Multiphase Systems. Int J Multiphase Flow 3:333-340
91. Gray WG (1983) Local Volume Averaging of Multiphase Systems Using A Non-Constant Averaging Volume. Int J Multiphase Flow 9(6):755-761
92. Gueyffier D, Li J, Nadim A, Scardovelli R, Zaleski S (1999) Volume-of-Fluid Interface Tracking with Smoothed Surface Stress Methods for Three-Dimensional Flows. J Comput Phys 152:423-456.
93. Hagesæther L, Jakobsen HA, Svendsen HF (1999) Theoretical analysis of fluid particle collisions in turbulent flow. Chem Eng Sci 54:4749-4755.
94. Heinbockel JH (2001) Introduction to Tensor Calculus and Continuum Mechanics. Trafford Publishing, Canada (ISBN 1553691334)
95. Han J, Tryggvason G (1999) Secondary breakup of axisymmetric liquid drops. I. Acceleration by a constant body force. Physics of Fluids 11(12):3650-3667
96. Harlow FH, Welch JE (1965) Numerical Calculation of Time-Dependent Viscous Incompressible Flow of Fluid with Free Surface. Physics and Fluids 8:2182-2189
97. Harlow FH, Amsden AA (1975) Numerical Calculation of Multiphase Fluid Flow. J Comput physics 17:19-52
98. Hassanizadeh M, Gray WG (1979) General conservation equations for multiphase systems: 1. Averaging procedure. Advances in Water Resources 2: 131-144

99. Hassanizadeh M, Gray WG (1979) General conservation equations for multi-phase systems: 2. Mass, momenta, energy, and entropy equations. *Advances in Water Resources* 2:191-203
100. Hassanizadeh M, Gray WG (1980) General conservation equations for multi-phase systems: 3. Constitutive theory for porous media flow. *Advances in Water Resources* 3:25-40
101. Hassanizadeh M, Gray WG (1987) High Velocity Flow in Porous Media. *Transport in Porous Media* 2:521-531
102. Hassanizadeh M, Gray WG (1990) Mechanics and thermodynamics of multi-phase flow in porous media including interphase boundaries. *Adv Water Resources* 13(4):169-186
103. Hidy GM, Broch JR (1970) *The Dynamics of Aerocolloidal Systems*. Pergamon, Oxford
104. Hinch EJ (1977) An average-equation approach to particle interactions in a fluid suspension. *J Fluid Mech* 83(4):695-720
105. Hinze JO (1975) *Turbulence*. Second Edition, McGraw-Hill, New York
106. Hirt CW (1968) Heuristic stability theory for finite difference equations. *J Comput Phys* 2:339-355
107. Hirt CW, Nichols BD (1980) Adding Limited Compressibility to Incompressible Hydrocodes. *J Comput Phys* 34:390-300
108. Hirt CW, Nichols BD (1981) Volume of Fluid (VOF) Method for the Dynamics of Free Boundaries. *J Comput Phys* 39:201-225
109. Holm DD, Kupersmidt BA (1986) A multipressure regulation for multiphase flow. *Int J Multiphase Flow*, 12(4):681-697
110. Howes FA, Whitaker S (1985) The Spatial Averaging Theorem Revisited. *Chem Eng Sci* 40(8): 1387-1392
111. Hyman JM (1984) Numerical Methods for Tracking Interfaces. *Physica* 12D:396-407.
112. Ishii M (1975) *Thermo-Fluid Dynamic Theory of Two-Phase Flow*. Eyrolles, Paris
113. Ishii M, Chawla TC (1979) Local drag laws in dispersed two-phase flows. Argonne National Laboratory Report NUREG/CR-1230, ANL-79-105, Argonne, Illinois, USA
114. Ishii M, Mishima K (1981) Study of two-fluid model and interfacial area. Argonne National Laboratory Report ANL-80-111, Argonne, Illinois, USA
115. Ishii M, Mishima K (1984) Two-Fluid Model and hydrodynamic Constitutive Equations. *Nuclear Engineering and Design* 82:107-126
116. Ishii M (1990) Two-fluid model for two-phase flow. *Multiphase Science and Technology* 5 (chap 1) Hemisphere, New York
117. Issa RI, Oliveira PJ (1995) Numerical Prediction of Turbulent Dispersion in Two-Phase Jet Flows. In: Celata GP, Shah RK (eds) *Two-Phase Flow Modelling and Experimentation*. pp. 421-428
118. Ivanov IB (1988) *Thin Liquid Films. Fundamentals and Applications*. Marcel Dekker Inc, New York and Basel
119. Jakobsen HA (1993) On the modelling and simulation of bubble column reactors using a two-fluid model. Dr Ing Thesis, Norwegian Institute of Technology, Trondheim, Norway.
120. Jakobsen HA, Sannæs BH, Grevskott S, Svendsen HF (1997) Modeling of Vertical Bubble Driven Flows. *Ind Eng Chem Res* 36 (10):4052-4074.

121. Jakobsen HA (2001) Phase Distribution Phenomena in Two-Phase Bubble Column Reactors. *Chem Eng Sci* 56(3):1049-1056
122. Jakobsen HA, Lindborg H, Handeland V (2002) A numerical study of the interactions between viscous flow, transport and kinetics in fixed bed reactors. *Computers and Chemical Engineering* 26:333-357
123. Jakobsen HA (2003) Numerical Convection Algorithms and Their Role in Eulerian CFD Reactor Simulations. *International Journal of Chemical Reactor Engineering* A1:1-15.
124. Jayatilleke CLV (1969) The Influence of Prandtl Number and Surface Roughness on the Resistance of the Laminar Sublayer to Momentum and Heat Transfer. *Prog Heat Mass Transfer* 1:193-329
125. Johansen ST (1990) On the Modelling of Dispersed Two-Phase Flows. Dr Techn thesis, The Norwegian Institute of Technology, Trondheim.
126. Joseph DD, Lundgren TS, Jackson R, Saville DA (1990) Ensemble Averaged and Mixture Theory Equations for Incompressible Fluid-Particle Suspensions. *Int J Multiphase Flow* 16 (1):35-42
127. Juric D, Tryggvason G (1996) A Front-Tracking Method for Dendritic Solidification. *J Comput Phys* 123:127-148
128. Juric D, Tryggvason G (1998) Computations of Boiling Flows. *Int J Multiphase Flow*. 24(3):387-410
129. Kolev NI (2002) *Multiphase Flow Dynamics 1: Fundamentals*. Springer, Berlin
130. Kuipers JAM, van Swaaij WPM (1997) Application of Computational Fluid Dynamics to Chemical Reaction Engineering. *Reviews in Chemical Engineering* 13 (3):1-118.
131. Kuo KK (1986) *Principles of Combustion*. John Wiley & Sons, New York
132. Lafaurie B, Nardone C, Scardovelli R, Zaleski S, Zanetti G (1994) Modelling Merging and Fragmentation in Multiphase Flows with SURFER. *J Comput Phys* 113:134-147.
133. Lafi AY, Reyes JN (1994). General particle transport equations. Final Report OSU-NE-9409. Department of Nuclear Engineering, Oregon State University
134. Lahey RT Jr, Cheng LY, Drew DA, Flaherty JE (1980) The effect of virtual mass on the numerical stability of accelerating two-phase flows. *Int J Multiphase Flow* 6:281-294
135. Lahey RT Jr, Drew DA (1989) The Three-Dimensional Time-and Volume Averaged Conservation Equations of Two -Phase Flow. *Advances in Nuclear Science and Technology* 20:1-69
136. Lahey RT Jr (1992) The prediction of phase distribution and separation phenomena using two-fluid models. In: Lahey RT Jr (ed) *Boiling Heat Transfer*. Elsevier Science Publishers BV
137. Lahey RT Jr, Drew DA (1992) On the Development of Multidimensional Two-Fluid Models for Vapor/Liquid Two-Phase Flows. *Chem Eng Comm* 118: 125-139
138. Laplace PS (1806) *Traité de Mécanique Céleste*. Supplement to book 10, Vol. IV. Paris: Gauthier-Villars, 1806. Annotated English translation by Nathaniel Bowditch (1839). Reprinted by New York: Chelsea Publishing Company, 1996
139. Laux H (1998) Modeling of dilute and dense dispersed fluid-particle flow. Dr Ing Thesis, Norwegian University of Science and Technology, Trondheim, Norway
140. Leonard BP, Drummond JE (1995) Why you should not use 'Hybrid', 'Power-Law' or related exponential schemes for convective modelling - There are much better alternatives. *Int J for Numerical Methods in Fluids* 20:421-442.

141. Li Y, Zhang J, Fan L-S (1999) Numerical simulation of gas-liquid-solid fluidization systems using a combined CFD-VOF-DPM method: bubble wake behavior. *Chem Eng Sci* 54:5101-5107.
142. Liljegren LM (1997) Ensemble-Average Equations of a Particulate Mixture. *J Fluids Engr* 119:428-434
143. Lopez de Bertodano M (1992) Turbulent Bubbly Two-Phase Flow in a Triangular Duct. PhD Thesis, Rensselaer Polytechnic Institute, Troy, NY
144. Lyckowski RW, Gidaspow D, Solbrig CW, Hughes ED (1978) Characteristics and stability analysis of transient one-dimensional two-phase flow equation and their finite difference approximations. *Nucl Sci Engrg* 66:378-396
145. Manninen M, Taivassalo V, Kallio S (1996) On the mixture model for multi-phase flow. Technical Research Center of Finland: VIT Publications, Espoo.
146. Mavrouniotis GM, Brenner H (1993) A Micromechanical Investigation of Interfacial Transport Processes. I. Interfacial Conservation Equations. *Phil Trans R Soc Lond A* 345:165-207
147. Mavrouniotis GM, Brenner H, Edwards DA, Ting L (1993) A Micromechanical Investigation of Interfacial Transport Processes. II. Interfacial Constitutive Equations. *Phil Trans R Soc Lond A* 345:209-228
148. Maxey MR, Riley JJ (1983) Equation of motion for a a mall rigid sphere in a non-uniform flow. *Phys Fluids* 26 (4):883-889.
149. Meier M, Andreani M, Smith B, Yadigaroglu G (1998) Numerical and Experimental Study of Large Stream-Air Bubbles Condensing in Water. *Proc Third Int Conf Multiphase Flow*, Lyon, June 8-12
150. Miller CA, Neogi P (1985) *Interfacial Phenomena: Equilibrium and Dynamic Effects*. Marcel Dekker, Inc., New York and Basel
151. Moeckel GP (1975) Thermodynamics of an Interface. *Arch ration Mech Analysis* 57:255-280
152. Mostafa AA, Mongia HC (1987) On the modeling of turbulent evaporating sprays: Eulerian versus Lagrangian approach. *Int J Heat Mass Transfer* 30 (12):2583-2593.
153. Ni J, Beckermann C (1990) A Two-Phase Model for Mass, Momentum, Heat, and Species Transport during Solidification. In: Charmchi M, Chyu MK, Joshi Y, Walsh SM (eds) *Transport Phenomena in Material Processing*, New York. ASME HTD-VOL. 132:45-56
154. Ni J, Beckermann C (1991) A Volume-Averaged Two-Phase Model for Transport Phenomena during Solidification. *Metallurgical Transactions B* 22B: 349-361
155. Nichols BD, Hirt CW (1975) Methods for Calculating Multi-Dimensional, Transient, Free Surface Flows Past Bodies. *Proceedings First Intern Conf Num Ship Hydrodynamics*, Gaithersburg, Md, October.
156. Nigmatulin RI (1979) Spatial averaging in the mechanics of heterogeneous and dispersed systems. *Int J of Multiphase Flow* 5:353-385
157. Nigmatulin RI, Lahey RT Jr, Drew DA (1996) On the Different Forms of Momentum Equations and on the Intra- and Interphase Interaction in the Hydromechanics of a Monodispersed Mixture. *Chem Eng Comm* 141-142: 287-302
158. Nobari MR, Jan Y-J, Tryggvason G (1996) Head-on collision of droplets - A numerical investigation. *Phys Fluids* 8(1):29-42
159. Pan Y, Suga K (2005) Numerical simulation of binary liquid droplet collision. *Phys Fluids* 17 (8):82105-082105-14

160. Patankar SV (1980) Numerical heat transfer and fluid flow. Series in Computational Methods in Mechanics and Thermal Sciences, Hemisphere publishing corporation, New York.
161. Pauchon C, Banerjee S (1986) Interface momentum interaction effects in the averaged multifield model. Part I: Void propagation in bubbly flows. *Int J Multiphase Flow* 12(4):559-573
162. Pauchon C, Banerjee S (1988) Interphase momentum interaction effects in the averaged multifield model, Part II: Kinematic waves and interfacial drag in bubbly flows. *Int J Multiphase Flow* 14(3):253-264
163. Poirier DR, Nandapurkar PJ, Ganesan S (1991) The Energy and Solute Conservation Equation for Dendritic Solidification. *Metallurgical Transactions B* 22B: 889-900
164. Popinet S, Zaleski S (1999) A Front-Tracking Algorithm for Accurate Representation of Surface Tension. *Int J Numer Meth Fluids* 30:775-793.
165. Prescott PJ, Incropera FP (1994) Convective Transport Phenomena and Macrosegregation During Solidification of a Binary Metal Alloy: I-Numerical Predictions. *J Heat Transfer* 116:735-749
166. Probstain RF (1994) *Physicochemical Hydrodynamics: An Introduction*, Second edition, John Wiley & Sons, Inc, New York
167. Prosperetti A, van Wijngaarden L (1976) On the characteristics of the equation of motion for bubbly flow and the related problem of critical flow. *Journal of Engineering Math* 10(2):153-162
168. Prosperetti A, Jones AV (1984) Pressure forces in dispersed two-phase flow. *Int Journal of Multiphase Flow* 10(4):425-440
169. Prosperetti A, Zhang DZ (1996) Disperse Phase Stress in Two-Phase Flow. *Chem Eng Comm* 141-142:387-398
170. Qian J, Tryggvason G, Law CK (1998) A Front Tracking Method for the Motion of Premixed Flames. *J Comput Phys* 144:52-69
171. Quintard M, Whitaker S (1993) Transport in Ordered and Disordered Porous Media: Volume-Averaged Equations, Closure Problems, and Comparisons with Experiments. *Chem Eng Sci* 48(14):2537-2564
172. Ramshaw JD, Trapp JA (1978) Characteristics, stability and short wavelength phenomena in two-phase flow equation systems. *Nucl Sci Engng* 66:93-102
173. Ransom VH, Ramshaw JD (1988) Discrete Modeling Considerations in Multiphase Fluid Dynamics. Japan - U.S. Seminar on Two-Phase Flow Dynamics, Kyoto, Japan, 15. July.
174. Raupach MR, Shaw RH (1982) Averaging Procedures for Flow within Vegetation Canopies. *Boundary Layer Meteorology* 22:79-90
175. Reeks MW (1991) On a kinetic equation for the transport of particles in turbulent flows. *Physics of Fluids A* 3:446-456
176. Reyes Jr JN (1989) Statistically derived conservation equations for fluid particle flows. Proc ANS Winter Meeting, Nuclear Thermal Hydraulics, 5th Winter Meeting
177. Reynolds O (1895) On the dynamical theory of incompressible viscous fluids and the determination of the criterion. *Philos Trans Roy Soc London A*186:123-164
178. Richtmyer RD, Morton KW (1957) *Difference Methods for Initial-Value Problems*. Second Edition, Interscience Publishers (John Wiley & Sons), New York
179. Rider WJ, Kothe DB (1995) Stretching and Tearing Interface Tracking Methods. AIAA paper 95-1717, pp. 806-816.

180. Rider WJ, Kothe DB (1998) Reconstructing Volume Tracking. *J Comput Phys* 141:112-152.
181. Roberts IF (1997) Conservation Equations, Two-Phase. *Int Encyclopedia of Heat and Mass Transfer*, pp. 223-230
182. Sanyal J, Vásquez S, Roy S, Dudukovic MP (1999) Numerical simulation of gas-liquid dynamics in cylindrical bubble column reactors. *Chem Eng Sci* 54:5071-5083
183. Scardovelli R, Zaleski S (1999) Direct Numerical Simulation of Free-Surface and Interfacial Flow. *Annu Rev Fluid Mech* 31:567-603
184. Schwartz MP, Turner WJ (1988) Applicability of the standard  $k-\epsilon$  turbulence model to gas-stirred baths. *Appl Math Modelling* 12:273-279
185. Scriven LE (1960) Dynamics of a fluid interface. *Chem Eng Sci* 12:98-108
186. Sethian JA (1996) *Level Set Methods*. Cambridge University Press, Cambridge.
187. Sha WT, Soo SL (1978) Multidomain Multiphase Fluid Mechanics. *Int J Heat Mass Transfer* 21:1581-1595
188. Sha WT, Soo SL (1979) Brief Communication: On the effect of  $p\nabla\alpha$  term in multiphase mechanics. *Int J Multiphase Flow* 5:153-158
189. Sha WT, Slattery JC (1980) Local Volume-Time Averaged Equations of Motion for Dispersed, Turbulent, Multiphase Flows. NUREG/CR-1491, ANL-80-51
190. Sha WT, Chao BT, Soo SL (1983) Averaging Procedures of Multiphase Conservation Equations. *Transactions of the American Nuclear Society* 45:814-816
191. Sha WT, Chao BT, Soo SL (1983) Time Averaging of Volume-Averaged Conservation Equations of Multiphase Flow. *AICHE Symposium Series* 79(225):420-426
192. Sha WT, Chao BT, Soo SL (1984) Porous-Media Formulation for Multiphase Flow with Heat Transfer. *Nuclear Engineering and Design* 82:93-106
193. Shyy W, Thakur S, Ouyang H, Liu J, Blosch E (1997) *Computational Techniques for Complex Transport Phenomena*. Cambridge University Press, Cambridge
194. Slattery JC (1967) Flow of Viscoelastic Fluids Through Porous Media. *AICHE J* 13(6):1066-1071
195. Slattery JC (1969) Single-Phase Flow through Porous Media. *AICHE J* 15(6):866-872
196. Slattery JC (1972) *Momentum, Energy, and Mass Transfer in Continua*. Second Edition, McGraw-Hill Kogakusha, LTD, Tokyo
197. Slattery JC (1980) Invited Review: Interfacial Transport Phenomena. *Chem Eng Sci* 4:149-166
198. Slattery JC, Flumerfelt RW (1982) Interfacial Phenomena. In: Hetsroni G (ed) *Handbook of Multiphase Systems*, Section 1.4, pp. (1-224) - (1-2246), McGraw-Hill, New York
199. Slattery JC (1990) *Interfacial Transport Phenomena*. Springer-Verlag, New York
200. Slattery JC (1999) *Advanced Transport Phenomena*. Cambridge University Press, New York
201. Sokolichin A, Eigenberger G, Lapin A, Lübbert A (1997) Dynamic numerical simulations of gas-liquid two-phase flows. Euler/Euler versus Euler/Lagrange. *Chem Eng Sci* 52 (4):611-626.

202. Sokolichin A, Eigenberger G (1999) Applicability of the standard  $k$ - $\epsilon$  turbulence model to the dynamic simulation of bubble columns: Part I. Detailed numerical simulations. *Chem Eng Sci* 54:2273-2284.
203. Sommerfeld M (2001) Validation of a stochastic Lagrangian modelling approach for inter-particle collisions in homogeneous isotropic turbulence. *Int J Multiphase Flow* 27:1829-1858
204. Soo SL (1967) *Fluid Dynamics of Multiphase Systems*. Blaisdell Publishing Company, Waltham, Massachusetts
205. Soo SL (1989) *Particles and Continuum: Multiphase Fluid Dynamics*. Hemisphere Publishing Corporation, New York
206. Soo SL (1990) *Multiphase Fluid Dynamics*. Science Press, Beijing and Gower Technical, Aldershot
207. Spalding DB (1977) The Calculation of Free-Convection Phenomena in Gas-Liquid Mixtures. ICHMT Seminar 1976. Published in: *Turbulent Buoyant Convection*, Hemisphere, Washington, pp. 569-586.
208. Spalding DB (1980) Numerical Computation of Multi-Phase Fluid Flow and Heat Transfer. In: Taylor C. et al. (eds) *Recent Advances in Numerical Methods in Fluids*. Pineridge Press, pp. 139-167.
209. Spalding DB (1980) Mathematical Methods in Nuclear Reactor Thermal Hydraulics. In: Lahey RT (ed) *Proceedings of ANS Meeting on Nuclear Reactor Thermal Hydraulics*, Saratoga, N. Y., pp. 1979-2023.
210. Spalding DB (1981) *IPSA 1981; New Developments and Computed Results*. HTS/81/2, Imperial College of Science and Technology, London, 1981.
211. Spalding DB (1985) Computer Simulation of Two-Phase Flows, with Special Reference to Nuclear-Reactor Systems. In: Lewis RW, Morgan K, Johanson JA, Smith WR (eds) *Computational Techniques in heat Transfer*, pp. 1-44.
212. Stewart HB, Wendroff B (1984) Two-Phase Flow: Models and Methods. *J Comput Phys* 56:363-409
213. Stuhmiller JH (1977) The Influence of interfacial pressure forces on the character of two-phase flow model equations. *Int J Multiphase Flow* 3:551-560
214. Sussman M, Smereka P, Osher S (1994) A Level-Set Approach for Computing Solutions to Incompressible Two-Phase Flow. *J Comput Phys* 114:146-159.
215. Sussman M, Smereka P (1997) Axisymmetric free boundary problems. *J Fluid Mech* 341:269-294.
216. Tayebi D, Svendsen HF, Jakobsen HA, Grislingås A (2001) Measurement Techniques and Data Interpretations for Validating CFD Multiphase Reactor Models. *Chem Eng Comm* 186:57-159
217. Thomas GB Jr, Finney RL (1996) *Calculus and Analytic Geometry*. Addison-Wesley Publishing Company, 9th Edition, Reading, Massachusetts
218. Tomiyama A, Miyoshi K, Tamai H, Zun I, Sakaguchi T (1998) A bubble tracking method for the prediction of spatial evolution of bubble flow in a vertical pipe. *Third International Conference on Multiphase Flow*, Lyon, France
219. Trapp JA (1986) The mean flow character of two-phase flow equations. *Int J Multiphase Flow* 12(2):263-276
220. Travis JR, Harlow FH, Amsden AA (1976) Numerical calculations of two-phase flows. *Nucl Sci Engng* 61:1-10
221. Tryggvason G, Bunner B, Esmaeeli A, Mortazavi S (1998) Direct numerical simulations of dispersed flows. *Third International Conference on Multiphase Flow*, ICMF'98, Lyon, France, June 8-12.

222. Tryggvason G (1999) Embedded Interface Methods Applications. In: Modelling and Computation of Multiphase Flows, Short Course, Zurich, Switzerland, March 8-12, 16B:1-27.
223. Tryggvason G (1999) Embedded Interface Methods Applications. In: Modelling and Computation of Multiphase Flows, Short Course, Zurich, Switzerland, March 8-12, 18B:1-24.
224. Tryggvason G, Bunner B, Esmaeeli A, Juric D, Al-Rawahi N, Tauber W, Han J, Nas S, Jan Y-J (2001) A Front-Tracking Method for the Computations of Multiphase Flow. *J Comput Phys* 169:708-759
225. Tryggvason G, Esmaeeli A, Al-Rawahi N (2005) Direct numerical simulations of flows with phase change. *Computers and Structures* 83:445-453
226. Ubbink O, Issa I (1999) A method for capturing sharp fluid interfaces on arbitrary meshes. *J Comput Phys* 153:26-50
227. Unverdi SO, Tryggvason G (1992) A Front-Tracking Method for Viscous, Incompressible, Multi-Fluid Flows. *J Comput Phys* 100:25-37.
228. Unverdi SO, Tryggvason G (1992) Computations of multi-fluid flows. *Physica D* 60:70-83, North-Holland
229. Vernier P, Delhaye JM (1968) General two-phase flow equations applied to the thermo-hydrodynamics of boiling water nuclear reactors. *Energie Primare* 4(1-2):
230. Voller VR, Brent AD, Prakash C (1989) The modelling of heat, mass and solute transport in solidification systems. *Int J Heat Transfer* 32(9):1719-1731
231. Wallis GB (1969) One-dimensional Two-phase Flow. McGraw-Hill Book Company, New York
232. Weatherburn CE (1927) *Differential Geometry of Three Dimensions*. Cambridge University Press, Cambridge
233. Whitaker S (1967) Diffusion and Dispersion in Porous Media. *AIChE J* 13(3):420-427
234. Whitaker S (1968) *Introduction to Fluid Mechanics*. Prentice-Hall, Inc., Englewood Cliffs
235. Whitaker S (1969) Fluid Motion in Porous Media. *Industrial and Engineering Chemistry*. 61(12): 15-28
236. Whitaker S (1973) The Transport Equations for Multiphase Systems. *Chem Eng Sci* 28:139-147
237. Whitaker S (1985) A Simple Geometrical Derivation of the Spatial Averaging Theorem. *Chemical Engineering Education*, pp. 18-21 and pp. 50-52
238. Whitaker S (1992) The species mass jump condition at a singular surface. *Chem Eng Sci* 47(7):1677-1685
239. Whitaker S (1999) *The Method of Volume Averaging*. Kluwer Academic Publishers, Dordrecht
240. White FM (1974) *Viscous Fluid Flow*. McGraw-Hill, New York
241. Willmore TJ (1961) *An Introduction to Differential Geometry*. Oxford University Press, Glasgow
242. Wright K, Cygan RT, Slater B (2001) Structure of the (1014) surfaces of calcite, dolomite and magnesite under wet and dry conditions. *Phys Chem Chem Phys* 3:839-844
243. Yadigaroglu G, Lahey RT Jr (1976) On the Various Forms of the Conservation Equations in Two-Phase Flow. *Int J Multiphase Flow* 2:477-494
244. Young T (1805) An essay on the cohesion of fluids. *Phil Trans Roy Soc London* 95:65-87

245. Zaleski S (1999) Multiphase-Flow CFD with Volume of Fluid (VOF) Methods. In: *Modelling and Computation of Multiphase Flows, Short Course, Zurich, Switzerland, March 8-12*, 15B/17B:1-43.
246. Zaprjanov Z, Tabakova S (1999) *Dynamics of Bubbles, Drops and Rigid Particles*. Kluwer Academic Publishers, Dordrecht
247. Zhang DZ, Prosperetti A (1994) Ensemble phase-average equations for bubbly flows. *Phys Fluids* 6(9):2956-2970
248. Zhang DZ, Prosperetti A (1994) Averaged equations for inviscid disperse two-phase flow. *J Fluid Mech* 267:185-219
249. Zhang DZ, Prosperetti A (1997) Momentum and Energy Equations for Disperse Two-Phase Flows and Their Closure for Dilute Suspensions. *Int J Multiphase Flow* 23(3):425-453
250. Zuber N, Findlay JA (1965) Average Volumetric Concentration in Two-Phase Flow Systems. *J Heat Transfer* 87:453-468

---

## Flows of Granular Materials

In this chapter the derivation of the governing macroscopic equations of granular flow are examined.

The standard references for the kinetic theory of granular flows consist of the papers by Savage and Jeffrey [65], Jenkins and Savage [31], Lun et al [49], Jenkins and Richman [32], Johnson and Jackson [35], Johnson et al [36], Ding and Gidaspow [16] and the book of Gidaspow [22]. In addition, several reviews of the kinetic theory of granular flow and papers presenting locally averaged equations of motion for a mixture of identical spherical particles might be suggested as supplementary reading. Among these reports are Anderson and Jackson [1], Campbell [10], Jenkins [34], Elghobashi [18], Boemer et al [9], Crow et al [12, 13], Sinclair [78], Hrenya and Sinclair [29], Jackson [30], Peirano and Leckner [60], and van Wachem et al [84, 85].

A *granular material* is defined as a collection of a large number of discrete solid particles in a vacuum. Granular flow might thus be referred to as a flow of a powder in a vacuum [22]. Nevertheless, at more relevant pressures the interstices between the particles are filled with at least one fluid, and thus, an industrial granular flow is a multiphase process. However, if the particles are closely packed or if they are much denser than the interstitial fluid, the particles alone, and not the fluid or the fluid-particle interactions, will play the greatest role in momentum transport within the material, in which case the interstitial fluid can be ignored in describing the flow behavior [10]. Flows of granular material are generally taken to fall into this limiting category and thus may be considered dispersed single-phase rather than multiphase flows. On the other hand, even so, for reactive systems like fluidized beds the interstitial fluid is normally of outmost importance because the interstitial fluid contains one or more of the reactants hence the transport processes within this phase has to be described in an appropriate manner to determine the chemical process operation.

In a granular material there are primarily three mechanisms by which the bulk stresses are generated. These are (i) dry friction, (ii) transport of momentum by particle translation like in dilute gases, and (iii) momentum

transport by particle interactions like in dense gases and liquids. In the past it was usually assumed that although all three mechanisms co-exist in most flow regimes, one of them will normally play a predominant role.

Depending on the local stress conditions, a granular material may behave either as an elastic solid or a fluid [10, 69]. The load supported by the elastic-solid systems is held locally by frictional bonds between the particles so the systems strength is limited to the loads that those bonds can support. When a sufficient number of the bonds have been overcome, the system will fail and begin to flow. The initial failure will consist of many-particle blocks moving relative to one another along shear bands that roughly follow stress characteristics through the material. If the motion occurs slowly, particles will stay in contact and interact frictionally with their neighbors over long periods of time. The failure will continue in this manner as long as the deformation remains fairly slow. This particle motion is characterized as the *quasi-static regime* of granular flow [10]. The dry friction stresses are of the quasi-static, rate independent, Coulomb, type as described in the soil mechanics literature [66, 68, 35, 36, 58, 79]. However, these quasi-static motions are not of primary interest for chemical reaction engineers and will thus be disregarded in the subsequent discussion. Nevertheless, there are several flows of practical interest that fall into the intermediate regime where both frictional contacts (1), particle translation (2) and particle-particle collisions (3) are all significant. To model such flows the momentum equation is normally extended including an extra stress so that the total stress is the linear sum of frictional, kinetic and collisional contributions, each calculated independently from constitutive expressions derived for the limits of pure frictional, pure kinetic, and pure collisional interactions, respectively. It is noted that the quasi-static stress models are still of empirical nature. Due to these additional stresses, the boundary conditions might also be adapted to the particular application. The other extreme is the *rapid-flow regime* which corresponds to high-speed flows, far beyond the initial failure [10]. In this case each particle moves freely instead of moving in many-particle blocks. This flow regime evolves naturally from the quasi-static regime if the motion becomes rapid enough to transfer enough energy to the particles in the vicinity of the local slip regions to break these particles free of their blocks. In this way the rapid flow regime regions might expand until every particle in the granular mass is moving independently. These flows are of great interest to chemical reactor engineers because the fluidized bed reactors are operated within this regime.

To model the latter type of flows an analogy between particle collisions in suspensions and molecular collisions in dense gases as described by the kinetic theory was proposed by Bagnold [2] in 1954. By employing a simple expression for the collision frequency of particles, Bagnold derived a relation for the repulsive pressure of particles for uniform shear flow. Nevertheless, the importance of the velocity fluctuations and the means by which they could be included in a properly formulated continuum theory were first exploited by Ogawa [56] and Ogawa et al [57].

Ogawa et al considered an analogy between the random motion of the granular particles and the thermal motion of molecules in the kinetic-theory picture of gases. In this view the velocity of each particle is decomposed into a sum of the mean velocity of the bulk material and an apparently random component to describe the motion of the particle relative to the mean. Furthermore, a fluctuation particle temperature, commonly referred to as the *granular temperature*, was defined as the mean kinetic energy of the particle velocity fluctuations. Moreover, they postulated that the mechanical energy of a granular flow is first transformed into random particle motion and then dissipated into internal energy.

Based on this hypothesis a balance law was formulated for the granular temperature that related the rate of change to the production by the mean flow shear, the heat like flux from one point to another in the flow, and the dissipation into thermal energy. The energy transport in granular flows can thus be interpreted as follows. The source of all the energy is the work done on the system, either by body forces or through the motion of the system boundaries. Shear work, as given by the product of the shear stress and the velocity gradient, performed on the system converts some of the kinetic energy of the mean motion into granular temperature which is the kinetic energy associated with the random particle velocities. Finally, the inelastic collisions between particles will dissipate away the granular temperature into thermodynamic heat. The magnitude of the granular temperature thus depends on the ratio of the temperature generation by shear work and its dissipation by collisional in-elasticity. To close the granular temperature equation the granular conductivity, granular dissipation and the mean granular stress must be related by constitutive assumptions to the mean density, mean velocity and the granular temperature in order to complete the theory.

In many ways the thermodynamic and granular temperatures play similar roles in governing the behavior of their respective systems. In particular, both temperatures generate pressures and govern the internal transport rates of mass, momentum, and energy.

Although no granular temperature equation was considered, Savage and Jeffrey [65] were the first to suggest that the kinetic theory for dense gases as proposed by Enskog [20] might be useful determining the stress tensor in a granular flow. In particular, Savage and Jeffery considered a collection of smooth, rigid, *elastic*, spherical particles in Couette flow. From elementary kinetic theory they recognize that in order to deduce explicit expressions for the stress tensor, it is necessary to determine the form of the complete pair-distribution function  $f^{(2)}$  at collision. It was assumed that the  $f^{(2)}$ -function can be expressed as a product of a configurational pair-correlation function and two single particle distribution functions. The configurational pair-correlation function represents a generalization of the more familiar radial distribution function. Bear in mind that the latter function is restricted to a gas at equilibrium in which there are no mean deformation so spatial homogeneity of the mean flow prevails. For non-equilibrium shear flows a

simple correction for anisotropy in the configurational pair-correlation function was made based on kinematic arguments. Furthermore, the single distribution function of each particle was approximated by the Maxwellian [32].

Jenkins and Savage [31] extended the preliminary kinetic theory of Savage and Jeffrey [65] considering slightly *inelastic* particles. Jenkins and Savage used Maxwell's [54] equations of transfer to derive local expressions for the balance of granular mass, granular linear momentum, granular temperature, and integral expressions for the stress, energy flux and energy dissipation terms therein. In order to evaluate these integrals and thereby close the transport equations it is again necessary to determine the complete pair-distribution function. In this case the preliminary distribution function proposed by Savage and Jeffrey [65] for elastic particles was modified reformulating the configurational pair-correlation function expression so that it depends linearly upon the rate of deformation. Besides, the granular temperature equation was taken into account to determine the local rate of change of the fluctuating energy considering the energy dissipation rate due to inelastic particle collisions. Moreover, to calculate the mean collisional rate of change of  $\psi$  per unit volume,  $\Delta(\psi)_{\text{Collision}}$ , several approximative closure relationships were introduced. Among these constitutive relations, the relative velocity component normal to the plane of contact is approximated and related to the corresponding component prior to the collision through (2.123). In addition, the complete pair-distribution function is approximated by a symmetric average obtained shifting the pair of spatial points at which it is evaluated through a first order Taylor expansion.

Lun et al [49] reviewed several granular flow theories for dense flows and proposed that the application of the classical granular theory might be extended making a unified model valid for both dilute and dense flows. A generalized model was thus established by incorporating the kinetic stresses and the kinetic fluctuation-energy flux in addition to the collisional stresses, the collisional fluctuation-energy flux and the collision rate of dissipation per unit volume in the classical dense flow formulation. The constitutive relations used were deduced assuming that the spherical particles are uniform, smooth, but slightly inelastic requiring that the coefficient of restitution is about unity. In addition, the component of relative velocity  $\mathbf{g}_{12}$  in the direction of  $\mathbf{k}$  was approximated by (2.123) in accordance with the work of Jenkins and Savage [31]. However, in contrast to previous work, in order to calculate the unknown fluxes by the concept of kinetic theory, Lun et al adopted the Enskog [20] dense gas pair-distribution function approximation. The collisional single distribution function therein was approximated using a scheme inspired by the Chapman-Enskog expansion method [11]. However, in this approach the parameters in the trail function were calculated by satisfying a few moment equations generated from an extended form of the Maxwell equation instead of using a Boltzmann type of equation.

It is emphasized that in the pioneering papers, mentioned above, simplified kinetic theories based on mechanically derived or intuitive relationships

were used to determine the distribution function in place of the Boltzmann equation. The complexity of formulating the Boltzmann equation accounting for the inter-particle collisions was a severe bottleneck that prevented the use of more rigorous kinetic theories describing the behavior of inelastic solid particles. In particular, the analogous results in kinetic theory of dense gases obtained using the reversibility of collisions are not valid anymore and must be re-derived.

A more elaborated extension of the kinetic theory of granular flows was proposed by Jenkins and Richman [32]. They showed that Grads [24] method of moments for determining the single particle distribution function of elastic molecular particles in dilute gases might be adapted and applied to dense systems of inelastic particles. By use of this method they extended the theory of Jenkins and Savage [31] and determined a supposedly more accurate form of the balance laws including the collisional transfers and productions of the velocity moments. Hence, as for the more familiar kinetic theory of a dilute gas, two distinct directions in the subsequent research on granular flow modeling emerged. One group of scientists followed closely the modeling ideas of Enskog [20] and solved the resulting Enskog equation by use of the Chapman-Enskog approximate method [11]. A second group of researchers followed roughly the modeling ideas of Enskog [20] but solved the Enskog like equations by the Grads [24] method of moments.

During the subsequent two or three decades a number of investigators include the drag into the governing equations for granular flows to generalize the treatment to multiphase flow [64, 16, 22, 42, 76]. In this case the interfacial momentum coupling is normally taken into account through the external force term. In general, the  $\mathbf{F}$  term includes the gravity, the external pressure gradient, the steady drag force, the added mass force, and several lift forces. The governing equations for the interstitial fluid phase are derived based on the continuum multi-fluid formulation and averaged in an appropriate manner as examined in sect 3.3.

Ding and Gidaspow [16], for example, derived a two-phase flow model starting with the Boltzmann equation for the distribution function of particles and incorporated fluid-particle interactions into the macroscopic equations. The governing equations were derived using the classical concepts of kinetic theory. However, to determine the constitutive equations they used the ad hoc distribution functions proposed by Savage and Jeffery [65]. The resulting macroscopic equations contain both kinetic - and collisional pressures but only the collisional deviatoric stresses. The model is thus primarily intended for dense particle flows.

Gidaspow [22] extended the work of Ding and Gidaspow [16] by deriving a modified set of approximative macroscopic conservation equations supposedly applicable for describing both dilute and dense granular flows. Again, following the classical concepts in kinetic theory, the Maxwell transport equation was formulated by the moment method starting out from the Boltzmann equation. Unlike the approach of Ding and Gidaspow [16], in this work the

kinetic and collisional transfer fluxes occurring in the governing equations were calculated in accordance with the Chapman-Enskog expansion method. However, each total transfer flux is approximated as a linear sum of the kinetic flux valid for dilute flows (i.e., as derived in accordance with the Enskog [20] dense gas approach) and the collisional flux contributions for dense flows. To determine the kinetic transfer fluxes for dilute suspensions the distribution function was determined from the Boltzmann equation with an inherent Enskog [20] dense gas collision operator considering *elastic* particles, whereas the collisional transfer fluxes were determined by approximating the distribution function from the modeled Boltzmann equation for dense suspensions consisting of *inelastic* particles.

The available continuum models for dispersed multi-phase flows thus follow one of two asymptotic approaches. The *dilute phase approach* is formulated based on the continuum mechanical principles in terms of the local conservation equations for each of the phases. A macroscopic model is then obtained by averaging the local equations based on an appropriate averaging procedure. In the *dense phase approach*, on the other hand, a kinetic theory description is adopted for the dispersed particulate phase (granular material), whereas an averaged continuum model formulation is adopted for the interstitial phase.

## 4.1 The Two-Fluid Granular Flow Model

The two-fluid granular flow model is formulated applying the classical Eulerian continuum concept for the continuous phase, while the governing equations of the particle phase are developed in accordance with the principles of kinetic theory. In this theory it is postulated that the particulate system can be represented considering a collection of identical, smooth, rigid spheres, adapting a Boltzmann type of equation. This microscopic balance describes the rate of change of the distribution function with respect to position and time.

The Boltzmann equation is generally expressed as [11]:

$$\frac{\partial f}{\partial t} + \mathbf{c} \cdot \nabla f + \nabla_{\mathbf{c}} \cdot (\mathbf{F}f) = \left( \frac{\partial f}{\partial t} \right)_{\text{Collision}} \quad (4.1)$$

The moment method can then be employed to derive a generalized equation of change for a mean particle property  $\langle \psi \rangle$  in the same manner as described in chap 2 for molecular systems. In particular, the generalized transport equation for  $\langle \psi(\mathbf{r}, t) \rangle$  is derived multiplying (4.1) by a microscopic quantity  $\psi(\mathbf{r}, \mathbf{c}, t)$  and integrating the resulting relation over the whole velocity space.

Suppose that  $\psi$  and  $f$  are expressed as functions of  $(\mathbf{r}, \mathbf{c}, t)$ , then a mathematical moment can be defined by the following ensemble average:

$$\langle \psi(\mathbf{r}, t) \rangle = \frac{1}{n(\mathbf{r}, t)} \int_{-\infty}^{\infty} \psi(\mathbf{r}, \mathbf{c}, t) f(\mathbf{r}, \mathbf{c}, t) d\mathbf{c} \quad (4.2)$$

where  $n$  is the number density of the particles. The moment  $\langle \psi(\mathbf{r}, t) \rangle$  denotes a macroscopic quantity.

To examine the derivation of the macroscopic equation throughly some further comments are needed. If we multiply (4.1) by  $\psi(t, \mathbf{r}, \mathbf{c})$  and there-after apply the chain rule to re-write the terms on the LHS, the intermediate result is:

$$\frac{\partial}{\partial t}(\psi f) - f \frac{\partial \psi}{\partial t} + \nabla \cdot (\mathbf{c} \psi f) - \mathbf{c} \cdot f \nabla \psi + \nabla_{\mathbf{c}} \cdot (\mathbf{F} \psi f) - (\mathbf{F} f) \cdot \nabla_{\mathbf{c}} \psi = \psi \left( \frac{\partial f}{\partial t} \right)_{\text{Collision}} \quad (4.3)$$

Integration over the whole velocity space yields:

$$\begin{aligned} & \frac{\partial}{\partial t} \int_{-\infty}^{\infty} (\psi f) d\mathbf{c} - \int_{-\infty}^{\infty} f \frac{\partial \psi}{\partial t} d\mathbf{c} + \nabla \cdot \int_{-\infty}^{\infty} (\mathbf{c} \psi f) d\mathbf{c} - \int \mathbf{c} \cdot f \nabla \psi d\mathbf{c} \\ & + \int_{-\infty}^{\infty} \nabla_{\mathbf{c}} \cdot (\mathbf{F} \psi f) d\mathbf{c} - \int_{-\infty}^{\infty} \mathbf{F} \cdot f \nabla_{\mathbf{c}} \psi d\mathbf{c} = \int_{-\infty}^{\infty} \psi \left( \frac{\partial f}{\partial t} \right)_{\text{Collision}} d\mathbf{c} \end{aligned} \quad (4.4)$$

The fifth term on LHS vanishes because  $[F_i f \psi]_{c_i=-\infty}^{c_i=\infty} = 0$ . It is assumed that the distribution function  $f$  converges to zero when the velocity in direction  $i$  becomes infinite.

In terms of moments on the form (4.2), relation (4.4) can be re-written as:

$$\begin{aligned} & \frac{\partial}{\partial t} (n \langle \psi \rangle) + \nabla \cdot (n \langle \mathbf{c} \psi \rangle) \\ & - n \left( \frac{\partial \langle \psi \rangle}{\partial t} + \langle \mathbf{c} \cdot \nabla \psi \rangle + \langle \mathbf{F} \cdot \nabla_{\mathbf{c}} \psi \rangle \right) = \Delta(\psi)_{\text{Collision}} \end{aligned} \quad (4.5)$$

in which  $\Delta(\psi)_{\text{Collision}} = \int \psi \left( \frac{\partial f}{\partial t} \right)_{\text{Collision}} d\mathbf{c}$  denotes the collisional rate of change of the macroscopic variable  $\langle \psi \rangle$ .

It is noted that in cases where the net external force  $\mathbf{F}$  is independent of  $\mathbf{c}$  it can be moved outside the averaging bracket. However, for granular flow the net external force is generally considered dependent on  $\mathbf{c}$  thus  $\mathbf{F}$  is kept inside the averaging operator.

#### 4.1.1 Collisional Rate of Change

In this section the derivation of the collision operators for dilute and dense suspensions are examined. Introductory the established formulas for dilute and dense gases consisting of elastic particles are outlined. Thereafter the kinetic theory of inelastic particles are considered.

It is explained in chap 2 that the Boltzmann equation is an equation of motion for the one-particle distribution function and is appropriate to a rare gas [86, 50]. In this particular case appropriate expressions for the collision

operator  $(\frac{\partial f}{\partial t})_{\text{Collision}}$  can be derived since the nature of the elastic interactions between the colliding particles is known. Enskog [20] extended the kinetic theory of dilute mono-atomic gases to slightly higher densities, as described in sect 2.11. In this approach Enskog adopted the molecular billiard ball model which assumes that the gas consists of a collection of identical, rigid, smooth and perfectly elastic spheres.

To elucidate the extended theory we refer to the derivation of the dilute gas collision operator and explain the important modifications that have to be introduced for dense gases. Basically, in order to calculate the collision rate of change we adopt similar principles as outlined for dilute gases in sects 2.4.3 and 2.4.2. However, a modified expression for the collision frequency is required.

To deduce the formula for the dense gas collision frequency a modified relation for the volume of the collision cylinder is required. As mentioned in chap 2, it is customary to consider the motion of particles 2 relative to the center of particles 1 (see Fig 2.2). For a binary molecular collision to occur the center of particle 2 must lie on the sphere of influence with radius  $d_{12}$  about the center of particle 1, see Fig 2.7. The radius of the sphere of influence is defined by (2.152). Besides, since the solid angle  $dk$  centered about the apse line  $\mathbf{k}$  is conveniently used in these calculations in which the billiard ball molecular model is adopted, it is also necessary to specify the direction of the line connecting the centers of the two particles at the instant of contact [86]. The two angles  $\theta$  and  $\phi$  are required for this purpose. Moreover, when the direction of the apse line lies in the range of  $\theta$ ,  $\phi$  and  $\theta + d\theta$ ,  $\phi + d\phi$ , at the instant of collision, the center of particle 2 must lie on the small rectangle  $da$  cut out on the sphere of influence of particle 1 by the angles  $d\theta$  and  $d\phi$ . The area of this rectangle is<sup>1</sup>:

$$da = (d_{12}d\theta)(d_{12}\sin\theta d\phi) = d_{12}^2 \sin\theta d\phi d\theta = d_{12}^2 dk \quad (4.6)$$

If such a collision occurs in a time  $dt$  so short that the possibility for the same particle to collide more than once during  $dt$  is negligible, then at the beginning of  $dt$  the particle must lie somewhere inside a cylinder with  $da$  as base. The sides of such a cylinder may not necessarily be perpendicular to the face  $da$ , hence the height is expressed as  $dl = (\mathbf{g}_{21} \cdot \mathbf{k}) dt = g_{21} dt \cos\theta$ . The volume of a single collision cylinder can thus be expressed by  $dv_{\text{single}} = dl \times da = [(\mathbf{g}_{21} \cdot \mathbf{k})dt] \times (d_{12}^2 dk)$ . Such a cylinder is associated with each of the  $f_1 d\mathbf{c}_1 d\mathbf{r}$  particles of the first kind having velocity within the range  $\mathbf{c}_1$  to  $\mathbf{c}_1 + d\mathbf{c}_1$  and being located in  $d\mathbf{r}$ . If  $da$  is small, it might be assumed that the cylinders do not overlap to any significant extent, so that the volume of all the cylinders  $dv_{\text{total}}$  is given by:

$$dv_{\text{total}} = (f_1 d\mathbf{c}_1 d\mathbf{r}) \times dv_{\text{single}} = f_1 (\mathbf{g}_{21} \cdot \mathbf{k}) d_{12}^2 dk d\mathbf{c}_1 d\mathbf{r} dt \quad (4.7)$$

<sup>1</sup> In the discussion of dilute gases in sect 2.4.2 the corresponding surface area element is determined by the product  $da = b db d\phi$ , as illustrated in Fig 2.10. For the billiard ball molecular model the link between the two surface element formulas when centered about the apse line is defined analogous to (2.159).

In many of these tiny cylinders there might be no particle of the second kind having velocity within the range  $\mathbf{c}_2$  to  $\mathbf{c}_2 + d\mathbf{c}_2$ . If  $da$  and  $d\mathbf{c}_2$  are sufficiently small, the possibility of two particles of type 2 in any of these cylinders can be neglected. Therefore, the total number of particles of type 2 in the whole gas volume  $dv_{\text{total}}$ , which we imagine consist of a set of tiny cylinders containing a particle of type 1, is determined by  $f_2 d\mathbf{c}_2 dv_{\text{total}}$ . In this way each collision cylinder in the gas which contains a particle of type 2 coincides with a collision of the specified type within  $d\mathbf{r}$  during the time period  $t$  to  $t + dt$ . Inserting the above expression for  $dv_{\text{total}}$  into  $f_2 d\mathbf{c}_2 dv_{\text{total}}$  and dividing by  $dt$ , the collision frequency can be calculated as:

$$N_{12} = f_1 f_2 (\mathbf{g}_{21} \cdot \mathbf{k}) d_{12}^2 dk d\mathbf{c}_1 d\mathbf{c}_2 d\mathbf{r} \quad (4.8)$$

This relation is consistent with (2.167), after dividing the latter relation by  $dt$ , and denotes the basis for the dense gas extensions made by Enskog as explained in sect 2.11.

To generalize the formulation of the collision frequency a collisional pair distribution function  $f^{(2)}(t, \mathbf{r}_1, \mathbf{c}_1, \mathbf{r}_2, \mathbf{c}_2)$  is sometimes introduced, following a slightly different approach than the one used in sect 2.11. This function is defined such that  $f^{(2)} d\mathbf{c}_1 d\mathbf{c}_2 d\mathbf{r}_1 d\mathbf{r}_2$  is the probability of finding a pair of particles 1 and 2 centered at  $\mathbf{r}_1, \mathbf{r}_2$  with a velocity  $\mathbf{c}_1, \mathbf{c}_2$  in the volume element  $d\mathbf{r}_1, d\mathbf{r}_2$  and the velocity range  $d\mathbf{c}_1, d\mathbf{c}_2$ , respectively.

For a dilute gas molecular chaos is assumed so the velocities of the two colliding particles are uncorrelated. The pair distribution function can then be expressed as the product of two single particle distribution functions  $f^{(2)} = f_1^{(1)} f_2^{(1)}$ . The number of binary collisions per unit time per unit volume  $N_{12}$  can then be expressed as follows:

$$N_{12} = f^{(2)}(t, \mathbf{r}_1, \mathbf{c}_1, \mathbf{r}_2, \mathbf{c}_2) (\mathbf{g}_{21} \cdot \mathbf{k}) d_{12}^2 dk d\mathbf{c}_1 d\mathbf{c}_2 d\mathbf{r} \quad (4.9)$$

A similar representation of the collision frequency is used in sect 2.4.3 deriving the Boltzmann equation for a dilute gas in a generalized manner.

In accordance with the ideas presented in sect 2.4.3, the corresponding dilute gas collision operator can be expressed analogous to (2.185). However, the operator is reformulated and defined in terms of  $\mathbf{k}$  because the billiard ball molecular model is adopted. The details of the transformation is explained in sect. 2.11. The result is:

$$\left(\frac{\partial f}{\partial t}\right)_{\text{Collision}} = \int [f'(\mathbf{r}, \mathbf{c}', t) f_1'(\mathbf{r}, \mathbf{c}'_1, t) - f(\mathbf{r}, \mathbf{c}, t) f_1(\mathbf{r}, \mathbf{c}_1, t)] d_{12}^2 (\mathbf{g} \cdot \mathbf{k}) dk d\mathbf{c}_1 \quad (4.10)$$

where the primed velocities are determined by (2.143) and (2.144).

Enskog [20] made two modifications to (4.9) in order to describe the frequency of collisions in a dense gas assumed to consist of rigid spheres, but the assumption of molecular chaos still prevails. Firstly, due to the finite size of

the colliding molecules, the centers of the two molecules are not at the same point any more. For two particles of equal diameters the collision contact point is now located at  $r + \frac{1}{2}d_{12}\mathbf{k}$ . The collision frequency expression is thus given by [20]:

$$N_{12} = f^{(2)}(t, \mathbf{r}, \mathbf{c}_1, \mathbf{r} + d_{12}\mathbf{k}, \mathbf{c}_2, t)(\mathbf{g}_{21} \cdot \mathbf{k})d_{12}^2dkd\mathbf{c}_1d\mathbf{c}_2d\mathbf{r} \quad (4.11)$$

Secondly, for a dense gas the volume of the molecules is comparable with the total volume occupied by the gas, so the free interstitial volume in which the center of any one molecule might be placed is reduced. The net effect is to increase the probability of a collision.

The pair distribution function is thus modified by a volume correction function [20] [11] (sects 16.2 to 16.4):

$$f^{(2)}(t, \mathbf{r}, \mathbf{c}_1, \mathbf{r} + d_{12}\mathbf{k}, \mathbf{c}_2) = \chi(\mathbf{r} + \frac{1}{2}d_{12}\mathbf{k})f^{(1)}(t, \mathbf{r}, \mathbf{c}_1)f^{(1)}(t, \mathbf{r} + d_{12}\mathbf{k}, \mathbf{c}_2) \quad (4.12)$$

where  $\chi$  is a quantity that is unity for ordinary gases, and increases with increasing density, becoming infinite as the gas approaches the state in which the molecules are packed so closely that motion is impossible (e.g. [11], Sect 16.2). The position of the point of collision can be expressed in different ways depending on the choice of origin, normally the center point of particle 1 is used.

The dense gas collision operator is also formulated in accordance with the ideas presented in sect 2.4.3, but in this case the generalized form (2.182) is adopted. After expressing the operator in terms of  $\mathbf{k}$ , the result is:

$$\begin{aligned} \left(\frac{\partial f}{\partial t}\right)_{\text{Collision}} &= \int_1 f'^{(2)}(\mathbf{r}', \mathbf{c}', \mathbf{r}'_1, \mathbf{c}'_1, t)(\mathbf{g}'_{21} \cdot \mathbf{k})d_{12}^2dkd\mathbf{c}_1 \\ &\quad - \int_1 f^{(2)}(\mathbf{r}, \mathbf{c}, \mathbf{r}_1, \mathbf{c}_1, t)(\mathbf{g}_{21} \cdot \mathbf{k})d_{12}^2dkd\mathbf{c}_1 \\ &= \int_1 \left(f'^{(2)}(\mathbf{g}'_{21} \cdot \mathbf{k}) - f^{(2)}(\mathbf{g}_{21} \cdot \mathbf{k})\right) d_{12}^2dkd\mathbf{c}_1 \end{aligned} \quad (4.13)$$

This operator formulation is similar to the one used in the Enskog equation (2.550). However, the simplifying assumption that the collisions are elastic is not yet introduced making the relation more general (i.e., at this stage  $\mathbf{g}'_{21}$  is not necessarily equal to  $\mathbf{g}_{21}$ ).

Savage and Jeffrey [65] and Jenkins and Savage [31] performed much of the pioneering work considering an extrapolation of the Enskog dense gas kinetic theory to granular flows. The collision operator of Enskog was modified because, as distinct from the elastic molecules, the particles are smooth but inelastic with a restitution coefficient  $e$ , ranging between zero and one [31]. On the other hand, the Enskog pair distribution function (4.12) was adopted in its original form. However, Savage and Jeffrey [65] associated the  $\chi$ -factor with a configurational pair-correlation function which for a gas at equilibrium reduces

to the radial distribution function denoting the ratio of the local number density at a distance  $r = |\mathbf{r}_2 - \mathbf{r}_1|$  from the central particle to the bulk number density. In other words, the radial distribution function,  $g_0 \geq 1$ , accounts for the increase of the binary collision probability when the suspension becomes denser. There are no way to determine an exact formula for this function, so numerous empirical parameterizations have been proposed.

Ding and Gidaspow [16], for example, proposed an empirical relation being a function of the particulate phase volume fraction to be used for granular flows in fluidized beds given by:

$$\chi(\mathbf{r} + \frac{1}{2}d_{12}\mathbf{k}) = g(\alpha_s) = \left[ 1 - \left( \frac{\alpha_s}{\alpha_{s,max}} \right)^{1/3} \right]^{-1} \quad (4.14)$$

To calculate the collisional rate of change for dense suspensions Gidaspow [22] adopted the dense gas collision operator (4.13), but in this case the particles are inelastic so  $\mathbf{g}'_{21}$  is related to  $\mathbf{g}_{21}$  through the empirical relation (2.123). The kinetic fluxes for dilute suspensions were determined adopting the dilute gas collision operator (4.10), valid for elastic particles, instead. For dense suspensions the kinetic fluxes were approximated by those deduced for dilute suspensions.

The collisional rate of change  $\Delta(\psi)_{\text{Collision}}$  of any particle property  $\psi$  is the integral over all possible binary collisions of the change in  $\psi$  in a particular collision multiplied by the probability frequency of such a collision. Hence, particle 1 gains  $\psi'_1 - \psi_1$  of the microscopic property  $\psi$  during the collision with particle 2. The primed and unprimed variables still refer to values of  $\psi$  after and before the collision. Thus, the net gain of  $\psi$  for particle 1 per unit volume and time for dilute systems becomes:

$$\Delta(\psi_1)_{\text{Collision}} = \int_{\mathbf{g}_{21} \cdot \mathbf{k} > 0} (\psi'_1 - \psi_1) f^{(2)}(t, \mathbf{r}, \mathbf{c}_1, \mathbf{r} + d_{12}\mathbf{k}, \mathbf{c}_2) (\mathbf{g}_{21} \cdot \mathbf{k}) d_{12}^2 d\mathbf{k} d\mathbf{c}_1 d\mathbf{c}_2 \quad (4.15)$$

where  $\mathbf{g}_{21} \cdot \mathbf{k} > 0$  indicates that the integration is to be taken over all values of  $\mathbf{k}$ ,  $\mathbf{c}_1$ , and  $\mathbf{c}_2$  considering only particles that are about to collide [31] [49] [32].

A similar expression for the collisional rate of change for particle 2 can be obtained. In this case we utilize the collision symmetry properties, so this relation is achieved by interchanging the labels 1 and 2 in (4.15) and replacing  $\mathbf{k}$  by  $-\mathbf{k}$ . As distinct from the previous analysis, to determine this probability frequency at the instant of a collision between particles labeled 1 and 2 we now take the center of the second particle to be located at position  $\mathbf{r}$  and the center of particle 1 to be at  $\mathbf{r} - d_{12}\mathbf{k}$ . This approach represents a collision dynamically identical but statistically different from the previous one [31] [49] [32]. The result is:

$$\Delta(\psi_2)_{\text{Collision}} = \int_{\mathbf{g}_{21} \cdot \mathbf{k} > 0} (\psi'_2 - \psi_2) f^{(2)}(\mathbf{r} - d_{12}\mathbf{k}, \mathbf{c}_1, \mathbf{r}, \mathbf{c}_2, t) (\mathbf{g}_{21} \cdot \mathbf{k}) d_{12}^2 d\mathbf{k} d\mathbf{c}_1 d\mathbf{c}_2 \quad (4.16)$$

Each of the integrals equals the collisional rate of change  $\Delta(\psi)_{\text{Collision}}$ , but a more symmetric expression of  $\Delta(\psi)_{\text{Collision}}$  might be achieved taking one half of the sum of (4.15) and (4.16) [31, 32].

The values of  $f^{(2)}$  separated by a distance  $d_{12}\mathbf{k}$  in (4.15) and (4.16) are related to each other by means of the Taylor series [49]:

$$f^{(2)}(t, \mathbf{r}, \mathbf{c}_1, \mathbf{r} + d_{12}\mathbf{k}, \mathbf{c}_2) = f^{(2)}(t, \mathbf{r} - d_{12}\mathbf{k}, \mathbf{c}_1, \mathbf{r}, \mathbf{c}_2) + (d_{12}\mathbf{k} \cdot \nabla) \sum_{m=0}^{\infty} \frac{(-d_{12}\mathbf{k} \cdot \nabla)^m}{(m+1)!} f^{(2)}(t, \mathbf{r}, \mathbf{c}_1, \mathbf{r} + d_{12}\mathbf{k}, \mathbf{c}_2) \quad (4.17)$$

By inserting  $f^{(2)}(t, \mathbf{r}, \mathbf{c}_1, \mathbf{r} + d_{12}\mathbf{k}, \mathbf{c}_2)$  from (4.17) into (4.15), adding the intermediate result to (4.16) and divide by 2, we obtain

$$\Delta(\psi)_{\text{Collision}} = \frac{1}{2} (\Delta(\psi_1)_{\text{Collision}} + \Delta(\psi_2)_{\text{Collision}}) = \Omega(\psi) - \nabla \cdot \Phi(\psi) \quad (4.18)$$

The source term  $\Omega(\psi)$  represents the loss of  $\psi$  caused by inelastic collisions. It is defined by:

$$\Omega(\psi) = \frac{d_{12}^2}{2} \int_{\mathbf{g}_{21} \cdot \mathbf{k} > 0} \Delta\psi f^2(\mathbf{r} - d_{12}\mathbf{k}, \mathbf{c}_1, \mathbf{r}, \mathbf{c}_2, t) (\mathbf{g}_{21} \cdot \mathbf{k}) d\mathbf{k} d\mathbf{c}_1 d\mathbf{c}_2 \quad (4.19)$$

with  $\Delta\psi = (\psi'_2 + \psi'_1) - (\psi_2 + \psi_1)$ .

The flux term represents the transfer of  $\psi$  during collisions. It is defined by:

$$\begin{aligned} \Phi(\psi) &= -\frac{d_{12}^3}{2} \int_{\mathbf{g}_{21} \cdot \mathbf{k} > 0} (\psi'_1 - \psi_1) \mathbf{k} \sum_{m=0}^{\infty} \frac{(-d_{12}\mathbf{k} \cdot \nabla)^m}{(m+1)!} \times \\ &\quad f^{(2)}(\mathbf{r}, \mathbf{c}_1, \mathbf{r} + d_{12}\mathbf{k}, \mathbf{c}_2, t) (\mathbf{g}_{21} \cdot \mathbf{k}) d\mathbf{k} d\mathbf{c}_1 d\mathbf{c}_2 \\ &\approx -\frac{d_{12}^3}{2} \int_{\mathbf{g}_{21} \cdot \mathbf{k} > 0} (\psi'_1 - \psi_1) \mathbf{k} f^{(2)}(\mathbf{r}, \mathbf{c}_1, \mathbf{r} + d_{12}\mathbf{k}, \mathbf{c}_2, t) (\mathbf{g}_{21} \cdot \mathbf{k}) d\mathbf{k} d\mathbf{c}_1 d\mathbf{c}_2 \end{aligned} \quad (4.20)$$

This relation represents a first order approximation to the flux since only the first term in the Taylor series is included.

To calculate the integrals defining the source term and the flux term, appropriate expressions for  $\Delta\psi$  and  $\psi'_1 - \psi_1$  have to be determined from an analysis of the inelastic binary particle collision dynamics.

### 4.1.2 Dynamics of Inelastic Binary Collisions

In this section the dynamics of inelastic binary particle collisions are examined. The theory represents a semi-empirical extension of the binary collision theory

of elastic particles described in sect 2.4.2. The aim is to determine expressions for the total change in the first and second moments of the particle velocity to be used deriving expressions for the collisional source (4.19) and flux (4.20) terms.

Consider an inelastic collision between two smooth identical spherical particles 1 and 2, of mass  $m$  and diameter  $d_p = d_{12}$  [32] [60]. If  $\mathbf{J}_{12}$  is the impulse of the force exerted by particle 1 on particle 2, the linear momentum balances over a collision relate the velocity vectors of the center of each sphere just before and after the collision through:

$$m\mathbf{c}_1 = m\mathbf{c}'_1 - \mathbf{J}_{12} \quad (4.21)$$

$$m\mathbf{c}_2 = m\mathbf{c}'_2 + \mathbf{J}_{12} \quad (4.22)$$

where  $\mathbf{c}'_1$  and  $\mathbf{c}'_2$  are the velocities of the particles just after the collision and  $\mathbf{c}_1$  and  $\mathbf{c}_2$  just before the collision.

The relative velocities of the centers of the spheres immediately before and after a collision are still given by (2.116).

For these inelastic particles it is required that the relative velocity component normal to the plane of contact,  $\mathbf{g}_{21} \cdot \mathbf{k}$  (before collision) and  $\mathbf{c}'_{21} \cdot \mathbf{k}$  (after collision) satisfy the empirical relation (2.123) [31]. If the restitution coefficient therein is equal to one, the collision is elastic, which means that there is no energy loss during collision. Otherwise the collision is inelastic, which means that there is energy dissipation during collision.

It is required that the component of the relative velocity perpendicular to the apse line should be unchanged in a collision, thus the impulse  $\mathbf{J}_{12}$  must act entirely in the  $\mathbf{k}$  direction. On this demand,  $\mathbf{J}_{12}$  can be determined from (4.21), (4.22) and (2.123). The impulse of the force exerted by particle 1 on particle 2 is given by:

$$\begin{aligned} 2\mathbf{J}_{12} &= m(\mathbf{c}_1 - \mathbf{c}_2) + m(\mathbf{c}'_2 - \mathbf{c}'_1) = m\mathbf{g}_{12} - m\mathbf{g}'_{12} \\ &= m(\mathbf{g}_{12} \cdot \mathbf{k})\mathbf{k} - m(\mathbf{g}'_{12} \cdot \mathbf{k})\mathbf{k} = m(1 + e)(\mathbf{g}_{21} \cdot \mathbf{k})\mathbf{k} \end{aligned} \quad (4.23)$$

The particle velocities just after collision can be expressed in terms of those just before collision in accordance with (4.21) and (4.22):

$$\mathbf{c}'_1 = \mathbf{c}_1 - \frac{1}{2}(1 + e)(\mathbf{g}_{12} \cdot \mathbf{k})\mathbf{k} \quad (4.24)$$

$$\mathbf{c}'_2 = \mathbf{c}_2 + \frac{1}{2}(1 + e)(\mathbf{g}_{12} \cdot \mathbf{k})\mathbf{k} \quad (4.25)$$

Expressions for the change in the velocity moments can thus be generated by repeated multiplication of the velocity quantities in (4.24) and (4.25). The change in the first and second moments are:

$$\mathbf{c}'_1 - \mathbf{c}_1 = -\frac{1}{m}\mathbf{J}_{12} = -\frac{1}{2}(1 + e)(\mathbf{g}_{21} \cdot \mathbf{k})\mathbf{k} \quad (4.26)$$

$$\mathbf{c}'_1 \mathbf{c}'_1 - \mathbf{c}_1 \mathbf{c}_1 = \frac{1}{2}(1+e)(\mathbf{g}_{12} \cdot \mathbf{k}) \left( \frac{1}{2}(1+e)(\mathbf{g}_{12} \cdot \mathbf{k}) \mathbf{k} \mathbf{k} - [\mathbf{k} \mathbf{c}_1 + (\mathbf{k} \mathbf{c}_1)^T] \right) \quad (4.27)$$

Similar expressions can be derived for the change in the velocity moments of particle 2.

The translational kinetic energy change during a binary particle collision  $\Delta E$  can be determined as the difference between the LHS and RHS of (2.108). After re-writing the result by use of (2.118), we get [22]:

$$2\Delta E = m_1 c_1'^2 + m_2 c_2'^2 - m_1 c_1^2 - m_2 c_2^2 = \frac{m_1 m_2}{m_c} (g_{12}'^2 - g_{12}^2) \quad (4.28)$$

Then, using (2.123) yields:

$$\Delta E = \frac{1}{2} \frac{m_1 m_2}{m_c} (e^2 - 1) (\mathbf{k} \cdot \mathbf{g}_{12})^2 \quad (4.29)$$

For the case of equal mass particles,  $m_1 = m_2 = m$ , the formula reduces to:

$$\Delta E = \frac{1}{4} m (e^2 - 1) (\mathbf{k} \cdot \mathbf{g}_{12})^2 \quad (4.30)$$

This expression coincides with the result of Jenkins and Savage [31].

The total change in the velocity moments can be deduced from (4.26) and (4.27), and expressed as:

$$\Delta(\mathbf{c}) = \mathbf{c}'_1 - \mathbf{c}_1 + \mathbf{c}'_2 - \mathbf{c}_2 = 0 \quad (4.31)$$

$$\begin{aligned} \Delta(\mathbf{c}\mathbf{c}) &= \mathbf{c}'_1 \mathbf{c}'_1 - \mathbf{c}_1 \mathbf{c}_1 + \mathbf{c}'_2 \mathbf{c}'_2 - \mathbf{c}_2 \mathbf{c}_2 \\ &= \frac{1}{2}(1+e)(\mathbf{g}_{12} \cdot \mathbf{k}) \left( (1+e)(\mathbf{g}_{12} \cdot \mathbf{k}) \mathbf{k} \mathbf{k} - [\mathbf{k} \mathbf{g}_{12} + (\mathbf{k} \mathbf{g}_{12})^T] \right) \end{aligned} \quad (4.32)$$

Similar expressions can also be derived for the fluctuating velocities.

### 4.1.3 Maxwell Transport Equation and Balance Laws

The Maxwell transport equation can be derived from (4.5) requiring that  $\psi(\mathbf{c})$  is a function of  $\mathbf{c}$  only. With (4.18), the Maxwell transport equation can be written as:

$$\frac{\partial}{\partial t} (n \langle \psi \rangle) + \nabla \cdot (n \langle \mathbf{c} \psi \rangle) - n \langle \mathbf{F} \cdot \nabla_{\mathbf{c}} \psi \rangle = \Omega(\psi) - \nabla \cdot \Phi(\psi) \quad (4.33)$$

in which  $\Omega(\psi)$  is given by (4.19) and  $\Phi(\psi)$  by (4.20). It is further noted that the terms  $\frac{\partial \psi}{\partial t}$  and  $\nabla \psi$  in (4.5) vanish because the local  $\psi(\mathbf{c})$  is now independent of  $t$  and  $\mathbf{r}$ .

**Continuity:**

Taking  $\psi = m$ , (4.33) yields the local form of the continuity equation for the granular material:

$$\frac{\partial \rho_d}{\partial t} + \nabla \cdot (\rho_d \mathbf{v}_d) = 0 \quad (4.34)$$

From (4.19) and (4.20) we conclude that  $\Omega(m) = \Phi(m) = 0$ .

**Momentum:**

Taking  $\psi = m\mathbf{c}$ , (4.33) yields the local form of the balance of linear momentum:

$$\frac{\partial}{\partial t}(\rho_d \mathbf{v}_d) + \nabla \cdot (\rho_d \langle \mathbf{c}\mathbf{c} \rangle) - \rho_d \langle \mathbf{F} \rangle = \Omega(m\mathbf{c}) - \nabla \cdot \Phi(m\mathbf{c}) \quad (4.35)$$

From (4.19) we conclude that  $\Omega(m\mathbf{c}) = 0$  because the  $m\mathbf{c}$  is a summational invariant (i.e., in a particle collision the momentum is conserved).

It is customary to introduce a total pressure tensor  $\mathbf{p}$  defined as the sum of a kinetic and a collisional pressure contribution:

$$\mathbf{p} = \mathbf{p}_{\text{kin}} + \mathbf{p}_{\text{coll}} = \rho_d \langle \mathbf{C}\mathbf{C} \rangle + \Phi(m\mathbf{c}) \quad (4.36)$$

The kinetic pressure term  $\mathbf{p}_{\text{kin}}$  can be deduced from the second term in the momentum balance after introducing the peculiar velocity (2.59). The second moment term is reformulated as follows:

$$\rho_d \langle \mathbf{c}\mathbf{c} \rangle = \rho_d \langle (\mathbf{C} + \mathbf{v}_d)(\mathbf{C} + \mathbf{v}_d) \rangle = \rho_d \langle \mathbf{C}\mathbf{C} \rangle + \rho_d \mathbf{v}_d \mathbf{v}_d \quad (4.37)$$

The last but one term on the RHS denotes kinetic pressure and the last term the convective momentum flux.

The collisional pressure term is defined in accordance with (4.20):

$$\begin{aligned} \mathbf{p}_{\text{coll}} &= \Phi(m\mathbf{c}) \\ &= -m \frac{d_{12}^3}{2} \int_{\mathbf{g}_{21} \cdot \mathbf{k} > 0} (\mathbf{c}'_1 - \mathbf{c}_1) \mathbf{k} f^{(2)}(\mathbf{r}, \mathbf{c}_1, \mathbf{r} + d_{12}\mathbf{k}, \mathbf{c}_2, t) (\mathbf{g}_{21} \cdot \mathbf{k}) d\mathbf{k} d\mathbf{c}_1 d\mathbf{c}_2 \end{aligned} \quad (4.38)$$

After introducing the derived quantities into the momentum balance, we get:

$$\frac{\partial}{\partial t}(\rho_d \mathbf{v}_d) + \nabla \cdot (\rho_d \mathbf{v}_d \mathbf{v}_d) - \rho_d \mathbf{F} = -\nabla \cdot \mathbf{p} \quad (4.39)$$

**The Granular temperature:**

Finally, taking  $\psi = \frac{1}{2}mc^2$  in (4.33), we get:

$$\frac{\partial}{\partial t} \left( \frac{\rho_d}{2} \langle c^2 \rangle \right) + \nabla \cdot \left( \frac{\rho_d}{2} \langle \mathbf{c} c^2 \rangle \right) - \frac{\rho}{2} \langle \mathbf{F} \cdot \nabla_{\mathbf{c}} (c^2) \rangle = \Omega \left( \frac{1}{2} m c^2 \right) - \nabla \cdot \mathbf{\Phi} \left( \frac{1}{2} m c^2 \right) \quad (4.40)$$

Introducing the peculiar velocity (2.59) we can re-write the terms to obtain more common forms. We first note that:

$$c^2 = \mathbf{c} \cdot \mathbf{c} = (\mathbf{C} + \mathbf{v}_d) \cdot (\mathbf{C} + \mathbf{v}_d) = C^2 + 2\mathbf{C} \cdot \mathbf{c} + v_d^2 \quad (4.41)$$

Then, we define the granular temperature which is given by the specific kinetic energy of the velocity fluctuations (i.e., the translational fluctuation energy):

$$\frac{3}{2}\theta = \frac{1}{2} \langle C^2 \rangle \quad (4.42)$$

It is noted that:

$$\mathbf{\Phi} \left( \frac{1}{2} m c^2 \right) = \mathbf{\Phi} \left( \frac{1}{2} m [C^2 + 2\mathbf{C} \cdot \mathbf{c} + v_d^2] \right) = \mathbf{v}_d \cdot \mathbf{p}_{\text{coll}} + \mathbf{q}_{\text{coll}} \quad (4.43)$$

since, in accordance with (4.20), it is customary to define:

$$\mathbf{\Phi} \left( \frac{1}{2} m C^2 \right) = \mathbf{q}_{\text{coll}} \quad (4.44)$$

$$\mathbf{\Phi} \left( \frac{1}{2} m [2\mathbf{C} \cdot \mathbf{c}] \right) = \mathbf{v}_d \cdot \mathbf{p}_{\text{coll}} \quad (4.45)$$

$$\mathbf{\Phi} \left( \frac{1}{2} m v_d^2 \right) = 0 \quad (4.46)$$

The last relationship is true because the macroscopic velocity is not changed in a microscopic particle collision as the microscopic particle momentum is conserved (i.e.,  $(v_d^2)' - v_d^2 = 0$ ).

The collisional source term  $\Omega(\frac{1}{2}mc^2)$  is given by (4.19) and expressed as:

$$\Omega \left( \frac{1}{2} m c^2 \right) = -\gamma \quad (4.47)$$

where  $\gamma$  is the rate of energy dissipation per unit volume due to inelastic collisions of smooth particles.

The kinetic part of the flux of fluctuation energy is defined by

$$\mathbf{q}_{\text{kin}} = \frac{1}{2} \rho \langle \mathbf{C} C^2 \rangle \quad (4.48)$$

Inserting these quantities into the Maxwell equation (4.33), in which  $\psi = \frac{1}{2}mc^2$ , the result is:

$$\begin{aligned} \frac{\partial}{\partial t} \left( \rho_d \left( \frac{3}{2} \theta + \frac{1}{2} v_d^2 \right) \right) + \nabla \cdot \left( \mathbf{q} + \rho \mathbf{v}_d \frac{3}{2} \theta + \mathbf{v}_d \cdot \mathbf{p} + \rho \mathbf{v}_d \frac{1}{2} v_d^2 \right) \\ = \rho \langle \mathbf{F} \cdot \mathbf{c} \rangle - \gamma \end{aligned} \quad (4.49)$$

where the total energy fluctuating flux is denoted by:

$$\mathbf{q} = \mathbf{q}_{\text{kin}} + \mathbf{q}_{\text{coll}} \quad (4.50)$$

An equation for the granular temperature can then be achieved by subtracting the mechanical energy equation from the above equation for the sum of the fluctuating and mean kinetic energy forms.

As shown for single phase flows in chap 1, the mechanical energy balance is obtained by taking the scalar vector product between the macroscopic velocity and the local momentum balance:

$$\mathbf{v}_d \cdot \left\{ \frac{\partial}{\partial t} (\rho_d \mathbf{v}_d) + \nabla \cdot (\rho_d \mathbf{v}_d \mathbf{v}_d) - \rho_d \mathbf{F} = -\nabla \cdot \mathbf{p} \right\} \quad (4.51)$$

Re-arranging the resulting relation gives:

$$\frac{\partial}{\partial t} (\rho_d \frac{1}{2} v_d^2) + \nabla \cdot (\rho_d \mathbf{v}_d \frac{1}{2} v_d^2) = -\mathbf{v}_d \cdot \nabla \cdot \mathbf{p} + \rho_d \mathbf{v}_d \cdot \mathbf{F} \quad (4.52)$$

A convenient short notation can be introduced in terms of the double dot tensor product [7]:

$$\mathbf{p} : \nabla \mathbf{v}_d = \nabla \cdot (\mathbf{p} \cdot \mathbf{v}_d) - \mathbf{v}_d \cdot \nabla \cdot \mathbf{p} \quad (4.53)$$

A convenient form of the macroscopic kinetic energy equation can be expressed as:

$$\frac{\partial}{\partial t} (\rho_d \frac{1}{2} v_d^2) + \nabla \cdot (\rho_d \mathbf{v}_d \frac{1}{2} v_d^2) = \mathbf{p} : \nabla \mathbf{v}_d - \nabla \cdot (\mathbf{p} \cdot \mathbf{v}_d) + \rho_d \mathbf{v}_d \cdot \mathbf{F} \quad (4.54)$$

The transport equation for the fluctuating kinetic energy expressed in terms of the granular temperature is achieved by subtracting the equation for the macroscopic kinetic energy from the equation for the sum of the fluctuating and macroscopic energy forms. The result is [16, 22]:

$$\begin{aligned} \frac{\partial}{\partial t} \left( \rho_d \frac{3}{2} \theta \right) + \nabla \cdot \left( \mathbf{v}_d \rho_d \frac{3}{2} \theta \right) = -\nabla \cdot \mathbf{q} - \mathbf{p} : \nabla \mathbf{v}_d \\ + \rho \langle \mathbf{F} \cdot \mathbf{c} \rangle - \rho \mathbf{v}_d \cdot \langle \mathbf{F} \rangle - \gamma \end{aligned} \quad (4.55)$$

The external force terms are retained in the given form to ensure that the effects of the interstitial fluid are included in a consistent manner. According to Reyes [64], Lafi and Reyes [42], Gidaspow [22], Simonin [76], among others, the net force exerted on a particle can be written on the form:

$$\mathbf{F} = \mathbf{F}_D - \frac{1}{\rho_d} \nabla p + \mathbf{g} \quad (4.56)$$

where the first term on the RHS is the steady drag term. The second term on RHS denotes the ratio of the macroscopic fluid pressure gradient and the density of the dispersed phase. The last term denotes the gravitational acceleration.

For granular flow (as distinct from the classical kinetic theory for a dilute gas) the net external force acting on the particle depends on the microscopic velocity because of the phase interaction terms introduced to consider the interstitial fluid behavior. However, the net force can be divided into two types of contributions, a set of external forces  $\mathbf{F}_e$  which are independent of  $\mathbf{c}$  and a separate steady drag force  $\mathbf{F}_D$ . Hence, the net force exerted on a particle is re-written as:

$$\mathbf{F} = \mathbf{F}_D + \mathbf{F}_e = \frac{1}{\tau_{cd}}(\mathbf{v}_c - \mathbf{c}) + \mathbf{F}_e \quad (4.57)$$

where  $\mathbf{F}_D = \frac{1}{\tau_{cd}}(\mathbf{v}_c - \mathbf{c})$  and  $\mathbf{F}_e = -\frac{1}{\rho_d}\nabla p + \mathbf{g}$ . The  $\mathbf{v}_c$  is the local instantaneous velocity of the interstitial fluid, and  $\tau_{cd}$  is the particle-to-fluid relaxation time.

For multiphase flows perturbed by the presence of particles to obtain a turbulence like behavior the local instantaneous velocity of the continuous phase can for example be decomposed adopting the Reynolds averaging procedure (i.e., other methods including time-, volume-, ensemble-, and Favre averaging have been used as well) and expressed as:  $\mathbf{v}_c = \mathbf{v}'_c + \langle \mathbf{v} \rangle_c$ , where  $\mathbf{v}'_c$  is the fluctuating component of the continuous phase velocity. Introducing the peculiar velocity for the dispersed phase this relation can be re-arranged as:

$$\mathbf{F} = \frac{1}{\tau_{cd}}(\langle \mathbf{v} \rangle_c - \mathbf{v}_d) + \frac{1}{\tau_{cd}}(\mathbf{v}'_c - \mathbf{C}) + \mathbf{F}_e \quad (4.58)$$

The second term on the RHS is often neglected due to a general lack of knowledge about the physics they represent.

#### 4.1.4 Transport Equation in Terms of Peculiar Velocity

In this section an alternative derivation of the governing equations for granular flow is examined. In this alternative method the peculiar velocity  $\mathbf{C}$ , instead of the microscopic particle velocity  $\mathbf{c}$ , is used as the independent variable in the particle property and distribution functions. The transformation of these functions and the governing equation follows standard mathematical procedures for changing the reference frame. The translational motion of an individual particle may be specified either by its microscopic velocity  $\mathbf{c}$  relative to a fixed or Galilean frame of reference, or by its velocity relative to a frame of reference moving with the local velocity of the granular material  $\mathbf{v}_d$ .

Experience has shown that one might benefit substantially from deriving the governing transport equations after having transformed the property and distribution functions so that they are dependent on the peculiar velocity variable (2.59) instead of the microscopic particle velocity  $\mathbf{c}$ . This means that the

basic functions  $\psi(\mathbf{r}, \mathbf{c}, t)$  and  $f(t, \mathbf{r}, \mathbf{c})$  in which  $(\mathbf{r}, \mathbf{c}, t)$  are the independent variables, have to be replaced by  $\psi(t, \mathbf{r}, \mathbf{C} + \mathbf{v}_d)$  and  $f(t, \mathbf{r}, \mathbf{C} + \mathbf{v}_d)$  where  $(t, \mathbf{r}, \mathbf{C})$  are now the independent variables. Compared to the previous derivation of the transport equations starting out from (4.5), the generalized balance formulation in the alternative frame is simpler because all the terms containing time and space derivatives of  $\psi$  vanish as the relevant properties are functions of  $\mathbf{C}$  only. This is particularly the case for the velocity moments of order 2 and higher because all the terms in the resulting equation appear directly in their desired form and do not require further manipulations.

To transform the mathematical operators when changing the reference frame, let  $f = f(\mathbf{r}, \mathbf{c}, t)$ ,  $f_C = f(\mathbf{r}, \mathbf{C}, t)$  and  $f(\mathbf{r}, \mathbf{c}, t) = f_C(\mathbf{r}, \mathbf{C}, t)$ . It is noted that by performing this frame transformation the interpretations of the mathematical operators  $\partial/\partial t$  and  $\nabla$  in the Boltzmann equation will change as well, because  $\mathbf{C}$ , not  $\mathbf{c}$ , is to be kept constant while performing the differentiation. Accordingly, due to the implicit dependence of  $f$  upon  $t$  and  $\mathbf{r}$  through the dependence of  $\mathbf{C}$  upon  $\mathbf{v}_d(\mathbf{r}, t)$  as expressed by (2.59), the chain rule theorem (e.g., [17], p 105 ; [11], pp. 48-49; [22]) has to be invoked to re-formulate the operators in an appropriate manner.

The chain rule provides a relation between the partial derivative of  $f$  with respect to the individual particle velocity  $\mathbf{c}$  and the partial derivative of  $f_C$  with respect to the peculiar velocity  $\mathbf{C}$ . To understand the forthcoming transformation it might be informative to specify explicitly the meaning of the partial derivatives.

In tensor notation we may write the theorem like:

$$\begin{aligned} \sum_i \frac{\partial f}{\partial c_i} \Big|_{t, r_i} &= \sum_i \frac{\partial f_C}{\partial C_i} \Big|_{t, r_i} \frac{\partial C_i}{\partial c_i} \Big|_{t, r_i} + \sum_i \frac{\partial f_C}{\partial r_i} \Big|_{t, C_i} \frac{\partial r_i}{\partial c_i} \Big|_{t, r_i} + \sum_i \frac{\partial f_C}{\partial t} \Big|_{r_i, C_i} \frac{\partial t}{\partial c_i} \Big|_{t, r_i} \\ &= \sum_i \frac{\partial f_C}{\partial C_i} \end{aligned} \tag{4.59}$$

where  $j \neq i$ . The terms  $\frac{\partial C_i}{\partial c_i} \Big|_{r_j, c_j}$ ,  $\frac{\partial r_i}{\partial c_i} \Big|_{r_j, c_j}$  and  $\frac{\partial t}{\partial c_i} \Big|_{r_j, c_j}$  are either zero by definition or calculated from (2.59)<sup>2</sup> which defines the relationships between the variables  $\mathbf{C}$ ,  $\mathbf{c}$ ,  $\mathbf{r}$ , and  $t$ .

In vector notation yields:

$$\nabla_c f = \nabla_C f_C \tag{4.60}$$

The chain rule can also be used to obtain a relation between the partial derivative of  $f$  with respect to time,  $t$ , and the partial derivative of  $f_C$  with respect to time,  $t$ . In tensor notation we may write the theorem like:

<sup>2</sup> It is noted that (2.59) can also be used in the opposite way too transforming the  $f_C$  back to  $f$ .

$$\begin{aligned}
\frac{\partial f}{\partial t}|_{r_i, c_i} &= \sum_i \frac{\partial f_C}{\partial C_i}|_{t, r_i} \frac{\partial C_i}{\partial t}|_{r_i, c_i} + \sum_i \frac{\partial f_C}{\partial r_i}|_{t, C_i} \frac{\partial r_i}{\partial t}|_{r_i, c_i} + \frac{\partial f_C}{\partial t}|_{r_i, C_i} \frac{\partial t}{\partial t}|_{r_i, c_i} \\
&= \sum_i \frac{\partial f_C}{\partial C_i}|_{t, r_i} \frac{\partial(c_i - v_{i,d})}{\partial t}|_{r_i, c_i} + 0 + \frac{\partial f_C}{\partial t}|_{r_i, C_i} \\
&= - \sum_i \frac{\partial f_C}{\partial C_i} \frac{\partial v_{i,d}}{\partial t} + \frac{\partial f_C}{\partial t}
\end{aligned} \tag{4.61}$$

The terms  $\frac{\partial C_i}{\partial t}|_{r_i, c_i}$ ,  $\frac{\partial r_i}{\partial t}|_{r_i, c_i}$  and  $\frac{\partial t}{\partial t}|_{r_i, c_i}$  are either zero by definition or calculated from (2.59) which defines the relationships between the variables  $\mathbf{C}$ ,  $\mathbf{c}$ ,  $\mathbf{r}$ , and  $t$ .

In vector notation yields:

$$\frac{\partial f}{\partial t} = \frac{\partial f_C}{\partial t} - \nabla_C f_C \cdot \frac{\partial \mathbf{v}_d}{\partial t} \tag{4.62}$$

To deduce a relation between the partial derivative of  $f$  with respect to the physical space coordinates,  $r_i$ , and the partial derivative of  $f_C$  with respect to the physical space coordinates,  $r_i$ , the chain rule is invoked again.

In tensor notation we may write the theorem like:

$$\begin{aligned}
\sum_i \frac{\partial f}{\partial r_i}|_{t, c_i} &= \sum_i \frac{\partial f_C}{\partial C_i}|_{t, r_i} \frac{\partial C_i}{\partial r_i}|_{t, c_i} + \sum_i \frac{\partial f_C}{\partial r_i}|_{t, C_i} \frac{\partial r_i}{\partial r_i}|_{t, c_i} + \sum_i \frac{\partial f_C}{\partial t}|_{r_i, C_i} \frac{\partial t}{\partial r_i}|_{t, c_i} \\
&= \sum_i \frac{\partial f_C}{\partial C_i}|_{t, r_i} \frac{\partial(c_i - v_{i,d})}{\partial r_i}|_{t, c_i} + \sum_i \frac{\partial f_C}{\partial r_i}|_{t, C_i} + 0 \\
&= - \sum_i \frac{\partial f_C}{\partial C_i} \frac{\partial v_{i,d}}{\partial r_i} + \sum_i \frac{\partial f_C}{\partial r_i}
\end{aligned} \tag{4.63}$$

The terms  $\frac{\partial C_i}{\partial r_i}|_{t, c_i}$ ,  $\frac{\partial r_i}{\partial r_i}|_{t, c_i}$  and  $\frac{\partial t}{\partial r_i}|_{t, c_i}$  are either zero by definition or calculated from (2.59) which defines the relationships between the variables  $\mathbf{C}$ ,  $\mathbf{c}$ ,  $\mathbf{r}$ , and  $t$ .

In vector notation yields :

$$\nabla f = \nabla f_C - \nabla_C f_C \cdot \nabla \mathbf{v}_d \tag{4.64}$$

The LHS of the Boltzmann equation (4.1) can thus be expressed as:

$$\frac{\partial f_C}{\partial t} - \nabla_C f_C \cdot \frac{\partial \mathbf{v}_d}{\partial t} + (\mathbf{C} + \mathbf{v}_d) \cdot (\nabla f_C - \nabla_C f_C \cdot \nabla \mathbf{v}_d) + \nabla_C \cdot (\mathbf{F} f_C) \tag{4.65}$$

Introducing the substantial derivative, defined by the average velocity  $\mathbf{v}_d$ , one obtains:

$$\frac{Df_C}{Dt} + \mathbf{C} \cdot \nabla f_C - \frac{D\mathbf{v}_d}{Dt} \cdot \nabla_C f_C - (\mathbf{C} \nabla_C f_C) : \nabla \mathbf{v}_d + \nabla_C \cdot (\mathbf{F} f_C) \tag{4.66}$$

Subsequently, a modified transport equation for a quantity  $\psi(\mathbf{C})$  can be derived by the moment method. To proceed we multiply the LHS of the modified Boltzmann equation (4.66) with  $\psi$  and thereafter integrate the resulting equation over the velocity space  $d\mathbf{C}$ . Integration over  $\mathbf{C}$  is equivalent to integration over  $\mathbf{c}$ , as the two vectors differ only by a vector which is independent of  $\mathbf{c}$  and  $\mathbf{C}$  and the integration is performed over the whole velocity space [39] (p 457). The various integral terms deduced from (4.66) can be transformed by means of the following relations:

$$\begin{aligned} \int_{-\infty}^{\infty} \psi \frac{Df_C}{Dt} d\mathbf{C} &= \frac{D}{Dt} \int_{-\infty}^{\infty} \psi f_C d\mathbf{C} - \int_{-\infty}^{\infty} f_C \frac{D\psi}{Dt} d\mathbf{C} \\ &= \frac{D}{Dt} n \langle \psi \rangle - n \left\langle \frac{D\psi}{Dt} \right\rangle \end{aligned} \tag{4.67}$$

$$\begin{aligned} \int_{-\infty}^{\infty} \psi \mathbf{C} \cdot \nabla f_C d\mathbf{C} &= \nabla \cdot \int_{-\infty}^{\infty} \psi \mathbf{C} f_C d\mathbf{C} - \int_{-\infty}^{\infty} f_C \nabla \cdot \mathbf{C} f_C d\mathbf{C} \\ &= \nabla \cdot n \langle \psi \mathbf{C} \rangle - n \langle \mathbf{C} \cdot \nabla \psi \rangle \end{aligned} \tag{4.68}$$

$$\begin{aligned} \int_{-\infty}^{\infty} \psi \nabla_C f_C d\mathbf{C} &= \int_{-\infty}^{\infty} \int_{-\infty}^{\infty} [\psi f_C]_{-\infty}^{\infty} dC_y dC_z - \int_{-\infty}^{\infty} f_C \nabla_C \psi d\mathbf{C} \\ &= -n \langle \nabla_C \psi \rangle \end{aligned} \tag{4.69}$$

Since  $\mathbf{C}$  is now regarded as independent of  $\mathbf{r}$ , the variable  $C$  is not included in the differentiation with respect to  $\mathbf{r}$  in (4.68) [11] (pp 48-49). In (4.69) integration by parts is performed and the first term vanishes because, by hypothesis,  $\psi f_C$  tends to zero as  $C_x$  tends to infinity in either direction.

By use of a similar argument we get:

$$\begin{aligned} \int_{-\infty}^{\infty} \psi \mathbf{C} \nabla_C f_C &= -n \langle \nabla_C (\psi \mathbf{C}) \rangle \\ &= -n \langle \psi \rangle \mathbf{e} - n \langle \mathbf{C} \nabla_C \psi \rangle \end{aligned} \tag{4.70}$$

where  $\mathbf{e}$  is the unit tensor.

Multiplying the RHS of the Boltzmann equation (4.1) with  $\psi d\mathbf{C}$  and thereafter integrating the resulting term over the velocity space, one obtains the rate of change by collisions in the property  $\psi$  summed over all the particles in a unit volume ([11], sect 3.11):

$$\int_{-\infty}^{\infty} \psi \left( \frac{\partial f}{\partial t} \right)_{\text{Collision}} d\mathbf{C} = \Delta(\psi)'_{\text{Collision}} \tag{4.71}$$

To complete the reformulation of the Boltzmann equation replacing the microscopic particle velocity with the peculiar velocity, the collisional rate of change term has to be modified accordingly. Jenkins and Richman [32] proposed the following approximate formula:

$$\begin{aligned}\Delta(\psi)_{\text{Collision}} &= \frac{1}{2} (\Delta(\psi_1)'_{\text{Collision}} + \Delta(\psi_2)'_{\text{Collision}}) \\ &= \Omega(\psi) - \nabla \cdot \Phi(\psi) - \Phi(\nabla_C \psi) : \nabla \mathbf{v}_d\end{aligned}\quad (4.72)$$

In the derivation of this expression, several manipulations are made [60]. The chain rule is applied, and the integral operator and the derivative operator in (4.17) are commuted. The order in which these operations are performed can be inverted because the Taylor series expansion is written for a fixed point in space. The third term in (4.72) occurs after the peculiar velocity is introduced. The symbol  $\Phi$  corresponds to the tensor equivalent of  $\Psi$  valid for the particular case in which the argument is a vector, both calculated in accordance with (4.20).

By use of the transformation formulas (4.66) to (4.70) and (4.72), the equation of change for the average property  $\langle \psi \rangle$  can be deduced from the Boltzmann equation (4.1):

$$\begin{aligned}\frac{D}{Dt} n \langle \psi \rangle + n \langle \psi \rangle \nabla \cdot \mathbf{v}_d + \nabla \cdot n \langle \psi \mathbf{C} \rangle - n \langle \mathbf{F} \cdot \nabla_C \psi \rangle \\ - n \langle \frac{D\psi}{Dt} \rangle - n \langle \mathbf{C} \cdot \nabla \psi \rangle + n \frac{D\mathbf{v}_d}{Dt} \cdot \langle \nabla_C \psi \rangle \\ + n \langle \mathbf{C} \nabla_C \psi \rangle : \nabla \mathbf{v}_d = \Omega(\psi) - \nabla \cdot \Phi(\psi) - \Phi(\nabla_C \psi) : \nabla \mathbf{v}_d\end{aligned}\quad (4.73)$$

In the particular case in which  $\psi(\mathbf{C})$  is a function of the peculiar velocity only, the given relation reduces to:

$$\begin{aligned}\frac{D}{Dt} n \langle \psi \rangle + n \langle \psi \rangle \nabla \cdot \mathbf{v}_d + \nabla \cdot n \langle \psi \mathbf{C} \rangle - n \langle \mathbf{F} \cdot \nabla_C \psi \rangle \\ + n \frac{D\mathbf{v}_d}{Dt} \cdot \langle \nabla_C \psi \rangle + n \langle \mathbf{C} \nabla_C \psi \rangle : \nabla \mathbf{v}_d \\ = \Omega(\psi) - \nabla \cdot \Phi(\psi) - \Phi(\nabla_C \psi) : \nabla \mathbf{v}_d\end{aligned}\quad (4.74)$$

By introducing the modified external force expression (4.58) into (4.74), the transport equation for the property  $\langle \psi \rangle$  can be re-written as:

$$\begin{aligned}\frac{D}{Dt} n \langle \psi \rangle + n \langle \psi \rangle \nabla \cdot \mathbf{v}_d = -\nabla \cdot [n \langle \psi \mathbf{C} \rangle + \Phi(\psi)] \\ - [n \langle \mathbf{C} \nabla_C \psi \rangle + \Phi(\nabla_C \psi)] : \nabla \mathbf{v}_d \\ + n \left( \mathbf{F}_e + \frac{1}{\tau_{cd}} (\langle \mathbf{v} \rangle_c - \mathbf{v}_d) - \frac{D\mathbf{v}_d}{Dt} \right) \cdot \langle \nabla_C \psi \rangle \\ + n \langle \frac{1}{\tau_{cd}} (\mathbf{v}'_c - \mathbf{C}) \cdot \nabla_C \psi \rangle + \Omega(\psi)\end{aligned}\quad (4.75)$$

in which we assume that the Maxwellian average of a turbulent quantity can be used to approximate a Reynolds averaged variable.

### The Mass Conservation Equation

The mass balance is obtained from (4.75) with  $\psi = m$ :

$$\frac{\partial}{\partial t} \alpha_d \rho_d + \nabla \cdot (\alpha_d \rho_d \mathbf{v}_d) = 0 \quad (4.76)$$

where  $\rho_d \alpha_d = nm$  is the local bulk density of the dispersed phase. All the terms like  $\Omega(m)$ ,  $\Phi(m)$  and  $\mathbf{\Phi}(m)$  vanish because  $m$  is an invariant and constant quantity.

### The Momentum Equation

The momentum balance is obtained with  $\psi = m\mathbf{C}$  in (4.75):

$$\alpha_d \rho_d \frac{D\mathbf{v}_d}{Dt} = -\nabla \cdot (\mathbf{p}_{\text{kin}} + \mathbf{p}_{\text{coll}}) - \frac{\alpha_d \rho_d}{\tau_{cd}} (\mathbf{v}_d - \langle \mathbf{v} \rangle_c) - \alpha_d \nabla p_d + \alpha_d \rho_d \mathbf{g} \quad (4.77)$$

where  $\mathbf{p}_{\text{kin}} = \alpha_d \rho_d \langle \mathbf{C}\mathbf{C} \rangle$  is the kinetic pressure tensor and  $\mathbf{p}_{\text{coll}} = \mathbf{\Phi}(m\mathbf{C})$  is the collisional pressure tensor of the granular material as defined by (4.20). These terms represent the transport of momentum by particle velocity fluctuations and by particle collisions, respectively.

The term  $\Omega(m\mathbf{C})$  defined by (4.19) becomes zero because  $m\mathbf{C}$  is an invariant quantity according to (4.31). The term  $\Phi(m)$  defined by (4.20) is equal to zero because  $m$  is a constant and doesn't change in a collision. The local instantaneous pressure of the continuous phase might be decomposed as the sum of a mean pressure  $\langle p \rangle$  and a pressure fluctuation  $p'$ . However, the pressure covariance terms are normally neglected in gas-solid flows [6].

### The Granular Temperature

A transport equation for the granular temperature is obtained with  $\psi = \frac{1}{2}mC^2$  in (4.75):

$$\begin{aligned} \frac{3}{2} \left( \frac{\partial}{\partial t} (\alpha_d \rho_d \theta) + \nabla \cdot (\alpha_d \rho_d \theta \mathbf{v}_d) \right) &= -\nabla \cdot (\mathbf{q}_{\text{kin}} + \mathbf{q}_{\text{coll}}) \\ &- (\mathbf{p}_{\text{kin}} + \mathbf{p}_{\text{coll}}) : \nabla \mathbf{v}_d - \frac{\alpha_d \rho_d}{\tau_{cd}} (3\theta - \langle \mathbf{v}'_c \cdot \mathbf{C} \rangle) - \gamma \end{aligned} \quad (4.78)$$

where  $\mathbf{q}_{\text{kin}} = \frac{1}{2} \alpha_d \rho_d \langle \mathbf{C}\mathbf{C}^2 \rangle$  is the kinetic heat flux and  $\mathbf{q}_{\text{coll}} = \mathbf{\Phi}(\frac{1}{2}mC^2)$  is the collisional heat flux. The first two terms on the RHS represent the transport of energy by particle velocity fluctuations and by particle collisions, respectively. The third and fourth terms represent production of energy by the mean velocity gradient. The fifth and sixth terms represent the different interactions with the continuous phase. The fifth term denotes a dissipation term due to the drag force ( $3\theta$ ), and the sixth term denotes production due

to the interaction with the fluid turbulence ( $\langle \mathbf{v}'_c \cdot \mathbf{C} \rangle$ ). The last term  $\Omega(\frac{1}{2}mC^2) = -\gamma$  represents the energy dissipation due to collisions.

A dissension is observed in the literature concerning whether the granular translational energy is representing a local fluid property or a continuum flow phenomenon. In one view it is noted that the properties reflected by the granular temperature  $\theta$  are quite different from those of the thermal temperature  $T$ . The granular temperature is not representing a noticeable sensible heat because the magnitude of the translational energy ( $\frac{1}{2}mC^2$ ) of granular flows is similar to the average translational kinetic energy ( $\frac{1}{2}m\mathbf{v}_d^2$ ). For comparison, in a gas the peculiar velocity of the molecules are much larger than the average gas velocity, i.e.,  $\mathbf{C}_{\text{Molecular}} \gg \langle \mathbf{v}_c \rangle$ . However, the translational energy associated with a granular material is assumed characterized by scales comparable to the particle size being considerable smaller than the microscopic length scales of the flow. Therefore, the particle fluctuations in granular flows is considered a local fluid property [48]. In this interpretation the granular temperature must not be confused with the turbulent kinetic energy which is a continuum flow phenomenon. In a second view, the particles are assumed to be characterized by scales comparable to the macroscopic length scales of the flow, thus the granular temperature is associated with the turbulent kinetic energy which is a continuum fluid flow phenomenon [15, 22, 19, 60].

### Granular Transport Coefficients- and Flux Closures

In this section the transport coefficients and flux closures derived by Ding and Gidaspow [16] and Gidaspow [22] are defined. For further details on the Enskog dense gas approach and the Chapman-Enskog approximate solution method the interested reader is referred to the original literature presented in chap 2, and in particular to the books of Gidaspow [22] and Chapman and Cowling [11], sects 7 and 16.

The granular material closures presented in this section lead to a typical, or even the standard reference, dense phase model used for simulating fluidized bed reactor flows.

### The Kinetic Pressure Tensor

By use of the Chapman-Enskog approximate solution method [11], the kinetic pressure tensor can be given by [22]:

$$\begin{aligned} p_{\text{kin}} &= \alpha_d \rho_d \langle \mathbf{C} \mathbf{C} \rangle = \alpha_d \rho_d \int \mathbf{C} \mathbf{C} f d\mathbf{C} = \alpha_d \rho_d \int \mathbf{C} \mathbf{C} f^0 (1 + \phi_1) d\mathbf{C} \\ &= \alpha_d (p_{\text{kin}} \mathbf{e} + \boldsymbol{\sigma}_{\text{kin}}) \end{aligned} \quad (4.79)$$

where

$$p_{\text{kin}} = \rho_d \theta \quad (4.80)$$

is the kinetic pressure.

The  $\boldsymbol{\sigma}_{\text{kin}}$  denotes the deviatoric pressure tensor defined by:

$$\boldsymbol{\sigma}_{\text{kin}} = -\frac{2}{(1+e)g_0} \left( 1 + \frac{4}{5}\alpha_d g_0(1+e) \right) 2\mu_{\text{dilute}} \mathbf{S} \quad (4.81)$$

The variable  $\mathbf{S}$  is the rate of strain (deformation) tensor given by:

$$\mathbf{S} = \frac{1}{2} (\nabla \mathbf{v}_d + (\nabla \mathbf{v}_d)^T) - \frac{1}{3} (\nabla \mathbf{v}_d : \mathbf{e}) \mathbf{e} \quad (4.82)$$

This pressure tensor closure was derived by Gidaspow [22] in accordance with the Enskog theory presented by Chapman and Cowling [11], chap 16. That is, with the restitution coefficient  $e$  equal to one, the  $\chi$  factor substituted by  $g_0$ , and  $b\rho = 4\alpha_d$  this relation corresponds to equation (16.34 – 2) in Chapman and Cowling [11].

It is further noted that in this context Gidaspow [22] refers to the dense gas approach of Enskog [20] using the phrase *a dilute gas solution for a non-Maxwellian distribution function*. This reflects the fact that the dense gas approach actually considers a gas only slightly denser than the dilute limit, as distinct from the kinetic theory of dense granular flows.

### The Collisional Pressure Tensor

Likewise, in accordance with the Enskog [20] dense gas approach, Gidaspow [22] proposed a closure for the collisional pressure tensor. By use of the Chapman-Enskog approximate solution method [11], the collisional pressure tensor can be written as:

$$\mathbf{p}_{\text{coll}} = \mathbf{p}_{\text{coll1}} + \mathbf{p}_{\text{coll2}} = \alpha_d (p_{\text{coll}} \mathbf{e} + \boldsymbol{\sigma}_{\text{coll}}) \quad (4.83)$$

where  $\mathbf{p}_{\text{coll1}}$  is given by:

$$\begin{aligned} \mathbf{p}_{\text{coll1}} &= \frac{2}{5} \alpha_d^2 \rho_d g_0 (1+e) (2 \langle \mathbf{C}\mathbf{C} \rangle + C^2 \mathbf{e}) \\ &= 2\alpha_d^2 \rho_d g_0 (1+e) \theta \mathbf{e} \\ &\quad - \frac{2\alpha_d}{(1+e)g_0} \left( 1 + \frac{4}{5}\alpha_d g_0(1+e) \right) \frac{4}{5} \alpha_d^2 \rho_d g_0 (1+e) 2\mu_{\text{dilute}} \mathbf{S} \end{aligned} \quad (4.84)$$

and, the  $\mathbf{p}_{\text{coll2}}$  is:

$$\mathbf{p}_{\text{coll2}} = -\frac{4}{3\sqrt{\pi}} \rho_d \alpha_d^2 d_{12} g_0 (1+e) \sqrt{\theta} \left( \frac{6}{5} \mathbf{S} + (\nabla \cdot \mathbf{v}_d) \mathbf{e} \right) \quad (4.85)$$

It is recognized that the first term in the formula for  $\mathbf{p}_{\text{coll1}}$  contains the collisional pressure, defined by:

$$p_{\text{coll}} = 2\alpha_d \rho_d g_0 (1+e) \theta \quad (4.86)$$

The collisional deviatoric pressure tensor consists of the remaining terms in  $\mathbf{p}_{\text{coll}}$  and is thus given by:

$$\begin{aligned} \boldsymbol{\sigma}_{\text{coll}} = & -\frac{2\alpha_d}{(1+e)g_0} \left(1 + \frac{4}{5}\alpha_d g_0(1+e)\right) \frac{4}{5}\alpha_d \rho_d g_0(1+e) 2\mu_{\text{dilute}} \mathbf{S} \\ & - \frac{4}{3\sqrt{\pi}} \rho_d \alpha_d d_{12} g_0(1+e) \sqrt{\theta} \left(\frac{6}{5}\mathbf{S} + (\nabla \cdot \mathbf{v}_d)\mathbf{e}\right) \end{aligned} \quad (4.87)$$

### The Total Pressure Tensor

The total pressure tensor contains both the kinetic and collisional contributions:

$$\mathbf{p} = \mathbf{p}_{\text{kin}} + \mathbf{p}_{\text{coll}} = \alpha_d(p_d \mathbf{e} + \boldsymbol{\sigma}_d) \quad (4.88)$$

Hence it follows that the total pressure of the dispersed phase is defined as the sum of the kinetic (4.80) and collisional (4.86) pressure contributions:

$$p_d = \rho_d \theta + 2\alpha_d \rho_d \theta(1+e)g_0 = \rho_d \theta [1 + 2(1+e)\alpha_d g_0] \quad (4.89)$$

The total deviatoric stress tensor can be written as:

$$\boldsymbol{\sigma}_d = -\mu_d (\nabla \mathbf{v}_d + (\nabla \mathbf{v}_d)^T) - \left(\mu_{B,d} - \frac{2}{3}\mu_d\right) (\nabla \cdot \mathbf{v}_d)\mathbf{e} \quad (4.90)$$

where

$$\mu_d = \frac{2\mu_{\text{dilute}}}{(1+e)g_0\alpha_d} \left(1 + \frac{4}{5}\alpha_d g_0(1+e)\right)^2 + \frac{4}{5}\alpha_d \rho_d d_{12} g_0(1+e) \sqrt{\frac{\theta}{\pi}} \quad (4.91)$$

The first term on the RHS in the viscosity closure denotes the kinetic contribution and dominates in the dilute regime. The second term on the RHS denotes the collisional contribution and dominates in the dense flow regime.

The normal component of the collisional deviatoric pressure tensor resembles the bulk viscosity term and is thus denoted by  $\mu_{B,d}$ :

$$\mu_{B,d} = \frac{4}{3}\alpha_d \rho_d d_{12} g_0(1+e) \sqrt{\frac{\theta}{\pi}} \quad (4.92)$$

The viscosity for the dilute limit can be written as:

$$\mu_{\text{dilute}} = \frac{5}{96}\rho_d d_{12} \sqrt{\pi\theta} \quad (4.93)$$

Except for the conversion to granular temperature, as performed by [22], this is the expression for the dilute gas viscosity given by the bracket integral (7.41-1) in Chapman and Cowling [11].

Using the given relation for  $\mu_{\text{dilute}}$  Laux [48] (sect 2.3.2) experienced numerical problems in regions of very dilute flow. The numerical problems

were connected with the non-zero dilute viscosity obtained when  $\alpha_d \rightarrow 0$ . These problems were avoided introducing a modified semi-empirical expression for  $\mu_{\text{dilute}}$ .

The modified dilute viscosity is defined by [48]:

$$\mu_{\text{dilute}} = \frac{30\sqrt{2}}{96} \rho_d \alpha_d \min |l_p, l_{p,\max}| \sqrt{\pi\theta} \quad (4.94)$$

This relation for  $\mu_{\text{dilute}}$  becomes zero when  $\alpha_d < \alpha_{d,\min}$ .

The modified dilute viscosity is approximated based on the relation  $\mu_{\text{dilute}} \propto \rho_B^d l_p \sqrt{\theta}$ . The bulk density is proportional to  $\alpha_d$ , whereas the mean free path  $l_p$  is inversely proportional to  $\alpha_d$ . A typical value,  $\alpha_{d,\min} = 1 \times 10^{-5}$ , was used to limit the mean free path in an unconfined flow. The limit  $l_{p,\max}$  was thus either given as a characteristic dimension of the flow geometry, or calculated from  $\alpha_{d,\min}$  as  $l_{p,\max} = \frac{1}{6\sqrt{2}} \frac{d_{12}}{\alpha_{d,\min}}$ .

### The Granular Heat Flux Vectors

A similar derivation can be made for the granular heat flux vectors [22]. The total granular heat flux is given by:

$$\mathbf{q}_d = \mathbf{q}_{\text{kin}} + \mathbf{q}_{\text{coll}} = -\alpha_d \Gamma_d \nabla \theta \quad (4.95)$$

where the granular conductivity is given by:

$$\Gamma_d = \frac{2k_{\text{dilute}}}{(1+e)g_0\alpha_d} \left[ 1 + \frac{6}{5}(1+e)g_0\alpha_d \right]^2 + 2\alpha_d \rho_d d_{12} g_0 (1+e) \sqrt{\frac{\theta}{\pi}} \quad (4.96)$$

As for the viscosity  $\mu_d$ , the first term on the RHS of the conductivity  $\Gamma_d$  closure denotes the kinetic contribution and dominates in the dilute regime. The second term on the RHS of the closure equation denotes the collisional contribution and dominates in the dense flow regime.

This relation corresponds to (9.272) in the book of Gidaspow [22]. An approximation of the dilute flow conductivity is given by Gidaspows equation (9.260). That is,

$$k_{\text{dilute}} = \frac{5}{2} \mu_{\text{dilute}} C_V = \frac{5}{2} \left( \frac{5\sqrt{\pi}}{96} \rho_p d_{12} \theta^{1/2} \right) \left( \frac{3}{2} \right) = \frac{75}{384} \sqrt{\pi} \rho_d d_{12} \theta^{1/2} \quad (4.97)$$

where  $C_V = \frac{3}{2}$  and  $\mu_{\text{dilute}}$  is given by (4.93).

### The Dissipation Term

The algebraic dissipation term in the equation for granular temperature (4.78) is defined in accordance with (4.19), and approximated by:

$$\gamma = -\Omega = 3(1-e^2)\alpha_d^2 \rho_d g_0 \theta \left( \frac{4}{d_{12}} \sqrt{\frac{\theta}{\pi}} - \nabla \cdot \mathbf{v}_d \right) \quad (4.98)$$

which corresponds to equation (9.213) in the book of Gidaspow [22].

### 4.1.5 Initial- and Boundary Conditions for the Granular Phase Equations

To solve the equations of granular flows, appropriate boundary conditions for the velocities and for the granular temperature are required. The boundary conditions proposed by Ding and Gidaspow [16] are generally adopted in most granular flow simulations.

At the *impermeable wall*, the no-slip condition is generally not appropriate for granular flows. Nevertheless, the granular phase velocity component normal to the wall is normally set to zero. However, the granular phase is usually allowed to slip along the wall. A velocity slip proportional to the velocity gradient at the wall is commonly applied:

$$v_{d,z}|_{\text{wall}} = -\lambda_d \frac{\partial v_{d,z}}{\partial n}|_{\text{wall}} \quad (4.99)$$

where the  $n$  denotes the direction normal to the wall. The slip parameter  $\lambda_d$  takes the value of the mean free path of the molecules.  $\lambda_d$  is normally estimated by:

$$\alpha_d \frac{4}{3} \pi \left(\frac{\lambda_d}{2}\right)^3 = \frac{\pi}{6} d_{12}^3 \quad (4.100)$$

with some simple manipulations we achieve

$$\lambda_d = \frac{d_{12}}{\alpha_d^{1/3}} \quad (4.101)$$

Although there might be a granular temperature flux through the wall, little is known about the magnitude of such a flux. Hence, a simple zero gradient boundary condition is normally used:

$$\left(\frac{\partial \theta}{\partial r}\right)_{\text{wall}} = 0 \quad (4.102)$$

The dispersed phase volume fraction normal gradient is set to zero.

The boundary value for the normal velocity at the *symmetry axis* is zero. The tangential velocity, volume fraction and granular temperature gradients normal to the symmetry axis are all set to zero. The *inlet* conditions for the fluidized bed are given in accordance with the operating conditions specified. In particular, a small but non-zero value is specified for the granular temperature, i.e.,  $\theta \approx 10^{-7} (m^2/s^2)$ . The dispersed phase volume fraction is set to zero at the inlet where solid-free gas enters the system. At the *outlet*, the normal gradients of all granular material quantities are zero as the mass flux is assumed to be continuous. The *initial* condition specifies a fluidized bed operating at the minimum fluidization state. The granular temperature is set equal to the inlet value everywhere inside the calculation domain.

## 4.2 Remarks on the Kinetic Theory of Granular Flows

The main advantage associated with the kinetic theory approach for dense suspensions is the appearance of two extra pressure terms in addition to the interstitial fluid phase pressure, one kinetic pressure tensor accounting for the transport phenomena due to the translational particle movement and one collisional pressure tensor accounting for the transport phenomena due to particle collisions.

The alternative dilute two-fluid modeling approach reflects the advantage of allowing the same averaging operators to be applied to both phases. In this way the governing equations for both phases contain consistent interfacial coupling terms. However, the dilute approach does not give rise to any of the two pressure tensors accounting for the transport phenomena caused by the particle movement and collisions. The dense phase two-fluid modeling concept, on the other hand, contain an inherent inconsistency as the dispersed granular material phase is averaged over the velocity space using the Maxwellian averaging approach while the Eulerian microscopic dilute phase equations are time-, volume- or ensemble averaged. The formulation of consistent phase interaction- and co-variance terms is thus a very complex task.

In particular, referring to the introduction of the external forces as presented in sect 4.1.3 there are still no complete consensus in the literature regarding the treatment of the interfacial coupling terms like the steady drag-, added mass- and lift forces. In one view it is considered convenient to split the net force exerted by the interstitial fluid on the particle into two different contributions: One virtual force applied by an *undisturbed flow* on a imaginary fluid particle which coincides with the solid particle in volume and shape, and a second contribution that represents the forces due to the perturbations in the flow. These flow disturbances are created by the presence of the particles. The phrase *undisturbed flow* thus refers to the flow that would be observed if the particle was not present. Neglecting the effects of the perturbations in the flow, the net force exerted on a particle (4.57) might be approximated by:

$$\tilde{\mathbf{F}} = \frac{1}{\tau_{cd}}(\tilde{\mathbf{v}}_c - \mathbf{c}) - \frac{1}{\rho_d}\nabla\tilde{p} + \mathbf{g} \quad (4.103)$$

where the quantities  $\tilde{p}_c$  and  $\tilde{\mathbf{v}}_c$  are the imaginary pressure and velocity fields of the undisturbed flow.

For undisturbed turbulent flows the local instantaneous velocity of the continuous phase have been decomposed in various ways, not necessarily in accordance with the familiar Reynolds - and Favre averaging procedures.

To explain the basic problem we use the Reynolds decomposition and averaging procedure, as an example. Introducing the peculiar velocity for the dispersed phase (4.103) can be re-arranged as:

$$\tilde{\mathbf{F}} = \frac{1}{\tau_{cd}}(\langle \tilde{\mathbf{v}} \rangle_c - \mathbf{v}_d) + \frac{1}{\tau_{cd}}(\tilde{\mathbf{v}}'_c - \mathbf{C}) - \frac{1}{\rho_d}\nabla\tilde{p} + \mathbf{g} \quad (4.104)$$

The interpretations of the velocity variables in the first and second terms on the RHS represent a severe problem due to a general lack of knowledge about the physics they represent. Besides, when the  $\mathbf{F}$  quantity in the Maxwell equation is substituted by this relation and Maxwellian averaged, the resulting covariances consist of velocity quantities which are averaged in an inconsistent manner (Maxwellian- versus time-, volume-, or ensemble averaging). For this reason other somewhat ad hoc decomposition procedures have been defined intending to achieve more consistent closures for these terms.

The granular flow modeling work of Simonin and co-workers [71, 73, 72, 15, 6, 74, 75, 26, 83, 87, 3, 88, 4, 4, 60, 89] is briefly outlined in the following illustrating the complexity of this task. The group is recognized for developing two-fluid models for industrial applications based roughly on the modeling ideas of Enskog [20] and the solution strategy of Grad [24]. Most of these model closures can be considered as extensions of, rather than alternatives to, the modeling approach of Gidaspow [22] taking into account the fluid-particle covariance term (i.e., the drift velocity) which is normally neglected employing the Chapman-Enskog approach. The closures of Simonin and co-workers are deduced by use of the statistical turbulence theories of Taylor [80], Hinze [27], Tchen [81], Csanady [14] and Yudine [90]. The work of Tchen [81] represents one of the first attempts to study the dispersion of particles in a steady and homogeneous turbulent flow field by use of the fluid Lagrangian two-point correlation function  $R_{ij}(\tau)$  and the gradient hypothesis. The turbulence dispersion coefficient needed to close the flux model is defined in terms of the correlation function and thus the fluid-particle velocity covariance (correlation tensor). Several additional assumptions were made in his derivation: (1) The particles are spherical and follow Stoke's law of resistance, (2) the particles are small compared to the smallest length scales of the fluid flow, and (3) during the motion of the particles, their neighborhood is formed by the same fluid. A few years later assumption (3) in the Tchen theory was assessed and found questionable. Yudine [90] and Csanady [14] studied the effect of turbulent diffusion of heavy particles in turbulent flows. In particular, the existence of the *crossing trajectory effect*<sup>3</sup> was recognized. Based on these classical analyzes Deutsch and Simonin [15] derived closure models for the particle velocity covariances, the fluid-particle velocity covariances, and the drift velocity intending to avoid assumption (3) in the theory of Tchen. An algebraic formula for the dispersion - or drift velocity computed along the particle trajectories was deduced for homogeneous isotropic turbulence<sup>4</sup>. Nevertheless, in the case of industrial gas-solid flows, most assumptions of these

<sup>3</sup> The crossing trajectory effect refers to the impact of the continuous change of the fluid eddy-particle interactions as the heavy particle trajectory might go through numerous eddies reflecting different flow properties. Hence it follows that the velocity history of heavy particles may differ from that of a marked fluid particle.

<sup>4</sup> Similar closure models for the drift velocity and the velocity co-variances have been derived from kinetic theory by Koch and co-workers [38, 39] and Reeks [62, 63].

models are still too restrictive and a more general formulation is necessary. The generalized formulation proposed in the subsequent work of Simonin and co-workers consists of separate transport equations for the drift velocity and the fluid-particle velocity correlation tensor. For dilute suspensions the derivation of the second order velocity moment closure follows a similar procedure as used for single phase flows deriving the Reynolds stress turbulence model. For dense suspensions similar transport equations are derived for the drift velocity and fluid-particle velocity correlation tensor based on the kinetic theory of granular flow approach. However, in another view the second order closure might be exaggerated in complexity, computationally expensive and impossible to validate. Besides, there are still no consensus regarding the physical meaning of these covariance terms [37]. The algebraic formulas proposed by Deutsch and Simonin [15] for the drift velocity supposedly valid for homogeneous isotropic turbulence of the interstitial fluid is not generally accepted but considered important by the inventors at least for particular applications. The second order closure of Simonin and co-workers is still only applied in academic research. For these reasons further details of the work of Simonin and co-workers are disregarded in this presentation.

A further comparison between the two-phase dilute formulation and the dense phase two-fluid model reveals another striking difference. The continuum mechanics modeling concepts give rise to a set of transport equations on the flux form, while the kinetic theory concepts as expressed in terms of the peculiar velocity give rise to transport equations defined by (4.75) on the advective- or non-flux form. The standard formulation using the local particle velocity  $\mathbf{c}$  defined by (4.33) leads to a set of equations on the flux form. Nevertheless, as long as there is no mass transfer between the phases, both forms of the dense phase equations are valid, as the continuity equation can be used to transform the equations in a consistent manner. However, when there is mass transfer fluxes between the phases as in chemical reactive flows, the models might differ considerably dependent on the starting point taken for re-writing the balance equations using the continuity equation.

Hence it follows that for multicomponent reactive mixtures the problem has to be re-considered deriving the governing equations again from scratch, this time in terms of an extended distribution function for molecules of a particular type. The multicomponent kinetic theory for a dilute gas has been considered by Hirschfelder et al [28]. Tham and Gubbins [82] extended the Enskog theory of dense, rigid sphere fluids to multicomponent systems.

In a series of papers Lathouwers and Bellan [43, 44, 45, 46] presented a kinetic theory model for multicomponent reactive granular flows. The model considers polydispered particle suspensions to take into account that the physical properties (e.g., diameter, density) and thermo-chemistry (reactive versus inert) of the particles may differ in their case. Separate transport equations are constructed for each of the particle types, based on similar principles as used formulating the population balance equations [61].

To describe the behavior of the multicomponent reactive granular material Lathouwers and Bellan started out from the work of Simonin [77] defining a single particle distribution function  $f_i^{(1)}(t, \mathbf{r}, \mathbf{c}, \mathbf{Y}, m)$  of particle type  $i$  such that  $f_i^{(1)}$  is the probable number of particles of type  $i$  having their center of mass in the region  $\mathbf{r}, \mathbf{r} + d\mathbf{r}$ , a velocity in the region  $\mathbf{c}, \mathbf{c} + d\mathbf{c}$ , mass fractions in  $\mathbf{Y}, \mathbf{Y} + d\mathbf{Y}$ , temperature in  $T, T + dT$ , and mass in the region  $m, m + dm$ . With only moderate mathematical complexity in derivation they established a set of equations governing reactive granular flows. The multicomponent model was applied to dense gas-solid reactive mixtures to investigate the performance and optimal operating conditions of biomass pyrolysis in fluidized bed. The main reason for using such a complex model was to enable incorporation of the phase change phenomena changing the particle mass along its trajectory.

However, to describe catalytic processes much simpler models might be sufficient because a catalyst is a substance that affects the reaction rate of a reaction but emerges from the the chemical process unchanged. In most cases like this a simple extension of the classical mono-disperse single component granular flow model, i.e., extending the model by introducing the reaction terms only, may be an option. Further work is thus needed to validate the performance of the granular flow models applied to different types of chemical reactive processes.

#### 4.2.1 Granular Flow Closure Limitations

There are many aspects of rapid granular flows that have barely been studied and require further considerations to provide appropriate closures for reactor flows.

The theoretical studies of rapid granular flows are generally based on the assumption that the energy dissipation in a binary particle collision is determined by a constant coefficient of restitution  $e$ , the ratio of the relative approach to recoil velocities normal to the point of impact on the particle. However, measurements show that the coefficient of restitution is a strong function of the relative impact velocity [10]. Physically, the energy dissipation relates to the plastic deformation of the particle's surface. Thus, a realistic microscopic model should include the deformation history of the particle's surface. However, such a model might become computationally demanding and thus not feasible.

Moreover, most theoretical studies performed so far are based on the assumption that the granular material is composed of uniformly sized disk or spheres. However, real materials may have a wide distribution of particle sizes affecting the properties of the flow.

Granular flows have a tendency to segregate according to size and/or density under the action of a body force such as gravity. Savage [67] made a review on the different mechanisms responsible for particle percolation, dispersion, and segregation. One such segregation effect is common in everyday experience and can be easily recognized. When a polydisperse mixture is agitated in

the presence of gravity the random particle motion is more likely to open a gap large enough for a small particle to fall into than one that can accommodate a large particle. Hence, the small particles migrate to the bottom of the flow, and the large particles migrate to the top. However, there is other phenomena associated with the deposition of sediments that results in the opposite behavior in which the finer particles are found in the top of the flow and the coarse ones are located at the bottom. Many similar phenomena have been identified. In fluidized beds in particular the axial segregation, due to particle diameters and/or density, is generally explained by the fact that smaller particles are more easily fluidized and will follow the gas more effectively than larger ones. Larger particles will not follow the gas effectively and start accumulating, particularly in the wall region where the gas velocity is very low. The radial particle segregation may have a similar origin. All these phenomena are caused by complex interactions between the particle sizes and densities that are not well understood, yet these mechanisms should be represented by the interaction terms of the individual phase equations. The important terms are thus the fluid particle steady drag-, the particle-particle steady drag-, the added mass-, and the transversal lift forces. Jenkins and Mancini [33] used the kinetic theory to derive balance laws and constitutive equations for plane flows of a dense, binary mixture of smooth, nearly elastic, circular disks. The disks may have different radii and masses and the coefficient of restitution, characterizing the energy dissipated in the collisions between like and unlike pairs, may be different. The collisional fluxes and sources of momentum and energy that appear in these equations involve the complete pair distribution function for colliding pairs of like and unlike disks. They assume that these distribution functions can be expressed as the product of the single particle distribution function for each disk and a factor that accounts for the effects of excluded area and collisional shielding. However, rather than determining the single particle distribution function as an appropriate solution to the kinetic equations governing their evolution, they were assumed to be Maxwellian. Equipartition of energy was also assumed, leading to equality of the granular temperatures of both particle phases. While such an assumption is found reasonable for mixtures of molecules experience elastic collisions it might not be true for inelastic solid particles. Gidaspow and co-workers (i.e., Gidaspow et al [23], Manger [51]) thus extended the kinetic theory to binary particle mixtures with unequal granular temperatures for the different particle phases. Manger [51] implemented the binary mixture model with two different granular temperatures into a 2D computer code to simulate segregation in a channel flow and concluded that the model can predict particle segregation induced by simultaneous changes in particle size and weight. However, no experimental validation of the model predictions were performed so further work was required on this topic. Hjertager and co-workers (i.e., Mathiesen et al [52] [53]) thus performed an experimental and computational investigation of the multiphase flow behavior in a circulating fluidized bed. In this work, the binary particle phase flow model developed by Gidaspow and co-workers [23]

[51] was generalized to  $N$  granular phases to enable a realistic description of the particle size and density distributions in gas-solid mixtures. Each granular phase is uniquely defined by a diameter, density and a restitution coefficient. A 2D model implemented in Cartesian coordinates with two, sometimes three, dispersed phases was applied to the circulating fluidized bed. The turbulence of the interstitial gas phase was modeled by use of a VLES turbulence closure. The model predictions were compared with literature data and their own measurements. In both experimental investigations Laser Doppler Anemometry and Phase Doppler Anemometry techniques were used to measure mean and fluctuating velocity, diameter and solid concentration, simultaneously. The model predictions were in fair agreement with the experimental data. However, there are still many aspects of particle segregation in granular flows that need further considerations. Lathouwers and Bellan [43] [44] [45] [46] [47] considered binary particle mixtures in their model investigating a multi-component reactive process operated in a fluidized bed reactor. However, the discussion focused mainly on the chemical process and no experimental validation of the particle segregation mechanisms were performed.

In addition, granular materials in industrial units operations will generally be highly angular. Yet all of the analyzes and most of the computer simulations have been performed for perfect spheres or disks.

Sphericity has been assumed in most studies for many reasons. In theoretical work and computer simulations it is easy to detect a collision of spherical particles, as particles are in contact whenever their centers are a distance of two radii apart. For non-spherical particles, the contact mechanisms become much more complicated, as the orientation of the particle, which changes as the particle rotates, must be taken into account. For this reason the assumption of spherical particles are normally considered a fair approximation for catalyst pellets.

Furthermore, for multicomponent reactive flows the sensible thermal energy or rather the thermal temperatures of the different phases are important variables for optimization, scale-up and design of the reactor units. Very few theoretical and experimental studies have focused on developing parameterizations for the thermal conductivity of granular materials. The work of Gelperin and Einstein [21] may be mentioned. However, the importance of these terms in fluidized bed simulations might not be crucial since the granular material advection processes generally dominate the heat transport.

Moreover, very few parameterizations are reported on the wall- and fluid-granular material convective thermal heat transfer coefficients. For introductory studies, the work of Natarajan and Hunt [55], Gunn [25], Kuibe and Broughton [40], Kuipers et al [41] and Patil et al [59] might be consulted. To enable validation and reliable predictions of non-isothermal non-adiabatic reactive granular flows the thermal conductivity and the convective heat transfer coefficients have to be determined with sufficient accuracy. For certain processes this may be an important task for future research in the field of granular flows in fluidized beds.

---

## References

1. Anderson TB, Jackson R (1967) A Fluid Mechanical Description of Fluidized Beds. I & EC Fundamentals 6 (4):527-539
2. Bagnold RA (1954) Experiments on a Gravity-Free Dispersion of Large Solid Spheres in a Newtonian Fluid Under Shear. Proc Roy Soc A225:49-63
3. Balzer G, Simonin O (1993) Extensions of Eulerian gas-solid flow modelling to dense fluidized bed prediction. In: Proc 5th Int Symp on refined flow modelling and turbulence measurements, ed Viollet PL, Paris, pp 417-424
4. Balzer G, Boelle A, Simonin O (1995) Eulerian gas-solid flow modelling of dense fluidized bed. Fluidization VIII, Int Symp of the Engineering Foundation, Tours, 14-19 May, pp 1125-1134
5. Barthod D, Del Pozo M, Mirgain C (1999) CFD-aided design improves FCC performance. Oil & Gas Journal 14:66-69
6. Bel Fdhila R, Simonin O (1992) 6th Workshop on Two-Phase Flow Predictions, Erlangen, FRG, pp. 264-273
7. Bird RB, Stewart WE, Lightfoot EN (2002) Transport phenomena. Second Edition, John Wiley & Sons, New York
8. Boelle A, Balzer G, Simonin O (1995) Second order prediction of the particle phase stress tensor of inelastic spheres in simple shear dense suspensions. Gas-Solid Flows, ASME FED 228:9-18
9. Boemer A, Qi H, Renz U, Vasquez S, Boysan F (1995) Eulerian computation of fluidized bed hydrodynamics - A comparison of physical models. Fluidized Bed Combustion - Volume 2 ASME 1995
10. Campbell CS (1990) Rapid Granular Flows. Annu Rev Fluid Mech 22:57-92
11. Chapman S, Cowling TG (1970) The Mathematical Theory of Non-Uniform Gases. Third edition, Cambridge Mathematical Library, Cambridge
12. Crowe CT, Chung JN, Troutt TR (1988) Particle Mixing in Free Shear Flows. Prog Energy Combust Sci 14:171-194
13. Crowe CT, Troutt TR, Chung JN (1996) Numerical Models for Two-Phase Turbulent Flows. Annu Rev Fluid Mech 28:11-43.
14. Csanady GT (1963) Turbulent Diffusion of Heavy Particles in the Atmosphere. J Atm Sci 20:201-208
15. Deutsch E, Simonin O (1991) Turbulence modification in multiphase flow. ASME FED 1:34-42

16. Ding J, Gidaspow D (1990) A bubbling fluidization model using kinetic theory of granular flow. *AIChE J* 36 (4):523-538
17. Edwards CH Jr, Penny DE (1982) *Calculus and Analytic Geometry*. Prentice-Hall Inc, Englewood Cliffs, New Jersey
18. Elghobashi SE (1994) On predicting particle laden turbulent flows. *Appl Sci Res* 52:309-329.
19. Enwald H, Peirano E, Almstedt AE (1996) Eulerian Two-Phase Flow Theory Applied to Fluidization. *Int J Multiphase Flow* 22:21-66 Suppl
20. Enskog D (1922) Kinetische Theorie der Wärmeleitung, Reibung und Selbstdiffusion in gewissen verdichteten Gasen und Flüssigkeiten. *Kungl Svenska Vet-Ak Handl* 63(4):1-44
21. Gelperin NI, Einstein VG (1971) Heat transfer in fluidized beds. In: *Fluidization*, ed, Davidson JF, Harrison D, Academic Press, London and New York, pp:471-568
22. Gidaspow D (1994) *Multiphase Flow and Fluidization-Continuum and Kinetic Theory Descriptions*. Academic Press, Harcourt Brace & Company, Publishers, Boston
23. Gidaspow D, Huilin L, Manger E (1996) Kinetic theory of multiphase flow and fluidization: Validation and extension to binary mixtures. In: *Nineteenth Int Cong of Theoretical and Appl Mech*, August, Kyoto, Japan, pp 25-31
24. Grad H (1949) On the kinetic theory of rarified gases. *Comm Pure and Appl Math* 2:331-407
25. Gunn DJ (1978) Transfer of heat or mass to particles in fixed and fluidized beds. *Int J Heat Mass Transfer* 21:467-476
26. He J, Simonin O (1993) Non-equilibrium prediction of the particle-phase stress tensor in vertical pneumatic conveying. *Gas-Solid Flows*, ASME FED 166, pp 253-263
27. Hinze JO (1975) *Turbulence*. 2nd edition, McGraw-Hill, New York
28. Hirschfelder JO, Curtiss CF, Bird RB (1954) *Molecular Theory of Gases and Liquids*. John Wiley & Sons, Inc., New York
29. Hrenya CM, Sinclair JL (1997) Effects of Particle-Phase Turbulence in Gas-Solid Flows. *AIChE J* 43 (4):853-869
30. Jackson R (1997) Locally averaged equations of motion for a mixture of identical spherical particles and a Newtonian fluid. *Chem Eng Sci* 52(15):2457-2469
31. Jenkins JT, Savage SB (1983) A Theory for Rapid Flow of Identical, Smooth, Nearly Elastic Spherical Particles. *J Fluid Mech* 130:187-202
32. Jenkins JT, Richman MW (1985) Grad's 13-Moment System for Dense Gas of Inelastic Spheres. *Arch Ratio Mech Anal* 87:355-377
33. Jenkins JT, Mancini F (1987) Balance Laws and Constitutive Relations for Plane Flows of a Dense, Binary Mixture of Smooth, Nearly Elastic, Circular Disks. *Journal of Applied Mechanics* 54:27-34
34. Jenkins JT (1992) Boundary Conditions for Rapid Granular Flow: Flat, Frictional Walls. *J Appl Mech - Trans ASME* 59:120-127
35. Johnson PC, Jackson R (1987) Frictional-collisional constitutive relations for granular materials, with application to plane shearing. *J Fluid Mech* 176:67-93
36. Johnson PC, Nott P, Jackson R (1990) Frictional-collisional equations of motion for particulate flows and their application to chutes. *J Fluid Mech* 210:501-535
37. Jung J, Gidaspow D, Gamwo IK (2006) Bubble Computation, Granular Temperatures, and Reynolds Stresses. *Chem Eng Comm* 193:946-975

38. Koch DL (1990) Kinetic theory for a monodispersed gas-solid suspension. *Phys Fluids A* 2:1711-1723
39. Koch DL, Sangani AS (1999) Particle pressure and marginal stability limits for a homogeneous monodisperse gas-fluidized bed: Kinetic theory and numerical simulations. *J Fluid Mech* 400:229-263
40. Kubie J, Broughton J (1975) A model of heat transfer in gas fluidized beds. *Int J Heat Mass Transfer* 18:289-299
41. Kuipers JAM, Prins W, van Swaaij WPM (1992) Numerical calculation of wall-to-bed heat transfer coefficients in gas-fluidized beds. *AIChE J* 38(7):1079-1091
42. Lafi AY, Reyes Jr JN (1994) General Particle Transport Equation. Report OSU-NE-9409, Department of Nuclear Engineering, Oregon State University, Oregon
43. Lathouwers D, Bellan J (2000) Modelling and simulation of bubbling fluidized beds containing particle mixtures. *Proc of the Comb Inst* 28:2297-2304
44. Lathouwers D, Bellan J (2001) Modelling of biomass pyrolysis for hydrogen production: The fluidized bed reactor. *Proc of the 2001 DOE Hydrogen Program Review*. NREL/CP-570-30535
45. Lathouwers D, Bellan J (2001) Modelling of dense gas-solid reactive mixtures applied to biomass pyrolysis in a fluidized bed. *Int Journal of Multiphase Flow* 27:2155-2187
46. Lathouwers D, Bellan J (2001) Yield optimization and scaling of fluidized beds for tar production from biomass. *Energy & Fuels* 15:1247-1262
47. Lathouwers D, Bellan J (2001) Modelling of dense gas-solid reactive mixtures applied to biomass pyrolysis in a fluidized bed. *Proc of the 2001 US DOE Hydrogen Program Review*. NREL/CP-570-28890
48. Laux H (1998) Modeling of Dilute and Dense Dispersed Fluid-Particle Flow. Dr Ing Thesis, Norwegian University of Science and Technology, Trondheim, Norway
49. Lun CKK, Savage SB, Jeffery DJ, Chepurniy N (1984) Kinetic Theories for Granular Flow: Inelastic Particles in Couette Flow and Slightly Inelastic Particles in a General Flow Field. *J Fluid Mech* 140:223-256
50. Liboff RL, (1998) *Kinetic Theory: Classical, Quantum, and Relativistic Descriptions*. Second Edition, John Wiley & Sons, Inc., New York
51. Manger E (1996) Modelling and Simulation of Gas/Solid Flow in Curvilinear Coordinates. Dr ing Thesis, Norwegian University of Science and Technology, Porsgrunn
52. Mathiesen V, Solberg T, Hjertager BH (2000) Predictions of gas/particle flow with an Eulerian model including a realistic particle size distribution. *Powder Technology* 112:34-45
53. Mathiesen V, Solberg T, Hjertager BH (2000) An experimental and computational study of multiphase flow behavior in a circulating fluidized bed. *Int J Multiphase Flow* 26:387-419
54. Maxwell JC (1866) On the dynamical theory of gases. *Phil Trans R Soc Lond* 157:49-88
55. Natarajan VVR, Hunt ML (1998) Kinetic theory analysis of heat transfer in granular flows. *Int J Heat Trnsfer* 41(13):1929-1944
56. Ogawa S (1978) Multitemperature Theory of Granular Materials. In: Cowin S, Satake M ed, *Proc US-Japan Seminar Continuum-Mechanical and Statistical Approaches in the Mechanics of Granular Materials*. Gakujutsu Bunken Fukyukai, Tokyo, Japan, p. 208

57. Ogawa S, Umemura A, Oshima N (1980) On the Equations of Fully Fluidized Granular Materials. *Z angew Math Phys* 31:483-493
58. Ocone R, Sundaresan S, Jackson R (1993) Gas-Particle Flow in a Duct of Arbitrary Inclination with Particle-Particle Interactions. *AIChE J* 39(8): 1261-1271
59. Patil DJ, Smit J, van Sint Annaland M, Kuipers JAM (2006) Wall-to bed heat transfer in gas-solid bubbling fluidized beds. *AIChE J* 52(1):58-74
60. Peirano E, Leckner B (1998) Fundamentals of Turbulent Gas-Solid Flows Applied to Circulating Fluidized Bed Combustion. *Proc Energy Combust Sci* 24:259-296
61. Ramkrishna D (2000) Population Balances. Academic Press, San Diego
62. Reeks MW (1992) On the continuum equations for dispersed particles in nonuniform flows. *Phys Fluids A* 4:1290-1303
63. Reeks MW (1993) On the constitutive relations for dispersed particles in nonuniform flows. I. Dispersion in simple shear flow. *Phys Fluids A* 5:750-761
64. Reyes Jr JN (1989) Statistically Derived Conservation Equations for Fluid Particle Flows. Nuclear Thermal Hydraulics 5th Winter meeting, Proc ANS Winter Meeting.
65. Savage SB, Jeffrey (1981) The Stress Tensor in a Granular Flow at High Shear Rates. *J Fluid Mech.* 110:255-272
66. Savage SB (1984) The Mechanics of Rapid Granular Flows. *Adv Appl Mech* 24:289-366
67. Savage SB (1987) Interparticle percolation and segregation in granular materials: A review. In: Selvadurai APS ed, *Developments in Engineering Mechanics*. Elsevier Science Publishers BV, Amsterdam, pp 347-363
68. Savage SB (1989) Flow of Granular Materials. In: Germain P, Piau M, Caillerie D (eds), *Theoretical and Applied Mechanics*. Elsevier Science Publishers B. V. (North-Holland)
69. Shahinpoor M (1983) *Advances in the Mechanics and the flow of Granular Materials*. Trans Tech Publications, Volume II, First edition, Clausthal-Zellerfeld, Germany
70. Shames IH (1962) *Mechanics of fluids*. McGraw-Hill, New York
71. Simonin O (1990) Eulerian formulation for particle dispersion in turbulent two-phase flows. Proc 5th workshop on two-phase flow predictions, Erlangen, FRG, pp 156-166
72. Simonin O, Viollet N, Méchitou N (1990) The modelling of turbulent recirculating high temperature flows loaded with particles. In: *Plasma jets in the development of new materials technology*, eds Solonenko OP, Fedorchenko AI, VSP publ, the Netherlands, pp 3-16
73. Simonin O, Viollet PL (1990) Prediction of an oxygen droplets pulverization in a compressible subsonic coflowing hydrogen flow. *Numer Methods for Multiphase Flows*, ASME FED 91:73-82
74. Simonin O, Balzer G, Deutsch E, Dalsecco S, Flour I, He J (1993) Numerical modelling of turbulent reactive two-phase flows with a dispersed phase. CFD applied to process engineering, IFP, Solaize, March 1993
75. Simonin O, Deutsch E, Minier JP (1993) Eulerian prediction of the fluid particle correlated motion in turbulent two phase flows. *App Sci Res* 51(1-2):275-283
76. Simonin O (1995) *Summerschool on Numerical Modelling and Prediction of Dispersed Two-Phase Flows*. IMVU, Meserburg, Germany
77. Simonin O (1996) *Combustion and turbulence in two-phase flows*. von Karman Lecture Series 1996-02, von Karman Institute for Fluid Dynamics.

78. Sinclair JL (1997) Hydrodynamic Modeling. In: Grace JR, Evidan AA, Knowlton TM, Blackie, London, pp. 149-180
79. Srivastava A, Sundaresan S (2003) Analysis of a frictional-kinetic model for gas-particle flow. *Powder Technology* 129:72-85
80. Taylor GI (1935) Statistical theory of turbulence: Parts I-III. *Proc R Soc London Ser A* 151:421-464
81. Tchen CM (1947) Mean value and correlation problems connected with the motion of small particles suspended in a turbulent fluid. PhD thesis, Delft University of Technology
82. Tham MK, Gubbins KE (1971) Kinetic theory of multicomponent dense fluid mixtures of rigid spheres. *J Chem Phys* 55:268-279
83. van Thai D, Minier JP, Simonin O, Freydier P, Olive J (1994) Multidimensional two-fluid model computation of turbulent dispersed two-phase flows. Numerical methods in multiphase flow ASME, Fluids Eng Div, FED 185:277-291
84. van Wachem BGM, Schouten JC, Krishna R, van den Bleek CM (1998) Eulerian Simulations of Bubbling Behaviour in Gas-Solid Fluidized Beds. *Computers Chem Engng* 22 Suppl:S299-S306
85. van Wachem BGM, Schouten JC, van den Bleek CM, Krishna R, Sinclair JL (2001) Comparative Analysis of CFD Models of Dense Gas-Solid Systems. *AIChE J* 47(5):1035-1051
86. Vincenti WG, Kruger CH Jr. (1967) *Introduction to Physical Gas Dynamics*. Second Printing, John Wiley and Sons, Inc., New York
87. Viollet PL, Simonin O, Olive J, Minier JP (1992) Modelling Turbulent two-phase flows in industrial equipment. In: *Computational methods in applied sciences*, ed Hirsh C, Elsevier Sciences, New York, pp 213-224
88. Viollet PL, Simonin O (1994) Modelling dispersed two-phase flows: Closure, validation and software development. *Appl Mech Rev* 47(6):S80-S84, Part 2, June
89. Wang Q, Squires KD, Simonin O (1998) Large eddy simulation of turbulent gas-solid flows in a vertical channel and evaluation of second-order models. *Int J Heat and Fluid Flow* 19:505-511
90. Yudine MI (1959) Physical considerations on heavy-particle diffusion. *Atmospheric diffusion and air pollution, Advantages in geophysics* 6, New York, Academic Press, pp 185-191

---

## Constitutive Equations

The macroscopic multi-phase models resulting from the local averaging procedures must be supplemented with state equations, constitutive equations, boundary and initial conditions. *The constitutive equations* specify how the phases interact with themselves and with each other. The closure laws or constitutive laws can thus be divided into three types [16]; *Topological, constitutive and transfer laws*, where the first type describes the spatial distribution of phase-specific quantities, the second type describes physical properties of the phases and the third type describes different interactions between the phases.

The accurate modeling of multiphase flows requires that the phase interaction terms given by the jump conditions and the turbulent like effects are correctly parameterized. This problem is very involved since not all of the phase interaction and phase change terms are independent. Most of the existing expressions are of empirical nature, thus experimental data are needed in order to develop and validate laws. Guiding principles for formulating closure laws are given by [31, 3, 35, 36, 37]:

1. The principle of *equipresence* states that if one variable is known to depend on one specific variable, then all other variables to be constituted must be allowed to depend on the same variable (i.e. unless another principle shows that a particular dependence cannot occur).

This principle prevents a priori prejudicing of the constitutive equations by selectively excluding certain dependencies. It is usually this principle which makes the general approach impractical, since it forces us to include dependencies for which there is no physical evidence. In practice, however, this principle has to be compromised.

2. The principle of *well-posedness* states that the description of the motion should be such that a solution to the initial boundary value problem exists and depends continuously on the initial and boundary conditions.

In mathematical terms this implies that all eigenvalues of the system of Partial Differential Equations, PDEs, are real.

3. The principle of *material frame indifference (objectivity)* states that variables, for which constitutive equations are needed, cannot depend on the coordinate frame (i.e., Euclidean space, plus time) in which the variables are expressed.
4. The principle of *coordinate invariance* states that constitutive rules must be stated in such a way that they do not depend on the coordinate system. One way to insure that this principle is satisfied is to work with dyadic or invariant notation as is common practice in the more mathematical engineering disciplines.
5. The *dimensional invariance* principle states that the constitutive equations must be dimensionally correct, and that arbitrary functional dependences can only occur through dimensionless variables.
6. The *phase separation* principle states that the bulk phase quantities should be functions of only the average variables for that phase.
7. The *correct low concentration limits* principle states that, in the limit as  $\alpha_k \rightarrow 0$ , the equations for the dispersed phases should approach the appropriate single particle equations, while the equations for the continuous phase should approach the correct equations for that single phase continuous fluid.
8. The *entropy inequality* principle must hold for all locations of the system. The closure law formulation is restricted by the second law of thermodynamics.

To be able to estimate the interfacial momentum, heat and mass transfer fluxes we need a firm understanding of the basic transport processes. A survey of the pertinent modeling concepts that may be adopted describing these phenomena in chemical reactors is given. Both the well known parameterizations used in the conventional reactor models (i.e., basically denoting a closed set of heat and species mass balances), and a few more rigorous formulations which rely on detailed information of the local flow patterns (i.e., for models that consist of a complete set of the governing balance equations for mass, momentum, heat, and species mass) are described. The latter group of model concepts may have the potential of improving the description of the interfacial fluxes in the more advanced multiphase reactor model formulations.

The primary interfacial closure laws were originally established in the context of the Lagrangian model formulation in which a single particle is surrounded by a continuous fluid of infinite extent. These concepts have later been adopted in the Eulerian models considering dilute non-colliding particulate flows. In this case a volume (space) averaged macroscopic model formulation is most convenient as this view allows of an intuitive physical interpretation of the coupling terms. In recent years the approximate Eulerian interfacial closure law parameterizations are adopted for the alternative macroscopic model formulations as well (even though the original physical interpretations of these closures may not be consistent with the different averaging methods).

## 5.1 Modeling of Multiphase Covariance Terms

The averaged multiphase equations do not contain enough information about the average of products to form a solvable set of equations. In addition, in contrast to single phase flows, the averaged multiphase equations also require some information about the interfacial phenomena occurring at a variety of time and length scales. On the other hand, in both situations the statistical studies of the equations always lead to a situation in which there are more unknowns than equations. This is a *closure* problem similar to that of single phase turbulence theory. In both the single phase and multiphase flow situations one has to make ad hoc assumptions to make the number of equations equal to the number of unknowns.

### 5.1.1 Turbulence Modeling Analogues

In this subsection an overview of the various formulations of the  $k - \epsilon$  turbulence models applied to multiphase flows is given.

In most multiphase modeling approaches the standard single phase  $k - \epsilon$  model formulation is adopted, with only minor modifications to account for the turbulence production and dissipation due to the existence of the dispersed phase. Only a few papers consider the consistent multiphase  $k - \epsilon$  models that can be formulated based on the multiphase equations following a procedure corresponding to the one we applied in sect 1.2.7 for single phase flows. It is noted that the various averaging procedures that might be applied formulating the governing multiphase equations can in specific cases give rise to different terms in the resulting  $k - \epsilon$  model equations, so the turbulence closures derived by use of the different averaging methods do not necessarily coincide (in particular comparing single- and multiple averaging operators).

For convenience a summary of a few important features of the single phase  $k - \epsilon$  model is repeated before the multiphase model extensions are introduced. It is stressed that the conventional form of the single phase  $k$ -equation is defined by (1.401). The corresponding transport equation for the dissipation rate  $\epsilon$  (1.404) is normally formulated empirically based on an analogy to the equation for turbulent kinetic energy (1.401). The latter equation possesses production and dissipation terms that are similar to those in the kinetic energy transport equation but are divided by the turbulence time scale of the energy containing eddies,  $\tau_t = \frac{k}{\epsilon}$  (i.e., the turbulent kinetic energy accumulated at the integral length scale of turbulence is approximated by an averaged  $k$  value for the whole spectrum of turbulence). Moreover, the turbulent kinetic energy production term is modeled based on the eddy viscosity hypothesis (1.380) which is an *isotropic* model for the Reynolds stress assuming that all the normal stresses are equal. In addition, the effective turbulent viscosity (1.406) is approximated by analogy with the kinetic theory of dilute gases (see, e.g., [92], pp 159-160; [116], pp 361-373; [160], pp 18-19). The dissipation rate  $\epsilon$  is estimated based on dimensional analysis (1.429).

A non-isotropic version of the eddy viscosity hypothesis is sometimes used in situations where such effects are essential and the particular flow in question is expected to be far from isotropic [93]. That is, when the turbulent kinetic energy is calculated, the Reynolds stresses can be approximated by:

$$\overline{\mathbf{v}'\mathbf{v}'} = \frac{2}{3}\mathbf{A}k - \nu_t(\nabla\bar{\mathbf{v}} + (\nabla\bar{\mathbf{v}})^T) \tag{5.1}$$

where  $\mathbf{A}$  is a turbulence anisotropy tensor which may be calculated by one of the various algebraic stress models available [108]. Naturally, for the case of isotropic turbulence  $\mathbf{A} = \mathbf{e}$ .

### A $k - \epsilon$ Model for Bubbly Flows: Bubble Induced Turbulence

To enable simulations of two-phase bubbly flows [67] [65] the single phase  $k - \epsilon$  model has been extended by including a semi-empirical production term to take into account the additional turbulence production induced by the bubbles' motion relative to the liquid (i.e., based on the idea of [128] [129]). In this approach it was assumed that the internal flow inside the dispersed phase (gas bubbles) does not affect the liquid phase turbulence. The shear work performed on the liquid by a single bubble, representing the additional turbulence production due to the bubble, was thus assumed to be equal to the product of the drag force and the relative velocity.

In vector notation the two-phase  $k - \epsilon$  model equations for incompressible flows (time averaged) were formulated as follows:

$$\frac{\partial}{\partial t}(\alpha_l \rho_l k) + \nabla \cdot (\alpha_l \rho_l \bar{\mathbf{v}}_l k) = \nabla \cdot (\alpha_l \frac{\nu_{l,t}}{\sigma_k} \nabla k) + \alpha_l (P_k + P_b - \rho_l \epsilon) \tag{5.2}$$

$$\frac{\partial}{\partial t}(\alpha_l \rho_l \epsilon) + \nabla \cdot (\alpha_l \rho_l \bar{\mathbf{v}}_l \epsilon) = \nabla \cdot (\alpha_l \frac{\nu_{l,t}}{\sigma_\epsilon} \nabla \epsilon) + \alpha_l \frac{\epsilon}{k} (C_1 (P_k + P_b) - C_2 \rho_l \epsilon) \tag{5.3}$$

in which  $P_k$  denotes the production of turbulence due to fluid shear and  $P_b$  represents the production of turbulence due to the relative bubble-liquid motion.

The turbulence production term due to the relative bubble-liquid motion per unit volume is expressed as:

$$P_b = C_b \bar{\mathbf{F}}_l \cdot (\bar{\mathbf{v}}_l - \bar{\mathbf{v}}_g) \tag{5.4}$$

In Cartesian index notation this term becomes:

$$P_b = C_b \sum_i \bar{F}_{l,i} (\bar{v}_{l,i} - \bar{v}_{g,i}) \tag{5.5}$$

where  $0 \leq C_b \leq 1$  is a parameter to be empirically determined. This parameter is expected to be related to bubble size and shape as well as the local

turbulent length scale. Note, however, that only the steady drag force part of the generalized drag force formulation has been included so far.

The fluid shear production term is usually expressed as:

$$P_k = \mu_{l,t}(\nabla \bar{\mathbf{v}}_l + (\nabla \bar{\mathbf{v}}_l)^T) : \nabla \bar{\mathbf{v}}_l \quad (5.6)$$

However, we recollect from the derivation of the single phase  $k$ -equation in sect 1.2.7 that the rigorous definition of this production term can be approximated by the generalized Boussinesq hypothesis, in the following manner (conveniently written in tensor notation):

$$P_k = -\rho_l \overline{v'_{l,i} v'_{l,j}} \frac{\partial \bar{v}_{l,i}}{\partial x_j} \approx -\left(\frac{2}{3} \rho_l k \delta_{ij} - \mu_{l,t} \left(\frac{\partial \bar{v}_{l,i}}{\partial x_j} + \frac{\partial \bar{v}_{l,j}}{\partial x_i}\right)\right) \frac{\partial \bar{v}_{l,i}}{\partial x_j} \quad (5.7)$$

This relation is usually further simplified by neglecting the normal stresses due to the assumption of a non-existing inverse cascade of turbulence. The shear production term is thus approximated by

$$P_k \approx \mu_{l,t} \left(\frac{\partial \bar{v}_{l,i}}{\partial x_j} + \frac{\partial \bar{v}_{l,j}}{\partial x_i}\right) \frac{\partial \bar{v}_{l,i}}{\partial x_j} \quad (5.8)$$

The two production terms  $P_k$  and  $P_b$  are normally added linearly in the turbulence model, because these mechanisms are assumed to be independent.

For steady-state simulations using Reynolds averaged models the turbulent kinetic energy variable  $k$  denotes a measure of the mean energy considering all time scales (i.e., for the whole energy spectrum). For a typical energy spectrum we know that most of the energy is accumulated on the larger scales of turbulence and very little on the smaller scales. Therefore, the  $k$ -quantity is sometimes used as a measure of the energy level on the integral scales (i.e., the larger energy containing scales).

Unsteady turbulent flow simulations using Reynolds averaged models have been discussed by [130] (chap 21) and [151] (Chap 6). The physical interpretation of the quantities used in these models has been a matter of discussion. Schlichting and Gersten [130] (chap 21) stated that these flow variables are interpreted as time average quantities whereby the time interval used in the averaging operator has been chosen large enough to include all turbulent fluctuations, but still small enough to contain no effect from the transient, or periodic, part. This concept is based on the assumption that the transient process occurs very slowly, or that the frequency of the oscillation is very small and lies outside the turbulent spectrum. Telionis [151] (Chap 6) discussed an extension of this approach, the triple decomposition, where the instantaneous quantities are decomposed into three parts. Note that in the standard Reynolds decomposition we split the instantaneous velocities into a time independent time average (mean) and a fluctuation, whereas in the triple decomposition approach the mean motion is also dependent on time. The mean is thus generally made up of a time independent part and a time dependent ordered part.

In other cases the application of this concept has been further extended simulating faster turbulent fluctuations that are within the turbulence spectrum. For such dynamic simulations, using Reynolds averaged models, the  $k$ -quantity represents the turbulent kinetic energy accumulated on the fraction of the spectrum that is represented by the modeled scales. Therefore, to compare the simulated results obtained with this type of models with experimental data, that is averaged over a sufficient time period to give steady-state data (representing the whole spectrum of turbulence), both the modeled and the resolved scales have to be considered [68].

Similarly, in our analysis of the dynamic multiphase flow pattern within chemical reactors we may need information on the size of eddies and on the scales of the coherent structures that can be observed within the flow. Unfortunately, in practice it is difficult to create a snapshot picture of the flow pattern in the reactors. Instead of observing a large region of space at an instant in time, we find it easier to make measurements at one point in space over a long time period. This approach is in accordance with the hypothesis of Taylor [150], as mentioned in sect 1.2.7. Taylor suggested that for quasi-steady single phase turbulent flows (i.e., homogeneous turbulence with respect to time), turbulence might be considered to be *frozen* as it advects past a sensor. Thus, the fluid velocity could be used to translate turbulence measurements determined as a function of time to their corresponding measurements in space. However, the approximate hypothesis is valid for the homogeneous fields only in which a constant mean velocity prevails, say  $\bar{v}_z$  in the the  $z$ -direction.

From sect 1.2.7 we reiterate that Taylor's simplification is useful for flow situations where the turbulent eddies evolve with a time scale longer than the time it takes an eddy to be advected past a fixed spatial point (e.g., the location of a sensor). If an eddy of diameter  $\lambda$  is advected at a mean velocity of magnitude,  $|\bar{v}|$ , (i.e., considering a uniform flow with mean velocity,  $\bar{v}$ , of low intensity, so that  $\bar{v} \gg \sqrt{v'^2}$ ) the time period,  $P$ , for it to pass by a stationary sensor is given by:

$$P = \frac{\lambda}{|\bar{v}|} \quad (5.9)$$

The Taylor hypothesis can also be stated in terms of a wavenumber,  $\kappa$ , and frequency,  $f$ :

$$\kappa = \frac{f}{|\bar{v}|} \quad (5.10)$$

where  $\kappa = \frac{2\pi}{\lambda}$ , and  $f = \frac{2\pi}{P}$ , for wavelength  $\lambda$  and wave period  $P$ . The dimensions of  $\kappa$  are radians per unit length, while  $f$  has dimensions of radians per unit time.

To satisfy the requirement that the turbulent properties of the flow within the eddy will not change significantly as the eddy advects past a sensor, the following criterion should be fulfilled:

$$\sigma_M \left\langle \frac{|\bar{v}|}{2} \right\rangle \quad (5.11)$$

where  $\sigma_M$ , the standard deviation of the magnitude of the velocity, is a measure of the intensity of turbulence. Thus, Taylor's hypothesis should be satisfactory when the turbulence intensity is small relative to the magnitude of the velocity.

The Taylor hypothesis has been further discussed by [144] (pp 5-7) and [59] (pp. 31-81) considering theories of double correlations between turbulence-velocity components, the features of the double longitudinal and lateral correlations in homogeneous turbulence, integral scales of turbulence, and Eulerian, Lagrangian and mixed Eulerian-Lagrangian correlations.

In this case it is usually assumed that [59] (p 46):

$$\frac{\partial}{\partial t} = -\bar{v}_z \frac{\partial}{\partial z} \quad (5.12)$$

Thus, Taylor's hypothesis is valid only if all terms on the right hand side of the  $z$ -component of the momentum equation (i.e., considering a homogeneous flow field that has a constant mean velocity given as  $\bar{v}_z$ ) are very small compared with the terms on the left hand side.

For steady-state simulations, considering the turbulence spectrum in terms of eddy size (length scale), the scales predicted by the  $k$ - $\epsilon$  model is thus much larger than the particle size. The inclusion of turbulence production due to the bubbles' relative motion is therefore based on the assumption of an inverse cascade of turbulence.

For dynamic simulations the  $k$ -quantity may represent scales less than or at the same order of magnitude as the particle size. In the cases where the extra turbulence production mechanisms represent scales larger than the ones represented by the modeled part of turbulence, no extra terms should be included in the turbulence model.

The physical interpretation that the particles may introduce a inverse cascade of turbulence has been confirmed numerically by [44] who used direct numerical simulations of arrays of bubbles (12 by 12 and 18 by 18) in 2D low Reynolds number bubbly flows to investigate the relative motion of several bubbles. They found that the bubbles produced eddies much larger than the bubble size. Those eddies kept growing until they were of the same size as the computational domain for the small (12 by 12) array. (For the 18 by 18 array the computation was stopped while the eddies were still growing, and not reached the size of the computational domain). Later studies on the the inverse energy cascade structure of turbulence in bubbly flows and on turbulence structures induced by bubble buoyancy by [106, 107] confirmed the findings of [44].

The given  $k$  -  $\epsilon$  turbulence model formulation has been used to determine the turbulence of the continuous phase in two-phase bubbly flow by several investigators on bubble columns (e.g., [65, 127]) and on stirred tank reactors (e.g., [49]).

### A $k - \epsilon$ for Bubbly Flows: Two Time Scales

Lopez de Bertodano et al [93] proposed a similar extension of the standard single-phase  $k - \epsilon$  model considering two time scales of turbulence to enable simulations of bubbly two-phase flows.

The basis for their model development was an analysis of the asymptotic behavior of both the modified single-phase  $k - \epsilon$  model described above, and a two-phase  $k - \epsilon$  model developed from the time averaged two-fluid model equations (i.e., by use of the time averaging operator outlined in sect 3.4.2 or alternatively by use of the generalized single averaging operator procedure discussed in sect 3.4.3). Two physical flows were analyzed: Bubbles rising in a still tank of liquid, and homogeneous decay of grid generated turbulence in bubbly flow.

The two-phase  $k - \epsilon$  model analyzed was based on the Favre averaged transport equation for turbulent kinetic energy developed by [73, 74]. The resulting transport equation for kinetic energy is similar to the one obtained from the single phase model (5.2), supporting the semi-empirical modification introduced in that model.

The formulation of a proper  $\epsilon$  - equation for the case of bubbly flow was found to be more severe. As a first approach they adopted the above equation developed from the single phase transport equations (5.3). However, analyzing the two physical situations mentioned above, they found that this model formulation fails to produce both the asymptotic value and the time constant of homogeneous decay of grid generated bubbly flow turbulence. That is, the modified single-phase model did not break down, but it gave rise to unphysical solutions for such cases.

Based on these observations [93] proposed a modified model containing two time constants, one for the liquid shear induced turbulence and a second one for the bubble induced turbulence. The basic assumption made in this model development is that the shear-induced turbulent kinetic energy and the bubble-induced turbulent kinetic energy may be linearly superposed in accordance with the hypothesis of [128, 129]. Note, however, that [82] observed experimentally that this assumption is only valid for void fractions less than 1 %, whereas for higher values there is an amplification in the turbulence attributed to the interactions between the bubbles. The application of this model to the high void fraction flows occurring in operating multiphase chemical reactors like stirred tanks and bubble columns is thus questionable.

Nevertheless, in the first step in the model derivation a transport equation for the bubble induced turbulent kinetic energy was postulated:

$$\frac{\partial}{\partial t}(\alpha_l \rho_l k_{\text{BI}}) + \nabla \cdot (\alpha_l \rho_l \bar{v}_l k_{\text{BI}}) = \nabla \cdot (\alpha_l \frac{\nu_{l,t}}{\sigma_k} \nabla k_{\text{BI}}) + \frac{1}{\tau_b} (k_{\text{BIa}} - k_{\text{BI}}) \quad (5.13)$$

where  $k_{\text{BIa}}$  denotes the asymptotic value of bubble induced turbulent kinetic energy,  $k_{\text{BI}}$  denotes the turbulence generated by the bubbles, and  $\tau_b$  denotes the time constant of the bubble.

Secondly, the standard single phase  $k$ -equation was adopted to describe the shear induced turbulence. Third, by adding these two transport equations, assuming that the bubble and shear induced turbulent kinetic energy contributions can be linearly superimposed, they obtained the following  $k$ -equation for the liquid phase:

$$\begin{aligned} \frac{\partial}{\partial t}(\alpha_l \rho_l k) + \nabla \cdot (\alpha_l \rho_l \bar{\mathbf{v}}_l k) = \nabla \cdot (\alpha_l \frac{\nu_{l,t}}{\sigma_k} \nabla k) + \alpha_l (P_{k,SI} - \rho_l \epsilon_{SI}) \\ + \frac{1}{\tau_b} (k_{BIa} - k_{BI}) \end{aligned} \quad (5.14)$$

To parameterize the new quantities occurring in these equations a few semi-empirical relations from the literature were adopted. The asymptotic value of bubble induced turbulent kinetic energy,  $k_{BIa}$ , is estimated based on the work of [3]. By use of the so-called *cell model* assumed valid for dilute dispersions, an average relation for the pseudo-turbulent stresses around a group of spheres in potential flow has been formulated. From this relation an expression for the turbulent normal stresses determining the asymptotic value for bubble induced turbulent energy was derived:

$$k_{BIa} = \alpha_g \frac{1}{2} C_V |\bar{\mathbf{v}}_l - \bar{\mathbf{v}}_g|^2 \quad (5.15)$$

Lopez de Bertodano [92] defined a time constant for the bubbles by:

$$\tau_b = \frac{d_b}{|\bar{\mathbf{v}}_l - \bar{\mathbf{v}}_g|} \quad (5.16)$$

whereas [93] redefined this definition to make the model consistent with the two-phase model of [74]:

$$\tau_b = \left( \frac{2}{3} \frac{C_V}{C_D} \right) \frac{d_b}{(|\bar{\mathbf{v}}_l - \bar{\mathbf{v}}_g|)} \quad (5.17)$$

This relation was obtained using the well-known expression for steady interfacial drag and the two formulations for bubble induced turbulence production (i.e., the one given by [74], and the other one defined by [93]).

At this point it is important to notice that the interfacial source and dissipation terms occurring in the  $k$ - equation above are consistent with the source and sink terms in the two-phase  $k$  - equation developed by [74]. Lopez de Bertodano et al [93] recognized that the terms  $\rho_l \epsilon_{SI} + \frac{k_{BI}}{\tau_b}$  are a linear superposition of shear and bubble induced dissipation. Similarly, the terms  $P_{k,SI} + \frac{k_{BIa}}{\tau_b}$  were found to denote the linear superposition of the shear and bubble induced sources of turbulence. Note that the latter term, i.e., by introducing the suggested parameterizations, is identical to the bubble induced source of turbulence ( $P_b$ ) which was taken to be proportional to the work done on the liquid by the bubbles as shown in equation (5.3). The  $k$  - equation used by [93] is thus identical to equation (5.3). The only modification

introduced into the modified single phase  $k - \epsilon$  model is that the production of bubble induced dissipation used in the  $\epsilon$  - equation, i.e.,  $\alpha_l \frac{\epsilon}{k} C_1 P_b$ , has been replaced by a bubble induced dissipation term arising from the above derivation,  $\epsilon_{\text{BI}} = -\frac{k_{\text{BIa}}}{\tau_b}$ . The  $\epsilon$  - equation used by Lopez de Bertodano et al [93] is then given by:

$$\frac{\partial}{\partial t}(\alpha_l \rho_l \epsilon) + \nabla \cdot (\alpha_l \rho_l \bar{\mathbf{v}}_l \epsilon) = \nabla \cdot (\alpha_l \frac{\nu_{l,t}}{\sigma_\epsilon} \nabla \epsilon) + \alpha_l \frac{\epsilon}{k} (C_1 P_k - C_2 \rho_l \epsilon) - \epsilon_{\text{BI}} \quad (5.18)$$

Lopez de Bertodano [92] stated that this simple modification has a big effect on the dynamic and the asymptotic behavior of the model. At a later stage, [93] also stated that the bubble induced time constant, which is proportional to the residence time of a bubble, is usually very short compared to the time constant of the shear induced turbulence. They concluded that for most practical cases the transport equation for bubble induced turbulence (5.13) can be reduced to  $k_{\text{BI}} = k_{\text{BIa}}$ .

Another important modification implemented is that [92] and [93] assumed that the idea of linear superposition may also be used for the viscosity. Sato et al [129] proposed that for bubbly flow the turbulent viscosity should be the sum of the single phase shear induced turbulent viscosity ( $\nu_{\text{SI}}$ ) and the bubble induced turbulent viscosity ( $\nu_{\text{BI}}$ ):

$$\nu_t = \nu_{\text{SI}} + \nu_{\text{BI}} \quad (5.19)$$

where the bubble induced viscosity is given by [129]:

$$\nu_{\text{BI}} = 1.2 \frac{d_b}{2} \alpha_g |\bar{\mathbf{v}}_l - \bar{\mathbf{v}}_g| \quad (5.20)$$

This simple model for bubble induced viscosity is a Prandtl mixing length model with the bubble radius as the mixing length and  $1.2 \alpha_g |\bar{\mathbf{v}}_l - \bar{\mathbf{v}}_g|$  as the mean eddy fluctuation (i.e.,  $\nu_{\text{BI}} = l_m \sqrt{\overline{v'^2}}$ ). The shear induced turbulent viscosity is still given by (1.406).

A few attempts to apply this model for the description of bubble column operation have been reported in the literature (e.g., [49]). However, no notable improvements were obtained compared to the single time-scale model.

## Turbulence Models for Gas-Solid Two-Phase Flows

Elghobashi [42] gives an overview of the challenges and progress associated with the task of numerically predicting solid particle-laden turbulent flows. The review covers the mathematical methods based on turbulence closure models as well as direct numerical simulation (DNS). The review is restricted to incompressible, isothermal flows without phase change or particle-particle collision. The flow situations where particle-particle collisions become important are discussed in chap 4 considering kinetic theory and granular flows.

In most gas-particle flow situations occurring in fluidized bed reactors, a standard  $k - \epsilon$  turbulence model is used to describe the turbulence in the continuous phase whereas a separate transport equation is formulated for the kinetic energy (or granular temperature) of the particulate phase [122, 42, 41, 165, 84, 52]. Further details on granular flows are given in chap 4.

### A Fairly Rigorous $k - \epsilon$ Model for Two-phase Flows

Elghobashi and Abou-Arab [40] did develop a modeled  $k - \epsilon$  turbulence model for two-phase flows. As basis the fairly rigorous instantaneous volume averaged momentum equation for the continuous phase was adopted (i.e., neglecting the spatial covariance terms), derived beforehand in accordance with the time - after volume averaging procedure described in sect 3.4.4. The conventional Reynolds averaging procedure was adopted for the time averaging process. Constitutive equations for the resulting time-averaged equations were suggested for the turbulent covariances up to third order.

However, to the author's knowledge, this model has not been applied for the prediction of multiphase reactors mostly due to the complexity of the suggested closure relations. On the other hand, this paper serves as a useful reference as the exact derivation of the  $k - \epsilon$  model equations are given and discussed. Parts of this modeling work have been adopted in many papers.

## 5.2 Interfacial Momentum Closure

Many authors have addressed the mathematical problem of averaging microscopic balance equations in order to derive macroscopic model formulations. However, the result is always a set of equations in which extra terms involving integrals over the microscopic domains remain. While various hypotheses may be made about interfacial closure laws expressing these extra terms as functions of the solution variables, it is not clear that such laws always exist, what form they should take and what approximations may be implied in their use.

One can thus state that the constitutive equations for the interfacial terms are the weakest link in a multi-fluid model formulation because of considerable difficulties in terms of experimentation and modeling on a macroscopic level. The main difficulties in modeling arise from the existence of interfaces between phases and discontinuities associated with them.

In practice one needs to provide appropriate formulations for the interfacial momentum closure laws using analytical expressions which are (to some extent) based on the general modeling principles presented in the introduction of this chapter, and that physically reproduce experimental results with reasonable fidelity. The formulations that will be given for various forces and effects will typically be applicable only for given ranges of particle-fluid conditions.

Introductorily we examine a generally accepted momentum balance formulation for a small (point) particle generally referred to as Newton's second law. The net force is conventionally split into the uncoupled effects of drag, gravity ( $\mathbf{f}_G$ ), body forces other than gravity ( $\mathbf{f}_E$ ), hydrostatic pressure force ( $\mathbf{f}_{hp}$ ), external pressure gradient force ( $\mathbf{f}_p$ ), pressure gradient term ( $\mathbf{f}_{pg}$ ), and wall interactions ( $\mathbf{f}_W$ ). The net drag force or *generalized drag* is usually split into the effects of steady drag ( $\mathbf{f}_D$ ), lift ( $\mathbf{f}_L$ ), virtual - or added mass ( $\mathbf{f}_V$ ), and Basset history force ( $\mathbf{f}_B$ ) terms. A fairly rigorous form of the Newton's second law can be expressed by [100, 7, 101, 96, 26, 94]:

$$\begin{aligned} \frac{d}{dt}(m_p \mathbf{v}_p) &= \sum_k \mathbf{f}_k \\ &\approx \mathbf{f}_D + \mathbf{f}_L + \mathbf{f}_V + \mathbf{f}_B + \mathbf{f}_G + \mathbf{f}_E + \mathbf{f}_{hp} + \mathbf{f}_p + \mathbf{f}_{pg} + \mathbf{f}_W \end{aligned} \quad (5.21)$$

This equation is referred to as the Basset [10] -Boussinesq [18]-Osceen [112] (BBO) equation.

The linear split of the net drag force acting on the particle is not always valid as there can be non-linear interactions between the various forces. Such interactions are not well understood, but are typically small enough to be neglected for many conditions [94].

For a particle moving in a fluid in motion the momentum equation might be extended including the so-called *pressure gradient force* term:

$$\mathbf{f}_{pg} = m_c \frac{D\mathbf{v}_c}{Dt} \quad (5.22)$$

which represents the force generated by the local pressure gradient in the fluid surrounding the particle due to fluid acceleration. In this model  $m_c$  denotes the mass of fluid enclosed in the volume of the particle. The pressure gradient term is naturally associated with the fluid acceleration as determined from the Navier-Stokes equation for the conveying fluid [22, 26].

For gas-rigid particle and gas-droplet flows, where the ratio of the continuous phase density to the dispersed particle material density is small ( $\sim 10^{-3}$ ), the RHS of the BBO equation is dominated by the steady drag ( $\mathbf{f}_D$ ) and the gravity ( $\mathbf{f}_G$ ) forces. For liquid-solid flows for which the densities are comparable a complete BBO equation might be required. For bubbly flows the important forces are  $\mathbf{f}_D$ ,  $\mathbf{f}_L$ ,  $\mathbf{f}_V$ ,  $\mathbf{f}_G$ , and  $\mathbf{f}_{hp}$ . It is noted that the virtual mass force is of particular importance in this case because the fluid phase density is much larger than the particle density ( $\sim 10^3$ ). In general, the steady drag and gravity forces are the predominant forces in multiphase flow systems, and as such it is helpful to consider the ratio of the other forces to either of these so that their inclusion or neglect can be properly decided.

The fluid-particle interaction closures applied in the modern single particle momentum balances originate from the classical work on the Newton's second law as applied to a small rigid sphere in an unsteady, non-uniform flow limited to Stokesian flow conditions ( $Re_P \ll 1$ ), as derived by Stokes [142] and

Basset [10]. The formulation of extended force expressions which are valid for larger particle Reynolds numbers to enable a more general description have later been the subject of much experimental and theoretical research. The fundamental modeling principles are outlined in the sequel.

In mathematical terms the total hydrodynamic surface force,  $\mathbf{f}_S$ , exerted by a continuous fluid on a particle is defined as [118] [11] (p. 404) [120, 14]:

$$\mathbf{f}_S = - \iint_A \mathbf{T} \cdot \mathbf{n} da \quad (5.23)$$

where  $\mathbf{T}$  is the total stress tensor for the continuous fluid and  $\mathbf{n}$  is the outward directed unit normal vector to the particle surface  $A$ .

The components  $f_{S,i}$  of the hydrodynamic force on the sphere are given by [120, 14]:

$$f_{S,i} = - \iint_A T_{ij} n_j da \quad (5.24)$$

where  $T_{ij}$  denotes the components of the total stress tensor,  $\mathbf{T}$ , in the  $x_i$ -direction acting on a surface element whose normal is in the  $x_j$ -direction, and  $n_j$  is the  $j^{\text{th}}$  component of the unit outward normal vector to the particle surface,  $A$ .

To evaluate the integral in the surface force definition (5.23), and to make the formulation consistent with the conventional momentum balance given (5.21), the conveying fluid pressure is decomposed into three contributions:

$$p_c = \rho_c \mathbf{g} \cdot \mathbf{r} + p_{c,\text{ext}} + p_{c,\text{dyn}} \quad (5.25)$$

The first term on the RHS corresponds to the hydrostatic pressure ( $p_{c,hp}$ ), the second represents any external pressure not induced by gravity ( $p_{c,\text{ext}}$ ), and the third ( $p_{c,\text{dyn}}$ ) denotes the dynamic pressure.

The surface force can then be rewritten as:

$$\begin{aligned} \mathbf{f}_S &= - \iint_{A_p} [(\rho_c \mathbf{g} \cdot \mathbf{r} + p_{c,\text{ext}} + p_{c,\text{dyn}}) \mathbf{e} + \boldsymbol{\sigma}_c] \cdot \mathbf{n} da \\ &= - \iiint_{V_p} \nabla \cdot (\rho_c \mathbf{g} \cdot \mathbf{r} + p_{c,\text{ext}}) \mathbf{e} dv - \iint_{A_p} (p_{c,\text{dyn}} \mathbf{e} + \boldsymbol{\sigma}_c) \cdot \mathbf{n} da \\ &= - V_p (\rho_c \mathbf{g} + \nabla p_{c,\text{ext}}) + \mathbf{f}_{\text{hydr}} = \mathbf{f}_{hp} + \mathbf{f}_p + \mathbf{f}_{c,\text{hydr}} \end{aligned} \quad (5.26)$$

this transformation is restricted to incompressible fluids and constant external pressure gradients.

The net hydrodynamic force, frequently also referred to as the generalized drag force, is usually further divided into numerous contributions like the steady drag, virtual mass, lift, and history forces:

$$\mathbf{f}_{c,\text{hydr}} \approx \mathbf{f}_D + \mathbf{f}_V + \mathbf{f}_L + \mathbf{f}_{\text{hist}} \quad (5.27)$$

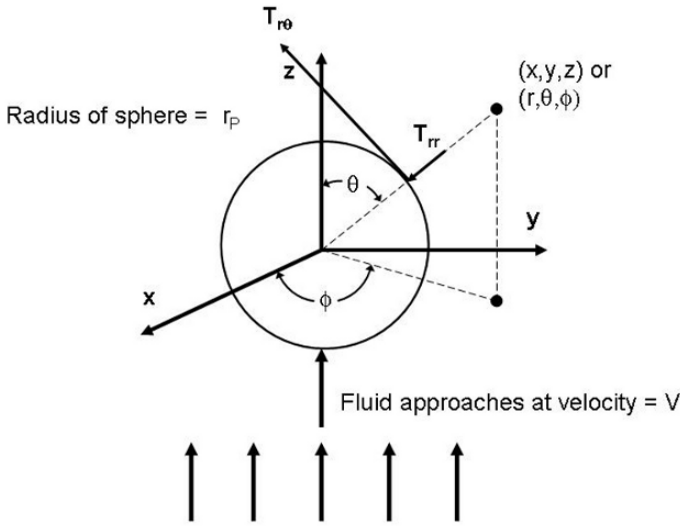


**Fig. 5.1.** Normal and shear stresses acting on the surface of a sphere, The stresses are due to the flow around the sphere with fluid velocity  $V\mathbf{e}_z$  far from the sphere.

In the general case the structure of the hydrodynamic force for incompressible fluids is generally retained.

The *steady drag* is the component of the hydrodynamic force acting on the particle surface in the continuous phase flow direction. One might, for example, imagine a uniform velocity in the  $z$ -direction as sketched in Fig 5.1, and describe the external flow using the Cartesian coordinate system, then the steady drag force is defined by [14, 30]:

$$f_{D,z} = - \iint_A p \mathbf{e}_z \cdot \mathbf{n} da - \iint_A \mathbf{n} \cdot \boldsymbol{\sigma} \cdot \mathbf{e}_z da \tag{5.28}$$

where  $p$  is the pressure,  $\mathbf{e}_z$  is the unit vector in the  $z$ -direction, and  $\boldsymbol{\sigma}$  is the viscous stress tensor. By use of vector and tensor identities, this expression may be rearranged to:

$$f_{D,z} = - \iint_A p n_z da - \iint_A \sigma_{zj} n_j da \tag{5.29}$$

The steady drag force may be split into two components, the *form drag* and the *friction drag*. The form drag, also called *pressure drag*, is the normal components of the total stress integrated over the surface area, while the friction drag consists of the surface integral of the shear components of the total stress. Consequently, the drag forces are defined as:

$$f_{D,z} = f_{D,\text{form}} + f_{D,\text{friction}} \quad (5.30)$$

The form and friction drag forces are given by:

$$f_{D,\text{form}} = - \iint_A p n_z da - \iint_A \sigma_{zz} n_z da \quad (5.31)$$

$$f_{D,\text{friction}} = - \iint_A (\sigma_{zx} n_x + \sigma_{zy} n_y) da \quad (5.32)$$

The *lift* force is the component of the hydrodynamic force acting on the particle surface normal to the direction of flow, say  $y$ -direction as we are considering a uniform fluid velocity in the  $z$ -direction [30]:

$$f_{L,y} = - \iint_A p \mathbf{e}_y \cdot \mathbf{n} da - \iint_A \mathbf{n} \cdot \boldsymbol{\sigma} \cdot \mathbf{e}_y da \quad (5.33)$$

where  $\mathbf{e}_y$  is the unit vector in the  $y$ -direction.

For applications in Eulerian model formulations the particles are assumed small and the dispersion is sufficiently dilute so that there is no significant particle-particle interactions [64] [65]. The net force on the particles per unit of mixture volume,  $\mathbf{F}_P$ , is then obtained by multiplying  $\mathbf{f}_P$  by the number density of particles,  $N_P$  (e.g., Albråten [1]):

$$\mathbf{F}_P = \mathbf{f}_P N_P \quad (5.34)$$

where  $\mathbf{f}_P$  is the net force on a single sphere.

It is noted that even though this relation (5.34) is often adopted when reactor modelers attempt to approximate the macroscopic interfacial momentum coupling terms in the averaged multi-fluid model formulations, such a closure is strictly not rigorous. That is, the given relation (5.34) is rigorous in itself but it is not strictly consistent with the coupling terms produced by the averaging procedures. Recollect that the average transfer terms are generally defined in terms of the difference between the total pressure and viscous stresses and their interfacial average counterparts so that these definitions deviate significantly from those used obtaining the classical solutions for the drag force components.

The number density of particles per unit mixture volume, can be expressed in terms of the volume fraction of the dispersed phase,  $\alpha_d$ , and the averaged particle volume,  $V_p$ :

$$N_p = \frac{\alpha_p}{V_p} = \frac{\text{Number of Particles}}{\text{Mixture Volume}} \quad (5.35)$$

where the volume fraction of the dispersed phase is given by:

$$\alpha_p = \frac{\text{Volume of particulate phase}}{\text{Mixture Volume}} = V_p N_p. \quad (5.36)$$

The average volume of a single particle is given by:

$$V_p = \left(\frac{\pi}{6}\right)d_V^3 \quad (5.37)$$

where  $d_V$  is the volume averaged particle diameter.

Indeed, several important length scales for a dispersed system can be defined [64].

The Sauter mean diameter:

$$d_S = \frac{6V_p}{A_S} \quad (5.38)$$

The drag diameter:

$$d_D = \frac{3V_p}{2A_P} \quad (5.39)$$

The equivalent diameter:

$$d_V = \left(\frac{6V_p}{\pi}\right)^{1/3} \quad (5.40)$$

and surface diameter:

$$d_A = \left(\frac{A_S}{\pi}\right)^{1/2} \quad (5.41)$$

in which  $A_S$  is the average surface area per particle, and  $A_P$  is the average projected area per particle on a plane normal to the flow. For spherical particles the above defined diameters are all equivalent. For a system with a distribution of particle sizes it is necessary to calculate the corresponding mean values for these parameters.

One can now define the interfacial area concentration or contact area  $a_S$  by:

$$a_S = N_p A_S \quad (5.42)$$

Using the given length scale definitions (5.38) to (5.41) the area concentration can be expressed in a number of forms:

$$a_S = \frac{6\alpha_P}{d_S} = \frac{6\alpha_P}{d_V} \left(\frac{d_A}{d_V}\right)^2 = \frac{6\alpha_P}{d_D} \left(\frac{d_D}{d_S}\right) \quad (5.43)$$

The ratio of the Sauter mean diameter to the drag diameter appears as a shape factor. It is noted that for non-spherical particles or for systems with a particle size distribution, the various shape factors may not be unity. However, for a distribution of spherical particles, the shape factor,  $\left(\frac{d_{PD}}{d_{PS}}\right)$ , is unity regardless of the particle size distribution. However, in most reactor simulations the shape factors have been set to unity for all multiphase systems.

Obtaining closed expressions describing the hydrodynamic forces experienced by rigid particles, drops or bubbles embedded in various flows has been a subject of active research since the first experimental studies of the drag force on spheres in viscous fluid were made by Newton in 1710 [141]. A brief survey of the important experimental observations, theory and the commonly used generalized drag force models is given in the following

subsections. Numerous review papers present the state-of-the-art concerning the steady drag, history, added mass and lift forces. The reviews by [22, 65, 96, 103, 26, 174, 143, 94, 97, 98, 99, 147] are recommended for complementary studies.

### 5.2.1 Drag force on a single rigid sphere in laminar flow

Stokes showed in 1851 that for very low Reynolds numbers ( $\text{Re}_P \ll 1$ ) the drag force can be found by theoretical analysis [142]:

$$f_D = 6\pi\mu_f r_p v_{\text{rel}} \quad (5.44)$$

which consists of one third *form drag* (due to pressure) and two thirds *friction drag* (due to shear stresses).

Due to its great importance in reactor simulations, a brief survey of the main steps involved in Stokes' solution of the Navier-Stokes equation for creeping motion about a smooth immersed rigid sphere is provided. The details of the derivation is not repeated in this book as this task is explained very well in many textbooks [169, 14, 103, 15].

Consider an incompressible creeping motion of a uniform flow of speed  $V = |\mathbf{v}| \approx |v_z \mathbf{e}_z|$  approaching a solid sphere of radius  $r_p$ , as illustrated in Fig 5.1. To describe the surface drag force in the direction of motion it is convenient to use spherical polar coordinates  $(r, \theta)$ , with  $\theta = 0$  in the  $z$ -direction. Moreover, we assumed symmetry about the  $z$ -axis (placing origin of the external Cartesian coordinate system for the bulk flow at the mass center of the sphere so that it coincides with the origin of the internal spherical coordinate system) reducing the continuity and Navier-Stokes equations significantly because all derivatives  $\partial/\partial\phi$  and all terms with  $v_\phi$  can be disregarded. The approximate 2D flow problem is then transformed by use of the Stokes stream function and solved analytically as the problem yields a product solution  $\psi(r, \theta) = f(r)g(\theta)$ . The two unknown velocity components  $v_r(r, \theta, \psi)$  and  $v_\theta(r, \theta, \psi)$  are related to the Stokes stream function and can thus be expressed in terms of  $(r, \theta)$  only, eliminating the stream function variable using the Stokian analytical solution  $\psi = \psi(\theta, r)$  for creeping motion past a sphere. With  $v_r(r, \theta)$  and  $v_\theta(r, \theta)$  known, the pressure  $p(r, \theta)$  is found by integrating the reduced form of the momentum equation neglecting all the inertia terms. The local surface problem is linked to the uniform bulk velocity through the boundary conditions, revealing the convenience of making the origins of the internal and external coordinate systems coincide. In view of the symmetry assumption adopted the fluid exerts a shear stress  $T_{r\theta}(r_p, \theta)$ , tangential to the particle surface, and a radial normal stress  $T_{rr}(r_p, \theta)$ , perpendicular to the surface. At any point on the surface of the sphere, both stresses have components in the direction of motion. It follows that at any point on the surface the normal stress has a component  $(-T_{rr}(r_p, \theta) \times \cos \theta)$  in the direction of motion. The drag force due to this stress is obtained from (5.29) by integration over the entire surface of the particle. Hence,

$$\begin{aligned}
f_{D,z}^{\text{Normal}} &= \int_0^{2\pi} \int_0^\pi \left[ -T_{rr}(r_p, \theta) \cos \theta \right] r_p^2 \sin \theta d\theta d\phi \\
&= 2\pi \int_0^\pi \left[ -\left( p - 2\mu \frac{\partial v_r}{\partial r} \right) \Big|_{r_p} \cos \theta \right] r_p^2 \sin \theta d\theta = 2\pi \mu r_p V
\end{aligned} \tag{5.45}$$

In most papers the contribution from the normal viscous stresses is assumed negligible compared to the pressure contribution [169, 22, 14, 15]. Nevertheless, Middleman [103] kept the normal viscous stress contributions<sup>1</sup> and after a lengthy exercise in calculus he shows that the the above mentioned simplification is valid. Actually, for any kind of flow pattern the normal viscous stresses are zero at fluid-solid boundaries for Newtonian fluids with constant density (i.e., in which the continuity equation reduces to  $\nabla \cdot \mathbf{v} = 0$ ) as a consequence of the no-slip boundary condition [15].

Likewise, the viscous shear component ( $T_{r\theta}(r_p, \theta) \times \sin \theta$ ) can be integrated to give a viscous force acting in the direction of the external flow.

$$\begin{aligned}
f_{D,z}^{\text{Shear}} &= \int_0^{2\pi} \int_0^\pi \left[ T_{r\theta}(r_p, \theta) \sin \theta \right] r_p^2 \sin \theta d\theta d\phi \\
&= 2\pi \int_0^\pi \left[ -\mu \left( r \frac{\partial}{\partial r} \left( \frac{v_\theta}{r} \right) + \frac{1}{r} \frac{\partial v_r}{\partial \theta} \right) \Big|_{r_p} \cos \theta \right] r_p^2 \sin \theta d\theta = 4\pi \mu r_p V
\end{aligned} \tag{5.46}$$

The total drag on the sphere in the direction of flow becomes

$$f_{D,z} = f_{D,z}^{\text{Normal}} + f_{D,z}^{\text{Shear}} = 2\pi \mu r_p V + 4\pi \mu r_p V = 6\pi \mu r_p V \tag{5.47}$$

This result is called the Stokes law. For a freely moving particle the interfacial drag formulation is normally modified and written as (5.44).

Except for the Stokes' regime<sup>2</sup>, an analytical description of the flow field is difficult. It has thus become common practice to apply a generalized steady drag force formulation intended to be valid for all flow regimes. Applying the principle of coordinate invariance, one intends to work with an invariant notation. Considering a particle motion in a continuous fluid the velocity relative to the surrounding fluid, and not only the fluid velocity as indicated by Stokes law, will determine an invariant drag force (i.e., an expression for the force that is independent of the coordinate system). This leads to the standard expression for the steady drag [64, 35, 120, 26]:

<sup>1</sup> It is not evident whether the normal viscous contribution should be regarded as a component of form drag or of skin friction.

<sup>2</sup> It is noted that Oseen [112], Proudman and Pearson [119], among others, extended Stokes' theoretical analysis to the narrow range  $\text{Re}_P < 5$  by including inertial effects in the flow field away from the particle surface.

$$\mathbf{f}_D^{\text{Steady}} = \frac{1}{2} C_D \rho_f A_P |\mathbf{v}_f - \mathbf{v}_p| (\mathbf{v}_f - \mathbf{v}_p) \quad (5.48)$$

where  $C_D$  is the drag coefficient.

For the problem of describing fluid flow past a rigid sphere, the relative importance of the convective acceleration term (also called the inertia term) and the linear viscous acceleration term can be assessed by dimensional arguments. Consider the drag force on a sphere falling or raising in the  $+z$ -direction within a stagnant fluid or the equivalent drag force exerted by a uniform flow, in the  $-z$ -direction, past a fixed sphere. Physically, these flows are characterized by the size of the sphere, for which we often take the particle diameter,  $d_P$ , as a natural measure, and by the terminal velocity,  $v_\infty$ . Therefore, we may expect  $\mathbf{v} \cdot \nabla \mathbf{v}$  to be of order  $v_\infty^2/d_P$ , and  $\nu \nabla^2 \mathbf{v}$  to be of order  $\nu v_\infty/d_P^2$ . This leads to the estimate:

$$\left| \frac{\mathbf{v} \cdot \nabla \mathbf{v}}{\nu \nabla^2 \mathbf{v}} \right| \sim \left| \frac{v_\infty^2/d_P}{\nu v_\infty/d_P^2} \right| \sim \left| \frac{v_\infty d_P}{\nu} \right| = Re_P \quad (5.49)$$

where  $Re_P$  is the particle Reynolds number.

From the  $z$ -component of the momentum equation it can be shown that the inertia term may be omitted if  $Re_P \ll 1$ . In other words, when the inertia term is not negligible, the drag formula given by Stokes law is no longer valid. The drag relation is thus modified by introducing a drag coefficient,  $C_D$ , defined by (e.g., [22, 120, 141, 103]):

$$C_D = \frac{f_{D,z}^{\text{Steady}}}{\frac{1}{2} \rho_f v_\infty^2 A_P} \quad (5.50)$$

This dependence of  $f_{D,z}^{\text{Steady}}$  on  $v_\infty$ ,  $d_P$ ,  $\mu$  and  $\rho_f$  may become more obvious writing the equations of motion for incompressible flow in dimensionless form (e.g., [14, 120, 169]).

The variables and terms in the governing equations are made dimensionless by introducing  $r' = r/d_P$ ,  $p' = p/(\rho v_\infty^2)$ ,  $\mathbf{v}' = \mathbf{v}/v_\infty$  and  $\nabla' = d_P \nabla$  into the equations:

$$\mathbf{v}' \cdot \nabla' \mathbf{v}' = -\nabla' p' + \frac{1}{Re_P} \nabla'^2 \mathbf{v}' = -\nabla' \cdot \mathbf{T}' \quad (5.51)$$

and

$$\nabla' \cdot \mathbf{v}' = 0 \quad (5.52)$$

The prime denotes dimensionless variables. The corresponding dimensionless boundary conditions may be written:  $\mathbf{v}'|_{r'=1/2} = 0$  and  $\lim_{r' \rightarrow \infty} \mathbf{v}' = -\mathbf{e}_z$ . At steady state conditions,  $\mathbf{v}'$  and  $p'$  are functions of position,  $\mathbf{r}'$ , only, and therefore the solutions of the equation with the suggested boundary conditions are functions of  $\mathbf{r}'$  and  $Re_P$  only. From the dimensionless momentum equation it follows that the normalized stress tensor can be expressed as:  $T'_{ij} = T_{ij}/(\rho v_\infty^2)$ . Thus, the drag force expression is also a function of  $\mathbf{r}'$  and  $Re_P$  only, as one recalls that the drag force was given by:

$$f_{D,z} = - \iint_A T_{zj} n_j dA \quad (5.53)$$

The dimensionless surface area can be given by:  $dA' = dA/(\pi d_{P,D}^2)$ . By inserting the dimensionless variables into the expression for the drag force, the drag force becomes:

$$f_{D,z} = - \iint_A \rho_f v_\infty^2 T'_{zj} n_j (\pi d_{P,D}^2) dA' \quad (5.54)$$

By non-dimensionalizing this equation one obtains

$$f'_{D,z} = \frac{F_{D,z}}{\rho_f v_\infty^2 (\pi d_{P,D}^2)} = - \iint_A T'_{zj} n_j dA' \quad (5.55)$$

where  $F'_{D,z}$  denotes the dimensionless drag.

Since the dimensionless variables only depend upon  $\mathbf{r}'$  and  $Re_P$ , it appears that the drag must be of the form:

$$f_{D,z} = d_{P,D}^2 \rho_f v_\infty^2 h(Re_P) \quad (5.56)$$

where  $h$  is a function of  $Re_P$  only. It has thus been shown that for a given geometry the steady drag force on the particle surface (i.e., integrated over the particle surface at  $r' = 1/2$ , so the dependency on  $\mathbf{r}'$  vanishes) only varies with the particle Reynolds number. The pre-factor 1/2 in the definition of  $C_D$  appears because it is often convenient to introduce the dynamic pressure, given by  $1/2 \rho v_\infty^2$  from the kinetic energy equation. The drag coefficient is based on the projected area normal to the flow rather than the entire surface area, because the area is the source of most of the drag that arise. The choice of area entering the formulation of the drag coefficient is a matter of convenience in practical applications. It follows from the definition of the drag coefficient (5.50) that  $C_D$  is a function of  $Re_P$  only, thus the drag force for any  $\rho$ ,  $v_\infty$  and  $A_P$  is established once the relation  $C_D = C_D(Re_P)$  is determined experimentally.

The *standard drag curve* refers to a plot of  $C_D$  as a function of  $Re_p$  for a smooth rigid sphere in a steady uniform flow field. The best fit of the cumulative data that have been obtained for this drag coefficient is shown in Fig 5.2. Numerous parameterizations have been proposed to approximate this curve (e.g., many of them are listed by [22]).

The variations in  $C_D$  have been examined and explained theoretically as summarized by [105, 22, 141, 26], among others. Table 5.1 summarizes briefly the phenomena that occur at different particle Reynolds numbers,  $Re_P$ . For very low Reynolds numbers,  $Re_P < 1$ , the Stokes law can be used as the inertial terms in the Navier-Stokes equations are negligible. With increasing Reynolds numbers the inertial forces become important and the actual

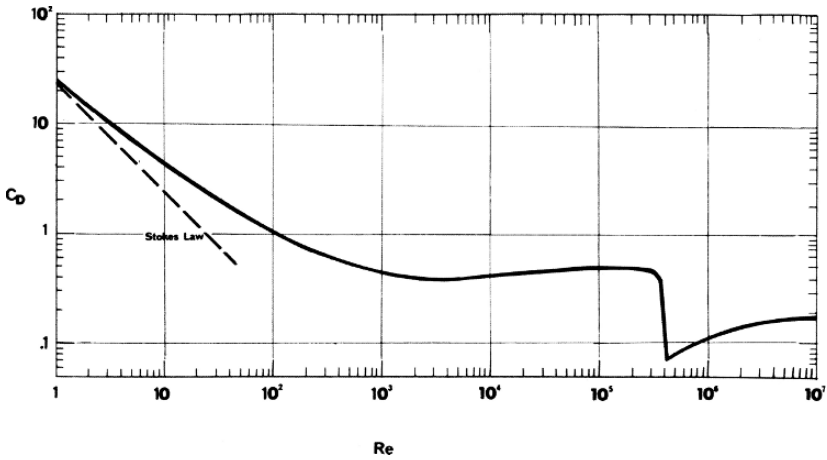


**Fig. 5.2.** The standard drag curve shows the drag coefficient of a rigid sphere as a function of particle Reynolds number. Reprinted from Clift et al [22] with permission from Elsevier.

drag coefficient is higher than what is predicted by Stokes drag formula. The Oseen [112] solution is considered valid for  $Re_P < 5$ . At  $Re_P \sim 10 - 100$  the flow begins to separate and form vortices behind the sphere. In this case the pressure in the wake is further reduced, so the form drag increases. Moreover, at about  $Re_P \sim 150$  the vortex system begins to oscillate and leaves the particle and forms a wake when  $Re_P \sim 500$  [141]. In Newton’s regime  $700 < Re_P < 2 \times 10^5$  the (form) drag coefficient is normally approximated by a constant value  $C_D \approx 0.44$ . Beyond  $Re_P \sim 3 \times 10^5$  Newton’s drag law is not valid anymore as this value is considered a critical Reynolds number, where the boundary layer becomes turbulent reducing the (form) drag significantly. However, if the particle is not smooth, this transition effect is blurred and less well defined.

Morsi and Alexander [105] provided a set of correlations for the drag coefficient as a function of particle Reynolds number which reproduce Fig 5.2

$Re_P < 1$	Stokes’ regime
$Re_P \geq 1$	Inertial effects become important
$Re_P \geq 10$	A vortex is formed
$Re_P$ increases	The vortex increases
$Re_P \geq 150$	The vortex starts oscillating
$Re_P \geq 500$	The vortex leaves the particle and forms a wake
$Re_P \geq 700$	Newton’s regime
$Re_P \geq 10^5$	Transition from laminar to turbulent boundary layer

**Table 5.1.** Formation of a vortex as  $Re_P$  increases.

fairly well in the  $Re_P$  range  $0 \leq Re_P < 5 \times 10^4$ . The experimental data available were divided into 8 regions in  $Re_P$ , and for each region they fitted a correlation of the form:

$$C_D = \frac{K_1}{Re_P} + \frac{K_2}{Re_P^2} + K_3 \quad (5.57)$$

The coefficients of (5.57) and the width of the regions were chosen to minimize the difference between the experimental and analytical curves.

The drag coefficient relations given are:

$$C_D = \begin{cases} \frac{24}{Re_P} & \text{for } 0 < Re_P < 0.1, \\ \frac{22.73}{Re_P} + \frac{0.0903}{Re_P^2} + 3.690 & \text{for } 0.1 < Re_P < 1, \\ \frac{29.1667}{Re_P} - \frac{3.8889}{Re_P^2} + 1.222 & \text{for } 1 < Re_P < 10, \\ \frac{46.50}{Re_P} - \frac{116.67}{Re_P^2} + 0.6167 & \text{for } 10 < Re_P < 100, \\ \frac{98.33}{Re_P} - \frac{2778}{Re_P^2} + 0.3644 & \text{for } 100 < Re_P < 1000, \\ \frac{148.62}{Re_P} - \frac{47500}{Re_P^2} + 0.357 & \text{for } 1000 < Re_P < 5000, \\ -\frac{490.546}{Re_P} + \frac{578700}{Re_P^2} + 0.46 & \text{for } 5000 < Re_P < 10000, \\ -\frac{1662.5}{Re_P} + \frac{5416700}{Re_P^2} + 0.5191 & \text{for } 10000 < Re_P < 50000 \end{cases} \quad (5.58)$$

These correlations are often used simulating particulate flows in chemical reactors.

### 5.2.2 Lift forces on a single rigid sphere in laminar flow

Rigid spheres sometimes experience a lift force perpendicular to the direction of the flow or motion. For many years it was believed that only two mechanisms could cause such a lift. The first one described is the so-called Magnus force which is caused by forced rotation of a sphere in a uniform flow field. This force may also be caused by forced rotation of a sphere in a quiescent fluid. The second mechanism is the Saffman lift. This causes a particle in a shear flow to move across the flow field. This force is not caused by forced rotation of the particle, as particles that are not forced to rotate also experience this lift (i.e., these particles may also rotate, but then by an angular velocity induced by the flow field itself).

#### Rotating spheres (Magnus force)

A rotating sphere in uniform flow will experience a lift which causes the particle to drift across the flow direction. This is called the Magnus effect (or force). The physics of this phenomenon are complex.

The rotation of a rigid sphere will cause the surrounding fluid to be entrained. When the sphere is placed in a uniform flow, this results in higher fluid velocity on one side of the particle, and lower velocity on the other side.

This gives an asymmetrical pressure distribution around the sphere. Originally this was thought to cause lift on the particle that move the particle towards the region of higher local velocity [22], see Fig 5.3.

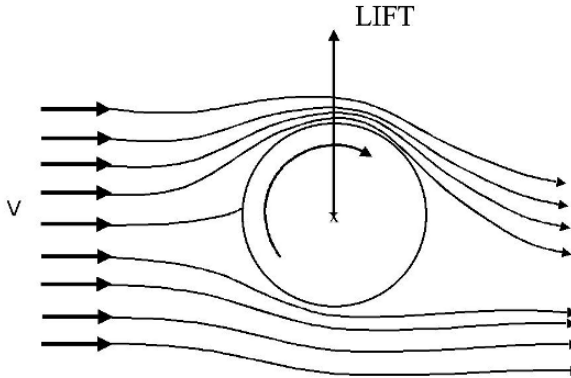


**Fig. 5.3.** The Magnus lift force on a rotating particle. The sketch illustrates the flow pattern induced by a rotating particle. The initial particle rotation is not caused by the flow.

Maccoll [95] studied the aerodynamics of a spinning sphere, and observed a negative Magnus effect when the ratio of the equatorial speed of the rotating sphere to the flow speed,  $v_{\text{equa}}/v$ , was less than 0.5.

Krahn [76] explained how the rotation of the sphere would cause the transition from laminar to turbulent boundary layers at different rotational velocities at the two sides of a sphere. The direction of the asymmetrical wake was explained based on the separation points for laminar and turbulent boundary layers. Krahn studied the flow around a cylinder. For a non-rotating cylinder the laminar boundary layer separates at  $82^\circ$  from the forward stagnation point, while the turbulent boundary layer separates at about  $130^\circ$ . Due to the rotation the laminar separation point will move further back, while the turbulent separation point will move forward. For some value of  $v_{\text{equa}}/v$  between 0 and 1 the laminar and turbulent separation points will be at equal distance from the stagnation point. The pressure on the turbulent side will be smaller than on the laminar side causing a negative Magnus force.

Taneda [148] studied a rotating sphere moving linearly in a quiescent liquid, and showed that when the Reynolds number was near  $2.5 \times 10^5$ , and  $v_{\text{equa}}/v < 0.6$  the particle would experience a negative lift force. This is close to the region where Swanson [145] found negative lifts for a rotating cylinder. Taneda found that the Magnus effect was caused by the asymmetric wake due to the rotation of the sphere. He showed that the negative lifts were due to the boundary layers changing from laminar to turbulent at different times

on the two sides of the rotating sphere, causing the wake to be distorted opposite to what is shown in Fig 5.3. It was also shown that disturbances in the main flow would cause the region of negative lift to contract, and shift to  $\text{Re}_p \sim 8.5 \times 10^4$ .

Swanson [145] reviewed the investigations of the Magnus force, and presented experimental drag and lift coefficients for an infinite, rotating cylinder at different Reynolds numbers and velocity ratios. For velocity ratios less than 0.55, and Reynolds numbers between  $12.8 \times 10^4$  and  $50.1 \times 10^4$  the cylinder would experience negative lift.

Rubinow and Keller [123] calculated the flow around a rotating sphere moving in a viscous fluid for small Reynolds numbers. They determined the drag, torque, and lift force (Magnus) on the sphere to  $O(\text{Re}_p)$ . The results were:

$$\mathbf{f}_D = -6\pi r_p \mu_c \mathbf{v}_{\text{rel}} \left(1 + \frac{3}{8} \text{Re}_p + O(\text{Re}_p)\right) \quad (5.59)$$

$$\mathbf{f}_L = \pi r_p^3 \rho_c \boldsymbol{\Omega} \times \mathbf{v}_{\text{rel}} (1 + O(\text{Re}_p)) \quad (5.60)$$

$$\mathbf{t} = -8\pi \mu_c r_p^3 \boldsymbol{\Omega} (1 + O(\text{Re}_p)) \quad (5.61)$$

Drew and Wallis [37] (p 61) examined the forces on spheres in two-phase suspensions based on theoretical analyzes. Their result included lift forces that give rise to a net transverse force on particle swarms if the group of spheres are translating and rotating as a unit. Note that this force is different from that due to rotation of each sphere.

Clift et al [22] summarized the measurements of drag and lift on rotating spheres, and concluded that the phenomena involved are so complex that drag and lift forces on rotating spheres should be determined experimentally.

### Spheres in shear flow (Saffman force)

A rigid sphere in shear flow experiences a force that moves the particle normal to the flow direction.

Segré and Silberberg [131, 132] showed experimentally that neutrally buoyant particles would migrate to, and concentrate at approximately 60% of the pipe radius in laminar flow. They used small tubes and relatively large particles.

Other workers have shown that initially non-rotating particles also experienced lateral motion [79, 80]. The shear flow thus gives rise to a lift force which is caused by the shear solely or rotation induced by the flow. Hence, these observations implied that a Magnus type of force was not adequate. Lawler and Lu [85] and Lahey [79, 80] gave an overview over lateral distributions of positive, neutrally, and negative buoyant particles. The result is sketched in Fig 5.4.

Subsequently Saffman [125, 126] derived an expression for the lift force on a particle in a shear flow, as illustrated in Fig 5.5. He incorporated three different Reynolds numbers defined by:

$$\text{Re}_\kappa = \frac{\kappa r_p^2}{\nu_c} \quad \text{Re}_P = \frac{v_{\text{slip}} r_p}{\nu_c} \quad \text{Re}_\Omega = \frac{\Omega r_p^2}{\nu_c} \quad (5.62)$$

and assumed that:

$$\text{Re}_\kappa \ll 1 \quad \text{Re}_\Omega \ll 1 \quad \text{Re}_P \ll \text{Re}_\kappa^{1/2} \quad (5.63)$$

That is, Saffman considered three different velocity scales. The conventional particle Reynolds number is expressed in terms of the relative fluid-particle velocity  $v_{\text{slip}}$ , the shear Reynolds number contains the fluid velocity gradient times the particle diameter ( $\frac{dv_z}{dy} d_p$ ), and the rotation Reynolds number contains the fluid rotational speed times the particle diameter ( $\Omega d_p$ ).

The lift force was found to

$$f_L = 6.46 \mu_c v_{z,c} \left( \frac{dv_{z,c}}{dy} \right)^{1/2} \frac{r_p^2}{\nu_c^{1/2}} \quad (5.64)$$

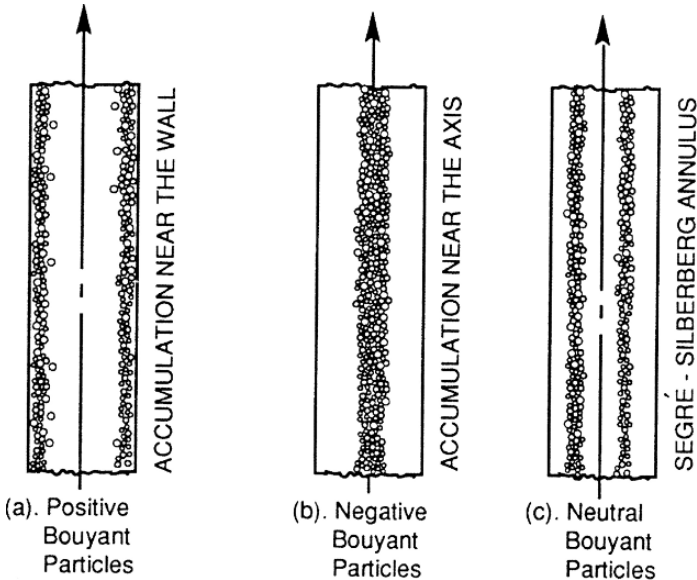


**Fig. 5.4.** Radial migration of particles in shear flow. Radial migration of positive, neutrally, and negative buoyant particles in shear flow. The figure illustrates the observations reported by Segré and Silberberg [131, 132], as sketched by Lawler and Lu [85] and Lahey [79, 80]. Reprinted from Lahey [80] with permission from Elsevier.

Saffman [125] (p 394) compared the Magnus force developed by Rubinow & Keller [123] with the shear force given above and showed that unless the rotational speed is much larger than the rate of shear  $\kappa = dv_z/dy$ , and for a freely rotating particle  $\Omega = \frac{1}{2} \frac{dv_z}{dy}$ , the lift force due to shear is an order of magnitude larger than the lift force due to forced rotation when the particle Reynolds number is small (for which these models are supposed to be valid).

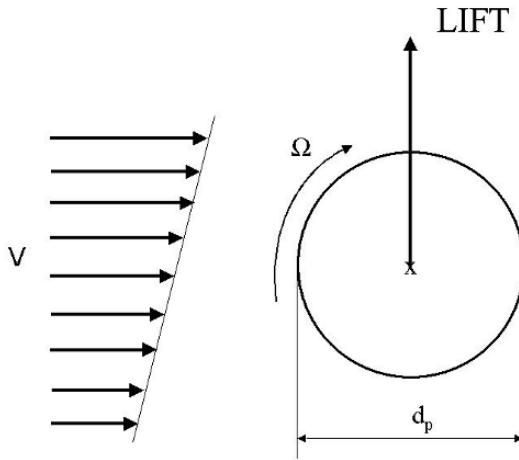


**Fig. 5.5.** The Saffman force on a particle in a shear flow. The sketch illustrates that this lift force is caused by the pressure distribution developed around the sphere due to particle rotation induced by the shear flow velocity gradient.

Lawler and Lu [85] reviewed the classical experimental observations on transversal migration of spherical particles and concluded that neither the original Magnus nor the Saffman force models are capable of explaining all these observations. They thus propose that the lift forces might be expressed in terms of the relative particle-fluid angular velocity rather than the absolute angular velocity of the particle as used in all the classical models. Crowe et al [26] also made similar extensions of the classical lift force models.

Dandy and Dwyer [30] computed numerically the three-dimensional flow around a sphere in shear flow from the continuity and Navier-Stokes equations. The sphere was not allowed to move or rotate. The drag, lift, and heat flux of the sphere was determined. The drag and lift forces were computed over the surface of the sphere from (5.28) and (5.33), respectively. They examined the two contributions to the lift force, the pressure contribution and the viscous contribution. While the viscous contribution always was positive, the pressure contribution would change sign over the surface of the sphere. The pressure

contribution to the lift was found to be negative for most of the Reynolds numbers and shear rates that were examined. The total lift was always found to be positive, and the results agreed well with those of Saffman [125, 126].

Auton [7], Thomas et al [152] and Auton et al [8] determined a lift force due to inviscid flow around a sphere. In an Eulerian model formulation this lift force parameterization is usually approximated for dilute suspensions, giving:

$$\mathbf{F}_L = C_L \rho_c \alpha_d (\mathbf{v}_c - \mathbf{v}_d) \times (\nabla \times \mathbf{v}_c) \quad (5.65)$$

For potential (inviscid) flow  $C_L = 0.5$ .

Drew and Lahey [33] derived the forces on a sphere in inviscid flow. They employed the objectivity principle which implies that the forces should be independent of coordinate system. They found the same formulation for the lift force as given by (5.65), but they stressed that it was not objective in that form. When written in combination with the virtual mass force as:

$$\begin{aligned} \mathbf{F}_{L,V} = \alpha_d C_V \rho_c [ & \left( \frac{\partial \mathbf{v}_c}{\partial t} + \mathbf{v}_c \cdot \nabla \mathbf{v}_c \right) - \left( \frac{\partial \mathbf{v}_d}{\partial t} + \mathbf{v}_d \cdot \nabla \mathbf{v}_d \right)] \\ & - \alpha_d \rho_c C_V (\mathbf{v}_c - \mathbf{v}_d) \times (\nabla \times \mathbf{v}_c) \end{aligned} \quad (5.66)$$

the combination was supposedly objective.

However, just after this paper was published, Acrivos pointed out in a personal communication with Drew and Lahey that a fundamental error had been made in the derivation. Therefore, in a corrigendum by Drew and Lahey [34] the conclusions regarding objectivity were modified to apply only approximately to a fluid with very small vorticity. In practice, the sum of the added mass and lift forces is thus not necessarily frame-indifferent when applied to reactor simulations.

### 5.2.3 Lift and drag on rigid spheres in turbulent flows

Spheres in turbulent flows have not been extensively studied, partly due to the difficulties in measuring.

Taneda [149] studied the flow past a sphere at particle Reynolds numbers between  $10^4$  and  $10^6$ , and found that the wake is not axisymmetric and that it rotates slowly and randomly about the stream-wise axis. The sphere is thus subject to a random side force.

Willetts and Murray [171] studied the lift on spheres fixed in turbulent flows. The spheres were located both near and far from a boundary. They found that particles near a wall experienced lift away from the wall, while a sphere in a shear flow away from a wall experienced a lift towards the wall. The forces were found to be of the same magnitude as the forces in laminar flow, and they were consistent with the laminar results of Segré and Silberberg [131, 132]. Spheres that were not close to a boundary, and not subjected to a velocity gradient, experienced randomly fluctuating instantaneous lift which was strongly associated with the wake deflection. They suggested that the lift

was caused by disturbances of the boundary layer separation line induced by small impinging eddies.

Lee and Durst [89] studied turbulent air-glass particles flow using Laser Doppler Anemometer (LDA) measurements, using particles with diameters 100, 200, 400, and 800  $\mu m$ . They found that the particles would lag behind the air more and more depending on particle size. An exception was that the two smaller particles sizes would have a larger upward velocity at the wall than the air. For the larger particles a particle free layer near the wall was seen. This layer was thicker than the viscous sublayer of the air. They also found that the large particles enhanced turbulence, while the small particles dampened it. The large particles would also cause the air velocity profile to be flatter. The root mean square axial fluctuating velocity was found to increase towards the wall with a sudden drop at the wall. Based on these observations they suggested a new theoretical approach based on the dynamic response characteristics of the particles to the fluid flow.

This new approach is described by Lee and Wiesler [90] and developed into a model that explains the transversal movement of particles as a result of the turbulent diffusion. The basis of their modeling is a particular form of the Maxey-Riley equation [100]:

$$\begin{aligned} \frac{\pi}{6} d_p^3 \rho_p \frac{d\mathbf{v}_p}{dt} &= 3\pi\mu_c d_p (\mathbf{v}_c - \mathbf{v}_p) \\ &+ \frac{\pi}{6} d_p^3 \rho_c \frac{d\mathbf{v}_c}{dt} \\ &+ \frac{1}{2} \frac{\pi}{6} d_p^3 \rho_c \left( \frac{d\mathbf{v}_c}{dt} - \frac{d\mathbf{v}_p}{dt} \right) \\ &+ \frac{3}{2} d_p^2 (\pi\rho_c\mu_c)^{(1/2)} \int_0^t \frac{\left( \frac{d\mathbf{v}_c}{dt'} - \frac{d\mathbf{v}_p}{dt'} \right)}{(t-t')^{(1/2)}} dt' \end{aligned} \quad (5.67)$$

They required that the turbulence should be locally isotropic and steady, that the particle Reynolds number should be small, that the particles concentration was small, and that the particle diameter should be much smaller than the length scale of the energy containing eddies for the diffusion controlled range of the model. The model is based on the ability of the particle to respond to the motion of the surrounding fluid. It depends on particle size and density, turbulence structure of the fluid, and transversal particle concentration differences.

Lee [86] examined earlier studies on cylinders in turbulent flow fields, and found in turbulent flow that the wake would decrease with increasing turbulence intensity, and then disappear, and the mean flow would behave in the same manner as for Stokes flow. He therefore proposed, and showed, that the drag on a particle in turbulent flow could be determined from a Stokes law with the molecular viscosity replaced by an effective viscosity calculated from the volumetric concentration of particles, the flow Reynolds number, the density ratio, and the Froude number. The Froude number, *determining the ratio between the initial- and gravity forces*, is defined as:

$$\text{Fr} = \frac{|\mathbf{v}_c|}{(d_p g)^{0.5}} \quad (5.68)$$

Lee and Börner [88] used LDA measurements to characterize the suspension turbulent flow to enable the calculation of the drag and lift forces. The results were in fair agreement with the measurements of Lee and Durst [89].

Based on the model of Lee and Wiesler [90] and the measurements of Lee and Börner [88] Lee [87] formulated a set of governing equations for the mean motion of particles in a suspension turbulent flow. The model contained both pseudo Stokes drag and pseudo Saffman forces which were expressed in terms of a modified viscosity, and supposedly valid for larger particle Reynolds numbers.

Yamamoto et al [173] studied lift and drag on cylinders and on spheres in linear shear turbulent flow in a vertical square duct. The cylinders had diameters from 4 to 10 mm, and the spheres had diameters from 20 to 30 mm. The approaching flow had center velocities of 12 to 19 m/s. They found that the lift near the center of the channel was always towards the low velocity side of the duct. For the circular cylinder they found that the lift coefficient varied with the radius, and it was negative near the wall. The lift increased with increasing velocity gradient, but the drag was little affected by the gradient. The fluctuating parts of the drag and lift forces were found to be small.

Clift et al [22] and Crowe et al [26] reviewed the literature considering the effects of free stream turbulence on the particle drag coefficient. Generally, in their view there are experimental data indicating that the free stream turbulence reduces the critical particle Reynolds number for the drag coefficient of a sphere. They further refer to several workers that investigated the effects of turbulence and proposed that the particle drag coefficient should be parameterized in terms of certain turbulence characteristics. In most cases two normalized parameters have been used to quantify the effect of the free stream turbulence on the particle drag, these are the relative turbulence intensity  $I_R = \sqrt{v'^2}/|\mathbf{v}_c - \mathbf{v}_p|$  and the ratio between the turbulent integral length scale and the particle diameter  $L_e/d_p$ . In most reports the effect of the turbulent length scale is found to be weak, whereas the relative turbulence intensity and the critical Reynolds number might be correlated.

However, there is generally considerable discrepancy in the data for the drag coefficient dependence on turbulence. The spread in the data obtained for the drag coefficient of a sphere in turbulent flows is indicated in Fig 5.6. For this reason the standard drag curve parameterizations are normally used and the effects of turbulence is disregarded.

To summarize, no firm conclusions regarding the impact of free stream turbulence on the drag and lift force coefficients can be drawn analyzing the available data. More detailed experiments are obviously needed to better understand the affect of turbulence on the drag and lift force coefficients.

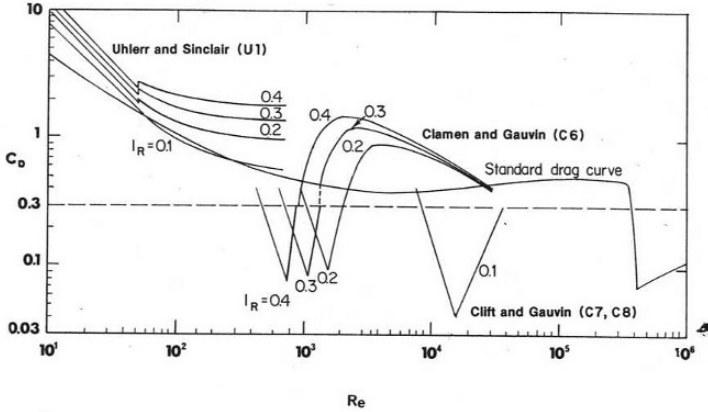


**Fig. 5.6.** Effect of relative turbulence intensity  $I_R$  on sphere drag coefficient  $C_D$ . Reprinted from Clift et al [22] with permission from Elsevier.

### 5.2.4 Drag force on bubbles

The interphase forces between bubbles and the surrounding liquid are more complex than the forces between rigid spheres and a surrounding liquid. This is because the gas in the bubbles may be circulating causing the interface to move as opposed to the surface of a rigid particle. The bubbles are deformable, and they may have different shapes depending on the different physical properties of the gas and of the surrounding fluid. The shape of bubbles or drops rising or falling unhindered in a liquid can be determined based on three dimensionless numbers.

The Eötvös number is *determining the ratio between the gravitational- and surface tension forces* (i.e., the Eötvös number is equal to the *Bond number*), and defined by:

$$Eo = \frac{g\Delta\rho d_p^2}{\sigma}, \tag{5.69}$$

the Morton number<sup>3</sup>:

$$Mo = \frac{g\mu_l^4\Delta\rho}{\rho_l^2\sigma^3}, \tag{5.70}$$

<sup>3</sup> This dimensionless group is often referred to as the *M-group* or the *property group* (Fan and Tsuchiya [45], p 19; Middleman [103], p 227). It is here called the *Morton number*,  $Mo$ , in accordance with the notation used by Clift et al [22] and Fan and Tsuchiya [45].  $Mo$  involves only physical properties of the surrounding medium for gas bubbles and the pressure field. A more general form for any fluid particles of density  $\rho_g$  can be given by  $\nabla p_S | \rho_l - \rho_g | \mu_l^4 / (\rho_l^3 \sigma^3)$  where  $\nabla p_S$  is the static pressure gradient in any pressure field and is replaced by  $\rho_l g$  in the gravitational field.

the particle Reynolds number (i.e., *determining the ratio between the initial- and the viscous forces*):

$$\text{Re}_P = \frac{\rho_l d_p v_{\text{slip}}}{\mu_l}, \quad (5.71)$$

and the Weber number (i.e., *determining the ratio between the initial- and surface tension forces*):

$$\text{We} = \frac{\rho_l v_{\text{slip}}^2 d_p}{\sigma}. \quad (5.72)$$

Only three of these numbers are independent, since the Eötvös number can be expressed as:

$$\text{Eo} = \frac{\text{Re}_P^4 \text{Mo}}{\text{We}^2} \quad (5.73)$$

Similarly, the Capillary number,  $Ca$ , *determining the ratio between the viscous- and surface tension forces*, is related to the Weber number,  $We$ , and particle Reynolds number,  $\text{Re}_P$ . That is, the Capillary number can be expressed as,  $Ca = \frac{We}{\text{Re}_P}$ .

When the Reynolds, Morton and Eötvös numbers are determined, the shape of bubbles or drops falling or rising unhindered in a liquid can be determined from the shape regime map in Fig 5.7. A similar map has been presented earlier by Grace et al [53].

### Bubbles or drops in creeping flow

The drag force acting on a spherical *bubble* in the Stokes flow regime (creeping flow) can be derived with only minor changes applying the same solution procedure as used for rigid spheres shown in sect 5.2.1. The difference between the two situations is just in the boundary conditions at the surface of the spherical object [14]. For bubbles the surface conditions at  $r = r_p$  are (1)  $v_r = 0$  and (2)  $T_{r\theta} \approx 0$ , meaning that we have neglected the gas viscosity of the bubble so there are no internal friction in the particle. With these boundary conditions one can find an analytical solution for the stream function  $\psi$ , and thus the velocity components  $v_r$  and  $v_\theta$ , and finally the pressure distribution around the particle are known. The  $rr$ -component of the total stress tensor at the surface of the bubble is therefore

$$\begin{aligned} f_{D,z}^{\text{Normal}} &= \int_0^{2\pi} \int_0^\pi \left[ -T_{rr}(r_p, \theta) \cos \theta \right] r_p^2 \sin \theta d\theta d\phi \\ &= 2\pi \int_0^\pi \left[ -\left( p - 2\mu \frac{\partial v_r}{\partial r} \right) \Big|_{r_p} \cos \theta \right] r_p^2 \sin \theta d\theta = 4\pi \mu r_p V \end{aligned} \quad (5.74)$$

Notice that  $\sigma_{rr} \neq 0$  on the surface of the bubble due to the prevailing free slip condition, in contrast to the rigid sphere case in which  $\sigma_{rr}$  vanishes on the surface due to the no-slip condition.

A similar solution for creeping flow past a spherical *droplet* of fluid were derived independently by Hadamard [55] and Rybczynski [124]. In this case the fluid stream has a velocity  $V$  at infinity and viscosity  $\mu_f$ , while the droplet has a viscosity  $\mu_p$  and a fixed interface. The boundary conditions at the droplet interface are (1) zero radial velocities and (2) equality of surface shear and

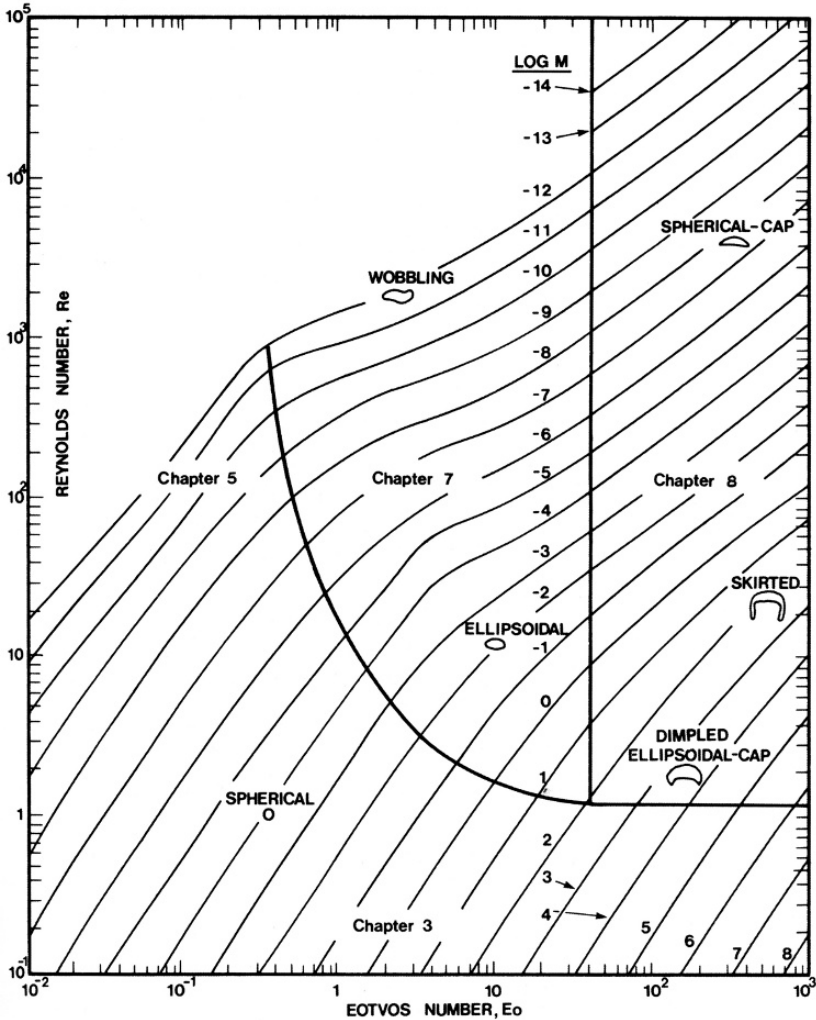


Fig. 5.7. Shape regimes for bubbles and drops in liquid. Reprinted from Clift et al [22] with permission from Elsevier.

tangential velocity on either side of the interface. The drag force on the droplet is then given by:

$$f_{D,z} = 6\pi\mu r_p V \frac{1 + \frac{2\mu_f}{3\mu_p}}{1 + \frac{\mu_f}{\mu_p}} \quad (5.75)$$

This drag force consists of contributions from pressure (form drag), deviatoric normal stress, and shear stress (friction drag).

The corresponding drag coefficient is given by:

$$C_D = \frac{f_{D,z}}{\frac{1}{2}\pi\rho_f V^2 r_p^2} = \frac{8}{\text{Re}_P} \left( \frac{2 + 3\frac{\mu_p}{\mu_f}}{1 + \frac{\mu_f}{\mu_p}} \right) \quad (5.76)$$

For  $\mu_p \gg \mu_f$ , this solution (5.75) coincides with Stokes' solution for a rigid sphere (5.47), whereas for  $\mu_p \ll \mu_f$ , this solution coincides with the solution for a spherical bubble in liquid (5.74). A liquid droplet in another liquid lies in between these limiting cases.

Langlois [83], White [169], Clift et al [22] and Zapryanov and Tabakova [174] give further details on the derivation of the viscous drag force on a small spherical droplet.

## Fluid spheres at higher Reynolds numbers

Fluid spheres in flow at higher Reynolds numbers behave different from rigid spheres.

As the Reynolds number increases, a wake is formed behind the fluid sphere or ellipsoid [22, 45]. The formation of a wake behind a fluid particle is delayed compared to a solid sphere due to the internal circulation of the gas. The recirculating wake may be completely detached from the fluid sphere. A secondary internal vortex will then not be formed. For smaller particle Reynolds numbers the wake is symmetrical, but as the Reynolds number increases further the vortex sheet breaks down to vortex rings. Further increase of the Reynolds number cause the vortex rings to shed asymmetrically, and the drop or bubble will show a rocking motion. This is one of the two types of secondary motion defined. The other is *oscillations* (shape dilations), and is also thought to be due to the vortex shedding.

In most systems the bubbles (or drops) with diameters between 1 and 15 mm are ellipsoidal. The terminal velocity of bubbles in water at 20°C has been measured by several researchers. The results are summarized in Fig 5.8.

The curves for the drag coefficient and the terminal velocity converge for small and large bubbles. This is likely to be because there is always some surface active contaminants present, even in distilled water, that will prevent the internal circulation of the smallest bubbles. For the large bubbles the surface tension forces are not important. Several different drag formulations are given based on the Reynolds number and the density ratio of the gas and liquid [54, 163, 78].

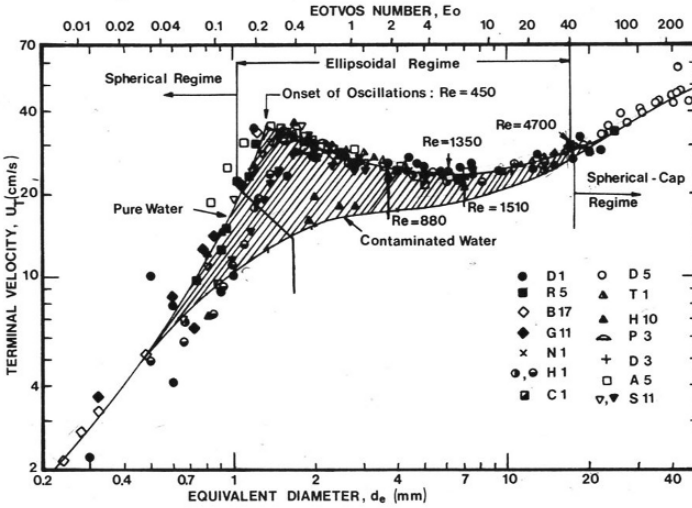


Fig. 5.8. Terminal velocity of air bubbles in water at 20°C. Reprinted from Clift et al [22] with permission from Elsevier.

The drag coefficient parameterizations proposed by Ishii and co-workers [62, 63, 64] for bubbles in liquid at different flow regimes are often used in reactor simulations. In the churn-turbulent regime they obtained:

$$C_D = \frac{8}{3}(1 - \alpha_g)^2 \tag{5.77}$$

and in the distorted bubble regime they gave:

$$C_D = \frac{2}{3}d_b \sqrt{\frac{g\Delta\rho}{\sigma}} \left\{ \frac{1 + 17.67(f(\alpha_g))^{6/7}}{18.67f(\alpha_g)} \right\}^2 \tag{5.78}$$

where:

$$f(\alpha_g) = (1 - \alpha_g)^{1.5} \tag{5.79}$$

More recently, Tomiyama and co-workers [154, 155, 156, 157] performed detailed experiments investigating the drag coefficient of a single bubble in a stagnant liquid. They proposed a drag coefficient parameterization which is split in three categories. These are pure, gently-contaminated, and contaminated systems, respectively.

For *pure* systems:

$$C_D = \max \left[ \min \left[ \frac{16}{Re_P} (1 + 0.15Re_P^{0.687}), \frac{48}{Re_P} \right], \frac{8}{3} \frac{Eo}{Eo + 4} \right] \tag{5.80}$$

For *gently-contaminated* systems:

$$C_D = \max \left[ \min \left[ \frac{24}{\text{Re}_P} (1 + 0.15 \text{Re}_P^{0.687}), \frac{72}{\text{Re}_P} \right], \frac{8}{3} \frac{Eo}{Eo + 4} \right] \quad (5.81)$$

For *contaminated* systems:

$$C_D = \max \left[ \frac{16}{\text{Re}_P} (1 + 0.15 \text{Re}_P^{0.687}), \frac{8}{3} \frac{Eo}{Eo + 4} \right] \quad (5.82)$$

where the Eötvös number  $Eo$  is defined as

$$Eo = \frac{g(\rho_c - \rho_d)d_P^2}{\sigma_I} \quad (5.83)$$

This parameterization of the drag coefficient for bubbles in stagnant liquids is very often used in the latest reports on bubbly flow simulations.

### 5.2.5 Lift force on bubbles

Experiments have shown that bubbles under certain conditions experience lift in the opposite direction to what would be predicted by rigid sphere analysis. Other mechanisms must therefore be important in determining the lift force on bubbles. Lift in turbulent flow is very complex, and few studies have been performed.

Several studies on the phase distribution in vertical bubbly flows in pipes and channels are performed, though, and many of these are reviewed by Jakobsen [65]. Typically, they describe how the bubbles will migrate towards the core of the column and rise there when the superficial gas velocity is larger than the small (0 to few cm/s) superficial liquid velocity. When the superficial liquid velocity is larger, the gas will tend to accumulate/peak at the wall. The core peaking of void is contradictory to the lift calculated from classical inviscid analyses [7] [152, 8]. To account for the net lift force acting on a particle swarm the classical lift force model (5.65) is normally adopted [152, 65]. In this case values of  $C_L$  from 0.01 up to 0.5 have been reported for different flow conditions. However, little or no knowledge on the mechanisms causing the changes in the parameter did exist until quite recently [65].

In a series of more recent papers, Tomiyama and co-workers (i.e., [154, 155, 156, 157]) performed detailed experiments investigating the transverse migration of single bubbles in simple shear flows and found that the transversal lift force coefficient depends on the Eötvös number. A net transverse force  $\mathbf{F}_L$  acting on a single bubble was proposed on the form (5.65). They further anticipated that the net lift force coefficient consists of three separate contributions accounting for the Magnus lift-, Saffman shear induced lift-, and lift caused by the slanted wake behind a deforming bubble, thus  $C_L = C_L^M + C_L^S + C_L^T$ . The Magnus force coefficient is  $C_L^M \sim 0$  when there is no forced particle rotation. For the Saffman type of shear induced lateral lift  $C_L^S = 0.5$  for potential (inviscid) flows [152].

Interpreting their data it was concluded that when  $EO$  is low, the bubble will migrate toward the pipe wall as explained with the classical shear-induced or Saffman type of lift force. On the other hand, when  $EO$  is high, the vortex behind a deformed bubble becomes slanted and for this reason the bubble migrates toward the pipe center. This implies that there is a third transversal lift force contribution caused by the interaction between the wake and external shear field.

Measurements performed under the experimental conditions of  $-5.5 \leq \log(Mo) \leq -2.8$  and  $1.6 \leq EO \leq 6$  were used as basis making an empirical parameterization for the net transverse lift force coefficient.

For  $EO < 4$ :

$$C_L = \min \left[ 0.288 \tanh(0.121 \text{Re}_P), 0.00105EO^3 - 0.0159EO^2 - 0.0204EO + 0.474 \right] \quad (5.84)$$

For  $4 \leq EO \leq 10$ :

$$C_L = 0.00105EO^3 - 0.0159EO^2 - 0.0204EO + 0.474 \quad (5.85)$$

For  $EO > 10$ :

$$C_L = -0.29 \quad (5.86)$$

This parameterization gives  $0 < C_L \leq 0.288$  for small bubbles that migrate towards the pipe wall and *negative* values for large distorted bubbles. The sign of  $C_L$  changes at  $d_p = 5.6$  (mm) from positive to negative.

In one of the latest studies reported by Tomiama et al [157] on the lift force the  $C_L$  value was found to be well correlated with  $\text{Re}_P$  in accordance with the given parameterization for small bubbles, whereas for intermediate and large bubbles  $C_L$  was considered a function of a modified Eötvös number  $EO_d$  (i.e., exchanging  $EO$  with  $EO_d$  in the above parameterization of  $C_L$ ). The  $EO_d$  is defined in terms of the maximum horizontal dimension of a bubble as a characteristic length:

$$EO_d = \frac{g(\rho_c - \rho_d)d_H^2}{\sigma_I} \quad (5.87)$$

To estimate  $d_H$  which occurs in the definition of  $EO_d$ , an empirical correlation of the aspect ratio  $E$  for spheroidal bubbles in a contaminated system was used:

$$E = \frac{d_V}{d_H} = \frac{1}{1 + 0.163EO^{0.757}} \quad (5.88)$$

where  $d_V$  is the maximum vertical dimension of a bubble.

Other lift forces might exist as well, in particular for wall bounded flows. To prevent the model inconsistency that small bubbles intend to penetrate through the pipe wall, as predicted by the conventional lift force (5.65), Antal et al [2] proposed the remedy of introducing an additional wall lift force that pushes the dispersed phase away from the wall toward the pipe center. The force was found to be:

$$\mathbf{F}_{L,d}^W = \frac{\alpha_d \rho_c |\mathbf{v}_{\parallel}|^2}{r_d} [C_{W1} + C_{W2} \left(\frac{r_d}{y_0}\right)] \mathbf{n}_W \quad (5.89)$$

where

$$\mathbf{v}_{\parallel} = (\mathbf{v}_d - \mathbf{v}_c) - [\mathbf{n}_W \cdot (\mathbf{v}_d - \mathbf{v}_c)] \mathbf{n}_W \quad (5.90)$$

$$C_{W1} = -0.104 - 0.06 v_{\text{slip}} \quad (5.91)$$

$$C_{W2} = 0.147 \quad (5.92)$$

$y_0$  is the distance between the wall and the particle and  $\mathbf{n}_W$  is the unit normal vector outward from the wall.

Later, Tomiyama [156, 154] observed a defect in the original model by Antal et al, namely, that a bubble located far from the wall is attracted to the wall. Based on a best fit of model simulations to experimental data from a square duct with wall-distance  $H$ , a modified wall force was given as:

$$\mathbf{F}_{L,d}^W = C_w \rho_c |\mathbf{v}_{\text{slip}} \cdot \mathbf{e}_z|^2 \mathbf{e}_r \quad (5.93)$$

where

$$C_w = C_{w2} \left( \frac{1}{y_0} - \frac{1}{H - y_0} \right) + \frac{C_{w3} d_V}{2} \left( \frac{1}{y_0^2} - \frac{1}{(H - y_0)^2} \right) \quad (5.94)$$

Subsequently, the original formulation by [2] has been modified in several ways to ensure that the wall force drop to zero at an appropriate distance from the wall [115, 66].

The modified wall lift force model used by Jakobsen et al [66] for the net force acting on the dispersed phase is given by:

$$\mathbf{F}_{L,d}^W = \max(0, C_{w1} + C_{w2} \frac{d_p}{y_0}) \alpha_d \rho_c \frac{|\mathbf{v}_d - \mathbf{v}_c|^2}{d_p} \mathbf{n}_W \quad (5.95)$$

in which the parameter values used, i.e.,  $C_{w1} = -0.1$  and  $C_{w2} = 0.35$ , are representing an empirical best fit to a set of experimental liquid velocity data for bubble columns (employing a finite grid resolution).

In another attempt to account for turbulence effects Jakobsen [65] performed turbulence modelling of the drag force, and showed that this procedure gave rise to a transversal force acting in the opposite direction compared to the classical lift force [7, 8, 152].

## Experiments and numerical simulations

Kariyasaki [70] studied bubbles, drops, and solid particles in linear shear flow experimentally, and showed that the lift force on a deformable particle is opposite to that on a rigid sphere. For particle Reynolds numbers between  $10^{-2}$  and 8 the drag coefficient could be estimated by Stokes' law. The terminal velocity was determined to be equal to that of a particle moving in a quiescent

liquid. The fluid particles would deform into airfoil shapes when submitted to shear flow.

Kariyasaki proposed to calculate the lift force from a balance of buoyancy, gravity, drag and lift, hence:

$$f_L = \frac{(f_{Buoy} - f_G)(v_{p,r} - v_{c,r})}{|\mathbf{v}_{slip}|} \quad (5.96)$$

The measured lift force on a solid particle compared well with the model of Saffman (5.64) when the shear Reynolds number was small, and with the model of Rubinow and Keller (5.60) when the shear Reynolds number was large. The shear Reynolds number was defined as:

$$\text{Re}_\kappa = \frac{\kappa d_V^2}{\nu_c} \quad (5.97)$$

where  $d_V$  is the equivalent volume diameter and the fluid shear is defined by  $\kappa = |\frac{dv_c}{dy}|$ . The lift force on the deformed fluid particle was assumed to be caused by the same mechanisms as those that create lift on a wing. The assumptions made in calculating the lift were:

1.  $|\kappa| \ll |\mathbf{v}_{slip}|/d_a$
2. The particle was shaped as a thin plate with a negligible volume.

The lift force was then expressed by:

$$f_L = 6.84\pi\rho_c \mathbf{v}_{slip}^2 d_V^2 D^2 \frac{\text{Re}_\kappa}{\text{Re}_\kappa^{1.2}} \quad (5.98)$$

where the deformation factor was given as

$$D = \frac{d_a - d_b}{d_a + d_b} = 0.43 \left( \frac{|\kappa| \rho_c \nu_c d_V}{\sigma} \right)^{0.6} \quad (5.99)$$

where  $d_a$  and  $d_b$  denote the major and minor axes of an ellipsoidal bubble.

Esmaceli et al [43] solved the full Navier–Stokes equations for a bubble rising in a quiescent liquid, or in a liquid with a linear velocity profile. The calculations were performed in 2-dimensional flow, but similar results have also been reported for 3-dimensional calculations. The surface tension forces were included, and the interface was allowed to deform. It was shown that deformation plays a major role in the lift on bubbles. Bubbles with a low surface tension have a larger Eötvös number, and are more prone to deform.

Fig 5.9 shows how two different bubbles rise in vertical shear flow with a non-dimensional shear rate:

$$G = \frac{\omega d_{\text{eff}}^2 \rho_c}{\mu_c} \quad (5.100)$$

where  $\omega$  is the mean vorticity and  $d_{\text{eff}}$  is the effective diameter of the bubble. For bubble (a) the Eötvös number is 0.78, and the Morton number is  $1.26 \times$

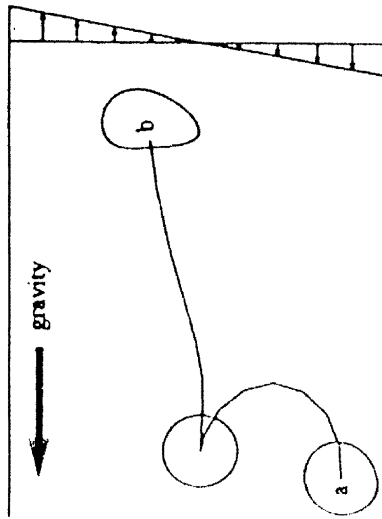


**Fig. 5.9.** Bubbles rising in vertical shear flow,  $G = 16$ . For bubble a  $Eo = 0.78$  and  $M = 1.2610^{-6}$ . For bubble b  $Eo = 6.24$  and  $M = 6.3110^{-4}$ . Reproduced from Esmaeeli et al [43] with permission from Elsevier.

$10^{-6}$ . For bubble (b) the Eötvös number is 6.24 and the Morton number is  $6.31 \times 10^{-4}$ . The bubbles have totally different motion depending on whether the bubble deforms or not. Bubble (a) does not deform significantly, and rotates with the flow as it rises, and eventually experiences a lift to the right. Bubble (b) deforms due to the shear and the upward motion. The bubble thus takes the form of an airfoil, and experiences lift to the left. The circulation of bubble (b) changes as the bubble deforms, and settles in the opposite direction of the circulation of bubble (a).

### 5.2.6 The Added mass or virtual mass force on a single rigid sphere in potential flow

The virtual mass effect relates to the force required for a particle to accelerate the surrounding fluid [65, 170, 26]. When a particle is accelerated through a fluid, the surrounding fluid in the immediate vicinity of the particle will also be accelerated at the expense of work done by the particle. The particle apparently behaves as if it has a larger mass than the actual mass, thus the net force acting on the particle due to this effect has been called virtual mass or added mass force. The steady drag force model does not include these transient effects.

To define the virtual mass force we postulate a Lagrangian force balance for the sphere:

$$m \frac{dV}{dt} = \left[ \frac{4}{3} \pi \rho_d r_P^3 + m_V \right] \frac{dV}{dt} = \sum_i f_i \quad (5.101)$$

in which the apparent mass can be expressed by:

$$m = \frac{4}{3}\pi\rho_{\text{fluid}}r_P^3 \left( \frac{\rho_d}{\rho_{\text{fluid}}} + \frac{m_V}{\frac{4}{3}\pi\rho_{\text{fluid}}r_P^3} \right) \tag{5.102}$$

where  $C_V = m_V/(\frac{4}{3}\pi\rho_{\text{fluid}}r_P^3)$  is the virtual mass or added mass force coefficient.

The magnitude of this added mass can be found by considering the change in kinetic energy of the fluid surrounding an accelerating particle. By equating the energy added to the fluid to an equivalent body energy, the virtual mass can be calculated. The kinetic energy of the surrounding fluid is given by:

$$E_{k,\text{fluid}} = \int \frac{1}{2}u_{\text{rel}}^2 dm = \frac{1}{2}m_V V^2 \tag{5.103}$$

where the integral is to be taken over all the fluid mass. The integration of the fluid kinetic energy can also be accomplished by a particle-surface integral involving the velocity potential [26].

Considering an initially stagnant fluid (see Fig 5.10),  $E_{k,\text{fluid}}$  denotes the kinetic energy added to the fluid by the particle movement (J),  $dm$  the fluid element (kg),  $v_{\text{rel}}$  the velocity of the fluid relative to the particle (m/s),  $m_V$  is the virtual mass (kg), and  $V$  is the velocity of the particle (m/s).

The motion of a sphere moving through a stagnant incompressible fluid is equivalent to the uniform fluid flow about a fixed sphere. For axisymmetrical potential flow the velocity components of the fluid can be obtained by use of the Stokes' stream function as explained by [26, 170]:

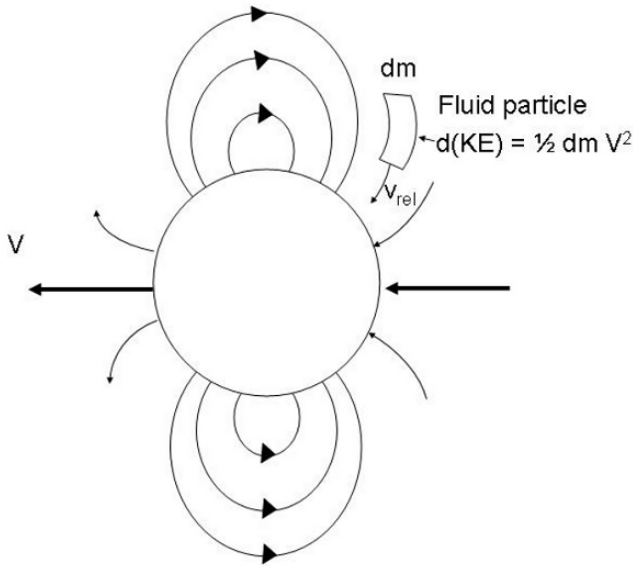


**Fig. 5.10.** Streamlines relative to a moving sphere.

$$\begin{aligned}
 v_r &= V \cos \theta \left( 1 - \frac{r_P^3}{r^3} \right) \\
 v_\theta &= -\frac{1}{2} V \sin \theta \left( 2 + \frac{r_P^3}{r^3} \right)
 \end{aligned}
 \tag{5.104}$$

where  $v_r$  denotes the fluid velocity in r-direction (m/s),  $v_\theta$  the fluid velocity in  $\theta$ -direction (m/s), and  $r_P$  is the radius of the sphere (m).

The velocity components relative to the moving sphere can be found by subtracting the sphere velocity  $v_{r,p} = V \cos \theta$  and  $v_{\theta,p} = -V \sin \theta$ . The relative velocity components are thus given by:

$$\begin{aligned}
 v_r &= -\frac{V r_P^3 \cos \theta}{r^3} \\
 v_\theta &= -\frac{V r_P^3 \sin \theta}{2r^3}
 \end{aligned}
 \tag{5.105}$$

The streamlines relative to the moving sphere are sketched in Fig 5.10.

The element of fluid mass  $dm$  relates to the volume element  $dV$ , as for incompressible fluids  $dm = \rho dV$  in which  $\rho$  is a constant. Since the fluid extend from the particle surface, it is convenient to express the mathematical problem in spherical coordinates. Fig 5.11 shows the spherical coordinates of an arbitrary point,  $P$ , in space. From Fig 5.12 the approximate volume of a rectangular block extending from the surface can be calculated as:

$$\Delta V = r_P \Delta \phi r \Delta \theta \Delta r = r \sin \theta \Delta \phi r \Delta \theta \Delta r
 \tag{5.106}$$

in which we have used the relation  $r_P = r \sin \theta$  considering the triangle  $OPQ$  in Fig 5.11.

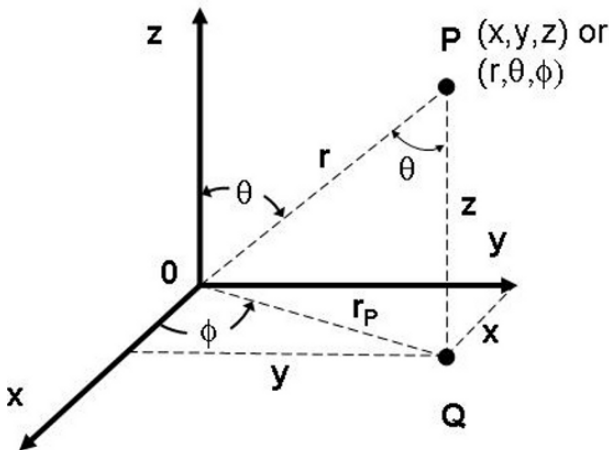


Fig. 5.11. Spherical polar coordinates.

In differential form the arbitrary fluid volume becomes:

$$dV = r^2 \sin \theta \, dr d\theta d\phi \quad (5.107)$$

So, the element of fluid mass  $dm$  is given by

$$dm = \rho dV = \rho(r \sin \theta)r \, dr d\theta d\phi \quad (5.108)$$

Inserting (5.108) and  $v_{rel}^2 = v_r^2 + v_\theta^2$  into (5.103), the integral can be evaluated to obtain the kinetic energy added to the fluid:

$$\begin{aligned} E_{k,fluid} &= \int \frac{1}{2} v_{rel}^2 dm = \int_0^{2\pi} \int_0^\pi \int_{r_P}^\infty \frac{1}{2} (v_r^2 + v_\theta^2) \rho(r \sin \theta)r \, dr d\theta d\phi \\ &= \int_0^{2\pi} \int_0^\pi \int_{r_P}^\infty \frac{1}{2} \left[ \left( -\frac{Vr_P^3 \cos \theta}{r^3} \right)^2 + \left( -\frac{Vr_P^3 \sin \theta}{2r^3} \right)^2 \right] \rho r^2 \sin \theta \, dr d\theta d\phi \\ &= \frac{\rho V^2 r_P^6}{2} \int_0^{2\pi} \int_0^\pi \int_{r_P}^\infty \left[ \frac{(\cos \theta)^2}{r^4} + \frac{(\sin \theta)^2}{4r^4} \right] \sin \theta \, dr d\theta d\phi \\ &= \frac{\rho V^2 r_P^6}{2} \int_0^{2\pi} \int_0^\pi \left[ (\cos \theta)^2 \left( -\frac{1}{3r^3} \right) + (\sin \theta)^2 \left( -\frac{1}{3r^3} \right) \frac{1}{4} \right]_{r_P}^\infty \sin \theta \, d\theta d\phi \\ &= \frac{\rho V^2 r_P^6}{2} \int_0^{2\pi} \int_0^\pi \left[ (\cos \theta)^2 \left( \frac{1}{3r_P^3} \right) + (\sin \theta)^2 \left( \frac{1}{3r_P^3} \right) \frac{1}{4} \right] \sin \theta \, d\theta d\phi \\ &= \frac{\rho V^2 r_P^3}{6} \int_0^{2\pi} \int_0^\pi \left( \cos^2 \theta \sin \theta + \frac{1}{4} (1 - \cos^2 \theta) \sin \theta \right) \, d\theta d\phi \\ &= \frac{\rho V^2 r_P^3}{6} \int_0^{2\pi} \left[ -\frac{1}{3} \cos^3 \theta + \frac{1}{4} \left( -\cos \theta + \frac{1}{3} \cos^3 \theta \right) \right]_0^\pi \, d\phi \\ &= \frac{\rho V^2 r_P^3}{6} \int_0^{2\pi} \left[ \frac{2}{3} + \frac{1}{4} \left( 2 - \frac{2}{3} \right) \right] \, d\phi = \frac{1}{3} \rho \pi r_P^3 V^2 \end{aligned} \quad (5.109)$$

The virtual mass  $m_V$  can now be derived from (5.109) and (5.103):

$$m_V = \frac{2}{3} \rho \pi r_P^3 = \frac{1}{2} \left( \frac{4}{3} \rho \pi r_P^3 \right), \quad (5.110)$$

It follows that the virtual mass force is given by: [97]:

$$f_{V,P} = \frac{1}{2} m_V \frac{dV}{dt} = \frac{1}{2} \rho_c \frac{\pi}{6} d_{P,V}^3 \frac{dV}{dt} \quad (5.111)$$

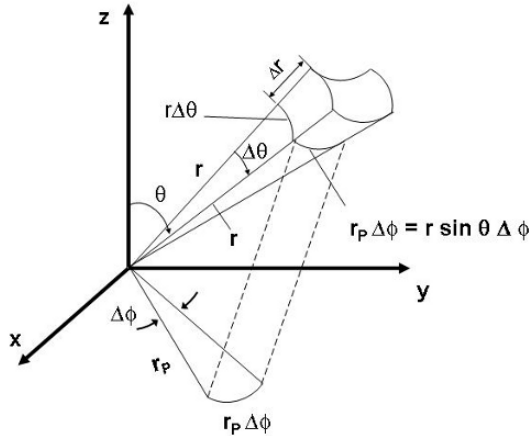


Fig. 5.12. Volume element represented in spherical polar coordinates.

The virtual mass coefficient for a sphere in an invicid fluid is thus  $C_V = \frac{1}{2}$ .

The basic model (5.111) is often slightly extended to take into account the self-motion of the fluid. In general the added mass force is expressed in terms of the relative acceleration of the fluid with respect to the particle acceleration.

Similar analyses can be performed for dispersed bodies other than spheres [26]. In these cases the basic equations are the same, but the mass of fluid displaced can be different.

It is emphasized that the virtual mass force accounts for the form drag (shape effects) due to the relative acceleration between the particle and the surrounding fluid.

**The Eulerian formulation of the added mass or virtual mass force acting on rigid spheres in potential flow**

In the Eulerian framework the virtual mass force valid for potential flows is normally expressed by [7, 152, 64, 33, 8]:

$$\mathbf{F}_V = \alpha_d \rho_c f_V \left( \frac{D\mathbf{v}_c}{Dt} - \frac{D\mathbf{v}_d}{Dt} \right) \tag{5.112}$$

where  $C_V$  is usually set to 0.5 as for a single sphere.

In bubbly flow simulations values ranging from 0.25 to 0.75 have been used for different bubble shapes and number densities of bubbles [65]. The added mass effect is obviously more important for light bubbles in liquids than for heavy solid particles or droplets in gas or liquid.

Alternative, and supposedly more advanced, added mass force and coefficient formulations have been presented and discussed in the literature [31, 32, 24, 164, 170, 19, 51, 94]. However, there are still controversis regarding the physics of added mass in particular considering dense dispersions [158].

### Oscillations of a sphere in viscous flow (History force)

The history force was discovered independently by Boussinesq [18] and Basset [10] in their study of the oscillations of a rigid sphere in a viscous flow.

While the virtual mass force accounts for the form drag on the particle due to relative acceleration between the particle and the surrounding fluid, the history term accounts for the corresponding viscous effects. Moreover, the history force originates from the unsteady diffusion of the vorticity around the particle so there is a delay in the boundary layer development as the relative velocity changes with time [96, 97, 22]. This means that when the relative velocity between the particle and the fluid varies, the vorticity present at the particle surface changes and the surrounding flow needs a finite time to readapt to the new conditions.

A general expression for  $\mathbf{f}_B$  in a uniform flow has been put in the form:

$$\mathbf{f}_B = \mu d_P \int_0^t K(t - \tau) \left( \frac{\partial \mathbf{v}_c}{\partial \tau} - \frac{\partial \mathbf{v}_d}{\partial \tau} \right) d\tau \quad (5.113)$$

where the kernel  $K(t - \tau)$  depends on the diffusion process of the vorticity.

The Basset's expression is found in the limit of unsteady Stokes flow for a *rigid sphere* and is given by:

$$K(t - \tau) = \frac{3}{2} \left[ \frac{\pi d_P^2}{\nu(t - \tau)} \right]^{1/2} \quad (5.114)$$

Substituting (5.114) into (5.113) the history force becomes [22, 174]:

$$\mathbf{f}_B = -6\pi\mu r_P^2 \frac{1}{\sqrt{\pi\nu}} \int_0^t \frac{\partial \mathbf{v}_p}{\partial \tau} (t - \tau)^{-1/2} d\tau \quad (5.115)$$

in which it is assumed that the fluid movement is negligible.

The case of a *bubble* is more complicated because of the different origin of the interfacial vorticity. For a rigid surface the vorticity comes from the no-slip condition, while on a bubble it is the vanishing of the shear stress on a curved surface that forces vorticity to be non-zero. For a bubble a closed expression of the kernel is defined by [104, 96]:

$$K(t - \tau) = 4\pi \exp[36\nu(t - \tau)/d_P^2] \operatorname{erfc}[36\nu(t - \tau)/d_P^2] \quad (5.116)$$

For a *drop*, the solution naturally depends on the ratio between the kinetic viscosities of the outer and inner fluids [146, 172, 21, 174]. A closed form of  $K(t - \tau)$  has not been obtained for this case [96].

Magnaudet [96] also compared the magnitudes of different history forces and concluded that the history force acting on a clean bubble is much smaller

than the corresponding one acting on a rigid sphere. The history force can be neglected in most cases considering bubbly flows.

The extension of the theory to non-uniform flows and to high Reynolds number flows is still controversial. Nevertheless, Clift et al [22] reviewed numerous investigations and claimed that the history term has a negligible effect on the mean motion of a particle in a turbulent fluid. The impacts on the fluctuations in particle motion might be more severe at high frequencies.

In multiphase reactor flow simulations the impacts of the history forces are normally neglected as the present understanding of these phenomena is far from complete.

### 5.2.7 Interfacial Momentum Transfer Due to Phase Change

The conventional formulas for the interfacial momentum transfer due to phase change are defined in sect 3.3 for the different averaging methods commonly applied in chemical reactor analysis. The modeling concepts usually adopted for the different averages are mathematically similar, so we choose to present a representative interfacial momentum transfer term in the framework of the volume averaging method described in sect 3.4.1.

In fluid mechanics the interfacial momentum transfer due to phase change (3.148) is normally expressed in terms of interfacial mass flux weighted quantities

$$\mathbf{M}_k^{\Gamma} = -\frac{1}{V} \int_{A_I} \rho_k \mathbf{v}_k (\mathbf{v}_k - \mathbf{v}_I) \cdot \mathbf{n}_k da \approx \Gamma_{V_k} \langle \mathbf{v}_k \rangle_{A_I}^{\Gamma} \quad (5.117)$$

The modeling of the interfacial mass transfer terms due to phase change  $\Gamma_{V_k}$  is discussed in sect 5.3, so only the  $\langle \mathbf{v}_k \rangle_{A_I}^{\Gamma}$  term is considered in this section.

For catalytic solid surfaces in packed beds and porous materials the speed of displacement of the interface is assumed to be zero,  $\mathbf{v}_I \cdot \mathbf{n}_k = 0$ . For this reason the interfacial momentum transfer due to phase change can be reduced to:

$$\mathbf{M}_k^{\Gamma} \approx -\frac{1}{V} \int_{A_I} \rho_k \mathbf{v}_k \mathbf{v}_k \cdot \mathbf{n}_k da \approx \Gamma_{V_k} \langle \mathbf{v}_k \rangle_{A_I}^{\Gamma} \quad (5.118)$$

The same model assumption is used for gas-liquid interfaces as well, since the interface is hypothetically pictured as being stagnant [47]. However, one or both of the bulk phases may move.

At catalytic solid surfaces there are normally no phase change, so the interfacial momentum transfer due to phase change simply vanishes. Hence,

$$\Gamma_{V_k} \langle \mathbf{v}_k \rangle_{A_I}^{\Gamma} = 0 \quad (5.119)$$

The rather blurry picture of the gas-liquid interface makes it very difficult to parameterize the  $\langle \mathbf{v}_k \rangle_{A_I}^{\Gamma}$  variable. Therefore, the interfacial momentum transfer due to phase change is generally neglected at these surfaces too. Further work is obviously required to improve our knowledge about these phenomena and to validate this model assumption.

### 5.3 Interfacial Heat and Mass Transfer Closures

In this section the classical heat and mass transfer theories are examined. The singular surface jump conditions for the primitive quantities, as derived in the framework of the standard averaging procedures, are approximated by the classical chemical engineering stagnant film theory normally used in chemical reactor models. The relevant transport phenomena solutions and the classical theories on heat and mass transfer considering both low- and high mass transfer rates are summarized in the subsequent subsections.

#### 5.3.1 Approximate Interfacial Jump Conditions

Fairly rigorous formulas for the interfacial heat and mass transfer terms are defined in sect 3.3 for the different averaging methods commonly applied in chemical reactor analysis. However, since the modeling concepts are mathematically similar for the different averages, we choose to examine these constitutive equations in the framework of the volume averaging method described in sect 3.4.1. This modeling framework is used extensively in chemical reactor analysis because the basic model derivation is intuitive and relatively easy to understand.

It has been pointed out that the macroscopic interfacial transfer terms occurring in the averaged model equations, as described in sect 3.3, represent approximate integral values of the averaged interfacial terms as proposed by Ishii [61] making a provisional model for *stratified flows* in nuclear reactor engineering. Specific application dependent constitutive equations and modeling concepts are thus required determining these terms for the different chemical systems, flow regimes, operating conditions, and so forth to reimpose the essential physics that were lost during the averaging process with an appropriate level of complexity.

For comparison we briefly display the standard macroscopic transfer functions resulting from the averaging process, before we introduce the particular constitutive equations normally applied in chemical reaction engineering. This might help to elucidate the connection between the conventional fluid mechanics modeling framework and the customary chemical reaction engineering interfacial coupling terms.

In the multiphase flow literature these integral terms are generally approximated as the product of the interfacial area concentration and a mean interfacial flux using the mean value theorem for integrals.

Using the mean value theorem the interfacial mass transfer rate due to phase change (3.144) becomes [61, 72, 12]:

$$\Gamma_{Vk} = -\frac{1}{V} \int_{A_I} \rho_k (\mathbf{v}_k - \mathbf{v}_I) \cdot \mathbf{n}_k da \approx a_I \langle \dot{m}_k \rangle_{A_I} \approx a_I \rho_k \langle v_{n,k}^{\text{rel}} \rangle_{A_I}$$

where  $\langle v_{n,k}^{\text{rel}} \rangle_{A_I}$  denotes the average interfacial velocity of phase  $k$ , relative to the velocity of phase  $k$  at the interface, normal to the interface and in a

direction outward of phase  $k$ . This means that  $\langle v_{n,k}^{\text{rel}} \rangle_{A_I}$  represents the normal interface velocity solely due to phase change.

Similarly, the interfacial heat transfer (3.175), as related to (3.201), and the species transfer (3.179) due to phase change are normally expressed in terms of interfacial mass flux weighted quantities

$$h_k^\Gamma = -\frac{1}{V} \int_{A_I} \rho_k h_k (\mathbf{v}_k - \mathbf{v}_I) \cdot \mathbf{n}_k da \approx \Gamma_{V_k} \langle h_k \rangle_{A_I}^\Gamma$$

$$J_{k,s}^\Gamma = -\frac{1}{V} \int_{A_I} \rho_k \omega_{k,s} (\mathbf{v}_k - \mathbf{v}_I) \cdot \mathbf{n}_k da \approx \Gamma_{V_k} \langle \omega_k \rangle_{A_I}^\Gamma$$

It is noted that in the general case the interface velocity is not equal to the neighboring phase velocities  $\mathbf{v}_I \neq \mathbf{v}_k$ .

The initial engineering applications of the two-fluid framework to model chemical reacting flows focused on combustion processes. Unlike the normal behavior of chemical reactors, in many of the homogeneous combustion applications the details of the chemical reaction kinetics are effectively ignored because the reactions are very fast and thus assumed to be in local instantaneous chemical equilibrium. That is, all the reactions are assumed to occur much faster than the turbulent micro-mixing. The rate determining step is thus the turbulent micro-mixing properties of the flow, so turbulence modeling was considered especially important. To describe heterogeneous systems like spray and solid particle combustion processes the two-fluid model has been considered useful [77] [111, 140, 137, 138]. It is noted that for these systems the burning rate  $\langle v_{n,k}^{\text{rel}} \rangle_{A_I}$ , i.e., the rate at which the particles shrink, is normally defined in accordance with the modeling approach explained by Ishii [61]. Moreover, in the combustion processes involving droplet vaporization the multicomponent mass diffusion and heating of the liquid phase are usually the rate-controlling phenomena determining the overall burning rate [138].

In recent years the conventional modeling framework has also been adopted for the description of multicomponent transport phenomena during metal alloy solidification [109, 110, 12].

In the field of chemical reaction engineering, on the other hand, the elementary modeling principles still being used in the modern fluid dynamic reactor models did not evolve from any averaging concept, since the classical reaction engineering models were postulated long before the averaging concepts were proposed. The present aim is thus to link the classical approach used in reactor analysis with the conventional fluid dynamic formulas given above.

Although many physical processes of interest to chemical reaction engineers involve absorption, heterogeneous reaction, surface mass transport, and interfacial mass transfer at moving and deforming interfaces, their main focus is concerned with the phenomena occurring at two particular types of interface systems. These are (1) the adsorption and reaction processes taking

place at catalytic solid surfaces and (2) the condensation/evaporation of fluid mixtures going on at gas-liquid interfaces.

In the case of adsorption and reaction at a fixed catalytic surface the speed of displacement of the interface is assumed to be zero<sup>4</sup> [167]. In this case the interfacial transfer terms due to phase change can be reduced to:

$$\Gamma_{V_k} = -\frac{1}{V} \int_{A_I} \rho_k (\mathbf{v}_k - \mathbf{v}_I) \cdot \mathbf{n}_k da \approx -\frac{1}{V} \int_{A_I} \rho_k \mathbf{v}_k \cdot \mathbf{n}_k da \quad (5.120)$$

$$h_k^I = -\frac{1}{V} \int_{A_I} \rho_k h_k (\mathbf{v}_k - \mathbf{v}_I) \cdot \mathbf{n}_k da \approx -\frac{1}{V} \int_{A_I} \rho_k h_k \mathbf{v}_k \cdot \mathbf{n}_k da \quad (5.121)$$

$$J_{k,s}^I = -\frac{1}{V} \int_{A_I} \rho_k \omega_{k,s} (\mathbf{v}_k - \mathbf{v}_I) \cdot \mathbf{n}_k da \approx -\frac{1}{V} \int_{A_I} \rho_k \omega_{k,s} \mathbf{v}_k \cdot \mathbf{n}_k da \quad (5.122)$$

where one of the phases represents a rigid solid which is in contact with the second one being a fluid phase. The interface is a catalytic surface at which chemical reactions can take place, and both the bulk phases are continuous. Further discussions and a fundamental description of the species mass transfer phenomena are given by Whitaker [167, 168].

In the case of phase change at gas-liquid mixtures interfaces profound understanding of (1) the thermodynamics of fluid mixtures, (2) phase equilibria, (3) heat transfer, and (4) mass transfer are required. The classical two-film theory concept of Colburn and Drew [23] is normally adopted [162, 15]. In this approach the interfacial transfer models are derived considering a *stagnant* surface or interface enclosed by two thin and stagnant hypothetical films. For dynamic (i.e., no global equilibrium) cases one imagines resistances to both heat and mass transfer through the films on both sides of the interface and that thermodynamic equilibrium prevails at the interface only, thereby the bulk phases are not necessarily uniform at steady state.

In this context it is emphasized that in chemical reaction engineering a detailed description of the movement of the interfaces have not been considered important even for gas-liquid systems, in the sense that the complexity of such an approach will lead to impracticable computational costs and little gain in understanding and physical modeling of the important chemical processes. Henceforth, if otherwise not explicitly stated, for the examination of the engineering heat and mass transfer theories both the hypothetical films and the embedded interface are assumed to be stagnant,  $\mathbf{v}_I \cdot \mathbf{n}_k = 0$ . However, the bulk phases may still move relative to each other.

It follows that the definitions of the interfacial heat and mass transfer fluxes are not stringent and to a certain extent based on fragmentary arguments, therefore the transfer coefficients can be interpreted in several ways [15, 139]. Basically, the transfer coefficients are either treated as an alternative model

<sup>4</sup> The fundamental analysis applies to packed and porous beds only, but in practice the same modeling approach is generally used for dispersed catalyst particles as well.

to the fundamental diffusion models (i.e., the Fourier's and Fick's laws) or the transfer coefficients are taking both diffusive and convective mechanisms into account through extended theories and/or empirical parameterizations. However, the distinction between these approaches is rather blurred so it is not always clear which of the fundamental transport processes that are actually implemented.

In an attempt to explain the chemical engineering modeling approach in a precise manner Bird et al [13, 15] proposed to distinguish between the definition of the transfer coefficients for problems with low- and high net mass transfer rates although no precise partition was made. It was assumed that for systems with a slightly soluble component, small diffusivities, and small net mass transfer rates the analytical expressions derived from pure diffusive flux considerations can be used. For high net mass transfer rates the transfer coefficients depend on the convective mass transport in addition to the diffusive mechanisms. To describe the transfer under such conditions, Bird et al adopted the approach of Colburn and Drew [23] consisting in replacing the analytical formula derived for pure diffusion through the hypothetical films by a similar but entirely empirical expression in which the pre-factor in front of the driving force is substituted by an empirical mass transfer coefficient. These mass transfer coefficients are assumed to be functions of the physical properties of the mixture and the conditions of the flow. Other theories, again, impose various semi-empirical convective effects and compare the classical stagnant film mass diffusion transport estimates with the extended mass transfer expressions. By similarity arguments one then postulate semi-empirical relationships between the transport and transfer coefficients. The impact of convection on the mass transfer coefficient are then supposedly lumped into the film thickness parameter [47]. It is hardly necessary to remark that prudence is required working with these concepts to make sure that the different formulas and the transfer coefficients are used in a consistent manner.

The advantage of working in terms of the traditional joint diffusive and convective flux concept is that the contribution of convection is automatically taken into account and we do not need separate models for the interfacial transfers due to phase change. The disadvantage is that the transfer coefficients show a more complicated dependence upon concentration and mass transfer rates. In a scientific view the loss in physical rigor might outweigh the possible gain in computational ease [139]. Nevertheless, in this work we follow the approach chosen in most chemical reactor analysis in which the transfer coefficients are defined in terms of the combined fluxes including both diffusive and convective contributions.

The combined volumetric species mass transfer rate across a hypothetical fluid film  $R_{n_{k,s}}$  represents the species mass transfer from a solid surface of area  $A_I$  and mass fraction  $\langle \omega_{k,s} \rangle_{A_I}$  to an adjacent moving fluid stream with mass fraction  $\langle \omega_{k,s} \rangle_{V_k}$ . For a binary fluid mixture the combined volumetric species mass transport rate is approximated by:

$$\begin{aligned}
 R_{\mathbf{n}_{k,s}} &= a_I \langle \mathbf{n}_{k,s} \rangle_{A_I} = J_{k,s}^j + J_{k,s}^\Gamma \approx a_I \rho_k \frac{D_{k,s}}{l_{k,s}} (\langle \omega_{k,s} \rangle_{A_I} - \langle \omega_{k,s} \rangle_{V_k}) \\
 &= a_I \rho_k k_{c,s} (\langle \omega_{k,s} \rangle_{A_I} - \langle \omega_{k,s} \rangle_{V_k})
 \end{aligned} \tag{5.123}$$

in which it is assumed that the mean interfacial flux is proportional to the difference between the interfacial average and the intrinsic volume average of the mass fraction.  $D_{k,s}$  is the binary diffusion coefficient in the phase denoted by  $k$ , and  $l_k$  is the thickness of the film on the phase  $k$  side of the interface. In this case  $J_{k,s}^\Gamma$  denotes the convective contributions to the interfacial species mass transfer flux, as no phase change takes place at these interfaces. If the no slip condition applies at the surface, the convective flux contribution is zero.

The surface average combined convective mass transfer flux  $\langle \mathbf{n}_{k,s} \rangle_{A_I}$  ( $kg/m^2s$ ) is generally approximated by:

$$\begin{aligned}
 \langle \mathbf{n}_{k,s} \rangle_{A_I} &= J_{k,s}^j + J_{k,s}^\Gamma \approx a_I \rho_k \frac{D_{k,s}}{l_{k,s}} (\langle \omega_{k,s} \rangle_{A_I} - \langle \omega_{k,s} \rangle_{V_k}) \\
 &= a_I \rho_k k_{c,s} (\langle \omega_{k,s} \rangle_{A_I} - \langle \omega_{k,s} \rangle_{V_k})
 \end{aligned} \tag{5.124}$$

It is further noted that the use of interfacial mass flux weighted transfer terms is generally not convenient treating multicomponent reactive systems, because the phase change processes are normally not modeled explicitly but deduced from the species composition dependent joint diffusive and convective interfacial transfer models. Moreover, the rigorous reaction kinetics and thermodynamic models of mixtures are always formulated on a molar basis.

Basically the fundamental convective heat transfer refers to the conductive flux mechanisms by which heat is transferred between a solid surface and a fluid moving over the surface in such a way that the fluid is stagnant at the wall because of the no slip behavior. The volumetric heat transfer rate  $R_{Q_k}$  ( $W/m^3s$ ) represents the heat transfer from a solid surface of area  $A_I$  and temperature  $\langle T_S \rangle_{A_I}$  to an adjacent moving fluid stream of temperature  $\langle T_k \rangle_{V_k}$  ( $K$ ). The volumetric heat transfer rate can be approximated by:

$$R_{Q_k} = -\frac{1}{V} \int_{A_I} \mathbf{q}_k \cdot \mathbf{n}_k da = a_I \langle \mathbf{q}_k \cdot \mathbf{n}_k \rangle \approx h_k^{\text{cond}} a_I (\langle T_S \rangle_{A_I} - \langle T_k \rangle_{V_k}) \tag{5.125}$$

The corresponding surface average convective heat transfer flux  $\langle \mathbf{q}_k \cdot \mathbf{n}_k \rangle_A$  is generally approximated by:

$$\left\langle \frac{\dot{Q}_k^{\text{cond}}}{A_I} \right\rangle_A = \langle \mathbf{q}_k \cdot \mathbf{n}_k \rangle_A \approx h_k^{\text{cond}} (\langle T_S \rangle_{A_I} - \langle T_k \rangle_{V_k}) \tag{5.126}$$

where  $h_k^{\text{cond}}$  is the heat transfer coefficient ( $Wm^2K$ ) associated with pure conduction at the wall.

Alternatively, the convective heat transfer rate may refer to the combined conductive and convective flux mechanisms by which heat is transferred between a solid surface and a fluid moving over the surface provided that the

fluid is not stagnant at the wall because of fluid-wall slip. In this case the volumetric heat transfer rate  $R_{Q_k}$  ( $W/m^3s$ ) is given by:

$$\begin{aligned} R_{Q_k} &= -\frac{1}{V} \int_{A_I} (\mathbf{q}_k + \rho_k h_k \mathbf{v}_k) \cdot \mathbf{n}_k da = a_I \langle (\mathbf{q}_k + \rho_k h_k \mathbf{v}_k) \cdot \mathbf{n}_k \rangle \\ &\approx h_k^{\text{cond, conv}} a_I (\langle T_S \rangle_{A_I} - \langle T_k \rangle_{V_k}) \end{aligned} \quad (5.127)$$

The corresponding surface average combined convective heat transfer flux is normally approximated by:

$$\begin{aligned} \left\langle \frac{\dot{Q}_k^{\text{cond, conv}}}{A_I} \right\rangle &= \left\langle \frac{\dot{Q}_k^{\text{cond}} + \dot{Q}_k^{\text{conv}}}{A_I} \right\rangle_A = \langle (\mathbf{q}_k + \rho_k h_k \mathbf{v}_k) \cdot \mathbf{n}_k \rangle_A \\ &\approx h_k^{\text{cond, conv}} (\langle T_S \rangle_{A_I} - \langle T_k \rangle_{V_k}) \end{aligned} \quad (5.128)$$

where  $h_k^{\text{cond, conv}}$  is the combined convective heat transfer coefficient accounting for conductive and convective heat transfer ( $W/m^2K$ ).

In both convective heat transfer definitions it is presumed that the solid surface is warmer than the fluid so that heat is being transferred from the solid to the fluid. Equations (5.125) and (5.127) are sometimes called *Newton's law of cooling* but are merely the defining equation for the  $h_k$  parameters [102, 60, 15].

The convective heat transfer coefficient generally depends on conditions in the boundary layer, surface geometry, fluid motion, and thermodynamic and transport properties of the fluid. A thorough examination of the heat transfer coefficient theory and many examples are given by Bird et al [15], Kays and Crawford [71], Middleman [102] and Incropera and DeWitt [60].

The approximate modeling approaches found to be suitable for the purpose of determining the interfacial heat and mass transfer fluxes in reactor analysis can be summarized as follows.

#### *Chemical Species Mass Transfer*

1. Considering a binary fluid mixture at a *catalytic solid surface* the species mass transport is approximated by the transfer flux across a hypothetical fluid film:

$$\begin{aligned} R_{n_{k,s}} &= a_I \langle \mathbf{n}_{k,s} \rangle_{A_I} = J_{k,s}^j + J_{k,s}^r \approx a_I \rho_k \frac{D_{k,s}}{l_{k,s}} (\langle \omega_{k,s} \rangle_{A_I} - \langle \omega_{k,s} \rangle_{V_k}) \\ &= a_I \rho_k k_{c,s} (\langle \omega_{k,s} \rangle_{A_I} - \langle \omega_{k,s} \rangle_{V_k}) \end{aligned} \quad (5.129)$$

The interfacial species mass jump balance (3.178) can now be expressed as:

$$R_{n_{\text{fluid},s}} + R_{n_{\text{solid},s}} \approx \rho_{\text{Bulk}} \langle R_{I,s} \rangle^m, \quad (5.130)$$

and we can eliminate the solid phase transfer term from the bulk phase transport equations [166].

In addition, the net diffusive mass flux for each phase vanishes for binary systems as  $\sum_s J_{k,s}^j = 0$  adopting Fick's law. Nevertheless, this diffusive flux definition is commonly used also for dilute pseudo-binary systems. In these particular cases the latter relationship is only approximate.

2. For a non-reactive two-phase *gas-liquid interface* the mass transport is approximated by the net transfer flux across the two stagnant fluid films. For each film we may write a transfer rate term on the form:

$$\begin{aligned} R_{n_{k,s}} &= J_{k,s}^j + J_{k,s}^I \approx a_I \rho_k \frac{D_{k,s}}{l_{k,s}} (\langle \omega_{k,s} \rangle_{A_I}^{\text{eq}} - \langle \omega_{k,s} \rangle_{V_k}) \\ &= a_I \rho_k k_{c,s} (\langle \omega_{k,s} \rangle_{A_I}^{\text{eq}} - \langle \omega_{k,s} \rangle_{V_k}) \end{aligned} \quad (5.131)$$

It is still assumed that the mean interfacial flux is proportional to the difference between the interfacial average and the intrinsic volume average of the mass fraction. In addition, the interfacial surface averaged concentrations are assumed to be in local instantaneous thermodynamic equilibrium.

For dilute mixtures Henry's law is frequently used to relate the interfacial concentrations:

$$\langle \omega_{g,s} \rangle_{A_I}^{\text{eq}} = \langle H_s \rangle_{A_I} \langle \omega_{l,s} \rangle_{A_I}^{\text{eq}} \quad (5.132)$$

where  $\langle H_s \rangle_{A_I}$  is a surface averaged value for a modified Henry's law constant for species  $s$  in the mixture. The conventional Henry's law is always defined on a mole basis.

When a similar expression for the second film is established, the interfacial concentrations can be eliminated (the derivation is shown in the subsequent subsections). Assuming there are no surface reactions in the hypothetical films or at the gas-liquid interface, the interfacial species mass jump balance (3.178) reduces to:

$$R_{n_{g,s}} + R_{n_{l,s}} = 0 \quad (5.133)$$

The net diffusive mass flux for each phase still vanishes for binary systems as  $\sum_s J_{k,s}^j = 0$  using Fick's law, whereas for dilute pseudo-binary systems the latter relationship is only approximate.

#### Mixture Mass Transfer

1. For *catalytic solid surfaces* the interfacial mass transfer rate is defined by (3.144) as:

$$\Gamma_{V_k} = \sum_s R_{n_{k,s}} = \sum_s (J_{k,s}^I + J_{k,s}^j) = \sum_s J_{k,s}^I = 0 \quad (5.134)$$

since the net rate of mass generation in phase  $k$  is given by the sum of the component mass transfer terms. In this case the convective and diffusive fluxes through the hypothetical film must cancel each other.

For a two-phase system the interfacial *mass* jump balance (3.143) is expressed as  $\Gamma_{Vg} = -\Gamma_{Vl} = 0$ .

2. For *gas-liquid interfaces* the interfacial mass transfer rate through each of the two films, is used to approximate (3.144), as expressed by:

$$\begin{aligned} \Gamma_{Vk} &= \sum_s R_{n_{k,s}} = \sum_s (J_{k,s}^{\Gamma} + J_{k,s}^j) = \sum_s J_{k,s}^{\Gamma} \\ &\approx a_I \rho_k \sum_s k_{c,s} (\langle \omega_{k,s} \rangle_{A_I}^{\text{eq}} - \langle \omega_{k,s} \rangle_{V_k}) \end{aligned} \quad (5.135)$$

That is, the net rate of mass generation in phase  $k$  is given by the sum of the component mass transfer fluxes for binary mixtures using Fick's law. For a two-phase system the interfacial *mass* jump balance (3.143) is expressed as  $\Gamma_{Vg} + \Gamma_{Vl} = 0$ .

Again, it is mentioned that the binary mass flux definitions given above are commonly used also for pseudo-binary systems. In these particular cases the above relationships are only approximate.

#### Mixture Heat Transfer

1. Similar constitutive equations are used to approximate the integrals representing the interfacial heat transfer rates by convection and conduction through the stagnant films in the vicinity of a catalytic solid surface. Hence, the film model can be used to approximate the interfacial heat transport (3.167) by:

$$\begin{aligned} R_{Q_k} &= -\frac{1}{V} \int_{A_I} (\mathbf{q}_k + \rho_k h_k \mathbf{v}_k) \cdot \mathbf{n}_k da = h_k^{\Gamma} + E_k^E \\ &\approx a_I h_k (\langle T_k \rangle_{A_I} - \langle T_k \rangle_k) \end{aligned} \quad (5.136)$$

The  $E_k^E$  contribution vanishes when the fluid is really stagnant at the interface (no slip).

The final form of the interfacial jump heat balance for a catalytic surface (3.173) yields:

$$R_{Q_g} + R_{Q_l} = E_g^E + h_g^{\Gamma} + E_l^E + h_l^{\Gamma} \approx \rho_{\text{Bulk}} \langle R_{I,s}(-\Delta H_R) \rangle_{A_I}^m \quad (5.137)$$

At the catalytic solid surfaces the interfacial heat transfer due to phase change vanishes, instead the convective contributions in (3.175) are incorporated into the convective heat transfer coefficients.

2. For gas-liquid systems involving phase change the mixture enthalpy consists of a sensible heat and a latent heat of vaporization. The corresponding heat jump condition (3.173) can be expressed as  $E_g^E + h_g^{\Gamma} + E_l^E + h_l^{\Gamma} \approx 0$ , or alternatively [138]:

$$\begin{aligned} &-\frac{1}{V} \int_{A_I} (\mathbf{q}_g + \rho_g \mathbf{v}_g h_g) \cdot \mathbf{n}_g \\ &= \frac{1}{V} \int_{A_I} (\mathbf{q}_l + \rho_l \mathbf{v}_l ([h_l - \Delta h_{lg,\text{mix}}^{\text{vap}}] + \Delta h_{lg,\text{mix}}^{\text{vap}})) \cdot \mathbf{n}_l da \end{aligned} \quad (5.138)$$

in which  $h_{lg,\text{mix}}^{\text{vap}}$  represents the net latent heat of vaporization of the multicomponent mixture ( $J/kg$ ).

In the chemical engineering community the interfacial heat balance concept proposed by Colburn and Drew [23] to treat the latent heat of vaporization term may be more familiar. A consistent expression for the net latent heat of vaporization of the multicomponent mixture  $h_{lg,\text{mix}}^{\text{vap}}$  in terms of the pure vapor  $s$  enthalpies  $h_{lg,s}^{\text{vap}}$  can be derived from the Colburn and Drew theory [23, 162, 9] (sect 4.1.8). In their two-film model approach the heat balance includes (1) the heat flux at the interface due to condensation  $R_{Q_{I,\lambda}}$ , (2) sensible heat loss by the gas film, and (3) sensible heat loss by the liquid film. The interfacial heat jump balance (3.173) is then approximated by:

$$R_{Q_i} \approx R_{Q_{I,\lambda}} - R_{Q_g} \quad (5.139)$$

neglecting the species mixing effects.

To be consistent with the mass transfer model, the interfacial heat transfer flux through each of the films consists of both conductive (3.167) and convective (3.175) contributions. The heat transfer terms are approximated by

$$\begin{aligned} R_{Q_k} &= -\frac{1}{V} \int_{A_I} (\mathbf{q}_k + \rho_k h_k \mathbf{v}_k) \cdot \mathbf{n}_k da = h_k^F + E_k^E \\ &\approx a_I h_k (\langle T_k \rangle_{A_I} - \langle T_k \rangle_k) \end{aligned} \quad (5.140)$$

That is, the interfacial heat transfer per unit volume is modeled as the product of the interfacial area concentration and a mean normal interfacial flux which is proportional to the difference between the interfacial average and the intrinsic volume average of the temperature of phase  $k$ .

The latent heat of vaporization for multicomponent mixtures is dependent upon the mixture composition and given by [138]:

$$\begin{aligned} R_{Q_{I,\lambda}} &= \frac{1}{V} \int_{A_I} \rho_l \mathbf{v}_l \Delta h_{lg,\text{mix}}^{\text{vap}} \cdot \mathbf{n}_l da = \frac{1}{V} \int_{A_I} \sum_s \rho_{l,s} \mathbf{v}_{l,s} \Delta h_{lg,s}^{\text{vap}} \cdot \mathbf{n}_l da \\ &= \frac{1}{V} \int_{A_I} \sum_s \frac{\mathbf{n}_{l,s} \cdot \mathbf{n}_l}{M_{w,s}} (\bar{h}_{g,s} - \bar{h}_{l,s}) da \\ &= \frac{1}{V} \int_{A_I} \sum_s \frac{\mathbf{n}_{l,s} \cdot \mathbf{n}_l}{M_{w,s}} \Delta \bar{h}_{lg,s} da \end{aligned} \quad (5.141)$$

The net latent heat of vaporization of the multicomponent mixture  $\Delta h_{lg,\text{mix}}^{\text{vap}}$  can thus be calculated from the following relation:

$$\Delta h_{lg,\text{mix}}^{\text{vap}} = \frac{\sum_s \frac{\mathbf{n}_{l,s} \cdot \mathbf{n}_l}{M_{w,s}} \Delta \bar{h}_{lg,s}}{\sum_s \mathbf{n}_{l,s} \cdot \mathbf{n}_l} = \frac{\sum_s \frac{\mathbf{n}_{l,s} \cdot \mathbf{n}_l}{M_{w,s}} \Delta \bar{h}_{lg,s}}{\mathbf{n}_{l,\text{tot}} \cdot \mathbf{n}_l} = \frac{\sum_s \frac{\mathbf{n}_{l,s} \cdot \mathbf{n}_l}{M_{w,s}} \Delta \bar{h}_{lg,s}}{\rho_l \mathbf{v}_l \cdot \mathbf{n}_l} \quad (5.142)$$

where  $\bar{h}_{g,s}$  is the partial molar enthalpy of component  $s$  in the gas, and  $\bar{h}_{l,s}$  is the partial molar enthalpy of component  $s$  in the liquid.  $\mathbf{n}_{l,s}$  denotes the liquid phase combined mass flux for species  $s$ , whereas  $\mathbf{n}_l$  is the outward directed unit vector for the liquid. For non-volatile/non-condensing species the convective and diffusive fluxes through the hypothetical films must be zero or cancel out.

For non-ideal multicomponent mixtures the multiphase flow calculation can be combined with a more rigorous thermodynamic equilibrium calculation to determine the mixture properties at the interface as discussed by [81, 69, 117].

However, describing the chemical reactor performance under industrial operation conditions the heat balance is normally dominated by the heat of reaction term, the transport terms and the external heating/cooling boundary conditions, hence for chemical processes in which the phase change rates are relatively small the latent heat term is often neglected.

Future work might consider extensions of these interfacial transfer concepts to ameliorate the simulation accuracy by utilizing the local information provided by the multi-fluid models. For multiphase reactive systems these processes can be rate determining, in such cases there are no use for advanced flow calculations unless these fluxes can be determined with appropriate accuracy.

### 5.3.2 Fundamental Heat and Mass Transport Processes

The molecular transport processes refer to the transfer of continuum properties by molecular movement through a medium which can be a fluid or a solid. Each molecule of a system has a given quantity of the property mass, energy and momentum associated with it. When concentration gradients exist in any of these property fields, a net transport occurs. In dilute fluids such as gases where the molecules are relatively far apart, the rate of transport of the property should be relatively fast since few molecules are present to block the transport by interaction. In dense fluids such as liquids the molecules are closer together and transport or diffusion proceeds more slowly. The molecules in solids are even more close-packed than in liquids and molecular migration is even more restricted. Therefore, the molecular diffusion coefficient for gases is larger than for liquids and solids.

The conventional parameterizations used describing molecular transport of mass, energy and momentum are the Fick's law (mass diffusion), Fourier's law (heat diffusion or conduction) and Newton's law (viscous stresses). The mass diffusivity,  $D_c$ , the kinematic viscosity,  $\nu$ , and the thermal diffusivity,  $\alpha$ , all have the same units ( $m^2/s$ ). The way in which these three quantities are analogous can be seen from the following equations for the fluxes of mass, momentum, and energy in one-dimensional systems [13, 135]:

$$j_{c,y} = -D_c \frac{d(\rho_c)}{dy} \quad (\text{Fick's law for constant } \rho) \quad (5.143)$$

$$q_y = -\alpha \frac{d(\rho C_p T)}{dy} \quad (\text{Fourier's law for constant } \rho C_p) \quad (5.144)$$

$$\sigma_{yx} = -\nu \frac{d(\rho v_x)}{dy} \quad (\text{Newton's law for constant } \rho) \quad (5.145)$$

where  $j_{c,y}$  is the flux of species  $c$  per area in  $kg/(sm^2)$ ,  $D_c$  is the mass diffusion coefficient in  $m^2/s$ ,  $\rho_c$  is the mass concentration of  $c$  in the mixture,  $q_y$  is the heat flux in  $J/(sm^2)$ ,  $\alpha = k/(\rho C_p)$  is the thermal diffusivity of the conducting medium,  $T$  is the temperature in  $K$ ,  $\tau_{yx}$  is the shear stress in  $kg/(sm^2)$ ,  $\nu$  is the kinematic viscosity coefficient and  $v_x$  is the  $x$ -velocity component in  $m/s$ .

Note that these analogies are less obvious in two- and three dimensional problems, however, because  $\sigma$  is a tensor quantity with nine components, whereas  $\mathbf{j}_c$  and  $\mathbf{q}$  are vectors with three components.

In general, there are more than one driving force involved producing diffusive transport for any one fluid property as examined in chap 2. The origin of molecular mass diffusion might be related a combination of one or more of the following non-equilibrium phenomena; concentration gradients, pressure gradients, thermal gradients or external forces.

Heat conduction is also related to atomic and molecular activity. Conduction may be viewed as the transfer of energy from the more energetic to the less energetic particles of a substance due to interactions between the particles. For a gas the temperature at any point in space is associated with the energy of molecules in proximity to the point. This energy is related to the random translational motion, as well to the internal rotational and vibrational motions, of the molecules. Higher temperatures are associated with an increase in molecular energies, and when neighboring molecules collide, a net transfer of energy from the more energetic to the less energetic molecules must occur. In the presence of a temperature gradient, energy transfer by conduction must then occur in the direction of decreasing temperature. We may speak of the net transfer of energy by random molecular motion as a diffusion of energy.

The situation is much the same in liquids, although the molecules are more closely spaced and the molecular interactions are stronger and more frequent. Similarly, in a solid, conduction may be attributed to atomic activity in the form of lattice vibrations. The modern view is to ascribe the energy transfer to lattice waves induced by atomic motions. In a non-conductor, the energy transfer is exclusively via these waves, in a conductor it is also due to the translational motion of the free electrons.

In reaction engineering the ordinary diffusion processes taking place close to an interface have been analyzed in two ways. First, as just mentioned, the interfacial transport fluxes can be described in a fundamental manner adopting the Fourier's and Fick's laws which are expressed in terms of the *transport coefficients* known as conductivity and diffusivity. Second, the interfacial

transport fluxes can alternatively be approximated in terms of the engineering *transfer coefficients* for convective heat and mass transport.

### 5.3.3 Mass Transport Described by Fick's law

This section contains a simple introduction to steady state and unsteady species mole (mass) diffusion in dilute binary mixtures. First, the physical interpretations of these diffusion problems are given. Secondly, the physical problem is expressed in mathematical terms relating the concentration profiles to the diffusion fluxes. Emphasis is placed on two diffusion problems that form the basis for the interfacial mass transfer modeling concepts used in reaction engineering.

The basic theory is reviewed in many textbooks on chemical reaction engineering [15, 6, 27, 102, 58]. These texts may be recommended for complementary studies.

Adolf Fick developed the law of diffusion by means of analogies with Fourier's work on thermal conduction [46]. Mathematically, the mass diffusion flux is thus expressed as:

$$\mathbf{j}_c = -\rho D_c \nabla \omega_c \quad (\text{Fick's law}) \quad (5.146)$$

This equation states that the flux of species is proportional to concentration gradient and occurs in the direction opposite to the direction of the concentration gradient of that species. The proportionality coefficient is the molecular diffusion coefficient.

This diffusion coefficient formulation is useful for fundamental studies where we want to know concentration versus position and time.

### Steady diffusion across a thin film with a fixed boundary

Consider a very thin film between two well-mixed fluids. Each of the fluids are dilute binary mixtures, consisting of the same solvent and solute having different concentrations. The solute diffuses from the higher concentrated solution into the less concentrated one.

The diffusion across this thin film is considered to be a steady-state problem. There are no concentration changes with time, as indicated in Fig 5.13.

To describe this problem in mathematical terms, either the differential species mass balance (1.39) can be reduced appropriately or alternatively a species mass shell balance over a thin layer,  $\Delta z$ , can be put up and combined with Fick's law. The resulting equation for steady diffusion in the thin layer is of course the same in both cases. The simple ordinary differential equation is integrated twice with the appropriate boundary conditions in order to get a relation for the concentration profile that is needed to determine the diffusive flux.

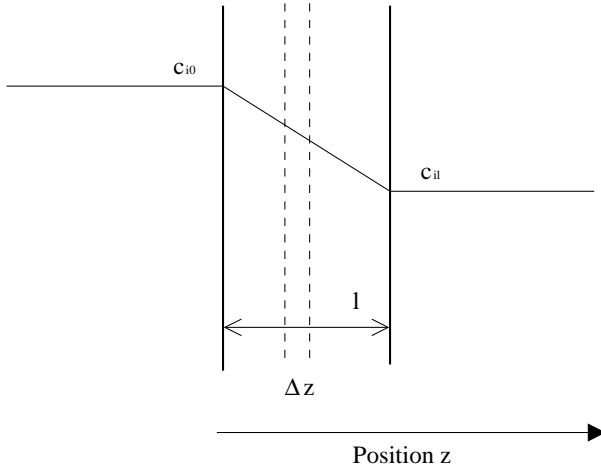


**Fig. 5.13.** Steady diffusion across a thin film.

Assuming that the diffusion coefficient is constant, the governing equations describing the problem are listed below:

The species mole balance<sup>5</sup>:

$$0 = -\frac{dJ_i^*}{dz} \quad (5.147)$$

The Fick's law for binary diffusion (i.e., in 1D):

$$J_i^* = -D \frac{dc_i}{dz} \quad (5.148)$$

Combining these relations we obtain the following differential equation:

$$0 = D \frac{d^2 c_i}{dz^2} \quad (5.149)$$

that can be solved using appropriate boundary conditions:

$$\begin{aligned} z = 0 & & c_i = c_{i0} \\ z = l & & c_i = c_{il} \end{aligned}$$

The solution of the above differential equation yields the concentration profile:

$$c_i = c_{i0} + \frac{1}{l}(c_{il} - c_{i0})z \quad (5.150)$$

The resulting concentration profile is linear and independent on the diffusion coefficient.

<sup>5</sup> The classical models are generally expressed in terms of diffusive mole fluxes.

The diffusive flux is then found by differentiating the concentration profile:

$$J_i^* = -D \frac{dc_i}{dz} = \frac{D}{l} (c_{i0} - c_{il}) \quad (5.151)$$

This flux formulation determine the basis for the basic film theory.

### Unsteady diffusion in a semi-infinite slab with a fixed boundary

Consider a volume of solution that start at an interface and extends a very long distance away from the interface. We want to describe how the concentration varies in the solution as a result of a concentration change at its interface. The concentration profile will change with time, as sketched in Fig 5.14.

To develop a model for this mathematical problem we can either simplify the differential species mass balance equation (1.39) appropriately or combine the transient shell species mass balance written for the thin layer  $\Delta z$  with Fick's law for binary diffusion. The resulting partial differential equation is called *Fick's second law*. A simple way to obtain a solution for this differential equation is to adopt the method of combination of variables. It is then necessary to define a new independent variable that enable us to transform the partial differential equation into an ordinary differential equation.

The equations describing the problem can be listed as follows:

The species mole balance:

$$\frac{\partial c_i}{\partial t} = -\frac{\partial J_i^*}{\partial z} \quad (5.152)$$

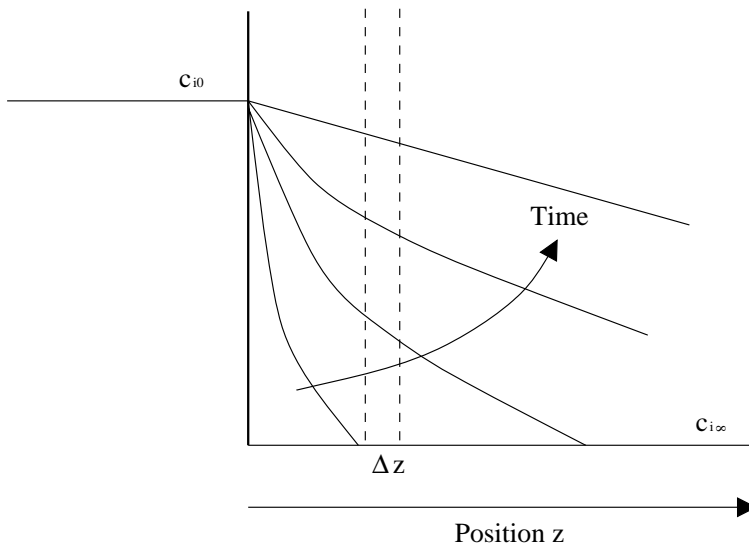


**Fig. 5.14.** Diffusion in a semi-infinite slab.

By use of the Fickian mole diffusion flux closure the Fick's second law is obtained:

$$\frac{\partial c_i}{\partial t} = D \frac{\partial^2 c_i}{\partial z^2} \quad (5.153)$$

The initial and boundary conditions needed are:

$$\begin{array}{lll} t = 0 & \text{all } z & c_i = c_{i\infty} \\ t < 0 & z = 0 & c_i = c_{i0} \\ t > 0 & z = \infty & c_i = c_{i\infty} \end{array}$$

The definition of the new independent variable is given as:

$$\zeta = \frac{z}{\sqrt{4Dt}} \quad (5.154)$$

Transforming Ficks second law and the initial and boundary conditions yield:

$$\frac{d^2 c_i}{d\zeta^2} + 2\zeta \frac{dc_i}{d\zeta} = 0 \quad (5.155)$$

and

$$\begin{array}{ll} \zeta = 0 & c_i = c_{i0} \\ \zeta = \infty & c_i = c_{i\infty} \end{array}$$

Two of the conditions have the same form after the transformation. However, the two reminding boundary conditions are sufficient solving the transformed ordinary differential equation.

The solution of the ordinary differential equation can be formulated as an error function. The concentrations profile is thus given as:

$$\frac{c_i - c_{i0}}{c_{i\infty} - c_{i0}} = 1 - \text{erf}(\zeta) = \frac{2}{\sqrt{\pi}} \int_0^\zeta e^{-\zeta^2} d\zeta \quad (5.156)$$

The flux can now be found by combining Ficks law for binary diffusion with the given concentration profile. The resulting flux relation can be expressed as:

$$J_i^* = \sqrt{\frac{D}{\pi t}} e^{-z^2/4Dt} (c_{i0} - c_{i\infty}) \quad (5.157)$$

The interfacial flux (i.e., the flux at  $z=0$ ) at a particular time,  $t$ , is given by:

$$J_i^* |_{z=0} = \sqrt{\frac{D}{\pi t}} (c_{i0} - c_{i\infty}) \quad (5.158)$$

Analysis of the results obtained for the unsteady problem shows that the predicted concentration profile is time and position dependent, and that the diffusive flux at the interface is proportional to the square root of the diffusion coefficient.

Before we leave this mathematical exercise it is emphasized that we did consider an semi-infinite slab to explain the physical basis of the more advanced interfacial heat and mass transfer concepts to be introduced shortly in sect 5.3.5. Moreover, it is noted that the boundary condition at  $z = \infty$  might be replaced by a more practical one at a bounded or semi-infinite distance from the interface. In this case the solution relies on the assumption that we are considering a finite time period so that the ambient concentration is kept unaltered. In other words, if the diffusion process proceeds only a relatively short time period after the change in concentration at the interface occurs, the ambient concentration at a semi-infinite distance from the interface will not change. On the other hand, after a longer time period the concentration profile slinther into the steady state limit. In this case the ambient concentration might be changed due to the diffusive mass transfer flux so the semi-infinite slab concept is not valid anymore. The penetration and surface renewal mass transfer models rely on the assumption that the residence time of the interfacial element is sufficiently short so the inherent diffusion processes can be descibed using a semi-infinite slab approximation.

### Unsteady diffusion in a semi-infinite slab with a moving boundary

For completeness we briefly outline in this subsection a generic analytical method of solution for a class of problems in unsteady-state linear diffusion, which involve two phases or regions separated by a moving plane interface.

In particular we examine situations in which diffusion occurs in two distinct regions separated by a moving boundary or interface [28, 25]. Moreover, the two regions are separated by a plane surface and diffusion takes place only in the direction perpendicular to this plane. The concentration is initially uniform in each region. The component mass diffusion may then result in a net movement of the matter in one or both regions relative to the interface.

In mathematical terms the position in medium 1 can be specified by a coordinate in the  $z_1$  system which is fixed with respect to medium 1, and position in medium 2 is specified by a coordinate in the  $z_2$  system, fixed with respect to medium 2. The media are thus separated at time  $t$  by the plane  $z_1 = Z_1$ ,  $z_2 = Z_2$ , which is initially at  $z_1 = z_2 = 0$ . Medium 1 occupies a semi-infinite slab of the space  $Z_1 < z_1 < \infty$ , medium 2 a semi-infinite slab of the space  $-\infty < z_2 < Z_2$ .

To adopt the conventional Fick's law of binary diffusion we assume that in both media one of the components present moves by diffusion relative to the  $z_1$  and  $z_2$  coordinates and is transferred from one medium to the other. The concentration of the diffusing component at time  $t$  is denoted by  $c_1$  at  $z_1$  and by  $c_2$  at  $z_2$ .

Fick's second law (5.155) is obeyed in the two media, and for simplicity we assume that the diffusion coefficient is constant and independent of the concentrations. At any time in the calculation the concentrations  $c_1(Z_1)$  and

$c_2(Z_2)$  at either side of the interface are assumed to be related by an equilibrium law, like for example the Henry's law for gas absorption. The diffusion component is conserved at the interface so a jump condition can be expressed as:

$$D_1\left(\frac{\partial c_1}{\partial z_1}\right)_{z_1=Z_1} - D_2\left(\frac{\partial c_2}{\partial z_2}\right)_{z_2=Z_2} + c_1(Z_1)\frac{dZ_1}{dt} - c_2(Z_2)\frac{dZ_2}{dt} = 0 \quad (5.159)$$

Since by assumption there is a constant proportionality between the rates of movement of the two media relative to the interface, it follows that:

$$Z_2 = \text{Constant} \times Z_1 \quad (5.160)$$

The solution to the diffusion problem has the same form as that for the conventional Fick's second law (5.156):

$$\frac{c_{1i\infty} - c_{1i}}{c_{1i\infty} - c_{1i0}} = 1 - \operatorname{erf}\left(\frac{z_1}{2\sqrt{D_1 t}}\right) \quad (5.161)$$

where  $c_{1\infty}$  and  $c_{10}$  are given by the initial and boundary conditions:

$$\begin{array}{lll} t = 0, & z_1 > 0, & c_{1i} = c_{1i\infty}, \\ t > 0, & z_1 = 0, & c_{1i} = c_{1i0}. \end{array}$$

Similarly, for medium 2 we get:

$$\frac{c_{2i(-\infty)} - c_{2i}}{c_{2i(-\infty)} - c_{2i0}} = 1 + \operatorname{erf}\left(\frac{z_2}{2\sqrt{D_2 t}}\right) \quad (5.162)$$

where  $c_{2i(-\infty)}$  and  $c_{20}$  are given by the initial and boundary conditions:

$$\begin{array}{lll} t = 0, & z_2 < 0, & c_{2i} = c_{2i(-\infty)}, \\ t > 0, & z_2 = 0, & c_{2i} = c_{2i0}. \end{array}$$

Eliminating the unknown interface quantities using the equilibrium relation and the rates of movement of the two media relative to the interface, the component mass jump condition can be used to calculate the position of the interphase.

Danckwerts [28] mentioned a few examples of chemical engineering processes that might be described in this way. However, in chemical reaction engineering this modeling approach is merely of mathematical interest, as it is rarely used for practical applications because of the numerous restrictions involved. For this reason the method is not further elucidated in this book.

### 5.3.4 Heat Transfer Described by Fourier's Law

Fourier's law of heat conduction states that heat transfer by molecular interactions at any point in a solid or fluid is proportional in magnitude and coincident with the direction of the negative gradient of the temperature field [48]:

$$\mathbf{q} = -k\nabla T \quad (\text{Fourier's law}) \quad (5.163)$$

Fourier's law is the simplest form of a general energy flux and is strictly applicable only when the system is uniform in all respects except for the temperature gradient, that is, there are no mass concentration gradients or gradients in other intensive properties.

In general, there could occur more than one driving force in a conductive transport process. Given a system with gradients of temperature, pressure, mass concentration, magnetic field strength, and so on, there is no a priori justification for ignoring the possibility that each of these gradients might contribute to the energy flux. The simplest expression that could describe this relationship would be a linear combination of terms, one for each of the existing potential gradients. Experience shows that there are, in fact, measurable *coupled* effects, such as energy fluxes due to mass concentration gradient, and that this general form of the linear rate equation is necessary under certain rare conditions. The relationships between the coefficients of this equation have been the subject of several investigations. This field of science is called irreversible thermodynamics [75].

### 5.3.5 Heat and Mass Transfer Coefficient Concepts

Fairly rigorous expressions for the interfacial heat and mass transfer terms are defined in sect 3.3 for the different averaging methods commonly applied in chemical reactor analysis. However, since the modeling concepts are analogous for the different averages, we choose to examine these constitutive equations in the framework of the volume averaging method described in sect 3.4.1. This modeling approach is used extensively in reactor analysis because the basic model derivation is intuitive and quite easy to understand.

Physically, the interfacial heat and mass transfer terms occurring in the averaged model equations described in sect 3.3 represent advection of an interfacial quantity of phase  $k$  due to the relative motion of the interface, as proposed by Ishii [61] making a provisional model for *stratified flows* in nuclear reactor engineering. It is noted that in these units bulky quantities of fluid mass are transferred across the interface due to phase change or various fragmentation/disintegration mechanisms (e.g., evaporation, condensation, boiling, liquid film fragmentation and disintegration, jet fragmentation, fluid particle fragmentation, etc.).

However, this modeling approach is not necessarily convenient for the purpose of describing dispersed reactive flows in general. The use of mass weighted interfacial fluxes is certainly not applicable treating multicomponent reactive systems since the rigorous reaction kinetics and thermodynamic models normally operates on a molar basis. Besides, in dynamic cases the classical interfacial heat and mass transfer theories (e.g., the hypothetical stagnant two-film model is commonly used) one imagines resistances to both heat and mass transfer on both sides of the interface, and that thermodynamic equilibrium prevails at the interface only, thereby the bulk phases are not necessarily

uniform at steady state. Moreover, it is emphasized that in these theories the interface is generally assumed to be stagnant,  $\mathbf{v}_I = 0$ . In reaction engineering the possibility of describing the movement of the interfaces is not considered important, in the sense that the complexity of such an approach will lead to impracticable computational costs and little gain in understanding and physical modeling of the important chemical processes.

The definitions of the heat and mass transfer fluxes are thus merely based on empirical arguments, so in the literature there are given more than one way to interpret the transfer coefficients [15, 139]. Basically, the transfer coefficients are either treated as an alternative model to the fundamental diffusion models (i.e., the Fourier's and Fick's laws) or the transfer coefficients are taking both diffusive and convective mechanisms into account through empirical parameterizations. However, in reaction engineering practice the distinction between these approaches is rather blurred so it is not always clear which of the fundamental transport processes that are actually implemented.

The advantage of working in terms of the traditional joint diffusive and convective flux concept is that the contribution of convection is automatically taken into account and we do not need separate models for the interfacial transfers due to phase change. The disadvantage is that the transfer coefficients show a more complicated dependence upon concentration and mass transfer rates.

In a scientific view the loss in physical rigor might outweigh the possible gain in computational ease [139]. Nevertheless, in most chemical reactor analysis the transfer coefficients are defined in terms of the combined fluxes including both diffusive and convective contributions [27].

In the following sections a survey of the elementary diffusion theories that are determining the basis for the mass transfer coefficient concepts is given. No heat and mass transfer models dealing with simultaneous chemical reactions are considered to maintain attention to the fundamental principles.

### **Mass Transfer in regions close to a stagnant Interface**

The description of the interfacial transport processes in terms of mass transfer coefficients is an approximate engineering concept that normally results in simpler mathematical problems than the alternative description in terms of the more fundamental Fick's law.

The definition of the mass transfer coefficient is thus based on an oversimplified picture of the actual physics. The mass transfer coefficient concept relies on the hypothesis that the changes in concentrations are limited to two hypothetical stagnant films, one on each side of the stagnant interface. The transfer flux is thus transferring mass between the interface and the well mixed bulk solution. The amount of matter transferred is expected to be proportional to the concentration difference and the interfacial area. The proportionality coefficient,  $k_c$ , is called the mass transfer coefficient. The mass transfer coefficient is usually defined by the following flux relation:

$$\langle N_i \rangle_{A_I} = k_c \left( \langle c_{i,k} \rangle_{A_I} - \langle c_{i,k} \rangle_{V_k} \right) \quad (5.164)$$

where  $\langle N_i \rangle_{A_I}$  is the flux at the interface in ( $mol/sm^2$ ),  $k_c$  is the mass transfer coefficient in (m/s), and  $(\langle c_{i,k} \rangle_{A_I} - \langle c_{i,k} \rangle_{V_k})$  is the concentration difference (driving force) in ( $mol/m^3$ ).

Correspondingly, the mean interfacial mass flux is assumed to be proportional to the difference between the interfacial average and the intrinsic volume average of the quantity determining the driving force of the fluxes [110, 109].

The species transfer can thus be expressed as a mass flux  $\langle N_{i,k} \rangle_{A_I}$  ( $kg/sm^2$ ) in line with (3.180), simply by multiplying the conventional mole flux by the molecular weight  $M_{\omega_i}$ :

$$\langle n_{i,k} \rangle_{A_I} = M_{\omega_i} \langle N_{i,k} \rangle_{A_I} = k_c \left( \langle \rho_{i,k} \rangle_{A_I} - \langle \rho_{i,k} \rangle_{V_k} \right) \quad (5.165)$$

where  $(\langle \rho_{i,k} \rangle_{A_I} - \langle \rho_{i,k} \rangle_{V_k})$  is the concentration difference (driving force) in ( $kg/m^3$ ).

It is noted that although the combined mole and mass fluxes are related as  $\mathbf{n}_s = M_{\omega_s} \mathbf{N}_s$ , when there are negligible convection fluxes as calculated either by mole or mass averaged velocities the corresponding diffusive fluxes are not necessarily related in the same way since:  $\mathbf{j}_s \neq M_{\omega_s} \mathbf{J}_s^* = \mathbf{j}_s^*$ .

The concentration difference can also be re-defined in different ways, thus there exists a variety of modifications of the basic mass transfer coefficient definition as well. Therefore, care should to be taken to ensure that the mass transfer coefficient parameterizations adopted for modeling purposes, correspond to the model formulation used.

The mass transfer coefficient concept is usually less accurate than Fick's law, but it is very useful for practical problems were only average concentrations are available.

### The Mole Flux Equation for an Ideal Gas

The driving force is usually defined as a concentration difference between the interface and the bulk phase. For gases, however, it is more common to use the pressure difference as the driving force. We can thus formulate two different definitions of the mass transfer flux, and then derive an expression for the relation between the concentration based and the pressure based mass transfer coefficients.

The flux is the same, so the definitions must be equal:

$$R_{n_{i,k}} = J_{i,k}^{\Gamma_{kV}} + J_{i,k}^j = M_{\omega_i} k_p \left( \langle p_{i,k} \rangle_{A_I} \frac{\langle T_k \rangle_{V_K}}{\langle T_k \rangle_{A_I}} - \langle p_{i,k} \rangle_{V_k} \right) \quad (5.166)$$

where  $k_c$  and  $k_p$  are the mass transfer coefficients defined with concentration and pressure as the driving force, respectively.  $\langle \rho_{i,k} \rangle_{A_I}$  and  $\langle \rho_{i,k} \rangle_{V_k}$  are the

mass concentrations at the interface and bulk-face in  $(\text{kg}/\text{m}^3)$ .  $\langle p_{i,k} \rangle_{A_I}$  and  $\langle p_{i,k} \rangle_{V_k}$  are the pressures at the interface and in the bulk phase having the unit  $(\text{Pa})$ .

The concentration and pressure are related by the equation of state for an ideal gas:

$$c = \frac{n}{V} = \frac{p}{RT} \quad (5.167)$$

where  $V$  is the volume in  $(\text{m}^3)$  and  $R$  is the universal gas constant in  $(\text{J}/\text{Kmol})$ .

The relation between the different mass transfer coefficients is:

$$k_p = \frac{k_c}{R\langle T_k \rangle_{V_k}} \quad (5.168)$$

It is thus possible to express the flux as:

$$\langle N_i \rangle_{A_I} = \frac{k_c}{R\langle T_k \rangle_{V_k}} \left( \langle p_{i,k} \rangle_{A_I} \frac{\langle T_k \rangle_{V_K}}{\langle T_k \rangle_{A_I}} - \langle p_{i,k} \rangle_{V_k} \right) \quad (5.169)$$

### Mass Transfer Across a Stagnant Interface

In the context of reactor technology, mass transfer across an interface means mass transfer from one well mixed bulk phase into another well mixed bulk phase. This case occurs more frequently than mass transfer from an interface into one bulk phase, which we have discussed above.

Mass transfer across an interface between two well mixed bulk phases can then be described in terms of the flux relation (henceforth for convenience we drop the averaging symbol):

$$N_i = K_c \Delta c_i \quad (5.170)$$

where  $N_i$  is the solute flux relative to the interface in  $(\text{mol}/\text{sm}^2)$ ,  $K_c$  is the overall mass transfer coefficient in  $(\text{m}/\text{s})$  and  $\Delta c_i$  is the concentration difference in  $(\text{mol}/\text{m}^3)$ .

Note that we can express the flux using either the concentration difference related to the phase at the left hand-side of the interface or the other concentration difference related to the phase at the right-hand side of the interface. *In this way two different overall mass transfer coefficients can be defined for the twophase mixture.*

To derive a relation for the overall mass transfer coefficient we consider a gas-liquid interface, as sketched in Fig 5.15. Formulate the expressions for the fluxes at both sides of the interface and relate the two unknown interfacial concentrations to each other by use of an equilibrium relation like Henrys law. The flux relations can then be combined in order to eliminate the interfacial concentrations obtaining an overall driving force.

It is further assumed that within the system containing the two stagnant 1D films steady state has been reached, so that the fluxes at both sides of

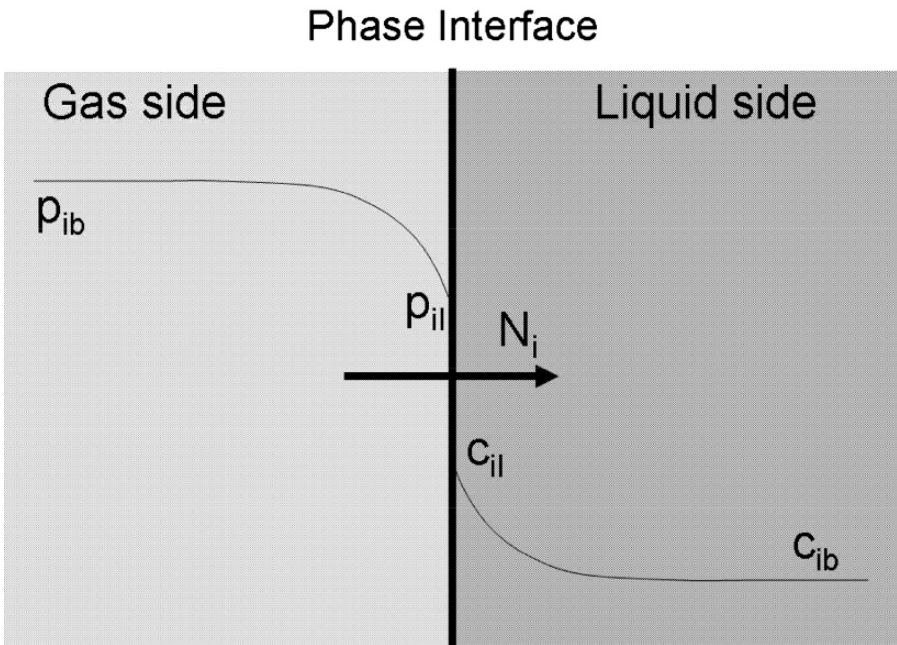


**Fig. 5.15.** Mass transfer across a gas - liquid interface.

the interface are equal. It is also assumed that the interface processes are in a state of thermodynamic equilibrium.

The species mole flux at the gas side can be expressed as:

$$N_i = k_g(p_{iI} - p_{ib}) \quad (5.171)$$

whereas the flux at the liquid side can be expressed as:

$$N_i = k_l(c_{ib} - c_{iI}) \quad (5.172)$$

The equilibrium processes at a dilute interface is usually described using Henry's law:

$$p_{iI} = H_i c_{iI} \quad (5.173)$$

where the  $H_i$  denotes the Henry law constant for species,  $i$ . The flux across the interface can be expressed in terms of the concentration difference at the liquid side:

$$N_i = K_L(c_{ib} - c_i^*) \quad (5.174)$$

where  $K_L$  is the overall *liquid-side* mass transfer coefficient.

The  $K_L$  coefficient is defined by:

$$K_L = \frac{1}{1/k_l + 1/k_g H_i} \quad (5.175)$$

and  $c_i^*$  is the hypothetical liquid phase concentration which would be in equilibrium with the bulk gas. This concentration is calculated from Henry's law:

$$c_i^* = \frac{p_{ib}}{H_i} \quad (5.176)$$

The flux across the interface could alternatively be expressed in terms of the gas side concentration difference:

$$N_i = K_G(p_i^* - p_{ib}) \quad (5.177)$$

where  $K_G$  is the overall *gas-side* mass transfer coefficient, given by:

$$K_G = \frac{1}{1/k_G + H_i/k_L} \quad (5.178)$$

and  $p_i^*$  is the hypothetical gas phase concentration which would be in equilibrium with bulk liquid:

$$p_i^* = H_i c_{ib} \quad (5.179)$$

### Parameterization of the Engineering Transfer Coefficients

In this section the formal mathematical concepts for deriving the engineering transfer coefficients are examined<sup>6</sup>.

The basic theory is thoroughly discussed by Astarita et al [6], Bird et al [15], Hines and Maddox [58], Cussler [27], Middleman [102], Arpaci et al [5], Sherwood et al [134] and Sideman and Pinczewski [135]. These texts might be recommended for supplementary studies.

Heat and mass transfer coefficients are usually reported as correlations in terms of dimensionless numbers. The exact definition of these dimensionless numbers implies a specific physical system. These numbers are expressed in terms of the characteristic scales.

Correlations for mass transfer are conveniently divided into those for fluid - fluid interfaces and those for fluid - solid interfaces. Many of the correlations have the same general form. That is, the Sherwood or Stanton numbers containing the mass transfer coefficient are often expressed as a power function of the Schmidt number, the Reynolds number, and the Grashof number.

---

<sup>6</sup> The methods of completely empirical experimentation and dimensional analysis are very important in engineering practice but excluded from this survey as these methods are well known and described in most introductory textbooks on unit operations in chemical engineering.

In principle *dimensional analysis* consists in an algebraic treatment of the symbols for units, and this method is sometimes considered intermediate between formal mathematical development and a completely empirical study.

These methods are used to attack problems for which no mathematical closure equations can be derived.

The formulation of the correlations can be based on dimensional analysis and/or theoretical reasoning. In most cases, however, pure curve fitting of experimental data is used. The correlations are therefore usually problem dependent and can not be used for other systems than the one for which the curve fitting has been performed without validation. A large list of mass transfer correlations with references is presented by Perry [113].

The dimensionless numbers commonly used in correlations of heat and mass transfer coefficients are listed below (e.g., [134], chap 5.2; [27], p 224; [60], pp 355-356):

The *Sherwood number*,  $Sh = k_c l/D$ , that determine the ratio between the effective mass transfer velocity and the molecular diffusivity (i.e., a dimensionless concentration gradient at the interface).

The *Nusselt number*,  $Nu = hl/k$ , that determine the ratio between the effective heat transfer velocity and the molecular conductivity (i.e., a dimensionless temperature gradient at the interface).

The *Stanton number* for mass,  $St_m = k_c/v_{z,av}$ , that determine the ratio between the mass transfer velocity and the flow velocity, a modified Sherwood number.

The *Stanton number* for heat,  $St_h = h/(C_P \rho v_{z,av}) = \frac{Nu}{Re Pr}$ , that determine the ratio between the convective heat transfer flux at the interface and the thermal capacity of the fluid, a modified Nusselt number.

The *Reynolds number*,  $Re = ul/\nu$ , that determine the ratio between the inertia force and the viscous force.

The *Lewis number*,  $Le = \alpha/D$ , that determine the ratio between the diffusivity of heat and the diffusivity of mass.

The *Prandtl number*,  $Pr = \nu/\alpha$ , that determine the ratio between the diffusivity of momentum and the diffusivity of heat.

The *Péclet number*,  $Pe = v_{z,av} l/D = Re Pr$ , that determine the ratio between the flow velocity and the mass diffusion velocity.

The *Schmidt number*,  $Sc = \nu/D$ , that determine the ratio between the kinetic viscosity or the diffusivity of momentum and the molecular diffusivity of mass.

The *Grashof number*,  $Gr = l^3 \Delta \rho g / \rho \nu^2$ , that determine the ratio between the buoyancy force and the viscous force for free convection problems.

where  $l$  is a characteristic length, which has to be chosen for the given system under consideration, and  $g$  is the gravitational acceleration.

The heat and mass transfer fluxes at the interface are influenced by the fluid dynamics of the phases near the interface. In most situations the flow in this region is so complicated that the governing equations cannot be solved without introducing simplifying assumptions. The fluid dynamic model adopted should, however, still be able to capture the main characteristics of the actual flow, as the heat and mass transfer coefficients may be very sensitive upon these variables.

We may now distinguish between two conceptually different approaches for incorporating the effects of the actual flow phenomena into the coefficient parameterizations. First, we have the semi-empirical chemical engineering theories using simplified relations determining imaginative flow patterns. These models are physical re-constructions, which are more easily analyzed than the actual flow situation. Unfortunately, these relations often contain several parameters that need to be fitted to experimental (input-output) data. Second, we have the more formal mechanical engineering approach that is based on analytical solutions of the governing equations for rather idealized flows systems. Although the resulting parameterizations are strictly only valid for the particular idealized flow system for which they were derived, the relations obtained are often successfully applied describing complex flows as well. For turbulent flows, most of the concepts available determining the fluxes close to solid surfaces were originally developed determining interfacial heat transfer fluxes for single component flow calculations. These concepts have later been extended to mass transfer problems by use of a so-called similarity hypothesis.

### The film theory

The film theory is the simplest model for interfacial mass transfer. In this case it is assumed that a stagnant film exists near the interface and that all resistance to the mass transfer resides in this film. The concentration differences occur in this film region only, whereas the rest of the bulk phase is perfectly mixed. The concentration at the depth  $l$  from the interface is equal to the bulk concentration. The mass transfer flux is thus assumed to be caused by molecular diffusion through a stagnant film essentially in the direction normal to the interface. It is further assumed that the interface has reached a state of thermodynamic equilibrium.

The mass transfer flux across the stagnant film can thus be described as a steady diffusion flux. It can be shown that within this steady-state process the mass flux will be constant as the concentration profile is linear and independent of the diffusion coefficient.

Consider a gas-liquid interface, as sketched in Fig 5.16. The mathematical problem is to formulate and solve the diffusion flux equations determining the fluxes on both sides of the interface within the two films. The resulting concentration profiles and flux equations can be expressed as:

*The concentration profile within the gas phase resembles (5.150) and is expressed in terms of species partial pressure:*

$$p_i = p_{i0} + \frac{z}{l_G}(p_{iI} - p_{i0}) \quad (5.180)$$

*The diffusive flux yields:*

$$J_i^* = -D_G \frac{dp_i}{dz} = \frac{D_G}{l_L}(p_{i0} - p_{iI}) \quad (5.181)$$

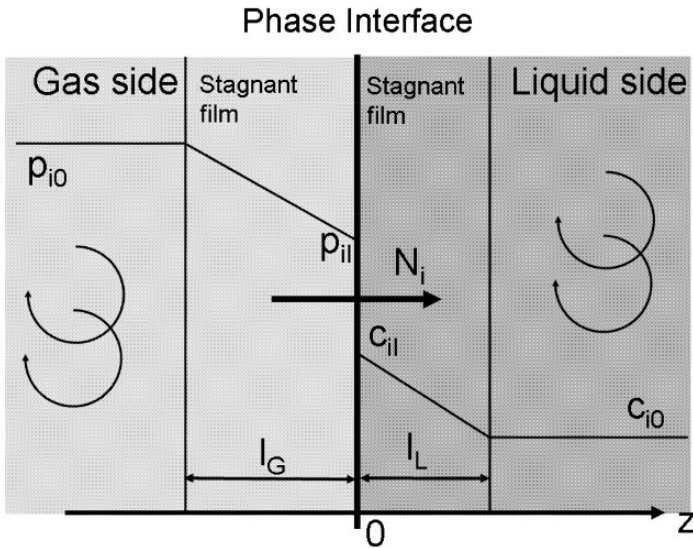


**Fig. 5.16.** Gas-liquid interface - Film theory.

The mole concentration profile within the liquid phase resembles (5.150) and is given by:

$$c_i = c_{iI} + \frac{z}{l_L}(c_{i0} - c_{iI}) \tag{5.182}$$

The corresponding diffusive flux yields:

$$J_i^* = -D_L \frac{dc_i}{dz} = \frac{D_L}{l_L}(c_{iI} - c_{i0}) \tag{5.183}$$

By comparing the equations determining the diffusive fluxes with the corresponding definitions of the mass transfer coefficients, we obtain the relationships between the mass transfer coefficients and the diffusion coefficients. As before we assume that the mass transfer rate is low, so that the flux is considered purely diffusive.

The definition of the mass transfer coefficient can thus be expressed as:

$$N_i = k_g(p_{i0} - p_{iI}) = k_l(c_{iI} - c_{i0}) \tag{5.184}$$

The corresponding diffusive flux can be expressed using Fick's law:

$$N_i = J_i^* = \frac{D_G}{l_G}(p_{i0} - p_{iI}) = \frac{D_L}{l_L}(c_{iI} - c_{i0}) \tag{5.185}$$

The relationships between the mass transfer and diffusion coefficients yield:

$$k_l = \frac{D_L}{l_L} \quad (5.186)$$

$$k_g = \frac{D_G}{l_G} \quad (5.187)$$

In dimensionless form, the relations can be expressed in terms of a Sherwood number:

$$Sh = \frac{k_c l}{D} \quad (5.188)$$

determining the ratio between the mass transfer and diffusion rates.

The film model can then be expressed as:

$$Sh = 1 \quad (5.189)$$

The result obtained from the film theory is that the mass transfer coefficient is directly proportional to the diffusion coefficient. However, the experimental mass transfer data available in the literature [6], for gas-liquid interfaces, indicate that the mass transfer coefficient should rather be proportional with the square root of the diffusion coefficient. Therefore, in many situations the film theory doesn't give a sufficient picture of the mass transfer processes at the interfaces. Furthermore, the mass transfer coefficient dependencies upon variables like fluid viscosity and velocity are not well understood. These dependencies are thus often lumped into the correlations for the film thickness,  $l$ . The film theory is inaccurate for most physical systems, but it is still a simple and useful method that is widely used calculating the interfacial mass transfer fluxes. It is also very useful for analysis of mass transfer with chemical reaction, as the physical mechanisms involved are very complex and the more sophisticated theories do not provide significantly better estimates of the fluxes. Even for the description of many multicomponent systems, the simplicity of the model can be an important advantage.

For heat transfer the film theory is the most commonly used model, and the physical picture of a laminar film in which the whole temperature difference is situated leads to a result analogous to the mass transfer coefficient model [5]. After integrating Fourier's law over the film, a comparison with the heat transfer coefficient model (5.126) yields:

$$q = \frac{k}{l}(T_S - T_f) \quad (5.190)$$

$$h = \frac{k}{l} \quad (5.191)$$

$$Nu = \frac{hl}{k} = 1 \quad (5.192)$$

where  $k$  denotes the conductivity of the fluid,  $l$  the film thickness,  $h$  the convective heat transfer coefficient, and  $T_S$  and  $T_f$  refer to the surface and fluid temperatures, respectively.

### The Surface-Renewal Theories

The surface-renewal models intend to provide an improved representation of the physical interface phenomena compared to the basic film theory. The surface-renewal models are based on the well known idea that turbulent flows consist of small fluid elements or eddies that may form discrete entities having certain characteristic flow properties. Within the interface region these fluid elements are arriving from the bulk phase and after residing at the interface for a period of time (the exposure time) they are replaced and mixed with the bulk fluid again, as sketched in Fig 5.17. The replacement of the eddies is caused by the turbulence properties of the flow. During the exposure time mass exchange between the fluid element on one side and the adjoining phase on the other side due to unsteady diffusion processes, and the interfacial element can be treated as a semi-infinite slab since the exposure time is less than the time required for diffusive transport across the whole slab. The bulk of both phases are assumed to be well mixed.

Excellent reviews on the surface-renewal theories are given by Sideman and Pinczewski [135], Astarita et al [6], and Thomson [153].

### The Penetration Theory

The penetration theory can be viewed as the original surface-renewal model. This model was formulated by Higbie [57]. This model is based on the assumption that the liquid surface contains small fluid elements that contact the gas

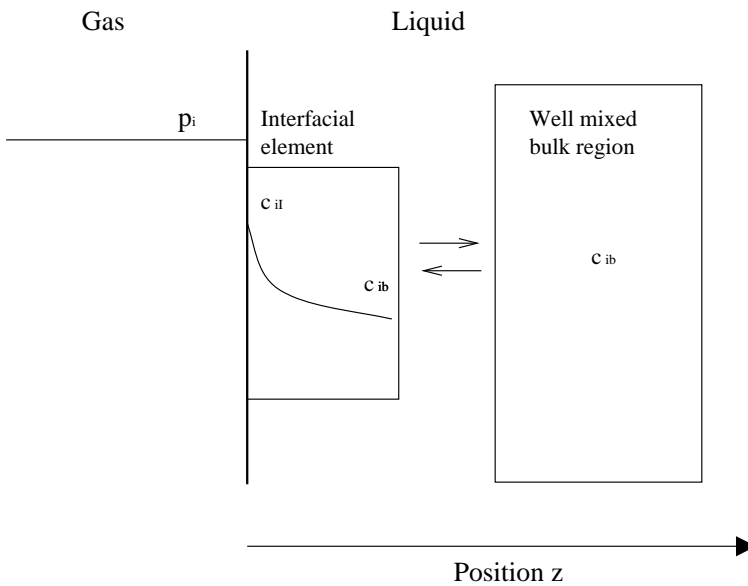


**Fig. 5.17.** The principles of Surface-Renewal theories.

phase for a time that is equal for all elements. After this contact time they penetrate into the bulk liquid and each element is then replaced by another element from the bulk liquid phase. The basic mechanism captured in this concept is that at short contact times, the diffusion process will be unsteady. Considering that the fluid elements may diffuse to an infinite extent into the liquid phase, the model formulation developed earlier for diffusion into a semi-infinite slab can be applied describing this system. After some time the diffusion process will reach a steady state, thus the penetration theory predictions will then correspond to the limiting case described by the basic film theory. However, when the transient flux development is determining a notable amount of the total flux accumulated, the two models will give rise to different mass transfer coefficients.

*The concentration profile resembles (5.156) and can be expressed by:*

$$\frac{c_i - c_{iI}}{c_i - c_{il}} = 1 - \operatorname{erf}\zeta = \frac{2}{\sqrt{\pi}} \int_0^\zeta e^{-\zeta^2} d\zeta \quad (5.193)$$

*and the diffusive flux can be expressed by:*

$$J_i^* = \sqrt{\frac{D}{\pi t}} e^{-z^2/4Dt} (c_i - c_{il}) \quad (5.194)$$

*where the instantaneous interfacial diffusion flux (i.e., at  $z = 0$ ) resembles (5.158) and is given by:*

$$J_i^*|_{z=0} = \sqrt{\frac{D}{\pi t}} (c_i - c_{il}) \quad (5.195)$$

This is the solution for an instantaneous flux rate at the interface, since we are considering dilute solutions any diffusion-induced convection can be neglected. This means that the total mole flux is equal to the diffusion flux, and that we can write the instantaneous mass transfer rate directly in the form derived for the diffusion flux:

$$N_i(t)|_{z=0} = \sqrt{\frac{D}{\pi t}} (c_i - c_{il}) \quad (5.196)$$

The instantaneous mass transfer rate is expressed as a function of time. In order to calculate an average mass transfer coefficient we need to average the instantaneous coefficient over the total exposure time period. To do this we need to know the age distribution function, which represents the fraction of elements having ages between  $t$  and  $t + dt$  at the surface. *In the penetration theory, it is assumed that all the elements reside at the interface for a time period of the same length.* As a consequence of this assumption the age distribution function is [6]:

$$E(t) = \frac{1}{t_e} \quad t \leq t_e \quad (5.197)$$

$$E(t) = 0 \quad t > t_e \quad (5.198)$$

where  $t_e$  is a fixed contact time (s).

The averaged mass transfer rate yields:

$$\langle N_i \rangle_{t_e} = \int_0^{t_e} N_i(t)|_{z=0} E(t) dt \quad (5.199)$$

$$\langle N_i \rangle_{t_e} = 2\sqrt{\frac{D}{\pi t_e}} (c_i - c_{il}) \quad (5.200)$$

Based on this model a relation between the mass transfer and diffusion coefficients can be expressed as:

$$k_c = 2\sqrt{\frac{D}{\pi t_e}} \quad (5.201)$$

The mass transfer coefficient parameterizations based on (5.201) can be written in terms of dimensionless groups. Two examples are listed here:

$$Sh = \frac{kl}{D} = \left(\frac{6}{\pi}\right)^{1/2} \left(\frac{lv_x}{\nu}\right)^{1/2} \left(\frac{\nu}{D}\right)^{1/2} \quad [27] \quad (5.202)$$

$$St = \frac{k}{v_x} = (const.) \left(\frac{\mu}{\rho D}\right)^{-1/2} \left(\frac{Lv_x \rho}{\mu}\right)^{-1/2} \quad [6] \quad (5.203)$$

The exposure time,  $t_e$ , equals the relationship between the penetration depth and the characteristic velocity. This theory predicts that the mass transfer coefficient is proportional to  $D^{1/2}$ , which indicates that the penetration model is more realistic than the film theory. This model contains a fitting parameter, the contact time  $t_e$ , into which all details on the true fluid dynamics are lumped.

An analogue heat transfer coefficient relation has been derived by the penetration concept. The heat transfer theory is reviewed by Thomson [153].

### The Danckwerts surface renewal model

The classical Danckwerts surface-renewal model is analogous to the penetration theory. The improvement is in the view of the eddy replacement process. *Instead of Higbie's assumption that all elements have the same residence time at the interface, Danckwerts [29] proposed to use an averaged exposure time determined from a postulated time distribution.* The residence time distribution of the surface elements is described by a statistical distribution function  $E(t)$ , defined so that  $E(t)dt$  is the fraction of the interface elements with age between  $t$  and  $t + dt$ . The rest of the formulation procedure is similar to that of the penetration model.

The normalized age distribution function was given by

$$E(t) = \frac{1}{\tau} \exp\left(-\frac{t}{\tau}\right) = s \exp(-st) \quad (5.204)$$

assuming that the rate of disappearance of surface elements of a certain age is proportional to the number of elements of the same age.  $s$  is the average surface renewal rate which is equal to the reciprocal of the average residence time of the elements  $\tau$ .

The averaged mass transfer rate is defined by:

$$N_i = \int_0^{t_e} n_i(t)|_{z=0} E(t) dt \quad (5.205)$$

$$N_i = \sqrt{\frac{D}{\tau}} (c_{il} - c_{ib}) \quad (5.206)$$

In this case the relation between mass transfer and diffusion coefficient can be expressed as:

$$k_c = \sqrt{\frac{D}{\tau}} = \sqrt{Ds} \quad (5.207)$$

The surface-renewal theory intends to provide a better representation of the physical mechanisms than the penetration theory, but it predicts the same dependency of the mass transfer coefficient upon the diffusion coefficient. The penetration theory can thus be looked upon as a special case of the surface renewal theory where the distribution function takes the form of (5.204). Moreover, both theories also contain an unknown fitting parameter and are thus in practice equivalent. For the quantitative determination of the transfer coefficient we need to relate  $s$ ,  $\tau$  or  $t_e$  to the measurable parameters of the system under consideration. For this reason these concepts have no predictive value.

The original Danckwerts model has later been extended to relate the renewal rate  $s$  to many flow parameters, and to account for the existence of the micro scale flow of the fluid within the individual eddies. Further modifications relate to the fact that not all the penetrating eddies reach the whole way to the interface. Many model extensions have thus been developed based on the basic surface-renewal concept. A review of these models is given by Sideman and Pinczewski [135]. The various extensions are motivated by the inherent assumptions regarding, the governing equations, the boundary conditions, the age distribution function and/or the mean contact time.

An analogue heat transfer coefficient relation has been derived by the surface renewal concept. The heat transfer theory is reviewed by Thomson [153].

## Laminar Boundary Layer Theory - The Integral Method

The integral boundary layer method for determining the transfer coefficients is explained in this section.

The basic boundary layer theory has been summarized in many textbooks in chemical engineering, among them the books of Hines and Maddox [58], Incropera De Witt [60], Cussler [27], Middleman [102] and Bird et al [15] are considered very informative.

While the film and surface-renewal theories are based on a simplified physical model of the flow situation at the interface, the boundary layer methods couple the heat and mass transfer equation directly with the momentum balance. These theories thus result in analytical solutions that may be considered more accurate in comparison to the film or surface-renewal models. However, to be able to solve the governing equations analytically, only very idealized flow situations can be considered. Alternatively, more realistic functional forms of the local velocity, species concentration and temperature profiles can be postulated while the functions themselves are specified under certain constraints on integral conservation. From these integral relationships models for the shear stress (momentum transfer), the conductive heat flux (heat transfer) and the species diffusive flux (mass transfer) can be obtained.

The prescribed shape of the velocity profile for the fluid flowing parallel to a flat plate may be expressed as:

$$v_x = a_0 + a_1 y + a_2 y^2 + a_3 y^3 \quad (5.208)$$

The parameters in this expression are assumed to be independent of  $y$  the direction normal to the plate, but may vary with  $x$  the direction parallel to the plate. The velocity profile need to fulfill the following boundary conditions (i.e., no slip and no pressure variation in the  $x$ -direction):

$$y = 0, \quad v_x = 0 \quad \frac{\partial^2 v_x}{\partial y^2} = 0 \quad (5.209)$$

$$y = \delta, \quad v_x = v_{x,0} \quad \frac{\partial v_x}{\partial y} = 0 \quad (5.210)$$

In this context the momentum boundary layer thickness  $y = \delta$  is conveniently defined as the point beyond which the velocity takes on its free stream value<sup>7</sup>.

The second condition stating that the velocity gradient vanishes at  $y = \delta$ , ensures that we obtain a continuous gradient as the velocity attains its free stream value.

Applying these boundary conditions we can determine the values for the parameters:

$$\begin{aligned} a_0 &= a_2 = 0 \\ a_1 &= \frac{3}{2} \frac{v_{x,0}}{\delta} \end{aligned}$$

---

<sup>7</sup> This definition merely represents a simplifying model assumption as opposed to the conventional definition in which the thickness of boundary layer  $\delta$  is arbitrarily taken as the distance away from the surface where the velocity reaches 99% of the free stream velocity

$$a_3 = -\frac{1}{2} \frac{v_{x,0}}{\delta^3}$$

These results give the following dimensionless velocity profile:

$$\frac{v_x}{v_{x,0}} = \frac{3}{2} \left(\frac{y}{\delta}\right) - \frac{1}{2} \left(\frac{y}{\delta}\right)^3 \quad (5.211)$$

The velocity gradient at the wall can then be expressed as:

$$\frac{\partial v_x}{\partial y} \Big|_{y=0} = \frac{3}{2\delta} \quad (5.212)$$

At this point it should be kept in mind that  $\delta$  is an unknown function of  $x$ . The velocity function,  $v_x(x, y)$ , is expressed in terms of the unknown function  $\delta(x)$ . The main advantage of the integral method is that it is easier to obtain a solution for  $\delta(x)$  than to solve the Navier Stokes equations for  $v_x(x, y)$ . A drawback is that we are using an approximate velocity field which to some extent reduces the accuracy of the result.

The next step in the procedure is to formulate mass and momentum balances for an element of the boundary layer, as sketched in Fig 5.18. The *mass balance* equates the net rate of mass flow across the two vertical boundaries to the rate of mass flow across the horizontal boundaries. Assuming no mass flow across the lower horizontal boundary, the mass balance becomes:

$$\int_0^l \rho v_x dy \Big|_x - \int_0^l \rho v_x dy \Big|_{x+\Delta x} - \rho v_{y,l} \Delta x = 0 \quad (5.213)$$

Dividing by  $\Delta x$  and letting  $\Delta x \rightarrow 0$ , gives a relation for  $v_y$ :

$$v_{y,l} = -\frac{d}{dx} \int_0^l v_x dy \quad (5.214)$$

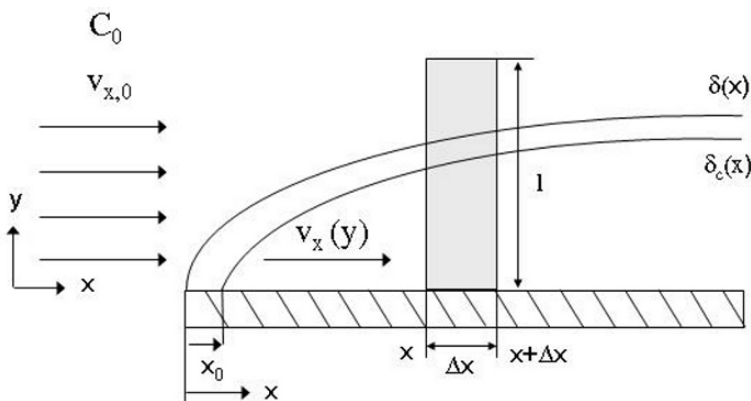


Fig. 5.18. Balance on fluid element of the laminar boundary layer.

The *momentum balance* states that any difference in x-directed momentum flow must be equal to the net x-directed shear force acting on the solid surface. This gives the momentum balance on the element:

$$\int_0^l \rho v_x^2 dy|_x - \int_0^l \rho v_x^2 dy|_{x+\Delta x} - \rho v_{x,l} v_{y,l} \Delta x = -\sigma_w \Delta x \quad (5.215)$$

Again, dividing by  $\Delta x$  and letting  $\Delta x \rightarrow 0$  gives:

$$-\sigma_w = -\frac{d}{dx} \int_0^l \rho v_x^2 dy - \rho v_{x,l} v_{y,l} \quad (5.216)$$

A combination of (5.214) and (5.216) eliminates  $v_{y,l}$ , and we may write:

$$-\sigma_w = \frac{d}{dx} \int_0^l (v_{x,l} - v_x) \rho v_x dy \quad (5.217)$$

Inside the boundary layer, the shear stress is given by Newton's law of viscosity:

$$-\sigma_w = \mu \frac{\partial v_x}{\partial y} \Big|_{y=0} \quad (5.218)$$

By combining (5.218), (5.217) and (5.212) we get:

$$\mu \frac{3}{2\delta} = \frac{d}{dx} \int_0^l (v_{x,l} - v_x) \rho v_x dy \quad (5.219)$$

By introducing the relation for the velocity profile (5.211) into (5.219) and performing the integration we get a differential equation for the boundary layer thickness. In this operation it is convenient to replace  $l$  by  $\delta$  in the upper limit of the integral. This problem reformulation is allowed as the integrand vanishes for  $l > \delta$  because  $v_x = v_{x,l} = v_{x,0}$ . The integral solution is [27, 102, 15]:

$$\delta \frac{d\delta}{dx} = \frac{140}{13} \frac{\mu}{\rho v_{x,0}}$$

This ODE is solved by introducing the following initial condition:

$$x = 0 \quad \delta = 0 \quad (5.220)$$

The solution is:

$$\frac{\delta}{x} = 4.64 \left( \frac{v_{x,0} x}{\nu} \right)^{-1/2} = 4.64 Re^{-1/2} \quad (5.221)$$

This means that *the fluid mechanics of the problem is solved*. The boundary layer thickness is given as a function of the distance  $x$  from the plate edge through (5.221). Hence, the velocity  $v_x$  can be calculated from (5.211).

To proceed determining an expression for the mass transfer coefficient, the same solution method is applied to the corresponding concentration boundary layer problem.

Again, a polynomial profile of third order is postulated for the unknown field:

$$c = a'_0 + a'_1 y + a'_2 y^2 + a'_3 y^3 \quad (5.222)$$

The parameters are evaluated by applying the concentration boundary conditions:

$$y = 0 \quad c = c_0 \quad \frac{\partial^2 c}{\partial y^2} = 0 \quad (5.223)$$

$$y = \delta_c \quad c = 0 \quad \frac{\partial c}{\partial y} = 0 \quad (5.224)$$

In this case we have defined a concentration variable that vanishes beyond the boundary layer. It is imagined a physical situation in which a species is dissolving from the surface of a plate and being transported by diffusion and convection into a fluid that does not contain this species except very near the plate, as sketched in Fig 5.18.

To satisfy these boundary conditions, the dimensionless concentration profile must have the form:

$$\frac{c}{c_0} = 1 - \frac{3}{2} \frac{y}{\delta_c} - \frac{1}{2} \left( \frac{y}{\delta_c} \right)^3 \quad (5.225)$$

The concentration gradient at  $y = 0$  can be expressed as:

$$\frac{\partial c}{\partial y} \Big|_{y=0} = -\frac{3c_0}{2\delta_c} \quad (5.226)$$

Next, a species mole (or mass) balance is made over the boundary layer element in Fig 5.18. The net rate of convection of the species across the vertical planes of the control volume must be balanced by the rate corresponding to the flux from the solid surface:

$$\int_0^l cv_x dy \Big|_x - \int_0^l cv_x dy \Big|_{x+\Delta x} - c_l v_{y,l} \Delta x = -n_w \Delta x \quad (5.227)$$

The species mole (mass) flux at the interface can be defined both in terms of Fick's first law and the mass transfer coefficient concepts:

$$-N_w = D \frac{\partial c}{\partial y} \Big|_{y=0} = -\frac{d}{dx} \int_0^{\delta_c} cv_x dy = -k_c (c_0 - c_{\delta_c}) \quad (5.228)$$

in which the upper integration limit  $y = l$  has been replaced by  $y = \delta_c$ . It is imagined that beyond the upper edge of the concentration boundary layer  $c = 0$  and  $v_{x,l} = 0$ , provided that the concentration boundary layer thickness is always thinner than the hydrodynamic boundary layer.

It occurs that  $v_x$  is a known function of  $x$  and  $y/\delta$  as given by (5.211) and (5.221),  $c$  is given in terms of  $y/\delta_c$  by (5.225) and the concentration gradient

at  $y = 0$  is given by (5.226), hence (5.228) yields a relationship between  $\delta_c$  and  $\delta$ . With the additional assumption that  $\delta_c \ll \delta$ , the species mole (mass) balance problem reduced to:

$$\frac{4}{3}x \frac{d}{dx} \left( \frac{\delta_c}{\delta} \right)^3 + \left( \frac{\delta_c}{\delta} \right)^3 \approx \frac{D}{\nu} = Sc^{-1} \quad (5.229)$$

where  $Sc$  is the Schmidt number.

Besides, if  $\delta_c$  is smaller than  $\delta$ , the former may also develop slower, thus the following boundary condition is induced [27]:

$$x = 0 \quad \frac{\delta_c}{\delta} = 0 \quad (5.230)$$

Integration now gives:

$$\left( \frac{\delta_c}{\delta} \right)^3 = \frac{D}{\nu} + bx^{-3/4} \quad (5.231)$$

Because  $(\frac{\delta_c}{\delta})$  does not become infinite as  $x$  approaches zero, the term containing  $x$  vanishes as  $b$  must be zero [13].

The momentum boundary layer thickness  $\delta$  can now be eliminated by use of (5.221):

$$\frac{\delta_c}{x} = 4.64 \left( \frac{\nu}{v_{x,0}x} \right)^{1/2} \left( \frac{D}{\nu} \right)^{1/3} = 4.64 Re^{-1/2} Sc^{-1/3} \quad (5.232)$$

Finally, the concentration boundary layer problem is almost solved as the mass transfer coefficient  $k_c$  can be calculated from (5.228):

$$-N_w = k_c c_0 = D \frac{\partial c}{\partial y} \Big|_{y=0} = -D \frac{3c_0}{2\delta_c} \quad (5.233)$$

Eliminating  $\delta_c$  by (5.232), we find:

$$N_w = 0.332 \frac{Dc_0}{x} \left( \frac{xv_{x,0}}{\nu} \right)^{1/2} \left( \frac{\nu}{D} \right)^{1/3} \quad (5.234)$$

Comparing this result with the first two terms in (5.233), we get a relation for the local value of the mass transfer coefficient:

$$\frac{k_c x}{D} = 0.332 \left( \frac{xv_{x,0}}{\nu} \right)^{1/2} \left( \frac{\nu}{D} \right)^{1/3} \quad (5.235)$$

By averaging over the plate length  $L$ , an average mass transfer coefficient is obtained  $\langle k_c \rangle_L = \frac{1}{L} \int_0^L k_c(x) dx$ . This quantity can be calculated from a relation expressed in terms of an averaged Shearwood number:

$$\langle Sh \rangle_L = \frac{\langle k_c \rangle_L L}{D} = 0.664 \left( \frac{Lv_{x,0}}{\nu} \right)^{1/2} \left( \frac{\nu}{D} \right)^{1/3} = 0.664 Re^{1/2} Sc^{1/3} \quad (5.236)$$

The integral method thus leads to a mass transfer coefficient which vary with the  $2/3$  power of the diffusion coefficient. This parameter dependency is between the linear one of the film theory and the square-root variation of the penetration and surface-renewal theories.

It is noted that the integral method gives only approximate values for the mass transfer coefficient as the model derivation is based on several simplifying assumptions regarding the concentration and velocity profiles. Nevertheless, the given relation has been confirmed by experiments for laminar boundary layer flows over a flat plate (e.g., [134], p 80 and p 201; [27], p 345).

Based on the boundary layer analysis for laminar flow past a plate we might suggest that the mass transfer coefficient generally depends on the Reynolds number and the Prandtl number:

$$Sh = A Re^m Sc^n \quad (5.237)$$

It is possible to show adopting an analogous procedure that for heat transfer the Nusselt number depends on the Reynolds and Prandtl number in a similar manner (e.g., [134], p. 160):

$$Nu = A Re^m Pr^n \quad (5.238)$$

The Reynolds analogy states that  $Sc = Pr = 1$ , indicating that the transfer coefficients are functions of  $Re$  only.

Each of the modified Reynolds analogy relations (5.237) and (5.238) includes an additional  $Sc$  and  $Pr$  dependency, respectively. These relationships are often referred to as the Chilton-Colburn analogies [20, 60] (p 364).

Experimental analyses show that (5.237) and (5.238) can be used for a number of convective heat and mass transfer systems, and might be sufficiently accurate even for problems involving complex geometries [60].

### **Turbulent Boundary Layer Theory - Eddy Viscosity Concept**

In this section the heat and mass transport coefficients for turbulent boundary layers are examined. In this case the model derivation is based on the governing Reynolds averaged equations. In these equations statistical covariances appear which involve fluctuating velocities, temperatures and concentrations. The nature of these terms is not known a priori and their effects must be estimated by semi-empirical turbulence modeling. The resulting parameterizations allow us to express the unknown turbulent fluctuations in terms of the mean flow field variables. It is emphasized that the Reynolds equations are not actually solved, merely semi-empirical relations are derived for the wall fluxes through the inner boundary layer.

Due to experimental difficulties, turbulence closures exist only for the turbulent momentum transport phenomena. In particular, approximate semi-empirical models for the turbulent viscosity parameter have been derived. To achieve constitutive relations for the corresponding heat and mass transport

properties further empiricism is introduced through the analogy theories for turbulent flows. The simplest of these analogies are frequently referred to as the *Reynolds analogy for turbulent flows*.

The basic *similarity hypothesis* states simply that the turbulent transport processes of momentum, heat and mass are caused by the same mechanisms, hence the functional properties of the transfer coefficients are similar. The different transport coefficients can thus be related through certain dimensionless groups. The closure problem is thus shifted and henceforth consist in formulating sufficient parameterizations for the turbulent Prandtl ( $Pr_t$ )- and Schmidt ( $Sc_t$ ) numbers.

The modeling procedure can be sketched as follows. First an approximate description of the velocity distribution in the turbulent boundary layer is required. The universal velocity profile called *the Law of the wall* is normally used. The local shear stress in the boundary layer is expressed in terms of the shear stress at the wall. From this relation a dimensionless velocity profile is derived. Secondly, a similar strategy can be used for heat and species mass relating the local boundary layer fluxes to the corresponding wall fluxes. From these relations dimensionless profiles for temperature and species concentration are derived. At this point the concentration and temperature distributions are not known. Therefore, based on the similarity hypothesis we assume that the functional form of the dimensionless fluxes are similar, so the heat and species concentration fluxes can be expressed in terms of the momentum transport coefficients and velocity scales. Finally, a comparison of the resulting boundary layer fluxes with the definitions of the heat and mass transfer coefficients, indicates that parameterizations for the engineering transfer coefficients can be put up in terms of the appropriate dimensionless groups.

The reports by Sideman and Pinczewski [135] and Arpaci and Larsen [4] provide extensive reviews of the analogy theories.

#### *Turbulent Flow Fields*

The application of Navier-Stokes equations to turbulent flows are described in sect 1.2.7. The Reynolds averaged equations for incompressible flows are normally adopted deriving the transfer coefficients for heat and mass.

For convenience the governing Reynolds averaged equations valid for fully developed turbulent boundary layer flow are listed below [169, 135]. In these equations several simplifications are made, in particular  $\frac{\partial}{\partial t} = 0$  and the dominant flow is in the  $x$ -direction so  $v_z = 0$ . Moreover, the diffusion in the  $x$ - and  $z$ -directions are neglected.

The continuity equation:

$$\frac{\partial \overline{v_x}}{\partial x} + \frac{\partial \overline{v_y}}{\partial y} = 0 \quad (5.239)$$

The momentum transport:

$$\rho \overline{v_x} \frac{\partial \overline{v_x}}{\partial x} + \rho \overline{v_y} \frac{\partial \overline{v_x}}{\partial y} = -\frac{\partial \overline{p}}{\partial x} + \frac{\partial}{\partial y} \left( \mu \frac{\partial \overline{v_x}}{\partial y} - \rho \overline{v'_x v'_y} \right) \quad (5.240)$$

The heat transport:

$$\rho C_p \overline{v_x} \frac{\partial \overline{T}}{\partial x} + \rho C_p \overline{v_y} \frac{\partial \overline{T}}{\partial y} = \frac{\partial}{\partial y} \left( k \frac{\partial \overline{T}}{\partial y} - \rho C_p \overline{T' v'_y} \right) \quad (5.241)$$

The species concentration transport:

$$\overline{v_x} \frac{\partial \overline{c}}{\partial x} + \overline{v_y} \frac{\partial \overline{c}}{\partial y} = \frac{\partial}{\partial y} \left( D \frac{\partial \overline{c}}{\partial y} - \overline{c' v'_y} \right) \quad (5.242)$$

The Reynolds transport terms (i.e., the terms of the kind  $\overline{v'_x v'_y}$ ,  $\overline{T' v'_y}$  and  $\overline{c' v'_y}$ ) are the mean rates of transport of momentum, heat, and mass across the corresponding CV-surfaces of the balanced element by the turbulent velocity fluctuations. This system of equations can not be solved because these terms are not known. We therefore need additional information regarding the Reynolds transport terms. We may postulate a model for the momentum transport terms, intending to relate the Reynolds transport stresses to the mean flow field variables.

*The gradient hypothesis*

The turbulent transport processes are often described as diffusive fluxes being proportional to the mean variable gradient of the transported quantities. The turbulent transport terms may then be expressed in a form analogous to their laminar equivalents in accordance with the hypothesis of Boussinesq [17].

The dominating turbulent fluxes can then be expressed as:

$$\sigma_t = \overline{v'_x v'_y} = -\mu_t \frac{\partial \overline{v_x}}{\partial y} \quad (5.243)$$

$$q_t = \rho C_p \overline{T' v'_y} = -k_t \frac{\partial \overline{T}}{\partial y} \quad (5.244)$$

$$N_t = \overline{c' v'_y} = -D_t \frac{\partial \overline{c}}{\partial y} \quad (5.245)$$

where  $\mu_t$  denotes the turbulent viscosity,  $k_t$  the turbulent conductivity, and  $D_t$  the turbulent diffusivity.

Although the Boussinesq's hypothesis does not determine a complete model for turbulence, its importance lies in the fact that it provides a relationship between the apriori unknown Reynolds transport terms and the mean flow field variables. To close the model it is necessary to specify the turbulent coefficients in terms of known quantities.

The molecular and turbulent transport coefficients may be added as a linear sum of independent contributions determining the effective transport coefficients.

The effective fluxes are thus given by:

$$\sigma = -(\mu + \mu_t) \frac{\partial \bar{v}_x}{\partial y} \quad (5.246)$$

$$q = -(k + k_t) \frac{\partial \bar{T}}{\partial y} \quad (5.247)$$

$$N_t = -(D + D_t) \frac{\partial \bar{c}}{\partial y} \quad (5.248)$$

In general, in fully developed turbulent flows the turbulent viscosity, conductivity and diffusivity vary from point to point in the flow field and are many magnitudes greater than the molecular coefficients.

The existing turbulence models consist of approximate relations for the  $\mu_t$ -parameter in (5.246). The Prandtl mixing-length model (1.356) represents an early algebraic (zero-equation) model for the turbulent viscosity  $\mu_t$  in turbulent boundary layers.

To determine the corresponding coefficients for heat and mass transfer we need some theoretical prerequisites which were introduced already in sect 1.3.4. However, it might be convenient to examine and partly repeat certain relationships before we proceed to the next section.

#### *Momentum Transfer:*

It has been shown that there exists a continuous change in the physical behavior of the turbulent momentum boundary layer with the distance from the wall. The turbulent boundary layer is normally divided into several regions and sub-layers. It is noted that the most important region for heat and mass transfer is the inner region of the boundary layer, since it constitutes the major part of the resistance to the transfer rates. This inner region determines approximately 10 – 20% of the total boundary layer thickness, and the velocity distribution in this region follows simple relationships expressed in the inner variables as defined in sect 1.3.4.

The ratio between the local shear stress in the boundary layer defined by (5.246) and the shear stress at the wall given by (1.359), yields:

$$\frac{\sigma}{\sigma_w} = \frac{-\rho(\nu + \nu_t) \frac{d\bar{u}}{dy}}{-\rho(v^*)^2} \quad (5.249)$$

This relation may be rewritten introducing the dimensionless inner variables:

$$\frac{\sigma}{\sigma_w} = \left(1 + \frac{\nu_t}{\nu}\right) \frac{du^+}{dy^+} = \varepsilon^+ \frac{du^+}{dy^+} \quad (5.250)$$

Since the shear in the inner region is assumed constant and equal to the shear stress at the wall (i.e.,  $\sigma \approx \sigma_w \approx \text{constant}$ ), we get:

$$\frac{dy^+}{du^+} = \varepsilon^+ = \left(1 + \frac{\nu_t}{\nu}\right) \quad (5.251)$$

For fully developed turbulent flow  $\frac{\nu_t}{\nu} \gg 1$ , the relation reduces to:

$$\frac{dy^+}{du^+} = \frac{\nu_t}{\nu} \quad (5.252)$$

If we combine this relationship with the Prandtl mixing length expression (1.356) in which the mixing length is approximated by  $l = \kappa y$ , we get the following dimensionless velocity gradient:

$$\frac{du^+}{dy^+} = \frac{1}{\kappa y^+} \quad (5.253)$$

After integration, the velocity distribution in the inner region of the boundary layer appears:

$$u^+ = \frac{1}{\kappa} \ln y^+ + G \quad (5.254)$$

The values of  $\kappa = 0.4$  and  $G = 5.1$  are recommended on the basis of extensive experimental data [169]. This equation is in satisfactory agreement with the experimental data for most parts of the inner region of the boundary layer (i.e., in the region where the Reynolds stress is of considerably greater magnitude than the viscous stress). Near the wall where the molecular viscosity effects predominate is called the viscous sub-layer and in that thin region the velocity profile is given by  $u^+ = y^+$ . A transition zone can be identified between the viscous sub-layer and the turbulent core where both molecular and turbulent transport mechanisms are significant. This layer is called a buffer zone. Numerous parameterizations of the velocity profile in the boundary layer exist on this form. Some of them are discussed by Sherwood [133] and listed by Sideman and Pinczewski [135]. The commonly used relationships were proposed by von Karman [161]. He defined the velocity profile in the form of empirical expressions relating  $u^+$  and  $y^+$  for three separate zones of the inner region.

- Viscous sub-layer,  $0 < y^+ < 5$ :

$$u^+ = y^+ \quad (5.255)$$

- Buffer zone,  $5 < y^+ < 30$ :

$$u^+ = 5.0 \ln y^+ - 3.05 \quad (5.256)$$

- Turbulent core,  $y^+ > 30$ :

$$u^+ = 2.5 \ln y^+ + 5.5 \quad (5.257)$$

These relations are often referred to as *the universal velocity profile* or the *law of the wall*.

*Analogies Between Mass, Heat and Momentum Transfer Fluxes*

A comparison of the partial differential equations for the conservation of heat, mass and momentum in a turbulent flow field (5.240), (5.241) and (5.242) shows that the equations are mathematically similar provided that the pressure term  $\frac{\partial P}{\partial x}$  in the momentum equation is negligible [135]. If the corresponding boundary conditions are similar too, the normalized solution of these equations will have the same form.

However, to solve the heat and mass transfer equations an additional modeling problem has to be overcome. While there are sufficient measurements of the turbulent velocity field available to validate the different  $\nu_t$  modeling concepts proposed in the literature, experimental difficulties have prevented the development of any direct modeling concepts for determining the turbulent conductivity  $\alpha_t$ , and the turbulent diffusivity  $D_t$  parameters. Nevertheless, alternative semi-empirical modeling approaches emerged based on the hypothesis that it might be possible to calculate the turbulent conductivity and diffusivity coefficients from the turbulent viscosity provided that sufficient parameterizations were derived for  $Pr_t$  and  $Sc_t$ .

The first model suggested for these dimensionless groups is named the Reynolds analogy. Reynolds suggested that in fully developed turbulent flow heat, mass and momentum are transported as a result of the same eddy motion mechanisms, thus both the turbulent Prandtl and Schmidt numbers are assumed equal to unity:

$$Pr_t = 1 \quad Sc_t = 1 \quad (5.258)$$

Provided that this hypothesis holds the heat and mass transfer rates can be estimated from the rate of momentum transport.

It is noted that Sideman and Pinczewski [135], among others, have examined this hypothesis in further details and concluded that there are numerous requirements that need to be fulfilled to achieve similarity between the momentum, heat and mass transfer fluxes. On the other hand, there are apparently fewer restrictions necessary to obtain similarity between heat and low-flux mass transfer. This observation has led to the suggestion that empirical parameterizations developed for mass transfer could be applied to heat transfer studies simply by replacing the Schmidt number ( $Sc_t = \frac{\nu_t}{D_t}$ ) by the Prandtl number ( $Pr_t = \frac{\nu_t}{\alpha_t}$ ) and visa versa.

To proceed we need to put up dimensionless relations for the heat and mass transfer fluxes in the turbulent boundary layer using a procedure analogous to the one applied for the momentum flux (5.249) in which the Boussinesq's turbulent viscosity hypothesis is involved.

*Heat Transport:*

Using Fourier's law, the ratio of the heat flux in the boundary layer (5.247) and the heat flux at the wall can be expressed as:

$$\frac{q}{q_w} = \frac{-(k + k_t) \frac{dT}{dy}}{q_w} \quad (5.259)$$

A dimensionless temperature,  $T^+$ , may be defined as:

$$T^+ = \frac{\bar{T} - T_w}{T^*} \quad (5.260)$$

Introducing dimensionless variables, we get:

$$\frac{q}{q_w} = -\frac{(k + k_t) \frac{T^* u^*}{\nu} \frac{dT^+}{dy^+}}{q_w} = \frac{-\rho C_P (\alpha + \alpha_t) \frac{T^* u^*}{\nu} \frac{dT^+}{dy^+}}{q_w} \quad (5.261)$$

In the latter relation the thermal diffusivity parameters,  $\alpha$  and  $\alpha_t$ , are defined by:

$$\alpha = \frac{k}{\rho C_P} \quad \text{and} \quad \alpha_t = \frac{k_t}{\rho C_P} \quad (5.262)$$

For convenience the corresponding Prandtl numbers,  $Pr$  and  $Pr_t$ , can be introduced:

$$\frac{q}{q_w} = \frac{-\rho C_P \left( \frac{1}{Pr} + \frac{1}{Pr_t} \frac{\nu_t}{\nu} \right) T^* u^* \frac{dT^+}{dy^+}}{q_w} \quad (5.263)$$

where

$$Pr = \frac{\nu}{\alpha} \quad \text{and} \quad Pr_t = \frac{\nu_t}{\alpha_t} \quad (5.264)$$

With the given sign convention, the heat flux at the wall can be expressed by:

$$q_w = -\rho C_P T^* u^* \quad (5.265)$$

which is merely the defining equation for the temperature scale.

The ratio of the heat fluxes (5.263) can then be expressed by:

$$\frac{q}{q_w} = \frac{-\rho C_P \left( \frac{1}{Pr} + \frac{1}{Pr_t} \frac{\nu_t}{\nu} \right) T^* u^* \frac{dT^+}{dy^+}}{-\rho C_P T^* u^*} = \left( \frac{1}{Pr} + \frac{1}{Pr_t} \frac{\nu_t}{\nu} \right) \frac{dT^+}{dy^+} \quad (5.266)$$

in which the dimensionless temperature is given by

$$T^+ = \frac{\bar{T} - T_w}{T^*} = -(\bar{T} - T_w) \frac{\rho C_P u^*}{q_w} = -(\bar{T} - T_w) \frac{C_P \sigma_w}{q_w u^*} \quad (5.267)$$

*Species Mole (Mass) Transport:*

Using Ficks law, the ratio of the species mole (mass) flux in the boundary layer (5.247) and the species mole (mass) flux at the wall can be expressed as:

$$\frac{N}{N_w} = -\frac{(D + D_t) \frac{d\bar{c}}{dy}}{N_w} \quad (5.268)$$

A dimensionless mole (mass) concentration,  $c^+$ , may be defined as:

$$c^+ = \frac{\bar{c} - c_w}{c^*} \quad (5.269)$$

Introducing the dimensionless variables, we get:

$$\frac{N}{N_w} = \frac{-(D + D_t) \frac{c^* u^*}{\nu} \frac{dc^+}{dy^+}}{N_w} \quad (5.270)$$

We may reformulate the relation by introducing the Schmidt numbers,  $Sc$  and  $Sc_t$ :

$$\frac{N}{N_w} = \frac{-\left(\frac{1}{Sc} + \frac{1}{Sc_t} \frac{\nu_t}{\nu}\right) c^* u^* \frac{dc^+}{dy^+}}{N_w} \quad (5.271)$$

where

$$Sc = \frac{\nu}{D} \quad \text{and} \quad Sc_t = \frac{\nu_t}{D_t} \quad (5.272)$$

With the given sign convention, the species mole (mass) flux at the wall can be defined as:

$$N_w = -c^* u^* \quad (5.273)$$

which is merely the definition equation for the concentration scale.

The ratio between the species mole (mass) fluxes can then be expressed:

$$\frac{N}{N_w} = \left(\frac{1}{Sc} + \frac{1}{Sc_t} \frac{\nu_t}{\nu}\right) \frac{dc^+}{dy^+} \quad (5.274)$$

where the dimensionless concentration is given by:

$$c^+ = \frac{\bar{c} - c_w}{c^*} = -(\bar{c} - c_w) \frac{u^*}{N_w} = -(\bar{c} - c_w) \frac{\sigma_w}{\rho N_w u^*} \quad (5.275)$$

The momentum, heat and species concentration equations (5.250), (5.266) and (5.274) may now be integrated to express the velocity, temperature, and concentration distribution in the turbulent boundary layer.

The velocity profile:

$$u^+ = \int_0^{y^+} \frac{\frac{\sigma}{1 + \frac{\nu_t}{\nu}}}{1 + \frac{\nu_t}{\nu}} dy^+ \quad (5.276)$$

The temperature profile:

$$T^+ = \int_0^{y^+} \frac{\frac{q}{\frac{1}{Pr} + \frac{1}{Pr_t} \frac{\nu_t}{\nu}}}{\frac{1}{Pr} + \frac{1}{Pr_t} \frac{\nu_t}{\nu}} dy^+ \quad (5.277)$$

The concentration profile:

$$c^+ = \int_0^{y^+} \frac{\frac{N}{N_w}}{\frac{1}{Sc} + \frac{1}{Sc_t} \frac{\nu_t}{\nu}} dy^+ \quad (5.278)$$

It is noted that the upper boundary of the integrals is taken as  $y = \delta > \delta_T$ , where  $\delta_T$  is the thickness of the thermal boundary layer for the temperature profile, and  $y = \delta > \delta_c$ , where  $\delta_c$  is the thickness of the concentration boundary layer for the concentration profile. Outside the boundary layers the free stream or completely mixed bulk quantities are set to  $T = T_0$  and  $c = c_0$ , respectively.

Therefore, by adopting the Reynolds analogy for turbulent flows (5.258) we get:

$$T_0^+ = (\bar{T}_W - \bar{T}_0) \frac{\rho C_p u^*}{q_W} = \int_0^{\delta^+} \frac{dy^+}{\frac{1}{Pr} + \frac{\nu_t}{\nu}} \quad (5.279)$$

$$c_0^+ = (\bar{c}_W - \bar{c}_0) \frac{u^*}{N_W} = \int_0^{\delta^+} \frac{dy^+}{\frac{1}{Sc} + \frac{\nu_t}{\nu}} \quad (5.280)$$

where  $\delta^+ = \delta u^* / \nu$  as can be derived from  $y^+ = y u^* / \nu$  when  $y = \delta$ .

Combining these two expressions with the definitions of dimensionless temperature (5.267) and concentration (5.275), and then rearranging these relations we obtain the general expressions for the heat and mass transfer coefficients.

The heat transfer coefficient:

$$h = \frac{q_W}{(\bar{T}_W - \bar{T}_0)} = \frac{\rho C_p u^*}{\int_0^{\delta^+} \frac{dy^+}{\frac{1}{Pr} + \frac{\nu_t}{\nu}}} \quad (5.281)$$

The mass transfer coefficient:

$$k_c = \frac{N_W}{(\bar{c}_W - \bar{c}_0)} = \frac{u^*}{\int_0^{\delta^+} \frac{dy^+}{\frac{1}{Sc} + \frac{\nu_t}{\nu}}} \quad (5.282)$$

Introducing the appropriate dimensionless groups:

$$Sh = \frac{k_c l}{D}, \quad Nu = \frac{hl}{k} \quad \text{and} \quad Re = \frac{\bar{u}l}{\nu} \quad (5.283)$$

we can generalize the resulting parameterizations for the heat and mass transfer coefficients as given by (5.284) and (5.286) below.

The dimensionless heat transfer coefficient yields [133, 135]:

$$Nu = \frac{\sqrt{\frac{f_F}{2}} Re Pr}{\int_0^{\delta} \frac{dy^+}{\frac{1}{Pr} + \frac{\nu_t}{\nu}}} \quad (5.284)$$

in which the friction velocity (1.359) is expressed in terms of the Fanning friction factor (3.479):

$$u^* = \sqrt{\frac{-\sigma_w}{\rho}} = \sqrt{\frac{f_F}{2}} \bar{u} \quad (5.285)$$

The dimensionless mass transfer coefficient yields [133] [135]:

$$Sh = \frac{\sqrt{\frac{f_F}{2}} Re Sc}{\int_0^\delta \frac{dy^+}{\frac{1}{Sc} + \frac{\nu_t}{\nu}}} \tag{5.286}$$

The introduction of different parameterizations for the turbulent viscosity parameter leads to different modifications of the correlations for the dimensionless numbers. By setting the viscous Prandtl and Schmidt number equal to unity and noting that the integral term in the denominator is simply the velocity  $u^+$  (5.276) that can also be expressed by  $u^+ = \frac{\bar{u}}{u^*} = \sqrt{\frac{2}{f_F}}$ , we get [133, 135]:

$$Sh = Nu = \frac{f_F}{2} Re \tag{5.287}$$

The latter relation may also be expressed in the form ([134], p 163; [60], p 364):

$$St_m = St_h = \frac{f_F}{2} \tag{5.288}$$

which is by many authors referred to as *the Reynolds analogy*. This relationship is based on the assumption that the Prandtl and Schmidt numbers (i.e. for laminar flow) are equal to unity. The given relation has been compared with experimental data and found to be appropriate for most common gases, but not for liquids [134]. For many common gasses  $D \approx \alpha \approx \nu$ , confirming the assumption that  $Pr$  and  $Sc$  are equal to unity [27] (p 510). However, for liquids these numbers may be significantly different. The need to extend the Reynolds analogy enabling a reliable description of liquid systems lead to the Chilton-Colburn relation [20], which was mentioned deriving the transfer coefficients for laminar flow in the previous section:

$$Sh = \frac{f_F}{2} Re Sc^{1/3} \tag{5.289}$$

and

$$Nu = \frac{f_F}{2} Re Pr^{1/3} \tag{5.290}$$

For Prandtl numbers other than unity, the integrals in (5.284) and (5.286) are split into parts depending upon the number of regions needed to appropriately reproduce the law of the wall. The simplest extension of the basic model is to split the integral into two parts, thus the expressions for  $Nu$  and  $Sh$  yield [133, 135]:

$$Nu = \frac{\sqrt{\frac{f_F}{2}} Re Pr}{\int_0^{y_1^+} \frac{dy_1^+}{\frac{1}{Pr} + \frac{\nu_t}{\nu}} + \int_{y_1^+}^{\delta^+} \frac{dy_1^+}{\nu}} \tag{5.291}$$

and

$$Sh = \frac{\sqrt{\frac{f_F}{2}} Re Sc}{\int_0^{y_1^+} \frac{dy_1^+}{\frac{1}{Sc} + \frac{\nu_T}{\nu}} + \int_{y_1^+}^{\delta^+} \frac{dy_1^+}{\frac{\nu_T}{\nu}}} \quad (5.292)$$

The analogy calculations with the turbulent Prandtl and Schmidt numbers other than unity are based on various empirical relations for these dimensionless parameters. However, comparisons with experimental data show that the parameter values of  $Sc = Pr = 1$  are good first approximations for most practical applications. No significant improvements have been obtained by the extended formulations.

Reviews of several extensions of the analogy theory are given in the reports by Sherwood [133] and Sideman and Pinczewski [135].

### Heat and Mass Transfer to the Surface of a Sphere

The mass transfer correlation determining the mass transfer to the surface of a sphere is commonly referred to as the Frössling equation [50]:

$$Sh = 2 + 0.6Re^{1/2}Sc^{1/3} \quad (5.293)$$

Based on Frössling's development, Ranz and Marshall [121] came to the well established conclusion that the heat transfer correlation can be expressed in an analogous manner:

$$Nu = 2 + 0.6Re^{1/2}Pr^{1/3} \quad (5.294)$$

If we study the heat transfer from the surface of a sphere with  $r = R$ , that is immersed in a stagnant fluid we have a process of steady conduction from the surface of the sphere ( $r = R$ ) through the fluid, radially outward to  $r = \infty$ . The radial conductive flux is:

$$q_r = -k \frac{dT}{dr} \quad (5.295)$$

When we have obtained steady state, the rate of heat transfer (flux times area) through the surrounding fluid is constant with respect to the radial position:

$$4\pi r^2 q_r = -4\pi k r^2 \frac{dT}{dr} = \text{Constant} \quad (5.296)$$

With the following boundary conditions:

$$T = T_R \quad r = R \quad (5.297)$$

$$T = T_0 \quad r = \infty \quad (5.298)$$

The solution to this problem is the temperature profile:

$$T = T_0 + (T_R - T_0) \frac{R}{r} \quad (5.299)$$

By inserting this temperature profile into the flux expression (5.295), we obtain the steady heat flux at the surface  $r=R$ :

$$q_R = k \frac{T_R - T_0}{R} \quad (5.300)$$

It is recollected that in according to Newton's law of cooling (5.125) the corresponding definition of the heat transfer coefficient can be expressed as:

$$q_R = h(T_R - T_0) \quad (5.301)$$

By comparing the given conductive heat flux relation with the corresponding definition of the heat transfer coefficient, it is customary to define the heat transfer coefficient by:

$$h = \frac{k}{R} \quad (5.302)$$

This  $h$  is the convective heat transfer coefficient for pure conduction (assuming no slip at the surface).

The dimensionless heat transfer coefficient, named the Nusselt number is defined by  $Nu = hd_p/k$ , and by combining this with (5.302) we get:

$$Nu = \frac{hd_p}{k} = \frac{2hR}{k} = 2 \quad (5.303)$$

This is the appropriate correlation to use when there is heat or mass (i.e., substitute  $Nu$  by  $Sh$ ) transfer from a sphere immersed in a stagnant film is studied,  $Nu = 2$ . The second term in (5.294) accounts for convective mechanisms, and the relation is derived from the solution of the boundary layer equations. For higher Reynolds numbers the Nusselt number is set equal to the relation resulting from the boundary layer analysis of a flat plate:

$$Nu = 0.6Re^{1/2}Pr^{1/3} \quad (5.304)$$

Bird et al [13] (p 647), Hines and Maddox [58] (chap 6.7), Cussler [27], Middleman [102] and Incropera and DeWitt [60] (p 415), among others, presents tabulated mass transfer correlations for various problems, including laminar/turbulent flow, single solid spheres and packed beds.

### 5.3.6 Heat Transfer by Radiation

In this section a brief introduction to the fundamental concepts of thermal radiation modeling is given. The main purpose of this survey is to elucidate the basic assumptions involved deriving the conventional engineering model of thermal radiation fluxes. To this end the thermal radiation flux is determined in terms of a heat transfer coefficient.

Explanations of radiation physics and more detailed descriptions of the concepts of thermal radiation can be found in the books by Long [91], Arpaci et al [5], Hagen [56], Incropera and DeWitt [60], Siegel and Howel [136], Eckert and Drake [39], among many others.

## Basic Definitions and Elementary Concepts of Thermal Radiation

Radiative heat transfer or thermal radiation is a distinctly separate mechanism from conduction and convection for the transport of heat. Thermal radiation is associated with the rate at which energy is emitted by the material as a result of its finite temperature. The mechanism of emission is related to energy released as a result of oscillations or transitions of the many electrons that constitute the material. These oscillations are, in turn, supported by the internal energy for this reason the temperature drops. The emission of thermal radiation is thus associated with thermally excited conditions within the matter.

Since radiation originates due to emission by matter its subsequent transport does not require the presence of any matter. Unlike convection and conduction, heat can thus be transferred by thermal radiation through vacuum. One theory views radiation as the propagation of electro-magnetic waves. Alternatively, radiation may be viewed as the propagation of a collection of particles termed photons or quanta. Planck [114] developed the quantum mechanics which can explain radiation in terms of particles (photon) traveling with the speed of light. The energy associated with each photon is given by:

$$E = h\nu = \frac{hc}{\lambda} \quad (5.305)$$

where  $h = 6.6262 \times 10^{-34}$  ( $J_s$ ) is the Planck constant.

Radiation also possesses the standard wave properties of frequency  $\nu$  and wavelength  $\lambda$ . For radiation propagating in a particular medium, the two properties are related by:

$$\lambda = \frac{c}{\nu} \quad (5.306)$$

where  $c$  is the speed of light in the medium. For propagation in a vacuum,  $c_0 = 2.998 \times 10^8$  ( $m/s$ ). The unit of wavelength is normally given in micrometer ( $\mu m$ ).

All states of matter (solids, liquids, and gases) emit thermal radiation. For gases and for semi-transparent solids, such as glass and salt crystals at elevated temperatures, emission is a volumetric phenomenon. That is, radiation emerging from a finite volume of matter is the integrated effect of local emission throughout the volume. In most solids and liquids, radiation emitted from interior molecules is strongly absorbed by adjoining molecules. Accordingly, radiation that is emitted from a solid or a liquid originates from molecules that are within a distance of approximately  $1 \mu m$  from the exposed surface. It is for this reason that emission from a solid or a liquid into an adjoining gas or a vacuum is viewed as a surface phenomenon.

Consider a heated enclosure with surface  $A$  and volume  $V$  filled with radiating material. If  $\mathbf{q}_A dA$  is defined as the radiant surface energy flux arriving at  $dA$  from a surface element  $dA_S$ , and the volumetric energy flux  $\mathbf{q}_V dV$

arrives at  $dA$  from a volume element  $dV$ , then the radiative energy flux from the entire enclosure arriving at  $dA$  is:

$$\mathbf{q}^{\text{rad}}dA = \int_{A_S} \mathbf{q}_{A_S}dA_S + \int_V \mathbf{q}_VdV \quad (5.307)$$

Radiation thus leads to energy balances in the form of integral equations. When radiation is combined with advection and conduction, the combination of integral and differential operators leads to integrodifferential equations which are more cumbersome to solve than partial differential equations (PDEs).

The energy in thermal radiation has in general a spectral distribution, as the radiation varies with the wavelength, and a directional distribution as the radiation also varies with angle. Actually, thermal radiation is the name given to electromagnetic radiation in the range of wavelengths  $0.1 < \lambda < 100\mu m$ . These spectral and directional dependencies severely complicates rigorous radiation analysis.

Before further details of the theory are considered an informative sketch of the general radiation flux modeling framework is required giving an introductory overview linking the conceptual fragments which constitute the overall theory. In most cases we will preferably focus on radiation from solid surfaces. Basically, as already mentioned, a material will emit radiation as a direct result of its temperature. This energy flux or emissive power is denoted by  $E$ . Also, radiation emitted from other objects can fall into a surface. This energy flux is termed irradiation and denoted by  $G$ . The irradiation generally interacts with a semitransparent medium and portions of this radiation are reflected, absorbed, and transmitted. The properties that determine the fractions of the irradiation that are distributed in each of these rays are called reflectivity, absorptivity and transmissivity, respectively. The total radiation leaving a surface is the sum of the reflected and emitted components and this is named radiosity indicated by the symbol  $J$ . The radiative behavior and properties of ideal (blackbody) and opaque materials are both important for the determination of the radiant flux from a real material. A property called emissivity is defined as the ratio of the radiation emitted by the real surface to the radiation emitted by a blackbody at the same temperature.

To get an idea about the spectral and directional complexity of the rigorous modeling of radiant heat transfer the variables that must be specified for the radiative properties are introduced. A functional notation is used to give explicitly the variables upon which a quantity depends. The most fundamental variables includes dependencies on wavelength, direction, and surface temperature. A total quantity does not have a spectral dependency. A hemispherical spectral variable does not have a directional dependency. A hemispherical total quantity has only a temperature dependency.

In the following radiation is treated as a electromagnetic phenomenon. The radiation emitted in any direction is normally defined in terms of a quantity called the intensity of radiation. There are two types of intensity, a spectral

intensity which refers to radiation in an interval  $d\lambda$  around a single wavelength  $\lambda$ , and the total intensity which refers to the combined radiation including all wavelengths.

The spectral intensity is defined as the energy per unit area normal to the direction of propagation, per unit solid angle about the direction, per metre of wavelength.

The solid angle is a 3D angle measured in steradian, as explained in sect 2.4.2. For convenience the defining arguments are briefly summarized this time with emphasis on applications to radiation heat transfer.

Consider emission from a differential element of area  $dA$  into a hypothetical hemisphere centered at a point on  $dA$ . The emission in a particular direction from an element of area  $dA$  is specified in terms of the zenith and azimuthal angles,  $\theta$  and  $\phi$ , respectively, of a spherical coordinate system Fig 5.11. A differential surface in space  $dA_S$ , through which this radiation passes, subtends a solid angle  $d\Omega$  when viewed from a point on  $dA$ .

From sect 2.4.2 we recall that the differential solid angle  $d\Omega$  is defined by a region between the rays of a sphere and is measured as the ratio of the element of area  $dA_S$  on the sphere to the square of the sphere's radius (see Figs 2.5 and 2.6 in which  $dA$  denotes any surface element):

$$d\Omega = \frac{dA_S}{r^2} = \frac{r \sin \theta r d\theta d\phi}{r^2} = \sin \theta d\theta d\phi \quad (5.308)$$

where the area  $dA_S$  is normal to the  $(\theta, \phi)$  direction and may be represented by:

$$dA_S = r^2 \sin \theta d\theta d\phi \quad (5.309)$$

for a spherical surface.

The rate at which emission from  $dA$  passes through  $dA_S$  can be expressed in terms of the spectral intensity  $I_{\lambda,e}$  of the emitted radiation.  $I_{\lambda,e}$  denotes the rate at which radiant energy is emitted at the wavelength  $\lambda$  in the  $(\theta, \phi)$  direction, per unit area of the emitting surface normal to this direction, per unit solid angle about this direction, and per unit wavelength interval  $d\lambda$  about  $\lambda$ . The area used to define  $I_{\lambda,e}$  is the component of  $dA$  perpendicular to the direction of the radiation,  $dA_p = dA \cos \theta$ , which denotes the projected area of  $dA$ . The spectral intensity is defined by:

$$I_{\lambda,e}(\lambda, \theta, \phi) = \frac{d\dot{Q}^{\text{rad}}}{dA \cos \theta d\Omega d\lambda} \quad (W/m^2 \text{ sr } \mu m) \quad (5.310)$$

in which  $d\dot{Q}_\lambda = (d\dot{Q}^{\text{rad}}/d\lambda)$  is the rate at which radiation of wavelength  $\lambda$  leaves  $dA$  and passes through  $dA_S$ .

The spectral heat flux associated with emission into any finite solid angle or any finite wavelength interval may be determined by integration over the hypothetical hemisphere above  $dA$ :

$$q_\lambda(\lambda) = \int_0^{2\pi} \int_0^{\pi/2} I_{\lambda,e}(\lambda, \theta, \phi) \cos \theta \sin \theta d\theta d\phi \quad (W/m^2 \mu m) \quad (5.311)$$

The total heat flux associated with emission in all directions and at all wavelengths is then:

$$q^{\text{rad}} = \int_0^{\infty} q_{\lambda}(\lambda) d\lambda = \int_0^{\infty} \int_0^{2\pi} \int_0^{\pi/2} I_{\lambda,e}(\lambda, \theta, \phi) \cos \theta \sin \theta d\theta d\phi d\lambda \quad (W/m^2) \quad (5.312)$$

The concept of *emissive power* is used to quantify the amount of radiation emitted per unit surface area. The hemispherical spectral emissive power  $E_{\lambda}$  is defined as the rate at which radiation of wavelength  $\lambda$  is emitted in all directions from a surface per unit wavelength  $d\lambda$  about  $\lambda$  and per unit surface area. It is thus related to the spectral intensity of the emitted radiation by:

$$E_{\lambda}(\lambda) = \int_0^{2\pi} \int_0^{\pi/2} I_{\lambda,e}(\lambda, \theta, \phi) \cos \theta \sin \theta d\theta d\phi = q_{\lambda}(\lambda) \quad (W/m^2 \mu m) \quad (5.313)$$

It is noted that  $E_{\lambda}(\lambda)$  is a flux based on the actual surface area, whereas  $I_{\lambda,e}$  is based on the projected area.

The total hemispherical emissive power  $E$  is the rate at which radiation is emitted per unit area at all possible wavelengths and directions:

$$E = \int_0^{\infty} E_{\lambda}(\lambda) d\lambda = \int_0^{\infty} \int_0^{2\pi} \int_0^{\pi/2} I_{\lambda,e}(\lambda, \theta, \phi) \cos \theta \sin \theta d\theta d\phi d\lambda \quad (W/m^2) \quad (5.314)$$

A diffuse emitter denotes a special case of a surface for which the intensity of the emitted radiation is independent of direction,  $I_{\lambda,e}(\lambda, \theta, \phi) \approx I_{\lambda,e}(\lambda)$ . In this case

$$E_{\lambda}(\lambda) = I_{\lambda,e}(\lambda) \int_0^{2\pi} \int_0^{\pi/2} \cos \theta \sin \theta d\theta d\phi \quad (5.315)$$

and

$$E = \int_0^{\infty} E_{\lambda}(\lambda) d\lambda = \pi I_e \quad (5.316)$$

The given concepts also apply to *incident radiation*. Such radiation originates from emission and reflection occurring at other surfaces and have spectral and directional distributions determined by the spectral intensity  $I_{\lambda,i}(\lambda, \theta, \phi)$ .

The *spectral irradiation* which encompasses radiation of wavelength  $\lambda$  incident from all directions is defined by:

$$G_{\lambda}(\lambda) = \int_0^{2\pi} \int_0^{\pi/2} I_{\lambda,i}(\lambda, \theta, \phi) \cos \theta \sin \theta d\theta d\phi \quad (W/m^2 \mu m) \quad (5.317)$$

The total irradiation  $G$  represents the rate at which radiation is incident per unit area from all directions and wavelengths:

$$G = \int_0^{\infty} G_{\lambda}(\lambda) d\lambda = \int_0^{\infty} \int_0^{2\pi} \int_0^{\pi/2} I_{\lambda,i}(\lambda, \theta, \phi) \cos \theta \sin \theta d\theta d\phi d\lambda \quad (W/m^2) \quad (5.318)$$

In the particular case in which the incident radiation is diffuse,  $I_{\lambda,i}$  is independent of  $\theta$  and  $\phi$ , thus:

$$G_{\lambda}(\lambda) = \pi I_{\lambda,i} \quad (5.319)$$

and

$$G = \pi I_i \quad (5.320)$$

The radiative flux termed *radiosity* accounts for the net radiant energy leaving a surface. The spectral radiosity  $J_{\lambda}$  represents the rate at which radiation of wavelength  $\lambda$  leaves a unit area of the surface, per unit wavelength interval  $d\lambda$  about  $\lambda$ .  $J_{\lambda}$  accounts for radiation leaving in all directions and is thus related to the intensity associated with emission and reflection  $I_{\lambda,e+r}(\lambda, \theta, \phi)$ . Therefore,

$$J_{\lambda}(\lambda) = \int_0^{2\pi} \int_0^{\pi/2} I_{\lambda,e+r}(\lambda, \theta, \phi) \cos \theta \sin \theta d\theta d\phi \quad (W/m^2 \mu m) \quad (5.321)$$

and the total radiosity  $J$  is:

$$J = \int_0^{\infty} J_{\lambda}(\lambda) d\lambda = \int_0^{\infty} \int_0^{2\pi} \int_0^{\pi/2} I_{\lambda,e+r}(\lambda, \theta, \phi) \cos \theta \sin \theta d\theta d\phi d\lambda \quad (W/m^2) \quad (5.322)$$

In the particular case that the surface is both a diffuse reflector and a diffuse emitter,  $I_{\lambda,\theta,\phi}$  is independent of  $\theta$  and  $\phi$ , hence:

$$J_{\lambda}(\lambda) = \pi I_{\lambda,e+r} \quad (5.323)$$

and

$$J = \pi I_{e+r} \quad (5.324)$$

The concept of *blackbody* is determining the basis for describing the radiation properties of real surfaces. The black body denotes an ideal radiative surface which absorb all incident radiation, being a diffuse emitter and emit a maximum amount of energy as thermal radiation for a given wavelength and temperature. The black body can be considered as a perfect absorber and emitter.

The spectral thermal radiative power  $E_{\lambda,b}$  emitted by a blackbody with wavelength  $\lambda$  can be related to the spectral radiation intensity  $I_{\lambda,b}$  as derived

by Planck [114] from considerations of quantum statistical thermodynamics. The relation is given by:

$$I_{\lambda,b}(\lambda, T) = \frac{2hc_0^2}{\lambda^5 [\exp(hc_0/\lambda kT) - 1]} \quad (W/m^2 \text{ sr } \mu m) \quad (5.325)$$

where  $T$  is the absolute temperature,  $h$  is Planck's constant,  $c_0$  is the velocity of electromagnetic radiation (i.e., speed of light in vacuum), and  $k$  is the Boltzmann constant. Hence it follows that:

$$E_{\lambda,b}(\lambda, T) = \pi I_{\lambda,b}(\lambda, T) = \frac{2\pi hc_0^2}{\lambda^5 [\exp(hc_0/\lambda kT) - 1]} \quad (W/m^2 \mu m) \quad (5.326)$$

The total emissive power emitted by a black body is obtained by integration over all wavelengths:

$$E_b = \int_0^{\infty} \pi I_{\lambda,b} d\lambda \quad (5.327)$$

The solution to this integral is called *the Stefan-Boltzmann law*:

$$E_b = \sigma \times T^4 \quad (W/m^2) \quad (5.328)$$

where  $\sigma$  is the Stefan-Boltzmann constant which is given by:

$$\sigma = \frac{8\pi^5 k^4}{15c^3 h^3} = 5.67 \times 10^{-8} \quad (W/m^2 K^4) \quad (5.329)$$

This relation is often used in engineering calculations.

The blackbody spectral and total intensities are independent of direction so that emission of energy into a direction at  $\theta$  away from the surface normal direction is proportional to  $\cos \theta$ . This is known as *Lambert's cosine law*.

For real surfaces *emissivity* is defined as the ratio of the radiation emitted by the surface to the radiation emitted by a blackbody at the same temperature. So, the emissivity specifies how well a real body radiates energy as compared with a blackbody. The directional spectral emissivity  $\epsilon_{\lambda,\theta}(\lambda, \theta, \phi, T)$  of a surface at temperature  $T$  is defined as the ratio of the intensity of the radiation emitted at the wavelength  $\lambda$  and the direction of  $\theta$  and  $\phi$  to the intensity of the radiation emitted by a blackbody at the same values of  $T$  and  $\lambda$ :

$$\epsilon_{\lambda,\theta}(\lambda, \theta, \phi, T) = \frac{I_{\lambda,e}(\lambda, \theta, \phi, T)}{I_{\lambda,b}(\lambda, T)} \quad (-) \quad (5.330)$$

In a similar manner, a total, directional emissivity  $\epsilon_{\theta}$  representing a spectral average of  $\epsilon_{\lambda,\theta}$  is defined by:

$$\epsilon_{\theta}(\theta, \phi, T) = \frac{I_e(\theta, \phi, T)}{I_b(T)} \quad (-) \quad (5.331)$$

A hemispherical spectral emissivity is a directional average of  $\epsilon_{\lambda,\theta}$  defined by:

$$\epsilon_{\lambda}(\lambda, T) = \frac{E_{\lambda}(\lambda, T)}{E_{\lambda,b}(\lambda, T)} = \frac{\int_0^{2\pi} \int_0^{\pi/2} I_{\lambda,e}(\lambda, \theta, \phi, T) \cos \theta \sin \theta d\theta d\phi}{\int_0^{2\pi} \int_0^{\pi/2} I_{\lambda,b}(\lambda, T) \cos \theta \sin \theta d\theta d\phi} \quad (-) \quad (5.332)$$

The *hemispherical total emissivity* represents an average of  $\epsilon_{\lambda,\theta}$  over all directional and wavelengths and is defined by:

$$\epsilon(T) = \frac{E(T)}{E_b(T)} \quad (-) \quad (5.333)$$

In the most general situation the irradiation interacts with a semitransparent medium. For a spectral component of irradiation, portions of this radiation can be reflected, absorbed, and transmitted:

$$G_{\lambda} = G_{\lambda,\text{ref}} + G_{\lambda,\text{abs}} + G_{\lambda,\text{trans}} \quad (W/m^2 \mu m) \quad (5.334)$$

where  $G_{\lambda,\text{ref}}$  is the reflected portion of the spectral irradiation,  $G_{\lambda,\text{abs}}$  is the absorbed portion of the spectral irradiation, and  $G_{\lambda,\text{trans}}$  is the transmitted portion of the spectral irradiation.

In general, the determination of these components is complex and can be strongly influenced by volumetric effects within the medium. However, in many engineering applications the medium is opaque to the incident radiation so that  $G_{\lambda,\text{trans}} \approx 0$  and the absorption and reflection processes are treated as surface phenomena.

The *absorptivity* is a property that determines the fraction of the irradiation that is absorbed by a surface. The directional spectral absorptivity of a surface is defined as the fraction of the spectral intensity incident in the direction of  $\theta$  and  $\phi$  that is absorbed by the surface:

$$\alpha_{\lambda,\theta}(\lambda, \theta, \phi, T) = \frac{I_{\lambda,i,\text{abs}}(\lambda, \theta, \phi, T)}{I_{\lambda,i}(\lambda, \theta, \phi, T)} \quad (-) \quad (5.335)$$

The *hemispherical total absorptivity*  $\alpha$  represents an integrated average over both direction and wavelength:

$$\alpha = \frac{G_{\text{abs}}}{G} = \frac{\int_0^{\infty} \alpha_{\lambda}(\lambda) G_{\lambda}(\lambda) d\lambda}{\int_0^{\infty} G_{\lambda}(\lambda) d\lambda} \quad (-) \quad (5.336)$$

where  $\alpha_{\lambda}(\lambda)$  is a hemispherical spectral absorptivity

$$\alpha_\lambda(\lambda) = \frac{G_{\lambda,\text{abs}}(\lambda)}{G_\lambda(\lambda)} = \frac{\int_0^{2\pi\pi/2} \int_0^{2\pi\pi/2} \alpha_{\lambda,\theta}(\lambda, \theta, \phi) I_{\lambda,i}(\lambda, \theta, \phi) \cos \theta \sin \theta d\theta d\phi}{\int_0^{2\pi\pi/2} \int_0^{2\pi\pi/2} I_{\lambda,i}(\lambda, \theta, \phi) \cos \theta \sin \theta d\theta d\phi} \quad (-) \quad (5.337)$$

Similar directional spectral reflectivity and transmissivity quantities can also be defined. These properties are normally given the symbols  $\rho$  and  $\tau$ . However, from the above discussion, it's apparent that the sum of the reflected, absorbed and transmitted components must equal the irradiance, and so we can write:

$$\rho G + \alpha G + \tau G = G \quad (W/m^2) \quad (5.338)$$

or  $\rho + \alpha + \tau = 1$ . As a rule of thumb, most gases have a high value of  $\tau$  as they transmit thermal radiation, and quite low values of  $\rho$  and  $\alpha$  as they reflect and absorb small amounts at moderate temperature and pressures. Most solids transmit little thermal radiation but reflect and absorb significant amounts. Since reactor analysis concerns radiation from solid surfaces in most cases, we get  $\rho + \alpha = 1$ . The radiosity  $J$  from a surface is thus given by:

$$J = E + \rho G = E + (1 - \alpha)G \quad (W/m^2) \quad (5.339)$$

Besides, according to *Kirchhoff's law*, the total hemispherical emissivity of the surface equals the total hemispherical absorptivity. Therefore,  $\epsilon = \alpha$ ,  $\epsilon_\lambda = \alpha_\lambda$ , and  $\epsilon_{\lambda,\theta} = \alpha_{\lambda,\theta}$ .

A *gray surface* may be defined as a surface for which  $\alpha_\lambda$  and  $\epsilon_\lambda$  are independent of  $\lambda$  over the relevant spectral regions of the irradiation and the surface emission.

$$\epsilon(T) = \frac{\epsilon_{\lambda,0}(T) \int_{\lambda_1}^{\lambda_2} E_{\lambda,T}(T) d\lambda}{E_b(T)} = \epsilon_{\lambda,0}(T) \quad (-) \quad (5.340)$$

and

$$\alpha(T) = \frac{\alpha_{\lambda,0}(T) \int_{\lambda_3}^{\lambda_4} G_\lambda(T) d\lambda}{G(T)} = \alpha_{\lambda,0}(T) \quad (-) \quad (5.341)$$

## Engineering Modeling of Thermal Radiation Fluxes

In this subsection we focus on the engineering modeling approach determining thermal radiation from plan solid surfaces. In this case the emitter is assumed to be diffuse and only hemispherical total radiation quantities are considered as calculated from the spectral counterparts by integration over all wavelengths and all directions.

Consider a solid that is initially at a higher temperature  $T_s$  than that of its surroundings  $T_{sur}$ , and around it there exist a vacuum, see Fig 5.19. The

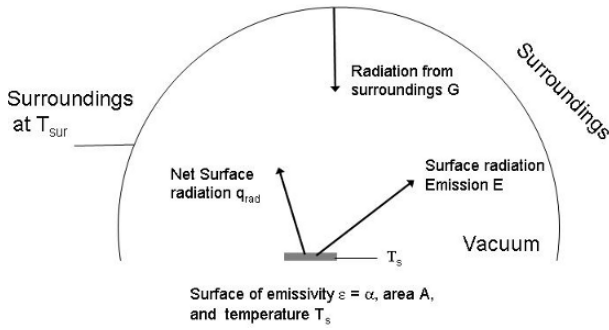


**Fig. 5.19.** Radiation cooling of a heated solid.

presence of the vacuum prevents energy loss from the surface of the solid by conduction or convection. However, experience has shown that the solid will cool and eventually achieve thermal equilibrium with its surroundings. This cooling is associated with a reduction in the internal energy stored by the solid and is a direct consequence of the emission of thermal radiation from the surface. In turn, the surface will receive and absorb radiation originating from the surroundings. But, since  $T_s > T_{sur}$  the net heat transfer rate by radiation  $\mathbf{q}^{rad}$  is from the surface, and the surface will be cooled until  $T_s$  reaches  $T_{sur}$ .

Radiation that is emitted by the surface originates from the thermal energy of matter bounded by the surface. The rate at which energy is released per unit area ( $W/m^2$ ) is determined by the surface emissive power  $E$ . For a blackbody the emissive power (representing a theoretical maximum rate) is prescribed by the Stefan-Boltzmann law:

$$E_b(T_s) = \sigma T_s^4 \quad (5.342)$$

where  $T_s$  is the absolute temperature ( $K$ ) of the surface.

The heat flux emitted by a real surface is of course less than that of a blackbody at the same temperature and is given by:

$$E = \epsilon \sigma T_s^4 \quad (5.343)$$

where  $\epsilon$  the emissivity of the surface. This quantity takes values in the range  $0 \leq \epsilon \leq 1$  and depends strongly on the surface material.

In this instance the irradiation  $G$  may originate from a special source, such as the sun, or from other surfaces to which the surface of interest is exposed. A portion, or all, of the irradiation may be absorbed by the surface, thereby increasing the thermal energy of the material. Since the rate at which radiant energy is absorbed per unit area is evaluated in terms of the surface radiative property termed the absorptivity  $\alpha$ , we get:

$$G_{abs} = \alpha G \quad (5.344)$$

where  $0 \leq \alpha \leq 1$ . If  $\alpha < 1$ , the surface is opaque and portions of the irradiation are reflected. If the surface is semitransparent, portions of the irradiation may also be transmitted.

A special case that occurs frequently in engineering practice involves radiation exchange between a small surface at  $T_s$  and a much larger, isothermal surface that completely surrounds the smaller one. The surroundings could be a furnace whose temperature  $T_{\text{sur}}$  differs from that of an enclosed surface ( $T_{\text{sur}} - T_s$ ). For such a condition, the irradiation may be approximated by emission from a blackbody at  $T_{\text{sur}}$ , in which case  $G = \sigma T_{\text{sur}}^4$ . If the surface is assumed to be one for which  $\alpha = \epsilon$  (a gray surface), the net rate of radiation heat transfer from the surface, is:

$$\dot{Q}^{\text{rad}} = \epsilon A E_b(T_s) - \alpha G A = \epsilon A \sigma (T_s^4 - T_{\text{sur}}^4) \quad (5.345)$$

This expression provides the difference between thermal energy that is released due to radiation emission and that which is gained due to radiation absorption.

There are many applications for which it is convenient to express the net radiation heat exchange in a form similar to Newton's law of cooling:

$$\langle \dot{Q}^{\text{rad}} \rangle_{A_I} = h^{\text{rad}} A (\langle T_s \rangle_{A_I} - \langle T_{\text{sur}} \rangle_V) \quad (5.346)$$

where the radiation heat transfer coefficient  $h_r$  is:

$$h^{\text{rad}} = \epsilon \sigma (\langle T_s \rangle_{A_I} + \langle T_{\text{sur}} \rangle_V) (\langle T_s \rangle_{A_I}^2 + \langle T_{\text{sur}} \rangle_V^2) \quad (5.347)$$

In this case we have linearized the radiation rate equation, making the heat rate proportional to a temperature difference rather than to the difference between two temperatures to the fourth power. Note, however, that  $h_r$  depends strongly on temperature, while the temperature dependence of the convection heat transfer coefficient,  $h$  is generally weak.

In reactor simulations where the bulk of the vessel contains a fluid the surface may also simultaneously transfer heat by convection to the adjoining fluid. The total rate of heat transfer from the surface is then given by:

$$\begin{aligned} \dot{Q}^{\text{cond,conv,rad}} &= h^{\text{cond,conv}} A (\langle T_s \rangle_{A_I} - \langle T_{\text{sur}} \rangle_V) + h^{\text{rad}} A (\langle T_s \rangle_{A_I} - \langle T_{\text{sur}} \rangle_V) \\ &= h^{\text{cond,conv}} A (\langle T_s \rangle_{A_I} - \langle T_{\text{sur}} \rangle_V) + \epsilon A \sigma (\langle T_s \rangle_{A_I}^4 - \langle T_{\text{sur}} \rangle_V^4) \end{aligned} \quad (5.348)$$

Note that most monoatomic and diatomic gases, as well as air, are transparent at low temperatures, thus we often assume that the radiation energy exchange among the enclosure surfaces is unaffected by the presence of these gases. At higher temperatures, gases no longer remain transparent and become to some degree opaque. Then they start participating in the energy exchange process by absorbing, and emitting this energy making the modeling problem much more complex since the radiation emerging from a finite volume of matter is an integrated effect of the local emission throughout the volume.

Radiation is relevant to many environmental (solar radiation) and industrial heating, cooling and drying processes. In chemical reaction engineering in particular thermal radiation is especially important for gas systems operating at high temperatures like chemical conversion processes that involve fossil fuel combustion. In addition to the thermal radiation from solid wall surfaces the gas radiation effects might be important describing the heat transport in furnaces of fired steam reformers [38]. Furthermore, the radiation energy emitted by flames in furnaces and combustion chambers depends not only on the gaseous emission, but also on the heated carbon (soot) particles formed within flames [5] (chaps 8-10). The radiation modeling and simulation approaches frequently applied in combustion engineering are reviewed by Viskanta and Mengüç [159].

---

## References

1. Albråten PJ (1982) The Dynamics of Two-Phase Flow. PhD thesis, Chalmers University of Technology, Göteborg, Sweden
2. Antal SP, Lahey RT Jr, Flaherty JE (1991) Analysis of phase distribution in fully developed laminar bubbly two-phase flow. *Int J Multiphase Flow* 17(5):635-652
3. Arnold GS (1988) Entropy and objectivity as constraints upon constitutive equations for two-fluid modeling of multiphase flow. PhD thesis, Rensselaer Polytechnic Institute, Troy, New York
4. Arpaci VS, Larsen PS (1984) *Convection heat Transfer*. Prentice-Hall, Inc, New Jersey
5. Arpaci VS, Kao S-H, Selamet A (1999) *Introduction to heat transfer*. Prentice Hall, Upper Saddle River
6. Astarita G, Savage DW, Biso A (1983) *Gas Treating with Chemical Solvents*. Wiley, New York
7. Auton TR (1983) *The Dynamics of Bubbles, Drops and Particles in Motion in Liquids*. PhD Thesis, University of Cambridge, Cambridge, UK
8. Auton TR, Hunt JCR, Prud'Homme M (1988) The force exerted on a body in inviscid unsteady non-uniform rotational flow. *J Fluid Mech* 197:241-257
9. Baehr HD, Stephan Karl (1998) *Heat and Mass Transfer*. Springer-Verlag, Berlin
10. Basset AB (1888) *A Treatise on Hydrodynamics Vol I*. Deighton, Bell and Co, London:George Bell and sons, Cambridge Republished: Dover Publications, Inc, Vol II, New York (1961)
11. Batchelor GK (1983) *An Introduction to Fluid Dynamics*. Cambridge University Press, Cambridge
12. Beckermann C, Viskanta R (1993) Mathematical modeling of transport phenomena during alloy solidification. *Appl Mech Rev* 46(1):1-27
13. Bird RB, Stewart WE, Lightfoot EN (1960) *Transport phenomena*. John Wiley & Sons, New York
14. Bird RB, Armstrong RC, Hassager O (1987) *Dynamics of polymeric liquids. Volume 1, Fluid mechanics*. John Wiley & Sons, New York
15. Bird RB, Stewart WE, Lightfoot EN (2002) *Transport phenomena. Second Edition*, John Wiley & Sons, New York

16. Bourè JA, Delhaye JM (1982) General Equations and Two-Phase Flow Modeling. In: Hetsroni G (ed) Handbook of Multiphase Systems, Section 1.2, pp. (1-36) - (1-95), McGraw-Hill, New York
17. Boussinesq J (1877) Essai sur la théorie des eaux courants. Mèm près par div savants à l'Acad Sci, Paris 23(1):1-680
18. Boussinesq J (1885) Sur ls résistance qu'oppose un liquide indéfini en repos, sans pesanteur, au mouvement varié d'une sphère solide qu'il mouille sur toute sa surface, quand les vitesses restent bien continues et asez faibles pour que leurs carrés et produits soient négligeables. C R Acad Sci Paris 100:935-937
19. Cai X, Wallis GB (1994) A more general cell model for added mass in two-phase flow. Chem Eng Sci 49(10):1631-1638
20. Chilton TH, Colburn AP (1934) Mass Transfer (Absorption) Coefficients. Ind Eng Chem 26(11):1183-1187
21. Chisnell RF (1987) The unsteady motion of a drop moving vertically under gravity. J Fluid Mech 176:443-464
22. Clift R, Grace JR, Weber ME (1978) Bubble, Drops, and Particles. Academic Press, New York
23. Colburn AP, Drew TB (1937) The Condensation of Mixed Vapors. Trans AIChE 33:197-215
24. Cook TH, Harlow FH (1986) Vortices in bubbly two-phase flow. Int J Multiphase Flow 12(1):35-61, 1986.
25. Crank J (1957) The Mathematics of Diffusion. Oxford University Press, Glasgow
26. Crowe CT, Sommerfeld M, Tsuji Y (1998) Multiphase Flows with Droplets and Particles. CRC Press, Boca Raton.
27. Cussler EL (1997) Diffusion: Mass Transfer in Fluid Systems. Second Edition, Cambridge University Press, Cambridge
28. Danckwerts PV (1950) Unsteady-state diffusion or heat conduction with moving boundary. Trans Faraday Soc 46(9):701-712
29. Danckwerts PV (1951) Significance of Liquid-Film Coefficients in Gas Absorption. Ind & Eng Chem 43(6):1460-1467
30. Dandy DS, Dwyer HA (1990) A sphere in shear flow at finite Reynolds number: Effect of shear on particle lift, drag, and heat transfer. Journal of Fluid Mechanics 216:381-410
31. Drew DA, Lahey RT Jr (1979) Application of general constitutive principles to the derivation of multidimensional two-phase flow equations. Int J Multiphase Flow. 5:243-264
32. Drew DA (1983) Mathematical Modeling of Two-Phase Flow. Ann Rev Fluid Mech 15:261-291
33. Drew DA, Lahey RT Jr (1987) The virtual mass and lift force on a sphere in rotating and straining inviscid flow. Int J Multiphase Flow 13 (1):113-121
34. Drew DA, Lahey RT Jr (1990) Some supplemental analysis concerning the virtual mass and lift force on a sphere in a rotating and straining flow. Int J Multiphase Flow 16:1127-1130
35. Drew DA (1992) Analytical Modeling of Multiphase Flows: Modern Developments and Advances. In: Lahey RT jr (ed) Boiling Heat Transfer, pp. 31-83, Elsevier Science Publishers BV, Amsterdam
36. Drew DA, Lahey RT Jr (1993) Analytical Modeling of Multiphase Flow. In: Roco MC (ed) Particulate Two-Phase Flow, Chapt. 16, pp. 509-566, Butterworth-Heinemann, Boston

37. Drew DA, Wallis GB (1994) Fundamentals of Two-Phase Flow Modeling. *Multiphase Science and Technology* 8:1-67
38. Dybkjær I (1995) Tubular reforming and autothermal reforming of natural gas - an overview of available processes. *Fuel Proc Techn* 42:42-107
39. Eckert ERG, Drake RM (1987) *Analysis of Heat and Mass Transfer*. Hemisphere, New York
40. Elghobashi SE, Abou-Arab TW (1983) A two-equation turbulence model for two-phase flows. *Phys Fluids* 26(4):931-938.
41. Elghobashi SE, Truesdell GC (1993) On the two-way interaction between homogeneous turbulence and dispersed solid particles. I: Turbulence modification. *Phys Fluids A5* (7):1790-1801
42. Elghobashi SE (1994) On predicting particle laden turbulent flows. *Appl Sci Res* 52:309-329.
43. Esmaeeli A, Ervin E, Tryggvason G (1994) Numerical simulations of rising bubbles. In: Blake JR, Boulton-Stone JM, Thomas NH (eds) *Bubble Dynamics and Interfacial Phenomena*. Kluwer Academic Publishers, Dordrecht
44. Esmaeeli A, Tryggvason G (1996) An Inverse Energy Cascade in Two-Dimensional Low Reynolds Number Bubbly Flows. *J Fluid Mech* 314:315-330
45. Fan F-S, Tsuchiya K (1990) *Bubble Wake Dynamics in Liquids and Solid-Liquid Suspensions*. Butterworth-Heinemann, Boston
46. Fick A (1855) Ueber Diffusion. *Ann der Physik* 94:59-86
47. Scott Fogler H (2006) *Elements of Chemical Reaction Engineering*. Fourth Edition, Prentice-Hall International, Inc, New Jersey
48. Fourier JB (1822) *Théorie analytique de la chaleur*. Chez Firmin Didot, père et fils, Paris
49. Friberg PC (1998) Three-dimensional modelling and simulation of gas/liquid flow processes in bioreactors. Dr. Ing. Thesis, Høgskolen i Telemark (HIT), Norwegian University of Science and Technology, Prossgrunn
50. Frössling N (1938) Über die Verdunstung fallender Tropfen. *Gerlands Beitr Geophys* 52:170-216
51. Geurst JA (1985) Virtual Mass in Two-Phase Bubbly Flow. *Physica* 129A: 233-261
52. Gidaspo D (1994) *Multiphase Flow and Fluidization-Continuum and Kinetic Theory Descriptions*. Academic Press, Harcourt Brace & Company, Publishers, Boston
53. Grace JR, Wairegi T, Nguyen TH (1976) Shapes and velocities of single drops and bubbles moving freely through immiscible liquids. *Transactions of the Institution of Chemical Engineers* 54:167-173
54. Grace JR, Weber ME (1982) Hydrodynamics of drops and bubbles. In: Hetsroni G (ed) *Handbook of Multiphase Systems*, Chap 1.3.9 pp 1-204-1-223 McGraw-Hill Book Company
55. Hadamard JS (1911) mouvement permanent lent d'une sphère liquide et visqueuse dans un liquide visqueux. *C R Acad Sci* 152:1735-1738
56. Hagen KD (2000) *Heat Transfer with Applications*. Prentice Hall, Upper Saddle River, New Jersey
57. Higbie R (1935) The rate of absorption of a pure gas into a still liquid during short periods of exposure. *Trans AIChE* 31:365-389
58. Hines AL, Maddox RN (1985) *Mass Transfer Fundamentals and Applications*. Prentice Hall PTR, New Jersey

59. Hinze JO (1975) Turbulence. Second Edition, McGraw-Hill, New York
60. Incropera FP, DeWitt DP (2002) Fundamentals of Heat and Mass Transfer. Fifth Edition, *John Wiley & Son*, New York
61. Ishii M (1975) Thermo-Fluid Dynamic Theory of Two-Phase Flow. Eyrolles, Paris
62. Ishii M, Zuber N (1978) Drag Coefficient and Relative Velocity in Bubbly, Droplet or Particulative Flows. *AIChE J* 25(5):843-854
63. Ishii M, Chawla TC (1979) Local drag laws in dispersed two-phase flows. Argonne National Laboratory Report NUREG/CR-1230, ANL-79-105, Argonne, Illinois, USA
64. Ishii M, Mishima K (1984) Two-Fluid Model and hydrodynamic Constitutive Equations. *Nuclear Engineering and Design* 82:107-126
65. Jakobsen HA (1993) On the modelling and simulation of bubble column reactors using a two-fluid model. Dr Ing Thesis, Norwegian Institute of Technology, Trondheim, Norway.
66. Jakobsen HA, Lindborg H, Dorao CA (2005) Modeling of Bubble Column Reactors: Progress and Limitations. *Ind Eng Chem Res* 44:5107-5151
67. Johansen ST, Boysan F (1988) Fluid Dynamics in Bubble Stirred Ladles: Part 2. Mathematical Modelling. *Met Trans B* 19:755-764
68. Johansson SH, Davidson L, Olsson E (1993) Numerical Simulation of Vortex Sheadding Past Triangular Cylinders at High Reynolds Number Using a  $k-\epsilon$  Turbulence Model. *Int J Numer Methods Fluids* 16:859-878
69. Jones JB, Dugan RE (1996) Engineering Thermodynamics. Prentice-Hall International, Inc., Englewood Cliffs
70. Kariyasaki A (1987) Behavior of a single gas bubble in a liquid flow with a linear velocity profile. In: Proceedings of the 1987 ASME-JSME Thermal Engineering Joint Conference, pp. 261-267, The American Society of Mechanical Engineers, New York
71. Kays WM, Crawford ME (1993) Convective Heat and Mass Transfer. Third Edition, McGraw-Hill, New York
72. Kolev NI (2002) Multiphase Flow Dynamics 1: Fundamentals. Springer, Berlin
73. Kataoka I, Serizawa A (1989) Basic Equations of Turbulence in Gas-Liquid Two-Phase Flow. *Int J Multiphase Flow* 15:1-13
74. Kataoka I, Besnard DC, Serizawa A (1992) Basic equation of turbulence and modeling of interfacial transfer terms in gas -liquid two-phase flow. *Chem Eng Comm* 118:221-236
75. Kjelstrup S, Bedeaux D (2001) Elements of irreversible thermodynamics for engineers. International Centre for Applied Thermodynamics, (ISBN: 975-97568-1-1), Istanbul
76. Krahn E (1956) Negative Magnus force. *J Aero Sci* 23:377-378
77. Kuo KK (1986) Principles of Combustion. John Wiley & Sons, New York
78. Kuo JT, Wallis GB (1988) Flow of bubbles through nozzles. *Int J Multiphase Flow* 14(5):547-564
79. Lahey RT Jr (1990) The analysis of phase separation and phase distribution phenomena using two-fluid models. *Nucl Eng Des* 122:17-40
80. Lahey RT Jr (1992) The prediction of phase distribution and separation phenomena using two-fluid models. In: Lahey RT Jr (ed) Boiling Heat Transfer. Elsevier Science Publishers BV
81. Laidler KJ, Meiser JH (1995) Physical Chemistry. Second Edition. Houghton Mifflin Company, Boston

82. Lance M, Bataille J (1991) Turbulence in the liquid phase of a uniform bubbly air-water flow. *J Fluid Mech* 222:95-118
83. Langlois WE (1964) *Slow Viscous Flow*. Macmillan, New York
84. Laux H (1998) Modeling of dilute and dense dispersed fluid-particle flow. Dr Ing Thesis, Norwegian University of Science and Technology, Trondheim, Norway
85. Lawler MT, Lu P-C (1971) The role of lift in radial migration of particles in a pipe flow. In: Zandi I (ed) *Advances in Solid-Liquid Flow in Pipes and its Applications*. Pergamon Press, Oxford, Chap 3, pp. 39-57
86. Lee SL (1987) Particle drag in a dilute turbulent two-phase suspension flow. *Int J Multiphase Flow* 13(2):247-256
87. Lee SL (1987) A unified theory on particle transport in turbulent dilute two-phase suspension flow-II. *Int J Multiphase Flow* 13(1):137-144
88. Lee SL, Börner T (1987) Fluid flow structure in a dilute turbulent two-phase suspension flow in a vertical pipe. *Int J Multiphase Flow* 13(2):233-246
89. Lee SL, Durst F (1982) On the motion of particles in turbulent duct flows. *Int J Multiphase Flow* 8(2):125-146
90. Lee SL, Wiesler MA (1987) Theory on transverse migration of particles in a turbulent two-phase suspension flow due to turbulent diffusion-I. *Int J Multiphase Flow* 13(1):99-111
91. Long CA (1999) *Essential Heat Transfer*. Longman, Malaysia
92. Lopez de Bertodano M (1992) *Turbulent Bubbly Two-Phase Flow in a Triangular Duct*. PhD Thesis, Rensselaer Polytechnic Institute, Troy, NY
93. Lopez de Bertodano M, Lahey RT Jr, Jones OC (1994) Development of a  $k-\epsilon$  Model for Bubbly Two-Phase Flow. *J Fluids Engineering* 116:128-134
94. Loth E (2000) Numerical approaches for motion of dispersed particles, droplets and bubbles. *Progress in Energy and Combustion Science* 26:161-223
95. Maccoll JW (1928) Aerodynamics of a spinning sphere. *J Roy Aero Soc* 32: 777-798
96. Magnaudet JJM (1997) *The Forces Acting on Bubbles and Rigid Particles*. ASME Fluids Engineering Division Summer Meeting, FEDSM97-3522
97. Magnaudet JJM, Eames I (2000) The Motion of High-Reynolds-Number Bubbles in Inhomogeneous Flows. *Annu Rev Fluid Mech* 32:659-708
98. Magnaudet JJM (2003) Small inertial effects on a spherical bubble, drop or particle moving near a wall in a time-dependent linear flow. *J Fluid Mech* 485:115-142
99. Magnaudet JJM, Takagi S, Legendre D (2003) Drag, deformation and lateral migration of a buoyant drop moving near a wall. *J Fluid Mech* 476:115-157
100. Maxey MR, Riley JJ (1983) Equation of motion for a small rigid sphere in a non-uniform flow. *Phys Fluids* 26 (4):883-889.
101. Maxey MR (1993) The equation of motion for a small rigid sphere in a nonuniform or unsteady flow. ASME , FED-Vol 166, Gas-Solid Flows
102. Middleman S (1998) *An Introduction to Mass and Heat Transfer: Principles of Analysis and Design*. John Wiley & Sons, Inc., New York
103. Middleman S (1998) *An Introduction to Fluid Dynamics: Principles of Analysis and Design*. John Wiley & Sons, Inc., New York
104. Morrison FA, Stewart MB (1976) Small Bubble Motion in an Accelerating Liquid. *J Appl Mech* 43:299-403
105. Morsi SA, Alexander AJ (1972) An investigation of particle trajectories in two-phase flow systems. *Journal of Fluid Mechanics* 55:193-208

106. Murai Y, Matsumoto Y, Song X-Q, Yamamoto F (2000) Numerical Analysis of Turbulent Structures Induced by Bubble Buoyancy. *JSME Int J Series B-Fluids and Thermal Engineering* 43 (2):180-187
107. Murai Y, Kitagawa A, Song X-Q, Ohta J, Yamamoto F (2000) Inverse Energy Cascade Structure of Turbulence in a Bubbly Flow (PIV measurement and results). *JSME Int J Series B-Fluids and Thermal Engineering* 43 (2):188-196
108. Naot D, Rodi W (1982) Calculation of secondary currents in channel flow. *Proc Am Soc Civ Engrs* 108 (HY8):948-968
109. Ni J, Beckermann C (1990) A Two-Phase Model for Mass, Momentum, Heat, and Species Transport during Solidification. In: Chermchi M, Chyu MK, Joshi Y, Walsh SM (eds) *Transport Phenomena in Material Processing*, New York. ASME HTD-VOL. 132:45-56
110. Ni J, Beckermann C (1991) A Volume-Averaged Two-Phase Model for Transport Phenomena during Solidification. *Metallurgical Transactions B* 22B: 349-361
111. Oran ES, Boris JP (1987) *Numerical Simulation of Reactive Flow*. Elsevier, New York
112. Oseen CW (1910) Über die Stokes'sche Formel und Über eine verwandte Aufgabe in der Hydrodynamik. *Ark Math Astron Fys* 6(29):1-20
113. Perry RH, Green DW (1984) *Chemical Engineer's Handbook*. Perry RH, Green DW (eds) 6. Edition, McGraw-Hill, New York
114. Planck M (1959) *The Theory of Heat Radiation*. Dover Publications, New York
115. Politano MS, Carrica PM, Conventi J (2003) A model for turbulent polydisperse two-phase flow in vertical channels. *Int J Multiphase Flow* 29:1153-1182
116. Pope S (2000) *Turbulent Flows*. Cambridge University Press, Cambridge
117. Prausnitz JM, Lichtenthaler RN, de Azevedo EG (1999) *Molecular Thermodynamics of Fluid-Phase Equilibria*. Third Edition, Prentice Hall PTR, New Jersey
118. Proudman J (1916) On the motion of solids in a liquid processing vorticity. *Proc Roy Soc A* 92:408-424
119. Proudman J, Pearson JRA (1957) Expansions at small Reynolds numbers for the flow past a sphere and a circular cylinder. *Journal of Fluid Mechanics* 2:237-262
120. Pruppacher HR, Klett JD (1978) *Microphysics of Clouds and Precipitation*. D. Reidel Publishing Company, Dordrecht, Holland
121. Ranz W, Marshall W (1952) "Evaporation from drops", Part I & II. *Chem Eng Prog* 48(3):141-180
122. Rizk MA, Elghobashi SE (1989) A Two-Equation Turbulence Model for Dispersed Dilute Confined Two-Phase Flows. *Int J multiphase Flow* 15(1):119-133
123. Rubinow SI, Keller JB (1961) The transverse force on a spinning sphere moving in a viscous fluid. *J Fluid Mech* 11:447-459
124. Rybczynski W (1911) O ruchu postepowym kuli ciekłej w osrodku lepkim. - Über die fortschreitende Bewegung einer flüssigen Kugel in einem zähen Medium. *Bull Int Acad Pol Sci Lett, Cl Sci Math Nat, Ser A*, pp. 40-46
125. Saffman PG (1965) The lift on a small sphere in a slow shear flow. *J Fluid Mech* 22:385-400
126. Saffman PG (1968) Corrigendum. *J Fluid Mech* 31:624

127. Sannæs BH (1997) Solids movement and concentration profiles in column slurry reactors. Dr. Ing. Thesis, Norwegian University of Science and Technology, Trondheim
128. Sato Y, Sekoguchi K (1975) Liquid velocity distribution in two-phase bubble flow. *Int J Multiphase Flow* 2:79-95
129. Sato Y, Sadatomi M, Sekoguchi K (1981) Momentum and heat transfer in two-phase bubble flow-I. Theory.-II A comparison between experimental data and theoretical calculations. *Int J Multiphase Flow* 7(6):167-190
130. Schlichting H, Gersten K (2000) *Boundary-Layer Theory*. Springer-Verlag, Berlin
131. Segré G, Silberberg A (1962) Behaviour of macroscopic rigid spheres in Poiseuille flow. Part 1. Determination of the local concentration by statistical analysis of particle passages through crossed light beams. *J Fluid Mech* 14:115-135
132. Segré G, Silberberg A (1962) Behaviour of macroscopic rigid spheres in Poiseuille flow. Part 2. Experimental results and interpretation. *J Fluid Mech* 14:136-157
133. Sherwood TK (1959) Mass, Heat, and Momentum Transfer between Phases. *Chem Eng Progr Symp Ser* 55(25):71-85
134. Sherwood TK, Pigford RL, Wilkie CR (1975) *Mass Transfer*. McGraw-Hill, New York
135. Sideman S, Pinczewski W (1975) Turbulent Heat and Mass Transfer at Interfaces: Transport Models and Mechanisms. In: Gutfinger C (ed) *Topics in Transport Phenomena: bioprocesses, mathematical treatment, mechanisms*. Hemisphere, Washington
136. Siegel R, Howell JR (2002) *Thermal Radiation Heat Transfer*. Fourth Edition, Taylor & Francis, New York
137. Sirignano WA (1986) The Formulation of Spray Combustion Models: Resolution Compared to Droplet Spacing. *Journal of Heat Transfer* 108:633-639
138. Sirignano WA (2000) *Fluid Dynamics and Transport of Droplets and Sprays*. Cambridge University Press, Cambridge
139. Slattery JC (1999) *Advanced Transport Phenomena*. Cambridge University Press, New York
140. Soo SL (1989) *Particles and Continuum: Multiphase Fluid Dynamics*. Hemisphere Publishing Corporation, New York
141. Soo SL (1990) *Multiphase Fluid Dynamics*. Science Press, Beijing and Gower Technical, Aldershot
142. Stokes GG (1851) On the effect of the internal friction of fluids on the motion of pendulums. Section II: Solution of the equations in the case of a sphere oscillating in a mass of fluid either unlimited, or confined by a spherical envelope concentric with the sphere in its position of equilibrium. *Trans Cambridge Phil Soc* 9 (pt II):8-106
143. Stone HA (2000) Philip Saffman and viscous flow theory. *J Fluid Mech* 409:165-183
144. Stull RB (1988) *An Introduction to Boundary Layer Meteorology*. Kluwer Academic Publishers, Dordrecht
145. Swanson WM (1961) The Magnus effect: A summary of investigations to date. *Transactions of the ASME Journal of Basic Engineering*, pp. 461-470
146. Sy F, Lightfoot EN (1971) Transient Creeping Flow Around Fluid Spheres. *AIChE J* 17(1):177-181

147. Takemura F, Magnaudet JJM (2003) The transverse force on clean and contaminated bubbles rising near a vertical wall at moderate Reynolds number. *J Fluid Mech* 495:235-253
148. Taneda S (1957) Negative Magnus effect. *Reports of Research Institute for Applied Mathematics* 5(29):123-128, Printed in Fukuoka
149. Taneda S (1978) Visual observations of the flow past a sphere at Reynolds numbers between  $10^4$  and  $10^6$ . *J Fluid Mech* 85:187-192
150. Taylor GI (1938) *The Spectrum of Turbulence*. Proc. Roy. Soc. London Series A 164:476-490
151. Telionis DP (1981) *Unsteady Viscous Flows*. Springer-Verlag, New York
152. Thomas NH, Auton TR, Sene K, Hunt JCR (1983) Entrapment and transport of bubbles by transient large eddies in multiphase turbulent shear flows. In: Stephens HS, Stapleton CA (eds) *International Conference on Physical Modelling of Multi-Phase Flows*, BHRA Fluid Engineering, pp. 169-184, Cranfield
153. Thomson WJ (2000) *Introduction to transport phenomena*. Prentice Hall, Upper Saddle River
154. Tomiyama A, Sou A, Zun I, Kanami N, Sakaguchi T (1995) Effects of Eötvös number and dimensionless liquid volumetric flux on lateral motion of a bubble in a laminar duct flow", In: Serizawa A, Fukano T, Bataille J (eds) *Advances in Multiphase Flow 1995*, pp. 3-15, Elsevier
155. Tomiyama A, Miyoshi K, Tamai H, Zun I, Sakaguchi T (1998) A bubble tracking method for the prediction of spatial evolution of bubble flow in a vertical pipe. *Third International Conference on Multiphase Flow, Lyon, France*
156. Tomiyama A (1998) *Struggle with Computational Bubble Dynamics*. *Third International Conference on Multiphase Flow, Lyon, France*
157. Tomiyama A, Tamai H, Zun I, Hosokawa S (2002) Transverse migration of single bubbles in simple shear flows. *Chem Eng Sci* 57:1849-1858
158. Torobin LB, Gauvin WH (1959) *Fundamental Aspects on Solid-Gas Flow. Part III: Accelerated Motion of a Particle in a Fluid*. *Can J Chem Engng* 37:224-236
159. Viscanta R, Mengic MP (1987) *Radiation Heat Transfer in Combustion Systems*. *Prog Energy Combust Sci* 13:97-160
160. Vincenti WG, Kruger CH Jr. (1967) *Introduction to Physical Gas Dynamics*. Second Printing, John Wiley and Sons, Inc., New York
161. von Kàrmàn T (1939) *Mechanische Ähnlichkeit Und Turbulenz*. *Proc 3rd Int Congress Appl Mech, Stockholm* 1:85
162. Vuddagiri SR, Eubank PT (1998) *Condensation of Mixed Vapors and Thermodynamics*. *AIChE J* 44(11):2526-2541
163. Wallis GB (1974) The terminal speed of single drops or bubbles in an infinite medium. *Int J Multiphase Flow* 1:491-511
164. Wallis GB (1989) *Inertial Coupling in Two-Phase Flow: Macroscopic Properties of Suspensions in an Inviscid Fluid*. *Multiphase Science and Technology* 5:239-361
165. Wang Y, Komori S, Chung MK (1997) *A Turbulence Model for Gas-Solid Two-Phase Flows*. *Journal of Chemical Engineering of Japan* 30(3):526-534
166. Whitaker S (1987) *Mass Transport and Reaction in Catalyst Pellets*. *Transport in Porous Media* 2:269-299
167. Whitaker S (1992) The species mass jump condition at a singular surface. *Chem Eng Sci* 47(7):1677-1685
168. Whitaker S (1999) *The Method of Volume Averaging*. Kluwer Academic Publishers, Dordrecht

169. White FM (1974) *Viscous Fluid Flow*. McGraw-Hill, New York
170. White FM (1999) *Fluid Mechanics*. Fourth Edition, McGraw-Hill, Inc., New York
171. Willetts BB, Murray CG (1981) Lift exerted on stationary spheres in turbulent flows. *J Fluid Mech* 105:487-505
172. Yang S-M, Leal LG (1991) A note on memory-integral contributions to the force on an accelerating spherical drop at low Reynolds number. *Phys Fluids A* 3(7):1822-1824
173. Yamamoto F, Koukawa M, Monya H, Teranishi A (1991) Particle lift and drag forces in linear turbulent shear flows. In: Sommerfeld M, Wennerberg D (eds) *Fifth Workshop on Two-Phase Flow Predictions: Proceedings*, pp. 323-332, Jülich, Forschungszentrum
174. Zapryanov Z, Tabakova S (1999) *Dynamics of Bubbles, Drops and Rigid Particles*. Kluwer Academic Publishers, Dordrecht

---

# APPLICATIONS

---

## Chemical Reaction Engineering

Chemical reaction engineering<sup>1</sup> (CRE) emerged as a methodology that quantifies the interplay between transport phenomena and kinetics on a variety of scales and allows formulation of quantitative models for various measures of reactor performance [3]. The ability to establish such quantitative links between measures of reactor performance and input and operational variables is essential in optimizing the operating conditions in manufacturing, for proper reactor design and scale-up, and in correct interpretation of data in research and pilot plant work.

A starting point for reaction engineers is the formulation of a reactor model for which the basis is the micro-scale species mass - and enthalpy balances. For practical applications the direct solution of these equations is too costly and simplifications or average representations are usually introduced.

The choice of averages (e.g., global reactor volume, cross sectional area or length) to which the balance equations are integrated over (averaged) determines the level of sophistication of the reactor model. It is very common in tubular reactors to have flow predominantly in one spatial direction, say  $z$ . The major gradients then occur in that direction. For many cases, then, the cross-sectional average values of concentration and temperature are used instead of the local values. In this way the one dimensional dispersion model is obtained. If the convective transport is completely dominant over the diffusive transport, the diffusive term may be neglected. The resulting equations are denoted the ideal Plug Flow Reactor (PFR) model. When the entire reactor can be considered to be uniform in both concentration and temperature (i.e., due to very large dispersion coefficients), one may neglect gradients in all spatial directions and integrate the equations globally over all spatial dimensions (assuming convective flows at the boundaries) leading to the ideal reactor model of the Continuous Stirred Tank Reactor (CSTR). The description of

---

<sup>1</sup> Recently a branch of CRE that is mainly focusing on transport phenomena and fluid flow analysis, rather than reaction kinetics, has emerged. By these groups the abbreviation *CRE* is frequently interpreted as *chemical reactor engineering*.

a real reactor, with intermediate levels of mixing, may require amplified information about the mixing. For such processes the dispersion models (DM), in which the mixing processes are described through the empirical dispersion parameters, might be useful. A classification of dispersion models for fixed-bed tubular reactors, for example, is given by Froment and Hofmann [7]. For more complex flow patterns more elaborated and complete models are required where the flow fields are described via the solution of the Navier-Stokes equations. The understanding of the complex flow phenomena involved as well as the solution of these vector equations make the problem much more difficult to analyze spending reasonable costs and efforts.

The advanced reactor models are discussed in the subsequent chapters, only a brief introduction to the idealized reactor models are presented in this chapter as these models are principal tools for chemical reaction engineers. In particular, the idealized models are easy to calculate, and they give the extreme values of the conversions between which those realized in a real reactor will occur provided there is no bypassing of reactants in the reactor.

## 6.1 Idealized Reactor Models

Basically, the processes taking place in a chemical reactor are chemical reaction, and mass, heat and momentum transfer phenomena. The modeling and design of reactors are therefore sought from employing the governing equations describing these phenomena [1]: the reaction rate equation, and the species mass, continuity, heat (or temperature) and momentum balance equations.

A fundamental aim in chemical reaction engineering is to be able to size reactors given the rate of reaction as a function of species composition and temperature. For practical applications chemical reaction engineers usually consider two extreme cases, either no mixing occurs in the reactor as the fluid elements move along parallel streamlines with equal velocity in the reactor or the mixing is complete and the fluid motion is complex and not ordered. By these two extremes approximations, the tubular plug flow (PFR) and the continuous stirred tank reactor (CSTR) models can be derived from the governing microscopic transport equations.

### 6.1.1 Plug Flow Reactor Models

To derive the plug flow reactor model for homogeneous systems we consider the single phase cross sectional averaged model formulation as derived in sect 1.2.7. The microscopic species mass balance reduces to (1.301) and the corresponding heat or temperature equation is given by (1.302). In chemical reaction engineering the non-ideal flow reactor model consisting of the species mass balance (1.301) and temperature equation (1.302) is named the axial dispersion model (ADM). If more than one phase exist, similar balance equations are needed for each of the phases. For two phase flow the cross sectional

average model equations (3.498) and (3.499) might be employed, as derived in sect 3.4.7. The latter non-ideal flow reactor model is often referred to as the heterogeneous axial dispersion model. Note also that in multiphase flow models, a distinction is made between the true local velocity, called the interstitial velocity ( $m/s$ ), and the velocity averaged over the whole cross section, called the superficial velocity ( $m^3/m^2s$ ).

Under plug flow conditions the convective transport is completely dominant over the diffusive mass transport term. The fluid moves like a plug and the diffusive term can be neglected. The conditions for plug flow are closely satisfied for narrow and long tubular reactors when the viscosity is low. However, this approximation is clearly best for fully developed turbulent flow, for which the velocity profiles are relatively flat. For dynamic conditions, the species mass balance is a PDE with  $z$  and  $t$  as the independent variables. The Eulerian species mass balance (1.301) reduces further to:

$$\frac{\partial}{\partial t}(\rho\omega_s) + \frac{\partial}{\partial z}(\rho v^S \omega_s) = R_s \quad (6.1)$$

Recall that the rate of generation for reaction  $r$  can be expressed independent of species, since this quantity is proportional to the extent of reaction (1.146), thus if only one reaction takes place:  $R_s = \nu_s M_{\omega_s} r_r$ .

Integration over a differential volume element in a tubular reactor gives:

$$\frac{\partial}{\partial t} \int_V \rho_s dv + A \int_z \frac{\partial}{\partial z} (\rho v^S \omega_s) dz = \int_V R_s dv \quad (6.2)$$

or

$$\frac{\partial M_s}{\partial t} + \int_z \frac{\partial \dot{m}_s}{\partial z} dz = \int_V R_s dv \quad (6.3)$$

in which  $M_s = \int_V \rho_s dv$  ( $kg$ ) and  $\dot{m}_s = \rho v^S \omega_s A$  ( $kg/s$ ).

For steady-state conditions the species mass balance equation is a first-order ODE with the  $z$ -coordinate as the only independent variable. The Eulerian species mass balance (6.1) becomes:

$$\frac{d}{dz}(\rho v^S \omega_s) = R_s \quad (6.4)$$

Multiplying the LHS of the species mass balance with the cross sectional area ratio  $A/A$ , gives:

$$\frac{d\dot{m}_s}{dV} = R_s \quad (6.5)$$

The standard plug flow model is written in terms of molar concentrations [8] [6], hence both sides of the relation above are divided by the molecular weight of species  $s$ ,  $M_{\omega_s}$ . The mole balance yields:

$$\frac{dF_s}{dV} = r_s \quad (6.6)$$

where  $F_s = \rho_s v^S A / M_{\omega_s}$  ( $mol/s$ ). This relation is named the *plug flow reactor* model.

The 1D total mass balance or continuity states that:

$$\frac{d}{dz}(\rho v^S) = 0 \quad (6.7)$$

This relation can be solved for the superficial velocity, provided that the density is known from a appropriate EOS. For gas mixtures the ideal gas law is often used, thus the changes in composition is taken into account through the average molecular mass of the mixture<sup>2</sup>. Moreover, the continuity equation can be integrated from the inlet  $z = 0$  to any level  $z = z$ , to show that the mass flux is constant in the tube  $(\rho v^S)|_z = (\rho v^S)|_{in} = \text{Constant}$  ( $kg/m^2s$ ). In particular, this integral relationship is frequently used to simplify the models, calculating the convective/advective flux terms from the known inlet values.

The plug flow model heat or temperature equation is deduced from the cross section averaged temperature equation (1.299). In many tubular reactor processes the heat conduction term in the  $z$ -direction is much smaller than the heat transport by convection. For such cases the conductive transport term can be neglected and the temperature equation reduces to:

$$\rho C_p \frac{\partial T}{\partial t} + \rho C_p v^s \frac{\partial T}{\partial z} = (-\Delta H_{r,s}) R_s / M_{\omega_s} + \frac{4U}{d_r} (T_{sur} - T) \quad (6.8)$$

For steady-state conditions the temperature equation becomes, after adopting the integrated continuity and multiplying the resulting relation with the cross section area  $A = \pi d_r^2 / 4$ ,

$$\dot{m} C_p \frac{dT}{dz} = (-\Delta H_{r,s}) A R_s / M_{\omega_s} + \pi d_r U (T_{sur} - T) \quad (6.9)$$

where  $\dot{m} = \rho v^S A = \rho_{in} v_{in}^S A$  ( $kg/s$ ). This relation is the heat balance for a single phase tubular reactor operating under plug flow conditions. This temperature equation is coupled with the species mass balances by the reaction term and through the mixture heat capacity term on the LHS.

The principal difference between reactor design calculations involving homogeneous reactions and those involving fluid-solid heterogeneous reactions is that for the latter, the reaction takes place on the surface of a catalyst. For the heterogeneous processes the reaction rate is normally based on mass of solid catalyst,  $W$ , rather than on reactor volume,  $V$ . For a fluid-solid heterogeneous process, the rate of reaction of a species  $s$  is defined as:

<sup>2</sup> In chap 1 it was shown that when the total mole balance is used instead, the reaction term does not always vanish on the RHS because the number of moles may change in a chemical process. This total molar balance can be obtained starting out from the species mass balance (6.4), after dividing by the molecular mass for each species to obtain a species mole balance and finally sum these equations for all species in the mixture.

$$r'_s = \text{mol s produced/s kg(catalyst)} \quad (6.10)$$

The mass of solid catalyst is used because the amount of catalyst is what is important to the rate of product formation. For a packed tubular reactor the governing plug flow balance equations are [8]:

$$\frac{d}{dz}(\rho v^s \omega_s) = \rho_B R'_s, \quad (6.11)$$

$$\dot{m} C_p \frac{dT}{dz} = (-\Delta H_{r,s}) A \rho_B R_s / M_{\omega_s} + \pi d_r U (T_{\text{sur}} - T), \quad (6.12)$$

$$\frac{dp_t}{dz} = f \frac{\rho_g (v^s)^2}{d_p} \quad (6.13)$$

The latter equation is used to calculate the pressure drop through the bed and is named the *Ergun equation* [4]. The  $\rho_B$  is the catalyst bulk density ( $\text{kg/m}^3$ ), and  $f$  is a friction factor ( $-$ ) for the packing. Ergun proposed the following parameterization for the friction factor:

$$f = \frac{1 - \varepsilon}{\varepsilon^3} \left[ 1.75 + \frac{150(1 - \varepsilon)}{Re_p} \right] \quad (6.14)$$

The following initial conditions are often used: at  $z = 0$ ,  $\rho_s = \rho_{s,0}$ ,  $T = T_0$ ,  $p_t = p_{t,0}$ . In this model  $d_p$  is the equivalent particle diameter.

### 6.1.2 Batch and Continuous Stirred Tank Reactors

Considering a well-mixed vessel, one may average the governing microscopic equations over all the spatial dimensions. For convenience, this operation is performed by further integrating the cross sectional averaged axial dispersion model equations over the remaining  $z$ -dimension. Moreover, due to the assumption of complete uniformity within the reactor, the diffusive transport terms vanish after integration of the balance equations because only convection/advection is considered at the inlet- and outlet boundaries. Nevertheless, one should keep in mind that the uniformity is actually created by the large level of mixing (large dispersion terms in the bulk of the reactor volume).

The reactor models considering *complete mixing* may be subdivided into batch and continuous types. In the continuous stirred tank reactor (CSTR) models, an entering fluid is assumed to be instantaneously mixed with the existing contents of the reactor so that it loses its identity. This type of reactor operates at uniform concentration and temperature levels. For this reason the species mass balances and the temperature equation may be written for the entire reactor volume, not only over a differential volume element. Under steady-state conditions, the species mass and heat balances reduce to algebraic equations.

For a CSTR which is completely mixed, we start from the averaged species mass (1.301) and heat (1.302) balance equations. No diffusive terms are retained as the reactor volume is assumed to be uniform in composition and temperature, as explained above. The resulting species mass balance yields:

$$\frac{\partial}{\partial t}(\rho\omega_s) + \frac{\partial}{\partial z}(\rho v^s \omega_s) = R_s \quad (6.15)$$

After global integration in  $z$  from the inlet to the outlet of the reactor and multiplying the resulting relation by the cross section area  $A$ , we get:

$$\frac{\partial}{\partial t}(\rho\omega_s V) + \int \frac{\partial \dot{m}_s}{\partial z} dz = R_s V \quad (6.16)$$

Let  $\dot{m}_s|_{\text{in}}$  and  $\dot{m}_s|_{\text{out}}$  represent, respectively, the inlet and outlet mass flow rates of species  $s$ , the following relation can then be obtained by use of Green's theorem:

$$\frac{dM_s}{dt} = \dot{m}_s|_{\text{out}} - \dot{m}_s|_{\text{in}} + R_s V \quad (6.17)$$

Under steady-state conditions, the simplified species mass balance reduces further to:

$$\dot{m}_s|_{\text{out}} - \dot{m}_s|_{\text{in}} + R_s V = 0 \quad (6.18)$$

The reactor model is preferably formulated in terms of mole numbers, so we may divide the relation by the molecular weight of the species  $s$ . The result is the algebraic mole balance:

$$F_s|_{\text{in}} - F_s|_{\text{out}} = R_s V \quad (6.19)$$

This mole balance is named the *continuous stirred tank reactor (CSTR)* model.

Integrating the temperature equation (1.302) over the entire reactor volume, we obtain:

$$MC_p \frac{\partial T}{\partial t} + \rho C_p v^s A \int \frac{\partial T}{\partial z} dz = V(-\Delta H_{r,s})R_s/M_{\omega_s} + \int \pi d_r U(T_{\text{sur}} - T) dz \quad (6.20)$$

in which  $M = \rho V$  (kg).

By use of the integrated continuity and assuming that the heat transfer term is not a function of  $z$ , the temperature equation can be modified to:

$$MC_p \frac{\partial T}{\partial t} + C_p(\rho v^s)|_{\text{in}} A \int \frac{\partial T}{\partial z} dz = V(-\Delta H_{r,s})R_s/M_{\omega_s} + A_h U(T_{\text{sur}} - T) \quad (6.21)$$

For steady-state conditions the transient term can be neglected, and by use of Green's theorem the relation reduces to:

$$C_p \dot{m}_{\text{in}}(T_{\text{out}} - T_{\text{in}}) = V(-\Delta H_{r,s})R_s/M_{\omega_s} + A_h U(T_{\text{sur}} - T) \quad (6.22)$$

in which the heat exchange surface of the reactor is denoted by  $A_h = \pi d_r L$ . This equation can be used calculating the temperature when the CSTR model is adopted.

In *batch reactors* the spatially uniform composition and temperature variables may vary with time, however, so first-order ODEs are obtained, with

time as the only independent variable. In a batch reactor no fluid is entering or leaving the reactor except at the time of loading or unloading, so the species mass balance (1.301) and the temperature equation (1.302), with no transport terms, can be integrated to yield:

$$\frac{d(\rho_s V)}{dt} = R_s V \quad (6.23)$$

or

$$\frac{dM_s}{dt} = R_s V \quad (6.24)$$

The classical batch reactor model is preferably formulated in terms of mole numbers,  $N_s$  (*mol*), so we may divide the relation by the molecular weight of the species  $s$ ,  $M_{\omega_s}$ . The resulting mole balance for the batch reactor yields:

$$\frac{dN_s}{dt} = r_s V \quad (6.25)$$

The batch reactor temperature equation is given by:

$$\dot{m}C_p \frac{dT}{dt} = (-\Delta H_{r,s})V R_s / M_{\omega_s} + (\pi d_r L)U(T_{\text{sur}} - T) \quad (6.26)$$

## 6.2 Simplified Reactor Models

In particular cases simplified reactor models can be obtained neglecting the insignificant terms in the governing microscopic equations (without averaging in space) [9]. For axisymmetrical tubular reactors, the species mass and heat balances are written in cylindrical coordinates. Himmelblau and Bischoff [9] give a list of simplified models that might be used to describe tubular reactors with steady-state turbulent flow. A representative model, with radially variable velocity profile, and axial- and radial dispersion coefficients, is given below:

$$v_z(r) \frac{\partial \rho_s}{\partial z} = \frac{\partial}{\partial z} (\rho D_{\text{eff},z}(r) \frac{\partial \omega_s}{\partial z}) + \frac{1}{r} \left[ \frac{\partial}{\partial r} (r \rho D_{\text{eff},r}(r) \frac{\partial \omega_s}{\partial r}) \right] + R_s \quad (6.27)$$

$$\rho C_p v_z(r) \frac{\partial T}{\partial z} = \frac{\partial}{\partial z} (k_{\text{eff},z}(r) \frac{\partial T}{\partial z}) + \frac{1}{r} \left[ \frac{\partial}{\partial r} (r k_{\text{eff},r}(r) \frac{\partial T}{\partial r}) \right] + R_s / M_{\omega_s} (-\Delta H_{r,s}) \quad (6.28)$$

with boundary conditions:

$$v_z(r) \rho_{s,\text{in}} = v_z(r) \rho_s(0, r) - \rho(0, r) D_{\text{eff},z}(r) \frac{\partial \omega_s(0, r)}{\partial z}, \quad (6.29)$$

$$\frac{\partial \omega_s(L, r)}{\partial z} = 0,$$

$$\frac{\partial \omega_s(z, 0)}{\partial r} = 0,$$

$$\frac{\partial \omega_s(z, R_r)}{\partial r} = 0$$

and

$$\rho_{\text{in}} C_{p,\text{in}} v_z(r) T_{\text{in}} = \rho(0, r) C_p(0, r) v_z(r) T(0, r) - k_{\text{eff},z}(r) \frac{\partial T(0, r)}{\partial z}, \quad (6.30)$$

$$\frac{\partial T(L, r)}{\partial z} = 0,$$

$$\frac{\partial T(z, 0)}{\partial r} = 0,$$

$$\frac{\partial T(z, R_r)}{\partial r} = -\frac{U}{k_r} \left( T(z, R_r) - T_{\text{wall}} \right)$$

For turbulent flow in pipes the velocity profile can be calculated from the empirical power law design formula (1.354).

Similar balance equations with purely laminar diffusivities can be used for a fully developed laminar flow in tubular reactors. The velocity profile is then parabolic, so the Hagen Poiseuille law (1.353) might suffice.

It is important to note that the important difference between the cross section averaged 1D axial dispersion model equations (discussed in the previous section) and the simplified 2D model equations (presented above) is that the latter is valid locally at each point within the reactor, whereas the averaged one simply gives a cross sectional average description of the axial composition and temperature profiles.

### 6.3 Chemical Reaction Equilibrium Calculations

The second law of thermodynamics is the basis for any equilibrium calculation. One way to state the second law is that all real processes occur spontaneously in the direction that increases the entropy of the universe<sup>3</sup> (system

<sup>3</sup> In classical thermodynamics a simple system is defined as a system that is macroscopically homogeneous, isotropic, and uncharged, that are large enough so that surface effects can be neglected, and that are not acted on by electric, magnetic, or gravitational fields [2]. A thermal reservoir is defined as a reversible heat source that is so large that any heat transfer of interest does not alter the temperature of the thermal reservoir. Such a thermal reservoir is a system enclosed by rigid impermeable walls and characterized by relaxation times sufficiently short so that all processes of interest therein are essentially quasi-static. Given two or more simple systems, they may be considered as constituting a single composite system. The composite system is termed closed if it is surrounded by a wall that is restrictive with respect to the total energy, the total volume, and the total mole numbers of each species of the composite system.

In the present outline the universe is considered a composite system, the system represents a simple subsystem and the surroundings a thermal reservoir.

plus surroundings). A spontaneous change occurs naturally (by itself) under specified conditions, without an ongoing input of energy from outside the system. In particular, a chemical reaction proceeding toward equilibrium is an example of a spontaneous change. For a thermodynamically reversible adiabatic process a quantitative statement of the second law can be formulated as [11]:

$$d\hat{S}_{\text{univ}} = d\hat{S}_{\text{sys}} + d\hat{S}_{\text{surr}} \geq 0 \quad (6.31)$$

Using this formulation two separate measurements of  $d\hat{S}_{\text{sys}}$  and  $d\hat{S}_{\text{surr}}$  are required to predict whether a reaction will be spontaneous at a particular temperature. Therefore, it is considered more convenient to have one criterion for spontaneity with reference to changes in the system only, which can be used to define an equilibrium state, without explicitly considering the environment. The Gibbs free energy ( $\hat{G}$ ) and the Helmholtz free energy<sup>4</sup> ( $\hat{F}$ ) functions have both been introduced especially, among other things, to provide such criteria for spontaneity as requested. Generally, the free energy change is a measure of the spontaneity of a process and of the useful energy available from the process. Moreover, the use of the Gibbs function is more common than the Helmholtz function because of the experimental convenience of specifying the  $T$  and  $p$  constraints (as compared with the alternative  $T$  and  $V$  constraints). Henceforth we continue to use the Gibbs function ( $\hat{G}$ ) exclusively, but the concepts might be recast into equivalent forms when appropriate to a particular situation [2].

By elementary theory we can show that the Gibbs function is defined in such a way that the free energy change criterion we are searching for (i.e.,  $d\hat{G}|_{T,p} = 0$ ) may be deduced from the second law of thermodynamics on the condition that  $T$  and  $p$  are constants. However, only a superficial summary of the fundamental theory is provided as the underlying ideas is quite involved.

For a thermodynamically reversible adiabatic process ( $T_{\text{sys}} = T_{\text{surr}}$ ) at constant pressure, the change in entropy of the surroundings can be expressed as [11]:

$$d\hat{S}_{\text{surr}} = -\frac{d\hat{H}_{\text{sys}}}{T_{\text{sys}}} \quad (6.32)$$

Substituting for  $d\hat{S}_{\text{surr}}$  in (6.31) gives a relationship that lets us focus solely on the system:

$$d\hat{S}_{\text{univ}} = d\hat{S}_{\text{sys}} - \frac{d\hat{H}_{\text{sys}}}{T_{\text{sys}}} \geq 0 \quad (6.33)$$

Multiplying both sides by  $(-T_{\text{sys}})$  gives:

$$-T_{\text{sys}}d\hat{S}_{\text{univ}} = -T_{\text{sys}}d\hat{S}_{\text{sys}} + d\hat{H}_{\text{sys}} \quad (6.34)$$

From the Gibbs equation,  $\hat{G} = \hat{H} - T\hat{S}$ , the change in the free energy of the system ( $d\hat{G}_{\text{sys}}$ ) at constant temperature and pressure is given by:

<sup>4</sup> The Helmholtz free energy is sometimes denoted by  $\hat{A}$  ( $J$ ).

$$d\hat{G}_{\text{sys}} = d\hat{H}_{\text{sys}} - T_{\text{sys}}d\hat{S}_{\text{sys}} \quad (6.35)$$

Combining this equation with the previous one, the result is:

$$-T_{\text{sys}}d\hat{S}_{\text{univ}} = -T_{\text{sys}}d\hat{S}_{\text{sys}} + d\hat{H}_{\text{sys}} = d\hat{G}_{\text{sys}} \quad (6.36)$$

In accordance with the second law interpretation, the sign of  $d\hat{G}_{\text{sys}}$  dictates whether a reaction is spontaneous or not. We reiterate that the second law states that if  $d\hat{S}_{\text{univ}} > 0$  the process is spontaneous, else if  $d\hat{S}_{\text{univ}} < 0$  the process is non-spontaneous, and if  $d\hat{S}_{\text{univ}} = 0$  the process is at equilibrium. Because  $d\hat{G}_{\text{sys}} = -T_{\text{sys}}d\hat{S}_{\text{univ}}$ , we can easily conclude that if  $d\hat{G}_{\text{sys}} < 0$  the process is spontaneous, else if  $d\hat{G}_{\text{sys}} > 0$  the process is non-spontaneous, and if  $d\hat{G}_{\text{sys}} = 0$  the process is at equilibrium.

Before we proceed with the conventional theory of chemical reaction equilibrium calculations, a few words might be required explaining the postulate given above that equivalent forms of the second law of thermodynamics can be preferable when appropriate to a particular situation.

Firstly, the reason why the particular  $\hat{G}(T, p, \mathbf{n})$  and  $\hat{F}(T, V, \mathbf{n})$  functions have been introduced to enable convenient equilibrium calculations, and no other state functions, must be seen in connection with historical requirements. The pioneers in classical thermodynamics experienced that in practice many chemical processes occur either in open vessels exposed to the atmosphere at constant temperature and pressure or in closed rigid vessels with diathermal walls at constant temperature and volume. In the latter case the ambient atmosphere acts as a thermal reservoir. The Gibbs energy function is thus conveniently defined in such a way that we can make use of the physical system property that at constant  $T$  and  $p$ , the system tends to move toward a state of minimum Gibbs energy for which  $d\hat{G}|_{T,p} = 0$ . It is emphasized that this system property represents a reformulation of the second law of thermodynamics which holds only when  $T$  and  $p$  are constants. In a similar manner, the Helmholtz energy function ( $\hat{F}$ ) is conveniently defined in such a way that we can make use of the physical system property that at constant temperature and volume, the system tends to move toward a state of minimum Helmholtz energy. Therefore, an alternative condition for chemical reaction equilibrium at constant  $T$  and  $V$  can be expressed as  $d\hat{F}|_{T,V} = 0$ . Again, it is emphasized that this system property represents a reformulation of the second law of thermodynamics which holds only when  $T$  and  $V$  are constants. Secondly, so far we have mentioned that the second law of thermodynamics provides several state functions governing the direction of natural processes. The particular state function appropriate to a given situation is governed by the choice of thermodynamic variables. In classical thermodynamics the most important state functions applied to equilibrium calculations are thus the entropy function, the Helmholtz function, and the Gibbs function. For each such state function, there is a statement of the second law of thermodynamics that include both the criterion for a natural process to occur and

for the equilibrium state. Thirdly, Callen [2] proved the equivalence of alternative formulations of the conditions of chemical equilibrium. Each of these alternative formulations can be convenient for particular problems. We recollect that the principle of maximum entropy is the conventional statement of the second law of thermodynamics. Callen postulated that this law may be generalized and expressed as an *extremum principle*. Moreover, he stated that the same extremum principle can be reformulated in several equivalent mathematical forms. In particular, the equivalence of the maximum entropy representation and the minimum energy representation has been examined. The reformulations of the novel extremum principle are written in terms of Legendre transformed energy and entropy functions representations. The Helmholtz and the Gibbs energies represent two such thermodynamic potentials which correspond to two particular Legendre transforms of the energy. In chap 2 it is explained that multiple equivalent formulations have been used in classical mechanics (i.e., the Newtonian, Lagrangian, and Hamiltonian mechanics) because certain problems are much more tractable in a Lagrangian formalism than in a Newtonian formalism, or *visa versa*. Another postulate of Callen [2] is that for particular problem formulations one of the equivalent representations of the equilibrium condition in thermodynamics may also be simpler to use than the conventional Gibbs energy condition. The main point now is that we may utilize these novel ideas enabling more efficient reactor simulations. In fluid dynamics chemical reaction equilibrium calculations are neither naturally occurring at uniform and constant  $T$  and  $p$  nor at uniform and constant  $T$  and  $V$  because a material control volume is not defined at particular  $T$ ,  $p$  or  $V$ . However, it is not trivial to design a more optimal state function for the control volume representation that will make future reactor simulations less computational demanding.

Meanwhile we still make use of the conventional theory, thus the chemical reaction equilibrium composition is usually found by minimizing the Gibbs energy constrained by the material balance. In this standard problem definition the values for the element-abundance vector  $\mathbf{b}$ , temperature  $T$ , pressure  $p$ , and the appropriate free energy data are thus assumed to be known. When designing numerical algorithms for calculating the unknown equilibrium composition of a mixture, it is customary to distinguish between two equivalent representations of the minimizing problem [14]:

1. The *stoichiometric formulation*, in which the constraints are incorporated through stoichiometric reaction equations. These procedures are sometimes referred to as the classical equilibrium constant methods because the equilibrium constant and the extent of reaction are the primary quantities.
2. The *non-stoichiometric formulation*, in which the stoichiometric equations are not used, instead the material balance constraints are treated by means of Lagrange multipliers. In these direct free energy minimization methods the problem is usually expressed as minimizing  $G$ , for fixed  $T$  and  $p$ , subject to the material balance constraint.

### 6.3.1 Stoichiometric Formulation

Generally the reaction equilibrium problem may be written:

$$\begin{aligned} \min \hat{G}(\mathbf{n}) &= \sum_{i=1}^q n_i \mu_i, \\ \text{subject to } \mathcal{A}\mathbf{n} &= \mathbf{b} \\ \text{and } n_i &\geq 0 \end{aligned} \quad (6.37)$$

In these equations  $\hat{G}(\mathbf{n})$  is the Gibbs energy function for the mixture and  $\mathbf{n} \in \mathcal{R}^q$  is a column vector (sometimes called the species-abundance vector) containing the unknown variables representing the number of moles of each of the  $q$  species (molecules) in the mixture.  $\mathcal{A} \in \mathcal{R}^{m \times q}$  is the predefined formula matrix. This coefficient matrix defines how the  $m$  elements in the mixture are distributed within the  $q$  species (molecules) that can exist in the system.  $m$  is the total number of elements in the mixture.  $\mathbf{b} \in \mathcal{R}^m$  is a column vector (sometimes called the element-abundance vector) containing the known values for the total amount of the different elements in the mixture.

In this formulation the solution task consist in identifying the species composition vector  $\mathbf{n}_{\text{eq}}$  that minimizes  $\hat{G}$ , for fixed  $T$  and  $p$ . The governing equations to be solved in the equilibrium calculations can be derived from the total differential of the state function. Assuming  $\hat{G} = \hat{G}(T, p, \mathbf{n})$ , the total differential of the Gibbs function can be expressed like:

$$d\hat{G} = \left( \frac{\partial \hat{G}}{\partial p} \right)_{T, \mathbf{n}} dp + \left( \frac{\partial \hat{G}}{\partial T} \right)_{p, \mathbf{n}} dT + \sum_i^q \left( \frac{\partial \hat{G}}{\partial n_i} \right)_{T, p, n_j, j \neq i} dn_i, \quad i = 1, 2, \dots, q \quad (6.38)$$

At equilibrium we require that  $d\hat{G}|_{T, p} = 0$ , hence the above differential reduces to:

$$d\hat{G} = \sum_i^q \left( \frac{\partial \hat{G}}{\partial n_i} \right)_{T, p, n_j, j \neq i} dn_i = 0, \quad i = 1, 2, \dots, q \quad (6.39)$$

However, the number of unknowns and thus the mathematical problem to be solved is still quite large even for systems in which only a few reactions occur. To reduce the number of unknown variables, it is convenient to introduce the extent of reaction quantity. For a specific stoichiometric equation defining a particular reaction, the extent of reaction is defined by:

$$\xi = \frac{n_i - n_{i,0}}{\nu_i} \quad (6.40)$$

By definition the stoichiometric coefficient is positive for a product and negative for a reactant.

For a system with  $r$  reactions a matrix notation may be more appropriate, hence the  $r$  stoichiometric equations and the species-abundance vector  $\mathbf{n}$  are related through the extent of reaction  $\boldsymbol{\xi}$  by:

$$\mathbf{n} = \mathbf{n}_0 + \sum_{j=1}^r \boldsymbol{\nu}_j \xi_j. \quad (6.41)$$

where  $\mathbf{n}_0$  represents any particular solution with an initial composition,  $\boldsymbol{\nu}_j$  is a stoichiometric vector, and  $\xi_j$  is the extent of reaction for reaction  $j$ . This relation is merely the definition equation for the extent of reaction  $\xi_j$ .

We may then re-define the Gibbs free energy function in terms of  $\boldsymbol{\xi}$  instead of  $\mathbf{n}$ . Hence, the modified state function definition yields:

$$\hat{G} = \hat{G}(T, p, \boldsymbol{\xi}) \quad (6.42)$$

In this case the solution task is to minimize  $\hat{G}$ , for fixed  $T$  and  $p$ , in terms of the extent of reaction  $\xi_j$  for the  $r$  reactions.

The total differential of the modified Gibbs energy function  $\hat{G} = \hat{G}(T, p, \boldsymbol{\xi})$  is examined to elucidate the necessary conditions for obtaining a minimum in the free energy function:

$$d\hat{G} = \left( \frac{\partial \hat{G}}{\partial p} \right)_{T, \boldsymbol{\xi}} dp + \left( \frac{\partial \hat{G}}{\partial T} \right)_{p, \boldsymbol{\xi}} dT + \sum_j^r \left( \frac{\partial \hat{G}}{\partial \xi_j} \right)_{T, p, \xi_k, k \neq j} d\xi_j, \quad j = 1, 2, \dots, r \quad (6.43)$$

By chain rule differentiation, the last term on the RHS of this relation can be re-written in terms of mole numbers:

$$d\hat{G} = \left( \frac{\partial \hat{G}}{\partial p} \right)_{T, \boldsymbol{\xi}} dp + \left( \frac{\partial \hat{G}}{\partial T} \right)_{p, \boldsymbol{\xi}} dT + \sum_j^r \sum_{i=1}^q \left( \frac{\partial \hat{G}}{\partial n_i} \right)_{T, p, n_k, k \neq i} \left( \frac{\partial n_i}{\partial \xi_j} \right)_{\xi_k, k \neq j} d\xi_j \quad (6.44)$$

The last term derived on the RHS can be further simplified by recognizing that:

$$\left( \frac{\partial \hat{G}}{\partial n_i} \right)_{T, p, n_k, k \neq i} = \mu_i \quad (6.45)$$

and

$$\left( \frac{\partial n_i}{\partial \xi_j} \right)_{\xi_k, k \neq j} = \nu_{ij} \quad (6.46)$$

At equilibrium, we again require that  $d\hat{G}_{T,p} = 0$ , hence (6.44) reduces to:

$$d\hat{G}_{T,p} = \sum_{j=1}^r \sum_{i=1}^q \nu_{ij} \mu_i d\xi_j = 0 \quad (6.47)$$

where  $\nu_{ij}$  is the stoichiometric coefficient of species  $i$  in reaction  $j$ .

From the relations (6.43) to (6.47) it is concluded that the necessary conditions for a minimum value of  $\hat{G}$  are:

$$\begin{aligned} \left(\frac{\partial \hat{G}}{\partial \xi_j}\right)_{T,p,\xi_k,k \neq j} &= \sum_{i=1}^q \left(\frac{\partial \hat{G}}{\partial n_i}\right)_{T,p,n_k,k \neq i} \left(\frac{\partial n_i}{\partial \xi_j}\right)_{\xi_k,k \neq j} \\ &= \sum_{i=1}^q \mu_i \nu_{ij} = 0, \quad j = 1, 2, \dots, r \end{aligned} \quad (6.48)$$

In this method the chemical equilibrium state is defined by the chemical equilibrium constant [10]. The chemical equilibrium constants can be derived from (6.48) provided that appropriate expressions are introduced for the chemical potential. A change in chemical potential for an isothermal process is related to a change in the fugacity of the species<sup>5</sup> [13]:

$$d\mu_i|_T = RT d \ln \hat{f}_i|_T \quad (6.49)$$

where  $\hat{f}_i$  is the fugacity of species  $i$  in the mixture.

If we integrate, at constant temperature, the given relation between the standard state and some arbitrary state, we obtain [13]:

$$\mu_i = \mu_i^0 + RT \ln \left( \frac{\hat{f}_i}{f_i^0} \right) \quad (6.50)$$

The fugacity of species  $i$  in the mixture  $\hat{f}_i$  can be defined in terms of the pure species fugacity  $f_i^{\text{pure}}$  through an activity coefficient  $\gamma_i$  or a fugacity coefficient  $\phi_i$  as will be explained shortly.

The ratio of the fugacities represents the activity,  $a_i = \hat{f}_i/f_i^0$ , hence we can re-write the above relation like:

$$\mu_i = \mu_i^0 + RT \ln (a_i) \quad (6.51)$$

Considering a single model reaction like:



we can derive an expression for the rate of change of the chemical potential:

$$\Delta\mu_R = \Delta\mu_R^0 + RT \ln \left( \frac{a_C^c a_D^d}{a_A^a a_B^b} \right) \quad (6.52)$$

The criterion for chemical reaction equilibrium is thus that the energy difference between reactants and products is zero,  $\Delta\mu_R = 0$ . Hence, we can define the equilibrium constant for the model reaction by:

<sup>5</sup> The American chemist G. N. Lewis (1875–1946) introduced the fugacity function (Latin *fugare*, to fly) as a measure of the pressure adjusted for the lack of ideality [11]. For an ideal gas the fugacity is equal to the pressure. For a non-ideal gas we normally define the standard state to correspond to unit fugacity,  $f_i^0 = 1$  (bar).

$$-\frac{\Delta\mu_R^0}{RT} = \ln \left( \frac{a_C^c a_D^d}{a_A^a a_B^b} \right)_{eq} = \ln K_{eq} \quad (6.53)$$

The relationship between the equilibrium constant and the change in the chemical potential for the reaction is sometimes called the van't Hoff equation [10].

An explicit expression for the chemical equilibrium constant is thus given by:

$$K_{eq} = \exp \left( -\frac{\Delta\mu_R^0}{RT} \right) \quad (6.54)$$

where  $\Delta\mu_R^0$  is the standard free energy change for the reaction at a given temperature  $T$  and a defined reference state.

This concept can be generalized and applied to a multicomponent mixture in which multiple reactions are taking place. In this case  $\Delta\mu_{R,j}^0$  is systematically expressed in terms of the reference chemical potentials by inserting (6.50) into (6.48). The result is:

$$\sum_{i=1}^q \left[ \nu_{ij} \mu_i^0 + \nu_{ij} RT \ln \left( \frac{\hat{f}_i}{f_i^0} \right) \right] = 0 \quad (6.55)$$

The measure of the change in chemical potential associated with reaction  $j$  is defined by  $\Delta G_{R,j}^0 = \Delta\mu_j^0 = \sum_{i=1}^q \nu_{ij} \mu_i^0$ . It is emphasized that this quantity is calculated from the stoichiometric coefficients of the reaction and not from the number of moles of the different species transformed by the reaction. Nevertheless, the  $\Delta G_{R,j}^0$  is frequently referred to as the standard Gibbs energy change for reaction  $j$ . The above relation can be re-written as:

$$\frac{\Delta G_{R,j}^0}{RT} = \frac{1}{RT} \sum_{i=1}^q \nu_{ij} \mu_i^0 = - \sum_{i=1}^q \nu_{ij} \ln \left( \frac{\hat{f}_i}{f_i^0} \right) = - \ln K_{eq,j} \quad (6.56)$$

In order to relate  $K_{eq,j}$  to the activities we rearrange the relation to obtain:

$$\ln K_{eq,j} = \sum_{i=1}^q \nu_{ij} \ln (a_i) = \ln (a_i)^{\sum_{i=1}^q \nu_{ij}} = \ln \prod_{i=1}^q a_i^{\nu_{ij}} \quad (6.57)$$

Hence, a non-linear equation for  $K_{eq,j}$  can easily be obtained:

$$K_{eq,j} = \prod_{i=1}^q a_i^{\nu_{ij}} \quad (6.58)$$

For most *liquid mixtures* the fugacity is not a strong function of pressure thus the fugacity ratio is approximately  $f_i^{\text{pure}}/f_i^0 \sim 1$ , thus for liquids the activity can be approximated as:

$$a_i = \frac{\gamma_i x_i f_i^{\text{pure}}}{f_i^0} \approx \gamma_i x_i \quad (6.59)$$

The corresponding equilibrium constant yields:

$$K_{eq,j} = \prod_{i=1}^q (\gamma_i x_i)^{\nu_{ij}} \quad (6.60)$$

The calculation of the equilibrium composition for a reactive liquid mixture requires specific excess models for the activity coefficient of every species [13]. Note that for ideal solutions the activity coefficient has a value of unity,  $\gamma_i = 1$ .

For *gas mixtures*<sup>6</sup> the fugacity of species  $i$  in the mixture  $\hat{f}_i$  is conventionally written:

$$\hat{f}_i = y_i f_i^{\text{pure}} = y_i \frac{f_i^{\text{pure}}}{p} p = y_i \phi_i p \quad (6.61)$$

The fugacity coefficient is defined as  $\phi_i = f_i^{\text{pure}}/p = \hat{f}_i/p_i$ , and is calculated from an appropriate EOS.

The corresponding equilibrium coefficient for reaction  $j$  in the mixture yields:

$$K_{eq,j} = \prod_{i=1}^q \left( \frac{\hat{f}_i}{f_i^*} \right) = \prod_{i=1}^q \left( \frac{y_i \phi_i p}{f_i^*} \right)^{\nu_{ij}} = \prod_{i=1}^q \left( \frac{y_i \phi_i p}{p^*} \right)^{\nu_{ij}} \quad (6.62)$$

in which  $f_i^* = p^* = 1$  (bar).  $p^*$  is the pressure at the reference state (ideal gas). For gases the standard state for  $\Delta G_{R,j}^0$  is thus 1 (bar).

This model represents the most frequently used description of chemical reaction equilibrium and should be familiar to most chemical engineering students. However, for multicomponent mixtures in which multiple reactions may take place, this type of non-linear problems may be cumbersome to solve numerically. One important obstacle is that the non-linear equilibrium constant definitions may give rise to multiple solutions, hence we have to identify which of them are the physical solutions. The stoichiometric formulation might thus be inconvenient for mixtures containing just a few species for which only a few reactions are taking place.

### 6.3.2 Non-stoichiometric formulation

In this case the chemical reaction equilibrium problem is expressed so that we are minimizing the free energy directly as formally defined by the fundamental statement (6.37). In mathematical terms (6.37) represents a constrained optimization problem. This type of problems is usually solved by the use of Lagrange multipliers.

A Lagrangian function for the equilibrium problem can be defined as<sup>7</sup>:

$$L(\boldsymbol{\lambda}, \mathbf{n}) \equiv \hat{G}(\mathbf{n}) - \boldsymbol{\lambda}^T (\mathcal{A}\mathbf{n} - \mathbf{b}) \quad (6.63)$$

<sup>6</sup> This approach can also be adopted for liquid mixtures provided that an appropriate EOS is available.

<sup>7</sup> The elements of Lagrangian mechanics are explained in chap 2.

In this framework the minimization problem is expressed as:

$$\min L(\boldsymbol{\lambda}, \mathbf{n}) \quad (6.64)$$

where  $\boldsymbol{\lambda} \in \mathcal{R}^m$  is a column vector of the Lagrange multipliers.

The Lagrangian function has a minimum when  $\nabla L = 0$ , in which the  $\nabla L$  operator is defined by a column vector consisting of the two elements:

$$\begin{aligned} \frac{\partial L}{\partial \mathbf{n}} &= \frac{\partial \hat{G}}{\partial \mathbf{n}} - \mathcal{A}^T \boldsymbol{\lambda} = \boldsymbol{\mu} - \mathcal{A}^T \boldsymbol{\lambda} = \mathbf{0} \\ \frac{\partial L}{\partial \boldsymbol{\lambda}} &= \frac{\partial \hat{G}}{\partial \boldsymbol{\lambda}} - (\mathcal{A}\mathbf{n} - \mathbf{b}) = -(\mathcal{A}\mathbf{n} - \mathbf{b}) = \mathbf{0} \end{aligned} \quad (6.65)$$

Notice that  $\partial \hat{G} / \partial \mathbf{n}$  equals the chemical potential vector  $\boldsymbol{\mu}$ , and  $\partial \hat{G} / \partial \boldsymbol{\lambda} = 0$ .

The solution of these equations may be obtained by use of the iterative Newton method. The Newton method can be derived from a second order Taylor expansion, which for the given Lagrangian ( $L$ ) gives:

$$\nabla L^{(k)} + \nabla^2 L^{(k)} \delta \mathbf{y}^{(k+1)} = \mathbf{0} \quad (6.66)$$

or more conveniently

$$\nabla^2 L^{(k)} \delta \mathbf{y}^{(k+1)} = -\nabla L^{(k)} \quad (6.67)$$

where  $\delta \mathbf{y} = (\delta \mathbf{n}, \delta \boldsymbol{\lambda})^T$  is a column vector containing the difference in the composition and Lagrange multiplier estimates for the iteration number  $k + 1$  and  $k$ .

The gradient and Laplace operators in (6.67) are applied to the Lagrangian (6.63). The gradient of the Lagrangian is defined by (6.65), whereas the Laplace operator applied to the Lagrangian is simply the divergence of the gradient of the Lagrangian. Hence, (6.67) can be re-written as:

$$\left[ \begin{array}{cc} \frac{\partial}{\partial \mathbf{n}^T} (\boldsymbol{\mu} - \mathcal{A}^T \boldsymbol{\lambda}) & \frac{\partial}{\partial \boldsymbol{\lambda}^T} (\boldsymbol{\mu} - \mathcal{A}^T \boldsymbol{\lambda}) \\ \frac{\partial}{\partial \mathbf{n}^T} (\mathbf{b} - \mathcal{A}\mathbf{n}) & \frac{\partial}{\partial \boldsymbol{\lambda}^T} (\mathbf{b} - \mathcal{A}\mathbf{n}) \end{array} \right]^{(k)} \begin{bmatrix} \delta \mathbf{n} \\ \delta \boldsymbol{\lambda} \end{bmatrix}^{(k+1)} = \begin{bmatrix} \mathcal{A}^T \boldsymbol{\lambda} - \boldsymbol{\mu} \\ \mathcal{A}\mathbf{n} - \mathbf{b} \end{bmatrix}^{(k)} \quad (6.68)$$

After performing the differentiation in the first parenthesis, the Newton method can be expressed as:

$$\begin{bmatrix} \mathcal{H} & -\mathcal{A}^T \\ -\mathcal{A} & \mathbf{0} \end{bmatrix}^{(k)} \begin{bmatrix} \delta \mathbf{n} \\ \delta \boldsymbol{\lambda} \end{bmatrix}^{(k+1)} = \begin{bmatrix} \mathcal{A}^T \boldsymbol{\lambda} - \boldsymbol{\mu} \\ \mathcal{A}\mathbf{n} - \mathbf{b} \end{bmatrix}^{(k)} \quad (6.69)$$

where  $\mathcal{H}$  is the Hessian matrix of  $G$ ,  $\mathcal{H} = \partial^2 G / \partial \mathbf{n} \partial \mathbf{n}^T = \partial \boldsymbol{\mu} / \partial \mathbf{n}^T$ . The Hessian matrix may be found by analytical differentiation or by a finite differences approximation of the derivative.

The matrix operations may be further simplified, as can be illustrated writing down the problem as two algebraic equations that need to be solved simultaneously:

$$\begin{aligned}\mathcal{H}^{(k)} \delta \mathbf{n}^{(k+1)} - \mathcal{A}^T \delta \boldsymbol{\lambda}^{(k+1)} &= \mathcal{A}^T \boldsymbol{\lambda}^{(k)} - \boldsymbol{\mu}^{(k)} \\ \mathcal{A}^T \delta \mathbf{n}^{(k+1)} &= \mathbf{b} - \mathcal{A} \mathbf{n}^{(k)}\end{aligned}\quad (6.70)$$

Moreover, since  $\delta \boldsymbol{\lambda}^{(k+1)} = (\boldsymbol{\lambda}^{(k+1)} - \boldsymbol{\lambda}^{(k)})$ , the equations reduce to:

$$\begin{aligned}\mathcal{H}^{(k)} \delta \mathbf{n}^{(k+1)} - \mathcal{A}^T \boldsymbol{\lambda}^{(k+1)} &= \mathcal{A}^T \boldsymbol{\lambda}^{(k)} - \mathcal{A}^T \boldsymbol{\lambda}^{(k)} - \boldsymbol{\mu}^{(k)} = -\boldsymbol{\mu}^{(k)} \\ \mathcal{A}^T \delta \mathbf{n}^{(k+1)} &= \mathbf{b} - \mathcal{A} \mathbf{n}^{(k)}\end{aligned}\quad (6.71)$$

The resulting iterative method formulation is called the Newton-Lagrange scheme:

$$\begin{bmatrix} \mathcal{H} & -\mathcal{A}^T \\ -\mathcal{A} & \mathbf{0} \end{bmatrix}^{(k)} \begin{bmatrix} \delta \mathbf{n} \\ \boldsymbol{\lambda} \end{bmatrix}^{(k+1)} = \begin{bmatrix} -\boldsymbol{\mu} \\ \mathcal{A} \mathbf{n} - \mathbf{b} \end{bmatrix}^{(k)}\quad (6.72)$$

Computational aspects, including advantages and disadvantages, of the solution of the chemical reaction equilibrium model formulation are discussed by Michelsen and Mollerup [12]. In particular, readers not familiar with the theory for constrained optimization can find a short introduction therein. A more extensive discussion of practical methods of optimization can be found in the book of Fletcher [5].

An important feature of the non-stoichiometric formulation is that no information about the reaction stoichiometry is required. However, the species that the mixture is composed of must be specified.

Note also that this type of chemical reaction equilibrium calculations is sometimes referred to as a *Gibbs reactor* simulation.

---

## References

1. Bird RB (1957) The equations of change and the macroscopic mass, momentum, and energy balances. *Chem Eng Sci* 6:123-181
2. Callen HB (1985) *Thermodynamics and an Introduction to Thermostatistics*. Second edition, John Wiley & Sons, New York
3. Duducovič MP (1999) Trends in Catalytic Reaction Engineering. *Catal Today* 48 (1-4):5-15
4. Ergun S (1952) Fluid Flow Through Packed Columns. *Chem Eng Prog* 48(2): 89-94
5. Fletcher R (1981) *Practical Methods of Optimization*. Volume 2: Constrained Optimization. John Wiley & Sons, Chichester
6. Fogler HS (2006) *Elements of Chemical Reaction Engineering*. Fourth edition, Pearson Education International, Massachusetts
7. Froment GF, Hofmann HPK (1987) Design of Fixed-Bed Gas-Solid Catalytic Reactors. In: Carberry JJ, Varma A (eds) *Chemical Reaction and Reaction Engineering*. Marcel Dekker Inc, New York and Basel, pp 373-440
8. Froment GF, Bischoff KB (1990) *Chemical Reactor Analysis and Design*. Second edition, John Wiley & Sons, Inc, New York
9. Himmelblau DM, Bischoff KB (1968) *Process Analysis and Simulation: Deterministic Systems*. John Wiley & Sons, Inc, New York
10. Jones JB, Dugan RE (1996) *Engineering Thermodynamics*. Prentice-Hall International, Inc., Englewood Cliffs
11. Laidler KJ, Meiser JH (1995) *Physical Chemistry*. Second Edition, Houghton Mifflin Company, Boston
12. Michelsen ML, Mollerup JM (2004) *Thermodynamic Models: Fundamentals & Computational Aspects*. Tie-Line Publications, Holte
13. Prausnitz JM, Lichtenthaler RN, de Azevedo EG (1999) *Molecular Thermodynamics of Fluid-Phase Equilibria*. Third Edition, Prentence Hall PTR, New Jersey
14. Smith WR, Missen RW (1982) *Chemical Reaction Equilibrium Analysis: Theory and Algorithms*. Second edition, John Wiley & Sons, New York

---

## Agitation and Fluid Mixing Technology

Many industrial processes rely on effective agitation and mixing of fluids. The application of agitators cover the areas of mining, hydrometallurgy, biology, petroleum, food, pulp and paper, pharmaceutical and chemical process industry. In particular, in these industries we find typical chemical reaction engineering processes like fermentation, waste water treatment, hydrogenation, polymerization, crystallization, flue gas desulfurization, etc [65, 21].

Generally, *agitation* refers to forcing a fluid by mechanical means to flow in a vessel. *Mixing* usually implies the taking of two or more separate phases, or two fluids, and causing them to be randomly distributed through one another.

There are a number of purposes for agitating fluids, the intension may for example be to optimize blending of two miscible liquids, dissolving solids in liquids, dispersing a gas in a liquid as fine bubbles, suspending fine solid particles in a liquid, and agitation of a liquid to increase heat transfer between the fluid and a coil or jacket in the vessel wall. Fluid mixing may also be important in reactors to ensure optimal operation conditions for some chemical systems requiring uniform temperature and species concentrations within the reactor volume. Fluid mixing and blending<sup>1</sup> devices may thus be important units both for reactive and non-reactive processes.

There are many ways to obtain mixing in a vessel. This chapter focuses on the turbulent impeller type of mixers, as they are frequently applied in the chemical process industries.

### 7.1 Tank Geometry and Impeller Design

There is not only one optimal or unique tank design for each kind of process, since several designs may satisfy the process specifications [65]. In order to simplify design and minimize costs, standard reactor designs are usually considered sufficient for most processes. Based on experience, it has been found

---

<sup>1</sup> In English literature the term *blending* are most commonly used describing mixing of miscible liquids, whereas the term *mixing* is used describing mixing of immiscible liquids, powders, etc [53].

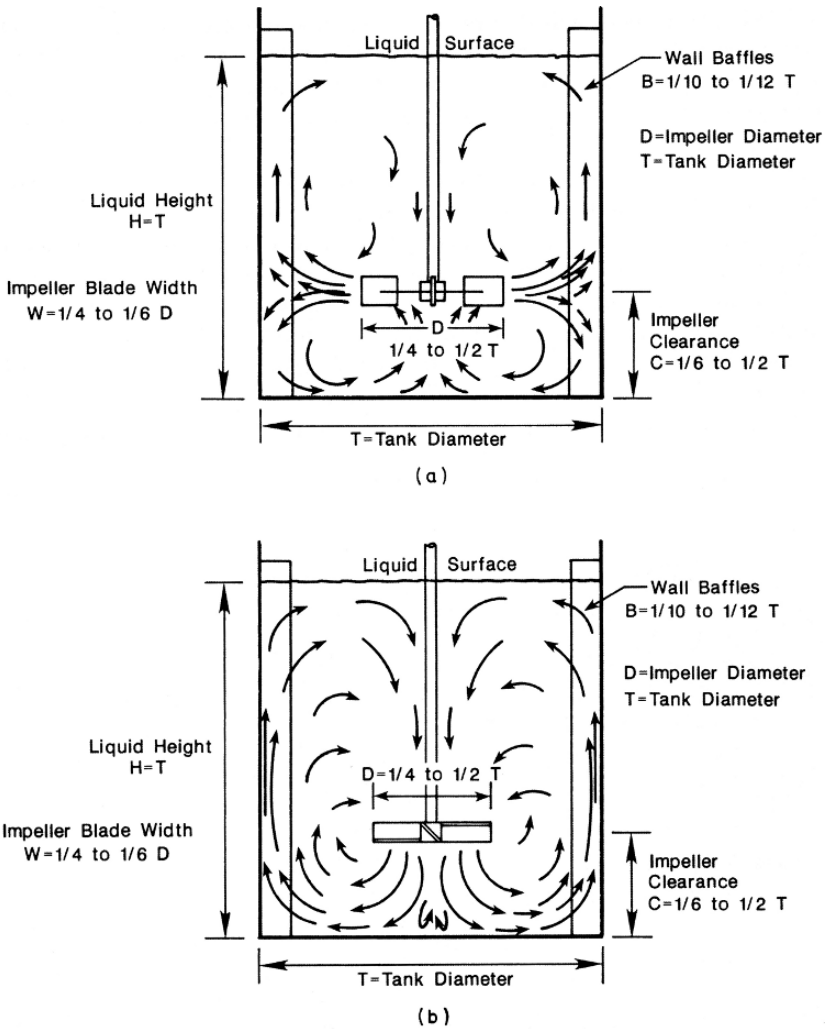
that for turbulent mixing using low viscosity fluids, the standard geometry shown in Fig 7.1 can be used. The standard tank is characterized by the diameter,  $T$ , liquid height  $H$ , impeller diameter  $D$ , impeller blade width  $W$ , clearance of impeller from the tank bottom  $C$  and the baffle width  $B$ . The standard tank is defined with four baffles placed  $90^\circ$  apart.

However, the standard tank does not reflect an optimized geometry for all processes performed in stirred tanks. The determination of an optimal geometry for a given process is very difficult, hence the standard geometry has been viewed as a reference geometry and as a point of departure for novel studies. For turbulent mixing, a liquid height to tank diameter ratio ( $H/T$ ) equal to 1 is often used as a base to describe the effect of geometry. No such standard tank geometry similar to the one used in turbulent mixing has been used for laminar mixing of high viscosity fluids.

Two different types of impellers for turbulent flow exist, radial impellers and axial impeller, as sketched in Fig 7.2. The radial impellers project the fluid radially out from the blade towards the tank wall. The flow splits at the tank wall, and approximately 50% of the fluid circulates towards the surface while the rest to the bottom, creating two regions of low mean velocity. The flow exiting the impeller blade forms a sharp velocity gradient with a strong peak at the impeller blade horizontal center line. Examples of radial flow impellers are disk style flat blade turbines (Rushton impellers) and curved blade turbines. Turbines that resemble multi-bladed paddle agitators with shorter blades are used at high speeds for liquids with a very wide range of viscosities. Normally, the turbines have four or six blades. Various types of paddle agitators are often used at low speeds between about 20 and 200 rpm. At low speeds mild agitation is obtained in an unbaffled vessel. At higher speeds baffles are used, since without baffles, the liquid is simply swirled around with little actual mixing. An anchor or gate paddle is often used with viscous liquids where deposits on walls can occur and to improve heat transfer to the wall.

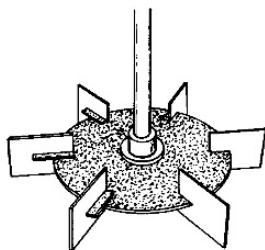
The axial impeller discharges fluid mainly axially, parallel to the impeller shaft. The fluid is pumped through the impeller, normally towards the bottom of the tank. Since the flow make a turn at the bottom, the velocity vectors fan out radially at approximately  $D/2$  beneath the impeller. Then, the flow moves along the bottom and rises near the tank wall. Analyzing the flow pattern, one can see that a back-flow eddy region is formed directly under the impeller. Upon examining the flow around the axial impeller one can also observe that a large contribution to the inlet flow enters radially at the tip of the impeller blade. This pattern is shown in Fig 7.1.

Examples of axial impellers are marine propeller and pitched blade turbine, shown in Fig 7.2. A three bladed marine type propeller is similar to the propeller blade used in driving boats. The propeller can be a side entering type in a tank or be clamped on the side of an open vessel in an off-center position. Axial flow impellers are used in blending and mixing of miscible liquids.

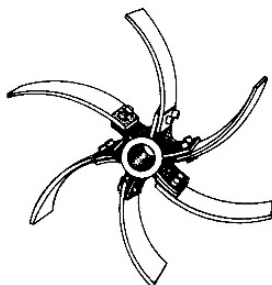


**Fig. 7.1.** Turbulent flow impellers. (a) The flow pattern produced by a radial impeller in a the standard tank geometry. (b) The flow pattern produced by an axial impeller in a standard tank geometry Tatterson [87]. By permission from Tatterson (personal communications, 2006).

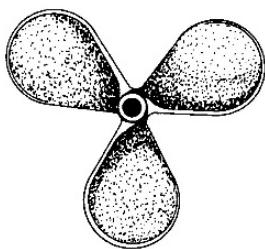
In turbulent mixing unwanted phenomena such as solid body rotation and central surface vortices may occur. In solid body rotation the fluid rotates as if it was a solid mass, and as a result little mixing takes place. At high impeller rotational speeds the centrifugal force of the impeller moves the fluid out to the walls creating a surface vortex. This vortex may even reach down to the impeller resulting in air entrainment into the fluid [87].

Radial Flow Impellers

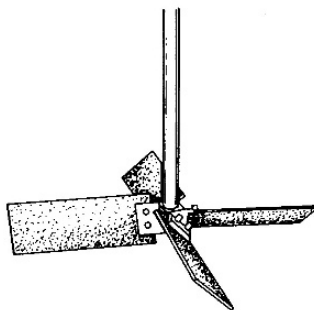
Disk Style Flat Blade Turbine  
Commonly Referred to as  
the Rushton Impeller



Sweptback or Curved Blade Turbine  
(a Spiral Turbine)

Axial Flow Impellers

Propeller



45° Pitched Blade Turbine

**Fig. 7.2.** Typical turbulent impellers [87]. By permission from Tatterson (personal communications, 2006).

The characteristic solid body rotation is the primary flow pattern in un-baffled tanks. To avoid these phenomena, baffles are installed in the tank. On wall baffles are sketched in Fig 7.1. Generally, baffles are placed in the tank to modify the flow and surface destroy vortices. Baffles mounted at the tank wall are most common, but also bottom baffles, floating surface baffles and disk baffles at the impeller shaft are possible. Often tank wall baffles are mounted a certain distance from the wall, as illustrated in Fig 7.3. This creates a different flow pattern in the tank. The purpose of installing baffles away from the wall is to avoid dead zones where liquid is seldom exchanged and where impurities accumulate. Experiments have confirmed that the flow patterns in baffled agitated tanks are different from the flow patterns in unbaffled agitated tanks. In baffled tanks the discharge flow dissipates partly in the bulk

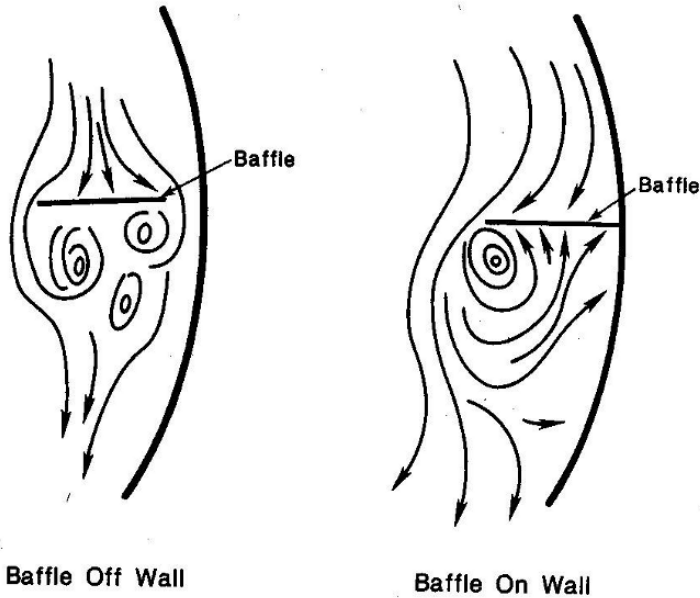


**Fig. 7.3.** Vortices in baffled tanks [87]. Left: Baffle off wall. Right: Baffle on wall. By permission from Tatterson (personal communications, 2006).

and turns axially near the tank wall. Baffles increase the axial circulation and reduce the tangential velocities. While the axial circulation dominates in the baffled tank, solid body rotation easily forms in an unbaffled tank. Due to the high tangential velocity in the unbaffled solid body rotation flow regime, the relative velocity between the fluid and the impeller becomes small, resulting in poorer mixing and circulation in unbaffled tanks compared to baffled tanks. The magnitude of the tangential velocity component is also reflected by the turbulence intensities. The radial and axial turbulence intensities are usually less than the turbulence intensities of the tangential velocity, indicating that the flow is non-isotropic, and that the mixing in the radial and axial directions is much lower than in the tangential direction [87].

In a tank with radial impellers, suitable baffles will produce strong top-to-bottom currents from the radial discharge. The installation of baffles generally increases the power consumption [65]. For axial flow impellers, the need for baffling is not as great as for radial flow impellers, thus axial flow impellers also consume less power than radial impellers. Baffles are normally used in turbulent mixing only.

For laminar mixing other impellers are used, some laminar impellers are sketched in Fig 7.4. To bring the fluid in the entire tank in motion, the diameter of these impellers usually approaches the tank diameter since the laminar

bulk flow is otherwise relatively low. Laminar impellers with diameter approaching the tank diameter are also called close-clearance impellers. Laminar mixers often have complex geometries, characterized by geometrical variables as the impeller diameter  $D$ , the blade width  $W$ , the pitch  $p$ , the impeller wall clearance  $C$ , and the off-bottom clearance  $C_b$ . In most applications, baffles are not needed and can in fact cause poor mixing behavior [87]. Examples of laminar impellers are helical ribbons, screws, helical ribbon screws and anchor impellers.

In many processes, multiple impellers are applied in order to obtain better mixing of a larger volume. In tall tanks where the liquid height to tank diameter ratio ( $H/T$ ) is greater than 1, the use of multiple impellers will cause better top-to-bottom circulation of the bulk. By using axial impellers, fluid can be pumped upward or downward in the tank into a new impeller's flow area. However, if the axial flow impellers are placed too close together, they may behave as a single larger impeller. A problem associated with multiple radial impellers is the formation of fluid cells or compartments around each impeller. Exchange of fluid mass between these fluid cells is poor resulting in poor mixing of the whole tank volume.

The viscosity of the fluid is one of several factors affecting the selection of the type of agitator ([27], pp 142-143). Based on experience the viscosity ranges for which the different agitators can be used might be indicated. Propellers are often used for viscosities of the fluid below about 3 ( $Pa s$ ), turbines may be used below about 100 ( $Pa s$ ), modified paddles such as anchor agitators are normally used above 50 ( $Pa s$ ) to about 500 ( $Pa s$ ), helical and ribbon type agitators are often used above this range to about 1000 ( $Pa s$ ) and have been used up to 25 000 ( $Pa s$ ). For viscosities greater than about 2.5 to 5 ( $Pa s$ ) and above, baffles are usually not needed since little swirling is present above these viscosities.

## 7.2 Fluid Shear Rates, Impeller Pumping Capacity and Power Consumption

An impeller is essentially a pump, although not a very efficient one. All the energy an impeller supplies to the fluid produces fluid flow and shear. In other words, a rotating impeller transports kinetic energy from the impeller blade to the surrounding fluid. Generally, approximately 80% of the mixing applications primarily require impeller pumping and mass flow of the batch, such as blending of liquids and solid suspension. These important applications include fermentation, particle degradation in emulsions, gas dispersion and polymerization [65]. For about 20% of the mixing applications, producing shear is the main requirement for mixing. Many industrial chemical reactive processes require primarily shear in order to provide contact between the reacting components on a molecular level.

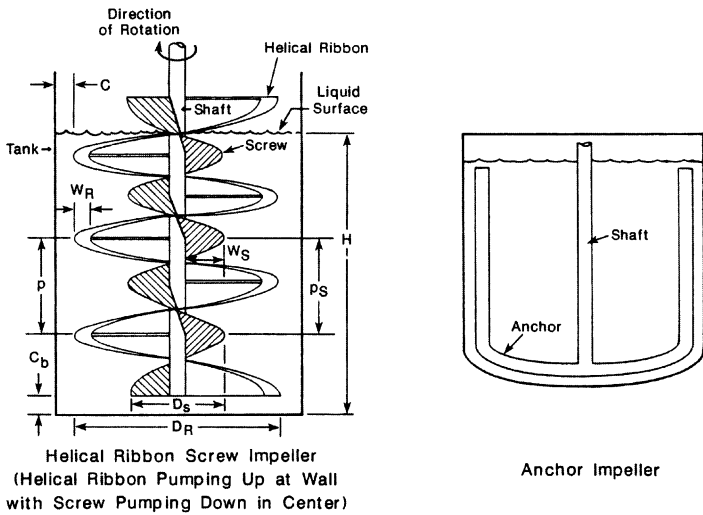
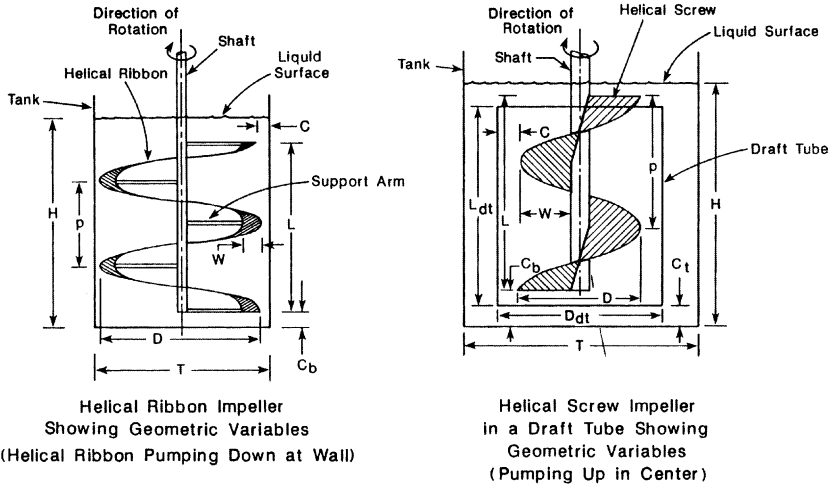


**Fig. 7.4.** Typical laminar impellers [87]. By permission from Tatterson (personal communications, 2006).

**7.2.1 Fluid shear rates**

Fig 7.5 shows a typical flow pattern produced by a radial impeller. As can be seen from the figure, the velocity of the fluid discharged from the middle of the impeller blade is highest. The shear rate is determined by the gradient of

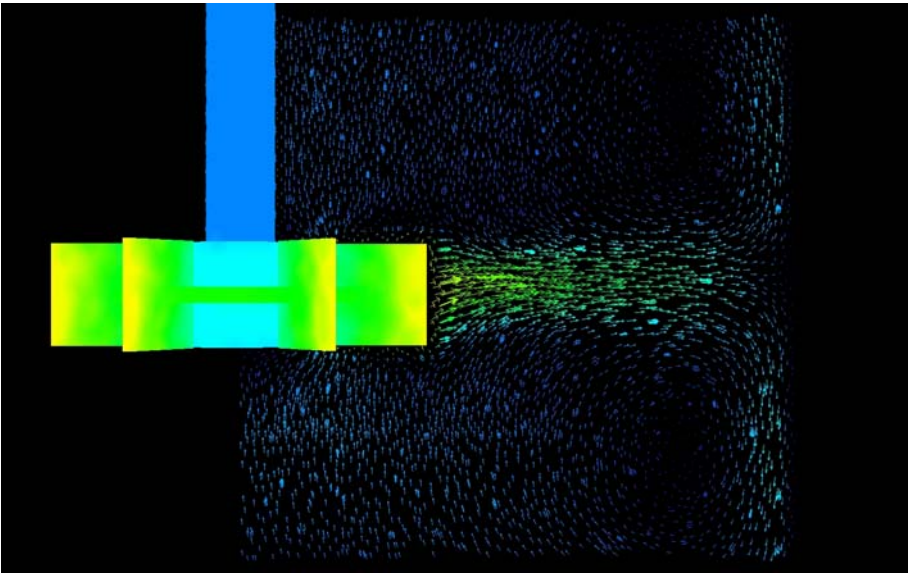


**Fig. 7.5.** Simulated stirred tank showing a typical flow pattern from a radial impeller. The figure is produced by a FLUENT simulation.

the velocity profile. The velocity gradient multiplied by the kinematic viscosity determines the shear stress. This force is responsible for dispersing gas, stretching liquid particles and intermixing small-scale fluid parcels [65].

To investigate how changes in impeller speed and impeller size influence on the fluid shear, the fluid discharge velocities from the impeller have been measured and simulated. The maximum shear rate obtained at the fluid boundary, as well as the average shear rate around the entire impeller can be calculated from these data. The maximum shear rates in the tank volume are generally found on the impeller blade. In a baffled tank, the shear rates decrease from impeller tip towards the tank wall and are decreasing with decreasing rotational speed.

### 7.2.2 Impeller Pumping Capacity

Axial turbines are pumping fluid axially in the tank creating a circulating flow pattern. The total volumetric turnover rate in the tank is the total circulation rate taking place in the tank. The pumping capacity,  $Q$ , of an impeller is the volumetric flow rate passing through the planes established by the impeller rotation. The entrained circulation rate is the difference between these two volumetric flow rates. In accordance with the continuity equation on integral form for an incompressible fluid, the volumetric flow rate  $Q$  is proportional to the fluid velocity multiplied by the flow area:

$$Q \propto vA \propto (\pi ND)D^2 \quad (m^3/s) \quad (7.1)$$

where the fluid velocity is assumed to be proportional to the impeller tip speed,  $v \propto v_t = (\pi ND)$ , and a size measure of the area is given by the square of the impeller diameter,  $A \propto D^2$ .

We may then introduce a proportionality coefficient,  $N_Q$ , defined as:

$$Q = N_Q ND^3 \quad (m^3/s) \quad (7.2)$$

where the flow or pumping number,  $N_Q$ , is a dimensionless group used to quantify the flow pattern in stirred tanks [65].  $N_Q$  varies with impeller type, tank geometry and flow regime.  $N$  is the stirring rate in RPM (rounds per minute).

The impeller Reynolds number is defined as:

$$Re = \frac{\rho v D}{\mu} = \frac{\rho (ND) D}{\mu} = \frac{\rho N D^2}{\mu} \quad (7.3)$$

A similar relation can be derived for radial impellers. Experiments have shown that for a disk style turbine the pumping number decreases with increasing impeller Reynolds number [87] (p 213), while for a propeller the pumping number seems to increase with increasing Reynolds number. Normally, empirical correlations expressed in terms of the impeller Reynolds number etc. are developed to estimate how the pumping number varies with impeller geometry.

### 7.2.3 Impeller Power Consumption

Impeller power draw is the power transfer from the impeller to the fluid causing fluid motion. This power is eventually dissipated by viscous dissipation into heat within the fluid. Power dissipation is often termed power consumption and is equal to the power draw at steady state according to a global or macro scale kinematic energy balance.

Several approaches have been applied estimating the power consumption. The traditional approach is to use dimensional analysis, creating power laws based on experimental data on torque<sup>2</sup> [87]. The power or Newton number has the same function as the pumping number, accounting for various effects on power consumption.

Impeller power consumption,  $P$ , is primarily a function of system characteristics like impeller speed,  $N$ , impeller diameter,  $D$ , impeller design, physical properties of fluid, vessel size and geometry, impeller location and baffle design. Through extensive experimental work, correlations determining the

---

<sup>2</sup> The torque or angular moment is defined as the tendency of a force to rotate the body to which it is applied. Torque is thus a force that affects rotational motion and is always specified with regard to the axis of rotation.

influence of these quantities upon power consumption have been established. The main purpose of such relations is to estimate the power draw for a given process, so that a tank geometry which maximizes impeller power draw can be designed and scaled to industrial units [87] (p 22). The power consumption,  $P$ , is given by:

$$P = N_p \rho N^3 D^5 \quad (W) \quad (7.4)$$

where  $N_p$  is the dimensionless Newton number and  $\rho$  is the density of the fluid. The dimensionless Newton number is a characteristic number for the effects of geometry and flow regime on the power consumption.

The power number in (7.4) is usually determined from suitable parameterizations which are functions of Reynolds number, Froude number, and geometry.

### 7.2.4 Fundamental Analysis of Impeller Power Consumption

Fundamental momentum and energy analyzes can be used to verify the relationships obtained by dimensional analysis. The theory might be of more general interest thus a brief outline is presented in this section.

#### Radial Impeller Power Consumption

In this analysis the moment of a force with respect to an axis, namely, *torque*, is important. Although the linear momentum equation can be used to solve problems involving torques, it is generally more convenient to apply the angular momentum equation for this purpose. By forming the moment of the linear momentum and the resultant force associated with each particle of fluid with respect to a point in an inertial coordinate system, a moment of moment equation that relates torque and angular momentum flow can be obtained.

Our starting point is the familiar Newton's second law for a single rigid particle:

$$\mathbf{f} = \frac{d(m\mathbf{v})}{dt} \quad (N) \quad (7.5)$$

The torque exerted by the force  $\mathbf{F}$  about a fixed point is [79]:

$$\mathbf{t} = \mathbf{r} \times \mathbf{f} \quad (Nm) \quad (7.6)$$

where  $\mathbf{r}$  is the radius vector from the fixed point to the point of application of  $\mathbf{r}$ .

From Newton's law of motion it is obvious that:

$$\mathbf{t} = \mathbf{r} \times \frac{d(m\mathbf{v})}{dt} \quad (Nm) \quad (7.7)$$

By convention the angular momentum vector  $\mathbf{h}$  is defined as the vector product of the radius vector to the particle and the linear momentum:

$$\mathbf{h} = \mathbf{r} \times (m\mathbf{v}) \quad (kg\ m^2/s) \quad (7.8)$$

Upon differentiating  $\mathbf{h}$  with respect to time, we get:

$$\frac{d\mathbf{h}}{dt} = \frac{d\mathbf{r}}{dt} \times m\mathbf{v} + \mathbf{r} \times \frac{d(m\mathbf{v})}{dt} = \mathbf{r} \times \frac{d(m\mathbf{v})}{dt} \quad (7.9)$$

The first term on the RHS vanishes because the cross product of two parallel vectors is zero (i.e.,  $m\frac{d\mathbf{r}}{dt} \times \mathbf{v} = m\mathbf{v} \times \mathbf{v} = 0$ ).

This relation expresses that the rate of change of angular momentum of a particle about a fixed point is equal to the torque applied to the particle ([95], p 130 and pp 158-159):

$$\mathbf{t} = \frac{d\mathbf{h}}{dt} \quad (Nm) \quad (7.10)$$

A similar analysis can be applied to a material control volume. If  $O$  is the point about which moments are desired, the angular momentum about  $O$  for the given system is expressed by:

$$\mathbf{H}_O = \int_{V(t)} \rho(\mathbf{r} \times \mathbf{v})\ dv \quad (kg\ m^2/s) \quad (7.11)$$

where  $\mathbf{r}$  is the position vector from  $O$  to the elemental volume  $dv$ , and  $\rho$  and  $\mathbf{v}$  are the fluid density and velocity of that element.

The torque on the material volume is then:

$$\mathbf{T}_O = \frac{D\mathbf{H}_O}{Dt} = \frac{D}{Dt} \int_{V(t)} \rho(\mathbf{r} \times \mathbf{v})\ dv \quad (Nm) \quad (7.12)$$

We can now relate the system formulation to an inertial control volume formulation using the Reynolds transport theorem (see App A):

$$\frac{D}{Dt} \int_{V(t)} \rho(\mathbf{r} \times \mathbf{v})\ dv = \int_V \frac{\partial}{\partial t} [(\mathbf{r} \times \mathbf{v})\rho]\ dv + \int_A (\mathbf{r} \times \mathbf{v})\rho\mathbf{v} \cdot \mathbf{n}\ da \quad (Nm) \quad (7.13)$$

For an Eulerian control volume, (7.12) becomes:

$$\mathbf{T}_O = \frac{\partial}{\partial t} \int_V (\mathbf{r} \times \mathbf{v})\rho\ dv + \int_A (\mathbf{r} \times \mathbf{v})\rho\mathbf{v} \cdot \mathbf{n}\ da \quad (Nm) \quad (7.14)$$

This relation is referred to as the *angular momentum theorem*. The first term on the RHS represents the rate of change of angular momentum of the fluid contained in the control volume, and the second term represents the net flux of angular momentum leaving the control volume. The sum is equal to the total torque applied to the mass of fluid that is contained in the control volume at time  $t$ .

For steady flows where the only external torque is applied by a shaft, the angular momentum equation reduces to:

$$\mathbf{T}_{\text{Shaft}} = \int_A (\mathbf{r} \times \mathbf{v}) \rho \mathbf{v} \cdot \mathbf{n} da \quad (Nm) \quad (7.15)$$

Furthermore, if there are only 1D inlets and outlets, the angular momentum flux terms evaluated on the control surface become:

$$\int_A (\mathbf{r} \times \mathbf{v}) \rho \mathbf{v} \cdot \mathbf{n} da = \sum (\mathbf{r} \times \mathbf{v})_{\text{Out}} \dot{m}_{\text{Out}} - \sum (\mathbf{r} \times \mathbf{v})_{\text{In}} \dot{m}_{\text{In}} \quad (7.16)$$

For 1D flows where the fluid enters the device at the radial location  $\mathbf{r}_1$  with a uniform absolute velocity  $\mathbf{v}_1$ , and leaving the pump at the radial location  $\mathbf{r}_2$  with a uniform absolute velocity  $\mathbf{v}_2$ , the relation reduces to:

$$T_{\text{Shaft}} = r_2 v_{\theta,2} \dot{m}_2 - r_1 v_{\theta,1} \dot{m}_1 \quad (Nm) \quad (7.17)$$

If the flow enters the impeller with purely axial absolute velocity, the entering fluid has no angular momentum and  $v_{\theta,1} = 0$ . The torque is then given by:

$$T_{\text{Shaft}} = r_2 v_{\theta,2} \dot{m}_2 = \rho Q r_2 v_{\theta,2} \quad (Nm) \quad (7.18)$$

This form of the angular momentum equation can be applied determining the dependence of torque on fluid pumping for a radial impeller. The control volume for radial flow impellers may be defined as a circular cylindrical volume encompassing the impeller plus some fluid surrounding the impeller. The fluid enters the impeller axially and exit radially. Tests have shown that the flow into the impeller has very little angular momentum. Therefore, only the flow exiting from the impeller must be considered for a radial impeller. The angular momentum balance (7.18) can be approximated as ([65], pp 158-159; [83], pp 413-414):

$$T_{\text{Shaft}} = r v_{\theta} \dot{m} = \frac{D}{2} v_{\theta} \dot{m} \quad (Nm) \quad (7.19)$$

where  $r$  has been set to  $D/2$ .

The mass flow rate  $\dot{m}$  is given by the radial component of the velocity exiting the impeller:

$$\dot{m} = \rho Q = \rho N_Q N D^3 = \rho \pi D H v_r \quad (kg/s) \quad (7.20)$$

The principal assumption required to link the angular momentum equation (7.19) and the continuity relation (7.20) is that the flow exiting the impeller is tangential to the blade attachment. Although this is not absolutely correct, it does make a reasonable first approximation [65]:

$$v_r = v \cos \phi \quad (7.21)$$

and

$$v_\theta = \pi ND - v \sin \phi \quad (7.22)$$

where  $\phi$  is the blade attachment angle,  $v$  is the fluid velocity parallel to the blade tip and  $H$  is the impeller blade height. Combining the latter two equations, we can express the tangential component of the flow from the impeller in terms of the tip speed and the impeller flow:

$$v_\theta = \pi ND - v_r \tan \phi \quad (7.23)$$

Using the continuity relation (7.20), the radial component of the velocity can be expressed as a function of the impeller flow number:

$$v_r = \frac{N_Q}{\pi \frac{H}{D}} ND \quad (7.24)$$

Substituting the expressions found for the two velocity components (7.23) and (7.24) into the continuity (7.20) and the angular momentum balance (7.19) gives an expression for the dependence of torque on fluid pumping:

$$P = N T_{\text{Shaft}} = \pi^2 \rho N_Q N^3 D^5 \left(1 - \frac{N_Q}{\pi^2 \frac{H}{D}} \tan \phi\right) = N_P \rho N^3 D^5 \quad (W) \quad (7.25)$$

where :

$$N_P = \frac{\pi}{2} N_Q \left(1 - \frac{N_Q}{\pi^2 \frac{H}{D}} \tan \phi\right) \quad (7.26)$$

The result deduced from the fundamental angular momentum equation coincides with the dimensional analysis. The fundamental equation provides additional information relating the dimensionless numbers  $N_P$  and  $N_Q$  to the impeller geometry.

### Propeller Power Consumption - Angular Momentum Analysis

The design of an axial propeller is based on the fundamental principles of airfoil theory. The device use airfoil sections to change the fluid pressure in order to produce a force, and the change in pressure occurs because the fluid momentum changes. The problem can be described using either the angular momentum equation or the total energy equation. The angular momentum equation analysis is presented first, the approach using the total energy equation is discussed in the next subsection. For chemical engineers the latter approach may seem more physically intuitive.

To simplify the analysis, we assume that the flow into the impeller has no preswirl. Tests have shown that this preswirl is quite small for most cases. Because of the impeller geometry and airfoil coordinate system, the lift and drag terms contribute both to the axial thrust<sup>3</sup> and to the torque forces. The

<sup>3</sup> Thrust is defined as the propulsive force developed by a jet-propelled motor.

propeller of a boat or a airplane is designed to produce thrust, and since the greatest contribution to thrust comes from the lift force  $F_L$ , the design goal is to maximize lift and minimize drag,  $F_D$ . Since the angle of the blade decreases with an increase in  $r$ , for a well designed propeller the propeller blade must be warped in order to obtain the optimum angle of attack along the length of the blade. This make it very difficult to estimate the resulting velocity profile around the whole surface of the blade, and it becomes very difficult to apply the same procedure as for radial devices. To obtain a reasonable estimate of the torque for axial devices we are forced to use the more complex procedure integrating the moment of inertia over the rigid blade surface.

By definition (e.g., [16], chap 14), the lift is normal to the relative fluid velocity,  $v_{\text{Relative}}$ , and the drag is the force acting parallel to the same velocity, as sketched in Fig 7.6. Thus one component of the lift force,  $dF_L \cos\theta$ , produces a positive thrust component<sup>4</sup>, and a component of the drag,  $dF_D \sin\theta$ , produces a negative thrust component:

$$dF_{\text{Thrust}} = dF_L \cos\theta - dF_D \sin\theta \quad (N) \quad (7.27)$$

In a similar manner, it can be shown that the tangential force for this blade element is given by:

$$dF_{\text{Tangential}} = dF_L \sin\theta + dF_D \cos\theta \quad (N) \quad (7.28)$$

The torque,  $T$ , opposing rotation of the propeller (and inducing fluid flow) is given by:

$$dT = r dF_{\text{Tangential}} = (dF_L \sin\theta + dF_D \cos\theta)r \quad (Nm) \quad (7.29)$$

Thus, the differential balance between the torque and the drag forces can be expressed as:

$$dT = r dF_D \quad (Nm) \quad (7.30)$$

assuming that  $\theta$  is very small so that  $\cos\theta \approx 1$  and  $\sin\theta \approx 0$ .

The steady drag force on the impeller blade section can, as a first approach, be formulated as:

$$F_D = \frac{1}{2} C_D \rho U^2 A \quad (N) \quad (7.31)$$

where  $A$  is the projected area or surface area of the body,  $\rho$  is the density of the fluid and  $U$  is the relative velocity between the blade and the fluid.

Using the differential force balance, the differential torque is given as:

$$dT = r dF_D = \frac{1}{2} C_D \rho U^2 W r dr \quad (7.32)$$

where  $W dr$  is the projected area of the blade section, and  $C_D$  is the average drag coefficient of the blade section.

<sup>4</sup> The work done by the impeller on the fluid is equal to the thrust multiplied by the distance [83](p 423), as is discussed in the subsequent section.

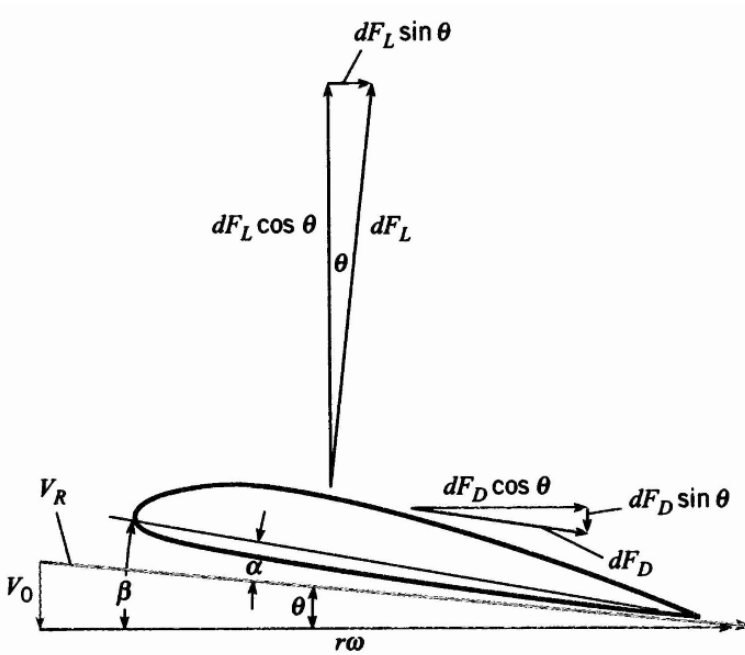


**Fig. 7.6.** Definition sketch for a propeller-blade element [16].  $V_R$ : Velocity of fluid relative to propeller section.  $F_L$ : Lift force normal to  $V_R$ .  $F_D$ : Drag force acting parallel to  $V_R$ .  $V_0$ : Speed of airplane and propeller.  $V_t = r\omega$ : Tangential velocity resulting from propeller rotation.  $r$ : Radial position on propeller.  $\omega$ : Angular speed of propeller.  $\theta$ : Angle between  $V_t$  and  $V_R$ .  $\alpha$  and  $\beta$ : Angular measures. Reproduced with permission from John Wiley & Sons, Inc, 2006.

Equating the relative velocity of the fluid to the blade with the impeller rotational speed ( $U = Nr$ ), assuming no pre-swirl, yields:

$$dT = \frac{1}{2}C_D\rho N^2Wr^3dr \tag{7.33}$$

Integrating over the impeller radius gives:

$$T = K\rho N^2WR^4 \tag{7.34}$$

For geometrically similar systems, the impeller radius,  $R$ , and the blade width,  $W$ , are proportional to the impeller diameter,  $D$ .

The torque may thus be approximated by:

$$T = K''\rho N^2D^5 \tag{7.35}$$

Hence, the power draw yields:

$$P = NT \approx K''' \rho N^3 D^5 \quad (W) \quad (7.36)$$

since power draw is the product of torque and the impeller rotational speed.

For laminar flow a similar differential force balance, balancing the drag force on a blade section and the torque can be formulated. For creeping flow inertial forces are not important and viscous forces completely dominates the flow.

The laminar steady drag force on the fluid can be written as  $F \propto \mu U D$ , where  $\mu$  is the fluid viscosity. Substituting  $U$  with  $\pi N D$  the power becomes  $P \propto \mu N^2 D^3$  or  $\frac{P}{\mu N^2 D^3} = K$ , where  $K$  is the Newton number for laminar flow.  $K$  can be rewritten as:

$$K = \frac{P}{\rho N^3 D^5} \times \frac{\rho N D^2}{\mu} = N_p Re \quad (-) \quad (7.37)$$

which shows that for laminar flow:

$$N_p \propto \frac{1}{Re} \quad (7.38)$$

This is in agreement with the observed change in power number under laminar flow conditions [87] (p 21-22).

### Propeller Power Consumption - Kinetic Energy Analysis

The application of impellers in mixing vessels denotes a kind of turbomachinery<sup>5</sup>. The principal difference between the two units is the feedback response which results from the fluid being contained in a vessel [65]. This has a major effect on the pumping capacity, the power draw, and the mechanical loads experienced by the structure. Nevertheless, the same broad principles may be applied to predict the impact of impeller geometry changes on the flow and power.

Two theoretical approaches can be applied to predict the head, power, efficiency, and flow rate of a pump or impeller. One way is to apply a simple 1D Euler flow formulation, and the alternative way is to apply more complex 3D models which account for viscous effects. In this section the derivation of the steady state 1D power equation is examined, starting out from the general microscopic energy balance [95] (chap 3.6 and 11.2), [62] (chap 5) and [100] (chap 5).

As explained in chap 1, for a fixed control volume the first law of thermodynamics can be written:

$$\dot{Q} + \dot{W} = \frac{DE}{Dt} = \frac{\partial}{\partial t} \int_V \hat{E} \rho dv + \int_A \hat{E} \rho (\mathbf{v} \cdot \mathbf{n}) da \quad (7.39)$$

<sup>5</sup> Turbomachines are dynamic fluid machines that add (for pumps) or extract (for turbines) flow energy.

The total stored energy,  $\hat{E}$ , per unit mass is considered to be the sum of three terms:

$$\hat{E} = e + \frac{1}{2}v^2 + (-\mathbf{g} \cdot \mathbf{r}) \quad (7.40)$$

If  $z$  is defined positive upwards,  $\mathbf{g} = -g\mathbf{e}_z$  and  $(-\mathbf{g} \cdot \mathbf{r}) = (g\mathbf{e}_z \cdot \mathbf{r}) = gz$ , thus:

$$\hat{E} = e + \frac{1}{2}v^2 + gz \quad (7.41)$$

The molecular internal energy,  $e$ , is a function of  $T$  and  $p$  for a single phase pure substance, whereas the potential and kinetic energies are kinetic properties.

The heat and work transfer terms need to be examined in detail. In chap 1,  $\dot{Q}$  was divided into conduction and radiation effects. Here we leave this term untouched and consider the work term in further detail.

The work term (i.e, the work transfer rate,  $\dot{W}$ , also called power) can be divided into three parts:

$$\dot{W} = \dot{W}_{\text{Shaft}} + \dot{W}_{\text{Pressure}} + \dot{W}_{\text{Viscous stresses}} \quad (7.42)$$

The work of gravitational forces has already been included as potential energy. Other types of work, e.g., those due to electromagnetic forces, are excluded in this analysis.

The shaft work isolates that portion of the work which is deliberately done by a machine (e.g., pump impeller, fan blade, piston, agitation impeller, etc.) protruding through the control surface into the control volume.

The power required to drive the pump is:

$$P_{\text{Shaft}} = \dot{W}_{\text{Shaft,Pump}} = \Omega_{\text{Shaft}} T_{\text{Shaft}} \quad (7.43)$$

where  $\Omega_{\text{Shaft}}$  is the shaft angular velocity and  $T_{\text{Shaft}}$  denotes the shaft torque. When shaft torque and rotation are in the same direction, we are dealing with a pump, otherwise the given turbomachine is a turbine.

The rate of work,  $\dot{W}$ , done by pressure forces occurs at the surface only, all work on internal portions of the material in the control volume is by equal and opposite forces and is self-canceling. The pressure work equals the pressure force on a small surface element,  $da$ , times the normal velocity component into the control volume:

$$d\dot{W}_{\text{Pressure}} = (pda)v_{n,in} = p(-\mathbf{v} \cdot \mathbf{n})da \quad (7.44)$$

The total pressure work is the integral over the control surface:

$$\dot{W}_{\text{Pressure}} = - \int_A p(\mathbf{v} \cdot \mathbf{n})da \quad (7.45)$$

If part of the control surface is the surface of a machine part, one prefers to delegate that portion of the pressure to the shaft work term,  $\dot{W}_{\text{Shaft}}$ , not

to  $\dot{W}_{\text{Pressure}}$ , which is primarily meant to isolate the fluid flow pressure work terms.

The shear work due to viscous stresses also occurs at the control surfaces, the internal work terms again being self-canceling, and consists of the product of each viscous stress (one normal and two tangential) and the respective velocity component:

$$d\dot{W}_{\text{Viscous stresses}} = (\boldsymbol{\sigma} \cdot \mathbf{n}) \cdot \mathbf{v} da \quad (7.46)$$

or

$$\dot{W}_{\text{Viscous stresses}} = \int_A (\boldsymbol{\sigma} \cdot \mathbf{n}) \cdot \mathbf{v} da \quad (7.47)$$

where  $(\boldsymbol{\sigma} \cdot \mathbf{n})$  is the stress vector on the elemental surface,  $da$ .

For all parts of the control surface which are *solid walls*,  $\mathbf{v} = 0$  from the viscous no-slip condition. Hence,  $\dot{W}_{\text{Viscous stresses}} = 0$  identically. If parts of the control volume surface denote the *surface of a machine*, the viscous work is contributed by the machine and should rather be absorbed in the term,  $\dot{W}_{\text{Shaft}}$ . At an inlet or outlet, the flow is approximately normal to the element  $da$ . Thus, the only viscous work term comes from the normal stress,  $\sigma_{nn}v_n da$ . Since viscous normal stresses are extremely small in most cases, it is customary to neglect viscous work at inlets and outlets of the control volume.

The net result of the above discussion is that the rate of work term essentially consists of:

$$\dot{W} = \dot{W}_{\text{Shaft}} - \int_A p(\mathbf{v} \cdot \mathbf{n}) da \quad (7.48)$$

Introducing these terms into the energy balance equation, we find that the pressure work term can be combined with the energy flux term since both involve surface integrals of  $(\mathbf{v} \cdot \mathbf{n})$ . The control volume energy equation thus becomes:

$$\dot{Q} + \dot{W}_{\text{Shaft}} = \frac{\partial}{\partial t} \int_V \hat{E} \rho dv + \int_A \left( \hat{E} + \frac{p}{\rho} \right) \rho (\mathbf{v} \cdot \mathbf{n}) da \quad (7.49)$$

The control volume surface integral can be expressed in terms of the enthalpy quantity,  $h = e + p/\rho$ . Then, the final form of the energy equation for a fixed control volume becomes:

$$\dot{Q} + \dot{W}_{\text{Shaft}} = \frac{\partial}{\partial t} \int_V \left( e + \frac{1}{2}v^2 + gz \right) \rho dv + \int_A \left( h + \frac{1}{2}v^2 + gz \right) \rho (\mathbf{v} \cdot \mathbf{n}) da \quad (7.50)$$

If the control volume has a series of 1D inlets and outlets, the surface integral reduces to a summation of outlet fluxes minus inlet fluxes:

$$\int_A \left( h + \frac{1}{2}v^2 + gz \right) \rho (\mathbf{v} \cdot \mathbf{n}) da = \sum \left( h + \frac{1}{2}v^2 + gz \right)_{\text{Out}} \dot{m}_{\text{Out}} - \sum \left( h + \frac{1}{2}v^2 + gz \right)_{\text{In}} \dot{m}_{\text{In}} \quad (7.51)$$

where the values of  $h$ ,  $\frac{1}{2}v^2$  and  $gz$  are taken to be averages over each cross section.

For steady flow with one inlet and outlet, both assumed 1D this equation further reduces to a relation used in many engineering analyzes. Let section 1 be the inlet and section 2 the outlet:

$$\dot{Q} + \dot{W}_{\text{Shaft}} = \sum (h + \frac{1}{2}v^2 + gz)_2 \dot{m}_2 - \sum (h + \frac{1}{2}v^2 + gz)_1 \dot{m}_1 \quad (7.52)$$

From continuity we find that,  $\dot{m}_{\text{In}} = \dot{m}_{\text{Out}} = \dot{m}$ , thus:

$$(h + \frac{1}{2}v^2 + gz)_1 = (h + \frac{1}{2}v^2 + gz)_2 - q - w_{\text{Shaft}} \quad (7.53)$$

where  $q = \dot{Q}/\dot{m} = dQ/dm$ , the heat transferred to the fluid per unit mass. Similarly,  $w_{\text{Shaft}} = \dot{W}_{\text{Shaft}}/\dot{m} = dW_{\text{Shaft}}/dm$ .

The steady flow energy equation states that the upstream stagnation enthalpy,  $H_1 = (h + \frac{1}{2}v^2 + gz)_1$ , differs from the downstream value  $H_2$  only if there is heat transfer or shaft work (i.e., neglecting viscous work) between section 1 and 2.

Each term in the latter equation has the dimensions of energy per unit mass, or velocity squared, which is a form commonly used by mechanical engineers. If we divide through by  $g$ , each term becomes a length, or a *head*, which is a form preferred by civil engineers. The traditional symbol for head is  $h$ , so we rewrite the head form of the energy equation in terms of internal energy:

$$\left(\frac{p}{\rho g} + \frac{e}{g} + \frac{v^2}{2g} + z\right)_1 = \left(\frac{p}{\rho g} + \frac{e}{g} + \frac{v^2}{2g} + z\right)_2 - h_q - h_{\text{Shaft}} \quad (7.54)$$

where  $h_q = q/g$  and  $h_{\text{Shaft}} = w_{\text{Shaft}}/g$  are the head forms of the heat added and shaft work, respectively. The term  $\frac{p}{\rho g}$  is called pressure head and the term  $\frac{v^2}{2g}$  is denoted velocity head.

A very common application of the steady flow energy equation is for low speed flow with no shaft work and negligible viscous work, such as liquid flow in pipes. For this case we may write the energy balance relation as:

$$\left(\frac{p}{\rho g} + \frac{v^2}{2g} + z\right)_1 = \left(\frac{p}{\rho g} + \frac{v^2}{2g} + z\right)_2 + \frac{e_2 - e_1 - q}{g} \quad (7.55)$$

The last term on the right is the difference between the available head upstream and downstream and is normally positive, representing the loss in head due to friction, denoted as  $h_{\text{Friction}}$ .

An important group of fluid mechanics problems involves 1D, incompressible, steady flow with friction and shaft work. Included in this category are constant density flows through pumps and agitators.

Thus, in low speed incompressible flow with one inlet and one exit, we may assume that the previous observation that  $\frac{e_2 - e_1 - q}{g}$  equals the loss in

head of available energy due to friction is still valid. Thus, we conclude that the energy equation can be expressed as:

$$\left(\frac{p}{\rho g} + \frac{v^2}{2g} + z\right)_2 = \left(\frac{p}{\rho g} + \frac{v^2}{2g} + z\right)_1 + h_{\text{Shaft}} - h_{\text{Friction}} \quad (7.56)$$

where  $h_{\text{Shaft}}$  is the head supplied and  $h_{\text{Friction}}$  the losses. This relation is sometimes called the mechanical energy equation or *the extended Bernoulli equation*.

If a turbine is in the control volume, the notation  $h_{\text{Shaft}} = -h_{\text{Turbine}}$  (with  $h_{\text{Turbine}} > 0$ ) is adopted. For a pump or an agitator in the control volume,  $h_{\text{Shaft}} = h_{\text{Pump}}$ . The quantity  $h_{\text{Turbine}}$  is termed the turbine head and  $h_{\text{Pump}}$  is the pump head. The loss term,  $h_{\text{Friction}}$ , is often referred to as head loss<sup>6</sup>.

The above equation may then be written in a more specific form:

$$\left(\frac{p}{\rho g} + \frac{v^2}{2g} + z\right)_2 = \left(\frac{p}{\rho g} + \frac{v^2}{2g} + z\right)_1 - h_{\text{Friction}} + h_{\text{Pump}} - h_{\text{Turbine}} \quad (7.57)$$

The  $h$ -terms are all positive, as friction loss is always positive in real flows, a pump adds energy, and a turbine extracts energy from the flow.

The loss term,  $h_{\text{Friction}}$ , is commonly correlated with flow parameters in pipes, valves, fittings, and other flow devices.

The pipe head loss may be calculated by the well known *Darcy-Weisbach equation* [94], valid for duct flows of any cross section and for laminar and turbulent flow:

$$h_{\text{Friction}} = f_D \frac{L}{d} \frac{v^2}{2g} \quad (7.58)$$

For laminar flow  $f_D$  can be found analytically,  $f_D = 64\mu/\rho vd$ , while for turbulent flows more approximate relations are used.

Assuming steady flow, the pump basically increases the Bernoulli head of the flow between point 1 and 2. Neglecting heat transfer, this change is denoted by  $H$ :

<sup>6</sup> In other contexts, the turbine head is sometimes written as  $h_T = -(h_{\text{Shaft}} - h_{\text{Friction}})_T$ , where the subscript  $T$  refers to the turbine component of the contents of the control volume only. The quantity  $h_T$  is the actual head drop across the turbine and is the sum of the shaft work head out of the turbine and the head loss within the turbine.

When a pump is in the control volume,  $h_P = (h_{\text{Shaft}} - h_{\text{Friction}})_P$  is often used where  $h_P$  is the actual head rise across the pump and is equal to the difference between the shaft work into the pump and the head loss within the pump. Notice that the  $h_{\text{Friction}}$  used for the turbine and the pump is the head loss within that unit only. When  $h_s$  is used in the extended Bernoulli equation,  $h_{\text{Friction}}$  involves all losses including those within the turbine, pump or compressor. When  $h_T$  or  $h_P$  is used for  $h_{\text{Shaft}}$ , then  $h_{\text{Friction}}$  includes all losses except those associated with the turbine or pump flows.

$$H = \left( \frac{p}{\rho g} + \frac{v^2}{2g} + z \right)_2 - \left( \frac{p}{\rho g} + \frac{v^2}{2g} + z \right)_1 = h_{\text{Pump}} - h_{\text{Friction}} \quad (7.59)$$

The net head  $H$  is a primary output parameter for any turbomachine. Usually  $v_1$  and  $v_2$  are about the same,  $z_2 - z_1$  is a meter or so, and the net pump head is essentially equal to the change in pressure head:

$$H \approx \frac{p_2}{\rho g} - \frac{p_1}{\rho g} = \frac{\Delta p}{\rho g} \approx h_{\text{Pump}} - h_{\text{Friction}} \quad (7.60)$$

The power delivered to the fluid yields:

$$\begin{aligned} P &= \dot{W}_{\text{Pump}} - \dot{W}_{\text{Pump, Friction}} = \dot{m}g(h_{\text{Pump}} - h_{\text{Friction}}) \\ &= (\rho v A)g(h_{\text{Pump}} - h_{\text{Friction}}) = \rho g Q(h_{\text{Pump}} - h_{\text{Friction}}) = Q\Delta p \end{aligned} \quad (7.61)$$

where the  $Q$  quantity in this relation is the volumetric flow rate.

The power draw (i.e., power transferred from the impeller to the fluid by the lift forces) will eventually dissipate to heat (through viscous dissipation in the fluid).

According to the  $z$ -component of the linear momentum equation, the thrust force from the impeller blade is balanced by the pressure difference over the pump [83] (p 423):

$$F_{\text{Thrust}} = \Delta p A = \rho g H A \quad (7.62)$$

The lift force is usually expressed as [16] (p 635):

$$F_{\text{Thrust}} = \frac{1}{2} C_L \rho U^2 A \propto \frac{1}{2} C_L \rho (ND)^2 A \quad (7.63)$$

Hence, the impeller power draw can be expressed as:

$$P = Q\Delta p \propto ND^3 [\rho (ND)^2] = \rho N^3 D^5 \quad (W) \quad (7.64)$$

Introducing a proportionality factor, the Newton number ( $N_P$ ), the following relation occurs:

$$P = N_P \rho N^3 D^5 \quad (W) \quad (7.65)$$

This relation determining the dependence of power draw on fluid pumping is identical to the expression we found earlier using the torque analysis. This result should be expected as the mechanical energy balance is not independent of the momentum equations, they basically provide the same information.

## 7.3 Turbulent Mixing

The study of mixing includes understanding of how gas, liquid and solid phases are transported in the tank, and how this transport is affected by the tank

and the impeller(s) geometry, as well as the operational conditions such as stirring rate and pumping capacity.

Many elements must be taken into consideration designing mixing devices, basically determining the geometry and size of the tank, what type of impeller to use, the size of the impeller, the size and geometry of heat transfer equipment and if baffles are needed.

Turbulent mixing includes phenomena on all scales in the turbulence spectra. For reactive mixtures the molecular scale phenomena are also pertinent. In the context of fluid mixing emphasis has been put on the scales assumed relevant to the process and to provide basic understanding of the controlling mechanisms of mixing. A common approach in practical reaction engineering is therefore to describe mixing on macro and micro scales only.

Micro mixing is mixing of individual molecules, while macro mixing is mixing of parcels, groups or aggregates of molecules. For a chemical reaction to take place, direct contact between the reacting molecules must be established. If the reactants  $A$  and  $B$  are introduced into an agitated tank, they will not react immediately because  $A$ -rich regions and  $B$ -rich regions are partially segregated in the tank. By means of shear from an impeller, a homogeneous mixture forms with time. However, before the fluids are completely mixed, reactions at different rates at different points in the reactor may occur, giving a non-uniform product, which may be unacceptable in an industrial process. In fact, this means that different fluid elements of one reactant do not experience mixing with the other reactant at a micro scale level at the same time. Therefore, for fast chemical reactions, an impeller producing high shear is recommended so that different reaction rates at different locations are avoided. The problems related to mixing of fluids are basically associated with fast reactions and all types of heterogeneous systems. Accordingly, for slow reactions, high shear mixing is not that important since the reactants have time to mix at a micro scale level in the whole tank volume before they react at all.

### 7.3.1 Studies on Turbulent Mixing

For non-reacting fluids the studies of turbulent mixing can be divided into three categories, the gross scale observations of the global flow pattern, fine scale analysis, and experimental studies on the whole turbulent energy spectra.

#### Gross Scale Studies

Gross-scale studies are concerned with the overall flow pattern in a tank with measurements of impeller pumping capacity and gross flow rate. Such studies can give qualitative and quantitative results good enough for initial selection of impeller type and may also provide information about the most advantageous design of the system. Circulation and mixing times are other important variables that may be determined in these studies.

### Fine Scale Studies

Three different theoretical approaches have been established describing turbulent flows in general, as outlined in sect 1.3. These methods are the direct numerical simulations (DNS), large eddy simulations (LES), and the Reynolds average Navier-Stokes (RANS) approach.

Only a few LES simulations have been reported describing the turbulent flow in single phase stirred tanks (e.g., [20, 77, 18]). The lattice-Boltzmann method is used in the more recent publications since this scheme is considered to be an efficient Navier-Stokes solver. Nevertheless, the computational requirements of these models are still prohibitive, therefore the application of this approach is restricted to academic research. No direct simulations of these vessels have been performed yet.

The Reynolds averaging approach has thus been found to represent a trade-off between accuracy and computational costs. Using the Reynolds averaging concept turbulence is interpreted as a waveform and described by the time averaged equations of motion and a turbulence closure. Two-equation turbulence models like the standard  $k$ - $\varepsilon$  and  $k$ - $\omega$  models are common but full Reynolds stress models have also been applied in rare cases.

For model validation measurements of instantaneous-, time average-, and fluctuating velocities, and turbulence energy are required.

### Experimental Studies on the Turbulence Energy Spectra

In this method correlations between various velocity fluctuations are used to determine the turbulent energy spectrum,  $E(k)$ , and several turbulence length scales. The correlations mentioned contain information about how velocities and other flow properties are statistically related in the turbulent flow. Turbulence measured at a fixed point can be described as a fluctuating waveform. If two instantaneous waveforms appear to have a corresponding behavior, they are said to be correlated. Equation (1.311) shows how velocity fluctuations at two points can be statistically correlated if the distance between the two points are small.

The velocity fluctuations  $v'_i(t, \mathbf{r})$  and  $v'_j(t, \mathbf{r} + \mathbf{x})$  are said to be correlated if  $R_{ij}(t, \mathbf{x})$  has a non-zero value, and uncorrelated if the Eulerian correlation tensor  $R_{ij}(t, \mathbf{x})$  is zero.

The  $R_{ij}(t, \mathbf{x})$  correlation can be normalized by introducing the rms velocity [8]. The Eulerian correlation function is defined by:

$$Q_{ij}(t, \mathbf{x}) = \frac{\overline{v'_i(t, \mathbf{r})v'_j(t, \mathbf{r} + \mathbf{x})}}{v_i^{\text{rms}}(t, \mathbf{r})v_j^{\text{rms}}(t, \mathbf{r} + \mathbf{x})} \quad (7.66)$$

By assuming isotropic turbulence the rms velocity components in all directions are equal, hence (7.66) becomes:

$$Q_{ii}(t, \mathbf{x}) = \frac{\overline{v'_i(t, \mathbf{r})v'_i(t, \mathbf{r} + \mathbf{x})}}{v_i^{\text{rms}}(t, \mathbf{r})v_i^{\text{rms}}(t, \mathbf{r} + \mathbf{x})} \quad (7.67)$$

To calculate  $Q_{ii}(t, \mathbf{x})$ , the  $v'_i$  terms must be determined. Therefore, the scalar function  $f(r)$  called the Eulerian correlation function for isotropic turbulence in sect 1.3, is introduced (e.g., [88], chap 8; [7], chap 8; [5], sect 3.4):

$$f(t, \mathbf{x}) = \frac{\overline{v'_p(t, \mathbf{r})v'_p(t, \mathbf{r} + \mathbf{x})}}{(v_p^{\text{rms}}(t, \mathbf{r}))^2} \quad (7.68)$$

in which the velocity fluctuations are measured in the direction  $p$  parallel to the vector of separation  $\mathbf{x}$ . Using the velocity components in the direction normal to  $\mathbf{x}$ , another correlation function  $g(t, \mathbf{x})$  is defined:

$$g(r) = \frac{\overline{v'_n(x)v'_n(t, \mathbf{r} + \mathbf{x})}}{(v_n^{\text{rms}})^2} \quad (7.69)$$

As explained in sect 1.2.7, from these correlations the turbulent energy spectra, and the micro and macro scales can be calculated. The values of the different correlations are determined experimentally by measuring mean velocities and velocity fluctuations at different locations in the agitated tank.

In sect 1.2.7 we showed that the dynamics of the one-point velocity correlation,  $\overline{v'_i v'_j}$ , for incompressible flows, can be expressed by four transport equations [41] (p 323). The analogous transport equation for the dynamics of the two-point velocity correlation,  $\overline{(v'_i)_A (v'_j)_B}$ , for the general case of inhomogeneous, non-isotropic turbulence can be formulated based on the equations for the fluctuating velocity components (i.e., obtained by subtracting the time averaged equation of motion from the corresponding instantaneous equation) referring to point  $A$ , multiplied by the fluctuating velocity component  $(v_j)_B$ , referring to point  $B$ . A similar equation can be formulated based on the equation for the fluctuating velocity components referring to point  $B$ , multiplied by  $(v_j)_A$ . The equation for  $Q_{ij}(r)$  is obtained by adding these two equations. The equation for the two-point velocity correlation predicts the energy transport by means of the velocity fluctuations between the two points  $A$  and  $B$ . In other words, it describes how the turbulence energy is spread out over different eddy sizes and the transfer mechanisms of the energy exchange through the energy cascade. By taking the Fourier transform of this equation, the equation for the energy spectrum  $E(k)$  is obtained ([41, 8]). A typical energy spectrum with essential features is illustrated in Fig 1.6. The physics represented by the spectra is explained in sect 1.3.2.

Several length scales of turbulence can also be determined from the measured correlation functions. The Eulerian length scales obtained from  $f(t, \mathbf{x})$  and  $g(t, \mathbf{x})$  are the longitudinal and transverse integral scales (1.312) and (1.313), respectively. These length scales are characteristics of the larger turbulence vortices in the flow.

The Taylor micro scales of turbulence can be calculated from the same functions  $f(t, \mathbf{x})$  and  $g(t, \mathbf{x})$  using (1.317) and (1.319), respectively. However, the resulting scales do not characterize any distinct group of turbulence vortices and are thus not very useful in describing micro mixing in stirred tanks.

Instead, the Kolmogorov micro-scales (1.328) to (1.330) characterize the dissipation scales of turbulence and might indicate the effectiveness of micro-mixing in the flow provided that the turbulent energy dissipation rate and the kinematic viscosity of the fluid is known. If the Kolmogorov micro length scale is much larger than the molecular scales, the molecules are not efficiently mixed by turbulent diffusion.

The mean energy dissipation rate can be calculated directly from the energy spectrum using (1.332). Moreover, for isotropic turbulence, the energy dissipation rate and the micro scale are related as expressed by (1.323). Caution is required using the dissipation rate calculated from a turbulence model like the  $k$ - $\varepsilon$  model as in this model the dissipation quantity is merely a tuning variable for the shear stresses in a pipe and not necessarily a true physical dissipation rate. The latter approach requires validation for any applications.

### 7.3.2 Flow Fields in Agitated Tanks

The flow fields in agitated tanks with different geometry and impellers have been studied by many researchers. Qualitative and quantitative observations have been reported for the discharge flow from the impeller, the flow near and around impeller and the flow in the bulk of the tank. The flow field is generally affected by impeller and tank geometry, number of blades, liquid height and fluid properties. Most studies of flow fields have been performed for a standard tank geometry.

In most investigations the discharge flow from a Rushton turbine in a baffled tank is considered, but also the discharge flow from pitched blade turbines, propellers and open flat blade turbines have been studied. The discharge flow patterns for three different impellers are illustrated in Fig 7.7.

The discharge flow from a Rushton turbine is characterized by two trailing vortices at the top and bottom of the blade, and a strong radial discharge flow in the middle. This pattern is discharged continuously, but a periodicity is observed. Away from the blade the pattern is disrupted, causing a significant increase in turbulent velocity fluctuations. The most efficient mixing occurs at the location where the discharge flow meets the bulk flow [87]. The magnitude of the maximum velocity in the profile is comparable with the impeller tip velocity,  $v_t$ . Experiments show that the radial discharge velocity profile is not symmetrical around the radial centerline.

The strong periodicity in the discharge flow velocity near the blade is caused by the trailing vortices shed by the impeller. In these vortices, the circumferential velocity is of the order of the impeller tip velocity,  $v_t$ , and the

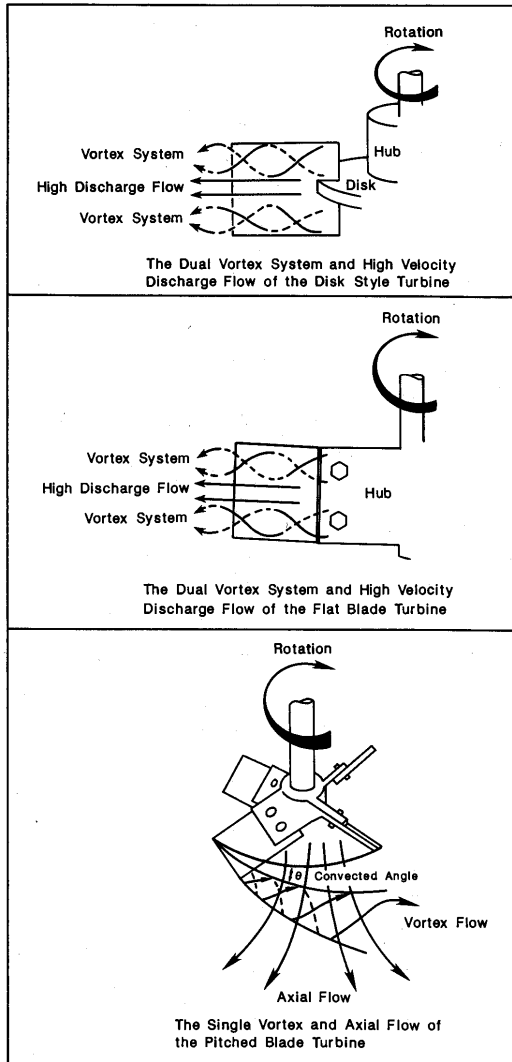


**Fig. 7.7.** The flow patterns around turbulent impellers [87]. By permission from Tatterson (personal communications, 2006).

diameter of a vortex is about half the blade width  $W$ . Vortices are found to exist all the way to the tank wall, but they do decay with radial distance from impeller.

The energy spectrum usually have a peak at the blade passing frequency, as shown by Mujumdar et al [61]. As the distance from the impeller increases, this peak weakens rapidly. This peak may be due to the presence of trailing vortices, but also influenced by the characteristic periodic component of the

impeller discharge flow. Experiments have also shown that the local energy dissipation rates decrease with radial distance from the impeller blade tip.

The discharge flow from a flat blade turbine (i.e., a paddle) is shown in Fig 7.7. The flow is similar to the flow from a disk style turbine, however, the flow pattern from the flat blade turbine is not as stable as that from the disk style turbine due to the absence of the disk. As for the Rushton turbine, the discharge flow is not symmetrical around the centerline of the blade. The energy spectra for the open flat blade turbine has a peak at the blade passing frequency, in addition to the standard  $-5/3$  and  $-7$  regions.

The flow pattern from a pitched blade turbine is shown in Fig 7.7. The flow pattern is dominated by a large axial flow through the impeller. This pumping does not provide any mixing of the fluid, but the mixing is accomplished by the vortex system formed from the blade tip. The flow from the pitched blade turbine spreads out both axially and radially. The flow pattern developed by a propeller is quite similar to that produced by the pitched blade turbine, but in the propeller discharge mostly axially.

Studies on the velocity flow fields near and around the impeller have primarily been focused on the turbulence structures and the behavior of the trailing vortices [92].

A trailing vortex system generated by a disk style turbine is shown in Fig 7.8. As can be seen from the figure, vortices along the top and bottom of the blade are formed. The centrifugal force of the blade throws the fluid outwards as the blade moves forward. This creates a mass deficit which causes the formation of a jet (the discharge flow) and the trailing vortices. The trailing vortices are continuously generated behind the blade, and upon leaving the blade, they have a short duration time before they break up. Upon exiting the blade, the vortex turns tangentially due to strong Coriolis forces. The axis of a vortex is not stationary from one blade passage to the next blade passage, but moves around in an erratic behavior.

The flow pattern around a pitched blade turbine is something similar to that for a Rushton turbine illustrated in Fig 7.8.

### 7.3.3 Circulation and mixing times in turbulent agitated tanks

Circulation times are measures of the average bulk fluid motion generated by the liquid pumping of the impeller in a stirred tank. Measurements of circulation and mixing times help us to understand the scalar transport in the tank.

Circulation times are associated with the tank's total volumetric flow rate, entrainment flow, and the pumping capacity of the impeller.

The mean circulation time,  $\theta_c$ , is given by the total tank volume divided by the pumping capacity [87, 64]:

$$\theta_c = \frac{V}{Q} \quad (7.70)$$

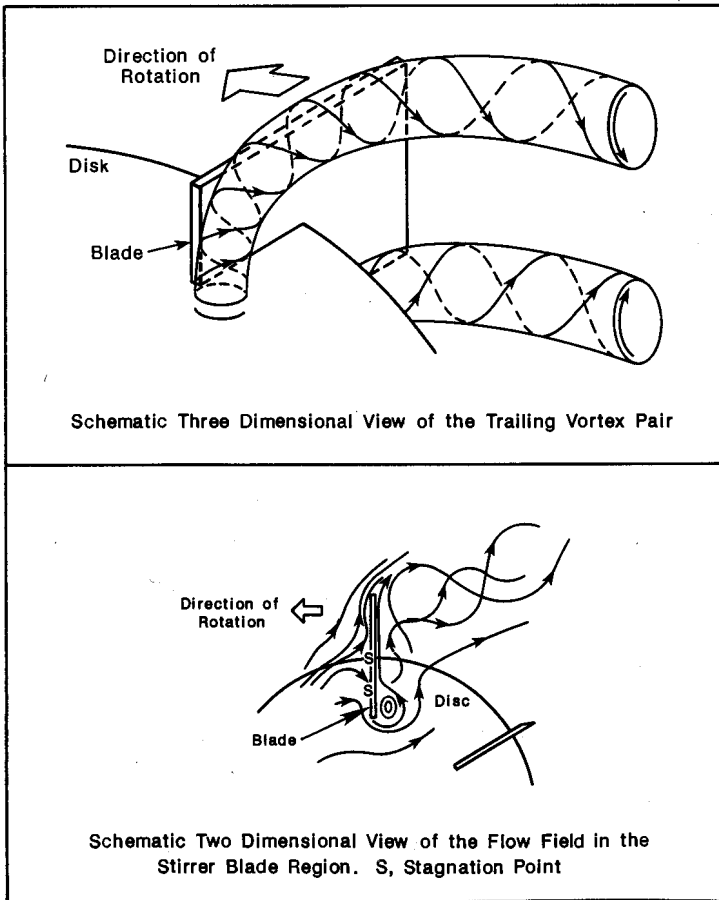


**Fig. 7.8.** The vortex system generated by a Rushton turbine [92]. Reprinted with permission from Elsevier.

The mean circulation time represents an average value for all the fluid elements in the tank and provide information on how fast the fluid parcels are transported around in the tank.

Mixing times are fundamental knowledge in reactor design and scale-up. Mixing times tell us when the whole tank volume is ideally mixed, or when a non-uniform system is made uniform. Generally, the impeller region is well mixed while the bulk fluid is not. To be able to mix all the bulk fluid of a tank, several tank volumes have to pass the impeller. Hence, the mixing time is usually considerably longer than the mean circulation time. To ensure sufficient mixing, the mixing time has to be shorter than the residence time of the species in the tank. The average residence time of material in a tank is

often considered to be the active volume of the tank divided by the volumetric flow rate. The differences between the residence and circulation times depend on the volumes of stagnant dead zones in the tank.

The number of revolutions needed to accomplish mixing is a function of the tank geometry, the impeller geometry, and of the rotational speed of the impeller. For a given geometry the relationship between impeller rotational speed and mixing time can be approximated as:

$$N\theta_m = K \quad (7.71)$$

where  $\theta_m$  is the mixing time,  $N$  the impeller speed and  $K$  a constant determined by the geometry and the size of the tank.

The mixing time is especially important upon scale-up since a larger tank will increase the mixing time, while a larger impeller will reduce the mixing time. These effects might be taken into account through the  $K$  function in (7.71) provided that a appropriate parameterization is available. The main parameters affecting the mixing times are the impeller rotational speed, the impeller and tank diameters, and the presence of baffles [87]. The mixing time is also affected by the presence of multiple impellers. However, for such vessel designs there are inconsistent mixing performance trends reported in the literature, so the mixing times need to be determined experimentally for each application.

### 7.3.4 Turbulent Reactive Flow in Stirred Tank

Turbulent reacting flow modeling is complicated by the fact that these flows contain a wide range of time and length scales (e.g., [71, 25, 26]; [2], chap 6 to 9). The rates of turbulent diffusion and convection (i.e., macro mixing) are controlled by the energy containing large scale eddies, generally several orders of magnitude larger than the molecular scale. Chemical reactions occur only if reactants are mixed on the molecular level. For non-premixed flows, molecular diffusion (i.e., micro mixing) occurs at intermediate and small scales and must occur before chemical reactions can take place.

Because of computational limitations, it is impossible to include a detailed description of all scales of interest simulating industrial reactors. The unresolved phenomena such as micro mixing and chemical reactions must be modeled. Due to the non-linear nature of the chemical reaction terms in the mass balance equation, these simplifications can lead to large errors in the model predictions for turbulent flows. In order to formulate appropriate models for reacting flows, one must understand the complex interactions between turbulence, molecular diffusion, and chemical kinetics. In general, the modeling process for turbulent reacting flows involves at least three steps [25]:

1. Modeling of the molecular diffusion-chemical reaction processes to predict the local reaction rate.

2. Modeling of the turbulent field in enough detail to approximate the rate controlling steps of turbulent mixing.
3. Modeling of local turbulent mixing of the heat and species concentrations.

The relative importance of the specific physical phenomena mentioned strongly depends on the type of flow under consideration. In this section, the discussion is limited to single-phase, constant density flows under isothermal conditions with constant viscosity and equal diffusivities. The emphasis is placed on the modeling of turbulent mixing and on the interactions between turbulent mixing and chemical reactions in non-premixed turbulent reacting flows.

The velocity field in these flows is governed by the incompressible Navier-Stokes equation (1.385) and the corresponding continuity relation (1.382). For incompressible fluids a generic transport equation for scalar species mass concentration fields can be deduced from (1.454) and expressed as:

$$\frac{\partial \omega_c}{\partial t} + \mathbf{v} \cdot \nabla \omega_c = D \nabla^2 \omega_c + S_{\omega_c} \quad (7.72)$$

In this equation  $D$  is the molecular diffusivity of binary systems, and  $S_{\omega_c}$  is the chemical source term for species  $c$ . The scalar fields are assumed to be passive scalars so that  $\omega_c$  has no significant influence on the momentum and continuity equations.

After suitable non-dimensional variables are substituted into the equations, following the same procedure as outlined in sect 1.2.5, the important dimensionless groups are obtained for the problem in question. These are the Reynolds number, the Schmidt number, the Peclet number,  $Pe = Re Sc = ul/D$ , and the Damköhler number,  $Da_I = lr/u$ . The  $u$  and  $l$  are the characteristic velocity and length scales, respectively, for the velocity field, and  $r$  denotes a characteristic chemical reaction rate.

Turbulence models are generally limited to fully developed high-Reynolds number flows. Gas-phase flows are normally characterized by  $Sc \approx 1$ , while for liquid phase flows,  $Sc \gg 1$ . The value of this Damköhler number indicates the relative rates of the mixing and chemical reaction rate time scales. Reactive flows might thus be divided into three categories: Slow chemistry ( $Da_I \ll 1$ ), fast chemistry ( $Da_I \gg 1$ ), and finite rate chemistry ( $Da_I \approx 1$ ).

The description of turbulent mixing of passive scalars is based on an extension of the turbulence theory developed for the momentum transfer processes, described in sect 1.2.7. In particular, the energy cascade idea introduced by Richardson [76] and the Kolmogorov hypotheses [47] are adopted.

However, there are important differences between the velocity and the passive scalar spectra (e.g., [68, 13, 14, 4, 8]). The spectra of passive scalars also varies for different systems depending on the value of  $Sc$ .

For large Reynolds number the kinetic energy spectrum of turbulence has the form  $E(k) \propto k^{-5/3}$  in inertial sub-range ranging from the energy containing integral scale  $k_0 = 2\pi/L$  to the Kolmogorov micro-scale

$k_K = (2\pi/\lambda_K) = 2\pi(\varepsilon/\nu^3)^{1/4}$ . Beyond the Kolmogorov micro scales the velocity spectrum has the form  $E(k) \propto k^{-7}$  [39, 80].

For mixtures where  $Sc \ll 1$ , the inertial convective subrange for passive scalars is specified by the wave number range  $k_{0,c} = 2\pi/L_c \ll k \ll k_C = 2\pi(\varepsilon/D^3)^{1/4}$ . The wave number of the largest scales for which the scalar has been spread out (i.e., the scale of segregation) is  $k_{0,c} = 2\pi/L_c$ . The integral scale of scalar segregation  $L_c$  can be estimated from an Eulerian scalar correlation function in analogy to the method used determining the integral scale of turbulence [8]. Since  $D \gg \nu$  the spectrum of concentration fluctuations in which  $E_c(k) \propto k^{-5/3}$  is not as extensive as the familiar inertial subrange for the velocity fluctuations [4, 8]. The scalar spectrum begins to fall off more rapidly at wave numbers near the Corrsin [13] micro-scale of turbulence  $k_C = 2\pi/\lambda_C = 2\pi(\varepsilon/D^3)^{1/4}$  as a result of larger effect of diffusion than of viscosity.

For mixtures where  $Sc \approx 1$ , the inertial-convective subrange of a scalar quantity spectrum and the inertial subrange of velocity spectrum are of comparable extent and end at the Kolmogorov scale ( $k_K$ ). That is, in both spectra the inertial subrange is specified by the wave number range  $k_0 \ll k \ll (\varepsilon/\nu^3)^{1/4}$ . Beyond the Kolmogorov scale both the scalar and velocity spectra fall off more rapidly than  $E \propto k^{-5/3}$  at the end of the inertia subrange as a consequence of molecular transport processes like viscosity and diffusion becoming important.

For mixtures with  $Sc \gg 1$  the classical turbulence theory for scalars fields predicts that the scalar spectrum has a shape similar to  $E(k)$  for  $k < k_K$ . For  $k_K < k < k_B$ , the so-called Batchelor spectrum [4] is found for which  $E_c(k) \propto k^{-1}$ , and for  $k > k_B$ , the scalar spectrum falls rapidly towards zero due to the effect of scalar dissipation by molecular diffusion, as illustrated in Fig 7.9. The Batchelor [4] wave number is of the order  $k_B \approx 2\pi(\varepsilon/\nu D^2)^{1/4}$ . Molecular

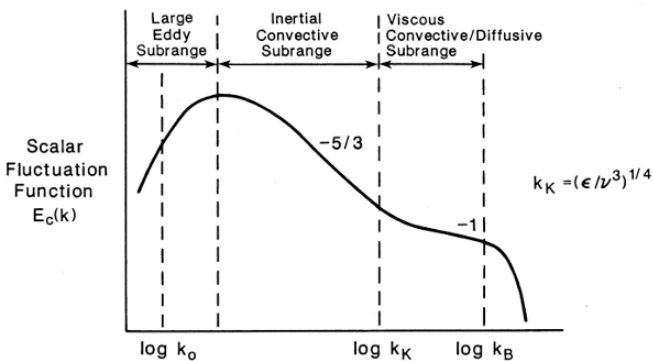


**Fig. 7.9.** The scalar spectrum in wave number space for systems in which  $Sc \gg 1$  [87]. By permission from Tatterson (personal communications, 2006).

diffusion occurs near the Batchelor scale  $\lambda_B = (\frac{\nu D^2}{\epsilon})^{1/4} = Sc^{-1/2} \lambda_K$ , defining the end of the Batchelor spectrum where  $E_c(k) \propto k^{-1}$ .

For gases the Schmidt number is close to unity so that no special attention is required for the higher wave numbers. Turbulent reactive gas flows might thus be sufficiently described using the relatively simple gradient hypothesis with a constant Schmidt number. However, from the above discussion it can be concluded that for liquids ( $Sc \gg 1$ ) momentum is transported much faster than mass in the viscous region of the spectrum. Due to this observation, turbulent reactive gas and liquid flows are usually modeled differently, as special emphasis has to be put on the liquid mixing properties avoiding the gradient hypothesis [78].

By far the most widely employed models for turbulent reactive flows in stirred tanks are based on the Reynolds averaged Navier Stokes (RANS) equation. This is a moment equation containing quantities that are averaged over the whole wave spectra, as explained in sect 1.2.7.

The Reynolds averaged equation for the scalar concentration fields can be deduced from (1.456) and written as:

$$\frac{\partial \overline{\omega_c}}{\partial t} + \overline{\mathbf{v}} \cdot \nabla \overline{\omega_c} = -\nabla \cdot (\overline{\mathbf{v}'\omega'_c}) + D_c \nabla^2 \overline{\omega_c} + \overline{S_c(\omega)} \quad (7.73)$$

Closure of the mean scalar field equation requires a model for the scalar flux term. This term represents the scalar transport due to velocity fluctuations in the inertial subrange of the energy spectrum and is normally independent of the molecular diffusivity. The gradient diffusion model is often successfully employed (e.g., [15, 78, 2]):

$$\overline{\mathbf{v}'\omega'_c} = -D_{t,i,j} \nabla \overline{\omega_c} \quad (7.74)$$

where  $D_{t,i,j}$  is a tensor that, in general, depends on the Reynolds stresses and mean velocity gradients. Using the  $k$ - $\epsilon$  model this tensor reduces to:

$$\overline{\mathbf{v}'\omega'_c} = -D_t \nabla \overline{\omega_c} \quad (7.75)$$

in which  $D_t = \mu_t/Sc$  in accordance with the Reynolds analogy for turbulent flow.

However, as discussed in chap 1.2.7, the gradient-diffusion models can fail because counter-gradient (or up-gradient) transport may occur in certain occasions [15, 85], hence a full second-order closure for the scalar flux (1.468) can be a more accurate but costly alternative (e.g., [2, 78]).

In scalar mixing studies and for infinite-rate reacting flows controlled by mixing, the variance of inert scalars is of interest since it is a measure of the local instantaneous departure of concentration from its local instantaneous mean value. For non-reactive flows the variance can be interpreted as a departure from locally perfect mixing. In this case the dissipation of concentration variance can be interpreted as mixing on the molecular scale. The scalar variance equation (1.462) can be derived from the scalar transport equation

(e.g., [2], chap 6.4). The relation contains three unknown covariance terms that need to be closed. These are the scalar and scalar variance flux terms, and the scalar dissipation. The flux terms are often macroscopic in nature and are usually modeled by the gradient hypothesis. The scalar dissipation rate describes the decay of scalar variance due to molecular diffusion and thus depends on the smaller scales of turbulence. The determination of the scalar dissipation term is discussed by Pope [71] (sect 5.7.3). A simple closure for the scalar dissipation term, suggested by Spalding [84] (A.1-11), assumes that the scalar mixing time is proportional to the turbulence time  $\tau_\omega \propto \tau_t$ . Hence, as a first approach we can approximate  $\varepsilon_\omega$  by:

$$\varepsilon_\omega = \frac{1}{2} C_\omega \overline{\omega'^2} / \tau_t \quad (7.76)$$

in which the decay time scale of the velocity fluctuations can be approximated by  $\tau_t = k/\varepsilon$ . The corresponding decay time scale of the scalar fluctuations is thus determined by  $\tau_\omega = \frac{1}{2} \overline{\omega'^2} / \varepsilon_\omega$ . The empirical constant  $C_\omega$  is usually taken to be 2.0.

More advanced dynamic models for  $\varepsilon_\omega$  have also been proposed [25, 26, 60]. In these models a separate transport equation is formulated, modeled and solved numerically to predict this variable field.

The most difficult term to close in (7.73) is the reaction rate terms denoted by  $\overline{S_c(\omega)}$ . To simulate turbulent reactive flows accurate modeling of this term is very important. For slow reactions (i.e.,  $Da_I \ll 1$ ) the turbulent mixing is completed before the reaction can take place thus an adequate closure is available:

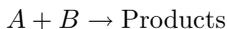
$$\overline{S_c(\omega)} = S_c(\bar{\omega}) \quad (7.77)$$

For very fast reactions local instantaneous chemical equilibrium might be assumed in the flow so that negligible turbulence-chemistry interactions prevail and the turbulence mixing behavior of a non-reactive but otherwise identical mixture can be adopted describing the evolution of the reactive process. The statistics of the reaction rate term can thus be predicted by the method of moments provided that an appropriate PDF for the turbulent mixing process is known. In this way the micro mixing models intend to restore some of the information that were lost in the averaging process. Such a procedure must require additional empirical information to determine the PDF. In particular, the mean concentration of the species can be calculated in terms of a presumed PDF estimated from a few of the lower moments of the local mixture fraction  $f$  (e.g., see [72], chap 12 and [2], chaps 6-9). The presumed PDFs are usually based on two moments, the mean mixture fraction  $\bar{f}$  and the variance about the mean  $\sigma^2 = \overline{(f')^2}$ . A typical presumed PDF can be represented by (i.e., the normal or Gaussian distribution):

$$\Phi(f) = \frac{1}{\sigma\sqrt{2\pi}} \exp\left[-\frac{(f - \bar{f})^2}{2\sigma^2}\right] \quad (7.78)$$

Other presumed PDFs exist as well. Each PDF has its own advantages and disadvantages, but none of them are generally applicable.

The use of the PDF is best illustrated by use of a simple example for a single irreversible second order reaction at isotherm conditions, defined by:



for which the reaction rate is given by:

$$r_{\text{products}} = kc_A c_B = \frac{k}{M_{w_A} M_{w_B}} \rho_A \rho_B \quad (7.79)$$

By performing Reynolds decomposition and time averaging the given reaction rate can be expressed as:

$$\overline{r_{\text{products}}} = k\overline{c_A c_B} = k(\overline{c_A c_B} + \overline{c'_A c'_B}) \quad (7.80)$$

In general the covariance term is non-zero, hence  $\overline{r_{\text{products}}} \neq r_{\text{products}}(\overline{c_A}, \overline{c_B})$ , since the average reaction term is not determined by the mean concentrations alone.

A proper closure strategy for the reaction rate thus depends on the ratio of the rate of reactions and the rate of mixing. In the previous case, considering very slow reactions the concentration fluctuations decay to zero before the reactions occur and no turbulence modeling is needed. The other extreme involves infinitely fast reactions so that local instantaneous chemical equilibrium prevails everywhere in the mixture. If the rate constant is very large ( $k \rightarrow \infty$ ), the reaction rate can only be finite when  $\overline{c_A c_B} + \overline{c'_A c'_B} \approx 0$ .

The concentration of  $A$  and  $B$  can then be related to the PDF of a passive scalar or tracer. Consider again the instantaneous transport equations for  $A$  and  $B$ , assuming equal diffusivity of both species, constant total molar concentration and that the molar average and mass average velocities are about equal we get:

$$\frac{\partial c_A}{\partial t} + \mathbf{v} \cdot \nabla c_A = D_{AB} \nabla^2 c_A + r_A(c_A, c_B) \quad (7.81)$$

and

$$\frac{\partial c_B}{\partial t} + \mathbf{v} \cdot \nabla c_B = D_{BA} \nabla^2 c_B + r_B(c_A, c_B) \quad (7.82)$$

Subtracting the latter relation from the previous one, the source term can be eliminated and we obtain a transport equation for a conserved scalar which behaves as a non-reacting tracer:

$$\frac{\partial(c_A - c_B)}{\partial t} + \mathbf{v} \cdot \nabla(c_A - c_B) = D_{AB} \nabla^2(c_A - c_B) \quad (7.83)$$

since  $r_B(c_A, c_B) = -r_A(c_A, c_B)$ .

By normalization, the mixture fraction is defined by:

$$f = \frac{c_A - c_B + c_{B0}}{c_{A0} + c_{B0}} \quad (7.84)$$

where  $c_{A0} + c_{B0}$  are the initial concentrations of the reactants  $A$  and  $B$  at the inlet and  $f$  is the mixture fraction denoting the normalized conserved scalar tracer. The mixture fraction is unity on the  $A$  inlet and zero on the  $B$  inlet.

The moment method states that given the probability density function  $\Phi$  of  $f$ , the average concentrations of the reactive scalars can be calculated by:

$$\frac{\overline{\rho_A}}{\rho_{A,0}} = \int_0^1 \frac{\rho_A(f)}{\rho_{A,0}} \Phi(f) df \quad (7.85)$$

$$\frac{\overline{\rho_B}}{\rho_{B,0}} = \int_0^1 \frac{\rho_B(f)}{\rho_{B,0}} \Phi(f) df \quad (7.86)$$

For the particular case of second-order kinetics the concentration covariance term is given by:

$$\overline{\rho'_A \rho'_B} = \int_0^1 \rho_A(f) \rho_B(f) \Phi(f) df \quad (7.87)$$

For instantaneous reactions the problem is thus reduced to the calculation of the presumed PDF of a passive scalar or tracer. A large number of alternative presumed PDFs have been listed and discussed by [2, 67, 60]. Each presumed PDF has its advantages and disadvantages, but none of them are generally applicable.

The concept of the full PDF approaches is to formulate and solve additional transport equations for the PDFs determining the evolution of turbulent flows with chemical reactions. These models thus require modeling and solution of additional balance equations for the one-point joint velocity-composition PDF. The full PDF models are thus much more CPU intensive than the moment closures and hardly tractable for process engineering calculations. These theories are comprehensive and well covered by others (e.g., [8, 2, 26]), thus these closures are not examined further in this book.

For finite rate chemical reaction processes neither of the asymptotic simplifications explained above are applicable and appropriate closures for  $\overline{S_c(\omega)}$  are very difficult to achieve.

The improvement in accuracy achieved by the complex closures compared to the simpler ones can also be questionable. Osenbroch [67] and Mortensen [60] successfully applied the combined particle image velocimetry (PIV)/planar laser induced fluorescence (PLIF) technique to measure the instantaneous velocity and reacting species concentration in mixing devices like a mixing channel, pipe, and multi-functional channel reactor. The measured

data was used to validate computational fluid dynamics simulations of reactive flows adopting numerous scalar mixing closures. Based on these studies it can be concluded that further work is needed developing sufficient models for the prediction of the turbulence-chemistry interaction processes occurring in chemical reactors.

## 7.4 Heat Transfer in Stirred Tank Reactors

The temperature in stirred tank reactors may be influenced by chemical or physical reactions within the tank. Cooling or heating devices might be required to control the process temperature. In many endothermic processes heat has to be added to raise and maintain the temperature of the bulk. In other exothermic processes heat is removed to avoid hot spots.

Heating and cooling of the process fluid are accomplished by heat transfer between the process fluid and a heating or cooling media that is circulated

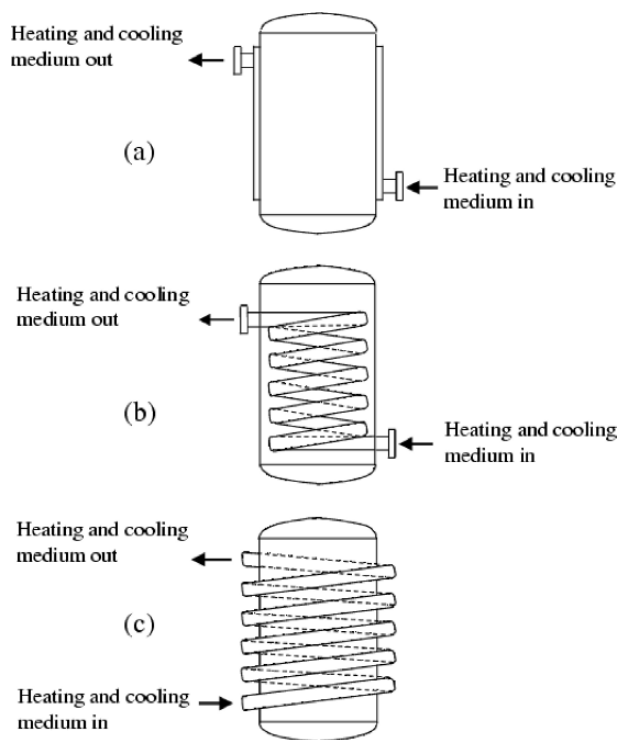


**Fig. 7.10.** Different heat transfer equipment. (a) Vessel with jacket. (b) Vessel with internal helical coil. (c) Vessel with external helical coil. Sketched after similar figures in [65, 40].

within a closed heat transfer surface. Different types of heat transfer equipment are used in industrial processes such as jackets, external or internal helical coils, as sketched in Fig 7.10.

Heat transfer from the bulk of the tank to the heat transfer medium can be calculated by the standard heat transfer model:

$$Q = U_0 A_0 \Delta T \quad (W) \quad (7.88)$$

where  $U_0$  is the overall heat transfer coefficient,  $A_0$  the heat transfer surface area and  $\Delta T$  the temperature driving force. An illustration of the heat transfer model is given in Fig 7.11.

The overall heat transfer resistance ( $1/U_0$ ) is calculated as the sum of the individual resistances in analogy to Ohm's law. The relationship between the overall resistance and the different contributions is expressed as:

$$\frac{1}{U} = \frac{1}{h_o} + \frac{l}{k} + \frac{1}{h_i} \frac{A_o}{A_i} + ff \quad (Km^2/W) \quad (7.89)$$

where  $h_o$  is the convective heat transfer coefficient at the process side,  $l$  is the thickness of the tank wall,  $k$  is the conductivity of the wall material and  $h_i$  is

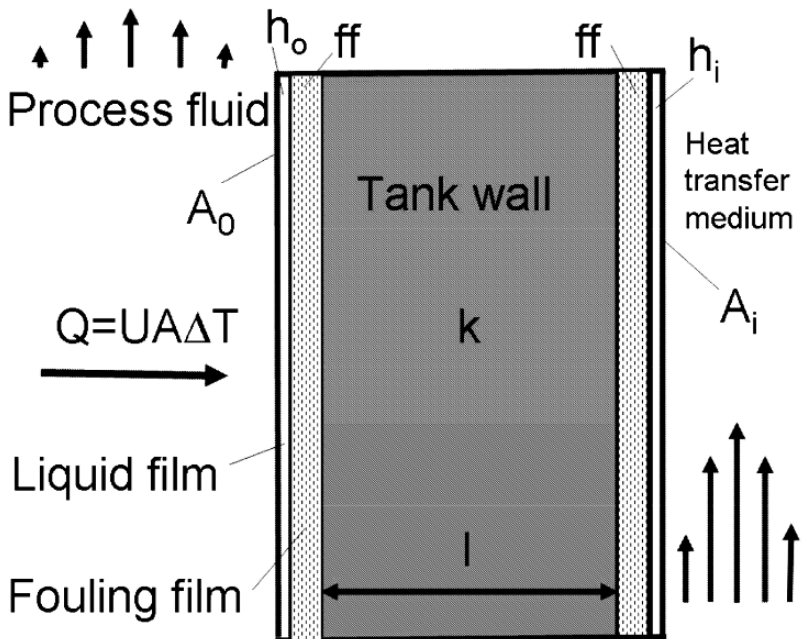


Fig. 7.11. A Sketch of the heat transfer flux model, determining the flux from the bulk of the tank to the heat transfer medium.

the convective heat transfer coefficient at the heat transfer liquid side related to a common heat transfer area basis, and  $ff$  is a fouling factor accounting for corrosion or dirt films on either side of the heat transfer surface [65].

The stirring and the resulting flow pattern inside the tank can be very important for the overall heat transfer resistance, because the performance of the reactor affects the heat transfer coefficient at the process side  $h_o$ . The other resistances are determined by the materials used and the properties of the cooling/heating media and are thus not influenced by the reactor performance.

To determine the process side heat transfer coefficient,  $h_o$ , empirical correlations for many impeller types and tank geometries have been established. The parameterizations are generally expressed in terms of dimensionless numbers, geometrical ratios and viscosity ratios (see e.g., [23, 65, 40] and references therein).

## 7.5 Scale-up of Single Phase Non-Reactive Turbulent Stirred Tanks

Mixing properties and flow fields in stirred tanks are usually studied on a laboratory scale. Practical scale-up of a stirred tank cannot be performed requiring that every individual mixing and fluid mechanical parameters in the small scale tank should be maintained in the larger one. Therefore, scale-up procedures for different types of processes have been determined through experience, testing and computational fluid dynamics simulations.

Over the years several guidelines have been developed for the optimal scale-up of stirred tanks, usually reflected through the concepts of geometric-, dynamic- and kinematic similarities [65]. *Geometric similarity* means that all the pertinent dimensions are similar and have a common constant ratio. *Kinematic similarity* requires that all the velocities at the two different scales have a common constant ratio. *Dynamic similarity* requires that all pertinent force ratios must have a common constant ratio.

The concepts of similarity suggest the use of dimensionless groups. There are, however, other process parameters that could be held constant. Such parameters could be, the blending time, the power per unit volume, the superficial gas velocity, the shear rates and the heat transfer coefficient. Which scale-up criteria that should be chosen depends on the actual process, since the sensitivity to each parameter appears to be different for the various processes.

A general trend is observed which might be used as a rule of thumb. In a small tank the blending time is relatively short, the pumping capacity is relatively high, the average shear rate is relatively high, and a smaller range of shear rates is observed compare to what is found in larger tanks. To obtain a similar flow pattern in a large scale tank, the geometry must change. Larger volumes require taller vessels, but not an equally larger diameter. When taller vessels are applied, the need for multiple impellers arises in order to obtain turbulent mixing in the whole volume.

When it comes to mixing in a laboratory scale unit, the content of the whole vessel is typically well mixed. At a larger scale, bulk mixing may be a problem. In a large tank, the fluid at the top of the vessel might participate irregularly in the general circulation. In the upper part turbulence is usually not well developed. However, experiments have shown that for fast reactions the product distribution can be unaffected by scale-up if the energy dissipation rate is held constant in the reaction zone. On the other hand, if local energy dissipation rate variations occur in the bulk, this may affect the micro mixing [87].

The integral length scales or macro scales of turbulence are generally of the same order of magnitude as the impeller blade width. In addition, the macro scale of turbulence is found to scale with the impeller size. This means that for a large scale vessel, larger eddies will form than in a small vessel. Consequently, large variations in velocities and concentrations can be expected in the vessel upon scale-up.

## 7.6 Mixing of Multi-Phase Systems

The previous sections describe how mixing is accomplished in a liquid phase. However, many industrial processes carried out in stirred tank reactors involve mixing of solids, gases and other liquids in a continuous liquid phase. The presence of a second phase will affect both the power consumption and the flow pattern in the tank. In the sequel, the mixing phenomena caused by the presence of gas bubbles, liquid droplets and solid particles are discussed.

### Gas-Liquid Dispersions.

To disperse gas, the gas is usually injected into the liquid from the bottom of the tank or near the impeller to enhance dispersion. Disk style turbines are found to be most convenient for gas dispersion because the disk disturbs the freely rising gas bubbles. The turbines with flat blades give radial flow and are very useful for gas dispersion where the gas is introduced just below the impeller at its axis and drawn up to the blades and chopped into fine bubbles.

With axial flow impellers, the upward flowing gas bubbles are allowed to rise near the shaft where the shear forces are small, so that the flow pattern and pumping effect is disrupted. Therefore, axial flow impellers are not very useful for gas dispersion [65].

How gas disperses in the liquid phase depends primarily on the impeller speed and the gas injection rate. The different flow regimes that may occur are illustrated in Fig 7.12.

The isothermal expansion power is the energy supplied to the system by the gas stream dispersing the gas in the liquid. When the power due to the impeller rotation is less than the isothermal expansion power of the gas, the flooded regime which is characterized by gas rising unhindered near the impeller shaft prevails. The distribution of gas in the tank is non-uniform.

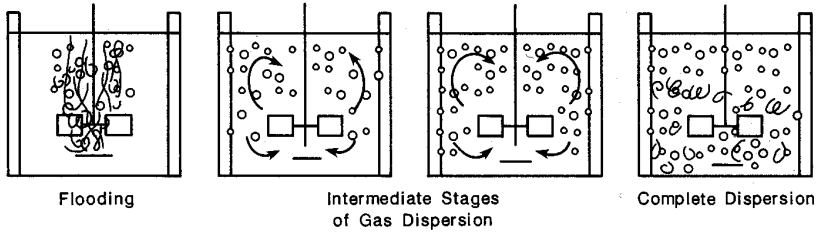


**Fig. 7.12.** Gas dispersion flow regimes [87]. By permission from Tatterson (personal communications, 2006).

When the mixer power is approximately equal to the gas stream energy, a surface picture may indicate a well-dispersed uniform flow of gas bubbles leaving the liquid phase. However, in the bulk of the tank the gas flow dominates the flow pattern. Radial impellers will help to disperse the gas bubbles towards the walls of the tank as the gas rises.

At a mixer power input of two to three times the gas stream energy, the flow pattern is controlled by the mixer [65]. If the mixer power is then increased

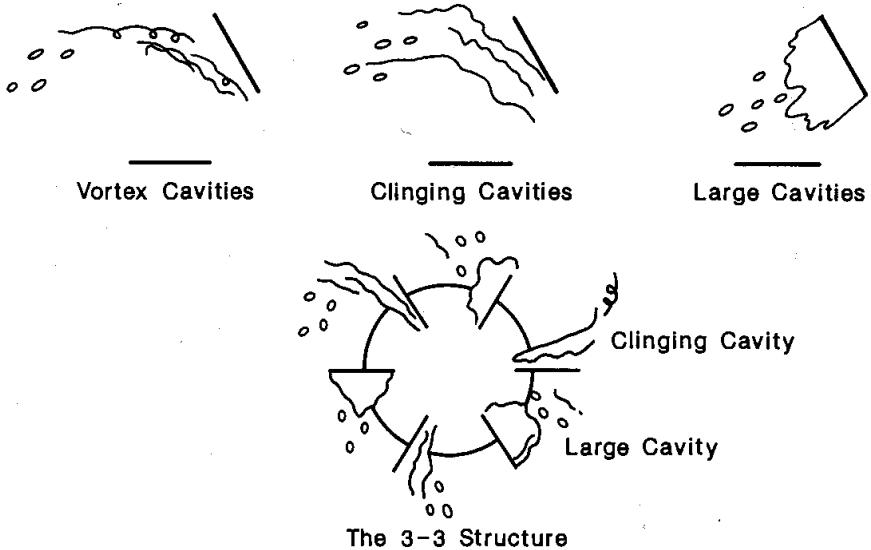


**Fig. 7.13.** Different types of cavities in gas dispersion systems [87]. The 3–3 cavity structure consists of three large cavities and three clinging cavities in a symmetrical pattern around a six-blade disk style turbine. By permission from Tatterson (personal communications, 2006).

to five times the gas expansion energy, the bubbles are driven down to the bottom of the tank, resulting in a completely uniform distribution of gas in the liquid phase.

Cavitation is a function of pressure drop occurring across the impeller blades, the fluid temperature and the vapor pressure of the fluid. If the fluid is near its boiling point, cavitation will occur with the turbulent impellers. Cavities are bubbles that are gathering behind the blades of a rotating impeller, these are characterized as vortex cavities, clinging cavities, large cavities and ragged cavities, and the 3 – 3 cavity structure. The different types of cavities are sketched in Fig 7.13. Vortex cavities may occur at very low gas rates, while large cavities can be found at high gas rates. Ragged cavities are large cavities at flooded conditions, and clinging cavities are intermediately between vortex and large cavities. The 3 – 3 structure is typically formed on a disk style turbine.

The purpose of most gas dispersion processes is to transfer gas into the liquid, sometimes to obtain a chemical reaction. The mass transfer rate across the gas-liquid interface can thus be the rate limiting step in the process, especially when the chemical reaction is fast. The rate of mass transfer is generally described by the mass transfer coefficients  $k_l$  and  $k_g$ , which are the coefficients for the liquid and the gas side, respectively. Usually, the gas side coefficient is neglected because the resistance to mass transfer on the liquid side is generally much higher than on the gas side.

The bubble size distribution is among the important factors controlling the interfacial mass transfer rate in gas liquid stirred tank reactors. This distribution is determined by a balance of coalescence and breakage rates. For this reason the trailing vortices play an important role in the gas dispersion processes in gas-liquid stirred tanks. This role stems from the vortex's ability to capture gas bubbles in the vicinity of the impeller, accumulate them inside the vortex and disperse them as small bubbles in the vortex tail. This ability is related to the high vorticity associated with the rotation of the vortex. Sudiyo [86] investigated bubble coalescence in a 2.6 liter stirred tank. Instantaneous velocity fields were measured using PIV and corresponding turbulent kinetic energy, dissipation rate, various length and time scales were estimated. A shadowgraph technique was employed to measure the bubble size distribution and the coalescence rate. The results show that bubble coalescence takes place mostly near the tank wall, especially on the leeward side of baffles. Moreover, the most important factors affecting coalescence are the gas volume fraction, fluctuation of liquid velocity, different rise velocities of bubbles, and trapping of bubbles in stationary and turbulent vortices. Andersson [1] investigated the breakage mechanisms of bubbles in a stirred tank with a high-speed imaging technique. It was observed that bubbles tend to generate unequal sized fragments. The measurements also showed that binary bubble breakage is frequent.

## Liquid-Liquid Emulsions

The dispersion of one liquid into another immiscible liquid occurs in the manufacture of many kinds of emulsion products.

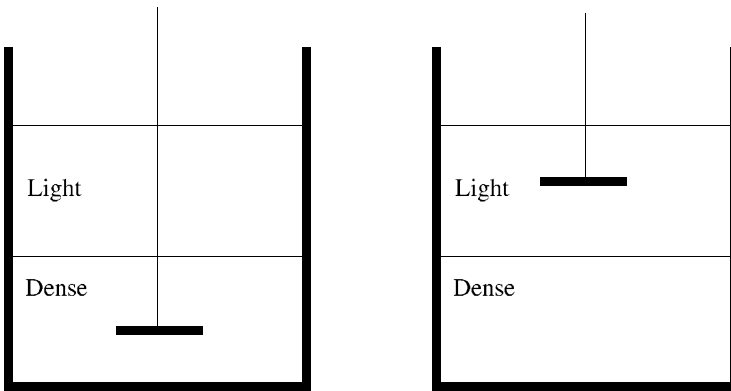
The design of a mixing equipment is usually based on experience with the type of product desired, and seldom upon model calculations of the actual drop sizes or interfacial areas. Reliable models for the drop size and interfacial area could be very useful as they may explain how changes in operating conditions or physical system variables will affect an operating system. However, it is very difficult in industrial applications to calculate the local drop sizes and drop size distributions. One of the difficulties is the wide variety of shear rates that exist in stirred tanks.

The shear rate affects the droplet size, and since the shear rate near the impeller is much higher than the shear rate in the bulk, a distribution of droplet sizes result. In the shear rate zone around the impeller, the dispersing zone, the droplets are teared apart, while in the coalescing zone throughout the rest of the tank the droplets are interacting resulting in larger droplets [65]. This makes the determination of an average droplet size difficult. However, some empirical correlations have been proposed for design purposes.

As the stirring speed increases, the peak in the distribution gets narrower and is moved towards smaller droplet sizes. This skewness in distribution is also a result of the interfacial tension between the two liquid phases. As the droplet size decreases, the interfacial tension is the dominating force. There is thus a minimum droplet size that can be achieved by the maximum shear stress near the impeller [33]. Andersson [1] investigated the breakage mechanisms of fluid particles with a high-speed imaging technique. Experiments of bubbles and droplets were made in the same vessel under identical operating conditions making a comparison between bubble and drop breakage dynamics possible. It was shown that bubbles tend to generate unequal sized fragments, whereas droplets form equal sized fragments. This difference was explained by an internal flow redistribution mechanism, active only for bubbles. The number of fragments produced upon breakage is also quite different for bubbles and droplets. For droplets breakage normally resulted in more than two fragments, whereas binary breakage is a common outcome for bubbles as mentioned in the previous section.

When operating liquid-liquid systems, it is important to know which one of the phases that is dispersed. If a tank is filled with 50% of each phase, the result will depend on how the mixing is performed. For void fractions of 20% of one liquid and 80% of the other, one can be quite sure that the 20% liquid will be dispersed because this phase could not possibly be the continuous phase.

Generally, to create a stable emulsion between a light and a dense liquid phase, the impeller should be placed in the phase which is going to be the continuous phase. With time, the other phase is then drawn into this phase. Figure 7.14 illustrates how to mix a light and a dense phase. There can be



Light phase dispersed in dense phase.

Dense phase dispersed in light phase.

**Fig. 7.14.** Methods for dispersion of a light and a dense liquid phase.

some practical problems dispersing the heavy phase in the light phase. If it is not sufficient to agitate in the light phase or optionally at the interface, it might be necessary to add the dense phase to the tank during agitation [65].

Like for gas-liquid dispersions, the liquid-liquid mass transfer flux is generally described by the mass transfer coefficient,  $k_l$ . One of the main factors limiting the mass transfer rate in industrial systems is impurities on the interface causing changes in the foam and settling characteristics of the system. Therefore, experimental data is always required to validate mass transfer models.

### Solid-Liquid Suspensions

The suspension of solids in a liquid is perhaps the most common application of stirred tanks. Usually, the solid particles are denser than the carrying fluid resulting in continuous settling of the particles towards the bottom of the tank. To avoid permanent settling of solids and to obtain a satisfactory mass transfer flux to the solid surface, mixing is provided to keep the solids in suspension.

To describe the solid-liquid suspension process, the settling velocity is one of the most important parameters. The settling velocity of a particle is obtained by measuring the falling velocity of an unhindered particle. A drag force will act on the falling particle, as explained in sect 5.2.1. This force can be described by an empirical correlation for the drag coefficient (5.50). The drag coefficient changes with flow regime. As can be seen from Fig 5.2, the drag coefficient decreases with increasing Reynolds number in the laminar regime, while it remains roughly constant under turbulent flow conditions.

The solids are kept in suspension if the pumping capacity of the impeller causes strong enough circulation of the liquid. In most processes, complete suspension of the particles is not required. Often, so-called off-bottom suspension is sufficient, which means that all particles are moving above the bottom of the tank with some vertical velocity. Radial flow impellers are usually not very effective in suspending solid particles. Actually, about three times more power is required for a radial turbine to provide the same degree of uniformity compared to an axial turbine. This is because the radial turbines pick up particles from the bottom of the tank by the suction side of the impeller, which is only half of the total flow from the impeller. Due to the appearance of an upper and a lower circulation zone, the contents of the two zones are not sufficiently mixed. Axial impellers are therefore most frequently used for the suspension of solids in stirred tanks [65].

In solid-liquid systems the size and shape of the baffles are important design parameters. The standard baffling is illustrated in Fig 7.1. As the solid concentration increases and the viscosity becomes high, narrower baffles (approximately  $1/24T$ ) placed a distance from the wall, should be used. This design is normally employed to avoid permanent settling of particles in the low velocity zones. In some processes such fillets (settled particles) can nevertheless be advantageous for the power consumption.

## Gas-Liquid-Solid Systems

Some industrial processes involve mixing of both gases, liquids and solids. In slurry stirred tank reactors the liquid phase is the continuous phase where gas is dispersed and solid is suspended. In many of the processes performed in tank reactors, the purpose of fluid mixing is to dissolve the gas in the liquid and transport the species from the gas phase to the surface of the solid particles. In most chemical processes the solid particles act as catalysts to promote a chemical reaction. However, in a few processes, like in polymerization, the solid particles are the product of the reaction.

The choice of impeller for three-phase systems is a compromise between dispersing gas in the liquid and suspending the particles in the liquid. We recall that the axial-flow impellers are usually used for solid-liquid systems, while radial impellers are used for gas-liquid systems. Introducing gas from the bottom of a tank containing a solid-liquid suspension will destroy the flow pattern created by an axial impeller. Therefore, radial impellers are usually more effective in three phase systems even if they require more power for the same level of suspension [65]. Another solution is to apply multiple impellers, one to fulfill the criterion for gas dispersion and another one to fulfill the criterion for solids suspension [87]. The existence of solid particles might also modify the interfacial area between gas and liquid compared to gas-liquid systems.

## 7.7 Governing Equations in Relative and Absolute Frames

In this section the governing equations employed in the different impeller model implementations are presented.

The fictitious forces are conventionally derived with the help of the framework of classical mechanics of a point particle. Newtonian mechanics recognizes a special class of coordinate systems called inertial frames. The Newton's laws of motion are defined in such a frame. A Newtonian frame (sometimes also referred to as a fixed, absolute or absolute frame) is undergoing no accelerations and conventionally constitute a coordinate system at rest with respect to the fixed stars or any coordinate system moving with constant velocity and without rotation relative to the inertial frame. The latter concept is known as the principle of Galilean relativity. Speaking about a rotating frame of reference we refer to a coordinate system that is rotating relative to an inertial frame.

The Laboratory framework is frequently assumed to be inertial and adequate for practical engineering problems on the earth although the laboratory framework is actually fixed to a rotating planet and is therefore strictly speaking an accelerated frame (i.e., this approximation is not valid for large scale ocean and atmospheric flows). To describe the fluid flow caused by the impeller motion in stirred tanks both rotating and laboratory frames have been employed.

For completeness it is mentioned that the transformations between different sets of coordinates describing the same motion, characterize a branch of classical mechanics named kinematics which is fundamentally mathematical methods, and is not based on physical principles.

### 7.7.1 Governing Eulerian Flow Equations in the Laboratory Frame

The general equations of continuity (1.26) and momentum (1.78) in vector notation are introduced in chap 1 employing a Laboratory frame. To describe the flow in the stirred vessels the governing equations are conveniently transformed and written in cylindrical coordinates<sup>7</sup> (e.g., [34]; [6], p 139 and p 555; [10]; [42]; [29], p 73; [95], pp 137-141):

*Continuity:*

$$\frac{\partial \rho}{\partial t} + \frac{1}{r} \frac{\partial}{\partial r} (\rho r v_r) + \frac{1}{r} \frac{\partial}{\partial \theta} (\rho v_\theta) + \frac{\partial}{\partial z} (\rho v_z) = 0 \quad (7.90)$$

*Momentum equation:*

The  $r$ -component:

---

<sup>7</sup> The laboratory frame equations can also be obtained from the rotational frame formulation, if we let  $\mathbf{\Omega} = 0$ .

$$\begin{aligned} \frac{\partial(\rho v_r)}{\partial t} + \frac{1}{r} \frac{\partial(r \rho v_r v_r)}{\partial r} + \frac{1}{r} \frac{\partial(\rho v_\theta v_r)}{\partial \theta} - \frac{\rho v_\theta v_\theta}{r} + \frac{\partial(\rho v_z v_r)}{\partial z} = \\ - \frac{\partial p}{\partial r} - \left( \frac{1}{r} \frac{\partial(r \sigma_{rr})}{\partial r} + \frac{1}{r} \frac{\partial \sigma_{\theta r}}{\partial \theta} - \frac{\sigma_{\theta\theta}}{r} + \frac{\partial \sigma_{zr}}{\partial z} \right) + \rho g_r \end{aligned} \quad (7.91)$$

The  $\theta$ -component:

$$\begin{aligned} \frac{\partial(\rho v_\theta)}{\partial t} + \frac{1}{r} \frac{\partial(r \rho v_r v_\theta)}{\partial r} + \frac{1}{r} \frac{\partial(\rho v_\theta v_\theta)}{\partial \theta} + \frac{\rho v_r v_\theta}{r} + \frac{\partial(\rho v_z v_\theta)}{\partial z} = \\ - \frac{1}{r} \frac{\partial p}{\partial \theta} - \left( \frac{1}{r} \frac{\partial(r \sigma_{r\theta})}{\partial r} + \frac{\sigma_{r\theta}}{r} + \frac{1}{r} \frac{\partial \sigma_{\theta\theta}}{\partial \theta} + \frac{\partial \sigma_{z\theta}}{\partial z} \right) + \rho g_\theta \end{aligned} \quad (7.92)$$

The  $z$ -component:

$$\begin{aligned} \frac{\partial(\rho v_z)}{\partial t} + \frac{1}{r} \frac{\partial(r \rho v_r v_z)}{\partial r} + \frac{1}{r} \frac{\partial(\rho v_\theta v_z)}{\partial \theta} + \frac{\partial(\rho v_z v_z)}{\partial z} = \\ - \frac{\partial p}{\partial z} - \left( \frac{1}{r} \frac{\partial(r \sigma_{rz})}{\partial r} + \frac{1}{r} \frac{\partial \sigma_{\theta z}}{\partial \theta} + \frac{\partial \sigma_{zz}}{\partial z} \right) + \rho g_z \end{aligned} \quad (7.93)$$

The nine components of the viscous stress tensor  $\boldsymbol{\sigma}$  are defined by:

$$\begin{aligned} \sigma_{rr} &= 2\mu \frac{\partial v_r}{\partial r} - \frac{2}{3}\mu \nabla \cdot \mathbf{v} & \sigma_{\theta r} &= \sigma_{r\theta} = \mu \left( \frac{1}{r} \frac{\partial v_r}{\partial \theta} + r \frac{\partial}{\partial r} \frac{v_\theta}{r} \right) \\ \sigma_{\theta\theta} &= 2\mu \left( \frac{1}{r} \frac{\partial v_\theta}{\partial \theta} + \frac{v_r}{r} \right) - \frac{2}{3}\mu \nabla \cdot \mathbf{v} & \sigma_{zr} &= \sigma_{rz} = \mu \left( \frac{\partial v_r}{\partial z} + \frac{\partial v_z}{\partial r} \right) \\ \sigma_{zz} &= 2\mu \frac{\partial v_z}{\partial z} - \frac{2}{3}\mu \nabla \cdot \mathbf{v} & \sigma_{z\theta} &= \sigma_{\theta z} = \mu \left( \frac{1}{r} \frac{\partial v_z}{\partial \theta} + \frac{\partial v_\theta}{\partial z} \right) \end{aligned}$$

It turns out that two fictitious forces occur in the momentum equation when written in cylindrical coordinates. The term  $\rho v_\theta v_r/r$  is an effective force in the  $\theta$ -direction when there is flow in both the  $r$ - and  $\theta$ -directions. The term  $\rho v_\theta^2/r$  gives the effective force in the  $r$ -direction resulting from fluid motion in the  $\theta$ -direction. These terms do *not* represent the familiar Coriolis and centrifugal forces due to the earth's rotation<sup>8</sup>. Instead, they arise automatically on transformation of the momentum equations from Cartesian to cylindrical coordinates and are thus not added on physical grounds (kinematics). Nevertheless, the  $\rho v_\theta^2/r$  term is sometimes referred to as a Coriolis force and the  $\rho v_\theta^2/r$  term is often called a centrifugal force. It is thus important to distinguish between the different types of fictitious forces.

### 7.7.2 Coriolis and Centrifugal Forces

In most textbooks the apparent forces, like the Coriolis and the centrifugal forces, are derived with the help of the framework of classical mechanics of a point particle.

<sup>8</sup> The virtual Coriolis and centrifugal forces due to the earth's rotation are normally added to  $g_\theta$  and  $g_r$ , as shown in (7.115).

To examine the elementary mathematical operations involved in Newtonian mechanics, for example, we describe the motion of a material particle by the Newton's second law of motion. The Newtonian frame of reference adopted is henceforth named  $\mathbf{O}$ . The moving relative reference frame is designated  $\bar{\mathbf{O}}$ . The basic task is thus to transform the Newton's second law of motion as formulated in an inertial frame of reference into a relative rotating frame of reference.

Let the translative velocity (i.e., the relative movement without any rotating component) of the reference frame  $\bar{\mathbf{O}}$  relative to  $\mathbf{O}$  be designated  $\mathbf{v}_0$ , and the angular velocity of  $\bar{\mathbf{O}}$  relative to  $\mathbf{O}$  denoted by  $\boldsymbol{\Omega}$ , as sketched in Fig 7.15. In the inertial frame in which  $\mathbf{e}_x, \mathbf{e}_y, \mathbf{e}_z$  are fixed orthogonal unit vectors, we define the vector of rotation and the rotational acceleration vector (in the common  $x$ - $y$  and  $\bar{x}$ - $\bar{y}$  plane):

$$\begin{aligned} \boldsymbol{\Omega} &= \Omega \mathbf{e}_z \\ \dot{\boldsymbol{\Omega}} &= \dot{\Omega} \mathbf{e}_z \end{aligned} \tag{7.94}$$

where  $\mathbf{e}_z$  is the unit vector in the  $z$ -direction (which is common to both systems of reference since the axes  $z$  and  $\bar{z}$  are parallel and normal to the figure plan). The quantities  $\mathbf{r}_0(t), \mathbf{v}_0(t)$  and  $\mathbf{a}_0(t)$  are time dependent functions relative to  $\mathbf{O}$ .

The vector  $\mathbf{r}$ , shown in Fig 7.15, can be determined in both coordinate systems  $\mathbf{O}$  and  $\bar{\mathbf{O}}$ :

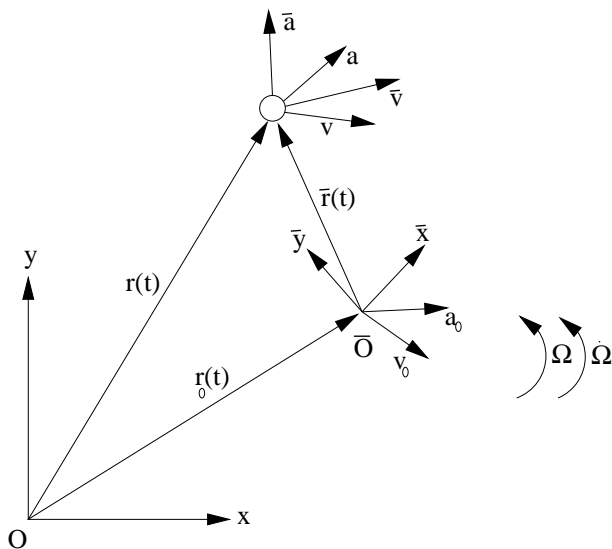


**Fig. 7.15.** Visualization of vectors of location, velocity and acceleration in the inertial and moving reference frames.

$$\mathbf{r} = \bar{\mathbf{r}} + \mathbf{r}_0 = r_x \mathbf{e}_x + r_y \mathbf{e}_y + r_z \mathbf{e}_z = \bar{r}_x \bar{\mathbf{e}}_x + \bar{r}_y \bar{\mathbf{e}}_y + \bar{r}_z \bar{\mathbf{e}}_z + \mathbf{r}_0 \quad (7.95)$$

A change of  $\bar{\mathbf{r}}$  with respect to time seen from  $\mathbf{O}$  then occurs as a result of both change of the components  $\bar{r}_x$ ,  $\bar{r}_y$  and  $\bar{r}_z$  in the moving relative frame and change of the unit vectors  $\bar{\mathbf{e}}_x$ ,  $\bar{\mathbf{e}}_y$  and  $\bar{\mathbf{e}}_z$ :

$$\begin{aligned} \dot{\bar{\mathbf{r}}} &= \frac{d(\bar{r}_x \bar{\mathbf{e}}_x)}{dt} + \frac{d(\bar{r}_y \bar{\mathbf{e}}_y)}{dt} + \frac{d(\bar{r}_z \bar{\mathbf{e}}_z)}{dt} \\ &= \frac{d\bar{r}_x}{dt} \bar{\mathbf{e}}_x + \bar{r}_x \frac{d\bar{\mathbf{e}}_x}{dt} + \frac{d\bar{r}_y}{dt} \bar{\mathbf{e}}_y + \bar{r}_y \frac{d\bar{\mathbf{e}}_y}{dt} + \frac{d\bar{r}_z}{dt} \bar{\mathbf{e}}_z + \bar{r}_z \frac{d\bar{\mathbf{e}}_z}{dt} \\ &= \bar{\mathbf{v}} + \boldsymbol{\Omega} \times \bar{\mathbf{r}} \end{aligned} \quad (7.96)$$

in which we have employed a set of predefined relations for the time derivatives of the unit vectors.

The time derivatives of the unit vectors referred above are defined by (similar to a planar movement of a solid body):

$$\frac{d\bar{\mathbf{e}}_x}{dt} = \boldsymbol{\Omega} \times \bar{\mathbf{e}}_x \quad (7.97)$$

$$\frac{d\bar{\mathbf{e}}_y}{dt} = \boldsymbol{\Omega} \times \bar{\mathbf{e}}_y \quad (7.98)$$

$$\frac{d\bar{\mathbf{e}}_z}{dt} = \boldsymbol{\Omega} \times \bar{\mathbf{e}}_z = 0 \quad (7.99)$$

These relationships can be derived recognizing that the unit vectors  $\bar{\mathbf{e}}_x$  and  $\bar{\mathbf{e}}_y$  in  $\bar{\mathbf{O}}$  are time dependent functions in  $\mathbf{O}$ , whereas  $\bar{\mathbf{e}}_z = \mathbf{e}_z$ .

A relation derived based on the same principles as used in (7.96) is valid for the velocity vector  $\bar{\mathbf{v}}$ :

$$\dot{\bar{\mathbf{v}}} = \bar{\mathbf{a}} + \boldsymbol{\Omega} \times \bar{\mathbf{v}} \quad (7.100)$$

From (7.95) we know that  $\mathbf{r} = \bar{\mathbf{r}} + \mathbf{r}_0$  (see Fig 7.15). By derivation of the position vector with respect to time, and using (7.96), we find that the velocity vector  $\mathbf{v}$  can be expressed by:

$$\mathbf{v} = \dot{\mathbf{r}} = \dot{\bar{\mathbf{r}}} + \dot{\mathbf{r}}_0 = \bar{\mathbf{v}} + \boldsymbol{\Omega} \times \bar{\mathbf{r}} + \mathbf{v}_0 \quad (7.101)$$

By derivation of (7.101) with respect to time, followed by use of (7.96) and (7.100), the acceleration  $\mathbf{a}$  can be expressed in terms of  $\bar{\mathbf{O}}$ :

$$\begin{aligned} \mathbf{a} = \dot{\mathbf{v}} &= \dot{\bar{\mathbf{v}}} + \frac{d\boldsymbol{\Omega}}{dt} \times \bar{\mathbf{r}} + \boldsymbol{\Omega} \times \dot{\bar{\mathbf{r}}} + \dot{\mathbf{v}}_0 \\ &= (\bar{\mathbf{a}} + \boldsymbol{\Omega} \times \bar{\mathbf{v}}) + \frac{d\boldsymbol{\Omega}}{dt} \times \bar{\mathbf{r}} + \boldsymbol{\Omega} \times (\bar{\mathbf{v}} + \boldsymbol{\Omega} \times \bar{\mathbf{r}}) + \dot{\mathbf{v}}_0 \\ &= \bar{\mathbf{a}} + 2\boldsymbol{\Omega} \times \bar{\mathbf{v}} + \frac{d\boldsymbol{\Omega}}{dt} \times \bar{\mathbf{r}} + \boldsymbol{\Omega} \times (\boldsymbol{\Omega} \times \bar{\mathbf{r}}) + \mathbf{a}_0 \end{aligned} \quad (7.102)$$

We can now illustrate the fictitious modifications required employing a relative frame in Newtonian mechanics. The Newton's second law of motion in the initial (i.e., non-rotating) reference frame, is defined by:

$$m\mathbf{a} = \mathbf{f} \quad (7.103)$$

in which  $m$  is the mass of our point on the object, and  $\mathbf{f}$  is the non-fictitious force acting on it. Note that, if these forces are Galilean invariant, the force definitions are equivalent in both reference frames. Making use of the relation (7.102) connecting the accelerations in the two frameworks, the apparent equation of motion of the point particle in the rotating reference frame takes the form:

$$m\bar{\mathbf{a}} = \mathbf{f} - m(2\boldsymbol{\Omega} \times \bar{\mathbf{v}} + \frac{d\boldsymbol{\Omega}}{dt} \times \bar{\mathbf{r}} + \boldsymbol{\Omega} \times (\boldsymbol{\Omega} \times \bar{\mathbf{r}}) + \mathbf{a}_0) \quad (7.104)$$

A comparison of equations (7.103) and (7.104) shows that the Newton's second law of motion in the inertial frame  $\mathbf{O}$  is identical in form to that in  $\bar{\mathbf{O}}$  except that the latter formulation contains several additional fictitious body forces. The term  $-2m\boldsymbol{\Omega} \times \bar{\mathbf{v}}$  is the Coriolis force, and  $-m\boldsymbol{\Omega} \times (\boldsymbol{\Omega} \times \bar{\mathbf{r}})$  designates the centrifugal force. No name is in general use for the term  $-\frac{d\boldsymbol{\Omega}}{dt} \times \bar{\mathbf{r}}$ . The acceleration  $-\mathbf{a}_0$  compensates for the translational acceleration of the frame.

### 7.7.3 Governing Eulerian Equations in a Rotating Frame

By use of the result obtained from Newtonian mechanics, relating the acceleration  $\mathbf{a}$  and  $\bar{\mathbf{a}}$ , we can convert (1.78), which is written in terms of  $\mathbf{O}$ , into a momentum balance as seen from an observer in  $\bar{\mathbf{O}}$ .

In fluid mechanics the time rate of change of a vector  $\boldsymbol{\psi}$  is then written as  $D\boldsymbol{\psi}/Dt = \bar{D}\boldsymbol{\psi}/\bar{D}t + \boldsymbol{\Omega} \times \boldsymbol{\psi}$  in analogy to the result from classical mechanics. The above relation for the generalized vector  $\boldsymbol{\psi}$  is applied to a fluid parcel's position  $\mathbf{r}$  and then to its velocity  $\mathbf{v}$ , leading to the relation:

$$\frac{D\mathbf{v}}{Dt} = \frac{\bar{D}\bar{\mathbf{v}}}{\bar{D}t} + 2\boldsymbol{\Omega} \times \bar{\mathbf{v}} + \frac{\bar{D}\boldsymbol{\Omega}}{\bar{D}t} \times \bar{\mathbf{r}} + \boldsymbol{\Omega} \times (\boldsymbol{\Omega} \times \bar{\mathbf{r}}) + \frac{D\mathbf{v}_0}{Dt} \quad (7.105)$$

Note that the rate of change of  $\boldsymbol{\Omega}$  is the same in the rotating frame as in an absolute frame [6].

Assuming that  $D\mathbf{v}/Dt$  is equal to the local force acting per unit mass on a fluid parcel, the apparent forces in the rotating frame are derived. The above derivation can be called a Lagrangian approach since it exploits the concept of the fluid parcel<sup>9</sup>. In this framework we define:

$$\mathbf{a} = \frac{D\mathbf{v}}{Dt} = \frac{\partial \mathbf{v}}{\partial t} + \mathbf{v} \cdot \nabla \mathbf{v} \quad (7.106)$$

and

<sup>9</sup> Recently, an Eulerian derivation of the Coriolis force has been reported by Kageyama and Hyodo [45]. They present a general procedure to derive the transformed equations in the rotating frame of reference based on the local Galilean transformation and rotational coordinate transformation of field quantities.

$$\bar{\mathbf{a}} = \frac{\bar{D}\bar{\mathbf{v}}}{Dt} = \frac{\partial\bar{\mathbf{v}}}{\partial t} + \bar{\mathbf{v}} \cdot \bar{\nabla}\bar{\mathbf{v}} \quad (7.107)$$

The momentum equation (1.78) in  $\mathbf{O}$  is then transformed from the flux form to the advective (non-flux) form:

$$\rho \left( \frac{\partial\mathbf{v}}{\partial t} + \mathbf{v} \cdot \nabla\mathbf{v} \right) + \mathbf{v} \left( \frac{\partial\rho}{\partial t} + \nabla \cdot (\rho\mathbf{v}) \right) = -\nabla p - \nabla \cdot \boldsymbol{\sigma} + \rho\mathbf{g} \quad (7.108)$$

The two terms in the second bracket is zero in accordance with the continuity equation (1.26).

Moreover, by use of (7.105) and (7.106), the substantial derivative in the inertial frame is transformed into the rotating framework:

$$\rho \left( \frac{\bar{D}\bar{\mathbf{v}}}{Dt} + 2\boldsymbol{\Omega} \times \bar{\mathbf{v}} + \frac{\bar{D}\boldsymbol{\Omega}}{Dt} \times \bar{\mathbf{r}} + \boldsymbol{\Omega} \times (\boldsymbol{\Omega} \times \bar{\mathbf{r}}) + \frac{D\mathbf{v}_0}{Dt} \right) = -\nabla p - \nabla \cdot \boldsymbol{\sigma} + \rho\mathbf{g} \quad (7.109)$$

The rate of deformation and the pressure are frame-indifferent (e.g., see [6], p 141; [54], p 400; [28, 31, 34]) so we can simply re-write the divergence operator and the stress terms into the rotating reference frame notation. The transformed momentum equation yields:

$$\rho \frac{\bar{D}\bar{\mathbf{v}}}{Dt} = \rho (-2\boldsymbol{\Omega} \times \bar{\mathbf{v}} - \boldsymbol{\Omega} \times (\boldsymbol{\Omega} \times \bar{\mathbf{r}})) - \bar{\nabla}p - \bar{\nabla} \cdot \bar{\boldsymbol{\sigma}} + \rho\bar{\mathbf{g}} \quad (7.110)$$

It is common practice to omit the bars as it is now understood that the equation is formulated in the rotating reference framework.

Greenspan [31] outline the transformation of the Eulerian equations governing the motion of an incompressible viscous fluid from an inertial to a rotational frame. The transformation of the Navier-Stokes equations simply results in adding the artificial forces in the momentum balance. The additional equations are apparently not changed as the substantial derivative of scalar functions are Galilean invariant so the form of the terms do not change.

Batchelor [6] and Ghil and Childress [28] examine the transformation of the governing Eulerian equations for compressible flows from an inertial to a rotational frame. As it turns out, only the momentum equation is actually effected by this transformation because the material or substantial derivative operator of scalar functions is invariant to rotation.

Of particular interest in the context of stirred tank reactor theory is the case of steadily rotating axes of reference ( $D\boldsymbol{\Omega}/Dt = 0$ ) without translating acceleration ( $D\mathbf{v}_0/Dt$ ). Equation (7.109) can then be written as:

$$\rho \frac{\bar{D}\bar{\mathbf{v}}}{Dt} = \rho (-2\boldsymbol{\Omega} \times \bar{\mathbf{v}} - \boldsymbol{\Omega} \times (\boldsymbol{\Omega} \times \bar{\mathbf{r}})) - \nabla p - \nabla \cdot \boldsymbol{\sigma} + \rho\mathbf{g} \quad (7.111)$$

To describe the flow in a stirred tank the governing equations are often written in cylindrical coordinates<sup>10</sup>, as listed in sect 7.7.1. The remaining

<sup>10</sup> Hansen [34] gives an informative derivation of the momentum equations in cylindrical coordinates employing an inertial frame.

task is thus to transform these governing Eulerian equations formulated in an inertial Laboratory frame into a relative rotating frame of reference. We outline this procedure by examining the transformation of the momentum equation components (7.91) to (7.93).

In the common case of  $\boldsymbol{\Omega}$  consisting only of a z-component orthogonal to the vector  $\bar{\mathbf{r}}$ , we define:

$$\boldsymbol{\Omega} = \begin{pmatrix} 0 & \bar{\mathbf{e}}_r \\ 0 & \bar{\mathbf{e}}_\theta \\ \bar{\Omega} & \bar{\mathbf{e}}_z \end{pmatrix} \quad (7.112)$$

The fictitious body forces in cylindrical coordinates are thus written as:

Coriolis force:

$$-2\boldsymbol{\Omega} \times \bar{\mathbf{v}} = -2 \begin{pmatrix} 0 & \bar{\mathbf{e}}_r \\ 0 & \bar{\mathbf{e}}_\theta \\ \bar{\Omega} & \bar{\mathbf{e}}_z \end{pmatrix} \times \begin{pmatrix} \bar{v}_r & \bar{\mathbf{e}}_r \\ \bar{v}_\theta & \bar{\mathbf{e}}_\theta \\ \bar{v}_z & \bar{\mathbf{e}}_z \end{pmatrix} = \begin{pmatrix} 2\bar{\Omega}\bar{v}_\theta & \bar{\mathbf{e}}_r \\ -2\bar{\Omega}\bar{v}_r & \bar{\mathbf{e}}_\theta \\ 0 & \bar{\mathbf{e}}_z \end{pmatrix} \quad (7.113)$$

Centrifugal force:

$$\begin{aligned} -\boldsymbol{\Omega} \times (\boldsymbol{\Omega} \times \bar{\mathbf{r}}) &= - \begin{pmatrix} 0 & \bar{\mathbf{e}}_r \\ 0 & \bar{\mathbf{e}}_\theta \\ \bar{\Omega} & \bar{\mathbf{e}}_z \end{pmatrix} \times \left[ \begin{pmatrix} 0 & \bar{\mathbf{e}}_r \\ 0 & \bar{\mathbf{e}}_\theta \\ \bar{\Omega} & \bar{\mathbf{e}}_z \end{pmatrix} \times \begin{pmatrix} \bar{r} & \bar{\mathbf{e}}_r \\ 0 & \bar{\mathbf{e}}_\theta \\ 0 & \bar{\mathbf{e}}_z \end{pmatrix} \right] \\ &= - \begin{pmatrix} 0 & \bar{\mathbf{e}}_r \\ 0 & \bar{\mathbf{e}}_\theta \\ \bar{\Omega} & \bar{\mathbf{e}}_z \end{pmatrix} \times \begin{pmatrix} 0 & \bar{\mathbf{e}}_r \\ \bar{\Omega}\bar{r} & \bar{\mathbf{e}}_\theta \\ 0 & \bar{\mathbf{e}}_z \end{pmatrix} \\ &= \begin{pmatrix} \bar{\Omega}^2\bar{r} & \bar{\mathbf{e}}_r \\ 0 & \bar{\mathbf{e}}_\theta \\ 0 & \bar{\mathbf{e}}_z \end{pmatrix} \end{aligned} \quad (7.114)$$

The components of these fictitious forces are usually added to the body force  $\mathbf{g}$  of momentum equation components (7.91) to (7.93). For the different components of the momentum equation we get:

$$\begin{aligned} g_r &= (\bar{\Omega}^2\bar{r} + 2\bar{\Omega}\bar{v}_\theta) \\ g_\theta &= (-2\bar{\Omega}\bar{v}_r) \\ g_z &= -g \end{aligned} \quad (7.115)$$

For turbulent flows the governing equations are usually Reynolds averaged. The resulting models are often closed by employing the eddy viscosity hypothesis. In these cases the laminar viscosity in the viscous stress terms are substituted with an effective viscosity  $\mu_{eff} = \mu + \mu_t$ . Moreover, the eddy viscosity is normally calculated using a kind of  $k-\epsilon$  model [50], as presented in sect 1.2.7. Using a rotating reference frame to model the impeller effects no additional covariance terms are occurring due to the fictitious terms.

## 7.8 Impeller Modeling Strategies

In this section the different impeller modeling strategies employed simulating the flow fields in stirred tanks are examined.

### 7.8.1 The Impeller Boundary Conditions (IBC) Method

The IBC method represents the traditional way to model the effect of the impeller in a stirred tank reactor. Harvey and Greaves [37, 38] were among the first to apply this method. Pericleous and Patel [69] used this method to simulate both tangential and axial agitators in chemical reactors. It is also noted that Gosman et al [30] simulated several two-phase flows in tanks stirred by Rushton turbines using a dynamic two-fluid model. However, the steady state condition is normally imposed and no moving reference frame, neither rotating nor translating, is considered. This means that all the transient terms, as well as the Coriolis- and centrifugal forces, vanish from the governing equations. Gravitation is the only body force considered. The rotating impeller is modeled by empirical boundary conditions being imposed on the surface of the impeller blades. For Rushton turbines, for example, empirical profiles for the physical quantities like  $v_r$ ,  $v_\theta$ ,  $v_z$ ,  $k$  and  $\epsilon$  as functions of  $z$  only (the method does not resolve the impeller region so only azimuthally uniform values are possible) were normally imposed on the vertical control surface  $\Sigma_v$  bounding the impeller-swept region in a stirred vessel [10], as illustrated in Fig 7.16. The flow field in the impeller region is computed as in any other part

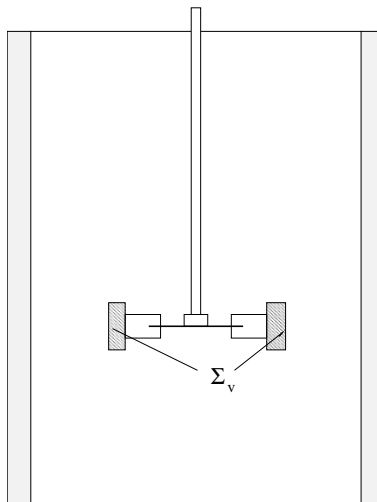


**Fig. 7.16.** Simulating the effect of a Rushton turbine on the flow one practice is to impose empirical profiles for the physical quantities like  $v_r$ ,  $v_\theta$ ,  $k$  and  $\epsilon$  on the vertical control surface  $\Sigma_v$  bounding the impeller-swept region in a stirred vessel [10].

of the computational domain. The shaft, hub and disc of the Rushton turbine (see Fig 7.16), excluding the impeller blades, are treated as solid volumes. For different impeller geometries (and in rare cases also for the Rushton turbine), the impeller region has been bounded by two surfaces, one horizontal and one vertical [73].

In order to reduce the computational efforts one may utilize symmetries in the problem so that only a part of the domain needs to be simulated, but the domain applied must still include at least one baffle. To determine appropriate boundary conditions for the impeller surface, experimental data are required. In fact the method relies on experimental data for each geometry and fluid in question. The need for such amounts of empirical information is the main limitation of the IBC method. Moreover, the reliability on the results of a simulation using the IBC method depends directly on the quality of the experimental data [10].

### 7.8.2 The Snapshot (SS) Method

Ranade and Van den Akker [74] introduced the *snapshot* method for simulating flows in baffled stirred tanks. The snapshot method has many similarities with the traditional IBC method but differs in that the effect of the impeller rotation is approximately modeled mechanistically and not deduced from empirical data analysis solely. The snapshot method thus represents an early attempt to improve on the main limitation associated with the IBC method.

The basic idea is to describe a snapshot of the flow in a stirred vessel with a fixed relative position of blades and baffles. It is assumed that the main flow characteristics of a stirred vessel at the particular time instant in question can be captured approximately from the solution of the steady-state equations, provided that artificial cell volume adjustments and momentum sources are implemented to represent the effect of the impeller rotation.

A particular simulation of the flow is performed using a fixed reference frame for a specific blade position. The snapshot model equations are thus basically the same as those used in the traditional IBC method. The modeling of the effects of the impeller rotation on the flow is based on a simple analysis of the physical problem [75]. In particular, the blade rotation causes suction of fluid at the rear side of the blades and equivalent ejection of fluid from the front side of the blades. These dynamic phenomena in the impeller region are thus modeled approximately by including apparent volume corrections (i.e., net time average effects) in the continuity equation for the computational cells attached to the front and rear sides of the impeller blades. In addition, since the impeller blades are treated as stationary walls, additional momentum source terms (i.e., net time average effects) representing the effect of shear caused by the rotating impeller blades are implemented for the computational cells attached to the edges of the impeller blades. These momentum sources are estimated for the contact area between the cell and impeller blade using an adjusted turbulence wall function model. Furthermore, empirical information

is required to quantify the size and location of the inner region where these artificial sources are needed. In the outer region the apparent effects of the transient terms are neglected as the flow is assumed to be in steady-state.

Simulating the flow generated by a Rushton turbine the governing equations are usually solved for half of the vessel volume due to symmetry considerations. The standard boundary conditions are implemented at the stationary wall, for the impeller shaft, disc and hub, an angular velocity corresponding to the impeller rotation speed was specified. The top fluid surface is assumed flat and modeled as a wall. Cyclic boundary conditions were imposed at the open surfaces of the solution domain. Simulations of flows generated by different impellers have also been performed requiring appropriate changes in the boundary conditions and calculation domain.

To achieve steady-state values for comparison with experimental data different calculations have to be carried out at different time instants representing an average for the different positions of the impeller blades relative to the baffles.

Ranade and Krishnan [75] reported an evaluation of the snapshot approach. It was concluded that the simulations captured most of the key features of near-impeller flows with fair accuracy.

Ranade and Van den Akker [74], for example, used the snapshot method for simulating gas-liquid flows in baffled stirred tanks using a time after volume averaged two-fluid model for incompressible flows (as described in sect 3.3). These multiphase simulations also predicted the near-impeller flows with fair accuracy. Most important, the cavities due to the accumulation of gas in the low-pressure region behind the impeller blades were detected.

Nevertheless, the artificial source term modeling approach has not been fully accepted as a predictive tool for simulating swirling flows. In one view the snapshot approach is not much better than the IBC method, because the artificial sources have to be validated for every case investigated requiring many costly experimental investigations. For this reason it will not be further assessed in this book.

### **7.8.3 The inner-outer (IO) method and the multiple reference frame approach (MRF)**

The inner-outer method was first presented by Brucato et al [9, 10]. This iterative procedure was proposed intending to design a relatively simple engineering simulation, which enable approximate predictions of the effect of the rotating impellers on the fluid motion in stirred tanks, without resorting to empirical source terms relying on experimental data. This procedure thus represents an advanced attempt to improve on the main limitation associated with the IBC method.

The model formulation is based on a simple physical analysis of the stirred tank problem which reveals the following characteristics. In the view of an observer fixed on the vessel wall, the impeller is rotating. On the other hand,

considering an observer following the impeller, the vessel itself appears to be rotating. In the *inner-outer* iterative procedure the whole vessel volume domain is thus subdivided into two overlapping zones. These are the inner domain containing the impeller and the outer one including the baffles. Accordingly, the global iterative procedure is also subdivided into two major steps.

In the first iterative step of this method the simulation of the flow in the inner domain is carried out using a model formulation considering a reference frame rotating with the impeller, with a first guess for the boundary conditions (e.g., initially a still fluid may suffice) imposed on the artificial surface  $\Sigma_2$  dividing the two sub-domains, as illustrated in Fig 7.17. Thus, (7.109) is to be solved taking the Coriolis- and centrifugal force into account. The steady state condition imposed on the simulation requires that the transient terms are neglected. The impeller region is resolved so physical boundary conditions are required implementing the actual surfaces. After the first trial flow field in the impeller region is obtained, the corrected values for the different quantities (e.g.,  $\mathbf{v}$ ,  $k$  and  $\varepsilon$ ) are imposed as boundary conditions on the inner surface  $\Sigma_1$  of the outer domain (Fig 7.18). Since the two frames are different, the information which is exchanged has to be adjusted for the relative motion and averaged over the azimuthal direction (due to an imposed symmetry requirement).

Thereafter, in the second step of the procedure the calculation is carried out using a model formulation considering a fixed laboratory reference frame

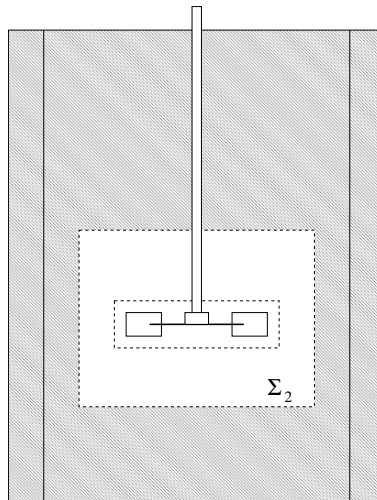


**Fig. 7.17.** Computational domain for the inner simulation, lined region is excluded from the domain. The figure is drawn based on a similar figure published by Brucato et al [10].

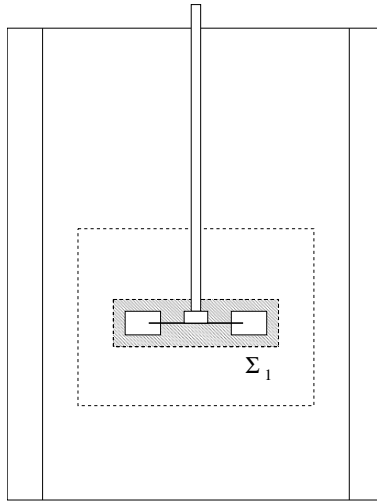


**Fig. 7.18.** Computational domain for the outer simulation, lined region is excluded from the domain. The figure is drawn based on a similar figure published by Brucato et al [10].

for the outer domain, in which the Coriolis- and centrifugal body forces are not included (i.e., except those for the earth's rotation). In this case the updated boundary conditions on the inner surface  $\Sigma_1$  of the outer domain (Fig 7.18) is employed. The baffle region is resolved so physical boundary conditions are required implementing the actual surfaces. Subsequent to obtaining convergence (at least performing a few iterations) on the outer part of the domain, a first iteration on the whole flow field has been achieved. After the results for the outer domain have been obtained, a new guess for the boundary conditions for the inner domain iteration can be imposed on surface  $\Sigma_2$ . A new estimate for the solution of the inner domain can then be calculated, and similar inner-outer iterations can be repeated until the whole calculation domain attains a satisfactory numerical convergence.

Simplified versions of the IO-method with no overlap between the inner and outer regions have been used by Marshall et al [55] and Luo et al [52]. Since there is no overlapping zone between the two regions, the solution is matched at the interface between the rotating and stationary regions. A general formula for transforming the interface velocity between the two frames of reference was given by [52]. However, the location of the interface may not be arbitrary, since in one view the concept requires that the surface has to be placed at a location where the flow variables do not change significantly with time or with  $\theta$ . Otherwise, a predictor-corrector approach may be needed in conjunction with the MRF method in order to find an optimal location of the interface. Notwithstanding, with a perfect first guess of the interface location

(or in particular cases for which the interface location is not of crucial importance) the multiple reference frame (MRF) method is computationally less expensive than the IO-method. For this reason the MRF-method has been implemented in most of the commercial CFD codes. It is further noted that in some commercial codes basically the same approach is known under the name the Multiple Rotating Reference Frame (MRRF).

To validate the predicted results several simulations have to be carried out specifying different positions of the impeller blades relative to the baffles to achieve average steady-state values for comparison with experimental data. This averaging procedure is analogous to the one used employing the snapshot method.

#### 7.8.4 The Moving Deforming Mesh (MDM) Technique

Perng and Murthy [70] introduced the moving deforming mesh technique for simulating unsteady flows in mixing vessels.

The model formulation used with moving meshes is of the arbitrary-Lagrangian-Eulerian (ALE) type. The integral form of the equations governing the incompressible Newtonian fluid in a time-varying control-volume  $V(t)$  is written as:

$$\frac{d}{dt} \int_{V(t)} dv = \oint_{A(t)} \mathbf{u} \cdot \mathbf{n} da \quad (7.116)$$

$$\frac{d}{dt} \int_{V(t)} \rho dv = \oint_{A(t)} \rho(\mathbf{u} - \mathbf{v}) \cdot \mathbf{n} da \quad (7.117)$$

$$\frac{d}{dt} \int_{V(t)} \rho \mathbf{v} dv = \oint_{A(t)} [\rho(\mathbf{u} - \mathbf{v})\mathbf{v} - \mathbf{T}_{\text{eff}}] \cdot \mathbf{n} da + \int_{V(t)} S_v dv \quad (7.118)$$

$$\frac{d}{dt} \int_{V(t)} \rho \psi dv = \oint_{A(t)} [\rho(\mathbf{u} - \mathbf{v})\psi - \mathbf{J}_{\text{eff}}] \cdot \mathbf{n} da + \int_{V(t)} S_\psi dv \quad (7.119)$$

where  $\mathbf{u}$  is the control volume surface velocity vector arising from the motion of the moving grid.  $S_v$  and  $S_\psi$  are the source terms for  $\mathbf{v}$  and  $\psi$  equations, respectively.  $d/dt$  is the total derivative.

A single mesh for both the moving and the stationary part is used in this approach. The grid attached to the rotor moves with it and causes the interfacial mesh to deform. When mesh deformation becomes acute, the grid is regenerated locally and the flow variables are transferred to the regenerated mesh. Fig 7.19 shows an illustrative example in which only a single row of cells are deformed. Regenerating the grid means, as indicated in the figure, *snapping* back the grid by one cell. At this point all the cells and grid nodes are renumbered and the procedure continues. Further details of the techniques for mesh deformation, regeneration and variable interpolation are explained by [70].

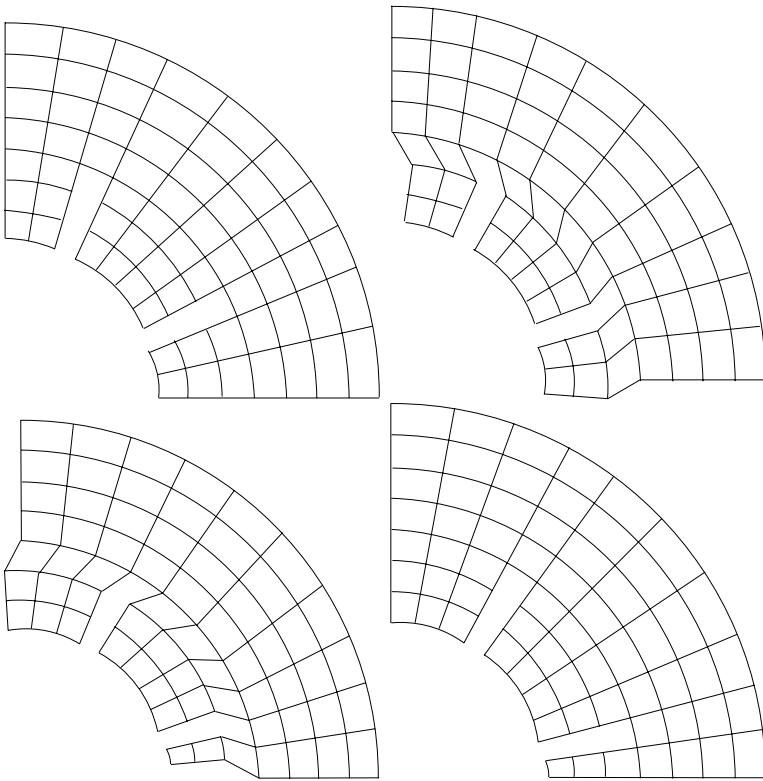


**Fig. 7.19.** Grid motion through deformation and snapping (from left to right) [70]: 1. initial grid, 2. grid moves and deforms, 3. the right boundary and cells are snapped to the left, 4. grid advances one cell distance. Reproduced with permission by John Wiley & Sons, Inc.

Note that this strategy may lose accuracy if the interface grid is allowed to deform excessively before regeneration.

To validate the predicted results only one time dependent simulation has to be carried out to achieve time and impeller region average values for comparison with experimental data and the steady-state results obtained by the IBC, IO and snapshot methods.

### 7.8.5 The Sliding Grid (SG) or Sliding Mesh (SM) Method

Murthy et al [63] were the first who used the sliding grid method for the simulation of unsteady flows in mixing vessels. The model formulation used with moving meshes is of the arbitrary-Lagrangian-Eulerian (ALE) type [70]. In this particular approach the flow domain is divided into two cylindrical, non-overlapping sub-domains, each gridded as a separate block. The outer

grid is fixed to the laboratory reference frame, the inner grid rotates with the impeller as illustrated in Fig 7.20 and Fig 7.21.

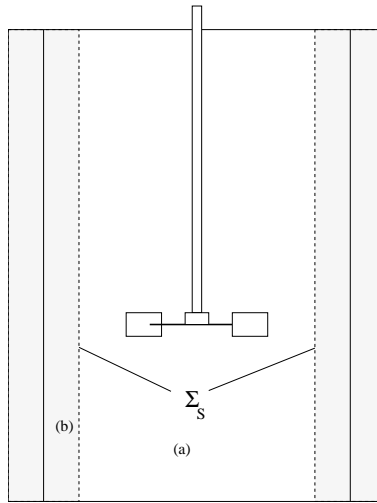


**Fig. 7.20.** Multiblock sliding grid approach. (a) = inner, rotating, block; (b) = outer, stationary, block;  $\Sigma_S$  = sliding interface. The figure is drawn based on a similar figure published by Brucato et al [10].

The governing equations for both the fixed and the rotating sub-domain grids are written with respect to the laboratory reference frame. In the inner domain the rotation of the grid is accounted for by transforming the total time derivative in the familiar Eulerian conservation equations into an Arbitrary-Eulerian-Lagrangian form similar to the model used in the MDM method [70]. The moving grid for the inner domain is allowed to slide relative to the stationary outer domain along a surface of slip. A conservative interpolation procedure is used to connect the necessary flow variables and face fluxes across this surface. Again, due to symmetry, the whole vessel does not need to be calculated. However, the domain must include an integer number of both blades and baffles.

To validate the predicted results only one of these time dependent simulations has to be carried out to achieve time (steady-state) and impeller region average values for comparison with experimental data and simulated results obtained by the IBC, IO and snapshot methods. This validation procedure is the same as the one used for the MDM method.

### 7.8.6 Model Validation

In order to validate the different approaches it is necessary to compare the results with experimental data. In addition, the IBC method relies on empirical

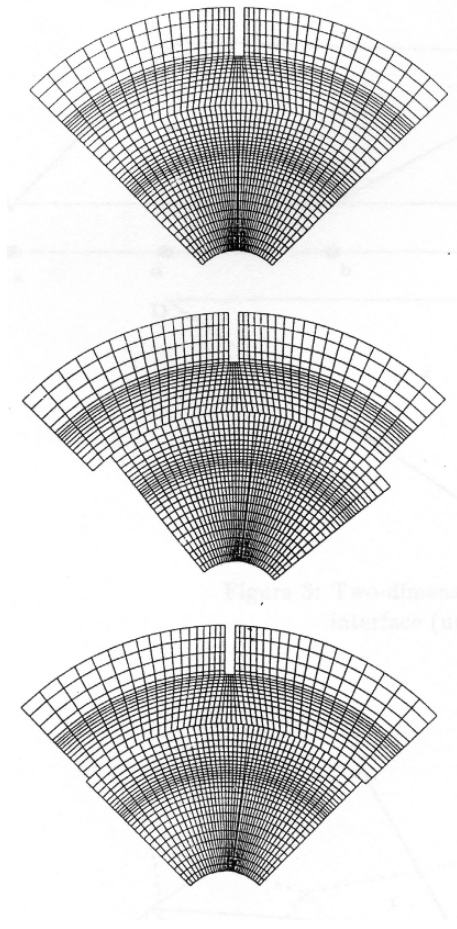


**Fig. 7.21.** Sliding grid motion [63]. Upper subfigure: sketch of the initial grid. Mid subfigure: Impeller grid rotation in clockwise direction. Lower subfigure: Cyclic rearrangement of impeller grid. Reproduced with permission by IChemE 2007.

data in order to implement the momentum source induced by the stirrer. Brucato et al [10] give a review of the different methods of measuring the velocity field. The most commonly used measurement technique is the Laser Doppler Velocimetry (LDV). Measurements for radial impellers were made for example by Dyster et al [19] who reported detailed mean and fluctuating velocity profiles in the impeller stream. Kemoun et al [46] used LDV to receive data in a closed surface surrounding the impeller. Another method that has been used to determine the velocities in the impeller region is to mount a hot wire on the rotating impeller, like Günkel and Weber [32] did for radial impellers. In addition, Van't Riet and Smith [89, 90] and Van't Riet et al [91] used a

camera mounted on a turntable rotating with the stirrer and obtained pictures of tracer particles relative to the rotating impeller.

Less experimental work has been performed for axial impellers. Kresta and Wood [48] performed LDV measurements of mean and fluctuating radial, axial and tangential velocities in cylindrical tanks with a 45°-pitched, four blade turbine at 400 rpm. A review of experimental investigations of turbulent flow in closed and free-surface unbaffled tanks stirred by radial impellers can be found in Ciofalo et al [12].

Experimental investigations of wall heat transfer in stirred tank reactors have been reported by Engeskaug et al [23], Oldshue [65], Hewitt et al [40], among others.

Harris et al [36] and Brucato et al [10] reviewed the status on modeling baffled stirred tank reactors. Simulations using the impeller boundary condition (IBC) method, the inner-outer approach, and the sliding mesh method were compared. Although reasonable flow predictions have been obtained for the liquid bulk by use of the IBC method, this approach is subject to the availability of velocities and turbulence data for formulating appropriate boundary conditions. This method is thus not feasible for multiphase flows and industrial scale reactors because of the difficulties in obtaining data for the boundary treatment. Moreover, the IBC method has no predictive value for the flow and turbulence in the impeller region, even its capabilities in predicting global parameters like the power and pumping numbers are limited.

The IO simulations confirmed that the IO procedure is capable of predicting the near impeller flow and turbulence fields with a reasonable accuracy, thus to some extent reducing the need for empirical information. Hence, the IO method is often preferred compared to the IBC method although it was 1 – 4 times more cpu demanding for one of the particular cases referred.

The SM method provides the advantage of enabling transient simulations for problems in which the flow and mixing phenomena occurring at impeller startup or as a consequence of changes in impeller rotational speed are of interest. The sliding mesh method generally provides more accurate results than the inner-outer approach, but in one of the cases referred it did also require a factor of four more computing time. The SM method also required 7 – 20 times larger cpu times than for the IBC runs for some problems.

Lane et al [49] did compare the performance of simulations with the SM and the MRF approach in predicting flow fields within a standard stirred tank equipped with a Rushton turbine. Reasonable agreement with experimental data in terms of mean velocities is obtained with both methods. Nevertheless, the MRF method provides a saving in computational time of about an order of magnitude.

Based on the impeller modeling analyses mentioned above, among other similar investigations, it is customarily concluded that for most industrial applications the MRF method is an appropriate simulation tool. The method represents a trade-off between accuracy and computational demands. However, the averaging process needed to obtain representative data in the im-

peller region is tedious as it requires many (several) similar simulations at different snapshots (representing different impeller blade positions).

In academia the SM method is considered a more fundamental method than the MRRF method because the former approach is transient and do not rely on a manual re-gridding of the geometry. The SM method has the potential of being predictive provided that the governing equations are solved with sufficient accuracy (i.e., for DNS). However, future work might improve on the direct fluid-impeller structure interaction mapping, enabling an efficient dynamic update of the impeller grid as the impeller moves and the flow evolves in a DNS without the interpolation costs of a sliding grid.

## 7.9 Assessment of Multiple Rotating Reference Frame Model Simulations

In this section a series of simulations of a standard vessel equipped with a Rushton turbine, as obtained by use of the Multiple Rotating Reference Frame (MRRF) method, are evaluated. The simulations are performed with the commercial software FLUENT [24]. The simulations were run with a resolution of 86950 cells. The turbulent effects are described by a modified (RNG)  $k$ - $\epsilon$  model<sup>11</sup> [97, 98, 99, 82, 66]. For model validation experimental LDA data characterizing a standard vessel of laboratory scale, as reported by Engeskaug [22], is used. The simulations considered in this section have been reported by Engeskaug [22], Druecker [17] and Jakobsen [43].

The stirred tank geometry used in these investigations:

- The tank diameter,  $T = 0.222$  (m)
- The liquid height in the vessel,  $H = T = 0.222$  (m)
- The impeller diameter,  $D = 0.076$  (m)
- The impeller blade width,  $W = 0.020$  (m)
- The impeller blade height,  $W = 0.020$  (m)
- The impeller clearance,  $C_b = 0.100$  (m)
- The width of wall baffles,  $B = 0.022$  (m)
- The wall baffles wall clearance,  $C_B = 0.011$  (m)
- The diameter of the impeller axis,  $T_I = 0.015$  (m)
- The thickness of the impeller blades is 1 (mm), the baffles 2 (mm) and of the Rushton Turbine's disc 3 (mm).
- The impeller rotates at 300 (rpm).

The grid used in these MRRF stirred tank simulations is shown in Fig 7.22.

The overall flow fields in a vertical layer between two baffles and in a horizontal layer at the disc axial level are shown as vector plots in Fig 7.23 and

---

<sup>11</sup> This turbulence model is similar to the standard  $k$ - $\epsilon$  model, but with altered model parameter values and the effect of swirl on turbulence is included in the RNG mode intending to enhance the accuracy of swirling flow simulations.

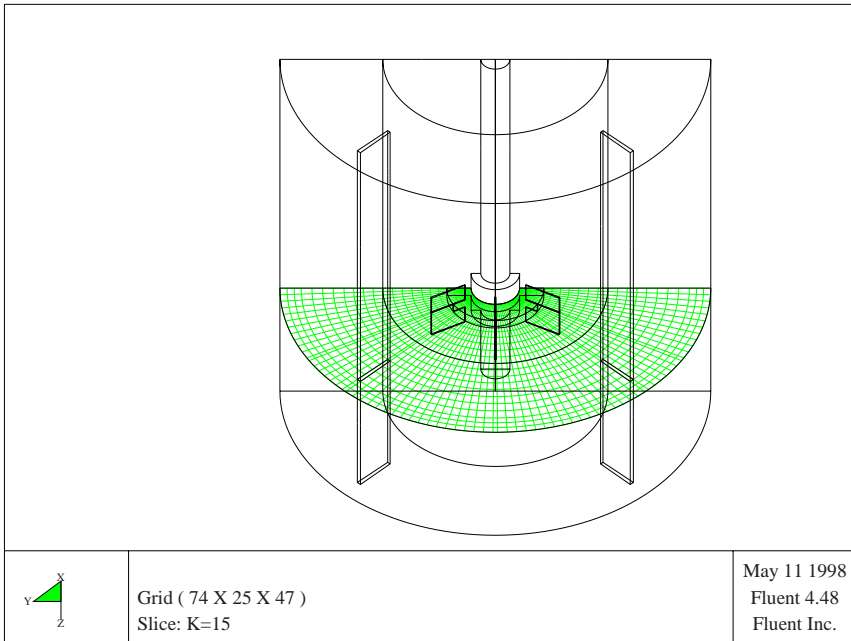


**Fig. 7.22.** A representative grid employed for the multiple rotating reference frame (MRRF) model simulations.

Fig 7.24. Sometimes it is more informative to present the corresponding speed or velocity magnitude quantity in a contour plot, for example to identify the location of the highest kinetic energy as shown in Fig 7.25 and Fig 7.26. Qualitatively the general flow field is described fairly well. The two main vortexes above and below the impeller can be identified and the highest speed occur at the impeller blade tips in agreement with the experimental observations.

A plot of the predicted turbulent kinetic energy at the disc axial level is shown in Fig 7.27. The turbulent kinetic energy values are questionable because the energy level is quite low in the impeller region where the velocity gradients are the largest.

In the following a quantitative comparison of the predicted velocity and turbulent kinematic energy profiles with experimental data is discussed. In each figure several graphs are compared. Considering velocities the meaning of the different lines are: The *blue line* denotes the experimental data [22] (Laser), the *black line* denotes MRRF simulations at high resolution (86950 cells) in which the sum of the residuals for each field is less than 0.001 (MRRF e-3), the *green line* denotes MRRF simulations at high resolution (86950 cells) in which the sum of the residuals for each field is less than 0.0001 (MRRF e-4), the *red line* denotes MRRF simulations at low resolution ( $\sim 50000$  cells) in which the sum of the residuals for each field is less than 0.0001 (MRRF

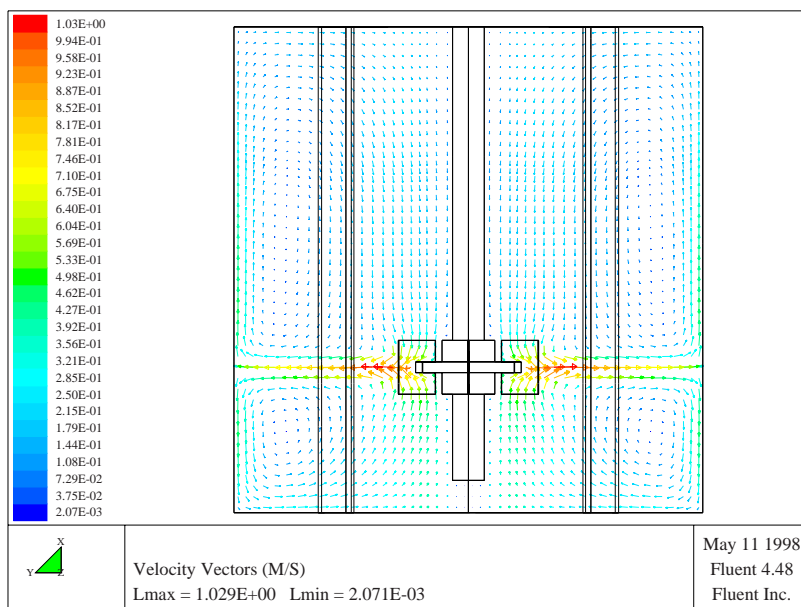


**Fig. 7.23.** Simulated velocity in a vertical plane of stirred tank reactor.

low res.), and the *pink line* represents the MRRF simulations of Engeskaug [22] at high resolution (86950 cells) in which the residuals for each field is less than 0.0001 (Engeskaug (MRRF)). Considering the turbulent kinetic energy the meaning of the different lines are modified: The *blue line* denotes the experimental data [22] (Laser), the *green line* denotes MRRF simulations at high resolution (86950 cells) in which the sum of the residuals for each field is less than 0.0001 (MRRF e-4), the *red line* denotes SM simulations at high resolution (86950 cells) in which the sum of the residuals for each field is less than 0.0001, the *black line* denotes SM simulations at low resolution ( $\sim 50000$  cells) in which the sum of the residuals for each field is less than 0.0001 (SM low res.), and the *pink line* represents the SM simulations of Engeskaug [22] at high resolution (86950 cells) in which the sum of the residuals for each field is less than 0.0001 (Engeskaug (MRRF)).

The radial velocity profiles (i.e., the three velocity components are given as azimuthal average functions of radial position in the vessel) obtained by the MRRF simulations for the axial level of the impeller are in good agreement with the experimental data both in the impeller region and in the area closer to the wall outside the impeller region, as can be seen from Fig 7.28, Fig 7.29 and Fig 7.30. However, the turbulent kinetic energy is not accurately predicted compared to the measured values, as shown in Fig 7.31. The highest turbulent kinetic energy values for the disc axial level are observed at the outer radius of the impeller where the impeller blades create the strongest swirls. The

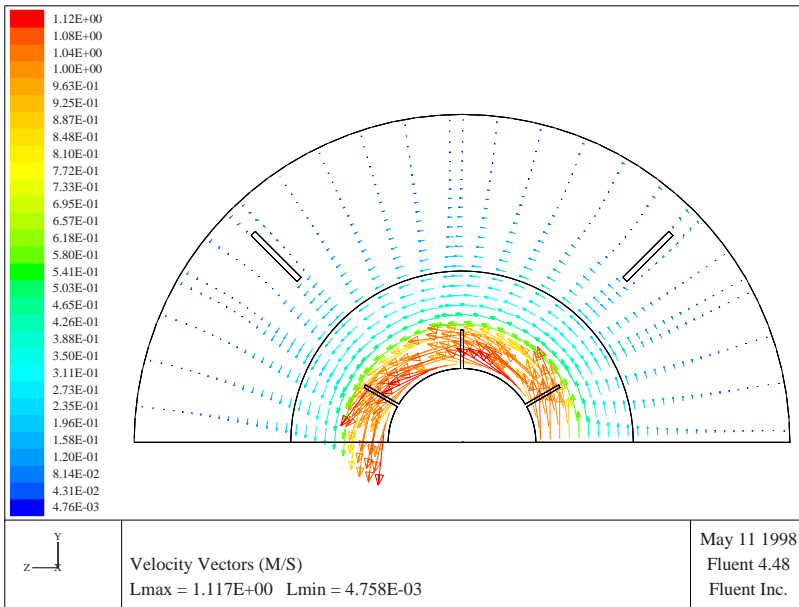


**Fig. 7.24.** Simulated velocity in a horizontal plane of stirred tank reactor.

simulated turbulent kinetic energy is much smaller than the experimental values over the whole cross section of the reactor. Below and above the disc the highest kinetic energy levels occur near the walls in the gap between the baffles and the walls (not shown).

Engeskaug [22] and Druecker [17] compared a compatible set of simulated sliding mesh (SM) and multiple rotating reference frame (MRRF) results with the experimental data. An identical numerical grid spacing was used for both methods, but in the SM method two non-overlapping sub-domains are sliding relative to each other whereas for the MRRF method the two subdomains are fixed. It was found that the MRRF and SM results are similar, but in most areas the MRRF velocity predictions were in better agreement with the experimental data than the SM results (not shown). On the other hand, quite surprisingly, the turbulent kinetic energy profiles are in most areas much better predicted with the SM method compared to the MRRF simulations (see Fig 7.31). However, it is difficult to determine if these differences in the predictions are due to the different averaging procedures applied to the simulated results, differences in the numerical model implementation, interpolation schemes, or differences in the two model formulations.

The computational time required by these impeller modeling methods were also compared. For baffled tanks the computational time required by these two impeller methods are quite similar as several MRRF simulations have to be run per one SM simulation because a manual change in the relative impeller-

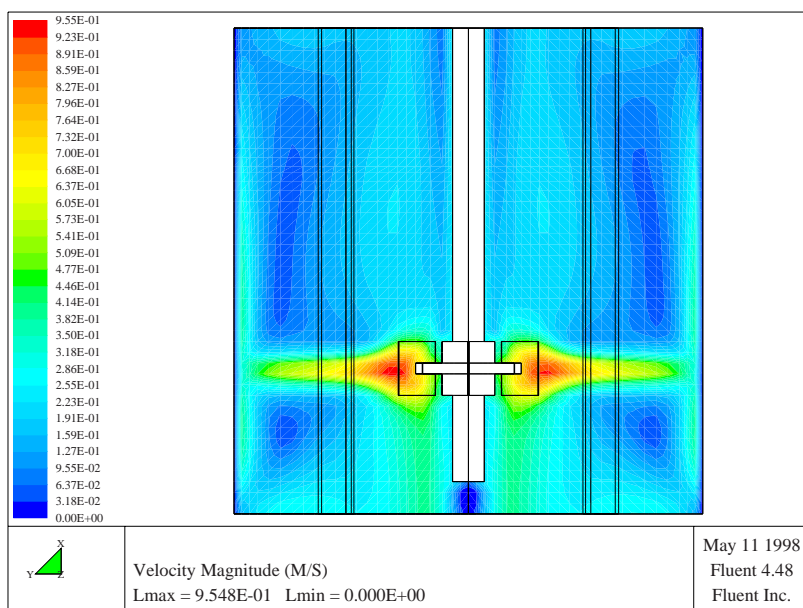


**Fig. 7.25.** Simulated velocity magnitude in a vertical plane of stirred tank reactor.

baffle positions are performed to resolve the flow in the impeller region. The SM simulations are time dependent so the results have to be averaged over a sufficient period in time. For unbaffled vessels only one MRRF simulation is required, so the MRRF method is significantly cheaper than the SM method in these cases.

The simulated results evaluated in this section are about ten years old, thus today the numerical resolution used in this work might be considered coarse. However, although the present computers allow better resolutions to be used in the simulations the status on stirred tank modeling is still very similar. For single phase flows the limiting steps are basically related to the turbulence modeling and the computational efficiency. For multi-phase flows additional limitations regarding the closure laws determining interfacial transfer fluxes, particle growth, particle coalescence and breakage processes, etc are prohibitive and make predictive simulations very difficult.

It is noted that in recent papers several extended turbulence models, i.e., the standard  $k-\varepsilon$  [50], RNG  $k-\varepsilon$  [97, 98, 99, 82, 66], realizable  $k-\varepsilon$  [81], Chen-Kim  $k-\varepsilon$  [11], optimized Chen-Kim  $k-\varepsilon$  [44], standard  $k-\omega$  [96],  $k-\omega$  shear-stress transport (SST) [56, 57, 58] and the standard Reynolds stress models, have been proposed and validated. However, little or no significant improvements have been achieved considering the predictivity of the turbulence models, although each of them may have minor advantages and disadvantages. A few

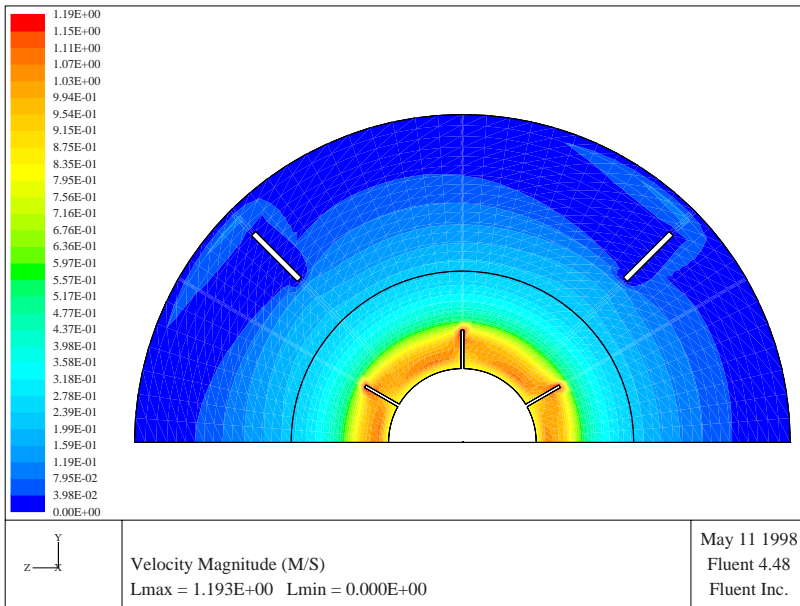


**Fig. 7.26.** Simulated velocity magnitude in a horizontal plane of stirred tank reactor.

recent investigations of the flow in stirred tanks are assessed to support this conclusion.

Jenne and Reuss [44] performed critical assessments of the use of  $k-\varepsilon$  turbulence models for simulations of turbulent single phase flow induced by the impellers in baffled/unbaffled stirred tanks. A standard configuration stirred-tank reactor equipped with a Rushton turbine was simulated by use of the PHOENICS code in which the effect of the impeller is described by the empirical source term method. The accuracy reflected by three  $k-\varepsilon$  turbulence models (i.e., the standard  $k-\varepsilon$ , Chen and Kim  $k-\varepsilon$ , RNG  $k-\varepsilon$  models) in predicting the mean flow and turbulence quantities is tested by 3D simulations. The different simulations were compared with experimental data, revealing that none of the possible  $k-\varepsilon$  models performs satisfactory reproducing a known flow field without an optimization of the model parameters for the vessel in question. By parameter fitting/tuning an optimized Chen-Kim  $k-\varepsilon$  turbulence model was obtained. By use of the optimized turbulence model fair agreement was achieved between measured flow details and the predicted results for vessels and impellers of somewhat different geometry.

Zakrzewska and Jaworski [101] performed single phase CFD simulations of turbulent jacket heat transfer in a Rushton turbine stirred vessel using the eight turbulence models mentioned above as implemented in FLUENT. In all simulations the boundary flow at the vessel wall was described by the

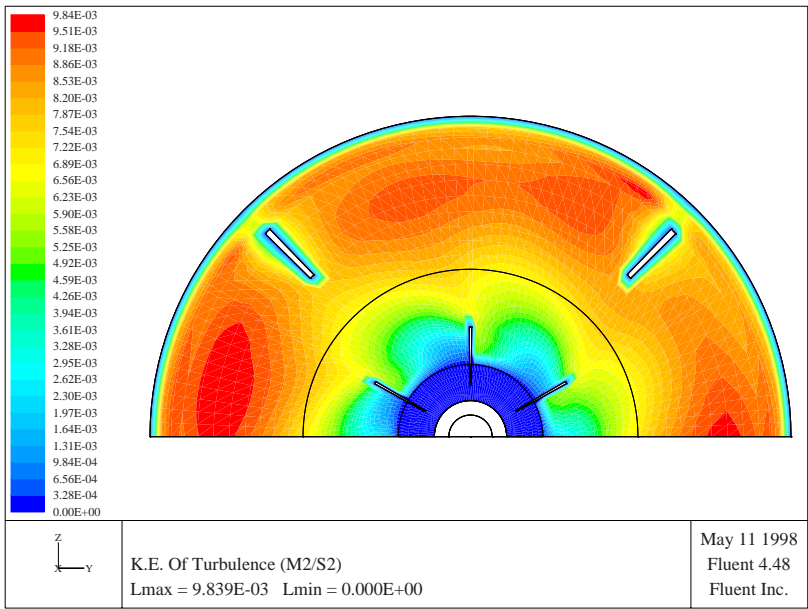


**Fig. 7.27.** Simulated turbulent kinetic energy in horizontal plane of stirred tank reactor.

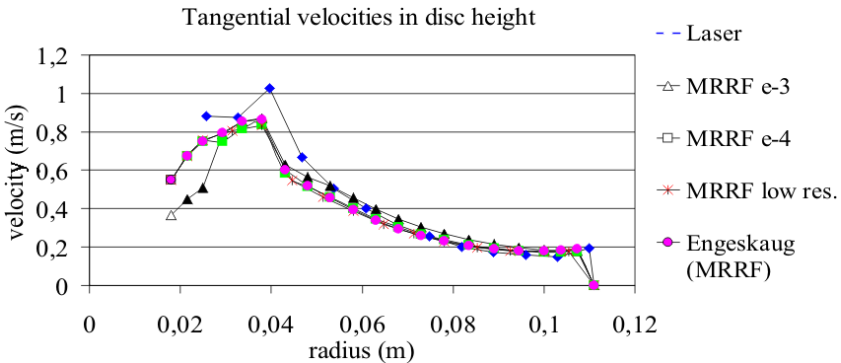


**Fig. 7.28.** Measured and simulated radial profiles of the tangential velocity component at the axial level of the disc.

standard logarithmic wall functions. The predicted values of the local heat transfer coefficient were compared with measured values. In these simulations the standard  $k-\varepsilon$ , the optimized Chen-Kim  $k-\varepsilon$  and the  $k-\omega$  SST model results were in fair agreement with experimental data, whereas the realizable  $k-\varepsilon$ , RNG  $k-\varepsilon$  and the Reynolds stress model were not recommended.

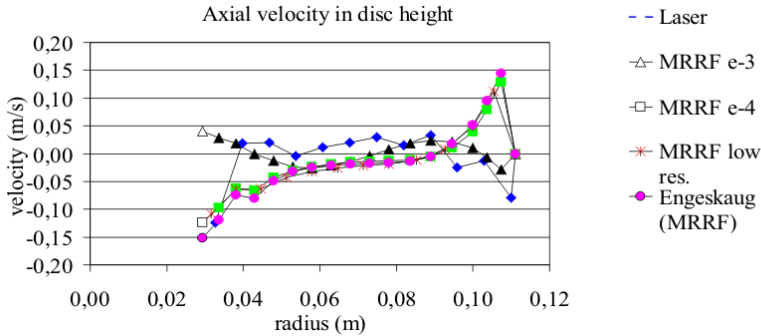


**Fig. 7.29.** Measured and simulated radial profiles of the axial velocity component at the axial level of the disc.

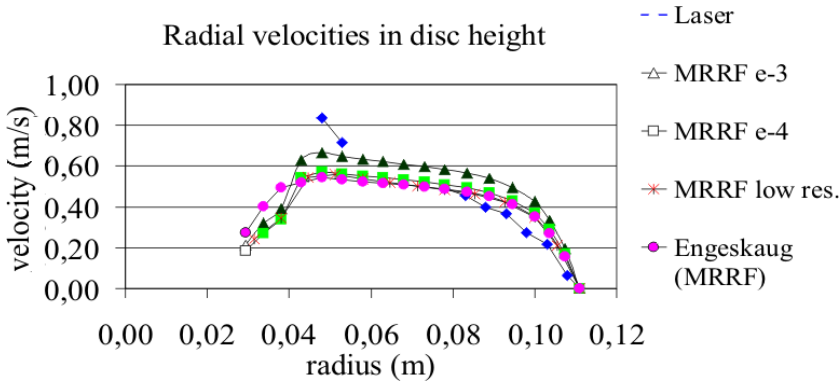


**Fig. 7.30.** Measured and simulated radial profiles of the radial velocity component at the axial level of the disc.

Haque et al [35] simulated turbulent flows with a free-surface in unbaffled agitated vessels using three turbulence models (i.e., the Reynolds stress, standard  $k-\varepsilon$  and  $k-\omega$  SST models) as implemented in CFX. In this case it appears that the SST model did perform better than the standard  $k-\varepsilon$  model, whereas some features of the flow structure and the mean velocity profiles were better predicted by the Reynolds stress model.

Lo [51] simulated two- and three phase isothermal non-reacting stirred tanks with two downward pumping  $45^\circ$  pitched -blade disc turbines and one curved-blade impeller at the bottom. Four or six baffles were placed at equal distance around the vessel wall. An Eulerian multiphase-population balance (MUltiple-SIze-Group, MUSIG) model was used as implemented in CFX. Turbulence of the continuous phase was modeled by the standard  $k-\varepsilon$  turbulence model, and an algebraic relation was used for the particle induced eddy vis-

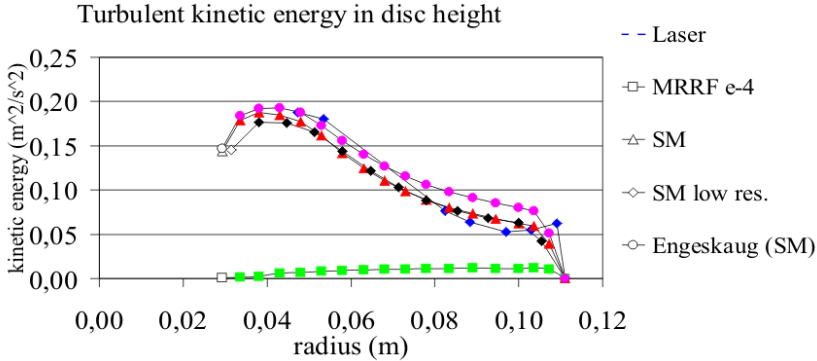


**Fig. 7.31.** Measured and simulated radial profiles of the turbulent kinetic energy at the axial level of the disc.

cosity. The sliding mesh impeller method was used. The phase distribution in the tanks were in fair agreement with experimental data. Comparisons of the measured and predicted shaft power were general within  $\pm 20\%$  deviation. No detailed evaluation of the performance of the turbulence model was reported.

A similar pseudo-two phase investigation was reported by Venneker et al [93] using the empirical source term impeller method in FLUENT. They simulated the turbulent flow pattern in a baffled agitated vessel equipped with a six-blade disc turbine and a ring sparger. The transport of bubbles throughout the vessel was simulated by a scaled single-phase flow field. The single phase turbulence field was modeled with the Reynolds stress model. Compared to LDA measurements the overall predictions were qualitatively correct, but the turbulent kinetic energy and energy dissipation rate fields need further improvements. Local gas fraction and bubble size distributions in the tank was described by a population balance model. Model predictions for the gas fractions in pseudoplastic Xanthan solutions were compared with local measurements and agreed fairly well qualitatively.

Basara et al [3] simulated single- and two-phase turbulent flows in stirred vessels equipped with six- and four blade Rushton-type turbines using the sliding mesh impeller method. To describe turbulence in the liquid phase a standard  $k-\varepsilon$  model was used for single phase calculations and an extended  $k-\varepsilon$  model was employed for the two-phase simulations. These simulations were performed in transient mode with 1 (*ms*) time steps. The whole calculation contains 3900 time steps, which means approximately 4s of real time and 17 complete rotations of the impeller. One such simulation took 13 days of CPU time using an Intel single processor with 2.6 (*GHz*). The flow pattern predictions were compared with experimental data and fair agreement was obtained. It was stated that the standard  $k-\varepsilon$  model over-predicted the

turbulence kinetic energy, and that might be achieved using more accurate turbulence models.

Moilanen et al [59] did use CFX to simulate two-phase aerated fermenters. A MRRF technique was employed to describe the impeller motion. The results obtained using two different turbulence closures were compared with experimental and visual observations. The two turbulence models tested were the standard  $k$ - $\varepsilon$  and the SST models. It was stated that the  $k$ - $\varepsilon$  model did behave unphysically in the bulk regions of the vessel by generating unreasonable turbulence properties. The SST model gave more reasonable results.

---

## References

1. Andersson R (2005) Dynamics of Fluid Particles in Turbulent Flows. CFD simulations, Model development and Phenomenological Studies. PhD Thesis, Chalmers University of Technology, Göteborg
2. Baldyga J, Bourne JR (1999) Turbulent Mixing and Chemical Reactions. John Wiley & Sons, Chichester
3. Basara B, Alajbegovic A, Beader D (2004) Simulation of single- and two-phase flows on sliding unstructured meshes using finite volume method. *Int J Numer Meth* 45:1137-1159
4. Batchelor GK (1959) Small-scale variation of convected quantities like temperature in turbulent fluid. Part 1. General discussion and the case of small conductivity. *J Fluid Mech* 5:113-133
5. Batchelor GK (1982) *The Theory of Homogeneous Turbulence*. Cambridge University Press, Cambridge
6. Batchelor GK (1983) *An Introduction to Fluid Dynamics*. Cambridge University Press, Cambridge
7. Biswas G, Eswaran V (2002) *TURBULENT FLOWS, Fundamentals, Experiments and Modeling*. Alpha Science International Ltd, Pangbourne
8. Brodkey RS (1967) *The Phenomena of Fluid Motion*. Addison-Wesley Publishing Company, Reading, Massachusetts
9. Brucato A, Ciofalo M, Grisafi F, Micale G (1994) Complete Numerical Simulation of Flow Fields in Baffled Stirred Vessels: the Inner-Outer Approach. Eight European Conference on Mixing, Cambridge (ISBN 0852953291)
10. Brucato A, Ciofalo M, Grisafi F, Micale G (1998) Numerical prediction of flow fields in baffled stirred vessels: A comparison of alternative modelling approaches. *Chem Eng Sci* 53(21):3653-3684
11. Chen YS, S.W.Kim SW (1987) Computation of turbulent flows using an extended  $k-\varepsilon$  turbulence closure model. NASA Report CR-179204
12. Ciofalo M, Brucato A, Grisafi F, Torraca N (1996) Turbulent Flow in Closed and Free-Surface Unbaffled Tanks Stirred by Radial Impellers. *Chem Eng Sci* 51(14):3557-3573
13. Corrsin S (1951) On the Spectrum of Isotropic Temperature Fluctuations in an Isotropic Turbulence. *J Applied Phys*
14. Corrsin S (1964) Further generalization of Onsager's cascade model for turbulent spectra. *Phys Fluids* 7:1156-1159

15. Corrsin S (1974) Limitations of Gradient Transport Models in Random Walks and in Turbulence. In: Landsberg HE, van Mieghem J (eds) *Advances in geophysics*, Academic Press, New York, 18A
16. Crowe CT, Elger DF, Roberson JA (2001) *Engineering Fluid Mechanics*. 7th Edition, John Wiley & Sons, Inc, New York
17. Druecker M (1999) Simulation of the Flow Field of Stirred Tank Reactors: Comparison Between Computational Results and Experiments. Studienarbeit summary report, Aachen, Germany
18. Derksen J, van den Akker HEA (1999) Large Eddy Simulations on the Flow Driven by a Rushton Turbine. *AIChE J* 45 (2):209-221
19. Dyster KN, Koutsakos E, Jaworski Z, Nienow AW (1993) An LDA study of the Radial Discharge Velocities Generated by a Rushton Turbine: Newtonian Fluids,  $Re \geq 5$ . *Trans. IChemE* 71A:11-23
20. Eggels JGM (1996) Direct and large-eddy simulation of turbulent fluid flow using the lattice-Boltzmann scheme. *Int J Heat and Fluid Flow* 17:307-323
21. *Handbook of Mixing Technology*. EKATO Rühr- und Mischtechnik GmbH, Schopfheim, Germany, (ISBN 3-00-0052 46-1), 2000.
22. Engeskaug R (1998) Modeling of chemical reactors with impellers. MSc Thesis, Høgskolen i Telemark, Norway
23. Engeskaug R, Thorbjørnsen E, Svendsen HF (2005) Wall Heat Transfer in Stirred Tank Reactors. *Ind Eng Chem Res* 44:4949-4958
24. FLUENT (1996) *FLUENT User's Guide*, Release 4.4, Volume 1-4, Fluent Inc, Lebanon (1996)
25. Fox RO (1996) Computational methods for turbulent reacting flows in the chemical process industry. *Revue de L'Institut Francais du petrole* 51 (2):215-243
26. Fox RO (2003) *Computational Models for Turbulent Reacting Flows*. Cambridge University Press, Cambridge
27. Geankoplis CJ (1993) *Transport Processes and Unit Operations*. Third edition, PTR Prentice Hall International Editions, Englewood Cliffs
28. Ghil M, Childress S (1987) *Topics in geophysical fluid dynamics: Atmospheric dynamics, dynamo theory, and climate dynamics*. Volume 60 of *Applied mathematical sciences*, Springer-Verlag, New-York
29. Gill AE (1982) *Atmosphere - Ocean Dynamics*. Academic Press Inc, San Diego
30. Gosman AD, Lekakou C, Polits S, Issa RI, Looney MK (1992) Multidimensional Modeling of Turbulent Two-Phase Flows in Stirred Vessels. *AIChE J* 38(12):1946-1956
31. Greenspan HP (1980) *The theory of rotating fluids*. Cambridge University Press, Cambridge
32. Günkel AA, Weber ME (1975) *Flow Phenomena in Stirred Tanks*. Part I: The Impeller Stream. *AIChE J* 21 (5):931-949
33. Hagesaether L (2002) Coalescence and break-up of drops and bubbles. Dr.ing. Thesis, The Norwegian University of Science and Technology, Trondheim
34. Hansen AG (1967) *Fluid Mechanics*. John Wiley and Sons Inc, New York
35. Haque AG, Mahmud T, Roberts KJ (2006) Modeling Turbulent Flows with Free-Surface in Unbaffled Agitated Vessels. *Ind Eng Chem Res* 45:2881-2891
36. Harris CK, Roekaerts D, Rosendal FJJ, Buitendijk FGJ, Daskopoulos PH, Vreenegoor AJN, Wang H (1996) Computational fluid dynamics for chemical reactor engineering. *Chem Eng Sci* 51:1569-1594

37. Harvey PS, Greaves M (1982) Turbulent Flow in an Agitated Vessel. Part I: A Predictive Model. *Trans IChemE* 60:195-200
38. Harvey PS, Greaves M (1982) Turbulent Flow in an Agitated Vessel. Part II: Numerical Simulation and Model Predictions. *Trans IChemE* 60:201-210
39. Heisenberg W (1948) Zur statistischen Theorie der Turbulenz. *Z Phys Bd* 124:628-657
40. Hewitt GF, Shires GL, Bott TR (1994) *Process Heat Transfer*, Chapter 31 (Heat Transfer in Agitated Vessels), CRC Press, Inc., pp. 937-954, Boca Raton
41. Hinze JO (1975) *Turbulence*. Second edition, McGraw-Hill, New York
42. Irgens F (1999) *Dynamikk*. Tapir Forlag, Fourth edition (in Norwegian)
43. Jakobsen HA (2001) Struggle on the modeling of swirling flow phenomena in multiphase chemical reactors. 426th EUROMECH & ERCOFTAC Colloquium on Swirling Flows. Bergen-Tromsø, September 16th - 20th. Printed in Book of abstracts.
44. Jenne M, Reuss M (1999) A critical assessment on the use of  $k$ - $\varepsilon$  turbulence models for simulation of the turbulent liquid flow induced by a Rushton-turbine in baffled stirred-tank reactors. *Chem Eng Sci* 54:3921-3941
45. Kageyama A, Hyodo M (2006) Euler derivation of the Coriolis force. *Geochem Geophys Geosyst* 7(2):1-5 ISSN:1525-2027
46. Kemoun A, Lusseyran F, Mahouast M, Mallet J (1994) Experimental Determination of the Complete Reynolds Stress Tensor in Fluid Agitated by a Rushton Turbine. *IChemE Symp Ser No 136*, pp. 399-406; Eight European Conference on Mixing, Cambridge (ISBN 0852953291)
47. Kolmogorov AN (1941) The local structure of turbulence in incompressible viscous fluid for very large Reynolds numbers. *Dokl Akad Nauk SSSR*, 30:299-303 (in Russian)
48. Kresta SM, Wood PE (1993) The Flow Field Produced by a Piched Blade Turbine: Characterisation of Turbulence and Estimation of the Sissipation Rate. *Chem Engng Sci* 48: 1761-1774
49. Lane GL, Schwartz MP, Evans GM (2000) Comparison of CFD Methods for Modeling of Stirred Tank. *Proc 10th European Conference on Mixing, Delft, the Netherlands, July*, pp 273-280
50. Launder BE, Spalding DB (1974) *The Numerical Computation of Turbulent Flows*. *Computer Methods in Applied Mechanics and Engineering*, No 3, pp 269-289
51. Lo S (2000) Some recent developments and applications of CFD to multiphase flows in stirred reactors. *Proc AMIF-ESF Workshop on Computing Methods for Two-Phase Flow, Aussois, France, 12-14 January*
52. Luo JY, Gosman AD, Issa RI, Middleton JC, Fitzgerald MK (1994) Full flow field computation of mixing in baffled stirred vessels. *Trans IChemE* 71(A):342-344
53. Lydersen A, Dahlø I (1988) *Ordbok for kjemiteknikk* (In Norwegian), Tapir Forlag, Trondheim
54. Malvern LE (1969) *Introduction to the Mechanics of a Continuous Medium*. Prentice-Hall, Inc, Englewood Cliffs
55. Marshall E, Haidari A, Subbiah S (1996) Paper presented at AIChE Annual Meeting, Chicago, November
56. Menter FR (1992) Improved Two-Equation  $k$ - $\varepsilon$  Turbulence Models for Aerodynamic Flows. NASA Technical Memorandum 103975

57. Menter FR (1994) Two-Equation Eddy-Viscosity Turbulence Models for Engineering Applications. *AIAA J* 32(8):1598-1605
58. Menter FR, Kuntz M, Langtry R (2003) Ten Years of Industrial Experience with the SST Turbulence Model. In: Hanjalic K, Y. Nagano, Tummers M (eds) *Turbulence, Heat and Mass Transfer 4*, Begell House Inc, New York, pp 625-632
59. Moilanen P, Laakonen M, Aittamaa J (2006) Modeling Aerated Fermenters with Computational Fluid Dynamics. *Ind Eng Chem Res* 45:8656-8663
60. Mortensen M (2005) *Mathematical Modeling of Turbulent Reactive Flows*. PhD Thesis, Chalmers University of Technology, Göteborg
61. Mujumdar AS, Huang B, Wolf D, Weber ME, Douglas WJM (1970) *Can J Chem Eng* 48:475-483
62. Munson BR, Young DF, Okiishi TH (2002) *Fundamentals of Fluid Mechanics*. Fourth Edition, John Wiley & Sons, Inc, New York
63. Murthy JY, Mathur SR, Choudhury D (1994) CFD Simulation of Flows in Stirred Tank Reactors Using a Sliding Mesh Technique. *ICHEME Symposium Series*, No. 136, pp. 341-348. Eight European Conference on Mixing, Cambridge (ISBN 0852953291)
64. Nienow AW (1997) On impeller circulation and mixing effectiveness in the turbulent flow regime. *Chem Eng Sci* 52 (15):2557-2565
65. Oldshue JY (1983) *Fluid Mixing Technology*. McGraw-Hill, New York
66. Orszag SA, Yakhot V, Flannery WS, Boysan F, Choudhury D, Maruzewski J, Patel B (1993) Renormalization Group Modeling and Turbulence Simulations. In: So RMS, Speziale CG, Launder BE (eds) *Near-Wall Turbulent Flows*, (pp 1031-1046) Elsevier Science Publishing BV.
67. Osenbroch LKH (2004) *Experimental and Computational Study of Mixing and Fast Chemical Reactions in Turbulent Liquid Flows*. PhD Thesis, Aalborg University, Esbjerg
68. Pao Y-H (1965) Structure of Turbulent Velocity and Scalar Fields at Large Wavenumbers. *Phys Fluids* 8 (6):1063-1075
69. Pericleous KA, Patel MK (1987) The Modelling of Tangential and Axial Agitators in Chemical Reactors. *PhysicoChemical hydrodynamics (PCH)*, 8(2):105-123, 1987.
70. Perng CY, Murthy JY (1993) A Moving-Deforming-Mesh Technique for Simulation of Flow in Mixing Tanks. *AIChE Meeting*, Miami Beach, FL (1992); *AIChE Symposium Series* 89(293):37-41
71. Pope S (1985) PDF Methods for turbulent reactive flows. *Prog Energy Combust Sci* 11:119-192
72. Pope S (2000) *Turbulent Flows*. Cambridge University Press, Cambridge, 2000.
73. Ranade VV, Joshi JB (1990) Flow generated by a disc turbine: Part II. Mathematical modelling and comparison with experimental data. *Trans IChemE* 68A:34-50
74. Ranade VV, Van den Akker HEA (1994) A Computational Snapshot of Gas-Liquid Flow in Baffled Stirred Reactors. *Chem Eng Sci* 49(24B):5175-5192
75. Ranade VV, Krishnan YTH (2002) CFD predictions of flow near impeller blades in baffled stirred vessels: Assessment of computational snapshot approach. *Chem Eng Comm* 198:895-922
76. Richardson LF (1922) *Weather Prediction by Numerical Process*. Cambridge University Press, Cambridge
77. Revstedt J, Fuchs L, Trägårdh C (1998) Large eddy simulations of the turbulent flow in a stirred reactor. *Chem Eng Sci* 53 (24):4041-4053

78. Rogers MM, Mansour NN, Reynolds WC (1989) An algebraic model for the turbulent flux of a passive scalar. *J Fluid Mech* 203:77-101
79. Sabersky RH, Acosta AJ, Hauptmann EG, Gates EM (1999) *Fluid Flow: A first course in fluid mechanics*. Fourth edition, Prentice Hall, London
80. Schlichting H, Gersten K (2000) *Boundary-Layer Theory*. Springer-Verlag, Berlin
81. Shih T-H, Liou WW, Shabbir A, Zhu J (1995) A New  $k-\varepsilon$  Eddy Viscosity Model for High Reynolds Number Turbulent Flows. *Comp Fluids* 24(3):227-238
82. Smith LM, Reynolds WC (1992) On the Yakhot-Orszag renormalization group method for deriving turbulence statistics and models. *Phys Fluids A* 4(2):364-390
83. Smits AJ (2000) *A Physical Introduction to Fluid Mechanics*. John Wiley & Sons, Inc, New York
84. Spalding DB (1971) Concentration fluctuations in a round turbulent free jet. *Chem Eng Sci* 26:95-107
85. Stull RB (1988) *An Introduction to Boundary Layer Meteorology*. Kluwer Academic Publishers, Dordrecht
86. Sudiyo R (2006) *Fluid Dynamics in Gas-Liquid Stirred Tank Reactors: Experimental and Theoretical Studies of Bubble Coalescence*. PhD Thesis, Chalmers University of Technology, Göteborg
87. Tatterson GB (1991) *Fluid Mixing and Gas Dispersion in Agitated Tanks*. McGraw-Hill, New York
88. Tennekes H, Lumley JL (1972) *A First Course in Turbulence*. MIT Press, Cambridge
89. Van't Riet K, Smith JM (1973) The behavior of gas-liquid mixtures near Rushton turbine blades. *Chem Engng Sci* 28:1031-1037, 1973.
90. Van't Riet K, Smith JM (1975) The Trailing Vortex System Produced by Rushton Turbine Agitators. *Chem Eng Sci* 30:1093-1105
91. Van't Riet K, Bruijn W, Smith JM (1976) Real and Pseudo-Turbulence in the Discharge Stream from a Rushton Turbine. *Chem Eng Sci* 31:407-412
92. Van't Riet K, Smith JM (1975) The trailing vortex system produced by Rushton turbine agitators. *Chem Eng Sci* 30:1093-1105
93. Venneker BCH, Derksen JJ, van den Akker HEA (2002) Population Balance Modeling of Aerated Stirred Vessels Based on CFD. *AIChE J* 48(4):673-685
94. Weisbach JL (1845) *Lehrbuch der Ingenieur-und Maschinenmechanik*, Braunschweig
95. White FM (1999) *Fluid Mechanics*, McGraw-Hill Inc, Fourth Edition, New York
96. Wilcox DC (1988) Reassessment of the Scale-Determining Equation for Advanced Turbulence Models. *AIAA J* 26(11):1299-1310
97. Yakhot A, Orszag S (1986) Renormalization Group Analysis of Turbulence: I. Basic Theory. *J Sci Comput* 1(1):3-51
98. Yakhot A, Smith LM (1992) The Renormalization Group, the  $\varepsilon$ -Expansion and Derivation of Turbulence Models. *J of Sci Comput* 7(1):35-60
99. Yakhot A, Orszag SA (1992) Development of turbulence models for shear flows by a double expansion technique. *Phys Fluids A* 4(7):1510-1520
100. Young DF, Munson BR, Okiishi TH (2001) *A Brief Introduction to Fluid Mechanics*. Second Edition, John Wiley & Sons, Inc, New York
101. Zakrzewska B, Jaworski Z (2004) CFD Modelling of Turbulent Jacket Heat Transfer in Rushton Turbine Stirred Vessel. *Chem Eng Technol* 27(3):237-242

## Bubble Column Reactors

In this chapter the elementary hydrodynamic characteristics of simple bubble columns are summarized. Different designs of bubble columns are sketched, and examples of their industrial applications are outlined. An overview of the status on Eulerian bubble column modeling is presented.

### 8.1 Hydrodynamics of Simple Bubble Columns

In its most simple form a bubble column reactor basically consists of a vertical cylinder with a gas distributor at the inlet, as sketched in Fig 8.1. Simple construction and lack of any mechanically operated parts are two characteristic aspects of the reactor. In general, the bubble column is an adaptable type of reactor which is reasonable in price and can be built in large sizes. The ratio between length and diameter may vary, but ratios between 3 and 10 are most common [28]. Units of 100–200 ( $m^3$ ) are regarded as very large in the chemical industry.

The liquid phase may be operated in batch mode or it may move co-currently or counter-currently to the flow of the gas phase. The gas usually enters at the bottom of the column through a gas distributor which may vary in design. The gas phase is dispersed by the distributor into bubbles entering a continuous liquid phase. In addition, reactive or catalytic particles may be suspended in the liquid phase.

The liquid flow rate passing through a bubble column is usually very low. The gas throughput on the other hand may vary widely according to the specified conversion level. The normal ranges of liquid and gas superficial velocities, based on empty reactor cross-sectional area, are in the region of 0 to 3 ( $cm/s$ ) and 3 to 25 ( $cm/s$ ), respectively.

The reactor may be cooled or heated by means of internal heat exchanges. One of the main features is very high heat transfer coefficients [68], thus ensuring a fairly uniform temperature throughout the reactor even with strong

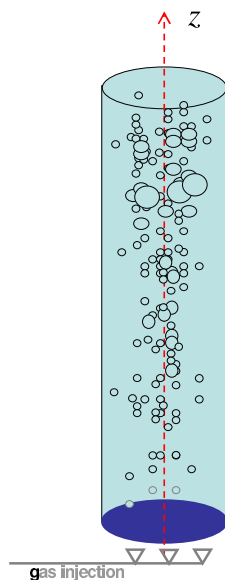


**Fig. 8.1.** A sketch of a simple bubble column.

exothermic/endothermic reactions. This is of special significance when reactions in which the selectivity is highly dependent on temperature are involved.

The rising gas bubbles entrain an amount of liquid with them which is considerably greater than that corresponding to the liquid throughput [28]. The larger bubbles plus entrained liquid tend to rise up through the center of the column. Thus, continuity will ensure that fluid returns down the column close to the wall, transporting smaller bubbles with it, forming a distinctive circulating flow pattern. Large bubble swarms with length scales of the same order as the column diameter are observed rising in a helical fashion towards the top of the column. However, averaged over a long period of time (in the order of 10 to 30 seconds) this transient circulation pattern vanishes. Yet non-uniform time averaged radial gas holdup and velocity profiles result despite a uniform initial distribution of gas across the whole cross-section of the reactor. The mean liquid axial velocity profiles have been found to be relatively stable with a general shape as shown in Fig 8.2. Nevertheless, a transient radial cross-exchange of fluid elements is superimposed on the mean axial circulation pattern, giving rise to a relatively high radial intermixing.

For water and dilute aqueous solutions the bubbles are generally uniformly distributed in the liquid at low gas flow rates [132]. The bubble size distribution is relatively narrow and the bubbles rise uniformly through the column. This is known as homogeneous flow and is sketched in Fig 8.3. Homogeneous bubbly flow may occur in small scale apparatus with superficial gas velocities below 5 ( $cm/s$ ).

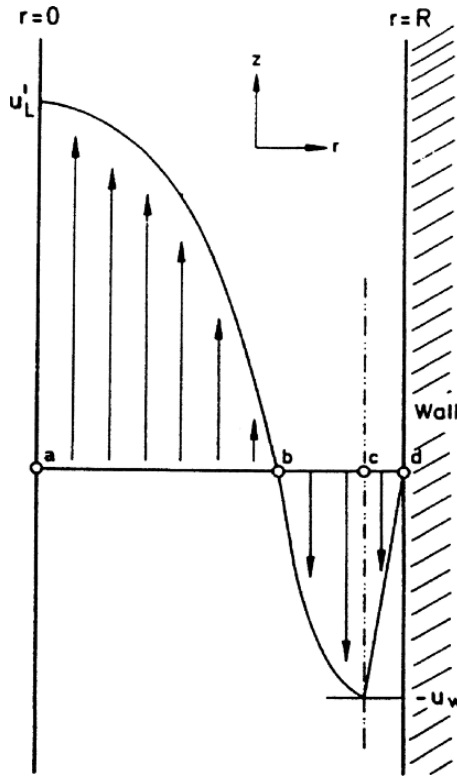


**Fig. 8.2.** Liquid flow profile in a simple bubble column [155]. Reproduced with permission. Copyright 1979 American Institute of Chemical Engineers (AIChE).

This state is not maintained when the gas passes more rapidly through the column. Coalescence and bubble breakage lead to a wider bubble size distribution. Large bubbles are formed and these may rise more rapidly than the smaller bubbles. This type of flow is referred to as heterogeneous, Fig 8.3, and is quite common as a result of the high gas rates frequently adopted in industry. For water and dilute aqueous solutions heterogeneous churn-turbulent flow may occur in columns with diameters larger than about 20 (*cm*) and when the superficial gas velocity exceeds about 7 (*cm/s*).

In narrow bubble columns the large bubbles in the heterogeneous zone are stabilized by the tube wall and move upwards through the column in a piston-like manner. These elongated bubbles or slugs fill practically the whole cross-section and continue to grow by collecting smaller bubbles continuously throughout their upward journey. This is known as slug flow, Fig 8.3, and for water and dilute aqueous solutions this regime is most likely to occur in tall appliances with column diameters of around 20 (*cm*) or less and with superficial gas velocities above 7 (*cm/s*).

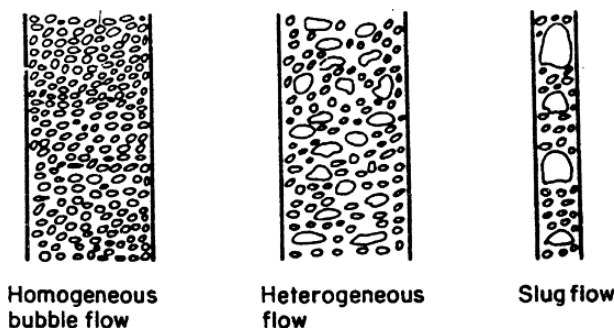


**Fig. 8.3.** Operating states in bubble columns. Figure depicted from Deckwer [28]. Copyright John Wiley & Sons Limited. Reproduced with permission.

Note that the flow chart is system dependent and may change somewhat for other mixtures and operating conditions [132].

Bubble columns have been found to work well when the gas throughput is high even in the case of the simple type shown in Fig 8.1, since the high rate of liquid circulation ensures that when any solids involved, such as catalyst, reagent or biomass are uniformly distributed [28]. However, liquid circulation does have the adverse effect of increasing the back-mixing and if conversion expectations are high, the reactor volume may increase accordingly. The effect of back-mixing on the conversion is of course dependent on the chemical reacting system in question. The short gas residence time, determined mainly by the bubble rise velocity, is a further disadvantage.

### 8.1.1 Experimental Characterization of Cylindrical Bubble Column Flow

The literature reporting measurements of gas and liquid velocities, flow patterns, and phase distribution of two-phase flow in pipes or cylindrical columns is extensive. Introductorily, a few essential observations are summarized.

Several thorough reviews on the characteristics of vertical bubbly flows have been reported [59, 62, 66, 104]. Bubble columns are usually operated at very low or zero liquid fluxes, and larger gas fluxes. Experimental investigations performed by several groups show that under these flow conditions, core peaking is the rule.

In a pioneering investigation, Serizawa [127, 128] measured the lateral void distribution as well as the turbulent axial liquid velocity fluctuations for bubbly air/water up-flows in a vertical pipe of diameter 60 (*mm*) inner diameter. They used electrical resistivity probes to measure the local void fraction, the bubble impaction rate, the bubble velocity and its spectrum. Turbulence quantities, such as the liquid phase mean velocity, and the axial turbulent fluctuations were measured using a hotfilm anemometer. A supplementary

experimental investigation of phase distribution phenomena in a 57.15 (*mm*) inner diameter pipe was performed by Wang et al [162]. By a hotfilm anemometer they measured the lateral void distribution as well as the mean and fluctuations in the axial liquid velocity for both bubbly up-flows and down-flows. To measure all components of the Reynolds stress tensor in the liquid phase, a special 3D conical probe was used. It was confirmed that the lateral void distribution is strongly influenced by the flow direction. Moreover, in this study it was also found that for up flows wall peaking become more pronounced for higher liquid flows, while liquid flow rate appeared to have little effect on the void fraction profiles for down flows.

Serizawa and Kataoka [129] made some interesting observations of phase distribution in bubbly flow in a 30 (*mm*) inner diameter circular tube. A variation of the phase distribution patterns as a function of the superficial liquid velocity (or liquid flux) was observed. In stagnant liquid (i.e., having zero superficial liquid velocity) no significant wall peaking was observed. The gas bubbles seemed to choose a pattern in the core of the tube, creating core peaking. For superficial liquid velocities ranging from 0.5 to 3.0 (*m/s*), wall peaking was observed. For superficial liquid velocities higher than 3.0 (*m/s*), they observed a gas phase maximum at a position shifting towards the tube center (intermediate peaking). Serizawa and Kataoka [129] also reviewed and interpreted data from other studies on two-phase flow phase distribution and sketched a rough flow regime map. Serizawa and Kataoka [129] concluded that there are three basic types of radial phase distributions. These are, wall peaking, intermediate peaking and core peaking. Other types of patterns are supposed to be a combination of these three regimes. Serizawa and Kataoka also speculated that the physical phenomena taking place in the region near walls were the governing mechanisms which dominate the whole picture of upward two-phase flow in pipes. It was further indicated that bubble size and shape might play an important role determining the lateral void distribution.

In a series of papers Žun [164, 165, 166, 167] studied the phase distribution of two-phase turbulent up-flows in a 25.4 (*mm*) square Plexiglas channel. The liquid (water) volumetric fluxes were between 0 and 0.97 (*m/s*). Air bubbles were generated on single nozzles, but about 50 different nozzle diameters were used to keep the bubbles size constant at different air and water flow rates. Ellipsoidal bubbles in the equivalent sphere diameter range from 0.6 to 5.3 (*mm*) with a distinctive intrinsic later space displacement were studied. The void fraction profiles were measured by micro-resistivity probes of 0.011 (*mm*) diameter. Žun found that the transition from wall to core void peaking would happen when the liquid flux was decreased. He also claimed that bubble size would be important in determining the phase distribution. Larger bubbles would cause core peaking, while smaller bubbles would cause wall peaking.

Hills [57] studied the radial variation of gas holdup and liquid velocity in a bubble column with diameter 138 (*mm*). The gas holdup was measured with a conductivity probe, while the liquid velocity was measured using a modified Pitot tube. He used three different gas distributors. The superficial

gas velocity was varied from 5 to 169 ( $mm/s$ ), while there was no net liquid flow through the column. He observed that the gas holdup was significantly larger (up to 35 % gas void fraction) in the center of the column than at the walls where it would typically fall off to between 0 and 10 % gas void fraction. He also found that, on average, the gas would rise in the center of the column giving large upward vertical liquid and gas velocities there, and down-flow along the wall. Large vortices were superimposed on the averaged pattern, thus the flow was not regular.

Menzel et al [98] found core peaking for all the gas fluxes they studied in their investigation, and the time averaged radially varying velocity component profiles have a maximum at the core of the column as shown in Fig 8.4. The column used had a diameter of 0.6 ( $m$ ), and a height of 5.44 ( $m$ ). The system considered was air-water. The water was operated in batch mode. The velocity measurements were performed with a hotfilm anemometer.

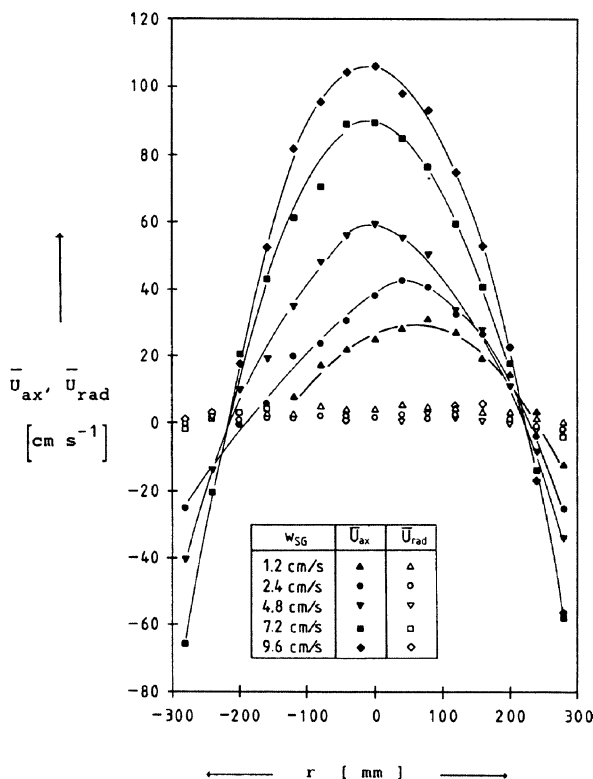


**Fig. 8.4.** Mean liquid velocities in axial and radial direction for different gas fluxes. Reproduced with permission [98]. Copyright 1990 American Chemical Society.

Torvik [154] also used a hotfilm anemometer and measured velocities, void fractions, and turbulent kinetic energy of a bubble column with diameter 0.29 (*m*) and height 4.52 (*m*). Both the air and the water were operated in continuous modes in the column. The liquid superficial velocity was low. Results at level 2.6 (*m*) above gas distributor at different gas velocities are shown in Fig 8.5.

Gasche [42], Gasche et al [43], Grienberger [46], Grienberger and Hofmann [47], Hillmer [55] and Hillmer et al [56] also studied the flow in two-phase bubble columns using a hotfilm anemometer.

Groen et al [48] measured the local and time-dependent behavior of the two-phase flow in a bubble column. Measurements with Laser Doppler Anemometry (LDA) and with glass fibre probes were performed in two air/water bubble columns of inner diameter 15 and 23 (*cm*), respectively. These measurements showed that the time averaged axi-symmetric liquid velocity profiles are a result of the passage of coherent structures (bubble swarms). It was concluded that considering the flow in a bubble column as stationary by far oversimplifies the actual phenomena present.

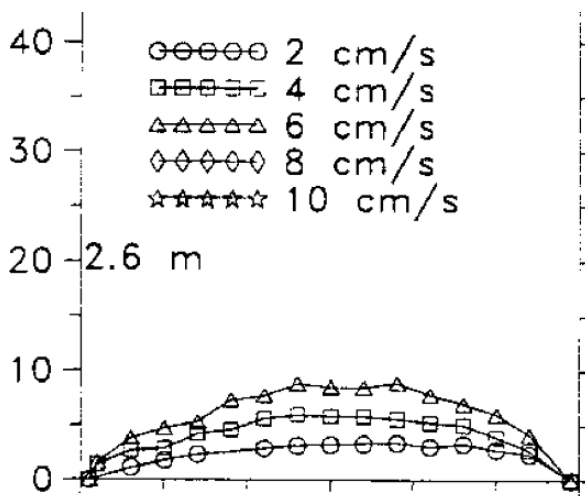


**Fig. 8.5.** Radial volume fraction profiles of gas at axial level 2.6 (*m*) above inlet in a two phase bubble column. The measurements are performed for five different superficial gas velocities. The figure is depicted from Torvik [154].

Lance and Bataille [78] studied grid-generated turbulent bubbly flow in a 45 (*cm*)  $\times$  45 (*cm*) rectangular pipe. Laser-Doppler and hotfilm anemometry were used for the experimental investigation. The high-frequency of spectra of the velocity components were determined by the power  $-8/3$ . A decade later Mudde et al [102] reported LDA-measurements characterizing 15 (*cm*) and

23 (*cm*) inner diameter bubble columns containing air-water mixtures with gas fractions ranging from 4% to 25%. The high-frequency of spectra of the axial and tangential velocity components did follow the Kolmogorov  $-5/3$  law. However, Harteveld [54] studied the accuracy of the estimation of turbulence power spectra from Laser Doppler Anemometry (LDA) signals in bubbly flows. It was found that the estimated spectra of bubble signals with reconstruction techniques give poor results. In other words, the power law of Lance and Bataille is probably more reliable than the one proposed by Mudde et al.

Recently, Garnier et al [40] performed experiments in a cylindrical column of 80 (*mm*) diameter and 310 (*mm*) height and reported that the vertical air/water bubbly flow is very uniform provided that a special design of the gas injection device is used. They used a gas injection device made of a regular array of 271 hollow needles, which are 126 (*mm*) long with a 0.62 (*mm*) internal diameter, through which gas bubbles were blown. The aim of the experiment was to produce a mono-disperse injection with as uniform as possible a distribution of void fraction. Garnier et al observed uniform flow up to 40% voidage and the radial void profiles were almost flat.

Harteveld et al [53, 104] reported similar experiments in a 15 (*cm*) diameter bubble column with gas fractions around 10%. A special sparger consisting of 561 needles was used to generate bubbles with a very narrow size distribution with a  $\sim 4.6$  (*mm*) equivalent diameter. When the sparging of the bubbles was uniform, the radial gas fraction profile was almost completely flat, but with a small peak at the wall. The flow was uniform and there was no large-scale liquid circulation. The turbulence levels are also low. If the outer ring of 0.75 (*cm*) thickness of needles was switched off, a weak circulation was observed but the flow was still stable and no large vortices were observed. Switching off a second ring so that the thickness of ungasped ring is about 1.6 (*cm*), the flow became strongly time dependent with the familiar large-scale circulation and the vortical structures present. It was later confirmed by experiments that the flow was stable at uniform gassing even up to gas fractions of 25%. These experiments clearly indicates that the sparger has a profound influence on the flow.

## 8.2 Types of Bubble Columns

Many different bubble column designs have been used over the years, all adapted to particular practical needs [133]. Figure 8.6 depicts a few of the modifications frequently used. A special case is the down-flow bubble column. In the column part of this reactor flow of the two phases is co-current from top to bottom as shown in Fig 8.6. The advantages of this type of reactor is that the relatively short gas residence times obtained in up-flow reactors, can be increased since the residence time is determined by the bubble rise velocity [28]. Furthermore, incorporation of additional perforated plates transforms the simple column, sketched in Fig 8.1, into a multistage cascade version, Fig 8.6. This redistribution of gas over the perforated plates intensifies mass transfer,

reduces the fraction of large bubbles and prevents back-mixing in both phases. Back-mixing is also decreased by filling the bubble column with a packing or by use of static mixers Fig 8.6. Multi-layer appliances, as obtained by incorporating cooling devices, prevent bulk circulation and a uniform gas flow can be achieved throughout the reactor, provided a suitable gas distributor is fitted [28]. Internal, axially oriented heat exchanger tubes may also increase the recirculation [10, 11].

Two main groups of bubble columns can be distinguished, these are simple bubble columns (Fig 8.1) and bubble columns with enforced circulation via a loop (Fig 8.6). Depending on the way in which the loop is realized, the latter group may be subdivided into bubble columns with internal or external loop. Compared to the types of bubble columns with reduced back-mixing

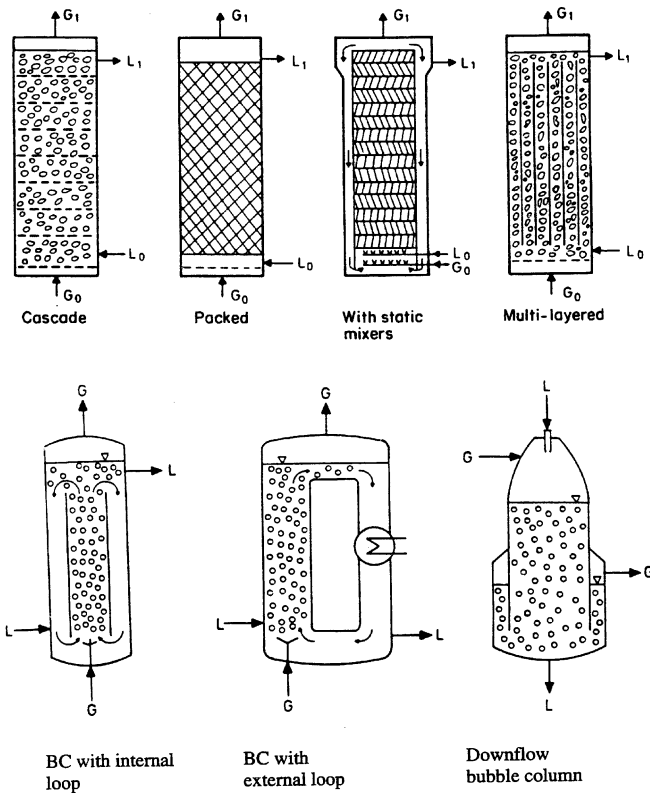


**Fig. 8.6.** Special types of bubble column reactors. Figures depicted from Onken [109] (Reproduced by permission from Verein Deutscher Ingenieure (VDI)- Gesellschaft Verfahrenstechnik und Chemieingenieurwesen 2007) and Deckwer [28] (Copyright John Wiley & Sons Limited. Reproduced with permission). Similar figures can also be found in Shah and Sharma [133] and Shah et al [132].

as described above, bubble columns with loop show more complex mixing behavior having a greater tendency of homogenizing the total reaction mixture. Loop reactors also permit the processing of large amounts of gas and provide a homogeneous flow zone. The homogeneous flow pattern is caused by directional fluid circulation being stabilized by means of an inserted loop eliminating complete radial transfer over the whole cross-sectional area. The high rate of circulation obtained gives shorter mixing times and hence a lack of any significant concentration gradient [28]. This is of special advantage for biotechnological processes in which it is important that the biomass is surrounded by material of constant composition. These reactors are thus often used in biotechnology, for instance as air-lift fermenters. In addition, these types of bubble column reactors can, compared to a stirred tank, decrease the shear stress induced cell damage for sensitive cultures.

In bubble columns with internal loop, the gas may either be supplied into the draft tube region or the annular region. If efficient degassing of the down-flowing liquid is required, the draft tube region is to be preferred with a conical widening of the top part of the bubble column allowing less turbulent liquid flow in this zone [109]. External loop bubble columns are often equipped with a pump for circulating the liquid. This may be necessary when a heat exchanger with a high pressure drop has been installed in the external loop (Fig 8.6). Alternatively, additional impulse for liquid circulation in the loop can be introduced, by feeding both the gas and liquid through a jet. Reactors with this type of gas sparging devices are called jet loop reactors.

In general, the gas may be dispersed in several ways, for instance through a perforated plate, sinter plate, or by various types of jets. Gas dispersion by use of a jet requires more energy compared to the distributor plates, but it may be advantageous if high utilization of the reacting gas is desired due to the high interfacial areas obtained [28]. Sintered plates produce small bubbles and a uniform bubble distribution. However, as sintered plates tend to become encrusted and clogged up and thus may cease to function, they are seldom used for process gas dispersion despite the advantages which they offer. Perforated plates with holes between 1 and 5 (*mm*) in diameter are thus commonly used. This kind of gas distributor plate gives rise to a more non-uniform bubble distribution, but is usually not associated with problems of deposits and encrustation. The bubble distribution in the inlet zone, caused by the construction of the gas distributor, have a decisive influence on gas holdup, interfacial area and the level of mass transfer [28].

### 8.3 Applications of Bubble Columns in Chemical Processes

Two-phase and slurry bubble columns are widely used in the chemical - and biochemical industry for carrying out gas-liquid and gas-liquid-solid (catalytic) reaction processes [27, 28, 29, 34, 35, 36, 117].

The surveys on applications of bubble columns in industrial processes given by Deckwer [28] and Onken [109] show that in many cases the simple type of bubble column is not used, but modifications, such as loop, multistage and down-flow bubble columns, depending on specific requirements of the individual process. Schügerl et al [126] describe special requirements associated with bio-processes. In the present summary of applications of the various types of bubble columns in chemical processes, the special use of bubble columns as bio-reactors at sterile conditions is excluded. However, aerobic fermentations can be considered as three-phase reactors [109], with suspended biomass as the third phase. The largest bubble column reactors that have been erected for fermentation processes operated at un-sterile conditions, referred to as the Bayer Tower Biology (simple bubble column) and the Biohoch Reactor Hoechst (jet loop reactor), have a volume of more than 10000 ( $m^3$ ) per reactor unit [109]. Moreover, for the aerobic treatment of small quantities of highly polluted effluents a process has been developed in which a down-flow bubble column is employed. This demonstrates that even for the same reactions different types of bubble columns may be suited, depending on the given conditions. Additional application examples of bubble column reactors are given in Table 8.1.

Bubble columns are also used for a number of conventional processes such as oxidation, hydrogenation, chlorination, chemical gas cleaning and also various bio-technological applications [28, 109, 132, 133, 126].

## 8.4 Modeling of Bubble Column Reactors

The historical development of bubble column modeling has been discussed by Deckwer [28] and Dudukovic [34]. Models for bubble column reactors can be divided into various categories according to the degree of mixing in each phase. Perfect mixing (CSTR), partial mixing (ADM) or no mixing (PFR) characteristics may be found in both gas and liquid phase. The mixing in the liquid phase is often more intense than within the gas phase due to the turbulent motion induced by the gas bubbles, hence the early bubble column models were defined using a simple and ideal CSTR model for the Liquid phase and a PFR model for the gas phase. However, the heterogeneous axial dispersion model (ADM), consisting of the mass (3.498) and heat (3.499) balances as assessed in chap 6, can be considered a more general formulation for both the gas and liquid (slurry) phases in bubble columns [168, 58, 133, 28].

For two-phase bubble columns the balance equations determining the liquid (slurry) phase axial dispersion model can be written as [133, 28]:

$$\frac{d(\rho_L v_L^S \omega_{i,L})}{dz} = \frac{d}{dz} \left( \varepsilon_L \rho_L D_{\text{eff,z,L}} \frac{d\omega_{i,L}}{dz} \right) + k_{L,i} a (\rho_{L,i}^* - \rho_{L,i}) + \varepsilon_L \sum_r \nu_{i,r} R_{L,r} \quad (8.1)$$

**Table 8.1.** Examples of Bubble Column Reactor Applications in the Chemical Process Industry.

Process	Type of Reactor	Reference
Partial Oxidation of ethylene to Acetaldehyde	BC with External Loop	Onken [109], Deckwer [28]
Oxidation of acetaldehyde to acetic acid	Cascade BC	Shah et al [132], Onken [109]
Oxidation of p-xylene to Dimethylterephthalate	BC with external loop or Cascade	Onken [109]
Hydrogenation of benzene to cyclohexane	Slurry BC with external loop	Onken [109], Deckwer [28]
Synthesis of hydrocarbons, Fischer-Tropsch synthesis in the liquid phase	Slurry BC	Dry [33], Deckwer [28], Shah et al [132]
Synthesis of Methanol	Slurry BC	Shah et al[132], Deckwer[28]
Oxychlorination of ethylene to 1,2-Dichloroethane	Packed BC	Onken [109], Deckwer [28]
Hydrolysis of phosgene	Downflow BC	Onken [109]
Ozonization of waste water	Downflow BC	Onken [109]
Biological waste water purification (aerobic)		Onken [109], Deckwer [28]
a) Bayer Tower Biology	Simple BC	
b) Biohoch Reactor	Jet internal loop BC	
c) Compact Reactor	Downflow BC	

---



---

 BC = Bubble Column.

$$\rho_L C_{P,L} v_L^S \frac{dT_L}{dz} = \frac{d}{dz} \left( \varepsilon_L k_{\text{eff},z,L} \frac{dT_L}{dz} \right) + 4 \frac{U}{d_t} (T_{\text{sur}} - T_L) + h_L a (T_G - T_L) + \varepsilon_L \sum_r (-\Delta H_r) R_{r,L} \quad (8.2)$$

For the gas phase the axial dispersion model is written as:

$$\frac{d(\rho_G v_G^S \omega_{i,G})}{dz} = \frac{d}{dz} \left( \varepsilon_G \rho_G D_{\text{eff},z,G} \frac{d\omega_{i,G}}{dz} \right) - k_{L,i} a (\rho_{L,i}^* - \rho_{L,i}) \quad (8.3)$$

$$\frac{d(\rho_G v_G^S)}{dz} = - \sum_i k_{L,i} a (\rho_{L,i}^* - \rho_{L,i}) \quad (8.4)$$

$$\rho_G C_{P,G} v_G^S \frac{dT_G}{dz} = \frac{d}{dz} \left( \varepsilon_G \lambda_{\text{eff},z,G} \frac{dT_G}{dz} \right) - h_L a (T_G - T_L) \quad (8.5)$$

The species balance equations are normally solved with the standard Danckwerts boundary conditions [26].

For the phase  $k (= G, L)$  the inlet boundary conditions at  $z = 0$  yield:

$$\rho_k(0) v_k^S(0) \omega_{i,k}(0) - \varepsilon_k(0) \rho_k(0) D_{\text{eff},k}(0) \frac{d\omega_{i,k}(0)}{dz} = v_{\text{in},k}^S \rho_{\text{in},k} \omega_{i,\text{in},k} \quad (8.6)$$

$$\rho_k(0) v_k^S(0) c_{p,k}(0) T_k(0) - \varepsilon_k(0) k_{\text{eff},k}(0) \frac{dT_k(0)}{dz} = \rho_{\text{in},k} v_{z,\text{in},k} c_{p,k} T_{\text{in},k} \quad (8.7)$$

$$v_G^S(0) = v_{z,\text{in},G} \quad (8.8)$$

The outlet boundary conditions at  $z = L$  yield:

$$\frac{d\omega_c(z=L)}{dz} = \frac{dT(z=L)}{dz} = 0 \quad (8.9)$$

where the superficial velocity is linked to the local velocity through  $v_k^S = v_k \varepsilon_k$ . The total pressure of the gas can be calculated from the ideal gas law:  $p_G = \rho_{G,i} RT_G / \overline{M}_\omega$ . For high pressure systems the operating pressure is dominated by the imposed pressure and is thus often assumed constant, whereas for atmospheric and low pressure processes the axial pressure profile is often dominated by the static pressure of the liquid phase,  $\frac{dp_L}{dz} = -\varepsilon_L \rho_L g_z$ . The pressures in the two phases are generally assumed to be equal,  $p_G \approx p_L$ . To close the interfacial mass transfer model a simple Henry's law equilibrium relation is frequently employed,  $\rho_{L,i}^* = M_{\omega_i} p_i / H_i = \rho_{G,i} RT_G / H_i$ .

In these balance equations all terms should be described at the same level of accuracy. It certainly does not pay to have the finest description of one term in the balance equations if the others can only be very crudely described. Current demands for increased selectivity and volumetric productivity require more precise reactor models, and also force reactor operation to churn turbulent flow which to a great extent is uncharted territory. An improvement in accuracy and a more detailed description of the molecular scale events describing the rate of generation terms in the heat- and mass balance equations has

in turn pushed forward a need for a more detailed description of the transport terms (i.e., in the convection/advection and dispersion/conduction terms in the basic mass- and heat balances).

Experimental evidence show that the liquid axial velocity is far from being flat and independent of the radial space coordinate [28], and the use of a cross-sectional average velocity variable seems not to be sufficient. The back mixing induced by the global liquid flow pattern was commonly accounted for by adjusting the axial dispersion coefficient accordingly. However, while (slurry) bubble column performance often can be fitted with an axial dispersion model, decades of research have failed to produce a predictive equation for the axial dispersion coefficient. Hence, research is in progress to quantify these based on first principles (e.g., see Jakobsen et al [62, 66], Joshi [67], Sokolichin et al [141], Rafique et al [117], Portela and Oliemans [115], and references therein). However, despite of their simple construction, the fluid dynamics observed in these columns is very complex. Even though the CFD modeling concepts have been extended over the last two decades in accordance with the rapid progress in computer performance, the model complexity required resolving all the important phenomena in these systems are still not feasible within reasonable time limits. The multi-fluid model is found to represent a trade-off between accuracy and computational efforts for practical applications.

Unfortunately, the present models are still on a level aiming at reasonable solutions with several model parameters tuned to known flow fields. For predictive purposes, these models are hardly able to predict unknown flow fields with reasonable degree of accuracy. It appears that the CFD evaluations of bubble columns by use of multi-dimensional multi-fluid models still have very limited inherent capabilities to fully replace the empirical based analysis (i.e., in the framework of axial dispersion models) in use today [63]. After two decades performing fluid dynamic modeling of bubble columns, it has been realized that there is a limit for how accurate one will be able to formulate closure laws adopting the Eulerian framework. In the subsequent sections a survey of the present status on bubble column modeling is given.

### 8.4.1 Fluid Dynamic Modeling

Considering modeling in further details the general picture from the literature is that the forces acting on the dispersed phase are [62]: Inertia-, gravity-, buoyancy-, viscous-, pressure-, lift-, wall-, turbulent stress-, turbulent dispersion-, steady drag- and added mass forces. In the latest papers performing 3D simulations, the force balances in vertical bubbly flows are found to be determined by only a few of these forces. The axial component of the momentum equation for the gas phase is dominated by the pressure- and steady drag forces only indicating that algebraic slip models may be sufficient [20, 105, 141], whereas most multi-fluid models also retain the inertia- and gravity (buoyancy) terms. The axial momentum balance for the liquid phase considers the inertia-, turbulent stress-, pressure-, steady drag- and gravity

forces. Only pressure and buoyancy forces are acting on a motionless bubble in a liquid at rest. In the radial- and azimuthal directions the force balances generally includes the steady drag force, i.e., a force that is opposing motion, while the pertinent forces causing motion are more difficult to define. In a very short inlet zone the wall friction is likely to induce a radial pressure gradient that pushes the gas bubbles away from the wall, whereas a few column diameters above the inlet the radial pressure gradient vanishes. It is still an open question whether or not this pressure gradient is sufficient to determine the phase distribution observed in these systems. It is expected that the presence of the wall induce forces that act on the dispersed particles further away from the inlet, but there is no general acceptance on the physical mechanisms and formulations of these forces. It is also a matter of discussion whether this wall effect should be taken into account indirectly through the liquid wall friction, or in view of the model averaging performed directly as a force in the gas phase equations.

In the generalized drag formulation the interfacial coupling is expressed as a linear sum of independent forces, this point of view is probably not valid when the void fraction exceeds a few percent. Moreover, the parameterizations used for the coefficients occurring in the interfacial closures vary significantly, especially at higher void fractions. Single particle drag -, added mass - and lift coefficients are most frequently used, whereas swarm corrections have been included in some codes. For higher void fractions other rather empirical corrections have been introduced as well [9]. Likewise, considering the multi-fluid model, the average interfacial momentum transfer terms containing the interfacial average pressure and viscous stresses (discussed in sect 3.3) are strictly not consistent with the fundamental singlephase forces presented in sect 5.2.

The interfacial coupling and wall forces are difficult to parameterize with sufficient accuracy. The steady drag component part of the generalized drag is the dominant interfacial force. In a few papers fair agreement with the available experimental data on the dynamic large scale circulating flow pattern in bubble columns have been achieved using this interfacial force solely [73, 66]. A variety of different formulations of this force, and especially on the drag coefficient, are reported in the literature valid for deformable and rigid spherical particles, extended for different flow regimes, swarm effects and pure and contaminated fluid systems. In several papers on bubble column flow modeling [12, 105] the drag coefficient correlations valid for non-deformable spheres [100, 125] have been adopted. For typical heterogeneous flow conditions these relations give rise to drag force coefficient values which are typically about 25% of the standard values for cap bubbles given by the parameterizations suggested by Tomiyama et al [149] (see sect 5.2.4). Jakobsen et al [66] did assess these spherical particle coefficient correlations in their 2D code and obtained completely flat profiles (i.e., no variation in the radial direction) for the axial velocities and the volume fraction. There was thus no circulation cells created in the column, which is in accordance with the experiments reported by Harteveld [53]. On the other hand, other 2D and 3D simulations reported

in the literature employing the drag coefficient correlations for spherical particles always give the anticipated dynamic circulating flow pattern that has become standard in the recent papers. It should be mentioned that in most of the latter simulations an additional wall friction force [94] acting on the gas phase is implemented (to be discussed shortly).

Implementing the added mass force has barely any influence on the steady state solution [30, 66]. Deen et al [30] explained this to some extent surprising result by the fact that the simulations soon reach a quasi-stationary state where there is only minor acceleration. The bubble jets observed close to the distributor plate are then disregarded. However, the convergence rate and thus the computational costs are often significantly improved implementing this force.

The primary effect of the transversal lift force is to push the gas bubbles radially inwards or outwards in the column depending on the sign of the lift coefficient. The force is usually modeled as though it is induced by a velocity gradient, and can therefore only reinforce or smooth out the existing gradients in the flow fields. For this reason other forces are important in the initial phase of the flow pattern development. Moreover, in the two-fluid model with a single average bubble size this force alone can not change a center peak flow pattern to a wall peak pattern or vice versa. However, using a multi-fluid model with a bubble size distribution the lift force might change a center peak flow pattern to a wall peak pattern or vice versa. Nevertheless, any interactions between the onset of the dynamic large-scale circulation flow pattern and the bubble coalescence and breakage mechanisms have not been demonstrated yet.

Effects similar to those of the lift force are observed when implementing the turbulent dispersion force using the gradient diffusion model. This dispersion force closure smoothes out sharp velocity gradients in the domain. If the model overestimates the diffusive effect, the velocity profiles may become completely flat over the column cross section.

The radial wall lift force proposed by Antal et al [2] requires a certain minimum resolution of the grid close to the wall. The values of the model coefficients are crucial for the development of the profiles since these parameters determine the magnitude of the force as well as the operative distance from the wall. The magnitude of the force is highest for larger bubbles, and the force is very sensitive to the bubble size. However, the force does not alter the flow development significantly except very close to the wall.

To ensure that the gas in upward bubbly flow migrates away from a triangular duct wall Lopez de Bertodano [94] introduced an axial friction force acting on the gas in the vicinity of the wall. Under bubble column flow conditions this friction force may significant affect the radial phase distribution provided that a sufficiently small steady drag force is employed [66]. The addition of the gas wall friction may for example alter a uniform or wall peaking flow regime into a center peaking behavior.

In several reports on bubble column modeling a constant gas density is employed. This assumption is not consistent for tall columns that are operated

at ambient outlet pressure. Similar inconsistency problems arise when reactive systems are simulated, as the gas density vary in accordance with the chemical process behavior. Moreover, interfacial mass transfer fluxes and chemical reactions often induce numerical stability problems and no proper convergence.

The flow of the continuous phase is considered to be initiated by a balance between the interfacial particle-fluid coupling - and wall friction forces, whereas the fluid phase turbulence damps the macroscale dynamics of the bubble swarms smoothing the velocity - and volume fraction fields. Temporal instabilities induced by the fluid inertia terms create non-homogeneities in the force balances. Unfortunately, proper modeling of turbulence is still one of the main open questions in gas-liquid bubbly flows, and this flow property may significantly affect both the stresses and the bubble dispersion [141].

It has been shown by Svendsen et al [144], among others, that the time averaged experimental data on the flow pattern in cylindrical bubble columns is close to axi-symmetric. Fair agreement between experimental - and simulated results are generally obtained for the steady velocity fields in both phases, whereas the steady phase distribution is still a problem. Therefore, it was anticipated that the 2D axi-symmetric simulations capture the pertinent time-averaged flow pattern that is needed for the analysis of many (not all) mechanisms of interest for chemical engineers. Sanyal et al [122] and Krishna and van Baten [72] for example stated that the 2D models provide good engineering descriptions, although they are not able to capture the high frequency unsteady behavior of the flow, and can be used for approximately predicting the low frequency time-averaged flow and void patterns in bubble columns.

The early 2D steady-state model proposed by Jakobsen [59] (outlined in app C) was able to capture the global flow pattern fairly well provided that a large negative lift force was included. However, after the first elaborated experimental studies on 2D rectangular bubble columns were published by Tzeng et al [153] and Lin et al [89], it was commonly accepted that time-average computations cannot provide a rational explanation of the transport processes of mass, momentum, and energy between the bubbles and liquid. The experimental data obtained was analyzed and sketches of their interpretations of the dynamic flow patterns in both 2D and 3D columns were given, as shown in Fig 8.7. It was concluded that a proper bubble column model should consider the transient flow behavior. A few years later Sokolichin and Eigenberger [138], Sokolichin et al [139], Sokolichin and Eigenberger [140] and Borchers et al [14] claimed that dynamic 3D models were needed to provide sufficient representations of the high frequency unsteady behavior of these flows. Very different dynamic flow patterns may result in quantitatively similar long-time averaged flow profiles. This limits the use of long-time averaged flow profiles for validation of bubbly flow models. van den Akker [156], among others, questioned the early turbulence modeling performed (or rather the lack of any) in these studies and argued that the apparently realistic simulations of the transient flow characteristics could be numerical modes rather than physical ones (see also Sokolichin et al [141]). Insufficiently fine grids

may have been used in the simulations resulting in numerical instabilities that could be erroneously interpreted as physical ones. However, after the observation of Sokolichin and Eigenberger was reported, intensive focus on these instability issues were put forward, mainly by researchers from the fluid dynamics community. The experimental data provided by Becker et al [7] and Becker et al [8], see Fig 8.8, still serve as a benchmark test and is often used for validation of dynamic flow models. The numerical investigations were restricted to bubbly flow hydrodynamics (i.e., no reactive systems were analyzed), where additional simplifications were made; isothermal conditions, no interfacial mass transfer, constant liquid density, gas density constant or depending on local pressure as described by the ideal gas law, neglecting bubble coalescence and breakage.

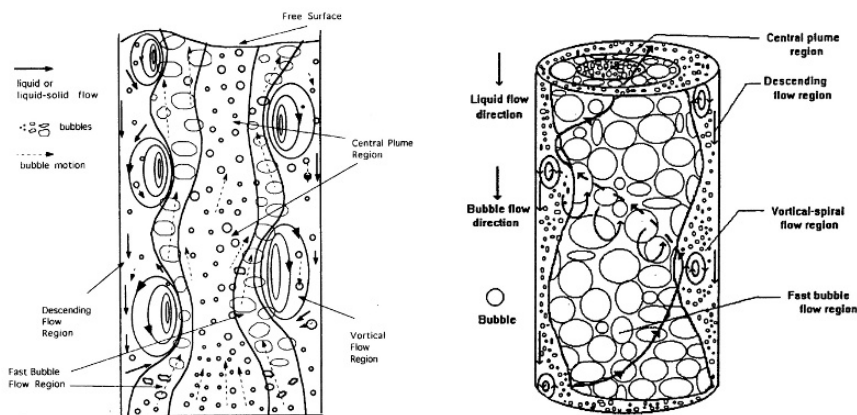


**Fig. 8.7.** Classification of regions accounting for the macroscopic flow structures: left, 2D bubble column[153]; right, 3D bubble column[22]. Reproduced with permission. Copyright 1993 and 1994 American Institute of Chemical Engineers (AIChE).

However, after the dynamic flow structures were observed bubble columns have generally been simulated using either 2D - or 3D dynamic models both for cylindrical [122, 74, 112, 107, 87, 88, 108, 12, 73] and rectangular 2D and 3D column geometries [105, 101, 103, 111, 73, 30, 17, 18, 12, 15, 141]. The gas is introduced both adopting uniform and localized feedings at the bottom of the column. Modeling of systems uniformly gassed at the bottom is more difficult than the modeling of partly aerated ones. Simulating systems with continuous liquid flow is also more difficult than keeping the liquid in batch mode. Finally, it is also noted that the different research groups applied both commercial codes (e.g., CFX, FLUENT, PHOENICS, ASTRID, NPHASE) and several in-house codes where the inherent choice of numerical methods, discretizations, grid arrangements and boundary implementations varies quite a lot. These numerical differences alter the solutions to some ex-

tent, so it should not be expected that the corresponding simulations will provide identical results. An open and unified research code available for all research groups could assist eliminating any misinterpretations of numerical modes as physical mechanisms, and *visa versa*.

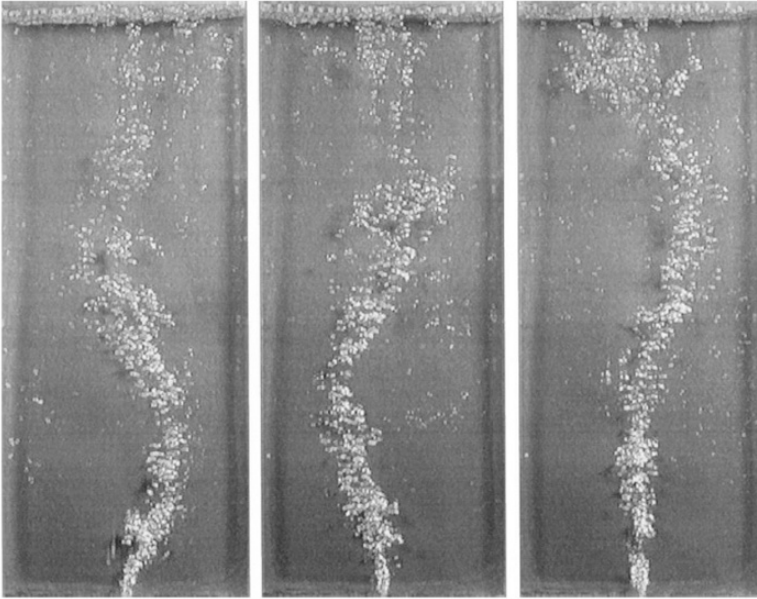


**Fig. 8.8.** Lateral movement of the bubble hose in a flat bubble column [8]. Reprinted with permission from Elsevier.

Considering the interfacial- and turbulent closures for vertical bubble driven flows, no extensive progress has been observed in the later publications. However, two diverging modeling trends seem to emerge due to the lack of understanding of the phenomena involved and on how to deal with these phenomena within an average modeling framework. One group of papers considers only phenomena that can be validated with the existing experimental techniques and thus contains a minimum number of terms and effects. The other group of papers include a large number of weakly founded theoretical hypothesis and relations intending to resolve the missing mechanisms.

### **Steady-State or Dynamic simulations, Closures, and Numerical Grid Arrangements**

Not only dynamic models have been adopted investigating these phenomena. Lopez de Bertodano [94] for example used a 3D steady finite volume method (FVM) (PHOENICS) with a staggered grid arrangement to simulate turbulent

bubbly two-phase flow in a triangular duct. In this study the lift-, the turbulent dispersion- and the steady drag forces were assumed dominant. Standard literature expressions were adopted for the drag- and lift forces, whereas a crude model for the turbulent dispersion force was developed. An extended  $k-\varepsilon$  model, considering bubble induced turbulence, was also developed for the liquid phase turbulence. It was proposed that the shear-induced turbulence and the bubble-induced turbulence could be superposed. The lift force was found essential to reproduce the experimentally observed wall void peaks satisfactorily. Anglart et al [1] adopted many of the same closures within a 2D steady version of the same code (PHOENICS) predicting low void bubbly flow between two parallel plates. They found satisfactory agreements with experimental data when applying drag-, added mass-, lift-, wall (lubrication)- and turbulent diffusion forces in their study. The extended  $k-\varepsilon$  model of Lopez de Bertodano [94] was applied for the liquid phase turbulence. In a more recent paper Antal et al [4] adopted very similar closures for 3D steady-state bubble column simulations using the NPHASE code. The NPHASE CMFD code employs a FVM on a collocated grid. A three field multi-fluid model formulation was used to simulate two-phase flow in a bubble column operating in the churn-turbulent flow regime. The gas phase was subdivided into two fields (i.e., small and large bubbles) to more accurately describe the interfacial momentum transfer fluxes. The third field was used for the liquid phase. The model results were validated against a few time averaged data sets for the liquid axial velocity and the gas volume fraction. Global flow patterns for all three fields and overall gas volume fractions were shown. The simulations were in fair agreement with the experimental observations. Using a 2D in-house FVM code with a staggered grid arrangement Dhotre and Joshi [31] predicted the flow pattern, pressure drop and heat transfer coefficient in bubble column reactors. The model used contained steady drag-, added mass- and lift forces, as well as a reduced pressure gradient formulated as an apparent form drag. Turbulent dispersion was accounted for by use of mass diffusion terms in the continuity equations. A low Reynolds number  $k-\varepsilon$  model was incorporated, broadly speaking constituting a standard  $k-\varepsilon$  model with modified treatment of the near-wall region. The turbulence model used contained an additional production term accounting for the large scale turbulence produced within the liquid flow field due to the movement of the bubbles. A semi-empirical mechanical energy balance for the gas-liquid system was required fulfilled. The simulated results were in very good agreement with experimental literature data on the axial liquid velocity, gas volume fraction, friction multiplier and heat transfer coefficient.

In a recent study Jakobsen et al [66] examined the capabilities and limitations of a dynamic 2D axi-symmetric two-fluid model for simulating cylindrical bubble column reactor flows. In their in-house code all the relevant force terms consisting of the steady drag, bulk lift, added mass, turbulence dispersion and wall lift were considered. Sensitivity studies disregarding one of the secondary forces like lift, added mass and turbulent dispersion at the time in otherwise

equivalent simulations were performed. Additional simulations were run with three different turbulence closures for the liquid phase, and no shear stress terms for the gas phase. A standard  $k - \epsilon$  model [86] was used to examine the effect of shear induced turbulence, case (a). In an alternative case (b), both shear- and bubble induced turbulence were accounted for by linearly superposing the turbulent viscosities obtained from the  $k - \epsilon$  model and the model of Sato and Sekoguchi [123]. A third approach, case (c), is similar to case (b) in that both shear and bubble induce turbulence contributions are considered. However, in this model formulation, case (c), the bubble induced turbulence contribution was included through an extra source term in the turbulence model equations [59, 62, 66]. The relevant theory is summarized in sect 5.1.

A comparison between the steady state profiles at axial levels  $z = 2.0$  ( $m$ ) and  $z = 0.3$  ( $m$ ) in the column employing the three turbulence closures (a), (b) and (c) was given as shown in Figs 8.9 and 8.10, respectively. The most important conclusion drawn from this investigation is that the assumption of cylindrical axi-symmetry in the computations prevents lateral motion of the dispersed gas phase and leads to an unrealistic radial phase distribution wherein the maximum void is away from the centerline, which is also reported by other authors [122, 73]. It is also worth noting that imposing the axi-symmetry boundary condition causes the liquid flow to develop very quickly and the long-time circulating pattern is reached within a few seconds (typically less than 5 seconds of real time) after the first gas has been flowing through the column. In contrast, the experimental data reported by Sanyal et al [122] and Pflieger and Becker [112] is characterized by a highly dynamic flow, with 3D vortical bubble swarms. For  $z = 2.0$  ( $m$ ) all the model versions gave reasonable velocities compared to the experimental data. For  $z = 0.3$  ( $m$ ) there were larger discrepancies between the simulated results and the experimental data. The voidage profiles observed in the experiments are lower than at  $z = 2.0$  ( $m$ ), while the profiles from the simulations are approximately the same. The discrepancy indicates that the physics in the bottom of the column is not sufficiently captured by the 2D model. At the axial level 0.3 ( $m$ ) above the inlet, Fig 8.10, the cross-sectional averaged void was overestimated by about 25 – 35%, thus the corresponding cross-sectional averaged gas velocity was underestimated. This is a strong indication that 3D effects are important at least in the inlet section. However, studies reported in the literature show that it can be very difficult to obtain reasonable time averaged radial void profiles even in 3D simulations [66]. Nevertheless, the deviation between the experimental data and the simulated results may also indicate that the inlet boundary conditions used, the phase distribution and the interfacial coupling are inaccurate and not in agreement with the real system.

Deen et al [30] used the lift force in addition to the steady drag- and added mass forces in their dynamic 3D-model to obtain the transversal spreading of the bubble plume which is observed in experiments. A prescribed zero void wall boundary was used forcing the gas to migrate away from the wall. The continuous phase turbulence was incorporated in two different ways, using

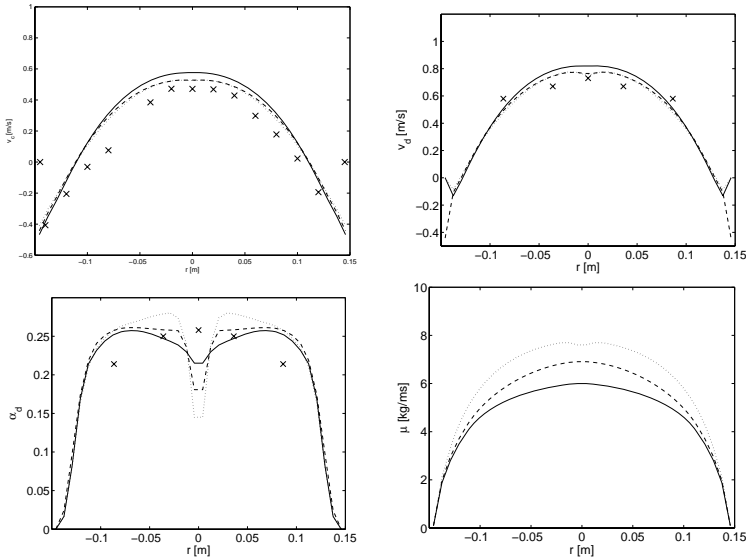


**Fig. 8.9.** Axial velocity-, gas voidage- and turbulent viscosity profiles as a function of column radius at the axial level  $z = 2.0$  (m) after 80 (s) (steady-state) employing the steady drag and added mass forces. Crosses: experimental data [61], continuous line: standard  $k-\varepsilon$  model, case (a), dotted line: standard  $k-\varepsilon$  model plus Sato model, case (b), dashed line: extended  $k-\varepsilon$  model, case (c). Grid resolution:  $20 \times 72$ , time resolution:  $2 \cdot 10^{-4}$  (s). Reprinted with permission from [66]. Copyright 2005 American Chemical Society.

either a standard  $k-\varepsilon$ - or a VLES model. The effective viscosity of the liquid phase was composed of three contributions, the molecular-, shear induced turbulent - and bubble induced turbulence viscosities. The calculation of the turbulent gas viscosity is based on the turbulent liquid viscosity as proposed by Jakobsen et al [62]. These simulations were performed using the commercial code CFX, thus a FVM on a collocated grid was employed. Sample results simulating a square 3D column at low void fractions using the 3D VLES model of Deen et al [30] are shown in Fig 8.11. Krishna and van Baten [73, 74] used a steady drag force as the only interfacial momentum coupling in their transient 2D- and 3D three fluid models with an inherent prescribed and fixed bi-modal distribution of the gas bubble sizes. The two bubble classes are denoted small and large bubbles. The small bubbles are in the range of 1–6 (mm), whereas the large bubbles are typically in the range of 20 – 80 (mm). A simplification made in the model is that there are no interactions or exchanges between the small and large bubble populations. A FVM on a non-staggered grid was used discretizing the equations (i.e., in CFX). No-slip conditions at the wall were used for both phases. A  $k-\varepsilon$  model was applied for the liquid phase turbulence, whereas no turbulence model was used for the dispersed phases. To prevent a

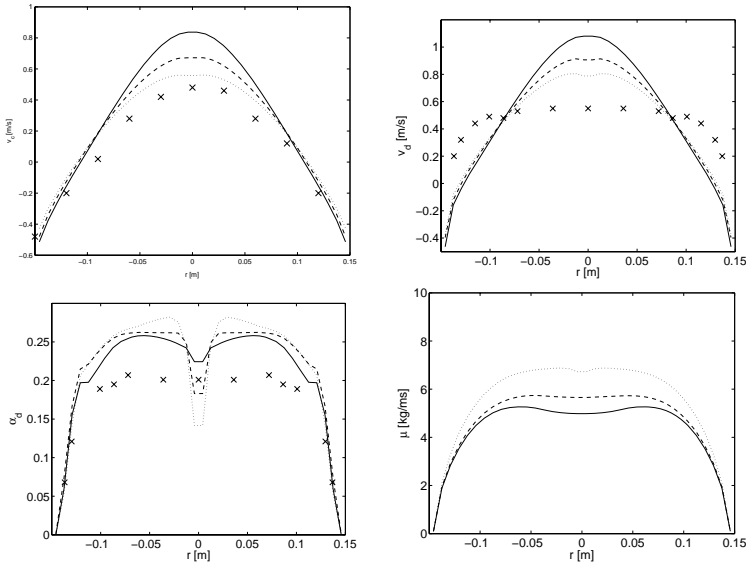


**Fig. 8.10.** Axial velocity-, gas voidage- and turbulent viscosity profiles as a function of column radius at the axial level  $z = 0.3$  (m) after 80 (s) (steady-state) employing the steady drag and added mass forces. Crosses: experimental data [61, 46], continuous line: standard  $k-\varepsilon$  model, case (a), dotted line:  $k-\varepsilon$  model plus Sato model, case (b), dashed line: extended  $k-\varepsilon$  model, case (c). Grid resolution:  $20 \times 72$ , time resolution:  $2 \cdot 10^{-4}$  (s). Reprinted with permission from [66]. Copyright 2005 American Chemical Society.

circulation pattern in which the liquid flows up near the wall and comes down in the core, the large bubble gas was injected on the inner 75% of the radius. The time averaged volume fraction- and velocity profiles calculated from the predicted 3D flow field were in reasonable agreement with experimental data. Lehr et al [88] used a similar three-fluid model (implemented in CFX), combined with a simplified population balance model for the bubble-size distribution. The simplified population balance relation used contained semi-empirical parameterizations for the bubble coalescence and breakage phenomena. It was concluded that the calculated long time average volume fractions, velocities, and also the interfacial area density were in good agreement with experimental data. Pflieger et al [111] applied a two-fluid model using the same code (CFX) to a 2D rectangular column with localized spargers. It was concluded that a 3D model including the steady drag force and a standard  $k-\varepsilon$  model is sufficient to correctly capture the unsteady behavior of bubbly flow with very low gas void fractions. The bubble swarm began its swinging motion after a certain time delay. Pflieger and Becker [112] and Bertola et al [12] used similar two-fluid models and FVMs on collocated grid arrangements (CFX and FLUENT, respectively) simulating both cylindrical and rectangular columns,

confirming the results found by Pflieger et al [111]. It should be noted, however, that Bertola et al [12] solved the  $k$ - $\epsilon$  turbulence model for both phases, whereas in the work of Pflieger and co-workers [111, 112] the dispersed phase was considered laminar. Mudde and Simonin [103] performed both dynamic 2D - and 3D simulations of a 2D rectangular column using a similar FVM on a collocated grid arrangement (ASTRID). Their two-fluid model contained an extended  $k - \epsilon$  turbulence model formulation for the liquid phase turbulence, and drag - and added mass forces. The dispersed phase turbulence was assumed steady and homogeneous and described by an extended Tchen's theory approach [145, 135, 136, 161]. This code predicted reasonable high frequency oscillating flows only when the added mass force was included, without this force low frequency almost steady flows were obtained. Using a FD algorithm Tomiyama et al [147] reported that the transient transversal migration of bubble plumes in vessels can be well predicted including steady drag-, added mass- and lift forces in their two-fluid model describing laminar flows containing very low void fractions (i.e., below 0.5%). Later, Tomiyama [148] and Tomiyama and Shimada [150] used the bubble induced turbulence model of Sato and Sekoguchi [123] and Sato et al [124] and an extended  $k - \epsilon$  model in their work on turbulent flows. In a recent paper Sokolichin et al [141] concluded that the model by Sato and Sekoguchi [123] for bubble induced turbulence overestimates the turbulent viscosity parameter and thus strongly underestimates the turbulence level in a number of test cases. Another disadvantage of this approach is associated with the local nature of the model, because it considers the increase of the turbulence intensity only locally in the reactor where the gas phase is actually present. In reality, the turbulence induced by the bubbles at some given point can spread and affect regions further away from the turbulence source. Oey et al [105] applied a 3D two-fluid model containing the steady drag-, added mass- and turbulent dispersion forces together with an extra source term in the  $k - \epsilon$  turbulence model accounting for the effects of the interface in their in-house staggered FVM code (ESTEEM). Due to the controversy in the literature regarding disperse phase turbulence, both laminar and turbulent gas simulations were made. In the turbulence case, the extended Tchen's theory approach was adopted. The liquid tangential velocity components close to the wall were found using wall functions, while no wall friction was taken into account for the dispersed phase. They found that in 3D the steady drag force was sufficient to capture the global dynamics of the bubble plume while the other forces moreover have secondary effects only.

Most of the studies mentioned above adopted a kind of  $k - \epsilon$  model to describe the liquid turbulence in the system, whereas there is less consensus regarding whether the dispersed phase should be considered turbulent or laminar, or even whether any deviating stress terms at all should remain in the dispersed phase equations. However, even the  $k - \epsilon$  model predictions are questioned by Deen et al [30] and Bove et al [15]. This group showed that only low frequency unsteady flow is obtained using the  $k - \epsilon$  model due to overestimation of the turbulent viscosity. These model predictions were found not to

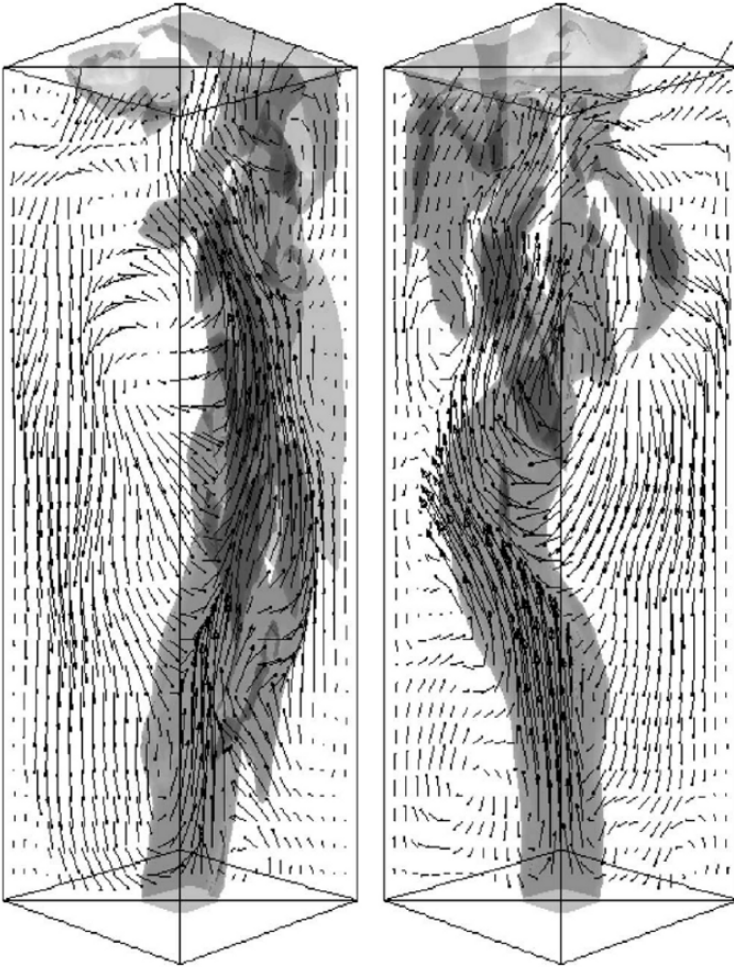


**Fig. 8.11.** Snapshots of the instantaneous isosurfaces of  $\alpha_d = 0.04$  and liquid velocity fields after 30 and 35 s, for the LES model [30]. Reprinted with permission from Elsevier.

be in satisfactory agreement with the more high frequent experimental results. On the other hand, when using a 3D Smagorinsky LES (Large Eddy Simulation) model instead, the strong transient movements of the bubble plume which are observed in experiments were captured.

Similarly, the majority of the investigations reported conclude that for both rectangular and cylindrical columns the high frequency instabilities are 3D and have to be resolved by the use of 3D models. Nevertheless, in a few recent papers [5, 6, 21] it has been shown that 2D mixture model formulations can be used to reproduce the time-dependent flow behavior of 2D bubble

columns. It has been found that the crucial physics can be captured by 2D models if suitable turbulence models are used. The predictions reported by Bech [5, 6] rely on the inclusion of a mass diffusion term in the dispersed phase continuity equation together with a appropriate zero- or two-equation turbulence model, while Cartland Glover and Generalis' [21] predictions rely on the inclusion of a Reynolds stress model. In the work of Bech [6] the  $k-\omega$  turbulence model gave a better qualitative prediction of the bubble plume than the standard  $k-\varepsilon$  model, due to the low-Reynolds number treatment of the former model. A simple mixing length turbulence model gave the best prediction of the meandering plume, even without any dispersion term.

A conclusion drawn in several papers investigating the fluid dynamics of the reactors is that the flow have to be about perfect before the chemistry related topics should be considered. Such an invidious statement may have been of severe hindrance for the development of integrated fluid dynamic reactor models of interest for chemical reaction engineers. However, there are several indications that the local high frequency dynamics and coherent structures of the flow are important determining the conversion in chemical reacting systems [141, 101, 18, 157, 53]. The mixing times predicted by steady flow codes are for example found not to be in accordance with experimental data, whereas mixing times predicted by high frequent transient flow codes are in fair agreement with the corresponding measurements. Nevertheless, the main limitation associated with these advanced reactor models is the tremendous CPU demands needed for the high frequency instabilities, making such 3D simulations not feasible for most research groups.

The interfacial and turbulence closures suggested in the literature also differ considering the anticipated importance of the bubble size distributions. It thus seemed obvious for many researchers that further progress on the flow pattern description was difficult to obtain without a proper description of the interfacial coupling terms, and especially on the contact area or projected area for the drag forces. The bubble column research thus turned towards the development of a dynamic multi-fluid model that is extended with a population balance module for the bubble size distribution. However, the existing models are still restricted in some way or another due to the large cpu demands required by 3D multi-fluid simulations.

## Multi-Fluid Models and Bubble Size Distributions

To gain insight on the capability of the present models to capture physical responses to changes in the bubble size distributions, a few preliminary analyzes have been performed adopting the multi-fluid modeling framework.

Lo [91, 92, 93] developed the extended two-fluid model named the MUSIG (MUltiple-SIze-Group) model in which the dispersed phase is divided into multiple groups. In the original two-fluid MUSIG model only one set of continuity and momentum equations are considered for the dispersed phase. The model describes the dynamic evolution of a number of bubble size groups in

space (typically  $\sim 15 - 20$  groups) and from the resulting size distribution a mean bubble size is determined. The mean bubble size, which is varying locally in the column, is used to calculate an improved estimate of the contact area and thus the momentum transfer terms (steady drag). However, since the two-fluid model is employed, the single gas velocity field limits the applicability of the model. In particular, effects such as segregation by size are difficult to describe. The performance of the original MUSIG model is thus limited to convectively dominated bubbly flows, since it is based on the assumption that a single velocity field can be applied for all bubble size groups [71].

To remove this model limitation entirely a complete multifluid model is required. For gas-liquid systems Reyes [121] and Lafi and Reyes [77] presented a detailed derivation of the mass, momentum and energy conservation equations for polydispersed systems following an approach analogous to the Boltzmann's transport equation. They derived a set of fluid particle conservation equations for the distribution of chemically non-reacting, spherical fluid particles dispersed in a continuous medium. Kocamustafaogullari and Ishii [70], following a similar approach, extended the application of the model to a general two-phase flow. An analogous modeling framework for dense gas-solid reactive mixtures in fluidized beds has been presented by Goldman and Sirovich [44], Simonin [137], Valiveti and Koch [158] and Lathouwers and Bellan [81, 82, 83, 84, 85]. In this case the governing transport equations are derived using kinetic theory concepts similar to those of dense gases. Important differences from classical kinetic theory are the inelasticity of collisions between macroscopic particles leading to dissipation, and the presence of an interstitial gas exerting drag on the particles, which leads to interaction terms in the averaged transport equations.

Based on these generalized theories the research group at FZ Rossendorf in Dresden [134, 39] developed a useful alternative to the original MUSIG model by extending the two-fluid model to a multifluid model with a limited number both of size ( $M$ ) and velocity ( $N$ ) phases (sometimes referred to as the  $N \times M$  MUSIG model). The dispersed phases can thus move with different velocities and the novel multifluid model might be capable of handling more complex flow situations. In particular, in the extended MUSIG model approach the dispersed phase is divided into a number of  $N$  velocity phases (or groups), where each of the velocity groups is characterized by its own velocity field. Moreover, the overall particle size distribution is represented by dividing the particle diameter range within each of the velocity groups into a number of  $M$  bubble size phases (or classes). The subdivision into groups and classes should preferably be based on the different physics of the particle motion. Considering bubbly flows with bubbles of different sizes, the different behaviour with respect to the lift or turbulent dispersion forces could be a suitable split up criterion for the velocity groups. Shi et al [134] assumed that for most cases 3 or 4 velocity groups are sufficient in order to capture the main phenomena in bubbly and slug flows. For simplicity the number of particle diameter classes within each of the velocity groups was equal and fixed to

a predefined value. The first numerical simulations were therefore performed using  $N = 3$  velocity phases and  $M = 7$  bubble size classes in each velocity group. An overall number of 21 bubble size classes was thus applied for the representation of the local bubble size distribution. This bubble size resolution was found to be appropriate for many bubbly flow problems.

Sha et al [130, 131] developed a similar multifluid model for the simulation of gas-liquid bubbly flow. To guarantee the conservation of mass the population balance part of the model was solved by the discrete solution method presented by Hagesaether et al [52]. The 3D transient simulations of a rectangular column with dimensions  $150 \times 30 \times 2000$  (mm) and the gas evenly distributed at the bottom were run using the commercial software CFX4.4. For the same bubble size distribution and feed rate at the inlet, the simulations were carried out as two, three, six and eleven phase flows. The number of population balance equations solved was 10 in all the simulations. It was stated that the higher the number of phases used, the more accurate are the results.

Carrica et al [20] developed a simplified multi-fluid model for the description of bubbly two-phase flow around a surface ship. In the momentum equations for the gas bubble phases or groups the inertia and shear stress terms were assumed to be negligible. The interfacial momentum transfer terms included for the different bubble groups are steady-drag, added mass, lift and turbulent dispersion forces. Algebraic turbulence models were used both for the liquid phase contributions and the for the bubble-induced turbulence. The two-fluid model was solved using a FVM on a staggered grid. In the population balance part of the model the intergroup transfer mechanisms included were bubble breakage, coalescence and the dissolution of air into the ocean. 15 size groups were used with bubble radius at normal pressure between 10 ( $\mu\text{m}$ ) and 1000 ( $\mu\text{m}$ ). It was found that intergroup transfer is very important in these flows both for determining a reasonable two-phase flow field and the bubble size distribution. The population balance was discretized using the multi-group approach. It was pointed out that the lack of validated kernels for bubble coalescence and breakage was limiting the accuracy of the model predictions. Politano et al [113] adapted the population balance model of Carrica et al [20] for the purpose of 3D steady-state simulation of bubble column flows. However, no details regarding the necessary model modifications were provided. In a later study by Politano et al [114] a 2D steady-state version of this model was applied for the simulation of polydisperse two-phase flow in vertical channels. The two-fluid model was modified using an extended  $k-\varepsilon$  model for the description of liquid phase turbulence. A two-phase logarithmic wall law was developed to improve on the boundary treatment of the  $k-\varepsilon$  model. The interfacial momentum transfer terms included for the different bubble groups are steady-drag, added mass, lift, turbulent dispersion and wall forces. The two-fluid model equations were discretized using a finite difference (FD) method. The bubble mass was discretized in three groups. The effect of bubble size on the radial phase distribution in vertical upward channels was

investigated. Comparing the model predictions with experimental data it was concluded that the model is able to predict the transition from the near-wall gas volume fraction peaking to the core peaking beyond a critical bubble size.

Tomiyama [148] and Tomiyama and Shimada [150] adopted a  $(N + 1)$ -fluid model for the prediction of 3D unsteady turbulent bubbly flows with non-uniform bubble sizes. Among the  $(N + 1)$ -fluids, one fluid corresponds to the liquid phase and the  $N$  fluids to gas bubbles. To demonstrate the potential of the proposed method, unsteady bubble plumes in a water filled vessel were simulated using both  $(3 + 1)$ -fluid and two-fluid models. The gas bubbles were classified and fixed in three groups only, thus a  $(3 + 1)$ - or four-fluid model was used. The dispersions investigated were very dilute thus the bubble coalescence and breakage phenomena were neglected, whereas the inertia terms were retained in the 3 bubble phase momentum equations. No population balance model was then needed, and the phase continuity equations were solved for all phases. It was confirmed that the  $(3 + 1)$ -fluid model gave better predictions than the two-fluid model for bubble plumes with non-uniform bubble sizes.

As mentioned earlier, three-fluid models have also been used by a few groups [73, 88]. Krishna and van Baten [73] solved the Eulerian volume-averaged mass- and momentum equations for all three phases. However, no interchange between the small and large bubble phases were included thus each of the dispersed bubble phases exchanges momentum only with the liquid phase. No population balance model was used as the bubble coalescence and breakage phenomena were neglected. Lehr et al [88] extended the basic three-fluid model including a simplified population balance model for the bubble-size distribution.

In most studies reported so far two-fluid models are used [20, 113, 91, 92, 93, 107, 17, 108], assuming that all the particles have the same average velocities. In other words, the possible particle collisions due to buoyancy effects are neglected even though these contributions have not been proven insignificant. This means that the two momentum equations for the two phases are solved together with the continuity equation of the liquid phase and the  $N$  population balance equations for the dispersed phases [20]. An alternative, often used adopting commercial CFD codes due to limited access to the solver routines, is to solve the full two-fluid model in the common way using the dispersed phase continuity equation together with the two momentum equations and the liquid phase continuity. Within the IPISA-like calculation loop the  $N - 1$  population balance equations are solved in another step considering additional transport equations for scalar variables. Unfortunately, using this approach it may be difficult to ensure mass conservation for the dispersed phase, and/or the last class can get negative concentrations. From the solution of the size distribution of the dispersed phase, the Sauter mean diameter is calculated. This diameter is then used computing the contact area, thus the two-way interaction between the flow and the bubble size distribution is established. When dilute dispersions are considered, the interfacial momentum

transfer fluxes due to particle collisions, coalescence and breakage phenomena are normally neglected. Politano et al [113] are the only ones that considered the interfacial momentum transfer fluxes between the bubble groups induced by bubble coalescence and breakage, but still the bubble collisions resulting in rebound were not taken into consideration.

Several recent studies indicate that algebraic slip models are sufficient modeling the flow pattern in bubble columns [20, 105, 141, 13], as the pressure and steady drag forces only dominate the axial component of the gas momentum balance. Therefore, the population balance model can be merged with an algebraic slip model to reduce the computational cost required for preliminary analysis [13]. Furthermore, adopting this concept the restriction used in the two-fluid model assuming that all the particles have the same velocity can be avoided. This means that only one set of momentum - and continuity equations for the mixture is solved together with the  $N$  population balance equations for the dispersed phases. The individual phase- and bubble class velocities are calculated from the mixture ones using algebraic relations.

Even simpler approaches are used solving a single transport equation for one moment of the population balance only, determining a locally varying mean particle size or the interfacial area density [70, 99, 87, 163].

The main contribution from the work of Luo [95, 96] was a closure model for binary breakage of fluid particles in fully developed turbulence flows based on isotropic turbulence - and probability theories. The author(s) also claimed that this model contains no adjustable parameters, a better phrase may be no additional adjustable parameters as both the isotropic turbulence - and the probability theories involved contain adjustable parameters and distribution functions. Hagesaether et al [49, 50, 51, 52] continued the population balance model development of Luo within the framework of an idealized plug flow model, whereas Bertola et al [13] combined the extended population balance module with a 2D algebraic slip mixture model for the flow pattern. Bertola et al [13] studied the effect of the bubble size distribution on the flow fields in bubble columns. An extended  $k$ - $\varepsilon$  model was used describing turbulence of the mixture flow. Two sets of simulations were performed, i.e., both with and without the population balance involved. Four different superficial gas velocities, i.e., 2, 4, 6 and 8 ( $cm/s$ ) were used, and the superficial liquid velocity was set to 1 ( $cm/s$ ) in all the cases. The population balance contained six prescribed bubble classes with diameters set to  $d_1 = 0.0038$  ( $m$ ),  $d_1 = 0.0048$  ( $m$ ),  $d_1 = 0.0060$  ( $m$ ),  $d_1 = 0.0076$  ( $m$ ),  $d_1 = 0.0095$  ( $m$ ) and  $d_1 = 0.0120$  ( $m$ ).

Figs 8.12 and 8.13 show simulated and experimental results with superficial gas velocity,  $v_g^s = 8$  ( $cm/s$ ). Fig 8.12 shows the axial and radial liquid velocity components, the axial gas velocity component and the gas fraction 2.0 ( $m$ ) above the column inlet. Fig 8.13 shows the number density in each class 2.0 ( $m$ ) above the inlet.

The results from the two simulations (i.e., with and without the population balance) are nearly identical. In both cases the simulated results are in

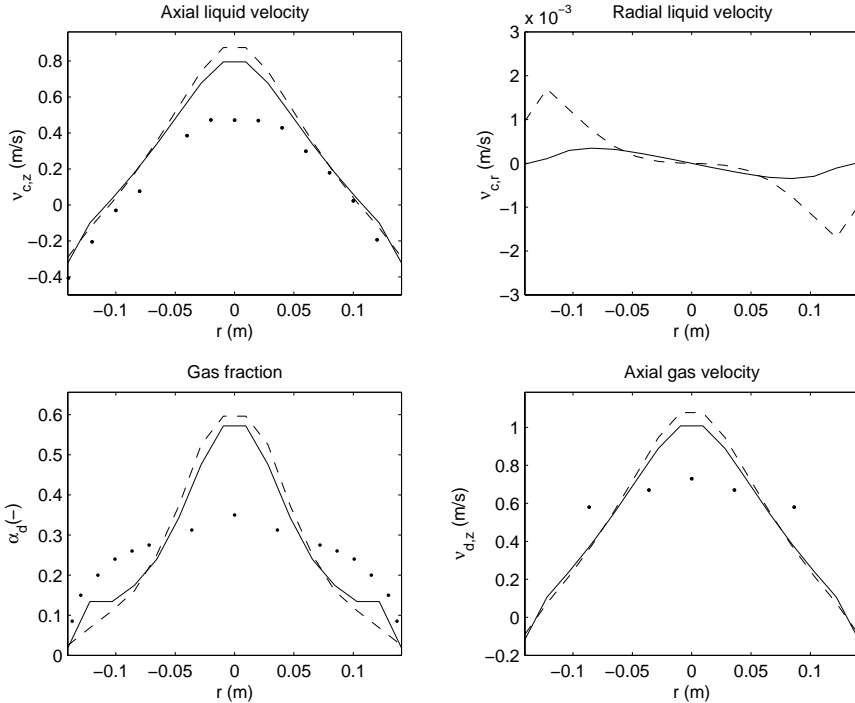


**Fig. 8.12.** Simulated results obtained with (continuous line —) and without (dashed line - - -) the population balance at the axial level 2 ( $m$ ) above the column inlet. ( $\cdot$ ) is experimental data [61].  $v_d^s = 8$  (cm/s). Reprinted with permission from Begell House Inc.

fair agreement with the experimental data, but in the center of the reactor the deviation between the simulated and experimental velocity and void fraction profiles are rather large. The number density 2.0 ( $m$ ) above the inlet is shown in Fig 8.13. In general, it was found that the initial bubble size was not stable and further determined by break-up and coalescence mechanisms. The simulation provides results in fair agreement with the experimental data for the classes 3 to 6 where the bubble number density is at the same order of magnitude as the experimental data. In bubble classes 1 and 2 the experimental bubble number densities are considerably underestimated in the simulations compared to the measured data.

However, in other cases the model predictions deviate much more from each other and were in poor agreement the experimental data considering the measurable quantities like phase velocities, gas volume fractions and bubble size distributions. An obvious reason for this discrepancy is that the breakage and coalescence kernels rely on ad-hoc empiricism determining the particle-particle and particle-turbulence interaction phenomena. The existing parameterizations developed for turbulent flows are high order functions of the local

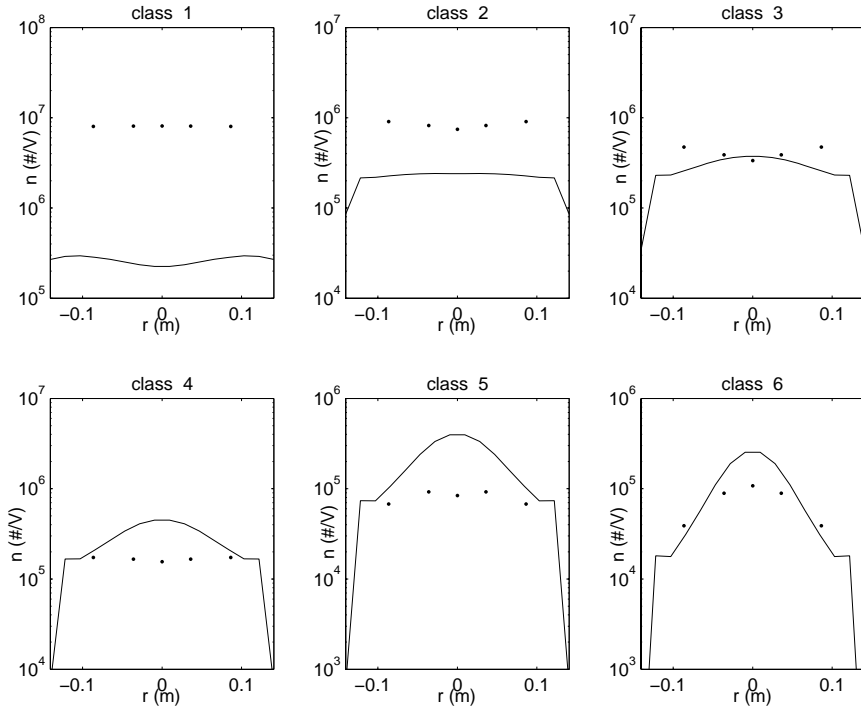


**Fig. 8.13.** The calculated bubble number density at axial level 2 ( $m$ ) above the column inlet. ( $\cdot$ ) is experimental data [61].  $v_d^s = 8$  (cm/s). Reprinted with permission from Begell House Inc.

turbulent energy dissipation rate that is often determined by the  $k$ - $\varepsilon$  turbulence model. This approach is not accurate enough [88, 108, 116], as this model variable (i.e.,  $\varepsilon$ ) merely represents a closure for the turbulence integral length scale with model parameters fitted to experimental data of idealized single phase flows. The population balance kernels are also difficult to validate on the meso scale level as the physical mechanisms involved (e.g., considering eddies and eddy - particle interactions) are vague and not clearly defined. If possible, the coalescence and breakage closures should be re-parameterized in terms of measurable quantities. Well planned experimental analysis of the meso scale phenomena are then required providing data for proper model validation.

### Initial- and Boundary Conditions

Initial- and boundary conditions are very important parts of any model formulation. However, there is still very limited knowledge regarding the formulation of proper boundary conditions even for simple bubble columns [63, 66, 156].

For implicate solutions and steady state problems the initial guess of the unknown fields are given physical values, as close to the expected solution as

possible. For very simple flow problems a uniform flow field may suffice in which some of the velocity components are set to zero.

For dynamic simulations initial values are specified for all the variable fields. For bubble column flows there is generally no gas in the column initially and thus no flow before the valves are opened ( $\alpha_c = 1$ ,  $\mathbf{v}_k = 0$ ). Using the  $k$ - $\varepsilon$  model the turbulent energy and dissipation rates are given low but non-zero values.

Inlet boundary conditions for the local gas volume fraction, bubble size distribution as well as the local gas velocity components are difficult to determine but numerous approximate conditions have been proposed in the literature [119, 12, 15]. For example, when the gas starts entering the column, uniform void - and velocity profiles for both phases might be specified at the inlet [66]. The inlet conditions for  $\alpha_k$  and  $v_{k,z}$  may also be determined using a 1D mass balance over the inlet plane, requiring that the relative velocity inside the column is determined by prescribed terminal velocities and a known (empirical) bubble size distribution. Superficial velocities for the liquid and dispersed phases are normally prescribed. This approach neglects the complex bubble trajectories, added mass- and turbulent production mechanisms within a short but important inlet zone [13]. Experimental investigations of the complex flows in the inlet zone of the column have been performed by several research groups [118, 41, 53]. Nevertheless, there is clearly a need for further studies as Hartevelde et al [53] demonstrated important discrepancies between their experimental observations and the model predictions reported in the literature regarding the onset of the important flow instabilities. A uniform aeration at the inlet did create a very small entrance region, and no large-scale circulation or coherent structures [53]. On the other hand, the general purpose flow simulators normally give a dynamic large-scale circulation flow pattern even with uniform distribution of gas at the inlet, because the current models are tuned to known flow fields and thus reveal insufficient predictive capabilities.

The specification of proper outlet boundary conditions is also a problem for these flows, as the recirculating motion of the liquid phase continues as long as gas bubbles are present at sufficiently high fluxes. Consistent formulations of such boundaries have not been reported so far [45]. When the liquid is operated in a continuous mode, Neuman conditions are frequently used for the scalar variables. For the velocity components Neuman conditions can be used as well, or a prescribed pressure boundary is preferred. However, at higher gas fluxes no inflow of gas can be allowed at the outlet boundary because the inflow fluxes are then generally unknown. If the column is operated in the heterogeneous flow regime, the recirculation motion is so strong that this boundary treatment often breaks down. This limitation restricts the use of explicit discretization schemes to situations with low gas fractions, or cases where the local recirculating flux contains very little gas.

For implicit solution methods other approximate and rather crude outlet conditions are sometimes used for the flow variables. In the commercial flow

codes the boundary is often idealized considering the liquid phase in batch mode only [119]. Following the experimental laboratory practice of keeping the height of the gas-liquid dispersion smaller than the actual column height, the top surface of the column can be modeled as an outlet for both the gas and liquid phases. It is anticipated that the solution of the model equations will determine the actual height of the gas-liquid dispersion and only gas will exit from the column outlet. Adopting this approach one has to ensure that the modeling closures are well posed and that the discretization scheme applied to the governing equations as well as the iterative solver used are capable of handling the steep gradients in the volume fraction and density profiles (discontinuities) that occur when the continuous phase change from being liquid below the gas-liquid interface and gas above it. Due to the large density difference between these phases, such an attempt very often leads to non-physical pressure and velocity values close to the interface and encounters severe convergence difficulties. In order to enhance the convergence behavior in the interface region, empirically adjusted and smoothed profiles of the continuous phase density profile and/or on the void fraction profile may help to maintain a fairly stable solution [110]. For incompressible flows this numerical approach could enforce mass conservation, whereas for reactive - and other density varying system's mass conservation may be a severe problem thus this boundary treatment should be avoided.

As numerical instabilities and inaccurate mass conservation are frequent solving problems containing sharp interfaces within the calculation domain, the solution domain is often restricted to the height of the gas-liquid dispersion. In this case the local liquid velocity components normal to the outlet plane are fixed at zero as there is no net fluxes through the column outlet cross section. The top surface of the solution domain is assumed to coincide with the free surface of the dispersion that may or may not be assumed flat. This assumption is rather crude as an exact value of the gas-liquid dispersion height is not known a priori. In order to induce apparently physical flow characteristics at the outlet, approximate boundaries are required for the other flow variables. The tangential shear stress and the normal fluxes of all scalar variables are set to zero at the free surface. The gas bubbles are free to escape from the top surface. In commercial codes this implementation may not be possible and further approximations have been proposed. In some cases the top surface of the dispersion is defined as an artificial inlet where the normal liquid velocity is set to zero and the normal gas velocity is set to an approximate terminal rise velocity. In other cases the top surface of the dispersion is modeled as a *no shear wall*. This boundary set both the gas and liquid velocities to zero. In order to represent escaping gas bubbles, an artificial gas sink is defined for all the grid cells attached to the top surface. A similar approach was used by Lehr et al [88]. The free surface, which was assumed to be located at the top of the column, was approximated by an apparent semi-permeable wall. In this way the gas could leave the system, whereas the liquid surface acts as a frictionless wall for the liquid. The liquid was considered to leave the system through an outflow at the periphery of the column.

Bove et al [15] specified an outlet pressure boundary instead, and the axial liquid velocity components were determined in accordance with a global mass balance. This approach is strictly only valid when the changes in liquid density due to interfacial mass transfer or temperature changes are negligible, as the local changes are not known a priori.

Furthermore, in many industrial systems the liquid phase is not operated in batch mode, a continuous flow of the liquid phase has to be allowed. However, due to numerical problems most reports on bubble column modeling introduce the simplifying assumption that the continuous phase is operated in batch mode. Further work is needed on the continuous mode boundary condition.

At an axi-symmetric boundary Neuman conditions are used for all the fields, except for the normal velocity component which is zero because the flow direction turns at this point. The assumption of cylindrical axi-symmetry in the computations prevents lateral motion of the dispersed gas phase and leads to an unrealistic radial phase distribution [73, 66]. Krishna and van Baten [73] obtained better agreement with experiments when a 3D model was applied. However, experience showed that it is very difficult to obtain reasonable time averaged radial void profiles even in 3D simulations.

To implement a wall boundary when a  $k$ - $\epsilon$  turbulence model closure is adopted for bubble driven flows in bubble columns, the conventional wall function approach used for the single phase flow is employed. The liquid velocity profile near the wall is thus assumed to be similar to the single phase flow profile and approximated by the classical logarithmic law of the wall, as described in sect 1.3.5. However, Troshko and Hassan [151, 152] claimed that this assumption is reasonable for dilute and downward bubbly flows, but not recommended for upwards bubble driven flows as found in bubble columns. A corresponding two-phase logarithmic wall law was derived intending to be in better agreement with experimental data on homogeneous bubbly flows. It is noted that when other turbulence closures are adopted, a variety of model specific wall boundary conditions have been designed.

### 8.4.2 Numerical Schemes and Algorithms

Significant improvements of the numerical methods have been obtained during the last decade, but the present algorithms are still far from being sufficiently robust and efficient. Further work on the numerical solution methods in the framework of FVMs should proceed along the paths sketched in the sequel.

Several schemes and algorithms for solving the fluid dynamic part of the model have been published. This work has been concentrated on several items. Most important, one avoids using the very diffusive first order upwind schemes discretizing the convective terms in the multi-fluid transport equations. Instead higher order schemes that are more accurate have been implemented into the codes [62, 139, 140, 65, 105, 66]. The numerical truncation errors induced by the discretization scheme employed for the convective terms may severely alter the numerical solution and this can destroy the physics reflected

by the model equations. Oey et al [105] and Jakobsen et al [66], for example, stated that accurate discretization schemes for the dispersed phase continuity equation and for the convection terms within the fluid momentum equations are crucial for accurate predictions of the dynamic flow development in bubble columns [105, 66]. Large discretization errors may change the flow developing from center to wall peaking or visa versa.

This finding reflects an important aspect of any multi-phase flow modeling, the numerical and modeling issues cannot be investigated (completely) separately as their interplay is of considerable importance [62, 63, 65, 66]. It is also well known that the strong coupling between the phasic equations prevents efficient and robust convergence for the implicit iteration process [106]. Exchanging the well known partial elimination algorithm (PEA) of Spalding [142, 143], reducing the interaction between the phasic velocities in the drag terms of the momentum equations, with a coupled solver [69, 75, 79, 80, 3, 76, 4, 146] that simultaneously iterates on one velocity component of all phases at the time seems to improve the numerical stability and the overall convergence rate [160]. In addition, the discretization schemes together with the solution algorithms lead to large sparse linear systems of algebraic equations that need to be solved. Previously the TDMA algorithm was applied to multi-dimensional problems determining a line-wise Gauss-Seidel approach. During the last decade there have been developments in full-field solvers along the lines of Krylov subspace methods and in the field of multigrid schemes [159, 79, 80, 160, 90]. These methods make effective use of sparsity and are efficient methods for the solution of large linear systems [90]. Furthermore, the original inter-phase-slip-algorithm (IPSA) of Spalding [142] was developed to introduce an implicit coupling between pressure and volume fractions. The algorithm contains an attempt to approximate the simultaneous change of volume fraction and velocity with pressure. However, most versions of the IPSA algorithm were merely extensions of the single phase SIMPLE approach, thus the pressure was computed by assuming that all the velocity components, but not the volume fraction variable, depend upon pressure changes. The pressure-volume fraction relationship was not considered in a satisfactory implicit manner. Therefore, the extension of the single phase pressure-velocity coupling to multi-fluid models leads to low convergence rates and pure robustness of the iterating procedure [59]. Another issue that makes the implication of multiphase reactor models difficult is that the conventional algorithms for incompressible flow are not applicable as for reactive flow systems the density is highly variable. Moreover, the overall solution strategy might also be re-designed to ensure that the algorithm conserves mass for all the phases and not only for the total mixture. Lately, numerical methods originally intended for multiphase models, rather than being extended single phase approaches, have been investigated [75, 80, 3, 76, 4, 146, 66]. A fully implicit coupling of the phasic continuity and compatibility equations within the framework of pressure-volume fraction-velocity correction schemes seems to have potentials if the resulting set of algebraic equations could be solved

by an efficient and robust parallel solver [76]. However, so far, severe stability problems have been identified within the iterative solution process. The numerical properties of the resulting set of algebraic equations are not optimized for robust solutions.

The capabilities of alternative methods like FEMs (e.g., [19]) and fully spectral methods (e.g., [32]) are still rarely explored.

### 8.4.3 Chemical Reaction Engineering

Based on the experimental and numerical analyzes discussed in the previous sections, it may seem evident that the current bubble column models have very limited inherent capabilities of predicting industrial bubble column flows with sufficient accuracy. However, after tedious adjustments of model parameters, boundary conditions, time and space resolutions, numerical implementations, and solution algorithms it is often possible to reproduce known flow fields to a certain extent. Dynamic and 3D flow patterns that upon averaging give profiles in fair agreement with experimental data can be achieved. The global liquid flow pattern is usually captured fairly well, whereas the corresponding gas fields are more questionable and difficult to evaluate due to the lack of reliable experimental data. Unfortunately, the possibility of achieving a completely erroneous steady-state flow pattern where the liquid flows up along the wall and down in the core of the column is present. Moreover, it is often difficult to reproduce the gas volume fraction fields with sufficient accuracy. The latter limitation would severely affect the contact areas, the interfacial heat- and mass transfer fluxes, the projected areas as well as the interfacial momentum transfer fluxes preventing reliable predictions of the performance of chemical processes. It can thus be concluded that a true predictive fluid dynamic model is not imminent.

However, even though there are obviously many open questions and shortcomings related to the fluid dynamic modeling of bubble columns, preliminary attempts have been performed predicting chemical reactive systems. For example, the early 2D models that were developed by Jakobsen [59, 144] to describe the global steady flow pattern were tested aiming at predicting chemical conversion of a reactive system operated in a bubble column [59, 64]. The system investigated was  $CO_2$  absorption in a methyldiethanolamine (MDEA) solution. The starting point for the numerical investigation was a steady two-fluid flow model tuned to the air/water system. This air/water model was then applied to the reactive system without re-tuning any model parameters but updating the physical properties in accordance with the reactive system. It was found that with this advanced reactor model both the global flow pattern, the interfacial mass transfer fluxes as well as the conversion were still difficult to predict due to the limited accuracy reflected by the interfacial coupling models and especially the relations used for the contact area (and the projected area). Several semi-empirical models for the locally varying mean bubble size and contact areas were suggested [59, 60] with limited success.

The accuracy of the experimental data used for model validation was also questioned.

According to Dudukovic et al [35], still no fundamental models for the interfacial heat- and mass transfer fluxes have been coupled successfully to the flow models and reliable reactor performance predictions based on these models are not imminent. The mechanisms of coalescence and breakage are far from being sufficiently understood yet. The physicochemical hydrodynamics determining the bubble coalescence and breakage phenomena may not be captured by any continuum model formulation. Therefore, the use of advanced fluid dynamic models might not significantly improve on the prediction of the interfacial transfer fluxes and thus the chemical conversion, as the pertinent physics on bubble, interface and molecular scales still have to be considered using empirical parameterizations.

In summary, one of the weakest links in modeling reactive systems operated in bubble columns is the fluid dynamic part considering multi-phase turbulence modeling, interfacial closures, and especially the impact and descriptions of bubble size and shape distributions. For reactive systems the estimates of the contact areas and thus the interfacial mass transfer rates are likely to contain large uncertainties.

#### 8.4.4 Multifluid Modeling Framework

Average multi-fluid models with approximate bubble coalescence and breakage rate closures<sup>1</sup> have been found to represent a trade-off between accuracy and computational efforts for practical applications. The multifluid model represents an extension of the well known two-fluid model and is described in detail by Reyes [121], Lafi and Reyes [77], Carrica et al [20], Pflieger et al [112], Lathouwers and Bellan [85], Pflieger et al [111], Tomiyama and Shimada [150], Fan et al [38] and Jakobsen et al [66]. To determine the multiphase flow solely (i.e., not including any reactive chemical processes) the governing equations consist of the continuity- and momentum equations for  $N + 1$  phases, one phase corresponds to the liquid phase and the remaining  $N$  phases are gas bubble size phases. In most recent papers ensemble average models are used.

The average multifluid model equations are outlined in the following together with the conventional interfacial closures that are frequently adopted in gas-liquid bubbly flow analyzes. The average multi-fluid continuity equation for phase  $k$  reads<sup>2</sup>:

$$\frac{\partial}{\partial t}(\alpha_k \rho_k) + \nabla \cdot (\alpha_k \rho_k \mathbf{v}_k) = \sum_{l=1}^N \Gamma_{k,l} \quad (8.10)$$

<sup>1</sup> The population balance modeling issues are discussed in chap 9.

<sup>2</sup> For simplicity, summarizing the governing transport equations, the averaging symbols are omitted.

where the novel term on the right hand side describes the net mass transfer flux to phase  $k$  from all the other  $l$  phases.

The phasic volume fractions must also satisfy the compatibility condition:

$$\sum_{k=1}^{N+1} \alpha_k = 1 \quad (8.11)$$

In a consistent manner the momentum balance for phase  $k$  yields:

$$\frac{\partial}{\partial t}(\alpha_k \rho_k \mathbf{v}_k) + \nabla \cdot (\alpha_k \rho_k \mathbf{v}_k \mathbf{v}_k) = -\alpha_k \nabla p - \nabla \cdot (\alpha_k \boldsymbol{\sigma}_k) + \alpha_k \rho_k \mathbf{g} + \sum_{l=1}^N \mathbf{M}_{k,l} \quad (8.12)$$

where the novel interfacial momentum transfer terms account for all the momentum transfer fluxes between phase  $k$  and the other  $N$  phases.

The limiting steps in the model development are the formulation of closure relations or closure laws determining turbulence effects, interfacial transfer fluxes and the bubble coalescence and breakage processes. When sufficiently dilute dispersions are considered, only particle - fluid interactions are significant and the two-fluid closures can be employed. In these particular cases, only the interaction between each of the dispersed gas phases ( $d$ ) and the continuous liquid phase ( $c$ ) is considered parameterizing the last term on the RHS of (8.12):

$$\begin{aligned} \sum_{l=1}^N \mathbf{M}_{d,l} &\approx \mathbf{M}_{d,c} = \alpha_c \mathbf{F}_d = -\alpha_c \mathbf{F}_c \\ &= \alpha_c \mathbf{F}_{D,d} + \alpha_c \mathbf{F}_{V,d} + \alpha_c \mathbf{F}_{L,d} + \alpha_c \mathbf{F}_{TD,d} + \alpha_c \mathbf{F}_{W,d} \end{aligned} \quad (8.13)$$

The steady drag-, added mass-, lift-, turbulent diffusion- and wall forces, respectively, are presented in sect 5.2. Moreover, the force terms for dilute dispersions are multiplied by the liquid fraction due to the reduced liquid volume available for considerable gas loadings [59].

The Lagrangian steady drag force on a single particle is commonly expressed by (5.48). For Eulerian model formulations one normally employs (5.34), hence for the multifluid models the standard steady drag force parameterization yields:

$$\mathbf{F}_{D,d} = -F_{D,d}(\mathbf{v}_d - \mathbf{v}_c) = -\frac{3}{4d_{s,d}} \alpha_d \rho_c C_{D,d} |\mathbf{v}_d - \mathbf{v}_c| (\mathbf{v}_d - \mathbf{v}_c) \quad (8.14)$$

The drag coefficient is frequently estimated using the relation suggested by Tomiyama et al [149], as described in sect 5.2.4.

The acceleration of the liquid in the wake of the bubbles can be taken into account through the added mass force given by (5.112), whereas the Eulerian lift force acting on the dispersed phase is normally expressed on the form (5.65).

In near-homogeneous, stationary flows, the turbulence in the continuous phase might cause the particles in the dispersed phases to be transported from regions of high concentration to regions of low concentration. This mechanism is often modeled as a gradient diffusion process. However, the particle motion in free shear layers is rather governed by the large-scale, rotating structures which represent a quasi-orderly, not stochastic, motion. In this particular case the turbulent particle dispersion cannot be regarded as a gradient diffusion process. In any case, the turbulence in the continuous phase may affect the migration of the dispersed phase particles. These turbulence-particle interaction mechanisms are collectively referred to as *turbulent dispersion*. The mechanisms and models for particle dispersion in turbulent flows have been reviewed by several researchers [23, 24, 120, 37, 16, 66]. Still there is no generally accepted model which is applicable to all flow conditions.

Nevertheless, the turbulent dispersion force acting on bubbles in turbulent liquid flow is commonly modeled using the gradient hypothesis (e.g., [20]):

$$\mathbf{F}_{TD,d} = -\frac{\nu_{c,t}}{\alpha_d S_{cb}} F_{D,d} \nabla \alpha_d = -\frac{3}{4d_{s,d}} \rho_c C_{D,d} |\mathbf{v}_d - \mathbf{v}_c| \frac{\nu_{c,t}}{S_{cb}} \nabla \alpha_d \quad (8.15)$$

where the bubble Schmidt number is defined as:  $S_{cb} = \frac{\nu_{c,t}}{\nu_b}$ , in which  $\nu_b (\approx \nu_{d,t})$  is interpreted as a bubble diffusivity.

An additional wall lift force that pushes the dispersed phase away from the wall was suggested by Antal et al [2]. Recently, the defect in the original model that a bubble located far from the wall is attracted to the wall, has been removed by Politano et al [114]. The modified wall lift force model used by Jakobsen et al [66] is given by (5.95).

The wall might also exert a friction force on the bubbles [97]. A wall boundary condition for the gas momentum equations that was formulated by Lopez de Bertodano [94] is thus sometimes used:

$$F_{d,w} = -C_{wb,d} \frac{\alpha_d \rho_c}{100d_{s,d}} |\mathbf{v}_c| v_{d,z} A_w \quad (8.16)$$

where  $C_{wb,d} = 1.0$  is a common value.

The mere presence of dispersed phases within a continuous phase can also affect turbulence within the continuous phase [25]. These effects are often named *turbulence modulation*. Large particles tend to increase the turbulence levels in the continuous phase, due to enhanced shear production in their wakes. However, large concentrations of small particles tend to decrease turbulence in the continuous phase. There is still no generally accepted model which is applicable to all flow conditions. Considering bubbly flows the standard (single phase)  $k - \varepsilon$  model is usually adopted as basis describing liquid phase turbulence in the Eulerian multiphase simulations. A few extensions of the standard  $k - \varepsilon$  model have also been used, accounting for bubble induced turbulence, as outlined in sect 5.1. There is, however, experimental evidence that the flow in bubble columns is highly anisotropic (e.g., see [98]). Nevertheless, complete Reynolds stress models are used in rare cases only due to their numerical stability limitations.

---

## References

1. Anglart H, Andersson S, Podowski MZ, Kurul N (1993) An Analysis of Multidimensional Void Distribution in Two-Phase Flows. Proc 6th Int Topical Meeting on Nuclear Reactor Thermal Hydraulics NURETH-6, Grenoble, October 5-8, 1:139-153
2. Antal SP, Lahey RT, Flaherty JE (1991) Analysis of Phase Distribution in Fully Developed Laminar Bubbly Two-Phase Flow. Int J Multiphase Flow 17(5):635-652
3. Antal SP, Ettore SM, Kunz RF, Podowski MZ (2000) Development of a Next Generation Computer Code for the Prediction of Multicomponent Multiphase Flows. Int Meeting on Trends in Numerical and Physical Modeling for Industrial Multiphase Flow, Cargese, France, September 27-29
4. Antal SP, Lahey Jr RT, Al-Dahhan MH (2004) Simulating Churn-Turbulent Flows in a Bubble Column using a Three Field, Two-Fluid Model. Paper presented at the 5th International Conference on Multiphase Flow, ICMF'04, Yokohama, Japan, May 30-June 4, Paper No. 182
5. Bech K (2004) Modeling of bubble-driven flow applied to electrolysis cells. CD-ROM of 5th Int Conf Multiphase Flow-ICMF'04, Yokohama, Japan, May 30-June 4, Paper No. 404
6. Bech K (2005) Dynamic simulation of a 2D bubble column. Chem Eng Sci 60(19):5294-5304.
7. Becker S, Sokolichin A, Eigenberger G (1994) Gas-Liquid Flow in Bubble Columns and Loop Reactors: Part II. Comparison of Detailed Experiments and Flow Simulations. Chem Eng Sci 49(24B):5747-5762.
8. Becker S, De Bie H, Sweeney J (1999) Dynamics flow behaviour in bubble columns. Chem Eng Sci 54(21):4929-4935.
9. Behzadi A, Issa RI, Rusche H (2004) Modelling of dispersed bubble and droplet flow at high phase fractions. Chem Eng Sci 59(4):759-770.
10. Berg S, Steiff A, Weinspach PM (1992) Gasphasenvermischung in Blasensäulen mit Einbauten. Chem Ing Tech 64(5):453-456
11. Bernemann K, Steiff A, Weinspach PM (1991) Zum Einfluß von längsangeströmten Rohrbündeln auf die großräumige Flüssigkeitsströmung in Blasensäulen. Chem Ing Tech 63(1):76-77

12. Bertola F, Vanni M, Baldi G (2003) Application of Computational Fluid Dynamics to Multiphase Flow in Bubble Columns. *Int J Chem Reactor Eng* 1:1-16, article A3
13. Bertola F, Grundseth J, Hagesaether L, Dorao C, Luo H, Hjarbo KW, Svendsen HF, Vanni M, Baldi G, Jakobsen HA (2005) Numerical Analysis and Experimental Validation of Bubble Size Distribution in Two-Phase Bubble Column Reactors. *Multiphase Science & Technology*, 17 (1-2):123-145
14. Borchers O, Busch C, Sokolichin A, Eigenberger G (1999) Applicability of the standard k-epsilon turbulence model to the dynamic simulation of bubble columns. Part II: Comparison of detailed experiments and flow simulations. *Chem Eng Sci* 54(24):5927-5935
15. Bove S, Solberg T, Hjertager BH (2004) Numerical Aspects of Bubble Column Simulations. *Int J Chem Reactor Eng* 2:1-24, Article A1
16. Burns AD, Frank T, Hamill I, Shi J-M (2004) The Favre Average Drag Model for Turbulent Dispersion in Eulerian Multi-Phase Flows. 5th Int Conf Multiphase Flow, Paper No. 392, CD-ROM of ICMF'04, Yokohama, Japan, May 30-June 4
17. Buwa VV, Ranade VV (2002) Dynamics of gas-liquid flow in a rectangular bubble column: Experimental and single/multigroup CFD simulations. *Chem Eng Sci* 57(22-23):4715-4736.
18. Buwa VV, Ranade VV (2003) Mixing in Bubble Column Reactors: Role of Unsteady Flow Structures. *Canadian J Chem Eng* 81(3-4):402-411.
19. Caia C, Mineev P (2004) A finite element method for an averaged multiphase flow model. *Int J Computational Fluid Dynamics* 18(2):111-123
20. Carrica PM, Drew D, Bonetto F, Lahey Jr RT (1999) A Polydisperse Model for Bubbly Two-Phase Flow Around a Surface Ship. *Int J Multiphase Flow* 25(2):257-305.
21. Cartland Glover GM, Generalis SC (2004) The modeling of buoyancy driven flow in bubble columns. *Chem Eng Proc* 43(2):101-115.
22. Chen RC, Reese J, Fan L-S (1994) Flow Structure in Three-Dimensional Bubble Column and Three-Phase Fluidized Bed. *AIChE J* 40:1093.
23. Crowe CT, Gore RA (1985) Particle dispersion by coherent structures in free shear flows. *Part Sci Technol J* 3:149-158
24. Crowe CT, Chung JN, Troutt TR (1988) Particle mixing in free shear flows. *Prog Energy Combust Sci* 14:171-194
25. Crowe CT (2000) On models for turbulence modulation in fluid-particle flows. *Int J Multiphase Flow* 26:719-727
26. Danckwerts PV (1953) Continuous flow systems: Distribution of Residence Times. *Chem Eng Sci* 2(1):1-18
27. Deckwer W-D, Schumpe A (1987) Bubble Columns - The state of the art and current trends. *Ind Chem Eng* 27(3):405-422
28. Deckwer W-D (1992) *Bubble Column Reactors*. John Wiley & Sons Ltd, Chichester
29. Deckwer W-D, Schumpe A (1993) Improved Tools for Bubble Column Reactor Design and Scale-up. *Chem Eng Sci* 48(5):889-911
30. Deen NG, Solberg T, Hjertager BH (2001) Large Eddy Simulation of the Gas-Liquid Flow in a Square Cross-Sectioned Bubble Column. *Chem Eng Sci* 56(21-22):6341-6349.

31. Dhotre MT, Joshi JB (2004) Two-Dimensional CFD Model for the Prediction of Flow Pattern, Pressure Drop and Heat Transfer Coefficient in Bubble Column Reactors. *Chemical Engineering Research and Design* 82(A6):689-707.
32. Dorao CA, Jakobsen HA (2006) A parallel time-space least squares spectral element solver for incompressible flow problems. *Applied Mathematics and Computation* doi:10.1016/j.amc.2006.07.009
33. Dry ME (1996) Practical and theoretical aspects of the catalytic Fisher-Tropsch process. *App Cat A: General* 138:319-344
34. Duducovič MP (1999) Trends in Catalytic Reaction Engineering. *Catalysis Today* 48(1-4):5-15
35. Duducovič MP, Larachi F, Mills PL (1999) Multiphase Reactors - Revised. *Chem Eng Sci* 54(13-14):1975-1995
36. Duducovič MP, Larachi F, Mills PL (2002) Multiphase Catalytic Reactors: A Perspective on Current Knowledge and Future Trends. *Catalysis Reviews-Science and Engineering* 44(1):123-246
37. Elghobashi S, Truesdell GC (1992) Direct simulation of particle dispersion in a decaying isotropic turbulence. *J Fluid Mech* 242:655-700
38. Fan R, Marchisio DL, Fox RO (2004) Application of the direct quadrature method of moments to polydisperse gas-solid fluidized beds. *Powder Technology*, 139(1):7-20
39. Frank T, Zwart PJ, Shi J-M, Krepper E, Lucas D, Rohde U (2005) Inhomogeneous MUSIG Model - a Population Balance Approach for Polydispersed Bubbly Flows. *Int Conf Nuclear Energy for New Europe 2005*, Bled, Slovenia, September 5-8
40. Garnier C, Lance M, Marié JL (2002) Measurement of local flow characteristics in buoyancy-driven bubbly flow at high void fraction. *Experimental Thermal and Fluid Science* 26:811-815
41. Geary NW, Rice RG (1991) Bubble Size Prediction for Rigid and Flexible Spargers. *AIChE J* 37(2):161-168.
42. Gasche H-E (1989) Moddierung von Blasensäulen. Dr ing thesis, Der Technischen Fakultät der Universität Erlangen-Nürnberg
43. Gasche H-E, Edinger C, Kömpel H, Hofmann H (1990) A fluid-dynamically based model of bubble column reactors. *Chem Eng & Tech* 13:341-349
44. Goldman E, Sirovich L (1967) *Physics of Fluids* 10(9):1928-1940
45. Gresho PM, Sani RL (1987) On pressure boundary conditions for the incompressible Navier-Stokes equations. *Int J Numer Methods Fluids* 7(10):1111-1145.
46. Grienberger J (1992) Untersuchung und Modellierung von Blasensäulen. Dr ing thesis, Der Technischen Fakultät der Universität Erlangen-Nürnberg
47. Grienberger J, Hofmann H (1992) Investigations and modelling of bubble columns. *Chem Eng Sci* 47(9-11):2215-2220
48. Groen JS, Oldeman RGC, Mudde RF, van den Akker HEA (1996) Coherent Structures and Axial Dispersion in Bubble Column Reactors. *Chem Eng Sci* 51(10):2511-2520
49. Hagesaether L, Jakobsen HA, Svendsen HF (1999) Theoretical Analysis of Fluid Particle Collisions in Turbulent Flow. *Chem Eng Sci* 54(21):4749-4755.
50. Hagesaether L, Jakobsen HA, Hjarbo K, Svendsen HF (2000) A Coalescence and Breakup Module for Implementation in CFD-codes. In: Pierucci S (ed) *European Symposium on Computer Aided Process Engineering - 10. Computer-Aided Chemical Engineering* 8:367-372, Elsevier Science, Amsterdam

51. Hagesaether L, Jakobsen HA, Svendsen HF (2002) A Model for Turbulent Binary Breakup of Dispersed Fluid Particles. *Chem Eng Sci* 57(16):3251-3267.
52. Hagesaether L, Jakobsen HA, Svendsen HF (2002) Modeling of the Dispersed-Phase Size Distribution in Bubble Columns. *Ind Eng Chem Res* 41(10):2560-2570.
53. Hartevelde WK, Mudde RF, van den Akker HEA (2003) Dynamics of a Bubble Column: Influence of Gas Distribution of Coherent Structures. *Can J Chem Eng* 81:389-394.
54. Hartevelde WK, Mudde RF, van den Akker HEA (2005) Estimation of turbulence power spectra for bubbly flows from Laser Doppler Anemometry signals. *Chem Eng Sci* 60:6160-6168
55. Hillmer G (1989) Experimentelle Untersuchung und Fluiddynamische Modellierung von Aufsprühsäulen. Dr ing thesis, Der Technischen Fakultät der Universität Erlangen-Nürnberg
56. Hillmer G, Weismantel L, Hofmann H (1994) Investigations and modelling of slurry bubble columns. *Chem Eng Sci* 49(6):837-843
57. Hills JH (1974) Radial non-uniformity of velocity and voidage in a bubble column. *Trans Inst Chem Eng* 52:1-52
58. Jakobsen HA (1988) Modeling of a bubble column. MSc thesis, the Norwegian Institute of Technology, Trondheim, Norway
59. Jakobsen HA (1993) On the modelling and simulation of bubble column reactors using a two-fluid model. Dr ing thesis, the Norwegian Institute of Technology, Trondheim, Norway
60. Jakobsen HA, Svendsen HF, Hjarbo KW (1993) On the prediction of local flow structures in internal loop and bubble column reactors using a two-fluid model. *Comp Chem Eng* 17S:S531-S536
61. Jakobsen HA, Hjarbo KW, Svendsen HF (1994) Bubble size distributions, bubble velocities and local gas fractions from conductivity measurements. Report STF21 F93103, SINTEF Applied Chemistry, Trondheim, Norway
62. Jakobsen HA, Sannæs BH, Grevskott S, Svendsen HF (1997) Modeling of Vertical Bubble Driven Flows. *Ind Eng Chem Res* 36 (10):4052-4074.
63. Jakobsen HA (2001) Phase distribution phenomena in two-phase bubble column reactors. *Chem Eng Sci* 56(3):1049-1056
64. Jakobsen HA, Bourg I, Hjarbo KW, Svendsen HF (2001) Interaction Between Reaction Kinetics and Flow Structure in Bubble Column Reactors. In: Jenssen CB et al (eds) *Parallel Computational Fluid Dynamics - Trends and Applications*, Elsevier Science B.V., pp 543-550, ISBN: 0-444-50673-X
65. Jakobsen HA (2003) Numerical Convection Algorithms and Their Role in Eulerian CFD Reactor Simulations. *Int J Chem Reactor Eng*, Article A1, 1: 1-18
66. Jakobsen HA, Lindborg H, Dorao CA (2005) Modeling of Bubble Column Reactors: Progress and Limitations. *Ind Eng Chem Res* 44:5107-5151
67. Joshi JB (2001) Computational flow modeling and design of bubble column reactors. *Chem Eng Sci* 56(21-22):5893-5933
68. Kast W (1962) Analyse Des Wärmeübergangs in blasensäulen. *Int J Heat Mass Transfer* 5:329-336
69. Kelly JM, Stewart CW, Cuta JM (1992) VIPRE-02 - A two-fluid thermal-hydraulics code for reactor core and vessel analysis: Mathematical modeling and solution methods. *Nuclear Technology* 100:246-259

70. Kocamustafaogullari G, Ishii M (1995) Foundation of the interfacial area transport equation and its closure relations. *Int J Heat Mass Transfer* 38(3):481-493
71. Krepper E, Lucas D, Prasser H-M (2005) On the modelling of bubbly flow in vertical pipes. *Nucl Eng Des* 235:597-611
72. Krishna R, van Baten JM (1999) Rise Characteristics of Gas Bubbles in a 2D Rectangular Column: VOF Simulations vs Experiments. *Int Comm Heat Mass Transfer* 26(7):965-974.
73. Krishna R, van Baten JM (2001) Scaling up Bubble column reactors with the aid of CFD. *Inst Chem Eng Trans IChemE* 79(A3):283-309.
74. Krishna R, van Baten JM (2002) Scaling up Bubble Column Reactors with Highly Viscous Liquid Phase. *Chem Eng Technol* 25(10):1015-1020.
75. Kunz RF, Siebert BW, Cope WK, Foster NF, Antal SP, Ettorre SM (1998) A coupled phasic exchange algorithm for three-dimensional multi-field analysis of heated flows with mass transfer. *Computers & Fluids* 27(7):741-768
76. Kunz RF, Yu W-S, Antal SP, Ettorre SM (2001) An Unstructured Two-Fluid Method Based on the Coupled Phasic Exchange Algorithm. American Institute of Aeronautics and Astronautics, AIAA-2001-2672, pp 1-13
77. Lafi AY, Reyes JN (1994). General particle transport equations. Final Report OSU-NE-9409. Department of Nuclear Engineering, Oregon State University
78. Lance M, Bataille J (1991) Turbulence in the liquid-phase of a uniform bubbly air water-flow. *J Fluid Mech* 222:95-118
79. Lathouwers D, van den Akker HEA (1996) A numerical method for the solution of two-fluid model equations. In: Numerical methods for multiphase flows. FED-Vol 236, ASME 1996 Fluids Engineering Division Conference, Volume 1, ASME 1996, pp 121-126
80. Lathouwers D (1999) Modeling and simulation of turbulent bubbly flow. PhD thesis, the Technical University in Delft, the Netherlands
81. Lathouwers D, Bellan J (2000) Modeling of dense gas-solid reactive mixtures applied to biomass pyrolysis in a fluidized bed. Proc of the 2000 U.S. DOE Hydrogen Program Review. NREL/CP-570-28890
82. Lathouwers D, Bellan J (2000) Modeling and simulation of bubbling fluidized beds containing particle mixtures. Proc of the Combustion Institute 28: 2297-2304
83. Lathouwers D, Bellan J (2001) Modeling of biomass pyrolysis for hydrogen production: The fluidized bed reactor. Proc of the 2001 U.S. DOE Hydrogen Program Review. NREL/CP-570-30535
84. Lathouwers D, Bellan J (2001) Yield Optimization and Scaling of Fluidized Beds for Tar Production from Biomass. *Energy & Fuels* 15:1247-1262
85. Lathouwers D, Bellan J (2001) Modeling of dense gas-solid reactive mixtures applied to biomass pyrolysis in a fluidized bed. *Int J Multiphase Flow* 27:2155-2187
86. Launder BE, Spalding DB (1972) *Mathematical Models of Turbulence*. Academic Press, London
87. Lehr F, Mewes D (2001) A transport equation for the interfacial area density applied to bubble columns. *Chem Eng Sci* 56:1159.
88. Lehr F, Millies M, Mewes D (2002) Bubble-Size Distributions and Flow Fields in Bubble Columns. *AIChE J* 48(11):2426-2443.
89. Lin T-J, Reese J, Hong T, Fan L-S (1996) Quantitative Analysis and Computation of Two-Dimensional Bubble Columns. *AIChE J* 42(2):301-318.

90. Lindborg H, Eide V, Unger S, Henriksen ST, Jakobsen HA (2004) Parallelization and performance optimization of a dynamic PDE reactor model for practical applications. *Computers and Chemical Engineering* 28:1585-1597
91. Lo S (1996) Application of the MUSIG model to bubbly flows. AEAT-1096, AEA Technology, June 1996
92. Lo S (2000) Some recent developments and applications of CFD to multiphase flows in stirred reactors. Proc of AMIF-ESF Workshop: Computing Methods for Two-Phase Flow. Aussois, France, 12-14 January
93. Lo S (2000) Application of population balance to CFD modeling of gas-liquid reactors. Proc of Trends in numerical and physical modelling for industrial multiphase flows, Corse, 27-29 September
94. Lopez de Bertodano M (1992) Turbulent Bubbly Two-Phase Flow in a Triangular Duct. PhD thesis, Rensselaer Polytechnic Institute, Troy, New York, USA
95. Luo H (1993) Coalescence, break-up and liquid circulation in bubble column reactors. Dr. ing. thesis, Department of Chemical Engineering, the Norwegian Institute of Technology, Trondheim, Norway
96. Luo H, Svendsen HF (1993) Theoretical Model for Drop and Bubble Breakup in Turbulent Dispersions. *AIChE J* 42(5):1225-1233.
97. Marié JL, Moussali E, Lance M (1991) A First Investigation of a Bubbly Stress Measurements. International Symposium on Turbulence Modification in Multiphase Flows, ASME/JSME Annual Meeting, Portland, Oregon, USA, 23-27 June
98. Menzel T, in der Weide T, Staudacher O, Wein O, Onken U (1990) Reynolds Shear Stress for Modeling of Bubble Column Reactors. *Ind Eng Chem Res* 29:988-994
99. Millies M, Mewes D (1999) Interfacial area density in bubbly flow. *Chem Eng and Proc* 38(4-6):307-319
100. Morsi SA, Alexander AJ (1972) An Investigation of Particle Trajectories in Two-Phase Flow Systems. *J Fluid Mech* 55:193-208.
101. Mudde RF, Lee DJ, Reese J, Fan L-S (1997) Role of Coherent Structures on Reynolds Stresses in a 2-D Bubble Column. *AIChE J* 43(4):913-926.
102. Mudde RF, Groen JS, van den Akker HEA (1997) Liquid velocity field in a bubble column: LDA experiments. *Chem Eng Sci* 52:4217-4224
103. Mudde RF, Simonin O (1999) Two- and three-dimensional simulations of bubble plume using a two-fluid model. *Chem Eng Sci* 54(21):5061-5069.
104. Mudde RF (2005) Gravity-Driven Bubbly Flows. *Annu Rev Fluid Mech* 37:393-423
105. Oey RS, Mudde RF, van den Akker HEA (2003) Sensitivity Study on Interfacial Closure Laws in Two-Fluid Bubbly Flow Simulations. *AIChE J* 49(7):1621-1636.
106. Oliveira PJ, Issa RI (1994) On the numerical treatment of interphase forces in two-phase flow. In: Crowe CT (ed) *Numerical Methods in Multiphase Flows*, FED-185:131-140, ASME
107. Olmos E, Gentric C, Vial C, Wild G, Midoux N (2001) Numerical simulation of multiphase flow in bubble column reactors. Influence of bubble coalescence and breakup. *Chem Eng Sci* 56(21-22):6359-6365.
108. Olmos E, Gentric C, Midoux N (2003) Numerical description of flow regime transitions in bubble column reactors by multiple gas phase model. *Chem Eng Sci* 58(10):2113-2121.

109. Onken U (1988) Bubble Column as Chemical Reactors. In: Bubble Columns, Preprints from the German/Japanese Symposium (by DVCV - Deutsche Vereinigung für Chemie- und Verfahrenstechnik, VDI - Gesellschaft Verfahrenstechnik und Chemie-ingenieurwesen), Schwerte/West-Germany, 13-15 June, 1988.
110. Padial NT, VanderHeyden WB, Rauenzahn RM, Yarbrow SL (2000) Three-dimensional simulation of a three-phase draft-tube bubble column. *Chem Eng Sci* 55(16):3261-3273.
111. Pflieger D, Gomes S, Gilbert N, Wagner H-G (1999) Hydrodynamic simulations of laboratory scale bubble columns fundamental studies of the Eulerian-Eulerian Modelling approach. *Chem Eng Sci* 54(21):5091-5099.
112. Pflieger D, Becker S (2001) Modeling and simulation of the dynamic flow behaviour in a bubble column. *Chem Eng Sci* 56(4):1737-1747.
113. Politano MS, Carrica PM, Larreteguy AE (2001) Gas/Liquid Polydisperse Two-Phase Flow Modeling for Bubble Column Reactors. Proc 3rd Mercosur Congress on Process Systems Engineering 1st Mercosur Congress on Chemical Engineering. 16-20/9/2001-Sante Fé.
114. Politano MS, Carrica PM, Converti J (2003) A model for turbulent polydisperse two-phase flow in vertical channels. *Int J Multiphase Flow* 29(7):1153-1182.
115. Portela LM, Oliemans RVA (2006) Possibilities and Limitations of Computer Simulations of Industrial Turbulent Dispersed Multiphase Flows. *Flow Turbulence Combust* 77:381-403
116. Prince MJ, Blanch HW (1990) Bubble Coalescence and Break-Up in Air-Sparged Bubble Columns. *AIChE J* 36(10):1485-1499
117. Rafique M, Chen P, Dudukovic MP (2004) Computational Modeling of Gas-Liquid Flow in Bubble Columns. *Reviews in Chemical Engineering* 20(3-4):225-375
118. Ramakrishnan S, Kumar R, Kuloor NR (1969) Studies in bubble formation -I: Bubble formation under constant flow conditions. *Chem Eng Sci* 24(4):731-747.
119. Ranade VV (2002) *Computational Flow Modeling for Chemical Reactor Engineering*, Academic Press; San Diego
120. Reeks MW (1992) On the continuum equations for dispersed particles in nonuniform flows. *Phys Fluids A* 4:1290-1303
121. Reyes Jr JN (1989) Statistically derived conservation equations for fluid particle flows. Proc ANS Winter Meeting. Nuclear Thermal Hydraulics, 5th Winter Meeting
122. Sanyal J, Vasquez S, Roy S, Dudukovic MP (1999) Numerical simulation of gas-liquid dynamics in cylindrical bubble column reactors. *Chem Eng Sci* 54(21):5071-5083.
123. Sato Y, Sekoguchi K (1975) Liquid Velocity Distribution in Two-Phase Bubbly Flow. *Int J Multiphase Flow* 2:79-95.
124. Sato Y, Sadotomi M, Sekoguchi K (1981) Momentum and Heat Transfer in Two-Phase Bubble Flow. *Int J Multiphase Flow* 7(2):167-177.
125. Schiller L, Naumann Z (1933) Über die grundlegenden Berechnungen bei der Schwerkraftaufbereitung. *Z Ver Deutsch Ing* 77:318-320
126. Schügerl K, Lücke J, Oels U (1977) Bubble Column Bioreactors. *Adv Biochem Eng* 7:1-84
127. Serizawa A (1974) Fluid dynamic characteristics of two-phase flow. PhD Thesis, Kyoto University, Japan

128. Serizawa A, Kataoka I, Michiyoshi I (1975) Turbulence structure of air-water bubbly flow-II: Local properties. *Int J Multiphase Flow* 2:235-246
129. Serizawa A, Kataoka I (1987) Phase distribution in two phase flow. Invited lecture, ICHMT Int Seminar on Transient Phenomena in Multiphase Flow, Dubrovnik, Yugoslavia, May 24-29, In: Afgan NH (ed) *Proc Transient Phenomena in Multiphase Flow*, Hemisphere Publ Corp, pp 179-224, 1988.
130. Sha Z, Laari A, Turunen I (2004) Implementation of Population Balance into Multiphase-Model in CFD Simulation of Bubble Column. *Proc of the 16th Int Congress of Chem Eng, Praha, Czech Republic* (paper E3.2)
131. Sha Z, Laari A, Turunen I (2006) Multi-Phase-Multi-Size-Group Model for the Inclusion of Population Balances into the CFD Simulation of Gas-Liquid Bubbly Flows. *Chem Eng Technol* 29(5):550-559
132. Shah YT, Kelkar BG, Godbole SP, Deckwer W-D (1982) Design parameter estimations for bubble column reactors. *AIChE J* 28(3):353-379
133. Shah YT, Sharma MM (1987) Gas-Liquid-Solid Reactors. In: Carberry JJ, Varma A (eds) *Chemical Reaction and Reaction Engineering*. Marcel Dekker Inc, New York and Basel, pp 667-734
134. Shi J, Zwart P, Frank T, Rohde U, Prasser H (2004). Development of a multiple velocity multiple size group model for poly-dispersed multiphase flows. *Annual Report 2004*. Institute of Safety Research, Forschungszentrum Rossendorf, Germany
135. Simonin O (1990) Eulerian formulation for particle dispersion in turbulent two-phase flows. In: Sommerfeld M, Wennerberg P (eds) *Fifth workshop on two-phase flow predictions*, pp. 156-166, Erlangen, Germany
136. Simonin O, Viollet PL (1990) Prediction of an Oxygen Droplet Pulverization in a Compressible Subsonic Co-flowing Hydrogen Flow. In: *Numerical Methods for Multiphase Flows*, ASME FED 91:73-82.
137. Simonin O (1996) Combustion and turbulence in two-phase flows. von Karman Lecture Series 1996-02, von Karman Institute for Fluid Dynamics
138. Sokolichin A, Eigenberger G (1994) Gas-liquid flow in bubble columns and loop reactors: Part I. Detailed modeling and numerical simulation. *Chem Eng Sci* 49(24B):5735-5746.
139. Sokolichin A, Eigenberger G, Lapin A, Lübbert A (1997) Dynamical numerical simulation of gas-liquid two-phase flows. Euler/Euler versus Euler/Lagrange. *Chem Eng Sci* 52(4): 611-626.
140. Sokolichin A, Eigenberger G (1999) Applicability of the  $k-\varepsilon$  turbulence model to the dynamic simulation of bubble columns: Part I. Detailed numerical simulations. *Chem Eng Sci* 54:2273.
141. Sokolichin A, Eigenberger G, Lapin A (2004) Simulation of Buoyancy Driven Bubbly Flow: Established Simplifications and Open Questions. *AIChE J* 50(1):24-45.
142. Spalding DB (1977) The calculation of free-convection phenomena in gas-liquid mixtures. ICHMT seminar 1976, In: *Turbulent Buoyant Convection*, Hemisphere, Washington, pp 569-586
143. Spalding DB (1980) Numerical computation of multiphase fluid flow and heat transfer. In: Taylor C et al (eds) *Recent Advances in Numerical Methods in Fluids*, Pineridge Press, pp 139-167
144. Svendsen HF, Jakobsen HA, Torvik R (1992) Local Flow Structures in Internal Loop and Bubble Column Reactors. *Chem Eng Sci* 47(13-14):3297-3304.

145. Tchen CM (1947) Mean value and correlation problems connected with the motion of small particles suspended in a turbulent fluid. PhD thesis, TU Delft, Netherlands
146. Tiwari P, Antal SP, Burgoyne A, Belfort G, Podowski MZ (2004) Multifield computational fluid dynamics model of particulate flow in curved circular tubes. *Theoret Comput Fluid Dynamics* 18:205-220
147. Tomiyama A, Matsouka T, Fukuda T, Sakaguchi T (1995) A Simple Numerical Method for Solving an Incompressible Two-Fluid Model in a General Curve-linear Coordinate System. *Advances in Multiphase Flow*, Elsevier, pp 241-252
148. Tomiyama A (1998) Struggle with computational bubble dynamics. Third International Conference on Multiphase Flow, CD-ROM of ICMF'98, Lyon
149. Tomiyama A, Miyoshi K, Tamai H, Zun I, Sakaguchi T (1998) A Bubble Tracking Method for the Prediction of Spatial-Evolution of Bubble Flow in a Vertical Pipe. Third International Conference on Multiphase Flow, CD-ROM of ICMF'98, Lyon
150. Tomiyama A, Shimada N (2001) A Numerical Method for Bubbly Flow Simulation Based on a Multi-Fluid Model. *Journal of Pressure Vessel Technology-Trans ASME* 123:510-516
151. Troshko AA, Hassan YA (2001) Law of the wall for two-phase turbulent boundary layers. *Int J Heat and Mass Transfer* 44(4):871-875
152. Troshko AA, Hassan YA (2001) A two-equation turbulence model of turbulent bubbly flows. *Int J Multiphase Flow* 27(11):1965-2000
153. Tzeng J-W, Chen RC, Fan L-S (1993) Visualization of Flow Characteristics in a 2D Bubble Column and Three-Phase Fluidized Bed. *AIChE J* 39(5):733-744
154. Torvik R (1990) Investigations of 2- and 3-Phase Bubble Columns. Dr Ing Thesis, Norwegian Institute of Technology, Trondheim, Norway
155. Ueyama K, Miyauchi T (1979) Properties of Recirculating Turbulent Two Phase Flow in Gas Bubble Column. *AIChE J* 25(2):258-266
156. van den Akker HEA (2000) Computational Fluid Dynamics: More Than a Promise to Chemical Reaction Engineering. Paper presented at the CHISA 2000 conference, Praha, Czech Republic
157. van den Akker HEA (1998) Coherent structures in multiphase flows. *Powder Technology* 100(2-3):123-136.
158. Valiveti P, Koch DL (1998) Instability of Sedimenting Bidisperse Particle Gas Suspensions. *Applied Scientific Research* 58:275-303
159. van Santen H, Lathouwers D, Kleijn CR, van den Akker HEA (1996) Influence of segregation on the efficiency of finite volume methods for the incompressible Navier-Stokes equations. FED-vol 238, Proc ASME 1996 Fluid Engineering Division Summer Meeting, Vol 3, pp 151-157
160. Vasquez SA, Ivanov VA (2000) A phase coupled method for solving multiphase problems on unstructured meshes. FEDSM2000-11281, Proc ASME FEDSM'00:ASME 2000 Fluids Engineering Division Summer Meeting, Boston, Massachusetts, June 11-15, pp 1-6
161. Viollet PL, Simonin O (1994) Modelling dispersed two-phase flows: Closure, validation and software development. *Applied Mechanics Reviews* 47:S80-S84.
162. Wang SK, Lee SJ, Jones Jr OC, Lahey Jr RT (1987) 3-D turbulence structure and phase distribution measurements in bubbly two-phase flows. *Int J Multiphase flow* 13(3):327-343
163. White AJ, Hounslow MJ (2000) Modelling droplet size distributions in poly-dispersed wet-stream flows. *Int J Heat Mass Transfer* 43(11):1873-1884.

164. Zun I (1980) The Transverse Migration of Bubbles Influenced by Walls in Vertical Bubbly Flow. *Int J Multiphase Flow* 6:583-588
165. Zun I (1985) The Role of Void Peaking in Vertical Two-Phase Bubbly Flow. 2nd Int Conf on Multi-phase Flow, London, paper C3. (ed) BHRA, The Fluid Engineering Centre, Cranfield, pp. 127-139
166. Zun I (1987) Transition From Wall Void Peaking to Core Void Peaking in Turbulent Bubbly Flow. Invited lecture, ICHMT Int Seminar on Transient Phenomena in Multiphase Flow, Dubrovnik, Yugoslavia, May 24-29 In: Afgan NH (ed) *Proc Transient Phenomena in Multiphase Flow*, Hemisphere Publ Corp, pp 225-245, 1988.
167. Zun I (1990) The Mechanism of Bubble Non-Homogeneous Distribution in Two-Phase Shear Flow. *Nucl Eng Des* 118:155-162
168. Üztürk S, Shah YT, Deckwer W-D (1988) Comparison of Gas and Liquid Phase Methanol Synthesis Processes. *Chem Eng J* 37:177-192

---

## The Population Balance Equation

The chemical engineering community began the first efforts that can be associated with the concepts of the population balance in the early 1960s.

The familiar application of population balance principles to the modeling of flow and mixing characteristics in vessels was formally organized by Danckwerts [17]. Certain distribution functions were then defined for the residence times of fluid elements in a process vessel. The residence time distribution function give information about the fraction of the fluid that spends a certain time in a process vessel. Himmelblau and Bishoff [35] describe how the residence time and other age distributions are defined, how they can be measured, and how they can be interpreted. This chapter thus focuses on the derivation and use of the general population balance equation (PBE) to describe the evolution of the fluid particle distribution due to the advection, growth, coalescence and breakage processes.

The historical derivation of the general population balance equation for countable entities is outlined. Two fundamental modeling frameworks emerge formulating the early population balances, in quite the same way as the kinetic theory of dilute gases and the continuum mechanical theory were proposed deriving the governing conservation equations in fluid mechanics. A third less rigorous approach is also used formulating the population balance directly on the macroscopic averaging scales, an analogue to the multiphase mixture models.

Considering dispersed two-phase flows, a few research groups adopted a statistical Boltzmann-type equation determining the rate of change of a suitable defined distribution function. Performing the Maxwellian averaging integrating all terms over the whole velocity space to eliminate the velocity dependence, one obtains the generic population balance equation. Rigorous closures are required for the unknown terms resulting from the averaging process. However, by employing the conventional Chapman-Enskog approximate expansion method solving the Boltzmann-type equation this theory provides rational means of understanding for the one way coupling between microscopic particle physics and the average macroscopic continuum properties.

Moreover, to represent complex problem physics an optimized choice of distribution function definition considering multiple internal coordinates in an environment of a particular state may be necessary, and novel closure required, making the approach rather demanding theoretically. The procedure sketched above has much in common with the granular theory of solid particles, outlined in chap 4. However, the majority of research groups within the chemical engineering community adopted an alternative approach based on a generalization of the classical continuum mechanical theory developing the population balance equation. On the other hand, the continuum theory gives only an average representation of the dispersed phase considering macroscopic scales several orders of magnitude larger than the microscopic particle dimensions and does not provide any information on the unresolved mechanisms that can be utilized formulating the population balance closures. In most cases, the balance principle is applied formulating a transport equation for the distribution function on the integral form. Generalized versions of the Leibnitz- and Gauss theorems are then required transferring the integral balance to the differential form. Thereafter, the governing microscopic continuum equations on the differential form are averaged to obtain a model formulation representing tractable volume and time resolutions. However, the averaging process also give rise to additional closure requirements. In the past, the time after volume averaging procedure was frequently used, being consistent with the time- after volume averaged multi-fluid model formulation discussed in sect 3.4.4. The third group of population balances are formulated on integral form directly on the averaging scales and then converted to the differential form employing the extended Leibnitz- and Gauss theorems. In this formulation, the closures are purely empirical parameterizations based on intuitive relationships rather than sound scientific principles.

The population balance concept was first presented by Hulburt and Katz [37]. Rather than adopting the standard continuum mechanical framework, the model derivation was based on the alternative Boltzmann-type equation familiar from classical statistical mechanics. The main problems investigated stem from solid particle nucleation, growth, and agglomeration.

Randolph [95] and Randolph and Larson [96], on the other hand, formulated a generic population balance model based on the generalized continuum mechanical framework. Their main concern was solid particle crystallization, nucleation, growth, agglomeration/aggregation and breakage.

Ramkrishna [93, 94] adopted the concepts of Randolph and Larson to investigate biological populations. An outline of the population balance model derivation from the continuum mechanics point of view was discussed.

Similar approaches are also frequently used in the theory of aerosols in which the gas is the continuous phase [122, 25], in chemical-, mechanical- and nuclear engineering describing multi-phase droplet flow dynamics [45, 46] and to incompressible bubbly two-phase flows [26].

In chemical engineering Coualoglou and Tavlarides [16] were among the first to introduce the simpler macroscopic formulation, describing the

interaction processes in agitated liquid-liquid dispersions. Drifting from the fundamental microscopic equations the closures became an integrated part of the discrete numerical discretization scheme adopted (i.e., there is no clear split between the numerical scheme and the closure laws).

Lee et al [66] and Prince and Blanch [92] adopted the basic ideas of Coualoglou and Tavlarides [16] formulating the population balance source terms directly on the averaging scales performing analysis of bubble breakage and coalescence in turbulent gas-liquid dispersions. The source term closures were completely integrated parts of the discrete numerical scheme adopted. The number densities of the bubbles were thus defined as the number of bubbles per unit mixture volume and not as a probability density in accordance with the kinetic theory of gases.

Luo [73] and Luo and Svendsen [74] extended the work of Coualoglou and Tavlarides [16], Lee et al [66] and Prince and Blanch [92] formulating the population balance directly on the macroscopic scales where the closure laws for the source terms were integrated parts of the discrete numerical scheme used solving the model equations.

Hagesæther et al [29, 30] and Wang et al [119] extended the breakage model of Luo and Svendsen [74] removing an internal limitation that the kernel was not taking into consideration that there is a physical lower limit for the particle size for which the breakage rate diminishes. Some of the shortcomings were removed from the original kernels by taking into account the energy distribution of the turbulent eddies, the effect of capillary pressure and the surface energy increase during bubble/droplet breakup.

Carrica et al [11] investigated compressible bubbly two-phase flow around a surface ship. They developed a population balance from kinetic theory using the particle mass as internal variable, whereas most earlier work on solid particle analysis used particle volume (or diameter). In flows where compressibility effects in the gas are important (as in the case of laboratory bubble columns operated at atmospheric conditions) the use of mass as an internal coordinate was found to be advantageous because this quantity is conserved under pressure changes. The use of a mass density form of the population balance derived based on the kinetic theory approach (i.e., instead of the more common number density) has also been discussed, having several advantages in reactor technology [90]. Millies and Mewes [82], Lehr and Mewes [67], Lehr et al [68], Pilon et al [87] and Lasheras [58] sketched a possible alternative formulation using particle volume (diameter) as the internal coordinate within the number density form of the population balance equation. In their approach several growth terms have to be considered expressing the effects of gas expansion due to changes in gas density in accordance with a suitable EOS. Both formulations are equivalent in the case of incompressible fluids.

In the work of Fleischer et al [23] and Hagesæther et al [28] one dimensional population balance formulations and closure laws very similar to those of Luo and Svendsen [74] were employed. In the bubbly flow simulations by Hagesæther et al [29, 30] and Wang et al [119, 120] the macroscopic population

balance formulation of Luo and Svendsen [74] was still adopted (no fluid dynamic calculations were performed) but with extended versions of the kernel functions.

Venneker et al [118] made an off-line simulation of the underlying flow and the local gas fractions and bubble size distributions for turbulent gas dispersions in a stirred vessel. The transport of bubbles throughout the vessel was estimated from a single-phase steady-state flow field, whereas literature kernels for coalescence and breakage were adopted to close the population balance equation predicting the gas fractions and bubble size distributions.

Several extensions of the two-fluid model have been developed and reported in the literature. Generally, the two-fluid model solve the continuity and momentum equations for the continuous liquid phase and one single dispersed gas phase. In order to describe the local size distribution of the bubbles, the population balance equations for the different size groups are solved. The coalescence and breakage processes are frequently modeled in accordance with the work of Luo and Svendsen [74] and Prince and Blanch [92].

Lehr and Mewes [67] included a model for a varying local bubble size in their 3D dynamic two-fluid calculations of bubble column flows performed by use of a commercial CFD code. A transport equation for the interfacial area density in bubbly flow was adopted from Millies and Mewes [82]. In deriving the simplified population balance equation it was assumed that a dynamic equilibrium between coalescence and breakage was reached, so that the relative volume fraction of large and small bubbles remain constant. The population balance was then integrated analytically in an approximate manner.

Extended two-fluid models have also been employed by Lo [70, 71, 72] developing the MUSIG model in the CFX-4 software, Buwa and Ranade [10] using the FLUENT software, Olmos et al [83, 84] using CFX4-3 with 10 bubble size classes, Chen et al [13] running 2D simulations using the FLUENT software with 16 bubble size classes, Chen et al [12] performed 3D simulations using the FLUENT software with 9 bubble size classes. Moreover, Laakkonen et al [55] simulated a laboratory scale stirred tank using the two-fluid MUSIG model in CFX5.7. Laakkonen et al adopted the simplified kernels of Lehr et al [68].

Chen et al [12] and Bertola et al [8] simulated mixtures consisting of  $N + 1$  phases by use of algebraic slip mixture models (ASMMs) which have been combined with a population balance equation. Each bubble size group did have individual local velocities which were calculated from appropriate algebraic slip velocity parameterizations. In order to close the system of equations, the mixture velocity was expressed in terms of the individual phase velocities. The average gas phase velocity was then determined from a volume weighted slip velocity superposed on the continuous phase velocity. Chen et al [12] also did run a few simulations with the ASMM model with the same velocity for all the bubble phases.

In order to improve the accuracy of the flow field simulation, a three-phase model was introduced by Krishna and co-workers [49, 50, 51, 52]. In

the three-phase models, the gas phase is divided into two bubble size groups. The momentum equations are employed for the two bubble groups and the liquid. For the two different bubble size groups, the drag coefficients are different. However, Krishna and co-workers [49, 50, 51, 52] did not include any population balance model to estimate the bubble coalescence and breakage phenomena, hence the size of the small and large bubbles was constant. Motivated by the work of Krishna et al [51, 52, 72, 50], Lehr et al [68] combined the three-fluid model in CFD 4.2 with the simplified population balance of Millies and Mewes [82] and Lehr and Mewes [67]. In this case the bubble size distribution is bimodal and the solutions of the balance equation for high superficial gas velocities result in two-fractions, one for the fraction with small and the other for the fraction with large bubble diameters. The flow field accuracy in cylindrical columns is considered better with a three phase model than that obtained by a two-fluid model [68]. However, the assumption of equilibrium between the coalescence and break-up processes may not be appropriate in bubble columns because of significant influence of convection.

To remove the two-fluid model limitations entirely a complete multi-fluid model is required. For gas-liquid systems Reyes [98] and Lafi and Reyes [57] presented a detailed derivation of the mass, momentum and energy conservation equations for polydispersed systems following an approach analogous to the Boltzmann's transport equation. They derived a set of fluid particle conservation equations for the distribution of chemically non-reacting, spherical fluid particles dispersed in a continuous medium. Kocamustafaogullari and Ishii [43], following a similar approach, extended the application of the model to a general two-phase flow. An analogous modeling framework for dense gas-solid reactive mixtures in fluidized beds has been developed by Simonin [108] and Lathouwers and Bellan [59, 60, 61, 62, 63].

Based on these generalized theories Shi et al [107] and Frank et al [24] developed a useful alternative to the original MUSIG model by extending the two-fluid model to a multi-fluid model with a finite number of size ( $M$ ) and velocity ( $N$ ) phases. This multi-fluid model is sometimes called the  $N \times M$  MUSIG model. In the extended MUSIG model approach the dispersed phase is divided into  $N$  velocity phases (or groups), where each of the velocity groups is characterized by its own velocity field. Moreover, the overall particle size distribution is represented by dividing the particle diameter range within each of the velocity groups into a number of  $M$  bubble size phases (or classes). The  $N \times M$  MUSIG model was built into CFX-10.

Sha et al [104, 105] developed a similar multi-fluid model for simulating gas-liquid bubbly flows in CFX4.4. However, slightly different distributions of the velocity fields and the particle size classes were allowed in these two codes. To guarantee the conservation of mass the population balance solution method presented by Hagesaether et al [29, 30] was adopted. For the same bubble size distribution and feed rate at the inlet, the simulations were run as two, three, six, and eleven phase flow. The number of the discrete population balance equations was ten for all the simulations.

## 9.1 Three Alternative Population Balance Frameworks

In the following sections three alternative approaches for deriving population balance models are outlined. Two of these population balance forms are formulated in accordance with the conventional continuum mechanical theory. First, a macroscopic balance is formulated directly on the averaging scales in terms of number density functions [92, 74]. A corresponding set of macroscopic source term closures are presented as well. Secondly, a more fundamental microscopic population balance is formulated in terms of number probability densities [95, 96, 35, 94]. The corresponding generalized source term closure formulation is then given without preference to any specific multiphase system. Nevertheless, emphasis is subsequently placed on bubbly flows [38]. A few source term closures for the bubble coalescence and breakage processes are then presented. The kernels given are frequently adopted describing the bubble size- and phase distributions in both two-phase bubble column- and stirred tank reactors. The microscopic balance is subsequently averaged using the familiar time after volume averaging procedure. In this approach the fairly general form of the constitutive relations adopted for the bubble coalescence and breakage phenomena are purely formulated based on physical reasoning and intuitive interpretations of the mechanisms involved. Further links to the discrete particle scale phenomena are usually expressed on the averaging scales extrapolating relationships and concepts from the kinetic theory of gases. The fundamental kinetic theory concept allows for the introduction of external forces determining the interaction between the fluid and the dispersed particles. In the third approach the generic population balance equation is derived by averaging a statistical Boltzmann-type of equation in line with the work of Reyes [98], Lafi and Reyes [57], Carrica et al [11] and Lasheras et al [58].

The fundamental derivation of the population balance equation is considered general and not limited to describe gas-liquid dispersions. However, to employ the general population balance framework to model other particulate systems like solid particles and droplets appropriate kernels are required for the particle growth, agglomeration/aggregation/coalescence and breakage processes. Many droplet and solid particle closures are presented elsewhere (e.g., [96, 122, 25, 117, 75, 76, 46]).

### 9.1.1 The Continuum Mechanical Approach

The formulations of the population balance equation based on the continuum mechanical approach can be split into two categories, the macroscopic- and the microscopic population balance equation formulations. The macroscopic approach consists in describing the evolution in time and space of several groups or classes of the dispersed phase properties. The microscopic approach considers a continuum representation of a particle density function.

In this book the macroscopic population balance equation formulation is presented following the original notation and nomenclature of Luo [73] and Luo and Svendsen [74].

The fundamental and thus more general microscopic population balance equation is formulated from scratch on the continuum scales using generalized versions of the Leibnitz- and Gauss theorems.

### The Macroscopic Population Balance Equation

In this section the macroscopic population balance formulation of Prince and Blanch [92], Luo [73] and Luo and Svendsen [74] is outlined. In the work of Luo [73] no growth terms were considered, the balance equation thus contains a transient term, a convection term and four source terms due to binary bubble coalescence and breakage.

The population equation was expressed as:

$$\frac{\partial n_i}{\partial t} + \nabla \cdot (\mathbf{v}_i n_i) = B_{B,i} - D_{B,i} + B_{C,i} - D_{C,i} \left( \frac{1}{sm^3} \right) \quad (9.1)$$

where  $n_i$  is the number density with units ( $m^{-3}$ ),  $\mathbf{v}_i$  is the mass average velocity vector, and the source terms express the bubble number birth and death rates per unit dispersion volume for bubbles of size  $d_i$  at time  $t$  due to coalescence and breakage, respectively. The source terms are assumed to be functions of bubble size  $d_i$ , bubble number  $n_i$  and time  $t$ .

The birth of bubbles of size  $d_i$  due to coalescence stems from the coalescence between all bubbles of size smaller than  $d_i$ . Hence, the birth rate for bubbles of size  $d_i$ ,  $B_{C,i}$ , can be obtained by summing all coalescence events that form a bubble of size  $d_i$ . This gives:

$$B_C(i) = \sum_{d_j=d_{\min}}^{d_i/2} \Omega_C(d_j : d_i - d_j) \left( \frac{1}{sm^3} \right) \quad (9.2)$$

where  $d_{\min}$  is the minimum bubble size and depends on the minimum eddy size in the system. The source term definition implies that bubbles of size  $d_j$  coalesce with bubbles of size  $(d_i - d_j)$  to form bubbles of size  $d_i$ . The upper limit of the sum stems from symmetry considerations or to avoid counting the coalescence between the same pair of bubble sizes twice.

Similarly, the death of bubbles of size  $d_i$  due to coalescence stems from coalescence between two bubbles in class  $d_i$  or between one bubble in class  $d_i$  and other bubbles. Hence, the bubble death rate for bubbles of size  $d_i$ ,  $D_C$ , can be calculated by:

$$D_C(i) = \sum_{d_j=d_{\min}}^{d_{\max}-d_i} \Omega_C(d_j : d_i) \left( \frac{1}{sm^3} \right) \quad (9.3)$$

where  $d_{\max}$  is the maximum bubble size in the system. The upper limit indicates that the bubble size formed by coalescence will not exceed  $d_{\max}$ .

The birth of bubbles of size  $d_i$  due to breakage stems from the breakage of all bubbles larger than  $d_i$ . The breakage birth rate,  $B_B$ , can be obtained by summing all the breakage events that form the bubbles of size  $d_i$ :

$$B_B(i) = \sum_{d_j=d_i}^{d_{\max}} \Omega_B(d_j : d_i) \left( \frac{1}{sm^3} \right) \quad (9.4)$$

The death of bubbles of size  $d_i$  due to breakage stems from breakage of the bubbles within this class, thus:

$$D_B(i) = \Omega_B(d_i) \left( \frac{1}{sm^3} \right) \quad (9.5)$$

The local gas volume fraction can be calculated by:

$$\alpha_g = \sum_{i=1}^N n_i \frac{\pi}{6} d_i^3 \quad (-) \quad (9.6)$$

Hagesæther et al [28, 29, 30] extended the model by Luo and Svendsen [74], but the resulting breakage model was still not completely conservative. To ensure number and mass conservation they thus adopted a numerical procedure redistributing the bubbles on pivot points in accordance with the discrete solution method [94].

### Macroscopic Source Term Closures

In accordance with the work of Coualoglou and Tavlarides [16] and Prince and Blanch [92], Luo [73] assumed that all the macroscopic source terms determining the death and birth rates could be defined as the product of a collision density and a probability. Thus modeling of bubble coalescence means modeling of a bubble-bubble collision density and a coalescence probability, whereas modeling of bubble breakage means modeling of an eddy-bubble collision density and a breakage probability.

Models for the collision densities were derived assuming that the mechanisms of the bubble-bubble and eddy-bubble collisions are analogous to collisions between molecules as in the kinetic theory of gases [16].

### Models for the Binary Bubble Coalescence Rate Sink, $\Omega_C(d_i : d_j)$

For the coalescence between bubbles of class,  $d_i$ , and bubbles of class,  $d_j$ , the binary coalescence rate sink is expressed as:

$$\Omega_C(d_i : d_j) = \omega_C(d_i : d_j) p_C(d_i : d_j) \left( \frac{1}{sm^3} \right) \quad (9.7)$$

### Models for the Bubble-Bubble Collision Density, $\omega_C(d_i : d_j)$

Although not necessary valid for bubble columns, the dispersions are considered sufficiently dilute so that only binary collisions need to be considered. A collision of two bubbles can occur when the bubbles are brought together by the surrounding liquid flow or by body forces like gravity. At least three sources of relative motion can be distinguished; motion induced by turbulence in the continuous phase, motion induced by mean velocity gradients, and buoyancy (or, more generally, body forces)- induced motion, arising from different bubble slip velocities, wake interactions or helical/zigzag trajectories [39]. However, most studies on bubble columns has been restricted considering only models for the contribution of turbulence to coalescence, the contributions from mean-velocity gradients and body forces are generally neglected without proper validation. The two last mentioned collision mechanisms are generally both significant, which greatly complicates the construction and validation of coalescence models.

The parameterization of the particle collision densities was obviously performed employing elementary concepts from the kinetic theory of gases, thus the derivation of the source term closures at the microscopic level have been followed by some kind of averaging and numerical discretization by a discrete numerical scheme [16, 92, 118].

Adopting elementary concepts from kinetic theory to derive a simple expression for the particle collision density one may consider a particle as it travels in a straight path from one collision to the next in a mono-disperse dispersion, as illustrated in Fig 9.1. Its speed and direction of motion changes with each collision. Further imagine that at a given instant all particles, but the one in question are frozen in position and this particle moves with an average speed,  $|\mathbf{v}_P|$ . At the instant of collision, the center to center distance of the two particles is  $d$ . Considering the relatively large bubbles in industrial bubble columns the total collision cross section of the target area of the spherical fluid particle<sup>1</sup> is  $\sigma_{AT} = \pi d^2$ . In time  $\Delta t$  the moving particle sweeps out a cylindrical volume of length  $|\mathbf{v}_P|\Delta t$  and cross section  $\pi d^2$ . Any particle whose center is in this cylinder will be struck by the moving particle. The number of collisions in the time  $\Delta t$  is  $f^{(1)}\pi d^2|\mathbf{v}_P|\Delta t$ , where  $f^{(1)}$  is assumed to be locally uniformly distributed in space.

---

<sup>1</sup> Smoluchowski [111], Williams and Loyalka [122], Friedlander [25] and Kolev [46] (p 170), among others, considered very small particles and interpreted the cross sectional area in a slightly different way representing an extrapolation of the concepts in kinetic theory of gases. In these analyzes the traveling particle is treated as a point in space without cross sectional area, thus the effective area becomes equal to the cross sectional area of the stagnant particle. This alternative cross sectional area approximation becomes:  $\sigma'_{AT} = \frac{1}{4}\pi d^2$ .

The effective swept volume rate<sup>2</sup>  $h_C(d)$  is given by:

$$h_C(d) = \sigma_{A_T} \mathbf{v}_p = \pi d^2 \mathbf{v}_p \quad \left( \frac{m^3}{s} \right) \quad (9.8)$$

where  $\sigma_{A_T} = \pi d^2$  is the total cross-sectional area of the collision tube.

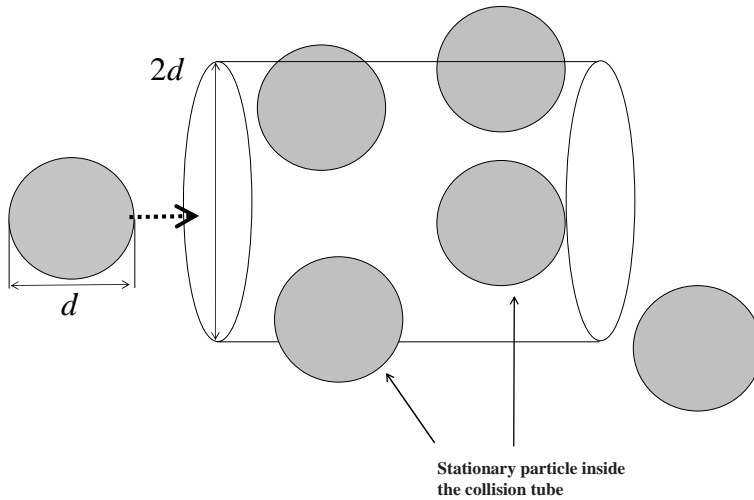


**Fig. 9.1.** A sketch of a collision tube of an entering bubble moving through the tube with speed  $|\mathbf{v}_p|$ . The bubbles within the tube are assumed to be frozen or stationary. Reprinted with permission from [38]. Copyright 2005 American Chemical Society.

In kinetic theory the collision density of a single particle is defined as the number of collisions per unit time and length (diameter):

$$\omega_f(d) = f^{(1)}(d)h_C(d) = f^{(1)}(d, t)\pi d^2|\mathbf{v}_p| \quad \left( \frac{1}{s[m]} \right) \quad (9.9)$$

This relation represents a rough collision density model for a dispersion containing only one type of particles.

Sometimes the collision density representing the number of collisions per unit mixture volume and per unit time and length<sup>2</sup> (diameter<sup>2</sup>) is a more convenient quantity. Multiplying the collision density of a single particle with the particle number density the modified collision density yields:

<sup>2</sup> The collision tube concept is familiar from the kinetic theory of gases. Consider a particle in such a tube, moving with a relative speed with respect to the other particles which are fixed. The particle in the tube sweeps a volume per unit time ( $m^3s^{-1}$ ). Venneker [118] named the rate of volume swept by the particle for the *effective swept volume rate*. Henceforth this name is used referring to this quantity.

$$\omega_{ff}(d) = h_C(d)f^{(1)}f^{(1)} = \frac{1}{2}f^{(1)}f^{(1)}\pi d^2|\mathbf{v}_P| \left( \frac{1}{m^3 s[m][m]} \right) \quad (9.10)$$

The factor  $\frac{1}{2}$  appears due to the fact that  $h(d)$  represents twice the number of collisions.

In accordance with the pioneering work of Smoluchowski [111], similar considerations can be repeated for dispersions containing two types of particles having diameters  $d, d'$  and particle densities  $f^{(1)}, f'^{(1)}$ . The resulting collision density yields:

$$\omega_C(d, d') = h_C(d, d')f^{(1)}f'^{(1)} = f^{(1)}f'^{(1)}\pi\left(\frac{d+d'}{2}\right)^2|\mathbf{v}_{\text{rel},d,d'}| \left( \frac{1}{m^3 s[m][m]} \right) \quad (9.11)$$

where the collision frequency is calculated using the mean collision diameter  $d_{dd'} \equiv (d+d')/2$ . Note that in this case the  $\frac{1}{2}$  factor is not included.

Kolev [46] discussed the validity of these relations for fluid particle collisions considering the obvious discrepancies resulting from the different nature of the fluid particle collisions compared with the random molecular collisions. The basic assumptions in kinetic theory that the molecules are hard spheres and that the collisions are perfectly elastic and obey the classical conservation laws do not hold for real fluid particles because these particles are deformable, elastic and may agglomerate or even coalesce after random collisions. The collision density is thus not really an independent function of the coalescence probability. For bubbly flow Colella et al [15] also found the basic kinetic theory assumption that the particles are interacting only during collision violated, as the bubbles influence each other by means of their wakes.

Prince and Blanch [92] modeled bubble coalescence in bubble columns considering bubble collisions due to turbulence, buoyancy, and laminar shear, and by analysis of the coalescence probability (efficiency) of collisions. It was assumed that the collisions from the various mechanisms are cumulative. The collision density resulting from turbulent motion was expressed as a function of bubble size, concentration and velocity in accordance with the work of Smoluchowski [111]:

$$\omega^T(d, d') \approx f^{(1)}f'^{(1)}\frac{\pi}{4}\left(\frac{d+d'}{2}\right)^2(\bar{v}_{t,d}^2 + \bar{v}_{t,d'}^2)^{1/2} \left( \frac{1}{m^3 s[m][m]} \right) \quad (9.12)$$

where the collision cross-sectional area is defined by:  $\sigma'_{AT} = \frac{\pi}{4}\left(\frac{d+d'}{2}\right)^2$ .

To calculate the collision density an estimate of the length of the relative velocity between a pair of unlike particles, taking into account the distribution of particle velocities, is required. From kinetic theory of gases, we know that  $\bar{v}_{\text{rel},1,2} = (\bar{v}_1^2 + \bar{v}_2^2)^{1/2}$  can be justified by a detailed calculation with the Maxwell distribution function (See Present [91], p 53 and p 79). However, this relation is not generally valid for bubble, drops and particles. The approximation:

$$|\bar{\mathbf{v}}_{\text{rel},t,d,d'}| \approx (\bar{v}_{t,d}^2 + \bar{v}_{t,d'}^2)^{1/2} \quad (9.13)$$

is questionable.

Estimates of the turbulent fluid particle velocities have been obtained using certain relations developed in the classical theory on isotropic turbulence due to Kolmogorov [47]. It is noted that the derivation of the population balance kernel closures are only approximate as the application of the classical turbulence relations, which were developed for continuous fluid velocity fluctuations or vortices, to describe discrete fluid particle flows are not always in accordance with the classical turbulence theory restrictions. The theory of Kolmogorov [47] states that within the inertial subrange of turbulence, where the distance  $\lambda$  between two points in the flow field is much smaller than the turbulence integral-scale  $L$  but much larger than the Kolmogorov micro-scale  $\eta$ , the second order velocity structure function is only a function of the turbulent energy dissipation rate  $\varepsilon$  and the distance  $\lambda$ ,

$$\overline{\delta v^2(\lambda)} = \overline{[v_z(z + \lambda) - v_z(z)]^2} = C(\varepsilon\lambda)^{2/3}. \quad (9.14)$$

This turbulence quantity is defined as the covariance of the difference in velocity between two points in physical space. The two-point velocity structure function should not be confused with the normal component of the Reynolds stresses, which is a one-point, one time, covariance of the velocity.

To estimate the average turbulent fluid particle velocity, the second-order structure function (9.14) is interpreted as an absolute particle velocity squared and defined for two points in the fluid separated by a distance equal to the bubble diameter  $d$ . The structure function is then given as  $\overline{\delta v^2(d)} = \overline{[v_z(z + d) - v_z(z)]^2}$ . If the magnitude of the diameter  $d$  lies within the inertial subrange of turbulence, the structure function can be calculated as  $\overline{\delta v^2(d)} = C(\varepsilon d)^{2/3}$ . The discrete absolute mean velocity of bubbles with diameter  $d_i$  is thus approximated as:

$$\bar{v}_{i,d_i}^2 \approx \overline{\delta v^2(d_i)} = C(\varepsilon d_i)^{2/3} \quad (9.15)$$

where  $C \approx \frac{27}{55} \Gamma(\frac{1}{3}) C_k \approx \frac{27}{55} \times 2.6789 \times 1.5 \approx 1.973$ . This relationship between the constant  $C$  and the Kolmogorov constant  $C_k$  (i.e., the parameter in the energy spectrum function for the inertial subrange) has been deduced from the power-law spectrum and the second-order structure function [89] (chap 6 and app G).

In this model approximation it is assumed that the eddy motion on the size of the bubble is primarily responsible for the relative motion between bubbles. Very small eddies do not contain sufficient energy to significantly affect the bubble motion, while eddies much larger than the bubbles transport groups of bubbles by fluid advection without leading to significant relative motion. Moreover, to make the problem feasible it is customary to assume that the turbulence is isotropic and that the bubble size lies in the inertial subrange of turbulence. However, the validity of using the Kolmogorov hypotheses describing bubbly flows is strictly not verified yet. The relationships from classical turbulence theory have simply been interpreted and extrapolated in a convenient manner. The Kolmogorov velocity second-order structure

function  $\overline{\delta v^2(d)}$  might for example appear as an estimate for an absolute turbulent bubble velocity in the inertial subrange of isotropic turbulence [92], in other cases the same structure function might be considered a relative bubble velocity in turbulent flow, or even employed as a measure of intra-bubble oscillations.

The collision density relation proposed by Prince and Blanch [92] for use in the framework of a discrete solution method was deduced from (9.12) and given as<sup>3</sup>,

$$\begin{aligned}\omega_C^T(d_i : d_j) &\approx n_i n_j \frac{\pi}{4} \left( \frac{d_i + d_j}{2} \right)^2 (\bar{v}_{i,d_i}^2 + \bar{v}_{i,d_j}^2)^{1/2} \\ &\approx 0.088 \pi n_i n_j (d_i + d_j)^2 \varepsilon^{1/3} (d_i^{2/3} + d_j^{2/3})^{1/2} \left( \frac{1}{sm^3} \right)\end{aligned}\quad (9.16)$$

The collision density formula was written in a discrete form consistent with the numerical scheme adopted. The number densities of the bubbles were thus defined as the number of bubbles per unit mixture volume and not as a probability density in accordance with the kinetic theory concept.

The buoyancy collision density  $\omega_C^B(d_i : d_j)$  has been expressed by (e.g., [73, 92], [122], p 164):

$$\omega_C^B(d_i : d_j) \approx n_i n_j \frac{\pi}{4} \left( \frac{d_i + d_j}{2} \right)^2 |\bar{v}_{r,d_i} - \bar{v}_{r,d_j}| \left( \frac{1}{sm^3} \right) \quad (9.17)$$

where  $\bar{v}_{r,d_i}$  is the rise velocity of the particle.

The functional form of the collision rate due to laminar shear is expressed by (e.g., [25], p 200; [122], p 170):

$$\omega_C^{LS}(d_i : d_j) \approx n_i n_j \frac{4}{3} \left( \frac{d_i + d_j}{2} \right)^3 \left( \frac{\overline{dv_c}}{dr} \right) \left( \frac{1}{sm^3} \right) \quad (9.18)$$

where  $\bar{v}_c$  is the continuous phase circulation velocity. The term  $\left( \frac{\overline{dv_c}}{dr} \right)$  is the average shear rate.

The net coalescence frequency of bubbles of diameter  $d_i$  and  $d_j$  was then calculated superposing the different bubble collisions mechanisms as a linear sum of contributions multiplied by a common efficiency [92]:

$$\Omega_C(d_i : d_j) = \left[ \omega_C^T(d_i : d_j) + \omega_C^B(d_i : d_j) + \omega_C^{LS}(d_i : d_j) \right] p_C(d_i : d_j) \left( \frac{1}{sm^3} \right) \quad (9.19)$$

Hagesæther et al [29, 30] adopted this approach modeling bubble column dispersions and found that with the choice of parameter values used in their

<sup>3</sup> Note that the parameter value used by Luo [73] is a factor of 4 larger than the one in (9.16). The reason for this deviation is that Luo used a different definition of the effective total cross-sectional area  $\sigma_{AT}$ .

analysis, the turbulent contribution dominated the collision rate for the bubbles in the system. However, the most important model parameter being the turbulent energy dissipation rate is difficult to compute and only crude estimates were obtained. To achieve approximate estimates for the macroscopic coalescence and breakage rates in bubble columns the macroscopic kernel values were calculated adopting a fixed global average value for the energy dissipation rate. The magnitude of the turbulent energy dissipation rate has been estimated by semi-empirical analysis of the kinetic energy transport in the column. Shah et al [106], for example, postulated that the global energy dissipation rate per unit mass in bubble columns can be calculated from the pressure drop experienced by the gas flow rate. This relationship was derived from a macroscopic mechanical energy balance assuming that the global work done by the pressure of surroundings on the bubble volume element moving with a constant and uniform gas velocity is balanced by the global energy dissipation rate term. The global energy dissipation function was then approximated by:

$$\mu\Phi_{\text{eff}}V \approx (v_G p|_{\text{out}} - v_G p|_{\text{in}})A \approx v_G A \Delta p|_{\text{global}} \approx v_G \rho_L g \alpha_L H_{GL} A \quad (J/s) \quad (9.20)$$

where  $H_{GL}$  is the suspension height,  $A$  the column cross section area,  $V = H_{GL}A$  the suspension volume, and  $\Delta p|_{\text{global}}$  the global pressure drop. The global specific energy dissipation rate is then obtained by dividing the dissipation function by the liquid mass:

$$\langle \varepsilon_G \rangle_{\text{global}} \approx \frac{\mu\Phi_{\text{eff}}V}{m_L} \approx \frac{v_G \rho_L g \alpha_L H_{GL} A}{\rho_L \alpha_L H_{GL} A} = v_G g \quad (J/kg \text{ s}) \quad (9.21)$$

Similar estimates of the turbulent energy dissipation rate per unit mass has been used by others as well [73, 68]. Nevertheless, the value of the energy dissipation rate has not been validated experimentally yet. For agitated vessels an analogous relation for the turbulent energy dissipation rate per unit mass has been reported by Prince and Blanch [92].

Hagesæther et al [29, 30] did not make any firm conclusion on the relative importance of the various collision density contributions, as the turbulent bubble velocity closures used by them are at best inaccurate.

In addition, as distinct from the approach of Prince and Blanch [92], Kolev [46] (p 174) argued that the frequency of coalescence of bubbles should rather be determined having individual efficiencies:

$$\begin{aligned} \Omega_C(d_i : d_j) = & \omega_C^T(d_i : d_j) p_C^T(d_i : d_j) + \omega_C^B(d_i : d_j) p_C^B(d_i : d_j) \\ & + \omega_C^{LS}(d_i : d_j) p_C^{LS}(d_i : d_j), \quad \left( \frac{1}{sm^3} \right) \end{aligned} \quad (9.22)$$

Kolev [46] (p 173) further assumed that for the coalescence processes induced by buoyancy and non-uniform velocity fields the forces leading to collisions inevitably act towards coalescence for contracting particle free path length.

Therefore, the probabilities must have the following values  $0 \leq p_C^T(d_i : d_j) \leq 1$  and  $p_C^B(d_i : d_j) = p_C^{LS}(d_i : d_j) \approx 1$ .

### Models for the Probability of Coalescence, $p_C(d_i : d_j)$

The expression for coalescence probability (sometimes named efficiency) of binary fluid particle collisions in dispersions is normally related to the physical phenomena that are considered to determine the overall coalescence process. The coalescence process in stagnant fluids is generally assumed to occur in three consecutive stages, as sketched in Fig 9.2. First, bubbles collide, trapping a small amount of liquid between them under the action of the continuous phase. Second, this liquid drains over a period of time from an initial thickness until the liquid film separating the bubbles reaches a critical thickness, under the action of the film hydrodynamics. The hydrodynamics of the film depends on whether the film surface is mobile or immobile, and the mobility, in turn, depends on whether the continuous phase is pure or a solution. Third, at this point, film rupture occurs due to film instability resulting in instantaneous coalescence.

The duration of the actual particle-particle interactions taking place in real flow situations in process vessels is however limited and may vary considerably in time and space. The net force which compresses the fluid particle must thus act for a sufficient time to ensure that the intervening film drains to the critical thickness so that film rupture and coalescence take place. In an early view it was postulated that for these processes to occur, the actual particle-particle collision (contact) time interval  $\Delta t_{\text{col}}$  must exceed the coalescence time interval  $\Delta t_{\text{coal}}$  of the coalescence processes,  $\Delta t_{\text{col}} > \Delta t_{\text{coal}}$ . The probability of coalescence was thus generally defined as a function of the ratio

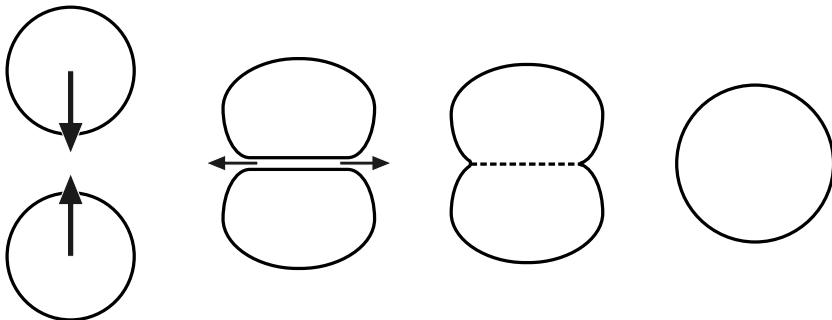


**Fig. 9.2.** A sketch of the three consecutive stages of the binary coalescence process. Two bubbles are approaching each other. The bubble surfaces deform and a thin liquid film is created between them. The liquid drains thinning the film, and hydrodynamic instabilities cause film rupture. The final result of binary bubble coalescence is a new larger bubble.

of the collision time interval  $\Delta t_{\text{col}}$  and the coalescence time interval,  $\Delta t_{\text{coal}}$  (e.g., [46], p 248):

$$p_C \propto f(\Delta t_{\text{col}}/\Delta t_{\text{coal}}) \quad (-) \quad (9.23)$$

The coalescence efficiency thus represents the fraction of particles that coalesce out of the total number of particles that have been colliding.

The functional relationship given by Ross and Curl [101] is often used modeling the fluid particle coalescence probability:

$$p_C \approx \exp(-\Delta t_{\text{coal}}/\Delta t_{\text{col}}) \quad (-) \quad (9.24)$$

The probability of oscillatory fluid particle coalescence which is induced by turbulent fluctuations, is generally expected to be determined by physical mechanisms on various scales. Coualaloglou and Tavlarides [16], Luo [73], Luo and Svendsen [74], Hagesæther et al [28, 29, 30], among others, adopted the same functional relationship as presented above describing these processes, basically because no extended models were available. However, modified relations for estimating the collision and coalescence time intervals were derived for these problems.

The coalescence time is usually estimated to be the time required for film drainage between the fluid particles. In most cases the complexity of the film draining phenomena involved is a severe problem for the modelers and may be best illustrated discussing briefly an early modeling attempt. Oolman and Blanch [85] derived an expression for the coalescence times in stagnant fluids by examining the time required for the liquid film between bubbles to thin from an initial thickness to a critical value where rupture occurs. The original model considers the flow rate of fluid from the liquid film by capillary pressure, augmented by the Hamaker contribution (reflecting the mutual attraction of fluid molecules on opposite sides of the liquid film) at very low film thicknesses, bubble deformation, and the changes in the concentration of surfactant species.

The liquid film drainage model was given by [85]:

$$-\frac{dh}{dt} = \left\{ \frac{8}{R_d^2 \rho_c} \left[ \frac{-4c}{RT} \left( \frac{d\sigma_I}{dc} \right)^2 + h^2 \left( \frac{2\sigma_I}{r_b} + \frac{A}{6\pi h^3} \right) \right] \right\}^{1/2} \quad (m/s) \quad (9.25)$$

where  $h$  is the film thickness ( $m$ ),  $R_d$  is the radius of the liquid disk between the coalescing bubbles ( $m$ ),  $R$  is the gas constant,  $T$  is the temperature ( $K$ ),  $A$  is the Hamaker constant ( $J$ ),  $\sigma_I$  is the surface tension ( $N/m$ ) and  $c$  is the concentration of a surfactant species ( $mol/m^3$ ).

To solve (9.25) sufficient initial conditions are required. In the work of Prince and Blanch [92] a rough estimate of the initial thickness of the films created in air-water systems was given to be  $h_0 = 1 \times 10^{-4}$  ( $m$ ). Likewise, the final film thickness was taken as  $h_f = 1 \times 10^{-8}$  ( $m$ ).

Prince and Blanch [92] thus obtained an estimate of the coalescence time for binary bubble collisions in bubble columns solving a simplified form of

(9.25). They considered that in practice several of the effects included in (9.25) are very cumbersome to determine and no analytical solution of the resulting equation is available. Several simplifying assumptions were therefore employed (e.g., no Hamaker contributions, no surface impurities, simplified interface geometry, etc.) making an analytical solution possible. A typical coalescence time  $\Delta t_{coal,ij}$  was found by integration,

$$\Delta t_{coal,ij} = \left( \frac{r_{ij}^3 \rho_c}{16\sigma_I} \right)^{1/2} \ln \left( \frac{h_0}{h_f} \right) \quad (s) \quad (9.26)$$

where  $r_{ij} = (r_{b,i}^{-1} + r_{b,j}^{-1})^{-1}/2$  denotes the equivalent bubble radius.

For dispersed flows Chesters [14] derived an extended estimate for the coalescence time  $\Delta t_{coal}$  considering drainage between deformable and fully mobile interfaces. This model is assumed to be valid for systems where the viscosity of the dispersed phase is sufficiently small so that the film drainage is controlled by the resistance induced by the film to deformation and acceleration. When the film drainage is further caused by inertia forces like turbulence stresses, the parallel film model reduces to  $h = h_0 \exp(-t/\Delta t_{coal})$ . In this formula  $\Delta t_{coal} = \rho_c \bar{v}_{rel} r^2 / 8\sigma_I$ . Assuming that the relations governing film drainage between unequal particles are the same as those between equal particles of equivalent radius [14], the given coalescence time relation has been used both for unequal and equal sized fluid particle collisions. Therefore, although many bubble collisions encountered in practice involve partial-fully mobile interfaces, Luo [73] approximated the coalescence time for equal and unequal bubbles in bubble column flows by:

$$\Delta t_{coal,ij} \approx 0.5 \frac{\rho_c \bar{v}_{rel,t,ij} d_i^2}{(1 + \xi_{ij})^2 \sigma_I} \quad (9.27)$$

The length of the relative velocity between a pair of unlike bubbles is approximated by a mean velocity representative for bubbles with size corresponding to the inertial subrange of isotropic turbulence (9.13):

$$\bar{v}_{rel,t,ij} = (\bar{v}_{t,i}^2 + \bar{v}_{t,j}^2)^{1/2} = \bar{v}_{t,i} (1 + \xi_{ij}^{-2/3})^{1/2}, \quad (9.28)$$

where  $\bar{v}_{t,i}$  is the discrete mean velocity of bubbles with diameter  $d_i$  was calculated from (9.15).

In a turbulent flow field the collision time  $\Delta t_{col}$  can be estimated by the time two bubbles of size  $d$  and  $d'$  will stay together before the turbulent fluctuations separate the bubbles again. Assuming that the collision time is proportional to the characteristic life time of an eddy with size in the inertial subrange of turbulence, Levich [69] determined the average collision time  $\Delta t_{col}$  between fluid particles in turbulent flow from dimensional analysis. In the inertial range of turbulence the energy dissipation rate might be approximated by  $\varepsilon \sim v^3/l_e$ . The characteristic life time of eddies with a given size  $l_e$  about the size of the mean collision diameter of the bubbles  $l_e \approx (d + d')/2$  is then  $\tau_l \sim l_e/v \sim l_e^{2/3} \varepsilon^{-1/3}$ . The average contact time was thus approximated as:

$$\Delta t_{\text{col}} \approx (d + d')^{2/3} \varepsilon^{-1/3}. \quad (9.29)$$

The accuracy reflected by the contact time relation obtained solely from dimensional considerations is generally not considered sufficient given the sensitivity of the coalescence probability to small changes in the approximate contact time. Moreover, little or no experimental data is available for model validation.

For bubble column flow Luo [73] intended to derive a more reliable collision time relation valid both for two unequal and equal sized fluid particles by investigating the fluid particle approach process by use of a simplified kinetic energy balance. Based on a simple parallel film model which disregards all external forces, an expression for the collision time was obtained:

$$\Delta t_{\text{col}} = 2t_{\text{max}} \approx (1 + \xi_{ij}) \sqrt{\frac{(\rho_d/\rho_c + C_V)}{3(1 + \xi_{ij}^2)(1 + \xi_{ij}^3)} \frac{\rho_c d_i^3}{\sigma_I}} \quad (9.30)$$

where  $\xi_{ij} = d_i/d_j$ ,  $C_V$  is the added mass coefficient, and  $t_{\text{max}}$  is the time between the first contact and the time when the film area between the two colliding bubbles reaches its maximum value.

In order to determine the mean turbulent approach velocity of bubbles causing bubble-bubble collisions, a series of questionable assumptions were made by Luo and Svendsen [74]. First, in accordance with earlier work on fluid particle coalescence the colliding bubbles were assumed to take the velocity of the turbulent fluid eddies having the same size as the bubbles [16, 92]. Luo and Svendsen [74] further assumed that the turbulent eddies in liquid flows may have approximately the same velocity as neutrally buoyant droplets in the same flow. Utilizing the experimental results obtained in an investigation on turbulent motion of neutrally buoyant droplets in stirred tanks reported by Kuboi et al [53, 54], the mean square droplet velocity was expressed by:

$$v_{\text{rms}}^2(d) = \overline{v^2}(d) = \beta(\varepsilon d)^{2/3} \quad (m^2/s^2) \quad (9.31)$$

where the parameter value  $\beta \approx 2.0$  was determined from the experimental data.

The experimental data also indicated that the turbulent velocity component distributions of droplets follow the Maxwellian distribution function, thus the mean droplet velocity was calculated as the mathematical average of the velocity distribution<sup>4</sup>:

$$\bar{v}_{\text{drops}} = \left(\frac{8v_{\text{rms}}^2(d)}{3\pi}\right)^{1/2} = \sqrt{\frac{16}{3\pi}}(\varepsilon d)^{1/3} = \sqrt{1.70}(\varepsilon d)^{1/3} \quad (m/s) \quad (9.32)$$

<sup>4</sup> Luo and Svendsen [74] did not distinguish between the experimentally determined relation (9.31) and the Kolmogorov structure function (9.14). In their work the theoretical parameter value  $C$  was calculated as  $C = (3/5)\Gamma(1/3)C_k \approx (3/5) \times 2.6789 \times 1.5 = 2.41$ . It follows that their mean droplet velocity estimate is  $\bar{v}_{\text{drops}} \approx \left(\frac{8\delta v^2(d)}{3\pi}\right)^{1/2} = \sqrt{8 \times C/(3\pi)}(\varepsilon d)^{1/3} = \sqrt{2.046}(\varepsilon d)^{1/3}$ .

It was further noticed that the value of the coefficient was sensitive to the density ratio between the continuous and dispersed phases,  $(\rho_d/\rho_c)$ . Moreover, in a recent study Brenn et al [9] investigated unsteady bubbly flow with very low void fractions and concluded that the velocity probability density functions of bubbles in liquid are better described using two superimposed Gaussian functions.

Hagesæther et al [27] derived a model for film drainage in turbulent flows and studied its predictive capabilities. It was concluded that the film drainage models are not sufficiently accurate, and that adequate data on bubbly flows are not available for model validation. For droplet flows it was found that the pure drainage process (without interfacial mass transfer fluxes) was predicted with fair accuracy, whereas no reliable coalescence criterion was found (similar conclusions were made by Klaseboer et al [41, 42]). Furthermore, it was concluded that a head on collisions are not representative for all possible impact parameters. Orme [86] and Havelka et al [32], among others, noticed that the impact parameter is of great importance for the droplet-droplet collision outcome in gas flows. However, no collision outcome maps have been published yet for bubble-bubble collisions.

Furthermore, according to the experimental analysis of liquid films formed upon single bubble impact with a free surface as reported by Doubiez [20], it is likely that a thin liquid film formed between two colliding bubbles ruptures after the collision when bubbles are actually already moving apart from each other. Millies and Mewes [82], Hagesæther [31], and Laari and Turunen [56] thus concluded that the film thinning time cannot be used to model the coalescence rate. Furthermore, Stewart [112] investigated experimentally bubble interaction in low-viscosity liquids and observed that the coalescence time is often much smaller than the contact time. Hence, the probabilistic hypotheses normally used for the calculation of the coalescence efficiency are questionable and presumably not valid. However, no complementary theory has been presented yet.

Saboni et al [102, 103] developed drainage models for partially mobile plane-films to describe film drainage and rupture during coalescence in liquid-liquid dispersions taking into account the interfacial-tension gradients generated by interfacial mass transfer. The resulting Marangoni forces were accelerating the film drainage which in general corresponds to dispersed to continuous phase transfer and diminish film drainage in the negative case. Similar effects might be expected to occur for the gas-liquid systems operated in bubble columns, but no detailed experimental analysis on gas-liquid dispersions has been reported yet.

### **Models for the Macroscopic Breakage Rate Source, $\Omega_B(d_i, d_j)$**

During the last decade considerable attention has been put on the macro-scale modeling of bubble breakage in gas-liquid dispersions (e.g., [92, 43, 99,

58, 119]). A brief outline of the important milestones are given in this subsection.

The fluid particle breakage controls the maximum bubble size and can be greatly influenced by the continuous phase hydrodynamics and interfacial interactions. Therefore, a generalized breakage mechanism can be expressed as a balance between external stresses (dominating component),  $\sigma$ , that attempts to disrupt the bubble and the surface stress,  $\sigma_I/d$ , that resists the particle deformation. Thus, at the point of breakage, these forces must balance,  $\sigma \approx \frac{\sigma_I}{d/2}$ . This balance leads to the prediction of a critical Weber number, above which the fluid particle is no longer stable. It is defined by [36]:

$$We_{cr} = \frac{\sigma d_{max}}{2\sigma_I} \quad (9.33)$$

where  $d_{max}$  is the maximum stable fluid particle, and  $\sigma$  reflects the hydrodynamic conditions responsible for particle deformation and eventual breakage.

In the case of turbulent flow, particle breakage is caused by velocity fluctuations resulting in normal stress variations along the particle surface,  $We_{cr} = \rho_c \overline{v_c^2} d_{max} / 2\sigma_I$ . In laminar flow, viscous shear in the continuous phase will elongate the particle and cause breakage,  $We_{cr} = \mu_c (\frac{\partial v_z}{\partial r}) d_{max} / 2\sigma_I$ . In the absence of net flow of the continuous phase such as rising bubbles in a liquid, the fluid particle breakage is caused by interfacial instabilities due to Raleigh-Taylor and Kelvin-Helmholtz instabilities [21]. In most bubble column analyzes the flow is considered turbulent and both the viscous – and interfacial instability effects are neglected basically without any further validation.

The fluid particle fragmentation phenomena in a highly turbulent flow are related to the fact that the velocity in a turbulent stream varies from one point to another (i.e., validated by two-point measurements [99]). Therefore, different dynamic normal stresses will be exerted at different points on the surface of the fluid particle. Under certain conditions, this will inevitably lead to deformation and breakage of the fluid particle.

According to Kocamustafaogullari and Ishii [43], the force due to the dynamic pressure may develop either through the local relative velocity around the particle, which appears because of inertial effects, or through the changes in eddy velocities over the length of the particle.

Most of the published literature on bubble breakage is derived from the theories of Kolmogorov [48] and Hinze [36]. In one phenomenological interpretation bubble breakage occurs through bubble interactions with turbulent eddies bombarding the bubble surface. If the energy of the incoming eddy is sufficiently high to overcome the surface energy, deformation of the surface results, which can finally lead to the formation of two or more daughter bubbles. For the bubble breakage to occur, the size of the bombarding eddies have to be smaller than or equal to the bubble size, since larger eddies only transport the bubble. In order to model the breakup process, the following simplifications are generally made [74]:

1. The turbulence is isotropic,
2. Only binary breakage of a bubble is considered,
3. The breakage volume ratio is a stochastic variable,
4. The occurrence of breakage is determined by the energy level of the arriving eddy,
5. Only eddies of a size smaller than or equal to the bubble diameter can cause bubble breakage.

The fundament of the macroscopic theories is the engineering interpretation considering the velocity fluctuations as imaginary discrete entities denoted fluid slabs or eddies. Following this concept a large number of eddies exist in the flow having a size (diameter) distribution ranging from the Kolmogorov micro scale up to the vessel dimensions.

The basic ideas for the model development of Luo and Svendsen [74] was adopted from an earlier paper by Coualoglou and Travlarides [16] considering droplet breakage in turbulent flows. In the model of Coualoglou and Travlarides [16] the breakage density was expressed as a product of an integral or average breakage frequency ( $\propto 1/t_b$ ) and an integral (average) breakage efficiency determining the fraction of particles breaking. The breakage time ( $t_b$ ) was determined from isotropic turbulence theory and the breakage efficiency was determined from a probable fraction of turbulent eddies colliding with the droplets that have kinetic energy greater than the droplet surface energy.

Prince and Blanch [92] further postulated that bubble breakage is a result of collisions between particles and turbulent eddies, and that the collision rate can be calculated following arguments from the kinetic theory of gases. A total breakage rate  $\Omega_B(d_i)$  for particles of size  $d_i$ , with units ( $1/sm^3$ ), was thus expressed as a product of an eddy-bubble collision rate  $\omega_B(d_i : \lambda_j)$  and a breakage probability (efficiency)  $p_B(d_i : \lambda_j)$ , thus  $\Omega_B(d_i) = \sum_{\lambda} \omega_B(d_i : \lambda_j) p_B(d_i : \lambda_j)$ . This breakage rate model thus depends on a predefined daughter particle size distribution.

Luo and Svendsen [74] modified the eddy-particle collision concept using an eddy number density (instead of an eddy number concentration) and argued that for a bubble to be fragmented each of the colliding eddies must have sufficient turbulent kinetic energy to overcome the increase in bubble surface energy, as illustrated in Fig 9.3. This is the so-called surface energy criterion for fluid particle breakage. Unlike the previous breakage models, the model by Luo and Svendsen [74] predicts the *partial breakage rate* for particles of size  $d_i$  breaking into the particular daughter particle sizes. In this way this breakage model does not require a predefined daughter particle size distribution function.

Luo and Svendsen [74] also used a second criterion stating that the size of the colliding eddies must be of the same order of magnitude as the bubble diameter or less. It was assumed that larger eddies will give the fluid particle a translational velocity solely, whereas eddies of scales comparable to the fluid particle can cause breakage.

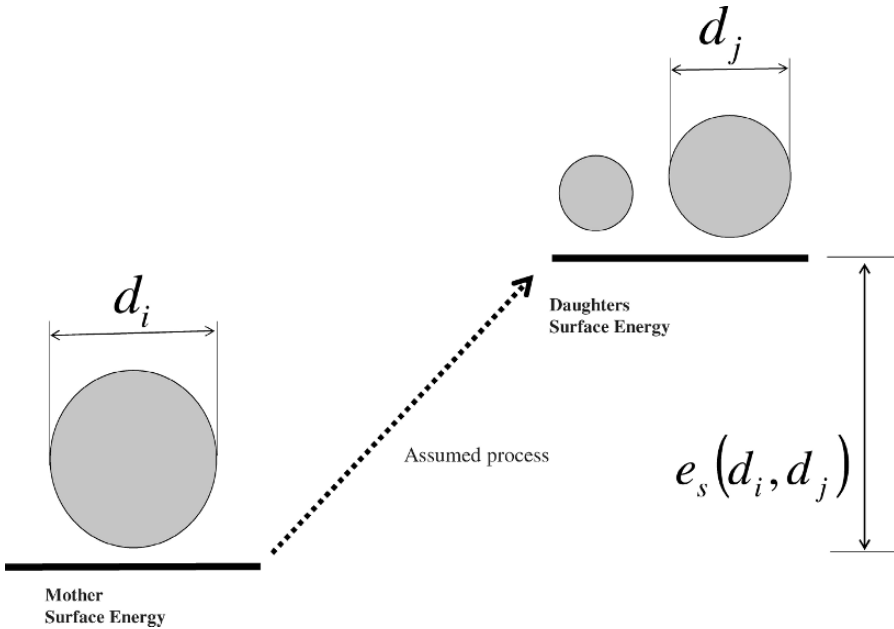


**Fig. 9.3.** A sketch of the bubble breakage surface energy balance. The mean kinetic energy of an eddy of size  $\lambda$  breaking a bubble of size  $d_i$ ,  $\bar{e}(d_i, \lambda)$ , is assumed to be larger than the increase of the bubble surface energy required breaking the parent bubble  $d_i$  into a daughter bubble  $d_j$  and a second corresponding daughter bubble,  $e_s(d_i, d_j)$ . Reprinted with permission from [38]. Copyright 2005 American Chemical Society.

A differential breakage density was then defined as a product of an eddy-bubble collision probability density  $\omega_{B,\lambda}^T(d_i, \lambda)$  and a breakage efficiency  $p_B(d_i : d_j, \lambda)$ , which both depended on the eddy size ( $\lambda$ ). The total breakage rate source for a bubble of size  $d_i$  yields:

$$\Omega_B(d_i) = \sum_{d_j=d_{\min}}^{d_{\max}} \Omega_B(d_i : d_j) \left( \frac{1}{sm^3} \right) \tag{9.34}$$

The individual rate breaking a parent bubble of size  $d_i$  into the daughter size classes  $d_j$  is expressed as:

$$\Omega_B(d_i : d_j) = \int_{\lambda_{\min}}^d \omega_B^T(d_i, \lambda) p_B(d_i : d_j, \lambda) d\lambda \left( \frac{1}{sm^3} \right) \tag{9.35}$$

The eddy-bubble collision probability density  $\omega_B^T(d_i, \lambda)$  has units  $(1/sm^3[m])$ . The upper integration limit for the eddy size is based on the model assumption

that only eddies of size smaller than or equal to the bubble diameter can cause bubble breakage. A bubble being dispersed in a large scale fluid eddy (larger than the bubble scale,  $d$ ) is assumed to be advected together with the eddies in the fluid. Unfortunately, the breakage frequency is found to be significantly sensitive to the choice of integration limits [29, 30, 58]. Note that no explicit breakage frequency was given.

Luo and Svendsen [74] considered the collision of eddies with a given velocity  $\bar{v}_\lambda$  bombarding a number  $n_i$  of locally frozen bubbles, as illustrated in Fig 9.4. The eddy-bubble collision probability density was computed as<sup>5</sup>:

$$\omega_B^T(d_i, \lambda) = n_i f_\lambda h_C(d_i, \lambda) = n_i f_\lambda \frac{\pi}{4} (d_i + \lambda)^2 \bar{v}_\lambda \left( \frac{1}{sm^3[m]} \right) \quad (9.36)$$

where  $f_\lambda$  is the number of eddies of size between  $\lambda$  and  $\lambda + d\lambda$  with units ( $1/m^3s[m]$ ), and  $\bar{v}_\lambda$  is the turbulent velocity of eddies of size  $\lambda$ .

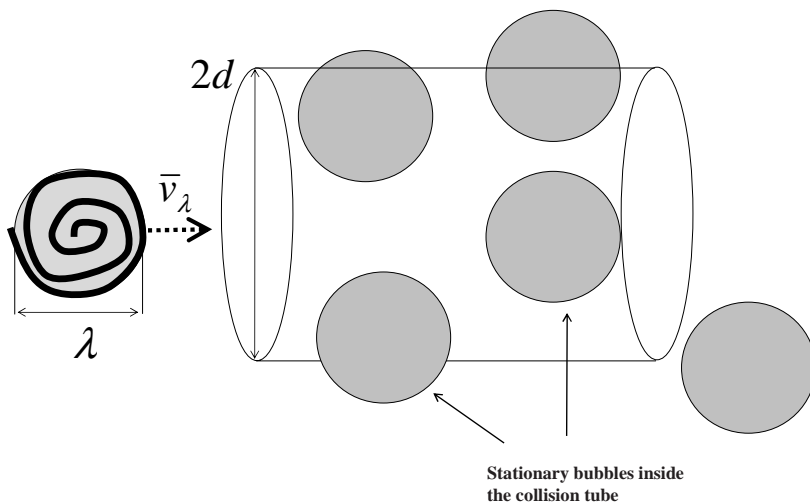


**Fig. 9.4.** A sketch of a collision tube of an entering eddy moving through the tube with a velocity  $\bar{v}_\lambda$ . The bubbles within the tube are assumed to be frozen or stationary. Reprinted with permission from [38]. Copyright 2005 American Chemical Society.

<sup>5</sup> Politano et al [88] adopted the kernel functionality of Luo and Svendsen but modified the definition of the effective collision cross-sectional area,  $\sigma_{AT} = \frac{\pi}{4} \left( \frac{d_i + \lambda}{2} \right)^2$ , in accordance with other work in nuclear engineering (e.g., Kolev [46], p 168).

The mean turbulent velocity of eddies with size  $\lambda$  in the inertial subrange of isotropic turbulence was assumed equal to the velocity of the neutrally buoyant droplets measured by Kuboi et al [53, 54]. Kuboi et al [53, 54] found that the turbulent velocity of droplets could be expressed by the Maxwell distribution function (9.32), thus the mean eddy velocity was approximated by:

$$\bar{v}_\lambda \approx \left(\frac{8\beta}{3\pi}\right)^{1/2} (\varepsilon\lambda)^{1/3} = \sqrt{1.70}(\varepsilon\lambda)^{1/3} \quad (m/s) \quad (9.37)$$

The  $\beta$  coefficient value in the droplet rms velocity relation (9.31) obtained by Kuboi et al [53, 54] is accidentally about the same as the  $C \approx \frac{27}{55} \Gamma(\frac{1}{3}) C_k$  value in the Kolmogorov structure function relation (9.14), that is  $\beta \approx C \approx 2.0$ . However, it was commented by Kuboi et al [53, 54] that the comparison of these relations cannot be very decisive, in view of the fact that there is a large difference between the processes and kind of fluid used to obtain these relations. Kuboi et al [53, 54] also investigated the particle-fluid density difference effect producing non-neutrally buoyant particle flows and concluded that the parameter value discussed above is very sensitive to the density ratio. Therefore, the application of the above relation as an approximation for the bubble velocity is highly questionable.

Furthermore, to employ (9.36), the number probability density of eddies of a particular size  $f_\lambda$  must be determined. Luo and Svendsen [74] assumed that the turbulence is isotropic and that the eddy size of interest lies in the inertial subrange. An expression for the number probability density of eddies as a function of wave length for these conditions were formulated adopting conceptual ideas from Azbel [2](p 85) and Azbel and Athanasios [3]. The turbulent energy spectrum function,  $E(k)$ , can be interpreted as the kinetic energy contained within eddies of wave numbers between  $k$  and  $k + dk$ , or equivalently, of size between  $\lambda$  and  $\lambda + d\lambda$ , per unit mass. A relationship between  $f_\lambda$  and  $E(k)$  can thus be obtained formulating an energy balance for eddies being interpreted both as discrete entities and as a wave function:

$$E_{\text{eddies}}(\lambda) = E_{\text{spectra}}(\lambda), \quad \left(\frac{J}{m^3[m]}\right) \quad (9.38)$$

thus

$$f_\lambda \left[ \frac{1}{2} (\rho_L \frac{\pi}{6} \lambda^3) \bar{v}_\lambda^2 \right] = E(k) \rho_L (1 - \alpha_g) \left( -\frac{dk}{d\lambda} \right), \quad \left(\frac{J}{m^3[m]}\right) \quad (9.39)$$

The functional form of the energy spectrum in the inertial subrange of turbulence is defined as (e.g., [89]):

$$E(k) = C_k \varepsilon^{2/3} k^{-5/3}, \quad \left(\frac{m^2}{s^2} [m]\right) \quad (9.40)$$

where  $C_k \approx 1.5$ .

To enable computation of the number density of eddies we need to eliminate the wave number  $k$  from the energy balance. The necessary relationship between the wave number and the size of the eddy (wave length) is given by  $k = 2\pi/\lambda$ , hence  $\frac{dk}{d\lambda} = -2\pi\lambda^{-2}$ . To be consistent with the previous assumptions the eddy velocity must be estimated from the experimental relation (9.37). The number density of eddies  $f_\lambda$  is thus defined by<sup>6</sup>:

$$f_\lambda = (1 - \alpha_g) \frac{24C_k}{\beta(2\pi)^{5/3}} \frac{1}{\lambda^4} = \frac{0.841(1 - \alpha_g)}{\lambda^4} \left( \frac{1}{m^3[m]} \right), \quad (9.41)$$

where  $\alpha_g$  is the volume fraction of dispersed phase.

The determination of the structure function parameter value  $C$  may represent a severe problem as several authors report very different estimates. For example, Luo [73] used  $C = \frac{3}{5}\Gamma(1/3)C_k = 2.41$ , Batchelor [7](p 123) defined  $C = \frac{9}{5}\Gamma(1/3)C_k = 7.23$ , Pope [89] (p 232) obtained another value  $C \approx 1.973$ , Martínez-Bazán et al [78] referred to Batchelor [6] and claimed that  $C \approx 8.2$ , Risso and Fabre [99] referred to Batchelor [5](p 120) and defined  $C = \frac{27}{55}\Gamma(1/3)C_k = 1,973$  which is the same value as given by Pope [89]. Lasheras et al [58] reviewed several breakage models, and pointed out that the value of this parameter is ranging from about  $C = 8 \times 2.41/(3\pi) = 2.045$  to  $C = 8.2$ .

Substituting the expression for the number density of eddies (9.41) into (9.36), the collision density for the eddies of size between  $\lambda$  and  $d\lambda$  with particles of size  $d_i$  can be expressed as:

$$\omega_B^T(d_i, \lambda) = \frac{\pi}{4}(0.841)\sqrt{1.70}(1 - \alpha_g)n_i(\varepsilon\lambda)^{1/3} \frac{(d_i + \lambda)^2}{\lambda^4} \left( \frac{1}{sm^3[m]} \right) \quad (9.42)$$

In dimensionless variables<sup>7</sup>,

$$\omega_B^T(\xi) = 0.861(1 - \alpha_g)(\varepsilon d_i)^{1/3} n_i \frac{(1 + \xi)^2}{d_i^2 \xi^{11/3}}, \quad (9.43)$$

where  $\xi = \lambda/d_i$ .

<sup>6</sup> Luo and Svendsen [74] did not distinguish between the value of the theoretical parameter  $C$  in the structure function relation (9.14) and the empirical parameter  $\beta = 2.0$  in the droplet rms velocity relation (9.31) when calculating the mean eddy velocity from (9.37). To reproduce the parameter value in the eddy number density relation used by Luo and Svendsen, the value of the  $\beta$  parameter is computed using the structure function relation (9.14) instead of the empirical relation (9.31). That is, they let  $\beta = \frac{8C}{3\pi}$ , and  $C = \frac{3}{5}\Gamma(1/3)C_k \approx \frac{3}{5} \times 2.6789 \times 1.5 = 2.41$ . The parameter in the eddy number density of eddies was thus approximated as:  $\frac{9C_k}{C^{25/3}\pi^{2/3}} = 0.822$ .

<sup>7</sup> Luo and Svendsen used the parameter values  $C = \frac{3}{5}\Gamma(1/3)C_k = 2.41$ , and  $(8C/3\pi) \approx 2.045$ , hence their parameter value in (9.43) becomes  $\frac{\pi}{4}(0.822)\sqrt{2.045} \approx 0.923$ .

To close the differential breakage density model (9.35) a *breakage probability* (efficiency) is needed. For each particular eddy hitting a particle, the probability for particle breakage was assumed to depend not only on the energy contained in the arriving eddy, but also on the minimum energy required to overcome the surface area increase due to particle fragmentation. The latter quantity was determined by the number and the sizes of the daughter particles formed in the breakage processes. In mathematical terms, the surface energy criterion was written:

$$e(d_i, \lambda) \geq e_s(d_i, d_j) \quad (9.44)$$

where  $e(d_i, \lambda)$  ( $J$ ) denotes the turbulent kinetic energy of an individual eddy of size  $\lambda$  breaking a bubble of size  $d_i$  and  $e_s(d_i, d_j)$  ( $J$ ) represents the increase of bubble surface energy required breaking the parent bubble  $d_i$  into a daughter bubble  $d_j$  and a second complement daughter bubble.

To determine the energy contained in eddies of different scales, a distribution function of the kinetic energy for eddies in turbulent flows is required. A Maxwellian distribution function may be a natural and consistent choice as the eddy velocity is assumed to follow this distribution [66], but Luo and Svendsen [74] preferred an empirical energy-distribution density function for fluid particles in liquid developed by Angelidou et al [1]. The turbulent kinetic energy distribution of eddies with size  $\lambda$  is approximated as follows:

$$p_e \left( e(d_i, \lambda) \right) = \frac{1}{\bar{e}(d_i, \lambda)} \exp \left[ - \frac{e(d_i, \lambda)}{\bar{e}(d_i, \lambda)} \right] \quad (9.45)$$

The probability density for a fluid particle with size  $d_i$  breaking with the larger daughter bubble  $d_j$  when hit by an eddy with size  $\lambda$  was then assumed equal to the probability of the arriving eddy of size  $\lambda$  having a turbulent kinetic energy greater than or equal to the minimum energy required for the particle breakage (9.44).

The conditional breakage probability function used by Luo and Svendsen thus yields<sup>8</sup>:

---

<sup>8</sup> Notice that this efficiency function is not necessary volume or mass conservative as Luo and Svendsen [74] did consider the breakage efficiency function being equal to the kinetic energy distribution function. It would probably be better to consider the breakage distribution function purely proportional to the empirical kinetic energy distribution function, and determine the probability constant by requiring bubble volume or mass conservation within the breakage process.

$$\begin{aligned}
 p_B(d_i : d_j, \lambda) &= \int_{e_s(d_i, d_j)}^{\infty} \frac{1}{\bar{e}(d_i, \lambda)} \exp \left[ -\frac{e(d_i, \lambda)}{\bar{e}(d_i, \lambda)} \right] de' \\
 &= 1 - \int_0^{e_s(d_i, d_j)} \frac{1}{\bar{e}(d_i, \lambda)} \exp \left[ -\frac{e(d_i, \lambda)}{\bar{e}(d_i, \lambda)} \right] de' \\
 &= 1 - \int_0^{\chi_c} \exp(-\chi) d\chi' = \exp(-\chi_c)
 \end{aligned} \tag{9.46}$$

where  $\chi = \frac{e(d_i, \lambda)}{\bar{e}(d_i, \lambda)}$  is a dimensionless energy ratio. In this ratio  $\bar{e}(d_i, \lambda)$  is the mean turbulent kinetic energy for eddies of size  $\lambda$  and  $e(d_i, \lambda)$  is the kinetic energy for an individual eddy of size  $\lambda$ , respectively.

In accordance with (9.44) the critical energy ratio for particle breakage to occur, was calculated from:

$$\chi_{cr} = \left( \frac{e(d_i, \lambda)}{\bar{e}(d_i, \lambda)} \right)_{cr} = \frac{e_s(d_i, d_j)}{\bar{e}(d_i, \lambda)} = \frac{3C_f \pi \sigma_I}{2\beta \rho_c \varepsilon^{2/3} d_i^{5/3} \xi^{11/3}}. \tag{9.47}$$

By use of (9.37) the mean kinetic energy of an eddy with size  $\lambda$ , was determined by<sup>9</sup>:

$$\bar{e}(d_i, \lambda) = \rho_c \frac{\pi}{6} \lambda^3 \frac{\bar{v}_\lambda^2}{2} = \rho_c \frac{2\beta}{3} \lambda^{11/3} \varepsilon^{2/3} = \rho_c \frac{2\beta}{3} \xi^{11/3} d_i^{11/3} \varepsilon^{2/3} \tag{9.48}$$

When a fluid particle with diameter  $d_i$  is broken up into a particle of size  $d_j$  and the complement particle of size  $(d_i^3 - d_j^3)^{1/3}$ , the increase in surface energy was given by:

$$\begin{aligned}
 e_s(d_i, d_j) &= \pi \sigma_I [d_j^2 + (d_i^3 - d_j^3)^{1/3} - d_i^2] \\
 &= \pi \sigma_I d_i^2 [f_{V_{ij}}^{2/3} + (1 - f_{V_{ij}})^{2/3} - 1] = C_f (f_{V_{ij}}) \pi \sigma_I d_i^2
 \end{aligned} \tag{9.49}$$

where  $C_f(f_{V_{ij}})$  is defined as the increase coefficient of surface area which depends only on the breakage volume fraction,  $f_{V_{ij}} = d_j^3/d_i^3$ . The  $e_s(d_i, d_j)$  function is symmetrical about the breakage volume fraction,  $f_{V_{ij}} = 0.5$ .

Combining (9.43), (9.46) and (9.35), the breakage density of one particle of size  $d_i$  that breaks into particles of sizes  $d_j$  and  $(d_i^3 - d_j^3)^{1/3}$  is given by<sup>10</sup>:

<sup>9</sup> Luo [73] employed (9.15) with  $C \approx 2.41$  and obtained  $\bar{e}(d_i, \lambda) = \rho_c \frac{\pi}{6} \lambda^3 \frac{\bar{v}_\lambda^2}{2} = \rho_c \frac{C\pi}{12} \lambda^{11/3} \varepsilon^{2/3} = \rho_c \frac{C\pi}{12} \xi^{11/3} d_i^{11/3} \varepsilon^{2/3}$ . Moreover, with this parameter value and bubble velocity estimate the critical energy ratio becomes  $\chi_{cr} \approx e_s(d_i, d_j)/\bar{e}(d_i, \lambda) = 12C_f \sigma_I / (C\rho_c \varepsilon^{2/3} d_i^{5/3} \xi^{11/3})$ .

<sup>10</sup> Luo and Svendsen [74] employed the parameter value  $(8C/3\pi) \approx 2.045$  instead, hence the parameter in (9.50) becomes 0.923.

$$\begin{aligned} \Omega_B(d_i : d_j) &= \int_{\lambda_{min}}^d \omega_B^T(d_i, \lambda) p_B(d_i : d_j, \lambda) d\lambda \left( \frac{1}{sm^3} \right) \\ &= 0.861(1 - \alpha_g) n_i \left( \frac{\varepsilon}{d_i^2} \right)^{1/3} \int_{\xi_{min}}^1 \frac{(1 + \xi)^2}{\xi^{11/3}} \exp\left(-\frac{3C_f \pi \sigma_I}{2\rho_c \beta \varepsilon^{2/3} d_i^{5/3} \xi^{11/3}}\right) d\xi \end{aligned} \quad (9.50)$$

where  $\xi_{min} = \frac{\lambda_{min}}{d}$ ,  $\frac{\lambda_{min}}{\lambda_d} \approx 11.4 - 31.4$  and  $\eta$  is the Kolmogorov micro-scale.

A severe limitation of the original breakage density closure of Luo and Svendsen [74] is that the model produces too many very small particles whatever numerical size resolution used, the model is thus not well posed. That is, using the surface energy criterion solely a maximum breakage probability is predicted when the breakage fraction approaches zero. This is not in agreement to the real physical situation [119]. Several contributions have focused on the modification of the basic model of Luo and Svendsen [74] intending to avoid this limitation (e.g., [29, 68, 119]).

Hagesæther et al [29] and Wang et al [119] extended the basic breakage model of Luo and Svendsen [74] assuming that when a fluid particle with size  $d_i$  is hit by an eddy of size  $\lambda$  having turbulent kinetic energy  $e(d_i, \lambda)$ , the daughter particle size is limited by a minimum value due to the capillary pressure and by a maximum value due to the increase of the surface energy.

The daughter bubble size is thus limited by two constraints. The capillary pressure constraint states that if the dynamic pressure of the turbulent eddy  $\frac{1}{2}\rho_c v_\lambda^2$  exceeds the capillary pressure  $\sigma_I/d''$ , the fluid particle is deformed and finally breaks up resulting in a minimum breakage fraction  $f_{V_{min}}$  (or bubble size  $d_{j,min}$ ) [69].  $d''$  denotes the diameter of the smaller daughter size (or two times the minimum radius of curvature). When breakage occurs, the dynamic pressure induced by the eddy turbulence kinetic energy satisfy the criterion:

$$\frac{1}{2}\rho_c v_\lambda^2 \geq \frac{\sigma_I}{d''} \quad (9.51)$$

The second constraint, often referred to as the surface area criterion [74], states that the eddy kinetic energy must be larger than the increase of the surface energy during the breakage as expressed by (9.44). This constraint results in a maximum breakage fraction  $f_{V_{max}}$  (or bubble size  $d_{j,max}$ ).

Lehr et al [68] derived a similar breakage density function using only the capillary constraint and assumed that the interfacial force on the bubble surface and the initial force of the colliding eddy balance each other. Contrary, Hagesæther et al [29] and Wang et al [119] assumed that during breakage the inertial force of the colliding eddy is often larger than the interfacial force and bubble deformation is strengthened until breakage occurs. Therefore, the force balance of Lehr et al [68] may not be satisfied during bubble breakage.

Politano et al [88] studied the equilibrium between coalescence and breakage in homogeneous flows with isotropic turbulence using a population balance

model. The population balance was solved using a multi-group approach. The daughter size distribution function was approximated by a uniform function, a delta function, and by the model proposed by Luo and Svendsen [74]. The breakage rate was calculated using either the model proposed by Luo and Svendsen [74] or the model proposed by Prince and Blance [92]. Significant differences in the resulting bubble breakage rate, and therefore in the bubble size distribution were observed comparing the model performance with experimental data on bubbly flows in an agitated tank. The model of Luo and Svendsen [74] was in very good agreement with the experimental data, whereas the model of Prince and Blanch [92] appears to over predict the bubble size.

Most of the macroscopic population balance kernels discussed are based on the eddy collision arguments that rely on the interpretation that turbulent flows consist of a collection of fluid slabs or eddies which are treated using relationships developed in the kinetic theory of gases. This engineering eddy concept is impossible to validate regarding eddy shape, the number densities and the breakage mechanisms discussed above. Further, the resulting breakage models require the specification of the minimum and maximum eddy sizes that are capable of causing particle breakage, as well as a criterion for the minimum bubble size  $d_{\min}$ . Finally, the macroscopic formulation is considered less fundamental and less general than the average microscopic one. An unfortunate consequence of this modeling framework is that a discrete numerical scheme for the particle size is embedded within the source term closures, thus optimizing the numerical solution procedure is not a trivial task.

### 9.1.2 The Microscopic Continuum Mechanical Population Balance Formulation

In this section the population balance modeling approach established by Randolph [95], Randolph and Larson [96], Himmelblau and Bischoff [35], and Ramkrishna [93, 94] is outlined. The population balance model is considered a concept for describing the evolution of populations of countable entities like bubble, drops and particles. In particular, in multiphase reactive flow the dispersed phase is treated as a population of particles distributed not only in physical space (i.e., in the ambient continuous phase) but also in an abstract property space [37, 95]. In the terminology of Hulburt and Katz [37], one refers to the spatial coordinates as external coordinates and the property coordinates as internal coordinates. The joint space of internal and external coordinates is referred to as the particle phase space. In this case the quantity of basic interest is a density function like the average number of particles per unit volume of the particle state space. The population balance may thus be considered an equation for the number density and regarded as a number balance for particles of a particular state.

A model describing the evolution of this density function must consider the various ways in which the particles of a specific state can either form or disappear from the system. The change of the density function with respect to

the external coordinates refers to motion through physical space, and that of internal coordinates refers to motion through an abstract property space (e.g., particle growth). The physical processes that can be described by terms on this form are collectively referred to as convective processes since they result from motion in particle phase space. This group of physical processes, which cause convective motion in particle phase space, may contribute to the rates of formation and disappearance of the specific particle types. The number of particles of a particular type can also change by processes that create new particles (*birth* processes) and destroy existing particles (*death* processes). In bubbly flow birth of new particles can occur both due to breakage and coalescence processes. The bubble breakage and coalescence processes also contribute to death processes, for a particle type that either breaks (into other particles) or coalesces with another particle no longer exists as such following the event. The phenomenological utility of population balance models lies in the convective processes as well as the birth- and death processes.

Following the notation of Ramkrishna [94] we let  $f^{(1)}(\mathbf{x}, \mathbf{r}, t)$  be the number of particles per unit volume of the particle phase space at time  $t$ , at location  $\mathbf{x} \equiv (x_1, x_2, \dots, x_d)$  in property space ( $d$  representing the number of different quantities associated with the particle) and  $\mathbf{r} \equiv (r_1, r_2, r_3)$  in physical space. This number density function is considered a smooth function of its arguments  $\mathbf{x}, \mathbf{r}$  and  $t$ , and  $f^{(1)}(\mathbf{x}, \mathbf{r}, t)$  can be differentiated as many times as desired with respect to any of its arguments. To describe the different convective processes separate velocities are defined for the internal coordinates,  $\mathbf{v}_x(\mathbf{x}, \mathbf{r}, \mathbf{Y}, t)$ , and for the external coordinates,  $\mathbf{v}_r(\mathbf{x}, \mathbf{r}, \mathbf{Y}, t)$ . It is thus possible to identify particle (number) fluxes. In this representation  $f^{(1)}(\mathbf{x}, \mathbf{r}, t)\mathbf{v}_r(\mathbf{x}, \mathbf{r}, \mathbf{Y}, t)$  designates the particle flux through physical space and  $f^{(1)}(\mathbf{x}, \mathbf{r}, t)\mathbf{v}_x(\mathbf{x}, \mathbf{r}, \mathbf{Y}, t)$  denotes the particle flux through internal coordinate space. The continuous phase variables are represented by a vector  $\mathbf{Y}(\mathbf{r}, t) \equiv (\mathbf{v}_c, \mathbf{v}_d, \alpha_c, \alpha_d, p, \rho_c, \rho_d, \dots)$  which is calculated from the governing transport equations and the problem dependent boundary conditions.

If  $dV_x$  and  $dV_r$  denote infinitesimal volumes in property space and physical space respectively located at  $(\mathbf{x}, \mathbf{r})$ , then the number of particles in  $dV_x dV_r$  is given by  $f^{(1)}(\mathbf{x}, \mathbf{r}, t)dV_x dV_r$ . The local (average) number density in physical space, that is, the total number of particles per unit volume of physical space, denoted  $N(\mathbf{r}, t)$ , is given by:

$$N(\mathbf{r}, t) = \int_{V_x} f^{(1)}(\mathbf{x}, \mathbf{r}, t) dV_x \quad (9.52)$$

For an arbitrary combined material volume element constituting a combined sub-volume  $V_{SV}(t)$  of the particle phase space the integral formulation of the population balance states that the only way in which the number of particles can change is by birth and death processes [95, 96, 35, 93, 94]. The system balance is thus written on the form:

$$\left\{ \begin{array}{l} \text{The Time Rate of Change} \\ \text{of } f^{(1)} \text{ in the Sub-volume } V_{SV}(t) \end{array} \right\} = \left\{ \begin{array}{l} \text{The Net Generation of } f^{(1)} \\ \text{Within the Sub-volume } V_{SV}(t) \end{array} \right\}$$

This modeling approach thus considers the balance principle to the number density function  $f^{(1)}(\mathbf{x}, \mathbf{r}, t)$  for an arbitrary combined material sub-volume  $V_{SV}(t)$  of the particle phase space  $V(t)$ :

$$\frac{D}{Dt} \int_{V_{SV}(t)} f^{(1)} dV' = \int_{V_{SV}(t)} (B - D) dV' \quad (9.53)$$

In this notation  $D/Dt$  represents a generalization of the substantial time derivative operator. The  $B - D$  terms are the net birth and death terms collectively representing the net rate of production of particles of state  $(\mathbf{x}, \mathbf{r})$  at time  $t$  in an environment of state  $\mathbf{Y}$ .

In accordance with the standard approach in continuum fluid mechanics, the abstract system or material control volume description is converted into a combined Eulerian framework by use of a generalization of the conventional Reynolds theorem. For general vector spaces the Reynolds theorem is written as [95, 96, 93, 94]:

$$\frac{D}{Dt} \int_{V_{SV}(t)} f^{(1)} dV' = \int_{V_{SV}} \frac{\partial f^{(1)}}{\partial t} dV' + \int_{A_{SA}} (\mathbf{v} f^{(1)}) \cdot \mathbf{n} dA' \quad (9.54)$$

where  $\mathbf{v}$  denotes the combined phase space velocity vector ( $\equiv \mathbf{v}_x + \mathbf{v}_r$ ) relative to a fixed combined control volume surface,  $dA' = dA'_x + dA'_r$  are local, infinitesimal surface areas in  $A = A_x + A_r$ , and  $\mathbf{n}$  denotes a combined normal unit vector ( $\equiv \mathbf{n}_x + \mathbf{n}_r$ ). Moreover,  $V$  is considered a combined abstract volume of a hypothetical continuous medium containing all the embedded particles within  $V_r$  and  $V_x$ . For convenience we use the compact notation  $dV' = dV'_x dV'_r$ ,  $V = V_x \cup V_r$ , and  $\int_V = \int_{V_x} \int_{V_r}$ .

Likewise, one imagines that the surface integral in (9.54) can be rewritten in terms of a volume integral using a generalization of the conventional Gauss' theorem:

$$\int_{A_{SA}} (\mathbf{v} f^{(1)}) \cdot \mathbf{n} dA' = \int_{V_{SV}} \nabla \cdot (\mathbf{v} f^{(1)}) dV' \quad (9.55)$$

By use of (9.54) the system balance (9.53) can be rewritten as a volume integral for a fixed combined control volume in particle phase space:

$$\int_{V_{SV}} \left( \frac{\partial f^{(1)}}{\partial t} + \nabla \cdot (\mathbf{v} f^{(1)}) - (B - D) \right) dV' = 0 \quad (9.56)$$

Since  $V_{SV}$  was arbitrary, (9.56) must be satisfied for any  $V_{SV}$ , hence a necessary condition for (9.56) to be true is that the integrand vanishes identically.

A differential population balance for the number density function  $f^{(1)}$  is thus achieved:

$$\frac{\partial f^{(1)}}{\partial t} + \nabla \cdot (\mathbf{v}f^{(1)}) - (B - D) = 0 \quad \left( \frac{1}{sm^3[\mathbf{x}]} \right) \quad (9.57)$$

Considering the fluid particle coalescence and breakage phenomena only, the net source  $B(\mathbf{x}, \mathbf{r}, \mathbf{Y}, t)$  and sink  $D(\mathbf{x}, \mathbf{r}, \mathbf{Y}, t)$  terms are given as:

$$B(\mathbf{x}, \mathbf{r}, \mathbf{Y}, t) = B_C(\mathbf{x}, \mathbf{r}, \mathbf{Y}, t) + B_B(\mathbf{x}, \mathbf{r}, \mathbf{Y}, t) \quad \left( \frac{1}{sm^3[\mathbf{x}]} \right) \quad (9.58)$$

$$D(\mathbf{x}, \mathbf{r}, \mathbf{Y}, t) = D_C(\mathbf{x}, \mathbf{r}, \mathbf{Y}, t) + D_B(\mathbf{x}, \mathbf{r}, \mathbf{Y}, t) \quad \left( \frac{1}{sm^3[\mathbf{x}]} \right) \quad (9.59)$$

The local population balance becomes:

$$\begin{aligned} \frac{\partial f^{(1)}(\mathbf{x}, \mathbf{r}, t)}{\partial t} + \nabla_r \cdot (f^{(1)}(\mathbf{x}, \mathbf{r}, t)\mathbf{v}_r) + \nabla_x \cdot (f^{(1)}(\mathbf{x}, \mathbf{r}, t)\mathbf{v}_x) \\ = B_B(\mathbf{x}, \mathbf{r}, \mathbf{Y}, t) - D_B(\mathbf{x}, \mathbf{r}, \mathbf{Y}, t) + B_C(\mathbf{x}, \mathbf{r}, \mathbf{Y}, t) - D_C(\mathbf{x}, \mathbf{r}, \mathbf{Y}, t). \end{aligned} \quad (9.60)$$

where  $f^{(1)}(\mathbf{x}, \mathbf{r}, t)$  is the bubble number probability density ( $1/m^3[\mathbf{x}]$ ), which varies with internal coordinates ( $\mathbf{x}$ ), spatial position ( $\mathbf{r}$ ) and time ( $t$ ).

The first term on the LHS of (9.60) describes the change of the particle number probability density with time. The second term designates the change in the particle number probability density due to convection. The third term represents the change in the bubble number probability density due to convection in the internal coordinates denoting several particle growth phenomena. Collectively the terms on the RHS denote a net source term, representing the change in the number probability density  $f^{(1)}$  due to particle breakup and coalescence. The  $B_B$  and  $D_B$  terms describe the birth and death rates of particles due to breakage, and the  $B_C$  and  $D_C$  terms account for the birth and death rates of particles due to coalescence.

To close this model formulation constitutive equations are required for both the growth and source term functions. This parameterization process is of great importance as it represents the weakest part of the population balance modeling. The detailed functionality of the closure relations and even the physical nature of these processes are generally unknown and require further attention. The complexity of the growth terms may also dependent on the choice of internal coordinates or particle properties used characterizing the dispersed phase. In most bubbly flow investigations the particle diameter (volume) is used, thus the gas expansion due to pressure-, temperature- and composition changes as well as interfacial mass transfer fluxes has to be incorporated through some kind of growth terms. Contrary, using particle mass as the internal coordinate, only the interfacial mass transfer fluxes has to be incorporated through this term.

It is still not common to solve the local population balance equations derived above by direct numerical simulations, instead some kind of averaging is

performed to enable solution with reasonable time and (physical) space resolutions. Another motivation for performing this averaging is to develop a PBE modeling framework that is consistent with the averaged multi-fluid model concept commonly used simulating multiphase flows. Adopting the conventional time after volume averaging procedure, the local transport equation is averaged over a physical averaging volume and thereafter in time. The result is:

$$\frac{\partial \overline{\langle f^{(1)}(\mathbf{x}, t) \rangle}}{\partial t} + \nabla_r \cdot (\overline{\langle f^{(1)}(\mathbf{x}, t) \rangle \langle \mathbf{v}_r \rangle}) + \nabla_x \cdot (\overline{\langle f^{(1)}(\mathbf{x}, t) \rangle \langle \mathbf{v}_x \rangle}) \quad (9.61)$$

$$= \overline{\langle B_B(\mathbf{x}, \mathbf{Y}, t) \rangle} - \overline{\langle D_B(\mathbf{x}, \mathbf{Y}, t) \rangle} + \overline{\langle B_C(\mathbf{x}, \mathbf{Y}, t) \rangle} - \overline{\langle D_C(\mathbf{x}, \mathbf{Y}, t) \rangle}$$

We may now introduce number density weighted average velocities, thus:

$$\overline{\langle f^{(1)}(\mathbf{x}, t) \rangle \langle \mathbf{v}_r \rangle} = \overline{\langle f^{(1)}(\mathbf{x}, t) \rangle} \overline{\langle \mathbf{v}_r \rangle}^f \quad (9.62)$$

and

$$\overline{\langle f^{(1)}(\mathbf{x}, t) \rangle \langle \mathbf{v}_x \rangle} = \overline{\langle f^{(1)}(\mathbf{x}, t) \rangle} \overline{\langle \mathbf{v}_x \rangle}^f \quad (9.63)$$

This approach makes the velocities in the population balance different from the mass- or phase weighted average velocities obtained solving the two-fluid model. This discrepancy is an argument for the formulation of a mass density population balance instead of a number balance to achieve a consistently integrated population balance within the two-fluid modeling framework.

We may also perform standard Reynolds decomposition of the variables and then time average the equation. The typical low order turbulence modeling of the resulting covariance terms gives rise to diffusive terms in the balance equation [25]. The physics involved in these terms is, however, not understood making this modeling issue a challenging task:

$$\overline{\langle f^{(1)}(\mathbf{x}, t) \rangle \langle \mathbf{v}_r \rangle} = \overline{\langle f^{(1)}(\mathbf{x}, t) \rangle} \overline{\langle \mathbf{v}_r \rangle} + \overline{\langle f^{(1)}(\mathbf{x}, t) \rangle' \langle \mathbf{v}_r \rangle'} \quad (9.64)$$

and

$$\overline{\langle f^{(1)}(\mathbf{x}, t) \rangle \langle \mathbf{v}_x \rangle} = \overline{\langle f^{(1)}(\mathbf{x}, t) \rangle} \overline{\langle \mathbf{v}_x \rangle} + \overline{\langle f^{(1)}(\mathbf{x}, t) \rangle' \langle \mathbf{v}_x \rangle'} \quad (9.65)$$

If an appropriate relation for the contact area as a function of the internal coordinates is available, the particle growth term due to interfacial mass transfer can be modeled in accordance with the well known film theory (although still of semi-empirical nature) and the ideal gas law [68]. The modeling of the source and sink terms due to fluid particle breakage and coalescence is less familiar and still on an early stage of development. Moreover, the existing theory is rather complex and not easily available. Further research is thus needed in order to derive consistent multifluid-population balance models.

### The Continuous Source Term Closures

In this section the conventional macroscopic continuum source term closures are presented and the standard constitutive relations are examined.

A fairly general framework has been formulated for the source terms considering particle breakage, fluid particle coalescence, solid particle agglomeration/aggregation and similar processes (e.g., [109, 80, 81, 37, 114, 43, 25, 94]). Detailed discussions of the particle breakage and coalescence modeling and the mathematical properties of the constitutive equations can be found in the papers by Barrow [4], Laurencot and Mischler [64, 65].

Considering the breakage terms, the physical breakage of the different particles are assumed to be independent of each other. The average loss rate of particles of state  $(\mathbf{x}, \mathbf{r})$  per unit time by breakage is normally written as:

$$D_B(\mathbf{x}, \mathbf{r}, \mathbf{Y}, t) = b_B(\mathbf{x}, \mathbf{r}, \mathbf{Y}, t) f^{(1)}(\mathbf{x}, \mathbf{r}, t) \quad (9.66)$$

where  $b_B(\mathbf{x}, \mathbf{r}, \mathbf{Y}, t)$  has the dimension of reciprocal time (1/s) and is often called the breakage frequency. It represents the fraction of particles of state  $(\mathbf{x}, \mathbf{r})$  breaking per unit time. The breakage processes are often considered of random nature, thus the modeling work usually adopt probabilistic theory.

The average production rate for particles of state  $(\mathbf{x}, \mathbf{r})$  originating from breakage of particles of all other particles states, considering both internal and external coordinates is frequently given by [94]:

$$B_B(\mathbf{x}, \mathbf{r}, \mathbf{Y}, t) = \int_{V_r, sV} \int_{V_x, sV} \nu(\mathbf{x}', \mathbf{r}', \mathbf{Y}, t) b_B(\mathbf{x}', \mathbf{r}', \mathbf{Y}, t) P_B(\mathbf{x}, \mathbf{r} | \mathbf{x}', \mathbf{r}', \mathbf{Y}, t) f^{(1)}(\mathbf{x}', \mathbf{r}', t) dV_r' dV_x' \quad (9.67)$$

where  $\nu(\mathbf{x}', \mathbf{r}', \mathbf{Y}, t)$  denotes the average number of particles formed from the breakage of a single particle of state  $(\mathbf{x}', \mathbf{r}')$  in an environment of  $\mathbf{Y}$  at time  $t$ .  $P_B(\mathbf{x}, \mathbf{r} | \mathbf{x}', \mathbf{r}', \mathbf{Y}, t)$  designates the probability density function for creating particles that have state  $(\mathbf{x}, \mathbf{r})$  from the breakage of a particle of state  $(\mathbf{x}', \mathbf{r}')$  in an environment of state  $\mathbf{Y}$  at time  $t$ . In the engineering literature it is commonly referred to as the daughter particle size distribution function [i.e., being a probability density with units  $(1/m^3[\mathbf{x}])$ ] denoting the size distribution of daughter particles produced upon breakage of a parent particle.

The integrand on the RHS represents the rate of formation of particles of state  $(\mathbf{x}, \mathbf{r})$  formed by breakage of particles of state  $(\mathbf{x}', \mathbf{r}')$ . That is, the number of particles of state  $(\mathbf{x}', \mathbf{r}')$  that breaks per unit time is  $b_B(\mathbf{x}', \mathbf{r}', \mathbf{Y}, t) f^{(1)}(\mathbf{x}', \mathbf{r}', t) dV_r' dV_x'$ . Multiplying the above expression by  $\nu(\mathbf{x}', \mathbf{r}', \mathbf{Y}, t)$  gives the number of new particles resulting from the breakage processes  $\nu(\mathbf{x}', \mathbf{r}', \mathbf{Y}, t) b_B(\mathbf{x}', \mathbf{r}', \mathbf{Y}, t) f^{(1)}(\mathbf{x}', \mathbf{r}', t) dV_r' dV_x'$  of which a fraction  $P_B(\mathbf{x}, \mathbf{r} | \mathbf{x}', \mathbf{r}', \mathbf{Y}, t) dV_r' dV_x'$  represents particles of state  $(\mathbf{x}, \mathbf{r})$ .

The probability density function  $P_B$  must satisfy the normalization condition (in the internal coordinates):

$$\int_{V_{x, sV}} P_B(\mathbf{x}, \mathbf{r} | \mathbf{x}', \mathbf{r}', \mathbf{Y}, t) dV_x' = 1 \quad (9.68)$$

Usually binary breakage is assumed for which  $\nu(\mathbf{x}', \mathbf{r}', \mathbf{Y}, t) = \nu = 2$ . However, experimental determination of this variable is recommended. The function  $P_B(\mathbf{x}, \mathbf{r}|\mathbf{x}', \mathbf{r}', \mathbf{Y}, t)$  should also be determined from experimental observations.

In addition, the  $\nu(\mathbf{x}', \mathbf{r}', \mathbf{Y}, t)$  and  $P_B(\mathbf{x}, \mathbf{r}|\mathbf{x}', \mathbf{r}', \mathbf{Y}, t)$  functions are not really independent, so it might be more convenient to define a *breakage yield redistribution function* as follows:

$$H_B(\mathbf{x}, \mathbf{r}|\mathbf{x}', \mathbf{r}', \mathbf{Y}, t) = \nu(\mathbf{x}', \mathbf{r}', \mathbf{Y}, t)P_B(\mathbf{x}, \mathbf{r}|\mathbf{x}', \mathbf{r}', \mathbf{Y}, t) \tag{9.69}$$

Dorao [18] and Dorao et al [19] introduced this function considering that (9.69) should reflect the property that:

$$\int_0^{\mathbf{x}'} H_B(\mathbf{x}, \mathbf{r}|\mathbf{x}', \mathbf{r}', \mathbf{Y}, t)\mathbf{x}^N d\mathbf{x} = \mathbf{x}'^N \tag{9.70}$$

where  $N$  represents the moment of the parent particle properties that are conserved.

In (9.67) the integral in physical space is strictly not appropriate as it is based on the assumption that a parent particle that is breaking at one location in physical space can produce daughter particles that occur elsewhere. It is obvious that the birthplace of the daughter particles should be at the same location as the parent particle did break. Ramkrishna [94](p 57) briefly mentioned this model limitation and that the given source term formulations have to be re-written for problems represented in the external coordinates. For this reason we have to extend the presentation requiring that the breakage is a local phenomena in physical space. An appropriate modification can be obtained by introducing a Dirac delta function  $\delta(\mathbf{r}' - \mathbf{r})$  within the physical space integral argument in the given source term definition. The breakage source term is then be reduced to:

$$B_B(\mathbf{x}, \mathbf{r}, \mathbf{Y}, t) = \int_{V_{x,SV}} \nu(\mathbf{x}', \mathbf{r}, \mathbf{Y}, t)b_B(\mathbf{x}', \mathbf{r}, \mathbf{Y}, t)P_B(\mathbf{x}, \mathbf{r}|\mathbf{x}', \mathbf{r}, \mathbf{Y}, t)f^{(1)}(\mathbf{x}', \mathbf{r}, t)dV'_x \tag{9.71}$$

in which  $P_B(\mathbf{x}, \mathbf{r}|\mathbf{x}', \mathbf{r}, \mathbf{Y}, t)$  is the daughter size distribution function ( $\frac{1}{|\mathbf{x}|}$ ).

The population balance source term due to coalescence is usually defined as [94]:

$$B_C(\mathbf{x}, \mathbf{r}, \mathbf{Y}, t) = \int_{V_{r,SV}} \int_{V_{x,SV}} \frac{1}{\delta} a_C(\tilde{\mathbf{x}}, \tilde{\mathbf{r}}; \mathbf{x}', \mathbf{r}', \mathbf{Y}) f^{(2)}(\tilde{\mathbf{x}}, \tilde{\mathbf{r}}; \mathbf{x}', \mathbf{r}', t) \frac{\partial(\tilde{\mathbf{x}}, \tilde{\mathbf{r}})}{\partial(\mathbf{x}, \mathbf{r})} \Big|_{\mathbf{x}', \mathbf{r}'} dV'_x dV'_r \tag{9.72}$$

where  $\delta$  represents the number of times identical pairs have been considered in the interval of integration, thus  $\frac{1}{\delta}$  corrects for the redundancy.

$a_C(\tilde{\mathbf{x}}, \tilde{\mathbf{r}}; \mathbf{x}', \mathbf{r}', \mathbf{Y}, t)$  denotes the coalescence frequency or the fraction of particle pairs of states  $(\tilde{\mathbf{x}}, \tilde{\mathbf{r}})$  and  $(\mathbf{x}', \mathbf{r}')$  that coalesce per unit time (1/s). The coalescence frequency is defined for an ordered pair of particles, although from a physical viewpoint the ordering of particle pairs should not alter the value of the frequency. In other words,  $a_C(\tilde{\mathbf{x}}, \tilde{\mathbf{r}}; \mathbf{x}', \mathbf{r}', \mathbf{Y}, t)$  satisfies a symmetry property:  $a_C(\tilde{\mathbf{x}}, \tilde{\mathbf{r}}; \mathbf{x}', \mathbf{r}', \mathbf{Y}, t) = a_C(\mathbf{x}', \mathbf{r}'; \tilde{\mathbf{x}}, \tilde{\mathbf{r}}, \mathbf{Y}, t)$ . It is thus essential to consider only one of the above order for a given pair of particles.

In order to proceed, it is necessary to assume that it is possible to solve for the particle state of one of the coalescing pair given those of the other coalescing particle and the new particle (as the three variables are not independent). Thus, given the state  $(\mathbf{x}, \mathbf{r})$  of the new particle, the state  $(\mathbf{x}', \mathbf{r}')$  of one of the two coalescing particles, the states of the other coalescing particle are known and denoted by  $[\tilde{\mathbf{x}}(\mathbf{x}, \mathbf{r}|\mathbf{x}', \mathbf{r}'), \tilde{\mathbf{r}}(\mathbf{x}, \mathbf{r}|\mathbf{x}', \mathbf{r}')]$ .

As in the classical kinetic theory of gases, the pair density function  $f^{(2)}$  is impossible to determine analytically and some closure approximation has to be made. In the population balance derivation we normally adopt a common assumption in kinetic theory and makes the coarse approximation:  $f^{(2)}(\tilde{\mathbf{x}}, \tilde{\mathbf{r}}; \mathbf{x}', \mathbf{r}', t) \approx \tilde{f}^{(1)}(\tilde{\mathbf{x}}, \tilde{\mathbf{r}}, t) f^{(1)}(\mathbf{x}', \mathbf{r}', t)$ . This assumption implies that there is no statistical correlation between particles of states  $(\mathbf{x}', \mathbf{r}')$  and  $(\tilde{\mathbf{x}}, \tilde{\mathbf{r}})$  at any instant  $t$ .

Again, as for the breakage source term, the integral in physical space is not appropriate for the coalescence source term neither as the present model is based on the assumption that two particles that are coalescing at a particular location in space can produce a new larger particle elsewhere. It is obvious that the birthplace of the particle should be at the same location as the parent particles did coalesce. Again, we may extend the given model requiring that coalescence is a local phenomena in physical space. This modification can be achieved by introducing a Dirac delta function  $\delta(\mathbf{r}' - \mathbf{r})$  within the physical space integral argument in the given source term definition.

The coalescence source term is then reduced to:

$$B_C(\mathbf{x}, \mathbf{r}, \mathbf{Y}, t) = \int_{V_{x,sv}} \frac{1}{\delta} a_C(\tilde{\mathbf{x}}, \mathbf{r}; \mathbf{x}', \mathbf{r}, \mathbf{Y}) f^{(2)}(\tilde{\mathbf{x}}, \mathbf{r}; \mathbf{x}', \mathbf{r}, t) \left. \frac{\partial(\tilde{\mathbf{x}}, \mathbf{r})}{\partial(\mathbf{x}, \mathbf{r})} \right|_{\mathbf{x}', \mathbf{r}} dV'_x \quad (9.73)$$

in which  $a_C(\tilde{\mathbf{x}}, \mathbf{r}; \mathbf{x}', \mathbf{r}, \mathbf{Y})$  denotes the coalescence frequency or the fraction of particle pairs of states  $(\tilde{\mathbf{x}}, \mathbf{r})$  and  $(\mathbf{x}', \mathbf{r})$  that coalesce per unit time multiplied by a differential volume ( $m^3/s$ ). This quantity coincides with the quantity referred to as the *swept volume rate* of the particle in the discrete macroscopic PBE formulation.

The sink term due to coalescence is usually defined as:

$$D_C(\mathbf{x}, \mathbf{r}, \mathbf{Y}, t) = \int_{V_r,sv} \int_{V_x,sv} a_C(\mathbf{x}', \mathbf{r}'; \mathbf{x}, \mathbf{r}, \mathbf{Y}) f^{(2)}(\mathbf{x}', \mathbf{r}'; \mathbf{x}, \mathbf{r}, t) dV'_x dV'_r \quad (9.74)$$

As for the integral source terms considered hitherto, the integral in physical space is not appropriate as it is based on the assumption that two particles that coalesce at a particular location in space can produce a larger particle elsewhere. Following the same procedure as described above, the sink term due to coalescence can be re-defined as:

$$D_C(\mathbf{x}, \mathbf{r}, \mathbf{Y}, t) = \int_{V_{x,SV}} a_C(\mathbf{x}', \mathbf{r}; \mathbf{x}, \mathbf{r}, \mathbf{Y}) f^{(2)}(\mathbf{x}', \mathbf{r}; \mathbf{x}, \mathbf{r}, t) dV'_x \quad (9.75)$$

To examine the derivation of the population balance source terms, the bubble diameter is henceforth chosen as the only internal coordinate (i.e.,  $x = d$ ) as it is the most frequent choice.

The local source terms are listed below:

$$B_B(d, \mathbf{r}, \mathbf{Y}, t) = \int_d^\infty \nu(d', \mathbf{r}, \mathbf{Y}) b_B(d', \mathbf{r}, \mathbf{Y}) P_B(d, \mathbf{r} | d', \mathbf{r}, \mathbf{Y}) f'^{(1)}(d', \mathbf{r}, t) dd' \quad (9.76)$$

$$D_B(d, \mathbf{r}, \mathbf{Y}, t) = b_B(d, \mathbf{r}, \mathbf{Y}) f^{(1)}(d, \mathbf{r}, t) \quad (9.77)$$

$$B_C(d, \mathbf{r}, \mathbf{Y}, t) = \frac{1}{2} \int_0^d a_C(\tilde{d}, \mathbf{r}; d', \mathbf{r}, \mathbf{Y}) \tilde{f}^{(1)}(\tilde{d}, \mathbf{r}, t) f'^{(1)}(d', \mathbf{r}, t) dd', \quad (9.78)$$

$$D_C(d, \mathbf{r}, \mathbf{Y}, t) = \int_0^\infty f^{(1)}(d, \mathbf{r}, t) a_C(d, \mathbf{r}; d', \mathbf{r}, \mathbf{Y}) f'^{(1)}(d', \mathbf{r}, t) dd' \quad (9.79)$$

All the source terms still have the common units,  $(1/sm^3[m])$ .

Comparing the source term expressions (9.76) to (9.79) with (9.2) to (9.5) it is clearly seen that only under particular conditions will the two formulations give rise to identical expressions for the source terms. The macroscopic formulation is explicitly expressed in terms of a discrete discretization scheme and is very difficult to convert to other schemes.

In the following sections examining the source term parameterizations, emphasis will be put on a selected number of the novel closures suitable for bubbly flow modeling.

### Coalescence Frequency Closures, $a_C(d, \mathbf{r}; d', \mathbf{r}, \mathbf{Y})$

Intuitively, bubble coalescence is related to bubble collisions. The collisions are caused by the existence of spatial velocity difference among the particles themselves. However, not all collisions necessarily lead to coalescence. Thus modeling bubble coalescence on these scales means modeling of bubble collision and coalescence probability (efficiency) mechanisms. The pioneering work on coalescence of particles to form successively larger particles was carried out by Smoluchowski [109, 110].

The more recent coalescence closures that were formulated directly within the macroscopic framework [77, 113, 92, 73] are frequently transformed and expressed in terms of probability densities and used within the average microscopic balance framework without further considerations employing a discrete numerical discretization scheme.

As for the collision density in the macroscopic model formulation, the average collision frequency of fluid particles is usually described assuming that the mechanisms of collision is analogous to collisions between molecules as in the kinetic theory of gases. The volume average coalescence frequency,  $a_C(d; d', \mathbf{Y})$ , can thus be defined as the product of an effective swept volume rate  $h_C(d; d', \mathbf{Y})$  and the coalescence probability,  $p_C(d; d', \mathbf{Y})$  (e.g., [16, 92, 114, 39, 46, 118]):

$$a_C(d, \mathbf{r}; d', \mathbf{r}, \mathbf{Y}) = h_C(d, \mathbf{r}; d', \mathbf{Y}) p_C(d, \mathbf{r}; d', \mathbf{Y}) \left( \frac{m^3}{s} \right) \quad (9.80)$$

This relation expresses that not all collisions lead to coalescence. The modeling of the coalescence processes thus means to find adequate physical expressions for  $h_C(d; d', \mathbf{Y})$  and  $p_C(d; d', \mathbf{Y})$ . Kamp et al [39], among others, suggested that microscopic closures can be formulated in line with the macroscopic population balance approach, thus we may define:

$$h_C(d, \mathbf{r}; d', \mathbf{Y}) = \frac{\pi}{4} (d + d')^2 (\bar{v}_{t,d}^2 + \bar{v}_{t,d'}^2) \left( \frac{m^3}{s} \right) \quad (9.81)$$

and

$$p_C(d, \mathbf{r}; d', \mathbf{Y}) = \exp\left(-\frac{\Delta t_{\text{coal}}}{\Delta t_{\text{col}}}\right) \quad (-) \quad (9.82)$$

where suitable continuous closures are needed for the model variables like the mean turbulent bubble approach velocities and the time scales. Multi-fluid models may provide improved estimates for the mean turbulent bubble approach velocities as individual velocity fields for each of the bubble phases are calculated. However, the existing closures for the time scales are very crude and need further considerations.

The coalescence terms in the average microscopic population balance can then be expressed in terms of the local effective swept volume rate and the coalescence probability variables:

$$B_C(d, \mathbf{r}, \mathbf{Y}, t) = \frac{1}{2} \int_0^d h_C(\tilde{d}, \mathbf{r}; d', \mathbf{Y}) p_C(\tilde{d}, \mathbf{r}; d', \mathbf{Y}) \tilde{f}^{(1)}(\tilde{d}, \mathbf{r}, t) f'^{(1)}(d', \mathbf{r}, t) dd' \quad (9.83)$$

$$D_C(d, \mathbf{r}, \mathbf{Y}, t) = f^{(1)}(d, \mathbf{r}, t) \int_0^\infty h_C(d, \mathbf{r}; d', \mathbf{Y}) p_C(d, \mathbf{r}; d', \mathbf{Y}) \tilde{f}^{(1)}(\tilde{d}, \mathbf{r}, t) dd' \quad (9.84)$$

It is noted that all the terms in the continuum population balance equation have common units,  $(1/m^3s[m])$ . By discretizing the continuous bubble number density in groups or classes, a PBE formulation equivalent to the discrete macroscopic framework is obtained.

### Models for the Breakage Frequency, $b_B(d, \mathbf{r})$

Formulating average microscopic source term closure laws for the breakage processes usually means to derive relations for the time after volume average breakage frequency,  $b_B(d)$ , the average number of daughter bubbles produced,  $\nu$ , and the average daughter particle size distribution,  $P_B(d|d')$ .

During the last decades a few models have been developed for the bubble breakage frequency,  $b_B(d)$ , under turbulent conditions ([58, 119]). Several different categories of breakage frequency models are distinguished in the literature; models based on reaction kinetic concepts (e.g., [101]), phenomenological models based on the turbulent nature of the system (e.g., [114]), and models based based on purely kinematic ideas (e.g., [78, 79]).

In an interesting attempt to overcome the limitations found in the turbulent breakage models described above Martínez-Bazán et al [78] (see also Lasheras et al [58]) proposed an alternative model in the kinetic theory (microscopic) framework based on purely kinematic ideas to avoid the use of the incomplete turbulent eddy concept and the macroscopic model formulation.

The basic premise of the model of Martínez-Bazán et al [78] is that for a bubble to break, its surface has to be deformed, and further, that this deformation energy must be provided by the turbulent stresses produced by the surrounding fluid. The minimum energy needed to deform a bubble of size  $d$  is its surface energy,

$$E_s(d) = \pi\sigma_I d^2 \quad (J) \quad (9.85)$$

The surface restoring pressure is ( $E_s$ /volume)

$$\sigma_s(d) = \frac{6E_s}{\pi d^3} = 6\frac{\sigma_I}{d} \quad (Pa). \quad (9.86)$$

The size of these bubbles is assumed to be within the inertial subrange of turbulence, thus the average deformation stress, which results from velocity fluctuations existing in the liquid between two points separated by a distance  $d$ , was estimated as:

$$\sigma_t(d) = \frac{1}{2}\rho_c \overline{\Delta v^2(d)} \quad (Pa) \quad (9.87)$$

where  $\overline{\Delta v^2(d)}$  is the mean value of the velocity fluctuations between two points separated by a characteristic distance  $d$ , and  $\rho_c$  is the density of the continuous phase.

When the turbulent stresses are equal to the confining stresses,  $\sigma_t(d) = \sigma_s(d)$ , a critical diameter,  $d_c$ , is defined such that bubbles with  $d < d_c$  are stable and will not break. A bubble  $d > d_c$  has a surface energy smaller

than the deformation energy  $\sigma_s(d) < \sigma_t(d)$ , and thus, the bubble deforms and may eventually breaks up in a time  $t_b$ . Martínez-Bazán et al [78] applied Kolmogorov's universal theory valid for homogeneous and isotropic turbulent flow to estimate the mean value of the velocity fluctuations,  $\Delta v^2(\bar{d}) = C(\varepsilon d)^{2/3}$ .

The critical diameter,  $d_c = (\frac{12\sigma_I}{C\rho})^{3/5}\varepsilon^{-2/5}$ , is defined by the crossing point of the two curves determined by  $\sigma_s(d)$  and  $\sigma_t(d)$ . Martínez-Bazán et al [78] postulated in accordance with Newton's law that the acceleration of the bubble interface during deformation is proportional to the difference between the deformation and confinement forces acting on it. In other words, the probability of breaking a bubble of size  $d$  in time  $t_b$  increases as the difference between the pressure produced by the turbulent fluctuations on the surface of the bubble,  $\frac{1}{2}\rho_c\Delta v^2(d)$ , and the restoring pressure caused by surface tension,  $6\sigma_I/d$ , increases. On the other hand, the breakage frequency should decrease to a zero limit value as this difference of pressures vanishes. Thus, the bubble breakage time can be estimated as:

$$t_b \propto \frac{d}{v_{\text{breakage}}} = \frac{d}{\sqrt{\Delta v^2(d) - 12\frac{\sigma_I}{\rho_c d}}} \quad (s) \quad (9.88)$$

where  $v_{\text{breakage}}$  is the characteristic velocity of the bubble breakage process. The breakage frequency  $b_B(d, \varepsilon)$  is given by:

$$b_B(d, \varepsilon) = \frac{1}{t_b} = K_g \frac{\sqrt{\Delta v^2(d) - 12\frac{\sigma_I}{\rho_c d}}}{d} = K_g \frac{\sqrt{\beta(\varepsilon d)^{2/3} - 12\frac{\sigma_I}{\rho_c d}}}{d} \quad (9.89)$$

the constant  $C = 8.2$  and the parameter  $K_g = 0.25$  was found experimentally for bubbly flows.

The breakage frequency is zero for bubbles of size  $d \leq d_c$ , and it increases rapidly for bubbles larger than the critical diameter,  $d > d_c$ . After reaching a maximum at  $d_{b_B, \text{max}} = (9/4)^{3/5}d_c \approx 1.63d_c$ , the breakage frequency decreases monotonically with the bubble size. The maximum breakage frequency, achieved at  $d_{b_B, \text{max}}$ , is given by  $b_{B, \text{max}}(\varepsilon) = 0.538K_g C^{1/2}\varepsilon^{3/5}(12\frac{\sigma_I}{\rho_c\beta})^{-2/5}$ .

Although this approach avoids the eddy concept, it is still restricted to homogeneous and isotropic turbulent flows, it contains several hypotheses that are not verified yet for bubble column flows, and contains a few additional adjustable parameters that need to be fitted to many sets of experimental data. Furthermore, this model concept was originally applied to systems (i.e., turbulent water jets, see e.g., Martínez-Bazán et al [78, 79]; Rodríguez-Rodríguez et al [100]; Eastwood et al [22]) where the turbulent dissipation rates are 2-3 orders of magnitude larger than what are observed in bubble columns. The bubble sizes considered were also very small, up to about 1 (mm) only. On the other hand, after careful investigations of the turbulent breakage processes in bubble columns it may be possible to extend the application of this approach to bubble column systems. The experimental techniques developed investigating breakage of bubbles on the centerline within the fully developed region of

turbulent water jets [100, 22] may initiate ideas on how to study these phenomena in bubble columns. The digital image-processing techniques used in these studies [100, 22] gives satisfactory results in very dilute two-phase flows, but the method is still questionable when the bubble concentration increases considerably as for bubble columns operated in the heterogeneous flow regime.

A severe drawback for the integrated two-fluid/population balance models is that all the kernels suggested in the literature are very sensitive to the turbulent energy dissipation rate ( $\varepsilon$ ). As mentioned earlier, the local  $\varepsilon$  variable is difficult to calculate from the  $k$ - $\varepsilon$  turbulence model since the equation for the dissipation rate merely represents a fit of a turbulent length scale to single phase pipe flow data. Therefore, further work is needed elucidating the mechanisms of bubble breakage in turbulent flows. However, an alternative to the eddy concept has been reported which may make the work on model validation easier. Perhaps the greatest advantages lies in the fact that this closure is formulated in the average microscopic modeling framework avoiding the limitations of the macro scale formulation.

It is finally remarked that working with the macroscopic and average microscopic model formulations, care should be taken as the discrete macroscopic breakage rate models ( $\Omega_B(d_i)$ ) are sometimes erroneously assumed equal to the average microscopic breakage frequency  $b_B(b)$ .

### Number of Daughter Bubbles Produced, $\nu$

In the average microscopic formulations this parameter determines the average number of daughter bubbles produced by breakage of a parent bubble of size  $d$ . The breakage of parent bubbles into two daughter bubbles is assumed in most investigations reported ( $\nu = 2$ ).

In a recent paper Risso and Fabre [99] observed that the number of fragments depended on the specific shape of the parent bubble during the deformation process and varies in a wide range. In their experiments a video processing technique was used making studies of two groups of bubbles, one group being of sizes in the range between 2 – 6 mm and the other of sizes in the range 12.4 – 21.4 mm. Two fragments were obtained in 48% of the cases, between 3 to 10 in 37% of the cases, and more than 10 fragments in 15% of the cases. The breakage process is certainly not purely binary. Implementing this effect instead of binary breakage is expected to significantly alter the number of smaller bubbles and the interfacial area concentration predicted by the population balance equation.

The experimental data of Risso and Fabre [99] also indicate that an equal size daughter distribution is more common for bubble breakage than an unequal one. Contrary, Hesketh et al [33, 34] investigated bubble breakage in turbulent flows in horizontal pipes and concluded that an unequal size daughter distribution is more probable than an equal size one. The daughter bubble size distribution model of Luo and Svendsen [74] rely on the assumption that unequal sized is more probable than equal size breakage in accordance with

the observations by Hesketh et al, as will be discussed in the next section. The deviating experimental observations indicate that further experimental investigations are needed determining reliable correlations for what physical systems and under which flow conditions the equal- and unequal breakage outcomes occur.

### Daughter Particle Distribution, $P_B(d, r|d')$

Among the papers adopting the average microscopic formulation, two of the earliest models for the daughter particle size distribution were proposed by Valentas et al [115, 116]. The daughter particle probability distribution functions suggested by Valentas et al [115, 116] were purely statistical relations. The first was a discrete model, in which a parent particle of diameter  $d$  is assumed to split into equally sized daughter particles of diameter  $d/\nu$ , where  $\nu$  is the number of daughter particles formed. The second model proposed by Valentas et al is a logical, continuous analogue of the discrete daughter particle pdf. In this case it is assumed that the daughter particle sizes are normally distributed about a mean value.

Ross and Curl [101], Coualoglou and Travlarides [16] and Prince and Blanch [92] argued that the particle breakage frequency should be a function of the difference in surface energy between a parent particle and the daughter particles produced, and the kinetic energy of a colliding eddy. Although Ross and Curl [101], Coualoglou and Travlarides [16] and Prince and Blanch [92] developed more physical models for the particle breakage frequency, the daughter particle size distributions still relied upon statistical relations.

Among the most widely used phenomenological models based on surface energy considerations is the one proposed by Tsouris and Tavlarides [114]. Their expression for the daughter particle pdf yields:

$$P_B(d|d') = \frac{e_{\min} + [e_{\max} - e(d')]}{\int_{d_{\min}}^d e_{\min} + [e_{\max} - e(d')] dd'} \left( \frac{1}{[m]} \right) \quad (9.90)$$

Considering binary breakage only, Tsouris and Tavlarides [114] postulated that the probability of formation of a daughter particle of size  $d'$  is inversely proportional to the energy required to split a parent particle of size  $d$  into a particle of size  $d'$  and its complementary particle of size  $\tilde{d} = (d^3 - d'^3)^{1/3}$ .

This energy requirement is proportional to the excess surface area generated by splitting the parent particle:

$$e(d') = \pi\sigma_I d'^2 + \pi\sigma_I \tilde{d}^2 - \pi\sigma_I d^2 = \pi\sigma_I d^2 \left[ \left( \frac{d'}{d} \right)^2 + \left[ 1 - \left( \frac{d'}{d} \right)^3 \right]^{2/3} - 1 \right] \quad (9.91)$$

To avoid the singularity present in their daughter size distribution model for  $d' = 0$  (i.e., the parent particle does not break), a minimum particle size was defined,  $d_{\min}$ . The excess surface area relation reaches a minimum

value when a particle of minimum diameter,  $d_{\min}$ , and a complementary one of maximum size,  $d_{\max} = (d^3 - d_{\min}^3)^{1/3}$ , are formed. The minimum energy,  $e_{\min}$ , is given by:

$$\epsilon(d_{\min}) = \pi\sigma_I d^2 \left[ \left( \frac{d_{\min}}{d} \right)^2 + \left[ 1 - \left( \frac{d_{\min}}{d} \right)^3 \right]^{2/3} - 1 \right] \quad (9.92)$$

This gives a minimum probability for the formation of two particles of the same size, and a maximum probability for the formation of a pair made up of a very large particle and a complementary very small one. The maximum energy corresponding to the formation of two particles of equal volumes or of diameters  $d' = (d^3 - d'^3)^{1/3} = d/2^{1/3}$  is  $e_{\max} = \pi\sigma_I d^2 [2^{1/3} - 1]$ .

Luo and Svendsen [74] derived a discrete expression for the breakage density of a particle of diameter  $d_i$  into two daughter particles of size  $d_j$  and  $(d_i^3 - d_j^3)^{1/3}$  respectively, using energy arguments similar to those employed by Tsouris and Tavlarides [114].

The significant difference between the Luo and Svendsen [74] model and its predecessors is that it gives both a partial breakage rate, that is, the breakage rate for a particle of size  $d_i$  splitting into a particle of size  $d_j$  and its complementary bubble, and an overall breakage rate. The previous surface energy models provided only an overall breakage rate. An expression for the daughter particle size distribution function can thus be calculated by normalizing the partial breakage rate by the overall breakage rate. As mentioned earlier, this variable was not required for the population balance closure but is rather a spin-off from the primary closures.

The Luo and Svendsen daughter particle size distribution is thus determined from the expression:

$$P_B(d_i|d_j) = \frac{\Omega_B(d_i : d_j)}{\Omega_B(d_i)} \quad (-) \quad (9.93)$$

Note that the units of the discrete daughter bubble size distribution variable are different from the units obtained deriving the continuous daughter size distribution function from the microscopic formulations ( $1/[m]$ ). It is thus not trivial how to adopt the model of Luo [73] within a more fundamental modeling approach.

However, like the model of Tsouris and Tavlarides [114], the model of Luo and Svendsen [74] predicted that the probability of breaking a parent particle into a very small particle and a complementary large particle is larger than the probability of equal size breakage, Fig 9.5. The distribution has a *U*-shape, with a minimum probability for the formation of two equally sized daughter particles and a maximum probability for the formation of a very large daughter particle and its complement  $d_{\min}$ .

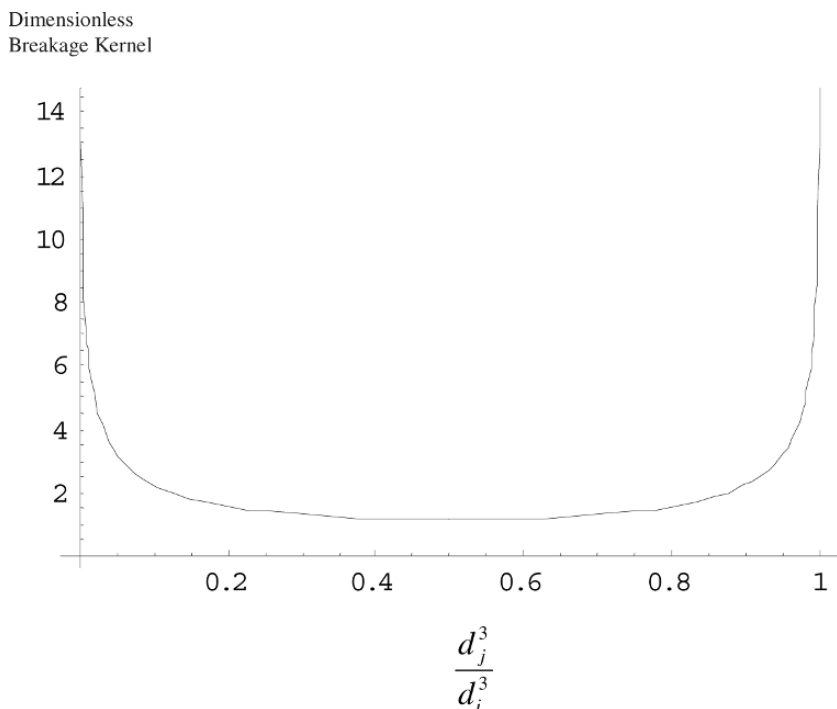


**Fig. 9.5.** A sketch of the breakage kernel of Luo and Svendsen [74]. An unequal daughter size distribution is predicted by this model. In this case the parent diameter size is,  $d_i = 0.006$  (m), and the turbulent energy dissipation rate is set at,  $\varepsilon = 1$  ( $m^2/s^3$ ). Reprinted with permission from [38]. Copyright 2005 American Chemical Society.

Although Hinze [36] and Risso and Fabre [99], among others, showed and discussed the diversity of shapes of the bubbles that can be found in turbulent flows, at present sufficient experimental data does not exist in the literature to assist in developing adequate daughter bubble probability density functions valid for bubble columns.

In an attempt to overcome the limitations found in the models for the daughter particle size distribution function described above based on the eddy collision concept, Martínez-Bazán et al [79] proposed an alternative statistical model based on energy balance principles. The model was originally intended for the prediction of air bubble breakage at the centerline of a high Reynolds number, turbulent water jet. It was assumed that when an air bubble is injected into the turbulent water jet, the velocity fluctuations of the underlying turbulence result in pressure deformation forces acting on the bubble's surface that, when greater than the confinement forces due to surface tension, will cause breakage.

The model assumes that when a parent particle breaks, two daughter particles are formed ( $\nu = 2$ ) with diameters  $d'$  and  $(d^3 - d'^3)^{1/3}$ . The validity of this assumption is supported by high-speed video images, given by Martínez-Bazán et al [79]. The diameters are related through the conservation of mass,  $(d^3 - d'^3)^{1/3} = d[1 - (d'/d)^3]^{1/3}$ . The particle-splitting process was not considered purely random, as the pressure fluctuations and thus the deformation stress ( $\sigma_t$ ) in homogeneous and isotropic turbulence are not uniformly distributed over all scales. It was further assumed that there is a minimum distance,  $d_{\min}$ , over which the turbulent stresses acting between two points separated by this distance,  $\frac{1}{2}\rho_c C(\varepsilon d_{\min})^{2/3}$ , are just equal to the confinement pressure due to surface tension:  $\sigma_t(d_{\min}) = \sigma_s(d)$ . In other words, at this distance, the turbulent pressure fluctuations are exactly equal to the confinement forces for a parent particle of size  $d$ . The probability of breaking off a daughter particle with  $d' < d'_{\min} = (\frac{12\sigma_I}{C\rho_c d})^{3/2}\varepsilon^{-1}$  should therefore be zero.

The fundamental postulate of the Martínez-Bazán et al [79] model is that the probability of splitting off a daughter particle of any size such that  $d'_{\min} < d' < d$  is proportional to the difference between the turbulent stresses over a length  $d'$  and the confinement forces holding the parent particle of size  $d$  together. For the formation of a daughter particle of size  $d'$ , the difference in stresses is given by  $\Delta\sigma_{t,d'} = \frac{1}{2}\rho_c C(\varepsilon d')^{2/3} - 6\sigma_I/d$ . For each daughter particle of size  $d'$ , a complementary daughter particle of size  $(d^3 - d'^3)^{1/3}$  is formed with a difference of stresses given by  $\Delta\sigma_{t,(d^3-d'^3)^{1/3}} = \frac{1}{2}\rho_c C(\varepsilon(d^3 - d'^3)^{1/3})^{2/3} - 6\sigma_I/d$ .

The model states that the probability of forming a pair of complementary daughter particles of size  $d'$  and  $(d^3 - d'^3)^{1/3}$  from splitting a parent particle of size  $d$  is related to the product of the excess stresses associated with the length scales corresponding to each daughter particle size. That is,

$$P_B(d/d') \propto [\frac{1}{2}\rho_c C(\varepsilon d')^{2/3} - 6\sigma_I/d][\frac{1}{2}\rho_c C(\varepsilon(d^3 - d'^3)^{1/3})^{2/3} - 6\sigma_I/d]. \quad (9.94)$$

Relating  $d'$  and  $(d^3 - d'^3)^{1/3}$  through the mass balance given above yields:

$$P_B(d/d') \propto (\frac{1}{2}\rho_c C(\varepsilon d)^{2/3})^2 [(d'/d)^{2/3} - (d_c/d)^{5/3}] [(1 - (d'/d)^3)^{2/9} - (d_c/d)^{5/3}] \quad (9.95)$$

or

$$P_B(d^*) \propto (\frac{1}{2}\rho_c C(\varepsilon d)^{2/3})^2 [d^{2/3} - \Lambda^{5/3}] [(1 - d^3)^{2/9} - \Lambda^{5/3}] \quad (9.96)$$

where  $\Lambda = d_c/d$ ,  $d_c$  is the critical diameter defined as  $d_c = (\frac{12\sigma_I}{C\rho_c})^{3/5}\varepsilon^{-2/5}$ .

The critical parent particle diameter defines the minimum particle size for a given dissipation rate of turbulent kinetic energy for which breakage can occur. The minimum daughter diameter defines the distance over which the turbulent normal stresses just balance the confinement forces of a parent particle of size  $d$ . The minimum diameter, therefore, gives the minimum length over which the underlying turbulence can pinch off a piece of the parent

particle. This length is not arbitrarily selected, rather, its determination is based on kinematics.

This model further assumes that the size of the parent particles is in the inertial subrange of turbulence. Therefore, it implies that  $d_{\min} \leq d' \leq d_{\max}$  provided that  $d_{\min} > \lambda_d$ , where  $\lambda_d$  is the Kolmogorov length scale of the underlying turbulence. Otherwise,  $d_{\min}$  is taken to be equal to  $\lambda_d$ . However, no assumption needs to be made about the minimum and maximum eddy size that can cause particle breakage. All eddies with sizes between the Kolmogorov scale and the integral scale are taken into account.

The daughter particle probability density function can be obtained from the probability expression given above by utilizing the normalization condition:

$$\int_{d_{\min}^*}^{d_{\max}^*} P(d^*)d(d^*) = 1.$$

The pdf of the ratio of diameters  $d^* = d'/d$ ,  $P_B^*(d^*)$ , can then be written as:

$$P_B^*(d^*) = \frac{[d^{*2/3} - \Lambda^{5/3}][(1 - d^{*3})^{2/9} - \Lambda^{*5/3}]}{\int_{d_{\min}^*}^{d_{\max}^*} [d^{*2/3} - \Lambda^{5/3}][(1 - d^{*3})^{2/9} - \Lambda^{*5/3}]d(d^*)} \quad (-) \quad (9.97)$$

Note that  $P_B(d'|d) = P_B^*(d^*)/d$ ,  $\Lambda = d_c/d = (d_{\min}/d)^{2/5}$ .

Contrary to the collision based phenomenological models for the daughter particle size distribution, this model predicts a symmetric distribution with the highest probability for equal size particle breakage in accordance with the pure statistical model of Konno et al [44], Fig 9.6.

In general, purely statistical models for the daughter particle size distribution lack physical support. As for the breakage frequency models, the existing daughter particle size models based on the eddy collision arguments rely on the assumption that turbulence consists of a collection of eddies that can be treated using relationships from the kinetic theory of gases. Martínez-Bazán et al [79], on the other hand, made a first approach developing an average microscopic kinematic/statistical model, where the physics were included through a daughter size distribution function expressed based on kinematic arguments. Alternatively, one may develop kinematic/statistical models where an effective daughter size distribution function represents an average of a large number of simulations of the physical breakage phenomena for a series of operating conditions.

The deviating experimental observations reported in the literature indicate that further experimental investigations are needed determining reliable correlations for which physical systems and under which flow conditions the equal- and unequal breakage outcomes occur.

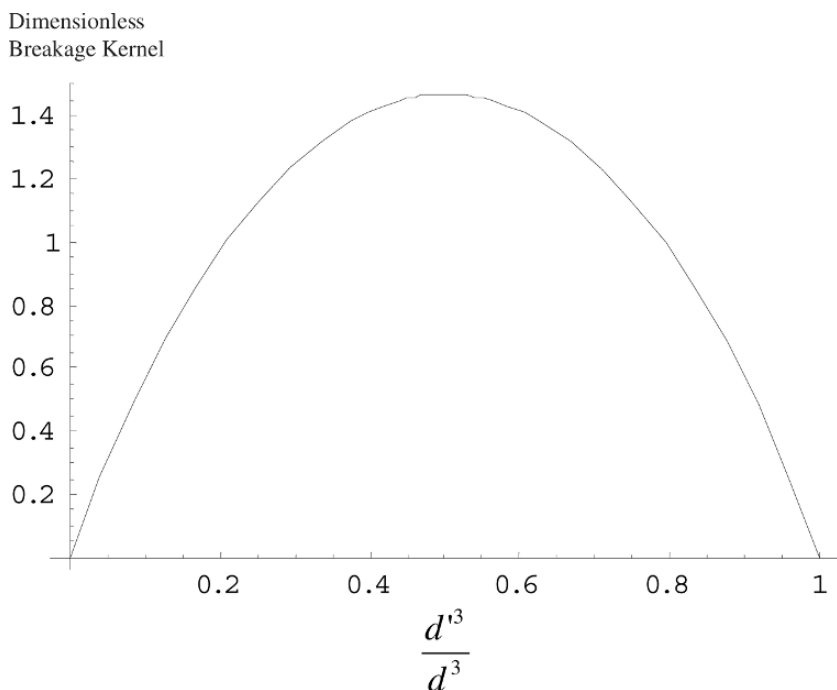


**Fig. 9.6.** A sketch of the breakage kernel of Konno et al [44]. An equal daughter size distribution is predicted by this model. The kernel by Martínez-Bazán et al [79] is quite similar to this one, but the shape of the profile is a little different close to the minimum and maximum  $\frac{d'^3}{d^3}$  values. Reprinted with permission from [38]. Copyright 2005 American Chemical Society.

### 9.1.3 The Statistical Mechanical Microscopic Population Balance Formulation

The statistical description of multiphase flow is developed based on the Boltzmann theory of gases [37, 121, 93, 11, 94, 58, 61]. The fundamental variable is the particle distribution function with an appropriate choice of internal coordinates relevant for the particular problem in question. Most of the multiphase flow modeling work performed so far has focused on isothermal, non-reactive mono-disperse mixtures. However, in chemical reactor engineering the industrial interest lies in multiphase systems that include multiple particle types and reactive flow mixtures, with their associated effects of mixing, segregation and heat transfer.

Defining a single distribution function,  $p(\mathbf{x}, \mathbf{r}, \mathbf{c}, t) d\mathbf{x} d\mathbf{r} d\mathbf{c}$ , as the probable number of particles with internal coordinates in the range  $d\mathbf{x}$  about  $\mathbf{x}$ , located in the spatial range  $d\mathbf{r}$  about the position  $\mathbf{r}$ , with a velocity range  $d\mathbf{c}$  about  $\mathbf{c}$ ,

at time  $t$ . A Boltzmann-type equation can be written to describe the temporal and spatial rate of change of the single distribution function,  $p$ :

$$\frac{\partial p}{\partial t} + \nabla_{\mathbf{r}} \cdot (\mathbf{c}p) + \nabla_{\mathbf{c}} \cdot (\mathbf{F}p) = -\nabla_{\mathbf{x}} \cdot \left\{ \frac{d\mathbf{x}}{dt} \right\} p + B'_B - D'_B + B'_C - D'_C + S' \quad (9.98)$$

where the rates of change of  $p$  with time due to breakage and coalescence are denoted by  $B'_B - D'_B + B'_C - D'_C$  with units  $(1/[\mathbf{x}](\mathbf{r})ms^{-1})$ . The force per unit mass acting on a particle is denoted by  $\mathbf{F}$ , and the rate of change with time of its internal coordinates is given by:  $\mathbf{v}_x$ .  $S'$  represents the rate of change of the distribution function caused by collisions which do not result in coalescence (i.e., rebound). Integrating over the whole particle velocity space to eliminate the particle velocity dependence, one obtains the following equation:

$$\frac{\partial f}{\partial t} + \nabla_{\mathbf{r}} \cdot (\mathbf{v}_r f) = -\nabla_{\mathbf{x}} \cdot (\mathbf{v}_x f) + B_B - D_B + B_C - D_C \quad \left( \frac{1}{[\mathbf{x}][\mathbf{r}]_s} \right) \quad (9.99)$$

where

$$f(\mathbf{x}, \mathbf{r}, t) = \int_{-\infty}^{\infty} p d\mathbf{c}. \quad (9.100)$$

The single distribution function  $f(\mathbf{x}, \mathbf{r}, t) d\mathbf{x} d\mathbf{r}$  thus denotes the probable number of particles within the internal coordinate space in the range  $d\mathbf{x}$  about  $\mathbf{x}$ , in the external (spatial) range  $d\mathbf{r}$  about  $\mathbf{r}$  at time  $t$ .  $\mathbf{v}_r$  is the mean velocity of all particles of properties  $\mathbf{x}$  at a location  $\mathbf{r}$  at time  $t$ . The velocity independent birth and death terms are defined by:

$$B_B - D_B + B_C - D_C = \int_{-\infty}^{\infty} (B'_B - D'_B + B'_C - D'_C) d\mathbf{c}. \quad (9.101)$$

Integrating the force term over the whole velocity space no net contribution appears explicitly in the population balance equation since the distribution function vanishes as the velocity approaches  $\pm\infty$ . Furthermore, the  $S'$ -term vanishes in the average equation as the number of particles is conserved during the rebound processes. Note, however, that the two last mentioned terms have direct effects on the size distribution as an consistent multi-fluid model developed from the Boltzmann equation (i.e., a granular model based on the population balance distribution function) would contain additional momentum transfer terms due to particle bouncing (e.g., a particle pressure contribution) and particle interactions with the wake of proceeding bubbles. These phenomena may also affect the coalescence and breakage processes, and may be accounted for by the corresponding closure laws.

To close the population balance problem, models are required for the growth, birth and death kernels. In the kinetic theory context, as distinct from the continuum mechanical approach, the continuum closure may be considered macroscopic in a similar manner as in the granular theory treating macroscopic particle properties.

### Using Particle Diameter as Inner Coordinate

For non-reactive, isothermal, particle mixtures it is customary to assume that all the relevant internal variables can be calculated in some way from the particle volume or diameter. It is natural to use the particle diameter as inner coordinate for the population balance analysis because this choice of inner coordinate coincides with the classical kinetic theory of gases. This inner coordinate is especially useful describing solid particle and incompressible fluid particle dispersions. A statistical description of dispersed multiphase flow can then be obtained by means of a distribution function  $f_{d_p}(d_p, \mathbf{r}, t)$ , defined so that the number of particles with diameters in the range  $d_p$  and  $d_p + d(d_p)$ , located in a volume  $d\mathbf{r}$  around a spatial location  $\mathbf{r}$  at time  $t$  is  $f(d_p, \mathbf{r}, t)d(d_p)d\mathbf{r}$ .

In this case the population balance (9.99) is usually expressed as:

$$\frac{\partial f}{\partial t} + \nabla_{\mathbf{r}} \cdot (\mathbf{v}f) = -\frac{\partial(Gf)}{\partial d_p} + B_B - D_B + B_C - D_C \quad \left( \frac{1}{[m](\mathbf{r})s} \right) \quad (9.102)$$

where  $G$  is a particle growth rate ( $m/s$ ).

To close the population balance problem, models are required for the growth, birth and death kernels. It is required that these kernels are consistent with the inner coordinate used. The coalescence and breakage kernels presented in this chapter are expressed in terms of the particle diameter.

### Using Particle Mass as Inner Coordinate

For flows where compressibility effects in a gas are important the use of the particle mass as internal coordinate may be advantageous because this quantity is conserved under pressure changes [11]. In this approach it is assumed that all the relevant internal variables can be derived from the particle mass, so the particle number distribution is described by the particle mass, position and time. Under these conditions, the dispersed phase flow fields are characterized by a single distribution function  $f(m, \mathbf{r}, t)$  such that  $f(m, \mathbf{r}, t)d\mathbf{r}dm$  is the number of particles with mass between  $m$  and  $m+dm$ , at time  $t$  and within  $d\mathbf{r}$  of position  $\mathbf{r}$ . Notice that the use of particle diameter and particle mass as inner coordinates give rise to equivalent population balance formulations in the case of describing incompressible fluids.

By taking the mass moments of the distribution function we define the following important multiphase flow parameters. The particle number density:

$$N(\mathbf{r}, t) = \int_0^{\infty} f(m, \mathbf{r}, t)dm; \quad (9.103)$$

The interfacial area density:

$$a(\mathbf{r}, t) = \int_0^{\infty} a(m, \mathbf{r})f(m, \mathbf{r}, t)dm; \quad (9.104)$$

where  $a(m, \mathbf{r})$  is the interfacial area of a particle having mass  $m$  at the location  $\mathbf{r}$ .

The particle mass density:

$$\rho_p^m(\mathbf{r}, t) = \rho_p(\mathbf{r}, t)\varepsilon_p(\mathbf{r}, t) = \int_0^\infty m f(m, \mathbf{r}, t) dm. \quad (9.105)$$

The dispersed phase volume fraction is related to the mass density by:

$$\varepsilon_p(\mathbf{r}, t) = \frac{\rho_p^m(\mathbf{r}, t)}{\rho_p(\mathbf{r}, t)} = \frac{\rho_p(\mathbf{r}, t)\varepsilon_p(\mathbf{r}, t)}{\rho_p(\mathbf{r}, t)} \quad (9.106)$$

where  $\rho_p(\mathbf{r}, t)$  is the local particle density which includes the effects of local pressure.

Assuming that the particle velocity for a given size is known,  $\mathbf{v} = \mathbf{v}(m, \mathbf{r}, t)$ , one may express a Boltzmann type of transport equation for the single distribution function:

$$\frac{\partial f(m, \mathbf{r}, t)}{\partial t} + \nabla_{\mathbf{r}} \cdot [\mathbf{v}_r(m, \mathbf{r}, t)f(m, \mathbf{r}, t)] + \frac{\partial}{\partial m} \left[ \frac{dm}{dt} f(m, \mathbf{r}, t) \right] = B_B(m, \mathbf{r}, t) - D_B(m, \mathbf{r}, t) + B_C(m, \mathbf{r}, t) - D_C(m, \mathbf{r}, t) \left( \frac{1}{[\text{kg}]m^3\text{s}} \right) \quad (9.107)$$

where  $B_B(m, \mathbf{r}, t)$ ,  $D_B(m, \mathbf{r}, t)$ ,  $B_C(m, \mathbf{r}, t)$  and  $D_C(m, \mathbf{r}, t)$  are the corresponding birth and death terms due to particle breakage and coalescence. The third term on the left hand side is related to the mass change of the particle that is caused by condensation, evaporation or dissolution.

Considering binary interactions only, as were assumed in the previous section, the particle breakage terms can be written as:

$$B_B(m, \mathbf{r}, t) = \int_m^\infty b(m, m''; m') f(m', \mathbf{r}, t) dm' = \int_m^\infty b(m, m' - m; m') f(m', \mathbf{r}, t) dm' \quad (9.108)$$

$$D_B(m, \mathbf{r}, t) = \int_0^m b(m, m''; m') f(m, \mathbf{r}, t) dm' = \int_0^m b(m, m' - m; m') f(m, \mathbf{r}, t) dm' \quad (9.109)$$

where  $b(m, m''; m')$  is the breakage frequency and represents the probability per unit time and mass that a particle of mass  $m'$  splits creating a particle of mass  $m''$  and a particle of mass  $m$ . As no mass is lost or gained in the breakage (and coalescence) processes, we have used the mass conservation principle  $m' = m'' + m$  to rewrite the particle breakage terms.

The corresponding coalescence terms yield:

$$B_C(m, \mathbf{r}, t) = \frac{1}{2} \int_0^m \omega_C(m - m'; m') p_C(m - m', m', \mathbf{r}, t) dm' \quad (9.110)$$

$$D_B(m, \mathbf{r}, t) = \int_0^{\infty} \omega_C(m', m) p_C(m, m', \mathbf{r}, t) dm' \quad (9.111)$$

where  $\omega_C$  denotes the collision density (i.e., probability per unit time) between bubbles of mass  $m'$  and  $m$ , and  $p_C$  is the coalescence probability denoting the probability of coalescence if a collision occurs. As for the breakage terms, the mass conservation principle  $m' = m'' + m$  has been implemented to rewrite the fluid particle coalescence terms.

The particles can change their mass if sublimation, condensation or evaporation occurs, or if mass is lost or gained due to interfacial mass transfer (mass diffusion). The interfacial mass transfer rate can be represented by use of the simple film model and expressed in terms of a mass transfer coefficient:

$$\frac{dm_i}{dt} = k_i a (\rho_i - \rho_i^*) V_{\text{mix}} \left( \frac{kg}{s} \right) \quad (9.112)$$

where  $k_i$  denotes the mass transfer coefficient ( $m/s$ ),  $a$  denotes the interfacial area ( $m^2/m^3$ ),  $\rho_i$  denotes the mass density of component  $i$  in the bulk of the phase, and  $\rho_i^*$  denotes the mass density of component  $i$  at the interface (i.e., for fluid particles it denotes the equilibrium mass density), and  $V_{\text{mix}}$  denotes the volume of the mixture.

The growth term thus yields:

$$\frac{\partial}{\partial m} \left[ \frac{dm}{dt} f(m, \mathbf{r}, t) \right] = \frac{\partial}{\partial m} \left[ \sum_i k_i a (\rho_i - \rho_i^*) V_{\text{mix}} f(m, \mathbf{r}, t) \right] \quad (9.113)$$

## Using Multiple Inner Coordinates

For non-isothermal, reactive multicomponent mixtures more advanced definitions of the distribution function is required. Adopting a kinetic theory modeling framework the dispersed particle phases might be separated on the basis of their physical properties (diameter, density, viscosity) or through their thermo-chemical properties (reactive versus inert particles). From chap 4 we reiterate that to enable the description of segregation effects a multi-fluid approach is required where the macroscopic balance equations are derived from the kinetic theory of granular flow using inelastic rigid-sphere models, thereby accounting for collisional transfer in high-density regions. Separate transport equations are constructed for each of the particle phases, as well as for the equilibration processes whereby momentum and energy are exchanged between the respective particle phases and the carrier fluid. Aimed at high-density suspensions, such as fluidized bed reactors, the relations obtained for the stress tensor are augmented by a model for frictional transfer, suitably extended to polydispersed systems. For reactive chemical processes the model are further extended to include heat and mass transfer, as well as chemical reactions.

To describe a chemical process in a fluid bed reactor Lathouwers and Bellan [61] introduced an extended form of the single-particle distribution function of particle phase  $i$  such that  $p_i^{(1)}(m, \mathbf{r}, \mathbf{c}, \mathbf{Y}, t)$  with  $\mathbf{Y} = \omega_c, T$  is the probable number of particles having their center of mass in the region  $\mathbf{r}, \mathbf{r} + d\mathbf{r}$ , a velocity in the region  $\mathbf{c}, \mathbf{c} + d\mathbf{c}$ , mass in the region  $m, m + dm$ , mass fractions in  $\omega_c, \omega_c + d\omega_c$ , temperature in  $T, T + dT$ , at time  $t$ .

The application of similar advanced distribution functions in the context of population balance analysis of polymerization processes is familiar in reaction engineering [40, 97]. However, the microscopic balance equations used for this purpose are normally averaged over the whole reactor volume so that simplified macroscopic (global) reactor analysis of the chemical process behavior is generally performed [35].

### The Continuous Source Term Closures

Only a few continuous source term closures are available, hence the discrete PBE model closures are used in practice. The macroscopic statistical mechanical PBE model thus coincides with the macroscopic PBE derived from continuum mechanical principles. In this way there are little or no differences in employing these two approaches. However, the formulation of the constitutive equations are strongly influenced by the concepts of kinetic theory of dilute gases. Nevertheless, the present closures are still at an early stage of development and future work should continue developing more reliable parameterizations of the kernels. These must be validated for the application in question.

---

## References

1. Angelidou C, Psimopoulos M, Jameson GJ (1979) Size Distribution Functions of Dispersions. *Chem Eng Sci* 34(5):671-676
2. Azbel D (1981) Two-phase flows in chemical engineering. Chambridge University Press, Chambridge
3. Azbel D, Athanasios IL (1983) A Mechanism of Liquid Entrainment. p 473, In: Cheremisinoff N (ed) *Handbook of Fluids in Motion*, Ann Arbor Science Publishers, Ann Arbor, MI
4. Barrow JD (1981) Coagulation with fragmentation. *Journal of physics A: Mathematical and General* 14:729-733
5. Batchelor GK (1953) *The Theory of Homogeneous Turbulence*. Cambridge University Press, Cambridge
6. Batchelor GK (1956) *The Theory of Homogeneous Turbulence*. Cambridge University Press, Cambridge
7. Batchelor GK (1982) *The Theory of Homogeneous Turbulence*. Cambridge University Press, Cambridge
8. Bertola F, Grundseth J, Hagesaether L, Dorao C, Luo H, Hjarbo KW, Svendsen HF, Vanni M, Baldi G, Jakobsen HA (2005) Numerical Analysis and Experimental Validation of Bubble Size Distribution in Two-Phase Bubble Column Reactors. *Multiphase Science & Technology* 17(1-2):123-145
9. Brenn G, Braeske H, Durst F (2002) Investigation of the unsteady two-phase flow with small bubbles in a model bubble column using phase-Doppler anemometry. *Chem Eng Sci* 57(24):5143-5159
10. Buwa VV, Ranade VV (2002) Dynamics of gas-liquid flow in a rectangular bubble column: Experimental and single/multigroup CFD simulations. *Chem Eng Sci* 57(22-23):4715-4736
11. Carrica PM, Drew D, Bonetto F, Lahey Jr RT (1999) A Polydisperse Model for Bubbly Two-Phase Flow Around a Surface Ship. *Int J Multiphase Flow* 25(2):257-305
12. Chen P, Dudukovic MP, Sanyal J (2005) Three-dimensional simulation of bubble column flows with bubble coalescence and breakup. *AIChE J* 51(3):696-712
13. Chen P, Sanyal J, Dudukovic MP (2005) Numerical simulation of bubble columns: effect of different breakup and coalescence closures. *Chem Eng Sci* 60:1085-1101

14. Chester AK (1991) The modelling of coalescence processes in fluid-fluid dispersions: A review of current understanding. *Trans IChemE* 69(A):259-270
15. Colella D, Vinci D, Bagatin R, Masi M, Bakr EA (1999) A study on coalescence and breakage mechanisms in three different bubble columns. *Chem Eng Sci* 54 (21):4767-4777
16. Coualoglou CA, Tavlarides LL (1977) Description of Interaction Processes in Agitated Liquid-Liquid Dispersions. *Chem Eng Sci* 32(11):1289-1297
17. Danckwerts PV (1953) Continuous Flow Systems: Distribution of Residence Times. *Chem Eng Sci* 2(1):1-18
18. Dorao CA (2006) High Order Methods for the Solution of the Population Balance Equation with Applications to Bubbly Flows. Dr ing thesis, Department of Chemical Engineering, The Norwegian University of Science and Technology, Trondheim
19. Dorao CA, Lucas D, Jakobsen HA (2007) Prediction of the Evolution of the Dispersed Phase in Bubbly Flow Problems. Accepted for publication, Applied Mathematical Modeling
20. Doubliez L (1991) The drainage and rupture of a non-foaming liquid film formed upon bubble impact with a free surface. *Int J Multiphase Flow* 17(6):783-803
21. Drazin PG, Reid WH (1981) *Hydrodynamic Stability*. Cambridge University Press, Cambridge
22. Eastwood CD, Armi L, Lasheras JC (2004) The breakup of immiscible fluids in turbulent flows. *J Fluid Mech* 502:309-333
23. Fleischer C, Bierdel M, Eigenberger G (1994) Prediction of Bubble Size Distributions in G/L-Contactors with Population Balances. Proc of Third German/Japanese Symposium on Bubble Columns, Schwerte, Germany, Jun 13-15, pp 229-235
24. Frank T, Zwart PJ, Shi J-M, Krepper E, Lucas D, Rohde U (2005) Inhomogeneous MUSIG Model - a Population Balance Approach for Polydispersed Bubbly Flows. *Int Conf Nuclear Energy for New Europe 2005*, Bled, Slovenia, September 5-8
25. Friedlander SK (2000) *Smoke, Dust, and Haze: Fundamentals of Aerosol Dynamics*, Second Edition, Oxford University Press, New York
26. Guido Lavalle G, Carrica PM, Clausse A, Qazi MK (1994) A bubble number density constitutive equation. *Nucl Engng Des* 152:213-224
27. Hagesaether L, Jakobsen HA, Svendsen HF (1999) Theoretical Analysis of Fluid Particle Collisions in Turbulent Flow. *Chem Eng Sci* 54(21):4749-4755
28. Hagesaether L, Jakobsen HA, Hjarbo K, Svendsen HF (2000) A Coalescence and Breakup Module for Implementation in CFD-codes. *Computer-Aided Chemical Engineering* 8:367-372
29. Hagesaether L, Jakobsen HA, Svendsen HF (2002) A Model for Turbulent Binary Breakup of Dispersed Fluid Particles. *Chem Eng Sci* 57(16):3251-3267
30. Hagesaether L, Jakobsen HA, Svendsen HF (2002) Modeling of the Dispersed-Phase Size Distribution in Bubble Columns. *Ind Eng Chem Res* 41(10): 2560-2570
31. Hagesaether L (2002) Coalescence and Break-up of Drops and Bubbles. Dr ing Thesis, Department of Chemical Engineering, The Norwegian University of Science and Technology, Trondheim

32. Havelka P, Gotaas C, Jakobsen HA, Svendsen HF (2004) Droplet Formation and Interactions under Normal and High pressures. Proc at the 5th Int Conf on Multiphase Flow, ICMF'04, Yokohama, Japan, May 30-June 4
33. Hesketh RP, Etchells AW, Russell TWF (1991) Experimental observations of bubble breakage in turbulent flows. *Ind Eng Chem Res* 30(5):835-841
34. Hesketh RP, Etchells AW, Russell TWF (1991) Bubble breakage in pipeline flows. *Chem Eng Sci* 46(1):1-9
35. Himmelblau DM, Bischoff KB (1968) *Process Analysis and Simulation: Deterministic Systems*. John Wiley & Sons Inc, New York
36. Hinze JO (1955) Fundamentals of the Hydrodynamic Mechanism of Splitting in Dispersion Processes. *AIChE J* 1(3):289-295
37. Hulburt HM, Katz S (1964) Some problems in particle technology: A statistical mechanical formulation. *Chem Eng Sci*, 19(8):555-574
38. Jakobsen HA, Lindborg H, Dorao CA (2005) Modeling of Bubble Column Reactors: Progress and Limitations. *Ind Eng Chem Res* 44:5107-5151
39. Kamp AM, Chesters AK, Colin C, Fabre J (2001) Bubble coalescence in turbulent flows: A mechanistic model for turbulence-induced coalescence applied to microgravity bubbly pipe flow. *Int J Multiphase Flow* 27(8):1363-1396
40. Kiparissides C (2006) Challenges in particulate polymerization reactor modeling and optimization: A population balance perspective. *J Process Control* 16:205-224
41. Klaseboer E, Chevallier JP, Masbernat O, Gourdon C (1998) Drainage of the liquid film between drops colliding at constant approach velocity. Proc of the Third International Conference on Multiphase Flow, ICMF98, Lyon, France, June 8-12
42. Klaseboer E, Chevallier JP, Gourdon C, Masbernat O (2000) Film drainage between colliding drops at constant approach velocity: Experimental and modeling. *Journal of Colloids and Interface Science* 229(1):274-285
43. Kocamustafaogullari G, Ishii M (1995) Foundation of the interfacial area transport equation and its closure relations. *Int J Heat Mass Transfer* 38(3):481-493
44. Konno M, Aoki M, Saito S (1980) Simulations model for break-up process in an agitated tank. *J Chem Eng Jpn* 13:67-73
45. Kolev NI (1993) Fragmentation and Coalescence Dynamics in Multi-phase Flows. *Experimental Thermal and Fluid Science* 6(3):211-251
46. Kolev NI (2002) *Multiphase Flow Dynamics 2: Mechanical and Thermal Interactions*. Springer, Berlin
47. Kolmogorov AN (1941) Local Structure of Turbulence in Incompressible Viscous Fluid for Very Large Reynolds Number. *it Dokl Akad Nauk SSSR* 30: 301-306
48. Kolmogorov AN (1949) On the Breakage of Drops in a Turbulent Flow. *Dokl Akad Nauk SSSR* 66:825-828
49. Krishna R, Urseanu MI, van Baten JM, Ellenberger J (1999) Influence of scale on the hydrodynamics of bubble columns operating in the churn-turbulent regime: experiments vs Eulerian simulations. *Chem Eng Sci* 54(21):4903-4911
50. Krishna R, van Baten JM, Urseanu MI (2000) Three-phase Eulerian simulations of bubble column reactors operating in the churn-turbulent regime: a scale up strategy. *Chem Eng Sci* 55(16):3275-3286
51. Krishna R, van Baten JM (2001) Scaling up Bubble column reactors with the aid of CFD. *Inst Chem Eng Trans IChemE* 79(A3):283-309.

52. Krishna R, van Baten JM (2001) Eulerian simulations of bubble columns operating at elevated pressures in the churn turbulent flow regime. *Chem Eng Sci* 56(21-22):6249-6258
53. Kuboi R, Komazawa I, Otake T (1972) Behavior of dispersed particles in turbulent liquid flow. *J Chem Eng Japan* 5:349-355
54. Kuboi R, Komazawa I, Otake T (1972) Collision and coalescence of dispersed drops in turbulent liquid flow. *J Chem Eng Japan* 5:423-424
55. Laakkonen M, Moilanen P, Alopaus V, Aittamaa J (2007) Modelling local bubble size distributions in agitated vessels. *Chem Eng Sci* 62:721-740
56. Laari A, Turunen I (2003) Experimental Determination of Bubble Coalescence and Break-up Rates in a Bubble Column Reactor. *The Canadian Journal of Chemical Engineering* 81(3-4):395-401
57. Lafi AY, Reyes JN (1994). General particle transport equations. Final Report OSU-NE-9409. Department of Nuclear Engineering, Oregon State University
58. Lasheras JC, Eastwood C, Martínez-Bazán C, Montañés JL (2002) A review of statistical models for the break-up of an immiscible fluid immersed into a fully developed turbulent flow. *Int J Multiphase Flow* 28(2):247-278
59. Lathouwers D, Bellan J (2000) Modeling of dense gas-solid reactive mixtures applied to biomass pyrolysis in a fluidized bed. Proc of the 2000 U.S. DOE Hydrogen Program Review. NREL/CP-570-28890
60. Lathouwers D, Bellan J (2000) Modeling and simulation of bubbling fluidized beds containing particle mixtures. Proc of the Combustion Institute 28:2297-2304
61. Lathouwers D, Bellan J (2001) Modeling of biomass pyrolysis for hydrogen production: The fluidized bed reactor. Proc of the 2001 U.S. DOE Hydrogen Program Review. NREL/CP-570-30535
62. Lathouwers D, Bellan J (2001) Yield Optimization and Scaling of Fluidized Beds for Tar Production from Biomass. *Energy & Fuels* 15:1247-1262
63. Lathouwers D, Bellan J (2001) Modeling of dense gas-solid reactive mixtures applied to biomass pyrolysis in a fluidized bed. *Int J Multiphase Flow* 27:2155-2187
64. Laurencot P, Mischler S (2002) The continuous coagulation-fragmentation equations with diffusion. *Arch Rational Mech Anal* 162:45-99
65. Laurencot P, Mischler S (2004) Modeling and computational methods for kinetic equations. Birkhäuser, Boston
66. Lee C-K, Erickson LE, Glasgow LA (1987) Bubble Breakup and Coalescence in Turbulent Gas-Liquid Dispersions. *Chem Eng Comm* 59(1-6):65-84
67. Lehr F, Mewes D (2001) A transport equation for the interfacial area density applied to bubble columns. *Chem Eng Sci* 56(3):1159-1166
68. Lehr F, Millies M, Mewes D (2002) Bubble-Size Distributions and Flow Fields in Bubble Columns. *AIChE J* 48(11):2426-2443
69. Levich VG (1962) *Physicochemical Hydrodynamics*. Prentice Hall, Englewood Cliffs, NJ
70. Lo S (1996) Application of population balance to CFD modelling of bubbly flow via the MUSIG model. AEA Technology, AEAT-1096.
71. Lo S (2000) Some recent developments and applications of CFD to multiphase flows in stirred reactors. Proc of AMIF-ESF Workshop: Computing Methods for Two-Phase Flow. Aussois, France, 12-14 January

72. Lo S (2000) Application of population balance to CFD modeling of gas-liquid reactors. Proc of Trends in numerical and physical modelling for industrial multiphase flows, Corse, 27-29 September
73. Luo H (1993) Coalescence, break-up and liquid circulation in bubble column reactors. Dr ing Thesis, the Norwegian Institute of Technology, Trondheim
74. Luo H, Svendsen HF (1996) Theoretical Model for Drop and Bubble Breakup in Turbulent Dispersions. *AIChE J* 42(5):1225-1233
75. Marchisio DL, Vigil RD, Fox RO (2003) Implementation of the quadrature method of moments in CFD codes for aggregation-breakage problems. *Chem Eng Sci* 58(15):3337-3351
76. Marchisio DL, Vigil RD, Fox RO (2003) Quadrature method of moments for aggregation-breakage processes. *Journal of Colloid and Interface Science* 258(2):322-334
77. Marrucci G (1969) A Theory of Coalescence. *Chem Eng Sci* 24(6):975-985
78. Martínez-Bazán C, Montañés JL, Lasheras JC (1999) On the breakup of an air bubble injected into a fully developed turbulent flow. Part 1. Breakup frequency. *J Fluid Mech* 401:157-182
79. Martínez-Bazán C, Montañés JL, Lasheras JC (1999) On the breakup of an air bubble injected into a fully developed turbulent flow. Part 2. Size PDF of the resulting daughter bubbles. *J Fluid Mech* 401:183-207
80. Melzak ZA (1957) A scalar transport equation. *Transactions of the American Mathematical Society* 85:547-560
81. Melzak ZA (1957) A scalar transport equation II. *Michigan Mathematical Journal* 4(3):193-206
82. Millies M, Mewes D (1999) Interfacial area density in bubbly flow. *Chemical Engineering and Processing* 38(4-6):307-319
83. Olmos E, Gentric C, Vial C, Wild G, Midoux N (2001) Numerical simulation of multiphase flow in bubble column reactors. Influence of bubble coalescence and breakup. *Chem Eng Sci* 56(21-22):6359-6365
84. Olmos E, Gentric C, Midoux N (2003) Numerical description of flow regime transitions in bubble column reactors by multiple gas phase model. *Chem Eng Sci* 58(10):2113-2121
85. Oolman TO, Blanch HW (1986) Bubble Coalescence in Stagnant Liquid. *Chem Eng Commun* 43(4-6):237-261
86. Orme M (1997) Experiments on Droplet Collisions, Bounce, Coalescence and Disruption. *Prog Energy Combust Sci* 23:65-79
87. Pilon L, Fedorov AG, Ramkrishna D, Viskanta R (2004) Bubble transport in three-dimensional laminar gravity-driven flow - mathematical formulation. *Journal of Non-Crystalline Solids* 336(2):71-83
88. Politano MS, Carrica PM, Baláño JL (2003) About bubble breakup models to predict bubble size distributions in homogeneous flows. *Chem Eng Comm* 190(3):299-321
89. Pope SB (2001) *Turbulent Flows*. Cambridge University Press, Cambridge
90. Prasher CL (1987) *Crushing and Grinding Process Handbook*. John Wiley & Sons Limited, Chichester
91. Present RD (1958) *Kinetic Theory of Gases*. McGraw-Hill, New York
92. Prince MJ, Blanch HW (1990) Bubble Coalescence and Break-Up in Air-Sparged Bubble Columns. *AIChE J* 36(10):1485-1499
93. Ramkrishna D (1985) The Status of Population Balances. *Revs Chem Eng* 3:49-97

94. Ramkrishna D (2000) Population Balances: Theory and Applications to Particulate Systems in Engineering. Academic Press, San Diego
95. Randolph AD (1964) A Population Balance for Countable Entities. *Can J Chem Eng* 42(6):280
96. Randolph AD, Larson MA (1988) Theory of Particulate Processes: Analysis and Techniques of Continuous Crystallization. Second Edition, Academic Press Inc, Harcourt Brace Jovanovich, Publishers, San Diego
97. Rawlings JB, Ray WH (1988) The Modeling of Batch and Continuous Emulsion Polymerization Reactors. Part I: Model Formulation and Sensitivity to Parameters. *Polymer Engineering and Science* 28(5):237-256
98. Reyes Jr JN (1989) Statistically derived conservation equations for fluid particle flows. Proc ANS Winter Meeting. Nuclear Thermal Hydraulics, 5th Winter Meeting
99. Risso F, Fabre J (1998) Oscillations and breakup of a bubble immersed in a turbulent field. *J Fluid Mech* 372:323-355
100. Rodríguez-Rodríguez J, Martínez-Bazán C, Montañés JL (2003) A novel particle tracking and break-up detection algorithm: application to the turbulent break-up of bubbles. *Meas Sci Technol* 14(8):1328-1340
101. Ross SL, Curl RL (1973) Measurement and models of the dispersed phase mixing process. Proc of Fourth Joint Chemical Engineering Conference, Paper 29b, Symposium Series 139, AIChE Press, Vancouver Canada September 9-12
102. Saboni A, Gourdon C, Chesters AK (1999) The influence of inter-phase mass transfer on the drainage of partially-mobile liquid films between drops undergoing a constant interaction force. *Chem Eng Sci* 54(4):461-473
103. Saboni A, Alexandrova S, Gourdon C, Chesters AK (2002) Inter-drop coalescence with mass transfer: Comparison of the approximate drainage models with numerical results. *Chemical Engineering Journal* 88(1-3):127-139
104. Sha Z, Laari A, Turunen I (2004) Implementation of Population Balance into Multiphase-Model in CFD Simulation of Bubble Column. Proc of the 16th Int Congress of Chem Eng, Praha, Czech Republic (paper E3.2)
105. Sha Z, Laari A, Turunen I (2006) Multi-Phase-Multi-Size-Group Model for the Inclusion of Population Balances into the CFD Simulation of Gas-Liquid Bubbly Flows. *Chem Eng Technol* 29(5):550-559
106. Shah YT, Kelkar BG, Godbole SP, Deckwer W-D (1982) Design parameter estimations for bubble column reactors. *AIChE J* 28(3):353-379
107. Shi J, Zwart P, Frank T, Rohde U, Prasser H (2004). Development of a multiple velocity multiple size group model for poly-dispersed multiphase flows. Annual Report 2004. Institute of Safety Research, Forschungszentrum Rossendorf, Germany
108. Simonin O (1996) Combustion and turbulence in two-phase flows. von Karman Lecture Series 1996-02, von Karman Institute for Fluid Dynamics
109. Smoluchowski M (1916) Drei vortrage uber diffusion, Brownsche molekularbewegung und koagulation von kolloidteilchen. *Phys Z* 17:557-585
110. Smoluchowski M (1917) Versuch einer mathematischen theorie der koagulationskinetik kolloider lösungen. *Z Physik Chem* 92:129-168
111. Smoluchowski M (1918) Versuch einer mathematischen theorie der koagulationskinetik kolloider lösungen. *Z Physik Chem*, Leipzig Band XCII, pp 129-168
112. Stewart CW (1995) Bubble Interaction in Low-viscosity Liquids. *Int J Multiphase Flow* 21(6):1037-1046

113. Thomas RM (1981) Bubble Coalescence in Turbulent Flows. *Int J Multiphase Flow* 7(6):709-717
114. Tsouris C, Tavlarides LL (1994) Breakage and Coalescence Models for Drops in Turbulent Dispersions. *AIChE J* 40:395-406
115. Valentas KJ, Bilous O, Amundson NR (1966) Analysis of Breakage in Dispersed Phase Systems. I & EC Fundamentals 5(2):271-279
116. Valentas KJ, Amundson NR (1966) Breakage and Coalescence in Dispersed Phase Systems. I & EC Fundamentals 5(4):533-542
117. Vanni M (2000) Approximate population balance equation for aggregation-breakage processes. *Journal of Colloid and Interface Science* 221(2):143-160
118. Venneker BCH, Derksen JJ, van den Akker HEA (2002) Population Balance Modeling of Aerated Stirred Vessels Based on CFD. *AIChE J* 48(4):673-685
119. Wang T, Wang J, Jin Y (2003) A novel theoretical breakup kernel function for bubbles/droplets in a turbulent flow. *Chem Eng Sci* 58(20):4629-4637
120. Wang T, Wang J, Jin Y (2005) Population Balance Model for Gas-Liquid Flows: Influence of Bubble Coalescence and Breakup Models. *Ind Eng Chem Res* 44:7540-7549
121. Williams FA (1985) *Combustion Theory: The fundamental theory of chemically reacting flow systems*. Second edition, Benjamin/Cummings, Menlo Park, CA
122. Williams MMR, Loyalka SK (1991) *Aerosol Science Theory and Practice: With Special Applications to the Nuclear Industry*. Pergamon Press, Oxford

## Fluidized Bed Reactors

In this chapter the characteristics of fluidized gas-solid suspensions are described, and the basic designs of fluidized bed reactors are sketched. Several modeling approaches that have been applied to described these units are outlined.

The term *fluidization* has been used in the literature to refer to dense-phase and lean-phase systems, as well as circulation systems involving fast fluidization, pneumatic transport or moving beds [56, 82]. The broad field of fluidization engineering thus deals with all these modes of contacting, but the two major groups of fluidized bed reactors are the dense phase and lean-phase reactors. Among the dense phase reactors, the bubbling bed reactor design is most common. The lean-phase flow regimes are employed in circulating bed reactors. The first industrial applications of the fluidized bed technology considered gasification of coal and the chemical fluid catalytic cracking (FCC) process. Today, the FCC process and circulating fluidized bed combustion (CFBC) are the major technologies for circulating fluidized beds.

Moving packed beds normally consist of a stack of catalyst particles inside a tube thus resembling a fixed bed. In a moving packed bed reactor, as distinct from fixed bed, the gravity force is generally utilized to shift the catalyst from top to bottom. However, other arrangements like upwards, horizontal and inclined beds exist as well. Therefore, the moving bed reactors have many of the same properties as fixed beds, but allow continuous regeneration of deactivated catalyst and lower pressure drop. Large scale operations of moving beds can thus be employed for rapidly deactivated catalysts [82]. Temperature gradients caused by extreme exothermic/endothermic reactions can also be minimized with appropriate solid circulation. Nevertheless, very little is known about the hydrodynamics, mixing, and transport characteristics of moving bed reactors. Moving beds are thus not considered further in this book.

## 10.1 Solids Classification

When gas is passed through a bed of solid particles, various types of flow regime are observed. Operating conditions, solid flux, gas flux and system configuration and the solid particle properties (e.g., mean size, size distribution, shape, density, and restitution coefficient) are factors that affect the prevailing flow regime. Geldart [49] investigated the behavior of solid particles of various sizes and densities fluidized by gases. From this study a four group classification of solids was proposed to categorize the bed behavior based on particle density and particle size:

- *Group A*: Solid particles having a small mean size  $30 < d_p < 100 \mu\text{m}$  [52, 142] and/or low particle density  $< \sim 1.4\text{g}/\text{cm}^3$ . These solids fluidize easily, with smooth fluidization at low gas velocities and bubbling/turbulent fluidization at higher gas velocities. Typical examples of this class of solid particles are catalysts used for fluid catalytic cracking (FCC) processes.
- *Group B*: Most solid particles of mean size  $100\mu\text{m} < d_p < 800\mu\text{m}$  [52] and density in the range  $1.4\text{g}/\text{cm}^3 < \rho_s < 4\text{g}/\text{cm}^3$ . These solids fluidize vigorously with formation of bubbles that may grow in size. Sand particles are representative for this group of solids.
- *Group C*: This class of solids includes very fine and cohesive powders. For most cases  $d_p < \sim 20\mu\text{m}$  [52]. With these particles normal fluidation is extremely difficult because inter-particle forces are greater than those resulting from the action of gas. Cement, face powder, flour, and starch are representative for this group of solids.
- *Group D*: These solid particles are large  $d_p > \sim 1\text{mm}$  [52] and/or dense, and spoutable. Large exploding bubbles or severe channeling may occur in fluidization of this type of solids. Drying grains and peas, roasting coffee beans, gasifying coals, and some roasting metal ores are representative for these solids.

Apart from density and particle size, several other solid properties, including angularity, surface roughness and composition may also significantly affect the quality of fluidization. However, in many cases Geldart's classification chart is still a useful starting point to examine fluidization quality of a specific gas-solid system.

## 10.2 Fluidization Regimes for Gas-Solid Suspension Flow

Most gas-solid systems experience a range of flow regimes as the gas velocity is increased. Several important gas-solid fluidization regimes for the chemical process industry are sketched in Fig 10.1. In dense fluidized beds regions of low solid density may be created. These gas pockets or voids are frequently referred to as bubbles.

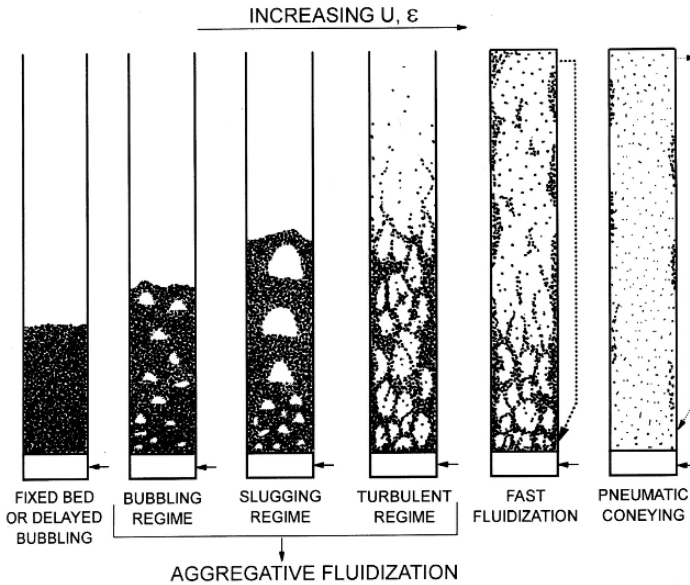


**Fig. 10.1.** The primary gas-solid flow-regimes [52, 58]. Reprinted with permission from the author 2007.

Each of the fluidization regimes has characteristic solids concentration profiles. A plot of the profile showing the solids concentration versus the height above the distributor for the bubbling bed regime of fluidization takes a pronounced s-shape. With increasing gas velocity the s-shape profile becomes less pronounced and is almost upright or uniform for the pneumatic conveying regime.

The main characteristics of the pertinent gas-solid flow regimes are [144, 56, 82, 47, 44]:

- *Fixed bed:* When a fluid is passing upward through a bed of fine particles at a low flow rate, and the fluid merely seeps through the void spaces between stationary particles.
- *Expanded bed:* With an increase in flow rate, a few particles vibrate and move apart in restricted ranges.
- *Minimum fluidization:* At a still higher velocity, a point is reached where all the particles are just suspended by the upward-flowing gas. At this point the frictional force between particle and fluid just counterbalances the weight of the particles, and the vertical component of the compressive force between adjacent particles disappears. The pressure drop through any section of the bed thus balance (approximately) the weight of fluid and particles in that section. Further increase in the gas velocity flow rate will not change the pressure drop noteworthy.

- *Smooth fluidization:* In fine particle A beds, a limited increase in gas flow rate above minimum fluidization can result in smooth, progressive expansion of the bed. Bubbles do not appear as soon as the minimum fluidization state is reached. There is a narrow range of velocities in which uniform expansion occurs and no bubbles are observed. Such beds are called a particulate fluidized bed, a homogeneously fluidized bed, or a smoothly fluidized bed. However, this regime does not exist in beds of larger particles of type B and D, in these cases bubbles do appear as soon as minimum fluidization is reached.
- *Bubbling fluidization:* An increase in flow rate beyond the point of minimum fluidization results in large instabilities with bubbling and channeling of gas. At higher flow rates, agitation becomes more violent and the movement of solids becomes more vigorous. Bubble coalescence and breakage take place, and with increasing gas velocity the tendency of bubble coalescence is normally enhanced. However, the bed does not expand much beyond its volume at minimum fluidization.
- *Slugging fluidization:* The gas bubbles coalesce and grow as they rise, and in a deep enough bed of small diameter they may eventually become large enough to spread across the vessel. Fine particles flow smoothly down by the wall around the rising void of gas. These voids are called axial slugs. For coarser particle beds, the portion of the bed above the bubble is pushed upward. Particles fall down from the slug, which finally disintegrates. Then another slug forms, and this unstable oscillatory motion is repeated. This is called a flat slug. Slugging normally occurs in long, narrow fluidized beds.
- *Turbulent fluidization:* This is often regarded as a transition regime from bubbling to lean phase fluidization. At relatively low gas velocities in this regime, bubbles are present. Moreover, when fine Geldart A particles are fluidized at a sufficiently high gas flow rate, the terminal velocity of the solids is exceeded, thus the upper surface of the bed becomes more diffuse with a large particle concentration in the freeboard, the solids entrainment becomes appreciable, and a turbulent motion of solid clusters and voids of gas of various sizes and shapes occurs. In contrast to the bubbling regime, in this regime the tendency for bubble breakage is enhanced as the gas velocity increases. For this reason the mean bubble size is significantly smaller than in the bubbling regime, hence the suspension becomes more uniform as the gas velocity further increases toward the lean phase fluidization regimes. However, for very high gas velocities within this regime pronounced radial gradients may occur, with a marked tendency for solids to be present in much greater concentration in the wall region, while the core of the column has a significantly smaller volume fractions of particles [56].
- *Dense phase fluidization:* Gas fluidized beds are considered dense phase fluidized beds as long as there is a clearly defined upper limit or surface to the dense bed. The dense-phase fluidization regimes include the smooth fluidization, bubbling fluidization, slugging fluidization, and turbulent

fluidization regimes. In a dense-phase fluidized bed the particle entrainment rate is low but increases with increasing gas velocity.

- *Spouting bed fluidization:* Spouting can occur when the fluidizing gas is injected vertically at a high velocity through a small opening into a bed of Geldart D particles. The gas jet penetrates the whole bed and form a dilute flow in the core region. A solids circulation pattern is created, as the particles carried upwards to the top of the core region by the fluidizing gas move downward in a moving bed mode in the annular region. The gross scale particle circulation induced by the axial spout gives rise to more regular and cyclic mixing behavior than in bubbling and turbulent fluidization.
- *Channeling:* In a fluidized bed channeling frequently occur if the gas distribution is nonuniform across the distributor. Channeling can also be caused by aggregation effects of cohesive Geldart C particles due to inter-particle contact forces.
- *Lean phase fluidization:* As the gas flow rate increases beyond the point corresponding to the disappearance of bubbles, a drastic increase in the entrainment rate of the particles occurs such that a continuous feeding of particles into the fluidized bed is required to maintain a steady solid flow. Fluidization at this state, in contrast to dense-phase fluidization, is generally denoted lean phase fluidization. Lean phase fluidization encompasses two flow regimes, these are the fast fluidization and dilute transport regimes.
- *Fast fluidization:* The fast fluidization regime is considered to be initiated when there is no longer a clear interface between a dense bed and a more dilute freeboard region. Instead, there is a continuous, gradual decrease in solids content over the whole height of the column. Particles are transported out of the top of the vessel and must be replaced by adding solids near the bottom. Clusters of particles move downwards near the wall, while gas and entrained dispersed particles move upward in the core of the vessel. The term clustering refers to the phenomenon that solids coalesce to form a larger pseudo-particle.
- *Dilute transport fluidization:* The gas velocity is so large that all the particles are carried out of the bed with the gas. This solid transport by gas blowing through a pipe is named pneumatic conveying. In vertical pneumatic transport, particles are always suspended in the gas stream mainly because the direction of gravity is in line with that of the gas flow. The radial particle concentration distribution is almost uniform. No axial variation of solids concentration except in the bottom acceleration section [58].

The model predictions of the transition borders between the different gas-solid flow regimes shown in Fig 10.1 are still not reliable. The borders are generally sharp and fairly well correlated for the minimum fluidization (mf) and minimum bubbling (mb) transitions, whereas the transitions at higher gas superficial velocities are diffuse and poorly understood.

The general flow regime diagram shown in Fig 10.2 illustrates the progression of changes in behavior of a bed of solids as the gas velocity is progressively increased. The letters A, B, C and D refer to the Geldart classification of solids.

### 10.3 Reactor Design and Flow Characterization

The fluidized bed reactors can roughly be divided into two main groups in accordance with the operating flow regimes employed. These two categories are named the dense phase and lean phase fluidized beds.

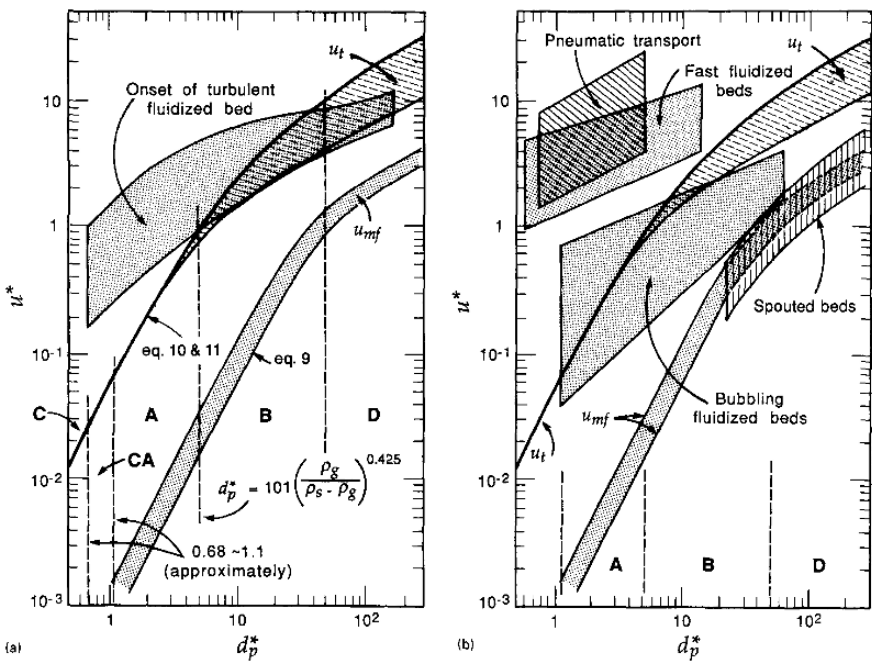


**Fig. 10.2.** Flow regime map of gas-solid contacting. In the figure notation the ordinate  $u^* = U_{in}^s [\rho_g^2 / \{\mu(\rho_p - \rho_g)g\}]^{1/3}$  is a dimensionless gas velocity, the abscissa  $d_p^* = d_p [\rho_g(\rho_p - \rho_g)g/\mu^2]^{1/3}$  a dimensionless particle size,  $u_t$  the terminal velocity of a particle falling through the gas (m/s), and  $u_{mf}$  the gas velocity at minimum fluidization (m/s). Reprinted from [83] with permission from Elsevier.

### 10.3.1 Dense-Phase Fluidized Beds

A dense phase fluidized bed generally consist of a gas distributor, a cyclone, a dipleg, a heat exchanger, an expanded section, and baffles [44]. A schematic representation of a dense phase fluidized bed reactor is shown in Fig 10.3.

At the bottom of the vessel is the gas distributor which yields the desired distribution of fluidizing gas and supports particles in the bed. A distributor with sufficient flow resistance to obtain a uniform distribution of gas across the bed is required, and sometimes caps are used to avoid gas jetting effects and plate clogging by fine particles. There are two basic designs of distributors, some for use when the inlet gas contains solids and others for use when the inlet gas is clean. For clean gases the distributor is designed to prevent back flow of solids during normal operation, and in many cases it is designed to prevent back flow during shutdown. Perforated plate distributors are widely used in industry because they are cheap and easy to fabricate [82]. However, the perforated plate distributors cannot be used under severe operating conditions, such as high temperature or highly reactive environment. The tuyere type of distributors are normally used in these situations,

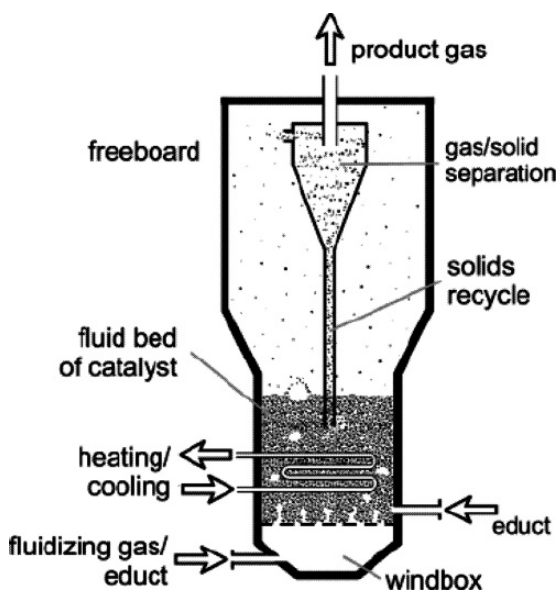


**Fig. 10.3.** A typical dense phase bubbling bed reactor design. The reactor consists of a gas distributor, an internal cyclone with solids recycle through a dipleg, and a heat exchanger. The freeboard section of the vessel is expanded and the heat exchanger may also function as a baffle. Reprinted with permission from [136]. Copyright 2004 American Chemistry Society.

but these are more expensive than perforated plates. The tuyere distributor design prevents solids from falling through the distributor. The high pressure drop porous plate distributors are commonly used in laboratory scale units to ensure even distribution of gas across the bed entrance.

A dense phase fluidized bed vessel has two zones, a dense phase having a distinct upper surface separating it from an upper dilute phase. The section of the vessel between the surface of the dense phase and the exit of the gas stream is called the *freeboard zone*. In vessels containing fluidized beds, the gas leaving the dense bed zone carries some suspended particles. Particle *entrainment* refers to the ejection of particles from the dense bed into the freeboard by the fluidizing gas. Particle *elutriation* refers to the separation of fine particles from a mixture of particles and their ultimate removal from the freeboard. The flux of solids leaving the freeboard with the gas is called *carry-over*. The entrained solids are normally separated from the outlet gas by internal or external cyclones and returned to the bed. In many cases several cyclones are combined to form a multistage cyclone system. A dipleg returns the particles separated by the internal cyclones into the vessel. The outlet of a dipleg may be located in the freeboard or immersed in the dense bed. A standpipe can be used to return the particles separated by the external cyclones into the dense bed. Sometimes a heat exchanger device is placed in the dense bed or the freeboard to control the temperature. The heat exchanger removes generated heat from or adds required heat to the fluidized bed by a cooling or heating fluid. An expanded freeboard section on the top of the vessel may be used to reduce the local gas velocity in the freeboard so that settling of the particles carried by the fluidizing gas can be efficiently achieved. Any internals other than diplegs can be employed as baffles to restrict flow, enhance the breakage of bubbles, promote gas-solid contact, and reduce particle entrainment.

The primary *bubbling fluidized bed* consists of gas bubbles flowing through a dense emulsion phase with gas percolating through the bed of solids. A fluidized bed reactor of this type designed for catalytic reactions operated in the bubbling bed regime has been shown in Fig 10.3. In many cases the particle entrainment rate is so low that the cyclone is considered superfluous.

In the *turbulent fluidized bed* larger amounts of particles are entrained precluding steady state operations. To maintain steady state operation the entrained particles have to be collected by cyclones and returned to the bed. For vessels operating in the turbulent fluidization regime internal cyclones may deal with the moderate rate of entrainment. This fluidization system, as sketched in Fig 10.4, is sometimes called a *fluid bed*. Since smooth and steady recirculation of solids through a solid trapping device is crucial for optimal operations of these units, Kunii and Levenspiel [82] included the turbulent fluidized beds in the reactor classification named circulating fluidized beds (i.e., the main lean-phase reactor design). However, this is not a conventional classification of the turbulent bed operation mode.

Bubbling and turbulent fluidized beds are operated with small granular or powdery non-friable catalysts. Rapid deactivation of the solids can then be

handled, and the efficient temperature control allows large scale operations. The main advantages of a turbulent fluidized bed over a standard bubbling fluidized bed are a more homogeneous fluidization that provides better contacting between gas and catalyst (i.e., low gas bypassing), and higher heat transfer coefficients between the suspension and heat transfer surfaces.

In design of fluidized bed systems the cross sectional area is determined by the volumetric flow of gas and the allowable or required fluidizing velocity of the gas at operating conditions. Generally, bed heights are not less than  $0.3\text{ m}$  or more than  $15\text{ m}$  [111]. For fluidized bed units operated at elevated temperatures refractory-lined steel is the most economical material.

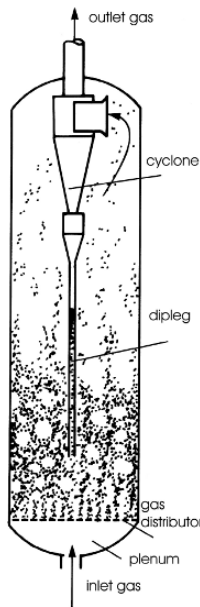


**Fig. 10.4.** A schematic representation of a turbulent fluidized bed. The illustration shows that in a turbulent fluidized bed entrainment is significant and an internal cyclone with solids recycle through a dipleg is required. Reprinted from [82] with permission from Elsevier.

### 10.3.2 Lean-Phase Fluidized Beds

The primary exploitation of the lean-phase fluidized beds is associated with the circulating fluidized bed (CFB) reactors.

The operation of circulating fluidized bed systems requires that both the gas flow rate and the solids circulation rate are controlled, in contrast to the gas flow rate only in a dense phase fluidized bed system. The solids circulation is established by a high gas flow.

The integral parts of a CFB loop are the riser, gas-solid separator, downcomer, and solids flow control device [44]. The CFB is thus a fluidized bed system in which solid particles circulate between the riser and the downcomer, as illustrated in Fig 10.5. The riser is the main component of the system. The name *riser* is generally used to characterize a tall vessel or column that provides the principal reaction zone. On average, the particles travel upwards (or rise) in the riser, though the motion at the wall may be downwards. The fluidized gas is introduced at the bottom of the riser, where solid particles from the downcomer are fed via a control device and carried upwards in the riser. The fast fluidization regime is the principal regime under which the CFB riser is operated. The particles exit at the top of the riser into the gas-solid separators which are normally cyclones. In lean-phase fluidized beds, the rate of entrainment is far larger than in turbulent fluidized beds, and bigger cyclone collectors outside the bed are usually necessary. The separated particles then flow to the downcomer and return to the riser. The entrance and exit geometries of the riser often significantly affect the gas and solid flow behavior in the reactor. The efficiency of the cyclones determine the particle size distribution and solids circulation rate in the system. The downcomer provides hold volume and a static pressure head for particle recycling to the riser. The downcomer can be a large reservoir which aids in regulating the solids circulation rate, a heat exchanger, a spent solid regenerator, hopper or a standpipe. The main task in achieving smooth operation of a CFB system is to control the solids recirculation rate to the riser. Several designs of valves for solids flow control are used. The solids flow control device serves two main functions, namely to seal the riser gas flow to the downcomer and to control the solids circulation rate. Rotary valves are effective sealing devices for solids discharge. The L-valve can act as a seal and as a solids-flow control valve. There are many other valve designs available to suit specific conditions. The riser cannot be considered as an isolated entity in the CFB loop because the pressure drop over the riser must be balanced by that imposed by the flow through its accompanying components such as the downcomer and the recirculation device.

In general, the high operating gas velocities for lean phase fluidization yield a short contact time between the gas and solid phases. Fast fluidized beds and co-current pneumatic transport are thus suitable for rapid reactions, but attrition of catalyst may be serious.

However, it is not always easy to distinguish between the flow behavior encountered in the fast fluidization and the transport bed reactors [56]. The transport reactors are sometimes called dilute riser (transport) reactors because they are operated at very low solids mass fluxes. The dense riser transport reactors are operated in the fast fluidization regime with higher solids mass fluxes. The transition between these two flow regimes appears to be gradual rather than abrupt. However, fast fluidization generally applies to a higher overall suspension density (typically 2 to 15% by volume solids) and to a situation wherein the flow continues to develop over virtually the entire

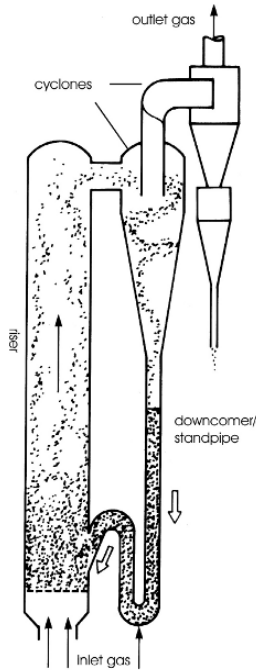


**Fig. 10.5.** A schematic representation of a circulating fluidized bed. The CFB loop consists of a riser, gas-solid cyclone separators, standpipe type of downcomer, and a non-mechanical solids flow control device. Reprinted from [82] with permission from Elsevier.

height of the reactor, whereas the flow usually associated with transport bed reactors tends to be more dilute (typically 1 to 5 % by volume solids) and uniform. However, in practice the differences in operation are generally small, hence the names are often used in an indistinguishable manner<sup>1</sup>. This regime overlap is also indicated in the regime map shown in Fig 10.2. The pertinent characteristics that distinguish the CFB from the dense phase fluidized beds and from the riser (transport) reactors are summarized in Table 10.1.

Advantages of the fast fluidization regime, relative to the dense phase fluidization regimes, include higher gas throughput per unit area, adjustable retention time of solids, limited axial dispersion of gas coupled with near uniformity of temperature and solids composition, reduced tendency for particles to undergo agglomeration, and possibility of staged addition of gaseous

<sup>1</sup> Berruti et al [13], for example, used the term CFB to generically describe systems like fast fluidized bed, riser reactor, entrained bed, transport bed, pneumatic transport reactor, recirculating solid riser, highly expanded fluid bed, dilute phase transported bed, transport line reactor and suspended catalyst bed in co-current gas flow.

reactants at different levels. Gas-solid contacting also tends to be very favorable. However, by increased overall reactor height and added complexity in designing and operating the recirculating loop the CFB systems tend to have higher capital costs than low-velocity systems, so that one or more of the above advantages must be very significant for this option to be viable. One of the most important factors inhibiting the commercialization of novel processes operated in risers is scale-up uncertainties arising from the complex hydrodynamic behavior of the CFB reactors.

**Table 10.1.** The key features that distinguish circulating fluidized bed reactors from low-velocity fluidized beds and from lean-phase transport reactors [58].

	Low-velocity FB Reactor	CFB Reactor	Transport Reactors
Particle residence times in Reactor	Minutes or hours	Seconds	Once through system
Flow regime	Bubbling, slugging or turbulent, distinct upper interface	Fast fluidization	Dilute transport
Superficial gas velocity	Less than 2 m/s	3 to 16 m/s	15 to 20 m/s
Mean particle diameter	0.03 to 3 mm	0.05 to 0.5 mm	0.02 to 0.08 mm
Net circulation of solids	0.1-5 $kg/m^2s$	15-1000 $kg/m^2s$	Up to $\sim 20 kg/m^2s$
Voidage	0.6-0.8	0.8-0.98	less than 0.99
Gas mixing	Intense	Intermediate	Little

A combination of a circulating fluidized bed riser reactor operating in the fast fluidization regime and a bubbling fluidized bed regenerator is frequently used in industry for heterogeneous catalyzed gas phase reactions in cases where the catalyst rapidly deactivates and has to be regenerated continuously. Such a catalytic circulating fluidized bed reactor design is sketched in Fig 10.6.

The most prominent chemical reactions operated within such a reactor design is the FCC process, which is widely used in the modern petroleum refinery industry. In this catalytic chemical process vaporized heavy hydrocarbons crack into lower-molecular-weight compounds. To explain the principal operating principles of this particular CFB unit, a FCC riser reactor can be divided into four parts from bottom to top according to their functions [45]: The prelift zone, the feedstock injection zone, the reaction zone, and the quenching zone. In the prelift zone, catalysts enter the riser reactor from the regenerator and are then conveyed by the prelift gas. In the feedstock injection zone, feed oil is introduced into the riser through the feed nozzles, and the heavy oil comes in contact with the high-temperature catalyst. Rapid reactions are then taking place in the reaction zone.

Apart from the mentioned application of CFB to the fluid catalytic cracking (FCC) process, circulating fluidized beds utilizing the fast fluidization regime have been used for a number of gas-solid reactions including calcination, combustion of a wide variety of fuels, gasification, and dry scrubbing of gas streams [56]. Applications for catalytic reactions can be taken to include the transport reactors employed in modern catalytic cracking operations in the petroleum industry and certain Fischer-Tropsch synthesis reactors.

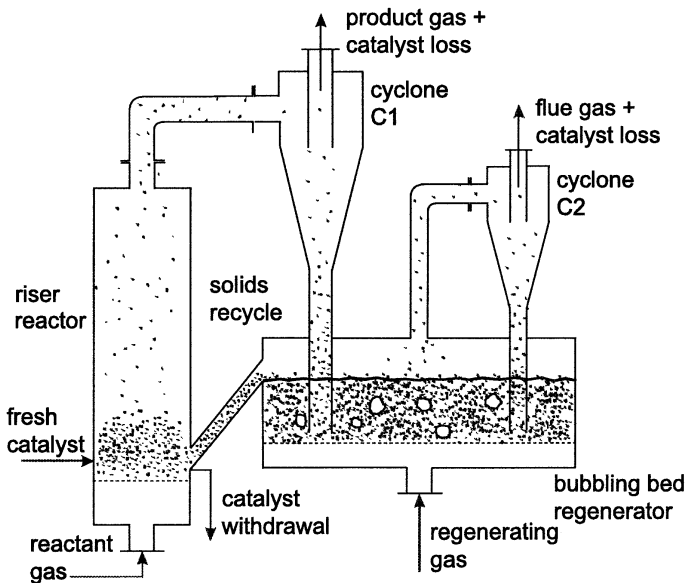


**Fig. 10.6.** A typical catalytic circulating bed reactor design. This CFB loop consists of a riser, gas-solid cyclone separators, and a downcomer. In this particular case the downcomer consists of a spend solid regenerator. Reprinted from [135] with permission from Elsevier.

Generally, to maximize profitability, the gas and solids residence times in CFBs are chosen to achieve the highest product yield per unit volume [14]. In FCC units, for example, a short and uniform catalyst residence time in the riser reactor, with reduced back-mixing, leads to better reactor performance by reducing the inventory of the deactivated catalyst in the riser. In other words, a uniform radial profile of solids velocity and little solids back-mixing in the riser is preferred, leading to shorter and more uniform solids residence times. In a FCC unit axial mixing is disadvantageous. For other catalytic reactions, lower gas velocities may be preferred because this gives higher solids holdup, thus maximizing the specific activity per unit volume [13].

Scale-up of CFBs is generally less of a problem than with bubbling beds [111]. Moreover, the higher velocity in CFB means higher gas throughput, which can minimize the reactor costs. Several CFB loop designs have been proposed for getting smooth steady state circulation of solids. Basically, there are two basic types of solids circulation loops distinct in that some include a reservoir of solids while others do not. The solids circulation loops which do not include a reservoir of solids (hopper) are less flexible in operation compared to the circulation systems with reservoirs.

### 10.3.3 Various Types of Fluidized Beds

Numerous types of fluidized bed reactor designs exist within each of the two categories mentioned in the previous subsection, some of them are illustrated in Fig 10.7. The key issues leading to re-design of the primary bubbling bed are also indicated.

### 10.3.4 Experimental Investigations

The first experimental investigations of bubbling bed fluidization led to the flow interpretation that the bubbles are flowing evenly through an essentially stagnant emulsion phase without affecting the flow of the emulsion phase. This picture of the bubbling bed hydrodynamics is named the two-phase theory [130, 29].

The subsequent experimental investigations on solids mixing and circulation in bubbling beds revealed that the bubbling phenomenon creates particle circulation patterns [5, 53, 82, 116]. Moreover, the axial and radial transport of solids within the fluidized bed influence many parameters governing the chemical process performance in these units. Most important, the heat transport within the bed is efficient due to the chaotic motion of solid particles having the property of high heat capacity compared to the fluidizing gas, making the bed close to isothermal.

Lin et al [90] were among the first to use the modern non-invasive Computer Automated Radioactive Particle Tracer (CARPT) technique to measure the Lagrangian solid particle motion in gas-solid bubbling fluidized beds. This advanced measuring technique determines the time-average solids velocity components in all three space dimensions simultaneously so that the derived Eulerian flow field map and various turbulence fields can be visualized. A number of experiments were conducted measuring mean velocity distributions for Geldart B glass beads of density  $2.5 \text{ (g/cm}^3\text{)}$  and diameters ranging from  $0.42 - 0.60 \text{ (mm)}$  in an air fluidized bed of  $13.8 \text{ (cm)}$  diameter, at various superficial air velocities ranging from  $32 - 89 \text{ (cm/s)}$ . The mean circulating flow patterns observed are summarily presented in Figs 10.8 (a)-(d). For bubbling fluidized beds consisting of Geldart A and B particles operating well above the minimum fluidization conditions the bubble flow will cause the solid particles to develop certain characteristic flow patterns. For a shallow

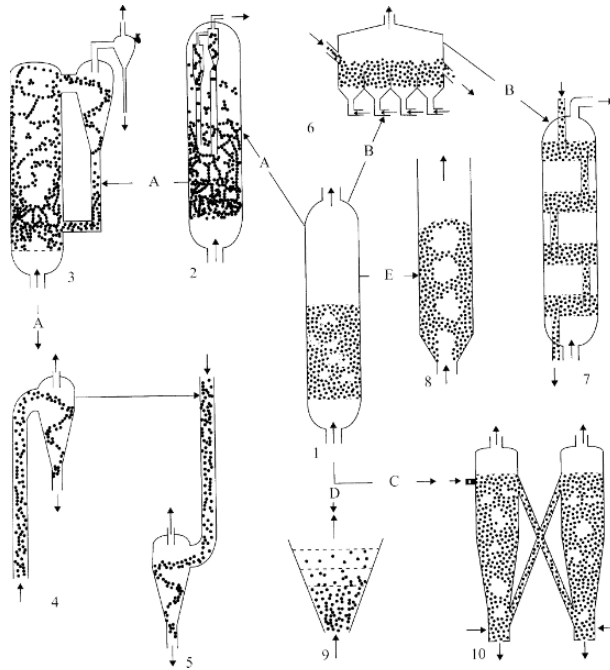


**Fig. 10.7.** Types of fluidized bed reactors [77]. Reprinted with permission from the authors.

<p>The primary fluidized bed reactor types:</p> <ul style="list-style-type: none"> <li>1: Bubbling Fluidized Bed</li> <li>2: Turbulent Fluidized Bed</li> <li>3: Circulating Fluidized Bed</li> <li>4: Riser</li> <li>5: Downer</li> <li>6: Cross-current Fluid Bed</li> <li>7: Counter-current Fluid Bed</li> <li>8: Spouted Fluidized Bed</li> <li>9: Floating Fluidized Bed</li> <li>10: Twin Fluidized Bed</li> </ul>	<p>The key issues leading to re-design of the conventional bubbling fluid bed:</p> <ul style="list-style-type: none"> <li>A: Higher gas velocity</li> <li>B: Counter-current contacting is beneficial</li> <li>C: Incompatible differences in desired environment</li> <li>D: Dusty environment</li> <li>E: Large particles/low gas load</li> </ul>
---	---

bed there is normally an upflow of particles near the wall and a downflow in the center of the bed at low gas velocities, as shown in Figs 10.8 (a) and (b). Increasing the gas velocity may reverse this flow pattern. In this case the bed apparently consists of one circulating cell just above the distributor similar to the one observed in shallow beds with upflow near the wall and down flow in the center. In the upper part of the bed the solids have an upward motion

in the center and downwards near the wall. This flow pattern is shown in Figs 10.8 (c) and (d). An additional advantage associated with the CARPT technique is that it can be used to characterize dense high flux suspensions as emphasized in industrial practice such as fluid catalytic cracking (FCC) units and CFB combustors. The CARPT measuring technique has thus been applied by Bhusarapu et al [14] investigating the solids velocity field in gas

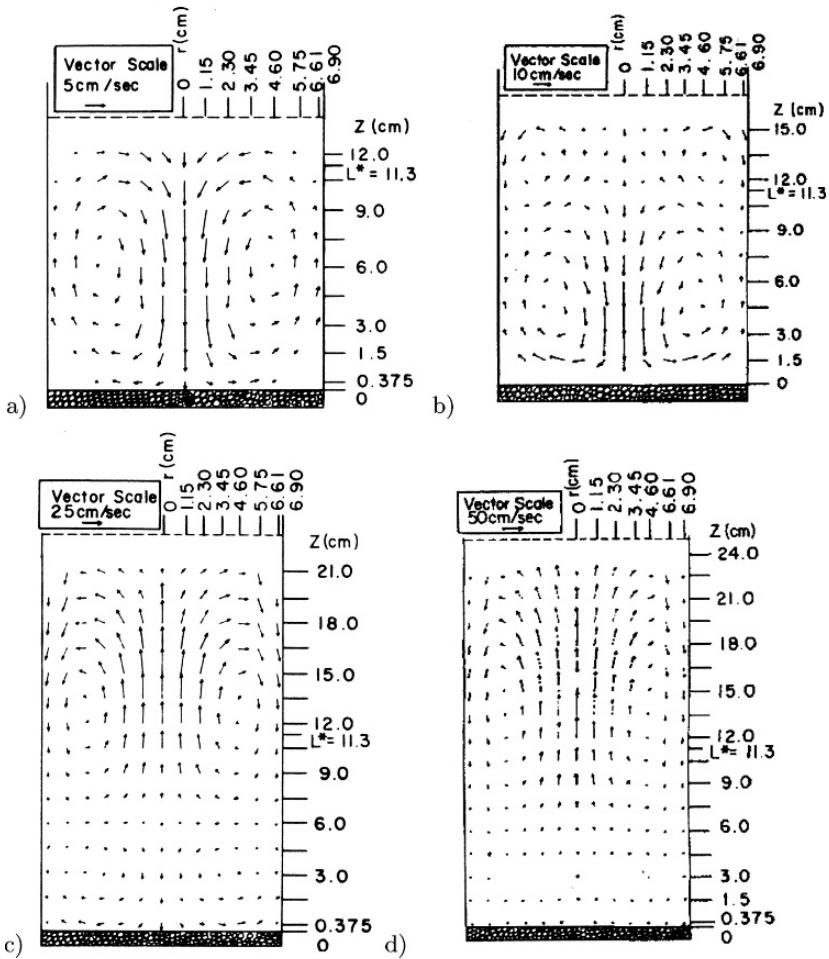


**Fig. 10.8.** Particle circulation patterns at various fluidizing velocities for a gas fluidized bed ID 13.8 (cm) consisting of 0.42 – 0.6 (mm) diameter glass beads [90].  $L^*$  denotes the static bed height. Case a)  $U_{in}^s = 32$  (cm/s) and  $U_{in}^s/U_{mf}^s = 1.65$ , Case b)  $U_{in}^s = 45,8$  (cm/s) and  $U_{in}^s/U_{mf}^s = 2.36$ , Case c)  $U_{in}^s = 64,1$  (cm/s) and  $U_{in}^s/U_{mf}^s = 3.41$ , and Case d)  $U_{in}^s = 89,2$  (cm/s) and  $U_{in}^s/U_{mf}^s = 4.6$ . Reprinted with permission of John Wiley & Sons Inc, Copyright 1985.

solid risers. Measurements were performed in two different risers at low and high solid fluxes at varying superficial gas velocity spanning both the fast-fluidized and dilute phase transport regimes.

Based on the experimental investigations reported in the literature, using both invasive and non-invasive techniques [129], it is recognized that most CFBs operating in the fast fluidization flow regime are subject to predominantly downflow of relatively dense suspensions along the outer wall while there is a net dilute upflow in the core [62, 99, 133, 73]. The fast fluidization regime is also characterized by a dense region at the bottom of the riser and a dilute region at the top. Due to the large reflux and density of the suspension, the temperature gradients are normally very small.

In vertical pneumatic transport the radial particle concentration distribution is almost uniform, but some particle strands may still be identified near the wall. Little or no axial variation of solids concentration except in the bottom acceleration section is observed [58]. The flow associated with transport bed reactors tends to be dilute (typically 1 to 5 % by volume solids) and uniform. By virtue of the smaller reflux and density of the suspension within the dilute pneumatic conveying regime, there might be larger temperature gradients than within the fast fluidization regime [56].

Optical techniques like laser doppler anemometry (LDA) can be used to obtain knowledge about the local solids hydrodynamics in CFB units close to walls at low solids fluxes [14]. Such LDA measurements of FCC particles in a riser in circulating fluidized bed have been reported by [119, 120].

An overview of sources of experimental data in the open literature characterizing the hydrodynamics of CFB risers can be found in [13]. These investigations might be useful for CFB riser model validation. However, despite the development of novel experimental techniques and many experimental investigations, there is still considerable uncertainty and disagreement with regard to the dependence of fine scale structures on the operating conditions. This dependency is important in scale-up, design, and optimization of these units.

## 10.4 Fluidized Bed Combustors

Although the scope of this book is the fluidized bed vessels used as chemical reactors, a brief outline of the combustor units representing the most widespread use of this technology is considered very useful in understanding the chemical reactor operation but also to orientate oneself in the vast literature on fluidization technology. Recent reviews of fluidized bed combustion systems are given by Anthony [2], Leckner [86], Longwell et al [93] and Issangya et al [67].

The popularity of fluidized bed combustion is due largely to the technology's fuel flexibility and the capability of meeting sulfur dioxide and nitrogen oxide emission requirements without the need for expensive flue-gas treatment.

In the early 1960s engineers in Britain and China considered fluidized bed combustion (FBC) to be an alternative future combustion technology to enable utilization of low-grade coal and oil shale fines, fuels that cannot be burned efficiently in conventional boiler furnaces [82]. Several power generation cycles utilizing the fluidization technology were commercialized [86, 18, 87]. The working principles of the conventional cycles can be outlined as follows. The fluidized bed boilers supply steam to a Rankine cycle. The efficiency of the electric power production has been further increased in a combined cycle with a pressurized FBC serving as the heat source for both the steam and the gas turbine cycle. More advanced cycles, such as the air blown gasification cycle and the integrated gasification combined cycle (IGCC), are currently being developed.

In a fluidized bed combustor the bed is made up primarily of inert material which may be ash, absorbent, or some other inert material such as sand. The technology's fuel flexibility arises from the fact that the fuel is present in the combustor at a low level and are burnt surrounded by these inerts [2]. The solid fuel normally represent between 0.5 and 5% of the total bed material. In general, almost any solid, liquid, slurry or gas containing carbon, hydrogen and sulfur can be used as fuels for energy production.

The first fluidized bed gasifiers were designed for burning coal. The second generation units were utilizing petroleum fuels. However, in order to compensate for the shortage of petroleum, the utilization of coal for combustion and gasification has again become dominating. Currently almost half of the total worldwide FBC capacity is primarily fueled by coals [87]. Other fossil fuels like oil and natural gas can also be burned effectively and efficiently in a CFB unit. Nevertheless, other combustable materials like petroleum coke, biomass and municipal waste are gaining in popularity. In particular, waste and biomass are used to replace a part of the coal as  $CO_2$ -neutral fuels. In addition, co-firing coal and petroleum coke can also be beneficial.

The first fluidized bed applications employed bubbling bed boilers, but problems with erosion of in-bed cooling tubes diverted the mainstream of development towards the circulating fluidized bed boiler [86]. The first circulating fluidized bed combustion (CFBC) systems were developed in the late 1970s by Ahlstrom Pyropower in Finland, Lurgi in Germany, and Studsvik Energiteknik in Sweden [18]. However, bubbling beds remain important for particular applications for which they have cost advantages.

Today the circulating fluidized bed (CFB) has become the dominating design for combustors operated at atmospheric pressure. Pressurized circulating fluidized bed combustors are under development for combined power cycle applications, but so far no clear advantages have been revealed yet. For this reason the existing commercial pressurized fluid bed systems are bubbling beds.

During the last decades several FBC technology's have become available for the combustion of coal and alternative fuels, with the trend that circulating

fluidized bed combustion (CFBC) is prevailing over bubbling fluidized bed combustion (BFBC) [4, 2].

One of the most attractive features of FBC, employing bubbling and circulating beds, is the potential to use a low cost sorbent to capture sulfur (in situ) within the fluidized bed in cases where high sulfur-fuels are burnt. The sorbent is typically limestone or dolomite (minerals composed of calcium and magnesium carbonates) and is fed to the bed either together with the fuel or as a separate solid stream [88, 3]. More than 90 % of the sulfur pollutants in coal can be captured by the sorbent. Low  $\text{NO}_x$  emissions is enforced since the fuel is burnt at temperatures of about 750 to 950°C, well below the threshold where nitrogen oxides form (i.e., nitrogen oxide pollutants are produced at about 1400°C). The environmental pollution by combustion ash containing residual sorbents must also be treated properly [80].

It should be mentioned that the combustion technology is not limited to these major designs. In catalytic fluidized bed combustion of low-sulfur natural gas, for example, powder catalysts are operated in the turbulent flow regime where the gas-solid contact is optimal so as to maintain a high combustion efficiency [46].

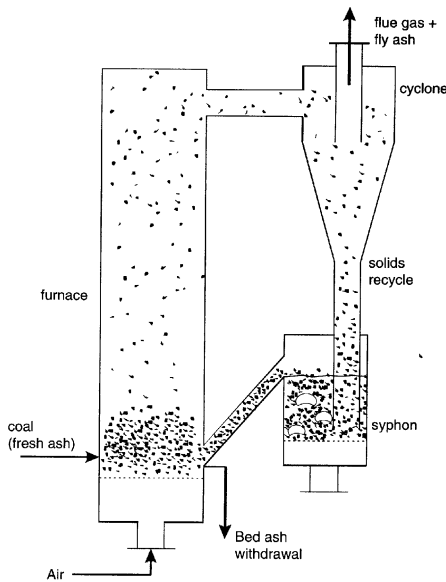


**Fig. 10.9.** A typical circulating fluidized bed combustor design [63]. The furnace (riser) is normally operated in the fast fluidization regime. The ash which is entrained from the furnace is separated from the flue gas in the cyclone. Most of the ash particles are sent into the syphon. The syphon is a small bubbling fluidized bed acting as a pressure lock. From the syphon the ash flows back into the riser. Reprinted with permission from Elsevier, copyright Elsevier 2007.

The fast fluidization regime is most often encountered in circulating fluidized beds where provision for continuous return of a significant flow of entrained solids is an integral part of the equipment. In combustion systems, the return is accomplished by capturing the entrained solids in one or more external cyclones or in impingement separators. These key features of a circulating fluidized bed combustion system are shown schematically in Fig 10.9. The captured particles are sent back to the base of the reactor (riser) through a vertical standpipe (downcomer), and then through a non-mechanical seal or a non-mechanical valve (mechanical valves are more common in FCC installations). The bottom section of the riser might also be tapered to prevent solids from sitting and agglomerating in the bottom section. In some cases, the solids pass through a separate low-velocity fluidized bed heat exchanger or a siphon only (equivalent to a catalyst regenerator in a FCC reactor installation) during their journey from cyclones capture to re-injection.

The design of CFB employed in chemical reactor engineering and circulating fluidized bed combustion may be distinguished by the aspect ratio ( $H/D$ ) of the riser [106, 67]. For chemical process analysis tall and narrow riser units with an aspect ratio of the order of 20 or higher is normally used. A chemical reactor utilizing the fast fluidization regime typically operates at high net solids fluxes for the purpose of producing product chemicals. A typical industrial scale CFB combustor is designed as larger units, with a lower aspect ratio typically less than 10, for the purpose of producing heat, electricity, fuel-gas or combinations of these.

The group B solids normally used in large scale CFBC and circulating fluidized bed gasification (CFBG) units consists of silica sand and/or primary ashes, and sorbent in the case of coal-fired units. We reiterate that the common FCC particles belongs to the Geldart group A. In particular, the particle sizes applied to fluid bed combustion are normally in the range 150 – 250 ( $\mu m$ ), whereas for catalytic cracking and other chemical processes finer particles with sizes in the range 60–70 ( $\mu m$ ) are used [67]. The flow pattern in CFB gasifiers and combustors is similar since the overall riser geometry, fluidization conditions and properties of the solids used are similar [106]. However, minor differences in the flow behavior can occur because of corner effects since combustors generally have a square or rectangular cross section and may partly have bare membrane tube walls, whereas the riser of a gasifier normally has a circular cross section with plane walls. Nevertheless, the flow pattern of the large CFB combustors and the gasifier units differs significantly from those of tall and narrow CFB reactor units (which normally have a circular cross section) due to the dissimilar operating conditions employed, so the abundant literature on CFBC and CFBG is seldom applicable for CFB reaction technology and visa versa. The important features of the two principal applications of the fast fluidization regime, the fluid catalytic cracking riser reactor and the solid fuel combustion vessel, are compared in Table 10.2.

Although considerable work has been done to understand the flow dynamics of CFBs, much of the CFB data reported are for low density CFB systems

representative of CFB combustors. Further work is thus required on high density systems to better understand the riser reactor behavior leading to more reliable scale-up of these units.

**Table 10.2.** Comparison of typical operating conditions for the two principal applications of fast fluidization: fluid catalytic cracking and circulating fluidized bed combustion [56, 67].

	FCC Riser Reactor	CFB Combustor
Particle density, ( $kg/m^3$ )	1100-1500	1800-2600
Mean particle diameter, ( $\mu m$ )	60-70	150-250
Particle size distribution	Broad	Broad
Geldart powder group	A	B
Inlet Superficial gas velocity, ( $m^3/m^2 s$ )	8-18	5-9
Exit temperature, ( $C$ )	500-550	850-900
Temperature uniformity	Gradients	Uniform
Pressure, ( $kPa$ )	150-300	110-120
Net Solid Flux, ( $kg/m^2 s$ )	400-1400	10-100
Suspension density, ( $kg/m^3$ )	50-80 at the top	10-40 at the top
Exit geometry	Various	Abrupt
Riser cross-section geometry	circular	rectangular/square
Riser diameter ( $m$ )	0.7-1.5	8-10
Height-to-diameter-ratio	> 20	< 5 - 10
Average solids residence time per pass ( $s$ )	2-4	20-40

Many of the modern combustion processes can be characterized by relatively low reaction rates compared to the modern catalytic processes operated in chemical reactors [67]. Therefore, these combustion processes do require lower gas velocities and higher solids circulation rates. On the other hand, many catalytic gas-phase reactions, including FCC, Fischer-Tropsch synthesis and oxidation of butane, utilize a relatively high gas velocity in the riser to promote plug flow operating conditions and short contact times between the gas and solids.

The solids residence time distribution (RTD) in the riser may thus be important in non-catalytic gas-solid reactions, as in a combustor, since this distribution characterizes the degree of solids mixing and provides information about the physical properties of the solid particles in the riser [14]. Moreover, lateral mixing and internal recirculation of solids in a CFB combustor are necessary to maintain uniform temperatures over the entire length of the riser. Hence, lateral and longitudinal mixing is advantageous in a CFB combustor.

Prediction of the flow and transport processes is crucial in modeling the heat transfer and combustion/gasification gas produced. The conventional modeling of bubbling and circulating fluidized bed coal combustors were outlined by Arena et al [4].

Saraiva et al [121] presented an extended model for a circulating atmospheric fluidized bed combustor (CAFBC) which included hydrodynamics for the fast section at the top of the bed as well a bubbling bed section at the bottom of the CAFBC. For the fast section of the bed, one dimensional momentum and energy balances were used to predict the temperature and velocity profiles for gas and particles throughout the reactor. The model contain species mass balances for five gas species including  $\text{SO}_2$ , as well as a model of  $\text{SO}_2$  retention by limestone particles. A bubbling bed model was considered to simulate the chemical process at the bottom of the combustor.

Recently, Pallarés and Johnsson [106] presented an overview of the macroscopic semi-empirical models used for the description of the fluid dynamics of circulating fluidized bed combustion units. They summarized the basic modeling concepts and assumptions made for each model together with the major advantages and drawbacks. In order to make a structured analysis of the processes involved, the CFBC unit is often divided into 6 fluid dynamical zones like the bottom bed, freeboard, exit zone, exit duct, cyclone and downcomer and particle seal, which have been shown to exhibit different fluid dynamical behavior.

## 10.5 Milestones in Fluidized Bed Reactor Technology

Fuel conversion in a fluidized bed was first introduced by Winkler who patented a gasifier in 1922 [137]. The first large-scale use of fluidized beds, the Winkler gas generator, was thus established for the process of gasification of coal in 1926 [82, 47]. These units were 13 (*m*) high, 12 (*m*<sup>2</sup>) in cross section and fed by powered coal to produce synthesis gas for the chemical industries<sup>2</sup>. A sketch of the pioneering Winkler gas generator is shown in Fig 10.10 (a). A number of more efficient bubbling bed and lean-phase CFB fluidization technologies for gasifying coal have been developed over the years [37]. An informative overview of the gasification chemistry, gasifier types and coal gasification reactor models is given by Denn and Shinnar [32].

In chemical reactor engineering, on the other hand, the fluidization technique is considered initiated by the cooperative work of the Standard Oil Development Co, the MW Kellogg Co, and Standard Oil of Indiana developing the first FCC unit. With war threatening in Europe and the Far East around 1940, the chemical engineering community in USA was urged to find new ways of transforming kerosene and gas oil into high-octane gasoline fuels. The real breakthrough of the fluidized bed technology was thus associated with the catalytic cracking of gas-oil into gasoline, first practiced in 1942 at the Baton Rouge refinery of Standard Oil of New Jersey (now Exxon) [82, 146].

---

<sup>2</sup> The gasification process involves conversion of coal and air (or oxygen) into a gaseous mixture of mainly  $\text{CO}$ ,  $\text{CO}_2$ ,  $\text{H}_2$ ,  $\text{H}_2\text{O}$ ,  $\text{CH}_4$  and  $\text{N}_2$ .

Before that, the catalytic cracking was carried out in fixed bed reactors<sup>3</sup> as commercialized in 1937. Catalytic cracking deposits carbonaceous products on the catalyst, causing rapid deactivation of the latter. To maintain the production capacity, the coke had to be burned off. This regeneration required switching the fixed bed reactor out of production. In order to eliminate the cycling, attempts were made to circulate the catalyst and burn off the coke in a separate vessel, the re-generator. Both the reactor and the regenerator were operated under transport conditions. A sketch of the pioneering FCC reactor is shown in Fig 10.10 (b). Today this reactor is classified as a CFB, but it was then called an upflow unit [97]. The term *circulating fluidized bed* was first applied to alumina calciners by Reh [113] in 1971.

The high turbulence created in the fluid-solid mixture leads to much higher heat transfer coefficients than those which can be obtained in fixed beds. The resulting uniformity of the fluidized bed makes it applicable for effecting catalytic reactions, especially highly exothermic and temperature sensitive reactions. However, the fluidization technology is much more complicated than that associated with fixed bed reactors.

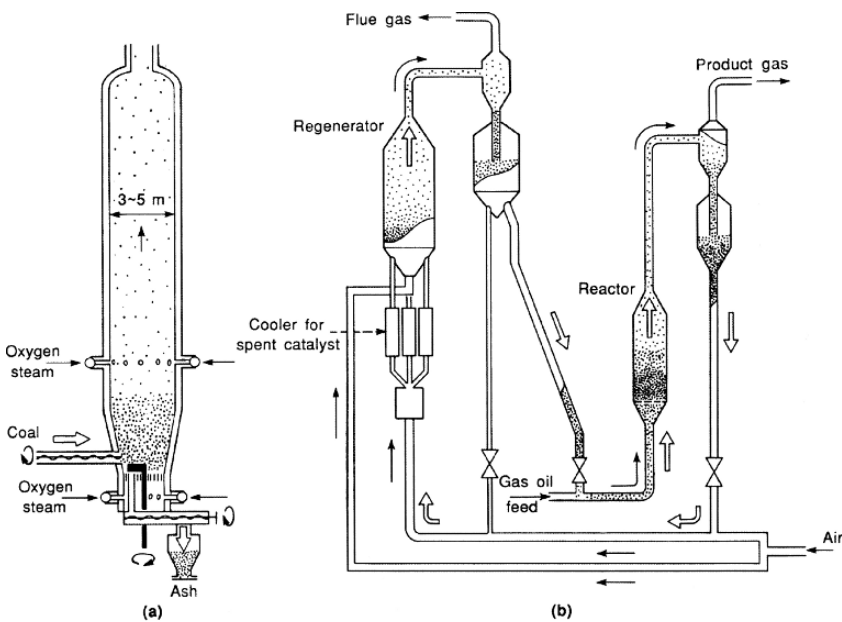


**Fig. 10.10.** Two pioneering fluidized bed reactors: (a) the Winkler gas generator; (b) the first large-scale pilot plant for fluid catalytic cracking. Reprinted from [82] with permission from Elsevier.

<sup>3</sup> This fixed bed process itself was already representing a major improvement over the earlier thermal-cracking methods yielding more gasoline of higher octane rating and less low-value, heavy fuel oil by-product [146].

For the low activity FCC catalysts then available, the bubbling bed design was a decided improvement over the first CFB reactor. Until the mid-1970s, virtually all FCC units maintained a dense phase bubbling or turbulent bed in the reactor vessel. A few of the second generation bubbling bed FCC reactors are still in operation [97].

The contemporary commercial reactors used for sulphide ore roasting, Fischer-Tropsch synthesis and acrylonitrile manufacture were routinely operated in the bubbling and turbulent fluidization regimes [56, 112].

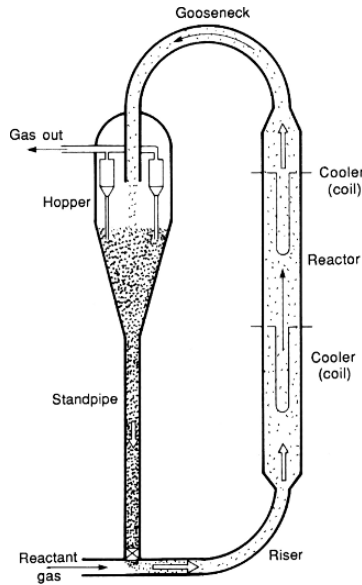
With the introduction of zeolites in the early 1960s, the FCC catalyst activity began to increase steadily [97]. By 1980 many units were again operating in a CFB mode to reduce the residence time of the gas reactants in the reactor. Today, by far the greatest use of CFB reactors is for the FCC process in petroleum refining.

There are processes in which the total amount of catalyst is entrained by the gas. The reactors then belong to the category of transport reactors. Examples are some of the present Fischer-Tropsch reactors for the production of hydrocarbons from synthesis gas and the modern catalytic cracking units. Fig 10.11 shows the Synthol circulating solids reactor. In the dilute side of the circuit, reactant gases carry suspended catalyst upward, and the fluidized bed and stand-pipe on the other side of the circuit provide the driving force for the smooth circulation of the solid catalyst. For the removal of heat, heat exchangers are positioned in the reactor.

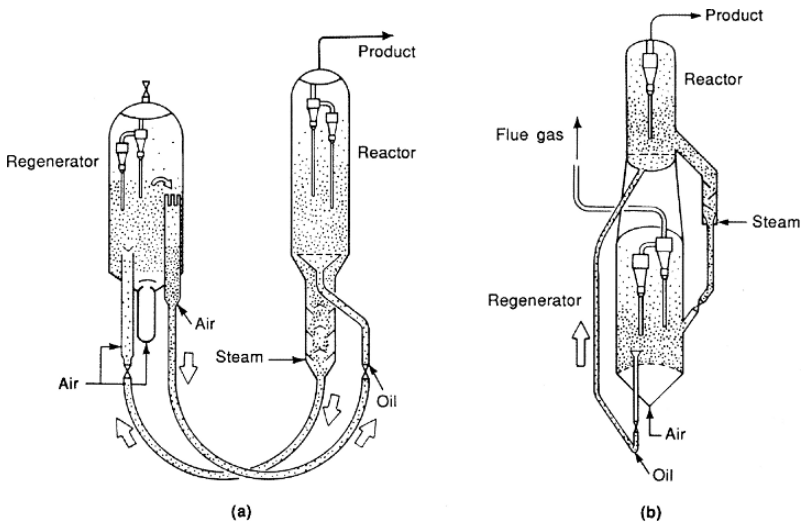
Fig 10.12(a) shows a Fluid Catalytic Cracking (FCC) unit (Exxon's model IV), in which the catalyst is circulating through a pair of U-tubes. Liquid oil is fed to the riser under the reactor, and on vaporization it reduces the bulk density of the up-going mixture and promotes the circulation of catalyst. The stacked unit in Fig 10.12(b) is an alternative design by Universal Oil Products Company. It uses a higher pressure in the re-generator than in the reactor, a single riser and a micro-spherical catalyst. Some of the synthetic crystalline zeolite catalyst introduced were so active that the cracking mainly or entirely took place in the riser, so that the reaction vessel caused over-cracking into undesired light gases and coke. In recent versions of the catalytic cracker, the catalyst is completely entrained in the riser-reactor to reduce the contact time.

Table 10.3 presents a few examples of industrial applications of fluidized beds for synthesis reactions. Other examples are given by [146, 82, 53, 58].

Other fluid bed applications have also used CFBs in preference to dense phase fluidized beds, but the use of CFBs is limited to situations where the higher capital and operational costs of higher gas velocity can be justified by significant process advantages. In many applications, a well designed dense phase fluidized bed may suffice and be less costly to construct and operate than a CFB.



**Fig. 10.11.** Synthol circulating fluid bed Fischer-Tropsch reactor. Reprinted from [82] with permission from Elsevier.



**Fig. 10.12.** FCC units in their middle stage of development. (a) Exxon's reactor model IV. (b) Alternative design by Universal Oil Products Company. Reprinted from [82] with permission from Elsevier.

**Table 10.3.** Industrial Applications of Fluidized Bed Catalytic Reactors [82].

Product or Reaction	Type
Fluidized bed catalytic cracking (FCC)	Riser reactor: FFB Regenerator: BB/FB
Phthalic anhydride	FB
Fischer-Tropsch synthesis	FFB
Vinyl acetate	FB
Acrylonitrile	BB/FB
Ethylene dichloride	BB/FB
Chloromethan	FB
Maleic anhydride	FB
Polymerization of olefines: Polyethylene (low density)	BB
Polymerization of olefines: Polypropylene	FB
<i>o</i> -cresol and 2,6-xylenol	FB
Calcination/roasting of ores	BB/FB
Inclination of solid waste	BB/FB

FB = fluidized bed; FFB = fast fluidized bed; BB = bubbling fluidized bed

## 10.6 Advantages and disadvantages

In general, fluidized beds are of special interest when a high degree of gas to solid contact coupled with large throughput of gas at fairly low pressure drop is needed.

In industry many different reactor designs are employed for the catalytic gas-solid processes, most important are the fixed bed, moving bed and fluidized bed designs. In fixed bed reactors the catalyst particles are arranged in a vessel, generally a vertical cylinder, with the flux of reactants and products passing through the stagnant bed. In moving bed reactors the bed can be removed either continuously or periodically in portions. The fluid circulation is similar to that in a fixed bed.

Among these vessels, the fixed bed reactors are the conventional workhorses for these processes. The fixed bed reactors are generally used for very slow or non-deactivating catalysts. For some of these processes serious temperature control problems limit the size of the reactor units. In the fixed bed units the catalyst particles must be fairly large and uniform, and with poor temperature control the catalyst may sinter and clog the reactor. Bubbling and turbulent fluidized beds are more suitable for small granular or powdery non-friable catalysts. Rapid deactivation of the solids can then be handled, and excellent temperature controlled allows large scale operations. In general, fluidized beds are of special interest when a high degree of gas to solid contact coupled with large throughput of gas at fairly low pressure drop is needed.

Comparing the fluidized bed and fixed bed reactor investment costs, physical characteristics and operation performance the important advantages and disadvantages of fluidized beds relative to fixed beds can be summarized as follows.

*Advantages of fluidized beds:*

- The ability to withdraw and reintroduce solids continuously.
- Possibility of continuous regeneration of the catalyst particles. This is particularly useful for chemical processes where the catalyst is rapidly deactivated.
- The rapid mixing of solids leads to close to isothermal conditions throughout the reactor. Low risk of hot spots, runaway and thermal instability. The fluidized bed is well suited for exothermic reactions.
- Low impact of internal and external diffusion phenomena because of the small particle size.
- Efficient gas-solid contacting. Heat and mass transfer rates between gas and particles are high when compared with fixed bed reactors.
- The convective heat transfer coefficients at the surfaces immersed in the bed are high. This property indicates that internal heat exchangers require relatively small surface areas.

*Disadvantages of fluidized beds:*

- For the same weight of catalyst, expansion of the bed requires an increase in reactor volume.
- The random movement of the particles causing back-mixing result in an overall reactor behavior that is closer to a CSTR than a plug flow reactor. In many chemical processes, this leads to an increase in the reaction volume and a loss of selectivity.
- The entrainment of solid particles necessitates the installation of a device (like a cyclone) for separating and recycling fines.
- Friable solids are pulverized and entrained by the gas and must be replaced.
- Erosion of internals, pipes, and vessels from abrasion by particles can be serious.
- Broad residence time distributions of solids due to intense mixing, erosion of the bed internals, and attrition of the catalyst particles.
- Broad residence time distributions of the gas due to dispersion and gas-bypass in the form of bubbles, especially when operated in the bubbling bed regime.
- Reactor hydrodynamics and modeling are complex. Scale-up and design thus presents serious challenges which limits the use of these reactors to applications that can justify the significant research and development efforts involved.

## 10.7 Chemical Reactor Modeling

Although many of the earliest fluidized beds were operated at high gas velocities, technical difficulties led to a decrease in superficial gas velocities in the early years [56]. At the same time, the academic research focused mainly on

the bubbles and slugs in fluidized beds. Call to mind that the characteristic nature of basic science guides academic researchers to proceed analyzing any problem in a systematic manner trying to understand the low velocity phenomena before the more complex high velocity flow patterns were studied. This naturally led to significant advances in the understanding of processes carried out at relatively low gas velocities, high-velocity processes and hydrodynamics were all simply ignored.

In recent years renewed interest in fluidized beds operated at high gas velocities (1.5 m/s or more) in hydrodynamic regimes beyond the bubbling and slugging regimes arise, firstly because some industrial fluid bed reactor processes were always operated at such high gas velocities. Secondly, the interest has been increased by the development of new circulating fluidized bed (5-10 m/s) and substantial external recycle of entrained solids. Larger units were constructed and operated to increase the profit and competitive ability.

### 10.7.1 Conventional Models for Bubbling Bed Reactors

In order to predict the performance of a chemical reactor information on the reaction kinetics, thermodynamics, heat and mass transfer, and flow patterns are generally required. For bubbling fluidized bed reactors in particular the flow and the phase interaction phenomena are the most challenging modeling tasks. In the early days, ideal flow models such as plug flow, continuous stirred tank or mixed flow, dispersion, and the tank in series approaches were assessed. Then, led by Toomey and Johnstone [130] a number of two-region models were proposed. The basic advantage of these models was that they enable the investigators to account for the observed non-homogeneity of dense fluidized beds, identifying the dilute *bubble* and the dense *emulsion* phases. The word phase in this context refers to a region which may include both gas and solid particles. These regions are distinguished from one another in terms of the volume fraction of solids, by physical appearance, and through their flow characteristics [54].

Two major discoveries in the understanding of the gas/solid interaction phenomena in bubbling fluidized beds were obtained in the 1960s [81]. Firstly, the Davidson and Harrison [29] analysis of the flow of gas within and in the vicinity of rising gas bubbles. Secondly, the Rowe and Partridge [115] and Rowe [116] finding that a rising bubble was accompanied by a wake of solids and that this was the main mechanism causing solids circulation in a dense fluidized bed.

These developments led to a novel type of reactor models, the hydrodynamic models, in which the bed behavior was based on the characteristics of the rising bubbles. Several models of this kind were derived for the industrial relevant fine particle suspensions in which the rising bubbles are surrounded by very thin clouds of circulating gas. Various combinations of assumptions have been used to represent the phase interaction phenomena in this region [81]:

- Two- or three phase models. In the three phase case the bubble, cloud, and emulsion phases are treated as separate regions. The three-phase model can be reduced to a two-phase model either by treating the bubble and cloud phases as a single region, or by treating the cloud and emulsion phases as a single region.
- The bubbles are spherical or non-spherical.
- The bubble wake region is accounted for or ignored.
- The simplest model versions consider one mean bubble size in the whole bed. The simple model can be extended so that bubbles are allowed to grow as they rise in the bed but are of the same size over the cross section of the bed at any level in the bed. The most advanced models are similar to the previous group of extended models but consider also a bubble size distribution at any level in the bed.
- The solids in the bubbles are considered or ignored.

A few of the early bubbling bed modeling approaches are assessed in the subsequent sub-sections. Reliable engineering models, at this simple level of complexity, can only be derived based on appropriate empirical information characterizing the important bed properties. The theory and typical parameterizations used to determine the relevant behavior of the gas and solids in the bubble, cloud, emulsion and wake regions are outlined.

### Pressure Drop and Minimum Fluidization Velocity

Increasing the gas flow just passing the point of minimum fluidization conditions the onset of particle fluidization will occur when the drag forces acting on the particles due to the upward moving gas are balanced by the weight of the solid particles [30].

The cross sectional average global pressure drop over a fluidized bed operated at minimum fluidization conditions is normally calculated by an extrapolation of the Ergun [42] equation (6.13) for fixed packed beds, the flow regime that is prevailing until the minimum fluidization flow rate has been reached, as described in chap 6:

$$-\frac{\Delta p_t}{L_{mf}} = f \frac{\rho_g (U_{mf}^s)^2}{d_p} \quad (10.1)$$

where  $f$  denotes an appropriate friction factor, as for example (6.14), and  $L_{mf}$  represents the height of the fixed bed at minimum fluidization conditions.

The weight of the cross sectional averaged bed at minimum fluidization is:

$$-\frac{\Delta p_t}{L_{mf}} = (1 - \varepsilon_{mf})(\rho_p - \rho_g)g \quad (10.2)$$

where  $\varepsilon_{mf}$  denotes the gas holdup (overall bed void fraction) in the bed at minimum fluidization (generally a measured characteristic of the bed packing).

The superficial gas velocity at minimum fluidization conditions  $U_{mf}^s$  is then found by combining the two relations for the pressure drop:

$$U_{mf}^s = \sqrt{\frac{d_p(1 - \varepsilon_{mf})(\rho_p - \rho_g)g}{\rho_g f}} \quad (10.3)$$

### Volumetric Gas Flow Rate and Bubble Rise Velocity

The volumetric gas flow rate to the bubble phase in a fluidized bed  $Q_b$  is defined as the average rate at which the bubble volume crosses any level in the bed [22]. However, the flow of gas in the bubble phase is generally greater than the volumetric gas flow rate in bubble because of the so-called bulk *throughflow* of gas into and out of each bubble (i.e., convective interfacial mass transfer).

A first estimate for  $Q_b$  is given by the *two-phase theory of fluidization*, proposed by Toomey and Johnstone [130] and developed by Davidson and Harrison [29, 30]. In this theory a bubbling fluidized bed consists of two zones or phases, referred to as the bubble phase consisting of pure gas and the emulsion phase consisting of uniformly distributed particles in a supporting gas steam. The emulsion phase is assumed to be operating at minimum fluidization conditions  $U_e^s \approx U_{mf}^s$ , while the bubble phase carries the remaining gas flow  $U_b^s \approx U_{in}^s - U_{mf}^s$ .

This simple model can then be used to estimate the volumetric gas flow rate in bubble phase as the excess gas flow above that required for minimum fluidization:

$$Q_b \approx (U_{in}^s - U_{mf}^s)A \quad (m^3/s) \quad (10.4)$$

where  $A$  is the cross sectional area of the bed ( $m^2$ ).

Experimental investigations indicate that the actual  $Q_b$  is 10–50% smaller than the value given by the simple two-phase model [22]. Nevertheless, the two-phase theory has been the basis for much work in fluidization technology. For example, knowing the bubble phase volumetric gas flow rate the average fraction of the bed area occupied by bubbles can be approximated as:

$$\varepsilon_b \approx \frac{Q_b}{Au_b} \approx \frac{U_{in}^s - U_{mf}^s}{u_b} \quad (-) \quad (10.5)$$

where  $u_b$  is the average rise velocity of bubbles in the bubbling bed.

Moreover, the simple two-phase theory results (10.4) and (10.5) can be adopted determining a first estimate of the *bed expansion*  $\Delta L = L - L_{mf}$  due to the bubble formation in dense beds. The expansion of the bed above its depth at minimum fluidization is obtained from the bubble phase volume balance:

$$A\Delta L = A \int_0^L (1 - \varepsilon_b)dz - A \int_0^{L_{mf}} (1 - \varepsilon_b)dz \approx \int_{L_{mf}}^L \frac{Q_b}{u_b} dz \quad (m^3) \quad (10.6)$$

provided that the average rise velocity of bubbles is known (since the  $L_{mf}$  and  $U_{in}^s$  parameters are normally specified and  $U_{mf}^s$  is calculated from suitable semi-empirical models).

The *rise velocity of a single bubble* rising in an emulsion phase unaffected by other bubbles and the walls is frequently calculated from an expression derived for gas liquid flow. Bubbles in a fluidized bed behave in many ways like bubbles in a low viscosity liquid [116, 82]. A small bubble is spherical, but a bubble becomes deformed with increasing size and the larger ones have a spherical capped shape. The smallest bubbles rise slowly. The larger bubbles generally rise faster. Bubbles flowing in series may coalesce to produce larger bubbles. Wall effects usually decreases the bubble rise velocity. However, in contrast to gas-liquid flow there is a high degree of gas interchange between the bubbles and the gas in the dense emulsion phase. Davies and Taylor [31] studied the rate of rise of large spherical cap bubbles of air through nitrobenzene or water. An approximate calculation showed that the velocity of rise of a single bubble is  $u_{bl,rise} = \frac{2}{3}(gR_n)^{1/2}$ . In this formula  $R_n$  is the radius of curvature at the nose of the gas bubble. Clift et al [23] (p 206) summarized the experimental rate of rise data for gas bubbles in liquids found in more recent publications.

For particular bubble Reynolds and Eötvös numbers,  $Re_b = \rho_g d_e u_{bl,rise} / \mu_g > 150$  and  $Eo = g \Delta \rho d_e^2 / \sigma_I \geq 40$ , the data on spherical cap bubbles indicate that a semi-empirical relation for the terminal velocity expressed in terms of the volume equivalent bubble diameter is appropriate [54]:

$$u_{bl,rise} \approx \left[ \frac{2}{3} \sqrt{\frac{R_n}{d_e}} \right] (g d_e)^{1/2} \approx 0.711 (g d_e)^{1/2} \quad (m/s) \quad (10.7)$$

where  $u_{bl,rise}$  denotes the rise velocity of a spherical cap bubble in liquid ( $m/s$ ), and  $d_e$  is the equivalent bubble diameter ( $m$ ). The term in the bracket is generally a weak function of  $Re_b$ , but for  $Re_b > 100$  the pre-factor is about constant. For gas-liquid flows the modified coefficient value is confirmed fairly well in several experimental investigations [28, 116, 138, 31].

Even though (10.7) is strictly valid in liquids, the formula is widely used for calculations of the ideal rise velocity of single bubbles in fluidized beds, when the ratio of bubble to bed diameters is  $d_b/d_t < 0.125$  [29, 82]:

$$u_{br,0} \approx 0.711 (g d_b)^{1/2} \quad (10.8)$$

However, experimental data on rise velocities in fluidized beds consisting of group A and B particles indicates that the pre-factor in (10.8) is about 2/3 as for a single spherical cap bubble in liquid. For group D particles the given pre-factor of 0.711 seems appropriate.

Wall effects are found to retard the single bubbles when  $d_b/d_t > 0.125$ . Kunii and Levenspiel [82] proposed that for  $0.125 < d_b/d_t < 0.6$  the rise velocity of a single bubble can be estimated from:

$$u_{br,0} \approx [0.711(gd_b)^{1/2}] \times 1.2 \times \exp\left(-1.49\frac{d_b}{d_t}\right) \quad (10.9)$$

For  $d_b/d_t > 0.6$ , the bed operates in the slugging regime which is not very interesting from a chemical reactor engineering point of view.

In reactor modeling we need to deal with the behavior of the bubbling bed as a whole rather than single rising bubbles. In extending the simple two-phase theory, Davidson and Harrison [29] proposed that the average velocity of bubbles in a freely bubbling bed can be approximated by <sup>4</sup>:

$$u_b = U_b^s + u_{br,0} \approx U_{in}^s - U_{mf}^s + u_{br,0} \quad (10.10)$$

where  $u_{br,0}$  is the ideal rise velocity of an isolated bubble of the same size (10.8).

This relation is not generally valid but considered to give a fair approximation of the average flow rate of bubbles when  $U_{in}^s$  is close to  $U_{mf}^s$  for all types of particles, and for all velocities of interest considering larger type B and type D particles. However, in large diameter beds consisting of fine particles and operated at higher gas velocities the real bubble rise velocity is several times the velocity predicted by (10.10). This deviation is primarily caused by the existence of preferred emulsion flow patterns [81, 82]. For small B and fine A particles the emulsion phase gas and solids are not really stagnant but develop distinct flow patterns, frequently referred to as *gulf streaming*, induced by the uneven rise or channeling of gas bubbles. In these gulf streaming patterns the bubbles rise in bubble rich regions with less friction thus a substantially higher mean bubble rise velocity occur in these zones. In small and narrow beds this flow pattern might be reduced or prevented by the wall friction. Several modified relations for the average bubble rise velocity in dense fluidized beds have been reported over the years, each of them valid for particular Geldart solids, bed designs and operating conditions. Kunii and Levenspiel [81], for example, proposed a correlation for Geldart A solids with  $d_t \leq 1$  (m):

$$u_b = 1.55 \left\{ (U_{in}^s - U_{mf}^s) + 14.1(d_b + 0.005) \right\} d_t^{0.32} + u_{br,0} \quad (m/s) \quad (10.11)$$

A similar correlation was given for Geldart B solids with  $d_t \leq 1$  (m):

$$u_b = 1.6 \left\{ (U_{in}^s - U_{mf}^s) + 1.13d_b^{0.5} \right\} d_t^{1.35} + u_{br,0} \quad (m/s) \quad (10.12)$$

### The Davidson-Harrison Model for Gas Flow Around Bubbles

The first model for the movement of both gas and solids and the pressure distribution around single rising bubbles was given by Davidson and Harrison

<sup>4</sup> This expression and the arguments for its use were first presented by Nicklin [102] for gas-liquid systems determining the rise velocity of a single bubble in a cloud of gas bubbles rising through a stagnant liquid, and later used by Davidson and Harrison [29] (p 28) for bubbles in fluidized beds.

[29] (Chap 4). Two versions of the model were developed, considering two- and three-dimensional fluidized beds. The theory is based on the following assumptions:

- There is no solids in a gas bubble. A three-dimensional bubble is spherical, whereas a two-dimensional bubble is cylindrical.
- As a bubble rises, the particles move aside, as would an incompressible inviscid fluid having the same bulk density as the whole bed at incipient fluidization  $\rho_s(1 - \varepsilon_{mf}) + \rho_g\varepsilon_{mf}$ .
- The gas flows in the emulsion phase as an incompressible viscous fluid. The relative velocity between the gas and the solid particles must satisfy Darcy's law:

$$\mathbf{v}_g - \mathbf{v}_s = -K\nabla p \quad (10.13)$$

where  $K$  is a permeability constant characteristic of the particles and the fluidizing fluid.

From potential flow theory, invoking the given model assumptions, the pressure distribution in the bed can be found by solving a Laplace equation. The boundary conditions used express that far from a single bubble an undisturbed pressure gradient exist as given by (10.2), and that the pressure in the bubble is constant. Then, after the pressure distribution is known the flow pattern for the solids and the gas in the vicinity of a rising bubble can be calculated. The solution shows that the pressure in the lower part of the bubble is lower than that in the surrounding bed, whereas in the upper part it is higher. For this reason the gas flows into the bubble from below and leaves at the top. A distinct difference in the gas flow pattern has been identified, depending on whether the bubble rises faster or slower than the emulsion gas. The gas flow pattern is thus classified dependent on the relative velocity between a single bubble  $u_{br,0}$  and the emulsion gas  $u_e = U_{mf}^s/\varepsilon_{mf}$  far from the bubble.

For slow bubbles ( $u_{br,0} < u_e$ ) in beds consisting of large particles the emulsion gas rises faster than the bubble, hence the faster rising emulsion gas shortcuts through the rising bubble on its way through the bed. The emulsion phase gas enters the bottom of the bubble and leaves at the top. Within the bubble an annular ring of gas is forced to circulate as it moves upwards with the bubble. For a fast bubble ( $u_{br,0} > u_e$ ) in beds consisting of small particles the emulsion gas rises slower than the bubble, but still the emulsion phase gas enters the bottom of the bubble and leaves at the top. However, since the bubble is rising faster than the emulsion gas, the gas leaving the top of the bubble is swept around and returns to the base of the bubble. The region around the bubble penetrated by this circulating gas is called the *cloud*. The rest of the gas in the bed does not mix with the recirculating gas but moves aside as the fast bubble with its cloud passes by. The cloud phase might be considered infinite in thickness at  $u_{br,0} = u_e$ , but thins with increasing bubble velocity. For very fast bubbles,  $u_{br,0}/u_e > 5$ , the cloud is very thin

and most of the gas stays within the bubble. In general slow cloudless bubbles occurs in beds of coarse particles (group D, or B) while fast bubbles with thin clouds are typically observed for group A and B particles at high gas velocities.

For a two-dimensional bed the cloud size is given by [29, 30]:

$$\frac{R_c^2}{R_b^2} = \frac{u_{br,0} + u_e}{u_{br,0} - u_e} \quad (10.14)$$

For a three-dimensional bed the cloud size is given by [29, 30]:

$$\frac{R_c^3}{R_b^3} = \frac{u_{br,0} + 2u_e}{u_{br,0} - u_e} \quad (10.15)$$

For a two-dimensional bed the ratio of cloud to bubble size is defined as [82]:

$$f_c = \frac{R_c^2}{R_b^2} \approx \frac{u_{br,0} + u_e}{u_{br,0} - u_e} \approx \frac{2u_e}{u_{br,0} - u_e} \approx \frac{2U_{mf}^s/\varepsilon_{mf}}{u_{br,0} - U_{mf}^s/\varepsilon_{mf}} \quad (10.16)$$

For a three-dimensional bed the ratio of cloud to bubble volume is defined as [82]:

$$f_c = \frac{R_c^3}{R_b^3} = \frac{u_{br,0} + 2u_e}{u_{br,0} - u_e} \approx \frac{3u_e}{u_{br,0} - u_e} \approx \frac{3U_{mf}^s/\varepsilon_{mf}}{u_{br,0} - U_{mf}^s/\varepsilon_{mf}} \quad (10.17)$$

These estimates for  $f_c$  are obtained considering the particular case when  $u_{br,0} \approx u_e$ .

The simple theory also provides estimates of the gas exchange between the bubble and the emulsion phase. For a two-dimensional bed of unit thickness the flow of gas through the bubble is  $v = 4u_e\varepsilon_{mf}r_b$ , and for a three-dimensional bed the flow of gas through the bubble is  $v = 3u_e\varepsilon_{mf}\pi r_b^2$ .

Rowe [116] and Davidson et al [30] summarized the experimental investigations of the properties of bubbles and clouds, explained the elementary theories using nice illustrations and provided pictures of the physical phenomena observed.

## The Wake Region

In an early study Rowe and Partridge [115] (see also [116]) did show that gas fluidized beds are characterized by the formation of bubbles which rise through denser bed zones of the bed and determine a gross scale gas and solid flow pattern.

It was observed that like a single bubble in liquid, a rising bubble in a fluidized bed drags a wake of material consisting of a gas-solid mixture up the bed behinds it. Close to the bottom of the bed, just above the gas distributor, solids are entrained by the rising bubbles to form the bubble wake. There is

also a continuous interchange of solids between the wake and emulsion as the bubble rise. At the top of the bed the wake solids rejoin the emulsion to move down the bed.

The bubble wake fraction is given by the volume ratio of the wake to the bubble:

$$f_w = \frac{V_w}{V_b} \quad (10.18)$$

The wake volume  $V_w$  is defined as the volume occupied by the wake within the sphere that circumscribes the bubble.

The wake fraction is normally determined from experimental analysis [82].

## Bubble Size

In bubbling fluidized beds there are several mechanisms affecting the bubbles properties [115, 116, 30, 82]. The main mechanisms determining the mean bubble size are bubble growth, bubble coalescence and bubble breakage. The primary bubble growth mechanism for a single bubble unaffected by other bubbles is gas transfer from the emulsion phase into the bubble. In a freely bubbling bed the main mechanism for bubble growth is bubble-bubble coalescence. Binary breakage of bubbles frequently occur as a result of small disturbances, often proceeded by a slight flattening of the bubble, initiated near the top of the roof of the bubble and these rapidly grow in a cutting edge of particles that may divide the parent bubble into two equal or unequal daughter bubbles. Later these daughter bubbles commonly re-combine either by gas leakage from one bubble to the other or because a small bubble falling behind the larger one is caught in its wake and coalescence.

Experiments have shown that in beds consisting of B type particles the bubbles increase steadily, whereas in beds consisting of type A particles the bubbles grow rapidly until they reach a stable size determined by a state of equilibrium between the coalescence and breakage processes [82].

When performing experimental investigations of bubble properties two dimensional beds have proved to be useful [55]. These two-dimensional columns are of rectangular cross section, the width being considerably greater than the thickness. The fluidized particles are contained in the gap between two transparent faces, separated by 2-3 *cm*. The bubbles span the bed thickness and are thus viewed. However, while these two-dimensional columns are useful for qualitative purposes, there are important quantitative differences between the two- and three dimensional fluid bed flow behavior. These differences arise from quantitative differences in rise velocities of isolated bubbles, bubble coalescence properties, bubble shape and wake characteristics, reduced solids mixing, etc. To characterize the bubble properties in three dimensional dense beds intrusive probes are normally used [129]. For modeling purposes it is important to distinguish between the relations obtained characterizing two- and three dimensional beds.

The equivalent bubble diameter  $d_e$ , defined as the diameter of a spherical bubble with a volume equal to the average bubble volume, is often used as a measure of bubble size. A representative relation for the equivalent bubble diameter in a three-dimensional bed with B particles supported by a perforated plate distributor was given by [134]:

$$d_e = d_{e,0}[1 + 27.2(U_{in}^s - U_{mf}^s)]^{1/3}(1 + 6.84z)^{1.21} \quad (m) \quad (10.19)$$

where  $d_{e,0}$  denotes the initial bubble size at the distributor, and  $z$  is the position above the distributor.

A more general relation for the equivalent bubble diameter in three-dimensional beds was derived by Darton et al [27]:

$$d_e = \frac{0.54}{g^{1/5}}(U_{in}^s - U_{mf}^s)^{2/5}(z + 4\sqrt{A_0})^{4/5} \quad (m) \quad (10.20)$$

where  $A_0$  is the *catchment area* for the bubble stream at the distributor plate, which characterize different distributors, and is usually the area of plate per orifice. For a porous plate distributor a typical value  $A_0 \approx 5.6 \times 10^{-5} (m^2)$  was proposed.

To determine the growth of circular bubbles in two-dimensional fluidized beds Lim et al [89] modified the relation of Darton et al [27] and proposed:

$$d_e = \left[ \frac{8(U_{in}^s - U_{mf}^s)(2^{3/4} - 1)}{\pi \lambda g^{1/2}} z + d_{e,0}^{3/2} \right]^{2/3} \quad (m) \quad (10.21)$$

where the initial equivalent bubble diameter just above the distributor is given by:

$$d_{e,0} = \left[ \frac{8(U_{in}^s - U_{mf}^s)A_0}{\pi \lambda g^{1/2}} \right]^{2/3} \quad (m) \quad (10.22)$$

The dimensionless proportionality constant  $\lambda \sim 2$  is related to the distance a bubble travels in a stream before coalescing with the adjacent stream to form a single stream of larger bubbles.

## The Basic Two-Phase Model

A number of fluidized bed reactor model versions are based on the cross sectional averaged two-phase transport equations as presented in sect 3.4.7. Due to the vigorous particle flow the fluidized beds are essentially isothermal, so no energy balance is generally required<sup>5</sup>. In addition, the necessary species mass (mole) balance can be deduced from (3.498). The solids are considered

<sup>5</sup> In particular cases, considering extremely exothermic or endothermic processes, a global CSTR heat balance may be employed to determine a uniform operating temperature and the necessary heating/cooling capacity.

to be completely mixed in the dense phase and is essentially stagnant, so only an overall mass balance is needed for the solid phase.

For the particular case of an irreversible gas solid catalyzed reaction with no accompanying volume change, the mass (mole) balance for a species A in the interstitial gas phase moving through the emulsion phase is frequently simplified assuming axially constant transport parameters (i.e.,  $f_e$ ,  $u_e$ ,  $D_e$ , and  $k_{be}$ ) [141, 142, 58]:

$$f_e \frac{\partial C_{Ae}}{\partial t} + f_e u_e \frac{\partial C_{Ae}}{\partial z} = f_e D_e \frac{\partial^2 C_{Ae}}{\partial z^2} + f_e k_{be} (C_{Ab} - C_{Ae}) + r_{Ae} \rho_e f_e \quad (10.23)$$

where  $C_{Ae}$  represents the cross sectional average mole concentration of A in the emulsion phase gas ( $kmol/m^3$ ),  $U_e^s = f_e u_e$  the superficial velocity of the emulsion phase gas ( $m^3/m^2 s$ ),  $u_e$  the interstitial emulsion gas velocity ( $m/s$ ),  $D_e$  an effective diffusivity for the emulsion gas ( $m^2/s$ ),  $k_{be}$  an interchange mass transfer rate coefficient per unit volume of bubble gas ( $m^3/m^3 s$ ),  $r_{Ae}$  reaction rate in emulsion phase ( $kmol/kg s$ ),  $f_e$  is the fraction of the bed gas volume taken by the emulsion gas ( $m^3/m^3$ ), and  $\rho_e$  the mass concentration of the catalyst particles in the emulsion phase ( $kg/m^3$ ).

The corresponding mass (mole) balance for species A in the bubble phase is:

$$f_b \frac{\partial C_{Ab}}{\partial t} + f_b u_b \frac{\partial C_{Ab}}{\partial z} = f_b D_b \frac{\partial^2 C_{Ab}}{\partial z^2} - f_b k_{be} (C_{Ab} - C_{Ae}) + r_{Ab} \rho_b f_b \quad (10.24)$$

where  $C_{Ab}$  represents the cross sectional average mole concentration of A in the bubble phase ( $kmol/m^3$ ),  $U_b^s = f_b u_b$  the superficial velocity of the bubble phase gas ( $m^3/m^2 s$ ),  $D_b$  an effective diffusivity for the bubble gas ( $m^2/s$ ),  $r_{Ab}$  reaction rate in bubble phase ( $kmol/kg s$ ),  $f_b$  the volume fraction of the bed gas taken by the bubble gas ( $m^3/m^3$ ), and  $\rho_b$  the mass concentration of the catalyst particles in the bubble phase ( $kg/m^3$ ).

### The Davidson-Harrison Two-Phase Model

The Davidson and Harrison [29, 30] bubbling bed reactor model represents one of the first modeling attempts that was based on bubble dynamics. The model rest on the following assumptions:

- The reactor operates at steady state, thus the transient terms in (10.23) and (10.24) disappear.
- The gas bubble are evenly distributed throughout the bed and are of equal size.
- The bubble phase gas flow can be described by a plug flow model, hence the bubble phase dispersion term in (10.24) vanishes.
- No solids in the bubbles, thus no catalytic reaction takes place in the bubble phase gas.

- The emulsion phase gas flows with a superficial velocity  $U_{mf}^s$  and is either considered completely mixed or plug flow.
- Gas is exchanged between the non-reactive bubble and the reactive emulsion phases by a combined molecular and convective transport flux.

Species mass balances were developed for the two phases and solved analytically for first order reactions. Thus, for the case of a completely mixed emulsion phase the concentration of a reactant leaving this phase is given by:

$$C_e = \frac{C_{in}(1 - f_b e^{-X})}{1 - f_b e^{-X} + \frac{kL_{mf}}{U^s}} \quad (10.25)$$

where  $X = K_{be}L/U_b^s$  is the interphase exchange parameter,  $L$  represents the bed height and  $U_b^s$  the bubble velocity, and  $f_b = 1 - U_{mf}^s/U^s$ .

For the bubble phase operated in plug flow:

$$C_b = C_e + (C_{in} - C_e)e^{-X} \quad (10.26)$$

The concentration of unconverted reactant  $C_{out}$  leaving the bed as a whole was then found from:

$$C_{out} = f_b C_b + (1 - f_b)C_e \quad (10.27)$$

The overall fraction of unconverted reactant becomes:

$$\frac{C_{out}}{C_{in}} = f_b e^{-X} + \frac{(1 - f_b e^{-X})^2}{1 - f_b e^{-X} + \frac{kL_{mf}}{U^s}} \quad (10.28)$$

For the case when the emulsion phase gas is in plug flow, the overall fraction unconverted reactant leaving the bed becomes:

$$\frac{C_{out}}{C_{in}} = \frac{1}{m_1 - m_2} \left[ m_1 e^{-m_2 L} \left( 1 - \frac{m_2 L U_{mf}^s}{X U^s} \right) - m_2 e^{-m_1 L} \left( 1 - \frac{m_1 L U_{mf}^s}{X U^s} \right) \right] \quad (10.29)$$

where  $m_1$  and  $m_2$  are obtained from:

$$2L(1 - f_b)m = \left( X - \frac{kL_{mf}}{U^s} \right) \pm \left[ \left( X - \frac{kL_{mf}}{U^s} \right)^2 - 4 \frac{kL_{mf}}{U^s} X (1 - f_b) \right]^{1/2} \quad (10.30)$$

In the latter expression  $m = m_1$  with the positive sign and  $m = m_2$  with the negative sign.

The details of the model derivation and the analytical solution can be found in [29, 141, 142, 141, 117]. It is noted that this model was developed before the importance of bubble clouds and wakes were realized.

Although this model is derived from first principles and uses a minimum of empirical information, the model predictions have been found to agree fairly well with experimental data in a number of cases and may thus be adequate for design purposes. However, the empirical relationships are derived from experiments with laboratory scale equipment, and this has caused the validity of their application to large industrial units to be questioned.

### The van Deemter Two-Phase Reactor Model

This model represents one of the first modeling approaches used to describe large industrial beds that has been fully documented and discussed in the open literature. The model was adopted by the Shell company designing a fluidized bed reactor for their solid catalyzed hydrogen chloride oxygen process. However, the model has many of the same limitations as the Davidson-Harrison model because it was developed before the importance of bubble clouds and wakes were realized.

The fairly general transport equations constituting the basic two-phase model, given in (10.23) and (10.24), were simplified making the van Deemter model specific assumptions [132, 142, 47]:

- The reactor operates at steady state, thus the transient terms disappear.
- The bubble gas flow can be described by a plug flow model, hence the bubble phase dispersion term vanishes.
- No solids in the bubbles so no catalytic reaction takes place in the bubble phase, thus the reaction term disappears in the bubble gas mole balance.

For a single reaction, a generic cross sectional average species mole balance for component A in the bubble phase gas can thus be written as:

$$f_b u_b \frac{dC_{Ab}}{dz} + f_b k_{be} (C_{Ab} - C_{Ae}) = 0 \quad \left( \frac{\text{kmol}}{\text{m}^3 \text{s}} \right) \quad (10.31)$$

The corresponding cross sectional average species mole balance for component A in the emulsion phase gas is written as:

$$f_e u_e \frac{dC_{Ae}}{dz} - f_b k_{be} (C_{Ab} - C_{Ae}) - f_e D_e \frac{d^2 C_{Ae}}{dz^2} + r_{Ae} \rho_e f_e = 0 \quad \left( \frac{\text{kmol}}{\text{m}^3 \text{s}} \right) \quad (10.32)$$

The overall outlet concentration  $C_{A,out}$  is calculated as:

$$U_{in}^s C_{A,out} = f_b u_b C_{Ab} + f_e u_e C_{Ae} \quad (10.33)$$

in which  $U_{in}^s$  denotes the overall superficial gas velocity ( $\text{m}^3/\text{m}^2 \text{s}$ ).

The model equations are normally solved applying the following initial and boundary conditions :

Bubble phase:

$$\text{Emulsion phase [26]: } \left. \begin{array}{l} -D_e \frac{dC_{Ae}}{dz} \Big|_{z=0} = u_e (C_{Ae}|_{z=0} - C_{Ae}) \\ \frac{dC_{Ae}}{dz} \Big|_{z=L} = 0 \end{array} \right\} \begin{array}{l} C_{Ab} = C_{Ab}|_{z=0} \end{array}$$

$$(10.34)$$

The undetermined model parameters like  $U_b^s$ ,  $u_b$ ,  $k_{be}$ ,  $D_e$ ,  $f_e$ ,  $f_b$ ,  $u_e$  and  $U_e^s$  were approximated from empirical correlations determined by experimental measurements.  $U_{in}^s$  and  $\varepsilon_{mf}$  are generally measured or specified, thus  $U_{mf}^s$  can be determined from (10.3).

A typical correlation for  $k_{be}$  is given by [117, 47]:

$$\frac{U_{in}^s}{f_b k_{be}} \approx (1.8 - \frac{1.06}{d_t^{0.25}})(3.5 - \frac{2.5}{Z^{1.4}}) \quad (m) \quad (10.35)$$

where  $Z$  is the total reactor height ( $m$ ).

The effective diffusivity in the emulsion phase may be approximated by [6]:

$$D_e \approx 0.35(gU_{in}^s)^{1/3}d_t^{4/3} \quad (m^2/s) \quad (10.36)$$

In the basic two-phase model a prescribed fraction of the total gas flow rate through the bed, which is coinciding with the minimum fluidization operating conditions, is assumed to move through the emulsion phase [130, 29]. The relative velocity between the interstitial gas and the solids in the emulsion phase is thus  $u_e = U_{mf}^s/\varepsilon_{mf}$ . The rest of the gas constitutes the bubble phase. The superficial bubble gas velocity is thus generally approximated as:

$$U_b^s = f_b u_b \approx U_{in}^s - U_{mf}^s \quad (m^3/m^2s) \quad (10.37)$$

Likewise, the superficial emulsion gas velocity is approximated as:

$$U_e^s = f_e u_e \approx U_{mf}^s = u_e \varepsilon_{mf} \quad (m^3/m^2s) \quad (10.38)$$

The average bubble rise velocity (10.10) is approximated by the bubble rise velocity among a swarm of bubbles [134]:

$$u_b = U_e^s - U_{mf}^s + u_{br,0} \approx u_{br,0} \approx K\sqrt{gd_b} \quad (10.39)$$

where  $K = 0.64$  when  $d_t < 0.1$  ( $m$ ),  $K = 1.6d_t^{0.4}$  when  $0.1 < d_t < 1.0$  ( $m$ ), and  $K = 1.6$  when  $d_t > 1.0$  ( $m$ ).

The flow pattern for solids is generally downward near the wall and upward in the central core. This particle movement also affects the gas flow in the emulsion phase. In this model the net rise velocity of solids is neglected, hence  $u_s = 0$ .

For a perforated plate distributor the bubble size might be approximated by (10.19).

### The Kunii-Levenspiel Three-Phase Model

The celebrated Kunii-Levenspiel [78, 79, 81, 82] (p 289) reactor model presented in this section was designed for the particular case of fast bubbles in vigorously bubbling beds which is relevant for industrial applications with Geldart A and AB solids. In such beds there are definite gross mixing patterns for the solid, downward near the wall and upward in the central core. This has a marked effect on the gas flow in the emulsion phase, which is also forced downward near the wall. However, based on experimental data analysis, Kunii

and Levenspiel found that at gas flow rates above  $U_{in}^s/U_{mf}^s \sim 6 - 11$  there are practically no net gas flow through the emulsion phase.

To take these observations into account a three phase model was proposed in which many ideas from the Davidson bubble theory, the Davidson-Harrison and the van Deemter reactor models were adapted. The Rowe cloud and wake observations were also considered. The basic model assumptions were:

- The bed is assumed to consist of three phases, the bubble, cloud and emulsion, with the wake region considered to be a part of the cloud phase.
- For industrial relevant operating conditions well above minimum fluidization,  $U_{in}^s \gg U_{mf}^s$  and practically all the moving gas is transported in the bubble phase. In this fast bubbling regime, for which  $u_b > 5U_{mf}^s/\varepsilon_{mf}$ , the clouds are very thin.
- Interchange mass transfer coefficients are used to account for the mass transfer between the phases.
- The rising bubbles contain no solid.
- The bubble phase operates under plug flow conditions.
- The cloud and emulsion phases are stagnant ( $u_e \approx u_c \approx 0$ ).
- Spherical bubbles of uniform size accompanied by wakes throughout the bed.
- First-order reaction is assumed. The catalytic reaction rate is given in accordance with modern literature [47].

For a single catalytic reaction, a generic cross sectional average species mole balance for component A in the bubble phase gas can be written as:

$$u_b \frac{dC_{Ab}}{dz} + k_{bc}(C_{Ab} - C_{Ac}) + r_{Ab}\rho_b = 0 \quad \left( \frac{kmol}{m^3s} \right) \quad (10.40)$$

where  $k_{bc}$  denotes the interchange coefficient determining the mass transfer between the bubble and cloud gas phases, referred to unit bubble gas volume ( $m^3/m^3s$ ), and  $C_{Ac}$  the molar concentration of species A in the cloud phase gas ( $kmol/m^3$ ).

For a single reaction a generic species mole balance for component A in the stagnant cloud phase gas is written as:

$$k_{bc}(C_{Ab} - C_{Ac}) = r_{Ac}\rho_c \frac{V_c}{V_b} + k_{ce}(C_{Ac} - C_{Ae}) \quad \left( \frac{kmol}{m^3s} \right) \quad (10.41)$$

where  $V_c$  denotes the volume of the cloud phase ( $m^3$ ),  $V_b$  the volume of the bubble phase ( $m^3$ ),  $\rho_c$  the mass concentration of the catalyst particles in the cloud phase ( $kg/m^3$ ), and  $k_{ce}$  denotes the interchange coefficient determining the mass transfer between the cloud and emulsion phases, referred to unit bubble volume ( $m^3/m^3s$ ).

For a single reaction a generic species mole balance for component A in the stagnant emulsion phase gas is written as:

$$k_{ce}(C_{Ac} - C_{Ae}) = r_{Ae}\rho_e \frac{f_e}{f_b} \approx r_{Ae}\rho_e \frac{1 - f_b}{f_b} \quad \left( \frac{\text{kmol}}{\text{m}^3\text{s}} \right) \quad (10.42)$$

In general, the model can be solved numerically with appropriate initial conditions for the plug flow ODE.

Bubble phase:

$$C_{Ab} = C_{Ab}|_{z=0} \quad (10.43)$$

The model can be solved analytically for first order reactions. Eliminating the unknown  $C_{Ac}$  and  $C_{Ae}$  concentrations from the model equations, we obtain:

$$f_b u_b \frac{dC_{Ab}}{dz} = K_r C_{Ab} \quad \left( \frac{\text{kmol}}{\text{m}^3\text{s}} \right) \quad (10.44)$$

where the overall rate coefficient  $K_r$  contains all the interfacial transfer resistances as well as the reaction resistance terms.

The overall rate coefficient  $K_r$  can be defined as [47]:

$$K_r = k \left[ \rho_b + \frac{1}{\frac{k}{k_{bc}} + \frac{1}{\rho_c \frac{V_c}{V_b} + \frac{1}{\frac{k}{k_{ce}} + \frac{1}{\rho_e \frac{(1-f_b)}{f_b}}}}} \right] \quad (1/s) \quad (10.45)$$

Integration over the whole reactor bed from  $z = 0$  to  $z = L$  gives:

$$C_{Ab} = C_{A,in} \exp\left(-\frac{K_r L}{U_b^s}\right) \quad \left( \frac{\text{kmol}}{\text{m}^3} \right) \quad (10.46)$$

The celebrated K-L model did gain its popularity because it is very simple, yet developed for large scale industrially relevant flows and considers most of the pertinent bubbling bed phenomena.

Over the years the range of uses of the K-L model has been extended to chemical processes that can not be described by first order kinetics. For these problems no analytical solution can be obtained so the resulting set of DAE equations are solved numerically. Gascon et al [48], for example, investigated the behavior of a two zone fluidized bed reactor for the propane dehydrogenation and n-butane partial oxidation processes employing the K-L model framework.

In any case the undetermined model parameters are determined from appropriate empirical correlations [78, 79, 81, 82]. The mass transfer coefficients, all based on unit bubble volume, can be obtained from:

$$k_{bc} = 4.5 \frac{u_{mf}^s}{d_b} + 5.85 \left( \frac{D_{Am}^{1/2} g^{1/4}}{d_b^{5/4}} \right) \quad (\text{m}^3/\text{m}^2\text{s}) \quad (10.47)$$

$$k_{ce} = 6.78 \left( \frac{\varepsilon_{mf} D_{Am} u_b}{d_b^3} \right)^{1/2} \quad (m^3/m^2 s) \quad (10.48)$$

where  $D_{Am}$  is the diffusivity for species A in the mixture ( $m^2/s$ ).

In the two-phase view the solids in the bubble phase is ignored ( $\varepsilon_b \approx 1$ ), thus the overall void fraction in the bubbling bed is:

$$\varepsilon_{ov} = f_b \varepsilon_b + (1 - f_b) \varepsilon_e \approx f_b + (1 - f_b) \varepsilon_e \quad (10.49)$$

If  $\varepsilon_{ov}$  and  $f_b$  are known from experiments,  $\varepsilon_e$  can be determined by this equation.

However, in many cases  $\varepsilon_{ov}$  and  $f_b$  are unknown, so  $\varepsilon_e$  cannot be determined in this way. For modeling purposes Kunii and Levenspiel [81] proposed some rough approximations. For beds of Geldart A solids,  $\varepsilon_e \approx \varepsilon_{mb}$ , whereas for beds of Geldart B and D solids,  $\varepsilon_e \approx \varepsilon_{mf}$ .

In the latter case, where  $\varepsilon_e \approx \varepsilon_{mf}$ , the volume balance over the bed can be written as:

$$1 - \varepsilon_{ov} \approx (1 - f_b)(1 - \varepsilon_{mf}) \quad (10.50)$$

The volume fraction of the bed consisting of bubbles  $f_b$  is determined by the prevailing flow regime. For fast bubbles in vigorously bubbling beds, where  $u_b > 5U_{mf}^s/\varepsilon_{mf}$  and  $U_{in}^s \gg U_{mf}^s$ , the clouds are thin and one may use the following approximation [81]:

$$f_b = \frac{V_b}{V_r} \approx \frac{U_{in}^s - U_{mf}^s}{u_b - U_{mf}^s} \approx \frac{U_{in}^s}{u_b} \quad (10.51)$$

The volume fraction of bed gas comprising the emulsion phase gas is:

$$f_e = 1 - f_b = \frac{u_b - U_{in}^s}{u_b - U_{mf}^s} \quad (10.52)$$

The distribution of solids in the three regions were defined by:

$$\gamma_b = \frac{V_{bs}}{V_b}, \quad \gamma_c = \frac{V_{cs}}{V_b}, \quad \gamma_e = \frac{V_{es}}{V_b} \quad (10.53)$$

A material balance for the solids and (10.50) then relates these  $\gamma$ -values:

$$f_b(\gamma_b + \gamma_c + \gamma_e) = 1 - \varepsilon_{ov} = (1 - \varepsilon_{mf})(1 - f_b) \quad (10.54)$$

hence

$$\gamma_e = \frac{(1 - \varepsilon_{mf})(1 - f_b)}{f_b} - \gamma_b - \gamma_c \quad (10.55)$$

Values of  $\gamma_c$  have been estimated considering a spherical bubble and accounting for the solids in both the cloud and wake regions:

$$\gamma_c = (1 - \varepsilon_{mf}) \left( \frac{V_c}{V_b} + \frac{V_w}{V_b} \right) \approx (1 - \varepsilon_{mf}) \left( \frac{3U_{mf}^s/\varepsilon_{mf}}{0.711(gd_b)^{1/2} - U_{mf}^s/\varepsilon_{mf}} + f_w \right) \quad (10.56)$$

where the volume of the cloud surrounding each of the fast rising bubbles is given by:

$$\frac{V_c}{V_b} \approx \frac{3U_{mf}^s/\varepsilon_{mf}}{0.711(gd_b)^{1/2} - U_{mf}^s} \quad (10.57)$$

Like bubbles in liquids, it might be expected that every rising bubble in fluidized beds has an associated wake of material rising behind it. The ratio of wake to bubble volume  $f_w = V_w/V_b$  has to be determined by experiments, but the void fraction of the wake is frequently assumed to be that of the emulsion phase.

Moreover, experiments in beds of uniformly sized bubbles indicates that  $\gamma_b \approx 0.001 \sim 0.01$ .

One may imagine that just above the distributor solid is entrained by the rising bubbles to form the bubble wake. This solid is carried up the bed with the bubbles at velocity  $u_b$  and is continually exchanged with fresh emulsion solid. At the top of the bed the wake solids rejoin the emulsion to move down the bed at velocity  $u_s$ . The upward velocity of gas flowing through the emulsion is thus:

$$u_e = \frac{u_{mf}}{\varepsilon_{mf}} - u_s \quad (10.58)$$

Under particular operating conditions the circulation of solids may then get high enough so that the gas flow is directed downward in the emulsion. However, in vigorous bubbling beds the rise velocity of solids is about zero:

$$u_s \approx 0 \quad (10.59)$$

The distribution of solids  $\gamma$  used in the original Kunii and Levenspiel model [82] can be linked to the bulk solid density in the following manner [47]. The bulk density of solids in the bubble phase yields:

$$\rho_b = \gamma_b \rho_s, \quad (10.60)$$

where  $\rho_s$  is the mass density of the solid catalyst material.

The bulk density of solids in the cloud and wake phases is given by:

$$\rho_c = \gamma_c \rho_s \frac{V_b}{V_c} \quad (10.61)$$

in which  $V_c$  is the volume of the cloud phase, and  $V_b$  is the volume of the bubble consisting of pure gas.

The bulk density of solids in the emulsion phase is obtained from:

$$\rho_e = \gamma_e \rho_s \frac{V_b}{V_e} = \gamma_e \rho_s \frac{f_b}{f_e} \approx \gamma_e \rho_s \frac{f_b}{1 - f_b} \quad (10.62)$$

In the latter relation the volume of the thin cloud phase is ignored.

### 10.7.2 Turbulent Fluidized Beds

Models for turbulent fluidized bed reactors are normally based on one dimensional gas flow, despite the significant radial density gradients observed experimentally [56, 57].

For reactors operated in the turbulent regime the following reactor modeling approaches have been proposed:

- The first modeling attempts employed one dimensional pseudo-homogeneous plug flow models for the gas phase. For first order reactions the model can be written as:

$$U_g^s \frac{dC}{dz} + k(1 - \varepsilon)C = 0 \quad \left( \frac{kmol}{m^3s} \right) \quad (10.63)$$

The customary initial condition is:

$$C = C_{in} \quad (10.64)$$

- For non-ideal flows the modeling approach has been extended adapting one dimensional pseudo-homogeneous axial dispersion models for the gas phase.

The latter model can be written as:

$$\frac{d}{dz} \left( D_{g,ax} \frac{dC}{dz} \right) + U_g^s \frac{dC}{dz} + k(1 - \varepsilon)C = 0 \quad \left( \frac{kmol}{m^3s} \right) \quad (10.65)$$

The boundary conditions are [26]:

$$C_{in} U_{g,in}^s = C U_g^s - D_{g,ax} \frac{dC}{dz} \quad \text{at} \quad z = 0 \quad (10.66)$$

$$\frac{dC}{dz} = 0 \quad \text{at} \quad z = L \quad (10.67)$$

The dispersion coefficient for the turbulent regime has been determined from correlations on the form:

$$D_{g,ax} \approx 0.84 \varepsilon_{ov}^{-4.445} \quad (m/s) \quad (10.68)$$

where  $\varepsilon_{ov}$  is the overall void fraction in the turbulent regime.

### 10.7.3 Circulating Fluidized Beds

For reactors operated in the fast fluidization and pneumatic conveying regimes the following modeling approaches have been used [57, 96, 13]:

- One dimensional pseudo-homogeneous plug flow models for the species in the gas phase.

For pneumatic conveying all the particles are evenly dispersed in the gas. This makes contacting ideal or close to ideal. The plug flow model is thus well suited for the dilute transport reactors, but has also been used for the denser fast fluidization regime neglecting gradients in the solids distribution. For first order reactions the model can be written as:

$$U_g^s \frac{dC}{dz} + k(1 - \varepsilon)C = 0 \quad \left( \frac{\text{kmol}}{\text{m}^3\text{s}} \right) \quad (10.69)$$

The initial condition is:

$$C = C_{in} \quad (10.70)$$

- One dimensional pseudo-homogeneous axial dispersion model for the species in the gas phase.

This model has been used for denser transport reactors and reactors operated in a dilute fast fluidization regime intending to account for the non-ideal flow behavior. For first order reactions the model can be written as:

$$\frac{d}{dz} \left( D_{ax} \frac{dC}{dz} \right) + U_g^s \frac{dC}{dz} + k(1 - \varepsilon)C = 0 \quad \left( \frac{\text{kmol}}{\text{m}^3\text{s}} \right) \quad (10.71)$$

The boundary conditions are [26]:

$$C_{in} U_{g,in}^s = C U_g^s - D_{ax} \frac{dC}{dz} \quad \text{at} \quad z = 0 \quad (10.72)$$

$$\frac{dC}{dz} = 0 \quad \text{at} \quad z = L \quad (10.73)$$

The dispersion coefficient was determined by correlations on the form:

$$D_{g,ax} \approx 0.1953 \times \varepsilon_{ov}^{-4.1197} \quad (\text{m/s}) \quad (10.74)$$

where  $\varepsilon_{ov}$  is the overall void-age in the reactor. This correlation is valid for all the regimes ranging from turbulent fluidization to pneumatic transport.

- Core/annulus models for the gas phase.  
Most state of the art CFB reactor models operated in the fast fluidization regime make use of the core/annulus approach, which dates back to the work of [17]. These models are based on the experimental data interpretation that two zones exist in the riser at every axial location, an upward moving dilute core phase and a dense annulus phase with high solids concentration. The gas was assumed to pass upward in plug flow through the central core. Some of this gas was exchanged with the outer annular region where the gas is stationary. Each of the two-regions was assumed to be radially uniform. An inter-region mass transfer coefficient and the radius of the core, both assumed to be independent of height, were obtained by fitting the models to experimental axial gas mixing data. The catalyst particles were assumed to be small enough so that both intra particle diffusion resistances and external particle mass transfer do not need to be

considered. Applying this model to a first order reaction with steady state operation leads to molar balances of the generic form [73]:

Core region:

$$U_g^s \left( \frac{R^2}{r_c^2} \right) \frac{dC_c}{dz} + \frac{2K}{r_c} (C_c - C_a) + k(1 - \varepsilon_{cs})C_c = 0 \quad \left( \frac{\text{kmol}}{\text{m}^3\text{s}} \right) \quad (10.75)$$

Annulus region:

$$\left( \frac{r_c^2}{R^2 - r_c^2} \right) \frac{2K}{r_c} (C_c - C_a) + k(1 - \varepsilon_{as})C_a = 0 \quad \left( \frac{\text{kmol}}{\text{m}^3\text{s}} \right) \quad (10.76)$$

where  $K$  and  $k$  are the cross flow mass transfer coefficient and first order kinetic rate constant, respectively. Furthermore, Kagawa et al [73] employed the following model parameters:  $k_c = k(1 - \varepsilon_c)$ ,  $k_a = k(1 - \varepsilon_a)$ ,  $r_c/R = 0.85$ ,  $\varepsilon_c = 0.6\langle\varepsilon_s\rangle_A$ ,  $\varepsilon_a = 2.0\langle\varepsilon_s\rangle_A$ , and  $U_c = U/0.85^2$ .

A common initial boundary condition is:

$$C_c = C_{in} \quad \text{at } z=0 \quad (10.77)$$

It is recognized that this model is formally analogous to the two-phase bubbling bed model, with the annulus replacing the stagnant dense phase and the dilute core replacing the bubble phase.

As the interest in high velocity fluidized beds operating in the turbulent, fast fluidization and pneumatic conveying regimes has grown, several attempts have been made to provide appropriate reactor models, often by extending the models originally devised for the bubbling bed reactors.

Kunii and Levenspiel [81] presented models for bubbling beds for all types of particles considering the lean phase freeboard and for fast fluidized beds. A freeboard entrainment reactor model was developed to account for the extra conversion taking place above dense bubbling beds. For fast fluidized bed reactors the vessel was divided into two zones, a lower dense zone and an upper free-board zone. Later, Kunii and Levenspiel [83, 84] deduced engineering models for determining the performance behavior of a CFB reactor extending the bubbling bed model by adjusting the parameters to the turbulent, fast fluidization and pneumatic conveying regimes.

### The Overall Pressure Balance Around a CFB Loop

In the CFB loop the pressure drop over the riser must be balanced by that imposed by the flow through its accompanying components such as the downcomer and the recirculation device. The pressure drops across the downcomer, the solids circulation and control device, and the riser are the major elements in the pressure balance around the CFB loop. The pressure drop balance is thus such that the sum of the control device, fluidized bed riser and cyclone

(piping) pressure drops must equal the downcomer and hopper pressure drops. The hopper pressure drop is usually negligible so that:

$$\Delta p_R + \Delta p_C + \Delta p_{CD} \approx \Delta p_D \quad (10.78)$$

A balance of the pressure around the CFB loop requires quantitative information for the pressure drops in each component. Typical design formulas for the pressure drop associated with the major components in a CFB loop can be outlined as follows [44, 20, 114, 1].

- Pressure Drop Across the Riser,  $\Delta p_R$ :

For the gas flow in the riser, kinetic energy in the gas phase is partially transferred to the solids phase through gas-particle interactions and is partially dissipated as a result of friction. Under most operating conditions in fluidized beds, gravitational effects dominate the overall gas phase energy consumption. Thus, neglecting the particle acceleration effects, the pressure drop in the riser can be approximated by the weight of the particles:

$$\Delta p_R = \int_0^L \rho_p \epsilon_p g dz = \rho_p \epsilon_p g L \quad (10.79)$$

where  $L$  is the riser height.

- Pressure Drop Through the Cyclone,  $\Delta p_C$ :

Cyclone pressure drop is essentially a consequence of the vortex energy, the solid loading and the gas-wall friction. The main contribution is the suspension vortex energy. Generally, the pressure drop through a cyclone is proportional to the velocity head and approximated by [111]:

$$\Delta p_C = k \rho_g (U_{g,in}^s)^2 \quad (10.80)$$

The value for the coefficient  $k$  may vary from 1-20, depending on the cyclone design [44].

- Pressure Drop Across the Downcomer,  $\Delta p_D$ :

The solids flow in the downcomer is either in a dense fluidized state or in a moving packed state.

The maximum pressure drop through in the downcomer is established when particles are fluidized, a state that can be expressed in terms of the pressure drop under the minimum fluidization condition as [44]:

$$\Delta p|_{D,max} = L_D (1 - \alpha_{g,mf}) \rho_p g \quad (10.81)$$

where  $L_D$  is the height of the solids in the downcomer.

- Pressure Drop Through the Solids Flow Control Devices,  $\Delta p_{CD}$ :

If the particles in the downcomer are fluidized, the pressure drop through the mechanical solids flow control device can be expressed as [72]:

$$\Delta p_{CD} = \frac{1}{2\rho_p(1 - \alpha_{g,mf})} \left( \frac{W_s}{C_0 A_0} \right)^2 \quad (10.82)$$

where  $W_s$  is the solids feeding rate and  $A_0$  is the opening area for the mechanical valve. The coefficient  $C_0 \sim 0.7 - 0.8$  over a variety of systems and control device opening configurations.

The solids flow rate can be controlled by non-mechanical valves such as an  $L$ -valve with a long horizontal leg. The overall pressure drop across an  $L$ -valve is normally calculated as a linear sum of two terms accounting for the pressure drop through the elbow and the pressure drop caused by the gas-solid flow in the horizontal leg [140]:

$$\Delta p_{CD} = \Delta p_{CD,elbow} + \Delta p_{CD,leg} = \frac{1}{2\rho_p(1 - \alpha_{g,mf})} \left( \frac{W_s}{C_0 A_0} \right)^2 \quad (10.83)$$

where  $C_0 = 0.5$ .

#### 10.7.4 Simulating Bubbling Bed Combustors Using Two-Fluid Models

In this section the application of multiphase flow theory to model the performance of fluidized bed reactors is outlined. A number of models for fluidized bed reactor flows have been established based on solving the average fundamental continuity, momentum and turbulent kinetic energy equations. The conventional granular flow theory for dense beds has been reviewed in chap 4. However, the majority of the papers published on this topic still focus on pure gas-particle flows, intending to develop closures that are able to predict the important flow phenomena observed analyzing experimental data. Very few attempts have been made to predict the performance of chemical reactive processes using this type of model.

#### Alternative Two-Fluid Model Closures

According to Enwald & Almstedt [40], the existing ensemble averaged two-fluid model closures for bubbling beds, developed by Simonin and co-workers (e.g., [123, 122, 33, 11, 64, 65, 7, 8, 126, 9, 100]), Drew [35], Drew and Lahey [36], and the group at Chalmers University of Technology (e.g., [39, 108, 109, 110, 40, 41]), are frequently divided into four different model classes.

With increasing model complexity, these model versions are:

- Constant Particle Viscosity (CPV) models.
- Particle Turbulence (PT) models.
- Particle and Gas Turbulence (PGT) models.
- Particle and Gas Turbulence with Drift Velocity (PGTDV) models.

The continuity and momentum equations that are common for these model versions are listed below. The model equations adopted for non-reactive mixtures can be deduced from the more general formulations (3.293) and (3.296), respectively.

The continuity equation used is expressed as:

$$\frac{\partial}{\partial t} \left( \alpha_k \langle \rho_k \rangle^{X_k} \right) + \nabla \cdot \left( \alpha_k \langle \rho_k \rangle^{X_k} \langle \mathbf{v}_k \rangle^{X_k \rho_k} \right) = 0 \quad (10.84)$$

The momentum equation employed is given by:

$$\begin{aligned} & \frac{\partial}{\partial t} \left( \alpha_k \langle \rho_k \rangle^{X_k} \langle \mathbf{v}_k \rangle^{X_k \rho_k} \right) + \nabla \cdot \left( \alpha_k \langle \rho_k \rangle^{X_k} \langle \mathbf{v}_k \rangle^{X_k \rho_k} \langle \mathbf{v}_k \rangle^{X_k \rho_k} \right) \\ & = -\nabla \cdot \left( \alpha_k \langle \mathbf{T}_k \rangle^{X_k} + \alpha_k \mathbf{T}_k^{Re, X_k} \right) + \alpha_k \langle \rho_k \rangle^{X_k} \mathbf{g} + \langle \mathbf{M}_{kI} \rangle \end{aligned} \quad (10.85)$$

In order to separate the average of products into products of average, weighted averaged values are commonly introduced. The phasic - and mass averages have been defined by (3.277) and (3.278), respectively. Hence, the instantaneous velocity is decomposed into a weighted mean component and a fluctuation component in accordance with (3.279).

The Reynolds stress tensor of phase  $k$  is given by:

$$\mathbf{T}_k^{Re, X_k} = \langle \rho_k \rangle^{X_k} \langle \mathbf{v}_k'' \mathbf{v}_k'' \rangle^{X_k \rho_k} \quad (10.86)$$

The total stress tensor is conventionally decomposed into a pressure term and a viscous stress term. The average total stress term in the momentum equations may thus be re-written as:

$$\begin{aligned} -\nabla \cdot (\alpha_k \langle \mathbf{T}_k \rangle^{X_k}) &= -\nabla \cdot [\alpha_k (\langle p_k \rangle^{X_k} \mathbf{e} + \langle \boldsymbol{\sigma}_k \rangle^{X_k})] \\ &= -\nabla (\alpha_k \langle p_k \rangle^{X_k}) - \nabla \cdot (\alpha_k \langle \boldsymbol{\sigma}_k \rangle^{X_k}) \end{aligned} \quad (10.87)$$

The viscous stress tensor of both phases can be modeled using the rigorous Newtonian strain-stress relation:

$$\langle \boldsymbol{\sigma}_k \rangle^{X_k} = -\mu_{B,k} \nabla \cdot \langle \mathbf{v}_k \rangle^{X_k \rho_k} \mathbf{e} - 2\mu_k (\langle \mathbf{S}_k \rangle^{X_k \rho_k} - \frac{1}{3} \nabla \cdot \langle \mathbf{v}_k \rangle^{X_k \rho_k} \mathbf{e}) \quad (10.88)$$

where  $\mu_{B,k}$  represents the bulk viscosity of phase  $k$  ( $kg/ms$ ).

The average strain rate tensor is defined by:

$$\langle \mathbf{S}_k \rangle^{X_k \rho_k} = \frac{1}{2} (\nabla \langle \mathbf{v}_k \rangle^{X_k \rho_k} + (\nabla \langle \mathbf{v}_k \rangle^{X_k \rho_k})^T) \quad (10.89)$$

It was explained in chap 4 that the particulate phase pressure,  $\langle p_p \rangle^{X_p}$ , consists of three effects, one kinetic contribution corresponding to momentum transport caused by particle velocity fluctuation correlations,  $\langle p_{p,kin} \rangle^{X_p}$ , one collisional contribution caused by particle interaction,  $\langle p_{p,coll} \rangle^{X_p}$ , and one being a contribution from the gas phase pressure,  $\langle p_g \rangle^{X_p}$ . The pressure in the particulate phase is thus given by:

$$\alpha_p \langle p_p \rangle^{X_p} = \alpha_p \langle p_{p,kin} \rangle^{X_p} + \alpha_p \langle p_{p,coll} \rangle^{X_p} + \alpha_p \langle p_g \rangle^{X_p} \quad (10.90)$$

The particulate phase total stress tensor can then be written as:

$$\begin{aligned}
 -\nabla \cdot (\alpha_p \langle \mathbf{T}_p \rangle^{X_p}) &= -\nabla \cdot (\alpha_p \langle p_{p,kin} \rangle^{X_p}) - \nabla \cdot (\alpha_p \langle p_{p,coll} \rangle^{X_p}) \\
 &\quad - \langle p_g \rangle^{X_p} \nabla \alpha_p - \alpha_p \nabla \langle p_g \rangle^{X_p} - \nabla \cdot (\alpha_p \langle \sigma_p \rangle^{X_p})
 \end{aligned} \tag{10.91}$$

The interfacial momentum transfer to phase  $k$  is defined by [36, 39]:

$$\langle \mathbf{M}_{kI} \rangle = \langle \mathbf{T}_k \cdot \nabla X_k \rangle \tag{10.92}$$

This relation can be reformulated adopting one out of several possible modeling approaches. The conventional continuum mechanical approach for re-writing the interfacial momentum transfer terms for dispersed flows was outlined in sect 3.4.3. Hence, an alternative approach for calculating the interfacial momentum transfer terms based on kinetic or probabilistic theories, as proposed by Simonin and co-workers, is examined in this section.

The gradient of the phase indicator function, which appears in (10.92), was defined by (3.288). The expression for  $\mathbf{M}_{kI}$  then becomes [36, 39]:

$$\langle \mathbf{M}_{kI} \rangle = \langle \mathbf{T}_k \cdot \nabla X_k \rangle = -\langle \mathbf{T}_k \cdot \mathbf{n}_k \delta_k \rangle \tag{10.93}$$

as we recall that  $\nabla X_k = (\partial X_k / \partial n) \mathbf{n}_k$ , where  $(\partial X_k / \partial n) = -\delta_k$ .

He & Simonin [65] argued that to find a relation for the drag force acting on a single sphere in a suspension, the velocity field of the undisturbed flow is needed. They derived a momentum equation for an undisturbed flow based on probabilistic arguments. Based on the momentum equations for the disturbed and undisturbed flow, they derived an expression for the interfacial momentum transfer. The interfacial momentum transfer term was thus decomposed as follows:

$$\begin{aligned}
 \langle \mathbf{T}_p \cdot \mathbf{n}_p \delta_p \rangle &= -\langle \mathbf{T}_g \cdot \mathbf{n}_g \delta_g \rangle = -\langle \tilde{\mathbf{T}}_g \cdot \mathbf{n}_g \delta_g \rangle - \langle \delta \mathbf{T}_g \cdot \mathbf{n}_g \delta_g \rangle \\
 &= \langle \tilde{\mathbf{T}}_g \cdot \nabla X_g \rangle - \langle \delta \mathbf{T}_g \cdot \mathbf{n}_g \delta_g \rangle \\
 &\approx \langle \tilde{p}_g \mathbf{e} \cdot \nabla X_g \rangle - \langle \delta \mathbf{T}_g \cdot \mathbf{n}_g \delta_g \rangle \\
 &= \langle \tilde{p}_g \nabla X_g \rangle - \langle \delta \mathbf{T}_g \cdot \mathbf{n}_g \delta_g \rangle \\
 &= \langle \tilde{p}_g \rangle \nabla \alpha_g + \langle \tilde{p}'_g \nabla X_g \rangle - \langle \delta \mathbf{T}_g \cdot \mathbf{n}_g \delta_g \rangle \\
 &\approx \langle p_g \rangle \nabla \alpha_g + \mathbf{F}_g
 \end{aligned} \tag{10.94}$$

where  $\tilde{\mathbf{T}}_g$  denotes the total stress tensor of the undisturbed flow. The undisturbed pressure is decomposed in accordance with the Reynolds procedure  $\tilde{p}_g = \langle \tilde{p}_g \rangle + \tilde{p}'_g$ .

The interfacial momentum transfer terms for the disturbed flow are approximated by the steady drag force:

$$\begin{aligned}
 \mathbf{F}_g &\approx -\langle \delta \mathbf{T}_g \cdot \mathbf{n}_g \delta_g \rangle \approx \langle X_p \rho_p \mathbf{v}_r / \tau_{gp} \rangle \approx \langle X_p \rho_p \rangle \langle \mathbf{v}_r \rangle^{X_p \rho_p} / \langle \tau_{gp} \rangle^{X_p \rho_p} \\
 &\approx \alpha_p \langle \rho_p \rangle^{X_p} \langle \mathbf{v}_r \rangle^{X_p \rho_p} / \langle \tau_{gp} \rangle^{X_p \rho_p}
 \end{aligned} \tag{10.95}$$

where  $\tau_{gp}$  is the particle relaxation time.

We reiterate that for a dispersed flow  $\mathbf{F}_p$  the macroscopic generalized drag force normally contains numerous contributions, as outlined in chap 5. However, for gas-solid flows the lift force  $\mathbf{f}_L$ , the virtual mass force  $\mathbf{f}_V$ , and the Basset history force  $\mathbf{f}_B$  components are usually neglected [39]. The conventional generalized drag force given by (5.27) thus reduces to:

$$\mathbf{F}_p \approx N_p(\mathbf{f}_D + \mathbf{f}_L + \mathbf{f}_V + \mathbf{f}_B) \approx N_p \mathbf{f}_D \quad (10.96)$$

where the forces in the brackets on the right hand side are the forces acting on a single particle in a suspension and  $N_p$  is the number of particles per unit volume.

The generalized drag force is then expressed as:

$$\mathbf{F}_g = -\mathbf{F}_p = -\frac{X_p \rho_p}{\tau_{gp}} (\mathbf{v}_g - \mathbf{v}_p) \quad (10.97)$$

in which the particle relaxation time  $\tau_{gp}$  is defined by:

$$\frac{1}{\tau_{gp}} = \frac{3}{4d_p} \frac{\rho_g}{\rho_p} C_D |\mathbf{v}_g - \mathbf{v}_p| \quad (10.98)$$

The averaged drag force was approximated by [8]:

$$\begin{aligned} \langle \mathbf{F}_g \rangle &= -\langle \mathbf{F}_p \rangle = \left\langle -\frac{X_p \rho_p}{\tau_{gp}} (\mathbf{v}_g - \mathbf{v}_p) \right\rangle \\ &\approx -\frac{3}{4d_p} \alpha_p \langle C_D \rangle^{X_p \rho_p} \langle \rho_g \rangle^{X_p} \langle |\mathbf{v}_r| \rangle^{X_p \rho_p} \langle \mathbf{v}_r \rangle^{X_p \rho_p} \end{aligned} \quad (10.99)$$

The average drag coefficient used is [51]:

$$\langle C_D \rangle^{X_p \rho_p} = \left( \frac{17.3}{\langle Re_p \rangle^{X_p \rho_p}} + 0.336 \right) \alpha_g^{-1.8} \quad (10.100)$$

An alternative parameterization for the drag coefficient is given by [34, 50].

The particle Reynolds number is given by:

$$\langle Re_p \rangle^{X_p \rho_p} = \frac{\langle \rho_g \rangle^{X_p} \langle |\mathbf{v}_r| \rangle^{X_p \rho_p} d_p}{\mu_g} \quad (10.101)$$

The average particle relaxation time is given by:

$$\langle \tau_{gp} \rangle^{X_p \rho_p} = \frac{4}{3} \frac{\langle \rho_p \rangle^{X_p} d_p}{\langle \rho_g \rangle^{X_g} \langle C_D \rangle^{X_p \rho_p} \langle |\mathbf{v}_r| \rangle^{X_p \rho_p}} \quad (10.102)$$

The resulting decomposition of the interfacial momentum transfer term is equivalent to the conventional closure outlined in sect 3.4.3, and adopted by several investigations on gas solids flow [64, 65, 39, 108]. Nevertheless, as for the conventional formulation, several simplifying assumptions are invoked in

this model closure as well. Most important, the viscous terms in the undisturbed flow were neglected, the average undisturbed pressure is approximated by the mean pressure of the bulk phase, and the terms involving correlations of the pressure fluctuations are negligible in gas-solid flows. Moreover, additional closures are needed for the stress tensors, the fluctuating terms and the mean relative velocity.

According to Bel F'dhila & Simonin [11], the average of the relative velocity between each particle and the surrounding fluid  $\mathbf{v}_r$  can be expressed as a function of the mean relative velocity and a drift velocity due to the correlation between the instantaneous distribution of the particles and the large scale turbulent fluid motion with respect to the particle diameter:

$$\langle X_p \rho_p \mathbf{v}_r \rangle = \langle X_p \rho_p \mathbf{v}_p \rangle - \langle X_p \rho_p \mathbf{v}_g \rangle \quad (10.103)$$

Introducing weighted velocity variables in the first and second term in this equation, while decomposing the instantaneous velocity in the third term into its weighted and fluctuating components, we obtain:

$$\langle X_p \rho_p \rangle \langle \mathbf{v}_r \rangle^{X_p \rho_p} = \langle X_p \rho_p \rangle \langle \mathbf{v}_p \rangle^{X_p \rho_p} - \langle X_p \rho_p \rangle \langle \mathbf{v}_g \rangle^{X_p \rho_p} - \langle X_p \rho_p \mathbf{v}_g'' \rangle \quad (10.104)$$

Dividing all terms by the factor  $\langle X_p \rho_p \rangle$ , we get:

$$\langle \mathbf{v}_r \rangle^{X_p \rho_p} = \langle \mathbf{v}_p \rangle^{X_p \rho_p} - \langle \mathbf{v}_g \rangle^{X_p \rho_p} - \langle X_p \rho_p \mathbf{v}_g'' \rangle / \langle X_p \rho_p \rangle \quad (10.105)$$

The last term on the right hand side of (10.105) is defined as the drift velocity:

$$\mathbf{v}_{\text{drift}} = \langle \mathbf{v}_g'' \rangle^{X_p \rho_p} = \langle X_p \rho_p \mathbf{v}_g'' \rangle / \langle X_p \rho_p \rangle \quad (10.106)$$

where  $\mathbf{v}_g''$  is the gas fluctuating velocity.

The term  $\langle |\mathbf{v}_r| \rangle^{X_p \rho_p}$  is the average relative velocity length that is approximated by [64, 65]:

$$\langle |\mathbf{v}_r| \rangle^{X_p \rho_p} \approx \sqrt{\langle \mathbf{v}_r \rangle^{X_p \rho_p} \cdot \langle \mathbf{v}_r \rangle^{X_p \rho_p} + \langle \mathbf{v}_r'' \cdot \mathbf{v}_r'' \rangle^{X_p \rho_p}} \quad (10.107)$$

where  $\mathbf{v}_r''$  is the fluctuating relative velocity.

The term  $\langle \mathbf{v}_r'' \cdot \mathbf{v}_r'' \rangle^{X_p \rho_p}$  is determined by:

$$\langle \mathbf{v}_r'' \cdot \mathbf{v}_r'' \rangle^{X_p \rho_p} = 2(k_p + k_g - k_{gp}) \quad (10.108)$$

where  $k_g$  represents the turbulent kinetic energy of the gas phase ( $m^2/s^2$ ),  $k_{gp}$  the gas-particle fluctuation covariance ( $m^2/s^2$ ),  $k_p = 3\theta_p/2$  the turbulent kinetic energy analogue of the particulate phase ( $m^2/s^2$ ), and  $\theta_p$  the granular temperature of the particle phase ( $m^2/s^2$ ).

### The Constant Particle Viscosity (CPV) model

The first attempts at describing the gas-particle flows in fluidized beds were performed using rather simple models neglecting both the Reynolds stresses,  $\mathbf{T}_k^{Re, X_k}$  in (10.86), and the kinetic pressure-gradient term,  $\alpha_p \langle p_{p, kin} \rangle^{X_p}$ , in (10.91). No turbulence models are thus used for any of the phases.

The momentum equation for the gas phase is thus given by:

$$\begin{aligned} \frac{\partial}{\partial t} \left( \alpha_g \langle \rho_g \rangle^{X_g} \langle \mathbf{v}_g \rangle^{X_g \rho_g} \right) + \nabla \cdot \left( \alpha_g \langle \rho_g \rangle^{X_g} \langle \mathbf{v}_g \rangle^{X_g \rho_g} \langle \mathbf{v}_g \rangle^{X_g \rho_g} \right) = \\ - \alpha_g \nabla \langle p_g \rangle^{X_g} - \nabla \cdot \left( \alpha_g \langle \boldsymbol{\sigma}_g \rangle^{X_g} \right) + \alpha_g \langle \rho_g \rangle^{X_g} \mathbf{g} + \langle \mathbf{F}_g \rangle \end{aligned} \quad (10.109)$$

The viscous stress tensor of the gas phase is modeled using a reduced form of the Newtonian strain-stress relation (10.88):

$$\langle \boldsymbol{\sigma}_g \rangle^{X_g} = -2\mu_g \left( \langle \mathbf{S}_g \rangle^{X_g \rho_g} - \frac{1}{3} \nabla \cdot \langle \mathbf{v}_g \rangle^{X_g \rho_g} \mathbf{e} \right) \quad (10.110)$$

The bulk viscosity is set to zero for the continuous gas phase, in line with what is common practice for single phase flows.

The momentum equation for the particulate phase is written as:

$$\begin{aligned} \frac{\partial}{\partial t} \left( \alpha_p \langle \rho_p \rangle^{X_p} \langle \mathbf{v}_p \rangle^{X_p \rho_p} \right) + \nabla \cdot \left( \alpha_p \langle \rho_p \rangle^{X_p} \langle \mathbf{v}_p \rangle^{X_p \rho_p} \langle \mathbf{v}_p \rangle^{X_p \rho_p} \right) = \\ - \nabla \cdot \left( \alpha_g \langle \mathbf{T}_p \rangle^{X_p} \right) + \alpha_p \langle \rho_p \rangle^{X_p} \mathbf{g} + \langle \mathbf{M}_{pI} \rangle = \\ - \nabla \left( \alpha_p \langle p_p \rangle^{X_p} \right) - \nabla \cdot \left( \alpha_p \langle \boldsymbol{\sigma}_p \rangle^{X_p} \right) + \alpha_p \langle \rho_p \rangle^{X_p} \mathbf{g} + \langle \mathbf{M}_{pI} \rangle = \\ - \nabla \left( \alpha_p \langle p_{p, coll} \rangle^{X_p} \right) - \alpha_p \nabla \langle p_g \rangle^{X_p} - \nabla \cdot \left( \alpha_p \langle \boldsymbol{\sigma}_p \rangle^{X_p} \right) + \alpha_p \langle \rho_p \rangle^{X_p} \mathbf{g} + \langle \mathbf{F}_p \rangle \end{aligned} \quad (10.111)$$

where  $\langle \mathbf{F}_p \rangle$  is given by (10.99) to (10.108). Since no turbulence closure is employed in the CPV model, (10.107) is approximated as:

$$\langle |\mathbf{v}_r| \rangle^{X_p \rho_p} \approx \sqrt{\langle \mathbf{v}_r \rangle^{X_p \rho_p} \cdot \langle \mathbf{v}_r \rangle^{X_p \rho_p}}, \quad (10.112)$$

and the average relative velocity vector (10.105) is approximated by:

$$\langle \mathbf{v}_r \rangle^{X_p \rho_p} = \langle \mathbf{v}_p \rangle^{X_p \rho_p} - \langle \mathbf{v}_g \rangle^{X_p \rho_p} \quad (10.113)$$

The particle collisional pressure-gradient term in (10.91) is approximated by [50]:

$$\nabla \langle \alpha_p \langle p_{p, coll} \rangle^{X_p} \rangle \approx -G(\alpha_g) \nabla \alpha_g \quad (10.114)$$

This term is often referred to as a particle-particle interaction force and has the effect of keeping the particles apart above a maximum possible particle packing. The particle-particle interaction coefficient  $G(\alpha_g)$  is named the modulus of elasticity. A survey of different particle-particle interaction force models are given by Massoudiet et al [98].

Enwald and Almstedt [40] adopted a relation for the particle-particle interaction force proposed by Bouillard et al [16]:

$$\nabla(\alpha_p \langle p_{p,coll} \rangle^{X_p}) \approx -G_0 \exp(-c(\alpha_g - \alpha^*)) \nabla \alpha_g \quad (10.115)$$

where  $G_0$ ,  $c$  and  $\alpha^*$  are empirical constants. Enwald and Almstedt [40] set  $\alpha^* = 0.46$  to limit the void-age from decreasing below this value. The other two constants were chosen as  $G_0 = 1.0$  ( $kg/ms^2$ ) and  $c = 500$ .

In the CPV model the viscous stress tensor for the particulate phase is modeled using a simplified version of the Newtonian strain-stress relation (10.88), similar to that employed for the gas phase:

$$\langle \boldsymbol{\sigma}_p \rangle^{X_p} = -2\mu_p \left( \langle S_p \rangle^{X_p \rho_p} - \frac{1}{3} \nabla \cdot \langle \mathbf{v}_p \rangle^{X_p \rho_p} \mathbf{e} \right) \quad (10.116)$$

In this particular model version, the bulk viscosity is set to zero for the particulate phase. The particle viscosity variable,  $\mu_p$ , is set to a constant value. Enwald and Almstedt [40] used a particle viscosity value of  $\mu_p \approx 1.0$  ( $kg/ms$ ), being representative for the experimental data presented by [24](p 77).

### The Particle Turbulence (PT) models

Over the years the CPV model has been shown not to be appropriate to represent important details of certain gas-particle flows. For this reason more rigorous closures have been developed for the total stress tensor of the particulate phase, intending to obtain better representations of the physical phenomena involved.

The PT model represents an extension of the basic CPV model and contains extended closures for the particle collisional pressure and the particle-particle velocity correlation terms, as well as simple attempts to account for some of the gas-particle interaction phenomena. For the gas phase, on the other hand, the same set of transport equations as for the CPV model are employed. The particulate phase continuity equation is also the same, but the momentum equation for the particulate phase is modified.

To model the particle velocity fluctuation covariances caused by particle-particle collisions and particle interactions with the interstitial gas phase, the concept of kinetic theory of granular flows is adapted (see chap 4). This theory is based on an analogy between the particles and the molecules of dense gases. The particulate phase is thus represented as a population of identical, smooth and inelastic spheres. In order to predict the form of the transport equations for a granular material the classical framework from the kinetic theory of

dense gases is used [21]. However, as explained by Peirano and Leckner [109], to derive the closure laws for the fluxes that occur in these equations the method of Grad [59] was preferred to that of Chapman-Enskog [21]. It is thus emphasized that the work of Simonin and co-workers is based on the results of Jenkins and Richman [69] that derived the necessary closure laws using the Grad's 13 moment system for a dense gas of inelastic spheres. It follows that the transport equations discussed in this section are derived from the classical results of the kinetic theory for dense gases [21], in combination with Grad's theory [59]. Bear in mind that in chap 4 the Chapman-Enskog method was used, so the closure laws obtained by Simonin and co-workers are similar but not completely identical to those given earlier.

Moreover, He & Simonin [64, 65] considered the early models developed by Jenkins and Richman [69] appropriate for granular flows in vacuum, but inaccurate in the dilute zones of the bed where the interstitial gas phase fluctuations may affect the particles. He & Simonin [64, 65] thus extended the kinetic theory of granular materials in vacuum to take into account the influence of the interstitial gas.

In the PT model the extended momentum balance for the particle phase yields:

$$\begin{aligned} \frac{\partial}{\partial t} \left( \alpha_p \langle \rho_p \rangle^{X_p} \langle \mathbf{v}_p \rangle^{X_p \rho_p} \right) + \nabla \cdot \left( \alpha_p \langle \rho_p \rangle^{X_p} \langle \mathbf{v}_p \rangle^{X_p \rho_p} \langle \mathbf{v}_p \rangle^{X_p \rho_p} \right) = \\ - \alpha_p \nabla \left( \langle p_g \rangle^{X_p} \right) - \nabla \left( \alpha_p [\langle p_{p,kin} \rangle^{X_p} + \langle p_{p,coll} \rangle^{X_p}] \right) \\ - \nabla \cdot \left( \alpha_p \langle \boldsymbol{\sigma}_p \rangle^{X_p} + \alpha_p \mathbb{T}_p^{Re, X_p} \right) + \alpha_p \langle \rho_p \rangle^{X_p} \mathbf{g} + \langle \mathbf{F}_p \rangle \end{aligned} \quad (10.117)$$

where  $\langle \mathbf{F}_p \rangle$  is given by (10.99) to (10.108). However, in accordance with the turbulence closure employed in the PT model, the relative velocity covariance term (10.108) therein is approximated by:

$$\langle \mathbf{v}_r'' \cdot \mathbf{v}_r'' \rangle^{X_p \rho_p} = 2k_p \quad (10.118)$$

Moreover, the average relative velocity vector (10.105) is approximated by (10.113), as for the CPV model, because the drift velocity is neglected.

The effective stress tensor of the particulate phase can be expressed by an analogy to Newton's law of viscosity for viscous fluids (10.88), adopting the well known gradient and Boussinesq hypotheses modeling the Reynolds stresses (10.86):

$$\begin{aligned} -\alpha_p \langle \boldsymbol{\sigma}_p \rangle^{X_p} - \alpha_p \mathbb{T}_p^{Re, X_p} = \alpha_p \mu_{B,p} \nabla \cdot \langle \mathbf{v}_p \rangle^{X_p \rho_p} \mathbf{e} \\ + 2\alpha_p \mu_{p,eff} \left( \langle \mathbf{S}_p \rangle^{X_p \rho_p} - \frac{1}{3} \nabla \cdot \langle \mathbf{v}_p \rangle^{X_p \rho_p} \mathbf{e} \right) \end{aligned} \quad (10.119)$$

In the PT model the particle pressure terms in (10.91) are modeled by:

$$-\nabla \left( \alpha_p [\langle p_{p,kin} \rangle^{X_p} + \langle p_{p,coll} \rangle^{X_p}] \right) = -\nabla \left( \alpha_p \langle \rho_p \rangle^{X_p} (1 + 2\alpha_p g_0 (1 + e)) \theta_p \right) \quad (10.120)$$

The transport equation for the granular temperature  $\theta_p$ , written in terms of the turbulent kinetic energy analogue of the particulate phase  $k_p$ , is given by [64, 65, 109]:

$$\begin{aligned} \frac{\partial}{\partial t} \left( \alpha_p \langle \rho_p \rangle^{X_p} k_p \right) + \nabla \cdot \left( \alpha_p \langle \rho_p \rangle^{X_p} \langle \mathbf{v}_p \rangle^{X_p} \rho_p k_p \right) = \\ \nabla \cdot \left( \alpha_p \langle \rho_p \rangle^{X_p} (K_p^{coll} + K_p^t) \nabla k_p \right) - \left( \alpha_p \langle \sigma_p \rangle^{X_p} + \alpha_p \langle \tau_p^{Re} \rangle^{X_p} \right) : \nabla \langle \mathbf{v}_p \rangle^{X_p} \rho_p \\ - \frac{\alpha_p \langle \rho_p \rangle^{X_p}}{\langle \tau_{gp} \rangle^{X_p} \rho_p} (2k_p - k_{gp}) + \alpha_p \langle \rho_p \rangle^{X_p} \frac{e^2 - 1}{3\tau_p^c} k_p \end{aligned} \quad (10.121)$$

where  $k_p = \frac{3}{2}\theta_p$  represents the turbulent kinetic energy analogue of the particulate phase ( $m^2/s^2$ ),  $K_p^{coll}$  the collisional diffusion coefficient ( $m^2/s$ ),  $K_p^t$  the turbulent diffusion coefficient ( $m^2/s$ ),  $e$  the restitution coefficient, and  $\tau_p^c$  the particle-particle collision time ( $s$ ). Furthermore, it is emphasized that the gas-particle covariance  $k_{gp}$  is set to zero in the PT-model.

The bulk viscosity  $\mu_{B,p}$  and the effective dynamic viscosity of the particulate phase  $\mu_{p,eff}$  are given by:

$$\mu_{B,p} = \frac{4}{3} d_p \alpha_p \langle \rho_p \rangle^{X_p} g_0 (1 + e) \sqrt{\frac{\theta_p}{\pi}} \quad (10.122)$$

$$\mu_{p,eff} = \langle \rho_p \rangle^{X_p} (\nu_p^{coll} + \nu_p^t) \quad (10.123)$$

in which  $\nu_p^{coll}$  and  $\nu_p^t$  are the collisional and turbulent viscosities of the particulate phase.

The collisional and turbulent viscosity values were calculated from [64, 65, 109]:

$$\nu_p^{coll} = \frac{4}{5} g_0 (1 + e) (\nu_p^t + d_p \sqrt{\frac{\theta_p}{\pi}}) \quad (10.124)$$

$$\nu_p^t = \left( \frac{2}{3} \frac{\tau_{gp}^t}{\langle \tau_{gp} \rangle} k_{gp} + \theta_p (1 + \alpha_p g_0 A) \right) / \left( \frac{2}{\langle \tau_{gp} \rangle^{X_p} \rho_p} + \frac{B}{\tau_p^c} \right) \quad (10.125)$$

where  $A = 2(1 + e)(3e - 1)/5$  and  $B = (1 + e)(3 - e)/5$ . The average particle relaxation time  $\langle \tau_{gp} \rangle^{X_p} \rho_p$  is obtained from (10.102). Moreover, it is emphasized that the gas-particle covariance  $k_{gp}$  and the interaction time between the particle motion and the gas phase velocity fluctuations  $\tau_{gp}^t$  are set to zero in the PT-model.

In the formulation of the transport equations, several characteristic time scales are defined. In this framework these time scales are considered fundamental in the classification and the understanding of the dominant mechanisms in the suspension flow. The particle relaxation time  $\tau_{gp}$  was already defined in (10.98). The particle-particle collision time  $\tau_p^c$ , is defined by:

$$\tau_p^c = \frac{d_p}{24\alpha_p g_0} \sqrt{\frac{\pi}{\theta_p}} \quad (10.126)$$

The radial distribution function  $g_0$  accounts for the probability of particle contact. A possible parameterization is given by [94]:

$$g_0 = (1 - \alpha_p/\alpha_{p,max})^{-2.5\alpha_{p,max}} \quad (10.127)$$

where  $\alpha_{p,max}$  is the maximum packing of the particulate phase ( $\approx 0.64$ ). Alternative parameterizations for  $g_0$  can be found in [34, 50, 95, 19, 104, 109].

The collisional and turbulent diffusion coefficients are modeled by [126, 109]:

$$K_p^t = \frac{\theta_p(1 + \alpha_p g_0 C)}{\left(\frac{9}{5\langle\tau_{gp}\rangle X_p \rho_p} + \frac{D}{\tau_p^c}\right)} \quad (10.128)$$

$$K_p^{coll} = \alpha_p g_0 (1 + e) \left(\frac{6}{5} K_p^t + \frac{4}{3} d_p \sqrt{\frac{\theta_p}{\pi}}\right) \quad (10.129)$$

where  $C = 3(1 + e)^2(2e - 1)/5$  and  $D = (1 + e)(49 - 33e)/100$ .

### The Particle and Gas Turbulence (PGT) model

The PGT model represents an extension of the PT models in that the gas turbulence is taken into account by including the Reynolds stress tensor in the momentum equation for the gas phase. The turbulence model used for the gas phase is similar to the standard single phase  $k$ - $\epsilon$  turbulence model presented in sect 1.3.5, although additional generation and dissipation terms may be added to consider the presence of particles. In the PGT model the drift velocity is neglected.

In the PGT momentum equations the average drag force  $\langle \mathbf{F}_p \rangle$  is given by (10.99) to (10.108). Moreover, the average relative velocity vector (10.105) is approximated by (10.113), as for the CPV and PT models, because the drift velocity is neglected in the PGT model too.

In the momentum equation for the gas phase the Reynolds stress tensor is approximated by the gradient and Boussinesq hypotheses and given by:

$$\begin{aligned} \mathbf{T}_g^{Re, X_g} &= \langle \rho_g \rangle^{X_g} \langle \mathbf{v}_g'' \mathbf{v}_g'' \rangle^{X_g \rho_g} \\ &= \frac{2}{3} \langle \rho_g \rangle^{X_g} k_g \mathbf{e} - 2\mu_g^t \left( \langle \mathbf{S}_g \rangle - \frac{1}{3} \nabla \cdot \langle \mathbf{v}_g \rangle^{X_g \rho_g} \mathbf{e} \right) \end{aligned} \quad (10.130)$$

where  $\mu_g^t$  is the dynamic turbulent viscosity of the gas phase. The viscous stress tensor used is given by (10.110).

Simonin and Viollet [122] calculated the dynamic viscosity for the gas phase from a modified  $k - \varepsilon$  model. The time scale of the large eddies of the gas phase flow was given by:

$$\tau_g^t = 3C_\mu k_g / (2\varepsilon_g) \quad (10.131)$$

The dynamic turbulent viscosity of the gas phase flow was given by  $\mu_g^t = 2\langle\rho_g\rangle^{X_g} k_g \tau_g^t / 3$ , in accordance with the standard single phase turbulence theory presented in sect 1.3.5.

The transport equation that was used for the turbulent kinetic energy of the gas phase is written as [122, 126, 8]:

$$\begin{aligned} \frac{\partial}{\partial t} \left( \alpha_g \langle \rho_g \rangle^{X_g} k_g \right) + \nabla \cdot \left( \alpha_g \langle \rho_g \rangle^{X_g} \langle \mathbf{v}_g \rangle^{X_g \rho_g} k_g \right) = \nabla \cdot \left( \alpha_g \frac{\mu_g^t}{\sigma_k} \nabla k_g \right) \\ - \alpha_g \mathbb{T}_g^{Re, X_g} : \nabla \langle \mathbf{v}_g \rangle^{X_g \rho_g} - \alpha_g \langle \rho_g \rangle^{X_g} \varepsilon_g + \Pi_{kg} \end{aligned} \quad (10.132)$$

where  $\Pi_{kg}$  represents the gas-particle interaction phenomena ( $kg/ms^3$ ). This interaction term is modeled by:

$$\Pi_{kg} = \frac{\alpha_p \langle \rho_p \rangle^{X_p}}{\langle \tau_{gp}^x \rangle^{X_p \rho_p}} \left( -2k_g + k_{gp} + \mathbf{v}_{drift} \cdot \langle \mathbf{v}_\tau \rangle^{X_p \rho_p} \right) \quad (10.133)$$

However, in the PGT model the drift velocity  $\mathbf{v}_{drift}$  is neglected and set to zero. The average particle relaxation time  $\langle \tau_{gp}^x \rangle^{X_p \rho_p}$  is obtained from (10.102).

The transport equation for the dissipation rate of the gas-phase turbulent kinetic energy is given by [122, 126, 8]:

$$\begin{aligned} \frac{\partial}{\partial t} \left( \alpha_g \langle \rho_g \rangle^{X_g} \varepsilon_g \right) + \nabla \cdot \left( \alpha_g \langle \rho_g \rangle^{X_g} \langle \mathbf{v}_g \rangle^{X_g} \varepsilon_g \right) = \nabla \cdot \left( \alpha_g \frac{\mu_g^t}{\sigma_\varepsilon} \nabla \varepsilon_g \right) - \\ \alpha_g \frac{\varepsilon_g}{k_g} \left( C_{\varepsilon 1} \alpha_g \mathbb{T}_g^{Re, X_g} : \nabla \langle \mathbf{v}_g \rangle^{X_g \rho_g} + C_{\varepsilon 2} \langle \rho_g \rangle^{X_g} \varepsilon_g \right) + \Pi_{\varepsilon g} \end{aligned} \quad (10.134)$$

where  $\Pi_{\varepsilon g}$  denotes the interaction term in the  $\varepsilon_g$  equation ( $kg/ms^4$ ). This interaction term is modeled by:

$$\Pi_{\varepsilon g} = C_{\varepsilon 3} \frac{\varepsilon_g}{k_g} \Pi_{kg} \quad (10.135)$$

The parameter values chosen in the gas phase turbulence model are the same as those used for the standard single phase  $k-\varepsilon$  model (see sect 1.3.5). The additional interaction term parameter is set at a fixed value,  $C_{\varepsilon 3} = 1.3$ , as suggested by Elghobashi and Abou-Arab [38].

For the particulate phase, the PT-model equations that were described in sect 10.7.4 are used with minor extensions. That is, in the PGT-model

the transport equation for  $k_p$  (10.121) contains the gas-particle fluctuation covariance,  $k_{gp}$ , to take into account the effect of the gas phase turbulence.

The effective particle phase viscosity is still obtained from (10.123). In addition, the turbulent viscosity of the particulate phase is calculated from (10.125) in which  $k_{gp}$  is obtained from a separate balance equation. The interaction time between the particle motion and the gas velocity fluctuations  $\tau_{gp}^t$ , is modeled as suggested by Csanady [25]:

$$\tau_{gp}^t = \frac{\tau_g^t}{\sqrt{1 + 1.45 \left( 3 \langle \mathbf{v}_r \rangle^{X_p \rho_p} \cdot \langle \mathbf{v}_r \rangle^{X_p \rho_p} / 2k_g \right)}} \quad (10.136)$$

The transport equation for the gas-particle fluctuation covariance is given by [126]:

$$\begin{aligned} \frac{\partial}{\partial t} \left( \alpha_p \langle \rho_p \rangle^{X_p} k_{gp} \right) + \nabla \cdot \left( \alpha_p \langle \rho_p \rangle^{X_p} \langle \mathbf{v}_p \rangle^{X_p \rho_p} k_{gp} \right) = \\ \nabla \cdot \left( \alpha_p \langle \rho_p \rangle^{X_p} \frac{\nu_{gp}^t}{\sigma_k} \nabla k_{gp} \right) - \alpha_p \langle \rho_p \rangle^{X_p} \langle \mathbf{v}_g'' \mathbf{v}_p'' \rangle : \nabla \langle \mathbf{v}_p \rangle^{X_p \rho_p} \\ - \alpha_p \langle \rho_p \rangle^{X_p} \langle \mathbf{v}'_g \mathbf{v}'_p \rangle : \nabla \langle \mathbf{v}_g \rangle^{X_g \rho_g} - \alpha_p \langle \rho_p \rangle^{X_p} \epsilon_{gp} + \Pi_{gp} \end{aligned} \quad (10.137)$$

where  $\nu_{gp}^t$  denotes the gas-particle turbulent viscosity ( $m^2/s$ ),  $\epsilon_{gp}$  the dissipation rate of the gas-particle fluctuation covariance ( $m^2/s^3$ ), and  $\Pi_{gp}$  the interaction term in the  $k_{gp}$  model ( $kg/ms^3$ ).

The dissipation rate of the gas-particle fluctuation covariance  $\epsilon_{gp}$  and the gas-particle turbulent viscosity  $\nu_{gp}^t$  are defined by:

$$\epsilon_{gp} = k_{gp} / \tau_{gp}^t \quad (10.138)$$

$$\nu_{gp}^t = k_{gp} \tau_{gp}^t / 3 \quad (10.139)$$

The gas-particle fluctuation correlation tensor  $\langle \mathbf{v}_g'' \mathbf{v}_p'' \rangle$  is expressed by:

$$\langle \mathbf{v}_g'' \mathbf{v}_p'' \rangle = \frac{1}{3} k_{gp} \mathbf{e} - \nu_{gp}^t \left( \langle \mathbf{S}_{gp} \rangle - \frac{1}{3} tr(\langle \mathbf{S}_{gp} \rangle) \mathbf{e} \right) \quad (10.140)$$

The average gas-particle strain rate tensor is given by:

$$\langle \mathbf{S}_{gp} \rangle = \frac{1}{2} \left( \nabla \langle \mathbf{v}_g \rangle^{X_g \rho_g} + (\nabla \langle \mathbf{v}_p \rangle^{X_p \rho_p})^T \right) \quad (10.141)$$

The interaction term in (10.137) is modeled by:

$$\Pi_{gp} = - \frac{\alpha_p \langle \rho_p \rangle^{X_p}}{\langle \tau_{gp}^x \rangle^{X_p \rho_p}} \left( \left( 1 + \frac{\alpha_p \langle \rho_p \rangle^{X_p}}{\alpha_g \langle \rho_g \rangle^{X_g}} \right) k_{gp} - 2k_g - 2 \frac{\alpha_p \langle \rho_p \rangle^{X_p}}{\alpha_g \langle \rho_g \rangle^{X_g}} k_p \right) \quad (10.142)$$

### The Particle and gas turbulence model with drift velocity (PGTDV) Model

The PGTDV model consists of the same equations as the PGT model described in sect 10.7.4, the only difference being that the drift velocity is considered in the PGTDV model. The drift velocity  $\mathbf{v}_{\text{drift}}$  is included in (10.105) and (10.133).

The drift velocity takes into account the dispersion effect due to the particle transport by the fluid turbulence. From the limiting case of particles with diameter tending towards zero, for which the drift velocity reduces to single turbulence correlation between the volumetric fraction of the dispersed phase and the turbulent velocity fluctuations of the continuous phase. The drift velocity:  $\mathbf{v}_{\text{drift}}$  is modeled as [33]:

$$\mathbf{v}_{\text{drift}} = D_{gp}^t \left( \frac{1}{\alpha_g} \nabla \alpha_g - \frac{1}{\alpha_p} \nabla \alpha_p \right) \quad (10.143)$$

Based on semi-empirical analysis, the fluid-particle turbulent dispersion tensor,  $D_{gp}^t$ , is expressed in terms of the covariance between the turbulent velocity fluctuations of the two phases and a fluid particle turbulent characteristic time:

$$D_{gp}^t = \tau_{gp}^t k_{gp} / 3 \quad (10.144)$$

The model assumes that the particles are suspended in a homogeneous field of gas turbulence.

It is mentioned, although not used in the model evaluation by Enwald and Almstedt [40], that a much simpler closure for the binary turbulent diffusion coefficient  $D_{gp}^t$  has been derived by Simonin [123] by an extension of Tchen's theory. This simple closure has been used by Simonin and Violette [124], Simonin and Flour [125] and Mudde and Simonin [100] simulating several dispersed two-phase flows.

### Initial and Boundary Conditions

To simulate a rectangular fluidized bed reactor the bed vessel dimensions have to be specified first. The vessel used for validation has a rectangular cross section [40]. The bed vessel was 0.3 (*m*) wide, 2.22 (*m*) high and 0.2 (*m*) deep.

Proper boundary conditions are generally required for the primary variables like the gas and particle velocities, pressures and volume fractions at all the vessel boundaries as these model equations are elliptic. Moreover, boundary conditions for the granular temperature of the particulate phase is required for the PT, PGT and PGTDV models. For the models including gas phase turbulence, i.e., PGT and PGTDV, additional boundary conditions for the turbulent kinetic energy of the gas phase, as well as the dissipation rate of the gas phase and the gas-particle fluctuation covariance are required. The

boundary conditions for the primary variables are normally specified adopting the standard single phase flow approaches. For some of the variables like the turbulence properties and the volume fractions one has to use empirical or semi-empirical information obtained from experiments to approximate the boundary values. The specification of the velocities at the inlet may require special attention to consider the different geometries of the gas distributors.

The initial conditions are generally specified in correspondence with the state of a fluidized bed operating at minimum fluidization conditions. The bed height at minimum fluidization conditions is then set to  $L_{mf}$ , and the gas volume fraction is set to  $\alpha_{mf}$  at the bed levels below  $L_{mf}$  and unity in the freeboard. The pressure profile in the bed is initialized using the Ergun [42] equation, whereas the pressure in the freeboard is set to the operational pressure at the outlet. The horizontal velocity components of both phases and the vertical particle velocity component are set to zero. The vertical interstitial gas velocity in the bed is normally initiated as  $U_{mf}^s/\alpha_{mf}$ , and  $U_{mf}^s$  in the freeboard.

The gas density is initiated by use of the ideal gas law requiring that the gas pressure, species composition and temperature are known. When turbulence is considered,  $k_g$ ,  $k_p$  and  $\epsilon_g$  are frequently set to small but non-zero values.  $k_{gp}$  is set to zero.

To obtain an asymmetrical flow, as observed for real cases, particular flow perturbations are generally introduced for a short time period as the flow develops in time from the start. Small jets at the bottom are often used for this purpose.

## Model Evaluations

Enwald and Almstedt [40] assessed the four different two-fluid model closures given above to investigate the effect of the gas phase turbulence, drift velocity and three dimensionality on the fluid dynamics of a bubbling fluidized bed. A few characteristics features of the different models were observed. The CPV model results generally deviated from those obtained by the more rigorous model versions. Nevertheless, the CPV model results were often in better agreement with the experimental data than the other model predictions. Comparing the PGT and PT model results it was observed that at atmospheric conditions the gas phase turbulence did not have any significant effect on the bed behavior. However, at higher pressures significant changes in the results were observed. Moreover, the drift velocity included in the most advanced model version PGTDV did not have any noticeable effect on the results at any pressure. Furthermore, strictly grid independent solutions were not obtained, and the three-dimensional effects were considered considerable.

### 10.7.5 Bubbling Bed Reactor Simulations Using Two-Fluid Models

The bubbling bed reactor flow investigation performed by Lindborg [91] and Lindborg et al [92] is assessed in this section.

The kinetic theory closures applied in the PGT model employed by Lindborg [91] are in many ways distinct from those examined by Enwald and Almstedt [40]. The model closures derived from kinetic theory and adopted by Lindborg [91] are consistent with the theory presented in chap 4. It is emphasized that these closures are derived using the Chapman-Enskog method, whereas Simonin and co-workers derived their closures using a combination of the Chapman-Enskog and Grad methods. Moreover, in the work by Lindborg et al the granular temperature is not considered a particle turbulence closure but a property of the granular material. Furthermore, the solid phase stress closure is extended considering the impact of the long term particle-particle interactions such as sliding or rolling contacts. This modification may be necessary for certain flow problems because the internal momentum transport closure derived from the kinetic theory of granular flows considers only the contributions from particle translation and short term particle-particle interactions. In particular dense flows at low shear rates the stress generation mechanism due to the long term particle-particle interactions in which large amounts of energy is dissipated, may be significant. The stress tensor closure proposed by Srivastava and Sundaresan [127] for the long term particle-particle interactions was adopted.

Srivastava and Sundaresan [127] calculated the total stress as a linear sum of the kinetic, collisional, and frictional stress components, where each of the contributions are evaluated as if they were alone. The extended particle pressure and viscosity properties are calculated as:

$$p_p = p_{p,kin} + p_{p,coll} + p_{p,fric} \quad (10.145)$$

$$\mu_p = \mu_{p,kin} + \mu_{p,coll} + \mu_{p,fric} \quad (10.146)$$

This model is supposed to capture the two extreme limits of granular flow, which are designating the rapid shear and quasi-static flow regimes. In the rapid shear flow regime the kinetic stress component dominates, whereas in the quasi-static flow regime the friction stress component dominates [127].

The frictional stress closure derived by Srivastava and Sundaresan [127] is based on the critical state theory of soil mechanics. Moreover, it was assumed that the granular material is non-cohesive and has a rigid-plastic rheological behavior. At the critical state the granular assembly deforms without volume change,  $\nabla \cdot \mathbf{v}_p = 0$ , and the frictional stress tensor equals the critical state frictional stress tensor. This particular frictional stress closure, which strictly speaking is valid only at the critical state, is frequently used as a simple representation of these stresses in the granular assembly even when  $\nabla \cdot \mathbf{v}_p \neq 0$ . In particular, based on a set of test simulations the simplified frictional stress closure was found adequate for bubbling fluidized bed simulations.

The critical state pressure is given by [70]:

$$p_{p,crit} = \begin{cases} F \frac{(\alpha_p - \alpha_{p,min})^r}{(\alpha_{p,max} - \alpha_p)^s} & \text{if } \alpha_p > \alpha_{p,min} \\ 0 & \text{if } \alpha_p \leq \alpha_{p,min} \end{cases} \quad (10.147)$$

where  $F$ ,  $r$  and  $s$  are empirical constants. The model asserts that the frictional interactions do not occur for particle volume fractions less than  $\alpha_{p,min}$ .

At the critical state, the solids frictional viscosity is given by:

$$\mu_{p,crit} = \frac{p_{p,crit}\sqrt{2}\sin\phi}{2\alpha_p\sqrt{S_p : S_p + \Theta_p/d_p^2}} \tag{10.148}$$

The parameters adopted in the work of Lindborg et al [92] were taken from Ocone et al [105]. Johnson et al [70] used a similar set of parameters. Both sets of parameter values are listed in table 10.4.

**Table 10.4.** Empirical parameters for frictional stresses.

		Ocone et al [105]	Johnson et al [70]
$\phi$	Angle of internal friction [°]	28	28.5
$F$	Constant [N/m <sup>2</sup> ]	0.5	0.5
$r$	Constant	2	2
$s$	Constant	3	5
$\alpha_{p,min}$	Lower volume fraction limit for friction	0.5	0.5

The solids frictional pressure and viscosity are thus approximated by:

$$p_{p,fric} \approx p_{p,crit} \tag{10.149}$$

$$\mu_{p,fric} \approx \mu_{p,crit} \tag{10.150}$$

The term  $\beta\langle\mathbf{v}'_g \cdot \mathbf{C}_p\rangle$  in the granular temperature equation is normally neglected due to a general lack of understanding of the physics represented by this term [34, 50]. In most cases, the closures found in the literature have no significant effect on the solution.

In one of the proposed modeling approaches the production of granular temperature represented by the gas-particle velocity covariance term is interpreted as a mechanism that breaks a homogeneous fluidized bed with no shearing motion into a non-homogeneous distribution. Koch [74] proposed a closure for these gas-particle interactions for dilute suspensions. Koch and Sagani [75] extended the closure of Koch [74] accounting for the dense suspensions effects. Lindborg et al [92] re-wrote the given closure in terms of the particle relaxation time for Stokes flow  $\tau_{gp} = \rho_p d_p^2 / 18\mu_g$  as:

$$\beta\langle\mathbf{v}'_g \cdot \mathbf{C}_p\rangle = \frac{\alpha_p \rho_p d_p |\mathbf{v}_p - \mathbf{v}_g|^2 R_s F^2}{4\tau_{gp}^2 \sqrt{\pi\theta_p}} \tag{10.151}$$

where  $R_s$  represents the energy source due to a specified mean force acting on the particles.

An expression for  $R_s$  obtained by a fit of lattice-Boltzmann simulations was used:

$$R_s = \frac{1}{g_0(1 + 3.5\sqrt{\alpha_p} + 5.9\alpha_p)} \quad (10.152)$$

By applying the  $F$  definition of Benyahia et al [12], the closure can be expressed as a function of the friction coefficient  $\beta$  instead of the dimensionless drag coefficient  $F$  [92]:

$$\beta \langle \mathbf{v}'_g \cdot \mathbf{C}_p \rangle = \frac{\beta^2 d_p |\mathbf{v}_p - \mathbf{v}_g|^2 R_s}{4\alpha_g^4 \alpha_p \rho_p \sqrt{\pi \theta_p}} \quad (10.153)$$

## The Governing Equations

For reactive flows the governing equations used by Lindborg et al [92] resemble those in sect 3.4.3, but the solid phase momentum equation contains several additional terms derived from kinetic theory and a frictional stress closure for slow quasi-static flow conditions based on concepts developed in soil mechanics. Moreover, to close the kinetic theory model the granular temperature is calculated from a separate transport equation. To avoid misconception the model equations are given below (in which the averaging symbols are disregarded for convenience):

The *continuity equation* for phase  $k$  ( $= g, p$ ) is:

$$\frac{\partial}{\partial t}(\alpha_k \rho_k) + \nabla \cdot (\alpha_k \rho_k \mathbf{v}_k) = M_{wCO_2} R_{k,CO_2} \quad (10.154)$$

The *momentum equation for the gas phase* is expressed as:

$$\frac{\partial}{\partial t}(\alpha_g \rho_g \mathbf{v}_g) + \nabla \cdot (\alpha_g \rho_g \mathbf{v}_g \mathbf{v}_g) = -\alpha_g \nabla p_g - \nabla \cdot (\alpha_g \boldsymbol{\sigma}_g) + \alpha_g \rho_g \mathbf{g} + \mathbf{M}_g \quad (10.155)$$

The single phase gas phase viscous stress tensor (1.69), in which the bulk viscosity of the gas is set to zero, is used. The resulting viscous stress model coincides with (10.110):

$$\boldsymbol{\sigma}_g = -\mu_g \left( \nabla \mathbf{v}_g + (\nabla \mathbf{v}_g)^T - \frac{2}{3} (\nabla \cdot \mathbf{v}_g) \mathbf{e} \right)$$

The drag force coefficient used was taken from Gibilaro et al [51]. From (10.100) and (10.101) a derived coefficient was defined by:

$$\beta = \left( \frac{17.3}{Re_p} + 0.336 \right) \frac{\rho_g |\mathbf{v}_p - \mathbf{v}_g|}{d_p} \alpha_p \alpha_g^{-1.8} \quad (10.156)$$

The *momentum equation for the solid phase* can be written as:

$$\frac{\partial}{\partial t}(\alpha_p \rho_p \mathbf{v}_p) + \nabla \cdot (\alpha_p \rho_p \mathbf{v}_p \mathbf{v}_p) = -\alpha_p \nabla p_g - \nabla \cdot \mathbf{p}_p + \alpha_p \rho_p \mathbf{g} + \mathbf{M}_p \quad (10.157)$$

The solids phase pressure tensor is modeled in accordance with (10.145). The pressure tensor is thus expressed as:

$$\mathbf{p}_p = - \left( -p_p + \alpha_d \mu_{B,d} \nabla \cdot \mathbf{v}_k \right) \mathbf{e} - \alpha_d \mu_d \left( \nabla \mathbf{v}_k + (\nabla \mathbf{v}_k)^T - \frac{2}{3} (\nabla \cdot \mathbf{v}_k) \mathbf{e} \right) \quad (10.158)$$

The solid phase pressure is calculated from (4.89) and (10.149):

$$\begin{aligned} p_p &= p_{p,kin} + p_{p,coll} + p_{p,fric} \\ &= \alpha_p \rho_p \Theta_p [1 + 2(1 - e)\alpha_p g_0] + p_{p,crit} \end{aligned} \quad (10.159)$$

The radial distribution function can be approximated from [95]:

$$g_0 = \frac{1 + 2.5\alpha_p + 4.5904\alpha_p^2 + 4.515439\alpha_p^3}{\left[ 1 - \left( \frac{\alpha_p}{\alpha_{p,max}} \right)^3 \right]^{0.67802}} \quad (10.160)$$

The solid phase bulk viscosity is calculated from (4.92):

$$\mu_{B,p} = \frac{4}{3} \alpha_p \rho_p d_p g_0 (1 + e) \sqrt{\frac{\Theta_p}{\pi}}$$

The particle phase viscosity is modeled in accordance with (10.146):

$$\begin{aligned} \mu_p &= \mu_{p,kin} + \mu_{p,coll} + \mu_{p,fric} \\ &= \frac{2\mu_p^{dilute}}{\alpha_p g_0 (1 + e)} \left[ 1 + \frac{4}{5} \alpha_p g_0 (1 + e) \right]^2 + \frac{4}{5} \alpha_p \rho_p g_0 (1 + e) \sqrt{\frac{\Theta_p}{\pi}} + \mu_{p,crit} \end{aligned} \quad (10.161)$$

The dilute particle viscosity is calculated from (4.93):

$$\mu_p^{dilute} = \frac{5}{96} \rho_p d_p \sqrt{\pi \Theta_p}$$

The *granular temperature equation for the particle phase* is written:

$$\begin{aligned} \frac{3}{2} \left[ \frac{\partial}{\partial t} (\alpha_p \rho_p \Theta_p) + \nabla \cdot (\alpha_p \rho_p \mathbf{v}_p \Theta_p) \right] &= - (\mathbf{p}_{p,kin} + \mathbf{p}_{p,coll} + \mathbf{p}_{p,fric}) : \nabla \mathbf{v}_p \\ &\quad - \nabla \cdot (-\alpha_p \Gamma_p \nabla \theta_p) \\ &\quad - 3\beta \Theta_p + \beta \langle \mathbf{v}'_c \cdot \mathbf{C}_d \rangle - \gamma_p \\ &\quad + \frac{3}{2} (M_{wCO_2} R_{p,CO_2}) \Theta_p \end{aligned} \quad (10.162)$$

The total heat flux is modeled in accordance with (4.95). Hence, the conductivity of the granular temperature is calculated from [50]:

$$\begin{aligned}\alpha_p \Gamma_p &= \alpha_p (\Gamma_{p,kin} + \Gamma_{p,coll}) \\ &= \frac{15}{2} \frac{\mu_p^{\text{dilute}}}{(1+e)g_0} \left[ 1 + \frac{6}{5} \alpha_p g_0 (1+e) \right]^2 + 2\alpha_p^2 \rho_p d_p g_0 (1+e) \sqrt{\frac{\Theta_p}{\pi}}\end{aligned}$$

The collisional energy dissipation term, as derived by [68], is given by (4.98):

$$\gamma_p = 3(1-e^2)\alpha_p^2 \rho_p g_0 \Theta_p \left[ \frac{4}{d_p} \sqrt{\frac{\Theta_p}{\pi}} - \nabla \cdot \mathbf{v}_p \right]$$

The term  $\beta \langle \mathbf{v}'_c \cdot \mathbf{C}_d \rangle$  is normally neglected due to a general lack of understanding of the physics represented by this term. However, to verify this assumption Lindborg et al [92] performed numerous simulations to study the influence of these phenomena as represented by the closure proposed by [75].

The *molecular temperature equation* for phase  $k$  ( $= g, p$ ) is defined by:

$$\begin{aligned}\sum_c \alpha_k \rho_k \omega_{k,c} C p_{k,c} \frac{\partial T_k}{\partial t} + \sum_c \alpha_k \rho_k \omega_{k,c} C p_{k,c} \mathbf{v}_k \cdot \nabla T_k = \\ \nabla \cdot (k_k \nabla T_k) + \sum_j (-\Delta H_{r,k,j}) R_{k,j} + Q_k\end{aligned}\quad (10.163)$$

For spherical particles the volumetric heat transfer coefficient is given as the product of the specific surface area and the interfacial heat transfer coefficient (10.177). The volumetric interfacial heat transfer coefficient is modeled by (10.178)

The *species mass balance* for phase  $k$  ( $= g, p$ ) yields:

$$\frac{\partial}{\partial t} (\alpha_k \rho_k \omega_{k,c}) + \nabla \cdot (\alpha_k \rho_k \mathbf{v}_k \omega_{k,c}) = \nabla \cdot (\alpha_k \rho_k D_{k,c} \nabla \omega_{k,c}) + M_{w_c} R_{k,c} \quad (10.164)$$

in which  $D_{k,c}$  represents an effective mass diffusion coefficient of species  $c$  in phase  $k$ .

## Initial and Boundary Conditions

Initially, there is no gas flow through the reactor, and the true volume fraction of solids in the bed is about that of maximum packing. However, Lindborg et al [92] adopted the customary approach of specifying the initial conditions in correspondence with the state of a bubbling bed operating at minimum fluidization conditions. The bed height at minimum fluidization conditions was thus set to an estimated value  $L_{mf}$ , and the gas volume fraction was set to  $\alpha_{mf}$  at the bed levels below  $L_{mf}$  and unity in the freeboard. The pressure

profile in the bed was initialized using the Ergun [42] equation, whereas the pressure in the freeboard is set to the operational pressure at the outlet. The horizontal velocity components of both phases and the vertical particle velocity component are set to zero. The vertical interstitial gas velocity in the bed is initiated as  $U_{in}^s/\alpha_{mf}$ , and  $U_{mf}^s$  in the freeboard.

The gas density was either initiated by a fixed value or calculated by use of the ideal gas law requiring that the gas pressure, species composition and temperature are known. When turbulence is considered,  $k_g$ ,  $k_p$  and  $\epsilon_g$  are frequently set to small but non-zero values. Typical levels of the turbulent kinetic energy and the dissipation rate are about  $10^{-5} (m^2s^{-2})$  and  $10^{-5} (m^2s^{-3})$ , respectively. The granular temperature is set at about  $10^{-5} (m^2s^{-2})$ .

To obtain an asymmetrical flow, as observed for real cases, particular flow perturbations are generally introduced for a short time period as the flow develops in time from the start. Heterogeneity was introduced by tilting the gravity vector by 1 % the first second if axi-symmetry is not assumed.

The governing equations are elliptic so boundary conditions are required at all boundaries. The normal velocity components for both phases are set to zero at the vertical boundaries. The wall boundary conditions for the vertical velocity component,  $k$  and  $\epsilon$  are specified in accordance with the standard wall function approach. The particle phase is allowed to slip along the wall following the boundary condition given by (4.99).

Uniform flow is assumed at inlet. The gas pressure is set at outlet. The particles are not allowed to leave the reactor. For the scalar variables, except pressure, Dirichlet boundary conditions are used at inlet, whereas Neumann conditions are employed at the other boundaries [92].

During start up the system is very unstable. To simplify the conditions in the reactor, reactants are gradually introduced after 5 seconds to avoid large variations of density in the gas phase.

## Cold Flow Reactor Simulations

In a bubbling bed flow assessment performed by Lindborg [91] and Lindborg et al [92], the CPV model was used to simulate the bed behavior in the cylindrical vessel investigated experimentally by Lin et al [90]. The elasticity modulus parameterization by Ettehadieh et al [43] was employed in these simulations:

$$G(\alpha_g) = -10^{-10.46\alpha_g+6.577} (Nm^{-2}) \quad (10.165)$$

A particular set of cold flow simulations were run with the physical properties and model parameters presented in table 10.5.

It was concluded that the CPV model is not able to reproduce the experimentally determined flow pattern, as is easily recognized by comparing Fig 10.8 and Fig 10.13, using a physical  $\mu_p$  value. The flow patterns predicted are in many ways opposite to the measured ones. The simulations may give an upward flow in the center region of the tube and downwards close to the wall,

**Table 10.5.** Physical properties and model parameters [92] (case 1).

		Cold Flow Simulations
$p_g^{\text{out}}$	Outlet pressure (atm)	1.0
$\rho_g$	Gas density (kg/m <sup>3</sup> )	1.21
$\mu_g$	Gas viscosity (kg/ms <sup>3</sup> )	$1.8 \times 10^{-5}$
$\rho_p$	Particle density (kg/m <sup>3</sup> )	2500
$d_p$	Particle diameter ( $\mu\text{m}$ )	500
$e$	Restitution coefficient	0.997
$\alpha_{p,max}$	Maximum particle packing	0.62
$\alpha_{p,mf}$	Particle volume fraction at minimum fluidization	0.58
$u_{p,mf}$	Minimum fluidization velocity (m/s)	0.19
$L_{mf}$	Bed height at minimum fluidization (m)	0.113
$H$	Column height (m)	0.3164
$D$	Reactor diameter (m)	0.1380
$\Delta r$	Lateral resolution (mm)	3.450
$\Delta z$	Axial resolution (mm)	2.825

whereas the measured data for the same case shows that the flow should be downwards in the center and upwards close to the wall and visa versa. Nevertheless, by increasing the particle viscosity artificially by a factor of about 5 the simulated flow patterns coincide much better with the observed ones. The deviation between the simulated and measured flow patterns may thus be explained by the limitations of the CPV model closures. However, the influence of the axi-symmetry boundary condition applied in the two-dimensional flow simulations is strictly not verified yet.

From the study by Enwald and Almstedt [40] it may be concluded that a PT model can be sufficient simulating bubbling fluidized bed reactors. However, it was shown by Lindborg et al [92] that the gas phase turbulence is important considering the species mixing within the gas phase. A PGT type of model was thus recommended for the purpose of simulating reactive flows in bubbling bed reactors. Moreover, using the (10.153) closure, the simulations performed by Lindborg et al [92] confirmed that the  $\beta \langle \mathbf{v}'_c \cdot \mathbf{C}_d \rangle$  term in the granular temperature equation has no significant effect on the solution and can be neglected.

Simulating the Lin et al data sets by use of a PGT model, Lindborg [91] and Lindborg et al [92] obtained good predictions of the flow as shown comparing the measured flow patterns Fig 10.8 and the predicted ones Fig 10.14. The gas bubbles generally form close to the gas distributor near the wall, and migrate towards the center as they rise. On their way up through the bed they withdraw particles into the wake and thereby create a gulf streaming circulation where the bubbles create a net upflow of solids in the low density regions and a downflow of solids in the dense regions. On average, at the lowest gas flow rate, descending particles are observed at the center of the vessel while ascending closer to the wall (case (a)). With increasing gas flow



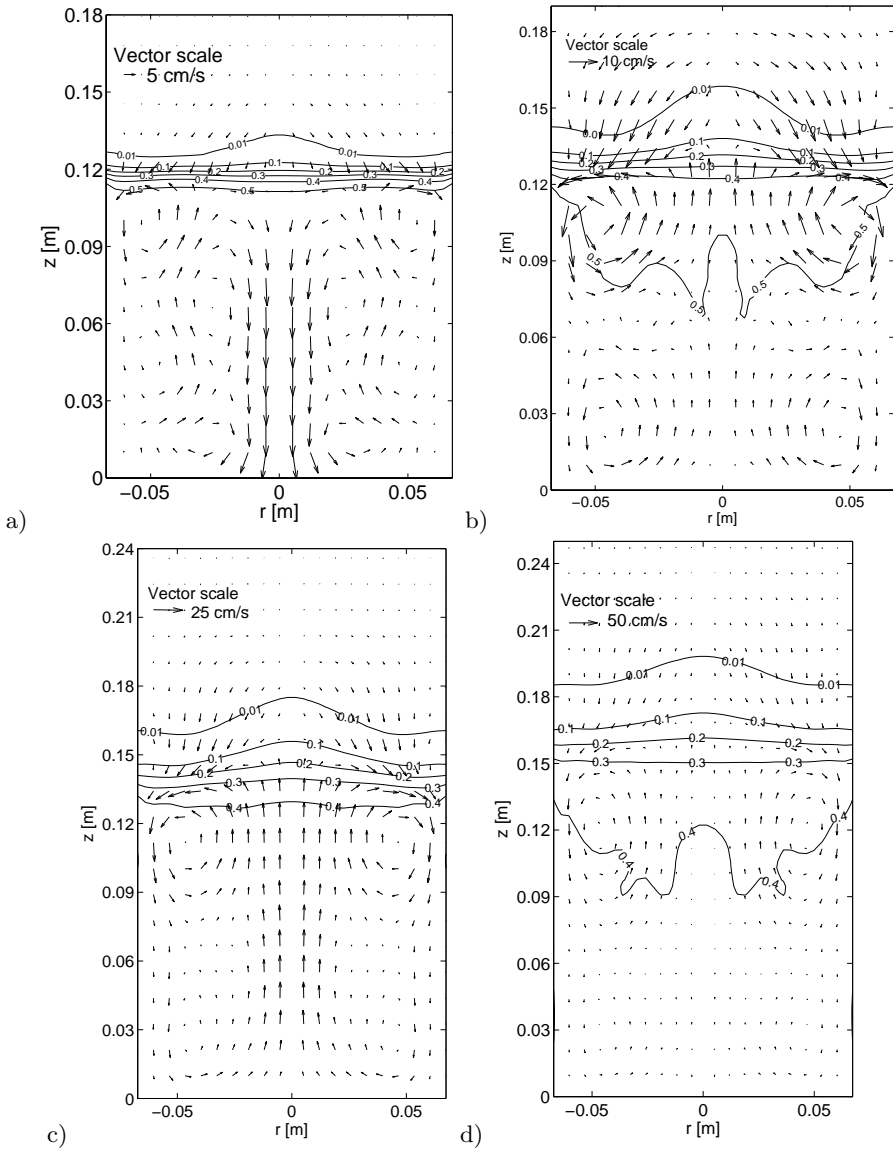


**Fig. 10.14.** Particle circulation patterns at various fluidizing velocities for a gas fluidized bed consisting of 0.42–0.6 (mm) diameter glass beads [90]. Simulated flow patterns obtained with the PGT model of Lindborg [91]. (a)  $U_{in}^s = 32$  (cm/s) and  $U_{in}^s/U_{mf}^s = 1.65$ , (b)  $U_{in}^s = 45.8$  (cm/s) and  $U_{in}^s/U_{mf}^s = 2.36$ , (c)  $U_{in}^s = 64.1$  (cm/s) and  $U_{in}^s/U_{mf}^s = 3.31$ , (d)  $U_{in}^s = 89.2$  (cm/s) and  $U_{in}^s/U_{mf}^s = 4.6$

rate the center-directed bubble migration is more pronounced, hence the solids circulation pattern gradually turns so that particles eventually ascend at the center and descend near the wall (cases (b)-(d)). Although the transition between the two main circulation patterns are not perfectly predicted, the particle motion dependence on the superficial gas velocity is captured very well since both the particle velocity magnitudes and circulation patterns coincide with the experimental data. In addition to the gas and solid motion in the bubbling bed, the bed expansion estimated from the same data corresponds quite well with the simulations. Moreover, the simulated mean bubble size and bubble rise velocity were in fair agreement with the frequently employed correlations given in the literature.

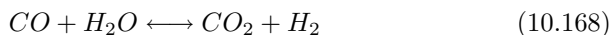
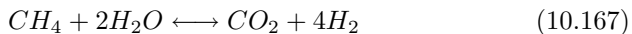
### Simulation of a Sorption Enhanced Steam reforming Process

Jørgensen [71] simulated a sorption enhanced steam reforming process employing an extended PGT model derived by Lindborg [91] and Lindborg et al [92]. The reactor configuration used operating the novel chemical process is defined in table 10.6.

**Table 10.6.** Circular axi-symmetric reactor configuration used by [71].

<b>Reactor configuration</b>	
Column height (m)	1.5
Reactor diameter (m)	0.25
Bed height at minimum fluidization (m)	0.5
Particle volume fraction at minimum fluidization	0.61
Outlet pressure (bar)	5
Inlet gas velocity (m/s)	0.1
Density dispersed phase (kg/m <sup>3</sup> )	1500
Numerical resolution (m)	0.0125
Grid resolution	122 × 12
Particle diameter (μm)	500

The kinetic model used for the conventional steam reforming process was taken from Xu and Froment [139]. The reaction takes place on a *Ni/MgAl<sub>2</sub>O<sub>4</sub>* catalyst. The kinetics can be described by three equations, where two are independent:



The rate equations are given by the following equations:

$$r_1 = \frac{k_1}{p_{H_2}^{2.5}} \frac{(p_{CH_4} p_{H_2O} - \frac{p_{H_2}^3 p_{CO}}{K_1})}{DEN^2} \quad (10.169)$$

$$r_2 = \frac{k_2}{p_{H_2}} \frac{(p_{CO} p_{H_2O} - \frac{p_{H_2} p_{CO_2}}{K_2})}{DEN^2} \quad (10.170)$$

$$r_3 = \frac{k_3}{p_{H_2}^{3.5}} \frac{(p_{CH_4} p_{H_2O}^2 - \frac{p_{H_2}^4 p_{CO_2}}{K_3})}{DEN^2} \quad (10.171)$$

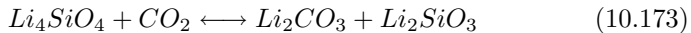
where

$$DEN = 1 + K_{CO} p_{CO} + K_{H_2} p_{H_2} + K_{CH_4} p_{CH_4} + K_{H_2O} p_{H_2O} / p_{H_2} \quad (10.172)$$

All equilibrium and kinetic constants are taken from Xu and Froment [139].

The removal of CO<sub>2</sub> from hot streams is considered a possible future technology for energy production. The sorption enhanced reaction process (SERP) has the potential to reduce the costs of hydrogen production by steam methane reforming, in addition to removing CO<sub>2</sub> from the product stream. In this process, a CO<sub>2</sub> acceptor is installed together with the catalyst for removal of CO<sub>2</sub> from the gas phase, and hence pushing the equilibrium limits toward a higher H<sub>2</sub> yield. The steam reforming process may thus be run at lower temperatures than conventional steam reforming (723-903 K), possibly reducing the investment and operational costs significantly [103].

The Lithium Silicate equilibrium reaction is:



The mathematical model for the sorption reactions is given by [118]:

$$\frac{dx}{dt} = k_1 (P_{CO_2} - P_{CO_2,eq})^{n_1} (1-x)^{n_2} \quad (10.174)$$

where  $x$  is the fractional conversion of the reaction, defined as  $x = q/q_{max}$ .  $q$  is defined as the mass of CO<sub>2</sub> adsorbed divided by mass adsorbent.  $q_{max}$  refers to maximum amount of CO<sub>2</sub> that can be adsorbed.

The temperature dependence of  $k_1$  is given by:

$$k_1 = k_{10} e^{-\frac{E_a}{R} (\frac{1}{T} - \frac{1}{T_0})} \quad (10.175)$$

The reaction rate for the sorption is then given by:

$$r_{ad} = \frac{q_{max}}{M_{wCO_2}} \frac{dx}{dt} \quad (10.176)$$

The parameters in the  $Li_4SiO_4$  sorption kinetics are given in table 10.7.

A review of the heat transfer characteristics of fluidized beds has been given by Yates [143]. It is generally accepted that the heat transfer between gas and particles is very efficient in fluidized beds as a result of the high surface area of the particle phase. The heat transfer fluxes between an immersed surface and the gas-fluidized bed material are more important from a practical design

**Table 10.7.** Parameters for the adsorption reaction kinetics [118].

	<i>Li<sub>4</sub>SiO<sub>4</sub></i>
$k_{10} \text{ (s}^{-1}\text{)}$	1.84e-4
$E_a \text{ (J/kmol)}$	1.1e8
$q_{max} \text{ (gCO}_2\text{/gadsorbent)}$	0.20
$n_1$	0.26
$n_2$	2

point of view. Due to the efficient particle mixing in fluidized bed vessels, these beds are frequently assumed to be operated in an isothermal mode. However, for particular processes, the effective conductivity of the bed material is required to predict possible temperature gradients within the bed.

The gas-particle interfacial heat transfer term in the temperature equations can be modeled by:

$$Q_g = -Q_p = -\frac{6\alpha_p k_g}{d_p^2} Nu_p (T_p - T_g) = h_v (T_p - T_g) \tag{10.177}$$

A large number of empirical correlations is available for estimating the Nusselt number in both packed- and fluidized beds. A Nusselt number correlation proposed by Gunn [60] was used. The Nusselt number parameterization represents a functional fit to experimental data for Reynolds number up to 10<sup>5</sup> in the porosity range 0.35 – 1:

$$Nu_p = (7 - 10\alpha_g + 5\alpha_g^2)(1 + 0.7Re_p^{0.2}Pr^{0.3}) + (1.33 - 2.4\alpha_g + 1.2\alpha_g^2)Re_p^{0.7}Pr^{0.3} \tag{10.178}$$

where

$$Nu_p = \frac{h_{gp}d_p}{k_g}, \quad Re_p = \frac{\alpha_g \rho_g |\mathbf{v}_g - \mathbf{v}_p|}{\mu_g} \quad \text{and} \quad Pr = \frac{\mu_g C_{p,g}}{k_g} \tag{10.179}$$

According to Natarajan and Hunt [101] the effective thermal conductivity of the solids phase  $k_p$  can be expressed as a linear sum of the kinetic- and molecular thermal conductivities:

$$k_p = k_{p,kin} + k_{p,m} \tag{10.180}$$

The kinetic conductivity for a two-dimensional system is calculated from a relation given by Hunt [66]:

$$k_{p,kin} = \rho_p C_{p,p} d_p \sqrt{\theta_p} \frac{\pi^{3/2}}{32\alpha_p g_0} \tag{10.181}$$

For gas-particle systems the molecular conductivities of the different phases are frequently calculated employing two semi-empirical relations deduced from the model of Zehner and Schlünder [145]. The original model of Zehner and

Schlünder was originally derived to describe the effective radial conductivity in fixed beds. By using a cell concept the heat is assumed to be transferred by molecular conduction both in a pure gas phase with surface fraction  $1 - \sqrt{\alpha_p}$ , and through a gas-solid bulk phase with the complementing portion of the surface fraction,  $\sqrt{\alpha_p}$ . Deviations from sphericity and inter-particle point-contacts were taken into account by further dividing the gas-solid bulk phase into a surface fraction,  $\phi$ , where heat is transferred through inter-particle contact and  $1 - \phi$  for heat transfer through the remaining surface [10]. However, in the two-fluid model framework it is necessary to separate the overall bulk thermal conductivity into individual conductivities for the gas and solid phases. Such a division has been proposed by Syamlal and Gidaspow [128]. This two-fluid model correlation has later been adopted for calculating the effective thermal conductivity of dense phase fluidized beds [15, 76, 107].

The effective thermal conductivity of the gas phase was given by:

$$k_{g,eff} = k_g \frac{(1 - \sqrt{\alpha_p})}{\alpha_g} \quad (10.182)$$

The solid phase molecular conductivity was determined by:

$$k_{m,p} = \frac{k_g}{\sqrt{\alpha_p}} (\phi A + (1 - \phi) \Lambda) \quad (10.183)$$

where

$$\Lambda = \frac{2}{(1 - B/A)} \left( \frac{(A - 1) B}{(1 - B/A)^2 A} \ln \left( \frac{A}{B} \right) - \frac{B - 1}{1 - B/A} - \frac{1}{2}(B + 1) \right) \quad (10.184)$$

The coefficients incorporated in these formulas are:

$$A = \frac{k_p}{k_g}, \quad B = 1.25 \left( \frac{\alpha_p}{\alpha_g} \right)^{10/9} \quad \text{and} \quad \phi = 7.26 \cdot 10^{-3} \quad (10.185)$$

The simulations were run with the feed gas composition presented in table 10.8. This composition represents a steam to carbon-ratio of 6. The feed gas enters the column with a temperature of 848K.

Fig 10.15 shows the composition field (mole fractions under dry conditions) in the reactor after 100 seconds. A rapid decrease in the methane and CO<sub>2</sub> mole fractions, and a steep increase in the H<sub>2</sub> mole fraction are observed. The endothermic steam methane reforming process reactions are fast, so most of the conversion is taking place immediately after the gas reactants enter the reactor. The CO<sub>2</sub>-sorption process is slower and takes place in the entire bed, removing CO<sub>2</sub> from the gas and thus shifting the chemical equilibrium limit for the SERP toward a higher H<sub>2</sub> yield compared to the conventional steam reforming process. The exothermic sorption reaction also reduces the temperature drop compared to the conventional steam methane reforming process. The temperature of the gas entering the vessel is 848 K.

In Fig 10.16 a) instantaneous fields of the solids volume fraction and velocity vectors after 50 seconds simulation time are shown. The black areas indicate locations where the solid fraction is below 0.2. It is seen that the solids in the bottom of the vessel have a tendency to move toward the center of the tube and rise at a radial position halfway between the wall and the center. The particles are moving down again away from the upflowing area both closer the wall and the center of the vessel.

In Fig 10.16 b) instantaneous fields of the dry  $H_2$  mole fraction and the gas velocity vectors after 10 seconds simulation time are shown. That is, the reactions were turned on 5 seconds after the flow was initiated. The hydrogen production is fast in the inlet zone and the hydrogen produced are transported toward the exit.

It is also seen that the gas bubbles created in the bottom of the vessel have a tendency to move toward the center of the tube and rise at a radial position halfway between the wall and the center. These bubbles carry some of the solids in their wakes producing the solids circulation pattern seen in (a).

There are no experimental data available for this process yet, so no firm validation has been performed. Nevertheless, the flow pattern is deemed to be reasonable and the chemical conversion is in fair agreement with those obtained in fixed bed simulations [118].

**Table 10.8.** Feed gas composition

Component	Weight fraction	Mole fraction
$CH_4$	0.129	0.143
$H_2O$	0.871	0.857

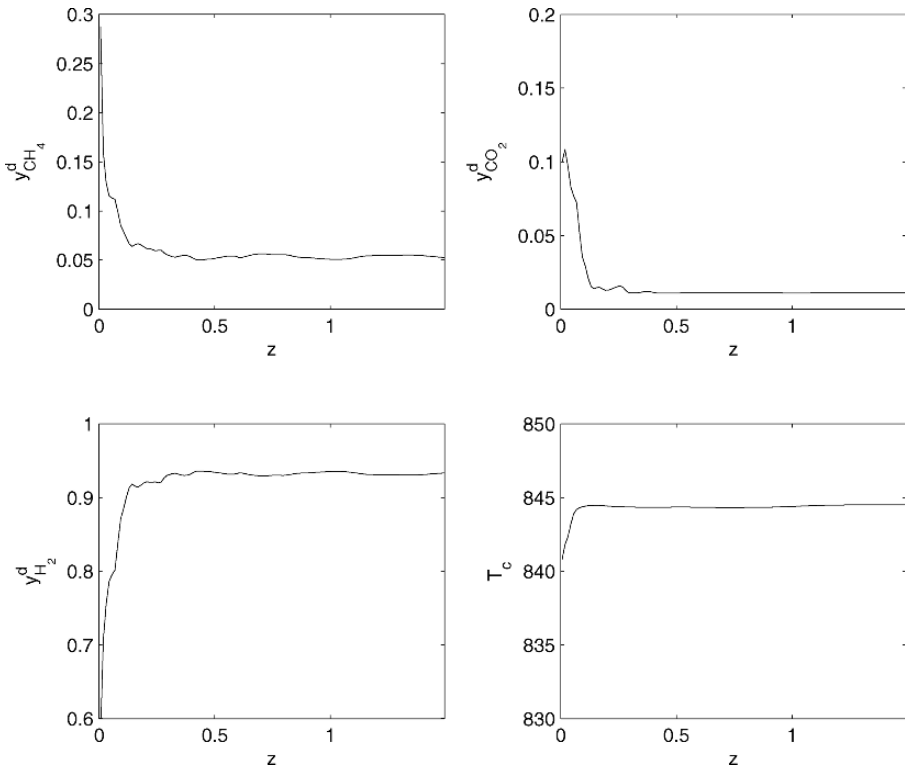


**Fig. 10.15.** Simulation of a chemical reactive mixture. Cross sectional average dry mole fraction profiles of  $\text{CH}_4$ ,  $\text{CO}_2$ ,  $\text{H}_2\text{O}$ ,  $\text{CO}$ ,  $\text{H}_2$  and temperature profile after 100 seconds. The results are averaged over the 2 last seconds to smooth the profiles.

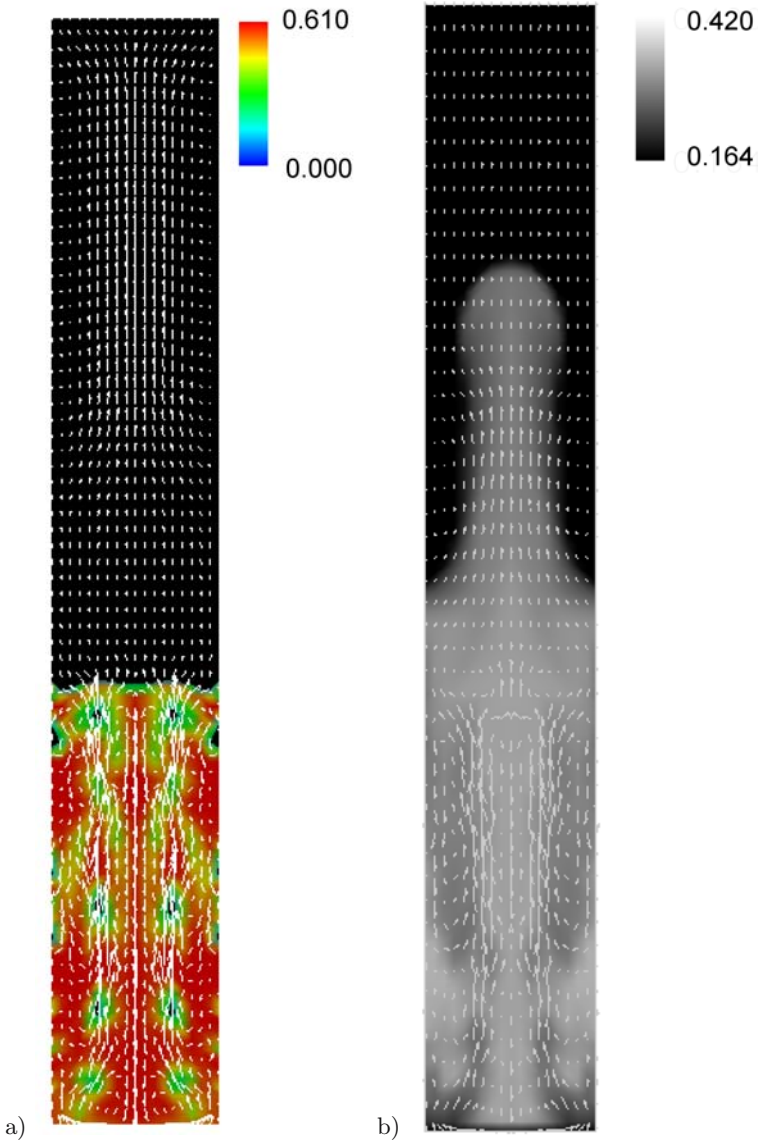


**Fig. 10.16.** Simulation of a chemical reactive mixture. (a) Instantaneous fields of the solids volume fraction and the particle velocity vectors after 50 seconds. (b) Contour plot of an instantaneous dry H<sub>2</sub> mole fraction field during start up of the process, 5 seconds after the reactants enter the column and 10 seconds after the start up of the flow. The consistent gas velocity vector field is given in the same plot.

---

## References

1. Alappat BJ, Rane VC (2001) Solids Circulation Rate in Recirculating Fluidized Bed. *J Energy Eng* 127(2):51-68
2. Anthony EJ (1995) Fluidized bed combustion of alternative solid fuels: Status, successes and problems of the technology. *Prog Energy Combust Sci* 21: 239-268
3. Anthony EJ, Jia L, Burwell SM, Najman J, Bulewicz EM (2006) Understanding the Behavior of Calcium Compounds in Petroleum Coke Fluidized Bed Combustion (FBC) Ash. *Journal of Energy Resources Technology* 128:290-299
4. Arena U, Chirone R, D'Amore M, Miccio M, Salatino P (1995) Some issues in modelling bubbling and circulating fluidized-bed coal combustors. *Powder Technology* 82:301-316
5. Baeyens J, Geldart D (1986) Solids Mixing. In: Geldart D (ed) *Gas Fluidization Technology*, Chap 5, pp 97-122, John Wiley & Sons, Chichester
6. Baird MHI, Rice RG (1975) Axial dispersion in large unbaffled columns. *Chem Eng J* 9:171-174
7. Balzer G, Simonin O (1993) Extension of Eulerian gas-solid flow modeling to dense fluidized beds. *Rapport HE-44/93.13*, Laboratoire National d'Hydraulique, EDF, Chatou, France
8. Balzer G, Boëlle A, Simonin O (1995) Eulerian gas-solid flow modelling of dense fluidized bed. *Fluidization VIII*, International Symposium of the Engineering Foundation, Tours, 14-19 May, pp 1125-1134
9. Balzer G, Simonin O (1996) Turbulent eddy viscosity derivation in dilute gas-solid turbulent flows. *8th Workshop on Two-Phase Flow Predictions*, 26-29 March, Merseburg, Germany
10. Bauer R, Schlünder EU (1978) Effective radial thermal conductivity of packings in gas flow. Part II. Thermal conductivity of the packing fraction without gas flow. *Int Chem Eng* 18:189-204
11. Bel F'dhila R, Simonin O (1992) Eulerian prediction of a turbulent bubbly flow downstream of a sudden pipe expansion. *Proc 6th Workshop on Two-Phase Flow Predictions*, Erlangen, FRG, March 30-April 2, pp 264-273
12. Benyahia S, Syamlal M, O'Brien T (2006) Extension of Hill-Koch-Ladd drag correlation over all ranges of Reynolds number and solids volume fraction. *Powder Technology* 162:166-174

13. Berruti F, Chaouki J, Godfroy L, Pugsley TS, Patience GS (1995) Hydrodynamics of Circulating Bed Risers: A Review. *Can J Chem Eng* 73:579-601
14. Bhusarapu S, Al-Dahhan MH, Dudukovic MP, Trujillo S, O'Hern TJ (2005) Experimental Study of the Solids Velocity Field in Gas-Solid Risers. *Ind Eng Chem Res* 44:9739-9749
15. Biyikli S, Tuzla K, Chen JC (1989) A phenomenological model for heat transfer in freeboard of fluidized beds. *Can J Chem Eng* 67:230-236
16. Bouillard JX, Lyczkowski RW, Folga S, Gidaspow D, Berry GF (1989) Hydrodynamics of Erosion of Heat Exchanger Tubes in Fluidized Bed Combustor. *Can J Chem Eng* 67(2):218-229
17. Brereton CMH, Grace JR, Yu J (1988) Axial Gas Mixing in a Circulating Fluidized Bed. In: eds Basu P, Large JF *Circulating Fluidized Bed Technology II*, Pergamon Press, New York, p 307
18. Brereton C (1997) Combustion performance. In: Grace JR, Avidan AA, Knowlton TM (eds) *Circulating Fluidized Beds*, First Edition, Blackie Academic & Professional, London, chap 10, pp 369-416
19. Carnahan NF, Starling KE (1969) Equation of State for Nonattracting Rigid Spheres. *Journal of Chemical Physics* 51(2):635-636
20. Chandel MK, Alappat BJ (2006) Pressure drop and gas bypassing in recirculating fluidized beds. *Chem Eng Sci* 61:1489-1499
21. Chapman S, Cowling TG (1970) *The Mathematical Theory of Non-Uniform Gases*. Cambridge Mathematical Library, Cambridge, third edition
22. Clift R (1968) Hydrodynamics of Bubbling Fluidized Beds. In: Geldart D (ed) *Gas Fluidization Technology*, Chap 4, pp 53-122, John Wiley & Sons Ltd, Chichester
23. Clift R, Grace JR, Weber ME (1978) *Bubble, Drops, and Particles*. Academic Press, New York
24. Clift R, Grace JR (1985) Continuous Bubbling and Slugging. In: eds Davidson JF, Clift R, Harrison D *Fluidization*, Academic Press, London
25. Csanady GT (1963) Turbulent diffusion of heavy particles in the atmosphere. *J Atm Sci* 20:201-208
26. Danckwerts PV (1953) Continuous Flow Systems: Distribution of Residence Times. *Chem Eng Sci* 2(1):1-18
27. Darton RC, LaNauze RD, Davidson FJ, Harrison D (1977) Bubble Growth due to Coalescence in Fluidized Beds. *Trans IChemE* 55:274-280
28. Davenport WG, Richardson FD, Bradshaw AV (1974) Spherical cap bubbles in low density liquids. *Chem Eng Sci* 22:1221-1235
29. Davidson JF, Harrison D (1963) *Fluidized Particles*. Cambridge University Press, Cambridge
30. Davidson JF, Harrison D, Darton RC, LaNauze RD (1977) The Two-Phase Theory of Fluidization and its Application to Chemical Reactors. In: eds Lapidus L, Amundson NR *Chemical Reactor Theory, A Review*. Prentice-Hall, Englewood Cliffs, New Jersey, pp 583-685
31. Davies RM, Taylor G (1950) The Mechanics of Large Bubbles Rising through Extended Liquids and through Liquids in Tubes. *Proc Roy Soc London Ser A, Mathematical and Physical Sciences*, 200(1062):375-390
32. Denn MM, Shinnar R (1987) Coal Gasification Reactors. In: Carberry JJ, Varma A (eds) *Chemical Reaction and Reactor Engineering*, Marcel Dekker Inc, New York, Chap 8, pp 499-543

33. Deutsch E, Simonin O (1991) Large Eddy Simulation applied to the motion of particles in steady homogeneous turbulence. *Turbulence Modification in Multiphase Flow*, ASME FED 1:34-42
34. Ding J, Gidaspow D (1990) A Bubbling Fluidization Model Using Kinetic Theory of Granular Flow. *AIChE J* 36(4):523-538
35. Drew DA (1983) Mathematical modeling of two-phase flow. *Ann Rev Fluid Mech* 15:261-291
36. Drew DA, Lahey RT Jr (1993) Analytical Modeling of Multiphase Flow. In: Ed Roco MC *Particulate Two-Phase Flow*, Butterworth-Heinemann, Boston, Chap 16, pp 509-566
37. Dry RJ, Beeby CJ (1997) Applications of CFB technology to gas-solid reactions. In: Grace JR, Avidan AA, Knowlton TM (eds) *Circulating Fluidized Beds*, First Edition, Blackie Academic & Professional, London, chap 12, pp 441-465
38. Elghobashi SE, Abou-Arab TW (1983) A two-equation turbulence model for two-phase flows. *Phys Fluids* 26:931-938
39. Enwald H, Peirano E, Almstedt A-E (1996) Eulerian Two-Phase Flow Theory Applied to Fluidization. *Int J Multiphase Flow* 22(Supplement):21-66
40. Enwald H, Almstedt AE (1999) Fluid dynamics of a pressurized fluidized bed: Comparison between numerical solutions from two-fluid models and experimental results. *Chem Eng Sci* 54:329-342
41. Enwald H, Peirano E, Almstedt A-E, Leckner B (1999) Simulation of a bubbling fluidized bed. Experimental validation of the two-fluid model and evaluation of a parallel multiblock solver. *Chem Eng Sci* 54:311-328
42. Ergun S (1952) Fluid Flow Through Packed Columns. *Chem Eng Prog* 48(2):89-94
43. Ettahadieh B, Gidaspow D, Lyczkowski RW (1984) Hydrodynamics of Fluidization in a Semicircular Bed with a Jet. *AIChE J* 30(4):529-536
44. Fan L-S, Zhu C (1998) *Principles of Gas-Solid Flows*. Cambridge University Press, Cambridge
45. Fan Y, Ye S, Chao Z, Lu C, Sun G, Shi M (2002) Gas-Solid Two-Phase Flow in FCC Riser. *AIChE J* 48(9):1869-1887
46. Foka M, Chaouki J, Guy C, Klvana D (1994) Natural Gas Combustion in a Catalytic Turbulent Fluidized Bed. *Chem Eng Sci* 49(24A):4269-4276
47. Froment GF, Bischoff KB (1990) *Chemical Reactor Analysis and Design*. John Wiley and Sons, New York, Second Edition
48. Gascón J, Téllez C, Herguido J, Jakobsen HA, Menéndez M (2006) Modeling of Fluidized Bed Reactors With Two Reaction Zones. *AIChE J* 52(11):3911-3923
49. Geldart D (1973) Types of gas fluidization. *Powder Technology* 7:285-292
50. Gidaspow D (1994) *Multiphase Flow and Fluidization-Continuum and Kinetic Theory Descriptions*. Academic Press, Harcourt Brace & Company, Publishers, Boston
51. Gibilaro LG, Di Felice RI, Waldran SP (1985) Generalized friction factor and drag coefficient correlations for fluid-particle interactions. *Chem Eng Sci* 40:1817-1823
52. Grace JR (1986) Contacting Modes and Behaviour Classification of Gas-Solid and Other Two-Phase Suspensions. *Can J Chem Eng* 64:353-363
53. Grace JR (1986) Fluid Beds as Chemical Reactors. In: Geldart D (ed) *Gas Fluidization Technology*, Chap 11, pp 285-339, John Wiley & Sons, Chichester
54. Grace JR (1986) Hydrodynamics of Bubbling Fluidized Beds. In: Geldart D (ed) *Gas Fluidization Technology*, Chap 4, pp 53-95, John Wiley & Sons, Chichester

55. Grace JR, Baeyens J (1986) Instrumentation and Experimental Techniques. In: Geldart D (ed) *Gas Fluidization Technology*, Chap 13, pp 415-462, John Wiley & Sons, Chichester
56. Grace JR (1990) High-Velocity Fluidized Bed Reactors. *Chem Eng Sci* 45(8):1953-1966
57. Grace JR, Lim KS (1997) Reactor modeling for high-velocity fluidized beds. In: Grace JR, Avidan AA, Knowlton TM (eds) *Circulating Fluidized Beds*, First Edition, Blackie Academic & Professional, London, chap 15, pp 504-524
58. Grace JR, Bi H (1997) Introduction to circulating fluidized beds. In: Grace JR, Avidan AA, Knowlton TM (eds) *Circulating Fluidized Beds*, First Edition, Blackie Academic & Professional, London, chap 1, pp 1-20
59. Grad H (1949) On the kinetic theory of rarified gases. *Comm Pure Appl Math* 2(4):331-407
60. Gunn DJ (1978) Transfer of heat or mass to particle in fixed bed and fluidized beds. *Int J Heat Mass Transfer* 21:467-476
61. Guo Q, Werther J (2004) Flow Behaviours in a Circulating Fluidized Bed with Various Bubble Cap Distributors. *Ind Eng Chem Res* 43:1756-1764
62. Hartge E-U, Li Y, Werther J (1986) Analysis of the local structure of the two phase flow in a fast fluidized bed. In: *CFB Technology*, Pergamon press, pp 153-160
63. Hartge E-U, Klett C, Werther J (2007) Dynamic Simulation of the Particle Size Distribution in a Circulating Fluidized Bed Combustor. *Chem Eng Sci* 62:281-293
64. He J, Simonin O (1993) Non-equilibrium prediction of the particle-phase stress tensor in vertical pneumatic conveying. *Gas-Solid Flows*, ASME FED 166: 253-263
65. He J, Simonin O (1994) Modélisation numérique des écoulements gaz-solides en conduite verticale. Rapport HE-44/94/021A, Laboratoire National d'Hydraulique, EDF, Chatou, France
66. Hunt ML (1997) Discrete element simulations for granular material flows: effective thermal conductivity and self-diffusivity. *Int J Heat Mass Transfer* 40:3059-3068
67. Issangya AS, Grace JR, Bai D, Zhu J (2000) Further measurements of flow dynamics in a high-density circulating fluidized bed riser. *Powder Technology* 111:104-113
68. Jenkins JT, Savage SB (1983) A theory for the rapid flow of identical, smooth, nearly elastic spherical particles. *J Fluid Mechanics* 130:187-202
69. Jenkins JT, Richman MW (1985) Grad's 13 moment system for a dense gas of inelastic spheres. *Arch Ratio Mech Anal* 87:355-377
70. Johnson PC, Nott P, Jackson R (1990) Frictional-collisional equations of motion for particulate flows and their application to chutes. *J Fluid Mech* 210: 501-535
71. Jørgensen V (2007) Numerical investigation of integrated reactor/separator designs for precombustion with carbondioxide capture. MSc Thesis, the Norwegian University of Science and Technology, Trondheim
72. Jones DRM, Davidson JF (1965) The Flow of Particles from a Fluidized Bed through an Orifice. *Rheol Acta* 4(3):180-192
73. Kagawa H, Mineo H, Yamazaki R, Yoshida K (1991) A gas-solid contacting model for fast-fluidized bed. In: eds Basu P, Horio M, Hasatani M *Circulating Fluidized Bed Technology III*, Pergamon, Oxford, pp 551-556

74. Koch DL (1990) Kinetic theory for a monodisperse gas-solid suspension. *Phys Fluids* A2:1711-1723
75. Koch DL, Sangani AS (1999) Particle pressure and marginal stability limits for a homogeneous monodisperse gas-fluidized bed: Kinetic theory and numerical simulations. *J Fluid Mechanics* 400:229-263
76. Kuipers JAM, Prins W, van Swaaij WPM (1992) Numerical calculation of wall-to-bed heat-transfer coefficients in gas-fluidized beds. *AIChE J* 38:1079-1091
77. Kuipers JAM, Hoomans BPB, van Swaaij WPM (1968) Hydrodynamic Models of Gas-Fluidized Beds and Their Role for Design and Operation of Fluidized Bed Chemical Reactors. In: Fan L-S, Knowlton TM (eds) *Proc of the Ninth Engineering Foundation Conference on Fluidization*, Engineering Foundation, New York, ISBN/ISSN: 0-939204-56-8
78. Kunii D, Levenspiel O (1968) Bubbling Bed Model for Kinetic Processes in Fluidized Beds. I & EC *Process Design and Development* 7(4):481-492
79. Kunii D, Levenspiel O (1968) Bubbling Bed Model. I & EC *Fundamentals* 7(3):446-452
80. Kunii D (1980) Chemical reaction engineering and research and development of gas solid systems. *Chem Eng Sci* 35:1887-1911
81. Kunii D, Levenspiel O (1990) Fluidized Reactor Models. 1. For Bubbling Beds of Fine, Intermediate, and large particles. 2. For the Lean Phase: Freeboard and Fast Fluidization. *Ind Eng Chem Res* 29:1226-1234
82. Kunii D, Levenspiel O (1991) *Fluidization Engineering*. Butterworth-Heinemann, Second edition, Boston
83. Kunii D, Levenspiel O (1997) Circulating fluidized-bed reactors. *Chem Eng Sci* 52(15):2471-2482
84. Kunii D, Levenspiel O (2000) The K-L reactor model for circulating fluidized beds. *Chem Eng Sci* 55:4563-4570
85. Lindborg H, Lysberg M and Jakobsen HA (2007) Practical validation of the two-fluid model applied to dense gas-solid flows in fluidized beds. *Chem Eng Sci* 62:5854-5869
86. Leckner B (1998) Fluid bed combustion: Mixing and pollutant limitation. *Prog Energy Combust Sci* 24:31-61
87. Lee YY (1997) Design considerations for CFB boilers. In: Grace JR, Avidan AA, Knowlton TM (eds) *Circulating Fluidized Beds*, First Edition, Blackie Academic & Professional, London, chap 11, pp 417-440
88. Li F, Zhai J, Fu X, Sheng G (2006) Characterization of Fly Ashes from Circulating Fluidized Bed Combustion (CFBC) Boilers Cofiring Coal and Petroleum Coke. *Energy & Fuels* 20:1411-1417
89. Lim KS, Gururajan VS, Agarwal PK (1993) Mixing of Homogeneous Solids in Bubbling Fluidized Beds: Theoretical Modelling and Experimental Investigation Using Digital Image Analysis. *Chem Eng Sci* 48(12):2251-2265
90. Lin JS, Chen MM, Chao BT (1985) A Novel Radioactive Particle Tracking Facility for Measurement of Solids Motion in Gas Fluidized Beds. *AIChE J* 31(3):465-473
91. Lindborg H (2007) Modeling and simulation of Chemical Reactor Flows. *Dr ing Thesis*, The Norwegian University of Science and Technology, Trondheim, In preparation
92. Lindborg H, Lysberg M, Jakobsen HA (2007) Practical Validation of the Two-Fluid Model Applied to Dense Gas-Solid Flows in Fluidized Beds. Submitted to *Chem Eng Sci* 2007

93. Longwell JP, Rubin ES, Wilson J (1995) Coal: Energy for the future. *Prog Energy Combust Sci* 21:269-360
94. Lun CKK, Savage SB (1986) The effect of an impact velocity dependent coefficient of restitution on stresses developed by sheared granular materials. *Acta Mechanica* 63:15-44
95. Ma D, Ahmadi G (1986) An equation of state for dense rigid sphere gases. *J Chem Phys* 84(6):3449-3450
96. Marmo L, Manna L, Rovero G (1995) Comparison among several predictive models for circulating fluidized bed reactors. In: Laguérie C, Large JF Preprints for Fluidization VIII, vol 1, pp 475-482
97. Matsen JM (1997) Design and scale-up of CFB catalytic reactors. In: Grace JR, Avidan AA, Knowlton TM (eds) *Circulating Fluidized Beds*, First Edition, Blackie Academic & Professional, London, chap 14, pp 489-503
98. Massoudi M, Rajagopal KR, Ekman JM, Mathur MP (1992) Remarks on the Modeling of Fluidized Systems. *AIChE J* 38(3):471-472
99. Monceaux L, Azzi M, Molodtsov Y, Large JF (1986) Overall and local characterization of flow regimes in circulating fluidized bed. In: *CFB Technology*, Pergamon press, pp 185-191
100. Mudde RF, Simonin O (1999) Two- and three-dimensional simulations of a bubble plume using a two-fluid model. *Chem Eng Sci* 54:5061-5069
101. Natarajan VVR, Hunt ML (1998) Kinetic theory analysis of heat transfer in granular flows. *International Journal of Heat and Mass Transfer*, 41: 1929-1944, 1998.
102. Nicklin DJ (1962) 2-Phase Bubble Flow. *Chem Eng Sci* 17(9):693-702
103. Ochoa-Fernández E, Rusten HK, Jakobsen HA, Magnus Rønning M, Holmen A, Chen D (2005) Sorption enhanced hydrogen production by steam methane reforming using  $\text{Li}_2\text{ZrO}_3$  as sorbent: Sorption kinetics and reactor simulation. *Catalysis Today* 106:41-46
104. Ogawa S, Umemura A, Oshima N (1980) On the Equations of Fully Fluidized Granular Materials. *J Applied Mathematics and Physics* 31:483-493
105. Ocone R, Sundaresan S, Jackson R (1993) Gas-Particle Flow in a Duct of Arbitrary Inclination with Particle-Particle Interactions. *AIChE J* 39(8): 1261-1271
106. Pallarés D, Johnsson F (2006) Macroscopic modelling of fluid dynamics in large-scale circulating fluidized beds. *Progress in Energy and Combustion Science* 32:539-569
107. Patil DJ, Smit J, van Sint Annaland M, Kuipers JAM (2006) Wall-to-bed heat transfer in gas-solid bubbling fluidized beds. *AIChE J* 52:58-74
108. Peirano E (1996) The Eulerian/Eulerian Formulation Applied to Gas-Particle Flows. Report A96-218, ISSN 0281-0034, Department of Energy Conversion, Chalmers University of Technology, Sweden
109. Peirano E (1998) Modelling and Simulation of Turbulent Gas-Solid Flow Applied to Fluidization. PhD thesis, Chalmers University of Technology, Sweden
110. Peirano E, Leckner B (1998) Fundamentals of turbulent gas-solid flows applied to circulating fluidized bed combustion. *Progress in Energy and Combustion Science* 24:259-296
111. Perry RH, Green DW (2007) Perry's chemical engineers' handbook. In: Green DW, Robert H. Perry RH (eds) McGraw-Hill, New York, Eighth Edition, ISBN: 0-07-142294-3

112. Ranade VV (2002) Computational Flow Modeling for Chemical Reactor Engineering. Academic Press, San Diego
113. Reh L (1971) Fluidized Bed Processing. *Chem Eng Prog* 67(2):58-63
114. Rodes MJ, Laussmann P (1992) A Study of the Pressure Balance Around the Loop of a Circulating Fluidized Bed. *Can J Chem Eng* 70:625-630
115. Rowe PN, Partridge BA (1965) An X-ray Study of Bubbles in Fluidized Beds. *Trans Instn Chem Engrs* 43:T157-T175
116. Rowe PN (1971) Experimental Properties of Bubbles. In: Davidson JF, Harrison D (eds), *Fluidization*, Chap4, pp 121-191 Academic Press, London
117. Rowe PN, Yates JG (1987) Fluidized-Bed Reactors. In: Carberry JJ, Varma A (eds) *Chemical Reaction and Reactor Engineering*, Marcel Dekker Inc, New York, Chap 7, pp 441-498
118. Rusten HK, Ochoa-Fernández E, Chen D, Jakobsen HA (2007) Numerical investigation of sorption enhanced steam methane reforming using  $\text{Li}_2\text{ZrO}_3$  as  $\text{CO}_2$ -acceptor. Submitted to *Ind Eng Chem Res* 2007
119. Samuelsen A, Hjertager BH (1996) An experimental and numerical study of flow patterns in a circulating fluidized bed reactor. *Int J Multiphase Flow* 22(3):575-591
120. Samuelsen A, Hjertager BH (1996) Computational Modeling of Gas/Particle Flow in a Riser. *AIChE J* 42(6):1536-1546
121. Saraiva PC, Azevedo JLT, Carvalho MG (1993) Mathematical Simulation of a Circulating Fluidized Bed Combustor. *Combust Sci and Tech* 93:223-243
122. Simonin O, Viollet PL (1989) Numerical study on phase dispersion mechanisms in turbulent bubbly flows. *Proc Int Conf on Mechanics of Two-Phase Flows*, 12-15 June, Taipei, Taiwan
123. Simonin O (1990) Eulerian formulation for particle dispersion in turbulent two-phase flows. In: Sommerfeld M, Wennerberg P Fifth Workshop on Two-phase Flow Predictions. Erlangen, FRG, pp 156-166
124. Simonin O, Viollet PL (1990) Prediction of an Oxygen Droplet Pulverization in a Compressible Subsonic Coflowing Hydrogen Flow. In: *Numerical Methods for Multiphase Flows*, ASME FED 91:73-82
125. Simonin O, Flour I (1992) An Eulerian Approach for Turbulent Reactive Two-Phase Flows Loaded with Discrete Particles. In: Sommerfeld M Sixth Workshop on Two-phase Flow Predictions. Erlangen, pp 61-62
126. Simonin O (1995) Two-fluid model approach for turbulent reactive two-phase flows. Summer school on numerical modelling and prediction of dispersed two-phase flows. IMVU, Merseburg, Germany
127. Srivastava A, Sundaresan S (2003) Analysis of a frictional-kinetic model for gas-particles flow. *Powder Technology* 129(1-3):72-85
128. Syamlal M, Gidaspow D (1985) Hydrodynamics of fluidization: Prediction of wall to bed heat transfer coefficients. *AIChE J* 31:127-135
129. Tayebi D, Svendsen HF, Jakobsen HA, Grislingås A (2001) Measurements Techniques and Data Interpretations for Validating CFD Multi Phase Reactor Models. *Chem Eng Comm* 186:57-159
130. Toomey RD, Johnstone HF (1952) Gaseous Fluidization of Solid Particles. *Chem Eng Prog* 48(5):220-226
131. Trambouze P, Euzen J-P (2004) *Chemical Reactors: From Design to Operation*. Institut Francais du Pétrole Publications, Paris
132. van Deemter JJ (1961) Mixing and contacting in gas-solid fluidized beds. *Chem Eng Sci* 13:143-154

133. Weinstein H, Shao M, Schnitzlein M (1986) Radial variation in solid density in high velocity fluidization. In: CFB Technology, Pergamon press, pp 201-206
134. Werther J (1978) Mathematical Modeling of Fluidized-Bed Reactors. Chem Ing Techn 50(11):850-860
135. Werther J, Hartge E-U (2004) A population balance model of the particle inventory in a fluidized-bed reactor/regenerator system. Powder Technology 148:113-122
136. Werther J, Hartge E-U (2004) Modeling of Industrial Fluidized-Bed Reactors. Ind Eng Chem Res 43:5593-5604
137. Winkler F (1922) Patentschrift Nr 37970, Reichspatentamt
138. Wu JC, Deluca RT, Wegener PP (1974) Rise speed of spherical cap bubbles at intermediate Reynolds number. Chem Eng Sci 29:1307-1309
139. Xu J, Froment GF (1989) Methane steam reforming, methanation and water-gas shift I. Intrinsic kinetics. AIChE J, 35:88-96
140. Yang W-C, Knowlton TM (1993) L-valve equations. Powder Technology 77: 49-54
141. Yates JG (1975) Fluidized bed reactors. The chemical Engineer, No 303, pp 671-677
142. Yates JG (1983) Fundamentals of Fluidized-bed Chemical Processes. Butterworths, London
143. Yates JG (1996) Effects of Temperature and Pressure on Gas-Solid Fluidization. Chem Eng Sci 51(2):167-205
144. Yerushalmi J (1981) Circulating Fluidized Bed Boilers. Fuel Processing Technology 5:25-63
145. Zehner P, Schlünder EU (1970) Wärmeleitfähigkeit von Schüttungen bei mäsigen Temperaturen. Chem Ing Tech 42:933-941
146. Zenz FA, Othmer DF (1960) Fluidization and Fluid-Particle Systems. Reinhold Publishing Corporation, New York

## Packed Bed Reactors

The discovery of solid catalysts led to a breakthrough of the chemical process industry. Today most commercial gas-phase catalytic processes are carried out in fixed packed bed reactors<sup>1</sup>. A fixed packed bed reactor consists of a compact, immobile stack of catalyst pellets within a generally vertical vessel. On macroscopic scales the catalyst bed behaves as a porous media. The fixed beds are thus employed as continuous tubular reactors in which the reactive species in the mobile fluid (gas) phase are reacting over the catalyst surface (interior or exterior) in the stationary packed bed. Compared to other reactor types or designs utilizing heterogeneous catalysts, the fixed packed bed reactors are preferred because of simpler technology and ease of operation.

### 11.1 Processes Operated in Packed Bed Reactors (PBRs)

Catalytic processes are carried out in several types of reactors like fixed bed, moving bed, trickle bed, two- and three phase fluidized beds, bubble columns, and stirred tanks. Examples of important fixed bed catalytic processes with only one fluid phase are given in Table 11.1. Other fixed bed processes with particular catalyst designs exist as well.

Several packed bed reactors are employed by the petroleum refining industries utilizing natural gas as feedstock. Different compositions of synthesis gas (mixtures of carbon monoxide and hydrogen) or syngas are important

---

<sup>1</sup> The word *fixed* is used to distinguish this particular reactor design from moving bed reactors. The moving bed reactors also consists of a stack of catalyst pellets inside a vessel. In this reactor the force of gravity causes the catalyst pellets to move with respect to the wall from top to bottom while maintaining their relative positions to one another. The moving bed thus offers the ability to withdraw catalyst for regeneration outside the reactor in a continuous mode. A survey of the moving bed technology is given by Trambouze and Euzen [12].

**Table 11.1.** Examples of fixed bed processes [3, 12].

Basic Chemical Industry	Petrochemical Industry	Petroleum Refining
Primary steam reforming	Ethylene oxide	Catalytic reforming
Secondary steam reforming	Ethylene dichloride	Isomerization
Carbon monoxide conversion	Vinylacetate	Polymerization
Carbon monoxide methanation	Butadiene	(Hydro)desulfurization
Ammonia synthesis	Maleic anhydride	Hydrocracking
Sulfuric acid synthesis	Phthalic anhydride	
Methanol synthesis	Cyclohexane	
Oxo synthesis	Styrene	
	Hydrodealkylation	

intermediate feedstocks for the production of large volume chemicals such as ammonia, methanol, hydrogen and synthetic hydrocarbon liquids. The fixed bed reactors used today are thus mainly large-capacity units due to the vast market demand.

## 11.2 Packed Bed Reactor Design

Typical for strongly exothermic processes is that at some location in the reactor an extreme temperature occur, frequently named the *hot spot*. In some processes with very strong exothermic reactions the hot spot temperature can raise beyond permissible limits. This phenomenon is called *runaway*. An important task in reactor design and operation is thus to limit the hot spot and avoid excessive sensitivity of the reactor performance to variations in the temperature. The value of the temperature at the hot spot is determined mainly by the reaction rate sensitivity to changes in temperature, the heat of reaction potential of the process, and the heat transfer potential of the heat exchanger units employed. A heat exchanger is characterized by the heat transfer coefficient and heat transfer areas.

The selection of an appropriate fixed bed reactor design for a given process is performed assessing the main limitations of these reactors. The fixed packed bed reactors can be malfunctioning due to in-proper temperature control, pressure drop for processes with low tolerance, and deactivation of the catalyst.

To optimize the performance of the fixed bed reactor operation several constructions of fixed bed reactors have been investigated over the years. Three of the most common reactor designs are:

- single-bed units
- multi-bed units
- multi-tube units

The single bed reactor is simply a vessel of relatively large diameter, as sketched in Fig 11.1. This simple reactor design is best suited for adiabatic

processes and not applicable for very exothermic or endothermic processes. If the reaction is very endothermic, the temperature change may be such as to extinguish the reaction before the desired conversion is attained. Strongly exothermic reactions, on the other hand, can lead to a temperature rise that is prohibitive due to its unfavorable influence on the equilibrium conversion, the product selectivity, the catalyst stability, and in extreme cases unsafe operation.

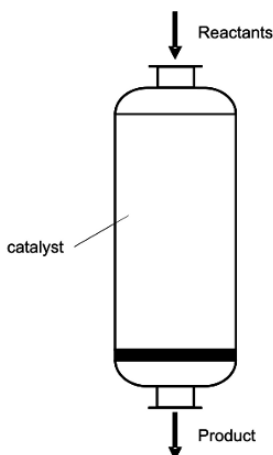


**Fig. 11.1.** Sketch of a single bed reactor.

For endothermic reactions the problem can be solved by dividing the reactor into multiple stages, with intermediate heat exchangers, defining a multi-bed reactor. In exothermic processes, the intermediate cooling may be achieved by mean of heat exchangers or by injection of cold feed. A schematic illustration of a multi-bed reactor is shown in Fig 11.2.

With very exothermic reactions the number of beds would have to be uneconomically large to limit the temperature increase per bed. This problem has been solved by introducing the multi-tube reactor. A schematic illustration of a multi-tube reactor is shown in Fig 11.3. A representative multi-tube reactor can contain hundreds or thousands of tubes with an inside diameter of a few centimeters [3]. The diameter is limited to this small size to avoid excessive temperature and hot spots.

The multi-tube reactor is more common than the other two fixed bed designs because many of the important heterogeneous catalytic processes require effective heat transfer between the mobile fluid, catalyst bed and heating/cooling media.

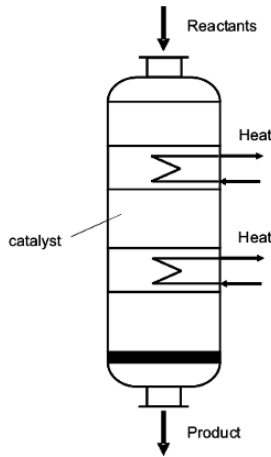


**Fig. 11.2.** Sketch of a multi-bed reactor.

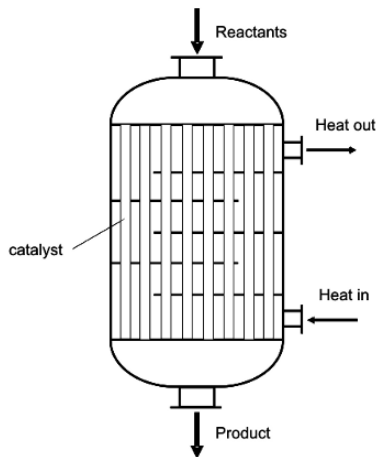


**Fig. 11.3.** Sketch of a multi-tube reactor.

### 11.3 Modeling and Simulation of Packed Bed Reactors

In industrial reactors there are normally gradients in the species mass concentrations, temperature, pressure and velocity in all space directions. The fundamental microscopic equations give a detailed description of all the known mechanisms involved. In the chemical reactor engineering approach we desire to eliminate the mechanisms that is not essential for the reactor performance from the equations to reduce the computational demand. An appropriate engineering packed bed reactor model is thus tailored for its main purpose. It is as simple as possible, but still include a sufficient representation of essential mechanisms involved.

The conventional classification of reactor models contains two main categories: The pseudo-homogeneous and heterogeneous models. The pseudo-homogeneous models are mixture models and do not account explicitly for the presence of catalyst, in contrast to the heterogeneous models which consist of separate conservation equations for the interstitial fluid and catalyst phases. The catalyst phase in this context refers to a region which may include both gas and solid material. The solids mass is stagnant and inert thus disregarded in both the pseudo-homogeneous and heterogeneous mass and momentum balances, but retained in the heat balances because the heat transfer processes are generally much more effective in the solid material than in the gas. The pseudo-homogeneous models are sufficient and can be used instead of heterogeneous models for processes where the intra-particle heat and mass transfer limitations are small. Heterogeneous models are required for processes with significant temperature and concentration differences between the phases.

The axial dispersion terms may be required to account for the mixing phenomena created by a non-ideal flow. However, the ideal plug flow model is often appropriate for packed bed reactors because the axial mixing is negligible compared to the convective flux for many processes.

The basis for the modeling of packed bed reactors are thus the cross sectional average homogeneous and heterogeneous model formulations. The homogeneous cross sectional average model equations were derived in sect 1.2.6 and simplified to the conventional single phase dispersion model in sect 1.2.7. The microscopic species mass balance reduces to (1.301) and the corresponding heat or temperature equation is given by (1.302). The heterogeneous two-phase cross sectional average model equations were derived in sect 3.4.6 and simplified to the two-phase dispersion model in sect 3.4.7. In this case the microscopic species mass balance reduces to (3.498) and the corresponding heat or temperature equation is given by (3.499). However, this formulation is used for the interstitial gas only. For the pellet similar equations are used for the gas in the pores, whereas the inert solid mass is disregarded in the species mass balances. The temperature equations for the pore gas and solid material are normally added together which collectively amount to a single mixture balance. The pseudo-homogeneous model equations are based on the classical mixture model derived in sect 3.4.5. In this concept the multiphase mixture is treated as a single homogeneous continuum. Thereby the balance principle can be applied to derive conservation laws for the macroscopic pseudo-fluid in analogy to the single phase formulation. The multiphase mixture properties are postulated or approximated by a volume fraction weighted sum of the phasic properties.

### 11.3.1 Fixed Bed Dispersion Models

The pseudo-homogeneous fixed bed dispersion models are divided into three categories: The axial dispersion model, the conventional two-dimensional dispersion model, and the full two-dimensional axi-symmetrical model formulation. The heterogeneous fixed bed dispersion models can be grouped in a similar way, but one dimensional formulations are employed in most cases.

Assuming that the bed packing is uniform, the local void fraction equals the overall holdup thus the void parameter can be canceled out in several model equations.

### Pseudo-Homogeneous Axial Dispersion Model

For reactive flows in packed beds a set of cross sectional average balance equations is written for the gas-solid multiphase mixture [3, 5].

Continuity for the interstitial gas phase:

$$\varepsilon \frac{\partial \rho_g}{\partial t} + \frac{\partial(\rho_g v_g^s)}{\partial z} = 0 \quad (11.1)$$

Momentum balance for the interstitial gas phase:

$$\frac{\partial}{\partial t}(\rho_g \frac{v_g^s}{\varepsilon}) + \frac{\partial}{\partial z}(\rho_g \frac{v_g^s v_g^s}{\varepsilon^2}) = -\frac{\partial p}{\partial z} - f \frac{\rho |v_g^s| v_g^s}{d_p} + 2 \frac{\partial}{\partial z}(\mu \frac{\partial v_g^s}{\partial z}) + \rho_g g_z - \frac{1}{2} \rho_g \frac{f_D}{d_t} |v_g^s| v_g^s \quad (11.2)$$

Within a porous body the flow of a fluid is resisted by viscous and geometric (tortuosity) effects. A porous media friction term is therefore added to the right hand side of the momentum equation. The physical meaning of different terms in the equation is explained in sect 3.4.6.

For flows through a porous packed bed the pressure drop is generally dominated by the bed friction and for fixed bed processes the velocity is normally not very large, hence the momentum balance for the bulk gas phase can be reduced to (6.13):

$$\frac{dp}{dz} = -f \frac{\rho_g (v_g^s)^2}{d_p} \quad (11.3)$$

Several parameterizations for the friction factor,  $f$ , are given in the literature. A parameterization valid for spheres over a relatively broad range of particle Reynolds numbers is frequently used [3]:

$$f = 6.8 \frac{(1 - \varepsilon)^{1.2}}{\varepsilon^3} Re_p^{-0.2} \quad \text{where} \quad Re_p = \frac{d_p \rho |v_g^s|}{\mu_g} \quad (11.4)$$

Species mass balance for the interstitial gas phase:

$$\varepsilon \frac{\partial(\rho_g \omega_c)}{\partial t} + \frac{\partial(\rho_g \omega_c v_g^s)}{\partial z} = \frac{\partial}{\partial z}(\rho_g D_{ez} \frac{\partial \omega_c}{\partial z}) + R_c \rho_{cat} (1 - \varepsilon) \quad (11.5)$$

Enthalpy balance for the gas-solid multiphase mixture:

$$\left( \varepsilon \rho_g C p_g + (1 - \varepsilon) \rho_{cat} C p_{cat} \right) \frac{\partial T}{\partial t} + \rho_g C p_g v_g^s \frac{\partial T}{\partial z} = \frac{\partial}{\partial z} (k_{ez} \frac{\partial T}{\partial z}) - \frac{4 U_i}{d_t} (T - T_a) + \sum_r (-\Delta H_{R,r}) r_r \rho_{cat} (1 - \varepsilon) \quad (11.6)$$

in which  $T_a$  represent the ambient temperature in the heating/cooling media.

In the current notation, the transport coefficients for heat and species mass are defined in terms of the superficial flow velocity. The species mass diffusivity – and the heat conductivity parameters may alternatively be expressed in terms of the interstitial gas flow velocity applying the following relations [3]:  $D_{ez} = \varepsilon D'_{ez}$  and  $k_{ez} = \varepsilon k'_{ez}$ .

The gas pressure or the gas mixture density can be calculated from an appropriate EOS, frequently the ideal gas law is employed in fixed bed simulations:

$$P = \rho_{mix}RT/M_{\omega_{mix}} \quad (11.7)$$

To solve these model equations appropriate initial and boundary conditions are required. Several conditions may be possible, a set of conditions for the rigorous case, in which (11.2) is used instead of (11.3), is listed below.

Initial conditions ( $t=0$ ):

Initially there is no flow in the reactor, the tube is filled with a stagnant gas mixture having prescribed composition and temperature. The bed packing has the same temperature as the gas.

$$\left. \begin{array}{l} \rho_g = \rho_{g,0} \\ v_g^s = v_{g,0}^s = 0 \\ p = p_0 \\ T = T_0 \\ \omega_c = \omega_{c,0} \end{array} \right\} \quad \text{for all } z \quad (11.8)$$

Boundary conditions ( $t > 0$ ):

$$\left. \begin{array}{l} \rho_g = \rho_{g,0} \\ v_g^s = v_{g,0}^s \\ T = T_0 \\ \omega_c = \omega_{c,0} \end{array} \right\} \quad \text{for } z = 0 \quad (11.9)$$

$$\frac{\partial \rho_c}{\partial z} = \frac{dT}{dz} = 0 \quad \text{and} \quad p = p_0 \quad \text{for } z = L \quad (11.10)$$

In specific cases the gas mixture is almost isotherm and the chemical process are not altering the mixture molecular mass very much, thus the system and transport properties may be considered constant. Otherwise, the system and transport properties have to be considered temperature and composition dependent and calculated from approximate parameterizations or kinetic theory relations.

### Pseudo-Homogeneous Two-dimensional Dispersion Model

The conventional two-dimensional pseudo-homogeneous reactor model consists of the continuity equation (11.1) and the simplified momentum equation (11.3) defined in connection with the pseudo-homogeneous dispersion model. The species mass and temperature equations are extended to 2D by adding postulated diffusion terms in the radial space dimension [3].

Species mass balance for the interstitial gas phase:

$$\varepsilon \frac{\partial(\rho_g \omega_c)}{\partial t} + \frac{\partial(\rho_g \omega_c v_g^s)}{\partial z} = \frac{\partial}{\partial z}(\rho_g D_{ez} \frac{\partial \omega_c}{\partial z}) + \frac{1}{r} \frac{\partial}{\partial z}(r \rho_g D_{er} \frac{\partial \omega_c}{\partial r}) + R_c \rho_{cat}(1 - \varepsilon) \tag{11.11}$$

Enthalpy balance for the gas-solid multiphase mixture:

$$\left( \varepsilon \rho_g C p_g + (1 - \varepsilon) \rho_{cat} C p_{cat} \right) \frac{\partial T}{\partial t} + \rho_g C p_g v_g^s \frac{\partial T}{\partial z} = \frac{\partial}{\partial z} \left( k_{ez} \frac{\partial T}{\partial z} \right) + \frac{1}{r} \frac{\partial}{\partial r} \left( k_{er} r \frac{\partial T}{\partial r} \right) + \sum_r (-\Delta H_{R,r}) r_r \rho_{cat} (1 - \varepsilon) \tag{11.12}$$

The gas pressure or the gas mixture density can be calculated from an appropriate EOS like (11.7).

To solve these model equations appropriate initial and boundary conditions are required. Several conditions may be possible, a frequently used a set of conditions for the classical formulation, in which (11.3) is used instead of (11.2), is listed below.

Initial conditions (t=0): Initially there is a steady-state flow in the reactor, and the tube contains a gas mixture having prescribed composition and temperature. The bed packing has the same temperature as the gas.

$$\left. \begin{aligned} \rho_g &= \rho_{g,0} \\ v_g^s &= v_{g,0}^s \\ p &= p_0 \\ T &= T_0 \\ \omega_c &= \omega_{c,0} \end{aligned} \right\} \text{ for all } z \text{ and } r \tag{11.13}$$

Boundary conditions (t > 0) are given as:

$$\left. \begin{aligned} \rho_g &= \rho_{g,0} \\ v_g^s &= v_{g,0}^s \\ p &= p_0 \\ T &= T_0 \\ \omega_c &= \omega_{c,0} \end{aligned} \right\} \text{ at } z = 0 \quad 0 \leq r \leq R \tag{11.14}$$

$$\frac{\partial \omega_c}{\partial z} = \frac{\partial T}{\partial z} = 0 \quad \text{at } z = L \quad 0 \leq r \leq R \tag{11.15}$$

$$\frac{\partial \omega_c}{\partial r} = 0 \quad \text{at } r = 0 \text{ and } r = R \quad \text{all } z \tag{11.16}$$

$$\frac{\partial T}{\partial r} = 0 \quad \text{at } r = 0 \quad \text{all } z \tag{11.17}$$

$$\frac{\partial T}{\partial r} = - \frac{U_i}{k_{er} \rho_g C_p} (T - T_a) \quad \text{at } r = R \quad \text{all } z \tag{11.18}$$

In the past many process simulations were performed keeping  $v_g^s$ ,  $\rho_g$ , and the system and transport properties constant to reduce the problem complexity [3].

This pseudo-homogeneous two-dimensional dispersion model formulation is strictly not consistent with the cross sectional averaging procedure outlined in sect 3.4.6 and sect 1.2.7 and should be treated with prudence and/or avoided.

### Full Pseudo-Homogeneous Two-Dimensional Axi-symmetric Model

A more rigorous pseudo-homogeneous two-dimensional axi-symmetric model can be obtained reducing the governing averaged equations, that can be derived using any of the local averaging procedures described in sect 3.4, for the particular axi-symmetric tube flow problem.

Continuity for the interstitial gas phase:

$$\frac{\partial \rho_g}{\partial t} + \frac{\partial(\rho_g v_{g,z})}{\partial z} + \frac{1}{r} \frac{\partial(r \rho_g v_{g,r})}{\partial r} = 0 \quad (11.19)$$

Momentum balances for the interstitial gas phase:

$$\begin{aligned} \frac{\partial}{\partial t}(\rho_g v_r) + \frac{1}{r} \frac{\partial}{\partial r}(r \rho_g v_r v_r) + \frac{\partial}{\partial z}(\rho_g v_z v_r) = \\ - \frac{\partial p}{\partial r} - f \frac{\rho |\mathbf{v}| v_r}{d_p} + \frac{2}{r} \frac{\partial}{\partial r}(r \mu \frac{\partial v_r}{\partial r}) + \frac{\partial}{\partial z}(\mu \frac{\partial v_r}{\partial z}) - 2 \mu \frac{v_r}{r^2} + \frac{\partial}{\partial z}(\mu \frac{\partial v_z}{\partial r}) \end{aligned} \quad (11.20)$$

and

$$\begin{aligned} \frac{\partial}{\partial t}(\rho_g v_z) + \frac{1}{r} \frac{\partial}{\partial r}(r \rho_g v_r v_z) + \frac{\partial}{\partial z}(\rho_g v_z v_z) = \\ - \frac{\partial p}{\partial z} - f \frac{\rho |\mathbf{v}| v_z}{d_p} + \rho_g g_z + \frac{1}{r} \frac{\partial}{\partial r}(r \mu \frac{\partial v_z}{\partial r}) + 2 \frac{\partial}{\partial z}(\mu \frac{\partial v_z}{\partial z}) + \frac{1}{r} \frac{\partial}{\partial r}(r \mu \frac{\partial v_r}{\partial z}) \end{aligned} \quad (11.21)$$

Species mass balances for the interstitial gas phase:

$$\begin{aligned} \frac{\partial(\rho_g \omega_c)}{\partial t} + \frac{\partial(\rho_g \omega_c v_{g,z})}{\partial z} + \frac{1}{r} \frac{\partial(r \rho_g \omega_c v_{g,r})}{\partial r} = \\ \frac{\partial}{\partial z}(\rho_g D'_{ez} \frac{\partial \omega_c}{\partial z}) + \frac{1}{r} \frac{\partial}{\partial r}(r \rho_g D'_{er} \frac{\partial \omega_c}{\partial r}) + R_c \rho_{cat} \frac{(1-\varepsilon)}{\varepsilon} \end{aligned} \quad (11.22)$$

Enthalpy balance for the gas-solid multiphase mixture:

$$\begin{aligned} \left( \rho_g C p_g + \frac{(1-\varepsilon)}{\varepsilon} \rho_{cat} C p_{cat} \right) \frac{\partial T}{\partial t} + \rho_g C p_g v_{g,z} \frac{\partial T}{\partial z} + \rho_g C p_g v_{g,r} \frac{\partial T}{\partial r} = \\ \frac{\partial}{\partial z}(k'_{ez} \frac{\partial T}{\partial z}) + \frac{1}{r} \frac{\partial}{\partial r}(r k'_{er} \frac{\partial T}{\partial r}) + \sum_r (-\Delta H_{R,r}) r_r \rho_{cat} \frac{(1-\varepsilon)}{\varepsilon} \end{aligned} \quad (11.23)$$

The gas pressure or the gas mixture density can be calculated from an appropriate EOS like (11.7).

The standard initial and boundary conditions for two-dimensional axisymmetric flows in a tube are generally used.

Initial conditions ( $t=0$ ): Initially there is no flow in the reactor ( $v_r = v_{r0} = v_z = v_{z0} = 0$ ), the tube is filled with stagnant gas having prescribed composition and temperature, as for the 2D dispersion model simulations.

Boundary conditions ( $t > 0$ ): The standard conditions for axis-symmetric flow in a 2D tube can be specified in the following manner. There is no flow through the reactor wall. The normal velocity component is set to zero at the symmetry boundary. Plug flow is assumed at the inlet. A prescribed pressure is specified at the reactor outlet. For the scalar variables Dirichlet boundary conditions are used at the inlet, whereas Neumann conditions are used at the other boundaries, as for the 2D dispersion model simulations.

### Full Heterogeneous Axial Dispersion Model

For reactive flows in packed porous beds a heterogeneous two-phase model consists of two sets of model equations, one set for the interstitial gas phase and one set for the pellet phase. The governing equations used by Rusten et al [11] are outlined below.

Continuity for the interstitial gas phase:

$$\varepsilon \frac{\partial \rho_g}{\partial t} + \frac{\partial(\rho_g v_g^s)}{\partial z} = 0 \quad (11.24)$$

Momentum balance for the interstitial gas phase:

$$\frac{\partial}{\partial t}(\rho_g \frac{v_g^s}{\varepsilon}) + \frac{\partial}{\partial z}(\rho_g \frac{v_g^s v_g^s}{\varepsilon^2}) = -\frac{\partial p}{\partial z} - f \frac{\rho |v_g^s| v_g^s}{d_p} + 2 \frac{\partial}{\partial z}(\mu \frac{\partial v_g^s}{\partial z}) + \rho_g g_z - \frac{1}{2} \rho_g \frac{f_D}{d_t} |v_g^s| v_g^s \quad (11.25)$$

Species mass balance for the interstitial gas phase:

$$\varepsilon \frac{\partial(\rho_g \omega_c)}{\partial t} + \frac{\partial(\rho_g \omega_c v_g^s)}{\partial z} = \frac{\partial}{\partial z}(\rho_g D_{ez} \frac{\partial \omega_c}{\partial z}) + a_s k_c \rho_g (\omega_{s,c} - \omega_c) \quad (11.26)$$

Enthalpy balance for the interstitial gas phase:

$$\left( \varepsilon \rho_g C p_g + (1 - \varepsilon) \rho_{cat} C p_{cat} \right) \frac{\partial T}{\partial t} + \rho_g C p_g v_g^s \frac{\partial T}{\partial z} = \frac{\partial}{\partial z} \left( k_{ez} \frac{\partial T}{\partial z} \right) - \frac{4 U_i}{d_t} (T - T_a) + a_s h (T_s - T) \quad (11.27)$$

Inside the pores of the catalyst pellets the convective terms are assumably not significant, hence the species mass balance equations for the porous gas are expressed by:

$$\varepsilon_p \frac{\partial \rho_g \omega_{p,c}}{\partial t} = \frac{1}{r^2} \frac{\partial}{\partial r} \left( r^2 \frac{D_{cm} \varepsilon_p}{\tau} \rho_g \frac{\partial \omega_{p,c}}{\partial r} \right) + (1 - \varepsilon_p) \rho_p R_c \quad (11.28)$$

The multicomponent diffusivities are generally calculated from the Wilke equation.  $\tau$  represents the tortuosity factor for the pellet.

The pellet temperature equation for the multiphase gas-solid mixture can be expressed as:

$$\begin{aligned}
 (\varepsilon_p \rho_g C_{p_g} + (1 - \varepsilon_p) \rho_p C_{p_p}) \frac{\partial T_p}{\partial t} &= \frac{1}{r^2} \frac{\partial}{\partial r} (r^2 k_{p,g} \frac{\partial T_p}{\partial r}) \\
 &+ (1 - \varepsilon_p) \rho_p \sum_r (-\Delta H_{R,r}) r_r
 \end{aligned} \tag{11.29}$$

The gas pressure or the gas mixture density can be calculated from an appropriate EOS like (11.7).

To solve these model equations appropriate initial and boundary conditions are required. Several conditions may be possible, a set of conditions for the rigorous case, in which (11.25) is used instead of (11.3), is listed below.

Initial conditions ( $t=0$ ): Initially there is no flow in the reactor, the tube is filled with a stagnant gas mixture having prescribed composition and temperature. The bed packing has the same temperature as the gas.

$$\left. \begin{aligned}
 v_g^s &= v_{g,0}^s = 0 \\
 \rho_g &= \rho_{g,0} \\
 p &= p_0 \\
 T &= T_0 \\
 \omega_c &= \omega_{c,0}
 \end{aligned} \right\} \quad \text{for all } z \text{ and } r \tag{11.30}$$

Boundary conditions ( $t > 0$ ):

$$\left. \begin{aligned}
 v_g^s &= v_{g,0}^s \\
 \rho_g &= \rho_{g,0} \\
 T &= T_0 \\
 \omega_c &= \omega_{c,0}
 \end{aligned} \right\} \quad \text{for } z = 0 \tag{11.31}$$

$$\frac{\partial \omega_c}{\partial z} = \frac{dT}{dz} = 0 \quad \text{and} \quad p = p_0 \quad \text{for } z = L \tag{11.32}$$

Neuman boundary conditions are used for the particle phase. These are generally defined for all  $z$  and  $t$ :

$$-\frac{D_{cm} \varepsilon_p}{\tau} \frac{\partial \omega_c}{\partial r} \Big|_{r=r_p} = k_c (\omega_{p,c} - \omega_c) \tag{11.33}$$

$$-k_{p,g} \frac{\partial T_p}{\partial r} \Big|_{r=r_p} = h (T_p - T) \tag{11.34}$$

$$\frac{\partial \omega_c}{\partial r} \Big|_{r=0} = 0 \tag{11.35}$$

$$\frac{\partial T_p}{\partial r} \Big|_{r=0} = 0 \tag{11.36}$$

### 11.3.2 Reactor Process Simulations

In the subsequent sections three examples of fixed bed reactor modeling are given, summarizing the work of Jakobsen et al [5] and Lindborg et al [7] investigating the steam methane reforming (SMR) and methanol production processes, and the simulations of the hydrogen production by sorption enhanced steam reforming of methane by Rusten et al [11].

#### Methanol Production Process

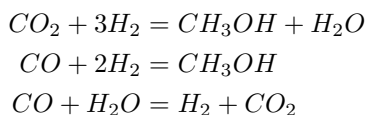
The last decades the discoveries of natural gas reserves are considerable, hence the oil and gas companies are looking into the economics and technical feasibility of building huge gas conversion plants to take fully advantage of the economics of scale [9]. Among the most interesting gas conversion processes are the methanol process, where natural gas is converted into fuel. It is expected that the methanol market will develop into a fuel market in the future. Methanol can be used as a hydrogen source in future automobiles based on fuel cell technology. It can also be used as an alternative to oil and LNG for power generation.

Model simulations of reactor operation are convenient in order to study:

- The effect on products of changes in feed and catalyst.
- Scale up from laboratory to industry scales.
- Optimization of the reactor performance.
- Optimization of the operating conditions.
- Interpretations of laboratory measurements.

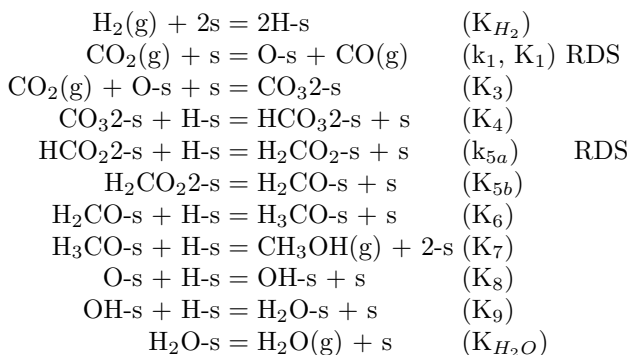
In this study the steady-state kinetic model for the methanol synthesis on a commercial Cu/ZnO/Al<sub>2</sub>O<sub>3</sub> catalyst developed by Vanden Bussche and Froment [13] are used.

The chemistry mechanism is based on three overall reactions:



The first and the second reaction are hydrogenation reactions of CO<sub>2</sub> and CO, respectively. The last reaction is the water gas shift reaction (WGS).

The reaction steps considered developing the reaction kinetics were given, and the rate determining steps (RDS) are indentified:



The kinetic rate models for the conversion of synthesis gas over a Cu/ZnO/Al<sub>2</sub>O<sub>3</sub> catalyst is thus given by:

$$r_{MeOH} = \frac{k'_{5a} K'_2 K_3 K_4 K_{H_2} p_{CO_2} p_{H_2} \left(1 - \frac{1}{K_1^*} \frac{p_{H_2O} p_{CH_3OH}}{p_{H_2}^3 p_{CO_2}}\right)}{\left(1 + \frac{K_{H_2O}}{K_8 K_9 K_{H_2}} \frac{p_{H_2O}}{p_{H_2}} + \sqrt{K_{H_2} p_{H_2}} + K_{H_2O} p_{H_2O}\right)^3} \quad (11.37)$$

$$r_{RWGS} = \frac{k'_1 p_{CO_2} \left(1 - K_3^* \frac{p_{H_2O} p_{CO}}{p_{H_2} p_{CO_2}}\right)}{1 + \frac{K_{H_2O}}{K_8 K_9 K_{H_2}} \frac{p_{H_2O}}{p_{H_2}} + \sqrt{K_{H_2} p_{H_2}} + K_{H_2O} p_{H_2O}} \quad (11.38)$$

The production of methanol is given by  $r_{MeOH}$  and the production of CO is given by the expression for the reversed water gas shift reaction  $r_{RWGS}$ .

These expressions can be re-written as:

$$r_{MeOH} = \frac{F_4 p_{CO_2} p_{H_2} \left(1 - \frac{1}{K_1^*} \frac{p_{H_2O} p_{CH_3OH}}{p_{H_2}^3 p_{CO_2}}\right)}{DENOM^3} \quad (11.39)$$

$$r_{RWGS} = \frac{F_5 p_{CO_2} \left(1 - K_3^* \frac{p_{H_2O} p_{CO}}{p_{H_2} p_{CO_2}}\right)}{DENOM} \quad (11.40)$$

The denominator is defined by:

$$DENOM = 1 + F_3 \frac{p_{H_2O}}{p_{H_2}} + F_1 \sqrt{p_{H_2}} + F_2 p_{H_2O} \quad (11.41)$$

The factors  $F_i$  were calculated from the Arrhenius or Van't Hoff equation:

$$F_i = A_i \times e^{\frac{B_i}{RT}} \quad (11.42)$$

in which  $B_i$  represents either the activation energy  $E$ , or the reaction enthalpy ( $-\Delta H$ ), or a combination of those. The parameter values for  $A_i$  and  $B_i$  are given in table 11.2.

**Table 11.2.** Parameters for the methanol synthesis

F <sub>1</sub>	$\sqrt{K_{H_2}}$	A <sub>1</sub>	0.499	(bar <sup>-1/2</sup> )
		B <sub>1</sub>	17197	(J/mol)
F <sub>2</sub>	K <sub>H<sub>2</sub>O</sub>	A <sub>2</sub>	6.62 × 10 <sup>-11</sup>	(bar <sup>-1</sup> )
		B <sub>2</sub>	124119	(J/mol)
F <sub>3</sub>	$\frac{K_{H_2O}}{K_8 K_9 K_{H_2}}$	A <sub>3</sub>	3453.38	(-)
		B <sub>3</sub>	-	(J/mol)
F <sub>4</sub>	$k'_{5a} K_2 K_3 K_4 K_{H_2}$	A <sub>4</sub>	1.07	(mol/kg <sub>cat</sub> /s/bar <sup>2</sup> )
		B <sub>4</sub>	36696	(J/mol)
F <sub>5</sub>	k' <sub>1</sub>	A <sub>5</sub>	1.22 × 10 <sup>10</sup>	(mol/kg <sub>cat</sub> /s/bar)
		B <sub>5</sub>	-94765	(J/mol)

To calculate the equilibrium constants K<sub>1</sub><sup>\*</sup> and K<sub>3</sub><sup>\*</sup>, the following expressions were applied:

$$\log_{10}(K_1^*) = \frac{3066}{T} - 10.592 \tag{11.43}$$

$$\log_{10}\left(\frac{1}{K_3^*}\right) = \frac{-2073}{T} + 2.029 \tag{11.44}$$

The rate of formation of the different components in the system is given as:

$$\begin{aligned} r_{CH_3OH} &= r_{MeOH} \\ r_{CO} &= -r_{RWGS} \\ r_{CO_2} &= r_{RWGS} - r_{MeOH} \\ r_{H_2} &= r_{RWGS} - 3r_{MeOH} \\ r_{H_2O} &= r_{MeOH} - r_{RWGS} \\ r_{N_2} &= 0 \\ r_{CH_4} &= 0 \end{aligned} \tag{11.45}$$

The reaction enthalpies were calculated from the the heat of formation for the species in the hydrogenation of CO<sub>2</sub> and water gas shift reactions. The overall process is strongly exothermic.

Due to the cooling requirement, the industrial scale fixed bed reactors used for this process are normally constructed based on the multi-tube design.

The operating conditions used for the methanol Bench Scale Reactor simulations are listed in the tables 11.3-11.5.

The pseudo-homogeneous two-dimensional dispersion model, consisting of (11.11) to (11.18) and the pressure drop relations (11.3) and (11.4), was solved for the methanol production process under non-adiabatic conditions.

The results from a simulation of the methanol process with external cooling (non-adiabatic process) are given in Fig 11.4. The predicted profiles show that methanol is produced at the expense of CO, CO<sub>2</sub> and H<sub>2</sub>. The temperature gradient at the reactor entrance is very steep. The temperature increases to about 550 K in the center of the tube, but near the walls the maximum

**Table 11.3.** Reactor Tube Data

	Methanol process
Inner tube diameter (m)	0.016
Outer tube diameter (m)	0.026
Tube length (m)	0.15
Temperature outside the wall (K)	523.2
Heat coefficient for the metal (J/msK)	52

**Table 11.4.** Catalyst data

	Methanol process
Catalyst density (kg/m <sup>3</sup> )	1775
Particle diameter (m)	0.0005
Void fraction in the bulk region	0.5

**Table 11.5.** Gas data

	Methanol process	
Mass fraction of CH <sub>4</sub>	0.1490	(6.00 mol%)
Mass fraction of CH <sub>3</sub> OH	0	(0.00 mol%)
Mass fraction of CO	0.1734	(4.00 mol%)
Mass fraction of CO <sub>2</sub>	0.2044	(3.00 mol%)
Mass fraction of H <sub>2</sub>	0.2564	(82.00 mol%)
Mass fraction of H <sub>2</sub> O	0	(0.00 mol%)
Mass fraction of N <sub>2</sub>	0.2168	(5.00 mol%)
Superficial inlet velocity (m/s)	0.0067184	
Inlet temperature (K)	493.2	
Inlet pressure (bar)	50	

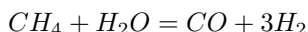
temperature is approximately 530 K. The temperature decreases further away from the reactor inlet, and the radial profiles are almost flat at  $z = 0.3$  meters downstream from the inlet.

Vanden Bussche and Froment [13] simulated an adiabatic Bench Scale Reactor using a pseudo-homogeneous one-dimensional model. Using a similar pseudo-homogeneous axial dispersion model Jakobsen et al [5] obtained axial concentration and temperature profiles that were hardly distinguishable from the pseudo-homogeneous one-dimensional model results of Vanden Bussche and Froment [13].

The adiabatic reactor case was used as a validation test for the two-dimensional model.

### Conventional Steam Methane Reforming

The most important reactions taking place in catalytic steam reforming are the endothermic methane steam reforming reaction and the parallel exothermic water gas shift reaction, respectively [4]:



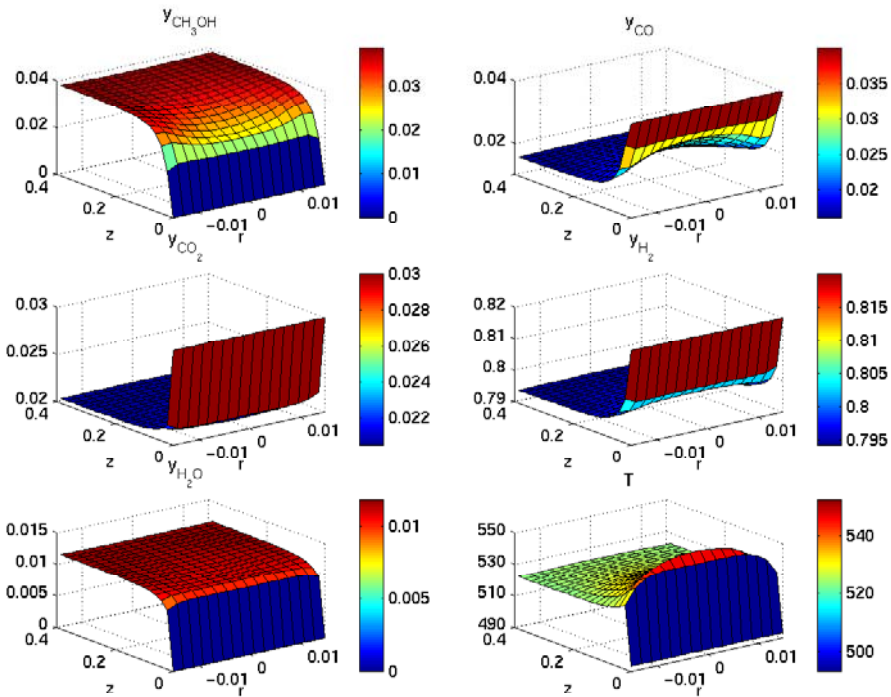
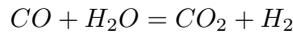
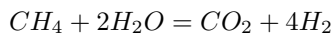


**Fig. 11.4.** Species mole fractions and temperature profiles predicted by the pseudo-homogeneous two-dimensional dispersion model. Note, as a 2D axisymmetric tube has been simulated, the model is solved for positive  $r$ -values only. Reprinted with permission by Elsevier [5].

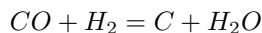


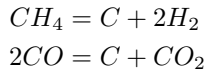
The endothermic  $\text{CO}_2$  reforming reaction is frequently considered:



These three reactions are not independent because the third reaction equals the sum of the other two reactions. The reactions are catalysed by pellets coated with nickel ( $\text{Ni}/\text{MgAl}_2\text{O}_3$ ) and are highly endothermic overall. The operating process conditions are typically 20-40 bar with inlet temperature of 300-650 °C and outlet temperature of 700-950 °C.

Coking reactions occur in parallel with the reforming reactions and are undesirable as they cause poisoning of the surface of the catalyst pellets. This leads to lower catalyst activity and the need for more frequently catalyst reloading. The coking reactions are the CO-reduction, methane cracking and Boudouard reaction, given by the respective equilibrium reactions [4]:





It can be seen from these reaction equations that low steam excess can lead to critical conditions causing coke formation, according to the principle of Le Chatelier.

The kinetics, physical data, correlations and operating conditions needed for the synthesis gas conversion process are taken from Froment and Bischoff [3], De Groote and Froment [1] and Xu and Froment [14, 15].

The most common reactor concept for steam reforming of natural gas is the fired steam reformer that is a multi-tube fixed bed design [2]. The Topsøe reformer design with tube and burner arrangement is shown in Fig 11.5. A Natural gas and the tail gas from the synthesis loop are burned in a firebox where several tubes packed with catalyst pellets are placed in rows with a number of 40 to 400 tubes. The reactor tubes are about 10-12 m long, with diameters of about 10 cm. The reactions for conversion of natural gas to syngas take place over the catalytic surfaces in the reactor tubes. The burners can be located in different places: On the roof, on the floor, on levelled terraces on the walls, or on the walls. The top fired reformer is characterized by a defiant peak in the tube wall temperature in the upper part of the reformer, and it has the highest heat flux where the metal temperature is at its maximum. The bottom fired type has an almost constant heat flux profile along the length of the tube. The terrace wall fired reformer is a modification of the bottom fired reformer and has some smaller problem with high metal temperatures. The side fired reformer has the most effective design and is also the most flexible reformer, both in design and in operation.

The operating conditions used in the simulations of the syngas process are listed in the tables 11.6-11.8.

For steam reforming, both heterogeneous and pseudo-homogeneous models have been used to simulate the process. However, since the steam methane reforming process is strongly intra-particle diffusion-controlled [3], an appropriate reactor simulation generally requires a heterogeneous model. Nevertheless, the use of pseudo-homogeneous models in which the diffusion resistances are taken into account through efficiency factors can also be a sufficient option provided that appropriate values of these factors are known.

The full pseudo-homogeneous 2D axi-symmetric model, consisting of (11.19) to (11.23), was used to simulate the synthesis gas process. The model was simulated with a grid  $17 \times 257$  for 3 seconds until the steady state solution was obtained. The time increment in the simulations was  $\Delta t = 10^{-3}$  s. To ensure mass conservation the convergence criteria was set to an error limit of  $10^{-18}$  of the residual error.

The results obtained from the 2D simulations with a uniform void distribution are given in Fig 11.6 and Fig 11.7.

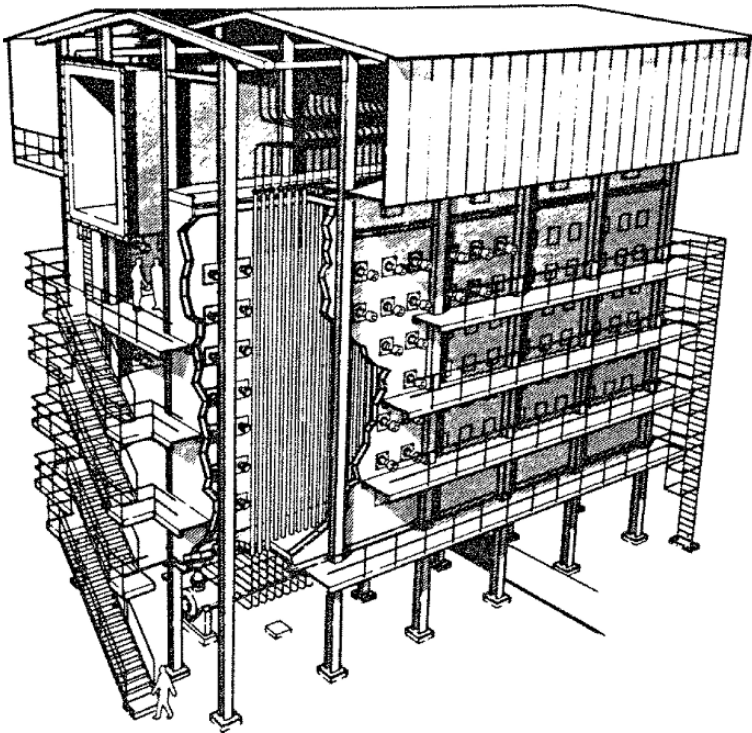


**Fig. 11.5.** The Topsøe reformer design with tube and burner arrangement. Reprinted from Rostrup-Nielsen [10] with permission from Springer.

**Table 11.6.** Reactor Tube Data

	Syngas process
Inner tube diameter (m)	0.102
Outer tube diameter (m)	0.132
Tube length (m)	8
Temperature outside the wall (K)	1100
Heat coefficient for the metal (J/msK)	52

**Table 11.7.** Catalyst data

	Syngas process
Catalyst density (kg/m <sup>3</sup> )	2355.2
Particle diameter (m)	0.0173
Void fraction in the bulk region	0.528

**Table 11.8.** Gas data

	Syngas process
Mass fraction of CH <sub>4</sub>	0.1911
Mass fraction of CO	0.0001
Mass fraction of CO <sub>2</sub>	0.0200
Mass fraction of H <sub>2</sub>	0.0029
Mass fraction of H <sub>2</sub> O	0.7218
Mass fraction of N <sub>2</sub>	0.0641
Superficial inlet velocity (m/s)	1.89
Inlet temperature (K)	793
Inlet pressure (bar)	29

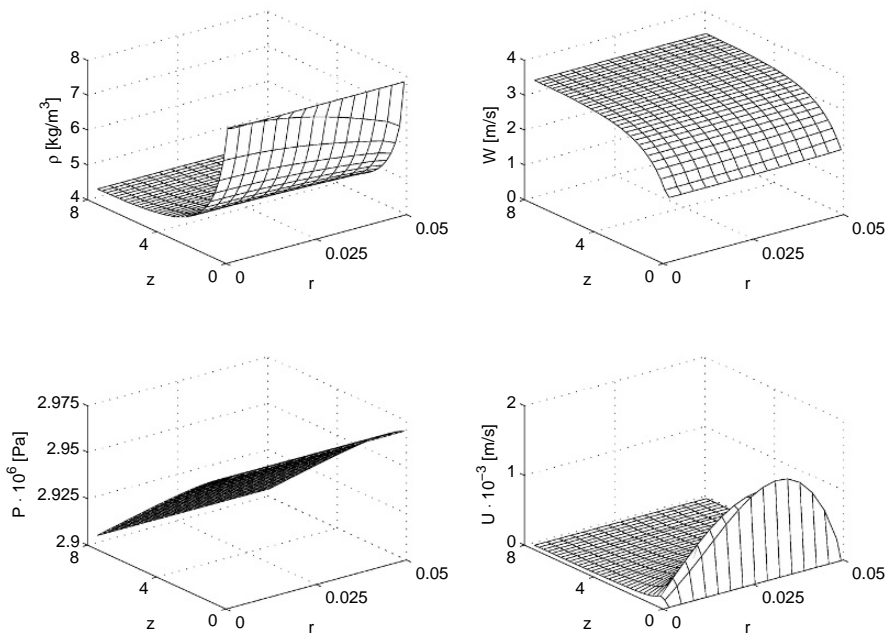


**Fig. 11.6.** Velocity, density, pressure and temperature profiles from a 2D simulation with a uniform void fraction profile. Reprinted with permission by Elsevier [7].

The axial velocity component is close to uniform and the radial velocity component is very small, hence the flow pattern can be characterized as plug flow.

In the synthesis gas process CO is produced from CH<sub>4</sub> and H<sub>2</sub>O. The reversed water gas shift reaction consumes CO in the z-interval from 0-1.5 m. The mole fraction of CO<sub>2</sub> is increasing from the reactor entrance and reaches

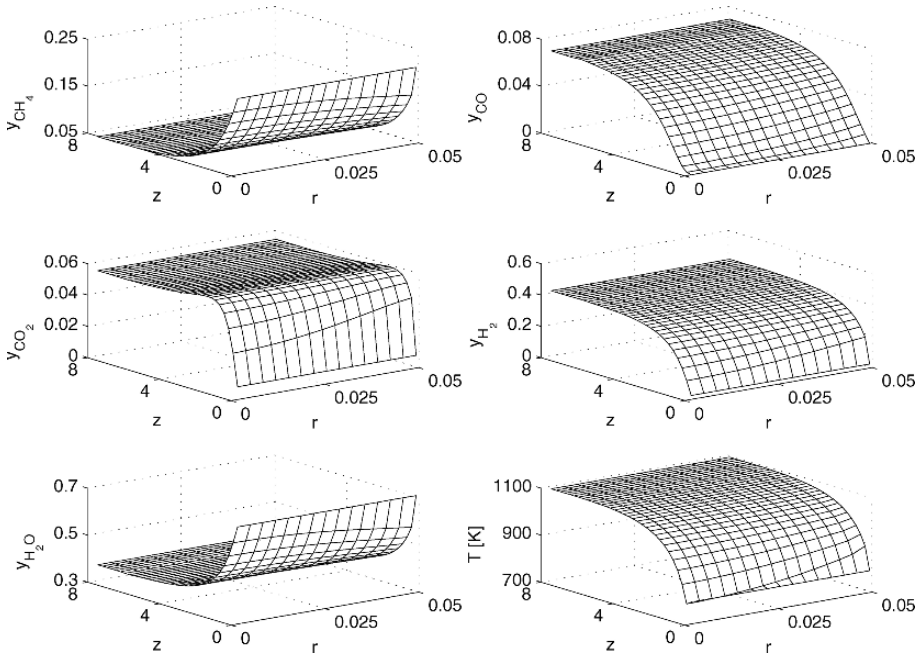


**Fig. 11.7.** Mole fraction profiles for the components from a 2D simulation with a uniform void fraction distribution. Reprinted with permission by Elsevier [7].

a maximum at a distance of 1.5 meters from the inlet. At  $z = 1.5$  m the reaction is reversed, and a maximum occurs in the  $CO_2$  profile. Then there is a slight decrease to the point where equilibrium is achieved.

A radial temperature gradient with a maximum at the wall is observed at the reactor entrance. Further away from the reactor entrance, the radial profile is flat. The mole fraction profiles also contain marked radial gradients within the first 1.5 meters of the reactor. The radial gradients observed in the species concentration profiles are caused by the limited heat flux added to the reactor through the wall. The reactions are endothermic and the heat transferred through the wall and/or from the wall into the bed is not sufficient to smooth out the temperature profile, thus the chemical conversion becomes non-uniform.

The use of a full 2D pseudo-homogeneous axi-symmetric model has the advantage, compared to the conventional 2D pseudo-homogeneous dispersion model, that it enables an evaluation of the influence of a non-uniform void distribution in the reactor.

To evaluate the importance of the radial variations in the void fraction profiles, simulations with prescribed radial variations in the bed structure were performed for the synthesis gas process. The velocity and pressure profiles were significantly altered. Higher void fractions at the wall induces less friction from

the bed, thus the gas flow increases and the pressure drop decreases. However, the influence on the temperature and mole fraction profiles were very small but noticeable. This particular process consists of very fast reactions that are very much controlled by the operational temperature, hence provided that sufficient heat is added the non-uniform bed packing has very little impact on the conversion.

A customary simplification is to run the conventional dispersion model simulations adopting prescribed values for the superficial velocity and the mixture density throughout the reactor, in conjunction with a linear pressure profile as represented by (11.3). The superficial velocity and the mixture density values are then generally set to the inlet values. However, solving the full 2D pseudo-homogeneous model formulation for the synthesis gas process, it is shown that the axial gradients predicted in the axial velocity component and mixture density profiles are considerable and should be taken into account. However, the chemical species concentration and temperature profiles obtained in the rigorous 2D simulations do not vary much from the corresponding results obtained by use of a conventional 2D pseudo-homogeneous dispersion model.

### Sorption Enhanced Steam Methane Reforming

Hydrogen is an important raw material in the chemical and petroleum industries. Large quantities are used in the manufacture of ammonia and methanol and in a variety of petroleum hydro treating processes. In addition, hydrogen might become a new generation clean energy source for transport, especially for fuel cell application, which would cause a huge increase in hydrogen demand.

Steam methane reforming (SMR) is currently the major process for large-scale production of hydrogen. For hydrogen production a more cost effective process is desirable. Within the last few years the concept of multi-functional reactors combining reaction and separation, especially the concept of sorption enhanced reaction process (SERP), have received increased attention. A CO<sub>2</sub>-acceptor can be installed together with catalyst to remove CO<sub>2</sub> from the gas phase, normal equilibrium limits of reforming and shift reactions are changed, and a product containing more than 98% H<sub>2</sub> (dry basis) is possible [8]. The steam reforming can be run at a much lower temperature (450-630 °C) than conventional steam reforming, which will significantly lower investment and operation cost.

A fixed bed reactor for production of hydrogen by sorption enhanced steam methane reforming (SE-SMR) using Li<sub>2</sub>ZrO<sub>3</sub> as CO<sub>2</sub>-acceptor was investigated by Rusten et al [11]:



The capture process is represented by an exothermic reaction (i.e.,  $\Delta H_{848K} = 15$  kJ/mol) contrary to the endothermic steam reforming and the heat of

sorption makes the need for external heating less than for the traditional steam reforming process.

An empirical parameterization of the sorption kinetics was employed:

$$\frac{dx}{dt} = k_1(p_{CO_2} - p_{eq,CO_2})^2(1 - x) \quad (11.46)$$

- The equilibrium partial pressure of CO<sub>2</sub>,  $p_{eq,CO_2}$ , was modeled using thermodynamical data [6].
- $x$  is the fractional conversion, defined by:

$$x = \frac{q}{q_{max}} \quad (11.47)$$

in which  $q$  is the mass of CO<sub>2</sub> captured per mass of lithium zirconate,  $q_{max}$  is  $q$  at maximum capture and is found to be 0.22 for this sample of Li<sub>2</sub>ZrO<sub>3</sub>.

- $k_1$  is the effective reaction rate constant for which an Arrhenius expression is used for the temperature dependence:

$$k_1 = k_{10}e^{-\frac{E}{R}(\frac{1}{T} - \frac{1}{T_0})} \quad (11.48)$$

The parameters in (11.48) have the values  $k_{10} = 8.07 \times 10^{-13}$  (s<sup>-1</sup>) and  $E = 7.7 \times 10^4$  (J/mol).

The sorption rate thus yields:

$$R_{cap} = R_{CO_2} = q_{max} \frac{dx}{dt} \left( \frac{kg}{kgs} \right) \quad (11.49)$$

Transient one-dimensional reactor models with axial dispersion were used to simulate the fixed bed reactor process. Transient models were chosen because the capture of CO<sub>2</sub> has a time-dependent nature, and the axial dispersion term was included because of the relatively low gas velocities that were used in the simulations.

Three different versions of the basic one dimensional model were developed, two heterogeneous models and a pseudo-homogeneous model. The difference in the two heterogeneous models is the way the sorbent was installed in the reactor bed. One model version considers that Li<sub>2</sub>ZrO<sub>3</sub> and the reforming catalyst are coated on two different particles, while in the other case there is one particle with both catalytic and capture properties. The steam methane reforming and the water-gas shift reaction kinetics are taken from Xu and Froment [14], but corrected for different properties of the catalyst.

Using the pseudo-homogeneous axial dispersion model as a reference, the governing equations are defined by (11.1) to (11.10).

The species mass balance (11.5) was solved for H<sub>2</sub>, CO, CH<sub>4</sub> and CO<sub>2</sub>. The mass fraction of H<sub>2</sub>O, the dominating species in the mixture, was calculated from (11.50).

$$\sum_{c=1}^5 \omega_c = 1 \quad (11.50)$$

To define the alternative model versions the effective reaction term  $S_c = M_{\omega_c} r_c \rho_{cat}(1 - \varepsilon) = R_c \rho_{cat}(1 - \varepsilon)$  in the basic model species mass balance is substituted with a modified source term  $S_c$  being different in the various model versions:

- For the heterogeneous one particle model, we can see from (11.26) that the source term is a conventional particle-bulk interstitial gas phase mass transfer term is defined by:

$$S_c = a_s k_c \rho_g (\omega_{s,c} - \omega_c) \quad (11.51)$$

- For the two-particle heterogeneous model the source term in the bulk gas phase equation is given as the sum of the conventional particle-bulk phase mass transfer terms for both the catalyst and CO<sub>2</sub>-acceptor particles. The net source term is thus defined by:

$$S_c = a_{s,cat} k_c \rho_g (\omega_{s,c}^{cat} - \omega_c) + a_{s,cap} k_c \rho_g (\omega_{s,c}^{cap} - \omega_c) \quad (11.52)$$

- For the pseudo-homogeneous model  $S_c$  represents an effective reaction rate. For CO<sub>2</sub> the source term for the pseudo-homogeneous model consists of two effective reaction rate terms, one for the reforming reactions and one for the CO<sub>2</sub>-capture kinetics:

$$S_{CO_2} = \frac{1 - \epsilon_b}{1 + \alpha \frac{\epsilon_p^{cap}}{\epsilon_p^{cat}}} (1 - \epsilon_p^{cat}) \rho_{cat} R_{CO_2} + \frac{1 - \epsilon_b}{1 - \frac{\epsilon_p^{cat}}{\epsilon_p^{cat} + \epsilon_p^{cap}} \alpha} (1 - \epsilon_p^{cap}) \rho_{cap} R_{CO_2, cap} \quad (11.53)$$

The  $\alpha$  represents the ratio between the solid mass of the CO<sub>2</sub>-acceptor and the catalyst.

For the other species, the capture rate is zero so the source terms in these equations reduce to the form:

$$S_c = \frac{1 - \epsilon_b}{1 + \alpha \frac{\epsilon_p^{cap}}{\epsilon_p^{cat}}} (1 - \epsilon_p^{cat}) \rho_{cat} R_c \quad (11.54)$$

The corresponding temperature equation for the interstitial gas is given by (11.6). To define the alternative model versions the effective heat of reaction term  $S_T = \rho_{cat}(1 - \varepsilon) \sum_r (-\Delta H_{R,r}) r_r$  in the basic model heat balance is substituted with a modified source term  $S_T$  being different in the various model versions:

- For the heterogeneous one particle model, we see from (11.27) that the source term equals the conventional particle-bulk gas phase heat transfer term, defined by:

$$S_T = a_s h (T_s - T) \quad (11.55)$$

- For the two-particle heterogeneous model the source term in the bulk gas phase equation is given as the sum of the conventional particle-bulk phase heat transfer terms for both the catalyst and CO<sub>2</sub>-acceptor particles.

$$S_T = a_{s,cat} h (T - T_s^{cat}) + a_{s,cap} h (T_s^{cap} - T) \quad (11.56)$$

- For the pseudo-homogeneous model  $S_T$  denotes an effective heat of reaction term. The source term for the pseudo-homogeneous model consists of two effective heat of reaction terms, one for the reforming reactions and one for the CO<sub>2</sub>-acceptor kinetics:

$$S_T = \frac{1 - \varepsilon_b}{1 + \alpha \frac{\varepsilon_p^{cap}}{\varepsilon_p^{cat}}} (1 - \varepsilon_p^{cat}) \rho_{cat} \sum_r^3 (-\Delta H_{R,r}) r_r \tag{11.57}$$

$$\frac{1 - \varepsilon_b}{1 - \frac{\varepsilon_p^{cat}}{\varepsilon_p^{cat} + \varepsilon_p^{cap} \alpha}} (1 - \varepsilon_p^{cap}) \rho_{cap} (-\Delta H_{cap}) R_{cap} / M_{\omega_{cap}}$$

The cross sectional average momentum and continuity equations were solved for the velocity and pressure, respectively. The pseudo-homogeneous continuity equation was written as:

$$\varepsilon_b \frac{\partial \rho_g}{\partial t} + \frac{\partial}{\partial z} (\rho_g v_g^s) = -R_{cap} \tag{11.58}$$

The net acceptor reaction  $R_{cap}$  is included in the continuity equation since the CO<sub>2</sub> mass captured is removed from the interstitial gas phase. The pseudo-homogeneous continuity equation was used for the heterogeneous models as well due to numerical convergency problems. A truly heterogeneous continuity equation should not contain the sorption reaction rate but the sum of all the species mass balance interfacial mass transfer terms. The sorption rate should then be included in the pellet continuity equation instead.

The heterogeneous momentum equation for the interstitial gas phase is written like (11.2).

The impact of two different ways of designing the packed bed were investigated, one case with one particle having both the sorbent and the catalyst properties, and a second case with two different particle types each of them having only one property.

The species mass balance for the gas mixture in the pellet pores are written on the form (11.28). To define the alternative model versions the effective reaction term  $S_c = R_c \rho_{cat} (1 - \varepsilon)$  in the basic model species mass balance is substituted with a modified source term  $S_c$  being different in the various model versions:

- For the model with one type of particle the term  $S_{CO_2}$  consists of both the reforming reaction rates and the capture reaction rate. The net source term in the  $S_{CO_2}$ -balance yields:

$$S_{CO_2} = \frac{1 - \varepsilon_p}{1 + \alpha} \rho_{cat} R_{CO_2} - \frac{1 - \varepsilon_p}{1 - \frac{1}{1 + \alpha}} \rho_{cap} R_{CO_2, cap} \tag{11.59}$$

For the other species the capture rate is zero, hence the effective reaction rate in the pellet reduces to:

$$S_c = \frac{1 - \varepsilon_p}{1 + \alpha} \rho_{cat} R_c \tag{11.60}$$

- In the model with two types of particles, (11.28) is solved for both of them. The catalyst particles are solved for all components, with the reforming kinetics. Like the equations for the bulk transport, (11.28) is solved for four components and  $H_2O$  is calculated from the sum of the mass fractions (11.50). The source term is then defined by:

$$S_c = (1 - \varepsilon_{p,cat})\rho_{cat}R_c \quad (11.61)$$

In the sorbent particle, all components but  $CO_2$  are inert, hence only one component equation is solved. The source term is defined by:

$$S_{CO_2} = -(1 - \varepsilon_{p,cap})\rho_{cap}R_{CO_2,cap} \quad (11.62)$$

The pellet temperature equation considering the multiphase gas-solid mixture was expressed on the form (11.29).

To define the two model versions the effective heat of reaction term  $S_T = (1 - \varepsilon_{p,cat})\rho_{cat} \sum_r (-\Delta H_{R,r})r_r$  in the basic pellet model heat balance is substituted with a modified source term  $S_T$ :

- For the model with one type of particle the  $S_T$  term consists of both the reforming heat of reaction and the capture heat of reaction. The net source term  $S_T$  yields:

$$S_T = \frac{1 - \varepsilon_p}{1 + \alpha} \rho_{cat} \sum_r^3 (-\Delta H_{R,r})r_r + \frac{1 - \varepsilon_p}{1 - \frac{1}{1+\alpha}} \rho_{cap} r_{CO_2,cap} (-\Delta H_{r,cap}) \quad (11.63)$$

- In the model with two types of particles, (11.29) is solved for both of them. For the catalyst particles the source term is defined by:

$$S_T = (1 - \varepsilon_{p,cat})\rho_{cat} \sum_r^3 (-\Delta H_{R,r})r_r \quad (11.64)$$

For the acceptor particles the source term is defined by:

$$S_T = (1 - \varepsilon_{p,cap})\rho_{cap}(-\Delta H_{R,cap})r_{CO_2,cap} \quad (11.65)$$

For the bulk gas phase Dirichlet boundary conditions were specified at the reactor inlet for all the variables, and Neuman boundary condition were employed at the outlet for all the variables except for the pressure which is specified by a Dirichlet boundary condition.

A tube reactor with dimensions given in Table 11.9 was simulated. A high ratio between  $CO_2$ -acceptor and catalyst was used because the reforming kinetics are fast compared to the sorption rate. The reactor was filled with steam (97 mole%) and a small amount of hydrogen at the desired temperature, 848 K, at startup. The input to the reactor was methane and steam, in which the steam to methane ratio is set to 6. A high steam to carbon ratio is necessary

to reach high conversions. Physical properties of the reactor and materials are given in Table 11.9. A typical set of reactor conditions are presented in Table 11.10. The inlet mass flux, which is set to  $0.77 \text{ kg/m}^2\text{s}$  in the simulations, corresponds to a superficial gas velocity of  $0.3 \text{ m/s}$ .

**Table 11.9.** Physical parameters used in the simulations

Pellet diameter, $d_p$	0.005 (m)
Reactor tube inner diameter, $d_t$	0.1 (m)
Reactor length, $L$	4 (m)
Gas holdup, $\varepsilon$	0.5 (-)
Tortuosity, $\tau$	3 (-)
Acceptor density, $\rho_{cap,p}$	2500 ( $\text{kg/m}^3$ )
Catalyst density, $\rho_{cat,p}$	2300 ( $\text{kg/m}^3$ )
Pellet effective conductivity, $k_{p,g}$	0.2 ( $\text{W/mK}$ )
Solids heat capacity, $Cp_p$	1000 ( $\text{J/kg K}$ )

**Table 11.10.** Standard reactor conditions

Prescribed outlet pressure, $P_{out}$	10 (bar)
Inlet Temperature, $T_f$	848 (K)
Wall temperature $T_w$	848 (K)
$\dot{m}_f$	0.77 ( $\text{kg/m}^2 \text{ s}$ )
Particle mass ratio= $m_{cap}/m_{cat}$ , $\alpha$	4 (-)

A measure used for the performance of the reactor is the dry hydrogen mole fraction, which is the hydrogen mole fraction of the gas after steam is removed. The dry mole fractions are calculated as:

$$y_c^{dry} = \frac{y_c}{1 - y_{H_2O}} \quad (11.66)$$

The dry hydrogen mole fractions at  $t = 200 \text{ s}$  predicted by the pseudo homogeneous, one-particle heterogeneous and two-particle heterogeneous models are shown in Fig 11.8. No significant differences were observed in the reactor performances as simulated by the three models. The pseudo-homogeneous model gives appropriate results for the particle size used. The capture of  $\text{CO}_2$  is the limiting step of the process. With larger particles the process may change behavior as the intra-particle diffusion resistance increases.

The conversion in the reactor decreases with larger particles. The effect is greater for the two-particle model and occurs at smaller particle sizes. The reason for this is that for two particles the  $\text{CO}_2$  have to diffuse out of the catalyst particle, through the bulk phase, and into the sorbent and this becomes

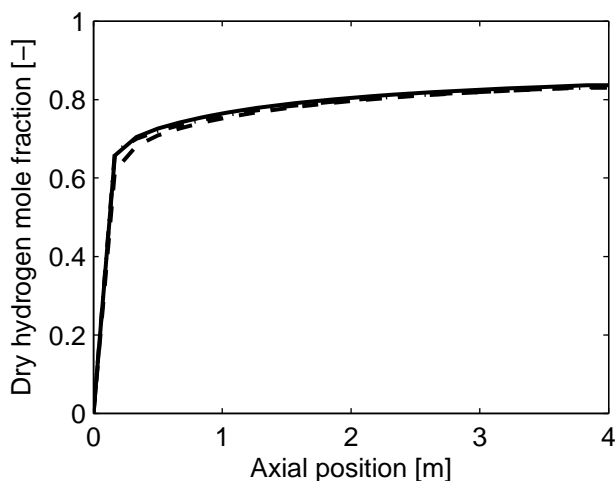


**Fig. 11.8.** Comparison in dry hydrogen mole fraction with pseudo-homogeneous model (—), one-particle heterogeneous model (· —) and two-particle heterogeneous model (— —) at  $t = 200$  s, standard conditions. Reprinted with permission from [11]. Copyright 2007 American Chemistry Society.

the limiting step. For one particle the diffusion to and from the bulk phase becomes the limiting step at larger particle diameters.

A tube reactor of 20 meters was simulated to show the performance of the reactor as a function of the length. The thermodynamic upper limit of hydrogen purity on dry basis at 10 bar total pressure and a temperature of 848 K with lithium zirconate as acceptor is 91 mole%. Very long reactors and low space velocities are required to reach the equilibrium composition due to the limitations of the  $\text{CO}_2$ -capture kinetics. A contour plot of the dry hydrogen fraction is shown in Fig 11.9. It is observed that a dry hydrogen mole fraction of 0.8 is reached just after 2 meters of the reactor, but to get close to the thermodynamical limit a significantly longer reactor is needed. At 10 meters a dry mole fraction of 0.88 is reached, but after ten more meters the dry hydrogen fraction has only increased by about 0.02 and equilibrium conversion is not reached. The main reason for this is the slow capture kinetics at low partial pressures of  $\text{CO}_2$ . A reaction order of 2 with respect to partial pressures of  $\text{CO}_2$  in (11.46) makes the process slow as it reaches the thermodynamical limitation.

The same tendency as with longer reactors is observed when lowering the gas velocity. Fig 11.10 shows dry hydrogen purity as function of axial position in a 4 meter long reactor at  $t = 200$  s, and the conversion is strongly dependent of the gas velocity. The  $\text{CO}_2$ -capture kinetics are dependent on the fractional conversion of the  $\text{CO}_2$ -acceptor. Thus, the sorption kinetics will be slower with time. This lead to lower conversion in the reactor as shown in Fig 11.11.

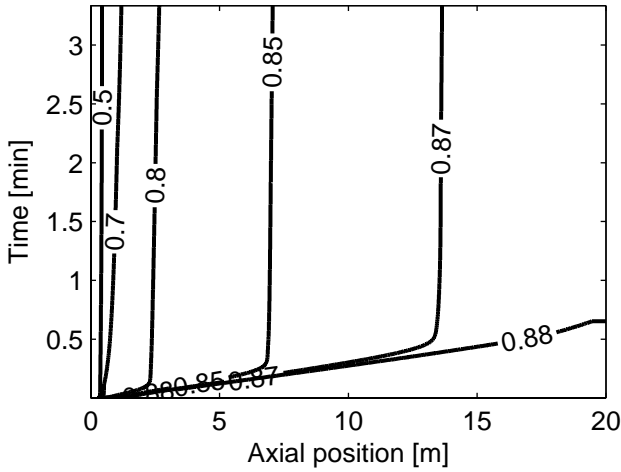


**Fig. 11.9.** Contour plots of the dry hydrogen mole fraction as function of time and axial position at standard conditions. Reprinted with permission from [11]. Copyright 2007 American Chemistry Society.

Fig 11.11 shows that a dry hydrogen mole fraction above 0.84 only is reached in the first minutes. After that the hydrogen content decreases, and after 50 minutes it is down to just above 70%, which is close to the thermodynamic limit for steam methane reforming without CO<sub>2</sub>-acceptor at these

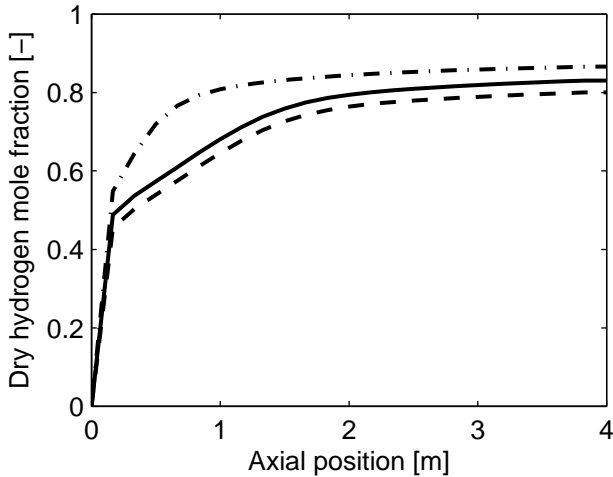


**Fig. 11.10.** Comparison in dry hydrogen mole fraction at different inlet superficial gas velocities.  $v_g^s = 0.6$  m/s (---), 0.3 m/s(—), 0.1 m/s (· —) at  $t = 200$  s. Reprinted with permission from [11]. Copyright 2007 American Chemistry Society.

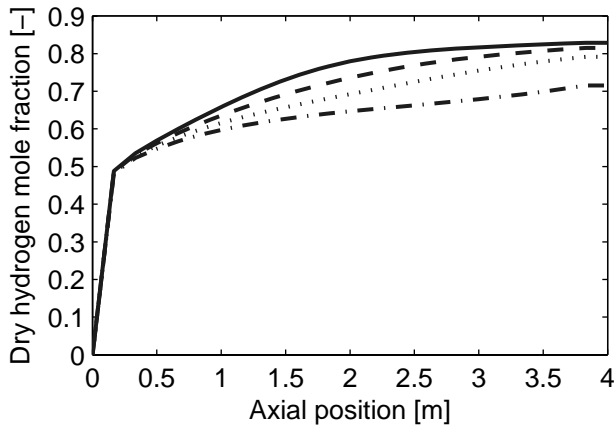


**Fig. 11.11.** Dry hydrogen mole fraction as a function of axial position at different times: (-) after 5 min, (- - -) after 20 min, (...) after 40 min, and (- · -) after 70 min). Reprinted with permission from [11]. Copyright 2007 American Chemistry Society.

conditions. The lower dry hydrogen mole fraction in the reactor is due to the decreasing capture kinetics. The decrease in kinetics is mainly because of the dependence of fractional conversion, but also because the temperature in the reactor is lowered. The reactor is heated with a constant temperature at the wall which is set equal to the inlet gas temperature. As observed in Fig 11.12 this is not sufficient to sustain the temperature in the reactor. This leads to

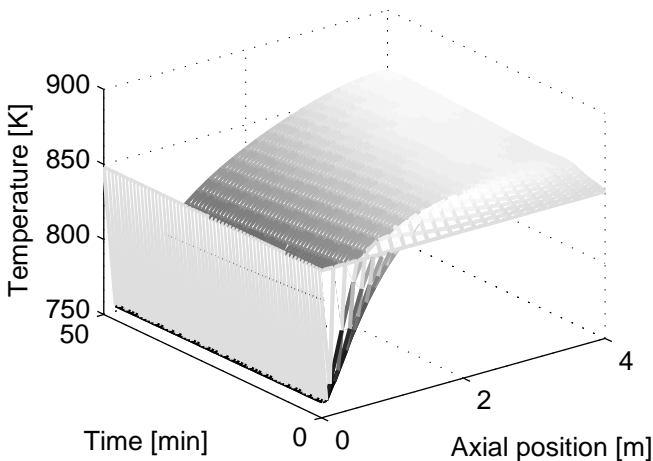


**Fig. 11.12.** Temperature in the reactor as function of time and axial position. Reprinted with permission from [11]. Copyright 2007 American Chemistry Society.

slower sorption kinetics and hence lower conversion. Dry hydrogen mole fractions over 90 % can be reached in SE-SMR with  $\text{Li}_2\text{ZrO}_3$  (s) as  $\text{CO}_2$ -acceptor, but require long reactors and low gas velocities. Simulations show that the kinetics of the  $\text{CO}_2$ -capture is the rate-determining step in the process at the given conditions and indicate that there are no significant intra-particle resistances. This means that a pseudo-homogeneous model with efficiency factor of one can be used instead of more rigorous heterogeneous models.

---

## References

1. De Groote AM, Froment GF (1995). Reactor Modeling and Simulation in Synthesis Gas Production. *Reviews in Chemical Engineering* 11(2):145-183.
2. Dybkjær I (1995) Tubular reforming and autothermal reforming of natural gas—an overview of available processes. *Fuel Processing Technology* 42:85-107
3. Froment GF, Bischoff KB (1990) *Chemical reactor analysis and design*. John Wiley & sons, New York, 2nd edition
4. Froment GF (2000) Production of synthesis gas by steam- and CO<sub>2</sub>-reforming of natural gas. *Journal of Molecular Catalysis A: Chemical* 163:147-156
5. Jakobsen HA, Lindborg H, Handeland V (2002) A numerical study of the interactions between viscous flow, transport and kinetics in fixed bed reactors. *Computers and Chemical Engineering*, 26:333-357
6. Knacke, O.; Kubaschewski, O.; Hesselmann, K.; Barin, I. *Thermochemical properties of inorganic substances*; Berlin: Springer Verlag, 1991.
7. Lindborg H, Eide V, Unger S, Henriksen ST, Jakobsen HA (2004) Parallelization and performance optimization of a dynamic PBE fixed bed reactor model for practical applications. *Computers and Chemical Engineering* 28: 1585-1597
8. Ochoa-Fernández E, Haugen G, Zhao T, Rønning M, Aartun I, Børresen B, Rytter E, Rønnekleiv M, Chen D (2006) Evaluation of potential CO<sub>2</sub> acceptors for application in hydrogen production by sorption enhanced steam reforming. *Am Chem Soc, Div Fuel Chem* 51:598-599
9. Olsvik O, Hansen R (1998) High Pressure Autothermal Reforming. *Studies in Surface Science and Catalysis* 119:875-882 Elsevier Science BV
10. Rostrup-Nielsen JR (1984) *Catalytic Steam Reforming*. Springer-Verlag, Berlin
11. Rusten HK, Ochoa-Fernández E, Chen D, Jakobsen HA (2007) Numerical investigation of sorption enhanced steam methane reforming using Li<sub>2</sub>ZrO<sub>3</sub> as CO<sub>2</sub>-acceptor. *Ind Eng Chem Res* 46(13):4435-4443
12. Trambouze P, Euzen J-P (2004) *Chemical Reactors: From Design to Operation*. Editions Technip, Paris ISBN 2-7108-0845-5
13. Vanden Bussche KM, Froment GF (1996). A Steady-State Kinetic Model for Methanol Synthesis and the Water Gas Shift Reaction on a Commercial *Cu/ZnO/Al<sub>2</sub>O<sub>3</sub>* Catalyst. *Journal of Catalysis* 161(156):1-10, Academic Press Inc

14. Xu J, Froment GF (1989). Methane Steam Reforming, methanation and Water-Gas Shift: I. Intrinsic Kinetics. *AIChE J* 35(1):88-96
15. Xu J, Froment GF (1989). Methane Steam Reforming, methanation and Water-Gas Shift: II. Diffusional Limitations and Reactor Simulations. *AIChE J* 35(1):97-103

---

## Numerical Solution Methods

In this chapter several numerical methods frequently employed in reactor engineering are introduced. To simulate the important phenomena determining single- and multiphase reactive flows, mathematical equations with different characteristics have to be solved. The relevant equations considered are the governing equations of single phase fluid mechanics, the multi-fluid model equations for multiphase flows, and the population balance equation.

Computers generally make the study of fluid flow easier, more effective and cheaper than using experimental analysis solely. Once the power of numerical simulations was recognized, the interest in numerical techniques increased dramatically and the work of developing numerical solution methods for the governing equations of fluid mechanics now constitutes a separate field of research known as *computational fluid dynamics* (CFD). In engineering practice, the basic conservation equations of fluid mechanics are normally solved by the Finite Difference- and the Finite Volume Methods. The CFD market is currently dominated by four codes CFX/ANSYS, FLUENT, PHOENICS and STAR-CD, that are all based on the finite volume method [201]. In this section, the elementary theory required for the effective use of this type of commercial codes to simulate single- and multiphase reactive flows in chemical reactors is outlined. However, this chapter is not primarily aimed at supporting those who have access to a commercial package, rather the theory is explored in greater depth so that the interested reader is able to start developing codes from scratch or to extend open source codes. Moreover, during the last decade the use of open source CFD codes (e.g., OPEN FOAM, CFDLIB, MFIX, etc) are continuously expanding both in academia and industry.

Other methods may be more appropriate for equations with particular mathematical characteristics or when more accurate, robust, stable and efficient solutions are required. The alternative spectral methods can be classified as sub-groups of the general approximation technique for solving differential equations named the *method of weighted residuals* (MWR) [51]. The relevant spectral methods are called the collocation -, Galerkin, Tau- and Least squares methods. These methods can also be applied to subdomains. The subdomain

methods are generally divided into two categories, named spectral element [34, 89], and finite element [75, 84, 35] methods. In the spectral element methods, the solution on each subdomain (or element) is approximated by a high order polynomial expansion. In the finite element methods, on the other hand, the solution on each element is normally approximated by a first order (low order) polynomial expansion [22]. A few commercial CFD codes based on the finite element method have entered the market (e.g., FIDAP<sup>1</sup>, COMSOL/FEMLAB<sup>2</sup>), but in general only research codes are developed based on the spectral methods.

A brief summary of the relevant methods are given in the introductory sections, then a more detailed description of the finite volume method is presented. The multi-fluid model is generally solved by methods that are representing extensions of the techniques used in single phase fluid dynamics. The main extensions are related to the treatment of the volume fraction-pressure-velocity coupling and the calculation of the phase distribution phenomena. The two-fluid- and multi-fluid models containing population balance models (PBEs) are solved adopting particular schemes for solving integro-differential equations.

## 12.1 Limitations of Numerical Methods

Due to the strong coupling and the non-linearity of the transport equations determining a reactor model, the usefulness of the numerical methods are conditional on being able to solve the set of PDE's accurately. This is difficult for most flows of engineering interest.

There are several reasons for observing differences between the computed results and experimental data. Errors arise from the modeling, discretization and simulation sub-tasks performed to produce numerical solutions. First, approximations are made formulating the governing differential equations. Secondly, approximations are made in the discretization process. Thirdly, the discretized non-linear equations are solved by iterative methods. Fourthly, the limiting machine accuracy and the approximate convergence criteria employed to stop the iterative process also introduce errors in the solution. The solution obtained in a numerical simulation is thus never exact. Hence, in order to validate the models, we have to rely on experimental data. The experimental data used for model validation is representing the reality, but the measurements

<sup>1</sup> FIDAP is a general purpose finite element code for simulating two-dimensional, axisymmetric, or three dimensional equations of viscous incompressible Newtonian or non-Newtonian fluid flow, including the effects of heat transfer.

<sup>2</sup> FEMLAB is an interactive FEM-based environment for modeling and solving scientific and engineering problems involving PDE's. This PDE Toolbox is a MATLAB toolbox which gives MATLAB the ability to solve 2D PDE's by the Finite Element Method, including meshing, preprocessing and post processing capabilities.

are also containing errors or uncertainties. These errors have to be taken into consideration comparing the experimental data and the model predictions.

A proper model validation procedure consists of a model verification part and a part where the model predictions are compared to experimental data [61]. The model verification may be performed by the *method of manufactured solutions*[147, 163]. The method of manufactured solutions consists in proposing an analytical solution, preferably one that is infinitely differentiable and not trivially reproduced by the numerical approximation, and the produced residuals are simply treated as source terms that produce the desired or prescribed solution. These source terms or residuals are referred to as the consistent forcing functions. This method can be used to confirm that there are no programming errors in the code and to monitor the truncation error behavior during the iteration process.

Visualization of numerical solutions is generally the most effective means of interpreting the huge amount of data produced by an unsteady reactor simulation. In many ways these movies resembles the informative weather forecasts on TV. However, there is the danger that an erroneous solution may look good but may not correspond to the actual boundary conditions, fluid properties, and so forth. Unexperienced users of commercial CFD codes must thus be careful. Nice color pictures and videos make a great impression but are of no value if they are not quantitatively or even qualitatively correct. Numerical results must therefore be examined critically before they are believed. In engineering practice, CFD simulations are thus commonly used as advanced learning aids because one may need to postulate expected trends and unknown physics, and estimate the numerical errors in a simulation to find realistic outcomes on which we base our process design decisions. Our physical understanding is then to a large extent improved by the work analyzing the actual flow problem to define a proper benchmark test for model validation, and not by the model predictions in itself solely.

## 12.2 Building Blocks of a Numerical Solution Method

The important ingredients of a numerical solution method are outlined in this section [141, 49, 201].

The basis for any numerical reactor performance simulation is a *mathematical model*, consisting of a set of ordinary differential-, partial differential- or integro-differential equations and initial and boundary conditions. An optimized solution method must then be designed for this particular set of equations.

The transport equations can be written in many different forms, depending on the *coordinate system* used. Generally, we may select the orthogonal curvilinear Cartesian-, cylindrical-, and spherical coordinate systems, or the non-orthogonal curvilinear coordinate systems, which may be fixed or moving. In reactor engineering we frequently apply the simple curvilinear

cylindrical – or Cartesian coordinates as most reactors have circular, quadratic or rectangular cross sectional geometries. Spherical coordinates are generally employed simulating the reactions and transport processes taking place in spherical catalyst pellets.

By *numerical grid* generation we define the discrete locations at which the variables are to be located. The numerical grid is essentially a discrete representation of the geometric domain on which the problem is solved. It divides the solution domain into a finite number of sub-domains named elements or grid volumes. For reactors with quadratic and rectangular cross sectional geometries structured (regular) grids are generally appropriate, but for the more complex geometries like cylindrical reactors unstructured grids may be required. The ill conditioned or singular points in origo at the center axis are difficult to deal with in an accurate manner employing a cylindrical coordinate representation. Similar problems may occur simulating the transport phenomena taking place in spherical catalyst pellets.

The selected mathematical model is represented by a *discretization method* for approximating the differential equations by a system of algebraic equations for the variables at some set of discrete locations in space and time. Many different approaches are used in reactor engineering<sup>3</sup>, but the most important of them are the simple finite difference methods (FDMs), the flux conservative finite volume methods (FVMs), and the accurate high order weighted residual methods (MWRs).

The *finite approximations* to be used in the discretization process have to be selected. In a finite difference method, approximations for the derivatives at the grid points have to be selected. In a finite volume method, one has to select the methods of approximating surface and volume integrals. In a weighted residual method, one has to select appropriate trial - and weighting functions. A compromise between simplicity, ease of implementation, accuracy and computational efficiency has to be made. For the low order finite difference- and finite volume methods, at least second order discretization schemes (both in time and space) are recommended. For the WRMs, high order approximations are normally employed.

The discretization process generally gives rise to a large system of non-linear algebraic equations, which has to be solved by an efficient and convergent *solution method*. For linear 1D problems discretized by the low order FDMs and FVMs the direct Tri-Diagonal-Matrix-Algorithm (TDMA) is frequently used [141, 202]. For multi-dimensional problems the *multigrid solvers* [20, 202, 207] and the Krylov sub-space methods like the *conjugate gradient solver*[70, 166] are quite efficient. The problems that are discretized by the low

<sup>3</sup> The high resolution lattice Boltzmann scheme, for example, is currently popular in the CFD research community performing LES and direct numerical simulations due to the simple implementation and high accuracy obtained, but this method is still under development and yet not suitable for multiphase reactive flows. The numerical scheme is constructed from and solves a kinetic theory representation of the actual flow. A good review can be found in Chen and Doolen [27].

order methods generally give rise to large systems of linear equations whose coefficient matrices are sparse<sup>4</sup>, thus a sparse matrix solver is required. Non-linear equations are solved by an iteration scheme and successive linearization of the equations.

A proper *convergence criterion* is important, from both the accuracy and efficiency points of view, because it is deciding when to stop the iterative process. Research codes are generally iterating until the machine accuracy is reached, whereas the commercial codes are less accurate as efficiency is commonly desired by the customers. In commercial CFD codes, a convergence criterion defined by the reduction of the normalized residual, as calculated from the initial guess variable values, by a factor of  $10^{-3}$  is frequently considered sufficient by contract research- and salespersons. However, for complex multiphase reactive flows this approach may easily lead to unphysical solutions.

## 12.3 Properties of Discretization Schemes

For most multiphase reactive flow problems, it is not possible to analyze all the operators in the complete solution method simultaneously. Instead the different operators of the method are analyzed separately one by one. The working hypothesis is that if the operators do not possess the desired properties solely, neither will the complete method. Unfortunately, the reverse is not necessarily true. In practical calculation we can only use a finite grid resolution, and the numerical results will only be physically realistic when the discretization schemes have certain fundamental properties. The usual numerical terminology employed in the CFD literature is outlined in this section [141, 202, 49].

A *consistent numerical scheme* produces a system of algebraic equations which can be shown to be equivalent to the original model equations as the grid spacing tends to zero. The *truncation error* represents the difference between the discretized equation and the exact one. For low order finite difference methods the error is usually estimated by replacing all the nodal values in the discrete approximation by a Taylor series expansion about a single point. As a result one recovers the original differential equation plus a remainder, which represents the truncation error.

A numerical solution method is said to be *stable* if the method does not magnify the errors that appear during the numerical solution process. This property is relevant as a consistent discretization scheme provides no guarantee that the solution of the discretized equation system will become an accurate solution of the differential equation in the limit of small step size. The stability of low order numerical schemes applied to idealized problems can be analyzed by the *von Neumann's method*. However, when solving relevant, non-linear and coupled reactor model equations with complex boundary

---

<sup>4</sup> A matrix which is  $n \times m$  with  $k$  non-zero entries is sparse if  $k \ll n \times m$ .

conditions, there are no methods available for stability analysis so we have to rely on experience and intuition.

A numerical method is *convergent* if the solution of the discretized equations tends to the exact solution of the differential equation as the grid spacing tends to zero. For simple problems convergence is frequently checked using numerical experiments repeating the calculation on a series of successively refined grids. If the method is stable and if all approximations used in the discretization process are consistent, we may experience that the solution does converge to a grid-independent solution. The overall order of the method can then be estimated from the convergence behavior of the error in the solution. For industrial multiphase reactive flows we generally do not have the computational resources available to perform numerical experiments repeating the calculation on a series of successively refined grids. In this case we are stuck and have to rely on experience, intuition, and experimental data.

In the cases where the transport equations to be solved express a conservation law, the numerical scheme should also both on a local and a global basis represent *conservative* properties. Conservative schemes are normally preferred. Numerical solution methods should also produce realistic results. In the absence of sources, the model equations require that the minimum and maximum values of the variables should be found on the boundaries of the domain. These conditions should be reflected by the numerical approximation as well. Only a few first order schemes guarantee the so-called *boundedness property*, but the higher-order schemes generally produce unbounded solutions. Closure models for the unresolved phenomena, which we cannot describe directly due to computational restrictions, should be designed to guarantee physically realistic solutions. Basically, this is a modeling issue, but models that are not *realizable* generally result in unphysical solutions or cause the numerical methods to diverge. In multiphase reactor models realizability is particularly important considering the interfacial coupling terms in the average multi-fluid models and the kernels in the population balance equation.

Numerical simulations of any non-linear reactive flow problem provide only approximate solutions. Errors in the solution might be introduced by mistakes when deriving the solution algorithm, in programming, and in setting up the boundary conditions. In addition, there are systematic errors caused by approximations in the model derivation, discretization, and convergence criteria [49]. An *accurate* solution is customarily said to be achieved when the overall truncation error in the solution is small and less than a prescribed threshold. From a Taylor series analysis this means that a fine grid resolution provides accurate solutions. The different errors may also cancel each other, so that sometimes a solution obtained on a coarse grid may agree better with the experiment than a solution on a finer grid, which by definition should be more accurate.

## 12.4 Initial and Boundary Condition Requirements

The formulation of initial- and boundary conditions for a given mathematical problem is of course basically a modeling issue, but models that are not solved with correct type, number and composition of conditions will result in unphysical solutions or cause the numerical methods to diverge. It is recognized that both the formulation of proper initial and/or boundary conditions for a given equation and the choice of an appropriate numerical method that can be used to solve a given PDE, are intimately tied to the mathematical character of the governing equations. The classification of a PDE problem may be difficult as the equation may be an initial value problem with respect to one variable and a boundary value problem in another. However, the overall classification of a PDE is generally governed by the behavior of the terms containing the highest order derivatives.

The elementary theory concerning the character of partial differential equations has developed mainly from the study of the simplified two dimensional, quasi-linear second order equation defined by [55, 174]:

$$a \frac{\partial^2 \psi}{\partial x^2} + b \frac{\partial^2 \psi}{\partial x \partial y} + c \frac{\partial^2 \psi}{\partial y^2} + d \frac{\partial \psi}{\partial x} + e \frac{\partial \psi}{\partial y} + f \psi + g = 0 \quad (12.1)$$

where  $a$ ,  $b$ ,  $c$ ,  $d$ ,  $e$ ,  $f$ , and  $g$  may be non-linear functions of the independent variables  $x$ ,  $y$ ,  $\psi$ ,  $\frac{\partial \psi}{\partial x}$  and  $\frac{\partial \psi}{\partial y}$ , but not of the second derivative of  $\psi$  (hence the term quasi-linear in the second derivative).

Based on mathematical analysis it has been found that the character of this equation changes depending upon the sign of the function<sup>5</sup>  $b^2 - 4ac$ :

$$\text{if } b^2 - 4ac \begin{cases} < 0 & \text{the equation is } \textit{elliptic} \\ = 0 & \text{the equation is } \textit{parabolic} \\ > 0 & \text{the equation is } \textit{hyperbolic} \end{cases} \quad (12.2)$$

A method for more advanced analysis of the eigenvalues of the governing equation matrix is examined by Flescher [53], Jiang [84], sect 4.7, Roache [158], among many others.

We generally distinguish between two principal categories of physical behavior, represented by equilibrium and marching problems [202]. The problems in the first category are governed by elliptic equations. Elliptic equations have no real characteristics. These problems, which are called *boundary-value problems*, require boundary conditions over the entire boundary of the calculation domain. An important feature of elliptic boundary value problems is that a disturbance in the interior of the solution changes the solution everywhere else. Many steady-state viscous fluid flow problems belong to this

<sup>5</sup> The names elliptic, parabolic, and hyperbolic that denote the different characters of the equation, have arisen by analogy with the conic sections of analytic geometry [208, 174].

group. Supersonic steady-state inviscid fluid flow problems may behave differently because the fluid velocity is greater than the propagation speed of disturbances and the pressure is unable to influence events in the upstream direction. Supersonic steady-state inviscid fluid flow problems are generally hyperbolic. Subsonic steady-state inviscid flows are normally elliptic because the pressure can propagate disturbances at the speed of sound, which is greater than the flow speed. The problems in the second category of physical behavior are governed by parabolic or hyperbolic equations. Most unsteady viscous fluid flow problems are parabolic, whereas many unsteady inviscid flow problems are hyperbolic with discontinuous solutions. It is noted that the viscous marching problems contain dissipation terms, whereas the inviscid marching problems contain no dissipation terms. Hyperbolic equations have two sets of real characteristics and arise in systems with finite propagation speeds. These problems, which are termed *initial-boundary-value problems*, may be classified as an initial value problem with respect to one variable and boundary value problems in the other variables. The spatial domain may or may not be bounded. If the spatial region is bounded, there may also be boundary conditions (one at each boundary). Otherwise, we have a pure *initial value problem*. An initial value problem requires only an initial condition at one boundary, that is within the domain of dependence of the solution. Thus, hyperbolic equations are always posed in domains that extend to infinity in a time like coordinate. Parabolic equations can be regarded as the limiting case of hyperbolic equations in which the propagation speed of the signals becomes infinite. Such equations are often obtained when it is assumed that the propagation speed (e.g., the speed of sound) is very large compared to any other velocity in the problem, so that the propagation speed may be set to infinity (e.g., the incompressible limit in gas dynamics). The initial and boundary conditions typically applied to parabolic equations are similar to those for hyperbolic problems with one important exception. Only one initial condition in time or space is necessary. This is related to the fact that there is only one set of characteristics. However, the spatial domain may be open or closed. In the case of a closed spatial domain, the boundary conditions are the same as those applied in the hyperbolic case. Recall, however, that for hyperbolic equations the signals propagate at a finite speed over a finite region. This property distinguishes hyperbolic equations from the two other types. Compressible flows at speeds close to and above the speed of sound exhibit shockwaves and it turns out that the inviscid flow equations are hyperbolic (i.e., not parabolic) at these speeds. The shockwave discontinuities are manifestations of the hyperbolic nature of such flows. Numerical solution algorithms for hyperbolic problems are designed for the need to allow for the possible existence of such discontinuities in the interior of the solution. In contrast algorithms designed for parabolic and elliptic problems assume infinite propagation speeds.

The mathematical character of the transport equations determining reactive flows are often too complicated to fit into the generalized form of the

quasi-linear second order PDE. For a reactive mixture the equations are often strongly coupled through the variable thermodynamic properties and transport coefficients, and may be elliptic, parabolic, hyperbolic or mixtures of all three types of equations, depending on the specific chemical process, flow conditions and geometry. For multiphase flows, additional complications are observed making the multi-fluid equations ill-posed under certain conditions, as mentioned in chap 3.5.

## 12.5 Discretization Approaches

In this section an outline of a selection of discretization methods frequently used in chemical reactor engineering is given.

### 12.5.1 The Finite Difference Method

The finite difference method is the oldest method for numerical solution of PDE's, presumably introduced by Euler in the 18th century [71, 49, 174, 167]. It is a convenient method to use for simple geometries.

The starting point for the FDM discretization is the transport equation in differential form. The first step in obtaining a numerical solution is to discretize the geometric domain by defining a numerical grid. The domain of interest is replaced by a set of discrete points. In FDMs the grid is normally structured. At each grid point, the differential equation is approximated by replacing the partial derivatives by approximations in terms of the nodal values of the functions. On staggered grids, interpolation is used to obtain variable values that are required at locations other than grid nodes. The result is one algebraic equation per grid node, in which the variable value at that and a few neighboring nodes appear as unknowns.

Taylor series expansions can be used to obtain approximations to the first and second order derivatives of the variables with respect to the coordinates. When necessary, these methods are used to obtain variable values at locations other than grid nodes (interpolation). The Taylor series expansion can be defined by:

$$\psi(z \pm \Delta z) \approx \psi(z) \pm \Delta z \left. \frac{\partial \psi}{\partial z} \right|_z + \frac{(\Delta z)^2}{2!} \left. \frac{\partial^2 \psi}{\partial z^2} \right|_z \pm \dots + \frac{(\Delta z)^k}{k!} \left. \frac{\partial^k \psi}{\partial z^k} \right|_z \quad (12.3)$$

By forming linear combinations of the values of the function at various grid points  $z$ ,  $z \pm \Delta z$ ,  $z \pm 2\Delta z$ , and so on, we can obtain approximations to the derivatives.

The truncation error is usually proportional to a power of the grid spacing  $\Delta x_i$  and/or the time step  $\Delta t$ . If the most important error term is proportional to  $(\Delta x_i)^n$  or  $(\Delta t)^n$  we call the method an  $n$ th-order approximation, often simply indicated by  $O(\Delta x_i^n)$  or  $O(\Delta t^n)$ , respectively.  $n > 0$  is required to

obtain an accurate solution as the grid spacing tends to zero. Ideally, all terms should be discretized with approximations of the same order of accuracy. However, certain terms may be dominant in a particular flow and it may be reasonable to treat them with more accuracy than the others. The order of the approximation tell us the rate at which the error decreases as the mesh spacing is reduced. It gives no information about the error on a single grid.

The simplest approximations for the first derivative are given below.

*Forward differences, first order explicit Euler method:*

$$\left. \frac{\partial \psi}{\partial z} \right|_z \approx \frac{\psi(z + \Delta z) - \psi(z)}{\Delta z} + O(\Delta z) \quad (12.4)$$

*Backward differences, first order implicit Euler method:*

$$\left. \frac{\partial \psi}{\partial z} \right|_z \approx \frac{\psi(z) - \psi(z - \Delta z)}{\Delta z} + O(\Delta z) \quad (12.5)$$

*Central differences, second order:*

$$\left. \frac{\partial \psi}{\partial z} \right|_z \approx \frac{\psi(z + \Delta z) - \psi(z - \Delta z)}{2\Delta z} + O(\Delta z^2) \quad (12.6)$$

The simplest approximation for the second derivative can be obtained in a similar manner.

*Central differences, second order:*

$$\left. \frac{\partial^2 \psi}{\partial z^2} \right|_z \approx \frac{\psi(z + \Delta z) - 2\psi(z) + \psi(z - \Delta z)}{(\Delta z)^2} + O(\Delta z^2) \quad (12.7)$$

Any approximation of the derivative of a function in terms of values of that function at a discrete set of points is called a *finite difference approximation*. There are several ways of constructing such approximations, the Taylor series approach illustrated above is frequently used in numerical analysis because it supplies the added benefit that information about the error is obtained. Another method uses interpolation to provide estimates of derivatives. In particular, we use interpolation to fit a smooth curve through the data points and differentiate the resulting curve to get the desired result. A collection of low order approximations (i.e., first to fourth order polynomial approximations) of first and second order derivative terms can be found in textbooks like [49, 50, 167].

At boundary nodes where the variable values are given by Dirichlet conditions, no model equations are solved. When the boundary condition involve derivatives as defined by Neumann conditions, the boundary condition must be discretized to provide the required equation. The governing equation is thus solved on internal points only, not on the boundaries. Mixed or Robin conditions can also be used. These conditions consist of linear combinations of the variable value and its gradient at the boundary. A common problem does arise when higher order approximations of the derivatives are used at

interior nodes in the vicinity of the boundaries, because these approximations may demand data at points beyond the boundary. It may then be necessary to use one-sided (i.e., upwind, and sometimes even down-wind) or lower order approximations for the derivatives at points close to the boundaries.

For many problems the solution changes rapidly in some parts of the solution domain and more gradually in others, hence it is required to use a grid in which the discretization points are more concentrated where the derivatives of the function are larger to distribute the error uniformly over the domain. On such non-uniform grids it is more difficult to construct finite difference approximations to derivatives and the errors tend to be larger. An introduction to finite difference approximations on non-uniform grids can for example be found in books like [49, 50, 71].

The main disadvantages of FDMs are low accuracy, low convergency rates and that the conservation is not enforced unless special care is taken. The restriction to simple geometries is a significant disadvantages in complex flows.

### 12.5.2 The Finite Volume Method

The finite volume method has become a very popular method of deriving discretizations of partial differential equations because these schemes preserve the conservation properties of the differential equation better than the schemes based on the finite difference method.

The FVM uses the integral form of the conservation or transport equations as its starting point. The solution domain is subdivided into a number of continuous grid of cell volumes, and the equations are applied to each cell volume. At the centroid of each cell volume lies a computational node at which the values are to be calculated. *Interpolation* is used to express variable values at the cell surface in terms of the nodal (cell volume-center) values. Surface and volume integrals are approximated using a suitable *quadrature formula*. As a result, one obtains an algebraic equation for each cell volume, in which a few of the neighboring nodal values appear. The FVM can accommodate any type of grid, so it is suitable for complex geometries. The method is conservative by construction, so long as the surface integrals which represent convective and diffusive fluxes are the same for the cell volumes sharing the boundary.

The main disadvantages of FVMs are low accuracy and low convergency rates. Compared to FDMs, the main disadvantage of the FVM is that methods of order higher than second are more difficult to develop in 3D because the FVM approach requires two levels of approximation considering the interpolation and integration processes. The FDM only requires approximations of the derivatives and interpolation.

### 12.5.3 The Method of Weighted Residuals

In some sense the method of weighted residuals (MWR) uses the integral form of the conservation or transport equations as its starting point. In particular,

the MWR is a general concept for minimizing a residual defined based on the integral form of the governing equations [51, 89].

The key elements of the MWR are the *expansion functions* (also called the trail-, basis- or approximating functions) and the *weight functions* (also known as test functions). The trial functions are used as the basis functions for a truncated series expansion of the solution, which, when substituted into the differential equation, produces the residual. The test functions are used to ensure that the differential equation is satisfied as closely as possible by the truncated series expansion. This is achieved by minimizing the residual, i.e., the error in the differential equation produced by using the truncated expansion instead of the exact solution, with respect to a suitable norm. An equivalent requirement is that the residual satisfy a suitable orthogonality condition with respect to each of the test functions.

The choice of test function distinguishes between the most commonly used spectral schemes, the Galerkin, tau, collocation, and least squares versions [22, 51, 84, 89] (see also [60, 132, 54, 17]). In the Galerkin approach, the test functions are the same as the trail functions, whereas in the collocation approach the test functions are translated Dirac delta functions centered at special, so-called collocation points. The collocation approach thus requires that the differential equation is satisfied exactly at the collocation points. Spectral tau methods are close to Galerkin methods, but they differ in the treatment of boundary conditions.

For particular problems, it is possible to formulate spectral methods starting out from variational principles [84, 89]. The variational methods provide a means to obtain approximate solutions to differential equations based on minimizing the functional of the equation. A variational method that is based on the principle of minimum potential energy, is known as the *Rayleigh-Ritz method* or just the Ritz method. Many attempts have been made to formulate variational principles patterned after Hamilton's principle (i.e., the *principle of least action*), which governs the equations of mechanics and dynamics of discrete particles as outlined in sect 2. The form of the Lagrangian is thus common to many of the variational principles and given by the kinetic energy minus the potential energy. However, the variational method cannot always be applied because there are no variational principle that can be employed for many problems.

The Galerkin method, on the other hand, represents a sub-class of the method of residuals and is always applicable because it does not depend on the existence of a variational principle. Hence, in some cases both the Rayleigh-Ritz method and the Galerkin method are applicable for the same problem. In these situations the Galerkin method is thus associated with the *variational principle*. In one view, the Galerkin methods may thus be interpreted as either variational principles or regular methods of weighted residual. To distinguish the two methods, a system of equations is said to be self-adjoint when we can formulate a variational principle for the corresponding problem. Because the Rayleigh-Ritz method is applicable only for equations with self-adjoint

operators, the Galerkin method is commonly considered a more universal approach to construction of spectral methods. The variational and Galerkin methods give identical results. However, the self-adjointness can be destroyed by combining the equations or by improper non-dimensionalization. There may be several ways to apply the Galerkin method, but only one of which corresponds to the variational methods. There is always a Galerkin method that corresponds to the variational method, but the reverse is not true.

*Orthogonal collocation* in the chemical engineering literature refers to the family of collocation methods with discretization grids associated to Gaussian quadrature methods [34, 204]. Spectral collocation methods for partial differential equations with an arbitrary distribution of collocation points are sometimes termed *pseudospectral* methods [22].

In one view the choice of trial functions is one of the features which distinguishes the spectral methods (SMs) from the spectral element Methods (SEMs). The finite element methods (FEMs) can thus be regarded as SEMs with linear expansion- and weight functions. The trial functions for spectral methods are infinitely differentiable global functions. In the case of spectral element methods, the domain is divided into small elements, and the trial function is specified in each element. The trial and test functions are thus local in character, and well suited for handling complex geometries.

It has been shown that several spectral-, spectral element-, finite volume-, and finite difference methods are related [51, 102, 89]. The comparison of MWR-, finite difference- and finite volume calculations may in some cases be best revealed through a spectral element method because in this framework the calculation domain is divided into small elements so the trial and test functions are local in character. The finite difference- and finite volume trial functions are likewise local [89]. With particular trial functions certain SEMs may be regarded as equivalent to finite difference methods. In other cases certain spectral element methods may be regarded as equivalent to particular finite volume methods [49, 141]. However, no formal mathematical generalization of these methods has been defined yet. Nevertheless, in engineering analysis and notation such a heuristic generalization may sometimes be useful, in which the FDMs and FVMs may be considered members of a broader class of methods called spectral- or spectral element methods.

The general method of weighted residuals is outlined next in terms of a simple one dimensional model example [51, 102, 89].

Let a linear differential operator  $D$  act on a function  $\psi$  to produce a function  $p$ .  $\psi(z)$  is the function sought.

$$D(\psi(z)) = p(z) \quad (12.8)$$

in  $\Omega$  which is the domain of the region governed by  $\psi(z)$ .

The solution is required to satisfy a set of boundary conditions:

$$G(\psi(z)) = 0 \quad (12.9)$$

on  $\Gamma$  representing the boundary of  $\Omega$ .

In the general method of residuals we desire to approximate  $\psi(z)$  by a function  $\tilde{\psi}(z; a_1, a_2, a_3, \dots, a_n)$ , which is a linear combination of the basis functions chosen from a linearly independent set. That is, the approximation of the solution is written as [62]:

$$\psi(z) \approx \tilde{\psi}(z; a_1, a_2, a_3, \dots, a_n) = \sum_{i=1}^n a_i \varphi_i(z) \tag{12.10}$$

in which  $n$  is the number of basis functions used.

The  $\tilde{\psi}(z; a_1, a_2, a_3, \dots, a_n)$  function has one or more unknown parameters,  $a_i$ , that are constant and satisfies exactly the boundary conditions.

Then, when substituted into the differential operator  $D$ , the result of the operations is not, in general,  $p(z)$ . Hence a residual error will exist:

$$R(z; a_1, a_2, a_3, \dots, a_n) = D(\tilde{\psi}(z; a_1, a_2, a_3, \dots, a_n)) - p(z) \neq 0 \tag{12.11}$$

The notation in the MWR is to force the residual to zero in some average sense over the domain. That is, the MWR requires that the parameters  $a_i$  are determined satisfying the integral:

$$\int_{\Omega} R(z; a_1, a_2, \dots, a_n) W_i(z) d\Omega = 0 \tag{12.12}$$

where  $W_i(z)$  are the  $n$  arbitrary weighting functions.

The number of weighting functions  $W_i(z)$  is exactly equal to the number of unknown constants  $a_i$  in  $\tilde{\psi}(z; a_1, a_2, a_3, \dots, a_n)$ . The result is a set of  $n$  algebraic equations for the unknown constants  $a_i$ .

There are several sub-groups of MWR methods, according to the particular choices for the weighting function  $W_i(z)$  employed. The performance of the resulting MWR is to a certain extent tied to the properties of the resulting coefficient matrix. To enable an efficient solution process it is desired that the coefficient matrix is symmetric, positive definite and characterized by a small condition number. At the same time the work needed to assemble the coefficient values should be minimized.

The most popular weighted residual methods are:

- collocation method

In this method, the weighting functions  $W_i(z)$  are taken from the family of Dirac  $\delta$  functions in the domain. That is,  $W_i(z) = \delta(z - z_i)$ . The Dirac  $\delta$  functions are defined such that:

$$\int_a^b \delta(z - z_i) dz = 1 \quad \text{for } z = z_i \tag{12.13}$$

$$\int_a^b \delta(z - z_i) dz = 0 \quad \text{for } z \neq z_i \tag{12.14}$$

Substitution of this choice of  $W_i(z)$  gives:

$$\int_{\Omega} R(z; a_1, a_2, \dots, a_n) \delta(x - x_i) d\Omega = 0 \quad \text{for } i = 1, 2, \dots, n \quad (12.15)$$

which when evaluated at  $n$  collocation points  $z_1, z_2, \dots, z_n$  results in  $n$  algebraic equations in  $n$  unknowns:

$$R(z_1; a_1, a_2, \dots, a_n) = 0 \quad (12.16)$$

$$R(z_2; a_1, a_2, \dots, a_n) = 0 \quad (12.17)$$

.

.

.

$$R(z_n; a_1, a_2, \dots, a_n) = 0 \quad (12.18)$$

Hence the integration of the weighted residual statement results in the forcing of the residuals to zero at specific points in the domain.

The collocation methods can be shown to give rise to symmetric, positive definite coefficient matrices that is characterized with a acceptable condition number for diffusion dominated problems or other higher order even derivative terms. For convection dominated problems the collocation method produces non-symmetric coefficient matrices that are not positive definite and characterized with a large condition number. This method is thus frequently employed in reactor engineering solving problems containing second order derivatives of smooth functions. A typical example is the pellet equations in heterogeneous dispersion models.

The work needed to assemble the coefficient values is generally minimized when the collocation points are chosen freely. However, better convergence performance is normally achieved by the orthogonal collocation methods because a more optimal distribution of the collocation points is achieved. In the orthogonal collocation methods (i.e., sometimes named by the synonym pseudospectral methods) the discretization points are chosen as the zeros in certain orthogonal polynomials. Because pseudospectral methods are generally implemented via orthogonal collocation, the pseudospectral and orthogonal collocation are essentially interchangeable<sup>6</sup>. Referring to

---

<sup>6</sup> In the historical survey of the spectral methods given by Canuto et al [22], it was assumed that Lanczos [101] was the first to reveal that a proper choice of trial functions and distribution of collocation points is crucial to the accuracy of the solution of ordinary differential equations. Villadsen and Stewart [203] developed this method for boundary value problems. The earliest applications of the spectral collocation method to partial differential equations were made for spatially periodic problems by Kreiss and Olinger [94] and Orszag [139]. However, at that time Kreiss and Olinger [94] termed the novel spectral method for the *Fourier method* while Orszag [139] termed it a *pseudospectral method*.

the orthogonal collocation method, researchers in some communities use the term pseudospectral method [60, 54, 1] while in the chemical engineering literature the term orthogonal collocation is normally used [204, 203].

- Least Squares method

The method of Least Squares (LS) requires that the integral  $I$  of the Square of the residuals  $R(z)$  is minimized:

$$I = \int_{\Omega} [R(z; a_1, a_2, \dots, a_n)]^2 d\Omega \quad (12.19)$$

In order to achieve a minimum of this scalar function, the derivatives of  $I$  with respect to all the unknown parameters must be zero. That is:

$$\begin{aligned} \frac{\partial I}{\partial a_i} &= \frac{\partial}{\partial a_i} \int_{\Omega} [R(z; a_1, a_2, \dots, a_n)]^2 d\Omega = \int_{\Omega} \frac{\partial}{\partial a_i} [R(z; a_1, a_2, \dots, a_n)]^2 d\Omega \\ &= 2 \int_{\Omega} R(z; a_1, a_2, \dots, a_n) \frac{\partial}{\partial a_i} R(z; a_1, a_2, \dots, a_n) d\Omega = 0 \end{aligned} \quad (12.20)$$

Compared to (12.12), the weight functions are found to be:

$$W_i(z) = 2 \frac{\partial}{\partial a_i} R(z; a_1, a_2, \dots, a_n), \quad i = 1, 2, \dots, n \quad (12.21)$$

The constant pre-factor 2 can be dropped, since it cancels out in the equation. Therefore, the weight functions for the Least Squares Method are just the derivatives of the residual with respect to the unknown constants:

$$W_i(z) = \frac{\partial R(z; a_1, a_2, \dots, a_n)}{\partial a_i}, \quad i = 1, 2, \dots, n \quad (12.22)$$

The determination of  $a_i$  is achieved from the solution of the general MWR integral statement (12.12):

$$\int_{\Omega} R(z; a_1, a_2, \dots, a_n) \frac{\partial R(z; a_1, a_2, \dots, a_n)}{\partial a_i} d\Omega = 0 \quad (12.23)$$

The Least squares method is generally applied to problems containing first order derivatives. A differential equation containing second order derivatives is thus re-written as a set of two equations containing only first order derivatives.

The LSMs can be shown to give rise to symmetric, positive definite coefficient matrices that are characterized with a acceptable condition number for convection dominated problems or other higher order odd derivative terms. For diffusion (even derivatives) dominated problems the LSMs still

produce symmetric and positive definite coefficient matrices but these are now generally characterized with large condition numbers. In particular, the errors in these LSM solutions grow faster with the condition number than the error induced by the other MWR methods.

The LSMs are thus generally best suited solving convection dominated problems. However, in reactor engineering a few successful attempts have been made applying this method to solve convection-diffusion problems, by reformulating the second order derivatives into a set of two first order derivative equations.

This method has been employed by Dorao [38] and Dorao and Jakobsen [39, 40, 41, 42, 43, 44] solving the population balance equation and single phase flow problems.

- Galerkin method

This method may be viewed as a modification of the Least Squares Method. In that is the case, rather than using the derivatives of the residual with respect to the unknown  $a_i$ , the derivative of the approximating function is used. That is, since the approximation of the  $\psi(z)$  function is (12.10), then the weight functions are:

$$W_i(z) = \frac{\partial \tilde{\psi}(z; a_1, a_2, \dots, a_n)}{\partial a_i}, \quad i = 1, 2, \dots, n \quad (12.24)$$

We note that these weights are identical to the original basis functions appearing in (12.10):

$$W_i(z) = \frac{\partial \tilde{\psi}}{\partial a_i} = \varphi_i(z), \quad i = 1, 2, \dots, n \quad (12.25)$$

The Galerkin methods have many of the same characteristics as the collocation methods because both of them give rise to symmetric, positive definite coefficient matrices that are characterized with a acceptable condition number for diffusion dominated problems. An important advantage is that the basis functions used in the Galerkin methods satisfy the boundary conditions (and sometimes other useful properties too). However, it may not always be feasible to require that the basis functions also satisfy the boundary conditions. The way around this problem is to derive formulas for the boundary coefficients requiring that the solution satisfies the boundary conditions instead of the PDEs. This method was invented by Cornelius Lanczos [101] in 1938 and is called the (Lanczos) tau method <sup>7</sup>. For convection dominated problems the Galerkin methods produce non-symmetric coefficient matrices that are not positive definite and characterized with a large condition number. Several upwind-like modifications of the original Galerkin method have been introduced (e.g., the Petrov-Galerkin method [35, 84]) to overcome this limitation. Nevertheless, this

---

<sup>7</sup> The (Lanczos) method was named the *tau* method because Lanczos used the letter  $\tau$  to represent the error.

method has rarely been employed in reactor engineering even for solving problems containing second order derivatives of smooth functions.

Fernandino et al [48] did study the use of Galerkin methods for solving typical convection-diffusion reaction engineering models expressed in spherical and cylindrical coordinate systems containing singular points at the origo. In particular, cylindrical and spherical coordinates can lead to a degeneracy in the global system of equations. This difficulty was removed by incorporating the factor  $r$  into the weight function which is introduced naturally by using Jacobi polynomials  $P_k^{\alpha,\beta}$  with  $\alpha = 0$  and  $\beta = 1, 2$ . In this way, an unified framework is obtained for treating the typical reactor geometries.

- Method of Moments

In this method, the weight functions are chosen from the family of polynomials. That is:

$$W_i(z) = z_i \quad i = 0, 1, 2, \dots, n - 1 \quad (12.26)$$

In the event that the basis functions for the approximation, the  $\varphi$ 's, were chosen as polynomials, then the method of moments may be identical to the Galerkin method.

In the finite element and spectral element methods the entire domain  $\Omega$  is divided into sub-domains or in a number of elements. Piecewise continuous trail (expansion) functions are defined for each element instead of using only one global trail function. Different continuity requirements for connecting the elements can be used.

### 12.5.4 The Finite Element Method

The finite element method originated in the 1950s from the needs for solving complex elasticity, structural analysis problems in civil engineering and aeronautical engineering. The standard nomenclature thus comes from the mechanics of solids, the field in which the method was first developed. The early development of the finite element method in these fields was based on the finite element form of the Rayleigh-Ritz method [84, 89, 35]. This method is based on an energy principle (i.e., the minimum total potential energy principle), and in these particular applications this concept provides a general, intuitive and physical basis that has a great appeal to structural engineers.

In the early 1970s, the standard finite element approximations were based upon the Galerkin formulation of the method of weighted residuals. This technique did emerge as a powerful numerical procedure for solving elliptic boundary value problems [102, 75, 53, 84, 50, 89, 17, 35]. The Galerkin finite element methods are preferable for solving Laplace-, Poisson- and diffusion equations because they do not require that a variational principle exists for the problem to be analyzed. However, the power of the method is still best utilized in systems for which a variational principle exists, and it

is the preferred method for such problems. In reactor modeling, the balance equations frequently used for analyzing the heat and species mass transport phenomena in porous catalyst pellets constitute an elliptic boundary value problem, provided there are no fluid convection through the pores of the particles. However, most of the classical reactor models consist of convection dominated species mass balances and temperature equations. For self-adjoint problems it is generally possible to define an energy norm of the Galerkin method that result in symmetric coefficient matrices. With regard to simulating convection-dominated transport phenomena by the finite element method, severe problems frequently occur due to the presence of non-symmetric convection operators. Solutions to convection dominated transport problems by the Galerkin method are thus often corrupted by spurious oscillations. These can only be removed by severe grid and time refinements. A remedy is to exchange the standard Galerkin formulation with alternative formulations, called stabilization techniques, avoiding these oscillations without requiring mesh or time step refinement. In recent years, generalized finite element methods of the Petrov-Galerkin type have been designed to produce stable and accurate results in the presence of highly convective effects. Adequate FEMs for solving convection-diffusion transport equations have thus been established and are to some extent used to simulate the performance of chemical reactor processes. However, very few single- and multiphase reactive flow models have been solved by the FEM yet.

The finite element method is similar to the finite volume method in that it describes the behavior of a continuum using a subdivision of the continuum domain into smaller subregions. In the FEM nomenclature each subregion of the domain is referred to as an *element* and the process of subdividing a domain into a finite number of simple elements is referred to as *discretization*. In 1D line element can be used. In 2D the elements are usually triangles or quadrilaterals, while in 3D tetrahedrals or hexahedrals are most often used.

The basic idea of the FEM is piecewise approximation, in which the solution of a complex problem is approximated by piecewise linear functions in each element. The function used to approximate the solution in each element is called the interpolation function, basis function, shape function or approximating function, depending upon the discipline in which the method is being applied. The overall accuracy of the finite element solution depends on the choice of the approximating function. Polynomial type of interpolation functions are most widely used in the finite element method literature. In selecting the order of the polynomials, a compromise has to be made between accuracy and computational effort. A higher order polynomial usually approximates an arbitrary function better, hence it may be desirable to use a higher order polynomial. However, a low order polynomial simplifies the computations. The simplest method of approximation is to assume a linear distribution of the unknown function within the element domain. Besides, the accuracy is normally low when using only a few large elements, more accurate solutions are generally obtained with a large number of small elements.

Computational costs, on the other hand, may increase significantly as the number of elements in a model increases. Thus, it may be more practical to use fewer elements, and ones that have a higher order of interpolation.

To illustrate the finite element method, the basic steps in the formulation of the standard Galerkin finite element method for solving a one-dimensional Poisson equation is outlined in the following.

The governing equations with boundary conditions are called the *strong form* of the problem. Let the strong form be defined by:

$$\frac{d^2\psi(z)}{dz^2} = p_0 \quad (12.27)$$

$$\psi(0) = 0 \quad (12.28)$$

$$\left. \frac{d\psi}{dz} \right|_{z=L} = 0 \quad (12.29)$$

The derivation of the governing FEM discretization equations is quite similar to the derivation of the spectral methods presented in the previous section.

The first task is to reformulate the problem into the *weak form*. The weak form is a variational statement of the problem in which we integrate against a weighting function. This has the effect of relaxing the problem, meaning that instead of finding an exact solution everywhere we are requiring a solution that satisfies the strong form in an average manner over the domain.

Following the MWR framework, the residual function can be defined as:

$$R(z) = \frac{d^2\tilde{\psi}(z)}{dz^2} - p_0 \quad (12.30)$$

Multiplying the residual function with a weighting function  $W(z)$ , we get the weak form:

$$\int_0^L R(z)W(z)dz = 0 \quad (12.31)$$

In the spectral form of the method we approximate  $\psi(z)$  by a function  $\tilde{\psi}(z; a_1, a_2, a_3, \dots, a_n)$ , representing a linear combination of the basis functions:

$$\psi(z) \approx \tilde{\psi}(z; a_1, a_2, a_3, \dots, a_n) = \sum_{i=1}^n a_i \varphi_i(z) \quad (12.32)$$

The  $a_i$  are constants and  $\varphi_i$  are linearly independent basis functions of  $z$ , which are chosen to satisfy the boundary conditions and  $n$  is the total number of basis functions used.

In the Galerkin method, the weights  $W_i(z)$  are taken to be the basis functions  $\varphi_i(z)$  used in the approximate solution of (12.32). In this case, the continuous residual function (12.30) can be approximated by:

$$\tilde{R}(z; a_1, a_2, a_3, \dots, a_n) = \frac{d^2\tilde{\psi}(z; a_1, a_2, a_3, \dots, a_n)}{dz^2} - p_0 \quad (12.33)$$

Thus, in the Galerkin method the weak form (12.31) becomes <sup>8</sup>:

$$\int_0^L \tilde{R}(z; a_1, a_2, \dots, a_n) \varphi_i(z) dz = 0, \quad i = 1, 2, \dots, n. \quad (12.34)$$

Equation (12.34) represents  $n$  simultaneous equations in the  $n$  unknowns  $a_1, a_2, \dots, a_n$ . Thus, the solution of (12.34) gives the approximation solution through (12.32).

Now we substitute the approximate solution (12.32) into the approximate weak form (12.34), the result is:

$$\int_0^L \left( \frac{d^2 \tilde{\psi}(z; a_1, a_2, a_3, \dots, a_n)}{dz^2} - p_0 \right) \varphi_j dz = \sum_{i=1}^n a_i \int_0^L \frac{d^2 \varphi_i}{dz^2} \varphi_j dz - \int_0^L p_0 \varphi_j dz \quad (12.35)$$

We can then use integration by parts to simplify the first term on the LHS of the equation:

$$\int_0^L \frac{d^2 \varphi_i}{dz^2} \varphi_j dz = \left. \frac{d\varphi_i}{dz} \varphi_j \right|_{z=0}^{z=L} - \int_0^L \frac{d\varphi_i}{dz} \frac{d\varphi_j}{dz} dz = - \int_0^L \frac{d\varphi_i}{dz} \frac{d\varphi_j}{dz} dz \quad (12.36)$$

where we have invoked the conditions that the basis functions and the first derivative of the basis functions vanish at the respective global boundaries. Hence, it is required that  $\varphi_j(0) = 0$  and  $\left. \frac{d\varphi_i}{dz} \right|_{z=L} = 0$ .

The weak form for the spectral method becomes:

$$- \sum_{i=1}^n a_i \int_0^L \frac{d\varphi_i}{dz} \frac{d\varphi_j}{dz} dz = \int_0^L p_0 \varphi_j dz \quad \text{for all } j = 1, 2, \dots, n \quad (12.37)$$

If a FEM is to be used instead, we need to replace the global basis functions with element basis functions. In this case, we need to discretize the domain. In general we may discretize  $z = [0, L]$  into  $K + 1$  elements with  $K$  internal node points in addition to the boundaries.

Next, we construct a finite dimensional subspace  $\Omega_h$  consisting of piecewise linear functions. We define subintervals of length  $\Delta z = z_{j+1} - z_j$ ,  $j = 1, 2, \dots, K$ . As parameters to describe how the function change over the subintervals, we choose the basis functions as the set of triangular functions defined as:

$$\varphi_j(z) = \begin{cases} \frac{1}{\Delta z} (z - z_{j-1}) & \text{for } z_{j-1} \leq z \leq z_j, \\ \frac{1}{\Delta z} (z_{j+1} - z) & \text{for } z_j \leq z \leq z_{j+1}, \\ 0 & \text{otherwise} \end{cases} \quad (12.38)$$

for  $j = 1, 2, \dots, K$ . Note that the basis functions have the following property:

<sup>8</sup> This is an  $L_2$  inner product. The orthogonality condition states that the residual is orthogonal to the space of basis functions.

$$\varphi_j(z) = \begin{cases} 1 & \text{if } i = j \\ 0 & \text{otherwise} \end{cases} \quad (12.39)$$

If the segments are equal, the interval  $[0, L]$  is divided into  $K + 1$  equal segments of length  $\Delta z$ . Each basis function is an isosceles triangle, displaced from the previous one by a distance equal to one-half of the length of the base line. This means that the solution to  $\psi$  between any two points  $z_j$  and  $z_{j+1}$  is approximated by a piecewise linear function:

$$\tilde{\psi} = a_j \left(1 - \frac{z - z_j}{z_{j+1} - z_j}\right) + a_{j+1} \left(\frac{z - z_j}{z_{j+1} - z_j}\right) \quad (12.40)$$

where  $a_j$  has the physical meaning of being the value of  $\psi$  at the nodes  $z = z_j$ .

The first-order derivatives of the basis functions are:

$$\frac{d\varphi_j(z)}{dz} = \begin{cases} \frac{1}{\Delta z} & \text{for } z_{j-1} \leq z \leq z_j, \\ \frac{1}{\Delta z} & \text{for } z_j \leq z \leq z_{j+1}, \\ 0 & \text{otherwise} \end{cases} \quad (12.41)$$

which have discontinuities for  $z = z_j$ ,  $j = 1, 2, \dots, K$ .

Introducing (12.38) into (12.37), we get:

$$\sum_{j=1}^n A_{ij} \tilde{\psi}_j = f_j \quad (12.42)$$

where  $A_{ij} = \int_0^L \frac{d\varphi_i}{dz} \frac{d\varphi_j}{dz} dz$  and  $f_j = \int_0^L p_0 \varphi_j dz$ .

The assembly of the complete system contributions to the discrete weak form results in a matrix equation of the form:

$$\mathcal{A} \tilde{\psi} = \mathbf{f} \quad (12.43)$$

where  $\tilde{\psi}$  is the vector of the unknown nodal values.

Due to the local nature of the basis functions chosen the system can be assembled based on local element contributions. The result is an element matrix equation of the form:

$$\mathcal{A}_e \tilde{\psi}_e = \mathbf{f}_e \quad (12.44)$$

where  $\tilde{\psi}_e$  is the vector of the unknown nodal values in element  $e$ , and  $\mathcal{A}_e$  and  $\mathbf{f}_e$  are the element characteristic matrix and vector, respectively.

It is important to note that in order to combine each element approximation of the field variable to obtain a global solution certain *continuity* conditions must be satisfied at the element boundaries. The value of the field variable at a node must be the same for each element that shares that node. Such an approximation is said to have  $C^0$  continuity. If the first derivatives of the field variable were continuous between elements, then the approximation would have  $C^1$  continuity. In general, with  $n$  the highest order derivative that

appears in the element equations, a function is  $C^n$  continuous if the derivatives up to the  $n$ -th order are continuous. The *compatibility* condition requires that  $C^{n-1}$  continuity exists at the element interfaces. The *completeness* condition requires that there is  $C^n$  continuity of the field variable within the element. It has been shown that the finite element solution will converge to the exact solution as the number of elements increases provided that the compatibility and completeness conditions are satisfied.

It is further noted that one may also proceed in the reverse order, starting out deriving a weak form for a generalized element  $e$  instead. In this case, the global system matrix  $\mathcal{A}$  and global system vector  $\mathbf{f}$  result from the assembly of element contributions. The addition of the element contributions to the appropriate locations in the global system matrix  $\mathcal{A}$  and global system vector  $\mathbf{f}$  can be represented through the action of an assembly operator acting on the local element matrix and nodal vector as follows:

$$\mathcal{A} = \sum_{e=1}^K \mathcal{A}_e \quad (12.45)$$

$$\mathbf{f} = \sum_{e=1}^K \mathbf{f}_e \quad (12.46)$$

where the summation sign indicates assembly over all finite elements. The summation does not indicate the usual algebraic summation, but is based on the requirement of compatibility at the element nodes. With the standard  $C^0$  continuity requirement at the element boundaries, this means that at the nodes where the elements are connected, the value of the unknown  $\psi_{e,i}$  is set to be equal for all the elements joining at the node.

In the implementation of the method one may thus either assemble information obtained on an element by element basis into a global representation of the problem or assemble the information from the complete system form instead. Some assembling techniques are outlined by Jiang [84], chap 15. Finally, standard numerical techniques may be used to solve the global system matrix equation for the unknown field variables.

### Basic Steps of a Standard Finite Element Analysis

- Discretization of the Continuum Calculation Domain.  
The continuum domain is generally replaced by a series of interconnected subdomains or elements. We must then determine which types of elements are appropriate for a given problem and the density of elements required to sufficiently approximate the solution.
- Selection of Interpolation Functions  
Once an element shape has been chosen, we must determine how the variation of the field variable across the element domain is to be represented or approximated. The method of approximating the solution across each

element is referred to as *element interpolation*. In most cases, a polynomial interpolation function is used. The number of nodes assigned to an element dictates the order of the interpolation function which can be used. The degree to which the approximate solution is sufficient to accurately model the problem is affected by the type of interpolation function used. The simplest method of approximation is to assume a linear distribution of the unknown function within the element domain.

- Find the Element Properties

Once the interpolation functions have been chosen, the field variables in the domain of the element are approximated in terms of the discrete values at the nodes.

The Galerkin finite element spatial discretization of the boundary value problem is formulated as an equivalent weak or variational form to the strong form of the boundary value problem.

A system of equations is formed which expresses the element properties in terms of the quantities at the nodes.

- Assembly the Element Properties

The assembly procedure combines each element approximation of the field variable with the specified compatibility and completeness requirements between the elements to form a piecewise approximation of the behavior over the entire solution domain.

A standard FEM require  $C^0$  continuity at the element boundaries.

- Apply the Boundary Conditions

The global system of equations created by the previous FEM steps cannot be solved, pending application of the boundary conditions.

- Solve the System of Equations

Once the boundary conditions have been applied to the assembled matrix of equations, standard numerical techniques can be used to solve the global system matrix equation for the unknown field variables. The matrix equations generated by the finite element process are often sparse and sometimes also symmetrical.

Among the basic attributes of the method are the ease in modeling complex geometries, the consistent treatment of differential type boundary conditions and the possibility to be programmed in a flexible and general purpose format.

## 12.6 Basic Finite Volume Algorithms Used in Computational Fluid Dynamics

The purpose of this section is to outline the design of the basic finite volume solution algorithms used in computational fluid dynamics. Other methods like finite difference, finite elements and spectral methods have been in widespread use in computational fluid dynamics for years. However, only finite volume

algorithms are examined in further details in this book, mainly because of length constraints.

The design of solution strategy for particular flow problems is strongly related to the mathematical characteristics of the governing equations. The mathematical nature of the governing equations for single phase flow was discussed in sect 12.4. For compressible flows, for which the pressure property equals the thermodynamic pressure, the continuity and momentum equations are strongly coupled to the energy equation through energy dissipation and reversible conversion of kinetic energy into internal energy. It follows that both the pressure gradient and the magnitude of the pressure are important properties in compressible flows. Transonic and greater Mach number flows usually exhibit shockwaves, which allow for nearly discontinuous changes in the flow field properties. The main difficulty encountered when constructing numerical methods for the compressible flow equations is thus the possible presence of discontinuities in the solution. One remedy devised to solve these equations is known as the shock-capturing methodology. One of the basic ingredients of the shock-capturing schemes is the high-resolution mechanism (implemented in the form of flux-limiters) that allows one to combine higher-order accuracy with shock-capturing capabilities to circumvent Gudunov's theorem [64]. The governing equations for compressible unsteady viscous flow collectively constitute an *incomplete parabolic* system of equations, as there are no second-order derivative terms in the continuity equation. The particular system form constituting the continuity, momentum, and temperature equations in addition to the ideal gas law is referred to as the *compressible Navier-Stokes equations*. The governing compressible equations for unsteady inviscid flows, called the *Euler equations*, are hyperbolic. This system admits discontinuous solutions, and it can also describe the transition from a subsonic flow (where  $|\mathbf{v}| < c$ ) to supersonic flow (where  $|\mathbf{v}| > c$ ), where  $c = (\gamma RT)^{1/2}$  is the speed of sound. The two basic sets of compressible equations are generally treated numerically within a generic system framework on the form of scalar convection laws [72, 4, 158, 173]. That is, the use of the *conservation form* of the unsteady governing conservation equations assures conservation of mass, momentum and energy so that the simulations performed may converge to physically valid solutions [105]. The solution of the generic conservation law form of all the governing equations (i.e., continuity, momentum, and energy) takes the form of a time-marching solution where the dependent flow field variables are solved progressively in steps of time. Note that in this formalism the computations provide the fluid density  $\rho$  and the flux variables  $\rho\mathbf{v}$  and  $\rho E$ , and not the primary variables  $\mathbf{v}$  and  $E$ . However, these methods are specifically designed for compressible flows and may become very inefficient when applied to incompressible flows [72, 158, 33]. In one view, the reason for this inefficiency is that in compressible flows the continuity equation contains a time derivative which drops out in the incompressible limit. As a result, the equations become extremely stiff in the limit of weak compressibility, necessitating the use of very small time steps or implicit methods. Another interpretation, of the same

effects, is that the compressible equations support sound waves which have a definite speed associated with them. As some information propagates at the flow velocity, the larger of the two velocities determines the allowable time step in an explicit method. In the low speed limit, one is forced to take a time step inversely proportional to the sound speed for any fluid velocity. This step size may be much smaller than the one a method designed for incompressible flows (which support sound waves that propagate at an infinite speed) might allow.

For incompressible flows, the pressure quantity acts as a surface force and the system of governing equations becomes parabolic (dynamic flow) or elliptic (steady-state flow), the continuity and momentum equations are not coupled to the energy equation because the fluid velocity is so low that no significant heat is produced thus the flow is isothermal. This means that only the pressure gradient, and not the magnitude of the pressure, is important characterizing the flow. Moreover, for these low Mach number flows, the pressure gradient required to force the fluid to move is so small that the density is not significantly affected. The density is thus almost constant and the transient term in the continuity equation drops out. For this reason, the continuity can no longer be considered as an equation for density but acts as a constraint on the velocity field. However, the pressure is closely connected to the velocity components in the continuity equation thus for a sequential solution of the equations, it is necessary to devise a mechanism to couple the continuity and momentum equations through the pressure field. It is further noted that for parabolic and elliptic equations the propagation speed of the signals is infinite. A Poisson-like equation for the pressure is frequently used to correct the intermediate velocity field and enforce continuity. In this formalism the computations provide the primary variables  $\rho$  and  $\mathbf{v}$ .

In computational fluid dynamics, the central part of a solution algorithm for the governing equations denotes the procedure used to resolve the coupling that arises between the pressure, density and velocity. Two families of algorithms, the *pressure-based methods* and *density-based methods*, have been developed for solving the governing equations for single phase flow. Pressure-based methods use a Poisson-like equation for updating the pressure instead of the continuity equation in the fundamental form, while density-based methods use the continuity equation to update density. For this reason, for compressible fluids an equation of state is used to provide density in pressure based schemes and pressure in density based schemes.

The pressure-based method was introduced by Harlow and Welch [67] and Chorin [30] for the calculation of unsteady incompressible viscous flows (parabolic equations). In Chorin's *fractional step method*, an incomplete form of the momentum equations is integrated at each time step to yield an approximate velocity field, which will in general not be divergence free, then a correction is applied to that velocity field to produce a divergence free velocity field. The correction to the velocity field is an orthogonal projection in the sense that it projects the initial velocity field into the divergence free

field without changing the vorticity. This step is called the projection step, and schemes that use this approach are often called *projection methods*. The original Chorin method was modified for use with finite volumes defined on a staggered grid by Kim and Moin [92]. An alternative to the basic projection method is the pressure correction method, which is similar to the basic projection method, but with the pressure gradient term retained in the momentum equations. The Poisson's equation is then solved for a pressure correction quantity which is used to correct the intermediate velocity field and enforce continuity. This approach was proposed by Patankar and Spalding [140] and Patankar [141].

In classical gas dynamics much research effort has been devoted to the development of accurate and efficient numerical algorithms suitable for solving flows in the different Mach number regimes. The magnitude of the Mach number dictates the type of algorithm to be employed in the solution procedure. The density-based methods are generally used for high Mach number flows, and the pressure-based methods for low Mach number flows. However, the fundamental equations of motion are uniformly valid as the Mach number ranges from zero (incompressible limit) to infinite (supersonic limit). During the years, many researchers have thus aimed at developing unified algorithms capable of solving flow problems in all the Mach number regimes. In any numerical method designed to be capable of predicting both incompressible and compressible fluid flows the pressure must play its dual role and act on both velocity and density to satisfy continuity. Several researchers have worked on extending the range of pressure-based methods, that were originally developed for incompressible flows at low Mach numbers, to high Mach numbers [78, 192, 87, 33, 172, 133, 121]. It is noted that Harlow and Amsden [68] developed one of the first pressure-based finite difference methods of this kind. On the other hand, the density-based methods were originally developed for compressible transonic flows and have been extended down to low Mach numbers through the use of preconditioning techniques [29, 184, 127, 100, 45].

Incompressible steady flows are commonly solved by pressure-based methods and methods based on the concept of artificial compressibility [183, 45]. The extension of pressure correction methods to steady flows, generally elliptic equations, has been performed by Patankar and Spalding [140] and Patankar [141]. The artificial compressibility method for calculating steady incompressible flows was proposed by Chorin [29]. In this method, an artificial compressibility term is introduced in the continuity equation, and the unsteady terms in the momentum equations are retained. Hence, the system of equations becomes hyperbolic and many of the methods developed for hyperbolic systems can be applied.

Generally, the design of modern solution algorithms for fluid flow problems is associated with the choice of primitive variables, the grid arrangement, and the solution approach [133]. In the class of pressure-based solution algorithms, both fully coupled and segregated approaches have been proposed. In the coupled approach, the discretized forms of the momentum and continuity

equations are linked together and the resulting system of equations is solved simultaneously [23]. This technique thus ensures a close connection between the velocity components and pressure, which may enhance the convergence rate and hence the efficiency of the method. However, the memory required to store the coefficients and variables at all grid nodes is often prohibitive for multidimensional flows. This storage problem may be alleviated by subdividing the domain into parts and solving the system of equations over each subdomain separately. However, these subdomain solvers artificially decouple the equations in the various parts of the domain and may thus lead to reduced convergence rates. In the segregated approach, the discretized equations are solved separately, but over the whole domain. This has the advantage of requiring considerably less computer storage than the semi-coupled method in addition to providing the flexibility of easily solving additional PDEs when needed. Two different grid arrangements have been used in implementations of the numerical methods, staggered grids [67] with different grid cell volumes for velocities and pressure and collocated grids [155, 125, 126] with the same grid cell volume for all variables. For the collocated variable schemes special interpolation procedures for evaluating the grid cell volume face velocities are required. The use of staggered grids [67], in which pressure is stored at the grid cell center and velocities at the grid cell faces, removes the need for interpolation of pressure in the momentum equations and of velocity in the continuity equation. The primary disadvantage of the staggered grid arrangement is the greater complexity associated with the use of different grid systems for the various variables, which becomes overwhelming in curvilinear coordinates.

Many other methods for solving flow problems can be devised. It is impossible to describe all of them here. In this book, emphasis is placed on describing elements of particular pressure-based methods originally developed for incompressible flows. The basic methods are extended and used to simulate reactive flows. The standard algorithms used to solve multi-fluid models are extensions of particular pressure-based methods for single phase flows.

## 12.7 Elements of the Finite Volume Method for Flow Simulations

In this section, a survey of the basic elements of the finite volume method, as applied to single phase flows, is provided [141, 201, 202, 49, 158]. The numerical issues considered are the approximations of surface and volume integrals, time discretizations, and space discretization of diffusive and convective (or advective) terms.

Consider the generic transport equation for the property  $\psi$  and assume that the velocity field and the fluid properties are known. The starting point for the FVM is the integral form of the balance equation:

$$\int_t \int_V \frac{\partial(\rho\psi)}{\partial t} dvdt + \int_t \int_A \rho\psi \mathbf{v} \cdot \mathbf{n} dadt = \int_t \int_A \Gamma_\psi \nabla\psi \cdot \mathbf{n} dadt + \int_t \int_V S_\psi dvdt \quad (12.47)$$

The finite volume integration of (12.47) over a grid volume is essentially the same for both steady and dynamic systems to treat convection, diffusion and source terms. The first observation is that for steady problems the transient term vanishes, and the finite volume integration consists of the space dimensions only. It makes sense to consider the common features first.

The first task is to discretize the domain. The computational domain is subdivided into a finite number of small grid cell volumes (GCVs) by a grid which defines both the grid cell volume boundaries and the computational nodes. Note that in the finite difference method, the grid defines the location of the computational nodes solely.

In the FVM a general 3D cell containing the central node  $P$  has six neighboring nodes identified as west, east, south, north, bottom and top nodes ( $W, E, S, N, B, T$ ), as sketched in Fig 12.2). The notation,  $w, e, s, n, b$  and  $t$  are used to refer to the west, east, south, north, bottom and top cell faces, respectively. The algorithms are illustrated using Cartesian grids.

The usual approach in the FVM is to define GCVs by a suitable grid and assign the computational node to the GCV center. However, one could as well define the nodal locations first and construct GCVs around them, so that GCV faces lie midway between nodes. The advantage of the first approach is that the nodal value represents the mean over GCV volume to higher accuracy (second order) than in the second approach, since the node is located at the centroid of the GCV. The advantage of the second approach is that CDS approximations of derivatives at GCV faces are more accurate when the face is midway between two nodes. The discretization principles are the same for both variants. One only has to take into account the relation between the various locations within the integration volume. The first variant is used more often than the second approach.

The transport equation on the integral form (12.47) applies to each GCV, as well as to the solution domain as a whole. If we employ consistent discretization schemes and sum the equations for all GCVs, the global transport equation is obtained, since the surface integrals over the inner GCV faces cancel out. To obtain an algebraic equation for each GCV, the surface and volume integrals need to be approximated using appropriate *quadrature formulas* [149, 50, 134, 93]. In some cases, depending on the approximations used, these equations are equal to those obtained from the FDM.

Special treatment of the boundary grid cells may be required for the implementation of boundary conditions. The volume integrals are calculated in the same way as for every GCV, but the fluxes through the GCV faces coinciding with the domain boundary require special treatment. These boundary fluxes must either be known, or be expressed as a combination of interior values and boundary data. The convective fluxes are normally prescribed at the

inflow boundary. Convective fluxes are zero at impermeable walls and symmetry planes, and are generally assumed to be independent of the coordinate normal to an outflow boundary. Diffusive fluxes are sometimes specified at a wall or boundary values of variables are prescribed.

### 12.7.1 Numerical Approximation of Surface and Volume Integrals

In Figs 12.1 and 12.2, typical 2D and 3D Cartesian cell volumes are shown together with the notation commonly used. In 3D the GCV surface is subdivided into six plane surfaces, denoted by lower case letters corresponding to their direction (*e*, *w*, *n*, *s*, *t*, and *b*) with respect to the central node *P*. The 2D case can be regarded as a special case of the 3D one in which the dependent variables are independent of *z*, hence the GCV surface is subdivided into four plane surfaces (*e*, *w*, *n*, and *s*). The net flux through the GCV boundary is the sum of integrals over the GCV faces:

$$\int_A f da = \sum_k \int_{A_k} f da \tag{12.48}$$

where *f* is the component of the convective ( $\rho\psi\mathbf{v} \cdot \mathbf{n}$ ) or diffusive ( $\Gamma_\psi\nabla\psi \cdot \mathbf{n}$ ) vector in the direction normal to the GCV face. The only unknown is  $\psi$ , since the velocity field and the fluid properties are assumed known. If the velocity field is not prescribed, it can be calculated from a more complex problem involving non-linear coupled equations, which are examined shortly.

To demonstrate the method, a representative GCV face labeled *e* in Fig 12.2 is considered. Analogous expressions can be derived for all faces by making appropriate index substitutions.

To calculate the surface integral in (12.48) accurately by a high order quadrature, the integrand *f* must be known at a large number of points on the surface *A<sub>e</sub>*. This information is generally not available, rather only the

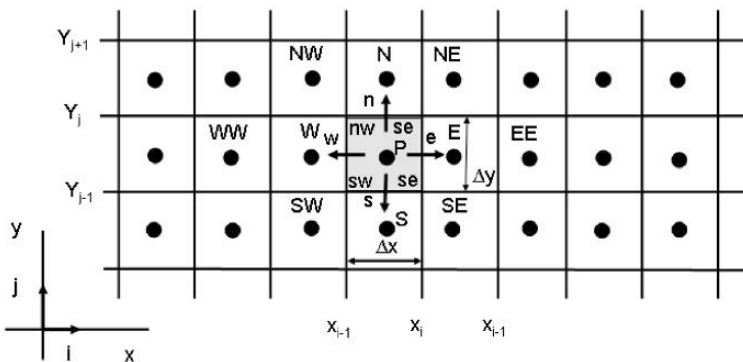


Fig. 12.1. A typical grid volume and the notation used for a Cartesian 2D grid.

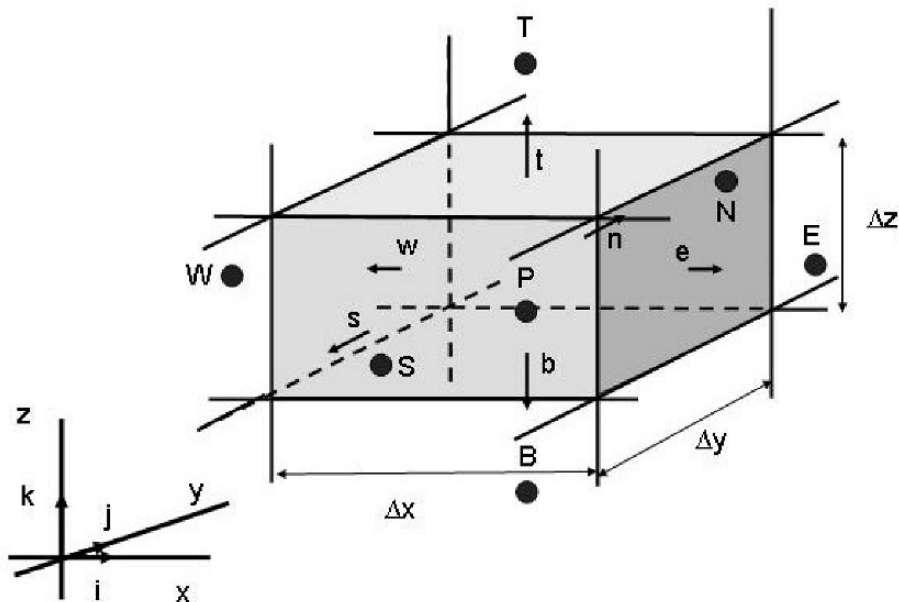


Fig. 12.2. A typical grid volume and the notation used for a Cartesian 3D grid.

nodal GCV center values are known so a low order quadrature approximation must suffice. The low order integral approximation consists in calculating the integral in terms of the variable values at one or only a few locations on the grid cell face. These cell face values are generally unknown and subsequently approximated by interpolation of the nodal GCV center values. The low order quadrature formula thus contains two levels of approximation.

Many quadrature formulas approximate the integral by a weighted sum of the values of the integrand at particular points on the interval of integration, that is, by [149, 50, 134, 93]:

$$\int_a^b f(x)dx = \sum_{i=1}^n w_i f(x_i) \tag{12.49}$$

where  $a \leq x_1 < x_2 < \dots < x_n \leq b$ . The numbers  $w_i$  are called the *weights* and the points  $x_i$  at which the function is evaluated are called the *abscissas*. Both the abscissas and weights depend on the method and on the number of intervals,  $n$ . A quadrature formula is defined by the prescription of the weights and abscissas.

One of the easiest ways to obtain useful quadrature formulas for our purpose is to use Lagrangian interpolation on an equally spaced mesh and integrate the result. This class of quadrature formulas is called the Newton-Cotes

formulas. The closed quadrature formulas includes the endpoints of the range of integration as abscissas, whereas the open quadrature formulas do not include the endpoints of the range of integration as abscissas.

The open formulas are not as accurate as the closed ones, hence most of the open formulas are rarely used. However, in engineering practice the simplest open formula, known as the *midpoint rule*, is frequently used as basis for the FVM.

The midpoint rule is obtained by a polynomial of order zero which passes through the midpoint assuming that the function is constant over the integral of integration. The surface integral can thus be approximated as a product of the mean value over the surface and the cell face area [49]. The integrand at the cell face center is frequently used as an approximation to the mean value over the surface. In this case the surface integral is written as:

$$F_e = \int_{A_e} f \, da = \langle f \rangle A_e \approx f_e A_e \quad (12.50)$$

This integral approximation is of second order, provided that the value of  $f$  at location  $e$  is known. However, the value of  $f$  is generally not available at cell faces, hence they have to be obtained by interpolation from the node values. In order to preserve the second order accuracy of the midpoint rule approximation of the surface integral, the value of  $f_e$  must be obtained with at least second order accuracy.

An alternative closed Newton-Cotes quadrature formula of second order can be obtained by a polynomial of degree 1 which passes through the end points. This quadrature formula is called the *trapezoid rule*. In 2D this surface integral approximation requires the integrand values at the GCV corners.

For higher order approximations of the surface integrals, the integrand is needed at more than two locations. To apply the fourth-order Simpson's rule approximation, the values of  $f$  are required at three locations, the cell face center  $e$  and, the two corners  $ne$  and  $se$ . In order to retain the fourth order accuracy of the surface integral approximation, the corner values have to be obtained by interpolation of the nodal values providing the same or higher order accuracy.

Several terms in the transport equations require *integration over the volume of a grid cell*. The midpoint rule is again the simplest second order approximation available. The second-order approximation thus consists in replacing the volume integral by the product of the mean value and the GCV. The mean value is approximated as the value at the GCV center:

$$S_P = \int_{GCV} s \, dv = \langle s \rangle \Delta V \approx s_P \Delta V \quad (12.51)$$

where  $s_P$  is the value of  $s$  at the GCV center. Since all the variables are available at node  $P$ , no interpolation is necessary.

Higher order approximations are possible but require the value of  $s$  at more locations than just the GCV center. If the intervals between the interpolation points are allowed to vary, other groups of quadrature formulas can be used, such as the Gaussian-, Clenshaw-Curtis- and Fejér quadrature formulas.

*It is noted that in engineering practice the simple second order midpoint approximation formulas are normally used for the surface and volume integrals.*

### 12.7.2 Solving Unsteady Problems

In transient problems the time coordinate must be discretized in a similar manner as the space coordinates [141, 66, 71, 72, 158, 49, 202]. The major difference between the space and time coordinates lies in the direction of influence. The time dependent variables will affect the flow only in the future, thus there is no backward influence. This has a strong influence on the choice of solution strategy.

In general, two different solution strategies can be adopted for the time coordinate and used together with the finite volume space discretization of the generic unsteady transport equation. In one approach, the standard finite volume space integration is subsequently followed by discretization of the resulting ordinary differential equation in time. This approach is named the *numerical method of lines* [167]. Numerical methods for solving ODEs are easily available in standard textbooks. However, a second alternative approach is commonly used in the basic textbooks on the finite volume method. In the standard finite volume discretization of the generic transport equation (12.47), integrations are performed over the GCV shown in Fig 12.2 and over the time interval from  $t$  to  $t + \Delta t$ . In this framework the time integrals have to be approximated by use of appropriate quadrature formulas. These formulas may not be as easily accessible as the differential methods. To illuminate this topic, henceforth we follow the standard finite volume approach integrating both in time and space.

Integration of the convective flux terms over the GCV surface gives:

$$\int_A \mathbf{n} \cdot (\rho \mathbf{v} \psi) dA = (\rho v_x \psi A)_e - (\rho v_x \psi A)_w + (\rho v_y \psi A)_n - (\rho v_y \psi A)_s + (\rho v_z \psi A)_t - (\rho v_z \psi A)_b \quad (12.52)$$

Integration of the diffusive flux terms over the GCV surface gives:

$$\int_A \mathbf{n} \cdot (\Gamma_\psi \nabla \psi) dA = (\Gamma_\psi A \frac{\partial \psi}{\partial x})_e - (\Gamma_\psi A \frac{\partial \psi}{\partial x})_w + (\Gamma_\psi A \frac{\partial \psi}{\partial y})_n - (\Gamma_\psi A \frac{\partial \psi}{\partial y})_s + (\Gamma_\psi A \frac{\partial \psi}{\partial z})_t - (\Gamma_\psi A \frac{\partial \psi}{\partial z})_b \quad (12.53)$$

Introducing these standard finite volume space integrations, and changing the order of integration in the rate of change term we get:

$$\begin{aligned}
 & \int_t^{t+\Delta t} (\rho v_x \psi A)_e dt - \int_t^{t+\Delta t} (\rho v_x \psi A)_w dt + \int_t^{t+\Delta t} (\rho v_y \psi A)_n dt - \int_t^{t+\Delta t} (\rho v_y \psi A)_s dt + \\
 & \int_t^{t+\Delta t} (\rho v_z \psi A)_t dt - \int_t^{t+\Delta t} (\rho v_z \psi A)_b dt = - \left[ \int_t^{t+\Delta t} \frac{d(\rho \psi)}{dt} dt \right] \Delta V + \\
 & \int_t^{t+\Delta t} (\Gamma_\psi A \frac{\partial \psi}{\partial x})_e dt - \int_t^{t+\Delta t} (\Gamma_\psi A \frac{\partial \psi}{\partial x})_w dt + \int_t^{t+\Delta t} (\Gamma_\psi A \frac{\partial \psi}{\partial y})_n dt - \int_t^{t+\Delta t} (\Gamma_\psi A \frac{\partial \psi}{\partial y})_s dt \\
 & + \int_t^{t+\Delta t} (\Gamma_\psi A \frac{\partial \psi}{\partial z})_t dt - \int_t^{t+\Delta t} (\Gamma_\psi A \frac{\partial \psi}{\partial z})_b dt + \int_t^{t+\Delta t} \langle S_\psi \rangle \Delta V dt
 \end{aligned} \tag{12.54}$$

In the framework of the FVM it is generally assumed that the transient term prevails over the whole grid volume. To make further progress we need approximate numerical techniques for evaluating the time integral from  $t_n$  to  $t_{n+1}$ .

It is observed that after the spatial terms have been approximated with appropriate discretizations, as outlined in the subsequent sections, the equation can be cast into the form of an ordinary differential equation on the form:

$$\int_{t_n}^{t_n+\Delta t} \frac{d\psi(t)}{dt} dt = \psi^{n+1} - \psi^n = \int_{t_n}^{t_n+\Delta t} f(t, \psi(t)) dt \tag{12.55}$$

where we have used the standard shorthand notation  $\psi^{n+1} = \psi(t_{n+1})$ .

Even though the time integration on the LHS is exact, the term on the RHS cannot be evaluated without knowing the solution<sup>9</sup> so some approximation is necessary. The time integral approximations are naturally viewed as obtained by use of some of the same quadrature rules as employed discussing the surface and volume integral approximations. However, there are more than one way to derive some of the time discretization methods considered in this section. Naturally, one way to derive these methods starts from the integrated form of differential equation, defining a quadrature problem. Nevertheless, another approach is to approximate the derivative in the differential equation, defining a numerical differentiation problem. Single-step

<sup>9</sup> In an attempt to find an exact formula for the integral, we may resort to the *mean value theorem* of calculus. This theorem states that if the integrand is evaluated at a particular known instant  $t = \tau$  between  $t_n$  and  $t_{n+1}$ , the integral is equal to  $f(\tau, \psi(\tau))\Delta t$ . However, in the present case the theorem is of little use since the instant  $\tau$  is unknown.

methods can thus be introduced in a natural way by means of Taylor series. The Taylor series method is conceptually simple and capable of high accuracy. Its basis is truncated Taylor Series about a particular point. The family of backward differentiation formulas, BDFs, are primarily viewed as arising from numerical differentiation [170]. These methods employ previously computed information at more than two points.

A brief survey of the different classes of ODE methods that are commonly applied solving the governing equations of fluid mechanics, is given in the following. The elementary notation and the basic properties of these ODE discretizations are briefly mentioned. Analysis of these methods can be found in numerous textbooks on the numerical solution of ordinary differential equations and will not be repeated here [156, 66, 170, 158, 134, 93, 28].

### Basic Single-Step Methods

The single-step methods<sup>10</sup> utilize the information at a single point on the solution curve to compute the next point. These methods are derived by use of low order quadrature formulas.

Four low order single-step approximations are frequently used:

- If the integral on the right side of (12.55) is estimated using the value of the integrand at the initial point, we get:

$$\psi^{n+1} = \psi^n + f(t_n, \psi^n)\Delta t \quad (12.56)$$

which is known as the first order *explicit* or *forward Euler* method.

- If the integral on the right side of (12.55) is estimated using the value of the integrand at the final point, we obtain the first order *implicit* or *backward Euler* Method:

$$\psi^{n+1} = \psi^n + f(t_{n+1}, \psi^{n+1})\Delta t \quad (12.57)$$

- If the integral on the right side of (12.55) is estimated using the value of the integrand at the midpoint point of the time interval, we obtain the *midpoint rule*:

$$\psi^{n+1} = \psi^n + f(t_{n+1/2}, \psi^{n+1/2})\Delta t \quad (12.58)$$

Depending on what further approximations are employed, the midpoint rule may give rise to single-step or multistep methods.

For example, the second order (two-step) *Leapfrog method* frequently used in meteorology and oceanography can be deduced from the midpoint rule [66, 49, 158]:

$$\psi^{n+1} = \psi^{n-1} + 2f(t_n, \psi^n)\Delta t \quad (12.59)$$

---

<sup>10</sup> In a few textbooks these methods are referred to as *two-level methods* because they involve the values of the unknown at two time levels [49].

- Finally, if the integral on the right side of (12.55) is estimated using a value of the integrand that is obtained by a straight line interpolation between the initial and final points, we get:

$$\psi^{n+1} = \psi^n + \frac{1}{2}[f(t_n, \psi^n) + f(t_{n+1}, \psi^{n+1})]\Delta t \quad (12.60)$$

This approximation is called the *trapezoid rule* and is the basis for the popular second order Crank-Nicholson method.

Several methods require the value of  $\psi(t)$  at some point other than  $t = t_n$  and these cannot be solved without further approximation or iteration. The class of methods that only require information from time level  $n$ , or previous time levels, is called *explicit* methods. The other class of methods that require information from time level  $n + 1$  and thus solved by an iterative procedure are named *implicit*. Explicit methods are relatively easy to program and use little computer memory and computation time per step but are unstable if the time step is large. On the other hand, implicit methods require iterative solution to obtain the values at the new time step. This makes them harder to program and they use more computer memory and time per time step, but they are more stable. Problems including a wide range of time scales are called *stiff*. In general, for stiff problems implicit methods tend to behave well, whereas explicit methods often become unstable. For a single small time step it is possible to use Taylor series to estimate the order of the error for the methods. The order determines the rate at which the error goes to zero as the step size goes to zero, and this only after the step size has become small enough.

## Runge-Kutta Methods

The *Runge-Kutta* methods are classified as a group of single-step methods that employs points between  $t_n$  and  $t_{n+1}$  to approximate the solution preferably with higher order accuracy. The Runge-Kutta methods are designed to imitate the desirable features of the Taylor series method, but with the replacement of the requirement for the evaluation of higher order derivatives of the original differential equation with the requirement to evaluate  $f(t, \psi)$  at some points within the step  $t_n$  to  $t_{n+1}$ . In one view, the Runge-Kutta methods arise from underlying quadrature formulas that use data only from  $[t_n, t_{n+1}]$ .

The basic idea of the Runge-Kutta methods is illustrated through a simple second order method that consists of two steps. The integration method is constructed by making an explicit Euler-like trail step to the midpoint of the time interval, and then using the values of  $t$  and  $\psi$  at the midpoint to make the real step across the whole time interval:

$$\psi_*^{n+1/2} = \psi^n + \frac{\Delta t}{2} f(t_n, \psi^n) \quad (12.61)$$

$$\psi^{n+1} = \psi^n + \Delta t f(t_{n+1/2}, \psi_*^{n+1/2}) \quad (12.62)$$

A major disadvantage with higher order Runge-Kutta methods is that the derivative must be calculated many times per time step, making these methods more expensive than midpoint methods of comparable order. However, the Runge-Kutta methods are more stable than the multistep methods of the same order and need no data other than the initial condition required by the differential equation itself (self-starting).

### Predictor-Corrector and Multistep Methods

Predictor-Corrector methods have been constructed attempting to combine the best properties of the explicit and implicit methods. The multistep methods are using information at more than two points. The additional points are ones at which data has already been computed. In one view, Adams methods arise from underlying quadrature formulas that use data outside of  $[t_n, t_{n+1}]$ , specifically approximate solutions computed prior to  $t_n$ .

Numerous predictor-corrector methods have been developed over the years. A simple second order predictor-corrector method can be constructed by first approximating the solution at the new time step using the first order explicit Euler method:

$$\psi_*^{n+1} = \psi^n + f(t_n, \psi^n) \Delta t \quad (12.63)$$

where the  $*$  indicates that this is not the final value of the solution at  $t_{n+1}$ .

Then, the solution is corrected by applying a second order trapezoid rule using  $\psi_*^{n+1}$  to compute the derivative:

$$\psi^{n+1} = \psi^n + \frac{1}{2} [f(t_n, \psi^n) + f(t_{n+1}, \psi_*^{n+1})] \Delta t \quad (12.64)$$

The formula is known both as the *improved Euler formula* and as *Heun's method* [170]. This method has roughly the stability of the explicit Euler method. Unfortunately, the stability may not be improved by iterating the corrector because this iteration procedure converges to the trapezoid rule solution only if  $\Delta t$  is small enough.

In order to construct higher-order approximations one must use information at more points. The group of multistep methods, called the *Adams methods*, are derived by fitting a polynomial to the derivatives at a number of points in time. If a Lagrange polynomial is fit to  $f(t_{n-m}, \psi^{n-m})$ ,  $f(t_{n-m+1}, \psi^{n-m+1})$ , ...,  $f(t_n, \psi^n)$ , and the result is used to compute the integrals in (12.55), we obtain an explicit method of order  $m + 1$ . Methods of this type are called *Adams-Bashforth* methods. It is noted that only the lower order methods are used for the purpose of solving partial differential equations. The first order method coincides with the explicit Euler method, the second order method is defined by:

$$\psi^{n+1} = \psi^n + \frac{1}{2} [3f(t_n, \psi^n) - f(t_{n-1}, \psi^{n-1})] \Delta t \quad (12.65)$$

and, the third order method is expressed by:

$$\psi^{n+1} = \psi^n + \frac{1}{12}[23f(t_n, \psi^n) - 16f(t_{n-1}, \psi^{n-1}) + 5f(t_{n-2}, \psi^{n-2})]\Delta t \quad (12.66)$$

If data at  $t_{n+1}$  is included in the interpolation polynomial, implicit methods, known as *Adams-Moulton* methods, are obtained. The first order method coincides with the implicit Euler method, and the second order method coincides with the trapezoid rule. The third order method is written as:

$$\psi^{n+1} = \psi^n + \frac{1}{12}[5f(t_{n+1}, \psi^{n+1}) + 8f(t_n, \psi^n) - f(t_{n-1}, \psi^{n-1})]\Delta t \quad (12.67)$$

The Adam-Bashforth methods are frequently used as predictors and the Adam-Moulton methods are often used as correctors. The combination of the two formulas results in predictor-corrector schemes.

The multistep methods are quite cheap as they require only one evaluation of the derivative per time step. However, these methods require data from many points prior to the current one, thus they cannot be started using only data at the initial point. One has to use other methods to get the calculation started. A common approach is to use a small step size and a lower order method to achieve the desired accuracy, and slowly increase the order as more data becomes available. Moreover, the multistep methods often give accurate solutions for some time and then begin to behave badly as they can produce non-physical solutions that may grow. A useful remedy for this problem is to restart the method at certain intervals. However, this trick may reduce the accuracy and/or the efficiency of the scheme.

### 12.7.3 Approximation of the Diffusive Transport Terms

In order to study the principles of spatial discretization, we consider the steady state diffusion of a property  $\psi$  in a one dimensional domain as sketched in Fig 12.3. In Cartesian coordinates the process is governed by:

$$\frac{d}{dx}(\Gamma_\psi \frac{d\psi}{dx}) + S_\psi = 0 \quad (12.68)$$

where  $\Gamma_\psi$  is a diffusion coefficient and  $S_\psi$  a source term. Boundary values of  $\psi$  at the end points are prescribed.

Considering the 1D system in x-direction, the west side face of the grid volume is referred to by  $w$  and the east side grid volume face by  $e$ . The distances between the nodes  $W$  and  $P$ , and between nodes  $P$  and  $E$ , are identified by  $\delta x_{WP}$  and  $\delta x_{PE}$ , respectively. Similarly, the distances between face  $w$  and point  $P$  and between  $P$  and face  $e$  are denoted by  $\delta x_{wP}$  and  $\delta x_{Pe}$ , respectively.

The key step of the finite volume method is the integration of the governing equation over the grid cell volume to yield a discretized equation at the nodal

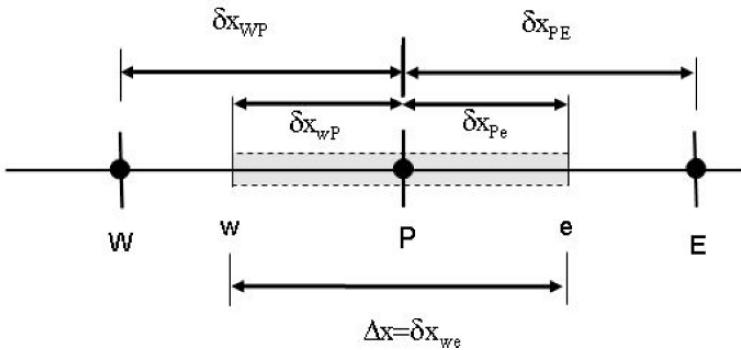


**Fig. 12.3.** A typical grid volume and the grid spacing notation used for a Cartesian 1D grid.

point  $P$ . By use of the Gauss theorem and the midpoint quadrature formula, we obtain:

$$\int_{\Delta V} \frac{d}{dx} \left( \Gamma_{\psi} \frac{d\psi}{dx} \right) dv + \int_{\Delta V} S_{\psi} dv = (\Gamma_{\psi} A \frac{d\psi}{dx})_e - (\Gamma_{\psi} A \frac{d\psi}{dx})_w + \langle S_{\psi} \rangle \Delta V \quad (12.69)$$

in which  $A$  is the cross section area of the GCV face,  $\Delta V$  is the grid cell volume and  $\langle S_{\psi} \rangle$  is the average value of  $S_{\psi}$  over the GCV.

In order to achieve useful forms of the discretized equation, the interface diffusion coefficient  $\Gamma_{\psi}$  and the property gradient  $d\psi/dx$  at the east  $e$  and west  $w$  faces are required. Linear approximations are frequently used to calculate the interface values and the gradients.

The linear profile approximation of the property gradient is second order and widely used for the evaluation of the diffusive fluxes in (12.68). For the diffusive flux at position  $e$ , the approximation is then written as:

$$\Gamma_{\psi,e} \left( \frac{\partial \psi}{\partial x} \right)_e \approx \Gamma_{\psi,e} \frac{(\psi_E - \psi_P)}{x_E - x_P} \quad (12.70)$$

The parameter value of  $\Gamma_{\psi,e}$  at the surface position  $e$  is determined by linear interpolation between points  $P$  and  $E$  (not formally derived yet, meanwhile we foresee the Taylor series expansion (12.97)). For uniform grids, and when the interface  $e$  is midway between the grid node points,  $\Gamma_{\psi,e}$  is approximated as the *arithmetic mean* of  $\Gamma_{\psi,P}$  and  $\Gamma_{\psi,E}$ , given by  $\Gamma_{\psi,e} \approx (\Gamma_{\psi,P} + \Gamma_{\psi,E})/2$ .

The source term  $\langle S_{\psi} \rangle$  may be a function of the dependent variable, hence a common practice in the FVM is to approximate the source term by means of a linear function,  $\langle S_{\psi} \rangle \approx S_{\psi,u} + S_{\psi,p} \psi_P$ . The discretized equation can then be approximated by:

$$\Gamma_{\psi,e} A_e \left( \frac{\psi_E - \psi_P}{\delta x_{PE}} \right) - \Gamma_{\psi,w} A_w \left( \frac{\psi_P - \psi_W}{\delta x_{WP}} \right) + (S_{\psi,u} + S_{\psi,p} \psi_P) \Delta V \quad (12.71)$$

This relation can be rearranged and written on the following algebraic form:

$$a_P \psi_P = a_W \psi_W + a_E \psi_E + S_{\psi,u} \Delta V \quad (12.72)$$

The corresponding coefficients are defined as:

$$a_W = \frac{\Gamma_{\psi,w}}{\delta x_{WP}} A_w \quad (12.73)$$

$$a_E = \frac{\Gamma_{\psi,e}}{\delta x_{PE}} A_e \quad (12.74)$$

$$a_P = \frac{\Gamma_{\psi,e}}{\delta x_{PE}} A_e + \frac{\Gamma_{\psi,w}}{\delta x_{WP}} A_w - S_{\psi,p} \Delta V = a_W + a_E - S_{\psi,p} \Delta V \quad (12.75)$$

The truncation error of the linear approximation of the property gradient  $(\frac{\partial \psi}{\partial x})_e$  can be calculated in terms of two Taylor series expansions around  $\psi_e$ .

The Taylor series expansion of  $\psi_P$  about  $\psi_e$  yields [202]:

$$\psi_P = \psi_e - \delta x_{eP} \left( \frac{\partial \psi}{\partial x} \right)_e + \frac{(\delta x_{eP})^2}{2} \left( \frac{\partial^2 \psi}{\partial x^2} \right)_e - \frac{(\delta x_{eP})^3}{6} \left( \frac{\partial^3 \psi}{\partial x^3} \right)_e + O((\delta x_{eP})^4) \quad (12.76)$$

The Taylor series expansion of  $\psi_E$  about  $\psi_e$  yields:

$$\psi_E = \psi_e + \delta x_{eE} \left( \frac{\partial \psi}{\partial x} \right)_e + \frac{(\delta x_{eE})^2}{2} \left( \frac{\partial^2 \psi}{\partial x^2} \right)_e + \frac{(\delta x_{eE})^3}{6} \left( \frac{\partial^3 \psi}{\partial x^3} \right)_e + O((\delta x_{eE})^4) \quad (12.77)$$

Subtracting the first expansion formula from the second one, recognizing that  $\delta_{EP} = \delta_{eP} + \delta_{eE}$ , the result is:

$$\begin{aligned} \psi_E - \psi_P &= (\delta x_{eP} + \delta_{eE}) \left( \frac{\partial \psi}{\partial x} \right)_e + \left( \frac{(\delta x_{eE})^2}{2} - \frac{(\delta x_{eP})^2}{2} \right) \left( \frac{\partial^2 \psi}{\partial x^2} \right)_e \\ &\quad + \left( \frac{(\delta x_{eE})^3}{6} + \frac{(\delta x_{eP})^3}{6} \right) \left( \frac{\partial^3 \psi}{\partial x^3} \right)_e + O((\delta x_{eE})^4) + O((\delta x_{eP})^4) \end{aligned} \quad (12.78)$$

The central difference approximation of the first derivative term becomes:

$$\begin{aligned} \left( \frac{\partial \psi}{\partial x} \right)_e &= \frac{\psi_E - \psi_P}{(\delta x_{eP} + \delta x_{eE})} - \left( \frac{(\delta x_{eE})^2 - (\delta x_{eP})^2}{2(\delta x_{eP} + \delta x_{eE})} \right) \left( \frac{\partial^2 \psi}{\partial x^2} \right)_e \\ &\quad + \left( \frac{(\delta x_{eE})^3 + (\delta x_{eP})^3}{6(\delta x_{eP} + \delta x_{eE})} \right) \left( \frac{\partial^3 \psi}{\partial x^3} \right)_e + O((\delta x_{eE})^4) - O((\delta x_{eP})^4) \end{aligned} \quad (12.79)$$

When the location  $e$  is midway between  $P$  and  $E$ , and for uniform grids, this scheme is of second order because the first error term on the RHS vanishes and the leading error term becomes proportional to the square of the grid spacing. When the grid is non-uniform, the leading error term is proportional to the grid spacing and is thus formally of first order.

### 12.7.4 Approximation of the Convective Transport Terms

An important aspect of Eulerian reactor models is the truncation errors caused by the numerical approximation of the convection/advection terms [82]. Very different numerical properties are built into the various schemes proposed for solving these operators. The numerical schemes chosen for a particular problem must be consistent with and reflect the actual physics represented by the model equations.

The transient equation describing the advection of a scalar property  $\psi$  yields:

$$\frac{\partial\psi}{\partial t} + \mathbf{v} \cdot \nabla\psi = 0 \quad (12.80)$$

The conservative form of the advection equation is obtained by use of the continuity equation, hence:

$$\frac{\partial(\rho\psi)}{\partial t} + \nabla \cdot (\mathbf{v}\rho\psi) = 0 \quad (12.81)$$

Numerical methods constructed based on the advective form (non-conservative form) of the transport operator are shape preserving, but not conservative [82]. Schemes constructed based on the conservative form (or flux form) of the transport operator are preferable when strict conservation is required.

The truncation error associated with convection/advection schemes can be analyzed by using the modified equation method [205]. By use of Taylor series all the time derivatives except the 1. order one are replaced by space derivatives. When the modified equation is compared with the basic advection equation, the right-hand side can be recognized as the error. The presence of  $\Delta x$  in the leading error term indicate the order of accuracy of the scheme. The even-ordered derivatives in the error represent the diffusion error, while the odd-ordered derivatives represent the dispersion (or phase speed) error.

Another method for analyzing the truncation error of advection schemes is the Fourier (or von Neumann method) [135, 174, 136]. This method is used to study the effects of numerical diffusion on the solution.

A Taylor series analysis on the 1D transport equation shows that the transient artificial viscosity coefficients for explicit upwind differencing is given by [157, 158]:

$$\nu_{\text{numerical}} = \frac{v\Delta x}{2}(1 - CFL) \quad (12.82)$$

whereas the implicit method gives:

$$\nu_{\text{numerical}} = \frac{v\Delta x}{2}(1 + CFL) \quad (12.83)$$

It can be noted that at least the explicit upwind method for the constant equation model gives the exact answer for  $CFL = 1$ , whereas the implicit upwind differencing method never does. The numerical viscosity of the implicit

method may increase a lot for  $CFL = 1$ . For this reason, many research codes for dynamic flows requiring high accuracy are solved using explicit time discretizations.

Over the years numerous discretization methods for the convection/advection terms have been proposed, some of them are stable for steady-state simulations solely, others were designed for transient simulations solely, but many techniques can be used for both types of problems.

In order to study properties of the schemes, we principally consider the steady state convection and diffusion of a property  $\psi$  with a source term in a one dimensional domain as sketched Fig 12.3 using a staggered grid for the velocity components so that the  $x$ -velocity components are located at the  $w$  and  $e$  GCV faces. Preliminary, we assume that the velocity is constant and constant fluid properties. The convective and diffusive processes are then governed by a balance equation of the form:

$$\frac{d}{dx}(\rho v_x \psi) = \frac{d}{dx}(\Gamma_\psi \frac{d\psi}{dx}) + S_\psi \quad (12.84)$$

where  $\rho$  denotes the mixture density and  $v_x$  the velocity component in the  $x$ -direction. Boundary values of  $\psi$  at the end points are prescribed.

The one dimensional flow must also satisfy the continuity equation:

$$\frac{d}{dx}(\rho v_x) = 0 \quad (12.85)$$

As for the pure diffusion problem, the key step of the finite volume method is the integration of the governing equations over the grid cell volume to yield a set of discretized equations at the nodal point  $P$ . By use of the Gauss theorem and the midpoint quadrature formula, we obtain:

$$(\rho v_x A \psi)_e - (\rho v_x A \psi)_w = (\Gamma_\psi A \frac{d\psi}{dx})_e - (\Gamma_\psi A \frac{d\psi}{dx})_w + \langle S_\psi \rangle \Delta V = 0 \quad (12.86)$$

The continuity yields:

$$(\rho v_x A)_e - (\rho v_x A)_w = 0 \quad (12.87)$$

In order to obtain useful forms of the discretized equations, the GCV surface terms at the east  $e$  and west  $w$  faces are required. As in the pure diffusion problem, the diffusive terms are approximated using linear approximations to calculate the surface values of the diffusion coefficients and the gradients. The result is:

$$F_e \psi_e - F_w \psi_w = D_e(\psi_E - \psi_P) - D_w(\psi_P - \psi_W) + S_{\psi,u} \Delta V \quad (12.88)$$

Temporarily, for convenience, we let the face values of the property  $\psi$  be unknown.

The continuity yields:

$$F_e - F_w = 0 \quad (12.89)$$

in which we have defined two variables  $F$  and  $D$  to represent the convective mass flux and the product of the diffusion conductance and cell face area  $F = \rho v_x A$  and  $D = \Gamma A / \delta x$ .

Let us temporarily assume that the velocity and density fields are known, hence  $F_w$  and  $F_e$  can be determined. By that means (12.88) reduces to a transport equation for the property  $\psi$  with only one unknown variable. However, in order to solve the convection-diffusion equation we need to approximate the transport property  $\psi$  at the  $e$  and  $w$  faces. A few classical convection/advection schemes are outlined in the subsequent sections.

### Upwind Differencing Scheme (UDS)

The first order explicit upwind scheme was introduced by Courant, Isaacson and Reeves [31], and later on several extensions to second order accuracy and implicit time integrations have been developed.

In the upwind scheme  $\psi_e$  is approximated by the  $\psi$  value at the node upstream of the surface location  $e$ :

$$\psi_e = \begin{cases} \psi_P & \text{if } (\mathbf{v} \cdot \mathbf{n})_e > 0, \\ \psi_E & \text{if } (\mathbf{v} \cdot \mathbf{n})_e < 0. \end{cases} \quad (12.90)$$

By use of the UDS, the coefficients in (12.88) can be defined as:

$$a_W = D_w + \max(F_w, 0) \quad (12.91)$$

$$a_E = D_e + \max(-F_e, 0) \quad (12.92)$$

$$a_P = a_W + a_E + (F_e - F_w) - S_{\psi,p} \Delta V \quad (12.93)$$

$$S_{\psi,u}^{UDS} \Delta V = S_{\psi,u} \Delta V \quad (12.94)$$

The main advantage of this scheme is that it satisfies the boundedness criteria unconditionally. A severe disadvantage associated with the UDS is that it is very numerically diffusive.

A Taylor series expansion about  $P$  gives (for Cartesian grid and  $(\mathbf{v} \cdot \mathbf{n})_e > 0$ ) [49]:

$$\psi_e = \psi_P + (x_e - x_P) \left( \frac{\partial \psi}{\partial x} \right)_P + \frac{(x_e - x_P)^2}{2} \left( \frac{\partial^2 \psi}{\partial x^2} \right)_P + O((x_e - x_P)^3) \quad (12.95)$$

The UDS approximation retains only the first term on the right hand side, hence the leading truncation error term is of first order in  $\delta x_{Pe} = (x_e - x_P)$  so it is a first order scheme.

The leading truncation error term obtained discretizing the convective terms in the convection-diffusion equation (12.88) by use of the UDS resembles a diffusive flux. For  $(\mathbf{v} \cdot \mathbf{n})_e > 0$ , the UDS for the convective flux at the location  $e$  becomes:

$$(\rho v_x A)_e \psi_e \approx (\rho v_x A)_e \psi_e - \frac{(\rho v_x A)_e \delta x_{Pe}}{2} \left( \frac{\partial \psi}{\partial x} \right)_P \quad (12.96)$$

in which the second term on the RHS represents the leading truncation error. In view of the diffusive form of this term, the numerical truncation error is sometimes named numerical-, artificial-, or false diffusion. The truncation error may be magnified in multidimensional problems if the flow is oblique to the grid.

### Central Difference Scheme (CDS)

Another classical approximation for the value at GCV face center is obtained by linear interpolation between the two nearest nodes. The linear interpolation corresponds to the central difference approximation of the first derivative in FDMs. At location  $e$  on a non-uniform Cartesian grid we have [49, 202]:

$$\psi_e \approx \psi_P + \frac{(x_e - x_P)}{(x_E - x_P)} (\psi_E - \psi_P) \quad (12.97)$$

On a uniform grid the geometric pre-factor equals  $1/2$  and the CDS reduces to the simple relation  $\psi_e \approx (\psi_P + \psi_E)/2$ . In this case, the coefficients in (12.88) are defined as:

$$a_W = D_w + \frac{F_w}{2} \quad (12.98)$$

$$a_E = D_e - \frac{F_e}{2} \quad (12.99)$$

$$a_P = a_W + a_E + (F_e - F_w) - S_{\psi,p} \Delta V \quad (12.100)$$

$$S_{\psi,u}^{CDS} \Delta V = S_{\psi,u} \Delta V \quad (12.101)$$

The main advantage of this scheme is that it is not numerically diffusive. However, the scheme is dispersive and a severe disadvantage associated with the CDS is that it does *not* always satisfy the boundedness criteria. The CDS may become unstable when  $F_e/D_e < 2$ , because the east coefficient will be negative. This scheme is thus conditionally stable. For this reason, the CDS may produce oscillatory solutions like all approximations of order higher than one.

For a non-uniform grid a Taylor series expansion of  $\psi_E$  about  $\psi_P$  is defined by:

$$\psi_E = \psi_P + (x_E - x_P) \left( \frac{\partial \psi}{\partial x} \right)_P + \frac{(x_E - x_P)^2}{2} \left( \frac{\partial^2 \psi}{\partial x^2} \right)_P + O((x_E - x_P)^3) \quad (12.102)$$

Using (12.102) to eliminate the first derivative in (12.95), the result is:

$$\psi_e = \psi_P + \frac{(x_e - x_P)}{(x_E - x_P)} (\psi_E - \psi_P) + \frac{(x_e - x_P)(x_E - x_P)}{2} \left( \frac{\partial^2 \psi}{\partial x^2} \right)_P + \dots \quad (12.103)$$

Comparing (12.97) and (12.103), it is seen that the leading truncation error term in CDS is proportional to the square of the grid spacing, hence the central difference scheme is second order accurate both on uniform and non-uniform grids.

### Quadratic Upwind Interpolation for Convective Kinematics (QUICK) Scheme

The quadratic upstream interpolation for convective kinetics (QUICK) scheme of Leonard [106] uses a three-point upstream-weighted quadratic interpolation for the cell face values. In the third order QUICK scheme the variable profile between  $P$  and  $E$  is thus approximated by a parabola using three node values. At location  $e$  on a uniform Cartesian grids,  $\psi_e$  is approximated as:

$$\psi_e = \begin{cases} \frac{6}{8}\psi_P + \frac{3}{8}\psi_E - \frac{1}{8}\psi_W & \text{if } (\mathbf{v} \cdot \mathbf{n})_e > 0, \\ \frac{6}{8}\psi_W + \frac{3}{8}\psi_P - \frac{1}{8}\psi_{WW} & \text{if } (\mathbf{v} \cdot \mathbf{n})_e < 0. \end{cases} \quad (12.104)$$

The main advantage of this scheme is that it is less numerically diffusive than the UDS. However, the scheme is dispersive and a severe disadvantage associated with the QUICK scheme is that it does *not* satisfy the boundedness criteria unconditionally. The QUICK scheme is therefore conditionally stable. The explicit QUICK scheme is unstable in the absence of diffusion.

The implicit QUICK scheme may become unstable due to the possible appearance of negative coefficients in the coefficient matrix, hence a reallocation of the terms in the coefficient matrix is required to alleviate these stability problems. To retain positive coefficients in the coefficient matrix the troublesome negative terms (possibly amongst others) are placed in the source term. One approach is to put the upwind coefficients into the coefficient matrix and the deviation between the upwind and QUICK coefficient values into the source term. The corresponding coefficients in (12.88) are defined as:

$$a_W = D_w + \max(F_w, 0) \quad (12.105)$$

$$a_E = D_e + \max(0, -F_e) \quad (12.106)$$

$$a_P = a_W + a_E + (F_e - F_w) - S_{\psi,p}\Delta V \quad (12.107)$$

$$S_{\psi,u}^{QUICK}\Delta V = (S_{\psi,u} + S_{\psi,u}^{DCS})\Delta V \quad (12.108)$$

By use of the *deferred correction method* some of the terms naturally belonging to the coefficient matrix are allocated to the source term because otherwise they may give rise to negative coefficients. The deferred correction method can only be applied when the scheme is being applied as part of an iterative loop structure. The iterative correction of these terms are thus deferred by one iteration, so at the  $\nu$ -th iteration the source term is evaluated using values known at the end of the previous  $(\nu-1)$ -th iteration. When convergence is reached, the solution is the same as without the deferred solution but the iterative process

is usually more stable. The method was first introduced by Khosla and Rubin [91], and later outlined by several authors like [115, 49, 202].

The deferred correction source (DCS) term obtained for the QUICK implementation can be defined by:

$$S_{\psi,u}^{DCS} = \frac{1}{8} \left[ (3\psi_P - 2\psi_W - \psi_{WW}) \max(F_w, 0) + (\psi_E + 2\psi_P - 3\psi_E) \max(F_e, 0) + (3\psi_W - 2\psi_P - \psi_E) \max(-F_w, 0) + (2\psi_E + \psi_{EE} - 3\psi_P) \max(-F_e, 0) \right] \tag{12.109}$$

The advantage of this approach is that the main coefficients are positive and satisfy the requirement for conservativeness, boundedness and transportiveness.

The deferred correction method can also be employed to improve the convergence properties of high order schemes, rewriting a high order flux approximation as the sum of a stable low order flux and a higher order correction in the following manner:

$$(F_e^H)^{\nu+1} = (F_e^L)^{\nu+1} + (F_e^H - F_e^L)^\nu \tag{12.110}$$

in which  $F_e^L$  denotes a low order scheme like the upwind scheme consisting of a small computational molecule, and  $F_e^H$  represents a high order scheme leading to a larger computational molecule. The term in the bracket is moved to the source term and calculated using values from the previous iteration.

The quadratic interpolation has a third order truncation error on both uniform and non-uniform grids [114, 49]. However, when this interpolation scheme is used in conjunction with the midpoint rule approximation of the surface integral, the overall approximation is still of second order accuracy (i.e., the accuracy of the quadrature approximation). Although the QUICK approximation is slightly more accurate than CDS, both schemes converge asymptotically in a second order manner and the difference are rarely large [49].

It can be shown that the leading truncation error associated with the QUICK scheme is proportional to the grid spacing in the power 3. It is noted that, for cases where  $(\mathbf{v} \cdot \mathbf{n})_e > 0$ , for a general GCV on a uniform grid the QUICK scheme determines the value of  $\psi_e$  at the grid cell face  $e$  by the first approximation in (12.104).

The three relevant Taylor series expansions about the  $e$  face value in a Cartesian grid are given by [202]:

$$\psi_P = \psi_e - \frac{\Delta x}{2} \left(\frac{\partial \psi}{\partial x}\right)_e + \frac{(-\frac{\Delta x}{2})^2}{2} \left(\frac{\partial^2 \psi}{\partial x^2}\right)_e + \frac{(-\frac{\Delta x}{2})^3}{6} \left(\frac{\partial^3 \psi}{\partial x^3}\right)_e + O\left(\left(\frac{\Delta x}{2}\right)^4\right) \tag{12.111}$$

$$\psi_E = \psi_e + \frac{\Delta x}{2} \left(\frac{\partial \psi}{\partial x}\right)_e + \frac{(\frac{\Delta x}{2})^2}{2} \left(\frac{\partial^2 \psi}{\partial x^2}\right)_e + \frac{(\frac{\Delta x}{2})^3}{6} \left(\frac{\partial^3 \psi}{\partial x^3}\right)_e + O\left(\left(\frac{\Delta x}{2}\right)^4\right) \tag{12.112}$$

$$\psi_W = \psi_e - \frac{3}{2}\Delta x \left(\frac{\partial\psi}{\partial x}\right)_e + \frac{(-\frac{3}{2}\Delta x)^2}{2} \left(\frac{\partial^2\psi}{\partial x^2}\right)_e + \frac{(-\frac{3}{2}\Delta x)^3}{6} \left(\frac{\partial^3\psi}{\partial x^3}\right)_e + O\left(\left(\frac{3}{2}\Delta x\right)^4\right) \quad (12.113)$$

If we add together  $\frac{3}{8} \times (12.112) + \frac{6}{8} \times (12.111) - \frac{1}{8} \times (12.113)$ , we obtain:

$$\psi_e = \frac{6}{8}\psi_P + \frac{3}{8}\psi_E - \frac{1}{8}\psi_W - \frac{3}{48}\Delta x^3 + O(\Delta x^4) \quad (12.114)$$

For non-uniform grids, the coefficients of the three nodal values involved in the interpolation are much more complex [49].

## Bounded High Resolution Convection schemes

A large number of numerical approximations to the convective fluxes have been proposed on structured grids within the framework of the finite volume method. The main challenge of the numerical approximation of hyperbolic transport equations is to obtain high accuracy of the solution in both discontinuous and smooth regions. The upwind scheme eliminate possible spurious oscillations in the neighborhood of sharp gradients and guarantee the resolution of discontinuities without wiggles. However, as already mentioned, the UDS possesses a strong numerical diffusion which spreads discontinuities over many grid nodes, hence it produces a low accuracy in the smooth region of the solution. The central difference scheme, on the other hand, gives good resolution in smooth regions, but introduces spurious oscillations near steep gradients that may lead to nonlinear instability. To avoid these difficulties, various high resolution schemes have been developed in recent years. These schemes, often called shock-capturing schemes in gas dynamics, are at least of second order accuracy in the smooth part of the solution and sharply resolve discontinuities without generating spurious oscillations. The high-resolution schemes often use flux/slope limiters to limit the gradient around shocks or discontinuities.

One such approach is based on the concepts of non-linear flux limiters introduced by van Leer [193] and Boris and Book [13]. The work of Boris and Book [13] and Zalesak [213] determine the basis for a group of methods called flux correction transport (FCT) schemes . The schemes of Smolarkiewicz [175] is representative for this group. In the FCT schemes a first order accurate monotone scheme is converted to a high resolution scheme by adding limited amounts of an anti-diffusive flux. The work of van Leer [193, 195], on the other hand, represents an extension of the ideas of Godunov [64] to higher order accuracy.

In 1959, Godunov [64] introduced a novel finite volume approach to compute approximate solutions to the Euler equations of gas dynamics that applies quite generally to compute shock wave solutions to non-linear systems of hyperbolic conservation laws. In the method of Godunov, the numerical approximation is viewed as a piecewise constant function, with a constant value on each finite volume grid cell at each time step and the time evolution

is determined by the exact solution of the Riemann problem (shock tube) at the inter-cell boundaries [72]. Solving the Riemann problem at the interface between grid cells gives a way to estimate the flux at the interface, and differencing these numerical fluxes gives a robust conservative shock-capturing method. This method is only first-order accurate, however, and introduces considerable numerical diffusion that tends to greatly smear out steep gradients. Nevertheless, the Godunov concept determines the basis for many finite volume methods that provides high accuracy numerical solutions to hyperbolic equations which can involve solutions that exhibit shocks, discontinuities or large gradients. Moreover, Godunov [64] proved the famous order barrier theorem stating that no linear convection scheme of second order accuracy or higher can be monotonic.

The remedy to achieve higher accuracy has been the use of non-linear discretizations, which adjust themselves according to the local solution so as to maintain a *bounded* behavior. The basic methodology of van Leer was published in a series of five papers in the journal of computational physics [198]. In this work, the oscillations are regarded as the result of oscillatory interpolation of the discrete initial values. The novel idea of van Leer [195] was to enforce non-oscillatory initial-value reconstruction by use of monotonicity preserving interpolation replacing the piecewise constant approximation of Godunov's scheme by reconstructed states, derived from cell-averaged states obtained from the previous time-step. For each cell, slope limited, reconstructed left and right states are obtained and used to calculate fluxes at the cell boundaries. Then, following Godunov, the van Leer's scheme includes fluxes derived from the solution of Riemann problems. When combined with higher-order reconstruction this leads to upwind-biased differencing. The first method based on the above principles was thus named MUSCL (Monotone Upstream Scheme for Conservative Laws). In a later paper, van Leer [196] introduced a computationally efficient alternative to the original Godunov algorithm by replacing the exact Riemann solver by Roe's approximate Riemann solver [159]. Henceforth, the Godunov-type schemes may be defined as non-oscillatory finite-volume schemes that incorporate the solution (exact or approximate) to Riemann's initial-value problems<sup>11</sup> [197].

These ideas of Godunov and van Leer were later generalized via the concept of total variation diminishing (TVD) schemes, introduced by Harten [69], whereby the variation of the numerical solution is controlled in a non-linear way, such as to forbid the appearance of any new extremum. Such methods give higher order accuracy without dispersive ripples.

Let  $\psi_i^n$  be a discrete approximation to  $\psi$  in the  $i$ -th GCV at time step  $n$ . The total variation (TV) at time step  $n$  is defined by:

$$TV^n = \sum_i |\psi_{i+1}^n - \psi_i^n| \quad (12.115)$$

---

<sup>11</sup> The conservation law together with piecewise constant data having a single discontinuity is known as the Riemann problem [117].

A convection/advection scheme is TVD if it ensures that  $TV^{n+1} \leq TV^n$ .

It is further noticed that in the sense of preserving monotonicity of the solution a difference between the limiting processes of TVD and FCT schemes lies in that the TVD schemes usually are of one step, while the FCT is of two steps. FCT schemes are widely used for simulating time-dependent flows, but are less suited for steady-state calculations and therefore have had little influence in computational fluid dynamics applied to chemical reactor engineering. The TVD schemes, on the other hand, can be easily implemented into standard CFD codes by means of the deferred correction approach using flux limiters without enlarging the stencil.

Some commonly used TVD limiters are:

- MC (Monotonic centered) limiter of van Leer [194]:

$$\phi(r) = (r + |r|)/(1 + r), \quad (12.116)$$

- MinMod limiter of Harten [69] (see also Sweby [182]):

$$\phi(r) = \text{MinMod}(r, 1) = \max(0, \min(r, 1)), \quad (12.117)$$

- SUPERBEE limiter of Roe [160, 161]:

$$\phi(r) = \max[0, \min(2r, 1), \min(r, 2)], \quad (12.118)$$

The use of first order down-winding (i.e.,  $\phi(r) = 2r$ ) in regions of high resolution curvature leads to an over-compressive behavior in smooth regions that may be responsible for artificial steepening of what should be weak gradients.

- MUSCL (Monotonic Upwind Scheme for Convective Laws) limiter of van Leer [194, 195]:

$$\phi(r) = \max[0, \min(2, 2r, (1 + r)/2)]. \quad (12.119)$$

- SMART (Sharp and Monotonic Algorithm for Realistic Transport) limiter of Gaskell and Lau [58]:

$$\phi(r) = \max[0, \min(4, \frac{3}{4} + \frac{1}{4}r, 2r)], \quad (12.120)$$

- QUICK (Quadratic Upstream Interpolation for Convective Kinematics) of Leonard [106, 107]:

$$\phi(r) = \frac{3}{4} + \frac{1}{4}r, \quad (12.121)$$

- ISNAS (Interpolation Scheme which is Non-oscillatory for Advected Scalars) of Zijlema [214]:

$$\phi(r) = \frac{1}{2}(r + |r|) \frac{r + 3}{(1 + r)^2}, \quad (12.122)$$

- SHARP (Simple High-Accuracy Resolution Program) scheme of Leonard [107]:

$$\phi(r) = \min[\max(0, 2r(r^{1/2} - 1)/(r - 1)), \max(\frac{3}{4}r + \frac{1}{4}, -\frac{5}{4})] \quad (12.123)$$

The SHARP and SMART schemes are monotone versions of the QUICK scheme.

The TVD limiters are functions of smoothness monitors determining the local gradient of the variable field. Several monitors were outlined by Yang and Przekwas [212]. Three of these monitors are [193, 161, 117]:

$$r_e = \frac{(\psi_{E-\sigma} - \psi_{P-\sigma})}{(\psi_E - \psi_P)} \quad (12.124)$$

$$r_e = \frac{(|v_{e-\sigma}| - \frac{\Delta t}{\Delta z} v_{e-\sigma}^2)(\psi_{E-\sigma} - \psi_{P-\sigma})}{[ (|v_e| - \frac{\Delta t}{\Delta z} v_e^2)(\psi_E - \psi_P) ]} \quad (12.125)$$

$$r_e = \frac{v_{e-\sigma}(\psi_{E-\sigma} - \psi_{P-\sigma})}{[v_e(\psi_E - \psi_P)]} \quad (12.126)$$

in which  $\sigma = \text{sign}(v_e)$ . The first of these monitors is most frequently used.

The face values of the property  $\psi$  can be constructed in the hybrid form of a non-linear sum of low order  $\psi^L$  and high order  $\psi^H$  approximations. For flow in the positive  $x$ -direction  $(\mathbf{v} \cdot \mathbf{n})_e > 0$ , the TVD value of  $\psi_e$  may be written as [212]:

$$\psi_e^{TVD} = \phi(r_e)\psi_e^H + (1 - \phi(r_e))\psi_e^L = \psi_e^L + \phi(r_e)(\psi_e^H - \psi_e^L) \quad (12.127)$$

The simplest TVD schemes are constructed combining the first-order (and diffusive) upwind scheme and the second order dispersive central difference scheme. These TVD schemes are globally second order accurate, but reduce to first order accuracy at local extrema of the solution.

In terms of the deferred correction method the corresponding coefficients in (12.88) are defined as:

$$a_W = D_w + \max(F_w, 0) \quad (12.128)$$

$$a_E = D_e + \max(0, -F_e) \quad (12.129)$$

$$a_P = a_W + a_E + (F_e - F_w) - S_{\psi,p}\Delta V \quad (12.130)$$

$$S_{\psi,u}^{TVD}\Delta V = (S_{\psi,u} + S_{\psi,u}^{DCS})\Delta V \quad (12.131)$$

The advantage of this approach is that the main coefficients are positive and satisfy the requirement for conservativeness, boundedness and transportiveness.

The deferred correction source (DCS) term obtained for the TVD implementation can be defined by:

$$S_{\psi,u}^{DCS} = \left[ \frac{1}{2} \phi(r_e^-) (\psi_E - \psi_P) \max(-F_e, 0) - \frac{1}{2} \phi(r_e^+) (\psi_E - \psi_P) \max(F_e, 0) \right. \\ \left. - \frac{1}{2} \phi(r_w^-) (\psi_P - \psi_W) \max(-F_w, 0) + \frac{1}{2} \phi(r_w^+) (\psi_P - \psi_W) \max(F_w, 0) \right] \quad (12.132)$$

The corresponding monitors for each face flux term equals the ratio of the upstream to the downstream gradient. For the  $e$  face, these are defined by:

$$r_e^+ = \frac{\psi_P - \psi_W}{\psi_E - \psi_P} \quad (12.133)$$

$$r_e^- = \frac{\psi_{EE} - \psi_E}{\psi_E - \psi_P} \quad (12.134)$$

The superscripts  $+$  and  $-$  are used to indicate the positive and negative flow directions.

Another approach to construct monotonic high-resolution convection schemes employs non-linear slope limiters around discontinuities to constrain the approximation of the grid cell face values, initially estimated on the basis of a higher-order approximation, to lie within specific limits. These non-linear slope limiters are generally designed based on the normalized-variable (NV) approach proposed by Leonard [109, 107] and further developed by Gaskell and Lau [58].

The normalized variable (NV) approach of Leonard [109, 107] uses the locally normalized variable  $\psi^*$  to predict the local behavior of the converted variable  $\psi$ :

$$\psi^* = \frac{\psi - \psi_U}{\psi_D - \psi_U} \quad (12.135)$$

where  $\psi_U$  is the upwind node value and  $\psi_D$  the downstream value. In terms of normalized variables,  $\psi_U^* = 0$  and  $\psi_D^* = 1$ . Let  $\psi_f^*$  be the normalized face value on the downstream GCV face. For locally monotonic node-values, the interpolative constraints on  $\psi_f^*$  are:

$$\psi_C^* \leq \psi_f^* \leq 1 \quad \text{for} \quad 0 \leq \psi_C^* \leq 1 \quad (12.136)$$

where  $\psi_C^*$  is the normalized central node value. The basic idea behind the universal limiter is that, for locally monotone node values, the normalized face values must lie between the upstream and downstream normalized node-values. Otherwise, the interpolative monotonicity would be destroyed.

In addition, to enforce local monotonicity in initially non-monotonic ranges (i.e.,  $\psi_C^* < 0$  or  $\psi_C^* > 1$ ),  $\psi_C^*$  must be corrected. A simple strategy is to use a first order UDS approximation that satisfies the limiter constraints, hence we can write:

$$\psi_f^* = \psi_C^* \quad \text{if} \quad \psi_C^* > 1 \quad \text{or} \quad \psi_C^* < 0 \quad (12.137)$$

Other higher-order functional relationships are possible [111, 114].

The normalized variable diagram [107, 109] was used as basis for development of the universal limiter. The universal limiter banishes unphysical oscillations without corrupting the accuracy of the underlying method.

The monotonic SHARP (Simple High-Accuracy Resolution Program) scheme of Leonard [107] consist in using the universal slope limiter concept for monotonic resolution to modify the standard third-order steady-state QUICK approximations of the face values. The SHARP scheme was the first multi-dimensional monotonic convection schemes designed with high accuracy based on the NV approach.

Later, Leonard [109] developed the 1D ULTIMATE (Universal Limiter for Transient Interpolation Modeling of Advective Transport Equations) scheme based on the NV approach. The ULTIMATE scheme consist of using an extended universal limiter for transient interpolation modeling of the advective transport equations. The ULTIMATE strategy was basically designed for explicit schemes of arbitrary high order. However, with minor modifications, the ULTIMATE strategy can be applied to steady-flow multi-dimensional simulations. The steady-state ULTIMATE scheme thus gives ULTRA-SHARP simulations of steady multi-dimensional flows containing discontinuities [108].

A cost-effective strategy for highly convective flows containing discontinuities, without distorting smooth profiles or clipping narrow local extrema was introduced by Leonard and Niknafs [110]. This scheme represents an extension of the transient ULTIMATE scheme. In smooth regions the unlimited third order QUICKEST (QUICK with Estimated Streaming Terms) scheme was used. In relatively large-gradient or strong-curvature regions, higher-order upwinding with the universal limiter was employed.

The ULTRA (Universal Limiter for Tight Resolution and Accuracy) approach of Leonard and Mokhtari [108, 111] was designed to guarantee monotonicity for high-resolution non-oscillatory multidimensional steady-state high-speed convective modeling.

The ULTIMATE 1D universal limiter of Leonard [109], was later extended to multi-dimensional flows by Thuburn [188]. The multi-dimensional method was designed for advected passive scalars in either compressible or incompressible flow and on arbitrary grids.

Recently, the flux limiters (FL) and the normalized variables (NV) design principles that are employed to construct non-linear high resolution convection schemes have been shown to lead to the same constraints on the fluxes [107, 189, 206]. However, three different boundedness criteria are frequently employed, these are the total variational diminishing (TVD) [69], positivity [141] and the convection boundedness criterion (CBC) [58]. Thus, although these schemes have slightly different conceptual bases, the two approaches lead to mathematically equivalent schemes [189]. In multidisciplinary research fields, it happens now and then that mathematically equivalent schemes are invented independently more than once, often with different conceptual bases [189].

It follows that the NV variable  $\psi_C^*$  is analogous to the TVD monitor  $r$  and the two quantities are related by the simple expression  $r = \psi_C^*/(1 - \psi_C^*)$  which allows the conversion of NV schemes to FL and visa versa [107, 109]. The two distinct notations did emerge because the same methods were derived independently in different communities of science and engineering.

### Other Convection/advection schemes

High-order convection/advection schemes are widely used in meteorological applications solving hyperbolic equations. For example, in European weather forecast models the explicit non-flux-based modified methods of characteristics have been very popular as they are very fast. Typical examples of this type of schemes are the semi-Lagrangian advection schemes of Bates and McDonald [9], McDonald [129] and McDonald [130]. These methods have an unrestricted time step advantage, but also an important disadvantage that they are not strictly conservative due to their non-flux-based formulation.

Moreover, in the last decades a lot of work has been focused on designing explicit schemes for passive scalars. These schemes have been applied solving the transport equations for the scalar variables in the the weather forecast models (e.g., [186]), and especially for the air pollution dispersion models solving the convection-diffusion equation (e.g., [187, 10, 85, 137]).

A large number of explicit numerical advection algorithms were described and evaluated for the use in atmospheric transport and chemistry models by Rood [162], and Dabdub and Seinfeld [32]. A requirement in air pollution simulations is to calculate the transport of pollutants in a strictly conservative manner. For this purpose, the flux integral method has been a popular procedure for constructing an explicit single step forward in time conservative control volume update of the unsteady multidimensional convection-diffusion equation. The second order moments (SOM) [164, 148], Bott [14, 15], and UTOPIA (Uniformly Third-Order Polynomial Interpolation Algorithm) [112] schemes are all derived based on the flux integral concept.

A limitation for long term dynamic simulations is the restrictions on the size of the time step for explicit schemes. The meteorological models are often solved applying operator splitting methods. The second order explicit two step method derived by MacCormack [120] from a combined space and time splitting discretization is sometimes used. The fractional step, time splitting and Strang splitting [181] techniques are more commonly used. In the ongoing quest for an explicit, single-time-step, conservative, flux-based, highly accurate, non-oscillatory finite volume scheme for multidimensional advection dominated flows, without restrictions on the time-step, Leonard et al [113] developed the NIRVANA (Non-oscillatory, Integrally Restricted, Volume-Averaged Numerical Advection) Scheme for one-dimensional advection.

The explicit operator splitting techniques based on sequential one-dimensional updates may contain large splitting errors. To reduce the splitting errors

associated with these splitting techniques, Leonard et al [116] developed the MACHO (Multidimensional Advective Conservative Hybrid Operator) and COSMIC (Conservative Operator Splitting for Multidimensions with Inherent Consistency) splitting strategies. These multidimensional methods have the unrestricted time step advantages of semi-Lagrangian schemes, but with the important additional attribute of strict conservation due to their flux-based formulation.

The fast and conservative versions of the flux-based modified method of characteristics may also be a useful for this purpose [157].

### 12.7.5 Brief Evaluation of Convection/Advection Schemes

The first order upwind scheme and several variations of this scheme are very diffusive and should be avoided. Much better results can be obtained with bounded higher-order schemes. The choice of smoothness monitor is not very important for the performance of the TVD schemes, whereas the choice of limiter can be crucial [82]. For some limiters, inherent oscillations, rather than being suppressed, are converted into a series of small monotonic steps, a phenomena known as *stair-casting* [109]. In general, the performance of most of the limiter functions has been found to be fairly similar giving solutions that are free from non-physical wiggles. The second- and third order schemes represent a trade-off between accuracy and computational time. Interpolation of order higher than third makes sense only if the integrals are approximated using higher-order quadrature formulas. Furthermore, since such schemes often produce oscillatory solutions when the grid is not sufficiently fine and are difficult to program, they are rarely used. The second- and third-order schemes are thus preferable, as the improved accuracy gained by higher order schemes are much more costly.

Implicit time integration schemes are not as efficient as the corresponding explicit schemes due to the computational time required on the iterative process. With larger time steps the accuracy of implicit schemes decrease rapidly. The widespread use of the implicit schemes with Courant numbers ten- or even hundredfold the magnitude of what is used in an explicit method, is not justifiable in the presence of gradients or steps in the convected variable.

## 12.8 Implicit Upwind Discretization of the Scalar Transport Equation

The governing transport equation for a scalar property  $\psi$  in an unsteady flow has the general form:

$$\frac{\partial(\rho\psi)}{\partial t} + \nabla \cdot (\rho\mathbf{v}\psi) = \nabla \cdot (I_\psi \nabla \psi) + S_\psi \quad (12.138)$$

To illustrate the principles of the finite volume method, as a first approach, the implicit upwind differencing scheme is used for a multi-dimensional problem. Although the upwind differencing scheme is very diffusive, this scheme is frequently recommended on the grounds of its stability as the preferred method for treatment of convection terms in multiphase flow and determines the basis for the implementation of many higher order upwinding schemes.

Introducing the standard finite volume space integrations and integrating over the time interval  $t_n$  to  $t_{n+1}$  using the implicit Euler approximation, we get:

$$\begin{aligned}
& [(\rho\psi)^{n+1} - (\rho\psi)^n] \frac{\Delta V}{\Delta t} + (\rho v_x \psi A)_e^{n+1} - (\rho v_x \psi A)_w^{n+1} \\
& \quad + (\rho v_y \psi A)_n^{n+1} - (\rho v_y \psi A)_s^{n+1} + (\rho v_z \psi A)_t^{n+1} - (\rho v_z \psi A)_b^{n+1} = \\
& (\Gamma_\psi A \frac{\partial \psi}{\partial x})_e^{n+1} - (\Gamma_\psi A \frac{\partial \psi}{\partial x})_w^{n+1} + (\Gamma_\psi A \frac{\partial \psi}{\partial y})_n^{n+1} - (\Gamma_\psi A \frac{\partial \psi}{\partial y})_s^{n+1} \\
& \quad + (\Gamma_\psi A \frac{\partial \psi}{\partial z})_t^{n+1} - (\Gamma_\psi A \frac{\partial \psi}{\partial z})_b^{n+1} + \langle S_\psi \rangle^{n+1} \Delta V
\end{aligned} \tag{12.139}$$

The upwind scheme is obtained by substituting the UDS approximation of the convective terms and central difference approximation of the diffusive terms into the equation.

For unsteady problems the discretized algebraic equation, for the upwind scheme example, is generally written:

$$\begin{aligned}
a_P^{n+1} \psi_P^{n+1} = & a_W^{n+1} \psi_W^{n+1} + a_E^{n+1} \psi_E^{n+1} + a_S^{n+1} \psi_S^{n+1} + a_N^{n+1} \psi_N^{n+1} \\
& + a_B^{n+1} \psi_B^{n+1} + a_T^{n+1} \psi_T^{n+1} + S_C^{n+1}
\end{aligned} \tag{12.140}$$

where

$$\begin{aligned}
a_P^{n+1} = & a_W^{n+1} + a_E^{n+1} + a_S^{n+1} + a_N^{n+1} + a_B^{n+1} + a_T^{n+1} \\
& - F_w^{n+1} + F_e^{n+1} - F_s^{n+1} + F_n^{n+1} - F_b^{n+1} + F_t^{n+1} - S_P^{n+1}
\end{aligned} \tag{12.141}$$

and

$$a_W^{n+1} = \max(F_w^{n+1}, 0) + D_w^{n+1} \tag{12.142}$$

$$a_E^{n+1} = \max(-F_e^{n+1}, 0) + D_e^{n+1} \tag{12.143}$$

$$a_S^{n+1} = \max(F_s^{n+1}, 0) + D_s^{n+1} \tag{12.144}$$

$$a_N^{n+1} = \max(-F_n^{n+1}, 0) + D_n^{n+1} \tag{12.145}$$

$$a_B^{n+1} = \max(F_b^{n+1}, 0) + D_b^{n+1} \tag{12.146}$$

$$a_T^{n+1} = \max(-F_t^{n+1}, 0) + D_t^{n+1} \tag{12.147}$$

$$S_C^{n+1} = (S_C^{n+1} + \frac{(\rho^n \phi^n)}{\Delta t}) \Delta V \tag{12.148}$$

$$S_P^{n+1} = (S_P^{n+1} - \frac{\rho^{n+1}}{\Delta t}) \Delta V \tag{12.149}$$

The quantities  $S_{C,\psi}$  and  $S_{P,\psi}$  arise from the source term linearization of the form:  $S_\psi = S_{C,\psi} + S_{P,\psi}\psi_P$ .

Higher-order integration schemes in time and space can be used to improve on the accuracy of the calculations, for example, using the higher order convection schemes presented above. For reactor simulations, any appropriate second- and third-order approximations are recommended.

## 12.9 Solution of the Momentum Equation

In this section, particular pressure-based methods designed to solve the momentum equation are outlined. The numerical methods for solving the momentum component equations differ considerably from those designed to solve the generic scalar transport equation, because the velocity is a vector quantity. The special treatment of the terms in the momentum equations that are different from those in the generic transport equation is summarized.

The survey of the numerical methods for single phase flow given here is, to a considerable extent, based on standard textbooks on CFD [141, 49, 202]. The elementary theory is included in this chapter to form a sound basis for the extended algorithms employed solving multiphase problems. The multiphase methods are presented in a sect 12.11.

### 12.9.1 Discretization of the Momentum Equations

The unsteady term in the momentum equation has the same form as the transient term in the generic transport equation and is discretized in the same manner.

The treatment of the convective term in the momentum equation basically follows that of the convective term in the generic equation. However, some extra linearization is required as the convective term in the momentum equation is non-linear in the velocity components.

The viscous shear stress terms in the momentum equation basically correspond to the diffusive term in the generic equation. However, since the momentum equation is a vector equation, the viscous term is more complicated than the generic diffusive term. The first part of the viscous shear stress term in the momentum equations corresponds formally to the diffusive term in the generic transport equation. This shear stress term can be discretized using the approaches described for the corresponding terms of the generic equation. The second viscous shear stress term has no analog in the generic equation but vanishes when the viscosity is constant due to continuity. On the other hand, when the viscosity is spatially variable, this term is non-zero. When solving the resulting algebraic equations, the latter term is conveniently placed as part of the source term. In reactor modeling the bulk viscosity term is normally set to zero for any single phase flow, as discussed in chap 1 and 2. An additional normal stress contribution may be considered for single phase flows, as

explained in chap 1. For incompressible flow with constant fluid properties, the viscous normal stress contributions vanish as can be shown by use of the continuity equation (the bulk viscosity term also vanishes for incompressible flow). In the particular cases when these terms are non-zero, the mean value approach is normally used thus these terms are assumed constant over the GCV and approximated by appropriate Taylor series expansions.

The momentum equation also contains a contribution from the pressure, which has no analog in the generic equation. This term is treated as a surface force. The pressure force term is thus approximated using the same quadrature rule as employed for the surface integrals in the generic transport equation. However, due to the close connection of the pressure and the continuity equation, the treatment of this term and the arrangement of variables on the grid play an important role in order to construct stable and accurate solution methods for the pressure-velocity coupling.

The body forces, like the gravity term, are integrated over the grid volume. Usually, the mean value approach is used, so that the value at the grid center is multiplied by the grid volume. The apparent forces that may occur in particular coordinate systems, are often considered as body forces and integrated in the same way as the gravity term.

### 12.9.2 Numerical Conservation Properties

In this section the numerical conservation properties of finite volume schemes for inviscid incompressible flow are examined<sup>12</sup>. Emphasis is placed on the theory of kinetic energy conservation. Numerical issues associated with the use of kinetic energy non-conservative schemes are discussed [158, 49, 47].

The approximations of the continuity and momentum equations by the finite volume method automatically ensure that mass and momentum are conserved by the discretized equations, provided that the surface fluxes for adjacent grid volumes are identical. These conservative properties are then valid both for a local grid cell and the overall calculation domain. Energy conservation is more difficult to deal with. In incompressible isothermal flow, the only energy form of significance is kinetic energy. In chap 1 it was shown that the kinetic energy equation can be derived by taking the scalar product of the momentum equation with the velocity. Furthermore, in contrast to compressible flow, for which there is a separate conservation equation for the total energy, in incompressible isothermal flows the momentum and energy balances are consequences of the same equation. This poses specific problems constructing proper solution methods for these flow situations. Principal

<sup>12</sup> The early meteorological finite difference studies of long-term numerical time integrations of the equations of fluid motion, which involve non-linear convection terms, revealed the presence of non-linear instabilities due to aliasing errors [143, 144, 7, 145, 210]. To avoid the occurrence of these non-linear instabilities, Arakawa [7] was the first to recognize the importance of the use of numerical schemes which conserve kinetic energy.

interest has thus be given to the kinetic energy balance for a macroscopic volume. The volume of interest may be either the entire calculation domain or a generic grid cell volume. If the local kinetic energy equation (1.124) obtained in sect 1.2.4 is integrated over a grid volume, we obtain, after using Gauss' theorem:

$$\begin{aligned} \frac{\partial}{\partial t} \int_V \left( \rho \frac{v^2}{2} \right) dv = & - \int_A \rho \frac{v^2}{2} \mathbf{v} \cdot \mathbf{n} da - \int_A p \mathbf{v} \cdot \mathbf{n} da + \int_A (\boldsymbol{\sigma} \cdot \mathbf{v}) \cdot \mathbf{n} da - \\ & \int_V (\boldsymbol{\sigma} : \nabla \mathbf{v} - p \nabla \cdot \mathbf{v} + \mathbf{v} \cdot \sum_{c=1}^N \rho_c \mathbf{g}_c) dv \end{aligned} \quad (12.150)$$

The first three terms on the RHS are integrals over the surface of the macroscopic volume. It is noted that the kinetic energy in the macroscopic volume is not changed by the action of convection and pressure. The fourth term on the RHS is an integral over the macroscopic volume. The first term in this volume integral disappears if the flow is inviscid. The second term is zero if the flow is incompressible. The third term is zero in the absence of body forces. In this particular case, the inviscid flow of energy through the grid cell surface and the work done by the pressure force acting at this surface are the only processes that can affect the kinetic energy within the macroscopic volume. The kinetic energy is thus globally preserved in this sense. If we run a simulation under the same extreme conditions, this energy property must be preserved by the numerical method as well. However, under the prevailing conditions, this property cannot be enforced separately because the kinetic energy balance is a consequence of the momentum conservation and not by an independent equation.

If a numerical method is energy conservative and the net energy flux through the surface is zero, then the overall kinetic energy in the domain does not grow with time. If such a method is used, the velocity at every point in the domain must remain bounded, hence the method reflect a kind of stability. Otherwise, if we devise a numerical scheme that is not strictly energy conservative, the net energy flux through the surface may not be zero and/or the overall kinetic energy in the domain can grow with time and create numerical instabilities in our simulations. In many of these schemes the leading truncation error in the kinetic energy equation has the form of an extra dissipation term. In low speed incompressible flows the addition to the internal energy is rarely significant but the loss of kinetic energy is often quite important to the flow. For compressible flows, both effects of the truncation error can be significant. The truncation errors in the time and spatial discretization methods can both destroy the energy conservation property. Kinetic energy preservation is thus especially important in computing unsteady flows. Typical examples are long-term time dependent geophysical flow simulations and dynamic turbulent simulations. For this reason, the interaction between dynamic model dissipation and numerical dissipation is a very important topic

in these fields of computational dynamics. For steady flows, energy conservation has generally got less attention. However, it is rather obvious that these truncation errors are analogous to the terms in the generic transport equation which we did refer to as *artificial diffusion* or *numerical diffusion*. For obvious reasons, in some fields of science the truncation error terms occurring in the kinetic energy equation are named *numerical dissipation* or *artificial dissipation*. In a broader view, in dynamics it is implied that when the pure convection/advection equation (which is free of physical diffusion) is solved for any property by a numerical approximation method that reduces the amplitude and changes the shape of the initial wave in a way analogous to a diffusional process, the method is said to contain numerical dissipation.

From the above discussion it may be inferred that for geophysical flow simulations and simulations of turbulent flow, using either direct numerical simulations (DNS) or large eddy simulations (LES), it is highly desirable to employ schemes that conserve mass, momentum, and kinetic energy [47]. However, many numerical methods approximate the transport of kinetic energy from the large scale vortices to the smaller ones in an erroneous manner. Hence, the kinetic energy stored at the smaller vortex scales may grow and the solution method can become unstable. In such situations some apparent dissipation that have no connection to physics are sometimes added to provide stability of numerical methods. It is noted that kinetic energy conservation is associated with numerical stability but not to the convergence or accuracy properties of a method. However, the physical dissipation used in the simulation is determined by the sum of the dynamic model dissipation and the apparent dissipation added.

### 12.9.3 Choice of Variable Arrangement on the Grid

In this section, attention is given to the numerical discretization of the finite volume calculation domain and the choice of variable arrangement on the grid.

In the coordinate discretization process one selects the node points in the domain at which the values of the unknown dependent variables are to be computed. In the finite volume method one also selects the location of the grid cell surfaces at which the property fluxes are determined. In this way the computational domain is sub-divided into a number of smaller, non-overlapping sub-domains. There are many variants of the distribution of the computational node points and grid cell surfaces within the solution domain. The grid arrangements associated with the finite volume discretization of the momentum equation are generally more complicated than the one employed for a scalar transport equation.

As a first approach, it may be natural to employ a *collocated* grid arrangement and store all the variables at the same set of grid points and to use the same grid volumes for all of them. In this case the number of coefficients that must be computed and stored is minimized, because many of the terms in each of the equations are essentially identical. However, it is not required that

all the variables share the same grid. A different arrangement has been shown to be advantageous. In the orthogonal curvilinear coordinates, the *staggered* grid arrangement introduced by Harlow and Welsh [67] offers several advantages over the collocated arrangement. The most important advantage of the staggered arrangement is that a stronger coupling between the velocities and the pressure is achieved. This helps to avoid some types of convergence problems and oscillations in the pressure and velocity fields [141]. In addition, several terms that require interpolation with the collocated arrangement, can be calculated to a second-order approximation without interpolation in the staggered arrangement. The numerical approximation on a staggered grid is also preserving the local and overall kinetic energy.

Other grid arrangements have not gained wide popularity in engineering studies of single- and multiphase flows. Numerous analysis of the impact of the grid arrangement on the accuracy and stability of numerical simulations have been performed in other branches of physical science. The arrangement of the grids is, for example, particularly important for dynamic flows in meteorology and oceanography. For further studies of the grid arrangements employed in these geophysical flows, the pioneering work of Arakawa and Lamb [8] may be considered.

#### 12.9.4 Calculation of Pressure

In this section, several strategies for determining the pressure in the incompressible flow limit is outlined for pressure-based methods. The extension of the pressure-correction approach to arbitrary Mach numbers is examined.

For pressure-based techniques, the lack of an independent equation for the pressure complicates the solution of the momentum equation. Furthermore, the continuity equation does not have a transient term in incompressible flows because the fluid transport properties are constant. The continuity reduces to a kinematic constraint on the velocity field. One possible approach is to construct the pressure field so as to guarantee satisfaction of the continuity equation. In this case, the momentum equation still determines the respective velocity components. A frequently used method to obtain an equation for the pressure is based on combining the two equations. This means that the continuity equation, which does not contain the pressure, is employed to determine the pressure. If we take the divergence of the momentum equation, the continuity equation can be used to simplify the resulting equation.

The Poisson equation for the pressure becomes:

$$\begin{aligned}\nabla \cdot (\nabla p) &= -\nabla \cdot \left[ \nabla \cdot (\rho \mathbf{v}\mathbf{v} + \boldsymbol{\sigma}) - \rho \mathbf{g} + \frac{\partial(\rho \mathbf{v})}{\partial t} \right] \\ &= -\nabla \cdot \left[ \nabla \cdot (\rho \mathbf{v}\mathbf{v} + \boldsymbol{\sigma}) \right] - \nabla \cdot (\rho \mathbf{g}) + \frac{\partial^2 \rho}{\partial t^2}\end{aligned}\tag{12.151}$$

in which the transient term is rewritten by use of the continuity equation.

For the case of constant fluid properties (e.g., density and viscosity), the equation reduces to:

$$\nabla \cdot (\nabla p) = -\nabla \cdot [\nabla \cdot (\rho \mathbf{v}\mathbf{v})] \quad (12.152)$$

This simplification is obtained by use of the continuity equation.

The Laplacian operator on the LHS of the pressure equation is the product of the divergence operator originating from the continuity equation and the gradient operator that comes from the momentum equations. The RHS of the pressure equation consists of a sum of derivatives of the convective terms in the three components of the momentum equation. In all these terms, the outer derivative stems from the continuity equation while the inner derivative arises from the momentum equation. In a numerical approximation, it is essential that the consistency of these operators is maintained. The approximations of the terms in the Poisson equations must be defined as the product of the divergence and gradient approximations used in the basic equations. Violation of this constraint may lead to convergence problems as the continuity equation is not appropriately satisfied.

Even though the original derivation of this method was based on the governing equations for incompressible flows, in which the fluid properties are constant, this concept can be adapted to many flows with variable fluid properties and weak compressibility.

### Explicit Projection Method for Unsteady Flow

In this section, an explicit time advance scheme for unsteady flow problems is outlined [30]. The momentum equation is discretized by an explicit scheme, and a Poisson equation is solved for the pressure to enforce continuity. The continuity is discretized in an implicit manner. In the original formulation, the spatial derivatives were approximated by finite difference schemes.

To illustrate the basic principles of the projection method, the semi-discretized momentum equations are written symbolically as:

$$\frac{\partial(\rho v_i)}{\partial t} = -\frac{\delta(\rho v_i v_j)}{\delta x_j} - \frac{\delta p}{\delta x_i} - \frac{\delta \sigma_{ij}}{\delta x_j} = -C_i - D_i - \frac{\delta p}{\delta x_i} \quad (12.153)$$

where  $\delta/\delta x$  represents a discretized spatial derivative, and  $C_i$  and  $D_i$  are shorthand notations for the convective and viscous terms.

For simplicity, the momentum equation (12.153) is solved with the explicit Euler method in time. Then, we obtain:

$$(\rho v_i)^{n+1} - (\rho v_i)^n = -\Delta t (C_i^n + D_i^n + \frac{\delta p^n}{\delta x_i}) \quad (12.154)$$

The velocity at time step  $n$  is used to compute  $C_i^n$  and  $D_i^n$ , whereas the pressure at time step  $n$  is used to compute the pressure gradient terms  $\delta p^n/\delta x_i$ .

This gives an estimate of  $\rho v_i$  at the new time step  $n + 1$ . However, in general, this velocity field does not satisfy the continuity equation. The continuity equation is generally discretized in an implicit manner:

$$\frac{\partial \rho}{\partial t} + \frac{\delta(\rho v_i)^{n+1}}{\delta x_i} = 0 \quad (12.155)$$

The transient term vanishes for incompressible flows, as the fluid properties are constant. The transient term is retained here to emphasize that this method can be applied for compressible flows as well. For compressible flow both velocity and density appear as dependent variables in the continuity equation. Nevertheless, the discrete form of the mass balance can still be interpreted as a constraint equation for pressure. Compressible and reactive variable density flows are considered shortly in the present section.

In the design of an approach to enforced continuity, we take the numerical divergence of (12.154). The result is:

$$\frac{\delta(\rho v_i)^{n+1}}{\delta x_i} - \frac{\delta(\rho v_i)^n}{\delta x_i} = -\Delta t \left[ \frac{\delta}{\delta x_i} (C_i^n + D_i^n + \frac{\delta p^n}{\delta x_i}) \right] \quad (12.156)$$

The first term is the divergence of the new mass fluxes, for which we must enforce continuity. The second term is known if continuity was enforced at time step  $n$ .

With minor manipulation, the result is a discrete Poisson equation for the pressure  $p^n$ :

$$\frac{\delta}{\delta x_i} \left( \frac{\delta p^n}{\delta x_i} \right) = -\frac{\delta}{\delta x_i} (C_i^n + D_i^n) + \frac{1}{\Delta t} \left[ \frac{\delta \rho}{\delta t} + \frac{\delta(\rho v_i)^n}{\delta x_i} \right] \quad (12.157)$$

In this relation, the operator  $\delta/\delta x_i$  outside the parentheses on the LHS is the divergence operator inherited from the continuity equation, while  $\delta p^n/\delta x_i$  is the pressure gradient from the momentum equation. The operator  $\delta\rho/\delta t$  is the time advancement of the continuity equation. If the pressure  $p^n$  satisfies the discrete Poisson equation, the velocity field at time step  $n + 1$  will fulfill continuity (and be divergence free for constant density flows).

The algorithm for time-integration of the momentum equation can then be sketched as follows:

1. Start with a velocity field  $v_i^n$  that satisfy continuity at time  $t_n$ .
2. Compute the convective  $C_i^n$  and viscous  $D_i^n$  terms and their divergences.
3. Solve the Poisson equation for the pressure  $p^n$ .
4. Compute the mass conservative velocity field at the new time step.
5. Go to the next time step.

Methods similar to this are commonly used to solve the momentum equation when an accurate time history of the flow is required. In these particular cases, more accurate time advancement methods than the first order Euler method must be used. Explicit methods are preferred for (fast) transient flows because

they are more accurate and less computationally demanding than implicit methods with the same time step size. To allow longer time steps to be used and for stability reasons, some of the terms may also be treated implicitly.

### Implicit Pressure-Correction Methods

In this section, an implicit pressure correction method is outlined [140, 141, 49, 202].

Implicit methods are preferred for slow-transient flows because they have less stringent time step restrictions than explicit schemes. However, the time step must still be chosen small enough so that an accurate history is obtained. It is further noted that implicit methods can also be used to solve steady problems. In this particular approach, we have to solve an unsteady form of the problem until a steady state is reached. For the artificial time integration, large time steps are often used intending to reach the steady state quickly.

If an implicit method is used to advance the momentum equation in time, the discretized equations for the velocities at the new time step are non-linear. Implicit methods thus require an iterative solution process. Several restrictions must be placed on the coefficient matrix to ensure a stable and efficient solution procedure, most important all the coefficients must be positive [141].

The discretized  $x$ -component of the momentum equation at the surface point  $e$ , for example, can be written as:

$$a_e^{n+1}v_{x,e}^{n+1} = \sum_{nb} a_{nb}^{n+1}v_{x,nb}^{n+1} + S_e^{n+1} - \left(\frac{\delta p^{n+1}}{\delta x}\right)_e \quad (12.158)$$

For convenience, explaining the solution methods, the pressure gradient term is written separately and not included in the source term. Furthermore, in this discrete momentum equation we have used the scalar grid notation. The index  $e$  refers to a surface point in the scalar grid used for the continuity equation, this surface point coincides with a velocity node in a staggered velocity grid. The index  $nb$  denotes the neighbor nodes that appears in the discretized momentum equation. The source term  $S_e$  contains all of the terms that may be explicitly computed in terms of  $v_x^n$  as well as any body force or other linearized terms that may depend on the  $v_x^{n+1}$  or other variables at the new time level.

When simulating unsteady flows and time accuracy is required, the iterations must be continued within each time step until the entire system of non-linear equations is satisfied in accordance with an appropriate convergence criterion. For steady flows, it is common either to take an infinite time step and iterate until the steady non-linear equations are satisfied, or march in time without requiring full satisfaction of the non-linear equations at each time step. However, both of these approaches may become unstable if the initial guesses are not sufficiently close to the exact solution, hence in some complex cases the time step must be restricted to ensure that the simulation does not diverge/explode.

For unsteady flows the system of non-linear equations are linearized in the iteration process within each time step, since all the solvers are limited to linear systems. The iterative process is thus performed on two different levels. The solver iterations are performed on provisional linear systems with fixed coefficients and source terms until convergence. Then, the system coefficients and sources are updated based on the last provisional solution and a new linearized system is solved. This process is continued until the non-linear system is converged, meaning that two subsequent linear systems give the same solution within the accuracy of a prescribed criterion. A standard notation used for the different iterations within one time step is that the coefficient and source matrices are updated in the *outer iterations*, whereas the *inner iterations* are performed on provisionally linear systems with fixed coefficients. On each outer iteration, the equations solved are on the form:

$$a_e v_{x,e}^{\nu*} = \sum_{nb} a_{nb} v_{x,nb}^{\nu*} + S_e^{\nu-1} - \left( \frac{\delta p^{\nu-1}}{\delta x} \right)_e \quad (12.159)$$

where  $v_{x,e}^{\nu*}$  represents a provisional value of  $v_{x,e}^{n+1}$ .

We normally drop the time step index  $n + 1$  and introduced an outer iteration counter  $\nu$ .  $v_x^\nu$  thus represents the current estimate of the solution  $v_x^{n+1}$ . At the beginning of each outer iteration, the two last terms on the right hand side of (12.159) are evaluated using the variables at the preceding outer iteration.

The components of the momentum equation are usually solved sequentially, meaning that the components of the momentum equation are solved one by one. Since the pressure used in these iterations has been obtained from the previous outer iteration or time step, the velocities computed from (12.159) do not generally satisfy the discretized continuity equation. The predicted velocities do not satisfy the continuity equation, so the  $v_{i,e}^{\nu*}$  at iteration  $\nu$  are not the final values of the velocity components. To enforce the continuity equation, the velocities need to be corrected. This is achieved by modifying the pressure field.

The solution algorithm for this class of methods are outlined in the following. The first task is to correct the velocity. In order to calculate the velocity correction, the velocity at the surface point  $e$  is obtained by solving the linearized momentum equations (12.159) for  $v_{x,e}^{\nu*}$ :

$$v_{x,e}^{\nu*} = \frac{S_e^{\nu-1} + \sum_{nb} a_{nb} v_{x,nb}^{\nu*}}{a_e} - \frac{1}{a_e} \left( \frac{\delta p^{\nu-1}}{\delta x} \right)_e \quad (12.160)$$

The next task is to correct the velocities so that they satisfy the continuity equation:

$$\frac{\delta \rho}{\delta t} + \frac{\delta(\rho v_i^\nu)}{\delta x_i} = 0 \quad (12.161)$$

which is achieved by correcting the pressure field. Recall that in the pressure-based methods the continuity is transformed to an equation for pressure or a

pressure correction quantity. The transient term in the continuity vanishes for incompressible flows, as the fluid properties are constant. The transient term is retained here to emphasize that this method can be applied for compressible flows as well. In this case, the discrete form of the mass balance can still be interpreted as a constraint equation for pressure. Compressible and reactive variable density flows are considered shortly in the present section.

The corrected velocities and pressure are linked by relations on the form:

$$v_{x,e}^\nu = \frac{S_e^{\nu-1} + \sum_{nb} a_{nb} v_{x,nb}^{\nu*}}{a_e} - \frac{1}{a_e} \left( \frac{\delta p^\nu}{\delta x} \right)_e \quad (12.162)$$

Continuity is then enforced by inserting the corresponding expressions for all the velocity components  $v_i^\nu$  into the continuity equation (12.161), to yield a discrete Poisson equation for the pressure:

$$\left[ \frac{\delta \rho}{\delta t} + \frac{\delta}{\delta x_i} (\rho v_i^\nu) \right]_P = \left[ \frac{\delta \rho}{\delta t} \right]_P + \frac{\delta}{\delta x_i} \left[ \rho \left( \frac{S^{\nu-1} + \sum_{nb} a_{nb} v_{i,nb}^{\nu*}}{a} - \frac{1}{a} \left( \frac{\delta p^\nu}{\delta x_i} \right) \right) \right]_P = 0 \quad (12.163)$$

or

$$\frac{\delta}{\delta x_i} \left[ \frac{\rho}{a} \left( \frac{\delta p^\nu}{\delta x_i} \right) \right]_P = \left[ \frac{\delta \rho}{\delta t} \right]_P + \frac{\delta}{\delta x_i} \left[ \rho \left( \frac{S^{\nu-1} + \sum_{nb} a_{nb} v_{i,nb}^{\nu*}}{a} \right) \right]_P \quad (12.164)$$

After solving the Poisson equation for the pressure, by use of (12.164), the final velocity field at the new iteration,  $v_i^\nu$ , is calculated from relations on the form (12.162). At this point, we have a velocity field which satisfies the continuity condition, but the velocity and pressure fields do not necessarily satisfy the momentum equations on the form (12.160). We begin another outer iteration and the process is continued until the velocity field which satisfies both the momentum and continuity equations is obtained.

In the most common family of methods constructed for correcting the pressure, a pressure-correction is used instead of the actual pressure. The velocities computed from the linearized momentum equations and the pressure  $p^{\nu-1}$  are taken as provisional values to which a small correction must be added:

$$v_i^\nu = v_i^{\nu*} + v_i' \quad \text{and} \quad p^\nu = p^{\nu-1} + p' \quad (12.165)$$

To initiate the iteration process a pressure field  $p^{\nu-1}$  is guessed. The discretized momentum component equations on the form like (12.160) are solved using the guessed pressure field to obtain the corresponding approximate values for the velocity components. Substitution of the correct pressure field into the momentum equations yields the correct velocity field. The discretized equations on the form (12.160) link the correct velocity fields with the correct pressure field. Subtraction of the approximate momentum equations from the exact ones (neglecting any changes in the source term  $S$ ), we obtain the necessary relations between the velocity and pressure corrections on the form:

$$v'_{x,e} = v_{x,e} - v_{x,e}^{\nu*} = \frac{\sum_{nb} a_{nb} v'_{x,nb}}{a_e} - \frac{1}{a_e} \left( \frac{\delta p'}{\delta x} \right)_e \quad (12.166)$$

Application of the discretized continuity equation (12.161) and velocity corrections on the form (12.166) produces the following pressure-correction equation:

$$\frac{\delta}{\delta x_i} \left[ \frac{\rho}{a} \left( \frac{\delta p'}{\delta x_i} \right) \right]_P = \left[ \frac{\delta \rho}{\delta t} \right]_P + \frac{\delta}{\delta x_i} \left[ (\rho v_i^{\nu*}) \right]_P + \frac{\delta}{\delta x_i} \left[ \left( \rho \frac{\sum_{nb} a_{nb} v'_{i,nb}}{a} \right) \right]_P \quad (12.167)$$

The velocity corrections at the neighbor nodes  $\sum_{nb} a_{nb} v'_{i,nb}$  are unknown at this point, so it is common practice to disregard them. The omission of these terms is the main approximation in this algorithm and the major reason why the resulting method does not converge very rapidly.

Once the pressure correction has been solved for, the velocities are updated using (12.165) and (12.166). This procedure is known as the SIMPLE (Semi-Implicit Method for Pressure-Linked Equations) algorithm [140, 141].

Another way of treating the last term in the pressure-correction equation (12.167) is to approximate it rather than neglecting it. One could approximate the velocity correction term  $\sum_{nb} a_{nb} v'_{i,nb}$  at the neighbor nodes by use of the center point velocity correction:

$$\sum_{nb} a_{nb} v'_{i,nb} \approx \sum_{nb} a_{nb} v'_{x,e} \quad (12.168)$$

In one view, the unknown velocity corrections at any node are approximated by a weighted mean of the neighbor values.

If we insert this approximation into (12.166), the following approximate relation between  $v'_x$  and  $p'$  is obtained:

$$v'_{x,e} = - \frac{1}{a_e + \sum_{nb} a_{nb}} \left( \frac{\delta p'}{\delta x} \right)_e \quad (12.169)$$

With this approximation the  $a$ -coefficient in front of the pressure gradient in (12.167) is replaced by  $a + \sum_{nb} a_{nb}$  and the last term disappears. This is known as the SIMPLEC (SIMPLE Consistent) algorithm [191].

An alternative method of this type is derived by neglecting  $\sum_{nb} a_{nb} v'_{x,nb}$  in the first correction step as in the SIMPLE method but following the correction with another corrector step. The second correction to the velocity  $v''_x$  is defined in analogy to (12.166):

$$v''_{x,e} = \frac{\sum_{nb} a_{nb} v'_{x,nb}}{a_e} - \frac{1}{a_e} \left( \frac{\delta p''}{\delta x} \right)_e \quad (12.170)$$

where  $\sum_{nb} a_{nb} v'_{x,nb}$  is approximated after  $v'_x$  has been calculated from (12.166) with  $\sum_{nb} a_{nb} v'_{x,nb}$  neglected. Application of the discretized continuity equation to correct velocities leads to a second pressure-correction equation on the form:

$$\frac{\delta}{\delta x_i} \left[ \frac{\rho}{a_P^{v_i}} \left( \frac{\delta p''}{\delta x_i} \right) \right]_P = \left[ \frac{\delta}{\delta x_i} \left( \rho \frac{\sum_{nb} a_{nb} v'_{i,nb}}{a} \right) \right]_P \quad (12.171)$$

This procedure is essentially a truncated iterative method for solving (12.167) with one correction only, so that the last term is treated explicitly. It is known as the PISO (Pressure Implicit with Splitting of Operators) algorithm [79].

The PISO algorithm solves the costly pressure correction equation twice, and under-relaxation is still required to stabilize the iteration process. However, this non-iterative method (only two outer corrections per time step) has been found to be quite efficient for certain single phase flows. An adapted, steady state version of the PISO algorithm has been deduced as well [202]. The original PISO algorithm can also be applied to steady state calculations starting with guessed initial conditions and solving as a transient problem for a long period of time until a steady solution is achieved.

Yet another similar method of this kind called SIMPLER (SIMPLE Revised) was proposed by Patankar [141] to improve the convergence rate, as compared to the SIMPLE procedure. In this method, the pressure-correction equation (12.167) is solved first with the last term neglected as in SIMPLE. The pressure correction so obtained is used only to correct the velocity field  $v_i^{\nu*}$  to obtain  $v_i^\nu$  so that it satisfies continuity by use of (12.166) in which the first term on the RHS is neglected. The new pressure field is calculated from pressure equation (12.164) using  $\sum_{nb} a_{nb} v_i^{\nu*}$  instead of  $\sum_{nb} a_{nb} v_i^{\nu}$ .

The convergence of the SIMPLE algorithm can be improved by under-relaxation so that only a portion of  $p'$  is added to  $p^{\nu-1}$  after the pressure-correction equation is solved:

$$p^\nu = p^{\nu-1} + \alpha_P p' \quad (12.172)$$

In the under-relaxation procedure, the under-relaxation parameter  $\alpha_P$  may take values in the range:  $0 \leq \alpha_P \leq 1$ . In particular cases, the SIMPLEC, SIMPLER and PISO approaches are more stable and do not require any under-relaxation of the pressure correction.

The solution algorithm for this class of methods can be summarized as follows:

1. Start calculation of the fields at the new time  $t_{n+1}$  using the latest solution  $v_i^n$  and  $p^n$  (i.e., the initial conditions are used when  $n = 1$ ) as starting estimates for  $v_i^{n+1}$  and  $p^{n+1}$ .
2. Assemble and solve the linearized algebraic equation systems for the velocity components (momentum equations) to obtain  $v_i^{\nu*}$ .
3. Assemble and solve the pressure-correction equation to obtain  $p'$ .
4. Correct the velocities and pressure to obtain the velocity field  $v_i^\nu$ , which satisfies the continuity equation, and the new pressure  $p^\nu$ .

For the PISO algorithm, solve the second pressure-correction equation and correct both velocities and pressure again.

For SIMPLER, solve the pressure equation for  $p^\nu$  after  $v_i^\nu$  is obtained above.

5. Return to step 2 and repeat, using  $v_i^{\nu}$  and  $p^{\nu}$  as improved estimates for  $v_i^{n+1}$  and  $p^{n+1}$ , until all corrections are negligible small.
6. Advance to the next time step.

To obtain the solution at the new time step in the implicit method, several outer iterations are performed. If the time step is small, only a few outer iterations per time step are necessary. For steady problems, the time step may be infinite and the under-relaxation parameter acts like a pseudo-time step.

Methods of this kind are quite efficient for solving single phase steady state problems.

### Pressure-Correction Method for Compressible Flow

In this section the pressure correction method for incompressible flow is extended to arbitrary Mach numbers [78, 87, 192, 33, 49].

The governing conservation equations for compressible flows are the continuity, momentum and energy equations. In addition, the pressure, density, and temperature are linked by an equation of state. It was shown in chap 1 that for compressible flows, the interactions between the mechanical and thermal processes are important. In particular, the viscous dissipation term may be a significant heat source and the conversion of internal energy to kinetic energy (and visa versa) by means of flow dilatation may also be significant. Most of the terms in the governing equations presented in chap 1 must then be retained. For low Mach number (almost) incompressible flows, however, the total energy or the heat equation can be approximated by a scalar transport equation for the temperature and only the transient, convection and heat conduction terms are important.

The discretization of the compressible flow equations can still be carried out using the same, or very similar, methods as already presented. However, the solution algorithms designed for incompressible (low Mach number) flow must be adapted to the novel (high Mach number) compressible properties of the governing equations. The relevant changes required are associated with the boundary conditions (since different conditions are required for hyperbolic equations compared to parabolic or elliptic equations), and the nature and treatment of the coupling between the density and the pressure. For compressible flows both velocity and density appear as dependent variables in the mass conservation equation. Nevertheless, the algebraic representation of mass conservation can still be interpreted as a constraint equation for pressure and the modified interpretation of the role of pressure for the segregated approach to solve compressible flow becomes that the pressure must influence the velocity through the momentum equation and the density through the equation of state such that together the resulting velocities and the resulting densities conserve mass.

To explain the modifications required to the pressure-correction equation previously presented for incompressible flow to deal with compressible flows,

we consider a segregated solution method, in which the linearized equations for the velocity components, pressure correction, temperature, and other scalar variables are known.

The velocities obtained by solving the linearized momentum equations on the form (12.160), by use of the previous outer iteration values for the pressure and the density, do not satisfy the mass conservation equations (12.161). When the mass fluxes computed from these velocities and the previous outer iteration density (denoted by  $F^*$ ) are inserted into the discretized continuity equation, we obtain:

$$\frac{(\rho^{\nu-1} - \rho^n)\Delta V}{\Delta t} + F_e^* + F_w^* + F_n^* + F_s^* + F_t^* + F_b^* = S_m^* \quad (12.173)$$

The imbalance  $S_m^*$  must be eliminated by a correction method.

In compressible flows, the mass flux depends on both the velocity component normal to the cell face and the variable density. To correct the mass flux imbalance, both the density and the velocity must be corrected. The corrected mass flux on the  $e$  face of a grid volume can be expressed as:

$$\begin{aligned} F_e^\nu &= (\rho^\nu v^\nu A)_e = (\rho^{\nu-1} + \rho')_e (v_x^{\nu*} + v'_x)_e A_e \\ &= (\rho^{\nu-1} v_x^{\nu*} A)_e + (\rho^{\nu-1} v'_x A)_e + (\rho' v_x^{\nu*} A)_e + (\rho' v'_x A)_e \end{aligned} \quad (12.174)$$

where  $\rho'$  and  $v'_{x,e}$  represent the density and velocity corrections, respectively.

The overall mass flux correction is defined as the sum of all the correction terms:

$$F'_e = (\rho^{\nu-1} v'_x A)_e + (\rho' v_x^{\nu*} A)_e + (\rho' v'_x A)_e \approx (\rho^{\nu-1} v'_x A)_e + (\rho' v_x^{\nu*} A)_e \quad (12.175)$$

The second order correction term is normally neglected as this term becomes zero more rapidly than the two first order correction terms.

The first of the two remaining terms in the mass flux correction is identical to the one obtained for incompressible flows (e.g., adopting the SIMPLE assumption in (12.166)):

$$(\rho^{\nu-1} v'_x A)_e = -(\rho^{\nu-1} A)_e \left( \frac{1}{a_e} \right) \left( \frac{\delta p'}{\delta x} \right)_e \quad (12.176)$$

The second term in the mass flux correction relation (12.175), is due to the compressibility effects. It involves the correction to the density at the grid cell volume face. If the SIMPLE method is to be extended to compressible flows, we must thus express the density correction in terms of the pressure correction to enable an efficient update of the density corrections in the pressure correction equation.

For one outer iteration, the temperature may be regarded as provisionally fixed, hence by use of the ideal gas law we may write:

$$\rho' \approx \left( \frac{\partial \rho}{\partial p} \right)_T p' = \frac{M_\omega}{RT} p' \quad (12.177)$$

When the solution is converged, all the variable corrections are zero. However, it is important that the connection between the density and pressure corrections becomes qualitatively correct, because the intermediate results may strongly influence the stability and convergence rate of the method.

The second correction term in the mass flux correction can then be written as:

$$(\rho' v_x^* A)_e = \left( \frac{(\frac{\partial \rho}{\partial p})_T F^*}{\rho^{\nu-1}} \right)_e p'_e \quad (12.178)$$

The overall mass flux correction on the  $e$  face of a grid volume is thus:

$$F'_e = -(\rho^{\nu-1} A)_e \left( \frac{1}{a_e} \right) \left( \frac{\delta p'}{\delta x} \right)_e + \left( \frac{(\frac{\partial \rho}{\partial p})_T F^*}{\rho^{\nu-1}} \right)_e p'_e \quad (12.179)$$

The value of  $p'$  at the cell face center and the normal component of the gradient of  $p'$  at the cell face center need to be approximated, using consistent convection schemes for the term that stems from the density correction and normally a central difference approximation to the term due to the velocity correction.

The continuity equation (12.173), which must be satisfied by the corrected mass fluxes and density, can now be written as:

$$\frac{\rho'_P \Delta V}{\Delta t} + F'_e + F'_w + F'_n + F'_s + F'_t + F'_b + S'_m = 0 \quad (12.180)$$

If (12.177) is used to express  $\rho'_P$  in terms of  $p'_P$  and the approximation (12.175) of the mass flux correction is substituted into the latter form of continuity equation, we obtain an algebraic system of equations for the pressure-correction:

$$a_P p'_P = \sum_{nb} a_{nb} p'_{nb} - S'_m \quad (12.181)$$

The coefficients in this equation depend on the approximations used for the gradients and cell face values of the pressure correction. The part which stems from the velocity correction is identical to that for the incompressible case. The second part depends on the approximation used for the term which corresponds to the convective contribution to the conservation equations. The presence of convective terms in the compressible pressure equation makes the solution unique.

It is noted that the given pressure-correction method can be applied for arbitrary Mach number flows. At low Mach numbers (almost incompressible flow), the Laplacian term dominates and we recover the Poisson equation. On the other hand, at high Mach number (highly compressible flow), the convective term dominates, reflecting the hyperbolic nature of the flow. Solving the pressure-correction equation is then equivalent to solving the continuity equation for density. Thus, the pressure correction method automatically adjusts

to the local nature of the flow and the same method can be applied to the entire flow. Using this unified method the standard boundary conditions applied for incompressible flows also hold for compressible flow and are treated in the same way as for incompressible flow simulations. However, in compressible flow additional boundary conditions are required. Most important, the total pressure must be prescribed.

### Pressure-Correction Methods for Reactive Flows

Most chemical reactor flows can be characterized as low Mach number flows. The governing equations for low Mach number reactive flows were derived in sect 1.2.5. Models for low Mach number reactive flows generally consist of the continuity, momentum, species mass and heat balances. The heat balance is generally expressed in terms of temperature. In general, for non-isothermal reactive low Mach number flows, the mixture density may vary due to changes in temperature, pressure and chemical composition. The temperature changes may be created by the chemical process through the chemical reactions, the heats of reaction, non-ideal fluid mixing, and the external heating or cooling devices. The thermodynamic pressure may be changed by external expansion or compression of the fluid mixture. The local pressure variations caused by the flow are generally very small in chemical reactors, except in the initial phase of flow in multiphase reactors and packed (porous) beds in which the axial pressure drop may be significant but not changing much after a short initial start-up period. The gravity force term may be important for tall liquid columns. The chemical composition can be changed by the chemical reactions in the process. In reactive processes, the fluid transport coefficients and the mixture thermodynamic properties vary basically due to changes in the chemical composition, temperature, thermodynamic pressure created by the chemical process, and not because of any particular flow phenomena.

The basic elements of the solution methods presented above for solving incompressible and compressible flows can be adapted for reactive flows as well. However, special attention must be attributed to the novel system characteristics that the multicomponent fluid mixture properties and temperature may change due to chemical reactions, non-ideal fluid mixing and external heat sources, although the low Mach number indicates that the transport properties should be about constant. Most important, an appropriate algorithm for reactive flows must enable accurate solutions of non-isothermal flows with changes in composition due to chemical reactions. For non-isothermal reactive flows, the interactions between the species mass balances, mixture continuity and momentum equations, and the heat or temperature equation must be considered and they are generally distinct from those of high Mach number compressible flow. In particular, the viscous dissipation term and the conversion of internal heat to kinetic energy (and visa versa) by means of flow dilatation can both be neglected in most cases. The heat equation can thus be approximated by a scalar transport equation for the enthalpy or the temperature

in which only the transient, convection/advection, heat conduction, heat of reaction and external heat source terms are important. To calculate the pressure for gas mixtures an appropriate EOS is needed to convert the density correction term into a pressure correction. The ideal gas law is often used. If the external pressure is changed, expansion or compression of the fluid mixture within the reactor take place. In this case, the conversion of internal heat to kinetic energy (and *visa versa*) by means of flow dilatation can not be neglected. A complete heat balance must be used. However, the present reactor simulations do not consider any variations of the external pressure during operation, another simulation with different operating conditions are performed instead. For many liquid mixtures the standard incompressible flow solvers can be adopted to solve isothermal reactive flows with negligible changes in the mixture density due to chemical reactions. No energy equation is then required as the flow and the chemical process are independent of temperature. To solve isothermal reactive flows with limited changes in the mixture density due to chemical reactions, a modified incompressible solver with no energy balance may be used. For chemical processes creating small temperature changes (for liquid mixtures in particular), the incompressible methods may be extended with a temperature equation provided that in all conservation laws temperature dependent transport coefficients and thermodynamic properties are considered.

## 12.10 Fractional Step Methods

The fractional step, or time splitting, concept is more a generic operator splitting approach than a particular solution method [30, 211, 124, 92, 49]. It is essentially an approximate factorization of the methods applied to the different operators in an equation or a set of equations. The overall set of operators can be solved explicitly, implicitly or by a combination of both implicit and explicit discretization schemes.

### Scalar Transport Equation

The fractional step concept is frequently used to solve scalar transport equations on the generic form [10, 85, 137]:

$$\frac{\partial(\rho\psi)}{\partial t} + \nabla \cdot (\mathbf{v}\psi) = \nabla(\Gamma_\psi \nabla\psi) + S_\psi \quad (12.182)$$

This balance equation is written on the conservative flux form, the non-conservative form of the equation is easily obtained by use of the continuity equation.

To illustrate the fractional step method, the explicit Euler advancement of the property  $\psi$  can be written in symbolic form:

$$(\rho\psi)^{n+1} = (\rho\psi)^n + (-C_\psi + D_\psi + S_\psi)^n \frac{\Delta t}{\Delta V} \quad (12.183)$$

where  $C_\psi$ ,  $D_\psi$ , and  $S_\psi$  represent the discretized form of the convective, diffusive, and source terms, respectively.

The fractional step, or time splitting, concept can be adapted to the discretized equation by splitting the discrete scalar equation into a three step method:

$$(\rho\psi)^* = (\rho\psi)^n - C_\psi^n \frac{\Delta t}{\Delta V} \quad (12.184)$$

$$(\rho\psi)^{**} = (\rho\psi)^* + D_\psi^n(\psi^*) \frac{\Delta t}{\Delta V} \quad (12.185)$$

$$(\rho\psi)^{n+1} = (\rho\psi)^{***} = (\rho\psi)^{**} + S_\psi^n(\psi^{**}) \frac{\Delta t}{\Delta V} \quad (12.186)$$

In this example the property  $\psi$  is advanced using the explicit Euler scheme for all the operators. However, both implicit and explicit methods can be employed. In order to take a larger time steps, implicit methods are generally preferred. The convective and diffusive terms can be further split into their components in the various coordinate directions, for example, by use of the Strang [181] operator factorization scheme.

### Incompressible Viscous Flow

The fractional-step concept can be used to solve the governing equations for the fluid motion as well. To illustrate the overall method with emphasis on the pressure-velocity coupling, a FVM variant of the fractional-step method used by Chorin [30], Fortin et al [56] and Andersson and Kristoffersen [3] for solving the unsteady Navier-Stokes and continuity equations for incompressible viscous flows is outlined. We consider the equations of motion of an incompressible viscous fluid:

$$\frac{\partial v_i}{\partial t} + \frac{\partial v_i v_j}{\partial x_j} = -\frac{\partial p}{\partial x_i} + \nu \frac{\partial^2 v_i}{\partial x_j \partial x_j} \quad (12.187)$$

and the continuity equation on the form:

$$\frac{\partial v_i}{\partial x_i} = 0 \quad (12.188)$$

By use of the explicit Euler scheme, the discrete form of the governing equations can be written as [3]:

$$\frac{v_i^{n+1} - v_i^n}{\Delta t} = -C_i^n - \beta \frac{\delta p^{n+1}}{\delta x_i} + D_i^n \quad (12.189)$$

It is assumed that the solution at time level  $n$  is known, satisfying the continuity equation.

The solution at the next time level  $n+1$  is then obtained from the discrete form of the above momentum equation subject to the continuity constraint on the form:

$$\frac{\delta v_i^{n+1}}{\delta x_i} = 0 \quad (12.190)$$

The time-splitting method can be adapted to the governing equations by splitting the momentum equation into two intermediate steps:

$$\left( \frac{v_i^* - v_i^n}{\Delta t} \right) \Delta V = -C_i^n + D_i^n - \beta \frac{\delta p^n}{\delta x_i} \quad (12.191)$$

$$\left( \frac{v_i^{n+1} - v_i^*}{\Delta t} \right) \Delta V = -\frac{\delta}{\delta x_i} (p^{n+1} - \beta p^n) \quad (12.192)$$

where  $\beta$  is a constant and  $v_i^*$  is an intermediate value of the velocity component. If  $\beta = 0$ , the intermediate velocity is advanced by the convective and viscous terms while the pressure term is ignored. By taking,  $\beta = 1$  instead, more information is carried over from  $v_i^n$  to  $v_i^*$  via the first step. Thus, if the solution tends to a steady state, the velocity  $v_i^{n+1}$  at the new time level becomes equal to  $v_i^*$ .

An essential feature of the two-step decomposition of the momentum equation is that the tentative velocity  $v_i^*$  can be calculated explicitly in the first step, while the new velocity  $v_i^{n+1}$  is related to the new pressure field in the second step. By taking the divergence of the equation in the second step, and making subsequent use of the implicit continuity equation, we obtain the Poisson equation for the potential function  $\phi^{n+1}$ :

$$\frac{\delta}{\delta x_j} \left[ \frac{\delta \phi^{n+1}}{\delta x_j} \right]_P = \frac{\Delta V}{\Delta t} \frac{\delta v_i^*}{\delta x_i} \quad (12.193)$$

where the potential function  $\phi$  is defined as:

$$\phi^{n+1} = p^{n+1} - \beta p^n \quad (12.194)$$

With  $\phi^{n+1}$  known from the solution of the Poisson equation, the pressure and velocities at the new time level  $n+1$  are obtained from:

$$p^{n+1} = p^n + \phi^{n+1} \quad (12.195)$$

$$v_i^{n+1} = v_i^* - \frac{\Delta t}{\rho^{n+1} \Delta V} \frac{\delta}{\delta x_i} \quad (12.196)$$

In application of the fractional step method to the incompressible Navier-Stokes equations, the pressure may be interpreted as a projection operator which projects an arbitrary vector field into a divergence-free vector field.

Fractional step methods have become quite popular. There are many variations of them, due to a vast choice of approaches to time and space discretizations, but they are all based on the principles described above. To

predict an accurate time history of the flow, higher order discretizations must be employed. Kim and Moin [92], for example, used a second order explicit Adams-Bashforth scheme for the convective terms and a second order implicit Crank-Nicholson scheme for the viscous terms. Boundary conditions for the intermediate velocity fields in time-splitting methods are generally a complex issue [92, 3].

### Chemical Reactive Flow

Jakobsen et al [81] and Lindborg et al [118] did apply similar algorithms for variable density flows to simulate the performance of chemical processes in fixed bed reactors. The fractional steps defining the elements of these algorithms are sketched in the following:

In a set of introductory steps, the mixture composition and the temperature are calculated. A set of scalar transport equations on the form (12.183) is generally solved for the species mass densities and the mixture enthalpy at the next time level  $n + 1$ . However, in reactor simulations, the enthalpy balance is frequently expressed in terms of temperature. The discrete form of the governing equations is thus written as:

$$\rho_c^{n+1} = \rho_c^n + (-C_c^n + D_c^{n+1} + S_c^{n+1}) \frac{\Delta t}{\Delta V} \quad (12.197)$$

$$T_c^{n+1} = T_c^n + (-A_T^n + D_T^{n+1} + S_T^{n+1}) \frac{\Delta t}{\Delta V} \quad (12.198)$$

where  $A$  is a shorthand notation for the advective terms.

The mixture density  $\rho^{n+1}$  is then obtained by the sum of the species densities  $\rho_c^{n+1}$ :

$$\rho^{n+1} = \sum_c \rho_c^{n+1} \quad (12.199)$$

In a set of intermediate steps, the evolution of the mixture pressure and velocity components are calculated. The variable density form of the Navier-Stokes equations are split into two intermediate steps.

$$\left( \frac{\rho^{n+1} v_i^* - (\rho v_i)^n}{\Delta t} \right) \Delta V = -C_i^n + D_i^n - \frac{\delta p^n}{\delta x_i} + S_i^n \quad (12.200)$$

$$\left( \frac{(\rho v_i)^{n+1} - (\rho^{n+1} v_i^*)}{\Delta t} \right) \Delta V = -\frac{\delta}{\delta x_i} (p^{n+1} - p^n) \quad (12.201)$$

where  $S$  represents the gravity term.

By taking the divergence of the momentum equation in the second step, we obtain the Poisson equation for the potential function  $\phi^{n+1}$ :

$$\frac{\delta}{\delta x_j} \left[ \frac{\delta \phi^{n+1}}{\delta x_j} \right]_P = \frac{\Delta V}{\Delta t} \left[ \frac{\delta (\rho^{n+1} v_i^*)}{\delta x_i} - \frac{\delta (\rho v_i)^{n+1}}{\delta x_i} \right] \quad (12.202)$$

The solution at the next time level  $n + 1$  is then obtained from the discrete form of the momentum equation subject to the continuity constraint on the form:

$$\frac{\delta\rho}{\delta t} + \frac{\delta(\rho v_i)^{n+1}}{\delta x_i} = 0 \quad (12.203)$$

The continuity equation for the reactive mixture is used to construct a stable approximation of the RHS of the Poisson equation for the potential function  $\phi$ . The transient term in the continuity equation may be approximated by an explicit high order scheme, or an implicit scheme can be used.

With  $\phi^{n+1}$  known from the solution of the Poisson equation, the pressure and velocities at the new time level  $n + 1$  are obtained from:

$$p^{n+1} = p^n + \phi^{n+1} \quad (12.204)$$

$$v_i^{n+1} = v_i^* - \frac{\Delta t}{\rho^{n+1} \Delta V} \frac{\delta\phi^{n+1}}{\delta x_i} \quad (12.205)$$

For reactive variable density flows, the pressure is interpreted as a projection operator which projects an arbitrary vector field into a vector field which fulfill the continuity equation.

For gas mixtures, the solution of the species mass balances, the temperature equation and the Navier-Stokes equations may be followed by a density update. For an ideal gas, the density changes may be determined by a complete differential of the density that is estimated by use of the ideal gas law in a new intermediate step:

$$\rho^{n+1,*} = \rho^{n+1} + \frac{p^n}{RT^n} (M_\omega^{n+1} - M_\omega^n) - \frac{\rho^n}{T^n} (T^{n+1} - T^n) + \frac{M_\omega^n}{RT^n} (p^{n+1} - p^n) \quad (12.206)$$

In order to allow longer time steps to be used, implicit schemes must be used for the  $C$ ,  $D$  and  $S$  operators in the first step of the momentum equation solution.

## 12.11 Finite Volume Methods for Multi-fluid Models

In this section, the path-breaking approximate implicit interface slip algorithm (IPSA) framework by Spalding [176, 177, 178] is outlined. Different designs of the basic algorithm for the novel multiphase properties are examined. A stable and efficient semi-implicit fractional step algorithm for the solution of unsteady two-fluid models is presented in the subsequent section. This particular numerical procedure has been used simulating bubble column flows. Finally, a summary of a similar semi-implicit fractional step algorithm for the solution of the unsteady two-fluid granular flow model equations is given. This particular numerical procedure has been employed describing reactive flow in fluidized beds.

### 12.11.1 Special Challenges in Solving the Two-fluid Model Equations

In this section, a survey of a selection of path-breaking procedures that have been designed for the numerical solution of the two-fluid model equations is given. It is emphasized that most of the standard procedures for solving multiphase problems represent more or less adequate extensions of the analogous procedures for single phase flow. The important procedure extensions required in order to solve the two-fluid model equations starting out from the standard single phase finite volume method algorithms, are pointed out and examined in further detail.

The basic discretization of the two-fluid model equations is similar to the approximations of the corresponding transport equations for single phase flow. A minor difference is that the two-fluid model equations contain the novel phase fraction variables that have to be approximated in an appropriate manner. More important, to design robust, stable and accurate solution procedures with appropriate convergence properties for the two-fluid model equations, emphasis must be placed on the treatment of the interface transfer terms in the phasic momentum, heat and mass transport equations. Because of these extra terms, the coupling between the different equations is even more severe for multiphase flows than for single phase flows.

A property of the finite volume method is that numerous schemes and procedures can be designed in order to solve the two-fluid model equations. In addition, the coupling terms can be approximated and manipulated in different ways. Besides, it is very difficult to predict the convergence and stability properties of novel solution methods. These aspects collectively increase the possibility of devising a numerical procedure which, when put to the test, does not converge.

In an early attempt to calculate the phase fractions in an approximate implicit volume fraction-velocity-pressure correction procedure, Spalding [176, 177, 178, 180] calculated the phase fractions from the respective phase continuity equations. However, experience did show that it was difficult to conserve mass simultaneously for both phases when the algorithm mentioned above was used. For this reason, Spalding [179] suggested that the volume fraction of the dispersed phase may rather be calculated from a discrete equation that is derived from a combination of the two continuity equations. An alternative form of the latter volume fraction equation, particularly designed for fluids with large density differences, was later proposed by Carver [26]. In this method the continuity equations for each phase were normalized by a reference mass density to balance the weight of the error for each phase.

Most of the present finite volume procedures that are used to solve the continuity and momentum equations are derived from the approximate implicit interphase slip algorithm (IPSA) framework proposed by Spalding [176, 177, 178, 180]. Rather than representing a particular algorithm and

discrete equations, the IPSA framework represents various extensions of the SIMPLE-like algorithms<sup>13</sup> that have been employed to solve the two-fluid model equations. Different procedure manipulations have been proposed to ensure high convergence rates depending on the coupling between the pressure, velocity and volume fractions and on the need of consideration of both fluids. The original IPSA of Spalding [176] was designed to comprise an approximate implicit coupling between the simultaneous changes of volume fraction and velocity with pressure. The pressure correction equation was designed from the two continuity equations in order to minimize the local imbalance in volume fractions as computed separately from the individual continuity equations. To improve the solution procedure mass conservation treatment for the individual phases and thus the convergence rate, Spalding [177, 178, 180] derived a pressure correction equation which contains a somewhat different attempt to approximate the simultaneous change of volume fraction and velocity with pressure for both phases. A similar third alternative IPSA pressure-correction equation was suggested by Carver [25]. For bubbly flows, Grienberger [63] argued that the two-fluid model contains only one pressure and thus designed a pressure-correction equation from the liquid continuity equation and the liquid velocity corrections formulas in the same way as for single phase flows [141].

One of the most important contributions of Spalding [176, 177] is the partial elimination algorithm (PEA). Due to the tight coupling between the velocities caused by the interface friction terms, manipulation of the discrete discretization equations for the velocity components was considered necessary to ensure sufficiently high convergence rates. The working principle of the PEA is thus to weaken the strong coupling between the phases through the partial elimination of the variables in the interphase coupling term. Linear algebra is basic to the computer solution of any kind of PDE problem. The mathematical impact of the partial elimination algorithm on the solver for the resulting system of algebraic equations is to reduce the effect of the strong coupling between the phasic momentum equations on the algebraic equations matrix condition number and thereby improve the convergence properties of the problem. Without this manipulation of the equations the condition number is very large as the matrix is almost singular. The PEA can also be generalized and applied to any of the two-fluid model equations that are strongly coupled, as illustrated in the following subsection.

No significant differences in convergence performance are generally observed assessing the above mentioned alternative schemes for the solution of the two-fluid model equations [80]. A main limitation associated with these procedures is that it is impossible to ensure that both the overall mixture continuity and the individual phase continuities are satisfied at the same time. In

---

<sup>13</sup> The velocity- and pressure correction equations in IPSA are frequently derived using the SIMPLEC method (i.e., the SIMPLE- Consistent approximation) by van Doormal and Raithby [191].

addition, to solve these problems, a more implicit treatment of the interphase coupling terms is required.

In the modern solution algorithms for the two-fluid model equations, the latter problem is generally relaxed by coupled strategies solving the corresponding transport equations of both phases simultaneously [90, 103, 104, 99, 98, 6, 119].

Numerous multiphase codes for dispersed flows have been developed to date, including both commercial multi-purpose codes and special purpose in-house codes. However, as indicated in the above summary, most of these codes have been originated as computational tools for multidimensional single-phase problems. Improved robustness and higher convergence rates are still important tasks for the code developers. A key feature of the next generation multiphase codes is that from the outset the software design has to be focused on the development of a reliable solver for multiphase flows with the capability to model an arbitrary number of fluid components and phases. One way to improve the convergence rate is to solve all the model equations simultaneously, at least all the momentum-, phase fraction- and pressure equations must be fully coupled in all the three space dimensions. The potential advantages of such a coupled treatment over a non-coupled or segregated approach are robustness, efficiency, generality and simplicity. The principal drawback is the higher storage needed for all the coefficients which did prevent such an algorithm to be used in the past.

## Solving Strongly Coupled Equations

In multiphase reactive flows, the interfacial transfer fluxes of momentum, heat and species mass are of great importance. These interfacial transfer fluxes are generally modeled as a product of the interfacial area concentration and a mean interfacial flux. It is normally assumed that the mean interfacial fluxes are, in turn, given as the product of the difference in the phase values of the primitive variables (driving force) multiplied by the transfer (proportionality) coefficients. Mathematically, a generic flux  $\mathbf{I}_k$  can be expressed on the form:

$$\mathbf{I}_k = K(\psi_l - \psi_k), \quad l \neq k \quad (12.207)$$

In multiphase reactor simulations, the momentum, heat and species mass balances may thus contain several terms that can be placed in this framework. However, in these problem solvers, the generalized proportionality coefficient  $K$  is usually derived from the steady drag force, and the convective heat and mass transfer fluxes, respectively.

Several strategies have been proposed to treat these interfacial coupling terms in the design of appropriate numerical solution methods. A simple way to implement these interphase coupling terms is to apply an explicit discretization scheme. Alternatively, an alternating direction implicit (ADI)-like method can be applied in which the current phase variable in the coupling term can



Although the interphase coupling terms are treated in a more implicit manner in this solution procedure, the weight of the intraphase coupling terms are weakened. A strong coupling between the phases diminishes the influence of the convection-diffusion coefficients, in particular for the lightest phase. The resulting solution of the equations for these phases is thus controlled primarily by the local value in the densest phase. An optimal solution procedure design must thus treat both the interphase- and intraphase coupling terms in an appropriate manner.

For this aim, Lindborg et al [119] used a coupled solver in combination with the partial elimination algorithm (PEA) proposed by Spalding [177]. The combined PEA-solver used in their work is outlined in the following.

From the discretized form of the generic transport equation (12.183), the interphase coupling terms can be singled out. With an implicit approximation of the interphase coupling terms, the terms in the discretized equation for the continuous phase can be rearranged and written as:

$$(a_{P,c} + K\Delta V)\psi_{P,c} = \sum_{nb} a_{nb,c}\psi_{nb,c} + S_c + K\psi_{P,d}\Delta V \quad (12.210)$$

For the dispersed phase, a similar equation yields:

$$(a_{P,d} + K\Delta V)\psi_{P,d} = \sum_{nb} a_{nb,d}\psi_{nb,d} + S_d + K\psi_{P,c}\Delta V \quad (12.211)$$

By using deferred estimates of the dispersed phase variable in the continuous phase equation and vice versa, the two equations can be solved sequentially using a standard equation solver. This procedure corresponds to the standard PEA implementation.

Alternatively, the dispersed phase variable in the continuous phase equation can be eliminated by use of the dispersed phase transport equation. Rearranging the continuous phase equation we get:

$$(a_{P,c} + f_d a_{P,d})\psi_{P,c} = \sum_{nb} a_{nb,c}\psi_{nb,c} + S_c + f_d \left( \sum_{nb} a_{nb,d}\psi_{nb,d} + S_d \right) \quad (12.212)$$

The corresponding equation representing the dispersed phase can be obtained with a corresponding procedure:

$$(a_{P,d} + f_d a_{P,c})\psi_{P,d} = \sum_{nb} a_{nb,d}\psi_{nb,d} + S_d + f_c \left( \sum_{nb} a_{nb,c}\psi_{nb,c} + S_c \right) \quad (12.213)$$

where

$$f_k = \frac{K\Delta V}{a_{P,k} + K\Delta V} \quad (12.214)$$

By implicit approximations of all the variables in both phases, the solution can now be obtained by solving the two sets of equations simultaneously.



$$\Gamma_{\psi,w} = (1 - f_w)\Gamma_{\psi,W} + f_w\Gamma_{\psi,P} \quad (12.217)$$

where the interpolation factor  $f_w$  is given by

$$f_w = \frac{\delta z_{W_w}}{\delta z_{W_w} + \delta z_{w_P}} \quad (12.218)$$

For a uniform grid the  $w$  is midway between the nodes,  $f_w = 0.5$  and the interpolated value of  $\Gamma_{\psi,w}$  reduces to the arithmetic mean of  $\Gamma_{\psi,W}$  and  $\Gamma_{\psi,P}$ :

$$\Gamma_{\psi,w} = \frac{1}{2}(\Gamma_{\psi,W} + \Gamma_{\psi,P}) \quad (12.219)$$

The linear interpolation approach cannot accurately treat the abrupt changes of diffusivity that may occur in some locations in multiphase reactors where the phase fractions change rapidly (e.g., across the transition zone from the dense bed to the freeboard section in a bubbling fluidized bed). To improve the interpolation procedure, one seeks an approximation of the diffusivity that gives an accurate approximation of the diffusive flux for cases with large changes in the material properties.

Consider that the grid cell volume surrounding the grid node  $P$  is filled with a material mixture of uniform diffusivity  $\Gamma_{\psi,P}$ , and the one around  $W$  with a material mixture of uniform diffusivity  $\Gamma_{\psi,W}$ . For the phase mixture between node  $P$  and  $W$ , a steady one dimensional analysis of the flux leads to [141]:

$$\Gamma_{\psi,w} = \left( \frac{1 - f_w}{\Gamma_{\psi,W}} + \frac{f_w}{\Gamma_{\psi,P}} \right)^{-1} \quad (12.220)$$

For uniform grids, the grid cell interface is placed midway between  $P$  and  $W$ , and  $f_w = 0.5$ , hence the interpolation reduced to the harmonic mean of  $\Gamma_{\psi,W}$  and  $\Gamma_{\psi,P}$ :

$$\Gamma_{w,\psi} = \frac{2\Gamma_{\psi,W}\Gamma_{\psi,P}}{\Gamma_{\psi,W} + \Gamma_{\psi,P}} \quad (12.221)$$

In bubbling fluidized bed reactor simulations harmonic mean values are normally used for the grid cell interface values of the scalar variable diffusivities [119]. Due to malfunctioning interpolation issues, the grid cell interface values of the diffusive momentum fluxes are generally approximated by arithmetic mean values. For bubble column and packed bed simulations arithmetic mean values can be used for the grid cell interface values of the generalized diffusivities, provided that no abrupt changes of diffusivity occur in any locations in the calculation domain.

### 12.11.2 Explicit Fractional Step Algorithm for Solving the Two-Fluid Model Equations Applied to Bubble Column Flow

In this section the solution method employed by Jakobsen et al [83] simulating bubble column flows is outlined.

The governing two-fluid model equations were discretized by a finite volume algorithm. A staggered grid arrangement was used. A fractional step scheme similar to those used by Tomiyama and Shimada [190] and Lathouwers [104] was employed. In particular, the single phase algorithms developed by Jakobsen et al [81] and Lindborg et al [118] for porous media were extended to two phase bubbly flows. Based on a semi-discrete formulation (discretized in time only) of the governing equations for incompressible fluids, the fractional steps defining the solution algorithm are sketched in the following:

1. First, intermediate volume fraction values were calculated solving the continuity equation for the dispersed phase by an explicit discretization scheme:

$$\int_V \left( \frac{\alpha_d^* \rho_d^n - \alpha_d^n \rho_d^n}{\Delta t} \right) dv = - \int_V \nabla \cdot (\alpha_d^n \rho_d^n \mathbf{v}_d^n) dv \quad (12.222)$$

The corresponding continuous phase volume fraction estimate is found by use of (8.11),  $\alpha_c^* = 1 - \alpha_d^*$ .

2. Intermediate velocity values were then obtained by solving the momentum balances without the interfacial coupling terms using explicit discretization schemes for all variables except for the volume fractions. The intermediate volume fraction estimates obtained in step 1 were used in all terms except from the convective terms:

$$\begin{aligned} \int_V \left( \frac{\alpha_k^* \rho_k^n \mathbf{v}_k^* - \alpha_k^n \rho_k^n \mathbf{v}_k^n}{\Delta t} \right) dv = & - \int_V \nabla \cdot (\alpha_k^n \rho_k^n \mathbf{v}_k^n \mathbf{v}_k^n) dv + \int_V \nabla \cdot (\alpha_k^* \boldsymbol{\sigma}_k^n) dv \\ & - \int_V \alpha_k^* \nabla p^n dv + \int_V \alpha_k^* \rho_k^n \mathbf{g} dv \end{aligned} \quad (12.223)$$

3. The lift force was approximated with an explicit Euler time discretization scheme:

$$\int_V \left( \frac{\alpha_k^* \rho_k^n \mathbf{v}_k^{**} - \alpha_k^n \rho_k^n \mathbf{v}_k^*}{\Delta t} \right) dv = \int_V \mathbf{F}_{L,k}^* dv \quad (12.224)$$

In this step the volume fractions were assumed independent of time.

The steady-drag, virtual mass, turbulent dispersion, and wall lift forces were approximated using a semi-implicit time discretization scheme:

$$\int_V \left( \left( \frac{\alpha_k^* \rho_k^n \mathbf{v}_k^{***} - \alpha_k^n \rho_k^n \mathbf{v}_k^{**}}{\Delta t} \right) - \alpha_c^* [\mathbf{F}_{D,k}^{***} + \mathbf{F}_{V,k}^{***} + \mathbf{F}_{TD,k}^{***} + \mathbf{F}_{W,k}^{***}] \right) dv = 0 \quad (12.225)$$

Like in the previous step, the volume fractions were assumed independent of time.

4. A Poisson equation for the pressure like variable  $\phi^{n+1}$  was derived from a discrete form of the momentum equation in which the volume fractions and densities were assumed independent of time:

$$\int_V \left( \frac{\alpha_k^* \rho_k^n \mathbf{v}_k^{n+1} - \alpha_k^* \rho_k^n \mathbf{v}_k^{***}}{\Delta t} \right) dv = - \int_V \alpha_k^* \nabla \phi^{n+1} dv \quad (12.226)$$

where  $\phi^{n+1} = p^{n+1} - p^n$ .

Applying the continuity divergence operator on the terms in this relation, and recognizing that the first divergence term in the resulting relation represents an extended estimate of the transient term in the continuity equation, yields:

$$\begin{aligned} \int_V \left( \frac{\nabla \cdot (\alpha_k^* \rho_k^n \mathbf{v}_k^{n+1}) - \nabla \cdot (\alpha_k^* \rho_k^n \mathbf{v}_k^{***})}{\Delta t} \right) dv = \\ \int_V \left( \frac{-\frac{\partial}{\partial t} (\alpha_k \rho_k^n) - \nabla \cdot (\alpha_k^* \rho_k^n \mathbf{v}_k^{***})}{\Delta t} \right) dv = - \int_V \nabla \cdot (\alpha_k^* \nabla \phi^{n+1}) dv \end{aligned} \quad (12.227)$$

The volume fraction variables were assumed to be time dependent in the semi-implicit discretization scheme used to solve the continuity equations. Considering the last two terms in the above relation, the transient term was then approximated by an explicit Euler time discretization scheme followed by volume integration in which the transient term was kept constant. If we thereafter multiply the resulting relation by  $\Delta t / \rho_k^n$ , the relation can be rewritten as:

$$\frac{\alpha_k^n - \alpha_k^{n+1}}{\Delta t} \Delta V - \frac{1}{\rho_k^n} \int_V \nabla \cdot (\alpha_k^* \rho_k^n \mathbf{v}_k^{***}) dv = - \frac{\Delta t}{\rho_k^n} \int_V \nabla \cdot (\alpha_k^* \nabla \phi^{n+1}) dv \quad (12.228)$$

If we take the sum of the corresponding equations for both phases and requiring that (8.11) is fulfilled both at time  $n$  and  $n+1$ , a Poisson equation for the pressure like variable is obtained:

$$\begin{aligned} - \frac{1}{\rho_d^n} \int_V \nabla \cdot (\alpha_d^* \rho_d^n \mathbf{v}_d^{***}) dv - \frac{1}{\rho_c^n} \int_V \nabla \cdot (\alpha_c^* \rho_c^n \mathbf{v}_c^{***}) dv \\ = - \frac{\Delta t}{\rho_d^n} \int_V \nabla \cdot (\alpha_d^* \nabla \phi^{n+1}) dv - \frac{\Delta t}{\rho_c^n} \int_V \nabla \cdot (\alpha_c^* \nabla \phi^{n+1}) dv \end{aligned} \quad (12.229)$$

5. The volume fraction values at the new time level  $n+1$  were obtained by solving the continuity equation for the dispersed phase using the latest estimate of the  $\alpha_k$  and  $\mathbf{v}_k$  variables:

$$\int_V \left( \frac{\alpha_d^{n+1} \rho_d^n - \alpha_d^n \rho_d^n}{\Delta t} \right) dv = - \int_V \nabla \cdot (\alpha_d^* \rho_d^n \mathbf{v}_d^{n+1}) dv \quad (12.230)$$

6. The remaining scalar transport equations, like the  $k$ - $\varepsilon$  turbulence model, are solved in the same way as the discrete scalar transport equation (12.183).

The fractional step concept applied to the scalar equations consists of successive applications of the methods for the different operators determining parts of the transport equations. The convective and diffusive terms are further split into their components in the various coordinate directions as explained in sect 12.9.4.

The convective terms were solved using a second order TVD scheme in space, and a first order explicit Euler scheme in time. The TVD scheme applied was constructed by combining the central difference scheme and the classical upwind scheme by adopting the smoothness monitor of van Leer [193] and the monotonic centered limiter [194]. The diffusive terms were discretized with a second order central difference scheme. The time-splitting scheme employed is of first order.

### 12.11.3 Implicit Fractional Step Method for Solving the Two-Fluid Granular Flow Model Equations Applied to Fluidized Bed Flow

In this section the solution method employed by Lindborg et al [119] simulating fluidized bubbling bed reactors is outlined.

The governing two-fluid equations for granular flows were discretized on a staggered grid arrangement using the finite volume method. A fractional-step scheme similar to those reported in the literature [104, 190, 83] is developed on the basis of the single-phase algorithms reported by Jakobsen et al [81, 118]. The fractional steps defining the algorithm are sketched in the following:

#### 1. Mixture composition calculation

For reactive mixtures, the species mass fractions at time level  $n + 1$  were calculated implicitly in accordance with the species mass balances on the generic form:

$$\int_V \left( \frac{\alpha_c^n \rho_c^n \omega_i^{n+1} - \alpha_c^n \rho_c^n \omega_i^n}{\Delta t} \right) dv = - \int_V \nabla \cdot (\alpha_c^n \rho_c^n \mathbf{v}_c^n \omega_i^{n+1}) dv + \int_V \nabla \cdot (\alpha_c^n \rho_c^n D_{m,i} \nabla \omega_i^{n+1}) dv + \int_V M_{\omega_i} R_i^{n+1} dv \quad (12.231)$$

The integration of the species transport equations was followed by a density update due to the change in the ideal gas mixture composition:

$$\rho_c^* = \rho_c^n + \frac{p^n}{RT_c} (M_{\omega_c}^{n+1} - M_{\omega_c}^n) \quad (12.232)$$

## 2. Temperature calculation

The chemical process and the external heating or cooling devices may give rise to temperature changes. The evolution of the temperature was thus computed as:

$$\begin{aligned} \int_V \alpha_k^n \rho_k^* C p_k \left( \frac{T_k^{n+1} - T^n}{\Delta t} \right) dv = & \\ & - \int_V \alpha_k^n \rho_k^* C p_k \mathbf{v}_k^n \cdot \nabla T_k^{n+1} dv + \int_V \nabla \cdot (k_k \nabla T_k^{n+1}) dv \quad (12.233) \\ & + \int_V \sum_r (-\Delta H_{R,r,k}) R_{r,k}^{n+1} dv + \int_V Q_k^{n+1} dv \end{aligned}$$

The solution of the heat balance is followed by a density update.

$$\rho_c^{**} = \rho_c^* + \frac{p^n M^{n+1}}{R} \left( \frac{1}{T_c^{n+1}} - \frac{1}{T_c^n} \right) \quad (12.234)$$

## 3. Volume fraction calculation - Iteration loop comprising steps 3-5

Estimates of the volume fraction values at the new time level  $n + 1$  were predicted by solving the dispersed phase continuity equation implicitly using the latest values of the dispersed phase velocity field:

$$\int_V \left( \frac{\alpha_d^\nu \rho_d^{n+1} - \alpha_d^n \rho_d^n}{\Delta t} \right) dv = - \int_V \nabla \cdot (\alpha_d^\nu \rho_d^{n+1} \mathbf{v}_d^\nu) dv + \int_V \Gamma_{V,d} dv \quad (12.235)$$

The corresponding continuous phase volume fraction value was calculated from (8.11),  $\alpha_c^\nu = 1 - \alpha_d^\nu$ .

## 4. Granular temperature calculation - Iteration loop comprising steps 3-5

An intermediate granular temperature field was computed by use of the latest estimates of the volume fraction- and velocity fields (i.e., calculated within the iteration loop):

$$\begin{aligned} \int_V \frac{3}{2} \left[ \frac{\alpha_d^\nu \rho_d^{n+1} \Theta^\nu - \alpha_d^n \rho_d^n \Theta^n}{\Delta t} \right] dv = & - \int_V \frac{3}{2} \nabla \cdot (\alpha_d^\nu \rho_d^{n+1} \mathbf{v}_d^\nu \Theta) dv \\ & + \int_V \boldsymbol{\sigma}_d^\nu : \nabla \mathbf{v}_d^\nu dv + \int_V \nabla \cdot (\Gamma_d \nabla \Theta^\nu) dv \quad (12.236) \\ & - \int_V 3\beta^\nu \Theta^\nu dv + \int_V \beta^\nu \langle \mathbf{C}_c \cdot \mathbf{C}_d \rangle^\nu dv - \int_V \gamma dv \end{aligned}$$

The particle pressure is then calculated based on the preliminary estimates of the volume fractions and the granular temperature:

$$p_d^\nu = \alpha_d^\nu \rho_d^{n+1} \Theta^\nu [1 + 2(1 - e) \alpha_d^\nu g_0^\nu] \quad (12.237)$$

5. *Particle pressure- and velocity correction - Iteration loop comprising steps 3-5*

A preliminary estimate of the dispersed phase velocity was obtained with a simplified form of the momentum equation, assuming that the particle pressure and drag forces are the dominant forces:

$$\int_V \left( \frac{\alpha_d^\nu \rho_d^{n+1} \mathbf{v}_d^{\nu+1} - \alpha_d^n \rho_d^n \mathbf{v}_d^n}{\Delta t} \right) dv = - \int_V \nabla p_d^\nu dv - \int_V K^\nu (\mathbf{v}_d^{\nu+1} - \mathbf{v}_c^{\nu+1}) dv \tag{12.238}$$

This simplification reduces the overall computational costs drastically. It was further assumed that the continuous phase momentum equation is dominated by the drag force only:

$$\int_V \left( \frac{\alpha_c^\nu \rho_c^{n+1} \mathbf{v}_c^{\nu+1} - \alpha_c^n \rho_c^n \mathbf{v}_c^n}{\Delta t} \right) dv = \int_V K^\nu (\mathbf{v}_d^{\nu+1} - \mathbf{v}_c^{\nu+1}) dv \tag{12.239}$$

An estimate of the continuous phase velocity was obtained by reformulating the equation:

$$\mathbf{v}_c^{\nu+1} = \frac{\alpha_c^n \rho_c^n \mathbf{v}_c^n + \Delta t K^\nu \mathbf{v}_d^{\nu+1}}{D} \tag{12.240}$$

where  $D = \alpha_c^\nu \rho_c^{n+1} + \Delta t K^\nu$ .

If (12.238) is solved with respect to the velocity estimate of the dispersed phase, followed by eliminating the unknown velocity of the continuous phase by use of (12.240), we get:

$$\mathbf{v}_d^{\nu+1} = \frac{\alpha_d^n \rho_d^n \mathbf{v}_d^n - \Delta t \nabla p_d^\nu + \Delta t K^\nu \alpha_c^n \rho_c^n \mathbf{v}_c^n / D}{\alpha_d^n \rho_d^n + \Delta t K^\nu (1 - \Delta t K^\nu / D)} \tag{12.241}$$

The steps 2 – 4 were performed in an iterating manner until the overall squared change in volume fraction  $\varepsilon = \sum_V (\alpha_d^{\nu+1} - \alpha_d^\nu)^2$  for two consecutive iterations was less than a predefined criterion typically of the order of the machine precision.

6. *Iterative velocity calculation* After the iteration loop in steps 3-5 is converged with the simplified momentum equation, improved velocity estimates were obtained from the complete momentum equation.

The discrete momentum balance was solved for the velocity using an implicit Euler discretization scheme:

$$\begin{aligned}
 \int_V \left( \frac{\alpha_k^{n+1} \rho_k^{new} \mathbf{v}_k^* - \alpha_k^n \rho_k^n \mathbf{v}_k^n}{\Delta t} \right) dv = \\
 - \int_V \nabla \cdot (\alpha_k^{n+1} \rho_k^{new} \mathbf{v}_k^n \mathbf{v}_k^*) dv \\
 + \int_V \nabla \cdot \boldsymbol{\sigma}_k^* dv - \int_V \alpha_k^{n+1} \nabla p^n dv \\
 + \int_V \alpha_k^n \rho_k^{new} \mathbf{g} dv + \int_V \mathbf{M}_k^* dv
 \end{aligned} \tag{12.242}$$

The density estimate  $\rho_k^{new}$  denotes the latest obtained density of phase  $k$ . In the dispersed phase  $\rho_d^{new} = \rho_d^{n+1}$ , while in the continuous phase  $\rho_c^{new} = \rho_c^{**}$ .

7. *Iterative gas pressure- and velocity corrections*

A gas pressure update was then performed to correct the pressure- and velocity fields:

$$\begin{aligned}
 \int_V \left( \frac{\alpha_k^{n+1} \rho_k^{new} \mathbf{v}_k^{n+1} - \alpha_k^{n+1} \rho_k^{new} \mathbf{v}_k^*}{\Delta t} \right) dv = \\
 - \int_V \alpha_k^{n+1} \nabla \delta p dv \pm \int_V K (\delta \mathbf{v}_l - \delta \mathbf{v}_k) dv, \quad l \neq k
 \end{aligned} \tag{12.243}$$

where the pressure correction  $\delta p = p^{n+1} - p^n$ , is obtained by solving the Poisson equation (the derivation is outlined below):

$$\begin{aligned}
 \sum_k \left( \frac{1}{\rho_k^0} \nabla \cdot (\alpha_k^{n+1} \rho_k^{new} G_k \nabla \delta p) \right) = \\
 \sum_k \left( \frac{1}{\rho_k^0} \nabla \cdot (\alpha_k^{n+1} \rho_k^{new} \mathbf{v}_k^*) \right) + \sum_k \left( \frac{1}{\rho_k^0} \frac{\partial}{\partial t} (\alpha_k \rho_k) \right) - \sum_k \left( \frac{\Gamma_k}{\rho_k^0} \right)
 \end{aligned} \tag{12.244}$$

When the pressure correction,  $\delta p$ , is known, the velocities of the dispersed and continuous phases were corrected according to (12.251) and (12.252), respectively.

Finally, the gas density is updated in accordance with the ideal gas law:

$$\rho_c^{n+1} = \rho_c^{**} + \frac{M_\omega^{n+1}}{RT_c^{n+1}} (p^{n+1} - p^n) \tag{12.245}$$

8. *Update of turbulence fields*

The  $k - \varepsilon$  turbulence model equations were discretized by an implicit fractional step scheme similar to (12.183).

### Summary of the algorithm

- Integration of species mass balance for the mass fractions including a density update due to change in mixture composition.
- Iterative loop solving for the particle volume fraction, granular temperature and velocity estimates.
- Re-calculation of the velocities by solving the full momentum equations.
- Iterative calculation of the gas pressure and velocities.
- Solution of turbulence model equations.

In the work of Lindborg et al [119], the resulting linear equation systems were solved with preconditioned Krylov subspace projection methods [166]. The Poisson equation was solved by a conjugate gradient (CG)-solver, while the other transport equations were solved using a bi-conjugate gradient (BCG)-solver which can handle also non-symmetric equations systems. The solvers were preconditioned with a Jacobi preconditioner.

### Derivation of the Poisson equation for the gas pressure

First, to balance the residual contributions from both phases, the continuity equations are normalized with respect to a constant representative density of the respective phases  $\rho_k^0$ . Then, we take the sum of the normalized continuity equations for the two phases. The result can be written as:

$$\sum_k \left( \frac{1}{\rho_k^0} \frac{\partial}{\partial t} (\alpha_k \rho_k) \right) + \sum_k \left( \frac{1}{\rho_k^0} \nabla \cdot (\alpha_k^{n+1} \rho_k^{new} \mathbf{v}_k^{n+1}) \right) = \left( \frac{\Gamma_k}{\rho_k^0} \right) \quad (12.246)$$

The velocity corrections  $\delta \mathbf{v}_k = \mathbf{v}_k^{n+1} - \mathbf{v}_k^*$  were introduced into (12.246):

$$\begin{aligned} \sum_k \left( \frac{1}{\rho_k^0} \frac{\partial}{\partial t} (\alpha_k \rho_k) \right) + \sum_k \left( \frac{1}{\rho_k^0} \nabla \cdot (\alpha_k^{n+1} \rho_k^{new} \delta \mathbf{v}_k) \right) \\ = - \sum_k \left( \frac{1}{\rho_k^0} \nabla \cdot (\alpha_k^{n+1} \rho_k^{new} \mathbf{v}_k^*) \right) \end{aligned} \quad (12.247)$$

The velocity corrections in (12.247) were then substituted by the pressure corrections employing appropriately defined pressure-velocity correction relationships. The pressure-velocity correction relationships were constructed by subtracting the discrete momentum equations with the pressure at the old time level  $n$  and the preliminary estimates for velocity fields (12.242) from the semi-implicit discretization of the momentum equation with the corrected pressure and the estimates for the velocity fields that satisfy the continuity equations. The desired relationships are the given on the form:

$$\int_V \frac{\alpha_k^{n+1} \rho_k^{n+1}}{\Delta t} \delta \mathbf{v}_k \, dv = - \int_V \alpha_k^{n+1} \nabla \delta p \, dv + \int_V K (\delta \mathbf{v}_l - \delta \mathbf{v}_k) \, dv, \quad l \neq k \quad (12.248)$$

Introducing a new variable  $T_k = \frac{\alpha_k^{n+1} \rho_k^{n+1}}{\Delta t}$  and rearranging these two relations to determine the velocity corrections for the two phases, we obtain:

$$\delta \mathbf{v}_c = \frac{K \delta \mathbf{v}_d - \alpha_c^{n+1} \nabla \delta p}{T_c + K} \quad (12.249)$$

$$\delta \mathbf{v}_d = \frac{K \delta \mathbf{v}_c - \alpha_d^{n+1} \nabla \delta p}{T_d + K} \quad (12.250)$$

Eliminating the continuous phase velocity correction in (12.250) by use of (12.249), the required pressure-velocity correction relation for the dispersed phase is achieved:

$$\delta \mathbf{v}_d = - \left[ \frac{\alpha_d^{n+1} T_c + K}{T_c T_d + K(T_c + T_d)} \right] \nabla \delta p = -G_d \nabla \delta p \quad (12.251)$$

where  $G_d = \frac{\alpha_d^{n+1} T_c + K}{T_c T_d + K(T_c + T_d)}$ .

By use of (12.251) eliminating the dispersed phase velocity in (12.249), the pressure-velocity correction relation for the continuous phase can be written as:

$$\delta \mathbf{v}_c = - \left[ \frac{\alpha_c^{n+1} + K G_d}{T_c + K} \right] \nabla \delta p = -G_c \nabla \delta p \quad (12.252)$$

where  $G_c = \frac{\alpha_c^{n+1} + \beta G_d}{T_c + K}$ .

A Poisson equation (12.244) was then obtained by inserting the pressure-velocity correction relationships into (12.247).

### Convergence Problems and Failure of Well-posedness of Granular theory closures

A common problem encountered when developing algorithms intended for simulation of fluidized beds is that numerical problems may occur in the dense regions of the domain. A high solids volume fraction restricts the fluctuating particle movement and thus reduces the granular temperature, which in turn reduces the solid pressure. As a result, local compactions may get even more compact. If the solids volume fraction approaches maximum packing, even small variations in the packing have extreme impact on the radial distribution function that instantly causes very steep gradients in the particle pressure, which in the worst case results in convergence problems. Thus, some kind of modification is commonly made in order to obtain convergence.

In the work by Lindborg et al [119], for example, the solid pressure is assumed to change its dependency from  $p_d^{kc}(\theta, \alpha_d)$  to  $p_d^{kc}(\alpha_d)$  if the temperature sinks below a certain threshold ( $\theta_{\text{crit}} = \max|\theta_{\text{min}}, \theta|$ ). The lower limit is dependent on the magnitude of the energy dissipation. A threshold value of  $\theta_{\text{min}} = 1 \times 10^{-6} \text{ m}^2/\text{s}^2$  was applied.

This model modification was not necessary when including frictional stresses since these mechanisms cause extra resistance to particle motion in

the dense areas and thereby reduce the probability of large, rapid fluctuations in the distribution function. In addition, the convergence rate is generally improved.

#### 12.11.4 Solution of Multi-fluid Models

The multi-fluid model framework is required to simulate chemical processes containing dispersed phases of multiple sizes. Two different designs of the multi-fluid model have emerged over the years representing very different levels of complexity. For dilute flows the dispersed phases are assumed not to interact, so no population balance model is needed. For denser flows a population balance equation is included to describe the effects of the dispersed phases interaction processes. Further details on the multi-fluid model formulations are given in chap 8 and chap 9.

To solve the multi-fluid model version without the population balance, a relatively simple generalization of the two-fluid IPSA algorithms to multiple dispersed phases [21] are often used [96, 142]. In the referred three-fluid models only two dispersed phases were included in the simulations. Tomiyama and Shimada [190] made a similar four-fluid model which was solved by a pressure-based finite difference algorithm similar to the single phase SMAC [2] or SOLA [73] methods. In recent years, coupled solver technology is employed in some codes solving the three-fluid models [21, 6].

No attempts has been made to solve the complete multi-fluid model version with a population balance for a continuous distribution of the dispersed phases together with the continuous phase equations. However, a few attempts have been made to solve the complete multi-fluid model version for a few dispersed phases only. In the Multi-Phase-Multi-Group Model [168, 169] and the  $N \times M$  MUSIG model [171, 57, 95],  $N$  particle size groups are used to describe the size distribution within the  $M$  phases (or velocity groups). The two model versions referred above were both implemented and solved in ANSYS CFX codes. However, the former model was solved using a multi-fluid algorithm that is similar to the IPSA procedures [176, 178, 179, 180], while the latter model was solved by a coupled solver for the velocities and pressure avoiding the SIMPLE-like approximation [21].

Bove [16] proposed a different approach to solve the multi-fluid model equations in the in-house code FLOTRACS. To solve the unsteady multi-fluid model together with a population balance equation for the dispersed phases size distribution, a time splitting strategy was adopted for the population balance equation. The transport operator (convection) of the equation was solved separately from the source terms in the inner iteration loop. In this way the convection operator which coincides with the continuity equation can be employed constructing the pressure-correction equation. The population balance source terms were solved in a separate step as part of the outer iteration loop. The complete population balance equation solution provides the

volume fractions of the dispersed phases. When the outer iteration loop was converged, a consistent solution of the dense multi-fluid model was achieved.

## 12.12 Numerical Solution of the Population Balance Equation

This part of the chapter is devoted to a few of the popular numerical discretization schemes used to solve the population balance equation for the (fluid) particle size distribution. In this section we discuss the *method of moments*, the *quadrature method of moments* (QMOM), the *direct quadrature method of moments* (DQMOM), the *discrete method*, the *class method*, the *multi-group method*, and the *least squares method*.

For the continuous microscopic formulations, the closures and the numerical discretizations are split so an optimal numerical solution method has to be found after the closure laws are derived. The numerical solution methods are in general problem dependent and optimized for particular applications. For the discrete macroscopic formulations, the closures and the numerical discretizations are not split thus the numerical solution method is determining a basis for the closure laws that are derived. The numerical solution method chosen is thus a part of the model closure and cannot be optimized for particular applications.

In mathematical terms the population balance equation (PBE) is classified as a non-linear partial integro-differential equation (PIDE). Since analytical solutions of this equation are not available for most cases of practical interest, several numerical solution methods have been proposed during the last two decades as discussed by Williams and Loyalka [209] and Ramkrishna [151].

In general, the numerical solution of PIDEs consists of a three step procedure. First the basic set of PIDEs is discretized in the internal coordinates and expressed as a set of partially differential equations (PDEs). The PDEs are then discretized in time and the physical space coordinates using standard PDE discretization techniques in a second step. Finally the resulting set of algebraic equations are solved by use of a suitable solver.

For most engineering calculations in the past, fluxes and integral results are considered sufficient interpreting growth-, agglomeration-, nucleation- and breakage data and for fitting the mechanistic kernels for solid particle suspensions. Therefore, only the first moments of the size density distribution function of the population (i.e., the mean, the standard deviation, etc.) are required. For the more complex fluid particle applications investigated in recent studies local or semi-local size distributions are required enabling better understanding of the physical phenomena involved and proper model validation. However, many of the present CFD codes still resort to integral formulations minimizing the computational time and memory requirements. It thus seems convenient to divide the numerical solution methods into two groups,

the methods solving the models for the moments of the size distribution and the methods solving the models for the size distribution itself.

### Methods for the Moments of the Distribution

Basically, the method of moments converts the set of PIDEs into a set of PDEs where each PDE represents a given moment of the population size density function. Defining the  $j$ -th moment of the population density function like

$$\mu_j = \int_0^\infty d^j f(\mathbf{r}, d, t) dd \tag{12.253}$$

The PBE can be reduced to a set of PDEs by integrating the basic transport equation over the whole particle size distribution,

$$\int_0^\infty \left[ \frac{\partial f}{\partial t} + \nabla_r \cdot (\mathbf{v}_r f) + \nabla_x \cdot (\mathbf{v}_x f) - D_C + B_C - D_B + B_B \right] d^j dd \quad \text{for } j = 0, 1, \dots \tag{12.254}$$

or in terms of the moments:

$$\frac{\partial \mu_j}{\partial t} + \int_0^\infty [\nabla_r \cdot (\mathbf{v}_r f)] d^j dd + \int_0^\infty [\nabla_x \cdot (\mathbf{v}_x f)] d^j dd = \int_0^\infty [D_C + B_C - D_B + B_B] d^j dd \tag{12.255}$$

for  $j = 0, 1, \dots$

Assuming that the convective velocities are independent of the property coordinate (i.e., the particle diameter), one may integrate by parts:

$$\begin{aligned} & \frac{\partial \mu_j}{\partial t} + d^j f \mathbf{v}_r |_0^\infty - \nabla_r \cdot \mathbf{v}_r \int_0^\infty j d^{j-1} f dd + d^j \mathbf{v}_x f |_0^\infty - \nabla_x \cdot \mathbf{v}_x \int_0^\infty j d^{j-1} f dd \\ & = \int_0^\infty [D_C + B_C - D_B + B_B] d^j dd, \text{ for } j = 0, 1, \dots \end{aligned} \tag{12.256}$$

Since the  $f(\mathbf{r}, d, t)$ -function goes to zero at the maximum and minimum boundaries, the equation can be simplified and rewritten as:

$$\frac{\partial \mu_j}{\partial t} - j \nabla_r \cdot (\mathbf{v}_r \mu_{j-1}) - j \nabla_x \cdot (\mathbf{v}_x \mu_{j-1}) = \int_0^\infty [D_C + B_C - D_B + B_B] d^j dd, \text{ for } j = 0, 1, \dots \tag{12.257}$$

with initial conditions  $\mu_j(r, d, t = 0) = \hat{\mu}_j(r, d)$  for  $j=0,1, \dots$

The mathematical model characteristics of the source terms, i.e.,  $D_C$ ,  $B_C$ ,  $D_B$  and  $B_B$ , determines whether the system of equations are closed or not.

To illustrate this problem a pure breakage process is considered, i.e.,  $D_C = B_C = 0$ , while  $D_B \neq 0$  and  $B_B \neq 0$ . In addition, as an example only, a generalized formulation of the breakage death term ( $D_B$ ) is analyzed in the following. Assuming that the breakage frequency,  $b_B(d)$ , can be represented by a polynomial relation like:  $b_B(d) = \sum_{i=0}^N b_{B_i} P_{B_i}(d)$ , where  $P_{B_i}(d) = d^i$ , integration of the source term gives:

$$\int_0^{\infty} b_{B_i} f(r, d, t) d^j dd = \sum_{i=0}^N b_{B_i} \int_0^{\infty} d^j f(r, d, t) d^j dd = \sum_{i=0}^N b_{B_i} \mu_{i+j} \quad (12.258)$$

This implies that higher order moments are introduced, thus the system of PDEs cannot be closed analytically. It is possible to show that similar effects will occur for the other source terms as well. This problem limits the application of the exact method of moments to the particular case where we have constant kernels only. In other cases one has to introduce approximate closures in order to eliminate the higher order moments ensuring that the transport equations for the moments of the particle size distribution can be expressed in terms of the lower order moments only (i.e., a modeling process very similar to turbulence modeling).

For bubbly flows most of the early papers either adopted a macroscopic population balance approach with an inherent discrete discretization scheme as described earlier, or rather semi-empirical transport equations for the contact area and/or the particle diameter. Actually, very few consistent source term closures exist for the microscopic population balance formulation. The existing models are usually solved using discrete semi-integral techniques, as will be outlined in the next sub-section.

Therefore, the approximate integral method is not widely used solving the population balance model for bubbly flows as the kernels involved for these systems are rather complex, thus it is very difficult to eliminate the higher order moments developing closures with sufficient accuracy.

Hounslow et al [74] suggested that the difficulty incurred by the inclusion of complex closures for the source terms investigating nucleation, growth and aggregation of particulate suspensions can be relaxed discretizing the population balance equation. The moments of the size distribution were calculated from the discrete data resulting from the simulations. However, the direct solution of the equations containing physical source term parameterizations by use of conventional finite difference techniques is complicated by the presence of the integral terms and results in computational loads far greater than is desirable. Hounslow et al. thus placed substantial emphasis on determining correctly both the moments and the particle size distribution. The novel numerical technique developed, later referred to as the class method, reinforces the conservative properties of a few lower order moments by transforming the

equation introducing a constant volume correction factor that was found valid for several cases. Further details will be given later on discussing the discrete semi-integral and differential methods in general. The class method containing volume correction factors has not been widely used for bubbly flows mainly due to the complexity of the bubble breakage closures.

When the population balance is written in terms of one internal coordinate (e.g., particle diameter or particle volume), the closure problem mentioned above for the moment equation has been successfully relaxed for solid particle systems by the use of a quadrature approximation.

In the quadrature method of moments (QMOM) developed by McGraw [131], for the description of sulfuric acid-water aerosol dynamics (growth), a certain type of quadrature function approximations are introduced to approximate the evolution of the integrals determining the moments. Marchisio et al [122, 123] extended the QMOM for the application to aggregation-breakage processes. For the solution of crystallization and precipitation kernels the size distribution function is expressed using an expansion in delta functions [122, 123]:

$$f(d, t) \approx \sum_{\alpha=0}^P \omega_{\alpha} \delta(d - d_{\alpha}) \quad (12.259)$$

where  $\omega_{\alpha}$  is the weight of the delta function centered at the characteristic particle size  $d_{\alpha}$ .

Defining the  $i$ -th moment of the population density function as

$$\mu_i = \int_0^{\infty} d^i f(d, t) dd \quad (12.260)$$

Using a quadrature rule in order to approximate the integral yields:

$$\mu_i = \int_0^{\infty} d^i f(d, t) dd \approx \sum_{\alpha=1}^P \omega_{\alpha}(t) d_{\alpha}^i \quad (12.261)$$

Inserting the same quadrature approximation to the source term integrals provides an approximate numerical type of closure avoiding the higher order moments closure problem on the cost of model accuracy [131]. This numerical approximation actually neglects the physical effects of the higher order moments. No reports applying this procedure to bubbly flows have been found so far.

## Methods for the Number Density Distribution

This group of methods contains a large variety of solution strategies, but only a few popular techniques like the finite volume (FVM) methods and the direct quadrature method of moments (DQMOM) will be discussed.

The main premise of these methods is that one in practice is not necessarily interested in the number density probability  $f_1$ , but rather in the number density  $N_i$  (i.e., the number of bubbles of a particular size or size interval per unit volume). The methods within this category either divide the size domain into finite regions on which the number density is integrated to provide balances between the number of particles in each bin, or solve the balance equations accurately for a limited number of discretization points on the size domain.

A group of discrete techniques is based on the conventional finite volume and finite difference concepts and can be classified as finite volume methods (FVM). The wide use of the FVMs to solve PBEs is due to the simple construction and their conservative characteristics, in a similar manner as the FVM is often preferred formulating the CFD discretization algorithms. That is, the flux of a given property leaving through one face of the grid volume must equal the flux entering the neighboring ones. Adopting this method thus enforces the conservation of the conservative quantities. The growth terms are simply treated as flux processes, whereas the coalescence and breakage processes are more difficult to handle as the particles can disappear and appear in different regions of the domain. In order to fulfill the conservation properties considering these processes, it is necessary to employ some kind of ad hoc numerical tricks analogue to the linear source term manipulations in the CFD algorithms. The different tricks employed in the literature on PBEs have been characterized determining the so-called discrete-, class- and multi-group methods.

Since either the discrete- or the multi-group FVMs are adopted in nearly all multi-fluid CFD simulations, emphasis in the next paragraph is placed on these two schemes as described by Ramkrishna [151] and Carrica et al [24]. In principle the discrete- and multi-group methods are very similar. A slight difference is observed in the way the number density is approximated. The discrete method approximate the functional values at discrete pivotal points within the size interval using delta functions, whereas the multi-group method divide the size spectrum into a number of continuous sub-integrals or groups. In addition, the mean value theorem is sometimes applied in different ways. The multi-group method substitutes the mean value of the population density in each interval in each integrand by  $f_i = N_i/(d_{i+1} - d_i)$  and withdraw this factor from the integral, whereas the discrete method can be based on the multi-group approach or alternatively derived by estimating the kernels at the pivots and assign the size interval definition to the remaining factors of the integrals. The two names used referring to these methods originate from the parallel historical development within two different fields of science. The discrete method was developed in chemical engineering investigating bio-populations, whereas the multi-group approach is developed in neutron- and nuclear reactor physics. A well established approach in nuclear engineering solving the neutron density transport equations resorts to the multiple energy group equations using transfer cross sections. Similar ideas were later used to

determine a detailed description of the dynamic interactions among groups of particles.

First, the dispersed phase is divided into size intervals according to some criteria, in this case we have chosen the bubble diameter  $d_i$ . The interval  $[d_i, d_{i+1}]$  is denoted  $I_i$  and the total number of particles in the interval  $I_i$  is:

$$N_i(t) \equiv \int_{d_i}^{d_{i+1}} f_i(d, t) dd. \tag{12.262}$$

The population balance is integrated in particle size over the subinterval:

$$\begin{aligned} & \int_{d_i}^{d_{i+1}} \frac{\partial f(d, t)}{\partial t} dd + \int_{d_i}^{d_{i+1}} \nabla \cdot (f(d, t) \mathbf{v}_p) dd \\ &= \int_{d_i}^{d_{i+1}} (B_B(d, t) - D_B(d, t) + B_C(d, t) - D_C(d, t)) dd. \end{aligned} \tag{12.263}$$

The class boundaries are independent of time and spatial position so the time derivation and the divergence operator can be moved outside the integral:

$$\begin{aligned} & \frac{\partial}{\partial t} \int_{d_i}^{d_{i+1}} f(d, t) dd + \nabla \cdot \int_{d_i}^{d_{i+1}} (f(d, t) \mathbf{v}) dd \\ &= \int_{d_i}^{d_{i+1}} (B_B(d, t) - D_B(d, t) + B_C(d, t) - D_C(d, t)) dd. \end{aligned} \tag{12.264}$$

The result of the integration is a balance equation for the number densities  $N_i$ , in terms of the unknown number density probability,  $f_1(d, t)$ , and is, hence, still unresolvable.

A number average particle velocity may be introduced to simplify the expression for the convective terms:

$$\int_{d_i}^{d_{i+1}} (f(d, t) \mathbf{v}) dd = \int_{d_i}^{d_{i+1}} f(d, t) dd \langle \mathbf{v} \rangle_{N_i} = N_i \langle \mathbf{v} \rangle_{N_i} \tag{12.265}$$

Inserting (12.262) and (12.265) into (12.264), yields:

$$\begin{aligned} & \frac{\partial N_i}{\partial t} + \nabla \cdot (N_i \langle \mathbf{v} \rangle_{N_i}) \\ &= \int_{d_i}^{d_{i+1}} (B_B(d, t) - D_B(d, t) + B_C(d, t) - D_C(d, t)) dd. \end{aligned} \tag{12.266}$$

The integrals (with respect to  $d'$ ) in the source terms (see (9.76) to (9.79)) are expressed as the sum of integrals over sub-intervals. Replacing the integral in all the source terms with a sum yields:

$$B_B(d, t) = \sum_{j=i}^M \int_{d_j}^{d_{j+1}} v(d') b_B(d') P_B(d|d') f_1(d', t) dd' \tag{12.267}$$

$$D_B(d, t) = b_B(d) f_1(d, t) \quad (12.268)$$

$$B_C(d, t) = \frac{1}{2} \sum_{j=0}^{i-1} \int_{d_{j+1}}^{d_j} a_C((d^3 - d'^3)^{1/3}, d') f_1((d^3 - d'^3)^{1/3}, t) f_1(d', t) dd' \quad (12.269)$$

$$D_C(d, t) = f_1(d, t) \sum_{j=0}^M \int_{d_j}^{d_{j+1}} a_C(d, d') f_1(d', t) dd' \quad (12.270)$$

The above expressions contain the continuous bubble number probability density,  $f(d, t)$ . The source terms must be expressed entirely in terms of the dependent variable  $N_i$ . This can be achieved by using the *mean value theorem* [151]. Note, as mentioned before, at this point the discrete method of Ramkrishna [151] may deviate slightly from the multi-group method.

The *mean value theorem* is used to cast the equations (12.267) to (12.270) entirely in terms of  $N_i$  and  $N_j$ . In each interval the variables are replaced by a mean value.

For example, using the discrete method the mean value theorem can be used to express that

$$\begin{aligned} \int_{d_i}^{d_{i+1}} D_C(d, t) dd &= \int_{d_i}^{d_{i+1}} f_1(d, t) \sum_{j=0}^M \int_{d_j}^{d_{j+1}} a_C(d, d') f_1(d', t) dd' dd \\ &\approx a_C(x_i, x_j) \int_{d_i}^{d_{i+1}} f_1(d, t) dd \sum_{j=0}^M \int_{d_j}^{d_{j+1}} f_1(d', t) dd' = N_i \sum_{j=0}^M a_C(x_i, x_j) N_j, \end{aligned} \quad (12.271)$$

where  $x_i$  and  $x_j$  are pivotal points in  $I_i$  and  $I_j$ , respectively. The pivot concentrates the particles in the interval at a single representative point. Thus one may write the number probability density  $f_1(d, t)$  as being given by:

$$f_1(d, t) = \sum_{i=0}^M N_i \delta(d - x_i). \quad \left( \frac{1}{m^3(m)} \right) \quad (12.272)$$

The RHS of equation (12.272) is zero for  $d \neq x_i$  and equals  $N_i$  when  $d = x_i$ .

Applying the *mean value theorem* on the source terms yields:

$$\int_{d_i}^{d_{i+1}} B_B(d, t) dd = \sum_{j=i}^M N_j v(x_j) b_B(x_j) \int_{d_i}^{d_{i+1}} P_B(d|x_j) dd \quad (12.273)$$

$$\int_{d_i}^{d_{i+1}} D_B(d, t) dd = b_B(x_i) N_i \quad (12.274)$$

$$\int_{d_i}^{d_{i+1}} B_C(d, t) dd = \frac{1}{2} \sum_{j=0}^{i-1} N_j \sum_{(x_j+x_k) \in I_i} N_k a_C(x_k, x_j) \tag{12.275}$$

$$\int_{d_i}^{d_{i+1}} D_C(d, t) dd = N_i \sum_{j=0}^M N_j a_C(x_i, x_j) \tag{12.276}$$

Inserting these expressions into (12.266) gives:

$$\begin{aligned} \frac{dN_i}{dt} + \nabla \cdot (N_i \langle \mathbf{v} \rangle_{N_i}) &= \sum_{j=i}^M N_j v(x_j) b_B(x_j) \int_{d_i}^{d_{i+1}} P_B(d|x_j) dd - b_B(x_i) N_i \\ &+ \frac{1}{2} \sum_{j=0}^{i-1} N_j \sum_{(x_j+x_k) \in I_i} N_k a_C(x_k, x_j) - N_i \sum_{j=0}^M N_j a_C(x_i, x_j), \quad i = 0, 1, \dots, M \end{aligned} \tag{12.277}$$

Equation (12.277) is not necessary conservative due to the finite (i.e., in practice rather coarse) size grid resolution, and some sort of numerical trick must be used to enforce the conservative properties. It is mainly at this point in the formulation of the numerical algorithm that the class method of Hounslow et al [74], the discrete method of Ramkrishna [151] and the multi-group approach used by Carrica et al [24], among others, differs to some extent as discussed earlier.

The problem in question is related to the birth terms only. In the discrete method of Ramkrishna [151], the formation of a bubble of size  $d'$  in size range  $(x_i, x_{i+1})$  due to breakage or coalescence is represented by assigning fractions  $\gamma_1(d, x_i)$  and  $\gamma_2(d, x_{i+1})$  to bubble population at pivots  $x_i$  and  $x_{i+1}$ , respectively. This is necessary because not all coalescence and breakage result in a bubble which has a legitimate size. For the non-valid daughter particles one has to distribute the new bubble in fractions  $\gamma_1(d, x_i)$  and  $\gamma_2(d, x_{i+1})$  of the two neighboring size pivots. To determine these two fractions, one needs two balance equations. The first balance equation relates to the total volume or mass of the bubbles, to ensure mass conservation. The second balance equation is the number balance for the bubbles involved in the breakage and coalescence processes.

The balances are thus written:

$$\gamma_1(d, x_i) V_{b,i}(d) + \gamma_2(d, x_{i+1}) V_{b,i+1}(d) = V_b(d) \tag{12.278}$$

$$\gamma_1(d, x_i) + \gamma_2(d, x_{i+1}) = 1 \tag{12.279}$$

Alternatively, the second balance equation is sometimes substituted by a bubble surface balance since one wants to ensure good estimates of the contact area. The surface area balance is stated like:

$$\gamma_1(d, x_i) a_{b,i} + \gamma_2(d, x_{i+1}) a_{b,i+1} = a_b(d) \quad (12.280)$$

The fractions  $\gamma_1(d, x_i)$  and  $\gamma_2(d, x_{i+1})$  need to be embedded in the source terms as part of the discretization procedure. Thus, the source terms are modified to:

$$\begin{aligned} \frac{dN_i}{dt} + \nabla \cdot (N_i \langle \mathbf{v} \rangle_{N_i}) &= \sum_{j=i}^M \gamma_1(d, x_i) N_j v(x_j) b_B(x_j) \int_{x_{i-1}}^{x_i} P_B(d|x_j) dd \\ &+ \sum_{j=i}^M \gamma_2(d, x_i) N_j v(x_j) b_B(x_j) \int_{x_i}^{x_{i+1}} P_B(d|x_j) dd - b_B(x_i) N_i \\ &+ \frac{1}{2} \sum_{j=0}^{i-1} N_j \sum_{(x_j+x_k) \in I_i} N_k \gamma_1(d, x_i) a(x_k, x_j) \\ &+ \frac{1}{2} \sum_{j=0}^{i-1} N_j \sum_{(x_j+x_k) \in I_{i-1}} N_k \gamma_2(d, x_i) a(x_k, x_j) - N_i \sum_{j=0}^M N_j a_C(x_i, x_j) \end{aligned} \quad (12.281)$$

The breakage function,  $P_B(d|d')dd$ , is the number of particles formed between size  $d'$  and  $d' + dd'$  divided by the total number of size  $d$  particles broken. At the pivots, the corresponding breakage function is defined as  $P_B(x_i|x_k)$ :

$$P_B(x_i|x_k) = \int_{x_{i-1}}^{x_i} P_B(d|x_k) dd + \int_{x_i}^{x_{i+1}} P_B(d|x_k) dd \quad (-) \quad (12.282)$$

The multi-group approach of Carrica et al [24] will be outlined next using particle mass as the internal coordinate. All the particles of mass between  $m_{g-1/2}$  and  $m_{g+1/2}$  are thus represented in a group,  $g$ , by a single particle mass,  $m_g$ .  $m_{g-1/2}$  and  $m_{g+1/2}$  are chosen such that a reasonable representation of the distribution is obtained.

Integrating the population balance equation between  $m_{g-1/2}$  and  $m_{g+1/2}$  one obtains:

$$\begin{aligned} \frac{\partial n_g(\mathbf{r}, t)}{\partial t} + \nabla_{\mathbf{r}} \cdot [\mathbf{v}_g(\mathbf{r}, t) n_g(\mathbf{r}, t)] + \left[ \frac{dm}{dt} f(m, \mathbf{r}, t) \right]_{m_{g-1/2}}^{m_{g+1/2}} = \\ \int_{m_{g-1/2}}^{m_{g+1/2}} [B_B(m, \mathbf{r}, t) - D_B(m, \mathbf{r}, t) + B_C(m, \mathbf{r}, t) - D_C(m, \mathbf{r}, t) + S(m, \mathbf{r}, t)] dm \end{aligned} \quad (12.283)$$

The average particle velocity in the group  $g$  can be calculated as:

$$\mathbf{v}_g(\mathbf{r}, t) = \frac{1}{n_g(\mathbf{r}, t)} \int_{m_{g-1/2}}^{m_{g+1/2}} \mathbf{v}(m, \mathbf{r}, t) f(m, \mathbf{r}, t) dm \tag{12.284}$$

The group number density is defined as:

$$n_g(\mathbf{r}, t) = \int_{m_{g-1/2}}^{m_{g+1/2}} f(m, \mathbf{r}, t) dm \tag{12.285}$$

Carrica et al [24] further assumed that the distribution function, the particle velocities, the particle mass exchange rate and the breakage and coalescence probability are assumed constant in each group. Under these restrictions, the balance equation yields:

$$\frac{\partial n_g}{\partial t} + \nabla_{\mathbf{r}} \cdot (\mathbf{v}_g n_g) = B_{B,g} - D_{B,g} + B_{C,g} - D_{C,g} + S_g - \left[ \frac{dm}{dt} f(m, \mathbf{r}, t) \right]_{m_{g-1/2}}^{m_{g+1/2}} \tag{12.286}$$

The growth terms need some further attention. Considering that for fluid particles the mass change rate (or an imaginary velocity in the internal coordinates) of the particle,  $\frac{dm}{dt}$ , is negative for the case of condensation or particle dissolution, and is positive in the case of evaporation or mass diffusion into the particle the distribution function was discretized using an upwinding approach.

In an imaginary finite volume approach the distribution function discretizations at the corresponding imaginary grid cell interface,  $g + 1/2$ , thus yield:

$$f_{g+1/2} \approx \frac{n_{g+1}}{m_{g+1} - m_g}, \quad \text{for } \frac{dm}{dt} < 0 \tag{12.287}$$

$$f_{g+1/2} \approx \frac{n_g}{m_{g+1} - m_g}, \quad \text{for } \frac{dm}{dt} > 0 \tag{12.288}$$

Consistent discretization schemes are used at the other grid cell interfaces.

For the case of condensation or particle dissolution, the growth terms can thus be expressed as:

$$\begin{aligned} \left[ \frac{dm}{dt} f(m, \mathbf{r}, t) \right]_{m_{g-1/2}}^{m_{g+1/2}} &= \left[ \frac{dm}{dt} f(m, \mathbf{r}, t) \right]_{m_{g+1/2}} - \left[ \frac{dm}{dt} f(m, \mathbf{r}, t) \right]_{m_{g-1/2}} \\ &\approx \left[ \frac{dm}{dt} \right]_{m_{g+1/2}} [f(m, \mathbf{r}, t)]_{m_{g+1/2}} - \left[ \frac{dm}{dt} \right]_{m_{g+1/2}} [f(m, \mathbf{r}, t)]_{m_{g+1/2}} \\ &\approx \left[ \frac{dm}{dt} \right]_{m_{g+1/2}} \frac{n_{g+1}}{m_{g+1} - m_g} - \left[ \frac{dm}{dt} \right]_{m_{g-1/2}} \frac{n_g}{m_g - m_{g-1}} \end{aligned} \tag{12.289}$$

For the case of evaporation or mass diffusion into the particle the discretization scheme is modified accordingly:

$$\begin{aligned}
 \left[ \frac{dm}{dt} f(m, \mathbf{r}, t) \right]_{m_{g-1/2}}^{m_{g+1/2}} &= \left[ \frac{dm}{dt} f(m, \mathbf{r}, t) \right]_{m_{g+1/2}} - \left[ \frac{dm}{dt} f(m, \mathbf{r}, t) \right]_{m_{g-1/2}} \\
 &\approx \left[ \frac{dm}{dt} \right]_{m_{g+1/2}} [f(m, \mathbf{r}, t)]_{m_{g+1/2}} - \left[ \frac{dm}{dt} \right]_{m_{g+1/2}} [f(m, \mathbf{r}, t)]_{m_{g+1/2}} \\
 &\approx \left[ \frac{dm}{dt} \right]_{m_{g+1/2}} \frac{n_g}{m_{g+1} - m_g} - \left[ \frac{dm}{dt} \right]_{m_{g-1/2}} \frac{n_{g-1}}{m_g - m_{g-1}}
 \end{aligned} \tag{12.290}$$

To generalize the mass loss (or gain) rate term formulation, a staggered grid arrangement is used shifting the velocity index notation:

$$\begin{aligned}
 \left[ \frac{dm}{dt} f(m, \mathbf{r}, t) \right]_{m_{g-1/2}}^{m_{g+1/2}} &= \left[ \frac{dm}{dt} f(m, \mathbf{r}, t) \right]_{m_{g+1/2}} - \left[ \frac{dm}{dt} f(m, \mathbf{r}, t) \right]_{m_{g-1/2}} \\
 &\approx \frac{n_{g+1}}{m_{g+1} - m_g} \min\left(\left[ \frac{dm}{dt} \right]_{m_{g+1}}, 0\right) - \frac{n_g}{m_g - m_{g-1}} \min\left(\left[ \frac{dm}{dt} \right]_{m_{g-1/2}}, 0\right) \\
 &\quad + \frac{n_g}{m_{g+1} - m_g} \max\left(\left[ \frac{dm}{dt} \right]_{m_{g+1/2}}, 0\right) - \frac{n_{g-1}}{m_g - m_{g-1}} \max\left(\left[ \frac{dm}{dt} \right]_{m_{g-1/2}}, 0\right)
 \end{aligned} \tag{12.291}$$

Introducing these approximations, the balance equation yields:

$$\begin{aligned}
 \frac{\partial n_g}{\partial t} + \nabla_{\mathbf{r}} \cdot (\mathbf{v}_g n_g) &= B_{B,g} - D_{B,g} + B_{C,g} - D_{C,g} + S_g \\
 &\quad - \frac{n_{g+1}}{m_{g+1} - m_g} \min\left(\left[ \frac{dm}{dt} \right]_{m_{g+1}}, 0\right) + \frac{n_g}{m_g - m_{g-1}} \min\left(\left[ \frac{dm}{dt} \right]_{m_{g-1/2}}, 0\right) \\
 &\quad - \frac{n_g}{m_{g+1} - m_g} \max\left(\left[ \frac{dm}{dt} \right]_{m_{g+1/2}}, 0\right) + \frac{n_{g-1}}{m_g - m_{g-1}} \max\left(\left[ \frac{dm}{dt} \right]_{m_{g-1/2}}, 0\right)
 \end{aligned} \tag{12.292}$$

The groups must be chosen so as to cover all the possible relevant masses, as estimated from the maximum and minimum particle sizes in the distribution for the problem in question. Furthermore, the group masses are determined by the constant lower and upper limit masses which are assumed to be  $m_{1-1/2}, m_{1+1/2}, \dots, m_{g-1/2}, m_{1+1/2}, \dots, m_{NG+1/2}$ , where  $NG$  is the total number of groups, and the average mass for each group is  $m_1, m_2, \dots, m_g, \dots, m_{NG}$ .

The particle volume fraction is related to the group number density by:

$$\alpha_g(\mathbf{r}, t) = \sum_{g=1}^{NG} \frac{m_g n_g(\mathbf{r}, t)}{\rho_g(\mathbf{r}, t)} \tag{12.293}$$

This multi-group model can be solved in combination with the multi-fluid model to calculate the dispersed phase velocity field for each group.

Furthermore, due to the limited internal coordinate resolution, the calculation of the coalescence and breakage terms requires some “trick” to enable an accurate determination of the mass of each group. The numerical implementation of the coalescence source terms is rather complex and requires a

model for the mass transfer between the groups. With the basic multi-group model assumptions we can define a group collision kernel as:

$$\int_{m_l} \int_{m_k} p_C(m, m') \omega_C(m, m') dm dm' \approx C_{kl} p_{C,kl} n_k n_l \tag{12.294}$$

The coalescence source term can then be calculated as:

$$B_{C,g} \approx \frac{1}{2} \sum_{k \leq l} C_{kl} p_{C,kl} X_{gkl} n_k n_l \tag{12.295}$$

where  $l$  is such that  $m_{g-1} < m_k + m_l < m_{g+1}$  and  $X_{gkl}$  is a matrix with components having a value between 0 and 1 that accounts for the fraction of mass that is transferred from the coalescence of two fluid particles from groups  $k$  and  $l$  to the group  $g$

$$X_{gkl} = \frac{m_k + m_l - m_g}{m_g - m_{g-1}}, \quad \text{when } (m_k + m_l < m_g) \tag{12.296}$$

and

$$X_{gkl} = \frac{m_k + m_l - m_{g+1}}{m_g - m_{g+1}}, \quad \text{when } (m_k + m_l > m_g) \tag{12.297}$$

If the group masses are chosen such as the mass interval is constant, the matrix  $X_{gkl}$  will be filled with 1 and 0, because the sum of the masses of any two groups will be coincident with the mass of other groups. However, if the group masses are chosen with non-constant intervals in mass, the daughter particle will generally not have a mass coincident with one of the group masses. In this model the particle mass is transferred to the two nearest groups to the sum of the masses  $k$  and  $l$  using a linear distribution. This implies that the total mass  $m_k + m_l$  will be distributed linearly between the groups  $g$  and  $g+1$ , or between the groups  $g-1$  and  $g$ .

On the same grounds, the losses due to coalescence can be calculated as:

$$D_{C,g} \approx \sum_{k=1}^{NG} C_{gk} p_{C,gk} n_g n_k \tag{12.298}$$

For the breakage sources, the procedure is similar. After integration of the population balance source terms we can write the particle breakage source terms for group  $g$  as:

$$B_{B,g} \approx \sum_{k=g}^{NG} b_k X_{gk} n_k \tag{12.299}$$

where  $b_k$  is the total breakage rate evaluated at the mass of group  $k$ . The matrix  $X_{gk}$  is defined using the same assumptions as in the case of the mass

conservation matrix  $X_{gkl}$  for the coalescence case, thus resulting in a mass conservation matrix of the form:

$$X_{gk} = 2 \frac{\frac{m_k}{2} - m_{g-1}}{m_g - m_{g-1}}, \quad \text{when } (m_{g-1} < \frac{m_k}{2} < m_g), \quad (12.300)$$

$$X_{gk} = 2 \frac{\frac{m_k}{2} - m_{g+1}}{m_g - m_{g+1}}, \quad \text{when } (m_{g+1} > \frac{m_k}{2} > m_g) \quad (12.301)$$

$$X_{gk} = 0, \quad \text{otherwise} \quad (12.302)$$

The sink terms are calculated as

$$D_{B,g} = b_g n_g \quad (12.303)$$

In the multi-group implementation, the particles of the minimum size group that were dissolving were considered lost.

In all the FVMs the smallest bubbles do not break up and the largest bubbles are not involved in the coalescence process. In order to cover a broad range in the bubble size distribution (i.e., mass, volume or diameter), a large number of classes, bins or groups are needed making these algorithms rather time consuming. However, these methods provide information on the bubble size distribution that is needed in the multi-fluid framework and can also be used for proper validation of the source term closures. The simpler method of moments containing transport equations for only a few moments like the mean bubble size, the variance, etc. cannot be used in a multi-fluid framework due to the lack of any bubble size resolution and can thus only be validated in an average sense even if experimental data on the size distribution is provided. For very simple distribution functions it may be possible to reconstruct the physical size distributions with sufficient accuracy utilizing the information provided by a few moments only (i.e., as provided by the moment models). However, as the existing integral models provide two to five moments only, it is believed that the complex bubble size distributions cannot be reproduced with sufficient accuracy. It is then an open question whether the computational costs solving transport equations for about 10-15 moments, ensuring sufficient accuracy, are less than the corresponding costs solving for the whole size distributions using spectral methods. Further work in our group continuous to elucidate this issue.

Another method representing an extension of the QMOM method has obtained increasing attention for particulate systems during the last years. According to Fan et al [46], one of the main limitations of the QMOM is that the solid phase is represented through the moments of the distribution, thus the phase-average velocity of the different solid phases must be used to solve the transport equations for the moments. Thus, in order to use this method in the context of multiphase flows, it is necessary to extend QMOM to handle cases where each particle size is convected by its own velocity. In order to address these issues, a direct quadrature method of moments (DQMOM) has

been formulated by Fan et al [46]. DQMOM is based on the direct solution of the transport equations for weights and abscissas of the quadrature approximation (i.e., being quadrature approximations for the moments). Moreover, each node of the quadrature approximation is treated as a distinct solid phase. DQMOM is thus used as a module in multi-fluid models describing polydisperse solid phases undergoing segregation, growth, aggregation and breakage processes in the context of CFD simulations.

Doraó and Jakobsen [40, 41] did show that the QMOM is ill conditioned (see, e.g., Press et al [149]) and not reliable when the complexity of the problem increases. In particular, it was shown that the high order moments are not well represented by QMOM, and that the higher the order of the moment, the higher the error becomes in the predictions. Besides, the nature of the kernel functions determine the number of moments that must be used by QMOM to reach a certain accuracy. The higher the polynomial order of the kernel functions, the higher the number of moments required for getting reliable predictions. This can reduce the applicability of QMOM in the simulation of fluid particle flows where the kernel functions can have quite complex functional dependences. On the other hand, QMOM can still be used in some applications where the kernel functions are given as low order polynomials like in some solid particle or crystallization problems.

There is still no reports published evaluating the behavior of this procedure for fluid particle flows. In practical applications, the stability problems are commonly adjusted by numerous tricks that reduce the accuracy of the method.

## Methods for the Continuous Distribution

This group of methods consists of a number of weighted residual methods that are based on spectral solution strategies, but only the least squares spectral method is discussed.

The main premise of these methods is to predict a continuous number density probability  $f_1$ . If the discrete number density  $N_i$  is of interest, it can be calculated from the solution of the continuous number density probability function.

The Least Squares Method (LSM) is a well established numerical method for solving a wide range of mathematical problems [84, 12, 150, 146]. The basic idea in the LSM is to minimize the integral of the square of the residual over the computational domain. In the case when the exact solutions are sufficiently smooth the convergence rate is exponential. In particular, the application of LSM to PBE as has been discussed by [38, 39, 36, 37].

The Least-Squares formulation is based on the minimization of a norm-equivalent functional. This method consists in finding the minimizer of the residual in a certain norm. Consider the following linear problem:

$$\mathcal{L}f(\xi) + g(\xi) = 0, \quad \text{in } \Omega \quad (12.304)$$

where  $\mathcal{L}$  is a linear first order differential operator. The norm-equivalent functional for equation (12.304) can be given by

$$\mathcal{J}(f; g) \equiv \frac{1}{2} \| \mathcal{L}f + g \|_{Y(\Omega)}^2 \quad (12.305)$$

with the norm  $\| \bullet \|_{Y(\Omega)}^2$  defined like:

$$\| \bullet \|_{Y(\Omega)}^2 = \langle \bullet, \bullet \rangle_{Y(\Omega)} = \int_{\Omega} \bullet \bullet \, d\Omega \quad (12.306)$$

in general the  $L^2$ -norm is used.

Based on variational analysis, the minimization statement is equivalent to: Find  $f \in X(\Omega)$  such that

$$\lim_{\epsilon \rightarrow 0} \frac{d\mathcal{J}(f + \epsilon v; g)}{d\epsilon} = 0 \quad \forall v \in X(\Omega) \quad (12.307)$$

where  $X(\Omega)$  is the space of the admissible functions. Consequently, the necessary condition can be written as:

Find  $f \in X(\Omega)$  such that

$$\mathcal{A}(f, v) = \mathcal{F}(v) \quad \forall v \in X(\Omega) \quad (12.308)$$

with

$$\mathcal{A}(f, v) = \langle \mathcal{L}f, \mathcal{L}v \rangle_{Y(\Omega)} \quad (12.309)$$

$$\mathcal{F}(v) = \langle g, \mathcal{L}v \rangle_{Y(\Omega)} \quad (12.310)$$

where  $\mathcal{A} : X \times X$  is a symmetric, continuous bilinear form, and  $\mathcal{F} : X$  a continuous linear form.

The discretization statement consists of searching the solution in a reduced subspace, i.e.  $f_N(\xi) \in X_N(\Omega) \subset X(\Omega)$ . Therefore,  $f_N$  can be expressed like:

$$f_N(\xi) = \sum_{l=0}^N f_l \varphi_l(\xi), \quad (12.311)$$

where  $\varphi_l(\xi)$  are basis functions. One possibility, the basis functions may consist of Lagrangian interpolants polynomials through the Gauss-Lobatto-Legendre (GLL) collocation points.

Inserting approximation (12.311) into equation (12.308), and choosing systematically  $v = \varphi_0, \dots, \varphi_N$ , we get the final algebraic system:

$$\mathcal{A} \mathbf{f} = \mathcal{F} \quad (12.312)$$

where the matrix  $\mathcal{A}$ , and vectors  $\mathcal{F}, \mathbf{f}$  are defined as:

$$[\mathcal{A}]_{ij} = \mathcal{A}(\varphi_j, \varphi_i) = \langle \mathcal{L}\varphi_j, \mathcal{L}\varphi_i \rangle_{Y(\Omega)} \quad (12.313)$$

$$[\mathcal{F}]_i = \mathcal{F}(\varphi_i) = \langle g, \mathcal{L}\varphi_i \rangle_{Y(\Omega)} \quad (12.314)$$

$$[\mathbf{f}]_i = f_i \quad (12.315)$$

The final system of equations is symmetric, positive definite, hence the solution of such a system can be obtained in an efficient way using standard matrix solvers like conjugate gradient method.

## 12.13 Solution of Linear Equation Systems

For steady-state models and models discretized by implicit schemes the result of a discretization process is a system of algebraic equations, which are linear or non-linear according to the nature of the partial differential equation(s) from which they are derived. However, all the existing equation solvers are designed for linear systems. In the non-linear case, the discretized equations must thus be solved in an iterative manner that involves guessing a solution, linearizing the equations about that solution, solving the linearized equations by a linear equation solver, and improving the solution. This process is repeated until a converged result is obtained. Although many procedures can be used to solve the algebraic equations, the available computer resources is a serious constraint. This means that, whether the equations are linear or not, efficient methods for solving linear systems of algebraic equations are required.

There are two basic families of solution techniques for linear algebraic equations: Direct- and iterative methods. A well known example of direct methods is Gaussian elimination. The simultaneous storage of all coefficients of the set of equations in core memory is required. Iterative methods are based on the repeated application of a relatively simple algorithm leading to eventual convergence after a number of repetitions (iterations). Well known examples are the Jacobi and Gauss-Seidel point-by-point iteration methods.

The discretization of the dynamic 3D multi-fluid model equations, for example, normally leads to a large number of sparse linear algebraic equations. Computer efficiency and storage are thus important aspects to consider when selecting an optimal solver for these problems. Direct methods are usually robust at the cost of large storage requirements. In contrast, iterative methods need less storage capacity while their performance may be problem dependent. Iterative solvers that take advantage of the sparsity of the discretization matrix are thus generally preferable for problems comprising a large number of variables.

### 12.13.1 Point-Iterative Methods

Consider a system of  $n$  equations and  $n$  unknowns in matrix form,  $\mathcal{A}\mathbf{x} = \mathbf{b}$ . This problem can be expressed in an element form where the coefficients of matrix  $\mathcal{A}$  can be seen explicitly:

$$\sum_{j=1}^n a_{ij}x_j = b_i \quad (12.316)$$

In the Jacobi method, we rearrange the system of equations to place the contribution due to  $x_i$  on the LHS of the  $i$ th equation and the other terms on the RHS, and we divide both sides of the equation by  $a_{ii}$ . The iteration equation for the *Jacobi method* is written as:

$$x_i^\nu = -\sum_{\substack{j=1 \\ j \neq i}}^n \frac{a_{ij}}{a_{ii}} x_j^{\nu-1} + \frac{b_i}{a_{ii}}, \quad i = 1, 2, 3, \dots, n \quad (12.317)$$

The iteration equation for the *Gauss-Seidel method* is obtained employing the last available values within the iteration process:

$$x_i^\nu = -\sum_{j=1}^{i-1} \frac{a_{ij}}{a_{ii}} x_j^\nu - \sum_{j=i+1}^n \frac{a_{ij}}{a_{ii}} x_j^{\nu-1} + \frac{b_i}{a_{ii}}, \quad i = 1, 2, 3, \dots, n \quad (12.318)$$

The convergence rate of the Jacobi and Gauss-Seidel methods depends on the properties of the iteration matrix. By experience, it has been found that these methods can be improved by the introduction of a relaxation parameter  $\alpha$ . Consider the Gauss-Seidel method, it can be rewritten as:

$$x_i^\nu = x_i^{\nu-1} - \alpha \left[ \sum_{j=1}^{i-1} \frac{a_{ij}}{a_{ii}} x_j^\nu - \sum_{j=i}^n \frac{a_{ij}}{a_{ii}} x_j^{\nu-1} + \frac{b_i}{a_{ii}} \right], \quad i = 1, 2, 3, \dots, n \quad (12.319)$$

When  $\alpha = 1$ , the original Gauss-Seidel method is recovered. Other values of the parameter  $\alpha$  yields different iterative sequences. If  $0 < \alpha < 1$  then the procedure is an under-relaxation method, else with  $\alpha > 1$  we have obtained an approach that is called the successive over-relaxation (SOR) technique.

Unfortunately, the optimum value of the relaxation parameter is problem and grid dependent, hence it is difficult to give precise guidance. Besides, the convergence rate of the point-iterative methods rapidly reduces as the grid is refined.

### 12.13.2 The Tri-Diagonal Matrix Algorithm (TDMA)

The matrices derived from partial differential equations are always sparse, i.e. most of their elements are zero. For one-dimensional systems the discretization process leads to tri-diagonal systems, a system with only three non-zero coefficients per equation. Since the systems are often very large we find that iterative methods are generally much more economical than direct methods.

Jacobi and Gauss-Seidel iterative methods are easy to implement in simple computer programs, but they can be slow to converge when the system of equations is large. Hence they are not considered suitable for CFD simulations.

The tri-diagonal matrix algorithm (TDMA) of Thomas [185] was commonly used in the period from the late 1960s to the early 1990s. The TDMA is a direct method for one-dimensional situations, but it can be applied iteratively, in a line-by-line fashion, to solve multi-dimensional problems (in a line wise Gauss-Seidel approach). There are, however, other algorithms which may be more robust concerning stability, but TDMA requires a minimum of storage and is often less expensive than the alternative techniques.

For convenience in presenting the TDMA algorithm, a somewhat different nomenclature will be used [141]. Suppose the grid points were numbered 1, 2, 3, ...,  $N$ , with points 1 and  $N$  denoting the boundary points. Consider a system of equations that has a tri-diagonal form:

$$a_i\phi_i = b_i\phi_{i+1} - c_i\phi_{i-1} + d_i \quad (12.320)$$

for  $i = 1, 2, 3, \dots, N$ . Thus, the variable  $\phi_i$  is related to the neighboring variables  $\phi_{i+1}$  and  $\phi_{i-1}$ . To account for the special form of the boundary-point equations, set  $c_1 = 0$  and  $b_N = 0$ , so that the variables  $\phi_0$  and  $\phi_{N+1}$  will not have any meaningful role to play. When the boundary values are given, these boundary point equations take a rather trivial form. For example, if  $\phi_1$  is given, we have  $a_1 = 0$ ,  $b_1 = 0$ ,  $c_1 = 0$ , and  $d_1 =$  the given value of  $\phi_1$ .

The basic equation above can be rewritten as:

$$\phi_i = \frac{b_i}{a_i}\phi_{i+1} - \frac{c_i}{a_i}\phi_{i-1} + \frac{d_i}{a_i} \quad (12.321)$$

These equations can be solved by forward elimination and back-substitution.

In *the forward elimination process* we seek a relation:

$$\phi_i = P_i\phi_{i+1} + Q_i \quad (12.322)$$

after we have just obtained

$$\phi_{i-1} = P_{i-1}\phi_i + Q_{i-1} \quad (12.323)$$

Substitution of equation (12.323) into (12.320) leads to:

$$a_i\phi_i = b_i\phi_{i+1} - c_i(P_{i-1}\phi_i + Q_{i-1}) + d_i \quad (12.324)$$

which can be rearranged to the form of equation (12.322). In other words, the coefficients  $P_i$  and  $Q_i$  is then given by:

$$P_i = \frac{b_i}{a_i - c_iP_{i-1}} \quad (12.325)$$

$$Q_i = \frac{d_i + c_iQ_{i-1}}{a_i - c_iP_{i-1}} \quad (12.326)$$

These are recurrence relations, since they give  $P_i$  and  $Q_i$  in terms of  $P_{i-1}$  and  $Q_{i-1}$ . At the boundary points we see that for  $i = 1$ ,  $P_1 = \frac{b_1}{a_1}$  and  $Q_1 = \frac{d_1}{a_1}$ , and for  $i = N$  we obtain  $P_N = 0$  and  $\phi_N = Q_N$ .

For the *back-substitution* we use the general form of the recurrence relationship (12.322).

The iterative procedure is considered to give a converged solution if the absolute normalized residuals for all the variables as well as the mass source  $b$  of the pressure correction equation are less than a prescribed small value, denoting the convergence criterion. The absolute normalized residual is defined as:

$$R_{\psi}^{\nu} = \frac{\sum_{\text{all nodes}} |\sum_{nb} a_{nb} \psi_{nb} + S_C - a_P \psi_P|^{\nu}}{F_{in,\psi}} \quad (12.327)$$

and for the pressure correction equation:

$$R_{\text{mass}}^{\nu} = \frac{\sum_{\text{all nodes}} |b|^{\nu}}{M_{in,\text{mass}}} \quad (12.328)$$

The  $F_{in,\psi}$  denotes the total inflow of the property  $\psi$  into the calculation domain and  $M_{in,\text{mass}}$  represents the total inflow of mass. The prescribed small threshold value used to define the convergence criterion is problem dependent and may vary with grid resolution. Nevertheless, the iteration is generally aborted when the normalized residuals for all the variables fall below  $10^{-3}$ .

Note that this solver fail to converge when applied to algebraic equation systems which are not diagonally dominant. For non-linear and multi-dimensional problems, the algorithm is used in a line-wise Gauss-Seidel approach. The convergence rate for linear multi-dimensional problems is generally severely degraded when only one dimension can be considered at the time, so multidimensional iterative algorithms may be preferable.

### 12.13.3 Krylov Subspace Methods

The conjugate gradient algorithm of Hestenes and Stiefel [70] and the bi-conjugate gradient algorithm of Fletcher [52] and their preconditioned versions [166] are presented in the following sections .

Consider a system of linear algebraic equations written on the form  $\mathcal{A}\mathbf{x} = \mathbf{b}$ . The basic idea of the Krylov subspace methods is to project a large problem onto a Krylov subspace by constructing a basis of the subspace. The Krylov subspace methods form an orthogonal basis of the sequence of successive matrix powers times the initial residual (the Krylov sequence). The approximations to the solution are then formed by minimizing the residual over the subspace formed. The projected subspace problem is solved by a standard well established technique before an approximate solution of the original problem is recovered from the solution of the projected problem. The numerous variants of the Krylov subspace methods arise from different choices of basis of the Krylov subspace. The prototype method in this class is the conjugate gradient method (CG). Another popular method in this class, the bi-conjugate gradient method (BCG) is more advanced and better suited

for solving problems giving rise to unsymmetric  $\mathcal{A}$ -matrices. Several extensions of the BCG-method have been developed (e.g., the Conjugate Gradient Squared (CGS) method, the bi-orthogonal Conjugate Gradient Stabilized (BCGSTAB), etc.), intending to reduce the the computational costs of the BCG method. The generalized minimal residual method (GMRES) proposed by Saad and Shultz [165] is also designed for unsymmetric matrices and is one of the most advanced methods in this class that among other things may treat nearly singular systems, but also one of the most computationally intensive methods.

In cases where iterative methods are employed to solve large, sparse linear systems, both the efficiency and robustness of these methods can be significantly improved by use of preconditioners. A preconditioner  $\mathcal{M}$  of a matrix  $\mathcal{A}$  is a matrix such that  $\mathcal{M}^{-1}\mathcal{A}$  has a smaller condition number than  $\mathcal{A}$ . The condition number associated with such a problem is a measure of that problem's amenability to digital computation, that is, how numerically well-posed the problem is. A problem with a low condition number is said to be well-conditioned, while a problem with a high condition number is said to be ill-conditioned. In particular, if  $\mathcal{M}$  is a symmetric, positive definite matrix<sup>14</sup> that approximates the original  $\mathcal{A}$  matrix but is easier to invert, the original problem  $\mathcal{A}\mathbf{x} = \mathbf{b}$  can be solved indirectly by solving  $\mathcal{M}^{-1}\mathcal{A}\mathbf{x} = \mathcal{M}^{-1}\mathbf{b}$ . However, the advanced preconditioners are generally more computationally expensive than the simpler ones. Although the number of iterations is normally reduced with increasing complexity of the preconditioner, the total computational cost may not necessarily be improved. An aim when designing appropriate preconditioners is to find a suitable balance between the computational time required by the preconditioner and the solver. One simple, but computationally inexpensive and effective preconditioner suitable for diagonally dominant matrices is the *Jacobi preconditioner*. This preconditioner contains only the diagonal elements of the  $\mathcal{A}$ -matrix:

$$\mathcal{M} = \text{diag}(\mathcal{A}) \quad (12.329)$$

More complex preconditioners are the incomplete LU-preconditioners (ILU) given on the form:

$$\mathcal{M} = \mathcal{L}\mathcal{U} \quad (12.330)$$

in which  $\mathcal{L}$  and  $\mathcal{U}$  are the lower- and upper triangular matrices, derived by Gauss-elimination where certain fill elements are ignored (hence the name incomplete).

The best known Krylov subspace method is the method of Conjugate Gradients (CG) by Hestenes and Stiefel [70]. If  $\mathcal{A}$  is symmetric positive definite, the solution of the problem  $\mathcal{A}\mathbf{x} = \mathbf{b}$  corresponds to determining a local minimum of the quadratic function:

<sup>14</sup> The matrix  $\mathcal{M}$  is symmetric if  $\mathcal{A} = \mathcal{A}^T$ . The matrix is said to be positive definite if the Euclidean inner product  $(\mathbf{x}, \mathcal{M}\mathbf{x}) > 0$  whenever  $\mathbf{x} \neq 0$  [166]. The Euclidean inner product between two vectors  $\mathbf{x}$  and  $\mathbf{y}$  is defined as  $(\mathbf{x}, \mathbf{y}) = \mathbf{x}^T \mathbf{y} = \sum_{i=1}^n x_i y_i$ .

$$f(\mathbf{x}) = \frac{1}{2}\mathbf{x}^T \mathcal{A}\mathbf{x} - \mathbf{b}^T \mathbf{x} \quad (12.331)$$

The basis used in this method is conjugate search directions and orthogonal residuals<sup>15</sup> which is equivalent to finding a minimum point along the search directions.

### The Conjugate Gradient Algorithm

In a linear system  $\mathcal{A}\mathbf{x} = \mathbf{b}$  where the matrix  $\mathcal{A}$  is symmetric and positive definite, the solution is obtained by minimizing the quadratic form (12.331). This implies that the gradient,  $f'(\mathbf{x}) = \mathcal{A}\mathbf{x} - \mathbf{b}$ , is zero. In the iteration procedure an approximate solution,  $\mathbf{x}_{m+1}$ , can be expressed as a linear combination of the previous solution and a search direction,  $\mathbf{p}_m$ , which is scaled by a scaling factor  $\alpha_m$ :

$$\mathbf{x}_{m+1} = \mathbf{x}_m + \alpha_m \mathbf{p}_m \quad (12.332)$$

An indication of how far the approximated solution is from the real solution is given by the residual:

$$\mathbf{r}_{m+1} = -f'(\mathbf{x}_{m+1}) = \mathbf{b} - \mathcal{A}\mathbf{x}_{m+1} = \mathbf{r}_m - \alpha_m \mathcal{A}\mathbf{p}_m \quad (12.333)$$

In order to determine scaling factor and thereby the step length, the quadratic function  $f(\mathbf{x}_{m+1})$  has to be minimized with respect to  $\alpha_m$ :

$$\frac{d}{d\alpha_m} f(\mathbf{x}_{m+1}) = f'(\mathbf{x}_{m+1})^T \frac{d\mathbf{x}_{m+1}}{d\alpha_m} = -\mathbf{r}_{m+1}^T \mathbf{p}_m = 0 \quad (12.334)$$

By using the definition the residual (12.333) in (12.334) and switching to the inner product notation  $\mathbf{r}_{m+1}^T \mathbf{p}_m = (\mathbf{r}_{m+1}, \mathbf{p}_m)$  results in:

$$\alpha_m = \frac{(\mathbf{r}_m, \mathbf{p}_m)}{(\mathcal{A}\mathbf{p}_m, \mathbf{p}_m)} \quad (12.335)$$

If the next search direction is a linear combination of the previous search direction scaled by a factor  $\beta_m$  and the residual  $\mathbf{r}_{m+1}$ :

$$\mathbf{p}_{m+1} = \mathbf{r}_{m+1} + \beta_m \mathbf{p}_m \quad (12.336)$$

a consequence of this relation and (12.334) is:

$$(\mathbf{r}_m, \mathbf{p}_m) = (\mathbf{r}_m, \mathbf{r}_m + \beta_{m-1} \mathbf{p}_{m-1}) = (\mathbf{r}_m, \mathbf{r}_m) \quad (12.337)$$

Then (12.335) becomes:

---

<sup>15</sup> If the matrix  $\mathcal{A}$  is symmetric, then two vectors  $\mathbf{x}$  and  $\mathbf{y}$  are conjugate or A-orthogonal if the A-inner product  $(\mathbf{x}, \mathbf{y})_{\mathcal{A}} = (\mathcal{A}\mathbf{x}, \mathbf{y}) = (\mathbf{x}, \mathcal{A}\mathbf{y}) = 0$  holds [166]. Vectors are orthogonal if  $(\mathbf{x}, \mathbf{y}) = 0$ .

$$\alpha_m = \frac{(\mathbf{r}_m, \mathbf{r}_m)}{(\mathcal{A}\mathbf{p}_m, \mathbf{p}_m)} \quad (12.338)$$

Moreover, it can be shown that the residuals are orthogonal when requiring conjugate search directions, i.e.  $(\mathbf{p}_m, \mathcal{A}\mathbf{p}_{m-1}) = (\mathcal{A}\mathbf{p}_m, \mathbf{p}_{m-1}) = 0$

$$\begin{aligned} (\mathbf{r}_{m+1}, \mathbf{p}_m) &= (\mathbf{r}_{m+1}, \mathbf{r}_m + \beta_{m-1}\mathbf{p}_{m-1}) \\ &= (\mathbf{r}_{m+1}, \mathbf{r}_m) + (\mathbf{r}_m - \alpha\mathcal{A}\mathbf{p}_m, \beta_{m-1}\mathbf{p}_{m-1}) \\ &= (\mathbf{r}_{m+1}, \mathbf{r}_m) = 0 \end{aligned} \quad (12.339)$$

The conjugacy constrain is also applied when determining the scaling factor,  $\beta_m$ , from (12.336):

$$\beta_m = -\frac{(\mathbf{r}_{m+1}, \mathcal{A}\mathbf{p}_m)}{(\mathbf{p}_m, \mathcal{A}\mathbf{p}_m)} \quad (12.340)$$

This equation can be reformulated by using (12.333), (12.339) and (12.338):

$$\begin{aligned} \beta_m &\stackrel{(12.333)}{=} \frac{1}{\alpha_m} \frac{(\mathbf{r}_{m+1}, \mathbf{r}_{m+1} - \mathbf{r}_m)}{(\mathbf{p}_m, \mathcal{A}\mathbf{p}_m)} \stackrel{(12.339)}{=} \frac{1}{\alpha_m} \frac{(\mathbf{r}_{m+1}, \mathbf{r}_{m+1})}{(\mathbf{p}_m, \mathcal{A}\mathbf{p}_m)} \\ &\stackrel{(12.338)}{=} \frac{(\mathbf{r}_{m+1}, \mathbf{r}_{m+1})}{(\mathbf{r}_m, \mathbf{r}_m)} \end{aligned} \quad (12.341)$$

Putting these relations together gives the following algorithm:

**ALGORITHM 1** The conjugate gradient (CG) algorithm.

$m = 0$

$\mathbf{p}_m = \mathbf{r}_m = \mathbf{b} - \mathcal{A}\mathbf{x}_m$

**while** not convergence **do**

$$\alpha_m = \frac{(\mathbf{r}_m, \mathbf{r}_m)}{(\mathcal{A}\mathbf{p}_m, \mathbf{p}_m)}$$

$$\mathbf{x}_{m+1} = \mathbf{x}_m + \alpha_m \mathbf{p}_m$$

$$\mathbf{r}_{m+1} = \mathbf{r}_m - \alpha_m \mathcal{A}\mathbf{p}_m$$

$$\beta_m = \frac{(\mathbf{r}_{m+1}, \mathbf{r}_{m+1})}{(\mathbf{r}_m, \mathbf{r}_m)}$$

$$\mathbf{p}_{m+1} = \mathbf{r}_{m+1} + \beta_m \mathbf{p}_m$$

$$m = m + 1$$

**end while**

The result is  $\mathbf{x}_{m+1}$ .

### 12.13.4 Preconditioning

Preconditioning is a technique which improves the condition number of a matrix and thereby increases the convergence rate of Krylov subspace methods. Thus, if the preconditioner  $\mathcal{M}$  is a symmetric, positive definite matrix, the original problem  $\mathcal{A}\mathbf{x} = \mathbf{b}$  can be solved indirectly by solving  $\mathcal{M}^{-1}\mathcal{A}\mathbf{x} = \mathcal{M}^{-1}\mathbf{b}$ . The the residual can then be written as:

$$\mathbf{z}_{m+1} = \mathcal{M}^{-1}\mathbf{r}_{m+1} = \mathbf{z}_m - \mathcal{M}^{-1}\alpha_m\mathcal{A}\mathbf{p}_m \quad (12.342)$$

Using this relation, the condition (12.334) can be expressed in terms of the  $\mathcal{M}$ -inner product:

$$(\mathbf{r}_{m+1}, \mathbf{p}_m) = (\mathcal{M}\mathbf{z}_{m+1}, \mathbf{p}_m) = (\mathbf{z}_{m+1}, \mathbf{p}_m)_{\mathcal{M}} = 0 \quad (12.343)$$

The new search direction is now a linear combination of the previous search direction and  $\mathbf{z}_{m+1}$ :

$$\mathbf{p}_{m+1} = \mathbf{z}_{m+1} + \beta_m\mathbf{p}_m \quad (12.344)$$

With the same procedures used in the previous section the scaling factors,  $\alpha_m$  and  $\beta_m$ , then becomes:

$$\alpha_m = \frac{(\mathbf{z}_m, \mathbf{z}_m)_{\mathcal{M}}}{(\mathcal{M}^{-1}\mathcal{A}\mathbf{p}_m, \mathbf{p}_m)_{\mathcal{M}}} = \frac{(\mathbf{z}_m, \mathbf{r}_m)}{(\mathcal{A}\mathbf{p}_m, \mathbf{p}_m)} \quad (12.345)$$

$$\beta_m = \frac{(\mathbf{z}_{m+1}, \mathbf{z}_{m+1})_{\mathcal{M}}}{(\mathbf{z}_m, \mathbf{z}_m)_{\mathcal{M}}} = \frac{(\mathbf{r}_{m+1}, \mathbf{z}_{m+1})}{(\mathbf{r}_m, \mathbf{z}_m)} \quad (12.346)$$

This result comprises an algorithm that can be summarized as follows:

**ALGORITHM 2** The preconditioned conjugate gradient (CG) algorithm

$m = 0$

$\mathbf{r}_m = \mathbf{b} - \mathcal{A}\mathbf{x}_m$

$\mathbf{p}_m = \mathbf{z}_m = \mathcal{M}^{-1}\mathbf{r}_m$

**while** not convergence **do**

$$\alpha_m = \frac{(\mathbf{z}_m, \mathbf{r}_m)}{(\mathcal{A}\mathbf{p}_m, \mathbf{p}_m)}$$

$$\mathbf{x}_{m+1} = \mathbf{x}_m + \alpha_m\mathbf{p}_m$$

$$\mathbf{r}_{m+1} = \mathbf{r}_m - \alpha_m\mathcal{A}\mathbf{p}_m$$

$$\mathbf{z}_{m+1} = \mathcal{M}^{-1}\mathbf{r}_{m+1}$$

$$\beta_m = \frac{(\mathbf{z}_{m+1}, \mathbf{r}_{m+1})}{(\mathbf{z}_m, \mathbf{r}_m)}$$

$$\mathbf{p}_{m+1} = \mathbf{z}_{m+1} + \beta_m\mathbf{p}_m$$

$$m = m + 1$$

**end while**

A weakness of the CG-method is the restriction to symmetric matrices. Thus, there is no guarantee for convergence when applying the algorithm to equation systems that are not symmetric. For that reason, for the flow models only the Poisson equation is normally solved using the CG-method, the other equations are solved using the bi-conjugate gradient method (BCG) of Fletcher [52] which is a generalization of the CG-method for solving systems of equations that are not necessarily symmetric or positive definite. With a doubling of the computational costs per iteration, non-symmetric systems can be converted into a symmetric system of double size:

$$\begin{bmatrix} 0 & \mathcal{A}_k \\ \mathcal{A}_k^T & 0 \end{bmatrix} \begin{bmatrix} \mathbf{x}_k^* \\ \mathbf{x}_k \end{bmatrix} = \begin{bmatrix} \mathbf{b}_k \\ \mathbf{b}_k^* \end{bmatrix} \quad (12.347)$$

However, since the expanded system is indefinite the minimization argument of the CG-method becomes ineffective. The CG-method is thus modified by replacing the orthogonal sequence of residuals by two mutually orthogonal sequences. In addition, the conjugacy constraint of the search directions is replaced by a corresponding conjugacy constraint of the two mutual search directions.

### The Bi-Conjugate Gradient Algorithm

The BCG-method is an extension of the CG-method for systems that are not symmetric or positive definite. Systems involving non-symmetric matrices, can be turned into symmetric systems on the form (12.347). Due to the indefinite matrix in this expanded system, the original CG-method is somewhat modified since the minimization argument becomes ineffective. The residual norm may even increase during iterations. With the following constrains:

$$(\mathbf{r}_{m+1}, \mathbf{r}_m^*) = (\mathbf{r}_m, \mathbf{r}_{m+1}^*) = 0 \quad (12.348)$$

$$(\mathcal{A}\mathbf{p}_{m+1}, \mathbf{p}_m^*) = (\mathcal{A}\mathbf{p}_m, \mathbf{p}_{m+1}^*) = 0 \quad (12.349)$$

the BCG-method can be derived in the same manner as the CG-method.

**ALGORITHM 3** The bi-conjugate gradient algorithm

$m = 0$

$\mathbf{p}_m^* = \mathbf{p}_m = \mathbf{r}_m^* = \mathbf{r}_m = \mathbf{b} - \mathcal{A}\mathbf{x}_m$

**while** not convergence **do**

$$\alpha_m = \frac{(\mathbf{r}_m, \mathbf{r}_m^*)}{(\mathbf{p}_m^*, \mathcal{A}\mathbf{p}_m)}$$

$$\mathbf{x}_{m+1} = \mathbf{x}_m + \alpha_m \mathbf{p}_m$$

$$\mathbf{r}_{m+1} = \mathbf{r}_m - \alpha_m \mathcal{A}\mathbf{p}_m$$

$$\mathbf{r}_{m+1}^* = \mathbf{r}_m^* - \alpha_m \mathcal{A}^T \mathbf{p}_m^*$$

$$\beta_m = \frac{(\mathbf{r}_{m+1}, \mathbf{r}_{m+1}^*)}{(\mathbf{r}_m, \mathbf{r}_m^*)}$$

$$\mathbf{p}_{m+1} = \mathbf{r}_{m+1} + \beta_m \mathbf{p}_m$$

$$\mathbf{p}_{m+1}^* = \mathbf{r}_{m+1}^* + \beta_m \mathbf{p}_m^*$$

$$m = m + 1$$

**end while**

The preconditioner is introduced in the same manner as in the CG-algorithm, leading to Algorithm 4.

**ALGORITHM 4** The preconditioned bi-conjugate gradient algorithm

$m = 0$

$\mathbf{r}_m^* = \mathbf{r}_m = \mathbf{b} - \mathcal{A}\mathbf{x}_m$

```

 $\mathbf{p}_m^* = \mathbf{p}_m = \mathbf{z}_m^* = \mathbf{z}_m = \mathcal{M}\mathbf{r}_m$ 
while not convergence do
   $\alpha_m = \frac{(\mathbf{z}_m, \mathbf{r}_m^*)}{(\mathbf{p}_m^*, \mathcal{A}\mathbf{p}_m)}$ 
   $\mathbf{x}_{m+1} = \mathbf{x}_m + \alpha_m \mathbf{p}_m$ 
   $\mathbf{r}_{m+1} = \mathbf{r}_m - \alpha_m \mathcal{A}\mathbf{p}_m$ 
   $\mathbf{r}_{m+1}^* = \mathbf{r}_m^* - \alpha_m \mathcal{A}^T \mathbf{p}_m^*$ 
   $\mathbf{z}_{m+1} = \alpha_m \mathcal{M}^{-1} \mathbf{r}_{m+1}$ 
   $\mathbf{z}_{m+1}^* = \alpha_m \mathcal{M}^{-1} \mathbf{r}_{m+1}^*$ 
   $\beta_m = \frac{(\mathbf{z}_{m+1}, \mathbf{r}_{m+1}^*)}{(\mathbf{z}_m, \mathbf{r}_m^*)}$ 
   $\mathbf{p}_{m+1} = \mathbf{r}_{m+1} + \beta_m \mathbf{p}_m$ 
   $\mathbf{p}_{m+1}^* = \mathbf{r}_{m+1}^* + \beta_m \mathbf{p}_m^*$ 
   $m = m + 1$ 
end while

```

The initial guess required in the iteration process is normally set equal to the variable values at the previous time step. The variable values at the current time level are expected to be close to the values at the previous time level. This is not necessarily true for the pressure correction due to the short time scales associated with the pressure. Thus, the initial guess for the pressure corrections are normally set to zero.

Both preconditioners are normally very robust and efficient, but the ILU-preconditioner can introduce small numerical perturbations due to floating point round-off error. Thus, simulations of symmetric problems may give non-symmetric results after some time. For this reason the Jacobi preconditioner is recommended.

### Convergence Criteria

The solver must stop when an acceptable accurate solution is found. A stop criterion must thus be defined by a sufficiently small residual value or preferably a norm<sup>16</sup> of the residual [166]. In the non-preconditioned CG-method it is natural to use the 2-norm since the euclidean inner product  $(\mathbf{r}, \mathbf{r})$  is already calculated as part of the algorithm. This is not the case neither in the preconditioned version of the CG-solver nor the BCG-methods. In these methods extra computations are thus required to calculate the stop criterion. For that reason, the less expensive infinity-norm is frequently used as stop criterion for these solvers. One possible criterion is that the norm of the residual must fall below a specific value  $|\mathbf{r}|_m < \epsilon$ . However, this criterion is difficult to use when employing the  $p$ -norm since this norm is grid dependent. Besides, the tolerance  $\epsilon$  has to be fit to the system under consideration since the residuals

<sup>16</sup> Several stop criteria can be defined in terms of different norms of the residual [166]. The general  $p$ -norm of a vector is defined as  $\|\mathbf{r}\|_p = (\sum_{i=1}^n |r_i|^p)^{1/p}$ . When  $p$  tends to infinity, the vector norm becomes  $\|\mathbf{r}\|_\infty = \max |\mathbf{r}|$ .

in the various systems may approach different values due to roundoff errors. The first issue may be solved by requiring the norm of the residual to fall below some small fraction of the norm of the initial residual  $\|\mathbf{r}_m\| < \epsilon\|\mathbf{r}_0\|$ . However, situations where the initial guess is close to the solution may cause infinite looping since the algorithm is not able to fulfill the stop criterion due to the roundoff errors. The most frequently used stop criterion is defined requiring that the norm of the residual must fall below a small fraction of the norm of the source term  $\|\mathbf{r}_m\| < \epsilon\|\mathbf{b}\|$ .

### 12.13.5 Multigrid Solvers

In this section the basic concepts of the multigrid solvers are outlined. Details of the advanced multigrid procedures may be found in the appropriate literature [18, 19, 65, 76, 77, 20, 207, 153, 154, 158, 202].

Multigrid acceleration of the Gauss-Seidel point-iterative method is currently used in many commercial CFD codes to solve the system of algebraic equations resulting from the discretization of the governing equations. For this reason, the basic principles and nomenclature must be known by the users of commercial codes and in particular for researchers that are making their own codes.

Consider a large system of algebraic equations arising from the discretization of the governing equations on a reactor flow domain:

$$\mathcal{A}\mathbf{x} = \mathbf{b} \quad (12.350)$$

If we solve this system with an iterative method, we obtain an intermediate solution  $\mathbf{x}^\nu$  after  $\nu$  iterations. This intermediate solution does not satisfy (12.350) exactly, and to determine the error in  $\mathbf{x}^\nu$  we define the residual as follows:

$$\mathbf{r}^\nu = \mathbf{b} - \mathcal{A}\mathbf{x}^\nu \quad (12.351)$$

In the multigrid concept it is essential to define an error vector  $\mathbf{e}$  as the difference between the true solution and the intermediate solution:

$$\mathbf{e}^\nu = \mathbf{x} - \mathbf{x}^\nu \quad (12.352)$$

Subtracting  $\mathcal{A}\mathbf{x}^\nu = \mathbf{b} - \mathbf{r}^\nu$ , i.e., a rearranged form of (12.351), from (12.350) gives the following relationship between the error and the residual vector:

$$\mathcal{A}\mathbf{e}^\nu = \mathbf{r}^\nu \quad (12.353)$$

The residual vector can then be calculated at any stage of the iteration process by substituting the intermediate solution into (12.351).

Multigrid methods are designed to exploit the inherent differences of the error behavior when performing iterations on grids of different sizes. It has been established theoretically that the solution error has components with a range of wavelengths that are multiples of the grid spacing. The iteration

methods cause rapid reduction of the error components with short wavelengths up to a few multiples of the grid spacing. However, the long-wavelength components of the error representing several multiples of the grid spacing tend to decay very slowly as the iteration count increases. The short-wavelength errors in a particular problem are thus effectively reduced on high resolution grids, whereas the long-wavelength errors decrease rapidly on low resolution grids. Besides, the computational cost of the iterations is larger on finer high resolution grids than on coarse low resolution grids. The extra cost due to iterations on the coarse grids may thus be offset by the benefit of the improved convergence rates.

The basic principles of multigrid solvers may be made clear by a brief sketch of a simple two-stage procedure comprising one fine ( $h$ ) and one coarse ( $2h$ ) grid. In principle, the fine grid solution can be transferred from the fine grid with spacing  $h$  onto any coarse grid with spacing  $ch$ , where  $c > 1$ . However, the process of transferring can be greatly simplified if we use a coarse grid with twice the mesh spacing of the fine grid.

*A two-stage procedure:*

1. *Fine grid iterations*

In this step we perform iterations on the finest grid with grid spacing  $h$  to generate an intermediate solution  $\mathbf{x}^\nu$  to system  $\mathcal{A}^h \mathbf{x} = \mathbf{b}$ . The number of iterations is normally chosen sufficiently large so that the short-wavelength oscillatory component of the error is reduced, but no attempt is made to eliminate the long-wavelength error component. The residual vector  $\mathbf{r}^{h,\nu}$  for the solution on this grid satisfies  $\mathbf{r}^{h,\nu} = \mathbf{b} - \mathcal{A}^h \mathbf{x}^{h,\nu}$  and the error vector  $\mathbf{e}^{h,\nu}$  is given by  $\mathbf{e}^{h,\nu} = \mathbf{x} - \mathbf{x}^{h,\nu}$ . The error and the residual is related through the formula:  $\mathcal{A}^h \mathbf{e}^{h,\nu} = \mathbf{r}^{h,\nu}$ .

2. *Restriction*

The solution is now transferred from the fine grid with spacing  $h$  onto the coarse grid with spacing  $2h$ . Due to the larger grid spacing of the coarse grid, the long-wavelength error observed on the fine grid now appears as a short-wavelength error on the new grid and will reduce rapidly.

Instead of solving for the solution vector  $\mathbf{x}^{2h,\nu}$  we work with the error equation  $\mathcal{A}^{2h} \mathbf{e}^{2h,\nu} = \mathbf{r}^{2h,\nu}$  on the coarse grid starting with an initial guess of  $\mathbf{e}^{2h,\nu} = \mathbf{0}$ .

To perform the solution process we need values of the residual vector and the matrix of coefficients. Given the values of  $\mathbf{r}^{h,\nu}$  on the fine grid we must use a suitable averaging or interpolation procedure to find the residual vector  $\mathbf{r}^{2h,\nu}$  on the coarse grid. The coefficients of matrix  $\mathcal{A}^{2h}$  can be recomputed from scratch on the coarser grid or evaluated from the fine grid grid coefficient matrix  $\mathcal{A}^h$  by use of a similar averaging/interpolation procedure as employed for the residual vector.

The cost per iteration on the coarse grid is generally less than on the fine grid, hence we may afford to perform a sufficient number of iterations to get a converged solution of the error vector  $\mathbf{e}^{2h,\nu}$ .

3. *Prolongation*

After obtaining the converged solution of the error vector  $\mathbf{e}^{2h,\nu}$  for the coarse grid, we need to transfer the solution back to the fine grid. However, we have fewer solution points in the coarse grid than nodes in the fine grid. A convenient interpolation operator is required to generate values for the prolonged error vector  $\tilde{\mathbf{e}}^{h,\nu}$  at intermediate points in the fine grid. Linear interpolation is commonly used for this purpose.

4. *Correction and final iterations*

Once we have calculated the prolonged error vector  $\tilde{\mathbf{e}}^{h,\nu}$  we may correct the intermediate fine grid solution by use of the formula:

$$\mathbf{x}^{\text{improved},\nu} = \mathbf{x}^{h,\nu} + \tilde{\mathbf{e}}^{h,\nu} \quad (12.354)$$

Because the long-wavelength error has been eliminated, the improved solution  $\mathbf{x}^{\text{improved},\nu}$  is generally closer to the true solution vector  $\mathbf{x}$ . However, several approximations were made, hence a few additional iterations are performed with the improved solution to iron out any errors that may have been introduced during the restriction and prolongation processes.

In practice, the illustrative two-stage procedure is replaced by more advanced multigrid cycles in which coarsening and refinement are used with special schedules of restriction and prolongation at different refinement levels. Common choices of multigrid cycles are the so-called V- and W-cycles.

The simple V-cycle consists of two legs. The calculation starts at the finest level. Iterations at any level are called relaxation. After a few relaxation sweeps on the finest level the residuals are restricted to the next coarse level and relaxation on that level the residuals are passed on to the next coarse level, and so on until the coarsest level is reached. After final relaxation on the coarsest level the prolongation steps are performed on the upward leg of the V-cycle until the finest level is reached. In the W-cycle additional restriction and prolongation sweeps are used at coarser levels to obtain better reduction of long-wavelength errors.

The residual  $r_i^\nu$  of the  $i$ -th equation after  $\nu$ -iterations can be defined as:

$$r_i^\nu = b_i - \sum_{j=1}^n a_{ij}x_j^\nu, \quad i = 1, 2, \dots, n \quad (12.355)$$

The average residual  $\bar{r}^\nu$  over all  $n$  equations in the system may be a useful indicator of the iterative convergence for a given problem:

$$\bar{r}^\nu = \frac{1}{n} |r_i^\nu| \quad (12.356)$$

If the iteration process is convergent the average residual tend to zero, since all contributing residuals  $r_i^\nu \rightarrow 0$  as  $\nu \rightarrow \infty$ . The average residual for a transported property  $\psi$  is frequently normalized considering the ratio of the average residual after  $\nu$  iterations and its value at the beginning of the iterations:

$$R_{\text{norm}}^{\nu} = \frac{\bar{r}^{\nu}}{\bar{r}^0} \quad (12.357)$$

The iteration is aborted when the normalized residuals for all the variables fall below  $10^{-3}$ .

### 12.13.6 Parallelization and Performance Optimization

Recent experimental studies on the flow structures of multi-phase chemical reactors like bubble column, fluidized bed and stirred tank reactors have provided insight and evidence of the dynamic nature of these systems. Transient multi-phase flow models are thus required to describe the multi-phase flow structure. Furthermore, due to the relatively high holdup of the dispersed phases in operating reactors, the Euler-Euler multi-fluid modeling framework has been adopted in most cases. An important inherent limitation of dynamic multiphase reactor flow simulations is the computational time requirements, making long time statistics intractable. To reduce the computational time of these reactor model simulations, performance optimization may be performed by selecting optimal solvers for the problem in question and by compiler optimization of the problem dependent code. For very large grids, the optimized code must be parallelized.

The compiler is the primary interface to the processor. High level languages like Fortran and C are translated into the level instructions that can be executed on the processor. Compiler optimization and instruction generation decisions can be influenced with compiler switches. These switches may correspond directly to individual modules for optimization, or influence settings of several modules. The compiler performs many optimizations on the source code based on various assumptions about the program. Typical assumptions are:

- The program is large (does not fit into the cache).
- The program does not violate language standards.
- The program is insensitive to roundoff errors.
- All data in the program is alias-ed, unless it can prove otherwise.

If one or more of the basic assumptions do not hold, the compiler should be tuned to the program by changing the compiler switches. Otherwise, the outcome may be erroneous. The source of the problem should be located, and the files where the problem occurs should be optimized with a less aggressive optimization.

For one-dimensional problems the direct TDMA algorithm is an efficient solver. In these cases the solver is computationally inexpensive and has the advantage that it requires a minimum amount of storage. For direct solvers, the number of operations to be performed to obtain the solution of a system of equations can be determined beforehand. However, for multi-dimension problems the TDMA algorithm is applied line by line on a selected plane

and then the calculation is moved to the next plane, scanning the domain plane by plane. The method is comprising a line-wise Gauss-Seidel iterative approach, hence the transfer of the boundary information into the calculation domain can be very slow. In these simulations the convergence rate depends on the sweep direction, with sweeping from upstream to downstream along the flow direction producing faster convergence than sweeping against the flow or parallel to the flow direction.

For multi-dimensional flow problems iterative methods are preferred compared to direct methods due to less storage requirements. However, the iterative methods generally converge slower than the direct methods and the number of operations to be performed to obtain the solution of a system of equations can generally not be determined beforehand. The convergence rates of the Jacobi and Gauss-Seidel point-iteration methods can be very slow when the system of equations is large. However, the multigrid acceleration techniques that have been developed recently do improve the convergence rates of these iterative solvers to such an extent that they are now commonly used in commercial codes. The Krylov subspace methods are used in many cases as their convergence rates are comparable with those of the multigrid solvers.

Lindborg et al [118] did evaluate the performance of several methods for solving the Poisson equations in dynamic 2D fixed bed reactor model simulations. The solvers evaluated were the TDMA-algorithm with and without a global block correction (multigrid) procedure [76, 77] and several variants of the CG and BCG Krylov subspace methods with and without preconditioners (Jacobi and ILU). Compiler optimization did have a larger impact on the computational time than the parallelization of the code. The BCG methods were considered the optimal Krylov subspace method alternatives as they are designed to solve problems on the form  $\mathcal{A}\mathbf{x} = \mathbf{b}$  with non-symmetric  $\mathcal{A}$  matrices. The GMRES methods are designed to solve problems on the same form and may be even more reliable and converge also for almost singular  $\mathcal{A}$  matrix systems but is also more complex to program and computational time intensive, hence not included in the test program. The CG-algorithms are also designed to solve problems on the same form and are much less computationally expensive for symmetric problems and may also converge for some non-symmetric problems. The plain and the preconditioned conjugated gradients algorithms were shown to be the best performing solvers in the test by Lindborg et al [118] solving the close to symmetric set of Poisson equations.

Parallel computers can be divided into two classes, based on whether the processors in the system have their own private memory or share a common memory. In a distributed memory system, the processors communicate with each other by sending and receiving messages through a communication network connecting all the processors. The problem to be solved must be explicitly partitioned by the programmer onto the various processors in such a way that load balancing is maintained and communication between processors is minimized and well ordered. For some problems it may not be easy or even

possible to find a satisfactory means of doing such a partitioning. From a programmers point of view, a shared memory multiprocessor is easier to program. All the processors share access to a common memory via a bus or a hierarchy of buses, and communicate with each other through shared variables in the common memory. This makes it possible for the compiler to find parallelism in scalar programs. The compiler analyzes data dependencies in each loop and if data updated is separate from data used for that update, that loop can be computed in parallel. However, this type of parallelization strategy is usually far from being optimal and explicit parallelism have to be introduced using compiler directives. The drawback with single memory device is limitations in performance, and as processors get faster it is harder to connect a considerable number of them to the same memory. To solve this problem, the shared memory is physically distributed to the nodes which may be a processor or a small group of processors. The memory elements have generally different access times to the processors in the system, hence the machines are called non-uniform memory access-machines (NUMA). The use of caches introduce a problem in finding the right copy of a variable among the multiple copies present in the concurrent hierarchical memory system. Some machines provides a full hardware support for keeping the caches coherent. These machines are called cache coherent non-uniform memory access-machines (CC-NUMA). Programs developed for distributed systems can also execute efficiently on shared memory machines, because shared memory permits an efficient implementation of message passing. The lifetime of supercomputers is relatively short, and when updating the computer, different machine architectures may be chosen. Hence, it is often chosen to program models in such a way that the model domain is explicitly partitioned onto the processors, making it portable between supercomputers of both architectures.

The scaling of the model performance with the number of processors is usually better with message passing programming (MPI; message passing interface) than with a compiler parallelized code (Open MP) for relatively small problems. However, the preference of the different programming techniques is under debate.

A widely used technique for partitioning the solution of a partial differential equation onto a number of processors is the *domain decomposition method* [128]. The space domain is divided into many sub-domains which have their own sub-boundaries. Each sub-domain is assigned to one processor such that the discretized equation system, which is split into sub-systems, one for each sub-domain, may be computed concurrently. This may decrease the convergence rate, but it offers more flexibility and, in most cases, yields a shorter computing time than global parallelization of the single domain solver. The method ensures reasonable load balancing, since the number of grid cells in each sub-domain is approximately equal and the work required for each grid cell is roughly the same.

Numerical algorithms, data structures and spatial data dependencies are thus important issues when parallelizing a code. It follows from the single- and

multi-fluid models and the standard numerical discretization schemes that the discretized equations may contain both explicit and implicit variable dependencies. The Explicit dependencies require local data communication only, whereas the implicit dependencies may require both local and global communication. The bottleneck in the Poisson equation algorithms is generally the pressure or pressure correction data communication that is required for every iteration performed within each time step of the integration.

Introduction of preconditioners on parallel architectures may not be as favorable as on a single processor due to extra communication costs. In the test by Lindborg et al [118], the CG Jacobi method was the most efficient algorithm tested for large computational loads. The optimal processor configuration for a tube with a large length to diameter ratio was shown to be the one which have all the processors in one line in the axial dimension, provided that the resolution in the radial direction is not too high.

---

## References

1. Alipanah A, Razzaghi M, Dehghan M (2007) Nonclassical pseudospectral method for the solution of brachistochrone problem. *Chaos, Solitons and Fractals* 34:1622-1628
2. Amsden AA, Harlow FH (1970) The SMAC Method: A Numerical Technique for Calculating Incompressible Fluid Flows. Los Alamos Scientific Laboratory Report 4370
3. Andersson HI, Kristoffersen R (1989) Numerical simulation of unsteady viscous flow. *Arch Mech* 41(2-3):207-223
4. Anderson JD Jr (1995) *Computational Fluid Dynamics: The basics with Applications*. McGraw-Hill Inc, New York
5. Antal SP, Ertorre SM, Kunz RF, Podowski MZ (2000) Development of a Next Generation Computer Code for the Prediction of Multicomponent Multiphase Flows. International Meeting on Trends in Numerical and Physical Modeling for Industrial Multiphase Flow, Cargese, France, September 27-29
6. Antal SP, Lahey Jr RT, Al-Dahhan MH (2004) Simulating Churn-Turbulent Flows in a Bubble Column using a Three Field, Two-Fluid Model. Paper presented at the 5th International Conference on Multiphase Flow, ICMF'04, Yokohama, Japan, May 30-June 4, Paper No 182
7. Arakawa A (1966) Computational Design for Long-Term Numerical Integration of the Equations of Fluid Motion: Two-Dimensional Incompressible Flow. Part I. *J Comput Phys* 1:119-143
8. Arakawa A, Lamb VR (1977) Computational design of the basic dynamical processes of the UCLA general circulation model. In: Chang J (ed) *Methods in Computational Physics*, Academic Press, New York, Vol 17, pp 173-265
9. Bates JR, McDonald A (1982) Multiply-Upstream, Semi-Lagrangian Advective Schemes: Analysis and Application to a Multi-Level Primitive Equation Model. *Mon Wea Rev* 110:1831-1842
10. Berge E, Jakobsen HA (1998) A regional scale multi-layer model for the calculation of long-term transport and deposition of air pollution in Europe. *Tellus B* 50(3):205-223
11. Bird RB, Stewart WE, Lightfoot EN (2002) *Transport phenomena*. Second Edition, John Wiley & Sons, New York
12. Bochev P (2001) *Finite Element Methods Based on Least-Squares and Modified Variational Principles*. Technical Report, POSTECH

13. Boris JP, Book DL (1973) Flux-Corrected Transport. I. SHASTA, A Fluid Transport Algorithm That Works. *Journal of Computational Physics*, 11:38-69
14. Bott A (1989) A positive definite advection scheme obtained by nonlinear renormalization of the advective fluxes. *Mon Wea Rev* 117:1006-1015
15. Bott A (1989) Reply. *Mon Wea Rev* 117:2633-2636
16. Bove S (2005) *Computational Fluid Dynamics of Gas-Liquid Flows Including Bubble Population Balances*. PhD thesis, Aalborg University Esbjerg, Danmark
17. Boyd JP (2001) *Chebyshev and Fourier spectral methods*. 2nd Edition, Dover, Mineola
18. Brandt A (1977) Multi-Level Adaptive Solutions to Boundary-Value Problems. *Mathematics of Computation* 31:333-390
19. Brandt A (1981) Multigrid solvers on parallel computers. In: Schultz MH (ed) *Elliptic Problem Solvers*, New York, Academic Press, pp 39-84
20. Briggs WL (1987) *A Multigrid Tutorial*. 2nd Edition, SIAM Publications
21. Burns A, Splawsky A, Lo S, Guetari C (2001) Application of coupled technology to CFD modeling of multiphase flows with CFX. In: Power H, Brebbia CA (eds) *Computational Methods in Multiphase Flow*, WIT Press, Southampton. *Proceedings of the 1st International Conference on Computational Methods in Multiphase Flow*, 14-16 March 2001, Orlando, Florida
22. Canuto C, Quarteroni A, Hussaini MY, Zang T (1988) *Spectral Methods in Fluid Mechanics*. Springer-Verlag, New York
23. Caretto LS, Curr RM, Spalding DB (1972) Two Numerical Methods for Three Dimensional Boundary Layers. *Comp Meth Appl Eng* 1:39-57
24. Carrica PM, Drew D, Bonetto F, Lahey Jr RT (1999) A Polydisperse Model for Bubbly Two-Phase Flow Around a Surface Ship. *Int J Multiphase Flow* 25(2):257-305
25. Carver MB (1981) Conservation and Pressure-Continuity Relationship in Multidimensional Two Fluid Computation. In: Vichnevetsky R (ed) *Advances in Computer Methods for Partial Differential Equations IV*. IMACS Press, pp 168-175
26. Carver MB (1984) Numerical Computation of Phase Separation in Two Fluid Flow. *J Fluids Eng* 106:147-153
27. Chen S, Doolen GD (1998) Lattice Boltzmann method for fluid flows. *Annu Rev Fluid Mech* 30:329-364
28. Cheney W, Kincaid D (2008) *Numerical Mathematics and Computing*. Thomson-Brooks/Cole Publishing Company, Belmont, California, 6th Edition
29. Chorin AJ (1967) A numerical method for solving incompressible viscous flow problems. *J Comput Phys* 2:12-26
30. Chorin AJ (1968) Numerical solution of the Navier-Stokes equations. *Math Comp* 22:745-762
31. Courant R, Isaacson E, Reeves M (1952) On the solution of nonlinear hyperbolic differential equations by finite differences. *Comm Pure and Applied Mathematics* 5:243-255
32. Dabdub D, Seinfeld JH (1994) Numerical Advective Schemes Used in Air Quality Models - Sequential and Parallel Implementation. *Atm Env* 28(20):3369-3385
33. Demirdžić I, Lilek Ž, Perić M (1993) A Collocated Finite Volume Method for Predicting Flows at all Speeds. *Int J Numer Methods Fluids* 16:1029-1050
34. Deville MO, Fischer PF, Mund EH (2002) *High-Order Methods for Incompressible Fluid Flow*. Cambridge University Press, Cambridge

35. Donea J, Huerta A (2003) Finite Element Methods for Flow Problems. John Wiley & Sons Ltd, Chichester
36. Dorao CA, Jakobsen HA (2005) An evaluation of selected numerical methods for solving the population balance equation. In: Fourth International Conference on CFD in the Oil and Gas, Metallurgical & Process Industries. SINTEF/NTNU Trondheim, Norway, 6-8 June
37. Dorao CA, Jakobsen HA (2005) Time-space least-squares spectral element method for population balance equations. In: Advances in Computational Methods in Science and Engineering 2005, ICCMSE, 21-26 October 2005, Greece. Lecture Series on Computer and Computational Sciences. Volume 4A, pp 171-174
38. Dorao CA (2006) High Order Methods for the Solution of the Population Balance Equation with Applications to Bubbly Flows. PhD thesis, Norwegian University of Science and Technology, Trondheim
39. Dorao CA, Jakobsen HA (2006) A least squares method for the solution of population balance problems. Computers and Chemical Engineering 30: 535-547
40. Dorao CA, Jakobsen HA (2006) Application of the least-squares method for solving population balance problems in  $R^{d+1}$ . Chem Eng Sci 61:5070-5081
41. Dorao CA, Jakobsen HA (2006) Numerical calculation of the moments of the population balance equation. Journal of Computational and Applied Mathematics 196:619-633
42. Dorao CA, Jakobsen HA (2007) A parallel time-space least-squares spectral element solver for incompressible flow problems. Applied Mathematics and Computation 185(1):45-58
43. Dorao CA, Jakobsen HA (2007) Time-space-property least squares spectral method for population balance problems. Chem Eng Sci 62(5):1323-1333
44. Dorao CA, Jakobsen HA (2007) Least-squares spectral method for solving advective population balance problems. Journal of Computational and Applied Mathematics 201(1):247-257
45. Drikakis D, Rider W (2005) High-Resolution Methods for Incompressible and Low-Speed Flows. Part II, Chapter 10, pp 173-208, Springer, Berlin, ISBN 978-3-540-22136-4
46. Fan R, Marchisio DL, Fox RO (2004) Application of the direct quadrature method of moments to polydisperse gas-solid fluidized beds. Powder Technology 139:7-20
47. Felten FN, Lund TS (2006) Kinetic energy conservation issues associated with the collocated mesh scheme for incompressible flow. J Comput Phys 215: 465-484
48. Fernandino M, Dorao CA, Jakobsen HA (2007) Jacobi Galerkin spectral method for cylindrical and spherical geometries. Chem Eng Sci, in press
49. Ferziger JH, Peric M (1996) Computational Methods for Fluid Dynamics. Springer, Berlin.
50. Ferziger JH (1998) Numerical Methods for Engineering Applications. Second edition, John Wiley & Sons Inc, New York
51. Finlayson BA (1972) The Method of Weighted Residuals and Variational Principles: with application in fluid mechanics, heat and mass transfer. Academic Press, New York
52. Fletcher R (1976) Conjugrate gradient methods for infinite systems. In: Proceedings of the Dundee Conference on Numerical Analysis, 1975, volume 506 of Lecture Notes in Mathematics, pp 73-89. Springer-Verlag, Berlin

53. Fletcher CAJ (1991) Computational Techniques for Fluid Dynamics. Vols I and II, Springer-Verlag, Berlin
54. Fornberg B (1998) A Practical Guide to Pseudospectral Methods. Cambridge University Press, Cambridge
55. Forsythe GE, Waso WR (1960) Finite-Difference Methods for Partial Differential Equations. John Wiley & Sons inc, New York
56. Fortin M, Peyert R, Temam R (1971) Résolution numérique des équations de Navier-Stokes pour un fluide incompressible. *J Méc* 10:357-390
57. Frank T, Zwart PJ, Shi J-M, Krepper E, Lucas D, Rohde U (2005) Inhomogeneous MUSIG Model - a Population Balance Approach for Polydispersed Bubbly Flows. *Int Conf Nuclear Energy for New Europe 2005*, Bled, Slovenia, September 5-8
58. Gaskell PH, Lau AKC (1988) Curvature-compensated Convective Transport: SMART, a new boundedness preserving transport algorithm. *Int J Numer Meth Fluids* 8:617-641
59. Gosman AD, Pun WM (1974) Calculation of recirculating flows. Report No HTS/74/2, Department of Mechanical Engineering, Imperial College, London
60. Gottlieb D, Orszag SA (1977) Numerical Analysis of Spectral Methods. SIAM, Philadelphia
61. Grace JR, Taghipour F (2004) Verification and validation of CFD models and dynamic similarity for fluidized beds. *Powder Technology* 139:99-110
62. Grandin H Jr (1991) Fundamentals of the Finite Element Method. Waveland Press, Inc, Prospect Heights, Illinois
63. Grienberger J (1992) Untersuchung und Modellierung von Blasensäulen. Dr ing Thesis, Der Technischen Fakultät der Universität Erlangen-Nürnberg, Germany
64. Gudunov SK (1959) A difference scheme for numerical calculation of discontinuous solutions of hydrodynamic equations. *Matematichaskiy Sbornik (Mathematics collection)*, 47(3):271-306 (in Russian). English Translation: US Joint Publications Research Service, JPRS-7225 (1960).
65. Hackbusch W (1985) Multigrid Methods and Applications. Springer, Berlin
66. Haltiner GJ, Williams RT (1980) Numerical Prediction and Dynamic Meteorology, 2nd Edition, Wiley, New York
67. Harlow FH, Welch JE (1965) Numerical Calculation of Time-Dependent Viscous Incompressible Flow of Fluid with Free Surface. *Physics and Fluids* 8:2182-2189
68. Harlow FH, Amsden AA (1971) A Numerical Fluid Dynamics Calculation Method for All Flow Speeds. *J Comput Phys* 8:197-213
69. Harten A (1983) High resolution schemes for hyperbolic conservation laws. *J Comput Phys* 49:357-393
70. Hestenes MR, Stiefel E (1952) Methods of Conjugate Gradients for Solving Linear Systems. *J Res NBS* 49(6):409-436
71. Hirsch C (1988) Numerical Computation of Internal and External Flows. Volume I: Fundamentals of Numerical Discretization. John Wiley & Sons, Chichester
72. Hirsch C (1990) Numerical Computation of Internal and External Flows. Volume II: Computational Methods for Inviscid and Viscous Flows. John Wiley & Sons, Chichester

73. Hirt CW, Nichols BD, Romero NC (1975) SOLA- A Numerical Solution Algorithm for Transient Fluid Flows. Los Alamos Scientific Laboratory Report 5852
74. Hounslow MJ, Ryall RL, Marshall VR (1988) A Discretized Population Balance for Nucleation, Growth, and Aggregation. *AIChE J* 34:1821-?
75. Hughes TJR (1987) *The Finite Element Method: Linear Static and Dynamic Finite Element Analysis*. Prentice-Hall Inc, Englewood Cliffs
76. Hutchinson BR, Raithby GD (1986) A Multigrid Based on the Additive Correction Strategy. *Numerical Heat Transfer* 9:511-537
77. Hutchinson BR, Galpin PF, Raithby GD (1988) Application of Additive Correction Multigrid to the Coupled Fluid Flow Equations. *Numerical Heat Transfer* 13:133-147
78. Issa RI, Lockwood FC (1977) On the Prediction of Two-Dimensional Supersonic Viscous Interactions Near Walls. *AIAA J* 15(2):182-188
79. Issa RI (1986) Solution of the Implicitly Discretised Fluid Flow Equations by Operator-Splitting. *J Comput Phys* 62:40-65
80. Jakobsen HA (1993) On the Modeling and Simulation of Bubble Column Reactors Using a Two-Fluid Model. Dr ing Thesis, the Norwegian Institute of Technology, Trondheim, Norway
81. Jakobsen HA, Lindborg H, Handeland V (2002) A numerical study of the interactions between viscous flow, transport and kinetics in fixed bed reactors. *Computers and Chemical Engineering* 26:333-357
82. Jakobsen HA (2003) Numerical Convection Algorithms and Their Role in Eulerian CFD Reactor Simulations. *International Journal of Chemical Reactor Engineering* A1:1-15
83. Jakobsen HA, Lindborg H, Dorao CA (2005) Modeling of Bubble Column Reactors: Progress and Limitations. *Ind Eng Chem Res* 44:5107-5151
84. Jiang B *The Least-Squares Finite Element Method: Theory and Applications in Computational Fluid Dynamics and Electromagnetics*. Springer, Berlin
85. Jonson JE, Bartnicki J, Olendrzynski K, Jakobsen HA, Berge E (1998) EMEP Eulerian model for atmospheric transport and deposition of nitrogen species over Europe. *Environmental Pollution* 102:289-298, Suppl 1
86. Karema H, Lo S (1999) Efficiency of interface coupling algorithms in fluidized bed conditions. *Computers & Fluids* 28:323-360
87. Karki KC, Patankar SV (1989) Pressure Based Calculation Procedure for Viscous Flows at All Speeds in Arbitrary Configurations. *AIAA J* 27(9):1167-1174
88. Karki KC, Patankar SV (2004) Application of the partial elimination algorithm for solving the coupled energy equations in porous media. *Numerical Heat Transfer, Part A* 45:539-549
89. Karniadakis GEM, Sherwin SJ (1999) *Spectral/hp Element Methods for CFD*. Oxford University Press, New York
90. Kelly JM, Stewart CW, Cuta JM (1992) VIPRE-02 - A two-fluid thermal-hydraulics code for reactor core and vessel analysis: Mathematical modeling and solution methods. *Nuclear Technology* 100:246-259
91. Khosla PK, Rubin SG (1974) A diagonally dominant second order accurate implicit scheme. *J Comput Fluids* 2:207-209
92. Kim J, Moin P (1985) Application of a Fractional-Step Method to Incompressible Navier-Stokes Equations. *J Comput Phys* 59:308-323
93. Kiusalaas J (2005) *Numerical Methods in Engineering with Python*. Cambridge University Press, New York

94. Kreiss H-O, Olinger J (1972) Comparison of accurate methods for the integration of hyperbolic equations. *Tellus* 24:199-215
95. Krepper E, Lucas D, Prasser H-M (2005) On the modelling of bubbly flow in vertical pipes. *Nucl Eng Des* 235:597-611
96. Krishna R, Urseanu MI, van Baten JM, Ellenberger J (1999) Influence of scale on the hydrodynamics of bubble columns operating in the churn-turbulent regime: experiments vs. Eulerian simulations. *Chem Eng Sci* 54:4903-4911
97. Krishna R, van Baten JM (2001) Scaling up Bubble column reactors with the aid of CFD. *Inst Chem Eng Trans IChemE* 79(A3):283-309.
98. Kunz RF, Yu W-S, Antal SP, Ertorre SM (2001) An Unstructured Two-Fluid Method Based on the Coupled Phasic Exchange Algorithm. Report AIAA-2001-2672, American Institute of Aeronautics and Astronautics, Herndon, VA
99. Kunz RF, Siebert BW, Cope WK, Foster NF, Antal SP, Ertorre SM (1998) A coupled phasic exchange algorithm for three-dimensional multi-field analysis of heated flows with mass transfer. *Computers & Fluids* 27(7):741-768
100. Kwak D, Kiris C, Dacles-Mariani J (1998) An Assessment of Artificial Compressibility and Pressure Projection Methods for Incompressible Flow Simulations. In (ed) Bruneau CH Sixteenth International Conference on Numerical Methods in Fluid Dynamics. Springer, Berlin, Volume 515. Proceedings of the Conference Held in Arcachon, France, 6-10 July 1998
101. Lanczos C (1938) Trigonometric Interpolation of Empirical and Analytical Functions. *J Math Phys* 17:123-199
102. Lapidus L, Pinder GF (1992) Numerical Solution of Partial Differential Equations in Science and Engineering. John Wiley & Sons, New York
103. Lathouwers D, van den Akker HEA. (1996) A numerical method for the solution of two-fluid model equations. In: Numerical methods for multiphase flows. FED-Vol 236, pp 121-126, ASME
104. Lathouwers D (1999) Modeling and simulation of turbulent bubbly flow. PhD thesis, the Technical University in Delft, the Netherlands
105. Lax PD (1954) Weak solutions of Nonlinear Hyperbolic Equations and Their Numerical Computation. *Communication on Pure and Applied Mathematics* 7:159-193
106. Leonard BP (1979) A stable and accurate convective modelling procedure based on quadratic upstream interpolation. *Comput Methods Appl Mech Eng* 19:59-98
107. Leonard BP (1988) Universal limiter for transient interpolation modeling of the advective transport equations: The ULTIMATE conservative difference scheme. Science report NASA-TM 100916 (ICOMP-88-11), NASA Lewis Research Center
108. Leonard BP, Mokhtari S (1990) Beyond first-order upwinding: The ULTRA-SHARP alternative for non-oscillatory steady-state simulation of convection. *International Journal of Numerical Methods in Engineering* 30:729-766
109. Leonard BP (1991) The ULTIMATE conservative difference scheme applied to unsteady one-dimensional advection. *Comput Methods Appl Mech Eng* 88:17-74
110. Leonard BP, Niknafs (1991) SHARP Monotonic Resolution of Discontinuities Without Clipping of Narrow Extrema. *Computers & Fluids* 19(1):141-154
111. Leonard BP, Mokhtari S (1992) ULTRA-SHARP solution of the Smith-Hutton problem. *Int J Num Heat Flow* 2:407-427

112. Leonard BP, MacVean MK, Lock AP (1995) The flux integral method for multidimensional convection and diffusion. *Applied Mathematical Modelling* 19:333-342
113. Leonard BP, Lock AP, MacVean MK (1995) The NIRVANA Scheme Applied to One-Dimensional Advection. *Int J Meth Heat Fluid Flow* 5:341-377
114. Leonard BP (1995) Order of accuracy of QUICK and related convection-diffusion schemes. *Appl Math Modelling* 19:640-653
115. Leonard BP, Drummond JE (1995) Why you should not use hybrid, power-law or related exponential schemes for convective modeling-There are much better alternatives. *Int J Numer Methods Fluids* 20:421-442
116. Leonard BP, Lock AP, MacVean MK (1996) Conservative Explicit Unrestricted-Time-Step Multidimensional Constancy-Preserving Advection Schemes. *Mon Wea Rev* 124:2588-2606
117. Le Veque RJ (1992) Numerical methods for conservation laws. Birkhauser Verlag, Basel
118. Lindborg H, Eide V, Unger S, Henriksen ST, Jakobsen HA (2004) Parallelization and performance optimization of a dynamic PDE reactor model for practical applications. *Computers and Chemical Engineering* 28:1585-1597
119. Lindborg H, Lysberg M, Jakobsen HA (2007) Practical validation of the two-fluid model applied to dense gas-solid flows in fluidized beds. *Chem Eng Sci* 62:5854-5869
120. MacCormack RW (1969) The effect of viscosity in hypervelocity impact cratering. AIAA paper no 69-354
121. Marchi CH, Maliska CR (1994) A Non-orthogonal Finite-Volume Method for the Solution of All Speed Flows Using Co-Located Variables. *Numerical Heat Transfer, Part B*, 26:293-311
122. Marchisio DL, Vigil RD, Fox RO (2003) Implementation of the quadrature method of moments in CFD codes for aggregation-breakage problems. *Chem Eng Sci* 58(15):3337-3351
123. Marchisio DL, Vigil RD, Fox RO (2003) Quadrature method of moments for aggregation-breakage processes. *Journal of Colloid and Interface Science* 258(2):322-334
124. Marchuk GI (1974) Numerical Methods in Weather Prediction. Academic Press, New York
125. Melaaen MC (1992) Calculation of Fluid Flows with Staggered and Nonstaggered Curvilinear Nonorthogonal Grids-the Theory. *Numerical Heat Transfer, Part B*, 21(1):1-19
126. Melaaen MC (1992) Calculation of Fluid Flows with Staggered and Nonstaggered Curvilinear Nonorthogonal Grids-a Comparison. *Numerical Heat Transfer, Part B*, 21(1):21-39
127. Merkle CL, Athavale M (1987) Time-Accurate Unsteady Incompressible Flow Algorithms Based on Artificial Compressibility. AIAA Paper 87-1137, AIAA Press Washington, DC
128. McBryan OA, van de Velde EF (1987) Hypercube algorithms and implementations. *SIAM Journal on Scientific and Statistical Computing* 8:5227-5287
129. McDonald A (1984) Accuracy of Multiply-Stream, Semi-Lagrangian Advective Schemes. *Mon Wea Rev* 112:1267-1275
130. McDonald A (1987) Accuracy of Multiply-Stream, Semi-Lagrangian Advective Schemes II. *Mon Wea Rev* 115:1446-1450

131. McGraw R (1997) Description of Aerosol Dynamics by the Quadrature Method of Moments. *Aerosol Science and Technology* 27:255-265
132. Mercier B (1989) An Introduction to the Numerical Analysis of Spectral Methods. Springer-Verlag, Berlin
133. Moukalled F, Darwish M (2000) A Unified Formulation of the Segregated Class of Algorithms for Fluid Flow at All Speeds. *Numerical Heat Transfer, Part B*, 37:103-139
134. Nakamura S (2002) Numerical Analysis and Graphic Visualization with MATLAB. Second Edition, Prentice Hall PTR, Upper Saddle River, New Jersey
135. O'Brien CG, Hyman MA, Kaplan S (1959) A study of the numerical solution of partial differential equations. *J Math Phys* 29:223-251
136. Odman MT (1997) A quantitative analysis of numerical diffusion introduced by advection algorithms in air quality models. *Atm Env* 31(13):1933-1940
137. Olendrzynski K, Jonson JE, Bartnicki J, Jakobsen HA, Berge E (2000) EMEP Eulerian model for acid deposition over Europe. *Int J Environment and Pollution* 14(1-6):391-399
138. Oliveira PJ, Issa RI (1994) On the numerical treatment of interphase forces in two-phase flow. In: Crowe CT (ed) *Numerical Methods in Multiphase Flows*, FED-Vol 185, pp 131-140, ASME Press, New York
139. Orszag SA (1972) Comparison of pseudospectral and spectral approximations. *Stud Appl Math* 51:253-259
140. Patankar SV, Spalding DB (1972) A Calculation Procedure for Heat, Mass and Momentum Transfer in Three-Dimensional Parabolic Flows. *Int J Heat Mass Transfer* 15:1787-1806
141. Patankar SV (1980) *Numerical heat transfer and fluid flow*. Hemisphere publishing corporation, New York
142. Pfleger D, Becker S (2001) Modeling and simulation of the dynamic flow behaviour in a bubble column. *Chem Eng Sci* 56(4):1737-1747.
143. Phillips NA (1956) The general circulation of the atmosphere: a numerical experiment. *Quart J Roy Meteorol Soc* 82:123-164
144. Phillips NA (1959) An example of non-linear computational instability. In: *The Atmosphere and Sea in Motion*, pp 501-504, Rockefeller Inst Press, New York, and Oxford University Press
145. Piacsek SA, Williams GP (1970) Conservation Properties of Convection Difference Schemes. *J Comput Phys* 6:392-405
146. Pontaza JP (2003) *Least-Squares Variational Principles and Finite Element Methods: Theory, formulations, and Models for Solid and Fluid Mechanics*. PhD thesis, Texas A & M University, USA
147. Post D, Kendall R (2003) Software project management and quality engineering practices for complex, coupled multiphysics, massively parallel computational simulations: Lessons learned from ASCI. *The International Journal of High Performance Computing Applications* 18(4):399-416
148. Prather MJ (1986) Numerical Advection by Conservation of Second Order Moments. *Journal of Geophysical Research*, 91(D6):6671-6681
149. Press WH, Teukolsky SA, Vetterling WT, Flannery BP (1992) *Numerical Recipes in Fortran 77. The Art of Scientific Computing*. 2. edition, Volume 1, Cambridge University Press
150. Proot MMJ (2003) *The Least-Squares Spectral Element Method*. PhD thesis, Delft University of Technology, the Netherlands

151. Ramkrishna D (2000) Population Balances: Theory and Applications to Particulate Systems in Engineering. Academic Press, San Diego
152. Rao SS (2002) Applied Numerical Methods for Engineers and Scientists. Prentice Hall, Upper Saddle River, NJ
153. Raw M (1994) A Coupled Algebraic Multigrid Method for the 3D Navier-Stokes Equations. In: Hackbusch W, Wittum G (eds) Fast Solvers for Flow Problems. Proceedings of the 10th GAMM-Seminar Kiel, January 14 to 16, 1994. Notes on Numerical Fluid Mechanics Vol 49, Vieweg-Verlag, Braunschweig, Wiesbaden, Germany
154. Raw M (1996) Robustness of Coupled Algebraic Multigrid for the Navier-Stokes Equations. Technical Paper AIAA 96-0297, AIAA Press, Washington, DC, Presented at 34th Aerospace Science Meeting & Exhibit, January 15-18, Reno, NV
155. Rhie CM, Chow WL (1983) Numerical Study of the Turbulent Flow Past an Airfoil with Trailing Edge Separation. AIAA J 21(11):1525-1532
156. Richtmyer RD, Morton KW (1967) Difference methods for initial value problems. Wiley, New York
157. Roache PJ (1992) A Flux-Based Modified Method of Characteristics. International Journal for Numerical Methods in Fluids 15:1259-1275
158. Roache PJ (1998) Fundamentals of Computational Fluid Dynamics. Hermosa Publishers, New Mexico
159. Roe PL (1981) Approximate Riemann solvers, parameter vectors and difference schemes. J Comput Phys 43:357-372
160. Roe PL (1985) Some contributions to the modeling of discontinuous flow. Lectures in Applied Mathematics 22:163-192
161. Roe PL (1986) Characteristic-based schemes for the Euler equations. Annual Reviews in Fluid Mechanics 18:337-365
162. Rood RB (1987) Numerical Advection Algorithms and Their Role in Atmospheric Transport and Chemistry Models. Reviews of Geophysics 25(1):71-100
163. Roy CJ (2005) Review of code and solution verification procedures for computational simulation. J Comput Phys 205:131-156
164. Russell GL, Lerner JA (1981) A Finite-Difference Scheme for the Tracer Transport Equation. Journal of Applied Meteorology 20:1483-1498
165. Saad Y, Shultz MH (1986) GMRES: A Generalized Minimal Residual Algorithm for solving Nonsymmetric Linear Systems. SIAM J Scientific and Stat Comp 7(3):856-869
166. Saad Y (2003) Iterative Methods for Sparse Linear Systems. 2nd Edition, SIAM, Philadelphia
167. Schiesser WE (1991) The Numerical Method of Lines: Integration of Partial Differential Equations. Academic Press, San Diego
168. Sha Z, Laari A, Turunen I (2004) Implementation of Population Balance into Multiphase-Model in CFD Simulation of Bubble Column. Proc of the 16th Int Congress of Chem Eng, Praha, Czech Republic (paper E3.2)
169. Sha Z, Laari A, Turunen I (2006) Multi-Phase-Multi-Size-Group Model for the Inclusion of Population Balances into the CFD Simulation of Gas-Liquid Bubbly Flows. Chem Eng Technol 29(5):550-559
170. Shampine LF (1994) Numerical solution of ordinary differential equations. Chapman & Hall, New York

171. Shi J, Zwart P, Frank T, Rohde U, Prasser H (2004). Development of a multiple velocity multiple size group model for poly-dispersed multiphase flows. Annual Report 2004. Institute of Safety Research, Forschungszentrum Rossendorf, Germany
172. Shyy W, Thakur SS, Ouyang H, Liu J, Blosch E (1998) Computational Techniques for Complex Transport Phenomena. Cambridge University Press, Cambridge
173. Sidilkover D (2002) Factorable Schemes for the equations of fluid flow. Applied Numerical Mathematics 41:423-436
174. Smith GD (1985) Numerical Solution of Partial Differential Equations: Finite Difference Methods. Third edition, Clarendon Press, Oxford
175. Smolarkiewicz PK (1983) A simple positive definite advection scheme with small implicit diffusion. Mon Wea Rev 11:479-486
176. Spalding DB (1977) The calculation of free-convection phenomena in gas-liquid mixtures. ICHMT seminar 1976. In: Turbulent Buoyant Convection, Hemisphere, Washington, pp 569-586
177. Spalding DB (1980) Numerical computation of multiphase fluid flow and heat transfer. In: Taylor C, Morgan K (Eds) Recent Advances in Numerical Methods in Fluids, Pineridge Press, pp 139-167
178. Spalding DB (1980) Mathematical Methods in Nuclear Reactor Thermal Hydraulics. In: Lahey RT (ed) Proc of ANS Meeting on Nuclear Reactor Thermal Hydraulics, Saratoga NY, pp 1979-2023
179. Spalding DB (1981) IPSA 1981: New Developments and Computed Results. Report HTS/81/2, Imperial College of Science and Technology, London
180. Spalding DB (1985) Computer Simulation of Two-Phase Flows, with Special Reference to Nuclear-Reactor Systems. In: Lewis RW, Morgan K, Johnson JA, Smith WR (eds) Computational Techniques in Heat Transfer, pp 1-44
181. Strang G (1968) On the Construction and Comparison of Difference Schemes. SIAM J Numer Anal 5(3):506-517
182. Sweby PK (1984) High resolution schemes using flux limiters for hyperbolic conservation laws. SIAM J Numer Anal 21(5):995-1011
183. Tamamidis P, Zhang G, Assanis DN (1996) Comparison of Pressure-Based and Artificial Compressibility Methods for Solving 3D Steady Incompressible Viscous Flows. J Comput Phys 124:1-13
184. The Duc N (2005) An Implicit Scheme for Incompressible Flow Computation with Artificial Compressibility Method. VNU Journal of Science, Mathematics-Physics, T-XXI (4):1-13
185. Thomas LH (1949) Elliptic Problems in Linear Differential Equations over a Network. Watson Sci Comput Lab Report, Columbia University, New York
186. Thuburn J (1993) Use of flux-limited scheme for vertical advection in a GCM. Q J R Meteorol Soc 119:469-487
187. Thuburn J (1995) Dissipation and Cascades to Small Scales in Numerical Models Using a Shape-Preserving Advection Scheme. Mon Wea Rev 123(6): 1888-1903
188. Thuburn J (1996) Multidimensional Flux-Limited Advection Schemes. Journal of Computational Physics 123:74-83
189. Thuburn J (1997) TVD Schemes, Positive Schemes, and the Universal Limiter. Mon Wea Rev 125(8):1990-1995

190. Tomiyama A, Shimada N (2001) A Numerical Method for Bubbly Flow Simulation Based on a Multi-Fluid Model. *Journal of Pressure Vessel Technology-Trans ASME* 123(4):510-516
191. van Doormal JP, Raithby GD (1984) Enhancement of the SIMPLE Method for Predicting Incompressible Fluid Flows. *Numer Heat Transfer* 7:147-163
192. van Doormal JP, Raithby GD, McDonald BH (1987) The Segregated Approach to Predicting Viscous Compressible Fluid Flows. *ASME J Turbomachinery* 109:268-277
193. van Leer B (1974) Towards the Ultimate Conservation Difference Scheme II. Monotonicity and Conservation Combined in a Second Order Scheme. *J Comput Phys* 14(4):361-370
194. van Leer B (1977) Towards the Ultimate Conservation Difference Scheme IV. A New Approach to Numerical Convection. *J Comput Phys* 23(3):276-299
195. van Leer B (1979) Towards the ultimate conservative difference scheme, V. *J Comp Phys* 32:101-136
196. van Leer B (1982) Flux-vector splitting for the Euler equations. In: *Lecture Notes in Physics*, Springer, Berlin 170:507-512
197. van Leer B (1997) Godunov's Method for Gas-Dynamics: Current Applications and Future Developments. *J Comput Phys* 132:1-2
198. van Leer B (2006) Upwind and High-Resolution Methods for Compressible Flow: From Donor Cell to Residual-Distribution Schemes. *Communications in Computational Physics* 1(2):192-206
199. van Santen H, Lathouwers D, Kleijn CR, van den Akker HEA (1996) Influence of segregation on the efficiency of finite volume methods for the incompressible Navier-Stokes equations. Presented at the 1996 ASME Fluids Engineering Division Summer Meeting, July 7-11, San Diego, California. In: *Proceedings of the ASME Fluid Engineering Division Conference, FED-238(3):151-157*
200. Vasquez SA, Ivanov VA (2000) A phase coupled method for solving multiphase problems on unstructured meshes. ASME 2000 Fluids Engineering Division Summer Meeting, Boston, Massachusetts, June 11-15. In: *Proceedings of ASME FEDSM'00*, paper FEDSM2000-11281, pp 1-6
201. Versteeg HK, Malalasekera W (1996) *An Introduction to Computational Fluid Dynamics: The Finite Volume Method*. Longman, Harlow
202. Versteeg HK, Malalasekera W (2007) *An Introduction to Computational Fluid Dynamics: The Finite Volume Method*. Pearson Prentice Hall, Harlow
203. Villadsen JV, Stewart WE (1967) Solution of boundary-value problems by orthogonal collocation. *Chem Eng Sci* 22:1483-1501
204. Villadsen J, Michelsen ML (1978) *Solution of Differential Equations Models by Polynomial Approximation*. Prentice-Hall, Englewood Cliffs
205. Warming RF, Hyett BJ (1974) The modified equation approach to the stability and accuracy analysis of finite-difference methods. *J Comp Phys* 14:159-179
206. Waterson NP, Deconinck H (2007) Design principles for bounded higher-order convection schemes-a unified approach. *J Comput Phys* 224:182-207
207. Wesseling P (1992) *An Introduction to Multigrid Methods*. John Wiley & Sons, New York
208. White FM (1974) *Viscous Fluid Flow*. McGraw-Hill, New York
209. Williams MMR, Loyalka SK (1991) *Aerosol Science Theory and Practice: With Special Applications to the Nuclear Industry*. Pergamon Press, Oxford

210. Wissink JG (2004) On unconditional conservation of kinetic energy by finite-difference discretizations of the linear and non-linear convection equation. *Computers & Fluids* 33:315-343
211. Yanenko NN (1974) *The Methods of Fractional Steps: The Solution of Problems of Mathematical Physics in Several Variables*. Springer-Verlag, Berlin
212. Yang HQ, Przekwas AJ (1992) A comparative study of advanced shock-capturing schemes applied to Burgers' equation. *J Comp Phys* 102:139-159
213. Zalesak ST (1979) Fully Multidimensional Flux-Corrected Transport Algorithms for Fluids. *J Comput Phys* 31:335-362
214. Zijlema M (1996) On the construction of a third-order accurate monotone convection scheme with applications to turbulent flows in general domains. *Int J Numer Methods Fluids* 22:619-641

**APPENDIX**

---

# APPENDIX

# A

---

## Mathematical Theorems

The mathematical theorems needed in order to derive the governing model equations are defined in this appendix.

### A.1 Transport Theorem for a Single Phase Region

The transport theorem is employed deriving the conservation equations in continuum mechanics.

The mathematical statement is sometimes attributed to, or named in honor of, the German Mathematician Gottfried Wilhelm Leibnitz (1646-1716) and the British fluid dynamics engineer Osborne Reynolds (1842-1912) due to their work and contributions related to the theorem. Hence it follows that the transport theorem, or alternate forms of the theorem, may be named the *Leibnitz theorem* in mathematics and *Reynolds transport theorem* in mechanics.

In a customary interpretation the Reynolds transport theorem provides the link between the system and control volume representations, while the Leibnitz's theorem is a three dimensional version of the integral rule for differentiation of an integral. There are several notations used for the transport theorem and there are numerous forms and corollaries.

#### A.1.1 Leibnitz's Rule

The *Leibnitz's integral rule* gives a formula for differentiation of an integral whose limits are functions of the differential variable [2, 36, 8, 16, 9, 3, 28, 33, 18]. The formula is also known as differentiation under the integral sign.

$$\frac{d}{dt} \int_{a(t)}^{b(t)} f(t, x) dx = \int_{a(t)}^{b(t)} \frac{\partial f(t, x)}{\partial t} dx + f(t, b) \frac{db}{dt} - f(t, a) \frac{da}{dt} \quad (\text{A.1})$$

The first term on the RHS gives the change in the integral because the function itself is changing with time, the second term accounts for the gain in area as

the upper limit is moved in the positive axis direction, and the third term accounts for the loss in area as the lower limit is moved. The formal derivation of the Leibnitz's rule can be found elsewhere [16, 3].

### A.1.2 Leibnitz Theorem

A three dimensional extension of the Leibnitz rule for differentiating an integral is relevant for the derivation of the governing transport equations<sup>1</sup>.

In the material (Lagrangian) representation of continuum mechanics a representative particle of the continuum occupies a point in the initial configuration of the continuum at time  $t = 0$  and has the position vector  $\boldsymbol{\xi} = (\xi_1, \xi_2, \xi_3)$ . In this  $\xi$ -space the coordinates are called the material coordinates. In the Eulerian representation the particle position vector in  $r$ -space is defined by  $\mathbf{r} = (r_1, r_2, r_3)$ . The coordinates  $r_1, r_2, r_3$  which gives the current position of the particle are called the spatial coordinates. Let  $\psi(\mathbf{r}, t)$  be any scalar, vector or tensor function of time and position and  $V(t)$  a material volume. We may then define a variable  $\Psi(t)$  as the volume integral [1]:

$$\Psi(t) = \int_{V(t)} (\rho\psi) dv \quad (\text{A.2})$$

It is desired to find an expression for differentiating the integral  $\Psi(t)$  with time:

$$\frac{D\Psi(t)}{Dt} = \frac{D}{Dt} \int_{V(t)} (\rho\psi)(\mathbf{r}, t) dv \quad (\text{A.3})$$

The integral is over the material volume  $V(t)$  that is a function of  $t$ , hence we cannot take the differentiation through the integration sign.

However, if the integration were with respect to a volume in the material  $\boldsymbol{\xi}$ -coordinates it would be possible to interchange the differentiation and integration, since  $D/Dt$  is defined as differentiation with respect to time keeping  $\boldsymbol{\xi}$  constant. A transformation of the volume from  $r$ -space to  $\xi$ -space allows us to do the desired operation. The position vector in  $r$ -space,  $\mathbf{r} = (r_1, r_2, r_3)$ , is transformed as  $\mathbf{r} = \mathbf{r}(\boldsymbol{\xi}, t)$  in  $\xi$ -space. If the coordinate system is changed from  $r$ -space to  $\xi$ -space, the volume element changes according to:

$$dv = \frac{\partial(r_1, r_2, r_3)}{\partial(\xi_1, \xi_2, \xi_3)} d\xi_1 d\xi_2 d\xi_3 = J dv_0 \quad (\text{A.4})$$

in which  $d\xi_1 d\xi_2 d\xi_3$  denotes the material volume  $dv_0$  about a given point  $\boldsymbol{\xi}$  at the initial instant.

<sup>1</sup> The theory has been outlined by Truesdell and Toupin [35] (p 347), Aris [1] (p 84), Malvern [20](p 210), Slattery [30] (p 17), Slattery [31](p 21), Bird et al [2](p 732), Fan and Zhu [15](p 167), Kundu [18](p 75), Delhaye and Achard [8](p 9), Delhaye [9](p 42), Bouré and Delhaye [4](p 1-37), Whitaker [36], Donea and Huerta [10](sects 1.3-1.4), Donea et al [11], and Collado [6].

The Jacobian determinant of transformation between the material and fixed coordinate systems, is defined by:

$$J = \frac{\partial(r_1, r_2, r_3)}{\partial(\xi_1, \xi_2, \xi_3)} = \frac{dv}{dv_0} \quad (\text{A.5})$$

The quantity  $J$  may be thought of as the ratio of an elementary material volume to its initial volume.

The differentiation of the integral  $\Psi(t)$  with respect to time can then be proven:

$$\begin{aligned} \frac{D\Psi}{Dt} &= \frac{D}{Dt} \int_{V(t)} (\rho\psi)(\mathbf{r}, t) dv = \frac{D}{Dt} \int_{V_0} (\rho\psi)(\mathbf{r}(\boldsymbol{\xi}, t), t) J dv_0 \\ &= \int_{V_0} \left( \frac{D(\rho\psi)}{Dt} J + (\rho\psi) \frac{DJ}{Dt} \right) dv_0 \\ &= \int_{V_0} \left( \frac{D(\rho\psi)}{Dt} + (\rho\psi)(\nabla \cdot \mathbf{u}) \right) J dv_0 \quad (\text{A.6}) \\ &= \int_{V(t)} \left( \frac{D(\rho\psi)}{Dt} + (\rho\psi)(\nabla \cdot \mathbf{u}) \right) dv \\ &= \int_{V(t)} \left( \frac{\partial(\rho\psi)}{\partial t} + \nabla \cdot ((\rho\psi)\mathbf{u}) \right) dv \end{aligned}$$

in which we have adopted, without proof, the following Lemma<sup>2</sup>:

$$\frac{DJ}{Dt} = J(\nabla \cdot \mathbf{u}) \quad (\text{A.7})$$

Applying the divergence theorem (A.19) to the second integral on the RHS of (A.6) we get a particular three dimensional form of the Leibnitz theorem:

$$\frac{D\Psi}{Dt} = \frac{D}{Dt} \int_{V(t)} (\rho\psi)(\mathbf{r}, t) dv = \int_{V(t)} \frac{\partial(\rho\psi)}{\partial t} dv + \int_{A(t)} (\rho\psi)\mathbf{u} \cdot \mathbf{n} da \quad (\text{A.8})$$

where  $A(t)$  is the surface of  $V(t)$ , and  $\mathbf{u}$  represents the velocity of the control surface with respect to the coordinate reference frame. This kinematical transport theorem is due to Reynolds [27]. For this reason it is sometimes referred to as the Reynolds theorem.

The given theorem can be extended to a general case considering an arbitrary geometric volume with a closed surface moving with an arbitrary velocity  $\mathbf{u}_S$ . Truesdell and Toupin [35] (p 347) presented the corollary that the above

<sup>2</sup> The proofs of the transport theorem are given by Slattery [32].

relation remains valid if we replace the derivatives with respect to time while following material particles,  $D/Dt$ , by derivatives with respect to time while following fictitious system particles  $d/dt$ , and the velocity vector for a material particle  $\mathbf{u}$  by the velocity vector for a fictitious system particle  $\mathbf{u}_S$ . Let us thus consider a geometric volume  $V_S(t)$ , not necessarily a material volume, which is moving in space and bounded by a closed surface  $A_S(t)$ . At a given point belonging to this surface,  $\mathbf{n}$  is the unit normal vector outwardly directed. The speed of the displacement of the surface at that point is denoted by  $\mathbf{u}_S \cdot \mathbf{n}$ . The generalized *Leibnitz theorem* enables the time derivative of the volume integral to be transformed into the sum of a volume integral and a surface integral [9, 4, 18]:

$$\frac{d}{dt} \int_{V_S(t)} (\rho\psi)(\mathbf{r}, t) dv = \int_{V_S(t)} \frac{\partial(\rho\psi)}{\partial t} dv + \int_{A_S(t)} (\rho\psi)\mathbf{u}_S \cdot \mathbf{n} da \quad (\text{A.9})$$

in which  $\mathbf{u}_S$  is the velocity of the points on the control volume surface with respect to the coordinate reference frame. Slattery [32] named this mathematical statement the *generalized transport theorem*. This kinematical transport theorem was asserted, not proven, by Reynolds [27].

Comparing (A.8) and (A.9) we note that to make these relations coincide the total time derivative must be specified equal to the substantial time derivative. In this way the substantial derivative may be considered a special kind of the total time derivative [2, 28], and thus the Reynolds transport theorem is a special kind of the Leibnitz theorem.

In the case that the integral boundaries are fixed, the surface integral vanishes because the surface velocity is zero [8, 9, 18, 14]:

$$\frac{d}{dt} \int_V f dv = \int_V \frac{\partial f}{\partial t} dv \quad (\text{A.10})$$

### A.1.3 Reynolds Theorem

In fluid mechanics the laws governing the fluid motion are expressed using both system concepts in which we consider a given mass of the fluid, and control volume concepts in which we consider a given volume [34, 16, 23, 37]. Basically the physical laws are defined for a system, thus we need a mathematical link between control volume and system concepts to convert the governing equations to apply to a specific region rather than to individual masses. The Reynolds transport theorem is precisely the analytical tool required to transform the laws from one representation to the other.

Let  $\Psi_{sys}(t)$  be an extensive property of the system at time  $t$ ,  $\psi(\mathbf{r}, t)$  is the corresponding intensive property. If  $V_{sys}(t)$  denotes a system material volume at time  $t$ ,  $CV$  a control volume, and  $CS$  the control volume surface, the extensive system property can be defined by:

$$\Psi_{sys}(t) = \int_{V_{sys}(t)} \rho\psi \, dv \quad (\text{A.11})$$

The corresponding extensive control volume property is defined by:

$$\Psi_{CV}(t) = \int_{CV} \rho\psi \, dv \quad (\text{A.12})$$

The system is defined by the fluid mass within the control volume at the initial time  $t$ . The values of the analogous extensive properties of the system and the fluid within control volume are thus equal at this time,  $\Psi_{sys}(t_0) = \Psi_{CV}(t_0)$ . A short time later a portion of the system fluid may have exited from the control volume and some of the surrounding fluid may have entered the control volume. Then we seek to determine how the rate of change of  $\Psi_{sys}$  within the system is related to the rate of change of  $\Psi_{CV}$  within the control volume at any instant. Based on a physical understanding of the concepts of the system and control volume motion, the kinematic Reynolds transport theorem relating system concepts to control volume concepts can be derived by geometrical analysis.

The most general form of the Reynolds transport theorem is defined for an arbitrary moving and deforming control volume [6]:

$$\frac{D\Psi_{sys}(t)}{Dt} = \frac{D}{Dt} \int_{V_{sys}(t)} \rho\psi \, dv = \frac{D}{Dt} \int_{CV(t)} \rho\psi \, dv + \int_{CS(t)} \rho\psi \mathbf{w} \cdot \mathbf{n} \, da \quad (\text{A.13})$$

in which  $\mathbf{w}$  is the velocity of the fluid at the control surface with respect to the control surface, and  $\rho$  is the fluid density.

For a fixed control volume, the integral limits are fixed thus the order of differentiation and integration may be interchanged, so the substantial derivative of the CV integral in (A.13) can be written in the equivalent form [37]:

$$\frac{D}{Dt} \int_{CV} \rho\psi \, dv = \int_{CV} \frac{\partial(\rho\psi)}{\partial t} \, dv \quad (\text{A.14})$$

Hence, for a fixed control volume, the Reynolds theorem (A.13) reduces to:

$$\frac{D\Psi_{sys}(t)}{Dt} = \frac{D}{Dt} \int_{V_{sys}(t)} \rho\psi \, dv = \int_{CV} \frac{\partial(\rho\psi)}{\partial t} \, dv + \int_{CS} \rho\psi \mathbf{v} \cdot \mathbf{n} \, da \quad (\text{A.15})$$

in which the velocity  $\mathbf{v}$  represents the velocity of the fluid at the control surface with respect to the control surface that coincides with the coordinate reference frame.

This form of the Reynolds transport theorem is a special version of the more general mathematical statement (A.13). However, the latter version is

particularly important because fixed control volumes are commonly employed in fluid mechanics and reactor modeling.

In chap 1 the derivation of the governing Eulerian equations for single phase flow is performed employing (A.15).

Let us now consider the Leibnitz theorem (A.8) and the Reynolds theorem (A.13). The volume integral on the RHS of the Reynolds theorem is defined over a control volume  $CV(t)$  which coincides with the geometric volume on the LHS of Leibnitz theorem at the considered instant  $t$  in time. At that instant the integrals cover precisely the same space, so we can substitute the Leibnitz theorem (A.8) expression for differentiating the integral into the Reynolds theorem (A.13). The Reynolds theorem can then be written as [6]:

$$\frac{D\Psi_{sys}(t)}{Dt} = \int_{CV(t)} \frac{\partial}{\partial t}(\rho\psi) dv + \int_{CS(t)} (\rho\psi)\mathbf{v} \cdot \mathbf{n} da \quad (\text{A.16})$$

The vector quantity  $\mathbf{v} = \mathbf{w} + \mathbf{u}$  represents the velocity of the fluid at the control surface with respect to the coordinate reference frame. This is the conventional Reynolds transport theorem.

## A.2 Gauss Theorem

In general, consider a geometric volume,  $V(t)$ , bounded by a closed surface,  $A(t)$ , which may either be material or not, moving or not. At a given point belonging to this surface  $A(t)$ , the unit normal vector  $\mathbf{n}$  is outwardly directed. For any scalar ( $f$ ), vector or tensor fields ( $\mathbf{f}$ ), Gauss theorem<sup>3</sup> enable a surface integral to be transformed into a volume integral according to the following relation:

### Gauss' theorem for a scalar

For single phase flows:

$$\oint_{A(t)} f\mathbf{n} da = \int_{V(t)} \nabla f dv \quad (\text{A.17})$$

For two phase flows we need to consider the interface, and a modified form of the theorem is applied (e.g., [8, 9]). Now we may consider a geometric volume,  $V_k(t)$ , bounded by a closed surface,  $A_k(t) + A_I(t)$ , which may either be material or not, moving or not. At a given point belonging to this surface  $A_k(t) + A_I(t)$ , the unit normal vector  $\mathbf{n}$  is outwardly directed.

$$\int_{A_k(t)} f\mathbf{n} da + \int_{A_I(t)} f\mathbf{n} da = \int_{V_k(t)} \nabla f dv \quad (\text{A.18})$$

<sup>3</sup> The Gauss' theorem is also known as the divergence theorem, Green's theorem, and Ostrogradsky's theorem [36]. In particular, the vector form of Gauss's theorem is normally referred to as the divergence theorem [18].

### Gauss' theorem for a vector or tensor

For single phase flows:

$$\oint_{A(t)} \mathbf{f} \cdot \mathbf{n} da = \int_{V(t)} \nabla \cdot \mathbf{f} dv \quad (\text{A.19})$$

For two phase flows we need to consider the interface, and a modified form of the theorem is applied. Now we may consider a geometric volume,  $V_k(t)$ , bounded by a closed surface,  $A_k(t) + A_I(t)$ , which may either be material or not, moving or not. At a given point belonging to this surface  $A_k(t) + A_I(t)$ , the unit normal vector  $\mathbf{n}$  is outwardly directed.

$$\int_{A_k(t)} \mathbf{f} \cdot \mathbf{n} da + \int_{A_I(t)} \mathbf{f} \cdot \mathbf{n} da = \int_{V_k(t)} \nabla \cdot \mathbf{f} dv \quad (\text{A.20})$$

## A.3 Surface Theorems

These theorems can be found in the books of [1, 22] [31] (p 73) [13], pp 48-52 and in the papers of [7] [5], pp 428-432, and pp 436-438.

### A.3.1 Leibnitz Transport Theorem for a Surface

The surface transport theorem ([31], p. 73) can be used to reformulate the term:

$$\frac{d_I}{dt} \int_{A_I(t)} \rho_I \psi_I da \quad (\text{A.21})$$

where  $\psi_I$  is any scalar-, vector-, or tensor function of time and position on the dividing surface. The indicated integration is to be performed over the dividing surface in its current configuration  $A_I$ . We allow  $A_I$  or the limits of the this integration to be a function of time. Slattery ([31], page 74) presents the surface transport theorem:

$$\frac{d_I}{dt} \int_{A_I(t)} (\rho_I \psi_I) da = \int_{A_I(t)} \left( \frac{d_I(\rho_I \psi_I)}{dt} + \rho_I \psi_I \nabla_I \cdot \mathbf{v}_I \right) da \quad (\text{A.22})$$

Note that this theorem can be reformulated into more generalized forms, but the formulation given here is used in most papers on reactor modeling.

### A.3.2 Gauss Theorem for a Surface

In a 3D space, the Gauss theorems enable the transformation of a surface integral into a volume integral. Similarly, in a 2D space, the Gauss theorems enable the transformation of a line integral into a surface integral. The surface divergence theorem can be expressed in a generic form as follows [13]:

$$\oint_{l_I(t)} \mathcal{R}_I \mathbf{N}_I dl = \int_{A_I(t)} \nabla_I \cdot (\mathbf{e}_I \mathcal{R}_I) da = \int_{A_I} \left( \nabla_I \mathcal{R}_I - (\nabla_I \cdot \mathbf{n}_I) \mathcal{R}_I \mathbf{n}_I \right) da \quad (\text{A.23})$$

where  $\mathcal{R}_I$  is a generic field of arbitrary tensorial order. The generic identity may be specialized by inserting a dot- or cross-product operational sign into identical tensorial positions on both sides of the equality sign. The scalar fields  $\mathcal{R}_I$  is defined by  $R_I \mathbf{N}_I$ .

The frequently used forms of the theorem are given as illustrative examples:

#### For interfacial vector fields

$$\oint_{l_I(t)} \mathbf{f}_I \cdot \mathbf{N}_I dl = \int_{A_I(t)} \nabla_I \cdot \mathbf{f}_I da \quad (\text{A.24})$$

where  $\mathbf{N}_I$  is the unit normal vector at a given point belonging to the curve  $l(t)$ , the boundary of  $A_I$ . The vector  $\mathbf{N}_I$  is directed outward the area  $A_I$  and located in the tangent plane.  $\nabla_I$  is the surface del operator.  $\mathbf{f}_I$  is a vector tangent to the surface  $A_I$ .

#### For interfacial tensor fields

$$\oint_{l_I(t)} \mathbf{f}_I \cdot \mathbf{N}_I dl = \int_{A_I(t)} \nabla_I \cdot \mathbf{f}_I da \quad (\text{A.25})$$

where  $\mathbf{f}_I$  is any interfacial tensor field.

#### For interfacial scalar fields

$$\oint_{l_I} f_I dl = \int_{A_I} \nabla_I \cdot (\mathbf{e}_I f_I) da = \int_{A_I} (\nabla_I f_I - (\nabla_I \cdot \mathbf{n}_I) f_I \mathbf{n}_I) da \quad (\text{A.26})$$

where  $f_I$  is any interfacial scalar field,  $\mathbf{e}_I$  is the dyadic idemfactor ([13], p 46), and  $\nabla_I \cdot \mathbf{n}_I$  is the surface divergence (equal to twice the mean curvature).

### Static Force Balance at a Fluid Interface

Brenner ([5], pp. 428-432, and pp. 436-438), Middleman [21] (pp. 39-42) and Edwards et al. ([13], pp. 48-52) address the basic nature of macro-scale interfacial force balances at an arbitrary curved fluid in the state of hydrostatic equilibrium (a state that serves as a standard from which non-equilibrium interfacial transport processes depart).

Analogous to 3D fluid continua, applying Newton second law the macro-scale fluid interfaces are acted upon by two fundamental types of forces, surface body forces per unit area,  $\mathbf{f}_I$ , and surface contact stress component,  $\mathbf{T}_I \cdot \mathbf{N}_I$ , being a force per unit length. The apparent surface body force densities denote forces originating outside of the 2D interface itself, whereas the apparent surface stresses denote forces acting lineally by virtue of intimate contact between adjacent 2D interfacial fluid elements.

Considering an interface existing in a state of hydrostatic equilibrium, an integral force balance over an element of area,  $A_I$ , lying on a fluid interface may be expressed as :

$$\int_{A_I} \mathbf{F}_I da + \oint_{l_I} \mathbf{T}_I \cdot d\mathbf{l} = 0 \quad (\text{A.27})$$

where  $d\mathbf{l} = \mathbf{N}_I d\mathbf{l}$  is an outwardly directed, differential line element to the closed contour  $l_I$  of the area domain  $A_I$ .

To derive the differential counterpart of the integral balance, starting from (A.27) we need to express the second term (line integral) as an area integral. Thereafter, analogous to the 3D approach used in chap. 1 deriving the governing conservation equations, the differential form emerges requiring that the resulting relation is valid for an arbitrary chosen surface domain so that the integrand itself must vanish.

To transform the line integral in (A.27) to a surface integral, the version of (A.23) that is defined inserting the dot product sign is relevant. Accordingly, introducing the dot product and a tensor field into (A.23), a specific version of the surface divergence theorem can be derived:

$$\begin{aligned} \oint_{l_I} \mathcal{R}_I \cdot d\mathbf{l} &= \int_{A_I} \nabla_I \cdot (\mathbf{e}_I \cdot \mathcal{R}_I) da = \int_{A_I} \nabla_I \cdot \mathcal{R}_I da \\ &= \int_{A_I} (\mathcal{R}_I \cdot \nabla_I \cdot \mathbf{e}_I + \mathbf{e}_I \cdot \nabla_I \cdot \mathcal{R}_I) da = \int_{A_I} (\mathcal{R}_I \cdot 2H_I \mathbf{n}_I + \nabla_I \cdot \mathcal{R}_I) da \end{aligned} \quad (\text{A.28})$$

where the following relationships have been used:  $\mathbf{e}_I^T = \mathbf{e}_I$ ,  $\mathbf{e}_I \cdot \nabla_I = \nabla_I$ ,  $\nabla_I \cdot \mathbf{e}_I = 2H_I \mathbf{n}_I$ , and  $\mathbf{n}_I \cdot \mathbf{T}_I = 0$ .

To proceed we need to determine the nature of the interface defining the surface pressure- or stress tensor. For the general non-equilibrium circumstances  $\mathbf{T}_I$  is a non-isotropic and non-symmetric tensor, containing six

independent components. Four of these components are analogous to the normal- and shear stresses in 3D fluids, while the so-called bending forces have no analog in ordinary 3D fluids. Fortunately, in practice most fluid interfaces are assumed to be inviscid and isotropic. For an isotropic interface existing in a state of hydrostatic equilibrium the surface-excess pressure tensor is given by  $\mathbf{T}_I = \sigma_I \mathbf{e}_I$ , where the scalar  $\sigma_I$  is the interfacial tension. This scalar quantity is an apparent macro-scale property of the physicochemical system, generally interpreted as the 2D analog of the thermodynamic pressure,  $p$ , for 3D continua. From thermodynamic analysis it is concluded that  $\sigma_I$  depends only upon macro-scale pressure, temperature and interfacial composition at the point  $\mathbf{r}_I$ .  $\mathbf{e}_I$  denotes the dyadic idem-factor ([13], p 46), defined as  $\mathbf{e}_I = \mathbf{e} - \mathbf{n}_I \mathbf{n}_I$ , with the dyadic  $\mathbf{e}$  being the 3D spatial idem-factor.

For the special case of  $\mathcal{R}_I = \mathbf{T}_I$ , (A.28) reduces to:

$$\begin{aligned} \oint_{l_I} \mathbf{T}_I \cdot d\mathbf{l} &= \int_{A_I} \nabla_I \cdot (\mathbf{e}_I \cdot \mathbf{T}_I) da = \int_{A_I} \nabla_I \cdot \mathbf{T}_I da = \int_{A_I} \nabla_I \cdot (\sigma_I \mathbf{e}_I) da \\ &= \int_{A_I} (\sigma_I \nabla_I \cdot \mathbf{e}_I + \mathbf{e}_I \cdot \nabla_I \sigma_I) da = \int_{A_I} (2H_I \sigma_I \mathbf{n}_I + \nabla_I \sigma_I) da \end{aligned} \tag{A.29}$$

Thereby, for an isotropic interfacial tensor existing in a state of hydrostatic equilibrium (A.27) yields,

$$\int_{A_I} (\mathbf{F}_I + \nabla_I \cdot \mathbf{T}_I) da = \int_{A_I} (\mathbf{F}_I + 2H_I \sigma_I \mathbf{n}_I + \nabla_I \sigma_I) da = 0 \tag{A.30}$$

As the choice of local surface domain,  $A_I$ , is arbitrary, and since the field variables  $\mathbf{F}_I(\mathbf{r}_I)$  and  $\mathbf{T}_I(\mathbf{r}_I)$  are independent of this choice, this requires at each point ( $\mathbf{r}_I$ ) that:

$$\mathbf{F}_I + \nabla_I \cdot \mathbf{T}_I = \mathbf{F}_I + \nabla_I \sigma_I + 2H_I \sigma_I \mathbf{n}_I = 0 \tag{A.31}$$

which constitutes the local surface force balance at a static fluid interface<sup>4</sup>. Nevertheless, the net surface tension force on a closed surface equals zero [26, 12, 25, 24].

<sup>4</sup> This is the analog of the corresponding hydrostatic equation:

$$\rho \mathbf{g} - \nabla \cdot \mathbf{T} = 0 \tag{A.32}$$

for a 3D fluid continuum, where the isotropic stresses are given by  $\mathbf{T} = p\mathbf{e}$ , with  $p = p(\mathbf{r})$  the thermodynamic pressure.

Note also that in typical textbooks on mechanical engineering this relation will be given as  $\mathbf{T} = -p\mathbf{e}$ , as the hydrostatic equation yields:

$$\rho \mathbf{g} + \nabla \cdot \mathbf{T} = 0 \tag{A.33}$$

Finally, we note that the surface body force term constitutes the sum of the surface-excess body force and the bulk-phase body force vector densities. The surface-excess body force is the 2D analog of continuum body forces in 3D fluids (e.g., gravitational force, electromagnetic force, etc). This force is often neglected. The bulk-phase body force has no counterpart for 3D fluids, as it denotes the stresses applied intimately at the interface by the surrounding 3D bulk phases. The normal component of this force equals the pressure difference between the two bulk phases, a relationship often referred to as the Young-Laplace equation.

---

## References

1. Aris R (1962) *Vectors, Tensors, and the Basic Equations of Fluid Mechanics*. Dover, Inc., New York
2. Bird RB, Stewart WE, Lightfoot EN (1960) *Transport phenomena*. John Wiley & Sons, New York
3. Bird RB, Stewart WE, Lightfoot EN (2002) *Transport phenomena*. Second Edition, John Wiley & Sons, New York
4. Bourè JA, Delhaye JM (1982) General Equations and Two-Phase Flow Modeling. In: Hetsroni G (ed) *Handbook of Multiphase Systems*, Section 1.2, pp. (1-36) - (1-95), McGraw-Hill, New York
5. Brenner H (1979) A Micromechanical Derivation of the Differential Equation of Interfacial Statics. *Journal of Colloid and Interface Science* 68 (3):422-439
6. Collado FJ (2007) Reynolds transport theorem for two-phase flow. *Appl Phys Lett* 90, 024101
7. Delhaye JM (1974) Jump Conditions and Entropy Sources in Two-Phase Systems: Local Instant Formulation. *Int J Multiphase Flow* 1:395-409
8. Delhaye JM, Achard JL (1977) On the averaging operators introduced in two-phase flow. In: Banerjee S, Weaver JR (eds) *Transient Two-phase Flow*. Proc. CSNI Specialists Meeting, Toronto, 3.-4. august
9. Delhaye JM (1981) Basic Equations for Two-Phase Flow Modeling. In: Bergles AE et al (eds) *Two-Phase Flow and Heat Transfer in the Power and Process Industries*. Hemisphere Publishing, Washington
10. Donea J, Huerta A (2003) *Finite Element Methods for Flow Problems*. John Wiley & Sons, Chichester
11. Donea J, Huerta A, Ponthot J-P, Rodríguez-Ferran A (2004) Arbitrary Lagrangian-Eulerian Methods. In: Stein E, de Borst R, Hughes TJR (eds) *Encyclopedia of Computational Mechanics*, Volume 1: Fundamentals, Chapter 14, pp 1-25, John Wiley & Sons Ltd ISBN: 0-470-84699-2
12. Edwards CH Jr, Penny DE (1982) *Calculus and Analytic Geometry*. Prentice-Hall Inc, Englewood Cliffs, New Jersey
13. Edwards DA, Brenner H, Wasan DT (1991) *Interfacial Transport Processes and Rheology*. Butterworth-Heinemann, Boston
14. Enwald H, Peirano E, Almstedt AE (1996) Eulerian Two-Phase Flow Theory Applied to Fluidization. *Int J Multiphase Flow* 22:21-66, Suppl.

15. Fan L-S, Zhu C (1998) Principles of Gas-Solid Flows. Cambridge University Press, Cambridge
16. Greenberg MD (1978) Foundations of Applied Mathematics. Prentice-Hall Inc, Englewood Cliffs
17. Kuiken GDC (1995a) Thermodynamics of Irreversible Processes. Applications to Diffusion and Rheology. John Wiley & Sons, Chichester
18. Kundu PK (1990) Fluid Mechanics. Academic Press Inc, San Diego
19. Kuo KK (1986) Principles of Combustion. John Wiley & Sons, New York
20. Malvern LE (1969) Introduction to the Mechanics of a Continuous Medium. Prentice-Hall, Inc, Englewood Cliffs
21. Middleman S (1998) An Introduction to Fluid Dynamics: Principles of Analysis and Design. John Wiley & Sons, Inc., New York
22. Miller CA, Neogi P (1985) Interfacial Phenomena: Equilibrium and Dynamic Effects. Marcel Dekker, Inc., New York and Basel
23. Munson BR, Young DF, Okiishi TH (2002) Fundamentals of Fluid Mechanics. John Wiley & Sons, New York, Fourth Edition
24. Ni J, Beckermann C (1990) A Two-Phase Model for Mass, Momentum, Heat, and Species Transport during Solidification. In: Charmchi M, Chyu MK, Joshi Y, Walsh SM (eds) Transport Phenomena in Material Processing, New York. ASME HTD-VOL. 132:45-56
25. Nobari MR, Jan Y-J, Tryggvason G (1996) Head-on collision of droplets - A numerical investigation. *Phys Fluids* 8(1):29-42
26. Prosperetti A, Jones AV (1984) Pressure forces in dispersed two-phase flow. *Int Journal of Multiphase Flow* 10(4):425-440
27. Reynolds O (1903) Papers on mechanical and physical subjects-the sub-mechanics of the Universe, Collected Work, Volume III, Cambridge University Press
28. Rosner DE (1986) Transport Processes in Chemically Reacting Flow Systems. Butterworths, Boston
29. Sandler SI (1999) Chemical and Engineering Thermodynamics. Third Edition, John Wiley & Sons, Inc., New York
30. Slattery JC (1972) Momentum, Energy, and Mass Transfer in Continua. McGraw-Hill Kogakusha LTD, Tokyo, Second Edition
31. Slattery JC (1990) Interfacial Transport Phenomena. Springer-Verlag, New York
32. Slattery JC (1999) Advanced Transport Phenomena. Cambridge University Press, Cambridge
33. Stull RB (1988) An Introduction to Boundary Layer Meteorology. Kluwer Academic Publishers, Dordrecht
34. Thompson PA (1972) Compressible-fluid dynamics. McGraw-Hill, Inc. New York
35. Truesdell C, Toupin RA (1960) The Classical Field Theories. In: Flügge S Handbuch der Physik Vol III/1, Principles of Classical Mechanics and Field Theory, Springer-Verlag, Berlin
36. Whitaker S (1968) Introduction to Fluid Mechanics. Prentice-Hall, Inc., Englewood Cliffs
37. White FM (1999) Fluid Mechanics. McGraw-Hill, Boston, Fourth Edition

## B

---

# Equation of Change for Temperature for a Multicomponent System

The equation of change for temperature can be derived from the enthalpy equation. For completeness, in this appendix we outline the procedure described by Bird et al ([2], Problem 19D.2., pp 608-609) and *Instructor's resource CD-ROM* to accompany *TRANSPORT PHENOMENA*, Second Edition, pp 19-15 and pp 19-16.

### B.1 The Problem Definition

In this appendix we will derive the equation of change for temperature:

$$\begin{aligned} \rho C_P \frac{DT}{Dt} = & -\nabla \cdot \mathbf{q} - \boldsymbol{\sigma} : \nabla \mathbf{v} + \sum_{c=1}^N \mathbf{J}_c \cdot \mathbf{g}_c - \frac{T}{\rho} \left( \frac{\partial \rho}{\partial T} \right)_{p,\omega} \frac{Dp}{Dt} \\ & + \sum_{c=1}^N \bar{h}_c \left( \nabla \cdot \left( \frac{\mathbf{J}_c}{M_{\omega_c}} \right) - \left( \frac{R_c}{M_{\omega_c}} \right) \right) \end{aligned} \quad (\text{B.1})$$

starting out from the enthalpy equation:

$$\rho \frac{Dh}{Dt} = -\nabla \cdot \mathbf{q} - \boldsymbol{\sigma} : \nabla \mathbf{v} + \sum_{c=1}^N \mathbf{J}_c \cdot \mathbf{g}_c + \frac{Dp}{Dt} \quad (\text{B.2})$$

In the next section the sequence of steps for the derivation of (B.1) from (B.2) will be described in detail.

### B.2 Deriving the Equation of Change for Temperature

For a closed system the enthalpy is given by  $\hat{H} = \hat{H}(P, T)$ , while for an open system that can exchange mass with its surroundings the total enthalpy depends also on the possible changes in masses  $M_c$  of each component  $c$ . This implies that for an open system the enthalpy is written as

$\hat{H} = \hat{H}(T, p, M_1, M_2, M_3, \dots, M_N)$ , where  $N$  is the number of chemical components. An extensive quantity can be divided by the mass of the system constituting a new variable defining a specific quantity ([3], p 103). The specific enthalpy (per unit mass) is then expressed as:

$$H = H(T, p, \omega_1, \omega_2, \omega_3, \dots, \omega_{N-1}) = \sum_{c=1}^N \omega_c \check{H}_c \quad (\text{B.3})$$

where the partial specific enthalpy of species  $c$  is given by  $\check{H}_c = (\frac{\partial \hat{H}}{\partial M_c})_{M', p, T} = (\frac{\partial(MH)}{\partial M_c})_{M', p, T}$ . Note also that these intensive quantities may be computed both per unit mass, per unit volume, or per mole.

In the given notation the LHS of (B.2) can be reformulated in terms of a complete differential if we consider the enthalpy per unit mass to be a thermodynamic function of  $T$ ,  $p$  and the first  $(N - 1)$  mass fractions:

$$dH = (\frac{\partial H}{\partial p})_{T, \omega'} dp + (\frac{\partial H}{\partial T})_{p, \omega'} dT + \sum_{c=1}^{N-1} (\frac{\partial H}{\partial \omega_c})_{p, T, \omega'} d\omega_c \quad (\text{B.4})$$

and then apply the principle of local instantaneous equilibrium:

$$\frac{Dh}{Dt} = (\frac{\partial h}{\partial p})_{T, \omega'} \frac{Dp}{Dt} + (\frac{\partial h}{\partial T})_{p, \omega'} \frac{DT}{Dt} + \sum_{c=1}^{N-1} (\frac{\partial h}{\partial \omega_c})_{p, T, \omega'} \frac{D\omega_c}{Dt} \quad (\text{B.5})$$

The capital letters for the quantities (e.g.,  $H = H(T, p, \omega_1, \omega_2, \omega_3, \dots, \omega_{N-1})$ ) indicate that we are considering the variable as a thermodynamic function, whereas the corresponding variables used in continuum mechanics are defined by lower case letters (e.g.,  $h = h(t, \mathbf{r}, T, p, \omega_1, \omega_2, \omega_3, \dots, \omega_{N-1})$ ).

Next, the term  $\frac{D\omega_c}{Dt}$  can be eliminated from (B.5) using the transport equation for the chemical species:

$$\rho \frac{D\omega_c}{Dt} = -\nabla \mathbf{J}_c + R_c \quad (\text{B.6})$$

The coefficient in front of  $\frac{D\omega_c}{Dt}$  in (B.5) is usually reformulated in terms of molar quantities known from thermodynamic theory. This is a rather complex task, thus a detailed description of this part of the model derivation is given shortly.

The theoretical basis for the model derivation used at this point originates from thermodynamics. The corresponding variables used in continuum mechanics are then defined in analogy to the thermodynamic quantities applying the principle of local instantaneous equilibrium, in line with the approach adopted above obtaining (B.5) from (B.4). Following the same approach, the thermodynamic quantities and relations needed in order to reformulate the coefficient in front of  $\frac{D\omega_c}{Dt}$  in (B.5) will be described before we introduce the corresponding extensions approved in continuum mechanic theory.

If we first consider the enthalpy variable as a thermodynamic quantity, the total enthalpy,  $\hat{H} = \hat{H}(T, p, M_1, M_2, M_3, \dots, M_N)$ , and the specific enthalpy (per unit mass),  $H = H(T, p, \omega_1, \omega_2, \omega_3, \dots, \omega_{N-1})$ , can be defined characterizing an open thermodynamic system. Since enthalpy is an extensive thermodynamic property, we may write:

$$\hat{H}(M_1, M_2, M_3, \dots, M_N) = MH(\omega_1, \omega_2, \omega_3, \dots, \omega_{N-1}) \quad (\text{B.7})$$

in which the  $M_\alpha$  are the masses of the various species,  $M$  is the sum of the  $M_\alpha$ 's, and  $\omega_\alpha = M_\alpha/M$  are the corresponding mass fractions. Both  $H$  and  $\hat{H}$  are understood to be functions of  $T$ ,  $p$  and as well as of composition (i.e.,  $T$  and  $p$  have been left out for simplicity in the mathematical manipulation below).

By use of the chain rule of partial differentiation we find for  $\alpha \neq N$ :

$$\begin{aligned} \left(\frac{\partial \hat{H}}{\partial M_\alpha}\right)_{M_\gamma} &= \sum_{\beta=1}^{N-1} \left(\frac{\partial(MH)}{\partial \omega_\beta}\right)_{\omega_\gamma, M} \left(\frac{\partial \omega_\beta}{\partial M_\alpha}\right)_{M_\gamma} + \left(\frac{\partial(MH)}{\partial M}\right)_{\omega_\gamma} \left(\frac{\partial M}{\partial M_\alpha}\right)_{M_\gamma} \\ &= M \sum_{\beta=1}^{N-1} \left(\frac{\partial H}{\partial \omega_\beta}\right)_{\omega_\gamma} \left(\frac{\partial(M_\beta/M)}{\partial M_\alpha}\right)_{M_\gamma} + H \left(\frac{\partial M}{\partial M}\right)_{\omega_\gamma} \cdot 1 \\ &= M \sum_{\beta=1}^{N-1} \left(\frac{\partial H}{\partial \omega_\beta}\right)_{\omega_\gamma} \left(\frac{1}{M} \frac{\partial M_\beta}{\partial M_\alpha} - \frac{M_\beta}{M^2} \frac{\partial M}{\partial M_\alpha}\right) + H \cdot 1 \cdot 1 \\ &= M \sum_{\beta=1}^{N-1} \left(\frac{\partial H}{\partial \omega_\beta}\right)_{\omega_\gamma} \left(\frac{\delta_{\alpha\beta}}{M} - \frac{M_\beta}{M^2}\right) + H \\ &= \sum_{\beta=1}^{N-1} \left(\frac{\partial H}{\partial \omega_\beta}\right)_{\omega_\gamma} \left(\delta_{\alpha\beta} - \frac{M_\beta}{M}\right) + H \end{aligned} \quad (\text{B.8})$$

The corresponding expression for  $\alpha = N$  can be found in a similar way:

$$\begin{aligned} \left(\frac{\partial \hat{H}}{\partial M_N}\right)_{M_\gamma} &= \sum_{\beta=1}^{N-1} \left(\frac{\partial(MH)}{\partial \omega_\beta}\right)_{\omega_\gamma, M} \left(\frac{\partial \omega_\beta}{\partial M_N}\right)_{M_\gamma} + \left(\frac{\partial(MH)}{\partial M}\right)_{\omega_\gamma} \left(\frac{\partial M}{\partial M_N}\right)_{M_\gamma} \\ &= M \sum_{\beta=1}^{N-1} \left(\frac{\partial H}{\partial \omega_\beta}\right)_{\omega_\gamma} \left(\frac{1}{M} \frac{\partial M_\beta}{\partial M_N} - \frac{M_\beta}{M^2} \frac{\partial M}{\partial M_N}\right) + H \cdot 1 \\ &= M \sum_{\beta=1}^{N-1} \left(\frac{\partial H}{\partial \omega_\beta}\right)_{\omega_\gamma} \left(-\frac{M_\beta}{M^2}\right) + H \\ &= \sum_{\beta=1}^{N-1} \left(\frac{\partial H}{\partial \omega_\beta}\right)_{\omega_\gamma} \left(-\frac{M_\beta}{M}\right) + H \end{aligned} \quad (\text{B.9})$$

The subscript  $\omega_\gamma$  means that all other mass fractions should be held constant.

Subtraction then gives for  $\alpha \neq N$ :

$$\begin{aligned}
 & \left(\frac{\partial \hat{H}}{\partial M_\alpha}\right)_{M_\gamma} - \left(\frac{\partial \hat{H}}{\partial M_N}\right)_{M_\gamma} \\
 &= \sum_{\beta=1}^{N-1} \left(\frac{\partial H}{\partial \omega_\beta}\right)_{\omega_\gamma} \left(\delta_{\alpha\beta} - \frac{M_\beta}{M}\right) + H - \left[\sum_{\beta=1}^{N-1} \left(\frac{\partial H}{\partial \omega_\beta}\right)_{\omega_\gamma} \left(-\frac{M_\beta}{M}\right) + H\right] \\
 &= \sum_{\beta=1}^{N-1} \left(\frac{\partial H}{\partial \omega_\beta}\right)_{\omega_\gamma} \left(\delta_{\alpha\beta} - \frac{M_\beta}{M} + \frac{M_\beta}{M}\right) \\
 &= \sum_{\beta=1}^{N-1} \left(\frac{\partial H}{\partial \omega_\beta}\right)_{\omega_\gamma} \delta_{\alpha\beta} = \left(\frac{\partial H}{\partial \omega_\alpha}\right)_{\omega_\gamma}
 \end{aligned} \tag{B.10}$$

In the last paragraph the coefficient of  $d\omega_c$  in (B.4) has been expressed in terms of species masses rather than species mass fractions by use of thermodynamic theory and a complete differential regarding the specific enthalpy to be a function of  $T$ ,  $p$  and the first  $(N-1)$  mass fractions. These species mass based functions may then more easily be converted to the appropriate molar quantities which we can obtain from thermodynamic models.

On the equivalent molar basis<sup>1</sup> the total enthalpy content (or the enthalpy)  $\hat{H}$  may be defined by  $\hat{H} = MH = n\underline{H}$ . This means that  $\hat{H}(T, p, M_1, M_2, M_3, \dots, M_N)$  may equivalently be written as  $\hat{H}(T, p, n_1, n_2, n_3, \dots, n_N)$ .

The specific molar enthalpy (per mole) is then expressed as:

$$\underline{H} = \underline{H}(T, p, x_1, x_2, x_3, \dots, x_{N-1}) = \sum_{c=1}^N x_c \overline{H}_c \tag{B.11}$$

where the partial (specific) molar enthalpy of species  $c$  is given by  $\overline{H}_c = \left(\frac{\partial \hat{H}}{\partial n_c}\right)_{n', p, T} = \left(\frac{\partial(n\underline{H})}{\partial n_c}\right)_{n', p, T}$ . Thus, we can easily see that  $\check{H}_c = \left(\frac{\partial \hat{H}}{\partial M_c}\right)_{M', p, T} = \frac{1}{M_{w_c}} \left(\frac{\partial \hat{H}}{\partial n_c}\right)_{n', p, T} = \frac{1}{M_{w_c}} \overline{H}_c$ . The specific molar enthalpy for an ideal gas is denoted by  $\underline{H}^*$ , and for ideal gases we have the following relations:  $\underline{H} = \underline{H}^* = \sum_{c=1}^N x_c \underline{H}_c^*$  and  $\overline{H}_c = \underline{H}_c^*$ .

The LHS of (B.2) can now be expressed as:

$$\begin{aligned}
 \rho \frac{Dh}{Dt} &= \rho \left( \frac{1}{\rho} - T \left( \frac{\partial(1/\rho)}{\partial T} \right)_{p, \omega} \right) \frac{Dp}{Dt} + C_P \frac{DT}{Dt} \\
 &+ \sum_{c=1}^{N-1} \left[ \left( \frac{\partial \hat{h}}{\partial M_c} \right)_{M'} - \left( \frac{\partial \hat{h}}{\partial M_N} \right)_{M'} \right] (-\nabla \cdot \mathbf{J}_c + R_c)
 \end{aligned} \tag{B.12}$$

<sup>1</sup> For further studies of these thermodynamic quantities the reader is referred to standard thermodynamic - and continuum mechanic textbooks [1, 2, 4, 5, 6, 3].

where we have applied the principle of local instantaneous equilibrium to obtain an expression for the coefficient in front of  $\frac{D\omega_c}{Dt}$  in (B.5) based on the result we obtained from thermodynamic theory as given in (B.10).

Because of the relations  $M_c = n_c M_{w_c}$  and  $\hat{h} = Mh = n\bar{h}$ , the differential quotients in the last term in (B.12) can be rewritten in terms of partial molar quantities:

$$\begin{aligned}
 \rho \frac{Dh}{Dt} &= \rho \left( \frac{1}{\rho} - T \left( \frac{\partial(\frac{1}{\rho})}{\partial T} \right)_{p,\omega} \right) \frac{Dp}{Dt} + \rho C_P \frac{DT}{Dt} \\
 &\quad + \sum_{c=1}^{N-1} \left[ \frac{1}{M_{w_c}} \left( \frac{\partial \hat{h}}{\partial n_c} \right)_{n'} - \frac{1}{M_{w_N}} \left( \frac{\partial \hat{h}}{\partial n_N} \right)_{n'} \right] (-\nabla \cdot \mathbf{J}_c + R_c) \\
 &= \rho \left( \frac{1}{\rho} - T \left( \frac{\partial(\frac{1}{\rho})}{\partial T} \right)_{p,\omega} \right) \frac{Dp}{Dt} + \rho C_P \frac{DT}{Dt} \\
 &\quad + \sum_{c=1}^{N-1} \left[ \frac{\bar{h}_c}{M_{w_c}} - \frac{\bar{h}_N}{M_{w_N}} \right] (-\nabla \cdot \mathbf{J}_c + R_c) \\
 &= \rho \left( \frac{1}{\rho} - T \left( \frac{\partial(\frac{1}{\rho})}{\partial T} \right)_{p,\omega} \right) \frac{Dp}{Dt} + \rho C_P \frac{DT}{Dt} \\
 &\quad + \sum_{c=1}^{N-1} \frac{\bar{h}_c}{M_{w_c}} (-\nabla \cdot \mathbf{J}_c + R_c) - \sum_{c=1}^{N-1} (-\nabla \cdot \mathbf{J}_c + R_c) \frac{\bar{h}_N}{M_{w_N}} \\
 &= \rho \left( \frac{1}{\rho} - T \left( \frac{\partial(\frac{1}{\rho})}{\partial T} \right)_{p,\omega} \right) \frac{Dp}{Dt} + \rho C_P \frac{DT}{Dt} \\
 &\quad + \sum_{c=1}^{N-1} \bar{h}_c \left( -\nabla \cdot \left( \frac{\mathbf{J}_c}{M_{w_c}} \right) + \left( \frac{R_c}{M_{w_c}} \right) \right) + (-\nabla \cdot \mathbf{J}_N + R_N) \frac{\bar{h}_N}{M_{w_N}} \\
 &= \rho \left( \frac{1}{\rho} - T \left( \frac{\partial(\frac{1}{\rho})}{\partial T} \right)_{p,\omega} \right) \frac{Dp}{Dt} + \rho C_P \frac{DT}{Dt} \\
 &\quad + \sum_{c=1}^{N-1} \bar{h}_c \left( -\nabla \cdot \left( \frac{\mathbf{J}_c}{M_{w_c}} \right) + \left( \frac{R_c}{M_{w_c}} \right) \right) + \bar{h}_N \left( -\nabla \cdot \left( \frac{\mathbf{J}_N}{M_{w_N}} \right) + \left( \frac{R_N}{M_{w_N}} \right) \right) \\
 &= \rho \left( \frac{1}{\rho} - T \left( \frac{\partial(\frac{1}{\rho})}{\partial T} \right)_{p,\omega} \right) \frac{Dp}{Dt} + \rho C_P \frac{DT}{Dt} + \sum_{c=1}^N \bar{h}_c \left( -\nabla \cdot \left( \frac{\mathbf{J}_c}{M_{w_c}} \right) + \left( \frac{R_c}{M_{w_c}} \right) \right)
 \end{aligned} \tag{B.13}$$

where we have used the relations that  $\sum_{c=1}^N \mathbf{J}_c = 0$  and  $\sum_{c=1}^N R_c = 0$ .

Inserted into (B.2) this result coincides with the temperature equation on the form (B.1).

---

## References

1. Bird RB, Stewart WE, Lightfoot EN (1960) Transport phenomena. John Wiley & Sons, New York
2. Bird RB, Stewart WE, Lightfoot EN (2002) Transport phenomena. Second Edition, John Wiley & Sons, New York
3. Kuiken GDC (1995a) Thermodynamics of Irreversible Processes. Applications to Diffusion and Rheology. John Wiley & Sons, Chichester
4. Kuo KK (1986) Principles of Combustion. John Wiley & Sons, New York
5. Rosner DE (1986) Transport Processes in Chemically Reacting Flow Systems. Butterworths, Boston
6. Sandler SI (1999) Chemical and Engineering Thermodynamics. Third Edition, John Wiley & Sons, Inc., New York

---

## Trondheim Bubble Column Model

The 2D steady-state two-fluid model presented in this section is based on the early work by Torvik and Svendsen [22], Svendsen et al [21], and Jakobsen [12]. The two-fluid model was derived based on the time-after volume averaging procedure, described in sect 3.4.4.

The model was later implemented in a commercial code PHOENICS. The input files specifying the calculations have been deposited in the PHOENICS library of two-phase flow examples [5]. This early bubble column model is included in this book because it is considered particularly useful for educational purposes.

The model derivation is outlined in Cartesian coordinates. The governing equations are then more conveniently written in vector notation (vector symbolism). For practical applications and simulations these vector equations are converted into cylindrical coordinates and finally reduced to the 2D axisymmetric bubble column problem. The axisymmetric model is discretized by use of the IPSA-SIMPLEC solution algorithm in sect C.4.1.

### C.1 Model Formulation

The elementary Two-fluid model derivation is outlined in this section.

#### Conservation of mass

The instantaneous volume averaged conservation of mass of the continuous liquid and dispersed gas phases were expressed as:

$$\frac{\partial}{\partial t}(\alpha_l \rho_l) + \nabla \cdot (\alpha_l \rho_l \mathbf{v}_l) = \Gamma_l \quad (\text{C.1})$$

$$\frac{\partial}{\partial t}(\alpha_g \rho_g) + \nabla \cdot (\alpha_g \rho_g \mathbf{v}_g) = \Gamma_g \quad (\text{C.2})$$

The void fractions must fulfill the compatibility condition:

$$\alpha_l + \alpha_g = 1 \quad (\text{C.3})$$

The mass exchange terms must satisfy the constraint:

$$\Gamma_l + \Gamma_g = 0 \quad (\text{C.4})$$

### Conservation of momentum

The instantaneous volume averaged Navier-Stokes equations for the two phases are:

$$\begin{aligned} \frac{\partial}{\partial t}(\alpha_l \rho_l v_{l,i}) + \frac{\partial}{\partial x_j}(\alpha_l \rho_l v_{l,j} v_{l,i}) = & -\alpha_l \frac{\partial p_l}{\partial x_i} + \frac{\partial}{\partial x_j} \left( \alpha_l \mu_l \left( \frac{\partial v_{l,i}}{\partial x_j} + \frac{\partial v_{l,j}}{\partial x_i} \right) \right) \\ & - \frac{\partial}{\partial x_j} \left( \delta_{ij} \alpha_l \left( \frac{2}{3} \mu_l - \mu_{bl} \right) \frac{\partial v_{l,k}}{\partial x_k} \right) \\ & + \rho_l \alpha_l g_i + F_{l,i}^C \end{aligned} \quad (\text{C.5})$$

$$\begin{aligned} \frac{\partial}{\partial t}(\alpha_g \rho_g v_{g,i}) + \frac{\partial}{\partial x_j}(\alpha_g \rho_g v_{g,j} v_{g,i}) = & -\alpha_g \frac{\partial p_g}{\partial x_i} + \frac{\partial}{\partial x_j} \left( \alpha_g \mu_g \left( \frac{\partial v_{g,i}}{\partial x_j} + \frac{\partial v_{g,j}}{\partial x_i} \right) \right) \\ & - \frac{\partial}{\partial x_j} \left( \delta_{ij} \alpha_g \left( \frac{2}{3} \mu_g - \mu_{bg} \right) \frac{\partial v_{g,k}}{\partial x_k} \right) \\ & + \rho_g \alpha_g g_i + F_{g,i}^C \end{aligned} \quad (\text{C.6})$$

where  $\mu_{bl}$  is the bulk viscosity of the liquid, and  $\mu_{bg}$  is the bulk viscosity of the gas.

The surface tension force was neglected so the interfacial momentum transfer terms satisfy:

$$\mathbf{F}_l^C + \mathbf{F}_g^C = 0 \quad (\text{C.7})$$

The pressure inside individual bubbles may vary, but this was assumed to have no relation to the flow of the continuous phase. The volume averaged pressure of the two phases were assumed to be equal,  $p_l = p_g$ . The dispersed phase approximation neglects internal flow inside the dispersed phases. The viscous terms of the gas equation were thus neglected. The bulk viscosity terms were also neglected since they are generally small, as discussed in chap 2. These assumptions and approximations simplify the momentum equations.

The instantaneous volume averaged liquid phase equation was written:

$$\begin{aligned} \frac{\partial}{\partial t}(\alpha_l \rho_l v_{l,i}) + \frac{\partial}{\partial x_j}(\alpha_l \rho_l v_{l,j} v_{l,i}) = & -\alpha_l \frac{\partial p}{\partial x_i} + \frac{\partial}{\partial x_j} \left( \alpha_l \mu_l \left( \frac{\partial v_{l,i}}{\partial x_j} + \frac{\partial v_{l,j}}{\partial x_i} \right) \right) \\ & - \frac{\partial}{\partial x_j} \left( \frac{2}{3} \delta_{ij} \alpha_l \mu_l \frac{\partial v_{l,k}}{\partial x_k} \right) + \rho_l \alpha_l g_i + F_{l,i}^C \end{aligned} \quad (\text{C.8})$$

The corresponding gas phase equation was written:

$$\frac{\partial}{\partial t}(\alpha_g \rho_g v_{g,i}) + \frac{\partial}{\partial x_j}(\alpha_g \rho_g v_{g,j} v_{g,i}) = -\alpha_g \frac{\partial p}{\partial x_i} + \rho_g \alpha_g g_i + F_{g,i}^C \quad (\text{C.9})$$

### Turbulence Modeling

Reynolds decomposition and time averaging were then applied to the instantaneous variables in the volume average model equations. However, it was assumed that none of the densities fluctuate. The terms of fluctuating quantities with order higher than two were considered small compared to those of first and second order and thus neglected.

Developed versions of the gradient and Boussinesq hypotheses were employed to model the second-order covariance terms. The liquid phase volume fraction-velocity covariance and the Reynolds stresses, for example, were approximated by:

$$\overline{\alpha'_l v'_{l,j}} = -\frac{\nu_{l,t}}{\sigma_{\alpha_l,t}} \frac{\partial \bar{\alpha}_l}{\partial x_j} \quad (\text{C.10})$$

and

$$\begin{aligned} \overline{v'_{l,j} v'_{l,i}} &= \sigma_{l,i,j}^t + \frac{2}{3} k \delta_{ij} \\ &= -\frac{\nu_{l,t}}{\sigma_{l,t}} \left( \frac{\partial \bar{v}_{l,i}}{\partial x_j} + \frac{\partial \bar{v}_{l,j}}{\partial x_i} - \frac{2}{3} \delta_{ij} \frac{\partial \bar{v}_{l,k}}{\partial x_k} \right) + \frac{2}{3} k \delta_{ij} \\ &= -\frac{\nu_{l,t}}{\sigma_{l,t}} \left( \frac{\partial \bar{v}_{l,i}}{\partial x_j} + \frac{\partial \bar{v}_{l,j}}{\partial x_i} \right) + \frac{2}{3} \delta_{ij} \left( \frac{\nu_{l,t}}{\sigma_{l,t}} \frac{\partial \bar{v}_{l,k}}{\partial x_k} + k \right) \end{aligned} \quad (\text{C.11})$$

The turbulent Schmidt numbers ( $\sigma_\psi^t$ ) were included for all variables that are modeled via the gradient and Boussinesq hypotheses. These Schmidt numbers were set to 1.0. The only exception was  $\sigma_\epsilon = 1.3$ .

### Turbulence Modeling of the Liquid Phase Continuity Equation

Time averaging the volume averaged liquid mass balance (C.1) gives for the transient term:

$$\overline{\frac{\partial}{\partial t}(\rho_l \tilde{\alpha}_l)} = \frac{\partial}{\partial t}(\rho_l \overline{(\alpha_l + \alpha'_l)}) = \frac{\partial}{\partial t}(\rho_l \bar{\alpha}_l) \quad (\text{C.12})$$

and for the convective terms:

$$\begin{aligned} \overline{\frac{\partial}{\partial x_i}(\rho_l \tilde{\alpha}_l \tilde{v}_{l,i})} &= \frac{\partial}{\partial x_i}(\rho_l \overline{(\alpha_l + \alpha'_l)(v_{l,i} + v'_{l,i})}) = \frac{\partial}{\partial x_i}(\rho_l (\bar{\alpha}_l \bar{v}_{l,i} + \overline{\alpha'_l v'_{l,i}})) \\ &= \frac{\partial}{\partial x_i}(\rho_l \bar{\alpha}_l \bar{v}_{l,i} - \rho_l \frac{\nu_{l,t}}{\sigma_{\alpha_l,t}} \frac{\partial \bar{\alpha}_l}{\partial x_i}) \end{aligned} \quad (\text{C.13})$$

### The Modeled Liquid Phase Continuity Equation

For none reactive flow calculations there are no mass exchange between the phases, the continuity equation was reduced to:

$$\frac{\partial}{\partial t}(\bar{\alpha}_l \rho_l) + \frac{\partial}{\partial x_i}(\bar{\alpha}_l \rho_l \bar{v}_{l,i}) = \frac{\partial}{\partial x_i} \left( \frac{\nu_{l,t}}{\sigma_{\alpha_l,t}} \frac{\partial \bar{\alpha}_l}{\partial x_i} \right) \quad (\text{C.14})$$

In vector notation:

$$\frac{\partial}{\partial t}(\bar{\alpha}_l \rho_l) + \nabla \cdot (\bar{\alpha}_l \rho_l \bar{\mathbf{v}}_l) = \nabla \cdot \left( \frac{\nu_{l,t}}{\sigma_{\alpha_l,t}} \nabla \bar{\alpha}_l \right) \quad (\text{C.15})$$

### Turbulence Modeling of the Liquid Phase Momentum Equation

Time averaging the volume averaged momentum balance (C.8) gives for the transient term:

$$\begin{aligned} \overline{\frac{\partial}{\partial t}(\tilde{\alpha}_l \rho_l \tilde{v}_{l,i})} &= \frac{\partial}{\partial t}(\rho_l \overline{(\alpha_l + \alpha'_l)(v_{l,i} + v'_{l,i})}) = \frac{\partial}{\partial t}(\rho_l (\bar{\alpha}_l \bar{v}_{l,i} + \overline{\alpha'_l v'_{l,i}})) \\ &\approx \frac{\partial}{\partial t}(\rho_l \bar{\alpha}_l \bar{v}_{l,i}) \end{aligned} \quad (\text{C.16})$$

The turbulent covariance terms were neglected. The transient term did serve as a means of under-relaxation.

Modeling the convection terms:

$$\begin{aligned} \overline{\frac{\partial}{\partial x_j}(\tilde{\alpha}_l \rho_l \tilde{v}_{l,j} \tilde{v}_{l,i})} &= \frac{\partial}{\partial x_j}(\rho_l \overline{(\alpha_l + \alpha'_l)(v_{l,j} + v'_{l,j})(v_{l,i} + v'_{l,i})}) \\ &= \frac{\partial}{\partial x_j}(\rho_l (\bar{\alpha}_l \bar{v}_{l,j} \bar{v}_{l,i} + \overline{\alpha'_l v'_{l,j} v'_{l,i}} + \overline{\alpha'_l v'_{l,i} v'_{l,j}} + \overline{\alpha_l v'_{l,j} v'_{l,i}})) \\ &= \frac{\partial}{\partial x_j} \left[ \bar{\alpha}_l \rho_l \bar{v}_{l,j} \bar{v}_{l,i} - \rho_l \frac{\nu_{l,t}}{\sigma_{\alpha_l,t}} \frac{\partial \bar{\alpha}_l}{\partial x_j} \bar{v}_{l,i} \right. \\ &\quad \left. - \rho_l \frac{\nu_{l,t}}{\sigma_{\alpha_l,t}} \frac{\partial \bar{\alpha}_l}{\partial x_i} \bar{v}_{l,j} - \bar{\alpha}_l \rho_l \frac{\nu_{l,t}}{\sigma_{l,t}} \left( \frac{\partial \bar{v}_{l,i}}{\partial x_j} + \frac{\partial \bar{v}_{l,j}}{\partial x_i} \right) \right. \\ &\quad \left. + \frac{2}{3} \delta_{ij} \bar{\alpha}_l \rho_l \left( \frac{\nu_{l,t}}{\sigma_{l,t}} \frac{\partial \bar{v}_{l,k}}{\partial x_k} + k \right) \right] \end{aligned} \quad (\text{C.17})$$

The time after volume averaged pressure-volume fraction term was modeled as:

$$\begin{aligned} \overline{\tilde{\alpha}_l \frac{\partial \tilde{p}}{\partial x_i}} &= \overline{(\alpha_l + \alpha'_l) \frac{\partial}{\partial x_i}(p + p')} = \bar{\alpha}_l \frac{\partial \bar{p}}{\partial x_i} + \overline{\alpha'_l \frac{\partial p'}{\partial x_i}} \\ &= \bar{\alpha}_l \frac{\partial \bar{p}}{\partial x_i} + \rho_l \frac{\nu_{l,t}}{\sigma_{\alpha_l,t}} \frac{\partial \bar{\alpha}_l}{\partial x_j} \frac{\partial \bar{v}_{l,i}}{\partial x_j} + \rho_l \bar{v}_{l,j} \frac{\partial}{\partial x_j} \left( \frac{\nu_{l,t}}{\sigma_{\alpha_l,t}} \frac{\partial \bar{\alpha}_l}{\partial x_i} \right) \end{aligned} \quad (\text{C.18})$$

The pressure-volume fraction covariance terms were deduced from the instantaneous steady state equations for conservation of mass and momentum of the continuous phase [12]. The instantaneous steady state continuity was written as:

$$\frac{\partial}{\partial x_i} \left( \rho_l (\bar{\alpha}_l \bar{v}_{l,i} + \bar{\alpha}'_l v'_{l,i} + \alpha'_l \bar{v}_{l,i} + \alpha'_l v'_{l,i}) \right) = 0 \quad (\text{C.19})$$

The time after volume averaged continuity equation became:

$$\frac{\partial}{\partial x_i} \left( \rho_l (\bar{\alpha}_l \bar{v}_{l,i} + \overline{\alpha'_l v'_{l,i}}) \right) = 0 \quad (\text{C.20})$$

The steady state equation for the instantaneous mass fluctuations was found by subtracting (C.20) from (C.19) giving:

$$\frac{\partial}{\partial x_i} \left( \rho_l (\bar{\alpha}_l v'_{l,i} + \alpha'_l \bar{v}_{l,i} + \alpha'_l v'_{l,i} - \overline{\alpha'_l v'_{l,i}}) \right) = 0 \quad (\text{C.21})$$

The instantaneous void fractions always satisfy (C.3), hence:

$$\bar{\alpha}_l + \alpha'_l + \bar{\alpha}_g + \alpha'_g = 1 \quad (\text{C.22})$$

Time averaging the instantaneous volume averaged compatibility relation gives:

$$\bar{\alpha}_l + \bar{\alpha}_g = 1 \quad (\text{C.23})$$

By subtracting the time averaged compatibility relation (C.23) from (C.22), the fluctuations were shown to satisfy:

$$\alpha'_l + \alpha'_g = 0 \quad (\text{C.24})$$

Since the two phases share the same pressure, the phasic pressure-volume fraction covariance terms were related through:

$$\overline{\alpha'_l \frac{\partial p'}{\partial x_i}} = -\overline{\alpha'_g \frac{\partial p'}{\partial x_i}} \quad (\text{C.25})$$

The pressure-volume fraction covariance terms appear with opposite signs in the equations for the gas and liquid phases. The pressure-volume fraction covariance terms thus describe momentum transfer fluxes between the phases.

A steady state equation for the instantaneous momentum fluctuations was found by subtracting the time averaged steady state equation from the instantaneous steady state equation. The resulting steady state relations were then simplified by the use of (C.22) and (C.24). The resulting equation was then multiplied through with  $\alpha'_l/\alpha_l$  and time averaged. Covariances of fluctuating quantities with order larger than two were assumed small compared to the other terms and thus neglected. The fluctuating interphase forces and viscous interaction terms were also neglected.

The factor:

$$\frac{\overline{\alpha_l'^2}}{\overline{\alpha_l^2}} \quad (\text{C.26})$$

is now a common factor for three of the remaining terms in the equation for the pressure–volume fraction covariance terms. By assuming that this pre-factor term was close to zero, all the terms with this prefactor factor were neglected. The pressure–volume fraction covariance terms were then approximated by:

$$\overline{\alpha_l' \frac{\partial p'}{\partial x_i}} = -\overline{\rho_l \alpha_l' v_{l,j}' \frac{\partial \bar{v}_{l,i}}{\partial x_j}} - \overline{\rho_l \bar{v}_{l,j} \alpha_l' \frac{\partial v_{l,i}'}{\partial x_j}} \quad (\text{C.27})$$

The first term on the RHS can be modeled using the gradient and Boussinesq hypotheses. The covariance within the second term was written as:

$$\overline{\alpha_l' \frac{\partial v_{l,i}}{\partial x_j}} = \frac{\partial}{\partial x_j} (\overline{\alpha_l' v_{l,i}'}) - \overline{v_{l,i}' \frac{\partial \alpha_l'}{\partial x_j}} \quad (\text{C.28})$$

A weakly justified approximation was then introduced [12]:

$$\overline{\alpha_l' \frac{\partial v_{l,i}}{\partial x_j}} \approx \frac{\partial}{\partial x_j} (\overline{\alpha_l' v_{l,i}'}) \quad (\text{C.29})$$

The final equation for the turbulent pressure–volume fraction covariance terms was then obtained:

$$\overline{\alpha_l' \frac{\partial p'}{\partial x_i}} = -\overline{\rho_l \alpha_l' v_{l,j}' \frac{\partial \bar{v}_{l,i}}{\partial x_j}} - \overline{\rho_l \bar{v}_{l,j} \frac{\partial}{\partial x_j} (\overline{\alpha_l' v_{l,i}'})} \quad (\text{C.30})$$

The closure is completed by use of the gradient and Boussinesq hypotheses on the form (C.10).

Time averaging the volume averaged gravity force yield:

$$\overline{\bar{\alpha}_l \rho_l g_i} = (\overline{\alpha_l} + \overline{\alpha_l'}) \rho_l g_i = \bar{\alpha}_l \rho_l g_i \quad (\text{C.31})$$

The time after volume averaged viscous shear terms became:

$$\begin{aligned} & \overline{\frac{\partial}{\partial x_j} (\tilde{\alpha}_l \mu_l (\frac{\partial \bar{v}_{l,i}}{\partial x_j} + \frac{\partial \bar{v}_{l,j}}{\partial x_i}))} \\ &= \frac{\partial}{\partial x_j} \left( \mu_l (\overline{\alpha_l} + \overline{\alpha_l'}) \left( \frac{\partial (v_{l,i} + v_{l,i}')}{\partial x_j} + \frac{\partial (v_{l,j} + v_{l,j}')}{\partial x_i} \right) \right) \\ &= \frac{\partial}{\partial x_j} \left( \mu_l \bar{\alpha}_l \left( \frac{\partial \bar{v}_{l,i}}{\partial x_j} + \frac{\partial \bar{v}_{l,j}}{\partial x_i} \right) + \overline{\mu_l \alpha_l' \left( \frac{\partial v_{l,i}'}{\partial x_j} + \frac{\partial v_{l,j}'}{\partial x_i} \right)} \right) \\ &\approx \frac{\partial}{\partial x_j} (\mu_l \bar{\alpha}_l (\frac{\partial \bar{v}_{l,i}}{\partial x_j} + \frac{\partial \bar{v}_{l,j}}{\partial x_i})) \end{aligned} \quad (\text{C.32})$$

and

$$\begin{aligned}
 -\frac{\partial}{\partial x_j} \left( \frac{2}{3} \delta_{ij} \tilde{\alpha}_l \mu_l \frac{\partial \tilde{v}_{l,k}}{\partial x_k} \right) &= -\frac{2}{3} \frac{\partial}{\partial x_i} \left( \mu_l (\alpha_l + \alpha'_l) \frac{\partial (v_{l,k} + v'_{l,k})}{\partial x_k} \right) \\
 &= -\frac{2}{3} \frac{\partial}{\partial x_i} \left( \mu_l \bar{\alpha}_l \frac{\partial \bar{v}_{l,k}}{\partial x_k} + \mu_l \alpha'_l \frac{\partial v'_{l,k}}{\partial x_k} \right) \\
 &\approx -\frac{2}{3} \frac{\partial}{\partial x_i} \left( \mu_l \bar{\alpha}_l \frac{\partial \bar{v}_{l,k}}{\partial x_k} \right)
 \end{aligned} \tag{C.33}$$

To make the notation used for the latter term consistent with the other equations, index  $j$  is substituted for  $k$  :

$$-\frac{\partial}{\partial x_j} \left( \frac{2}{3} \delta_{ij} \tilde{\alpha}_l \mu_l \frac{\partial \tilde{v}_{l,j}}{\partial x_j} \right) \approx -\frac{2}{3} \frac{\partial}{\partial x_i} \left( \mu_l \bar{\alpha}_l \frac{\partial \bar{v}_{l,j}}{\partial x_j} \right) \tag{C.34}$$

In abbreviated form the viscous shear can thus be written as:

$$\overline{\tilde{F}_{l,i}^V} = \overline{F_{l,i}^V} + \overline{F_{l,i}^{V'}} \tag{C.35}$$

in which the  $\overline{F_{l,i}^{V'}}$  terms are ignored. The modeled viscous term was thus approximated as:

$$\overline{\tilde{F}_{l,i}^V} \approx \overline{F_{l,i}^V} \approx \frac{\partial}{\partial x_j} \left( \mu_l \bar{\alpha}_l \left( \frac{\partial \bar{v}_{l,i}}{\partial x_j} + \frac{\partial \bar{v}_{l,j}}{\partial x_i} \right) \right) - \frac{2}{3} \frac{\partial}{\partial x_i} \left( \mu_l \bar{\alpha}_l \frac{\partial \bar{v}_{l,j}}{\partial x_j} \right) \tag{C.36}$$

The time averaged interphase forces were modeled as:

$$\overline{\tilde{F}_{l,i}^C} = \overline{F_{l,i}^C} + \overline{F_{l,i}^{C'}} \tag{C.37}$$

It is noted that  $\overline{F_{l,i}^{C'}}$  is made up of terms which are of order higher than one in the fluctuating quantities, so by time averaging they are not zero. The interphase forces and the turbulence modeling of the drag force are described shortly in this section.

### The Modeled Liquid Phase Momentum Equation

After all the modeled terms were substituted into the averaged conservation equation for momentum, the balance equation became:

$$\begin{aligned}
 & \underbrace{\frac{\partial}{\partial t}(\bar{\alpha}_l \rho_l \bar{v}_{l,i})}_{\text{Transient term}} + \underbrace{\frac{\partial}{\partial x_j}(\bar{\alpha}_l \rho_l \bar{v}_{l,j} \bar{v}_{l,i})}_{\text{Convection term}} = \\
 & \underbrace{\frac{\partial}{\partial x_j} \left( \rho_l \frac{\nu_{l,t}}{\sigma_{\alpha_l,t}} \frac{\partial \bar{\alpha}_l}{\partial x_j} \bar{v}_{l,i} + \rho_l \frac{\nu_{l,t}}{\sigma_{\alpha_l,t}} \frac{\partial \bar{\alpha}_l}{\partial x_i} \bar{v}_{l,j} + \bar{\alpha}_l \rho_l \frac{\nu_{l,t}}{\sigma_{l,t}} \left( \frac{\partial \bar{v}_{l,i}}{\partial x_j} + \frac{\partial \bar{v}_{l,j}}{\partial x_i} \right) \right)}_{\text{From convection term}} \\
 & - \underbrace{\frac{\partial}{\partial x_j} \left( \frac{2}{3} \delta_{ij} \bar{\alpha}_l \rho_l \left( k + \frac{\nu_{l,t}}{\sigma_{l,t}} \frac{\partial \bar{v}_{l,k}}{\partial x_k} \right) \right)}_{\text{From convection term}} - \underbrace{\bar{\alpha}_l \frac{\partial \bar{p}}{\partial x_i} - \rho_l \frac{\nu_{l,t}}{\sigma_{\alpha_l,t}} \frac{\partial \bar{\alpha}_l}{\partial x_j} \frac{\partial \bar{v}_{l,i}}{\partial x_j}}_{\text{From pressure term}} \\
 & - \underbrace{\rho_l \bar{v}_{l,j} \frac{\partial}{\partial x_j} \left( \frac{\nu_{l,t}}{\sigma_{\alpha_l,t}} \frac{\partial \bar{\alpha}_l}{\partial x_i} \right)}_{\text{From pressure term}} + \underbrace{\rho_l \bar{\alpha}_l g_i}_{\text{Gravity term}} \\
 & + \underbrace{\frac{\partial}{\partial x_j} \left( \bar{\alpha}_l \mu_l \left( \frac{\partial \bar{v}_{l,i}}{\partial x_j} + \frac{\partial \bar{v}_{l,j}}{\partial x_i} \right) \right) - \frac{\partial}{\partial x_i} \left( \frac{2}{3} \bar{\alpha}_l \mu_l \frac{\partial \bar{v}_{l,k}}{\partial x_k} \right)}_{\text{Viscous terms}} + \underbrace{\overline{F_{l,i}^C} + \overline{F_{l,i}^{C'}}}_{\text{Interphasial forces term}}
 \end{aligned} \tag{C.38}$$

The viscous terms were joined with the turbulent diffusion terms that come from the modeling of the convection terms. The notations  $\mu_{l,\text{eff}} = \mu_l + \frac{\mu_{l,t}}{\sigma_{l,t}}$  and  $\nu_{l,\text{eff}} = \nu_l + \frac{\nu_{l,t}}{\sigma_{l,t}}$  are used, giving:

$$\begin{aligned}
 & \frac{\partial}{\partial t}(\bar{\alpha}_l \rho_l \bar{v}_{l,i}) + \frac{\partial}{\partial x_j}(\bar{\alpha}_l \rho_l \bar{v}_{l,j} \bar{v}_{l,i}) = \\
 & \frac{\partial}{\partial x_j} \left( \rho_l \frac{\nu_{l,t}}{\sigma_{\alpha_l,t}} \frac{\partial \bar{\alpha}_l}{\partial x_j} \bar{v}_{l,i} + \rho_l \frac{\nu_{l,t}}{\sigma_{\alpha_l,t}} \frac{\partial \bar{\alpha}_l}{\partial x_i} \bar{v}_{l,j} + \bar{\alpha}_l \rho_l \nu_{l,\text{eff}} \left( \frac{\partial \bar{v}_{l,i}}{\partial x_j} + \frac{\partial \bar{v}_{l,j}}{\partial x_i} \right) \right) \\
 & - \frac{\partial}{\partial x_i} \left( \frac{2}{3} \bar{\alpha}_l \rho_l \left( k + \nu_{l,\text{eff}} \frac{\partial \bar{v}_{l,k}}{\partial x_k} \right) \right) - \bar{\alpha}_l \frac{\partial \bar{p}}{\partial x_i} - \rho_l \frac{\nu_{l,t}}{\sigma_{\alpha_l,t}} \frac{\partial \bar{\alpha}_l}{\partial x_j} \frac{\partial \bar{v}_{l,i}}{\partial x_j} \\
 & - \rho_l \bar{v}_{l,j} \frac{\partial}{\partial x_j} \left( \frac{\nu_{l,t}}{\sigma_{\alpha_l,t}} \frac{\partial \bar{\alpha}_l}{\partial x_i} \right) + \rho_l \bar{\alpha}_l g_i + \overline{F_{l,i}^C} + \overline{F_{l,i}^{C'}}
 \end{aligned} \tag{C.39}$$

These equations can be written in vector notation giving:

$$\begin{aligned}
 & \frac{\partial}{\partial t}(\bar{\alpha}_l \rho_l \bar{\mathbf{v}}_l) + \nabla \cdot (\bar{\alpha}_l \rho_l \bar{\mathbf{v}}_l \bar{\mathbf{v}}_l) = \\
 & \nabla \cdot \left( \rho_l \frac{\nu_{l,t}}{\sigma_{\alpha_l,t}} \nabla \bar{\alpha}_l \bar{\mathbf{v}}_l + \rho_l \frac{\nu_{l,t}}{\sigma_{\alpha_l,t}} \bar{\mathbf{v}}_l \nabla \bar{\alpha}_l + \bar{\alpha}_l \rho_l \nu_{l,\text{eff}} (\nabla \bar{\mathbf{v}}_l + (\nabla \bar{\mathbf{v}}_l)^T) \right) \\
 & - \nabla \cdot \left( \frac{2}{3} \bar{\alpha}_l \rho_l (k + \nu_{l,\text{eff}} \nabla \cdot \bar{\mathbf{v}}_l) \right) - \bar{\alpha}_l \nabla \bar{p} - \rho_l \frac{\nu_{l,t}}{\sigma_{\alpha_l,t}} \nabla \bar{\alpha}_l \cdot \nabla \bar{\mathbf{v}}_l \\
 & - \rho_l \bar{\mathbf{v}}_l \cdot \nabla \left( \frac{\nu_{l,t}}{\sigma_{\alpha_l,t}} \nabla \bar{\alpha}_l \right) + \rho_l \bar{\alpha}_l \mathbf{g} + \overline{\mathbf{F}_l^C} + \overline{\mathbf{F}_l^{C'}}
 \end{aligned} \tag{C.40}$$

This equation can be transformed into cylindrical coordinates as shown shortly in this appendix. The resulting equations in 2D cylindrical are listed in sect C.4.

### The Modeled Gas Phase Continuity Equation

The continuity equation was modeled in an identical manner to that of the liquid phase. The result is:

$$\frac{\partial}{\partial t}(\bar{\alpha}_g \rho_g) + \frac{\partial}{\partial x_i}(\bar{\alpha}_g \rho_g \bar{v}_{g,i}) = \frac{\partial}{\partial x_i} \left( \frac{\mu_{g,t}}{\sigma_{\alpha_g,t}} \frac{\partial \bar{\alpha}_g}{\partial x_i} \right) \quad (\text{C.41})$$

In vector notation this is:

$$\frac{\partial}{\partial t}(\bar{\alpha}_g \rho_g) + \nabla \cdot (\bar{\alpha}_g \rho_g \bar{\mathbf{v}}_g) = \nabla \cdot \left( \frac{\mu_{g,t}}{\sigma_{\alpha_g,t}} \nabla \bar{\alpha}_g \right) \quad (\text{C.42})$$

### The Modeled Gas Phase Momentum Equation

The turbulence modeling of the transient and convective terms of the momentum balance (C.9) gives analogous results to that of the liquid phase. The pressure term is determined from [12]:

$$\overline{\alpha'_g \frac{\partial p'}{\partial x_i}} = -\overline{\alpha'_l \frac{\partial p'}{\partial x_i}} \quad (\text{C.43})$$

The gravitational and interphase forces are also analogous to those of the liquid phase.

The momentum balance was thus be written as:

$$\begin{aligned} & \underbrace{\frac{\partial}{\partial t}(\bar{\alpha}_g \rho_g \bar{v}_{g,i})}_{\text{Transient term}} + \underbrace{\frac{\partial}{\partial x_j}(\bar{\alpha}_g \rho_g \bar{v}_{g,j} \bar{v}_{g,i})}_{\text{Convection term}} = \\ & \underbrace{\frac{\partial}{\partial x_j} \left( \rho_g \frac{\nu_{g,t}}{\sigma_{\alpha_g,t}} \frac{\partial \bar{\alpha}_g}{\partial x_j} \bar{v}_{g,i} + \rho_g \frac{\nu_{g,t}}{\sigma_{\alpha_g,t}} \frac{\partial \bar{\alpha}_g}{\partial x_i} \bar{v}_{g,j} + \bar{\alpha}_g \rho_g \frac{\nu_{g,t}}{\sigma_{g,t}} \left( \frac{\partial \bar{v}_{g,i}}{\partial x_j} + \frac{\partial \bar{v}_{g,j}}{\partial x_i} \right) \right)}_{\text{From convection term}} \\ & - \underbrace{\frac{\partial}{\partial x_j} \left( \frac{2}{3} \delta_{ij} \bar{\alpha}_g \rho_g (k + \frac{\nu_{g,t}}{\sigma_{g,t}} \frac{\partial \bar{v}_{g,k}}{\partial x_k}) \right)}_{\text{From convection term}} - \underbrace{\bar{\alpha}_g \frac{\partial \bar{p}}{\partial x_i}}_{\text{From pressure term}} + \rho_l \frac{\nu_{l,t}}{\sigma_{\alpha_l,t}} \frac{\partial \bar{\alpha}_l}{\partial x_j} \frac{\partial \bar{v}_{l,i}}{\partial x_j} \\ & + \underbrace{\rho_l \bar{v}_{l,j} \frac{\partial}{\partial x_j} \left( \frac{\nu_{l,t}}{\sigma_{\alpha_l,t}} \frac{\partial \bar{\alpha}_l}{\partial x_i} \right)}_{\text{From pressure term}} + \underbrace{\rho_g \bar{\alpha}_g g_i}_{\text{Gravity term}} + \underbrace{\overline{F_{g,i}^C} + \overline{F_{g,i}^{C'}}}_{\text{Interphasial forces term}} \end{aligned} \quad (\text{C.44})$$

In vector notation this equation becomes:

$$\begin{aligned} & \frac{\partial}{\partial t}(\bar{\alpha}_g \rho_g \bar{\mathbf{v}}_g) + \nabla \cdot (\bar{\alpha}_g \rho_g \bar{\mathbf{v}}_g \bar{\mathbf{v}}_g) = \\ & \nabla \cdot \left( \rho_g \frac{\nu_{g,t}}{\sigma_{\alpha_g,t}} \nabla \bar{\alpha}_g \bar{\mathbf{v}}_g + \rho_g \frac{\nu_{g,t}}{\sigma_{\alpha_g,t}} \bar{\mathbf{v}}_g \nabla \bar{\alpha}_g + \bar{\alpha}_g \rho_g \frac{\nu_{g,t}}{\sigma_{\alpha_g,t}} (\nabla \bar{\mathbf{v}}_g + (\nabla \bar{\mathbf{v}}_g)^T) \right) \\ & - \nabla \cdot \left( \frac{2}{3} \bar{\alpha}_g \rho_g (k + \frac{\nu_{g,t}}{\sigma_{\alpha_g,t}} \nabla \cdot \bar{\mathbf{v}}_g) \right) - \bar{\alpha}_g \nabla \bar{p} + \rho_l \frac{\nu_{l,t}}{\sigma_{\alpha_l,t}} \nabla \bar{\alpha}_l \cdot \nabla \bar{\mathbf{v}}_l \\ & + \rho_l \bar{\mathbf{v}}_l \cdot \nabla \left( \frac{\nu_{l,t}}{\sigma_{\alpha_l,t}} \nabla \bar{\alpha}_l \right) + \rho_g \bar{\alpha}_g \mathbf{g} + \overline{\mathbf{F}}_g^C + \overline{\mathbf{F}}_g^{C'} \end{aligned} \quad (\text{C.45})$$

The mass and momentum conservation equations are written in cylindrical coordinates in a later section in this appendix.

### The Liquid Phase Turbulence Model

The  $k - \epsilon$  model is chosen as the turbulence model [14]. It is assumed that the turbulence inside the dispersed phase (gas bubbles) does not affect the liquid phase turbulence. Both  $k$  and  $\epsilon$  are determined from transport equations, as described in sect 5.1.

In vector notation the equations are:

$$\frac{\partial}{\partial t}(\bar{\alpha}_l \rho_l k) + \nabla \cdot (\bar{\alpha}_l \rho_l \bar{\mathbf{v}}_l k) = \nabla \cdot (\bar{\alpha}_l \frac{\mu_{l,t}}{\sigma_k} \nabla k) + \bar{\alpha}_l (P_k + P_b - \rho_l \epsilon) \quad (C.46)$$

and

$$\frac{\partial}{\partial t}(\bar{\alpha}_l \rho_l \epsilon) + \nabla \cdot (\bar{\alpha}_l \rho_l \bar{\mathbf{v}}_l \epsilon) = \nabla \cdot (\bar{\alpha}_l \frac{\mu_{l,t}}{\sigma_\epsilon} \nabla \epsilon) + \bar{\alpha}_l \frac{\epsilon}{k} (C_{\epsilon 1} (P_k + P_b) - C_{\epsilon 2} \rho_l \epsilon) \quad (C.47)$$

with

$$P_k = \mu_{l,t} (\nabla \bar{\mathbf{v}}_l + (\nabla \bar{\mathbf{v}}_l)^T) : \nabla \bar{\mathbf{v}}_l \quad (C.48)$$

and

$$P_b = C_b \bar{\mathbf{F}}_{D,l} \cdot (\bar{\mathbf{v}}_l - \bar{\mathbf{v}}_g) \quad (C.49)$$

The  $C_b$  parameter takes values between 0 and 1, and generally depends on bubble size and shape, and on the turbulent length scale. The empirical coefficients in the turbulence model were kept equal to the standard values for the original single phase model.

### Interphase Forces

The interphase forces considered were steady drag, added (virtual) mass and lift. The steady drag force on a collection of dispersed bubbles with a given average diameter was described by (5.48) and (5.34). The transversal lift force was determined by the conventional model (5.65), whereas the added mass force was approximated by (5.112).

Jakobsen [12] used a drag coefficient formulation for the bubbles formulated by Johansen and Boysan [13] based on the terminal velocities for ellipsoidal bubbles given by Clift et al [7].

$$C_D = \frac{0.622}{\frac{1.0}{E_o} + 0.235} \quad (C.50)$$

By applying turbulence modeling to the drag force, negative transversal forces arise. The resulting transversal force was written as [12]:

$$\overline{F_{T,g}^i} = \frac{3}{4} \overline{\alpha_l} \overline{\alpha_g} \frac{\mu_l}{d_S^2} C_D \frac{C_\tau}{(1 + \frac{\tau_L}{t_P})} \left( \frac{d_S}{\nu_l} \right)^2 \frac{(\overline{v_l} - \overline{v_g})_k}{Re_P} (-\nu_{l,t} \left( \frac{\partial \overline{v_{l,i}}}{\partial x_k} + \frac{\partial \overline{v_{l,k}}}{\partial x_i} \right)) (1 - \delta_{ik}) \quad (\text{C.51})$$

where  $\overline{Re_P}$  is the time averaged turbulent particle Reynolds number:

$$\overline{Re_P} = \frac{d_S \sqrt{(v_{l,i} + v'_{l,i} - v_{g,i} - v'_{g,i})^2}}{\nu_l} \quad (\text{C.52})$$

### Variable Local Bubble Size Model

Jakobsen [59] developed a simple model for the bubble size postulating that the bubble diameter was proportional to the turbulence length scale determined by the  $k$ - $\varepsilon$  turbulence model. The bubble diameter was thus approximated by:

$$d_s = C_{\text{SMD}} \frac{k^{\frac{3}{2}}}{\varepsilon} \quad (\text{C.53})$$

in which  $C_{\text{SMD}} = 0.04$  was considered a constant system parameter tuned to the air-water system.

## C.2 Tensor Transformation Laws

Thus far the two-fluid model has been derived in Cartesian coordinates. However, for working problems it is often more natural to use curvilinear coordinates like cylindrical and spherical coordinates. In reactor modeling cylindrical coordinates are of particular interest because many reactors have the shape of a tube.

In this section we are thus primarily interested in knowing how to convert the various differential operations written in Cartesian coordinates into vector notation and from thence into curvilinear coordinates. The first operation is relatively easy to perform since the elementary operators can be found in many introductory textbooks on fluid mechanics. The second operation can also be achieved in a rigorous manner provided that we know, for the coordinate being used, two mathematical characteristics<sup>1</sup>: The expressions for  $\nabla$  and the spatial derivatives of the unit vectors in curvilinear coordinates.

In the following subsections we define the formulas that are necessary to convert the equations from the general vector notation to cylinder coordinates. Finally, the governing equations for the two-fluid model are given in cylinder coordinates.

<sup>1</sup> The textbooks by Bird et al [3], Aris [2], Malvern [15], Slattery [17], Irgens [10] [11] and Borisenko and Tarapov [6] may be consulted for thoroughgoing studies of the extensive theory of vector and tensor analysis.

### C.2.1 Curvilinear Coordinate Systems

The position of a point  $P$  in any coordinate system may be specified by three coordinates. To determine these we must first establish a frame of reference by taking any point  $\mathbf{O}$  as the origin and drawing through it three lines, the coordinates. A reference frame with origin  $\mathbf{O}$  consists of three base vectors pointing in three different directions which do not all lie in the same plane. The set of three base vectors is called a basis. A coordinate system is said to be curvilinear if its coordinate curves are not straight lines. A characteristic property of curvilinear coordinate systems is that the orientation of the axes vary from point to point. Considering the general non-orthogonal curvilinear coordinate systems the base vectors are not orthogonal and need not be the same at different points in space. In these non-orthogonal curvilinear coordinate systems, two distinct frames of basis vectors exist at any point. One frame follows the coordinate lines, i.e., the covariant basis vectors are tangents to the coordinate curves. In the other frame, the contravariant basis vectors are normal to the coordinate surface. The orthogonal curvilinear coordinates can be considered a special case of the non-orthogonal curvilinear coordinates. These orthogonal coordinate systems are characterized by tangential basis vectors to the coordinate lines which are mutually perpendicular at every point. In this book only orthogonal coordinate systems are considered. The Cartesian coordinate system is defined by three mutually orthogonal unit vectors with equal units of measurement. The unit vectors may then be thought of as lines of unit length lying along the three axes. The orthogonal curvilinear coordinate systems, like the cylindrical and spherical coordinates, are defined by three mutually orthogonal unit vectors with unequal units of measurement.

Considering a generalized orthogonal coordinate system, the orthogonal curvilinear coordinates are defined as  $q_\alpha$ . In this  $\mathbf{O}$ -system the base vectors  $\mathbf{e}_\alpha$  are defined as unit vectors along the coordinates. The position of the point  $P$  is given by the coordinates, or by the position vector  $\mathbf{r} = \mathbf{r}(q_\alpha, t)$ .

### C.2.2 The Tensor Concept

A *scalar* is a quantity associated with a point in space, whose specification requires just one number. For example, the fluid density, mass fraction, temperature, pressure and work are all scalar quantities. Scalars can be compared only if they have the same physical dimensions. Scalars measured in the same system of units are said to be equal if they have the same magnitude and sign. A *vector* is an entity that possesses both magnitude and direction and obeys certain laws. For example, velocity, acceleration, force are all vectors. Two vectors are equal if they have the same direction and the same magnitude. Moreover, a direction has to be specified in relation to a given frame of reference and this frame of reference is just as arbitrary as the system of units in which the magnitude is expressed. We distinguish therefore between the vector as an entity and its components which allow us to reconstruct it in a

particular system of reference. *Second-order tensors* (also called second-rank tensors<sup>2</sup>) are next in order of complexity after scalars and vectors. Scalars and vectors are both special cases of the more general mathematical entity called a *tensor of order  $n$* , whose specification in any given coordinate system requires  $3^n$  numbers for 3D tensors, these are called the components of the tensor. In this way, we may consider that scalars are tensors of order 0, with  $3^0 = 1$  components, and vectors are tensors of order 1, with  $3^1 = 3$  components. By a second-order tensor is thus meant a quantity uniquely specified by  $3^2 = 9$  numbers denoting the components of the tensor. Higher-order tensors can naturally be defined too, but the second-order tensors are the ones of primary interest in this book. For brevity, we often use the word tensor to mean second-order tensor. The stress tensor is customarily considered the primary tensor in fluid mechanics. A fluid stress has the units of a force per unit area. This tensor is thus an entity associated with two directions (those of the force and the normal to the area). The Cauchy's stress principle establishes that the stress in fluids can be represented by a tensor (e.g., Aris [2], chap 5; Borisenko and Tarapov [6], sect 2.4.2; Slattery [17], sect 2.2.2). Basically, Cauchy's stress principle asserts that  $\mathbf{f}/\delta A$ , tends towards a finite limit as  $\delta A \rightarrow 0$ . This limit is called the stress vector. To elucidate the nature of the stress system at a point  $P$  one considers a fluid element with shape like a small tetrahedron with three of its faces perpendicular to the coordinate axes, while the fourth has an area  $\delta A$  with normal  $\mathbf{n}$ . The three faces are mutually orthogonal and coincide with a set of Cartesian coordinate planes intersecting at  $\mathbf{z}$ . By the law of action and reaction, the stress forces acting on the inside faces of the tetrahedron are equal and opposite to those acting on the outside faces. Applying the principle of local equilibrium then shows that if the tetrahedral fluid element shrink in volume toward a point  $P$ , the net surface force will approach zero. It follows that the stress vector can be re-written as  $\mathbf{f} = -(\mathbf{f}_1 n_1 + \mathbf{f}_2 n_2 + \mathbf{f}_3 n_3)$ . With the convention that  $-T_{mk}$  is the  $k$ th component of the stress vector acting upon the positive side of the plane  $z_m = \text{constant}$ , we project  $\mathbf{f}$  onto the axes of the system:

$$\mathbf{f} = -n_i T_{ij} \mathbf{e}_j, \quad (\text{C.54})$$

where  $T_{ij}$  is a matrix of nine stress components constituting a tensor. This allow us to write (C.54) as:

$$\mathbf{f} = -\mathbf{n} \cdot \mathbf{T} \quad (\text{C.55})$$

Thus, in order to describe completely the state of stress at a point in a continuum, we must specify the stress tensor  $\mathbf{T}$ .

A key property of a tensor is the *transformation law* of its components. This law expresses the way in which the tensor components in one coordinate system are related to its components in another coordinate system. The precise

---

<sup>2</sup> The rank of a particular tensor is the number of array indices required to describe such a quantity.

form of this transformation law is a consequence of the physical or geometric meaning of the tensor.

### C.2.3 Coordinate Transformation Prerequisites

In this section we explain how to determine  $\nabla$  and the spatial derivatives of the unit vectors in cylindrical coordinates.

In Cartesian coordinates the position vector is given by:

$$\mathbf{r} = x\mathbf{e}_x + y\mathbf{e}_y + z\mathbf{e}_z \quad (\text{C.56})$$

The nabla operator yields:

$$\nabla = \frac{\partial}{\partial x}\mathbf{e}_x + \frac{\partial}{\partial y}\mathbf{e}_y + \frac{\partial}{\partial z}\mathbf{e}_z \quad (\text{C.57})$$

The gradient of a scalar field  $\psi$  is defined by:

$$\nabla\psi = \frac{\partial\psi}{\partial x}\mathbf{e}_x + \frac{\partial\psi}{\partial y}\mathbf{e}_y + \frac{\partial\psi}{\partial z}\mathbf{e}_z \quad (\text{C.58})$$

The divergence of a vector field  $\mathbf{v}$  is defined by:

$$\nabla \cdot \mathbf{v} = \frac{\partial v_x}{\partial x} + \frac{\partial v_y}{\partial y} + \frac{\partial v_z}{\partial z} \quad (\text{C.59})$$

The divergence of a tensor field  $\boldsymbol{\sigma}$  is defined by:

$$\nabla \cdot \boldsymbol{\sigma} = \sum_i \frac{\partial}{\partial x_i} \mathbf{e}_i \cdot (\boldsymbol{\sigma}_{jk} \mathbf{e}_j \mathbf{e}_k) = \sum_k \mathbf{e}_k \frac{\partial}{\partial x_i} \boldsymbol{\sigma}_{ik} \quad (\text{C.60})$$

The Laplacian of a scalar field  $\psi$  is defined by:

$$\nabla^2\psi = \frac{\partial^2\psi}{\partial x^2} + \frac{\partial^2\psi}{\partial y^2} + \frac{\partial^2\psi}{\partial z^2} \quad (\text{C.61})$$

The Curl of a vector field  $\mathbf{v}$  is defined by:

$$\nabla \times \mathbf{v} = \begin{vmatrix} \mathbf{e}_x & \mathbf{e}_y & \mathbf{e}_z \\ \frac{\partial}{\partial x} & \frac{\partial}{\partial y} & \frac{\partial}{\partial z} \\ v_x & v_y & v_z \end{vmatrix} \quad (\text{C.62})$$

The governing equations can be transformed directly from Cartesian coordinates into cylindrical coordinates without considering the vector notation. In this appendix the relationships between the Cartesian coordinates and the cylindrical coordinates are defined solely, but the method of coordinate transformation is generic and can thus be applied to any orthogonal coordinate system.

In cylindrical coordinates, instead of locating a point in space by  $x, y, z$  as in Cartesian coordinates, we designate the coordinates of the point by  $r, \theta, z$ . The Cartesian coordinates are related to the cylindrical coordinates by [3]:

$$x = r \cos \theta, \quad y = r \sin \theta, \quad z = z \quad (\text{C.63})$$

To convert the derivatives of scalars with respect to  $x, y, z$  into derivatives with respect to  $r, \theta, z$ , the chain rule of partial differentiation is used. The derivative operators are thus related as:

$$\frac{\partial}{\partial x} = \cos \theta \frac{\partial}{\partial r} - \frac{\sin \theta}{r} \frac{\partial}{\partial \theta}, \quad \frac{\partial}{\partial y} = \sin \theta \frac{\partial}{\partial r} + \frac{\cos \theta}{r} \frac{\partial}{\partial \theta}, \quad \frac{\partial}{\partial z} = \frac{\partial}{\partial z} \quad (\text{C.64})$$

Trigonometrical arguments lead to the following relations between the unit vectors:

$$\mathbf{e}_r = \cos \theta \mathbf{e}_x + \sin \theta \mathbf{e}_y, \quad \mathbf{e}_\theta = -\sin \theta \mathbf{e}_x + \cos \theta \mathbf{e}_y, \quad \mathbf{e}_z = \mathbf{e}_z \quad (\text{C.65})$$

From these equations one can derive the formulas required for the spatial derivatives of the unit vectors  $\mathbf{e}_r, \mathbf{e}_\theta, \mathbf{e}_z$ .

The given trigonometrical relationships may also be solved for  $\mathbf{e}_x, \mathbf{e}_y, \mathbf{e}_z$ , giving:

$$\mathbf{e}_x = \cos \theta \mathbf{e}_r - \sin \theta \mathbf{e}_\theta, \quad \mathbf{e}_y = \sin \theta \mathbf{e}_r + \cos \theta \mathbf{e}_\theta, \quad \mathbf{e}_z = \mathbf{e}_z \quad (\text{C.66})$$

To obtain the formula for  $\nabla$  in cylindrical coordinates we employ the definition of the  $\nabla$ -operator in Cartesian coordinates (C.57), eliminate the Cartesian unit vectors by (C.66) and eliminate the Cartesian derivative operators by (C.64). The resulting formula for the  $\nabla$  operator in cylindrical coordinates can then be used to calculate all the necessary differential operators in cylindrical coordinates provided that the spatial derivatives of the unit vectors  $\mathbf{e}_r, \mathbf{e}_\theta, \mathbf{e}_z$  are used to differentiate the unit vectors on which  $\nabla$  operates.

The spatial derivatives of the unit vectors  $\mathbf{e}_r, \mathbf{e}_\theta, \mathbf{e}_z$  can be determined from (C.65):

$$\frac{\partial}{\partial r} \mathbf{e}_r = 0 \quad \frac{\partial}{\partial r} \mathbf{e}_\theta = 0 \quad \frac{\partial}{\partial r} \mathbf{e}_z = 0 \quad (\text{C.67})$$

$$\frac{\partial}{\partial \theta} \mathbf{e}_r = \mathbf{e}_\theta \quad \frac{\partial}{\partial \theta} \mathbf{e}_\theta = -\mathbf{e}_r \quad \frac{\partial}{\partial \theta} \mathbf{e}_z = 0 \quad (\text{C.68})$$

$$\frac{\partial}{\partial z} \mathbf{e}_r = 0 \quad \frac{\partial}{\partial z} \mathbf{e}_\theta = 0 \quad \frac{\partial}{\partial z} \mathbf{e}_z = 0 \quad (\text{C.69})$$

By use of (C.56), (C.63) and (C.68) the position vector can be transformed into cylindrical coordinates:

$$\mathbf{r} = r \mathbf{e}_r(\theta) + z \mathbf{e}_z \quad (\text{C.70})$$

### C.2.4 Orthogonal Curvilinear Coordinate Systems and Differential Operators

In this section the relevant differential operators are defined for generalized orthogonal curvilinear coordinate systems.

Let  $(q_1, q_2, q_3)$  be curvilinear orthogonal coordinates connected with the Cartesian coordinates  $(x, y, z)$  by the vector relation  $\mathbf{r} = \mathbf{r}(q_1, q_2, q_3)$ , where  $\mathbf{r}$  is the radius vector of the point  $P$  considered. The Cartesian coordinates are then related to the generalized curvilinear coordinates by:

$$x = x(q_1, q_2, q_3), \quad y = y(q_1, q_2, q_3), \quad z = z(q_1, q_2, q_3) \quad (\text{C.71})$$

If the Jacobian is nonzero,

$$\frac{\partial(x, y, z)}{\partial(q_1, q_2, q_3)} \neq 0, \quad (\text{C.72})$$

then

$$q_1 = q_1(x, y, z), \quad q_2 = q_2(x, y, z), \quad q_3 = q_3(x, y, z) \quad (\text{C.73})$$

form a basis for the orthogonal curvilinear coordinate system.

The basis vectors (not necessarily unit vectors) in the generalized curvilinear coordinate system are defined as (e.g., [1], p 193; [24], p 6; [3], p 737):

$$\mathbf{g}_\alpha = \frac{\partial \mathbf{r}}{\partial q_\alpha} = \frac{\partial \mathbf{r}}{\partial x_k} \frac{\partial x_k}{\partial q_\alpha} = \frac{\partial x_k}{\partial q_\alpha} \mathbf{e}_k \quad \text{or} \quad \mathbf{e}_k = \frac{\partial q_\alpha}{\partial x_k} \mathbf{g}_\alpha \quad (\text{C.74})$$

where  $x_k$  is the Cartesian coordinates, and  $\mathbf{g}_\alpha$  are the tangent basis vectors which are tangents to the coordinate lines.

From these basis vectors we can define the Lamé coefficients denoting the length of the basis vectors (also named *scale factors*) and expressed by:

$$h_{q_\alpha} = |\mathbf{g}_\alpha| = \left| \frac{\partial \mathbf{r}}{\partial q_\alpha} \right| = h_\alpha = \sqrt{\mathbf{g}_\alpha \cdot \mathbf{g}_\alpha} = \sqrt{\frac{\partial \mathbf{r}}{\partial q_\alpha} \cdot \frac{\partial \mathbf{r}}{\partial q_\alpha}} = \sqrt{\frac{\partial x_k}{\partial q_\alpha} \frac{\partial x_k}{\partial q_\alpha}} \quad (\text{C.75})$$

thus the unit tangent vectors to the coordinate lines  $q_\alpha$  can be determined by:

$$\mathbf{e}_\alpha = \frac{\mathbf{g}_\alpha}{|\mathbf{g}_\alpha|} = \frac{\mathbf{g}_\alpha}{\sqrt{g_\alpha g_\alpha}} = \frac{\mathbf{g}_\alpha}{h_\alpha} \quad (\text{C.76})$$

For orthogonal coordinate systems, we can write:

$$\sqrt{\mathbf{g}_\alpha \cdot \mathbf{g}_\beta} = \sqrt{\frac{\partial x_k}{\partial q_\alpha} \frac{\partial x_k}{\partial q_\beta}} = 0, \quad \text{for } \alpha \neq \beta. \quad (\text{C.77})$$

We may then present a generalization of (C.75), the relation for  $h_\alpha$ :

$$\sqrt{\frac{\partial x_k}{\partial q_\alpha} \frac{\partial x_k}{\partial q_\beta}} = h_\alpha \delta_{\alpha\beta} \quad (\text{C.78})$$

Moreover, since:

$$\frac{\partial q_\alpha}{\partial q_\beta} = \frac{\partial q_\alpha}{\partial x_k} \frac{\partial x_k}{\partial q_\beta} = \delta_{\alpha\beta} \quad (\text{C.79})$$

the equality relation between the last two terms in the above expression can be rewritten as:

$$\left( \frac{\partial q_\alpha}{\partial x_k} \right) = \left( \frac{\partial x_k}{\partial q_\alpha} \right)^{-1} \quad (\text{C.80})$$

Combining the latter three relationships, we obtain:

$$\left( \frac{\partial q_\alpha}{\partial x_k} \frac{\partial q_\beta}{\partial x_k} \right) = \left( \frac{\partial x_k}{\partial q_\alpha} \frac{\partial x_k}{\partial q_\beta} \right)^{-1} = \frac{1}{h_\alpha^2} \delta_{\alpha\beta} \quad (\text{C.81})$$

In Cartesian coordinates the position vector (C.56) is expressed in terms of the unit base vectors  $\mathbf{e}_x, \mathbf{e}_y, \mathbf{e}_z$ , hence a position vector increment  $d\mathbf{r}$  between two infinitely close points yields:  $d\mathbf{r} = dx\mathbf{e}_x + dy\mathbf{e}_y + dz\mathbf{e}_z$ . The base vectors  $g_\alpha$  in the curvilinear system, called the natural basis of the curvilinear system (also called covariant base vectors), is defined such that the same position vector increment  $d\mathbf{r}$  is given in terms of the curvilinear increments  $dg_\alpha$  by:  $d\mathbf{r} = dg_\alpha \mathbf{e}_\alpha$ . The distance element in curvilinear coordinate systems is then computed as the square of the element of arc length between the two infinitely close points:

$$(ds)^2 = |d\mathbf{r}|^2 = d\mathbf{r} \cdot d\mathbf{r} = g_{\alpha\gamma} dq_\alpha dq_\gamma \quad (\text{C.82})$$

where  $g_{\alpha\gamma} = \mathbf{e}_\alpha \cdot \mathbf{e}_\gamma$  is called the metric tensor.

The basic quantities describing an orthogonal coordinate system are the metric coefficients  $h_1 = \sqrt{g_{11}}$ ,  $h_2 = \sqrt{g_{22}}$ ,  $h_3 = \sqrt{g_{33}}$ , which satisfy the formula:

$$(ds)^2 = d\mathbf{r} \cdot d\mathbf{r} = (h_1 dq_1)^2 + (h_2 dq_2)^2 + (h_3 dq_3)^2 \quad (\text{C.83})$$

For the cylindrical coordinates the metric coefficients can be determined from (C.75):

$$h_r = \sqrt{\frac{\partial \mathbf{r}}{\partial r} \cdot \frac{\partial \mathbf{r}}{\partial r}} = 1, \quad h_\theta = \sqrt{\frac{\partial \mathbf{r}}{\partial \theta} \cdot \frac{\partial \mathbf{r}}{\partial \theta}} = r, \quad h_z = \sqrt{\frac{\partial \mathbf{r}}{\partial z} \cdot \frac{\partial \mathbf{r}}{\partial z}} = 1 \quad (\text{C.84})$$

using the following relations

$$\frac{\partial \mathbf{r}}{\partial r} = \mathbf{e}_r, \quad \frac{\partial \mathbf{r}}{\partial \theta} = r \frac{\partial \mathbf{e}_r}{\partial \theta} = r \mathbf{e}_\theta, \quad \frac{\partial \mathbf{r}}{\partial z} = \mathbf{e}_z \quad (\text{C.85})$$

which are deduced from (C.70).

The del operator can then be written in a generalized form using (C.56), (C.74) and (C.81):

$$\begin{aligned} \nabla &= \mathbf{e}_k \frac{\partial}{\partial x_k} = \left( \frac{\partial q_\alpha}{\partial x_k} \mathbf{g}_\alpha \right) \left( \frac{\partial}{\partial q_\beta} \frac{\partial q_\beta}{\partial x_k} \right) = \sum_\alpha \left( \frac{1}{h_\alpha^2} \delta_{\alpha\beta} \right) \mathbf{g}_\alpha \frac{\partial}{\partial q_\beta} \\ &= \sum_\alpha \frac{1}{h_\alpha^2} \mathbf{g}_\alpha \frac{\partial}{\partial q_\alpha} = \sum_\alpha \frac{1}{h_\alpha} \mathbf{e}_\alpha \frac{\partial}{\partial q_\alpha} \end{aligned} \quad (\text{C.86})$$

where  $\mathbf{e}_k$  denotes the unit vectors in the Cartesian coordinate system and  $\mathbf{e}_\alpha = \frac{\mathbf{g}_\alpha}{h_\alpha}$  is the unit tangent vectors to the coordinate lines  $q_\alpha$ .

The resulting expression for the nabla operator (C.86) are then employed to deduce the transformation formulas for the gradient, divergence, and curl operators in any orthogonal curvilinear coordinate system [11]:

$$\nabla\psi = \sum_{\alpha} \frac{1}{h_{\alpha}} \mathbf{e}_{\alpha} \frac{\partial\psi}{\partial q_{\alpha}} \quad (\text{C.87})$$

$$\nabla \cdot \mathbf{v} = \sum_{\alpha} \frac{1}{h_{\alpha}} \mathbf{e}_{\alpha} \cdot \frac{\partial(v_{\beta} \mathbf{e}_{\beta})}{\partial q_{\alpha}} \quad (\text{C.88})$$

$$\text{curl}(\mathbf{v}) = \text{rot}(\mathbf{v}) = \nabla \times \mathbf{v} = \sum_{\alpha} \frac{1}{h_{\alpha}} \mathbf{e}_{\alpha} \times \frac{\partial(v_{\beta} \mathbf{e}_{\beta})}{\partial q_{\alpha}} \quad (\text{C.89})$$

$$\nabla \mathbf{v} = \sum_{\alpha} \frac{1}{h_{\alpha}} \mathbf{e}_{\alpha} \frac{\partial(v_{\beta} \mathbf{e}_{\beta})}{\partial q_{\alpha}} \quad (\text{C.90})$$

$$\nabla \cdot \boldsymbol{\sigma} = \sum_{\alpha} \frac{1}{h_{\alpha}} \mathbf{e}_{\alpha} \frac{\partial(\sigma_{\beta\gamma} \mathbf{e}_{\beta} \mathbf{e}_{\gamma})}{\partial q_{\alpha}} \quad (\text{C.91})$$

in which the vector  $\mathbf{v}$  is presented in terms of its physical components  $v_{\alpha}$  in such a way that:

$$\mathbf{v} = v_{\alpha} \mathbf{e}_{\alpha} \quad (\text{C.92})$$

where  $\mathbf{e}_{\alpha}$  is the unit tangent vector to the coordinate lines in the orthogonal  $q_{\alpha}$ -system.

The orthogonal curvilinear unit vectors just introduced obey certain laws, which are used in the subsequent paragraphs. The scalar or dot product of two unit vectors yields:

$$\mathbf{e}_{\alpha} \cdot \mathbf{e}_{\beta} = \delta_{\alpha\beta} \quad (\text{C.93})$$

The vector or cross product of two unit vectors is defined by:

$$\mathbf{e}_{\alpha} \times \mathbf{e}_{\beta} = \sum_{\gamma=1}^3 \epsilon_{\alpha\beta\gamma} \mathbf{e}_{\gamma} \quad (\text{C.94})$$

Many formulas in tensor analysis are expressed compactly in terms of the *Kronecker delta*,  $\delta_{\alpha\beta}$ , and the *alternating unit tensor*,  $\epsilon_{\alpha\beta\gamma}$ . These entities are defined as:

$$\delta_{\alpha\beta} = \begin{cases} +1 & \text{if } \alpha = \beta \\ 0 & \text{if } \alpha \neq \beta \end{cases} \quad (\text{C.95})$$

$$\epsilon_{\alpha\beta\gamma} = \begin{cases} +1 & \text{if } \alpha\beta\gamma = 123, 231, \text{ or } 312 \\ -1 & \text{if } \alpha\beta\gamma = 321, 132, \text{ or } 213 \\ 0 & \text{if any two indices are alike} \end{cases} \quad (\text{C.96})$$

### C.2.5 Differential Operators in Cylindrical Coordinates

In this section the cylindrical coordinate transforms are deduced from the formulas presented in the preceding subsections.

From (C.92) we recognize that a vector in cylindrical coordinates yields:

$$\mathbf{v} = v_r \mathbf{e}_r + v_\theta \mathbf{e}_\theta + v_z \mathbf{e}_z \quad (\text{C.97})$$

where  $\mathbf{e}_r$ ,  $\mathbf{e}_\theta$ , and  $\mathbf{e}_z$  are the unit vectors in the radial, azimuthal, and axial directions respectively.

The nabla-operator is given by (C.86):

$$\nabla = \sum_{\alpha} \frac{1}{h_{\alpha}} \mathbf{e}_{\alpha} \frac{\partial}{\partial q_{\alpha}} = \mathbf{e}_r \frac{\partial}{\partial r} + \mathbf{e}_{\theta} \frac{1}{r} \frac{\partial}{\partial \theta} + \mathbf{e}_z \frac{\partial}{\partial z} \quad (\text{C.98})$$

#### Gradient of a scalar

The gradient of a scalar  $\psi$  is:

$$\text{grad}(\psi) = \nabla \psi = \sum_{\alpha} \frac{1}{h_{\alpha}} \mathbf{e}_{\alpha} \frac{\partial \psi}{\partial q_{\alpha}} = \mathbf{e}_r \frac{\partial \psi}{\partial r} + \mathbf{e}_{\theta} \frac{1}{r} \frac{\partial \psi}{\partial \theta} + \mathbf{e}_z \frac{\partial \psi}{\partial z} \quad (\text{C.99})$$

which is a vector.

#### Divergence of a vector

If  $\mathbf{v}$  is a vector, the divergence of  $\mathbf{v}$  is:

$$\begin{aligned} \text{div}(\mathbf{v}) &= \nabla \cdot \mathbf{v} = \sum_{\alpha} \frac{1}{h_{\alpha}} \mathbf{e}_{\alpha} \cdot \frac{\partial}{\partial q_{\alpha}} (v_{\beta} \mathbf{e}_{\beta}) \\ &= \mathbf{e}_r \cdot \frac{\partial}{\partial r} (v_{\beta} \mathbf{e}_{\beta}) + \mathbf{e}_{\theta} \frac{1}{r} \cdot \frac{\partial}{\partial \theta} (v_{\beta} \mathbf{e}_{\beta}) + \mathbf{e}_z \cdot \frac{\partial}{\partial z} (v_{\beta} \mathbf{e}_{\beta}) \\ &= \frac{\partial v_r}{\partial r} + \mathbf{e}_{\theta} \frac{1}{r} \cdot \frac{\partial}{\partial \theta} (v_r \mathbf{e}_r + v_{\theta} \mathbf{e}_{\theta}) + \frac{\partial v_z}{\partial z} \\ &= \frac{\partial v_r}{\partial r} + \mathbf{e}_{\theta} \frac{1}{r} \cdot \left( v_r \frac{\partial \mathbf{e}_r}{\partial \theta} + \mathbf{e}_r \frac{\partial v_r}{\partial \theta} + \frac{\partial}{\partial \theta} (v_{\theta} \mathbf{e}_{\theta}) \right) + \frac{\partial v_z}{\partial z} \quad (\text{C.100}) \\ &= \frac{\partial v_r}{\partial r} + \mathbf{e}_{\theta} \frac{1}{r} \cdot \left( v_r \mathbf{e}_{\theta} + \mathbf{e}_r \frac{\partial v_r}{\partial \theta} + \frac{\partial}{\partial \theta} (v_{\theta} \mathbf{e}_{\theta}) \right) + \frac{\partial v_z}{\partial z} \\ &= \frac{\partial v_r}{\partial r} + \frac{1}{r} \left( v_r + \frac{\partial v_{\theta}}{\partial \theta} \right) + \frac{\partial v_z}{\partial z} \\ &= \frac{1}{r} \frac{\partial}{\partial r} (r v_r) + \frac{1}{r} \frac{\partial v_{\theta}}{\partial \theta} + \frac{\partial v_z}{\partial z} \end{aligned}$$

which is scalar.

### Gradient of a vector

Let  $\mathbf{v}$  represent a vector, the gradient of  $\mathbf{v}$  is:

$$\begin{aligned}
 \text{grad}(\mathbf{v}) &= \nabla \mathbf{v} = \sum_{\alpha} \frac{1}{h_{\alpha}} \mathbf{e}_{\alpha} \frac{\partial}{\partial q_{\alpha}} (v_{\beta} \mathbf{e}_{\beta}) \\
 &= \mathbf{e}_r \frac{\partial}{\partial r} (v_r \mathbf{e}_r + v_{\theta} \mathbf{e}_{\theta} + v_z \mathbf{e}_z) \\
 &\quad + \frac{1}{r} \mathbf{e}_{\theta} \frac{\partial}{\partial \theta} (v_r \mathbf{e}_r + v_{\theta} \mathbf{e}_{\theta} + v_z \mathbf{e}_z) \\
 &\quad + \mathbf{e}_z \frac{\partial}{\partial z} (v_r \mathbf{e}_r + v_{\theta} \mathbf{e}_{\theta} + v_z \mathbf{e}_z) \\
 &= \mathbf{e}_r \mathbf{e}_r \frac{\partial v_r}{\partial r} + \mathbf{e}_r \mathbf{e}_{\theta} \frac{\partial v_{\theta}}{\partial r} + \mathbf{e}_r \mathbf{e}_z \frac{\partial v_z}{\partial r} \\
 &\quad + \frac{1}{r} \mathbf{e}_{\theta} \mathbf{e}_r \frac{\partial v_r}{\partial \theta} + \frac{1}{r} \mathbf{e}_{\theta} \mathbf{e}_{\theta} v_r + \frac{1}{r} \mathbf{e}_{\theta} \mathbf{e}_{\theta} \frac{\partial v_{\theta}}{\partial \theta} - \frac{1}{r} \mathbf{e}_{\theta} \mathbf{e}_r v_{\theta} + \frac{1}{r} \mathbf{e}_{\theta} \mathbf{e}_z \frac{\partial v_z}{\partial \theta} \\
 &\quad + \mathbf{e}_z \mathbf{e}_r \frac{\partial v_r}{\partial z} + \mathbf{e}_z \mathbf{e}_{\theta} \frac{\partial v_{\theta}}{\partial z} + \mathbf{e}_z \mathbf{e}_z \frac{\partial v_z}{\partial z} \\
 &= \mathbf{e}_r \mathbf{e}_r \frac{\partial v_r}{\partial r} + \mathbf{e}_r \mathbf{e}_{\theta} \frac{\partial v_{\theta}}{\partial r} + \mathbf{e}_r \mathbf{e}_z \frac{\partial v_z}{\partial r} \\
 &\quad + \mathbf{e}_{\theta} \mathbf{e}_r \frac{\partial}{\partial \theta} \left( \frac{1}{r} \frac{\partial v_r}{\partial \theta} - \frac{1}{r} v_{\theta} \right) + \mathbf{e}_{\theta} \mathbf{e}_{\theta} \left( \frac{1}{r} \frac{\partial v_{\theta}}{\partial \theta} + \frac{1}{r} v_r \right) + \mathbf{e}_{\theta} \mathbf{e}_z \frac{1}{r} \frac{\partial v_z}{\partial \theta} \\
 &\quad + \mathbf{e}_z \mathbf{e}_r \frac{\partial v_r}{\partial z} + \mathbf{e}_z \mathbf{e}_{\theta} \frac{\partial v_{\theta}}{\partial z} + \mathbf{e}_z \mathbf{e}_z \frac{\partial v_z}{\partial z}
 \end{aligned} \tag{C.101}$$

The product is a second-order tensor, or a dyadic product.

### Divergence of a second-order tensor

The unit dyads may be multiplied with each other and with the unit vectors:

$$\mathbf{e}_{\alpha} : \mathbf{e}_{\beta} = \delta_{\alpha\kappa} \delta_{\beta\gamma} \tag{C.102}$$

$$\mathbf{e}_{\alpha} \mathbf{e}_{\beta} \cdot \mathbf{e}_{\gamma} = \mathbf{e}_{\alpha} \delta_{\beta\gamma} \tag{C.103}$$

$$\mathbf{e}_{\alpha} \cdot \mathbf{e}_{\beta} \mathbf{e}_{\gamma} = \delta_{\alpha\beta} \mathbf{e}_{\gamma} \tag{C.104}$$

$$\mathbf{e}_{\alpha} \mathbf{e}_{\beta} \cdot \mathbf{e}_{\gamma} \mathbf{e}_{\kappa} = \delta_{\beta\gamma} \mathbf{e}_{\alpha} \mathbf{e}_{\kappa} \tag{C.105}$$

Then, if  $\mathbf{A}$  is a second order tensor, or a dyad, the divergence of  $\mathbf{A}$  is:

$$\begin{aligned}
 \operatorname{div}(\mathbf{A}) = \nabla \cdot \mathbf{A} &= \sum_{\alpha} \frac{1}{h_{\alpha}} \frac{\partial}{\partial q_{\alpha}} (A_{\gamma\kappa} \mathbf{e}_{\gamma} \mathbf{e}_{\kappa} \cdot \mathbf{e}_{\alpha}) \\
 &= \frac{\partial}{\partial r} (A_{\gamma\kappa} \mathbf{e}_{\gamma} \mathbf{e}_{\kappa}) \cdot \mathbf{e}_r + \frac{1}{r} \frac{\partial}{\partial \theta} (A_{\gamma\kappa} \mathbf{e}_{\gamma} \mathbf{e}_{\kappa}) \cdot \mathbf{e}_{\theta} + \frac{\partial}{\partial z} (A_{\gamma\kappa} \mathbf{e}_{\gamma} \mathbf{e}_{\kappa}) \cdot \mathbf{e}_z \\
 &= \frac{\partial}{\partial r} (A_{\gamma\kappa}) \mathbf{e}_{\gamma} \mathbf{e}_{\kappa} \cdot \mathbf{e}_r + A_{\gamma\kappa} \frac{\partial}{\partial r} (\mathbf{e}_{\gamma} \mathbf{e}_{\kappa}) \cdot \mathbf{e}_r \\
 &\quad + \frac{1}{r} \frac{\partial}{\partial \theta} (A_{\gamma\kappa}) \mathbf{e}_{\gamma} \mathbf{e}_{\kappa} \cdot \mathbf{e}_{\theta} + \frac{1}{r} A_{\gamma\kappa} \frac{\partial}{\partial \theta} (\mathbf{e}_{\gamma} \mathbf{e}_{\kappa}) \cdot \mathbf{e}_{\theta} \\
 &\quad + \frac{\partial}{\partial z} (A_{\gamma\kappa}) \mathbf{e}_{\gamma} \mathbf{e}_{\kappa} \cdot \mathbf{e}_z + A_{\gamma\kappa} \frac{\partial}{\partial z} (\mathbf{e}_{\gamma} \mathbf{e}_{\kappa}) \cdot \mathbf{e}_z \\
 &= \frac{\partial}{\partial r} (A_{rr}) \mathbf{e}_r + \frac{\partial}{\partial r} (A_{\theta r}) \mathbf{e}_{\theta} + \frac{\partial}{\partial r} (A_{zr}) \mathbf{e}_z \\
 &\quad + \frac{1}{r} \frac{\partial}{\partial \theta} (A_{r\theta}) \mathbf{e}_r + \frac{1}{r} \frac{\partial}{\partial \theta} (A_{\theta\theta}) \mathbf{e}_{\theta} + \frac{1}{r} \frac{\partial}{\partial \theta} (A_{z\theta}) \mathbf{e}_z \\
 &\quad + \frac{1}{r} A_{kr} \mathbf{e}_k + \frac{1}{r} A_{k\theta} \left( \frac{\partial \mathbf{e}_k}{\partial \theta} \cdot \mathbf{e}_{\theta} \right) \\
 &\quad + \frac{\partial}{\partial z} (A_{rz}) \mathbf{e}_r + \frac{\partial}{\partial z} (A_{\theta z}) \mathbf{e}_{\theta} + \frac{\partial}{\partial z} (A_{zz}) \mathbf{e}_z \\
 &= \frac{\partial}{\partial r} (A_{rr}) \mathbf{e}_r + \frac{\partial}{\partial r} (A_{\theta r}) \mathbf{e}_{\theta} + \frac{\partial}{\partial r} (A_{zr}) \mathbf{e}_z \\
 &\quad + \frac{1}{r} \frac{\partial}{\partial \theta} (A_{r\theta}) \mathbf{e}_r + \frac{1}{r} \frac{\partial}{\partial \theta} (A_{\theta\theta}) \mathbf{e}_{\theta} + \frac{1}{r} \frac{\partial}{\partial \theta} (A_{z\theta}) \mathbf{e}_z \\
 &\quad + \frac{1}{r} A_{rr} \mathbf{e}_r + \frac{1}{r} A_{\theta r} \mathbf{e}_{\theta} + \frac{1}{r} A_{zr} \mathbf{e}_z + \frac{1}{r} A_{\theta\theta} \mathbf{e}_{\theta} - \frac{1}{r} A_{\theta\theta} \mathbf{e}_r \\
 &\quad + \frac{\partial}{\partial z} (A_{rz}) \mathbf{e}_r + \frac{\partial}{\partial z} (A_{\theta z}) \mathbf{e}_{\theta} + \frac{\partial}{\partial z} (A_{zz}) \mathbf{e}_z \\
 &= \mathbf{e}_r \left[ \frac{\partial}{\partial r} (A_{rr}) + \frac{1}{r} \frac{\partial}{\partial \theta} (A_{r\theta}) + \frac{1}{r} A_{rr} - \frac{1}{r} A_{\theta\theta} + \frac{\partial}{\partial z} (A_{rz}) \right] \\
 &\quad + \mathbf{e}_{\theta} \left[ \frac{\partial}{\partial r} (A_{\theta r}) + \frac{1}{r} \frac{\partial}{\partial \theta} (A_{\theta\theta}) + \frac{1}{r} A_{\theta r} + \frac{1}{r} A_{r\theta} + \frac{\partial}{\partial z} (A_{\theta z}) \right] \\
 &\quad + \mathbf{e}_z \left[ \frac{\partial}{\partial r} (A_{zr}) + \frac{1}{r} \frac{\partial}{\partial \theta} (A_{z\theta}) + \frac{1}{r} A_{zr} + \frac{\partial}{\partial z} (A_{zz}) \right] \\
 &= \mathbf{e}_r \left[ \frac{1}{r} \frac{\partial}{\partial r} (r A_{rr}) + \frac{1}{r} \frac{\partial}{\partial \theta} (A_{r\theta}) + \frac{\partial}{\partial z} (A_{rz}) - \frac{1}{r} A_{\theta\theta} \right] \\
 &\quad + \mathbf{e}_{\theta} \left[ \frac{1}{r} \frac{\partial}{\partial r} (r A_{\theta r}) + \frac{1}{r} \frac{\partial}{\partial \theta} (A_{\theta\theta}) + \frac{\partial}{\partial z} (A_{\theta z}) + \frac{1}{r} A_{r\theta} \right] \\
 &\quad + \mathbf{e}_z \left[ \frac{1}{r} \frac{\partial}{\partial r} (r A_{zr}) + \frac{1}{r} \frac{\partial}{\partial \theta} (A_{z\theta}) + \frac{\partial}{\partial z} (A_{zz}) \right]
 \end{aligned} \tag{C.106}$$

which is a vector.

## The Laplacian of a Scalar Field

If we take the divergence of the gradient of the scalar function  $\psi$ , as is done for the pressure field formulating an equation for the pressure, we obtain:

$$\begin{aligned}
 \nabla^2 \psi &= \nabla \cdot \nabla \psi = \nabla \cdot \text{grad}(\psi) \\
 &= (\mathbf{e}_r \frac{\partial}{\partial r} + \mathbf{e}_\theta \frac{1}{r} \frac{\partial}{\partial \theta} + \mathbf{e}_z \frac{\partial}{\partial z}) \cdot (\mathbf{e}_r \frac{\partial \psi}{\partial r} + \mathbf{e}_\theta \frac{1}{r} \frac{\partial \psi}{\partial \theta} + \mathbf{e}_z \frac{\partial \psi}{\partial z}) \\
 &= \frac{\partial^2 \psi}{\partial r^2} + \mathbf{e}_r \frac{\partial}{\partial r} \cdot \mathbf{e}_\theta \frac{1}{r} \frac{\partial \psi}{\partial \theta} + \mathbf{e}_\theta \frac{1}{r} \frac{\partial}{\partial \theta} \cdot \mathbf{e}_r \frac{\partial \psi}{\partial r} + \frac{1}{r^2} \frac{\partial^2 \psi}{\partial \theta^2} + \frac{\partial^2 \psi}{\partial z^2} \\
 &= \frac{\partial^2 \psi}{\partial r^2} + (\mathbf{e}_r \cdot \frac{1}{r} \frac{\partial \psi}{\partial \theta} \frac{\partial \mathbf{e}_\theta}{\partial r}) + \mathbf{e}_r \cdot \mathbf{e}_\theta \frac{\partial}{\partial r} (\frac{1}{r} \frac{\partial \psi}{\partial \theta}) \\
 &\quad + \mathbf{e}_\theta \frac{1}{r} \cdot \frac{\partial}{\partial \theta} (\mathbf{e}_r \frac{\partial \psi}{\partial r}) + \frac{1}{r^2} \frac{\partial^2 \psi}{\partial \theta^2} + \frac{\partial^2 \psi}{\partial z^2} \tag{C.107} \\
 &= \frac{\partial^2 \psi}{\partial r^2} + \mathbf{e}_\theta \frac{1}{r} \cdot (\frac{\partial \alpha}{\partial r} \frac{\partial \mathbf{e}_r}{\partial \theta} + \mathbf{e}_r \frac{\partial}{\partial \theta} \frac{\partial \psi}{\partial r}) + \frac{1}{r^2} \frac{\partial^2 \alpha}{\partial \theta^2} + \frac{\partial^2 \psi}{\partial z^2} \\
 &= \frac{\partial^2 \psi}{\partial r^2} + \mathbf{e}_\theta \frac{1}{r} \cdot \frac{\partial \alpha}{\partial r} \mathbf{e}_\theta + \frac{1}{r^2} \frac{\partial^2 \psi}{\partial \theta^2} + \frac{\partial^2 \psi}{\partial z^2} \\
 &= \frac{\partial^2 \psi}{\partial r^2} + \frac{1}{r} \frac{\partial \psi}{\partial r} + \frac{1}{r^2} \frac{\partial^2 \psi}{\partial \theta^2} + \frac{\partial^2 \psi}{\partial z^2} \\
 &= \frac{1}{r} \frac{\partial}{\partial r} (r \frac{\partial \psi}{\partial r}) + \frac{1}{r^2} \frac{\partial^2 \psi}{\partial \theta^2} + \frac{\partial^2 \psi}{\partial z^2}
 \end{aligned}$$

The result is a scalar.

## The Curl of a Vector Field

$$\begin{aligned}
 \text{curl}(\mathbf{v}) &= \text{rot}(\mathbf{v}) = \nabla \times \mathbf{v} = \sum_{\alpha} \frac{1}{h_{\alpha}} \mathbf{e}_{\alpha} \times \frac{\partial(v_{\beta} \mathbf{e}_{\beta})}{\partial q_{\alpha}} \\
 &= \mathbf{e}_r \times \frac{\partial(v_{\beta} \mathbf{e}_{\beta})}{\partial r} + \frac{1}{r} \mathbf{e}_{\theta} \times \frac{\partial(v_{\beta} \mathbf{e}_{\beta})}{\partial \theta} + \mathbf{e}_z \times \frac{\partial(v_{\beta} \mathbf{e}_{\beta})}{\partial z} \\
 &= \mathbf{e}_r \times \frac{\partial}{\partial r} (v_r \mathbf{e}_r + v_{\theta} \mathbf{e}_{\theta} + v_z \mathbf{e}_z) + \frac{1}{r} \mathbf{e}_{\theta} \times \frac{\partial}{\partial \theta} (v_r \mathbf{e}_r + v_{\theta} \mathbf{e}_{\theta} + v_z \mathbf{e}_z) \\
 &\quad + \mathbf{e}_z \times \frac{\partial}{\partial z} (v_r \mathbf{e}_r + v_{\theta} \mathbf{e}_{\theta} + v_z \mathbf{e}_z) \\
 &= \mathbf{e}_r \times (v_r \frac{\partial \mathbf{e}_r}{\partial r} + \frac{\partial v_r}{\partial r} \mathbf{e}_r + v_{\theta} \frac{\partial \mathbf{e}_{\theta}}{\partial r} + \frac{\partial v_{\theta}}{\partial r} \mathbf{e}_{\theta} + v_z \frac{\partial \mathbf{e}_z}{\partial r} + \frac{\partial v_z}{\partial r} \mathbf{e}_z) \\
 &\quad + \frac{1}{r} \mathbf{e}_{\theta} \times (v_r \frac{\partial \mathbf{e}_r}{\partial \theta} + \frac{\partial v_r}{\partial \theta} \mathbf{e}_r + v_{\theta} \frac{\partial \mathbf{e}_{\theta}}{\partial \theta} + \frac{\partial v_{\theta}}{\partial \theta} \mathbf{e}_{\theta} + v_z \frac{\partial \mathbf{e}_z}{\partial \theta} + \frac{\partial v_z}{\partial \theta} \mathbf{e}_z) \\
 &\quad + \mathbf{e}_z \times (v_r \frac{\partial \mathbf{e}_r}{\partial z} + \frac{\partial v_r}{\partial z} \mathbf{e}_r + v_{\theta} \frac{\partial \mathbf{e}_{\theta}}{\partial z} + \frac{\partial v_{\theta}}{\partial z} \mathbf{e}_{\theta} + v_z \frac{\partial \mathbf{e}_z}{\partial z} + \frac{\partial v_z}{\partial z} \mathbf{e}_z)
 \end{aligned}$$

$$\begin{aligned}
&= \mathbf{e}_r \times \left( \frac{\partial v_r}{\partial r} \mathbf{e}_r + \frac{\partial v_\theta}{\partial r} \mathbf{e}_\theta + \frac{\partial v_z}{\partial r} \mathbf{e}_z \right) \\
&\quad + \frac{1}{r} \mathbf{e}_\theta \times \left( v_r \mathbf{e}_\theta + \frac{\partial v_r}{\partial \theta} \mathbf{e}_r - v_\theta \mathbf{e}_r + \frac{\partial v_\theta}{\partial \theta} \mathbf{e}_\theta + \frac{\partial v_z}{\partial \theta} \mathbf{e}_z \right) \\
&\quad + \mathbf{e}_z \times \left( \frac{\partial v_r}{\partial z} \mathbf{e}_r + \frac{\partial v_\theta}{\partial z} \mathbf{e}_\theta + \frac{\partial v_z}{\partial z} \mathbf{e}_z \right) \\
&= \mathbf{e}_r \times \left( \frac{\partial v_\theta}{\partial r} \mathbf{e}_\theta + \frac{\partial v_z}{\partial r} \mathbf{e}_z \right) + \frac{1}{r} \mathbf{e}_\theta \times \left( \frac{\partial v_r}{\partial \theta} \mathbf{e}_r - v_\theta \mathbf{e}_r + \frac{\partial v_z}{\partial \theta} \mathbf{e}_z \right) \\
&\quad + \mathbf{e}_z \times \left( \frac{\partial v_r}{\partial z} \mathbf{e}_r + \frac{\partial v_\theta}{\partial z} \mathbf{e}_\theta \right)
\end{aligned}$$

The vector or cross product of two unit vectors was defined by (C.94), hence in cylindrical coordinates the following relations are valid:

$$\mathbf{e}_r \times \mathbf{e}_\theta = \epsilon_{r\theta\gamma} \mathbf{e}_\gamma = \epsilon_{r\theta z} \mathbf{e}_z = \mathbf{e}_z \quad (\text{C.108})$$

$$\mathbf{e}_r \times \mathbf{e}_z = \epsilon_{rz\theta} \mathbf{e}_\theta = -\mathbf{e}_\theta \quad (\text{C.109})$$

$$\mathbf{e}_\theta \times \mathbf{e}_r = \epsilon_{\theta r z} \mathbf{e}_z = -\mathbf{e}_z \quad (\text{C.110})$$

$$\mathbf{e}_\theta \times \mathbf{e}_z = \epsilon_{\theta z r} \mathbf{e}_r = \mathbf{e}_r \quad (\text{C.111})$$

$$\mathbf{e}_z \times \mathbf{e}_r = \epsilon_{z r \theta} \mathbf{e}_\theta = \mathbf{e}_\theta \quad (\text{C.112})$$

$$\mathbf{e}_z \times \mathbf{e}_\theta = \epsilon_{z \theta r} \mathbf{e}_r = -\mathbf{e}_r \quad (\text{C.113})$$

Introducing these relations into the above expression for the *Curl* operator gives:

$$\begin{aligned}
\text{curl}(\mathbf{v}) &= \frac{\partial v_\theta}{\partial r} \mathbf{e}_z - \frac{\partial v_z}{\partial r} \mathbf{e}_\theta - \frac{1}{r} \frac{\partial v_r}{\partial \theta} \mathbf{e}_z + \frac{v_\theta}{r} \mathbf{e}_z + \frac{1}{r} \frac{\partial v_z}{\partial \theta} \mathbf{e}_r + \frac{\partial v_r}{\partial z} \mathbf{e}_\theta - \frac{\partial v_\theta}{\partial z} \mathbf{e}_r \\
&= \mathbf{e}_r \left( \frac{1}{r} \frac{\partial v_z}{\partial \theta} - \frac{\partial v_\theta}{\partial z} \right) + \mathbf{e}_\theta \left( \frac{\partial v_r}{\partial z} - \frac{\partial v_z}{\partial r} \right) + \mathbf{e}_z \left( \frac{\partial v_\theta}{\partial r} - \frac{1}{r} \frac{\partial v_r}{\partial \theta} + \frac{v_\theta}{r} \right) \\
&= \mathbf{e}_r \left( \frac{1}{r} \frac{\partial v_z}{\partial \theta} - \frac{\partial v_\theta}{\partial z} \right) + \mathbf{e}_\theta \left( \frac{\partial v_r}{\partial z} - \frac{\partial v_z}{\partial r} \right) + \mathbf{e}_z \left( \frac{1}{r} \frac{\partial (r v_\theta)}{\partial r} - \frac{1}{r} \frac{\partial v_r}{\partial \theta} \right)
\end{aligned}$$

### C.2.6 Differential Operators Required for the Two-fluid Model

In this section the governing equations are transformed from vector notation to cylindrical coordinates.

#### Gradient of a scalar

The pressure gradient is one of the gradients of a scalar variable that are part of the equations in question. In cylindrical coordinates it is determined as:

$$\nabla \bar{p} = \frac{\partial \bar{p}}{\partial r} \mathbf{e}_r + \frac{1}{r} \frac{\partial \bar{p}}{\partial \theta} \mathbf{e}_\theta + \frac{\partial \bar{p}}{\partial z} \mathbf{e}_z \quad (\text{C.114})$$

### Divergence of a vector

In all the scalar equations a convective term on the form  $\nabla \cdot (\bar{\alpha}_l \rho_l \bar{\mathbf{v}}_l)$  is included. In cylindrical coordinates this term is expressed as:

$$\nabla \cdot (\bar{\alpha}_l \rho_l \bar{\mathbf{v}}_l) = \frac{1}{r} \frac{\partial}{\partial r} (r \bar{\alpha}_l \rho_l \bar{v}_{l,r}) + \frac{1}{r} \frac{\partial}{\partial \theta} (\bar{\alpha}_l \rho_l \bar{v}_{l,\theta}) + \frac{\partial}{\partial z} (\bar{\alpha}_l \rho_l \bar{v}_{l,z}) \quad (\text{C.115})$$

### Divergence of a gradient

In the scalar equations there are also terms like  $\nabla \cdot (\frac{\mu_{l,t}}{\sigma_t} \nabla \bar{\alpha}_l)$ . This term is identical in form to the previous one, since the gradient is just a vector. In cylindrical coordinates the term is written as:

$$\nabla \cdot (\frac{\mu_{l,t}}{\sigma_t} \nabla \bar{\alpha}_l) = \frac{1}{r} \frac{\partial}{\partial r} (r \frac{\mu_{l,t}}{\sigma_t} \frac{\partial \bar{\alpha}_l}{\partial r}) + \frac{1}{r} \frac{\partial}{\partial \theta} (\frac{\mu_{l,t}}{\sigma_t} \frac{1}{r} \frac{\partial \bar{\alpha}_l}{\partial \theta}) + \frac{\partial}{\partial z} (\frac{\mu_{l,t}}{\sigma_t} \frac{\partial \bar{\alpha}_l}{\partial z}) \quad (\text{C.116})$$

### Divergence of a dyad

Generally, the divergence of a dyad or 2. order tensor, say  $\boldsymbol{\sigma}$ , is transformed as:

$$\begin{aligned} \nabla \cdot \boldsymbol{\sigma} = & \left( \frac{1}{r} \frac{\partial}{\partial r} (r \boldsymbol{\sigma}_{rr}) + \frac{1}{r} \frac{\partial}{\partial \theta} (\boldsymbol{\sigma}_{\theta r}) - \frac{1}{r} \boldsymbol{\sigma}_{\theta\theta} + \frac{\partial}{\partial z} (\boldsymbol{\sigma}_{zr}) \right) \mathbf{e}_r \\ & + \left( \frac{1}{r} \frac{\partial}{\partial \theta} (\boldsymbol{\sigma}_{\theta\theta}) + \frac{1}{r} \frac{\partial}{\partial r} (r \boldsymbol{\sigma}_{r\theta}) + \frac{1}{r} \boldsymbol{\sigma}_{\theta r} + \frac{\partial}{\partial z} (\boldsymbol{\sigma}_{z\theta}) \right) \mathbf{e}_\theta \\ & + \left( \frac{1}{r} \frac{\partial}{\partial r} (r \boldsymbol{\sigma}_{rz}) + \frac{1}{r} \frac{\partial}{\partial \theta} (\boldsymbol{\sigma}_{\theta z}) + \frac{\partial}{\partial z} (\boldsymbol{\sigma}_{zz}) \right) \mathbf{e}_z \end{aligned} \quad (\text{C.117})$$

The dyad  $\bar{\mathbf{v}} \bar{\mathbf{v}}$  is symmetric. In cylindrical coordinates  $\nabla \cdot (\bar{\alpha} \rho \bar{\mathbf{v}} \bar{\mathbf{v}})$  is given as:

$$\begin{aligned} \nabla \cdot (\bar{\alpha} \rho \bar{\mathbf{v}} \bar{\mathbf{v}}) = & \left( \frac{1}{r} \frac{\partial}{\partial r} (r \bar{\alpha} \rho \bar{v}_r \bar{v}_r) + \frac{1}{r} \frac{\partial}{\partial \theta} (\bar{\alpha} \rho \bar{v}_\theta \bar{v}_r) - \frac{1}{r} \bar{\alpha} \rho \bar{v}_\theta \bar{v}_\theta + \frac{\partial}{\partial z} (\bar{\alpha} \rho \bar{v}_z \bar{v}_r) \right) \mathbf{e}_r \\ & + \left( \frac{1}{r} \frac{\partial}{\partial \theta} (\bar{\alpha} \rho \bar{v}_\theta \bar{v}_\theta) + \frac{1}{r} \frac{\partial}{\partial r} (r \bar{\alpha} \rho \bar{v}_r \bar{v}_\theta) + \frac{1}{r} \bar{\alpha} \rho \bar{v}_\theta \bar{v}_r + \frac{\partial}{\partial z} (\bar{\alpha} \rho \bar{v}_z \bar{v}_\theta) \right) \mathbf{e}_\theta \\ & + \left( \frac{1}{r} \frac{\partial}{\partial r} (r \bar{\alpha} \rho \bar{v}_r \bar{v}_z) + \frac{1}{r} \frac{\partial}{\partial \theta} (\bar{\alpha} \rho \bar{v}_\theta \bar{v}_z) + \frac{\partial}{\partial z} (\bar{\alpha} \rho \bar{v}_z \bar{v}_z) \right) \mathbf{e}_z \end{aligned} \quad (\text{C.118})$$

The terms similar to  $\nabla \cdot (\frac{\mu_{l,t}}{\sigma_{\alpha,t}} \nabla \bar{\alpha} \bar{\mathbf{v}})$  are also divergences of a dyad.  $\nabla \bar{\alpha} \bar{\mathbf{v}}$  is not symmetric.

$$\begin{aligned}
\nabla \cdot (\frac{\mu_{l,t}}{\sigma_{\alpha,t}} \nabla \bar{\alpha} \bar{\mathbf{v}}) = & \\
& \left( \frac{1}{r} \frac{\partial}{\partial r} (r \frac{\mu_{l,t}}{\sigma_{\alpha,t}} \frac{\partial \bar{\alpha}}{\partial r} \bar{v}_r) + \frac{1}{r} \frac{\partial}{\partial \theta} (\frac{\mu_{l,t}}{\sigma_{\alpha,t}} \frac{1}{r} \frac{\partial \bar{\alpha}}{\partial \theta} \bar{v}_r) - \frac{\mu_{l,t}}{\sigma_{\alpha,t}} \frac{1}{r^2} \frac{\partial \bar{\alpha}}{\partial \theta} \bar{v}_\theta + \frac{\partial}{\partial z} (\frac{\mu_{l,t}}{\sigma_{\alpha,t}} \frac{\partial \bar{\alpha}}{\partial z} \bar{v}_r) \right) \mathbf{e}_r \\
& + \left( \frac{1}{r} \frac{\partial}{\partial \theta} (\frac{\mu_{l,t}}{\sigma_{\alpha,t}} \frac{1}{r} \frac{\partial \bar{\alpha}}{\partial \theta} \bar{v}_\theta) + \frac{1}{r} \frac{\partial}{\partial r} (r \frac{\mu_{l,t}}{\sigma_{\alpha,t}} \frac{\partial \bar{\alpha}}{\partial r} \bar{v}_\theta) + \frac{\mu_{l,t}}{\sigma_{\alpha,t}} \frac{1}{r^2} \frac{\partial \bar{\alpha}}{\partial \theta} \bar{v}_r + \frac{\partial}{\partial z} (\frac{\mu_{l,t}}{\sigma_{\alpha,t}} \frac{\partial \bar{\alpha}}{\partial z} \bar{v}_\theta) \right) \mathbf{e}_\theta \\
& + \left( \frac{1}{r} \frac{\partial}{\partial r} (r \frac{\mu_{l,t}}{\sigma_{\alpha,t}} \frac{\partial \bar{\alpha}}{\partial r} \bar{v}_z) + \frac{1}{r} \frac{\partial}{\partial \theta} (\frac{\mu_{l,t}}{\sigma_{\alpha,t}} \frac{1}{r} \frac{\partial \bar{\alpha}}{\partial \theta} \bar{v}_z) + \frac{\partial}{\partial z} (\frac{\mu_{l,t}}{\sigma_{\alpha,t}} \frac{\partial \bar{\alpha}}{\partial z} \bar{v}_z) \right) \mathbf{e}_z
\end{aligned} \tag{C.119}$$

The term  $\nabla \cdot (\frac{\mu_{l,t}}{\sigma_{\alpha,t}} \bar{\mathbf{v}} \nabla \bar{\alpha})$  is very similar to the previous one:

$$\begin{aligned}
\nabla \cdot (\frac{\mu_{l,t}}{\sigma_{\alpha,t}} \bar{\mathbf{v}} \nabla \bar{\alpha}) = & \\
& \left( \frac{1}{r} \frac{\partial}{\partial r} (r \frac{\mu_{l,t}}{\sigma_{\alpha,t}} \bar{v}_r \frac{\partial \bar{\alpha}}{\partial r}) + \frac{1}{r} \frac{\partial}{\partial \theta} (\frac{\mu_{l,t}}{\sigma_{\alpha,t}} \bar{v}_\theta \frac{\partial \bar{\alpha}}{\partial r}) - \frac{\mu_{l,t}}{\sigma_{\alpha,t}} \frac{1}{r^2} \bar{v}_\theta \frac{\partial \bar{\alpha}}{\partial \theta} + \frac{\partial}{\partial z} (\frac{\mu_{l,t}}{\sigma_{\alpha,t}} \bar{v}_z \frac{\partial \bar{\alpha}}{\partial r}) \right) \mathbf{e}_r \\
& + \left( \frac{1}{r} \frac{\partial}{\partial \theta} (\frac{\mu_{l,t}}{\sigma_{\alpha,t}} \bar{v}_\theta \frac{1}{r} \frac{\partial \bar{\alpha}}{\partial \theta}) + \frac{\partial}{\partial r} (\frac{\mu_{l,t}}{\sigma_{\alpha,t}} \bar{v}_r \frac{1}{r} \frac{\partial \bar{\alpha}}{\partial \theta}) + \frac{1}{r^2} \frac{\mu_{l,t}}{\sigma_{\alpha,t}} \bar{v}_r \frac{\partial \bar{\alpha}}{\partial \theta} + \frac{\mu_{l,t}}{\sigma_{\alpha,t}} \frac{1}{r} \bar{v}_\theta \frac{\partial \bar{\alpha}}{\partial r} \right. \\
& \quad \left. + \frac{\partial}{\partial z} (\frac{\mu_{l,t}}{\sigma_{\alpha,t}} \bar{v}_z \frac{1}{r} \frac{\partial \bar{\alpha}}{\partial \theta}) \right) \mathbf{e}_\theta \\
& + \left( \frac{1}{r} \frac{\partial}{\partial r} (r \frac{\mu_{l,t}}{\sigma_{\alpha,t}} \bar{v}_r \frac{\partial \bar{\alpha}}{\partial z}) + \frac{1}{r} \frac{\partial}{\partial \theta} (\frac{\mu_{l,t}}{\sigma_{\alpha,t}} \bar{v}_\theta \frac{\partial \bar{\alpha}}{\partial z}) + \frac{\partial}{\partial z} (\frac{\mu_{l,t}}{\sigma_{\alpha,t}} \bar{v}_z \frac{\partial \bar{\alpha}}{\partial z}) \right) \mathbf{e}_z
\end{aligned} \tag{C.120}$$

In cylindrical coordinates the term  $\nabla \cdot (\bar{\alpha} \mu \nabla \bar{\mathbf{v}})$  is expressed as:

$$\begin{aligned}
\nabla \cdot (\bar{\alpha} \mu \nabla \bar{\mathbf{v}}) = & \\
& \left( \frac{1}{r} \frac{\partial}{\partial r} (r \bar{\alpha} \mu \frac{\partial \bar{v}_r}{\partial r}) + \frac{1}{r} \frac{\partial}{\partial \theta} (\bar{\alpha} \mu (\frac{1}{r} \frac{\partial \bar{v}_r}{\partial \theta} - \frac{\bar{v}_\theta}{r})) - \frac{1}{r} \bar{\alpha} \mu (\frac{1}{r} \frac{\partial \bar{v}_\theta}{\partial \theta} + \frac{\bar{v}_r}{r}) \right. \\
& \quad \left. + \frac{\partial}{\partial z} (\bar{\alpha} \mu \frac{\partial \bar{v}_r}{\partial z}) \right) \mathbf{e}_r \\
& + \left( \frac{1}{r} \frac{\partial}{\partial \theta} (\bar{\alpha} \mu (\frac{1}{r} \frac{\partial \bar{v}_\theta}{\partial \theta} + \frac{\bar{v}_r}{r})) + \frac{1}{r} \bar{\alpha} \mu (\frac{1}{r} \frac{\partial \bar{v}_r}{\partial \theta} - \frac{\bar{v}_\theta}{r}) + \frac{1}{r} \frac{\partial}{\partial r} (r \bar{\alpha} \mu \frac{\partial \bar{v}_\theta}{\partial r}) \right. \\
& \quad \left. + \frac{\partial}{\partial z} (\bar{\alpha} \mu \frac{\partial \bar{v}_\theta}{\partial z}) \right) \mathbf{e}_\theta \\
& + \left( \frac{1}{r} \frac{\partial}{\partial r} (r \bar{\alpha} \mu \frac{\partial \bar{v}_z}{\partial r}) + \frac{1}{r} \frac{\partial}{\partial \theta} (\bar{\alpha} \mu \frac{\partial \bar{v}_z}{\partial \theta}) + \frac{\partial}{\partial z} (\bar{\alpha} \mu \frac{\partial \bar{v}_z}{\partial z}) \right) \mathbf{e}_z
\end{aligned} \tag{C.121}$$

The divergence of the transpose of the gradient of a vector  $\nabla(\bar{\alpha}\mu(\nabla\bar{\mathbf{v}})^T)$  in cylindrical coordinates is written:

$$\begin{aligned} \nabla \cdot (\bar{\alpha}\mu(\nabla\bar{\mathbf{v}})^T) = & \\ & \left( \frac{1}{r} \frac{\partial}{\partial r} (r\bar{\alpha}\mu \frac{\partial\bar{v}_r}{\partial r}) + \frac{1}{r} \frac{\partial}{\partial\theta} (\bar{\alpha}\mu \frac{\partial\bar{v}_\theta}{\partial r}) - \frac{1}{r} \bar{\alpha}\mu \left( \frac{1}{r} \frac{\partial\bar{v}_\theta}{\partial\theta} + \frac{\bar{v}_r}{r} \right) + \frac{\partial}{\partial z} (\bar{\alpha}\mu \frac{\partial\bar{v}_z}{\partial r}) \right) \mathbf{e}_r \\ & + \left( \frac{1}{r} \frac{\partial}{\partial r} (r\bar{\alpha}\mu \left( \frac{1}{r} \frac{\partial\bar{v}_r}{\partial\theta} - \frac{\bar{v}_\theta}{r} \right)) + \frac{1}{r} \frac{\partial}{\partial\theta} (\bar{\alpha}\mu \left( \frac{1}{r} \frac{\partial\bar{v}_\theta}{\partial\theta} + \frac{\bar{v}_r}{r} \right)) + \frac{1}{r} \bar{\alpha}\mu \frac{\partial\bar{v}_\theta}{\partial r} \right. \\ & \quad \left. + \frac{\partial}{\partial z} (\bar{\alpha}\mu \frac{1}{r} \frac{\partial\bar{v}_z}{\partial\theta}) \right) \mathbf{e}_\theta \\ & + \left( \frac{1}{r} \frac{\partial}{\partial r} (r\bar{\alpha}\mu \frac{\partial\bar{v}_r}{\partial z}) + \frac{1}{r} \frac{\partial}{\partial\theta} (\bar{\alpha}\mu \frac{\partial\bar{v}_\theta}{\partial z}) + \frac{\partial}{\partial z} (\bar{\alpha}\mu \frac{\partial\bar{v}_z}{\partial z}) \right) \mathbf{e}_z \end{aligned} \quad (\text{C.122})$$

### Gradient of a vector

The gradient of  $\bar{\mathbf{v}}$  is part of the momentum equations. In cylindrical coordinates it is expressed as:

$$\begin{aligned} \nabla\bar{\mathbf{v}} = & \frac{\partial\bar{v}_r}{\partial r} \mathbf{e}_r \mathbf{e}_r + \frac{\partial\bar{v}_\theta}{\partial r} \mathbf{e}_r \mathbf{e}_\theta + \frac{\partial\bar{v}_z}{\partial r} \mathbf{e}_r \mathbf{e}_z \\ & + \left( \frac{1}{r} \frac{\partial\bar{v}_r}{\partial\theta} - \frac{\bar{v}_\theta}{r} \right) \mathbf{e}_\theta \mathbf{e}_r + \left( \frac{1}{r} \frac{\partial\bar{v}_\theta}{\partial\theta} + \frac{\bar{v}_r}{r} \right) \mathbf{e}_\theta \mathbf{e}_\theta + \frac{1}{r} \frac{\partial\bar{v}_z}{\partial\theta} \mathbf{e}_\theta \mathbf{e}_z \\ & + \frac{\partial\bar{v}_r}{\partial z} \mathbf{e}_z \mathbf{e}_r + \frac{\partial\bar{v}_\theta}{\partial z} \mathbf{e}_z \mathbf{e}_\theta + \frac{\partial\bar{v}_z}{\partial z} \mathbf{e}_z \mathbf{e}_z \end{aligned} \quad (\text{C.123})$$

### The dot product $\nabla\bar{\alpha} \cdot \nabla\bar{\mathbf{v}}$

In cylindrical coordinates this term is written as:

$$\begin{aligned} \nabla\bar{\alpha} \cdot \nabla\bar{\mathbf{v}} = & \left( \frac{\partial\bar{\alpha}}{\partial r} \frac{\partial\bar{v}_r}{\partial r} + \frac{1}{r} \frac{\partial\bar{\alpha}}{\partial\theta} \left( \frac{1}{r} \frac{\partial\bar{v}_r}{\partial\theta} - \frac{\bar{v}_\theta}{r} \right) + \frac{\partial\bar{\alpha}}{\partial z} \frac{\partial\bar{v}_r}{\partial z} \right) \mathbf{e}_r \\ & + \left( \frac{\partial\bar{\alpha}}{\partial r} \frac{\partial\bar{v}_\theta}{\partial r} + \frac{1}{r} \frac{\partial\bar{\alpha}}{\partial\theta} \left( \frac{1}{r} \frac{\partial\bar{v}_\theta}{\partial\theta} + \frac{\bar{v}_r}{r} \right) + \frac{\partial\bar{\alpha}}{\partial z} \frac{\bar{v}_\theta}{z} \right) \mathbf{e}_\theta \\ & + \left( \frac{\partial\bar{\alpha}}{\partial r} \frac{\partial\bar{v}_z}{\partial r} + \frac{1}{r} \frac{\partial\bar{\alpha}}{\partial\theta} \frac{1}{r} \frac{\partial\bar{v}_z}{\partial\theta} + \frac{\partial\bar{\alpha}}{\partial z} \frac{\partial\bar{v}_z}{\partial z} \right) \mathbf{e}_z \end{aligned} \quad (\text{C.124})$$

### The dot product $\bar{\mathbf{v}} \cdot \nabla \left( \frac{\mu_{l,t}}{\sigma_{\alpha,t}} \nabla \bar{\alpha} \right)$

In cylindrical coordinates this term is written as:

$$\begin{aligned}
 & \bar{\mathbf{v}} \cdot \nabla \left( \frac{\mu_{l,t}}{\sigma_{\alpha,t}} \nabla \bar{\alpha} \right) \\
 &= \left( \bar{v}_r \frac{\partial}{\partial r} \left( \frac{\mu_{l,t}}{\sigma_{\alpha,t}} \frac{\partial \bar{\alpha}}{\partial r} \right) + \bar{v}_\theta \frac{1}{r} \frac{\partial}{\partial \theta} \left( \frac{\mu_{l,t}}{\sigma_{\alpha,t}} \frac{\partial \bar{\alpha}}{\partial r} \right) - \bar{v}_\theta \frac{1}{r^2} \frac{\mu_{l,t}}{\sigma_{\alpha,t}} \frac{\partial \bar{\alpha}}{\partial \theta} + \bar{v}_z \frac{\partial}{\partial z} \left( \frac{\mu_{l,t}}{\sigma_{\alpha,t}} \frac{\partial \bar{\alpha}}{\partial r} \right) \right) \mathbf{e}_r \\
 &+ \left( \bar{v}_r \frac{\partial}{\partial r} \left( \frac{\mu_{l,t}}{\sigma_{\alpha,t}} \frac{1}{r} \frac{\partial \bar{\alpha}}{\partial \theta} \right) + \bar{v}_\theta \frac{1}{r} \frac{\mu_{l,t}}{\sigma_{\alpha,t}} \frac{\partial \bar{\alpha}}{\partial r} + \bar{v}_\theta \frac{1}{r} \frac{\partial}{\partial \theta} \left( \frac{\mu_{l,t}}{\sigma_{\alpha,t}} \frac{1}{r} \frac{\partial \bar{\alpha}}{\partial \theta} \right) + \bar{v}_z \frac{\partial}{\partial z} \left( \frac{\mu_{l,t}}{\sigma_{\alpha,t}} \frac{1}{r} \frac{\partial \bar{\alpha}}{\partial \theta} \right) \right) \mathbf{e}_\theta \\
 &+ \left( \bar{v}_r \frac{\partial}{\partial r} \left( \frac{\mu_{l,t}}{\sigma_{\alpha,t}} \frac{\partial \bar{\alpha}}{\partial z} \right) + \bar{v}_\theta \frac{1}{r} \frac{\partial}{\partial \theta} \left( \frac{\mu_{l,t}}{\sigma_{\alpha,t}} \frac{\partial \bar{\alpha}}{\partial z} \right) + \bar{v}_z \frac{\partial}{\partial z} \left( \frac{\mu_{l,t}}{\sigma_{\alpha,t}} \frac{\partial \bar{\alpha}}{\partial z} \right) \right) \mathbf{e}_z
 \end{aligned} \tag{C.125}$$

## C.3 Two-Fluid Equations in Cylindrical Coordinates

By use of the transformations defined above, the governing 3D equations are written in cylindrical coordinates.

### Liquid Phase Continuity Equation in Cylindrical Coordinates

$$\begin{aligned}
 & \frac{\partial}{\partial t} (\bar{\alpha}_l \rho_l) + \frac{1}{r} \frac{\partial}{\partial r} (r \bar{\alpha}_l \rho_l \bar{v}_{l,r}) + \frac{1}{r} \frac{\partial}{\partial \theta} (\bar{\alpha}_l \rho_l \bar{v}_{l,\theta}) + \frac{\partial}{\partial z} (\bar{\alpha}_l \rho_l \bar{v}_{l,z}) = \\
 & \frac{1}{r} \frac{\partial}{\partial r} \left( r \frac{\mu_{l,t}}{\sigma_{\alpha,t}} \frac{\partial \bar{\alpha}_l}{\partial r} \right) + \frac{1}{r} \frac{\partial}{\partial \theta} \left( \frac{\mu_{l,t}}{\sigma_{\alpha,t}} \frac{\partial \bar{\alpha}_l}{\partial \theta} \right) + \frac{\partial}{\partial z} \left( \frac{\mu_{l,t}}{\sigma_{\alpha,t}} \frac{\partial \bar{\alpha}_l}{\partial z} \right)
 \end{aligned} \tag{C.126}$$

### Liquid Phase Radial Momentum Balance in Cylindrical Coordinates

$$\begin{aligned}
 & \frac{\partial}{\partial t} (\bar{\alpha}_l \rho_l \bar{v}_{l,r}) \\
 &+ \frac{1}{r} \frac{\partial}{\partial r} (r \bar{\alpha}_l \rho_l \bar{v}_{l,r} \bar{v}_{l,r}) + \frac{1}{r} \frac{\partial}{\partial \theta} (\bar{\alpha}_l \rho_l \bar{v}_{l,\theta} \bar{v}_{l,r}) - \frac{1}{r} \bar{\alpha}_l \rho_l \bar{v}_{l,\theta} \bar{v}_{l,\theta} + \frac{\partial}{\partial z} (\bar{\alpha}_l \rho_l \bar{v}_{l,z} \bar{v}_{l,r}) = \\
 & \frac{1}{r} \frac{\partial}{\partial r} \left( r \frac{\mu_{l,t}}{\sigma_{\alpha,t}} \frac{\partial \bar{\alpha}_l}{\partial r} \bar{v}_{l,r} \right) + \frac{1}{r} \frac{\partial}{\partial \theta} \left( \frac{\mu_{l,t}}{\sigma_{\alpha,t}} \frac{1}{r} \frac{\partial \bar{\alpha}_l}{\partial \theta} \bar{v}_{l,r} \right) - \frac{1}{r^2} \frac{\mu_{l,t}}{\sigma_{\alpha,t}} \frac{\partial \bar{\alpha}_l}{\partial \theta} \bar{v}_{l,\theta} \\
 &+ \frac{\partial}{\partial z} \left( \frac{\mu_{l,t}}{\sigma_{\alpha,t}} \bar{v}_{l,r} \frac{\partial \bar{\alpha}_l}{\partial z} \right) + \frac{1}{r} \frac{\partial}{\partial r} \left( r \frac{\mu_{l,t}}{\sigma_{\alpha,t}} \frac{\partial \bar{\alpha}_l}{\partial r} \bar{v}_{l,r} \right) + \frac{1}{r} \frac{\partial}{\partial \theta} \left( \frac{\mu_{l,t}}{\sigma_{\alpha,t}} \bar{v}_{l,\theta} \frac{\partial \bar{\alpha}_l}{\partial r} \right)
 \end{aligned}$$

$$\begin{aligned}
& -\frac{1}{r^2} \frac{\mu_{l,t}}{\sigma_{\alpha_{l,t}}} \bar{v}_{l,\theta} \frac{\partial \bar{\alpha}_l}{\partial \theta} + \frac{\partial}{\partial z} \left( \frac{\mu_{l,t}}{\sigma_{\alpha_{l,t}}} v_{l,z} \frac{\partial \bar{\alpha}_l}{\partial r} \right) + \frac{1}{r} \frac{\partial}{\partial r} \left( r \bar{\alpha}_l \mu_{l,\text{eff}} \frac{\partial \bar{v}_{l,r}}{\partial r} \right) \\
& + \frac{1}{r} \frac{\partial}{\partial \theta} \left( \bar{\alpha}_l \mu_{l,\text{eff}} \left( \frac{1}{r} \frac{\partial \bar{v}_{l,r}}{\partial \theta} - \frac{\bar{v}_{l,\theta}}{r} \right) \right) - \frac{1}{r} \bar{\alpha}_l \mu_{l,\text{eff}} \left( \frac{1}{r} \frac{\partial \bar{v}_{l,\theta}}{\partial \theta} \right. \\
& + \left. \frac{\bar{v}_{l,r}}{r} \right) + \frac{\partial}{\partial z} \left( \bar{\alpha}_l \mu_{l,\text{eff}} \frac{\partial \bar{v}_{l,r}}{\partial z} \right) + \frac{1}{r} \frac{\partial}{\partial r} \left( r \bar{\alpha}_l \mu_{l,\text{eff}} \frac{\partial \bar{v}_{l,r}}{\partial r} \right) + \frac{1}{r} \frac{\partial}{\partial \theta} \left( \bar{\alpha}_l \mu_{l,\text{eff}} \frac{\partial \bar{v}_{l,\theta}}{\partial r} \right) \\
& - \frac{1}{r} \bar{\alpha}_l \mu_{l,\text{eff}} \left( \frac{1}{r} \frac{\partial \bar{v}_{l,\theta}}{\partial \theta} + \frac{\bar{v}_{l,r}}{r} \right) + \frac{\partial}{\partial z} \left( \bar{\alpha}_l \mu_{l,\text{eff}} \frac{\partial \bar{v}_{l,z}}{\partial r} \right) \\
& - \frac{\partial}{\partial r} \left( \frac{2}{3} \bar{\alpha}_l \rho_l (k + \nu_{l,\text{eff}} \left( \frac{1}{r} \frac{\partial}{\partial r} (r \bar{v}_{l,r}) + \frac{1}{r} \frac{\partial \bar{v}_{l,\theta}}{\partial \theta} + \frac{\partial \bar{v}_{l,z}}{\partial z} \right)) \right) \\
& - \bar{\alpha}_l \frac{\partial \bar{p}}{\partial r} - \frac{\mu_{l,t}}{\sigma_{\alpha_{l,t}}} \left( \frac{\partial \bar{\alpha}_l}{\partial r} \frac{\partial \bar{v}_{l,r}}{\partial r} + \frac{1}{r} \frac{\partial \bar{\alpha}_l}{\partial \theta} \left( \frac{1}{r} \frac{\partial \bar{v}_{l,r}}{\partial \theta} - \frac{\bar{v}_{l,\theta}}{r} \right) + \frac{\partial \bar{\alpha}_l}{\partial z} \frac{\partial \bar{v}_{l,r}}{\partial z} \right) \\
& - \bar{v}_{l,r} \frac{\partial}{\partial r} \left( \frac{\mu_{l,t}}{\sigma_{\alpha_{l,t}}} \frac{\partial \bar{\alpha}_l}{\partial r} \right) - \bar{v}_{l,\theta} \frac{1}{r} \frac{\partial}{\partial \theta} \left( \frac{\mu_{l,t}}{\sigma_{\alpha_{l,t}}} \frac{\partial \bar{\alpha}_l}{\partial r} \right) + \bar{v}_{l,\theta} \frac{1}{r^2} \frac{\mu_{l,t}}{\sigma_{\alpha_{l,t}}} \frac{\partial \bar{\alpha}_l}{\partial \theta} \\
& - \bar{v}_{l,z} \frac{\partial}{\partial z} \left( \frac{\mu_{l,t}}{\sigma_{\alpha_{l,t}}} \frac{\partial \bar{\alpha}_l}{\partial r} \right) + \bar{\alpha}_l \rho_l g_r + \overline{F_{l,r}^C} + \overline{F_{l,r}^{C'}}
\end{aligned} \tag{C.127}$$

### Liquid Phase Azimuthal Momentum Balance in Cylindrical Coordinates

$$\begin{aligned}
& \frac{\partial}{\partial t} (\bar{\alpha}_l \rho_l \bar{v}_{l,\theta}) \\
& + \frac{1}{r} \frac{\partial}{\partial r} (r \bar{\alpha}_l \rho_l \bar{v}_{l,r} \bar{v}_{l,\theta}) + \frac{1}{r} \frac{\partial}{\partial \theta} (\bar{\alpha}_l \rho_l \bar{v}_{l,\theta} \bar{v}_{l,\theta}) + \frac{1}{r} \bar{\alpha}_l \rho_l \bar{v}_{l,\theta} \bar{v}_{l,r} + \frac{\partial}{\partial z} (\bar{\alpha}_l \rho_l \bar{v}_{l,z} \bar{v}_{l,\theta}) = \\
& \frac{1}{r} \frac{\partial}{\partial r} \left( r \frac{\mu_{l,t}}{\sigma_{\alpha_{l,t}}} \frac{\partial \bar{\alpha}_l}{\partial r} \bar{v}_{l,\theta} \right) + \frac{\mu_{l,t}}{\sigma_{\alpha_{l,t}}} \frac{1}{r^2} \frac{\partial \bar{\alpha}_l}{\partial \theta} \bar{v}_{l,r} + \frac{1}{r} \frac{\partial}{\partial \theta} \left( \frac{\mu_{l,t}}{\sigma_{\alpha_{l,t}}} \frac{1}{r} \frac{\partial \bar{\alpha}_l}{\partial \theta} \bar{v}_{l,\theta} \right) \\
& + \frac{\partial}{\partial z} \left( \frac{\mu_{l,t}}{\sigma_{\alpha_{l,t}}} \bar{v}_{l,\theta} \frac{\partial \bar{\alpha}_l}{\partial z} \right) + \frac{\partial}{\partial r} \left( \frac{\mu_{l,t}}{\sigma_{\alpha_{l,t}}} \frac{1}{r} \frac{\partial \bar{\alpha}_l}{\partial \theta} \bar{v}_{l,r} \right) + \frac{1}{r^2} \frac{\mu_{l,t}}{\sigma_{\alpha_{l,t}}} \bar{v}_{l,r} \frac{\partial \bar{\alpha}_l}{\partial \theta} + \frac{1}{r} \frac{\mu_{l,t}}{\sigma_{\alpha_{l,t}}} \bar{v}_{l,\theta} \frac{\partial \bar{\alpha}_l}{\partial r} \\
& + \frac{1}{r} \frac{\partial}{\partial \theta} \left( \frac{\mu_{l,t}}{\sigma_{\alpha_{l,t}}} \bar{v}_{l,\theta} \frac{1}{r} \frac{\partial \bar{\alpha}_l}{\partial \theta} \right) + \frac{\partial}{\partial z} \left( \frac{\mu_{l,t}}{\sigma_{\alpha_{l,t}}} \bar{v}_{l,z} \frac{1}{r} \frac{\partial \bar{\alpha}_l}{\partial \theta} \right) + \frac{1}{r} \frac{\partial}{\partial r} \left( r \bar{\alpha}_l \mu_{l,\text{eff}} \frac{\partial \bar{v}_{l,\theta}}{\partial r} \right) \\
& + \frac{1}{r} \frac{\partial}{\partial \theta} \left( \bar{\alpha}_l \mu_{l,\text{eff}} \left( \frac{1}{r} \frac{\partial \bar{v}_{l,\theta}}{\partial \theta} + \frac{\bar{v}_{l,r}}{r} \right) \right) + \frac{1}{r} \bar{\alpha}_l \mu_{l,\text{eff}} \left( \frac{1}{r} \frac{\partial \bar{v}_{l,r}}{\partial \theta} - \frac{\bar{v}_{l,\theta}}{r} \right) + \frac{\partial}{\partial z} \left( \bar{\alpha}_l \mu_{l,\text{eff}} \frac{\partial \bar{v}_{l,\theta}}{\partial z} \right) \\
& + \frac{1}{r} \frac{\partial}{\partial r} \left( r \bar{\alpha}_l \mu_{l,\text{eff}} \left( \frac{1}{r} \frac{\partial \bar{v}_{l,r}}{\partial \theta} - \frac{\bar{v}_{l,\theta}}{r} \right) \right) + \frac{1}{r} \frac{\partial}{\partial \theta} \left( \bar{\alpha}_l \mu_{l,\text{eff}} \left( \frac{1}{r} \frac{\partial \bar{v}_{l,\theta}}{\partial \theta} + \frac{\bar{v}_{l,r}}{r} \right) \right) + \frac{\bar{\alpha}_l \mu_{l,\text{eff}}}{r} \frac{\partial \bar{v}_{l,\theta}}{\partial r}
\end{aligned}$$

$$\begin{aligned}
 & + \frac{\partial}{\partial z} (\bar{\alpha}_l \mu_{l,\text{eff}} \frac{1}{r} \frac{\partial \bar{v}_{l,z}}{\partial \theta}) - \frac{\partial}{\partial \theta} (\frac{2}{3} \bar{\alpha}_l \rho_l (k + \nu_{l,\text{eff}} (\frac{1}{r} \frac{\partial}{\partial r} (r \bar{v}_{l,r}) + \frac{1}{r} \frac{\partial \bar{v}_{l,\theta}}{\partial \theta} + \frac{\partial \bar{v}_{l,z}}{\partial z}))) \\
 & - \bar{\alpha}_l \frac{\partial \bar{p}}{\partial \theta} - \frac{\mu_{l,t}}{\sigma_{\alpha_{l,t}}} (\frac{\partial \bar{\alpha}_l}{\partial r} \frac{\partial \bar{v}_{l,\theta}}{\partial r} + \frac{1}{r} \frac{\partial \bar{\alpha}_l}{\partial \theta} (\frac{1}{r} \frac{\partial \bar{v}_{l,\theta}}{\partial \theta} + \bar{v}_{l,r}) + \frac{\partial \bar{\alpha}_l}{\partial z} \frac{\partial \bar{v}_{l,\theta}}{\partial z}) \\
 & - \bar{v}_{l,r} \frac{\partial}{\partial r} (\frac{\mu_{l,t}}{\sigma_{\alpha_{l,t}}} \frac{1}{r} \frac{\partial \bar{\alpha}_l}{\partial \theta}) - \bar{v}_{l,\theta} \frac{1}{r} \frac{\mu_{l,t}}{\sigma_{\alpha_{l,t}}} \frac{\partial \bar{\alpha}_l}{\partial r} - \bar{v}_{l,\theta} \frac{1}{r} \frac{\partial}{\partial \theta} (\frac{\mu_{l,t}}{\sigma_{\alpha_{l,t}}} \frac{1}{r} \frac{\partial \bar{\alpha}_l}{\partial \theta}) \\
 & - \bar{v}_{l,z} \frac{\partial}{\partial z} (\frac{\mu_{l,t}}{\sigma_{\alpha_{l,t}}} \frac{1}{r} \frac{\partial \bar{\alpha}_l}{\partial \theta}) + \bar{\alpha}_l \rho_l g_r + \overline{F_{l,\theta}^C} + \overline{F_{l,\theta}^{C'}}
 \end{aligned} \tag{C.128}$$

### Liquid Phase Axial Momentum Balance in Cylindrical Coordinates

$$\begin{aligned}
 & \frac{\partial}{\partial t} (\bar{\alpha}_l \rho_l \bar{v}_{l,z}) + \frac{1}{r} \frac{\partial}{\partial r} (r \bar{\alpha}_l \rho_l \bar{v}_{l,r} \bar{v}_{l,z}) + \frac{1}{r} \frac{\partial}{\partial \theta} (\bar{\alpha}_l \rho_l \bar{v}_{l,\theta} \bar{v}_{l,z}) + \frac{\partial}{\partial z} (\bar{\alpha}_l \rho_l \bar{v}_{l,z} \bar{v}_{l,z}) = \\
 & \frac{1}{r} \frac{\partial}{\partial r} (r \frac{\mu_{l,t}}{\sigma_{\alpha_{l,t}}} \frac{\partial \bar{\alpha}_l}{\partial r} \bar{v}_{l,z}) + \frac{1}{r} \frac{\partial}{\partial \theta} (\frac{\mu_{l,t}}{\sigma_{\alpha_{l,t}}} \frac{1}{r} \frac{\partial \bar{\alpha}_l}{\partial \theta} \bar{v}_{l,z}) + \frac{\partial}{\partial z} (\frac{\mu_{l,t}}{\sigma_{\alpha_{l,t}}} \frac{\partial \bar{\alpha}_l}{\partial z} \bar{v}_{l,z}) \\
 & + \frac{1}{r} \frac{\partial}{\partial r} (r \frac{\mu_{l,t}}{\sigma_{\alpha_{l,t}}} \frac{\partial \bar{\alpha}_l}{\partial z} \bar{v}_{l,r}) + \frac{1}{r} \frac{\partial}{\partial \theta} (\frac{\mu_{l,t}}{\sigma_{\alpha_{l,t}}} \frac{\partial \bar{\alpha}_l}{\partial z} \bar{v}_{l,\theta}) + \frac{\partial}{\partial z} (\frac{\mu_{l,t}}{\sigma_{\alpha_{l,t}}} \frac{\partial \bar{\alpha}_l}{\partial z} \bar{v}_{l,z}) \\
 & + \frac{1}{r} \frac{\partial}{\partial r} (r \bar{\alpha}_l \mu_{l,\text{eff}} \frac{\partial \bar{v}_{l,z}}{\partial r}) + \frac{1}{r} \frac{\partial}{\partial \theta} (\bar{\alpha}_l \mu_{l,\text{eff}} \frac{\partial \bar{v}_{l,z}}{\partial \theta}) + \frac{\partial}{\partial z} (\bar{\alpha}_l \mu_{l,\text{eff}} \frac{\partial \bar{v}_{l,z}}{\partial z}) \\
 & + \frac{1}{r} \frac{\partial}{\partial r} (r \bar{\alpha}_l \mu_{l,\text{eff}} \frac{\partial \bar{v}_{l,r}}{\partial z}) + \frac{1}{r} \frac{\partial}{\partial \theta} (\bar{\alpha}_l \mu_{l,\text{eff}} \frac{\partial \bar{v}_{l,\theta}}{\partial z}) + \frac{\partial}{\partial z} (\bar{\alpha}_l \mu_{l,\text{eff}} \frac{\partial \bar{v}_{l,z}}{\partial z}) \\
 & - \frac{\partial}{\partial z} (\frac{2}{3} \bar{\alpha}_l \rho_l (k + \nu_{l,\text{eff}} (\frac{1}{r} \frac{\partial}{\partial r} (r \bar{v}_{l,r}) + \frac{1}{r} \frac{\partial \bar{v}_{l,\theta}}{\partial \theta} + \frac{\partial \bar{v}_{l,z}}{\partial z}))) \\
 & - \bar{\alpha}_l \frac{\partial \bar{p}}{\partial z} - \frac{\mu_{l,t}}{\sigma_{\alpha_{l,t}}} (\frac{\partial \bar{\alpha}_l}{\partial r} \frac{\partial \bar{v}_{l,z}}{\partial r} + \frac{1}{r^2} \frac{\partial \bar{\alpha}_l}{\partial \theta} \frac{\partial \bar{v}_{l,z}}{\partial \theta} + \frac{\partial \bar{\alpha}_l}{\partial z} \frac{\partial \bar{v}_{l,z}}{\partial z}) \\
 & - (\bar{v}_{l,r} \frac{\partial}{\partial r} (\frac{\mu_{l,t}}{\sigma_{\alpha_{l,t}}} \frac{\partial \bar{\alpha}_l}{\partial z}) + \bar{v}_{l,\theta} \frac{1}{r} \frac{\partial}{\partial \theta} (\frac{\mu_{l,t}}{\sigma_{\alpha_{l,t}}} \frac{\partial \bar{\alpha}_l}{\partial z}) + \bar{v}_{l,z} \frac{\partial}{\partial z} (\frac{\mu_{l,t}}{\sigma_{\alpha_{l,t}}} \frac{\partial \bar{\alpha}_l}{\partial z})) \\
 & + \bar{\alpha}_l \rho_l g_z + \overline{F_{l,z}^C} + \overline{F_{l,z}^{C'}}
 \end{aligned} \tag{C.129}$$

### Turbulence Model

The transport equation for turbulent kinetic energy in cylindrical coordinates is written as:

$$\begin{aligned}
 & \frac{\partial}{\partial t} (\bar{\alpha}_l \rho_l k) + \frac{1}{r} \frac{\partial}{\partial r} (r \bar{\alpha}_l \rho_l \bar{v}_{l,r} k) + \frac{1}{r} \frac{\partial}{\partial \theta} (\bar{\alpha}_l \rho_l \bar{v}_{l,\theta} k) + \frac{\partial}{\partial z} (\bar{\alpha}_l \rho_l \bar{v}_{l,z} k) = \\
 & \frac{1}{r} \frac{\partial}{\partial r} (r \bar{\alpha}_l \frac{\mu_{l,\text{eff}}}{\sigma_k} \frac{\partial k}{\partial r}) + \frac{1}{r} \frac{\partial}{\partial \theta} (\bar{\alpha}_l \frac{\mu_{l,\text{eff}}}{\sigma_k} \frac{1}{r} \frac{\partial k}{\partial \theta}) + \frac{\partial}{\partial z} (\bar{\alpha}_l \frac{\mu_{l,\text{eff}}}{\sigma_k} \frac{\partial k}{\partial z}) \\
 & + \bar{\alpha}_l (P_k + P_b - \rho_l \varepsilon)
 \end{aligned} \tag{C.130}$$

The transport equation for the turbulent energy dissipation rate in cylindrical coordinates is written as:

$$\begin{aligned} \frac{\partial}{\partial t}(\bar{\alpha}_l \rho_l \varepsilon) + \frac{1}{r} \frac{\partial}{\partial r}(r \bar{\alpha}_l \rho_l \bar{v}_{l,r} \varepsilon) + \frac{1}{r} \frac{\partial}{\partial \theta}(\bar{\alpha}_l \rho_l \bar{v}_{l,\theta} \varepsilon) + \frac{\partial}{\partial z}(\bar{\alpha}_l \rho_l \bar{v}_{l,z} \varepsilon) = \\ \frac{1}{r} \frac{\partial}{\partial r}(r \bar{\alpha}_l \frac{\mu_{l,\text{eff}}}{\sigma_\varepsilon} \frac{\partial \varepsilon}{\partial r}) + \frac{1}{r} \frac{\partial}{\partial \theta}(\bar{\alpha}_l \frac{\mu_{l,\text{eff}}}{\sigma_\varepsilon} \frac{1}{r} \frac{\partial \varepsilon}{\partial \theta}) + \frac{\partial}{\partial z}(\bar{\alpha}_l \frac{\mu_{l,\text{eff}}}{\sigma_\varepsilon} \frac{\partial \varepsilon}{\partial z}) \\ + \bar{\alpha}_l \frac{\varepsilon}{k} (C_1(P_k + P_b) - C_2 \rho_l \varepsilon) \end{aligned} \quad (\text{C.131})$$

where

$$\begin{aligned} P_k = 2\mu_{l,t} \left[ \left( \frac{\partial \bar{v}_{l,r}}{\partial r} \right)^2 + \left( \frac{1}{r} \frac{\partial \bar{v}_{l,\theta}}{\partial \theta} + \frac{\bar{v}_{l,r}}{r} \right)^2 + \left( \frac{\partial \bar{v}_{l,z}}{\partial z} \right)^2 \right] + \\ \mu_{l,t} \left[ \left( \frac{\partial \bar{v}_{l,z}}{\partial r} + \frac{\partial \bar{v}_{l,r}}{\partial z} \right)^2 + \left( \frac{1}{r} \frac{\partial \bar{v}_{l,z}}{\partial \theta} + \frac{\partial \bar{v}_{l,\theta}}{\partial z} \right)^2 + \left( \frac{\partial \bar{v}_{l,\theta}}{\partial r} + \left( \frac{1}{r} \frac{\partial \bar{v}_{l,r}}{\partial \theta} - \frac{\bar{v}_{l,\theta}}{r} \right) \right)^2 \right] \end{aligned} \quad (\text{C.132})$$

and

$$P_b = C_b \left( \overline{F_{D,r}}(\bar{v}_{g,r} - \bar{v}_{l,r}) + \overline{F_{D,\theta}}(\bar{v}_{g,\theta} - \bar{v}_{l,\theta}) + \overline{F_{D,z}}(\bar{v}_{g,z} - \bar{v}_{l,z}) \right) \quad (\text{C.133})$$

## Gas phase equations in cylindrical coordinates

The gas phase continuity and momentum equations are almost identical to those for the liquid phase, and are not repeated to save space.

## C.4 The 2D Axi-Symmetric Bubble Column Model

### Liquid phase equations in cylindrical coordinates:

In an axi-symmetric case the liquid phase continuity equation simplifies to:

$$\begin{aligned} \frac{\partial}{\partial t}(\bar{\alpha}_l \rho_l) + \frac{1}{r} \frac{\partial}{\partial r}(r \bar{\alpha}_l \rho_l \bar{v}_{l,r}) + \frac{\partial}{\partial z}(\bar{\alpha}_l \rho_l \bar{v}_{l,z}) = \\ \frac{1}{r} \frac{\partial}{\partial r} \left( r \frac{\mu_{l,t}}{\sigma_{\alpha_{l,t}}} \frac{\partial \bar{\alpha}_l}{\partial r} \right) + \frac{\partial}{\partial z} \left( \frac{\mu_{l,t}}{\sigma_{\alpha_{l,t}}} \frac{\partial \bar{\alpha}_l}{\partial z} \right) \end{aligned} \quad (\text{C.134})$$

The corresponding radial liquid phase momentum balance reduces to:

$$\begin{aligned}
 & \frac{\partial}{\partial t}(\bar{\alpha}_l \rho_l \bar{v}_{l,r}) + \frac{1}{r} \frac{\partial}{\partial r}(r \bar{\alpha}_l \rho_l \bar{v}_{l,r} \bar{v}_{l,r}) + \frac{\partial}{\partial z}(\bar{\alpha}_l \rho_l \bar{v}_{l,z} \bar{v}_{l,r}) = \\
 & \quad \frac{1}{r} \frac{\partial}{\partial r} \left( r \frac{\mu_{l,t}}{\sigma_{\alpha_{l,t}}} \frac{\partial \bar{\alpha}_l}{\partial r} \bar{v}_{l,r} \right) + \frac{\partial}{\partial z} \left( \frac{\mu_{l,t}}{\sigma_{\alpha_{l,t}}} \frac{\partial \bar{\alpha}_l}{\partial z} \bar{v}_{l,r} \right) \\
 & \quad + \frac{1}{r} \frac{\partial}{\partial r} \left( r \frac{\mu_{l,t}}{\sigma_{\alpha_{l,t}}} \frac{\partial \bar{\alpha}_l}{\partial r} \bar{v}_{l,r} \right) + \frac{\partial}{\partial z} \left( \frac{\mu_{l,t}}{\sigma_{\alpha_{l,t}}} \frac{\partial \bar{\alpha}_l}{\partial r} \bar{v}_{l,z} \right) \\
 & \quad + \frac{1}{r} \frac{\partial}{\partial r} (r \bar{\alpha}_l \mu_{l,\text{eff}} \frac{\partial \bar{v}_{l,r}}{\partial r}) - \frac{1}{r} \bar{\alpha}_l \mu_{l,\text{eff}} \frac{\bar{v}_{l,r}}{r} + \frac{\partial}{\partial z} (\bar{\alpha}_l \mu_{l,\text{eff}} \frac{\partial \bar{v}_{l,r}}{\partial z}) \\
 & \quad + \frac{1}{r} \frac{\partial}{\partial r} (r \bar{\alpha}_l \mu_{l,\text{eff}} \frac{\partial \bar{v}_{l,r}}{\partial r}) - \frac{1}{r} \bar{\alpha}_l \mu_{l,\text{eff}} \frac{\bar{v}_{l,r}}{r} + \frac{\partial}{\partial z} (\bar{\alpha}_l \mu_{l,\text{eff}} \frac{\partial \bar{v}_{l,z}}{\partial r}) \\
 & \quad - \frac{\partial}{\partial r} \left( \frac{2}{3} \bar{\alpha}_l \rho_l (k + \nu_{l,\text{eff}} \left( \frac{1}{r} \frac{\partial}{\partial r} (r \bar{v}_{l,r}) + \frac{\partial \bar{v}_{l,z}}{\partial z} \right)) \right) \\
 & \quad - \bar{\alpha}_l \frac{\partial \bar{p}}{\partial r} - \frac{\mu_{l,t}}{\sigma_{\alpha_{l,t}}} \left( \frac{\partial \bar{\alpha}_l}{\partial r} \frac{\partial \bar{v}_{l,r}}{\partial r} + \frac{\partial \bar{\alpha}_l}{\partial z} \frac{\partial \bar{v}_{l,r}}{\partial z} \right) \\
 & \quad - (\bar{v}_{l,r} \frac{\partial}{\partial r} \left( \frac{\mu_{l,t}}{\sigma_{\alpha_{l,t}}} \frac{\partial \bar{\alpha}_l}{\partial r} \right) + \bar{v}_{l,z} \frac{\partial}{\partial z} \left( \frac{\mu_{l,t}}{\sigma_{\alpha_{l,t}}} \frac{\partial \bar{\alpha}_l}{\partial r} \right)) \\
 & \quad + \bar{\alpha}_l \rho_l g_r + \overline{F_{l,r}^C} + \overline{F_{l,r}^{C'}}
 \end{aligned} \tag{C.135}$$

Using the product rule of calculus a few terms cancel out and the equation yields:

$$\begin{aligned}
 & \frac{\partial}{\partial t}(\bar{\alpha}_l \rho_l \bar{v}_{l,r}) + \frac{1}{r} \frac{\partial}{\partial r}(r \bar{\alpha}_l \rho_l \bar{v}_{l,r} \bar{v}_{l,r}) + \frac{\partial}{\partial z}(\bar{\alpha}_l \rho_l \bar{v}_{l,z} \bar{v}_{l,r}) = \\
 & \quad \frac{\bar{v}_{l,r}}{r} \frac{\partial}{\partial r} \left( r \frac{\mu_{l,t}}{\sigma_{\alpha_{l,t}}} \frac{\partial \bar{\alpha}_l}{\partial r} \right) + \bar{v}_{l,r} \frac{\partial}{\partial z} \left( \frac{\mu_{l,t}}{\sigma_{\alpha_{l,t}}} \frac{\partial \bar{\alpha}_l}{\partial z} \right) \\
 & \quad + \frac{1}{r} \frac{\partial}{\partial r} (r \bar{\alpha}_l \mu_{l,\text{eff}} \frac{\partial \bar{v}_{l,r}}{\partial r}) - \frac{1}{r} \bar{\alpha}_l \mu_{l,\text{eff}} \frac{\bar{v}_{l,r}}{r} + \frac{\partial}{\partial z} (\bar{\alpha}_l \mu_{l,\text{eff}} \frac{\partial \bar{v}_{l,r}}{\partial z}) \\
 & \quad + \frac{1}{r} \frac{\partial}{\partial r} (r \bar{\alpha}_l \mu_{l,\text{eff}} \frac{\partial \bar{v}_{l,r}}{\partial r}) - \frac{1}{r} \bar{\alpha}_l \mu_{l,\text{eff}} \frac{\bar{v}_{l,r}}{r} + \frac{\partial}{\partial z} (\bar{\alpha}_l \mu_{l,\text{eff}} \frac{\partial \bar{v}_{l,z}}{\partial r}) \\
 & \quad - \frac{\partial}{\partial r} \left( \frac{2}{3} \bar{\alpha}_l \rho_l (k + \nu_{l,\text{eff}} \left( \frac{1}{r} \frac{\partial}{\partial r} (r \bar{v}_{l,r}) + \frac{\partial \bar{v}_{l,z}}{\partial z} \right)) \right) \\
 & \quad + \frac{\mu_{l,t}}{\sigma_{\alpha_{l,t}}} \frac{\partial \bar{\alpha}_l}{\partial r} \left[ \frac{1}{r} \frac{\partial}{\partial r} (r \bar{v}_{l,r}) + \frac{\partial \bar{v}_{l,z}}{\partial z} \right] - \bar{\alpha}_l \frac{\partial \bar{p}}{\partial r} \\
 & \quad + \bar{\alpha}_l \rho_l g_r + \overline{F_{l,r}^C} + \overline{F_{l,r}^{C'}}
 \end{aligned} \tag{C.136}$$

Assuming axi-symmetry the azimuthal liquid phase momentum balance vanishes completely.

The liquid phase axial momentum balance becomes:

$$\begin{aligned}
\frac{\partial}{\partial t}(\bar{\alpha}_l \rho_l \bar{v}_{l,z}) + \frac{1}{r} \frac{\partial}{\partial r}(r \bar{\alpha}_l \rho_l \bar{v}_{l,r} \bar{v}_{l,z}) + \frac{\partial}{\partial z}(\bar{\alpha}_l \rho_l \bar{v}_{l,z} \bar{v}_{l,z}) = \\
\frac{1}{r} \frac{\partial}{\partial r}(r \frac{\mu_{l,t}}{\sigma_{\alpha_{l,t}}} \frac{\partial \bar{\alpha}_l}{\partial r} \bar{v}_{l,z}) + \frac{\partial}{\partial z}(\frac{\mu_{l,t}}{\sigma_{\alpha_{l,t}}} \frac{\partial \bar{\alpha}_l}{\partial z} \bar{v}_{l,z}) \\
+ \frac{1}{r} \frac{\partial}{\partial r}(r \frac{\mu_{l,t}}{\sigma_{\alpha_{l,t}}} \frac{\partial \bar{\alpha}_l}{\partial z} \bar{v}_{l,r}) + \frac{\partial}{\partial z}(\frac{\mu_{l,t}}{\sigma_{\alpha_{l,t}}} \frac{\partial \bar{\alpha}_l}{\partial z} \bar{v}_{l,z}) \\
+ \frac{1}{r} \frac{\partial}{\partial r}(r \bar{\alpha}_l \mu_{l,\text{eff}} \frac{\partial \bar{v}_{l,z}}{\partial r}) + \frac{\partial}{\partial z}(\bar{\alpha}_l \mu_{l,\text{eff}} \frac{\partial \bar{v}_{l,z}}{\partial z}) \\
+ \frac{1}{r} \frac{\partial}{\partial r}(r \bar{\alpha}_l \mu_{l,\text{eff}} \frac{\partial \bar{v}_{l,r}}{\partial z}) + \frac{\partial}{\partial z}(\bar{\alpha}_l \mu_{l,\text{eff}} \frac{\partial \bar{v}_{l,z}}{\partial z}) \\
- \frac{\partial}{\partial z}(\frac{2}{3} \bar{\alpha}_l \rho_l (k + \nu_{l,\text{eff}} (\frac{1}{r} \frac{\partial}{\partial r}(r \bar{v}_{l,r}) + \frac{\partial \bar{v}_{l,z}}{\partial z}))) \\
- \bar{\alpha}_l \frac{\partial \bar{p}}{\partial z} - \frac{\mu_{l,t}}{\sigma_{\alpha_{l,t}}} (\frac{\partial \bar{\alpha}_l}{\partial r} \frac{\partial \bar{v}_{l,z}}{\partial r} + \frac{\partial \bar{\alpha}_l}{\partial z} \frac{\partial \bar{v}_{l,z}}{\partial z}) \\
- (\bar{v}_{l,r} \frac{\partial}{\partial r} (\frac{\mu_{l,t}}{\sigma_{\alpha_{l,t}}} \frac{\partial \bar{\alpha}_l}{\partial z}) + \bar{v}_{l,z} \frac{\partial}{\partial z} (\frac{\mu_{l,t}}{\sigma_{\alpha_{l,t}}} \frac{\partial \bar{\alpha}_l}{\partial z})) \\
+ \bar{\alpha}_l \rho_l g_z + \overline{F_{l,z}^C} + \overline{F_{l,z}^{C'}}
\end{aligned} \tag{C.137}$$

Using the product rule of calculus a few terms cancel out and the equation yields:

$$\begin{aligned}
\frac{\partial}{\partial t}(\bar{\alpha}_l \rho_l \bar{v}_{l,z}) + \frac{1}{r} \frac{\partial}{\partial r}(r \bar{\alpha}_l \rho_l \bar{v}_{l,r} \bar{v}_{l,z}) + \frac{\partial}{\partial z}(\bar{\alpha}_l \rho_l \bar{v}_{l,z} \bar{v}_{l,z}) = \\
\bar{v}_{l,z} \frac{1}{r} \frac{\partial}{\partial r}(r \frac{\mu_{l,t}}{\sigma_{\alpha_{l,t}}} \frac{\partial \bar{\alpha}_l}{\partial r}) + \bar{v}_{l,z} \frac{\partial}{\partial z}(\frac{\mu_{l,t}}{\sigma_{\alpha_{l,t}}} \frac{\partial \bar{\alpha}_l}{\partial z}) \\
+ \frac{\mu_{l,t}}{\sigma_{\alpha_{l,t}}} \frac{\partial \bar{\alpha}_l}{\partial z} (\frac{1}{r} \frac{\partial}{\partial r}(r \bar{v}_{l,r}) + \frac{\partial \bar{v}_{l,z}}{\partial z}) \\
+ \frac{1}{r} \frac{\partial}{\partial r}(r \bar{\alpha}_l \mu_{l,\text{eff}} \frac{\partial \bar{v}_{l,z}}{\partial r}) + \frac{\partial}{\partial z}(\bar{\alpha}_l \mu_{l,\text{eff}} \frac{\partial \bar{v}_{l,z}}{\partial z}) \\
+ \frac{1}{r} \frac{\partial}{\partial r}(r \bar{\alpha}_l \mu_{l,\text{eff}} \frac{\partial \bar{v}_{l,r}}{\partial z}) + \frac{\partial}{\partial z}(\bar{\alpha}_l \mu_{l,\text{eff}} \frac{\partial \bar{v}_{l,z}}{\partial z}) \\
- \frac{\partial}{\partial z}(\frac{2}{3} \bar{\alpha}_l \rho_l (k + \nu_{l,\text{eff}} (\frac{1}{r} \frac{\partial}{\partial r}(r \bar{v}_{l,r}) + \frac{\partial \bar{v}_{l,z}}{\partial z}))) \\
- \bar{\alpha}_l \frac{\partial \bar{p}}{\partial z} + \bar{\alpha}_l \rho_l g_z + \overline{F_{l,z}^C} + \overline{F_{l,z}^{C'}}
\end{aligned} \tag{C.138}$$

A generalized transport equation for a scalar quantity in the liquid phase can be formulated as:

$$\begin{aligned}
\frac{\partial}{\partial t}(\bar{\alpha}_l \rho_l \bar{\phi}_l) + \frac{1}{r} \frac{\partial}{\partial r}(r \bar{\alpha}_l \rho_l \bar{v}_{l,r} \bar{\phi}_l) + \frac{\partial}{\partial z}(\bar{\alpha}_l \rho_l \bar{v}_{l,z} \bar{\phi}_l) = \\
\frac{1}{r} \frac{\partial}{\partial r}(r \bar{\alpha}_l \Gamma_{\phi_l,\text{eff}} \frac{\partial \bar{\phi}_l}{\partial r}) + \frac{\partial}{\partial z}(\bar{\alpha}_l \Gamma_{\phi_l,\text{eff}} \frac{\partial \bar{\phi}_l}{\partial z}) + \bar{S}_{\phi_l}
\end{aligned} \tag{C.139}$$

The particular scalar transport equation for the liquid phase turbulent kinetic energy is written:

$$\begin{aligned} \frac{\partial}{\partial t}(\bar{\alpha}_l \rho_l k) + \frac{1}{r} \frac{\partial}{\partial r}(r \bar{\alpha}_l \rho_l \bar{v}_{l,r} k) + \frac{\partial}{\partial z}(\bar{\alpha}_l \rho_l \bar{v}_{l,z} k) = \\ \frac{1}{r} \frac{\partial}{\partial r}(r \bar{\alpha}_l \frac{\mu_{l,\text{eff}}}{\sigma_k} \frac{\partial k}{\partial r}) + \frac{\partial}{\partial z}(\bar{\alpha}_l \frac{\mu_{l,\text{eff}}}{\sigma_k} \frac{\partial k}{\partial z}) + \bar{\alpha}_l (P_k + P_b - \rho_l \varepsilon) \end{aligned} \quad (\text{C.140})$$

where

$$P_k = \mu_{l,t} (2[(\frac{\partial \bar{v}_{l,r}}{\partial r})^2 + (\frac{\partial \bar{v}_{l,z}}{\partial z})^2 + (\frac{\bar{v}_{l,r}}{r})^2] + (\frac{\partial \bar{v}_{l,r}}{\partial z} + \frac{\partial \bar{v}_{l,z}}{\partial r})^2) \quad (\text{C.141})$$

and

$$P_b = C_b (\bar{F}_{D,z} (\bar{v}_{g,z} - \bar{v}_{l,z}) + \bar{F}_{D,r} (\bar{v}_{g,r} - \bar{v}_{l,r})) \quad (\text{C.142})$$

The particular transport equation for the liquid phase turbulent energy dissipation rate is written:

$$\begin{aligned} \frac{\partial}{\partial t}(\bar{\alpha}_l \rho_l \varepsilon) + \frac{1}{r} \frac{\partial}{\partial r}(r \bar{\alpha}_l \rho_l \bar{v}_{l,r} \varepsilon) + \frac{\partial}{\partial z}(\bar{\alpha}_l \rho_l \bar{v}_{l,z} \varepsilon) = \\ \frac{1}{r} \frac{\partial}{\partial r}(r \bar{\alpha}_l \frac{\mu_{l,\text{eff}}}{\sigma_\varepsilon} \frac{\partial \varepsilon}{\partial r}) + \frac{\partial}{\partial z}(\bar{\alpha}_l \frac{\mu_{l,\text{eff}}}{\sigma_\varepsilon} \frac{\partial \varepsilon}{\partial z}) + \bar{\alpha}_l \frac{\varepsilon}{k} (C_1 (P_k + P_b) - C_2 \rho_l \varepsilon) \end{aligned} \quad (\text{C.143})$$

### Gas phase equations in cylindrical coordinates:

The gas phase mass balance equation for the axisymmetric case is:

$$\begin{aligned} \frac{\partial}{\partial t}(\bar{\alpha}_g \rho_g) + \frac{1}{r} \frac{\partial}{\partial r}(r \bar{\alpha}_g \rho_g \bar{v}_{g,r}) + \frac{\partial}{\partial z}(\bar{\alpha}_g \rho_g \bar{v}_{g,z}) = \\ \frac{1}{r} \frac{\partial}{\partial r}(r \frac{\mu_{g,t}}{\sigma_{\alpha_{g,t}}} \frac{\partial \bar{\alpha}_g}{\partial r}) + \frac{\partial}{\partial z}(\frac{\mu_{g,t}}{\sigma_{\alpha_{g,t}}} \frac{\partial \bar{\alpha}_g}{\partial z}) \end{aligned} \quad (\text{C.144})$$

The radial gas phase momentum balance equation is:

$$\begin{aligned} \frac{\partial}{\partial t}(\bar{\alpha}_g \rho_g \bar{v}_{g,r}) + \frac{1}{r} \frac{\partial}{\partial r}(r \bar{\alpha}_g \rho_g \bar{v}_{g,r} \bar{v}_{g,r}) + \frac{\partial}{\partial z}(\bar{\alpha}_g \rho_g \bar{v}_{g,z} \bar{v}_{g,r}) = \\ \frac{1}{r} \frac{\partial}{\partial r}(r \frac{\mu_{g,t}}{\sigma_{\alpha_{g,t}}} \frac{\partial \bar{\alpha}_g}{\partial r} \bar{v}_{g,r}) + \frac{\partial}{\partial z}(\frac{\mu_{g,t}}{\sigma_{\alpha_{g,t}}} \frac{\partial \bar{\alpha}_g}{\partial z} \bar{v}_{g,r}) \\ + \frac{1}{r} \frac{\partial}{\partial r}(r \frac{\mu_{g,t}}{\sigma_{\alpha_{g,t}}} \frac{\partial \bar{\alpha}_g}{\partial r} \bar{v}_{g,r}) + \frac{\partial}{\partial z}(\frac{\mu_{g,t}}{\sigma_{\alpha_{g,t}}} \frac{\partial \bar{\alpha}_g}{\partial r} \bar{v}_{g,z}) \\ + \frac{1}{r} \frac{\partial}{\partial r}(r \bar{\alpha}_g \frac{\mu_{g,t}}{\sigma_{g,t}} \frac{\partial \bar{v}_{g,r}}{\partial r}) - \frac{1}{r} \bar{\alpha}_g \frac{\mu_{g,t}}{\sigma_{g,t}} \frac{\bar{v}_{g,r}}{r} + \frac{\partial}{\partial z}(\bar{\alpha}_g \frac{\mu_{g,t}}{\sigma_{g,t}} \frac{\partial \bar{v}_{g,r}}{\partial z}) \end{aligned}$$

$$\begin{aligned}
& + \frac{1}{r} \frac{\partial}{\partial r} (r \bar{\alpha}_g \frac{\mu_{g,t}}{\sigma_{g,t}} \frac{\partial \bar{v}_{g,r}}{\partial r}) - \frac{1}{r} \bar{\alpha}_g \frac{\mu_{g,t}}{\sigma_{g,t}} \frac{\bar{v}_{g,r}}{r} + \frac{\partial}{\partial z} (\bar{\alpha}_g \frac{\mu_{g,t}}{\sigma_{g,t}} \frac{\partial \bar{v}_{g,z}}{\partial r}) \\
& - \frac{\partial}{\partial r} (\frac{2}{3} \bar{\alpha}_g \rho_g (k + \frac{\nu_{g,t}}{\sigma_{g,t}} (\frac{1}{r} \frac{\partial}{\partial r} (r \bar{v}_{g,r}) + \frac{\partial \bar{v}_{g,z}}{\partial z}))) \\
& - \bar{\alpha}_g \frac{\partial \bar{p}}{\partial r} + \frac{\mu_{l,t}}{\sigma_{\alpha_{l,t}}} (\frac{\partial \bar{\alpha}_l}{\partial r} \frac{\partial \bar{v}_{l,r}}{\partial r} + \frac{\partial \bar{\alpha}_l}{\partial z} \frac{\partial \bar{v}_{l,r}}{\partial z}) \\
& + \bar{v}_{l,r} \frac{\partial}{\partial r} (\frac{\mu_{l,t}}{\sigma_{\alpha_{l,t}}} \frac{\partial \bar{\alpha}_l}{\partial r}) + \bar{v}_{l,z} \frac{\partial}{\partial z} (\frac{\mu_{l,t}}{\sigma_{\alpha_{l,t}}} \frac{\partial \bar{\alpha}_l}{\partial r}) \\
& + \bar{\alpha}_g \rho_g g_r + \overline{F_{g,r}^C} + \overline{F_{g,r}^{C'}}
\end{aligned} \tag{C.145}$$

Assuming axi-symmetry the azimuthal gas phase momentum balance vanishes completely.

The axial gas phase momentum balance equation is:

$$\begin{aligned}
\frac{\partial}{\partial t} (\bar{\alpha}_g \rho_g \bar{v}_{g,z}) + \frac{1}{r} \frac{\partial}{\partial r} (r \bar{\alpha}_g \rho_g \bar{v}_{g,r} \bar{v}_{g,z}) + \frac{\partial}{\partial z} (\bar{\alpha}_g \rho_g \bar{v}_{g,z} \bar{v}_{g,z}) = \\
\frac{1}{r} \frac{\partial}{\partial r} (r \frac{\mu_{g,t}}{\sigma_{\alpha_{g,t}}} \frac{\partial \bar{\alpha}_g}{\partial r} \bar{v}_{g,z}) + \frac{\partial}{\partial z} (\frac{\mu_{g,t}}{\sigma_{\alpha_{g,t}}} \frac{\partial \bar{\alpha}_g}{\partial z} \bar{v}_{g,z}) \\
+ \frac{1}{r} \frac{\partial}{\partial r} (r \frac{\mu_{g,t}}{\sigma_{\alpha_{g,t}}} \frac{\partial \bar{\alpha}_g}{\partial z} \bar{v}_{g,r}) + \frac{\partial}{\partial z} (\frac{\mu_{g,t}}{\sigma_{\alpha_{g,t}}} \frac{\partial \bar{\alpha}_g}{\partial z} \bar{v}_{g,z}) \\
+ \frac{1}{r} \frac{\partial}{\partial r} (r \bar{\alpha}_g \frac{\mu_{g,t}}{\sigma_{g,t}} \frac{\partial \bar{v}_{g,z}}{\partial r}) + \frac{\partial}{\partial z} (\bar{\alpha}_g \frac{\mu_{g,t}}{\sigma_{g,t}} \frac{\partial \bar{v}_{g,z}}{\partial z}) \\
+ \frac{1}{r} \frac{\partial}{\partial r} (r \bar{\alpha}_g \frac{\mu_{g,t}}{\sigma_{g,t}} \frac{\partial \bar{v}_{g,r}}{\partial z}) + \frac{\partial}{\partial z} (\bar{\alpha}_g \frac{\mu_{g,t}}{\sigma_{g,t}} \frac{\partial \bar{v}_{g,z}}{\partial z}) \\
- \frac{\partial}{\partial z} (\frac{2}{3} \bar{\alpha}_g \rho_g (k + \frac{\nu_{g,t}}{\sigma_{g,t}} (\frac{1}{r} \frac{\partial}{\partial r} (r \bar{v}_{g,r}) + \frac{\partial \bar{v}_{g,z}}{\partial z}))) \\
- \bar{\alpha}_g \frac{\partial \bar{p}}{\partial z} + \frac{\mu_{l,t}}{\sigma_{\alpha_{l,t}}} (\frac{\partial \bar{\alpha}_l}{\partial r} \frac{\partial \bar{v}_{l,z}}{\partial r} + \frac{\partial \bar{\alpha}_l}{\partial z} \frac{\partial \bar{v}_{l,z}}{\partial z}) \\
+ (\bar{v}_{l,r} \frac{\partial}{\partial r} (\frac{\mu_{l,t}}{\sigma_{\alpha_{l,t}}} \frac{\partial \bar{\alpha}_l}{\partial z}) + \bar{v}_{l,z} \frac{\partial}{\partial z} (\frac{\mu_{l,t}}{\sigma_{\alpha_{l,t}}} \frac{\partial \bar{\alpha}_l}{\partial z})) \\
+ \bar{\alpha}_g \rho_g g_z + \overline{F_{g,z}^C} + \overline{F_{g,z}^{C'}}
\end{aligned} \tag{C.146}$$

A generalized transport equation for a scalar quantity in the gas phase can be formulated:

$$\begin{aligned}
\frac{\partial}{\partial t} (\bar{\alpha}_g \rho_g \bar{\phi}_g) + \frac{1}{r} \frac{\partial}{\partial r} (r \bar{\alpha}_g \rho_g \bar{v}_{g,r} \bar{\phi}_g) + \frac{\partial}{\partial z} (\bar{\alpha}_g \rho_g \bar{v}_{g,z} \bar{\phi}_g) = \\
\frac{1}{r} \frac{\partial}{\partial r} (r \bar{\alpha}_g \Gamma_{\phi_g,t} \frac{\partial \bar{\phi}_g}{\partial r}) + \frac{\partial}{\partial z} (\bar{\alpha}_g \Gamma_{\phi_g,t} \frac{\partial \bar{\phi}_g}{\partial z}) + \bar{S}_{\phi_g}
\end{aligned} \tag{C.147}$$

#### C.4.1 Discretization of the Trondheim Bubble Column Model

In this section the *Trondheim Bubble Column model* is discretized using the finite volume technique on a staggered grid. The Trondheim Bubble Column

model consists of a two-dimensional two-fluid model written in cylindrical coordinates. The governing equations are defined in appendix C.

In the first subsection, the discretization of the continuity equations is outlined. The discretization of these equations follows the basic principles as outlined earlier for single phase flow. In the second subsection the generic part of the discretization procedure, being similar for all the transport equations, is outlined for a generalized variable  $\psi$  of phase  $k$ . The discretization concepts applied are the same as those used for the generic equation for single phase flow. In the third section the discretization scheme used for the volume fraction is presented. The volume fraction of the gas phase is calculated using a combination of the two continuity equations based on a scheme given by Spalding [20]. In the fourth section the discretization procedure used for the momentum equations is presented. The momentum equation was solved using the SIMPLEC method (the SIMPLE- Consistent approximation) by van Doormal and Raithby [23], and the PEA method (Partial Elimination Algorithm) by Spalding [18, 19]. The pressure-correction was calculated by use of the liquid phase continuity equation only, based on the scheme given by Grienberger [9] and the single phase algorithm of Patankar [16].

The two-fluid model discretization procedure outlined in this appendix is to a large extent based on the single phase flow algorithm implemented in the pioneering TEACH-T code [8]. In order to simulate two phase bubble driven flow in bubble columns, the original TEACH-T code was extended to enable solution of the two-fluid model described previously in this appendix.

### Uniform Staggered Grid Arrangement

The first step in any discretization procedure is to define the grid to be used by dividing the computational domain into a number of grid cells and distribute the variables on the grid. In this work a uniform staggered grid arrangement was used as sketched in Fig C.1 using the scalar cell notation.

The indices of the nodes (i,j) vary between 1 and NI and 1 and NJ in the  $z$ - and  $r$ - directions, respectively. Boundary nodes are located at  $i = 1, NI$  and  $j = 1, NJ$ , thus the equations are solved in the range  $2 < i < NI - 1$  and  $2 < j < NJ - 1$ .

#### *Scalar Grid Cell Definition*

The uniform distance between two node points in the *axial direction* is given by:

$$\Delta z = \frac{\text{Height of reactor}}{(\text{number of discretization points} - 2)} = \frac{L}{NI - 2} \quad (\text{C.148})$$

The location of the different points in the  $z$ -direction can then be calculated as follows, for  $i > 1$ :

$$z_i = z_{i-1} + \Delta z \quad \text{where} \quad z_1 = -\Delta z/2 \quad (\text{C.149})$$

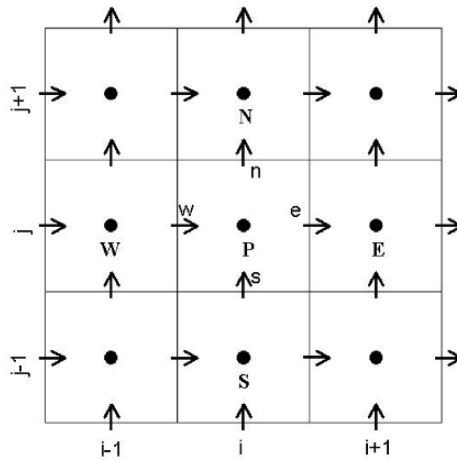


**Fig. C.1.** Staggered Cartesian grid arrangement in the scalar cell notation. The scalar variables are located in the cell centers, while the velocity components are centered around the cell faces. The velocity components are located in the centers of their own grid cell volumes (not shown) which are staggered in one dimension compared to the scalar grid.

For  $i \geq 1$ :

$$\delta z_{EP,i} = z_{i+1} - z_i, \tag{C.150}$$

$$\delta z_{PW,i} = z_i - z_{i-1} \tag{C.151}$$

$$\delta z_{EW,i} = \frac{1}{2}(\delta z_{EP,i} + \delta z_{PW,i}) \tag{C.152}$$

The uniform distance between two node points in the *radial direction* is given by:

$$\Delta r = \frac{\text{Radius of reactor}}{(\text{number of discretization points} - 2)} = \frac{R}{NJ - 2} \tag{C.153}$$

The location of the node points in the *r*-direction can then be calculated as follows, for  $j > 1$ :

$$r_j = r_{j-1} + \Delta r \quad \text{where} \quad r_1 = -\Delta r/2 \tag{C.154}$$

For  $j \geq 1$ :

$$\delta r_{NP,j} = r_{j+1} - r_j, \tag{C.155}$$

$$\delta r_{PS,j} = r_j - r_{j-1} \tag{C.156}$$

$$\delta r_{NS,j} = \frac{1}{2}(\delta r_{NP,j} + \delta r_{PS,j}) \tag{C.157}$$

In cylindrical coordinates, a typical three dimensional volume integral of a function  $\psi(r, \theta, z)$  would be of the form [4](A 8):

$$\int_{z_1}^{z_2} \int_{\theta_1}^{\theta_2} \int_{r_1}^{r_2} \psi(r, \theta, z) r dr d\theta dz \quad (\text{C.158})$$

Integration can also be performed on one of the surfaces of the coordinate system. In cylindrical coordinates there are three different kinds of surfaces, defined by keeping one of the coordinates constant at the time:

$$\int_{z_1}^{z_2} \int_{\theta_1}^{\theta_2} \psi(r_0, \theta, z) r_0 d\theta dz, \quad \text{On the surface } r = r_0. \quad (\text{C.159})$$

$$\int_{z_1}^{z_2} \int_{r_1}^{r_2} \psi(r, \theta_0, z) dr dz, \quad \text{On the surface } \theta = \theta_0. \quad (\text{C.160})$$

$$\int_{\theta_1}^{\theta_2} \int_{r_1}^{r_2} \psi(r, \theta, z_0) r dr d\theta, \quad \text{On the surface } z = z_0. \quad (\text{C.161})$$

In two-dimensional problems, the volume and surface integrals reduce accordingly. The scalar grid cell surface areas and cell volume are defined as follows:

$$A_w = A_e = r_p \times \delta r_{NS,j} = r_j \times \frac{1}{2}(\delta r_{NP,j} + \delta r_{PS,j}), \quad (\text{C.162})$$

$$A_n = r_n \times \delta z_{EW,i} = r_{j+1}^v \times \frac{1}{2}(\delta z_{EP,i} + \delta z_{PW,i}), \quad (\text{C.163})$$

$$A_s = r_s \times \delta z_{EW,i} = r_j^v \times \frac{1}{2}(\delta z_{EP,i} + \delta z_{PW,i}) \quad (\text{C.164})$$

and

$$\Delta V = r_p \times \delta z_{EW,i} \times \delta r_{NS,j} = r_j \times \frac{1}{2}(\delta z_{EP,i} + \delta z_{PW,i}) \times \frac{1}{2}(\delta r_{NP,j} + \delta r_{PS,j}) \quad (\text{C.165})$$

#### *Staggered Axial Velocity Component (w) Grid Cell Definition*

The location of the different points in the  $z$ -direction are calculated as follows, for  $i > 1$ :

$$\Delta z^w = \frac{1}{2}(z_i + z_{i-1}) \quad \text{where } z_1^w = 0 \quad (\text{C.166})$$

For  $i \geq 1$ :

$$\delta z_{EP,i}^w = z_{i+1}^w - z_i^w, \quad (\text{C.167})$$

$$\delta z_{PW,i}^w = z_i^w - z_{i-1}^w, \quad (\text{C.168})$$

$$\delta z_{EW,i}^w = \frac{1}{2}(\delta z_{EP,i}^w + \delta z_{PW,i}^w) \quad (\text{C.169})$$

The radial position of the grid for the axial velocity component ( $w$ ) coincides with that of the scalar grid cell.

The staggered axial velocity component grid cell surface areas and cell volume are defined by:

$$A_w = A_e = r_p \times \delta r_{NS,j} = r_p \times \frac{1}{2}(\delta r_{NP,j} + \delta r_{PS,j}), \quad (\text{C.170})$$

$$A_n = r_n \times \delta z_{EW,i}^w = r_{j+1}^v \times \frac{1}{2}(\delta z_{EP,i}^w + \delta z_{PW,i}^w), \quad (\text{C.171})$$

$$A_s = r_s \times \delta z_{EW,i}^w = r_j^v \times \frac{1}{2}(\delta z_{EP,i}^w + \delta z_{PW,i}^w) \quad (\text{C.172})$$

and

$$\Delta V = r_p \times \delta z_{EW,i}^w \times \delta r_{NS,j} = r_j \times \frac{1}{2}(\delta z_{EP,i}^w + \delta z_{PW,i}^w) \times \frac{1}{2}(\delta r_{NP,j} + \delta r_{PS,j}) \quad (\text{C.173})$$

#### *Staggered Radial Velocity Component ( $v$ ) Grid Cell Definition*

The axial position of the grid cell for the radial velocity component ( $v$ ) coincides with that of the scalar grid cell defined above.

The location of the different points in the  $r$ -direction can then be calculated as follows, for  $j > 1$ :

$$r_j^v = \frac{1}{2}(r_j + r_{j-1}) \quad \text{where} \quad r_1 = 0 \quad (\text{C.174})$$

For  $j \geq 1$ :

$$\delta r_{NP,j}^v = r_{j+1}^v - r_j^v, \quad (\text{C.175})$$

$$\delta r_{PS,j}^v = r_j^v - r_{j-1}^v \quad (\text{C.176})$$

$$\delta r_{NS,j}^v = \frac{1}{2}(\delta r_{NP,j}^v + \delta r_{PS,j}^v) \quad (\text{C.177})$$

For the radial velocity component ( $v$ ) grid cell, the surface areas and cell volume are defined by:

$$A_w = A_e = r_p^v \times \delta r_{NS,j}^v = r_j^v \times \frac{1}{2}(\delta r_{NP,j}^v + \delta r_{PS,j}^v), \quad (\text{C.178})$$

$$A_n = r_n \times \delta z_{EW,i} = r_{j+1} \times \frac{1}{2}(\delta z_{EP,i} + \delta z_{PW,i}), \quad (\text{C.179})$$

$$A_s = r_s \times \delta z_{EW,i} = r_j \times \frac{1}{2}(\delta z_{EP,i} + \delta z_{PW,i}) \quad (\text{C.180})$$

and

$$\Delta V = r_p^v \times \delta z_{EW,i} \times \delta r_{NS,j}^v = r_j^v \times \frac{1}{2}(\delta z_{EP,i} + \delta z_{PW,i}) \times \frac{1}{2}(\delta r_{NP,j}^v + \delta r_{PS,j}^v) \quad (\text{C.181})$$

To discretize the governing equations using the finite volume method, the differential equations are written on the integral form by integrating over a

grid cell volume. The volume integrals of the convective and diffusive flux terms are transformed into surface integrals by use of the Gauss theorem. It is further assumed that the source term is constant throughout the grid cell volume, and the fluxes are uniform over the cell faces. The resulting semi-discrete equation is then integrated over a time step. After the integrations all the terms are divided by the time step length  $\Delta t$ . The transient term is approximated by the midpoint rule, hence it is considered an average value representative for the whole grid cell volume. The order of the time and volume integration is interchangeable.

The solution of the discretized forms of the governing equations can be based on general geometrical dimensions such as  $\delta z_{EP}$ ,  $\delta z_{PW}$ ,  $\delta r_{NP}$  and  $\delta r_{PS}$  which are valid for non-uniform grids as well as for uniform grids. However, the implementation of the discretized equations on uniform grids into a computer code can be simplified adopting a grid dependent notation which is faster to compute.

### C.4.2 The Continuity Equation

The phasic continuity equations are defined by:

$$\frac{\partial}{\partial t}(\alpha_k \rho_k) + \frac{1}{r} \frac{\partial}{\partial r}(r \alpha_k \rho_k v_k) + \frac{\partial}{\partial z}(\alpha_k \rho_k w_k) = \frac{1}{r} \frac{\partial}{\partial r}(r \Gamma \frac{\partial \alpha_k}{\partial r}) + \frac{\partial}{\partial z}(\Gamma \frac{\partial \alpha_k}{\partial z}) + S$$

The continuity equation is re-written on the integral form, integrated in time and over a grid cell volume in the non-staggered grid for the scalar variables sketched in Fig C.2. The transient terms are discretized with the implicit Euler scheme.

$$\begin{aligned} & \frac{((\alpha_k \rho_k)_P - (\alpha_k \rho_k)_P^o) \Delta V}{\Delta t} + \Delta z((r \alpha_k \rho_k v_k)_n - (r \alpha_k \rho_k v_k)_s) \\ & + r_p \Delta r((\alpha_k \rho_k w_k)_e - (\alpha_k \rho_k w_k)_w) = \Delta z((r \Gamma \frac{\partial \alpha_k}{\partial r})_n - (r \Gamma \frac{\partial \alpha_k}{\partial r})_s) \quad (\text{C.182}) \\ & + r_p \Delta r((\Gamma \frac{\partial \alpha_k}{\partial z})_e - (\Gamma \frac{\partial \alpha_k}{\partial z})_w) + S \Delta V \end{aligned}$$

The gradient terms were then approximated by the central difference scheme. For simplicity, the variables  $\delta_{rPN}$ ,  $\delta_{rSP}$ ,  $\delta_{zPE}$ ,  $\delta_{zWP}$ ,  $A$ ,  $C$ ,  $D$  and  $F$  are commonly introduced. The resulting equation can thus be written as:

$$\begin{aligned} & \frac{(\alpha_k \rho_k)_P \Delta V}{\Delta t} + C_n - C_s + C_e - C_w = \frac{(\alpha_k \rho_k)_P^o \Delta V}{\Delta t} + D_n(\alpha_{k,N} - \alpha_{k,P}) \\ & - D_s(\alpha_{k,P} - \alpha_{k,S}) + D_e(\alpha_{k,E} - \alpha_{k,P}) - D_w(\alpha_{k,P} - \alpha_{k,W}) + S \Delta V \end{aligned} \quad (\text{C.183})$$

The novel variables are defined as follows:

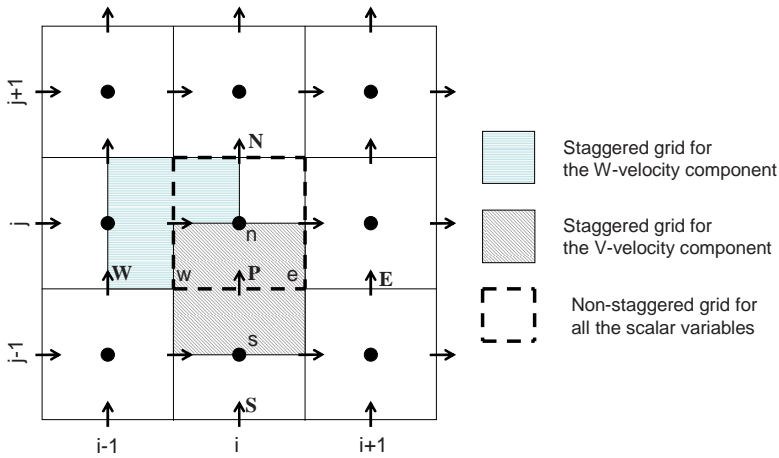


**Fig. C.2.** A sketch of a scalar Cartesian grid cell showing the distribution of the variables in the grid and the configuration of the staggered velocity grids. In cylindrical coordinates equivalent grid cells can be defined.

$$\begin{aligned}
 C_n &= A_n F_n = A_n (\alpha_k \rho_k v_k)_n, \\
 C_s &= A_s F_s = A_s (\alpha_k \rho_k v_k)_s, \\
 C_e &= A_e F_e = A_e (\alpha_k \rho_k w_k)_e, \\
 C_w &= A_w F_w = A_w (\alpha_k \rho_k w_k)_w
 \end{aligned}
 \tag{C.184}$$

The  $C$ -variables represent the convective fluxes through the grid cell surfaces and are normally approximated by the central difference scheme.

$$\begin{aligned}
 D_n &= A_n \frac{\Gamma_n}{\delta r_{NP}}, \\
 D_s &= A_s \frac{\Gamma_s}{\delta r_{PS}}, \\
 D_e &= A_e \frac{\Gamma_e}{\delta z_{EP}}, \\
 D_w &= A_w \frac{\Gamma_w}{\delta z_{PW}}
 \end{aligned}
 \tag{C.185}$$

The  $D$ -variables represent the generalized diffusion conductance and are related to the diffusive fluxes through the grid cell surfaces. In order to approximate these terms the gradients of the transported properties and the diffusion coefficients  $\Gamma$  are required. The property gradients are normally approximated by the central difference scheme. In a uniform grid the diffusion coefficients are obtained by linear interpolation from the node values (i.e., using arithmetic mean values):

$$\begin{aligned}
 \Gamma_n &= \frac{1}{2}(\Gamma_P + \Gamma_N), \\
 \Gamma_s &= \frac{1}{2}(\Gamma_P + \Gamma_S), \\
 \Gamma_e &= \frac{1}{2}(\Gamma_P + \Gamma_E), \\
 \Gamma_w &= \frac{1}{2}(\Gamma_P + \Gamma_W)
 \end{aligned} \tag{C.186}$$

We can re-organize (C.183) to:

$$C_n - C_s + C_e - C_w = \text{transient} + mC_1 + mC_2 \tag{C.187}$$

where

$$\begin{aligned}
 \text{transient} &= \frac{(\alpha_k \rho_k)_P^o \Delta V}{\Delta t} - \frac{(\alpha_k \rho_k)_P \Delta V}{\Delta t} \\
 mC_1 &= D_n \alpha_{k,N} + D_s \alpha_{k,S} + D_e \alpha_{k,E} + D_w \alpha_{k,W} \\
 mC_2 &= -(D_n + D_s + D_e + D_w) \alpha_{k,P}
 \end{aligned} \tag{C.188}$$

The *LHS* of (C.187) can be recognized as part of the  $a_P$ -factor of the discretized equations for all the other variables. To keep the  $a_P$ -coefficient always positive during the iterative process, the LHS terms can be substituted by the RHS terms.

### C.4.3 The Generalized equation

$$\begin{aligned}
 \frac{\partial}{\partial t}(\alpha_k \rho_k \psi_k) + \frac{1}{r} \frac{\partial}{\partial r}(r \alpha_k \rho_k v_k \psi_k) + \frac{\partial}{\partial z}(\alpha_k \rho_k w_k \psi_k) \\
 = \frac{1}{r} \frac{\partial}{\partial r}(r \alpha_k \rho_k \frac{\mu_{k,t}}{\sigma_{\alpha_k,t}} \frac{\partial \Phi}{\partial r}) + \frac{\partial}{\partial z}(\alpha_k \rho_k \frac{\mu_{k,t}}{\sigma_{\alpha_k,t}} \frac{\partial \Phi}{\partial z})
 \end{aligned}$$

The finite volume discretization of the generalized multi-fluid equation coincides with the corresponding equation for single phase flows as outlined in the preceding subsections.

#### The Transient term

The transient term is discretized using the implicit Euler scheme.

$$\begin{aligned}
 \int_{\Delta V} \int_{\Delta t} \frac{\partial}{\partial t}(\alpha_k \rho_k \psi_k) dt dz r dr &= \left[ (\alpha_k \rho_k \psi_k)_P - (\alpha_k \rho_k \psi_k)_P^o \right] \Delta V \\
 &= \frac{\Delta V}{\Delta t} (\alpha_k \rho_k \psi_k)_P \Delta t - \frac{\Delta V}{\Delta t} (\alpha_k \rho_k \psi_k)_P^o \Delta t \\
 &= \frac{\Delta V}{\Delta t} (\alpha_k \rho_k \psi_k)_P \Delta t - a_P^o \psi_{k,P}^o \Delta t
 \end{aligned} \tag{C.189}$$

where

$$a_P^o = \frac{\Delta V}{\Delta t} (\alpha_k \rho_k)_P^o \tag{C.190}$$

**The Convection terms**

Radial direction:

$$\begin{aligned}
 \int_{\Delta t \Delta V} \int \frac{1}{r} \frac{\partial}{\partial r} (r \alpha_k \rho_k v_k \psi_k) dz r dr dt &= \Delta z [(r \alpha_k \rho_k v_k \psi_k)_n - (r \alpha_k \rho_k v_k \psi_k)_s] \Delta t \\
 &= A_n (\alpha_k \rho_k v_k \psi_k)_n \Delta t - A_s (r \alpha_k \rho_k v_k \psi_k)_s \Delta t \\
 &= A_n F_n \psi_n \Delta t - A_s F_s \psi_s \Delta t \\
 &= C_n \psi_n \Delta t - C_s \psi_s \Delta t
 \end{aligned} \tag{C.191}$$

where

$$\begin{aligned}
 F_n &= (\alpha_k \rho_k v_k)_n \\
 F_s &= (\alpha_k \rho_k v_k)_s
 \end{aligned} \tag{C.192}$$

Axial direction:

$$\begin{aligned}
 \int_{\Delta t \Delta V} \int \frac{\partial}{\partial z} (\alpha_k \rho_k w_k \psi_k) dz r dr dt &= r \Delta r [(\alpha_k \rho_k w_k \psi_k)_e - (\alpha_k \rho_k w_k \psi_k)_w] \Delta t \\
 &= A_e (\alpha_k \rho_k w_k \psi_k)_e \Delta t - A_w (\alpha_k \rho_k w_k \psi_k)_w \Delta t \\
 &= A_e F_e \psi_e \Delta t - A_w F_w \psi_w \Delta t \\
 &= C_e \psi_e \Delta t - C_w \psi_w \Delta t
 \end{aligned} \tag{C.193}$$

where

$$\begin{aligned}
 F_e &= (\alpha_k \rho_k w_k)_e \\
 F_w &= (\alpha_k \rho_k w_k)_w
 \end{aligned} \tag{C.194}$$

**The Diffusion terms**

The the diffusion terms are discretized using the central-difference scheme.

Radial direction:

$$\begin{aligned}
 \int_{\Delta t \Delta V} \int \frac{1}{r} \frac{\partial}{\partial r} (r \alpha_k \frac{\mu_{k,eff}}{\sigma_\psi} \frac{\partial \psi_k}{\partial r}) r dr dz dt \\
 &= \Delta z [(r \alpha_k \frac{\mu_{k,eff}}{\sigma_\psi} \frac{\partial \psi_k}{\partial r})_n - (r \alpha_k \frac{\mu_{k,eff}}{\sigma_\psi} \frac{\partial \psi_k}{\partial r})_s] \Delta t \\
 &= A_n \Gamma_n \left( \frac{\psi_{k,N} - \psi_{k,P}}{\delta_{rPN}} \right) \Delta t - A_s \Gamma_s \left( \frac{\psi_{k,P} - \psi_{k,S}}{\delta_{rSP}} \right) \Delta t \\
 &= D_n (\psi_{k,N} - \psi_{k,P}) \Delta t - D_S (\psi_{k,P} - \psi_{k,S}) \Delta t
 \end{aligned} \tag{C.195}$$

where

$$\begin{aligned}
 \Gamma_n &= (\alpha_k \frac{\mu_{k,eff}}{\sigma_\psi})_n \quad \text{and} \quad \Gamma_s = (\alpha_k \frac{\mu_{k,eff}}{\sigma_\psi})_s \\
 D_n &= \frac{A_n \Gamma_n}{\delta_{rPN}} \quad \text{and} \quad D_s = \frac{A_s \Gamma_s}{\delta_{rSP}}
 \end{aligned} \tag{C.196}$$

Axial direction:

$$\begin{aligned}
 &\int_{\Delta t \Delta V} \frac{\partial}{\partial z} (\alpha_k \frac{\mu_{k,eff}}{\sigma_\psi} \frac{\partial \psi_k}{\partial z}) dz r dr dt \\
 &= r_p \Delta r (\alpha_k \frac{\mu_{k,eff}}{\sigma_\psi} \frac{\partial \psi_k}{\partial z})_e \Delta t - r_p \Delta r (\alpha_k \frac{\mu_{k,eff}}{\sigma_\psi} \frac{\partial \psi_k}{\partial z})_w \Delta t \\
 &= A_e \Gamma_e \left( \frac{\psi_{k,E} - \psi_{k,P}}{\delta_{zEP}} \right) \Delta t - A_w \Gamma_w \left( \frac{\psi_{k,P} - \psi_{k,W}}{\delta_{zWP}} \right) \Delta t \\
 &= D_e (\psi_{k,E} - \psi_{k,P}) \Delta t - D_w (\psi_{k,P} - \psi_{k,W}) \Delta t
 \end{aligned} \tag{C.197}$$

where

$$\begin{aligned}
 \Gamma_w &= (\alpha_k \frac{\mu_{k,eff}}{\sigma_\psi})_w \quad \text{and} \quad \Gamma_e = (\alpha_k \frac{\mu_{k,eff}}{\sigma_\psi})_e \\
 D_e &= \frac{A_e \Gamma_e}{\delta_{zEP}} \quad \text{and} \quad D_w = \frac{A_w \Gamma_w}{\delta_{zWP}}
 \end{aligned} \tag{C.198}$$

### The Source terms

The the source terms are approximated by the midpoint rule, in which  $S$  is considered an average value representative for the whole grid cell volume.

### Upwind Discretized Form of the Generalized Equation

After the given approximations of the terms have been substituted into the generic equation, and dividing all the terms by  $\Delta t$ , the balance equation yields:

$$\begin{aligned}
 &\frac{\Delta V}{\Delta t} (\alpha_k \rho_k)_P \psi_{k,P} - a_P^o \psi_{k,P}^o + C_n \psi_{k,n} - C_s \psi_{k,s} + C_e \psi_{k,e} - C_w \psi_{k,w} = \\
 &D_n (\psi_{k,N} - \psi_{k,P}) - D_s (\psi_{k,P} - \psi_{k,S}) + D_e (\psi_{k,E} - \psi_{k,P}) - D_w (\psi_{k,P} - \psi_{k,W}) \\
 &+ S \Delta V
 \end{aligned} \tag{C.199}$$

By use of the upwind scheme for the convective terms, the generalized transport equation becomes:

$$\begin{aligned}
 &\left( \frac{\Delta V}{\Delta t} (\alpha_k \rho_k)_P + a_N + a_S + a_E + a_W + C_n - C_s + C_e - C_w - S_{P,1} \Delta V \right) \psi_{k,P} \\
 &= a_N \psi_{k,N} + a_S \psi_{k,S} + a_E \psi_{k,E} + a_W \psi_{k,W} + S_{C,1} \Delta V + a_P^o \psi_{k,P}^o
 \end{aligned} \tag{C.200}$$

The discretized equation can then be written on the standard algebraic form:

$$a_P \psi_P = a_N \psi_N + a_S \psi_S + a_E \psi_E + a_W \psi_W + b \quad (\text{C.201})$$

in which the coefficients are defined as follows:

$$\begin{aligned} a_N &= D_n + \max[-C_n, 0] \\ a_S &= D_s + \max[C_s, 0] \\ a_E &= D_e + \max[-C_e, 0] \\ a_W &= D_w + \max[C_w, 0] \\ b &= S_{C,1} + a_P^0 \psi_{k,P}^0 \\ a_P &= \frac{\Delta V}{\Delta t} (\alpha_k \rho_k)_P + a_N + a_S + a_E + a_W + C_n - C_s + C_e - C_w - S_{P,1} \Delta V \end{aligned} \quad (\text{C.202})$$

To avoid negative coefficients, the relation for the coefficient  $a_P$  can be modified using the continuity equation (C.187). The result is:

$$a_P = \frac{(\alpha_k \rho_k)_P^0 \Delta V}{\Delta t} + a_N + a_S + a_E + a_W + mC_1 + mC_2 - S_{P,1} \Delta V \quad (\text{C.203})$$

The negative  $mC_2$ -term must then be moved to the RHS of the discretized transport equation and included as part of the  $b$ -term (multiplied with  $\psi_k^0$ , the value at the previous iteration). The alternative  $a_P^*$  and  $b^*$  coefficients are defined by:

$$\begin{aligned} b^* &= -mC_2 \psi_{k,P}^0 + S_{C,1} + a_P^0 \psi_{k,P}^0 \\ a_P^* &= \frac{\Delta V}{\Delta t} (\alpha_k \rho_k)_P^0 + a_N + a_S + a_E + a_W + mC_1 - S_{P,1} \Delta V \end{aligned} \quad (\text{C.204})$$

#### C.4.4 The liquid phase radial momentum balance

The radial momentum balance is given in (C.135).

$$\begin{aligned} \frac{\partial}{\partial t} (\alpha_l \rho_l v_l) + \frac{1}{r} \frac{\partial}{\partial r} (r \alpha_l \rho_l v_l v_l) + \frac{\partial}{\partial z} (\alpha_l \rho_l w_l v_l) = \\ \frac{v_l}{r} \frac{\partial}{\partial r} \left( r \frac{\mu_{l,t}}{\sigma_{\alpha_l,t}} \frac{\partial \alpha_l}{\partial r} \right) + v_l \frac{\partial}{\partial z} \left( \frac{\mu_{l,t}}{\sigma_{\alpha_l,t}} \frac{\partial \alpha_l}{\partial z} \right) \\ + \frac{1}{r} \frac{\partial}{\partial r} \left( r \alpha_l \mu_{l,\text{eff}} \frac{\partial v_l}{\partial r} \right) - \frac{1}{r} \alpha_l \mu_{l,\text{eff}} \frac{v_l}{r} + \frac{\partial}{\partial z} \left( \alpha_l \mu_{l,\text{eff}} \frac{\partial v_l}{\partial z} \right) \\ + \frac{1}{r} \frac{\partial}{\partial r} \left( r \alpha_l \mu_{l,\text{eff}} \frac{\partial v_l}{\partial r} \right) - \frac{1}{r} \alpha_l \mu_{l,\text{eff}} \frac{v_l}{r} + \frac{\partial}{\partial z} \left( \alpha_l \mu_{l,\text{eff}} \frac{\partial w_l}{\partial r} \right) \\ - \frac{\partial}{\partial r} \left( \frac{2}{3} \alpha_l \rho_l [k + \nu_{l,\text{eff}} \left( \frac{1}{r} \frac{\partial}{\partial r} (r v_l) + \frac{\partial w_l}{\partial z} \right)] \right) \\ + \frac{\mu_{l,t}}{\sigma_{\alpha_l,t}} \frac{\partial \alpha_l}{\partial r} \left[ \frac{1}{r} \frac{\partial}{\partial r} (r v_l) + \frac{\partial w_l}{\partial z} \right] - \alpha_l \frac{\partial p}{\partial r} \\ + \alpha_l \rho_l g_r + F_{l,r}^C + \overline{F_{l,r}^{C'}} \end{aligned} \quad (\text{C.205})$$

In the FVM, the integral form of the momentum equation is used. The differential equation is thus integrated in time and over a grid cell volume in the staggered grid for the  $v$ -velocity sketched in Fig C.4.4.

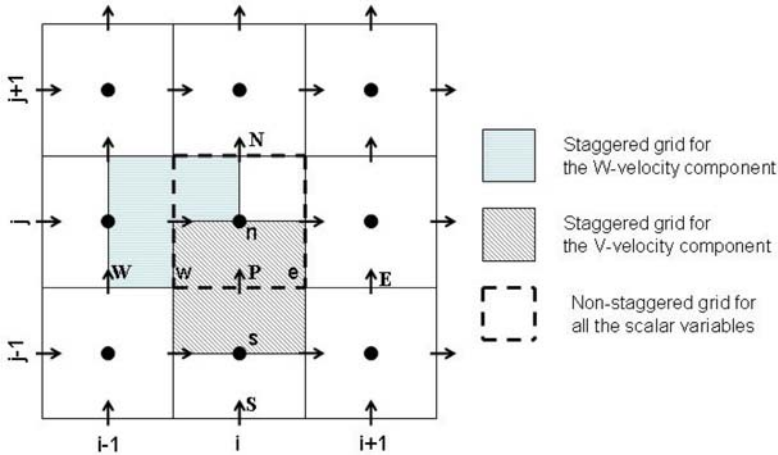


**Fig. C.3.** A sketch of the staggered  $v$ -grid cell in Cartesian coordinates. The figure shows the distribution of the variables in this grid, and the configuration of the staggered  $w$ -velocity grid and the non-staggered scalar grid. In cylindrical coordinates equivalent grid cells can be defined.

**The transient term**

$$\int_{\Delta V} \int_t^{t+\Delta t} \frac{\partial}{\partial t} (\alpha_l \rho_l v_l) dt dV = \left[ (\alpha_l \rho_l v_l)_P - (\alpha_l \rho_l v_l)_P^o \right] \Delta V \tag{C.206}$$

To approximate the scalar grid cell variables  $\alpha$  and  $\rho$  at the staggered velocity grid cell nodes, arithmetic interpolation is needed:

$$(\alpha_l \rho_l v_l)_P = \frac{1}{2} \left[ (\alpha_{l,P} \rho_{l,P}) + (\alpha_{l,S} \rho_{l,S}) \right] v_{l,P} \tag{C.207}$$

$$(\alpha_l \rho_l v_l)_P^o = \frac{1}{2} \left[ (\alpha_{l,P} \rho_{l,P})^o + (\alpha_{l,S} \rho_{l,S})^o \right] v_{l,P}^o \tag{C.208}$$

**The convection terms**

The locations of the node points in the staggered grid for the  $v$ -velocity are shown in Fig C.4.4.

Radial direction:

$$\begin{aligned} \int_{\Delta t \Delta V} \int \frac{1}{r} \frac{\partial}{\partial r} (r \alpha_l \rho_l v_l v_l) r dr dz dt &= \Delta z \left[ (r \alpha_l \rho_l v_l)_n v_{l,n} - (r \alpha_l \rho_l v_l)_s v_{l,s} \right] \Delta t \\ &= C_n v_{l,n} \Delta t - C_s v_{l,s} \Delta t \end{aligned} \quad (\text{C.209})$$

To approximate the scalar grid cell mass fluxes at the staggered velocity grid cell surface points, arithmetic interpolation is frequently used:

$$\begin{aligned} C_n &= A_n \frac{1}{2} [F_N + F_P] \\ C_s &= A_s \frac{1}{2} [F_P + F_S] \\ F_N &= (\alpha_l \rho_l v_l)_N = \frac{1}{2} [\alpha_{l,N} \rho_{l,N} + \alpha_{l,P} \rho_{l,P}] v_{l,N} \\ F_P &= (\alpha_l \rho_l v_l)_P = \frac{1}{2} [\alpha_{l,P} \rho_{l,P} + \alpha_{l,S} \rho_{l,S}] v_{l,P} \\ F_S &= (\alpha_l \rho_l v_l)_S = \frac{1}{2} [\alpha_{l,S} \rho_{l,S} + \alpha_{l,SS} \rho_{l,SS}] v_{l,S} \end{aligned} \quad (\text{C.210})$$

Axial direction:

$$\begin{aligned} \int_{\Delta t \Delta V} \int \frac{\partial}{\partial z} (\alpha_l \rho_l w_l v_l) dz r dr dt &= [(r \Delta r \alpha_l \rho_l w_l)_e v_{l,e} - (r \Delta r \alpha_l \rho_l w_l)_w v_{l,w}] \Delta t \\ &= C_e v_{l,e} \Delta t - C_w v_{l,w} \Delta t \end{aligned} \quad (\text{C.211})$$

To approximate the scalar grid cell mass fluxes at the staggered velocity grid cell surface points, arithmetic interpolation is frequently used:

$$\begin{aligned} C_e &= A_e \frac{1}{2} [F_E + F_{SE}] \\ C_w &= A_w \frac{1}{2} [F_W + F_{SW}] \\ F_E &= (\alpha_l \rho_l u)_E = \frac{1}{2} [\alpha_{l,E} \rho_{l,E} + \alpha_{l,P} \rho_{l,P}] u_{l,E} \\ F_{SE} &= (\alpha_l \rho_l u)_{SE} = \frac{1}{2} [\alpha_{l,S} \rho_{l,S} + \alpha_{l,SE} \rho_{l,SE}] u_{l,SE} \\ F_W &= (\alpha_l \rho_l u)_W = \frac{1}{2} [\alpha_{l,P} \rho_{l,P} + \alpha_{l,W} \rho_{l,W}] u_{l,P} \\ F_{SW} &= (\alpha_l \rho_l u)_{SW} = \frac{1}{2} [\alpha_{l,S} \rho_{l,S} + \alpha_{l,SW} \rho_{l,SW}] u_{l,S} \end{aligned} \quad (\text{C.212})$$

### The Diffusion terms

The location of the node points in the staggered grid for the  $v$ -velocity are shown in Fig C.4.4.

Radial direction:

$$\begin{aligned}
 \int_{\Delta t \Delta V} \frac{1}{r} \frac{\partial}{\partial r} (r \alpha_l \mu_{l,eff} \frac{\partial v_l}{\partial r}) r dr dz dt &= \Delta z [(r \alpha_l \mu_{l,eff} \frac{\partial v_l}{\partial r})_n - (r \alpha_l \mu_{l,eff} \frac{\partial v_l}{\partial r})_s] \Delta t \\
 &= A_n \Gamma_n \left[ \frac{v_{l,N} - v_{l,P}}{\delta r_{NP}} \right] \Delta t - A_s \Gamma_s \left[ \frac{v_{l,P} - v_{l,S}}{\delta r_{PS}} \right] \Delta t \\
 &= D_n (v_{l,N} - v_{l,P}) \Delta t - D_s (v_{l,P} - v_{l,S}) \Delta t
 \end{aligned} \tag{C.213}$$

To approximate the scalar grid cell mass fluxes at the staggered velocity grid cell surface points, arithmetic interpolation is frequently used:

$$\begin{aligned}
 D_n &= \frac{A_n \Gamma_n}{\delta r_{NP}} \\
 D_s &= \frac{A_s \Gamma_s}{\delta r_{PS}} \\
 \Gamma_n &= (\alpha_l \mu_{l,eff})_n = \alpha_{l,P} \mu_{l,eff,P} \\
 \Gamma_s &= (\alpha_l \mu_{l,eff})_s = \alpha_{l,S} \mu_{l,eff,S}
 \end{aligned} \tag{C.214}$$

Axial direction:

$$\begin{aligned}
 \int_{\Delta t \Delta V} \frac{\partial}{\partial z} (\alpha_l \mu_{l,eff} \frac{\partial v}{\partial z}) dz r dr dt &= [r_p \Delta r (\alpha_l \mu_{l,eff} \frac{\partial v}{\partial z})_e - r_p \Delta r (\alpha_l \mu_{l,eff} \frac{\partial v}{\partial z})_w] \Delta t \\
 &= A_e \Gamma_e \left[ \frac{v_{l,E} - v_{l,P}}{\delta z_{EP}} \right] \Delta t - A_w \Gamma_w \left[ \frac{v_{l,P} - v_{l,W}}{\delta z_{PW}} \right] \Delta t \\
 &= D_e (v_{l,E} - v_{l,P}) \Delta t - D_w (v_{l,P} - v_{l,W}) \Delta t
 \end{aligned} \tag{C.215}$$

To approximate the scalar grid cell mass fluxes at the staggered velocity grid cell surface points, arithmetic interpolation is frequently used:

$$\begin{aligned}
 D_e &= \frac{A_e \Gamma_e}{\delta z_{EP}} \\
 D_w &= \frac{A_w \Gamma_w}{\delta z_{PW}} \\
 \Gamma_e &= (\alpha_l \mu_{l,eff})_e \\
 &= \frac{1}{4} [\alpha_{l,P} \mu_{l,eff,P} + \alpha_{l,E} \mu_{l,eff,E} + \alpha_{l,S} \mu_{l,eff,S} + \alpha_{l,SE} \mu_{l,eff,SE}] \\
 \Gamma_w &= (\alpha_l \mu_{l,eff})_w \\
 &= \frac{1}{4} [\alpha_{l,P} \mu_{l,eff,P} + \alpha_{l,W} \mu_{l,eff,W} + \alpha_{l,S} \mu_{l,eff,S} + \alpha_{l,SW} \mu_{l,eff,SW}]
 \end{aligned} \tag{C.216}$$

**The source terms**

The the source terms are approximated by the midpoint rule, in which  $S$  is considered an average value representative for the whole grid cell volume. The derivatives are represented by an abbreviated Taylor series expansion, usually a central difference expansion of second order is employed.

Term 1 on the RHS of the momentum equation:

$$\int \int_{\Delta t \Delta V} \frac{v_l}{r} \frac{\partial}{\partial r} \left( r \frac{\mu_{l,t}}{\sigma_{\alpha_{l,t}}} \frac{\partial \alpha_l}{\partial r} \right) dV dt = \frac{v_{l,P} \Delta V \Delta t}{r_P^v \frac{1}{2} (\delta r_{NP} + \delta r_{PS})} \left[ \left( r \mu_{l,t} \frac{\partial \alpha_l}{\partial r} \right)_n - \left( r \mu_{l,t} \frac{\partial \alpha_l}{\partial r} \right)_s \right] \tag{C.217}$$

This term is implemented through the source term  $S_C$  as:

$$S_{C,1} = \frac{v_{l,P} \Delta V \Delta t}{r_P^v \frac{1}{2} (\delta r_{NP} + \delta r_{PS})} \left[ r_P \mu_{l,P} \left( \frac{\partial \alpha_l}{\partial r} \right)_n - r_S \mu_{l,S} \left( \frac{\partial \alpha_l}{\partial r} \right)_s \right] \tag{C.218}$$

To approximate derivatives of scalar grid cell variables and scalar grid cell variables at the staggered velocity grid cell surface points, arithmetic interpolation is frequently used:

$$\begin{aligned} \left( \frac{\partial \alpha_l}{\partial r} \right)_n &= \frac{(\alpha_l)_N - (\alpha_l)_P}{\delta r_{NP}} = \frac{\frac{1}{2}(\alpha_{l,N} + \alpha_{l,P}) - \frac{1}{2}(\alpha_{l,P} + \alpha_{l,S})}{\delta r_{NP}} \\ \left( \frac{\partial \alpha_l}{\partial r} \right)_s &= \frac{(\alpha_l)_P - (\alpha_l)_S}{\delta r_{PS}} = \frac{\frac{1}{2}(\alpha_{l,P} + \alpha_{l,S}) - \frac{1}{2}(\alpha_{l,S} + \alpha_{l,SS})}{\delta r_{PS}} \end{aligned} \tag{C.219}$$

Term 2 on the RHS of the momentum equation:

$$\int \int_{\Delta t \Delta V} v_l \frac{\partial}{\partial z} \left( \frac{\mu_{l,t}}{\sigma_{\alpha_{l,t}}} \frac{\partial \alpha_l}{\partial z} \right) dV dt = \frac{v_{l,P} \Delta V \Delta t}{\frac{1}{2} (\delta z_{EP} + \delta z_{PW})} \left[ \left( \frac{\mu_{l,t}}{\sigma_{\alpha_{l,t}}} \frac{\partial \alpha_l}{\partial z} \right)_e - \left( \frac{\mu_{l,t}}{\sigma_{\alpha_{l,t}}} \frac{\partial \alpha_l}{\partial z} \right)_w \right] \tag{C.220}$$

This term is implemented through the source term  $S_C$  as:

$$S_{C,2} = \frac{v_{l,P} \Delta V \Delta t}{\frac{1}{2} (\delta z_{EP} + \delta z_{PW})} \left[ (\mu_l)_e \left( \frac{\partial \alpha_l}{\partial z} \right)_e - (\mu_l)_w \left( \frac{\partial \alpha_l}{\partial z} \right)_w \right] \tag{C.221}$$

To approximate derivatives of scalar grid cell variables and scalar grid cell variables at the staggered velocity grid cell surface points, arithmetic interpolation is frequently used:

$$\begin{aligned} \left( \frac{\partial \alpha_l}{\partial z} \right)_e &= \frac{(\alpha_l)_E - (\alpha_l)_P}{\delta z_{PE}} = \frac{\frac{1}{2}(\alpha_{l,E} + \alpha_{l,SE}) - \frac{1}{2}(\alpha_{l,E} + \alpha_{l,SE})}{\delta z_{PE}} \\ \left( \frac{\partial \alpha_l}{\partial z} \right)_w &= \frac{(\alpha_l)_P - (\alpha_l)_W}{\delta z_{WP}} = \frac{\frac{1}{2}(\alpha_{l,P} + \alpha_{l,S}) - \frac{1}{2}(\alpha_{l,W} + \alpha_{l,SW})}{\delta z_{WP}} \\ (\mu_l)_e &= \frac{1}{4} (\mu_{l,P} + \mu_{l,E} + \mu_{l,S} + \mu_{l,SE}) \\ (\mu_l)_w &= \frac{1}{4} (\mu_{l,P} + \mu_{l,W} + \mu_{l,S} + \mu_{l,SW}) \end{aligned} \tag{C.222}$$

The 3rd and 6th terms on the RHS of the momentum equation are identical and are approximated as follows:

$$\begin{aligned} & \int_{\Delta t \Delta V} \frac{1}{r} \frac{\partial}{\partial r} (r \alpha_l \mu_{l,eff} \frac{\partial v_l}{\partial r}) dV dt \\ &= \frac{\Delta V \Delta t}{r_P^v \frac{1}{2} (\delta r_{NP}^v + \delta r_{PS}^v)} [(r \alpha_l \mu_{l,eff} \frac{\partial v_l}{\partial r})_n - (r \alpha_l \mu_{l,eff} \frac{\partial v_l}{\partial r})_s] \end{aligned} \quad (C.223)$$

This term is implemented through the source term  $S_C$  as:

$$S_{C,3} = \frac{\Delta V \Delta t}{r_P^v \frac{1}{2} (\delta r_{NP}^v + \delta r_{PS}^v)} \left[ r_P \alpha_{l,P} \mu_{l,P} \left( \frac{v_{l,N} - v_{l,P}}{\delta r_{NP}^v} \right) - r_S \alpha_{l,S} \mu_{l,S} \left( \frac{v_{l,P} - v_{l,S}}{\delta r_{PS}^v} \right) \right] \quad (C.224)$$

The scalar grid cell variables at the staggered velocity grid cell surface points coincide with center nodes, hence no interpolation is needed.

The 4th and 7th terms on the RHS of the momentum equation are identical. They are approximated as follows:

$$\begin{aligned} & -2 \int_{\Delta t \Delta V} \frac{1}{r} \alpha_l \mu_{l,eff} \frac{v_l}{r} dV dt = -2 (\alpha_l \mu_{l,eff})_P \frac{v_{l,P}}{r_P^{2,v}} \Delta V \Delta t \\ &= -2 \times \frac{1}{2} (\alpha_{l,P} \mu_{l,eff,P} + \alpha_{l,S} \mu_{l,S}) \frac{v_{l,P}}{r_P^{2,v}} \Delta V \Delta t \end{aligned} \quad (C.225)$$

This term is implemented through the source term  $S_p$  as:

$$S_{P,1} = -2 \times \frac{1}{2} (\alpha_{l,P} \mu_{l,eff,P} + \alpha_{l,S} \mu_{l,S}) \frac{1}{r_P^{2,v}} \Delta V \Delta t \quad (C.226)$$

To approximate scalar grid cell variables at the staggered velocity grid cell surface points, arithmetic interpolation is used:

$$(\mu_l)_P = \frac{1}{2} (\mu_{l,P} + \mu_{l,S}) \quad (C.227)$$

The 5th term on the RHS of the momentum equation:

$$\begin{aligned} & \int_{\Delta t \Delta V} \frac{\partial}{\partial z} (\alpha_l \mu_{l,eff} \frac{\partial v_l}{\partial z}) dV dt \\ &= \frac{\Delta V \Delta t}{\frac{1}{2} (\delta z_{EP} + \delta z_{PW})} [(\alpha_l \mu_{l,eff} \frac{\partial v_l}{\partial z})_e - (\alpha_l \mu_{l,eff} \frac{\partial v_l}{\partial z})_w] \end{aligned} \quad (C.228)$$

This term is implemented through the source term  $S_C$  as:

$$S_{C,4} = \frac{\Delta V \Delta t}{\frac{1}{2} (\delta z_{EP} + \delta z_{PW})} [(\alpha_l \mu_l)_e \left( \frac{\partial v_l}{\partial z} \right)_e - (\alpha_l \mu_l)_w \left( \frac{\partial v_l}{\partial z} \right)_w] \quad (C.229)$$

To velocity derivatives are approximated by use of the central difference scheme:

$$\begin{aligned} \left(\frac{\partial v_l}{\partial z}\right)_e &= \frac{v_{l,E} - v_{l,P}}{\delta z_{PE}} \\ \left(\frac{\partial v_l}{\partial z}\right)_w &= \frac{v_{l,P} - v_{l,W}}{\delta z_{WP}} \end{aligned} \tag{C.230}$$

The 8th term on the RHS of the momentum equation:

$$\begin{aligned} &\int \int_{\Delta t \Delta V} \frac{\partial}{\partial z} (\alpha_l \mu_{l,eff} \frac{\partial w_l}{\partial r}) dV dt \\ &= \frac{\Delta V \Delta t}{\frac{1}{2}(\delta z_{PW} + \delta r_{EP}^v)} \left[ (\alpha_l \mu_{l,eff} \frac{\partial w_l}{\partial r})_e - (\alpha_l \mu_{l,eff} \frac{\partial w_l}{\partial r})_w \right] \end{aligned} \tag{C.231}$$

This term is implemented through the source term  $S_C$  as:

$$S_{C,5} = \frac{\Delta V \Delta t}{\frac{1}{2}(\delta z_{PW} + \delta r_{EP}^v)} \left[ \Gamma_e \frac{(w_{l,E} - w_{l,SE})}{\frac{1}{2}(\delta r_{NP}^v + \delta r_{PS}^v)} - \Gamma_w \frac{(w_{l,P} - w_{l,S})}{\frac{1}{2}(\delta r_{NP}^v + \delta r_{PS}^v)} \right] \tag{C.232}$$

Term 9A on the RHS of the momentum equation:

$$- \int \int_{\Delta t \Delta V} \frac{\partial}{\partial r} \left( \frac{2}{3} \alpha_l \rho_l k \right) dV dt = - \frac{2 \Delta V \Delta t}{3 \times \frac{1}{2}(\delta r_{NP}^v + \delta r_{PS}^v)} [(\alpha_l \rho_l k)_n - (\alpha_l \rho_l k)_s] \tag{C.233}$$

This term is implemented through the source term  $S_C$  as:

$$S_{C,6} = \frac{2 \Delta V \Delta t}{3 \times \frac{1}{2}(\delta r_{NP}^v + \delta r_{PS}^v)} [\alpha_{l,P} \rho_{l,P} k_P - \alpha_{l,S} \rho_{l,S} k_S] \tag{C.234}$$

The scalar grid cell variables at the staggered velocity grid cell surface points coincide with center nodes, hence no interpolation is needed.

Term 9B on the RHS of the momentum equation:

$$\begin{aligned} &- \int \int_{\Delta t \Delta V} \frac{\partial}{\partial r} \left( \frac{2}{3} \alpha_l \rho_l \nu_{l,eff} \frac{1}{r} \frac{\partial (rv_l)}{\partial r} \right) dV dt \\ &= - \frac{2 \Delta V \Delta t}{3 \times \frac{1}{2}(\delta r_{NP}^v + \delta r_{PS}^v)} \left[ \left( \frac{\alpha_l \mu_{l,eff}}{r} \frac{\partial (rv_l)}{\partial r} \right)_n - \left( \frac{\alpha_l \mu_{l,eff}}{r} \frac{\partial (rv_l)}{\partial r} \right)_s \right] \end{aligned} \tag{C.235}$$

This term is implemented through the source term  $S_C$  as:

$$S_{C,7} = - \frac{2 \Delta V \Delta t}{3 \times \frac{1}{2}(\delta r_{NP}^v + \delta r_{PS}^v)} \left[ \frac{\alpha_{l,P} \mu_{l,eff,P}}{r_P} \frac{\partial (rv_l)}{\partial r} \Big|_n - \frac{\alpha_{l,W} \mu_{l,eff,W}}{r_S} \frac{\partial (rv_l)}{\partial r} \Big|_s \right] \tag{C.236}$$

where

$$\begin{aligned}\frac{\partial(rv_l)}{\partial r}\Big|_n &= \frac{(rv_l)_N - (rv_l)_P}{\delta r_{NP}^v} = \frac{r_N^v v_{l,N} - r_P^v v_{l,P}}{\delta r_{NP}^v} \\ \frac{\partial(rv_l)}{\partial r}\Big|_s &= \frac{(rv_l)_P - (rv_l)_S}{\delta r_{PS}^v} = \frac{r_P^v v_{l,P} - r_S^v v_{l,S}}{\delta r_{PS}^v}\end{aligned}\quad (\text{C.237})$$

Term 9C on the RHS of the momentum equation:

$$\begin{aligned}- \int \int_{\Delta t \Delta V} \frac{\partial}{\partial r} \left( \frac{2}{3} \alpha_l \rho_l v_{l,eff} \frac{\partial w_l}{\partial z} \right) dV dt \\ = - \frac{2 \Delta V \Delta t}{3 \times \frac{1}{2} (\delta r_{NP}^v + \delta r_{PS}^v)} \left[ (\alpha_l \mu_{l,eff} \frac{\partial w_l}{\partial z})_n - (\alpha_l \mu_{l,eff} \frac{\partial w_l}{\partial z})_s \right]\end{aligned}\quad (\text{C.238})$$

This term is implemented through the source term  $S_C$  as:

$$\begin{aligned}S_{C,8} = - \frac{2 \Delta V \Delta t}{3 \times \frac{1}{2} (\delta r_{NP}^v + \delta r_{PS}^v)} \left[ \alpha_{l,P} \mu_{l,eff,P} \frac{(w_{l,E} - w_{l,P})}{\frac{1}{2} (\delta z_{EP} + \delta z_{PW})} \right] \\ + \frac{2 \Delta V \Delta t}{3 \times \frac{1}{2} (\delta r_{NP}^v + \delta r_{PS}^v)} \left[ \alpha_{l,W} \mu_{l,eff,W} \frac{(w_{l,P} - w_{l,W})}{\frac{1}{2} (\delta z_{EP} + \delta z_{PW})} \right]\end{aligned}\quad (\text{C.239})$$

Term 10 on the RHS of the momentum equation:

$$\int \int_{\Delta t \Delta V} \frac{\mu_{l,t}}{\sigma_{\alpha,t}} \frac{\partial \alpha_l}{\partial r} \left( \frac{1}{r} \frac{\partial}{\partial r} (rv_l) + \frac{\partial w_l}{\partial z} \right) dV dt = \left( \frac{\mu_{l,t}}{\sigma_{\alpha,t}} \frac{\partial \alpha_l}{\partial r} \right)_P \left[ \frac{1}{r} \frac{\partial}{\partial r} (rv_l) + \frac{\partial w_l}{\partial z} \right]_P \Delta V \Delta t \quad (\text{C.240})$$

This term is implemented through the source term  $S_C$  as:

$$S_{C,9} = \frac{\frac{1}{2} \left( \frac{\mu_{l,t,P}}{\sigma_{\alpha,t}} + \frac{\mu_{l,t,S}}{\sigma_{\alpha,t}} \right)}{\sigma_{\alpha,t}} \left( \frac{\partial \alpha_l}{\partial r} \right)_P \left[ \frac{1}{r_P^v} \frac{(r_P v_n - r_S v_s)}{\delta r_{PS}^v} + \left( \frac{\partial w_l}{\partial z} \right)_P \right] \Delta V \Delta t \quad (\text{C.241})$$

To approximate derivatives of velocity variables and scalar grid cell variables at the staggered velocity grid cell node points, arithmetic interpolation is frequently used:

$$\begin{aligned}\left( \frac{\partial \alpha_l}{\partial r} \right)_P &= \frac{(\alpha_l)_n - (\alpha_l)_s}{\frac{1}{2} (\delta r_{NP}^v + \delta r_{PS}^v)} = \frac{\alpha_{l,P} - \alpha_{l,S}}{\frac{1}{2} (\delta r_{NP}^v + \delta r_{PS}^v)} \\ (\mu_l)_P &= \frac{1}{2} (\mu_{l,P} + \mu_{l,S}) \\ \left( \frac{\partial w_l}{\partial z} \right)_P &= \frac{(w_l)_e - (w_l)_w}{\frac{1}{2} (\delta z_{PW} + \delta z_{EP})} = \frac{\frac{1}{2} (w_E + w_{SE}) - \frac{1}{2} (w_P + w_S)}{\frac{1}{2} (\delta z_{PW} + \delta z_{EP})}\end{aligned}\quad (\text{C.242})$$

**Pressure force:**

$$-\int_{\Delta t \Delta V} \alpha_l \frac{\partial p}{\partial r} dV dt = -\frac{1}{2}(\alpha_{l,P} + \alpha_{l,S}) \frac{(P_P - P_S)}{\frac{1}{2}(\delta r_{NP}^v + \delta r_{PS}^v)} \Delta V \Delta t \quad (\text{C.243})$$

This term is implemented through the source term  $S_C$  as:

$$S_{C,10} = -(\alpha_l)_P \frac{(P_P - P_S)}{\delta r_{PS}} \Delta V \Delta t \quad (\text{C.244})$$

To approximate scalar grid cell variables at the staggered velocity grid cell node points, arithmetic interpolation is frequently used:

$$(\alpha_l)_P = \frac{1}{2}(\alpha_{l,P} + \alpha_{l,S}) \quad (\text{C.245})$$

**Gravity force:**

There is no gravity force in radial direction.

**Added Mass force:**

$$\begin{aligned} & - \int_{\Delta t \Delta V} \alpha_l \alpha_g \rho_l f_v [w_l \frac{\partial v_l}{\partial z} + v_l \frac{\partial v_l}{\partial r} - (w_g \frac{\partial v_g}{\partial z} + v_g \frac{\partial v_g}{\partial r})] dV dt = \\ & - f_v (\alpha_l)_P (\alpha_g)_P (\rho_l)_P [w_l \frac{\partial v_l}{\partial z} + v_l \frac{\partial v_l}{\partial r} - (w_g \frac{\partial v_g}{\partial z} + v_g \frac{\partial v_g}{\partial r})]_P \Delta V \Delta t \end{aligned} \quad (\text{C.246})$$

This term is implemented through the source term  $S_C$  as:

$$\begin{aligned} S_{C,11} = & -f_v \frac{1}{2}(\alpha_{l,P} + \alpha_{l,S}) \frac{1}{2}(\alpha_{g,P} + \alpha_{g,S}) \frac{1}{2}(\rho_{l,P} + \rho_{l,S}) \times \\ & [w_l \frac{\partial v_l}{\partial z} + v_l \frac{\partial v_l}{\partial r} - (w_g \frac{\partial v_g}{\partial z} + v_g \frac{\partial v_g}{\partial r})]_P \Delta V \Delta t \end{aligned} \quad (\text{C.247})$$

To approximate derivatives of velocity variables and scalar grid cell variables at the staggered velocity grid cell node points, arithmetic interpolation is frequently used:

$$\begin{aligned} (\alpha_l)_P &= \frac{1}{2}(\alpha_{l,P} + \alpha_{l,S}) \\ (w_l)_P &= \frac{1}{4}(v_{l,P} + v_{l,S} + v_{l,E} + v_{l,SE}) \\ \left(\frac{\partial v_l}{\partial r}\right)_P &= \frac{v_{l,n} - v_{l,s}}{\frac{1}{2}(\delta r_{NP}^v + \delta r_{PS}^v)} = \frac{\frac{1}{2}(v_{l,P} + v_{l,N}) - \frac{1}{2}(v_{l,P} + v_{l,S})}{\frac{1}{2}(\delta r_{NP}^v + \delta r_{PS}^v)} \\ \left(\frac{\partial v_l}{\partial z}\right)_P &= \frac{v_{l,e} - v_{l,w}}{\frac{1}{2}(\delta z_{PW} + \delta z_{EP})} = \frac{\frac{1}{2}(v_{l,P} + v_{l,E}) - \frac{1}{2}(v_{l,P} + v_{l,W})}{\frac{1}{2}(\delta z_{PW} + \delta z_{EP})} \end{aligned} \quad (\text{C.248})$$

**Transversal force:**

$$\begin{aligned}
 & - \int_{\Delta t \Delta t} \alpha_l \alpha_g \rho_l C_L (w_l - w_g) \frac{\partial w_l}{\partial r} dV dt = \\
 & - (\alpha_l)_P (\alpha_g)_P (\rho_l)_P C_L \Delta w_P \left( \frac{\partial w_l}{\partial r} \right)_P \Delta V \Delta t
 \end{aligned} \tag{C.249}$$

This term is implemented through the source term  $S_C$  as:

$$S_{C,12} = -\frac{1}{2}(\alpha_{l,P} + \alpha_{l,S}) \frac{1}{2}(\alpha_{g,P} + \alpha_{g,S}) \frac{1}{2}(\rho_{l,P} + \rho_{l,S}) C_L \Delta w_P \left( \frac{\partial w_l}{\partial r} \right)_P \Delta V \Delta t \tag{C.250}$$

To approximate derivatives of velocity variables and scalar grid cell variables at the staggered velocity grid cell node points, arithmetic interpolation is used:

$$\begin{aligned}
 (\alpha_l)_P &= \frac{1}{2}(\alpha_{l,P} + \alpha_{l,S}) \\
 \Delta w_P &= (w_l - w_g)_P \\
 &= \frac{1}{4}(w_{l,P} - w_{g,P} + w_{l,E} - w_{g,E} + w_{l,S} - w_{g,S} + w_{l,SE} - w_{g,SE}) \\
 \left( \frac{\partial w_l}{\partial r} \right)_P &= \frac{w_{l,n} - w_{l,s}}{\frac{1}{2}(\delta r_{NP}^v + \delta r_{PS}^v)} = \frac{\frac{1}{2}(w_{l,P} + w_{l,E}) - \frac{1}{2}(w_{l,S} + w_{l,SE})}{\frac{1}{2}(\delta r_{NP}^v + \delta r_{PS}^v)} \\
 C_L &= f_L - \frac{3}{4} \frac{\nu_{l,t}}{\nu_l} \frac{C_D C_\tau}{(1 + \frac{\tau_L}{t_p}) \overline{Re}_p}
 \end{aligned} \tag{C.251}$$

**Steady drag force:**

$$\int_{\Delta t \Delta V} \frac{3}{4} \alpha_l \alpha_g \rho_l \frac{C_D}{d_S} |\mathbf{v}_l - \mathbf{v}_g| (v_l - v_g) dV dt \approx (K)_P (v_{l,P} - v_{g,P}) \Delta V \Delta t \tag{C.252}$$

To approximate scalar grid cell variables at the staggered velocity grid cell node points, arithmetic interpolation is used:

$$\begin{aligned}
 (K)_P &= \frac{1}{2}(K_P + K_S) \\
 K_P &= \left[ \frac{3}{4} \alpha_l \alpha_g \rho_l \frac{C_D}{d_S} |\mathbf{v}_l - \mathbf{v}_g| \right]_P = [\alpha_l \alpha_g C_W]_P = \frac{3}{4} \alpha_{l,P} \alpha_{g,P} \rho_{l,P} \left( \frac{C_D}{d_S} \right)_P |\mathbf{v}_l - \mathbf{v}_g|_P
 \end{aligned} \tag{C.253}$$

and the relative speed at the center node in the staggered  $v$ -grid cell volume is approximated by:

$$|\mathbf{v}_l - \mathbf{v}_g|_P \approx \left[ \frac{1}{2}(w_{l,P} + w_{l,S}) - \frac{1}{2}(w_{g,P} + w_{g,S}) \right]^2 + \left[ \frac{1}{2}(v_{l,P} + v_{l,W}) - \frac{1}{2}(v_{g,P} + v_{g,W}) \right]^2 \Bigg]^{1/2} \quad (\text{C.254})$$

To deal with the strong coupling between the phasic momentum equations, the *partial elimination algorithm* (PEA)-method proposed by Spalding [18, 19] is frequently used.

To outline the PEA-method, the discretized momentum equations for the gas phase at the  $e$  location in the staggered grid for the  $w$  variable (i.e., between the P and E grid points in the scalar grid) is re-written pulling the drag force out of the source term:

$$a_{g,n}v_{g,n} = \sum_{nb} a_{g,nb}v_{g,nb} + K(v_{l,n} - v_{g,n})\Delta V + S_g \quad (\text{C.255})$$

One part of the drag term is put on the LHS of the equation, thus we may write:

$$v_{g,n}(a_{g,n} + K\Delta V) = \sum_{nb} a_{g,nb}v_{g,nb} + K\Delta V v_{l,n} + S_g \quad (\text{C.256})$$

The  $v_{g,n}$  is then given by:

$$v_{g,n} = \frac{\sum_{nb} a_{g,nb}w_{g,nb} + K\Delta V v_{l,n} + S_g}{a_{g,n} + K\Delta V} \quad (\text{C.257})$$

In the same way we can write for the liquid velocity (shown shortly):

$$v_{l,n} = \frac{\sum_{nb} a_{l,nb}v_{l,nb} + K\Delta V v_{g,n} + S_l}{a_{l,n} + K\Delta V} \quad (\text{C.258})$$

Combining these two equations to take out  $v_{l,n}$  in the gas calculations and  $v_{g,n}$  in the liquid calculations we get:

$$v_{g,n} = \frac{\sum_{nb} a_{g,nb}v_{g,nb} + K\Delta V \frac{\sum_{nb} a_{l,nb}v_{l,nb} + K\Delta V v_{g,n} + S_l}{a_{l,n} + K\Delta V} + S_g}{a_{g,n} + K\Delta V} \quad (\text{C.259})$$

and

$$v_{l,n} = \frac{\sum_{nb} a_{l,nb}v_{l,nb} + K\Delta V \frac{\sum_{nb} a_{g,nb}v_{g,nb} + K\Delta V v_{l,n} + S_g}{a_{g,n} + K\Delta V} + S_l}{a_{l,n} + K\Delta V} \quad (\text{C.260})$$

In the equation for phase  $k$  all the  $v_{k,n}$  terms can be regrouped on the left, hence for  $k = g, l$  we get:

$$v_{g,n}(a_{g,n} + K\Delta V - \frac{(K\Delta V)^2}{a_{l,n} + K\Delta V}) = \sum_{nb} a_{g,nb}v_{g,nb} + K\Delta V \frac{\sum_{nb} a_{l,nb}v_{l,nb} + S_l}{a_{l,n} + K\Delta V} + S_g \quad (\text{C.261})$$

$$\begin{aligned}
 v_{l,n}(a_{l,n} + K\Delta V - \frac{(K\Delta V)^2}{a_{g,n} + K\Delta V}) = \sum_{nb} a_{l,nb}v_{l,nb} \\
 + K\Delta V \frac{\sum_{nb} a_{g,nb}v_{g,nb} + S_g}{a_{g,n} + K\Delta V} + S_l
 \end{aligned} \tag{C.262}$$

This means that the modified coupling terms  $K\Delta V \frac{\sum a_{k,i}v_{k,i} + S_k}{a_{k,n} + K\Delta V}$  and  $K\Delta V - \frac{(K\Delta V)^2}{a_{k,n} + K\Delta V}$  must be calculated separately for the momentum balance components in each phase, then transferred and employed in the corresponding equation for the other phase. In particular, after the coupling terms have been received from the phase where they are calculated, the modified terms are added to the source  $S_e$  and the coefficient  $a_e$  terms in the other phase, respectively. In this case,  $S_k$  denotes the sum of all source terms except the drag force.

### Algebraic discretization equation

Finally, after dividing all the terms by  $\Delta t$ , the discretized equation can be written on the standard algebraic form:

$$a_P v_{l,P} = a_N v_{l,N} + a_S v_{l,S} + a_E v_{l,E} + a_W v_{l,W} + b_{v_l} \tag{C.263}$$

in which the coefficients are defined by:

$$\begin{aligned}
 a_N &= D_n + \max[-C_n, 0] \\
 a_S &= D_s + \max[C_s, 0] \\
 a_E &= D_e + \max[-C_e, 0] \\
 a_W &= D_w + \max[C_w, 0] \\
 b &= \sum_m S_{C,m} + a_P^0 v_{l,P}^0 \\
 a_P &= \frac{\Delta V}{\Delta t} (\alpha_l \rho_l)_P + a_N + a_S + a_E + a_W + C_n - C_s + C_e - C_w - \sum_q S_{P,q} \Delta V
 \end{aligned} \tag{C.264}$$

To avoid negative coefficients, the relation for the coefficient  $a_P$  can be modified using the continuity equation (C.187). The negative  $mC_2$ -term is then moved to the RHS of the discretized transport equation and included as part of the  $b$ -term. The alternative  $a_P^*$  and  $b^*$  coefficients are defined by:

$$\begin{aligned}
 b^* &= -mC_2 v_{l,P}^v + \sum_m S_{C,m,l} + a_P^0 v_{l,P}^0 \\
 a_P^* &= \frac{\Delta V}{\Delta t} (\alpha_l \rho_l)_P^0 + a_N + a_S + a_E + a_W + mC_1 - \sum_q S_{P,q,l} \Delta V
 \end{aligned} \tag{C.265}$$

### C.4.5 The Liquid phase axial momentum balance

The axial component of the momentum balance is given in (C.137).

$$\begin{aligned}
 \frac{\partial}{\partial t}(\alpha_l \rho_l w_l) + \frac{1}{r} \frac{\partial}{\partial r}(r \alpha_l \rho_l v_l w_l) + \frac{\partial}{\partial z}(\alpha_l \rho_l w_l w_l) = \\
 w_l \frac{1}{r} \frac{\partial}{\partial r}(r \frac{\mu_{l,t}}{\sigma_{\alpha_{l,t}}} \frac{\partial \alpha_l}{\partial r}) + w_l \frac{\partial}{\partial z}(\frac{\mu_{l,t}}{\sigma_{\alpha_{l,t}}} \frac{\partial \alpha_l}{\partial z}) \\
 + \frac{\mu_{l,t}}{\sigma_{\alpha_{l,t}}} \frac{\partial \alpha_l}{\partial z} (\frac{1}{r} \frac{\partial}{\partial r}(r v_l) + \frac{\partial w_l}{\partial z}) \\
 + \frac{1}{r} \frac{\partial}{\partial r}(r \alpha_l \mu_{l,\text{eff}} \frac{\partial w_l}{\partial r}) + \frac{\partial}{\partial z}(\alpha_l \mu_{l,\text{eff}} \frac{\partial w_l}{\partial z}) \\
 + \frac{1}{r} \frac{\partial}{\partial r}(r \alpha_l \mu_{l,\text{eff}} \frac{\partial v_l}{\partial z}) + \frac{\partial}{\partial z}(\alpha_l \mu_{l,\text{eff}} \frac{\partial w_l}{\partial z}) \\
 - \frac{\partial}{\partial z}(\frac{2}{3} \alpha_l \rho_l (k + \nu_{l,\text{eff}} (\frac{1}{r} \frac{\partial}{\partial r}(r v_l) + \frac{\partial w_l}{\partial z}))) \\
 - \alpha_l \frac{\partial p}{\partial z} + \alpha_l \rho_l g_z + F_{l,z}^C + \overline{F_{l,z}^{C'}}
 \end{aligned} \tag{C.266}$$

In the FVM, the integral form of the momentum equation is used. The differential equation is thus integrated in time and over a grid cell volume in the staggered grid for the  $w$ -velocity sketched in Fig C.4.

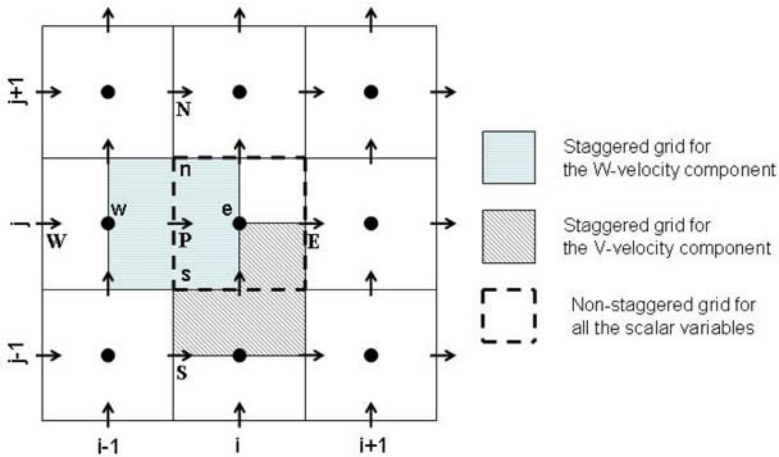


**Fig. C.4.** A staggered Cartesian  $w$ -grid cell, the distribution of the variables in this grid and the configuration of the staggered  $v$ -velocity grid cell and the non-staggered scalar grid. In cylindrical coordinates equivalent grid cells can be defined.

### The Transient term

$$\int_{\Delta V} \int_t^{t+\Delta t} \frac{\partial}{\partial t} (\alpha_l \rho_l w_l) dt dV = \left[ (\alpha_l \rho_l w_l)_P - (\alpha_l \rho_l w_l)_P^o \right] \Delta V \quad (\text{C.267})$$

To approximate the scalar grid cell variables  $\alpha$  and  $\rho$  at the staggered velocity grid cell nodes, arithmetic interpolation is needed:

$$(\alpha_l \rho_l w_l)_P = \frac{1}{2} [(\alpha_{l,P} \rho_{l,P}) + (\alpha_{l,W} \rho_{l,W})] w_{l,P} \quad (\text{C.268})$$

$$(\alpha_l \rho_l w_l)_P^o = \frac{1}{2} [(\alpha_{l,P} \rho_{l,P})^o + (\alpha_{l,W} \rho_{l,W})^o] w_{l,P}^o \quad (\text{C.269})$$

### The convection term

The locations of the node points in the staggered grid for the  $w$ -velocity component are shown in Fig C.4.

Radial direction:

$$\begin{aligned} \int_{\Delta t \Delta V} \int \frac{1}{r} \frac{\partial}{\partial r} (r \alpha_l \rho_l v_l w_l) r dr dz dt &= \Delta z [(r \alpha_l \rho_l v_l w_l)_n - (r \alpha_l \rho_l v_l w_l)_s] \Delta t \\ &= C_n u_{l,n} \Delta t - C_s u_{l,s} \Delta t \end{aligned} \quad (\text{C.270})$$

To approximate the scalar grid cell mass fluxes at the staggered velocity grid cell surface points, arithmetic interpolation is frequently used:

$$\begin{aligned} C_n &= A_n F_n = A_n \frac{1}{2} [F_N + F_{NW}] \\ C_s &= A_n F_n = A_s \frac{1}{2} [F_S + F_{SW}] \\ F_N &= (\alpha_l \rho_l v_l)_N = \frac{1}{2} [\alpha_{l,N} \rho_{l,N} + \alpha_{l,P} \rho_{l,P}] v_{l,N} \\ F_{NW} &= (\alpha_l \rho_l v_l)_{NW} = \frac{1}{2} [\alpha_{l,W} \rho_{l,W} + \alpha_{l,NW} \rho_{l,NW}] v_{l,NW} \\ F_S &= (\alpha_l \rho_l v_l)_S = \frac{1}{2} [\alpha_{l,S} \rho_{l,S} + \alpha_{l,P} \rho_{l,P}] v_{l,P} \\ F_{SW} &= (\alpha_l \rho_l v_l)_{SW} = \frac{1}{2} [\alpha_{l,W} \rho_{l,W} + \alpha_{l,SW} \rho_{l,SW}] v_{l,W} \end{aligned} \quad (\text{C.271})$$

Axial direction:

$$\begin{aligned} \int_{\Delta t \Delta V} \int \frac{\partial}{\partial z} (\alpha_l \rho_l w_l w_l) dz r dr dt &= [r_p \Delta r (\alpha_l \rho_l w_l w_l)_e - r_p \Delta r (\alpha_l \rho_l w_l w_l)_w] \Delta t \\ &= C_e u_{l,e} \Delta t - C_w u_{l,w} \Delta t \end{aligned} \quad (\text{C.272})$$

To approximate the scalar grid cell mass fluxes at the staggered velocity grid cell surface points, arithmetic interpolation is frequently used:

$$\begin{aligned} C_e &= A_e F_e = A_e \frac{1}{2} [F_E + F_P] \\ C_w &= A_w F_w = A_w \frac{1}{2} [F_P + F_W] \\ F_E &= (\alpha_l \rho_l w_l)_E = \frac{1}{2} [\alpha_{l,P} \rho_{l,P} + \alpha_{l,E} \rho_{l,E}] w_{l,E} \\ F_P &= (\alpha_l \rho_l w_l)_P = \frac{1}{2} [\alpha_{l,P} \rho_{l,P} + \alpha_{l,W} \rho_{l,W}] w_{l,P} \\ F_W &= (\alpha_l \rho_l w_l)_W = \frac{1}{2} [\alpha_{l,W} \rho_{l,W} + \alpha_{l,W} \rho_{l,W}] w_{l,W} \end{aligned} \quad (\text{C.273})$$

### The diffusion terms

The locations of the node points in the staggered grid for the  $w$ -velocity are shown in Fig C.4.

Radial direction:

$$\begin{aligned} \int_{\Delta t \Delta V} \int \frac{1}{r} \frac{\partial}{\partial r} (r \alpha_l \mu_{l,eff} \frac{\partial w_l}{\partial r}) r dr dz dt \\ &= \left[ (\Delta z r \alpha_l \mu_{l,eff} \frac{\partial w_l}{\partial r})_n - (\Delta z r \alpha_l \mu_{l,eff} \frac{\partial w_l}{\partial r})_s \right] \Delta t \\ &= A_n \Gamma_n \left( \frac{w_{l,N} - w_{l,P}}{\delta r_{NP}} \right) \Delta t - A_s \Gamma_s \left( \frac{w_{l,P} - w_{l,S}}{\delta r_{PS}} \right) \Delta t \\ &= D_n (w_{l,N} - w_{l,P}) \Delta t - D_s (w_{l,P} - w_{l,S}) \Delta t \end{aligned} \quad (\text{C.274})$$

To approximate the scalar grid cell mass fluxes at the staggered velocity grid cell surface points, arithmetic interpolation is frequently used:

$$\begin{aligned} D_n &= \frac{A_n \Gamma_n}{\delta r_{NP}} \\ D_s &= \frac{A_s \Gamma_s}{\delta r_{PS}} \\ \Gamma_n &= (\alpha_l \mu_{l,eff})_n = \frac{1}{4} (\alpha_{l,P} \mu_{l,P} + \alpha_{l,N} \mu_{l,N} + \alpha_{l,W} \mu_{l,W} + \alpha_{l,NW} \mu_{l,NW}) \\ \Gamma_s &= (\alpha_l \mu_{l,eff})_s = \frac{1}{4} (\alpha_{l,P} \mu_{l,P} + \alpha_{l,S} \mu_{l,S} + \alpha_{l,W} \mu_{l,W} + \alpha_{l,SW} \mu_{l,SW}) \end{aligned} \quad (\text{C.275})$$

Axial direction:

$$\begin{aligned}
 & \int_{\Delta t \Delta V} \frac{\partial}{\partial z} (\alpha_l \mu_{l,eff} \frac{\partial w_l}{\partial z}) dz r dr dt \\
 &= [r_p \Delta r (\alpha_l \mu_{l,eff} \frac{\partial w_l}{\partial z})_e - r_p \Delta r (\alpha_l \mu_{l,eff} \frac{\partial w_l}{\partial z})_w] \Delta t \\
 &= A_e \Gamma_e \left( \frac{w_{l,E} - w_{l,P}}{\frac{1}{2}(\delta z_{PW} + \delta z_{EP})} \right) \Delta t - A_w \Gamma_w \left( \frac{w_{l,P} - w_{l,W}}{\frac{1}{2}(\delta z_{PW} + \delta z_{EP})} \right) \Delta t \\
 &= D_e (w_{l,E} - w_{l,P}) \Delta t - D_w (w_{l,P} - w_{l,W}) \Delta t
 \end{aligned} \tag{C.276}$$

To approximate the scalar grid cell mass fluxes at the staggered velocity grid cell surface points, arithmetic interpolation is frequently used:

$$\begin{aligned}
 D_e &= \frac{A_e \Gamma_e}{\frac{1}{2}(\delta z_{PW} + \delta z_{EP})} \\
 D_w &= \frac{A_w \Gamma_w}{\frac{1}{2}(\delta z_{PW} + \delta z_{EP})} \\
 \Gamma_e &= (\alpha_l \mu_{l,eff})_e = \alpha_{l,P} \mu_{l,P} \\
 \Gamma_w &= (\alpha_l \mu_{l,eff})_w = \alpha_{l,W} \mu_{l,W}
 \end{aligned} \tag{C.277}$$

### The source terms

The the source terms are approximated by the midpoint rule, in which  $S$  is considered an average value representative for the whole grid cell volume. The derivatives are represented by an abbreviated Taylor series expansion, usually a central difference expansion of second order is employed.

Term 1 on the RHS of the momentum equation:

$$\begin{aligned}
 & \int_{\Delta t \Delta V} w_l \frac{1}{r} \frac{\partial}{\partial r} \left( r \frac{\mu_{l,t}}{\sigma_{\alpha_{l,t}}} \frac{\partial \alpha_l}{\partial r} \right) dV dt \\
 &= \frac{w_P}{r_P} \left[ \left( r \frac{\mu_{l,t}}{\sigma_{\alpha_{l,t}}} \frac{\partial \alpha_l}{\partial r} \right)_n - \left( r \frac{\mu_{l,t}}{\sigma_{\alpha_{l,t}}} \frac{\partial \alpha_l}{\partial r} \right)_s \right] \frac{\Delta V \Delta t}{\frac{1}{2}(\delta r_{NP} + \delta r_{PS})}
 \end{aligned} \tag{C.278}$$

This term is implemented through the source term  $S_C$  as:

$$S_{C,1} = \frac{w_P}{r_P} \left[ r_N^v \left( \frac{\mu_{l,t}}{\sigma_{\alpha_{l,t}}} \right)_n \left( \frac{\partial \alpha_l}{\partial r} \right)_n - r_P^v \left( \frac{\mu_{l,t}}{\sigma_{\alpha_{l,t}}} \right)_s \left( \frac{\partial \alpha_l}{\partial r} \right)_s \right] \frac{\Delta V \Delta t}{\frac{1}{2}(\delta r_{NP} + \delta r_{PS})} \tag{C.279}$$

To approximate derivatives of scalar grid cell variables and scalar grid cell variables at the staggered velocity grid cell surface points, arithmetic interpolation is frequently used:

$$\begin{aligned} \left(\frac{\partial \alpha_l}{\partial r}\right)_n &= \frac{(\alpha_l)_N - (\alpha_l)_P}{\delta r_{NP}} = \frac{\frac{1}{2}(\alpha_{l,N} + \alpha_{l,NW}) - \frac{1}{2}(\alpha_{l,P} + \alpha_{l,W})}{\delta r_{NP}} \\ \left(\frac{\partial \alpha_l}{\partial r}\right)_s &= \frac{(\alpha_l)_P - (\alpha_l)_S}{\delta r_{PS}} = \frac{\frac{1}{2}(\alpha_{l,P} + \alpha_{l,W}) - \frac{1}{2}(\alpha_{l,S} + \alpha_{l,SW})}{\delta r_{PS}} \end{aligned} \quad (\text{C.280})$$

Term 2 on the RHS of the momentum equation:

$$\int_{\Delta t \Delta V} \int w_l \frac{\partial}{\partial z} \left( \frac{\mu_{l,t}}{\sigma_{\alpha_{l,t}}} \frac{\partial \alpha_l}{\partial z} \right) dV dt = w_{l,P} \left[ \left( \frac{\mu_{l,t}}{\sigma_{\alpha_{l,t}}} \frac{\partial \alpha_l}{\partial z} \right)_e - \left( \frac{\mu_{l,t}}{\sigma_{\alpha_{l,t}}} \frac{\partial \alpha_l}{\partial z} \right)_w \right] \frac{\Delta V \Delta t}{\delta z_{PW}} \quad (\text{C.281})$$

This term is implemented through the source term  $S_C$  as:

$$S_{C,2} = w_{l,P} \frac{\Delta V \Delta t}{\delta z_{PW}} \left( \frac{\mu_{l,t,P}}{\sigma_{\alpha_{l,t}}} \left( \frac{\partial \alpha_l}{\partial z} \right)_e - \frac{\mu_{l,t,W}}{\sigma_{\alpha_{l,t}}} \left( \frac{\partial \alpha_l}{\partial z} \right)_w \right) \quad (\text{C.282})$$

where

$$\begin{aligned} \left(\frac{\partial \alpha_l}{\partial z}\right)_e &= \frac{(\alpha_l)_E - (\alpha_l)_P}{\frac{1}{2}(\delta z_{PW} + \delta z_{EP})} = \frac{\frac{1}{2}(\alpha_{l,E} + \alpha_{l,P}) - \frac{1}{2}(\alpha_{l,P} + \alpha_{l,W})}{\frac{1}{2}(\delta z_{PW} + \delta z_{EP})} \\ \left(\frac{\partial \alpha_l}{\partial z}\right)_w &= \frac{(\alpha_l)_P - (\alpha_l)_W}{\frac{1}{2}(\delta z_{PW} + \delta z_{EP})} = \frac{\frac{1}{2}(\alpha_{l,P} + \alpha_{l,W}) - \frac{1}{2}(\alpha_{l,W} + \alpha_{l,WW})}{\frac{1}{2}(\delta z_{PW} + \delta z_{EP})} \end{aligned} \quad (\text{C.283})$$

Term 3 on the RHS of the momentum equation:

$$\begin{aligned} \int_{\Delta t \Delta V} \int \left[ \frac{\mu_{l,t}}{\sigma_{\alpha_{l,t}}} \frac{\partial \alpha_l}{\partial z} \left( \frac{1}{r} \frac{\partial}{\partial r} (rv_l) + \frac{\partial w_l}{\partial z} \right) \right] dV dt \\ = \left( \frac{\mu_{l,t}}{\sigma_{\alpha_{l,t}}} \frac{\partial \alpha_l}{\partial z} \right)_P \left( \frac{1}{r_P} \frac{(rv_l)_n - (rv_l)_s}{\frac{1}{2}(\delta r_{NP} + \delta r_{PS})} + \left( \frac{\partial w_l}{\partial z} \right)_P \right) \Delta V \Delta t \end{aligned} \quad (\text{C.284})$$

This term is implemented through the source term  $S_C$  as:

$$\begin{aligned} S_{C,3} &= \left( \frac{\mu_{l,t}}{\sigma_{\alpha_{l,t}}} \frac{\partial \alpha_l}{\partial z} \right)_P \left( \frac{1}{r_P} \frac{r_N^v \frac{1}{2}(v_{l,N} + v_{l,NW}) - r_P^v \frac{1}{2}(v_{l,P} + v_{l,W})}{\frac{1}{2}(\delta r_{NP} + \delta r_{PS})} \right) \Delta V \Delta t \\ &+ \left( \frac{\mu_{l,t}}{\sigma_{\alpha_{l,t}}} \frac{\partial \alpha_l}{\partial z} \right)_P \left( \frac{\partial w_l}{\partial z} \right)_P \Delta V \Delta t \end{aligned} \quad (\text{C.285})$$

To approximate derivatives of scalar grid cell variables and scalar grid cell variables at the staggered velocity grid cell surface points, arithmetic interpolation is frequently used:

$$\begin{aligned} (\mu_{l,t})_P &= \frac{1}{2}(\mu_{l,P} + \mu_{l,W}) \\ \left(\frac{\partial \alpha_l}{\partial z}\right)_P &= \frac{(\alpha_l)_e - (\alpha_l)_w}{\delta z_{PW}} = \frac{\alpha_{l,P} - \alpha_{l,W}}{\delta z_{PW}} \\ \left(\frac{\partial w_l}{\partial z}\right)_P &= \frac{w_{l,e} - w_{l,w}}{\delta z_{PW}} = \frac{\frac{1}{2}(w_{l,P} + w_{l,E}) - \frac{1}{2}(w_{l,P} + w_{l,W})}{\delta z_{PW}} \end{aligned} \quad (\text{C.286})$$

Term 4 on the RHS of the momentum equation:

$$\begin{aligned} & \int_{\Delta t \Delta V} \int \frac{1}{r} \frac{\partial}{\partial r} (r \alpha_l \mu_{l,eff} \frac{\partial w_l}{\partial r}) dV dt \\ &= \frac{\Delta V \Delta t}{r_P} \left[ (\alpha_l r \mu_{l,eff} \frac{\partial w_l}{\partial r})_n - (\alpha_l r \mu_{l,eff} \frac{\partial w_l}{\partial r})_s \right] \end{aligned} \quad (C.287)$$

This term is implemented through the source term  $S_C$  as:

$$S_{C,4} = \frac{\Delta V \Delta t}{r_P} \left[ \Gamma_n r_N^v \left( \frac{w_{l,N} - w_{l,P}}{\delta r_{NP}} \right) - \Gamma_s r_P^v \left( \frac{w_{l,P} - w_{l,S}}{\delta r_{PS}} \right) \right] \quad (C.288)$$

Term 5th and 7th terms on the RHS of the momentum equation are identical and both of them are approximated as follows:

$$\int_{\Delta t \Delta V} \int \frac{\partial}{\partial z} (\alpha_l \mu_l \frac{\partial w_l}{\partial z}) dV dt = \frac{\Delta V \Delta t}{\delta z_{PW}} \left[ (\alpha_l \mu_l \frac{\partial w_l}{\partial z})_e - (\alpha_l \mu_l \frac{\partial w_l}{\partial z})_w \right] \quad (C.289)$$

This term is implemented through the source term  $S_C$  as:

$$S_{C,5} = \frac{\Delta V \Delta t}{\delta z_{PW}} \left[ \alpha_{l,P} \mu_{l,P} \frac{(w_{l,E} - w_{l,P})}{\frac{1}{2}(\delta z_{EP} + \delta z_{PW})} - \alpha_{l,W} \mu_{l,W} \frac{(w_{l,P} - w_{l,W})}{\frac{1}{2}(\delta z_{EP} + \delta z_{PW})} \right] \quad (C.290)$$

The staggered velocity grid cell surface points coincide with center nodes in the scalar grid, so no interpolation is needed.

Term 6 on the RHS of the momentum equation:

$$\begin{aligned} & \int_{\Delta t \Delta V} \int \frac{1}{r} \frac{\partial}{\partial r} (r \alpha_l \mu_{l,eff} \frac{\partial v_l}{\partial z}) dV dt \\ &= \frac{\Delta V \Delta t}{r_P} \left[ (\alpha_l r \mu_{l,eff} \frac{\partial v_l}{\partial z})_n - (\alpha_l r \mu_{l,eff} \frac{\partial v_l}{\partial z})_s \right] \end{aligned} \quad (C.291)$$

This term is implemented through the source term  $S_C$  as:

$$S_{C,6} = \frac{\Delta V \Delta t}{r_P} \left[ \Gamma_n r_N^v \left( \frac{v_{l,N} - v_{l,NW}}{\delta z_{PW}} \right) - \Gamma_s r_P^v \left( \frac{v_{l,P} - v_{l,W}}{\delta z_{PW}} \right) \right] \quad (C.292)$$

Term 8A on the RHS of the momentum equation:

$$\begin{aligned} - \int_{\Delta t \Delta V} \int \frac{\partial}{\partial z} \left( \frac{2}{3} \alpha_l \rho_l k_l \right) dV dt &= - \frac{2}{3} \frac{\Delta V \Delta t}{\delta z_{PW}} [(\alpha_l \rho_l k_l)_e - (\alpha_l \rho_l k_l)_w] \\ &= - \frac{2}{3} \frac{\Delta V \Delta t}{\delta z_{PW}} \left[ \alpha_{l,P} \rho_{l,P} k_{l,P} - \alpha_{l,W} \rho_{l,W} k_{l,W} \right] \end{aligned} \quad (C.293)$$

This term is implemented through the source term  $S_C$  as:

$$S_{C,7} = \frac{2}{3} \frac{\Delta V \Delta t}{\delta z_{PW}} [\alpha_{l,W} \rho_{l,W} k_W - \alpha_{l,P} \rho_{l,P} k_P] \quad (C.294)$$

The staggered velocity grid cell surface points coincide with center nodes in the scalar grid, so no interpolation is needed.

Term 8B on the RHS of the momentum equation:

$$\begin{aligned} & - \int_{\Delta t \Delta V} \int \frac{\partial}{\partial z} \left( \frac{2}{3} \alpha_{l,P} \rho_{l,eff} \frac{1}{r} \frac{\partial(rv_l)}{\partial r} \right) dV dt \\ & = - \frac{2\Delta V \Delta t}{3 \delta z_{PW}} \left[ \left( \frac{\alpha_{l,P} \rho_{l,eff}}{r} \frac{\partial(rv_l)}{\partial r} \right)_e - \left( \frac{\alpha_{l,P} \rho_{l,eff}}{r} \frac{\partial(rv_l)}{\partial r} \right)_w \right] \end{aligned} \quad (C.295)$$

This term is implemented through the source term  $S_C$  as:

$$S_{C,8} = - \frac{2\Delta V \Delta t}{3 \delta z_{PW}} \left[ \frac{\alpha_{l,P} \mu_{l,eff,P}}{r_P} \frac{\partial(rv_l)}{\partial r} \Big|_e - \frac{\alpha_{l,W} \mu_{l,eff,W}}{r_P} \frac{\partial(rv_l)}{\partial r} \Big|_w \right] \quad (C.296)$$

The staggered velocity grid cell surface points coincide with center nodes in the scalar grid, so no interpolation is needed for the scalar grid variables.

The velocity derivatives are approximated by central difference discretizations:

$$\begin{aligned} \frac{\partial(rv_l)}{\partial r} \Big|_e &= \frac{(rv_l)_{ne} - (rv_l)_{se}}{\frac{1}{2}(\delta r_{NP} + \delta r_{PS})} = \frac{r_N^v v_{l,N} - r_P^v v_{l,P}}{\frac{1}{2}(\delta r_{NP} + \delta r_{PS})} \\ \frac{\partial(rv_l)}{\partial r} \Big|_w &= \frac{(rv_l)_{nw} - (rv_l)_{sw}}{\frac{1}{2}(\delta r_{NP} + \delta r_{PS})} = \frac{r_{NW}^v v_{l,NW} - (r_P^v v_{l,W})}{\frac{1}{2}(\delta r_{NP} + \delta r_{PS})} \end{aligned} \quad (C.297)$$

Term 8C on the RHS of the momentum equation:

$$\begin{aligned} & - \int_{\Delta t \Delta V} \int \frac{\partial}{\partial z} \left( \frac{2}{3} \alpha_{l,P} \rho_{l,eff} \frac{\partial w_l}{\partial z} \right) dV dt \\ & = - \frac{2\Delta V \Delta t}{3 \delta z_{PW}} \left[ \left( \alpha_{l,P} \rho_{l,eff} \frac{\partial w_l}{\partial z} \right)_e - \left( \alpha_{l,P} \rho_{l,eff} \frac{\partial w_l}{\partial z} \right)_w \right] \end{aligned} \quad (C.298)$$

This term is implemented through the source term  $S_C$  as:

$$\begin{aligned} S_{C,9} &= - \frac{2\Delta V}{3 \delta z_{PW}} \alpha_{l,P} \mu_{l,eff,P} \frac{(w_{l,E} - w_{l,P})}{\frac{1}{2}(\delta z_{EP} + \delta z_{PW})} \\ &+ \frac{2\Delta V}{3 \delta z_{PW}} \alpha_{l,W} \mu_{l,eff,W} \frac{(w_{l,P} - w_{l,W})}{\frac{1}{2}(\delta z_{EP} + \delta z_{PW})} \end{aligned} \quad (C.299)$$

The staggered velocity grid cell surface points coincide with center nodes in the scalar grid, so no interpolation is needed for the scalar grid variables. The velocity gradients are approximated by central difference expansions.

**Pressure force**

$$-\int_{\Delta t \Delta V} \alpha_l \frac{\partial p}{\partial z} dV dt = -\frac{1}{2}(\alpha_l)_P \frac{(P_P - P_W)}{\delta z_{PW}} \Delta V \Delta t \quad (\text{C.300})$$

This term is implemented through the source term  $S_C$  as

$$S_{C,10} = -\frac{1}{2}(\alpha_{l,P} + \alpha_{l,W}) \frac{P_P - P_W}{\delta z_{PW}} \Delta V \quad (\text{C.301})$$

To approximate scalar grid cell variables at the staggered velocity grid cell node points, arithmetic interpolation is frequently used:

$$(\alpha_l)_P = \frac{1}{2}(\alpha_{l,P} + \alpha_{l,W}) \quad (\text{C.302})$$

**Gravity force**

$$\int_{\Delta t \Delta V} \alpha_l \rho_l g dV dt = g(\alpha_l \rho_l)_P \Delta V \Delta t \quad (\text{C.303})$$

This term is implemented through the source term  $S_C$  as:

$$S_{C,11} = g \frac{1}{2}(\alpha_{l,P} \rho_{l,P} + \alpha_{l,W} \rho_{l,W}) \Delta V \Delta t \quad (\text{C.304})$$

To approximate scalar grid cell variables at the staggered velocity grid cell node points, arithmetic interpolation is frequently used:

$$(\alpha_l \rho_l)_P = \frac{1}{2}(\alpha_{l,P} \rho_{l,P} + \alpha_{l,W} \rho_{l,W}) \quad (\text{C.305})$$

**Added Mass force**

$$\begin{aligned} & \int_{\Delta t \Delta V} -\alpha_l \alpha_g \rho_l f_v \left[ (w_l \frac{\partial w_l}{\partial z} + v_l \frac{\partial w_l}{\partial r}) - (u_g \frac{\partial u_g}{\partial z} + v_g \frac{\partial u_g}{\partial r}) \right] dV dt \\ &= -f_v (\alpha_l)_P (\alpha_g)_P (\rho_l)_P \times \\ & \quad \left[ (w_l (\frac{\partial w_l}{\partial z}) + (v_l) (\frac{\partial w_l}{\partial r})) - (w_g (\frac{\partial w_g}{\partial z}) + (v_g) (\frac{\partial w_g}{\partial r})) \right]_P \Delta V \Delta t \end{aligned} \quad (\text{C.306})$$

This term is implemented through the source term  $S_C$  as:

$$\begin{aligned} S_{C,12} = & -f_v \frac{1}{2}(\alpha_{l,P} + \alpha_{l,W}) \frac{1}{2}(\alpha_{g,P} + \alpha_{g,W}) \frac{1}{2}(\rho_{l,P} + \rho_{l,W}) \times \\ & \left[ w_l \frac{\partial w_l}{\partial z} + v_l \frac{\partial w_l}{\partial r} - (w_g \frac{\partial u_g}{\partial z} + (v_g) \frac{\partial u_g}{\partial r}) \right]_P \Delta V \Delta t \end{aligned} \quad (\text{C.307})$$

To approximate scalar grid cell variables at the staggered  $w$ -velocity grid cell center node point, arithmetic interpolation is frequently used. The radial velocity component is discretized in the staggered  $v$ -grid cell volume and need to be interpolated to the  $w$ -grid cell center node point. The derivatives of the  $w$ -velocity component is approximated by a central difference scheme. When needed, arithmetic interpolation is used for the velocity components as well.

$$\begin{aligned}
 (\alpha_g)_P &= \frac{1}{2}(\alpha_{g,P} + \alpha_{g,W}) \\
 (\rho_l)_P &= \frac{1}{2}(\rho_{l,P} + \rho_{l,W}) \\
 (v_l)_P &= \frac{1}{4}(v_{l,P} + v_{l,N} + v_{l,W} + v_{l,NW}) \\
 \left(\frac{\partial w_l}{\partial r}\right)_P &= \frac{w_{l,n} - w_{l,s}}{\frac{1}{2}(\delta r_{NP} + \delta r_{PS})} = \frac{\frac{1}{2}(w_{l,P} + w_{l,N}) - \frac{1}{2}(w_{l,P} + w_{l,S})}{\frac{1}{2}(\delta r_{NP} + \delta r_{PS})} \\
 \left(\frac{\partial w_l}{\partial z}\right)_P &= \frac{w_{l,e} - w_{l,w}}{\delta z_{PW}} = \frac{\frac{1}{2}(w_{l,P} + w_{l,E}) - \frac{1}{2}(w_{l,P} + w_{l,W})}{\delta z_{PW}}
 \end{aligned} \tag{C.308}$$

The corresponding terms for the gas phase are discretized in the same way.

### Steady Drag force

The steady drag term is treated in the same way as described for the radial velocity component.

### Algebraic discretization equation

After dividing all the terms by  $\Delta t$ , the discretized equation can be written on the standard algebraic form:

$$a_P w_{l,P} = a_N w_{l,N} + a_S w_{l,S} + a_E w_{l,E} + a_W w_{l,W} + b_{w_l} \tag{C.309}$$

in which the coefficients are defined by:

$$a_N = D_n + \max[-C_n, 0]$$

$$a_S = D_s + \max[C_s, 0]$$

$$a_E = D_e + \max[-C_e, 0]$$

$$a_W = D_w + \max[C_w, 0]$$

$$b = \sum_m S_{C,m} + a_P^0 v_{l,P}^0$$

$$a_P = \frac{\Delta V}{\Delta t} (\alpha_l \rho_l)_P + a_N + a_S + a_E + a_W + C_n - C_s + C_e - C_w - \sum_q S_{P,q} \Delta V \tag{C.310}$$

To avoid negative coefficients, the relation for the coefficient  $a_P$  can be modified using the continuity equation (C.187). The negative  $mC_2$ -term is then moved to the RHS of the discretized transport equation and included as part

of the  $b$ -term. The alternative  $a_P^*$  and  $b^*$  coefficients are defined by:

$$\begin{aligned}
 b^* &= -mC_2w_{l,P}^{\nu} + \sum_m S_{C,m,l} + a_P^0w_{l,P}^0 \\
 a_P^* &= \frac{\Delta V}{\Delta t}(\alpha_l\rho_l)_P^0 + a_N + a_S + a_E + a_W + mC_1 - \sum_q S_{P,q,l}\Delta V
 \end{aligned} \tag{C.311}$$

#### C.4.6 The gas phase radial momentum balance

The radial component of the momentum balance for the gas phase is given in (C.145):

$$\begin{aligned}
 &\frac{\partial}{\partial t}(\alpha_g\rho_gv_g) + \frac{1}{r}\frac{\partial}{\partial r}(r\alpha_g\rho_gv_gv_g) + \frac{\partial}{\partial z}(\alpha_g\rho_gw_gv_g) = \\
 &\quad \frac{1}{r}\frac{\partial}{\partial r}\left(r\frac{\mu_{g,t}}{\sigma_{\alpha_{g,t}}}\frac{\partial\alpha_g}{\partial r}v_g\right) + \frac{\partial}{\partial z}\left(\frac{\mu_{g,t}}{\sigma_{\alpha_{g,t}}}\frac{\partial\alpha_g}{\partial z}v_g\right) \\
 &\quad + \frac{1}{r}\frac{\partial}{\partial r}\left(r\frac{\mu_{g,t}}{\sigma_{\alpha_{g,t}}}\frac{\partial\alpha_g}{\partial r}v_g\right) + \frac{\partial}{\partial z}\left(\frac{\mu_{g,t}}{\sigma_{\alpha_{g,t}}}\frac{\partial\alpha_g}{\partial r}w_g\right) \\
 &\quad + \frac{1}{r}\frac{\partial}{\partial r}\left(r\alpha_g\frac{\mu_{g,t}}{\sigma_{g,t}}\frac{\partial v_g}{\partial r}\right) - \frac{1}{r}\alpha_g\frac{\mu_{g,t}}{\sigma_{g,t}}\frac{v_g}{r} + \frac{\partial}{\partial z}\left(\alpha_g\frac{\mu_{g,t}}{\sigma_{g,t}}\frac{\partial v_g}{\partial z}\right) \\
 &\quad + \frac{1}{r}\frac{\partial}{\partial r}\left(r\alpha_g\frac{\mu_{g,t}}{\sigma_{g,t}}\frac{\partial v_g}{\partial r}\right) - \frac{1}{r}\alpha_g\frac{\mu_{g,t}}{\sigma_{g,t}}\frac{v_g}{r} + \frac{\partial}{\partial z}\left(\alpha_g\frac{\mu_{g,t}}{\sigma_{g,t}}\frac{\partial w_g}{\partial r}\right) \\
 &\quad - \frac{\partial}{\partial r}\left(\frac{2}{3}\alpha_g\rho_g\left(k + \frac{\nu_{g,t}}{\sigma_{g,t}}\left(\frac{1}{r}\frac{\partial}{\partial r}(rv_g) + \frac{\partial w_g}{\partial z}\right)\right)\right) \\
 &\quad - \alpha_g\frac{\partial p}{\partial r} + \frac{\mu_{l,t}}{\sigma_{\alpha_{l,t}}}\left(\frac{\partial\alpha_l}{\partial r}\frac{\partial v_l}{\partial r} + \frac{\partial\alpha_l}{\partial z}\frac{\partial v_l}{\partial z}\right) \\
 &\quad + v_l\frac{\partial}{\partial r}\left(\frac{\mu_{l,t}}{\sigma_{\alpha_{l,t}}}\frac{\partial\alpha_l}{\partial r}\right) + w_l\frac{\partial}{\partial z}\left(\frac{\mu_{l,t}}{\sigma_{\alpha_{l,t}}}\frac{\partial\alpha_l}{\partial r}\right) \\
 &\quad + \alpha_g\rho_gg_r + F_{g,r}^C + \overline{F_{g,r}^C}
 \end{aligned}$$

In the FVM, the integral form of the momentum equation is used. The differential equation is thus integrated in time and over a grid cell volume in the staggered grid for the  $v$ -velocity.

The transient, convective and diffusive terms are discretized just like the corresponding terms in the liquid phase (i.e., see sect C.4.4).

#### The source terms

The the source terms are approximated by the midpoint rule, in which  $S$  is considered an average value representative for the whole grid cell volume. The derivatives are represented by an abbreviated Taylor series expansion, usually a central difference expansion of second order is employed.

Term 1 on the RHS of the momentum equation is split into two parts, term 1a and term 1b:

$$\frac{1}{r} \frac{\partial}{\partial r} \left( r \frac{\mu_{g,t}}{\sigma_{\alpha_{g,t}}} \frac{\partial \alpha_g}{\partial r} v_g \right) = -v_g \frac{\partial}{\partial r} \left( \frac{\mu_g}{\sigma_{\alpha_{g,t}}} \frac{\partial \alpha_l}{\partial r} \right) - \frac{1}{r} \frac{\mu_g}{\sigma_{\alpha_{g,t}}} \frac{\partial \alpha_l}{\partial r} \frac{\partial}{\partial r} (rv_g) \quad (\text{C.311})$$

By use of (8.11), the gas-volume fractions has been substituted with the liquid volume fraction. The gradient of the gas phase volume fraction is thus related to the liquid phase volume fraction in accordance with:

$$\nabla \alpha_g = \nabla(1 - \alpha_l) = -\nabla \alpha_l \quad (\text{C.312})$$

Term 1a on the RHS of the momentum equation:

$$\begin{aligned} & \int_{\Delta t \Delta V} \int -v_g \frac{\partial}{\partial r} \left( \frac{\mu_g}{\sigma_{\alpha_{g,t}}} \frac{\partial \alpha_l}{\partial r} \right) dV dt \\ &= -\frac{v_{g,P} \Delta V \Delta t}{\frac{1}{2}(\delta r_{NP} + \delta r_{PS})} \left[ \left( \frac{\mu_g}{\sigma_{\alpha_{g,t}}} \frac{\partial \alpha_l}{\partial r} \right)_n - \left( \frac{\mu_g}{\sigma_{\alpha_{g,t}}} \frac{\partial \alpha_l}{\partial r} \right)_s \right] \end{aligned} \quad (\text{C.313})$$

This term is implemented through the source term  $S_C$  as:

$$S_{C,1} = -\frac{v_{g,P} \Delta V \Delta t}{\frac{1}{2}(\delta r_{NP} + \delta r_{PS})} \left[ \mu_{g,P} \left( \frac{\partial \alpha_l}{\partial r} \right)_n - \mu_{g,S} \left( \frac{\partial \alpha_l}{\partial r} \right)_s \right] \quad (\text{C.314})$$

The staggered velocity grid cell surface points coincide with center nodes in the scalar grid, so no interpolation is needed for the scalar grid variables. The scalar gradient terms in the staggered velocity cell volume are approximated by central difference expansions and arithmetic interpolation:

$$\begin{aligned} \left( \frac{\partial \alpha_l}{\partial r} \right)_n &= \frac{(\alpha_l)_N - (\alpha_l)_P}{\delta r_{NP}} = \frac{\frac{1}{2}(\alpha_{l,N} + \alpha_{l,P}) - \frac{1}{2}(\alpha_{l,P} + \alpha_{l,S})}{\delta r_{NP}} \\ \left( \frac{\partial \alpha_l}{\partial r} \right)_s &= \frac{(\alpha_l)_P - (\alpha_l)_S}{\delta r_{PS}} = \frac{\frac{1}{2}(\alpha_{l,P} + \alpha_{l,S}) - \frac{1}{2}(\alpha_{l,S} + \alpha_{l,SS})}{\delta r_{PS}} \end{aligned} \quad (\text{C.315})$$

Term 1b on the RHS of the momentum equation:

$$-\int_{\Delta t \Delta V} \int \frac{1}{r} \frac{\mu_g}{\sigma_{\alpha_{g,t}}} \frac{\partial \alpha_l}{\partial r} \frac{\partial}{\partial r} (rv_g) dV dt = -\left( \frac{1}{r} \frac{\mu_g}{\sigma_{\alpha_{g,t}}} \frac{\partial \alpha_l}{\partial r} \right)_P \frac{[(rv_g)_n - (rv_g)_s]}{\frac{1}{2}(\delta r_{NP} + \delta r_{PS})} \Delta V \Delta t \quad (\text{C.316})$$

This term is implemented through the source term  $S_C$  as:

$$S_{C,2} = -\frac{(\mu_g)_P}{r_P^v} \left( \frac{\partial \alpha_l}{\partial r} \right)_P \frac{r_P \frac{1}{2}(v_{g,P} + v_{g,N}) - r_S \frac{1}{2}(v_{g,P} + v_{g,S})}{\frac{1}{2}(\delta r_{NP} + \delta r_{PS})} \Delta V \Delta t \quad (\text{C.317})$$

The scalar variables at the staggered velocity grid cell surface points is usually obtained by arithmetic interpolation. The scalar gradient terms in the staggered velocity cell volume are approximated by central difference expansions.

The scalar properties at the staggered grid cell surface points coincide with the scalar grid central nodes.

$$\begin{aligned} (\mu_g)_P &= \frac{1}{2}(\mu_{g,P} + \mu_{g,S}) \\ \left(\frac{\partial \alpha_l}{\partial r}\right)_P &= \frac{(\alpha_l)_n - (\alpha_l)_s}{\frac{1}{2}(\delta r_{NP} + \delta r_{PS})} = \frac{\alpha_{l,P} - \alpha_{l,S}}{\frac{1}{2}(\delta r_{NP} + \delta r_{PS})} \end{aligned} \quad (\text{C.318})$$

Term 2 on the RHS of the momentum equation is split into two parts, term 2a and term 2b:

$$\frac{\partial}{\partial z} \left( \frac{\mu_{g,t}}{\sigma_{\alpha_{g,t}}} \frac{\partial \alpha_g}{\partial z} v_g \right) = -v_g \frac{\partial}{\partial z} \left( \frac{\mu_{g,t}}{\sigma_{\alpha_{g,t}}} \frac{\partial \alpha_l}{\partial z} \right) - \frac{\mu_{g,t}}{\sigma_{\alpha_{g,t}}} \frac{\partial \alpha_l}{\partial z} \frac{\partial v_g}{\partial z} \quad (\text{C.319})$$

Term 2a on the RHS of the momentum equation:

$$\begin{aligned} &\int_{\Delta t} \int_{\Delta V} -v_g \frac{\partial}{\partial z} \left( \frac{\mu_{g,t}}{\sigma_{\alpha_{g,t}}} \frac{\partial \alpha_l}{\partial z} \right) dV dt \\ &= -\frac{v_{g,P} \Delta V}{\frac{1}{2}(\delta z_{PW} + \delta z_{EP})} \left[ \left( \frac{\mu_{g,t}}{\sigma_{\alpha_{g,t}}} \frac{\partial \alpha_l}{\partial z} \right)_e - \left( \frac{\mu_{g,t}}{\sigma_{\alpha_{g,t}}} \frac{\partial \alpha_l}{\partial z} \right)_w \right] \end{aligned} \quad (\text{C.320})$$

This term is implemented through the source term  $S_C$  as:

$$S_{C,3} = -\frac{v_{g,P} \Delta V}{\frac{1}{2}(\delta z_{PW} + \delta z_{EP})} \left[ \left( \frac{\mu_{g,t}}{\sigma_{\alpha_{g,t}}} \frac{\partial \alpha_l}{\partial z} \right)_e - \left( \frac{\mu_{g,t}}{\sigma_{\alpha_{g,t}}} \frac{\partial \alpha_l}{\partial z} \right)_w \right] \quad (\text{C.321})$$

To approximate the scalar variables at the staggered velocity grid cell surface points, arithmetic interpolation is frequently applied. The derivatives are approximated by a central difference scheme.

$$\begin{aligned} \left(\frac{\partial \alpha_l}{\partial z}\right)_e &= \frac{(\alpha_l)_E - (\alpha_l)_P}{\delta z_{EP}} = \frac{\frac{1}{2}(\alpha_{l,E} + \alpha_{l,SE}) - \frac{1}{2}(\alpha_{l,E} + \alpha_{l,SE})}{\delta z_{EP}} \\ \left(\frac{\partial \alpha_l}{\partial z}\right)_w &= \frac{(\alpha_l)_P - (\alpha_l)_W}{\delta z_{PW}} = \frac{\frac{1}{2}(\alpha_{l,P} + \alpha_{l,S}) - \frac{1}{2}(\alpha_{l,W} + \alpha_{l,SW})}{\delta z_{PW}} \\ (\mu_g)_e &= \frac{1}{4}(\mu_{g,P} + \mu_{g,E} + \mu_{g,S} + \mu_{g,SE}) \\ (\mu_g)_w &= \frac{1}{4}(\mu_{g,P} + \mu_{g,W} + \mu_{g,S} + \mu_{g,SW}) \end{aligned} \quad (\text{C.322})$$

Term 2b on the RHS of the momentum equation:

$$\int_{\Delta t} \int_{\Delta V} -\frac{\mu_{g,t}}{\sigma_{\alpha_{g,t}}} \frac{\partial \alpha_l}{\partial z} \frac{\partial v_g}{\partial z} dV dt = -\left( \frac{\mu_{g,t}}{\sigma_{\alpha_{g,t}}} \frac{\partial \alpha_l}{\partial z} \right)_P \frac{(v_{g,e} - v_{g,w})}{\frac{1}{2}(\delta z_{EP} + \delta z_{PW})} \Delta V \Delta t \quad (\text{C.323})$$

This term is implemented through the source term  $S_C$  as:

$$S_{C,4} = -(\mu_{g,t} \frac{\partial \alpha_l}{\partial z})_P \frac{\frac{1}{2}(v_{g,P} + v_{g,E}) - \frac{1}{2}(v_{g,P} + v_{g,W})}{\frac{1}{2}(\delta z_{EP} + \delta z_{PW})} \Delta V \Delta t \quad (\text{C.324})$$

where

$$\begin{aligned} \left(\frac{\partial \alpha_l}{\partial z}\right)_P &= \frac{(\alpha_l)_e - (\alpha_l)_w}{\frac{1}{2}(\delta z_{EP} + \delta z_{PW})} \\ &= \frac{\frac{1}{4}(\alpha_{l,P} + \alpha_{l,E} + \alpha_{l,S} + \alpha_{l,SE}) - \frac{1}{4}(\alpha_{l,P} + \alpha_{l,W} + \alpha_{l,S} + \alpha_{l,SW})}{\frac{1}{2}(\delta z_{EP} + \delta z_{PW})} \end{aligned} \quad (\text{C.325})$$

Term 3 on the RHS of the momentum equation is split into two parts, term 3a and term 3b:

$$\frac{1}{r} \frac{\partial}{\partial r} \left( r \frac{\mu_{g,t}}{\sigma_{\alpha_{g,t}}} \frac{\partial \alpha_g}{\partial r} v_g \right) = -\frac{v_g}{r} \frac{\partial}{\partial r} \left( r \frac{\mu_{g,t}}{\sigma_{\alpha_{g,t}}} \frac{\partial \alpha_l}{\partial r} \right) - \frac{\mu_{g,t}}{\sigma_{\alpha_{g,t}}} \frac{\partial \alpha_l}{\partial r} \frac{\partial v_g}{\partial r} \quad (\text{C.326})$$

Term 3a on the RHS of the momentum equation:

$$\int_{\Delta t} \int_{\Delta V} -\frac{v_g}{r} \frac{\partial}{\partial r} \left( r \frac{\mu_{g,t}}{\sigma_{\alpha_{g,t}}} \frac{\partial \alpha_l}{\partial r} \right) dV dt = -\frac{v_{g,P}}{r_P^v} \left[ \frac{(r \frac{\mu_{g,t}}{\sigma_{\alpha_{g,t}}} \frac{\partial \alpha_l}{\partial r})_n - (r \frac{\mu_{g,t}}{\sigma_{\alpha_{g,t}}} \frac{\partial \alpha_l}{\partial r})_s}{\frac{1}{2}(\delta r_{NP} + \delta r_{PS})} \right] \Delta V \Delta t \quad (\text{C.327})$$

This term is implemented through the source term  $S_C$  as

$$S_{C,5} = -\frac{v_{g,P}}{r_P^v} \left[ \frac{r_P \frac{\mu_{g,t,P}}{\sigma_{\alpha_{g,t}}} \left(\frac{\partial \alpha_l}{\partial r}\right)_n - r_S \frac{\mu_{g,t,S}}{\sigma_{\alpha_{g,t}}} \left(\frac{\partial \alpha_l}{\partial r}\right)_s}{\frac{1}{2}(\delta r_{NP} + \delta r_{PS})} \right] \Delta V \Delta t \quad (\text{C.328})$$

where

$$\begin{aligned} \left(\frac{\partial \alpha_l}{\partial r}\right)_n &= \frac{(\alpha_l)_N - (\alpha_l)_P}{\delta r_{NP}} = \frac{\frac{1}{2}(\alpha_{l,N} + \alpha_{l,P}) - \frac{1}{2}(\alpha_{l,P} + \alpha_{l,S})}{\delta r_{NP}} \\ \left(\frac{\partial \alpha_l}{\partial r}\right)_s &= \frac{(\alpha_l)_P - (\alpha_l)_S}{\delta r_{PS}} = \frac{\frac{1}{2}(\alpha_{l,P} + \alpha_{l,S}) - \frac{1}{2}(\alpha_{l,S} + \alpha_{l,SS})}{\delta r_{PS}} \end{aligned} \quad (\text{C.329})$$

Term 3b on the RHS of the momentum equation:

$$\int_{\Delta t} \int_{\Delta V} -\frac{\mu_{g,t}}{\sigma_{\alpha_{g,t}}} \frac{\partial \alpha_l}{\partial r} \frac{\partial v_g}{\partial r} dV dt = -\left(\frac{\mu_{g,t}}{\sigma_{\alpha_{g,t}}}\right)_P \left(\frac{\partial \alpha_l}{\partial r}\right)_P \frac{(v_{g,n} - v_{g,s})}{\frac{1}{2}(\delta r_{NP} + \delta r_{PS})} \Delta V \quad (\text{C.330})$$

This term is implemented through the source term  $S_C$  as:

$$S_{C,6} = -\left(\frac{\mu_{g,t}}{\sigma_{\alpha_{g,t}}}\right)_P \left(\frac{\partial \alpha_l}{\partial r}\right)_P \frac{\frac{1}{2}(v_{g,N} + v_{g,P}) - \frac{1}{2}(v_{g,P} + v_{g,S})}{\frac{1}{2}(\delta r_{NP} + \delta r_{PS})} \Delta V \Delta t \quad (\text{C.331})$$

where the staggered grid variables are expressed in terms of the node values in the scalar grid:

$$\begin{aligned} (\mu_g)_P &= \frac{1}{2}(\mu_{g,P} + \mu_{g,S}) \\ \left(\frac{\partial \alpha_l}{\partial r}\right)_P &= \frac{(\alpha_l)_n - (\alpha_l)_s}{\frac{1}{2}(\delta r_{NP} + \delta r_{PS})} = \frac{\alpha_{l,P} - \alpha_{l,S}}{\frac{1}{2}(\delta r_{NP} + \delta r_{PS})} \end{aligned} \quad (\text{C.332})$$

Term 4 on the RHS of the momentum equation is split into two parts, term 4a and term 4b:

$$\frac{\partial}{\partial z} \left( \frac{\mu_{g,t}}{\sigma_{\alpha_{g,t}}} \frac{\partial \alpha_g}{\partial r} w_g \right) = -w_g \frac{\partial}{\partial z} \left( \frac{\mu_{g,t}}{\sigma_{\alpha_{g,t}}} \frac{\partial \alpha_l}{\partial r} \right) - \frac{\mu_{g,t}}{\sigma_{\alpha_{g,t}}} \frac{\partial \alpha_l}{\partial r} \frac{\partial w_g}{\partial z} \quad (\text{C.333})$$

Term 4a on the RHS of the momentum equation:

$$\int \int_{\Delta t \Delta V} -w_g \frac{\partial}{\partial z} \left( \frac{\mu_{g,t}}{\sigma_{\alpha_{g,t}}} \frac{\partial \alpha_l}{\partial r} \right) dV dt = -w_{g,P} \left[ \frac{\left(\frac{\mu_{g,t}}{\sigma_{\alpha_{g,t}}} \frac{\partial \alpha_l}{\partial r}\right)_e - \left(\frac{\mu_{g,t}}{\sigma_{\alpha_{g,t}}} \frac{\partial \alpha_l}{\partial r}\right)_w}{\frac{1}{2}(\delta z_{EP} + \delta z_{PW})} \right] \Delta V \Delta t \quad (\text{C.334})$$

This term is implemented through the source term  $S_C$  as:

$$S_{C,7} = -(w_g)_P \left[ \frac{\left(\frac{\mu_{g,t}}{\sigma_{\alpha_{g,t}}} \frac{\partial \alpha_l}{\partial r}\right)_e - \left(\frac{\mu_{g,t}}{\sigma_{\alpha_{g,t}}} \frac{\partial \alpha_l}{\partial r}\right)_w}{\frac{1}{2}(\delta z_{EP} + \delta z_{PW})} \right] \Delta V \Delta t \quad (\text{C.335})$$

where the staggered grid variables are expressed in terms of the node values in the scalar grid:

$$(w_g)_P = \frac{1}{4}(v_{g,P} + v_{g,S} + v_{g,E} + v_{g,SE}) \quad (\text{C.336})$$

Term 4b on the RHS of the momentum equation:

$$\int \int_{\Delta t \Delta V} -\frac{\mu_{g,t}}{\sigma_{\alpha_{g,t}}} \frac{\partial \alpha_l}{\partial r} \frac{\partial w_g}{\partial z} dV dt = -\left(\frac{\mu_{g,t}}{\sigma_{\alpha_{g,t}}} \frac{\partial \alpha_l}{\partial r}\right)_P \left[ \frac{(w_g)_e - (w_g)_w}{\frac{1}{2}(\delta z_{EP} + \delta z_{PW})} \right] \Delta V \Delta t \quad (\text{C.337})$$

This term is implemented through the source term  $S_C$  as:

$$\begin{aligned} S_{C,8} &= -\left(\frac{\mu_{g,t}}{\sigma_{\alpha_{g,t}}} \frac{\partial \alpha_l}{\partial r}\right)_P \left[ \frac{(w_g)_e - (w_g)_w}{\frac{1}{2}(\delta z_{EP} + \delta z_{PW})} \right] \Delta V \Delta t \\ &= -\left(\frac{\mu_{g,t}}{\sigma_{\alpha_{g,t}}} \frac{\partial \alpha_l}{\partial r}\right)_P \left[ \frac{\frac{1}{2}(v_{g,E} + v_{g,SE}) - \frac{1}{2}(v_{g,P} + v_{g,S})}{\frac{1}{2}(\delta z_{EP} + \delta z_{PW})} \right] \Delta V \Delta t \end{aligned} \quad (\text{C.338})$$

The 5th and 8th terms on the RHS of the radial component of the momentum equation for the gas phase are identical and discretized in the same way as the corresponding terms in the liquid phase equation, as discussed in sect C.4.4.

$$\int_{\Delta t \Delta V} \frac{1}{r} \frac{\partial}{\partial r} \left( r \alpha_g \frac{\mu_{g,t}}{\sigma_{\alpha_{g,t}}} \frac{\partial v_g}{\partial r} \right) dV dt = \frac{\Delta V \Delta t}{r_P^v} \left[ \frac{(r \alpha_g \frac{\mu_{g,t}}{\sigma_{\alpha_{g,t}}} \frac{\partial v_g}{\partial r})_n - (r \alpha_g \frac{\mu_{g,t}}{\sigma_{\alpha_{g,t}}} \frac{\partial v_g}{\partial r})_s}{\frac{1}{2}(\delta r_{NP} + \delta r_{PS})} \right] \quad (\text{C.339})$$

This term is implemented through the source term  $S_C$  as:

$$S_{C,9} = \frac{\Delta V \Delta t}{r_P^v} \frac{r_P \alpha_{g,P} \mu_{g,P} \left( \frac{\partial v_g}{\partial r} \right)_n - r_S \alpha_{g,S} \mu_{g,S} \left( \frac{\partial v_g}{\partial r} \right)_s}{\frac{1}{2}(\delta r_{NP} + \delta r_{PS})} \quad (\text{C.340})$$

in which the scalar variables at the staggered grid surface are expressed in terms of the node values in the scalar grid. The derivatives of staggered grid variables are approximated by use of the central difference scheme:

$$\begin{aligned} \left( \frac{\partial v_g}{\partial r} \right)_n &= \frac{v_{g,N} - v_{g,P}}{\delta r_{NP}} \\ \left( \frac{\partial v_g}{\partial r} \right)_s &= \frac{v_{g,P} - v_{g,S}}{\delta r_{PS}} \end{aligned} \quad (\text{C.341})$$

The 6th and 9th terms on the RHS of the radial component of the momentum equation for the gas phase are identical and discretized in the same way as the corresponding terms in the liquid phase equation, as discussed in sect C.4.4.

$$\begin{aligned} -2 \int_{\Delta t \Delta V} \frac{1}{r} \alpha_g \frac{\mu_{g,t}}{\sigma_{\alpha_{g,t}}} \frac{v_g}{r} dV dt &= -2 \left( \alpha_g \frac{\mu_{g,t}}{\sigma_{\alpha_{g,t}}} \right)_P \frac{v_{g,P}}{r_P^{2,v}} \Delta V \Delta t \\ &= -2 \times \frac{1}{2} \left( \alpha_{g,P} \frac{\mu_{g,t,P}}{\sigma_{\alpha_{g,t}}} + \alpha_{g,S} \frac{\mu_{g,t,S}}{\sigma_{\alpha_{g,t}}} \right) \frac{v_{g,P}}{r_P^{2,v}} \Delta V \Delta t \end{aligned} \quad (\text{C.342})$$

This term is implemented through the source term  $S_P$  as:

$$S_{P,1} = -2 \times \frac{1}{2} \left( \alpha_{g,P} \frac{\mu_{g,t,P}}{\sigma_{\alpha_{g,t}}} + \alpha_{g,S} \frac{\mu_{g,t,S}}{\sigma_{\alpha_{g,t}}} \right) \frac{\Delta V \Delta t}{r_P^{2,v}} \quad (\text{C.343})$$

in which the scalar variables at the staggered grid surface are expressed in terms of the node values in the scalar grid.

Term 7 on the RHS of the radial momentum equation is discretized in the same way as the corresponding term in the liquid phase equation, as discussed in sect C.4.4. The formulation is not repeated here.

Term 10 on the RHS of the radial momentum equation is discretized in the same way as the corresponding term in the liquid phase equation, as discussed in sect C.4.4.

$$\begin{aligned}
 & \int_{\Delta t \Delta V} \frac{\partial}{\partial z} \left( \alpha_g \frac{\mu_{g,t}}{\sigma_{\alpha_{g,t}}} \frac{\partial w_g}{\partial r} \right) dV dt \\
 &= \frac{\Delta V \Delta t}{\frac{1}{2}(\delta z_{PW} + \delta z_{EP})} \left[ \left( \alpha_g \frac{\mu_{g,t}}{\sigma_{\alpha_{g,t}}} \frac{\partial w_g}{\partial r} \right)_e - \left( \alpha_g \frac{\mu_{g,t}}{\sigma_{\alpha_{g,t}}} \frac{\partial w_g}{\partial r} \right)_w \right] \\
 &= \frac{\Delta V \Delta t}{\frac{1}{2}(\delta z_{PW} + \delta z_{EP})} \left[ \Gamma_e \frac{(w_{g,E} - w_{g,SE})}{\frac{1}{2}(\delta r_{NP} + \delta r_{PS})} - \Gamma_w \frac{(w_{g,P} - w_{g,S})}{\frac{1}{2}(\delta r_{NP} + \delta r_{PS})} \right]
 \end{aligned} \tag{C.344}$$

This term is implemented through the source term  $S_C$  as:

$$S_{C,10} = \frac{\Delta V \Delta t}{S_{EW,P}} \left[ \Gamma_e \frac{(w_{g,E} - w_{g,SE})}{\frac{1}{2}(\delta r_{NP} + \delta r_{PS})} - \Gamma_w \frac{(w_{g,P} - w_{g,S})}{\frac{1}{2}(\delta r_{NP} + \delta r_{PS})} \right] \tag{C.345}$$

in which the scalar variables at the staggered grid surface are expressed in terms of the node values in the scalar grid.

Term 11A on the RHS of the radial momentum equation is discretized in the same way as the corresponding term in the liquid phase equation, as discussed in sect C.4.4.

$$- \int_{\Delta t \Delta V} \frac{\partial}{\partial r} \left( \frac{2}{3} \alpha_g \rho_g k \right) dV dt = - \frac{2}{3} \frac{\Delta V \Delta t}{\frac{1}{2}(\delta r_{NP} + \delta r_{PS})} \left( (\alpha_g \rho_g k)_n - (\alpha_g \rho_g k)_s \right) \tag{C.346}$$

This term is implemented through the source term  $S_C$  as:

$$S_{C,11} = \frac{2}{3} \frac{\Delta V}{\frac{1}{2}(\delta r_{NP} + \delta r_{PS})} [\alpha_{g,P} \rho_{g,P} k_P - \alpha_{g,S} \rho_{g,S} k_S] \tag{C.347}$$

in which the scalar variables at the staggered grid surface are expressed in terms of the node values in the scalar grid.

Term 11B on the RHS of the radial momentum equation is discretized in the same way as the corresponding term in the liquid phase equation, as discussed in sect C.4.4.

$$\begin{aligned}
 & - \int_{\Delta t \Delta V} \frac{\partial}{\partial r} \left( \frac{2}{3} \alpha_g \rho_g \frac{\mu_{g,t}}{\sigma_{\alpha_{g,t}}} \frac{1}{r} \frac{\partial (rv_g)}{\partial r} \right) dV dt \\
 &= - \frac{2}{3} \frac{\Delta V}{\frac{1}{2}(\delta r_{NP} + \delta r_{PS})} \left[ \left( \frac{\alpha_g \frac{\mu_{g,t}}{\sigma_{\alpha_{g,t}}}}{r} \frac{\partial (rv_g)}{\partial r} \right)_n - \left( \frac{\alpha_g \frac{\mu_{g,t}}{\sigma_{\alpha_{g,t}}}}{r} \frac{\partial (rv_g)}{\partial r} \right)_s \right]
 \end{aligned} \tag{C.348}$$

This term is implemented through the source term  $S_C$  as:

$$S_{C,12} = - \frac{2}{3} \frac{\Delta V}{\frac{1}{2}(\delta r_{NP} + \delta r_{PS})} \left[ \frac{\alpha_{g,P} \frac{\mu_{g,t,P}}{\sigma_{\alpha_{g,t}}}}{r_P} \left( \frac{\partial (rv_g)}{\partial r} \right)_n - \frac{\alpha_{g,W} \frac{\mu_{g,t,W}}{\sigma_{\alpha_{g,t}}}}{r_S^*} \left( \frac{\partial (rv_g)}{\partial r} \right)_s \right] \tag{C.349}$$

where

$$\begin{aligned} \left(\frac{\partial(rv_g)}{\partial r}\right)_n &= \frac{(rv_g)_N - (rv_g)_P}{\delta r_{NP}} = \frac{r_N^v v_{g,N} - (r_P^v v_{g,P})}{\delta r_{NP}} \\ \left(\frac{\partial(rv_g)}{\partial r}\right)_s &= \frac{(rv_g)_P - (rv_g)_S}{\delta r_{PS}} = \frac{r_P^v v_{g,P} - (r_S^v v_{g,S})}{\delta r_{PS}} \end{aligned} \quad (\text{C.350})$$

Term 11C on the RHS of the radial momentum equation is discretized in the same way as the corresponding term in the liquid phase equation, as discussed in sect C.4.4.

$$\begin{aligned} \int_{\Delta t \Delta V} \int -\frac{\partial}{\partial r} \left( \frac{2}{3} \alpha_g \rho_g \frac{\mu_{g,t}}{\sigma_{\alpha_{g,t}}} \frac{\partial w_g}{\partial z} \right) dV dt \\ = -\frac{2}{3} \frac{\Delta V \Delta t}{\frac{1}{2}(\delta r_{NP} + \delta r_{PS})} \left[ \left( \alpha_g \frac{\mu_{g,t}}{\sigma_{\alpha_{g,t}}} \frac{\partial w_g}{\partial z} \right)_n - \left( \alpha_g \frac{\mu_{g,t}}{\sigma_{\alpha_{g,t}}} \frac{\partial w_g}{\partial z} \right)_s \right] \end{aligned} \quad (\text{C.351})$$

This term is implemented through the source term  $S_C$  as:

$$\begin{aligned} S_{C,13} &= -\frac{2}{3} \frac{\Delta V}{\frac{1}{2}(\delta r_{NP} + \delta r_{PS})} \left[ \alpha_{g,P} \frac{\mu_{g,t,P}}{\sigma_{\alpha_{g,t}}} \frac{(w_{g,E} - w_{g,P})}{\frac{1}{2}(\delta z_{EP} + \delta z_{PW})} \right] \\ &\quad + \frac{2}{3} \frac{\Delta V}{\frac{1}{2}(\delta r_{NP} + \delta r_{PS})} \left[ \alpha_{g,W} \frac{\mu_{g,t,W}}{\sigma_{\alpha_{g,t}}} \frac{(w_{g,P} - w_{g,W})}{\frac{1}{2}(\delta z_{EP} + \delta z_{PW})} \right] \end{aligned} \quad (\text{C.352})$$

Term 13A on the RHS of the momentum equation:

$$\int_{\Delta t \Delta V} \int \frac{\mu_{l,t}}{\sigma_{\alpha_{l,t}}} \frac{\partial \alpha_l}{\partial r} \frac{\partial v_l}{\partial r} dV dt = \left( \frac{\mu_{l,t}}{\sigma_{\alpha_{l,t}}} \frac{\partial \alpha_l}{\partial r} \frac{\partial v_l}{\partial r} \right)_P \Delta V \Delta t \quad (\text{C.353})$$

This term is implemented through the source term  $S_C$  as:

$$S_{C,14} = \frac{1}{2} \left( \frac{\mu_{l,t,P}}{\sigma_{\alpha_{l,t}}} + \frac{\mu_{l,t,S}}{\sigma_{\alpha_{l,t}}} \right) \left( \frac{\partial \alpha_l}{\partial r} \frac{\partial v_l}{\partial r} \right)_P \Delta V \Delta t \quad (\text{C.354})$$

in which the scalar variables at the staggered grid center node are obtained by arithmetic interpolation of the node values in the scalar grid. Moreover, the velocity gradient is approximated by use of the central difference scheme and the surface values are obtained by arithmetic interpolation of the node values in the staggered velocity grid.

$$\left( \frac{\partial v_l}{\partial r} \right)_P = \frac{v_{l,n} - v_{l,s}}{\frac{1}{2}(\delta r_{NP} + \delta r_{PS})} = \frac{\frac{1}{2}(v_{l,P} + v_{l,N}) - \frac{1}{2}(v_{l,P} + v_{l,S})}{\frac{1}{2}(\delta r_{NP} + \delta r_{PS})} \quad (\text{C.355})$$

Term 13B on the RHS of the momentum equation:

$$\int_{\Delta t \Delta V} \int \frac{\mu_{l,t}}{\sigma_{\alpha_{l,t}}} \frac{\partial \alpha_l}{\partial z} \frac{\partial v_l}{\partial z} dV dt = \Delta V \Delta t \left( \frac{\mu_{l,t}}{\sigma_{\alpha_{l,t}}} \frac{\partial \alpha_l}{\partial z} \frac{\partial v_l}{\partial z} \right)_P \quad (\text{C.356})$$

This term is implemented through the source term  $S_C$  as:

$$S_{C,15} = \Delta V \Delta t \left( \frac{\mu_{l,t}}{\sigma_{\alpha_{l,t}}} \frac{\partial \alpha_l}{\partial z} \right)_P \frac{\frac{1}{2}(v_{l,E} + v_{l,P}) - \frac{1}{2}(v_{l,P} + v_{l,W})}{\frac{1}{2}(\delta z_{EP} + \delta z_{PW})} \quad (\text{C.357})$$

where

$$\begin{aligned} \left( \frac{\partial \alpha_l}{\partial z} \right)_P &= \frac{(\alpha_l)_e - (\alpha_l)_w}{\frac{1}{2}(\delta z_{EP} + \delta z_{PW})} \\ &= \frac{\frac{1}{4}(\alpha_{l,P} + \alpha_{l,E} + \alpha_{l,S} + \alpha_{l,SE}) - \frac{1}{4}(\alpha_{l,P} + \alpha_{l,W} + \alpha_{l,S} + \alpha_{l,SW})}{\frac{1}{2}(\delta z_{EP} + \delta z_{PW})} \end{aligned} \quad (\text{C.358})$$

Term 14 on the RHS of the momentum equation:

$$\int_{\Delta t \Delta V} v_l \frac{\partial}{\partial r} \left( \frac{\mu_{l,t}}{\sigma_{\alpha_{l,t}}} \frac{\partial \alpha_l}{\partial r} \right) dV dt = v_{l,P} \left[ \frac{(\mu_{l,t} \frac{\partial \alpha_l}{\partial r})_n - (\mu_{l,t} \frac{\partial \alpha_l}{\partial r})_s}{\frac{1}{2}(\delta r_{NP} + \delta r_{PS})} \right] \Delta V \Delta t \quad (\text{C.359})$$

This term is implemented through the source term  $S_C$  as:

$$S_{C,16} = v_P \left[ \frac{\mu_{l,P} (\frac{\partial \alpha_l}{\partial r})_n - \mu_{l,S} (\frac{\partial \alpha_l}{\partial r})_s}{\frac{1}{2}(\delta r_{NP} + \delta r_{PS})} \right] \Delta V \Delta t \quad (\text{C.360})$$

in which the scalar variables at the staggered grid center node are obtained by arithmetic interpolation of the node values in the scalar grid.

Term 15 on the RHS of the momentum equation:

$$\int_{\Delta t \Delta V} w_l \frac{\partial}{\partial z} \left( \frac{\mu_{l,t}}{\sigma_{\alpha_{l,t}}} \frac{\partial \alpha_l}{\partial r} \right) dV dt = (w_l)_P \left[ \frac{(\frac{\mu_{l,t}}{\sigma_{\alpha_{l,t}}} \frac{\partial \alpha_l}{\partial r})_e - (\frac{\mu_{l,t}}{\sigma_{\alpha_{l,t}}} \frac{\partial \alpha_l}{\partial r})_w}{\frac{1}{2}(\delta z_{EP} + \delta z_{PW})} \right] \Delta V \Delta t \quad (\text{C.361})$$

This term is implemented through the source term  $S_C$  as:

$$S_{C,17} = (w_l)_P \left[ \frac{(\mu_{l,t} \frac{\partial \alpha_l}{\partial r})_e - (\mu_{l,t} \frac{\partial \alpha_l}{\partial r})_w}{\frac{1}{2}(\delta z_{EP} + \delta z_{PW})} \right] \Delta V \Delta t \quad (\text{C.362})$$

## Pressure force

The pressure force term is treated in the same way as described for the radial liquid velocity component.

## Added mass force

The added mass force term is treated in the same way as described for the radial liquid velocity component.

**Transversal force**

The transversal force term is treated in the same way as described for the radial liquid velocity component.

**Steady drag force**

The steady drag force term is treated in the same way as described for the radial liquid velocity component.

**Algebraic discretization equation**

After dividing all the terms by  $\Delta t$ , the discretized equation can be written on the standard algebraic form:

$$a_P v_{g,P} = a_N v_{g,N} + a_S v_{g,S} + a_E v_{g,E} + a_W v_{g,W} + b_{v_g} \quad (\text{C.363})$$

in which the coefficients are defined by:

$$\begin{aligned} a_N &= D_n + \max[-C_n, 0] \\ a_S &= D_s + \max[C_s, 0] \\ a_E &= D_e + \max[-C_e, 0] \\ a_W &= D_w + \max[C_w, 0] \\ b &= \sum_m S_{C,m} + a_P^0 v_{g,P}^0 \\ a_P &= \frac{\Delta V}{\Delta t} (\alpha_g \rho_g)_P + a_N + a_S + a_E + a_W + C_n - C_s + C_e - C_w - \sum_q S_{P,q} \Delta V \end{aligned} \quad (\text{C.364})$$

To avoid negative coefficients, the relation for the coefficient  $a_P$  can be modified using the continuity equation, as shown for the liquid phase equations. The alternative  $a_P^*$  and  $b^*$  coefficients are defined by:

$$\begin{aligned} b^* &= -m C_2 v_{g,P}^v + \sum_m S_{C,m,g} + a_P^0 v_{g,P}^0 \\ a_P^* &= \frac{\Delta V}{\Delta t} (\alpha_g \rho_g)_P^0 + a_N + a_S + a_E + a_W + m C_1 - \sum_q S_{P,q,g} \Delta V \end{aligned} \quad (\text{C.365})$$

### C.4.7 The gas phase axial momentum balance

The axial momentum balance for gas is given in (C.146).

$$\begin{aligned}
 \frac{\partial}{\partial t}(\alpha_g \rho_g w_g) + \frac{1}{r} \frac{\partial}{\partial r}(r \alpha_g \rho_g v_g w_g) + \frac{\partial}{\partial z}(\alpha_g \rho_g w_g w_g) = \\
 \frac{1}{r} \frac{\partial}{\partial r} \left( r \frac{\mu_{g,t}}{\sigma_{\alpha_{g,t}}} \frac{\partial \alpha_g}{\partial r} w_g \right) + \frac{\partial}{\partial z} \left( \frac{\mu_{g,t}}{\sigma_{\alpha_{g,t}}} \frac{\partial \alpha_g}{\partial z} w_g \right) \\
 + \frac{1}{r} \frac{\partial}{\partial r} \left( r \frac{\mu_{g,t}}{\sigma_{\alpha_{g,t}}} \frac{\partial \alpha_g}{\partial z} v_g \right) + \frac{\partial}{\partial z} \left( \frac{\mu_{g,t}}{\sigma_{\alpha_{g,t}}} \frac{\partial \alpha_g}{\partial z} w_g \right) \\
 + \frac{1}{r} \frac{\partial}{\partial r} \left( r \alpha_g \frac{\mu_{g,t}}{\sigma_{g,t}} \frac{\partial w_g}{\partial r} \right) + \frac{\partial}{\partial z} \left( \alpha_g \frac{\mu_{g,t}}{\sigma_{g,t}} \frac{\partial w_g}{\partial z} \right) \\
 + \frac{1}{r} \frac{\partial}{\partial r} \left( r \alpha_g \frac{\mu_{g,t}}{\sigma_{g,t}} \frac{\partial v_g}{\partial z} \right) + \frac{\partial}{\partial z} \left( \alpha_g \frac{\mu_{g,t}}{\sigma_{g,t}} \frac{\partial w_g}{\partial z} \right) \\
 - \frac{\partial}{\partial z} \left( \frac{2}{3} \alpha_g \rho_g (k + \frac{\nu_{g,t}}{\sigma_{g,t}} (\frac{1}{r} \frac{\partial}{\partial r}(r v_g) + \frac{\partial w_g}{\partial z})) \right) \\
 - \alpha_g \frac{\partial p}{\partial z} + \frac{\mu_{l,t}}{\sigma_{\alpha_{l,t}}} \left( \frac{\partial \alpha_l}{\partial r} \frac{\partial w_l}{\partial r} + \frac{\partial \alpha_l}{\partial z} \frac{\partial w_l}{\partial z} \right) \\
 + (v_l \frac{\partial}{\partial r} (\frac{\mu_{l,t}}{\sigma_{\alpha_{l,t}}} \frac{\partial \alpha_l}{\partial z}) + w_l \frac{\partial}{\partial z} (\frac{\mu_{l,t}}{\sigma_{\alpha_{l,t}}} \frac{\partial \alpha_l}{\partial z})) \\
 + \alpha_g \rho_g g_z + F_{g,z}^C + \overline{F_{g,z}^C}
 \end{aligned}$$

The transient, convective and the diffusive terms are discretized just like the corresponding terms in the liquid phase as shown in sect C.4.5. Only the novel source terms found only in the axial gas phase momentum equation are considered in this section.

#### The source terms

The the source terms are approximated by the midpoint rule, in which  $S$  is considered an average value representative for the whole grid cell volume. The derivatives are represented by an abbreviated Taylor series expansion, usually a central difference expansion of second order is employed.

Term 1 on the RHS of the momentum equation is split into two parts, term 1a and term 1b:

$$\frac{1}{r} \frac{\partial}{\partial r} \left( r \frac{\mu_{g,t}}{\sigma_{\alpha_{g,t}}} \frac{\partial \alpha_g}{\partial r} w_g \right) = -\frac{w_g}{r} \frac{\partial}{\partial r} \left( r \frac{\mu_{g,t}}{\sigma_{\alpha_{g,t}}} \frac{\partial \alpha_l}{\partial r} \right) - \frac{\mu_{g,t}}{\sigma_{\alpha_{g,t}}} \frac{\partial \alpha_l}{\partial r} \frac{\partial w_g}{\partial r} \quad (\text{C.366})$$

Term 1a on the RHS of the momentum equation:

$$\begin{aligned}
 & - \int_{\Delta t \Delta V} \frac{w_g}{r} \frac{\partial}{\partial r} \left( r \frac{\mu_{g,t}}{\sigma_{\alpha_{g,t}}} \frac{\partial \alpha_l}{\partial r} \right) dV dt \\
 & = - \frac{w_{g,P} \Delta V \Delta t}{r_P \frac{1}{2} (\delta r_{NP} + \delta r_{PS})} \left[ \left( r \frac{\mu_{g,t}}{\sigma_{\alpha_{g,t}}} \frac{\partial \alpha_l}{\partial r} \right)_n - \left( r \frac{\mu_{g,t}}{\sigma_{\alpha_{g,t}}} \frac{\partial \alpha_l}{\partial r} \right)_s \right]
 \end{aligned} \tag{C.367}$$

This term is implemented through the source term  $S_C$  as:

$$S_{C,1} = - \frac{w_{g,P} \Delta V \Delta t}{r_P \frac{1}{2} (\delta r_{NP} + \delta r_{PS})} \left[ r_N^v \left( \frac{\mu_{g,t}}{\sigma_{\alpha_{g,t}}} \right)_n \left( \frac{\partial \alpha_l}{\partial r} \right)_n - r_P^v \left( \frac{\mu_{g,t}}{\sigma_{\alpha_{g,t}}} \right)_s \left( \frac{\partial \alpha_l}{\partial r} \right)_s \right] \tag{C.368}$$

where

$$\begin{aligned}
 (\mu_{l,t})_n &= \frac{1}{4} (\mu_{l,P} + \mu_{l,N} + \mu_{l,W} + \mu_{l,NW}) \\
 (\mu_{l,t})_s &= \frac{1}{4} (\mu_{l,P} + \mu_{l,S} + \mu_{l,W} + \mu_{l,SW}) \\
 \left( \frac{\partial \alpha_l}{\partial r} \right)_n &= \frac{(\alpha_l)_N - (\alpha_l)_P}{\delta r_{NP}} = \frac{\frac{1}{2} (\alpha_{l,N} + \alpha_{l,NW}) - \frac{1}{2} (\alpha_{l,P} + \alpha_{l,W})}{\delta r_{NP}} \\
 \left( \frac{\partial \alpha_l}{\partial r} \right)_s &= \frac{(\alpha_l)_P - (\alpha_l)_S}{\delta r_{PS}} = \frac{\frac{1}{2} (\alpha_{l,P} + \alpha_{l,W}) - \frac{1}{2} (\alpha_{l,S} + \alpha_{l,SW})}{\delta r_{PS}}
 \end{aligned} \tag{C.369}$$

Term 1b on the RHS of the momentum equation:

$$- \int_{\Delta t \Delta V} \frac{\mu_{g,t}}{\sigma_{\alpha_{g,t}}} \frac{\partial \alpha_l}{\partial r} \frac{\partial w_g}{\partial r} dV dt = - \left( \frac{\mu_{g,t}}{\sigma_{\alpha_{g,t}}} \frac{\partial \alpha_l}{\partial r} \right)_P \frac{(w_{g,n} - w_{g,s})}{\frac{1}{2} (\delta r_{NP} + \delta r_{PS})} \Delta V \Delta t \tag{C.370}$$

This term is implemented through the source term  $S_C$  as:

$$S_{C,2} = - \frac{1}{2} \left( \frac{\mu_{g,t,P}}{\sigma_{\alpha_{g,t}}} + \frac{\mu_{g,t,W}}{\sigma_{\alpha_{g,t}}} \right) \left( \frac{\partial \alpha_l}{\partial r} \right)_P \left[ \frac{\frac{1}{2} (w_P + w_N) - \frac{1}{2} (w_P + w_S)}{\frac{1}{2} (\delta r_{NP} + \delta r_{PS})} \right] \Delta V \Delta t \tag{C.371}$$

where

$$\begin{aligned}
 \left( \frac{\partial \alpha_l}{\partial r} \right)_P &= \frac{(\alpha_l)_n - (\alpha_l)_s}{S_{NS,P}} \\
 &= \frac{\frac{1}{4} (\alpha_{l,P} + \alpha_{l,N} + \alpha_{l,W} + \alpha_{l,NW}) - \frac{1}{4} (\alpha_{l,P} + \alpha_{l,S} + \alpha_{l,W} + \alpha_{l,SW})}{\frac{1}{2} (\delta r_{NP} + \delta r_{PS})}
 \end{aligned} \tag{C.372}$$

Term 2 on the RHS of the momentum equation is split into two parts, term 2a and term 2b:

$$\frac{\partial}{\partial z} \left( \frac{\mu_{g,t}}{\sigma_{\alpha_{g,t}}} \frac{\partial \alpha_g}{\partial z} w_g \right) = -w_g \frac{\partial}{\partial z} \left( \frac{\mu_{g,t}}{\sigma_{\alpha_{g,t}}} \frac{\partial \alpha_l}{\partial z} \right) - \frac{\mu_{g,t}}{\sigma_{\alpha_{g,t}}} \frac{\partial \alpha_l}{\partial z} \frac{\partial w_g}{\partial z} \quad (\text{C.373})$$

Term 2a on the RHS of the momentum equation:

$$-\int_{\Delta t \Delta V} w_g \frac{\partial}{\partial z} \left( \frac{\mu_{g,t}}{\sigma_{\alpha_{g,t}}} \frac{\partial \alpha_l}{\partial z} \right) dV dt = -w_{g,P} \left[ \frac{\left( \frac{\mu_{g,t}}{\sigma_{\alpha_{g,t}}} \frac{\partial \alpha_l}{\partial z} \right)_e - \left( \frac{\mu_{g,t}}{\sigma_{\alpha_{g,t}}} \frac{\partial \alpha_l}{\partial z} \right)_w}{\delta z_{PW}} \right] \Delta V \Delta t \quad (\text{C.374})$$

This term is implemented through the source term  $S_C$  as:

$$S_{C,3} = -w_{g,P} \left[ \frac{\frac{\mu_{g,t,P}}{\sigma_{\alpha_{g,t}}} \left( \frac{\partial \alpha_l}{\partial z} \right)_e - \frac{\mu_{g,t,W}}{\sigma_{\alpha_{g,t}}} \left( \frac{\partial \alpha_l}{\partial z} \right)_w}{\delta z_{PW}} \right] \Delta V \Delta t \Delta t \quad (\text{C.375})$$

where

$$\begin{aligned} \left( \frac{\partial \alpha_l}{\partial z} \right)_e &= \frac{(\alpha_l)_E - (\alpha_l)_P}{\frac{1}{2}(\delta z_{PW} + \delta z_{EP})} = \frac{\frac{1}{2}(\alpha_{l,E} + \alpha_{l,P}) - \frac{1}{2}(\alpha_{l,P} + \alpha_{l,W})}{\frac{1}{2}(\delta z_{PW} + \delta z_{EP})} \\ \left( \frac{\partial \alpha_l}{\partial z} \right)_w &= \frac{(\alpha_l)_P - (\alpha_l)_W}{\frac{1}{2}(\delta z_{PW} + \delta z_{EP})} = \frac{\frac{1}{2}(\alpha_{l,P} + \alpha_{l,W}) - \frac{1}{2}(\alpha_{l,W} + \alpha_{l,W})}{\frac{1}{2}(\delta z_{PW} + \delta z_{EP})} \end{aligned} \quad (\text{C.376})$$

Term 2b on the RHS of the momentum equation:

$$-\int_{\Delta t \Delta V} \frac{\mu_{g,t,P}}{\sigma_{\alpha_{g,t}}} \frac{\partial \alpha_l}{\partial z} \frac{\partial w_g}{\partial z} dV dt = -\left( \frac{\mu_{g,t,P}}{\sigma_{\alpha_{g,t}}} \frac{\partial \alpha_l}{\partial z} \right)_P \frac{(w_{g,e} - w_{g,w})}{\delta z_{PW}} \Delta V \Delta t \quad (\text{C.377})$$

This term is implemented through the source term  $S_C$  as:

$$S_{C,4} = -\frac{1}{2} \left( \frac{\mu_{g,t,P}}{\sigma_{\alpha_{g,t}}} + \frac{\mu_{g,t,W}}{\sigma_{\alpha_{g,t}}} \right) \left( \frac{\partial \alpha_l}{\partial z} \right)_P \left[ \frac{\frac{1}{2}(w_{g,E} + w_{g,P}) - \frac{1}{2}(w_{g,P} + w_{g,W})}{\delta z_{PW}} \right] \Delta V \Delta t \quad (\text{C.378})$$

where

$$\left( \frac{\partial \alpha_l}{\partial z} \right)_P = \frac{(\alpha_l)_e - (\alpha_l)_w}{\delta z_{PW}} = \frac{(\alpha_l)_P - (\alpha_l)_W}{\delta z_{PW}} \quad (\text{C.379})$$

Term 3 on the RHS of the axial momentum equation is split into two parts, term 3a and term 3b:

$$\frac{1}{r} \frac{\partial}{\partial r} \left( r \frac{\mu_{g,t}}{\sigma_{\alpha_{g,t}}} \frac{\partial \alpha_g}{\partial z} v_g \right) = -v_g \frac{\partial}{\partial r} \left( \frac{\mu_g}{\sigma_{\alpha_{g,t}}} \frac{\partial \alpha_l}{\partial z} \right) - \frac{1}{r} \frac{\mu_g}{\sigma_{\alpha_{g,t}}} \frac{\partial \alpha_l}{\partial z} \frac{\partial}{\partial r} (rv_g) \quad (\text{C.380})$$

Term 3a on the RHS of the momentum equation:

$$-\int_{\Delta t \Delta V} v_g \frac{\partial}{\partial r} \left( \frac{\mu_g}{\sigma_{\alpha_{g,t}}} \frac{\partial \alpha_l}{\partial z} \right) dV dt = -(v_g)_P \left[ (\mu_g \frac{\partial \alpha_l}{\partial z})_n - (\mu_g \frac{\partial \alpha_l}{\partial z})_s \right] \frac{\Delta V \Delta t}{\frac{1}{2}(\delta r_{NP} + \delta r_{PS})} \quad (\text{C.381})$$

This term is implemented through the source term  $S_C$  as:

$$S_{C,5} = -v_{g,P} \left[ (\mu_g \frac{\partial \alpha_l}{\partial z})_n - (\mu_g \frac{\partial \alpha_l}{\partial z})_s \right] \frac{\Delta V \Delta t}{\frac{1}{2}(\delta r_{NP} + \delta r_{PS})} \quad (\text{C.382})$$

where

$$\begin{aligned} (v_g)_P &= \frac{1}{4}(v_{g,P} + v_{g,N} + v_{g,W} + v_{g,NW}) \\ (\mu_{l,t})_n &= \frac{1}{4}(\mu_{l,P} + \mu_{l,N} + \mu_{l,W} + \mu_{l,NW}) \\ (\mu_{l,t})_s &= \frac{1}{4}(\mu_{l,P} + \mu_{l,S} + \mu_{l,W} + \mu_{l,SW}) \\ \left( \frac{\partial \alpha_l}{\partial z} \right)_n &= \frac{\frac{1}{2}(\alpha_{l,P} + \alpha_{l,N}) - \frac{1}{2}(\alpha_{l,W} + \alpha_{l,NW})}{\delta z_{PW}} \\ \left( \frac{\partial \alpha_l}{\partial z} \right)_s &= \frac{\frac{1}{2}(\alpha_{l,P} + \alpha_{l,S}) - \frac{1}{2}(\alpha_{l,W} + \alpha_{l,SW})}{\delta z_{PW}} \end{aligned} \quad (\text{C.383})$$

Term 3b on the RHS of the axial momentum equation:

$$-\int_{\Delta t \Delta V} \frac{1}{r} \frac{\mu_{g,t}}{\sigma_{\alpha_{g,t}}} \frac{\partial \alpha_l}{\partial z} \frac{\partial}{\partial r} (rv_g) dV dt = -\left( \frac{\mu_{g,t}}{\sigma_{\alpha_{g,t}}} \frac{\partial \alpha_l}{\partial r} \right)_P \left[ \frac{(rv_l)_n - (rv_l)_s}{\frac{1}{2}(\delta r_{NP} + \delta r_{PS})} \right] \Delta V \Delta t \quad (\text{C.384})$$

This term is implemented through the source term  $S_C$  as:

$$S_{C,6} = -\frac{\frac{1}{2}(\frac{\mu_{g,t,P}}{\sigma_{\alpha_{g,t}}} + \frac{\mu_{g,t,S}}{\sigma_{\alpha_{g,t}}})}{r_P} \left( \frac{\partial \alpha_l}{\partial r} \right)_P \left[ \frac{\frac{1}{2}(v_N + v_{NW}) - \frac{1}{2}(v_P + v_W)}{\frac{1}{2}(\delta r_{NP} + \delta r_{PS})} \right] \Delta V \Delta t \quad (\text{C.385})$$

where

$$\begin{aligned} \left( \frac{\partial \alpha_l}{\partial r} \right)_P &= \frac{(\alpha_l)_n - (\alpha_l)_s}{\delta r_{NP} + \delta r_{PS}} \\ &= \frac{\frac{1}{4}(\alpha_{l,P} + \alpha_{l,N} + \alpha_{l,W} + \alpha_{l,NW}) - \frac{1}{4}(\alpha_{l,P} + \alpha_{l,S} + \alpha_{l,W} + \alpha_{l,SW})}{\delta r_{NP} + \delta r_{PS}} \end{aligned} \quad (\text{C.386})$$

Term 4 on the RHS of the axial momentum equation is split into two parts, term 4a and term 4b:

$$\frac{\partial}{\partial z} \left( \frac{\mu_{g,t}}{\sigma_{\alpha_{g,t}}} \frac{\partial \alpha_g}{\partial z} w_g \right) = -w_g \frac{\partial}{\partial z} \left( \frac{\mu_{g,t}}{\sigma_{\alpha_{g,t}}} \frac{\partial \alpha_l}{\partial z} \right) - \frac{\mu_{g,t}}{\sigma_{\alpha_{g,t}}} \frac{\partial \alpha_l}{\partial z} \frac{\partial w_g}{\partial z} \quad (\text{C.387})$$

Term 4a on the RHS of the momentum equation:

$$-\int \int_{\Delta t \Delta V} w_g \frac{\partial}{\partial z} \left( \frac{\mu_{g,t}}{\sigma_{\alpha_{g,t}}} \frac{\partial \alpha_l}{\partial z} \right) dV dt = -w_{g,P} \left[ \frac{\left( \frac{\mu_{g,t}}{\sigma_{\alpha_{g,t}}} \frac{\partial \alpha_l}{\partial z} \right)_e - \left( \frac{\mu_{g,t}}{\sigma_{\alpha_{g,t}}} \frac{\partial \alpha_l}{\partial z} \right)_w}{\delta z_{PW}} \right] \Delta V \Delta t \quad (\text{C.388})$$

This term is implemented through the source term  $S_C$  as:

$$S_{C,7} = -w_{g,P} \left[ \frac{\left( \frac{\mu_{g,t,P}}{\sigma_{\alpha_{g,t}}} \frac{\partial \alpha_l}{\partial z} \right)_e - \left( \frac{\mu_{g,t,W}}{\sigma_{\alpha_{g,t}}} \frac{\partial \alpha_l}{\partial z} \right)_w}{\delta z_{PW}} \right] \Delta V \Delta t \quad (\text{C.389})$$

Term 4b on the RHS of the momentum equation:

$$-\int \int_{\Delta t \Delta V} \frac{\mu_{g,t}}{\sigma_{\alpha_{g,t}}} \frac{\partial \alpha_l}{\partial z} \frac{\partial w_g}{\partial z} dV dt = -\left( \frac{\mu_{g,t}}{\sigma_{\alpha_{g,t}}} \frac{\partial \alpha_l}{\partial z} \right)_P \left[ \frac{w_{g,e} - w_{g,w}}{\delta z_{PW}} \right] \Delta V \Delta t \quad (\text{C.390})$$

This term is implemented through the source term  $S_C$  as:

$$S_{C,8} = -\frac{1}{2}(\mu_{g,P} + \mu_{g,W}) \left( \frac{\partial \alpha_l}{\partial z} \right)_P \left[ \frac{\frac{1}{2}(w_{g,E} + w_{g,P}) - \frac{1}{2}(w_{g,P} + w_{g,W})}{\delta z_{PW}} \right] \Delta V \Delta t \quad (\text{C.391})$$

The 5th to 9th terms on the RHS of the axial component of the gas momentum equation are discretized in the same way as the corresponding equations in the liquid phase equation, discussed in sect C.4.5.

Term 11A on the RHS of the axial momentum equation:

$$\int \int_{\Delta t \Delta V} \frac{\mu_{l,t}}{\sigma_{\alpha_{l,t}}} \frac{\partial \alpha_l}{\partial r} \frac{\partial w_l}{\partial r} dV dt = \left( \frac{\mu_{l,t}}{\sigma_{\alpha_{l,t}}} \frac{\partial \alpha_l}{\partial r} \frac{\partial w_l}{\partial r} \right)_P \Delta V \Delta t \quad (\text{C.392})$$

This term is implemented through the source term  $S_C$  as:

$$S_{C,14} = \frac{1}{2} \left( \frac{\mu_{l,t,P}}{\sigma_{\alpha_{l,t}}} + \frac{\mu_{l,t,W}}{\sigma_{\alpha_{l,t}}} \right) \left( \frac{\partial \alpha_l}{\partial r} \right)_P \left( \frac{\partial w_l}{\partial r} \right)_P \Delta V \Delta t \quad (\text{C.393})$$

where

$$\left( \frac{\partial w_l}{\partial r} \right)_P = \frac{w_{l,n} - w_{l,s}}{\frac{1}{2}(\delta r_{NP} + \delta r_{PS})} = \frac{\frac{1}{2}(w_{l,P} + w_{l,N}) - \frac{1}{2}(w_{l,P} + w_{l,S})}{\frac{1}{2}(\delta r_{NP} + \delta r_{PS})} \quad (\text{C.394})$$

Term 11B on the RHS of the axial momentum equation:

$$\int_{\Delta t \Delta V} \int \frac{\mu_{l,t}}{\sigma_{\alpha_{l,t}}} \frac{\partial \alpha_l}{\partial z} \frac{\partial w_l}{\partial z} dV dt = \left( \frac{\mu_{l,t}}{\sigma_{\alpha_{l,t}}} \frac{\partial \alpha_l}{\partial z} \frac{\partial w_l}{\partial z} \right)_P \Delta V \Delta t \quad (\text{C.395})$$

This term is implemented through the source term  $S_C$  as:

$$S_{C,15} = \frac{1}{2} \left( \frac{\mu_{l,t,P}}{\sigma_{\alpha_{l,t}}} + \frac{\mu_{l,t,W}}{\sigma_{\alpha_{l,t}}} \right) \left( \frac{\partial \alpha_l}{\partial z} \right)_P \left( \frac{\partial w_l}{\partial z} \right)_P \Delta V \Delta t \quad (\text{C.396})$$

Term 12 on the RHS of the axial component of the momentum equation:

$$\int_{\Delta t \Delta V} \int v_l \frac{\partial}{\partial r} \left( \frac{\mu_{l,t}}{\sigma_{\alpha_{l,t}}} \frac{\partial \alpha_l}{\partial z} \right) dV dt = \frac{(v_l)_P \Delta V \Delta t}{\frac{1}{2}(\delta r_{NP} + \delta r_{PS})} \left[ \left( \frac{\mu_{l,t}}{\sigma_{\alpha_{l,t}}} \frac{\partial \alpha_l}{\partial z} \right)_n - \left( \frac{\mu_{l,t}}{\sigma_{\alpha_{l,t}}} \frac{\partial \alpha_l}{\partial z} \right)_s \right] \quad (\text{C.397})$$

This term is implemented through the source term  $S_C$  as:

$$S_{C,16} = \frac{(v_l)_P \Delta V \Delta t}{\frac{1}{2}(\delta r_{NP} + \delta r_{PS})} \left[ \frac{\mu_{l,t,P}}{\sigma_{\alpha_{l,t}}} \left( \frac{\partial \alpha_l}{\partial r} \right)_n - \frac{\mu_{l,t,S}}{\sigma_{\alpha_{l,t}}} \left( \frac{\partial \alpha_l}{\partial r} \right)_s \right] \quad (\text{C.398})$$

Term 13 on the RHS of the axial component of the momentum equation:

$$\int_{\Delta t \Delta V} \int w_l \frac{\partial}{\partial z} \left( \frac{\mu_{l,t}}{\sigma_{\alpha_{l,t}}} \frac{\partial \alpha_l}{\partial z} \right) dV dt = \frac{w_{l,P} \Delta V \Delta t}{\delta z_{PW}} \left[ \left( \frac{\mu_{l,t}}{\sigma_{\alpha_{l,t}}} \frac{\partial \alpha_l}{\partial z} \right)_e - \left( \frac{\mu_{l,t}}{\sigma_{\alpha_{l,t}}} \frac{\partial \alpha_l}{\partial z} \right)_w \right] \quad (\text{C.399})$$

This term is implemented through the source term  $S_C$  as:

$$S_{C,17} = \frac{w_{l,P} \Delta V}{\delta z_{PW}} \left[ \frac{\mu_{l,t,P}}{\sigma_{\alpha_{l,t}}} \left( \frac{\partial \alpha_l}{\partial z} \right)_e - \frac{\mu_{l,t,W}}{\sigma_{\alpha_{l,t}}} \left( \frac{\partial \alpha_l}{\partial z} \right)_w \right] \quad (\text{C.400})$$

### Pressure force term

The pressure force term in the axial component of the gas momentum equation is discretized in the same way as described when considering the liquid momentum equation in sect C.4.5.

### Gravity force term

The gravity force term in the gas momentum equation is discretized in the same way as described when considering the liquid momentum equation in sect C.4.5.

### Virtual mass force term

The virtual mass force term in the gas momentum equation is discretized in the same way as described when considering the liquid phase momentum equation in sect C.4.5.

### Steady drag force term

The steady drag force term in the axial component of the gas momentum equation is treated in the same way as described when considering the liquid momentum equation, as discussed in sect C.4.5.

### Algebraic discretization equation

After dividing all the terms by  $\Delta t$ , the discretized equation can be written on the standard algebraic form:

$$a_P w_{g,P} = a_N w_{g,N} + a_S w_{g,S} + a_E w_{g,E} + a_W w_{g,W} + b_{w_g} \quad (\text{C.401})$$

in which the coefficients are defined by:

$$\begin{aligned} a_N &= D_n + \max[-C_n, 0] \\ a_S &= D_s + \max[C_s, 0] \\ a_E &= D_e + \max[-C_e, 0] \\ a_W &= D_w + \max[C_w, 0] \\ b &= \sum_m S_{C,m} + a_P^0 w_{g,P}^0 \\ a_P &= \frac{\Delta V}{\Delta t} (\alpha_g \rho_g)_P + a_N + a_S + a_E + a_W + C_n - C_s + C_e - C_w - \sum_q S_{P,q} \Delta V \end{aligned} \quad (\text{C.402})$$

To avoid negative coefficients, the relation for the coefficient  $a_P$  can be modified using the continuity equation, as shown for the liquid phase equations. The alternative  $a_P^*$  and  $b^*$  coefficients are defined by:

$$\begin{aligned} b^* &= -m C_2 w_{g,P}^\nu + \sum_m S_{C,m,g} + a_P^0 w_{g,P}^0 \\ a_P^* &= \frac{\Delta V}{\Delta t} (\alpha_g \rho_g)_P^0 + a_N + a_S + a_E + a_W + m C_1 - \sum_q S_{P,q,g} \Delta V \end{aligned} \quad (\text{C.403})$$

### C.4.8 The Turbulent Kinetic Energy

The equation for the turbulent kinetic energy is discretized in accordance with the generalized equation in sect C.4.3, with  $\psi = k$  and phase  $k = l$ .

#### The source terms

The the source terms are approximated by the midpoint rule, in which  $\langle S \rangle$  is considered an average value representative for the whole grid cell volume. The derivatives are represented by an abbreviated Taylor series expansion, usually a central difference expansion of second order is employed.

$$\int_{\Delta t \Delta V} \alpha_l (P_k + P_b - \rho_l \varepsilon) dV dt = \alpha_l (P_k + P_b - \rho_l \varepsilon) \Delta V \Delta t \quad (\text{C.404})$$

where

$$S_{C,1} \Delta V \Delta t = [\alpha_{l,P} P_k \Delta V + \alpha_{l,P} P_b] \Delta V \Delta t \quad (\text{C.405})$$

$$S_{p,1} \Delta V \Delta t = \alpha_{l,P} \rho_{l,P} \varepsilon \Delta V \Delta t \quad (\text{C.406})$$

in which the production terms are approximated as:

$$\begin{aligned} P_k &= \mu_{l,t,P} (2[(\frac{\partial v_l}{\partial r})_P^2 + (\frac{\partial w_l}{\partial z})_P^2 + (\frac{v_l}{r})_P^2] + (\frac{\partial v_l}{\partial z} + \frac{\partial w_l}{\partial r})_P^2) \\ (\frac{\partial v_l}{\partial r})_P &= \frac{(v_l)_n - (v_l)_s}{\frac{1}{2}(\delta r_{NP} + \delta r_{PS})} = \frac{v_{l,N} - v_{l,S}}{\frac{1}{2}(\delta r_{NP} + \delta r_{PS})} \\ (\frac{\partial w_l}{\partial z})_P &= \frac{(w_l)_e - (w_l)_w}{\frac{1}{2}(\delta_{PW} + \delta_{EP})} = \frac{w_{l,E} - w_{l,P}}{\frac{1}{2}(\delta_{PW} + \delta_{EP})} \\ (\frac{v_l}{r})_P &= \frac{\frac{1}{2}(v_{l,P} + v_{l,N})}{\frac{1}{2}(r_P^v + r_N^v)} \\ (\frac{\partial v_l}{\partial z})_P &= \frac{\frac{1}{4}(v_{l,P} + v_{l,E} + v_{l,N} + v_{l,NE}) - \frac{1}{4}(v_{l,P} + v_{l,W} + v_{l,N} + v_{l,NW})}{\frac{1}{2}(\delta_{PW} + \delta_{EP})} \\ (\frac{\partial w_l}{\partial r})_P &= \frac{\frac{1}{4}(w_{l,P} + w_{l,E} + w_{l,N} + w_{l,NE}) - \frac{1}{4}(w_{l,P} + w_{l,W} + w_{l,N} + w_{l,NW})}{\frac{1}{2}(\delta r_{NP} + \delta r_{PS})} \end{aligned} \quad (\text{C.407})$$

and

$$\begin{aligned} P_b &= C_d [F_{D,z}((w_g)_P - (w_l)_P) + F_{D,r}((v_g)_P - (v_l)_P)] \\ &= C_d \left[ F_{D,z} \left( \frac{1}{2}(w_{g,P} + w_{g,E}) - \frac{1}{2}(w_{l,P} + w_{l,E}) \right) \right. \\ &\quad \left. + F_{D,r} \left( \frac{1}{2}(v_{g,P} + v_{g,N}) - \frac{1}{2}(v_{l,P} + v_{l,N}) \right) \right] \end{aligned} \quad (\text{C.408})$$

### Algebraic discretization equation

After dividing all the terms by  $\Delta t$ , the discretized equation can be written on the standard algebraic form:

$$a_P k_{l,P} = a_N k_{l,N} + a_S k_{l,S} + a_E k_{l,E} + a_W k_{l,W} + b_{k_l} \quad (\text{C.409})$$

in which the coefficients are defined by:

$$\begin{aligned}
 a_N &= D_n + \max[-C_n, 0] \\
 a_S &= D_s + \max[C_s, 0] \\
 a_E &= D_e + \max[-C_e, 0] \\
 a_W &= D_w + \max[C_w, 0] \\
 b &= \sum_m S_{C,m} + a_P^0 k_{l,P}^0 \\
 a_P &= \frac{\Delta V}{\Delta t} (\alpha_l \rho_l)_P + a_N + a_S + a_E + a_W + C_n - C_s + C_e - C_w - \sum_q S_{P,q} \Delta V
 \end{aligned} \tag{C.410}$$

To avoid negative coefficients, the relation for the coefficient  $a_P$  can be modified using the continuity equation, as shown for the liquid phase velocity equations. The alternative  $a_P^*$  and  $b^*$  coefficients are defined by:

$$\begin{aligned}
 b^* &= -m C_2 k_{l,P}^0 + \sum_m S_{C,m} + a_P^0 k_{l,P}^0 \\
 a_P^* &= \frac{\Delta V}{\Delta t} (\alpha_l \rho_l)_P^0 + a_N + a_S + a_E + a_W + m C_1 - \sum_q S_{P,q,l} \Delta V
 \end{aligned} \tag{C.411}$$

The convective and diffusive fluxes are approximated in the following way:

$$\begin{aligned}
 C_n &= A_n (\alpha_l \rho_l v_r)_n = A_n \frac{1}{2} (\alpha_N \rho_N + \alpha_P \rho_P) v_{r,N} \\
 C_s &= A_s (\alpha_l \rho_l v_r)_s = A_s \frac{1}{2} (\alpha_P \rho_P + \alpha_S \rho_S) v_{r,P} \\
 C_e &= A_e (\alpha_l \rho_l v_z)_e = A_e \frac{1}{2} (\alpha_E \rho_E + \alpha_P \rho_P) v_{z,E} \\
 C_w &= A_w (\alpha_l \rho_l v_z)_w = A_w \frac{1}{2} (\alpha_P \rho_P + \alpha_W \rho_W) v_{z,P} \\
 D_n &= \frac{A_n \Gamma_n}{\delta r_{NP}} \\
 D_s &= \frac{A_s \Gamma_s}{\delta r_{PS}} \\
 D_e &= \frac{A_e \Gamma_e}{\delta z_{EP}} \\
 D_w &= \frac{A_w \Gamma_w}{\delta z_{PW}} \\
 \Gamma_n &= \left( \frac{\mu_{l,eff}}{\sigma_k} \right)_n = \frac{1}{2\sigma_k} (\alpha_N \mu_N + \alpha_N \mu_N) \\
 \Gamma_s &= \left( \frac{\mu_{l,eff}}{\sigma_k} \right)_s = \frac{1}{2\sigma_k} (\alpha_P \mu_P + \alpha_S \mu_S) \\
 \Gamma_w &= \left( \frac{\mu_{l,eff}}{\sigma_k} \right)_w = \frac{1}{2\sigma_k} (\alpha_W \mu_W + \alpha_P \mu_P) \\
 \Gamma_e &= \left( \frac{\mu_{l,eff}}{\sigma_k} \right)_e = \frac{1}{2\sigma_k} (\alpha_P \mu_P + \alpha_W \mu_W)
 \end{aligned} \tag{C.412}$$

### C.4.9 The Turbulent Kinetic Energy Dissipation Rate

The equation for the turbulent energy dissipation rate is discretized in accordance with the generalized equation in sect C.4.3, with  $\psi = \epsilon$  and phase  $k = l$ .

#### The source term

The source terms in the equation for the turbulent kinetic energy dissipation rate are implemented through the source terms  $S_P$  and  $S_C$  in the following way:

$$\int_{\Delta t \Delta V} \alpha_l \frac{\epsilon}{k} (C_1(P_k + P_b) - C_2 \rho_l \epsilon) dV dt = [\alpha_l \frac{\epsilon}{k} (C_1(P_k + P_b) - C_2 \rho_l \epsilon)]_P \Delta V \Delta t \quad (\text{C.413})$$

where

$$S_{C,1} \Delta V \Delta t = [\alpha_l \frac{\epsilon}{k} C_1 P_k + \alpha_l \frac{\epsilon}{k} C_1 P_b]_P \Delta V \Delta t \quad (\text{C.414})$$

$$S_{p,1} \Delta V \Delta t = [\alpha_l \rho_l C_2 \frac{\epsilon}{k}]_P \Delta V \Delta t \quad (\text{C.415})$$

The production terms  $P_k$  and  $P_b$  are defined in section C.4.8.

#### Algebraic discretization equation

After dividing all the terms by  $\Delta t$ , the discretized equation can be written on the standard algebraic form:

$$a_P \epsilon_{l,P} = a_N \epsilon_{l,N} + a_S \epsilon_{l,S} + a_E \epsilon_{l,E} + a_W \epsilon_{l,W} + b_{\epsilon_l} \quad (\text{C.416})$$

in which the coefficients are defined by:

$$a_N = D_n + \max[-C_n, 0]$$

$$a_S = D_s + \max[C_s, 0]$$

$$a_E = D_e + \max[-C_e, 0]$$

$$a_W = D_w + \max[C_w, 0]$$

$$b = \sum_m S_{C,m} + a_P^0 k_{l,P}^0$$

$$a_P = \frac{\Delta V}{\Delta t} (\alpha_l \rho_l)_P + a_N + a_S + a_E + a_W + C_n - C_s + C_e - C_w - \sum_q S_{P,q} \Delta V \quad (\text{C.417})$$

To avoid negative coefficients, the relation for the coefficient  $a_P$  can be modified using the continuity equation, as shown for the liquid phase velocity equations. The alternative  $a_P^*$  and  $b^*$  coefficients are defined by:

$$\begin{aligned}
 b^* &= -mC_2\varepsilon_{l,P}^\nu + \sum_m S_{C,m} + a_P^0\varepsilon_{l,P}^0 \\
 a_P^* &= \frac{\Delta V}{\Delta t}(\alpha_l\rho_l)_P^0 + a_N + a_S + a_E + a_W + mC_1 - \sum_q S_{P,q,l}\Delta V
 \end{aligned} \tag{C.418}$$

The convective and diffusive fluxes are approximated in the following way:

$$\begin{aligned}
 C_n &= A_n(\alpha_l\rho_lv_r)_n = A_n\frac{1}{2}(\alpha_N\rho_N + \alpha_P\rho_P)v_{r,N} \\
 C_s &= A_s(\alpha_l\rho_lv_r)_s = A_s\frac{1}{2}(\alpha_P\rho_P + \alpha_S\rho_S)v_{r,P} \\
 C_e &= A_e(\alpha_l\rho_lv_z)_e = A_e\frac{1}{2}(\alpha_E\rho_E + \alpha_P\rho_P)v_{z,E} \\
 C_w &= A_w(\alpha_l\rho_lv_z)_w = A_w\frac{1}{2}(\alpha_P\rho_P + \alpha_W\rho_W)v_{z,P} \\
 D_n &= \frac{A_n\Gamma_n}{\delta r_{NP}} \\
 D_s &= \frac{A_s\Gamma_s}{\delta r_{PS}} \\
 D_e &= \frac{A_e\Gamma_e}{\delta z_{EP}} \\
 D_w &= \frac{A_w\Gamma_w}{\delta z_{PW}} \\
 \Gamma_n &= \left(\frac{\mu_{l,eff}}{\sigma_\epsilon}\right)_n = \frac{1}{2\sigma_\epsilon}(\alpha_N\mu_N + \alpha_P\mu_P) \\
 \Gamma_s &= \left(\frac{\mu_{l,eff}}{\sigma_\epsilon}\right)_s = \frac{1}{2\sigma_\epsilon}(\alpha_P\mu_P + \alpha_S\mu_S) \\
 \Gamma_w &= \left(\frac{\mu_{l,eff}}{\sigma_\epsilon}\right)_w = \frac{1}{2\sigma_\epsilon}(\alpha_W\mu_W + \alpha_P\mu_P) \\
 \Gamma_e &= \left(\frac{\mu_{l,eff}}{\sigma_\epsilon}\right)_e = \frac{1}{2\sigma_\epsilon}(\alpha_P\mu_P + \alpha_W\mu_W)
 \end{aligned} \tag{C.419}$$

#### C.4.10 The Volume fraction

The gas volume fraction is calculated from the continuity equation for phase  $k$  which is discretized by the scheme proposed by Spalding [20].

The continuity equation for phase  $k$  ( $k = l, g$ ) is derived in appendix C:

$$\begin{aligned}
 \frac{\partial}{\partial t}(\alpha_k\rho_k) + \frac{1}{r}\frac{\partial}{\partial r}(r\alpha_k\rho_kv_{k,r}) + \frac{\partial}{\partial z}(\alpha_k\rho_kv_{k,z}) = \\
 \frac{1}{r}\frac{\partial}{\partial r}\left(r\frac{\mu_{k,t}}{\sigma_{\alpha_k,t}}\frac{\partial\alpha_k}{\partial r}\right) + \frac{\partial}{\partial z}\left(\frac{\mu_{k,t}}{\sigma_{\alpha_k,t}}\frac{\partial\alpha_k}{\partial z}\right) + S
 \end{aligned}$$

In the FEM, this equation is integrated in time and over a grid cell volume. The resulting terms are then approximated in accordance with the approach

presented for the generalized equation. The derivatives of the volume fraction in the diffusive terms are approximated by central differences and for the convection terms the upwind scheme is employed.

The discretized liquid phase continuity equation ( $k = l$ ) can then be expressed as:

$$\begin{aligned} & \alpha_{l,P} \left[ \frac{\rho_l \Delta V}{\Delta t} + (\max[C_n, 0] + D_n) + (\max[-C_s, 0] + D_s) \right. \\ & \quad \left. + (\max[C_e, 0] + D_e) + (\max[-C_w, 0] + D_w) \right] \\ & = \frac{(\alpha_l \rho_l)_P^o \Delta V}{\Delta t} + \alpha_{l,N} (\max[-C_n, 0] + D_n) + \alpha_{l,S} (\max[C_s, 0] + D_s) \\ & \quad + \alpha_{l,E} (\max[-C_e, 0] + D_e) + \alpha_{l,W} (\max[C_w, 0] + D_w) + S \Delta V \end{aligned} \quad (\text{C.420})$$

where

$$\begin{aligned} C_n &= A_n F_n = A_n (\rho_l v_l)_n = A_n v_{r,N} \frac{1}{2} (\rho_{l,P} + \rho_{l,N}) \\ C_s &= A_s F_s = A_s (\rho_l v_l)_s = A_s v_{r,P} \frac{1}{2} (\rho_{l,P} + \rho_{l,S}) \\ C_e &= A_e F_e = A_e (\rho_l w_l)_e = A_e w_{l,E} \frac{1}{2} (\rho_{l,P} + \rho_{l,E}) \\ C_w &= A_w F_w = A_w (\rho_l w_l)_w = A_w w_{l,P} \frac{1}{2} (\rho_{l,P} + \rho_{l,W}) \end{aligned} \quad (\text{C.421})$$

and

$$\begin{aligned} D_n &= \frac{A_n \Gamma_n}{\delta r_{NP}} \\ D_s &= \frac{A_s \Gamma_s}{\delta r_{PS}} \\ D_e &= \frac{A_e \Gamma_e}{\delta z_{EP}} \\ D_w &= \frac{A_w \Gamma_w}{\delta z_{PW}} \\ \Gamma_n &= \left( \frac{\mu_{l,t}}{\sigma_{\alpha_{l,t}}} \right)_n = \frac{1}{2} \left( \frac{\mu_{l,t,P}}{\sigma_{\alpha_{l,t}}} + \frac{\mu_{l,t,N}}{\sigma_{\alpha_{l,t}}} \right) \\ \Gamma_s &= \left( \frac{\mu_{l,t}}{\sigma_{\alpha_{l,t}}} \right)_s = \frac{1}{2} \left( \frac{\mu_{l,t,P}}{\sigma_{\alpha_{l,t}}} + \frac{\mu_{l,t,S}}{\sigma_{\alpha_{l,t}}} \right) \\ \Gamma_w &= \left( \frac{\mu_{l,t}}{\sigma_{\alpha_{l,t}}} \right)_w = \frac{1}{2} \left( \frac{\mu_{l,t,P}}{\sigma_{\alpha_{l,t}}} + \frac{\mu_{l,t,W}}{\sigma_{\alpha_{l,t}}} \right) \\ \Gamma_e &= \left( \frac{\mu_{l,t}}{\sigma_{\alpha_{l,t}}} \right)_e = \frac{1}{2} \left( \frac{\mu_{l,t,P}}{\sigma_{\alpha_{l,t}}} + \frac{\mu_{l,t,E}}{\sigma_{\alpha_{l,t}}} \right) \end{aligned} \quad (\text{C.422})$$

For convenience two new variables  $m$  and  $S_{l,1}$  are introduced, hence the equation can be written in a more compact form:

$$\alpha_{l,P} \sum_i m_{l,i,out} - \sum_i \alpha_{l,i,in} m_{l,i,in} - S_{l,1} = R_l = 0 \quad (\text{C.423})$$

where

$$\begin{aligned} \sum_i m_{l,i,out} &= \frac{\rho_l \Delta V}{\Delta t} + (\max[C_n, 0] + D_n) + (\max[-C_s, 0] + D_s) \\ &\quad + (\max[C_e, 0] + D_e) + (\max[-C_w, 0] + D_w) \\ \sum_i \alpha_{l,i,in} m_{l,i,in} &= \alpha_{l,N} (\max[-C_n, 0] + D_n) + \alpha_{l,S} (\max[C_s, 0] + D_s) \\ &\quad + \alpha_{l,E} (\max[-C_e, 0] + D_e) + \alpha_{l,W} (\max[C_w, 0] + D_w) \\ S_{l,1} &= \frac{(\alpha_l \rho_l)_P^o \Delta V}{\Delta t} \end{aligned} \quad (\text{C.424})$$

A similar equation can be obtained for the gas phase as well. If both equations are solved for  $\alpha_P$  yields:

$$\alpha_{l,P} + \alpha_{g,P} = \frac{\sum_i \alpha_{l,i,in} m_{l,i,in} + S_l}{\sum_i m_{l,i,out}} + \frac{\sum_i \alpha_{g,i,in} m_{g,i,in} + S_g}{\sum_i m_{g,i,out}} = 1 \quad (\text{C.425})$$

With minor manipulation of the equation, we get:

$$\begin{aligned} \sum_i m_{l,i,out} &= \\ &= \frac{(\sum_i \alpha_{l,i,in} m_{l,i,in} + S_l) \sum_i m_{g,i,out} + (\sum_i \alpha_{g,i,in} m_{g,i,in} + S_g) \sum_i m_{l,i,out}}{\sum_i m_{g,i,out}} \end{aligned} \quad (\text{C.426})$$

This relation is used to substitute for the  $\sum_i m_{l,i,out}$  term in (C.423), hence we get:

$$\begin{aligned} \alpha_{l,P} &\left[ \frac{(\sum_i \alpha_{l,i,in} m_{l,i,in} + S_l) \sum_i m_{g,i,out} + (\sum_i \alpha_{g,i,in} m_{g,i,in} + S_g) \sum_i m_{l,i,out}}{\sum_i m_{g,i,out}} \right] \\ &= \sum_i \alpha_{l,i,in} m_{l,i,in} + S_l \end{aligned} \quad (\text{C.427})$$

### Algebraic discretization equation

The algebraic equation that must be solved for the gas volume fraction variable can thus be written as:

$$a_P \alpha_{l,P} = a_N \alpha_{l,N} + a_S \alpha_{l,S} + a_E \alpha_{l,E} + a_W \alpha_{l,W} + S_l \quad (\text{C.428})$$

in which the coefficients are defined as follows:

$$\begin{aligned} a_N &= D_n + \max[-C_n, 0] \\ a_S &= D_s + \max[C_s, 0] \\ a_E &= D_e + \max[-C_e, 0] \\ a_W &= D_w + \max[C_w, 0] \\ S_C &= \frac{(\alpha_l \rho_l)_P \Delta V}{\Delta t} + S \Delta V \\ a_P &= \frac{(\sum_i \alpha_{l,i,in} m_{l,i,in} + S_l) \sum_i m_{g,i,out} + (\sum_i \alpha_{g,i,in} m_{g,i,in} + S_g) \sum_i m_{l,i,out}}{\sum_i m_{g,i,out}} \end{aligned} \quad (\text{C.429})$$

#### C.4.11 The Pressure-Velocity Correction Equations

The pressure correction equation is derived from the liquid continuity equation and the liquid velocity correction equation formulas. The SIMPLE Consistent (SIMPLEC) -approximation proposed by van Doormal and Raithby [23] is used to derive the velocity correction formulas.

The continuity equation for the liquid phase is given in appendix C. The discretization of this equation is discussed in sect C.4.10. The discretized form of the continuity equation thus yields:

$$\begin{aligned} &\frac{[(\alpha_l \rho_l)_P - (\alpha_l \rho_l)_P^*] \Delta V}{\Delta t} + \\ &A_n (\alpha_l \rho_l v_{l,r})_n - A_s (\alpha_l \rho_l v_{l,r})_s + A_e (\alpha_l \rho_l v_{l,z})_e - A_w (\alpha_l \rho_l v_{l,z})_w \\ &= D_n (\alpha_{l,N} - \alpha_{l,P}) - D_s (\alpha_{l,P} - \alpha_{l,S}) + D_e (\alpha_{l,E} - \alpha_{l,P}) - D_w (\alpha_{l,P} - \alpha_{l,W}) \\ &+ S \Delta V \end{aligned} \quad (\text{C.430})$$

The pressure correction is given by the difference between the correct pressure,  $p$ , and the guessed pressure,  $p^*$ . The velocity correction  $v'$  is given by the difference between the correct velocity,  $v$ , and the guessed velocity  $v^*$ :

$$\begin{aligned} p &= p^* + p' \\ u &= u^* + u' \end{aligned} \quad (\text{C.431})$$

The relationship between the liquid velocity correction at the grid cell surface  $e$  and the pressure corrections, i.e., the velocity correction formula, is given as:

$$w'_{l,e} = \frac{A_e \alpha_{l,e} (p'_P - p'_E)}{a_{l,e} - \sum_{nb} a_{nb}} = d_e (p'_P - p'_E) \quad (\text{C.432})$$

where

$$d_e = \frac{A_e \alpha_{l,e}}{a_{l,e} - \sum_{nb} a_{l,nb}} \quad (\text{C.433})$$

The correction formulas for the liquid velocity components in the other directions, as well as the corresponding correction formulas for the gas phase, can be deduced in a similar manner.

### Algebraic discretization equation

The transport equation for the pressure corrections is obtained substituting all the velocity components in (C.430) by the sum of the guessed and corrected velocities, and then substituting the velocity corrections by the corresponding pressure corrections employing the liquid phase velocity correction formulas. The resulting algebraic equation to be solved is written:

$$a_P p'_P = a_N p'_N + a_S p'_S + a_E p'_E + a_W p'_W + b \quad (\text{C.434})$$

where the coefficients are given as:

$$\begin{aligned} a_N &= A_n (\alpha_l \rho_l)_n d_n = A_n d_n \frac{1}{2} (\alpha_{l,P} \rho_{l,P} + \alpha_{l,N} \rho_{l,N}) \\ a_S &= A_s (\alpha_l \rho_l)_s d_s = A_s d_s \frac{1}{2} (\alpha_{l,P} \rho_{l,P} + \alpha_{l,S} \rho_{l,S}) \\ a_E &= A_e (\alpha_l \rho_l)_e d_e = A_e d_e \frac{1}{2} (\alpha_{l,P} \rho_{l,P} + \alpha_{l,E} \rho_{l,E}) \\ a_W &= A_w (\alpha_l \rho_l)_w d_w = A_w d_w \frac{1}{2} (\alpha_{l,P} \rho_{l,P} + \alpha_{l,W} \rho_{l,W}) \\ a_P &= a_N + a_S + a_E + a_W \\ b &= \frac{((\alpha_l \rho_l)_P - (\alpha_l \rho_l)_P^o) \Delta V}{\Delta t} \\ &\quad - A_n (\alpha_l \rho_l v_{l,r}^*)_n + A_s (\alpha_l \rho_l v_{l,r}^*)_s - A_e (\alpha_l \rho_l v_{l,z}^*)_e + A_w (\alpha_l \rho_l v_{l,z}^*)_w \\ &\quad + D_n (\alpha_{l,N} - \alpha_{l,P}) - D_s (\alpha_{l,P} - \alpha_{l,S}) \\ &\quad + D_e (\alpha_{l,E} - \alpha_{l,P}) - D_w (\alpha_{l,P} - \alpha_{l,W}) + S_C \Delta V \end{aligned} \quad (\text{C.435})$$

---

## References

1. Anderson DA, Tannehill JC, Pletcher RH (1984) Computational Fluid Mechanics and Heat Transfer. Hemisphere, New York
2. Aris R (1962) Vectors, Tensors, and the Basic Equations of Fluid Mechanics. Dover, Inc., New York
3. Bird RB, Stewart WE, Lightfoot EN (1960) Transport phenomena. John Wiley & Sons, New York
4. Bird RB, Stewart WE, Lightfoot EN (2002) Transport phenomena. Second Edition, John Wiley & Sons, New York
5. Boisson N, Malin MR (1996) Numerical Prediction of two-phase flow in bubble columns. *Int J Numer Meth Fluids* 23:1289-1310
6. Borisenko AI, Tarapov IE (1979) Vector and tensor analysis with applications. Translated and edited by Silverman RA, Dover Publication Inc, New York
7. Clift R, Grace JR, Weber ME (1978) Bubble Drops, and Particles. Academic Press, New York
8. Gosman AD, Ideriah FJK (1976) TEACH-T: a general computer program for two dimensional turbulent recirculating flows. London: Mechanical Engineering Department, Imperial College
9. Grienberger J (1992) Untersuchung und Modellierung von Blasensäulen. Dr ing Thesis, Der Technischen Fakultät der Universität Erlangen-Nürnberg, Germany
10. Irgens F (1982) Kontinuumsmekanikk Del III: Tensoranalyse. Tapir, Trondheim
11. Irgens F (2001) Kontinuumsmekanikk. Institutt for mekanikk, thermo- og fluidodynamikk, Norges teknisk- naturvitenskapelige universitet, Trondheim
12. Jakobsen HA (1993) On the modelling and simulation of bubble column reactors using a two-fluid model. Dr ing thesis, the Norwegian Institute of Technology, Trondheim, Norway
13. Johansen ST, Boysan F (1988) Fluid Dynamics in Bubble Stirred Ladles: Part 2. Mathematical Modelling. *Met Trans B* 19:755-764
14. Launder BE, Spalding DB (1972) Mathematical Models of Turbulence. Academic Press, London
15. Malvern LE (1969) Introduction to the Mechanics of a Continuum Medium. Prentice-Hall Inc, Englewood Cliffs
16. Patankar SV (1980) Numerical heat transfer and fluid flow. Hemisphere publishing corporation, New York

17. Slattery JC (1972) Momentum, Energy, and Mass Transfer in Continua. McGraw-Hill Book Company, New York
18. Spalding DB (1977) The calculation of free-convection phenomena in gas-liquid mixtures. ICHMT seminar 1976. In: Turbulent Buoyant Convection, Hemisphere, Washington, pp 569-586
19. Spalding DB (1980) Numerical computation of multiphase fluid flow and heat transfer. In: Taylor C, Morgan K (Eds) Recent Advances in Numerical Methods in Fluids, Pineridge Press, pp 139-167
20. Spalding DB (1981) IPSA 1981: New Developments and Computed Results. Report HTS/81/2, Imperial College of Science and Technology, London
21. Svendsen HF, Jakobsen HA, Torvik R (1992) Local Flow Structures in Internal Loop and Bubble Column Reactors. Chem Eng Sci 47(13-14):3297-3304.
22. Torvik R, Svendsen HF (1990) Modeling of slurry reactors - a fundamental approach. Chem Eng Sci 45(8):2325-2332
23. van Doormal JP, Raithby GD (1984) Enhancement of the SIMPLE Method for Predicting Incompressible Fluid Flows. Numer Heat Transfer 7:147-163
24. Zapryanov Z, Tabakova S (1999) Dynamics of bubble, drops and rigid particles. Kluwer academic publishers, Dordrecht

---

# Index

- activity coefficient, 674
- affinity, thermodynamic forces, 64
- agitation, 679
- algebraic-slip mixture model, 467
- angular momentum balance, 67
- apse-line, 232
- averaging, 394
  - area averaging, 86, 90, 93, 473
  - ensemble averaging, 118, 429
  - Maxwellian, 211, 246, 249
  - statistics, 118
  - time averaging, 118, 419
  - time- after volume averaging, 441
  - volume averaging, 118, 397
- balance equations, 6
- balance laws, 7
- balance principle, 12
- BBGKY-hierarchy, 207
- Bernoulli equation, 82
- billiard ball model, 208
- blending, 679
- Boltzmann equation, 218, 245, 246
- Boltzmann stosszahlansatz, 223
- breakage probability, 832
- bubble wall friction force, 796
- bulk expansion coefficient, 69
- Capillary number, 573
- Carnot cycle, 191
- Cauchy equation, 250
- centrifugal force, 195
- centripetal force, 195
- chemical reaction engineering, CRE, 336
- chemical reaction equilibrium, 666
- Chilton-Colburn relation, 633
- classical thermodynamics, 36
- closure law
  - constitutive, 543
  - topological, 543
  - transfer, 543
- coalescence time, 822
- coefficient of restitution, 228
- collision cylinder, 244
- collision frequency, 243
- collision time, 823
- complete differential, 54
- compressible
  - flow, 3
  - fluid, 4
- concentration diffusion, 20
- configuration space, 203
- conservative forces, 45
- constitutive equations, 7, 543
- continuous stirred tank reactor model, CSTR, 337
- continuous surface force, CSF, 352
- continuum hypothesis, 319
- continuum mechanics, 5
- continuum surface stress, CSS, 352
- control volume
  - arbitrary Lagrangian-Eulerian (ALE), 10
  - Eulerian, 10
  - Lagrangian, 10

- material, 10
- control volume approach, 8, 11
- Coriolis force, 195
- curvature
  - mean curvature of surface, 348
  - principal curvatures of a surface, 349
  - principal radii of curvature, 349
- curvilinear coordinate systems, 1158
  
- Damköhler number, 708
- Dankwerts boundary conditions, 665, 769, 905, 912
- Darcy friction factor, 479
- Darcy-Weisbach equation, 698
- degrees of freedom, 197
- diffusion barrier, 271
- diffusion mixture model, 469
- diffusion velocity, 263
- dilute gas, 192, 318
- dirac delta function, 350
- Dirichlet boundary conditions, 994
- dispersed flows, 339
- dispersion reactor models, 337
  - axial, 98
  - heterogeneous, 484, 957
  - homogeneous, 957
  - pseudo-homogeneous, 485
- distribution function, 190, 210
- drift-flux model, 472
- Dufour effect, 42, 266
- dusty gas model, 274
  
- Eötvös number, 572
- eddy viscosity hypothesis, 545
- effective swept volume rate, 816
- elastic collision, 209
- embedded interface method, EI, 344, 362
- ensemble, 203
- Enskog equation, 246, 248, 323
- Enskog expansion method, 256
- equations of transfer, 191
- equipartition theorem, 217
- ergodic hypothesis, 119, 189
- Euler equations, 215, 258
- Eulerian-Eulerian models, 340
- Eulerian-Lagrangian models, 340
- excess property, 372
- extent of reaction, 56, 670
  
- Fanning friction factor, 86, 92, 479
- Fick's law of viscosity, 597
- fluid mechanics, 3
- fluidization, 867
  - CPV model, 920
  - drift velocity, 919, 927
  - flow regimes, 869
  - Geldart classification of particles, 868
  - gulf streaming, 898
  - PGT model, 924
  - PGTDV model, 927
  - PT model, 921
  - riser, 876
  - transport reactor, 876
- forced diffusion, 21
- form drag, 556, 559
- Fourier's law, 597
- free surface flow, 349
- friction drag, 556, 559
- front tracking method, FT, 344
- fugacity, 672
- fugacity coefficient, 674
  
- Galilean transformation, 64
- Galileo law, 194
- Gauss' theorem, 1130
  - divergence theorem, 1130
  - Green's theorem, 1130
  - Ostrgradsky's theorem, 1130
  - surface, 1132
- generalized coordinates, 196, 197
- generalized drag force, 554, 555, 558
- generalized Eulerian transport equation, 12
- generalized transport theorem, 379
- generalized velocities, 197
- Gibbs-Duhem equation, 295
- granular flow, 503
- granular material, 503
- granular temperature, 505
  
- H-theorem, 223, 252, 253
- Hagen-Poiseuille law, 122
- Hamiltonian variational principle, 198
- heat of reaction, 58
- heat transfer models, 588
- heaviside function, 358
- high resolution models, 340
- history force, 586

- hydraulic diameter, 92
- ideal gas law, 218
- ill-posed model system, 486
- incompressible, 3
  - flow, 4, 68
  - fluids, 4
- inelastic collision, 209
- interface model
  - macroscopic 2D dividing surface, 370
  - microscopic 3D transition region, 370
- interfacial coupling, 341
  - four way, 341
  - one way, 341
  - two way, 341
- irreversible thermodynamics, 37
  - transport properties, 309
- isentropic, 84
- isothermal compressibility, 69
- jump condition formulation, 344
- kinetic theory, 189
- kinetic theory of dense gases, 319, 510
- Knudsen number, 367
- Lagrange multiplier, 669
- least squares method, 996
- Leibnitz theorem, 1128
- Leibnitz' theorem
  - surface, 1131
- Leibnitz's integral rule, 1125
- level set method, LS, 344, 357
- lift force, 557
- Liouville equations, 205
- Liouville theorem, 205, 218
- local equilibrium, 223
- Mach number, 72
- macro mixing, 707
- Magnus lift force, 564
- maker and cell method, MAC, 344, 345
- mass transfer models, 588
  - film theory, 612
  - Frössling equation, 634
  - laminar boundary layer theory, 618
  - penetration theory, 615
  - surface-renewal theory, 615
  - turbulent boundary layer theory, 624
- Maxwell-Stefan equations, 269
- Maxwellian molecules, 191, 209
- Maxwellian velocity distribution, 254
- mean free path, 5, 309, 312
  - concept, 191
- mean value theorem, 1083
- mechanics, 187
  - chaos, 188
  - classical, 187
  - continuum, 188
  - dynamics, 188
  - fluid, 188
  - Hamiltonian, 194, 201
  - Hamiltonian integral principle, 197
  - kinematics, 188
  - kinetics, 188
  - Lagrangian, 194, 197
  - Newton, 194
  - Newtonian, 194
  - non-linear dynamics, 188
  - quantum, 187
  - solid, 188
  - statics, 188
  - statistical, 188, 203
- method of manufactured solutions, 987
- micro mixing, 707
- mixed or Robin boundary conditions, 994
- mixing, 679
- mixture model, 463
- molar heat of formation, 59
- molecular chaos, 223
- moment equations, 191
- momentum balance, 25
- Morton number, 572
- moving bed, 867
- multifluid model, 343, 391
- multiphase control volume, 372
- mutual diffusion, 315
- Navier-Stokes equations, 262
- Neumann boundary conditions, 994
- Newton's first law, 194, 195
- Newton's law of cooling, 593
- Newton's law of viscosity, 597
- Newton's second law, 194, 340, 554
- Newton's third law, 194, 195, 342
- normal stresses, 214
- numerical methods

- approximation function, 996
- arithmetic mean values, 1067
- basis function, 996
- boundary-value problems, 991
- boundedness, 990
- central difference scheme, 1028
- class method, 1077
- collocation method, 996, 998
- convergent, 990
- deferred correction method, 1029
- density-based methods, 1010
- discrete method, 1077
- domain decomposition parallelization method, 1107
- FCT schemes, 1031
- finite difference method, 993
- finite volume method, 995
- fractional step methods, 1010
- Galerkin method, 996, 1001
- Gauss-Seidel point iteration method, 1093
- harmonic mean values, 1067
- initial value problem, 992
- initial-boundary-value problems, 992
- Jacobi point iteration method, 1093
- Jacobi preconditioner, 1096
- Krylov subspace methods, 1095
- least squares method, 1000, 1077, 1090
- method of lines, 1017
- method of moments, 1002, 1077
- method of weighted residuals, 985, 995
- multi-group method, 1077
- multigrid solvers, 1102
- multistep methods, 1021
- numerical accuracy, 990
- numerical stability, 989
- ODE solution methods, 1019
- orthogonal collocation, 997
- predictor-corrector methods, 1021
- pressure-based methods, 1010
- projection methods, 1011
- quadrature formulas, 1013
- quadrature method of moments, 1077
- QUICK scheme, 1029
- Rayleigh-Ritz method, 996
- Runge-Kutta methods, 1020
- strong form, 1004
- tau method, 996
- test function, 996
- trail function, 996
- TVD schemes, 1032
- upwind differencing scheme, 1027
- von Neumann method, 989
- weak form, 1004
- weight function, 996
- Nusselt number, 611
- osmotic diffusion, 271
- packed bed reactor
  - hot spot, 954
  - runaway, 954
- partial molar enthalpy, 58
- partial specific enthalpy, 58
- particle Reynolds number, 573
- peculiar velocity, 212
- perimeter, 92
- phase change, interfacial momentum transfer closure, 587
- phase space, 210
- phase trajectory, 203
- plug flow reactor model, PFR, 337
- pressure diffusion, 21
- pressure tensor, 214
- radii of curvature, 378
- reactor flow characteristics, 338
- realizable models, 990
- reduced mass, 227, 230, 242
- reverse diffusion, 271
- reversible adiabatic, 84
- Reynolds number, 611
- Saffman lift force, 564
- scalar quantity, 1158
- scattering cross section, 235, 236
- self-diffusion, 315
- separated flows, 339
- shear stresses, 214
- Sheerwood number, 611
- solid angle, 233
- Soret effect, 42, 266
- specific chemical potentials, 62
- specific enthalpy, 52
- specific entropy, 39
- specific molar enthalpy, 57

- speed of sound, 72
- standard drag curve, 562
- Stanton number, 611
- state vector, 210
- statistical thermodynamics, 189
- steady drag force, 556
- steady flow, 68
- superficial velocity, 484
- surface tension, 382
  - static force balance, 1133
- surface theorem, 379
- symmetry of stress tensor, 67
- system approach, 8
  
- temperature equation, 1143
- tensor quantity, 1159
- tensor transformation laws, 1157
- thermal diffusion, 21
- thermal radiation, 635
  - absorptivity, 642
  - blackbody, 640
  - emissivity, 641
  - gray surface, 643
  - incident, 639
  - irradiation, 639
  - Kirchhoff's law, 643
  - Lambert's cosine law, 641
  - radiosity, 640
  - Stefan-Boltzmann law, 641
- thermodynamic pressure, 214
- thermodynamics, 36, 39
  - entropy, 191
  - first law, 40
  - second law, 61, 63, 191
- torque, 566, 687, 688
- transport properties, 309
- turbulence
  - $k$ - $\varepsilon$  model, 139
  - auto-covariance, 106
  - autocorrelation coefficient, 106
  - Batchelor spectrum, 709
  - Boussinesq turbulent viscosity hypothesis, 626
  - buffer layer, 125
  - coherent structures, 102
  - cross-term stress, 169
  - definitions, 99
  - dispersion force, 796
  - eddy concept, 105
  - eddy turnover time, 112
  - energy cascade, 106
  - energy dissipation rate, 110, 112
  - energy spectrum, 103, 115
  - Eulerian longitudinal integral length scale, 109
  - Eulerian transverse integral length scale, 109
  - friction velocity, 124
  - gradient transport hypothesis, 161, 626
  - homogeneous turbulence, 108
  - inner wall layer, 124
  - intensity, 120
  - isotropic turbulence, 108
  - Kolmogorov five-third law, 116
  - Kolmogorov hypotheses, 113
  - Kolmogorov microscales, 114
  - Kolmogorov similarity hypothesis, 114
  - Kolmogorov structure function, 116
  - Kolmogorov two-third-law, 116
  - Kolmogorov-Prandtl relationship, 142
  - Lagrangian integral time scale, 106
  - Lagrangian microscale, 106
  - large eddy simulation, LES, 161
  - law of the wall, 127, 628
  - Leonard stresses, 169
  - local isotropic turbulence, 113
  - log-law sublayer, 125
  - longitudinal autocorrelation function, 108
  - mixing length, 105
  - modulation, 796
  - one-point two-time correlation, 106
  - outer wall layer, 124
  - overlap wall region, 124
  - passive scalar spectra, 708
  - power law velocity profile, 122
  - Prandtl's Mixing length model, 123
  - residual stresses, 169
  - Reynolds analogy, 629
  - Reynolds averaging, 104, 129
  - Reynolds stress models, 133
  - rms-velocity, 110
  - Smagorinsky constant, 172
  - Smagorinsky eddy-viscosity model, 171
  - standard  $k$ - $\varepsilon$  model parameters, 143

- statistical theory, 104
- sub-grid-scale, SGS, 164
- Taylor's hypothesis, 111
- transverse autocorrelation function, 108
- turbulent dispersion, 796
- two-point correlation function, 108
- universal velocity profile, 628
- velocity-defect law, 127
- viscous sub-layer, 125
- wall functions, 150
- turbulent impeller, 680
- two-fluid
  - continuity, 384
  - energy balance, 387
  - internal energy, 387
  - momentum balance, 385
  - species mass balance, 385
- variable density flow, 75
- vector quantity, 1158
- velocity distribution function, 190
- virtual mass force, 581
- viscous stress tensor, 29
- volume of fluid method, VOF, 344, 346
  - Piecewise Linear Interface Construction, PLIC, 351
  - Simple Line Interface Calculation, SLIC, 351
  - SOLA-VOF method, 349
- wall lift force, 796
- Weber number, 573
- well-posed model system, 486
- well-posedness, 485
- whole field formulation, 344, 350
- Wilke equation, 273